ISBN: 978-3-95450-168-7 doi:10.18429/JACoW-IPAC2015-MOXGB2

COMMISSIONING AND OPERATION OF 12GeV CEBAF *

A. Freyberger† for the CEBAF Commissioning Team, JLab, Newport News, VA 23606, USA

Abstract

The Continuous Electron Beam Accelerator Facility (CEBAF) located at the Thomas Jefferson National Accelerator Laboratory (JLAB) has been recently upgraded to deliver continuous electron beams to the experimental users at a maximum energy of 12 GeV, three times the original design energy of 4 GeV. This paper will present an overview of the upgrade, referred to as the *12GeV upgrade*, and highlights from recent beam commissioning results.

INTRODUCTION

The Continuous Electron Beam Accelerator Facility, CEBAF, designed for 4 GeV continuous electron beams for nuclear physics, was the first large scale implementation of SRF technology. The CEBAF design included 42 cryomodules with each cryomodule containing 8 SRF cavities to achieve the design energy of 4 GeV. CEBAF reached design energy in 1995. The cryomodules were evenly divided among two linacs, North and South, connected by magnetic spreaders, arcs and recombiner sections. The energy reach of 6 GeV of CEBAF was establish in 2000; CEBAF operated at energies up to 6 GeV until 2012.

The beam parameters for 6 GeV configuration can be found in Table 1. CEBAF supported simultaneous beam delivery to three experimental end-stations; each end-station receiving beams with energy a multiple of the one-pass energy, beam currents from sub 1nA to 190 μA and beam polarization greater than 85%. During 6GeV operations 178 experiments were performed by the experimental users.

THE 12GeV UPGRADE

An experimental case to upgrade CEBAF to 12 GeV was made at the start of the 21st century. *Mission need* was granted in 2004 by the Department of Energy for Jefferson to develop a design for a 12 GeV capable CEBAF. This design was completed and construction started in 2009, construction overlapped with 6 GeV beam operations for work that did not impact CEBAF operations. Construction that did impact CEBAF was interleaved with 6 GeV operations, notably the arc magnet upgrade during the 2011 shutdown. 6 GeV beam operations terminated in 2012, and the accelerator tunnel portion of the upgrade was sufficiently complete by the end of 2013 to start of beam commissioning activities.

The 12GeV upgrade design retained the same footprint as the original 4GeV CEBAF allowing for the new accelerator to use the existing tunnel with the addition of the new extraction line transporting beam to the new end-station, Hall-D. In order to achieve the 12 GeV energy requirement, the design called for:

- A new Arc10 that would enable an additional pass of energy gain in the North linac, 11 linac traverses versus 10 traverses for 6 GeV CEBAF.
- Additional cryomodules in each linac contributing 500MeV of energy gain, increasing the total energy gain to 1100 MeV/linac from 600 MeV/linac.

The beam parameters from for the 12GeV design can be found in Table 1. The main difference with the 6GeV beam parameters, aside from beam energy, is the increase in beam emittance and energy spread due to the copious synchrotron radiation effects in the high energy arcs.

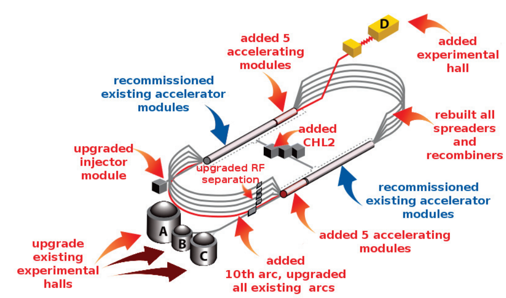

Figure 1: High level overview of the 12GeV upgrade

The scope of the accelerator upgrade is graphically presented in Figure 1.

Injector

The doubling of the CEBAF race-track energy requires that the injector energy be increased in order to maintain the same ratio of injection to one-pass energy. This energy increase was accomplished by replacing an original CEBAF cryomodule, denoted as C20, with a new cryomodule that provides 108 MeV in energy gain, denoted as C100. In addition the laser drive has been modified to allow for subharmonics of 499MHz in order to support the new 5-pass separation system. Details on the injector modifications and results of beam commissioning can be found in [1].

Linac

The ten cryomodules, C100s, that provide in total 1000 MeV per pass of additional energy gain were installed in five empty zones that existed at the end of each linac. The existing 20 cryomodules per linac from 6GeV CEBAF are an integral part of the new 12GeV CEBAF; 1200 MeV of energy is required from these modules to achieve the design energy of 12 GeV. During the upgrade, the linacs were warmed to 300 K to allow for the required cryogenic upgrades. Once the cryomodules were returned to the 2 K operating temperature

* Authored by Jefferson Science Associates, LLC under U.S. DOE Contract No. DE-AC05-06OR23177. The U.S. Government retains a non-exclusive, paid-up, irrevocable, world-wide license to publish or reproduce this manuscript for U.S. Government purposes.
† freyberg@jlab.org

Content from this work may be used under the terms of the CC BY 3.0 licence (© 2015). Any distribution of this work must maintain attribution to the author(s), title of the work, publisher, and DOI.

ISBN: 978-3-95450-168-7 doi:10.18429/JACoW-IPAC2015-MOXGB3

Content from this work may be used under the terms of the CC BY 3.0 licence (© 2015). Any distribution of this work must maintain attribution to the author(s), title of the work, publisher, and DOI.

LHC COMMISSIONING AT HIGHER ENERGY

P. Collier, F. Bordry, J. Wenninger, CERN, Geneva, Switzerland

Abstract

The LHC has just come to the end of its first Long Shutdown (LS1) and preparations are underway to prepare for Run 2 data taking at 13 TeV centre of mass energy. After briefly recalling the major work undertaken during the 2-year long LS1, details will be given of the cool-down and hardware commissioning phase where each individual superconducting circuit is individually qualified for operation at nominal current. For the main dipole circuits this phase was completed with a quench training campaign in order to operate reliably at the required field. In parallel to the training campaign a rigorous cold checkout has been used to qualify the machine as an ensemble and to establish the conditions necessary for beam operation. The details of this phase will be given together with associated dry runs and beam injection tests. Finally, the latest news will be presented concerning the beam commissioning of the machine in preparation for first physics operation, which will hopefully begin in June.

INTRODUCTION

Between 2009 and early 2013 the LHC was delivering beam to the experiments almost continuously, with only relatively short end of year technical stops to perform essential maintenance. This mode of operation was triggered by the need for a major shutdown to consolidate the inter-magnet bus-bar splices before operation at nominal energy could be considered [1]. The time required to plan, prepare and organize this long shutdown (LS1) allowed three years of operation of the LHC at an intermediate energy, first at 3.5 TeV, then, in 2012, at 4 TeV.

During this first run a total of 30 fb^{-1} were delivered to the large general purpose experiments, using ~1400 bunches spaced by 50 ns to deliver a peak luminosity of over $7x10^{+33} cm^{-2}s^{-1}$. During this period there were also highly successful runs with Pb^{82+} heavy ion collisions as well as proton-lead operation during the final month.

LS1 lasted almost 26 months, beam-to-beam, and involved a huge amount of activity in the machine tunnel. Most activities were planned, but some were unexpected and others were added later [2]. Some of these are described below.

LHC LONG SHUTDOWN 1

The main priorities in LS1 were to prepare the machine for high-energy operation and to perform maintenance and consolidation to ensure reliable operation through the second long run, i.e. up to the next long shutdown scheduled for 2018. In addition to these main themes there were many additional activities to repair and upgrade individual systems. Major modifications to the control system itself as well as the operational software and databases were also foreseen. As a result it rapidly became clear that the LHC would be essentially a new machine when it restarted. Careful consideration was given from an early stage into the re-commissioning process and this was built into the overall planning.

Unfortunately only a few of the major planned and unexpected activities can be described here.

Super-Conducing Magnet and Circuit Consolidation (SMACC)

As soon as the machine was warm the SMACC activities could begin. Each interconnect in the machine was opened and the high-current bus-bars measured and inspected. Where necessary the joint was machined or repaired. Shunts were then applied across the joints and the whole junction encased in an insulating box. After suitable QA checks and measurements, the interconnect was re-closed [3]. With ~1700 interconnects and 10,170 high current splices this represented a huge workload over the shutdown, especially with an unexpectedly high number of splices (30%) needing to be completely re-made.

In addition to the splice repair a total of 18 cryo-magnets were removed from the machine and replaced by spares. These all had known unconformities: either showing high internal resistance, or having broken quench heaters. In total over 1 million hours were worked in the tunnel on these machine related activities.

Reliable Operation

During the first run of the LHC a problem with radiation-induced failures in electronic equipment was diagnosed and progressive mitigation measures used to keep single-event upsets at a reasonable level. During LS1 major works were undertaken to relocate, or shield electronics in several parts of the machine. The relocation often involved local civil engineering works, followed by major cabling campaigns to relocate the electronic equipment into more favourable locations. Over 100 control and power racks were moved. For the QPS system, which cannot be relocated, new cards were designed having a number of radiation-tolerant features and over 1000 cards in the tunnel were replaced [4].

To be reliable the major systems of the LHC needed maintenance. An example is the cryogenic system where some stations had been running for close to 5 years. A complete overhaul of the warm and cold compressors was undertaken as well as major interventions on the cryogenic lines and valve boxes. In addition, the opportunity was taken to repair several small leaks in the cryogenic feed lines (QRL).

An additional unexpected activity became apparent once the whole system had been warmed up. Several

ISBN: 978-3-95450-168-7 doi:10.18429/JACoW-IPAC2015-MOYGB3

COMMISSIONING OF NSLS-II*

F. Willeke, BNL, Upton, NY 11973, USA

Figure 1: Aerial view of NSLS-II.

Abstract

NSLS-II, the new 3rd generation light source at BNL was designed for a brightness of 10^{22} photons s^{-1} mm^{-2} $mrad^{-2}$ $(0.1\%BW)^{-1}$. It was constructed between 2009 and 2014. The storage ring was commissioned in April 2014 which was followed by insertion device and beamline commissioning in the fall of 2014. All ambitious design parameters of the facility have already been achieved except for commissioning the full beam intensity of 500mA which requires more RF installation. This paper reports on the results of commissioning.

NSLS-II OVERVIEW

The NSLS at BNL was the pioneer of the 3rd Generation Light Sources which provided a wealth of scientific results which have shaped the landscape of synchrotron radiation based science. However, the high demands on the performance of synchrotron light sources in the future motivated constructing a new machine which would enable spatial resolution of 1 nm and energy resolution of 0.1 meV. This mission was acknowledged by the Department of Energy in 2005 when the design of the new machine began. The goals require a beam brightness of B = 10^{22} photons s^{-1} mm^{-2} $mrad^{-2}$ $(0.1\%BW)^{-1}$. The corresponding beam parameters are a beam current of 500 mA, a sub-nm horizontal emittance with < 1% emittance ratio. Furthermore, state-of- the- art and beyond small gap undulators are needed to generate the ultra-bright photon beams. With full beam intensity, NSLS-II will be the brightest synchrotron at present.

The facility has the following topology: The ~800 m circumference ring building houses the accelerator tunnel (width 3.7m, height 3.2m) and the 17m wide experimental floor. Power supplies, vacuum equipment, diagnostics and controls are placed on the 86 cm thick tunnel roof. The ratchet shield wall is 100 cm thick.

* Work supported by DOE under contract No.DE-AC02-98CH10886.

The injector complex with the 200 MeV s-band LINAC and the 158 m circumference 3 GeV Booster Synchrotron is placed inside the ring. Also on the inside of the ring are five service buildings with mechanical utilities and HVAC systems as well as the RF-Cryogenic complex. The cooling tower and the central DI water system are in the center of the ring. On the outside of the ring building are five laboratory-office- buildings, each with 145 seats and several laboratory spaces. (See Figure 1.)

ACCELERATOR LATTICE

NSLS-II has a double bend achromat lattice with 30 cells on a 792 m circumference. The dipole magnets are long and weak (l = 3.69 m, B = 0.4 tesla) which allows obtaining close to DBA minimum beam emittance with moderate peak beta-values (30 m) and chromaticities >- 3. The gentle bends also imply low energy loss per turn (286 keV/e/turn). These are favorable conditions to increase radiation damping by adding six 3.4m long, 1.85 Tesla damping wigglers thereby increasing radiation damping and reducing emittance by more than a factor of two. The beam emittance obtained this way is only 0.9 nm rad. The straight sections for insertion devices alternate between long (9.3m, 3m vertical beta) and short (6.6m, 1m vertical beta). The damping wigglers weakly break the 15-fold symmetry to 3-fold symmetry. Three of the long straight sections are needed for injection and six superconducting RF cavities (including two passive units; for details see [1].)

TIMELINE

The mission of NSLS-II was acknowledged in 2005 by the DOE (CD-0) which was followed swiftly by the completion of the conceptual design and the establishment of a cost and schedule baseline (CD-1 in 2007 and CD-2 in 2008). Civil construction started in June 2009 after CD-3 was granted. Two years later, in the spring of 2011, the first part of the ring building was ready for accelerator installation which was completed by

Content from this work may be used under the terms of the CC BY 3.0 licence (© 2015). Any distribution of this work must maintain attribution to the author(s), title of the work, publisher, and DOI.

ISBN: 978-3-95450-168-7 doi:10.18429/JACoW-IPAC2015-MOAB1

HIGH BEAM INTENSITY HARP STUDIES AND DEVELOPMENTS AT SNS*

W. Blokland, ORNL, Oak Ridge, TN, USA

Abstract

The Spallation Neutron Source (SNS) Harp consists of 30 wires for each of the horizontal, vertical, and diagonal planes. The purpose of the harp is to measure the position, profile, and peak density of the high intensity beam coming out of the accumulator ring and going onto the spallation target. The data-acquisition hardware is now over ten years old and many of the electronics parts are obsolete. Occasionally, the electronics must be rebooted to reset the sample-and-hold circuitry. To evaluate options for a new system, the signals from the harp were studied. This paper will describe these studies' results, the design, and initial results of the new and simpler data-acquisition system.

INTRODUCTION

The harp was built as a removable instrument to measure the horizontal, vertical, and diagonal position and profile of an up to 1.4 MW, 1 GeV proton beam 10 meters in front of the target, using thirty 100 µm tungsten wires per plane, see Fig. 1 and [1,2].

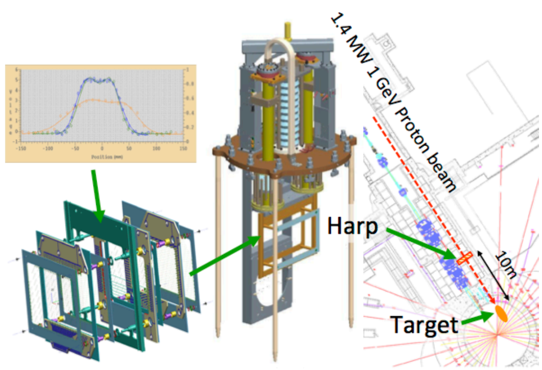

Figure 1: Harp actuator and profiles.

Initially, the harp was only to be inserted during tune-up, but the mechanism to insert and retract the harp was not strong enough and the harp is now left inserted at all times, allowing us to monitor the beam profile during full power production runs. The data-acquisition system consists of low-pass filters, amplifiers, and two sample-and-hold circuits per wire to integrate the charge intercepted and to integrate the baseline charge, followed by digitizer boards, see [3]. The analysis uses a single or double super-Gaussian function fit to derive the position and RMS width of the beam, see [4].

The data-acquisition electronics, designed and implemented by LANL, is now well over 10 years old and occasionally locks up and requires a manual reset. Many of the electronic parts are now obsolete and a redesign would be required to replace the electronics. Another issue is that the signal strength during production beam intensity saturates the sample-and-hold circuits. To avoid this saturation, we sample later, well into the signal decay to minimize the signal distortion.

STUDIES

To study the harp system and determine the requirements for a new data-acquisition system, we made the harp signal available for studies. An interconnect was placed between the diagonal plane cable from the harp and the electronics to allow us to temporarily disconnect a single wire from the electronics and route the signal to a scope for studies.

Wire Signal Strength

The first study was to determine the amount of charge intercepted by the wires to help define the requirements for a new data-acquisition system.

The instant current created by the proton beam charges up the long cable from the harp to the upstairs service building, while a 1 MOhm resistor discharges the charge as shown in Fig. 2.

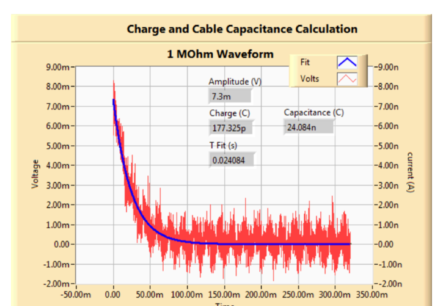

Figure 2: Wire charge measurement.

By fitting the discharge curve, we can approximate the total charge received, the peak voltage, and the capacitance of the cable. In this particular case, 2.5 µC beam, the measured charge was 177 pC, with a peak voltage 7.3 mV, giving a cable capacitance of C=Q/V=177pC/7.3 mV or about 24 nF. Given the beam pulse duration of 670 ns and assuming a flattop longitudinal profile, the instantaneous current is 0.26 mA.

We extrapolate the maximum expected voltage and current for the full intensity beam of 21 µC to be around 60 mV and 2.2 mA.

*ORNL/SNS is managed by UT-Battelle, LLC, for the U.S. Department of Energy under contract DE-AC05-00OR22725

Content from this work may be used under the terms of the CC BY 3.0 licence (© 2015). Any distribution of this work must maintain attribution to the author(s), title of the work, publisher, and DOI.

ISBN: 978-3-95450-168-7 doi:10.18429/JACoW-IPAC2015-MOAB2

OVERVIEW OF BEAM INSTRUMENTATION FOR THE CADS INJECTOR I PROTON LINAC*

Y.F. Sui#, J.S. Cao, H.Z. Ma, L.D.Yu, Y. Zhao, Q.Y. Deng, J. He, X.Y. Zhao, Q. Ye, J.H. Yue, L. Wang, IHEP, 100049, China
Key Laboratory of Particle Acceleration Physics and Technology, IHEP, Chinese Academy of Sciences

Abstract

The injector I of China Accelerator Driven Subcritical system (C-ADS), which is composed of an ECR ion source, a low energy beam transport line (LEBT), a radio frequency quadrupole accelerator (RFQ), a medium energy beam transport line (MEBT) and cryomodules with SRF cavities to boost the beam energy up to 10 MeV. The injector linac will be equipped with beam diagnostics to measure the beam position, the transverse profile and emittance, the beam energy as well as beam current and beam losses. Though many of that are conventional design, they can provide efficient operation of injector linac. This paper gives an overview of C-ADS linac beam instrumentation.

INTRODUCTION

The Chinese ADS project is aimed to solve the nuclear waste problem and the resource problem for nuclear power plants in China. With its long-term plan lasting until 2030th, the project will be carried out in 3 phases: Phase I of R&D facility, Phase II of experiment facility and Phase III of industry demonstration facility. The driver linac of the CADS consists of two injectors to ensure its high reliability. Each of the two injectors will be a hot-spare of the other. Although the two injectors that are installed in the final tunnel will be identical, two different design schemes, named injector I and II respectively are being pursued in parallel by the Institute of High Energy of Physics (IHEP) and the Institute of Modern Physics (IMP). [1] The Injector I ion source is based on ECR technology. The beam will be extracted with an energy of 35 keV. The ion source will be followed by a Low Energy Beam Transportline (LEBT), which consists of 2 solenoids, a fast chopper system and a set of beam diagnostics including CTs and faraday cup. A Radio Frequency Quadrupole (RFQ) will accelerate the beam up to 3.2 MeV and will be followed by the first Medium Energy Beam Transport line (MEBT1), fully instrumented and also equipped. The next section is two cryogenic modules named CM1 and CM2 with seven cold beam position monitors in each, which accelerate beam up to about 10 MeV. The last section is the second Medium Energy Beam Transport line (MEBT2). The drift tubes between magnets provide the gap for diagnostics.

The injector I linac is equipped with beam diagnostics to measure the beam position, the transverse profile, the beam emittance, the beam energy as well as beam current and beam losses. This will provide efficient operation of drive linac and ensure the beam loss at a low level. A list of the different type of monitors using in the injector I linac is presented in Table 1.

Table 1: List of beam instrumentation in C-ADS linac

Device	Accuracy	Resolution	Quantity
Beam position monitor	±100um	30 um	25
Wire scanner	±0.5mm	50 um	4
Beam emittance unit	10%	-	2
Beam current monitor	1.5%	0.01mA	5
Beam loss monitor	1%	-	8
Beam energy monitor	±1deg	0.5deg	3
IPM	1mm	200 um	1
Electron scanner	1mm	300um	1

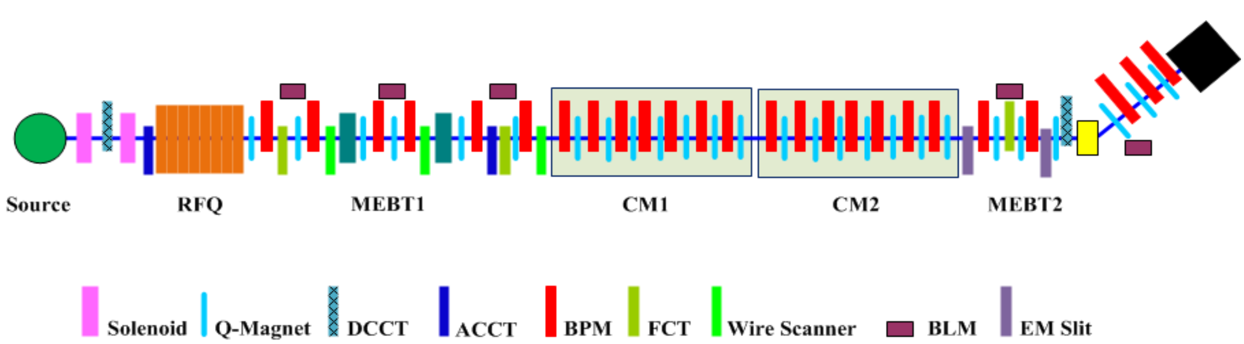

Figure 1: Beam instrumentation layout in C-ADS linac.

*Work supported by China ADS Project (XDA03020000) and the National Natural Science Foundation of China (NO. 11205172, NO. 11475204)

Content from this work may be used under the terms of the CC BY 3.0 licence (© 2015). Any distribution of this work must maintain attribution to the author(s), title of the work, publisher, and DOI.

ISBN: 978-3-95450-168-7 doi:10.18429/JACoW-IPAC2015-MOAB3

Content from this work may be used under the terms of the CC BY 3.0 licence (© 2015). Any distribution of this work must maintain attribution to the author(s), title of the work, publisher, and DOI.

COMMISSIONING RESULTS OF THE NEW BPM ELECTRONICS OF THE ESRF BOOSTER SYNCHROTRON*

M. Cargnelutti, Instrumentation Technologies, Solkan, Slovenia
B. K. Scheidt, ESRF, Grenoble, France

Abstract

The 75 BPM stations of the Booster Synchrotron of the ESRF have been equipped with new RF electronics from December 2014. This new BPM system is based on the commercial Libera Spark system and now provides beam position data at various output rates, and with a possible time resolution even below that of the orbit-turn time (1 us). All modules are situated inside the Booster tunnel and powered by an Ethernet cable. This implies that the RF cables from the BPM blocks are less then 3m and only a single trigger signal in daisy chain is sufficient to keep the 75 stations in turn-by-turn phase over the full energy ramping (200 MeV to 6 GeV) time of typically 50 ms. The high sensitivity of the system yields excellent performance at very low beam currents down to 10uA. Full results of the system, including the application as a high quality betatron tune monitor, will be presented.

INTRODUCTION

This paper presents the measurements achieved during the commissioning of the new BPM electronics readout system for the ESRF booster synchrotron. The advantages of installing of the electronics in the tunnel and their integration in the control system are also described.

The ESRF booster ring accelerates the electron beam coming from the 200 MeV linear pre-injector up to the extraction energy of 6 GeV in a 50 ms period, with 10 Hz cycling frequency. In case of "long-pulse" operation mode, 352 bunches with a maximum current of 5 mA are injected in the storage ring, which operates with 200 mA current. Other operation modes enable multi-single bunch configurations with 1 to 5 bunches and currents up to 0.5 mA. The 300 m ring contains 75 BPM blocks with 60 mm diameter and four buttons with a diameter of 10 mm [1].

The 25 years old BPM electronics are now replaced with the Libera Spark system provided by Instrumentation Technologies. The instrument is a cost-effective network attached device which digitizes and buffers the 4 RF signals from the BPM with 14-bit 125 MHz ADCs. The raw data is later processed in the FPGA delivering position, sum, I&Q and strength signals at Turn-By-Turn rate (1 MSa/s) [2]. This enables the study of the beam properties over the full acceleration cycle, with optional time-domain processing for single-bunch fill pattern [3].

INSTALLATION IN THE TUNNEL

The decision to install all 75 units inside the Booster tunnel was taken after a series of radiation dosimetry, that showed globally low radiation doses as expected. The units are located underneath the girders of the dipoles by means of a simple support. At only a few locations, where radiation doses are stronger (i.e. injection & extraction zones) the unit will be protected against radiation damage by a (slightly) different position and additional Lead shielding. The RF cables (RG-223) are only 3 m long between BPM block and the unit. This installation inside the tunnel yielded a significant cost reduction for this RF cabling, and also an important increase of the sensitivity and resolution of the BPM system since the attenuation of otherwise long (typically 50 m) RF cables is avoided. The installation of cables and units was carried out in 2 weeks, according with the time slots when the tunnel was accessible and during the weekly machine stops.

Data acquisition from all 75 stations is triggered with a daisy-chained signal which travels around the machine in less than 2 µs. To align all the data acquisitions at the same ADC sample a delay setting in the FPGA is used. No machine reference signal is provided to the device since the short acceleration cycle doesn't call for a PLL to control the ADCs sampling rate over time. This simplifies the interface making the instrument affordable without compromising the TBT performance.

CONTROL SYSTEM INTEGRATION

Libera Spark can be accessed through a SCPI-like interface over Ethernet (100 MbE and 1 GbE). Every unit is integrated in the TANGO control system through individual Device Servers (DS) running on a dedicate server. On top of them a "grouping" server collects data from all the stations providing global attributes both for parameters and signals – see Fig. 1. GUIs and Matlab functions enable the end user to control the system.

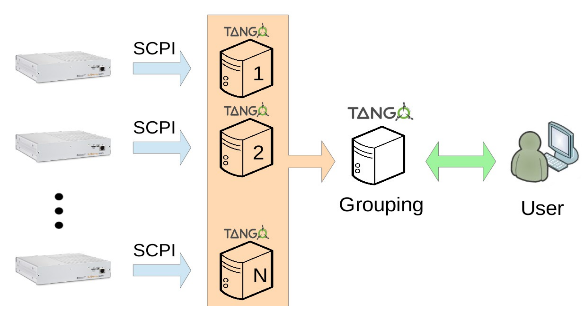

Figure 1: Control System integration architecture.

COMMISSIONING RESULTS

This chapter presents the data acquired from the ESRF booster ring with the new BPM electronics. Since 2 BPM blocks were dedicated to other measurements, only the acquisitions from 73 stations will be presented.

*This project has received funding from the European Union's Seventh Framework Programme for research, technological development and demonstration under grant agreement no 289485

ISBN: 978-3-95450-168-7 doi:10.18429/JACoW-IPAC2015-MOBB1

Content from this work may be used under the terms of the CC BY 3.0 licence (© 2015). Any distribution of this work must maintain attribution to the author(s), title of the work, publisher, and DOI.

STATUS OF PROTON BEAM COMMISSIONING AT THE MEDAUSTRON ION BEAM THERAPY CENTRE

A. Garonna#, M. Kronberger, T. Kulenkampff, C. Kurfürst, L. Penescu, M. Pivi, C. Schmitzer, A. Wastl, F. Osmic, P. Urschütz, EBG MedAustron, Wr. Neustadt, Austria

Abstract

The MedAustron accelerator (Wiener Neustadt, Austria) will deliver clinical beams of protons (60 - 250 MeV) and carbon ions (120 - 400 MeV/n) to three ion beam therapy irradiation rooms (IR). Clinical beams and proton beams up to 800 MeV will be provided in a fourth IR, dedicated to non-clinical research. A slow-extracted proton beam of maximum clinical energy reached for the first time the IR3 in October 2014, thus providing the technical proof-of-principle of the entire accelerator chain. The main characteristics of the MedAustron accelerator system are presented, along with the results obtained along the ongoing commissioning.

INTRODUCTION

MedAustron is a synchrotron-based ion beam therapy centre. The accelerator supports beam rigidities up to 6.4 Tm. The accelerator layout is shown in Fig. 1. Its design [1] originates from those of PIMMS [2] and CNAO [3]. The injector produces beams of H_3^+ or C^{4+}, which are chopped with a fast electrostatic deflector, then bunched and pre-accelerated to 7 MeV/n with a Radiofrequency Quadrupole (RFQ) and an IH-DTL linac. In the Medium Energy Beam Transfer line (MEBT), the beam is stripped to H^+ or C^{6+} before injection into the synchrotron. The synchrotron has a superperiod of 2 with non-dispersive regions for injection and the Radiofrequency (RF) cavity. After acceleration, the beam is extracted via the third-integer resonance in the High Energy Beam Transfer Line (HEBT). Since last year [4-5], the installation of accelerator components for proton treatments in the two horizontal beam lines of IR2 and IR3 has been completed and a first beam of protons at 62.5 MeV reached IR3 in October 2014. Beam commissioning is currently resuming and passing the torch to medical commissioning.

INJECTOR AND MEBT

The commissioning of the beam from the source to the end of the MEBT has been completed at the end of 2014 with very positive results, in terms of intensity, transmission and stability. The main contributors to this progress have been: the extensive work on the IH stability (cooling and setpoint adjustment), optimization of the IH quadrupole strengths, steering at the source exit and in the matching section between RFQ and linac and finally, the increase of the RFQ output energy. The appropriate choice of the operation point of the linac was critical in stabilizing the energy of the beam injected into the ring. A summary is shown in Table 1.

adriano.garonna@medaustron.at

Table 1: Results of Commissioning up to the MEBT

Parameter	Performance
S1 current	650 μA
Linac exit current (H_3^+)	290 μA ± 3 %
Transmission through RFQ+Linac	45 %
MEBT exit current (H^+)	805 μA ± 2%
Transmission through MEBT	93 %
Energy Stability	± 0.1 %

SYNCHROTRON INJECTION

Multi-turn Injection

The injection in the ring is performed in 16 turns via a linearly decaying π orbit bump of 41 mm horizontal amplitude with 100 μs linear decay time. The resulting horizontal RMS geometric beam emittance is around 8 μm and the maximum injected number of particles is $6 \cdot 10^{10}$ protons, corresponding to 6 effective injection turns. Without orbit correction, the measured beam closed orbit errors are within ± 7 mm in the horizontal (H) plane and ± 2 mm in the vertical (V) plane.

RF Capture

The debuncher phase and amplitude were adjusted by measuring the time-of-flight coming from the phase probes in the MEBT and by maximizing the debunching time of a 1 μs injected beam pulse length. The results were confirmed by empty-bucket measurements and show that the RMS injected momentum spread can thus be decreased from $1.6 \cdot 10^{-3}$ to $0.5 \cdot 10^{-3}$.

The capture RF frequency (~ 470 kHz) was chosen by maximizing locally the signal on the current transformer and the sigma signal on the pickups. The voltage is adiabatically ramped to 170 V over 150 ms.

Beam Instability

With injected intensities over $1 \cdot 10^{10}$ protons (1 mA), erratic and strong beam losses were observed, with both unbunched and bunched beam. The variability of this effect is very strong in time. The common patterns are beam losses of nearly 90 % in around 100-300 ms, starting 0.1 to 3 s, when using an artificially prolonged injection flat-bottom (FB). These losses are correlated with coherent beam orbit oscillations in the V plane, with characteristic frequencies ~120 kHz and exponential rise times of 0.1 - 0.3 s, see Fig. 2.

ISBN: 978-3-95450-168-7 doi:10.18429/JACoW-IPAC2015-MOBB2

FABRICATION OF TESLA-SHAPE 9-CELL CAVITIES AT KEK FOR STUDIES ON MASS-PRODUCTION IN COLLABORATION WITH INDUSTRIES

T. Saeki# and H. Hayano, KEK, 1-1 Oho, Tsukuba, Ibaraki, Japan

Abstract

The construction of the new Center-of-Innovation (COI) building started at KEK from 2014 for the studies of mass-production of Superconducting-RF (SRF) accelerators in collaboration with industries. The COI building is sitting next to the existing KEK-STF building and includes various SRF facilities like clean-room for cavity-string assembly, cryomodule-assembly facility, cryogenic system, vertical-test, cryomodule-test, input-coupler processing, cavity Electro-Polishing (EP) facilities, and control-room/office-rooms in the dimension of 80 m x 30 m. The purpose of these new SRF facilities is to establish a close collaboration between SRF researchers and industries in order to prepare for the upcoming small- and middle-scale SRF programs, and also large-scale future SRF projects, like ILC. This article reports the fabrication of four TESLA-shape 9-cell cavities for the commissioning of these new facilities the details of the new SRF facilities.

INTRODUCTION

KEK and several industry companies: Mitsubishi Heavy Industry (MHI), Hitachi, Toshiba, Mitsubishi Electronic, Kyocera, Fujikura, etc. obtained a new budget from "Ministry of Education, Culture, Sports, Science and Technology of Japan" (MEXT) in 2012. The title of new budget is "New Project for Creating a Market for EARTH-CLEANER Products in Collaboration with Industries and Laboratories / Universities". In the program of the budget, we proposed to produce new innovations to realize sustainable societies on the earth by the accelerator science in collaboration among laboratories, universities, and industries. In order to keep the earth sustainable, we need to solve the serious problems such as "pollution of the earth", "warming of the earth", "energy crisis", "natural resources shortage", etc. Here, the situation created the needs for "new energy network system", "integration of power plant and water/air cleaner" and so on, which clean the environment of the earth. The new project by the budget utilizes the Superconducting Accelerator and Quantum Beam Technology, and create a new market for these "EARTH CLEANER" products. Finally, the goal of the project is to challenge the realization of global/sustainable environment on the earth. After the proposal and budget were successfully approved, we started the construction of new SRF building at KEK, which is so-called Center-of-Innovation (COI) building. Various SRF facilities were planned to be installed in the COI building to realize the innovations to create the EARTH-CLEANER products. We started the construction of COI building at KEK from 2014 and finished the construction in January 2015.

VARIOUS SRF FACILITIES IN COI BUIDING

Figure 1 shows the picture of the existing Superconducting Test Facility (STF) and new COI buildings, and the bird view of these two buildings at KEK.

Figure 1: The picture of STF and COI buildings and the bird view of these two buildings.

The new COI building includes various SRF facilities like clean-room for cavity-string assembly, cryomodule-assembly facility, cryogenic system, vertical-test, cryomodule-test, input-coupler processing, cavity Electro-Polishing (EP) facilities, and control-room/office-rooms in the dimension of 80 m x 30 m. The layout plan of these facilities in the COI building is shown in Figure 2.

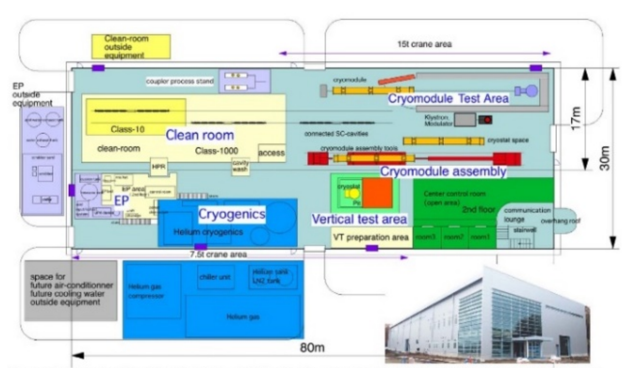

Figure 2: The layout plan of SRF facilities in the COI building.

#takayuki.saeki@kek.jp

Content from this work may be used under the terms of the CC BY 3.0 licence (© 2015). Any distribution of this work must maintain attribution to the author(s), title of the work, publisher, and DOI.

ISBN: 978-3-95450-168-7 doi:10.18429/JACoW-IPAC2015-MOAC1

AWAKE, THE PROOF-OF-PRINCIPLE R&D EXPERIMENT AT CERN

M. Bernardini, T. Bohl, C. Bracco, A. Butterworth, S. Cipiccia, H. Damerau, S. Doebert, E. Gschwendtner, V. Fedosseev, E. Feldbaumer W. Hofle, A. Pardons, A. Petrenko, J. Schmidt, M. Turner, H. Vincke, CERN, Geneva, Switzerland
P. Muggli, MPP Munich, Germany

Abstract

The Advanced Proton Driven Plasma Wakefield Acceleration Experiment (AWAKE) is a proof-of-principle R&D experiment at CERN. It is the world's first proton driven plasma wakefield acceleration experiment, using a high-energy proton bunch to drive plasma wakefields for electron beam acceleration. The AWAKE experiment will be installed in the former CNGS facility and will use the 400 GeV proton beam bunches from the SPS, which will be sent to a plasma source. An electron beam will be injected into the plasma cell to probe the accelerating wakefield. Challenging modifications in the area and new installations are required for AWAKE. First proton beam to the experiment is expected late 2016. The accelerating electron physics will start late 2017.

This paper gives an overview of the project from physics and engineering point of view, it describes the main activities and the milestones.

INTRODUCTION

In the baseline design of the AWAKE experiment at CERN, an LHC-type proton bunch of 400GeV/c (but with higher intensity of $3\cdot 10^{11}$ protons/bunch) will be extracted from the CERN SPS (see Fig. 1) and sent along the 750m long proton beam line towards a plasma cell, which will be installed in the former CNGS area.

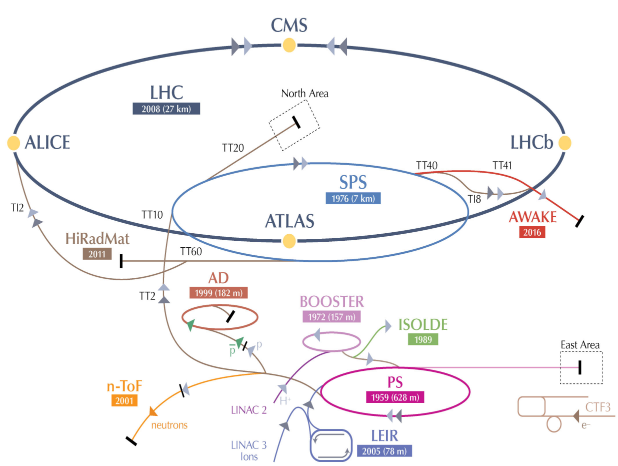

Figure 1: Layout of the CERN accelerator chain.

The proton beam will be focused to $\sigma_{x,y} = 200\,\mu$m near the entrance of the 10 m long Rubidium vapour plasma cell with an adjustable density in the 10^{14} - 10^{15} cm^{-3} range. When the proton bunch with an rms bunch length of $\sigma_z = 12$ cm (400 ps) enters the plasma cell, it undergoes the self-modulation instability (SMI) [1] i.e. the development a long bunch of protons into a series of micro-bunches that resonantly drive large wakefields. The effective length and period of the modulated beam is set by the plasma wavelength (for AWAKE typically λ_{pe} = 1mm). A high power (~4.5 TW) laser pulse [2] co-propagating and co-axial with the proton beam, will be used to ionize the neutral gas in the plasma cell and also generates the seed of the proton bunch self-modulation. Several diagnostics tools [3] will be installed downstream of the plasma cell to measure the proton bunch self-modulation effects. In the AWAKE master schedule the experimental evidence for the self-modulation instability corresponds to Phase 1, which foresees the following milestones: installation during 2015 until Q1 2016, hardware and beam commissioning in Q2/Q3 2016 and physics from Q4 2016.

In Phase 2 AWAKE aims at the first demonstration of proton driven plasma wakefield acceleration of an electron witness beam; an electron beam of $1.2\cdot 10^9$ electrons, which will be injected at 10 – 20 MeV/c into the plasma cell, will serve as witness beam and will be accelerated in the wake of the proton bunch and the accelerated electron bunch properties will be measured with an electron spectrometer. In Phase 2 the milestones are: installation during Q1 and Q2 2017, alternate with SMI physics, hardware and beam commissioning from Q3 to Q4, Physics from Q1 until the start of the CERN Long Shutdown 2 in Q3 2018.

AWAKE AT CERN

The AWAKE experiment is installed in the former CNGS facility. The conversion of the CNGS area into the AWAKE area started in January 2014 and challenging modifications are currently put in place. The following chapters describe the different activities and status of the systems of the AWAKE facility.

Proton Beam Line

The existing CNGS proton beam line is modified only in its last ~80 m, i.e. in the matching section and in the final focusing part in order to comply with the AWAKE requirements. The laser beam is merged with the proton beam at a distance of ~20 m from the plasma cell by adding a proton beam chicane to integrate the laser mirror. An offset of 19.9 mm exists between the proton and the laser beam axis, enough clearance to avoid intercepting protons and inducing losses. The proton and laser beams are made co-axial over the full length of the plasma cell, in particular the 3 σ proton beam envelope (~0.6 mm) must be contained in the 1σ laser spot size (~1

Content from this work may be used under the terms of the CC BY 3.0 licence (© 2015). Any distribution of this work must maintain attribution to the author(s), title of the work, publisher, and DOI.

ISBN: 978-3-95450-168-7 doi:10.18429/JACoW-IPAC2015-MOBC1

TOWARDS ULTRA-LOW BETA* IN ATF2

M. Patecki*, A. Aloev, D. Bett, M. Modena, R. Tomás, CERN, Geneva, Switzerland
E. Marin, G. White, SLAC†, California, USA
K. Kubo, T. Okugi, T. Tauchi, N. Terunuma, KEK and SOKENDAI, Ibaraki, Japan

Abstract

The Accelerator Test Facility 2 (ATF2) has already demonstrated the feasibility of Final Focus Systems based on the local chromaticity correction scheme and its focusing capabilities by reaching a vertical beam size at the virtual Interaction Point (IP) of less than 50 nm. The level of chromaticity in ATF2 is comparable with the expected chromaticity in ILC, but 5 times lower than in a design of CLIC. ATF2 gives the unique possibility to test CLIC chromaticity level by reducing the vertical beta function at the IP by a factor of 4 (the inverse proportionality of chromaticity with beta function value at IP is assumed). The experience collected by tuning of a more challenging machine would be beneficial for both ILC and CLIC projects.

Simulations show that the multipolar errors and final doublet fringe fields spoil the IP beam sizes at ATF2. Either increasing the value of the horizontal beta function or installing a pair of octupole magnets mitigate the impact of these aberrations. This paper summarizes the studies towards the realization of the ultra-low beta* optics in ATF2 and reports on the progress of the construction of the octupoles.

INTRODUCTION

In the future linear colliders (CLIC [1], ILC [2]) the high collision rate is achieved by colliding the beams demagnified to the nanometer size in the interaction point (IP). Strong quadrupole magnets, called final doublet (FD), are used for the beam focusing at the IP, but they also introduce the chromatic effect which causes that the off-momentum particles are not focused exactly at the focal point, leading to larger spot sizes at the IP. In the ATF2 [3], which is a Final Focus System (FFS) test facility, the IP vertical beam size is expected to be 450 nm without correcting the chromaticity and 37 nm if the chromaticity is compensated. This shows the importance of the chromaticity correction.

A novel scheme [4], based on local chromaticity correction in the FD, is tested in ATF2. Its operating principle has been already experimentally validated by measuring a beam size of about 45 nm [5–7]. Therefore, the local chromaticity correction scheme is considered as a baseline for CLIC and ILC FFS. However, the level of chromaticity in ATF2 is comparable with the ILC expectation, but a factor 5 lower than in case of CLIC. For this reason, the ultra-low β^* [8] project is studied in ATF2, reducing the value of β^* by a factor 4, set the chromaticity to be comparable with CLIC (see Table 1). Larger tuning difficulties are expected under these more demanding conditions. Experiencing with higher chromatic lattice would benefit to both CLIC and ILC.

The chromaticity roughly scales as $\zeta_y \sim L^*/\beta_y^*$, so it can be increased by decreasing the β_y^* value, initially by a factor 2 to test a halfway moderated step and finally by a factor 4, which brings the chromaticity level close to CLIC. This will cause the β_y function increase in the FFS, especially in the FD which makes the beam more sensitive to the magnetic imperfections as e.g. multipolar errors, fringe fields, and other aberrations. Some of these issues were already addressed and mitigated in order to make the ultra-low β^* project feasible [9, 14].

MULTIPOLE COMPONENTS AND FRINGE FIELDS OF THE ATF2 MAGNETS

The decrease of the IP β_y value causes that the β_y function in the Final Focus region increases, as shown in Fig. 1. As a consequence, the beam size is larger in the FF and therefore the particles (especially in the tails) are more sensitive to any aberrations and imperfections. It was reported in [9] that carefully measured multipole components [10, 11] of the ATF2 magnets are setting the main limitation in reaching the low beam size for the ultra-low β^* optics. From the simulations, where all multipole components are represented as thin multipoles with integrated gradient corresponding to the measurements, the vertical IP beam size (in rms sense) is $\sigma_y^* = 27$ nm, which is not satisfactory. The impact of the magnetic multipole components was calculated using a MAPCLASS2 [12] code including a high-order transfer map given by PTC [13].

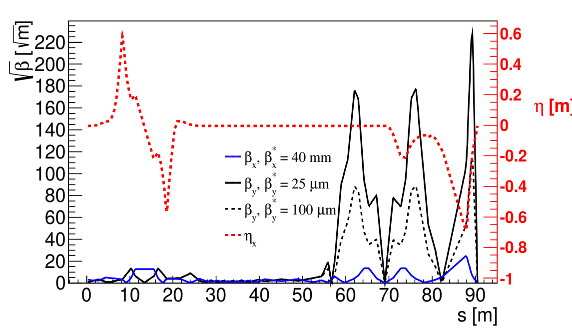

Figure 1: β functions and dispersion along the ATF2 beam line in case of nominal β_y^* and ultra-low β_y^* optics. β_x^* is increased by a factor 10 to minimize horizontal to vertical coupling.

Another limitation in reaching the low beam size in case of ultra low β optics is the magnetic fringe fields of the

---

* mpatecki@cern.ch, also at Warsaw University of Technology, Faculty of Physics, Koszykowa 75, 00-661 Warsaw, Poland

† Work supported in part by the US Department of Energy contract DE-AC02-76SF00515

Content from this work may be used under the terms of the CC BY 3.0 licence (© 2015). Any distribution of this work must maintain attribution to the author(s), title of the work, publisher, and DOI.

ISBN: 978-3-95450-168-7 doi:10.18429/JACoW-IPAC2015-MOBC2

HIGH-PERFORMANCE SIMULATIONS OF COHERENT SYNCHROTRON RADIATION ON MULTICORE GPU AND CPU PLATFORMS *

B. Terzić†, A. Godunov, K. Arumugam, D. Ranjan, M. Zubair
Old Dominion University, Norfolk, VA 23529, USA

Abstract

Coherent synchrotron radiation (CSR) is an effect of self-interaction of an electron bunch as it traverses a curved path. It can cause a significant emittance degradation and microbunching. We present a new high-performance 2D, particle-in-cell code which uses massively parallel multicore GPU/GPU platforms to alleviate computational bottlenecks. The code formulates the CSR problem from first principles by using the retarded scalar and vector potentials to compute the self-interaction fields. The speedup due to the parallel implementation on GPU/CPU platforms exceeds three orders of magnitude, thereby bringing a previously intractable problem within reach. The accuracy of the code is verified against analytic 1D solutions (rigid bunch).

INTRODUCTION

Coherent synchrotron radiation (CSR) can lead to a host of deleterious effects, such as increase in emittance and energy spread and microbunching instability. First step in mitigating these adverse effects is developing a code for high-fidelity numerical simulation of CSR. Numerical simulations of the CSR effects based on Greens function approach have proven to be extremely challenging because of the following features of simulation: (i) large memory requirement associated with storing the history of the beam bunch; (ii) difficulty to accurately account for retardation; (iii) large cancellation between $\boldsymbol{E}$ and $\boldsymbol{B}$ fields in Lorentz force; (iv) sensitivity to numerical noise, exacerbated by presence of gradients in relevant equations; (v) the manner in which self-interactions scale. In this paper, we present a new, 2D particle-in-cell code for modeling CSR and other collective effects in an electron beam using state-of-the-art computing platforms. The proposed method is optimized to run efficiently on different computing platforms such as GPUs, multicore CPUs and on hybrid CPU-GPU. This adaptation of the code design to the new computing architectures results in unprecedented efficiency and fidelity.

EQUATIONS OF MOTION

The dynamics of electron beams is captured by the Lorentz force:

$$\frac{d}{dt}(\gamma m_e \boldsymbol{v}) = e(\boldsymbol{E} + \boldsymbol{\beta}\times\boldsymbol{B}), \tag{1}$$

where the relativistic $\boldsymbol{\beta}$ and γ, velocity $\boldsymbol{v}$, electric field $\boldsymbol{E}$ and magnetic field $\boldsymbol{B}$ given as, respectively,

$$\boldsymbol{\beta} \equiv \boldsymbol{v}/c, \quad \gamma = \frac{1}{\sqrt{1+\boldsymbol{\beta}^2}}, \quad \boldsymbol{v}(\boldsymbol{p}) = \frac{\boldsymbol{p}/m_e}{\sqrt{1+\boldsymbol{p}\cdot\boldsymbol{p}/(m_e c)^2}}, \tag{2a}$$

$$\boldsymbol{E} = -\nabla\phi - \frac{1}{c}\frac{\partial \boldsymbol{A}}{\partial t}, \qquad \boldsymbol{B} = \nabla\times\boldsymbol{A}. \tag{2b}$$

ϕ and $\boldsymbol{A}$ the *retarded scalar and vector potentials*, respectively, which are computed by integration of the charge distribution ρ and charge current density $\boldsymbol{J}$ over the *retarded time* $t' = t - |\boldsymbol{r}-\boldsymbol{r}'|/c$:

$$\begin{bmatrix}\phi(\boldsymbol{r},t)\\ \boldsymbol{A}(\boldsymbol{r},t)\end{bmatrix} = \int_0^\infty \begin{bmatrix}\rho(\boldsymbol{r}',t-\frac{\boldsymbol{r}-\boldsymbol{r}'}{c})\\ \boldsymbol{J}(\boldsymbol{r}',t-\frac{\boldsymbol{r}-\boldsymbol{r}'}{c})\end{bmatrix}\frac{d^2\boldsymbol{r}'}{|\boldsymbol{r}-\boldsymbol{r}'|}, \tag{3a}$$

$$\begin{bmatrix}\rho(\boldsymbol{r},t)\\ \boldsymbol{J}(\boldsymbol{r},t)\end{bmatrix} = \int_0^\infty \begin{bmatrix}1\\ \boldsymbol{v}(\boldsymbol{p})\end{bmatrix} f(\boldsymbol{r},\boldsymbol{p},t)d\boldsymbol{p}. \tag{3b}$$

$\boldsymbol{r}$ are the particle coordinates, $\boldsymbol{p}$ the particle momentum and $f(\boldsymbol{r},\boldsymbol{p},t)$ is the beam's particle distribution function (DF) in phase space, m_e is electron mass, c the speed of light. It is important to note that $\boldsymbol{E} = \boldsymbol{E}^{\text{ext}}+\boldsymbol{E}^{\text{self}}$, $\boldsymbol{B} = \boldsymbol{B}^{\text{ext}}+\boldsymbol{B}^{\text{self}}$. $\boldsymbol{E}^{\text{ext}}$ and $\boldsymbol{B}^{\text{ext}}$ are external electromagnetic (EM) fields fixed by the accelerator lattice. $\boldsymbol{E}^{\text{self}}$ and $\boldsymbol{B}^{\text{self}}$ are the EM fields from the bunch self-interaction, which depend on the history of the bunch charge distribution ρ and current density $\boldsymbol{J}$ via the retarded scalar and vector potential ϕ and $\boldsymbol{A}$.

As can be seen from Eq. (3a), computation of the retarded potentials requires integration over the history of the charge distribution and current density. It points to the main computational bottlenecks of the CSR simulations: (i) data storage for the time-dependent beam quantities (ρ and $\boldsymbol{J}$); (ii) numerical treatment of retardation and singularity in the integral equation for retarded potentials; and (iii) accurate and efficient multidimensional integration in the equation for retarded potentials.

MODEL

Vlasov-Maxwell equations in CSR simulations can be solved either directly, by sampling the entire phase space of the DF, on a grid or in a appropriate basis [1], or by using a particle tracking approach (*e.g.*, [2, 3]). Computational requirements associated with sampling the entire phase space limit the direct solvers to low dimensions (usually 1D). Tracking methods are less restrictive owing to the fact that the sampling of the phase space is done only through simulation particles. This allows the study in higher-dimensional systems, which gives them a clear advantage and makes them a preferred method for modeling CSR effects [4]. We

* Work supported by the Jefferson Science Associates Project No. 712336 and the U.S. Department of Energy Contract No. DE-AC05-06OR23177 (B.T. and K.A), and of the Modeling and Simulation Graduate Research Fellowship Program by Old Dominion University 2013-2015 (K.A).
† bterzic@odu.edu

Content from this work may be used under the terms of the CC BY 3.0 licence (© 2015). Any distribution of this work must maintain attribution to the author(s), title of the work, publisher, and DOI.

ISBN: 978-3-95450-168-7 doi:10.18429/JACoW-IPAC2015-MOBC3

Content from this work may be used under the terms of the CC BY 3.0 licence (© 2015). Any distribution of this work must maintain attribution to the author(s), title of the work, publisher, and DOI.

ELECTRON LENSES FOR EXPERIMENTS ON NONLINEAR DYNAMICS WITH WIDE STABLE TUNE SPREADS IN THE FERMILAB INTEGRABLE OPTICS TEST ACCELERATOR*

G. Stancari†, K. Carlson, M. W. McGee, L. E. Nobrega, A. L. Romanov, J. Ruan, A. Valishev, Fermilab, Batavia IL, USA, D. Noll, IAP, Frankfurt am Main, Germany

Abstract

Recent developments in the study of integrable Hamiltonian systems have led to nonlinear accelerator lattice designs with two transverse invariants. These lattices may drastically improve the performance of high-power machines, providing wide tune spreads and Landau damping to protect the beam from instabilities, while preserving dynamic aperture. To test the feasibility of these concepts, the Integrable Optics Test Accelerator (IOTA) is being designed and built at Fermilab. One way to obtain a nonlinear integrable lattice is by using the fields generated by a magnetically confined electron beam (electron lens) overlapping with the circulating beam. The parameters of the required device are similar to the ones of existing electron lenses. We present theory, numerical simulations, and first design studies of electron lenses for nonlinear integrable optics.

INTRODUCTION

The study of neutrinos and rare processes in particle physics requires high-power accelerators to provide primary beams. The performance of these machines is limited by several factors, including tolerable losses and beam halo, space-charge effects, and instabilities. A possible path towards high-intensity rings includes these steps: developing theories and models describing high-intensity circular machines; carrying out related proof-of-principle experiments; and designing a new kind of rapid-cycling synchrotron based on nonlinear optics, wide tune spreads to suppress instabilities, and possibly self-consistent or compensated space-charge dynamics.

In particular, the Integrable Optics Test Accelerator (IOTA, Fig. 1) is a small storage ring (40 m circumference) being built at Fermilab [1–3]. Its main purposes are the practical implementation of nonlinear integrable lattices in a real machine, the study of space-charge compensation in rings, and a demonstration of optical stochastic cooling.

The concept of nonlinear integrable optics applied to accelerators involves a small number of special nonlinear focusing elements added to the lattice of a conventional machine in order to generate large tune spreads while preserving dynamic aperture [4]. The concept may have a profound impact in the design of high-intensity machines by providing improved stability to perturbations and mitigation of collective instabilities through Landau damping.

The effect of nonlinear lattices on single-particle dynamics will be investigated during the first stage of IOTA operations using pencil beams of electrons at 150 MeV with 10^9 particles/bunch, transverse rms geometrical equilibrium emittance in the range 0.01–0.04 μm, bunch lengths of a few centimeters, and a relative momentum spread of 1.4×10^{-4}. The goal of the project is to demonstrate a nonlinear tune spread of about 0.25 without loss of dynamic aperture in a real accelerator. The beam is generated by the photoinjector currently being operated at the Fermilab Advanced Superconducting Test Accelerator (ASTA) facility [5].

It was shown that one way to generate a nonlinear integrable lattice is with specially segmented multipole magnets [4]. There are also two concepts based on electron lenses: (a) axially symmetric thin kicks with a specific amplitude dependence [6–8]; and (b) axially symmetric kicks in a long solenoid [9, 10]. These concepts use the electromagnetic field generated by the electron beam distribution to provide the desired nonlinear transverse kicks to the circulating beam.

Electron lenses are pulsed, magnetically confined, low-energy electron beams whose electromagnetic fields are used for active manipulation of circulating beams [11, 12]. One of the main features of an electron lens is the possibility to control the current-density profile of the electron beam (flat, Gaussian, hollow, etc.) by shaping the cathode and the extraction electrodes. Electron lenses were developed for beam-beam compensation in colliders [13], enabling the first observation of long-range beam-beam compensation effects by tune shifting individual bunches [14]. They were used for many years during regular Tevatron collider operations for cleaning uncaptured particles from the abort gap [15]. One of the two Tevatron electron lenses was used for experiments on head-on beam-beam compensation in 2009 [16], and for exploring hollow electron beam collimation in 2010–2011 [17, 18]. Electron lenses for beam-beam compensation were built for RHIC at BNL, showing considerable improvements in luminosity [19–21]. Current areas of research on electron lenses include applications for the upgrades of the Large Hadron Collider: as halo monitors and scrapers [22], as charged current-carrying ‘wires’ for long-range beam-beam compensation [23, 24], and as tune-spread generators for Landau damping of instabilities before collisions.

In this paper, we describe the concept of electron lenses for nonlinear integrable optics and present the main design considerations for the Fermilab IOTA ring.

* Fermilab is operated by Fermi Research Alliance, LLC under Contract No. DE-AC02-07CH11359 with the United States Department of Energy. Report number: FERMILAB-CONF-15-136-AD-APC.
† Email: ⟨stancari@fnal.gov⟩.

ISBN: 978-3-95450-168-7 doi:10.18429/JACoW-IPAC2015-MOAD1

DEVELOPMENT OF HIGH GRADIENT RF SYSTEM FOR J-PARC UPGRADE

C. Ohmori, K. Hara, K. Hasegawa, M. Nomura, T. Shimada, F. Tamura, M. Toda, M. Yamamoto, M. Yoshii, KEK and JAEA J-PARC Center, 2-4 Shirakata-Shirane, Tokai, Ibaraki 319-1195, Japan
A. Schnase, GSI, 64291 Darmstadt, Germany

Abstract

A new 5-cell cavity has been developed for the upgrade of the J-PARC Main Ring. In the cavity, high impedance magnetic alloy, Finemet ®-FT3L, cores are loaded. The cavity was installed and has been used for the 320 kW beam operation. The cavity is operated with the RF voltage of 70 kV which is two times higher voltage than the present cavities. Eight more cavities will be assembled and installed in the next two years to increase the repetition rate of the Main Ring. This paper describes the status of cavity operation under the beam loading and status of the mass production of the cavities.

INTRODUCTION

We have been working for the development of magnetic alloy loaded RF system for high intensity proton ring for twenty years. In the first ten years, we have finished basic R&Ds on high field gradient [1], on the technique to control bandwidth [2], and on cut core configuration [3]. The water-proof coating [4] was developed to use magnetic alloys in water tanks. The high gradient RF systems were installed in the J-PARC RCS and MR [5, 6]. At the same time, the technology is also used for medical applications [7] and heavy ion acceleration [8].

In the last ten year, we have improved water-proof coating [4] and protection of cut surfaces of cut cores [9] to afford a stable operation. Now, J-PARC has delivered 500 kW beam to the Material and Life Science Facility and 320 kW for the T2K long base line neutrino experiment. We also worked for R&D of higher gradient RF systems to increase the repetition rate of the MR for the J-PARC upgrade. The key technology of high gradient RF is the development of magnetic alloy core with higher impedance to reduce the power consumption in the cavity. A magnetic annealing oven was constructed leasing a large spectrometer magnet from a high energy experiment during a short rental period of one year [10]. Based on the success of the proof-of-principle production of high impedance magnetic alloy cores, a dedicated magnetic annealing system was developed. The production by the dedicated system shows about 10 % improving on the core impedance because of an optimum magnetic field value and improvements of ribbon winding and insulation [11]. Although the magnetic oven which J-PARC made is designed for the production of large size cores, it is also reported that characteristics of the FT3L cores made by the oven is better than that of commercially available cores for medium size (330 mm) [12].

The dedicated magnetic annealing system was moved to a company according to the contract to produce FT3L in 2013. In these two years, 280 FT3L cores with the outer diameter of 800 mm were produced using the KEK-made production system. These 280 FT3L cores are manufactured for water-proof coating and cut core configuration. For the J-PARC upgrade to deliver 750 kW beam to the T2K experiment, all cavities in the MR will be replaced with new FT3L cavities to accelerate 2×10^{14} protons with 1.3 second cycle. Although the cavities are replaced, the final stage amplifiers and power supplies can be used. According to the power upgrade beyond 750 kW, the power supplies will be modified to increase the capability to drive the power.

5-CELL CAVITY

The first five-cell cavity was constructed and installed in 2014. Each cell consists of two sets of water tanks. Three cut cores are installed in a water tank. The cut core is covered by epoxy water-proof coating for the direct water cooling in the water tank. Between two water tanks, a ceramic gap for acceleration is located. The impedance of each cavity cell is 1450 Ω and it is higher than 1300 Ω of the proof-of-principle FT3L cell installed in 2012 because of the improvements of core impedance since the production of the FT3L cores in 2011 [11]. Before the installation, two sets of high power tests were performed with a total voltage of 80 kV for 1000 hours. It is a standard procedure to test a cavity with higher voltage and higher power dissipation for several hundreds hours before an installation to the tunnel. After the power test, the cavity was disassembled and status of the FT3L cores was investigated. The detail is described in the reference [13]. After re-assembling, the cavity was taken down to the MR tunnel by a crane as shown in Fig. 1 [13]. After the installation, the gap voltage of 14 kV has been generated. A total voltage of 70 kV which corresponds to two times higher voltage than the present cavity is generated.

Figure 2 shows the upgrade plan of the RF system. The upper figure shows the status before installation of the FT3L cavities. The lower figure shows the layout after replacement. Three sets of the 5-cell cavity will be installed in a long straight section where 4 sets of the present 3-cell cavity are installed. Two sets of FT3L cavity will be 4-cell type instead of 5-cell one to fit to short straight sections. Adopting the FT3L material for the cavity, the cavity impedance becomes about 40% higher and the length of the cavity cell is about 500 mm which is 90 mm shorter than the present cavity. The total length of the 5-cell cavity is about 700 mm longer than the present 3-cell cavity and 3 sets of the 5-cell cavity fit to

Content from this work may be used under the terms of the CC BY 3.0 licence (© 2015). Any distribution of this work must maintain attribution to the author(s), title of the work, publisher, and DOI.

ISBN: 978-3-95450-168-7 doi:10.18429/JACoW-IPAC2015-MOAD2

RF BREAKDOWN OF 805 MHz CAVITIES IN STRONG MAGNETIC FIELDS*

D. Bowring, A. Kochemirovskiy, M. Leonova, A. Moretti, M. Palmer, D. Peterson, K. Yonehara, FNAL, Batavia, IL 60150, USA
B. Freemire, P. Lane, Y. Torun, IIT, Chicago, IL 60616, USA
D. Stratakis, BNL, Upton, NY 11973, USA
A. Haase, SLAC, Menlo Park, CA 94025, USA

Abstract

Ionization cooling of intense muon beams requires the operation of high-gradient, normal-conducting RF structures in the presence of strong magnetic fields. We have measured the breakdown rate in several RF cavities operating at several frequencies. Cavities operating within solenoidal magnetic fields $B > 0.25$ T show an increased RF breakdown rate at lower gradients compared with similar operation when $B = 0$ T. Ultimately, this breakdown behavior limits the maximum safe operating gradient of the cavity. Beyond ionization cooling, this issue affects the design of photoinjectors and klystrons, among other applications. We have built an 805 MHz pillbox-type RF cavity to serve as an experimental testbed for this phenomenon. This cavity is designed to study the problem of RF breakdown in strong magnetic fields using various cavity materials and surface treatments, and with precise control over sources of systematic error. We present results from tests in which the cavity was run with all copper surfaces in a variety of magnetic fields.

INTRODUCTION

Strong, external magnetic fields have been shown to have an effect on the rate and extent of RF breakdown in normal-conducting cavities [1, 2]. The impetus for these studies was the design of ionization cooling channels for a future muon accelerator. Muons must be cooled quickly due to their relatively short lifetime. Ionization cooling – the only cooling method viable on muon-appropriate timescales – requires the operation of copper cavities in multi-Tesla external, solenoidal magnetic fields [3].

A model has been proposed to explain the effect of strong magnetic fields on RF breakdown rates [4]. In this model, field emission current from asperities (or other irregularities) on a cavity's surface is focused by the external solenoidal magnetic field into "beamlets" with current densities between 10^3 and 10^5 A/m^2 depending on field strengths, cavity geometry, etc. These beamlets may persist over multiple RF periods, causing cyclic fatigue and damage on cavity walls and contributing to an increased breakdown probability. Increases in solenoid field strength beyond some threshold value ($B \approx 0.5$ T in this context) produce negligible changes in beamlet current density due to space charge effects.

* Work supported by Fermilab Research Alliance, LLC under Contract No. DE-AC02-07CH11359.

Breakdown probabilities may therefore be reduced by careful surface preparation, which reduces the number of defects causing surface electric field enhancement. Note also that the problem is mitigated by using cavity materials with long radiation lengths, such as beryllium. Low-Z materials should allow beamlets to exit the cavity without depositing energy in cavity walls and contributing to material fatigue and damage.

Breakdown behavior consistent with this model has been observed in several RF cavities. The relevant methodology and results are described here.

EXPERIMENTAL SETUP AND RF MEASUREMENTS

Work was performed at the MuCool Test Area (MTA) at the south end of the Fermilab Linac. The MTA is an experimental hall optimized for R&D related to muon ionization cooling [5]. RF power is available in the hall at 201 MHz (4.5 MW) and at 805 MHz (12 MW). RF structures can be operated at high power inside the 44 cm diameter bore of a 5 Tesla superconducting solenoid. A data acquisition system (DAQ) automates the collection of data from six oscilloscopes and a wide array of instrumentation [6]. The DAQ also detects breakdown sparks in real time by examining (a) the time derivative of a cavity pickup probe voltage signal; (b) the time derivative of power reflected from the cavity; and (c) light from a spark, transmitted through an optical fiber and detected by a photomultiplier tube. Cavities are prepared and inspected inside a class-100 portable clean room.

A spark rate of 1 in 10^5 RF pulses defines the maximum "safe" operating gradient of a cavity. Higher breakdown probabilities lead to lower cooling channel efficiencies.

The All-Seasons Cavity

RF breakdown may be suppressed by pressurizing cavities with gas, which gas can also serve as an ionization cooling medium [7]. Furthermore, for "traditional" evacuated cavities, there is some interest in studying the dependence of breakdown probabilities on cavity materials and surface preparations [4, 8]. Muons, Inc. has designed, built, and tested a cavity suitable for R&D on these various ideas – "a cavity for all seasons" [9]. The so-called All-Seasons cavity (ASC) is shown in Fig. 1. It has replaceable walls, can be pressurized up to 100 atm or evacuated to 3×10^{-8} Torr, and is fed with a coaxial power coupler.

Content from this work may be used under the terms of the CC BY 3.0 licence (© 2015). Any distribution of this work must maintain attribution to the author(s), title of the work, publisher, and DOI.

ISBN: 978-3-95450-168-7 doi:10.18429/JACoW-IPAC2015-MOAD3

RELATIVE ALIGNMENT WITHIN THE MAX IV 3 GeV STORAGE RING MAGNET BLOCKS

J. Björklund Svensson*, M. Johansson, MAX IV Laboratory, Lund, Sweden

Abstract

Unlike the discrete magnet scheme of previous 3rd generation light sources, the magnet elements of the MAX IV storage rings are integrated in precision-machined magnet blocks. By analyzing the rotating coil measurements made by the magnet suppliers, we determined the relative alignment between consecutive magnet elements, which was found to be <10 μm RMS for all magnet block types in both horizontal and vertical direction. This article presents our analysis and results for the full magnet production series.

INTRODUCTION

The MAX IV synchrotron radiation facility [1], currently being built on the outskirts of Lund, Sweden, will house two electron storage rings; one smaller and one larger, at 1.5 and 3 GeV, respectively [2]. The magnet design concept [3], with magnet blocks containing several different magnets, will be used for both storage rings. The two halves of these magnet blocks are each CNC machined out of a single block of iron (2.3-3.4 m long), and together, they work as both supporting structure and return yoke for the magnets, see Figure 1. The different magnet block types for the 3 GeV ring are called M1, U1, U2, U3, U4, U5 and M2 and are placed in that order in the achromats. The production of these magnet blocks, including all field measurements, was entirely outsourced to industry[1], based on a technical specification and full set of drawings [4] provided by MAX-lab.

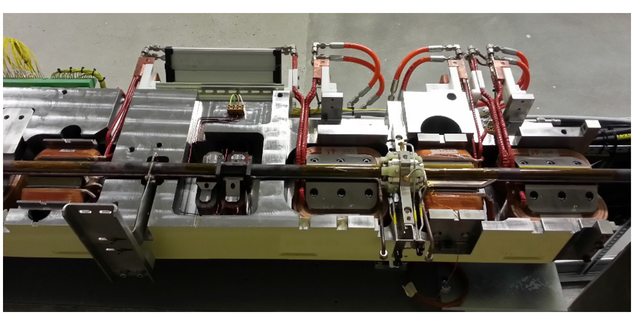

Figure 1: U3 bottom yoke half in achromat 16 with vacuum chamber in place, upstream side, viewed from the outside of the ring. Magnet elements from right to left (particle direction): QF, SFi, QF, Corr y/x, SD.

The MAX IV magnet block design assumes that the magnetic center location for each magnet depends only on the position of the pole surfaces [3]. This means that the alignment accuracy of individual magnets within each block is given by the mechanical tolerances of the top and bottom yoke halves (±0.02 mm over the whole block length), the loose quadrupole pole tips (±0.01 mm) and the sextupole and octupole yoke halves (±0.02 mm), as well as the respective assembly tolerances. Based on this assumption, no requirement of measuring magnetic center locations relative to the mechanical reference surfaces with high accuracy was made in the technical specification. However, from the provided field measurements, we could calculate the relative alignment between consecutive magnet elements within each magnet block.

The technical specification required measurement of the magnetic field strength as well as the harmonic content to characterize the magnets. Both magnet manufacturers decided to measure the harmonic content with rotating coils, and because of limited accessibility inside the magnet blocks they produced rotating coil shafts fitted with multiple coils placed at different positions along the shaft. These were used to measure several consecutive magnets, which then allowed us to evaluate the relative alignment since the magnets could be considered to have been measured within a common local coordinate system defined by the shaft. Several different rotating coil shafts were produced because of the differences in magnet layout between block types. A brief summary of the elements measured by each rotating coil shaft can be found in Table 1.[2]

Table 1: Elements Measured by Each Rotating Coil Assembly

Coil assembly	Magnet elements
"M1/M2 long"	OXX - QFe - OXY - QDe
"M1/M2 short"	OYY - SDe
"U3"	QF - SFi - QF - SD
"U1..U5 long"	QFm - SFm - QFm/ QF - SFo - QF
"U1..U5 short"	SD

MAGNETIC CENTERS FROM ROTATING COIL MEASUREMENTS

Displacements from Harmonic Content

To calculate the displacement of the rotating coil axis from the magnet center, one can use the feed-down of the main magnetic field components. Eq. 9.72 in [5] relates the

* jonas.bjorklund_svensson@maxlab.lu.se

[1] Danfysik A/S, Taastrup, Denmark: 60 pcs M1, M2 and U3. Scanditronix Magnet AB, Vislanda, Sweden: 80 pcs U1, U2, U4 and U5.

[2] The corrector magnets present in some of these setups were also measured, but are not listed since they were not used for this evaluation. The "U1..U5 long" measurements also include a SD magnet, but since this rotating coil shaft has an extra bearing in the middle to counteract sag, the SD can not be considered as being in the same coordinate system.

Content from this work may be used under the terms of the CC BY 3.0 licence (© 2015). Any distribution of this work must maintain attribution to the author(s), title of the work, publisher, and DOI.

ISBN: 978-3-95450-168-7 doi:10.18429/JACoW-IPAC2015-MOBD1

Content from this work may be used under the terms of the CC BY 3.0 licence (© 2015). Any distribution of this work must maintain attribution to the author(s), title of the work, publisher, and DOI.

PRELIMINARY DESIGN OF THE HIGH-LUMINOSITY LHC BEAM SCREEN WITH SHIELDING*

V. Baglin, C. Garion, R. Kersevan, CERN, Geneva, Switzerland

Abstract

A new beam screen is needed in the High-Luminosity LHC (HL-LHC) final focusing magnets. Such an essential vacuum component, while operating in the range 40-60 K, has to ensure the vacuum performance and to prevent the beam-induced heating from reaching the cold bore which is at 1.9 K. In addition, it has to shield the cold mass from physics debris coming from the nearby beam collision points. To such purpose, energy absorbers made of tungsten alloy are installed onto the beam screen in the vacuum system. In this contribution, the proposed mechanical design is shown; it covers different thermomechanical aspects such as the behaviour during a magnet quench and the heat transfer from the tungsten absorbers to the cooling tubes. Assembly and manufacturing tolerances are also considered to evaluate the impact on the aperture. Results obtained with a short prototype assembly test are discussed.

INTRODUCTION

The beam screen is a complex object with a variety of functions [1]. HL-LHC beam screens are to be inserted into the separation dipole (D1) and the inner triplet (IT) quadrupoles (Q1 to Q3) of the LHC long straight sections 1 and 5. The main purpose is to intercept the beam induced heat load before it reaches the cold mass. It has also to shield the cold bore inner surface from direct particle impingement, which would lead to important outgassing while assuring high effective pumping speed on the cold bore toward pumping slots to fulfil vacuum requirements. It is equipped with shielding made of tungsten alloy to absorb the particle debris generated in the collision points [2].

The beam screen with shielding has to withstand the Lorentz' forces induced by eddy currents during a quench. The temperature of the beam screen must be actively controlled in a given temperature range: 40-60 K, where vacuum stability is guaranteed [1]. The system must be compatible with the global LHC impedance and with the machine aperture.

DESIGN OF THE BEAM SCREEN WITH SHIELDING

Preliminary design relied on the soldering of the absorbers made of tungsten alloy (Inermet® 180) on the beam screen shell [3]. This concept raises few critical aspects:

- Feasibility: how to accommodate the large differential thermal contraction between the tungsten alloy (around 0.09% at 50 K) and the beam screen shell in stainless steel (around 0.29 % at 50 K).
- Manufacturing: the brazing has to be done under vacuum and requires therefore a long furnace. The risk to have a bad brazing of one element is not negligible and would lead to the reject of the whole beam screen.
- Assembly: The tolerances obtained after brazing are not well managed. In addition, the beam screen obtained after the brazing of the tungsten alloy blocks would be very stiff and difficult to insert into the cold bore. This would require large assembly tolerances.

A concept based on a mechanical assembly of the tungsten absorbers is proposed here (Fig. 1). As for the standard LHC beam screen, the shell is perforated with oblong holes to provide sufficient pumping speed of the desorbed gas. The cooling is provided by four tubes, whose diameter depends on the type of magnet (external diameter of 16 mm and 10 mm for the Q1 and Q2-D1, respectively). The tungsten blocks are positioned on the beam screen by pins, welded onto the shell. Dedicated slots are used on one side of the block to allow differential thermal contraction; an overlap is used to reduce the number of pins. Elastic rings, in titanium grade 5, block the tungsten shields onto the beam screen. Copper strips are installed between the absorbers and the cooling tubes to assure a good heat transfer.

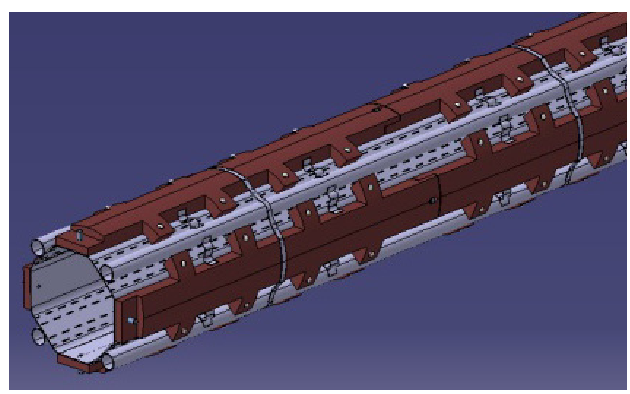

Figure 1: New beam screen design.

THERMAL MECHANICAL BEHAVIOR OF THE BEAM SCREEN

Self-weight Deformation

The weight of the tungsten absorbers is rather high (53 kg/m for the Q1 beam screen). The self-weight deformation has been assessed. The vertical deformation

*Research supported by the High Luminosity LHC project.

ISBN: 978-3-95450-168-7 doi:10.18429/JACoW-IPAC2015-MOBD2

Content from this work may be used under the terms of the CC BY 3.0 licence (© 2015). Any distribution of this work must maintain attribution to the author(s), title of the work, publisher, and DOI.

DESIGN AND PROTOTYPING OF HL-LHC DOUBLE QUARTER WAVE CRAB CAVITIES FOR SPS TEST*

S. Verdú-Andrés#, J. Skaritka, Q. Wu, B. P. Xiao, BNL, Upton, NY 11973, USA
S. Belomestnykh, I. Ben-Zvi, BNL, Upton, NY 11973, USA; SBU, Stony Brook, NY 11790 USA
L. Alberty, K. Artoos, R. Calaga, O. Capatina, T. Capelli, F. Carra, R. Leuxe, N. Kuder, C. Zanoni, CERN, Geneva, Switzerland
Z. Li, SLAC, Menlo Park, CA 94025, USA, A. Ratti, LBNL, Berkeley, CA 94707, USA

Abstract

The LHC high luminosity project envisages the use of the crabbing technique for increasing and levelling the LHC luminosity. Double Quarter Wave (DQW) resonators are compact cavities especially designed to meet the technical and performance requirements for LHC beam crabbing. Two DQW crab cavities are under fabrication and will be tested with beam in the Super Proton Synchrotron (SPS) at CERN by 2017. This paper describes the design and prototyping of the DQW crab cavities for the SPS test.

INTRODUCTION

The LHC luminosity upgrade would significantly increase the potential to discover new physics from rare events. Bunch crabbing is one of the proposed techniques for increasing and levelling the LHC luminosity [1].

The first phase of the crab cavity program was to validate the design by demonstrating the nominal deflecting voltage. The first prototype of a DQW crab cavity was successfully cold tested at BNL in 2014 [2].

The next phase of the program envisages testing of the crab cavities with proton beams in SPS by 2017. A prototype cryomodule will host two fully dressed DQW crab cavities. The tests will try to crab bunches of proton beams for the first time ever.

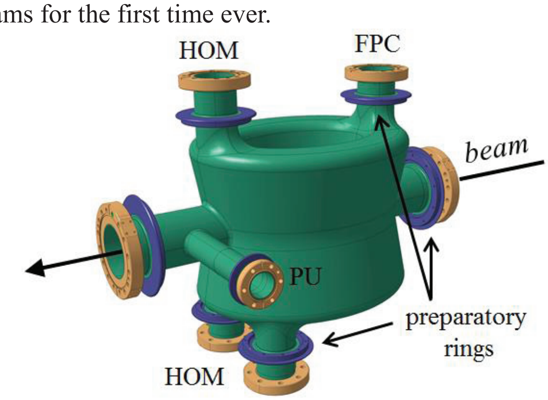

Figure 1: Bare SPS DQWCC with flanges and rings.

*Work supported by US DOE through Brookhaven Science Associates LLC under contract No. DE-AC02-98CH10886 and the US LHC Accelerator Research Program (LARP) and by EU FP7 HiLumi LHC – Grant Agreement 284404. This research used resources of the National Energy Research Scientific Computing Center, which is supported by US DOE under contract No. DE-AC02-05CH11231.
#sverdu@bnl.gov

DQW CRAB CAVITY FOR SPS TESTS

Optimization of the cavity body and port tubes was discussed in previous papers [3,4] and focused on reducing residual accelerating voltage and peak surface fields while respecting clearance requirements for the adjacent LHC beam pipe.

Position of the flanges has been carefully chosen to reduce the dissipative losses in the copper RF-seal gaskets while respecting space constraints of the cryomodule.

Figure 1 shows a bare DQW crab cavity with flanges and preparatory rings. Table 1 summarizes the main geometric and electromagnetic properties of the SPS DQW crab cavities.

Table 1: Properties of SPS DQWCC

Geometrical parameter *(at 300K)*		**Unit**
Cavity length L	352	mm
Cavity width W	288	mm
Cavity height H (w/o ports)	286	mm
Beam pipe diameter	84	mm
Port diameter	62	mm
Electromagnetic quantity *(Microwave Studio [5] simulations)*		**Unit**
Crab mode frequency f_0	400	MHz
Nearest mode frequency f_1	570	MHz
Deflecting voltage V_t (1)	3.34	MV
Deflecting gradient V_t/L_{cavity} (2)	9.5	MV/m
Accelerating voltage V_{acc} (2)	15	kV
Electric field center offset	0.23	mm
Peak surface electric field E_{pk} (2)	37	MV/m
Peak surface magnetic field B_{pk} (2)	72	mT
Stored energy U (2)	10	J
R_t/Q	429	Ω
Geometric factor G	87	Ω

(1) Nominal deflecting voltage per cavity [6].
(2) For a nominal deflecting voltage Vt of 3.34 MV.

ISBN: 978-3-95450-168-7 doi:10.18429/JACoW-IPAC2015-MOBD3

DEVELOPMENT OF A 9 MHz 15 kW SOLID-STATE CW AMPLIFIER FOR RHIC

Shane Dillon, Tomco Technologies, Adelaide, Australia

Abstract

This paper describes the technical details of the development of a high-power solid-state amplifier for Brookhaven Laboratory. The amplifier must withstand short duration events of 100% full-power reflection, and also must guarantee delivery of continuous power into any load impedance at any angle.

INTRODUCTION

This paper describes some of the technical considerations in the design of a 9MHz 15kW CW amplifier for use in RHIC at Brookhaven National Laboratory (BNL). A total of six of these 15kW amplifiers will be commissioned, driving "gap cap" cavities [1].

The amplifier uses modular solid-state architecture and 6th Generation LDMOS power transistors. In the 15kW system, six 2.5kW amplifier units are combined via a 6:1 combiner unit to give a single 15kW output. The RF amplifier rack is located within the accelerator tunnel close to the cavity, and the associated switchmode DC power supply is located remotely to minimise the risk of damage due to ionizing radiation. A failsafe opto-isolated interlock link was designed to accommodate this requirement. The amplifier system has extensive control and monitoring functions and is equipped with three different control interfaces: it can be controlled locally via front panel push-buttons, or remotely via a wired parallel (PLC) interface or an Ethernet connection.

DESIGN CONSIDERATIONS

The major specifications of the amplifier are listed in Table 1. The requirement for the amplifier to supply significant amounts of forward power to mismatched loads presented a number of design challenges: Since circulators are not an option at 9MHz, the amplifier had to be capable of withstanding the mismatch in its own right, while remaining stable and well behaved under all load conditions.

To meet these specifications several key design factors had to be simultaneously optimised, namely: forward power, thermal management, stability, and parts count.

Forward Power

As a first approximation, the maximum power that a push-pull transistor pair can produce is limited to $2V_{dc}^2/R_L$, where V_{dc} is the DC supply voltage (fixed at 50 volts), and R_L is the load resistance presented across the transistor drains. Thus, if R_L is very large it becomes impossible to achieve the required output power. At the other extreme, if R_L is very small the available output power becomes very large, but as described later, there is a risk of destroying the device due to excessive die temperature. The various measures that were taken to address this issue are described in the following paragraphs.

Table 1: Basic Specifications

<table>
<tr><td>Frequency</td><td colspan="8">9MHz ±10% minimum</td></tr>
<tr><td>Power</td><td colspan="8">15kW CW minimum</td></tr>
<tr><td>Gain/phase Linearity</td><td colspan="8">±1dB maximum and ±10° maximum from 15W to 15kW output</td></tr>
<tr><td>Harmonics</td><td colspan="8"><-30dBc at rated power</td></tr>
<tr><td>Stability</td><td colspan="8">Unconditionally stable over entire load space and dynamic range</td></tr>
<tr><td rowspan="2">Forward power at worst-case phase</td><td>SWR</td><td>1</td><td>1.5</td><td>2</td><td>3</td><td>5</td><td>10</td><td>∞</td></tr>
<tr><td>kW (min.)</td><td>15</td><td>15</td><td>12</td><td>9</td><td>6</td><td>4.5</td><td>3</td></tr>
<tr><td>Load transients</td><td colspan="8">Withstands 100% reflection at full rated power for at least 100µs</td></tr>
</table>

Thermal Management

Reflected power acts to disrupt the operating point of the transistor and affect its efficiency. For example, it can result in a very low impedance load being presented to the transistor, forcing the transistor to carry high current whilst simultaneously having a large voltage across it. This results in very high heat dissipation in the silicon die, which unless properly managed can lead to overheating and permanent destruction of the transistor. Safe operation hinges on minimising the thermal resistance between the power transistor and the cooling water. Therefore, a great deal of care was taken in the mechanical design to ensure a very low thermal resistance and a solid electrical connection from the flange to the earth.

Stability

Since the amplifier is required to operate into all phase angles of any possible VSWR, there is significant potential for amplifier instability. There is also a risk of that circuit elements might form high Q resonances with the load reactance. This can produce large gain variations and possible oscillations if any suitable feedback path exists. It can also result in damage to components such as harmonic filter capacitors or coupling capacitors.

Parts Count

In order to maximize the expected MTBF of the system, every effort was made to minimise the parts

Content from this work may be used under the terms of the CC BY 3.0 licence (© 2015). Any distribution of this work must maintain attribution to the author(s), title of the work, publisher, and DOI.

ISBN: 978-3-95450-168-7 doi:10.18429/JACoW-IPAC2015-MOPWA001

INSTABILITY THRESHOLDS AND TUNE SHIFT ESTIMATION FOR SIRIUS

F. H. Sá*, L. Liu, X. R. Resende, N. Milas, LNLS, Campinas, Brazil

Abstract

In this work we present the evaluation of longitudinal and transverse instability thresholds as well as tune shifts for Sirius using time and frequency domain codes that are being developed in-house and take into account various effects on the beam instability, such as bunch by bunch feedback system, quadrupolar impedances from undulator chambers and tune spreads.

INTRODUCTION

This contribution is a continuation of the work presented at IPAC14 [1], where we detailed the construction of the impedance budget for Sirius and used a frequency domain code based on the solution of the Linearized Vlasov Equation for equally spaced Gaussian bunches [2, 3] to calculate thresholds for single and coupled bunch instabilities. After analyzing the results we concluded that: a) Due to the strength of the coupled bunch instability induced by the chamber wall, a transverse bunch by bunch feedback system will operate from start for safety; b) With a small positive absolute chromaticity (maximum of 1.5 in both planes) it is possible to get a strong damping of the chamber wall instability. This motivated us to include this value in our dynamic aperture and lifetime optimizations [4]; c) The thresholds for intra-bunch instabilities in the three planes are relatively low and can compromise some operation modes.

The last item motivated us to implement a single bunch tracking code to better characterize the intra-bunch dynamics. Even though the chromaticity and the interplay between coupled and single bunch instabilities were taken into account in the frequency domain code, other important effects such as potential well distortion, third harmonic cavity, tune shift with amplitude, quadrupolar impedances and the bunch by bunch feedback were not considered. The simultaneous action of these forces changes significantly the behavior of each bunch, which can increase or decrease the thresholds.

The effects described above also influence the multi-bunch dynamics and consequently the coupled bunch motion. However, they are generally of a stabilizing nature due to the introduction of tune spreads. For this reason we decided to focus on the single bunch dynamics first. The implementation of a multi-bunch tracking code will be performed later.

SINGLE BUNCH TRACKING CODE

The single bunch tracking code is presently implemented using MATLAB® but an implementation using C/C++ is planned to gain speed in the simulations.

* fernando.sa@lnls.br

Haissinski Equation Solver

The code is organized in two parts. First an equilibrium distribution in four dimensions is generated. In the transverse plane an exponential distribution of emittances and a uniform distribution of phases are used. In the longitudinal plane there are two options: a) generate energy deviations with a Gaussian distribution with the input value of the energy spread and longitudinal positions following the distribution determined by the input potential well (which can be arbitrary); b) solve the Haissinski equation, taking into account the input potential well and wakes to get the new equilibrium distribution to generate the particle's longitudinal positions and the new potential well.

The Haissinski equation solver may also change the value of the energy spread, because its algorithm first tries to solve the equation with the input value. If convergence is not achieved, it increases the value of the energy spread by a small amount and iterates again. This procedure is repeated until an equilibrium state is found [5, 6]. The new value of energy spread is then used to generate the energy deviation distribution.

Macro Particles Tracking

The second part of the code is the tracking itself. The one turn map is approximated by the following set of equations:

$$\begin{aligned}
J &= \frac{(x-\eta_x\delta)^2}{\beta_x} + (x'-\eta_x'\delta)^2\,\beta_x \\
\phi &= 2\pi\left(\nu_0 + \xi\delta + AJ\right) \\
\begin{pmatrix} x \\ x' \end{pmatrix} &= \begin{pmatrix} \cos\phi & \beta_x\sin\phi \\ -\frac{1}{\beta_x}\sin\phi & \cos\phi \end{pmatrix}\begin{pmatrix} x-\eta_x\delta \\ x'-\eta_x'\delta \end{pmatrix} + \begin{pmatrix} \eta_x \\ \eta_x' \end{pmatrix}\delta \\
\tau &= \tau - T_0\alpha\delta \qquad (1)\\
\delta &= \delta + \frac{V(\tau)}{E_0} + K_{W_L}(\tau) \\
x' &= x' + K_{W_T}(x,\tau) + K_F(\langle x\rangle)
\end{aligned}$$

where J is the transverse action, A is the tune shift with the action coefficient, τ is the relative position of the particle ahead of the synchronous particle and K_{W_T}, K_{W_L} and K_F are the collective kicks generated by the transverse and longitudinal wakes and the feedback system, respectively. The other terms have the usual interpretation. When the longitudinal dynamics is solved with the Haissinski equation solver and the effect of the longitudinal wakes is considered in the longitudinal potential used in the tracking, K_{W_L} is zeroed to be consistent.

The wakes are generated from the Fourier Transform of the impedances, multiplied by the betatron function at the point where the kick is given, summed and passed to the tracking code as a table for interpolation. However,

Content from this work may be used under the terms of the CC BY 3.0 licence (© 2015). Any distribution of this work must maintain attribution to the author(s), title of the work, publisher, and DOI.

ISBN: 978-3-95450-168-7 doi:10.18429/JACoW-IPAC2015-MOPWA002

Content from this work may be used under the terms of the CC BY 3.0 licence (© 2015). Any distribution of this work must maintain attribution to the author(s), title of the work, publisher, and DOI.

TRANSITION TO SPACE-CHARGE LIMITED FLOW IN CROSSED-FIELD DEVICES *

S. Marini†, F. B. Rizzato, and R. Pakter, UFRGS, Porto Alegre, Brazil

Abstract

This work presents a fully kinetic description to model the electron flow in the electronic crossed-field configuration observed in a smooth-bore magnetron. Through this model, it has been observed that, according to the electromagnetic field, the injection temperature and the charge density, the electron flow can be classified in two different stationary modes: magnetic insulation mode where most of the electrons returning to the cathode after a transient time and Child-Langmuir mode where most of the electrons reach the anode after a transient time. Focusing on magnetic insulated mode, it has been found that charge density and injection temperature define whether electrons are accelerated (accelerating regime) or decelerated (space-charge limited regime) on the cathode. Besides, when the injection temperature is relatively low (high), a small charge increase causes (does not cause) an abrupt transition between accelerating and space-charge limited regime. Basing on the results, it was possible to identify a critical temperature that separates abrupt and continuous behavior. The results have been verified by using self-consistent computer simulations.

INTRODUCTION

Describing the electron flow in presence of crossed electric and magnetic fields is fundamental for the development of several advanced applications in areas ranging from microwave sources [1] to space propulsion [2]. The study of the electron dynamics in such field configuration was pioneered by Hull [3] who showed that a magnetic field might limit the particle flow from the cathode to the anode. This result was based on a single-particle model that assumes given external electromagnetic fields. Nowadays, a large number of papers have investigated the equilibrium and stability of these systems by explicitly taking into account the particles self-fields [4–6]. The self-fields may play a major role in the dynamics since they can also limit the particles flow from the cathode to the anode as the current density exceeds a certain threshold and a space-charge limited (SCL) regime emerges [7, 8]. However, given the complexity that long ranged self-fields add to the problem, the large majority of the theoretical analysis done so far are based on models that assume the electron flow is either completely cold or is a fluid with postulated equation of state. These fluid models might not properly take into account thermal effects. Because of it, recently we have developed a fully kinetic model to investigate thermal effects in crossed-field configuration observed in a smooth-bore magnetron [9]. Here, we review the theoretical framework and compare it against simulations with different injection distributions at the cathode.

* This work was partially supported by CNPq and FAPERGS, Brazil, and by the US-AFOSR under the grant FA9550-09-1-0283
† marini@ufrgs.br

THE PHYSICAL MODEL

The model and field configuration of a smooth-bore magnetron is shown in Fig. 1. There are two plates separated by a distance L along the y axis. The one localized at $y = 0$ is a thermionic cathode kept at zero electrical potential and the one localized at $y = L$ is an anode kept at V_0 electrical potential. As consequence of the electrical potential difference in the gap region between the plates, there is an uniform electric field $\mathbf{E}_0 = -(V_0/L)\hat{\mathbf{y}}$. Besides, in gap region there is an uniform constant magnetic field $\mathbf{B}_0 = -B_0\hat{\mathbf{z}}$, consolidating the crossed-field configuration.

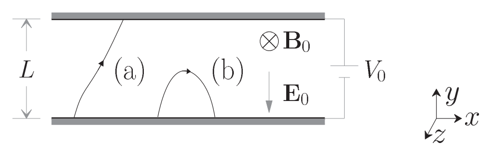

Figure 1: Model and field configuration of a smooth-bore magnetron. The curves correspond to the trajectories of test electrons emitted from the thermal cathode with vanishing velocities. In the case (a) $V_0 > V_H$ and in the case (b) $V_0 < V_H$.

At instant of time $t = 0$, the thermionic cathode starts to emit electrons, which enter in gap region. These are accelerated by the electric field $\mathbf{E}_0$ along the y direction while they are deflected along clockwise direction on $x-y$ plane by the magnetic field $\mathbf{B}_0$. In Fig. 1 is also shown two trajectories of test electron under external fields influence. Assuming the test electron enters the gap region with vanishing velocities, it is observed that, whether electrical potential satisfies the condition $V_0 > V_H$– where $V_H = eB_0^2L^2/2m$ is called potential Hull and m and e are the mass and electric charge of the electron– the test electron has enough energy to reach the anode, as illustrated in detail (a) of the Fig. 1. On the other hand, whether $V_0 < V_H$ the test electron has not enough energy to reach the anode and the magnetic field deflects the test electron to cathode, as illustrated in detail (b) of the Fig. 1. In the smooth-bore magnetron system, there is a spatial symmetry and it is assumed the thermal cathode emits infinite charges sheets parallel to $x - z$ plane instead of single particles. Consequently, the particle distribution function on phase space $f(\mathbf{r}, \mathbf{p}, t)$ only depends on the y spatial coordinate and its evolution is dictated by Vlasov equation [10]

$$\frac{df}{dt} = \frac{\partial f}{\partial t} + \frac{\partial H}{\partial p_y}\frac{\partial f}{\partial y} - \frac{\partial H}{\partial y}\frac{\partial f}{\partial p_y} = 0, \tag{1}$$

ISBN: 978-3-95450-168-7 doi:10.18429/JACoW-IPAC2015-MOPWA003

OPTIMAL GENERALIZED FINITE DIFFERENCE SOLUTION TO THE PARTICLE-IN-CELL PROBLEM

X. Wang, Stony Brook University, Stony Brook, NY 11794, USA
R. Samulyak, Stony Brook University, Stony Brook, NY 11794, USA and BNL, NY 11973, USA
X. Jiao, Stony Brook University, Stony Brook, NY 11794, USA
K. Yu, Stony Brook University, Stony Brook, NY 11794, USA

Abstract

A new adaptive Particle-in-Cloud (AP-Cloud) method for obtaining optimal numerical solutions to the Vlasov-Poisson equation has been proposed. The traditional particle-in-cell (PIC) method, commonly used for solving this problem, is not optimal in terms of the balance of errors of the differential operator discretization and source integration; it is also inaccurate when the particle distribution is highly non-uniform. Our method replaces the Cartesian grid in the traditional PIC with adaptive computational nodes or particles, to which the charges from the physical macroparticles are assigned by a weighted least-square approximations. The partial differential equation is then discretized using a generalized finite difference (GFD) method and solved with fast linear solvers. The density of computational particles is chosen adaptively, so that the error from GFD and that from the source integration are balanced and the total error is approximately minimized. The method is independent of geometrical shape of computational domains and free of artificial parameters. Results of verification tests using electrostatic problems of particle beams with halo and comparison of accuracy and solution time of the AP-Cloud method with the traditional PIC are presented.

ERROR ANALYSIS OF TRADITIONAL PIC METHOD

Particle-in-cell [1] (PIC) is the traditional method for solving both the Vlasov-Poisson and Vlasov-Maxwell problems. In this work, we focus on the Vlasov-Poisson equation using an example of the electrostatic space charge problem for particle beams.

In PIC, the charge density at grid point $\rho(x^j)$ is estimated from the distribution of particles by interpolating particle charges to mesh nodes. Then the Poisson equation

$$\Delta\varphi = \rho \tag{1}$$

subject to a Dirichlet or Neumann boundary condition is discretized on the mesh. Performing error analysis of the PIC method, we can show that the total error is

$$O\left(\sqrt{\frac{\rho(x^i)}{Nh^D}} + \rho(x^i)h^2\right),$$

where N is the number of physical macroparticles, h is the cell size, and D is the space dimension. The error is minimized if

$$h = O\left(\frac{1}{N\rho(x^j)}\right)^{\frac{1}{4+D}},$$

which is impossible if a uniform mesh is used for a highly nonuniform particle distribution.

AP-CLOUD METHOD

Adaptive Particle-in-Cloud (AP-Cloud) method can be viewed as a meshless and adaptive version of PIC. We use computational particles instead of Cartesian grid, the distribution of which is derived using an error balance criterion. Instead of the finite difference discretization of the Laplace operator, we use the framework of weighted least squares approximation, also known as the generalized finite-difference (GFD) [2]. The framework includes interpolation, least squares approximation, and numerical differentiation on a stencil in the form of cloud of computational particles in a neighborhood of the point of interest. It is used for the charge assignment scheme, numerical differentiation, and interpolation of solutions.

The Particle-in-Cloud method operates as follows:

- Given a distribution of physical macro-particles, optimally select a subset of computational nodes (particles) from this distribution by constructing an octree and applying the error balance criterion
$$h = O\left(\frac{1}{N\rho(x^j)}\right)^{\frac{1}{2k+D-2}}$$
where h is the local averaged distance between computational macro-particles and k is the order of interpolation polynomial in the GFD method.
- Place computational particles on the boundary
- Enforce the 2:1 balance of inter-particle distances in the case of extreme density changes. The 2:1 balance requires that the difference between the levels of refinement of two neighbors is at most one, improving the smoothness in the placement of computational particles.
- Assign physical states to computational nodes and approximate differential operators in the location of computational nodes using GFD.
- Solve the corresponding linear system using a

Content from this work may be used under the terms of the CC BY 3.0 licence (© 2015). Any distribution of this work must maintain attribution to the author(s), title of the work, publisher, and DOI.

ISBN: 978-3-95450-168-7 doi:10.18429/JACoW-IPAC2015-MOPWA004

REFORMULATION OF THE ACTION AND PHASE JUMP METHOD TO OBTAIN MAGNETIC ERRORS IN THE LHC IRS*

Alba-Carolina Garcia-Bonilla , Javier Fernando Cardona†
Universidad Nacional de Colombia, Bogotá, Colombia

Abstract

One of the major problems when doing the commissioning of an accelerator is to identify and correct the linear components of magnetic errors. The Action and Phase Jump Technique is one of the available methods to perform this task. For this method to work, it is necessary to have one BPM measurement at the Interaction Region (IR), the region where the magnetic error is evaluated. In some cases, this BPM measurement become the biggest source of uncertainty when the action and phase jump technique is used. In this paper, a new formulation based on this method is presented. This new formulation doesn't make any use of BPM measurements at the IR, thereby allowing more robust error estimations. Quadrupole errors in the LHC lattice are estimated with this new formulation, using both, simulated data and LHC experimental data. A comparison with the previous formulation is included. The results on simulated data show that the reformulation leads to a reduction in the uncertainty, while for the experimental case, the reduction is not so clear. Explanations for this behavior and possible remedies will also be discussed.

INTRODUCTION

One of the main goals during commissioning of accelerators like LHC is to reduce the magnetic errors. The Action and Phase Jump Analysis Technique, also called Action and Phase method, or just APJ, is one of the available methods to perform magnetic error corrections. This method is based on the theoretical principle of preservation of the Action and Phase variables in absence of a magnetic error. The corrections are made locally and specially at the Interaction Regions (IR) of an accelerator. Its theoretical development is presented in the first part of [1].

Experimental studies using this method have been already presented. Different tests were run at RHIC in Brookhaven, for example using closed-orbit [2] or first turn orbit [3] data. In LHC, preliminary analysis had been done using turn-by-turn (TBT) orbits, these are [4] and [5].

In this paper, a reformulation of the APJ technique for linear error corrections will be presented. First, theoretical expressions will be shown and then a comparison between the previous and the new formulation, using simulated orbits, will be discussed. Finally, the results of proposed corrections using LHC data are reported.

* Thanks to Fundación Para la Promoción de la Investigación y la Tecnología del Banco de la República and DIB (División de Investigación de Bogotá)
† jcardona@unal.edu.co

THEORETICAL REFORMULATION FOR THE ACTION AND PHASE ANALYSIS

With the APJ method, the variables of Action (J) and Phase (δ) are measured from orbit data around the accelerator and then three regions are identified: the region which contains the magnetic error, a region (or subsection of the accelerator) before the error, and a region after the error. To calculate the magnetic errors the method uses the J and δ from the region before and after the error, and one transverse position from the error region.

The transverse position at the error region is inferred from one BPM measurement at the IR as described in [6]. In some cases, this BPM measurement can become the biggest source of uncertainty when the action and phase jump technique is used, because it is a single measurement while the other quantities involved to estimate the magnetic error are obtained from multiple measurements.

Keeping the theoretical framework of the Action and Phase method, given in [1], new equations are introduced that mainly start by changing equation (15) from that paper (the strength of the magnetic error), and ends in new equations for the magnetic errors estimations, which changes equations (22), (25) and (26).

The reformulation implies the following procedure. Equation (15) in [1] is

$$\sqrt{2J_0 + 2J_1 - 4\sqrt{J_0 J_1}\cos(\delta_1 - \delta_0)}/\sqrt{\beta_{z,i}(s_\theta)} = \theta_z \quad (1)$$

where J_n, δ_n are the average of the Action and Phase variables, for the region before $n = 0$ and after $n = 1$ the error, θ_z is the strength of the magnetic error, and $\beta_{z,i}(s_\theta)$ is the beta-function at the longitudinal position of the error. In addition, in terms of the multipolar components of the magnetic field, the strength of the magnetic error is written as equations (19) and (29) from [1], these are:

$$\begin{aligned}
\theta_x &= \mathbf{B}_0 - \mathbf{B}_1 x(s^\varepsilon) + \mathbf{A}_1 y(s^\varepsilon) + 2\mathbf{A}_2 x(s^\varepsilon) y(s^\varepsilon) + \\
&\quad + \mathbf{B}_2[-x^2(s^\varepsilon) + y^2(s^\varepsilon)] + \ldots \\
\theta_y &= \mathbf{A}_0 - \mathbf{A}_1 x(s^\varepsilon) + \mathbf{B}_1 y(s^\varepsilon) + 2\mathbf{B}_2 x(s^\varepsilon) y(s^\varepsilon) + \\
&\quad + \mathbf{A}_2[x^2(s^\varepsilon) - y^2(s^\varepsilon)] + \ldots.
\end{aligned} \quad (2)$$

where $\mathbf{B}_i$ and $\mathbf{A}_i$ are quantities related with the multipolar expansion of the magnetic field, and $x(s^\varepsilon)$, $y(s^\varepsilon)$ are the transverse coordinates of the orbit at the error position.

When several errors are present, equation (1) can be rewritten as:

$$\sqrt{2J_0 + 2J_1 - 4\sqrt{J_0 J_1}\cos(\delta_1 - \delta_0)} = \sum_i [\theta_{z,i}\sqrt{\beta_{z,i}(s_\theta)}] \quad (3)$$

Content from this work may be used under the terms of the CC BY 3.0 licence (© 2015). Any distribution of this work must maintain attribution to the author(s), title of the work, publisher, and DOI.

ISBN: 978-3-95450-168-7 doi:10.18429/JACoW-IPAC2015-MOPWA005

COMPARISON BETWEEN DIGITAL FILTERS AND SINGULAR VALUE DECOMPOSITION TO REDUCE NOISE IN LHC ORBITS USED FOR ACTION AND PHASE JUMP ANALYSIS*

Alba-Carolina Garcia-Bonilla, Javier Fernando Cardona†, UNAL, Bogota, Colombia

Abstract

One of the initial difficulties to apply the Action and Phase Jump (APJ) analysis to LHC orbits was the high level of noise present in the BPM measurements. On the other hand, the unprecedented number of turns for LHC allows us to use all sort of filters. In this paper, we evaluate the effectiveness of digital filters like the band-pass filter and compare them with a filter based on Singular Value Decomposition, when magnetic error estimations are made using a recent version of the APJ method. First, mainly results on simulated orbits with noise are presented, and then, plots and results are shown for the filters effect on experimental data. The analysis indicates that a combination of filters leads to measurements with the least uncertainty.

INTRODUCTION

The Large Hadron Collider (LHC) is a machine designed to have two beams of particles, which encounter each other in four points along a ring of 26.7 Km. The LHC system is capable of running and measuring all 2808 bunches of the beam. For this task, the Beam Position Monitors (BPMs) have a much wider bandwidth than previous colliders [1].

A requirement for optical measurements is that each beam uses only one single bunch for security reasons. Therefore, with the wide bandwidth of the BPMs, the measurements have a considerable amount of noise when compared to others accelerators.

On the other hand, the unprecedented number of turns available per measurement in the LHC allows us to use all sort of filters to drastically reduce such noise, some of which have been already presented [2–5].

In this paper, we evaluate the effectiveness of digital filters like the band-pass filter and compare them with a filter based on Singular Value Decomposition, which is currently used in the LHC. First, the results of the filters and its combinations on simulated orbits are presented, and then, results from experimental data with the same filters are shown.

The technique used to measure the magnetic errors is the Action and Phase Jump Analysis (APJ), in particular, the new formulation, explained in [6].

DIFFERENT WAYS TO REDUCE NOISE

During this investigation, initially, we studied the effectiveness of the dual band-pass filter (described in [2]) in reducing the noise. This, by using the signal-to-noise (STN) ratio quantity, which is independent of the technique used to obtain the magnetic errors. Trials to separate the noise from the signal were performed, like taking the difference of the orbit with and without noise after using the filter. Generally, the filters change the output signal amplitude, so we applied the filter for both, the signal before adding noise and the signal with noise to have a comparison.

It was found that generally the noise is reduced more faster than the amplitude, as the bandwidth ($\Delta\omega$) of the dual pass-band filter decreases. Sometimes there was an optimum $\Delta\omega$ which was different depending on the magnetic error[1].

Also, we developed studies for the sensitivity of the band-pass filter with frequency. Initially, fictitious sinusoidal signals with fraction frequencies between 0.0 and 0.5 (like in the real accelerator) were used, and it is found that the filter is effective at any of these frequencies. Actually, the filter changes a bit the Fourier frequency at the points closer to the central band but this is not a problem to obtain the magnetic errors as proposed. Later this was corroborate with some Mad-X simulations for the LHC.

Therefore, the most convenient way to apply the band-pass filter is to do a simulation curve to establish a range for the optimal band-width according to the experimental conditions. The type of curves proposed are discussed later.

To reduce noise on turn-by-turn orbits in the LHC, the filters that have been used are: a filter based on the average of many orbits (*Prom*) [3], a dual band-pass filter (*Band*) [2], and a filter based on singular value decomposition (*Svd*) [4], Combinations of these filters can be built and the following cases are analyzed:

1. Prom
2. Band
3. Svd
4. BandProm
5. SvdProm
6. BandSvdProm
7. SvdBandProm

Composed names like "BandProm" means that the band-pass filter is applied and then the "Prom" filter.

RESULTS ON SIMULATIONS

The comparison between the studied filters are based on the exactness and precision of the measurements obtained from LHC orbits using the APJ method.

Although it is not possible to compare a simulation with the experimental data because not all what is happening in reality can be modeled in the simulation, a simulation close

* Thanks to *Fundación Para la Promoción de la Investigación y la Tecnología del Banco de la República* and *DIB (División de Investigación de Bogotá).*

† jfcardona@unal.edu.co

[1] During these studies, the most effective bandwidth changes according with the type of error, the transverse plane used, and even more with the amount of noise

Content from this work may be used under the terms of the CC BY 3.0 licence (© 2015). Any distribution of this work must maintain attribution to the author(s), title of the work, publisher, and DOI.

ISBN: 978-3-95450-168-7 doi:10.18429/JACoW-IPAC2015-MOPWA006

Content from this work may be used under the terms of the CC BY 3.0 licence (© 2015). Any distribution of this work must maintain attribution to the author(s), title of the work, publisher, and DOI.

CORE-HALO LIMIT AS AN INDICATOR OF HIGH INTENSITY BEAM INTERNAL DYNAMICS

P.A.P. Nghiem*, M. Valette, N. Chauvin, N. Pichoff, D. Uriot
CEA/DSM/IRFU, Centre de Saclay, 91191 Gif-sur-Yvette cedex, France

Abstract

The dynamics of high-intensity beams is mainly governed by their internal space charge forces. These forces induce emittance growth and halo generation. They contribute to shape the beam density profile. As a consequence, a careful analysis of this profile can help revealing the internal dynamics of the beam. This paper recalls the precise core-halo limit determination proposed earlier, then studies its behaviour through a wide range of beam profiles and finally shows its relevance as an indicator of the limit separating the two specific space charge field regimes of the core and the halo.

INTRODUCTION

In high intensity accelerators, the outermost part of the beam, although tenuous, is often the object of great attention. Indeed, the halo is the main contributor to particle losses downstream, which must be maintained under specified levels. There is nevertheless no consensus on a definition of the halo [1]. Yet there is a real need of precisely and quantitatively defining halo. Simulations of halo generation and halo growth all need to know how much halo has been generated or how much it has grown. For halo measurement or halo cleaning there is a need to know what to measure and what to clean.

In this paper, we first recall the existing definitions of halo and study their relevance through a great variety of different density profiles. Then we point out the particular relevance of the definition we proposed earlier by showing that it is a good indicator of the beam internal dynamics.

EXISTING DEFINITIONS

Halo definitions often consist in comparing beam characteristics somewhere "far from" and "close to" beam centre. Are considered the ratio of particles contained in n times rms emittance to those contained in rms emittance, or the ratio of emittance containing x% of particles to rms emittance, with generally n>3 and x> 90%. But to be relevant, n or x must be adjusted to each particular density profile, according to visual inspection in most cases. This makes difficult studies of halo evolution that comes with beam shape evolution.

To our knowledge, there exist only two definitions able to be applied to any density profile.

The first one, widely used, stated that halo can be characterised by the parameter h, defined as ratio of the fourth to the square of the second invariant moment [2]. This corresponds to the profile kurtosis or "peakedness". Thus, the higher the kurtosis is, the larger the halo would be. This definition, valid for a 1D projection, was later extended to a 2D phase space [3].

The second definition started from considering the extreme case of a uniform core surrounded by a tenuous halo, where the core-halo limit is indisputably at the foot of the discontinuity in density ρ, i.e. where there is an infinite change in the slope of ρ. For a more general case of continuously varying density, it is proposed that the core-halo limit is where there is the biggest change in slope, that is where the second derivative ρ" is maximal [4, 5]. Once this limit precisely known, it is then possible to define the parameters PHS and PHP, which are respectively the Percentage of Halo Size and Percentage of Halo Particles.

The relevance of the parameters h, PHS and PHP can be studied through their behaviour for a great variety of different density profiles.

FOR DIFFERENT DENSITY PROFILES

For this study, without lack of generality, it is enough to consider the cases of cylindrically symmetric beam where the density profile depends only on the radius, ρ(r). For the sake of comparison, we state that the beam external limit is where density decreases down to 10^{-6} of its maximum.

Let us consider first the large family of density profiles described by the Generalized Gaussian functions:

$$\rho(r) = \rho_0 e^{-\left|\frac{r}{\alpha\sqrt{2}}\right|^{\beta}}. \tag{1}$$

For given parameters ρ_0 and α (both fixed to 1 here), different profiles can be described by varying continuously β from ∞ (uniform) to 2 (Gaussian), and even ≤ 1 (sharply convex). The first six graphs of Fig. 1 shows some typical examples of such profiles ρ together with its second derivative ρ" of which the location of maximum marks the core-halo limit (black curves). The first graph of Fig. 2 gives the corresponding h, PHS, PHP. The regular decrease of all these parameters would let us think that h on one side and PHS, PHP on the other are compatible for this type of density profile [6]. The h parameter would combine the two information of halo size and halo particles, while PHS and PHP can analyse them separately. However, for more particular profiles like triangular or parabolic ones (two last graphs of Fig. 1), the kurtosis of the first profile is three times bigger than that of the second, while PHS=PHP=0 for both profiles, meaning no halo, as expected for profiles decreasing abruptly to zero.

The cases of a core and a halo described by the sum of two Gaussians can also be examined:

* phu-anh-phi.nghiem@cea.fr

ISBN: 978-3-95450-168-7 doi:10.18429/JACoW-IPAC2015-MOPWA007

THE SARAF-LINAC BEAM DYNAMICS

N. Pichoff, B. Dalena, D. Uriot, CEA/IRFU, Gif-sur-Yvette, France

Abstract

SNRC and CEA collaborate to the upgrade of the SARAF Accelerator to 5 mA CW 40 MeV deuteron and proton beams (Phase 2). This paper presents the beam dynamics in the reference design of the SARAF-LINAC, from the 4 m long 176 MHz RFQ to the HWR Superconducting linac's end. The beam losses, mostly in longitudinal direction, estimated from error studies, are compared with acceptable losses defined for hands-on maintenance.

INTRODUCTION

Israeli's SNRC solicited CEA (France) to contribute to the development of phase 2 of the SARAF accelerator [1].

In order to deliver 5 mA beams of deuteron up to 40 MeV and protons up to 35 MeV, CEA proposed a SARAF-LINAC reference design made of:

- an optional 4-vane RFQ bunching and accelerating 5 mA-cw beams from 20 keV/u to 1.3 MeV/u,
- a MEBT measuring, cleaning and matching the beam to
- a superconducting linac accelerating the beams to 40 MeV deuteron or 35 MeV proton,
- and the associated local control systems.

This design is based on beam dynamics calculations made with TraceWIN codes package developed at CEA [2] where the beam is represented by about 1M macro-particles.

RFQ SIMULATIONS

The initial beam will be delivered by SARAF's source and LEBT built during phase 1. Measurements 1.4 m upstream the RFQ exhibit that the beam RMS normalized emittance is around (and even below) 0.2 π.mm.mrad [3]. Therefore, we considered as simulation input deuteron and proton beams of 0.2 π.mm.mrad rms emittance with a Gaussian distribution truncated to ±4 sigmas (Fig.1). In the reference design [1], the 3.85 m long, 4-vane RFQ proposed by CEA is considered. It has:

- a constant 4 mm average radius R0, except at entrance and exit where it is increased to 6 mm in a few cells to reduce the input/output beam con/divergence.
- a constant voltage limited to 70 kV corresponding to a peak field of 1.6 Kp,
- a maximum sine vane modulation of 2.

The input energy is 20 keV/u and the output energy is 1.3 MeV/u. The matched beams density profiles are plotted on Fig. 2. The exit beam phase-space distribution of deuteron beam is plotted in Fig. 3. Please note that all the densities plotted in this paper are in logarithm scale.

Good transmission, low longitudinal emittance (Table 1) and no transverse emittance growth are observed.

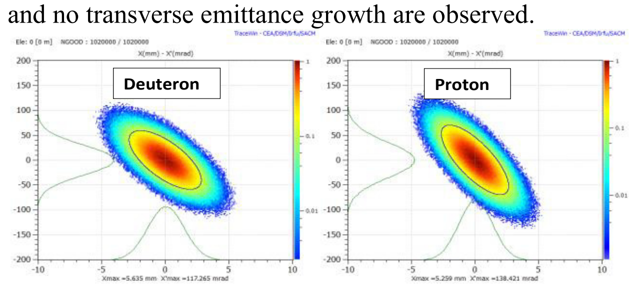

Figure 1: Input beam (x,x') distributions (matched to RFQ).

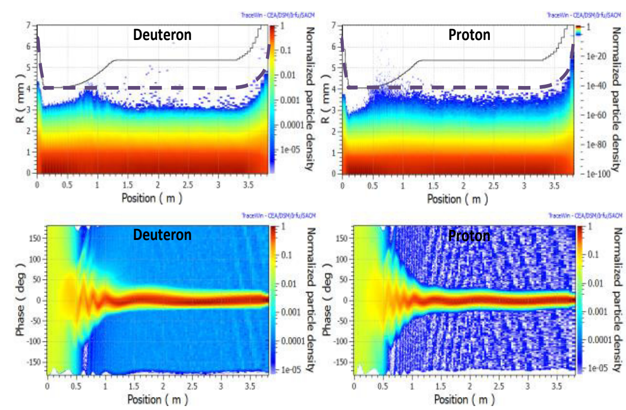

Figure 2: Matched beam density profiles in the RFQ.

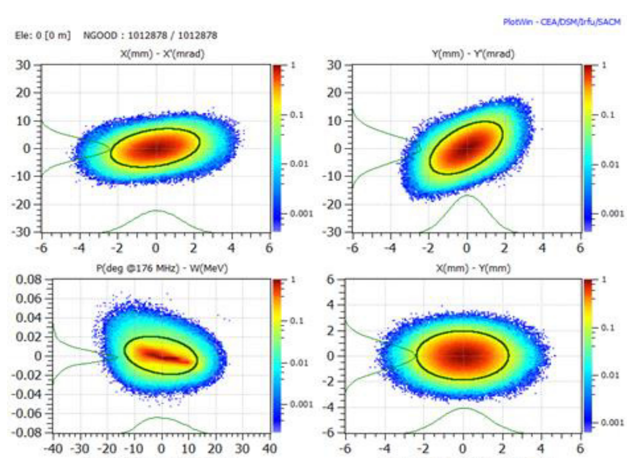

Figure 3: Deuteron beam phase-space distributions at RFQ exit.

Table 1: RFQ Performances

Particle	Transmission	Long. Rms emittance π.mm.mrad (π.°.keV/u)
Deuteron	99.3% (70 kV)	0.161 (31.8)
Proton	99.9% (50 kV)	0.194 (38.4)

© Content from this work may be used under the terms of the CC BY 3.0 licence (© 2015). Any distribution of this work must maintain attribution to the author(s), title of the work, publisher, and DOI.

ISBN: 978-3-95450-168-7 doi:10.18429/JACoW-IPAC2015-MOPWA008

STATUS OF TRACEWIN CODE*

D. Uriot#, N. Pichoff
CEA-Saclay/DSM/Irfu/SACM, Gif-sur-Yvette, France

Abstract

Well known in the community of high-intensity linear accelerators, the transport code TraceWin is able to simulate a beam from the source to the target using either simple linear model or multiparticle simulations including 2D or 3D space-charge. Continuously developed at CEA Saclay since 15 years, it is today the reference code for projects such IFMIF, ESS, MYRRHA, SPIRAL2, IPHI, SARAF... The accuracy of his predictions associated with an original and powerful GUI and its numerous features have made its success, with a community of 200 users worldwide in 45 laboratories. It is now used on a larger perimeter that its initial skills. The aim of this paper is to summarize the TraceWin capabilities, including implemented last ones.

INTRODUCTION

The TraceWin code was initially developed to fulfil the special requirement of high intensity linear accelerators. It has been maintained by CEA Saclay, France for more than 15 years. Since 2009, it is distributed under a CEA commercial license, required for each identified user to pay an annual symbolic financial contribution. Due to this special status allowing users to request specific developments and our willingness to help them as fast as possible, the code has been gradually enriched with new features and advanced tools to finally become a global tool box oriented to accelerator design and realistic simulations.

One of the main specificity of TraceWin, probably unique in the plethora of existing codes, is to make possible to run different models with various levels of sophistication. Thus, model complexity can be gradually increased from envelope optic with hard edge linearized elements and space-charge to massive tracking 3D simulations using PIC space-charge, field maps, and use of automatic tuning procedures in realistic (imperfect) accelerators.

MAIN FEATURES

Software

Six versions of the software are available for 32 and 64 bits Mac, Linux and Windows operating systems. They all use common very powerful GUI, figure 1, allowing to compute, print and plot all quantities of interest of the accelerator and the beam. A free limited version for test or the last full version release can be downloaded at http://irfu.cea.fr/Sacm/logiciels/index3.php. Six associated batch versions and a dedicated server allow automatic run of the code on a multicore computer network.

*http://irfu.cea.fr/Sacm/logiciels/
#didier.uriot@cea.fr

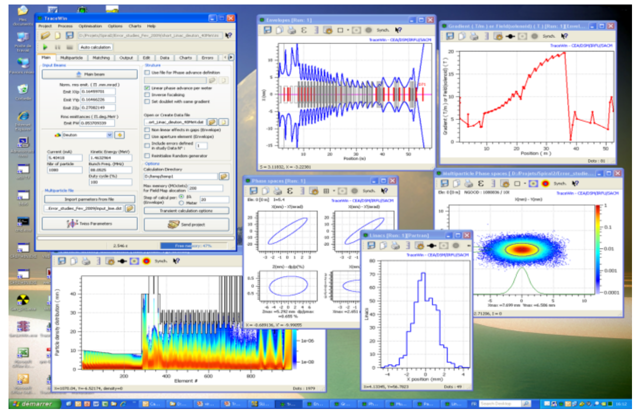

Figure 1: TraceWin screenshot example.

Even if originally dedicated to high intensity proton linacs, it is today used for more exotic applications, like electron machine, spectrometer, ILC IP [1]… A simulation with up to 10^8 particles can be easily made on a multicore desktop in one day.

TraceWin Main Features

Here are the main features of TraceWin code:

- a full documentation including examples,
- electrons and ions transport, with distribution generated/red in several format,
- envelopes and macro-particle tracking modes on multi-core machines,
- fully compatible with the free independent beam plot/analysis tool: PlotWin [2],
- a wide range of elements (see next page) with possible user-defined ones,
- linear and PIC 2D and 3D space-charge routines with possible user-defined ones,
- automatic beam tuning procedures (possibility to use diagnostics),
- dynamics charts allowing to visualize machine and beam behaviors during matching and tuning,
- beam scattering on residual gas,
- H- stripping on residual gas or in magnetic field,
- possible transport of two beams in the same structure,
- exhaustive error studies using a Monte-Carlo approach, based on a client/server architecture and a statistical analysis module,
- Halo [3] and beam loss analysis with location of particle loss.
- transient time module (figure 2),
- acceptance calculation,
- Hofmann stability diagram.

Content from this work may be used under the terms of the CC BY 3.0 licence (© 2015). Any distribution of this work must maintain attribution to the author(s), title of the work, publisher, and DOI.

ISBN: 978-3-95450-168-7 doi:10.18429/JACoW-IPAC2015-MOPWA009

CHANNELING RADIATION EXPERIMENT AT FERMILAB ASTA

D. Mihalcea, Northern Illinois University, DeKalb, IL 60115, USA
D. R. Edstrom, Fermilab, Batavia, IL 60510, USA
P. Piot, Northern Illinois University, DeKalb, IL 60115, USA
and Fermilab, Batavia, IL 60510, USA
W. Rush, Kansas University, Lawrence, KS 66045, USA
T. Sen, Fermilab, Batavia, IL 60510, USA

Abstract

Electron beams with moderate energy ranging from 4 to 50 MeV can be used to produce x-rays through the Channeling Radiation (CR) mechanism. Typically, the x-ray spectrum from these sources extends up to 140 keV and this range covers the demand for most practical applications. The parameters of the electron beam determine the spectral brilliance of the x-ray source. The electron beam produced at the Fermilab new facility Advanced Superconducting Test Accelerator (ASTA) meets the requirements to assemble an experimental high brilliance CR x-ray source. In the first stage of the experiment the energy of the beam is 20 MeV and due to the very low emittance ($\approx$ 100 nm) at low bunch charge (20 pC) the expected average brilliance of the x-ray source is about 10^9 photons/[s-(mm-mrad)^2-0.1%BW]. In the second stage of the experiment the beam energy will be increased to 50 MeV and consequently the average brilliance will increase by a factor of five. Also, the x-ray spectrum will extend from about 30 keV to 140 keV.

INTRODUCTION

Channeling radiation (CR) is generated by charged beams (typically electrons or positrons) passing through a crystal parallel with a crystallographic plane [1]. Electrons may oscillate perpendicular to the plane and generate CR which propagates in the same direction as the incident beam. The frequency of the CR is given by $\omega = 2\gamma^2\omega_0/(1+\gamma^2\theta^2)$ and depends on beam energy (the relativistic factor γ) on crystal lattice (ω_0) and on the observation angle θ. Due to $\propto \gamma^2$ beam energy dependence the CR can reach the x-ray domain even for moderate electron energy (4 to 50 MeV) which means that relatively small accelerators can be used to build compact x-ray sources [2].

For beam energies below about 100 MeV, the X-ray spectrum consists of discrete lines and an accurate description of the CR requires a quantum mechanical calculation. Still, some of the classical interpretations are valid and offer an understanding of the requirements for the incident electron beam. In planar channeling the beam electrons oscillate quasi harmonically perpendicular to a certain crystal plane. Since the electron oscillation amplitude is limited by the inter-planar distances, the kinetic energy associated with the transverse motion can be related to the maximum potential energy V_{max}. The angle of the incident electrons is limited by a critical channeling angle related to V_{max}: $\Psi_c = \sqrt{\frac{V_{max}}{pv}}$ where p and v are electron momentum and velocity respectively. With diamond as the crystal material, the depth of the potential in the (1,1,0) channeling plane is 23.8 eV. Hence the critical angle at 20 MeV is 1.54 mrad while at 50 MeV, it is 0.98 mrad. The value of the critical angle measured at SLAC [3], for diamond and electron beam energy of 23 GeV is 44 μrad. Scaling this value with beam energy as $E^{-1/2}$ yields 0.94 mrad at 50 MeV, in good agreement with the theoretical value.

The figure of merit of the CR x-ray source is given by the spectral brilliance $B = dN/[(d\omega/\omega)\cdot d\Omega\cdot dA\cdot dt]$ defined as the number of photons per second emitted within solid angle $d\Omega$, from area dA, and within a relative spectral bandwidth $d\omega/\omega$. The expression for spectral brilliance in terms of electron beam parameters [4] can be written as::

$$B_{av} = \frac{I_{av}}{e}\cdot\frac{\gamma^2 Y\cdot\sigma_e'^2\times 10^{-3}}{\epsilon_n^2\cdot\Delta E_\gamma/E_\gamma}Erf[\frac{\psi_C}{\sigma_e'}] \quad (1)$$

where I_{av} is the average electron beam current, e elementary electron charge, γ Lorentz factor, Y photon yield per electron and unit solid angle, σ_e', electron beam angular spread, ϵ_n normalized transverse emittance and $\Delta E_\gamma/E_\gamma$ relative spectral bandwidth and the error function accounts for the fraction of the beam within the critical angle.

The average current (over one second) I_{av} in Eq. 1 is proportional with charge per micro-pulse q, laser sampling rate f_L, RF duration pulse ΔT_{RF} and the RF repetition rate R:

$$I_{av} = q\cdot f_L\cdot\Delta T_{RF}\cdot R \quad (2)$$

In this paper we briefly present the relevant components of Fermilab ASTA beamline, preparations for the experiment and the expectations for CR properties as they are derived from theoretical models applied to our specific beam properties. Previous high brightness channeling experiments were reported [5] from the Elbe facility at Helmholtz-Zentrum Dresden-Rossendorf (HZDR) in Germany.

EXPERIMENTAL SETUP

At ASTA the nominal values for the parameters in Eq. 2 are: bunch charge q = 3.2 nC, laser sampling rate f_L = 3 MHz, macro-pulse duration ΔT_{RF} = 1.0 ms and repetition rate T = 5 Hz. The nominal energy is 50 MeV but in the first stage of the experiment "CAV1" (Fig. 1) will not be installed and the kinetic energy will be about 20 MeV. The

Content from this work may be used under the terms of the CC BY 3.0 licence (© 2015). Any distribution of this work must maintain attribution to the author(s), title of the work, publisher, and DOI.

ISBN: 978-3-95450-168-7 doi:10.18429/JACoW-IPAC2015-MOPWA010

EMITTANCES OF THE CORE AND OF THE HALO

Matthieu Valette, Phu Anh Phi Nghiem, CEA/IRFU, Gif-sur-Yvette 91191 France

Abstract

In high intensity accelerators, the beam is often space charge dominated. The density profile then takes a shape very different from a Gaussian one, with a more or less sharp core and a more or less compact halo. Furthermore, the core and the halo can be differently focused and thus differently oriented in the phase spaces. In these conditions, classically characterizing the beam by a global set of RMS values, namely Emittance and Twiss parameters, is not enough meaningful. This paper extends the core-halo limit defined earlier in 1D real space [1] to the 2D phase space, allowing to define for the very first time Emittances and Twiss parameters for the core and the halo separately. Applications to some typical beam distributions are given as an example of more appropriate beam characterization for high intensity linacs.

THE CORE-HALO ISSUES

In high intensity linacs, the space charge induces strong self-repelling electric forces on the particle beam. These nonlinear internal forces can lead to emittance growth and halo formation, two linked phenomena leading to an increased beam size and particle losses on the beam pipe. As beam power increases with beam energy and intensity, the beam power rapidly increases in high intensity linacs; furthermore, with increasing halo proportion, the power stored in it can become significant. A special attention should thus be brought to the halo behaviour and not only to the beam core. Halo quality is also important in high intensity machines.

A common practice in the design or the tuning of an accelerator is to minimize global emittance growth, but halo quality is also important in high intensity machines. Halo scraping equipment is frequently installed to limit the extension of the halo. However a widespread definition of what and where the halo is has yet to be agreed upon [2]. It is also true that a definition for halo has to suit each experiment's application, constraint and typical beam profile.

Regarding beam dynamics, the central dense core and the surrounding thinner halo are subject to different space charge force regimes [3]. As a consequence their dynamics are different and need to be studied separately.

Gaussian-like beam distributions are very common in accelerators and defining the halo as particles further than a certain number of standard deviations in this case is only natural. In high intensity linacs though, the low energy and thus high perveance makes the beam sensible to space charge effects. As a consequence beam distributions are often far from Gaussian.

A precise determination of the core-halo limit is thus needed and was proposed in [1, 4]. Such a limit allows to know whether a particle is part of the halo or not and to study the specific characteristics of the core and the halo.

A PRECISE DETERMINATION OF THE CORE-HALO LIMIT

We will here recall the one dimensional criterion defined to determine the precise location of the core-halo limit. This criterion originated from considering the extreme case of a uniform core surrounded by a tenuous halo, where the core-halo limit is indisputably at the foot of the discontinuity in density ρ, i.e. where there is an infinite change in the slope of ρ. For a more general case of continuously varying density, it is proposed that the core-halo limit is where there is the biggest change in slope, that is where the second derivative ρ'' is maximal [1, 4]. Once this limit precisely known, it is then possible to define the parameters PHS and PHP, which are respectively the Percentage of Halo Size and Percentage of Halo Particles.

The interest of such a limit is that it corresponds to a transition from two different space charge fields [3].

A TWO DIMENSIONAL EXTENSION OF THE METHOD

The work presented here is an extension of the previously mentioned criterion to two dimensional distributions $\rho(x,y)$ in any phase space. The general algorithm used to determine such a two dimensional core-halo limit is detailed and applications to some examples are displayed.

The two dimensional distribution is first converted into a two dimensional histogram. The "good" number of bins is given by: $NbBins = SizeRatio * \sqrt[4]{NbParticle}$, where *SizeRatio* was fixed to 3.0 by calibration of the algorithm on various distributions. This allows keeping statistical noise to a constant level, as explained in [5].

Several zooms or rescaling are then performed in order to maximize resolution. The Twiss parameters (for a phase-space distribution) or covariance matrix (for a general case) are calculated and the histogram is shifted to normalised coordinates in order to have a round beam. Another set of zooms and rescaling is then done before starting the so called “wheel” algorithm.

Around the centroid of the beam, cross sections of the beam with regular angles in normalised coordinates are performed. This would allow having iso-density curves perpendicular to the cross sections in case of elliptically symmetric beams. The length of the cross section on each side of the centre is then adjusted to maximise resolution. The interpolated local densities are converted to a one-dimensional histogram with the same number of bins as

Content from this work may be used under the terms of the CC BY 3.0 licence (© 2015). Any distribution of this work must maintain attribution to the author(s), title of the work, publisher, and DOI.

ISBN: 978-3-95450-168-7 doi:10.18429/JACoW-IPAC2015-MOPWA011

THE DAMPING OF TRANSVERSE COHERENT INSTABILITIES BY HARMONIC CAVITIES

F. Cullinan*, R. Nagaoka, Synchrotron SOLEIL, Gif-sur-Yvette, France
G. Skripka, P. F. Tavares, MAX IV Laboratory, Lund, Sweden

Abstract

At nonzero chromaticity, the threshold current due to transverse coupled bunch instabilities in an electron storage ring is defined by intrabunch head-tail motion of higher than zeroth order. Multibunch tracking simulations predict that this threshold can be increased to several times its original value through the introduction of bunch lengthening harmonic cavities. One previously suggested explanation is the narrower spectra of the elongated bunches but reliable estimates for the threshold currents are not obtainable for anything other than rigid beam motion since the usual Sacherer formalism is not directly applicable to beams in a non-harmonic potential. A new scheme has been developed in which the decay time of a higher than zeroth order transverse head-tail mode may be estimated by taking into account the synchrotron tune spread generated by the harmonic cavity potential. This scheme is presented along with the results of numerical simulations performed in order to confirm the analytical predictions and justify the assumptions made. The extension of the scheme to more complex scenarios is also discussed.

INTRODUCTION

Many present and future light sources based on an electron storage ring make use of passive or active harmonic cavities (HCs) [1] [2] [3]. In most cases, these are used to lengthen the electron bunches, thus reducing the impact of intrabeam scattering and allowing for a higher beam current while maintaining the same small transverse emittance. HCs work by modifying the radio frequency (RF) potential in which the electron bunches are confined longitudinally. Since the potential is no longer quasi-harmonic, the synchrotron tune of a single particle is no longer approximately independent of its amplitude of synchrotron oscillation. The stronger amplitude dependence results in a large tune spread within a bunch and Landau damping of longitudinal instabilities [4].

The use of harmonic cavities has important consequences in the transverse plane, particularly regarding head-tail motion. A head-tail mode describes coherent motion within a bunch. At the lowest order ($m = 0$), this is a dipole oscillation of the whole bunch while at higher order, there is a change in betatron phase along the bunch so that there is some longitudinal structure to the transverse oscillation with nodes and antinodes. The effect of nonzero chromaticity is to add a further modulation of the transverse motion at the chromatic frequency, shifting its spectrum in the frequency domain. Head-tail motion is important for multibunch instabilities since the collective motion of multiple bunches is strongly linked to the overall motion of each individual bunch.

A HC lengthened bunch corresponds to a narrower range of frequencies and so a small positive chromaticity is more effective in decoupling the zeroth order head-tail mode from the damaging impedance at negative frequency, so called head-tail damping. Frequency domain calculations therefore show a significant improvement in coupled bunch instability threshold currents for the $m = 0$ mode [5]. As the chromaticity is increased further, for a single RF system, the threshold current would then be limited by the presence of a first order head-tail mode which is not damped since its spectrum peaks at a negative frequency. However, because of the synchrotron tune spread from the HC-modified potential, the higher than zeroth order head tail modes will no longer remain coherent indefinitely as they would in a harmonic potential. Studies of this regime with HCs are therefore, at present, limited to multiple particle tracking and although these simulations show that an improvement in the current threshold is maintained [6], it can no longer be attributed solely to the lengthening of the bunch. This paper attempts to quantify the contribution of the synchrotron tune spread.

THEORY

The position of a particle in longitudinal phase space can be expressed using cartesian coordinates τ and δ where the former is the arrival time with respect to the synchronous particle ($\tau > 0$ refers to the head of the bunch) and the latter is the energy deviation normalised by the design energy. Using, as an approximation, a sinusoidal oscillation at synchrotron tune Q_s, the motion of a particle in longitudinal phase space can be expressed as

$$\tau = \hat{\tau}\cos(\omega_s(\hat{\tau})t + \psi_0) \quad (1)$$

$$\delta = -\frac{\dot{\tau}}{\alpha_c} = \frac{\omega_s(\hat{\tau})}{\alpha_c}\hat{\tau}\sin(\omega_s(\hat{\tau})t + \psi_0) \quad (2)$$

where $\hat{\tau}$ is the synchrotron amplitude, ψ_0 is the synchrotron phase at $t = 0$, α_c is the momentum compaction factor and $\omega_s = Q_s\omega_0$ is the angular synchrotron frequency for angular revolution frequency ω_0. ω_s has been expressed as a function of the amplitude $\hat{\tau}$ so that the equations can approximate nonharmonic potentials, ignoring the inevitable harmonics that these introduce.

Longitudinal phase space can be normalised and converted into convenient polar coordinates (r, θ) by multiplying the δ coordinate by $\alpha_c/\omega_s(r)$. A particle's synchrotron amplitude and phase can then be determined from its position in synchrotron phase space. Under the current approximation, $\hat{\tau} = r$ and $\psi_0 = \theta - \omega_s(\hat{\tau})t$ [7].

* francis.cullinan@synchrotron-soleil.fr

Content from this work may be used under the terms of the CC BY 3.0 licence (© 2015). Any distribution of this work must maintain attribution to the author(s), title of the work, publisher, and DOI.

ISBN: 978-3-95450-168-7 doi:10.18429/JACoW-IPAC2015-MOPWA012

STUDY OF OPTIMAL MBA LATTICE STRUCTURES FOR THE SOLEIL UPGRADE

R. Nagaoka, P. Brunelle, F. Cullinan, X.-N. Gavaldà, A. Loulergue, A. Nadji, L.S. Nadolski, M.-A. Tordeux, Synchrotron SOLEIL, Gif-sur-Yvette, France

Abstract

Within the context of a future upgrade of SOLEIL, the present paper reports on the low emittance lattice design studies made using 7BA and 6BA cells in the SOLEIL ring. With this combination of the MBA lattices, it is found that the horizontal emittance in the range below 200 pm·rad can be achieved by basically keeping the optical functions in the straight sections unchanged as in the previous 5BA-4BA solutions. In particular, a solution giving the horizontal emittance of 145 pm·rad with the use of longitudinal gradient bends (LGBs) is shown. On the other hand, the required transverse gradients in quadrupoles and combined dipoles as well as the chromaticities increase significantly as anticipated. Future directions including the ways to improve the encountered difficulties are considered.

INTRODUCTION

SOLEIL is the French third generation light source routinely operated for users since 2007 with a low emittance electron beam of 3.91 nm·rad in high intensity multibunch and temporal structure (e.g. 8 bunches) modes (cf. Table 1) [1]. After nearly 9 years of successful operation, a series of feasibility study is launched towards a possible future upgrade of the lattice with a significantly lower emittance. The approach taken is to employ whatever useful methods in lowering the emittance by fully respecting the geometric constraints such as the circumference of the ring and the available straight sections, so not to impact the existing insertion device based beamlines.

Table 1: Main SOLEIL Parameters as of Today

Energy	2.75 GeV
Circumference	354.097 m
Nominal current	430 mA (multibunch mode), 8×12 mA (8-bunch mode)
Horizontal emittance ε_x	3.91 nm rad
Adjusted emittance ratio	1%
Betatron tunes (ν_x, ν_z)	(18.174, 10.232)
RF frequency f_{RF}	352.2 MHz

As a first of such studies, the use of longitudinal field variations of superbends was attempted in a 4BA cell, finding a zero dispersion solution with the horizontal emittance ε_x of 0.98 nm·rad [2]. A particularity of SOLEIL is the short straight sections (SDCs) inserted between the dipoles of half of the 16 double-bend (DB) cells, to provide 8 additional straight sections for users. The SDCs however tend to limit the number (M) of dipoles introduced in those cells. Here we shall refer to cells with and without SDCs as SDM-SDC-SDM and SDL-SDM, respectively. In the second studies, a combination of 5- and 4BA was followed [3,4], where the use of longitudinal gradient bends (LGBs) allowed the emittance to reach 440 pm·rad [4]. In the framework of developing an optimal MBA lattice for SOLEIL, the axis towards the limit of the achievable lowest emittance must also be pursued. An approximate formula for the theoretical minimum emittance (TME) in a ring composed of alternating M_1BA and M_2BA cells may be given by

$$\varepsilon_x^{TME} = \frac{1}{8\sqrt{15}}\frac{C_q\gamma^2}{J_x}\theta_0^3\cdot\left\{\frac{1}{\left[2+(M_1-2)3^{1/3}\right]^3}+\frac{1}{\left[2+(M_2-2)3^{1/3}\right]^3}\right\}, \quad (1)$$

where θ_0 denotes the total bending angle per cell and other symbols have their usual meanings [5]. The above expression extends the derivation found in Ref. 6 for a MBA cell composed of 2 outer dispersion suppressing dipoles and (M-2) inner dipoles, all having the same field but differing in length between the two groups. The TME condition is imposed on each dipole. The optimal ratio between the inner and outer dipoles lengths to minimize the emittance is found to be $1/3^{1/3} \approx 0.69$ and is applied in the formula. Plotting the emittance for several different values of M_1 and M_2 in proportion to the relation given by Eq. 1, by normalizing the $M_1 = M_2 = 2$ case to the present SOLEIL value, suggests that an emittance lower than 200 pm·rad could be reached if a combination of 7BA and 6BA is considered (Fig. 1).

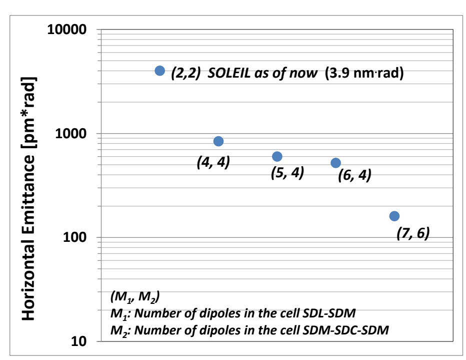

Figure 1: An estimate of attainable emittance in a lattice composed of alternating M_1BA and M_2BA using Eq. 1.

In the following, application of a 7BA-6BA lattice in the SOLEIL ring and obtained solutions are presented.

LATTICE STRUCTURE CONSIDERED

As already said, the SOLEIL ring with its extended DB lattice is optimized to provide as much as 46% of its

Content from this work may be used under the terms of the CC BY 3.0 licence (© 2015). Any distribution of this work must maintain attribution to the author(s), title of the work, publisher, and DOI.

ISBN: 978-3-95450-168-7 doi:10.18429/JACoW-IPAC2015-MOPWA013

MODELING AND MEASUREMENTS OF SPIN DEPOLARIZATION

N. Carmignani, F. Ewald, L. Farvacque, B. Nash, P. Raimondi, ESRF, Grenoble, France

Abstract

An electron bunch in a storage ring becomes spin polarized due to the Sokolov-Ternov effect. The beam may then be depolarized by applying a horizontal magnetic field oscillating in resonance with the spin tune. This technique has been used to measure the electron energy at numerous synchrotrons. In this paper, we report on modeling and measurements of the polarization and depolarization process at the ESRF. We report the results of a Matlab based parallelized spin tracking code that we developed for these studies. We show the change in depolarization resulting as different physical effects are added to the model.

SPIN DYNAMICS

Each electron in a beam has a spin which may be represented as a point on a sphere $\vec{S}_j$. The polarization of the beam may then be defined as $\vec{P} = \frac{1}{N}\sum_j \vec{S}_j$, where N is the number of particles.

An electron beam becomes spontaneously polarized due to the Sokolov-Ternov effect in which spin flips induced by synchrotron radiation cause preferentially polarization in the direction opposite to the magnetic field of the dipole magnets [1].

As the electron passes through magnetic fields it receives transverse orbital kicks $\theta_{x,y,\mathrm{orbit}} = (-\Delta y', \Delta x')$ [1]. The corresponding spin kick is then given by

$$\Delta\theta_{x,y,\mathrm{sp}} = a\gamma\Delta\theta_{x,y,\mathrm{orbit}} \tag{1}$$

where $a = (g-2)/2 = 0.0011596$ with g the anomalous magnetic moment of the electron and γ is the relativistic energy factor. Thus the net result of the dipoles in one revolution around the ring is to rotate the spin vector about the y axis by the spin tune $\nu_{sp} = a\gamma$.

After equilibration, the spins in the ring will continue to precess at the spin tune frequency. We now consider adding a vertical oscillating magnetic kicker to the ring with the goal of depolarization. The vertical orbit kick is given by

$$\theta_{orbit} = \theta_k \cos(\omega_k t) \tag{2}$$

Then, using Eqn (1), we get the kick to the spin by an angle

$$\theta_{x,sp} = a\gamma\theta_k \cos(\omega_k t) \tag{3}$$

Here we may also define the tune of the kicker, by dividing the kicker frequency by the revolution frequency

$$\nu_k = \frac{\omega_k}{\omega_0} \tag{4}$$

[1] Note that we use the coordinates (x, y, z) where y is vertical, z is the direction of the particle orbit, and x points out of the ring.

The polarization reduces the scattering cross section of the electrons and increases the Touschek lifetime. This latter can be calculated via:

$$\frac{1}{\tau_t(|\vec{P}|)} = \frac{1}{\tau_t(0)} + Q|\vec{P}|^2 \qquad Q < 0 \tag{5}$$

where the expression for Q can be found in reference [2] and depends on the lattice functions and momentum acceptance. The polarization evolves with time as:

$$\vec{P}(t) = \vec{P}_{max}\left(1 - e^{-\frac{t}{\tau_p}}\right) \tag{6}$$

with τ_p being the polarization time.

POLARIZATION AND DEPOLARIZATION AT THE ESRF

For the ESRF, the theoretical polarization time is τ_p = 15.6 min (using equation 4 in section 2.7.7 in reference [1]). If we assume the Sokolov-Ternov maximum polarization of $P_{ST} = 0.9238$ and a constant momentum acceptance of 2.5%, we obtain a lifetime increase of 15.1%.

The polarization at the ESRF was measured using the Touschek lifetime, as given by equation (5) and (6). The result is shown in figure 1. Fitting the curve, we obtain $\tau_p = 15.9 \pm 0.6$ min and $\Delta\tau_t/\tau_t = 0.150 \pm 0.005$ [3]. These values are very close to the theoretical ones, which is an indication that the final polarization P_{max} is close to the Sokolov-Ternov value.

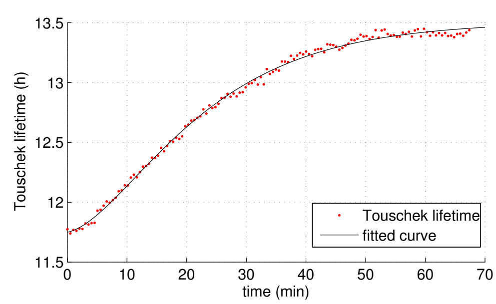

Figure 1: Polarization measurement at the ESRF via Touschek lifetime. The Touschek lifetime has been normalized to account for current and bunch length change and the measured vacuum lifetime has been subtracted.

The method of resonant spin depolarization allows a precise measurement of electron beam energy [4] [5]. We tried to apply this technique at the ESRF, however, the observed frequency range leading to depolarization was orders of magnitudes wider (~ 20 kHz) than expected (few Hz), see figure 2. This result and the difficulty of defining the correct experimental parameters motivated a more careful analysis of the depolarization process. A code based on AT [2] was written

[2] ATfastring function [6] was used for tracking speed.

Content from this work may be used under the terms of the CC BY 3.0 licence (© 2015). Any distribution of this work must maintain attribution to the author(s), title of the work, publisher, and DOI.

ISBN: 978-3-95450-168-7 doi:10.18429/JACoW-IPAC2015-MOPWA014

NEW FUNCTIONALITY FOR BEAM DYNAMICS IN ACCELERATOR TOOLBOX (AT)

B.Nash, N.Carmignani, L.Farvacque, S.M. Liuzzo,
T.Perron, P.Raimondi, R.Versteegen, S.White, ESRF, Grenoble, France

Abstract

Accelerator Toolbox is a widely used code for beam dynamic simulations based on Matlab. To continue the development of the code in a collaborative manner, a SourceForge project and SVN repository called *atcollab* has been established. Here we describe the contributions to *atcollab* from the ESRF beam dynamics group. Additional modules have been developed: general matching (*atmatch*), improved plotting (*atplot*), Touschek lifetime computation via the Piwinski formula, nonlinear dynamics computations such as resonance driving terms, improved reporting of lost particles and improvements and additions to the integration routines. One example of the latter includes diffusion due to quantum fluctuations. Modeling of collective effects may now be performed using pass methods representing a variety of impedance models. Finally, routines to replace the full ring with a compact representation have been developed, facilitating studies in which many turns and many particles are required.

INTRODUCTION

Accelerator Toolbox (AT) is a Matlab [1] based tool box for accelerator simulation originally created by Andrei Terebilo during the late 1990's at SLAC [2, 3]. The latest release of AT from SLAC is 1.3. AT is widely used at accelerator facilities around the world. We describe the status of the developments made by the ESRF beam dynamics group, outlining our approach and some of the additions since AT 1.3. We have made an effort to maintain backwards compatibility throughout these changes.

WORKING WITH LATTICE STRUCTURES

Consistent with the original design of AT, a storage ring lattice is a Matlab structure where each element contains a link to a pass method[1] together with the relevant data to describe the element. Particles may then be tracked through the lattice structure using the function called *atpass* which is a compiled C language Mex Function for purposes of speed.

Element Creation Functions

Element creation functions exist to aid in the creation of a valid lattice structure. Previous versions of AT included many of these, but within a global variable structure. These have been modified to allow direct output of the lattice elements. As an example, QF=atquadrupole('QF1',0.94,0.39,'QuadMPoleFringePass') produces a quadrupole element structure with length 0.94 m and $k = \frac{1}{B\rho}\frac{\mathrm{d}B_y}{\mathrm{d}x} = 0.39m^{-2}$ using the pass method QuadMPoleFringePass. These elements may then be strung together to create a lattice structure.

[1] A pass method, or integrator is a function that maps initial phase space to final phase space in an element.

Class Field

The field 'Class' has been added to each element to facilitate element finding. The classes are 'Drift', 'Bend', 'Quadrupole', 'Sextupole', 'Multipole', 'ThinMultipole', 'Wiggler', 'KickMap', 'RFCavity', 'QuantDiff', 'Aperture', 'Monitor', 'Corrector', 'Solenoid', 'Matrix66', 'RingParam'. As an example, the indices of all sextupoles may be simply found using the command 'indsext=findcells(ring,'Class','Sextupole')'. The 'RingParam' element may contain global parameters describing the ring such as the electron energy or the ring periodicity, in case only one period is represented in the structure.

Lattice Manipulation Functions

We create functions to make changes to a lattice. Examples include misalignments and multipole errors. Additional function for setting elements properly include functions for setting cavities, turning radiation on and off, etc. The element creation functions output a lattice element directly. The lattice manipulation functions work directly with lattice structures. Working this way, rather than with a global variable THERING or FAMLIST as in AT 1.3, allows multiple ring structures to be stored simultaneously and more easily compared.

Plotting

A new plotting routine has been developed called *atplot*. It allows the plotting of arbitrary functions around the ring, together with the lattice synoptic. Examples are shown in Fig. 1 and 2. In Fig. 1, we see a plot of the varying dipole strength in sliced dipoles, together with the $\mathcal{H}_x$ function. This visualization allows understanding of how emittance may be minimized. In Fig. 2, we plot the geometric Hamiltonian driving terms throughout a lattice cell for the ESRF upgrade lattice. These have been computed using code from Elegant [4] interfaced to AT via MEX.

Matching

The function *atmatch* [5] allows general linear and nonlinear matching of an AT lattice structure. For optics matching the routine uses the function *atlinopt* (with a single call for all matching conditions), however generic Matlab functions may be used both to define variables (matching knobs) or conditions to be achieved, such as emittance reduction,

Content from this work may be used under the terms of the CC BY 3.0 licence (© 2015). Any distribution of this work must maintain attribution to the author(s), title of the work, publisher, and DOI.

ISBN: 978-3-95450-168-7 doi:10.18429/JACoW-IPAC2015-MOPWA015

LATTICE CORRECTION USING LOCO FOR THE THOMX STORAGE RING*

I. Chaikovska†, C. Bruni, S. Chancé, A. Variola, J. Zhang
Laboratoire de l'Accélérateur Linéaire, CNRS-IN2P3, Université Paris-Sud XI, Orsay, France
A. Loulergue
SOLEIL, Gif-sur-Yvette, France

Abstract

ThomX is a compact Compton based X-ray source under construction at LAL in Orsay (France). The ThomX accelerator facility is composed by a 50-70 MeV linac driven by 3 GHz RF gun, a transfer line and a 18 meters long Storage Ring (SR). The Compton backscattering at each revolution between the 1 nC electron bunch and the ~25 mJ laser pulses stacked in the Fabry-Perot cavity results in the production of $\sim 10^{13}$ photons per second with energies in the X-ray regime. This high flux of the X-rays strongly depends on the quality (beam sizes) of the electron beam at the interaction point. To guarantee this, a good knowledge and quality of the linear lattice of the ThomX SR are required. Nowadays, LOCO (Linear Optics from Closed Orbits) is a well-known and widely used algorithm to measure and restore the linear optics of the SRs and ensure the designed performances. Comparing the measured and model orbit response matrices, the linear lattice can be restored by retuning the quadrupole gradients. In this paper, we report on the LOCO analysis of the ThomX SR taking into account simulated misalignment, calibration and field errors.

INTRODUCTION

ThomX is a demonstrator proposed by a collaboration of French institutions and one company to build an accelerator based compact X-ray (up to 90 keV) source in Orsay [1]. The main goal of the project is to deliver a stable and a high energy X-ray flux generated by the Compton backscattering process. Low energy, compactness and lack of the operation experience make such type of the machine very difficult to operate and, especially, to commission. At present, the ThomX machine is under construction. Layout of the ThomX accelerator facility including the Photoinjector, Transfer Line, Storage Ring (SR) and Extraction Line is shown on Figure 1.

First, to ensure a high flux X-ray production, linear optics of the ThomX SR has to be measured and controlled. Broken symmetry of the optics due to the field, calibration and misalignment errors usually leads to the resonant excitation which can strongly affect the beam dynamics and so the X-ray generation in the ring. Therefore, it is very important to identify and correct the linear optics (quadrupole gradient) errors in the ThomX SR.

In this framework, the analysis of the machine optics is usually performed by using the trajectories or closed orbit information organized in terms of the Orbit Response Matrices (ORM).

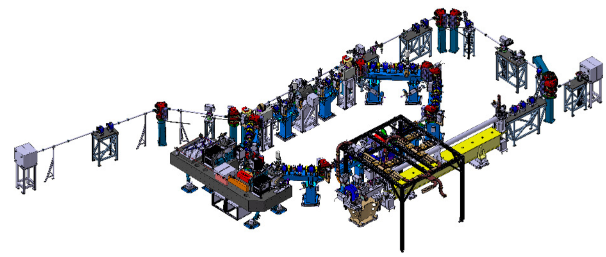

Figure 1: Layout of the ThomX facility.

THOMX STORAGE RING

ThomX SR design is based on a Double Bend Achromat (DBA) optics with a two-fold symmetry including eight 45° dipoles, 24 quadrupoles and 12 sextupoles (see Figure 2). This design accommodates two long straight sections and two short sections between the dipoles where potentially two interaction points can be located. Some of the ThomX SR parameters are listed in Table 1.

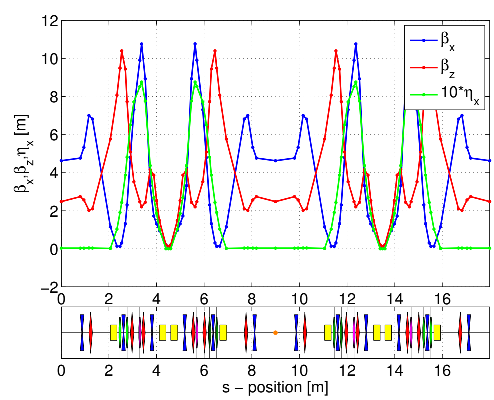

Figure 2: ThomX storage ring nominal optics: horizontal beta function (blue), vertical beta function (red), and horizontal dispersion (green).

The SR has 12 Beam Position Monitors (BPMs) and 12 correctors integrated in the sextupoles for both the horizontal and the vertical planes. The 24 quadrupoles are divided in 6 families and foreseen to have individual power supplies.

The Linear Optics from Closed Orbit (LOCO) code [2] is widely used to correct errors in the linear optics of the storage rings and transport lines. This paper will describe

* Work supported by the EQUIPEX program, the Ile-de-France region, CNRS-IN2P3 and Université Paris Sud XI
† chaikovs@lal.in2p3.fr

Content from this work may be used under the terms of the CC BY 3.0 licence (© 2015). Any distribution of this work must maintain attribution to the author(s), title of the work, publisher, and DOI.

ISBN: 978-3-95450-168-7 doi:10.18429/JACoW-IPAC2015-MOPWA016

INCREASING THE DYNAMIC AND MOMENTUM APERTURES OF THE THOMX RING BY MEANS OF OCTUPOLE CORRECTORS*

J. Zhang†, P. Bambade, A. Faus-Golfe*, H. Monard
LAL, Université Paris 11, IN2P3/CNRS, 91898 Orsay, France
IFIC (CSIC-UV), Valencia, Spain*
A. Loulergue, Synchrotron SOLEIL, St-Aubin, 91192 Gif-sur-Yvette, France

Abstract

The electron ring of the compact Compton-backscattering X-ray source ThomX which is being built at LAL featured with a small circumference of 18 meters and a low beam energy 50-70 MeV, and its long term single particle dynamics is dominated by the non linear effects in the transverse and longitudinal planes. In this paper, we study the feasibilities to reduce the sextupole resonances and then increase the dynamic aperture and momentum aperture of the ThomX ring, using octupoles correctors.

INTRODUCTION

The compact Compton-backscattering X-ray source ThomX is under construction by a collaboration of seven institutes and an industry partner at LAL-Orsay, France. The accelerator part of this X-ray source is composed of an electron photon-gun, a linac, and a ring; and is featured with the compact size of 10 m long and 7 m wide, and the high average flux of 10^{11} to 10^{13} photons/second. However, the small size of the ring of 18 circumference and the low electron beam energy 50-70 MeV determine that the beam dynamics in the ThomX ring is dominated by the non-linear effect, which is a common issue for the future generation circular accelerators, like the low emittance light sources and the high luminosity colliders. For such type of accelerators, the dynamic aperture (DA) is normally smaller than the vacuum chamber size, and the momentum aperture (MA) is limited by the non linear motions of the off momentum particles.

DA AND MA OF THE THOMX RING

Quadrupole fringe fields (FFs) show no obvious effects on the beam dynamics, but the sextupole-like second order dipole FFs contribute greatly to the vertical chromaticities [1], and the sextupoles and the multipole field errors in the main magnets (dipoles, quadrupoles, sextupoles) in the ring are the main sources of the non linear effects of the ThomX machine, and they reduced the DA and the MA which have nontrival effects on the injection efficiency and the beam storage time in the ring.

In the final version of the ThomX ring lattice, there are 12 sextupoles which are composed of one family focusing sextupoles and two families defocusing sextupoles. The DA is reduced to around 15 mm in the horizontal plane x and 20 mm in the vertical plane z, which are respectively 30 times of the horizontal beam size σ_x and 57 times of the vertical beam size σ_z at the injection point of the ring; the MA is around ±3%, which is much larger than the final beam energy spread 0.6% after 20 ms storage time.

Table 1: Relative systematic multipole field errors in the ThomX ring, with the unit 10^{-4} at 18 mm radial position. From the OPERA-3D simulations.

Pole N	Inner dip.	Outer dip.	Quad.	Sext.
6	+8.5	-16	-	
8	+0.1	-0.7	-	
10	+3	-6	-	
12	-	-	+2	-
18	-	-	-	-4
20	-	-	-6	-
28	-	-	-9	-
30	-	-	-	-0.9

Furthermore, the engineering construction of the magnets introduces high order magnetic field errors, which deteriorate the DA and MA of the ThomX ring. With the systematic multipole field errors shown in Table 1 [2], the DA is reduced to around 13 mm (25 times of σ_x) in x and to 10 mm (29 times of σ_z) in z, which is smaller than the physical vacuum chamber size of 20 mm in x and 14 mm in z, while larger than the scaled chamber size of 12 mm in x and 7 mm in z; the MA is reduced to -1.8% and 2% (Fig. 1 and 2), which is comparable to the energy momentum acceptance ±2% limited by the vacuum chamber size.

Although from the simulation, the DA and MA (Fig. 1 and 2) seems to be sufficient for the operation mode of the ThomX ring with sextupoles and systematic multipole field errors, in the real ThomX machine, there will be other sources of perturbations that can reduce the DA and MA, such as the random multipole field errors, the systematic and random misalignment errors, power supply ripples, ground vibrations, thermal expansions of the ring, etc. As a result, one needs to further optimize the DA and MA of the machine.

HAMILTONIAN AND SEXTUPOLE RESONANCE TERMS

To optimize the DA and MA of the ThomX ring, one powerful method is the analysis of the Hamiltonian resonance

* Work is supported by ANR-10- EQPX-51 and ANR-11-IDEX-0003-02, and also by grants from Région Ile-de-France.
† zhangj@lal.in2p3.fr

Content from this work may be used under the terms of the CC BY 3.0 licence (© 2015). Any distribution of this work must maintain attribution to the author(s), title of the work, publisher, and DOI.

ISBN: 978-3-95450-168-7 doi:10.18429/JACoW-IPAC2015-MOPWA017

DESIGN STATUS OF THE ESSνSB SWITCHYARD

E. Bouquerel* on the behalf of the ESSνSB Collaboration
IPHC, Université de Strasbourg, CNRS/IN2P3, F-67037 Strasbourg, France

Abstract

The feasibility of the distribution of 5 MW proton beam power pulsed at 70 Hz onto a 4-target station for the production of neutrino super beams is discussed. To deflect and focus the beam having a magnetic rigidity of 11.0 Tm onto the targets, different configurations of beam switchyard are proposed and compared. The number of dipoles and quadrupoles composing this system is defined for each scenario. The length, the aperture, the magnetic fields and the field gradients of these optical elements are determined. The code TraceWin is used to simulate and optimize the envelopes of the beam along the beam lines. The transverse emittances at the exit of the system are shown.

INTRODUCTION

The next generation of neutrino beams are based on multi MW scale proton drivers. The proposal for the ESSνSB (European Spallation Source Neutrino Super Beam) project has been submitted to H2020 Design Study and is led by the Neutrino Group of the IPHC (Institut Pluridisciplinaire Hubert Curien) of Strasbourg and the University of Uppsala. It foresees the use of the ESS linac currently being constructed at Lund, to accelerate H^- ions (2.5 GeV, 5 MW, 70 Hz) and produce neutrino super beams [1]. It succeeds the studies made by the FP7 Design Study EUROν [2], regarding future neutrino facilities. The primary proton beam-line completing the linac will consist of an accumulator ring and a switchyard to distribute the protons onto the different targets composing the horn system (4 targets of 15 mm radius). The BSY (beam switchyard) is one of the key systems of the project. Its efficiency and reliability directly impact the production of yields of secondary particles.

Table 1: Beam Parameters for EUROν and ESSνSB [1]

Parameter	EUROν	ESSνSB
Particle	H^-	H^-
Proton kinetic energy (GeV)	4.5	2.5
Pulse intensity (mA)	40	62.5
Avg beam power (MW)	4	5
Beam rigidity (Tm)	17.85	11.02
Macro-pulse length (linac) (ms)	2.86	0.715
Pulse length (accu.) (μs)	1.5	1.5
Pulse repetition rate (Hz)	50	70

Preliminary studies were done on such system within EUROν [3]. Although the horn requires similar conditions as for EUROν, the parameters of the primary beam being different from those used for this previous project (Table 1) implies considering an upgrade or even new solutions for the distribution of the protons onto the horn system.

*Elian.Bouquerel@iphc.cnrs.fr

SPLITTING AND DISTRIBUTING THE PROTONS

Different Configurations Investigated

Besides the configuration studied for EUROν (labelled "config1" in this paper), other scenarios to deflect the beam onto the horn system have been recently under considerations. Among several layouts, two new configurations, in addition to config1, could be seriously retained for further detailed studies. These new solutions will be labelled "config2" and "config2a" respectively. The selection criteria relied on the number of magnetic elements necessary, on the type of operation (i.e. simple or bi-polar devices) and on the prospective of beam dump requirements.

Deflecting Elements

Although kicker technology was raised for config1 in the framework of the EUROν Design Study, the rise and fall times of few ms and the repetition rates of 17.5 Hz (35 Hz according to the configuration) needed by each device would actually allow the use of simple classical dipoles (O- and H-types), to deflect the protons onto the 4 target axes [4]. This would have the advantage of making easier the design of both the magnets and the power supplies, thus reducing their cost.

BEAM FOCUSSING SYSTEM

Beam Parameter Definition

The normalised rms transverse emittances of the beam extracted from the ESS linac are foreseen to be 0.33 μm [5]. The charge exchange injection with high power beam requires a modest number of foil hits during the phase space painting, resulting in a larger emittance than the injected beam. Therefore transverse emittances at the exit of the accumulator will be much larger than the one at the end of the ESS linac. Current studies suggest the emittances of the beam coming from the accumulator to be of several tenths of μm [6]. In the following, the normalised transverse emittances of the proton beam are assumed to be 225 μm (99.7%) and the rms momentum dispersion 0.1%. The required beam size at the target station is 4 mm rms.

Content from this work may be used under the terms of the CC BY 3.0 licence (© 2015). Any distribution of this work must maintain attribution to the author(s), title of the work, publisher, and DOI.

ISBN: 978-3-95450-168-7 doi:10.18429/JACoW-IPAC2015-MOPWA018

Content from this work may be used under the terms of the CC BY 3.0 licence (© 2015). Any distribution of this work must maintain attribution to the author(s), title of the work, publisher, and DOI.

LOSS FACTOR AND IMPEDANCE ANALYSIS OF WARM COMPONENTS OF BERLINPRO*

H.-W. Glock[1,2], M. Abo-Bakr[1], J. Kolbe[1], F. Pflocksch[1], C. Potratz[2], Andreas Schälicke[1]
[1] Helmholtz-Zentrum Berlin für Materialien und Energie (HZB), BESSY II, Berlin, Germany
[2] Compaec e.G., Rostock, Germany

Abstract

The ongoing component design for the HZB 50 MeV, 100 mA ERL project bERLinPro is accompanied by loss factor and impedance computations. A list of accelerator components that are likely to induce geometric wake fields including bellows, collimators, tapers, shutter valves etc. is given. Loss factors and impedance spectra, both calculated using CST-ParticleStudio®, are presented. Scaling of the loss factors with respect to the bunch length is calculated on base of the numerical simulations and is used to extrapolate down to a rms bunch length of 0.6 mm, which is hard to reach directly in numerical simulations.

INTRODUCTION

Future single-pass accelerators, in particular high-brilliant next-generation light sources or colliders for high-energy physics, will demand for beam power levels hardly to be maintained by classical set-ups, which dump the beam with most of its kinetic energy. This led to the "energy recovery linac" concept with a recirculation of the used beam through the accelerating cavities, where it is decelerated by a proper choice of the beam-to-field-phase to a small fraction of its maximum kinetic energy. Thus the beam feeds back the accelerating cavity mode, which in turn accelerates a fresh beam. Such a mode of operation will be most effectively applied to a high current, continuously operated (cw) accelerator with low loss, i.e. super-conducting cavities. It is the aim of the bERLinPro project [1] (cf. Fig. 1), now under construction at HZB, to demonstrate energy recovery operation with a cw (1.3 GHz repetition rate), 50 MeV, 100 mA, $\sigma_t < 2$ ps bunch length, low-emittance beam.

This demands for a careful analysis of all beam line components according to their potential to excite wake fields. This paper is focussed on so-called geometric wakes; effects of coherent synchrotron radiation (CSR), resistive walls or surface roughness are only cited for comparison. Since the bunch spectrum reaches far above 100 GHz most wakes are able to propagate through the machine, in principle causing a strong rf-coupling between individual components. It would demand for excessive supercomputing capabilities to compute the field interaction with each other and the beam for such a long chain of coupled components, which – even if available – would not be practicable for any design optimisation. Thus the two following figures of merit, computable for every single component, were used (cf. Fig. 2, Tab. 1): a) the loss factor; b) the impedance close to the beam-harmonic frequencies of N·1.300 GHz.

*Work supported by German Bundesministerium für Bildung und Forschung, Land Berlin, and grants of the Helmholtz Association.
hans.glock@helmholtz-berlin.de, glock@compaec.de

SIMULATION TECHNIQUE

All simulations were performed with the wakefield solver of CST ParticleStudio® [2], running on a dedicated workstation (2x Intel Xeon E5 2643v2-6-core, 3.50 GHz, Intel S2600 board, 256 GB of DDR3-1866 RAM). The solver uses an explicit time stepping scheme on a hexahedral mesh. In most cases 15 mesh lines were applied longitudinally per bunch rms length $\sigma_s = c\cdot\sigma_t$ of Gaussian shaped bunches. σ_s usually was chosen as 1 mm (computed impedance spectra up to 100 GHz), 3 mm and 5 mm. The number of mesh cells was in most cases up to a few 10^8, largest possible meshes reached $1.3\cdot10^9$ cells. Indirect wake integration was used (option "indirect interfaces"), mostly applied to on-axis beams. As a trade-off between spectral resolution versus grid dispersion error and computation time typically a wake length of 10 m was computed for at least one of the three bunch lengths. In most cases two more runs were performed with a wake length of 200 mm, which is sufficient for the program to determine the loss factor.

LOSS FACTOR DEPENDENCY ON BUNCH LENGTH

Due to its infinitely extended spectrum, which cannot be handled numerically, it is not possible to compute a point charge's wake potential (at least not with bandwidth-limited discretizing approaches). Instead the wakes of Gaussian shaped bunches were simulated, giving wake potentials and loss factors depending on the bunch rms length. Computing various objects (many of them not shown here) and comparing their bunch-length dependent loss factors in a double-logarithmic viewgraph heuristically led to the observation of a loss factor scaling according to:

$$k_{loss}(\sigma) = k_{loss}(\sigma_0)\left(\frac{\sigma}{\sigma_0}\right)^{-\alpha} \tag{1}$$

ISBN: 978-3-95450-168-7 doi:10.18429/JACoW-IPAC2015-MOPWA019

Content from this work may be used under the terms of the CC BY 3.0 licence (© 2015). Any distribution of this work must maintain attribution to the author(s), title of the work, publisher, and DOI.

STATUS OF THE ROBINSON WIGGLER PROJECT AT THE METROLOGY LIGHT SOURCE

T. Goetsch*, J. Feikes, M. Ries, G. Wüstefeld, HZB, Berlin, Germany

Abstract

The beam lifetime in electron storage rings concerns machines running in decay mode as well as machines doing top-up. A standard procedure to increase the lifetime is via bunch lengthening as the lifetime depends on the electron density in the bunch. Bunch lengthening is typically achieved with higher harmonic (Landau) cavities. As noted in [1], there are several advantages in using a different approach: it is possible to increase the bunch length by installing a Transverse Gradient (Robinson) Wiggler, which allows to transfer damping between the horizontal and the longitudinal plane. While increasing the bunch length, the horizontal emittance is being reduced yielding advantages regarding the source size depending on the magnet optics. At the Metrology Light Source, a primary source standard used by Germanys national metrology institute (Physikalisch-Technische Bundesanstalt) [2], such a scheme is being investigated. The current state of the project including dynamic aperture effects and synchrotron radiation issues of the device is being presented in the following.

INTRODUCTION

The lifetime at the MLS is Touschek dominated and it is 6 h for a beam current of 150 mA. To improve the lifetime, the prospects of installing a Robinson Wiggler (RW) are being investigated. The RW transfers damping between the horizontal and the longitudinal plane. Therefore, it will allow tuning of the energy spread σ_δ, and by that the bunch length σ_s as $\sigma_s \propto \sigma_\delta$. Hence, the bunch density can be decreased via bunch lengthening, resulting in an increased lifetime. Increasing the bunch length is usually achieved by installing higher harmonic (Landau) cavities. Installing a RW at the MLS is an option, as the users of the synchrotron radiation are not as sensitive to an increased energy spread as in other facilities.

THEORY

The damping partition number D describes how the damping is divided between the horizontal and the longitudinal plane. It is the ratio between the fourth and the second synchrotron radiation integral, I_4 and I_2:

$$D = \frac{I_4}{I_2}, \tag{1}$$

$$I_2 = \oint \frac{1}{\rho^2} \mathrm{d}s, \tag{2}$$

$$I_4 = \oint \left(\frac{\eta_x}{\rho^3} + \frac{2\eta_x k_1}{\rho} \right) \mathrm{d}s, \text{ with } k_1 = \frac{1}{B\rho} \frac{\partial B_y}{\partial x}, \tag{3}$$

* tobias.goetsch@helmholtz-berlin.de

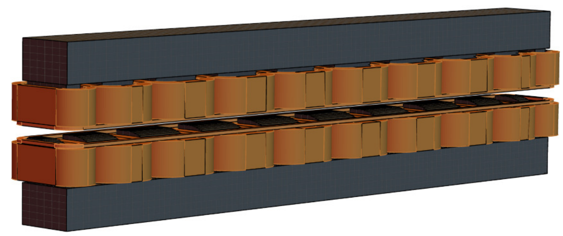

Figure 1: Robinson Wiggler as described in RADIA [3]. The poles have a hyperbolic shape in the horizontal direction, giving rise to a linear, horizontal field gradient (comp. Fig. 4). Field and gradient depend on the current in the coils.

where ρ is the bending radius, η_x is the horizontal dispersion function and k_1 is a horizontal gradient to the field. The damping partition D can be manipulated by introducing a magnetic field B and a gradient $\partial B/\partial x$ simultaneously in a dispersive section. The contribution to I_4 is negative when choosing B and $\partial B/\partial x$ to be of opposite sign (for a positive dispersion). Chains of alternating combined function magnets yield such fields (compare Fig. 1).

In Fig. 2 the development of σ_x, the averaged beam width along the circumference, the hor. emittance ε_x, the bunch length σ_s (and with that the energy spread σ_δ) and the beam lifetime $\tau_{1/2}$ are shown as a function of the damping partition D. The lifetime includes gas lifetime, the different quantum lifetimes and the Touschek lifetime. The gas lifetime was assumed to be constant with a value of $\tau_{\mathrm{gas}} = 25$ h, which is the result of measurements performed in 2013.

The lifetime is calculated for two scenarios: τ_1 represents the lifetime calculated for a constant vertical source size, independent of the horizontal emittance; τ_2 represents the lifetime as it would be for a constant emittance coupling between the horizontal and the vertical plane of $\varepsilon_y/\varepsilon_x = 0.5$ %. The graphs show that for $D = -1.75$, a lifetime improvement between 60 % (τ_2) and 100 % (τ_1) seems achievable.

DESIGN STATUS

Number of Poles and Drift Correction

As the available space for the device is limited to 1740 mm, the maximum length of an individual pole is defined by the number of pole pairs. The longer a pole, the higher the achievable fields. But the longer the poles the larger the particles amplitude. Taking the constraints at the MLS into account, the optimum seems to be 9 to 10 poles (including end poles). In order to preserve the aperture, it is worthwhile to have the beam oscillating around the central

ISBN: 978-3-95450-168-7 doi:10.18429/JACoW-IPAC2015-MOPWA020

LONGITUDINAL STABILITY OF SHORT BUNCHES IN STORAGE RINGS WITH STRONG LONGITUDINAL FOCUSING*

P. Kuske#, Helmholtz-Zentrum Berlin, Germany

Abstract

In the BESSY VSR project, the variable bunch length storage ring, two high gradient accelerating structures at 1.5 and 1.75 GHz will be phased such that long and short bunches can be stored simultaneously. The longitudinal stability of the short bunches is investigated taking into account the shielded CSR- and a purely inductive impedance. Multi particle tracking studies and numerical solutions of the Vlasov-Fokker-Planck equation show that threshold currents for short bunches do not follow the simple scaling law which was found for long bunches. The inductive impedance can even lower the thresholds for the instability. With an 80 times increased accelerating gradient and reasonable assumptions on the inductive impedance for shorter bunches stable operation can be expected with bunches 1.8 ps long (RMS-value) and 0.8 mA current. According to the calculations and operating in a dedicated low-α mode will produce stable 40 μA bunches with 400 fs length.

INTRODUCTION

At the 3rd generation synchrotron radiation light source BESSY II shorter light pulses are requested by a growing number of users. Laser slicing is operated routinely and produces pulses as short as 100fs FWHM. Operating in the short bunch, low-α mode delivers bunches shorter than 6 ps FWHM. This is offered for up to 3 weeks per year. Slicing and low-α mode suffer both from a too low intensity. One way to increase the intensity of light pulses, or overcome the quite low stable bunch currents, is the increase of the longitudinal RF-focusing. This produces shorter bunches and shifts threshold currents to higher values. A neat way to produce short bunches without sacrificing flux or brilliance for other users was proposed by G. Wüstefeld, et al. [1]: long and short bunches can be stored simultaneously with proper phasing of two super-conducting high gradient accelerating structures operating at 1.5 and 1.75 GHz, 3 and 3.5 times the fundamental 500 MHz-RF-system. Most of the charge will be stored in long bunches producing most of the photon flux and, at the same time, a few short bunches carrying charge just below their instability threshold will emit the desired short light pulses. The purpose of this paper is to analyse the longitudinal stability of these short bunches.

MODEL OF SHIELDED CSR

For very short bunches the coherent synchrotron radiation (CSR) is dominating the longitudinal beam dynamics. In the calculations presented here the model of the steady-state CSR theory for bunches moving on a circle with radius ρ is used. This is justified by the fact that the BESSY dipoles are long enough so that the light emitted from a trailing electron at the entrance of the dipole can overtake the bunch and interact with the electrons at the head of the bunch [2] already inside the dipole magnet. The slippage length is a factor of 3 to 14 longer than the length of the investigated bunches. Bunches are not yet short enough to assume that the interaction takes place in free-space. Shielding effects of the nearby dipole vacuum chamber have to be taken into account. This is done with the wake function derived by J. Murphy, et al. [3] for the model of two perfectly conducting infinite parallel plates separated by 2h.

Some of the results of the simulations and also the observations are easier to understand within the impedance picture of the shielded CSR-interaction first derived by R. Warnock [4] and later expressed in scaled parameters by Y. Cay [5]. The resulting CSR-impedance is presented in Figure 1. The plates suppress the impedance at low frequencies and at higher frequencies the impedance approaches the free-space values. In between a resonance-like enhancement appears. The frequency of the maximum as deduced from the Olver expansion of the impedance [6] is located around $n_{max} = \omega/\omega_0 = \omega\rho/c = 2/3^{1/2}(\pi\rho/2h)^{3/2}$. This broad resonance has features of a broad-band resonator and can create similar instabilities.

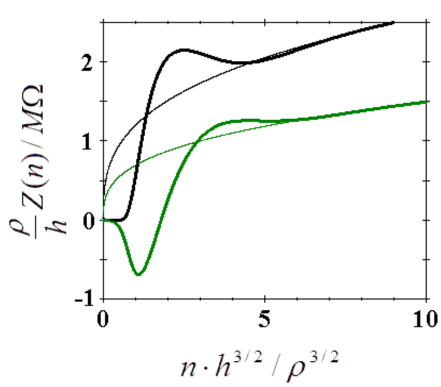

Figure 1: Scaled real part (black) and imaginary part (green) of the CSR impedance in free space (thin lines) and shielded by two infinite perfectly conducting parallel plates (thick lines).

Based on the shielded CSR-model, K. Bane, et al. [7] found a very simple scaling law valid for a large range of parameters, except for bunch lengths with 1/σ in the neighbourhood of this resonance. In this region the strong instability turns into a weak instability and threshold currents are dramatically reduced. BESSY VSR will produce bunches with a length in the critical region.

*Work supported by the BMBF and the Land Berlin
#peter.kuske@helmholtz-berlin.de

Content from this work may be used under the terms of the CC BY 3.0 licence (© 2015). Any distribution of this work must maintain attribution to the author(s), title of the work, publisher, and DOI.

ISBN: 978-3-95450-168-7 doi:10.18429/JACoW-IPAC2015-MOPWA021

TRANSVERSE RESONANCE ISLAND BUCKETS AT THE MLS AND BESSY II

M. Ries *, J. Feikes, T. Goetsch, P. Goslawski, J. Li, M. Ruprecht, A. Schälicke, G. Wüstefeld †
HZB, Berlin, Germany

Abstract

By operating the Metrology Light Source (MLS) near horizontal resonances (ΔQ_x = 1/2, 1/3 or 1/4), two, three or four resonance island buckets may be populated for beam storage. This paper presents experimental results and operational experience such as tuning the machine for high current, controlling inter-bucket diffusion rates, improving overall lifetime and extraction of radiation pulses with sub-revolution repetition rate. First approaches to transfer this mode of operation to the BESSY II storage ring will also be presented.

INTRODUCTION

The MLS is an electron storage ring operated as a dedicated light source for metrology applications of the Physikalisch-Technische Bundesanstalt (PTB). By design, it is equipped with additional families of sextupole and octupole magnets to manipulate nonlinear beam dynamics [1, 2]. Therefore, the MLS is ideally suited to investigate nonlinear beam dynamics in the transverse plane.

Transverse resonance island buckets form when a machine is operated in the vicinity of a resonance and suitable amplitude dependent tune shift is present. The existence of these island buckets is well known and described for long time, e.g. [3]. An application is multi-turn extraction at CERN [4]. However, island buckets are not yet exploited for user operation at electron storage rings.

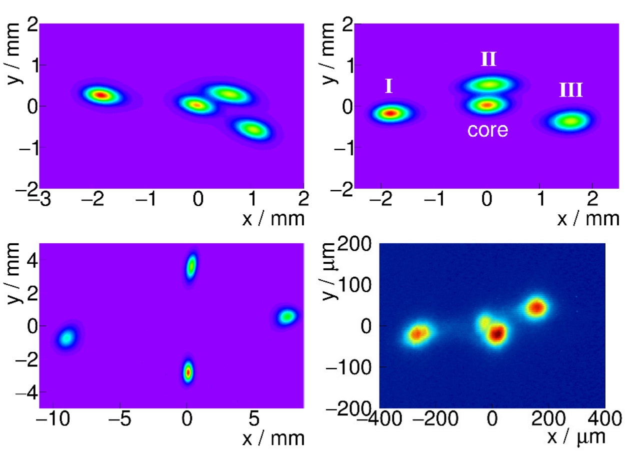

Figure 1: Source point imaging measurements from island bucket operation near horizontal resonances ΔQ_x = 1/3 (top) and 1/4 (bottom left) at the MLS and BESSY II (bottom right).

* markus.ries@helmholtz-berlin.de
† gwuestefeld@gmx.de

Figure 1 exemplarily shows transverse electron distributions measured using a source point imaging system. The MLS was successively operated near horizontal resonances $\Delta Q_x = f_x/f_{\text{rev}} = 1/3$ (top) and 1/4 (bottom left). Skew quadrupole magnets were used to introduce vertical separation for the purpose of visualization. The upper measurements were taken simultaneously at two different locations along the circumference. The position of the islands can be manipulated by changing quadrupole and sextupole currents. Islands stored near the ΔQ_x = 1/4 resonance are shown bottom left, with large off-axis fixed points. The core beam was not populated.

Studies for island bucket operation are also performed at the BESSY II storage ring, an example measurement is shown in the bottom right part. Resonance island buckets may provide an elegant way of beam separation – see next section – for the BESSY VSR project [5].

MULTIPLE BEAMS & SEPARATION

Two intrinsic characteristics of island buckets seem to be of special interest for application at light sources. First, island buckets offer the possibility to store two distinct user beams simultaneously, e.g. homogeneous fill and pseudo single bunch. Second, island bucket and core beams are separated in space and/or in angle in the plane corresponding to the resonance.

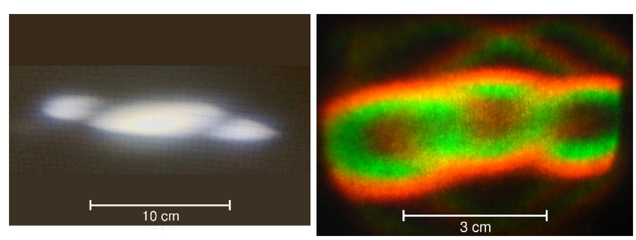

Figure 2: Photon beam separation in divergent parts of user beamlines shown for bending magnet radiation (left) and undulator radiation (right).

The separation in electron phase space translates to the generated photon beams. Figure 2 shows photon beams generated by island buckets in a bending magnet (left) and an undulator straight (right) in divergent parts of the user beamlines. The former image was taken with simultaneously populated island bucket and core beam. In contrast, the latter image was measured with exclusively populated island buckets. At the position of the undulator two islands are characterized by fixed points at ($x_{\text{FP}} \approx 0, \pm x'_{\text{FP}}$), whereas the third island is at ($x_{\text{FP}}, x'_{\text{FP}} \approx 0$). The achieved photon beam separation is in the order of cm, which is an accessible range

Content from this work may be used under the terms of the CC BY 3.0 licence (© 2015). Any distribution of this work must maintain attribution to the author(s), title of the work, publisher, and DOI.

ISBN: 978-3-95450-168-7 doi:10.18429/JACoW-IPAC2015-MOPWA022

INFLUENCE OF TRANSIENT BEAM LOADING ON THE LONGITUDINAL BEAM DYNAMICS AT BESSY VSR*

M. Ruprecht†, P. Goslawski, A. Jankowiak, A. Neumann, M. Ries, G. Wüstefeld,
HZB, Berlin, Germany
T. Weis, TU Dortmund University, Dortmund, Germany

Abstract

BESSY VSR, a scheme where 1.7 ps and 15 ps long bunches (rms) can be stored simultaneously in the BESSY II storage ring has recently been proposed [1]. The strong longitudinal bunch focusing is achieved by superconducting high gradient RF cavities. If the bunch fill pattern exhibits a significant inhomogeneity, e.g. due to gaps, transient beam loading causes a distortion of the longitudinal phase space which is different for each bunch. The result are variations along the fill pattern in synchronous phase, synchrotron frequency and bunch shape. This paper presents investigations of transient beam loading and depicts the consequences on bunch length, phase stability and longitudinal multi-bunch oscillations for the projected setup of BESSY VSR.

INTRODUCTION

The upgrade proposal BESSY VSR [2] is based on the idea that the superposition of the voltage of two different higher harmonic cavity systems will allow to store short and long bunches simultaneously. In order to separate the synchrotron radiation from single bunches by means of a mechanical chopper, they need to be placed in the center of gaps in the bunch fill pattern. Therefore, the fill pattern is proposed to have two 100 ns gaps as depicted in Fig. 2, which gives rise to potentially strong transient beam loading.

TRACKING CODE

A tracking code written in C++ has been developed which uses one macro-particle per bunch for the calculations presented here. The cavity-bunch interaction is calculated by means of phasor addition and active cavities are controlled by a feedback loop which does not act within a revolution but acts quickly from one revolution to another. This simplified method is sufficient to evaluate the effects of beam dynamics discussed in this paper. Related studies, with a focus on RF control are given in [3].

Experimental Verification at BESSY II

Transient beam loading can readily be observed at BESSY II as it is typically operated with a 200 ns gap in the fill pattern and the 1.5 GHz Landau cavities set to bunch lengthening mode. Figure 1 shows an example of measurements at BESSY II compared to simulations performed with the tracking code used in this paper. Both, the data of the synchronous phase position of each bunch, measured in ps with respect to the nominal equidistant bucket reference, and the individual synchrotron frequencies was taken by the diagnostics of bunch-by-bunch feedback systems [4].

The agreement of simulation and measurement can be considered satisfying. Despite some deviation, all major features, such as magnitude of phase transient, magnitude and shape of the synchrotron frequencies are predicted by the simulation. The deviations are expected to stem from uncertainties from both the measurements and the input parameters to the simulation, such as quality factors Q, the shunt impedances R_s^c and the tuning settings. Investigations towards identification and improving the accuracy are ongoing.

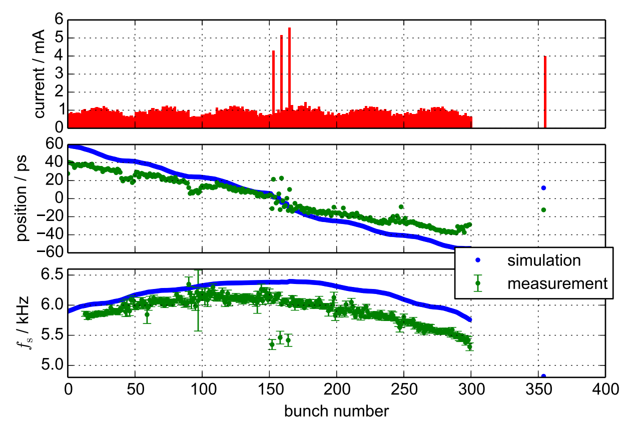

Figure 1: Comparison between simulation and measurements of synchronous phase position of each bunch (center), measured in ps w.r.t. the nominal equidistant bucket reference, and synchrotron frequency (bottom) at BESSY II for a given fill pattern (top). Error bars show a statistical error only.

BESSY VSR SETUP

In BESSY VSR, the storage ring will be equipped with four 5-cell SC cavities, two at 1.5 GHz and two at 1.75 GHz. In this simulation, the normalized shunt impedance[1] is set to $R_s^c/Q = 250\,\Omega$ per cavity. In order to accelerate the approach of the equilibrium state in this simulation, the quality factor of the cavities is set to $Q = 4 \times 10^5$ and the radiation damping time to $\tau = 4 \times 10^{-4}$ s. The 1.5 GHz and 1.75 GHz system are tuned to $\Delta f = -11.3$ kHz and $\Delta f = 15.3$ kHz respectively to compensate for the average

* Work supported by German Bundesministerium für Bildung und Forschung, partly under contract 05K13PEB, and Land Berlin.
† martin.ruprecht@helmholtz-berlin.de

[1] Given in circuit definition: $R_s^c = V_{acc}^2/(2P_{diss})$ with V_{acc} the maximum effective accelerating voltage and P_{diss} the dissipated power.

Content from this work may be used under the terms of the CC BY 3.0 licence (© 2015). Any distribution of this work must maintain attribution to the author(s), title of the work, publisher, and DOI.

ISBN: 978-3-95450-168-7 doi:10.18429/JACoW-IPAC2015-MOPWA023

PRESERVING INFORMATION OF THE THREE SPATIAL ELECTRON BEAM DIMENSIONS IN ONE STREAK CAMERA MEASUREMENT *

M. Switka and W. Hillert, ELSA, Bonn, Germany

Abstract

At the pulse stretcher and storage ring ELSA a streak camera is used for the analysis of visible synchrotron radiation. It functions as fast time resolving beam diagnostic apparatus, capable of visualizing dynamics down to the picosecond time regime. The optical beamline splits the photon beam into two parts and projects both electron beam images onto the streak camera, one of them with transversely perpendicular orientation and slight displacement. Thereby it provides simultaneous imaging of both transverse planes. Thus, the information of bunch and beam dynamics of all three dimensions is preserved and can be observed in slow sweep or synchroscan operation. Characteristics and exemplary measurements, demonstrating the capabilities and limits of this technique, are presented.

INTRODUCTION

Since commissioning of the ELSA streak camera beamline was completed in 2013 [1], the natural reduction of three-dimensional spatial information to two dimensions due to the streaking action turned out to be of hindrance as both, horizontal and vertical beam responses were of interest. In the initial setup the change of the observation plane was possible by insertion of a Dove prism. However, simultaneous observation of both transverse planes could not be performed. Therefore a dual imaging beamline was installed and initially tested [2] by coupling a horizontal and a vertical beam image onto the streak camera's input optics. Due to the promising results, attention was drawn to the addition of two beamline extensions. First, the possibility to adjust the difference of photon propagation time between the two imaging beams was added. Secondly, independent remote positioning of both photon beams enabled to account for transverse electron beam orbit displacements. The remote positioning capability also ensures optimum utilization of the available space on the CCD matrix, especially in synchroscan mode.

THE OPTICAL SYSTEM

The evacuated synchrotron radiation (SR) beamline frontend is approximately 12 m long and serves as differential vacuum pumping section in order to achieve a pressure 1-2 orders of magnitude below synchrotron vacuum. As the primary reflecting mirror is fully exposed to the x-ray beam, mirror surface reactions with residual gas are suppressed [3]. The mirror couples the visible part of the SR spectrum out of the accelerator's plane through a vertical chicane onto an optical table housing the optical components. An overview of the beam optics assembly is given in Fig. 1.

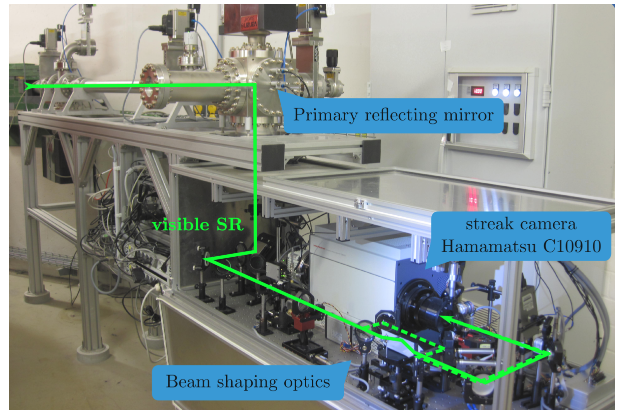

Figure 1: Photograph of the optical diagnostics beamline's back-end including the vertical chicane and the optical setup. The optical path (green) is guided through beam shaping optical elements half-way around the streak camera.

Table 1: ELSA & Source Point Parameters

Parameter	Value
Beam energy E	0.5–3.5 GeV
Revolution period T_{rev}	548 ns
Cavity RF frequency f_{RF}	499.67 MHz
Natural emittance ϵ_x	18–900 nm· rad
Bunch length σ_s	14–91 ps
Beam size ($8\sigma_x$ at source point)	3.1–21.9 mm

Requirements for Image Magnification

ELSA's electron beam dimensions are in the order of millimeters transversely and several ten picoseconds longitudinally. The accelerator properties and the resulting source point parameters are listed in Table 1.

Since longitudinal resolution capabilities are intrinsic properties of any streak camera, the aforegoing beamline is designed to provide sufficient resolution of transverse beam dynamics. The optics therefore match the expected electron beam size with the smallest field stop aperture which is identified as the photocathode of the operating streak camera Hamamatsu C10910 with a size of $0.15 \times 4.41\,\text{mm}^2$ [4]. The requirement for minimum beam demagnification at the photocathode is therefore

$$M_{\text{cathode}} \lesssim h_i/h_o \approx 10^{-2},$$

where $h_i = 150\ \mu\text{m}$ is the maximum allowable field size due to the aperture and $h_o \approx 22$ mm the maximum expected source size. The inequation takes into account that transverse beam oscillations enlarge the effective source size.

* Work supported by the DFG within CRC/TRR16.

Content from this work may be used under the terms of the CC BY 3.0 licence (© 2015). Any distribution of this work must maintain attribution to the author(s), title of the work, publisher, and DOI.

ISBN: 978-3-95450-168-7 doi:10.18429/JACoW-IPAC2015-MOPWA024

ESTIMATION OF THE ION DENSITY IN ACCELERATORS USING THE BEAM TRANSFER FUNCTION TECHNIQUE*

D. Sauerland†, W. Hillert, ELSA, Bonn, Germany
A. Meseck, Helmholtz-Zentrum Berlin, Germany

Abstract

The ELSA stretcher ring of Bonn University serves external hadron physics experiments with a quasi continuous electron beam of up to 3.2 GeV energy. Ions, being generated by collisions of the circulating electrons with the residual gas molecules, accumulate inside the beam potential, causing *incoherent* tune shifts and *coherent* beam instabilities. Detailed measurements were carried out in which ion dynamics is studied in dependence of beam energy and current, filling patterns and bias voltages of the ion clearing electrodes. By measuring the beam transfer function using a broadband transversal kicker, we were able to derive an estimate of the average ion density from the shift and broadening of the tune peak. In this contribution first results of these measurements are presented.

INTRODUCTION

The **El**ectron **S**tretcher **A**ccelerator (ELSA) is a three stage electron accelerator, consisting of a linear accelerator, a booster synchrotron, and the fast-ramping stretcher ring (see Figure 1). It is capable of providing polarized and unpolarized electrons with an energy of up to 3.2 GeV for hadron physics experiments.

An energy dependent equilibrium beam emittance in the stretcher ring is caused by damping due to synchrotron radiation. Thus the resulting transversal beam dimensions are scaling with the beam energy as well, which is shown in Table 1 in which also important operating parameters of the stretcher ring are presented. This energy dependency has an observable impact on the occurrence of transversal beam instabilities when storing high beam currents. Investigations have shown that these instabilities are mainly caused by trapped ions [1]. Since the dynamics of ion generation and motion in circular accelerators is i.a. influenced by the size of the beam, these instabilities arise in the horizontal and in the vertical plane at different beam energies. The growth rates of these instabilities scale with the ion density and may lead to beam losses during operation. In order to reduce the density of trapped ions, several ion clearing measures are applied at ELSA. To evaluate their efficiency, it is essential to develop a technique to estimate the average ion density. For this purpose an approach using beam transfer functions (BTF) was developed and will be discussed in this contribution.

* funded by the BMBF, Germany under grant 05K13PDA
† sauerland@physik.uni-bonn.de

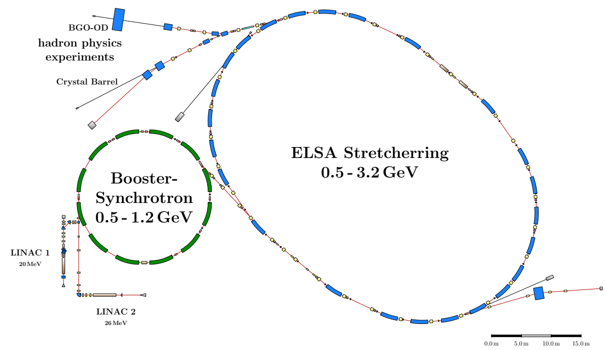

Figure 1: ELSA facility, status 2015

Table 1: Main Operating Parameters of ELSA

Energy	1.2 to 3.2 GeV
Beam current	up to 200 mA
Harmonic number	274
Revolution frequency	1.824 MHz
Horizontal tune (typ.)	4.612
Vertical tune (typ.)	4.431
Horizontal emittance	131 to 752 nm rad
Horizontal betafunction	betw. 2.4 and 17.3 m
Vertical betafunction	betw. 2.4 and 18.5 m
Coupling between planes	~ 7.2 %
1-σ bunch length	18.5 to 80 ps
Pressure (avg.)	$5.5 \cdot 10^{-8}$ mbar

ION EFFECTS IN CIRCULAR ACCELERATORS

Production, Accumulation and Impact of Ions

In an accelerator the passing electron beam continuously produces charged ions. Their composition mainly depend on the partial pressures of the different residual gas species and their corresponding ionization cross-sections. The electron beam forms an attractive potential wherein the positively charged ions can be trapped.

Once the ions are trapped, the beam's repulsive electrical field caused by space charge is reduced by the superimposed space charge field of the accumulated ions, while the focussing magnetic field generated by the beam remains constant as the ions are moving nonrelativistic. This results in a decreased defocussing of the electrons whose strength is dependent on their position inside the bunch. Thus an accumulation of ions causes an *incoherent* tune shift in the transversal planes which increases for higher ion densities.

Additionally trapped ions perform transversal oscillations inside the beam's potential around the barycenter of the

Content from this work may be used under the terms of the CC BY 3.0 licence (© 2015). Any distribution of this work must maintain attribution to the author(s), title of the work, publisher, and DOI.

ISBN: 978-3-95450-168-7 doi:10.18429/JACoW-IPAC2015-MOPWA025

Content from this work may be used under the terms of the CC BY 3.0 licence (© 2015). Any distribution of this work must maintain attribution to the author(s), title of the work, publisher, and DOI.

SIMULATION OF LASER COOLING OF HEAVY ION BEAMS AT HIGH INTENSITIES

L. Eidam*, TEMF, TU Darmstadt, Germany
O. Boine-Frankenheim, GSI Helmholtzzentrum für Schwerionenforschung GmbH (GSI), Germany
D. Winters, GSI Helmholtzzentrum für Schwerionenforschung GmbH (GSI), Germany

Abstract

In the past the principle of Doppler laser cooling was investigated and verified in storage rings in the low energy regime. Within the FAIR project the laser cooling will be applied to high intensity and high energy beams for the first time. The laser cooling results in a further increase of the longitudinal phase space density and in non-Gaussian longitudinal beam profiles. In order to ensure stable operation and optimize the cooling process the interplay of the laser force and high intensity effects has to be studied numerically. This contribution will identify constrains of the cooling scheme for an efficient reduction of momentum spread. For high beam energies the scattering of photons has to be treated stochastically instead of using averaged forces. The modeling of the laser force in a particle in cell tracking code will be discussed.

INTRODUCTION

Laser cooling produces ultra cold ion beams by intersecting laser light anti parallel with the particle beam. The momentum kick of the absorbed photon always points in direction of the laser beam, whereas the emission is isotropically distributed. For many scattering events the effect of the emission vanishes and the directional force of the absorption remains as shown in Fig. 1. Indeed this process requires a precise matching of the laser wavelength in the particle frame to the energy of the atomic transition. For available laser light sources this fact assigns a constrain on the beam velocity depending on the chosen transition as discussed in ref. [1].

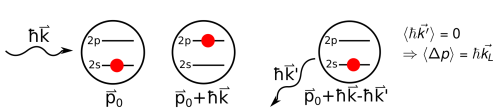

Figure 1: Sketch of a scattering event. Directional absorption and isotropic emission of photons leads to net force used for laser cooling.

The laser force requires a counteracting force to cool an ion beam. A second laser in opposite direction is the most efficient way for ion traps and low energy storage rings. For higher beam energies the best solution is given by capturing the particles in a rf bucket. The narrow laser force does not interact simultaneously with all ions in a hot particle bunch. Therefore the position of the laser force is scanned in order to damp continuously the synchrotron oscillation of all particles as shown in Fig. 2.

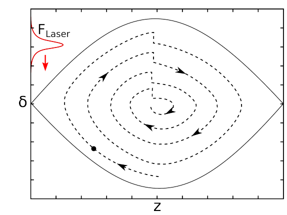

Figure 2: Sketch of the cooling process for a hot ion beam in a rf bucket. The laser force is scanned to damp continuously the synchrotron oscillation of all particles.

MODELING OF THE LASER FORCE

The influence of the laser force on the particle dynamic cannot be described by a cooling rate because of its strong non-linearity. In order to determine cooling equilibriums and optimize the general cooling process the longitudinal particle dynamics are solved numerically. For simplicity, the study contains only longitudinal dynamics assuming that the transverse motion is unaffected by the laser cooling.

The cooling force in the laboratory frame (LF) is given by the momentum change of one scattering event times the scattering rate.

$$F^{cool} = \Delta p^{LF} \cdot k \tag{1}$$

As shown in Fig. 1 the momentum change is given by the difference of the momentum of the incoming and outgoing photon:

$$\begin{aligned} \Delta p^{LF} &= \Delta p^{LF}_{in} - \Delta p^{LF}_{out} && (2)\\ &= -\frac{\hbar\omega^{LF}}{c_0} - \frac{\hbar\omega^{LF}}{c_0}\frac{U_i+\beta}{1-\beta} && (3)\\ &= -\frac{\hbar\omega^{LF}}{c_0}\gamma^2(1+\beta)\cdot(1+U_i) && (4) \end{aligned}$$

Where U_i is a random number between -1 and 1 that describes the projection of the isotropically radiated photon on the longitudinal axes. Note that the Lorentz boost of the outgoing photon provides a kick that is approximately $2\gamma^2$ higher than the incoming photon.

The scattering rate is given by the occupation of the excited state divided by its lifetime:

$$k = \frac{1}{\tau} \cdot \rho_{ee} \tag{5}$$

For simulations the ion-photon interaction is reduced to an atomic two level system in an electromagnetic mode and

* L.Eidam@gsi.de

ISBN: 978-3-95450-168-7 doi:10.18429/JACoW-IPAC2015-MOPWA026

DEMONSTRATION OF FLAT ION BEAM-CREATION AND -INJECTION INTO A SYNCHROTRON

L. Groening, S. Appel, L. Bozyk, Y. El-Hayek, M. Maier, C. Xiao, GSI, 64291 Darmstadt, Germany

Abstract

An ion beam with different horizontal and vertical emittances has been created from a beam with initially equal emittances. This round-to-flat adoption has been accomplished without any beam loss. In the set-up the beam passes through a stripping foil placed inside a solenoid followed by a skewed quadrupole triplet. The amount of beam flatness has been controlled by setting the solenoid field strength only. Increase of the product of the two transverse emittances is purely due to the stripping process that occurs anyway along an ion linac. Beams with different amounts of flatness were injected into a synchrotron applying horizontal multi-turn injection. The efficiency of injection increased as smaller as the horizontal emittance was set by the round-to-flat adaptor.

INTRODUCTION

For heavy-ion synchrotrons an efficient Multi-Turn Injection (MTI) from the injector linac is crucial in order to reach the specified currents using the available machine acceptance. The FAIR Heavy-ion synchrotrons are operated with intermediate charge state ions in order to increase the space charge limit. Therefore, stripping injection is not an option and the MTI has to respect Liouville's theorem for the chosen charge state - avoiding the already occupied phase space area. To achieve the space charge limit the multiplication of the injected current should be as large as possible. The beam loss during the MTI must not exceed the limits determined by machine protection and by the vacuum requirements. Especially for low energy and intermediate charge state ions, the beam loss can cause a degradation of the vacuum and a corresponding reduction of the beam lifetime.

One consequence of single-plane MTI is that the effective acceptance in the injection plane (usually the horizontal one) is reduced w.r.t. the acceptance in the other transverse plane. However, the two transverse emittances of the injected beam are generally similar to equal. The case may rise that the injected beam emittance is within the vertical acceptance budget but not within the horizontal acceptance budget for high MTI performance, although the product of its two emittances is lower than the product of the two effective acceptances. The MTI performance is thus reduced due to a not favourable emittance partitioning of the injected beam rather than by the product of its two emittances. Re-partitioning of the beam emittances, i.e. round-to-flat transformation would help to eliminate this reduction in injection efficiency. The latter has been proposed already for electrons by [1].

FLAT BEAM CREATION

Strict definition of rms-emittances is given through the transverse beam second moments matrix

$$C = \begin{bmatrix} \langle xx \rangle & \langle xx' \rangle & \langle xy \rangle & \langle xy' \rangle \\ \langle x'x \rangle & \langle x'x' \rangle & \langle x'y \rangle & \langle x'y' \rangle \\ \langle yx \rangle & \langle yx' \rangle & \langle yy \rangle & \langle yy' \rangle \\ \langle y'x \rangle & \langle y'x' \rangle & \langle y'y \rangle & \langle y'y' \rangle \end{bmatrix} \tag{1}$$

with

$$\epsilon_u := \sqrt{< u^2 >< u'^2 > - < uu' >^2}, \tag{2}$$

where u stands either for x or y as the particle coordinate. The prime denotes the derivative w.r.t. the longitudinal coordinate. The eigen-emittances [2] are the two emittances to which the rms-emittances can be reduced if all inter-plane correlation moments are removed:

$$\varepsilon_1 = \frac{1}{2}\sqrt{-tr[(CJ)^2] + \sqrt{tr^2[(CJ)^2] - 16det(C)}} \tag{3}$$

$$\varepsilon_2 = \frac{1}{2}\sqrt{-tr[(CJ)^2] - \sqrt{tr^2[(CJ)^2] - 16det(C)}}, \tag{4}$$

where

$$J = \begin{bmatrix} 0 & 1 & 0 & 0 \\ -1 & 0 & 0 & 0 \\ 0 & 0 & 0 & 1 \\ 0 & 0 & -1 & 0 \end{bmatrix}. \tag{5}$$

The square root of the determinant of C (Equ. 1) is equal to the 4d-rms-emittance of the beam and equal to the product of the two eigen-emittances. The amount of inter-plane correlation is quantified through the coupling parameter

$$t = \frac{\varepsilon_x \varepsilon_y}{\varepsilon_1 \varepsilon_2} - 1 \geq 0\,. \tag{6}$$

Figure 1 depicts the EMittance Transfer EXperiment (EMTEX) beam line that performs the desired round-to-flat adoption. It comprises two doublets to provide a small double waisted beam spot in the center of a subsequent solenoid where a charge state stripping foil is inserted. It causes

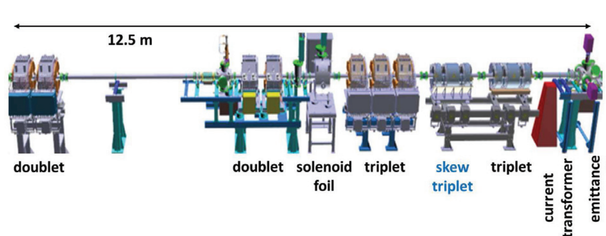

Figure 1: Beam line of EMTEX (Emittance Transfer Experiment).

Content from this work may be used under the terms of the CC BY 3.0 licence (© 2015). Any distribution of this work must maintain attribution to the author(s), title of the work, publisher, and DOI.

ISBN: 978-3-95450-168-7 doi:10.18429/JACoW-IPAC2015-MOPWA027

GENERIC SETTINGS GENERATION FOR FAIR: FIRST EXPERIENCE AT SIS18

H. Liebermann, J. Fitzek, R. Mueller, D. Ondreka,
GSI Helmholtzzentrum für Schwerionenforschung GmbH, Darmstadt, Germany

Content from this work may be used under the terms of the CC BY 3.0 licence (© 2015). Any distribution of this work must maintain attribution to the author(s), title of the work, publisher, and DOI.

Abstract

The accelerators of the FAIR facility will be operated using a new control system presently under design at GSI. One of its major components, the module for settings generation and management is based on the framework LSA developed at CERN. Its task is the provision and administration of set values for all devices in the FAIR facility. The set values for any accelerator are derived from a machine model, implemented by accelerator physicists using the features of the LSA framework. In view of the large number of accelerators in the FAIR facility, the aim is to develop a generic model, applicable to any of those machines. This requires the introduction of an additional logical layer on top of the LSA framework, ensuring the coherence of the modeling strategy across all accelerators. Following this design concept, a prototype of the FAIR settings management system has been realized at GSI, providing support for a large number of operation modes relevant for the later operation of FAIR. The prototype has been used extensively during recent machine experiments with the synchrotron SIS18, performed both to benchmark the machine model and to support further machine developments for FAIR.

INTRODUCTION

The FAIR facility comprises ten circular accelerators and a large number of beam transport lines. The planned operation schemes require a coordinated activity of the accelerators in order to achieve a high degree of parallel operation to optimize the facility's duty cycle. Consequently, each circular accelerator must be represented by a suitable machine model parameterized in terms of the physics parameters describing the functionality of the machine. The machine models have to be integrated into the control system to allow for the calculation of set values and timing events consistent with the planned operation schemes.

The FAIR control system will employ the software framework LSA developed at CERN to implement the settings generation and management component. The machine models will therefore be implemented using the features of the LSA framework. LSA itself, as a data-driven framework, provides excellent support for the storage of data related to devices and ion optical layout of accelerators. Moreover, it comes with generic concepts for the implementation of machine models as well as algorithms for the generation, modification, and persistance of set values. However, within the limits of the framework, it is completely up to the users of the framework to choose a particular representation for a certain machine.

At CERN, this freedom has, mostly for historical reasons, led to the existence of a heterogeneous collection of machine models (basically one model per machine) employing different philosophies and using the LSA structures in different ways. In essence, this means that each model is defined and maintained by a different group of machine experts. For FAIR, we aim at creating generic machine models that can be used for any circular accelerator. This is possible since the same fundamental principles of accelerator physics apply to each ring. Special features of individual rings can then be added on top of the common structures. This strategy will greatly reduce the implementation and maintenance effort for the machine models for FAIR. In addition, the machine experts implementing the models automatically share a common knowledge about all machines, which increases the resources for troubleshooting during operation.

In this paper, we first discuss our strategy for implementing generic machine models using LSA, giving two important examples. Then, we report on recent results obtained using a prototype of the settings management system for FAIR to control the existing synchrotron SIS18.

GENERIC MODELS

In the context of an accelerator control system, we define a *machine model* loosely as the collection of all input parameters and algorithms used to implement the calculation of hardware set values, according to the desired operation of the machine and based on a theoretical description in terms of accelerator physics equations. The input parameters of the machine model should allow the control of the accelerator in terms of physics quantities (e.g., tunes, magnet strengths, bucket size). This is particularly important in a facility like FAIR, where beams of different mass, charge states and energies are routinely produced in alternating cycles.

The LSA framework provides generic structures for implementing machine models. Physics quantities and hardware set values are represented as *parameters*. Parameters are grouped according to their *parameter type*, describing the physics category of the parameter. For instance, each quadrupole magnet has a strength value represented by a parameter of the same parameter type KL. A *setting* is a value of a parameter associated with a certain machine cycle. The task of the machine model is the calculation of hardware settings from the settings of the physics parameters.

The rules for calculations among the parameters are expressed explicitly in terms of *relations* between pairs of parameters, i.e., *parent* and *child*. A set of relations between parameters is called a *parameter hierarchy*. There is typically one parameter hierarchy per accelerator or beam trans-

ISBN: 978-3-95450-168-7 doi:10.18429/JACoW-IPAC2015-MOPWA028

RESONANCE COMPENSATION FOR HIGH INTENSITY BUNCHED BEAM

G. Franchetti, S. Aumon, F. Kesting, H. Liebermann, C. Omet, D. Ondreka, R. Singh
GSI, Darmstadt, Germany

Abstract

Mitigation of periodic resonance crossing induced by space charge is foreseen via classic resonance compensation. The effect of the space charge is, however, not obvious on the effectiveness of the compensation scheme. In this proceeding we report on the experimental campaign performed at SIS18 to investigate experimentally the effect of space charge on the resonance compensation. The experimental results and their consequences are discussed.

INTRODUCTION

Long term beam loss are due to several factors, but lattice nonlinearities and high intensity certainly rank among the main causes for long term beam loss. In fact, numerical and experimental studies have shown that periodic resonance crossing induced by space charge in a bunched beam is a deleterious effect for beam survival [1,2]. The focus in the mentioned studies was on one dimensional resonances: in Ref. [1] with $4Q_x = 25$, and in Ref. [2] with $3Q_x = 13$. The underlying mechanism leading to beam loss is explained, for 1D resonances, in terms of instantaneous stable islands in the two-dimensional phase space and their crossing of particles orbits [3].

Detailed studies for SIS100 have shown that in the injection scenario of the uranium ions, random components of magnet nonlinearities excite a significant web of resonances including 2D resonances [4], the simpler of which is the $Q_x + 2Q_y = N$. The details of the periodic resonance crossing induced by space charge for coupled resonances have never been studied due to its complexity. In fact, while for 1D resonances the mechanism is relatively well understood, for 2D resonances it is not, as the dynamics is now fully 4-dimensional in phase space. Indication of this complexity have been observed in the experimental campaign at the CERN-PS in 2012, where space charge studies near the resonance $Q_x + 2Q_y = 19$ have shown that beam profiles for some machine tunes acquired an anomalous asymmetry. In this scenario new nonlinear dynamics objects called fix-lines play a similar role as the fixed points for the crossing of the 1D resonances. A full study of the fix-lines is reported in Ref. [5].

In SIS100 operational requirements do no allow beam loss to exceed ~ 5%, and the issue of whether a resonance compensation may be carried out for a long term storage of a high intensity bunched beam or not is of high relevance. Recent numerical studies have shown that resonance compensation in simulations using a *frozen space charge* model has a beneficial effect on long term beam loss [4,6,7]. However, it remains to be established if this procedure is effective in a real high intensity bunched beam. In fact, resonance compensation is obtained by creating an artificial driving term that counteract the driving term of the machine nonlinearities. This procedure relies on the assumption that a resonance is excited mainly by a single harmonics. While this assumption works well in standard operational regimes for low intensity beams, it is not obvious what are the consequences for multiple periodic resonance crossing induced by space charge. For these reasons at GSI a campaign for testing the effectiveness of a resonance compensation in presence of space charge has been undertaken.

THIRD ORDER RESONANCE MITIGATION

Figure 1 shows the resonance chart of SIS18 after the recent re-alignment of the accelerator magnets. The apparent mismatch of some of the resonance lines with the theoretical solid lines is due to small systematic tune-shifts present in the machine model used by the control system. The third

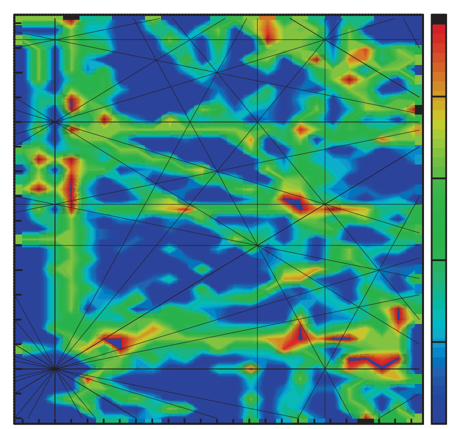

Figure 1: Resonances of SIS18 measured on the 16/7/2014 after the magnets re-alignment. This picture have been obtained by using SISMODI control system.

order resonance $Q_x + 2Q_y = 11$, visibly excited, is of particular interest because a similar resonance will affect the SIS100 for the preliminary working point for ions (example for the uranium beam scenario at the working point $Q_x = 18.84, Q_y = 18.73$) and fast extraction [8].

This resonance strength was estimated by measuring beam loss while the resonance is crossed with linear ramp from $Q_y = 3.45$ to $Q_y = 3.35$ in 1 second keeping $Q_x =$

Content from this work may be used under the terms of the CC BY 3.0 licence (© 2015). Any distribution of this work must maintain attribution to the author(s), title of the work, publisher, and DOI.

ISBN: 978-3-95450-168-7 doi:10.18429/JACoW-IPAC2015-MOPWA029

Content from this work may be used under the terms of the CC BY 3.0 licence (© 2015). Any distribution of this work must maintain attribution to the author(s), title of the work, publisher, and DOI.

INVESTIGATIONS OF THE SPACE-CHARGE-LIMITED EMISSION IN THE L-BAND E-XFEL PHOTOINJECTOR AT DESY-PITZ*

Y. Chen†, E. Gjonaj, A. Tsakanian, H. De Gersem, T. Weiland
TEMF, Technische Universitaet Darmstadt, Schlossgartenstrasse 8, 64289 Darmstadt, Germany
C. Hernandez-Garcia, M. Krasilnikov, F. Stephan
Deutsches Elektronen-Synchrotron DESY, Platanenallee 6, 15738 Zeuthen, Germany

Abstract

This paper discusses the numerical modelling of electron bunch emission for an L-band normal conducting RF photogun. The main objective is clarifying the discrepancies between measurements and simulations performed for the European X-ray Free Electron Laser (E-XFEL) injector at DESY-PITZ. An iterative beam dynamics simulation procedure is proposed for the calculation of the total extracted bunch charge under the assumption that the emission source operates at the space-charge limit of the gun. This algorithm has been implemented in the three-dimensional full electromagnetic PIC Solver of the CST Particle Studio ő (CST-PS) [1]. Simulation results are in good agreements with measurements for a series of operation parameters. Further comparisons with a conventional Poisson-solver-based (PSB) tracking algorithm demonstrates the great significance of transient electromagnetic field effects for the beam dynamics in high brightness electron sources.

INTRODUCTION

For the operation of Free Electron Lasers (FELs), high quality electron beams characterized by high brightness and extremely low transverse emittance, are required. An L-band normal conducting (copper) RF photoinjector was particularly designed and optimized at PITZ for the generation of such high quality electron beams for the European X-ray Free Electron Laser (E-XFEL) and the Free Electron Laser in Hamburg (FLASH) [2]. Hereby, a crucial role plays the modelling of electron bunch emission as well as the simulation of the space-charge dominated beam dynamics in the gun.

It has been previously reported [3] that for specific machine conditions, comparatively large discrepancies between simulations and measurements are found. In particular, the total extracted bunch charge at an RMS beam size of 0.3 mm is much higher than predicted in the simulations. One source of discrepancy was identified in [4]. It was shown that in conventional Poisson-solver-based (PSB) tracking codes, the magnetic space-charge field contribution is neglected. For high current beams, this contribution becomes important due to the fast electron bunch expansion during emission. In order to take into account the impact of these magnetic space-charge fields, beam dynamics simulations based on the solution of the full set of Maxwell equations are necessary. Yet another important modelling issue, however, is the computation of the total charge extracted from the cathode when the injector is operated close to or at the space-charge limit. This quantity depending on various machine parameters is not a priori known. In this paper we propose a self-consistent simulation procedure which is able to predict very accurately space-charge field dominated photoemission in RF electron sources.

Investigations of the space-charge-limited emission will be performed specifically with parameters of significance experimentally obtained for the PITZ photoinjector project. The main components of the PITZ injector are a 1.6 cell copper RF gun cavity with a cesium-telluride photocathode, CDS booster cavity, cathode laser system, and multiple beam diagnostic systems. The electron beam is extracted as the photocathode is illuminated by the UV laser pulse at the wavelength of 257 nm, and then accelerated by a 1.3 GHz RF field excited in the gun cavity. A main solenoid and a bucking solenoid are additionally applied for beam focusing and space-charge emittance compensation. A detailed description of this setup can be found in [2].

BUNCH EMISSION MODELLING AT THE SPACE-CHARGE LIMIT

A sketch of the total bunch charge extraction based on experimental observations [3] is shown in Fig. 1. The top curve shows the total space-charge-limited bunch charge at each gun launch phase when operating the emission source exactly at the space-charge limit. As for below the space-charge limit, the emission becomes a combination of two emission regimes, the space-charge-limited (SCL) and the quantum-efficiency-limited (QEL). The QEL regime in the combined emission case is marked out by the trapezoid area. The total charge in this regime depends on conditions of the emission source instead of the applied RF field at the cathode. As shown, the maximum extracted charge is apparently given by the flat-top region in the gun phase range. However, the charge extraction below this flat level (i.e., the rise / fall edge) is still limited by the space-charge field. This is because the space charge limits there are lower than the maximum total charge produced by the emission source.

In the following we propose a self-consistent simulation procedure specifically to calculate the total SCL bunch charge extracted from the cathode. Using a set of gun launch phases, the bunch emission simulation is performed initially with a sufficiently large total bunch charge depending on specific machine parameters (f.i., 2 nC in this paper). After

* Work supported by DESY Hamburg and Zeuthen sites. PITZ: Photo Injector Test Facility at Zeuthen, Berlin, Germany
† chen@temf.tu-darmstadt.de

ISBN: 978-3-95450-168-7 doi:10.18429/JACoW-IPAC2015-MOPWA030

SIMULATIONS OF ELECTRON CLOUD LONG RANGE WAKEFIELDS *

F.B. Petrov, O. Boine-Frankenheim, TEMF, TU-Darmstadt, Darmstadt, Germany

Abstract

A typical approach to electron cloud simulations is to split the problem in two steps: buildup simulations and instability simulations. In the latter step the cloud distribution is usually refreshed after each full interaction with the bunch. This approach does not consider multibunch effects. We present studies of the long range electron cloud wakefields generated in electron clouds after interaction with relativistic proton bunch trains. Several pipe geometries - relevant to CERN accelerators - with and without external magnetic field are considered. Using simple examples we show that the long range wakefields depend significantly on the secondary emission curve as well as on the pipe geometry. Additivity of electron cloud wakefields is studied as well.

INTRODUCTION

Relativistic bunches penetrating electron clouds induce transverse and longitudinal wakes. Transverse wakefields cause instabilities and emittance growth [1]. Whereas longitudinal wakefields are responsible for energy loss and synchronous phase shift [2, 3]. In many cases researchers look for the first unstable bunch in bunch trains. For this purpose one performs scans over electron cloud density. Typically, the electron cloud is assumed to be a very nonlinear object. Thus, most of the beam tracking studies utilize particle-in-cell electron cloud distributions.

In this contribution we investigate the parameters of transverse and longitudnal electron cloud wakefields for CERN-like conditions. We compare the results of 2D and 3D codes. We investigate single-bunch electron cloud wakefields induced by transversely perturbed proton bunches. Moreover, we investigate multi-bunch electron cloud wakefields induced by $k = 0$ bunch mode in bunch trains. The aim is to identify possible regimes where electron cloud representation can be simlified for future beam tracking simulations.

SIMULATION MODEL

For our simulations we utilize two codes: openECLOUD [4] and commercial Vsim [5]. The first code is the electron cloud buildup code from TU-Darmstadt. It utilizes 2D Poisson solver; electron cloud is represented as a 2D slice; the interaction with the beam is purely transverse; stainless steel and copper material models are implemented according to Ref. [6]. For all the simulation we assume rigid, frozen bunches. We take pipe parameters of the super proton synchrotron (SPS) and the large hadron collider (LHC) (set Table 1).

Table 1: Simulation Parameters

Parameter	Value
Bunch length, $\sigma_z[m]$	0.1
Bunch radius, $\sigma_r[m]$	0.01
Bunch spacing, $T[ns]$	25
Bunch population, N_i	10^{11}, 2×10^{11}
Round pipe radius, $R[m]$	0.02
LHC pipe dimensions, $l_x/l_y[m]$	0.044/0.036
SPS MBB dimensions, $l_x/l_y[m]$	0.1218/0.0485
Dipole field, $B[T]$	0.1
Wall materials	copper, stainless steel

SINGLE-BUNCH WAKEFIELDS

In this section we investigate the single-bunch electron cloud wakefields for several bunch parameters. The aim is to indicate the conditions where electron coud wakefields show any linearity.

Figure 1 shows the comparison between the wakefields calculated with openECLOUD and Vsim (3D electromagnetic). The bunch is offcentered as a whole ($k = 0$ head-tail mode), electron cloud fills the cylindrical pipe uniformly. The left plot shows the transverse wakefields obtained directly from the simulations. The right plot shows the longitudinal wakefields. In case of openECLOUD this field is obtained during the data postprocessing. For this purpose we take the derivative of 2D potential with respect to z. One can see that the agreement between the two codes is very good.

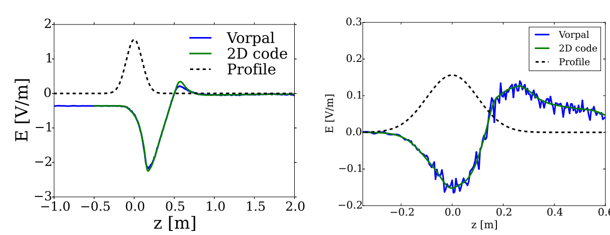

Figure 1: Electron cloud transverse (left) and longitudinal (right) wakefields simulated with Vsim and openECLOUD codes for $N_i = 2 \times 10^{11}$.

Next we analyze the wakefields due to the harmonically excited bunches. All the following simulations are performed using the openECLOUD code. The transverse displacement as a function of longitudinal coordinate is given as follows:

$$\Delta x_k = A_x \sin \frac{2k\pi z}{\lambda_z} \quad (1)$$

, where k is the mode number, A_x is the amplitude, z is the longitudinal coordinate, λ_z is the bucket length. Figure 2 shows the transverse electric fields induced by several

Content from this work may be used under the terms of the CC BY 3.0 licence (© 2015). Any distribution of this work must maintain attribution to the author(s), title of the work, publisher, and DOI.

ISBN: 978-3-95450-168-7 doi:10.18429/JACoW-IPAC2015-MOPWA031

A NEW APPROACH FOR RESISTIVE WAKEFIELD CALCULATIONS IN TIME DOMAIN

A. Tsakanian#, E. Gjonaj, H. De Gersem, T. Weiland, TU-Darmstadt/TEMF, Darmstadt, Germany
M. Dohlus, I. Zagorodnov, DESY, Hamburg, Germany

Abstract

We report on a new numerical technique for the computation of the wakefields excited by ultra-short bunches in the structures with walls of finite conductivity. The developed 3D numerical method is fully time domain. It is based on special Staggered Finite Volume Time Domain (SFVTD) method and has no numerical dispersion in all three axial directions simultaneously. The resistive boundary model applies Surface Impedance Boundary Condition (SIBC) evaluation in time domain and covers boundary effects like frequency dependent conductivity, surface roughness and metal oxidation. A good agreement between numerical simulation and perturbation theory is obtained.

INTRODUCTION

Electromagnetic wakefields due to the finite conductivity of cavity walls are one of the main concerns in the design of electron accelerators. These so called resistive wall wakefields are the largest contributor to beam coupling impedances in the high energy sections of the accelerator where extremely short electron bunches are operated [1]. For an estimation of these contributions one relies (almost) exclusively on numerical simulations, since wakefield measurements within the high-vacuum accelerator chamber are very cumbersome.

Conventional methods for the solution of Maxwell's equations in the time domain, however, will usually fail for this class of problems. This is primary due to the extremely high frequency of wakefields resulting in large numerical dispersion errors. These errors tend to accumulate in the course of the simulation as, e.g., short electron bunches of μm-length propagate over several meters within the accelerator.

To cope with this problem, specialized low-dispersion techniques have been proposed [2]. The SFVTD method introduced in [3] is one of them. It represents a volume-integral based formulation with very appealing numerical properties. The dispersion error of SFVTD is substantially smaller than that of the conventional FDTD technique. The crucial property, however, is that the method can be operated at a maximum stable time step corresponding to the 1D-CFL stability limit. Applying SFVTD at this so called 'magic' time step provides the exact, dispersion-free solution for all electromagnetic waves propagating along the three main axis directions (cf. [3]).

In order to take into account resistive and/or rough wall wakefields in such simulations, however, an appropriate implementation of broadband SIBC for SFVTD is needed. In the following, this task is accomplished by combining the ADE technique with a particular time stepping scheme. This latter allows to maintain the numerical dispersion and stability properties of the original SFVTD which are necessary for this type of simulations.

THE SFVTD METHOD

The basic idea of the SFVTD discretization is depicted in Fig. 1. Fields and currents are allocated component-wise on the faces of a Cartesian mesh. For each of these components a unique control volume enclosing the corresponding mesh face is introduced. Alternatively, one may think of three secondary, staggered meshes which are obtained by shifting the original mesh along the x-, y- and z-directions, respectively.

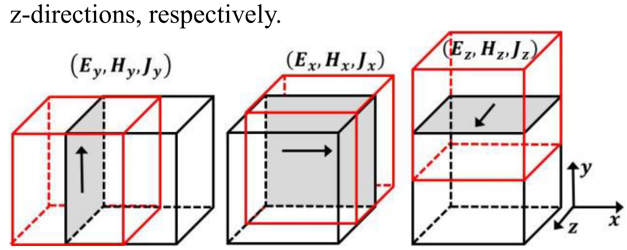

Figure 1: Allocation of fields and currents on mesh cells (black) and corresponding control volumes (red) of SFVTD.

A discretization of Maxwell's equations is obtained by applying the generalized Stokes' theorem for each of the 6 field components on the corresponding control volumes. A detailed derivation of these equations is given in [3]. Here, we begin with the semi-discrete form of SFVTD:

$$\boldsymbol{M}_\mu \frac{d\boldsymbol{h}}{dt} = -\boldsymbol{C}\boldsymbol{e} \ , \tag{1}$$

$$\boldsymbol{M}_\varepsilon \frac{d\boldsymbol{e}}{dt} = \boldsymbol{C}^T \boldsymbol{h} - \boldsymbol{j} \, . \tag{2}$$

In (1), (2), $\boldsymbol{e}$, $\boldsymbol{h}$ and $\boldsymbol{j}$ represent volume averages over the control volumes of the electric, magnetic and current field components, respectively. The matrices, $\boldsymbol{C}$, $\boldsymbol{M}_\varepsilon$ and $\boldsymbol{M}_\mu$ are the *curl*- and *mass*-operators of the method resulting from this particular choice of integration volumes on the mesh. The particular form of these matrices determines the numerical properties of the SFVTD method such as the low numerical dispersion and the large bound of stability.

In figure 2 are presented the numerical phase velocity behavior of the plane wave versus its propagation direction. Both, SFVTD and conventional FDTD methods are evaluated at their stability limits, i.e. FDTD - $c\Delta t_{2D} = \Delta/\sqrt{2}$, $c\Delta t_{3D} = \Delta/\sqrt{3}$, SFVTD - $c\Delta t_{2D,3D} = \Delta$.

Content from this work may be used under the terms of the CC BY 3.0 licence (© 2015). Any distribution of this work must maintain attribution to the author(s), title of the work, publisher, and DOI.

6th International Particle Accelerator Conference IPAC2015, Richmond, VA, USA JACoW Publishing
ISBN: 978-3-95450-168-7 doi:10.18429/JACoW-IPAC2015-MOPWA032

ASPECTS OF SRF CAVITY OPTIMIZATION FOR BESSY-VSR UPGRADE*

T. Galek†, J. Heller, K. Brackebusch, T. Flisgen, U. van Rienen, Universität Rostock, Germany
B. Isbarn, B. Riemann, M. Sommer, T. Weis, Technische Universität Dortmund, Germany

Abstract

In this work we present a preliminary study of a long chain of cavities and some aspects involved in the optimization procedure. It is important to numerically model and optimize the SRF cavities with respect to external quality factors of the most dangerous higher order modes. BESSY-VSR is an upgrade scheme for the existing BESSY II storage ring aiming to simultaneously support variable electron pulse lengths. Currently, BESSY II supports long 15 ps bunches in the standard user optics configuration and short 1.5 ps bunches in a so-called low-α optics mode. In order to develop BESSY II into a variable electron pulse length storage ring, additional two sets of SRF higher-harmonic cavities will be installed. The present RF acceleration system operates at 0.5 GHz and the additional 3rd harmonic and 3rd sub-harmonic cavities will operate at 1.5 GHz and 1.75 GHz, respectively. These cavities are essential to produce short 1.5 ps bunches with a design current of up to 0.8 mA per bunch. The total current in the storage ring is limited by the higher order mode damping capabilities of the SRF cavities.

END-GROUP OPTIMIZATION

The design of the cavity used in this work is similar to the bERLinPro [1] energy recovery linac main cavity. It is characterized by spline-nose cavity to beam-pipe transition and threefold waveguide higher order mode (HOM) couplers. One of the waveguide HOM couplers is replaced by a coaxial input coupler as shown in Fig. 1. The Cornell mid-cell based on TESLA design and used in the bERLinPro cavity was selected for this study. The mid-cell design was scaled to the operational frequency of 1.5 GHz and 1.75 GHz. The results of a comparison between Cornell mid-cell and other mid-cell designs were discussed previously elsewhere [2].

Field Flatness in Cavities

Usually, in the optimization procedure of the end-groups of a superconducting radio frequency (SRF) cavity one can aim at multiple optimization targets like minimum magnetic and electric surface fields, operational frequency, maximum accelerating gradient (R/Q) and field flatness. In this work the optimization focused only on the operational frequency and field flatness. Typically the E-field flatness is of a concern. The E-field flatness on the beam axis is defined as [3]

$$\eta_{E_z} = \left(1 - \frac{\sigma_{E_{z,\text{peak}}}}{\mu_{E_{z,\text{peak}}}}\right) \times 100\%, \tag{1}$$

where $\mu_{E_{z,\text{peak}}}$ is the mean value of the peak electric field component $E_z(z)$ on the beam axis in the direction of the beam in every cell and $\sigma_{E_{z,\text{peak}}}$ is the standard deviation.

The BESSY-VSR higher harmonic cavities will not operate close to the maximum achievable electric field gradient, thus the electric peak surface fields and field assisted emission become less of a concern. This allows to focus on peak magnetic surface fields that contribute to magnetic quenches. The H-field flatness is even more of an issue in cavities with mid-cell designs that have relatively large iris

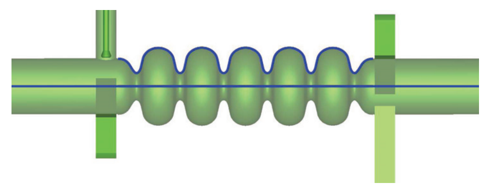

Figure 1: Example of 5-cell 1.5 GHz cavity model. The blue profile lines along the beam axis and along the cavity's boundary are used to evaluate E- and H-field patterns, respectively.

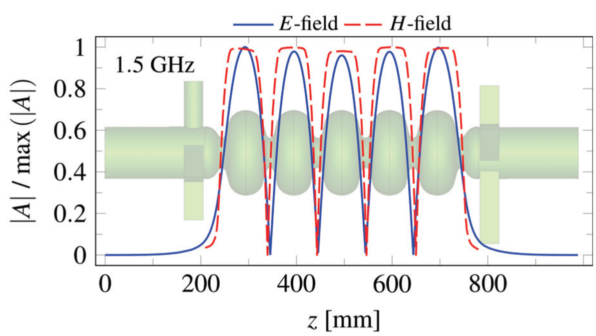

Figure 2: Normalized E- (solid blue line) and H-field (dashed red line) patterns along profiles depicted in Fig. 1 for 1.5 GHz cavity.

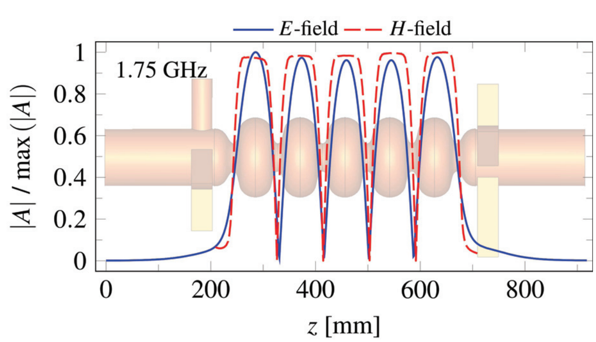

Figure 3: Normalized E- (solid blue line) and H-field (dashed red line) patterns along profiles depicted in Fig. 1 for 1.75 GHz cavity.

* Work supported by Federal Ministry for Research and Education BMBF under contract 05K13HR1.
† Corresponding author: tomasz.galek@uni-rostock.de

Content from this work may be used under the terms of the CC BY 3.0 licence (© 2015). Any distribution of this work must maintain attribution to the author(s), title of the work, publisher, and DOI.

ISBN: 978-3-95450-168-7 doi:10.18429/JACoW-IPAC2015-MOPWA033

YACS - A NEW 2.5D FEM EIGENMODE SOLVER FOR AXISYMMETRIC RF-STRUCTURES *

B.D. Isbarn†, B. Riemann, M. Sommer, T. Weis
TU Dortmund University (DELTA), Center for Synchrotron Radiation, Dortmund, Germany

Abstract

Most feasibility studies for modern accelerator concepts, including superconducting multicell RF-cavity-resonators in circular accelerators, depend on computing a large number of eigenmode frequencies and field patterns to obtain typical figures of merit. This task includes computationally intensive studies. To obtain the full eigenfrequency spectra most of these studies are performed in 3D, require a great amount of computation resources and thus are limited to a few hundred or thousand eigenmodes. To overcome this issue, some codes make use of the axisymmetric geometry of most of the RF-cavity-resonator structures and solve the problem in 2D. Solving in 2D however reduces the eigenmode spectra to eigenmodes with no azimuthal dependencies (so called monopole modes). Due to the lack of freely available and easy to use 2.5D eigenmode solvers which are able to solve for the full 3D field in a reduced 2.5 dimensional problem, we developed yet another cavity solver (Yacs), a simple FEM based solver capable of solving for the full 3D eigenmodes of axisymmetric problems while only requiring a fraction of the computation resources required by most modern 3D codes.

INTRODUCTION

Numerical calculation of resonant eigenmodes with the eigenfrequency $\omega \in \mathbb{C} \setminus \{0\}$ in a rf-structure usualy involves solving the vector Helmholtz equation for the electric field that arises from the Maxwell equations in a bounded domain $\Omega \subset \mathbb{R}^3$

$$\nabla \times \left(\underline{\mu}^{-1} \nabla \times \boldsymbol{E}\right) - \omega^2 \underline{\epsilon} \boldsymbol{E} = \boldsymbol{0} \,. \tag{1}$$

Closed-form solutions of (1) can only be obtained for simple geometries like cylindrical or spherical resonators.

The Sparse Eigenvalue Problem

In the case of an axisymmetric problem domain we may use spherical coordinates and expand the azimuthal component of the electric field by a Fourier series

$$\boldsymbol{E}\left(\boldsymbol{r}\right) = \sum_{m=0}^{\infty} \boldsymbol{E}_m^{(c)}\left(r,z\right) \cos\left(m\theta\right) + \boldsymbol{E}_m^{(s)}\left(r,z\right) \sin\left(m\theta\right) \,. \tag{2}$$

Due to the pairwise orthogonality of the Fourier basis functions we receive a decoupled problem and can solve for each mulipole mode m individually. Applying the finite element method on the problem stated in (1) together with the azimuthal fourier series expansion (2) we can approximate (1) with a sparse generalized eigenvalue system. This has allready been discussed thoroughly in earlier works [1]. The resulting sparse generalized eigenvalue system is described by

$$\begin{pmatrix} \underline{\boldsymbol{K}}^{pp} & \underline{\boldsymbol{K}}^{p\theta} \\ \underline{\boldsymbol{K}}^{p\theta^T} & \underline{\boldsymbol{K}}^{\theta\theta} \end{pmatrix} \begin{pmatrix} \hat{\boldsymbol{E}}_p \\ \hat{\boldsymbol{E}}_\theta \end{pmatrix} = \omega^2 \begin{pmatrix} \underline{\boldsymbol{M}}^{pp} & 0 \\ 0 & \underline{\boldsymbol{M}}^{\theta\theta} \end{pmatrix} \begin{pmatrix} \hat{\boldsymbol{E}}_p \\ \hat{\boldsymbol{E}}_\theta \end{pmatrix} \tag{3}$$

$$\underline{\boldsymbol{K}} \hat{\boldsymbol{E}} = \omega^2 \underline{\boldsymbol{M}} \hat{\boldsymbol{E}} \tag{4}$$

with

$$\begin{aligned}
\underline{\boldsymbol{K}}_{ij}^{pp} &= \langle \mu_\theta^{-1} r \nabla_p \times \boldsymbol{\phi}_i, \nabla_p \times \boldsymbol{\phi}_j \rangle + m^2 \langle \mu_p^{-1} r^{-1} \boldsymbol{\phi}_i, \boldsymbol{\phi}_j \rangle \\
\underline{\boldsymbol{K}}_{ij}^{p\theta} &= m \langle \mu_p^{-1} r^{-1} \boldsymbol{\phi}_i, \boldsymbol{\nabla}_p \psi_j \rangle \\
\underline{\boldsymbol{K}}_{ij}^{\theta\theta} &= \langle \mu_p^{-1} r^{-1} \boldsymbol{\nabla}_p \psi_i, \boldsymbol{\nabla}_p \psi_j \rangle \\
\underline{\boldsymbol{M}}_{ij}^{pp} &= \langle \epsilon_p r \boldsymbol{\phi}_i, \boldsymbol{\phi}_j \rangle \\
\underline{\boldsymbol{M}}_{ij}^{\theta\theta} &= \langle \epsilon_\theta r^{-1} \psi_i, \psi_j \rangle
\end{aligned}$$

where $\underline{\boldsymbol{K}}$ and $\underline{\boldsymbol{M}}$ are typically referred to as stiffness- resp. mass-matrices, p (in-plane) denotes operations and vectors with respect to the $\hat{\boldsymbol{r}}$ and $\hat{\boldsymbol{z}}$ direction, while $\boldsymbol{\phi}_x$ together with ψ_x refer to the global mapping of the basis functions with $\boldsymbol{\phi}_x$ referring to the vector-valued in-plane component and ψ_x referring to the out of plane scalar component.

IMPLEMENTATION

The primary part of the FEM code has been developed in C++ using state-of-the-art numerical libraries to achieve maximum performance and reliability. The meshing of the problem domain is performed with Triangle [2], general dense and sparse algebra is done using Eigen v3 [3] and solving the sparse generalized eigenvalue problem has been realized with ARPACK [4] in conjunction with UMFPACK [5]. The latter is used for solving sparse linear systems. In this first iteration of Yacs we solely use first order basis functions for expanding the trial and test functions.

Boundary Conditions

In the case of solving multipole modes, we artifically introduce PEC boundary conditions on the rotation axis and thus force the electrical field parallel to the rotation axis to vanish. In order to avoid the singular terms for $r = 0$ in (3), we use a Gauss quadrature scheme that only evaluates points inside the domain and avoids those points on the boundary of the domain.

BENCHMARK

All the benchmarks presented in the following were performed on a simple $\nu = 500\,\mathrm{MHz}$ pillbox cavity for which

* Work supported by the BMBF under contract no. 05K13PEB
† benjamin.isbarn@tu-dortmund.de

Content from this work may be used under the terms of the CC BY 3.0 licence (© 2015). Any distribution of this work must maintain attribution to the author(s), title of the work, publisher, and DOI.

ISBN: 978-3-95450-168-7 doi:10.18429/JACoW-IPAC2015-MOPWA034

COUPLED-BUNCH INSTABILITY SUPPRESSION USING RF PHASE MODULATION AT THE DELTA STORAGE RING*

M. Sommer†, M. Höner, B. Isbarn, S. Khan, B. Riemann, T. Weis
Center for Synchrotron Radiation (DELTA), TU Dortmund University, Dortmund, Germany

Abstract

In this paper, a feedback-based method to measure the damping rates of multibunch modes at the 1.5-GeV electron storage ring DELTA operated by the TU Dortmund University is presented and the influence of an RF modulation on these damping rates is analyzed. For this purpose, the amplitude as well as the frequency of the modulation was varied. The suppression of coupled-bunch instabilities could be observed with a modulation frequency slightly below twice and three times the synchrotron frequency. However, the determination of damping rates for high modulation amplitudes using the presented method is problematic.
In addition, the decrease of beam quality using RF phase modulation was investigated and the increase of bunch length was measured as a function of the modulation amplitude.

INTRODUCTION

The upcoming upgrade of BESSY II, called BESSY-VSR [1], involves the utilization of superconducting multicell RF-resonators to provide short and long bunches simultaneously. The residual impedances of the cavities may cause collective multibunch instabilities at the frontier of stability available from current bunch-by-bunch feedback systems. Hence, other damping methods have to be considered, e.g. a modulation of the radio frequency (RF) of the accelerating cavity. The effects of RF phase modulation in circular accelerators date back to the early 1990's [2] [3]. In 2008, a modulation had been applied at the 1.5-GeV electron storage ring DELTA operated by the TU Dortmund University (see Fig. 1 and Table 1) in order to suppress longitudinal instabilities [4] [5]. In 2011, a digital bunch-by-bunch feedback system [6] was installed for beam diagnostics purposes [7]. This system is able to suppress the aforementioned instabilities succesfully, without the application of the RF phase modulation. During user operation, the RF modulation is routinely in operation to increase the beam lifetime by up to 20% due to the reduction of the mean electron density and, thus, the rate of Touschek scattering [8]. To get a deeper understanding of the suppression of instabilities by RF phase modulation, the bunch-by-bunch feedback system is used to determine the damping rates of all coupled-bunch modes.

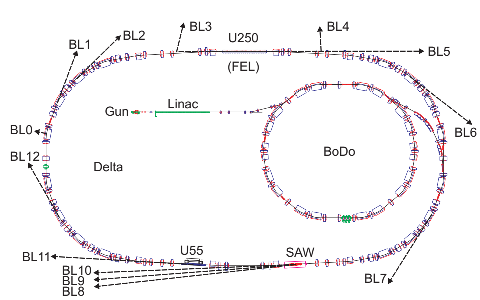

Figure 1: Overview of the DELTA facility including the storage ring and its booster synchrotron BoDo.

Experimental Setup

To extract the horizontal, vertical and longitudinal position of every bunch, a combination of a beam position monitor and a hybrid network is used. The horizontal and vertical differential signals as well as the sum signal are sent to the feedback frontend, where they are filtered, attanuated and digitized. By applying a 24-tap FIR filter on consecutive input data, the output signals are created, which are converted to analog signals driving the power amplifiers and the corresponding kicker structures. In addition, the processing units include a frequency generator, which allows to send a dedicated RF signal to the beam, for example to excite a specific multibunch mode [9].
The modulation of the RF phase of the accelerating cavity is realized by an external system. It mainly consists of electrical phase shifters and a signal generator with variable frequency and amplitude (for detailed information see [5]).The signal modulation of the DELTA RF master generator is given by

$$U_{\mathrm{RF}}(\omega) = U_0 \sin\left(\omega_{\mathrm{RF}} t + a \cdot \sin\left(\omega_{\mathrm{mod}} t\right)\right)$$

with the amplitude U_0, the RF frequency ω_{RF}, the modulation amplitude a and the modulation frequency ω_{mod}. At the signal generator, the modulation frequency $f_{\mathrm{mod}} = \omega_{\mathrm{mod}}/2\pi$ can be set directly and the modulation amplitude a can be set via input signal U_{mod} from 0 V up to 3 V. The standard settings for user operation are $U_{\mathrm{mod}} = 0.7$ V and $\omega_{\mathrm{mod}} \approx 2 \cdot \omega_s$, with the synchrotron frequency $f_s = \omega_s/2\pi$.

Table 1: Storage Ring Parameters

parameter	value
revolution frequency	2.6 MHz
RF frequency	500 MHz
nominal RF power loss	26 kW
maximum beam current (multibunch)	130 mA
maximum beam current (single bunch)	20 mA
synchrotron frequency	15.2 - 16.4 kHz
fractional horizontal tune	0.10 - 0.20
fractional vertical tune	0.20 - 0.30

* Work supported by the BMBF under contract no. 05K13PEB
† malte.sommer@tu-dortmund.de

Content from this work may be used under the terms of the CC BY 3.0 licence (© 2015). Any distribution of this work must maintain attribution to the author(s), title of the work, publisher, and DOI.

ISBN: 978-3-95450-168-7 doi:10.18429/JACoW-IPAC2015-MOPWA035

TWO GENERAL ORBIT THEOREMS FOR EFFICIENT MEASUREMENTS OF BEAM OPTICS

B. Riemann*, A. Ferrarotto, P. Hartmann, B.D. Isbarn, S. Koetter, M. Sommer, P. Towalski, T. Weis
DELTA, Dortmund, Germany

Abstract

Closed-orbit perturbations and oscillating beam solutions in storage rings are closely related. While techniques exist to fit accelerator models to closed-orbit perturbations or to oscillation data, the exploitation of their relation has been limited. In this work, two orbit theorems that allow an efficient computation of optical parameters in storage rings with older hardware are derived for coupled linear beam motion. The monitor theorem is based on an uncoupled case study described by the author in an earlier work [1] and has been generalized as well as simplified in mathematical abstraction to provide a reliable and computationally stable framework for beam optics measurements. It is based on a closed-orbit measurement utilizing 4 dipole correctors (2 for each plane). The corrector theorem allows to obtain parameters of these dipole correctors using two turn-by-turn monitors at almost arbitrary positions in the ring (which do not need to be located in a drift space), so that it possible to uniquely resolve closed orbits into optical parameters without sophisticated lattice models.

INTRODUCTION

To express the orbit theorems in a reasonable and straightforward way, we need to describe coupled optics in the linear phasor model, instead of the polar-like Courant-Snyder parameters. Then, the two orbit theorems are formulated and verified by experimental data obtained using the mapping method, a diagnostic method containing both theorems.

LINEAR PHASOR MODEL

In a storage ring, a closed orbit exists. For any working setup, the particle motion around this orbit is bound and undamped in good approximation. From these assumptions, we can linearize the bound motion around the orbit as a $M = 3$-dimensional harmonic oscillator. In the following, we will not consider synchrotron motion ($M = 2$).

Beam Oscillation (Turn-by-Turn)

The deviations $\vec{r}$ from the closed orbit at each turn n at a given longitudinal position s_j can be modeled [2] as ($\Re$: real part)

$$\vec{r}_n(s_j) = \sum_m^M \Re\left\{\vec{R}_{jm} e^{in\mu_m}\right\}, \tag{1}$$

where the phase advances μ_m correspond to betatron tunes, while $\vec{R}_{jm}$ are vectors of complex oscillation amplitudes (phasors) that we will call *monitor vectors* in the following. The monitor vectors are related to the Mais-Ripken parameterization of beam optics [3] [4] and are a fully coupled representation of spatial linear beam motion.

Closed-Orbit Perturbation (Orbit Response)

The closed orbit can be defined by a fixpoint of the linear transfer map at a given position. The map has a zero-order term $\vec{t}_k$, which corresponds to a dipole kick, and a first-order term which is the transfer matrix $\mathbf{T}_k$. If we assume that the kick is located directly before the corrector, we obtain the closed orbit vector $\langle\vec{r}\rangle$ at position $\tilde{s}_k$ by the equation system

$$\vec{t}_k = (\mathbf{1} - \mathbf{T}_k)\langle\vec{r}\rangle_{jk}$$

A computation [2] including the knowledge that the spatial parts of the eigenvectors of $\mathbf{T}$ are indeed the forementioned monitor vectors $\vec{R}_{jm}$, while the eigenvalues are $e^{i\mu_m}$, leads to a phasor expression for the closed-orbit perturbation

$$\langle\vec{r}\rangle_{jk} = \Re\left\{\sum_m \vec{R}_{jm} E^*_{jkm} D^*_{km}\right\}, \tag{2}$$

The phase jump coefficients $E_{jkm} = \exp\{i\mu/2\ \mathrm{sign}(s_j - \tilde{s}_k)\}$ hold numbers on the complex unit circle. These coefficients occur as closed orbits are ring-periodic, and may be interpreted as correcting the "fractional tune" of the betatron oscillations. The corrector parameter D_{km} is a complex quantity that represents the coupling of a given dipole error or corrector k to each oscillation mode m.

ORBIT THEOREMS

Both orbit theorems are based on solving systems of equations for all monitors $1 \le j \le J$, or the subset of all turn-by-turn capable monitors $1 \le f \le F$, and correctors k. In brief, the first theorem obtains the corrector parameters D_{km} from closed-orbit perturbations turn-by-turn data at monitors f. Then, the second theorem is used to obtain $\vec{R}_{jm}$ at all monitors j.

Corrector Theorem

In a first step towards the knowledge of spatial optical parameters at all BPMs, we state that

- it is possible to compute D_{km} from a set of closed orbit data and turn-by-turn data at $F \ge 2$ turn-by-turn capable monitors

* bernard.riemann@tu-dortmund.de

Content from this work may be used under the terms of the CC BY 3.0 licence (© 2015). Any distribution of this work must maintain attribution to the author(s), title of the work, publisher, and DOI.

ISBN: 978-3-95450-168-7 doi:10.18429/JACoW-IPAC2015-MOPWA036

STATUS OF INJECTION STUDIES INTO THE FIGURE-8 STORAGE RING

J.F. Wagner*, A. Ates, M. Droba, O. Meusel, H. Niebuhr, D. Noll, U. Ratzinger
Goethe University, Frankfurt am Main, Germany

Abstract

The ongoing investigations on the design of the Figure-8 Storage Ring [1] at Frankfurt University focus on the beam injection. The research includes simulations as well as a scaled down experiment. The studies for an optimized adiabatic magnetic injection channel, starting from a moderate magnetic field up to a maximum of 6 Tesla, with a realistic field model of toroidal coils due to beam dynamics with space charge will be shown. For the envisaged ExB-kicker system the simulations deal with beam potential constraints and a multi-turn injection concept in combination with an adiabatic magnetic compression. To investigate the concept of the beam injection into a toroidal magnetic field, a scaled down room temperature experiment is implemented at the university. It is composed of two 30 degree toroidal segments, two volume ion sources, two solenoids and two different types of beam detectors. The experiment is used to investigate the beam transport and dynamics of the laterally injected and "circulating" beam through the magnetic configuration. To set up the injection experiment, theoretical calculations and beam simulations with bender [2] are used.

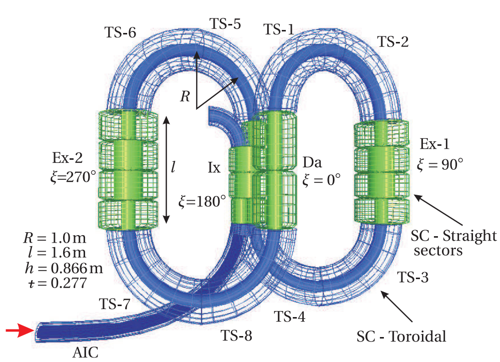

Figure 1: Figure-8 Storage Ring with the proposed adiabatic injection channel (AIC).

INTRODUCTION

The Figure-8 storage ring (*F8SR*) concept is under development at Frankfurt University. Different from traditional storage rings, a guiding longitudinal magnetic field confines the charged particle beam continuously with high transverse momentum acceptance. Due to the strong magnetic field level (B=6 T), high current low energy proton (W~150 keV) and ion beams of several amperes can be confined. Many characteristic features and key components were developed in the past. The current developments are concentrated on the design of a realistic injection system and test campaign in scaled down experiments.

* j.wagner@iap.uni-frankfurt.de

SIMULATIONS OF THE INJECTION SYSTEM

An injection system composed of an adiabatic magnetic compression channel and an **E**×**B**-kicker was designed and 3D multi particle simulations with realistic static magnetic and electric fields were performed.

The shape of the injection channel follows the curve of a hyperbolic spiral $R(\theta) = \frac{a}{\theta}$ within the interval of the parameter $\theta \in [\frac{\pi}{3} : \pi]$, see Fig. 1 (AIC). The channel has a length of L=4 m and a minimum radius R_1 of 1 m, hence a=π. The chosen channel geometry was implemented in the design code *segments* with solenoidal coils of decreasing distance $\sim \frac{1}{\theta}$ and constant current . The results of a Biot-Savart solver delivers a smooth ascending magnetic field, see Fig. 2 (blue). Concerning the curvature κ the channel

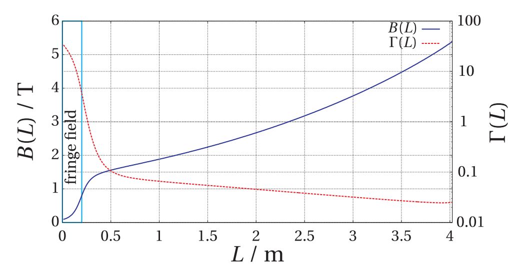

Figure 2: Rise of the magnetic flux and the adiabatic condition, on axis along the injection channel.

provides a small value at the entrance to avoid an instant kick to the injected beam. At the junction to the ring a high curvature keeps the perturbation of the ring flux low. For an adiabatic magnetic compression the magnetic field has to obey the condition for the parameter Γ in Eq. (1)

$$v_{\parallel}\frac{\Delta B}{\Delta s} < B\frac{\omega_c}{2\pi} = \frac{|q|B^2}{2\pi m} \rightarrow \Gamma = v_{\parallel}\frac{\Delta B}{\Delta s}\frac{2\pi m}{|q|B^2} < 1 \qquad (1)$$

The calculated Γ shows that this condition is fulfilled along the whole proposed injection channel. The only exception can be found at the magnet fringe at the beginning. Single particle tracking in *segments* with protons at E_{kin}=150 keV injected on axis show an expected rise of the transversal velocity $v_{\perp}$ due to the $\mathbf{R} \times \mathbf{B}$-drift with an acceptable ratio to the parallel velocity. The off plane drift amounts to 17 mm. Field maps of the whole injection system area were exported to the multi-particle code *bender* and simulations were qualitatively confirmed, see Fig. 3.

Further, an $\mathbf{E} \times \mathbf{B}$-kicker system with two fixed and two movable electrodes with a total length of 1170 mm, at a gap width of 30 mm and 90 kV voltage, i.e. E=3 MV/m, were integrated into the simulations. Single particle tracking shows the velocity components in Fig. 4. The increase in $v_{\perp}$ occurs respectively to the shift of the magnetic flux due to the

Content from this work may be used under the terms of the CC BY 3.0 licence (© 2015). Any distribution of this work must maintain attribution to the author(s), title of the work, publisher, and DOI.

ISBN: 978-3-95450-168-7 doi:10.18429/JACoW-IPAC2015-MOPWA037

Content from this work may be used under the terms of the CC BY 3.0 licence (© 2015). Any distribution of this work must maintain attribution to the author(s), title of the work, publisher, and DOI.

MIRROR SYMMETRIC CHICANE-TYPE EMITTANCE EXCHANGE BEAMLINE WITH TWO DEFLECTING CAVITIES

V.Balandin*, W.Decking, N.Golubeva, DESY, Hamburg, Germany

Abstract

In this paper we present the conceptual design of a mirror symmetric chicane-type beamline with two dipole-mode cavities for transverse-to-longitudinal emittance exchange.

INTRODUCTION

Optical systems for transverse-to-longitudinal emittance exchange (EEXs) were initially proposed in application to the free electron lasers for transverse emittance reduction in an electron beam with a smaller longitudinal emittance [1]. Since then EEXs involving single transverse deflecting cavity (TDC) were in great details studied theoretically and experimentally, and many interesting applications of such beamlines were suggested [2–6].

Among all EEXs chicane-type beamlines are of keen interest, because they do not alter the beam propagation direction. To our knowledge, the first design of such EEX was presented in [6] and, in minimal configuration, can be seen in Fig. 1 (beamline one). Besides TDC and four dipoles, this beamline includes fundamental (accelerating) mode cavity (FMC) to cancel the longitudinal acceleration in the TDC (the so-called thick-lens effect) and two quadrupoles (green ellipses) to reverse the dispersion at the TDC location.

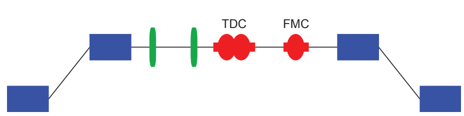

Figure 1: Schematic of non-symmetric chicane-type EEX.

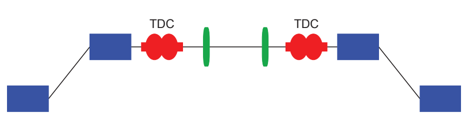

Figure 2: Schematic of symmetric chicane-type EEX.

The beamline one demonstrates two features which are common to all EEXs with a single TDC. First, such EEXs cannot be mirror symmetric with respect to the TDC center and, second, without involvement of at least one FMC the emittance exchange cannot be made exact even on the level of the linear beam dynamics. One of the ways to overcome these limitations was found in [7] where properties of EEXs utilizing two TDCs instead of one were investigated. In this paper we detail some results of [7] and present a mirror symmetric chicane-type EEX with two TDCs which does not require additional FMCs for compensation of the thick-lens effect. Schematic of this beamline (again, in minimal configuration) can be seen in Fig. 2 (beamline two), and there are the following similarities and differences in comparison with the beamline one:

- Quadrupoles in the beamline one are used for the reversion of the entrance dogleg dispersion and both are horizontally focusing. Quadrupoles in the beamline two have similar purpose and also must provide dispersion sign change, but in this case between the TDC centers. Besides that, they have an additional duty and work for suppression of the thick-lens effect, which allows to avoid usage of FMCs.
- With equal dispersions generated by the entrance dogleg, the total transverse deflection required is equal for both beamlines. It means that the strength of each TDC in the beamline two is two times smaller than the strength of the single TDC in the beamline one.
- The mirror symmetry of the beamline two automatically cancels part of nonlinear aberrations in the beamline map.

MATRICES AND SYMMETRIES

In the deriving conditions for a beamline to be an EEX, we consider the linear symplectic dynamics in the horizontal and longitudinal degrees of freedom and ignore the vertical degree of freedom, which (on the linear level) is assumed to be decoupled from the two others. Still, for convenience, we index elements of the 4×4 horizontal-longitudinal transport matrices as if these matrices were extracted from the complete three degrees of freedom 6×6 matrices, where the first degree of freedom is horizontal, the second is vertical, and the longitudinal comes as the third.

Transport Matrices

From the assumptions made it follows that the horizontal-longitudinal matrix of a magnetostatic system has the form

$$M = \begin{bmatrix} m_{11} & m_{12} & 0 & m_{16} \\ m_{21} & m_{22} & 0 & m_{26} \\ m_{51} & m_{52} & 1 & m_{56} \\ 0 & 0 & 0 & 1 \end{bmatrix}, \qquad (1)$$

and, as concerning the TDC matrix, we take it in the commonly used approximation

$$R(\kappa, l_c, q) = \begin{bmatrix} 1 & l_c & \kappa l_c/2 & 0 \\ 0 & 1 & \kappa & 0 \\ 0 & 0 & 1 & 0 \\ \kappa & \kappa l_c/2 & q\kappa^2 l_c & 1 \end{bmatrix}, \qquad (2)$$

where l_c is the cavity length, κ is the deflecting strength, and q is the energy gain factor. The particular value of q depends from the cavity design and, for example, for the n-cell pillbox resonator satisfies $1/6 < q \leq 1/4$.

Approximations made in the equations of motion in order to obtain matrix (2) include among others the neglection of the terms of the order $O(\gamma_0^{-2})$, where γ_0 is the Lorentz factor of the reference particle. To be consistent with this, we

* vladimir.balandin@desy.de

ISBN: 978-3-95450-168-7 doi:10.18429/JACoW-IPAC2015-MOPWA038

SENSITIVITY OF LINAC OPTICS TO FOCUSING AND ENERGY ERRORS

V.Balandin*, W.Decking, N.Golubeva, DESY, Hamburg, Germany

Abstract

The ability to control beam optics in the presence of such imperfections as focusing and energy gain errors is essential for a successful operation of high brightness electron linacs providing beams for free-electron lasers. We characterize the cumulative effect of these imperfections using the value of mismatch parameter calculated at the linac exit and show how it depends on the design of the focusing lattice.

INTRODUCTION

Control of the optics matching is one of the key ingredients for a successful operation of modern high brightness electron linacs providing beams for free-electron lasers (FELs). Available operational experience indicates that in order to optimize FEL signal at different wavelengths or to fine-tune the FEL wavelength, empirical adjustment of the machine parameters is often required and, therefore, the sensitivity of the beamline optics to small changes in the beam energy and in the magnet settings becomes one of the important issues which affects both, the final performance and the reproducibility of the results after breaks in operation. This fact was quickly recognized when the FLASH facility at DESY started its regular user operation in August 2005. In a little while after that the simple criteria for comparison of the optics sensitivities was introduced, new (lower sensitivity) optics for the FLASH beamline was developed and brought in operation in spring 2006, and has shown a superior performance with respect to the previous setup of the transverse focusing [1]. Later on this criteria also has been usefully adopted as a part of the optics redesign strategy during commissioning of the FERMI@Elettra FEL facility [2].

The purpose of this paper is to give some generalizations and provide details of the derivation of the optics sensitivity criteria which were missing in [1], and practical examples and discussions of the application strategies can be found in the papers [1] and [2].

DYNAMICAL VARIABLES AND TWISS PARAMETERS

We consider the linear beam dynamics with acceleration in one degree of freedom (lets say, horizontal) and use the variables $z = (x, q)^{\top}$ for the description of the horizontal beam oscillations. We assume that evolution of these variables along the linac is described by the linear equation

$$dz \,/\, d\tau \;=\; F(\tau)\, z, \tag{1}$$

where the independent variable τ is the longitudinal position. As concerning the physical meaning of the variables z, we do not see any particular reasons to specify it at this point, because, first, there is no single commonly accepted transverse coordinates for description of the beam dynamics in the linacs and, second, the main object of our study (the mismatch parameter) is, up to some extend, independent on the coordinate system choice.

As often, we introduce the Twiss (or Courant-Snyder) parameters using the second central moments of the particle distribution and define them as follows

$$\beta = \langle x^2 \rangle \,/\, \epsilon, \quad \alpha = -\langle xq \rangle \,/\, \epsilon, \quad \gamma = \langle q^2 \rangle \,/\, \epsilon, \tag{2}$$

where

$$\epsilon \;=\; \sqrt{\langle x^2 \rangle \langle q^2 \rangle - \langle xq \rangle^2} \tag{3}$$

is the rms emittance. With this definition, the Twiss matrix

$$\Sigma \;=\; \begin{bmatrix} \beta & -\alpha \\ -\alpha & \gamma \end{bmatrix}, \quad \det(\Sigma) \;=\; 1 \tag{4}$$

satisfies the linear differential equation

$$d\Sigma \,/\, d\tau \;=\; JH\Sigma \;-\; \Sigma HJ, \tag{5}$$

where J is the 2×2 symplectic unit matrix and the 2×2 symmetric matrix H is defined by the expression

$$H(\tau) \;=\; \tfrac{1}{2}\mathrm{tr}[F(\tau)]\, J \;-\; JF(\tau). \tag{6}$$

The solution of Eq. (5) is given by the formula

$$\Sigma(\tau) = M(\tau)\, \Sigma(0)\, M^{\top}(\tau), \tag{7}$$

where the symplectic matrix M satisfies the equation

$$dM \,/\, d\tau = JHM, \quad M(0) = I, \tag{8}$$

and the rms emittance ϵ evolves according to the rule

$$\frac{\epsilon(\tau)}{\epsilon(0)} = \det\left[A(\tau)\right] = \exp\left(\int_0^{\tau} \mathrm{tr}[F(\xi)]\, d\xi\right), \tag{9}$$

where A is the fundamental matrix solution of the Eq. (1). Because the matrices M and A are connected by the relation

$$M(\tau) = \frac{1}{\sqrt{\det\left(A(\tau)\right)}} \cdot A(\tau), \tag{10}$$

and because for an arbitrary 2×2 matrix X

$$X\, J\, X^{\top} = X^{\top} J\, X = \det(X)\, J, \tag{11}$$

the transport rule (7) can also be written as follows

$$[\Sigma(\tau) J] = A(\tau)\; [\Sigma(0) J]\; A^{-1}(\tau). \tag{12}$$

Alternatively, the matrices M and A can be expressed using Σ and ϵ, if they are known, in the familiar forms

$$M(\tau) \;=\; T^{-1}(\tau)\, R[\mu(\tau)]\, T(0), \tag{13}$$

$$A(\tau) \;=\; \sqrt{\epsilon(\tau)/\epsilon(0)} \cdot T^{-1}(\tau)\, R[\mu(\tau)]\, T(0), \tag{14}$$

where

* vladimir.balandin@desy.de

Content from this work may be used under the terms of the CC BY 3.0 licence (© 2015). Any distribution of this work must maintain attribution to the author(s), title of the work, publisher, and DOI.

ISBN: 978-3-95450-168-7 doi:10.18429/JACoW-IPAC2015-MOPWA039

EMITTANCE REDUCTION POSSIBILITIES IN THE PETRA III MAGNET LATTICE

V. Balandin, W. Decking, N. Golubeva*, R. Wanzenberg
DESY, Hamburg, Germany

Abstract

PETRA III is a third generation light source at DESY that has been operated as a user facility since 2010 with a horizontal emittance of 1 nm · rad at a beam energy of 6 GeV. Recently an upgrade for additional photon beamlines has been carried out, and the recommissioning of PETRA III started in February 2015 [1]. Because the current optics solution for the upgraded storage ring predicts about 20% increase in the horizontal emittance, it motivates us to study a question whether or not there are optics modifications which allow the reduction of the emittance without significant changes in the present magnet arrangement. In this paper we present the results of the first look at this problem mostly limiting our consideration to the capabilities of the linear optics of the separate storage ring parts.

STORAGE RING OVERVIEW

The current layout of the PETRA III storage ring [2,3] is shown in Fig. 1, and one sees that it does not look like a conventional synchrotron light source constructed from large number of identical cells accommodating insertion devices. This is a result of a long history of the modifications of the facility. The former electron-positron collider PETRA has been turned into a pre-accelerator PETRA II for HERA, and then, after the shutdown of HERA, PETRA II has been converted into the synchrotron light source.

PETRA II has consisted of four identical quadrants, each of them mirror symmetric with respect to the center of a straight section. Therefore one octant (half of quadrant or one eight of the ring) has reflected all lattice and optics properties of the machine. For PETRA III [2] it was decided to accommodate all insertion devices in one octant. The octant extending from North-East to East was redesigned, and the FODO lattice was replaced by a sequence of the double-bend achromat (DBA) cells (in the following we will refer to this section as the "new octant"). Besides that, for the additional emittance reduction, twenty 4 m long damping wigglers were installed in the straight sections West and North. As concerning the chromaticity correction, no sextupoles were placed in the DBA lattice, and the chromaticity correction was performed globally using old sextupoles in the remaining seven octants [4].

In the recent upgrade [3] two new experimental halls were built, one in the North and one in the East, each housing 5 new photon beamlines. In order to accommodate new insertion devices, the part of the hardware of arcs in two old octants is removed and replaced by DBA-like cells (the extensions North and East), and for the rest of these arcs (shortened octant arcs) the FODO structure is kept. No new sextupoles are added but several old sextupoles are uninstalled that leads to some reduction of the dynamic aperture (∼ 20% predicted, which is acceptable).

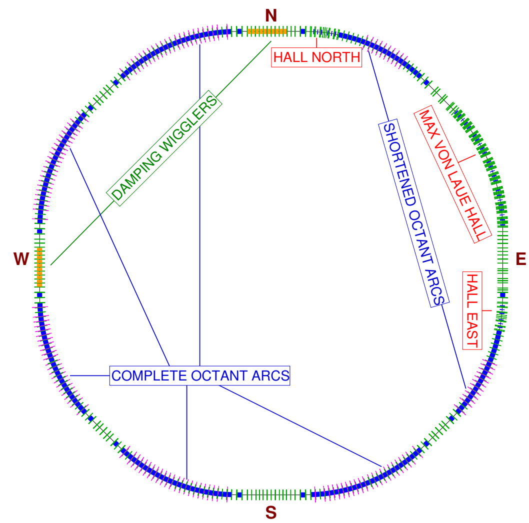

Figure 1: Layout of the PETRA III ring. Blue, green and red colors mark dipole, quadrupole and sextupole magnets, respectively. Yellow rectangles in the straight sections West and North indicate locations of the damping wigglers.

Contribution of Different Ring Sections to the Horizontal Emittance

One of the main figures of merit of the synchrotron light source quality is the value of the horizontal emittance which can be calculated as follows

$$\varepsilon_x \; [nm \cdot rad] \; = \; 1470 \left(E \; [GeV] \right)^2 \cdot \frac{I_5}{J_x \, I_2}, \qquad (1)$$

where I_2 and I_5 are the second and the fifth synchrotron radiation integrals, respectively, and J_x is the horizontal damping partition factor.

Table 1: Emittance Contributions of Ring Sections

Section	I_2	I_5
Old Octant Arcs	0.027 (9.5%)	3.29e-6 (48%)
New Octant	0.031 (11%)	1.70e-6 (25%)
Extension North	0.0057 (2.1%)	8.57e-7 (12.5%)
Extension East	0.0058 (2.1%)	8.05e-7 (11.8%)
Wigglers	0.211 (75.4%)	1.95e-7 (2.85%)
Total	0.280	6.84e-6

The contribution of different sections of the ring to the emittance is summarized in Table 1, where only the values of I_2 and I_5 are shown, because PETRA III contains no gradient dipoles and therefore $J_x \approx 1$. The value of I_2 is defined only by the reference orbit curvature and does not depend on the lattice functions. This means that the relative

* nina.golubeva@desy.de

Content from this work may be used under the terms of the CC BY 3.0 licence (© 2015). Any distribution of this work must maintain attribution to the author(s), title of the work, publisher, and DOI.

ISBN: 978-3-95450-168-7 doi:10.18429/JACoW-IPAC2015-MOPWA040

VIRTUAL CAVITY PROBE GENERATION USING CALIBRATED FORWARD AND REFLECTED SIGNALS

S. Pfeiffer*, V. Ayvazyan, J. Branlard, Ł. Butkowski, H. Schlarb and C. Schmidt,
DESY, Hamburg, Germany
R. Rybaniec, ISE, Warszawa, Poland

Abstract

The European X-ray free electron laser requires a high-precision control of accelerating fields to ensure a stable photon generation. Its low level radio frequency system, based on the MicroTCA.4 standard, detects the probe, forward and reflected signals for each cavity. While the probe signal is used to control the accelerating fields, a combination of the forward and reflected signals can be used to compute a virtual probe, whose accuracy is comparable to the directly sampled probe. This requires the removal of cross-coupling effects between the forward and reflected signals. This paper presents the precise generation of a virtual probe using an extended method of least squares. The virtual probe can then be used for precise field control in case the probe signal is missing or corrupted. It can also be used to detect any deviation from the nominal probe profile.

INTRODUCTION

The Free Electron LASer (FLASH) at the *"Deutsches Elektronen Synchrotron"* in Hamburg is a facility for research with tunable laser light. It provides its users a pulsed light in the X-ray range with tunable wavelength down to 4.2 nm generated by SASE processes. Electron bunch trains of variable length and frequency with a repetition rate of 10 Hz are accelerated to about 1.2 GeV. Each pulse is enabled for about 1.4 ms, meanwhile up to 2400 bunches with a maximum repetition rate of 3 MHz are injected. In order to provide stable and reproducible photon pulses a precise acceleration field control is needed. During the last years, several control strategies for vector-sum regulation, i.e. the sum of up to 16 cavities and its RF field probes, were developed and included in the Low-Level RF (LLRF) controller. Hereby learning feedforward (LFF) minimizes repetitive amplitude and phase errors from pulse to pulse [1], whereas the multiple input multiple output (MIMO) controller acts within the pulse [2]. The necessary RF field regulation requirements are reached and below a relative amplitude error of 0.01 % and an absolute phase error of 0.01 degree. Besides the detection of the cavity probe signal, the forward and reflected signals of each cavity at the waveguide distribution is measured, as depicted in Fig. 1. In this paper, it is shown that the latter can be used to generate a virtual probe signal usable for system health detection and failure classification. If the real probe detection fails, the virtual probe can still be used to drive the system and ensure the amplitude and phase regulation requirements.

* sven.pfeiffer@desy.de

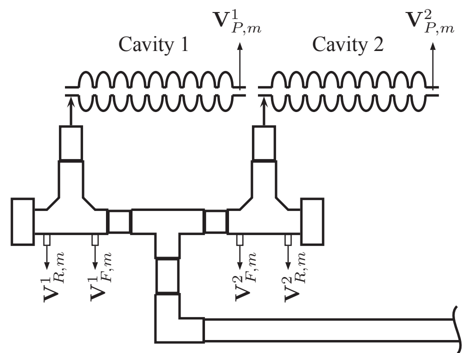

Figure 1: Waveguide distribution as example for the first accelerator module ACC1 at FLASH with depicted complex probe ($\mathbf{V}^c_{P,m}$), forward ($\mathbf{V}^c_{F,m}$) and reflected ($\mathbf{V}^c_{R,m}$) signal measurement for 2 out of 8 cavities, i.e. $c = 1, 2$.

THEORETICAL APPROACH

The main goal of this contribution is to calibrate the measured (index m) complex forward ($\mathbf{V}_{F,m} \in \mathbb{C}$) and complex reflected ($\mathbf{V}_{R,m} \in \mathbb{C}$) signals to the calibrated (index c) $\mathbf{V}_{F,c} \in \mathbb{C}$ and $\mathbf{V}_{R,c} \in \mathbb{C}$, respectively. An example for signal detection is shown in Fig. 2. As can be seen, the forward

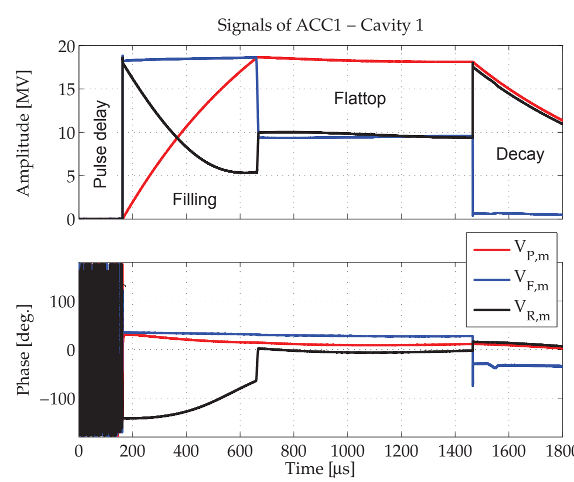

Figure 2: Measured probe, forward and reflected signals (pre-calibrated by (1)) for a standard RF pulse with $Q_L \ll Q_0$ for $\beta \gg 1$.

signal shows an amplitude value which is non-zero during decay, although the RF drive is switched off. A measurement calibration can overcome the imperfection of the signal detection, mainly caused by signal couplings at the pick-up, also visible in the reflected signal.

Content from this work may be used under the terms of the CC BY 3.0 licence (© 2015). Any distribution of this work must maintain attribution to the author(s), title of the work, publisher, and DOI.

ISBN: 978-3-95450-168-7 doi:10.18429/JACoW-IPAC2015-MOPWA041

INVESTIGATION OF RADIATION DAMAGE OF INSERTION DEVICES AT PETRA III DUE TO PARTICLE LOSSES USING TRACKING RESULTS WITH SIXTRACK

G. K. Sahoo#, M. Bieler, J. Keil, A. Kling*, G. Kube, M. Tischer, R. Wanzenberg
Deutsches Elektronen-Synchrotron, Notkestraße 85, Hamburg, Germany
*Institute of Dual Cooperative Studies, Osnabrück University of Applied Sciences, Kaiserstraße 10b, Lingen, Germany

Abstract

PETRA III is a 3rd generation synchrotron light source dedicated to users at 14 beamlines with 30 instruments since 2009. The horizontal beam emittance is 1 nmrad while a coupling of 1% amounts to a vertical emittance of 10 pmrad. Some undulators and wiggler devices have accumulated total radiation doses of about 100 kGy. Doses measured regularly by Thermo Luminescent Dosimeters (TLDs) are monitored, which lead to inspect the magnetic field of all insertion devices in the PETRA tunnel. We are investigating particle losses with tracking simulation using SixTrack to gain a certain understanding of the radiation damage of the insertion devices. The goal is to develop a strategy to protect the insertion devices from further radiation damage.

INTRODUCTION

PETRA III [1, 2] is a 3rd generation synchrotron light source operating with electrons at beam energy of 6 GeV which is an upgrade of the previous machine PETRA II. The horizontal beam emittance of 1 nmrad is achieved using 20 damping wigglers each of 4 m length, while a coupling of 1% amounts to a vertical emittance of 10 pmrad. The machine is dedicated to users at 14 beamlines with 30 end-stations. Parts of PETRA III [3] have recently been rebuilt to accommodate 12 new beam lines including a super luminescence in near UV beamline providing bending magnet radiation. PETRA III operates with several filling modes, such as 40, 60, 240, 480 and 960 bunches with a beam current of 100 mA.

The insertion devices (IDs) and other accelerator components are expected to experience extreme radiation in synchrotron light sources especially where higher beam energies, beam currents and smaller gaps are in place. It is worth to mention that, permanent magnets operating under conditions of high radiation are especially susceptible to demagnetization [4] caused by direct and scattered radiation induced by electrons, positrons, high-energy photons and neutrons. Serious demagnetization has been observed in some of the operating light sources such as ESRF, where insertion devices experienced field losses of as much as 8% [5] and at the APS [6]. Here we report a partial demagnetization profiles which is not linear along the device [7, 8] in some of the IDs in PETRA III caused by radiation, similar loss patterns are also clearly seen in tracking results. To protect the IDs additional collimators have been installed at PETRA III.

gajendra.kumar.sahoo@desy.de

OBSERVATION OF RADIATION DAMAGE OF INSERTION DEVICES

Inspection of the magnetic structures and in-situ magnetic peak field measurements revealed a partial demagnetization of devices exhibiting performance losses. Some results of these measurements are summarized in Fig. 1 [7]. Devices located upstream in canted straight sections as PU02 and PU08 are damaged at the entrance end of the magnet structure while the downstream located device PU03 is damaged at the exit end (Fig. 1a). The measured decrease of the peak field is attributed to radiation damage and is most likely caused by particle losses.

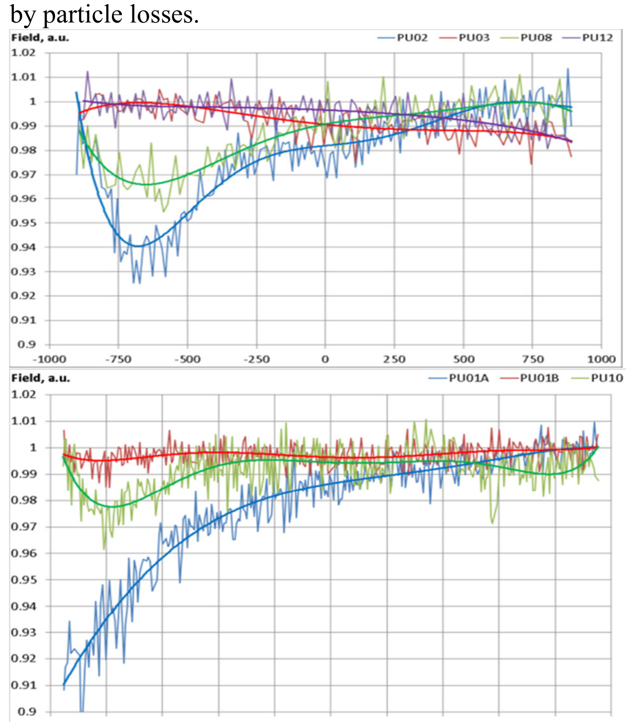

Figure 1: Recently measured longitudinal normalized peak field variation of (a) 2 m devices, (b) 5 m devices installed in PETRA III verses longitudinal position in mm.

A similar situation is observed for the 5 m long devices (Fig. 1b). In sector 1, the upstream device PU01a is strongly damaged at the upstream end. The 5 m device PU10 also confirms the damage pattern observed at the 2 m devices installed in the canted straight sections. PU10 is installed in a standard (not canted) straight section. PU10 shows signs of demagnetization at the entrance and

Content from this work may be used under the terms of the CC BY 3.0 licence (© 2015). Any distribution of this work must maintain attribution to the author(s), title of the work, publisher, and DOI.

ISBN: 978-3-95450-168-7 doi:10.18429/JACoW-IPAC2015-MOPWA042

SUB-fs ELECTRON BUNCH GENERATION USING MAGNETIC COMPRESSOR AT SINBAD

J. Zhu[#1,2], R. Assmann[1], U. Dorda[1], J. Grebenyuk[1], B. Marchetti[1]
[1] DESY, Hamburg, Germany
[2] University of Hamburg, Hamburg, Germany

Abstract

In order to achieve high quality electron beams by laser-driven plasma acceleration with external injection, sub-fs bunches with a few fs arrival-time jitter are required. SINBAD (Short Innovative Bunches and Accelerators at DESY) is a proposed dedicated accelerator research and development facility at DESY. One of the baseline experiment at SINBAD is ARES (Accelerator Research Experiment at SINBAD), which will provide ultra-short electron bunches of 100 MeV to one or two connected beam lines. We present start-to-end simulation studies of sub-fs bunch generation at ARES using a magnetic compressor with a slit. In addition, the design of a dogleg with tunable R_{56} for the second beamline is also presented.

INTRODUCTION

Plasma-Wakefield Accelerators (PWFA) can produce acceleration gradients up to 100 GV/m [1], which makes them promising candidates for compact accelerators and novel light sources. SINBAD (Short and INnovative Bunches and Accelerators at DESY) is a proposed dedicated research facility where Laser-driven Plasma Wakefield Acceleration (LWFA) with external injection will be explored by using ultra-short electron bunches generated at ARES (Accelerator Research Experiment at SINBAD) [2]. External injection allows precise manipulation of phase-spaces of electron bunches and thereby provides possibilities to optimise the subsequent acceleration and transport inside the plasma.

ARES will consist of a compact photo-injector providing ultra-short electron bunches to one of the two connected beamlines [3]. The ~5-MeV electron bunches generated by the 1-1/2 cell S-band photocathode RF-gun are accelerated by two S-band travelling-wave RF-structures (TWS) to around 100 MeV. A third S-band TWS is foreseen in the future to boost electron bunches to higher energy, which will reduce the impact of the space-charge effects on bunch compression and final focus before the plasma cell. Downstream of the photo-injector the beamline includes quadrupole magnets and a magnetic chicane bunch compressor (BC) with a slit located in the middle of it. Ultra-short bunches at ARES can be produced by both velocity bunching and magnetic compression. In order to deliver ultra-short bunches to the second beamline, a dogleg section is also foreseen.

#jun.zhu@desy.de

MAGNETIC CHICANE WITH A SLIT

Since it is difficult to directly compress the pulse duration of an electron bunch generated at a photo-injector to sub-fs in one compression stage even with a high-harmonic cavity, the slit method is employed in our design, as shown in Fig. 1 [4]. The coherence synchrotron radiation (CSR) at the chicane can be reduced by using a weak chicane and a large initial correlated energy spread. Because the slit only allows the central slice of the whole bunch to pass, the energy spread of the compressed bunch remains small enough. Likewise, the emittance of the final bunch will not be affected by the chromatic aberration from quadrupoles upstream of the chicane. More importantly, the bunch arrival-time jitter downstream of the chicane will be reduced if the chicane is weak [5], which is vitally important for plasma acceleration with external injection [6]. On the other hand, the R_{56} should be large enough in order to compress the bunch with a reasonable chirp. As a result, R_{56}=-10 mm was chosen in the current design.

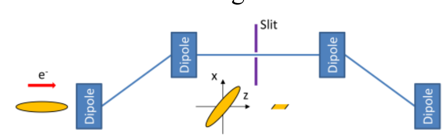

Figure 1: Schematic of the magnetic chicane with a slit.

Start-to-end Simulation

The start-to-end (S2E) simulation of the beam dynamics at ARES were performed with ASTRA [7] and IMPACT-T [8]. The electron bunch was first transported to the end of the linac by using ASTRA with 2D cylindrical-symmetric space-charge effects, and then the rest part was simulated by using IMPACT-T with 3D space-charge effects and 1D CSR effect. The photocathode laser is assumed to follow a Gaussian longitudinal distribution with rms duration of 3 ps, and a uniform transverse laser intensity distribution was taken at the photocathode. The two TWSs are operated at the same gradient and phase in order to minimize the bunch arrival-time jitter [5]. The chirp of the bunch at the linac exit is approximately -1/R_{56} in order to fully compress the bunch. The final longitudinal phase-spaces (LPS) and the current profiles 0.4 m downstream of the last dipole magnet with two different initial bunch charges are shown in Fig. 2, and the parameters of the final bunches are summarized in table 1. The results indicate that sub-fs electron bunch with charge of several pC is achievable at ARES. However, it is found that the bunch starts to

Content from this work may be used under the terms of the CC BY 3.0 licence (© 2015). Any distribution of this work must maintain attribution to the author(s), title of the work, publisher, and DOI.

ISBN: 978-3-95450-168-7 doi:10.18429/JACoW-IPAC2015-MOPWA043

FEL SIMULATIONS WITH OCELOT

I. Agapov *, G. Geloni, European XFEL GmbH, Hamburg, Germany
S. Tomin, NRC Kurchatov Institute, Moscow, Russia, and European XFEL GmbH, Hamburg, Germany
M. Dohlus, I. Zagorodnov, DESY, Hamburg, Germany

Abstract

OCELOT has been developed as a multiphysics simulation tool for FEL and synchrotron light source studies. In this work we highlight recent code developments focusing on electron tracking in linacs taking into account collective effects and on x-ray optics calculations.

INTRODUCTION

OCELOT has been developed as a multiphysics python-based simulation and on-line control framework for free electron laser (FEL) and synchrotron light source studies. Overview of its design and application areas can be found e.g. in [1]. FEL simulations comprise electron beam dynamics, FEL process proper, and interaction of radiation with optics components. OCELOT is a framework to account for all such processes, by including native physics models or interfacing to third-party codes. FEL calculations heavily rely on *Genesis 1.3* [2], while for other physics processes native models of various complexity exist. In this work we focus on recent code developments in two application areas not discussed in [1]: electron beam dynamics with space charge effects and x-ray optics. Accounting for space charge effects is necessary to extend the application area to low energy electron transport. The other major physics process which has to be taken into account for electron beam dynamics in FELs is Coherent Synchrotron radiation (CSR). A corresponding solver for OCELOT is being introduced and will be discussed elsewhere. The x-ray optics module has been largely driven by the needs of self-seeded FEL and some crystal optics simulations. This paper discusses calculations of crystal reflectivity and transmissivity in the optics module. Ray tracing and Fourier optics methods have also been introduced but are not discussed here.

SPACE CHARGE EFFECTS

OCELOT has been recently extended for particle tracking with collective effects. A three-dimensional Poisson solver to take into account the space charge forces has been included. In the near future additional modules for coherent synchrotron radiation and wakefields will be included in the code as well. The tracking of particles is done in the same way as, for example, in Elegant [3]. Quadrupoles, dipoles, sextupoles, radiofrequency (RF) cavities and so on are modelled by linear or nonlinear maps. The focusing effect of RF cavities is taken into account according to [4]. The space charge forces are calculated by solving the Poisson equation in the bunch frame. Then the Lorentz transformed electromagnetic field is applied as a kick in the laboratory frame.

* ilya.agapov@xfel.eu

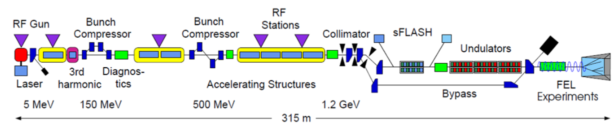

Figure 1: FLASH1 layout.

For the solution of the Poisson equation we use an integral representation of the electrostatic potential by convolution of the free-space Green's function with the charge distribution. The convolution equation is solved with the help of the Fast Fourier Transform (FFT). The same algorithm for solution of the 3D Poisson equation is used, for example, in ASTRA [5]. However, ASTRA solves equations of motion directly with a Runge-Kutta method, while in OCELOT particles are tracked using maps.

In this Section beam dynamics simulations for FLASH [6] using OCELOT are presented. FLASH is a high-gain FEL operating in the wavelength range of 4.2 - 45 nm. The layout of the facility is shown in Fig. 1. The formation of the electron bunch is carried out in two bunch compressors and seven TESLA-type 1.3 GHz superconducting accelerator modules. Each 12 m long module contains eight cavities. A special superconducting 3.9 GHz module built at FNAL has been installed in 2010 to improve the quality of the accelerated electron beam. The initial low-energetic part (14 meters from cathode of the gun) of the facility up to the third harmonic module was simulated with ASTRA since gun simulation is not presently possible in OCELOT. Then OCELOT was used to track the beam up to the entrance of the undulator section (203 meters from the cathode). The beam was tracked with and without taking space charge into account. The impact of space charge on the beam optics is shown in Fig. 2, where beta functions in the vertical plane without space charge (gray solid line) and with space charge (black points) are compared. A considerable mismatch is seen, which of course can be corrected. Such correction is not shown here since the focus is on benchmarking OCELOT with ASTRA.

The results of simulating the same setup with ASTRA is shown in Fig. 3. A slight disagreement between the two simulations is related to the fact that only first order maps were used for quadrupoles in OCELOT (higher order maps are presently used only for sextupoles and octupoles). This is also confirmed by cross-checks with Elegant. Higher order corrections to quadrupole and bending magnet maps are now being introduced in OCELOT as well. The current profile at the undulator entrance is shown in Fig. 4, where results obtained with OCELOT and ASTRA are compared.

Content from this work may be used under the terms of the CC BY 3.0 licence (© 2015). Any distribution of this work must maintain attribution to the author(s), title of the work, publisher, and DOI.

ISBN: 978-3-95450-168-7 doi:10.18429/JACoW-IPAC2015-MOPWA044

QUASI-FROZEN SPIN METHOD FOR EDM DEUTERON SEARCH*

Yu. Senichev#, A. Lehrach, B. Lorentz, R. Maier, IKP, Forschugszentrum Jülich, Germany
S. Andrianov, A. Ivanov, St. Petersburg State University, St. Petersburg, Russia
S. Chekmenev, III. Physikalisches Institut, RWTH Aachen, Aachen, Germany
M. Berz, E. Valetov, Michigan State University, East Lansing, MI 48824, USA
on behalf of the JEDI Collaboration and JARA-FAME (Forces and Matter Experiments)

Abstract

To search for proton Electric Dipole Moments (EDM) using proton storage ring with purely electrostatic elements, the concept of frozen spin method has been proposed [1]. This method is based on two facts: in the equation of spin precession, the magnetic field dependence is entirely eliminated, and at the "magic" energy, the spin precession frequency coincides with the precession frequency of the particle momentum. In case of deuteron we have to use the electrical and magnetic field simultaneously as will be explained later, keeping the frozen spin direction along the momentum as in the pure electrostatic ring. In this article, we suggest the concept of the quasi-frozen spin, in which the spin oscillates around the momentum direction within the half value of the advanced spin phase in magnetic arcs, each time returning back in electrostatic arcs. Due to the low value of the anomalous magnetic moment of deuteron, an effective contribution to the expected EDM effect is reduced only by a few percent compared with frozen spin method.

INTRODUCTION

The frozen spin method [1] is based on the fact that at a certain so-called "magic" energy, the particle spin begins to rotate with the frequency of the momentum and is always directed along the momentum. Under this condition, the signal growth of presumably existing electric dipole moment is maximized. This is clearly evident from the T-BMT equations:

$$\begin{aligned}
&\frac{d\vec{S}}{dt} = \vec{S}\times\left(\vec{\omega}_G + \vec{\omega}_{edm}\right)\\
&\vec{\omega}_G = -\frac{e}{m}\left\{G\vec{B} + \left(\frac{1}{\gamma^2-1} - G\right)\frac{\vec{\beta}\times\vec{E}}{c}\right\}\\
&\vec{\omega}_{edm} = \frac{e\eta}{m}\left(\vec{\beta}\times\vec{B} + \frac{\vec{E}}{c}\right)\\
&G = \frac{g-2}{2},
\end{aligned} \tag{1}$$

where G is the anomalous magnetic moment, g is the gyromagnetic ratio, ω_G is the spin precession frequency due to the magnetic dipole moment (hereinafter called MDM precession) relative to the momentum, ω_{edm} is the spin precession frequency due to the electrical dipole moment (hereinafter called EDM precession), and η is the dimensionless coefficient defined by the relation $d = \eta e\hbar / 4mc$ in (1).

It is reasonable to implement the frozen spin method in a purely electrostatic machine with electrical deflectors holding a beam on orbit. The advantages of purely electrostatic machines are especially evident at the "magic" energy, where

$$G - \frac{1}{\gamma_{mag}^2 - 1} = 0, \tag{2}$$

and the spin oriented in the longitudinal direction rotates in horizontal plane with the same frequency as the momentum, which is $\omega_G = 0$ [2].

However, this method cannot be used for deuterons having the negative anomalous magnetic moment $G = -0.142$, which follows from condition (2). Therefore, the only possible method in this case is a storage ring with both electric and magnetic fields [3]. It was proposed to store a longitudinally polarized deuteron beam of 1 GeV/c total momentum in an electro-magnetic storage ring of 0.5 T, where they minimize ω_G. It should be small, but not zero. This can be done by applying a radial electric field of magnitude to cancel the $G \cdot B$ contribution to ω_G in Eq. (1):

$$E_r = \frac{GBc\beta\gamma^2}{1 - G\beta^2\gamma^2} \approx GBc\beta\gamma^2 \tag{3}$$

However, studying the proton spin-orbital dynamics in a purely electrostatic ring [4], we realized that the condition (2) is feasible only for the reference particle. For all other particles the spin is not frozen and changes in time. In addition, condition (3) forcibly couples the values of the electric and magnetic fields, assuming both of them exist in each element. Firstly, the latter determines the rate of EDM signal increase, and secondly, it complicates the design of the element with incorporated E and B field.

QUASI-FROZEN SPIN CONCEPT

Thus, the only requirement of the "frozen" spin condition is to maximize the EDM signal growth. However, if the spin oscillates in the horizontal plane with respect to frozen spin direction with amplitude Φ_s, then the EDM growth decreases proportionally to the

*Work supported by BMBF International Cooperation (Grant Number RUS 11/043) and Jülich-Aachen Research Alliance JARA-FAME.
#y.senichev@fz-juelich.de

Content from this work may be used under the terms of the CC BY 3.0 licence (© 2015). Any distribution of this work must maintain attribution to the author(s), title of the work, publisher, and DOI.

ISBN: 978-3-95450-168-7 doi:10.18429/JACoW-IPAC2015-MOPWA045

Content from this work may be used under the terms of the CC BY 3.0 licence (© 2015). Any distribution of this work must maintain attribution to the author(s), title of the work, publisher, and DOI.

FIRST TESTS OF A BEAM TRANSPORT SYSTEM FROM A LASER WAKEFIELD ACCELERATOR TO A TRANSVERSE GRADIENT UNDULATOR*

C. Widmann[1]†, V. Afonso Rodriguez[1], S. Kuschel[3], M. Nicolai[2], R. Rossmanith[3], A. Sävert[2], M. B. Schwab[2], W. Werner[1], M. C. Kaluza[2,3], A. Bernhard[1], A.-S. Mueller[1]
[1]Karlsruhe Institute of Technology (KIT), Germany; [2]Friedrich Schiller University Jena, Germany; [3]Helmholtz Institute Jena, Germany

Abstract

An experimental setup for the generation of monochromatic undulator radiation at the laser wakefield accelerator (LWFA) in Jena using a transverse gradient undulator (TGU) is planned. Proper matching of the betatron functions and the dispersion of the electron beam to the undulator is essential. Therefor a beam transport system with strong focusing magnets and chromatic correction of the magnets is required.

As a first step, a linear beam transport system without chromatic correction was assembled at the LWFA. With this setup the electron beam's dispersion and the beta function of one selected energy are matched to the required parameters at the TGU. This contribution presents the experimental results of these measurements.

INTRODUCTION

A challenging but essential part of any experimental setup at a laser wakefield accelerator (LWFA) is the beam transport system. One has to match the electrons of the LWFA to the parameters required by the experiment. Due to the relative energy spread of the LWFA-generated bunches of some percent a chromatic correction is necessary. At the same time the large initial divergence of some milli-radian required strong focusing with compact magnets.

For the generation of monochromatic undulator radiation at the LWFA using a transverse gradient undulator (TGU) a dogleg chicane is required for matching the beam parameters and the dispersion. In the chicane the electron bunch is dispersed in the deflection plane of the undulator, i.e. the x-z-plane, and the resulting lateral distribution of the electron energy is matched to the flux density amplitude $B_y(x)$ of the undulator with a transverse gradient dB_y/dx. So a broadening of the radiation spectra is prevented such that electrons of different energies emit radiation at the same wavelength [1, 2].

Several studies were performed to optimize the layout of a beam transport system to the TGU [3, 4]. In this measurement campaign such a beam transport system was set up to demonstrate that it is possible to transport a LWFA-generated bunch with a complex transport system and to match the beam parameters required for the undulator. As a first step a linear system was assembled consisting of six quadrupoles to focus the beam and two dipoles for generating the dispersion. The transverse beam profiles were measured with scintillating screens. For measuring the spectra an electron spectrometer was integrated in the setup.

In this contribution the results of a first experiment are presented. The parameters of the LWFA and of the magnets and the alignment procedure is described in the next section. Thereafter some magnet configurations and the measured beam profiles are presented and compared to simulations performed with *elegant* [5] and MADX [6].

EXPERIMENTAL SETUP

The experiment was performed at the JETI-40 laser system in Jena. The laser pulse with an energy of 700 mJ and a pulse duration of 27 fs was focused by a f/12 off-axis parabolic mirror to a spot size of 12 μm^2 (FWHM). This results in a peak intensity of $I_L = 9.1 \cdot 10^{18}$ W/cm^2. The target was a gas cell of 3.0 mm length. A gas mixture of 95% helium and 5% nitrogen was used.

The beam transport system consisted of six in-house built quadrupoles [7] installed inside the vacuum chamber and two commercially available dipole magnets [8], which were inside an air-box as they are not designed for in-vacuum use. A sketch of the setup is shown in Fig. 1. The yoke length of the quadrupoles is 80 mm and the gradient at the maximum current of 5 A is 35 T/m for the quadrupoles with the slightly larger size (Q2 and Q5) and 29 T/m for the quadrupoles with the more compact design (Q1, Q3, Q4 and Q6). The dipoles with rectangular pole shape and a pole length of 50 mm have a maximum field of 460 mT.

All quadrupoles are mounted on motorized vertical translation stages for alignment in x, the deflection plane. The four compact quadrupoles have an additional horizontal translation stage for alignment in y. Quadrupole four to six are inclined by the deflection angle of 24.5 mrad. The dipoles are mounted at a fixed height without inclination.

For measuring the electron beam profile a scintillating screen, which was placed under an angle of 45° to the beam axis, could be placed at three different positions along the beam line at 0.7 m, 1.8 m and 2.9 m distance from the electron source (marked as screen 1 to 3 in Fig. 1).

The electron spectrometer consists of a permanent dipole magnet, which deflects the electrons to a scintillating screen. The range corresponding to an electron energy of 3 MeV to

* This work is partially funded by the German Federal Ministry for Education and Research under contract no. 05K10VK2 and 05K10SJ2 and by the Helmholtz Association on the framework of the ARD program.
† christina.widmann@kit.edu

ISBN: 978-3-95450-168-7 doi:10.18429/JACoW-IPAC2015-MOPWA046

LATTICE AND BEAM DYNAMICS OF THE ENERGY RECOVERY MODE OF THE MAINZ ENERGY-RECOVERING SUPERCONDUCTING ACCELERATOR MESA*

D. Simon†, K. Aulenbacher, R. Heine, F. Schlander
Institut für Kernphysik, Johannes Gutenberg-Universität Mainz,
D-55128 Mainz, Germany

Abstract

The Mainz Energy-recovering Superconducting Accelerator (MESA) is a proposed multi-turn energy recovery linac for particle physics experiments [1, 2]. It will be built at the Institute for Nuclear Physics (KPH) at Mainz University. Because of the multi-turn energy recovery mode, there are particular demands on the beam dynamics. We present the current status of the lattice development.

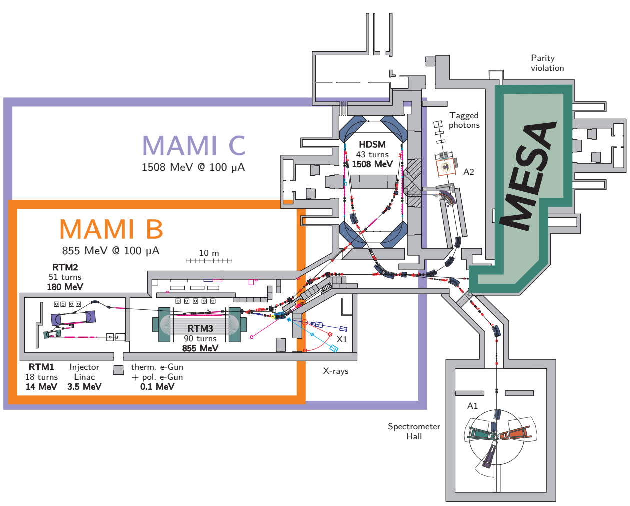

Figure 1: Floor plan of the MAMI facility. Space intended for MESA is marked in green.

INTRODUCTION

The MESA accelerator will be a CW-electron beam accelerator and will operate in two modes: an energy recovery mode (ER) with currents up to 1 mA (up to 10 mA in stage-2) and a polarized external beam mode (EB) with up to 150 μA. As presented in [3], MESA will be a double-sided recirculating linac with vertical stacking of the return arcs similar to a proposal for the LHeC ERL test facility [4]. A normal conducting linac with an extraction energy of 5 MeV will be used as injector. The linear lattice was designed with our own matrix optics program "Beam Optics" and also with Mad X [5]. To allow for space charge effects and pseudo-damping of the TESLA 9-cell cavities [6], the lattice was additionally simulated with PARMELA [7].

As shown in Fig. 3, MESA consists of:

- a 100 keV polarized photo-cathode electron gun [8],
- a normal conducting injector linac with an extraction energy of 5 MeV [2, 9],
- two superconducting linac modules with an energy gain of 25 MeV each [10],
- four spreader sections for separating and recombining the beam [3] vertically,
- five 180° arcs for beam recirculation,
- two chicanes for the injection and extraction of the 5 MeV beam,
- an 180° bypass arc for ER mode incorporating the internal experiment and a chicane to adjust the path-length (not shown in Fig. 3),
- a beam line to the external experiment.

SPACE CONSTRAINTS

MESA will be built in three existing halls formerly used for Experiments at the Mainz Microtron (MAMI) [11] (as shown in Fig. 1). These halls are located 10 m underground. Therefore alteration of the building is a challenge, due to the building statics. The main accelerator will be located in two of these halls; the third is appointed for the experiments. Due to the space restrictions, the lattice for MESA was optimized for a footprint area of circa 7.7 m × 27 m [3].

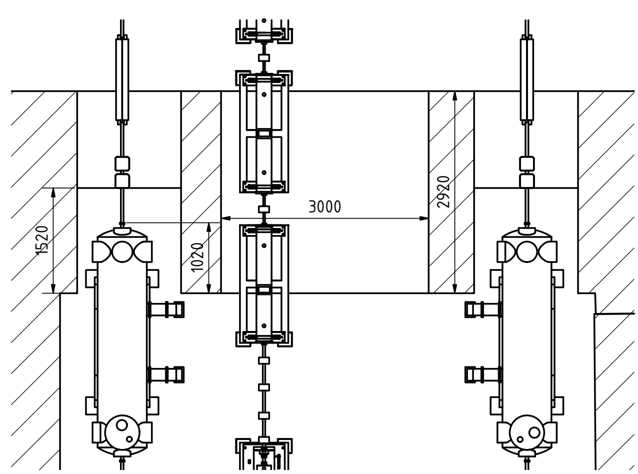

Figure 2: Sketch of the top view of the walls including the cryomodules and the injector linac (old concept).

* Work supported by the German Federal Ministry of Education and Research (BMBF) and German Research Foundation (DFG) under the Cluster of Excellence "PRISMA"
† simon@kph.uni-mainz.de

Content from this work may be used under the terms of the CC BY 3.0 licence (© 2015). Any distribution of this work must maintain attribution to the author(s), title of the work, publisher, and DOI.

ISBN: 978-3-95450-168-7 doi:10.18429/JACoW-IPAC2015-MOPWA047

START TO END SIMULATION OF HIGH CURRENT INJECTOR USING TRACEWIN CODE

Sarvesh Kumar, Abanimohan Mandal
Inter University Accelerator Centre, New Delhi, INDIA

Abstract

High Current Injector (HCI) is an alternate injector to superconducting linac at IUAC in addition to pelletron. It consists mainly of high temperature superconducting ECR ion source (PKDELIS), radio frequency quadrupole (RFQ) and a drift tube linac (DTL). The ions of mass to charge (A/q) ratio of 6 are analysed initially and accelerated through RFQ and DTL to a total energy of 1.8 MeV/u. The different energy regimes connecting the accelerating stages are named as low, medium and high energy beam transport section (LEBT, MEBT and HEBT). The energy spread of beam increases from 0.02% at ECR source to 0.5% at the LINAC entrance. An ion beam of normalized transverse and longitudinal emittance of 0.3 pi mm-mrad and 3 keV/u-ns has been considered at the start for the simulation of ion optics using TRACEWIN code. The whole beam transport system has been designed using GICOSY, TRANSPORT and TRACE 3D codes piecewise and TRACEWIN code is used to simulate whole ion optics from start to end including acceleration stages such as RFQ and DTL. Simulation results shows that beam can be injected through LEBT, MEBT and HEBT into LINAC without significant emittance growth and beam loss.

HIGH CURRENT INJECTOR

The ECR ion source [1,2,3] provides intense ion beams of high charge states which is the main requirement for nuclear physics experiments for better statistics and maximum energy gain from LINAC [4]. The beam optics calculations have been done piecewise [5] using different codes earlier and presently performed using TRACEWIN code [6] from start to end in envelope mode within framework of linear beam optics regime. A normalised longitudinal emittance of 3keV/u-ns and normalised transverse emittance of 0.3 pi mm-mrad has been assumed at the ECR ion source to design the whole system.

LEBT SECTION

The LEBT section consists of an electrostatic einzel lens (EL) and an electrostatic quadrupole doublet (EQD) so that all the ions follow same trajectory independent of their mass which are analysed as mass to charge ratio of 6 using a large acceptance analysing magnet [7] (AM). These ions are followed by a combination of electrostatic quadrupole triplet (EQT) and electrostatic accelerating section (AS) to transversely focus across the RF gap of a 12.125 MHz multiharmonic buncher. The input (i) and output (o) ion beam parameters for designing the individual LEBT, MEBT and HEBT section which connects the acceleration stages like high voltage DECK, RFQ [8] and DTL [9] are given in Table-1 where all twiss parmeters are in unit of mm/pi-mrad and all emittances (100%) are in unit of pi-mm-mrad.

Table 1: Ion Beam Parameters of Beam Transport Sections

Parameters	LEBT	MEBT	HEBT
α_{xi}, β_{xi}, ε_{xi}	0,1.0 0.3	0.62,0.05 0.46	-0.44,0.98 0.46
α_{xo}, β_{xo}, ε_{xo}	1.72,0.14 0.46	2.2,0.53 0.46	0.14,0.84 0.38
α_{yi}, β_{yi}, ε_{yi}	0,1.0 0.3	-0.59,0.22 0.3	-0.1,1.1 0.3
α_{yo},β_{yo}, ε_{yo}	1.73,0.14 0.3	2.2,0.45 0.3	0.02,0.97 0.3
α_{zi}, β_{zi}, ε_{zi}	0,22.5 1.31	-2.2,1.1 1.36	-9.1, 18.6 1.36
α_{zo}, β_{zo}, ε_{zo}	-0.05,0.2 1.36	-2.8,0.54 1.36	2.8,2.1 1.32
ME/q^2 (amu.MeV)	0.108	6.48	64.8
E (MeV/u)	0.003	0.180	1.8

These ions are bunched using a RF voltage of around 500V to the entrance of RFQ and transversely focussed using a set of four air cooled magnetic quadrupoles (MQS). The particles are bunched with a repetition rate of 83 ns and squeezed to a bunch width within 5 ns. The RFQ provides bunching, focusing to the injected ions from LEBT section and acceleration to an energy around 180 keV/u. The horizontal and vertical beam envelope for this section followed by RFQ section is shown in Fig. 1. The ion optical design of RFQ has been studied by TRACK code previously.

MEBT SECTION

This section matches the beam from RFQ to DTL. It consists of a set of magnetic quadrupoles and a spiral buncher for transverse and time focusing at the entrance of DTL respectively. The ion optical design of DTL has been studied using LANA code previously.

Content from this work may be used under the terms of the CC BY 3.0 licence (© 2015). Any distribution of this work must maintain attribution to the author(s), title of the work, publisher, and DOI.

ISBN: 978-3-95450-168-7 doi:10.18429/JACoW-IPAC2015-MOPWA048

TRANSVERSE EMITTANCE MEASUREMENT FOR LOW ENERGY ION BEAMS USING QUADRUPOLE SCAN METHOD

Sarvesh Kumar, Abanimohan Mandal
Inter University Accelerator Centre, New Delhi, India

Abstract

Low energy ion beam facility (LEIBF) at IUAC consists of all permanent magnet 10 GHz electron cyclotron resonance (ECR) ion source (NANOGAN) along with 400 kV high voltage accelerating platform, a switching cum analysing magnet and electrostatic quadrupoles. Intense low energy ion beams puts tremendous challenge to transport from ion source to target with minimum emittance growth and beam losses. The normalized emittance of analysed ion beam is measured using electrostatic quadrupole scan method for various source parameters like RF power and injection pressure of gas etc. It is attributed to beam rotation induced by ECR axial magnetic field, effect of ion temperature in plasma, nonlinear electric fields and space charge etc. which play a significant role in emittance growth.

INTRODUCTION TO LEIBF

The new low energy ion beam facility (LEIBF) [1] at the Inter-University Accelerator Centre (IUAC) is a facility dedicated to provide multiply charged ion beams at a wide range of energies (a few keV to a few tens of MeV) for experiments in Atomic, Molecular and Materials Sciences. This facility consists of an all permanent magnet (NdFeB) 10 GHz electron cyclotron resonance (ECR) ion source (NANOGAN) [2] installed on a high voltage platform (400 kV) for obtaining multiply charged intense ions and the analysed beam is transported to the three beam lines along 75deg., 90deg. and 105 deg. angles using a switching cum analysing magnet. The beam tuning parameters of various ion beams are verified experimentally within first order linear beam optics analysis. The emittance is measured for various parameters of NANOGAN using quadrupole scan method in 90 deg. beam line. Standard beam dynamics and 3D field computation codes have been used to design beam transport element. The whole system has been installed and tested and facility is being used by scientific users.

ECR ION SOURCE AND LOW ENERGY BEAM TRANSPORT

The ECR ion source [3, 4] acts as prominent injector into heavy ion accelerators as they can produce the broad range of intense ions in multiple charge states for maximum energy gain in linear accelerators. Simultaneously, they are also used as a compact facility in low energy regime to perform implantation experiments on target samples. The magnetic confinement necessary to sustain the ECR plasma makes the ion density distribution across the extraction aperture inhomogeneous and charge state dependent. Thus it is necessary to characterize the extracted beam in terms of its emittance and transmission along the beam lines. The ion beam parameters from the exit of ECR ion source taken for beam optics simulations are given in Table 1.

Table 1: Ion Beam Parameters

Parameters	Values
Emittance ε (π mm-mrad)	100
Extraction Energy (E) keV/q	30
Max. ME/q^2 along 75°, 90° and 105° lines (MeV.amu)	44.68, 30.37 22.96

The beam is extracted using 30kV dc potential and focussed by a combination of electrostatic quadrupole doublet (EQD), 400kV accelerating section (AS) and an electrostatic quadrupole triplet (EQT) directly to object point of switching magnet (SW). The beam optics for the whole facility in 90 deg. line is shown in Fig. 1 using code TRANSPORT [5]. Different colour envelopes corresponds to different charge states of Ar ion beam. Based on this beam optics, the whole facility is installed and commissioned. Transverse emittance measurements of analysed beam have been performed using electrostatic quadrupole scan method.

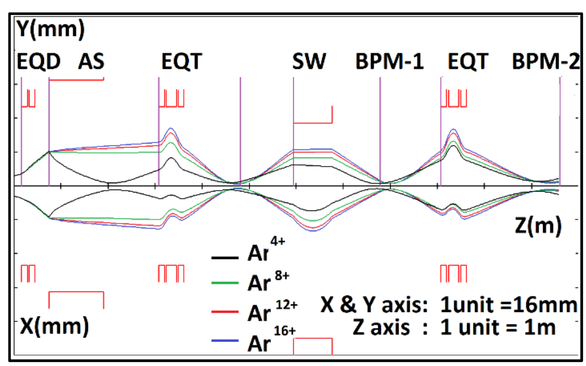

Figure 1: Beam optics of LEIBF in 90° line using TRANSPORT code for charge states of Ar ion beam at the energy of q*210 keV.

QUADRUPOLE SCAN METHOD

The two beam profile monitors before and after the EQT in 90 deg. line are used to measure the emittance using quadupole scan method [6, 7]. It is based upon linear transformations of beam phase space and

Content from this work may be used under the terms of the CC BY 3.0 licence (© 2015). Any distribution of this work must maintain attribution to the author(s), title of the work, publisher, and DOI.

ISBN: 978-3-95450-168-7 doi:10.18429/JACoW-IPAC2015-MOPWA049

SIMULATION OF CRAB WAIST COLLISIONS IN DAΦNE WITH KLOE-2 INTERACTION REGION*

M. Zobov, A. Drago, A. Gallo, C. Milardi, INFN/LNF, Frascati, Italy
D. Shatilov, BINP, Novosibirsk, Russia
A. Valishev, FNAL, Batavia, IL, USA

Abstract

After the successful completion of the SIDDHARTA experiment run with crab waist collisions, the electron-positron collider DAΦNE has started routine operations for the KLOE-2 detector. The new interaction region also exploits the crab waist collision scheme, but features certain complications including the experimental detector solenoid, compensating anti-solenoids, and tilted quadrupole magnets. We have performed simulations of the beam-beam collisions in the collider taking into account the real DAΦNE nonlinear lattice. In particular, we have evaluated the effect of crab waist sextupoles and beam-beam interactions on the DAΦNE dynamical aperture and energy acceptance, and estimated the luminosity that can be potentially achieved with and without crab waist sextupoles in the present working conditions. A numerical analysis has been performed in order to propose possible steps for further luminosity increase in DAΦNE such as a better working point choice, crab sextupole strength optimization, correction of the phase advance between the sextupoles and the interaction region. The proposed change of the e^- ring working point was implemented and resulted in a significant performance increase.

INTRODUCTION

DAΦNE is an accelerator complex the main element of which is a double ring electron-positron collider operating at the c.m. energy of the Φ-resonance (1.02 GeV) [1].

The implementation of the Crab Waist collision scheme (CW) has led to the achievement of the record peak luminosity L=4.5×10^{32} cm^{-2}s^{-1} while working for the SIDDHARTA experiment [2]. This success has led to a decision to reinstall the upgraded KLOE detector, KLOE-2, exploiting the advantages of the CW scheme. For this purpose, the KLOE interaction region (IR) was carefully redesigned [3], and in 2013 the KLOE detector has been upgraded with new layers in the inner part of the apparatus [4]. The new KLOE-2 IR is much more complex as compared to the SIDDHARTA IR because the collisions take place inside the detector solenoid, IR has rotated quadrupoles and additional compensator solenoids.

At present, the luminosity of 1.9×10^{32} cm^{-2}s^{-1} has been achieved to be compared with 1.5×10^{32} obtained in the previous KLOE run [5]. Table 1 summarizes the most relevant machine and beam parameters. It is worth noting that the performance is mostly limited by collective effects such as electron cloud, microwave instability, feedback system noise, etc. [6]. An extensive campaign of experimental and simulation studies is in progress in order to fully exploit the CW potential and push the luminosity to higher values.

Numerical simulations of beam-beam effects with the weak-strong particle tracking code Lifetrac proved to be very efficient for the detailed understanding of the crab-waist collision scheme, and for the collider performance optimization [7,8]. The goal of the present work was to implement the complete model of DAΦNE with the KLOE-2 IR in weak-strong beam-beam simulation and apply the modeling to guide parameter optimization.

In addition to the value for the DAΦNE program, the studies represent a unique opportunity to benchmark the numerical tools against the experimental data to enable further application towards the High Luminosity upgrade of the LHC.

Table 1: DAΦNE Machine and Beam Parameters during 2015 Operation with KLOE-2 Detector (April 2015)

Parameter	Value
Number of bunches	95
Bunch spacing	2.7 ns
Full horizontal crossing angle	50 mrad
Number of electrons / bunch	2.05×10^{10}
Number of positrons / bunch	2.05×10^{10}
Electron emittance, r.m.s. (x,y)	0.28, 0.0021 μm
Positron emittance, r.m.s. (x,y)	0.28, 0.0021 μm
Momentum spread, r.m.s.	5.5×10^{-4}
Bunch length, r.m.s. (e^-, e^+) σ_z	1.55, 1.6 cm
Electron betatron tunes (ν_x,ν_y)	0.130, 0.170
Positron betatron tunes (ν_x,ν_y)	0.098, 0.130
Damping decrements (x,y,z)	(1.1, 1.1, 2.2) ×10^{-5}
Beta-function at IP (x,y)	25, 0.84 cm
Beam-beam parameter, e^+ (x,y)	0.011, 0.04

* Research supported by DOE via the US-LARP program and by EU FP7 HiLumi LHC - Grant Agreement 284404.

Content from this work may be used under the terms of the CC BY 3.0 licence (© 2015). Any distribution of this work must maintain attribution to the author(s), title of the work, publisher, and DOI.

ISBN: 978-3-95450-168-7 doi:10.18429/JACoW-IPAC2015-MOPWA050

BEAM DYNAMICS STUDIES TO DEVELOP A HIGH-ENERGY LUMINOSITY MODEL FOR THE LHC

G. Campogiani, University of Rome “La Sapienza”, Rome Italy and CERN, Geneva, Switzerland
Y. Papaphilippou, CERN, Geneva, Switzerland

Abstract

Luminosity, the key figure of merit of a collider as the LHC, depends on the brightness of the colliding beams. This makes the intensity dependent beam-beam effect the dominant performance limiting factor at collision. The parasitic interactions due to the electromagnetic mutual influence of the beams in the interaction region of a collider induce a diffusive behaviour in the tails of the beam. The evolution of charge density distribution is studied to model the beam tails evolution in order to characterize beam lifetime and luminosity. To achieve this, tools are developed for tracking distributions of arbitrary number of single particles interacting with the opposing strong-beam, to analyse the halo formation processes due to the combined effect of beam-beam and machine non-linearities. This paper presents preliminary results of the simulations, both for the LHC Run I and nominal LHC parameters. The former will be used to benchmark simulations while the latter aims at supporting luminosity estimate for the Run II.

INTRODUCTION

The figure of merit of a collider is the (istantaneous) luminosity $\mathcal{L}$, defined as the proportionality factor between the cross-section σ_p and the rate of events per seconds $\frac{dR}{dt}$, and corresponds to the volume of overlap integral of the beams charge density distributions in the interaction region times the number of bunches, the revolution frequency and the product of the population in each of the opposing bunches. In the simplifying assumption of round ($\sigma_x = \sigma_y$), symmetric, equally populated beams colliding head-on and with Gaussian charge density distribution, the ideal luminosity formula is the following

$$\mathcal{L}(t) = \frac{n_b f_{rev} N^2(t)}{4\pi\sigma_x(t)\sigma_y(t)} = \mathcal{L}_0(t)$$

where N is the number of particles in each of the colliding bunches, $\sigma_{x,y} = \sqrt{\beta^*_{x,y}\epsilon_n/\gamma_{rel}}$ is the beam transverse size, $\gamma_{rel} = (1-(\frac{v}{c})^2)^{-1/2}$ is the relativistic gamma, ε_n is the normalised transverse emittance, n_b is the number of bunches per beam and f_{rev} is the revolution frequency.

In the real machine additional effects reducing luminosity are present: the presence of a crossing angle, the hour-glass effect due to the spatial modulation of the betatron function when $\sigma_s \gg \beta^*$, where σ_s is the bunch length, and an offset in the position of the beams at the interaction point. Thus, a more realistic expression for the instantaneous luminosity is [1]

$$\mathcal{L}(t) = \Lambda(t)N^2(t)$$
$$\Lambda(t) = \frac{n_b f_{rev}}{4\pi}\frac{\gamma_{rel}}{\beta^*\varepsilon_n}H(\frac{\sigma_s(t)}{\beta*})F(\theta_c,\sigma^*(t),\beta^*)$$

where $H(\sigma_s(t),\beta^*)$ is the reduction factor due to the hour-glass effect and $F(\sigma_s(t),\beta^*)$ is the geometrical reduction factor due to the presence of a crossing angle θ_c that reduces the geometrical intersecting volume of the colliding beams with respect to the head-on one. This form of the expression of luminosity is convenient to highlight its dependence on beam intensity, while the other factors are included in the $\Lambda(t)$ term.

It is evident how, for a fixed energy value, such as the collision one, the easiest way to increase the luminosity would be to increase the ratio of $\frac{N}{\varepsilon_n}$ which is proportional to the beam brightness. From injection to collision energy, several phenomena interplay to cause emittance growth, and in particular intra-beam scattering (IBS). Once the beams reach the maximum energy level and are brought into collision, the intensity dependent long-range beam-beam effect is dominant, putting a limit to performance optimization. This phenomenon is due to the non-linear lens behaviour of the electromagnetic field of one beam on the other one in the interaction region, both in the collision point (head-on) and at a distance from the design interaction point (long-range).

The parasitic encounters drive beam-halo formation. Our aim is to study the beam dynamics of the halo through numerical simulations, to characterize beam lifetime and luminosity evolution at hight energy. To reach this goal, the evolution of charge density distributions in the beam is analyzed, by tracking particles through a symplectic integrator that includes the beam-beam effect as a thin-kick in the transverse phase-space. The final goal is to find ways to better characterise the beam lifetime and be able to predict the component of luminosity evolution due to beam-beam effect through numerical simulations based on detailed beam dynamics models.

Table 1: Summary of Machine Optics and Beam Parameters Used in the Simulations

Parameter	Run I	nominal
E_{kin}[TeV]	4	7
ε_n[μm-rad]	2.5	3.75
$\beta^*_{x,y}$[cm]	60	50
bunch spacing [ns]	50	25
$\frac{\Delta p}{p}$	0	0
N	1.6	1.15

SIMULATIONS PARAMETERS

We have used MAD [2] to generate the LHC machine optics from Run I and the nominal LHC parameters, with

Content from this work may be used under the terms of the CC BY 3.0 licence (© 2015). Any distribution of this work must maintain attribution to the author(s), title of the work, publisher, and DOI.

ISBN: 978-3-95450-168-7 doi:10.18429/JACoW-IPAC2015-MOPWA052

Content from this work may be used under the terms of the CC BY 3.0 licence (© 2015). Any distribution of this work must maintain attribution to the author(s), title of the work, publisher, and DOI.

FORMATION OF A UNIFORM ION BEAM BASED ON NONLINEAR FOCUSING AND ITS APPLICATIONS AT THE JAEA TIARA CYCLOTRON

Yosuke Yuri, Takahiro Yuyama, Tomohisa Ishizaka,
Ken-ichi Yoshida, Ikuo Ishibori, Susumu Okumura
Takasaki Advanced Radiation Research Institute, Japan Atomic Energy Agency,
1233 Watanuki-machi, Takasaki, Gunma, Japan

Abstract

A formation/irradiation technique of large-area uniform ion beams based on nonlinear focusing of multipole magnets has been developed toward advanced research and efficient industrial applications at the TIARA AVF cyclotron facility of Japan Atomic Energy Agency. The formation procedure of the uniform beam has been established as follows: An ion beam extracted from the cyclotron is multiply scattered with a thin foil so that the transverse beam intensity distribution can be smoothed into a Gaussian-like one, prerequisite to the formation of a highly uniform beam. Then, the tail of the Gaussian-like distribution is folded into the inside by the nonlinear force of octupole magnets and eventually the distribution can be made uniform on a target. We have realized large-area uniform beams of ^{1}H, ^{12}C, ^{40}Ar, and ^{129}Xe typically over 100 cm^2 in area and below 10% in uniformity. Such uniform beams have enabled the suppression of local target heating and efficient low-fluence irradiation, and been applied to radiation degradation testing of space-use solar cells and a study on functional materials.

INTRODUCTION

The ion accelerator complex TIARA (Takasaki Ion Accelerators for Advanced Radiation Application) is an accelerator facility in Japan Atomic Energy Agency (JAEA), dedicatedly constructed for the advanced research and development (R&D) on material, biological and medical sciences and their applications [1]. The complex consists of four accelerators: An azimuthally-varying-field (AVF) cyclotron (*K* number of 110 MeV), a 3-MV tandem accelerator, a 3-MV single-ended accelerator and a 400-kV ion implanter.

A theoretical and experimental R&D study has been carried out on the formation of a large-area uniform beam with multipole magnets using ion beams from the AVF cyclotron for various applications [2-4]. The uniform-beam formation is based on the transformation of the transverse beam intensity distribution by means of the nonlinear focusing force produced mainly by octupole magnets [5]. It is possible to make the intensity distribution uniform by folding the tail of the Gaussian beam distribution with octupole magnets in a properly-designed beam transport line.

Recently, we have established the tuning procedure of the uniform-beam formation and then achieved the primary objective (to form a uniform region 100-cm^2 in area with a uniformity below 10%) using several species of ion beams from the cyclotron. In these proceedings, the latest R&D results and application examples of the uniform beam are reported.

BEAM TUNING PROCEDURE IN THE BEAM TRANSPORT SYSTEM

The schematic view of the cyclotron facility in TIARA is illustrated in Fig. 1. The main elements for the uniform-beam formation are a thin scattering foil for conditioning the prerequisite beam, octupole magnets for beam tail folding and a target station for beam measurement and utilization. The tuning procedure in the beam transport system for the efficient uniform-beam formation has been determined as follows through the beam optics design, tracking simulation, and repeated experiments.

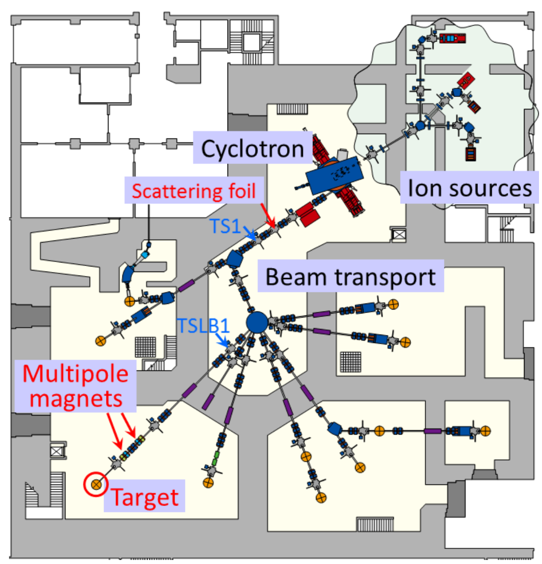

Figure 1: Schematic view of the JAEA AVF cyclotron facility. There are four ion sources, which can generate various ions from proton to osmium. A scattering foil is mounted at the first straight section after the cyclotron. The gray squares on the beam lines correspond to the beam diagnostic stations (labelled as TS1 and TSLB1) equipped with a silt, a wire profile monitor, a phosphor screen, and a Faraday cup. Multipole (sextupole and octupole) magnets have been installed in one of the beam lines for the formation of a uniform beam.

First, the transverse beam size and position are adjusted to the diameter (30 mm) of the scattering foil and the beam waist is formed at the diagnostic station TS1 using

ISBN: 978-3-95450-168-7 doi:10.18429/JACoW-IPAC2015-MOPWA053

EMITTANCE PRESERVATION IN SUPERKEKB INJECTOR

S. Kazama*, M. Satoh, H. Sugimoto, M. Yoshida, Y. Ogawa
High Energy Accelerator Research Organization (KEK), Tsukuba, Ibaraki, 305-0801, Japan

Abstract

Injector linac at KEK is now under the way to produce high current and low emittance beams for SuperKEKB. The target luminosity for SuperKEKB is 40 times higher than that of KEKB. A short-range transverse wakefield and a dispersive effect at the linac cause an emittance growth, and a longitudinal wakefield effect enlarges an energy spread of the beams. In this paper, we presented simulation studies concerning the emittance preservation and the energy spread issues. As a candidate for the mitigation of the emittance dilution originating from the transverse wakefield, a so-called "offset injection" method using steering coils is considered. It is demonstrated that the offset injection remarkably improves the emittance preservation.

INTRODUCTION

SuperKEKB is an electron-positron collider with an energy of 7 GeV and 4 GeV, respectively. The target luminosity is $8\times10^{35}\mathrm{cm}^2\mathrm{s}^{-1}$, which is 40 times higher than that of KEKB [1]. SuperKEKB main ring therefore requires a high current and low emittance beam. These parameters are summarized in Table 1. In order to meet the requirement, photo-cathode RF guns are now installed at the injector linac for the electron beam. For the production of a low emittance positron beam, a damping ring is now under construction. Since the target emittance is quite small compared to that of KEKB, much more attention should be paid to the emittance growth through the linac. The Short-range wakefield and the dispersive effect are considered to be the major sources of the emittance dilution. In this paper, we report on a design study on SuperKEKB injector for high current, low emittance, and low energy spread beams. We mainly report on simulation studies concerning the emittance preservation issues and how to suppress the increase of the energy spread. All simulation presented in this paper is performed with elegant [2].

Table 1: Required parameters for SuperKEKB

	Phase 2 (e^+/e^-)	**Phase 3** (e^+/e^-)
Bunch charge [nC]	2 / 2	4 / 5
Vertical emittance [mm mrad]	20 / 20	20 / 20
Horizontal emittance [mm mrad]	100 / 50	100 / 50
Energy spread [%]	0.1	0.1

* kazama@post.kek.jp

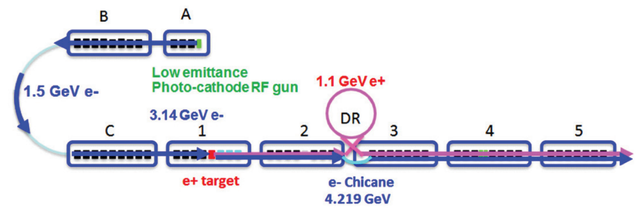

Figure 1: Schematic of SuperKEKB injector linac.

TRACKING SIMULATION

Figure 1 shows a schematic of SuperKEKB injector linac. The linac is mainly composed of 9 sections. In this paper, simulation is performed from C-sector to 5-sector for simplicity.

Condition of Simulation

The initial particle distribution in the longitudinal direction at the C-sector is a Gaussian of 10 ps bunch length (FWHM) with 2 or 5 nC charge and 1.5 GeV energy. The distributions of transverse phase space and energy spread are both assumed to be Gaussian. The initial emittance in the horizontal and vertical directions and the energy spread are set to be 10 mm mrad and 0.1 %, respectively. Longitudinal monopole and transverse dipole wakefield are incorporated in the simulation with an analytical expression of the wake functions [3]. Long-range wakefield effects are not taken into account in the simulation. The electron beam is approximated by 10^5 macro particles. For the study of the effect of misalignment on the emiitance growth, alignment errors for quadrupole magnet and acceleration tube are considered, and their distributions are assumed to be Gaussian.

EMITTANCE PRESERVATION

Short-Range Wakefield and Misalignment

When a bunch of electron beam passes through a misaligned accelerating structure, the head particles in the bunch will interact with the beam pipe and leave a wakefield to the tail particles. The induced wakefield can deflect the trailing particles further away from the axis, resulting in an increase of the projected beam emittance. A small amount of misalignment and a short bunch length can reduce the transverse wakefield strength. However, the short bunch length causes the strong longitudinal wakefield, resulting in a large energy spread. Therefore, the bunch length has to be optimized with a detailed simulation. The dependence of the bunch length on the energy spread will be discussed in the next section. To achieve the required emittance, the magnitude of the misalignment must be kept as small as possible. Figure. 2 shows a simulated vertical emittance at

Content from this work may be used under the terms of the CC BY 3.0 licence (© 2015). Any distribution of this work must maintain attribution to the author(s), title of the work, publisher, and DOI.

ISBN: 978-3-95450-168-7 doi:10.18429/JACoW-IPAC2015-MOPWA054

EFFECT OF NUMBER OF MACRO PARTICLES ON RESOLUTION IN PHASE SPACE DISTRIBUTION

T. Miyajima*, KEK, Tsukuba, Ibaraki 305-0801, Japan

Abstract

In order to analyze charged particle beam in an accelerator, a beam model is used to reduce number of degrees of freedom, e.g. charged disk model, charged cylinder model and macro-particle model. In numerical simulation, the macro-particle model, which has same mass-to-charge ratio, is widely used, since it does not require any symmetry of beam shape. However, the estimation of proper number of macro-particles is one of the important issues. In order to study the effect of the number of macro-particles for the numerical model, we defined a simple transformation to generate reduced distribution. The transformation was applied for one dimensional and two dimensional particle distributions. The static electric fields due to the transformed distributions were calculated. As a result, we confirmed the effectiveness of the transformation.

INTRODUCTION

In an accelerator, the motion of a charged particle beam which consists of N particles can be described by a trajectory on $6N$ dimension phase space. Since an actual beam contains enormous number of particles, for example $N \sim 4.8 \times 10^8$ electrons in an Energy Recovery Linac with 77 pC operation, degree of freedom in a simulation and a theoretical analysis is reduced using an approximation. In order to analyze the charged particle beam, a beam model is used to reduce number of degrees of freedom, e.g. charged disk model, charged cylinder model and macro-particle model [1]. The macro-particle model, which does not depend on the symmetry in the beam, is versatile method to describe it.

In numerical simulation, the macro-particle model, which has same mass-to-charge ratio, is widely used, since it does not require any symmetry of beam shape. However, the estimation of proper number of macro-particles is one of the important issues, since it affects the resolution of the phase space distribution of the beam. Then, we define a transformation to reduce macro-particles, and study the relation between the number of macro-particles and the resolution in the phase space. In this paper, we report the transformation and static electric fields calculated by the transformed distribution about an electron beam for one and two dimensional distributions.

MACRO PARTICLE MODEL

The equation of motion of an electron in electro-magnetic field, $\boldsymbol{E}$ and $\boldsymbol{B}$, is

$$c\frac{m_e}{e}\frac{d(\gamma\boldsymbol{\beta})}{dt} = \boldsymbol{E} + \boldsymbol{v} \times \boldsymbol{B}, \qquad (1)$$

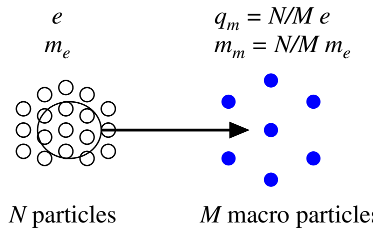

Figure 1: Description of charged particle beam by macro-particle model. The mass-to-charge ratio is a conserved quantity.

where, m_e and e are the mass and the charge of an electron, c is the speed of light, $\boldsymbol{v}$ is the speed of the electron, $\beta = v/c$ and $\gamma = 1/\sqrt{\beta^2 - 1}$. Here, the electron beam consists of N electrons. In order to describe the electron beam by the macro-particle model with$M$ macro-particles, we have to preserve the mass-to-charge ratio. As shown in Fig. 1, the macro-particle contains $a(= N/M)$ electrons, and the mass and charge are $m_m = am_e$, $q_m = ae$, respectively. The equation of motion of the single macro-particle is

$$c\frac{m_m}{q_m}\frac{d(\gamma\boldsymbol{\beta})}{dt} = \boldsymbol{E} + \boldsymbol{v} \times \boldsymbol{B}. \qquad (2)$$

It is the same equation as the single electron, Eq. (1), because $m_e/e = m_m/q_m$. Therefore, the description of the beam motion by macro-particle model corresponds to an approximation by M charged particles with the mass, am_e, and the charge, ae. However, we have to select proper number of macro-particles, which preserves the property of the original beam, because the replacement by the macro-particles causes the loss of information about the beam. In order to study this mechanism, we introduce a transformation, particle pair transformation, to describe the replacement by the macro-particle in the next section.

PARTICLE PAIR TRANSFORMATION

In this section, we define a particle pair transformation to describe the replacement of an particle distribution by macro-particles. The original distribution consists of n_0 macro-particles with the mass, m_{m0}, and the charge, q_{m0}. The procedure of the transformation has the following five steps.

1. Calculate the center of the original particle distribution.
2. Choose the most distant particle from the center, and the nearest neighbor particle from it.
3. Calculate the average position about the above two particles.
4. Replace the two particles by a new macro-particle with $m_{m1} = 2m_{m0}$ and $q_{m1} = 2q_{m0}$ on the average position.

* tsukasa@post.kek.jp

Content from this work may be used under the terms of the CC BY 3.0 licence (© 2015). Any distribution of this work must maintain attribution to the author(s), title of the work, publisher, and DOI.

ISBN: 978-3-95450-168-7 doi:10.18429/JACoW-IPAC2015-MOPWA055

STUDY OF EMITTANCE GROWTH CAUSED BY SPACE CHARGE AND LATTICE INDUCED RESONANCES

Kazuhito Ohmi, KEK, Tsukuba, Japan

Abstract

Emittance growth and beam loss in high intensity circular proton accelerators are one of the most serious issue which limit their performance. The emittance growth is caused by linear and nonlinear resonances of betatron/synchrotron oscillation due to lattice and space charge nonlinear force. The resonances are induced by errors in many cases. The space charge effects have been studied by computer simulations. Simulations with taking into account errors at random are consuming. We should first understand which resonances are serious. Resonance strength and resonance width induced by space charge and lattice nonlinearity is discussed with integrals along a ring like the radiation integrals. Emittance growth is evaluated by model with the resonance width to understand the mechanism.

INTRODUCTION

Particles move with experience of electro-magnetic field of lattice elements and space charge. We study slow emittance growth arising in a high intensity circular proton ring. We assume that the beam distribution is quasi-static, and each particle moves in the filed of the quasi-static distribution. Actually we concern about beam loss of 0.1-1% during a long term ($\approx$ 10,000 turns) in J-PARC MR. A halo is formed by the nonlinear force due to the electro-magnetic field. The halo, which consists of small part of whole beam, does not affect potential. Particle motion is described by a single particle Hamiltonian in the averaged field. This picture is not self-consistent for a distortion of beam distribution due to space charge force. Hamiltonian is separated by three parts for (1) linear betatron/synchrotron motion (μJ) (2) nonlinear component of the lattice magnets (U_{nl}) and (3) space charge potential (U).

$$H = \mu J + U_{nl} + U_{sc}. \tag{1}$$

where Hamiltonian is represented by action variables J and ϕ, which are Courant-Snyder invariant ($W = 2J$) and betatron phase, respectively.

Hamiltonian is expanded by Fourier series,

$$H = \mu J + U_{00(J)} + \sum_{m_x, m_y \neq 0} U_{m_x,m_y}(J)\exp(-im_x\phi_x - im_y\phi_y) \tag{2}$$

where Phase space structure near resonances are characterized by the resonance width. It is determined by their strength and tune slope for amplitude as follows [1],

$$\Delta J_x = 2\sqrt{\frac{U_{m_x,m_y}}{\Lambda}} \qquad \Lambda = \frac{\partial^2 U_{00}}{\partial J_x^2}. \tag{3}$$

EVALUATION OF RESONANCE WIDTH

Resonances Due to Space Charge Force

We first discuss the space charge potential U_{sc} [2]. Beam distribution is assumed to be Gaussian in transverse determined by emittance and Twiss parameters. U contains linear component, which gives a tune shift and Twiss parameter distortion. Twiss distortion is given by solving an envelope equation including linear space charge force self-consistently.

$$U_{sc} = \int ds' U_{sc}(s') = \frac{\lambda_p r_p}{\beta^2\gamma^3}\oint ds' \tag{4}$$
$$\int_0^\infty \frac{1 - \exp\left(-\frac{\beta_x(s')X(s,x')}{2\sigma_x^2+u} - \frac{\beta_y(s')Y(s,s')}{2\sigma_y^2+u}\right)}{\sqrt{2\sigma_x^2+u}\sqrt{2\sigma_x^2+u}} du$$

X and Y are normalized betatron coordinates at s' as

$$\begin{aligned} X(s,s') &= \sqrt{2J_x}\cos(\varphi_x(s') + \phi_x(s)) \\ Y(s,s') &= \sqrt{2J_y}\cos(\varphi_y(s') + \phi_y(s)). \end{aligned} \tag{5}$$

where $\varphi_{x,y}(s')$ is the betatron phase difference between s and s'.

The Fourier component, which correspond to resonance strength, is given by

$$U_{m_x,m_y}(J_x,J_y) = \frac{\lambda_p r_p}{\beta^2\gamma^3}\oint ds \int_0^\infty \frac{du}{\sqrt{2\sigma_x^2+u}\sqrt{2\sigma_y^2+u}}$$
$$\Big[\delta_{m_x0}\delta_{m_y0} - \exp(w_x - w_y)(-1)^{(m_x+x_y)/2}$$
$$I_{m_x/2}(w_x)I_{m_y/2}(w_y)e^{-im_x\varphi_x - im_y\varphi_y}\Big]. \tag{6}$$

The tune slope $\partial^2 U_{00}/\partial J_x^2$ in Eq.(3) induced by space charge potential is obtained as follows. The tune slope is evaluated by $U_{00}(J_x,J_y)$ in Eq.(7).

$$U_{00}(J_x,J_y) = \frac{\lambda_p r_p}{\beta^2\gamma^3}\oint ds \int_0^\infty \frac{d\eta}{\sqrt{2+\eta}\sqrt{2r_{yx}+\eta}}$$
$$(1 - e^{-w_x-w_y}I_0(w_x)I_0(w_y)). \tag{7}$$

where $r_{yx} = \sigma_y^2/\sigma_x^2$ and

$$w_x = \frac{\beta_x J_x/\sigma_x^2}{2+\eta}. \qquad w_y = \frac{\beta_y J_y/\sigma_y^2}{2+\eta/r_{yx}}. \tag{8}$$

$$\frac{\partial}{\partial J_x} = \frac{\beta_x/\sigma_x^2}{2+\eta}\frac{\partial}{\partial w_x}. \qquad \frac{\partial}{\partial J_y} = \frac{\beta_y/\sigma_x^2}{2r_{yx}+\eta}\frac{\partial}{\partial w_y}. \tag{9}$$

Content from this work may be used under the terms of the CC BY 3.0 licence (© 2015). Any distribution of this work must maintain attribution to the author(s), title of the work, publisher, and DOI.

ISBN: 978-3-95450-168-7 doi:10.18429/JACoW-IPAC2015-MOPWA056

Content from this work may be used under the terms of the CC BY 3.0 licence (© 2015). Any distribution of this work must maintain attribution to the author(s), title of the work, publisher, and DOI.

TRANSVERSE MULTI-PASS BEAM BREAKUP SIMULATION FOR KEK ERL LIGHT SOURCE

S.Chen*, M.Shimada, N.Nakamura, D.Zhou, KEK, Oho 1-1, Tsukuba, 305-0801, Japan
K. Liu, S. Huang, IHIP, Peking University, Beijing 100871, China

Abstract

In this paper, simulation results of the transverse multi-pass beam breakup for KEK ERL light source are presented.

INTRODUCTION

An X-ray synchrotron light source based on a multi-GeV ERL is under design in KEK, which is expect to be a successor of the existing synchrotron light sources of Photon Factory in KEK [1]. A preliminary design report of this project has been published in 2012 [2,3]. An average beam current up to 100mA is required for KEK ERL light source. It is known that the multi-pass transverse beam breakup could be a possible limitation to the average current. It is primarily contributed by a positive feedback between the recirculated bunch with transverse offset and insufficiently damped dipole HOMs in superconducting cavity. If the average current is larger than a certain value which is called threshold current, exponential growth of HOM power and transverse oscillation amplitude will occur and thus cause beam breakup. A two-dimensional analytical formula for the multi-pass BBU threshold current is [4]

$$I_{th} = -\frac{2pc}{e(\frac{\omega}{c})(\frac{R_d}{Q})Q_{ext}M_{12}^{*}\sin(\omega T_r)}, \qquad (1)$$

where (R_d/Q) is the shunt impedance of the dipole mode in the cavity, Q_{ext} is the external quality factor, ω is the HOM frequency, T_r is the bunch recirculating time, and

$$M_{12}^{*} = T_{12}\cos^2\theta + \frac{1}{2}(T_{14}+T_{23})\sin 2\theta + T_{34}\sin^2\theta,$$

where T_{ij} are the elements of the pass-to-pass transport matrix and θ is the polarization angle of the dipole HOM.

Eq. 1 shows the main determinants of multi-pass BBU instability in an ERL. This formula only valids in the case of single cavity, single HOM and $M_{12}^{*}\sin(\omega T_r) < 0$. In real cases, the situation is more complicated. It's necessary to use simulation codes to compute the BBU threshold current. In this paper, the code *bi* [5] based on particle tracking is used to simulate the multi-pass BBU effect of KEK ERL light source. Some features of the BBU of high energy ERLs are then discussed based on the simulation results.

KEK 3-GeV ERL LIGHT SOURCE

Several linac configurations have been designed for KEK ERL light source. In this paper, we are referring two of them. One configuration consists of 28 cryomodules with 8 cavities in each cryomodule. The cavity gradient is about 13.4 MV/m and the full energy is about 3.01 GeV [2]. The other configuration consists of 34 cryomodules of the same structure. The cavity gradient is about 12.5 MV/m and the full energy is about 3.41 GeV [6].

To improve the dipole HOM damping, a 9-cell KEK-ERL mode-2 cavity (shown in Fig. 1) with a larger iris diameter compared with TESLA-type cavity and two large beam pipes to provide stronger HOM damping [7]. Several major dipole HOMs in the mode-2 cavity are listed in Table 1. A previous work shows the BBU threshold current of more than 600 mA can be achieved when applying this type of cavity to a 5-GeV ERL configuration [8].

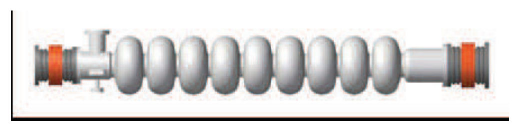

Figure 1: 1.3 GHz 9-cell KEK-ERL mode-2 cavity

Table 1: Major Dipole HOMs in KEK-ERL 9-cell Cavity

f GHz	Q_e	R/Q Ω/cm^2	$(R/Q)Q_e/f$ $\Omega/cm^2/GHz$
1.835	1.1010×10^3	8.087	4852
1.856	1.6980×10^3	7.312	6691
2.428	1.6890×10^3	6.801	4732
3.002	2.9990×10^4	0.325	3246
4.011	1.1410×10^4	3.210	9135
4.330	6.0680×10^5	0.018	2522

BBU SIMULATION RESULTS

Lattice Configuration

The focusing effect of the RF field in the superconducting cavity is considered in the simulation. The Rosenzweig's form of the transport matrix for a pure π-mode standing-wave cavity [9] is applied in the simulation, i.e.,

$$M_{cav} = \begin{pmatrix} \cos\alpha - \sqrt{2}\sin\alpha & \sqrt{8}\frac{\gamma_i}{\gamma'}\sin\alpha \\ -\frac{3}{\sqrt{8}}\frac{\gamma'}{\gamma_f}\sin\alpha & \frac{\gamma_i}{\gamma_f}\left[\cos\alpha + \sqrt{2}\sin\alpha\right] \end{pmatrix}, \qquad (2)$$

where $\alpha = \frac{1}{\sqrt{8}}\ln\frac{\gamma_f}{\gamma_i}$, $\gamma_{i(f)}$ is the initial (final) relativistic factor of the particle, $\gamma' = qE_0\cos(\Delta\phi)/m_0c^2$ where E_0 is the maximum particle energy gain from the RF cavity and $\Delta\phi$ is the phase of acceleration.

* chensi@post.kek.jp

ISBN: 978-3-95450-168-7 doi:10.18429/JACoW-IPAC2015-MOPWA057

SPACE CHARGE SIMULATION AND MATCHING AT LOW ENERGY SECTION OF J-PARC LINAC

S. Artikova, Y. Kondo, T. Morishita, JAEA, Tokai-Mura, Japan

Abstract

An intensity upgrade of Japan Proton Accelerator Research Complex (J-PARC) included the installation of a new ion source (IS) and a radio-frequency quadrupole (RFQ) which to be used at first stage of acceleration. The linac is divided into two sections on the basis of operating frequencies and three sections on the basis of family of RF cavities to be used for the acceleration of 50 mA beam of H^- ions from 50 keV to 400 MeV. Low energy part of linac consists of an IS, a two-solenoid beam transport (LEBT) and the RFQ. The transition from one section to another can limit the acceptance of the linac if these are not matched properly in both longitudinal and transverse plane. Initially, we have calculated the acceptance of the RFQ at zero current in which space charge effects are not considered. In addition, a particle tracking technique is employed to study the space charge effects in LEBT of the J-PARC linac after the intensity upgrade in order to match the beam to the RFQ. Also, RFQ tank level and intervene voltage calibration factor is determined by comparing the simulation results of the beam transmission with the test measurement of tank level vs. transmission.

INTRODUCTION

J-PARC - the Japan Proton Accelerator Research Complex is a high intensity proton accelerator facility located at Tokai village in Japan [1]. A new linac front-end had been installed for intensity upgrade in 2014, July-September [2]. It consists of a 50 keV IS, a two-magnetic solenoid based LEBT and 324 MHz RFQ accelerating H^- beam to 3 MeV. To support commissioning of J-PARC linac, General Particle Tracing (GPT) code [3] is used for H^- beam dynamics simulations. The particle tracking technique using 3D field-maps is a convenient tool to study the charged particle dynamics in electromagnetic fields. The goal is to optimize beam quality and transmission through the accelerator and to prepare the beam for the next section. For high intensity, low energy ion beams the electric field created by space charge reveals defocusing effect and is non-linear as induced by the non-uniform distribution of charge density. This defocusing effect can be compensated by transporting the low energy beam in space charge neutralization regime. Here we discuss the process of creating a partially-neutralized beam and examine the effects of space charge on the beam emittance. For optimizing the beam matching to the RFQ transverse emittance measurements are also used in simulations. RFQ acceptance with zero current and taking into account the space charge is determined. RFQ tank level and intervene voltage calibration factor is found by comparing the simulation results of the beam transmission with the measurement of tank level vs. transmission.

LEBT

Low energy part of linac consists of an IS, LEBT and the RFQ. The length of LEBT is approximately 566 mm. It consists of two short solenoid magnets, a gate valve and a diagnostic chamber which has a vacuum partition plate with an orifice of 15 mm. The solenoid magnets can produce a magnetic flux of 1.1 T. Solenoid based magnetic focusing transport system has been confirmed to be superior for the injection of the RFQ used to accelerate H^- beams. In the transport of high current low energy ion beams the space charge forces are most prominent. In the LEBT, the H^- beam traverses a region containing H_2 background. The vacuum level at upstream and downstream of LEBT is 3×10^{-3} Pa and 2×10^{-5} Pa, relatively. H^- beam and H_2 interaction is possible in two channels: detachment of an electron from the beam and ionization of the H_2. The compensation of space charge effects by charge neutralization using secondary particles produced in the interaction between ion beam and residual gas can significantly reduce the required focal strength and reduce emittance degradation.

Transverse Beam Emittance Measurement from IS Test Stand

At IS test stand a slit-and-grid emittance-meter located after the first solenoid and measurements for 66 mA beam were taken. The horizontal and vertical emittances are measured by using two sets of W-slit emittance monitors, each of them is composed of a movable slit and a movable Faraday-Cup with slit (FCS) [4]. Each slit has an opening of 0.1 mm. The measured emittance is visualized by randomly plotting dots, whose number is proportional to the current detected by the FCS and is normalized to make the total number 10 000, in each mesh area defined by the moving steps (0.2 mm and 2 mrad) and the positions of the slit and the FCS. 3D raw data analysis is shown in Fig. 1. To suppress the background noise, an arbitrary threshold is applied to cut off some data. Obviously, this can effect the tail of the beam. Gray area shows where the intensity is higher than the threshold and the main part of particles are situated approximately in this area. The knowledge of beam phase space at the IS exit is essential for transverse matching of the beam into the RFQ. For this reason, an algorithm to reconstruct the beam phase space distribution from emittance measurement developed and can be used to find the optimized solenoid settings for transverse matching. 3D field maps of solenoid magnets and the RFQ are calculated by CST EM Studio Suite.

Content from this work may be used under the terms of the CC BY 3.0 licence (© 2015). Any distribution of this work must maintain attribution to the author(s), title of the work, publisher, and DOI.

ISBN: 978-3-95450-168-7 doi:10.18429/JACoW-IPAC2015-MOPWA058

MEASUREMENT RESULTS OF THE IMPEDANCE OF THE RF-CAVITY AT THE RCS IN J-PARC

Y. Shobuda, H. Harada, H. Hotchi, J-PARC Center, Ibaraki, Japan

Abstract

The kicker impedance dominates at the RCS in J-PARC. Recently, we observe beam instabilities, which are not explained by the kicker. As a candidate causing the beam instability, the impedance of the RF-cavity is measured. The longitudinal impedance is measured by stretching a single-wire inside the cavity. On the other hand, the measurement of the transverse impedance is done by horizontally shifting the single-wire, due to the accuracy problem. The measured impedance is too low to explain the beam instability.

INTRODUCTION

The Rapid Cycling Synchrotron (RCS) in Japan Proton Accelerator Research Complex (J-PARC) [1] is a machine, where protons are accelerated from 400 MeV to 3 GeV during 20 ms. The injection beam from the LINAC is accumulated there during 500 μs in synchronization with the excitation of the injection bump magnets [2].

The role of the RCS is to deliver the proton beam to the Material and Life Science Facility (MLF)-target as well as to work as the injector to the main ring in J-PARC. Main objective of the RCS is to routinely supply one mega-watt beam (8.3×10^{13} particles per a pulse with the repetition rate 25 Hz) to the MLF-target.

Let us consider a situation that 8.3×10^{13} particles per a pulse are accelerated, where the chromaticity is corrected only at the injection energy. When the bunching factor of the beam and the tune-tracking are inadequately manipulated during the ramping process [3], we can observe beam instabilities [4]. However, the characteristic of the beam behavior can be understood by assuming that the cause of the instability mainly attributes to the kicker impedance. In this sense, the RCS is characterized by the machine where the kicker impedance dominates, from an impedance point of view [3–7].

At the high intensity proton beam, the space charge effects produce large tune spreads. Thereby, some particles cross resonance lines, which are the source of the particle losses. In order to avoid the particle loss, the typical horizontal and the vertical operation tunes of the RCS are chosen to be $\nu_x = 6.45$ and $\nu_y = 6.42$, respectively, at the injection period [8].

To make matters worse, the resonance lines severely restrict the allowable operation region near the present tunes ($\nu_x = 6.45, \nu_y = 6.42$) at the RCS. Accordingly, a trial was done to change the operation tunes to the other ones ($\nu_x = 5.86, \nu_y = 5.86$). This is because significant resonance structures cannot exist there from a viewpoint of magnetic error sources.

Contrary to our expectations, significant beam instabilities are observed under the operation tunes.

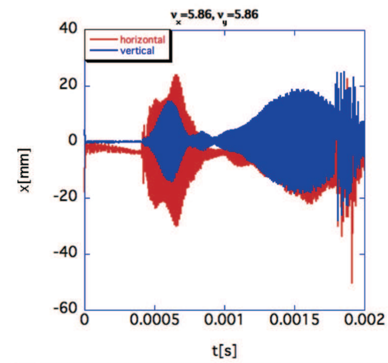

Figure 1: Beam instability observed at $\nu_x = \nu_y = 5.86$.

The measured results are shown in Fig. 1. The horizontal and the vertical axes show the acceleration period and the transverse position of the beam, respectively. The red and the blue lines show the horizontal and the vertical beam positions, respectively. The chromaticity is corrected only at the injection energy by quarter against the full chromaticity correction. The particle per a bunch is only 1.32×10^{13}, which is equivalent to 316 kW beam. Considering 1MW-equivalent beam is already achieved at the RCS [8], the impedance source is incredibly huge. To tell the truth, the beam power is weaker and the conditions (partial correction of the chromaticity) may rather stabilize the beam.

The results in Fig. 1 demonstrate that the beam becomes unstable around 1.5 ms. However, the injection bump magnets are perfectly turned off at that time. Consequently, it is hard to consider that the instability attributes to the field errors due to the injection bump magnet [9, 10]. Moreover, the beam instability is not related to x-y coupling, because the instability occurs even when one of the transverse tunes sits on $\nu_x = 5.86$ or $\nu_y = 5.86$ lines, independently.

Now, it is necessary to review the impedance source causing the unexpected beam instabilities, and to specify the impedance source along the RCS. As a first step, let us measure the impedance of RF-cavity. In the next section, let us see the measurement scheme and the results.

MEASUREMENTS

A schematic picture of RF-cavity is shown in Fig. 2. Four chambers are connected through three ceramic breaks (red). The chambers are surrounded over six Magnetic Alloy cores (blue). The inner radius of the chamber is 123.5 mm.

Content from this work may be used under the terms of the CC BY 3.0 licence (© 2015). Any distribution of this work must maintain attribution to the author(s), title of the work, publisher, and DOI.

ISBN: 978-3-95450-168-7 doi:10.18429/JACoW-IPAC2015-MOPWA059

DYNAMIC APERTURE STUDIES FOR THE FCC-ee*

L. Medina†, Universidad de Guanajuato, Leon, Mexico
R. Martin, Humboldt-Universität zu Berlin, Germany
R. Tomas, F. Zimmermann, CERN, Geneva, Switzerland

Abstract

Dynamic aperture (DA) studies have been conducted on the latest *Future Circular Collider – ee* (FCC-ee) lattices as a function of momentum deviation. Two different schemes for the interaction region are used, which are connected to the main arcs: the crab waist approach, developed by BINP, and an update to the CERN design where the use of crab cavities is envisioned. The results presented show an improvement in the performance of both designs.

INTRODUCTION

The FCC-ee is a proposed high luminosity e^+e^- collider [1,2] with a center-of-mass energy from 90 to 350 GeV. The ring has separate beam pipes for electrons and positrons, which intersect at two or four interaction points (IPs). The FCC-ee is a potential intermediate step in a global study towards a 100 TeV hadron collider –the FCC-hh– sharing the same 100 km tunnel. A first parameter set, used as a basis for the design study, has been published [3]. One of the main constraints of the FCC-ee design is the imposed limit of 50 MW of synchrotron radiation per beam. Four operation energies have been proposed, with beam energies of 45 , 80 , 120 , and 175 GeV, corresponding to the Z pole, the WW threshold, the HZ cross-section maximum, and the top pair threshold, respectively.

The present DA studies have been performed for the lattice at a beam energy of 175 GeV, for which the off-momentum DA is most critical.

Table 1: Lattices Under Study

Opt.	Ring	Interaction Region	Comments
1	R-v14	CW-v13	Crab off
2	R-v14	CW-v14	Crab off, set 1
3	R-v14	CW-v14	Crab off, set 2
4	R-v14	CW-v14	Crab on, set 2
5	R-v16	CW-v14	Crab off, set 2
6	R-v16	Small crossing angle	Crab cavity

LATTICES

Six main lattices, called options 1 to 6 in Table 1, have been studied. In our model, the main arc is enclosed by the left and right sides of the interaction region (IR), with the interaction point located at their respective ends; the complete ring is a sequence of four of this structures (i.e. 4 IPs). Each of the main arcs is composed of three arcs and two RF cavity sections. Ring versions 14 (R-v14) and 16 (R-v16) differ in the structure of the basic arc cell, the number and position of the arc sextupoles, and the horizontal phase advance attained, namely 90° for R-v14, and 79.2° for R-v16 [4]. A set of quadrupole strengths for the basic arc cells of R-v16 with 90° phase advance is also available, but this configuration has not been explored.

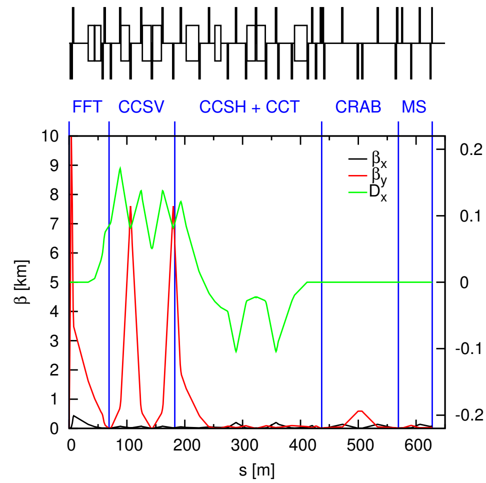

(a) Crab waist scheme.

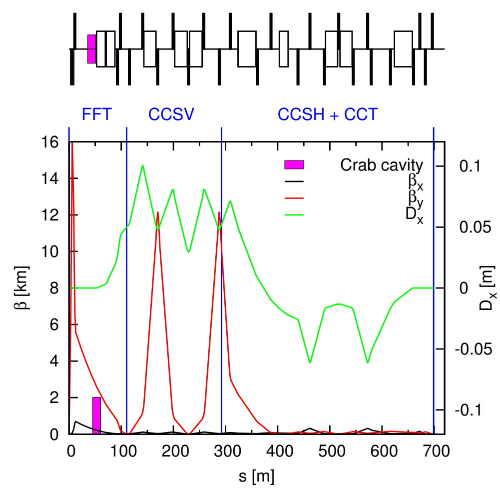

(b) Small crossing angle scheme.

Figure 1: General layout and optical functions of the IR.

The first design for the IR follows a crab waist (CW) scheme [5, 6]; the advantage of such approach is the higher luminosity at the lower beam energies. Its general layout and beta functions are shown in Fig. 1a, and consists of a final telescope (FFT), dedicated chromaticity correction sections for both transverse planes (CCSV and CCSH), a chromaticity correction telescope (CCT) that also provides

* Work supported by the Beam Project (CONACYT, Mexico).
† lmedinam@cern.ch

Content from this work may be used under the terms of the CC BY 3.0 licence (© 2015). Any distribution of this work must maintain attribution to the author(s), title of the work, publisher, and DOI.

ISBN: 978-3-95450-168-7 doi:10.18429/JACoW-IPAC2015-MOPWA060

Content from this work may be used under the terms of the CC BY 3.0 licence (© 2015). Any distribution of this work must maintain attribution to the author(s), title of the work, publisher, and DOI.

THE COUPLING IMPEDANCE MEASUREMENT OF THE FAST EXTRACTION KICKER IN CSNS/RCS *

Liangsheng Huang#, Yudong Liu, Sheng Wang, CSNS/IHEP, CAS, Dongguan, 523803, China

Abstract

The Rapid Cycling Synchrotron of the China Spallation Neutron Source is a high intensity proton accelerator. In order to high intensity beam operation, the beam coupling impedance of the extracted kicker must be controlled. The measurement of longitudinal and transverse coupling impedance of the fast extraction kicker is described.

INTRODUCTION

The electromagnetic interaction of a charged particle beam with its surroundings in the accelerator is conveniently described by the coupling impedances of its components. Coupling impedance and its instability budget are the important part of designing of a high intensity accelerator. Impedance measurement on the bench is a useful method to study the impedance [1] [2].

China Spallation Neutron Source (CSNS) is a high intensity proton accelerator based facility, which consists of an H- Linac, a Rapid Cycling Synchrotron (RCS) and two beam transport lines [3]. It accumulates and accelerate proton beam from 80 MeV to 1.6 GeV. The bunch length is range from 460 ns on injection to 80 ns on extraction. To achieve high beam current, the impedance must be carefully studied. The extraction kicker is the vital component devoted to the impedance. There are eight fast extraction kickers and the No. 2 kicker is measured. Figure 1 shows the kicker system. The main part of the kicker is the window-frame geometry ferrite with the material of CMD5005 [4]. The side strap connects the upper and lower busbar plates, and the busbar and the window-frame ferrite are located in a vacuum vessel, 0.58 m length. The power of the magnet comes from the PFN via the 130 m length cable. It is difficult to theoretically calculate the impedance for the complicated structure. Thus studying the impedance by measurement is a relevant method.

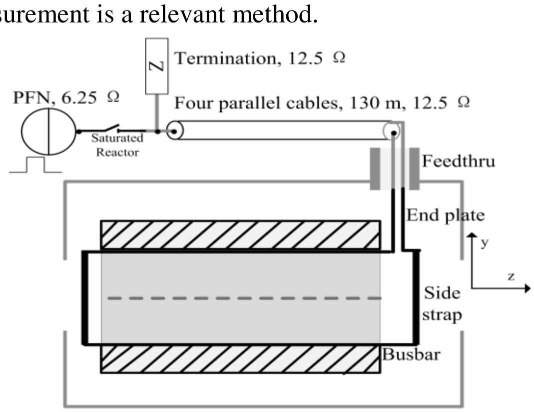

Figure 1: The extraction kicker system.

MEASUREMENT METHOD

The assign of measurement is measure longitudinal and vertical impedance of the kicker system on range from 1 MHz to 100 MHz. Figure 2 shows the schematics of longitudinal impedance measurement with coaxial transmission line and transverse impedance measurement by the twin-wire and the loop method. The copper wire with 0.5 mm diameter is stretched in the Device Under Test (DUT) with the appropriate resistor for matching to the 50 Ω cables at both ends, and the matching resistor is mounted by 35 mm sucobox [5]. The Vector Network Analyzer (VNA, Agilent E5071C) is connected to measure the S_{21} and the input impedance. Four attenuators with 6 dB between the hybrid and the DUT are applied in the transverse impedance measurement by the twin-wire. The differential-mode signal in transverse measurement can be obtained by Hybrid ZFSCJ-2-1-N [6].

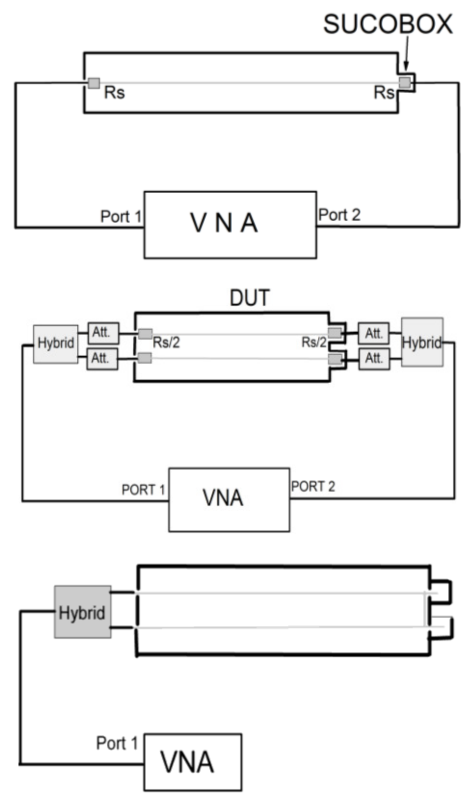

Figure 2: The schematics of longitudinal impedance measurement (coaxial transmission line, top) and transverse impedance measurement (twin-wire, middle and loop method, bottom).

The longitudinal and transverse coupling impedance in the measurement can be obtained as formulas

* Supported by National Natural Science Foundation of China (11175193, 11275221)
# huangls@ihep.ac.cn

ISBN: 978-3-95450-168-7 doi:10.18429/JACoW-IPAC2015-MOPWA061

ADS INJECTOR I FREQUENCY CHOICE AT IHEP

Fang Yan, Shilun Pei, Huiping Geng, Cai Meng, Huafu Ouyang, Yaliang Zhao
Key Laboratory of Particle Accleration Physics and Technology, Institute of High Energy Physics (IHEP), Chinese Academy of Science, Beijing 100049, China

Abstract

The China ADS driver linac is composed of two major parts: the injector and the main linac. There are two frequency choices for the injector: 325 MHz and 162.5 MHz. The former choice is benefit for the same frequency with the front end of the main linac. For half frequency choice, to obtain the same longitudinal acceptance of the main linac comparing with 325 MHz injector, the tune depression of the beam reaches the lower design limit of 0.5, no current upgrade opportunity is reserved; contrarily to get the same space charge effect, 16 more cavities would be the cost to get the same acceptance. However the disadvantage of the 325 MHz injector choice is the bigger power density of the copper structure CW RFQ and the smaller longitudinal acceptance of the SC section. The details of the comparing for the two frequency choices are introduced and presented.

INTRODUCTION

The China ADS driver linac is proposed to accelerate the CW proton beam up to 1.5 GeV with average beam current of 10mA. It consist two major components: the injector and the main linac as shown in Fig. 1. The injector part accelerate beam up to 10 MeV. The main linac boosts the energy from 10 MeV to 1.5 GeV. The injector is composed of an ECR source, a LEBT, a four vane type copper structure RFQ, a LEBT and a Superconducting (SC) linac. The MEBT1 undertakes the matching between the RFQ and SC section. There are two design strategies for the injector. Injector I scheme is on basis of 325 MHz RFQ and β=0.12 SC spoke cavity with same frequency. Injector II scheme is on basis of 162.5 MHz RFQ and SC Half Wave Resonator (HWR) structure with same frequency. Injector I scheme is benefit for the same frequency with the front end of main linac while Injector II has a frequency jump.

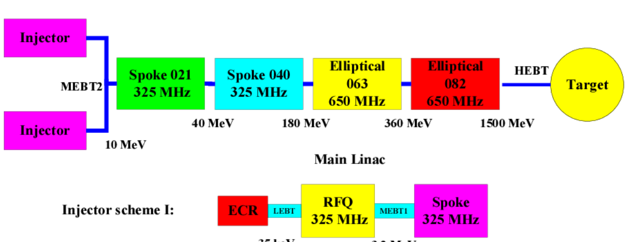

Figure 1: The general layout of the ADS linac in China.

*Work supported by Chinese Academy of Science (CAS) strategic Priority Research Program-Future Advanced Nuclear Fission Energy (Accelerator-Driven Sub-critical System).
#yanfang@ihep.ac.cn

The frequency jump has effects to the linac design on two aspects. On the one hand, 325 MHz choice is benefited for attenuated space charge effect comparing with half frequency if the longitudinal beam size out of injector kept the same for both frequency choices. The space charge effect is very crucial for the ADS applications (with final beam power of MW magnitude). Because nonrelativistic proton beam with stronger space charge effect is more sensitive to the mismatch and has bigger possibility inducing parameter/structure and coupling resonances and finally leading to halo growth and particle losses. Although space charge effect for 10 mA average current is not so strong, higher current upgrading opportunity is necessary to be kept for the future power upgrading.

On the other hand, if keeping the space charge effect to be the same, the longitudinal beam size out of the injector has to be increased for the 162.5 MHz choice. Bigger longitudinal beam size means more cavities numbers. To keep the same acceptance, the 325 MHz choice is benefit for less cavities leading to less cost at the whole downstream linac. However there are also drawbacks for the 325 MHz RFQ and SC linac of the injector. Finally 325 MHz is adopted for the ADS injector I at IHEP. The advantages and disadvantages of this choice will be introduced.

ADVANTAGES

The utmost design goal of a high intensity linac is controlling the beam loss along the linac as low as possible. The commonly acceptance of the beam loss rate is 1 W/m considering hands on maintenance. The higher the final beam power is, the more challenging to realize it. For China ADS project, the designed beam power on target is 15 MW, this means that the particle loss rate has to be controlled down to the magnitude of 1×10^{-8} /m at high energy part, this request is much higher than existing high intensity accelerators. To control the beam loss in design stage, on the one hand is keeping big enough acceptances. On the other hand is choosing a reasonable range for the tune depression of the beam.

Space Charge Effect

One important design principle for high current linac is to keep the tune depression of the beam bigger than 0.5 [1-2]. If half frequency is chosen for the China ADS injector, the particle charge in one bunch would be doubled under the condition that the longitudinal beam size keeping the same. For different average currents, the tune depressions are calculated for two different frequencies as shown in Table 1 on basis of the first SC

Content from this work may be used under the terms of the CC BY 3.0 licence (© 2015). Any distribution of this work must maintain attribution to the author(s), title of the work, publisher, and DOI.

ISBN: 978-3-95450-168-7 doi:10.18429/JACoW-IPAC2015-MOPWA062

OPTIMIZATION OF THE MOMENTUM BANDWIDTH FOR FINAL FOCUS SYSTEM IN CEPC*

S. Bai[#], Y.W. Wang, D. Wang, H.P. Geng, J. Gao, T.J. Bian, M. Xiao, F. Su, IHEP, Beijing, China

Abstract

With the discovery of the higgs boson at around 125GeV, a circular higgs factory design with high luminosity ($L \sim 10^{34}\ cm^{-2}s^{-1}$) is becoming more popular in the accelerator world. To achieve such high luminosity, a final focus system in non-local chromaticity correction scheme with very low β functions at the interaction point is designed. The narrow momentum bandwidth is a crucial problem of this kind of design. It is shown that by introducing additional sextupoles the momentum acceptance of the CEPC final focus system can be increased by about a factor of four.

INTRODUCTION

With the discovery of a Higgs boson at about 125 GeV, the world high-energy physics community is investigating the feasibility of a Higgs Factory, a complement to the LHC for studying the Higgs [1]. There are two ideas now in the world to design a future higgs factory, a linear 125 × 125 GeV e^+e^- collider and a circular 125 GeV e^+e^- collider. From the accelerator point of view, the circular 125 GeV e^+e^- collider, due to its low budget and mature technology, is becoming the preferred choice to the accelerator group in China. In order to achieve high luminosity ($L \sim 10^{34}\ cm^{-2}s^{-1}$), the beam dimensions at the interaction point have to be extremely small, typically $\sigma_x^*\sigma_y^* \sim 10^{-11}\ cm^2$. This requires, in addition to small beam emittances, a beam-optical system which produces very low β functions at the interaction point. Unavoidably, the natural chromaticity of such a system becomes very large and its compensation difficult. On the other hand, high luminosity and overall efficiency of the collider calls for a high bunch intensity which in turn increases the momentum spread within a bunch due to the longitudinal wakefields in the linac. It is therefore clear that a large momentum acceptance of the final focus system (usually defined as the range of δp/p for which the spot size at the interaction point varies by less than a factor of two) is highly desirable.

In this paper, the limitation of the momentum bandwidth is first analyzed. An improved chromaticity correction section is achieved by adding Brinkmann sextupoles. The momentum bandwidth of the final focus system is then increased by a factor of four. The performance of the optimized system is investigated with particle tracking simulations.

*Work supported by the National Natural Science Foundation of China (NSFC, Project 11175192) and in part by the CAS Center for Excellence in Particle Physics (CCEPP).
#baisha@ihep.ac.cn

-I TRANSFORMATION MATRIX BREAKDOWN

The CEPC final focus system are designed that the chromatic aberrations caused by the final focus doublet are compensated with a two-family non-interleaved sextupole distribution (Fig. 1). Each family consists of two identical sextupoles connected by a $-I$ transformer. The non-interleaved scheme of the sextupoles almost cancels the pure geometric aberrations from the sextupoles except for the aberrations produced by the finite thickness of the sextupoles.

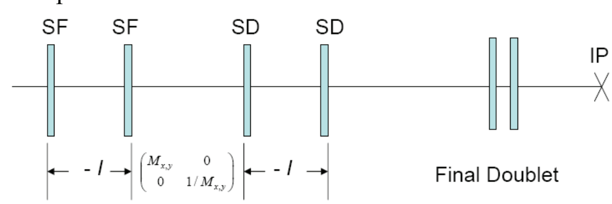

Figure 1: Sextupole families.

The increase of the vertical beam size due to the thickness l_s of the sextupole is written as [2]:

$$\Delta_y \equiv \frac{\Delta\sigma_y^{*2}}{\sigma_y^{*2}} = \frac{5}{12}\frac{k'^4\beta_y^4\varepsilon_{Ny}^2 l_s^2}{\gamma^2} \tag{1}$$

Where k', l_s and β_y are the strength, thickness of the SD sextupole and the vertical β function at the sextupole.

HIGH ORDER ANALYSIS IN CEPC FFS

Due to the breakdown of the $-I$, the non-linear kicks for off-momentum particles are no longer cancelled. The aberrations which caused by this will degrade the momentum acceptance for off-momentum particles. We analyzed the high-order aberrations of CEPC final focus system with different energy spread using a code called MAPCLASS [3] which is developed in CERN.

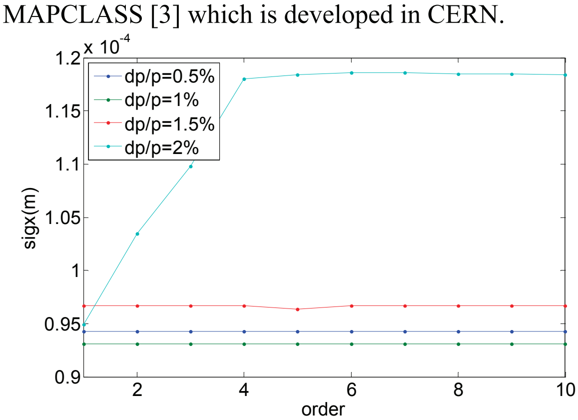

Figure 2: Order analysis of horizontal in CEPC FFS.

Content from this work may be used under the terms of the CC BY 3.0 licence (© 2015). Any distribution of this work must maintain attribution to the author(s), title of the work, publisher, and DOI.

ISBN: 978-3-95450-168-7 doi:10.18429/JACoW-IPAC2015-MOPWA065

Content from this work may be used under the terms of the CC BY 3.0 licence (© 2015). Any distribution of this work must maintain attribution to the author(s), title of the work, publisher, and DOI.

UNIFORMIZATION OF THE TRANSVERSE BEAM PROFILE BY A NEW TYPE NONLINEAR MAGNET*

Shengdong Gu# and Weibin Liu, Key Laboratory of Particle Acceleration Physics and Technology, Institute of High Energy Physics, Chinese Academy of Sciences, 19(B) Yuquan Road, Beijing 100049, China

Abstract

The uniform transverse profile beam is desirable in many beam applications. One method to get this type of beam distribution is using octupoles, but loss of particles in the halo will be produced by this method. To reduce the beam loss, a new type of magnet is proposed in this paper. The field in the middle region of the new type magnet is similar to the octupole magnet field, but the rate of rise decline quickly in the edge. So that the particle in the edge experience a lower magnet field compared with the octupole, and this would result in less particle loss. We also add a mechanical structure on the new type magnet to make it possible to adjust the size of middle region. So that the magnet can adapt to different transverse dimensions of the beam, and this would further reduce particle loss. Some numerical simulations have been done respectively with the octupole and the new type of magnet. The simulation results show that the new type of magnet could get the uniform distribution of particle beam with less particle loss. We are processing a magnet now, and an experiment to test the magnet will be arranged on CPHS.

INTRODUCTION

The beam with uniform spatial distributions is required in several practical applications such as irradiation of targets for isotope production, uniform irradiation of detectors for improved efficiency, irradiation of biological samples and materials. A general method to get a transverse uniform beam from a Gaussian profile beam is utilizing odd-order nonlinear focusing magnets. Many people have theoretically studied uniformization of the transverse beam profile with multipole magnets [1-4].

Yuri et al. have theoretically studied uniformization of the transverse beam profile using nonlinear-focusing forces produced by multipole magnets. They get distribution at the target is related to that at the multipole magnet position as follows [1],

$$\rho_t = \rho_0 \left(\frac{dx_t}{dx_0}\right)^{-1}$$
$$= \frac{\rho_0}{M_{11} - \frac{\alpha_0}{\beta_0} M_{12} - M_{12} \sum_{n=3}^{\infty} \frac{K_{2n}}{(n-2)!} {x_0}^{n-2}}$$
$$= \frac{\rho_0}{M_{11} - \frac{\alpha_0}{\beta_0} M_{12} - M_{12} \sum_{n=3}^{\infty} \frac{K_{2n}}{(n-2)!} {x_0}^{n-2}}$$

*Work supported by National Natural Science Foundation of China (11175195).
#gushengdong@ihep.ac.cn

Where $M_{ij} (i, j = 1,2)$ are the elements of M**.** M is the transmission matrix. Where K_{2n} is the 2n-pole integrated strength of the multipole magnet and the magnet is assumed to be a thin lens for simplicity's sake. Where ρ_0 and ρ_t are the particle density functions in the real space at the initial and at the target. Where β_0 and β_t are the beta functions at the initial and at the target. The initial particle distribution can be transformed into a different one at the target by using the nonlinear magnetic field.

Many beam distributions ρ_0 are Gaussian or can be fitting with Gaussian. After some algebraic transformation we can get all of the odd-order nonlinear fields are needed for transformation of an ideal Gaussian beam into a totally uniform beam. But the realistic case is that the multipole magnet produces only one nonlinear component. So we usually use the octupole magnet to get the uniform distribution beam. But loss of particles in the halo will be produced by this method. To reduce the beam loss, a new type of magnet is proposed in this paper.

THE NEW TYPE OF MAGNET

The new type magnet is shown in Figure 1. The top is the mode of the Opera 3D. And the bottom is the section of the central plane. To get a uniform distribution beam, the field in the middle region of the new type magnet is similar to the octupole magnet field. But the rate of rise decline quickly in the edge in the new type magnet. So that the particle in the edge experience a lower magnet field compared with the octupole, and this would result in less particle loss. We also add a mechanical structure on the new type magnet to make it possible to adjust the size of middle region.

Opera 3D is used for the new magnet design. The magnetic field of the new type magnet is compared with the magnet of the octupole for the distance between the C-type dipoles equal to 0.2m in the top of Figure 2. The magnetic field profiles are plotted at the centre plane. As we have mentioned, we would add a mechanical structure on the new type magnet to make it possible to adjust the size of middle region. The new magnet is separated for three parts (two C type dipoles and the shield block). The distance between the two dipoles can be changed with the mechanical structure. And the size of the middle region, the octupole-like region, can be changed with the distance change. The Figure 2 give the change of the magnet field with the distance from the centre. As shown in the Figure 2, the top figure is plotted while the distance is the minimum and the right figure is plotted while the distance is the maximum. While the distance is the minimum, the size of the middle region is also the minimum. The

ISBN: 978-3-95450-168-7 doi:10.18429/JACoW-IPAC2015-MOPWA066

SIMULATION ON BUILDUP OF ELECTRON CLOUD IN RAPID CYCLING SYNCHROTRON OF CHINA SPALLATION NEUTRON SOURCE *

Liu Yu-Dong#, Li Kai-Wei, Wang Sheng, Huang Liang-Sheng
IHEP, CAS，Beijing 100049, China

Abstract

Electron cloud interaction with high energy positive beam are believed responsible for various undesirable effects such as vacuum degradation, collective beam instability and even beam loss in high power proton circular accelerator. An important uncertainty in predicting electron cloud instability lies in the detail processes on the generation and accumulation of the electron cloud. The simulation on the build-up of electron cloud is necessary to further studies on beam instability caused by electron cloud. China Spallation Neutron Source (CSNS) is the largest scientific project in building, whose accelerator complex includes two main parts: an H- linac and a rapid cycling synchrotron (RCS). The RCS accumulates the 80Mev proton beam and accelerates it to 1.6GeV with a repetition rate 25Hz. During the beam injection with lower energy, the emerging electron cloud may cause a serious instability and beam loss on the vacuum pipe. A simulation code has been developed to simulate the build-up, distribution and density of electron cloud in CSNS/RCS.

INTRODUCTION

In high intensity proton circular accelerator, the electron cloud effect has been considered as one of the main sources of beam instability, which can lead to the uncontrolled beam loss [1]. This electron proton instability has been observed and confirmed in many commission proton circular accelerators, such as LANL PSR [2], KEK Booster [3], CERN PS [4] and SNS in ORNL [5]. The primary electrons produced by proton losses at the chamber surface attracted and accelerated by the body of bunch then released at the bunch tail or bunch spacing. The secondary electrons are produced and amplified when the accelerated electron hitting the chamber wall. This secondary electron multipacting attributes to the main source of electron cloud.

Table 1: The main parameters of the RCS/CSNS

Parameters	Injection	Extraction
Circumference C (m)	227.92	227.92
Energy E (GeV)	0.08	1.6
Bunch Population N_p (10^{13})	1.56	1.56
Revolution Frequency ω (MHz)	3.20	6.78
Bunch length σ_p (m)	48.931	22.285
Beam transverse size σ_x, σ_y (cm)	1.5, 1.5	1.2, 1.2
Pipe radius b (cm)	10	10

*Work supported by National Natural Science Foundation of China (11275221, 11175193)
#liuyd@mail.ihep.ac.cn

A high intensity proton accelerator facility as neutron source proposed in past ten years and is being built in China, which is named China Spallation Neutron Source (CSNS) [5]. The facility is equipped with an H- linac and a rapid cycling synchrotron (RCS). A simulation code has been developed and benchmarked to ascertain detailed establishment of electron cloud in CSNS/RCS. The physical mechanism on primary electron production, its dynamics, secondary electron emission and electron accumulation is described in section II of this paper. By tracking dynamics of electrons with physical model in section II, a simulation code for obtaining distribution and density of electron cloud has been developed and benchmarked with other machines. With the beam parameters of RCS/CSNS, the process of electron cloud buildup is studied in different simulation conditions such as average beam loss rate, secondary electron yield, transverse and longitudinal beam profile, and beam intensity. Most of the simulations are performed in a field-free region mainly. The comprehensive simulation on electron cloud in RCS/CSNS gives the quantitative relation between electron density and beam parameters which is meaningful to the construction of RCS/CSNS.

PHYSICAL MODEL

The electron sources in proton circular accelerator may be classified into (1) electrons stripped at injection region; (2) electrons produced by proton loss incident the vacuum chamber; (3)secondary electron emission process; and (4) electrons produced by residual gas ionization. The stripped electrons generated near the stripping foil, which can be absorbed by installing a special collector at the injection region [7]. The yield of ionization electrons is determined by the ionization cross section and vacuum pressure in beam chamber. Because of the lower vacuum pressure about 10^{-7} Pa and ionization cross section for CO and H_2 approximately 1.3 MBar and 0.3 MBar, the ionization electrons can be neglected in simulation. In the electron dynamic tracking for RCS/CSNS, the primary electrons produced by proton losses and secondary electrons are considered.

These striking electrons may produce secondary electrons if their energy is high enough. The fraction between the emission electrons from pipe surface and the total incident electrons is defined as secondary electrons yield (SEY). If SEY is above 1, the electrons multipacting will happen. Actually, the secondary electrons include two types: elastic backscattered electrons and true secondary electrons. The yields of the true secondary electrons and elastic backscattered electrons can be expressed with formula (1) and (2) [8], respectively. In formula, δ_{max} is the

Content from this work may be used under the terms of the CC BY 3.0 licence (© 2015). Any distribution of this work must maintain attribution to the author(s), title of the work, publisher, and DOI.

ISBN: 978-3-95450-168-7 doi:10.18429/JACoW-IPAC2015-MOPWA067

THEORY OF TRANSVERSE IONIZATION COOLING IN A LINEAR CHANNEL

Ming Xiao*, Jie Gao, Teng Yue
Key Laboratory of Particle Acceleration Physics and Technology,
Institute of High Energy Physics, Chinese Academy of Sciences, Beijing, China

Abstract

Ionization cooling is the most hopeful method to reduce the emittance of muon beams, which plays an important role in neutrino factory and muon collider. Within the moment-equation approach, we present a way to derive the formulae of emittance in transverse under linear channel. All heating and coupling terms are reserved in the deriving process. From our formulae, it is a way to achieve a small emittance by designing the cooling channel compact to make the beta function changing sharply.

INTRODUCTION

The physics potentials of neutrino factories and muon colliders have stimulated worldwide studies of the feasibility of high-energy muon accelerators. Ionization cooling of particles proposed a long time ago in [1]. Ionization cooling theory is being studied for a very long time. And this cooling channel is developed to reduce the emittance of muon beam for envisioned neutrino factory and muon collider. Basic concept of this proposal is that the friction force acting to the particle moving through the absorber, directed against instant velocity of particle. As the longitudinal component of momentum lost in absorber could be restored by the longitudinal electric field in a RF cavity, the loss of transverse component is not, so this process resulting emittance reduction. This process is similar to the one with radiation losses; in some sense excitation of betatron oscillation while emitting the quanta in a channel with nonzero dispersion is similar to the (multiple) scattering in absorber.

Ionization cooling in a quadrupole channel has been discussed extensively by many authors, especially Neuffer's cooling formulae in [2]. Neuffer's formulae of transverse cooling theory is

$$\epsilon_{xn} = \frac{\beta_\perp E_s^2}{2\beta E_\mu L_{rad}|\mathrm{dE/ds}|} \tag{1}$$

where $\beta_\perp$ stands for the betatron function, E_μ is the particle energy, L_{rad} is radiation length.

And, Wang and Kim have developed coupled cooling equations including dispersion, wedges, solenoids, and symmetric focussing [3][4][5][6].

SINGLE PARTICLE DYNAMICS

We consider an idealized uncoupled quadrupole channel with quadrupole strength $K(s)$; horizontal bending radius ρ. Using the standard Frenet-Serret coordinates $\{x, y, s\}$, the Hamiltonian can be written as

$$\begin{aligned} H =& \frac{1}{2}\{P_x^2 + [K(s) + \frac{1}{\rho^2}]x^2\} + \frac{1}{2}[P_y^2 - K(s)y^2] - \frac{\delta x}{\rho} \\ &+ \frac{1}{2}[\frac{1}{\gamma_0^2}\delta^2 + V(s)z^2] + \eta[xP_x + yP_y] + \eta_x xz \\ &- \sqrt{\chi}(\xi_x x + \xi_y y) - \sqrt{\chi_\delta}\xi_z z \end{aligned} \tag{2}$$

where $\{x, P_x\}$, $\{y, P_y\}$ are the horizontal and vertical canonical variables, and $\{z, \delta\}$ are the longitudinal canonical variables. And γ_0 is the Lorentz factor of the reference particle, $K(s)$ is the quadrupole strength, $\rho(s)$ is the horizontal bending radius, $V(s)$ is the RF focusing strength, δ is momentum deviation from the nominal momentum, η is a positive quantity characterizing the cooling force from energy loss, χ is the projected mean-square angular deviation per unit length due to multiple scattering, $\xi_{(x,y,z)}$ is uncorrelated unit stochastic quantities describing the fluctuation forces due to multiple scattering and energy straggling.

From eq.(2), one could get the equations of motion directly. Because the forces are linear, we use the Fokker-Plank equations to study the phase-space distribution.

FORMULAE OF TRANSVERSE IONIZATION COOLING IN A LINEAR CHANNEL

According to eq.(2), horizontal and vertical motions in the two transverse planes are uncoupled. It is sufficient to treat only the x phase space dynamics, so the Hamiltonian simplifies into the form:

$$H = \frac{1}{2}[P_x^2 + K_x(s)x^2] + \eta x P_x - \sqrt{\chi}\xi_x x \tag{3}$$

where $K_x(s) = K(s) + \frac{1}{\rho^2}$.

Then the single-particle equations of motion according to eq.(3) are:

$$\frac{\mathrm{d}x}{\mathrm{d}s} = \frac{\partial H}{\partial P_x} = P_x + \eta x \tag{4}$$

$$\frac{\mathrm{d}P_x}{\mathrm{d}s} = -\frac{\partial H}{\partial x} = -K_x(s)x - \eta P_x + \sqrt{\chi}\xi_x \tag{5}$$

After some algebra within eq.(4) and eq.(5), we obtained the second-order beam moments in x plane:

$$\langle x^2\rangle' = 2(\langle xP_x\rangle + \langle \eta x\rangle) \tag{6}$$

$$\langle xP_x\rangle' = \langle P_x^2\rangle - \langle K_x(s)x^2\rangle + \langle\sqrt{\chi}x\xi_x\rangle \tag{7}$$

$$\langle P_x^2\rangle' = -2(\langle K_x(s)xP_x\rangle + \langle\eta P_x^2\rangle - \langle\sqrt{\chi}P_x\xi_x\rangle) \tag{8}$$

* xiaoming@ihep.ac.cn

Content from this work may be used under the terms of the CC BY 3.0 licence (© 2015). Any distribution of this work must maintain attribution to the author(s), title of the work, publisher, and DOI.

ISBN: 978-3-95450-168-7 doi:10.18429/JACoW-IPAC2015-MOPWA069

Content from this work may be used under the terms of the CC BY 3.0 licence (© 2015). Any distribution of this work must maintain attribution to the author(s), title of the work, publisher, and DOI.

UPGRADES ON A SCALABLE SOFTWARE PACKAGE FOR LARGE SCALE BEAM DYNAMIC SIMULATIONS

X. Dong[1], R. Zhao[1], Ch. Li[2], Y. Zhao[2], Zh. Wang[3], K. Du[1], J. Xu[1], Y. He[3] and Q. Qin[2]
[1]Institute of Software, Chinese Academy of Sciences,
4# ZHONGGUANCUN South 4th Street, Beijing, 100190, China
[2]Institute of High Energy Physics, Chinese Academy of Sciences,
Beijing, 100049, China
[3]Institute of Modern Physics, Chinese Academy of Sciences,
509 Nanchang Road, Lanzhou, 730000, China

Abstract

Scalable software package for beam dynamics simulation are playing more and more important role in precise design and optimization of the linear accelerator. In this paper, recent upgrades (version 2.0) on LOCUS3D, which is a parallel software developed for beam dynamics simulation, are introduced. The numerical methods are kept as before, but whole structure of the software has been rebuilt. These upgrades include optimized software structure, more reasonable arrangements of components, and capability of simulating several different kinds of particles with different charge states and masses. It also provides suitable structures for extension to use modern heterogeneous supercomputers. Standard accelerator devices have been tested again for this new version. The new software can run on several different platforms, such as INSPUR cluster, TIANHE-2, and BG/P at ANL. At last, some simulation results for DTL with large number of particles will be shown.

INTRODUCTION

Many beam dynamics codes [1-5] have been developed for beam dynamics simulations, but few of them were designed and developed specifically for efficiently use of the newly emerged software and hardware technologies for large supercomputers. LOCUS3D [6] was developed for meeting this purpose in 2013. It solves the Poisson's equation for the space charge effect, and the time integration algorithm uses sub-steps for effects of electric and magnetic fields separately. After several years of successful simulations, several places need improvements to meet more broad requirements.

In this paper, we explain several upgrades on the LOCUS3D. These upgrades include new data structure, software structure, and future extension for heterogeneous supercomputers. The new data structure setup new relations between different elementary classes, such as PtcSet, Bunch, Device and Solver etc. The new relation is based on natural relation between these concepts, which make them easier to be used for building applications in BDS. The new software structure separates functions based on different classes by different levels. High-level functions are built on low-level functions, and are made from them. Furthermore, new software structure provides extension, which can easy use the heterogeneous supercomputers in the future. These upgrades require new particle initialization module, time integration module, Poisson solver module, parallel model and parallel I/O module. The new version has been tested to simulate beam dynamics in the basic accelerator devices, such as multi-pole lenses, solenoid, and Drift Tube Linac (DTL). The parallel Poisson solver has been successfully redeveloped and benchmarked on the new Solver class. Besides the FFT Poisson solver, other numerical methods can easily build alternative solver under new software structure. This upgrade makes LOCUS3D more suitable to meet various demands exist in design and modelling of linear accelerators. Accelerator physicists and engineers can easily have features that satisfy their requirements. The paper will introduce the new data and software structure first, and then give benchmark and simulation results.

NUMERICAL METHOD

The numerical methods are similar, and can be divided into two parts: particle tracking and electromagnetic (EM) field computation, including external fields and space charge (SC) fields. Particle tracking is designed to have different time integration schemes for choices [7], which can be realised easily based on the new software structure. A parallel Poisson solver using Fast Fourier Transform (FFT) [8] has been developed for SC field computation. Currently LOCUS3D uses sub-steps to separates the effects of electric and magnetic fields, which is similar to the algorithm of BEAMPATH code. But it has many differences from B6EAMPATH, such as units of quantities, Poisson solver, parallel model, etc. Detail information can be found in our previous paper, which will be omitted in the following sections.

UPGRADE STRUCTURES

LOCUS3D was designed from beginning to be parallel software for complete beam dynamics simulations. It is based on MPI library, and object-oriented C++ language. It targets on modern supercomputers, such as TIANHE, BG/P, etc. After several years of successful running, we are upgrading it for many places in order to make its structure more reasonable in nature, easier for extension for simulating complex physics and for using modern supercomputers.

ISBN: 978-3-95450-168-7 doi:10.18429/JACoW-IPAC2015-MOPWA072

EMITTANCE EXCHANGE BEAMLINE DESIGN IN THU ACC LAB

Qiang Gao[1,2,#], Jiaru Shi[1,*], Huaibi Chen[1], Yingchao Du[1], Wenhui Huang[1], Wei Gai[1,2]
[1] Tsinghua University, Beijing 100084,China, [2] Argonne National Laboratory, Lemont, IL 60439, USA

Abstract

Emittance exchange (EEX) provides a novel tool to enhance the phase space manipulation techniques. This study presents a beamline design for exchanging the transverse and longitudinal emittance of an electron bunch based on the Tsinghua Thomson scattering experimental facility. This beamline consists of a 2.856 GHz half-one-half cell deflecting cavity with no axis offset and two doglegs. In this paper, by optimizing the beam envelope parameters for Tsinghua Thomson scattering source, we report the theoretical analysis and a good particle tracking simulation result about emittance exchange and longitudinal shaping.

INTRODUCTION

Since the emittance exchange (EEX) concept was firstly came up with in 2002 [1], lots of researches have been developed to optimize the exchange result for different applications. Theoretical analysis for identical dogleg-type exchanger presented an exact result contrast to chicane-type in 2006 [2]. A proof-of-principle transverse and longitudinal emittance exchange experiment conducted at Fermi Lab demonstrates the feasibility of EEX theory [3]. Although the initial motivation for EEX aims to attain an optimized transverse emittance for FEL, a significant innovation proposed in [2] and [4] which provide a novel tool for advanced phase space manipulation really extends the application of EEX and incites a new term research in bunch shaping for many kinds of accelerators. In the wakefield acceleration, a short and low energy but high current drive beam can create high gradient fields to accelerate trailing bunch. A novel shaped drive bunch to enhance the transformer ration which can extremely increase the acceleration efficiency has been proposed in Argonne AWA group based on EEX [5]. Now the experiment to achieve this specific shaped bunch is being conducted at Argonne. A similar beam shaping using emittance exchanger is presented in LANL [6].

Tsinghua University has been constructed a Thomson Scattering X-ray (TTX) beamline in 2009 [7], which aims at an ultra-fast, high flux, and tuneable X-ray source for advanced imaging applications. Based on this experimental facility, we design an EEX beamline to use RF deflecting cavity for bunch longitudinal shaping. Whether to shape electron bunch for wakefield accelerator or for tuneable subpicosecond electron bunch train generation [8], this EEX technique can be the spectacular tool in accelerator physics.

This paper is organised in three parts, firstly we report the theoretical design of EEX beamline based on TTX, and secondly we introduce the half-one-half deflecting cavity designed for EEX, finally the particle tracking simulation of emittance exchange and bunch shaping using this beamline is presented.

gao-q12@mails.tsinghua.edu.cn
* shij@tsinghua.edu.cn

ANALYTIC TRANSFER MATRIX

Generally, two identical doglegs sperated by a deflecting cavity consist the main components of EEX beamline. The transfer matrix of dogleg and deflecting cavity in first order can be written as

$$M_{DL}=\begin{bmatrix}1 & L_{DL}/2 & 0 & \eta\\ 0 & 1 & 0 & 0\\ 0 & \eta & 1 & \xi/2\\ 0 & 0 & 0 & 1\end{bmatrix}, M_C=\begin{bmatrix}1 & L_C & kL_C/2 & 0\\ 0 & 1 & k & 0\\ 0 & 0 & 1 & 0\\ k & kL_C/2 & k^2L_C/n & 1\end{bmatrix} \quad (1)$$

Where L_{DL},η,ξ,L_c,k denote respectively the whole length of two doglegs, dispersion, compression of one dogleg, and length, dimensionless strength of deflecting cavity. The factor n is related to the effective deflecting cavity length, and n equals 4 for one pill-box cavity. When particles pass through the dogleg, their horizontal and longitudinal momentum has an impact of dispersion η on their longitudinal and horizontal position respectively. Similarly, deflector relates the initial longitudinal and horizontal position to final horizontal and longitudinal momentum. On the condition that $1+k\eta=0$, this dogleg type EEX transfer matrix is

$$M_{EEX}=M_{DL}M_CM_{DL}=\begin{bmatrix}0 & \frac{L_C}{n} & m_{13} & m_{14}\\ 0 & 0 & k & \frac{k\xi}{2}\\ \frac{k\xi}{2} & m_{32} & \frac{k^2\xi L_C}{2n} & \frac{k^2\xi^2L_C}{4n}\\ k & m_{42} & \frac{k^2L_C}{n} & \frac{k^2\xi L_C}{2n}\end{bmatrix} \quad (2)$$

Where m_{ab} represents the function of parameters in expression (1). In order to achieve the exact phase space exchange (PSEX), additional quadrupoles are needed before the first dogleg so that we can shape the bunch to some specific shape. Figure 1 is the schematic of this beamline. In our design, by using four quadrupoles, we can transform the left bottom sub matrix of matrix M to an approximate identical matrix, so the final transfer matrix of our beamline can be written as

$$M_{PSEX}=\begin{bmatrix}0 & m_{12} & m_{13} & m_{14}\\ 0 & 0 & m_{23} & m_{24}\\ m_{31} & 0 & \sim 0 & \sim 0\\ 0 & 1/m_{31} & \frac{k^2L_C}{n} & \frac{k^2\xi L_C}{2n}\end{bmatrix} \quad (3)$$

Where ~0 denotes a small quantity approximating zero. Eq.3 explains that on the first order approximation, initial

Content from this work may be used under the terms of the CC BY 3.0 licence (© 2015). Any distribution of this work must maintain attribution to the author(s), title of the work, publisher, and DOI.

ISBN: 978-3-95450-168-7 doi:10.18429/JACoW-IPAC2015-MOPJE001

EFFECT ON BEAM DYNAMICS FROM WAKEFIELDS IN TRAVELLING WAVE STRUCTURE EXCITED BY BUNCH TRAIN

D. Wang[1, 2], W. Gai[1], C. Jing[1,3], J. Power[1], J. Qiu[1,3], C.Tang[2]
[1] Argonne National Laboratory, IL, 60439, USA
[2] Tsinghua University, Beijing, 100084, China
[3] Euclid Tech. labs LLC, IL, 60439, USA

Abstract

Electron bunch train technology is used to excited coherent high power RF radiation in travelling wave (TW) structures. This article concentrates on the analytical expression of wakefields excited by bunch train in TW structures and the effects of wakefields on beam dynamics. We focus on the first monopole mode and the first dipole mode wakefields. The long range wake function has a linear decrease which agrees well with the ABCi simulations. Taking example of the 11.7 GHz wakefields structure at the Argonne Wakefield Accelerator (AWA) facility, with 1.3 GHz interval drive electron bunch train, we have done the beam dynamics simulation with a point to point (P2P) code. Results shows the effects of wakefields on the energy distribution and the transverse instability for each sub-bunch.

INTRODUCTUION

Electron bunch train is used as drive beam to resonantly excited wakefields in travelling wave (TW) structure. In the two beam accelerator scheme in linear accelerators [1], driven beam is usually consists of *ps* sub-bunches, and the interval between bunches is the RF periods. The beam dynamics of the drive beam is affected by both the self-wake of each bunch and the long range wake from the head bunches. A lot of tracking codes can be applied to study the self-wake effect by means of a convolution integral or sum, based on the mesh technology, such as in ASTRA [2]. For the case of long range wake field effect caused by the head bunches, since the bunch interval is much longer than the bunch length, sub-bunches are always taken as point particles in order to reduce mesh and computation cost [3].

When concern about the motion of each particles in the drive beam, due to bunch instability such as beam break up (BBU) issue, we have to calculate the interaction between the wakefields and all the particles, thus a point to point (P2P) beam dynamics simulation code is desired. This paper starts from the analysis expression of the first monopole and the first dipole mode wake fields in TW structure. Taking the 11.7 GHz X-band TW PETS as an example, with drive bunch train of 1.3 GHz interval at the Argonne Wakefields Accelerator (AWA) facility, the P2P simulations show the longitudinal and transverse wake effects on each sub-bunch.

WAKEFIELDS IN TRAVELLING WAVE STRUCTURE

The Gradient of a Single Mode Wakefield

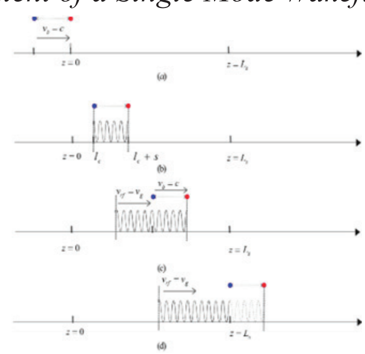

Figure 1: Single mode wakefields in TW structure.

When a drive particle with charge Q_d (red dot shown in Fig. 1) passing through a PETS of length L_s, wakefields is generated. Ignoring the attenuation, the electric field has constant gradient along Z direction for a single mode wake [4]. Once we know the parameters of the structure at certain mode, including the R over Q, relative group velocity β_g, and wake frequency ω, we can figure out the gradient. The gradient of the first monopole mode (TM_{01}) wake field is:

$$E^{//}_{w01}(s) = 2Q_d \cdot \kappa_{01} \cdot \cos\left(\frac{\omega_{01}s}{c}\right) \cdot H(s) \cdot Boolean(s \le L^{01}_w) \qquad (1)$$

Here k_{01} is the loss factor of TM_{01} mode, H(s) is the Heavenside step function and L^{01}_W is the duration of the wake field. The $Boolean(s \le L^{01}_W)$ in Eq. 1 declares the finite duration of wakefields in finite TW structure. For clarity we will omit the *Boolean* word in the following discussion. The duration of the wake is:

$$L^{01}_w(s) = L_S(1/\beta^{01}_g - 1) \qquad (2)$$

Loss factor in Eq. 1 is defined with the group velocity modification in TW structure

$$\kappa_{01} = \frac{\omega_{01}}{4}\left(\frac{R}{Q}\right)_{01}\frac{1}{(1-\beta^{01}_g)}$$

The loss factor of the structure and the drive particle charge determine the amplitude of the wakefield as a constant of $2Q_d \cdot k_{01}$.

Linear Decrease of the Wake Function

Wake function is used to describe the integrated wake field effect along the whole structure. The definition is

$$w_{//}(s) = -\frac{1}{Q_d}\int_0^L dz \cdot [E^{//}_W(s,z,t)]_{t=(z+s)/c} \qquad (3)$$

Content from this work may be used under the terms of the CC BY 3.0 licence (© 2015). Any distribution of this work must maintain attribution to the author(s), title of the work, publisher, and DOI.

ISBN: 978-3-95450-168-7 doi:10.18429/JACoW-IPAC2015-MOPJE003

MEASURING DUKE STORAGE RING LATTICE USING TUNE BASED TECHNIQUE*

Wei Li[1,2†], Jingyi Li[1], Hao Hao[2], Stepan F. Mikhailov[2], Victor Popov[2], Ying K. Wu[2]
[1]NSRL, University of Science and Technology of China, Anhui, 230029, China
[2]DFELL/TUNL, and Department of Physics, Duke University, NC, 27708, USA

Abstract

The Duke electron storage ring is a dedicated driver for oscillator Free-Electron Lasers (FELs). A 34 m long straight section of the storage ring is used to host up to four FEL wigglers in several different configurations. A total of six wigglers, two planar OK-4 wigglers and four helical OK-5 wigglers, are available for FEL research. The storage ring magnetic lattice has to be designed with great flexibility to enable the storage ring operation with different FEL wigglers, at various wiggler settings, and for different electron beam energies. Since 2012, the storage ring has demonstrated all designed characteristics in terms of lattice flexibility and tuning. This work is aimed at gaining better understanding of the real storage ring lattice by performing a series of measurements of the beta-functions along the storage ring. Unlike the LOCO technique, the β-functions in the quadrupoles are directly measured with good accuracy using a tune measurement system. We will describe our experimental design and techniques, and measurement procedures. We will also report our preliminary results for the lattice characterization.

INTRODUCTION

The Duke electron storage ring is a dedicated driver for oscillator Free-Electron Lasers (FELs). This facility consists of three accelerators, a linac pre-injector (0.16 GeV), a booster injector (0.16 – 1.2 GeV), and an electron storage ring (0.24 – 1.2 GeV). In the south part of the storage ring, a 34 m long straight section is used to host up to four FEL wigglers in several different configurations. Two planar OK-4 wigglers and four helical OK-5 wigglers, are available for FEL research. To enable the storage ring operation with different FEL wigglers at various wiggler settings, and for different electron beam energies, the storage ring magnetic lattice has to be designed with great flexibility. The storage ring with a number of new wiggler configurations has demonstrated all designed characteristics in terms of lattice flexibility and tuning since 2012 [1]. This work is aimed at gaining better understanding of the real storage ring lattice by performing a series of measurements of the β-functions along the storage ring. This technique is different from the LOCO technique, β-functions in the quadrupoles are measured directly with good accuracy measurement using transverse feedback system [2, 3]. We will introduce β measurement method and measurement system, discuss tune changes related with beam current decay, influence of quadrupole hysteresis on β measurements, describe our experimental design and preliminary measurement results for the lattice characterization.

* Work supported by US Department of Energy grant DE-FG02-97ER41033.
† weili@fel.duke.edu

MEASUREMENT METHOD AND SYSTEM

In a storage ring that quadrupole strength change can be controlled independently, β functions at the location of the quadrupole can be measured directly. A change in the quadrupole strength will cause a tune change proportional to the β-function at the quadrupole, we can measure β-functions by measuring the tune changes [4]. The relation between β-function and the changes in tune is given by:

$$\Delta\nu_{x,y} = \frac{1}{4\pi}\int_{quad}(\Delta K_1)_{x,y}\,\beta_{x,y}\,ds$$

$$\text{or } \left\langle \beta_{x,y} \right\rangle = \frac{4\pi\Delta\nu_{x,y}}{(\Delta K_1)_{x,y} L_{eff}}$$

where ν is the measured betatron tune, K_1 is the quadrupole strength, L_{eff} is the effective length of the quadrupole, and the measured $\langle\beta\rangle$ is the average β at the location of the quadrupole.

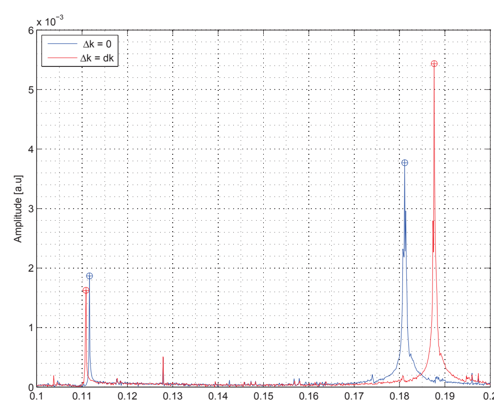

Figure 1: Tune signals measured with a network analyzer system, with a 638 MeV beam. The blue line is the nominal tune, the red line is the tune signal after a quadrupole is changed by $\triangle K_1$. The fractional nominal tune is [0.11, 0.18], the left peaks show the horizontal tune ν_x and the right peaks show the vertical tune ν_y.

This method of β-function measurement is based on tune measurements. The basic approach to measure the betatron tune of the electron beam is to excite the beam and measure its response. Two sets of tune measurement systems are

Content from this work may be used under the terms of the CC BY 3.0 licence (© 2015). Any distribution of this work must maintain attribution to the author(s), title of the work, publisher, and DOI.

ISBN: 978-3-95450-168-7 doi:10.18429/JACoW-IPAC2015-MOPJE006

ELECTRON GUN LONGITUDINAL JITTER：SIMULATION AND ANALYSIS *

Liu Ming-shan, Pei Shi-Lun, Chi Yun-long, Sui Yan-feng, IHEP, Cas Beijing 100049, China

Abstract

Electron gun timing longitudinal jitter is fatal not only for electron beam performance but also for positron yield in routine operation of Beijing Electron Positron Collider (BEPCII) Linac, which has been observed many times practically. We simulated longitudinal jitter effect of electron gun using PARMELA during one cycle and analyzed its results about beam performance including average energy, energy spread, emittance and longitudinal phase of reference particle. It is concluded that longitudinal jitter of gun trigger time is seriously for maintaining good beam performance and stable operation, which also gives a salutary lesson to any other longitudinal jitter which can affect beam bunching in pre-injector.

INTRODUCTION

In 2006, the sub-harmonic bunching (SHB) system was installed on BEPCII linac pre-injector to obtain single bunch per beam pulse and to increase positron beam injection rate[1] from linac to storage ring, which is composed of electron gun, two sub-harmonic bunchers (SHB1 & SHB2), one 4-cell travelling wave buncher and a standard 3-m long accelerating structure[2-3] as shown in Fig. 1.

Figure 1: Schematic of the pre-injector.

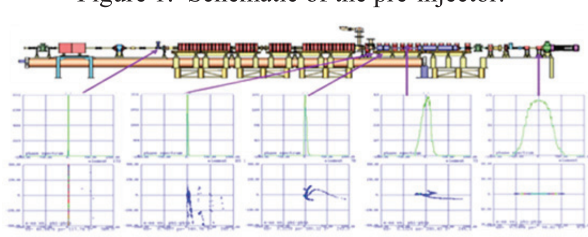

Figure 2: Schematic and simulation of bunching process.

Figure 2 is schematic of beam bunch process and simulation results at every bunch unit calculated by PARMELA when SHB system was designed[4]. The beam macro-pulse width at gun exit is 1ns FWHM with 1.6ns bottom width, after velocity modulation by SHB1 and SHB2, the beam length is ~900ps and 500ps at their exits without any real acceleration while it is ~60ps and ~10ps at buncher and A0 exit, respectively, beam energy is about 50MeV at A0 exit[3-5], which can be measured by an analysis magnet installed at A0 accelerator exit[6]. During bunch process, any variation in longitudinal sequence between pre-injector cells can be called longitudinal jitter that may deteriorate beam performance to some extent.

In order to ensure expected bunching results, physical tolerances in pre-injector were studied[7] when SHB system was designed, which are listed in Table 1. The electron gun is powered by a high voltage power supply and triggered by signal from timing system. SHBs are derived by independent power supplies with 142.8MHz and 571.2MHz microwave signals, As for buncher and A0 accelerator whose microwave comes from the 1st klystron, any perturbation of power and phase of its exporting microwave also give variation to beam performance. In other sense, timing stabilization between bunch cells in pre-injector was vital, any variation of them can cause longitudinal jitter.

Table 1: Physical Tolerance in the Pre-injector[8]

Jitter	Tolerance
Electron gun timing	±50ps
Electron gun high voltage	±0.4%
SHB phase	±1.5%
SHB power	±1.5%
Buncher phase	±2%
A0 accelerator phase	±2%

LONGITUDINAL JITTER MEASUREMENT

In electron gun trig system, electrons are emitted started by Trig On button and optimized by adjusting Delay or Fine Delay button in following operating interface as illustrated in Fig. 3. The units of them are nano-second and pico-second, respectively.

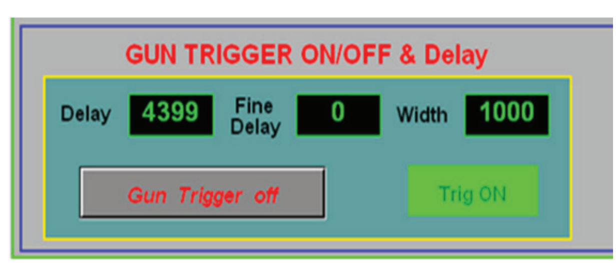

Figure 3: Operating interface of electron gun trigger.

For beam instrumentation, a beam current transformer (BCT1) is installed at gun exit, a beam current transformer(BCT2),a beam position monitor(BPM) and an Analysis Magnet are installed after A0 exit in sequence to measure beam parameters. The beam current and time

Content from this work may be used under the terms of the CC BY 3.0 licence (© 2015). Any distribution of this work must maintain attribution to the author(s), title of the work, publisher, and DOI.

ISBN: 978-3-95450-168-7 doi:10.18429/JACoW-IPAC2015-MOPJE008

SUPPRESSION OF MICROBUNCHING INSTABILITY VIA A TRANSVERSE GRADIENT UNDULATOR

D. Huang*, C. Feng, H. Deng, D. Gu, Q. Gu, Z. Zhao
Shanghai Institute of Applied Physics, Shanghai 201800, China

Abstract

The microbunching instability in the linear accelerator (linac) of a free-electron laser facility has always been a problem that degrades the electron beam quality. In this paper, a quite simple and inexpensive technique is proposed to smooth the electron beam current profile to suppress the instability. By directly adding a short undulator with transverse gradient field right after the injector to couple the transverse spread into the longitudinal direction, additional density mixing in the electron beam is introduced to smooth the current profile, which results in the reduction of the gain of the microbunching instability. The magnitude of the density mixing can be easily controlled by turning the strength of the undulator magnet field. Theoretical analysis and numerical simulations demonstrate the capability of the proposed technique in the accelerator of an X-Ray free-electron laser.

INTRODUCTION

X-Ray free-electron lasers (FELs) are being developed to serve as ultra-short, tuneable, intensity radiation sources for advanced user applications. In the recent years, the successful user operation of the first FEL facilities in soft and hard x-Ray regimes announced the birth of the x-Ray laser. High intensity electron beams of sub-picosecond (sub-ps) length typically required for x-Ray FELs are usually obtained by compressing longer beams in magnetic bunch compressors at relativistic energies. The bunch compressor manipulates longitudinal phase space of the electron beam with a considerable energy chirp by introducing the dependence of particle's longitudinal position on their relative energy. The bunch length therefore can be significantly compressed by the compressor. However, in the compression process, the initial small energy and density perturbation in the electron bunch can be amplified with a large gain factor in many cases, which will increase the fragmentation of the longitudinal phase space and dilute the emittance. This process of amplification is usually known as the microbunching instability, and it will seriously degrade the FEL performance thereafter.

The microbunching instability can be suppressed by various techniques that rely on the electron beam manipulation. The idea of using a transverse gradient undulator (TGU) to mitigate the effects of electron beam energy spread in FEL oscillators has been initially described in reference [1]. Recently, this idea has been applied to laser-plasma accelerator driven high-gain FELs. It is found later that TGU is a functional device that provides an additional measure for manipulating the electron beam via transverse-to-longitudinal phase space coupling. One of the applications of this manipulation technique is to perform the phase merging effect for significantly improving the frequency up-conversion efficiency of a seeded FEL. In this paper, a quite simple and inexpensive technique based on the transverse-to-longitudinal phase space coupling is proposed and studied for suppression the microbunching instability of the electron beam. It is found that by directly adding a TGU after the injector in a linac, the gain of the microbunching instability in the electron beam can be effectively suppressed. Compared with the previous techniques, this method is quite simple and could be easily applied on all existing FEL facilities in addition to the laser heater. Moreover, the change of the chromaticity introduced by the scheme in this paper is ignorable and the transverse emittance of the beam is preserved well enough throughout the whole linac lattice after transverse matching, which is considered as another great advantage.

*huangdazhang@sinap.ac.cn

METHODS

The schematic layouts of the proposed technique are shown in Figure 1. In Figure 1(a), a short TGU is added after accelerating section L1 and another one is added after L2 in the linac, the linear energy chirp of the beam exists in both the locations. In Figure 1(b), one TGU is placed right after the injector where there is no energy chirp. The selections of the locations of TGUs will be discussed later on in this paper.

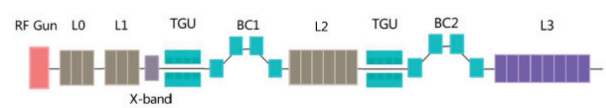

(a) Double TGU scheme

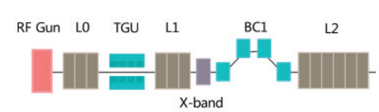

(b) Single TGU scheme

Figure 1: (Color) Layouts of two TGU schemes.

TGU, like what described by its own name, is an undulator with transverse gradient between magnetic poles. Such a device can be realized by canting the poles of an regular undulator and the gradient is usually made in the horizontal direction. Because electrons at different horizontal positions feel different magnetic fields, the path length of an electron traversing TGU depends on its transverse coordinate at the entrance of TGU. Because of

Content from this work may be used under the terms of the CC BY 3.0 licence (© 2015). Any distribution of this work must maintain attribution to the author(s), title of the work, publisher, and DOI.

ISBN: 978-3-95450-168-7 doi:10.18429/JACoW-IPAC2015-MOPJE009

LATTICE DESIGN OF THE SSRF-U STORAGE RING

S.Q. Tian, M.Z. Zhang, Q.L. Zhang, B.C. Jiang, Z.T. Zhao
Shanghai Institute of Applied Physics, Shanghai 201800, P. R. China

Content from this work may be used under the terms of the CC BY 3.0 licence (© 2015). Any distribution of this work must maintain attribution to the author(s), title of the work, publisher, and DOI.

Abstract

Multi-Bend Achromatic (MBA) cell has been well known to significantly reduce the beam emittance of the synchrotron radiation light sources in the past two decades. With the great development of the high gradient magnets, the small-aperture vacuum chamber and the precise alignment, the ultimate-emittance ring based on MBA lattice became practical in recent years. We present a preliminary lattice design for the upgraded SSRF storage ring based on a 7BA lattice in this paper. The circumference and the number of the straight sections are preserved for the existing tunnel. The beam emittance is desired toward diffraction-limited of X-ray, as much as possible.

INTRODUCTION

SSRF has been operated for users experiments since 2009. It has 13 beamlines now, and about 40 beamlines will serve users around 2020 [1]. The storage ring of SSRF has 20 DBA cells (four folds), and the beam emittance is 3.9 nm.rad on the beam energy of 3.5 GeV. In the past several years, worldwide discussion about the diffraction-limited light source of X-ray was frequently made. The beam emittance of many synchrotron light sources is designed to reach the order of 100 pm.rad, and lots of operated machines have the same upgrade considerations or plans [2]. In order to increase the photon brightness by a factor of about 100, SSRF has a preliminary upgrade plan (SSRF-U) to reduce the beam emittance by a factor of 10, reduce the beam energy to 3.0 GeV, and appropriately increase the beam current. In the following section, the lattice design of the SSRF-U storage ring is presented.

LATTICE AND BEAM PARAMETERS

The lattice of the SSRF-U storage ring is based on 7BA, because it is a good tradeoff between the emittance reduction and the cell lengthening. There are 20 cells and four folds, the same as SSRF. The upgrade ESRF-type [3] structure with beta and dispersion bump is applied due to its very effective chromaticity correction. There are only focusing quadrupoles in the arc cells, and all the defocusing gradients are provided by the combined dipoles. Six sextupoles are installed in the sections of the two beta and dispersion bumps of each cell in order to correct the chromaticity, and four harmonic sextupoles to correct the high order geometric aberrations. The maximum gradients of the quadrupole and sextupole are 80 T/m and 4000 T/m^2, respectively.

Figure 1 plots the liner optics of the SSRF-U storage ring, and Table 1 summarizes the main lattice parameters. A triplet of quadrupole beside the long straight section increase the horizontal beta function at the injection point to 25, in order that a sufficient dynamic aperture for beam injection can be obtained. The working point is optimized to be 43.22 in the horizontal plane and 17.32 in the vertical plane, and the natural emittance reaches down to 202.5 pm.rad with the beam energy of 3 GeV. Due to the IBS effect, the horizontal emittance will increase by about 37.7%, with the coupling of 10%, the RF frequency of 500MHz and the bunch current 0.4mA/bunch. A third harmonic cavity will reduce the horizontal emittance growth to 13.4%. The energy loss per turn in bare lattice is 0.44 MeV, and a RF voltage of about 2 MV can compensates the beam. The length of 5.6m of the standard straight section is left for IDs.

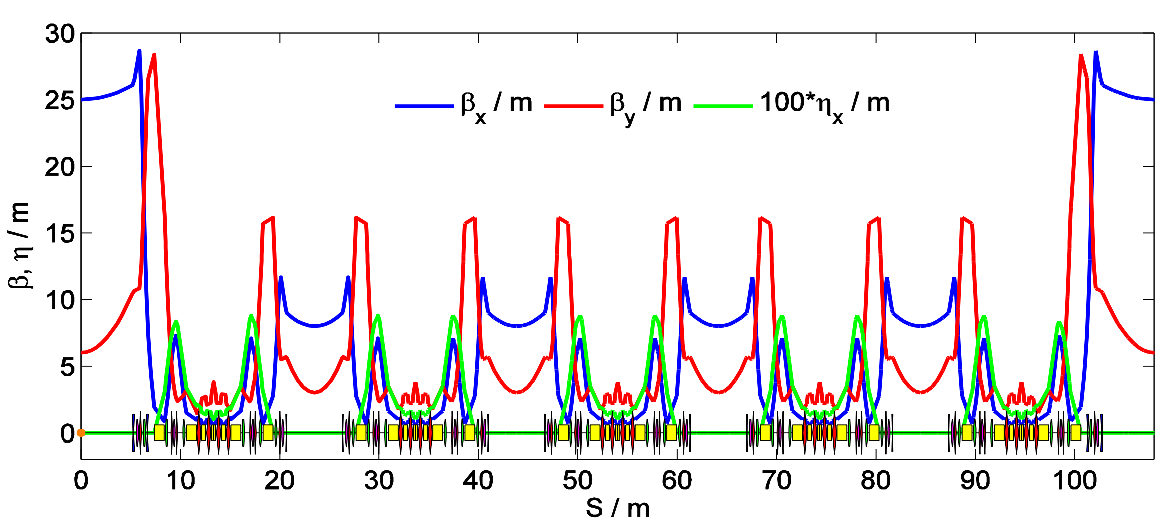

Figure 1: The linear optics of one fold of the SSRF-U storage ring.

ISBN: 978-3-95450-168-7 doi:10.18429/JACoW-IPAC2015-MOPJE015

COMPENSATIONS OF DEPU EFFECTS AT THE SSRF STORAGE RING

M.Z. Zhang, Q.L. Zhang, S.Q. Tian, B.C. Jiang, M. Zhang, J.H. Tan
Shanghai Institute of Applied Physics, Shanghai 201800, P. R. China

Abstract

A pair of Apple-II type EPU (DEPU) is installed in the SSRF storage ring. They introduce closed orbit distortion, tune shift, coupling, reduction of the dynamic aperture and so on. The distortions and the compensations of these effects are described in this paper. Feedforward tables of corrector coils, quadrupole and skew quadrupoles are used to correct the COD, tune shifts and coupling, respectively. Sextupole optimization is used to correct the dynamic aperture.

INTRODUCTION

Shanghai Synchrotron Radiation Facility (SSRF) [1] is a dedicated third generation synchrotron light source with nominal energy of 3.5 GeV. A beam line (named 'Dream Line') of Angle Resolved Photoemission Spectroscopy (APRES) and Photoemission Electron Microscope (PEEM) has been built and installed at SSRF [2]. In order to get very wide photon energy and reduce the heat load to optics instrument simultaneously, two Apple-II type EPUs (DEPU) are used. The lower energy photon from 20 to 200eV is produced by U58 whose period is 58mm and minimal gap is 17mm. The higher energy photon from 200 to 2000eV is produced by U148 whose period is 148mm and minimal gap is 22mm.

EPU is widely used in the synchrotron radiation sources. The effects and compensations are well studied in many labs over the world [3]. There are many effects are introduced by the EPU [4][5]: closed orbit distortion, tune shift, reduction of the dynamic aperture, coupling. The effects and compensation on the real machine are described in this paper.

CLOSED ORBIT DISTORTION

The COD results from the nonzero 1st order integral fields (dipole errors) [5]. The dipole errors vary with the gaps and block position. The integral field of U148 and U58 both are about 200Gs-cm. The peak-to-peak values of the orbit distortion between the gap of 160mm and 22mm are 150um and 80um in horizontal and vertical plane. The large distortion affect the photon position and thus flux not only the dream line but also other beam lines. The integral fields also changes when the frame and shifts changed. Figure 1 shows the orbit positions vary with the shift position. The standard deviation of orbit distortion (COD) varies from 0 um to 25 um in horizontal and vertical plane. The maximum of orbit distortion introduced by frame position is about 200um at the edge of U148. Figure 2 shows the orbit distortion before and after correction when the gap of U58 varies, it rises rapidly when the gap is less than 60mm, the maximum value is 60 and 120um in horizontal and vertical plane. It seems to be in reverse to the square of the gap and consistent with theoretical calculation.

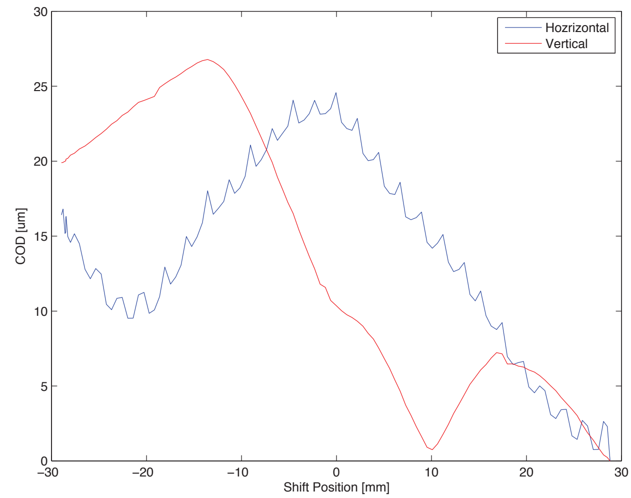

Figure 1: COD varies with the shift position.

There are 2 correction coils in each plane at the entrance exit of DEPU. In order to increase the tuning speed, one select analogy power supply. Scanning the correctors' strength with different gaps and shifts makes a feed forward table. Controller varies the power supply settings when it detects the gap change. This work takes lots of time to get the table data and tests at more and more gaps and shifts are still needed.

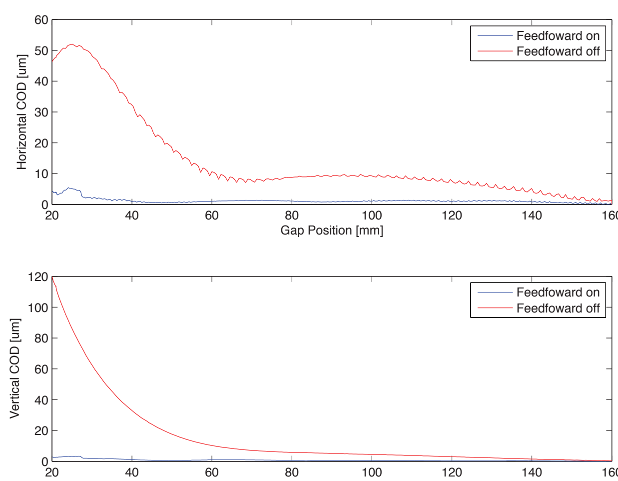

Figure 2: The CODs in both planes before and after correction during gap variation.

The feedforward reduces the COD to 5um. But it's still larger than the requirement of beam position stability. Slow and fast orbit feedbacks are needed during the daily operation to correction these distortions.

Content from this work may be used under the terms of the CC BY 3.0 licence (© 2015). Any distribution of this work must maintain attribution to the author(s), title of the work, publisher, and DOI.

ISBN: 978-3-95450-168-7 doi:10.18429/JACoW-IPAC2015-MOPJE016

START-TO-END SIMULATION FOR RAON SUPERCONDUCTING LINAC

Hyojae Jang, Ji-Ho Jang and Hyunchang Jin, IBS, Daejeon, Korea

Abstract

An ion accelerator, RAON is going to be built in Daejeon, Korea by Rare Isotope Science Project(RISP) team in Institute of Basic Science(IBS). The linac part of RAON consists of two low energy linacs, one high energy linac and two bending section for transporting accelerated low energy ions to high energy linac. It is planned to accelerate many diverse ions like proton, carbon, calcium, uranium, etc. which have different A/q values. Consequently the lattice design for each ion and to investigate beam dynamics issues for each case are one of the important topics for this project. For enhancement of beam acceleration a study to suppress emittance growth and to maximize the longitudinal acceptance is conducted while designing the RAON lattice. In this presentation the designed linac lattices for various ions and start-to-end simulation results will be described.

INTRODUCTION

Nowadays the importance of an ion accelerator is increasing as it is an essential tool for research of medical, nuclear, material, science and many other areas. Since 2009 Rare Isotope Science Project (RISP) project has been going on in Korea to build an ion accelerator which can generate high-power ion beams and rare isotopes. [1]- [2] For acceleration of stable ions, electron cyclotron resonance ion source (ECR-IS) is going to be used while electron beam ion source (EBIS) and ECR-IS are going to be used as ion sources of isotope separation on-line (ISOL) system which will generate rare isotopes. Because the ions from these systems have various charge states they will be filtered to desired charge states in low energy beam transport (LEBT). Radio frequency quadrupole (RFQ) and medium energy transport (MEBT) will be installed after LEBT for beam acceleration and bunching. Superconducting linear accelerators start immediately after MEBT. They consist of two low superconducting energy linacs (SCL1 and SCL3), one high energy superconducting linac (SCL2), two bending section for bridging of linacs and one 120m beam transport for transporting high energy ions to high energy beam transport of IF(In-flight Fragment seperator) system. The layout of RAON superconducting linear accelerators is shown in Fig. 1. SCL1 accelerates stable ion beams while SCL3 accelerates rare isotope. Ions from low energy linacs are transported to high energy linac, SCL2. In this transport there are two charge strippers and charge selection selections between SCL1 and SCL2 and between SCL3 and SCL2. The charge state of ions become higher and it leads to the enhancement of acceleration efficiency. To provide high quality ion beams, RAON adopted superconducting cavity and normal conducting quadrupole doublet structure for linac lattice. The Bunch frequency of the linear accelerator is 81.25 MHz. There are four kinds of cavities in RAON. Quarter wave resonators (QWR) will be used at the first part of low energy linac and this section is called as SCL11 and SCL31. Half wave resonators (HWR) are going to be used for the rest of low energy linac and this section is called as SCL12 and SCL32. In high energy linacs (SCL2) two kinds of single spoke resonators (SSR) which have dfferent geometrical betas are going to be used and they are called as SCL21 and SCL22. Selected optimum betas were β_g=[0.047,0.12,0.3,0.51]. Also the accelerating voltages according to beam beta are shown in Fig. 2.

Each period in linac consists of a cryomodule containing superconducting cavities, one quadrupole doublet and a beam box which will be used for vacuum pumping, installing the diagnostics. Also recently transport line for transporting high energy is designed. In this section there are two cryomodules which are similar to the cryomodules used in SCL22 section. Summarized parameters of each linac section for stable ion acceleration are summarized in Table 1.

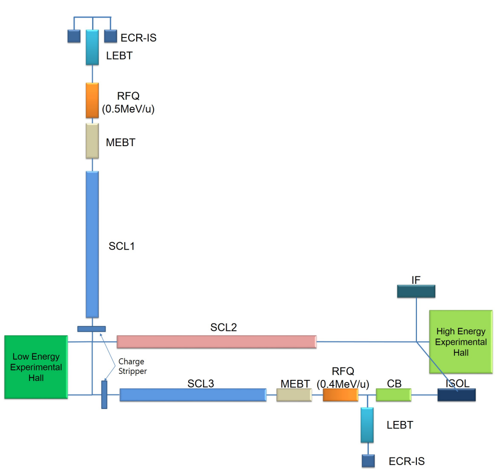

Figure 1: Layout of RAON superconducting linacs.

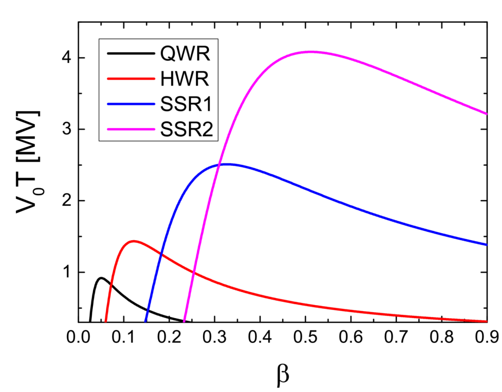

Figure 2: Effective accelerating voltage of cavities in RAON superconducting linac.

Content from this work may be used under the terms of the CC BY 3.0 licence (© 2015). Any distribution of this work must maintain attribution to the author(s), title of the work, publisher, and DOI.

ISBN: 978-3-95450-168-7 doi:10.18429/JACoW-IPAC2015-MOPJE017

ERROR ANALYSIS AND CORRECTION AT THE MAIN LEBT OF RAON HEAVY ION ACCELERATOR

Hyunchang Jin, Ji-Ho Jang, In-Seok Hong, and Hyo-Jae Jang
Institute for Basic Science, Yuseong-daero 1689-gil, Yuseong-gu, Daejeon, Korea

Abstract

The main Low Energy Beam Transport (LEBT) section of Rare isotope Accelerator Of Newness (RAON) heavy ion accelerator is designed to transport the ion beams which are generated by Electron Cyclotron Resonance Ion Source (ECR-IS) to the Radio Frequency Quadrupole (RFQ). In the main LEBT, one or two beams are selected among a variety of ion beams to meet the beamline experiment requirements such as beam charge and current. In a uranium beam case, two charge-state, 33+ and 34+, beams are chosen and transported to the RFQ. For transportation of two charge-state beams, beams can be seriously affected by dipole kick or unexpected dispersion caused by magnet errors. These effects of magnet or cavity errors lead to beam loss at the main LEBT or RFQ. Therefore, the effect to the beam orbit and size should be identified and the research for reducing such effect should be required in the main LEBT. In this paper, we will examine the orbit distortion and beam size growth caused by magnet errors and discuss the correction of errors by using correctors and BPMs.

INTRODUCTION

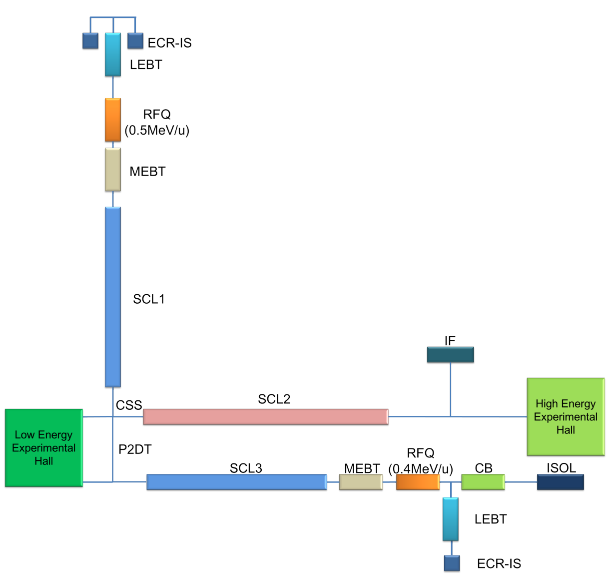

Figure 1: Schematic view of RAON heavy ion accelerator.

The RAON heavy ion accelerator [1] proposed by Rare Isotope Science Project (RISP) is in progress to become one of the world leading facilities as a rare isotope accelerator. At the RAON accelerator, the rare isotopes can be generated with two ways; one way is the isotope separation on line (ISOL) system [2] and the other is the projectile fragmentation in the in-flight fragmentation (IF) system [3]. In a wide range of science programs, we can use these rare isotopes.

For a uranium beam case, the beam generated by electron cyclotron resonance ion source (ECR-IS) with a beam energy of 10 keV/u reaches to an energy 200 MeV/u and a power 400 MW at the IF system to produce a high-intensity rare isotopes. For this process, RAON accelerator will use a low energy superconducting linac (SCL1) and a high energy superconducting linac (SCL2) [4]. The beams generated by the ECR-IS passes through the low energy beam transport (LEBT), the radio frequency quadrupole (RFQ), and the medium energy beam transport (MEBT) before entering the SCL1. The schematic layout of RAON accelerator is shown in Fig. 1.

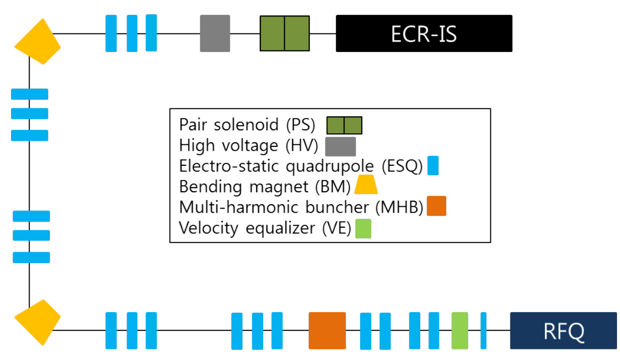

Figure 2: Layout of the main LEBT.

The main LEBT consists of many components: a pair solenoid (PS), high voltage platform (HV), 20 electro-static quadrupoles (ESQ), two 90-degree bending magnets, a multi-harmonic buncher (MHB), and a velocity equalizer (VE). All the components of it can be error sources of orbit distortion and the error of ESQs is a dominant source. The schematic layout of main LEBT is shown in Fig. 2.

We have developed the graphical user interface (GUI) for the error analysis and correction in RAON accelerator by using a multi-particle beam simulation code, DYNAC [5], and a computing language program, MATLAB [6]. In this paper, we will present the orbit distortion induced by magnet errors and correction to the errors by using correctors and beam-position monitors (BPMs) in the main LEBT.

PROCEDURE FOR ERROR ANALYSIS AND CORRECTION

With the lattice information, the orbit trajectory is calculated with and without errors by using the DYNAC code. The whole procedure of error analysis and correction with DYNAC and MATLAB programs is listed in Table 1.

Content from this work may be used under the terms of the CC BY 3.0 licence (© 2015). Any distribution of this work must maintain attribution to the author(s), title of the work, publisher, and DOI.

ISBN: 978-3-95450-168-7 doi:10.18429/JACoW-IPAC2015-MOPJE019

CATEGORIZATION AND ESTIMATION OF POSSIBLE DEFORMATION IN EMITTANCE EXCHANGE BASED CURRENT PROFILE SHAPING

Gwanghui Ha, Moohyun Cho, Won Namkung, POSTECH, Pohang, Gyeongbuk 790-784, KOREA
Wei Gai, Kwang-Je Kim, John Gorham Power, Argonne National Laboratory, Argonne, IL 60439, USA

Abstract

Bunches with shaped current profiles can be used to increase the transformer ratio in the beam-driven collinear wakefield acceleration. Shaped current profiles can be generated with an emittance exchange (EEX) and controlled by the incoming beam parameters as well as the EEX beam line parameters. The ideal bunch shape, predicted from first order theory in the absence of collective effects, is deformed in the real case. In this paper, we categorize the sources of deformation with a deformation parameter and observe their deformation pattern on the current profile.

CATEGORIZATION OF DEFORMATION

Perturbation theory can be used to categorize the deformations of the bunch shape that arise with the emittance exchange (EEX) based bunch shaping. We define the ideal bunch shape, $N_0(\mathrm{z})$, as that which occurs under the ideal conditions of zero emittance, thin-lens deflecting cavity, first-order beam dynamics, and the absence of collective effects [1]. In this case, there is perfect linear relationship between the initial horizontal position (x_i) and the final longitudinal position ($z_f^0 = \{k\xi - s(\eta + k\xi(L+D))\}x_i$). The actual bunch shape, $N(\mathrm{z})$, is deformed from the ideal when realistic effects are included. In this paper, we characterize the deformation patterns in order to improve the beamline design. We analyse the deformation of an ideal single triangle current profile and determine how the deformation affects the transformer ratio (TR).

Single Particle Treatment

The final bunch position (z_f) can be treated as a perturbation to the ideal bunch position (z_f^0) by adding perturbation terms.

$$z_f = z_f^0 + \sum C_m \prod X_n, \tag{1}$$

where C_m are the perturbation coefficients of the beam parameters $X_n \in \{x_i, x_i', y_i, y_i', z_i, \delta_i\}$. Based on the polynomial form of Eq. (1), there are three categories. (1) random deformation where all X_n are not correlated to x_i This deformation spreads the particle from its ideal position without any preferred direction. The thick-lens effect from the deflecting cavity ($\frac{L_c}{6}\kappa^2\xi z_i + \frac{L_c}{6}\kappa^2\xi^2\delta_i$) belongs to this category since z_i and δ_i are not correlated to x_i [1]. (2) correlated-random deformation contains at least one X_n which is and is not correlated to x_i. This deformation makes a similar effect like the random perturbation, but it changes the shape of the current profile in the different way. Since a divergence after the deflecting cavity ($x_2' = \kappa z_i + \kappa\xi\delta_i$) is not correlated to x_i, and an energy spread after the deflecting cavity ($\delta_2 = \kappa x_i + \kappa(L+L_{bc})x_i{}'$) is correlated to x_i, the second order term $\mathrm{T}_{526}x_2'\delta_2$ is the one of the correlated random deformation terms [2]. (3) correlated random deformation only has X_n which is correlated to x_i. Since all parameters are correlated to x_i, particles move to the specific position based on its original position. This collective movement makes the strongest deformation to the current profile.

EEX BASED SHAPING DEFORMATION PATTERNS

Each major deformation categories can be further separated into several minor cases depending on the sign of the coefficients and the order of beam parameter terms. By considering up to the second order for the random and the correlated-random case, and the third order for the correlated case, there are total ten minor deformation cases.

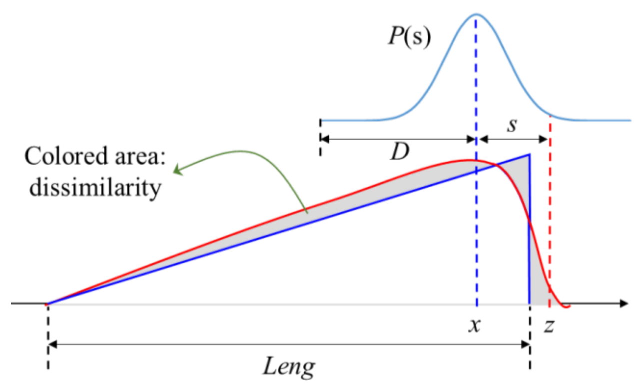

Figure 1: Definition of parameters

Deformed Density Profile

We define a perturbation function (which is similar to the probability density function) in order to analyse the cases. If s is the distance between two positions, $P(s \equiv z - x)ds$ indicates what portion of particles in position $[x, x+dx]$ moves to z (Fig. 1). This function satisfies $\int_{-\infty}^{\infty} P(s)ds = 1$. Also, the deformed profile related to the ideal profile, $N_0(x)$, can be expressed

$$N(z) = \int_{-\infty}^{\infty} N_0(x)P(z-x)dx. \tag{2}$$

Content from this work may be used under the terms of the CC BY 3.0 licence (© 2015). Any distribution of this work must maintain attribution to the author(s), title of the work, publisher, and DOI.

ISBN: 978-3-95450-168-7 doi:10.18429/JACoW-IPAC2015-MOPJE020

Content from this work may be used under the terms of the CC BY 3.0 licence (© 2015). Any distribution of this work must maintain attribution to the author(s), title of the work, publisher, and DOI.

HIGH RESOLUTION LONGITUDINAL PROPERTY MEASUREMENT USING EMITTANCE EXCHANGE BEAM LINE

Gwanghui Ha, Moohyun Cho, and Won Namkung, POSTECH, Pohang, Gyeongbuk 790-784, KOREA
Wei Gai, Kwang-Je Kim, and John Gorham Power, Argonne National Laboratory, Argonne, IL 60439, USA

Abstract

Most longitudinal diagnostics intentionally introduce a transverse-longitudinal correlation since it is difficult to measure longitudinal properties directly. This correlation is introduced in order to observe longitudinal properties on a transverse screen, but the initial transverse components of the beam limit the resolution of the measurement. It is possible to overcome this resolution limit with an emittance exchange beam line in which the transverse properties after the exchanger only depend on longitudinal properties at its entrance. We present a new concept for measuring longitudinal properties with an emittance exchange beamline and preliminary simulation results.

RESOLUTION LIMIT OF THE DEFLECTING CAVITY MEASUREMENT

Since it is difficult to measure the longitudinal density profile of an electron bunch directly, the longitudinal profile is often transformed into the transverse profile. An example is a transverse deflecting cavity (TDC) followed by a screen (Fig. 1). The TDC applies a time-dependent-transverse-kick to the bunch. The particles in the bunch obtain an additional transverse momentum depending on its arrival time at the TDC. Because the strength and the direction of this momentum kick varies with arrival time, the transverse position of each particle at the measurement screen is proportional to the longitudinal position inside the bunch. Therefore, we can estimate the bunch length by measuring the transverse beam size.

The transverse beam size at the screen downstream of the TDC (Fig. 1) is not an exact representation of the initial bunch length. The bunch's finite transverse size and divergence before the TDC contributes to the transverse beam size at the screen. To minimize the contribution of the initial transverse parameters, the quadrupole is used in front of the TDC. If all beam parameters at X_1 are well-known, then the beam size at the screen can be calculated using the linear transport matrix given in Eq. (1).

$$\mathrm{R} = \begin{bmatrix} 1 & L_c + D + D' & \kappa\left(\frac{L_c}{2} + D\right) & 0 \\ 0 & 1 & k & 0 \\ 0 & 0 & 1 & 0 \\ \kappa & \frac{L_c}{2}\kappa & \frac{L_c}{4}\kappa^2 & 1 \end{bmatrix}, \quad (1)$$

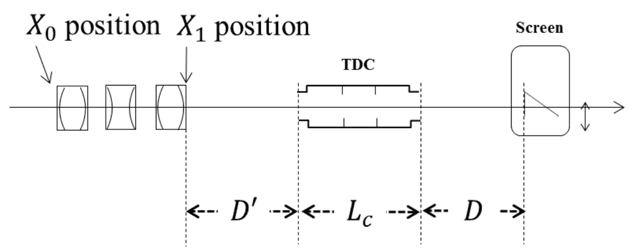

Figure 1: Typical TDC measurement configuration.

where κ is the deflecting cavity kick strength ($= \frac{\mathrm{eV}}{E}\frac{2\pi}{\lambda}$).

According to Eq. (1), the rms transverse beam size at the screen position in terms of $\mathrm{X}_1 = (x_1, x_1', z_1, \delta_1)$ is

$$\sigma^2_{\mathrm{x,screen}} = \sigma^2_{x,1} + L^2\sigma^2_{x',1} + 2L\sigma_{xx',1} + \kappa^2 L'\sigma^2_{z,1}. \quad (2)$$

where L is $L_c + D + D'$ and L' is $\frac{L_c}{2} + D$. The first three terms are due to the initial transverse parameters, while the last term is due to the bunch length. Two parameters from Eq. (2) determine the resolution. The first parameter, the scaling factor, determines the beam size at the screen due to the initial bunch length. Therefore, $\kappa L'$ in Eq. (2) is the scaling factor and a larger value improves the resolution. The second is the TDC-off transverse beam size. When the TDC is off, only the first three terms in Eq. (2) remain and the TDC-off size is the square root of those terms. The smaller the TDC-off size is the better the resolution.

To minimize the TDC-off size, the focal length of the quadrupole is adjusted to $\frac{1}{\mathrm{f}} = -\left(\frac{1}{L} + \frac{\sigma_{xx',0}}{\sigma^2_{x,0}}\right)$ (a thin-lens single quadrupole is assumed for simple calculation instead of triplet). The corresponding minimum TDC-off size become

$$\sigma_{\mathrm{x,min,screen}} = \frac{\varepsilon_{x,0}}{\sigma_{x,0}}(D + D' + L_c). \quad (3)$$

The resolution of a TDC-based measurement is the ratio of the minimum TDC-off size to the scaling factor.

$$\mathrm{Resolution} = \frac{\varepsilon_{\mathrm{x},0}(D+D'+L_c)}{\sigma_{x,0}\kappa\left(D+\frac{L_c}{2}\right)}. \quad (4)$$

Unfortunately, most of resolution related terms in Eq. (4) has a clear limit. A small emittance and large beam size enhance the resolution, but the emittance does not change

ISBN: 978-3-95450-168-7 doi:10.18429/JACoW-IPAC2015-MOPJE022

PHYSICAL MODEL OF PARTIAL RF DISCHARGE IN ISOCHRONOUS CYCLOTRONS

V.S. Dyubkov, National Research Nuclear University "MEPhI", Moscow, Russia*
S.A. Korenev, Siemens Healthcare, Knoxville, TN 37932, USA

Abstract

The physical model of partial RF discharge, based on the residual gases molecules ionization by detached electrons produced in collisions of negative hydrogen ions with residual gases, as well as electro-dissociation of H^- ions in isochronous cyclotrons, is proposed in this paper. The following problems are discussed in this article: the influence of magnetic field on the properties of partial RF discharge, the analysis of conductivity of RF plasma (partial RF discharge), the results of proposed model application for 11 MeV Eclipse cyclotrons.

INTRODUCTION

A partial electrical discharge is the first stage of forming the radiofrequency (rf) discharge in the cavities (cavity consists of dee and cooper surfaces of magnet valleys) of isochronous cyclotron which takes place before full breakdown (the so called crowbar). The main question of the discharge appearance is a question of origin of preliminary electrons that initiate rf discharge. The vacuum conditions in isochronous cyclotrons with internal ion source have large influence on loses of H^- ions. The time of processes of forming the rf partial discharge is not stable and stochastic. The analysis of existing rf discharge in charged particle accelerators [1, 2] shows that the used physical models cannot hitherto describe partial discharge appearance in low energy isochronous cyclotrons (for instance, 11 MeV Siemens Eclipse cyclotron). The partial discharge can lead to full rf discharge and consequently determines the time of irradiation. One can point, for example, that decreasing the total time of irradiation on the 15% leads to reduction of short-lived isotope activity on the 15% ultimately. A new physical model of partial discharge for isochronous cyclotrons with internal ion source is presented in this paper. Furthermore, the paper has practical aspect related to efficiency of medical radioisotopes production during target irradiation by protons.

PHYSICAL MODEL OF PARTIAL RF DISCHARGE

The main idea of proposed physical model is based on the ionization of residual gas molecules by electrons. These freed electrons appear due to stripping and electrodissociation of H^- ions. The ionization result in formation of plasma clouds between dees and trimbars with enough conductivity to decrease rf voltage (Fig. 1). This proposal makes a difference from other models of electrical discharge presented in Ref. [3]. Waveforms illustrating the partial discharge and crowbar are shown in Fig. 2. Curves in Fig. 2a are cyclotron magnet current (CH1) and a signal on RF probe (CH2) correspondingly.

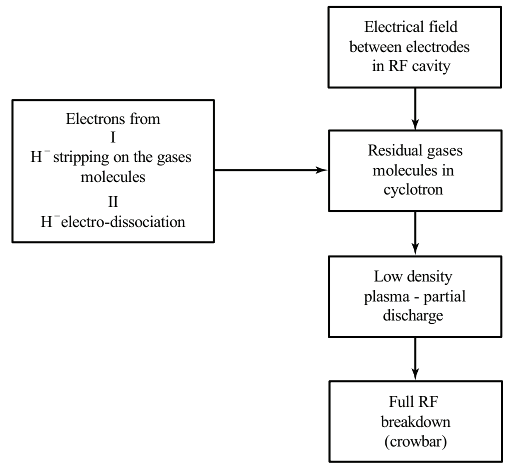

Figure 1: Physical model structure of forming the RF discharge in cyclotron cavity.

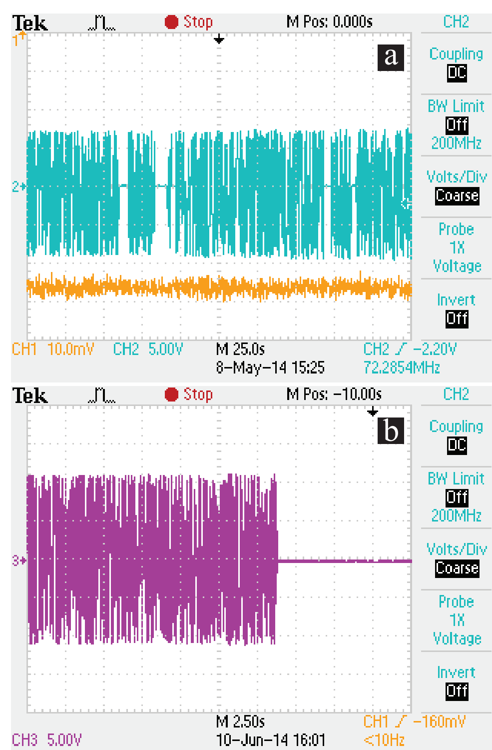

Figure 2: The waveforms of RF partial discharge (a); RF partial discharge & full electrical one (b).

* vsdyubkov@mephi.ru

Content from this work may be used under the terms of the CC BY 3.0 licence (© 2015). Any distribution of this work must maintain attribution to the author(s), title of the work, publisher, and DOI.

ISBN: 978-3-95450-168-7 doi:10.18429/JACoW-IPAC2015-MOPJE023

Content from this work may be used under the terms of the CC BY 3.0 licence (© 2015). Any distribution of this work must maintain attribution to the author(s), title of the work, publisher, and DOI.

3D COMPUTER SIMULATIONS OF THE ULTRARELATIVISTIC BEAM DYNAMICS IN SUPER COLLIDERS*

M.A. Boronina, V.A. Vshivkov, ICM&MG SB RAS, Novosibirsk, Russia
G.I. Dudnikova, ICT SB RAS, Novosibirsk, Russia

Abstract

The problem of numerical modeling of beam-beam interaction with high relativistic factor ($\sim 10^4$) is considered. We present a 3D self-consistent simulation model based on particle-in-cell method. The mixed Euler-Lagrangian decomposition is used in the parallel algorithm for achieving good load balancing and reducing communication costs. Stable regimes of beam dynamics, depending on the beams configuration (beta-function, emittance, energy, currents and relative offset) can be found on the base of the model. In the calculations we used grid 100×100×100 with 10^8 macro-particles, the number of processors depends highly on the beam shape.

INTRODUCTION

We present a new PIC code for mathematical modeling of the collective ultrarelativistic beam dynamics with the aim to achieve large luminosities. The high relativistic factors of the beam particles ($\gamma \sim 10^3$-10^5) lead to the luminosity restriction, the negative effects can be reduced by optimization of the beam configuration.

The standard slice approach represents the slices rearrangement, each slice of one beam impacts on the counter beam particles by two-dimensional forces. The approach is widely used for cyclic accelerators, where the beam deformations are not strong, the computations of a single interaction are fast, number of slices 5-50 and number of macro-particles in the bunch 10^5 provide sufficient accuracy [1]. The single collision of ultrarelativistic beams of high densities may lead to a strong compression and even disruption of the bunch, and in this case longitudinal resolution must be adequate to the number of pinches. The longitudinal effects cannot be simulated by a quasi-3D model, but in the case of critical beam densities such as in ILC they may play significant role, and the redistribution of energy may cause ruinous consequences. The fine resolution requires an appropriate number of macro-particles in the beam (10^8-10^{10}). A monoprocessor machine allows performing 3D simulations with maximum $2 \cdot 10^6$ macro-particles, and new efficient parallel algorithms are needed to simulate the critical regimes of the ultrarelativistic beams interaction.

In our parallel 3D algorithm we apply the particle-in-cell (PIC) method and the leap-frog scheme [2,3] to solve Vlasov-Liouville equation the three-dimensional set of Maxwell's equations. The three-dimensional nature of interaction together with the new special methods for initial and boundary conditions computations [4] allow automatically account for above difficulties and demonstrate good results.

MATHEMATICAL MODEL

We consider the motion of counter beams in a rectangular domain in Cartesian coordinates. The positron/electron beams are focused by the external focusing field and move in the self-consistent electromagnetic fields. The boundaries of the computational domain are located very close to the beams, in the near wave zone, no radiation effects are considered [5]. We use Vlasov kinetic equation for the distribution function of the particles and the three-dimensional set of Maxwell's equations to describe the beam dynamics. In dimensionless variables, which are obtained from the characteristic beam length $L = 1$ cm and the characteristic particle speed $v = c = 299792.458$ km/s, the equations may be rewritten in the following form:

$$\frac{\partial f_{+,-}}{\partial t} + \mathbf{v}_{+,-}\frac{\partial f_{+,-}}{\partial \mathbf{r}} + \mathbf{F}_{+,-}\frac{\partial f_{+,-}}{\partial \mathbf{p}} = 0$$

$$\begin{aligned} rot\mathbf{E} &= -\frac{1}{c}\frac{\partial \mathbf{H}}{\partial t}, \\ rot\mathbf{H} &= \frac{4\pi}{c}\mathbf{j} + \frac{1}{c}\frac{\partial \mathbf{E}}{\partial t}, \\ div\mathbf{E} &= 4\pi\left(n_- e^- + n_+ e^+\right), \\ div\mathbf{H} &= 0. \end{aligned}$$

The Lorentz's force can be calculated from the following equation for each particle:

$$\mathbf{F}_{+,-} = e^{+,-}\left(\mathbf{E} + \mathbf{v}_{+,-} \times \mathbf{H} / c\right)$$

and the particle moment:

$$\mathbf{p}_{+,-} = \gamma_{+,-} m_e \mathbf{v}_{+,-}$$

$$\gamma_{+,-} = 1 \Big/ \sqrt{1 - \left|\mathbf{v}_{+,-}\right|^2 / c^2}$$

*Work supported by RFBR Grants 14-01-31088, 14-01-00392, 14-07-00241.

6th International Particle Accelerator Conference IPAC2015, Richmond, VA, USA JACoW Publishing
ISBN: 978-3-95450-168-7 doi:10.18429/JACoW-IPAC2015-MOPJE026

Content from this work may be used under the terms of the CC BY 3.0 licence (© 2015). Any distribution of this work must maintain attribution to the author(s), title of the work, publisher, and DOI.

REVISION OF THE IMPEDANCE MODEL FOR THE INTERPRETATION OF THE SINGLE BUNCH MEASUREMENTS AT ALBA

T.F. Günzel and U.Iriso, ALBA Synchrotron, Cerdanyola de Vallés, Spain

Abstract

Recently [1] we were able to explain 65% of the measured vertical single bunch detuning with the developed transverse impedance model. In this note we show the improvements of the impedance model we could achieve in the meantime. We included a better bunch length parametrisation of all contributions. Moreover, the geometrical impedance of several vacuum chamber elements was recalculated with GdfidL [2] and the impedance of a couple of elements neglected so far was included in the budget. ImpedanceWake2D [3] was used for the computation of the (resistive) wall impedance.

INTRODUCTION

In the past at different accelerators significant differences between the computed and measured single bunch detuning were observed [4, 5]. However, the work [6] shows that achieving an agreement is not impossible. An accurate computation of the impedance gains importance as the construction of ultralow emittance sources pushes the instability thresholds to limits which are hardly feasible. This note describes the work carried out to carefully benchmark impedance measurements with the computated impedance at the ALBA storage ring. On one side, measurements were taken varying different machine parameters like the RF-voltage and the gap of the in-vacuum undulators. On the other hand, careful simulations using GdfidL and Impedance-Wake2D(IW2D) were carried out using an experimental bunch parametrisation.

IMPROVEMENT OF THE IMPEDANCE MODEL

The key point of this work consists in the upgrade of the underlaying vertical impedance model. The model contains two parts, the impedance of geometrical origin – also called broadband impedance – and impedance related to the resistivity of the vacuum chamber walls and that part of space charge that only depends on the chamber extension – the wall impedance. The broadband impedance (BBI) is computed by simulation of electromagnetic wake fields in corresponding vacuum chambers with the program GdfidL [2] whereas the wall impedance is computed analytically. For this work the wall impedance was computed for the first time with ImpedanceWake2D.

Wall Impedance

IW2D allows to calculate the wall impedance for a round or fully flat beam pipe consisting of n different material layers of constant thickness. Table 1 shows the list of chambers analyzed by IW2D. The code solves the Maxwell equations exactly and should be therefore best adapted to the problem (this is only partly true as no chamber wall is an assembly of layers of exactly constant thickness).

Comparing the impedance spectra of IW2D with those of the RW-models of the precedent work [1] rather good agreement was found even for multi-layer chamber walls. Actually, IW2D computes in the range $f \in [5, 50]$GHz an imaginary part slightly smaller than the one given by the traditional RW-formula for mono-layers (Fig. 1) as well as for most multi-layer chamber walls.[1] The real part was slightly higher though.

Table 1: Vacuum Chambers Analyzed by IW2D

Chamber type	**Assumed Layers**
In-vac undulator(open/closed)	Cu/Ni/CoSm
NEG-coated Al-chamber	NEG/Al/Air
Ti-coated ceramic chamber	Ti/Al_2O_3/Air/Ferrit
Wiggler chamber	Cu/Air
Cavities	Cu/Air
Different SS[2]-chambers	SS/Air

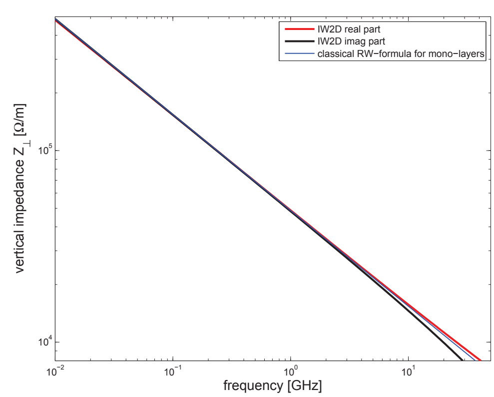

Figure 1: wall impedance of std vacuum chamber. At high frequency the imaginary part is smaller than both the real part and the one given by the classical RW-formula for mono-layers.

Geometrical Impedance

For the improvement of the geometrical impedance a revision of the geometrical models of the taper-dominated geometries and their annexes (table 2) was done. Furthermore, element geometries were equipped with the missing pump grids and their wake-fields simulated. They are all finally decomposed in monopolar, dipolar and quadrupolar

[1] formulas based on the work of [7]
[2] SS: stainless steel

ISBN: 978-3-95450-168-7 doi:10.18429/JACoW-IPAC2015-MOPJE027

Content from this work may be used under the terms of the CC BY 3.0 licence (© 2015). Any distribution of this work must maintain attribution to the author(s), title of the work, publisher, and DOI.

BEAM-BASED IMPEDANCE CHARACTERIZATION OF THE ALBA PINGER MAGNET

U. Iriso, T.F. Günzel, ALBA-CELLS, Cerdanyola de Vallès, Spain
E. Koukovini-Platia, H. Bartosik, G. Rumolo, CERN, Geneva, Switzerland

Abstract

The ALBA pinger magnet consists on two short kickers (for horizontal and vertical planes) installed in a single Titanium coated ceramic vacuum chamber. Single bunch measurements in the vertical plane were performed in the ALBA Synchrotron Light Source before and after the pinger installation, and by comparing the Transverse Mode Coupling Instability (TMCI) thresholds for zero chromaticity, we infer the pinger impedance and compare it with the model predictions.

INTRODUCTION

Coupling impedance calculations are a key issue when designing an accelerator, in particular for electron light sources, where the presence of numerous Insertion Devices (IDs) with very small gaps can limit the circulating beam intensity in the machine. Often, these IDs are not made of a single material, but they are composed of different materials in different layers. Therefore, it is important to evaluate the reliability of the computer codes that evaluate the impedance of these devices before their installation.

At ALBA, a pinger magnet has been installed during the summer shutdown of 2014 [1]. The pinger magnet is a multilayer structure composed by a ceramic vacuum chamber of 6.5 mm thickness, with an inner Titanium (Ti) coating of only 400 nm. This vacuum chamber is surrounded with a ferrite yoke [1], and between the ceramic and the ferrite there is a gap of 1 mm width for air cooling. This structure is exactly the same as the one used for the four injection kickers installed since day-1, with the only difference in the ferrite thickness surrounding the ceramic chambers [2].

Figure 1: Vertical (left) and horizontal (right) pinger magnet installed at ALBA during summer 2014. The ceramic chamber (in white) is visible between the two structures used for the vertical (left) and horizontal (right) excitations.

Figure 1 shows a picture of the pinger magnet, where the ceramic chamber is visible in the middle. The same vacuum chamber (780 mm in length) is used for the horizontal (left) and vertical kick excitations (right). The difference for each structure consists in the position of the Copper (Cu) electrodes, which are located on left/right for the horizontal excitation, and top/bottom for the vertical.

The goal of these studies is to infer the pinger magnet impedance based on beam measurements and compare it with results using different computer simulation codes (GdfidL, CST, and IW2D [3–5]). Beam-based impedance characterization of the pinger magnet are based on Transverse Mode Coupling Instability (TMCI) studies: by analysing the machine detuning and instability thresholds before the pinger installation (Autumn 2013) and after (Autumn 2014) we can infer the contribution of the new installed element to the total machine impedance.

BEAM-BASED MEASUREMENTS

TMCI Theory

Assuming a Gaussian beam bunch with N_b particles and rms length of σ_τ, the complex frequency shift in betatron frequency for the $l = 0$ mode is expressed by [6]

$$\Omega - \omega_\beta = -iZ_{\text{eff}} \frac{N_b e c^2}{4\sqrt{\pi}(E/e)T_0\omega_\beta\sigma_\tau}, \tag{1}$$

where $\omega_\beta = Q_\beta\omega_0$ the angular betatron frequency, Q_β is the betatron tune (including the integer part), ω_0 is the angular revolution frequency, E is the beam energy, c is the speed of light, and e the electron charge. The term Z_{eff} is the effective impedance of the machine, defined as:

$$Z_{\text{eff}} = \frac{\sum \beta_i Z_i}{\langle\beta\rangle}, \tag{2}$$

where Z_i, β_i refers to the impedance and beta function of the machine element i, respectively. Equation 1 shows that the imaginary part of Z_{eff} causes a tune shift with increasing bunch current, which allows to infer the total machine impedance, as already performed in other machines [6–8].

While the vertical detuning is proportional to $\text{Im}(Z_{\text{eff}})$, the threshold at which the instability occurs decreases with increasing the impedance (approximately like $1/Z_{\text{eff}}$). In general, there is no readily available formula relating the intensity threshold and the impedance, and this has to be inferred using computer simulation codes including bunch lengthening effects.

In the following, we focus our studies on the vertical plane because the pinger transverse aperture is 80 × 24 mm (horizontal × vertical), and thus the effect is much more critical in the vertical plane.

ISBN: 978-3-95450-168-7 doi:10.18429/JACoW-IPAC2015-MOPJE028

Content from this work may be used under the terms of the CC BY 3.0 licence (© 2015). Any distribution of this work must maintain attribution to the author(s), title of the work, publisher, and DOI.

DETAILED CHARACTERIZATION OF ALBA QUADRUPOLES FOR BETA FUNCTION DETERMINATION

Z.Martí*, J.Campmany, J. Marcos, V.Massana,
CELLS-ALBA Synchrotron, Cerdanyola del Vallès, Spain
X.Nuel, SOLEIL, Gif-sur-Yvette, France

Abstract

Beta function value at quadrupoles for a circular accelerator can be determined using the relationship between the machine tune and quadrupole strength variations. ALBA Storage Ring quadrupoles were measured during manufacturing, to be sure that their performance fitted the specifications. However, measurements were carried out at a limited number of current settings and do not allow an accurate determination of the beta function value. In fact, less than 1% error in the calibration of the hysteresis curve slope is required, and therefore new detailed measurements of the hysteresis cycle are needed. In order to make these magnetic measurements, the spare quadrupoles existing at ALBA have been used. In this paper we present the results of beta function values determination using this method for ALBA Storage Ring.

INTRODUCTION

Linear optic functions like beta functions are a common figure of merit to evaluate the performance of circular accelerators. At ALBA, the beta functions are measured using both an orbit response matrix method and Turn by Turn (TbT) data analysis [1–4]. Despite they agree at the level of $1-2\%$ rms, both methods are limited by characteristic systematic measurement errors.

On one side, the orbit response matrix method, in particular the Local Optics from Closed Orbit, known as LOCO, suffers from systematic errors as it is completely model dependent. As shown in [2] the systematic contribution to the beta beating is around 1% rms.

On the other side, the unknown gains of the BPM during the TbT acquisition can introduce considerable systematic measurement errors. Recently it has been shown that the gain issue may be solved using the phase information of the TbT data, achieving agreements with LOCO around 1% rms [5].

Given the limited accuracy of these two methods, at ALBA it has been decided to measure the beta function values also by measuring the tune changes due to quadrupole change. If the quadrupole integrated strength change $\Delta\, kL$ is small, the tune change can be expressed as follows, [6]

$$\Delta Q_{x,y} = \pm \frac{\left\langle \beta_{x,y} \right\rangle}{4\pi} \Delta kL, \tag{1}$$

where L is the length of the quadrupole and $\left\langle \beta_{x,y} \right\rangle$ the corresponding plane average beta function along the quadrupole that has been varied. This allows to measure the averaged beta function at each quadrupole. Assuming that the magnet calibration $kL(I)$ as a function of the current set point I is precisely known, Eq. (1) can be expressed as:

$$\left\langle \beta_{x,y} \right\rangle = \pm \frac{4\pi \Delta Q_{x,y}}{\Delta I \partial (kL)/\partial I}, \tag{2}$$

This well known technique encounters some difficulties:

1. It requires a very good knowledge of the calibration curves of the quadrupoles as it depends on its derivative.
2. The hysteresis effects after the quadrupole change may spoil subsequent measurements.
3. The measurement is limited by the tune jitter. The present ALBA performance is 2×10^{-4} rms. [4]
4. It is a very slow measurement.

As it is shown in this paper, the first three points can be greatly compensated. However, it is clearly a very slow measurement not suited for normal operation optics control. Nevertheless it could constitute a good bench mark method.

The paper is separated mainly in two sections. The first section describes the recent precise magnetic measurements of spare quadrupoles and the corresponding data processing. The second part describes the measurements done during this year dedicated machine time and how that agrees with LOCO beta functions at the quadrupoles position.

MAGNETIC MEASUREMENTS

The ALBA Storage Ring includes 112 quadrupoles, all of them with the same iron cross section, and which can be divided into four groups depending on the length of the iron yoke: 200, 260, 280 and 500 mm. All quadrupoles were magnetically characterized by the manufacturer (BINP) during the production process [7]. The harmonic content of each magnet was determined for 5–6 current settings between the maximum one (either 200 or 225 Amp depending on the iron length) and 50 Amp. From this data an average transfer function curve $GL(I)$ providing the integrated gradient strength for each iron yoke length as a function of the current setting was obtained.

In order to increase the accuracy of the $GL(I)$ curves, four spare quadrupoles —one for each iron yoke length— have been measured in detail at ALBA magnetic measurements laboratory. Measurements have been carried out on a rotating coil bench, using a shaft based on printed circuit coils designed and manufactured at ALBA, with a diameter

* zeus@cells.es

ISBN: 978-3-95450-168-7 doi:10.18429/JACoW-IPAC2015-MOPJE029

A LINEAR ACCELERATOR SIMULATION FRAMEWORK

J. Snuverink, John Adams Institute at Royal Holloway, University of London, Egham, UK
N. Fuster-Martinez, IFIC (CSIC-UV), Valencia, Spain
J. Pfingstner, CERN, Geneva, Switzerland and University of Oslo, Oslo, Norway

Abstract

Many good tracking tools are available for simulations for linear accelerators. However, several simple tasks need to be performed repeatedly, like lattice definitions, beam setup, output storage, etc. In addition, complex simulations can become unmanageable quite easily. A high level layer would therefore be beneficial. We propose LinSim, a linear accelerator framework with the codes PLACET and GUINEA-PIG. It provides a documented well-debugged high level layer of functionality. Users only need to provide the input settings and essential code and / or use some of the many implemented imperfections and algorithms. It can be especially useful for first-time users. Currently the following accelerators are implemented: ATF2, ILC, CLIC and FACET. This paper discusses the framework design and shows its strength in some condensed examples.

INTRODUCTION

When simulating linear accelerators or transport lines, one encounters repeating tasks that are basically the same for each simulation such as:

- Setting up the model of the beamline and the beam
- Specifying and saving simulation parameters
- Implementing a scripting structure to simulate typical scenarios
- Implementing of correction techniques
- Implementing imperfections such as ground motion and component imperfections
- Maintaining scripts to ease computing on a server farm
- Evaluating the results
- Performing backups and keeping track of changes

All these tasks are usually repeated for each simulation project that is started. As a result, there are a large number of implementations of very similar code in each beam physics team, which reduces the productivity significantly.

Instead of this approach, a unified simulation framework for linear accelerators based on PLACET [1, 2] and GUINEA-PIG [3], named LinSim, is described in this paper. It automates the mentioned tasks and takes a large (re)implementation burden away from the user. The user needs only to specify simulation settings and to add the minimal specific code for the given problem.

Additionally, many correction techniques (e.g. orbit feedbacks, IP feedbacks, dispersion free steering, wakefield alignment, and many other) are already implemented or need to be implemented only once, which increases productivity and leads to well debugged code.

Furthermore, LinSim includes more features than would usually be written, e.g. consistency input parameter checks, automated settings storing to be able to reproduce the results at a later stage, revision control, scripts for analysis of results and many others. This helps to increase the productivity of the user. Especially (but not only) for newcomers, LinSim is an enormous starting help, since they don't have to know all the details of the already provided simulation scripts.

FRAMEWORK STRUCTURE

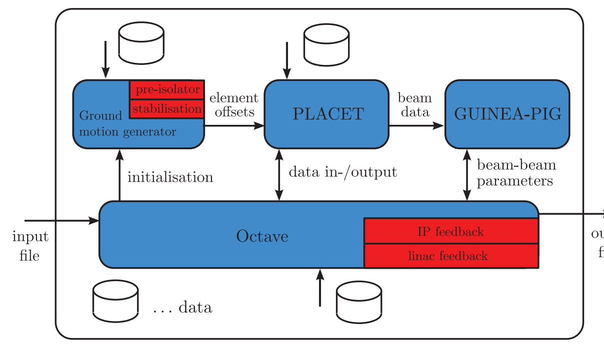

Figure 1: Internal structure of LinSim, where scripts (written in Tcl and Octave) interface the simulation codes PLACET, a ground motion generator, and GUINEA-PIG. An input file is used to control the simulations that use additional data such as lattice files and created standardised output files.

The structure of the framework is illustrated in Fig. 1. It consists of a set of scripts written in Tcl [4] and Octave [5] that interface different simulation codes: PLACET is used for the beam tracking, a ground motion simulator [6] (which has been ported to C++ and is now included in PLACET) generates realistic element misalignments, and GUINEA-PIG facilitates beam-beam simulations. Several types of imperfections are implemented and can be turned on and off. Also, many algorithms for the correction of these imperfections, e.g. beam-based alignment and orbit feedbacks, have been put in place. LinSim also provides the lattice, beam and additional information for the accelerators ATF2 [7], CLIC [8], FACET [9], and ILC [10].

SIMULATION STRUCTURE

A typical simulation consists of two components as depicted in Fig. 2. The first part is a set of provided scripts that make up LinSim itself, together with provided lattice files and additional data as, e.g. orbit response matrices. The entry point to LinSim is the script `run.tcl`, which is executed with PLACET. The second element of a simulation is the user specific test, which consists of two files: a settings file and a code file (e.g. `test_settings.tcl` and

Content from this work may be used under the terms of the CC BY 3.0 licence (© 2015). Any distribution of this work must maintain attribution to the author(s), title of the work, publisher, and DOI.

ISBN: 978-3-95450-168-7 doi:10.18429/JACoW-IPAC2015-MOPJE030

NON-LINEAR DYNAMICS MODEL FOR THE ESS LINAC SIMULATOR

E. Laface* ESS, Lund, Sweden

Abstract

The ESS Proton Linac will run a beam with 62.5 mA of current. In the first meters of the accelerator, the non-linear space-charge force dominates the dynamics of the beam. The Drift Tube Linac, the Spoke resonators and the elliptical cavities, which are responsible for the 99.8% of the total energy gained by the beam along the accelerator, produce a significant longitudinal non-linear force on the proton beam. In this paper, we introduce a new theory to transport the probability density function of the beam under the effect of non-linear forces. A model based on this theory can be implemented in the ESS Linac Simulator for the fast simulations to be performed during the operations of the proton Linac.

INTRODUCTION

The success of the Courant-Snyder theory with particle accelerators is due to the simple connection between the dynamics of one particle and the dynamics of a beam. A single particle is fully described by the vector of its coordinates and momenta at a given time:

$$\vec{v} = (q_1 q_2 \dots q_n p_1 p_2 \dots p_n)^T . \tag{1}$$

If $\mathcal{H}$ is the Hamiltonian, the equations of motion can be expressed as

$$\frac{d}{dt}\vec{v} = S \cdot \vec{\partial}\mathcal{H} \tag{2}$$

where $\vec{\partial}$ and S are defined as

$$\vec{\partial} = (\partial/\partial q_1 \partial/\partial q_2 \dots \partial/\partial q_n \partial/\partial p_1 \partial/\partial p_2 \dots \partial/\partial p_n)^T \tag{3}$$

$$S = \begin{pmatrix} 0 & I \\ -I & 0 \end{pmatrix}. \tag{4}$$

When the Hamiltonian is quadratic in coordinates and momenta, $\mathcal{H} = f({q_i}^2, {p_i}^2)$, it can be written as $\vec{\partial}H = A \cdot \vec{v}$, where A is a matrix. The equations of motion become

$$\frac{d}{dt}\vec{v} = S \cdot A \cdot \vec{v} \tag{5}$$

with the solution

$$\vec{v}(t) = e^{tSA} \cdot \vec{v}(0) \tag{6}$$

$$M(t) = e^{tSA} \tag{7}$$

$$\vec{v}(t) = M(t) \cdot \vec{v}(0). \tag{8}$$

In this case, $M(t)$ is the transport matrix that effects the changes of coordinates and momenta for each linear element of the accelerator.

Because of the linear nature of Eq. (8), it is possible to use the same matrix $M(t)$ to transport the r.m.s. of a bunch of particles using equation [1]:

$$\begin{pmatrix} \sigma_x^2 & \sigma_x\sigma_{x'} \\ \sigma_x\sigma_{x'} & \sigma_{x'}^2 \end{pmatrix}_t = M \begin{pmatrix} \sigma_x^2 & \sigma_x\sigma_{x'} \\ \sigma_x\sigma_{x'} & \sigma_{x'}^2 \end{pmatrix}_0 M^T \tag{9}$$

here we only consider one dimension, using the standard notation $x = q_x$ and $x' = \frac{p_x}{p_z}$, where q_x and p_x are the respective conjugate coordinate and momentum in the horizontal plane x and p_z is the momentum in the direction of motion of the particles.

When the force is non-linear, $\mathcal{H} \neq f({q_i}^2, {p_i}^2)$, Eqs. (8) and (9) are no longer valid. In the following sections, we will show how to construct a general solution for the equations of motion of a bunch of particles, starting from the solution of the equation for a single particle, generalising the Eq. (9) for the case of non-linear forces.

BEAM DENSITY

Let us assume that we were able to solve the equation of motion in (2) in the case of a non-linear force, that is, when $\mathcal{H} \neq f({q_i}^2, {p_i}^2)$. We will then have an equation of motion for a single particle in the form

$$\vec{v}(t) = f(\vec{v}(0)) \tag{10}$$

where f is

$$f : \mathbb{R}^{2n} \to \mathbb{R}^{2n} \tag{11}$$

with n coordinates and momenta; for all the practical cases $n = 3$.

In order to pass from the single-particle solution to one with many particles, we start by considering an invariant of a beam: the number of particles. This number will not change along the accelerator unless the losses are a significant fraction of the total number of particles. If ρ_{ps} is the probability density function of the beam in the phase space, the number of particles can be expressed as:

$$N = \int_{\mathbb{R}^{2n}} \rho_{ps} dq_1 dq_2 \dots dq_n dp_1 dp_2 \dots dp_n. \tag{12}$$

We know from the Liouville theorem that if the dynamics is symplectic then the volume of the phase space is preserved. Thus, any dynamics that apply it will keep the quantity $dq_1 dq_2 \dots dq_n dp_1 dp_2 \dots dp_n$ constant. On the other hand, we also know that the number of particles is preserved in the physical space and in the momentum space separately:

$$N = \int_{\mathbb{R}^n} \rho_r dq_1 dq_2 \dots dq_n \tag{13}$$

$$N = \int_{\mathbb{R}^n} \rho_m dp_1 dp_2 \dots dp_n \tag{14}$$

where ρ_r and ρ_m are the beam density in the real space and in the momentum space, respectively. These two integrals are invariant all along the machine and we can express this invariance by saying that at any time t the following

* Emanuele.Laface@esss.se

Content from this work may be used under the terms of the CC BY 3.0 licence (© 2015). Any distribution of this work must maintain attribution to the author(s), title of the work, publisher, and DOI.

ISBN: 978-3-95450-168-7 doi:10.18429/JACoW-IPAC2015-MOPJE031

Content from this work may be used under the terms of the CC BY 3.0 licence (© 2015). Any distribution of this work must maintain attribution to the author(s), title of the work, publisher, and DOI.

FIELD MAP MODEL FOR THE ESS LINAC SIMULATOR

E. Laface* ESS, Lund, Sweden
I. List, Cosylab, Ljubljana, Slovenia

Abstract

The proton beam driving the spallation process at the European Spallation Source, in Lund, will be accelerated and delivered onto a tungsten target by a linac. This linac is composed of four different families of accelerating structures: a drift tube linac, a section of spoke resonators and two sections of elliptical cavities for the particles' medium and high relativistic β. These structures provide 99.8% of the total energy gained by the beam along the accelerator. It is necessary, then, to have an accurate model describing the physics of the cavities in the ESS Linac Simulator (ELS), which is the online model that will simulate the accelerator during operation. Here, we present an RF-cavity model based on the field maps that we implemented in ELS, showing a maximum 10% deviation from TraceWin in the horizontal, vertical and longitudinal planes.

INTRODUCTION

In order to accurately model the accelerating components used in the ESS Proton Linac, the beam physics team is adopting a description of the electromagnetic field based on one-dimensional maps. Each spoke resonator and RF cavity is characterized by a file containing the value of the longitudinal electric field measured along the axis of symmetry (z axis). This field has a sinusoidal behaviour in the inner part of a cavity and an exponential decay on the two ends, as described in [1].

These field maps are then used to calculate the matrix representing the linear part of the equations of motion of a particle subjected to each field. The result is used to transport the beam envelope by applying the matrix of the linear elements to the covariant matrix of the beam.

To calculate the equations of motion we used two different approaches: the first evaluates the contribution of each step of the field map on the variation of the x', y' and z' momenta components for a particle, applying it as thin kicks. With this method, more precise cavity sampling improves accuracy. The second approach is to integrate the field in a certain number of cells (the NCell method), using the Transit Time Factor [2] to evaluate the proper phase and energy changes between cells. Each cell is then treated as a thin accelerating gap in the middle of a drift.

Both methods are then compared with the code used for the design of the ESS Proton Linac—TraceWin [3]—which can simulate the same kind of field maps.

* Emanuele.Laface@esss.se

FIELD MAPS

The transversal normalized momenta can be written in the paraxial approximation as

$$x' = \frac{dx}{ds} = \frac{dx/dt}{ds/dt} \approx \frac{p_x}{p_s} \tag{1}$$

$$y' = \frac{dy}{ds} = \frac{dy/dt}{ds/dt} \approx \frac{p_y}{p_s} \tag{2}$$

we will evaluate x', noting that the same treatment is valid for y'. The variation of momentum in x is given by

$$\begin{aligned}\frac{dx'}{ds} &\approx \frac{d(p_x/p_s)}{ds} = \frac{d(p_x/p_s)}{dt}\frac{dt}{ds} = \frac{\dot{p}_x p_s - p_x \dot{p}_s}{p_s^2}\frac{dt}{ds} \\ &\approx \frac{1}{\beta_s c}\frac{\dot{p}_x - x'\dot{p}_s}{p_s} = \frac{\dot{p}_x - x'\dot{p}_s}{\gamma_s \beta_s^2 mc^2}\end{aligned} \tag{3}$$

where β_s and γ_s are the relativistic parameters of the particle traveling in the s direction and the dot represents the time derivative.

The $\dot{p}_x$ and $\dot{p}_z$ components can be evaluated in terms of the Lorentz force

$$\frac{d\vec{p}}{dt} = q\left(\vec{E} + \frac{\vec{p}}{\gamma m} \times \vec{B}\right) \tag{4}$$

and, again using the paraxial approximation $p_z \approx p_s$, which is valid for the transverse plane, we have

$$\dot{p}_x = q\left(E_x + \frac{p_y B_z - p_z B_y}{\gamma m}\right) \approx q\left(E_x + p_s \frac{y' B_z - B_y}{\gamma m}\right) \tag{5}$$

and

$$\dot{p}_s = q\left(E_z + \frac{p_x B_y - p_y B_x}{\gamma m}\right) \approx q\left(E_z + p_s \frac{x' B_y - y' B_x}{\gamma m}\right) \tag{6}$$

where the quantities $x' B_y$ and $y' B_x$ are always zero because the velocity is parallel to the magnetic field, then

$$\dot{p}_s = qE_z. \tag{7}$$

Substituting Eqs. (5) and (7) into (3) we have

$$\frac{dx'}{ds} = \frac{q}{\gamma_s \beta_s^2 mc^2}\left(E_x + p_s \frac{y' B_z - B_y}{\gamma m} - x' E_z\right). \tag{8}$$

For our model, we are interested in the linear part of the fields where the following equations hold

$$E_x = \frac{\partial E_x}{\partial x} x, \quad E_y = \frac{\partial E_y}{\partial y} y \tag{9}$$

$$E_z = E_{z0}(s)\cos(\omega t + \phi) \tag{10}$$

$$B_x = \frac{\partial B_x}{\partial y} y, \quad B_y = \frac{\partial B_y}{\partial x} x \tag{11}$$

$$B_z = 0 \tag{12}$$

and where ω is the frequency of the cavity and ϕ is the phase. Substituting these equations into Eq. (8), we have

$$\frac{dx'}{ds} = \frac{q}{\gamma_s \beta_s^2 mc^2}\left(\frac{\partial E_x}{\partial x} x - \beta_s c \frac{\partial B_y}{\partial x} x - x' E_z\right). \tag{13}$$

ISBN: 978-3-95450-168-7 doi:10.18429/JACoW-IPAC2015-MOPJE032

A STEERING STUDY FOR THE ESS NORMAL CONDUCTING LINAC

R. Miyamoto*, ESS, Lund, Sweden

Abstract

Construction of the European Spallation Source is rapidly progressing in Lund, Sweden, and preparations for commissioning of its proton linac has been underway for some time now. Accurate adjustment of accelerator components to achieve ideal beam parameters is the key to maximizing performance and safe operation for any machine. This paper presents a study of beam steering for the normal conducting part of the proton linac of ESS.

INTRODUCTION

The European Spallation Source (ESS) will be a neutron source based on a 5 MW proton linac. The facility is currently under construction in Lund, Sweden and preparations for the beam commissioning are also progressing. For such a high power machine, it is the key to successful commissioning and operation to minimize beam losses and protect its components by properly adjusting the electromagnetic elements and achieving ideal beam parameters. Figure 1 shows a schematic layout of the linac of ESS and some of the high level parameters. The initial part of the linac is consist of normal conducting structures and this paper presents a study of beam steering in this part of the linac as a part of the ongoing preparations for the beam commissioning. The ion source (IS) and radio frequency quadrupole (RFQ) have nothing to adjust the beam trajectory. The low energy beam transport (LEBT) has only two dipole magnet steerers and thus the steering in the LEBT is relatively simple. Therefore, the focus of this paper is on the steering in the medium energy beam transport (MEBT) and drift tube linac (DTL).

STEERING IN MEBT

Figure 2 shows the zero current phase advances of transverse planes within the MEBT, together with a lattice schematic. This lattice is a version in 2014 [1] and has ten identical quadrupoles and an additional one surrounding the chopper. Each of ten quadrupoles is equipped with a dual-plane BPM and additional coils to produce dipole fields and steer the beam in both plane. Please note that, after evaluations in terms of beam dynamics and engineering design, it has been decided that the chopper and the quadrupole around it is separated. Hence, from the next version, the same quadrupole as other ten will be placed right after the chopper and the numbers of BPMs and steerers per plane will be increased to eleven. To identify which BPMs and steerers are essential to achieve a good steering, cases with reduced numbers of BPMs and steerers were studied and the yellow markers in Fig. 2 represent the BPM locations of one such cases with six BPMs and steerers per plane. The

* ryoichi.miyamoto@esss.se

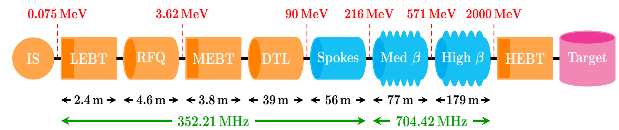

Figure 1: Schematic of the linac of ESS. Sections of superconducting cavities are in blue and those of normal conducting structures are in orange.

steerers used in this case are ones in quadrupole numbers 1, 2, 5, 7, 9, and 10.

Figure 3 shows RMS trajectories in the MEBT and the initial part of the DTL after the steering is applied to one thousand linacs with errors in the lattice elements and the parameters of the beam out of the RFQ. The layout of BPMs and steerers in the DTL used in this calculation is the new one, which is discussed in the next section. In 2014, a campaign of studies about impacts of the lattice element errors on beam quality and beam losses was conducted [2–4] and the values referred to as *tolerances* in these articles are used as the errors in this calculation. The exceptions are the dynamic errors of the cavities and inaccuracy in BPMs, to observe the effects of just the layout and the algorithm of steering. The calculations of the trajectories were done with the TraceWin code [5]. For the MEBT, the steering was done with the simplest way of minimizing the position at one BPM with one steering and performing this process one by one from the first steerer to the last (referred to as *one-to-one steering* in the following). If the layout of BPMs and steerers is adequate, this method should provide a reasonably good steering and this is indeed the case as seen in Fig. 3, even for the layout of the reduced numbers of the BPMs and steerers. The anticipated inaccuracy of the BPMs is on the order from a few hundred μm to a half mm so this will have a larger impact in the real machine. Please note that there is a small peak around ~1.2 m on the horizontal plane. This

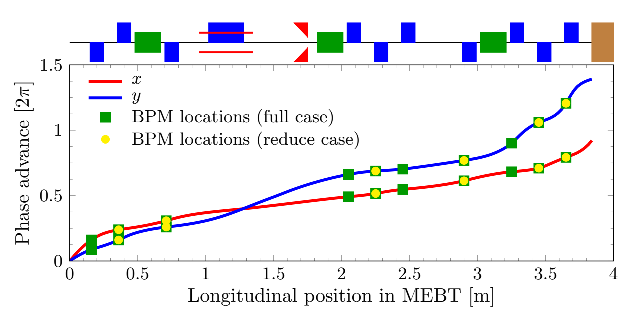

Figure 2: Zero current phase advances within the MEBT and a MEBT lattice schematic, where the blue boxes above (below) the line are the focusing (defocusing) quadrupoles, green boxes are the buncher cavities, and the red lines and triangles are the chopper and its dump.

Content from this work may be used under the terms of the CC BY 3.0 licence (© 2015). Any distribution of this work must maintain attribution to the author(s), title of the work, publisher, and DOI.

ISBN: 978-3-95450-168-7 doi:10.18429/JACoW-IPAC2015-MOPJE033

Content from this work may be used under the terms of the CC BY 3.0 licence (© 2015). Any distribution of this work must maintain attribution to the author(s), title of the work, publisher, and DOI.

COUPLED ORBIT RESPONSE COEFFICIENTS WITH CONSTANT REVOLUTION TIME

V. Ziemann, Uppsala University, Uppsala, Sweden

Abstract

We calculate orbit response coefficients for arbitrarily coupled lattice which keep the orbit length constant as is needed to maintain synchronicity with a radio-frequency system.

INTRODUCTION

In a circular accelerator the orbit correction system and diagnostic tools such as CALIF [1] or LOCO [2] rely on the knowledge of how steering magnets affect the beam position measured at beam position monitors (BPM). Historically the so-called response coefficients C^{ij} or response matrix elements between steering magnet labeled j and BPM i can be expressed in terms of TWISS parameters or transfer matrices by

$$C^{ij} = R^{ij}(1 - R^{jj})^{-1} \tag{1}$$

where R^{ij} is the transfer matrix from location j to location i and R^{jj} is the full-turn matrix starting at location j. Equation 1 does not constrain the revolution time, despite the fact that for example a horizontal steering magnet with kick angle θ^j lengthens the circumference by $D^j\theta^j$, where D^j is the dispersion at the steering magnet [3, 4]. This can be accommodated in the response coefficient by an additional term to Eq. 1 containing the dispersion at the location of the steering magnet and the BPM

$$C^{ij}_{12} = \left[R^{ij}\left(1 - R^{jj}\right)^{-1}\right]_{12} - \frac{D^i D^j}{\eta C} \tag{2}$$

with the ring circumference C and the the phase slip factor η.

In this note we generalize this expression to the fully coupled case.

COUPLED CASE

The six-dimensional full-turn matrix R^{jj} starting at location j maps the orbit vector $\vec{x} = (x, x', y, y', \tau, \delta)$ onto itself after one turn. If there is a perturbation vector $\vec{v}$ present at location j the requirement for a periodic solution reads

$$\vec{x} = R^{jj}\vec{x} + \vec{v}\,. \tag{3}$$

Note that the requirement to have equal entries in the arrival time and energy location, constrains the revolution time to be constant. The solution to this equation is given by $\vec{x} = (1 - R^{jj})^{-1}\vec{v}$ and the top left 4×4 part of $(1 - R^{jj})^{-1}$ is the response matrix which constrains the revolution time. This is well-known and used for example in the accelerator toolbox [5] to determine the closed orbit.

In order to find a generalized version of Eq. 2 and express the response coefficients in terms of the dispersions we need to split Eq. 3 in a transverse and longitudinal part. To achieve this we write the matrix R^{jj} in terms of its 2×2 sub-matrices

$$R^{jj} = \begin{pmatrix} A & B & C \\ D & E & F \\ G & H & I \end{pmatrix} \tag{4}$$

and split the equation into a transverse and a longitudinal part

$$\begin{aligned} |x\rangle &= \hat{R}\,|x\rangle + \begin{pmatrix} C \\ F \end{pmatrix}\begin{pmatrix} \tau \\ \delta \end{pmatrix} + |v\rangle \\ \begin{pmatrix} \tau \\ \delta \end{pmatrix} &= (G, H)\,|x\rangle + I\begin{pmatrix} \tau \\ \delta \end{pmatrix}\,. \end{aligned} \tag{5}$$

here $|x\rangle$ denotes the transverse part of the closed orbit vector $\vec{x}$. Solving the second, longitudinal equation for τ and δ, inserting in the first equation and collecting terms we arrive at

$$\left[1 - \hat{R} - \begin{pmatrix} C \\ F \end{pmatrix}(1 - I)^{-1}(G, H)\right]|x\rangle = |v\rangle \tag{6}$$

The matrix in the square brackets is the inverse of the response matrix c^{jj}. To express it in terms of the dispersion we first need to identify the dispersions in a coupled ring. It is given by the periodic orbit vector subjected to the perturbation defined by the $R_{i,6}$ matrix elements, namely

$$|D\rangle = \hat{R}\,|D\rangle + \begin{pmatrix} R_{16} \\ R_{26} \\ R_{36} \\ R_{46} \end{pmatrix}. \tag{7}$$

Consequently we introduce the dispersion-like quantities with a tilde on top

$$\begin{pmatrix} \tilde{C} \\ \tilde{F} \end{pmatrix} = (1 - R)^{-1}\begin{pmatrix} C \\ F \end{pmatrix}. \tag{8}$$

and note that the right column of $\tilde{C}$ and $\tilde{F}$ contains the dispersions. This leads to

$$\left[1 - \begin{pmatrix} \tilde{C} \\ \tilde{F} \end{pmatrix}(1 - I)^{-1}(G, H)\right]|x\rangle = (1 - R)^{-1}|v\rangle \tag{9}$$

and the special form of the matrix in the square brackets permits us to explicitly calculate its inverse with the result

$$|x\rangle = \left[1 + \begin{pmatrix} \tilde{C} \\ \tilde{F} \end{pmatrix} Q\,(1 - I)^{-1}(G, H)\right](1 - R)^{-1}|v\rangle \tag{10}$$

where Q is given by

$$Q = \left[1 - (1 - I)^{-1}\left(G\tilde{C} + H\tilde{F}\right)\right]^{-1}. \tag{11}$$

ISBN: 978-3-95450-168-7 doi:10.18429/JACoW-IPAC2015-MOPJE034

LOW EMITTANCE TUNING FOR THE CLIC DAMPING RINGS*

J. Alabau-Gonzalvo, F. Antoniou, Y. Papaphilippou, CERN, Geneva, Switzerland

Abstract

A study on the sensitivity of the CLIC Damping Ring lattice to different sources of misalignment is presented. Dipole and quadrupole rolls, quadrupole and sextupole vertical offsets are considered, as well as the impact of a finite BPM resolution. The result of this study defines a low emittance tuning procedure and establishes alignment tolerances to preserve the vertical emittance below the design value (1 pm·rad). Non-linear dynamics studies including dynamic aperture and frequency maps are shown and synchrotron radiation effects are discussed.

INTRODUCTION

The design of the Damping Ring (DR) for a future linear collider foresees unprecedent small emittances. For the CLIC DRs, the zero-current equilibrium vertical emittance is $\gamma\epsilon_y$ = 3.7 nm·rad as compared to the target of 5 nm·rad, providing enough margin for the observed growth due to IBS at the nominal current [1]. This corresponds to an ultralow vertical emittance of around 0.7 pm·rad at the DR energy of 2.86 GeV.

Alignment of the magnetic elements is crucial for reaching this ultra-low vertical emittance. The goal of this study is to define a correction procedure for a realistic machine in order to achieve the design emittance, thus identifying the target misalignment tolerances.

The CLIC DR is a racetrack lattice with Theoretical Minimum Emittance cells in the arcs and superconducting wigglers in the long straight sections. The lattice has BPMs located near the quadrupoles in the straight section FODO cells and in points of alternated high and low dispersion and beta functions in the arcs corresponding to a total of 358 monitors along the machine. Alternated horizontal and vertical orbit correctors are installed close to the straight section quadrupoles, and additional windings in the sextupoles are used for correcting both planes in the arcs, with a total of 320 vertical and 312 horizontal orbit correction knobs. Skew quadrupole correctors are installed as well as additional windings in the sextupoles. The first section of this paper explains the main differences between the previous low emittance tuning and the actual one. The results before and after applying BPM finite resolution are presented in the second section. Lastly, the non-linear behaviour of the lattice is studied with dynamic aperture (DA) and frequency maps.

* The research leading to these results has received funding from the European Commission under the FP7 Research Infrastructures project EuCARD-2, grant agreement no.312453.

LOW EMITTANCE TUNING

As introduced in previous studies [2], four kinds of misalignment are being considered:

- Quadrupole vertical offsets
- Quadrupole transverse rolls
- Dipole transverse rolls
- Sextupole vertical offsets

With respect to the previous low emittance tuning studies the coupling correction procedure has evolved in order to make it more realistic by including BPM finite resolution. Previously, the correcting method cancelled the $\langle xy\rangle$ element from the one turn transfer matrix in each BPM. This parameter was taken directly from MADX [3] and the explicit dependence with the BPM resolution is not straightforward. Now the coupling is corrected along with the dispersion and it is made directly from position measurements taken from the monitors. The response submatrix corresponding to the coupling (C) is built by measuring the change in the beam vertical position at every BPM (Δ_y) when each skew quadrupole is sequentially activated (k_{skew}), while the beam is being horizontally kicked at a fixed point:

$$\begin{pmatrix} \Delta y \\ w \cdot \Delta D_y \end{pmatrix} = \begin{pmatrix} C \\ w \cdot D \end{pmatrix} \cdot (k_{skew}) \qquad (1)$$

The algorithm foresees a weight w between dispersion and coupling correction. The optimization of this weight has been done for each kind of misalignment looking at the value that minimised the vertical emittance. The chosen optimal weight is $w = 2.1$, which corresponds to the optimal correction of the coupling due to vertical quadrupole offset since the lattice is most sensible to it.

SIMULATION RESULTS

Once the correction is applied, the four coupling elements of the one turn transfer matrix are visibly flattened and the maximum error in the dispersion is lowered by a factor 8. The beta beating is also lowered from a maximum value of 5.6% to a 0.13%. The maximum pole tip field after 200 misaligned lattices (using a set of RMS errors equal to the found tolerances, see next section) was 0.03 T for an aperture of 20 mm, which is well within the feasible limits.

Simulations have been done averaging over 200 machines for each of the four misalignment considered, which were distributed according to a 2.5σ truncated Gaussian.

Figure 1 shows the result of applying each error independently. The geometrical vertical emittance as a function of the RMS error is plotted for the uncorrected lattice in solid red line and for the corrected in solid light blue. The

Content from this work may be used under the terms of the CC BY 3.0 licence (© 2015). Any distribution of this work must maintain attribution to the author(s), title of the work, publisher, and DOI.

ISBN: 978-3-95450-168-7 doi:10.18429/JACoW-IPAC2015-MOPJE035

Content from this work may be used under the terms of the CC BY 3.0 licence (© 2015). Any distribution of this work must maintain attribution to the author(s), title of the work, publisher, and DOI.

AN EXTENDED SPS LONGITUDINAL IMPEDANCE MODEL

José E. Varela, T. Argyropoulos, T. Bohl, F. Caspers, J. F. Esteban Müller, J. Ghini, A. Lasheen, D. Quartullo, B. Salvant, E. Shaposhnikova, C. Zannini, CERN, Geneva, Switzerland

Abstract

Longitudinal multi-bunch instability in the CERN SPS with a very low intensity threshold is a serious limitation for the future doubling of bunch intensity required by the HL-LHC project. A complete and accurate impedance model is essential to understand the nature of this instability and to plan possible cures. This contribution describes the current longitudinal impedance model of the SPS. Electromagnetic simulations and bench measurements were used to build the model. The contribution from each element is described and compared to the total machine impedance. Together with relevant beam measurements and simulations, the analysis of the different sources of impedance is used to identify the source of the longitudinal instability limiting the SPS performance so that the responsible elements can be acted upon.

INTRODUCTION

At the end of the LHC Run 1 in 2012 the beam with 25 ns bunch spacing and with an intensity of 1.3×10^{11} p/b was successfully accelerated in the SPS. However, for the intensity of HL-LHC ($\sim 2.5 \times 10^{11}$), the SPS bunches will be too long for the LHC capture with the existing 400 MHz RF system. This limitation comes from beam loading and longitudinal beam instabilities in the SPS. As a part of the LHC Injectors Upgrade (LIU) project [1], instabilities were studied by means of beam measurements and simulations [2,3]. The simulations rely on having an accurate impedance model of the machine. This paper describes the current status of the SPS longitudinal impedance model which was recently updated with the contribution from the vacuum flanges [4]. This model is then used in macroparticle simulations and the results are compared to beam measurements.

LONGITUDINAL IMPEDANCE MODEL

The longitudinal impedance model of the SPS currently accounts for the accelerating and Landau cavities, the extraction kickers, the vacuum flanges, the Beam Position Monitors (BPM), the pumping ports, the so-called Y-chambers, the beam scrapers and resistive wall as well as space charge impedance at low energy. The main contributors are the accelerating cavities, the extraction kickers and the vacuum flanges. Recently, the focus has been put on the accurate characterization of the Higher Order Modes (HOM) of the RF cavities and on the electrostatic and magnetic septa.

Cavities

The SPS has two RF systems, four 200 MHz Traveling Wave Cavities (TWC) and two 800 MHz TWC. The existing impedance model for the fundamental pass-band of the cavities is [5]

$$Z(\omega) = R\left[\left(\frac{\sin(\tau/2)}{\tau/2}\right)^2 - 2j\frac{\tau - \sin(\tau)}{\tau^2}\right], \qquad (1)$$

with $\tau = (\omega - \omega_0)l/v_g(\omega)$, where l is the length of the cavity, $v_g(\omega)$ is the frequency dependent group velocity and R the impedance at the center frequency ω_0. This model assumes perfect main coupler matching to the traveling wave inside the cavity. It has to be highlighted that the dependence on frequency of the group velocity is specially important for the 200 MHz cavities, as it introduces a significant asymmetry in the impedance spectrum.

There are two $\sim$ 16 m and $\sim$ 20 m long 200 MHz cavities. They have $R = 875$ kΩ and $R = 1.4$ MΩ, respectively. The 800 MHz cavities are $\sim$ 3 m long and are modeled with $R = 970$ kΩ. Finally, there is one known longitudinal HOM in the 200 MHz cavities at 629 MHz. With the existing HOM damping, this HOM can be described as a resonator with $R = 108$ and 86 kΩ and $R/Q = 430$ and 346 Ω for the long and short cavities, respectively.

The black lines in Fig. 1 show the modulus of the total longitudinal impedance of the SPS in both linear and logarithmic scales. The two biggest peaks, at 200 and 800 MHz, are the contributions from the fundamental pass-bands of the cavities.

Kickers

The SPS kickers are the biggest source of longitudinal broadband impedance. A fast extraction kicker system was

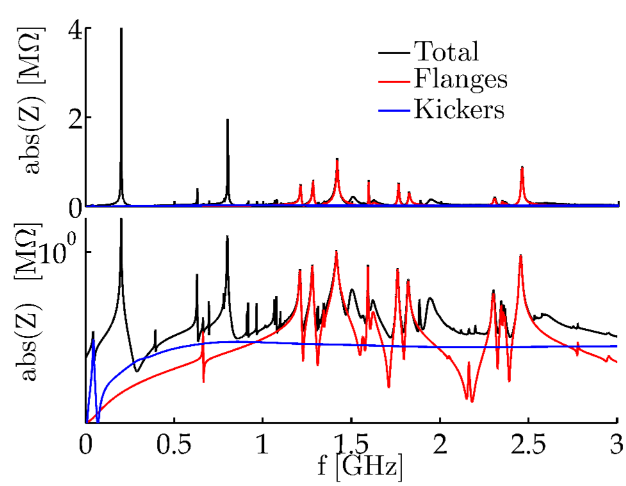

Figure 1: Modulus of the current longitudinal impedance of the SPS. The red and blue traces show the contribution of the vacuum flanges and the kickers, respectively. The top and bottom plots show the impedance in linear and logarithmic scale, respectively.

ISBN: 978-3-95450-168-7 doi:10.18429/JACoW-IPAC2015-MOPJE036

LONGITUDINAL IMPEDANCE CHARACTERIZATION OF THE CERN SPS VACUUM FLANGES

José E. Varela, CERN, Geneva, Switzerland

Abstract

This contribution describes the thorough studies carried out to characterize the longitudinal impedance of the CERN SPS vacuum flanges, which are believed to be the main source of LHC beam instability. Around 600 high-impedance flanges of 12 different types have been identified. Not only, full-wave electromagnetic field simulations, but also RF measurements have been used to evaluate the impedance of these elements. The R/Q of the relevant resonances was measured using the well-known bead-pull technique. In particular, a subset of ~ 150 flanges has been found to be the source of a high-impedance resonance at 1.4 GHz, also observed in beam measurements. Two possible ways of reducing the impedance of these elements are currently under consideration and will be briefly discussed here.

INTRODUCTION

Longitudinal multi-bunch instability in the CERN SPS with a very low intensity threshold is a serious limitation for the future doubling of bunch intensity required by the HL-LHC project. During the past years, a lot of effort has been put into studying this instability by means of beam dynamics simulations [1]. Self-evidently, these simulations rely on having an accurate impedance model of the machine. This contribution describes the longitudinal coupling impedance of the elements which are believed to be the source of the instability.

The longitudinal coupling impedance of the interconnects between the different types of vacuum chambers in the SPS was already studied by G. Dôme in 1973 [2]. As a result, cylindrical resistors were placed all around the ring to damp the resonances created by the aforementioned interconnects. In 2001, around 800 pumping ports were shielded in a huge impedance reduction campaign as they were limiting the performance of the SPS [3]. Currently, the multi-bunch instability threshold is reached at $\sim 3 \times 10^{10}$ p/b. To reach the nominal intensity of 1.15×10^{11} both, the 800 MHz cavities and controlled longitudinal emittance blow up are used. The SPS bunches will be too long for the LHC to capture for the requested intensity of HL-LHC (2.5×10^{11}). As part of the LHC Injectors Upgrade (LIU) project [4], one of the potential cures for this problem is to reduce the impedance of the vacuum flanges [5].

LONGITUDINAL COUPLING IMPEDANCE CHARACTERIZATION

Classification of the Vacuum Flanges

The vacuum flanges in the SPS can be divided in two main groups depending on the vacuum chambers that they interconnect. Small (83 mm inner diameter) circular cross-section chambers are referred to as QD beam pipes. Similarly, elliptical and quasi-rectangular cross sections are named QF and MBA beam pipes. Flanges interconnecting two QD vacuum chambers, as the one shown in Fig. 1 (a), belong to group I. On the other hand, flanges interconnecting any combination of MBA and QF chambers, see Fig. 1 (b) and (c), belong to group II. Groups I and II contain approximately 400 and 240 flanges respectively. Each group is further divided into six different flange types. Finally, a number of flanges in the SPS have an enamel coating. The enamel is used to electrically isolate both sides of the flange. These flanges are part of the grounding scheme of the SPS which minimizes the effect of eddy currents.

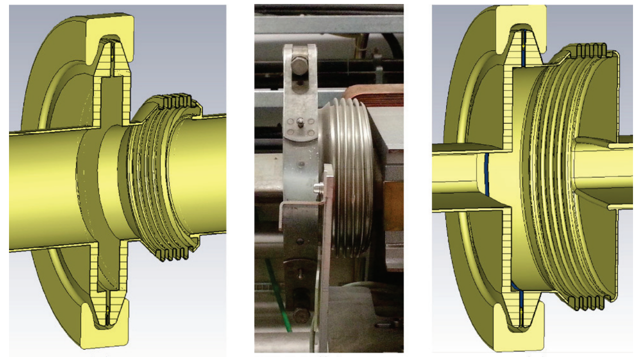
(a) (b) (c)

Figure 1: SPS vacuum flanges. (a) Model of a QD-QD flange. (b) Photo of a QF-MBA flange in the SPS. (c) Model of an MBA-MBA flange.

Simulations

All the aforementioned types have been modeled using official SPS layouts and simulated using HFSS [6], CST [7] or both. As analogous to the method used to calculate beam-loading in the CLIC main Linac [8], an on-axis plane wave was used as a source to calculate the beam induced field inside the enameled interconnects. Non-enameled flanges were characterized using both the aforementioned method and the wake field solver of CST. The enamel coating was modeled as a 0.2 mm thick layer with relative permeability $\epsilon_r = 3$ and dielectric losses tan$\delta = 0.01$. Finally, a conductivity of $\sigma = 1.35 \times 10^6$ S/m was used for the beam pipes and bellows to model the 304L/316L stainless steel.

Flanges belonging to group II are responsible for a set of resonances around 1.4 GHz. The enameled flanges are open and inhomogeneous resonators. Radiation losses were found to be dominant in all enameled flanges of group II. On top of this, these flanges have damping resistors inside. The damping resistors are hollow alumina cylinders with

Content from this work may be used under the terms of the CC BY 3.0 licence (© 2015). Any distribution of this work must maintain attribution to the author(s), title of the work, publisher, and DOI.

ISBN: 978-3-95450-168-7 doi:10.18429/JACoW-IPAC2015-MOPJE037

STUDY AND COMPARISON OF MODE DAMPING STRATEGIES FOR THE UA9 CHERENKOV DETECTOR TANK

A. Danisi, A. Masi, R. Losito, F. Caspers, C. Vollinger, B. Salvant, CERN, Geneva, Switzerland
T. Demma and P. Lepercq, LAL, Orsay, France

Abstract

In the framework of the UA9 experiment, the Cherenkov detector is useful to measure the amount of particles deflected by a bent crystal, proving the crystal collimation principle. The tank used to host this device is taken as a case study for an in-depth analysis of different damping strategies for electromagnetic modes which otherwise would give rise to important beam-coupling impedance contributions. Such strategies involve the use of ferrite, damping resistors and a mode-coupler, a solution which intercepts the modes inside the cavity but damps the related power outside the vacuum tank (potentially avoiding heating). Such solutions are discussed through experimental measurements and the relative quality factor is taken as a figure of merit.

INTRODUCTION

The UA9 experiment aims at the use of bent crystals instead of carbon jaws to achieve beam collimation. The UA9 experimental layout [1] includes many critical devices such as precision piezo-goniometers for crystal positioning, beam-loss monitors and Cherenkov detectors. The Cherenkov detector is installed using a special vacuum tank with four apertures.

From the beam-coupling impedance viewpoint, these apertures can give rise to resonances which could de-stabilize the beam. Many techniques are available to date [2]-[4] in order to decrease the quality factor of unwanted cavity resonances. This paper takes the UA9 Cherenkov detector (CD) as a case study for investigation on different damping techniques, based on ferrite insertions, damping ceramic resistors and mode couplers. The study is performed with experimental measurements carried out on a 1:1 scale replica of the Cherenkov vacuum tank.

THE CASE STUDY

The UA9 CD vacuum tank for use in the SPS is depicted in Fig. 1. It can be seen as a central cylindrical cavity with four smaller cylindrical cavities (ends), disposed on two perpendicular directions. Along the z direction, instead, is the beam path.

The vacuum tank is made of 316 LN steel and does not present any object in the central cavity. The detector bar is mounted on one of the four ends [5], whereas the other three ends remain available for diagnostic equipment.

A fast simulation of the UA9 CD tank using Microwave Studio has shown that two particular modes are of interest when considering the beam-coupling impedance issues of this device: the first one is at about 922 MHz and the second one is at about 1.32 GHz. Both are TM modes associated with the central cavity and are characterized by the quality factors listed in Table 1 (void cavity).

A way of decreasing or even vanishing the quality factors and shunt impedances of parasitic cavity resonances is to re-design the structure, so as to avoid the occurrence of such resonances (e.g. use of uniform-diameter sectors, RF shielding, elimination of unused empty spaces). When this step is not possible due to other design issues, i.e., when the re-design for impedance-related issues leads to unacceptable changes, passive countermeasures have to be considered.

EXPERIMENTAL RESULTS

Measurements Setup

Measurements have been carried out in transmission. The two beam pipe outputs and the four apertures of the vacuum tank have been sealed with aluminium flanges. Two small antennas mounted on coaxial assemblies, have been inserted axially and connected to a Vector Network Analyser (VNA) for the measurement of the S_{21} scattering parameter (Fig. 2).

Given the excitation scheme (axial linear antenna), mostly TM modes will be excited. The two probes are largely undercoupled so as not to perturb the configuration of the electromagnetic fields in the original uncoupled vessel. [6].

For each resonance peak measured on the S_{21} parameter, a preliminary check (through the Smith chart) has been done in order to maintain under-coupling conditions of the probes. Successively, the quality factor [4], [6] has been measured directly with the VNA.

Different damping strategies have been tested for this

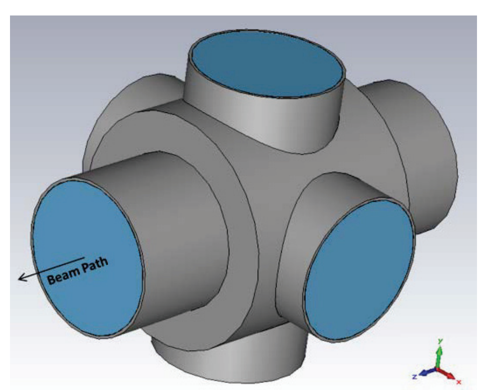

Figure 1: UA9 Cherenkov detector vacuum tank adopted as a case study.

Content from this work may be used under the terms of the CC BY 3.0 licence (© 2015). Any distribution of this work must maintain attribution to the author(s), title of the work, publisher, and DOI.

ISBN: 978-3-95450-168-7 doi:10.18429/JACoW-IPAC2015-MOPJE038

Content from this work may be used under the terms of the CC BY 3.0 licence (© 2015). Any distribution of this work must maintain attribution to the author(s), title of the work, publisher, and DOI.

IMPEDANCE STUDIES OF THE LHC INJECTION KICKER MAGNETS FOR HL-LHC

H. Day*, M.J. Barnes, L. Coralejo Feliciano, CERN, Geneva, Switzerland

Abstract

The LHC injection kicker magnets (MKIs) experienced strong heating during the first operational run, identified as being caused by power loss due to wakefields induced by circulating beam. Studies of the beam coupling impedance of the beam screen, a series of conductors embedded in a ceramic tube placed in the aperture of the ferrite yoke to screen the ferrite from the beam, resulted in new design offering improved screening: this is predicted to reduce the heating to acceptable levels for operation with 25ns beam during run 2 of the LHC. However higher beam intensities proposed for HL-LHC operation are predicted to again cause strong heating to occur. Further studies have been carried out to reduce the beam induced power loss by optimising the beam screen design, some key results and findings of which are presented here.

INTRODUCTION

The injection kicker magnets (MKIs) are fast pulsed transmission line kicker magnets, which have a ceramic tube inserted into the aperture of the ferrite yoke: this supports a number of screen conductors, designed to provide a good conducting path for the image currents of the circulating beam. One end of the screen is directly connected to the beam pipe whilst the other is capactively coupled to the beam pipe in order to preserve the fast field rise time of the magnet. Beam-induced heating, due to high circulating beam current, leads to high temperatures being observed in devices in the LHC, including the MKIs [1]. In one non-conforming MKI this lead to problems as the temperature of the ferrite yoke occassionally rose above it's Curie temperature (≈120°C) necessitating 2-3 hours waiting time between fills. Substantial work has been done to reduce the power deposited by reducing the beam coupling impedance of the device - a revised beam screen was implemented on all magnets during long shutdown 1 (LS1) which is predicted to reduce the power loss to <52W/m (see Table 1) and the temperature is <80°C [2], comfortably below the Curie temperature.

The planned high luminousity upgrade of the LHC (called HL-LHC) will involve a doubling of the beam current in the LHC under current nominal parameters [3] - this is predicted to lead again to a four fold increase in the power loss to all devices in the LHC unless counter-measures are taken. To this end further improvements to the beam screen have been studied in order to reduce the power loss into the magnet whilst continuing to ensure both good high voltage (HV) performance and good field quality during pulsing.

Building on the previous success a new design has been proposed to satisfy competing needs of low rates of electrical breakdown, during magnet pulsing, and a low beam coupling impedance to reduce the power lost into the structure by wakefields; in addition to meet strict requirements for magnet operation for field rise time and flat top ripple [4].

* hugo.day@hep.manchester.ac.uk

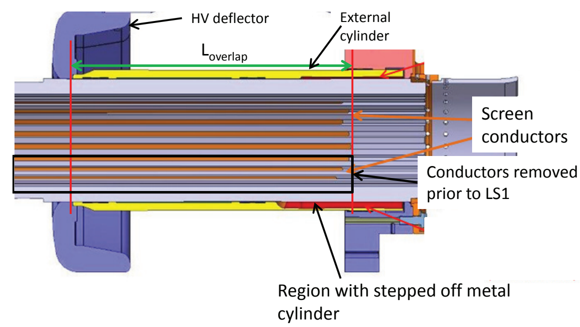

Figure 1: Cross-section of the beam screen of the MKI. Conductors circled in red weren't in place prior to long-shutdown 1.

CHANGES TO BEAM SCREEN DESIGN

Past work on the beam screen of the MKI has focused on improving the screening of the ferrite yoke from the beam by increasing the number of screen conductors in the beam screen to the full compliment of 24 - during the first run of the LHC only 15 screen conductors were in place, positioned closest to the return busbar (see Fig. 1), due to issues with surface flashover during magnet pulsing [5].

A revised beam screen was designed that reduced the electric field strength during magnet pulsing sufficiently to allow 24 conductors to be installed for post-LS1 [4], shown in Fig. 1. This is predicted to substantially reduce in the power loss in the MKIs post LS1, by a factor of more than 3 relative to the non-conforming MKI pre-LS1 (≈160W/m), even accounting for the increased beam current with the change to 25ns bunch separation. However this is not expected to be sufficient for HL-LHC operation, which will see a much higher beam current than nominal LHC operation (see Table 2) and is predicted to see power losses comparable to that which caused the non-conforming magnet to heat beyond it's Curie temperature during run 1 of the LHC [6], thus necessitating further modifications.

Previous work had showed that the beam coupling impedance of the MKI with a well shielded ferrite yoke is resonant in nature, with the frequency of the resonances, f_{res}, determined by the length of the overlap between the screen conductors on the internal face of the ceramic tube

ISBN: 978-3-95450-168-7 doi:10.18429/JACoW-IPAC2015-MOPJE039

GENERALISED TRUNCATED POWER SERIES ALGEBRA FOR FAST PARTICLE ACCELERATOR TRANSPORT MAPS

L. Deniau, C. I. Tomoiagă, CERN, Geneva, Switzerland

Abstract

A new Generalised Truncated Power Series Algebra (GTPSA) has been developed for extending, simplifying and optimising the transport maps used by particle accelerator simulation codes. TPSA are intensively used in optics code to describe transport maps of the elements constituting the particle accelerator to any order. GTPSA extend the degrees to inhomogeneous ones, where separate degrees can be specified for each variable and constrained by two total orders, one for map variables and one for ordinary variables. This allows tracking inhomogeneous planes of the 6D phase space with many extra variables. A complete set of new formulas and data structures have been derived to address the problem of memory consumption required for efficient computation of high order TPSA, including generalised indexing, multiplication and composition of inhomogeneous multivariate polynomials. The implementation has been benchmarked against well established libraries for the common subset with TPSA, and outperforms all of them for supported differential algebra operators on low and high orders, and high number of variables.

INTRODUCTION

TPSA packages are intensively used in optics code to describe transport maps of the elements constituting the particle accelerator to any order [1,2]. Most of the known fast multiplication algorithms working for univariate polynomials do not straightforwardly extend to several variables [3], and therefore the brute force approach remains the most efficient one for *truncated* power series. The performance improvements have to come from other kind of optimizations [4–7].

Notations

The TPSA are multivariate polynomials $P(\vec{z}) \in \mathbb{K}[\vec{z}]$, $\vec{z} = \{z_1, ..., z_n\}$ truncated at order d, where the commutative ring is generally $\mathbb{R}$ or $\mathbb{C}$. A multivariate polynomial is defined by the sum of all the monomials of order d or less:

$$P(\vec{z}) = \sum_{i=1}^{N} a_i \prod_{j=1}^{n} z_j^{\alpha_{ij}}, \quad \sum_{j=1}^{n} \alpha_{ij} \le d, \tag{1}$$

where the number N of coefficients a_i is given by:

$$N = C(n+d, n) = C(n+d, d) = \frac{(n+d)!}{n!d!}. \tag{2}$$

The binomial coefficient C is symmetric in variables and orders, hence a TPSA package can deal equivalently with high orders and low number of variables or low orders and high number of variables. The number N_i of monomials of order i with $0 \le\ i \le\ d$ or equivalently of monomials in the variable z_j^{d-i} with $1 \le\ j \le\ n$ can be calculated from the recurrence property of the binomial coefficient:

$$\begin{aligned} N_i &= C(n+i, n) - C(n+i-1, n) \\ &= C(n+i, n-1). \end{aligned} \tag{3}$$

Representations

The (unordered) sum of the monomials in (1) can be ordered in two practical forms:

1. By the **product of univariate polynomials** in the variables z_i, which is used by the indexing function:

$$P(\vec{z}) = \prod_{i=1}^{n} P(z_i) = \sum_{i=0}^{d} \sum_{j=1}^{N_{d-i}} a_{ij} \vec{z}_{ij}. \tag{4}$$

The monomial $\vec{z}_{ij}$ associated with the coefficient a_{ij} are generated recursively from $z_k \times \{z_{k+1}, ..., z_n\}$, e.g. the outer sum over i corresponds to the variable z_1. As an example, a multivariate polynomial of order 3 with variables $\{z_1, z_2, z_3\}$ can be represented by the series:

$$\begin{aligned} P(\vec{z}) =& a_1 z_1^0 z_2^0 z_3^0 + \\ & a_2 z_1^0 z_2^0 z_3^1 + a_3 z_1^0 z_2^0 z_3^2 + a_4 z_1^0 z_2^0 z_3^3 + \\ & a_5 z_1^0 z_2^1 z_3^0 + a_6 z_1^0 z_2^1 z_3^1 + a_7 z_1^0 z_2^1 z_3^2 + \\ & ... + a_{20} z_1^3 z_2^0 z_3^0. \end{aligned} \tag{5}$$

2. By the **sum of homogeneous multivariate polynomials** in the orders $i = \sum_{k=1}^{n} \alpha_{ik}$, , which is used by the storage of the a_{ij} and by the optimized multiplication:

$$P(\vec{z}) = \sum_{i=0}^{d} P_i(\vec{z}) = \sum_{i=0}^{d} \sum_{j=1}^{N_i} a_{ij} \vec{z}_{ij}. \tag{6}$$

The monomial $\vec{z}_{ij}$ associated with the coefficient a_{ij} are generated recursively from $P_1 \times P_{i-1}$. As an example, a multivariate polynomial of order 3 with variables $\{z_1, z_2, z_3\}$ can be represented by the series:

$$\begin{aligned} P(\vec{z}) =& a_1 z_1^0 z_2^0 z_3^0 + \\ & a_2 z_1^0 z_2^0 z_3^1 + a_3 z_1^0 z_2^1 z_3^0 + a_4 z_1^1 z_2^0 z_3^0 + \\ & a_5 z_1^0 z_2^0 z_3^2 + a_6 z_1^0 z_2^1 z_3^1 + a_7 z_1^0 z_2^2 z_3^0 + \\ & ... + a_{20} z_1^3 z_2^0 z_3^0. \end{aligned} \tag{7}$$

Generalization

The GTPSA extends the TPSA by splitting the variables in two kinds $\vec{z} = \{\vec{x}, \vec{k}\}$, where the **map variables** $\vec{x} = \{x_1, ..., x_v\}$ with $v \ge\ 1$ are present in both the map and the (G)TPSA of the map variables, and where the **knob variables** $\vec{k} = \{k_{v+1}, ..., k_n\}$ with $n - v \ge\ 0$ are only present in the GTPSA of the map variables.

Content from this work may be used under the terms of the CC BY 3.0 licence (© 2015). Any distribution of this work must maintain attribution to the author(s), title of the work, publisher, and DOI.

ISBN: 978-3-95450-168-7 doi:10.18429/JACoW-IPAC2015-MOPJE042

Content from this work may be used under the terms of the CC BY 3.0 licence (© 2015). Any distribution of this work must maintain attribution to the author(s), title of the work, publisher, and DOI.

LONGITUDINAL INJECTION SCHEMES FOR THE CERN PS BOOSTER AT 160 MeV INCLUDING SPACE CHARGE EFFECTS

V. Forte*, CERN, Geneva, Switzerland - Université Blaise Pascal, Clermont-Ferrand, France
E. Benedetto, A. Lombardi, CERN, Geneva, Switzerland
D. Quartullo, CERN, Geneva, Switzerland - Ministère des Affaires étrangères, France

Abstract

In the frame of the LHC Injectors Upgrade project, the CERN PS Booster will be equipped with a H- injection system at 160 MeV to tailor the initial transverse and longitudinal profiles. We are here reviewing the different multi-turn longitudinal injection schemes, from the beam dynamics point of view, taking into account the needs of the large variety of the PSB users, spanning in intensity from 5e9 to about 1.6e13 protons per bunch. The baseline of the longitudinal injection has always been the longitudinal stacking with central energy modulation: this scheme has the advantage of filling uniformly the RF bucket and mitigate transverse space charge, but it requires at least 40 turns of injection. A simpler injection protocol without energy modulation is here analyzed in detail to find the optimum initial conditions in terms of bucket filling and reduction of transverse and longitudinal space charge effects, with the advantage of minimizing the number of turns for the LHC beams. Simulations with space charge of the longitudinal injection process from different Linac4 trains are presented to fix possible longitudinal injection scenarios during the future commissioning and operation with Linac4.

INTRODUCTION

The transverse space charge in the CERN PS Booster (PSB) is one of the main bottle-necks for the machine beam dynamics. In the framework of the CERN LHC Injectors Upgrade project (LIU) project, the machine will be equipped with a new H- charge-exchange injection at 160 MeV, substituting the present 50 MeV proton multiturn injection. The Linac4 chopper will give the opportunity to tailor the longitudinal beam profiles in a way to minimize the space charge effects in terms of losses and longitudinal/transverse emittances. The PSB has to produce large variety of beams and we here consider the production of the 2 most important ones: the high intensity and large emittance beam for ISOLDE experiment and the LHC high brightness beam [1]. For ISOLDE we will inject 100 turns [2] and use the baseline scheme proposed already by C. Carli and R. Garoby [3]: in this way the energy modulation in the Linac4 requires at least 40 turns to complete this longitudinal painting scheme.

This is the reason why for the standard LHC beams (I=29.55e11 p.), 20 turns injection [4], for which it is important to minimize the number of foil hits and blow-up due to the scattering at the screen, we consider no energy modulation. The main concern of this solution is the inhomogeneities and beating of the bunch shape, leading to a dense core and less populated tails [3]. However this regulation becomes more practical in control room during the commissioning of the machine.

Several simulations have been run through the ESME [5] and PyOrbit [6] codes with Linac4 realistic bunches to evaluate the parameters of possible initial unmodulated injections in a double RF accelerating bucket for the first 10 ms after injection: it is possible, in simulation, to vary the bunch length (in reality with the chopper) and/or the energy spread ΔE (in reality with the debuncher) of the injected beams. The choice of using PyOrbit for pure longitudinal studies goes in the direction of using the code as baseline for 6D tracking including transverse-longitudinal space charge effects. Finally PyOrbit and BlonD [7] have been compared to estimate the contribution of space charge effects for the unmodulated injection scheme, after an initial benchmark between the two codes.

LONGITUDINAL PAINTING SCHEME WITH ENERGY MODULATION

A longitudinal painting scheme with energy modulation has been selected as preferred one for high intensity beams, because it makes possible a uniform population of the initial accelerating RF bucket and, therefore, a reduction of the line density [protons/m] and an increase of the bunching factor, which are favorable conditions for reduced transverse space charge effects. This scheme aims at filling the 80% of the double RF accelerating bucket through a series of small energy spread (0.1 MeV) beams which are injected at different central energy. The central energy is modulated in time in a triangular way between ±1 MeV. Figure 1 shows the bucket at the end of the filling, before the full filamentation phase. As said, this method requires at least 40 turns to be completed.

THE UNMODULATED INJECTION

The longitudinal machine settings for the simulations are shown in Table 1. Figure 2 shows the three initial tested values of energy spread from Linac4: 113 keV, 336 keV and 592 keV rms. Figure 3 shows that the solution at 336 keV (halfway) is preferable, as it minimizes the peak line density due to the rotation in the longitudinal phase space of the mismatched beam, with respect to the 113 keV case (Fig. 4). Figure 5 represents the peak line density evolution turn-by-turn for the two cases.

On the other side, at 592 keV rms, the beam has a very large energy spread (over the acceptance). In this case, to

* vincenzo.forte@cern.ch

ISBN: 978-3-95450-168-7 doi:10.18429/JACoW-IPAC2015-MOPJE043

DESIGN AND OPTIMIZATION OF ELECTROSTATIC DEFLECTORS FOR ELENA

D. Barna, University of Tokyo, Japan
W. Bartmann, M. Fraser, R. Ostojic, CERN, Switzerland

Abstract

The ELENA ring [1] will decelerate the antiprotons ejected from the Antiproton Decelerator (AD) at 5.3 MeV down to 100 keV kinetic energy. The slow antiprotons will be delivered to experiments using electrostatic beamlines, consisting of quadrupoles, correctors and deflectors. An extensive simulation study was carried out to find solutions to minimize the aberrations of the deflectors. These solutions will be presented together with the actual design of these devices.

INTRODUCTION

At low particle energies electrostatic devices have many advantages over magnetic ones, for example the absence of remanent magnetic fields, no need for cooling, cheap and simple production. Following a cost-performance analysis, electrostatic beamlines were chosen for ELENA.

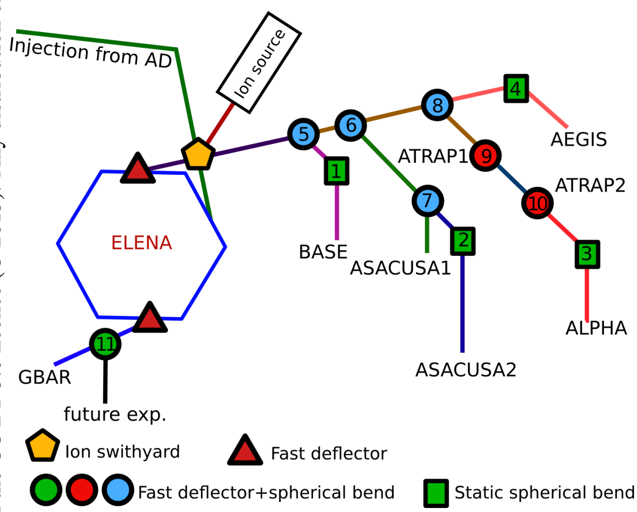

Figure 1: Layout of the ELENA transfer lines.

The schematic layout of the ELENA transfer lines is shown in Fig. 1. Due to the constraints given by the existing experiments and other equipment already present in the AD hall, the angles of the different bends could not be made equal. However, they can be arranged into groups with nearly equal angles. In order to facilitate the design, manufacturing and spare part management, identical electrode structures will be used at these positions with slightly different voltage settings to account for the different bending angles. In most cases the deflectors will have custom vacuum chambers to match the actual angle of the beamline.

The deflectors of the ELENA transfer lines can be grouped into following types (Table 1):

1. Fast switch (FS) combinations: ELENA will deliver 4 antiproton bunches with a spacing of about 1 µs in a single extraction. These bunches will be distributed among 4 experiments running simultaneously using fast switches in the beamlines. This functionality is realized by a combination of a fast electrostatic deflector [2] (the same device which is used for ejection from the ring) and a static deflector. The fast deflector has a rise time <1 µs and gives an initial kick of 220 mrad. The static deflector gives the remaining deflection. The fast switches can be further classified into two groups:
   (a) Horizontal fast switches (HFS at positions 5, 6, 7, 8 and 11 in Fig. 1) - these devices deflect the beam in the horizontal plane by a total angle between 45.7° and 48.1°.
   (b) Vertical fast switches (VFS at positions 9 and 10 in Fig. 1) - these devices deflect the beam vertically to ATRAP1 and ATRAP2.
2. Standalone static deflectors will deflect the beam by an angle between 45.77° and 50.42° at positions 1, 2, 3 and 4 in Fig. 1.

Table 1: List of Electrostatic Deflectors

Pos. in Fig. 1	Tot. defl. [deg]	Type	Electrode angle [deg]	Range [deg]
1,2 3 4	48.1 50.42 45.77	Static Static Static	48	±2.3
5,6,7 8	48.08 45.76	HFS HFS	34.3	±1.2
9,10	90	VFS	77.4	0
11	t.b.d.	HFS	t.b.d.	0

OPTIMIZATION OF ELECTRODES

The mechanical aperture (*A* in Fig. 2a) was chosen to be 65 mm - slightly larger than the value adopted for the beamlines in general (60 mm) due to the following reasons: the fringe field of the device deflects the particles already outside of the electrodes, and the central particle trajectory deviates from the nominal arc towards the bending center. Also, the same device will be used for slightly different bending angles, which gives a further excursion of the central particle trajectory from the nominal arc. A larger aperture

Content from this work may be used under the terms of the CC BY 3.0 licence (© 2015). Any distribution of this work must maintain attribution to the author(s), title of the work, publisher, and DOI.

ISBN: 978-3-95450-168-7 doi:10.18429/JACoW-IPAC2015-MOPJE044

BEAM DYNAMICS STUDIES OF THE ELENA ELECTROSTATIC TRANSFER LINES

M.A. Fraser*, W. Bartmann, R. Ostojic, CERN, Geneva, Switzerland
D. Barna, University of Tokyo, Tokyo, Japan

Abstract

The low-energy ELENA ring at the Antiproton Decelerator (AD) facility at CERN will lower the kinetic energy of antiproton beams from 5.3 MeV to 100 keV, significantly increasing the antiproton trapping efficiency at the experiments. The antiprotons from ELENA will be distributed to two experimental areas housing several different experiments through a system of electrostatic transfer lines totalling 90 m in length. A significant optimisation of the electrostatic optical elements (deflectors, quadrupoles, and correctors) has been carried out to improve the beam quality delivered to the experiments and facilitate installation of the beam lines into the AD hall. A general overview of the beam optics is presented, including end-to-end particle tracking and error studies from the extraction point in the ELENA ring to the experiments.

INTRODUCTION

The installation of the ELENA synchrotron [1] at CERN's AD facility will lower the kinetic energy of antiproton beams to 100 keV. A network of transfer lines has been designed to distribute the low energy antiproton beam to eight different experiments. The system is presently undergoing the first stage of installation in the AD hall. The layout of the transfer lines is shown in Fig. 1 and the relevant ELENA beam parameters for discussion in this paper are collected in Table 1. The transfer lines exploit electrostatic optical elements and are built up in a modular way from a series of standardised blocks: electrostatic quadrupole doublets with integrated correctors, beam position monitors, fast electric deflectors and electrostatic deflectors. After an initial optimisation of the orientation of the ELENA ring the transfer lines have been integrated and the geometry of the lines fixed in the AD hall. The fast deflectors located at each branch permit different bunches within the same bunch train extracted from ELENA to be distributed simultaneously to up to four experiments.

DESIGN OVERVIEW

The initial beam line design [2] was carried out using electrostatic beam line elements represented as transfer matrices and implemented in MADX [3]. The transfer matrices were computed by tracking test particles in the field maps generated using the finite element electromagnetic field solver COMSOL [4, 5]. The higher-order (non-linear) field components were carefully optimised in each device as described elsewhere in these proceedings [6]. The design evolved in several iterations, evaluating each time the effects of changes in the layout, or in the design of the optical elements, on the beam quality. The final validation of the transfer line design was achieved with end-to-end particle tracking in the field maps of all elements from the ELENA ring to the experiment, in the presence of errors and imperfections.

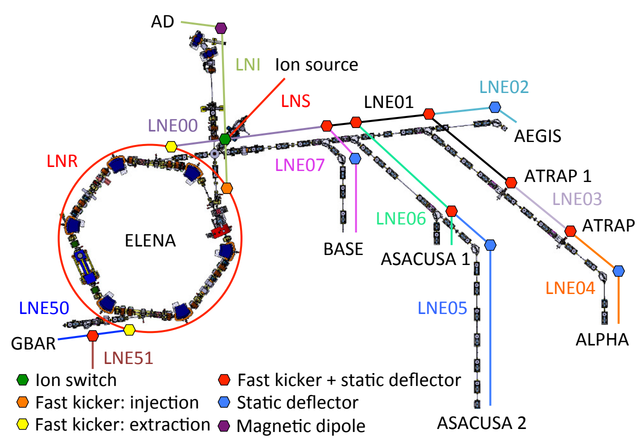

Figure 1: Layout of the ELENA transfer line network.

Table 1: ELENA Beam Parameters

Parameter	Injection	Extraction
Kinetic energy, W [MeV]	5.3	0.1
Reduced velocity, β	0.1064	0.0146
Magnetic rigidity [Gm]	3329	457
Electric rigidity [kV]	10570	200
No. of bunches	1	1 - 4
Emit. (95%) H / V [mm mrad]	< 15 / 15	6 / 4
Momentum spread (95%)	1×10^{-3}	2.5×10^{-3}
Intensity [$\bar{\text{p}}$]	3.0×10^{7}	1.8×10^{7}
Bunch length [m]	~12.7	1.3

The basic layout of the lines is determined by a FODO focusing structure with a cell length of 3.1 m and a phase advance of 90 deg per cell. The quadrupoles are housed in the same doublet assembly in order to standardise production; in the FODO sections only one of the quadrupoles in the assembly is powered, whereas in the matching sections both are powered.

Each doublet assembly contains separated horizontal and vertical correctors between the quadrupoles, giving two correctors per plane in each cell and good control over the beam trajectory. This is particularly important in areas where stray field from experimental equipment will play a role in beam tuning.

* mfraser@cern.ch

Content from this work may be used under the terms of the CC BY 3.0 licence (© 2015). Any distribution of this work must maintain attribution to the author(s), title of the work, publisher, and DOI.

ISBN: 978-3-95450-168-7 doi:10.18429/JACoW-IPAC2015-MOPJE045

FIXED POINTS IN PRESENCE OF SPACE CHARGE IN CIRCULAR PARTICLE ACCELERATORS

S. S. Gilardoni, M. Giovannozzi, A. Huschauer, CERN, Geneva, Switzerland
S. Machida, C. R. Prior, S. L. Sheehy, STFC/RAL, Didcot, UK

Abstract

Recent measurements performed in the framework of the multi-turn extraction (MTE) studies at the CERN Proton Synchrotron showed a dependence of the position of beamlets obtained by crossing a stable transverse resonance on the total beam intensity. This novel observation has triggered a number of studies aiming at understanding the source of the observed effect. In this paper the results of numerical simulations performed in different conditions are discussed in detail.

INTRODUCTION

The Multi-Turn Extraction (MTE) at the CERN Proton Synchrotron (PS) is a novel technique [1, 2] proposed to replace the existing extraction from the PS to the Super Proton Synchrotron (SPS) so as to allow long runs compatible with delivering good quality high intensity beams.

The MTE extraction is based on beam trapping in stable islands of the transverse phase-space: the beam is split in five beamlets by crossing a fourth-order resonance and, once sufficiently separated in the horizontal plane, each beamlet is extracted on five consecutive PS turns towards the SPS. The adiabaticity of the trapping process requires a long extraction flat top. During the splitting process, realised at 14 GeV/c for the specific CERN application, the horizontal chromaticity and the beam $\Delta p/p$ are kept both as small as possible, to assure that the largest fraction of the particles crosses the resonance all at the same moment. The beam is kept bunched during the entire capture process to precisely control the radial position, i.e., the energy, for the different reasons described in [3]. The position of the beamlets at the end of the trapping process should depend only upon the distance in tune from the resonance and the amplitude-dependent tune shift, thus from the value of the quadrupolar, sextupolar and octupolar fields introduced to create and control the islands' size and separation.

During normal operation, the total beam intensity can vary between 1×10^{13} and 3×10^{13} protons per pulse, depending on the needs of the SPS users. The intensity is usually kept constant for a certain period of time, usually days, and changed upon users requests. During the MTE commissioning period, as reported in [3], it was noticed that the position of the beamlets, i.e., the position of the stable fixed point in the horizontal phase space, changes significantly and in a measurable way with the intensity. In particular, the final position of the beamlets was found to be a linear function of the total beam intensity, whereas the four beamlets and the beam core sizes did not show any measurable change, as shown for example in Fig. 1. The observed effect suggested

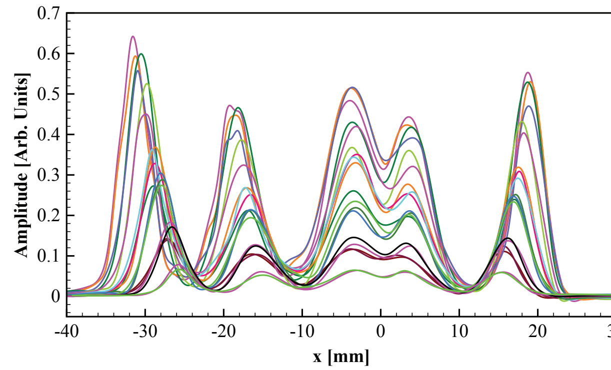

Figure 1: Example of islands profiles measured by a wire scanner and for different intensity [3]. The displacement of the islands centers with intensity is apparent.

as being generated by the superposition of two different components, i.e., the direct space charge between the beamlets and the beam core, and the beamlets interaction with the image charges on the vacuum chamber walls. Also the finite resistivity of the vacuum chamber was proposed to introduce a relevant effect.

This paper presents a first attempt to disentangle the different sources that might cause the observed change of beamlet position, and in particular space charge.

SIMPLE MODEL WITH DIRECT SPACE CHARGE

The incoherent tune shift due to the direct space charge is always negative so that the fixed points in the horizontal phase space move inward when the amplitude-dependent tune shift due to nonlinear elements has negative sign (Fig. 2). That is not the case of the experimental observation where the beamlets move outward with beam intensity [3].

SIMULATIONS WITH FROZEN SPACE CHARGE

In order to simulate the space charge effects, we consider the frozen space charge model of a coasting beam. The charge distribution and total charge of each beamlet are fixed at the beginning of the simulations and redistribution or beam loss is not considered. More specifically, the charge distribution is Gaussian in both horizontal and vertical directions and all the beamlets including that at the centre have the same charge. We calculate, however, the position of beamlets self-consistently including the space charge effects among them. When the distance among the beamlets in real space is more than the beam size of each of them, the

Content from this work may be used under the terms of the CC BY 3.0 licence (© 2015). Any distribution of this work must maintain attribution to the author(s), title of the work, publisher, and DOI.

ISBN: 978-3-95450-168-7 doi:10.18429/JACoW-IPAC2015-MOPJE046

Content from this work may be used under the terms of the CC BY 3.0 licence (© 2015). Any distribution of this work must maintain attribution to the author(s), title of the work, publisher, and DOI.

INFLUENCE OF THE ALIGNMENT OF THE MAIN MAGNETS ON RESONANCES IN THE CERN PROTON SYNCHROTRON

A. Huschauer, S. S. Gilardoni, R. Wasef, CERN, Geneva, Switzerland

Abstract

During the Long Shutdown 1 seven out of the one hundred combined function main magnets were removed from the tunnel to conduct maintenance. After reinstallation, the entirety of the main magnets was aligned to the reference positions and within the first week of operation of the accelerator, a beam-based alignment campaign was performed to reduce the excursions of the closed orbit. In order to further investigate and understand the source of betatronic resonances, which, already in 2011, were found to be excited by the bare machine, tune diagram measurements before and after this beam-based magnet alignment were conducted. In both cases the same resonances were found to be present; however, after the alignment, an overall increase of their strengths was observed. In this paper we present the corresponding measurement results and discuss the direct impact on the daily operation of the accelerator.

INTRODUCTION

The CERN Proton Synchrotron (PS) plays a crucial role among the accelerators in the injector chain of the Large Hadron Collider (LHC) and will provide beam to the LHC at least until 2035. Therefore, reliable performance of the accelerator components is required and extensive maintenance measures are being undertaken accordingly. This especially concerns the refurbishment of the combined-function main magnets, which are continuously subject to ionizing radiation and pulsed magnetic forces leading to degradation of these elements. In the framework of the PS main magnet consolidation program, 51 out of 100 main units (MUs) underwent maintenance between 2005 and 2009 [1] and, more recently, seven MUs were refurbished during the Long Shutdown 1 (LS1), which took place from 2013 to 2014. Before the restart of the accelerator complex after the LS1, all MUs were aligned to their reference positions. Subsequently, a beam-based realignment campaign was conducted to reduce the excursion of the closed orbit, and the effect on the betatronic resonances, which are supposedly excited by magnetic errors in the main magnets, was investigated.

The applied measurement technique, which was first proposed in [2], is based on measuring beam loss while keeping the tune constant in one plane and changing it dynamically in the other. These measurements lead to a graphical representation of the tune diagram and the underlying procedure is described in detail in [3].

In order to control the working point, two independent systems are available in the PS: the Low Energy Quadrupoles (LEQ), and the Pole Face Windings (PFW) in combination with the Figure of Eight Loop (F8L) [3, 4]. For the measurements presented in this paper, the PFW and the F8L were used, as these circuits provide larger flexibility compared to the LEQ. A single bunch with large transverse emittance and small direct space charge tune spread was required to increase the sensitivity of the measurement technique by filling the aperture at maximum. The beam parameters, which are summarized in Table 1, show that the maximum tune spreads (computed using the Laslett formula considering the variation of the optical machine parameters [5]) were basically kept constant for both cases. This is important, as it allows direct comparison of the tune scans before and after the realignment.

Furthermore, it was important to perform all measurements at injection kinetic energy of 1.4 GeV to reduce the radiological impact of the losses, as several people were required to access the machine to realign the main magnets.

MEASUREMENT RESULTS

In Fig. 1 the tune diagrams resulting from the measurements before and after the realignment are shown. In total four plots are depicted, corresponding to scans where either the horizontal or the vertical tune was kept constant.

Even though the MUs were aligned to their reference positions during the LS1, the measurements before the realignment revealed the same excited resonances as previous scans (see [3]), such as the lines $3q_y = 1$ and $2q_x + q_y = 1$. The measurements after the realignment, shown in Figs. 1c and 1d, confirm this observation, but the strengths of the various resonances appear to have increased.

Comparison of the Figs. 1a and 1c further reveals that, before the realignment, the vertical tune could be set closer to the integer resonance. In fact, the first measured line

Table 1: Comparison between Beam Parameters before and after the Realignment. The measurements were taken at extraction energy in the PS Booster.

Parameter	before	after
Intensity [10^{10} p]	120	130
Bunch length (4σ) [ns]	166	168
Relative momentum error (1σ) [10^{-3}]	0.85	0.97
Horizontal normalized emittance (1σ) [π mm mrad]	9.6	9.4
Vertical normalized emittance (1σ) [π mm mrad]	5.0	5.2
Horizontal tune spread	0.065	0.069
Vertical tune spread	0.093	0.10

ISBN: 978-3-95450-168-7 doi:10.18429/JACoW-IPAC2015-MOPJE047

CHROMATICITY DEPENDENCE OF THE TRANSVERSE EFFECTIVE IMPEDANCE IN THE CERN PROTON SYNCHROTRON

S. Persichelli*, CERN, Geneva, Switzerland and University La Sapienza, Rome, Italy
M. Migliorati, University La Sapienza, and INFN-Roma1, Rome, Italy
N. Biancacci, S. Gilardoni, A. Huschauer, E. Métral, B. Salvant, R. Wasef,
CERN, Geneva, Switzerland

Abstract

The current knowledge of the transverse beam coupling impedance of the CERN Proton Synchrotron (PS) has been established with beam-based measurements at different energies. The transverse coherent tune shift as a function of the beam intensity has been measured in order to evaluate the total effective imaginary part of the transverse impedance in the accelerator at the energies of 7, 13 and 25 GeV. Measurements have been performed changing the vertical chromaticity for each vertical tune scan with intensity. The data analysis revealed an increase of impedance with chromaticity for all the considered energies. The transverse impedance can be compared with the previously evaluated theoretical impedance budget taking into account the individual contribution of several machine devices.

INTRODUCTION

Coherent Transverse Tune Shift

The number of betatron oscillations per turn of the bunch center of mass is called coherent betatron tune, and it is defined as

$$Q_0 = \frac{\omega_\beta}{\omega_0}, \tag{1}$$

where ω_0 is the machine angular revolution frequency and ω_β is the angular betatron frequency. To perform tune measurements, a chirp signal is used to excite the beam, and the variation of the intensity of the bunch allows to observe a tune shift that is linear with the measured intensity. The transverse tunes can be measured in the PS with a Base Band Tune system based on diode detectors, known as the BBQ [1]. The transverse position of the bunch is acquired every turn by a beam position monitor (BPM). High amplitude short pulses measured by the BPM are then sent to a diode detector, which converts the modulation of the BPM pulses, related to beam oscillations, into a signal in the audio frequency range. This signal is then processed in order to deliver the tune content. BBQ measurements are performed here on a single circulating bunch of particles.
Measuring the tune shift with intensity gives information on the total reactive transverse impedance. For a Gaussian bunch of r.m.s. bunch length σ_z traveling with velocity $v = \beta c$, the coherent tune shift with intensity ΔQ is proportional to the imaginary part of the total (driving plus detuning) transverse effective impedance Z_t^{eff} by [2]

$$\Delta Q = -\frac{\beta e I_0}{4\sigma_z\sqrt{\pi}\omega_0^2\,\gamma\,Q_0\,m_0}\Im\left\{Z_t^{eff}\right\}, \tag{2}$$

where I_0 is the bunch current, Q_0 is the unperturbed betatron tune, γ is the relativistic factor, e the particle charge and m_0 the particle mass at rest. The effective transverse impedance is defined as the impedance weighted by the transverse bunch power spectrum centered at the chromatic frequency ω_ξ:

$$Z_t^{eff} = \frac{\sum\limits_{p=-\infty}^{\infty} Z_t(\omega')h(\omega'-\omega_\xi)}{\sum\limits_{p=-\infty}^{\infty} h(\omega'-\omega_\xi)}, \tag{3}$$

where $\omega' = \omega_0(p+Q_0)$ with p an integer, $\omega_\xi = \omega_0\,Q_0\,\xi/\eta$, with ξ the chromaticity and η the slippage factor, and the power spectrum of the Gaussian zero azimuthal bunch mode is $h(\omega) = \exp-(\omega^2\sigma_z^2/c^2)$. If the bunch length does not change with intensity, Eq. 2 predicts a tune shift linear with bunch intensity, with a slope proportional to the imaginary part of the transverse total effective impedance.

Chromaticity

The tune variation with the momentum is a machine parameter called chromaticity, defined as

$$\xi = \frac{\Delta Q/Q_0}{\Delta p/p_0}, \tag{4}$$

where p_0 is the particle momentum on the nominal closed orbit and Δp is the momentum deviation. Chromaticities in the PS can be measured by acquiring the tune shift while varying $\Delta p/p_0$. Introducing a radial offset, we generate a momentum offset that lead to a variation of the revolution frequency. The tune can be written as a Taylor series of $\frac{\Delta p}{p_0}$

$$Q\left(\frac{\Delta p}{p_0}\right) = Q_0 + Q'\frac{\Delta p}{p_0} + \frac{Q''}{2!}\left(\frac{\Delta p}{p_0}\right)^2 + \ldots + \frac{Q^n}{n!}\left(\frac{\Delta p}{p_0}\right)^n, \tag{5}$$

where

$$Q' = \frac{\Delta Q}{\Delta f/f_0} \tag{6}$$

and Q^n are the higher order terms. The chromaticity is computed applying a polynomial fit on the measured data: from the linear term we can calculate the linear chromaticity as

$$\xi = \frac{Q'}{Q_0}. \tag{7}$$

* serena.persichelli@cern.ch

Content from this work may be used under the terms of the CC BY 3.0 licence (© 2015). Any distribution of this work must maintain attribution to the author(s), title of the work, publisher, and DOI.

ISBN: 978-3-95450-168-7 doi:10.18429/JACoW-IPAC2015-MOPJE048

ELECTRON-CLOUD STUDIES FOR TRANSVERSELY SPLIT BEAMS

S. S. Gilardoni, M. Giovannozzi, G. Iadarola, G. Rumolo, CERN, Geneva, Switzerland
N. Pradhan, CERN, Geneva, Switzerland and University of Mississippi, MS, USA

Abstract

Recently, resonance crossing has been proposed as a means of manipulating the transverse beam distribution. This technique has application, among other topics, to injection and extraction schemes. Moreover, the transversely split beams might also be used as a mitigation measure of electron-cloud effects. The results of detailed numerical simulations are discussed in this paper, possibly opening new options for scrubbing of beam pipes in circular accelerators.

TRANSVERSE BEAM SPLITTING

In recent years, a novel beam manipulation has been proposed, which is based on beam splitting by resonance crossing in the horizontal plane [1, 2]. The process is based on the use of non-linear beam dynamics. Stable islands are created by means of sextupole and octupole magnets, which are responsible for making the beam dynamics non-linear. An adiabatic tune variation is then applied so that a given resonance is crossed. During the resonance crossing stage particles can be trapped into the islands and transported to high amplitudes. The net result is to split the beam in the horizontal phase space so that from the initial single Gaussian multiple quasi-Gaussian distributions are generated. Examples of this process for the case of the third- and fourth-order resonance are shown in Fig. 1 and 2, respectively.

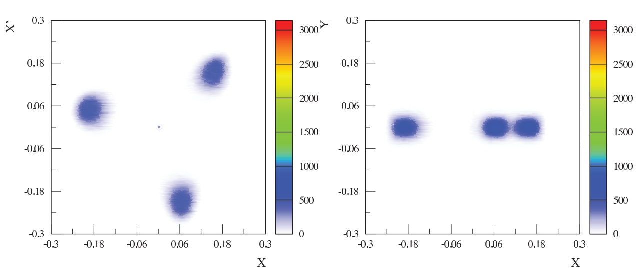

Figure 1: Phase space portraits of the final beam distribution after crossing the third-order resonance. Two of the six projections of the 4D transverse phase space are shown here, namely horizontal phase space (left), and physical space (right). The three beamlets are clearly visible in both the horizontal and physical space.

The difference between the two cases is striking and it can be summarised as follows: for an unstable resonance of order n the beam is split in n Gaussian beamlets with the centre of phase space almost completely depleted. Whereas in case of a stable resonance of order n, $n + 1$ Gaussian beamlets are created. This is a consequence of the stability of the resonance, which makes it possible for the beam at the centre of phase space to remain there, thus creating an additional beamlet. It is worth stressing the intrinsically different properties of the beamlets at non-zero amplitude with respect to the one at the origin. Indeed, while the beamlet around the origin represents a structure with periodicity equal to one machine turn, the other beamlets represent a single structure that winds up around the ring and closes up in a periodic way after n machine turns.

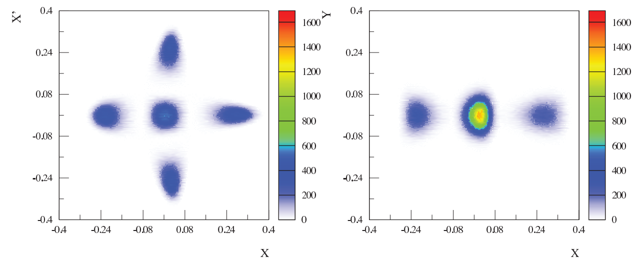

Figure 2: Phase space portraits of the final beam distribution after crossing the fourth-order resonance. Two of the six projections of the 4D phase space are shown, namely horizontal phase space (left), and physical space (right). The five beamlets are visible in the horizontal phase space, while the effect of projection is visible in the physical space.

It is also clear that properties like emittance and intensity are by definition the same for the n beamlets away from the centre as they are indeed one single structure. On the other hand, whenever it exists, the central beamlet does not need to have the same properties as the external ones. This implies that an additional degree of freedom is available (for the case of stable resonances) when defining the protocol for crossing the resonance. In fact, one can control the sharing of both emittance and intensity between the two phase space structures.

The technique of beam splitting had been originally proposed to perform multi-turn extraction from the CERN PS machine [1–6], but soon afterwards it has been realised that many more applications could be based on resonance crossing. Indeed, this technique could be time-reversed so to envisage a multi-turn injection based on beamlets' merging [7]. Such an approach would be very appealing as it allows beam shaping, which is a very interesting aspect in view of mitigating space charge effects [8]. Furthermore, the stability of the fourth-order resonance has been studied in detail proposing a method to turn it into an unstable resonance in view of generating a split beam with only four beamlets [9].

In parallel, detailed experimental studies have been performed at the PS [6] in view of an operational implementation of the novel technique to transfer beam from the PS to the SPS [10]. On a different front, intense efforts were devoted to the more theoretical aspect of the beam splitting with the goal of understanding the detail of the splitting process in a quantitative way with the help of adiabatic theory [11].

Content from this work may be used under the terms of the CC BY 3.0 licence (© 2015). Any distribution of this work must maintain attribution to the author(s), title of the work, publisher, and DOI.

ISBN: 978-3-95450-168-7 doi:10.18429/JACoW-IPAC2015-MOPJE049

BENCHMARKING THE CERN-SPS TRANSVERSE IMPEDANCE MODEL WITH MEASURED HEADTAIL GROWTH RATES

C. Zannini, H. Bartosik, G. Iadarola, G. Rumolo, B. Salvant (CERN, Geneva)

Content from this work may be used under the terms of the CC BY 3.0 licence (© 2015). Any distribution of this work must maintain attribution to the author(s), title of the work, publisher, and DOI.

Abstract

The latest SPS transverse impedance model includes kicker magnets, wall impedance, transition pieces (e.g. flanges and vacuum chamber discontinuities), beam position monitors and RF cavities. The model has already been successfully benchmarked against coherent tune shift and transverse mode coupling instability measurements. In this paper we present measurements of the headtail growth rates for a wide range of negative chromaticities and for two different configurations of machine optics (nominal and low gamma transition). The measurement results are compared with HEADTAIL simulations using the wake fields obtained from the SPS transverse impedance model.

INTRODUCTION

In the framework of the SPS upgrade project an accurate impedance model is needed in order to determine its effect on the beam stability and assess the impact of the new devices to be installed in the machine, with both the present and future beam parameters [1]. The SPS impedance model is obtained by summing the contributions of the different devices along the machine (β-weighted for the transverse impedance). Analytical models, 3-D simulations and bench measurements are used to estimate these contributions. The SPS impedance model is dynamical because it needs to be updated to include newly identified impedance sources as well as modifications of installed elements or new elements.

THE LATEST SPS IMPEDANCE MODEL

The present version of the SPS transverse impedance model, which we present here, includes the following contributions:

- Kicker magnets. They are likely to be the most important impedance source in the SPS. In a very simple approximation a SPS ferrite loaded kicker can be modelled as two parallel plates of ferrite. For this simple geometrical model all the impedance terms (longitudinal, driving and detuning horizontal and vertical impedances) have been calculated analytically. CST 3D simulations were found to be in very good agreement with the analytical results. The excellent agreement between analytical model and numerical simulations can be read as an important benchmark for the simulation code in the correct solution of electromagnetic problems involving dispersive materials such a ferrite. In the framework of an improvement of the kicker impedance model we performed a step by step simulation study starting from the simplest model and introducing one by one the new features that make the model gradually closer to reality. This approach allows for a good understanding of the different contributions brought to the kicker impedance by the different aspects. First, the ferrite is assumed to be C-shaped and the whole finite length device is inserted in the vacuum tank and equipped with an inner conductor [2]. In order to further approach a more realistic model other aspects have to be included: the cell longitudinal structure, also called segmentation, which determines a significant increase of the beam coupling impedance for the SPS injection kickers (due to the short cell length) and the serigraphy for the SPS extraction kickers. All the details about the SPS kicker impedance model can be found in Ref. [3];
- Wall (resistive wall and indirect space charge), based on analytical calculation taking into account the different SPS vacuum chambers [3];
- Beam position monitors, based on CST 3D simulations [4];
- RF cavities, based on CST 3D simulations [5];
- Broadband impedance from step transitions, based on the information for the SPS flanges collected during the task force for the identification of the longitudinal impedance source responsible of the impedance peak at 1.4 GHz observed during beam measurements [6]. The broadband impedance of the SPS transitions has been calculated as:

$$Z_{transitions} = \sum_{i=1}^{N} Z_i \, n_i \qquad (1)$$

where N is the number of different transition types, Z_i is the β-weighted broadband impedance of the transition i and n_i is the number of occurrences of the transition type i. The broadband impedance contribution of each type of transition has been obtained by means of CST 3D EM simulations.

Figure 1 shows the full SPS impedance model including all the impedance sources analyzed weighted by the respective length and beta functions for the horizontal and vertical driving and detuning impedances [3].

BENCHMARKING THE SPS TRANSVERSE IMPEDANCE MODEL

The model has been found to reproduce with very good accuracy coherent tune shift measurements in both trans-

ISBN: 978-3-95450-168-7 doi:10.18429/JACoW-IPAC2015-MOPJE050

TRANSVERSE IMPEDANCE MODEL OF THE CERN-PSB

C. Zannini, G. Iadarola, K. Li, G. Rumolo, CERN, Geneva
B. Jones, STFC, Rutherford
T.L. Rijoff, CERN, Geneva; TU Darmstadt, Darmstadt

Abstract

In the framework of the PS-Booster upgrade project an accurate impedance model is needed in order to determine the effect on the beam stability and assess the impact of the new devices before installation in the machine. This paper describes the PSB impedance model which includes resistive wall, indirect space charge, flanges, step transitions, ejection kicker including cables, injection kickers and cavities. Each impedance contribution has been computed for different energies in the PSB cycle. Measurements of the coherent tune shifts have been performed and compared to calculations based on the impedance model.

INTRODUCTION

A first attempt to build the PSB impedance model was made in the PhD thesis of D. Quatraro [1] where the attention was focused on the model of the wall impedance, which includes resistive wall and indirect space charge, and on the estimation of the so called "broadband impedance" (i.e. the measured impedance after the removal of the wall impedance) at different energies. These studies led to the conclusion that at injection about 50% of the measured tune shift can be attributed to indirect space charge and that the broadband impedance decreases with the relativistic beta. A more detailed impedance model of the PSB could help to explain the behavior of the measured tune shift at different energies. Presently, there is an ongoing effort to build such an impedance model and continuously refine it according to the modifications in the machine or new understanding.

PSB IMPEDANCE MODEL

The latest version of the impedance model includes resistive wall, indirect space charge, vacuum pipe discontinuities, ejection kicker including cables, injection kickers and FINEMET cavities. For each accelerator element the horizontal and vertical driving and detuning impedances have been calculated [2].

Indirect Space Charge

Up to now the indirect space charge impedance was estimated assuming the PSB to have an elliptic beam pipe (half height $h = 32$ mm and half width $w = 80$ mm) for 1/3 of the circumference, and a circular one for the remaining 2/3 (radius $r = 80$ mm) [1]. However, since the indirect space charge impedance is expected to play a major role, a more accurate calculation based on the PSB aperture model has been performed. For a circular chamber the indirect space charge impedance has been analytically calculated [3]. The calculation has been extended to the different PSB vacuum chambers by using the appropriate form factors [4], which have been numerically estimated with the simulation method for non-relativistic beta described in Ref. [5] for CST Particle Studio [6]. For the dipole chambers the form factors have been found very close to the rectangular chamber case [7], while a form factor of 1.4 has been estimated for the quadrupole chambers. More details on the PSB indirect space charge impedance model can be found in Ref. [4].

Table 1: Main parameters of the resistive wall calculation for the different vacuum chambers: thickness of the wall, electrical conductivity of the wall and background material.

	Wall thick [mm]	Wall (σ_{el}) [10^6S/m]	BG
Dipoles	0.4	0.77	Iron
Quadrupoles	1.5	1.3	Iron
Straight sections	1.0	1.3	Vacuum

Resistive Wall

In Ref. [1] the resistive wall impedance was estimated approximating the PSB elliptic beam pipe with a circular pipe with radius $r = h$, and considering the circular pipe for the rest of the accelerator. For the stainless steel an electrical conductivity $\sigma_{el} = 10^6$ S/m and a relative permeability $\mu_r = 8$ were used. Here we present a more accurate calculation based on the aperture model that accounts for the different PSB vacuum chambers. The calculation has been performed with the new code TLwall based on a transmission line model [2]. In Tab. 1 the main parameters used for the calculation are summarized. As an example, Fig. 1 shows the generalized horizontal and vertical resistive wall impedance of the PSB at kinetic energy of 160 MeV. The largest contribution to the resistive wall impedance is given by the bending magnets due to the very thin wall (0.4 mm). Due to the very thin layer, assuming an electrical conductivity of 7.7 10^5 S/m, the skin depth becomes larger than the wall thickness for frequencies below 2 MHz. Therefore, below this frequency the impedance becomes strongly dependent on the background material [4]. The iron has been modeled as a silicon-steel similarly to the SPS case [2]. The dispersion model for the permeability μ has been obtained as:

$$\mu = \mu_0 \, \mu_r(\boldsymbol{B}) = \mu_0 \left(1 + \frac{\mu_i(\boldsymbol{B})}{1 + jf/f_{rel}}\right) \quad (1)$$

with $f_{rel} = 10$ kHz [8]. The relative permeability μ_r is a function of the magnetic field $\boldsymbol{B}$ and thus of the particle momentum. The behaviour of μ_i as a function of $\boldsymbol{B}$ can be found in Ref. [9]. The variation of the resistive wall impedance due to the variation of μ_r during the PSB cycle has been estimated to be lower than 5%.

Content from this work may be used under the terms of the CC BY 3.0 licence (© 2015). Any distribution of this work must maintain attribution to the author(s), title of the work, publisher, and DOI.

ISBN: 978-3-95450-168-7 doi:10.18429/JACoW-IPAC2015-MOPJE051

EFFECT OF ELECTRON CLOUD IN QUADRUPOLES ON BEAM INSTABILITY

G. Iadarola* A. Axford, H. Bartosik, K. Li, G. Rumolo, CERN, Geneva, Switzerland

Abstract

Both simulations and machine experience at the CERN Super Proton Synchrotron (SPS) and Large Hadron Collider (LHC) have shown that the electron cloud has a lower build up threshold in quadrupoles than in dipoles and field free regions. As a consequence, while beam induced scrubbing can efficiently suppress the electron cloud in both dipoles and field free regions, a residual electron cloud can still survive in the quadrupoles and potentially degrade the beam quality. To study this effect, a PyECLOUD module for electron tracking in quadrupole fields including effects of secondary emission at the vacuum chamber has been implemented in PyHEADTAIL. With this module, the effect of the electron cloud in quadrupoles on beam stability and beam quality preservation can be assessed, as well as its impact on future LHC and HL-LHC operation.

INTRODUCTION

Electron cloud (EC) effects have been observed at the SPS throughout the years in which this machine has been prepared to become injector for the LHC, and at the LHC itself during the first three years of beam operation (Run 1, 2010–2012), becoming more and more severe while reducing the bunch spacing [1].

At the SPS, the EC has been identified as a main performance limitation since the early years of 2000. At that time a severe pressure rise was observed all around the machine together with transverse beam instabilities, significant losses and emittance blow-up on the trailing bunches of the train. Since 2002, scrubbing runs with 25 ns beams were carried out almost every year of operation in order to condition the inner surfaces of the vacuum chambers and therefore mitigate the EC. Since 2011, no important beam degradation due to EC can be observed on the cycle timescale for four batches of 72 bunches with $N \approx 1.35\times10^{11}$ p/b and normalized transverse emittances of about 3 μm (r.m.s.). However, for higher intensities, an EC driven transverse instability is observed after the injection of batches beyond the first one, leading to emittance blow up and particle losses on the trailing bunches of the injected trains. This can be due to a recrudescence of the EC both in the regions with dipole field (because of the stripes moving to out to unscrubbed regions) and in quadrupole regions, where the threshold for EC build up becomes lower due to the higher bunch intensities. Pinning down the main origin of these instabilities is crucial to decide on the future strategy of coating some parts of the SPS with low Secondary Electron Yield (SEY) material [2]. This depends not only on the multipacting thresholds in the different chambers and magnetic field configurations, but also on how much they individually contribute to render the beam unstable.

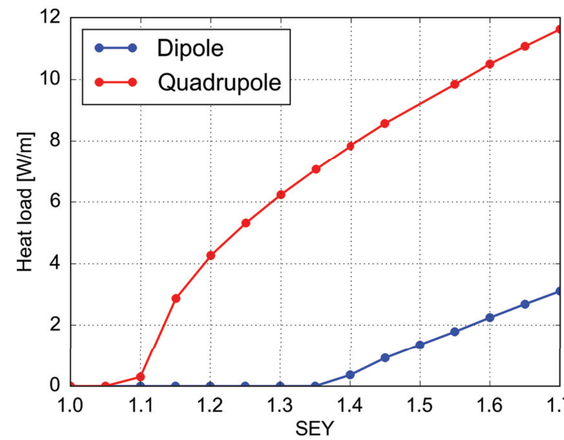

Figure 1: Heat load in the dipole and quadrupole magnets in the LHC arcs as a function of the SEY of the beam screen.

At the LHC, the EC effects could be successfully mitigated with 50 ns beams through beam induced scrubbing. This bunch spacing could be used for most of the integrated luminosity production with 7–8 TeV Center of Mass (CoM) energy in 2011–12. After the long shutdown 1 (LS1) the LHC will be able to run at 13 TeV CoM energy and the design bunch spacing of 25 ns will be used to reach the design luminosity within the pileup limits accepted by the LHC experiments. In the test runs on 2011 and 2012, the 25 ns beam, due to its significantly lower multipacting threshold, suffered from strong EC effects [1]. Thanks to the scrubbing effect, a decrease of the SEY resulted in a substantial reduction of the heat load in the cryogenic sections and of the dynamic pressure rise in the warm regions. Heat load measurements from the cryogenic system showed that up to 80% of the energy lost by the beam was deposited on the beam screens of the cryogenic arcs. Since in the LHC arcs each beam screen cooling circuit extends over a full half cell (three 15 m long dipoles and one 3 m long quadrupole plus multipoles), the individual contributions of the different magnets to the heat load cannot be disentangled. However, simulations carried out with the PyECLOUD code [1] show that the multipacting threshold in the arc quads is much lower than in the dipoles, as illustrated in Fig. 1. For SEY of 1.35, the EC can be suppressed in the arc dipoles, but not in the quadrupoles,which have a multipacting threshold of 1.1. This suggests that, even after significant scrubbing, the quadrupoles are likely to remain important contributors to the integrated EC along the LHC. Measurements from the Stand Alone Modules (SAM), which are magnets equipped with dedicated cryostats for which heat load detection is available, confirmed that the quadrupoles exhibit a much

* Giovanni.Iadarola@cern.ch

Content from this work may be used under the terms of the CC BY 3.0 licence (© 2015). Any distribution of this work must maintain attribution to the author(s), title of the work, publisher, and DOI.

ISBN: 978-3-95450-168-7 doi:10.18429/JACoW-IPAC2015-MOPJE052

OBSERVATIONS OF AN ANOMALOUS OCTUPOLAR RESONANCE IN THE LHC

F. Carlier, R. Tomás, E. Hamish Maclean, R. Westenberger,
J. Maria Coello de Portugal, A.S. Langner, T. Persson,
CERN, Geneva, Switzerland

Abstract

While linear LHC dynamics are mostly understood and under control, non-linear beam dynamics will play an increasingly important role in the challenging regimes of future LHC operation. In 2012, turn-by-turn measurements of large betatron excitations of LHC Beam 2 at injection energy were carried out. These measurements revealed an unexpectedly large spectral line in the horizontal motion with frequency $-Q_x - 2Q_y$. Detailed analyses and simulations are presented to unveil the nature of this spectral line.

INTRODUCTION

Linear beam dynamics in the LHC is currently well understood [1–4]. Nonlinear dynamics will play an increasingly important role in the challenging regimes of future LHC operation. Nonlinearities in circular accelerators can significantly affect the dynamic aperture [5, 6] and can lead to poor beam lifetime. Understanding these nonlinearities and their underlying sources is therefore important to improve the performance of the machine. Great progress has been made in recent years in this field in the LHC [7–12].

Spectral analysis of turn-by-turn data obtained from beam position monitors after large betatron excitations provide accurate measurements of the main tunes and secondary spectral lines related to specific resonant driving terms. Such measurements of resonant driving terms can provide insight on the presence machine nonlinearities. The theory of resonant driving terms is extensively discussed in [13–16].

In 2012, turn-by-turn measurements of large betatron excitations of LHC Beam 2 at injection energy were carried out [11]. These measurements revealed an unexpectedly large spectral line in the horizontal motion with frequency $-Q_x - 2Q_y \approx 0.1$, whose amplitude is well above model expectations. Details of these measurements can be found in [11]. This spectral line, later referred to as the (-1,-2) spectral line only appears for large diagonal excitations with nominal kick amplitudes higher than $5\sigma_{x,\text{nom}}$ and $4\sigma_{y,\text{nom}}$. This paper presents observations of the (-1,-2) spectral line and possible sources.

OBSERVATIONS

Figure 1 shows the complex spectra of turn-by-turn data for a measurement and multiparticle tracking simulation with 5000 particles for 1000 turns in the horizontal plane with measured kick amplitudes of $8.2\sigma_{x,\text{nom}}$ and $6.5\sigma_{y,\text{nom}}$. The large (-1,-2) line is observed in the measurement spectrum at $freq \approx 0.1$ corresponding to the generating term f_{2020} related to the $2Q_x + 2Q_y = p$ resonance, while its conjugate (1,2) line, corresponding to f_{1102}, is not visible. Furthermore, the amplitude of the (-1,-2) line reaches 8% of the main horizontal tune amplitude, while in tracking simulation it is not visible. Though other spectral lines are correctly reproduced from the model (0,1), (1,1), the discrepancy between model and measurement indicate a clear lack of understanding of the machine at such large betatronic excitations.

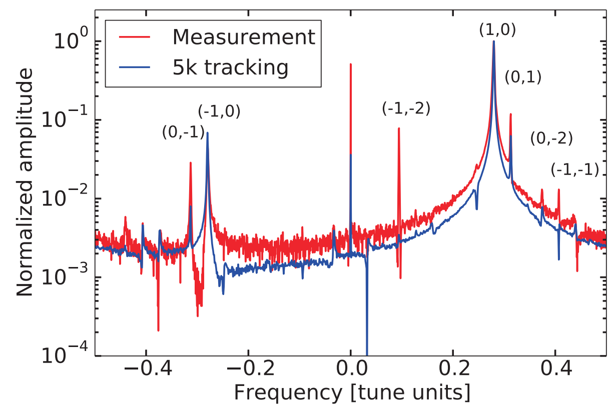

Figure 1: Complex spectra amplitude of $h_x^- = x - ip_x$ reconstructed from two BPM signals at BPM.12L1.B2 from the LHC with $8.2\sigma_{x,\text{nom}}$ and $6.5\sigma_{y,\text{nom}}$ measured kick amplitudes. A large amplitude is observed at $freq \approx 0.1$, but not at -0.1.

Further observations of the (-1,-2) line show its frequency is linear with the calculated frequency from the main tunes as it is shown in Fig. 2. This result confirms that the (-1,-2) line is not an artifact unrelated to the beam.

The decoherence of the (-1,-2) line over the number of turns is shown in Fig. 3. The measured (-1,-2) line cleary decoheres much slower than the main horizontal tune. This result motivates the study of possible surviving lines [15] as part of the cause of the large measured amplitude.

Anharmonicities for first and second order amplitude detuning have been calculated in 2012 [12]. These can be used to calculate the amplitude detuning for specific frequencies. Figure 4 shows the amplitude detuning for the (-1,-2) line for different anharmonicities than in [12], but still within the error margins of the measurements. The obtained amplitude detuning for the (-1,-2) line shows a saddle point on the diagonal of the $(2J_x, 2J_y)$-plane where the gradient is zero. A beam kicked near this critical point would have zero amplitude detuning for the (-1,-2) line and therefore a decreased

Content from this work may be used under the terms of the CC BY 3.0 licence (© 2015). Any distribution of this work must maintain attribution to the author(s), title of the work, publisher, and DOI.

ISBN: 978-3-95450-168-7 doi:10.18429/JACoW-IPAC2015-MOPJE053

NSLS-II BEAM LIFETIME MEASUREMENTS AND MODELING*

Boris Podobedov#, Weixing Cheng, Yoshiteru Hidaka, Hsiao-Chaun Hseuh, Guimei Wang,
Brookhaven National Laboratory, Upton, NY 11973-5000, USA

Content from this work may be used under the terms of the CC BY 3.0 licence (© 2015). Any distribution of this work must maintain attribution to the author(s), title of the work, publisher, and DOI.

Abstract

NSLS-II is a recently constructed 3 GeV synchrotron light source with design horizontal emittance values in sub-nm range. Achieving good beam lifetime is critically important for NSLS-II as it is closely tied to such important operational aspects as top-off injection frequency, injector components wear, radiation protection and control, and others. In this paper we present lifetime-related commissioning results and describe our present understanding of beam lifetime at NSLS-II.

INTRODUCTION

At 500 mA design beam current the beam lifetime in the NSLS-II ring is expected to be Touschek-dominated [1]; contributions from gas scattering could also be significant, especially when small gap in-vacuum undulators are in operation.

Direct measurements of just the Touschek lifetime are not possible, as the combined lifetime due to all of the effects is always measured. However, contributions due to gas scattering can be separated from the Touschek effect as they generally do not depend on beam dimensions (ignoring ion trapping) and only depend on the total beam current through current-dependent outgassing rates. These rates could be measured, and, at low beam intensity their current-dependence is negligible. Touschek lifetime, on the other hand, has a strong dependence on beam dimensions and is inversely proportional to single-bunch current.

For a simplified model of constant gas pressure, gas scattering lifetime results in the exponential time dependence of the total beam current,

$$I(t) = I(0)\,\mathrm{Exp}(-t/\tau), \qquad (1)$$

where two separate processes are responsible for the decay. Elastic gas-scattering lifetime is given by [2]

$$\frac{1}{\tau_{el}} = \frac{4r_e^2 Z^2 \pi n c}{2\gamma^2}\left[\frac{\langle\beta_x\rangle}{A_x} + \frac{\langle\beta_y\rangle}{A_y}\right], \qquad (2)$$

where $A_{x,y}$ are horizontal and vertical acceptances, given by the minimum value of aperture, a(s), squared and divided by the beta function at that location, $A=\min(a(s)^2/\beta(s))$, n and Z are the concentration and the atomic number of the residual gas ions.

Lifetime due to inelastic gas-scattering, or Bremsstrahlung, is given by [2]

$$\frac{1}{\tau_{brem}} = \frac{16 r_e^2 Z^2 n c}{411}\ln\left[\frac{183}{Z^{1/3}}\right]\left[-\ln\varepsilon_{acc} - \frac{5}{8}\right], \qquad (3)$$

where ε_{acc} is the limiting momentum acceptance.

Touschek scattering process leads to the non-exponential decay of single-bunch current,

$$I_b(t) = \frac{I_b(0)}{1 + t/\tau_{tous\_1/2}}, \qquad (4)$$

where $\tau_{tous\_1/2}$ is the so-called Touschek half-life (but also called Touschek lifetime below), given by [3]

$$\frac{1}{\tau_{tous\_1/2}} = \frac{\sqrt{\pi}\, r_e^2 c N_b}{\gamma^3}\left\langle \frac{C(\zeta)}{\sigma'_x V \varepsilon_{acc}^2}\right\rangle, \qquad (5)$$

where N_b is the number of electrons per bunch, $C(\zeta) = -\frac{3}{2}e^{-\zeta} + \frac{\zeta}{2}\int_\zeta^\infty \ln(u)\frac{e^{-u}}{u}\,du + \frac{1}{2}(3\zeta - \zeta\ln\zeta + 2)\int_\zeta^\infty \frac{e^{-u}}{u}\,du$, $\zeta = \left[\varepsilon_{acc}/\gamma\sigma'_x\right]^2$, V is the beam volume, and the brackets denote averaging over the ring circumference.

For short time intervals, the current decay is relatively small, which is what is happening during top-off operations or during typical lifetime measurements. In such instances both (1) and (4) are well approximated by a linear time-dependence, so the total lifetime is given by

$$\tau_{total} = 1/(\tau_{el}^{-1} + \tau_{brem}^{-1} + \tau_{tous\_1/2}^{-1}). \qquad (6)$$

In NSLS-II ring the standard (total) beam lifetime measurements are performed by linearly fitting the decaying beam current signal, measured by DCCT, over the specified time interval (typically 5 minutes). The lifetime is simply the average current over this interval divided by the fitted slope. However, for low beam currents we found the DCCT-derived lifetime to be too noisy, especially when we could not afford long averaging times. This is why the so-called "BPM lifetime" measurement was implemented as well. Instead of the DCCT signal, it uses the average sum signal from 180 BPMs, resulting in much lower noise, even when the time averaging is performed over 30s or shorter intervals. This is the measured lifetime reported below.

MEASUREMENTS AND ANALYSIS

Phase I Commissioning

We start with the single bunch measurements from 05/08/14 as well as the 20-bunch train data from 05/11/14 (both data sets are with emittance coupling corrected to an estimated value of $\kappa=\varepsilon_y/\varepsilon_x=0.32\%$). The RF cavity voltage at the time was 1.9 MV (close to the maximum allowed) corresponding to the momentum acceptance of $\varepsilon_{RF}=2.5\%$. The measured lifetime vs. single bunch current is plotted in Fig.1 (circles). Note that the trends vs.

* Work supported by DOE contract DE-AC02-98CH10886.
# boris@bnl.gov

ISBN: 978-3-95450-168-7 doi:10.18429/JACoW-IPAC2015-MOPJE054

DEVELOPMENTS OF THE SEGMENT-BY-SEGMENT TECHNIQUE FOR OPTICS CORRECTIONS IN THE LHC

A. Langner* [1,2], J. Coello de Portugal[2], P. Skowronski[2], R. Tomás[2]
[1]University of Hamburg, Germany, [2]CERN, Geneva, Switzerland

Abstract

Optics correction algorithms will become even more critical for the operation of the LHC at 6.5 TeV. For the computation of local corrections the segment-by-segment technique is used. We present improvements to this technique and an advanced error analysis, which increase the sensitivity for finding local corrections. Furthermore, we will investigate limitations of this method for lower β* optics as they will be used in the high-luminosity LHC (HL-LHC) upgrade.

INTRODUCTION

The segment-by-segment technique (SbS) was developed at the LHC for the computation of optics corrections for local, strong error sources [1]. The concept is to run MAD-X [2] in a part of the accelerator in between two beam position monitor (BPM) locations. The optical functions which were derived from measured turn-by-turn data of the BPMs are the start parameters for this simulation. For optics corrections the simulated phase advances between BPMs are compared to the measured ones, as they are more directly observable than e.g. the β-function. Possible correction settings aim at eliminating the deviations in the phase advance. This method has been very successful at finding local optics corrections for the LHC, where it was once even able to identify a cable swap between the two beam apertures in a quadrupole which caused an unexpectedly large β-beating [3, 4]. SbS was also successfully tested at RHIC and is fully implemented there [5].

Another purpose of SbS is the propagation of optical functions from the BPM positions to other lattice elements. This allows for example to derive the β-function at the interaction points (β*). It has also been used to propagate the optical functions to beam wire scanners for an emittance study [6] and to collimators for a comparison to beam sizes as they are measured in beam-based collimator alignment [7]. These studies require very precisely measured β-functions and improvements to SbS were required to comply with these demands. Recent improvements related to SbS include an improved measurement of the β-function from BPM turn-by-turn data [8] which results in significantly more precise start parameters for the SbS simulation.

Furthermore, an automatic routine has been developed to match the measured and simulated phase advances for finding optics corrections [9, 10]. In the following sections we will show improvements in the error analysis for SbS and also present a comparison of simulated local optics corrections for LHC and HL-LHC, which shows a possible limitation of SbS for lower β* optics.

* andy.langner@cern.ch

IMPROVED ERROR ANALYSIS

Phase Advance

The β-beating propagation can be described by an oscillation with constant amplitude A which propagates with twice the betatron oscillation frequency

$$\frac{\Delta\beta}{\beta}(s) = A \cdot \sin(2 \cdot \phi(s) + \phi_0). \tag{1}$$

$\phi(s) + \phi_0$ is the phase of the betatron oscillation at the position s and ϕ_0 the initial phase for $s = 0$. Using Eq. (1) one can approximate the deviation of the phase $\Delta\phi$ due to the β-beating at the start of the segment. Error propagation on $\Delta\phi$ using the uncertainties σ_{β_0} and σ_{α_0} of the optical functions at the start of the segment leads to the uncertainty of the propagated phase

$$\begin{aligned}\sigma^2_{\phi(s)} =& \left(\frac{1}{2}(\cos(2\phi(s)) - 1)\frac{\alpha_0}{\beta_0} + \frac{1}{2}\sin(2\phi(s))\frac{1}{\beta_0}\right)^2 \sigma^2_{\beta_0} + \\ &\left(\frac{1}{2}(\cos(2\phi(s)) - 1)\right)^2 \sigma^2_{\alpha_0},\end{aligned} \tag{2}$$

where α_0 and β_0 are the initial α- and β-function at the start of the segment. The computation of uncertainties for the phase advance in the simulation, which were not regarded before, allow for a better calculation of optics corrections, since the uncertainties can be considered as weights when matching the measured and simulated phase advances. This feature is part of the automatic matching routine [10].

β- and α-function

The same approach as for the phase advance uncertainty can also be used for other optical function. The uncertainties of the propagated α- and β-function at the position s (α_s and β_s) are shown in Eqs. (3-4).

$$\begin{aligned}\sigma^2_{\beta_s} =& \left[\beta_s \sin(2\phi(s))\frac{\alpha_0}{\beta_0} + \beta_s \cos(2\phi(s))\frac{1}{\beta_0}\right]^2 \sigma^2_{\beta_0} + \\ &\left[\beta_s \sin(2\phi(s))\right]^2 \sigma^2_{\alpha_0}.\end{aligned} \tag{3}$$

$$\begin{aligned}\sigma^2_{\alpha_s} =& \left[\alpha_s \sin(2\phi(s))\frac{\alpha_0}{\beta_0} + \alpha_s \cos(2\phi(s))\frac{1}{\beta_0} - \right. \\ &\left. \cos(2\phi(s))\frac{\alpha_0}{\beta_0} + \sin(2\phi(s))\frac{1}{\beta_0}\right]^2 \sigma^2_{\beta_0} + \\ &\left[\cos(2\phi(s)) - \alpha_s \sin(2\phi)\right]^2 \sigma^2_{\alpha_0}.\end{aligned} \tag{4}$$

Content from this work may be used under the terms of the CC BY 3.0 licence (© 2015). Any distribution of this work must maintain attribution to the author(s), title of the work, publisher, and DOI.

ISBN: 978-3-95450-168-7 doi:10.18429/JACoW-IPAC2015-MOPJE055

DESIGN OF AN INTENSE MUON SOURCE WITH A CARBON AND MERCURY TARGET

Diktys Stratakis, J. Scott Berg, BNL*, Upton, NY 11973, USA
David Neuffer, Fermilab†, Batavia, IL, USA
Xiaoping Ding, University of California, Los Angeles, CA, USA

Abstract

In high-intensity sources, muons are produced by firing high energy protons onto a target to produce pions. The pions decay to muons which are captured and accelerated. In the present study, we examine the performance of the channel for two different target scenarios: one based on liquid mercury and another one based on a solid carbon target. We produce distributions with the two different target materials and discuss differences in particle spectrum near the sources. We then propagate the distributions through our capture system and compare the full system performance for the two target types.

INTRODUCTION

In this paper we will first discuss the particle distributions created from a C target and a Hg target. We will describe our muon capture and initial cooling scenario, and then present results of simulation of that front end system.

PARTICLE DISTRIBUTIONS

We produce particle distributions from mercury and carbon targets under similar conditions. A proton bunch hits a target, with the relevant parameters described in Table 1. The target is in a field that peaks near 20 T at the center of the beam-target crossing, and tapers down to 2 T just under 5 m downstream, and continues at that field downstream from that point. The solenoids that produce this field are described in Table 2; the choice of this field profile was based on [1]. A beam pipe with an inner radius of 13 cm surrounds the target and extends downstream to 85 cm from the beam-target crossing point. Downstream from there, the beam pipe has an inner radius of 23 cm. Particle production computations were performed using MARS15(2014) [2, 3].

We found that the choice of event generator parameters for nuclear inelastic interactions had a significant impact on particle production, as shown in Fig. 1. In contrast to [4, 5], but like [6], these studies use IQGSM=1, the current MARS15(2014) default [3]. Pion production per unit of proton power in mercury is notably higher than in carbon for lower pion energies, but the production rapidly becomes

Table 1: Parameters of the target and incident proton beam. Carbon target parameters are taken from [6], without the dump, with the target radius increased to 10 mm, and a corresponding increase in the proton beam size. For mercury, the target, proton beam, and solenoid axis lie in the same plane at the crossing point, with the proton beam to the outside. The optimization process for obtaining the target geometry is described in [4].

Material	**C**	**Hg [5]**
Target Radius (mm)	10.00	4.04
RMS Beam Size (mm)	2.5	1.212
Target Tilt (mrad)	65	127
Crossing Angle (mrad)	0	20.6
Proton Energy (GeV)	6.75	8
Geometric Emittance (µm)	5	0

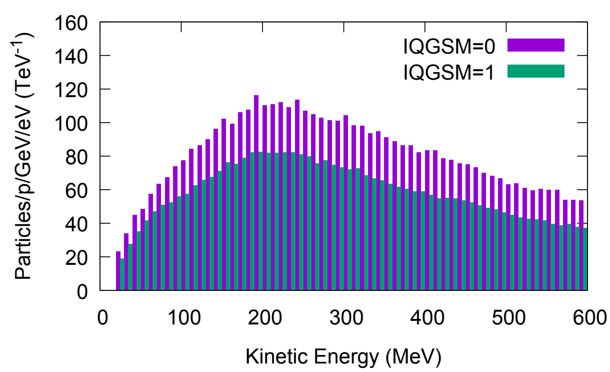

Figure 1: Spectrum of positive pions from carbon, 2 m downstream from the beam-target crossing, for different values of IQGSM in MARS15(2014) [3]: IQGSM=0 is the default value used in older MARS versions, and was used in [4, 5]; IQGSM=1 is the current default value in MARS and was used in [6] and elsewhere in this study. Values are divided by proton beam energy in GeV and histogram bin width.

closer above 250 MeV (Figs. 2 and 3). The differences are much larger for negative than for positive pions. Thus the particle capture system should be optimized differently for a mercury than for a carbon target due to the lower-energy spectrum in mercury. Furthermore, the difference in the spectral shape between positive and negative pions in mercury requires that the optimal capture parameters for positive and negative particles will be different, and some application-

* This manuscript has been authored by employees of Brookhaven Science Associates, LLC under Contract No. DE-SC0012704 with the U.S. Department of Energy. The United States Government retains a non-exclusive, paid-up, irrevocable, world-wide license to publish or reproduce the published form of this manuscript, or allow others to do so, for United States Government purposes.

† Operated by Fermi Research Alliance, LLC under Contract No. DE-AC02-07CH11359 with the United States Department of Energy.

Content from this work may be used under the terms of the CC BY 3.0 licence (© 2015). Any distribution of this work must maintain attribution to the author(s), title of the work, publisher, and DOI.

ISBN: 978-3-95450-168-7 doi:10.18429/JACoW-IPAC2015-MOPJE056

Content from this work may be used under the terms of the CC BY 3.0 licence (© 2015). Any distribution of this work must maintain attribution to the author(s), title of the work, publisher, and DOI.

OMC SOFTWARE IMPROVEMENTS IN 2014

J. Coello de Portugal, F. Carlier, A. Langner,
T. Persson, P. Skowronski, R. Tomás, CERN, Geneva, Switzerland

Abstract

We present the LHC Optics Measurement and Corrections (OMC) software developments done during 2014 on stability, performance and usability. This software is used to analyze turn-by-turn data and compute optics corrections to get the best performance of the LHC. The main developments have been an automatic local correction script to get faster and more accurate corrections in the interaction regions, a self contained test for the whole software package to avoid mistakes during the software development and the improvements in the software quality and efficiency of the Segment-by-segment technique script. We also present a study of the code quality in its current status.

DESCRIPTION OF THE SOFTWARE

The OMC software targets to measure and correct several optics parameters of the LHC. As the machine has very tight tolerances, a good control of the optics is critical for machine protection and performance.

The purpose of the software is to analyze turn-by-turn data measured during the LHC operation. Using an improved Fourier analysis [1] the spectra of the measured signal is obtained and from the spectrum the machine parameters can be computed [2–4]. This data is compared then to the nominal model of the machine and the differences are corrected so it behaves as close as possible to the designed machine.

This set of compiled programs and scripts is gathered into a GUI (*Graphical User Interface*) programmed in Java. The GUI lets the users take advantage of the software suite without having to know in depth its operating details. The chain of operations needed to analyze, compute corrections of turn-by-turn data and upload them to the machine can be done in minutes using the OMC GUI.

AUTOMATIC CORRECTIONS

During the 2012 run, the Segment-by-segment technique was used with good success to locally correct the optics at regions of importance as the interaction points [5–8]. This technique was used to identify beating in the phase advance between BPMs as phase advance is independent of BPM calibration [9]. However, these corrections were done mostly manually, fitting the phase deviation curve by varying the strength of the correctors and rerunning the scripts to watch the results. This method is slow and lacks of precision and thus, an automatic way of computing this correction has been developed.

Segment-by-segment

The Segment-by-segment technique divides the machine in a certain number of smaller segments and treats them as standalone beam lines. In absence of errors and given the measured initial conditions, the propagation of the phase advance between BPMs using the reference model should behave as that of the measured machine. The differences found in the propagations can be more easily corrected taking only these small segments into account.

Automatic Matching

To perform the automatic correction of the phase advances in a given segment, the Segment-by-segment script has to be run for both beams, as quadrupole magnets which are shared by both beams may also be used for computing corrections. Therefore, for automatic corrections, the matching script in Segment-by-segment needs to run for both beams simultaneously. After that, the MAD-X simulation software [10] is used to match the phase deviations at each measurement point:

1. A set of variables is given to MAD-X, representing the different strengths of the corrector magnets in the chosen segment.

2. The program is provided with a set of constraints, representing the deviations in the phase advance between each BPM in the region of interest:

$$\Delta\phi_{n+1} = \phi_{n+1}^{meas} - \phi_{n}^{meas} - (\phi_{n+1}^{mod} - \phi_{n}^{mod}) \qquad (1)$$

3. Then, MAD-X will try to find a configuration of the variables that satisfies the constraints as precisely as possible, using a least square minimization technique.

4. Once the phase deviation is reproduced with the desired accuracy, the resulting magnet strength corrections are flipped in sign to counteract that deviation.

If MAD-X finds a configuration of strengths that overpowers some magnet, the user can deactivate it, forcing the matching script to find another configuration. Also, if the measurement in some BPM is thought to be wrong or misleading, the algorithm can be told to ignore this matching point. Furthermore, the algorithm takes the errors in the phase measurements into account, giving less importance to those that have highest errors.

The automatic matching procedure takes around 20 seconds until it finds a solution, performing much faster and more precisely than manually. This new feature is integrated in the OMC GUI (Fig. 1).

TRACKING TEST

As 2014 has been a year of improvements not only in the performance but also in the precision and usability of the

ISBN: 978-3-95450-168-7 doi:10.18429/JACoW-IPAC2015-MOPJE057

OPTICS MEASUREMENT USING THE N-BPM METHOD FOR THE ALBA SYNCHROTRON

A. Langner* [1,2], G. Benedetti [3], M. Carlà [3], J. Coello de Portugal [2], U. Iriso [3], Z. Martí [3], R. Tomás [2]
[1] University of Hamburg, Germany, [2] CERN, Geneva, Switzerland,
[3] ALBA-CELLS Synchrotron, Cerdanyola del Vallès, Spain

Abstract

The N-BPM method which was recently developed for the LHC has significantly improved the precision of optics measurements that are based on beam position monitor (BPM) turn-by-turn data. The main improvement is owed to the consideration of correlations for statistical and systematic error sources, as well as increasing the amount of BPM combinations for one measurement. We present how this technique can be applied at light sources like ALBA, and compare the results with other methods.

INTRODUCTION

Linear optics from closed orbit (LOCO) [1] is the standard method for optics measurements and corrections at the ALBA synchrotron [2]. Turn-by-turn measurements can provide faster optics measurements than LOCO and are of great interest also for other light sources [3–5]. Recently, efforts have been put in developing optics measurements based on BPM turn-by-turn data at ALBA. However, previous measurements showed discrepancies of the measured β-beating in comparison to LOCO of 4-10 % [6]. Also at SOLEIL significant discrepancies were observed when comparing the β-beating from turn-by-turn measurements to LOCO and an optics correction study at SLS found an inferior performance of turn-by-turn measurements compared to LOCO. Studies in ESRF [7] show that the model which arises from a fit to the phase advances from turn-by-turn data is superior to their standard orbit response matrix (ORM) based model. However, this approach could not become operational for technical reasons. One method to infer the β-function uses the phase advance of the betatron oscillation between three BPMs [8, 9]. The phase advance can be derived from the BPM turn-by-turn data while an oscillation has been excited on the beam.

Previous attempts of optics measurements from turn-by-turn data at LHC and SOLEIL used only neighboring BPMs for the analysis because the effect of systematic errors for larger ranges of BPMs would quickly deteriorate the results. The N-BPM method overcomes this limitation by performing a detailed analysis of systematic and statistical errors and their correlations [10]. This allows to consider more BPM combinations for the analysis and therefore to use more information when probing the β-function at one BPM position. This is especially useful if neighboring BPMs have phase advances which are not well suited for a measurement. Optimal phase advances in between two BPMs are $45° + n_1 \cdot 90°$, and phase advances of $n_2 \cdot 180°, (n_1, n_2) \in \mathbb{N}^2$ should be avoided. The phase advances of consecutive BPMs are shown in Fig. 1 for the nominal ALBA lattice. In the vertical plane there are many consecutive BPMs with small phase advance, and considering BPMs combinations within a larger range of BPMs would allow for better phase advances for the measurement.

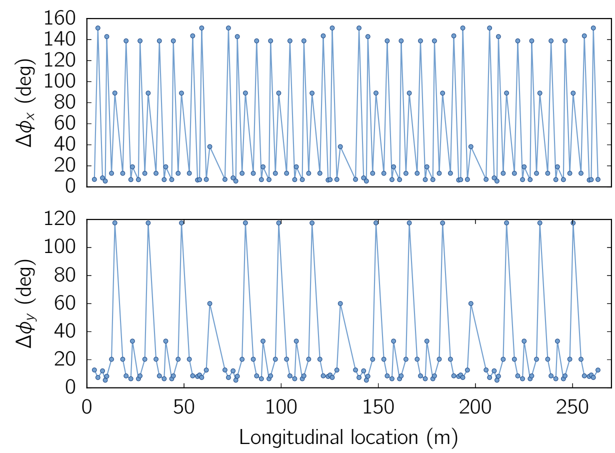

Figure 1: Phase advances of consecutive BPMs in the nominal model.

SYSTEMATIC ERRORS

For the N-BPM method it is crucial to consider model uncertainties and their correlations for the β-function measurement. They can be derived for example in a Monte-Carlo simulation where the error sources are varied within their uncertainty and the impact on the measurement is observed. The calculation of systematic errors is based on the uncertainties of magnetic measurements and alignment uncertainties, which can be found in Table 1. The Monte-Carlo simulation was performed for 1,000 iterations and the error sources were varied randomly following a Gaussian distribution.

We perform Monte-Carlo simulations separately for each contribution to study how much each error source is contributing to the total systematic error, cf. Fig 2. The dominant contribution comes from quadrupolar gradient errors (b_2), and transverse misalignment of sextupole magnets. For the horizontal plane the quadrupole b_2 errors have a larger effect than the dipole b_2, which is the opposite in the vertical plane. This is because β_y is much larger at the dipole magnets than β_x.

The systematic errors can furthermore be assessed separately for different BPM combinations. In Table 2 the aver-

* andy.langner@cern.ch

Content from this work may be used under the terms of the CC BY 3.0 licence (© 2015). Any distribution of this work must maintain attribution to the author(s), title of the work, publisher, and DOI.

ISBN: 978-3-95450-168-7 doi:10.18429/JACoW-IPAC2015-MOPJE058

Content from this work may be used under the terms of the CC BY 3.0 licence (© 2015). Any distribution of this work must maintain attribution to the author(s), title of the work, publisher, and DOI.

FLUKA MODELING OF THE ESS ACCELERATOR

L. Lari, L.S. Esposito, ESS, Lund, Sweden and CERN, Geneva, Switzerland
M. Eshraqi, L. Tchelidze, ESS, Lund, Sweden
F. Cerutti, A. Mereghetti, CERN, Geneva, Switzerland

Abstract

In order to evaluate the energy deposition and radiation issues concerning the ESS accelerator, a FLUKA model of the machine has been created. The geometry of the superconducting beam line is built according to the machine optics, described in the TraceWin file and the CATIA drawings of the beam elements, using the LineBuilder tool developed at CERN. The objective is to create a flexible FLUKA model that is able to be adapted to the optimization of the optics, design modifications and machine integration constraints. Preliminary results are also presented.

INTRODUCTION

The European Spallation Source (ESS) is a high-energy and a high-intensity accelerator-driven facility, currently under construction at Lund, in Sweden [1]. The ESS superconducting linac is designed to accelerate protons up to 2 GeV (kinetic energy) and to provide an average beam power of 5 MW on target. Table 1 summarizes the main accelerator parameters, while the general layout of the ESS linear accelerator is shown in Fig. 1.

Table 1: Key Parameters of the ESS Proton Linac

Average Beam Power	5 MW
Peak Beam Power	125 MW
Beam on target	> 95% availability
Proton kinetic energy	2 GeV
Pulse frequency	2.86 ms
Pulse frequency	14 Hz
Peak current	62.5 mA

The proton beam from the Ion Source is transported through a Low Energy Beam Transport (LEBT) section to the Radio Frequency Quadrupole (RFQ) for bunching and acceleration. At the extraction of the RFQ, the beam is transported and matched to the normal conducting Drift Tube Linac (DTL) through a Medium Energy Beam Transport (MEBT) section. Downstream of the 5 DTL tanks, the beam enters the superconducting part of the linac, where it is accelerated via superconducting radio frequency cavities, constructed from niobium and immersed in liquid helium at a nominal temperature of 2K. The first superconducting section contains 13 cryomodules each containing a pair of double spoke cavities. The spoke section is followed by two sections of elliptical cavities, medium-β and high-β, where β is the ratio of the proton speed to the speed of the light. In this section, the cryomodules contains 4 elliptical cavities each, for a total of 9 cryomodules for the medium-β and 21 for the high-β respectively. Finally, after acceleration, the beam is transported via the High Energy Beam Transport (HEBT) to the target.

METHODOLOGY

The effect of prompt radiation and induced radioactivity are planned to be studied with Monte-Carlo simulations. For the low energy part of the ESS linac including the DTLs included, the MCNPX code is used [2], while in the more energetic part of the accelerator (at energies outside of the neutron resonance regions), the calculations are performed with MARS [3,4] and/or FLUKA codes [5,6].

In particular, FLUKA is used to address all questions for which a detailed accelerator geometry is needed, such as activation of beam line elements and it will be used to benchmark some MARS shielding results. For this reason, a detailed FLUKA model of the ESS accelerator is in progress, starting from the last DTLs until the target and including tunnel and gallery buildings as well as stubs between tunnel and gallery, and tunnel emergency exits (see Fig. 2 for a representation of the model).

The FLUKA model of the beam line follows automatically the lattice sequence described in the official TraceWin optics output file, thanks to the LineBuilder [7]. In case of future possible hardware, footprint or optics changes, the coupling between TraceWin and LineBuilder makes possible to generate a new model, if the geometry of each element is available in FLUKA.

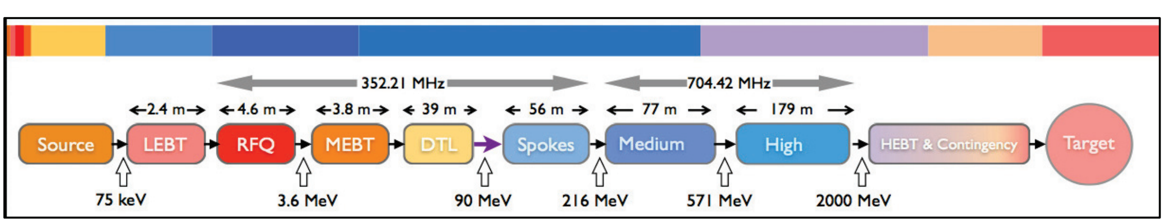

Figure 1: Schematic block diagram of the ESS accelerator lattice (bottom) and corresponding proportional length of the different sections (top). The blue items are superconducting (i.e. the spoke resonators, the medium and high β elliptical cavities), while the other items are normal conducting.

ISBN: 978-3-95450-168-7 doi:10.18429/JACoW-IPAC2015-MOPJE059

Content from this work may be used under the terms of the CC BY 3.0 licence (© 2015). Any distribution of this work must maintain attribution to the author(s), title of the work, publisher, and DOI.

TESTS OF WAKEFIELD-FREE STEERING AT ATF2

A. Latina, J. Pfingstner, D. Schulte, CERN, Geneva, Switzerland
J. Snuverink, Royal Holloway, University of London, Egham, UK
N. Fuster, IFIC, Valencia, Spain
E. Adli, University of Oslo, Oslo, Norway

Abstract

Charge-dependent effects on the orbit and on the beam size affect the performance of the Accelerator Test Facility (ATF2) in a non-negligible way. Until now small beam sizes have only been achieved running with a beam charge significantly smaller than the nominal value. These detrimental effects on the beam have been attributed to wakefields, in the cavity BPMs, in the multi-Optical Transition Radiation (OTR) systems as well as in other components of the beamline. The successful tests of a Wakefield-free Steering (WFS) algorithm at FACET have encouraged performing tests of the same correction scheme at ATF2. The performance of the algorithm has been simulated in detail, including several realistic imperfection scenarios, including charge-dependent BPMs resolution, and incoming injection error and position jitters, which are described in this paper. Tests of Dispersion-free Steering (DFS) and of WFS have been performed at ATF2 during December 2014. The results are discussed here.

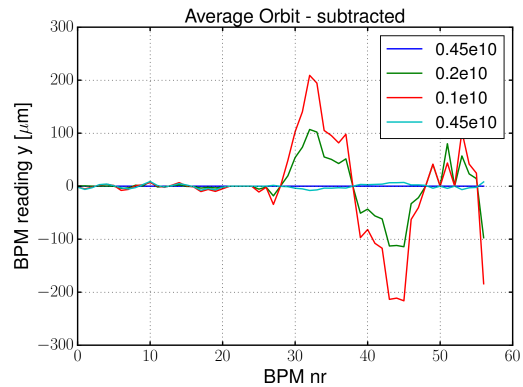

Figure 1: Example of a current-dependent beam orbit. The orbits are displayed relative to charge 4.5×10^9 particles per bunch.

INTRODUCTION

ATF2 [1] is a scaled demonstrator for the final focus system of future linear lepton colliders, the so-called local chromaticity correction scheme [2]. ATF2 is built as an extension of the ATF complex at KEK (Japan). The beam from a low emittance damping ring is extracted into the ATF2 beamline.

Effects depending on the beam current affecting the orbit and especially the beam-size, have repeatedly been reported for the ATF2, preventing it from achieving the target nominal beam-size at the focal point and from running at its fullest nominal beam current of 10^{10} electrons per bunch [3, 4]. Figure 1 shows the average beam orbit for different intensities with respect to the orbit with a bunch charge of 4.5×10^9 particles, as it was measured in April 2013. A beam orbit that changes with the bunch charge can be symptom of the presence of strong wakefields induced by some beamline components.

Techniques such as Dispersion-free steering and Wakefield-free steering have proven to be effective in reducing dispersive and wakefield effects on the orbit, and in most of the cases also managed to significantly reduce the emittance growth associated with such effects [5, 6]. These successes motivated the tests we are reporting about in this paper.

SIMULATION

The extraction line of the ATF2 was simulated using the code PLACET [7]. Wakefield effects were added at the cavity BPMs according to the calculations performed in [4]. Several static and dynamic imperfections were considered in the simulation: element misalignment, BPM resolution, and time-dependent effects such as pulse-to-pulse random variations in beam energy, position, and angle at injection. These jittering quantities were meant to assess stability and robustness of the algorithm in a realistic dynamic environment. 100 misalignment seeds were simulated with a RMS misalignment for magnets and BPMs of 100 μm. 55 BPMs were used for the steering, together with 11 correctors in both the vertical and horizontal plane. WFS was applied in 3 iterations with weights of $\beta = 5$ and $\omega = 26$. An explanation of the function of β and ω, as well as details on the implementation of WFS, can be found in [6]. The fact that the resolution of the BPMs drops with a lower charge was taken into account. Two beam charges of 8×10^9 and 5×10^9 particles per bunch were chosen as test beams for WFS, since these two values of the charge don't compromise excessively the BPM resolution, see Fig. 2, which shows the measured BPM resolution of a cavity BPM typical of the ATF2 [8].

The results of the simulations are shown in Fig. 3, where the final emittance after correction is plotted as a function of the weight parameter ω, for DFS and for WFS in combination with DFS respectively. Figure 4 shows the profile of the relative emittance growth along the beamline. Each of these results is the average of the 100 random seeds previously mentioned.

ISBN: 978-3-95450-168-7 doi:10.18429/JACoW-IPAC2015-MOPJE060

Content from this work may be used under the terms of the CC BY 3.0 licence (© 2015). Any distribution of this work must maintain attribution to the author(s), title of the work, publisher, and DOI.

BBA AND COUPLING CORRECTION AT CLIC RTML

Yanliang Han, Lianliang Ma, Shandong University, Jinan, China
Andrea Latina, Daniel Schulte, CERN, Geneva, Switzerland

Abstract

The CLIC Ring To Main Linac (RTML) must transport the electron and the positron bunches through more than 20 km of beamlines with minimal emittance growth. The turnaround loops (TAL) are one of the most critical sections. In this paper a study of the Beam-Based Alignment (BBA) techniques in the Turnaround loop (TAL) of the CLIC RTML is presented. In order to reduce the emittance growth, the one-to-one(1:1) and dispersion-free steering (DFS) corrections have been tested. The results showed that the emittance growth budgets can be met both in the horizontal and vertical planes. The impact of coupling errors due to magnets roll on the emittance has also been studied and a coupling correction scheme has been designed. By inserting the correction scheme into the RTML dispersive region, the vertical emittance can be largely compressed. While this coupling correction result is very preliminary and more further studies are needed.

INTRODUCTION

CLIC is one of the future accelerators designed for the particle physics after LHC. The concept of two-beam acceleration can provide colliding beam energy up to 3 TeV [1]. The RTML section is the part of CLIC that connects the damping rings and the main linacs. The sketch of the RTML is shown in Fig. 1 [1]. The RTML sections for electrons and positrons are composed by the same subsystems (two bunch compressors, booster linac, central arc, vertical transfer, long transfer line, and turnaround loops), with the difference that there is no spin rotator in the positron line. In this paper we will focus on the electron RTML, and in particular the TAL. The TAL is a complex subsection featuring a lattice that must be achromatic, isochronous while minimizing ISR emittance growth.

In order to guarantee a luminosity of the order of 2×10^{34} cm^{-2}s^{-1}, CLIC accepts a very strict emittance growth budget for the RTML. The normalized emittances are respectively 500 and 5 nm·rad for horizontal and vertical plane at the entrance of RTML, and they should be smaller than 600 and 10 nm · rad at its exit [1]. Pre-alignment of dipoles and quadrupoles has been considered to be of the order of 100 μm, assuming the BPM resolution of 1 μm [1]. These values are such that BBA must be used in order to preserve the small emittances to magnets errors.

It must also be noticed that, at the entrance of the RTML, the vertical emittance is only 1% of the horizontal emittance. This implies that even very small coupling between horizontal and vertical plane will introduce large emittance growth in the vertical plane. It is known that it is hard in technique to align the rotation errors less than 100 μrad. So, a coupling correction scheme must be envisaged.

In this paper, we will use the CLIC beam tracking software PLACET, which is intended to simulate the dynamics of a beam in the presence of wakefields [2] in order to assess the performance of BBA in the TAL, and the impact of coupling errors on the beam quality.

BBA IN THE TURNAROUND LOOPS

The turnaround loops feature the most complex lattice in RTML so it is also very difficult to do the BBA. The dipoles are selected as the correctors and one dipole is added after each quadrupole. We used a gaussian distribution to misalign the lattice, with σ_{pos} denoting the standard deviation. All the quadrupoles and Beam Position Monitor (BPM) are misaligned. BPM also has a resolution $\sigma_{\text{res}} = 1$ μm. One-to-one (1:1) and DFS are used to improve the orbit. The 1:1 is a simple and faster algorithm which is often used first to correct the misalignment errors. We use the Eq. 1 to get strength of the dipole correctors for the 1:1 correction.

$$\theta = \min||\Delta\mathbf{u} - \mathbf{R}\theta||_2^2 + \beta^2||\theta||_2^2; \qquad (1)$$

Here, θ is the strength of the dipole correctors. $\Delta\mathbf{u} = \mathbf{u}-\mathbf{u}_0$ represent the beam position difference recorded by BPMs between misalignment machine and perfect machine. $\mathbf{R}$ is the response matrix between the dipole correctors and the BPMs. β is damping factor which is used to avoid the large fluctuation of corrector strength.

In the real world, BPMs always have non-zero resolution and alignment errors, we need DFS to correct this. The strength of correctors are got according to Eq. 2.

$$\theta = \min||\Delta\mathbf{u} - \mathbf{R}_1\theta||_2^2 + \omega^2||\Delta\eta - \mathbf{D}\theta||_2^2 + \beta^2||\theta||_2^2 \qquad (2)$$

Here, $\Delta\mathbf{u}$ has the same meaning as in Eq. 1 and $\mathbf{R}_1$ is same as $\mathbf{R}$. ω is weight factor. $\Delta\eta = \Delta\mathbf{u}_{\text{dis}}$ - $\Delta\mathbf{u}$ represent the dispersion recorded by BPMs, here $\Delta\mathbf{u}_{\text{dis}}$ denote beam position difference between misalignment machine and perfect machine for the beam with energy $E_0(1+\delta)$, E_0 is the nominal beam energy. In this study, we set the δ to be 0.5%. $\mathbf{D}$ is the dispersion response matrix.

Simulation Setup

The effectiveness of One-to-one correction (1:1) and DFS depends on the response matrix. In order to compute numerically the response matrix $\mathbf{R}$ and the dispersion response matrix $\mathbf{D}$, a bunch containing 100’000 particles was used. Such a large number of particles was chosen to average out the stochastic effects of the synchrotron radiation emission.

BBA was tested for different σ_{pos} misalignment levels, simulating 100 different random machines. The final observables were the average emittance, and the 90% percentile of the distribution of 100 final emittances. BBA was

ISBN: 978-3-95450-168-7 doi:10.18429/JACoW-IPAC2015-MOPJE062

TESTING ASPECTS OF ADVANCED COHERENT ELECTRON COOLING TECHNIQUE

Vladimir N. Litvinenko[1,2], Yichao Jing[2,1], Igor Pinayev[2], Gang Wang[2,1], Roman Samulyak[3] and Daniel Ratner[4]
[1] Department of Physics and Astronomy, Stony Brook University, Stony Brook, NY 11794, USA
[2] Collider-Accelerator Department, Brookhaven National Laboratory, Upton, NY 11973, USA
[3] Department of Applied Mathematics, Stony Brook University, Stony Brook, NY 11794, USA
[4] SLAC Accelerator Laboratory, Menlo Park, CA 94025, USA

Abstract

An advanced version of the Coherent-electron Cooling (CeC) based on the micro-bunching instability was proposed in [1]. This approach promises significant increase in the bandwidth of the CeC system and, therefore, significant shortening of cooling time in high-energy hadron colliders. In this paper we present our plans of simulating and testing the key aspects of this proposed technique using the set-up of the coherent-electron-cooling proof-of-principle experiment at BNL [2].

INTRODUCTION

In contrast to electron and positron beams, hadron beams in all present-day colliders do not have a strong natural damping mechanism to reduce their energy spreads and emittances. Cooling hadron beams transversely and longitudinally at the energy of collision may significantly increase the luminosity of high-energy hadron colliders and future electron-hadron colliders, such as RHIC, eRHIC [3] and even the LHC/LHeC. Coherent electron Cooling (CeC) [4] promises to deliver cooling of hadron beam with damping rates exceeding that of the existing cooling techniques by many orders of magnitude. The original CeC scheme is based on the amplified electrostatic interactions between electrons and hadrons using FEL as a broadband amplifier [4]. Bandwidth of FEL-based CeC is measured in THz compared with GHz for a traditional microwave stochastic cooling. It is well known that bandwidth of the amplifier determines the maximum cooling rate of the system. The bandwidth of the FEL-based CeC it determined by the duration of the FEL response – so called Green's function [5]. Typical bandwidth of FEL amplifier is a small portion (~ 0.1% to few %) of the FEL frequency. Using micro-bunching as an amplification mechanism [1] promises to extend the CeC bandwidth by additional one to two orders of magnitude. This makes this approach very interesting to explore.

Since the CeC is a novel concept, it first must be demonstrated experimentally before we rely upon it for upgrading present colliders. We are building at BNL a dedicated device, called CeC Proof-of-Principle experiment, supported by DoE Nuclear Physics office grant [2]. It is designed to demonstrate FEL-based CeC using 22 MeV electron beam.

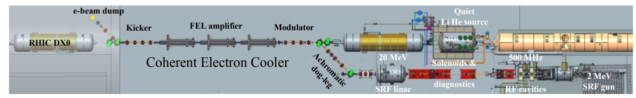

Figure 1: 3D rendering of the CeC demonstration set-up in the RHIC's IP2. It includes the following equipment: 112 MHz SRF gun; 500 MHz RF buncher/pre-accelerator; 20 MeV 704 MHz SRF module; electron beam transport magnets (dipoles, quadrupoles, solenoids, trims); helical FEL wigglers; beam dump; and RHIC DX-, D0-, and triplet-magnets. The electron beam is merged with the ion beam using an achromatic dog-leg, cools the ions in the CeC, and then is discarded into a beam dump.

We are extending this test, using NSF support, to demonstration of the key component of the micro-bunching-based CeC: specifically, demonstrating the amplification of the imprint of the hadron beam density modulation.

COHERENT ELECTRON COOLING

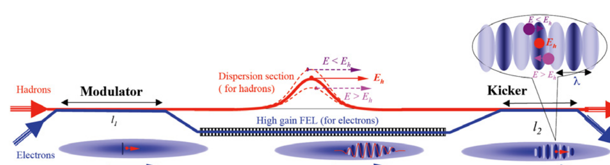

Figure 2: A general schematic of the classical Coherent Electron Cooler comprising three sections: A modulator, an FEL amplifier plus a dispersion section, and a kicker. For clarity, the size of the FEL wavelength, λ, is exaggerated grossly.

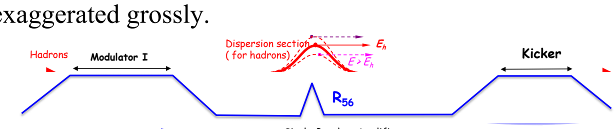

Figure 3: A CeC with an enhanced bunching by a single strong-field buncher. The scheme requires that the electron beam has special qualities [6-7,1].

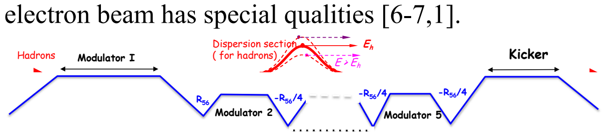

Figure 4: A layout of a CeC using a micro-bunching instability as an amplifier [1].

Content from this work may be used under the terms of the CC BY 3.0 licence (© 2015). Any distribution of this work must maintain attribution to the author(s), title of the work, publisher, and DOI.

ISBN: 978-3-95450-168-7 doi:10.18429/JACoW-IPAC2015-MOPJE063

ORBIT CORRECTION IN THE CERN PS BOOSTER*

M. McAteer, E. Benedetto, C. Carli, G.P. Di Giovanni, B. Mikulec, R. Tomás
CERN, Geneva, Switzerland

Abstract

Prior to the Long Shutdown of 2013-2014 (LS1), control of the closed orbit in the four rings of the CERN PS Booster (PSB) was achieved by adjusting the alignment of several focusing quadrupoles. After a set of orbit corrector dipoles was installed, a major realignment campaign was undertaken to remove these intentional quadrupole offsets and any other magnet misalignments. This paper summarizes the effects of the magnet realignment on the closed orbit in the PSB and the results of closed orbit correction with corrector dipoles.

INTRODUCTION

The PSB is the first synchrotron in the LHC injector chain, accelerating proton beams from 50 MeV to 1.4 GeV in about 500 milliseconds. It is composed of four vertically stacked rings and accelerates four beams simultaneously, which are recombined before being transferred to the Proton Synchrotron. The lattice has a 16-fold periodic structure with two bending magnets and an F-D-F focusing triplet in each period. The four rings share the same bending and focusing magnets, which each have four gaps through which the four beam pipes pass. Each period also contains a multipole corrector magnet stack with an integrated beam position monitor (BPM), and a horizontal and a vertical orbit corrector dipole, but hardware limitations allow for only four orbit correctors per plane per ring to be used at any given time.

These orbit corrector dipoles were not available in the PSB until 2012, and they were not used operationally until after LS1. Prior to this, closed orbit distortion was minimized by introducing horizontal, vertical, and tilt alignment offsets to certain quadrupole magnets [1]. During LS1 an alignment survey was made and a major realignment campaign was undertaken in order to correct both random magnet alignment errors and the intentional quadrupole offsets previously used for orbit correction. In total, about ninety horizontal, vertical, or tilt magnet adjustments were made.

After the shutdown, some final magnet alignment adjustments were made in order to reduce the closed orbit distortion, and then the orbit was further corrected using corrector dipoles and the console application YASP (Yet Another Steering Program) [2].

MAGNET REALIGNMENT

At the beginning of LS1, a tunnel survey was completed to determine the alignment of the main bending magnets, the triplet quadrupoles, and elements containing both beam position monitors and multipole corrector magnets. Figure 1

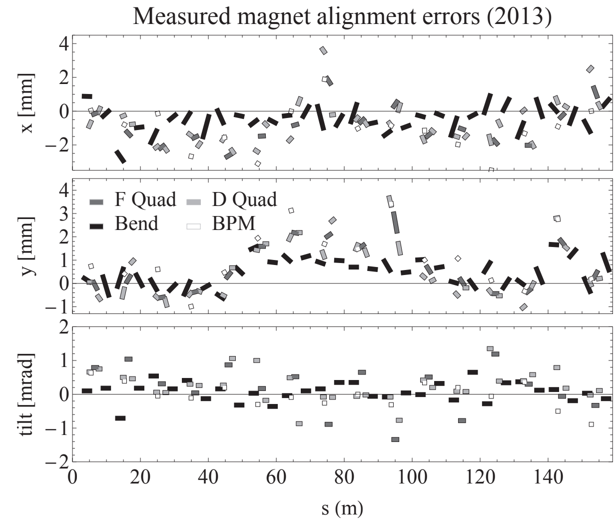

Figure 1: Initial measured alignment of bending magnets, quadrupoles, and BPM stacks, showing the transverse displacement of the ends of each element and the rotation around the longitudinal axis.

shows the measured horizontal and vertical positions of each magnet and its tilt around the longitudinal axis. To reduce aperture restrictions, a realignment strategy was formulated to minimize transverse magnet offsets and jumps between adjacent magnets, while keeping the number of hours of work in the tunnel reasonably low for radiation safety reasons.

All quadrupoles and BPMs with a radial displacement of more than 1 mm from the reference position or from the adjacent quadrupole were realigned to zero. The bending magnets have a large horizontal aperture, so they were not realigned radially. However, the bending magnets have a small vertical aperture which creates one of the main aperture restrictions in the vertical plane. Moving these magnets carries a risk of damaging them, so instead of aligning the bends and quads to the vertical reference position, the quadrupoles were aligned to a smooth curve fit to the vertical position of the bends. Quadrupole magnets and BPMs whose vertical position was more than 1 mm from this curve were moved to lie on the curve. The vertical position of bending magnets was adjusted only in a few cases where there was a jump of more than 1 mm between the position of adjacent bends.

All quadrupoles and BPMs with a tilt of more than 0.3 mrad, and all bending magnets with a tilt of more than 0.5 mrad, were corrected to zero. Note that the radial position measurements refer to the position of the magnet at beam level on Ring 3, which is the third ring up from the ground. When the magnet tilt is adjusted, the physical pivot point is at ground level. Therefore, in order to keep the ra-

* This research project supported by a Marie Curie Early Initial Training Network Fellowship of the European Community's Seventh Framework Programme under contract number (PITN-GA-2011-289485-OPAC)

Content from this work may be used under the terms of the CC BY 3.0 licence (© 2015). Any distribution of this work must maintain attribution to the author(s), title of the work, publisher, and DOI.

ISBN: 978-3-95450-168-7 doi:10.18429/JACoW-IPAC2015-MOPJE064

Content from this work may be used under the terms of the CC BY 3.0 licence (© 2015). Any distribution of this work must maintain attribution to the author(s), title of the work, publisher, and DOI.

BEAM IMPEDANCE OPTIMIZATION OF THE TOTEM ROMAN POTS

N. Minafra[1] on behalf of the TOTEM Collaboration
[1]INFN sez. di Bari, Italy and CERN, Geneva, Switzerland

Abstract

The TOTEM experiment has been designed to measure the total proton-proton cross section and to study elastic and diffractive scattering at the LHC energy. The measurement requires detecting protons at distances as small as 1 mm from the beam center: TOTEM uses Roman Pots (RP), special beam pipe insertions, to move silicon detectors close to the beams to detect particles very near the beam axis. In the first period of running of the LHC no problems were detected with retracted Roman Pots and during insertions in special runs; however, during close insertions to highest intensity beam, impedance heating has been observed. After the LS1 the LHC beam current will increase and the equipment that can interact with the beam needed to be optimized. A new RP, optimized to minimize the beam coupling, has been designed with the help of CST Particle Studio; a prototype has been used to test the simulation results in the laboratory with wire and probe measurements. Furthermore, in both the old and the new RPs, new ferrites have been installed. The new ferrite material has a higher Curie temperature than the one used before LS1 and a thermal treatment at 1000°C has been applied to reduce the out-gassing.

IMPEDANCE SIMULATIONS

A particle beam can induce resonances in any cavity created by the vacuum chamber. When the geometry of the vacuum chamber is too complex, analytical models can not be used to predict the impact of these resonances on the beam and on the environment. Thus, software like CST Particle Studio [1] are used to numerically simulate the evolution of the electromagnetic field inside the cavity after the passage of a particle beam.

A Roman Pot (RP) is a movable part of the beam pipe that allows the positioning of a detector up to a few millimeters from the beam without interfering with the primary vacuum. Especially for equipment that can approach the beam so closely, the impedance has to be optimized and numerical simulations were a key part of the development [2].

The interaction between the beam and the cavity can be harmful for the beam itself, introducing instabilities, but can also damage the equipment, for example due to excessive beam induced heating.

To foresee the instabilities it is useful to compute Z^{eff}, the impedance effectively felt by the beam; the imaginary part of the effective longitudinal impedance $(\Im Z_{\mathrm{long}}/n)^{\mathrm{eff}}$, where $n = f/f_{\mathrm{rev}}$ is the harmonic number, is an indication of the dispersion of the beam through the cavity.

In a similar way, it is possible to compute the power lost by the beam and transferred to the cavity [3] [4]:

$$P_{loss} = 2\,I^2 \sum_{p=1,\,\ldots,\,\infty} PS(pM' f_{\mathrm{rev}})\,\Re[Z_{\mathrm{long}}(p\,M'\,f_{\mathrm{rev}})] \quad (1)$$

where, $PS(f)$, f_{rev}, M' and I are the power spectrum, the revolution frequency and the number of buckets of the LHC;Z_{long} is the simulated longitudinal impedance.

The goal of the optimization is to reduce both heating and effective impedance.

OPTIMIZATION OF THE DESIGN

Before the Long Shutdown 1 (LS1) all Totem RP installed in the LHC were box shaped, as shown in Fig. 1. This design has several mechanical advantages; for instance, the relatively small size of the detector housing does not require the separation between the detector and the primary vacuum to be thicker than 150 μm, reducing the secondary particles shower produced inside the steel and reducing the minimum possible distance of the detector from the beam.

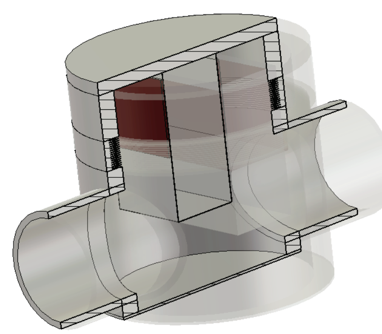

Figure 1: Before LS1 all Totem Roman Pots were box shaped. The empty space between the RP and the flange resonate at low frequency (~ 500 MHz).

However, from a RF point of view, the box RP has a considerable amount of empty space between the detector housing and the vacuum flange that resonates at low frequency (~ 500 MHz). This lead to the introduction of planes of ferrite [5].

Moreover, some of the time-of-flight detectors proposed for the the future upgrade require more longitudinal space inside the RP [6]. The new RP has been designed to increase the space available for the detector, together with reducing the impedance.

The simple solution of having a detector housing that uses all the available space would be ideal; however, the RP needs to be safely inserted and retracted and mechanical constraints and tolerances have to be considered.

ISBN: 978-3-95450-168-7 doi:10.18429/JACoW-IPAC2015-MOPJE065

CONTRIBUTION OF OPTICAL ABERRATIONS TO SPOT-SIZE INCREASE WITH BUNCH INTENSITY AT ATF2

M. Patecki*, R. Tomás, F. Zimmermann, CERN, Geneva, Switzerland
G. White, SLAC, California, USA
K. Kubo, S. Kuroda, T. Naito, T. Okugi, T. Tauchi, N. Terunuma, KEK and SOKENDAI, Ibaraki, Japan

Abstract

A primary goal of ATF2 (Accelerator Test Facility 2) at KEK is to demonstrate an unprecedentedly low vertical beam size at the interactateck ion point (IP) of about 37 nm. Measurements over the past years indicate that the ATF2 vertical beam size, achieved after tuning, strongly rises with bunch intensity. This increase could have several different origins. For example, it could be due to wake fields occurring between the ATF damping ring and the IP, and/or be due to changes in the transverse emittances and energy spread in the damping ring, which are known to increase with intensity as a result of intrabeam scattering (IBS). In this paper we address the second possibility. Past measurements and simulations of the IBS effects in the ATF damping ring and in the extraction line are used to model the intensity-dependent initial emittances and energy spread at the entrance of the final focus. Using this model, particle tracking simulations predict the IP vertical beam size growth expected from the known optical aberrations for initial beam parameters corresponding to varying bunch intensities. We consider both the nominal final-focus optics and a relaxed optics with ten times increased horizontal IP beta function, which has also been used in operation. Comparing simulation results with emittance measurements at different locations allows us to draw some conclusions about the impact of IBS in the damping ring on the IP spot size, and about possible single-bunch wakefields in the ATF2.

INTRODUCTION

Between the end of 2012 and the spring of 2014 a significant reduction of the vertical beam size was achieved [3] at ATF2 [1, 2]. This improvement coincided with two major modifications: (1) an increase of the horizontal beta function at the focal point, β_x^*, by a factor of 10 (in the following called the "$10\beta_x$ optics"), and (2) a 10-fold reduction of the bunch intensity .

The $10\beta_x$ optics decreases the horizontal beam size at almost all the quadrupole magnets of the ATF2 final-focus system, which minimizes the effect of most optical imperfections (e.g. x-y coupling, residual sextupole aberrations) on the vertical beam size at the IP [4]. In parallel, the lower bunch charge weakens single-bunch wake fields [5], and it also minimizes the emittance and momentum spread of the incoming beam, extracted from the damping ring.

In this paper we investigate the IP vertical beam size as a function of beam charge in ATF2 using MAD-X [6] simulations based on the PTC [7] tracking routines. Both the design optics and the relaxed $10\beta_x$ optics are considered. The latter optics is actually in use.

Our simulations do not include any wake fields in the extraction line or in the final focus, but they do take into account the measured dependence of the danping-ring transverse emittance and momentum spread on the bunch charge. Our simulations also incorporate the measured high-order imperfections of the final-focus magnets, i.e. their multipolar field errors. On the other hand, off-center field errors of damping-ring magnets [8] or the nonlinear components of the septum field affecting the kicked beam during extraction are not considered.

INTENSITY-DEPENDENT SPOT SIZE

In 2003 the dependence of the ATF damping-ring emittance and momentum spread on the beam intensity was measured [9, 10]. Figures 2a and b summarize the emittance measurements (grey bands). The measured growth of the momentum spread with rising bunch intensity [10], shown in Fig. 1 (upper curve), is included in all our simulations. The strong intensity dependence of the emittance, and, especially, of the momentum spread, is due to IBS [10].

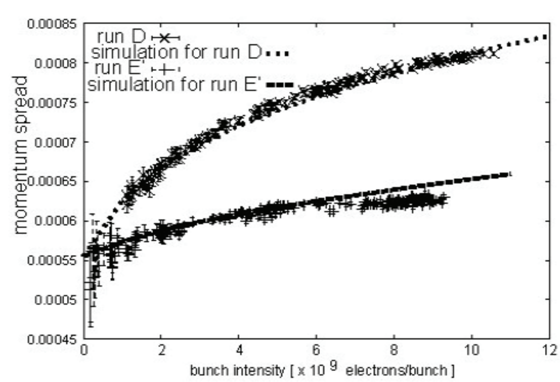

Figure 1: Measured rms momentum spread in the damping ring as a function of the bunch charge compared with IBS simulations [10]. The upper curve was obtained in standard operation, far from the coupling resonance, and it is used for our simulations.

We next examine how this beam emittance increase affects the IP vertical beam size. Three cases are considered: The first case assumes the beam emittances measured in the damping ring (DR). In the second case a constant increment is added to model the emittance of the beam extracted from

* mpatecki@cern.ch, also at Warsaw University of Technology, Faculty of Physics, Koszykowa 75, 00-661 Warsaw, Poland

Content from this work may be used under the terms of the CC BY 3.0 licence (© 2015). Any distribution of this work must maintain attribution to the author(s), title of the work, publisher, and DOI.

ISBN: 978-3-95450-168-7 doi:10.18429/JACoW-IPAC2015-MOPJE066

SINGLE AND MULTI-BUNCH END-TO-END TRACKING IN THE LHeC

D. Pellegrini, EPFL, Lausanne, Switzerland and CERN, Geneva, Switzerland
A. Bogacz, JLab, Newport News, VA 23606, USA
A. Latina, D. Schulte, CERN, Geneva, Switzerland

Abstract

The LHeC study aims at delivering an electron beam for collision with the LHC proton beam. The current baseline design consists of a multi-pass superconductive energy-recovery linac operating in a continuous wave mode. The high current beam (~100 mA) in the linacs excites long-range wake-fields between bunches of different turns, which induce instabilities and might cause beam losses. PLACET2, a novel version of the tracking code PLACET, capable to handle recirculation and time dependencies, has been employed to perform the first LHeC end-to-end tracking. The impact of long-range wake-fields, synchrotron radiation, and beam-beam effects has been assessed. The simulation results and recent improvements in the lattice design are presented and discussed in this paper.

INTRODUCTION

The current baseline design for the LHeC electron is sketched in Fig. 1. Each of the two 1 km long superconducting linacs provide a total acceleration of 10 GeV. The injection energy is 500 MeV. In order to reach the collision energy of 60 GeV, the electrons are recirculated three times. This is accomplished employing beam spreaders and recombiners placed at each end of the linacs. They allow to vertically separate the beams at the different energies routing them to the corresponding arcs. Arc2 and Arc4 are equipped with bypasses to avoid the interference with the detector. After the collision with the LHC proton or ion beam, the electron beam is decelerated in further three turns, allowing to increase the beam current and luminosity while limiting the power consumption [1]. The machine is operated continuously and bunches at different turns are interleaved in the linacs. An up-to-date beam parameter list can be found in [2].

The full LHeC lattice consisting of the two linacs and the six arcs has been imported into PLACET2 which allows to simulate recirculating machines [3]. A single-bunch end-to-end tracking simulation has been set up to evaluate the impact of synchrotron radiation and beam-beam effect. We verified the beam transport to the dump and we identified the lattice sections that could be improved. Moreover, since PLACET2 natively supports simultaneous multibunch tracking, it has been possible to investigate the impact of the transverse long range wakefields.

Progress has also been made with the machine design including the detector bypasses in Arc2 and Arc4. Details of the design will be presented.

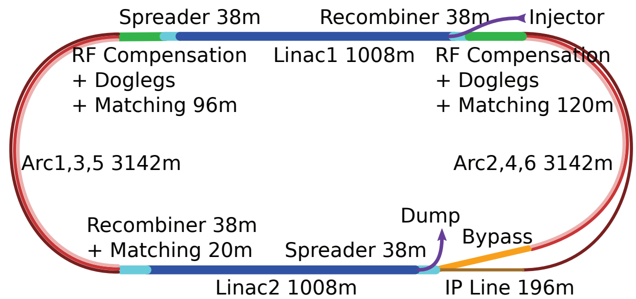

Figure 1: Scheme of the LHeC electron facility.

MACHINE MODELLING

The two linacs and the six arcs, properly connected together, have been imported in PLACET2. This code implements the recirculation in a realistic way. Each element is defined only once and its phase is computed accordingly to the beam time of flight. Although progress is being made, a complete, detailed design of the whole machine is not yet available and small footprint variations are still expected. For this reasons and for convenience the lengths of the arcs are adjusted artificially. Another simplification was applied to the IR, where the squeezing is implemented with a matrix, the beam-beam effect is then computed by GUINEA-PIG [4]. It has been found that the synchrotron radiation has a big impact in the spreader and recombiner sections and in the doglegs for path length adjustments. For the time being, in order to proceed with this study, the above effects have been ignored. The second harmonic RF, required to re-integrate the synchrotron radiation energy loss, is currently modelled as a thin element. No multipolar magnets are currently in the lattice, however higher order beam dynamics arise both from RF cavities and from the fringe fields in the dipole magnets.

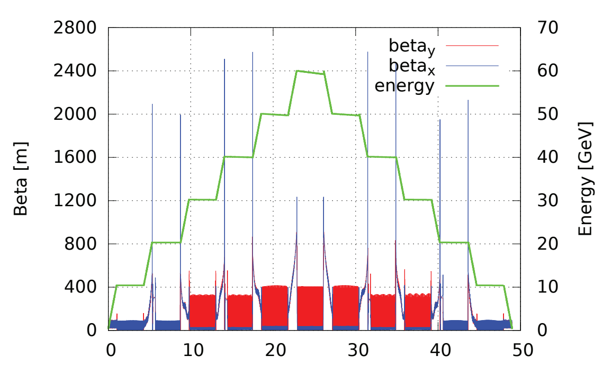

Figure 2: Beta functions and energy profile obtained following a bunch in the whole LHeC lattice.

Content from this work may be used under the terms of the CC BY 3.0 licence (© 2015). Any distribution of this work must maintain attribution to the author(s), title of the work, publisher, and DOI.

ISBN: 978-3-95450-168-7 doi:10.18429/JACoW-IPAC2015-MOPJE067

Content from this work may be used under the terms of the CC BY 3.0 licence (© 2015). Any distribution of this work must maintain attribution to the author(s), title of the work, publisher, and DOI.

APPLICATIONS OF PLACET2 TO THE CTF3 COMBINER RING

D. Pellegrini, EPFL, Lausanne, Switzerland and CERN, Geneva, Switzerland
D. Gamba, A. Latina, R. Corsini, CERN, Geneva, Switzerland

Abstract

The CTF3 Combiner Ring (CR) is an isochronous ring that employs RF-injection to combine multiple bunch trains (up to five) into a single one with higher bunch frequency. The length of the CR plays a critical role in obtaining the correct structure of the recombined train. PLACET2: the new recirculating version of the code PLACET, is particularly suited to simulate the operational scenario. In order to validate this code, two different case studies have been considered: ring-length variations due to optics scaling and vertical instabilities due to bunch-to-bunch wakefield effects. The response of the ring length to the optics scaling has been measured during the last CTF3 run. The instability has been compared with previous studies. The results are presented and discussed.

INTRODUCTION

At CTF3 the acceleration of an electron test beam is powered by an high-current electron drive beam that is decelerated in apposite power extraction units operating at 12 GHz [1]. The drive beam trains of bunches at 12 GHz are produced from longer, 1.5 GHz pulses, applying a factor 8 recombination. A first factor 2 is obtained in the delay loop [2]. The beam is then injected in the combiner ring using RF-deflectors. At every turn, new bunches are injected and interleaved with the one already turning.

The MAD-X model of the CTF3 combiner ring has been imported in PLACET2: the novel version of PLACET capable to handle recirculation [3]. A first measurement of the ring length response to the optics scaling has been performed and compared with the simulation. This has three main motivations: test the code predictions on a real machine, improve the understanding of the combiner rings optics, and demonstrate the possibility to manipulate the ring length possibly going beyond the capabilities of the wiggler magnet installed in the ring. This is particularly important to ensure a regular time structure of the combined beam that is crucial for an efficient deceleration.

The multi-bunch tracking capabilities of PLACET2 have been exploited reproducing the instability that was observed during the commissioning of the combiner ring, caused by a vertical mode trapped in the RF-deflectors.

METHODOLOGY OF THE LENGTH MEASUREMENT

The combiner ring length is measured using a button pickup or BPR: the beam-induced signal is multiplied by an external reference 3 GHz sine function. The phase slippage of the beam arrival time with respect to the 3 GHz reference becomes evident turn after turn as a modulation of the output signal. In the frequency domain the revolution frequency, f_{rev}, and its harmonics split into two sidebands whose distance, d_s, is determined by the fractional length, L_f, of the ring:

$$L_f = \pm \frac{d_s}{2 f_{rev}} \frac{c}{f_{ref}} \quad (1)$$

where c is the speed of light and f_{ref} is the 3 GHz reference frequency. The sign depends on the sidebands crossing; it can be determined empirically by varying the wiggler, whose effect on the fractional length is well understood.

The ideal machine setup for this measure consists of a 3 GHz beam from the gun, bypassing the delay loop. However, in order to not disturb other experiments, a factor 2 combined beam in the delay loop was kept. The train length was 140 ns, filling half of the ring and leaving enough time to completely switch off the RF deflector after the initial injection kick. The beam was kept circulating for approximately 100 turns.

The signal from the BPR was collected with an oscilloscope. The FFT of the signal was saved for the off-line analysis. A small dedicated C++ program has been written to clean the spectra, identify the peaks and compute the fractional length averaging over the available harmonics.

The quadrupoles and the dipoles currents where scaled independently monitoring the length variation. The data collected also comprehend a scan of the wiggler magnet.

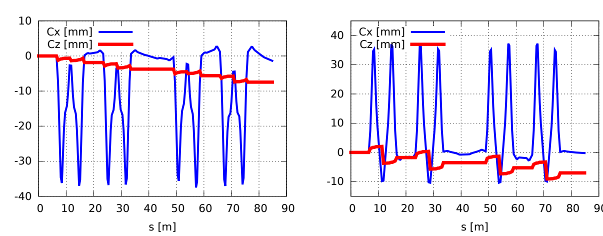

Figure 1: Horizontal and longitudinal bunch position computed for one turn in the combiner ring for two different scalings of the optics: left Q@95%, D@105%; right Q@105%, D@95%.

SIMULATION AND LOSSES

PLACET2 easily allows to track the bunch centroid in the reference frame of the ideal particle. Figure 1 shows the horizontal and longitudinal positions of a bunch for two possible scalings of the dipoles (D) and the quadrupoles (Q). Both the configurations decrease the length of the ring.

When scaling the optics by few percent, part of the beam may hit the vacuum chamber and be lost. This can affect the centroid position altering the result of the measurement.

ISBN: 978-3-95450-168-7 doi:10.18429/JACoW-IPAC2015-MOPJE068

PLACET2: A NOVEL CODE FOR BEAM DYNAMICS IN RECIRCULATING MACHINES

D. Pellegrini, EPFL, Lausanne, Switzerland and CERN, Geneva, Switzerland
A. Latina, D. Schulte, CERN, Geneva, Switzerland

Abstract

Efforts have been taken to enable the simulation of recirculating machines in PLACET. The new version, PLACET2, allows handling multiple interconnected beamlines in order to obtain a realistic model of a machine. Two new elements, injectors and dumps, have been introduced and are active components of any working machine. Trains of bunches are routed through beamlines and tracked simultaneously in a parallel manner. Tracking through time-dependent elements is possible, and care is made to preserve the correct time-structure of the beam in case of beam recombination. This allows straightforward computations of multi-bunch effects arising with high-charge and shortly spaced bunch trains, even with variable train structure. The main features of the code are presented together with its working principles and its key ideas. Two case studies are introduced: LHeC and the CTF3 combiner ring.

INTRODUCTION

The parameters of the electron beams achievable adopting recirculation techniques outperform linacs in terms of average current, but also rings in terms of the longitudinal emittance.

Today we find a flourishing number of Energy Recovery Linacs projects. Many low energy machines like ALICE in England, the cERL in Japan and the JLab FEL in the USA are already operating, but the spectrum extends to the energy frontier with studies like the LHeC and the eRHIC.

Energy recovery and multi-pass linacs are not the only kind of machines that exploits beam recirculation. CTF3 at CERN routinely applies it to fold a train of bunches on itself achieving currents up to 30 A and bunch frequency of 12 GHz. The Drive Beam Complex, a key component of the CLIC technology, will adopt the same concepts to reach a current of 100 A.

The complexity of both the topology and the operation of those machines is a big obstacle for traditional tracking codes, which describe the machines as sequences of elements and/or adopt a very rigid definition of the beam. Single-bunch start-to-end simulations with these codes requires can be pursued unrolling the lattice, however the evaluation of multi-bunch effects, that may be critical, is not feasible.

For these reasons we decided to take advantages from the experience maturated with the developing of the tracking code PLACET [1], to create a new version that allows to set up realistic simulations of the operation of recirculating machines: PLACET2. A new tracking core has been entirely written from scratch in the latest C++ standards. Efforts are being taken to implement the same physics effects handled by PLACET and more. In the next sections we will give an overview of the new-developed concepts and up-to-date code functionalities that provide to our users a powerful tool to tackle these new challenges in accelerator physics.

OVERVIEW OF THE FEATURES AND FUNCTIONALITIES

PLACET2 is developed with a wide spectrum of machines in mind, in particular ERLs like the LHeC [2], but also peculiar lattices like the CLIC Drive Beam Complex [3]. It offers a great tunability of the trade-off between speed and accuracy. On one hand the beam can be represented using multiple models, on the other hand the lattice is implemented in an innovative way that allows to split the thick element cores in order to insert the desired physical effects at the required computational precision.

PLACET2 tracks many bunches simultaneously in recirculating lattices. The bunches enter each beamline in the correct time sequence. This makes possible to compute multibunch effects.

The most common accelerator components are implemented in PLACET2. The initial global phases of time dependent elements are locked by default to the first passing bunch, this resolves any synchronization issues in an automatic manner and relieves the user from tedious initializations. Elements can be misaligned and have apertures, with the possibility to track losses. Physical effects currently include the synchrotron radiation and the multi-bunch long-range-transverse wakefields.

With a bunch-based beam structure, the beam properties can be computed and monitored in any location of the simulated machine. This allows great flexibility. Moreover it is possible to set up a bunch to collect its properties such as orbit and Twiss functions, along its path in the machine.

Although PLACET2 is entirely written in C++, a TCL scripting interface similar to the one of PLACET is provided using SWIG [4]. Recently an Octave interface have also been added following the mechanism developed for PLACET.

COMPONENTS OF PLACET2

PLACET2 adopts an intuitive way to describe a machine based on traditional concepts, but with expanded capabilities and new elements such as injectors, dumps and joints, which allows to simulate the recirculation.

Beam PLACET2 represents the beam as a collection of bunches. Bunches can be routed independently through multiple beamlines, and are recombined together where the beamlines join. PLACET2 is designed to support many

Content from this work may be used under the terms of the CC BY 3.0 licence (© 2015). Any distribution of this work must maintain attribution to the author(s), title of the work, publisher, and DOI.

ISBN: 978-3-95450-168-7 doi:10.18429/JACoW-IPAC2015-MOPJE069

GENERAL FUNCTIONALITY FOR TURN-DEPENDENT ELEMENT PROPERTIES IN SIXTRACK*

K. Sjobak†, H. Burkhardt, R. De Maria, A. Mereghetti, A. Santamaría García
CERN, Geneva, Switzerland

Abstract

In order to facilitate studies of how dynamically changing element attributes affect the dynamics of the beam and beam losses, the functionality for dynamic kicks (DYNK) of SixTrack has been significantly extended. This functionality can be used for the simulation of dynamic scenarios, such as when crab cavities are switched on, orbit bumps are applied, optics are changed, or failures occur. The functionality has been extended with a more general and flexible implementation, such that arbitrary time-dependent functions can be defined and applied to different attributes of families or individual elements, directly from the user input files. This removes the need for source code manipulation, and it is compatible with LHC@Home which offers substantial computing resources from volunteers. In this paper, the functionality and implementation of DYNK is discussed, along with examples of application to the HL-LHC crab cavities.

INTRODUCTION

SixTrack is a 6D single particle tracking code [1,2], which is routinely used at CERN to study the dynamic aperture and collimation system in high-energy circular machines like the LHC. There are also a large number of tools built around SixTrack, both for analyzing the results and for handling very large numbers of initial conditions. For this reason, SixTrack is the natural tool to use for studying fast failure scenarios at the HL-LHC, and for other transient phenomena at other similar machines.

Functionality for applying dynamic kicks (DYNK) – i.e. time-dependent machine element parameters – was therefore added to the code [3, 4] and significantly extended. It makes it possible for the user to specify the functional form of these parameters directly in the input file, or to load them from a file. This eliminated the need for multiple private code forks, freeing up and focusing developer resources. The specification of the functions, to which elements they should be applied, and when they should be applied, is done using a simple mini-language. Some examples of this language are given below, and a full description is given on the TWIKI page [5].

DYNK currently supports setting the strength of all the standard thin elements, and also setting the voltage, phase, and frequency of crab cavities. It also supports a wide variety of functions, which may use the turn number or the output of other functions as input. It is also possible for the functions to store and retrieve data from memory, as is used for pseudo random number generating functions that stores the random seed between turns, and when loading the functions as tables from files. There is also an option to output the setting of the affected elements at every turn to a file. In order to work with LHC@Home [6], which is used for large tracking campaigns, DYNK supports checkpointing and restarting from a checkpoint. It interacts correctly with the collimation routines, including resetting the elements and generating exactly the same values for each pass of 64 particles. The ripple module is made redundant by DYNK, which can exactly reproduce its results, and is therefore removed.

* Research supported by EU FP7 HiLumi LHC – Grant Agreement 284404
† kyrre.ness.sjoebaek@cern.ch

IMPLEMENTATION

In order to make DYNK work, there are two main components: a function parser and evaluator, and a setter and getter for the element properties. Additionally, there are hooks for calling DYNK in the tracking loops, and for initialization before the start of tracking. The data storage for the functions are provided by one master table (one row per function) and a "free memory" for each of the major data types (integers, floats and strings).

This architecture is very easily extendable, making adding support for new types of functions a matter of adding a few lines to the parser and evaluator. Similarly, new elements or element attributes can be supported by adding them to the setter and getter functions – the difficulty of this is determined by the complexity of the memory structures and initialization scheme used for that element.

EXAMPLE USE CASES

Some examples for the use of DYNK are provided below. All of these are ran using the HL-LHC v1.1 lattice [7] with vertical crab cavities around the first interaction point (IP1, ATLAS). The beam was sampled at IP1 as a Gaussian distribution using the nominal HL-LHC parameters, cropped so to only include particles inside of the RF bucket.

The crab cavities closing the bump (at s=153.6, 154.6, 160.2 and 161.2 m, relative to IP1) are in this simulation called CRAB_IP1_R1$\cdots$4, while the cavities creating the bump (at s=26494.3, 26495.3, 26500.9 and 26501.9 m) are called CRAB_IP1_L1$\cdots$4. Their frequencies are set to 400.8 MHz, i.e. the same as for the accelerating cavities. The standard voltages of the closing- and opening cavities opening cavities are calculated using Eq. 4 from [8]. For the opening cavities, it is assumed that the transverse betatron β-function and phase advance is the same for all the cavities, while the voltage of each of the closing cavities are chosen such that they cancel the symmetrically positioned opening

Content from this work may be used under the terms of the CC BY 3.0 licence (© 2015). Any distribution of this work must maintain attribution to the author(s), title of the work, publisher, and DOI.

ISBN: 978-3-95450-168-7 doi:10.18429/JACoW-IPAC2015-MOPJE070

Content from this work may be used under the terms of the CC BY 3.0 licence (© 2015). Any distribution of this work must maintain attribution to the author(s), title of the work, publisher, and DOI.

REDUCTION OF E-CLOUD IN PARTICLE ACCELERATORS BEAM PIPES STUDIED BY RADIO-FREQUENCY MULTIPACTING

R. Leber, F. Caspers, P. Costa Pinto, M. Taborelli, CERN, Geneva, Switzerland

Abstract

For a given beam structure, chamber geometry and magnetic field configuration, the electron cloud, (EC), intensity depends on the Secondary Electron Yield, (SEY), of the inner walls of the beam pipe. The observed reduction of the EC intensity as a function of the time of exposure to the beam, often called conditioning, is attributed to the growth of a low SEY carbon film due to the bombardment of electrons from the cloud itself. The full mechanism for the growth of carbon is not yet fully understood, but it depends on the dose of electrons and their energy. As the SEY of the beam pipe surface decreases, the flux of electrons from the EC also decrease and the conditioning decelerates. In the present paper we study the time evolution of the conditioning in stainless steel and copper beam pipes. The EC is induced by Radio-Frequency, (RF), multipacting using a coaxial resonator. Strip detectors are used to monitor the intensity of the EC. After each conditioning cycle, the SEY of beam pipes is measured and the growth of carbon analysed by X-ray Photoelectron Spectroscopy. The influence of the bias voltage, the composition of the base pressure with injection of C_2H_2 and $C_{12}H_{26}$, and the resilience of the conditioning after air exposure are tackled.

EXPERIMENTAL SETUP

The RF resonator to induce electron multipacting, (MP), consists of a tungsten wire drawn along the axis of a one meter long liner with a cross section similar to a CERN-SPS Main Bending magnet of type B (MBB) beam pipe. The liner is inserted in a cylindrical vacuum chamber, which is itself enclosed in a dipole magnet. The vacuum system is unbaked and operates at ~$1x10^{-7}$ mbar. The RF signal is generated by a Vector Network Analyzer (VNA); it is amplified and injected in the resonator. The network is matched to a frequency close to 100 MHz. To maximize the MP intensity, the dipole magnetic field is set close to cyclotron resonance (~43 Gauss). The RF excitations, (shots), are applied in power ramps from -30 dBm to -10 dBm in 30s, followed by a 90s pause to avoid overheating the wire. A measurement run consists of several thousands of shots and lasts several days. A DC bias voltage can be applied to the wire and is superimposed to the RF excitation. During the runs the pressure, the reflected RF power, and the MP current can be measured. Further details on the set-up can be found in [1]. The total pressure is measured by a cold cathode gauge and the partial pressures with a Residual Gas Analyser (RGA). The MP current distribution along the axis of the beam pipe is measured using a collector with 47 transversal stripes, (8 mm width, spaced by 0.17 mm, and bundled to 16 channels). The collector is separated from the beam pipe volume by a grid with a transparency of 7% to minimize the influence of the measurements on the MP process. The current on each channel is registered for every shot and the electron dose received by the beam pipe surface is calculated by correcting with the grid transparency. A similar strip detector with longitudinal stripes is used to measure the transversal distribution of the MP. Details about the strip detectors can be found in [2] [3]. Stainless steel (316LN) and electroplated copper liners were studied. Samples for SEY measurement (10 mm x 300 mm) are made of the same material of the liners and exposed to the MP in the beam pipe. Reference samples are placed in the same vacuum system but not exposed to MP. Before each measurement run, the liner and the samples are etched and cleaned following standard CERN procedures. At the end of the run, the system is vented to the laboratory air and the samples transferred to the SEY/XPS system for measurement [4].

RESULTS AND DISCUSSION

Effect of the Bias Voltage

It was observed that positive bias voltages enhance the MP and negative bias values below -100 V, suppress it completely. For positive bias from 0 V to 1000 V the MP current increases linearly. This might be an indication that the bias voltage increases the energy of the electrons hitting the walls, so that it approaches the SEY peak value. Figure 1 (top) shows the time evolution of the average of the doses measured in all the channels of the strip detector during one RF shot for stainless steel liners at 0 V and 1000 V bias and for a copper liner at 1000 V. To allow a direct comparison between the two voltages, during the 1000 V bias conditioning some points were measured by applying 0 V. The runs lasted 11 days. The current and dose per shot with the 1000 V bias is always the highest and it induces also a faster conditioning. After 3 days conditioning at 1000 V, no more MP could be observed at 0 V bias. After 11 days at 0 V the MP still remains (with a dose per shot ~$5x10^{-8}$ C/mm^2). This is due to the fact that at higher bias voltage the cumulated dose increases faster in time. Nevertheless, Fig. 1 (bottom) shows that the conditionings obtained with the two bias voltages have the same dose dependence.

For all runs, full suppression of the MP was never achieved. The system approaches asymptotically the SEY threshold for MP. We remark that the distribution of the MP intensity along the liner changes during the conditioning process, probably due to the fact that the RF electromagnetic field is not uniform and the electron dose

ISBN: 978-3-95450-168-7 doi:10.18429/JACoW-IPAC2015-MOPJE071

NEW ELECTRON CLOUD DETECTORS FOR THE CERN PROTON SYNCHROTRON

C. Yin Vallgren, P. Chiggiato, S. Gilardoni, H. Neupert, M. Taborelli#, CERN, Geneva, Switzerland

Abstract

Electron cloud (EC) has already been observed during normal operation of the PS using classical shielded button pick-up detectors in drift sections. In the context of the LHC Injector Upgrade (LIU project), similar measurements are also needed for the combined function magnets of the machine, where the access to the vacuum chamber is strongly limited by the presence of the yoke. Two new electron cloud detectors have been studied, developed, and installed during the Long Shutdown (LS1) in one of such magnets. The first is based on current measurement by using a shielded button-type pick-up with a special geometry to reach the bottom surface of the vacuum pipe embedded in the magnet. The second one relies on a newly developed measurement method based on detection of the photons, which are emitted by cathodoluminescence from the electron cloud impinging on the vacuum chamber walls. Part of the emitted photons is collected through a quartz window by a Micro-Channel Plate Photomultiplier Tube (MCP-PMT). First results obtained during machine development runs show the feasibility of the photon detection scheme. The results are discussed and compared with pick-up measurements.

INTRODUCTION

The direct measurement of the electron cloud (e-cloud) current in an accelerator implies to collect part of the electrons arriving to the beam-pipe. The collected electrons no longer contribute to the e-cloud development and therefore the measurement slightly perturbs the electron multipacting. Such measurements are more difficult in a magnetic field, since the dedicated vacuum beam pipe must have sufficient space to host the collector electrode without aperture restrictions for the machine [1]. In order to follow the e-cloud effect in the Proton Synchrotron (PS) accelerator at CERN in the context of the LHC Injector Upgrade program, we explored the development of a device which can monitor the signal of the electrons without collecting them directly. Such a device was implemented in one of the standard combined function magnets of the PS accelerator.

PRINCIPLE OF OPERATION

The principle of operation is the detection of cathodoluminescence [2, 3] photons produced by electrons impinging on a metallic surface. The decay of the secondary electrons to lower energy states, after the excitation by the primary electrons in the solid, occurs partly by photon emission. Figure 1 illustrates the spectrum of the photons obtained with an electron beam of 300eV, 9μA (area 2 mm^2) impinging on a stainless steel 316LN as-received surface (same material as the wall of the PS vacuum pipes). The beam energy is representative of the electrons of the e-cloud impinging on the accelerator wall. The light emitted by the sample is collected by a spectrometer (Andor Shamrock 303i, CCD Andor iDus 420) in air from a quartz viewport attached to a dedicated UHV chamber hosting the sample and the electron gun. The cold BaO cathode (nominal operating T=1150 K) of the gun aims at minimizing the black body radiation in the near UV region, where the

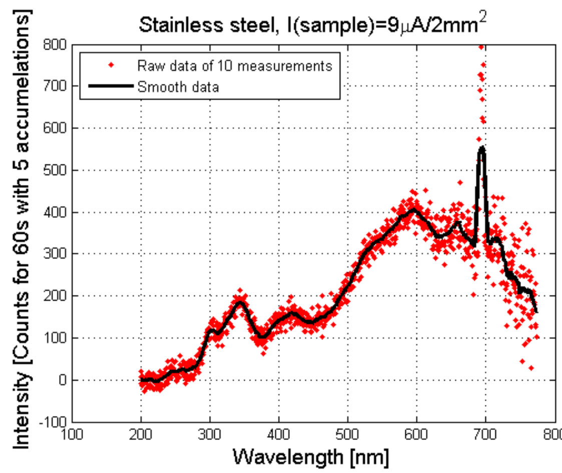

Figure 1: Typical spectrum obtained with e-gun.

cathodoluminescence is expected [2,3]. Most of the cathode radiation is indeed above 700 nm. This is proved by the fact that the signal in the range shown in figure 1 vanishes when the electron beam is deviated away from the sample. As expected the intensity is found to be proportional to the primary current impinging on the sample. A Monte Carlo simulation shows that the efficiency of collection due to the solid angle of the setup is only 0.04% (assuming isotropic emission). From this value and the measured integrated intensity between 200nm and 700nm we obtain a yield of $5x10^{-11}$ ph/e which is compatible with the literature values [2, 3].

SETUP FOR THE PS AND TESTS IN THE LABORATORY

The setup installed in the PS is shown in the scheme in Fig. 2. After the quartz viewport of the vacuum chamber the light is collected by a UV compatible optical system and brought to a PMT. The PMT (Photonis PP0365G) is robust with respect to parallel magnetic fields up to 2T and is placed in order to be parallel to the fringe field of the magnet. It has a nominal efficiency of 30% at 200-400 nm decreasing from 20% to 3% in the range 400 to 700

#mauro.taborelli@cern.ch

Content from this work may be used under the terms of the CC BY 3.0 licence (© 2015). Any distribution of this work must maintain attribution to the author(s), title of the work, publisher, and DOI.

ISBN: 978-3-95450-168-7 doi:10.18429/JACoW-IPAC2015-MOPJE072

SIMULATIONS AND MEASUREMENTS OF LONGITUDINAL COUPLED-BUNCH INSTABILITIES IN THE CERN PS

L. Ventura, M. Migliorati, CERN, Geneva, Switzerland, Univ. Sapienza and INFN-Roma1, Rome, Italy
H. Damerau, G. Sterbini, CERN, Geneva, Switzerland

Abstract

Among various and challenging objectives of the LHC Injectors Upgrade project (LIU), one aim is to double the beam intensity of the CERN Proton Synchrotron (PS) in order to achieve the integrated luminosity target of the High-Luminosity LHC project (HL-LHC). A known limitation to reach the required high intensity is caused by the longitudinal coupled-bunch oscillations developing above the transition energy. The unwanted oscillations induce large bunch-to-bunch intensity variations not compatible with the specifications of the future LHC-type beams. A wide-band longitudinal damper has been installed in the PS to suppress these instabilities and is going to be commissioned. A measurement campaign of coupled-bunch oscillations has been launched to substantiate the extrapolations and predictions for the future High Luminosity LHC beam with the final aim to determine the maximum intensity that could be provided to the LHC. In parallel a Simulink© model of the PS is going to be implemented to predict the machine behavior in the parameter space of LIU and to be used during the beam commissioning and optimization of the feedback system.

INTRODUCTION

The Proton Synchrotron (PS) [1] is the LHC injector where the longitudinal structure of the beam train serving LHC is established. RF systems at multiple harmonics between $h = 7$ and $h = 458$ provide the flexibility required for the longitudinal bunch splitting [2]. After the beam is accelerated above transition energy [3], dipolar longitudinal coupled-bunch (CB) instabilities are observed [4, 5]. The machine longitudinal impedance changes according to the dynamic tuning of the main accelerating cavities along the magnetic cycle. During the ramp all cavities are tuned at $h = 21$ and the longitudinal impedance is maximized, thus causing a crosstalk among bunches. Presently this instability is cured by a controlled longitudinal emittance blow-up at injection energy and dedicated feedback at 15 f_{rev} and 20 f_{rev}. From the present bunch population of $1.3 \cdot 10^{11}$ p/b (72 bunches in $h = 84$), the LIU project [6] aims to reach $2.6 \cdot 10^{11}$ p/b [7]. This makes the present counter measurement (blow-up) inadequate to control the instability, producing, during the splitting at top energy, a bunch-by-bunch intensity variation not compatible with the required LHC luminosity performance.

In the following we assume as working hypothesis that the train of equidistant bunches is regularly distributed along the machine azimuth (to compare with the nominal filling pattern with 18 bunches in $h = 21$). Under this condition, the bunches are not sortable from the physical point of view (circulant symmetry). Assuming in addition that the CB oscillations can be described by a linear approximation, the circulant matrix formalism [8] becomes the ideal mathematical tool to analyze the dipolar coupled-bunch oscillations. The purpose of the study is to develop an algorithm to analyze the longitudinal profiles of the bunch train and, using the circulant matrices formalism, to perform the mode analysis of the system to study its stability. In addition a Simulink© [9] model of the PS and the new damper cavity is being implemented to take into account the non idealities of the system, i.e. the limited voltage of the damper cavity, the noise level of the longitudinal pickup (PU), the errors introduced by the quantization and sampling of the low level electronics of the feedback.

THE CIRCULANT MATRIX FORMALISM

A $2n_b \times 2n_b$ circulant matrix, $\mathbf{F}$, has the general form

$$\mathbf{F} = \begin{pmatrix} f_1 & \dots & f_2 \\ \dots & \dots & \dots \\ f_{2n_b} & \dots & f_1 \end{pmatrix}. \tag{1}$$

The evolution in the normalised longitudinal phase space of n_b bunches from turn n to turn $n+1$ can be linearly approximated by the following

$$\begin{pmatrix} x_1 \\ \Delta p_1/p \\ \dots \\ \dots \\ x_{n_b} \\ \Delta p_{n_b}/p \end{pmatrix}_{n+1} = \mathbf{M} \times \begin{pmatrix} x_1 \\ \Delta p_1/p \\ \dots \\ \dots \\ x_{n_b} \\ \Delta p_{n_b}/p \end{pmatrix}_{n}, \tag{2}$$

where $\mathbf{M}$ is a stationary block circulant matrix where each block represents a rotation matrix. This paper will discuss how to derive the $\mathbf{M}$ matrix starting from the measurement data from the longitudinal PU. Once $\mathbf{M}$ is known, the stability of the system described in Eq. 2 can be investigated by its eigenvalues if the matrix can be put in diagonal form. Since we consider a perturbative approach, it is possible to assume that all the bunches in the system have the same synchrotron tune Q_s. Therefore each bunch position x_i and each bunch momentum deviation $\Delta p_i/p$ can be written as

$$x_i = \Re\left\{a_i e^{j\phi_i} \cdot e^{j2\pi Q_s \times n}\right\} \tag{3}$$

$$\Delta p_i/p = \Im\left\{a_i e^{j\phi_i} \cdot e^{j2\pi Q_s \times n}\right\} \tag{4}$$

where $i \in \{1, \dots, n_b\}$, a_i and ϕ_i are the amplitude and the phase of the longitudinal bunch oscillation. The dynamic

Content from this work may be used under the terms of the CC BY 3.0 licence (© 2015). Any distribution of this work must maintain attribution to the author(s), title of the work, publisher, and DOI.

ISBN: 978-3-95450-168-7 doi:10.18429/JACoW-IPAC2015-MOPJE073

THE EXTREME BEAMS INITIATIVE IN EuCARD-2*

K. Aulenbacher, JGU, Mainz, Germany; M. Biagini, INFN-LNF Italy; M. Eshraqi, ESS, Lund, Sweden; G. Franchetti, J. Struckmeier, GSI, Germany; F. Zimmermann, CERN, Switzerland

Abstract

EuCARD-2 [1] is an Integration Activity on accelerator R&D co-funded within the European Union's 7th Framework Program. The Extreme Beams (XBEAM) network of EuCARD-2 extends, and goes beyond the scope of, the previous Networking Activities of CARE-HHH and EuCARD [2] EuroLumi. XBEAM addresses, and pushes, all accelerator frontiers: luminosity, energy, beam power, beam intensity, and polarization. This is realized through five tasks, which are focusing on Coordination and Communication, Extreme Colliders (XCOLL), Extreme Performance Rings (XRING), Extreme SC Linacs (XLINAC), and Extreme Polarization (XPOL), respectively. This presentation reports the major achievements of the XBEAM activity from 2013 to 2015, and outlines the further plans through 2017.

OVERVIEW

The EuCARD-2 network on Extreme Beams ("XBEAM") aims at advancing on all accelerator frontiers, in particular luminosity, energy, beam power, beam intensity, and polarization. On the high energy and luminosity frontier it is supporting the HL-LHC crab cavity development and the studies of a Future Circular Collider, both of which became official projects thanks to activities in EuCARD, as well as plans for lepton-hadron colliders, and the preparation of SuperKEKB commissioning. At the high-intensity frontier, it is advancing projects like FAIR, the PSI cyclotron enhancement, and the ISIS upgrade, as well as preparing the ESS linac commissioning. Polarization management is improved both at high energy (LHeC, eRHIC, FCC, ILC, CLIC) and for low-energy precision experiments, such as electron storage rings for electric dipole measurements. XBEAM includes the five tasks shown in Table 1. Detailed information can be found on the XBEAM web site at http://cern.ch/xbeam.

In the first 2 years of the EuCARD-2 project, XBEAM has organised or co-organised more than fifteen workshops, as summarized in Table 2. These workshops addressed key questions for extreme colliders, extreme performance rings, extreme linacs, and extreme polarization. The XBEAM workshop achievements were complemented by a proactive outreach and dissemination effort, including numerous invited presentations at high-level conferences, workshops, or universities, several articles in the Accelerating News, the CERN Courier, and the ICFA Newsletter, plus two EuCARD-2 monographs. Some expert exchanges complete the picture.

*Work supported by European Commission under the FP7 Capacities project EuCARD-2, grant agreement 312453

Table 1: The Five Tasks of EuCARD-2 XBEAM

Task	Coordinators
1. Coordination and Communication	F. Zimmermann (CERN) and G. Franchetti (GSI)
2. Extreme Colliders (XCOLL)	M. Biagini (INFN) and F. Zimmermann (CERN)
3. Extreme Performance Rings (XRING)	G. Franchetti and J. Struckmeier (both GSI)
4. Extreme SC Linacs (XLINAC)	M. Eshraqi (ESS)
5. Extreme Polarization (XPOL)	K. Aulenbacher (JGU Mainz)

EXTREME COLLIDERS

XCOLL, together with the earlier AccNet-EuroLumi activity of EuCARD, has helped revive the idea of large high-energy circular lepton ("Higgs factory") and hadron colliders. The development and proposals started by AccNet and continued by XCOLL workshops have led to the launch, in February 2014, of an official 5-year "Future Circular Collider" (FCC) study, under a mandate from the CERN Directorate and from ECFA. The SuperKEKB B-factory soon to be commissioned in Japan will test and demonstrate the feasibility of several important features for these proposed future colliders. Impedance issues are one particular concern for both large lepton and hadron colliders, and have been investigated at a dedicated workshop co-organised by XCOLL. The scope of the LHeC study has been extended to include the integration of an electron-hadron collider option within the FCC complex. Novel compact crab cavities, earlier promoted at several workshops in the framework of CARE-HHH and EuCARD-AccNet, have now become a baseline ingredient for the LHC luminosity upgrade. Their continued development is being followed up by EuCARD-2 XBEAM XCOLL. These crab cavities may also be of interest for LHeC and FCC.

EXTREME PERFORMANCE RINGS

XRING has created discussion forums around critical areas of research for advanced storage rings. The first of these has focused on a topic relevant for FAIR, at the workshop "Beam dynamics meets Magnets" in Darmstadt. Experiences at J-PARC and LHC have provided examples for different working models with the following outcome: 1) According to LHC experience and benchmarking of the LHC dynamic aperture [1] theoretical models can correctly predict beam behaviour when the magnets parameters are well known. 2) Only for the LHC project the magnets characterization were determined by the beam-dynamics requirements, whereas in all other projects (J-PARC, RHIC) the beam dynamics calculations primarily studied the effect of given magnetic

Content from this work may be used under the terms of the CC BY 3.0 licence (© 2015). Any distribution of this work must maintain attribution to the author(s), title of the work, publisher, and DOI.

ISBN: 978-3-95450-168-7 doi:10.18429/JACoW-IPAC2015-MOPJE074

Content from this work may be used under the terms of the CC BY 3.0 licence (© 2015). Any distribution of this work must maintain attribution to the author(s), title of the work, publisher, and DOI.

OPTIMIZING SLS-2 NONLINEARITIES USING A MULTI-OBJECTIVE GENETIC OPTIMIZER

M. P. Ehrlichman*, M. Aiba, A. Streun, Paul Scherrer Institut, Villigen, Switzerland

Abstract

An upgrade to the SLS is currently under development. This upgrade will likely utilize the same hall and same machine circumference, 288 m, of the SLS. Achieving a sufficiently low emittance with such a small circumference requires tight focusing and low dispersion. These conditions make chromaticity correction difficult and minimization of 1st and 2nd order non-linear driving terms does not yield sufficient dynamic aperture and Touschek lifetime. In this proceeding, we discuss the multi-objective genetic optimization method implemented at SLS to aid the design of a chromaticity correction scheme for SLS-2.

INTRODUCTION

An upgrade to the `SLS`, which we will refer to as `SLS-2` in this paper, is under development [1]. The upgrade is envisioned as a complete replacement of the SLS storage ring while keeping the same hall, shielding, and booster. The beamline locations will be kept, but the beamlines themselves may be upgraded. The `SLS-2` will utilize small vacuum chambers, as pioneered by `MAX-IV`, to obtain higher field strengths, and also longitudinal gradient bends and anti-bends [2] to reduce the horizontal emittance from 5.6 nm to approximately 130 pm. The new ring will maintain the 12 cell topology of the existing SLS. 3-fold periodic lattices, like the existing SLS, and also 12-fold periodic lattices have been considered.

The new lattice uses strong quadrupole fields which induce a large chromaticity. This, in combination with small dispersion, necessitates a scheme of strong chromatic sextupoles to correct the chromaticity. These strong sextupoles generate strong nonlinearities which must in turn be compensated using harmonic sextupoles and octupoles.

Layout constraints prevent zeroing resonant driving terms (RDTs) beyond 1st order (in sextupole strength). Therefore, the optimal map has some combination driving terms and tune shift terms of 2nd order and higher. In fact, the optimal map may even have non-zero 1st order terms. Weighting 1st, 2nd, and higher order RDTs to obtain the best map, and locating the global minimum, is not straightforward. This is especially so given that RDTs are only a heuristic for the actual objectives, which are acceptance and lifetime.

An application of perturbation theory to 1st and 2nd order terms as described in [3] yields only marginally acceptable dynamic aperture (DA) and beam lifetime. We find that the direct genetic optimizer described in this proceeding consistently does better. For example, the direct optimizer finds high order corrections to the tune footprint far away from the closed orbit.

Elements of the traditional approach are maintained in our genetic optimization scheme. Chromatic and harmonic sextupoles and octupole locations are set by hand taking into consideration β-functions and phase advances. The working point is positioned considering the locations of low order resonances such that the tune footprint does not cross any dangerous resonances.

Features of the optimization scheme described here are: 1) It does not use RDTs. 2) It requires only moderate computing resources, typically about 12 hours on 64 PC cores. 3) A robust constraint system. 4) It seems to reliably converge to the global minimum. 5) Does not require seeding.

SYSTEM

The accelerator physics simulation is developed using the `Bmad` [4] subroutine library. The multi-objective genetic optimization scheme is the `aPISA` extension [5] to the PISA framework [6]. The sorting algorithm is `aspea2`, a version of the spea2 [7] sorting algorithm modified to support dominance constraints. The parallelization is implemented using Fortran COARRAYs, which are implemented as a high level layer on top of MPI. The computing resource is a Linux cluster running SGE consisting of distributed Intel Xeon compute nodes. The scheme is naturally load-balancing and works fine in heterogeneous environments.

The results from the optimizer are portable to other codes, in particular `OPA` [8], for further analysis. Effort in this project includes understanding the usage and modeling differences of different calculation codes so as to keep the development process consistent and flexible.

OPTIMIZATION PROBLEM

The goal of the optimization problem is to maximize injection acceptance and maximize the Touschek lifetime. Injection acceptance is maximized by maximizing the on-energy DA. The Touschek lifetime is maximized by maximizing the momentum aperture. However, the element-by-element momentum aperture is expensive to calculate. Therefore, instead of calculating the momentum aperture we calculate the off-momentum DA and constrain the chromatic tune footprint. As will be shown later, we find this is an effective and efficient proxy for maximizing the Touschek lifetime.

Objectives

Three objectives are used by the optimizer. The objective function, depicted for $N_{angle} = 7$ in Fig. 1, is calculated as

* michael.ehrlichman@psi.ch

ISBN: 978-3-95450-168-7 doi:10.18429/JACoW-IPAC2015-MOPJE075

TRACKING THROUGH ANALYTIC QUADRUPOLE FRINGE FIELDS WITH GPT

S.B. van der Geer, M.J. de Loos, Pulsar Physics (PP), The Netherlands
B.D. Muratori, STFC Daresbury Laboratory and Cockcroft Institute, U.K.

Abstract

In the early design stages it is customary to work with a highly simplified analytic model to describe a beamline. Dipoles and quadrupoles are often based on hard-edged approximations. This is not only unrealistic, it also significantly slows down time-domain spacecharge tracking codes such as the General Particle Tracer (GPT) code. The underlying reason for the poor performance is that, despite the fact that the simple hard-edged field equations are fast to evaluate, they force the integration process to use excessively small step sizes near the field discontinuities in order to achieve the desired accuracy. In other words, the apparently simple equations turn out to be the most difficult ones to evaluate numerically. An obvious solution is to switch to field-maps, but this is not practical in the early design stages. In this contribution we show a new solution implemented in the GPT code based on analytical expressions for the fringes where the transverse size of the magnet is properly taken into account. In addition to producing more realistic results, the smooth fields increase tracking speed by over an order of magnitude for typical cases.

INTRODUCTION

Time domain simulations codes such as GPT [1, 2], PARMELA and ASTRA are essential tools for the design and understanding of high-brightness charged particle accelerators. The physics included in these codes is a particularly good match for injector / RF-photogun simulations producing pulsed, high-brightness, high-charge beams. The way the simulation codes operate is by tracking a large number of sample particles through the superposition of external fields and spacecharge fields. At each step in the simulation the codes maintain a collection of sample particles, where all particles are stored at the same time. This ensures self-consistent results for Coulomb interactions, even when the beam shape changes on relatively short time-scales. A simulation step involves the calculation of all electromagnetic fields due to external beamline components at the position of all sample particles, in addition to calculating the fields due to space charge. These fields are fed into an Ordinary Differential Equation (ODE) solver to solve the relativistic equations of motion, thereby advancing the entire population in time.

Regardless of the exact integration scheme, it is important to have the correct timestep length. On the one hand, a very small timestep gives accurate results at the costs of excessive CPU time. On the other hand, a very large timestep gives incorrect results. The best operating mode is arguably with the largest timestep possible, giving results which are 'barely good enough'. Finding the right balance is difficult, and this is further complicated by the fact that the optimal timestep varies greatly along the beamline. Very small steps must be taken during the emission process and in beamline components with large gradients, whereas very large steps can be taken in relatively constant or zero field regions.

Problems arise when part of the beamline is modelled with hard-edge approximations. It might be that the fringes capture relevant physics, and with ever brighter sources these effects become increasingly important. Furthermore, tiny integration steps need to be taken during the crossing of the interface to maintain sufficient accuracy. For just one particle this could be acceptable, but all particles have to be tracked together to get self-consistent results. Consequently, a timestep reduction for one particle crossing the interface of a hard-edged beamline component implies in a timestep reduction for all other particles as well. This significantly slows down simulation speed, especially for long bunches where there is always some particle crossing some interface. This is the problem we address in this paper, in particular for quadrupoles.

One solution to the problem of requiring small time-steps crossing a hard-edge interface is to split the trajectory in two halves at the interface: Neither half contains any discontinuities, and the simulation speed is restored. However, this solution misses relevant physics captured in the fringe fields, it requires non-trivial interpolation of the spacecharge fields to a set of intermediate timesteps, and it involves extra bookkeeping that makes misaligning beamline components in 3D prohibitively difficult. Another solution is to use realistic field maps, not containing these discontinuities. This restores the missing physics, it solves the problems arising from discontinuities, but it is often rather unpractical in the early design stages when fast parameter scans are required. Furthermore, field-maps are intrinsically based on interpolations causing a whole list of potential problems of their own.

The conceptually easiest and arguably best solution that solves all issues mentioned above is to track through a simple continuously differentiable equation for the fields, Maxwell compatible, including the fringes. Inspired by the analytical fringe fields of dipoles [3], we show in the next section how such expressions can be derived for higher order multipoles. The subsequent section presents the results of a GPT implementation of these expressions for the case of quadrupoles. Although the equations are far more complicated than the hard-edge counterparts, we will show that the overall GPT simulation speed is significantly improved.

Content from this work may be used under the terms of the CC BY 3.0 licence (© 2015). Any distribution of this work must maintain attribution to the author(s), title of the work, publisher, and DOI.

ISBN: 978-3-95450-168-7 doi:10.18429/JACoW-IPAC2015-MOPJE076

MULTI-OBJECTIVE GENETIC OPTIMIZATION WITH THE GENERAL PARTICLE TRACER (GPT) CODE

S.B. van der Geer, M.J. de Loos, Pulsar Physics, Eindhoven, The Netherlands

Abstract

In a typical design process there are a large number of variables, external constraints, and multiple conflicting objectives. Examples of the latter are short pulse, high charge, low emittance and low price. The classical solution to handle such problems is to combine all objectives into one merit function. This however implicitly assumes that the tradeoffs between all objectives are a-priori known. Especially in the early design stages this is hardly ever the case. A popular solution to this problem is to switch to multi-objective genetic optimization algorithms. This class of algorithms solves the problem by genetically optimising an entire population of sample solutions based on selection and recombination operators. The output, the so-called Pareto front, only includes solutions that are fully optimized where no objective can be improved without degrading any other. Here we present numerical studies and practical test runs of the genetic optimizer built into the General Particle Tracer (GPT) code [1].

INTRODUCTION

GDFMGO is a new multi-objective global optimizer for the GPT code. Its internal algorithm evolves a population of candidate solutions towards the so-called Pareto-front. This front is defined as the set of points where it is impossible to improve one objective without making at least one other objective worse. The final result is a set of points equally spaced at or near the Pareto front, where each point is fully optimized in all its variables.

The Pareto front samples, for the given objectives, the optimal combination of variables. For two objectives and ten variables, the Pareto front is a line through two dimensional objective space and ten dimensional variable space. In other words, the original problem of having to choose the best combination of ten variables has been reduced to the one dimensional problem of selecting where on the line you want to be. This collapse of dimensionality makes multi-objective optimization such a powerful tool for decision making. Its power does not come from providing the 'the best' solution, but from reduction of the dimensionality of the problem and simultaneously providing insight in tradeoffs between the different objectives.

GDFMGO starts with a fixed size population of candidate solutions with variables either chosen randomly in a user specified interval or read from file. Typically this initial population is very poor in terms of the objectives, and probably in violation of a number of constraints if present. The idea is to create improved candidate solutions based on the solutions already present, while gradually removing the worst ones. This process is repeated over and over again, and slowly the population as a whole evolves in the desired direction. Global convergence properties come from the fact that the population is pushed gently towards the Pareto front instead of steepest descent into a potential local minimum. Although there are plenty of pathological cases where this does not work, in practice the algorithm finds the global optimum in a impressively large number of cases with the default parameters.

The key ingredients of the algorithm are a) creation of new candidate solutions based on the existing ones, b) ranking the solutions such that the worst can be removed and c) a stopping criterion. They are described in detail below.

New Species

New random samples are created from the existing population. The mechanism we use is known as Differential Evolution (DE) [2]. To create a new combination of variables **p**, first four random species from the population are selected. We denote them **u**, **v**, **w** and **x**. Subsequently, an intermediate point **t** is calculated from **u**, **v** and **w** using: $\mathbf{t} = \mathbf{w} + s\,(\mathbf{u} - \mathbf{v})$.

The idea is that the new point is close to the existing **w**, but offset with the direction from **v** to **u**. To enforce convergence, the direction is slightly reduced by a scale factor s that must be below 1. In practice using this intermediate point **t** as the new point already works very well. However, when the entire candidate solution lies on a hyperplane in all variables there is no escape from this plane thereby stalling the algorithm. This is where the last selected point **x** comes into play, where there is a mutation probability (1-ρ) that variables are selected from **x** instead of from **t**. To avoid duplicating **x** at least one of the variables must come from **t**. In equations:

$$cr = \text{random\_int}[1,n]$$
$$p_i = \begin{cases} t_i & \text{random}[0,1] < \rho \quad \vee \quad i = cr \\ x_i & \text{otherwise} \end{cases}$$

A lower ρ increases global convergence properties at the cost of a slower convergence rate. In practice neither the scale factor s nor the mutation rate ρ are critical parameters and the defaults of 0.6 and 0.9 respectively work fine in most cases.

New candidate solutions are added until the population size is doubled. Then the population is ranked and trimmed to the original size again. How this is done is the subject of the next section.

Content from this work may be used under the terms of the CC BY 3.0 licence (© 2015). Any distribution of this work must maintain attribution to the author(s), title of the work, publisher, and DOI.

ISBN: 978-3-95450-168-7 doi:10.18429/JACoW-IPAC2015-MOPJE077

PROGRESS ON SIMULATION OF FIXED FIELD ALTERNATING GRADIENT ACCELERATORS

S. L. Sheehy*, JAI/Oxford and STFC/ASTeC/RAL, UK
D. J. Kelliher, S. Machida, C. R. Prior, C. Rogers, STFC/ASTeC/RAL, UK
M. Haj Tahar, F. Meot, BNL, USA
Y. Ishi, T. Uesugi, Y. Kuriyama, M. Sakamoto, Y. Mori, KURRI, Japan
A. Adelmann, PSI, Switzerland

Abstract

Fixed Field Alternating Gradient accelerators have been realised in recent decades thanks partly to computational power, enabling detailed design and simulation prior to construction. We review the specific challenges of these machines and the range of different codes used to model them including ZGOUBI, OPAL, SCODE and a number of in-house codes from different institutes. The current status of benchmarking between codes is presented and compared to the results of recent characterisation experiments with a 150 MeV FFAG at KURRI in Japan. Finally, we outline plans toward ever more realistic simulations including space charge, material interactions and more detailed models of various components.

INTRODUCTION

Fixed Field Alternating Gradient (FFAG) accelerators have potential to provide high intensity hadron beams for various applications. This arises from the combination of strong focusing to reach high energies with a fixed magnetic field which enables a high repetition rate and high average current. In 2013 a collaboration was formed to focus effort in the FFAG community on this topic. The collaboration aims to undertake a series of experiments to progress toward high intensity operation of the 150 MeV proton scaling FFAG accelerator at Kyoto University Research Reactor Institute (KURRI) in Japan. Relevant parameters of the accelerator can be found in Ref. [1].

At the same time a simulation campaign has been established to benchmark relevant simulation codes. This campaign aims to provide reliable tools for FFAG modelling and to help understand the results of the experiments as they progress. After short description of the codes used, we will discuss present benchmarking efforts.

SIMULATION CODES

The beam orbit in an FFAG moves radially with momentum, as in a cyclotron. Simulation codes which assume a central orbit independent of momentum are unsuitable for studying FFAGs as they do not reproduce the correct dynamics. There are a few codes which remove the constraint of the existence of the central orbit: OPAL, Zgoubi, SCODE, MAUS and EARLIETIMES, which we have selected to perform our benchmarking.

* suzie.sheehy@stfc.ac.uk

OPAL

OPAL (Object Oriented Particle Accelerator Library) [2] is an open source C++ framework for general particle accelerator simulations including 3D space charge, short range wake fields and particle-matter interaction. OPAL is based on IPPL (Independent Parallel Particle Layer) which adds parallel capabilities. The main functions inherited from IPPL are: structured rectangular grids, fields, parallel FFT and particles with the respective interpolation operators. Massive parallelism (up to 65000 processors) makes it possible to tackle the largest problems in the field.

ZGOUBI

Zgoubi is a ray-tracing code which can track particles through electric and magnetic fields introduced as field maps or as analytic elements. It has excellent flexibility in the choice of elements, and includes complex geometries with high-order multipole and combined-function magnets as analytic elements. For this reason it has been adopted as one of the main simulation codes in the FFAG community [3].

SCODE

SCODE was developed specifically for the simulation of FFAG accelerators. Some of the modules such as the space charge module and the single particle tracking module with time as the independent variable are imported from another code, Simpsons [4]. Space charge calculation in 2.5D and frozen model are available. Simple models of multiple scattering in the transverse direction and energy loss due to foil scattering are also included. Recently, tracking based on 3D magnetic field maps has been added.

MAUS

MAUS (MICE Analysis User Software [5] is a tracking and reconstruction code base on Geant4 [6]. MAUS provides a framework for accelerator raytracing using custom field map routines, the Geant4 material physics libraries and the capability to plug-in realistic diagnostic modelling.

KURRI In-house Code EARLIETIMES

EARLIETIMES [7] was developed at KURRI for the purpose of design and beam commissioning of the KURRI FFAG accelerator complex. It uses a 4th order Runge-Kutta algorithm to find the closed orbit in a 3D magnetic field calculated by external software e.g. TOSCA. EARLIETIMES treats this closed orbit as a reference orbit, which can be

Content from this work may be used under the terms of the CC BY 3.0 licence (© 2015). Any distribution of this work must maintain attribution to the author(s), title of the work, publisher, and DOI.

ISBN: 978-3-95450-168-7 doi:10.18429/JACoW-IPAC2015-MOPJE078

BEAM DELIVERY SIMULATION - RECENT DEVELOPMENTS AND OPTIMISATION*

J. Snuverink†, S. T. Boogert, H. Garcia-Morales, S. M. Gibson, R. Kwee-Hinzmann, L. J. Nevay,
John Adams Institute at Royal Holloway, University of London, Egham, UK
L.C. Deacon, University College London, London, UK

Abstract

Beam Delivery Simulation (BDSIM) is a particle tracking code that simulates the passage of particles through both the magnetic accelerator lattice as well as their interaction with the material of the accelerator itself. The Geant4 toolkit is used to give a full range of physics processes needed to simulate both the interaction of primary particles and the production and subsequent propagation of secondaries. BDSIM has already been used to simulate linear accelerators such as the International Linear Collider (ILC) and the Compact Linear Collider (CLIC), but it has recently been adapted to simulate circular accelerators as well, producing loss maps for the Large Hadron Collider (LHC). In this paper the most recent developments, which extend BDSIM's functionality as well as improve its efficiency are presented. Improvement and refactorisation of the tracking algorithms are presented alongside improved automatic geometry construction for increased particle tracking speed.

INTRODUCTION

Many particle accelerators need to predict and minimise beam losses throughout the machine to avoid damage, radioactivation of the beamline elements and background radiation. Beam loss simulation studies often make use of several codes for different features. Typically, a fast tracking code is used to record positions where particles hit a collimator or the beam pipe, and these positions are then input into a detailed radiation transport code. Obviously, this approach is not ideal. For example, the geometry description capabilities of such codes are rarely equivalent as the fast tracking code usually has a very limited description of the geometry, the data must be transferred between the two codes, particles that scatter back into the beam pipe might not be considered, etc. For the greatest accuracy, a combined approach is required that allows both efficient transport of particles in the accelerator as well as particle interaction with surrounding material.

For this purpose BDSIM [1, 2] has been developed. BDSIM is a flexible, open source C++ particle tracking code that uses the Geant4 framework [3]. Geant4 gives access to many electromagnetic and hadronic interaction models as well as powerful geometry description and visualisation tools. For fast beam tracking inside the beam pipe efficient tracking routines are implemented.

For its input BDSIM deploys a MAD-like input syntax, which has the advantage of an easy, fast and accurate conversion from existing lattices. Additional keywords allow for a more detailed geometry and material description.

BDSIM was originally developed for the simulation of linear colliders such as the International Linear Collider (ILC) and the Compact Linear Collider (CLIC), see e.g. [4, 5]. In recent years it has been adapted to accommodate circular accelerators as well [6, 7]. BDSIM is in active development and is currently utilised for several accelerators, e.g. AWAKE [8], CLIC [9], ILC [10] and HL-LHC [11].

This paper gives an overview of the latest code developments. More information and the source code can be found on the BDSIM website [12].

GEOMETRY

For accurate background studies it is important to have the right amount of detail in the description of the geometry and material. The geometry will be of particular relevance in simulation studies for laserwire diagnostics and other Compton-photon based diagnostics, whose specification is highly dependent on their detector background environment. The geometry of poles in comparison to a generic cylinder of material for example, allows the passage of radiation between the poles significantly further along the machine.

A beamline element like a quadrupole can have many different designs and consist of various geometry components. However, it will have a beam pipe geometry (round, rectangular, ellipse, etc.), a magnet geometry (cylindrical, with poles, etc.), and possibly a supporting plinth or girder. Previously, the creation of the simulation world in BDSIM was done in a single pass in the direction of the beam, element by element. This meant that a quadrupole also needed to create beam loss monitors situated in the vicinity, a part of the tunnel, and even surrounding soil. Such a philosophy is suitable if one works with only one a few types of geometry and structures, but becomes unmanageable when one wants to add new geometry types or new structures.

To simplify the already large beamline element class `BDSAcceleratorComponent`, a more basic base class `BDSGeometryComponent` has been created. This improved geometry class hierarchy allows for a plug and play nature of components, which is normally not provided with the Geant4 toolkit where the user must take care to comprehend the geometry description and avoid geometrical overlaps.

* Research supported by FP7 HiLumi LHC - grant agreement 284404 and by the STFC via the JAI3 grant.
† jochem.snuverink@rhul.ac.uk

Content from this work may be used under the terms of the CC BY 3.0 licence (© 2015). Any distribution of this work must maintain attribution to the author(s), title of the work, publisher, and DOI.

ISBN: 978-3-95450-168-7 doi:10.18429/JACoW-IPAC2015-MOPJE079

Content from this work may be used under the terms of the CC BY 3.0 licence (© 2015). Any distribution of this work must maintain attribution to the author(s), title of the work, publisher, and DOI.

TRACKING STUDIES IN THE LHeC LATTICE

E. Cruz-Alaniz, D. Newton, Univ. Liverpool/Cockcroft Institute, UK
R. Tomás, CERN, Switzerland

Abstract

The Large Hadron Electron Collider (LHeC) is a proposed upgrade of the LHC to provide electron-proton collisions and explore a new regime of energy and luminosity for nucleon-lepton scattering. A nominal design has previously been presented, featuring a lattice and optical configuration to focus one of the proton beams of the LHC (reaching a value of β^*=10 cm) and to collide it head-on with an electron beam to produce collisions with the desired luminosity of L=10^{33} cm^{-2}s^{-1}. The proton beam optics is achieved with the aid of a new inner triplet of quadrupoles at L^*=10 m from the interaction point and the extension of the Achromatic Telescopic Squeezing (ATS) Scheme used for the High Luminosity-LHC project. In this work, particle tracking is performed in a thin lens approximation of the LHeC proton lattice to compute the dynamic aperture and perform frequency map analysis for different types of chromatic correction schemes, in order to find the one who will provide the most beam stability and to study the effects of nonlinearities.

INTRODUCTION

The LHeC interaction region (IR), first proposed in [1] contemplates the implementation of a new set of quadrupoles closer to the interaction point (IP), called the inner triplet (IT), at a distance L^* from the interaction point 2 (IP2) to achieve head-on electron-proton collisions at a luminosity of L=10^{33} cm^{-2}s^{-1}. In order to change the trajectory of the proton beams, the polarity of the two dipoles close to the IP (D1 and D2) must be reversed, compared to the present polarity, and the strength of D2 should be 1.21 stronger and the one of D1 3.43 stronger.

A first integration of the LHeC IR into the HL-LHC lattice, was done in [2] with an extension of the Achromatic Telescopic Squeezing Scheme (ATS), successfully applied for the HL-LHC lattice in [3]. This extension was done in the arc 23 performing a telescopic squeeze to further reduce the value of β^* in IP2 while leaving the HL-LHC insertions (IP1 and IP5) with round optics undisturbed. Achieving a value of $\beta^* = 10$ cm for IP2 and β^*=15 cm in IP1 and IP5.

The flexibility of this design was studied in [4] in terms of minimising β^* to study the reach in luminosity, and in terms of increasing L^* to reduce the synchrotron radiation.

Using a thin lens version of this LHeC lattice, tracking studies can be done to study the stability of the beam for the nominal case with β^*=10 cm and L^*=10 m.

CHROMATIC CORRECTION

One of the characteristics of the ATS is the locality of the chromatic correction of the inner triplet by using one single arc of sextupoles of either side of the small β^* insertions. However, in the LHeC case, the achromaticity is broken due to the telescopic squeeze in arc 12 shared by both IP1 and IP2. In this section, three different chromatic corrections are studied using a thin lens version of the lattice to study the impact of each correction scheme on the stability of the beam.

These chromatic corrections are performed by a matching procedure in MADX. The first correction, named "LHC-like" takes as 2 variables the strengths of the focussing and defocussing families of sextupoles, to fix as constraints the global values of the horizontal and vertical chromaticity (dqx, dqy) to a value of 2. The second correction, named "LHeC-like" increases the number of variables to allow every family of sextupoles to vary independently, accounting for 32 variables (2 for every arc of the LHC), to adjust not only the global value of the chromaticities to 2 as the previous case, but also to adjust the horizontal and vertical Montague functions (Wx and Wy) below 200 in the collimation insertions interaction region 3 (IR3) and interaction region 7 (IR7). Finally the third correction, named "second order", takes the same variables and constraints as the LHeC-like correction but adds as further constraints the variation of the horizontal and vertical chromaticity with momentum below a value of 7.

Figures 1 and 2 illustrate the change of tune over momentum for the three different chromatic corrections. The presence of nonlinearities is clear, specially for the cases LHC-like and LHeC-like, with the first one having a larger variation in the tune. On the other side, the second order correction is linear for the vertical tune, although for the horizontal tune, this linearity was not achieved for the whole momentum spread.

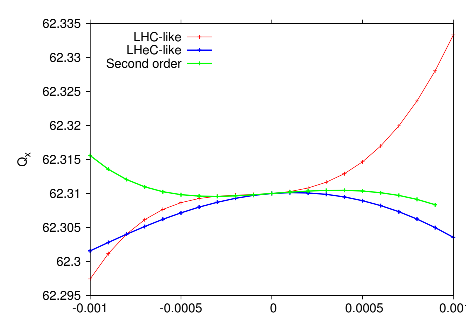

Figure 1: Q_x vs δ_p for three different chromatic corrections: LHC-like, LHeC-like and second order.

Figure 3 shows the chromatic variation over momentum

ISBN: 978-3-95450-168-7 doi:10.18429/JACoW-IPAC2015-MOPJE081
Content from this work may be used under the terms of the CC BY 3.0 licence (© 2015). Any distribution of this work must maintain attribution to the author(s), title of the work, publisher, and DOI.

LONGITUDINAL STABILITY IN MULTI-HARMONIC ACCELERATING CAVITIES

L.R. Carver*, R.M. Jones, School of Physics and Astronomy, University of Manchester
& The Cockcroft Institute of Science and Technology, UK
Y. Jiang, J.L. Hirshfield, Yale University, New Haven, CT 06511, USA

Abstract

Accelerating cavities that excite multiple modes at integer harmonics of the fundamental frequency can potentially be used to limit the effects of rf breakdown and pulsed surface heating at high accelerating gradients. Understanding the longitudinal stability and the acceptance of such a cavity is important to their development and use. The general Hamiltonian for longitudinal stability in multi harmonic cavities is derived and the particle dynamics are explored.

INTRODUCTION

A multi-harmonic cavity that operates at high gradients could act as an alternative cavity design for CLIC. Cavities of this type have unconventional surface electric and magnetic field profiles that can potentially lower the surface field emission and/or pulsed surface heating without compromising the gradient [1]. Two particular phenomena found in multi-harmonic cavities provide the main motivation for their use: (a) the anode-cathode effect, which can be found in an asymmetric multi-harmonic cavity that relies on fields pointing into one wall (cathode-like) to be significantly smaller than fields pointing away (anode-like) from the same wall. This effect will raise the work function barrier to supress field and secondary emission, and (b) a reduction in the surface heating by lowering the average $H_{\parallel}^2$ along the surface.

For cavities of this type to be used in an accelerator, the effect of the additional mode on a bunch of traversing particles needs to be explored. To achieve this, a Hamiltonian is derived that describes the behaviour of particles with small deviations from the synchronous particle in energy and/or phase. Typical formalisms of this kind only account for a single TM_{010} mode which follow a $\cos(kz)$ longitudinal distribution [2, 3] (where k is the wave number and z is the longitudinal coordinate) and not for a combination of modes with different longitudinal field profiles.

Harmonic rf systems are often used to linearise the energy gain [4] and reduce the energy spread of the bunch [5, 6]. These typically require an additional cavity operating in a TM_{010} mode with a frequency that is an integer harmonic of the main cavities. Here however, we excite two modes simultaneously within one cavity.

The first section presents tracking results for a particle traversing a linac and this is compared with the Hamiltonian found in literature. In subsequent sections, a general Hamiltonian for multi-harmonic cavities is derived and applied to two seperate modal configurations.

* Lee.Carver@manchester.ac.uk

SINGLE MODE PARTICLE TRACKING

The electric field of a TM_{010} standing wave in a cavity with amplitude E_0 is

$$E_T = E_0 \cos(kz)\cos(\omega t + \phi). \tag{1}$$

where ϕ is the phase of the field when the particle is at $z = 0$, ω is the angular frequency and $k = 2\pi/\beta_s\lambda$. The energy gain of a charge q as it crosses a single cavity gap g is given by

$$W = qE_0 \int_{-g/2}^{g/2} \cos(kz)\cos(\omega t + \phi)dz \tag{2}$$

The energy relative to the synchronous particle is $w = W - W_s$. The relevant differential equations in terms of the Hamiltonian H are given by [2]

$$\frac{dw}{ds} = qE_1 T(\beta)(\cos(\phi) - \cos(\phi_s)) = -\frac{\partial H}{\partial \phi} \tag{3}$$

and

$$\frac{d\phi}{ds} = -2\pi \frac{w}{\gamma_s^3 \beta_s^3 mc^2 \lambda} = \frac{\partial H}{\partial w}, \tag{4}$$

where $V_0 = E_0 \int_{-g/2}^{g/2} \cos(kz)dz$. and T is the transit time factor given by

$$T(\beta) = \frac{\int_{-g/2}^{g/2} \cos(kz)\cos(\frac{\omega z}{\beta c})dz}{V_0}, \tag{5}$$

with $E_1 = V_0/g$. For the synchronous particle, T remains constant as the cavity gap increases with β_s. For negligibly small acceleration rates, the differential equations can be integrated, and the Hamiltonian is

$$H = \frac{\pi}{\beta_s^3 \gamma_s^3 mc^2 \lambda} w^2 + qE_1 T[\sin\phi - \phi\cos(\phi_s)], \tag{6}$$

where β_s and γ_s refer to the velocity and gamma factor of the synchronous particle.

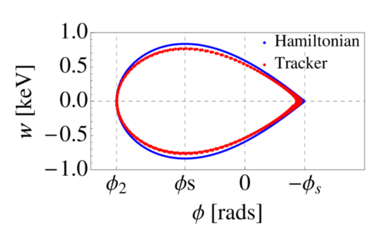

Figure 1: Comparison of Hamiltonian with particle tracked according to Eq. 2.

ISBN: 978-3-95450-168-7 doi:10.18429/JACoW-IPAC2015-MOPJE082

Content from this work may be used under the terms of the CC BY 3.0 licence (© 2015). Any distribution of this work must maintain attribution to the author(s), title of the work, publisher, and DOI.

ANALYTICAL APPROACH TO THE BEAM-BEAM INTERACTION WITH THE HOURGLASS EFFECT

M. Crouch, University of Manchester/ The Cockcroft Institute, U.K.
B. D. Muratori, ASTeC, STFC Daresbury Laboratory, and The Cockcroft Institute, U.K.
R. B. Appleby, University of Manchester/ The Cockcroft Institute, U.K.

Abstract

The hourglass effect arises due to a coupling between the longitudinal and transverse bunch planes. This coupling will result in a charge density distribution that will vary parabolically through the Interaction Point (IP). Here a method of analytically determining the electric field a particle receives from a charge density distribution which varies parabolically when centred at the IP, is derived for a 2D transverse model of a Gaussian bunch.

INTRODUCTION.

The High Luminosity Large Hadron Collider (HL-LHC) seeks to reach even higher luminosities than previously achieved. An increased luminosity can lead to a saturation or "pile up" in the machine detectors. To avoid pile up in the detectors, luminosity levelling has been proposed which aims to hold the luminosity constant over the duration of a physics run. One proposed method of levelling the luminosity is to reduce the β-function at the IP as the bunch intensity decays due to proton burn off.

One of the benefits of levelling by this method is it is operationally easy to implement and the longitudinal vertex density remains fixed when there is no crossing angle. The flat beam option is an alternative operational scenario for the HL-LHC when there are no crab cavities installed. To reach high luminosities without crab cavities, small β^* is required to generate high luminosities. The final levelling step of the flat beam option will give a β-function at the IP of $\beta^*_{x,y} = 0.3/0.075$ m. In this scenario, the β-function in the vertical plane at the end of a physics run will be comparable to the length of the bunch. When the length of the bunch is comparable to the transverse bunch size, a coupling between the planes is introduced, which results in the bunch varying parabolically at the IP. This coupling will result in a deviation from a Gaussian distribution in the longitudinal coordinate as the bunch passes through the IP. Such a deviation will result in some particles not colliding at the minimum β^*, which will hence lead to a reduction in luminosity. This is known as the hourglass effect.

Here, a new approach is applied to the beam-beam interaction to obtain analytical solutions for the electric field of a bunch that is centred at the IP undergoing a parabolic variation due to the hourglass effect. From the electric field in the rest frame of the bunch, one can later obtain the force a test particle experiences when the counter rotating bunch is centred at the IP.

THEORY

Starting from Maxwell's equations, which when expressed in full are given by,

$$\partial_y B_z - \partial_z B_y = \mu\left(J_x + \epsilon\partial_t E_x\right), \tag{1}$$
$$\partial_x B_z - \partial_z B_x = -\mu\left(J_y + \epsilon\partial_t E_y\right), \tag{2}$$
$$\partial_x B_y - \partial_y B_x = \mu\left(J_z + \epsilon\partial_t E_z\right), \tag{3}$$
$$\partial_y E_z - \partial_z E_y = -\partial_t B_x, \tag{4}$$
$$\partial_x E_z - \partial_z E_x = \partial_t B_y, \tag{5}$$
$$\partial_x E_y - \partial_y E_x = -\partial_t B_z, \tag{6}$$
$$\partial_x B_x + \partial_y B_y + \partial_z B_z = 0, \tag{7}$$
$$\partial_x E_x + \partial_y E_y + \partial_z E_z = \frac{\rho(x,y,z)}{\epsilon_0}. \tag{8}$$

If these equations are written in the rest frame of the bunch, the problem can be treated as electrostatic, assuming that there are no external magnetic fields in the rest frame. This provides an appropriate starting point and is one that is applied in the original derivation given by Bassetti-Erskine [1]. Maxwell's equations in the transverse planes are then given by

$$\partial_x E_y - \partial_y E_x = 0, \tag{9}$$
$$\partial_x E_x + \partial_y E_y = \frac{\rho(x,y)}{\epsilon_0}, \tag{10}$$

Since the charge density distribution, ρ, is known and is given by a Gaussian distribution, one is able to solve this system of equations to obtain the transverse electric field experienced by a particle as it traverses the electric field of a counter rotating bunch. Following the method proposed by Muratori *et al*, [2], one attempts to solve these non-linear coupled partial differential equations using an expression with a number of unconstrained functions, which in turn, will reduce to the well known Bassetti-Erskine (BE) equation. This method can then be extended for a charge density distribution that has a parabolic dependence on the longitudinal coordinate.

The BE equation for radially symmetric beams with fixed transverse beam sizes is well known and is obtained through solving Poisson's equation for a Gaussian source. Poisson's equation relating the scalar potential φ to the charge density distribution is given by,

$$\nabla^2\varphi = \frac{\rho}{\epsilon_0}. \tag{11}$$

Solving this using the Green's function method as introduced by S.Kheifets [3] allows the radial electric field to be

ISBN: 978-3-95450-168-7 doi:10.18429/JACoW-IPAC2015-MOPJE083

IMPLICATIONS OF MANUFACTURING ERRORS ON HIGHER ORDER MODES AND ON BEAM DYNAMICS IN THE ESS LINAC

A. Farricker*, R. M. Jones, School of Physics and Astronomy, Univ. of Manchester, Manchester, UK
and The Cockcroft Institute of Science and Technology, Daresbury, UK
S. Molloy, ESS AB, Lund, Sweden

Abstract

The European Spallation Source (ESS) in Lund, Sweden, will be a facility for fundamental physics studies of atomic structure using a spallation source of unparalleled brightness. To achieve this end, protons will be accelerated up to 2 GeV using a suite of cavities. Here we focus on the medium beta (β=0.67) elliptical superconducting cavities and we assess the influence of potential errors in fabrication to shift eigenmode frequencies onto an harmonic of the bunch frequency. If this occurs, and countermeasures are not adopted, the beam quality will be appreciably diluted. We provide details on the geometrical parameters which are particularly sensitive to frequency errors from intensive finite element simulations of the electromagnetic fields. A circuit model is also employed to rapidly assess the shift in the eigenmodes from their anticipated design values due a variety of potential errors.

INTRODUCTION

The ESS is a material science research facility currently under construction in Lund, Sweden. It will provide an unparalleled neutron flux for neutron based experiments by colliding a 5 MW (average) proton beam with a solid Tungsten target [1]. To achieve this a superconducting (SC) linear accelerator (linac) will accelerate a 2.86 ms, 62.5 mA beam up to a final energy of 2 GeV. The beam will have a bunch frequency of 352.21 MHz and have a repetition rate of 14 Hz. The SC linac will consist of 146 SC cavities of which 26 are two-spoke resonators (β = 0.50), 36 medium-beta (β = 0.67) and 84 high-beta (β = 0.86) [2].

The introduction of a charged particle beam into an accelerating cavity results in the excitation of a wakefield. This has both longitudinal and transverse components which can be decomposed into a series of modes. Beam excited higher order modes (HOMs) can cause significant dilution in the beam quality as well as increased levels of beam loss by moving bunches outside the stable RF bucket. The affects of HOMs can be reduced by coupling out the radiation and damping them with appropriate absorbing materials. In the ESS, as the bunch charge (174 pC) is relatively small, the transverse HOMs are small enough [3] such that damping them by these means is considered unnecessary. Also the longitudinal HOMs have relatively small loss factors [4] and their impact on beam dynamics is in general quite benign. However, if the frequency of a longitudinal HOMs is close to an harmonic of the bunch frequency, it can have a detrimental impact on the beam quality and can give rise to enhanced cryogenic load.

In summary, due to the low bunch charge and frequency of the cavities the magnitude of the field excited will be small [5]. However if a monopole mode is resonantly excited due to lying on a harmonic of the bunch frequency (machine line) the induced voltage can build up significantly and have severe impact on the beam and also on the cryogenic system of the accelerator. Here we investigate this issue.

This situation can be avoided through carefully tuning the geometry of the cavity such that no mode below the cut-off frequency of the beam pipe (1.688 GHz) is within a specified frequency of a machine line, both in the design and production stages. In this case, 5 MHz is chosen as the tolerance.

This paper is arranged such that the first section considers the impact of geometrical errors in single cells. The following section assesses the change in the mode frequencies of complete cavities due to these geometric errors –both random and systematic are analysed. The last section entails a set of final remarks.

CELL FREQUENCY SENSITIVITY

The cavities in the medium-beta section of the ESS linac consist of six-cell elliptical cavities operating at a frequency of 704.42 MHz with an accelerating gradient of 15 MV/m and with a prescribed quality factor, $Q < 5 \times 10^5$. The medium beta cavities are particularly important as the transition in the accelerating frequency and also a large increase in gradient compared to the spoke cavities. These two issues will make the beam particularly sensitive to dilution effects from beam excited HOMs in these cavities.

The ESS elliptical cavities will be fabricated from high purity Niobium shaped using the deep drawing process. It is anticipated that the deviation of the internal shape will be at the 0.3 mm level. These deviations from the design will result in each cavity having HOMs at different frequencies and this shift may be large enough to move a mode to a machine line.

In the present series of simulations we use a quiet generic geometry for the medium beta cavity, driven by considerations of size, iris diameter, cell coupling, surface fields and field flatness; close, but by no means identical to the structure designed by CEA Saclay. A typical trapped HOM in this cavity is illustrated in Fig. 1.

To study, in detail, the effects of changes in geometry on the resonant frequencies of the individual cells we have simulated a cell with the code HFSS [6] in which we vary the

* aaron.farricker@manchester.ac.uk

Content from this work may be used under the terms of the CC BY 3.0 licence (© 2015). Any distribution of this work must maintain attribution to the author(s), title of the work, publisher, and DOI.

ISBN: 978-3-95450-168-7 doi:10.18429/JACoW-IPAC2015-MOPJE084

Content from this work may be used under the terms of the CC BY 3.0 licence (© 2015). Any distribution of this work must maintain attribution to the author(s), title of the work, publisher, and DOI.

PARTICLE-IN-CELL SIMULATIONS OF A PLASMA LENS AT DARESBURY LABORATORY

K. Hanahoe, O. Mete, G. Xia, University of Manchester, Manchester, UK
Cockcroft Institute, Daresbury, UK
D. Angal-Kalinin, J. Jones, STFC/DL/ASTeC/Cockcroft Institute, Daresbury, UK
J. Smith, Tech-X UK Ltd, Daresbury Innovation Centre, Daresbury, UK

Abstract

Feasibility of a focusing element using the transverse fields provided by a plasma cell was studied numerically. In this paper, an experimental set up is proposed for various beam parameters available from the VELA and CLARA beam lines at Daresbury Laboratory. 2D simulation results from VSim [1], and expected results from planned measurement stations are presented. Field properties and the advantages and disadvantages of such an instrument compared to conventional focusing elements are discussed.

INTRODUCTION

Focusing of a particle beam is conventionally carried out using quadrupole magnets, either normal or superconducting, or solenoids. For final focus elements in particle colliders, the smallest possible beam size at the interaction region is desirable to achieve the highest possible luminosity. A plasma lens provides a possible means of achieving extremely large focusing gradients in both transverse directions simultaneously, but also provides a new set of challenges to overcome [2]. Study of plasma lenses using the electron beam from VELA and CLARA will provide results for comparison with previous experiments performed elsewhere and will provide a groundwork for further experiments using present and proposed accelerator test facilities at Daresbury Laboratory.

EXPECTED FOCUSING GRADIENTS

When a negatively charged particle bunch enters a plasma, the space charge force expels electrons from the path of the bunch. This leaves the bunch propagating in a region of net positive charge. If the background plasma density n_p is larger than the density of the bunch n_b (the overdense regime), the plasma left behind will completely neutralize the bunch. If n_p is lower than n_b (the underdense regime), the plasma electrons will be completely expelled leaving behind an ion channel. Applying Gauss's and Ampère's laws, the forces due to the electric and magnetic fields on a particle of charge q at a radius r within a homogenous, cylindrical bunch of charge density ρ_b and current density j, travelling at velocity v_b, can be calculated:

$$F = q\left(\frac{\rho_b r}{2\epsilon_0} + v_b \frac{\mu_0 r j}{2}\right) \tag{1}$$

In the overdense regime the net force on the particle is due to the magnetic field and is proportional to r. For comparison with magnetic quadrupoles, this can be quoted as a magnetic field gradient G:

$$G = \frac{B}{r} = \frac{\mu_0 j}{2} \tag{2}$$

Reasonable parameters for a future linear collider before final focus, with a peak beam current of 3.2 kA [3] and transverse bunch size of 100 µm, give a magnetic field gradient of 100 kT m $^{-1}$. In the underdense regime, more realistic for very high density beams, the focusing gradient will be smaller by, to a first approximation, a factor of n_p/n_b. This can still lead to very large focusing gradients compared to conventional magnets e.g. 200 T m^{-1} for quadrupoles for an LHC upgrade [4].

EFFECT OF ABERRATIONS

Compared to conventional magnets, plasma lenses have a significant disadvantage of increasing the emittance of the beam during focusing. This is caused by two main factors: the deviation of the focusing force from linearity in r, the spherical aberration, and the variation in focusing force with longitudinal position in the bunch, the longitudinal aberration. Scattering from plasma particles is not expected to be a significant source of emittance growth over the length scale of a plasma lens [5]. The emittance growth due to the spherical aberration can be calculated by considering the force on a particle at a distance from the axis of $r = 1\sigma_r$, being focused to a focal length f, in a beam of initial beta function β_0 and emittance ϵ_0 [6]. The fractional deviation in focusing strength from linearity, $\frac{\Delta K}{K}$ leads to a deviation from expected angular deflection of $\delta\theta$ given by:

$$\delta\theta = \frac{\sqrt{\beta_0\epsilon_0}}{f}\frac{\Delta K}{K} \tag{3}$$

The effective emittance ϵ_{eff} due to the spherical aberrations is given by:

$$\epsilon_{\text{eff}} = \sqrt{\epsilon_0^2 + \beta_0\epsilon_0\delta\theta^2} \tag{4}$$

The longitudinal aberration requires consideration of the phase space of the bunch as it passes through the lens. The head of the bunch enters an unperturbed plasma, and as such its space charge is not neutralized and it sees no net focusing force. Moving back along the bunch, the focusing force seen by slices of the beam will be proportional to the perturbation in plasma density. Focusing corresponds to a rotation of the phase space of the bunch, and non-uniform focusing will lead to smearing out of the phase space.

ISBN: 978-3-95450-168-7 doi:10.18429/JACoW-IPAC2015-MOPMA001

COMPARISON OF MEASUREMENTS AND SIMULATIONS OF SINGLE BUNCH INSTABILITIES AT DIAMOND

M. Atay[2], R.T. Fielder[1], I. Martin[1] and R. Bartolini[1,2]
[1]Diamond Light Source, Oxfordshire, UK
[2]John Adams Institute, University of Oxford, Oxfordshire, UK

Abstract

The single bunch dynamics in the Diamond storage ring has been analysed with a multiparticle tracking code and compared with the results of a wealth of diagnostics under development at Diamond. The interplay of various wakefield sources has been studied and it has been found that the THz spectrum can be reproduced in many cases with simple impedance models, both below and above the bursting threshold.

INTRODUCTION

The study of single bunch instabilities in modern light sources has been fostered by the user requirements to operate the storage rings with short electron bunches for the generation of short X-ray pulses or coherent THz radiation. Diamond has developed a number of low-alpha optics tailored to different users' requirements [1] attempting to optimize either the short X-ray pulse operation ($\alpha \sim 10^{-5}$) or the coherent THz radiation ($\alpha \sim 4{\cdot}10^{-6}$) [2]. This process has also stimulated the development of advanced THz diagnostics and data collection techniques described in a companion paper [3]. Numerous measurements has been carried out in the past to investigate the rich phenomenology associated to the single bunch instabilities, under different machine conditions, both below and above the instability thresholds. At the same time we have developed a macroparticle tracking code in order to gain a better insight in the mechanism driving the instabilities with the aim of reproducing the complex dynamics and guide further optimisation of the machine performance. The tracking code has been specifically tailored to replicate the data available from our diagnostics, such as THz spectrograms, streak camera images, BPM data and FTIR spectra. We present the first preliminary results of the comparisons between the measurements and tracking simulations and address the issues met.

TRACKING CODE

The beam dynamics in presence of wakefields can be described with various numerical techniques [4]. We have chosen to develop a multiparticle tracking code to study the single bunch dynamics with the influence of wakefields in 6-dimensional phase space, extending the capabilities of the code "sbtrack" [5]. While the original code was written in C, it was later translated to MATLAB to exploit its graphical capability. A number of wakefields have been implemented: most notably resistive wall (RW), coherent synchrotron radiation (CSR), shielded CSR [6] and any number of broad band resonators (BBR). The last option allows the implementation of the wakefields as computed from CST Microwave studio [7] or Gdfidl [8] by fitting a number of BBR models to the most prominent modes.

The code integrates the 6D equations of motion of the electron in the presence of the RF potential, synchrotron radiation damping and diffusion. The link to the full accelerator tracking with AT is under development, although the first tests resulted in prohibitively long computation times. The different impedance models used and the construction of the overall impedance model are described in more details below.

The output of the tracking code is the phase space evolution of the 6D macroparticle distribution on a turn by turn basis This is post-processed to extract all the relevant data that can be measured in the machine, such as tuneshifts, rise time or damping time of the instabilities, turn-by-turn and orbit data, THz emission power, spectrograms and streak camera images. All those quantities can be computed and measured as a function of the single bunch current and the various different machine parameters.

BUILDING THE IMPEDANCE MODEL

The code uses several different types of wakefields. The wake function of the broad band resonator (BBR) model is given by [4]

$$W(z) = 2\alpha R_s e^{\alpha z/c}\left(\cos\frac{\bar{\omega}z}{c} + \frac{\alpha}{\bar{\omega}}\sin\frac{\bar{\omega}z}{c}\right) \tag{1}$$

where $\alpha = \omega_R/2Q$, $\bar{\omega} = \sqrt{\omega_R^2 - \alpha^2}$, Q is a quality factor, ω_R is a resonance frequency and R_s is a shunt impedance. The CSR model is described in [6] and the shielding is taken into account as follows:

$$W(z) = -\frac{2\pi R}{4\pi\varepsilon_0} e N_e \left(\int_0^\infty \frac{2}{(3R^2)^{1/3}} \frac{d\rho(z-z')}{dz} \frac{dz'}{z'^{1/3}} - \right. \\ \left. -\frac{1}{2h^2}\int_{-\infty}^{\infty} \rho(z-z')dz' G_2\left[\frac{1}{2h}\left(\frac{R}{h}\right)^{1/2} z'\right]dz'\right) \tag{2}$$

where 2h is the gap between the shielding plates and R is the bending magnet radius. Purely resistive and purely inductive impedances have also been implemented to be able to accurately characterize the impedance of the storage ring, according to the respective wake functions:

Content from this work may be used under the terms of the CC BY 3.0 licence (© 2015). Any distribution of this work must maintain attribution to the author(s), title of the work, publisher, and DOI.

ISBN: 978-3-95450-168-7 doi:10.18429/JACoW-IPAC2015-MOPMA002

OPTIMISING THE DIAMOND DDBA UPGRADE LATTICE FOR LOW ALPHA OPERATION

I.P.S. Martin, Diamond Light Source, Oxfordshire, U.K.
R. Bartolini, Diamond Light Source, Oxfordshire, U.K., and
John Adams Institute, University of Oxford, U.K.

Abstract

The Diamond storage ring will be upgraded during 2016 by replacing one of the existing double bend achromat (DBA) cells with a double-DBA (DDBA) cell [1]. One requirement of the upgrade is that following the installation of the new cell, Diamond should continue to offer dedicated user time in 'low alpha' mode [2]. In this paper we describe the particular challenges relating to this task, and present the lattice design and optimisation studies undertaken so far. The paper concludes by discussing preliminary studies of adding a second DDBA cell into the storage ring.

INTRODUCTION

An upgrade of the Diamond storage ring in 2016 will replace one of the existing DBA cells with a single DDBA cell, thereby creating space for an additional insertion device beamline. At present, the Diamond storage ring is operated for several periods each year in a dedicated 'low-alpha' optics [2], and it is the intention to continue to offer this mode following the upgrade. A comparison of the magnet layout before and after the upgrade is shown in Fig. 1.

The existing low alpha lattice has been in operation since 2010, serving both short-pulse x-ray users on the I06 'Nanoscience' ID beamline and THz users on the B22 'MIRIAM' bending magnet beamline. Part of the success of this mode of operation is down to the combination of having both low emittance and low momentum compaction, achieved by allowing the dispersion to become negative only within the bending magnets [3]. The lattice is operated with negative momentum compaction α_1, as this is found to reduce the bunch lengthening with current and causes the leading edge of the bunch profile to become sharper, enhancing the CSR gain at shorter wavelengths.

In this paper we present the adaptation of the low alpha lattice for the DDBA upgrade. This work includes optimisation of the linear and nonlinear optics, analysis of the lattice sensitivity to errors, and an assessment of the likely injection efficiency and lifetime. The paper concludes with preliminary studies of adding a second DDBA cell to the storage ring.

LATTICE OPTIMISATION

Design Constraints

The inclusion of a single DDBA cell presents a number of challenges for the optimisation. Firstly, whilst the inclusion of four gradient sector-bends helps to keep the cell

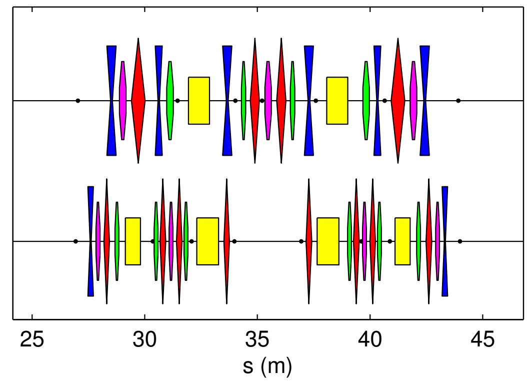

Figure 1: Existing DBA (top) and new DDBA (bottom) cell.

compact, the fixed defocussing gradient reduces the flexibility to tune it to different optics. As a result, the adjacent quadrupoles must also be powered with large gradients, increasing the natural chromaticity of the ring. The need to match the DDBA cell to the adjacent DBA cells leads to a higher dispersion than is otherwise the case with multi-bend achromat lattices designed for low emittance. However, the dispersion function within the cell is still relatively small compared with the remainder of the ring, and does not provide an obvious location to correct the added natural chromaticity locally. Similarly, the ability to correct for the second-order momentum compaction α_2 scales with $-S\eta_x^3$ [4], again requiring the sextupole strength S to increase in the remaining DBA cells.

The final, and perhaps most significant difficulty is in the loss of symmetry of the storage ring. In contrast to the nominal user optics, the low alpha lattice has so far been operated without powering the two mini-beta sections [5], thereby maintaining the 6-fold symmetry of the lattice. The inclusion of a DDBA cell clearly breaks this symmetry, with natural consequences on the sensitivity to errors.

Optimisation Techniques

Optimisation of the lattice is an iterative process, primarily carried out using the parallel version of elegant [6, 7]. Initially, the linear optics are adjusted using the 'particle swarm' option in the parallel optimisation module, having applied a number of constraints. Following this, the nonlinear optics are explored using a Multi-Objective Genetic Algorithm (MOGA) [8].

The constraints for the linear optics include fixing α_1 to the desired value, placing limits on the maximum β-functions around the ring, maximising β_x at the injection

Content from this work may be used under the terms of the CC BY 3.0 licence (© 2015). Any distribution of this work must maintain attribution to the author(s), title of the work, publisher, and DOI.

ISBN: 978-3-95450-168-7 doi:10.18429/JACoW-IPAC2015-MOPMA003

RECONSTRUCTION OF ELECTRON BUNCH MOTION DURING CSR BURSTS USING SYNCHRONISED DIAGNOSTICS

I.P.S. Martin, C. Bloomer, L.M. Bobb, A. Finn, G. Rehm, Diamond Light Source, Oxfordshire, U.K.
R. Bartolini, Diamond Light Source, Oxfordshire, U.K.
John Adams Institute, University of Oxford, U.K.

Abstract

Above a certain threshold current, electron bunches become unstable and emit bursts of coherent synchrotron radiation (CSR). The character and periodicity of these bursts vary with bunch current, RF voltage and lattice momentum compaction. In this paper we describe recent measurements taken at Diamond of how the electron bunch longitudinal profile and energy vary during a burst, and correlate this with CSR emission at a range of wavelengths.

INTRODUCTION

The onset of microbunching instabilities in storage rings is a well known phenomenon [1, 2]. These occur when the current stored in an electron bunch exceeds a certain threshold value, at which point the interaction of the bunch with its own wakefields is sufficiently strong to cause density modulations to occur within the bunch. These in turn increase the amplitude of the wakefields, giving rise to an instability. For a given storage ring, the current threshold is found to vary both with RF voltage and momentum compaction.

In recent years the subject of CSR-driven microbunching has received considerable attention due to its detrimental effects both in rings and in linac bunch compressors [3–9]. In the case of rings, this attention has been mainly focussed on rings with positive momentum compaction, with little experimental evidence for negative momentum compaction lattices. Such data would provide a useful benchmark against which numerical simulations could be compared [10], as well be valuable for its wider academic interest. It is also of particular relevance for Diamond Light Source, as the ring is regularly operated in a negative low-alpha configuration for the generation of both coherent THz radiation and short x-ray pulses [11].

In this paper we describe recent measurements taken at Diamond Light Source in low-alpha mode that characterise the electron bunch motion during CSR bursts. These are correlated with mm-wave emissions recorded using a selection of Schottky Barrier Diodes, thus giving further insight into the underlying electron beam dynamics.

CSR BURST DETECTION

The microbunching instability primarily affects the longitudinal phase space of the electron bunch. As such, the most important observables to measure are the electron bunch length, bunch arrival time and bunch energy. Ideally one would also like to measure the internal bunch structure and energy spread during a burst; however, this is not yet possible using the diagnostics available at Diamond.

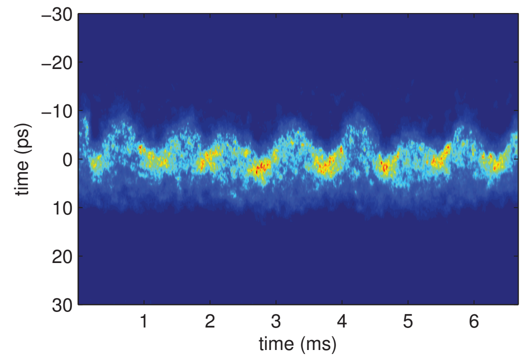

Figure 1: Streak camera image capturing CSR bursts for $\alpha_1 = -4.6 \times 10^{-6}$, $V_{RF} = 3.4$ MV, $I_{bunch} = 39.5\mu$A.

The electron bunch length and arrival time is recorded using an Optronis dual-sweep streak camera [12]. In recent years, the performance of this camera at Diamond has been optimised by the introduction of a fully reflective front-end optics and pinhole located upstream of the camera, alongside a post-processing of the recorded images by deconvolving them with the measured point-spread function [13]. An example of one such measurement is shown in Fig. 1.

The electron bunch energy is measured indirectly using the turn-by-turn BPM system. During a burst the electron bunch loses energy to the radiation field, causing it to undergo coherent synchrotron oscillations. This energy deviation can be measured from the transverse offset at positions of high dispersion, assuming the dispersion amplitude is known. The picture is slightly complicated by the presence of additional betatron oscillations. However, by averaging across BPMs of similar dispersion, and by filtering out the high-frequency betatron contributions, the mean energy deviation of the bunch can be recovered.

Whilst it is not possible to directly observe the internal structure of the electron bunches at Diamond, the detection of the accompanying CSR bursts using Schottky Barrier Diodes (SBDs) serves as a useful proxy. The detectors used during these measurements have sensitivity bandwidths of 33-50 GHz, 60-90 GHz, 90-140 GHz, 140-220 GHz, 220-330 GHz, 330-500 GHz and 500-750 GHz. These frequencies correspond to periods in the range 1.3-30 ps, and the detectors at the higher frequency end of the range in particular should be sensitive to sub-structure appearing within the electron bunch. The SBD array used during these studies is described in more detail in a companion paper [14].

Content from this work may be used under the terms of the CC BY 3.0 licence (© 2015). Any distribution of this work must maintain attribution to the author(s), title of the work, publisher, and DOI.

ISBN: 978-3-95450-168-7 doi:10.18429/JACoW-IPAC2015-MOPMA004

NUMERICAL OPTIMIZATION OF ACCELERATORS WITHIN oPAC

C.P. Welsch#

Cockcroft Institute, Daresbury, UK and The University of Liverpool, Liverpool, UK
on behalf of the oPAC Consortium

Abstract

Powerful simulation tools are required for every accelerator and light source to study the motion of charged particles through electromagnetic fields during the accelerator design process, to optimize the performance of machine diagnostics and to assess beam stability and non-linear effects. The Optimization of Particle Accelerators (oPAC) Project is funded by the EU within the 7th Framework Program and currently supports 23 Fellows that are based at institutions across Europe. This large network carries out R&D that closely links beam physics studies with the development of diagnostics and beyond state-of-the-art simulation tools. This contribution presents selected research outcomes from oPAC, including the numerical optimization of beam loss monitor locations along the European Spallation Source's 5 MW proton linac, results from tracking studies for the LHeC lattice that allow beam stability to be assessed, and multi-objective optimization of the linear and non-linear beam dynamics of the synchrotron SOLEIL. In addition, an overview of recent and future oPAC events is given.

INTRODUCTION

oPAC – Optimization of Particle Accelerators – is a Training Network funded by the European Union [1]. With a budget of almost €6M shared between 12 beneficiary partners over a 4-year period, it brings together 34 institutions across the industry and academia to provide formation on particle accelerators to a total of 23 early stage researchers. The main objective of the oPAC network is to train the next generation of accelerator scientists and engineers for the increasingly demanding community of accelerator facilities while strengthening the bonds within this community. oPAC is also strongly engaged in raising public awareness on the importance of particle accelerators for society, through their applications in health, industry, security, energy, and fundamental knowledge.

Each of the Fellows is developing a project set in one of the following topics: research of beam dynamics, development of beam diagnostics, numerical simulation tools, and accelerator control and data acquisition systems. In addition to the research in their home institution, the Fellows undertake secondments in any of the other partner institutions, complementing their formation and fostering collaborative research. Moreover, the Fellows receive regularly specific training on complementary skills and techniques through a series of topical workshops and schools that are held at different venues across the network. The Fellows together with the central management team are also carrying out an intensive program of outreach and dissemination, through the internet and social media, but also through the organization of events and participation in conferences, trade fairs, exhibitions, etc.

*This project has received funding from the European Union's Seventh Framework Programme for research, technological development and demonstration under grant agreement no 289485.
#carsten.welsch@cockcroft.ac.uk

RESEARCH

As outlined before research within the network is carried out across four thematic work packages. The following subsections highlight progress made by three exemplar Fellows across these work packages.

Beam Loss Monitoring at ESS

The linear accelerator of ESS will produce a 5 MW proton beam. Beam of this power must be strictly monitored by a specialized Beam Loss Monitoring (BLM) system to detect any abnormal losses and to ensure that operational losses do not exceed a limit of 1 W/m. In order to optimize the detectors layout in terms of their numbers and locations a series of beam loss simulations was performed using the MARS Monte Carlo code. Different loss scenarios were considered and yielded an indication of the energy deposition along the ESS linac.

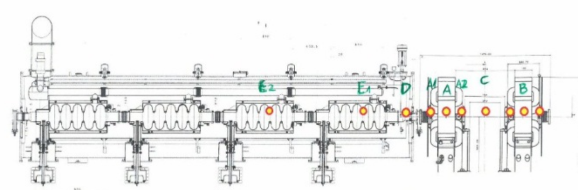

Figure 1: Loss point locations.

Different beam loss simulations were performed for four different energies in the ESS cold linac, ranging from 220-2,000 MeV [2]. For all of these energies 10 different possible locations along a cryomodule-quadrupole doublet were chosen, see Fig.1. At these locations three points on the beam pipe were considered as possible loss points. Losses were then simulated for 3 different angles: 1 mrad, 3 mrad and 1°. The power deposited in air around a loss was used as primary indicator for suitable BLM locations as it is proportional to the BLM signal within certain limits. For more accurate results, an approach using particle flux-to-generated charge converters shall be applied in the future. BLMs were placed around the cryomodule-quad assemblies in a way that optimizes three figures of merit: Distinguishability of individual losses, volume coverage and sensitivity. The aim is to avoid missing any loss (full volume coverage), ability to differentiate between individual losses, and detecting even smallest losses which are just above the noise level.

Content from this work may be used under the terms of the CC BY 3.0 licence (© 2015). Any distribution of this work must maintain attribution to the author(s), title of the work, publisher, and DOI.

ISBN: 978-3-95450-168-7 doi:10.18429/JACoW-IPAC2015-MOPMA005

NON-INVASIVE BEAM PROFILE MONITORING

C.P. Welsch[#1], T. Cybulski[1], A. Jeff[1,3], V. Tzoganis[1,2], H. Zhang[1]
[1] Cockcroft Institute and The University of Liverpool, UK
[2] RIKEN, Nishina Center, Wako, Japan
[3] CERN, Geneva, Switzerland

Abstract

Highest energy and intensity accelerators require new approaches to transverse beam profile monitoring as many established techniques will no longer work due to the high power stored in their beam. In addition, many accelerator applications such as ion beam cancer therapy or material irradiation would benefit significantly from the availability of non-invasive beam profile monitors. Research in the QUASAR Group has focused on this area over the past 5 years. Two different approaches were successfully developed: Firstly, a supersonic gas jet-based monitor was designed and commissioned. It enables the detection of the 2-dimensional transverse beam profile of essentially any charged particle beam with negligible disturbance of the primary beam and accelerator vacuum. Secondly, a monitor based on the Silicon strip VELO detector, originally developed for the LHCb experiment, was tested as an online beam monitor at the Clatterbridge Cancer Center in the UK. The design of both monitors and results from measurements are presented in this contribution.

INTRODUCTION

Least intrusive beam profile measurement techniques that allow continuous operation of an accelerator whilst providing comprehensive information about the particle beam would be ideal for many applications, ranging from high energy/high intensity accelerators such as the LHC at CERN and its future upgrades or the high power proton driver linac at ESS where conventional diagnostics would simply not work. Various non-invasive methods have been developed for the determination of the transverse beam profile. These include Ionization Profile Monitors (IPM) [1] which are based on the collection of the ions produced by impact ionization of rest gas by the main beam and the Beam Induced Fluorescence Monitor (BIF) [2] which relies on the detection of the light produced from the excited residual gas. IPM's are truly non-invasive devices which can operate parasitically if the residual gas pressure is sufficiently high and offer very good spatial resolution down to 100 µm and time resolution in the order of 10 ms with a fast camera or a few µs with a fast readout system. However they are usually limited to high energy accelerators. BIF's are parasitical as well, but require higher residual gas pressures in excess of 10^{-6} mbar and longer signal integration times.

*Work supported by the EU under grant agreement 215080 and 289485, HGF and GSI under contract number VH-HG-328, the STFC Cockcroft Institute Core Grant No. ST/G008248/1, and a RIKEN-Liverpool studentship.
#carsten.welsch@cockcroft.ac.uk

Gas Jet-based Beam Profile Monitor

A possible approach to overcome these limitations is to utilize a cold (< 20 K) neutral supersonic gas jet shaped into a thin curtain. The core of this monitor consists of an expansion of a room temperature high pressure gas (1-10 bars) into vacuum through a nozzle with 30 µm diameter, resulting in an adiabatic expansion and the formation of a jet with a very stable and cold inner core.

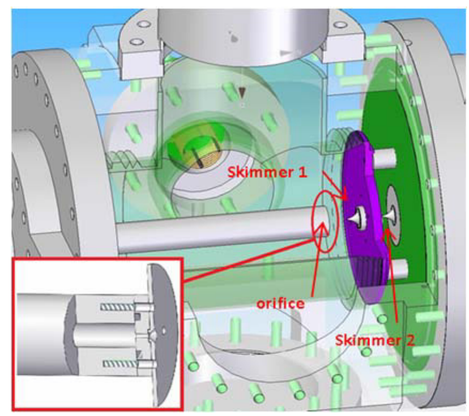

Figure 1: CAD drawing of the nozzle chamber where the first two skimmers are highlighted.

This jet is then further shaped by several skimmers. The first part of the experimental setup is illustrated in Fig. 1. Skimmers separate several differentially pumped vacuum chambers through which the jet passes until it reaches a final "reaction chamber", held at a pressure of 10^{-9}-10^{-12} mbar [3]. When entering this chamber the jet has already been shaped by a final rectangular skimmer into a curtain that crosses the primary beam to be analyzed under an angle of 45°. In this interaction impact ionization of the jet particles occurs and the resulting ions are imaged by a moderate electric field of some kV/m onto a position-sensitive double layer Micro Channel Plate (MCP) detector. The MCP provides signal amplification of up to 10^6. Finally, the resulting beam profile is observed by a Phosphor screen-camera combination that is mounted on the top of the reaction chamber, see Fig. 2.

At low energies of the primary beam the extraction electric field can lead to its displacement when passing through the reaction chamber. This is compensated by deflecting electric fields before and after the interaction region (not shown in the figure).

Content from this work may be used under the terms of the CC BY 3.0 licence (© 2015). Any distribution of this work must maintain attribution to the author(s), title of the work, publisher, and DOI.

ISBN: 978-3-95450-168-7 doi:10.18429/JACoW-IPAC2015-MOPMA006

Content from this work may be used under the terms of the CC BY 3.0 licence (© 2015). Any distribution of this work must maintain attribution to the author(s), title of the work, publisher, and DOI.

MODELING RF FEEDBACK IN ELEGANT FOR BUNCH-LENGTHENING STUDIES FOR THE ADVANCED PHOTON SOURCE UPGRADE *

T. Berenc, M.Borland, ANL, Argonne, IL 60439, USA

Abstract

The proposed Advanced Photon Source (APS) multi-bend achromat (MBA) lattice includes a passive bunch-lengthening cavity to alleviate lifetime and emittance concerns. Feedback in the main radio-frequency (rf) system affects the overall impedance presented to the beam in this double rf system. To aid beam stability studies, a realistic model of rf feedback has been developed and implemented in `elegant` and `Pelegant`.

INTRODUCTION

Many existing and planned storage ring light sources employ harmonic bunch-lengthening cavities [1–3]. For the required tuning in bunch-lengthening mode, the harmonic cavity contributes to Robinson mode growth which opposes the damping provided by the main rf cavities [4]. RF feedback on the main rf modifies the apparent impedance to the beam and hence influences Robinson instabilities [5]. Direct rf feedback can easily be accounted for by simply reducing the cavity shunt impedance and quality factor.

However, rf feedback systems rarely consist of, nor always include, pure direct rf feedback. They can work in either amplitude and phase (amp/phase) polar coordinates or in-phase and quadrature (I/Q) cartesian coordinates. They can also include integral feedback and other frequency shaping effects and need not be implemented symmetrically.

Including realistic rf feedback in particle tracking is essential to capture the interaction of the beam with the rf system as depicted in Fig. 1. Thus, a flexible framework for including rf feedback in `elegant` [6] and `Pelegant` [7,8] has been developed. This has allowed rf feedback to be included in APS upgrade tracking studies [9].

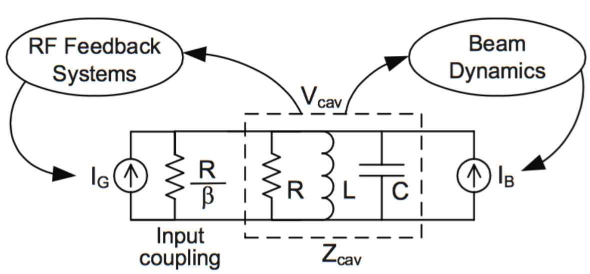

Figure 1: Interaction of beam, cavity, and rf systems.

SYSTEM MODEL

Figure 2 represents the rf feedback model added to `elegant`. The interaction between the beam current and the rf cavity is still modeled using `elegant`'s `RFMODE` element. However, instead of using a fixed generator voltage, the generator voltage is determined by amp/phase rf feedback. I/Q and combination feedback as shown are planned but not yet implemented.

The rf system signals are represented at baseband using a time-varying complex-envelope. For example, the total cavity voltage is $v_{cav}(t) = Re\left\{\mathbf{V_{cav}}(t)e^{j\omega_{rf}t}\right\}$ where $j = \sqrt{-1}$, ω_{rf} is the rf drive frequency, and $\mathbf{V_{cav}}(t) = V_I(t) + jV_Q(t)$ is the complex envelope with I/Q components $V_I(t)$ and $V_Q(t)$ respectively. The amp/phase are $|\mathbf{V_{cav}}|(t) = \sqrt{V_I^2(t) + V_Q^2(t)}$ and $\angle\mathbf{V_{cav}}(t) = \text{atan2}\left\{V_Q(t), V_I(t)\right\}$.

Filters are provided to separately process the amplitude and phase errors with respect to reference setpoints. The outputs of these filters affect the generator current which drives a cavity I/Q state-space model to obtain the generator induced voltage. To facilitate initial conditions or feed-forward, a nominal generator current $\mathbf{I_{G_o}}$ is provided.

Feedback Filters

The feedback filters are implemented as difference equations of the form

$$y[n] = \frac{1}{b_0}\sum_{i=1}^{r} b_i y[n-i] + \frac{1}{b_0}\sum_{i=0}^{m} a_i x[n-i] \quad (1)$$

where $y[n]$, $x[n]$ are respectively the filter output and input at sample n, and $y[n-i]$, $x[n-i]$ are past outputs and inputs from time $(n-i)T$ where T is the sample period equal to an integer number of rf buckets. Four parallel filter blocks, each with an unlimited number of a_i and b_i filter coefficients can be supplied to `elegant` for both the amplitude and phase feedback.

Various methods exist to transform an analog filter (like that used at APS) to a digital one [10]. The bilinear transform produces a good match for an integrator.

Generator Induced Cavity Voltage

I/Q modulation of the drive current, $I_G(t) = I_I(t)\cos\omega_{rf}t - I_Q(t)\sin\omega_{rf}t$, produces I/Q modulation of the cavity voltage. In general, the I/Q components of $\mathbf{V_{cav}}$ will each contain a response to both I/Q components of $\mathbf{I_G}$. The cavity state-space equations [11–13], when discretized using the zero-order hold method [10], become

$$\begin{bmatrix} V_I(n) \\ V_Q(n) \end{bmatrix} = \mathcal{A}\begin{bmatrix} V_I(n-1) \\ V_Q(n-1) \end{bmatrix} + \mathcal{B}\begin{bmatrix} I_I(n-1) \\ I_Q(n-1) \end{bmatrix} \quad (2)$$

The matrices $\mathcal{A}$ and $\mathcal{B}$ are given as

$$\mathcal{A} = e^{-\sigma T}\begin{bmatrix} \cos\Delta\omega T & -\sin\Delta\omega T \\ \sin\Delta\omega T & \cos\Delta\omega T \end{bmatrix} \quad (3)$$

* Work supported by the U.S. Department of Energy, Office of Science, Office of Basic Energy Sciences, under Contract No. DE-AC02-06CH11357.

ISBN: 978-3-95450-168-7 doi:10.18429/JACoW-IPAC2015-MOPMA007

TRACKING STUDIES OF A HIGHER-HARMONIC BUNCH-LENGTHENING CAVITY FOR THE APS UPGRADE *

M. Borland, T. Berenc, R. Lindberg, A. Xiao, ANL, Argonne, IL 60439, USA

Abstract

The Advanced Photon Source (APS) multi-bend achromat (MBA) lattice will require a bunch-lengthening cavity to decrease the effects of Touschek scattering on the beam lifetime and of intrabeam scattering on the beam emittance. Using `elegant`, we've performed tracking studies of a passive, i.e. beam-driven, fourth-harmonic cavity in the MBA lattice, including the longitudinal impedance of the ring. Studies include investigating optimal detuning, simulation of transients after loss of a bunch, simulation of effects of bunch population variation, simulation of possible non-uniform filling patterns, and simulation of filling from zero. Realistic amplitude and phase feedback of the main rf cavities is also taken into account.

INTRODUCTION

The APS MBA lattice [1] has an emittance of under 70 pm at 6 GeV. Because of the short (12.5 ps rms) zero-current bunch length, use of a higher-harmonic cavity (HHC) to lengthen the bunch is needed to reduce IBS-related emittance growth and improve the Touschek lifetime.

The HHC provides bunch lengthening by reducing the local slope of the total accelerating voltage. In the case of a passive HHC, the cavity is detuned to the positive side of harmonic n of the main rf system frequency. The voltage induced in the HHC by the beam then has a phase that reduces the slope of the time-dependent total voltage. The induced voltage and bunch shape can be computed in a self-consistent fashion as in [2].

However, such results ignore potential well distortion and the longitudinal impedance, which can best be included using a tracking code. Tracking can also include self-consistent, time-dependent interaction of the beam with the cavity mode, particularly important for a passive system, as well as higher-order beam transport effects.

SIMULATION METHODS

`Pelegant` [3, 4] was used for the tracking simulations. Although the needed features have existed in `elegant` [5] for over a decade, we took advantage of recent improvements to parallel performance [1], diagnostics, and implementation of rf feedback [6].

Eight beamline elements were used: `ILMATRIX` provides fast single-turn beam transport that incorporates longitudinal, chromatic, and transverse nonlinearities. `SREFFECTS` provides lumped simulation of synchrotron radiation. `WATCH` and `HISTOGRAM` provide bunch-by-bunch diagnostic data. `CHARGE` provides the ability via the `modulate_elements` command to achieve a quiet start by slowly ramping the beam current. `RFMODE` simulates a beam- and (optionally) generator-driven cavity mode. This is used for both the 352-MHz ($Q_L = 9.1 \times 10^3$, $R_a/Q = 208\Omega$) main cavities and the 4^{th} harmonic cavity. A feedback model is used to maintain the main cavity voltage [6]. This element implicitly includes the short-range wake resulting from the fundamental cavity modes. It can also be used for including cavity HOMs [7]. `ZLONGIT` simulates the short-range wake, using an impedance model based on the conceptual vacuum system design (an older version of that presented in [8]).

BASIC RESULTS

The passive HHC [9] has $R_a/Q = 108\Omega$ and two free parameters: the detuning $\Delta f_h > 0$ of the resonance from the harmonic condition and the loaded quality factor Q_L. Earlier studies showed that using $Q_L = 6 \times 10^5$ or greater gave improved stability in the presence of irregular fill patterns, so this value is used throughout.

Starting with $\Delta f_h \gg f_h/Q_L$ and progressively decreasing the detuning, increasing voltage is induced until the ideal bunch lengthening condition is achieved. Further reduction results in splitting of the bunch. Figure 1 shows the bunch duration and energy spread as a function of the detuning for two fill patterns. The difference between results for the two patterns stems from the microwave instability (MWI), which impacts 48-bunch mode significantly, lengthening the bunch to 35 ps rms even in the absence of the HHC. The MWI is also slightly suppressed by the lengthening of the bunch. Nominally, ideal lengthening to 50 ps rms occurs at about $\Delta f_h = 16.5$ kHz, which agrees well with the simulation results for 324 bunches.

Figure 2 shows the longitudinal profiles averaged over 2000 turns for two detuning values. For 48 bunches, Δf_h can be reduced beyond what is possible for 324 bunches without creating a strongly double-humped shape, a curious benefit of being well above the MWI threshold. Turn-by-turn longituidinal profiles can be used to compute the Touschek lifetime using the program `touschekLifetime` along with local momentum acceptance results [1], providing higher-fidelity results than would be obtained from using the rms bunch duration [10]. Since these show that $\Delta f_h = 13.50$ kHz is benefical, subsequent simulations concentrate on that value.

TRANSIENTS FOLLOWING BUNCH LOSS

The inclusion of rf feedback in the simulations allows realistic modeling of fault conditions, such as a swap-out fail-

* Work supported by the U.S. Department of Energy, Office of Science, Office of Basic Energy Sciences, under Contract No. DE-AC02-06CH11357

Content from this work may be used under the terms of the CC BY 3.0 licence (© 2015). Any distribution of this work must maintain attribution to the author(s), title of the work, publisher, and DOI.

ISBN: 978-3-95450-168-7 doi:10.18429/JACoW-IPAC2015-MOPMA008

Content from this work may be used under the terms of the CC BY 3.0 licence (© 2015). Any distribution of this work must maintain attribution to the author(s), title of the work, publisher, and DOI.

SIMULATION OF GAS SCATTERING LIFETIME USING POSITION- AND SPECIES-DEPENDENT PRESSURE AND APERTURE PROFILES *

M. Borland, J. Carter, H. Cease, and B. Stillwell, ANL, Argonne, IL 60439, USA

Abstract

When computing gas scattering lifetime for storage rings, it is common to use the average pressure, even though it is known that the pressure varies with location in the ring and varies differently for different gas species. In addition, other simplifications are commonly made, such as assuming that the apertures in the horizontal and vertical planes are independent and assuming that the momentum acceptance can be characterized by a single value. In this paper, we describe computation of the elastic and bremsstrahlung scattering lifetimes that includes species-specific gas pressure profiles computed with Synrad+ and Molflow+. The computations make use of the detailed shape of the dynamic acceptance and the position-dependent momentum acceptance computed with `elegant`. Comparisons are made to simpler methods for the multi-bend achromat upgrade lattice for the Advanced Photon Source.

INTRODUCTION

Particles in storage rings undergo scattering from residual gas atoms, which may result in particle loss when the scattering places a particle outside the physical or dynamical acceptance of the ring. In this paper, we outline an elaboration of lifetime calculations for elastic and inelastic gas scattering that removes common assumptions. E.g., it is common to assume that the elastic gas scattering lifetime is limited in the vertical plane only, that the momentum acceptance is constant around the ring, and that the vacuum pressure is constant around the ring. The present calculations use results from Molflow+ and Synrad+ [1,2], which allow computing species-specific pressure profiles. They also use dynamic acceptance (DA) and local momentum acceptance (LMA) [3,4]. results from `elegant` [5].

A general form for the lifetime is (compare [6])

$$\frac{1}{\tau} = \frac{c}{L}\sum_{g=1}^{G}\sum_{a=1}^{C_g}\int_0^L \sigma_{g,a}(s)S_{g,a}n_g(s)ds, \tag{1}$$

where L is the length of the ring (or a periodic unit), G is the number of molecular gas constituents, C_g is the number of atomic components of gas g, $\sigma_{g,a}(s)$ is the out-scattering cross section for atomic component a of gas g at location s, $S_{g,a}$ is the number of atoms of type a in a molecule of gas g, and $n_g(s)$ is the number density of gas g at location s, which is related to the partial pressure $p_g(s)$ by $n_g(s) = \frac{p_g(s)}{k_b T}$.

* Work supported by the U.S. Department of Energy, Office of Science, Office of Basic Energy Sciences, under Contract No. DE-AC02-06CH11357.

The out-scattering cross section is given by

$$\sigma_{g,a}(s) = \int_{q_1(s)}^{q_2(s)} \frac{d\sigma_{g,a}}{dq}dq \tag{2}$$

where q is the scattering coordinate, q_1 is the maximum surviving value of q, and q_2 is the physically-limiting value of q. E.g., for elastic scattering, q is the change in slope of the particle trajectory, q_1 is the maximum change that will keep the particle within the acceptance, and $q_2 = \infty$. For gas bremsstrahlung, q is the change in fractional momentum deviation δ, q_1 is the momentum acceptance, and $q_2 = 1$.

ELASTIC NUCLEAR SCATTERING

Elastic scattering from atomic nuclei is described by the Rutherford cross section [7]

$$\frac{d\sigma_{g,a}}{d\Omega} = \frac{Z_{g,a}^2 r_e^2}{4\gamma^2}\frac{1}{\sin^4\frac{\theta}{2}} \equiv \frac{E_{g,a}}{\sin^4\frac{\theta}{2}}, \tag{3}$$

where $Z_{g,a}$ is the atomic number, r_e is the classical electron radius, and γ is the relativistic factor. The scattering angle θ is assumed to be large compared to the angular divergence of the particle beam. While the cross section does not depend on azimuthal angle ϕ, the out-scattering cross section may, because the maximum surviving angle $\hat{\theta}$ depends on the position in the ring, whether the scattering occurs mostly in the horizontal or vertical plane, and on the beta functions at the scattering location. The local value of the out-scattering cross section may thus be written

$$\sigma_{g,a}(s) = \int_0^{2\pi}\int_{\hat{\theta}(s,\phi)}^{\pi} \frac{d\sigma_{g,a}}{d\Omega} d\theta \sin\theta d\phi. \tag{4}$$

Performing the integral over θ gives

$$\sigma_{g,a}(s) = E_{g,a}I_e(s), \tag{5}$$

where

$$I_e(s) = \int_0^{2\pi}\frac{2}{\tan^2\frac{1}{2}\hat{\theta}(\phi,s)}d\phi. \tag{6}$$

In low emittance storage rings, the transverse aperture is determined by some combination of beam dynamics and physical aperture limits, i.e., by the "dynamic acceptance" or DA. Typically the DA is determined by tracking particles for many turns starting at $s = 0$, giving a set of (x, y) pairs at the aperture limit that trace out the DA contour. If $(x_0(\phi), y_0(\phi))$ for $\phi : [0, 2\pi]$ gives the DA contour at $s = 0$, then the beta functions β_x and β_y may be used to write

$$\hat{\theta}(s,\phi) = \left[\frac{x_0^2(\phi)}{\beta_x(s)\beta_x(0)} + \frac{y_0^2(\phi)}{\beta_y(s)\beta_y(0)}\right]^{\frac{1}{2}}, \tag{7}$$

ISBN: 978-3-95450-168-7 doi:10.18429/JACoW-IPAC2015-MOPMA009

IMPROVEMENTS IN MODELING OF COLLECTIVE EFFECTS IN ELEGANT*

M. Borland, R. Lindberg, A. Xiao, ANL, Argonne, IL 60439, USA

Abstract

elegant has long had the ability to model collective effects, including beam-driven cavity modes, short-range wakes, coherent synchrotron radiation, and intrabeam scattering. Recently, we made improvements specifically targeting simulations that require multiple bunches in storage rings. The ability to simulate long-range, non-resonant wakes was added, which can be used, for example, to study the effect of the resistive wall wake on multibunch instabilities. We also improved the implementation of short-range and resonant wakes to make them more efficient for multibunch simulations. Finally, improvements in the parallel efficiency were made that allow taking advantage of larger parallel resources.

INTRODUCTION

elegant [1] has long had the ability to simulate collective effects, starting with the addition of impedances and rf cavity modes in the early 1990s, in support of the design of the APS Positron Accumulator Ring [2]. In the late 1990s, wakefields and coherent synchrotron radiation were added, primarily in response to the needs of free-electron laser projects, e.g., [3] These features were subsequently implemented in the parallel version, Pelegant, [4, 5]. More recently, intrabeam scattering [6, 7] and Touschek scattering [8, 9] simulation were added. To confidently design a next-generation accelerator, such as the multi-bend achromat (MBA) upgrade for the Advanced Photon Source (APS) [10, 11], further improvements were needed.

The primary factor driving the recent improvements was the need for a bunch-lengthening higher-harmonic cavity (HHC) in the new ring [12] and the need for high-fidelity simulations including a multi-bunch beam and the impedance of other structures in the ring [13, 14]. Although this could be done with earlier versions of elegant and Pelegant, improved performance was needed for simulations with many bunches. Part of the issue is that inclusion of the short-range impedance necessitates the use of a large number of simulation particles in each bunch, which coupled with a desire to simulate as many as 324 bunches, makes for challenging computations.

In addition, because of the narrow beam pipe in the upgraded machine, we need to simulate multi-turn, non-resonant wakes, e.g., resistive wall wakes. This capability is new to elegant and Pelegant, which previously could only simulate single-turn wakes. Multi-turn collective effects could previously only be simulated using resonant modes.

With these improvements came the need for enhanced diagnostics, specifically the need for more convenient bunch-by-bunch diagnostics.

WAKE AND RF CAVITY SIMULATION

Bunch Mode Simulations

In order to minimize changes to the structure of the code, the bunched-mode feature was added by making use of the existing particleID property of each particle. In particular, the user may declare that different blocks of particle ID values correspond to distinct bunches. This requires use of the sdds_beam command and is documented in the manual. In brief, the user may either provide the entire multi-bunch beam as an SDDS file, or else provide a file specifying the phase space for a single bunch and request that it be duplicated n times. In the latter case, the spacing of the duplicates should also be specified. In the former case, the beam can be generated by a previous elegant run using the bunched_beam to specify the bunch properties and the bunch_frequency parameter of the run_control command to specify the interval between bunches. For more complex bunch patterns, the manual provides detailed instructions on preparing a beam file.

Given a properly prepared beam file, bunched-mode simulation is automatic for FRFMODE, FTRFMODE, IBSCATTER, LRWAKE, RFMODE, WAKE, TRFMODE, TRWAKE, ZLONGIT, ZTRANSVERSE elements. It may be turned off for any element by setting the BUNCHED_BEAM_MODE parameter to 0. Bunched mode simulation is presently not implemented for CSRCSBEND, CSRDRIFT, and LSCDRIFT.

For the diagnostic elements WATCH and HISTOGRAM, bunch-by-bunch output is obtained using the START_PID and END_PID parameters to specify the range of particle ID values to include in the output. For large numbers of bunches, one may typically select only a few bunches for output, so the setup is not too tedious. Creation of a parameter file for use with load_parameters is a convenient way to configure large numbers of diagnostic elements.

In a parallel code, a natural choice for domain decomposition is that each bunch is handled by a single core. However, this is suboptimal as it forces processors to wait in line to process bunches through elements that have effects on following bunches (e.g., rf modes or long-range wakes). In addition, this choice limits the size of computational resources that can be used. In Pelegant, these issues are avoided because bunches are shared among processors, with all processors working together on each bunch in turn. One minor

* Work supported by the U.S. Department of Energy, Office of Science, Office of Basic Energy Sciences, under Contract No. DE-AC02-06CH11357.

Content from this work may be used under the terms of the CC BY 3.0 licence (© 2015). Any distribution of this work must maintain attribution to the author(s), title of the work, publisher, and DOI.

ISBN: 978-3-95450-168-7 doi:10.18429/JACoW-IPAC2015-MOPMA010

COMMISSIONING SIMULATIONS FOR THE APS UPGRADE LATTICE*

V. Sajaev, M. Borland, ANL, Argonne, IL 60439, USA

Abstract

A hybrid seven-bend-achromat lattice that features very strong focusing elements and a relatively small vacuum chamber has been proposed for the APS upgrade. Achieving design lattice parameters during commissioning will need to be accomplished quickly in order to minimize dark time for APS users. The paper will describe start-to-end simulation of the machine commissioning beginning from first-turn trajectory correction, progressing to orbit and lattice correction, and culminating in evaluation of the nonlinear performance of the corrected lattice.

INTRODUCTION

Several existing synchrotron light source facilities are considering replacing operating storage rings in order to increase the brightness of delivered photon beams. These light sources have large user communities who insist that facility "dark time" is minimized. APS, for example, is targeting 12 months for removal, installation, and commissioning. Of this 12 month period, only three months are set aside for commissioning of the new multi-bend achromat ring.

The proposed lattice [1] has natural emittance that is 40 times smaller than the present APS ring, which is achieved by much stronger focusing than in the present ring. For example, maximum quadrupole strengths increase nearly five-fold in the new lattice. Stronger focusing inevitably leads to larger natural chromaticity and thus a nearly seven-fold increase in sextupole strength is needed, resulting in rather small dynamic aperture and short lifetime even for the ideal lattice. Misalignments of the strong quadrupoles generate large orbit errors, which in the presence of very strong sextupoles leads to huge lattice and coupling errors. Add to this smaller vacuum chamber gaps that are required to achieve high gradients in the magnets, and the required rapid commissioning seems doubtful. In this paper, we address this issue using a highly realistic simulation of the commissioning.

SIMULATION PROCEDURE

While the effect of individual lattice imperfections on accelerator performance can be estimated or calculated analytically, including all errors together is beyond the realm of analytical estimations. To understand how various errors combine together and impact commissioning, a start-to-end simulation of machine commissioning was performed taking into account as many errors as possible. All simulations were done using `elegant` [2]. Table 1 gives the list of errors included in the simulations (official specification for girder alignment is 100 μm which was found to be equally workable in earlier runs).

* Work supported by the U.S. Department of Energy, Office of Science, Office of Basic Energy Sciences, under Contract No. DE-AC02-06CH11357.

Table 1: Rms Values for Various Errors Used for Start-to-end Commissioning Simulation

Girder misalignment	50 μm
Elements within girder	30 μm
Dipole fractional strength error	$1 \cdot 10^{-3}$
Quadrupole fractional strength error	$1 \cdot 10^{-3}$
Dipole tilt	0.4 mrad
Quadrupole tilt	0.4 mrad
Sextupole tilt	0.4 mrad
Initial BPM offset error	500 μm
BPM gain error	5%
BPM orbit measurement noise	1 μm
Corrector calibration error	5%

The simulation procedure closely follows the steps that will be performed during commissioning. We assume that before setting up the lattice, the betatron tunes are adjusted away from integer and coupling resonances (the design fractional tunes are 0.12 in both planes, they are adjusted to 0.18 and 0.24). The procedure consists of the following major steps: (1) Generate errors for all elements according to Table 1 using Gaussian distributions with 2σ cut off. (2) Correct trajectory until closed orbit is found. If needed, optimize tunes and low-order beta function harmonics. (3) Correct closed orbit down to acceptable level. (4) Correct optics and coupling.

The entire simulation procedure was automated, allowing commissioning to be simulated for 200 different error sets. The procedure was able to correct orbit and optics in 98% of all cases. The correction results were statistically analyzed for residual orbit and lattice perturbations, correctors strengths, emittances, etc. For each error set, various performance measures (e.g., rms horizontal beta error) are computed. These are then histogrammed over all error sets. Before presenting such results, we first discuss the detailed commissioning procedure.

Trajectory Correction

Simple estimations show that in order to expect a reasonable probability of the closed orbit not exceeding the vacuum chamber dimensions, magnet alignment tolerances must be three times tighter than in Table 1. Since this is considered prohibitively expensive, trajectory correction will need to be performed first in order to find a closed orbit.

Trajectory correction consists of two steps. First, `elegant`'s one-to-best method is applied, wherein steering is performed by pairing one corrector with the BPM that has the best response to this corrector. Only four correctors

Content from this work may be used under the terms of the CC BY 3.0 licence (© 2015). Any distribution of this work must maintain attribution to the author(s), title of the work, publisher, and DOI.

ISBN: 978-3-95450-168-7 doi:10.18429/JACoW-IPAC2015-MOPMA011

Content from this work may be used under the terms of the CC BY 3.0 licence (© 2015). Any distribution of this work must maintain attribution to the author(s), title of the work, publisher, and DOI.

EVALUATION OF POWER SUPPLY AND ALIGNMENT TOLERANCES FOR THE ADVANCED PHOTONS SOURCE UPGRADE*

V. Sajaev, ANL, Argonne, IL 60439, USA

Abstract

A hybrid seven-bend-achromat lattice that features very strong focusing elements and provides an electron beam with very low emittance has been proposed for the Advanced Photon Source upgrade [1, 2]. In order to be able to maintain stable operation, tight tolerances are required for various types of errors. Here we describe an evaluation of the effects of various errors, including magnet power supplies, alignment, and vibration.

STATIC RANDOM ERRORS

Examples of static errors are power supply calibration errors, alignment errors, etc. The effect of these errors in most cases can be measured and corrected. Two types of static errors are distinguished: initial errors (errors expected during commissioning) and reproducibility errors (errors after turning power supplies off and then back on). Table 1 gives goals for various machine parameters.

Table 1: Goals for Initial Errors and Reproducibility in High-Level Machine Parameters Driven by Static Errors

	Initial error	Reproducibility
Energy	10^{-3}	10^{-4}
Orbit	2 mm	0.1 mm
Betatron tune	0.1	0.01
Beta functions	20%	2%
Chromaticity	1 unit	0.1 unit

When a dipole power supply current changes, the energy and orbit of the electron beam change. To calculate the sensitivity of the energy offset to such errors, an `elegant` [3] simulation was used. 200 sets of dipole fractional errors with 10^{-5} rms were generated, then the orbit was calculated and corrected. Two different orbit correction configurations were tested. The results are shown in Fig. 1, left. The distribution width varies by about a factor of two, so the energy error depends little on whether orbit correction is running or not. The amplifying effect of powering dipoles in series on the energy error is significant, as Fig. 1 (right) shows. The resulting allowable initial dipole errors are $2 \cdot 10^{-3}$. Initial orbit distortion is generated by dipole errors and quadrupole misalignments, while orbit errors after a shutdown result from dipole and corrector reproducibility errors. The orbit requirements in Table 1 were chosen to ensure that the initial orbit fits inside the vacuum chamber. This leads to unrealistic requirements for individual quadrupole alignment of 10 µm. To relax this requirement, a single-turn trajectory

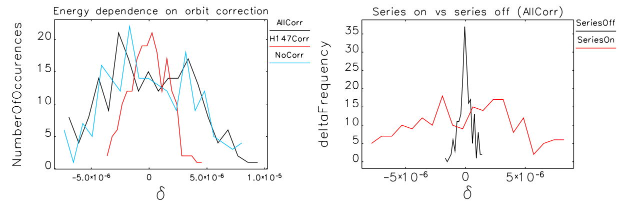

Figure 1: Left: Distribution of Energy Errors for Two Different Orbit Correction Configurations (Black and Red) and without Orbit Correction (Blue). Right: Comparison of Energy Errors for the Cases When M1 and M2 Dipoles Powered in Series or Separately.

correction will be used to obtain the first closed orbit. For orbit reproducibility after shutdowns, all of the error budget is assigned to dipoles and correctors. This gives $\Delta\alpha/\alpha = 10^{-4}$ for dipoles and $\Delta\theta/\theta = 7 \cdot 10^{-3}$ for correctors, assuming an equally split error budget.

Betatron tune errors come from quadrupole gradients, beam energy, and orbit inside sextupoles. Initial tune errors will be dominated by the orbit in sextupoles. Simple estimations show that 1-mm rms orbit errors in sextupoles will produce a tune error of 0.9. Therefore, during commissioning, after the first closed orbit has been established, the tune will need to be corrected. Despite this need for early tune correction, it is still advisable to limit tune error contributions from quadrupoles and dipoles. The effect of quadrupole errors can be estimated using a simple expression, while the effect of dipole errors is more complex and was obtained from simulations. Assuming that the tune error budget of 0.1 is distributed equally between quadrupoles and dipoles, the requirements for the initial errors are: $\Delta K_1/K_1 = 3 \cdot 10^{-3}$ and $\Delta\alpha/\alpha = 1.2 \cdot 10^{-3}$.

Initial beta function errors are expected to be dominated by the orbit errors in sextupoles. If the quadrupole contribution is limited to 20% beta beating, a simple simulation of beta function errors due to random quadrupole errors results in an initial quadrupole error requirement of $1 \cdot 10^{-3}$.

Chromaticity errors are generated by sextupole errors and by lattice errors. Simulations show that chromaticity errors after the beam is first stored have an rms of five units due to lattice errors. After orbit correction, the chromaticity error decreases to one unit rms. The contribution from sextupole strength errors is required to be one unit as well. Simple calculation results in the initial error requirement of $2.7 \cdot 10^{-2}$. Table 2 summarizes tolerances for random static errors.

VARIABLE ERRORS

Variable errors can be split in several parts according to their frequency spectrum: "slow" (slower than 100 seconds), "fast" (between 0.01 Hz and 1 kHz), and "very fast" (faster than 1 kHz). The required limits on the varying errors are

* Work supported by the U.S. Department of Energy, Office of Science, Office of Basic Energy Sciences, under Contract No. DE-AC02-06CH11357.

ISBN: 978-3-95450-168-7 doi:10.18429/JACoW-IPAC2015-MOPMA012

INTRA-BEAM AND TOUSCHEK SCATTERING COMPUTATIONS FOR BEAM WITH NON-GAUSSIAN LONGITUDINAL DISTRIBUTIONS*

A. Xiao†, M. Borland, ANL, Argonne, IL 60439, USA

Abstract

Both intra-beam scattering (IBS) and the Touschek effect become prominent for multi-bend-achromat- (MBA-) based ultra-low-emittance storage rings. To mitigate the transverse emittance degradation and obtain a reasonably long beam lifetime, a higher harmonic rf cavity (HHC) is often proposed to lengthen the bunch. The use of such a cavity results in a non-gaussian longitudinal distribution. However, common methods for computing IBS and Touschek scattering assume Gaussian distributions. Modifications have been made to several simulation codes that are part of the `elegant` [1] toolkit to allow these computations for arbitrary longitudinal distributions. After describing these modifications, we review the results of detailed simulations for the proposed hybrid seven-bend-achromat (H7BA) upgrade lattice [2] for the Advanced Photon Source.

INTRODUCTION

The natural emittance of next-generation storage ring light sources will be reduced by more than an order of magnitude compared to present rings. As a consequence, the Coulomb scattering rate among particles, which is inversely proportional to the bunch volume, increases rapidly. The small angle multiple scattering process (IBS effect) significantly increases beam emittance at the operating current, and limits benefits obtained from a ultra-low emittance machine. The large angle single scattering process (Touschek effect) puts more particles outside the rf acceptance, resulting in a much shorter beam lifetime.

To mitigate these problems, an HHC is often proposed to lengthen the bunch. Due to the distortion of the rf potential well, the particles are no longer Gaussian-distributed longitudinally. To accurately simulate beam scattering effects, all of our original beam scattering simulation tools—developed based on the assumption of Gaussian distributions—have been updated to allow arbitrary distributions. This paper first describes the technique used to deal with non-Gaussian distributed beam, then gives calculation results from the original and new methods for the same Gaussian distributed bunch to verify the code. The results of detailed simulations for the H7BA lattice with HHC are presented at the end.

TOUSCHEK SCATTERING

The Touschek scattering rate R is given by Eq. 28 in [3] and is an integral of the local scattering rate over all beam coordinates:

$$R = 2\beta c \int P_1 P_2 \sigma \chi dV, \tag{1}$$

where βc is the particle's velocity, σ is the Møller cross-section transformed into the laboratory system, χ is the half angle between the scattered particles' momenta vectors $\vec{p_1}$ and $\vec{p_2}$, $P_{1,2}$ is bunch density function, and dV is given by

$$dV = d\Delta s_1 dx_{\beta 1} dy_{\beta 1} d\Delta p_{s1} d\Delta p_{s2} dx'_{\beta 1} dx'_{\beta 2} dy'_{\beta 1} dy'_{\beta 2}. \tag{2}$$

The density function P is well known for a Gaussian distributed beam, giving an analytical expression for R [3]. For a non-Gaussian beam, the integral is less straightforward. One option is the Monte-Carlo integration method [4], which is already coded in `elegant`. However, this method is computationally-demanding, and we elected to also enhance the faster-running `touschekLifetime` program. The quantity $\sigma\chi$ is dependent on the momenta and thus on the transverse coordinates owing to $x-p_x$ and $y-p_y$ correlations. In general, there is less correlation between $s - p_s$ in a storage ring, thus the integral over ds can be done separately, i.e., the beam can be sliced longitudinally.

For each longitudinal slice, particles are Gaussian distributed in all dimensions except in s, which is approximately uniformly distributed. One can show that the scattering rate R_U for a uniform longitudinal distribution of length L is related to the rate R_G for a Gaussian distrubtion with $\sigma_s = L$ by

$$R_U = 2\sqrt{\pi} R_G. \tag{3}$$

Since R_G is already computed by `touschekLifetime`, relation 3 is used to calculate the scattering rate from each slice $R_{U,m}$. The total scattering rate will be the sum of $R_{U,m}$ over all slices m, giving a lifetime

$$\frac{1}{T_l} = \left\langle \frac{R}{N_0} \right\rangle = \left\langle \frac{\sum_m R_{U,m}}{\sum_m N_m} \right\rangle, \tag{4}$$

where N_m is the population of slice m.

To verify the code, the total local scattering rate of a Gaussian distributed bunch was calculated with slicing (21 slices) and without slicing. Results shown in Fig.1 agree very well with one another.

INTRA-BEAM SCATTERING

A similar slicing technique can be used for IBS calculations. Since IBS is a multiple scattering process and the beam emittance is diluted over time, the equilibrium beam emittance results from the interplay of many factors, such as synchrotron radiation damping, quantum excitation, and beam optics. The standalone `ibsEmittance` tool is

* Work supported by the U.S. Department of Energy, Office of Science, Office of Basic Energy Sciences, under Contract No. DE-AC02-06CH11357.

† xiaoam@aps.anl.gov

Content from this work may be used under the terms of the CC BY 3.0 licence (© 2015). Any distribution of this work must maintain attribution to the author(s), title of the work, publisher, and DOI.

ISBN: 978-3-95450-168-7 doi:10.18429/JACoW-IPAC2015-MOPMA013

Content from this work may be used under the terms of the CC BY 3.0 licence (© 2015). Any distribution of this work must maintain attribution to the author(s), title of the work, publisher, and DOI.

EXPERIENCE WITH ROUND BEAM OPERATION AT THE ADVANCED PHOTON SOURCE *

A. Xiao†, L. Emery, V. Sajaev, B. Yang, ANL, Argonne, IL 60439, USA

Abstract

Very short Touschek lifetime becomes a common issue for next-generation ultra-low emittance storage ring light sources. In order to reach a longer beam lifetime, such a machine often requires operating with a vertical-to-horizontal emittance ratio close to an unity, i.e. a “round beam”. In tests at the APS storage ring, we determined how a round beam can be reached experimentally. Some general issues, such as beam injection, optics measurement and corrections, and orbit correction have been tested also. To demonstrate that a round beam was achieved, the beam size ratio is calibrated using beam lifetime measurement.

INTRODUCTION

It is foreseen that the brightness from a next-generation storage ring based light source can be improved by several orders with an ultra-low emittance lattice design. One of the biggest challenges associated with an ultra-low emittance storage ring is the necessarily much shorter beam lifetime. In many cases, the lifetime is so short that the beam can only satisfy operational requirements under a “round beam” operation scenario. A good example of how the beam lifetime varies with beam size ratio can be seen from the proposed APS upgrade MBA lattice design [1], and is illustrated in Fig. 1.

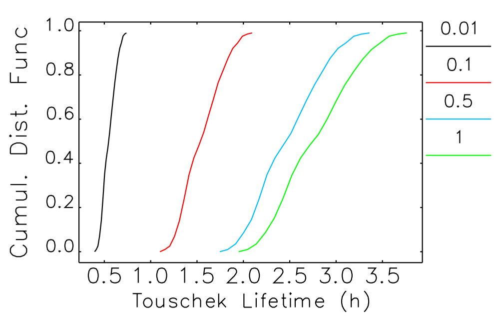

Figure 1: Cumulative distribution functions for the Touschek lifetime from the 100 error ensembles of H7BA optics at different emittance ratios (legend).

A round beam can be achieved in two ways. One is introducing strong skew quadrupoles in the lattice. This method not only couples the x and y beam motion, but also couples optical functions. This scheme could generate difficulty for routine machine operations procedures such as orbit correction, optics measurement and correction, etc. Another way to obtain a round beam is to operate machine at the difference resonance (equal fractional betatron tunes). This way, the coupling coefficient does not need to be large; real machine imperfections with weak skew elements installed in the ring could be enough. Thus the beam operation will be close to a normal decoupled regime of operation, and the x and y optical functions can still be treated separately. The x and y moments (from random process of synchrotron radiation) would simply exchange their values internally due to the resonance effect.

To test the idea of a round beam generation and related operational issues at the coupling resonance, experiments had been performed at the APS storage ring, and results are compared with simulation for the calibrated machine model [2]. We had measured beam lifetime, off-axis injection efficiency, optical response matrix, etc. at different machine coupling coefficients. Beam emittances are calculated from beam sizes measured using dipole synchrotron radiation. The existing vertical beam size measurement system is configured for measurement of only small beam sizes, and does not respond to the round beam conditions that we need to confirm. Thus we used Touschek lifetime at lowered rf voltage to estimate the vertical beam size.

SIMULATION STUDY ON COUPLING RESONANCE

A simple theory for weak betatron coupling can be found in [3]. Assuming that a particle is excited in the x plane, the presence of coupling will cause an interchange of the oscillation energy between the two planes, as shown in Fig. 2. The interchange period T and modulation factor S are given by

$$T = \frac{1}{f_{\rm rev}\sqrt{\Delta^2 + |C|^2}}, \tag{1}$$

$$S = \frac{E_T}{E_{max}} = \frac{|C|^2}{\Delta^2 + |C|^2}, \tag{2}$$

where $f_{\rm rev}$ is particle’s revolution frequency, $\Delta = (\nu_x - \nu_y)$ is separation of uncoupled tunes, and $|C|$ is the machine coupling coefficient, which indicates the strength of the x-y coupling. From Eq. 2 a full x-y energy modulation (round beam) can be reached when $\Delta = 0$. In a real machine, Δ can not be made exactly zero for many reasons, such as tune spread inside the bunch, PS noise, etc. Therefore, we need to test that the round beam can be reached when $\Delta^2 \ll |C|^2$.

Thus the allowable Δ variation range for keeping S above a certain level (for example, $S > 0.9$) depends on $|C|$. If $|C|$ is large, then machine tolerances on various errors are also large, and the oscillation energy is interchanged between x

* Work supported by the U.S. Department of Energy, Office of Science, Office of Basic Energy Sciences, under Contract No. DE-AC02-06CH11357.
† xiaoam@aps.anl.gov

ISBN: 978-3-95450-168-7 doi:10.18429/JACoW-IPAC2015-MOPMA014

DESIGN OF SUPERCONDUCTING CW LINAC FOR PIP-II *

A. Saini†, V. Lebedev, J.F. Ostiguy, N.Solyak, V. Yakovlev, Fermilab, IL 60510, USA

Abstract

Proton Improvement Plan (PIP) -II is a proposed roadmap to upgrade existing proton accelerator complex at Fermilab. It is primarily based on construction of superconducting (SC) linear accelerator (linac) that would be capable of operating in continuous wave (CW) mode. This paper presents reference design layout and beam optics of SC linac and discusses some of the underlying requirements and motivations.

INTRODUCTION

An ambitious program is proposed to develop a high intensity proton beam facility that would support, over the next two decades, a world-leading neutrino program and rich variety of high intensity frontier particle physics experiments at Fermilab. This program, referred to as Proton Improvement Plan -II (PIP-II), is primarily based on construction of 800 MeV SC linac that would provide flexible platform for further enhancement of the existing Fermilab accelerator complex. A schematic of PIP-II facility is shown in Fig 1. A detailed description of site layout is presented elsewhere [1].

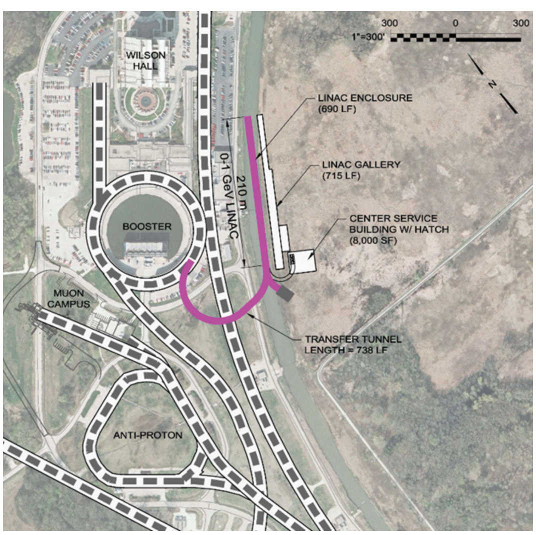

Figure 1: Schematic of PIP-II facility.

To reconcile a stringent budgetary situation and an immediate requirement for high beam power by existing operating experiments, we plan to expedite construction by leveraging the existing Fermilab infrastructure. In particular, the cryogenic infrastructure of the now decommissioned Tevatron will be re-purposed for the PIP-II SC linac. While the machine is designed to be fully compatible with continuous wave (CW) operation, limitations in the capacity of the Tevatron system will require that the linac initially operate in pulsed mode. Success of the PIP-II facility depends critically on the robustness of the SC linac design. While the reference design parameters [1] have been established, the optics is still evolving to incorporate technical constraints and to address issues that may potentially cause degradation of beam quality and result in beam losses. In this paper we discuss baseline configuration of PIP-II SC linac and present results of preliminary beam optics studies.

LINAC ARCHITECTURE

A schematic of linac baseline configuration is shown in Fig 2. It consists of room temperature front-end and SC linac. Each superconducting section in Fig 2 is represented by optimal beta of respective cavities except LB and HB section which are shown for geometrical beta of corresponding cavities. The room temperature front-end is composed of

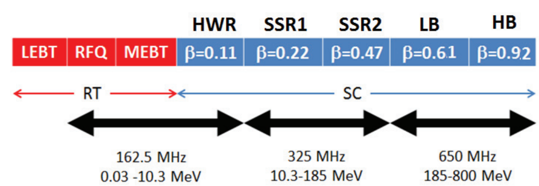

Figure 2: Technology map of PIP-II linac.

an ion source, a low energy beam transport (LEBT) section, an RFQ and a medium energy beam transport (MEBT) section. The DC ion source delivers a nominal current of 5 mA at 30 keV. The beam is transported through the LEBT and matched to the RFQ. The RFQ operates at a frequency of 162.5 MHz and accelerates the beam up to 2.1 MeV. The beam then enters the MEBT where it gets chopped to acquire the time structure required to drive different experiments.

The H^- ion is non-relativistic at kinetic energy of 2.1 MeV and its velocity changes rapidly with acceleration along linac. In order to achieve efficient acceleration SC linac employs several families of accelerating cavities optimized for specific range of velocities. On the basis of these families, SC linac is segmented into five sections. The first SC section is based on Half Wave Resonators (HWR) operating at frequency of 162.5 MHz.

The choice of this frequency was motivated by several factors, including reducing transverse RF defocusing. It can be observed from equation 1 [2] that RF kick is directly proportional to the frequency. Operation at lower frequency helps making maximum use of the available accelerating gradient in cavities. HWR section accelerates the beam from 2.1 MeV to 10.3 MeV. It is required eight HWR cavities assembled in single cryomodule to cover this energy range.

$$\Delta(\gamma\beta r') = -\frac{\pi E_0 T L sin(\phi)}{mc^2\gamma_s^2\beta_s^2\lambda} r \tag{1}$$

* Work supported by US DOE under contract DE- AC02-76CH03000.
† asaini@fnal.gov

Content from this work may be used under the terms of the CC BY 3.0 licence (© 2015). Any distribution of this work must maintain attribution to the author(s), title of the work, publisher, and DOI.

ISBN: 978-3-95450-168-7 doi:10.18429/JACoW-IPAC2015-MOPMA015

APPLICATIONS OF AN MPI ENHANCED SIMULATED ANNEALING ALGORITHM ON NUSTORM AND 6D MUON COOLING*

A. Liu†, Fermilab, Batavia, IL, 60510, USA

Abstract

The nuSTORM decay ring is a compact racetrack storage ring with a circumference ~480 m using large aperture (⌀ = 60 cm) magnets. The design goal of the ring is to achieve a momentum acceptance of 3.8±10% GeV/c and a phase space acceptance of 2000 μm·rad. The design has many challenges because the acceptance will be affected by many nonlinearity terms with large particle emittance and/or large momentum offset. In this paper, we present the application of a meta-heuristic optimization algorithm to the sextupole correction in the ring. The algorithm is capable of finding a balanced compromise among corrections of the nonlinearity terms, and finding the largest acceptance. This technique can be applied to the design of similar storage rings that store beams with wide transverse phase space and momentum spectra. We also present the recent study on the application of this algorithm to a part of the 6D muon cooling channel. The technique and the cooling concept will be applied to design a cooling channel for the extracted muon beam at nuSTORM in the future study.

INTRODUCTION

The nuSTORM decay ring shares the production straight and part of the arc with a pion beamline, so that the pions can be injected into the ring without fast kickers but through an Orbit Combination Section (OCS) [1–3]. The design aims at achieving a momentum acceptance of 3.8±10% GeV/c ($\delta = \Delta P/P \in \pm 0.1$) and a phase space acceptance of 2000 μm·rad (denoted as 2 mm in the rest of the paper). Because of the large δ, a large linear chromaticity can cause resonance crossings for many times. Moreover, the productivity of neutrinos in the decay ring critically rely on a large ratio of the production straight length to the circumference of the ring. Accordingly, an arc design with combined function magnets was proposed to achieve small linear chromaticities and reduce the arc length. The schematic layout of the nuSTORM facility and the linear optics of the decay ring is shown in Fig. 1 and Fig. 2.

Many nonlinearity terms in the decay ring become significant with the large particle emittance and the momentum offset, and thus need to be corrected, primarily by sextupoles. However, using sextupoles in the arcs of the ring is constrained because of the space and the maximum field limits. Octupolar fields can also be added in the design, but the two limits still apply. Also, adding more higher order nonlinear fields stimulates more nonlinear resonances. Therefore, nonlinear fields that are above sextupolar are not considered in the correction scheme.

* Work supported by DOE under contract DE-AC02-07CH11359
† aoliu@fnal.gov

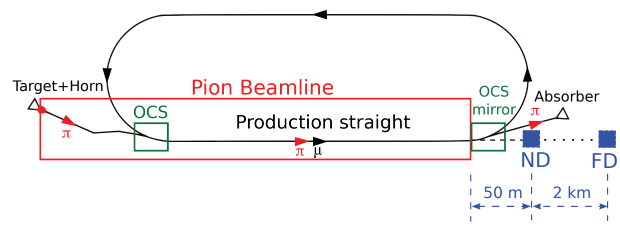

Figure 1: The layout of nuSTORM facility.

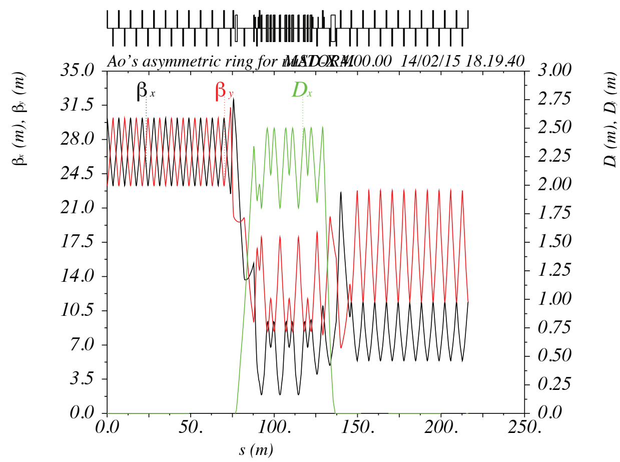

Figure 2: The linear optics of the proposed ring design with combined function magnets in the arcs.

The natural higher order nonlinearities combine with those induced by the sextupoles and play significant roles in the beam stability. Therefore, choosing and correcting the most significant terms as done conventionally in other designs does not work the most efficiently. In order to find the balance among corrections of all the nonlinearities that limit the acceptance of the beam, it is straightforward to apply a numerical algorithm to find the best configuration. This is a single objective optimization, which is to maximize the acceptance of a muon beam with a 2 mm Gaussian transverse admittance, and a uniform momentum spread within 3.8 ± 10% GeV/c. The variables are the strengths, lengths, and locations of the sextupolar fields. Since the concept of "sextupole families" does not apply in this design, namely all the variables are independent of each other, a meta-heuristic algorithm that thoroughly searches the parameter space for the global optimum can be implemented.

The Simulated Annealing (SA) algorithm is known for its efficiency in performing a satisfactory global search, especially when limited computing resources are available [4]. In the SA algorithm, each set of variables determines a "state"

Content from this work may be used under the terms of the CC BY 3.0 licence (© 2015). Any distribution of this work must maintain attribution to the author(s), title of the work, publisher, and DOI.

ISBN: 978-3-95450-168-7 doi:10.18429/JACoW-IPAC2015-MOPMA016

COUPLER RF KICK IN THE INPUT 1.3 GHz ACCELERATING CAVITY OF THE LCLS-II LINAC

A. Lunin#, N. Solyak, A. Sukhanov, and V. Yakovlev, FNAL, Batavia, IL 60510, USA*

Abstract

Main and HOM couplers break the cavity axial symmetry, distort RF field and, thus, create a transverse kick, even for a particle moving along the cavity axes. Dependence of a kick on the RF phase causes beam emittance dilution and degrade the FEL radiation quality. The transverse kick is most dangerous for a beam passing through the first accelerating structure of a linac, where particles energy is low. In this paper we analyse the coupler RF kick in the first accelerating structure of the LCSL-II linac.

INTRODUCTION

The 1.3 GHz ILC accelerating structure is chosen as a baseline for the LCLS-II linac. The cavity contains 9 elliptical cells, a main power coupler, and two HOM couplers, upstream and downstream, see Figure 1.

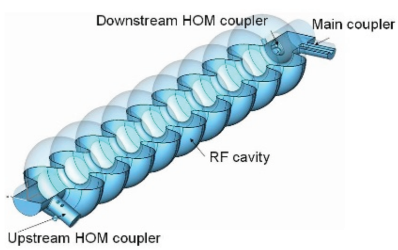

Figure 1: The 1.3 GHz ILC accelerating cavity with main and HOM couplers.

Main and HOM couplers break the cavity axial symmetry, distort electromagnetic field and, thus, create a transverse kick, even for a particle moving along the cavity axes. Dependence of the kick on the RF phase causes beam emittance dilution and may degrade the FEL radiation quality [1, 2]. Bellow we analyze a coupler RF kick in the first accelerating structure of the LCLS-II linac [3]. Beam and cavity parameters relevant to the coupler kick and emittance growth calculations are listed in the Table 1.

Table 1: Parameters for the RF Kick Simulations

Bunch transverse size, rms, σ_t	1 [mm]
Bunch length, rms, σ_z	1 [mm]
Input beam energy, E_{inp}	0.75 [MeV]
Accelerating gradient	12 [MeV/m]
Operating frequency	1.3 [GHz]
Cavity Q-external	4E7

*Operated by Fermi Research Alliance, LLC, under Contract DE-AC02-07CH11359 with the U.S. DOE.
#lunin@fnal.gov

GENERAL

The longitudinal component of electric field near the cavity axis is few orders of magnitude larger than the transverse one. Therefore, any misalignment of mesh elements in respect to the axis may result in appearance of a nonzero transverse projection of the longitudinal component and, thus, produce spurious transverse components of electric field. Since a magnetic field is usually derived from the solution of an electric field we have the same problem for an accurate magnetic field representation near the cavity axis. The remedy is use a regularized mesh with the elements aligned to the cavity axis. The regular mesh pattern near the cavity axis and the vertical component of electric field are shown in Figure 2 as a result of ANSYS HFSS simulation [4].

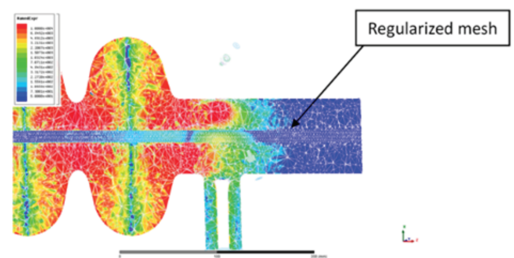

Figure 2: Map of the vertical electric field component E_y.

The transverse RF kick is the total beam transverse momentum change along the trajectory. For a low relativistic beam which is moving not along a straight line, dependence of the transverse momentum on the accelerating gradient becomes non-linear. Therefore we characterize RF kick in this case as a non-normalized transverse kick accumulated along the actual beam trajectory at a given accelerating gradient:

$$V_x = \Delta P_x \frac{c}{e_0} = \int_{t_1}^{t_2} (E_x - \beta_z Z_0 H_y) e^{i(\omega t + \varphi_s)} dt \tag{1}$$

where t_2-t_1 is the beam transit time, β_z is the longitudinal beam velocity as a fraction of speed of light, φ_s is the synchronous RF phase, e_0 is electron charge and c is the speed of light. The beam tracking in the accelerating structure is realized with MATHCAD script using the paraxial approximation for particles motion [5, 6].

CAVITY RF FOCUSING

A beam RF focusing at the entrance of first accelerating structure, where particles energy is low, is not fully compensated by defocussing forces at its exit [7]. Thus, the structure itself is producing a non-zero net

Content from this work may be used under the terms of the CC BY 3.0 licence (© 2015). Any distribution of this work must maintain attribution to the author(s), title of the work, publisher, and DOI.

ISBN: 978-3-95450-168-7 doi:10.18429/JACoW-IPAC2015-MOPMA017

NUMERICAL SIMULATIONS OF TRANSVERSE MODES IN GAUSSIAN BUNCHES WITH SPACE CHARGE*

Alexandru Macridin, James Amundson, Eric Stern, Fermilab, Batavia, Illinois, USA

Abstract

The transverse modes and the intrinsic Landau damping in Gaussian bunched beams with space charge are numerically investigated. The evolution of the phase space density is calculated with the Synergia accelerator modeling package and analyzed with Dynamic Mode Decomposition (DMD) method. DMD is a relatively new technique used to calculate mode dynamics in both linear and nonlinear systems. The properties of the first three space charge modes, including their shape, damping rates and tune shifts are calculated over the entire range of the space charge interaction.

INTRODUCTION

Landau damping provides an important mechanism for stabilizing beam propagation. The mechanism operates via an energy exchange between the potentially unstable coherent mode and some resonant particles. A necessary condition for the Landau damping mechanism is the existence of resonant particles with a continuous frequency spectrum around the coherent frequency. In accelerators, aside from the tune spread due to nonlinear lattice elements, there is a tune spread caused by the space charge interaction which plays an important and not-well-understood role in the damping mechanism. Here we neglect the nonlinear lattice effects and focus only on the intrinsic effect of space charge on the transverse modes of a Gaussian bunch. The beam dynamics are investigated over the entire range of the interaction, from no space charge to the strong space charge limit.

The effect of space charge on the head-tail modes was first addressed by Blaskiewicz [1] who showed that space charge can improve beam stability. The strong space charge regime for bunches of arbitrary shape was addressed analytically in [2, 3]. The mode shapes, tune shifts and damping rates were calculated for Gaussian bunches. A numerical investigation of the transverse modes in longitudinal Gaussian bunches with K-V transverse distribution using particle tracking simulations was done by V. Kornilov *et al.* [4]. Our simulations for bunches with K-V charge distribution (not shown here) are in agreement with the ones in Ref [4].

ANALYTICAL RESULTS

The tune shift for a particle propagating through a lattice and experiencing a transverse space charge force $\frac{eE_x}{\gamma^2}$ is [5]

$$\Delta Q_{sc} = \frac{e}{m\gamma^3\beta^2c^2}\frac{1}{4\pi}\oint \beta(s)\frac{\partial E_x}{\partial x}(\bar{x},s)ds\ . \tag{1}$$

where $\beta(s)$ is the lattice beta function.

We define the transverse displacement density as

$$X(z,u,s) = \frac{\int dxdp_xdydp_y\, x\rho(x,p_x,y,p_y,z,u,s)}{\rho(z,u)} \tag{2}$$

where $\rho(x,p_x,y,p_y,z,u,s)$ is the density in phase space with z being the longitudinal position relative to the reference particle and $u = \frac{\delta p}{p}$ being the relative momentum spread. Following Ref [3] and defining $X(z,u)$ such as

$$X(z,u,s) = X(z,u)e^{(-i\omega_0 Qs - i\chi z)} \tag{3}$$

where ω_0 is the reference particle angular velocity and χ is the effective chromaticity one gets the equation of motion

$$(Q - Q_\beta)X(z,u) + iQ_s\frac{\partial X}{\partial\theta}(z,u) = -\Delta Q_{sc\ eff}(z)(X(z,u) - \bar{X}(z))\ , \tag{4}$$

with θ being the synchrotron oscillation phase. $\Delta Q_{sc\ eff}(z)$ is the effective space charge tune shift. For a Gaussian beam we define the space charge parameter as

$$q_{eff} = \frac{\Delta Q_{sc\ eff\ max}}{Q_s} = 0.52\frac{\Delta Q_{sc\ max}}{Q_s} \tag{5}$$

where $\Delta Q_{sc\ max}$ is the maximum tune shift (at the beam center) and Q_s is the synchrotron tune. This definition is in agreement with the one in Ref [2]. For a Gaussian beam the effective tune shift is about 0.52 smaller than the maximum tune shift [2]. In order to determine q_{eff} we numerically calculate the integral in Eq. 1 using the electric field from the simulation.

When the space charge is zero there is a simple solution to Eq. 4,

$$X(z,u) \equiv X(r,\theta) = R(r)e^{im\theta}\ , \tag{6}$$

with r and θ being the amplitude and the phase of the synchrotron oscillation. The tune shift is given by

$$Q - Q_\beta = mQ_s \tag{7}$$

for integer m. The modes are defined by the angular number m and are radially degenerate.

Large q_{eff} requires solutions which are weakly dependent on u, i.e. $X(z,u) \approx X(z)$. A detailed calculation of the modes properties is presented in [2, 3]. The strong space charge modes form an orthogonal set

$$\int X_k(z)X_m(z)\rho(z) = \delta_{km}, \tag{8}$$

where k and m represent mode numbers. For the mode k the tune shift is $\frac{\nu_k Q_s}{q_{eff}}$ (the values of ν_k are tabulated in [2]), while the Landau damping is $\lambda_k = \frac{k^4 2\pi Q_s}{q_{eff}^3}$.

* Work supported by U.S. Department of Energy contract DE-AC02-07CH11359.

Content from this work may be used under the terms of the CC BY 3.0 licence (© 2015). Any distribution of this work must maintain attribution to the author(s), title of the work, publisher, and DOI.

ISBN: 978-3-95450-168-7 doi:10.18429/JACoW-IPAC2015-MOPMA018

SIMULATION OF MULTIPACTING IN SC LOW BETA CAVITIES AT FNAL*

Gennady Romanov#, Paolo Berrutti, Timergali N. Khabiboulline, Fermilab, Batavia, Illinois, USA

Abstract

Proton Improvement Plan-II at Fermilab is a plan for improvements to the accelerator complex aimed at providing a beam power capability of at least 1 MW on target at the initiation of LBNE (Long Base Neutrino Experiment) operations. The central element of the PIP-II is a new 800 MeV superconducting linac, injecting into the existing Booster. Multipacting affects superconducting RF cavities in the entire range from high energy elliptical cavities to coaxial resonators for low-beta applications. This work is focused on multipacting study in the low-beta 325 MHz spoke cavities; namely SSR1 and SSR2, which are especially susceptible to the phenomena. The extensive simulations of multipacting in the cavities with updated material properties and comparison of the results with experimental data helped us to improve overall reliability and accuracy of these simulations. Our practical approach to the simulations is described in details. For SSR2, which has a high multipacting barrier right at the operating power level, some changes of the cavity shape to mitigate this harmful phenomenon are proposed.

INTRODUCTION

Proton Improvement Plan-II [1] at Fermilab is a plan for improvements to the accelerator complex aimed at providing a beam power capability of at least 1 MW on target at the initiation of LBNE (Long Base Neutrino Experiment) operations. The central element of the PIP-II is a new 800 MeV superconducting linac, injecting into the existing Booster. The PIP-II 800 MeV linac is a derivative of the Project X Stage 1 design as described in the Project X Reference Design Report [2]. A room temperature (RT) section accelerates H^- ions to 2.1 MeV and creates the desired bunch structure for injection into the superconducting (SC) linac. Five superconducting cavity types operating at three different frequencies are required for acceleration to 800 MeV.

The electron multiplication on surfaces exposed to an oscillating electromagnetic field causes the phenomenon of multipacting, which is a serious obstacle to be avoided for normal operation of particle accelerator and their RF components. In worst cases this phenomena, described in many accelerators, can completely prevent normal operation of an accelerating cavity.

Multipacting affects superconducting RF cavities in the entire range from high energy elliptical cavities to coaxial resonators for low-beta applications. This work is focused on multipacting study in the low-beta structures; namely 325 MHz Single-Spoke Resonators: SSR1 (β=0.22) and SSR2 (β=0.47).

Study of MP in SSR2 was a primary goal of this work along with sharpening of simulation technique. SSR2 is currently under development for PIP-II linac [3]. The design has been finalized recently, and the preliminary simulations indicated strong MP in the cavity. It was necessary to understand at what level this resonator is affected by multipacting, what critical gradients are, where the MP develops in the cavity geometry and what can be done to mitigate this harmful phenomena.

Multipacting in the SSR1 cavity has been studied already [4], and the results have been compared with experimental data on multipacting barriers found during the vertical test of the SSR1 cavity [5]. In this work the MP simulations in the SSR1 cavity were repeated by two reasons. First, a new secondary emission yield (SEY) data for niobium became available – the previous simulations of the SSR1 used SEY for copper, that allows defining RF power levels of MP, but is not correct to evaluate intensity and exact boundaries of MP discharge. Second, 12 SSR1 cavities were manufactured and tested at high power level since then, and rich experimental data on the MP behaviour in SSR1 during RF conditioning was accumulated [6]. Comparison of the MP simulations that used updated material properties with experimental data helped us to evaluate overall reliability and accuracy of our simulation technique.

NEW IN SIMULATION SET UP

There are a number of numerical simulation codes for predicting multipactor, each with various pros and cons. Our choice is still CST Studio Suite because it smoothly combines flexible and developed modelling, electromagnetic field simulation, multi-particle tracking, adequate post-processing and advanced probabilistic emission model (Furman-Pivi model [7]), which is very important capability in multipactor simulations. In general we follow earlier established simulation procedure [4, 8] but several new features have been added.

CST Particle Studio (PS) offers two solvers for particle tracking; this time both were used in our MP simulations. One of them is the Gun Solver & Particle Tracking solver (TRK) which is used to compute trajectories of charged particles within RF fields and optionally electrostatic or/and magnetostatic fields. Other one is the Particle-In-Cell solver (PIC) that computes the charged particles motion in self-consistent transient fields. Usually the space charge effects are not taken into account in MP simulations, so just simple particle tracking in electromagnetic fields was used for both solvers.

PIC solver can use only imported field maps, while TRK solver has its own eigenmode solver, but it also can

*Operated by Fermi Research Alliance, LLC under Contract No. DE-AC02-07CH11359 with the United States Department of Energy.
#gromanov@fnal.gov

Content from this work may be used under the terms of the CC BY 3.0 licence (© 2015). Any distribution of this work must maintain attribution to the author(s), title of the work, publisher, and DOI.

ISBN: 978-3-95450-168-7 doi:10.18429/JACoW-IPAC2015-MOPMA019

SIMULATION OF THE FERMILAB RECYCLER FOR LOSSES AND COLLIMATION*

E. Stern, R. Ainsworth, J. Amundson, B. Brown, Fermilab, Batavia, IL 60510, USA

Abstract

Fermilab has recently completed an upgrade to the complex with the goal of delivering 700 kW of beam power as 120 GeV protons to the NuMI target. A major part of boosting beam power is to shorten the beam cycle by accumulating up to 12 bunches of 0.5×10^{11} protons in the Recycler ring through slip-stacking during the Main Injector ramp. This introduces much higher intensities into the Recycler than it has had before. Meeting radiation safety requirements with high intensity operations requires understanding the effects of space charge induced tune spreads and resulting halo formation, and aperture restrictions in the real machine to develop a collimation strategy. We report on initial simulations of slip-stacking in the Recycler performed with Synergia.

INTRODUCTION

Fermilab has recently completed an upgrade to the complex [1] with the goal of delivering 700 kW of beam power as 120 GeV protons to the NuMI target. Possible methods for increasing beam power are increasing the intensity of individual bunches and move beam bunches through the accelerator chain at a faster rate. Since we are already producing bunches close to the intensity limit that we can transport, we will be reducing the cycle time from 2.2 s to 1.33 s. Previously, the Main Injector combined one set of six booster batches each containing 80 beam bunches were combined with an additional set of six batches using the slip-stacking [2] procedure at 8 GeV. The resulting set of batches were then accelerated to 120 GeV for extraction to the NuMI target. Both the accumulation/slip-stacking and the ramping are time consuming operations. We will instead perform the accumulation and slip-stacking in the Recycler ring while the Main Injector performs its ramp.

The Recycler [3] is a permanent magnet based proton storage ring originally constructed to accumulate antiprotons during the Tevatron Run II era. As such it was not anticipated that it would have experience significant space charge problems. Injecting high intensity proton bunches now introduces space charge tune shifts causing possible resonance excitation, halo production and resulting particle loss. The slip-stacking procedure is inherently messy as it involves the transport of bunches at different mimatched momenta in the ring while at the same time the chromaticity has to be kept at large negative values to suppress a head-tail instability. To understand the dynamics of the machine and develop a plan for collimation and halo reduction we have initiated a campaign of simulation of the Recycler dynamics including the slip-stacking and true locations and sizes of machine apertures with the Fermilab developed beam dynamics code Synergia [4, 5].

* Work supported by U.S. Department of Energy contract DE-AC02-07CH11359

SYNERGIA

Synergia is developed and maintained at Fermilab by the Accelerator Simulations group within the Scientific Computing Division to provide detailed high fidelity simulations of particle accelerators or storage rings specializing in space charge and wakefield collective effects. Synergia is a Particle-in-Cell (PIC) based code that tracks macro-particles through the lumped elements of the accelerator. Synergia simulates the usual single particle optics from produced by magnetic elements as well as RF cavities. Space charge and impedance kicks are applied at locations around the ring using the split-operator method. So that realistic particle losses can be simulated, apertures may be associated with each element. The Synergia aperture model includes rectangular and elliptical apertures of arbitrary size and transverse offset as well as arbitrary user defined polygonal apertures. To achieve statistically meaningful results in a reasonable time, Synergia has been designed from the beginning to take advantage of multiprocessing systems such as Linux clusters and supercomputers.

RECYCLER SIMULATION MACHINE MODEL

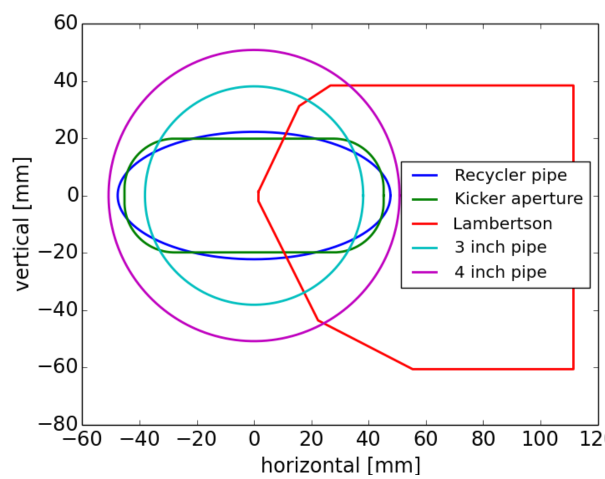

Figure 1: Apertures in the Recycler.

The Recycler machine lattice is described by a MAD file [6, 7] incorporating the measured multipoles for the magnet body and shim correctors. Synergia reads and interprets the same MAD description. The lattice functions for the Recycler calculated by Synergia are identical to those calculated by MAD. The apertures in the recycler are: 3" diameter pipe,

Content from this work may be used under the terms of the CC BY 3.0 licence (© 2015). Any distribution of this work must maintain attribution to the author(s), title of the work, publisher, and DOI.

ISBN: 978-3-95450-168-7 doi:10.18429/JACoW-IPAC2015-MOPMA020

Content from this work may be used under the terms of the CC BY 3.0 licence (© 2015). Any distribution of this work must maintain attribution to the author(s), title of the work, publisher, and DOI.

MEASUREMENT AND CORRECTION OF THE FERMILAB BOOSTER OPTICS WITH LOCO*

C.Y. Tan†, V. Lebedev, A.K. Triplett, Fermilab, Batavia, IL 60510, USA,
M. McAteer, CERN, Geneva, Switzerland

Abstract

The optics of the original Booster lacked the ability for full optics correction and it was not until 2009 when new optics corrector packages were installed between gradient magnets that this ability became available. The optics correction method that is chosen is called LOCO (Linear Optics from Closed Orbits) that measures the orbit response from every beam position monitor (BPM) in the ring from every kick of every dipole corrector. The large data set collected allows LOCO to not only calculate the quadrupole and skew quadrupole currents that both reduces beta beatings and corrects coupling, it also finds the dipole kicker strengths, BPM calibrations and their tilts by minimizing the difference between the measured and ideal orbit response of the beam. The corrected optics have been loaded into Booster and it is currently being tested to be eventually used in normal operations.

INTRODUCTION

The Fermilab Booster is a rapid cycling synchrotron that accelerates protons from 400 MeV to 8 GeV in 33 ms to supply beam to the rest of the complex for high energy physics. Booster has been operational since 1971 [1] but it was not until 2009 that new optics corrector packages were installed between the gradient magnets that the ability to completely correct its optics for the entire ramp became available. Fig. 1 shows an example of a corrector package that contains dipole correctors in both planes, a normal quadrupole, a skew quadrupole, normal sextupole, a skew sextupole, and beam position monitors in both planes.

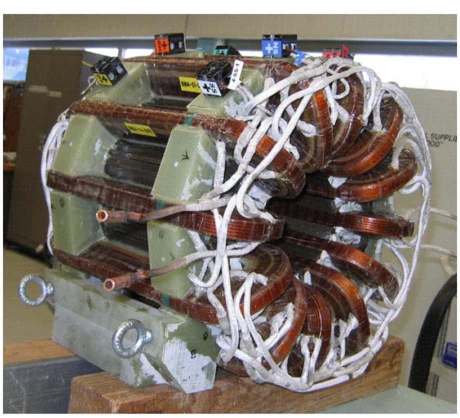

Figure 1: A Booster corrector magnet package before potting.

The method that has been chosen to correct Booster optics is called LOCO (Linear Optics from Closed Orbits) and has been adapted to the peculiarities of Booster which will be discussed below. This method has been successfully used to correct the optics of other machines, for example the NSLS (National Synchrotron Light Source) X-Ray ring from which LOCO originated. [2]

BOOSTER LOCO

The principle of LOCO is the measurement of the orbit of the beam (i.e. orbit response) at every BPM as each dipole kicker in the ring is used to consecutively 1-bump the beam up the ramp at predefined breakpoints. Mathematically, the process can be parameterized as measuring the orbit response $\Delta x_i/\Delta\theta_j$ of the beam at BPM i due to the kick from kicker j of a fully decoupled machine at each breakpoint:

$$\begin{aligned}\frac{\Delta x_i}{\Delta\theta_j} &= \frac{\sqrt{\beta_i\beta_j}}{2\sin\pi\nu_x}\cos(|\psi_i-\psi_j|-\pi\nu_x)- \\ &\frac{D_i}{D_{\mathrm{RPOS}}}\frac{\sqrt{\beta_{\mathrm{RPOS}}\beta_j}}{2\sin\pi\nu_x}\cos(|\psi_{\mathrm{RPOS}}-\psi_j|-\pi\nu_x)\end{aligned} \tag{1}$$

where $\Delta\theta_j$ is the size of the dipole kick from the jth kicker, Δx_i is the change in position at BPM i and $\beta_{i,j}$ are the beta functions at BPM i or kicker j respectively, $\psi_i-\psi_j$ is the phase advance between these two elements, and ν_x is the horizontal betatron tune. The RPOS device here is the radial feedback monitor. The beta function β_{RPOS} and dispersion D_{RPOS} (measured separately) at RPOS is required in the formula because Booster uses radial feedback and thus the dispersion function has a large efect on the response. The same formula without the dispersion term is used when the vertical plane orbit response is considered by appropriately replacing horizontal β's for vertical ones.

It is obvious that the same equation, Eq. 1, is found when the "measurement" comes from the lattice model. Clearly, both these methods will yield different values for $\Delta x_i/\Delta\theta_j$ and so a χ^2 error can be defined and it is

$$\chi^2=\sum_{i,j}\left[\left(\frac{\Delta x_i}{\Delta\theta_j}\right)_{\text{measured}}-\left(\frac{\Delta x_i}{\Delta\theta_j}\right)_{\text{model}}\right]^2\frac{1}{\sigma_{ij}^2} \tag{2}$$

where σ_{ij} is the statistical error taken at the 95% confdence interval of the slope in the linear fit of the measured orbit response at the ith BPM from a set of kicks using the jth kicker. The use of slopes as the response rather than absolute positions is one reason why LOCO is a successful method.

In principle, LOCO minimizes the χ^2 error, but in practice Eq. 2 is not directly used in the algorithm as the measure. An equivalent measure is defined instead so that a linear algebra

* Operated by Fermi Research Alliance, LLC under Contract No. DE-AC02-07CH11359 with the United States Department of Energy.
† cytan@fnal.gov

ISBN: 978-3-95450-168-7 doi:10.18429/JACoW-IPAC2015-MOPMA022

NUMERICAL ANALYSIS OF PARASITIC CROSSING COMPENSATION WITH WIRES IN DAΦNE*

A. Valishev, FNAL, Batavia, IL 60510, USA, D. Shatilov, BINP, Novosibirsk, Russia
C. Milardi, M. Zobov, INFN/LNF, Frascati, Italy

Abstract

Current bearing wire compensators were successfully used in the 2005-2006 run of the DAΦNE collider to mitigate the detrimental effects of parasitic beam-beam interactions. A marked improvement of the positron beam lifetime was observed in machine operation with the KLOE detector. In view of the possible application of wire beam-beam compensators for the High Luminosity LHC upgrade, we revisit the DAΦNE experiments. We use an improved model of the accelerator with the goal to validate the modern simulation tools and provide valuable input for the LHC upgrade project.

INTRODUCTION

The long-range (also referred to as the parasitic) beam-beam interactions in colliders occur when the two particle beams moving in a common vacuum chamber and separated transversely, interact via the electromagnetic field. Such interactions may be a significant factor limiting the performance of multi-bunch particle colliders: for example, they were shown to impact the luminosity lifetime and increase particle losses during the Tevatron collider Run II [1]. At the Tevatron, the beams collided head-on in two high-luminosity Interaction regions (IR), and were separated by means of electrostatic separators in the rest of the machine, where each bunch experienced 70 parasitic interactions with the separation ranging from 6 to 10 of the beam σ. It was shown that four collisions at the smallest separation of 6 σ were responsible for the dramatic degradation of lifetime of both beams [2]. At the LHC, the beams collide at an angle in the experimental IRs and move in separate vacuum chambers in the arcs. Still, the number of parasitic crossings in the common sections is up to 120 with 25 ns bunch spacing at the nominal transverse separation of 9.5 σ [3]. Experiments during the LHC Run 1 have shown that with ½ the nominal number of bunches (bunch spacing of 50 ns), the onset of high losses is at the transverse separation of ≈5 σ for nominal bunch intensity [4]. The HL-LHC upgrade demands a two-fold increase in the total beam current [5], which leads to a significant enhancement of the long-range beam-beam effects [6]. As a consequence, the transverse separation of the two beams, and hence the crossing angle, has to be increased (to 12.5 σ in the baseline scenario), which in turn leads to several undesired effects: the geometric loss of luminosity, increased pile-up density, and the demand for large-aperture final focus magnets.

Compensator devices in the form of current-bearing wires (also referred to as the Beam-Beam Long-Range Compensators, BBLRC) were proposed as a way to mitigate the long-range beam-beam effects [7], and since were extensively studied both theoretically [8-10] and experimentally [11,12]. A remarkable demonstration of the effectiveness of BBLRC for improvement of collider performance was achieved during the 2005-2006 operation of DAΦNE at INFN/LNF (Frascati, Italy). The application of BBLRC devices during the KLOE run resulted in approximately 50% improvement of the average luminosity integration rate [13].

Numerical simulations of beam-beam effects with the weak-strong particle tracking code Lifetrac [14] guided the design of DAΦNE beam-beam compensation. Over the past decade, the code functionality has been considerably expanded. The most important additions include the implementation of Frequency Map Analysis (FMA) [15] and the ability to perform tracking in detailed machine lattices. The goals of the present work are to revisit the results of DAΦNE beam-beam compensation experiment using the modern computing tools, and demonstrate the predictive power of Lifetrac simulations with BBLRC for future applications.

EXPERIMENTAL DATA

We compiled a comprehensive set of machine and beam parameters during the 2005-2006 run with the KLOE detector (see Tab. 1). The collider performance data relevant to the BBLRC experiments is presented in Figs. 1, 2 showing the time dependence of electron and positron intensities, luminosity, and the beam-beam related portion of positron losses for the cases of BBLRC turned off and on, respectively. The beam-beam related loss rate $\dot{N}_{BB}$ was derived from the total loss rate $\dot{N}$ according to the following consideration:

$$\dot{N} = \dot{N}_{Lum} + \dot{N}_T + \dot{N}_{BB}$$

where $\dot{N}_{Lum} = \sigma_{tot} L$ is the luminous loss rate (σ_{tot} = 0.048 barn), $\dot{N}_T$ is the Touschek loss rate, and the losses due to scattering on the residual gas are vanishingly small. The typical positron loss rate in the experimental runs was about 2×10^9 s^{-1} (corresponding beam intensity lifetime $\tau\approx10^3$ s), and was dominated by the Touschek and beam-beam effects with luminous losses being a relatively minor contribution at about 5×10^6 s^{-1}. The highlighted time intervals in Figs. 1, 2 are the data samples used for comparison with the beam-beam simulation as they represent stable beams in weak-strong

* Research supported by DOE via the US-LARP program and by EU FP7 HiLumi LHC - Grant Agreement 284404.

Content from this work may be used under the terms of the CC BY 3.0 licence (© 2015). Any distribution of this work must maintain attribution to the author(s), title of the work, publisher, and DOI.

ISBN: 978-3-95450-168-7 doi:10.18429/JACoW-IPAC2015-MOPMA024

A PARALLEL PARTICLE-PARTICLE, PARTICLE-MESH SOLVER FOR STUDYING COULOMB COLLISIONS IN THE CODE IMPACT-T*

Chad Mitchell† and Ji Qiang
LBNL, Berkeley, CA 94720, USA

Abstract

In intense charged-particle beams, the presence of Coulomb collisions can result in growth of the beam slice energy spread and emittance that cannot be captured correctly using traditional particle-in-cell codes. Particle-particle, particle-mesh solvers take a hybrid approach, combining features of N-body and particle-in-cell solvers, to correctly capture the effect of short-range particle interactions with less computing time than direct N-body solvers. We describe the implementation and benchmarking of such a solver in the code IMPACT-T for beam dynamics applications.

INTRODUCTION

Coulomb collisions can play a significant role in the dynamics of low emittance, high-intensity beams for applications such as high-brightness photoinjectors, electron microscopy, and storage ring light sources [1, 2]. Short-range fluctuations in the fields seen by each particle can result in a growth of emittance and energy spread that is not captured by traditional accelerator particle-in-cell codes, which assume a smooth (mean-field) model of the beam space-charge seen by each particle.

These effects can be captured by N-body solvers that directly compute the Coulomb particle-particle interactions for every particle pair [3]. However, the successful use of these solvers is limited to beams with extremely low bunch charge, since computing times scale as $O(N_p^2)$, where N_p is the number of particles per bunch. In cosmology, plasma physics and molecular dynamics, such collisional many-body problems have been treated successfully [4, 5] using particle codes with improved scaling ($O(N_p \log N_p)$ or better) including tree codes [6] and particle-particle, particle-mesh (P^{3}M) solvers [7]. The application of these methods to charged-particle beams is relatively new in the context of accelerator systems. In this paper, we describe the implementation of a parallel P^{3}M solver in the photoinjector code IMPACT-T [8].

THE P^{3}M SOLVER

The solver is based on the algorithm described in Chapter 8 of [7]. In the reference frame in which the bunch centroid is at rest, the Coulomb force on a particle at location $\mathbf{x}_i$ due to a particle at location $\mathbf{x}_j$ is expressed in terms of the displacement $\mathbf{r}_{ij} = \mathbf{x}_i - \mathbf{x}_j$ as:

$$\mathbf{F}(\mathbf{r}_{ij}) = \frac{q^2 \mathbf{r}_{ij}}{4\pi\epsilon_0 |\mathbf{r}_{ij}|^3} = \mathbf{F}^S(\mathbf{r}_{ij}) + \mathbf{F}^L(\mathbf{r}_{ij}). \quad (1)$$

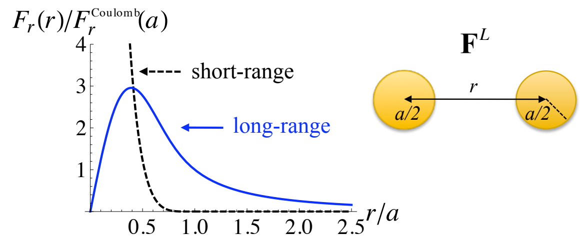

Figure 1: Short-range and long-range contributions to the Coulomb force between two particles (1) for a given cutoff radius a used by a P^{3}M solver in IMPACT-T.

Both $\mathbf{F}^S$ and $\mathbf{F}^L$ are radial forces determined by the interparticle distance $r = |\mathbf{r}_{ij}|$ and a parameter a known as the *cutoff radius*. The long-range contribution $\mathbf{F}^L$ is the smooth, nonsingular force between two spherically-symmetric distributions of charge q and radius $a/2$ whose centroids are separated by distance r, while the short-range contribution $\mathbf{F}^S$ satisfies $\mathbf{F}^S(r) = 0$ for $r > a$. See Figure 1. We use expressions for $\mathbf{F}^S$ and $\mathbf{F}^R$ corresponding to the S2 shape function described in (8-3) of [7].

The net long-range force acting on each particle is computed in the beam rest frame by solving on a mesh for the long-range contribution to the corresponding electric and magnetic fields. This is done using an FFT-based convolution procedure [7, 8]. The net short-range force acting on each particle is computed in the beam rest frame by directly summing the short-range forces due to all other particles in the beam. To reduce computing time, in addition to the potential mesh, a second *chaining cell* mesh is introduced whose cells have side $HC \geq a$. At each timestep, particles are sorted according to chaining cell location. During the short-range force computation, the solver needs to sum only over the subset of particles that lie within the current chaining cell or its nearest neighbors. The long-range and short-range force computations are each parallelized using domain decomposition [4, 5].

The cutoff radius a is typically chosen as 3-4 times the side H of a potential mesh cell. In the limit $a \to 0$ for fixed H, one has $\mathbf{F}^S \to 0$ and the P^{3}M computation is equivalent to a particle-in-cell computation (approximating a mean-field model), while in the limit $a \to \infty$ for fixed H, one has $\mathbf{F}^L \to 0$ and the P^{3}M computation is equivalent to a direct N-body simulation (all collisional effects are included).

* Work supported by the U.S. Department of Energy under Contract No. DE-AC02-05CH11231.
† ChadMitchell@lbl.gov

Content from this work may be used under the terms of the CC BY 3.0 licence (© 2015). Any distribution of this work must maintain attribution to the author(s), title of the work, publisher, and DOI.

ISBN: 978-3-95450-168-7 doi:10.18429/JACoW-IPAC2015-MOPMA025

CSR INDUCED MICROBUNCHING GAIN ESTIMATION INCLUDING TRANSIENT EFFECTS IN TRANSPORT AND RECIRCULATION ARCS*

C. -Y. Tsai#, Department of Physics, Virginia Tech, VA 24061, USA
D. Douglas, R. Li, and C. Tennant, Jefferson Lab, Newport News, VA 23606, USA

Abstract

The coherent synchrotron radiation (CSR) of a high brightness electron beam traversing a series of dipoles, such as transport or recirculation arcs, may result in the microbunching instability (μBI). To accurately quantify the direct consequence of this effect, we further extend our previously developed semi-analytical Vlasov solver [1] to include more relevant coherent radiation models than the steady-state free-space CSR impedance, such as the entrance and exit transient effects derived from upstream beam entering to and exiting from individual dipoles. The resultant microbunching gain functions and spectra for our example lattices are presented and compared with particle tracking simulation. Some underlying physics with inclusion of these effects are also discussed.

FREE-SPACE CSR IMPEDANCES

For an ultrarelativistic beam traversing an individual dipole, the steady-state CSR impedance in free space can be expressed as [2,3]

$$Z_{CSR}^{ss}\left(k(s);s\right)=\frac{-ik(s)^{1/3}A}{\left|\rho(s)\right|^{2/3}} \tag{1}$$

where $k = 2\pi/\lambda$ is the modulation wave number, ρ is the bending radius, and the constant $A \approx -0.94 + 1.63i$.

Prior to reaching steady-state interaction, the beam entering a bend from a straight section would experience the so-called entrance transient state, where the impedance can be obtained by Laplace transformation of the corresponding wakefield [4,5]

$$Z_{CSR}^{ent}\left(k(s);s\right)=\frac{-4}{s^*}e^{-4i\mu(s)}+\frac{4}{3s^*}\left(i\mu(s)\right)^{1/3}\Gamma\left(\frac{-1}{3},i\mu(s)\right) \tag{2}$$

where $\mu(s) = k(s)z_L(s)$, s^* the longitudinal coordinate measured from dipole entrance, $z_L=\left(s^*\right)^3/24\rho^2$ and Γ the upper incomplete Gamma function.

In addition, there are exit CSR transient effects as the beam exits from a dipole. For the case with fields generated from an upstream electron (at retarded time) propagating across the dipole to downstream straight section, i.e. Case C of Ref. [6], the corresponding impedance can be similarly obtained by Laplace transformation:

$$Z_{CSR}^{exit}\left(k(s);s\right)=\frac{-4}{L_b+2s^*}e^{\frac{-ik(s)L_b^2}{6|\rho(s)|^2}\left(L_b+3s^*\right)} \tag{3}$$

where s^* is the longitudinal coordinate measured from dipole exit and L_b is the dipole length.

Instead of performing Laplace transformation of the wakefield expression for the case with fields generated from an electron (at retarded time) within a dipole propagating downstream the straight section, here we use Bosch's expression [7] for the exit transient impedance:

$$Z_{CSR}^{drif}(k(s);s)\approx\begin{cases}\frac{2}{s^*},\ \text{if}\ \rho^{2/3}\lambda^{1/3}\le s^*\le\lambda\gamma^2/2\pi\\ \frac{2k(s)}{\gamma^2},\ \text{if}\ s^*\ge\lambda\gamma^2/2\pi\\ 0,\ \text{if}\ s^*<\rho^{2/3}\lambda^{1/3}\end{cases} \tag{4}$$

where s^* is the longitudinal coordinate measured from dipole exit. This expression assumes the exit impedance comes primarily from coherent edge radiation in the near-field region (i.e. $z < \lambda\gamma^2$), and in our simulation we only include such transient effects [Eq. (3) and (4)] right after a nearest upstream bend. Here we note that these CSR models are valid only when the wall shielding effect is negligible. The wall shielding effect becomes important when the distance from the beam orbit to the walls h is to satisfy $h\le\left(\rho\lambda^2\right)^{1/3}$. We further note that the above impedance models, Eqs. (1-3), assume the beam is at ultrarelativistic energy. It is interesting to examine how the above models deviate for non-ultrarelativistic beams, and this is currently under study in parallel [8].

NUMERICAL METHODS

To quantify the μBI in a single-pass system, we would estimate the microbunching amplification factor G (or, gain) by two methods. One is to solve the linearized Vlasov equation [9] using given impedance models [e.g. Eqs. (1-4)]. The other, served as a benchmarking tool, is by ELEGANT tracking [10,11]. For the former, we actually solve the general form of Volterra integral equation [9,12]

$$g_k(s)=g_k^{(0)}(s)+\int_0^s K(s,s')g_k(s')ds' \tag{5}$$

where the kernel function is particularly expressed as

$$K(s,s')=\frac{ik}{\gamma}\frac{I(s)}{I_A}C(s')R_{56}(s'\to s)Z\left(kC(s'),s'\right)\times[\text{Landau damping}] \tag{6}$$

for the [Landau damping] term

$$[\text{Landau damping}]=\exp\left\{\frac{-k^2}{2}\left[\varepsilon_{x0}\left(\beta_{x0}R_{51}^2(s,s')+\frac{R_{52}^2(s,s')}{\beta_{x0}}\right)+\sigma_\delta^2R_{56}^2(s,s')\right]\right\} \tag{7}$$

with

$R_{56}(s'\to s)=R_{56}(s)-R_{56}(s')+R_{51}(s')R_{52}(s)-R_{51}(s)R_{52}(s')$ and $R_{5i}(s,s')=C(s)R_{5i}(s)-C(s')R_{5i}(s')$. Here the kernel function $K(s,s')$ describes CSR effect, $g_k(s)$ the resultant bunching factor as a function of the longitudinal position

* This material is based upon work supported by the U.S. Department of Energy, Office of Science, Office of Nuclear Physics under contract DE-AC05-06OR23177.
#jcytsai@vt.edu

Content from this work may be used under the terms of the CC BY 3.0 licence (© 2015). Any distribution of this work must maintain attribution to the author(s), title of the work, publisher, and DOI.

ISBN: 978-3-95450-168-7 doi:10.18429/JACoW-IPAC2015-MOPMA026

PROPOSED CAVITY FOR REDUCED SLIP-STACKING LOSS

J. Eldred, Department of Physics, Indiana University, Bloomington, IN 47405, USA
R. Zwaska, FNAL, Batavia, IL 60510, USA

Abstract

This paper employs a novel dynamical mechanism to improve the performance of slip-stacking. Slip-stacking in an accumulation technique used at Fermilab since 2004 which nearly double the proton intensity. During slip-stacking, the Recycler or the Main Injector stores two particles beams that spatially overlap but have different momenta. The two particle beams are longitudinally focused by two 53 MHz 100 kV RF cavities with a small frequency difference between them. We propose an additional 106 MHz 20 kV RF cavity, with a frequency at the double the average of the upper and lower main RF frequencies. In simulation, we find the proposed RF cavity significantly enhances the stable bucket area and reduces slip-stacking losses under reasonable injection scenarios. We quantify and map the stability of the parameter space for any accelerator implementing slip-stacking with the addition of a harmonic RF cavity.

INTRODUCTION

Slip-stacking is integral to high-intensity operation at Fermilab and will likely play a central role in upgrades to the accelerator complex [1–3]. Particle loss in the slip-stacking process is a limiting factor on ultimate performance [1,4]. Single-particle dynamics associated with slip-stacking contribute directly to the particle losses. Our previous work [5] has introduced new tools for characterizing the stable phase-space boundary of slip-stacking and evaluating particle loss in slip-stacking scenarios. A recommendation provided in this work, an upgrade of the Booster cycle-rate from 15-Hz to 20-Hz, has subsequently been incorporated into the Proton Improvement Plan (PIP-II) [1,6]. In this paper, we propose the addition of a new 106 MHz 20 kV RF cavity to further reduce particle losses from the single-particle longitudinal dynamics of slip-stacking.

BACKGROUND

Slip-stacking is a particle accelerator configuration that permits two high-energy particle beams of different momenta to use the same transverse space in a cyclic accelerator (see [7] and [4]). The potential beam intensity of a synchrotron is doubled through the application of this technique. The two beams are longitudinally focused by two RF cavities with a small frequency difference between them. Each beam is synchronized to one RF cavity and perturbed by the other RF cavity. The proposed harmonic RF cavity has a frequency equal to twice the average of the upper and lower frequency.

This paper follows the research program outlined in [5]. Prior work in the single-particle dynamics of slip-stacking can be found in [8–10]. Fermilab has implemented slip-stacking operationally since 2004 [4,10,11] and is currently applied to neutrino production for Neutrinos at Main Injector (NuMI) experiments [12–14].

Beam-loading effects can impact the effectiveness of slip-stacking. A summary of beam-loading research can be found in [5] and draws upon work on beam-loading conducted for the slip-stacking in the Fermilab Main Injector [15–18].

STABILITY WITH HARMONIC RF

The equations of motion for a single particle under the influence of two main RF cavities with frequencies separated by Δf and a harmonic RF cavity at twice the average frequency is given by:

$$\begin{aligned} \dot{\phi} &= 2\pi f_{rev} h\eta\delta \\ \dot{\delta} &= f_{rev} V_\delta [\sin(\phi) + \sin(\phi - \Delta f t) + \lambda \sin(2\phi - \Delta f t)]. \end{aligned} \tag{1}$$

where V_δ is the maximum change in δ during a single revolution under the action of a single cavity [19] and λ is the ratio of the harmonic RF voltage to the main RF voltage.

Broadly speaking, slip-stacking is complicated by the fact that the two RF systems will interfere and reduce the stable bucket area. To quantify this, the literature [5,8–10] has identified the importance of the slip-stacking parameter

$$\alpha_s = \frac{\Delta f}{f_s} \tag{2}$$

as the criterion for effective slip-stacking. Here f_s is the single-RF synchrotron frequency (see [20]). The further the buckets are away from each other in phase-space, the higher α_s is and the less interference there is. Our numerical simulation results show that a negative value of λ (bunch-lengthening mode) can counteract the interference effect that arises as the α_s decreases.

We create a stability map [5] for each value of the slip-stacking parameter α_s and the harmonic voltage ratio λ. We map the stability of initial particle positions by integrating the equations of motion for each initial position. Each position is mapped independently and only the single particle dynamics are considered. A particle is considered lost if its phase with respect to each of the first RF cavity, the second RF cavity, and the average of the two RF cavities, is larger than a certain cut-off (we used $3\pi/2$). Figure 1 shows an example of a stability without a harmonic RF cavity and with a harmonic RF cavity.

The bucket area is computed as the product of the total number of ultimately surviving points and the cell area. The slip-stacking area factor $F(\alpha_s, \lambda)$ is the defined to be the ratio between the slip-stacking bucket area to that of a single-

Content from this work may be used under the terms of the CC BY 3.0 licence (© 2015). Any distribution of this work must maintain attribution to the author(s), title of the work, publisher, and DOI.

ISBN: 978-3-95450-168-7 doi:10.18429/JACoW-IPAC2015-MOPMA027

ELECTRON CLOUD MEASUREMENTS IN FERMILAB MAIN INJECTOR AND RECYCLER

J. Eldred, Department of Physics, Indiana University, Bloomington, IN 47405, USA
M. Backfish, C. Y. Tan, R. Zwaska, FNAL, Batavia, IL 60510, USA

Abstract

This conference paper presents a series of electron cloud measurements in the Fermilab Main Injector and Recycler. A new instability was observed in the Recycler in July 2014 that generates a fast transverse excitation in the first high intensity batch to be injected. Microwave measurements of electron cloud in the Recycler show a corresponding dependence on the batch injection pattern. These electron cloud measurements are compared to those made with a retarding field analyzer (RFA) installed in a field-free region of the Recycler in November. RFAs are also used in the Main Injector to evaluate the performance of beampipe coatings for the mitigation of electron cloud. Contamination from an unexpected vacuum leak revealed a potential vulnerability in the amorphous carbon beampipe coating. The diamond-like carbon coating, in contrast, reduced the electron cloud signal to 1% of that measured in uncoated stainless steel beampipe.

BACKGROUND

Electron cloud instabilities have been observed in a variety of modern proton accelerators [1–5]. Electron cloud was first observed in the Fermilab Main Injector in 2006 [6] and in the Fermilab Recycler in 2014 [7].

During the build-up of electron cloud, the particle beam causes the transverse acceleration of stray electrons which then scatter additional electrons from the beampipe. The number of electrons increase exponentially until a saturation is reached. The secondary electron yield (SEY) of a surface is the ratio of the average number of electrons scattered from the surface to the number of electron impacting the surface. The density of the electron cloud depends critically on beam intensity and SEY of the inner surface of the beampipe [8–10].

ELECTRON CLOUD MEASUREMENTS IN FERMILAB RECYCLER

Beginning in July 2014, a fast intensity-induced transverse instability was observed in the Recycler and limited operation until November. The instability has the unusual feature of selectively impacting the first high-intensity batch. A detailed description of the instability is given in [7]. The threshold of the instability is sensitive to batch intensity and bunch length, but recent studies in the Recycler demonstrated that the threshold of the instability was not sensitive to the azimuthal spacing of batches. Consequently, the prevailing theory is that the instability is caused by the electron cloud that is trapped [11, 12] in the gradient focusing dipoles of the Recycler [13]. In response to the instability, the electron cloud in the Recycler has been measured by retarding field analyzers (RFAs) and the dispersion of microwaves.

Microwave Measurements of the Recycler

The presence of electron cloud was measured in the Recycler by transmitting a microwave signal between a pair of two “split-plate” BPMs [14]. These studies follow the technique implemented in the Main Injector by Crisp et. al. in [15] and also by others elsewhere [16–18].

The first microwave measurement in the Recycler was conducted on August 20, 2014 by temporarily repurposing two Recycler BPMs (VP201 and VP203). During this measurement, the first batch was operating at an intensity of $\sim 3.6e12$ and subsequent batches at an intensity of $\sim 4.5e12$ per batch. During the pre-scheduled shutdown period from September 5 to October 23, spare Recycler BPMs (VP130 and VP202) were dedicated to the microwave experiment on a permanent basis. The second microwave measurement of the Recycler was conducted on December 18, 2014 using the new measurement location. At this time, the beampipe in the Recycler had conditioned and the instability no longer limited the operation of the Recycler. During the second measurement, the six batches each had an intensity of $\sim 4.4e12$.

A schematic of the electronic setup used for these studies is shown in Figure 1. The use of split-plate BPMs as improvised microwave antennas results in a ~ -80 dB transmission loss. Due to differences in the transmission spectrum at the two measurement locations [19], the second measurement was made at a carrier frequency of 2.060 GHz whereas the first measurement was made at 1.977 GHz.

The density of the electron cloud is modulated by the revolution harmonics of the proton beam (~90 KHz) and therefore the carrier frequency is phase-modulated (PM) in the presence of the electron cloud. Consequently, the electron cloud signal is seen as 90kHz sidebands on either side of the carrier frequency [7, 15]. The contribution that each batch makes to the sideband is $2\pi/7$ out of phase with the contribution made by the adjacent batch. This creates a possible ambiguity between changes in the density of the electron cloud and changes in the distribution of the electron cloud.

Figure 2 and Figure 3 show the first and second microwave measurement of the Recycler respectively. Each figure plots the average spectral power of the lower sideband frequency as a function of time within the Recycler cycle. The sharp feature in the beginning of each batch injection is composed of several sharp peaks, each declining in height with respect to the previous peak. The peaks are spaced at half-synchrotron period intervals and coincide with the minimums of the bunch length oscillation. The peaks in the

Content from this work may be used under the terms of the CC BY 3.0 licence (© 2015). Any distribution of this work must maintain attribution to the author(s), title of the work, publisher, and DOI.

ISBN: 978-3-95450-168-7 doi:10.18429/JACoW-IPAC2015-MOPMA028

Content from this work may be used under the terms of the CC BY 3.0 licence (© 2015). Any distribution of this work must maintain attribution to the author(s), title of the work, publisher, and DOI.

CHROMATICITY & DISPERSION IN NONLINEAR INTEGRABLE OPTICS*

S. D. Webb†, D. L. Bruhwiler, RadiaSoft, LLC, Boulder, CO 80304, USA
S. Nagaitsev, A. Valishev‡, Fermilab, Batavia, IL 60510, USA
V. V. Danilov, Oak Ridge National Lab, Oak Ridge, TN 37831, USA

Abstract

Proton accumulator rings and other circular hadron accelerators are susceptible to intensity- driven parametric instabilities because the zero-current charged particle dynamics are characterized by a single tune. Landau damping can suppress these instabilities, which requires energy spread in the beam or introducing nonlinear magnets such as octupoles. However, this approach reduces dynamic aperture. Nonlinear integrable optics can suppress parametric instabilities independent of energy spread in the distribution, while preserving the dynamic aperture. This novel approach promises to reduce particle losses and enable order-of-magnitude increases in beam intensity. In this paper we present results, obtained using the Lie operator formalism, on how chromaticity and dispersion affect particle orbits in integrable optics. We conclude that chromaticity in general breaks the integrability, unless the vertical and horizontal chromaticities are equal. Because of this, the chromaticity correcting magnets can be weaker and fewer correcting magnet families are required, thus minimizing the impact on dynamic aperture.

INTRODUCTION

Nonlinear integrable optics [1] is a concept for mitigating collective instabilities in intense beams using specially designed magnetic elements which introduce large tune spreads with integrable, bounded motion. The lattices which use nonlinear integrable optics are fundamentally different from conventional uses of strong focusing. In conventional strong focusing lattices, nonlinearities introduced by, for example, octupoles for Landau damping are small perturbations on the overall linear dynamics. This is to minimize their impact on the dynamic aperture. For lattices using nonlinear integrable optics, the nonlinear elliptic potential is a dominant part of the dynamics which introduces a large tune spread. This requires particular design considerations to implement properly.

The design of these lattices requires special considerations to ensure that the dynamics remains as close to integrable as possible. In the original treatment of this work, which considers transverse dynamics in the absence of collective effects and zero energy spread, the lattice required a drift section with equal vertical and horizontal beta functions. This was the first design consideration for a nonlinear integrable lattice.

In this proceeding we introduce two additional design criteria based on a study of off-momentum dynamics. Using a Lie map [2] formalism, we derive an expression for the single turn transfer map including the elliptic potential and chromatic and linear dispersive effects. As a result of this calculation, we conclude that chromaticity serves to both modify the invariants and, if not carefully managed, ruin the integrability. Similarly, dispersion through the elliptic element drift breaks the invariant potential. Because the calculations are too elaborate for this proceeding, we here simply state the key results. The detailed work may be found in [3].

BERTRAND-DARBOUX EQUATION

Because the specific conditions of the Bertrand-Darboux equation [4, 5] are critical for understanding the conclusions of this work, we summarize the results here. This is a partial differential equation for a two-dimensional potential $V(x, y)$ which has an invariant of the motion quadratic in the momenta. That is, the Hamiltonian $H = {}^1\!/_2(p_x^2 + p_y^2) + V(x, y)$ has a second invariant (aside from the Hamiltonian itself) given by the form

$$\begin{aligned} I = p_x^2 A(x, y) + p_y^2 B(x, y) + p_x p_y C(x, y) + \dots \\ \dots + p_x D(x, y) + p_y E(x, y) + F(x, y). \end{aligned} \tag{1}$$

First, and importantly, we note that H is isotropic in the momenta – the coëfficients of p_x and p_y are equal. This is not generally true; a Hamiltonian for a ring with different vertical and horizontal tunes will have differing coëfficients.

The resulting Bertrand-Darboux differential equation is given by

$$\begin{aligned} xy\left(\frac{\partial^2 V}{\partial x^2} - \frac{\partial^2 V}{\partial y^2}\right) + \dots \\ \dots + (y^2 - x^2 + c^2)\frac{\partial^2 V}{\partial x \partial y} + 3y\frac{\partial V}{\partial x} - 3x\frac{\partial V}{\partial y} = 0. \end{aligned} \tag{2}$$

Here we note two more features required of the potential: (1) that the partial differential equation is linear in V and therefore the sum of any set of potentials V_i which satisfy this will have an associated invariant and (2) that only specifically $x^2 + y^2$ satisfies the differential equation, and not x^2 or y^2 individually. Because of (1), a strong focusing lattice with a nonlinear element can form an integrable potential of this form. Because of (2), said strong focusing lattice must have equal vertical and horizontal tunes, a

---

* Work supported by the U.S. Department of Energy, Office of Science, Office of High Energy Physics under Awards Number DE-SC0011340.
† swebb@radiasoft.net
‡ valishev@fnal.gov

ISBN: 978-3-95450-168-7 doi:10.18429/JACoW-IPAC2015-MOPMA029

EXPERIENCES SIMULATING NONLINEAR INTEGRABLE OPTICS*

S.D. Webb†, D.L. Bruhwiler, R. Kishek, RadiaSoft, LLC, Boulder, CO 80304, USA
S. Nagaitsev, A. Valishev, Fermilab, Batavia, IL 60510, USA
V.V. Danilov, Oak Ridge National Lab, Oak Ridge, TN 37831, USA

Abstract

With increasing interest in the nonlinear integrable optics, it is important that early experiences with simulating the lattices be shared to save time and point out potential difficulties in the simulations. We present here some details of simulating the nonlinear integrable lattices. We discuss correctly implementing and testing the elliptic element kicks, and the limits of the thin lens approximation. We also discuss generating a properly matched bunch in the transverse phase space, and how to analyze the resulting computational data from simulations.

INTRODUCTION

Nonlinear integrable optics [1] is a concept for mitigating collective instabilities in intense beams. It has generated considerable interest in the field, and multiple groups and institutions have begun contributing to the research. Because of the novel form of the potential, they require special considerations for beam matching, calculating the kick in a drift-kick symplectic tracking code, and analyzing the results of simulations.

At the moment, the nonlinear element is implemented and benchmarked in Synergia [2], LIFETRAC, PyORBIT [3], and MAD-X [4] by way of PTC [5]. Please contact the authors if you plan to implement the nonlinear element in your tracking code. As the collaboration grows and the number of implementations expands, it is important to keep track of updates and changes and compare computational results. By sharing post-processing scripts and source code, we hope to minimize the redundant effort required for new researchers to begin studying nonlinear integrable optics.

MATCHED DISTRIBUTIONS

The Hamiltonian described by eqns. (10) and (18) in the original paper by Danilov and Nagaitsev [1] is an invariant of the single-particle motion in a nonlinear integrable lattice. As is well-known, any distribution which is a pure function of the invariants is itself an invariant of the motion – it is a matched beam. Any computational study of a nonlinear integrable lattice must start with, at the minimum, a beam properly matched in the transverse direction including the elliptic potential. Early attempts at simple linear matching showed severe mismatch in the nonlinear lattice, leading to large excursions of single particle orbits.

* Work supported by the U.S. Department of Energy, Office of Science, Office of High Energy Physics under Awards Number DE-SC0011340 and Number DE-SC0009531.
† swebb@radiasoft.net

The Hamiltonian in the normalized coördinates is given by

$$\mathcal{H} = \frac{\hat{p}_x^2}{2} + \frac{\hat{p}_y^2}{2} + \frac{\hat{x}^2}{2} + \frac{\hat{y}^2}{2} + t\mathcal{U}(\hat{x}, \hat{y}) \qquad (1)$$

where $\mathcal{U}$ is the normalized elliptic potential given by eqn. (18) of [1]. Here, the overhat denotes the usual Courant-Snyder normalization of the momenta and coördinates. Thus, a function of $\mathcal{H}$ will be matched to a lattice with zero collective effects and zero longitudinal-transverse coupling (i.e. the zero chromaticity limit).

The generalization of the Kapchinskij-Vladimirskij distribution [6] is a delta function in the generalized emittance $f(\varepsilon) = \delta(\varepsilon - \varepsilon_0)$ for a beam where every particle has its Hamiltonian equal to a single emittance, $\mathcal{H}_i = \varepsilon_0$. To generate this delta function distribution, it is convenient to pick a magnitude of the transverse momentum, $\hat{p}_0$, at random, limited to the range $\hat{p}_0 \in [0, \sqrt{2\varepsilon_0})$. Then, solve for $\hat{x}$ and $\hat{y}$ in the nonlinear equation

$$\frac{1}{2}\left(\hat{x}^2 + \hat{y}^2\right) + t\mathcal{U}(\hat{x}, \hat{y}) = \varepsilon_0 - \frac{\hat{p}_0^2}{2} \qquad (2)$$

One method of doing this is to pick an angle at random from $\theta \in [0, 2\pi)$ and solve for the radius using a numerical root finding algorithm. Another method, what we call the “lemming method”, is to pick random values of $\hat{x}$ and $\hat{y}$ from inside some bounding box and walk the point in $\hat{x}$ at fixed $\hat{y}$ until it solves the origin. Either method should generate a uniform distribution in the $\hat{x} - \hat{y}$ plane, filling the isoenergetic contours in Fig. (1).

To generate a general distribution in $\mathcal{H}$, generate the distribution as a Riemann sum of delta functions on the desired distribution function. Thus, $f(\varepsilon)$ is a Riemann sum of K-V distributions. Specifically, consider the unit-normalized distribution $f(\varepsilon)$, such that

$$\int_0^\infty d\varepsilon\; f(\varepsilon) = 1 \qquad (3)$$

and a total of N particles. Then on a finite interval from $\varepsilon' - \Delta\varepsilon/2$ to $\varepsilon' + \Delta\varepsilon/2$, there will be $N f(\varepsilon')\Delta\varepsilon$ total particles. If there are $N_{\text{macro.}}$ macroparticles with weight w, then there will be $N_{\text{macro.}} w f(\varepsilon')$ macroparticles with $\mathcal{H} = \varepsilon'$. Thus, a way to generate the arbitrary distribution $f(\varepsilon)$, we can approximate this with a large number of KV distributions with the proper number of macroparticles in each sub-distribution.

To invert the generated coördinates to real coördinates, generate a uniformly random angle θ for the momentum and

Content from this work may be used under the terms of the CC BY 3.0 licence (© 2015). Any distribution of this work must maintain attribution to the author(s), title of the work, publisher, and DOI.

ISBN: 978-3-95450-168-7 doi:10.18429/JACoW-IPAC2015-MOPMA030

MULTISYMPLECTIC INTEGRATORS FOR ACCELERATOR TRACKING CODES*

S. D. Webb†, D. L. Bruhwiler, RadiaSoft, LLC, Boulder, CO 80304, USA

Abstract

It has been long understood that long time single particle tracking requires symplectic integrators to keep the simulations stable. In contrast, space charge has been added to tracking codes without much regard for this. Indeed, multisymplectic integrators are a promising new field which may lead to more stable and accurate simulations of intense beams. We present here the basic concept, through a spectral electrostatic field solve which is suitable for adapting into existing tracking codes. We also discuss the limitations of current algorithms, and suggest directions for future development for the next generations of high intensity accelerators.

INTRODUCTION

Integrating single-particle orbits in storage rings using symplectic integration has been a staple of the accelerator field for decades[1]. The fundamental idea of symplectic integrators is: if the continuous equations of motion derive from an action principle, then so too should their discretization.

Keeping in this idea, recent work in the plasma-based accelerator field [2, 3] has expanded on early work [4, 5, 6] generalizing the idea of symplectic integration to field theories such as Maxwell's equations. Conventional particle-in-cell algorithms have discretized the particle motion and field solvers individually, then used charge deposition and force interpolation to enforce energy or momentum conservation. The difficulty with this approach is that conservation laws are encoded in the action principle, and arise from Noether's Theorem. Thus, momentum or energy conservation should be a natural result of the discretization of the continuum Lagrangian, not an *ad hoc* addition to impose certain physical constraints.

These ideas have a clear application to studying beam physics with intense space charge, or other dynamical effects over the long term. One can roughly understand non-symplectic versus symplectic integrators as being similar to secular versus canonical perturbation theory. In the secular theory, the expansion over a parameter ε is only valid for small times, so that $|\varepsilon t| \ll 1$. Canonical perturbation theory is valid for all time, so long as ε is small. As applied to accelerators, this means that a non-symplectic integrator will only give reliable results over time scales short compared to the space-charge tune shift (for example). Thus, a non-symplectic space charge simulation is likely only reliable for $n \propto (\Delta Q_{\text{SC}})^{-1}$ turns, with additional scaling for the step size such that $n \to \infty$ as $h \to 0$.

We here present the basic concepts of multisymplectic integration using a Lagrangian approach. We discuss this first schematically, then using a specific example – a spectral electrostatic particle-in-cell algorithm. We conclude with a discussion of future work required to implement these ideas in accelerator tracking codes.

MULTISYMPLECTIC INTEGRATION

The current literature in the field deals primarily with Lagrangians, as the plasma physics community generally thinks in terms of the tangent space (position and velocity) rather than the cotangent space (coördinates and momenta). However, the geometric structures (symplectic 2-form, conserved momenta, etc.) have a clear translation between Lagrangian and Hamiltonian treatments, so the basic principles will be the same.

The so-called Low Lagrangian [7] can be written generally as

$$\begin{aligned} L = \int d\mathbf{x}_0 d\mathbf{v}_0 \Big[T\left(\frac{\partial \mathbf{x}}{\partial t}(\mathbf{x}_0, \mathbf{v}_0)\right) + \dots \\ \dots - q\varphi + \frac{q}{c}\frac{\partial \mathbf{x}}{\partial t}\cdot \mathbf{A}\Big] f(\mathbf{x}_0, \mathbf{v}_0) + \dots \\ \dots + \frac{1}{16\pi}\int d\mathbf{x} F_{\mu\nu}F^{\mu\nu} \end{aligned} \tag{1}$$

where T is the kinetic energy term and $F_{\mu\nu} = \partial_\mu A_\nu - \partial_\nu A_\mu$ is the antisymmetric electromagnetic tensor. We note that the conservation of phase space density implies that $f(\mathbf{x}_0, \mathbf{v}_0) = f(\mathbf{x}, \mathbf{v}, t)$. Variation with respect to the individual vector potential components A, and the position $\mathbf{x}$, lead to the familiar Lorentz force law and Maxwell's equations, assuming we are using the conventional coördinate systems (Cartesian, cylindrical, spherical...). The specific application for accelerator coördinates will diverge from these familiar forms.

The first step in discretizing this Lagrangian is to discretize the spatial components of the fields. Thus, each component of the 4-vector potential

$$A = \sum_\sigma \Psi_\sigma(\mathbf{x}) a_\sigma(t) \tag{2}$$

over some set of indices σ. These could be finite elements, structured finite elements (which lead to finite difference equations), Fourier decompositions, eigenmodes formulations, or a variety of other possibilities. Similarly, we dis-

* Work supported by the U.S. Air Force Office of Scientific Research, Young Investigator Program, under contract no. FA9550-15-C-0031.
† swebb@radiasoft.net
[1] see, e.g., [1] for an overview of the history and literature of this topic.

Content from this work may be used under the terms of the CC BY 3.0 licence (© 2015). Any distribution of this work must maintain attribution to the author(s), title of the work, publisher, and DOI.

ISBN: 978-3-95450-168-7 doi:10.18429/JACoW-IPAC2015-MOPMA031

SIMULATIONS OF DIAMOND DETECTORS WITH SCHOTTKY CONTACTS*

G. I. Bell†, D. Dimitrov, S. Zhou, D. Meisner, J. Cary, D. Smithe, Tech-X Corp, Boulder, CO, 80303, USA
J. Smedley, Brookhaven National Lab, Upton, NY, 11973, USA
E. Muller, M. Gaowei, Stony Brook University, Stony Brook, NY, 11794, USA

Abstract

We present simulations of semiconductor devices using the code VSim (formerly Vorpal). The 3D simulations involve the movement and scattering of electrons and holes in the semiconductor, voltages which may be applied to external contacts, and self-consistent electrostatic fields inside the device. Particles may experience a Schottky barrier when moving between the semiconductor and a metal contact. Example devices include MOSFETs as well as a diamond X-ray detector. Our code VSim includes scattering models for GaAs and diamond, and runs in parallel on thousands of processors. We compare our simulation results with experimental results from a prototype diamond X-ray detector.

INTRODUCTION

Diamond is a promising material for use in X-ray and particle detectors [1]. Figure 1 shows the experimental

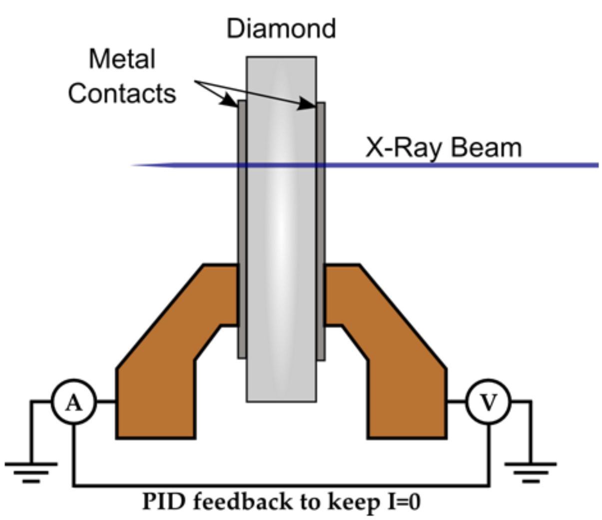

Figure 1: Schematic of an experimental X-ray detector.

setup, using a thin sheet of diamond 90 μm thick. When an X-ray photon passes through this thin diamond sheet, it may be absorbed, creating an electron-hole pair. The electron and hole scatter inelastically in diamond, creating many more secondary electrons and holes. Further relaxation of low energy charge carriers is dominated by scattering with phonons.

If a voltage bias is applied between the metal contacts, the generated electrons and holes drift in opposite directions and become separated. Diffusion also affects both charge carriers, and with the voltages applied experimentally (up to 8 V across the metal contacts) the effects of drift and diffusion are similar in magnitude. A charge carrier will drift at a constant rate due to the applied field, while the average distance traveled as a result of diffusion scales as the square root of the elapsed time. When these charge carriers reach the metal contacts, they may be absorbed, generating a net current. In order to reach the metal contacts, electrons and holes must cross a potential barrier.

Modeling this detector requires that we resolve widely disparate time scales. In order to accurately model the high-energy electrons produced in the initial X-ray absorption, we must resolve the mean time between inelastic collisions, on the order of 10^{-17} seconds. On the other hand the low energy electrons and holes interact with phonons much less frequently, about once every 10^{-14} seconds. Finally, the time needed for an electron or hole to drift or diffuse across 90 μm is around 10^{-8} seconds (10 ns). There are nine orders of magnitude between the smallest time scale of the simulation and the final time, so we can't simulate all these processes for 10 ns.

In contrast to the experiments, in these simulations we consider the delta-function response of the detector to a single photon—or, for better statistics, many photons all absorbed by the device at time $t = 0$.

SIMULATION OF A DIAMOND DETECTOR WITHOUT BARRIERS

In order to understand the role played by a Schottky barrier (which can prevent charge carriers from exiting through the metal contacts) we first simulate a diamond detector without barriers.

Our 3D simulations of the diamond detector use a domain of size $90 \times 20 \times 20$ μm, and we use periodic boundaries in y and z. The electrostatic field is calculated at each time step by doing a Poisson solve based on the current charge density, with boundary conditions in x using the applied voltage difference.

We consider 500 photons, each with an energy of 3 KeV, and absorbed by the diamond detector at $t = 0$. In diamond 3 KeV X-rays have an absorption length of 31.6 μm [2]. In order to determine the initial x position of the primary elec-

* This work is supported by the US DOE Office of Science, department of Basic Energy Sciences, grant numbers DE-SC0006246 and DE-SC0007577.
† gibell@txcorp.com

Content from this work may be used under the terms of the CC BY 3.0 licence (© 2015). Any distribution of this work must maintain attribution to the author(s), title of the work, publisher, and DOI.

ISBN: 978-3-95450-168-7 doi:10.18429/JACoW-IPAC2015-MOPMA033

Content from this work may be used under the terms of the CC BY 3.0 licence (© 2015). Any distribution of this work must maintain attribution to the author(s), title of the work, publisher, and DOI.

MODELING ELECTRON EMISSION AND SURFACE EFFECTS FROM DIAMOND CATHODES*

D. A. Dimitrov, J. R. Cary, D. Smithe, C. Zhou, Tech-X Corp., Boulder, CO 80303, USA
I. Ben-Zvi, T. Rao, J. Smedley, E. Wang, BNL, Upton, NY 11973, USA

Abstract

We developed modeling capabilities, within the Vorpal particle-in-cell code, for three-dimensional (3D) simulations of surface effects and electron emission from semiconductor photocathodes. They include calculation of emission probabilities using general, piece-wise continuous, space-time dependent surface potentials, effective mass and band bending field effects. We applied these models, in combination with previously implemented capabilities for modeling charge generation and transport in diamond, to investigate the emission dependence on applied electric field in the range from approximately 2 to 17 MV/m along the [100] direction. The simulation results were compared to experimental data when using different emission models, band bending effects, and surface-dependent electron affinity. Simulations using surface patches with different levels of hydrogenation lead to the closest agreement with the experimental data.

INTRODUCTION

High-average current and high-brightness electron beams are needed in advanced applications such as ultra-high Free-Electron Lasers, electron cooling of hadron accelerators, and Energy-Recovery Linac light sources. Semiconductor cathodes with negative electron affinity are known [1] to have good quantum efficiency (QE) (10% achieved experimentally) properties. To address the high brightness requirements for these applications, a new design for a photoinjector with a diamond amplifier was proposed [2] and is currently being investigated (see, e.g. [3–5] and references therein).

The operation of the diamond-amplifier cathode consists of using first a primary beam of electrons, accelerated to about 10 keV, (or photons with similar energies) to impact a diamond sample. The energetic primary electrons scatter inelastically generating secondary electrons. These electrons, and their related holes, relax their energies initially by producing more electron-hole pairs and later by scattering with phonons.

In applied electric field, the generated electrons and holes drift in opposite directions and are separated. The secondary electrons are transported towards a diamond surface with a negative electron affinity (NEA). Part of these electrons are then emitted into the accelerating cavity of an electron gun. The NEA is used to enhance the emission. Two orders of magnitude charge amplification (number of emitted electrons relative to the number of injected primary ones) has been observed in different experiments [4,5].

* We are grateful to the U.S. DoE Office of Basic Energy Sciences for supporting this work under grants DE-SC0006246 and DE-SC0007577.

Investigation of the phenomena involved in using diamond for generation of amplified electron beams via simulations requires modeling of secondary electron generation, charge transport, and electron emission. We have now implemented models for these processes in the Vorpal computational framework [6, 7].

MODELING ELECTRON EMISSION

The overall modeling approach involves three main steps shown in the simplified digram in Fig. 1. First, creation of (secondary) electrons in the conduction band and holes in the valence band is started by inelastic scattering with highly energetic primary electrons. Next, the free electrons and holes relax their energies via inelastic scattering (creating more electron-hole pairs and/or emission/absorption of phonons). Field is applied causing electrons to drift towards the band bending region (BBR) that ends with a (usually hydrogenated) negative electron affinity surface. In the final step, the electrons are emitted or reflected when they attempt to cross the diamond-vacuum interface.

For the secondary electron generation, we used our implementation of the Tanuma–Powell-Penn model. For modeling charge transport, we used a Monte Carlo approach. Detailed description of these modeling capabilities is provided in Ref. [6]. Recently, we implemented several emission mod-

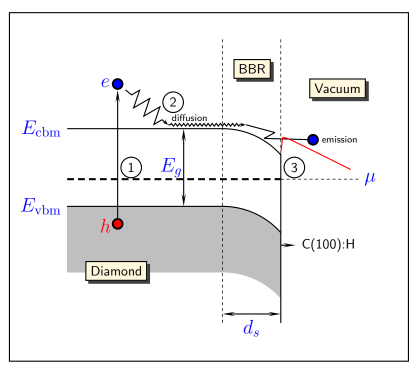

Figure 1: Three main processes are modeled: electron-hole generation, charge transport, and electron emission from surfaces with different potentials and band bending regions.

els and started using them to study electron emission from semiconductor cathodes [7] (and references therein for use of these models to investigate electron emission from GaAs). For the results presented here, we used our implementation of the transfer matrix (TM) model for calculation of emission probabilities and a surface potential energy that includes the effect of the image charge:

$$V(x) = \chi - Fx - Q/x, \tag{1}$$

ISBN: 978-3-95450-168-7 doi:10.18429/JACoW-IPAC2015-MOPMA035

CURRENT STATUS OF THE GPU-ACCELERATED ELEGANT *

J.R. King, I.V. Pogorelov†, Tech-X Corporation, Boulder, CO 80303, USA
M. Borland, R. Soliday, Argonne National Laboratory, Argonne, IL 60439, USA
K. Amyx, Sierra Nevada Corporation, Centennial, CO 80112, USA

Abstract

Efficient implementation of general-purpose particle tracking on GPUs can result in significant performance benefits to large-scale tracking simulations and direct (tracking-based) accelerator optimization techniques. This paper is an update on the current status of our work on accelerating Argonne National Lab's particle accelerator simulation code ELEGANT using CUDA-enabled GPUs. We summarize the performance of beamline elements ported to GPU, and discuss optimization techniques for some important collective effects kernels. We also present the latest results of scaling studies with realistic lattices of the GPU-accelerated version of the code.

INTRODUCTION

ELEGANT is an open-source, multi-platform code used for design, simulation, and optimization of FEL driver linacs, ERLs, and storage rings [1, 2]. The parallel version, Pelegant [3, 4], uses MPI for parallelization. Several "direct" methods of simultaneously optimizing the dynamic and momentum aperture of storage ring lattices have recently been developed at Argonne [5]. These new methods typically require various forms of tracking the distribution for over a thousand turns, and so can benefit significantly from faster tracking capabilities.

Graphics processing units (GPUs) offer unparalleled general purpose computing performance, at low cost and at high performance per watt, for large problems with high levels of parallelism. Unlike general purpose processors, which devote significant on-chip resources to command and control, pre-fetching, caching, instruction-level parallelism, and instruction cache parallelism, GPUs devote a much larger amount of silicon to maximizing memory bandwidth and raw floating point computation power.

Our main goals for this project are (1) to port a wide variety of beamline elements to GPUs so that ELEGANT users can take advantage of the high performance that GPUs can provide, (2) support CUDA-MPI hybrid parallelism to leverage existing GPU clusters, and (3) maintain 'silent support' so that GPU-accelerated elements can be used without additional input from the user.

* Work supported by the DOE Office of Science, Office of Basic Energy Sciences grant No. DE-SC0004585, and in part by Tech-X Corporation. This research used resources of the Oak Ridge Leadership Computing Facility, which is a DOE Office of Science User Facility supported under Contract DE-AC05-00OR22725.

† ilya@txcorp.com

BEAMLINE ELEMENT PERFORMANCE

In this section we present a list of the particle beamline elements fully ported to the GPU, and rough estimates of their acceleration compared to the reference CPU code, comparing an NVIDIA Tesla K20c GPU to an Intel Core i7-3770K CPU in simulations with a few million particles.

QUAD and DRIFT: Quadrupole and drift elements, implemented as a transport matrix, up to 3^{rd} and 2^{nd} order, respectively: $\sim$ 100x acceleration, achieving particle data bandwidth of 80 gb/s and over 200 GFLOPS in double precision.

CSBEND: A canonical kick sector dipole magnet with exact Hamiltonian (computationally intensive): Nearly 30x acceleration due to its high arithmetic intensity.

KQUAD, KSEXT, MULT: A canonical kick quadrupole, sextupole, and multipole elements using 4^{th} order symplectic integration: 45x acceleration.

EDRIFT: An exact drift element: Roughly 20x acceleration (purely bandwidth bound).

RCOL: Rectangular collimator: 60x acceleration if particles are removed from simulation.

LSCDRIFT: Longitudinal space charge impedance: $\sim$ 45x acceleration using optimized histogram calculation.

CSRCSBEND: A canonical kick sector dipole with coherent synchrotron radiation: Over 50x acceleration using optimized histogram calculation.

RFCW: RF cavity element, a combination of a first-order matrix RF cavity with exact phase dependence (RFCA), longitudinal wake (WAKE) and transverse wake (TRWAKE) specified as a function of time lag behind the particle, and LSCDRIFT: over 30x acceleration, convolution-based wake elements being the primary bottleneck.

SCRAPER: A one-side collimation element: a 14.5x acceleration with intensive random number generation.

MATTER: A Coulomb-scattering and energy-absorbing element simulating material in the beam path: an acceleration of 23x.

OPTIMIZATION OF COLLECTIVE-EFFECTS KERNELS

In this section we briefly summarize some of our results on optimization of the collective-effects elements. A more detailed discussion can be found in [6].

Histogram Computation

Most collective effects elements in ELEGANT require computing a histogram, which is difficult on a GPU because of the thread contention problem. Thread-safe atomic operations do not provide a practical solution to this problem

Content from this work may be used under the terms of the CC BY 3.0 licence (© 2015). Any distribution of this work must maintain attribution to the author(s), title of the work, publisher, and DOI.

ISBN: 978-3-95450-168-7 doi:10.18429/JACoW-IPAC2015-MOPMA037

Content from this work may be used under the terms of the CC BY 3.0 licence (© 2015). Any distribution of this work must maintain attribution to the author(s), title of the work, publisher, and DOI.

ELECTRON CLOUD BUILDUP AND DISSIPATION MODELS FOR PIP-II *

S. A. Veitzer†, Tech-X Corporation, Boulder, CO, 80303 USA
P. H. Stoltz, Tech-X Corporation, Boulder, CO, 80303 USA

Abstract

Buildup of electron plasmas in accelerator cavities can cause beam degradation and limit performance in high-intensity circular particle accelerators. This is especially important in machines such as the LHC, and PIP-II, where mitigation techniques such as beam scrubbing in order to decrease the SEY are expensive and time consuming. Modeling of electron cloud buildup and dissipation can provide understanding as to the potential negative effects of electron clouds on beam properties, as well as estimates of the mitigation required to maintain accelerator performance and beam quality as accelerators move to higher intensity configurations. We report here on simulations of electron cloud buildup and dissipation for geometry, beam and magnetic field configurations describing the Recycler at Fermilab. We perform electrostatic simulations in 3D with VSim PIC, including the effects of space charge and secondary electrons. We quantify the expected survival rate of electrons in these conditions, and argue that improvements in reducing the SEY is unlikely to mitigate the electron cloud effects.

ELECTRON CLOUD SURVIVAL RATE IN CIRCULAR ACCELERATORS

In circular accelerators, electron clouds may build up from very low densities as trains of bunches pass through the accelerator. As each bunch passes, electrons experience the potential of the beam and are accelerated through the center of the beam pipe to the opposite wall. Typically they will gain enough energy to produce secondary electrons, which are in turn accelerated by the next bunch.

This process produces a build up of an electron plasma, which saturates at a density that is some large fraction of the linear charge density of the beam [1], depending on the bunch length and the cross-sectional size of the beam pipe. At saturation, electrons near the beam pipe walls are shielded from the beam potential by other electrons, and are not significantly accelerated to produce more secondaries. Also, electrons that are accelerated by the passing beam encounter space charge due to these electrons and so impact the walls with lower energy, which can reduced overall secondary yields.

Electron clouds dissipate during the period of time when there are no bunches crossing, as they drift to beam pipe walls with energies low enough that they do not produce significant secondary electrons. The dissipation typically occurs very swiftly, with the number of electrons decreasing exponentially. However, without the influence of additional bunch crossings, some electrons will have very low energies, and will drift for long enough that they are present when the first bunch in the beam returns.

ELECTRON CLOUD BUILD UP AND DISSIPATION NUMERICAL MODELS

Electron cloud build up has previously been modeled using a variety of high-performance Particle-In-Cell (PIC) codes, including Vorpal [1–3], WARP coupled with POSINST [4–6] and others. Build up simulations have typically focussed on the saturation density, and dynamics of electron cloud evolution under different magnetic field configurations e.g. [7], and the effects of different wall materials on overall cloud densities e.g. [8]. Here, we focus on the build up and dissipation aspects of electron clouds, in order to understand the survival rate of electrons over more than a single revolution period.

We use the plasma simulation package VSim [9], which employs the Vorpal simulation engine [10] to model electron cloud build up, dynamics, and dissipation. Our models use the following physical parameters, corresponding to the Fermilab Recycler storage ring. We simulate the crossing of 504 Gaussian-shaped bunches (84 bunches per batch and 6 batches per beam) with bunch lengths of 60 cm, bunch spacing of 18.94 ns, beam radius of 3.0 mm, and 5.25×10^{10} protons/bunch. The bunches cross during the first 9.545 μs of the simulation, followed by 1.5265 μs where there is no beam, for a total revolution period of 11.0723 μs.

The beam pipe cross-section is elliptical with major radius $a = 0.047$ m and minor radius $b = 0.022$ m. We simulate $l = 0.50$ m of beam pipe in the longitudinal (beam axis) direction. We apply an external magnetic field that is primarily a dipole field with an additional quadrupole component,

$$
\begin{aligned}
B_x &= 0.0 && (1)\\
B_y &= B_0 + Gz && (2)\\
B_z &= Gy, && (3)
\end{aligned}
$$

where $B_0 = 0.1375$ T and $G = 0.3355$ T/m, x is the longitudinal direction, and y and z are the transverse directions. We seed the simulation with a low-density, randomly distributed electron cloud. We examine the dependence of build up time and saturation density with initial seed density in section below. We use the Furman-Pivi secondary electron yield model [11] for stainless steel, with max(SEY) = 2.05 at a primary energy of $E_{\text{max}} = 292.0$ eV.

* This work was performed under the auspices of the Department of Energy as part of the ComPASS SCiDAC-2 project (DE-FC02-07ER41499), and the SCiDAC-3 project (DE-SC0008920).
† veitzer@txcorp.com

ISBN: 978-3-95450-168-7 doi:10.18429/JACoW-IPAC2015-MOPMA039

SECONDARY ELECTRON YIELD MEASUREMENT AND ELECTRON CLOUD SIMULATION AT FERMILAB

Yichen Ji, Linda Spentzouris, Department of Physics, Illinois Institute of Technology, IL 60616, USA
Robert Zwaska, FNAL, Batavia, IL 60510, USA

Abstract

Fermilab Main Injector is upgrading the accelerator to double the beam intensity from 24e12 protons to 48e12 protons, which brings the accelerator into a regime where electron cloud effects may limit the accelerator performance. In fact, an instability that could be caused by electron cloud effects has already been observed in the Recycler [1, 2].

Secondary Electron Yield (SEY) is an important property of the vacuum chamber material that has great influence on the process of building up free electrons. The Main Injector of the Fermilab accelerator complex offers the opportunity to measure SEY and conditioning effects in the environment of a running accelerator, since samples of these materials are located at the beampipe wall. The SEY of stainless steel (SS316L) and TiN coated SS316L in the proximity of the proton beam were measured and compared.

A series of simulation studies of electron cloud build up were done for the Main Injector and Recycler using the code POSINST. Parametric studies were done to determine the maximum electron density vs. peak SEY at different beam intensities in the Fermilab Main Injector. Threshold simulations of electron cloud density versus SEY were extended from Main Injector to include the Recycler Ring [3]. It was found that the electron cloud density around the beam depends on bunch location within the bunch train.

SEY MEASUREMENT

The Secondary Electron Yield (SEY) measures on average how many electrons are emitted when one electron hits the beam chamber surface. SEY is generally dependent on the incident electron energy, E, and the incident angle, θ. The SEY of different materials and coatings has been studied for many years; however, the effect of the accumulated dose under actual accelerator conditions has only been studed recently [4].

SEY Test Stand

The SEY measurement stand was originally designed and built by Cornell. Modifications were made to adapt it to the Main Injector, reduce background, and improve signal level for the Main Injector tunnel conditions [4, 5].

The measurement stand has two different arms so that two samples can be exposed to the same dose for comparison. The arms are protected by faraday boxes to eliminate leakage current. Each sample is a small curved piece that sits on the vacuum chamber wall. They are retracted from the vacuum chamber on an electrically isolated arm during measurements. Two Kimball Physics ELG-02 electron guns were installed and are directed towards the sample at a 15° angle, which will increase the measured SEY by 1% compared to normal incidence, according to the Furman-Pivi probabilistic model [6]. The electron guns scan over an energy spectrum of 45 eV to 1545 eV with a 1 mm diameter spot on a 3 × 3 grid. A Keithley 6487 pico-Ammeter is used to indirectly measure the SEY of the sample. A bias voltage must be applied during measurements and the pico-Ammeter is also used to apply this bias voltage.

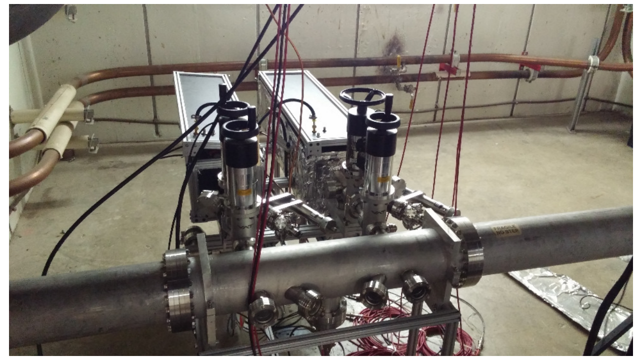

Figure 1: The SEY test stand.

A typical measurement generally takes 6 to 8 hours, which includes transportation of the DAQ-control computer, equipment set-up and warm-up and then the actual measurement. The test stand vacuum vessel is grounded during measurements. The gun was set to to deliver 0.5 to 1.0 nA beam at 300 eV. The primary current I_p is measured by applying a +150 V bias voltage that recaptures all secondary electrons. The total current I_t is measured by applying -20 V that repels all low energy secondary electrons. Then the secondary emission current is given by $I_{SEY} = I_t - I_p$. The SEY can be calculated by the following equation.

$$SEY = \frac{I_{SEY}}{I_p} = \frac{I_t - I_p}{I_p} \tag{1}$$

Leakage Current

Due to the low signal current measured, the bias voltage induced leakage current can cause a very high background during a measurement. The leakage current can reach as high as tens of nano-Amperes and must be compensated when calculating the SEY from the data. High leakage current generally occurred when the ceramic (used to isolate the vacuum vessel from the sample) got wet due to moisture from the surrounding atmosphere, or there were excessive vibrations around the testing stand, or current leakage from the wire to the faraday box. The following modifications were made to control the leakage current:

1. Implementation of a faraday box.

Content from this work may be used under the terms of the CC BY 3.0 licence (© 2015). Any distribution of this work must maintain attribution to the author(s), title of the work, publisher, and DOI.

ISBN: 978-3-95450-168-7 doi:10.18429/JACoW-IPAC2015-MOPMA040

ANALYSIS OF BEAM TRANSVERSE INSTABILITIES AT FERMILAB

T. Zolkin*, The University of Chicago, Chicago, IL 60637, USA

Abstract

The transverse beam dynamics in Fermilab Recycler ring has been analyzed using *SCHARGEV* Vlasov solver. In the first part of paper we discuss how *SCHARGEV* analyses collective instabilities for Gaussian bunch with strong space charge in resistive impedance environment. In the second part the bunched beam dynamics is studied depending on head-tail phase and damper gain. An example for Fermilab Recycler is presented.

SSC THEORY AND BUROV EQUATION

For transverse oscillations of bunched beams, a parameter of the space charge strength is a ratio of the maximal space charge tune shift to the synchrotron tune. When this parameter is large, the transverse oscillations are described by a one-dimensional integro-differential **Burov equation**

$$\nu\, y + \frac{1}{Q_{\rm eff}}\frac{\mathrm{d}}{\mathrm{d}\,\tau}\left(u^2\frac{\mathrm{d}\,y}{\mathrm{d}\,\tau}\right) = \varkappa\, N\left(\hat{W}+\hat{D}\right), \quad \left.\frac{\mathrm{d}\,y}{\mathrm{d}\,\tau}\right|_{\tau\to\pm\infty} = 0,$$

derived in [1]. *SCHARGEV* Vlasov solver is based on numerical solution of the equation above and for more details see [2].

Below we will consider the case of Gaussian bunch which corresponds to a thermal equilibrium when the bunch length is much shorter than the rf wavelength [3]. In this case the Sturm-Liouville problem for no-wake case leads to the **Burov-Balbekov functions** [1, 4]:

$$\begin{cases} \bar{y}''(\tau) + \nu\, e^{-\tau^2/2}\,\bar{y}(\tau) = 0, \\ \bar{y}'(\pm\infty) = 0, \end{cases}$$

where the natural system of units is employed: the distance τ is measured in units of the RMS bunch length σ, and, eigenvalues ν_k is measured in units of $u^2/\sigma^2 Q_{\rm eff}(0) = Q_s^2/Q_{\rm eff}(0)$. First eight eigenfunctions, $\bar{y}_k(\tau)$, are plotted in Fig. 1.

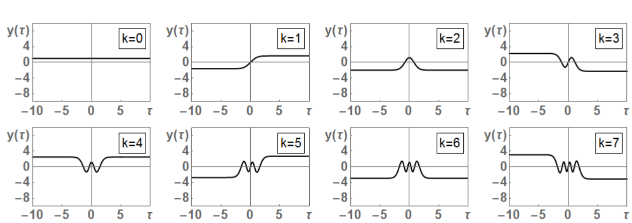

Figure 1: The first 8 eigenfunctions of the Gaussian bunch, $\bar{y}_k(\tau)$. The modes do not depend on the chromaticity, except the common head-tail phase factor $\exp(-i\zeta\tau)$.

* zolkin@uchicago.edu

DIPOLE MOMENTS AND DAMPER

For further discussion we need to introduce the bunch dipole moments defined as functions of the head-tail phase:

$$I_k(\zeta) = \int_{-\infty}^{\infty} \rho(\tau)\bar{y}_k(\tau)e^{i\zeta\tau}\,\mathrm{d}\tau : \quad I_k^*(\zeta) = (-1)^k I_k(\zeta),$$

where $\rho(\tau) = \int_{-\infty}^{\infty} f(v,\tau)\,\mathrm{d}v = (2\pi)^{-1/2}\exp(-\tau^2/2)$ is the normalized line density of the beam. First four of them are plotted in Fig. 2.

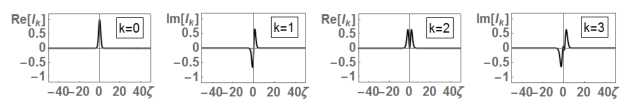

Figure 2: The first 4 bunch dipole moments for the Gaussian bunch as a function of the head-tail phase, $I_k(\zeta)$. Only real or imaginary part is plotted for even and odd ks respectively.

Matrix elements of an operator of the linear bunch by bunch damper can be constructed as a direct product of a set of dipole moment functions

$$\hat{G}_{lm}(\zeta) = \int_{-\infty}^{\infty}\int_{-\infty}^{\infty} \rho(\tau)\rho(\sigma)\bar{y}_l(\tau)\bar{y}_m(\sigma)e^{i\zeta(\tau-\sigma)}\,\mathrm{d}\sigma\,\mathrm{d}\tau$$
$$= I_l(\zeta)I_m^*(\zeta) = (-1)^m I_l(\zeta)I_m(\zeta),$$

(same matrix describes the couple bunch wake terms for sufficiently separated bunches).

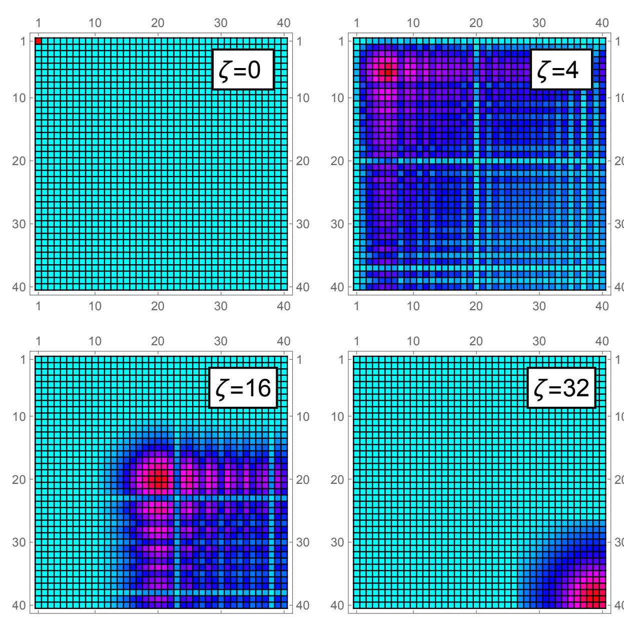

Figure 3: Absolute value of 40 by 40 dipole moments direct product matrices, $\hat{G}_{lm}$, plotted for different values of the head-tail phase ($\zeta = 0, 4, 16, 32$).

Content from this work may be used under the terms of the CC BY 3.0 licence (© 2015). Any distribution of this work must maintain attribution to the author(s), title of the work, publisher, and DOI.

ISBN: 978-3-95450-168-7 doi:10.18429/JACoW-IPAC2015-MOPMA041

EXPERIMENTAL OBSERVATION OF HEAD-TAIL MODES FOR FERMILAB BOOSTER*

T. Zolkin†, The University of Chicago, Chicago, IL 60637, USA
A. Burov‡, V. Lebedev§, FNAL, Batavia, IL 60510, USA

Abstract

The Fermilab Booster is known to suffer from beam transverse instabilities. An experimental attempt of head-tail modes extraction from the stable beam motion by periodic excitement of betatron motion has been performed. The shapes of head-tail modes have been successfully obtained while eigenfrequencies separation from the betatron tune were too small to be resolved. The qualitative agreement between the theory and an experimental data has been demonstrated. This is an important step towards the understanding of general theory of collective instabilities for strong space charge case, which is a rather typical case for hadron machines.

INTRODUCTION

The goal of experiment was an observation and decomposition of head-tail modes. Usually head-tail modes can be observed when beam is in an unstable regime. Here we used a different approach studying the stable beam motion and exciting a betatron motion by pinging a beam every 100 turns [1]. Further analysis of collected data allowed to resolve the spatial structure of intra-bunch modes. Obtained experimental results have been interpreted according to the existing theory of collective beam motion and they do coincides with existing qualitative picture of beam motion in a Booster. This experimental activity is a very important step in order to build the bridge from theoretical expectations to real machine life; it should help with the further understanding of collective instabilities and possible ways to suppress them or move further the transverse mode coupled instability mode threshold.

FERMILAB BOOSTER

The FNAL Booster accelerator is a proton synchrotron, originally designed and constructed in the beginning of 1970's to match the beam from the linear accelerator to the Fermilab Main Ring, see Fig. (1). Since the 70's the whole accelerator complex has undergone many changes. At the present time, Booster accumulates the 400 MeV proton beam from the LINAC and then gives an intermediate boost to the beam energy. Booster was build as a fast cycling machine operating at 15 Hz which goes through repeated acceleration cycles delivering extracted 8 GeV beam pulses (referred to as a batch) to different experiments or filling the Main Injector ring which is about seven times larger. A multiple turn injection system increases the Booster intensity; it allows to stack successive turns of LINAC beam layered on top of each other. LINAC provides Booster with 400 MeV debunched H^- ion beam. The H^- ions and circulating beam passes through the stripping foil, which removes electrons of the ions and made of a thin layer of carbons. Operationally, the practical limit for maximum intensity is about 7 to 8 turns; fractional turns are not used normally.

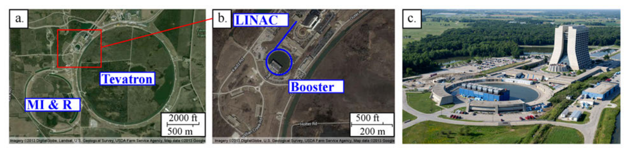

Figure 1: (a.), (b.) Satellite images of the Fermilab site showing Linear Accelerator (LINAC), Booster, Main Injector (MI), Recycler (R) and Tevatron ring. (c.) Photo of the Fermilab Willson Hall, LINAC and Booster.

Booster lattice consists of 96 combined function magnets which are arranged in 24 superperiods of the FOFDOOD-type cells; each superperiod containing two horizontally focusing magnets (F magnet) and two horizontally defocussing magnets (D magnet), along with short (O) and long (OO) straight sections, 1.2 and 6 meters respectively. All magnets are combined function magnets which bend the beam (a dipole magnet function) and focuses the beam either horizontally or vertically (a quadrupole function) and are powered by a resonant power supply with sinusoidal current waveform.

SSC THEORY FOR GAUSSIAN BUNCH

Below we will consider the case of Gaussian bunch which has a special practical importance; it corresponds to a thermal equilibrium when the bunch length is much shorter than the rf wavelength, in which case the longitudinal distribution function is

$$f(v,\tau) = \frac{N_\mathrm{b}}{2\,\pi\,\sigma\,u(\tau)}\,e^{-v^2/2\,u^2-\tau^2/2\,\sigma^2}.$$

The equation describing strong space charge no-wake head-tail modes for a bunch with Gaussian distribution [2]

$$y''(\tau) + \nu\,e^{-\tau^2/2}\,y(\tau) = 0, \qquad y'(\pm\infty) = 0,$$

leads to **Burov-Balbekov functions**, $y_k^0(\tau)$. The natural system of units is employed: the distance τ is measured in units of the RMS bunch length σ, and, eigenvalues ν_k is measured in units of $u^2/\sigma^2 Q_\mathrm{eff}(0) = Q_s^2/Q_\mathrm{eff}(0)$.

* FNAL is operated by Fermi Research Alliance, LLC under Contract No. De–AC02–07CH11359 with the United States Department of Energy.
† zolkin@uchicago.edu
‡ burov@fnal.gov
§ val@fnal.gov

Content from this work may be used under the terms of the CC BY 3.0 licence (© 2015). Any distribution of this work must maintain attribution to the author(s), title of the work, publisher, and DOI.

ISBN: 978-3-95450-168-7 doi:10.18429/JACoW-IPAC2015-MOPMA043

LONGITUDINAL BUNCH SHAPING AT PICOSECOND SCALES USING ALPHA-BBO CRYSTALS AT THE ADVANCED SUPERCONDUCTING TEST ACCELERATOR*

B.L. Beaudoin, Institute for Research in Electronics & Applied Physics, University of Maryland, College Park, MD 20742-3511, USA

D. Edstrom Jr., A.H. Lumpkin, J. Ruan, J. Thangaraj, Fermi National Accelerator Laboratory, Batavia, IL 60510-5011, USA

Abstract

The Integrable Optics Test Accelerator (IOTA) electron injector at Fermilab will enable a broad range of experiments at a national laboratory in order to study and develop solutions to the limitations that prevent the propagation of high intensity beams at picosecond lengths. One of the most significant complications towards increasing short-beam intensity is space-charge, especially in the vicinity of the gun. A few applications that require a longitudinally shaped electron beam at high intensities are for, the generation of THz waves and dielectric wakefields, each of which will encounter the effects of longitudinal space-charge. This paper investigates the effects of longitudinal space-charge on alpha-BBO UV laser shaped electron bunches in the vicinity of the 1½cell 1.3 GHz cylindrically symmetric RF photocathode gun.

INTRODUCTION

The IOTA electron linac is currently being built and commissioned at Fermilab. As of March 27, 2015 they commissioned the electron linac up to 20 MeV, a laboratory record for maximum electron energy achieved [1]. The work presented in this paper seeks to answer the question: *How do density perturbations evolve and affect the electron beams 6-D beam phase-space brightness in a linear accelerator under various beam and machine conditions, such as acceleration?*

The University of Maryland Charged Particle Beam Laboratory has pioneered the ability of generating controlled perturbations to understand longitudinal space-charge an intense beams [2]. These controlled perturbations have ranged from grid modulations of a thermionic gun to UV laser focused onto the dispenser cathode, in-turn extracting additional current through photoemission and thus modulating a local region of the longer beam bunch [3-9]. This work intends to extend these studies to pico-second high current bunch lengths in the MeV range.

IOTA LASER & ELECTRON LINAC

IOTA facility houses a superconducting high intensity electron linear accelerator (linac). The first stage of the facility has generate and transported a 20 MeV intense electron beam (shown in Fig. 1 below) using the accelerating cavity CAV2 [10]. Additional cavities are installed in the tunnel and conditioned that will allow the accelerator to transport up to 250 MeV electron beams.

Currently the electron linac is running with a Cs_2Te cathode for commissioning of the gun RF systems. A Cs_2Te photocathode is illuminated with an ultraviolet (263 μm) laser pulse, producing bunch trains at a repetition rate of 1-5 Hz and a frequency of 3 MHz for a 1 ms macro-pulse duration [11-12]. The number of bunches can be anywhere from 1-3000 depending on the beam charge.

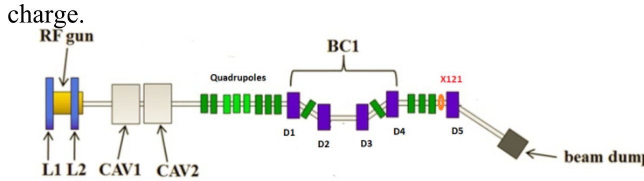

Figure 1: The 50 MeV electron beamline showing the RF gun followed by CAV1 and CAV2 that will accelerate the beam to 50 MeV. The green boxes show the quadrupoles used to focus the beam. The purple boxes are the dipoles that are used to bend the electron beam. D5 is the spectrometer dipole that is used in measuring the energy spectrum of the bunch. X121 is an Optical Transition Radiation (OTR) monitor that will be used to measure the current profile of the electron beam [11].

The photoinjector consists of a 1½ cell 1.3 GHz (L-band) cylindrical-symmetric RF gun injecting beam into the linac at nominally 5 MeV. By changing the gradient inside the RF gun, were able to generate beam energies ranging from 2-to-5 MeV.

TEMPORAL PULSE STACKING

The generation of longitudinally uniform electron beams can be achieved utilizing UV birefringent crystals by temporally stacking the incident laser pulse. The method of using birefringent crystals for temporal pulse stacking was developed at the Argonne Wakefield Accelerator (AWA) facility to generate 83-167 GHz electron bunch trains from an RF photocathode gun [13].

When a short laser pulse is incident on a birefringent crystal at a particular angle, the pulse will split into two pulses (or two rays), with different polarizations. The two pulses also separate in time as a result of the different group velocities. This separation in time can be calculated using Eqn. 1 below:

$$\Delta t = L\left(\frac{1}{v_{ge}} - \frac{1}{v_{go}}\right) \quad (1)$$

*Work supported by the University Research Association Inc. Operated by the Fermi Research Alliance, LLC under Contract No. DE-AC02-07CH11359 with the United States Department of Energy

Content from this work may be used under the terms of the CC BY 3.0 licence (© 2015). Any distribution of this work must maintain attribution to the author(s), title of the work, publisher, and DOI.

ISBN: 978-3-95450-168-7 doi:10.18429/JACoW-IPAC2015-MOPMA044

BARRIER SHOCK COMPRESSION WITH LONGITUDINAL SPACE-CHARGE*

B.L. Beaudoin, I. Haber, R.A. Kishek, Institute for Research in Electronics & Applied Physics, University of Maryland, College Park, MD 20742, USA

Abstract

Synchrotrons and storage rings routinely employ RF barrier buckets as a means of accumulating charge to increase the peak intensity and preserve longitudinal emittance while minimizing emittance growth [1-3]. This was shown in the main injector and recycler at Fermilab as well as the SIS-18 at GSI Helmholtz center for heavy ion research. The RF cavities typically used are ferrite loaded magnetic alloys with low Q to maximize bandwidth and generate single pulses, either as delta functions, triangular or half/full period sine waves.

The University of Maryland Electron Ring (UMER) group is studying a novel scheme of bunch compression in the presence of longitudinal space charge. It has been analytically shown through 1-D computations that the presence of space-charge considerably improves the efficiency of the barrier compression by taking advantage of the shock-front that launches when the barrier moves into a space-charge dominated beam. In this paper, we summarize the initial results of the study.

INTRODUCTION

The University of Maryland Electron Ring is a storage ring that accesses high intensities through the use of low momentum high-current electron beams. The machine is capable of injecting various beam currents ranging from 0.6-to-104 mA (shown in Table 1) and has since propagated a new low current beam of approximately 50 µA in Nov 2014 [4]. This beam is still undergoing full characterization.

Table 1: Beam Parameters vs Injected Current

Current (mA)	Emittance (mm-mr)	c_s (1×10^6 x m/s)
0.05	TBD	0.066
0.6	7.6	0.285
6.0	25.5	0.766
21.0	30.0	1.27
78.0	58.9	1.90
104.0	64.0	2.03

Longitudinal space-charge causes the ends of the beam to axially expand, filling the ring with charge [5-6]. In order to overcome the longitudinal space-charge forces, a barrier bucket system was developed to prevent the expansion, allowing us to store the beam for more than 1000 turns [5]. The barrier bucket system consists of two independently operated burst mode modulators, where the first modulator applies an 8 ns FWHM negative voltage pulse to the head of the bunch and the other applies the equivalent positive pulse to the tail of the bunch. Both modulators are synchronized to injection and operate at the revolution frequency of the beam. Figure 1 below illustrates the voltage pulses (red), the beam current (black) from the wall current monitor in the ring as well as the synchronization between them. Note in this figure the voltage pulses are applied every fifth turn.

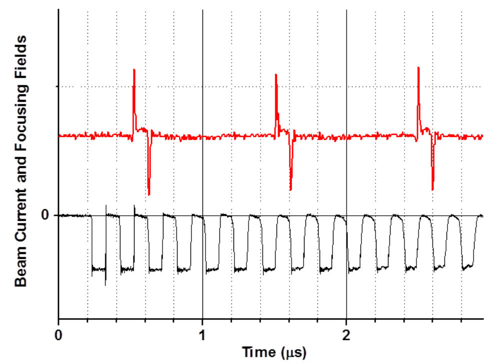

Figure 1: Synchronization between the barrier bucket fields (red) and beam current (black) from the wall-current monitor in the ring.

Once the barrier bucket fields are initiated, the beam can be stored for as long as required for a given experiment, limited by the average power that the pulse modulators can drive the low Q cavity. The modulators are capable of storing the 0.6 mA beam for more than 1000 turns. The barrier fields are not perfectly matched to the beam edges, resulting in space-charge waves induced at the edges of the beam that bounce from edge to edge during a long store of charge [5].

Various barrier bucket compression schemes have been explored in the past, to produce more intense beams for neutrino based programs demanding high intensity hadron beams [1]. A few schemes that have been explored are: barrier flip-flop, adiabatic compression and momentum stacking. Each of these schemes compresses the total charge in order to increase the peak current with little consideration for longitudinal emittance growth and especially when intense longitudinal space-charge forces are considered.

This paper summarizes both the computational and experimental progress on this novel method of compression with intense space-charge.

NOVEL METHOD OF LONGITUDINAL COMPRESSION

This method of compression utilizes longitudinal space-charge to assist with the compression of the beam,

*Work supported by the US Dept. of Energy, Office of High Energy Physics.

Content from this work may be used under the terms of the CC BY 3.0 licence (© 2015). Any distribution of this work must maintain attribution to the author(s), title of the work, publisher, and DOI.

ISBN: 978-3-95450-168-7 doi:10.18429/JACoW-IPAC2015-MOPMA045

CONCEPTUAL DIFFICULTIES OF A THERMODYNAMICS DESCRIPTION OF CHARGED-PARTICLE BEAMS *

Santiago Bernal, Institute for Research in Electronics and Applied Physics, University of Maryland, College Park, MD, 20742, USA

Abstract

We review the existing phenomenological theories of emittance growth with and without entropy terms and re-examine the condition for thermal equipartitioning in an unbunched charged-particle beam. The model incorporates linear space charge and a uniform-focusing lattice. Because of non-extensitivity of the transverse ("thermal") energy and the absence of a classical heat bath, we conclude that a rigorous classical thermodynamics treatment of charged-particle beams is not possible. In particular, the postulated relationships between the rms emittance and temperature and entropy must be qualified.

INTRODUCTION

Lapostolle suggested some 45 years ago [1] that a thermodynamic model may apply to the observed emittance exchanges between degrees of freedom in intense charged-particle beams (e.g., proton linacs at CERN). He went further to comment that heat flow may occur between degrees of freedom corresponding to different temperatures; under these circumstances, entropy would increase and emittance blow up in an irreversible manner.

Since Lapostolle's work, phenomenological theories of emittance growth have been developed by Wangler, Reiser, and others [2, 3]. Furthermore, a connection between rms emittance and entropy had been suggested by Lawson, Lapostolle and Gluckstern in 1973 [4]. Although the original work by Wangler et al does not address reversibility, an extension of the theory by O'Shea [5] predicts a connection between entropy changes and reversible and irreversible rms emittance growth. However, a thermodynamic framework for describing beam dynamics has neither been theoretically examined in detail nor tested in simulations.

Recent work by Hofmann and Boine-Frankenheim [6] emphasizes computational aspects of emittance and entropy growth. Their simulation studies focus on the role of grid resolution and numerical collisions on (6D) rms emittance and entropy growth in 3D beams confined by a periodic potential. Moreover, Hofmann and Boine-Frankenheim compare the numerical results to the predictions of a stochastic model developed by Struckmeier [7] based on temperature anisotropy and the effect of using macro-particles.

ENTROPY AND EMITTANCE GROWTH

In the phenomenological theory of Wangler et al [2, 3], the rate of change of normalized rms emittance (squared) in an unbunched beam is described by the equation

$$\frac{d\tilde{\varepsilon}_n^2}{dz} = -\frac{1}{8}\beta^2\gamma^2 \left\langle x^2 \right\rangle K \frac{d}{dz}\left[\frac{U(z)}{W_0}\right], \tag{1}$$

where z is the axial coordinate, $U(z) = W - W_u$ the difference between field energies per unit length of the actual beam distribution and the equivalent uniform distribution, i.e., the Kapchinskij-Vladimirskij (K-V) beam [3], and W_0 is the space-charge field energy per unit length inside the boundary of the equivalent K-V beam. The excess energy $U(z)$, or *free energy*, is available for the beam to thermalize. The symbol K represents the generalized beam perveance, which is proportional to current; $\left\langle x^2 \right\rangle = \left\langle y^2 \right\rangle$ is the squared rms transverse dimension at z, and the rest of the quantities have the standard meanings from special relativity.

No statement about *reversibility* is made in the original derivation of eq. (1). In O'Shea's work [5], though, eq. (1) is qualified as one *valid when the entropy change is zero* and, therefore, when the rms emittance change is in principle *reversible* by the application of *appropriate* forces. The reversibility, however, will depend on our ability to apply corrective forces with the same fine resolution that lead us to conclude that no entropy growth occurred. In many practical situations, this resolution is not possible and, hence, we must conclude that entropy in fact increased and emittance change is irreversible.

The normalized information entropy, S_n, in O'Shea's work is related to the normalized transverse rms emittance. For a 2-D beam we have [4]:

$$S_n(z) \equiv \frac{S_2(z)}{k_B N L} = \ln[\tilde{\varepsilon}_n(z)] + \ln[C(z)] - \ln[A_2], \tag{2}$$

where k_B is Boltzmann's constant, N is the number of beam particles per unit length, L, the bunch's length, is $L >>$ transverse dimension. $C(z)$ depends on the form of the phase-space particle distribution at z, and A_2 corresponds to the size of the grid cell for the computation, or the experimental resolution of the measuring device. Equation (2) tells us that it is possible to have rms emittance growth while entropy remains constant because the evolution of $C(z)$ may compensate for the growth. By the same token, it is possible for rms emittance to decrease while entropy increases. The value of $C(z)$ at $z = 0$, the start of the simulation or experiment, is denoted by C_0. For the widely used K-V distribution, for example, $C_0 = \pi$; for a thermal (Gaussian) distribution, $C_0 = \sqrt{2}\pi^{3/2}$ [4], more than twice the value for the K-V distribution.

* Work supported by U.S. Department of Energy

Content from this work may be used under the terms of the CC BY 3.0 licence (© 2015). Any distribution of this work must maintain attribution to the author(s), title of the work, publisher, and DOI.

ISBN: 978-3-95450-168-7 doi:10.18429/JACoW-IPAC2015-MOPMA046

SIMULATIONS AND EXPERIMENTS IN SUPPORT OF OCTUPOLE LATTICE STUDIES AT THE UNIVERSITY OF MARYLAND ELECTRON RING *

K. Ruisard, B. Beaudoin, I. Haber, T. Koeth
University of Maryland, College Park, MD, USA

Abstract

We present plans for a nonlinear lattice at the University of Maryland Electron Ring (UMER). Theory predicts that a strong nonlinear lattice can limit resonant behavior without reducing dynamic aperture if the nonlinear fields preserve integrability or quasi-integrability. We discuss plans for a quasi-integrable octupole lattice, based on the work of Danilov and Nagaitsev. We use Elegant and the WARP PIC code to estimate the octupole-induced tune spread. We discuss improvements to the ring in support of octupole lattice experiments, including generation and detection of emittance-dominated, negligible space charge beams.

INTRODUCTION

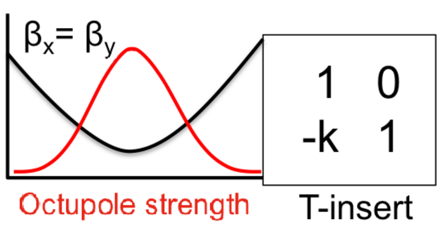

Figure 1: Toy model of quasi-integrable octupole lattice.

Conventional accelerators are based on Courant and Snyder's theory of the alternating-gradient synchrotron, developed in 1952 [1]. In an AG focusing lattice, particles oscillate transversely with a characteristic tune. Unfortunately, this system is susceptible to coherent resonances which lead to beam loss and halo growth. Thin lens octupoles for Landau damping limit coherent resonances, but introduce unbounded chaotic orbits leading to particle losses and limiting achievable beam intensity.

A novel approach by Danilov and Nagaitsev suggests an integrable but highly nonlinear lattice as an alternative to the standard AG synchrotron [2]. In a nonlinear lattice with a large amplitude-dependent tunes spread, particles that are resonantly driven to higher amplitudes will decohere from that resonance and have only limited amplitude growth. Effectively, the beam is immune to coherent resonances. This nonlinear detuning is also shown to mitigate halo growth driven by beam envelope mismatch [3].

The fully integrable elliptic potential willl be tested at Fermilab's IOTA ring [4]. Danilov and Nagaitsev also consider the case in which the nonlinear field is purely octupolar. Particles contained in an octupole potential that scales as $V(s) \propto {}^{1}/_{\beta^3(s)}$ will conserve a single invariant of transverse motion, the normalized Hamiltonian, and particle orbits will be chaotic but bounded. The nonlinear optics program at UMER will test this quasi-integrable lattice by incorporating octupole magnets into the existing ring framework.

This paper describes the progress being made towards the UMER octupole lattice design and experiments. The simulation effort is focused on identifying an operating point for the lattice that maximizes beam tune spread with acheivable octupole fields. Experimental work includes demonstration of a negligible space charge beam for future lattice studies.

* This work is supported by the NSF Graduate Research Fellowship and the NSF Accelerator Science Program

NONLINEAR UMER LATTICE

The theory of quasi-integrable nonlinear optics assumes a symmetric beam is propagating in nonlinear fields that are scaled longitudinally with the inverse of the envelope function [2]. External focusing must be provided for a bounded envelope function. To achieve this in a ring, a nonlinear channel will installed over a symmetric beam waist, and the remaining linear lattice has a transfer function equivalent to a thin x-y symmetric focusing lens. This is shown schematically in Fig. 1.

UMER is a 10 keV, 11.52 meter storage ring that supports electron beams with variable tune depressions $({}^{\nu}/_{\nu_0} = 0.85 - 0.15)$ for the study of space charge dominated beam dynamics. The ring lattice is 36 FODO cells composed of printed circuit quadrupoles and dipoles. To modify UMER as a nonlinear optics test bed, we will superimpose an octupole channel onto the existing lattice, as shown in

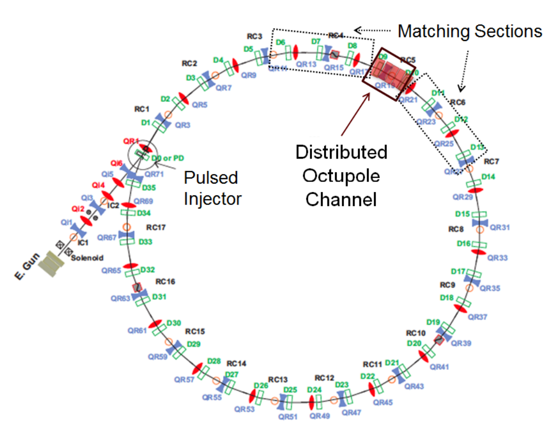

Figure 2: UMER lattice showing quadrupole and dipole elements, with overlay of future octupole channel.

Content from this work may be used under the terms of the CC BY 3.0 licence (© 2015). Any distribution of this work must maintain attribution to the author(s), title of the work, publisher, and DOI.

ISBN: 978-3-95450-168-7 doi:10.18429/JACoW-IPAC2015-MOPMA047

Content from this work may be used under the terms of the CC BY 3.0 licence (© 2015). Any distribution of this work must maintain attribution to the author(s), title of the work, publisher, and DOI.

NONLINEAR BEAM DYNAMICS STUDIES OF THE NEXT GENERATION STRONG FOCUSING CYCLOTRONS AS COMPACT HIGH BRIGHTNESS, LOW EMITTANCE DRIVERS*

S. Assadi#, P. McIntyre, A. Sattarov, Texas A&M University, College Station, TX 55057, USA
N. Pogue, PSI, 5234 Villigen, Switzerland

Abstract

The Strong Focusing Cyclotron development at Texas A&M University has evolved from stacks of cyclotrons to a single layer high brightness, low emittance device to produce greater than 10 mA of proton beam to a desired target at 800 MeV. The latest design has a major geometric design optimization of strong focusing quadrupoles and a modified algorithm of high gradient cavities. These optimizations address the turn separation and interaction of radially neighbouring bunches and produced a reduced the number of turns necessary to reach the desired final energy under control conditions. In this paper, we present the new design, the physics of nonlinear synchrobetatron coupling, mvh+nvv=p causing beam blow-up in other form of cyclotrons and how this work has resolved it. The cavity beam loading, and space charge effects of multi turns at low energies to reduce losses, are discussed.

INTRODUCTION

The Accelerator Research Lab at Texas A&M University is developing designs for a strong-focusing cyclotron (SFC) as a high-current (10 mA CW) proton driver for fundamental physics, ADS fission, production of medical isotopes, and as a spallation source for neutron damage studies. Challenges associated with high power, high brightness linear accelerators, such as minimizing particle losses, space charge and beam stability, are also obstacles from the SFC. Cyclotrons have additional degrees of complexity as the multi-bunches pass through the cavities and have coulomb and Wakefield interactions. We report on three studies in this paper: (1) better understanding of proposed cavity by modelling stiffened cavity after additional corrugations, (2) initial corona and multipacting studies of the new cavity, and lastly wakefield studies of uncoupled and coupled bunches traversing through SFC cavity with a realistic 6D initial bunch distribution.

BEAM DYNAMCIS

The world-record CW beam power for a proton accelerator today is the PSI isochronous cyclotron [1], which produces 2.2 mA CW at 590 MeV. Two issues pose the main limits to its beam current: succeeding orbits overlap strongly so the defocusing action of space charge is exacerbated; and it has only weak focusing so that the betatron tunes migrate throughout acceleration and cross multiple resonances. We solve both problems in the SFC, see Fig. 1, by incorporating two new elements:

- superconducting ó-wave slot-geometry cavities that provide sufficient energy gain per turn to fully separate the orbits;
- beam transport channels that provide alternating-gradient strong focusing to maintain constant betatron tunes throughout acceleration.

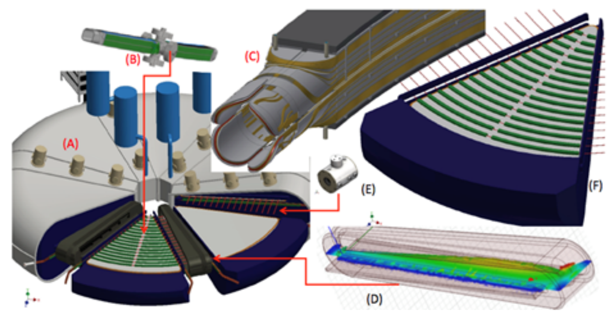

Figure 1: Strong-focusing cyclotron: a) cutaway showing the proton orbits, warm-iron flux return, (B) Beam Position Monitors between every two quad-channel. (C) quad channel composed of corrector and MgB2 4.2 cm bore magnet, (D) electric field distribution in the superconducting slot-geometry ½ wave cavity, (e) twenty five cm long 500 Watt instrumented beam dump at extraction channel, and (f) cold-iron flux plate with FD pairs of arc beam transport channels defining each equilibrium orbit.

Our initial simulations show that one such 800 MeV SFC could deliver > 10 mA continuously (cw) so that a high-current proton beam could be available for the above-mentioned purposes. In Ref. [2] we addressed the versatilities of quad focusing and added correctors allowing one to compensate for out of tolerance magnets by 100 times of other cyclotrons or 1% of main field. Additionally it has been shown the system can accept the loss of one of the ten cavities. In this paper we attempt to address the cavity and demonstrated a deep understanding of the self-field and beam coupling in the cavity.

SRF Cavity

The original straight cavity designed for SFC-800 MeV did not incorporate any corrugations in its calculations, although they were planned to be inserted based on the experience at BNL [3].

*Work supported by Texas A&M University and HiTek ESE LLC.
#assadi@tamu.edu

ISBN: 978-3-95450-168-7 doi:10.18429/JACoW-IPAC2015-MOPMA049

DEVELOPMENT OF A SINGLE-PASS AMPLIFIER FOR AN OPTICAL STOCHASTIC COOLING PROOF-OF-PRINCIPLE EXPERIMENT AT FERMILAB'S * IOTA FACILITY

M. B. Andorf[1], V. A. Lebedev[2], and P. Piot[1,2],
[1]Department of Physics and Northern Illinois Center for Accelerator & Detector Development, Northern Illinois University DeKalb, IL 60115, USA
[2]Accelerator Physics Center, Fermi National Accelerator Laboratory, Batavia, IL 60510, USA

Abstract

Optical stochastic cooling (OSC) is a method of beam cooling which is expected to provide cooling rates orders of magnitude larger than ordinary stochastic cooling. Light from an undulator (the pickup) is amplified and fed back onto the particle beam via another undulator (the kicker). Fermilab is currently exploring a possible proof-of-principle experiment of the OSC at the integrable-optics test accelerator (IOTA) ring. To implement effective OSC a good correction of phase distortions in the entire band of the optical amplifier is required. In this contribution we present progress in experimental characterization of phase distortions associated to a Titanium Sapphire crystal laser-gain medium (a possible candidate gain medium for the OSC experiment to be performed at IOTA). We also discuss a possible option for a mid-IR amplifier.

INTRODUCTION

An Optical Stochastic Cooling experiment (OSC) is planned to take place at the Advanced Superconducting Test Accelerator (ASTA) in the Integrable Optics Test Accelerator (IOTA) ring at Fermilab [1]. OSC is a beam cooling technique capable of providing damping rates orders of magnitude larger than the conventional and widely implemented microwave stochastic cooling. In OSC a particle passes through an undulator (the pickup) and radiates; see Fig. 1. This radiation is amplified while the particle is delayed via a magnetic chicane. The particle and amplified radiation then meet in a second undulator (the kicker) with a relative phase in such a way to provide a corrective longitudinal kick [2] [3].

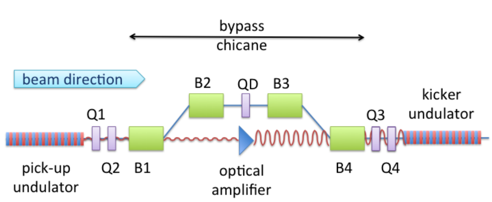

Figure 1: Schematics of the OSC insertion. The labels "Qx", "Bx" respectively correspond to quadrupole and dipole bending magnets.

* M. A. is financially supported by a Great-Journey Assistantship from Northern Illinois University. V. L and P.P are supported by the Fermi Research Alliance, LLC under Contract No. DE-AC02-07CH11359 with the US DOE.

The chicane is only capable of providing a few millimeters of delay and thus puts a serious constraint on the optical amplifier (OA) design. A single-pass OA was suggested in [4] using Titanium Sapphire (Ti:Sapph) as the gain medium with a center wavelength of 780 nm.

The Cooling rate is inversely proportional to the bandwidth of the system. Since the undulator bandwidth can be made quite large, the system bandwidth is determined by the OA and so a gain material with a large bandwidth is desirable. Ti:Sapph is a promising candidate gain material because it is capable of providing a large amount of gain for a short signal delay over a large bandwidth.

This paper discusses progress made in the development of a single pass OA using Ti:Sapph, specifically steps toward characterizing the possibility of phase distortions in the amplification process. Additionally Cr:ZnSe is suggested as an alternative gain medium.

PHASE MEASUREMENTS

Technique

If a gain material of thickness T and index of refraction n is inserted into one leg of an interferometer, the relative phase of light passing through can be written as

$$\phi = k[\Delta L + Tn(\lambda)] \tag{1}$$

with ΔL being the path length difference between the two legs, $k \equiv \frac{2\pi}{\lambda}$ and λ is the wavelength of the radiation. The path length difference can be written as $\Delta L = C - Tn(\lambda_o)$ with C being a constant and λ_o a fixed wavelength. The index of refraction can also be Taylor expanded around λ_o. Doing so up to second order and inserting the expression for the path length difference into Eq. (1) yields

$$\phi = kT\left[\frac{C}{T} + \frac{dn}{d\lambda}(\lambda - \lambda_o) + \frac{1}{2}\frac{d^2n}{d\lambda^2}(\lambda - \lambda_0)^2\right] \tag{2}$$

Dividing the above expression by kT results in a quadratic equation in $(\lambda - \lambda_o)$. The linear portion of this equation results in a net delay of the optical pulse and thus can be compensated for by the chicane. The non-linear portion results in a modification of the pulse shape and is not able to be compensated by the chicane. It is this coefficient $a = \frac{d^2n}{d\lambda^2}$ that needs to be measured during the amplification process. This is done by measuring the phase as a function of wavelength and performing a least squares fit.

Content from this work may be used under the terms of the CC BY 3.0 licence (© 2015). Any distribution of this work must maintain attribution to the author(s), title of the work, publisher, and DOI.

ISBN: 978-3-95450-168-7 doi:10.18429/JACoW-IPAC2015-MOPMA050

SMOOTH FAST MULTIPOLE METHOD FOR SPACE CHARGE TRACKING: AN ALTERNATE TO PARTICLE-IN-CELL

A. Gee*,[1] and B. Erdelyi†,[1,2]

[1]Physics Department, Northern Illinois University, DeKalb, IL 60115, USA
[2]Physics Division, Argonne National Laboratory, Argonne, IL 60439 , USA

Abstract

The fast multipole method (FMM) algorithm was developed by Greengard and Rokhlin in 1987 [1]. As one of the top ten algorithms of the 20th century, it has been applied in a wide range of fields. The FMM complexity is $O(N)$, where N is the number of particles, allowing for large-scale simulations. However, it includes all the two-body collisional forces, in contrast to other methods such as the popular particle in-cell (PIC) methods. While collisionality can be very important, many applications require only the mean field effects. PIC is frequently used in this regime. Due to recent concerns of unphysical effects of grids, interpolation and other approximations in PIC codes, an alternative based on different underlying assumptions would prove enlightening. For these cases, a smoothed or softened FMM using a Plummer-like smoothing parameter holds much promise. Unfortunately, the original FMM algorithm based on analytic expansions of the $\frac{1}{r}$-like potentials does not allow for Plummer softening. We present our new soft-FMM employing differential algebras (DA) to obtain the modified expansions. We also compare the performance of the smoothed DA-FMM with examples from PIC simulations.

INTRODUCTION

Algorithms to solve the N-body problem have advanced greatly in recent years. With increasing interest in high intensity beams, tracking codes must efficiently simulate collective effects, particularly space charge. Particle in-cell (PIC) is the standard class of methods for the accelerator and beam community. Since all PIC methods share the basic assumptions [2], comparing PIC codes would not distinguish unphysical behavior, which are well-known to exist due to numerical noise, interpolation errors, grid heating, etc. An alternative method based on completely different assumptions would prove insightful.

Of recently developed methods, the fast multipole method (FMM) shows great promise. We present the smoothed FMM as an alternative to PIC. Previously, we implemented the FMM using a differential algebraic (DA) framework. With the DA method, we reformulated the FMM in real Cartesian space and made it kernel independent. However, while PIC estimates the mean fields, the FMM includes all collisional effects. Since close encounters lead to strong collisions, unphysical in this context, we introduced Plummer-like smoothing or softening into the FMM. This technique could not be done with the original FMM, but the kernel independence based on the DA framework allows computational cost in the smooth FMM to be near the same as the original FMM. With appropriate softening parameter, the FMM can estimate the mean fields to be used for space charge tracking. This paper illustrates the behavior of the smoothed FMM for transverse space charge and compares it to theory, the method of statistical moments (MoM) [3], and a widely-used representative PIC code.

SMOOTHED DA-FMM IN CARTESIAN FORM

The smoothed 2D Coulomb potential at (x, y) due to a source at (x_0, y_0) of unit charge with smoothing parameter λ is given by (1), or alternatively by (2). (1) and its derivative are used for particle-particle interactions.

$$\Phi(x, y, \lambda) = -\frac{1}{2}\log\left((x-x_0)^2 + (y-y_0)^2 + \lambda^2\right) \quad (1)$$

$$= -\frac{1}{2}\left\{\log\left(x^2+y^2+\lambda^2\right) + \log\left[1 + \frac{x_0^2+y_0^2}{x^2+y^2+\lambda^2} - 2\frac{xx_0+yy_0}{x^2+y^2+\lambda^2}\right]\right\} \quad (2)$$

Far multipole expansion

We can separate (2) as $\Phi(x, y, \lambda) = \Phi_T + \Phi_M$, where Φ_T only depends on the target position. We expand Φ_M in (2) from the origin. Let $r^2 \equiv x^2 + y^2 + \lambda^2$. We define DA variables, $d_x = \frac{x}{r^2}$, $d_y = \frac{y}{r^2}$, $d_\lambda = \frac{\lambda}{r^2}$, and $d_r^2 = \frac{1}{r^2} = d_x^2 + d_y^2 + d_\lambda^2$. Substituting these into the second log term of (2), we have the form for the smooth multipole expansion Φ_M, given in (3).

$$\Phi_M(x, y, d_x, d_y, \lambda, d_\lambda) = -\frac{1}{2}\log[1 + (x_0^2+y_0^2)d_r^2 - 2(x_0d_x + y_0d_y)] \quad (3)$$

The DA framework allows efficient expansion of Φ_M in terms of the DA variables. Thus, we will get a Taylor series in d_x, d_y, d_λ describing the multipole expansion, which we may evaluate using the DA variables defined earlier.

Multipole-to-multipole translation

To remap (3) to a new multipole center, (x_m, y_m), we redefine the DA variables as $d_{x_2} = \frac{x_2}{r_2^2}$, $d_{y_2} = \frac{y_2}{r_2^2}$, $d_{\lambda_2} = \frac{\lambda}{r_2^2}$,

* agee1@niu.edu
† berdelyi@niu.edu

Content from this work may be used under the terms of the CC BY 3.0 licence (© 2015). Any distribution of this work must maintain attribution to the author(s), title of the work, publisher, and DOI.

ISBN: 978-3-95450-168-7 doi:10.18429/JACoW-IPAC2015-MOPMA051

Content from this work may be used under the terms of the CC BY 3.0 licence (© 2015). Any distribution of this work must maintain attribution to the author(s), title of the work, publisher, and DOI.

GENERATION OF MODULATED BUNCH USING A MASKED CHICANE FOR BEAM-DRIVEN ACCELERATION EXPERIMENTS AT ASTA

Y. M. Shin, Department of Physics, Northern Illinois University, Dekalb, IL 60115, USA and Accelerator Physics Center (APC), FNAL, Batavia, IL 60510
A. Green, Department of Physics, Northern Illinois University, Dekalb, IL 60115, USA
D. J Crawford, Accelerator Physics Center (APC), FNAL, Batavia, IL 60510
P. R. G. Piot, Department of Physics, Northern Illinois University, Dekalb, IL 60115, USA and Accelerator Physics Center (APC), FNAL, Batavia, IL 60510
D.R. Broemmelsiek, Accelerator Physics Center (APC), FNAL, Batavia, IL 60510
A. Lumpkin, Accelerator Division (AD), FNAL, Batavia, IL 60510

Abstract

Density modulations on electron beams can improve machine performance of beam-driven accelerators and FELs with resonance beam-wave coupling. The beam modulation is studied with a masked chicane by the analytic model and simulations with the beam parameters of the Advanced Superconducting Test Accelerator (ASTA) in Fermilab. With the chicane design parameters (bending angle of 18°, bending radius of 0.95 m and R_{56} ~ - 0.19 m) and a nominal beam of 3 ps bunch length, the analytic model showed that a slit-mask with slit period 900 μm and aperture width 300 μm induces a modulation of bunch-to-bunch spacing ~100 μm to the bunch with 2.4% correlated energy spread. With the designed slit mask and a 3 ps bunch, particle-in-cell (PIC) simulations, including nonlinear energy distributions, space charge force, and coherent synchrotron radiation (CSR) effect, also result in beam modulation with bunch-to-bunch distance around 100 μm and a corresponding modulation frequency of 3 THz. The beam modulation has been extensively examined with three different beam conditions, 2.25 ps (0.25 nC), 3.25 ps (1 nC), and 4.75 ps (3.2 nC), by tracking code Elegant. The simulation analysis indicates that the sliced beam by the slit-mask with 3 ~ 6% correlated energy spread has modulation lengths about 187 μm (0.25 nC), 270 μm (1 nC) and 325 μm (3.2 nC). The theoretical and numerical data proved the capability of the designed masked chicane in producing modulated bunch train with micro-bunch length around 100 fs.

INTRODUCTION

We have been investigating the masked chicane technique [1 – 3] with the available beam parameters such as the 50 MeV photoinjector of the Advanced Superconducting Test Accelerator (ASTA), which is currently being constructed and commissioned in Fermilab [4]. Downstream of the ASTA 50 MeV photoinjector beamline, a magnetic bunch compressor, consisting of four rectangular dipoles, is adopted and a slit-mask is designed and inserted in the middle. Based on this slit-masked chicane, the bunching performance and the ability of sub-ps microbunch generation are studied.

In order to evaluate bunching performance with nominal beam parameters, the masked chicane has been analyzed by the linear bunching theory in terms of bunch-to-bunch distance and microbunch length. Elegant code is employed to examine the theoretical model with the ASTA nominal beam parameters (RMS bunch length $\sigma_{z,i}$ is 3 ps and energy ratio τ is around 0.1). The Particle-In-Cell (PIC) simulation (CST-PS) includes space charge and CSR effect and nonlinear energy distribution over macro-particle data. For Elegant simulations, bunch charge distribution and the beam spectra are mainly investigated with three different bunch charges, 0.25 nC, 1 nC, and 3.2 nC, under two RF-chirp conditions of minimum and maximum energy spreads. The corresponding bunch length for the maximally chirped beam is 2.25, 3.25, and 4.75 ps and the correlated energy spread is 3.1, 4.5, and 6.2 % respectively for bunch charge of 0.25 nC, 1 nC, and 3.2 nC

ANALYTIC DESIGN

The designed chicane consists of four dipoles and a slit mask with slit spacing, *W*, and aperture width, *a*, is inserted in the middle of the bunch compressor (dispersion region). Before the beam is injected into the masked chicane, a positive linear energy-phase correlation is imposed by accelerating the beam off the crest of the RF wave in the linear accelerator. The chicane disperses and re-aligns the particles with respect to their energies in phase space. The input beam is then compressed and the phase space ellipse is effectively rotated toward the vertical. In the middle of the chicane, the beam is partially blocked by the transmission mask and holes are introduced in the energy-phase ellipse. In the second half of the chicane, the beam is deliberately over-bunched and the beam ellipse is slightly rotated past the vertical. In this step, the linear energy-phase correlation is preserved by over-bunching, accompanied with a steeper phase-space slope. Consequently, the projection of the beam ellipse on the time axis generates

*Work supported by the DOE contract No.DEAC02-07CH11359 to the Fermi Research Alliance LLC

ISBN: 978-3-95450-168-7 doi:10.18429/JACoW-IPAC2015-MOPMA052

IMPLEMENTATION OF QUADRUPOLE-SCAN EMITTANCE MEASUREMENT AT FERMILAB'S ADVANCED SUPERCONDUCTING TEST ACCELERATOR (ASTA)

A. T. Green, Department of Physics, Northern Illinois University, Dekalb, IL 60115, USA
Y. M. Shin, Department of Physics, Northern Illinois University, Dekalb, IL 60115 and
Accelerator Physics Center (APC), FNAL, Batavia, IL 60510

Abstract

Transverse emittance measurements based on the quadrupole scan technique have been widely used to characterize the beam phase space parameters in linear accelerators. This paper discusses the implementation of the technique at the Advanced Superconducting Test Accelerator (ASTA) at Fermilab. We plan on deploying a flexible implementation that permits an operator to select a quadrupole with associated analyzing screen to measure the beam emittance. Our implementation utilizes Python scripts combined with Fermilab's control system ACNet and ELEGANT tracking code. We also discuss the applicability of the quadrupole scan method at 20.3 MeV at an operating charge of 250 pC at ASTA. Some preliminary measurements will also be presented.

INTRODUCTION

The Advanced Superconducting Test Accelerator (ASTA) has been constructed and commissioned in Fermilab and it is currently scheduled to build a high energy beamline (150 – 300 MeV) by adding a cryomodule with construction plan of the Integrable Optics Test Accelerator (IOTA) ring by 2016. Most recently, 20 MeV of electron beam energy was successfully demonstrated in the ASTA injector beamline and it is planned to increase the beam energy up to 50 MeV with the schedule to add a capture cavity downstream of the photoinjector. Along with the timeline of the construction/commissioning schedules, it is necessary to assure a beam monitoring technique for a full scale transverse and longitudinal phase-space characterization of a commissioned beam, which enables to precisely operate the machine. Instantaneous monitoring of beam parameters is highly required for preserving the beam emittance along the beamline. We have been working on the idea of developing a real-time emittance monitoring system based on a quadruple-scan technique [1,2]. Our plan is to design a Python script programmed with a quad-scan algorithm and to implement it in the ASTA beamline control system (ACNet console). We expect that successful development of a designed system will allow a beamline operator to trace temporal profiles of transverse beam parameters and also to systematically control the dynamics using quadrupoles installed in the ASTA beamline.

*Work supported by the DOE contract No.DEAC02-07CH11359 to the Fermi Research Alliance LLC.

BEAM DYNAMICS

Emittance is an important property of charged particle beams, allowing for a description of beam quality and the comparison of beams. Generally, emittance can be described in six-dimensional phase space $[x, y, z, p_x, p_y, p_z]$ as the spread of density of particles in the beam. In many cases, the transverse emittance is of particular interest and the six-dimensional phase space is split into subspaces comprised of (x, p_x) and (y, p_y) [1].

The area occupied by the particles of interest may be considered as being bound by an ellipse and can mathematically be described by the following beam matrix:

$$\Sigma_{beam} = \begin{bmatrix} \Sigma_{11} & \Sigma_{12} \\ \Sigma_{21} & \Sigma_{22} \end{bmatrix}. \quad (1)$$

Figure 1 shows the beam ellipse and the physical interpretation of its physical components. In the figure, x and x' are the position and angle of the particles, respectively.

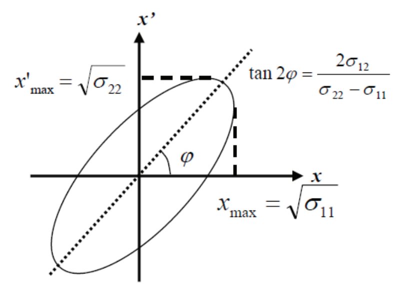

Figure 1: Beam ellipse with physical interpretation of the physical components [1].

Using the beam matrix, the geometrical emittance can then be defined as:

$$\epsilon = \pi\sqrt{\Sigma_{beam}} \quad (2)$$

The beam ellipse and matrix can also be expressed in terms of the Courant-Snyder parameters:

$$\epsilon = \gamma x^2 + 2\alpha x x' + \beta x'^2, \quad (3)$$

where $\gamma = \Sigma_{22}/\epsilon$, $\alpha = -\Sigma_{12}/\epsilon$, and $\beta = \Sigma_{11}/\epsilon$ [3].

A more complete description of the emittance may be given as the root mean square emittance (ϵ_{rms}). With this description, the moments of the particle distribution in phase space can be related to the beam matrix elements by [1]:

Content from this work may be used under the terms of the CC BY 3.0 licence (© 2015). Any distribution of this work must maintain attribution to the author(s), title of the work, publisher, and DOI.

ISBN: 978-3-95450-168-7 doi:10.18429/JACoW-IPAC2015-MOPMA053

CHARACTERIZING BETATRON TUNE KNOBS AT DUKE STORAGE RING *

H. Hao†, S. Mikhailov, V. Popov, Y.K. Wu, TUNL, Duke University, Durham, NC 27708, USA
J. Li, University of Science and Technology of China, Hefei, Anhui 230029, China

Abstract

A good control of the electron beam betatron tune is critical for the operation of a storage ring. As the driver for Duke free-electron lasers (FELs) and the High Intensity Gamma-ray Source (HIGS), the Duke storage ring is operated in a wide energy range (0.3 GeV – 1.2 GeV), with several different electromagnetic wiggler configurations. This creates the challenge of controlling the betatron tune in a global manner. As the the first step, the feedforward tune compensation schemes were designed and implemented to the real-time computer control system to compensate the tune change caused by the wiggler field. To further increase the flexibility of the operation, a set of tune knob schemes are designed for various wiggler configurations. The β function changes caused by these knobs are constrained within the south straight section where the tune knob is located, minimizing the impact on the electron beam dynamics (i.e. injection and lifetime). The tune and β function measurements show a good agreement with the calculation. In addition, it is found that some tune knob schemes are effective for new wiggler configurations that are not originally designed for.

INTRODUCTION

In the operation of a storage ring based light source, it is necessary to have a good control of the storage ring lattice, i.e. the ability to vary the betatron tunes in a desired way. This type of control is usually realized using the tune knob, a scheme to vary a set of quadrupoles simultaneously in a way such that the global tunes can be changed as needed. As the driver for Duke free-electron lasers (FELs) and the High Intensity Gamma-ray Source (HIGS) [1] [2], the Duke storage ring is operated in a wide energy range from 0.3 GeV to 1.2 GeV, with several different electromagnetic wiggler configurations. The vasitility of the Duke storage ring opeation creates the challenge of designing a set of betatron tune knobs to work with different lattice configurations. As part of the wiggler switchyard upgrade project in 2012, a set of tune knobs were designed on top of the lattices with wiggler focusing compensations [3]. The knobs were implemented into the EPICS control system in a feedforward manner [4]. The tune knobs have been used for the HIGS γ-ray operation since 2012. In this paper, we report the quantitative investigation of effectiveness of these tune knobs and document a set of calibrations to improve the usefulness of the tune knobs.

* Work supported by US Department of Energy grant DE-FG02-97ER41033.
† haohao@fel.duke.edu

DESIGN OF THE TUNE KNOB

A tune knob is realized by changing the the strength of a set of quadrupoles in the storage ring. To minimize the impact on the beam dynamics of the Duke storage ring, e.g. the injection, the β fucntion changes introduced by the quadrupole variations are constrained within the 34-meter-long south straight section (SSS). The lattice at two ends are required to match with the arc lattice when the quadrupoles are varied. To preserve the beam dynamics, the symmetry of the lattice also should be preserved whenever possible.

For the HIGS γ-ray operation, the electron beam energy, FEL wiggler strength and configuration are varied in a wide range to produce high-flux γ-ray photon beams for a variety of nuclear physics experiments. To cover such wide range of operation, a number of tune knobs are designed for 6 commonly used wiggler configurations, with the wiggler strength varying from zero to its maximum setting. The horizontal (or vertical) tune knobs are designed to control tune only in one direction, with a minimum impact on the tunes in the other direction. The complete tune knob to change both ν_x and ν_y is realized by simply adding together the two independent knobs in the two directions. Numerical computation shows that this design could simultaneously control tunes (ν_x, ν_y) in both directions.

CALIBRATION OF THE TUNE KNOBS

The calibration of tune knobs requires a large number of tune measurements. A transverse feedback (TFB) based tune measurement technique was used to reduce the tune measurement time [5]. In the measurement, the electron beam is excited by a pseudo white noise signal with a finite bandwidth which covers the frequency range of betatron tunes. The turn-by-turn BPM signal of the transverse orbit motion is recorded by the TFB. By using the fast Fourier transform (FFT), the betatron tune can be identified. Compared to the conventional network analyzer based method that we also use, the TFB based tune measurement technique reduces the measurement time by a factor of 3, with an improved tune resolution. In the operation of Duke storage ring, the tune variation cannot reach the maximum designed tune knob values of ±0.1 due to the betatron tune resonances. One of the resonances is the horizontal integer resonance $\nu_x = 9$; another one is the difference resonance $\nu_x - \nu_y = 5$. In our measurements, the tune knob variation is limited within ±0.05, which is more than adequate to cover the tune variation for HIGS operation.

Content from this work may be used under the terms of the CC BY 3.0 licence (© 2015). Any distribution of this work must maintain attribution to the author(s), title of the work, publisher, and DOI.

ISBN: 978-3-95450-168-7 doi:10.18429/JACoW-IPAC2015-MOPMA054

START-TO-END SIMULATION OF FREE-ELECTRON LASERS

C.C. Hall, H.P. Freund, S.G. Biedron, S.V. Milton
Colorado Sate University, Fort Collins, CO 80523, USA

Abstract

Start-to-end (S2E) modeling of free-electron lasers (FELs) normally requires the use of multiple codes to correctly capture the physics in each region of the machine. Codes such as PARMELA, IMPACT-T or MICHELLE, for instance, may be used to simulate the injector. From there the linac and transport line may be handled by codes such as DIMAD, ELEGANT or IMPACT-Z. Finally, at the FEL a wiggler interaction code such as GENESIS, GINGER, or MINERVA must be used. These codes may be optimized to work with a wide range in magnitude of macro-particle numbers (from 10^4-10^8 in different codes) and have different input formats. It is therefore necessary to have translator codes to provide a bridge between each section. It is essential that these translators be able to preserve the statistical properties of the bunch while raising or lowering the number of macro-particles used between codes. In this work we show a suite of such translators designed to facilitate S2E simulations of an FEL with a new wiggler code, MINERVA, and use these codes to provide benchmarking of MINERVA against other common wiggler simulation codes.

INTRODUCTION

The simulation of an FEL including the injector, linac, beam transport, and undulator requires modeling of the electron beam in a variety of regimes, all of which have differing dominant effects. To accurately perform these start-to-end simulations it is normally necessary to use of variety of codes, each of which is adapted to accurate simulation in a particular regime. It is therefore necessary to be able pass the beam distribution from one code onto another. Unfortunately, these codes often use a variety of conventions for representing the distribution and in the case of macro-particle based codes there is often great disparity in the number of macro-particles necessary for effective simulation. In this paper we describe a set of software tools built to provide translation between the particle tracking codes PARMELA [1], DIMAD [2], and ELEGANT [3] to the undulator simulation code MINERVA [4]. In particular we look at the use of an ELEGANT output to perform an FEL simulation in MINERVA.

MINERVA

MINERVA is a new FEL code under development capable of modeling a large range of FEL configurations, including seeded and self-amplified spontaneous emission (SASE) amplifiers and FEL oscillators (through interface with the optical propagation code OPC [5]). The formulation used in MINERVA describes the particles and fields in three spatial dimensions and includes time dependence as well. Electron trajectories are integrated using the complete Newton-Lorentz force equations. No wiggler-averaged-orbit approximation is made. The magnetostatic fields can be specified by analytical functions for a variety of analytic undulator models (such a planar or helical representations), quadrupoles, and dipoles. These magnetic field elements can be placed in arbitrary sequences to specify a variety of different transport lines. The electromagnetic field is described by a modal expansion. For free-space propagation, MINERVA uses Gaussian optical modes, while waveguide modes are used when the wavelength is comparable to the dimensions of the drift tube. As a result, MINERVA can treat both long and short wavelength FELs. A combination of the Gaussian and waveguide modes is also possible when there is partial guiding at, for example THz frequencies.

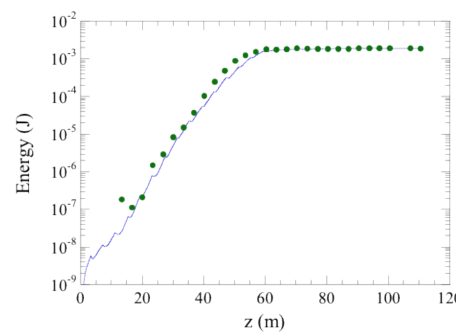

Figure 1: Comparison between experimental data for the LCLS (Green dots) and simulation in MINERVA (blue line).(LCLS data courtesy of P. Emma and H.-D. Nuhn.)

Particle loading is done in a deterministic way using Gaussian quadrature that preserves a quiet start for both the fundamental and all harmonics. Shot noise is included using the usual Poisson statistics algorithm [6] so that MINERVA is capable of simulating SASE FELs; however, provision is made for enhanced shot-noise due to various levels of micro-bunching.

Shown in Fig. 1 is a comparison between measured and simulated pulse energies for the LCLS SASE FEL. The simulation results represent an average over an ensemble of runs performed with different noise seeds

ELEGANT

The code ELEGANT, ELEctron Generation And Tracking is a macro-particle code that can track particles in 6-D phase space using matrices, canonical-kick elements, numerically integrated elements, or a combination of techniques [3]. Of particular importance to linac-based FEL design, ELEGANT includes a 1-D coherent synchrotron radiation (CSR) model [7]. This allows for modeling the impact of CSR in the

Content from this work may be used under the terms of the CC BY 3.0 licence (© 2015). Any distribution of this work must maintain attribution to the author(s), title of the work, publisher, and DOI.

ISBN: 978-3-95450-168-7 doi:10.18429/JACoW-IPAC2015-MOPMA055

Content from this work may be used under the terms of the CC BY 3.0 licence (© 2015). Any distribution of this work must maintain attribution to the author(s), title of the work, publisher, and DOI.

MUSIM, A GRAPHICAL USER INTERFACE FOR MULTIPLE SIMULATION PROGRAMS

Thomas J. Roberts*, Muons, Inc., Batavia, IL 60510, USA
Paul Guèye, Hampton University, Hampton, VA 23668, USA

Abstract

MuSim is a new user-friendly program designed to interface to many different particle simulation codes, regardless of their data formats or geometry descriptions. It presents the user with a compelling graphical user interface that includes a flexible 3-D view of the simulated world plus powerful editing and drag-and-drop capabilities. All aspects of the design can be parameterized so that parameter scans and optimizations are easy. It is simple to create plots and display events in the 3-D viewer (with a slider to vary the transparency of solids), allowing for an effortless comparison of different simulation codes. Simulation codes: G4beamline [1], MAD-X [2], and MCNP [3]; more will be coming. Many accelerator design tools and beam optics codes were written long ago, with primitive user interfaces by today's standards. MuSim is specifically designed to make it easy to interface to such codes, providing a common user experience for all, and permitting the construction and exploration of models with very little overhead. For today's technology-driven students, graphical interfaces meet their expectations far better than text-based tools, and education in accelerator physics is one of our primary goals.

OVERVIEW

MuSim is designed to make it easy to construct, simulate, and analyze all types of particle simulations, using any supported simulation code. As shown in Fig. 1, the user interface is 100% graphical and offers advanced user features not available in any other particle-simulation program. It has a flexible 3-D viewer that displays the system as it is constructed, and into which Library objects can be simply dragged and dropped (objects can also be placed at specific positions and orientations). The basic abstraction is based on solid objects placed into the world and/or each other, which is much more flexible and intuitive than the geometry specifications of some simulation codes like MCNP. Along with the parameterization of any aspect of the simulation, this makes simulation decks far more modifiable and maintainable. There is a comprehensive Help system that follows user navigation, and a slider for solid transparency (easily see inside them).

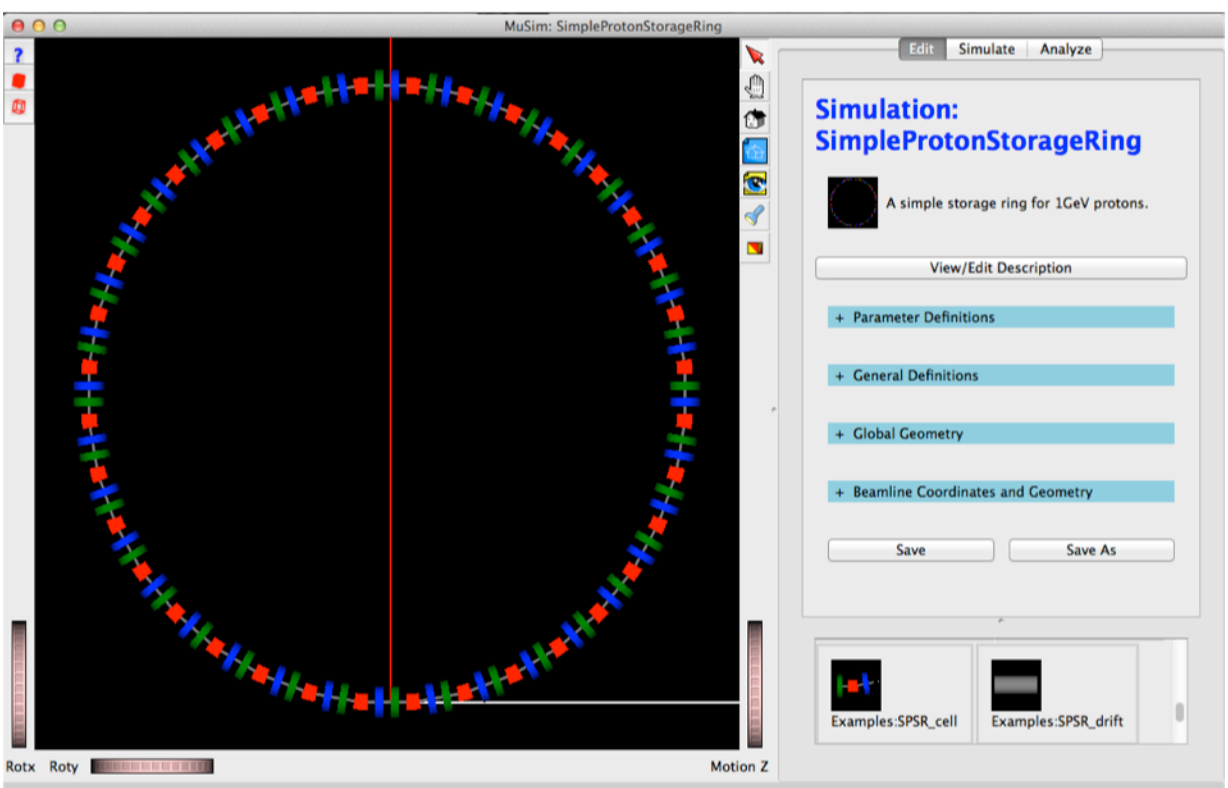

Figure 1: MuSim editing a simulation named "SimpleProtonStorageRing".

* tjrob@muonsinc.com

ISBN: 978-3-95450-168-7 doi:10.18429/JACoW-IPAC2015-MOPMA056

MEASUREMENT AND MODELING OF SINGLE BUNCH WAKE FIELD EFFECTS IN CESR*

J. Calvey, ANL, Argonne, IL 60439, USA
M. Billing, W. Hartung, J. Perrin, D. Rubin, D. Sagan, S.T. Wang, CLASSE, Ithaca, NY 14853

Abstract

Short-range wake fields have been incorporated into a Bmad-based particle tracking code to assess their contribution to current-dependent emittance growth, tune shift, and single bunch instabilities. The wakes are computed for CESR vacuum components using T3P. Simulation results are compared with measurements of bunch length, vertical beam size, and coherent tune shift. Additionally, we use movable scrapers to vary the transverse wake and measure the effect on the beam. We show that a vertical emittance increase at high current may be due to a transverse monopole wake produced by pumping slots in the beam pipe.

INTRODUCTION

The interaction of the electric field from an ultra-relativistic beam of charged particles with its environment, commonly known as its wake field, can cause a variety of problems in particle accelerators, including instabilities, distortion of the bunch's phase space, and beam loss [1]. This effect has been previously studied at the Cornell Electron Storage Ring (CESR) [2–4]. However, two recent developments at CESR have generated a renewed interest in wake field effects: the observation of a vertical emittance blowup at high single bunch current [5], and the installation of a small aperture chamber for a new undulator [6] (which is expected to have a strong transverse wake).

To investigate these effects, we have modified an existing particle tracking code designed for intra-beam scattering (IBS) studies [5] to include wakes. This paper will describe our methodology for calculating the wake fields and how their effect on the beam is simulated. It will then compare these simulations to measurements at 2.1 GeV of bunch lengthening, tune shifts, and emittance growth.

METHODOLOGY

We simulate the effect of wake fields on the beam using a particle tracking code, which makes extensive use of the Bmad software library [7]. The bunch is modeled as a distribution of macroparticles, and tracked through a realistic lattice for several radiation damping times. The single particle wake (i.e. the wake of a point charge) is added to each impedance element, and the effect on the bunch is calculated using a "pseudo-mode" formalism (described below).

Wakes for a given accelerator element are calculated using the ACE3P electromagnetic simulation suite, developed at SLAC [8]. First, the three-dimensional structure of the element is constructed using the finite element mesh toolkit CUBIT [9]. Next, the longitudinal wake for a given bunch is calculated using the time domain wake field solver T3P, which is part of ACE3P.

The primary sources of longitudinal impedance in CESR are sliding joints, horizontal separators, RF cavities, and tapers into and out of the RF sectors. Fig. 1 shows the CUBIT model of the separator. Because this element has approximate top-down and left-right symmetry, only one quarter is modeled, which saves on computation time. Fig. 2 compares the longitudinal wake calculated by T3P for each of the major CESR elements. Although the wake for a single sliding joint is small, there are approximately 100 of them in CESR, so they collectively represent the largest longitudinal impedance.

In principle, we can obtain the single particle wake by deconvolving the wake calculated by T3P from the bunch distribution. However, numerical inaccuracies will cause this calculation to diverge at high frequency, so we suppress any high frequency structure in the wake. While we verify that re-convolving our single particle wake with the bunch spectrum gives us our original wake back, the lack of high frequency information will limit the reliability of the simulation at distance scales short compared to the bunch length.

Once the single particle wake is obtained, it is decomposed as a sum of "pseudo-modes" of the form $A_i \cos(\omega_i t + \phi_i)$ where A_i, ω_i and ϕ_i are parameters of the i^{th} pseudo-mode and are chosen to best reproduce the calculated wake. During tracking, each macroparticle in the bunch adds to the amplitude of each mode, and is kicked by the wake generated by the macroparticles in front of it. By expressing the wake in terms of modes that can be added together at different phases, we avoid having to calculate the effect of each macroparticle on every other one. Thus the computation time scales linearly with the number of particles, rather than quadratically.

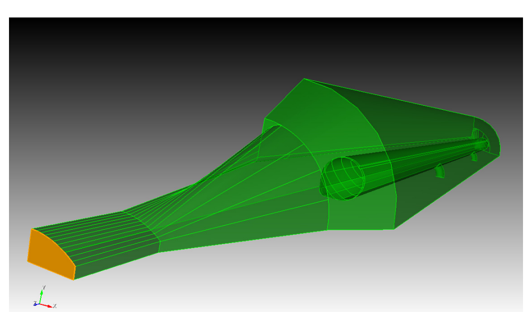

Figure 1: CUBIT quarter model of the horizontal separator.

* Work supported by NSF PHY-1416318 and NSF DMR 1332208. This research used resources of the National Energy Research Scientific Computing Center, which is supported by the Office of Science of the U.S. Department of Energy under Contract No. DE-AC02-05CH11231.

Content from this work may be used under the terms of the CC BY 3.0 licence (© 2015). Any distribution of this work must maintain attribution to the author(s), title of the work, publisher, and DOI.

ISBN: 978-3-95450-168-7 doi:10.18429/JACoW-IPAC2015-MOPMA057

SPACE-CHARGE NEUTRALIZATION OF 750-keV PROTON BEAM IN LANSCE INJECTOR LINE*

Y.K. Batygin#, LANL, Los Alamos, NM 87545, USA

Abstract

The 750-keV low-energy beam transport of the Los Alamos Neutron Science Center (LANSCE) linac consists of two independent beam lines for simultaneous injection of H^+ and H^- beams into the linear accelerator. Space charge effects play an important role in the beam transport therein. A series of experiments were performed to determine the level of proton beam space charge neutralization by residual gas ionization, and time required for neutralization. Study was performed as emittance scans between pairs of emittance measurement stations. The value of compensated space charge was determined through comparison of results of measurements and simulations using macroparticle method and envelope code. Obtained results provide new setup for beam tuning in transport beamline.

750 keV H^+ LANSCE BEAM TRANSPORT

The H^+ beam injector includes a duoplasmatron proton source mounted at 750 keV Cockroft-Walton accelerating column and low-energy beam transport line (LEBT). The 750 keV LEBT (see Fig. 1) consists of a quadrupole lattice, 81° and 9° bending magnets, RF prebuncher, diagnostics and steering magnets to prepare beam for injection into the Drift Tube Linac (DTL). Slit-collector beam emittance measurements at 750 keV are performed at three locations: 1) TAEM1 (just after the Cockroft - Walton column), 2) TAEM2 after pre-buncher, and 3) TDEM1 (before the entrance to the DTL).

BEAM EMITTANCE SCANS

Ionization of residual gas by transported particles is an important factor of low-energy beam transport. Typical pressure measured by ion gauges along the transport channel is 9×10^{-7} Torr. A series of beam emittance scans along 750 keV proton beam transport were performed to determine time and level of space charge neutralization of the beam, value of effective beam current under space–charge neutralization, and the value of effective beam emittance. Measurements were done as pair measurements between each pair of emittance stations TAEM1–TAEM2, TAEM2–TDEM1. Measurements were performed with an ion source pulse length of 825 µs. The emittance was sampled within 50 μs of the ion source pulse being delayed at τ = 10 – 400 µs after beginning of beam pulse. The value of proton beam current at 750 keV was 15.2 mA.

*Work supported by US DOE under contract DE-AC52-06NA25396
#batygin@lanl.gov

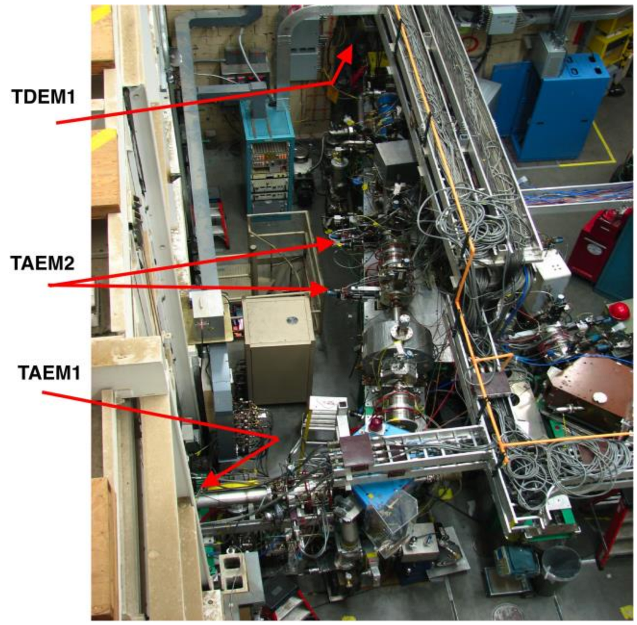

Figure 1: Layout of 750-keV proton Low Energy Beam Transport of LANSCE linear accelerator.

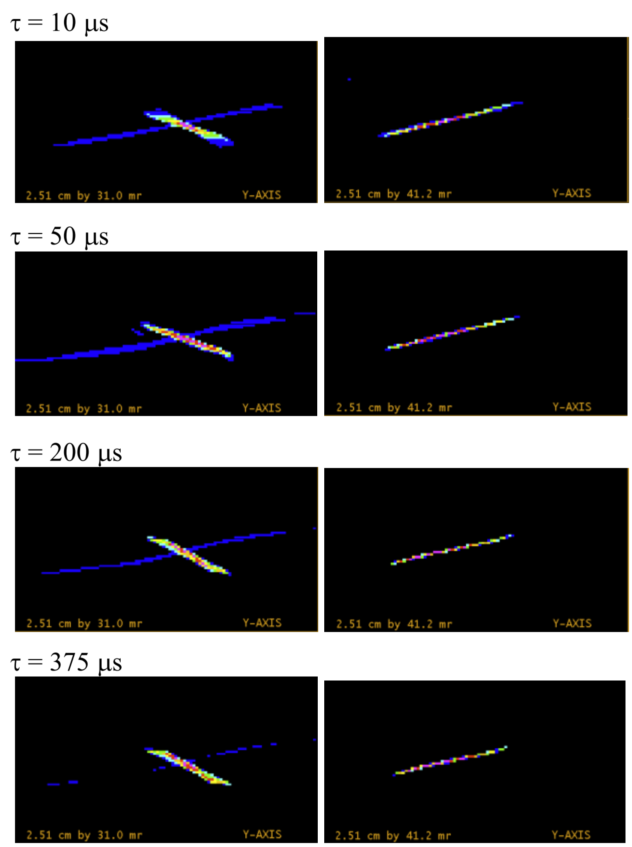

Figure 2: Variation of vertical beam emittance along the beam pulse: (left) TAEM1, (right) TAEM2.

Content from this work may be used under the terms of the CC BY 3.0 licence (© 2015). Any distribution of this work must maintain attribution to the author(s), title of the work, publisher, and DOI.

ISBN: 978-3-95450-168-7 doi:10.18429/JACoW-IPAC2015-MOPMA058

Content from this work may be used under the terms of the CC BY 3.0 licence (© 2015). Any distribution of this work must maintain attribution to the author(s), title of the work, publisher, and DOI.

EFFECT OF SPHERICAL ABERRATION ON BEAM EMITTANCE GROWTH*

Y.K. Batygin#, LANL, Los Alamos, NM 87545, USA

Abstract

Spherical aberration in axially symmetric magnetic focusing lenses results in an S-shape figure of beam emittance. Filamentation of beam emittance in phase space is a fundamental property of a beam affected by aberrations. An analytical expression for effective beam emittance growth due to spherical aberration is obtained. Analysis is extended for intial emittance growth in drift space and within a focusing channel, induced by beam space charge.

BEAM EMITTANCE GROWTH IN AXI-AL-SYMMETRIC LENS

Beam dynamics in an axially-symmetric field may be severely affected by spherical aberrations, which results in beam emittance growth. Magnetic field of the focusing lens can be approximated as

$$B(z) = \frac{B_o}{1+(z/d)^n} , \qquad (1)$$

where B_o is the peak field, and d is the characteristic length. Parameter $n = 2$ corresponds to the well-known Glazer model [1] for short length/diameter lenses, while in many cases the field of a solenoid is better approximated by $n = 4$, which yields a flatter distribution.

Let us estimate the emittance growth of a beam during its passage through the lens. We assume that the position of the particle is not changed while crossing the lens, and only the slope of the particle trajectory is altered. The transformation of particle variables before $(r_o,\ r_o^{'})$ to after $(r,\ r^{'})$ lens-crossing is given by [2]:

$$r = r_o , \qquad r' = r_o^{'} - \frac{r}{f}(1 + C_\alpha r^2) , \qquad (2)$$

where $f = (4/D)(mc\beta\gamma/qB_o)^2$ is the focal length of the lens, D is the effective length of the lens, and C_α is the spherical aberration coefficient. For the Glazer model $D = (\pi/2)d$, $C_\alpha = 0.25 d^{-2}$, and for $n = 4$ $D = d3\pi/4\sqrt{2}$, $C_\alpha = (5/12)d^{-2}$ [3]. In many applications, the spherical aberration coefficient can be expressed through solenoid sizes as $C_\alpha = 5/(S+2a)^2$, where $2a$ is the pole piece diameter and S is the solenoid pole gap width [4].

Suppose that the initial phase space volume of the beam with radius R is bounded by the ellipse

$$\frac{r_o^2}{R^2}\ni + \frac{r_o^{'2}}{\ni}R^2 = \ni , \qquad (3)$$

where $\ni$ is the unnormalized beam emittance. To find the deformation of the boundary of the beam phase space after passing through the lens, let us substitute the inverse transformation $r_o = r$, $r_o^{'} = r' + (r/f)(1 + C_\alpha r^2)$ into the ellipse equation, Eq. (3). The boundary of the new phase space volume, occupied by the beam after passing through the lens at phase plane $(r,\ r^{'})$ is given by:

$$\frac{r^2}{R^2}\ni + \frac{R^2}{\ni}\left(r' + \frac{r}{f} + C_\alpha\frac{r^3}{f}\right)^2 = \ni . \qquad (4)$$

Let us introduce new variables $(T,\ \psi)$ arising from the transformation:

$$\frac{r}{R} = \sqrt{T}\cos\psi , \qquad \left(r' + \frac{r}{f}\right)\frac{R}{\ni} = \sqrt{T}\sin\psi . \qquad (5)$$

In terms of the new variables, the shape of the beam emittance after lens-crossing is

$$T + 2\upsilon T^2 \sin\psi\cos^3\psi + T^3\upsilon^2\cos^6\psi = 1 , \qquad (6)$$

where the following notation is used

$$\upsilon = \frac{C_\alpha R^4}{f\ni} . \qquad (7)$$

Without nonlinear perturbations, $\upsilon = 0$, and Eq. (6) describes a circle in phase space. Conversely, if $\upsilon \neq 0$, Eq. (6) describes an S – shape distorted figure of beam emittance (see Fig. 1). Accordingly, filamentation of beam emittance in phase space is a fundamental property of a beam affected by aberrations.

Being symplectic in nature, the transformation, Eq. (2), conserves phase-space area. However, the effective area occupied by the beam, increases as a result of the encounter. Let us determine the increase in effective beam emittance as a square of the product of minimum and maximum values of T:

$$\frac{\ni_{eff}}{\ni} = \sqrt{T_{\min}T_{\max}} . \qquad (8)$$

The values T_{max}, T_{min} are determined numerically from Eq. (6). Dependence of the emittance growth on the parameter υ is shown in Fig. 2.

Qualitatively, this relationship can be approximated by the function:

*Work supported by US DOE under contract DE-AC52-06NA25396
#batygin@lanl.gov

ISBN: 978-3-95450-168-7 doi:10.18429/JACoW-IPAC2015-MOPMA059

LORENTZ BOOSTED FRAME SIMULATION OF LASER WAKEFIELD ACCELERATION USING HYBRID YEE-FFT SOLVER IN QUASI-3D GEOMETRY

P. Yu*, A. Davidson, A. Tableman, V. K. Decyk, F. S. Tsung, W. B. Mori, UCLA, CA 90024, USA
X. Xu, W. Lu, Tsinghua University, Beijing 100084, China
J. Vieira, L. O. Silva, Instituto Superior Técnico, Lisbon, Portugal
R. A. Fonseca, ISCTE - Instituto Universitário de Lisboa, Portugal
F. Fiuza, SLAC National Accelerator Laboratory, CA 94025, USA

Abstract

We present results from a preliminary study on modeling Laser wakefield acceleration (LWFA) with OSIRIS in a Lorentz boosted frame using a quasi-3D algorithm. In the quasi-3D algorithm, the fields and currents are expanded into azimuthal harmonics and only a limited number of harmonics are kept. Field equations in (r, z) space are solved for a desired number of harmonics in ϕ. To suppress the numerical Cerenkov instability (NCI) that inevitably arises due to the relativistic plasma drift in the simulation, we use a hybrid Yee-FFT solver in which the field equations are solved in (k_z, r) space, where $\hat{z}$ is the drifting direction. Preliminary results show that high fidelity LWFA boosted frame simulations can be carried out with no evidence of the NCI. Good agreement is found when comparing LWFA boosted frame simulations in the full 3D geometry against those in the quasi-3D geometry. In addition, we discuss how the moving window can be combined with the hybrid Yee-FFT solver to further speed up the simulation. The results indicate that unprecedented speed ups for LWFA simulations can be achieved when combining the Lorentz boosted frame technique, the quasi-3D algorithm, and a moving window.

INTRODUCTION

Laser wakefield acceleration (LWFA) [1] offers the potential to construct compact accelerators that have numerous potential applications including the building blocks for a next generation linear collider and for compact light sources. Due to the strong nonlinear effects that are present in LWFA [2], particle-in-cell (PIC) simulations play a very important role in LWFA research. The PIC algorithm follows the self-consistent interactions of particles through the forces directly calculated from solving the full set of Maxwell equations with the currents and charge densities calculated from the particle trajectories. However, using a standard PIC code to study LWFA in a nonlinear regime can be very CPU-time consuming, e.g. a 10GeV stage run takes approximately 30 million CPU hours. While computing resources now exist to do a few of such simulations, it is not possible to do parameter scans in full three-dimensions (3D).

Recently, there has been much research focused on performing simulations in a Lorentz boosted frame with a plasma drifting towards the laser with a Lorentz factor γ_b [3, 4]. So long as there is no reflected light, then the effective time and space scales to be resolved in a numerical simulation may be minimized. The increase in time step and decrease in the plasma length in this frame lead to savings of factors of γ_b^2 as compared to a lab frame simulation using the so-called moving window [5]. Another reduced model that has been recently proposed is to expand the fields in azimuthal mode numbers m and truncate the expansion [6]. This can reduce modeling a 3D problem with low azimuthal asymmetry into the similar computational cost as using a 2D $r - z$ code. The quasi-3D algorithm was implemented into OSIRIS [7] including a new charge conserving current deposit for improved accuracy [8].

It was pointed out in [9, 10] that it would be intriguing to combine the two methods. Similarly to full PIC simulations in cartesian geometry, it was found [9] that in cylindrical geometry, one of the obstacles that needs to be overcome the numerical Cerenkov instability (NCI) [11], that arises due to the inevitable numerical coupling between the Langmuir modes (main and aliasing) and electromagnetic (EM) modes in relativistically drifting plasma frame [12–14]. This makes clear that Lorentz invariance is not strictly true in a PIC code [15, 16]. However, while the multi-dimensional NCI theory in 2D/3D Cartesian coordinates has been well studied, there is currently no dispersion relation for the NCI in the quasi-3D geometry.

In cartesian geometry several ideas have been proposed to minimize and in some cases essentially eliminate the NCI [10, 13–15, 17]. For example, theory and simulations show how to eliminate the NCI through the use of FFT (spectral) solvers and additional strategies including filters [15]. Recently, it was proposed and demonstrated that a hybrid Yee-FFT solver could also be used to greatly minimize the NCI and that this scheme can be used to suppress the NCI in quasi-3D geometry [10] . In this solver, the Maxwell equation is solved in (k_z, r) space, where $\hat{z}$ is the drifting direction of the plasma for each azimuthal mode number. In this way, the fastest growing modes of the NCI at $(\mu, \nu_1) = (0, \pm 1)$ can be well suppressed by filtering the current in k_z space. Here μ and ν_1 refer the time and space aliased modes [14]. Furthermore, the highly localized $(\mu, \nu_1) = (0, 0)$ NCI modes have similar patterns to that of a 2D spectral solver in Cartesian coordinate, and can be suppressed by reducing the simulation time step, or using a local dispersion modification that accurately eliminate the $(\mu, \nu_1) = (0, 0)$ NCI modes [15].

* tpc02@ucla.edu

Content from this work may be used under the terms of the CC BY 3.0 licence (© 2015). Any distribution of this work must maintain attribution to the author(s), title of the work, publisher, and DOI.

ISBN: 978-3-95450-168-7 doi:10.18429/JACoW-IPAC2015-MOPMA060

IMPEDANCE MEASUREMENT FOR THE SPEAR3 STORAGE RING*

Xiaobiao Huang†, James J. Sebek, SLAC, Menlo Park, CA 94025, USA

Abstract

We studied the transverse impedance of the SPEAR3 storage ring with tune shift vs. beam intensity, head-tail instability and transverse mode coupling instability measurements. By taking measurements under different machine conditions, we probed the frequency dependence of the impedance, from which an impedance model was built. This model is consistent with instability measurements and previous bunch lengthening results.

INTRODUCTION

Impedance of a storage ring is an important factor that determines the performance of the machine. For an operational machine, knowledge of the machine impedance helps one to understand the machine performance and provides input for upgrade considerations.

SPEAR3 is a third generation storage ring light source. Table 1 shows a list of selected parameters relevant to this study. Great care was given to controlling the machine impedance during the design and building phases. Consequently the ring is passively stable under normal operation conditions.

Table 1: Selected Parameters of SPEAR3

Parameters	Value	Unit
Energy	3	GeV
Circumference	234.1	m
Current	500	mA
Tune $\nu_{x,y}$	14.106, 6.177	
RF gap voltage	2.85	MV
Bunch length σ_{z0}	6.3	mm
Phase slippage η	1.62×10^{-3}	
Synchrotron tune ν_s	0.0093	

During the 2014 and 2015 runs, we took various beam-based measurements in order to determine the transverse impedance of the machine. These include tune shifts vs. bunch current measurements, head-tail instability measurements and single bunch current threshold measurements. Machine conditions, such as momentum compaction factor, chromaticities, fill pattern, and RF gap voltages were changed as needed to probe the spectrum of the impedance. We tried to interpret the measured impedance with a model that includes resistive wall impedance and a broad-band resonator.

In the following we will show measurements and calculations and discuss the impedance model.

TUNE SHIFT MEASUREMENT

Vertical Plane

The betatron tune shift of a storage ring is related to the transverse impedance through [1, 2]

$$\frac{\Delta\nu_\beta}{\Delta I_b} = \frac{R}{4\sqrt{\pi}(E/e)\sigma_z}\sum_i \beta_i \mathrm{Im}\{Z^{\mathrm{eff}}_{\perp,i}\}, \qquad (1)$$

where I_b is the bunch current, R the average ring radius, E/e beam energy in eV, σ_z the bunch length, β the beta function, $Z^{\mathrm{eff}}_{\perp,i}$ the effective impedance, and $\mathrm{Im}\{\cdot\}$ represents taking the imaginary part. The summation over i is for sections of the ring whose beta functions and impedance contributions may differ. The effective impedance is defined as

$$Z^{\mathrm{eff}}_{\perp} = \frac{\sum_p Z_\perp(\omega_p)h(\omega_p-\omega_\xi)}{\sum_p h(\omega_p-\omega_\xi)}, \qquad (2)$$

where $\omega_p = (p+\nu_\beta)\omega_0$, ν_β the betatron tune, ω_0 the angular revolution frequency, $\omega_\xi = \xi\omega_0\nu_\beta/\eta$, ξ the chromaticity, η the phase slippage factor, and $h(\omega)$ the spectral power density function for the $m = 0$ azimuthal mode. For a Gaussian beam, $h(\omega) = e^{-\omega^2\sigma_t^2}$, with $\sigma_t = \sigma_z/c$, c being the speed of light.

We measured tune shifts vs. bunch current for various machine conditions. Data for the vertical plane are shown in Figure 1. The vertical chromaticity was corrected to zero for the low emittance (LE) lattice data. One of the LE data points was measured with the RF gap voltage reduced to 1.40 MV in order to increase the bunch length. The LE data points at 2.85 MV were taken with 1, 6, 10, and 12 bunches filled, respectively. The low alpha data (LA4) were taken in a lattice for which the momentum compaction factor is reduced to 2.73×10^{-4}. The vertical chromaticity was $\xi = 0.62$ for the low alpha lattice because we had exhausted our sextupole knobs for second order alpha control. The low alpha measurements were repeated on two shifts, each time with RF gap voltage settings of 3.2, 2.4, 2.1 and 1.4 MV, respectively. All data points were taken with the in-vacuum undulator BL12-2 gap open.

Using the data in Figure 1 and Eq. (1) we can calculate the total effective impedance for the ring under the smooth optics approximation,

$$\mathrm{Im}Z^{\mathrm{eff}}_{\perp} = \frac{1}{R/\nu_y}\sum_i \beta_i \mathrm{Im}\{Z^{\mathrm{eff}}_{\perp,i}\}. \qquad (3)$$

The total impedance includes the contribution of resistive wall (RW) impedance, which can be directly calculated, knowing the geometry and surface material of the vacuum chamber. For SPEAR3, the vacuum chamber height in the arcs and in straight sections without insertion devices (ID) is 34 mm. At the ID straight sections, the height ranges from

* Work supported by DOE Contract No. DE-AC02-76SF00515
† xiahuang@slac.stanford.edu

Content from this work may be used under the terms of the CC BY 3.0 licence (© 2015). Any distribution of this work must maintain attribution to the author(s), title of the work, publisher, and DOI.

ISBN: 978-3-95450-168-7 doi:10.18429/JACoW-IPAC2015-MOPMN001

LINEAR OPTICS AND COUPLING CORRECTION WITH TURN-BY-TURN BPM DATA*

Xiaobiao Huang†, SLAC, Menlo Park, CA 94025, USA
Xi Yang, BNL, Upton, Long Island, NY 11973, USA

Abstract

We propose a method to measure and correct storage ring linear optics and coupling with turn-by-turn BPM data. The independent component analysis (ICA) is used to obtain the amplitudes and phase advances of the betatron normal modes, which are compared to their counterparts derived from the lattice model. By fitting the model to the data with quadrupole and skew quadrupole variables, the linear optics and coupling of the machine can be obtained. Simulation demonstrates that errors in the lattice and BPM parameters can be recovered with this method. Experiments on the NSLS-II storage ring show that it can find the same optics as the linear optics from closed orbit (LOCO) method.

INTRODUCTION

The linear optics of a storage ring is often distorted by various error sources such as systematic and random errors of quadrupole magnets, feed-down effect from orbit offsets in sextupole magnets, and perturbations by insertion devices. The machine with distorted optics has large beta beating and phase advance deviation, which would have a negative impact on the nonlinear beam dynamics performance, resulting in reduced dynamic aperture and/or Touschek lifetime. There is also a need to accurately implement the design optics in order to deliver certain beam properties to users or to facilitate beam diagnostics and beam protection systems. Therefore, optics correction is of crucial importance for storage ring operation. The uncorrected machine may also have a large linear coupling, which needs to be corrected in order to reduce the vertical emittance.

The LOCO method [1] is widely used for both linear optics and coupling correction for storage rings. It fits the measured orbit response matrix data to a lattice model, from which one can derive the required quadrupole and skew quadrupole adjustments for optics and coupling correction. This method is very effective if care is taken to avoid the weakly constrained directions of parameter space from having large contributions in the corrections [2]. A main disadvantage of the LOCO method is that it is time consuming to measure the orbit response matrix. Depending on the size of the ring and the ramp rate of the corrector magnets, the time for measuring the orbit response matrix may vary from 10 min to a few hours.

Similar to the orbit response matrix, turn-by-turn (TBT) BPM data taken when beam undergoes coherent betatron oscillation contain valuable information of the linear optics of the machine. Taking TBT BPM data requires only a few seconds and is nearly non-invasive to the beam. There have been previous proposals and experimental studies on the use of TBT BPM data to measure and correct optics [3–6]. There have also been studies that utilize TBT BPM data to correct linear coupling [7, 8]. These methods typically treat in-plane optics correction and coupling correction separately, despite the fact that TBT BPM data contain optics and coupling error information simultaneously, much the same as the orbit response matrix data.

In this study we propose a method to simultaneously measure and correct linear optics and coupling with TBT BPM data. Similar to LOCO, quadrupole and skew quadrupole variables in the lattice model are varied to fit the measured data, resulting in a calibrated lattice model. The independent component analysis (ICA) method is employed to retrieve the normal mode components for each BPM, which are then compared to model calculations.

In the following we will give a description of the method and present simulation and experimental results.

DESCRIPTION OF THE METHOD

With linear coupling, the beam motion observed on each plane of a BPM is a combination of two normal modes. The ICA can separate the normal modes simultaneously for all BPMs and obtain the beam motion at each BPM in a form [3]

$$\begin{aligned} x_n &= A\cos\Psi_1(n) - B\sin\Psi_1(n) + c\cos\Psi_2(n) - d\sin\Psi_2(n), \\ y_n &= a\cos\Psi_1(n) - b\sin\Psi_1(n) + C\cos\Psi_2(n) - D\sin\Psi_2(n), \end{aligned} \tag{1}$$

where x_n and y_n are observed beam positions for the x and y planes at the n'th turn, respectively, $\Psi_{1,2}(n) = 2\pi\nu_{1,2}n + \psi_{1,2}$, and $\nu_{1,2}$ and $\psi_{1,2}$ are the tunes and initial phases of the normal modes. Note that $\psi_{1,2}$ are equal for all BPMs.

On the other hand, the phase space coordinates $X = (x, x', y, y')^T$ are related to the normal mode coordinates

$$\Theta = \begin{pmatrix} \sqrt{2J_1}\cos\Phi_1 \\ -\sqrt{2J_1}\sin\Phi_1 \\ \sqrt{2J_2}\cos\Phi_2 \\ -\sqrt{2J_2}\sin\Phi_2 \end{pmatrix} \tag{2}$$

via a transformation $X = P\Theta$, where $J_{1,2}$ and $\Phi_{1,2}$ are the action and phase variables for the two normal modes, respectively [9]. Explicitly,

$$\begin{aligned} x &= p_{11}\sqrt{2J_1}\cos\Phi_1 + \sqrt{2J_2}(p_{13}\cos\Phi_2 - p_{14}\sin\Phi_2), \\ y &= \sqrt{2J_1}(p_{31}\cos\Phi_1 - p_{32}\sin\Phi_1) + p_{33}\sqrt{2J_2}\cos\Phi_2, \end{aligned} \tag{3}$$

where we have made use of the fact that $p_{12} = p_{34} = 0$ by definition of P and $\Phi_{1,2}$. The phase variables $\Phi_{1,2}$ advance

* Work supported by DOE Contract No. DE-AC02-76SF00515
† xiahuang@slac.stanford.edu

Content from this work may be used under the terms of the CC BY 3.0 licence (© 2015). Any distribution of this work must maintain attribution to the author(s), title of the work, publisher, and DOI.

ISBN: 978-3-95450-168-7 doi:10.18429/JACoW-IPAC2015-MOPMN002

ADVANCES IN PARALLEL FINITE ELEMENT CODE SUITE ACE3P*

Lixin Ge, Kwok Ko, Oleksiy Kononenko, Zenghai Li, Cho-Kuen Ng[1], Liling Xiao,
SLAC, Menlo Park, CA 94025, USA
Ji Qiang, LBNL, Berkeley, CA 94720, USA

Abstract

New capabilities in SLAC's parallel finite element electromagnetics simulation suite ACE3P are reported. These include integrated electromagnetic (Omega3P), thermal and mechanical (TEM3P) modules for multi-physics modeling, an interface to particle-material interaction codes for calculation of radiation effects due to dark current generation (Track3P), and coupled electromagnetic (ACE3P) and beam dynamics (IMPACT) simulation. Results from these applications are presented.

INTRODUCTION

SLAC has developed the electromagnetics simulation suite **ACE3P** (**A**dvanced **C**omputational **E**lectro-magnetics **3D** **P**arallel), consisting of modules in frequency and time domains [1]. These massively parallel codes are based on the high-order finite-element method so that geometries of complex structures can be represented with high fidelity through conformal grids, and high solution accuracies can be obtained using high-order basis functions in finite elements. **ACE3P** consists of the following modules: **Omega3P**, an eigensolver for cavity mode (damping) calculations; **S3P**, a frequency-domain solver to calculate S-parameters of rf components; **T3P**, a time-domain solver for transients and wakefield computations; **Track3P**, a particle tracking code for multipacting and dark current studies; **Pic3P**, a particle-in-cell code for self-consistent particle and field interactions; **TEM3P**, a multi-physics code for integrated electromagnetic, thermal and mechanical effects. Running on DOE supercomputing facilities, these six applications modules have been applied to a wide range of modeling and simulation problems for accelerators [2].

Recent advances in the modeling capabilities of **ACE3P** have been focused on enhancing the multi-physics module **TEM3P** and the integration of **ACE3P** modules with other application codes. The major improvements include

- Benchmarking **TEM3P** thermal calculations for a realistic 3D structure against measurement;
- Development of a mechanical eigensolver in **TEM3P** to determine mechanical modes of a superconducting (SRF) cavity to facilitate the investigation of microphonics [3];
- Development of an electro-mechanical analysis tool to decompose the Lorentz force displacement into those of the mechanical modes of an SRF cavity;
- Integration of **ACE3P** with the beam dynamics code **IMPACT** for realistic calculation of beam emittance in accelerator structures and systems;
- Interface of **ACE3P** to particle-material interaction codes such as Geant4 and Fluka for evaluating radiation effects in accelerators.

In the following sections, simulation results from these applications are presented.

THERMAL CALCULATIONS FOR LCLS-II COUPLER

The LCLS-II adopts the TTF3 coaxial fundamental power coupler with modest modifications to make it suitable for CW operation. The coupler consists of a cold section and a warm section made of different kinds of materials with a thin copper coating at the warm side. The fully 3D geometry of the coupler is modeled using **TEM3P** to determine the temperature distribution along the feedthrough of the coupler [4]. The temperature distribution shown in Fig. 1 is obtained for using 6 kW power for the standing wave on resonance. The maximum temperature is found at the bellows located near the central region of the coupler, and it agrees well with the value from high power tests at Fermilab, as shown in Fig. 2 [5].

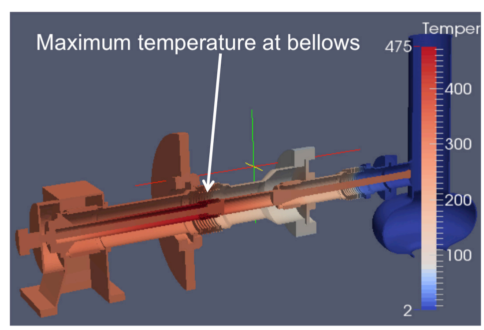

Figure 1: Temperature distribution in TTF3 coupler calculated using TEM3P.

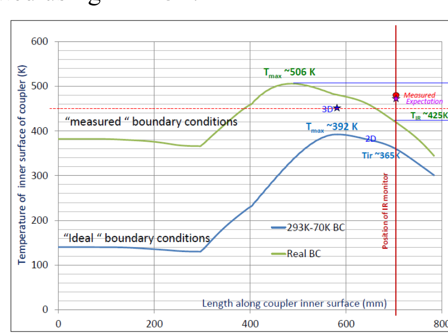

Figure 2: Temperature along the inner conductor with the red dot showing the agreement of simulation and measurement.

* This work was supported by DOE Contract No. DE-AC02-76SF00515.
[1]cho@slac.stanford.edu

Content from this work may be used under the terms of the CC BY 3.0 licence (© 2015). Any distribution of this work must maintain attribution to the author(s), title of the work, publisher, and DOI.

ISBN: 978-3-95450-168-7 doi:10.18429/JACoW-IPAC2015-MOPMN003

DYNAMIC APERTURE STUDIES FOR THE LHC HIGH LUMINOSITY LATTICE*

R. de Maria, M. Giovannozzi, E. McIntosh, CERN, Geneva, Switzerland
Y. Cai, Y. Nosochkov†, M-H. Wang, SLAC, Menlo Park, CA 94025, USA

Abstract

Since quite some time, dynamic aperture studies have been undertaken with the aim of specifying the required field quality of the new magnets that will be installed in the LHC ring in the framework of the high-luminosity upgrade. In this paper the latest results concerning the specification work will be presented, taking into account both injection and collision energies and the field quality contribution from all the magnets in the newly designed interaction regions.

INTRODUCTION

The low-β optics of the high luminosity LHC [1] demands very stringent requirements on the field quality (FQ) of the new large aperture interaction region (IR) magnets: the inner triplet (IT) quadrupoles, the D1 and D2 separation dipoles, and the Q4 and Q5 matching quadrupoles. Specifications of the FQ of these magnets have been studied based on dynamic aperture (DA) calculations with the goal of reaching an acceptable minimum DA ($\simeq 10\sigma$) while being realistically close to the expected magnet FQ. The latter is based on magnet design or scaling from existing magnets FQ. In this paper, the impact of the latest FQ estimate of the IT and Q4 quadrupoles, and the D2 dipoles on DA at collision and injection energies is analyzed, and the necessary adjustments to this FQ are proposed.

The DA study was done for the latest HLLHCV1.0 lattice [2]. Nominally, the so-called `round` beam optics at collision energy was used, where $\beta^*_{x,y}$ = 15 cm at the interaction points IP1 and IP5. In this study, we extend the simulations to other lattice options with different values of β^* which will be described in more detail later. The DA of these lattices was also studied for an extended range of machine linear chromaticity ξ from +2 (nominal) to +18.

The DA was obtained using SixTrack [3,4] with the following set-up: 10^5 turns, 11 x-y phase space angles, 30 particle pairs per $2\,\sigma$ amplitude step, 60 random error seeds, normalized emittance of 3.75 μm, $\Delta p/p = 2.7\cdot10^{-4}$ and $7.5\cdot10^{-4}$ at 7 TeV (collision) and 450 GeV (injection) beam energy, respectively. The machine errors included the arc field errors based on measured FQ of the existing magnets, and the IR magnet field errors based on the latest FQ specifications. The simulations included the correction of tune, chromaticity, coupling and orbit, the use of b_3, b_4, b_5 correctors in the arc dipoles, as well as the IT non-linear field correctors up to the 6th order [5]. Beam-beam effects were not included in this study.

* Research supported by DOE via the US-LARP program and by EU FP7 HiLumi LHC - Grant Agreement 284404
† yuri@slac.stanford.edu

LATEST FIELD QUALITY

The FQ of LHC magnets is defined by [6]

$$B_y + iB_x = 10^{-4} B_N \sum_{n=N}^{\infty} (b_n + ia_n) \left(\frac{x+iy}{r_0}\right)^{n-1}, \quad (1)$$

where the a_n, b_n coefficients are determined at a reference radius r_0, and B_N is the main field at r_0. Furthermore, each a_n and b_n is composed of the mean (a_{nm}, b_{nm}), uncertainty and random terms, where the uncertainty and random values are randomly generated based on their Gaussian sigmas a_{nu}, b_{nu} and a_{nr}, b_{nr}, respectively (see, e.g., Ref. [5]).

The FQ tables for the new IR magnets can be found at the official LHC repository [7]. The recent updates include the new FQ estimates for the IT and Q4 quadrupoles, and for the D2 dipoles.

D2 and Q4 Magnets

The new estimate of the D2 FQ is referred to as `D2_errortable_v5` and includes an update to several b_n coefficients at both the collision and injection energies [8]. The impact of the D2 FQ at collision energy was verified previously [9] and found acceptable since it improved the minimum DA to DA$_{\text{min}} = 9.85\,\sigma$. It has been designated the new D2 FQ specification. The updated D2 FQ coefficients at injection energy are shown in Table 1. The new non-zero b_2 term affects the linear optics. In machine operation the IR focusing errors are expected to be compensated. However, due to lack of such correction in the simulations, this term was set to zero to avoid its impact on the DA. With this assumption, the effect of the updated D2 FQ on DA at injection energy was found negligible and, hence, this FQ is acceptable as a new D2 specification. In this case, the DA$_{\text{min}} = 9.92\,\sigma$.

Table 1: Updated Coefficients of the D2 FQ at Injection Energy (r_0 = 35 mm). Old Values are Shown for Reference

	b_{2m}	b_{3m}	b_{4m}	b_{6m}	b_{7m}	b_{8m}	b_{9m}
Old	0	3.8	-8.0	0	0.1	0	0.02
New	5.0	-19.0	2.0	2.0	1.3	1.0	0.52

The new estimate of Q4 FQ is referred to as `Q4_errortable_v2` and it affects all the field coefficients. In this update, the high order terms (n>9) are reduced at the expense of somewhat larger low order coefficients. Also, new non-zero systematic terms are introduced: b_{6m}, b_{14m} at collision energy and b_{6m}, b_{10m}, b_{14m} at injection. On the other hand, the corresponding uncertainty and random terms b_{nu}, b_{nr} of order n=6,10,14 are cancelled. The SixTrack calculations showed negligible impact of this Q4 FQ

Content from this work may be used under the terms of the CC BY 3.0 licence (© 2015). Any distribution of this work must maintain attribution to the author(s), title of the work, publisher, and DOI.

ISBN: 978-3-95450-168-7 doi:10.18429/JACoW-IPAC2015-MOPMN004

CSR IMPEDANCE FOR NON-ULTRARELATIVISTIC BEAMS*

R. Li#, Thomas Jefferson National Accelerator Facility, Newport News, VA 23606, USA
C.-Y. Tsai, Department of Physics, Virginia Tech, VA 24061, USA

Abstract

For the analysis of the coherent synchrotron radiation (CSR) induced microbunching gain in the low energy regime, such as when a high-brightness electron beam is transported through a low-energy merger in an energy-recovery linac (ERL) design, it is necessary to extend the existing CSR impedance expression in the ultrarelativistic limit to the non-ultrarelativistic regime. This paper presents our analysis of CSR impedance for general beam energies.

INTRODUCTION

Modern accelerator designs often demand the generation and transport of high brightness electron beams. For these designs it is important to have accurate estimation of the coherent synchrotron radiation (CSR) effects on the degradation of the beam phase space quality. The analytical expressions of CSR wakefield are often utilized in time-domain particle tracking. For example, in ELEGANT, CSR effects are modelled for ultrarelativistic beams using CSR wakefield obtained for the steady-state interaction [1] or for the transient-state interaction [2]. On the other hand, the analytical expression of CSR impedance is necessary for the frequency-domain analysis, such as for the Vlasov anslysis of the microbunching gain [3,4]. For ultrarelativistic bunch in free space, the CSR impedance is given by [3,4]

$$Z(k) = -iA\, k^{1/3} R^{-2/3} \tag{1}$$

For

$$A = -2\pi[Bi'(0)/3 + iAi'(0)] = -0.94 + 1.63i \tag{2}$$

where Ai and Bi are Airy functions.

The designs of low-energy mergers in ERLs requires the knowledge of CSR interaction at low energy and also LSC interaction on a curved orbit. For time-domain particle tracking with codes such as GPT [5] or TStep [6], the study of CSR wakefields are extended from ultrarelativistic regime [1,2] to the low energy regime [7,8]. Similarly, to apply the Vlasov analysis of microbunching gain [3,4] in the frequency domain for the low energy regime, we need to extend the CSR impedance in Eq. (1) to the low energy regime. In the following we present our analysis of the steady-state CSR impedance for general beam energies. The impedance expression reduces to Eq. (1) under ultrarelativistic approximation. In addition, it is shown that the real part of the CSR impedance is consistent with the synchrotron-radiation power loss spectrum given by Schwinger [9]. Note that an existing expression of CSR impedance in free space for general beam energies was presented earlier [10], which takes different form from our expression. Relation between the two will be established in our coming-up studies.

ANALYSIS OF CSR IMPEDANCE FOR GENERAL BEAM ENERGIES

Consider a rigid line bunch, with the longitudinal density distribution $\lambda(z)$, moving at velocity v on a circular orbit with radius R. We will start with the longitudinal wakefield on the bunch as a result of steady-state CSR interaction in free space, and obtain the impedance from the Fourier transform of the CSR wakefield.

First, the electric field on a particle at (s,t), due to the CSR interaction from all other particles in the bunch, is expressed in terms of the retarded potentials

$$\vec{E} = -\nabla\Phi - \frac{\partial\vec{A}}{c\partial t},$$

$$\Phi(s,t) = \int_{-\infty}^{\infty} ds' \frac{\rho(s',t')}{|\vec{r}(s)-\vec{r}(s')|}, \quad \vec{A}(s,t) = \int_{-\infty}^{\infty} ds' \frac{\vec{\beta}(t')\rho(s',t')}{|\vec{r}(s)-\vec{r}(s')|}.$$

Here the retarded time is

$$t' = t - |\vec{r}(s)-\vec{r}(s')|/c$$

and the longitudinal charge density distribution is

$$\rho(s,t) = e\lambda(z) \quad \text{for} \quad z = s-\beta ct.$$

The energy loss rate for the particle per unit path length is

$$e\hat{\beta}\cdot\vec{E} = -e\frac{d\Phi}{vdt} + e\left(\frac{\partial\Phi}{v\partial t} - \vec{\beta}\cdot\frac{\partial\vec{A}}{v\partial t}\right).$$

For the rigid line bunch on the circular orbit, we have

$$\vec{\beta} = (\beta_r,\beta_\theta,\beta_z) = (0, v/c, 0) \quad \text{and} \quad \frac{d\Phi}{dt} = 0.$$

The longitudinal wakefield on the particle is subsequently

$$E_\theta = -\left(\frac{\partial\Phi}{\partial z} - \vec{\beta}\cdot\frac{\partial\vec{A}}{\partial z}\right),$$

in which

$$\Phi - \vec{\beta}\cdot\vec{A} = e\int_{-\infty}^{\infty} ds' \frac{(1-\beta^2)+\beta^2\left[1-\cos\left((s-s')/R\right)\right]}{|\vec{r}(s)-\vec{r}(s')|}\lambda(z')$$

for $z' = z-(s-s')+\beta|\vec{r}(s)-\vec{r}(s')|$.

Using Fourier expansion,

$$\lambda(z) = \int_{-\infty}^{\infty} dk\lambda(k)e^{ikz}, \quad E_\theta(z) = -e\int_{-\infty}^{\infty} dk\, Z(k)\lambda(k)e^{ikz}, \tag{3}$$

we obtain the CSR impedance

* This material is based upon work supported by the U.S. Department of Energy, Office of Science, Office of Nuclear Physics under contract DE-AC05-06OR23177.

lir@jlab.org

Content from this work may be used under the terms of the CC BY 3.0 licence (© 2015). Any distribution of this work must maintain attribution to the author(s), title of the work, publisher, and DOI.

ISBN: 978-3-95450-168-7 doi:10.18429/JACoW-IPAC2015-MOPMN007

AN ALTERNATE RING-RING DESIGN FOR eRHIC

Yuhong Zhang, Thomas Jefferson National Accelerator Facility, Newport News, VA 23606, USA

Abstract

I present here a new ring-ring design of eRHIC. It utilizes high repetition rate colliding beams and is likely able to deliver the performance to meet the requirements of the science program with low technical risk and modest accelerator R&D. The expected performance includes high luminosities over multiple collision points and a broad CM energy range with a maximum value up to 2×10^{34} $cm^{-2}s^{-1}$ per detector, and polarization higher than 70% for the colliding electron and light ion beams. This new design calls for reuse of decommissioned facilities in the US, namely, the PEP-II high energy ring and one section of the SLAC linac as a full energy injector.

INTRODUCTION

A polarized electron-ion collider (EIC) in a CM energy range up to 100 GeV/n is envisioned as a future facility for nuclear science research in the US [1]. Presently, both BNL and JLab are engaged in design studies for this future collider [2,3,4,5]. Since the beginning in 2001, the EIC design studies have been focused on achieving superior performance. The EIC science program [1] requires high luminosity (above 10^{33} $cm^{-2}s^{-1}$ per detector) over a broad CM energy range with a wide array of fully stripped ion species up to lead or uranium, and high polarization (>70%) for both colliding electron and light ion beams. Both ring-ring and linac(ERL)-ring collider scenarios have been adopted respectively for MEIC (the JLab design [4,5]) and eRHIC (the BNL design [3]).

The MEIC design is based on a very high bunch repetition rate for both colliding beams and strong final focusing to achieve a luminosity close to 10^{34} $cm^{-2}s^{-1}$ per detector [6]. The design concept was formulated more than 10 years ago and is still considered the best approach for MEIC. Recently, the reuse of the PEP-II high energy ring for the MEIC electron collider ring has been integrated into the present baseline [5].

eRHIC started with a ring-ring collider design [2] and advanced to the present ERL-ring collider design [3] around 2007 to maximize luminosity. This design is very innovative and introduces a set of new and advanced concepts and schemes, and relies on several yet-to-be-demonstrated technologies [3]. These include a high current polarized electron source based on a multi-cathode Gatling gun; high energy high current multi-pass ERL based on FFAG-type recirculation beam lines; space charge compensation; and coherent electron cooling. While these concepts and technologies are expected to improve the eRHIC performance, they do require R&D effort for development and proto-typing, and for proof-of-principle demonstrations.

In this paper I propose an alternate eRHIC design based on a ring-ring scenario and the same luminosity concept used in the MEIC design. This design has the potential to reach high luminosities and polarization while requiring modest accelerator R&D. I also include a discussion on implementation issues and the required accelerator R&D.

* yzhang@jlab.org

DESIGN CONCEPT

Design Strategy

I choose a ring-ring collider scenario as the basis of this alternate eRHIC design since it is technically a conservative approach compared to an ERL-ring design but still able to deliver very high luminosities. The design supports simultaneous operation of multiple detectors, thus increases science productivity. This is different from an ERL-ring design where an electron bunch is allowed to collide only once (at one of the detectors) due to a large beam-beam disruption, so the detectors can only be operated alternately.

The strategy for high luminosity has been demonstrated already in the B-factories [6] and has been adopted for the MEIC design since 2002 [4]. The concept involves specific design choices of colliding beams, interaction region (IR) and beam cooling. Namely, (1) both colliding beams have a high bunch repetition rate, very small bunch lengths, bunch charges and transverse emittances; (2) the IR has very strong final focusing to attain very small beam spots at collision points; it also has an implementation of crab crossing of colliding beams to support high bunch repetition; (3) electron cooling is responsible for reduction of the proton or ion beam six-dimensional emittances.

New Design Baseline

The following key elements are proposed as the new ring-ring eRHIC baseline

- *Electron collider ring*: the PEP-II high energy ring;
- *Ion collider ring*: one of the RHIC rings;
- *Electron full energy injector*: a section of the SLAC warm linac;
- *Ion injector*: the RHIC ion complex

Reuse of the PEP-II high energy ring includes the entire magnet set and the vacuum chamber as well as the RF system. This results in a 476 MHz bunch repetition rate of the electron beam in the collider ring. Following this approach, no major new facility is required.

RHIC Upgrade

I further propose to upgrade RHIC and its injectors

- To support high bunch repetition rates;
- To support multi-phased electron cooling;
- To improve the RHIC polarized ion beam operation.

To match bunch structure of the electron beam, the RF system of RHIC (and part of AGS) should be rebuilt to support 476 MHz frequency. This provides an

Content from this work may be used under the terms of the CC BY 3.0 licence (© 2015). Any distribution of this work must maintain attribution to the author(s), title of the work, publisher, and DOI.

ISBN: 978-3-95450-168-7 doi:10.18429/JACoW-IPAC2015-MOPMN008

SPACE CHARGE STUDIES IN FFAG USING THE TRACKING CODE ZGOUBI

M. Haj Tahar*, F. Méot, N. Tsoupas, BNL, Upton, Long Island, New York, USA

Abstract

A method is implemented in Zgoubi that allows the computation of space charge effects in 2D distributions and with some restrictions in 3D distributions. It relies on decomposing field maps or analytical elements into slices and applying a space charge kick to the particles. The aim of this study is to investigate the accuracy of this technique, its limitations/advantages by comparisons with other linear/nonlinear computation methods and codes, and to apply it to high power fixed field ring design studies.

INTRODUCTION

Accelerator Driven Systems are still in the early development stage. One of the main challenges is the average beam current required in order to achieve high transmutation rates. By choosing the effective multiplication factor as to accommodate any possible positive reactivity insertion during the operation of the reactor, it can be shown that the minimum average beam current is ~ 10 mA. So, in order to investigate the possible benefits of FFAGs for Accelerator Driven Systems, one has to develop techniques to understand and master the space charge effects.

IMPLEMENTATION

Zgoubi [1] is a ray-tracing code which can track particles through electric and magnetic fields introduced as field maps or as analytic elements. We carry out a self consistent multi-particle simulation that is based on the space charge KV model [2] : the beam is supposed to have a uniform distribution with elliptical cross section, and a constant linear charge density. In that case, the free-space self-field solution within the beam is:

$$E_x = -\frac{\partial \phi}{\partial x} = \frac{\lambda}{\pi \epsilon_0} \frac{x}{(r_x + r_y) r_x} \tag{1}$$

$$E_y = -\frac{\partial \phi}{\partial y} = \frac{\lambda}{\pi \epsilon_0} \frac{y}{(r_x + r_y) r_y} \tag{2}$$

The kick received transversly by the particles after each integration step Δs is thus given by:

$$\Delta x' = \frac{2Q}{(r_x + r_y) r_x} x \Delta s \tag{3}$$

$$\Delta y' = \frac{2Q}{(r_x + r_y) r_y} y \Delta s \tag{4}$$

where Q is the generalized pervance term defined by, $Q = \frac{q\lambda}{2\pi\epsilon_0 m_0 c^2 \beta^2 \gamma^3}$. So, in order to evaluate the space charge force, one has to evaluate the beam radii and vice-versa.

* mhajtahar@bnl.gov

Slicing

If we cut the magnet into thin slices, we may assume that the beam radii do not change much within each slice. Thus, each particle will experience a transverse space charge kick given by the formula (3) and (4) above. The main assumption here is that each particle in the beam does not see its immediate neighbors, but the smooth potential which is derived from the bunch (with uniform distribution) as a whole. Taking the statistical averages (rms quantities) is the natural way to derive analytically the evolution of such quantities as the beam emittance or the beam edge radius. Here we restrict ourselves to the KV model for which we define:

$$r_x = 2 < x^2 >^{1/2} \tag{5}$$

$$\epsilon_x = 4[< x^2 >< x'^2 > - < xx' >^2]^{1/2} \tag{6}$$

Given that the space charge forces are linear, the rms edge emittance in this model is constant and represents the maximum Courant-Snyder invariants. This was successfully checked. Also, the transverse particle equation of motion (when dispersion is neglected and only valid within the beam) is given by [3]:

$$x''(s) + \left(\kappa_x(s) - \frac{2Q}{[r_x(s) + r_y(s)] r_x(s)}\right) x(s) = 0 \tag{7}$$

If we consider a KV beam composed of N particles and with zero rms emittance, such as x_i(s=0)=x_i and x_i'(s=0)=0 $\forall i \in [\![1 \,;\, N]\!]$. Then the envelope edge radius in a drift is given by:

$$r_x(s) = x_i^{max} \cosh\left[\left(\frac{2Q}{r_{x0}(r_{x0} + r_{y0})}\right)^{1/2} \times s\right] \tag{8}$$

where r_{x0} and r_{y0} are the envelope edge radii at the entrance of the drift. Fig. 1 shows a comparison of the axial beam envelope in a drift obtained from tracking with the analyti-cal formula (8). Similar tests were performed in quadrupole element which gave agreement as well. A natural test of the convergence of this method is to vary the number of slices until the beam envelope stabilizes: Fig. 2 below illustrates the convergence in a drift element (which is easy to picture). This result can be interpreted in the following way: it shows the speed at which the space charge force evolves in a KV beam (in a drift).

SPACE CHARGE EFFECTS IN SCALING FFAG

Analytical Model of the 150 MeV KURRI FFAG

The current work is a first step to understand the space charge effects in the 150 MeV scaling FFAG at KURRI in

Content from this work may be used under the terms of the CC BY 3.0 licence (© 2015). Any distribution of this work must maintain attribution to the author(s), title of the work, publisher, and DOI.

ISBN: 978-3-95450-168-7 doi:10.18429/JACoW-IPAC2015-MOPMN009

CROSS-PLATFORM AND CLOUD-BASED ACCESS TO MULTIPLE PARTICLE ACCELERATOR CODES VIA APPLICATION CONTAINERS*

D.L. Bruhwiler#, R. Nagler, S.D. Webb, RadiaSoft, Boulder, CO 80304, USA
G. Andonian, M.A. Harrison, S. Seung, RadiaBeam Technologies, Santa Monica, CA 90404, USA
T. Shaftan, BNL, Upton, NY 11973, USA
P. Moeller, Bivio Software, Boulder, CO 80303, USA

Abstract

Particle accelerator and radiation modeling codes focus on specific problems, rely on complicated command-line interfaces, are sometimes limited to a small number of computing platforms, and can be difficult to install. There is also a growing need to use two or more codes together for end-to-end design or for complicated sub-systems. RadTrack [1,2] is a lightweight cross-platform GUI for such codes, based on the Qt framework [3] and PyQt [4] bindings for Python. RadTrack is designed to support multiple codes, placing no burden on the corresponding development teams. Elegant [5] and the Synchrotron Radiation Workshop (SRW) [6-9] are supported now in a pre-beta stage, and support for GENESIS 1.3 [10,11] is under development. These codes are being containerized via the open source Docker platform [12] for use in the cloud. The open source Vagrant [13] and Virtual Box [14] are used for MacOS and Windows. We discuss RadTrack and our vision for cloud computing.

RADTRACK USER TESTING

In preparation for an upcoming beta test program, user testing of RadTrack was conducted at the IPAC conference in Richmond, VA on May 4 and 5, 2015. In order to ensure the entire team has access to user feedback, we are using Screenflick [15] on the Mac and BB Flashback [16] on Windows to record user actions, audio and video. These videos have been invaluable in discovering basic user interaction (UX) issues. We are now improving the workflow to be more intuitive for end-users.

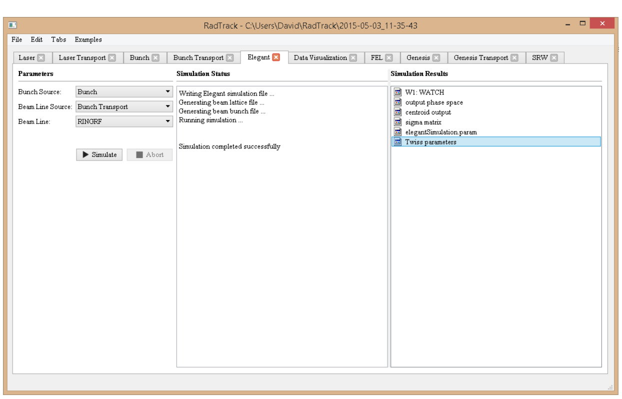

Figure 1: RadTrack Qt widget for Elegant simulations.

The use case presented to test subjects was to build a FODO accelerator lattice from scratch, beginning with a 65 MeV electron beam, and to simulate the problem with Elegant. Figure 1 shows the widget for Elegant modeling. This Tab manages the selection of an accelerator lattice and a beam description, shows runtime output, then provides easy access to the resulting output files for visualization.

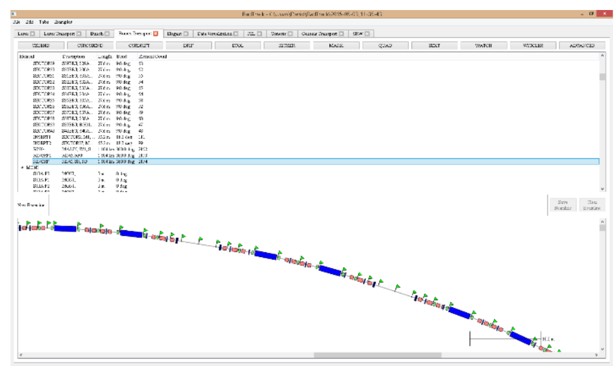

Figure 2: RadTrack Qt widget for drag-and-drop construction and visualization of particle accelerator lattices.

Figure 2 shows the bunch transport tab, which parses Elegant lattice files to present a graphical representation of the beamline. Drag-and-drop features enable interactive modification of existing lattices or rapid creation of new beamlines. The Elegant tab can use the bunch transport tab directly, or parse a specified lattice file. The user can create multiple bunch transport tabs.

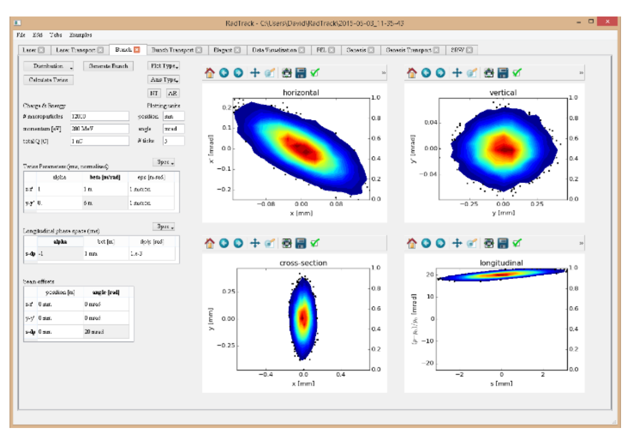

Figure 3: RadTrack Qt widget for interactive specification and visualization of particle beams.

*Work funded by DOE Basic Energy Sciences grant DE-SC0006284.
bruhwiler@radiasoft.net

Content from this work may be used under the terms of the CC BY 3.0 licence (© 2015). Any distribution of this work must maintain attribution to the author(s), title of the work, publisher, and DOI.

ISBN: 978-3-95450-168-7 doi:10.18429/JACoW-IPAC2015-MOPMN010

Content from this work may be used under the terms of the CC BY 3.0 licence (© 2015). Any distribution of this work must maintain attribution to the author(s), title of the work, publisher, and DOI.

NON-LINEAR MAGNETIC INSERTS FOR THE INTEGRABLE OPTICS TEST ACCELERATOR*

F. H. O'Shea, R. Agustsson, Y.-C. Chen and E. Spranza,
RadiaBeam Technologies, 1717 Stewart St., Santa Monica, California, USA
D. W. Martin and J. D. McNevin
RadiaBeam Systems, 1717 Stewart St., Santa Monica, California, USA

Abstract

We present here a status update of the manufacture and magnetic measurements of the non-linear inserts for the Integrable Optics Test Accelerator. RadiaBeam Technologies is designing the 2-meter structure from magnetic field specifications, including pole design, measurement systems and alignment fiducialization. Herein, we will describe the current state of the project.

STATE OF THE PROJECT

The goal of the Integrable Optics Test Accelerator (IOTA) is to serve as a proof of principle experiment of the integrable optics technique. Briefly, the technique seeks to improve accelerator intensity by deliberately violating the assumption of linear motion that has two invariants: particle emittance and energy [1, 2]. The IOTA ring will be constructed at the Advanced Superconducting Test Accelerator facility at Fermi National Lab [3]. While a great many of the components for the IOTA ring are being recommissioned from other projects, the non-linear inserts are entirely new and must be designed exclusively for the IOTA ring because the magnetic field of the insert depends on the configuration of the other optical elements in the ring.

Unlike magnets typically found in circular accelerators, both the magnetic field strength and the mechanical aperture of the non-linear insert are explicit functions of the longitudinal coordinate [1–3]. To reduce the complexity of manufacturing the magnets for this insert and allow flexibility for assembly, we have decided to segment the insert such that the magnetic field properties are constant along a fixed short length of the insert, but the magnetic properties vary between segments along the length of the insert in accordance with the requirements of the integrable optics theory. An example of a segmented prototype can be seen in Fig. 1. The constraints on the field quality are specified by tracking simulations to be:

1. The magnetic axes of all of the segments may not deviate from each other by more than 50 μm.

2. The field may not deviate from the theoretical field by more than 1% within some good field region.

3. The good field region should cover as much of the physical aperture as practicable.

* Work supported by DOE under contract DE-SC0009531.

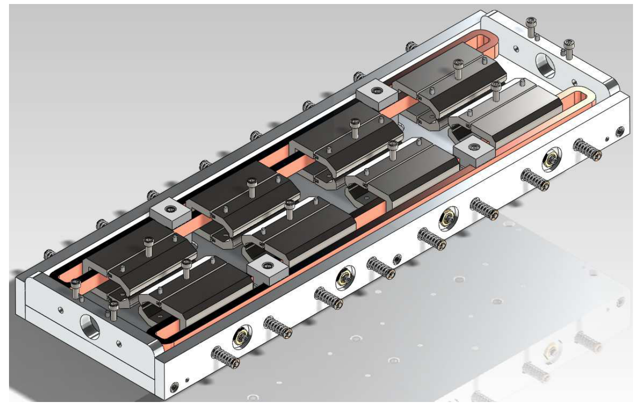

Figure 1: Isometric view of the initial IOTA insert prototype. A plate on top has been hidden to show detail below. The copper items are the excitation coils, the dark grey items are the steel poles and return yokes, and light grey items are aluminum.

In previous proceedings we reported the construction of an initial prototype to test a simple tuning mechanism to allow adjustment of the magnetic fields in the insert [4]. RadiaBeam Technologies is now moving forward with the design of a full scale prototype non-linear insert that will be installed on the IOTA ring. We have advanced the design of the full scale prototype to take advantage of the experience gained during manufacture of the initial prototype. In addition to reporting the results of the magnetic measurement of the initial prototype, we report on the design and engineering strategy for the full scale insert. Specifically, we cover the design of the vacuum system, a manufacturing strategy for the magnets, and the alignment technique we will use to align the many segments of the insert.

MEASUREMENT OF THE PREVIOUS PROTOTYPE

Previously, we had planned to measure the magnetic field of the initial prototype insert (see Fig. 1) via a custom Hall probe bench to accommodate the very small aperture of the magnets [4]. This measurement system was constructed, but it turned out to be impractical. The very small Hall probes, of total size in the mm range, required very fine wires which easily broke. In addition, the connections to the Hall effect sensor were sensitive to movement and produced spurious signals on the order of the measurement signal. As a result, we decided on a more conventional rotating

ISBN: 978-3-95450-168-7 doi:10.18429/JACoW-IPAC2015-MOPMN012

Content from this work may be used under the terms of the CC BY 3.0 licence (© 2015). Any distribution of this work must maintain attribution to the author(s), title of the work, publisher, and DOI.

SPACE CODE FOR BEAM-PLASMA INTERACTION

K. Yu*, Stony Brook University, Stony Brook, NY 11794, USA
R. Samulyak#, Stony Brook University, Stony Brook, NY 11794 and BNL, Upton, NY 11973, USA

Abstract

A parallel particle-in-cell code SPACE has been developed for the simulation of electromagnetic fields, relativistic particle beams, and plasmas. The algorithms include atomic processes in the plasma, proper boundary conditions, an efficient method for highly-relativistic beams in non-relativistic plasma, support for simulations in relativistic moving frames, and special data transfer algorithm from the moving to the laboratory frame that collects particles and fields in the lab frame without time shift due to the Lorentz transform, enabling data analysis and visualization. Plasma chemistry algorithms implement atomic physics processes such as the generation and evolution of plasma, recombination of plasma, and electron attachment on dopants in dense neutral gas. Benchmarks and experimental validation tests are also discussed. The code has been used for the simulation of processes relevant to the eRHIC program at BNL and the high pressure RF cavity (HPRF) program at Fermilab.

INTRODUCTION

Direct numerical simulation of plasma in the presence of atomic processes such as generation and recombination of charged particles is a complex multiscale problem. Plasma number density may change by orders of magnitude during relevant time scales, creating difficulties in representing secondary plasma particles by macroparticles within the Particle-in-Cell (PIC) method. Another difficulty is in the presence of different time scale, as in the case of plasmas interacting with relativistic particle beams. Evolution of atomic physics processes may be orders of magnitude longer compared to passing times of short relativistic bunches.

Novel algorithms for the simulation of plasma undergoing atomic processes and relativistic particle beams have been developed and implemented in SPACE, a parallel electromagnetic PIC code. The code has been applied to a number of problems relevant to advanced particle cooling mechanisms.

SUMMARY OF SPACE CODE

PIC Method for Maxwell's Equations

The system of Maxwell's equations in the presence of moving charges is written as

$$\frac{\partial \boldsymbol{B}}{\partial t} = -\nabla \times \boldsymbol{E} \quad (1a)$$

$$\frac{\partial \boldsymbol{E}}{\partial t} = -\frac{1}{\epsilon_0 \mu_0}\nabla \times \boldsymbol{B} - \frac{1}{\epsilon_0}\mathbf{J} \quad (1b)$$

$$\nabla \cdot \boldsymbol{E} = \frac{\rho}{\epsilon_0} \quad (1c)$$

$$\nabla \cdot \boldsymbol{B} = 0 \quad (1d)$$

The Maxwell equations are discretized using the finite difference time domain (FDTD) [1] with second order accuracy in space and time. Electric charges are represented by discrete macroparticles coupled with electromagnetic fields by the action of Lorentz forces and electric currents.

When one solves Maxwell's equations analytically, solving Eq. (1a) and Eq. (1b) is sufficient: if Eq. (1c) and Eq. (1d) are satisfied at initial time, they remain invariants of motion at later time. Due to numerical truncation errors, this property may be violated. To resolve this problem, a special rigorous charge conservation method was developed within the PIC framework in [2]. This algorithm, implemented in the SPACE code, requires solving numerically the Poisson problem (Eq. (1c)) only once for obtaining consistent initial conditions. Then only the first two Maxwell's equations (Eq. (1a) and Eq. (1b)) and the Newton-Lorentz equation are solved numerically at each time step. A schematic of processes occurring at each time step is depicted in Fig. 1. The computational sequence is of fields and particle coordinates is shown in Fig. 2. We also implemented modifications of the Boris scheme [3] proposed in [4] for dealing with rapidly accelerating particles for which the relativistic factor is not constant.

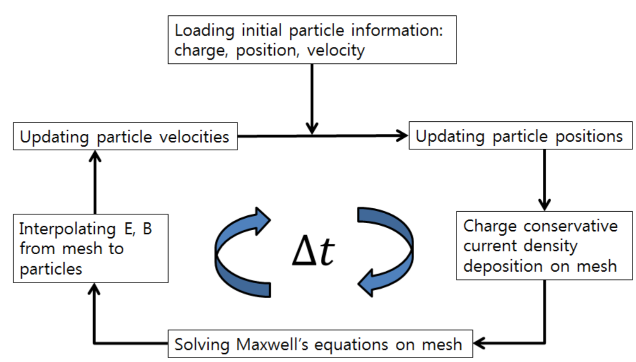

Figure 1: Schematic of one time step of SPACE code.

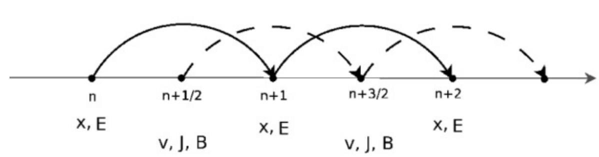

Figure 2: Computation sequence along time step

Code Structure and Properties

The code is developed in C++ utilizing the advantages of Objected-Oriented Programming. The code is

* kwangmin.yu@stonybrook.edu
# rosamu@bnl.gov

ISBN: 978-3-95450-168-7 doi:10.18429/JACoW-IPAC2015-MOPMN013

SIMULATION OF BEAM-INDUCED PLASMA IN GAS FILLED CAVITIES

K. Yu*, Stony Brook University, Stony Brook, NY 11794, USA
R. Samulyak#, Stony Brook University, Stony Brook, NY 11794 and BNL, Upton, NY 11973, USA
A. Tollestrup, K. Yonehara, Fermilab, Batavia, IL 60510, USA
B. Freemire, Illinois Institute of Technology, Chicago, IL 60616, USA
M. Chung, UNIST, Ulsan, Korea

Abstract

Understanding of the interaction of muon beams with plasma in muon cooling devices is important for the optimization of the muon cooling process. SPACE, a 3D electromagnetic particle-in-cell (EM-PIC) code, is used for the simulation support of the experimental program on the hydrogen gas filled RF cavity in the Mucool Test Area (MTA) at Fermilab. We have investigated the plasma dynamics in the RF cavity including the process of power dump by plasma (plasma loading), recombination of plasma, and plasma interaction with dopant material. By comparison with experiments in the MTA, simulations suggest several unknown properties of plasma such as the effective recombination rate, the electron attachment time on dopant molecule, and the ion – ion recombination rate in the plasma.

INTRODUCTION

When a beam passes through a dense hydrogen gas filled RF (HPRF) cavity, the beam energy ionizes the gas. The induced plasma gains energy from the RF electric field applied to cavity. This effect is called plasma loading. The induced plasma undergoes complicated recombination processes. If a small amount of dopant (molecular oxygen) is added to the hydrogen gas, plasma electrons attach to dopant molecules, creating negatively charges ions and causing ion-ion recombination processes. These processes have been studied by experiments at the MuCool Test Area at Fermilab [1,2,3]. Simulation study has been used to compare the experiment results with the mathematical model and uncover unknown or uncertain properties from the experiments. Even though the recombination rate, attachment time, and ion-ion recombination are measured in experiments, the range of measurements is restricted in narrow region. Benchmarked with experimental data, simulations suggest those rates for a large experimental range. To enable such simulations, new algorithms to resolve plasma chemistry and plasma loading have been developed and implemented in SPACE [4].

ATOMIC PHYSICS IN GAS-FILLED CAVITY

Plasma Formation

As an intense proton beam propagates in the HPRF cavity, it generates plasma by ionization due to collision of beam particles with neutral gas molecules [5,6]. When the cavity is filled with pure hydrogen gas, the plasma is formed by electrons and hydrogen ion clusters. If dopant such as oxygen is added in the gas, electrons quickly attach to dopant molecules, creating negative ions [5,7]. The formation of plasma follows the beam shape because plasma particles are generated along beam particle trajectories, and the plasma particles cannot move far away from their initial position due to collisions with the dense neutral gas. The plasma column preserves its form as time evolves (Fig. 7), even though the density of plasma changes by successive beam injections and atomic processes such as electron ion recombination, electron attachment, and ion-ion recombination in the cavity.

Plasma Loading

The energy loss by one plasma pair during one RF cycle, dw, is introduced [1,3] based on the electron or ion drift velocity (v) or mobility (μ), and the external RF field ($E_0 \sin(\omega t)$):

$$dw = \mathrm{q}\int_0^T (v_e + v_+ + v_-)\, E_0 \sin(\omega t)\, dt = \mathrm{q}\int_0^T (\mu_e + \mu_+ + \mu_-)\, E_0^{\,2} \sin^2(\omega t)\, dt \quad (1)$$

where subscripts "e", "+", and "-" denote electron, positive ion (hydrogen), negative ion (oxygen), respectively, and T and E_0 are the period and peak magnitude of the RF cycle. The external electric field E_0 in Eq. (1) has spatial distribution related to the geometry of the cavity [3]. Even though E_0 is not constant in space, we can assume it is constant for each specific plasma pair during one RF cycle since plasma charges cannot move far away from their initial positions. But different plasma pair in different position may have different E_0. Spatial distribution of E_0 is implemented in the SPACE code. Analytic computation of Eq. (1) was compared with experiments in [1,2,5]. Numerical simulation results are compared with experiments in Fig. 2.

The power delivered to gas in cavity by plasma loading is given by

$$\mathrm{P} = \frac{(V_{peak} - V)V}{R} - CV\frac{dV}{dt} \quad (2)$$

where R, C, and V_{peak} denote the shunt impedance, capacity of the cavity, and the peak RF voltage, respectively [1,3]. In simulations, the total power is computed and E_0 (V in Eq. (2)) is updated at every time step. Functions implementing the electron drift velocity

* kwangmin.yu@stonybrook.edu
# rosamu@bnl.gov

Content from this work may be used under the terms of the CC BY 3.0 licence (© 2015). Any distribution of this work must maintain attribution to the author(s), title of the work, publisher, and DOI.

ISBN: 978-3-95450-168-7 doi:10.18429/JACoW-IPAC2015-MOPMN015

Content from this work may be used under the terms of the CC BY 3.0 licence (© 2015). Any distribution of this work must maintain attribution to the author(s), title of the work, publisher, and DOI.

SIMULATION OF BEAM-INDUCED PLASMA FOR THE MITIGATION OF BEAM-BEAM EFFECTS

J. Ma, Stony Brook University, Stony Brook, New York 11794, USA
R. Samulyak, Brookhaven National Laboratory, Upton, New York 11973, USA
K. Yu, Stony Brook University, Stony Brook, New York 11794, USA
V. N. Litvinenko, Brookhaven National Laboratory, Upton, New York 11973, USA
G. Wang, Brookhaven National Laboratory, Upton, New York 11973, USA

Abstract

One of the main challenges in the increase of luminosity of circular colliders is the control of the beam-beam effect. In the process of exploring beam-beam mitigation methods using plasma, we evaluated the possibility of plasma generation via ionization of neutral gas by proton beams, and performed highly resolved simulations of the beam-plasma interaction using SPACE, a 3D electromagnetic particle-in-cell code. The process of plasma generation is modelled using experimentally measured cross-section coefficients and a plasma recombination model that takes into account the presence of neutral gas and beam-induced electromagnetic fields. Numerically simulated plasma oscillations are consistent with theoretical analysis. In the beam-plasma interaction process, high-density neutral gas reduces the mean free path of plasma electrons and their acceleration. A numerical model for the drift speed as a limit of plasma electron velocity was developed. Simulations demonstrate a significant reduction of the beam electric field in the presence of plasma. Preliminary simulations using fully-ionized plasma have also been performed and compared with the case of beam-induced plasma.

PLASMA GENERATION

We study the process of plasma generation by the proton beam ionization of neutral matter, such as molecular hydrogen gas. We use the following parameters relevant to the Relativistic Heavy Ion Collider (RHIC) at the Brookhaven National Laboratory.

Table 1: Proton Beam Structure

Energy	30 GeV
Normalized emittance	2e-6 m rad
Beta function	10 m
Number of protons per bunch	2e+11
Bunch duration	5 ns
Number of bunches	110
Bunch arrival interval	110 ns

Energy loss of an incident particle in matter by ionization is described by the Bethe-Bloch formula. But since the amount of energy absorbed by excitation processes is not precisely known, we use an empirical formula and experimentally measured ionization cross-sections. The evolution of the plasma density is given as

$$\frac{dn_e}{dt} = \frac{dN_p}{dt}\sigma L n_{gas} - \beta_r n_e n_i \qquad (1)$$

where dn_e/dt is the ionization rate, dN_p/dt is the inflow of protons in the elementary volume, L is the volume length, n_{gas}, n_e, and n_i are number densities of neutral gas, plasma electrons, and plasma ions, respectively, and β_r is the recombination coefficient. The ionization cross section σ of energetic particles in molecular hydrogen was experimentally measured in [1].

The recombination of plasma is strongly affected by the presence of neutral gas with much bigger density than the plasma density, and the electric field of the proton beam. The recombination coefficient is an empirical coefficient [2, 3] evaluated as

$$\beta_r = c_1 X^{-c_2}$$

Here $X = E/P$ is the ratio of electric field and hydrogen pressure, and c_1 and c_2 are empirical numerical coefficients. We use results of measurements of plasma recombination in high-pressure hydrogen gas filled RF cavity at Fermilab [2, 3] to evaluate the recombination coefficient.

In the initial stage of plasma generation, recombination is negligible because of low plasma density, as shown in Figure 1. In this section, long-time evolution of plasma was obtained by numerically integrating equation (1). Fully resolved 3D PIC simulations are presented in the next section.

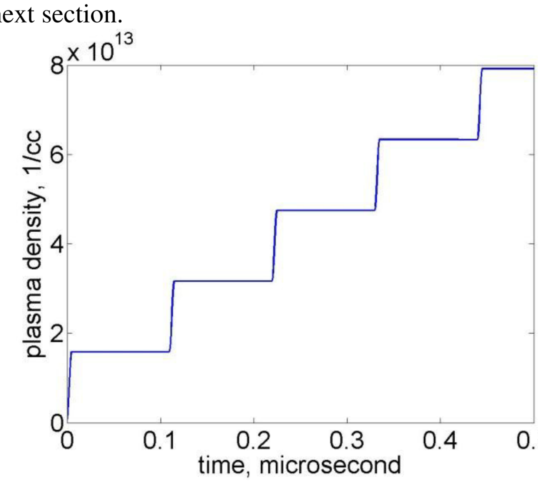

Figure 1: Plasma density evolution corresponding to first five bunches of proton beam.

ISBN: 978-3-95450-168-7 doi:10.18429/JACoW-IPAC2015-MOPMN016

DECOHERENCE DUE TO SECOND ORDER CHROMATICITY IN THE NSLS-II STORAGE RING*

G. Bassi†, A. Blednykh, J. Choi, V. Smaluk, BNL, Upton, NY 11973-5000, USA

INTRODUCTION

We study decoherence effects due to second order chromaticity for small amplitude kicks, in order to estimate the energy spread from TbT data. The measurements are taken for the bare lattice (no Damping Wigglers and Insertion devices) of the NSLS-II storage ring, since the long transverse radiation damping time $\tau_x = 54$ allows the study of decoherence effects on shorter time scales. To minimize the chromatic damping/antidamping from the slow-head tail effect, we used a short train of 50 bunches distributed over consecutive rf-buckets with an average current $I_0 = 1$mA, high enough to obtain a good BPM signal. The vertical and horizontal betatron motion have been excited independently with pinger magnets. In this contribution we limit the discussion to the horizontal case. A more detailed analysis discussing the vertical case, together with the transition to kicks of larger amplitudes to characterize decoherence with amplitude effects will be addressed in our future work. Decoherence studies have been done by independently exciting horizontal and vertical betatron oscillations with pingers, from small values of the pinger voltage for good BPM signal, to larger values in order to excite betatron oscillations of amplitude (peak to peak) 2mm. Larger betatron oscillations have been induced to clearly show the transition from decoherence due to second order chromaticity to decoherence with amplitude. Decoherence due to chromaticity and nonlinearities and beam energy spread measurements have been discussed in [1, 2].

DECOHERENCE DUE T0 LINEAR CHROMATICITY

Although in this contribution we discuss measurements for negligible linear chromaticity, in a small kick regime dominated by second order chromaticity, the decoherence due to nonzero linear chromaticity can be used as well to accurately estimate important beam parameters such as the synchrotron tune and the energy spread, based on the direct analysis of TbT data or on the analysis of their spectra. Of course, in second order chromaticity can not be made negligible, both effects (linear chromaticity and second order chromaticity) must be studied simultaneously. This case introduces little complications, for example formulae cannot eventually be put in closed form, however, as shown in the next Section, it does not prevent to estimate beam parameters. A formula for the decoherence of TbT data due to linear chromaticity is well known [3–5]. A derivation of the formula is given in Appendix. Here we discuss its use to estimate the synchrotron tune and energy spread from

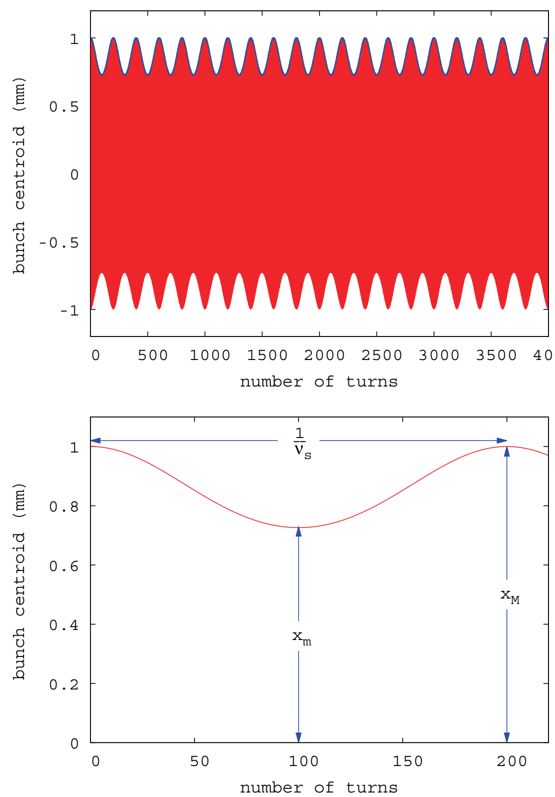

Figure 1: Top frame: evolution of the bunch centroid $\langle x(t)\rangle$. Bottom frame: enlargement of the top frame illustrating how the synchrotron tune and energy spread can be extracted from the signal of TbT data.

TbT data. Assuming for the betatron frequency ω a linear dependence on the relative energy deviation δ

$$\omega(t) = \omega_\beta + \xi\omega_0\delta(t), \tag{1}$$

where ξ is the linear chromaticity, the time evolution of the kicked (at t=0) bunch centroid $\langle x(t)\rangle$ reads (see Appendix)

$$\langle x(t)\rangle = \langle x_0\rangle e^{-2\frac{\xi^2\sigma_\delta^2}{\nu_s^2}\sin^2\frac{\omega_s t}{2}} \cos\omega_\beta t, \tag{2}$$

where η is the slippage factor, ω_s the synchrotron frequency, $\nu_s = \omega_s/\omega_0$ the synchrotron tune, σ_δ the energy spread and $\sigma_{z0} = \eta c/(\omega_s\sigma_\delta)$ the bunch length, where c is the speed of light. The top frame of Fig. 1 shows the evolution of the bunch centroid $\langle x(t)\rangle$ where its envelope shows a modulation with a characteristic wavelength and amplitude as given by Eq. 2. For illustration purposes, the linear chromaticity ξ has been chosen equal to 4. The bottom frame of Fig. 1 shows an enlargement of the top frame, and illustrates how the synchrotron tune and energy spread can be extracted from the signal of TbT data. The synchrotron tune

* Work supported by DOE contract DE-SC0012704
† gbassi@bnl.gov

Content from this work may be used under the terms of the CC BY 3.0 licence (© 2015). Any distribution of this work must maintain attribution to the author(s), title of the work, publisher, and DOI.

ISBN: 978-3-95450-168-7 doi:10.18429/JACoW-IPAC2015-MOPMN018

Content from this work may be used under the terms of the CC BY 3.0 licence (© 2015). Any distribution of this work must maintain attribution to the author(s), title of the work, publisher, and DOI.

A GENERIC FORMULATION FOR EMITTANCE AND LATTICE FUNCTION EVOLUTION FOR NON-HAMILTONIAN SYSTEMS WITH STOCHASTIC EFFECTS

J. Scott Berg, BNL*, Upton, NY 11973, USA

Abstract

I describe a generic formulation for the evolution of emittances and lattice functions under arbitrary, possibly non-Hamiltonian, linear equations of motion. The average effect of stochastic processes, which would include ionization interactions and synchrotron radiation, is also included. I first compute the evolution of the covariance matrix, then the evolution of emittances and lattice functions from that. I examine the particular case of a cylindrically symmetric system, which is of particular interest for ionization cooling.

INTRODUCTION

I describe a general formulation for the evolution of the first and second moments of a beam distribution. Similar formulations have been presented before ([1–3] are some examples). What is of interest here is the definition of the stochastic behavior in terms of probabilities, the direct computation of the evolution of generalized lattice functions (really the symplectic normalizing transformation of the second moment matrix) and emittances, and the definition of a metric for mismatch of those lattice functions.

MATHEMATICAL FORMULATION

$\psi(z, s)$ is the distribution function for particles in the phase space coordinates z at a point s along a reference curve. We define the first and second moments of this distribution

$$\boldsymbol{a}(s) = \int z\,\psi(z, s)\,dz \tag{1}$$

$$\Sigma(s) = \int [z - \boldsymbol{a}(s)][z - \boldsymbol{a}(s)]^T \psi(z, s)\,dz \tag{2}$$

The deterministic motion of a particle is described by

$$\frac{dz}{ds} = \boldsymbol{f}(z, s) \tag{3}$$

The stochastic part of the motion is described such that $\rho(\boldsymbol{x}, z, s) d\boldsymbol{x}\, ds$ is the probability that, for a particle at z in phase space and in the interval $[s, s + ds)$, the particle is displaced in phase space by a value in the phase space volume of size $d\boldsymbol{x}$ at $\boldsymbol{x}$. Then the continuity equation is

$$\frac{\partial\psi}{\partial s} + \boldsymbol{\nabla} \cdot [\psi(z, s)\boldsymbol{f}(z, s)] = \int \psi(z - \boldsymbol{x}, s)\rho(\boldsymbol{x}, z - \boldsymbol{x}, s)\,d\boldsymbol{x} - \psi(z, s)\int \rho(\boldsymbol{x}, z, s)\,d\boldsymbol{x}. \tag{4}$$

From this one can determine the evolution of the moments. The system acts as though it were governed by a deterministic vector field $\boldsymbol{g}$ such that

$$\frac{dz}{ds} = \boldsymbol{g}(z, s) = \boldsymbol{f}(z, s) + \int \boldsymbol{x}\,\rho(\boldsymbol{x}, z, s)\,d\boldsymbol{x} \tag{5}$$

Then

$$\frac{d\boldsymbol{a}}{ds} = \int \boldsymbol{g}(z, s)\psi(z, s) \tag{6}$$

$$\begin{aligned}\frac{d\Sigma}{ds} = &\int [z - \boldsymbol{a}(s)]\boldsymbol{g}(z, s)^T \psi(z, s)\,dz \\ &+ \int \boldsymbol{g}(z, s)[z - \boldsymbol{a}(s)]^T \psi(z, s)\,dz \\ &+ \int \boldsymbol{x}\boldsymbol{x}^T \rho(\boldsymbol{x}, z, s)\psi(z, s)\,d\boldsymbol{x}\,dz\end{aligned} \tag{7}$$

If $\boldsymbol{g}(z, s) = \boldsymbol{g}_0(z) + JH(s)z$, with J the antisymmetric symplectic metric (H is symmetric only for a Hamiltonian system),

$$\frac{d\boldsymbol{a}}{ds} = \boldsymbol{g}_0(s) + JH(s)\boldsymbol{a}(s) \tag{8}$$

$$\begin{aligned}\frac{d\Sigma}{ds} = &JH(s)\Sigma(s) - \Sigma(s)H^T(s)J \\ &+ \int \boldsymbol{x}\boldsymbol{x}^T \rho(\boldsymbol{x}, z, s)\psi(z, s)\,d\boldsymbol{x}\,dz\end{aligned} \tag{9}$$

As long as Σ is positive definite (its definition insures that it is positive *semi*-definite), then one can find a symplectic A such that

$$\Sigma(s) = A(s)E(s)A^T(s) \tag{10}$$

where E is diagonal with pairs of equal diagonal elements, which are the emittances. A contains the generalized versions of the Courant-Snyder functions that describe the *distribution*. For a distribution "matched" to a lattice, A will by definition refer to the generalization of the corresponding functions for the *lattice*. If the emittances are distinct, the right hand side of A can be multiplied by any block-diagonal rotation with 2×2 blocks (there is more freedom when some emittances are equal).

* This manuscript has been authored by employees of Brookhaven Science Associates, LLC under Contract No. DE-SC0012704 with the U.S. Department of Energy. The United States Government retains a non-exclusive, paid-up, irrevocable, world-wide license to publish or reproduce the published form of this manuscript, or allow others to do so, for United States Government purposes.

ISBN: 978-3-95450-168-7 doi:10.18429/JACoW-IPAC2015-MOPMN019

UNDERSTANDING THE EFFECT OF SPACE CHARGE ON INSTABILIIES*

M. Blaskiewicz†, BNL, Upton NY 11973 USA
A. Chao, SLAC, Stanford University, Stanford CA 94309 USA
Y.H. Chin, KEK, Ibaraki, Japan

Abstract

The combined effect of space charge and wall impedance on transverse instabilities is an important consideration in the design and operation of high intensity hadron machines as well as an intrinsic academic interest. This study explores the combined effects of space charge and wall impedance using various simplified models in an attempt to produce a better understanding of their interplay.

TWO PARTICLE MODEL

The simplest nontrivial model including the space charge force requires two macroparticles [1, 2]. We consider vertical motion and use $\theta = s/R$ as the dynamical variable, it increases by 2π each turn. When particle two leads particle one during the synchrotron oscillation one has:

$$y_1'' = -\nu^2 y_1 + K(y_1 - y_2) + W y_2 \tag{1}$$
$$y_2'' = -\nu^2 y_2 + K(y_2 - y_1), \tag{2}$$

where ν is the unperturbed betatron tune, $'$ denotes $d/d\theta$, K creates the space charge tune shift and W is the wake strength. Indicies are reversed during the second half of the synchrotron oscillation. To proceed we use the single sideband approximation. Assume

$$y_i(\theta) = \hat{y}_i(\theta)\exp(-iA\theta),$$

insert these in eq (1) and(2), and neglect terms proportional $\hat{y}_i''$. Setting $A^2 = \nu^2 - K$ gives

$$\hat{y}_1' = -i\frac{K-W}{2A}\hat{y}_2 \tag{3}$$
$$\hat{y}_2' = -i\frac{K}{2A}\hat{y}_1 \tag{4}$$

Set $\kappa = \sqrt{(K-W)/K}$ and $b_0 = K\kappa/2A$ so that

$$\hat{y}_1(\theta) = \cos(b_0\theta)\hat{y}_{10} - i\kappa\sin(b_0\theta)\hat{y}_{20} \tag{5}$$
$$\hat{y}_2(\theta) = \cos(b_0\theta)\hat{y}_{20} - \frac{i}{\kappa}\sin(b_0\theta)\hat{y}_{10}, \tag{6}$$

where $\hat{y}_{10}$ and $\hat{y}_{20}$ are intial conditions.When b_0 is imaginary we use $\cos(ix) = \cosh(x)$ and $\sin(ix) = i\sinh(x)$. Setting $\theta = \pi/\nu_s$ with ν_s the synchrotron tune yields the map for the first half of the synchrotron oscillation. Reversing the roles of particle 2 and 1 yields the map for the second half. Concatenating the maps yields a two by two matrix with unit determinant. The trace of the full matrix is

$$Tr(M_0) = 2\cos^2(b_0\pi/\nu_s) - \left\{\kappa^2 + 1/\kappa^2\right\}\sin^2(b_0\pi/\nu_s). \tag{7}$$

Let λ be an eigenvalue of M. Then $Tr(M) = \lambda + 1/\lambda$ and the system is unstable if $|Tr(M)| > 2$.

AN ALTERNATE SOLUTION

By neglecting the terms proportional to $\hat{y}''$ in the previous section we introduced errors in the tunes appearing in the transport matrix. These can be avoided without sacrificing a simple closed form solution. We start off by diagonalizing equations (1) and (2). Set $z = y_1 + \alpha y_2$, where α is an unknown constant. One gets

$$z'' = -A^2 z - \alpha K\kappa y_1 - (K-W)y_2.$$

Now introduce another unknown constant β and demand $\beta z = \alpha K\kappa y_1 - (K-W)y_2$. This gives $\alpha = \pm\kappa$ and $\beta = \alpha K$.The new equations of motion are

$$z_1'' = -(A^2 + K\kappa)z_1 \qquad z_2'' = -(A^2 - K\kappa)z_2 \tag{8}$$

with $z_1 = y_1 + \kappa y_2$ and $z_2 = y_1 - \kappa y_2$. Define

$$B_1 = \sqrt{A^2 + K\kappa}, \qquad B_2 = \sqrt{A^2 - K\kappa}.$$

Now, assume κ is real and positive along with the Bs. We deal with imaginary κ later. Approximate

$$\hat{z}_m(\theta) \equiv z_m(\theta) + iz_m'(\theta)/A = \hat{z}_m(0)e^{-iB_m\theta}, \tag{9}$$

where we would divide by B_m instead of A for an exact solution. To the same level of approximation one has

$$\hat{y}_1 = (\hat{z}_1 + \hat{z}_2)/2, \qquad \hat{y}_2 = (\hat{z}_1 - \hat{z}_2)/2\kappa.$$

Now define

$$\bar{B} = (B_1 + B_2)/2, \qquad b = (B_1 - B_2)/2.$$

The map during the first half of the synchrotron oscillation is

$$\hat{y}_1(\theta) = e^{-i\bar{B}\theta}\left[\cos(b\theta)\hat{y}_{10} - i\kappa\sin(b\theta)\hat{y}_{20}\right] \tag{10}$$
$$\hat{y}_2(\theta) = e^{-i\bar{B}\theta}\left[\cos(b\theta)\hat{y}_{20} - \frac{i}{\kappa}\sin(b\theta)\hat{y}_{10}\right] \tag{11}$$

Apart from the overall phase evolution due to $\exp(-i\bar{B}\theta)$ and the small difference between b and b_0 these equations

* This work was supported by United States Department of Energy Contracts DE-SC0012704 and DE-AC02-76SF00515.
† blaskiewicz@bnl.gov

Content from this work may be used under the terms of the CC BY 3.0 licence (© 2015). Any distribution of this work must maintain attribution to the author(s), title of the work, publisher, and DOI.

ISBN: 978-3-95450-168-7 doi:10.18429/JACoW-IPAC2015-MOPMN020

Content from this work may be used under the terms of the CC BY 3.0 licence (© 2015). Any distribution of this work must maintain attribution to the author(s), title of the work, publisher, and DOI.

LONGITUDINAL IMPEDANCE OF RHIC*

M. Blaskiewicz†, J.M. Brennan, K. Mernick
BNL, Upton, NY 11973, USA

Abstract

The longitudinal impedance of the two RHIC rings has been measured using the effect of potential well distortion on longitudinal Schottky measurements. For the blue RHIC ring $Im(Z/n) = 1.5 \pm 0.2\Omega$. For the yellow ring $Im(Z/n) = 5.4 \pm 1\Omega$.

INTRODUCTION

In a storage ring the net RF voltage per turn is that supplied by the RF cavities plus the voltage due to parasitic impedances. The parasitic voltage changes the incoherent spectrum [1, 2, 3]. The broad band impedance can be characterized by an inductance L. Let τ denote the arrival time of a particle with respect to the synchronous particle. The net voltage per turn is

$$V(\tau) = V_{rf}(\tau) - L dI/d\tau$$

where I is the instantaneous beam current. Consider a single RF harmonic operating above transition. Particles near the center of the bunch have the largest synchrotron frequency and the voltage there is

$$V \approx -\hat{V}_{rf}\omega_{rf}\tau - L\ddot{I}\tau$$

where $\hat{V}_{rf}$ is the amplitude of the RF voltage, ω_{rf} is the angular Rf frequency, and $\ddot{I}$ is the second derivative of the beam current with respect to time evaluated in the center of the bunch. The parasitic voltage modifies the small amplitude synchrotron frequency

$$f_s = f_{s0}\left(1 + \frac{L\ddot{I}}{\hat{V}_{rf}\omega_{rf}}\right)^{1/2} \approx f_{s0}\left(1 + \frac{L\ddot{I}}{2\hat{V}_{rf}\omega_{rf}}\right), \tag{1}$$

where f_{s0} is the small amplitude synchrotron frequency with no impedance and the approximation is excellent for our parameters. The inductance satisfies $j\omega_0 L = Z/n$ where ω_0 is the angular revolution frequency and Z/n is the impedance divided by the revolution harmonic. For space charge $Im(Z/n) < 0$ and for wall impedances $Im(Z/n) > 0$. Of course the actual value of Z/n varies with frequency and can change in sign, but for RHIC the root mean square bunch length is $\gtrsim$30 cm while the vacuum chamber radius is $\sim$ 3 cm. Therefore, all resonant wavelengths are short compared to the bunch length and only the inductive part of the parasitic impedance creates significant voltage for stable beams.

* This work was supported by United States Department of Energy Contract DE-SC0012704
† blaskiewicz@bnl.gov

DATA ACQUISITION AND ANALYSIS

The data were obtained during an accelerator physics experiment on June 4, 2014. Figure 1 shows the blue fill pattern at the beginning of the experiment. The gold ions were accelerated to 100 GeV/nucleon and stored in the $h = 360$ (28 MHz) RF system. The spectrum analyzer was gated so that each of the 5 different batches of bunch intensity were measured individually. As time progressed intrabeam scattering and losses provided a natural spread in bunch parameters. The values of $\ddot{I}$ were obtained by averaging the bunch profiles in each group and fitting a parabolic cap to the top 30%. Wall current monitor data were acquired every 5 minutes and linear interpolation in time was used to align the wall current monitor data to the spectrum analyzer data. Some spectrum analyzer data are shown in figure 2. As is clear from the figure the peaks move, but the effect is fairly subtle. To analyze these data we fit parabolas to the top 3 points around each of the peaks and measured the difference between the location of the positive and negative synchrotron sidebands. The difference was divided by twice the order of the synchrotron mode and we obtained 12 independent estimates of synchrotron frequency for each spectrum. Data from the different synchrotron lines were analyzed independently. At this point two different techniques were employed. In the first technique we assumed a two dimentsional (2d) fitting function

$$f_s(k) = a_1 + a_2\ddot{I}(k) + \text{error}, \tag{2}$$

where a_1 and a_2 are fit parameters and index k characterizes a particular measurement. Linear least squares was used to obtain the $a_i s$ and equation(1) was used to obtain L and subsequently $Im(Z/n)$. In the second technique we assumed a three dimensional (3d) fitting function

$$f_s(k) = a_1 + a_2\ddot{I}(k) + a_3 t_{spec}(k) + \text{error}, \tag{3}$$

where $t_{spec}(k)$ was the time at which the spectra were acquired. This accounts for smooth, uncontrolled drifts in the machine parameters. Figures 4 and 5 show the least squares results for Z/n.

Figures 4 and 5 show clear discontinuities in the measured values of Z/n. We ascribe these to the presence of coherent modes and assume the low lying synchrotron modes are primarily influenced. Hence we took the average values of Z/n over the regions shown as the actual values of Z/n. Both lines fall within the one sigma errors for most of the data, so we take the average as a best estimate. For the blue RHIC ring $Im(Z/n) = 1.5\pm0.2\Omega$. For the yellow ring $Im(Z/n) = 5.4 \pm 1\Omega$. Previous results for the yellow

ISBN: 978-3-95450-168-7 doi:10.18429/JACoW-IPAC2015-MOPMN021

NSLS-II STORAGE RING BPM BUTTON DEVELOPMENT*

A. Blednykh#, B. Bacha, G. Bassi, W. Cheng, C. Hetzel, B. Kosciuk, D. Padrazo, O. Singh,
BNL, NSLS-II, Upton, NY, 11973-5000, USA

Abstract

The NSLS-II BPM Button design and its development process have been presented. Subjects discussed include BPM impedance optimization, design and construction, production, BPM selection and a first temperature measurement at 200mA average current within 1200 bunches.

IMPEDANCE OPTIMIZATION

Two types of BPM (beam position monitor) Buttons have been installed in the NSLS-II storage ring; the large aperture and the small aperture BPM Buttons. The large aperture BPM Button located on the multipole vacuum chambers of $12.5mm$ half-aperture, six BPMs per cell, 180 BPM assemblies total [1]. During the BPM Button optimization process we paid attention to: BPM Button heating due to trapped modes which are generated in the gap between the housing and the button [2]; heat transfer analysis; proper choice of the button and housing materials; dielectric materials choice from good thermal conductivity and low electrical conductivity point of views; impedance optimization process.

The large aperture BPM assemblies are located on the multipole vacuum chambers with antechamber slot of 10mm high. The standard BPM assembly consists of two BPM Flanges. Each BPM Flange, top and bottom, includes two BPM Buttons mounted into one flange as it shown in Fig. 1.

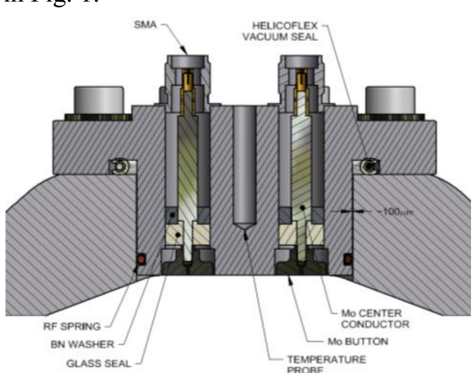

Figure 1: BPM Flange fixed to vacuum vessel. The clearance of the BPM Flange $\sim 100\mu m$ from the contact vacuum chamber surface.

The NSLS-II large aperture BPM button is chosen with a diameter of 7mm to satisfy horizontal and vertical BPM sensitivity requirements and to reduce heat load. It produces smaller geometric loss factor compared with a larger button diameter. The button thickness is chosen to be 2mm. The gap between the housing and the button is $250\mu m$. The BPM Button is made from molybdenum, which has an electrical conductivity $\sigma_{Mo} = 17 \times 10^6\ S/m$ is much larger than the conductivity of stainless steel material chosen for the BPM Flange $\sigma_{StSt} = 1.5 \times 10^6\ S/m$. Due to different material selection, trapped mode power will be predominantly dissipated in the BPM Flange rather than in well-conducted button [3]. Due to excitation of resonant modes in the buttons, the kick factor and the loss factor depend very strongly on the BPM button geometry. Several types of modes can be generated in the button geometry by a passing bunch. A coaxial TEM-mode (signal) propagates through the button and the feedthrough to the BPM electronics. If the feedthrough is matched well to 50 Ohm, there will be no TEM-modes reflected back to the chamber. Coaxial cavity type modes TE_{m1p}-mode (H_{m1p}-mode) where *m* and *p* are *1, 2, 3, k* (field variation in azimuthal and longitudinal directions). These modes then can be seen by the beam at frequencies defined by the cut-off frequency. The cut-off frequency for H_{m1}-mode like in a coaxial waveguide can be defined as

$$f_c^{H_{m1}} \approx \frac{1}{\sqrt{\varepsilon_r}} \frac{c}{\pi} \frac{m}{(r_1 + r_2)}, \qquad (1)$$

Where r_1 and r_2 are the radii of the inner and outer conductors, *m=1, 2, 3, k* and ε_r is relative permittivity (dielectric constant). As can be seen from Fig. 2, there are two types of dielectric materials present in the button geometry. It is 7070 glass (SiO2) for the vacuum seal and a Boron Nitride (BN) disc installed on the ambient side of the glass seal to improve the heat transfer from the pin to the stainless flange.

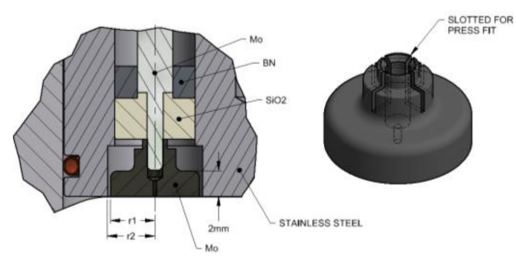

Figure 2: Internal button details with press fit connection.

The longitudinal wake potential for a 3mm Gaussian bunch and its Fast Fourier Transform are shown in Figs. 3,4. For the numerical calculation "port" boundary condition was specified at the end of the button. In this case the TEM-mode propagates out of the button without reflection. The first lowest mode is H_{11}-Mode (TE_{11}-mode). It is trapped in a gap between the housing and the button due to the button shape at frequency $f_{H11} = 13.4GHz$, which is slightly above the cut-off frequency $f_c^{H11} = 13.2GHz$ ($r_1 = 3.5mm$ and $r_2 = 3.75mm$). The peak at frequency $25.95GHz$ corresponds to the same type of mode with $m = 2$ (H_{21}-Mode). Two other peaks were identified at frequencies $15.43GHz$ and

* Work supported by DOE contract DE-SC0012704.
#blednykh@bnl.gov

Content from this work may be used under the terms of the CC BY 3.0 licence (© 2015). Any distribution of this work must maintain attribution to the author(s), title of the work, publisher, and DOI.

ISBN: 978-3-95450-168-7 doi:10.18429/JACoW-IPAC2015-MOPMN024

STUDY OF NSLS-II DYNAMIC APERTURE TOLERANCES WITH RESPECT TO FIELD AND ORBIT ERRORS *

J. Choi†, G. Wang, T. Shaftan, BNL, Upton, NY 11973, USA

Abstract

As the emittance of synchrotron light sources moves towards diffraction limit, magnet tolerances for reaching dynamic aperture for high injection efficiency and long lifetime become more stringent. Once nonlinear families are designed and the machine is built, a machine operator may ask to which accuracy the linear optics and orbit should be corrected so to achieve reasonable dynamic aperture. We also studied the relations of the non-linear elements and beta-beat to the dynamic apertures by simulating NSLS-II storage ring lattice and the paper shows the results.

INTRODUCTION

As the emittance of synchrotron light sources moves towards diffraction limit, the more and more strong quadrupoles are required. The strong quadrupole field generates high linear chromaticity and to correct the chromaticity, in turn, strong sextupoles are also required. The nonlinearity from the sextupoles can create resonance excitation, and the excitation from the strong sextupoles can critically reduce the dynamic aperture (DA). The poor dynamic aperture directly impact the injection efficiency and lifetime and the normal operation will not be possible. The most traditional strategy is canceling the sextupole effects by making the lattice symmetric. Then the dynamic aperture can be recovered by lattice symmetry restoration [1]. However, as the chromatic sextupole strengths become too big to cancel each other using phase differences, geometric sextupoles are introduced in non-dispersive region to cancel out the effect of chromatic sextupoles [2]. And the symmetry becomes even more important. The usual measure of the symmetry breaking is the beta beating.

Because the dynamic aperture is so an important issue, many efforts are invested to secure it at every step of the lattice design. There are many reviews [3] and studies [4]. Many methods including analytic analysis [5] and simulations are used for the design as well as for improving the running machine. Usually, the simulation is accompanied by the frequency map analysis [6] from which we can see the quality of the DA. Also, the driving terms [7] are used to obtain the good dynamic aperture, and there are some computer tools [8] for this purpose.

Even if the dynamic aperture is good with the given sextupoles, there are many imperfections from magnets and insertion devices are added to the lattice. In general, if the linear lattice is robust, i.e. the twiss parameters are well optimized, the effect of the non-linear disturbance can be far more reduced. Therefore, we not only focus on removing the effect of the sextupoles [9] but, more importantly, we should design and maintain the robust lattice.

As the state of art synchrotron radiation source targeting sub-nanometer emittance with damping wigglers, NSLS-II storage ring is quite a robust lattice [10], as the result of the huge efforts, Still, the dynamic aperture is changing frequently from known as well as unknown reasons. To keep it big enough for the high injection efficiency and long lifetime, the machine parameters should be routinely checked and corrected. Those parameters include beta beating, tune, phase advance, dispersion and chromaticity. Among these parameters, beta beating, which is coming from the symmetry breaking, is primarily corrected for the recovery of the dynamic aperture.

The major linear errors which can break the symmetry is quadrupole field errors and sextuple alignment errors. In this paper, only by simulations, we analyzed the effects of these errors imposed on NSLS-II bare lattice. From the analysis, we want to find the relations between errors, beta beatings, and DA variations.

We'd like to mention that the error numbers in this paper have nothing to do with design specifications nor measured data. They are chosen just for convenience. The design specifications can be found in the design report [10].

QUADRUPOLE FIELD ERROR

The 792 m NSLS-II storage ring have 30 cells and 15 super periods. Each cell has 10 quadrupoles and the total number is 300 with all independent power supplies. We assigned gaussian random errors to these quadrupoles where the rms of the errors are 0.03%, 0.04%,..., 0.09%, 0.1% and, for each rms value, 10 sets of errors are generated. For each simulation, we obtained the area of the dynamic aperture and its ratio to that of the bare lattice is used as the figure of merit. To minimize the distraction, we also assume that the beta beating is corrected to at least 10% and when it is bigger than 10% the points are ignored.

Figure 1 shows the results of those precesses. The marks in Fig. 1(a) are the horizontal and vertical beta beatings of the sampled lattices. The colors of the marks represent the given rms values for the samples. Here, especially when the beta beating is bigger than 2% in the horizontal direction, the beta beating is very loosely related to the rms of the errors. That is, even though beta beating correction is necessary to reduce the field errors, it does not guarantee the reduction of the errors. Similarly, from Fig. 1(b), where the color means the relative dynamic aperture to the bare lattice, the big dynamic aperture does not necessarily mean the low beta beating and vice versa.

* Work supported by DOE contract No: DE-AC02-98CH10886
† jchoi@bnl.gov

Content from this work may be used under the terms of the CC BY 3.0 licence (© 2015). Any distribution of this work must maintain attribution to the author(s), title of the work, publisher, and DOI.

ISBN: 978-3-95450-168-7 doi:10.18429/JACoW-IPAC2015-MOPMN025

Content from this work may be used under the terms of the CC BY 3.0 licence (© 2015). Any distribution of this work must maintain attribution to the author(s), title of the work, publisher, and DOI.

LOCAL IMPEDANCE ESTIMATION OF NSLS-II STORAGE RING WITH BUMPED ORBIT*

J. Choi†, Y. Hidaka, G. Bassi, A. Blednykh, BNL, Upton, NY 11973, USA

Abstract

As the newly constructed 3rd generation light source, NSLS-II is expected to provide synchrotron radiation of ultra high brightness and flux with advanced insertion devices. To minimize the beam emittance, damping wigglers are used and there is a small aperture located at the straight section with the damping wiggler and whose vacuum chamber is coated with non-evaporable getter (NEG). We used the local bump method to find the effect on the beam from the narrow aperture and this paper discusses the results.

INTRODUCTION

To reduce the electron beam emittance as well as to serve as broadband sources of very bright and high flux x-rays, 1.8T damping wigglers (DW) are installed at NSLS-II storage ring. As the first stage, 3 sets of the wigglers are installed where each set consists of 2 wigglers of 3.5 m. Most of the NSLS-II storage ring uses extruded aluminum vacuum chambers and their apertures are ±38 mm in the horizontal direction and ±12.5 mm in the vertical direction. However, the damping wiggler chambers have vertical apertures of ±5.75 mm with tapers. The narrow gap results in very limited linear conductance and, in this case, lumped pumps at the ends of the chamber will not be enough for the desired vacuum. To simplify the pumping system design, narrow-gap chambers as the DW chambers are NEG coated and the damping wiggler chambers are also included.

As the emittance of the synchrotron radiation source approaches the diffraction limit, and the vacuum chambers are becoming extremely narrow, the NEG coating is seriously considered for the solution of the vacuum system. However, there are concerns about its impact on the resistive wall impedance. Various studies have been undertaken and more are being underway, including the experience reports [1] [2], calculations and experiments [3] [4]. Also, some analytical methods to calculate the impedance of the layered structure are developed [5-9]. However, because of the uncertainties in NEG coating, the impedance from the calculation or simulation can be far from the real value. Therefore accurate impedance measurement at the NEG coated location is even more important than the measurements for the conventional cases.

The local transverse impdedance will change the transverse kick factor and the focussing effect will shift the phase at the location. If the dependence of the phase advance on the beam current is found, the local kick factor can be obtained [10] [11]. Like a quadrupole, if we make a local orbit bump, the transverse kick factor will generate closed orbit distortion, and by comparing the changes in the closed orbit between high and low beam current, the kick factor can also be obtained [12] [13]. We used the local bump methods to measure the kick factor at the NEG coated damping wiggler ID chamber. Because we are interested in the effect of the vertical narrow gap, all the measurements in this paper are regarding the vertical direction.

LOCAL ORBIT BUMP

To measure the local effect on the closed orbit using a local bump, it is very important to make a clean flat bump without any significant leak. To completely contain a local bump within a long straight where the damping wiggler is installed, only 2 upstream and 2 downstream regular correctors can be used. Given the maximum corrector strength (1 mrad) and their locations in the lattice, a phase space scan in a model found the maximum feasible height of a vertical position bump at the long straight to be 2 mm. A Python module and its frontend interactive script (as an IPython notebook) have been developed to create a local bump of an arbitrary target height/angle. This code can work both in online (actual machine) and offline (simulation using PyTracy) modes. This allows an operator to reliably and quickly create a large-amplitude bump by pre-computing corrector setpoint values for a desired bump in the offline mode, loading these values into the machine, and finally fine-tuning the bump online. With this software, a local bump with 1.8-mm vertical height was successfully created for the purpose of the impedance measurement. The leakage of the bump was minimized after multiple iterations of orbit correction using SVD. The maximum and RMS difference between the achieved orbit and the target orbit around the ring (180 regular BPMs) was 34.7 μm (~1.9 % of the target height) and 12.4 μm (0.7 %), respectively. Figure 1 shows the resulting local bump together with the generated bump with simulation. The simulated bump will be used to estimate the local impedance with fiitting.

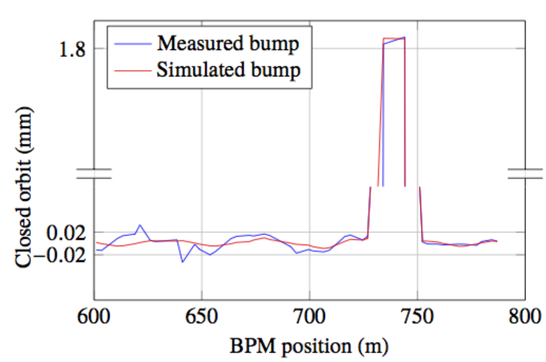

Figure 1: Local bump in the DW28.

* Work supported by DOE contract No: DE-AC02- 98CH10886
† jchoi@bnl.gov

ISBN: 978-3-95450-168-7 doi:10.18429/JACoW-IPAC2015-MOPMN027

OPTIMIZATION OF DYNAMIC APERTURE FOR HADRON LATTICES IN eRHIC

Yichao Jing*, Vladimir N. Litvinenko, Dejan Trbojevic, BNL, Upton, NY 11973, USA

Abstract

The potential upgrade of the Relativistic Heavy Ion Collider (RHIC) to an electron ion collider (eRHIC) involves numerous extensive changes to the existing collider complex. The expected very high luminosity is planned to be achieved at eRHIC with the help of squeezing the beta function of the hadron ring at the IP to a few cm, causing a large rise of the natural chromaticities and thus bringing with it challenges for the beam long term stability (Dynamic aperture). We present our effort to expand the DA by carefully tuning the nonlinear magnets thus controlling the size of the footprints in tune space and all lower order resonance driving terms. We show a reasonably large DA through particle tracking over millions of turns of beam revolution.

INTRODUCTION

The potential upgrade of the Relativistic Heavy Ion Collider (RHIC) to an electron ion collider (eRHIC) [1] involves numerous extensive changes to the existing collider complex. A high intensity electron energy recovery linac (ERL) will be added to the existing RHIC facility to collide with the strongly cooled hadron beams. The expected very high luminosity will be achieved with the help of squeezing the beta function of the hadron ring at the interaction points (IP) by at least 10-fold to a few cm, from the existing RHIC operating lattices. This will cause a large rise of the chromaticities and potentially undermines the beam's long term stability (Dynamic aperture).

It is well know that modern storage rings (both hadron rings and lepton rings) employs nonlinear magnets (sextupoles, octupoles, etc.) to correct the chromaticities from negative to small positive numbers to avoid microwave instabilities to develop. The natural chromaticities in the storage ring, i.e., the chromaticities rising from pure linear magnets (dipoles, quadrupoles), can be expressed as

$$C_x = -\frac{1}{4\pi}\int \beta_x(s)K_x(s)ds, \tag{1}$$

and

$$C_y = -\frac{1}{4\pi}\int \beta_y(s)K_y(s)ds. \tag{2}$$

Furthermore, the chromaticities rising from the IRs can be conveniently expressed as

$$C_{IR} = -\frac{2\Delta s}{4\pi\beta^*} \approx -\frac{1}{2\pi}\sqrt{\frac{\beta_{max}}{\beta^*}}, \tag{3}$$

where Δs is the distance from the IP to the first focusing magnet. Thus by squeezing the β^* 10-fold, the β_{max} increases

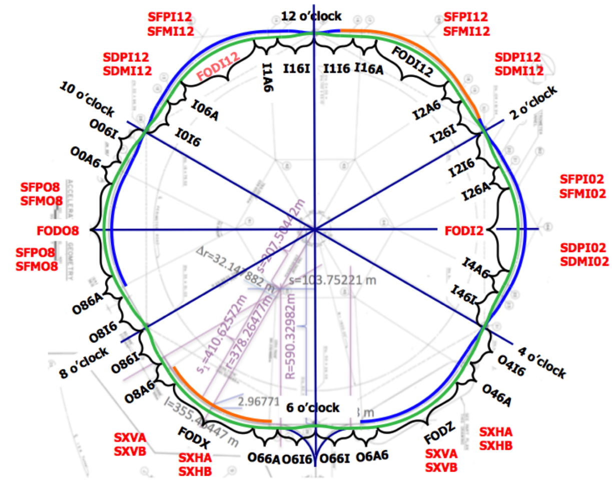

Figure 1: A schematic layout of hadron lattice for eRHIC as a rearrangements of the current operating RHIC lattice. Sextupoles families are indicated in red characters.

10 times and C_{IR} gains a 10 times of growth. This can be the dominant contribution to the total natural chromaticities in strongly focused colliders. For eRHIC, the β^* for hadron lattice is 5 cm (down from 65 cm for RHIC), which results in $C_{IR} \approx 50$, about 2 times of the chromaticities in all the ARCs. Thus the total chromaticities C_{tot} become about 70-80 for one IP and 120-140 for two IPs.

We employ strong sextupole families to correct such high chromaticities. A schematic in Fig. 1 shows the layout of eRHIC sextupole families as the rearrangements of the existing RHIC layout for higher energy and new IR designs. At the mean time, the buses of sextupole power supplies are proposed to be rewired to form more families (24 families) of independent knobs for chromatic terms corrections (detailed in following sections).

DYNAMIC APERTURE OPTIMIZATION

As mentioned above, the sextupole strengths are strong (about 2 times of the running RHIC's setup) for eRHIC due to the high chromaticities rising from strongly focused IRs. This generates strong chromatic aberration and high resonance driving terms (RDTs). Resonance driving terms, as a direct product from normal forming the one turn map of the storage ring whose schematic drawing can be found in Fig. 2, has an indirect impact on the particle's long term stability know as dynamic aperture (DA).

The direct relation between RDTs and DA is not known since the particle revolution in phase space and x-y real space in existence of nonlinear elements is highly chaotic.

* yjing@bnl.gov

Content from this work may be used under the terms of the CC BY 3.0 licence (© 2015). Any distribution of this work must maintain attribution to the author(s), title of the work, publisher, and DOI.

ISBN: 978-3-95450-168-7 doi:10.18429/JACoW-IPAC2015-MOPMN028

Content from this work may be used under the terms of the CC BY 3.0 licence (© 2015). Any distribution of this work must maintain attribution to the author(s), title of the work, publisher, and DOI.

DESIGN OF BUNCH COMPRESSING SYSTEM WITH SUPPRESSION OF COHERENT SYNCHROTRON RADIATION FOR ATF UPGRADE

Yichao Jing*, Mikhail Fedurin, Diktys Stratakis, BNL, Upton, NY 11973, USA

Abstract

One of the operation modes for Accelerator Test Facility (ATF) upgrade is to provide high peak current, high quality electron beam for users. Such operation requires a bunch compressing system with a very large compression ratio. The CSR originating from the strong compressors generally could greatly degrade the quality of the electron beam. In this paper, we present our design for the entire bunch compressing system that will limit the effect of CSR on the e-beam's quality. We discuss and detail the performance from the start to end simulation of such a compressor for ATF.

INTRODUCTION

Accelerator Test Facility (ATF) is ungoing an upgrade to provide users with wider spectrum of possiblities and choices. One of the most interesting applications is biology and material science which requires high charge and peak current. Such applications would make ATF become prime source for cutting edge research in photon sciences [1]. This requires a relatively higher energy (semi-GeV) electron beam with high peak current (kA) and low emittance.

The beam lines, which resembles High-gain Free electron lasers (FELs), usually are comprised of a low peak current electron beam generated at sources for acceleration and a strong bunch compressor to compress such a low peak current to a kA-level peak current for the users and other beamlines. In linac based SASE FELs, this compression usually is distributed in multiple stages along the beam transport at different energies of the beam. The linacs between two stages, in addition, could be used to accelerate the electron beam to higher energy and to prepare the electron beam for the next stages of compression. In such a way, each buncher's compression factor could be reduced (e.g. via a partial rotation in longitudinal phase space) so resulting in an overall lowering of emittance growth. Further more, the phase and strengths between different stages could be tuned for optimal performance. However, if a single stage compression can be achieved (without sacrifice of beam qualities), it benefits the layout of ATF and its upgrade. Further more, many different beam lines (for different users) can be installed downstream to such compressor to share the high quality electron beam. However, one concern of a single bunch compression scheme is CSR which could greatly degrade the quality of the e-beam [2–4].

In this paper, we present our design for a bunch compressor that will limit the effect of CSR on the e-beam's quality. We further perform the start-to-end (S2E) simulation to show our findings from a study of such a compressing scheme.

* yjing@bnl.gov

C-SHAPE CHICANE VS ZIGZAG CHICANE

A traditional approach to e-beam compression is to use a C-shape compensated chicane comprised of four dipole magnets. In such a chicane, the paths' lengths, as well as the transit time through the chicane, depend on the particles' energy. In combination with the correlated energy spread (chirp), this entails a rotation in longitudinal phase space. The emittance growth originates mostly from the third and forth magnets, where the beam is already compressed and the peak current is high. This growth in transverse emittance reflects the fact that the CSR wake depends both on longitudinal position within the bunch, as well as on the azimuth along the beamline. The head of the bunch gains energy while the tail part loses energy [5]. Furthermore, the location-dependent energy variation $\delta E(z, s)$ induced by CSR wakes engender transverse coordinate- and angular- displacements via non-zero $R_{16}(s, s_2)$ and $R_{26}(s, s_2)$ induced in the chicane. At the end of the chicane, the transverse displacement and the angle deviation will be non-zero.

The coordinate and the angular displacement that depend on longitudinal position of the particle result in a smearing in the transverse phase space, and also in the growth of the projected emittance. Figure 1 illustrates this smearing effect, comparing the plots of the transverse phase space before and after the chicane, which indicites a typical few fold of emittance growth for a C-shape chicane.

As a remedy for the above problem, i.e., the displacement in the transverse plane due to the longitudinal energy variation induced by CSR wakes, we propose to use two consequent chicanes with reversed bending directions, i.e., a Zig-Zag type compressor [6] as is shown in Fig. 2. The opposite signs of the dispersion functions should allow us to decouple the longitudinal and transverse degrees of freedom. We expect that in our scheme the transverse phase space displacement caused by CSR in the 1st chicane could be, at least, partially reversed in 2nd chicane. Thus, the resulting emittance growth due to CSR effects could be greatly reduced. Since bunch length is shorter, correspondingly CSR wake is stronger in the second chicane, and the energy change also is larger. The cancellation of the CSR effect naturally requires a weaker second chicane compared to the first one. In addition, we could better align the transverse phase-space displacements originating from two chicanes by adjusting phase advance between them.

ISBN: 978-3-95450-168-7 doi:10.18429/JACoW-IPAC2015-MOPMN029

SPIN RESONANCE STRENGTH CALCULATION THROUGH SINGLE PARTICLE TRACKING FOR RHIC*

Y. Luo, Y. Dutheil, H. Huang, F. Meot, V. Ranjbar
Brookhaven National Laboratory, Upton, NY, USA

Abstract

The strengths of spin resonances for the polarized-proton operation in the Relativistic Heavy Ion Collider are currently calculated with the code DEPOL, which numerically integrates through the ring based on an analytical approximate formula. In this article, we test a new way to calculate the spin resonance strengths by performing Fouier transformation to the actual transverse magnetic fields seen by a single particle traveling through the ring. Comparison of calculated spin resonance strengths is made between this method and DEPOL.

INTRODUCTION

The Relativistic Heavy Ion Collider (RHIC) at Brookhaven National Laboratory is the only high energy collider in the world to collide polarized protons with the particle energy up to 255 GeV. Polarization is the average value of the projection of the spins of particles in a bunch on the average spin direction. To maintain a high polarization during the beam transfer from the injectors to RHIC and on the acceleration and at store of RHIC, we need to have a good knowledge of all the spin resonance strengths on the way.

The strengths of spin resonances are normally numerically calculated based on analytical approximate formula. For an example, DEPOL [1] numerically integrates through the ring based on known magnetic fields and linear Twiss parameters. However, DEPOL itself does not calculate the linear optics. The linear optics parameters have been imported from other codes such as MADX. To improve the accuracy of resonance strength calculation, sometime we may need to split each magnet into several slices.

SimTrack [2] is a compact c++ library for beam optics calculation and particle tracking based on symplectic integration. It has been extensively used for dynamic aperture calculation with beam-beam interaction in RHIC. Recently we implemented proton spin tracking into this code [3]. Since SimTrack tracks particles in steps through each magnet, the particle coordinates and the magnetic fields the particles feel are all transparent to the users. Therefore it is possible to calculate the spin resonance strength through particle tracking.

* This work was supported by Brookhaven Science Associates, LLC under Contract No. DE-AC02-98CH10886 with the U.S. Department of Energy.

SPIN RESONANCES

Thomas-BMT equation describes the particle's spin motion in the presence of magnetic and electric fields,

$$\frac{d\mathbf{S}}{dt} = \mathbf{S} \times \mathbf{\Omega}, \tag{1}$$

$$\mathbf{\Omega} = \frac{e}{\gamma m}\left[(1+G\gamma)\mathbf{B}_{\perp} + (1+G)\mathbf{B}_{||}\right]. \tag{2}$$

$\mathbf{S}$ is the 3-dimensional spin vector in the particle's frame. $\mathbf{B}_{\perp}$ and $\mathbf{B}_{||}$ are the magnetic fields perpendicular and parallel to the particle velocity. It is convenient to use the path length s of the reference particle as the independent variable, then Eq. (1) turns to

$$\frac{d\mathbf{S}}{ds} = \mathbf{S} \times \mathbf{F}, \tag{3}$$

$$\mathbf{F} = \frac{\sqrt{(1+\frac{x}{\rho})^2 + x'^2 + y'^2}}{1+\delta}\frac{\mathbf{\Omega}}{(B\rho)_0}, \tag{4}$$

where $(B\rho)_0$ is the magnetic rigidity for the reference particle, ρ is the curvature for the reference particle on which the local coordinate system is built.

To study the polarization loss for a single particle when it crosses a single spin resonance, we would like to use the spinor equations where the bending angle θ is used as the independent variable. Then Eq. (3) is re-written as

$$\frac{d\mathbf{S}}{d\theta} = \mathbf{n} \times \mathbf{S}, \tag{5}$$

where $\mathbf{n} = -G\gamma\hat{y} - F_x\hat{x} - F_s\hat{s}$, $G\gamma$ is the spin tune for the reference particle. Defining $\xi = F_x - iF_s$ and expanding it in Fourier series, we have

$$\xi = \sum_K \epsilon_K e^{-iK\theta}. \tag{6}$$

Here ϵ_K is the strength of spin resonance. There are two important types of spin resonances: imperfection and intrinsic resonances. For imperfection resonances, $G\gamma = K$, K is an integer. For intrinsic resonances, $G\gamma = K \pm \mu_y$, μ_y is the fractional vertical tune.

According to Eq. (4) and Eq. (6), we have [4]

$$\epsilon_k = \frac{1}{2\pi}\oint\left[(1+G\gamma)\frac{B_x}{(B\rho)_0} - i(1+G)\frac{B_{||}}{(B\rho)_0}\right]e^{iK\theta}ds. \tag{7}$$

where B_x and $B_{||}$ are the projections of the magnetic fields seen by the particle. In Ref. [1, 4], ϵ_k can be presented with particle's coordinates as $\epsilon_k =$

$$-\frac{1}{2\pi}\oint\left[1+G\gamma)(\rho y'' + iy') - i\rho(1+G)(\frac{y}{\rho})'\right]e^{iK\theta}d\theta. \tag{8}$$

Content from this work may be used under the terms of the CC BY 3.0 licence (© 2015). Any distribution of this work must maintain attribution to the author(s), title of the work, publisher, and DOI.

ISBN: 978-3-95450-168-7 doi:10.18429/JACoW-IPAC2015-MOPMN030

Content from this work may be used under the terms of the CC BY 3.0 licence (© 2015). Any distribution of this work must maintain attribution to the author(s), title of the work, publisher, and DOI.

PROTON SPIN TRACKING WITH SYMPLECTIC INTEGRATION OF ORBIT MOTION*

Y. Luo, Y. Dutheil, H. Huang, F. Meot, V. Ranjbar
Brookhaven National Laboratory, Upton, NY USA

Abstract

Symplectic integration had been adopted for orbital motion tracking in code SimTrack. SimTrack has been extensively used for dynamic aperture calculation with beam-beam interaction for the Relativistic Heavy Ion Collider (RHIC). Recently proton spin tracking has been implemented on top of symplectic orbital motion in this code. In this article, we will explain the implementation of spin motion based on Thomas-BMT equation, and the benchmarking with other spin tracking codes currently used for RHIC. Examples to calculate spin closed orbit and spin tunes are presented too.

INTRODUCTION

The Relativistic Heavy Ion Collider (RHIC) is capable of colliding heavy ions and polarized protons. In the polarized proton operation, the Figure of Merit (FOM) is LP^2 and LP^4 for the single and double spin programs. Here L is luminosity and P is polarization. Polarization is the average value of the projection of the spins of particles in a bunch on the average spin direction. Spin is a 3-D vector associated with the particle's magnetic moment. To improve the FOM in the polarized proton operation, many efforts had been made to understand through numeric simulations the mechanisms of polarization loss in the RHIC's injector-Alternating Gradient Synchrotron (AGS) , and during during injection, energy acceleration, and physics store in RHIC.

Currently there are two main codes for spin simulation calculations at Brookhaven National Laboratory: one is SPINK [1] developed by A. Luccio, and the other is Zgoubi [2] developed by F. Meot. Since the spin motion is linked to the magnetic fields the particles feel on their orbits, therefore we need an accurate modeling of orbit motion. SPINK does not have its own orbit motion tracker. It uses the first and second order matrices generated with MADX. Zgoubi is a ray-searching code, which tracks particle's orbit motion directly based on Lorentz equation. The particles position, velocity, and the magnetic fields are all expanded to 5th and higher order. Orbit motion tracking in both codes is not symplectical. For a long term tracking, especially for proton accelerators like RHIC, symplecticity is crucial to avoid the unphysical results from numeric simulations.

SimTrack [3] is a compact c++ library for linear optics calculation and particle tracking for circular accelerators. It adopts the 4th order symplectic integration to transfer particles through magnets. Its optics transport in magnets had been benchmarked with Tracy-II. Its 6-D symplectic beam-beam interaction was benchmarked with SixTrack. Since 2009, SimTrack had been extensively used for particle tracking with beam-beam interaction for RHIC. For an example, simulation results from SimTrack showed that the non-luminous particle loss in the gold-gold ion collision is due to limited off-momentum dynamic aperture. SimTrack is also used to simulate head-on beam-beam compensation with electron lenses in RHIC.

In this article we first introduce symplectic integration of orbit motion and its application in SimTrack. Then we implement proton spin tracking based on Thomas-BMT equation. Examples of benchmarking of spin tracking with Zgoubi are presented. In the end, we show some examples to calculate the spin closed orbit, spin tune, and to simulate a single spin resonance crossing.

SYMPLETIC ORBIT TRACKING

Symplectic integration is one kind of numeric integrations to solve differential equations. Different from other methods, symplectic integration will preserve the symplectic condition of particle motion governed by a Hamiltian. R. Ruth invented the forth order symplectic integrator for a splitable Hamitonian [4],

$$H(p,q) = H_1(p) + H_2(q). \tag{1}$$

Here p, q are the canonical positions and momenta. In each step of integration, the solution of particle orbit motions is given by

$$\begin{aligned} e^{-:H:} = {} & e^{:-c_1 L H_1/2:} e^{:-d_1 L H_2:} e^{:-c_2 L H_1/2:} e^{:-d_2 L H_2:} \\ & e^{:-c_2 L H_1/2:} e^{:-d_1 L H_2:} e^{:-c_1 L H_1/2:} + O(L^5), \end{aligned} \tag{2}$$

where $c_{1,2}$ and $d_{1,2}$ are coefficients given in Ref. [4].

Symplectic integration has been used with an expanded Hamiltonian in many codes, where H_1 represents a drift and H_2 a thin magnetic kick. The expanded Hamiltonian is a good approximation for high energy accelerators where the particle's velocity is very close to the speed of light. Eq. (2) also can be used for solvable Hamiltonians H_1 and H_2, where H_1 normally represents an ideal bending maget and H_2 a thin magnetic kick.

In SimTrack, both expanded and exact Hamiltonians are implemented. With the expanded Hamiltonian, the computing time will be shorter than that with the exact Hamiltonian. Expanded Hamiltonian is normally used for particle tracking in RHIC at store energies. However, for a low

* This work was supported by Brookhaven Science Associates, LLC under Contract No. DE-AC02-98CH10886 with the U.S. Department of Energy.

ISBN: 978-3-95450-168-7 doi:10.18429/JACoW-IPAC2015-MOPHA001

TRANSVERSE BUNCH BY BUNCH FEEDBACK OPERATIONS AT THE AUSTRALIAN SYNCHROTRON LIGHT SOURCE

R. Dowd, M. Atkinson, M. J. Boland, G. S. LeBlanc,
Y-R. E. Tan, K. Zingre, Australian Synchrotron, Clayton, Australia

Abstract

The Australian Synchrotron light source has recently put in operation its transverse bunch-by-bunch feedback system during user beam mode. Getting to the stage of stable operation has been a long road and this paper will outline the many difficulties that were encountered. Chief among these are the apparent strong, high frequency, vertical resonances that appear when the storage ring's three in-vacuum undulators are closed to specific gaps. The behaviour of these resonances and their effects on achieving stable feedback operation will be explored in detail.

INSTABILITY SOURCES

The vacuum chamber of the Australian Synchrotron storage ring is stainless steel and therefore a major source of resistive wall impedance. The impedance effects have been measured previously [1] with the strongest effect in the vertical plane due to the aspect ratio of the vacuum chamber. The main instability sources have been the in-vacuum undulators (IVUs). The storage ring contains two 3-metre long IVUs (IVU03 and IVU13) that close down to a 6.6 mm pole gap and one 2 metre undulator (IVU05) that closes to 6 mm. While these devices have copper wakefield shields with flexible transitions at either end, they have been the source of very strong, high frequency resonances at particular gap positions that cause primarily vertical instabilities. The high frequency nature of these instabilities poses a much stronger challenge to the successful operation of the transverse feedback system than the resistive wall effects.

IVU Resonance Mapping

Attempts to map out these resonances in order to understand their source have been conducted. These resonance maps are difficult to obtain without the beam becoming so unstable that we experience beam loss and so may be incomplete, however they do show a strong pattern of instability mode number vs. IVU gap, with the instability mode increasing by 1 for every 0.3 mm of gap change. Table 1 and Figure 1 show one such mapping, performed at low chromaticity. Later measurements performed at lower chromaticity indicate this pattern of instabilities continues into the 8-9 mm gap range.

The regular repetition of the instability at gaps of every 0.3 mm suggests a trapped mode resonance in the IVU chamber. On a simple analysis of a vertical resonance between the two pole faces however, a change in IVU gap of 0.3 mm does not correspond to a frequency change of 1 revolution harmonic (1.38 MHz), which is implied by the unit

Table 1: IVU gap setting vs peak resonance mode number. The relative spacing of the resonance modes is also shown

IVU05 Pole Gap (mm)	Peak Instability Mode	Δ (mm)
7.59 - 7.62	220	
7.28 - 7.32	221	0.30
6.98 - 7.04	222	0.28
6.68 - 6.74	223	0.30
6.40 - 6.47	224	0.27
6.12 - 6.15	225	0.32

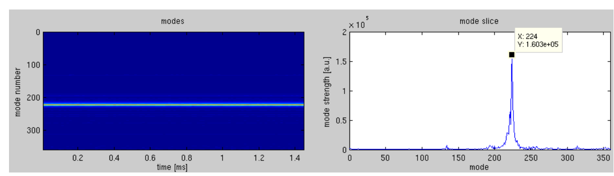

Figure 1: Instability Mode analysis of IVU05 at 6.4mm gap. Mode 224 is the strongest mode, but the neighbouring modes are also excited, indicating a resonance with width of multiple revolution harmonics.

change in instability mode number. The type of resonance is still not clear to us, although there are some possibilities, including a fast ion instability, or a situation similar to a klystron instability [6] (due to the similar geometry of the IVU device to a klystron tube).

FEEDBACK SYSTEM

Overview

While the transverse feedback system used at the Australian synchrotron has been described in detail previously [2],[3], and only a brief overview will be presented for clarity. Signals from a BPM block are sent through a hybrid mixing unit to produce X and Y signals which are sent to a mixing front-end unit, where the signal is mixed with a 1.5 GHz clock down to base band.

The mixing unit then sends the baseband signal to a pair of feedback processing units. The feedback units and frontend were supplied from Instrumentation Technologies [4].

The output waveforms are then fed through 100 W broadband amplifiers and sent to the storage ring stripline kickers. A programmable delay line before the amplifiers allows for timing of the output pulses in 20 ps steps in order coincide the peaks of the correction pulses with the arrival of the electron bunches. The overall system architecture is shown in Figure 2.

Content from this work may be used under the terms of the CC BY 3.0 licence (© 2015). Any distribution of this work must maintain attribution to the author(s), title of the work, publisher, and DOI.

ISBN: 978-3-95450-168-7 doi:10.18429/JACoW-IPAC2015-MOPHA002

OPERATIONAL APPLICATIONS - A SOFTWARE FRAMEWORK USED FOR THE COMMISSIONING OF THE MedAustron ACCELERATOR

A. Wastl*, M. Hager, M. Regodic, EBG MedAustron, Wiener Neustadt, Austria

Abstract

MedAustron is a synchrotron-based cancer therapy and non-clinical research center located in Austria. Its accelerator is currently being commissioned prior to first medical treatment. During the tuning of the machine, many iterations of measurements involving several parameter changes are performed in order to optimize the accelerator's performance. An operation and measurement software framework called 'Operational Application Framework' (OpApp) has been developed for this purpose. It follows a modular approach and provides basic methods like 'write to file' or 'measure beam position monitor'. By appropriately combining modules, *OpApps* performing automatized measurements and complex procedures can be created. A detailed description of the setup as well as examples of use are provided here.

INTRODUCTION

The MedAustron accelerator complex includes up to four ion sources, a linear accelerator, a synchrotron and beam transfer lines guiding the beam to four irradiation rooms. Currently the accelerator commissioning is focusing on proton beams for two clinical horizontal irradiation rooms (energy range : 60 -250 MeV). For patient treatment clinical cycles of protons and carbon ion beams of 255 different energies have to be provided to three irradition rooms.

OPERATING ENVIRONMENT

Accelerator commissioning, hardware installation and software development are processes performed in parallel leading to a very dynamic working environment. Commissioning requires repetitive measurements based on complex measurement procedures to be performed in order to verify several beam and accelerator parameters. To automatize this work the MedAustron Accelerator Control System (MACS) has constantly being extended with dedicated software tools. These tools interact with the Accelerator Control System and its sub-systems like the timing system, power converter controllers, RF systems or beams diagnostic devices.

MedAustron and CERN have developed a software infrastructure that communicates with the different systems. However, even with this infrastructure the development of commissioning tools face very specific challenges: the tools have to be flexible enough to adapt to new operation modalities of the accelerator components. Furthermore, in the course of commissioning the quantity of tools provided in different programming language increase causing the duplication of code and additional effort of maintenance.

A NEW FRAMEWORK

During the commissioning phase, flexible software applications are required that can quickly be adjusted to the changing environment, new features requested by users or to work around problems. To address these requirements an own software architecture, called 'Operational Applications' (OpApps) has been developed at MedAustron. The OpApp architecture enforces the use of small re-usable modules like setting of a control values or acquiring a beam diagnostic measurement. The basic modules can be combined to bigger modules and eventually to powerful applications.

The main domain of OpApps is the provision of configuration data and the measurement of the resulting beam. The according functionality is:

- Generate cycle dependent settings like current setpoints and waveforms from optical settings such as the magnet strength
- Deploy settings to accelerator devices
- Request the generation of beam
- Acquire beam diagnostic measurements
- Store data as files or a database entry

Optical computations and advanced analysis functionality are currently not part of the OpApps. In order to close the beam commissioning cycle (Fig. 1) a thought-through concept for the storage of measurement data has been developed. The concept defines a schema for file names, folder structures and the meta-data to be included. Sophisticated analysis modules such as the CERN ALOHA [1] program or in-house Python tools access the stored data and process it. The outcome of analysis and optical computations is fed back into Operational Applications via input files.

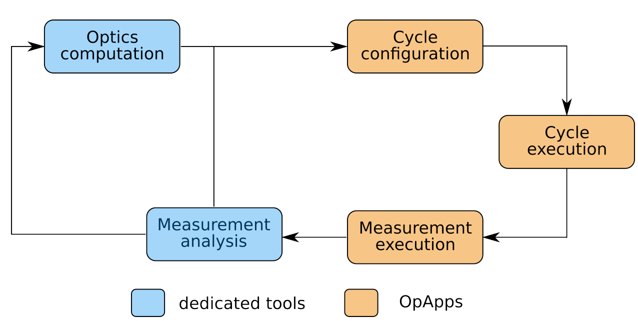

Figure 1: Commissioning tools cycle.

* alexander.wastl@medaustron.at

Content from this work may be used under the terms of the CC BY 3.0 licence (© 2015). Any distribution of this work must maintain attribution to the author(s), title of the work, publisher, and DOI.

ISBN: 978-3-95450-168-7 doi:10.18429/JACoW-IPAC2015-MOPHA003

STATUS OF ATF2 IP-BPM PROJECT

O.R. Blanco, CERN, Geneva, Switzerland and LAL, U-PSUD, CNRS/IN2P3, Orsay, France
P. Bambade, F. Bogard, P. Cornebise, S. Wallon
LAL, U-PSUD, CNRS/IN2P3, Orsay, France
N. Blaskovic Kraljevic, D.R. Bett, T. Bromwich, P.N. Burrows, G.B. Christian, C. Perry
John Adams Institute for Accelerator Science at University of Oxford, UK
S. Araki, KEK, Tsukuba, Japan
Y. Honda, K. Kubo, S. Kuroda, T. Naito, T. Okugi, T. Tauchi, N. Terunuma
KEK, Tsukuba, Japan and School of High Energy Accelerator Science, SOKENDAI, Ibaraki, Japan
E.-S. Kim, S. Jang, Kyungpook National University, S. Korea

Abstract

The efforts during the second half of 2014 towards nanometric beam position measurement and stabilization at the Interaction Point (IP) section of the Accelerator Test Facility (ATF) at KEK are presented. Recent improvements to the beam position monitor (BPM) data analysis and processing electronics, as well as the installation of a new set of C-Band BPMs, are reviewed.

INTRODUCTION

The main objective of the Accelerator Test Facility (ATF) at the High Energy Accelerator Research Organization (KEK) in Tsukuba, Japan, is to serve as an R&D platform for the technology required for linear accelerators, in particular the International Linear Collider (ILC). The ATF has already achieved a record minimum vertical beam emittance [1, 2], and so attention moves to the next step: reduction in the vertical beam size at the IP. Beam size reduction using local chromaticity correction is explored at the ATF in an extension of the original beam line known as ATF2 [3, 4]. The ATF2 lattice is the final focus system (FFS) of the ILC scaled down to 100 m and exists to demonstrate two goals: (**goal 1**) a vertical beamsize at the IP of 37 nm (**goal 2**) stabilization of the beam position at the IP to the level of a few nanometres.

In 2014 a vertical beam size of about 55 nm was measured at ATF2 [5]. Subsequently, a smaller beam size, of down to 44 nm, has been achieved [6] through systematic tuning. This demonstrates the local chromaticity correction method, though only at charges below 0.1×10^{10} particles per bunch.

The identified issue of intensity dependence is currently being explored by the ATF2 collaboration. However, even at low intensities the beam size remains above the designed 37 nm. Possible causes are: (1) increase of the incoming beam emittance throughout the ATF2 line, (2) systematic errors and resolution limitations on the beam size monitor (IPBSM), (3) beam drift beyond the tolerable margin and (4) undetected optics mismatch.

The last two issues can be addressed by measuring the beam trajectory in the IP region after the final doublet. In addition, looking forward to **goal 2**, high resolution beam position measurement is a requirement for beam stabilization.

BPM SYSTEM DESCRIPTION

A set of three cavities, two upstream and one downstream of the nominal IP, are used to measure the beam trajectory in the IP region and thus provide enough information to reconstruct the bunch position and angle at the IP.

The three cavities (IPA, IPB and IPC) are rectangular and resonate in the TM_{210} mode at 5.7 GHz in the horizontal plane and TM_{120} at 6.4 GHz in the vertical plane. They have a design decay time of 20 ns and sensitivities to bunch position of 2.2 μV/nm/nC (horizontal) and 3.7 μV/nm/nC (vertical). Two additional cylindrical cavities, one per resonant frequency, are placed downstream of the IP to measure the bunch charge and to downmix the C-Band frequency signals; these are the reference cavities.

Each position measurement cavity has two output ports in antiphase per plane connected to independent processing electronics to downmix the signals, separate them into two orthogonal components called I and Q, and set the gain according to beam charge conditions. A set of remotely-controllable attenuators, variable between 0-70 dB in steps of 10 dB, is used to increase the linear range of electronics at the expense of resolution.

The acquisition system samples the two downmixed orthogonal waveforms per cavity per plane over the decay time. This amounts to 14 simultaneous channels: I and Q waveforms for both x and y for each of the three position measurement cavities plus the charge signal from each reference cavity.

A local beam-based feedback system has been installed at the IP in order to stabilise the beam position. This system comprises a stripline kicker just upstream of the IP chamber, a fast kicker amplifier and a digital feedback controller. The feedback can be driven by any of the three IPBPM raw output signals or a linear combination of the signals from any two BPMs. The system is designed for operation on a bunch train of two or more bunches, separated by greater than 150–200 ns, where the measurement of the first bunch provides the input to the feedback system and the correction is applied to subsequent bunches.

Content from this work may be used under the terms of the CC BY 3.0 licence (© 2015). Any distribution of this work must maintain attribution to the author(s), title of the work, publisher, and DOI.

ISBN: 978-3-95450-168-7 doi:10.18429/JACoW-IPAC2015-MOPHA004

OIDE LIMIT MITIGATION STUDIES

O. R. Blanco*, CERN, Geneva, Switzerland and LAL, U-PSUD, CNRS/IN2P3, Orsay, France
P. Bambade, LAL, U-PSUD, CNRS/IN2P3, Orsay, France
R. Tomas, CERN, Geneva., Switzerland

Abstract

Particle radiation when traversing a focusing quadrupole limits the minimum achievable beam size, known as the Oide limit. This effect may be compensated by a pair of multipoles which reduce the impact of the energy loss in the vertical beam size. Simulations in PLACET using the CLIC 3 TeV QD0 and L^* show a reduction of $(4.3 \pm 0.2)\%$ in the vertical beam size.

INTRODUCTION

In order to achieve higher luminosity, it is necessary to reduce the beam size to compensate the lower frequency collisions in linear accelerators compared with collider rings [1], radiation effects plays an important role in the presence of strong focusing required for the IP small beam size. This document addresses the radiation phenomenon called Oide effect [2].

The Oide effect is caused by the interaction of charged particles with the magnetic field from quadrupoles. Radiation in a focusing magnet, schematically represented as QD0 in Fig. 1, changes the energy of the particle and modifies the focusing effect. This results in a limit on the minimum beam size specially relevant in the vertical plane.

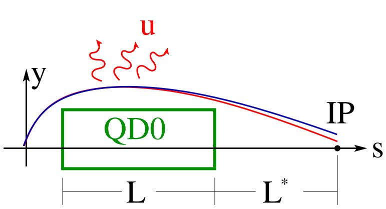

Figure 1: Designed particle trajectory in blue and the trajectory of a particle due to radiation in the quadrupole in red.

The beam size growth due to radiation is added quadratically to the linear beam size $\sigma_0^2 = \epsilon\beta$ where β represents the optical beta function and ϵ is the emittance. Therefore, $\sigma^2 = \sigma_0^2 + \sigma_{oide}^2$. The beam size contribution is [2],

$$\sigma_{oide}^2 = \frac{110}{3\sqrt{6\pi}} r_e \frac{\lambda_e}{2\pi} \gamma^5 F(\sqrt{k}L, \sqrt{k}L^*) \left(\frac{\epsilon}{\beta^*}\right)^{5/2} \tag{1}$$

where $F(\sqrt{k}L, \sqrt{k}L^*)$ is a double integral solved in [3], λ_e is the Compton wavelength of the electron, r_e is the electron radius, γ is the relativistic factor, β^* is the twiss parameter function at the observation point, in this case the IP; and, k, L, and L^* are the quadrupole gradient, the quadrupole length and the distance to the IP.

* blanco@lal.in2p3.fr

Although the total contribution to beam size depends on lattice and beam parameters, the minimum achievable beam size is given by [2],

$$\sigma_{y\ \min} = \left(\frac{7}{5}\right)^{\frac{1}{2}} \left[\frac{275}{3\sqrt{6\pi}} r_e \frac{\lambda_e}{2\pi} F(\sqrt{K}L, \sqrt{K}L^*)\right]^{\frac{1}{7}} (\epsilon_{Ny})^{\frac{5}{7}} \tag{2}$$

where $\epsilon_N = \gamma\epsilon$ is the normalized emittance, showing the independence from beam energy.

The only possibility to reduce the beam size is by changing the value of F, by modifying the magnet parameters, or to minimize the beam emittance. However, using the ILC 500 GeV [4], CLIC 500 GeV and CLIC 3 TeV [5] parameters, it is possible to conclude from Table 1 that the contribution to beam size is significant for CLIC 3 TeV.

Δy DUE TO RADIATION

Particle tracking from the imput of QD0 to the IP for CLIC 3 TeV with and without radiation, using PLACET [6], allows one to compute the effects of radiation on the six dimentional phase space. Figure 2 shows the current transverse distribution of particles at the IP. To compensate the adverse effects a compensation system would ideally remove the position change due to radiation $\Delta y = y_{\text{rad}} - y_0$.

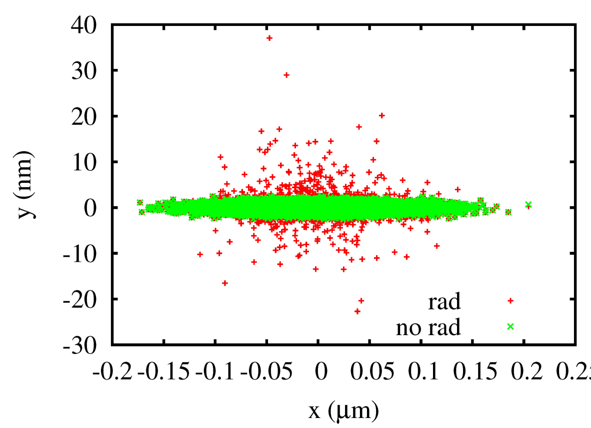

Figure 2: CLIC 3 TeV beam at the IP after tracking QD0 with and without radiation.

Although the average radiation effect is zero, $\langle\Delta y\rangle = 0$ because of the cubic term $(y_0')^3$ as stated by Oide [2], the correlation between $\Delta y, y'$ is not zero. The correlation expression is shown in Eq. (3).

$$\langle\Delta y, y_0'\rangle = \frac{2}{3} r_e \gamma^3 G(\sqrt{K}L, \sqrt{K}L^*)(y_0')^3 \tag{3}$$

Content from this work may be used under the terms of the CC BY 3.0 licence (© 2015). Any distribution of this work must maintain attribution to the author(s), title of the work, publisher, and DOI.

ISBN: 978-3-95450-168-7 doi:10.18429/JACoW-IPAC2015-MOPHA006

A SLOW RF-LASER FEEDBACK FOR PHIL PHOTOINJECTOR

N. Elkamchi, V. Chaumat, V. Soskov, LAL, Orsay, France

Abstract

PHIL [1] is a low energy (E<5 MeV) and high current (1nC/bunch) electron beam accelerator at LAL. It uses a laser beam to extract electron bunch from a copper cathode at a repetition frequency of 5Hz.

The stability of the beam charge at PHIL is a key issue for the successful operation of the physic experiences that use the machine. It is also one of the most important specifications of a laser driven high current RF gun.

Two Integrated Current Transformers (ICT) and back-end electronics are used to monitor the stability of the beam charge at PHIL, with an accuracy of about 1pC [2].

At PHIL, the electron beam charge is quite stable, but we often note a slow charge drift on long duration experiences.

Several types of jitter can impact the stability of the beam charge. The fluctuations of the RF power or the RF to laser relative phase drift could have significant influence on the machine stability, due to temperature variations and electronic components overheating.

To correct the phase drift, we describe, in this work, a method based on slow analog-digital feedback loop between the RF wave in the gun (3GHz) and the synchronization signal of the laser (75MHz).

It allows maintaining the jitter between the laser pulse and the RF wave stable at a very low value (1° of 3GHz). As a result, the electron beam charge will be maintained at a stable level, to meet the requirements of users.

ACCELERATOR DESCRIPTION

Photoinjector

PHIL is a test facility at the Laboratoire de l'accélérateur linéaire (LAL), Orsay. The main goal of the accelerator is testing photoinjection as part of research and development of advanced RF gun.

The principal beam line of the machine is devoted to beam characterization (bunch length, transverse emittance) and standard instrumentation testing. A second beam line is used to analyze the energy distribution using a dipole (figure1).

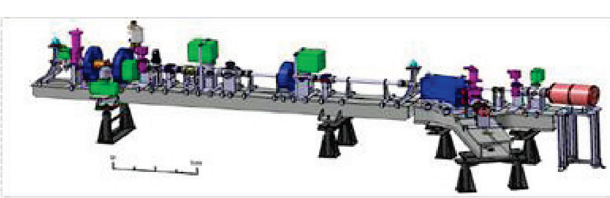

Figure 1: Drawing of PHIL beamlines. Blue boxes are magnetic elements; orange is the RF gun, green boxes stand for vacuum pumps.

Table 1: Specifications of PHIL [3]

Energy, Mev	Energy spread %	Charge , single pulse, nC	Frequency, GHz	Repetition rate, Hz	Pulse duration, ps	Emittance πmmmrad
5	< 1	0.01-2	3	5	5-10	< 5

In addition to research and development activities, PHIL is open to physics experiences that need low energy and well-defined electron beams for detector calibration.

RF Chain

The primary goal of the RF chain at PHIL is to generate and amplify the 3GHz signal destined to electron beam acceleration. It has also the role of synchronizing the laser oscillator and diagnostic facilities (figure 2).

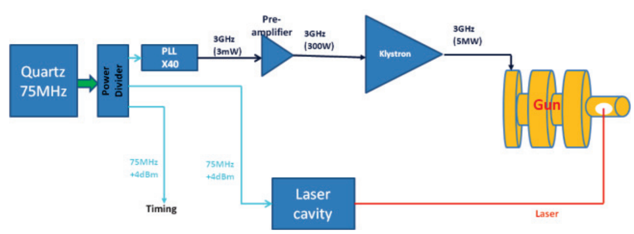

Figure 2: Drawing of PHIL RF chain and synchronization system.

It consists essentially of a quartz oscillator generating a reference signal at 75MHz turned into 3GHz via a PLL. A pre-amplifier and a klystron amplify the RF signal to reach 5MW in the gun.

The reference signal is also used to lock the laser oscillator and to generate 5Hz pulse frames for synchronizing diagnostic systems.

PHASE DRIFT AT PHIL

In photoinjector based accelerator, an accurate synchronization between the RF wave and the laser beam is highly required. This allows having an uniform electron beam with a stable charge value [4].

The RF gun of PHIL is a 2,5 cells [5].It is designed to get a maximum axial electromagnetic field at the cathode level (z=0) (figure 3) when it is hit by the laser pulse. The electromagnetic field can be adjusted using a phase shifter in low level RF electronics, to change the characteristics of the beam (charge, energy, dark current).

Content from this work may be used under the terms of the CC BY 3.0 licence (© 2015). Any distribution of this work must maintain attribution to the author(s), title of the work, publisher, and DOI.

ISBN: 978-3-95450-168-7 doi:10.18429/JACoW-IPAC2015-MOPHA007

MODELING / MEASUREMENT COMPARISON OF SIGNAL COLLECTION IN DIAMOND SENSORS IN EXTREME CONDITIONS

V. Kubytskyi*, S. Liu, P. Bambade, LAL, Université Paris-Sud, CNRS/IN2P3, Orsay, France

Abstract

Such unique properties like radiation hardness, low dark current, good signal to noise ratio make single crystal Diamond Sensors (DS) excellent devices for measurements of beams in a wide range of conditions. Here we present a study of charge collection dynamics in a DS subjected to intensities from 1 to 10^9 Minimum Ionizing Particles (MIP). We developed a model based on the numerical solution of the 1D drift-diffusion equations, using the Scharfetter-Gummel discretization scheme. Inhomogeneity of the space-charge distribution together with the externally applied electric field are taken into account by analytically solving the Poisson equation at each discrete time step. We identified two regimes of charge collection. The first corresponds to $1 - 10^6$ MIPs, in this case the externally applied electric field is negligibly perturbed by space-charge effects during the separation of the electron/hole clouds. The second corresponds to intensities larger than 10^7 MIPs, where the space-charge effects significantly slow down the charge collection due to large concentrations of electron/hole pairs in the DS volume. The results of our modeling are in qualitative agreement with the experimental data acquired at the PHIL photo-injector electron beam facility at LAL. Our model allows optimising DS parameters to achieve desired charge collection times for different beam intensities.

INTRODUCTION

When charged particles pass trough the material it ionises the material along the track which results in the creation of electron hole pairs. In the case of diamond, 1 MIP creates on average 36 electron-hole pairs per micrometer. Applying external electric field to the diamond force the electrons and holes to move in opposite directions, this process is usually called charge collection. According to Shockley-Ramo theorem [1] the motion of these charges creates an electric current on the electrodes which can be amplified if it is necessary and measured with an oscilloscope.

However when the diamond sensor is subjected to the beam where the number of electrons (MIPs) can be as large as 10^8 electrons or more, the charge collection becomes nonlinear and it can be strongly slowed down (see [2]) for the following reasons: First, is the space charge effect that becomes important when the clouds of electron and holes are separated in the external electric field, which creates an opposite electric field to the applied one inside the sensor. Second, is the voltage drop due to the strong current which passes trough the resistive load in the readout channel.

In this paper we construct a Diamond Sensor model which includes these effects in a consecutive manner. Modeling of charge collection in diamond sensors subjected to extreme conditions is of great importance for the device parameter specification during the design and for calibration during operation.

* kubytsky@lal.in2p3.fr

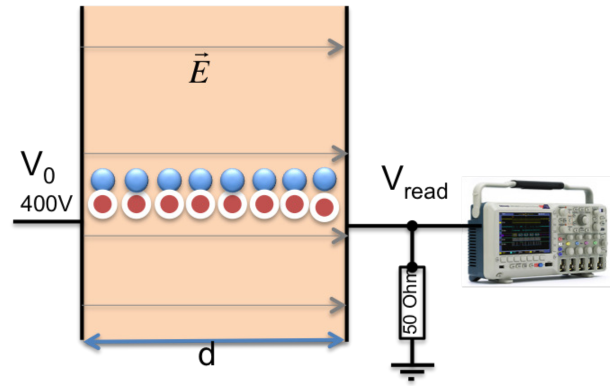

Figure 1: Schematic representation of diamond detector with electronics for data acquisition. Electrons (blue circles) and holes (red circles) pairs are created along the track of the incident MIP.

MODELLING OF CHARGE COLLECTION

Let us consider the 1D case where the detector has a finite thickness and is infinite in the lateral directions. In this case the Poisson equation can be solved analytically, giving the electric field inside the material:

$$E(x,t) = -\frac{V}{d} - \frac{q}{\varepsilon_0 d}\int_0^d\int_0^x (p-n)dx'dx + \frac{q}{\varepsilon_0}\int_0^x (p-n)dx', \tag{1}$$

where

$$V = V_0 - V_{read} \tag{2}$$

is the difference of potentials applied to the diamond due polarising potential V_0 and voltage drop on the reading electrode V_{read}; n and p are electrons and holes densities, d is the thickness of the diamond; q is the elementary charge and ε_0 is dielectric constant.

In order to obtain temporal evolution of charge densities in the volume of the diamond we are solving the drift-diffusion equations [3]:

$$\frac{\partial J_n}{\partial x} - q\frac{\partial n}{\partial t} = \frac{n}{\tau_n} \quad \text{with } J_n = qn\mu_n E + qD_n\frac{\partial n}{\partial x}, \tag{3}$$

$$\frac{\partial J_p}{\partial x} + q\frac{\partial p}{\partial t} = -\frac{p}{\tau_p} \quad \text{with } J_p = qp\mu_p E + qD_p\frac{\partial p}{\partial x}, \tag{4}$$

where, correspondingly for electrons and holes, J_n and J_p are electric current densities; μ_n and μ_p are the mobilities; D_n , D_p diffusion constants and τ_n , τ_p lifetimes.

Content from this work may be used under the terms of the CC BY 3.0 licence (© 2015). Any distribution of this work must maintain attribution to the author(s), title of the work, publisher, and DOI.

ISBN: 978-3-95450-168-7 doi:10.18429/JACoW-IPAC2015-MOPHA008

INVESTIGATION OF BEAM HALO USING IN VACUUM DIAMOND SENSOR AT ATF2*

S. Liu, P. Bambade, F. Bogard, P. Cornebise, V. Kubytskyi, C. Sylvia, LAL, Université Paris-Sud, CNRS/IN2P3, Orsay, France
A. Faus-Golfe, N. Fuster-Martínez, IFIC (CSIC-UV) , Valencia, Spain
T. Tauchi, N. Terunuma, KEK and SOKENDAI, Tsukuba, Japan

Abstract

Beam halo transverse distribution measurements are of great importance for the understanding of background sources of the nano-meter beam size monitor at the interaction point (IPBSM) of ATF2 [1,2]. One of the most critical issues for the beam halo measurement is to reach high dynamic range. Two *in vacuum* diamond sensor beam halo scanners (DSv) with four strips each have been developed for the investigation of beam halo transverse distributions at ATF2. The first DSv was installed for horizontal beam halo scanning after the interaction point (IP) of ATF2, in Nov. 2014. It aims to measure the beam halo distribution with large dynamic range ($\sim 10^6$), and investigate the possibility of probing the Compton recoil electrons produced in the interaction with the IPBSM laser beams. Studies to characterize the DS performance and measurements of horizontal beam halo performed in Nov.-Dec. 2014 are presented.

INTRODUCTION

The investigation of beam halo transverse distribution is an important issue for beam loss and background control in ATF2 and in Future Linear Colliders (FLC). A DSv was installed downstream of the IP, 1.35 m from the BDUMP bending magnet exit at ATF2, to study the beam halo transverse distribution and the spectrum of the Compton recoil electrons produced in the interaction with the IPBSM laser beams at ATF2. In order to measure the beam core, beam halo and Compton recoil electrons simultaneously, a large dynamic range of $> 10^6$ is needed [3]. Previous beam halo measurements using wire scanners have only reached a dynamic range of $\sim 10^4$ [1,4,5]. However, a single crystalline CVD (sCVD) diamond sensor is not only sensitive to single electron but also tested to have a linear response up to 10^7 electrons [6]. Therefore, two sCVD DSv have been developed for our measurements.

Since the signal strength is proportional to the metallised effective surface on diamond, DSv with four strips was designed to help cover this large dynamic range [6]. The two strips for beam halo scanning are on the outer sides, with a dimension of 1.5 mm× 4 mm and the other two in the center are for beam core scanning with a dimension of 0.1 mm×4 mm. After characterising the DSv, beam core and halo transverse horizontal distributions were measured in Nov.-Dec. 2014. Beam core measurements were used for the normalisation of the beam halo distribution.

* Work supported by Chinese Scholarship Council, CNRS and P2IO LABEX

EXPERIMENTAL SETUP

For the *in vacuum* application a ceramic PCB is used. The ceramic PCB uses silver-platinum conductor produced in thick-film technology. The PCB with the diamond sensor in the center is shown in Fig.1 (left), a low pass filter together with charging capacitors are mounted on the backside of the PCB [6].

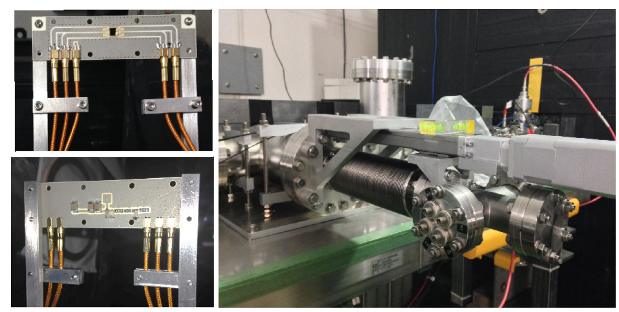

Figure 1: Layout of the DSv with the frontside (upper left) and backside (lower left) of the PCB and the motor used for the scan (right).

The DSv were fabricated by the CIVIDEC company [7] and the first set of it was installed in vacuum horizontally with a holder to scan beam and beam halo in the horizontal plane. The mechanical design was done and fabricated at LAL as shown in Fig 1 (right). The whole setup is 744mm long and it can be oriented either horizontally or vertically to scan in different axes.

Data Acquisition System

In order to transfer the signal from the DSv installed in the post-IP region to the IP laser room, where the oscilloscope is located, we have chosen a high quality LDF1-50 1/4 inch thick Heliax low density foam coaxial cable (more than 20m). For the bias voltage supply we used the Keithley 2410 sourcemeter, which can supply a bias voltage of ±1000 V. The whole data acquisition system is connected via Ethernet cables to the PC located in the control room. On the PC, Matlab is installed and used for system control and data taking. The oscilloscope we used is an Agilent oscilloscope with a sampling rate of 4 GS/s and an analogue bandwidth of 1 GHz. The motor we used for the DSv scan control is a stepper motor EMMS-ST-42-S-SEB-G2. The resolution of the steps is 10 μm and the reproducibility accuracy is 3μm. The mover precision was set as 50 μm for our experiment and the maximum scan range is 110 mm.

Content from this work may be used under the terms of the CC BY 3.0 licence (© 2015). Any distribution of this work must maintain attribution to the author(s), title of the work, publisher, and DOI.

ISBN: 978-3-95450-168-7 doi:10.18429/JACoW-IPAC2015-MOPHA009

SINGLE-SHOT ELECTRO-OPTIC SAMPLING COMBINED WITH PHOTONIC TIME-STRETCH: DETAILED RESULTS AT SOLEIL

E. Roussel, C. Evain, M. Le Parquier, C. Szwaj*, S. Bielawski,
PhLAM/CERLA, Villeneuve d'Ascq, France
L. Manceron, J.-B. Brubach, M.-A. Tordeux, J.-P. Ricaud, L. Cassinari,
M. Labat, M.-E Couprie, P. Roy, Synchrotron SOLEIL, Gif-Sur-Yvette, France

Abstract

Single-shot recording of pulses is possible with high repetition rates (more than 80 MHz), as was demonstrated in the framework of a PhLAM-SOLEIL collaboration [1]. This can be achieved by a relatively simple upgrade of existing setups based on spectral encoding. The strategy consists to encode the sub-picosecond information into the time domain, but at a slower scale (nanoseconds), using dispersion in a long optical fiber. Then the information is recorded by a photodiode connected to an oscilloscope. Here, we present guidelines for the practical realization of the electro-optical setup, as well as a performance analysis. In particular, we analyze the temporal resolution and compare it to the classical electro-optical sampling setup.

INTRODUCTION

The past decade has seen the rapid development of CSR studies in many storage rings. Despite the large amount of experimental observations, e.g. the recordings of coherent THz bursts, lack of direct observation of the electron bunch and its microstructures is a main issue to the test and the development of the theoretical models. Even though first real time measurements of CSR pulses using a YBCO superconductor-based detector at UVSOR-III have been successfully achieved [2, 3], a majority of storage rings emits coherent synchrotron radiation at higher frequencies than the state-of-the-art oscilloscope bandwidth (currently 65 GHz), e.g. ≈ 300 GHz at SOLEIL [4], ≈ 250 GHz at ANKA [5], ≈ 500 GHz at ELETTRA [6].

The electro-optic sampling (EOS) technique offers the possibility to measure THz electric fields with a sub-picosecond resolution. This technique has already been applied in storage rings [7–9]. However, to date, used methods based on electro-optic detection do not fulfill the requirements for a single-shot detection of CSR pulses at high-repetition rate, i.e. in the tens of megahertz (typical order of magnitude of electron bunch revolution frequency).

At first, we recall the principle of the spectrally-encoded electro-optic (EO) technique for the single-shot detection of THz CSR pulses. Then, we show the potential interest of photonic time-stretch [10, 11], well-known in optics and photonics, for the EO techniques to overcome the limitation of acquisition rate needed in storage rings, in particular we compare the performance with the classical spectral-encoding Finally, we present experimental data obtained at SOLEIL using the time-stretch EO strategy.

SPECTRALLY ENCODED ELECTRO-OPTIC DETECTION

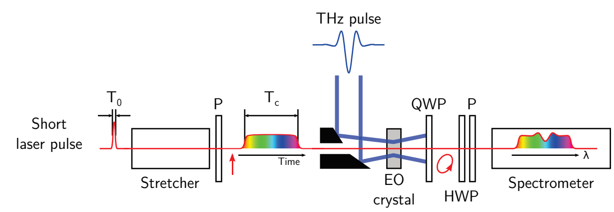

Figure 1: Schematic drawing of spectrally encoded electro-optic detection.

The spectrally-encoded electro-optic detection technique (EOSD) allows single-shot measurements of THz pulses (Fig. 1). In this technique, a probe laser pulse is stretched in a dispersive material or using a grating stretcher to a duration similar to the THz pulse duration before co-propagating in the EO crystal. In these conditions, the instantaneous frequency in the laser pulse varies with time. Thus, a modulation in time of the laser pulse induces the same modulation in the optical spectrum. The THz pulse induces a time dependent birefringence in the EO crystal through the Pockels effect and this anisotropy modulates the polarization state of the probe laser pulse which is converted into an amplitude modulation by a series of quarter-wave plate (QWP), half-wave plate (HWP) and a polarizer (P). The temporal modulation of the laser pulse is retrieved by measuring the spectrum of the laser pulse using a spectrometer and a photodiode array detector. The temporal resolution T_{min} of the EOSD is limited and is given by [12] $T_{min} = \sqrt{T_0 T_C}$, with T_0 the bandwidth-limited pulse duration (i.e. the pulse duration before the stretcher) and T_C the chirped probe laser pulse duration.

Even though the spectrally encoded EOSD allows single-shot measurements, the acquisition rate is limited by the speed of the current camera of at best around hundred kilohertz.

PHOTONIC TIME-STRETCH

Principle

The principle of time-stretch process is simple and consists in slowing down a signal before the detection. A practi-

* christophe.szwaj@univ-lille1.fr

Content from this work may be used under the terms of the CC BY 3.0 licence (© 2015). Any distribution of this work must maintain attribution to the author(s), title of the work, publisher, and DOI.

ISBN: 978-3-95450-168-7 doi:10.18429/JACoW-IPAC2015-MOPHA010

Content from this work may be used under the terms of the CC BY 3.0 licence (© 2015). Any distribution of this work must maintain attribution to the author(s), title of the work, publisher, and DOI.

RF FEEDBACK AND DETUNING STUDIES FOR THE BESSY VARIABLE PULSE LENGTH STORAGE RING HIGHER HARMONIC SC CAVITIES*

A. Neumann†, P. Echevarria, P. Goslawski, M. Ries, M. Ruprecht, A. Vélez , G. Wüstefeld
Helmholtz-Zentrum Berlin, 12489 Berlin, Germany

Abstract

For the feasibility of the BESSY VSR upgrade project of BESSY II two higher harmonic systems at a factor of 3 and 3.5 of the ring's RF fundamental of 500 MHz will be installed in the ring. Operating in continuous wave at high average accelerating field of 20 MV/m and phased at zero-crossing, the superconducting cavities have to be detuned within tight margins to ensure stable operation and low power consumption at a loaded Q of 5×10^7. The field variation of the cavities is mainly driven by the repetitive transient beam-loading of the envisaged complex bunch fill pattern in the ring. Within this work combined LLRF-cavity and longitudinal beam dynamics simulation will demonstrate the limits for stable operation, especially the coupling between synchrotron oscillation and RF feedback settings. Further impact by beam current decay and top-up injection shots are being simulated.

CHALLENGES FOR VSR SRF CW CAVITY OPERATION

To simultaneously create RF buckets for long and short pulses two higher harmonic RF systems have to be operated in zero-crossing at 1.5 and 1.75 GHz respectively [1, 2]. With respect to both bucket types the 1.5 GHz cavities will work in the focusing regime, whereas the 1.75 GHz cavities will be defocusing for the long buckets where the latter carry the majority of the average beam current. Table 1 shows the required RF parameters for an continuous fill pattern of the storage ring. In order to achieve the desired bunch shortening the average accelerating field will be E_{acc} 20 MV/m. This scheme implies several challenges for the stable operation of the higher harmonic system. The required power for a given cavity voltage V_{cav}, normalized shunt impedance $R/Q = V_{cav}^2/(\omega U)$, average beam current I_{b0} and accelerating phase ϕ_{acc} is [3]:

Table 1: RF system parameters for an even beam pattern without clearance gaps in the storage ring and two 5 cell cavities per higher harmonic.

Parameter per cavity	1.5 GHz	1.75 GHz
Voltage (MV)	10	8.7
E_{acc} (MV/m)	20.0	20.0
Q_L	5×10^7	4.3×10^7
R/Q TM$_{010}$-$\pi(\Omega)$	500	500
ϕ_{acc} (degree)	90	-90
Δf for beam-loading (kHz)	-11.25	15.3
Average P_f (kW)	1.49	1.0
Voltage 0.5 GHz	1.5 MV	

$$P_f \approx \frac{V_{cav}^2}{\frac{R}{Q}Q_L}\frac{1}{4}\times \tag{1}$$

$$\left\{\underbrace{\left(1+\frac{\frac{R}{Q}Q_L I_{b0}}{V_{cav}}\cos\phi_{acc}\right)^2}_{\text{resistive}}+\underbrace{\left(\frac{\Delta f}{f_{1/2}}+\frac{\frac{R}{Q}Q_L I_{b0}}{V_{cav}}\sin\phi_{acc}\right)^2}_{\text{reactive}}\right\},$$

where $\Delta f/f_{1/2}$ is the ratio of expected peak detuning to cavity half-bandwidth $f_{1/2} = f_{rf}/(2Q_L)$. Assuming the reactive beam loading can be compensated and controlled as

$$\Delta f = -\frac{R}{Q}\frac{f_{rf}I_{b0}}{2V_{cav}}\sin\phi_{acc}, \tag{2}$$

the cavity can be treated as a zero-beam CW SRF cavity operated at potentially high loaded Q to allow for low average forward power level at the coupler. This would reduce the problem to control any unwanted detuning by microphonics and coupled Lorentz-force detuning. Operation at comparable cavity voltages of a TESLA cavity at loaded Q up to 2×10^8 with low residual phase errors below 0.02 deg has been already demonstrated [4]. The optimum Q_L is then given by $\frac{1}{2} f_{rf}/\Delta f$, here about 5×10^7.

Tuning and Ramping the Cavities

In order to inject from the current booster synchrotron into the short bunches, the higher harmonic cavities (HHC) need to be ramped down to about ≤ 0.1MV [5]. As shown in Figure 1 that would require hundreds of kHz, only achievable by slow coarse tuners and such lead to a too long dark time for short pulse users. Also by the shorter lifetime of the short buckets that tuning would be performed with a high duty cycle posing the danger of mechanical stress, tuner failure or even vacuum leakage. For fast piezo tuners the typical range is far below the one needed for the field ramp. Thus an upgrade of the injection is currently discussed at HZB. At the VSR working point a power of about one kW is required to maintain the cavity voltage. The RF power overhead up to a level of 13 kW will allow one effect of the following at a time:

- A factor of three of the expected peak detuning of 20 Hz, thus $4 \times f_{1/2}$
- A not well synchronized top-up injection with a current jump of 1.5 mA

* Work supported by German Bundesministerium für Bildung und Forschung, Land Berlin, and grants of Helmholtz Association
† Axel.Neumann@helmholtz-berlin.de

ISBN: 978-3-95450-168-7 doi:10.18429/JACoW-IPAC2015-MOPHA012

Content from this work may be used under the terms of the CC BY 3.0 licence (© 2015). Any distribution of this work must maintain attribution to the author(s), title of the work, publisher, and DOI.

A NEW FPGA BASED TIMING SYSTEM AT ELSA

D. Proft* and W. Hillert, ELSA, Bonn, Germany

Abstract

At the electron stretcher facility ELSA a beam intensity upgrade from 20 mA to 200 mA is in progress. Investigations showed, that the maximum beam current is currently limited by excitation of beam instabilities. For separated characterization of single bunch instabilities from multi-bunch ones, a high beam current stored in a single revolving bunch is required. These high beam currents can only be achieved by accumulation of many shots from the injector.

The existing timing system is not capable of single bunch injection and accumulation in the main stretcher ring. Therefore a new FPGA based timing system, synchronized to the RF system of the accelerator, has been developed which will completely supersede the existing one. Simultaneously the "slow" timing system, providing trigger signals for the typically 6 s long accelerator cycle, is also modernized using a similar FPGA based solution to achieve a much better duty cycle during standard operation.

In this contribution the FPGA designs laying the focus on the single bunch accumulation will be presented.

ELSA

The electron stretcher facility ELSA (see Fig. 1) is a three stage accelerator consisting of two linear accelerators and a fast ramping booster synchrotron which are utilized as injector for the main storage ring. In the storage ring electrons can be accumulated by multiple injections of the booster, post-accelerated to a maximum energy of 3.2 GeV and then be extracted to one of the hadron physics experiments *Crystal Barrel* or *BGO-OD*. The typical cycle length is 6 s consisting of 400 ms injection time and 2×300 ms acceleration/deceleration time. The extraction takes place during the remaining 5 s, where the electrons are extracted using a third integer resonance, resulting in a constant electron current of typically up to 2 nA at the experiments.

Motivation

The ELSA stretcher ring is currently operated with a maximum current of 20 mA. That allows for an extraction of currents of about 2 nA during an extraction time of typically 5 s. The experiments desire an increase of this current by a factor of 10. In order to preserve the duty factor of $> 80\,\%$ the intensity of the beam accumulated in the storage ring has to be increased by one order of magnitude to 200 mA.

The maximum beam current that can be stored is limited by emerging beam instabilities. These can be classified in single- and multi bunch instabilities. The latter ones are damped by the installed three dimensional bunch-by-bunch feedback system [1] whereas the investigation of single bunch instabilities requires the accumulation of a single bunch in the accelerator.

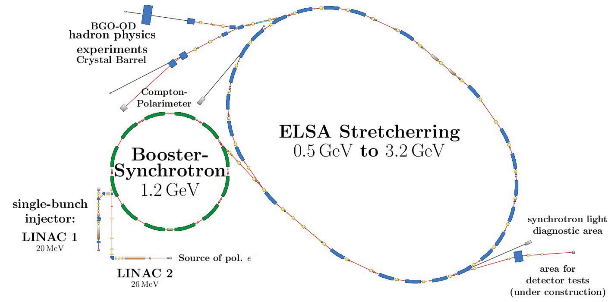

Figure 1: Sketch of the electron stretcher facility ELSA.

At the moment this can only be achieved by excitation and subsequently removing all unwanted bunches of a homogeneously filled accelerator ring. Unfortunately the attainable current per single bunch is then limited to approximately 800 µA/bunch by multi bunch instabilities occurring during injection.

To workaround these limitations a new high current single bunch injector, LINAC1 [2], is currently under construction. In the *short pulse mode* only a single bucket in the booster synchrotron can be filled whereas in *long pulse mode* it is capable of filling the whole synchrotron with a high intensity beam.

Besides the ability to accumulate electrons into a single bunch in the stretcher ring it will also be possible to produce any arbitrary filling pattern in the stretcher ring by successive injection into different buckets. This is in particular very helpful for investigations of instabilities caused by trapped ions [3].

CURRENT TIMING SYSTEM

The timing system can be separated into two different branches. The so-called *fast timing* system is operated at 50 Hz line frequency generating trigger signals for timing the injector (gun and linear accelerator) and accumulation in the stretcher ring. Due to the fluctuating line frequency the acceleration cycle in the booster synchrotron is not static. The trigger for the injector (gun and LINAC) is generated by a premagnetized peaking strip[1] placed in the magnet gap of the booster's dipole.

With the current setup there is no synchronization to the revolution clock, therefore the filled bucket in the booster synchrotron is unknown. In addition the transfer to the stretcher ring is not synchronized as well, making it impossible to accumulate electrons in a single bucket or even produce a requested filling pattern.

* proft@physik.uni-bonn.de

[1] ferromagnetic material with an almost rectangular hysteresis loop

ISBN: 978-3-95450-168-7 doi:10.18429/JACoW-IPAC2015-MOPHA013

SUPERCONDUCTING RADIO FREQUENCY CAVITY DEGRADATION DUE TO ERRANT BEAM*

C. Peters, A. Aleksandrov, W. Blokland, M. Crofford, D. Curry, C. Deibele, G. Dodson, J. Galambos, G. Johns, A. Justice, S. Kim, T. Pelaia, M. Plum, and A. Shishlo, Spallation Neutron Source, Oak Ridge National Laboratory, Oak Ridge, TN, 37831, USA

Abstract

In 2009, the Superconducting Radio Frequency (SRF) cavities at the Spallation Neutron Source (SNS) began to experience significant operational degradation [1]. The source of the degradation was found to be repeated striking of cavity surfaces with errant beam pulses. The Machine Protection System (MPS) was designed to turn the beam off during a fault condition in less than 20 μseconds [2] as these errant beam pulses were not unexpected. Unfortunately an improperly operating MPS was not turning off the beam within the designed 20 μseconds, and the SRF cavities were being damaged. The MPS issues were corrected, and the SRF performance was restored with cavity thermal cycling and RF processing. However, the SRF cavity performance has continued to degrade, though at a reduced rate compared to 2009. This paper will detail further study of errant beam frequency, amount lost per event, causes, and the corrective actions imposed since the initial event.

INTRODUCTION

The SNS Linac consists of an ion source, Low Energy Beam Transport (LEBT), Radio Frequency Quadrupole (RFQ), Medium Energy Beam Transport (MEBT), Drift Tube Linac (DTL), Coupled Cavity Linac (CCL), and Superconducting Linac (SCL). This paper will focus on the ion source, LEBT, RFQ, DTL, CCL, and SCL. The DTL and CCL will be referred to as the Normal-conducting Linac (NCL).

ERRANT BEAM

An errant beam is a beam pulse that is not normal. The beam current may be higher or lower than expected, or the beam pulse may be shorter or longer than expected. Errant beam produces beam loss. The beam loss can be abrupt from a fast shift in beam parameters or slow with small amounts of beam loss over an extended period of time. The beam may hit cavity surfaces causing gas or particulate desorption. The gas or particle desorption can create an environment for arcing, multipacting, or field emission.

MACHINE PROTECTION SYSTEM

The major task of the MPS is to turn off the beam. Individual equipment detects fault conditions and send a signal to the MPS to interrupt beam operation. The MPS does this function by turning off the ion source RF timing gate (the ion source decays in about 20 μseconds) and the RFQ timing gate (the RFQ decays in about 1 μsecond), and the entire beam is deflected outside the entrance aperture of the RFQ for 20 μseconds (the response for beam deflection is about 1 μsecond). The design maximum turn off time for the MPS is 20 μseconds [2]. This does not include the time for fault detection by individual equipment.

INITIAL EVENT

In 2009 the SCL began experiencing increased amounts of downtime [1]. Multiple cavities required running with reduced gradients, and some had to be turned off completely. This reduction in gradient significantly impacted the overall beam availability as well as the peak beam energy. The initial investigation determined that there were significant amounts of beam loss in the SCL near the cavities that experienced operational issues. Experts suspected the MPS was not working properly.

Measurements were done to verify the proper turn off time of the MPS. It was found that it was not working properly, and in some cases entire beam pulses were transported during fault conditions. The issue was found quickly and repaired, and SCL operation was restored with thermal cycling and RF processing.

CONTINUED DEGRADATION

Though the problems with the MPS in 2009 were corrected the SCL cavity performance continued to degrade due to errant beams, although gradients could be restored to their original values by thermal cycling and RF processing during maintenance periods. Figure 1 shows the short beam trip rate and beam energy from October 2010 to October 2012. It shows that there were typically 40 short trips per day, but in some cases up to 80 trips per day. Much of these trips were errant beam trips. It also shows that the beam energy decreased during the same time. Twice during 2012 the beam energy had to be reduced due to issues with SCL cavity performance. Some cavities had to be removed from the Linac to be repaired.

Content from this work may be used under the terms of the CC BY 3.0 licence (© 2015). Any distribution of this work must maintain attribution to the author(s), title of the work, publisher, and DOI.

ISBN: 978-3-95450-168-7 doi:10.18429/JACoW-IPAC2015-MOPHA014

MAGNETIC FIELD PARAMETRIZATION FOR EFFICIENT SPIN TRACKING WITH POLE*

J. F. Schmidt†, W. Hillert, ELSA, Bonn, Germany

Abstract

The new spin dynamics simulation suite POLE is designed to perform systematic studies of beam depolarization in circular accelerators with short storage times or fast energy ramps. It is based on spin tracking using a Runge-Kutta algorithm with adaptive step width. POLE can approximate the magnetic fields of the accelerator with a Fourier series to reduce computing time. Therefore, the magnetic field distribution is simplified with frequency filters by a C++ library before the spin tracking. The versatile library deals with import and export of lattices and particle trajectories from MAD-X and ELEGANT . The derived magnetic field distributions can be interpolated, Fourier transformed and accessed easily by applications. This contribution discusses advantages and disadvantages of the frquency filtering concept.

INTRODUCTION

The new spin dynamics simulation suite POLE is designed to perform systematic studies of beam depolarization in circular accelerators with short storage times or fast energy ramps. This includes the crossing of depolarizing resonances and the impact of synchrotron radiation on short time scales (up to seconds). The intention is to develop open source tools that are also usable for other facilities.

Spin motion in an accelerator is described by the Thomas-BMT equation [1]. So, its numerical integration is an obvious approach for spin tracking. Neglecting electric fields perpendicular to the beam axis, the Thomas-BMT equation for an electron spin $\vec{S}(t)$ can be written as

$$\frac{\mathrm{d}}{\mathrm{d}t}\vec{S} \approx c \cdot \vec{S} \times \left[(1+\gamma a)\vec{\tilde{B}}_{\perp} + (1+a)\vec{\tilde{B}}_{\parallel}\right] \qquad (1)$$

with the gyromagnetic anomaly $a = (g_s - 2)/2$, the Lorentz factor $\gamma(t)$ and the energy normalized magnetic field

$$\vec{\tilde{B}}(t) := \frac{e}{p(t)} \cdot \vec{B}(t) \qquad (2)$$

parametrized by the time t. All the information about the accelerator lattice, beam optics settings and also beam dynamics are contained in the magnetic field $\vec{\tilde{B}}(t)$ experienced by the particles. Hence, the major task for efficient spin tracking is to implement a suitable magnetic field parametrization and an according integration algorithm.

The basis for POLE is a C++ accelerator lattice library developed at ELSA. It allows to work with lattice information and particle tracking results from MAD-X and ELEGANT within any C++ code. Building on this, magnetic field parametrizations can be tested and compared. The first approach realized for POLE was a frequency filtering of the magnetic fields to balance spin tracking accuracy against computing time [2]. Advantages and disadvantages of this approach are discussed in this contribution.

* Work supported by BMBF
† schmidt@physik.uni-bonn.de

C++ LATTICE LIBRARY

The C++ accelerator lattice library developed at ELSA basically provides two data structures. One represents a lattice consisting of individual elements of different types (e.g. dipole, cavity, quadrupole or kicker) stored by their position in the accelerator. The second structure implements arbitrary physical quantities, which are defined as a function of the position in the accelerator. They can have integer or floating point data type, including two or three dimensional quantities. Common examples are Twiss parameters or the closed orbit. A schematic of the library is shown in Figure 1. Lattice information can be accessed at an arbitrary position. Interpolation and Fourier transformation of the physical quantities are included using the GNU scientific library.

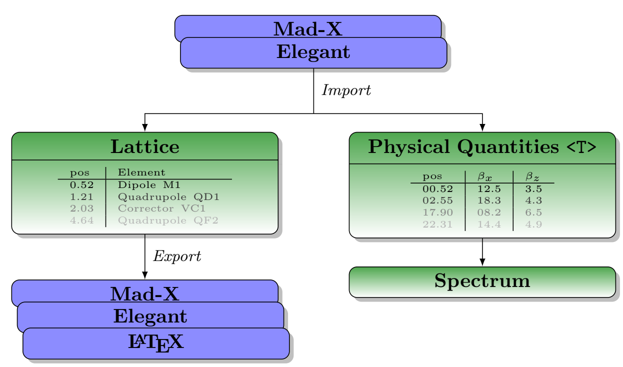

Figure 1: Schematic of the C++ accelerator lattice library.

Both data structures can be imported from the established simulation tools MAD-X and ELEGANT . Lattice definitions for these widespread tools exist for many accelerators and can be made available in any C++ program with about two lines of code. Of course, a lattice can also be constructed and modified within C++ . Additionally, the library provides a lattice export, which also facilitates the automatic lattice conversion between MAD-X and ELEGANT . Automated drawings of an accelerator can be made with a LaTeXexport using the tikz-palattice package [3]. A shared library version will be published as open source software soon.

Content from this work may be used under the terms of the CC BY 3.0 licence (© 2015). Any distribution of this work must maintain attribution to the author(s), title of the work, publisher, and DOI.

ISBN: 978-3-95450-168-7 doi:10.18429/JACoW-IPAC2015-MOPHA015

MEASUREMENT OF MOMENTUM COMPACTION FACTOR VIA DEPOLARIZING RESONANCES AT ELSA*

J. F. Schmidt†, W. Hillert, M. Schedler, J.-P. Thiry, ELSA, Bonn, Germany

Abstract

Measuring beam depolarization at energies in close proximity to a depolarizing integer resonance is an established method to determine the beam energy of a circular accelerator. This technique offers high accuracy due to the small resonance widths. Thus, also other accelerator parameters related to beam energy can be measured based on this method. This contribution presents a measurement of the momentum compaction factor with a high precision of 10^{-4}. It was performed at the 164 m stretcher ring of the Electron Stretcher Facility ELSA at Bonn University, which provides a polarized electron beam of up to 3.2 GeV.

MEASUREMENT PRINCIPLE

Precise knowledge of key accelerator parameters is important for the analysis of numerous beam dynamics measurements and user experiments as well as to adjust the accelerator model.

One essential parameter is the beam energy. An established method to precisely determine the beam energy in a storage ring is based on spin polarization measurements. If both a polarized beam and polarimetry are available, a decrease of polarization at certain, theoretically well known beam energies can be observed. The characteristic energy of such a depolarizing resonance can be determined experimentally by measuring polarization at various storage energies around the expected resonance. The small energy width of these resonances allows for an energy measurement with a precision of $\Delta E/E \lesssim 10^{-4}$.

Building on this procedure, other accelerator parameters can be measured with likewise precision, if they are related to beam energy. One example is the momentum compaction factor. Recently, it was measured at the ELSA stretcher ring at Bonn University using a polarized electron beam.

DEPOLARIZING RESONANCES

In a flat circular accelerator (without solenoids) the stable spin axis, also known as invariant spin axis, usually points in vertical direction due to the strong vertical guiding fields of the bending magnets. The spins of revolving electrons precess around this axis γa times per turn according to the Thomas-BMT equation [1]. The spin tune $Q_{\text{spin}} = \gamma a$ is given by the gyromagnetic anomaly $a = (g_s - 2)/2$ of the electron and the Lorentz factor γ and thus depends linearly on beam energy. Only the projection of the polarization on the invariant spin axis can be preserved, since the finite energy width of the beam implies a spin tune spread, that leads to a spin spreading in the precession plane.

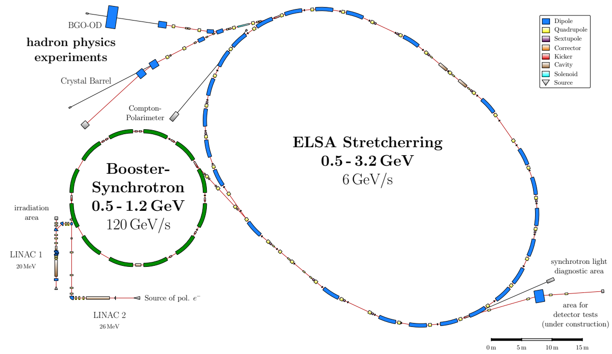

Figure 1: The Electron Stretcher Facility ELSA in Bonn.

The electrons experience horizontal magnetic fields along their trajectories occurring with specific spatial frequencies, which are related to the accelerator lattice and beam dynamics. On the one hand, magnet misalignments and vertical closed orbit distortions cause revolution harmonic contributions, which are not present in an ideal accelerator. On the other hand, betatron motion causes contributions of the quadrupole magnets depending on the betatron tunes.

Usually, spin precession around these horizontal magnetic fields averages out due to the changing phase relationship between these fields and the precession around the vertical axis. However, for certain beam energies the spin tune is in phase with one of the horizontal field contributions and the spin motion results in an additional precession around the horizontal fields. On such a depolarizing resonance, the stable spin axis is aligned completely within the horizontal plane and a beam stored at this energy has zero vertical polarization.

Though, the resonance energy can be determined experimentally by measuring vertical polarization at several energies in close proximity to the resonance. The measurements presented below use one of the so called integer resonances, which occur every 440 MeV at spin tunes

$$\gamma a = n \in \mathbb{N}\,. \qquad (1)$$

In this case, the theoretically expected resonance energy is known precisely, because it only depends on the gyromagnetic anomaly a of the electron. For that reason, the corresponding beam energy can be precisely determined by this method. Integer resonances are driven by revolution harmonic horizontal field distributions. They are mostly generated by vertical closed orbit displacements in the quadrupole magnets and rotations of the bending dipole magnets around the beam axis.

When crossing a depolarizing resonance on an energy ramp, the preserved vertical polarization decreases with the strength of the resonance driving fields and increases

* Work supported by DFG
† schmidt@physik.uni-bonn.de

Content from this work may be used under the terms of the CC BY 3.0 licence (© 2015). Any distribution of this work must maintain attribution to the author(s), title of the work, publisher, and DOI.

ISBN: 978-3-95450-168-7 doi:10.18429/JACoW-IPAC2015-MOPHA019

IMPLEMENTATION OF A HIGH LEVEL PHASE CONTROLLER FOR THE SUPERCONDUCTING INJECTOR OF THE S-DALINAC*

T. Bahlo†, C. Burandt, F. Hug, N. Pietralla
Institut für Kernphysik, TU Darmstadt, Darmstadt, Germany

Abstract

The S-DALINAC is a recirculating electron accelerator with a design energy of 130 MeV. Before entering the 40 MeV main accelerator the electron beam passes both, a normal-conducting injector beamline for beam preparation and a superconducting 10 MeV injector beamline for preacceleration. The phase of the beam which is injected into the main accelerator is crucial for the efficiency of the acceleration process and the minimization of the energy spread. Due to thermal drifts of the normal-conducting injector cavities this injection phase varies by about 0.2 degree over a timescale of an hour. In order to compensate for these drifts, a high level phase controller has been implemented. It adjusts the phase measured at an rf-monitor at the exit of the superconducting injector by changing the phase of a prebuncher in the normal-conducting injector beamline. We will present the used hardware, the control algorithm as well as measurements showing the phase stabilization achieved by this controller.

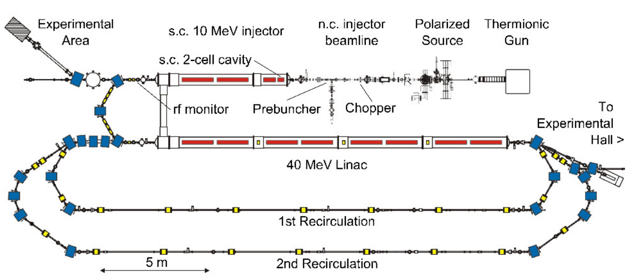

Figure 1: Floor plan of the S-DALINAC.

MOTIVATION

The Superconducting DArmstadt LINear ACcelerator S-DALINAC (see Fig. 1) is a recirculating electron accelerator with a design energy of 130 MeV that delivers electron beams with beam currents between several nA and 60 μA in cw-mode for nuclear and astrophysical experiments since 1987 [1]. The beam can be provided either thermionically and therefore unpolarized or by the photo effect from the Spin Polarized INjector SPIN [2] with a polarization of up to 86%. After beam preparation in the normal-conducting part of the injector including chopper and prebuncher cavities the electrons enter the superconducting 10 MeV injector beamline where they get preaccelerated by niobium cavities working at a resonance frequency of 3 GHz. The preaccelerated electron beam can then either be used to produce bremsstahlung for nuclear resonance fluorescence experiments at the Darmstadt High Intensity Photon Setup DHIPS [3] or be injected into the 40 MeV main accellerator. By recirculating the beam up to two times the maximum energy of 130 MeV can be reached.

It has been shown that the energy spread of the beam can be reduced significantly by using a non-isochronous recirculating mode [4]. In this case the remaining energy spread heavily depends on the correct injection phase into the main accelerator. A phase mismatch of 2° can increase the relative energy spread from $8 \cdot 10^{-5}$ to $3 \cdot 10^{-4}$. Experience shows that the beam phase behind the superconducting injector drifts and oscillates over several hours. An example measurement of the unadjusted beam phase can be seen in Fig. 2. This dynamic might either be caused by instabilities of the high voltage supply of the source or could come from thermal drifts of the normal-conducting beam preparation cavities. To compensate for these drifts a high-level phase controller has been developed.

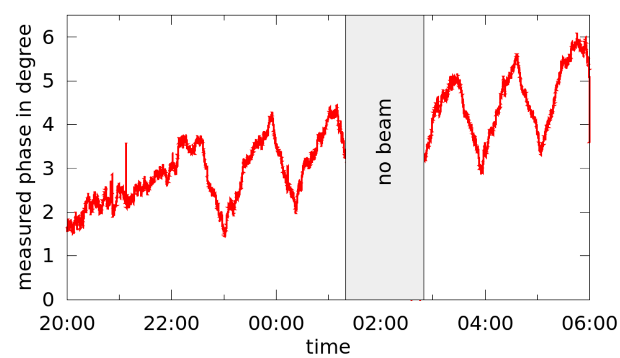

Figure 2: Measured beam phase behind the s.c.-injector with visible phase drift and oscillation.

PHASE ADJUSTMENT DEVICES

To adjust the beam phase behind the s.c. injector three devices have been tested:

Chopper

The chopper cavity converts continuous beams into bunched beams by forcing the electrons on a cone shaped trajectory and slipping them over an aperture. In this manner the chopper defines the reference phase of the beam and therefore of every adjacent rf device.

Prebuncher

The prebuncher decelerates the early electrons inside a bunch and accelerates the later ones in order to longitudi-

* This work has been supported by the DFG through CRC 634
† tbahlo@ikp.tu-darmstadt.de

Content from this work may be used under the terms of the CC BY 3.0 licence (© 2015). Any distribution of this work must maintain attribution to the author(s), title of the work, publisher, and DOI.

ISBN: 978-3-95450-168-7 doi:10.18429/JACoW-IPAC2015-MOPHA020

AUTOMATED TRANSVERSE BEAM EMITTANCE MEASUREMENT USING A SLOW WIRE SCANNER AT THE S-DALINAC*

P. Dijkstal#, M. Arnold, C. Burandt, F. Hug, N. Pietralla,
Institut für Kernphysik, TU Darmstadt, 64289 Darmstadt, Germany

Abstract

The superconducting linear accelerator S-DALINAC of the Institute for Nuclear Physics (IKP) from TU Darmstadt provides electron beams of up to 130 MeV in cw mode [1]. In order to improve beam simulations, it is planned to observe the transverse beam emittance at different locations along the beam line. A system of slow wire scanners in combination with quadrupole variation is foreseen to accomplish this task. For a first test a wire scanner was installed in the 250 keV section behind the thermionic electron gun of the S-DALINAC. A procedure to automatize measurements was developed and integrated in the EPICS-based control system [2]. We will show the status of the work on the automatized control and the results of first emittance measurements. A report on future plans will be given.

INTRODUCTION

The S-DALINAC consists of a 10 MeV injector and a 40 MeV main linac, both equipped with elliptical cavities operating in liquid helium at 2 K on a frequency of 3 GHz. Both, a thermionic and a polarized source [3] for electrons are available. The final energy is reached by using up to two recirculation paths. The current layout of the S-DALINAC is shown in Fig. 1.

Several locations are interesting for emittance measurements. It is desired to observe the emittance in between the accelerating sections and also in the extraction beam line. Additionally, two scraper systems will be in use in the near future [4, 5] and will certainly affect the emittance as well. To calculate the emittance with the method of quadrupole variation, one has to repeatedly measure the beam profile for different quadrupole currents. A wire scanner was available for this purpose from previous measurements at the polarized source [6]. The main task was to develop an automatized procedure to obtain the emittance. It should be easy to use and applicable for other locations at the S-DALINAC as well.

QUADRUPOLE VARIATION

The idea of emittance measurement with quadrupole variation is briefly recapitulated here. Detailed information can be found in many standard works on beam dynamics (e.g. [7]). In one transverse direction, a beam is commonly described with the two-dimensional σ matrix. The square root of the determinant of this matrix yields the emittance.

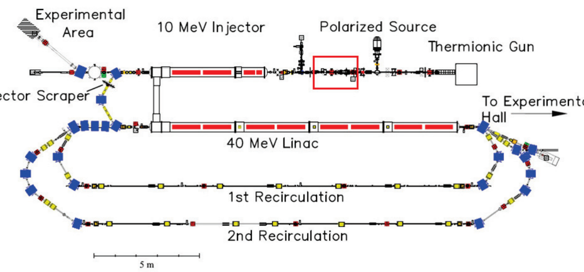

Figure 1: The section where the first emittance measurements took place is indicated with the red rectangle in this floor plan of the S-DALINAC.

$$\sigma = \begin{pmatrix} \langle x^2 \rangle & \langle xx' \rangle \\ \langle xx' \rangle & \langle x'^2 \rangle \end{pmatrix} \quad (1)$$

$$\epsilon = \sqrt{\det \sigma} \quad (2)$$

For sections that only consist of drift spaces, quadrupoles and dipoles, a transport matrix R can be defined which allows to transform the σ matrix from location a to b.

$$\sigma_b = R\,\sigma_a\,R^T \quad (3)$$

The matrix entry σ_{11} at the location of the wire scanner is easily accessible experimentally as it is the square of the beam width. In this work, a Gaussian distribution is assumed and the beam size is defined as one standard deviation. After several measurements of the profile for different quadrupole currents, a set of linear equations can be formed as the measured beam widths and the transport matrices R change. All entries of the σ matrix at the position of the quadrupole can then be determined numerically.

MEASUREMENT SETUP

The devices used for the first emittance measurements are shown in Fig. 2. The wire scanner consists of two perpendicular tungsten wires within a frame and is moved through the beam under an angle of 45° by a linear actuator. Therefore the profile in both transverse dimensions is recorded by the same device (see Fig. 3). The resulting current on the wires is picked up directly. Additionally, a linear potentiometer is attached which measures the current position of the wire scanner. Both these quantities are necessary to calculate the beam profile and have been available as EPICS process variables. A power supply for the linear actuator was developed and integrated in EPICS as well.

The quadrupole is part of a triplet in the low energy section following the electron gun. The field distribution was

* This work has been supported by the DFG through CRC 634 and by the EPS-AG through the EPS-AG student grant program.
# pdijkstal@ikp.tu-darmstadt.de

Content from this work may be used under the terms of the CC BY 3.0 licence (© 2015). Any distribution of this work must maintain attribution to the author(s), title of the work, publisher, and DOI.

ISBN: 978-3-95450-168-7 doi:10.18429/JACoW-IPAC2015-MOPHA021

BUNCH-BY-BUNCH LONGITUDINAL RF FEEDBACK FOR BEAM STABILIZATION AT FAIR*

K. Groß†, TEMF, TU Darmstadt, Germany
U. Hartel, U. Laier, D. Lens, K.-P. Ningel, S. Schäfer, B. Zipfel, GSI, Darmstadt, Germany
H. Klingbeil, GSI, Darmstadt, Germany; TEMF, TU Darmstadt, Germany

Abstract

To damp undesired longitudinal oscillations of bunched beams, the main synchrotron SIS100 of FAIR (Facility for Antiproton and Ion Research) will be equipped with a bunch-by-bunch feedback system. This helps to stabilize the beam, to keep longitudinal emittance blow-up low and to minimize beam losses. The proposed LLRF (low level radio frequency) topology of the closed loop feedback system is described. In some aspects, it is similar to the beam phase control system [1] developed at GSI Helmholtzzentrum für Schwerionenforschung GmbH. The differences and challenges are pointed out, which are mainly the bunch-by-bunch signal processing followed by the generation of a correction voltage in dedicated feedback cavities. The adapted topology was verified at SIS18 during beam time in 2014 using LLRF prototype subsystems and the two existing ferrite-loaded acceleration cavities. The experimental setup to damp coherent longitudinal dipole oscillations is presented and evaluated with focus on the realized modifications, including ongoing and pending investigations. Finally, the current status of the longitudinal feedback system for FAIR is summarized.

LLRF TOPOLOGY

Overview

Longitudinal coherent bunched beam modes can be classified by two numbers [2], the phase plane periodicity of individual bunches $m = 1$ (dipole), 2 (quadrupole), 3 (sextupole), ...with the oscillation frequencies $m\omega_{\mathrm{syn}}$, where ω_{syn} is the synchrotron frequency, and the coupled bunch mode number $n = 0, 1, 2, \ldots, M-1$ quantifying the phase shift $2\pi n/M$ between oscillations of adjacent bunches for M equidistant identical bunches. In order to damp rigid bunch oscillations with $m = 1$ and $n = 0$ the beam phase control system acts on the phase of the standard acceleration cavities. Within the scope of the longitudinal feedback (LFB) system higher order inner bunch modes, in particular quadrupole oscillations ($m = 2$), will be included using multiple filters with different settings based on the mode frequency $m\omega_{\mathrm{syn}}$. Arbitrary phase advances (mode number n) are covered by means of bunch-by-bunch signal processing and dedicated broadband kicker cavities.

Figure 1 gives a module-based overview of LLRF for the LFB system.

* Work supported by the German Federal Ministry of Education and Research (BMBF) under the project 05P12RDRBF.
† gross@temf.tu-darmstadt.de

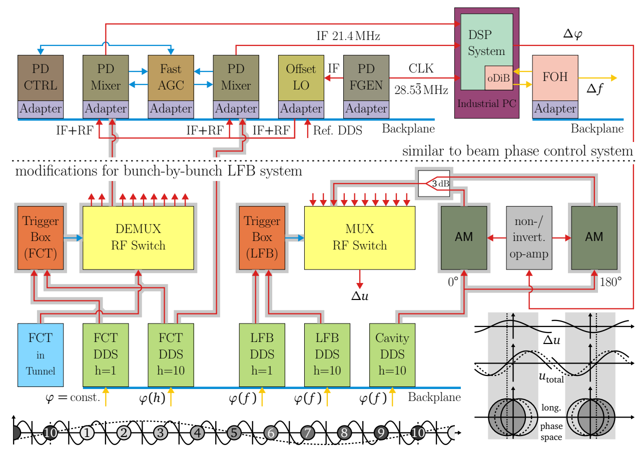

Figure 1: Sketch of LLRF of beam phase control system (top) with modifications for the LFB system (center) and principles of operation (bottom).[1]

Bunch-by-Bunch Operation

The bunch-by-bunch signal processing is based on trigger units and fast RF switches for de-multiplexing (DEMUX) of the beam current as well as multiplexing (MUX) of the correction signal for the kicker cavities. The working principle of the trigger unit is illustrated in Fig. 1 (bottom left) for operation below transition energy. It relies on an RF harmonic[2] to change over to the next bunch and the revolution harmonic as reset. This allows unambiguous assignment of the bunches for the variety of ion species and energies at GSI as well as an arbitrary choice of harmonic numbers[3]. Copies of the setup are used to determine the excitation and the required correction voltage for each bunch. Thus, the multiplexed LLRF correction signal Δu comprises the calculated control outputs from all DSP (digital signal processor) systems, i.e. for all of the bunches.

In contrast to electron machines and storage rings, where bunch-by-bunch LFB systems are well-established, special attention has to be paid to the synchronization due to fast ramp rates and a considerable frequency span. Therefore, the gray-shaded paths are cut to length to reach all interaction points with the same time delay. The phase $\varphi(f)$ of the DDS

[1] Abbreviations not mentioned in the text: PD - Phase Detector (historical), CTRL - ConTRoLer, LO - Local Oscillator, FGEN - Frequency GENerator, CLK - CLocK, FOH - Fiber Optical Hub

[2] The phase of the gap voltages (and thus of the bunches) is locked to that of the reference signals from DDS modules by means of local DSP systems.

[3] adjusting $\varphi(h)$, as the point of measurement is naturally defined as phase with respect to one revolution, but independent of the (revolution) frequency (cf. $\varphi(f)$)

Content from this work may be used under the terms of the CC BY 3.0 licence (© 2015). Any distribution of this work must maintain attribution to the author(s), title of the work, publisher, and DOI.

ISBN: 978-3-95450-168-7 doi:10.18429/JACoW-IPAC2015-MOPHA023

OBSERVATION OF COHERENT PULSES IN THE SUB-THz RANGE AT DELTA*

C. Mai†, P. Ungelenk‡, F.H. Bahnsen, M. Bolsinger, S. Hilbrich, M. Höner, M. Huck, S. Khan, A. Meyer auf der Heide, R. Molo, H. Rast, G. Shayeganrad
Center for Synchrotron Radiation (DELTA), TU Dortmund University, 44227 Dortmund, Germany
M. Brosi, B. Kehrer, A.-S. Müller, M.J. Nasse, P. Schönfeldt, P. Schütze, S. Walther,
Karlsruhe Institute of Technology (KIT), 76131 Karlsruhe, Germany
H. Huck, Deutsches Elektronen-Synchrotron Zeuthen, 15738 Zeuthen, Germany

Abstract

Coherent ultrashort THz pulses induced by a laser-electron interaction are routinely produced and observed at DELTA, a 1.5-GeV synchrotron light source operated by the TU Dortmund University. The turn-by-turn evolution of the radiation spectrum is known to shift to the sub-THz regime after the initial laser-electron interaction. Recently, an ultrafast YBCO-based THz detector has been permanently installed and a Schottky diode has been tested at the THz beamline. Measurements with these detectors showing the temporal evolution of the coherent signals after several revolutions are presented. Furthermore, the concept of a recently designed Fourier-transform spectrometer optimized for the sub-THz region is shown.

INTRODUCTION

The 1.5-GeV electron storage ring DELTA operated by the TU Dortmund University is a light source with a circumference of 115.2 m and a revolution frequency of 2.6 MHz. Since 2011, a source for ultrashort VUV and THz pulses based on the coherent harmonic generation (CHG) principle [1, 2] was commissioned. At this source, 40-fs Ti:sapphire laser pulses interact with a short slice of an electron bunch in the first section of the electromagnetic undulator U250, causing an energy modulation of the electrons. The energy modulation is converted into a density modulation forming microbunches by a dispersive section (center of the U250). In the last part of the U250, the microbunches emit coherent VUV radiation at harmonics of the laser wavelength. Energy-dependant path-length differences in the subsequent bending magnets lead to the formation of a sub-picosecond dip in the longitudinal electron density which gives rise to coherent THz radiation. The filling pattern of the storage ring during the operation of the short-pulse facility is a single bunch or a hybrid pattern in which a single bunch is injected in addition to a multi-bunch train.

A dedicated THz beamline (BL5a) for the extraction of the pulses is part of the DELTA short-pulse facility [3]. The beamline uses telescopes consisting of toroidal aluminium mirrors to transfer the THz radiation over the radiation shielding wall to an optical table. The THz laboratory is equipped with an indium-antimonide hot-electron bolometer, an ultrafast detector (<17 ps FWHM response time) [4, 5] based on the high-temperature superconductor $YBa_2Cu_3O_7$ (YBCO) and a Fourier-transform spectrometer with an Si composite bolometer.

Optimization of the laser-electron interaction relies on THz radiation as a diagnostics tool to improve the spatial and temporal laser-electron overlap. In addition, the THz radiation allows for the investigation of the turn-by-turn evolution of the density modulation induced by the ultrashort laser pulse [6, 7]. Particle-tracking simulations based on *elegant* [8] showed that the electron density modulation is present for at least 10 revolutions after the initial laser electron interaction [6, 9]. Recently, coherent THz pulses were observed for even more revolutions by means of an ultrafast oscilloscope. Furthermore, in cooperation with the Karlsruhe Institute of Technology (KIT), a Schottky diode sensitive in the sub-THz range was used to detect the laser-induced radiation at DELTA.

DETECTION OF MULTI-REVOLUTION RADIATION PULSES

As a first device for the detection of coherent pulses at the THz beamline, a liquid-helium cooled InSb hot-electron bolometer has been used [3, 10]. Because the signal repetition time is 384 ns when DELTA is operated in single-bunch mode, the InSb detector with a rise time of 350 ns is not fast enough for the investigation of the temporal evolution of the laser-induced density modulation. After first test measurements with an NbN hot-electron bolometer (<160 ps response time) and a YBCO detector (see above) [6, 7], an ultrafast YBCO detector was permanently installed at DELTA.

Figure 1 shows the response of the YBCO detector to coherent THz radiation at BL5a at DELTA acquired with an ultrafast Keysight Z-Series DSA-Z 634A real-time oscilloscope providing a bandwidth of 63 GHz at a sampling rate of 160 GS/s. Due to the high bandwidth, weak signals after several revolutions are not broadened by the readout. Hence, the coherent signals were acquired for up to 20 turns after the laser-electron interaction. Previous simulations of the evolution of the electron density distribution and spectral measurements showed that only the first turn has a significant spectral content above 1 THz [6, 7, 9]. Accordingly, the in-

* Work supported by the BMBF (05K13PEC).
† carsten.mai@tu-dortmund.de
‡ peter.ungelenk@tu-dortmund.de

Content from this work may be used under the terms of the CC BY 3.0 licence (© 2015). Any distribution of this work must maintain attribution to the author(s), title of the work, publisher, and DOI.

ISBN: 978-3-95450-168-7 doi:10.18429/JACoW-IPAC2015-MOPHA024

A NOVEL TRANSVERSE DEFLECTING CAVITY FOR SLICE DIAGNOSTICS AT BERLINPRO*

A. Ferrarotto, B. Riemann, T. Weis, DELTA Dortmund Germany,
T. Kamps, H.-W. Glock, J. Völker, HZB Berlin Germany

Abstract

BERLinPro [1], [2] is an energy-recovery linac project to be realized at the Helmholtz-Zentrum Berlin (HZB) for an electron beam with 1 mm mrad normalized emittance and 100 mA average current. The initial beam parameters are determined by the performance of the electron source, an SRF photo-electron injector. The development of this SRF photon-electron injector is a main task of BERLinPro. Especially the beam emittance is basically defined by the SRF photogun. For beam diagnostics time dependent effects from the RF curvature and space charge must be taken into account and a sophisticated slice diagnostics is required [3]. To perform this type of diagnostics a transverse deflecting cavity has been designed, characterized and is presently under construction. This single cell cavity operates in a TM_{110}-like mode at 1.3 GHz optimized for high transverse shuntimpedance of appr. 3.2 MΩ by a concentration of fields near the beam axis. The cavity has a novel geometry that allows for an operation with both polarizations of the TM_{110}-mode. The layout of the deflecting cavity will be presented together with the results of the low RF characterization.

INTRODUCTION

The Energy Recovery Linac (ERL) project BERLinPro should provide an electron beam with an average current of 100 mA and a normalized emittance of 1 mmmrad. The electron beam should be produced in a SRF photogun operating at 1.3 GHz repetition rate in CW mode. The beam emittance is basically defined by the SRF photogun.
A SRF gun with 100 mA average current and an emittance of 1 mm mrad has never been demonstrated. As part of the development process of such a SRF gun GunLab was designed as a test facility to characterize beam parameters of SRF photoinjectors. The main challenge of GunLab is to characterize the full six-dimensional phase space as a function of drive laser and RF parameters [4]. For usage in GunLab a novel type of transversal deflecting cavity (TCAV) for slice emittance measurements [5] in horizontal and vertical direction was designed. The development process of this novel TCAV is described in this paper.

TRANSVERSE DEFLECTING CAVITIES

Typically deflecting cavities make use of a TM_{110}-like mode in a modified cylinder geometry to apply transverse momentum to particle beams. This transverse momentum

$$\Delta p_\perp = e\left|\int_{-\infty}^{\infty} B_\perp(z)\, e^{i\frac{k}{\beta}z} dz - \frac{i}{\beta c} E_\perp(z)\, e^{i\frac{k}{\beta}z} dz\right| \quad (1)$$

$$= e\left|\frac{1}{\omega}\int_{-\infty}^{\infty} \vec{\nabla}_\perp E_z(z)\, e^{ikz} dz\right| \quad (2)$$

depends on the transverse components of the electric and magnetic fields on the cavity axis acting on the particle beam. z represents the coordinate along the cylinder axis, $k = \omega/c$ represents the wave number, e the electric charge of the particles, c the speed of light and ω represents the RF angular frequency. The transverse momentum is related to the transverse deflection voltage

$$V_\perp = \frac{\Delta p_\perp c}{e} \quad (3)$$

and to the transverse shunt impedance

$$Z_\perp = \frac{V_\perp^2}{2P} = \frac{V_\perp^2 Q}{2\omega U} \quad (4)$$

with the quality factor Q of the transverse deflecting mode and the electromagnetic energy U stored in this mode.

TWO POLARIZATIONS

The theory of cylinder resonators shows that the TM_{110}-mode has two polarizations, rotated by 90 degrees. In a perfectly symmetric resonator, there are both polarizations degenerated with arbitrary spatial orientation. Usually the symmetry of the resonator is broken by inserting protrusions. This asymmetry splits the resonance frequencies and fixes the orientation of the two polarizations. The orientation of the polarization determinates the plane of transverse deflection. Depending on their actual shape, the protrusions also increase the electric and magnetic fields on the cavity axis. For use in GunLab we need a transversal deflection in both transversal planes to reconstruct the full six dimensional phase space as a function of drive laser and RF parameters. Thus we designed a novel type of transverse deflecting cavity which is able to make use of both polarizations of the TM_{110}-Mode at the same resonance frequency. To select the actual polarization we use two plungers as shown in Figure 1. The plunger which protrudes deeper inside the resonator determines the polarizations and by that the planes of transverse deflection.

* Work supported by BMBF under contract no. 05K10PEA

Content from this work may be used under the terms of the CC BY 3.0 licence (© 2015). Any distribution of this work must maintain attribution to the author(s), title of the work, publisher, and DOI.

ISBN: 978-3-95450-168-7 doi:10.18429/JACoW-IPAC2015-MOPHA025

CONTROL SYSTEM FOR THE FRANZ FACILITY

Suha Alzubaidi#, O. Meusel, U. Ratzinger, C. Wagner, IAP, Frankfurt am Main, Germany

Abstract

The Frankfurt Neutron Source at the Stern- Gerlach Zentrum (FRANZ) will use the reaction of ^{7}Li(p,n)^{7}Be to produce an intense neutron beam. The neutron energy will be between 10 and 500 keV depending on the primary proton beam, which is variable between 1.8 and 2.2 MeV. A volume type ion source will be used to deliver a 120 keV proton beam with currents up to 200 mA. Like any other facility, FRANZ will need a powerful and reliable control system that also allows monitoring the whole accelerator target areas and experiments. Also interlock and safety systems have to be included to protect personnel from radiation hazards associated with accelerator operations and accompanying experiments. The FRANZ control system is still under development. The ion source will be the first element to be controlled, and to gain experience. A test ion source will be used for testing and examining the performance of this control system. The plasma properties, filament ageing and an internal control loop for stable beam production with respect to controlling issues will be discussed.

INTRODUCTION

In this paper, the control system of the FRANZ facility and of all its components will be discussed. On the one hand it controls the operation status of each component permanently, on the other hand it delivers data relevant for service and personal security maintenance. This system deals with all "slow" tasks of FRANZ while there will be rf control systems and fast control loops on the ns to µs scale separately.

The FRANZ proton driver consists of a volume type ion source delivering a 200 mA d.c proton beam at an energy of 120 keV. The proton beam will be transported to the low energy beam transport (LEBT) which consists of four solenoids and a chopper system for producing beam pulses of 100 ns with a repetition rate around 250 kHz.The main acceleration of the proton beam will be provided by a radio-frequency quadrupole (RFQ) working at 175 MHz with an output energy of about 700 keV followed by an IH-DTL for achieving 2.0 MeV beam energy which may be varied by ±0.2 MeV in the following 5 gap rebuncher of the CH-type. In a next project step, a Mobley- type bunch compressor will be realized where 9 rf linac bunches will pass in individual paths and will be focused on the neutron production target within 1 ns. The neutron production target is a solid Li target. Figure 2 shows a scheme of the FRANZ facility [1-2].

FRANZ CONTROL SYSTEM

In the FRANZ facility a "Mesh Networked Data Acquisition and Control System (MNDACS)" is used as a control System [3-4]. It is a Java based control system which is developed in house by C. Wagner. It consists of a kernel that manages all device drivers, graphical user interface (GUI) and driver abstraction layer (DAL) and provides the access to devices with local drivers or drivers loaded at different computers (see Fig. 1). The project approach is to build a mesh system to tolerate control unit breakdowns with a load balancing between units.

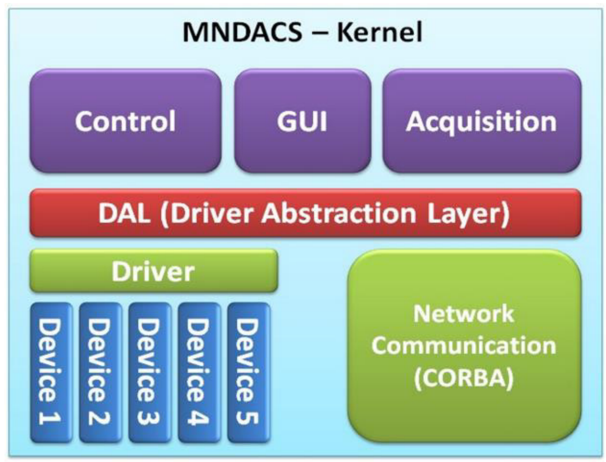

Figure 1: Program architecture of MANDACS.

The FRANZ control system consists of two basic layouts; the high level control and the data acquisition through the Ethernet layout, and the low level layout for the interlock and security system like emergency shutdown (see Fig. 3). All the devices will be connected to the TCP/IP Ethernet, which will be used as a physical communication backbone. To prevent software induced device outage, the number of computers will be as low as possible.

The network topology for FRANZ is shown in Fig. 4, where 1 Gbe links are used between devices and computers. At the FRANZ control system, three types of communications are used:

- Devices directly connected to the network (if possible).
- Connected through a converter in case of having a common interface like RS232.
- Connected through a computer in case of using an interface like USB.

#s.alzubaidi@iap.uni-frankfurt.de

Content from this work may be used under the terms of the CC BY 3.0 licence (© 2015). Any distribution of this work must maintain attribution to the author(s), title of the work, publisher, and DOI.

ISBN: 978-3-95450-168-7 doi:10.18429/JACoW-IPAC2015-MOPHA026

PRESENT AND FUTURE OPTICAL-TO-MICROWAVE SYNCHRONIZATION SYSTEMS AT REGAE FACILITY FOR ELECTRON DIFFRACTION AND PLASMA ACCELERATION EXPERIMENTS

M. Titberidze *, F. Grüner, A.R. Maier, B. Zeitler, University of Hamburg, CFEL, Hamburg, Germany
H. Schlarb, M. Felber, T. Lamb, C. Sydlo, K. Flöttmann, U. Mavric, J. Müller, DESY, Hamburg, Germany
S. Epp, Max Planck Institute for the Structure and Dynamics of Matter, Hamburg, Germany
E. Janas, Warsaw University of Technology, Warsaw, Poland

Abstract

Relativistic Electron Gun for Atomic Explorations (REGAE) is a Radio Frequency (RF) driven linear accelerator. It uses frequency tripled short photon pulses (~ 35 fs) from the Titanium Sapphire (Ti:Sa.) Laser system in order to generate electron bunches from a photo-cathode. The electron bunches are accelerated up to ~ 5 MeV kinetic energy and compressed down to sub-10 fs using the so called ballistic bunching technique. REGAE currently is used for electron diffraction experiments (by Prof. R.J.D. Miller's Group). In near future within the collaboration of Laboratory for Laser- and beam-driven plasma Acceleration (LAOLA), REGAE will also be employed to externally inject electron bunches into laser driven linear plasma waves. Both experiments require very precise synchronization (sub-50 fs) of the photo-injector laser and RF reference. In this paper we present experimental results of the current and new optical to microwave synchronization systems in comparison. We also address some of the issues related to the current system and give an upper limit in terms of its long-term performance.

INTRODUCTION

Ultrafast Electron Diffraction (UED) as well as planned external laser plasma wave injection experiments at REGAE require stable (sub-picosecond) electron beam arrival at the target chamber [1–3]. Mainly, two sub-systems of the accelerator - Low-Level RF (LLRF) system and injector laser - play a significant role to deliver low jitter electron bunches. Since REGAE is a normal conducting S-band accelerator, it uses a 2.997 GHz radio frequency (RF) signal for electron beam acceleration and bunching. This 2.997 GHz reference signal from a RF Master Oscillator (MO) is distributed to the LLRF system and injector laser synchronization system. The LLRF system controls the amplitude and phase of the RF reference signal while the laser synchronization system ensures the stability of the laser beam arrival on a photocathode. Figure 1 shows the layout of the REGAE facility including its sub-systems.

Different schemes can be employed to synchronize optical lasers to a microwave reference [4–8]. Currently, REGAE is using a so called down conversion (DWC) based setup to synchronize a 83.25 MHz repetition rate Ti:Sa. laser to the 2.997 GHz reference signal from the MO [9]. Later, this DWC based scheme will be replaced by a new balanced Mach-Zehnder Modulator (MZM) based synchronization setup which is currently under development [3]. It has been shown that the short term locking performance of the DWC based setup is in the order of ~ 20 fs RMS [9]. In this paper we show that the long term locking performance of the DWC based scheme is limited by AM/PM effects and environmental dependencies of the RF reference and optical components. We also present for the first time the long term detector stability of the new single output MZM based setup and its potential for synchronizing the Ti:Sa. lasers to microwave signals or vice versa.

LONG TERM PERFORMANCE OF DWC BASED SETUP

Description of the DWC Locking Setup

Long term out-of-loop (OOL) measurements have been carried out while the Ti:Sa. laser oscillator was locked to the RF reference using the DWC setup.

Some part of the light from the Ti:Sa. laser oscillator has been coupled into the pigtailed fiber collimator connected to a fast 10 GHz bandwidth photodiode (EOT4000F). This photodiode converts laser pulses to electric signals producing an RF frequency comb, containing a fundamental frequency of 83.25 MHz and its corresponding harmonics. The 36th harmonic of the repetition rate is filtered out using a 3.0 GHz RF bandpass filter and is further amplified. This filtered signal is used to downconvert the reference frequency of 3.025 GHz derived from the Local Oscillator (LO) generation box, which receives the reference 2.997 GHz signal from the MO. The downconversion and digitalization is done by employing a commercially available MicroTCA standard boards from Struck GmbH. The DWC board provides an intermediate frequency (IF) of ~ 25 MHz which is sampled by the 125 MS/s SIS 8300 ADC board. After digitalization, the digital IF signal is further processed by the controller firmware, where amplitude and phase information is extracted using a so called digital IQ demodulation technique. The obtained phase error information is fed to a piezo driver acting on a piezo mirror inside the laser cavity to match the frequency and phase of the reference signal. More details about controller firmware and the FPGA signal processing chain can be found [9].

* mikheil.titberidze@desy.de

Content from this work may be used under the terms of the CC BY 3.0 licence (© 2015). Any distribution of this work must maintain attribution to the author(s), title of the work, publisher, and DOI.

ISBN: 978-3-95450-168-7 doi:10.18429/JACoW-IPAC2015-MOPHA027

TRANSVERSE EMITTANCE MEASUREMENT AT REGAE

M. Hachmann, K. Floettmann, DESY, Hamburg, Germany

Abstract

The linear accelerator REGAE at DESY produces short and low charged electron bunches, on the one hand to resolve the excitation transitions of atoms temporally by pump probe electron diffraction experiments and on the other hand to investigate principal mechanisms of laser plasma acceleration. For both cases a high quality electron beam is required which can be identified with a small beam emittance. A standard magnet scan is used for the emittance measurement which is in case of a low charged bunch most sensitive to the beam size determination (2$^{\text{nd}}$ central moment of a distribution). Therefore the diagnostic and a routine to calculate proper central moments of an arbitrary distribution will be introduced and discussed.

INTRODUCTION

The Relativistic Electron Gun for Atomic Exploration (REGAE, Fig. 1) at DESY is a small 5 MeV linear accelerator with a bunch charge range of a few to some hundreds fC. The beam energy is delivered by an S-band photo-injector cavity. In addition to the gun a 4-cell buncher cavity is installed. It is designed for velocity bunching down to 10 fs. Due to the low energy a beam optics consisting of solenoids is sufficient. They are compact and focusing in both directions simultaneously.

The machine is built for two types of experiments: first a time-resolved electron diffraction experiment in order to make atomic transitions 'visible' [1] and secondly investigations of new plasma-wakefield acceleration schemes [2]. Both experiments require a low transverse beam emittance down to 10 nm (normalized emittance). Hence, there are two challenges: generate such a high quality electron bunch and measure this quality for a low-charge bunch with high precision which is discussed below.

Due to the small energy spread as well as in first approximation negligible space charge effects a phase advance method can be utilized for the emittance measurement. For this purpose a charge sensitive detector system was developed which has the required spatial resolution to measure the beam profile despite the unavoidable noise and background signals.

EMITTANCE MEASUREMENT VIA A SOLENOID SCAN

Phase Advance Method

A commonly used method to determine the transverse emittance of an electron bunch is a magnet scan. Here the phase advance between a magnet and a downstream screen is changed by varying the magnet current. Analyzing the RMS beam size as function of the focusing strength yields the emittance. Alternatively, it is possible to measure the beam size at different positions without any additional change of the optics. At REGAE the first method is used.

Assuming a small energy spread the *trace space emittance* is determined as

$$\epsilon_x = \sqrt{\langle x^2\rangle \langle x'^2\rangle - \langle x\, x'\rangle^2}$$

and is related in the following way to the *normalized emittance*: $\epsilon_x = \frac{1}{\beta\gamma}\epsilon_{n,x}$ with $\beta = v/c$, the Lorentz factor γ and the velocity v. Furthermore, $\langle\rangle$ denotes the central moment of a distribution, in this case the 2$^{\text{nd}}$ central moment where the square root is normally called RMS: $\langle x^2\rangle = x_{rms}^2$.

In order to measure the transverse beam emittance the envelope equation can be used [3]:

$$x_{rms}{}^2 = \begin{pmatrix} R_{11}{}^2 & 2\,R_{11}\,R_{12} & R_{12}{}^2 \end{pmatrix}^{\top} \begin{pmatrix} a_1 \\ a_2 \\ a_3 \end{pmatrix} \qquad (1)$$

$$\text{with}\quad a_1 = x_{0,rms}{}^2$$
$$a_2 = x_{0,rms}(x_{0,rms})'$$
$$a_3 = \frac{\epsilon_x{}^2}{x_{0,rms}{}^2} + (x_{0,rms})'^2.$$

x_{rms} denotes the RMS beam size at the screen, $x_{0,rms}$ the beam size and $(x_{0,rms})'$ the envelope slope at the position of the solenoid. In order to calculate the RMS beam size a Gaussian fit is often used. But the width of the normal distribution is only equal to the RMS if the beam profile is really normal distributed. In any other case this assumption doesn't hold which causes false results. It is important to emphasize that Eq. 1 only holds for RMS quantities. But the calculation of the RMS is difficult because the whole signal has to be taken into account which means the beam signal as well as background and noise. A post-processing routine for images will be introduced in the next section.

Taking Eq. 1 as a model describing the beam size development at a certain position in dependence of varying phase advances, the emittance can be found with the method of least squares.

Detector System at REGAE

For the diffraction experiment at REGAE a highly sensitive detector system is installed which is able to detect single electrons. This detector combined with the solenoids Sol45 or Sol67 (Fig. 1) can be used for the emittance measurements. The detector contains a CsI-crystal-screen which is evaporated onto light guides, called FOS (Fiber Optics Scintillator), and a charge sensitive Electron Multiplying CCD (EMCCD). The overall spatial resolution of this detector system is ∼ 20 µm/pixel. A schematic layout is shown in Fig. 2. The FOS is orientated perpendicular to the beam propagation. To avoid high energy photons or electrons hitting the EMCCD camera a mirror reflects the visible light

Content from this work may be used under the terms of the CC BY 3.0 licence (© 2015). Any distribution of this work must maintain attribution to the author(s), title of the work, publisher, and DOI.

ISBN: 978-3-95450-168-7 doi:10.18429/JACoW-IPAC2015-MOPHA028

OPERATION OF NORMAL CONDUCTING RF GUNS WITH MicroTCA.4

M. Hoffmann*, V. Ayvazyan, J. Branlard, Ł. Butkowski, M. Grecki, U. Mavrič, M. Omet, S. Pfeiffer, H. Schlarb, C. Schmidt, DESY, Hamburg, Germany
A. Piotrowski, FastLogic, Łódź, Poland; W. Fornal, R. Rybaniek, WUT-ISE, Warszawa, Poland

Abstract

During the last half year, the MicroTCA.4 based single cavity LLRF control system was installed and commissioned at several normal conducting facilities at DESY (FLASH RF gun, REGAE, PITZ RF gun and Booster, and XFEL RF gun). First tests during the last year show promising results in optimizing the system for high speed digital LLRF feedbacks, i.e. reducing system latency, increasing the internal controller processing speed, testing new control schemes, and optimizing controller parameters. In this contribution we will present results and gained experience from the commissioning phase and the first time period of real operation.

INTRODUCTION

The well known problem with normal conducting cavities is the temperature dependency of the resonance frequency, which introduces the main source for RF field fluctuations. The stability of the temperature defines the stability of the cavity field. For the RF gun cavities used at FLASH, XFEL and PITZ, the temperature coefficient is about 20 kHz/K. The required RF field stability is 0.01 % in amplitude and 0.01° in phase. The stabilization of the temperature for the RF guns at FLASH, XFEL and PITZ is quite challenging, because of the long RF pulses of typically 500 to 800 μs, which represents a massive heat load of typical 20 kW to the cooling system. In case of an interlock, the heat load has to be absorbed by the cooling system in a short time, while during normal operation the system has to be very accurate and keep the temperature of the gun constant below 0.03 K peak-to-peak. A further disturbance source comes from the the driving chain primary the klystron. Its stability is mainly defined by the stability of the modulator high voltage. The task of the RF controller is to suppress these disturbances. Temperature fluctuations are a slow effect, which degrades the pulse-to-pulse stability, while the klystron high voltage stability can be seen even within the RF pulse. During the commissioning phase of the new MicroTCA.4 based LLRF system at the FLASH, XFEL and PITZ gun, the main source of disturbances turned out to be quite different from facility to facility.

CONTROLLER DESIGN FOR RF GUNS

Due to the high bandwidth of normal conducting cavities of about 60 kHz (compared to superconducting cavities with about 200 Hz), the latency in the control loop of a normal conducting system is critical for the feedback controller design. It introduces a phase roll-off over the frequency, which makes the proportional feedback unstable at high feedback gains. One method to compensate this effect is the integration of a lead-lag element. The lead-lag element increases the phase margin of the closed loop transfer function in a certain frequency range, which allows to shift the area of instability to slightly higher controller gain. Additionally, it introduces an integrative part to the controller, which increases the feedback gain at lower frequencies and therefore to higher disturbance rejection. In our standard controller

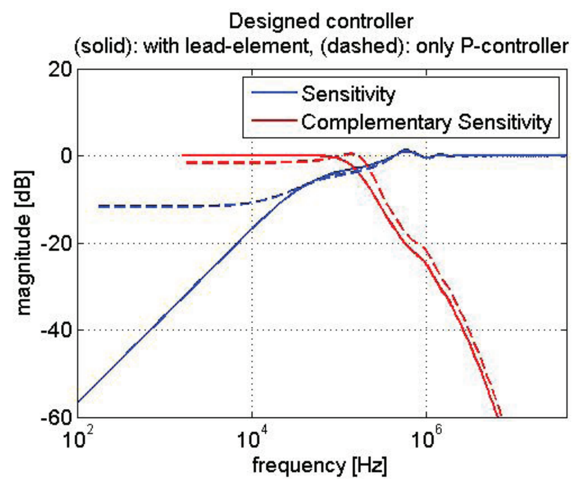

Figure 1: Sensitivity (S) and complementary sensitivity (T) function of the designed controller for the FLASH gun with lead-lag element (solid) and P-controller (dashed).

firmware, a two dimensional multiple input multiple output (MIMO) controller with second order transfer functions for each path is implemented [1]. This MIMO structure allows to compensate coupling between the real and imaginary part of the cavity field. Nevertheless, for the RF guns the main diagonal transfer functions are configured as a lead-lag element with an additional low pass filter. The low pass filter simply helps to reduce the loop back of the measurement noise, since the cavity bandwidth is just a few tens of kHz, while the detection bandwidth is several MHz. Fig. 1 shows an implementation example of the sensitivity function (S) and the complementary sensitivity function (T) of this controller. S describes the suppression of the disturbances. The S and T of a simple proportional feedback controller are shown in Fig. 1, for comparison purposes. In the low frequency regime the effect of the integrative part of the lead-lag element is clearly visible.

FLASH RF GUN

The FLASH gun is running since January 2015 with the new MicroTCA.4 based LLRF system. The system was running in parallel, already commissioned and tested during the

* m.hoffmann@desy.de

Content from this work may be used under the terms of the CC BY 3.0 licence (© 2015). Any distribution of this work must maintain attribution to the author(s), title of the work, publisher, and DOI.

ISBN: 978-3-95450-168-7 doi:10.18429/JACoW-IPAC2015-MOPHA029

OPERATION EXPERIENCES WITH THE MICROTCA.4–BASED LLRF CONTROL SYSTEM AT FLASH

M. Omet*, V. Ayvazyan, J. Branlard, Ł. Butkowski, M. Grecki, M. Hoffmann, F. Ludwig, U. Mavrič, S. Pfeiffer, K. Przygoda, H. Schlarb, C. Schmidt, H. Weddig, B. Yang, DESY, Hamburg, Germany,
K. Czuba, K. Oliwa, I. Rutkowski, R. Rybaniec, D. Sikora, W. Wierba, M. Żukociński, ISE, Warszawa, Poland,
W. Cichalewski, D. Makowski, DMCS, Łódź, Poland,
A. Piotrowski, FastLogic, Łódź, Poland.

Abstract

The Free–Electron Laser in Hamburg (FLASH) at Deutsches Elektronen–Synchrotron (DESY), Hamburg Germany is a user facility providing ultra–short, femtosecond laser pulses down to the soft X–ray wavelength range. For the precise regulation of the radio frequency (RF) fields within the 60 superconducting cavities, which are organized in 5 RF stations, digital low level RF (LLRF) control systems based on the novel MicroTCA.4 standard were implemented in 2013. With the newly installed system, an outstanding LLRF performance was achieved so far, positively impacting the FLASH stability and operation capabilities. Also valuable experiences with failures potentially due to radiation, overheating, and ageing as well as with the general operation of the control system could be gained. These have a direct impact on the operation and on the performance of FLASH and will allow future improvements. The lessons learned are not only important for FLASH but also in the scope of European X–ray Free–Electron Laser (XFEL), which will be operated with the same LLRF control system.

INTRODUCTION

The Deutsches Elektronen–Synchrotron (DESY) in Hamburg is currently building the European X–ray Free Electron Laser (E-XFEL) [1,2]. This hard X-ray light source will generate up to 27000 coherent laser pulses per second with a duration of less than 100 fs and a wavelength down to 0.05 nm. For this, electrons have to be accelerated to 17.5 GeV using a 2 km particle accelerator based on superconducting radio frequency technology. Precision regulation of the RF fields inside the accelerating cavities is essential to provide a highly reproducible and stable electron beam. RF field regulation is done by measuring the stored electromagnetic field inside the cavities. This information is further processed by the feedback controller to modulate the driving RF source, using a low level RF system. Detection and real-time processing are performed using most recent FPGA techniques. Special calibration and fast processing techniques of the RF signals inside the system are required. Performance increase demands a powerful and fast digital system, which was found with the Micro Telecommunications Computing Architecture (MicroTCA.4) [3], offering the following advantages. It combines a high precision of measurements and with a low latency processing. It is designed for the parallel processing of a huge number of RF signals. The system standard is very compact. High reliability and availability is assured with redundancy and radiation resistance due to shielding. A further feature is the capability of remote software upgrades and maintenance. Modularity and scalability permit easy hardware system upgrades.

DESY currently is operating the free electron laser (FLASH) [4], which is a user facility of the same type as XFEL but at a significantly lower maximum electron energy of 1.2 GeV. The LLRF system for FLASH is equal to the one of XFEL, which allows testing, developments and performance benchmarks in advance of the XFEL commissioning [5].

This fact is highly beneficial in preparation for the XFEL commissioning and operation. The FLASH LLRF system is successfully operated for about 2 years in the MicroTCA.4 framework demonstrating its capability of running a highly performing field regulation. They key question to be answered are:

1. What lessons have been learned for setup and commissioning of the LLRF system?
2. What problems have to be considered for operating the XFEL LLRF with MicroTCA.4 LLRF?
3. What efforts have to be addressed to further improve the system?

In the following these questions are to be discussed with the experience gained at FLASH. Due to the long operation at this facility, a large number of bug fixes could be achieved which is already beneficial since directly applicable to XFEL. Furthermore, vice versa FLASH benefits to a large extent, since requirements of the XFEL LLRF system are directly transferred to FLASH improving its performance.

SETUP AND COMMISSIONING OF THE LLRF SYSTEM

The LLRF system as well as all other subcomponents for the European XFEL main linac are installed within the accelerator tunnel which has a major impact of the system

* mathieu.omet@desy.de

Content from this work may be used under the terms of the CC BY 3.0 licence (© 2015). Any distribution of this work must maintain attribution to the author(s), title of the work, publisher, and DOI.

ISBN: 978-3-95450-168-7 doi:10.18429/JACoW-IPAC2015-MOPHA030

COMMISSIONING OF THE LOW-NOISE MTCA.4-BASED LOCAL OSCILLATOR AND CLOCK GENERATION MODULE*

U. Mavrič, J. Branlard, M. Hoffmann, F. Ludwig, H. Schlarb, DESY, Hamburg, Germany
A. Rohlev, TSR Engineering, Triest, Italy
D. R. Makowski, A. Mielczarek, P. Perek, TUL-DMCS, Łodz, Poland

Abstract

Within the Helmholtz Validation Fund Project "MicroTCA.4 for Industry", DESY together with collaboration partners from industry and research developed a compact fully MicroTCA chassis-integrated local RF oscillator module. The local oscillator and clock generation module generates a low noise local oscillator out of the global reference that is distributed over the accelerator. The module includes a splitting section which provides 9 local oscillator signals which are distributed over the RF-Backplane to the rear-transition modules. Similarly, the clock signal is also generated out of a single reference input by means of low-noise dividers. The clock is then fan-out to 22 differential lines that are routed over the RF backplane to the rear-transition modules. The functional block is implemented such that it fits in the rear slots 15 and 14 of a standard MTCA.4 crate. In the paper the commissioning results measured on the L3 low-level RF stations of the European XFEL will be presented.

SYSTEM ARCHITECTURE

The basic RF field detection scheme for the XFEL imposes specific requirements on the local oscillator (LO) and clock (CLK) generation circuits. The main design parameters are large number of tap-points and performance in terms of phase and amplitude stability. The decision was taken that each crate will have its own LO and CLK generation module. If one LO/CLK generation circuit would be serving multiple crates, this would cause issues with cable-drifts and reliability. On the other hand, having one LO/CLK generation circuits per one down-converter unit (8 field detectors) would increase the performance that could be achieved by vector-sum processing gain. The last option will be investigated in the future.

The LO/CLK module presented in this paper is located in the rear side of a standard MTCA.4 crate in slot 15. It uses a dedicated RF backplane [1] for distributing the LO and CLK signals. This reduces the amount of cables needed. The crate environment provides also the power, hardware management and data communication to the module.

One of the main functions of the LO/CLK generation module for the XFEL is to provide the local oscillator (LO) frequency at 1354 MHz. The LO frequency is generated by means of splitters and dividers as shown in Fig. 1.

* This work has partly been funded by the Helmholtz Validation Fund Project MTCA.4 for Industry.

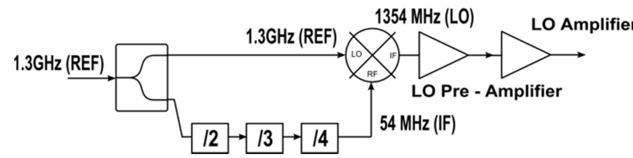

Figure 1: Generation of the local oscillator frequency.

Even if other architectures such as PLL-based circuits cover a wider frequency range of possible LO frequencies the method using dividers-only can practically achieve a lower residual phase noise while keeping the circuit simple. Because of the high number of tap-points the RF power before the splitting has to be in the order of 1 W which represents also a challenge in terms of shielding and DC power dissipation.

The generation of the CLK signals is implemented via simple clock dividers. The reasons for such architecture are similar to the ones for the LO generation.

HARDWARE OVERVIEW

The module is composed of several subsystems. The carrier hosts the RF splitting section, the CLK signal generation, the digital management section, the application processing unit and the low-noise linear regulators. Other functionalities such as DC/DC converters, the temperature controllers and the local oscillator generation are moved off the carrier board on daughter cards and connected to the main board through multi-pin connectors.

Carrier Board

The carrier board's primary function is frequency and clock distribution to the RF back plane (see Fig. 2). The 25 PECL differential clocks can be activated individually. The LO (1.354 GHz), CAL (1.3 GHz), and REF (1.3 GHz) signals are distributed via small 'RF-Mezzanine' cards that are directly soldered to the Carrier. Each RF-Mezzanine card provides a 1:9 signal fan-out as well as individual fixed attenuators and an absorptive RF switch for each signal. By swapping RF-Mezzanine cards frequency distribution up to 6 GHz can be achieved without altering the supporting carrier hardware.

The carrier also provides DC power generation for the system via a shielded 'DC/DC-Mezzanine' card that hosts two 8 A switch-mode convertors. One convertor provides a 5.9 V output used by the numerous LDO's on both RF and carrier card, the other convertor provides a 5.0 V output used exclusively for temperature control via thermoelectric controllers (TEC's) and Peltier elements.

Content from this work may be used under the terms of the CC BY 3.0 licence (© 2015). Any distribution of this work must maintain attribution to the author(s), title of the work, publisher, and DOI.

ISBN: 978-3-95450-168-7 doi:10.18429/JACoW-IPAC2015-MOPHA031

Content from this work may be used under the terms of the CC BY 3.0 licence (© 2015). Any distribution of this work must maintain attribution to the author(s), title of the work, publisher, and DOI.

IMPLEMENTATION OF A DIAGNOSTIC PULSE FOR BEAM OPTICS STABILITY MEASUREMENTS AT FLASH

F. Mayet, R. Assmann, S. Schreiber, M. Vogt, DESY, Hamburg, Germany

Abstract

In order to monitor long-term stability of beam optics, simple and at the same time minimally invasive procedures are desirable. Using selectively kicked bunches, betatron phase advance, as well as potential growth of the betatron oscillation amplitude and the Twiss parameters alpha and beta can be extracted from BPM data. If done periodically, this data can be compiled into a long-term history that is accessible via the control system. This way it is possible to identify potential sources of beam optics errors. At FLASH the procedure could be implemented as a server/client tool. Since the whole procedure takes less than five seconds, operation is not disturbed significantly. In this work the possible implementation of the procedure is presented. It is also shown how the history data can be evaluated in order to infer possible beam optics error sources.

INTRODUCTION

The high-gain free-electron laser FLASH at DESY, Germany produces ultra-short X-ray pulses with a duration less than 30 fs FWHH. These pulses are generated by the SASE process using a high brightness electron beam, which can be tuned to energies between 350 MeV and 1.25 GeV. This corresponds to a photon wavelength range between roughly 52 nm and 4 nm. Electron bunches are created by a laser-driven photoinjector and then accelerated by seven 1.3 GHz superconducting accelerator modules (*TESLA-type*). X-ray pulses are then generated inside the 27 m long undulator section. [1–3]

Since FLASH is a user facility, the long-term stability of the beam optics is crucial for all connected user experiments and the operation of the new second beamline FLASH2. In addition to that the seeding experiment sFLASH also demands for high beam optics stability. In [4] a simple procedure to monitor the beam optics routinely and at the same time minimally invasive was proposed. This work presents the actual implementation of the procedure at FLASH, as it is planned to be deployed during beamtime in the second half of 2015.

METHOD

The diagnostic pulse method is based on the idea of extracting beam optics stability information by measuring kicker magnet induced betatron oscillations of selected pulses periodically. These oscillations are measured by all available beam position monitors downstream the location of the kick. An online tool then analyzes the data. This way a long-term history of beam optics stability can be compiled.

The aim of the method is to reveal the cause of beam optics errors by correlating the long-term beam optics stability history with recorded machine parameters, or other events. A detailed description of the method can be found in [4].

IMPLEMENTATION

For the implementation of the method two schemes are possible. Table 1 shows the two possible scenarios at FLASH.

Fast Kicker

The first scheme is based on fast single bunch kickers. The main advantage of this scheme is the fact that it is minimally invasive and can potentially be run in the backround without disturbing any user experiments. At FLASH an appropriate fast kicker would be a dark current kicker at the beginning of the linac ($s = 0.45$ m). This device would then act as the only betatron oscillation inducing device (*DC-Kicker Scheme*). Being a sinusoidal kicker running resonantely at 1 MHz, the kicker can only be used in *single bunch mode*. Due to space constraints the installation of a second kicker is currently not possible. Since the DC-kicker only acts on the y-plane, information about the x-plane cannot be recorded. Because of the missing second kicker data analysis must rely on the *zero-crossing method*, as described in [4].

Slow Steerers

The second scheme (*Steerer Scheme*) relies on the use of two slow steerer magnets. By choosing a suitable set of steerers ($\approx \pi/2$ phase advance distance), it is possible to perform a complete trajectory fit. This then enables the extraction of beam optics parameters (like Twiss parameters β and α - see [4] for details). If two suitable sets of steerers are chosen, both the x and y plane data can be taken. First test measurements showed that in this scheme the whole procedure takes roughly 5 seconds. Therefore this scheme must be considered invasive, which is the main disadvantage. Two implementations of the *Steerer Scheme* are possible. The first one is an easy to use control panel and the other one is the integration of the diagnostic pulse measurement into the routinely performed shift documentation. This documentation already involves running several diagnostics and documentation related scripts. The diagnostic pulse measurement would then be added as another plug-in script to be run. Because of the invasive nature of the *Steerer Scheme*, currently the control panel is the favored approach.

Software

Independent of the choice of scheme, the implemenation of the diagnostic pulse measurement and beam optics stability history is based on a server/client concept. At FLASH many of the machine components are controlled via the DOOCS control system [5]. Therefore the diagnostic pulse

ISBN: 978-3-95450-168-7 doi:10.18429/JACoW-IPAC2015-MOPHA032

Content from this work may be used under the terms of the CC BY 3.0 licence (© 2015). Any distribution of this work must maintain attribution to the author(s), title of the work, publisher, and DOI.

ALL-OPTICAL SYNCHRONIZATION OF PULSED LASER SYSTEMS AT FLASH AND XFEL

J. Müller*, C. Sydlo, M. Schäfer, M. Felber, F. Zummack, M. K. Czwalinna, S. Schulz, H. Schlarb, B. Schmidt, DESY, Hamburg, Germany

Abstract

The all-optical laser synchronization at FLASH and XFEL provides femtosecond-stable timing of the FEL X-ray photon pulses and associated optical laser pulses (photo-injector laser, seed laser, pump-probe laser, etc.). Based on a two-color balanced optical cross-correlation scheme a high-precision measure of the laser pulse arrival time is delivered, which is used for diagnostic purposes as well as for the active stabilization of the laser systems. In this paper, we present the latest installations of our all-optical synchronization systems at FLASH and the recent developments for the upcoming European XFEL that will ensure a reliable femtosecond-stable timing of FEL and related pulsed laser systems.

INTRODUCTION

The free-electron laser in Hamburg (FLASH) and the upcoming European XFEL as fourth-generation linac-based light sources are capable of producing X-ray pulses with a duration of a few femtoseconds. Particulary for time-resolved pump-probe experiments and the externally seeded operation mode it is mandatory to achieve a synchronization of the external laser systems with an accuracy on the same timescale. One possibility to fullfill the requirements of a femtosecond-precise synchronization is a laser-based infrastructure [1]. Already in operation at FLASH and currently in the installation phase at XFEL the transmission of a highly stable periodic train of laser pulses to the critical subsystems over actively stabilized optical fibers is used and provides a time-stable reference signal to the corresponding end-stations [2]. This laser pulse train can be utilized directly for diagnostic purposes like in the bunch arrival time monitors [3]. Another application is the high-precision synchronization of external pulsed laser systems using a two-color balanced optical cross-correlation scheme [4]. The first prototypes for the actual system at FLASH were installed in 2007. Meanwhile, this optical synchronization system has grown to a key part of the facility. Further improvements of the system, particulary with regard to the European XFEL, focus on reliability and maintainablity of the subsystems. As one result we show here the first version of a new engineered design for laser-to-laser synchronization that is based on the well-proven all-optical laser synchronization setup currently running at several locations at FLASH.

* jost.mueller@desy.de

LASER-TO-LASER SYNCHRONIZATION

One essential key feature of the optical synchronization systems at FLASH and XFEL is the laser-to-laser (L2L) synchronization of external pulsed laser systems. This is based on a two-color balanced optical cross correlation scheme [4] that delivers a high-precision measure of the timing error between the reference and the laser pulse. Here, a twofold sum-frequency generation process in a nonlinear crystal provides a pure timing-sensitive error signal that is not affected by amplitude fluctuations of the two input signals. The principle of the balanced optical cross-correlation is shown in Fig. 1. To lock the laser repetition rate to the reference the error signal can be fed back within an electronic control loop that tunes the laser cavity length. The initialization of the synchronization process requires an additional RF-based pre-locking with a locking stability in the order of the used pulse widths.

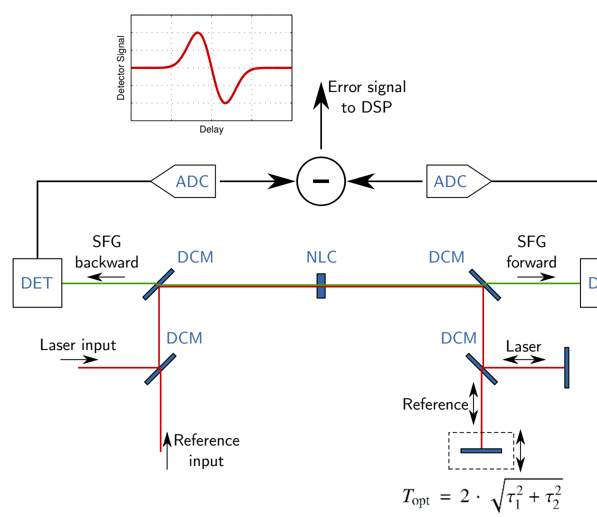

Figure 1: Principle of the balanced optical cross-correlator.

Current & Future Installations

So far we are operating three L2L-based synchronization setups at FLASH. The all-optical synchronization of the pump-probe laser system has brought great improvement regarding the jitter performance between pump-probe and FEL pulses [5]. A facility-wide timing jitter between pump-probe and FEL pulses could be shown to be below 30 fs (rms) [5]. Beside this, the injector laser system at FLASH is also equipped with an optical cross-correlator whereat no fast synchronization but a slow drift feedback is used to lock the laser to the optical reference. And meanwhile we also upgraded the synchronization system of the Ti:Sapphire

ISBN: 978-3-95450-168-7 doi:10.18429/JACoW-IPAC2015-MOPHA033

PHYSICAL PARAMETER IDENTIFICATION OF CROSS-COUPLED GUN AND BUNCHER CAVITY AT REGAE

Ayla S. Nawaz*, Herbert Werner, TUHH, Hamburg, Germany
Matthias Hoffmann, Sven Pfeiffer, Holger Schlarb, DESY, Hamburg, Germany

Abstract

A reasonable description of the system dynamics is one of the key elements to achieve high performance control for accelerating modules. This paper depicts the system identification of a cross-coupled pair of cavities for the Relativistic Electron Gun for Atomic Exploration - REGAE. Two normal conducting copper cavities driven by a single RF source accelerate and compress a low charge electron bunch with sub 10 fs length at a repetition rate up to 50 Hz. It is shown how the model parameters of the cavities and the attached radio frequency subsystem are identified from data generated at the REGAE facility.

INTRODUCTION

High field stability in phase and amplitude is the primary concern for the control of gun and buncher cavities at REGAE [1], a collaboration of the Center for Free-Electron Laser Science CFEL, the Max Planck Society, the University of Hamburg and DESY. Both the gun - a 1.5 cell cavity and the buncher - a 4 cell cavity are powered by the same klystron, Fig. (1).

The input to the klystron is modified through the feed forward tables. The required complex signal is implemented for the real and for the imaginary part separately. Power division after the klystron is obtained with the help of a T-shunt. It supplies the gun with 2/3 of the total power and the buncher with the remaining 1/3. It can be reasonably assumed, that the usage of one klystron for both the gun and the buncher cavity leads to cross-couplings between the two systems.

Signal detection, which is based on a MicroTCA.4 system standard [2], takes place in the gun and buncher respectively. For this the electromagnetic fields are measured by pick up antennas. The produced complex signal is then down converted to the intermediate frequency of 25 MHz and sampled with a frequency of 125 MHz. Results are then stored for the real and imaginary parts separately. The behaviour of the real and imaginary parts of the signals in the system can therefore be identified separately, though not independently, resulting in a two by two MIMO system for the gun as well as for the buncher. The frequency difference between the operating mode in each cavity, i.e. the π-mode, and the higher order modes lies between 2 MHz and 9.5 MHz. This difference is not enough to assume no influence of the higher order modes on the total field. The resulting electromagnetic field in the cavities is therefore a superposition of all the excited modes. This means that in the case of the gun one extra mode will be excited. In the case of the buncher there will be three extra modes. This behaviour is taken into consideration in the following system identification.

* ayla.nawaz@tu-harburg.de

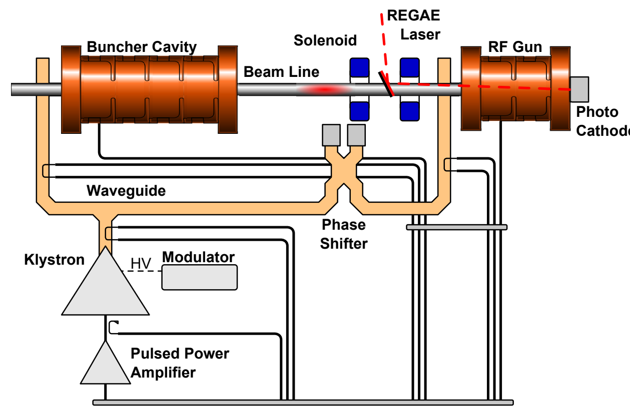

Figure 1: General cavity system set-up.

The system identification is obtained with the assumption that the cross-couplings between the gun and the buncher are negligible - case A and have to be taken into account - case B. It is shown that a consideration of the cross-couplings results in a higher accuracy of the acquired system model.

In the following the procedure of the system identification for the REGAE cavity system is explained. The used excitation signals, assumed model orders and time delays for the system are explained. Finally the results of a cross validation with the identified system model is discussed.

IDENTIFICATION

For the excitation of the system a pseudo random binary signal (PRBS) is used. This assures persistent excitation for the relevant frequency range. Two uncorrelated PRB-signals are used to excite the I and the Q channel of the input signal. The values for that are stored in the discrete time domain vector $u_I(k)$ and $u_Q(k)$ respectively. Accordingly in the frequency domain as $U_I(z)$ and $U_Q(z)$. The measured outputs are collected in the discrete time vector of $y_I(k)$ and $y_Q(k)$ and accordingly in the frequency domain as $Y_I(z)$ and $Y_Q(z)$. The general structure of the MIMO system is given by

$$\begin{bmatrix} Y_I(z) \\ Y_Q(z) \end{bmatrix} = \begin{bmatrix} G_{II}(z) & G_{IQ}(z) \\ G_{QI}(z) & G_{QQ}(z) \end{bmatrix} \begin{bmatrix} U_I(z) \\ U_Q(z) \end{bmatrix}, \quad (1)$$

representing the dependencies between the two inputs $U_I(z), U_Q(z)$ and the resulting outputs $Y_I(z), Y_Q(z)$ of the system. The z specifies the system as discrete. The parameters in the transfer functions $G_{II}(z), G_{IQ}(z), G_{QI}(z)$ and $G_{QQ}(z)$ are the unknowns. They are determined by the system identification.

Content from this work may be used under the terms of the CC BY 3.0 licence (© 2015). Any distribution of this work must maintain attribution to the author(s), title of the work, publisher, and DOI.

ISBN: 978-3-95450-168-7 doi:10.18429/JACoW-IPAC2015-MOPHA034

HIGH VOLTAGE RTM PIEZO DRIVER FOR XFEL SPECIAL DIAGNOSTICS*

K. Przygoda#, M. Felber, C. Gerth, M. Heuer, E. Janas, U. Mavric, P. Peier, H. Schlarb, B. Steffen, C. Sydlo, DESY, Hamburg, Germany
T. Kozak, P. Predki, DMCS, Lodz, Poland

Abstract

High voltage RTM Piezo Driver (PZD) has been developed to support special diagnostic (SD) applications foreseen for XFEL facility. The RTM Piezo Driver is capable of driving 4 piezo actuators with voltages up to ±80 V [1]. The solid state power amplifiers are driven using 18-bit DACs and sampling rates of 1 MSPS. The bandwidth of the driver is remotely tuneable using programmable low pass filters. The 4-channel Piezo Driver unit provides the information of piezo output voltage and current. Three independent test setups have been built to test 4-channel Piezo Driver performance. In the paper we are presenting EOD laser lock to 1.3 GHz FLASH master oscillator using bipolar piezo stretcher (fine tuning). The piezo motor based course tuning has been applied for the long term laser stability measurements. The unipolar piezo actuator operation has been demonstrated for the Origami Onefive laser locked to 1.3 GHz LAB MO. The preliminary results of active stabilization of 3.6 km fibre link laboratory setup are shown.

INTRODUCTION

In accelerator facilities, especially free-electron lasers (FEL), the use of mode locked lasers is most common approach, e.g. for electro-optical diagnostics (EOD), as photo-cathode lasers, seeding, Beam Arrival and Beam Position Monitors (BAM, BPM) or pump-probe experiments [2].

The repetition rate of the laser train pulses is typically a sub-harmonic of the main RF synchronization signal. At European XFEL the main reference signal is at 1.3 GHz while the lasers run in a range between 54 MHz and 216 MHz. In order to synchronize the laser to the accelerator reference a piezo element within a laser cavity is applied. The main approach is to use a loop filter (digital or analog) driving a high output voltage and current power amplifier in order to minimize a phase difference between reference and the laser.

The accelerator reference signal needs to be also distributed over different places of the machine. The main idea is to encode the reference timing information in the precise rate of an optical pulse trains using master laser oscillator (MLO). The MLO optical signal is next transmitted to different accelerator locations (e.g. RF Gun, main linac or undulator sections) using fibre laser connections. The fibre lasers needs to be actively stabilized using stretcher in a fibre due to temperature drifts and microphonics. The typical active fibre link stabilization is done using balanced optical cross-correlator (OXC) that compares the optical signal of the transmitter (e.g. MLO) and receiver (e.g. Probe Laser) and minimize its phase difference using analog or digital feedback loop. The block diagram of the laser synchronization and special diagnostic applications foreseen for XFEL machine are shown in Fig. 1.

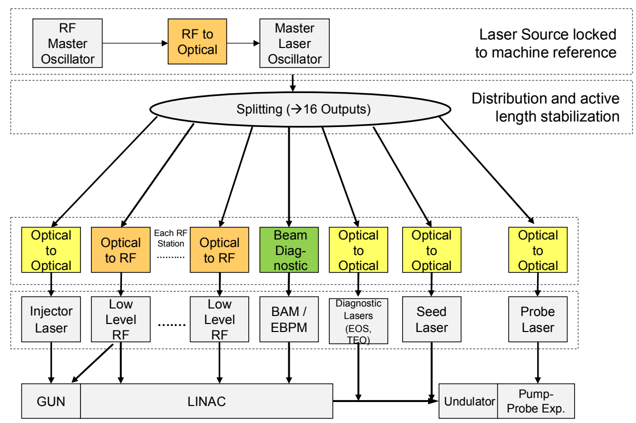

Figure 1: The block diagram of XFEL laser synchronization and special diagnostics.

The 2 laser sources locked to machine reference are foreseen for XFEL facility installation. The both MLO applications based on unipolar piezo actuator will occupy two 4-channel RTM Piezo Drivers (one channel per RTM). When considering optical signal distribution over XFEL accelerator a total of 24 fibre link connections with a length between 20 m and 3 km will be established. The bipolar piezo based fibre stretcher applications will consume 6 RTM Piezo Drivers (4 channels per RTM). The 4 electro-optical bunch length diagnostic (EOD) setups will use both bipolar (fine tuning) and unipolar (coarse tuning) piezo elements. The EOD lasers will occupy 4 Piezo Driver units. The 2 channels per module will be driven.

HIGH VOLTAGE PIEZO DRIVER APPLICATIONS

The 3 test stands have been established to check piezo driver performance for precise synchronization of optical lasers and special diagnostic applications [3].

MLO Synchronization

The Master laser oscillator application is based on Origami-15 onefive ultra-low noise femtosecond laser

*This project is supported by Grant No. HVF-0016 "MTCA.4 for Industry" awarded by the Helmholtz Validation Fund
#konrad.przygoda@desy.de

Content from this work may be used under the terms of the CC BY 3.0 licence (© 2015). Any distribution of this work must maintain attribution to the author(s), title of the work, publisher, and DOI.

ISBN: 978-3-95450-168-7 doi:10.18429/JACoW-IPAC2015-MOPHA035

BEAM OPTICS MEASUREMENTS AT FLASH2

M. Scholz, J. Zemella, M. Vogt, DESY, Hamburg, Germany

Abstract

FLASH2 is a newly build second beamline at FLASH, a soft X-ray FEL at DESY, Hamburg. Unlike the existing beamline FLASH1, it is equipped with variable gap undulators. This beamline is currently being commissioned. Both undulator beamlines of FLASH are driven by a common linear accelerator. Fast kickers and a septum are installed at the end of the linac to distribute the electron bunches of every train between FLASH1 and FLASH2. A specific beam optics in the extraction arc with horizontal beam waists in the bending magnets is mandatory in order to mitigate effects from coherent synchrotron radiation (CSR). We performed various beam optics measurements to ensure that the conditions for FEL operation at FLASH2 are fulfilled. Here we will show results of measurements.

INTRODUCTION

The existing superconducting single-pass high-gain SASE FEL FLASH (Free-electron LASer in Hamburg) at DESY, Hamburg [1] delivers photons in the wavelength range from 4.2 nm to 52 nm. The photons generated in the fixed gap SASE undulators can be delivered to five experimental stations one at a time. A second undulator beamline was attached to the linac during the last three years and is now under commissioning [1, 2]. The FEL will continue to be referred as FLASH and the two beamlines are named FLASH1 and FLASH2. Fast kickers and a DC Lambertson-Septum, installed behind the FLASH linac, allow to distribute the beam either to FLASH1 or to the extraction arc leading to FLASH2. The final angle between FLASH1 and FLASH2 is 12°. Strong bending magnets in the extraction arc require specific Twiss functions in order to mitigate emittance growth due to CSR [2, 3]. The FLASH2 undulator beamline is equipped with variable gab undulators [4] for SASE and reserves space for future seeding options. The extraction to a proposed third beamline hosting a plasma wake field experiment is considered in the beamline layout at the end of the FLASH2 arc.

DISPERSION MEASUREMENT AND MATCHING

The linear dispersion describes the derivative of the transverse beam position w.r.t. the relative momentum offset:

$$\eta_{x,y} = \frac{\Delta(x, y)}{\Delta p/p_0} \tag{1}$$

where $\eta_{x,y}$ describes the dispersion in horizontal or vertical plane, $\Delta(x, y)$ is the horizontal respectively the vertical beam offset caused by the dispersion and $\Delta p/p_0$ is the relative momentum offset.

In the extraction arc leading to the FLASH2 undulator beamline the beam is deflected in horizontal plane. However, due to the use of a Lambertson septum that requires a vertical offset – realized with two vertical kickers and additional kicks applied by quadrupole magnets – the vertical dispersion in the FLASH2 extraction arc is not zero. The extraction was designed such that the dispersion in each plane is closed after the last bending magnet deflecting in that plane. The FLASH2 design dispersion functions are shown in the lower plot in Fig. 1.

Two methods for closing the dispersion were quickly identified: First, one can adjust the strength of the dipoles in the extraction arc or, secondly, one can change the focusing strength of the quadrupole magnets in the dispersive section. However, both methods come along with a large number of possible optimization variables. It would be preferable to have a solution with a small number of parameters that can then be scanned until the (horizontal) dispersion is closed.

The results from different beam energy models in FLASH (the vector sum of the accelerating modules and two different models employing dispersive measurements) are not fully consistent. Thus a potential energy scaling error is an obvious candidate for causing the major part of the residual dispersion leaking out of the extraction arc. A wrong scaling of the main magnets plus steerer corrections to hit the reference trajectory can lead to spurious dispersion from the arc.

The approach is to correct the energy scaling of the extraction arc which will automatically close the dispersion of the arc. The only optimization parameter in this procedure is the design beam energy. We setup the arc for different beam energies within a range of ± 10 MeV and measured the horizontal dispersion (which is large than the vertical). This was repeated until the dispersion was closed. Since this method is convenient and since it worked, it is now the default procedure to close the horizontal dispersion in the FLASH2 extraction arc.

The plots in Fig. 2 show the results of the dispersion measurement after the optimization procedure was completed. As one can see the vertical dispersion is not perfectly closed but the remaining dispersion is small. It is planned to correct this in future measurements with the two vertical dipoles installed downstream the last horizontal bends or with quads located at positions were the horizontal dispersion is already closed.

BEAM OPTICS MEASUREMENT AND MATCHING

The design beta functions of the FLASH2 beamline including the injector, the linac, the extraction arc, the matching section as well as the undulator section are shown in the upper plot in Fig. 1.

Content from this work may be used under the terms of the CC BY 3.0 licence (© 2015). Any distribution of this work must maintain attribution to the author(s), title of the work, publisher, and DOI.

ISBN: 978-3-95450-168-7 doi:10.18429/JACoW-IPAC2015-MOPHA037

VISIBLE LIGHT DIAGNOSTICS AT THE ANKA STORAGE RING

B. Kehrer*, A. Borysenko, E. Hertle, N. Hiller, M. Holz, A.-S. Müller, P. Schönfeldt, P. Schütze
Karlsruhe Institute of Technology (KIT), Karlsruhe, Germany

Abstract

Synchrotron radiation in the visible light range is a versatile diagnostics tool for accelerator studies. At the ANKA storage ring of the Karlsruhe Institute of Technology (KIT), we have a dedicated visible light diagnostics beamline and two additional beam ports close to the radiation's source point. The visible light diagnostics beamline hosts a time-correlated single photon counting unit to measure the bunch filling pattern and a streak camera for longitudinal diagnostics. Recently, the beamline has been extended with a fast gated intensified camera to study transverse instabilities. The synchrotron light monitor ports were previously used for direct source imaging. Due to the diffraction limit the vertical beam size could not be resolved. One of the two ports has recently been equipped with a double-slit to allow for interferometric measurements of the vertical beam size.

In this paper we give an overview of the different setup modifications and present first results.

MOTIVATION

ANKA, the synchrotron light source at KIT can be operated in two different modes. In the normal user operation mode the machine is operated with an energy of 2.5 GeV and a filling pattern consisting of a sequence of bunches ('train') followed by a gap. In the short bunch mode with an energy of 1.3 GeV the lattice is changed to lower the momentum compaction factor α_c. By tuning the bunch length down (to the order of picoseconds), coherent synchrotron radiation (CSR) is emitted. Depending on the beam current, this radiation is either emitted constantly or in the so called bursts with a strong temporal fluctuation of the intensity. This latter mode requires a dedicated set of measurement tools for tracking the relevant parameters to gain further insight into accelerator physics. The charge distribution plays a vital role for these processes, either as the charge distributed over the bunches (filling pattern) or as the temporal and spatial profile of the different bunches. Incoherent synchrotron radiation can be used as diagnostics tool as its intensity is proportional to the bunch charge and thus the light pulse directly represents the charge distribution. Using the visible range simplifies the handling of the required components. At ANKA we have a dedicated visible light diagnostics beamline housing a set of experimental setups, additionally two dedicated beam ports for source point imaging are in use.

VISIBLE LIGHT DIAGNOSTICS BEAMLINE

The beamline is located at a 5° port front end at a dipole magnet. Two off-axis paraboloid and two planar mirrors transport the light onto the optical table where they form an intermediate image that is rotated by 90 degrees relative to the beam. To allow parallel measurements for the different setups the light is split into spectral regions by using two consecutive short pass filters (see Fig. 1). Using those filters allows the realization of a dispersion-free beam path for the streak camera as this would deform the temporal shape of the light pulses otherwise.

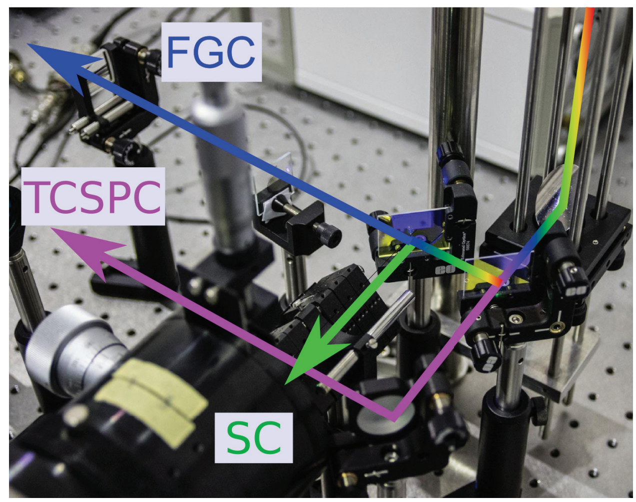

Figure 1: Picture of the of the setup for distributing the incoming light to the three different experiments (TCPSC: Time-correlated single photon counting, SC: Streak camera, FGC: Fast gated intensified camera) by using a sequence of two short pass filters (λ = 400 nm and λ = 500 nm).

Time-Correlated Single Photon Counting

For precise measurements of the filling pattern we use the time-correlated counting of single photons. The setup consists of a single photon avalanche diode (id100-20 from IDquantique [1]) and a histogramming device (PicoHarp 300 from PicoQuant [2]). The timing resolution of the setup is defined by the detector with a typical resolution of 40 ps, whilst the PicoHarp300 is operated with a channel width of 8 ps. To avoid deformations of the histogram due to too much events falling into the dead time we operate with count rates below $5\cdot10^5$ 1/s. The combination of the small sensitive area of the detector (20 μm diameter) and an iris lens mounted on the detector's C-mount leads to a good suppression of background light and thus we can operate the setup without any additional background light shielding. As the absorption depth of the photons in the solid state detector becomes smaller with decreasing wavelengths [3] we use a narrow bandpass filter (center wavelength 400 nm) to suppress the resulting diffusion tail in the histogram (see Fig. 2). This

* benjamin.kehrer@kit.edu

Content from this work may be used under the terms of the CC BY 3.0 licence (© 2015). Any distribution of this work must maintain attribution to the author(s), title of the work, publisher, and DOI.

ISBN: 978-3-95450-168-7 doi:10.18429/JACoW-IPAC2015-MOPHA038

STUDIES FOR A WAKEFIELD-OPTIMIZED NEAR-FIELD EO SETUP AT THE ANKA STORAGE RING

P. Schönfeldt*, A. Borysenko, N. Hiller, B. Kehrer, A.-S. Müller,
Karlsruhe Institute of Technology, Karlsruhe, Germany

Abstract

ANKA, the synchrotron light source of the Karlsruhe Institute of Technology (KIT), is the first storage ring with a near-field single-shot electro-optical (EO) bunch profile monitor inside its vacuum chamber. Using the method of electro-optical spectral decoding, the current setup made it possible to study longitudinal beam dynamics (e.g. microbunching) occurring during ANKA's low-alpha-operation with sub-ps resolution (granularity). However, the setup induces strong wake-fields spanning the distance between consecutive bunches which cause heat load to the in-vacuum setup for high beam currents. This heat load in turn leads to a laser misalignment thus preventing measurements during multi-bunch operation. Fortunately, the EO setup also allows us to directly study these wake-fields so simulation results can be compared to measurement data. This paper reviews a possible redesign of the setup, aiming to reduce the effects of the wakefield.

INTRODUCTION

An in-vacuum setup for for electro-optical bunch profile measurements is in regular operation at the ANKA storage ring since its installation in 2013 [1]. The measurement is based on the Pockels effect – a crystal becomes birefringent when it is exposed to an electric field. When a laser pulse is sent through the crystal, this birefringence then turns the linear polarization of a laser pulse into an elliptical one. At ANKA, a 5 mm thick Gallium Phosphide (GaP) crystal and a near-infrared laser (central wavelength 1030 nm) are used.

There are two possible measurement options: Electro optical sampling can be used to span time ranges of multiple nanoseconds. Here a short laser pulse is delayed with respect to the bunch arrival time and samples the electric field inside the electro optical crystal over many revolutions. Electro optical spectral decoding on the other hand allows to measure the bunch profile in a single shot. Here a long, chirped laser pulse is used. Afterwards one can reconstruct the time information by using a single shot spectrometer [2]. Using this mode it is possible to resolve substructures on the electron bunch, that only persist for a small number of revolutions [3].

Until now, the usage is limited to single-bunch operation. During the first measurements that were performed during multi-bunch operation, a decrease of the signal intensity was observed. The reason is that the laser has to be coupled into an optical fiber after passing the free space part inside the vacuum chamber. This step is very sensitive already to small misalignments, but the setup itself generates long ranging wakefields which cause the setup to heat up and makes misalignments unavoidable [4]. To overcome this limitation, a wakefield-optimized near-field EO setup is designed from scratch. A second design goal is a fast decrease of the wakefields' amplitude, to minimize biases when measuring electron bunches with a spacing of 2 ns.

For simulation and design, *CST Particle Studio* [5] is used. Its wakefield solver assumes a gaussian bunch shape (RMS bunch length σ_z) and can derive time dependent electromagnetic fields at defined points in space. Furthermore it computes the impedance and the integral over the longitudinal wake potential [6]

$$k_l = \frac{1}{\sqrt{2\pi}\sigma_z} \int_{-\infty}^{\infty} W_{\parallel} \exp\left(-\frac{s^2}{2\sigma_z^2}\right) \mathrm{d}s, \tag{1}$$

which is called the wake loss factor. To calculate the power an electron bunch looses by traveling through the structure, the correlation $P = k_l \times Q_b^2 \times f$ can be used, where Q_b is the bunch charge, and f the frequency bunches are passing by.

THE INSTALLED SETUP

The setup currently in operation has been designed by PSI and DESY for electro-optical bunch length measurements at SwissFEL and the European X-FEL [2]. The in vacuum part consists of a holder for the electro optical GaP crystal and a prism with a silver coated surface, which serves as a mirror.

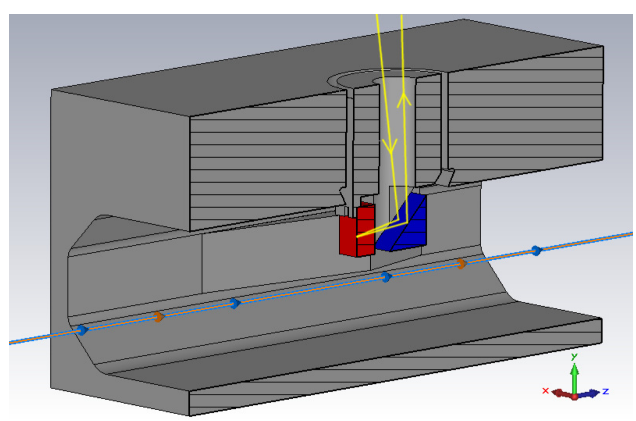

Figure 1: Cut through the beam pipe and the installed EO setup. The electron beam travels from the left to the right, the laser (yellow) enters from the top, is reflected at the mirror (blue), transverses the GaP crystal (red), is reflected at its back side and then travels back the same way.

* patrik.schoenfeldt@kit.edu

Content from this work may be used under the terms of the CC BY 3.0 licence (© 2015). Any distribution of this work must maintain attribution to the author(s), title of the work, publisher, and DOI.

ISBN: 978-3-95450-168-7 doi:10.18429/JACoW-IPAC2015-MOPHA039

Content from this work may be used under the terms of the CC BY 3.0 licence (© 2015). Any distribution of this work must maintain attribution to the author(s), title of the work, publisher, and DOI.

A FAST GATED INTENSIFIED CAMERA SETUP FOR TRANSVERSAL BEAM DIAGNOSTICS AT THE ANKA STORAGE RING

P. Schütze*, A. Borysenko, E. Hertle, N. Hiller, B. Kehrer, A.-S. Müller, P. Schönfeldt
Karlsruhe Institute of Technology (KIT), Karlsruhe, Germany

Abstract

ANKA, the synchrotron light source at Karlsruhe Institute of Technology (KIT), can be operated in different modes including the short bunch operation with bunch lengths compressed to a few picoseconds. In this mode, coherent synchrotron radiation (CSR) is emitted leading to beam instabilities. For gaining further insight into those processes, a setup based on a fast gated intensified camera was installed recently at the visible light diagnostics beamline of the ANKA storage ring. The experimental layout consists of an optical setup, which magnifies the image of the beam in the horizontal and demagnifies it in the vertical plane to obtain a projection of the horizontal beam shape, the camera itself and a fast scanning galvanometric mirror that sweeps this image across the sensor. This allows the tracking of the horizontal bunch size and position over many turns.

In this paper we present the setup and show first measurement results.

INTRODUCTION

The synchrotron light source ANKA, located at the Karlsruhe Institute of Technology (KIT), can be operated at energies from 0.5 GeV up to 2.5 GeV. In addition to normal operation at 2.5 GeV, a short bunch operation at 1.3 GeV is regularly offered [1]. By lowering the momentum compaction factor α_c, bunch lengths of a few picoseconds are reached, leading to the emission of coherent synchrotron radiation (CSR) in the high GHz and THz range. Furthermore in short bunch operation micro-bunching instabilities and thus strong bursts of THz radiation occur. Their periodicity and power strongly depend on the bunch current. Various investigations of micro-bunching instabilities were performed at the ANKA storage ring, characterizing the coherent radiation bursts [2] and the corresponding longitudinal bunch profile [3].

The measurement setup presented in this paper, based on an idea of J. Corbett [4], will allow the observation of the horizontal bunch profile on a single turn base. It can be used for the observation of transverse bunch profile fluctuations, e.g. during micro-bunching instabilities.

EXPERIMENTAL SETUP

Optical Setup

The experiment is under commissioning at ANKA's visible light diagnostics beamline, which is located at a 5° port front end at a dipole magnet. There are various experiments located at the beamline, such as Time-Correlated Single Photon Counting (TCSPC) and a streak camera. The optical beam path from the source point to the fast gated intensified camera is shown in Fig. 1. A cooled planar mirror is used to filter the visible range from the synchrotron radiation spectrum. After passing through an optical chicane, the visible spectrum is split into three wavelength regions for the different experiments by using dichroic mirrors. This separation is performed directly after the second off-axis paraboloid mirror and is not shown in the drawing. For the fast gated intensified camera blue light in the range from 400 nm to 500 nm is used. More information on the other experiments carried out at this beamline can be found in [5].

The optical chicane contains two off-axis paraboloid mirrors of different focal lengths, creating a real image of the incoherent synchrotron radiation, directly representing the bunch's transverse charge distribution. It is shown in the upper part of Fig. 2.

Being the smallest aperture in this setup, the diaphragm leads to a diffraction limit of about 150 μm in the vertical plane, compared to a vertical beam size of less than 100 μm [6]. Thus, this experiment is exclusively designed for monitoring the horizontal bunch profile. To gain sensitivity in the horizontal plane, the image is stretched by two cylindrical lenses of different focal lengths. The resulting image can be seen in Fig. 2.

The last planar mirror in front of the camera will be a fast rotating, galvanometric mirror. To track the horizontal bunch profiles over many turns, this mirror sweeps the stretched images over the camera sensor, fast enough (> 500 deg/s) to place the images of consecutive turns clearly separate next to each other. A schematic scheme is shown in Fig. 3.

Fast Gated Intensified Camera

The existing transverse beam profile monitors at ANKA have a slow acquisition rate (> 50 Hz) and a relatively long exposure time (typically hundreds of μs to 1 s). Thus they are integrating over many bunches and bunch revolutions due to the minimum bunch spacing of 2 ns and a bunch revolution frequency of 2.7 MHz.

In order to observe the horizontal beam profile of a single bunch for a single turn, a fast gated intensified camera (Andor iStar 340T [7]) was installed. The optical gate with a width of less than 2 ns allows the imaging of single synchrotron radiation pulses even in a multibunch environment, since the bunch spacing at ANKA is 2 ns. A maximum gate repetition rate of 500 kHz enables the imaging of the synchrotron radiation pulse of a certain bunch at every 6th turn for the tracking of the bunch profile on fast timescales.

* paul.schuetze@student.kit.edu

ISBN: 978-3-95450-168-7 doi:10.18429/JACoW-IPAC2015-MOPHA040

Content from this work may be used under the terms of the CC BY 3.0 licence (© 2015). Any distribution of this work must maintain attribution to the author(s), title of the work, publisher, and DOI.

FIRST RESULTS OF ENERGY MEASUREMENTS WITH A COMPACT COMPTON BACKSCATTERING SETUP AT ANKA*

C. Chang, E. Bründermann, E. Hertle, N. Hiller, E. Huttel, A.-S. Müller, M. J. Nasse, M. Schuh, J. L. Steinmann, Karlsruhe Institute of Technology (KIT), Karlsruhe, Germany, H.-W. Hübers, H. Richter, Deutsches Zentrum für Luft- und Raumfahrt (DLR), Berlin, Germany

Abstract

An electron energy measurement setup based on the detection of Compton backscattered photons, generated by laser light scattered off the relativistic electron beam, has been proposed and developed for operation at the ANKA storage ring of the Karlsruhe Institute of Technology (KIT). In contrast to conventional methods based on head-on collisions, the setup at ANKA is, for the first time, realized in a transverse configuration where the laser beam hits the electron beam at an angle of ~90°. This makes it possible to achieve a relatively low-cost and very compact setup since it only requires a small side-port instead of a straight section. This development could benefit storage rings with restricted space or where no straight sections are available, for example due to interferences with existing beamlines. The setup and the first measurement results are presented in the paper.

MOTIVATION

The ANKA storage ring [1] is operated from 0.5 GeV to 2.5 GeV. In the short bunch operation mode, typically at 1.3 and 1.6 GeV, coherent THz synchrotron radiation is generated [2]. Previously, precise energy calibration at 2.5 GeV was successfully achieved by resonant spin depolarization [3]. For lower energies, however, this technique requires very long measurement times. Here Compton Back-Scattering (CBS) is more suitable as it does not require a polarized electron beam. So far, several facilities have reported energy measurements based on CBS using a head-on collision geometry ($\varphi=\pi$) with relative accuracies reaching 10^{-4} to a few 10^{-5} [4-9]. Compared to the traditional CBS method, we have for the first time developed and measured with a transverse configuration ($\varphi=\pi/2$). This setup has several advantages: It is very compact and can therefore also be used at rings with restricted space. Furthermore, the transverse setup reduces the energy of Compton edge photons by a factor of two, which either makes measurements and detector calibration much easier, or enlarges the measurable range of a specific setup considerably. The transverse configuration can in principle also be converted easily into a versatile laser wire diagnostics tool.

*Work supported by the European Union under contract PITN-GA-2011-289191

METHOD PRINCIPLE

If monochromatic (laser) photons (energy E_L) scatter off of relativistic electrons (energy E_e), the scattered photons with energy E_s follow the kinematics illustrated in Eq. 1 and Fig. 1, where φ is the collision angle between the incoming laser and the electrons and θ is the scattering angle between the scattered photons and the initial electrons. The electron velocity divided by the speed of light is denoted by β:

$$E_s = \frac{E_L(1-\beta\cos\varphi)}{1-\beta\cos\theta+E_L/E_e[1-\cos(\theta-\varphi)]}. \quad (1)$$

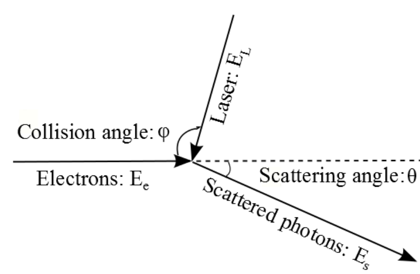

Figure 1: Scheme of CBS.

For θ=0, the energy of the scattered photons reaches its maximum E_{max} and forms a sharp cut-off edge (Compton edge) in the energy spectrum.

For typical CBS measurements at storage rings we have $E_e \gg mc^2 \gg E_L$ (mc^2 is the electron rest energy) and φ>0. The electron beam energy E_e can then be determined from the known values of mc^2 and E_L, and the measured φ and E_{max} using

$$E_e \approx \frac{mc^2}{2\sin\frac{\phi}{2}}\sqrt{\frac{E_{max}}{E_L}}. \quad (2)$$

Its relative uncertainty can be calculated as

$$\frac{\sigma_{E_e}}{E_e} = \sqrt{[\frac{\sigma_{E_L}}{2E_L}]^2+[\frac{\sigma_\phi}{2\tan(\phi/2)}]^2+[\frac{\sigma_{E\max}}{2E_{\max}}]^2}. \quad (3)$$

Here σ_{E_L}/E_L is the relative uncertainty of the average laser photon energy.

ISBN: 978-3-95450-168-7 doi:10.18429/JACoW-IPAC2015-MOPHA041

LASER WIRE BASED TRANSVERSE EMITTANCE MEASUREMENT OF H$^-$ BEAM AT SPALLATION NEUTRON SOURCE*

Y. Liu#, A. Aleksandrov, C. Long, A. Menshov, A. Zhukov
Spallation Neutron Source, Oak Ridge National Laboratory, Oak Ridge, TN 37831, USA

Abstract

A laser wire based transverse emittance measurement system has been developed at the Spallation Neutron Source (SNS). The system enables a nonintrusive measurement of the transverse emittance in both directions on a 925 MeV/1 MW hydrogen ion (H$^-$) beam at the high energy beam transport (HEBT) beam line.

INTRODUCTION

Conventional particle beam emittance measurement techniques such as the slit-and-collector or pepper-pot methods are generally intrusive and cannot be applied to full spec high-brightness particle beams [1, 2]. At the Spallation Neutron Source (SNS), we have developed a laser based, nonintrusive emittance measurement system at the high energy beam transport (HEBT) beam line [3].

The SNS laser emittance measurement setup consists of a laser wire scanner in the HEBT beam line and a metallic wire scanner in the linac dump beam line. The laser light slices out a narrow neutralized hydrogen beam (H^0) through the photodetachment process. The H^0 beam is transmitted through a downstream dipole and separated from the rest of the beam. The titanium wires measure the distribution of the H^0 beam released from the laser slit. The system has been applied to the emittance measurement of a 925 MeV/1 MW neutron production H$^-$ beam.

SYSTEM DESCRIPTION

A schematic of the laser based emittance measurement system is shown in Fig. 1. The emittance measurement setup is located about 40 meters away from the beginning of the SNS HEBT beam line. The expected beam emittance at this location is about 0.5 mm·mrad. The setup consists of two parts: a laser wire scanner (laser slit) and a conventional metallic wire scanner. The laser wire scanner is installed right before the first of eight 11.25° C-type dipoles which turn the H$^-$ beam to the accumulator ring. These dipoles also separate the neutralized hydrogen beam (H^0) from the main beam trajectory and direct the H^0 beam to the linac dump beam line. A metallic wire scanner is installed in the linac dump beam line, about 11.6 meters downstream of the laser wire station. The wire scanner measures the distribution of the H^0 beam released from the laser slit. Since the laser wire only interacts with a very tiny portion (~10^{-7}) of the ion beam and the wire scanner is interacting with an off-line H^0 beam, the entire measurement is effectively nonintrusive and can be conducted parasitically on a neutron production H$^-$ beam.

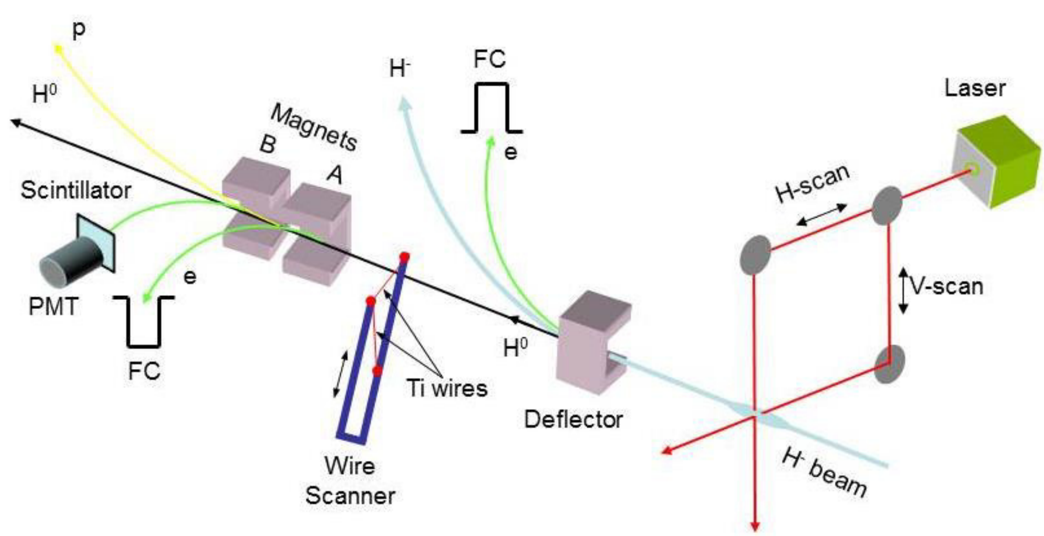

Figure 1: Schematic of laser wire based H$^-$ beam emittance measurement system. FC: Faraday cup, PMT: photomultiplier tube, Magnets A and B deflects electrons for FC and scintillator detection schemes, respectively.

*Work supported by U.S. Department of Energy under contract DE-AC05-00OR22725.
liuy2@ornl.gov.

Content from this work may be used under the terms of the CC BY 3.0 licence (© 2015). Any distribution of this work must maintain attribution to the author(s), title of the work, publisher, and DOI.

ISBN: 978-3-95450-168-7 doi:10.18429/JACoW-IPAC2015-MOPHA042

Content from this work may be used under the terms of the CC BY 3.0 licence (© 2015). Any distribution of this work must maintain attribution to the author(s), title of the work, publisher, and DOI.

ONLINE STUDIES OF THz-RADIATION IN THE BURSTING REGIME AT ANKA

M. Brosi*, M. Caselle, E. Hertle, N. Hiller, A. Kopmann, A.-S. Müller, P. Schönfeldt, M. Schwarz, J. L. Steinmann, M. Weber, KIT, Karlsruhe, Germany

Abstract

The ANKA storage ring of the Karlsruhe Institute of Technology (KIT) operates in the energy range from 0.5 to 2.5 GeV and generates brilliant coherent synchrotron radiation in the THz range with a dedicated bunch length reducing optic. The producing of radiation in the so-called THz-gap is challenging, but this intense THz radiation is very attractive for certain user experiments. The high degree of compression in this so-called low-alpha optics leads to a complex longitudinal dynamics of the electron bunches. The resulting micro-bunching instability leads to time dependent fluctuations and strong bursts in the radiated THz power. The study of these fluctuations in the emitted THz radiation provides insight into the longitudinal beam dynamics. Fast THz detectors combined with KAPTURE, the dedicated KArlsruhe Pulse Taking and Ultrafast Readout Electronics system developed at KIT, allow the simultaneous measurement of the radiated THz intensity for each bunch individually in a multi-bunch environment. This contribution gives an overview of the first experience gained using this setup as an online diagnostics tool.

INTRODUCTION

ANKA is a synchrotron radiation source located in Karlsruhe, Germany, and is operated by the Karlsruhe Institute of Technology. It consists of a 110.4 m long electron storage ring, which can operate at energies ranging from 0.5 GeV up to 2.5 GeV. Beside the standard user operation a special operation mode is provided to the research community. This so called low-alpha mode allows the reduction of the bunch length down to a few picoseconds by making use of an adaptable magnet optics. Additionally, the pattern in which the RF-buckets are filled can be chosen ranging from a single electron bunch up to custom filing patterns provided by the Bunch-by-Bunch feedback system [1].

The short bunch length of a few picoseconds in the low-alpha operation mode leads to an increase in the emitted power in the lower THz band due to the coherent emission of synchrotron radiation for wavelengths in the order of or longer than the emitting structure. Partially, coherent synchrotron radiation (CSR) is also emitted for (slightly) shorter wavelength than expected by the bunch length. This happens above a certain bunch current when a modulation of the longitudinal phase space is induced by the CSR impedance. This effect in the longitudinal particle distribution is called micro-bunching instability [2]. Due to the temporally changing/evolving nature of these substructures the emitted power in the THz regime fluctuates strongly with characteristic frequencies. The frequency of the fluctuations depends on the bunch current as well as on the parameters of the longitudinal beam dynamics, such as the RF-voltage, the synchrotron frequency and the momentum compaction factor [3]. The fluctuations of the radiated power in the THz regime are often referred to as bursts, while the whole effect is called bursting. For user experiments relying on stable intensity, it is necessary to know for each machine setting above which bunch current the micro-bunching instability occurs and bursting starts.

To detect and monitor bursting, the peak-intensity of the emitted THz pulse of each bunch at each turn is recorded using a fast THz detector combined with a dedicated data acquisition system. The peak-intensity of each bunch, recorded in one measurement, for approximately 2.7 million consecutive turns, is called the bunch's THz signal in the following. For the measurements described below, a zero-biased quasi-optical broadband Schottky diode detector from ACST [4] was combined with the KArlsruhe Pulse Taking and Ultrafast Readout Electronics system (KAPTURE) [5], which was developed for this purpose. This combination opens up the possibility to simultaneously measure the THz signal of each individual bunch in a multi-bunch fill, over an almost unlimited number of turns (see Fig. 1).

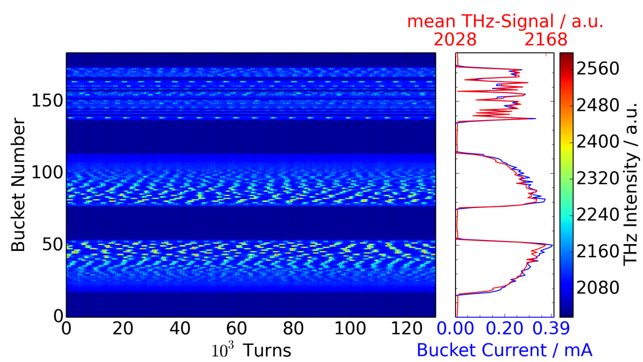

Figure 1: The peak-intensity of the THz pulses of all 184 RF-buckets is displayed over 130 thousand consecutive turns and shows strong fluctuations caused by bursting. A typical measurement takes one second and contains 2.7 million turns. The graph to the right shows the filling pattern.

This setup allows us to study the potential influence of a multi-bunch environment on the bursting behavior of each bunch. Furthermore, if these multi-bunch influences are known, then the information from all bunches with different currents in a multi-bunch fill can be used to speed up measurements like a characterization of different machine set-

* miriam.brosi@kit.edu

ISBN: 978-3-95450-168-7 doi:10.18429/JACoW-IPAC2015-MOPHA043

PROPERTIES OF TRANSITION- AND SYNCHROTRON RADIATION AT FLUTE

M. Schwarz*, A.-S. Müller, KIT, Karlsruhe, Germany
M. Schmelling, MPIK, Heidelberg, Germany

Abstract

FLUTE (Ferninfrarot Linac Und Test Experiment) is a 41 MeV linear accelerator currently under construction at KIT. It is aimed at accelerator physics and THz radiation research. For this reason the machine will cover a wide range of bunch charges (1 pC up to 3 nC) and lengths (1 fs to 300 fs). One aim of FLUTE is the study of different mechanisms for the generation of intense THz pulses, such as transition- (TR) or synchrotron radiation (SR). In this contribution, we calculate and compare various pulse properties, such as spectra, and electric fields, for both TR and SR.

MOTIVATION

Coherent radiation is emitted by electron bunches whenever the wavelength in question is larger than the bunch length. The test facility FLUTE [1] aims to produce bunches with charges 1 pC and bunch lengths 1 fs. In this paper, we compare our own semi-analytic methods for calculating the electric field of a coherent THz pulse [2] with analytic results and standard numerical methods. Next, we apply it to compute the electric field pulse of a simulated bunch profile for synchrotron- (SR) and transition radiation (TR).

RADIATION FROM ULTRA-SHORT BUNCHES

A bunch consists of N particles at positions t_i. Assuming that each particle emits a pulse with electric field $E_0(t)$ the field of the entire bunch is given by the superposition of the individual pulses

$$E(t) = \sum_{i=0}^{N-1} E_0(t - t_i)\,.$$

Here, we are only interested in the coherent field, and thus, ignoring the transverse bunch size, approximate the bunch by a continuous normalized longitudinal density $\rho(t)$. The field of the pulse is then a convolution of the single particle pulse $E_0(t)$ and the bunch profile $\rho(t)$

$$E(t) = \int_{-\infty}^{\infty} E_0(t-\tau)\rho(\tau)\,\mathrm{d}\tau\,.$$

It is more convenient to solve the convolution in the frequency domain

$$\varepsilon(t) \equiv \int_0^{\infty} \tilde{E}_0(\omega)\,\tilde{\rho}(\omega)\,\mathrm{e}^{-\mathrm{i}\omega t}\mathrm{d}\omega\,, \tag{1a}$$

$$E(t) = N\,\mathrm{Re}\left[\mathrm{e}^{-\mathrm{i}\phi}\varepsilon(t)\right]\,. \tag{1b}$$

* markus.schwarz@kit.edu

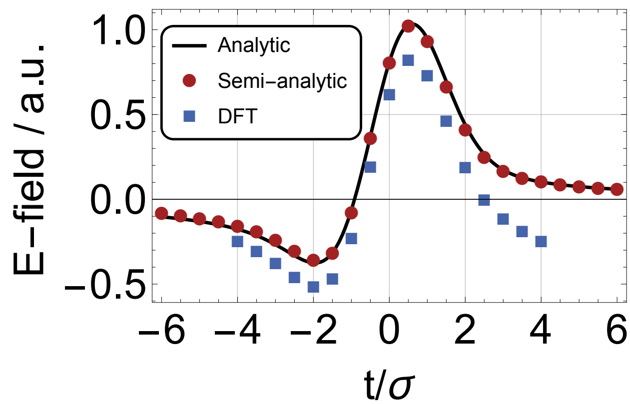

Figure 1: Electric field of a synchrotron radiation pulse emitted by a Gaussian bunch, calculated according to Eq. (1). Eq. (1) was solved analytically (continuous curve) [3], employing the discrete Fourier transform (DFT, boxes), and our own semi-analytic code (circles) [2]. Compared to the analytic result, the DFT method yields both a wrong peak field and pulse shape.

Here and in the following, a ~ above a symbol denotes its representation in the frequency domain. The phase ϕ is a property of the emission process, and determines whether the pulse is single or "half" cycle. Setting $\phi = 0, 180°$ yields a "half" cycle pulse whereas $\phi = \pm 45$ or $\pm 135°$ leads to a single cycle pulse.

The main problem is to solve Eq. (1a) for different spectra $\tilde{E}_0$ and general bunch profiles ρ. A standard way of computing the convolution would be to sample the bunch profile at reasonably many points, and use the discrete Fourier transform (DFT) to both obtain $\tilde{\rho}$ and subsequently compute Eq. (1a). That this procedure only asymptotically, i.e. for many sampling points and a large time interval, yields the correct result is demonstrated in Fig. 1 for a Gaussian bunch emitting low-frequency synchrotron radiation, $\tilde{E}_0(\omega) \sim \omega^{1/6}$. To apply the DFT, the profile was sampled by 17 equidistant data points in the interval $[-4\sigma, 4\sigma]$, containing more than 99.9% of the bunch. The boxes in Fig. 1 depict the result obtained by using the DFT. Notice that it is limited to times given by the sampling interval. The continuous curve shows the analytic result [3]. Here, the DFT gives a peak field that is about 22% too low, and the wrong shape at large (positive) times[1].

One reason for the discrepancy is that the integral $\int_{-\infty}^{\infty} E(t)\,\mathrm{d}t$ needs to vanish [4]. Thus, a positive peak needs to be balanced by a negative tail. The analytic calculation is

[1] An agreement better than 1% requires a sampling interval $\pm 50\sigma$ and ten times as many data points.

Content from this work may be used under the terms of the CC BY 3.0 licence (© 2015). Any distribution of this work must maintain attribution to the author(s), title of the work, publisher, and DOI.

ISBN: 978-3-95450-168-7 doi:10.18429/JACoW-IPAC2015-MOPHA044

TESTING A DIGITAL BEAM POSITION STABILIZATION FOR THE P2-EXPERIMENT AT MESA*

M. Dehn, K. Aulenbacher, J. Diefenbach, F. Fichtner, R. Herbertz, W. Klag
Institut für Kernphysik, Universität Mainz, Germany

Abstract

The Mainz Energy-recovering Superconducting Accelerator (MESA) will be built at the institute for nuclear physics at Mainz University. Besides the multi-turn energy recovery mode an external beam mode is foreseen to provide 155 MeV electrons of 85% polarization at 150 μA for parity violating experiments. To achieve the required stability of the main beam parameters a dedicated digital position stabilization is currently developed and tested at the Mainz Microtron (MAMI).

INTRODUCTION

MESA as illustrated in Fig. 1 will provide the opportunity to study precision physics at lower energies but higher beam currents than the accelerator cascade of the Mainz Microtron (MAMI) [1, 2]. The main parameters of the new accelerator are listed in Table 1.

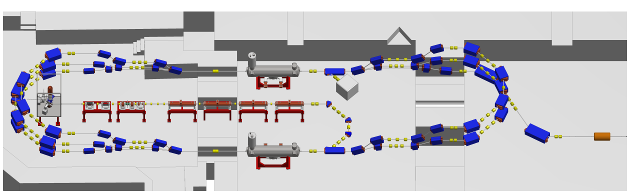

Figure 1: Illustration of MESA.

Table 1: MESA Operation Modes

Parameter stage 1 (2)	EB	ER
Energy [MeV]	155	105
Beam current	150 μA	1 mA (10 mA)
Bunch charge [pC]	0.12	0.77 (7,7)
max. Beam power [kW]	22.5	105 (1050)

Since the very beginning of MAMI (see Fig. 2) RF cavity monitors are used to acquire beam positions and relative phase as well as the intensity of the electron beam [3].

While running the machine for experiments the monitor system delivers CW signals. To optimize the position and phase of the electron beam through the microtrons pulsed beam of high intensity is used to increase sensitivity while reducing the amount of beam losses [4].

* Work supported by the German Federal Ministry of Education and Research (BMBF) and German Research Foundation (DFG) under the Collaborative Research Center 1044 and the Cluster of Excellence "PRISMA"

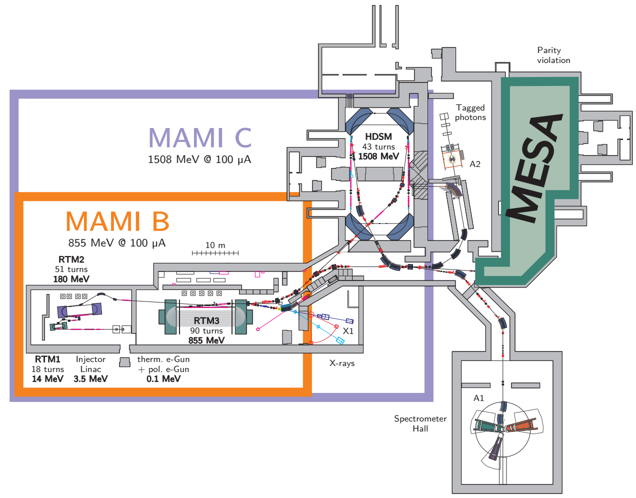

Figure 2: Floor plan of the MAMI accelerator. The space for MESA currently available is marked in green. The test setup at MAMI is installed next to the RTM3 where the beam has an energy of 180 MeV – similar to the external mode with 155 MeV of MESA.

HIGH PRECISION PHYSICS

For high precision parity violating experiments the electron beam has a certain polarization $\vec{P}$. The parity violating asymmetry $A_{LR} = \frac{n_L - n_R}{n_L + n_R}$ with the two counting rates n_L and n_R is determined by switching the helicity of the electron beam (usually $\vec{P}_L \rightarrow \vec{P}_R$). Modern experiments like the MOLLER experiment at Jefferson Lab or the P2-Experiment at MESA test asymmetries in the order of 10^{-8} with a precision of a few percent [5, 6]. If for any reason there are smallest inaccuracies while the helicity is switched there is an unwanted helicity dependend modification of the counting rates. This leads to a systematic error called "false asymmetry". To actively minimize this effect different stabilization systems are required, in our case the most important parameters to stabilize are beam intensity, position, angle and relative energy.

Parity Violating Experiments at MAMI

The A4 experiment at MAMI was performed using four RF beam position monitors (horizontal and vertical) together with four fast steerer magnets (both planes also) to achieve a sufficient suppression of helicity correlated position fluctuations of the beam. Another RF monitor is used to measure and stabilize the beam intensity very close to the electron source, another one right upstream of the target monitors the beam intensity for the experimental run control. For a single experiment at 315 MeV at 20 μA and approximately

Content from this work may be used under the terms of the CC BY 3.0 licence (© 2015). Any distribution of this work must maintain attribution to the author(s), title of the work, publisher, and DOI.

ISBN: 978-3-95450-168-7 doi:10.18429/JACoW-IPAC2015-MOPHA045

DEVELOPMENTS AND PERFORMANCE OF THE LLRF SYSTEM OF THE S-BAND FERMI LINAC

A. Fabris[#], F. Gelmetti, M. Milloch, M. Predonzani, Elettra, Trieste, Italy

Abstract

The requirements on beam quality of the FERMI Free Electron Laser (FEL) linac impose challenging specifications on the stability of the RF fields that can only be met using reliable and high performance state of the art LLRF systems. The system installed in FERMI has met these requirements and is routinely operational for the machine on a 24/7 basis. The completion of the deployment of the LLRF units in 2015 increases the capabilities of the system, adding further measurements channels and monitoring, and allowing new functionalities. This paper provides an overview of the results achieved with the LLRF system of FERMI and an outlook of the further developments that are being implemented or planned.

INTRODUCTION

FERMI, the Italian seeded FEL located in Trieste, consists of two FEL lines, FEL-1 and FEL-2, covering the wavelength range between 20 and 100 nm and between 4 and 20 nm. Both the two FEL lines are now open to external users [1]. The accelerator is based on a 1.5 GeV S-band linac [2]. FEL generation requires very high beam stability and for the S-band RF system this translates in a specification of a stability in RF phase and amplitude within 0.1° rms and 0.1% rms respectively [3]. In addition to a careful design of all the parts of the system, from modulators supplies to cables and waveguides temperature stabilization, meeting these targets requires a high performing LLRF system. The LLRF system measures the RF signals and, according to the requirements and taking into account the beam feedbacks, controls the RF drive to the klystron. The system implemented in FERMI is an all-digital system specifically designed in collaboration with Lawrence Berkeley National Laboratory [4].

SYSTEM DESCRIPTION

Fourteen 3 GHz 45 MW peak RF plants are installed to power sixteen accelerating sections, the RF gun and the three RF deflectors. Two more accelerating sections will be added at beginning of 2016. An additional power plant is installed to provide a hot-spare backup solution for the first two. The basic hardware unit is the LLRF chassis. The layout foresees one of them for each RF powered component of the machine, whether it is an accelerating section or gun or deflector. In case of plants which power more than one section, one chassis will act as the master, controlling the RF drive to the klystron, besides monitoring the corresponding section parameters, while the second one will act as a slave chassis primarily providing information to the master, for example the RF measurements of the second section.

Hardware

The LLRF chassis basically includes the RF front end (RFFE), the processing board (AD board), the OCXO and all power supplies (see Fig. 1) [5]. The RFFE performs the conversion between RF (3 GHz) an IF (99 MHz) signals and hosts all the frequency dependent components. The AD board, which implements a Virtex5 FPGA, performs all controls, diagnostics and system communication. The chassis has five RF inputs and two RF outputs. The inputs signals are the reference, the klystron output, the cavity input forward, the cavity input reflected and the cavity load signals. The outputs channels are used for the driving signal to the klystron and to generate a calibration signal. Each LLRF unit is designed to be beam feedback ready.

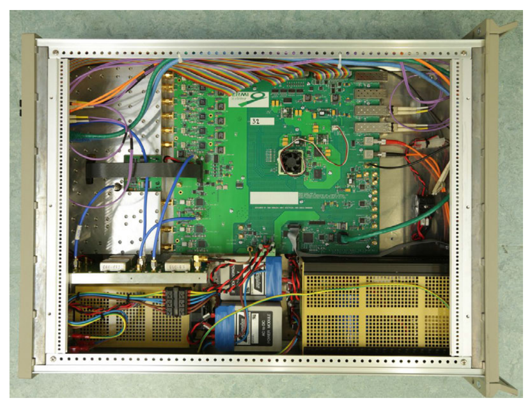

Figure 1: LLRF chassis.

A block diagram of a complete LLRF for a one klystron/two sections plant is shown in Fig. 2. The scheme shows as well the interconnections of the LLRF units with the other systems of the machine. All the components of the LLRF for each plant are installed in a temperature controlled EMC shielded IP65 rack. The temperature is kept stable better than ± 0.2 °K by means of an air/water heat exchanger. Also all the cables between racks and accelerating structures are installed in an insulated environment.

Firmware

The firmware presently in operation [6] implements all the basic loops needed: amplitude, phase, cable calibration, local oscillator phase drift and phase reference locking loops. All these are feed-forward loops. In addition, the control of the SLED phase reversal and phase modulation is also implemented through the LLRF firmware.

[#]alessandro.fabris@elettra.eu

Content from this work may be used under the terms of the CC BY 3.0 licence (© 2015). Any distribution of this work must maintain attribution to the author(s), title of the work, publisher, and DOI.

ISBN: 978-3-95450-168-7 doi:10.18429/JACoW-IPAC2015-MOPHA046

!CHAOS STATUS AND EVOLUTION

C. Bisegni, S. Caschera, G. Di Pirro, L. G. Foggetta, R. Gargana, E. Gioscio, D. Maselli, G. Mazzitelli, A. Michelotti, R. Orrù, S. Pioli, F. Spagnoli, A. Stecchi, M. Tota, INFN-LNF, Frascati (RM), Italy, and C. Di Giulio, INFN-ROMA2, Rome, Italy

Abstract

A synthesis of the "!CHAOS: a cloud of controls" project and its application to accelerators and large experiments will be presented. We will describe here how the !CHAOS project has evolved from a candidate for the SuperB accelerator control system to a facility for IT distributed infrastructures. !CHAOS is currently, not only suitable for accelerators and large High Energy Physics (HEP) experiments, but is also applicable to other contexts, such as social and industrial applications. Preliminary results achieved on an accelerator use case are discussed.

INTRODUCTION

!CHAOS project started as candidate of Distributed Control Systems (DCS) and Slow Control of the SuperB accelerator and detector [1], with the ambition to be a prototype of innovative DCS standards. Today, the project is supported by the MIUR (Italian Ministry of University and Research) and INFN to develop a national infrastructure prototype of high performing services devoted to devices and polyfunctional sensors distributed on LAN and WAN [2,3].

!CHAOS exploits the new high performance web technologies by strongly increasing control system performances and services, preserving scalability, redundancy and reliability, as well as the abstraction of processes at any level obtained by:

- key/value database (KVDB) implemented as distributed memory object caching systems (DOC).
- using non-relational databases, in a specific document database.
- optimizing and embedding high performance e/o standard inter process communication and handling (RPC/direct I-O/Events).
- abstracting data structure through binary data serialization (BSON)
- embedding COTS and, in general, open hardware, in order to minimize costs and integration time
- making "Controls as a services" to be responsive to new trends of IT technologies and the request of industries and society.

Moreover, the !CHAOS DCS architecture embeds by design the Data Acquisition (DAQ) topology and object data concepts which make the project able to handle Big Analog Data and their Variety, Volume, Velocity, Value and Visibility. The scope of the project is therefore to study and realize a prototype of a dynamic, on-demand Cloud-based infrastructure able to handle the "five V" for data collected from analog devices.

Finally, the project foresees applications on different use cases: accelerator DCS, building automation and environmental controls, integration in embedded devices like CRIO National Instruments, BPM Libera, Beagle Bone, etc… In March 2015 a second test [4] of !CHAOS accelerator DCS has been performed at the Frascati Beam Test Facility (BTF) [5], successfully replacing the original DCS for the monitoring and control of the beam transport magnets by integrating at the same time BTF DAQ functionalities.

ACCELERATOR USE CASE @ BTF

The BTF is a beam transfer line, part of the DAFNE complex, optimized for the production of single electron/positron in the rage 25-700 MeV mainly used for HEP detectors testing and calibration [6]. The high intensity LINAC beam, intercepted by a pulsed magnet, is attenuated by Cu target and a set of scrapers. Six quadrupoles, two 45^0 bending magnets and horizontal/vertical slits permits to select beam quality, the proper momentum and multiplicity down to single particle (Fig. 1).

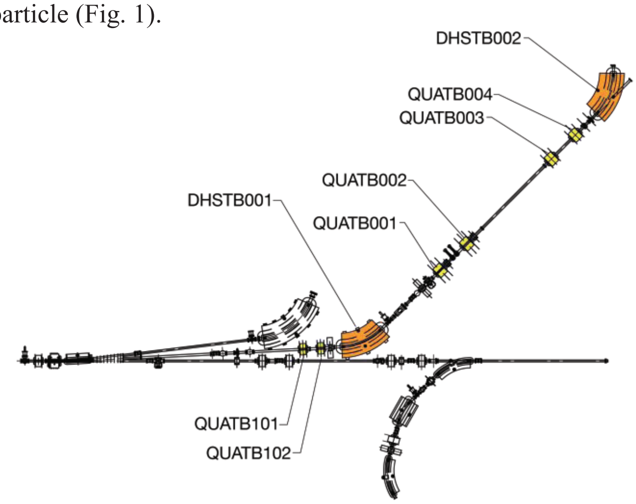

Figure 1: Beam Test Facility layout.

The test consisted in monitoring and controlling the transfer-line magnets and the facility DAQ devoted to acquire the x-y scintillating fiber system profile detector [7] and the glass lead calorimeters monitoring and acquiring single particle position and energy.

The scope of the test was to exploit the !CHAOS framework in a real operating condition, test the IT infrastructure and the Graphical User Interface (GUI), verify the stability and capability of the information service – Meta Data Service (MDS) and storing – the !CHAOS Data Service (CDS).

Content from this work may be used under the terms of the CC BY 3.0 licence (© 2015). Any distribution of this work must maintain attribution to the author(s), title of the work, publisher, and DOI.

ISBN: 978-3-95450-168-7 doi:10.18429/JACoW-IPAC2015-MOPHA047

RF SYSTEM DESIGN FOR THE TOP-IMPLART ACCELERATOR

V. Surrenti, G. Bazzano, P. Nenzi, L. Picardi,C. Ronsivalle, ENEA,Frascati, Italy
F. Ambrosini, La Sapienza University, Roma, Italy

Abstract

In the ENEA-Frascati research center a linear accelerator for proton therapy is under development in the framework of TOP-IMPLART Project carried out by ENEA in collaboration with ISS and IRE-IFO. The machine is based on a 7 MeV injector operating at a frequency of 425 MHz followed by a sequence of 2997.92 MHz accelerating modules. Five 10 MW klystrons will be used to power all high frequency structures up to a beam energy of 150 MeV. The maximum repetition frequency is 100 Hz and the pulse duration is 4 µs. The RF amplitude and phase stability requirements of the accelerating field are within ±2% and ±2 degrees respectively. For therapeutic use the beam energy will be varied between 85 and 150 MeV by switching off the last modules and varying the electric field amplitude in the last module switched on. Fast control of the RF power supplied to the individual structures allows an energy variation on a pulse by pulse basis; furthermore the system must be able to control the RF phase between accelerating structures. This work describes the RF power distribution scheme and the RF phase and amplitude monitoring system implemented into an embedded control system.

THE TOP-IMPLART ACCELERATOR

A RF proton linear accelerator is under realization in the framework of the TOP-IMPLART (Intensity Modulated Proton Linear Accelerator for RadioTherapy) Project leaded by ENEA in collaboration with the Italian Institute of Health (ISS) and Regina Elena National Cancer Institute IFO-Rome [1].The project is devoted to the realization of a protontherapy centre to be sited at IFO based on a 230 MeV accelerator. The first segment up to 150 MeV has been funded by Regione Lazio and is under realization and test at ENEA-Frascati [2]. It is composed (fig.1) by a low frequency (425 MHz) injector (ACCSYS-HITACHI PL7 model, RFQ+DTL) and a high frequency (2997.92 MHz) booster (SCDTL up to 35 MeV and CCL up to the final energy).

A LINAC-based proton therapy facility can provide, like synchrotron-based facility, both energy and intensity active modulation. However synchrotron accelerators typically vary the beam energy in no less than 1-2 seconds (the time it takes to complete a whole acceleration cycle), while LINAC can in principle vary the energy on a pulse by pulse basis, i.e. within a few milliseconds, without the need to dump the accelerated beam.

To guarantee patient safety through the correct actuation of the desired machine settings, some subsystems are identified as "critical", namely those systems actively responsible for the energy, intensity and spot size of the beam. To this end, the critical subsystems will provide the dose delivery system with an acknowledgment of their status on successful completion of the new settings, thus allowing beam acceleration in the next pulse.

THE RF SYSTEM

The block scheme of the TOP IMPLART RF system up to 150 MeV is shown in figure 1. The high power part foresees the use of a number of identical RF plants each based on a 10 MW klystron (TH2157) and its power supply (modulator). The power is split in 4 or 2 parts depending on the needs of the fed structures. Tight controls are used to stabilize the phase among the several klystron outputs. The energy is varied by changing the power of the klystrons supplying the accelerator structure. The TOP-IMPLART aims at changing the beam energy as quickly as possible, although, as in other protontherapy plants the limiting factor is the velocity of changing the beam transport line magnetic elements, that limits the repetition frequency to 100 Hz.

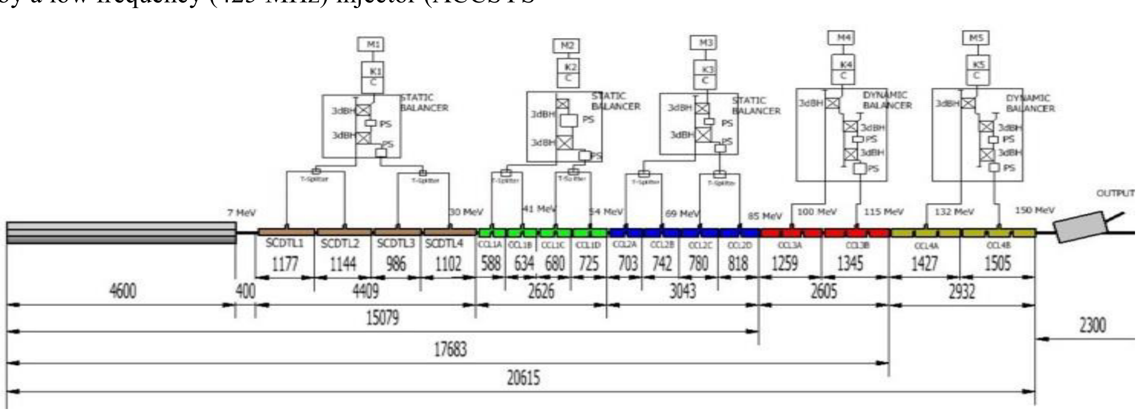

Figure 1: Block scheme of TOP-IMPLART RF system.

Content from this work may be used under the terms of the CC BY 3.0 licence (© 2015). Any distribution of this work must maintain attribution to the author(s), title of the work, publisher, and DOI.

ISBN: 978-3-95450-168-7 doi:10.18429/JACoW-IPAC2015-MOPHA048

BEAM OPTIMIZATION OF THE DAΦNE BEAM TEST FACILITY*

L. Foggetta and B. Buonomo INFN/LNF, Frascati, Rome, Italy
P. Valente INFN, Roma, Rome, Italy

Abstract

The DAΦNE Beam Test Facility delivers electron and positron beam with a wide spread of parameters in charge, energy, transverse dimensions and time width. Thanks to the recent improvements of the diagnostics, all the beam parameters have been measured and optimized. In particular we report here some results on beam transverse size, divergence, and position stability for different energy and intensity configurations. After the upgrade of the electronic gun of the DAΦNE LINAC, the pulse time width and charge distribution have been also characterized.

DAΦNE BEAM TEST FACILITY (BTF)

The BTF (Beam Test Facility) is part of the DAΦNE accelerator complex: it is composed of a transfer line driven by a pulsed magnet allowing the diversion of electrons or positrons, usually injected into to the DAΦNE damping ring, from the high intensity LINAC [1] towards a 100 m^2 experimental hall. The facility can provide runtime tuneable electrons and positrons beams in a defined range of different parameters: energy (up to 750 MeV for e^- and 540 MeV for e^+), charge (up to 10^{10} e^-/bunch) and pulse length (1.4–40 ns). The bunch delivery rate is depending on the DAΦNE injection frequency (25 or 50 Hz) with a duty cycle also according to the DAΦNE injection requirements.

Two major modes of operations are possible, depending on the user needs. The high intensity mode is operated when the LINAC beam is directly steered in the BTF hall with a fixed energy (i.e. the LINAC one) and with a reduced capability in multiplicity selection (typically from 10^{10} down to 10^4 particles/bunch). In the low intensity mode of operation, a step copper target, allowing the selection of three different radiation lengths (1.7, 2 or 2.3 X_0), is inserted in the initial portion of the BTF line for intercepting the beam. This produces a secondary beam with a continuous full-span energy (from LINAC energy down to 50 MeV) and multiplicity (down to single particle/bunch) selection range. In the single particle mode, the multiplicity per bunch delivered to the users follows a Poisson distribution (Figure 1). A pulsed dipole magnet at the end of the LINAC allows alternating the beam between the DAΦNE damping ring and the test beam area, thus keeping a pretty high BTF duty cycle, assuring at least about 20 bunches per second during the positron injection in DAΦNE accumulator when BTF operates in low intensity regime, 28 on average for a complete e^+/e^- injection cycle.

* This work is partially supported by FP7 Research infrastructures project AIDA, grant agreement no. 262025

GENERAL DAQ AND STANDALONE DIAGNOSTICS OVERVIEW

BTF DAQ

BTF DAQ is composed mainly of one data producer and two data consumers: one for online diagnostics and one for data storing. The DAQ hardware configuration is NIM/VME based and controlled by VMIC VMIVME 7750 (Intel PIII, 1,3Ghz, 0.5Gb RAM). The acquisition software, hosted in DAΦNE data control system environment (DAΦNE DCS), is written in LabVIEW® LV7.0 and a shared memory is provided for the system, based on MemCached protocol[2], in order to handle the new standalone USB/ETH/Serial based diagnostics elements. The BTF-DAQ is a dynamic composition of different modules, that can be switched on and off at run-time according to the user beam monitoring needs. A standard BTF configuration includes:

- Delay Programmable Unit
- Scaler, Peak sensing ADC, QDC, TDC
- BTF custom detectors electronics
- Digital I/O

The mostly used detectors, stably readout by the BTF DAQ front-end, are the fiber transverse beam profile hodoscope and a lead glass calorimeter[3]. The consumer software is also hosted in the DAΦNE DCS and it is normally used for online monitoring of the BTF beam and data storage.

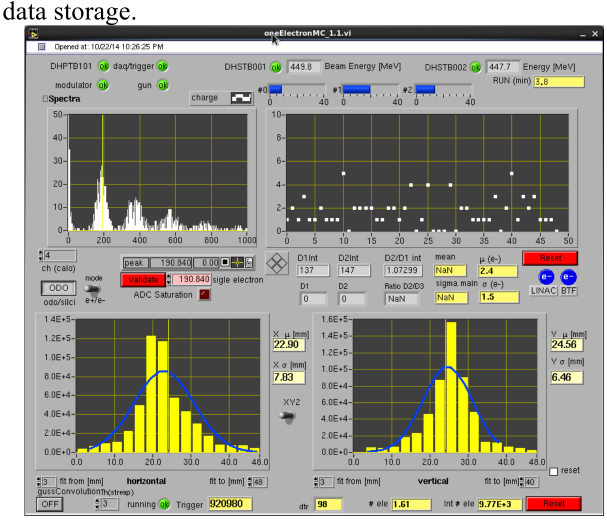

Figure 1: BTF DAQ data (Calorimeter on top and Hodoscope on the bottom) displayed in the BTF DCS diagnostics display software.

MEMCACHED

MemCached (MC) is an Ethernet based in-memory key-value store for arbitrary data (strings, objects). In the

Content from this work may be used under the terms of the CC BY 3.0 licence (© 2015). Any distribution of this work must maintain attribution to the author(s), title of the work, publisher, and DOI.

ISBN: 978-3-95450-168-7 doi:10.18429/JACoW-IPAC2015-MOPHA049

Content from this work may be used under the terms of the CC BY 3.0 licence (© 2015). Any distribution of this work must maintain attribution to the author(s), title of the work, publisher, and DOI.

EVOLUTION OF DIAGNOSTICS AND SERVICES OF THE DAΦNE BEAM TEST FACILITY

L. Foggetta and B. Buonomo INFN/LNF, Frascati, Rome, Italy
P. Valente INFN Roma, Rome, Italy

Abstract

The DAΦNE Beam Test Facility (BTF) is operational in Frascati since 2003. In the last years the beam diagnostics tools have been completely renewed and the services for users have been largely improved. We describe here the new transverse beam diagnostics based on new GEM TPC detectors and MEDIPIX, the new BTF network layout, the renewed DAQ system including the BCM detectors, the data caching system based on MEMCACHED and the integration of the new sub-systems in the new data-logging. All other services, such as the environmental monitoring system, vacuum system, payload remote handling, and gas distribution have been also improved.

THE DAΦNE BEAM TEST FACILITY (BTF)

The BTF (Beam Test Facility) is part of the DAΦNE accelerator complex: it is composed of a transfer line driven by a pulsed magnet allowing the diversion of electrons or positrons, usually injected into to the DAΦNE damping ring, from the high intensity LINAC [1] towards a 100 m^2 experimental hall. The facility can provide runtime tuneable electrons and positrons beams in a defined range of different parameters: energy (up to 750 MeV for e^- and 540 MeV for e^+), charge (up to 10^{10} e^-/bunch) and pulse length (1.4–40 ns) [2]. The bunch delivery rate is depending on the DAΦNE injection frequency (25 or 50 Hz) with a duty cycle also according to the DAΦNE injection requirements. Two major modes of operations are possible, depending on the user needs. The high intensity mode is operated when the LINAC beam is directly steered in the BTF hall with a fixed energy (i.e. the LINAC one) and with a reduced capability in multiplicity selection (typically from 10^{10} down to 10^4 particles/bunch). In the low intensity mode of operation, a step copper target, allowing the selection of three different radiation lengths (1.7, 2 or 2.3 X_0), is inserted in the initial portion of the BTF line for intercepting the beam. This produces a secondary beam with a continuous full-span energy (from LINAC energy down to 50 MeV) and multiplicity (down to single particle/bunch) selection range. A pulsed dipole magnet at the end of the LINAC allows alternating the beam between the DAΦNE damping ring and the test beam area, thus keeping a pretty high BTF duty cycle, assuring at least about 20 bunches per second during the injection in DAΦNE accumulator when BTF operates in low intensity regime. A large fraction of the tests required electron or positron beam, with a 10% of allocation for the tagged-photon beam and a few shifts dedicated to neutron production.

BTF TOWARD USERS' NEEDS

Some Classes of Users

Such a kind of versatility is very interesting for a wide community of experimental HEP groups: at least one half of the users have used the facility for detector-testing purposes, covering almost all the possible detection techniques:

- Calorimeters: homogenous (NaI, CsI, PbWO, LYSO, YAP: Belle-II, CMS, KLOE-2, Linear collider, Mu2e, BGO-OD); sampling (KLOE, AMS, LUMI, Linear collider, NA62, MICE, etc.);
- Gas detectors: GEM/Micromegas (LHCb, ATLAS, UA9, Siddharta, KLOE-2), drift chamber/tubes (Super-B, MEG, TPS), RPC (Linear collider);
- Silicon detectors: micro-strip (AGILE, Insulab), pixel (ALICE, MIMOSA, Linear collider);
- Scintillating/Fluorescence detectors: MEG, neutron detection, fiber-trackers (MEG, BES-III, Plasmon-X), AIRFLY (Auger);
- Cerenkov detectors: RICH (LHCb, JLAB12), threshold (UA9)
- Nuclear emulsion: OPERA.

In addition, experiments looking at specific beam-induced effects were carried on:

- Beam diagnostics: fluorescence flag, WCM diagnostics calibration, emittance measurement
- Thermo-acoustic effect: RAP (gravitational wave detection)
- Beam-induced radiation: C-SPEED, AMY
- Crystal channelling and parametric radiation emission.

In the last 10 years of operation, the DAΦNE Beam-Test Facility has delivered an average of 220 beam-days/year. The facility usually allocates slots of 1 week, Monday to Monday, and operates 24/7. More complex experimental setups of course required much longer beam-periods (i.e. up to five months of total allocation for the AGILE satellite pay-load in 2005; the beam was not delivered 100% of this period, however). Occasionally, two teams were present together, profiting of the possibility of parasitizing each other.

DETECTOR, DIAGNOSTIC, SCIENTIFIC INSTRUMENTATION AND DAQ IMPROVEMENTS

BTF Computing and Control Service

A complete new design of the BTF networking service offered to the users has been deployed, in accordance to

ISBN: 978-3-95450-168-7 doi:10.18429/JACoW-IPAC2015-MOPHA050

ONLINE SPILL INTENSITY MONITORING FOR IMPROVING EXTRACTION QUALITY AT CNAO

M. Caldara, Department of Engineering and Applied Sciences, University of Bergamo, Italy
E. Rojatti, Department of Physics, University of Pavia, Italy
J. Bosser, G. M. A. Calvi, L. Lanzavecchia, A. Parravicini, C.Viviani, CNAO Foundation, Pavia, Italy

Abstract

The CNAO Foundation is the first Italian center for deep hadrontherapy with Protons and Carbon Ions, performing treatments since September 2011. The extracted beam energy and intensity can vary over a wide range (60-250 MeV for Protons and 120-400 MeV/u for Carbon Ions, 4e6÷1e10 pps); the beam intensity uniformity during the slow extraction process is a fundamental requirement for achieving accurate and fast treatments. CNAO developed an online Fast Intensity Monitor (FIM), not perturbing the extracted beam, capable of measuring beam intensity with a bandwidth of 50kHz and a resolution of 1%. It consists of a thin (0.8 μm) metallic foil that emits secondary electrons when traversed by the beam. The electrons are multiplied by a Channeltron device, polarized at high voltage versus ground. The Channeltron output current is amplified and converted in a Pulse Width Modulated (PWM) signal, which is then decoupled and transmitted to the equipment room, where an FPGA implements a servo-spill. The work presents the detector, the floating electronics, the preliminary measurements with beam and the integration in a closed loop on the synchrotron air-core quadrupole obtaining promising results.

INTRODUCTION

CNAO is one of the four accelerators worldwide capable to perform hadrontherapy with both Protons and Carbon Ions; nowadays more than 400 patients completed the treatments, two third of them with carbon ions [1]. The active dose delivery treatment by rasterscan technique, presently used at CNAO, is the most advanced method in hadrontherapy machines for achieving accurate treatments of target volumes. The beam is directed to each tumor voxel by controlling fast magnets deflectors and the beam energy for transversal position and longitudinal penetration respectively. A uniform beam extracted intensity is favourable because it gives a higher intensity without risk of beam aborts, leading to faster treatments and thus more patients. In order to minimize the spill intensity ripple during the slow extraction, a feedback loop acting on the synchrotron fast quadrupoles [2] or on the RF Knock-Out exciter are the most diffused techniques [3-4]. A fast, accurate, high resolution and not-interceptive beam intensity measurement is essential in each servo-spill system.

MATERIALS AND METHOD

FIM Detector

In order not to perturb the beam, an ultra-thin metallic foil is the only material that can be traversed by the accelerated particles [5]; a secondary emission electrons principle is the signal origin, followed by electrons collection into a Channeltron (CEM) device [6], a single channel electron multiplier. The mechanical arrangement of the foil with respect to the beam path (Fig.1) is a compromise between secondaries yield maximization and beam perturbation minimization (α=45deg). By raising the angle between the foil and the beam trajectory, the foil thickness crossed by the beam and thus beam perturbation increases. Secondary emitted electrons angular distribution follows Lambert Law, namely it is proportional to cos(θ) (Fig.1). In consequence, if the CEM is installed on the foil perpendicular axis the number of collected electrons will be maximized. To be conservative, a foil input/output pneumatic actuator has been foreseen on the FIM instrument. The FIM monitor will be installed in the CNAO common extraction line; to get the results presented in this paper, the FIM has been installed at beam isocenter, in the treatment room.

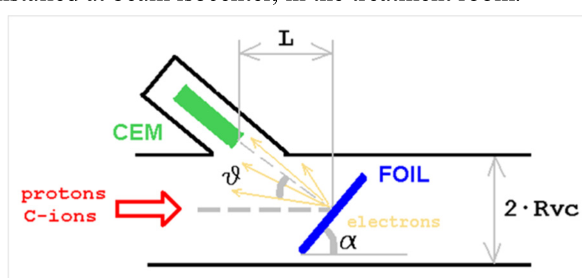

Figure 1: FIM detector mechanical layout; R_{vc} (33 mm) is vacuum chamber radius, L is 42mm.

Electronics and Processing

The CEM output electrons are attracted to an output collector, polarized to a higher voltage than the CEM output; being the beam-generated signal quasi-dc, the readout electronics cannot be AC coupled to the output collector, thus it needs to work at floating high potential with respect to ground. The system block diagram is depicted in Fig. 2. The electronics input signal is a current, thus the conversion into a voltage is implemented

Content from this work may be used under the terms of the CC BY 3.0 licence (© 2015). Any distribution of this work must maintain attribution to the author(s), title of the work, publisher, and DOI.

ISBN: 978-3-95450-168-7 doi:10.18429/JACoW-IPAC2015-MOPHA051

SCINTILLATING FIBERS USED AS PROFILE MONITORS FOR THE CNAO HEBT LINES

E. Rojatti*, Department of Physics, University of Pavia, Pavia, Italy
J. Bosser, CERN, Geneva, Switzerland and CNAO, Pavia, Italy
G. Calvi, L. Lanzavecchia, A. Parravicini, M. Pullia, C. Viviani, CNAO, Pavia, Italy
M. Haguenauer, Department of Physics, Detector Technology Group, CERN, Geneva, Switzerland
P. Poilleux, Department of Physics, CMS Users Group, CERN, Geneva, Switzerland
M. Caldara, Department of Engineering and Applied Sciences, University of Bergamo, Bergamo, Italy

Abstract

The CNAO (Centro Nazionale di Adroterapia Oncologica, Pavia, Italy) is the first Italian center using Proton and Carbon ion beams for radioresistant tumors therapy. Scintillating fibers detectors are used in the HEBT (High Energy Beam Transfer) lines of the CNAO accelerator in order to monitor the therapeutic beam parameters. Twenty SFHs (Scintillating Fibers Harp) and one QPM (Qualification Profile Monitor) have been already installed for the beam transverse profiles measurement. One SFP (Scintillating Fibers plus Photodiodes) prototype, that is a SFH upgrade project, has been assembled and tested on beam. One WD (Watch Dog) detector, not already installed, has been assembled and tested to check the beam position at the HEBT end through the intensity of the beam tails. The present work describes the beam detectors, their achieved performances and the most recent beam measurements.

HEBT LINES LAYOUT

The HEBT [1] (High Energy Beam Transfer) is the extraction line of the CNAO [2] accelerator. It consists of three horizontal and one vertical transfer lines, coming from one first common sector (called H sector) and reaching three different treatment rooms.

The energy range of particles running in the HEBT line is 60 to 250 MeV/u for Protons, and 120 to 400 MeV/u for Carbon ions. The beam is slowly extracted from the synchrotron so that the spill length is settable from 1 to 10 seconds. The nominal intensities per spill are 1×10^{10} for Protons and 4×10^{8} for Carbon ions.

SFH AND QPM: DETECTORS OVERVIEW

The SFH (Scintillating Fibers Harp) and the QPM [3] (Qualification Profile Monitor) are detectors based on grids of adjacent scintillating fibers, installed in the HEBT lines for the beam profiles measurement (position and width). They have been both designed and built by the *LLR (Louis Leprince Ringuet) laboratory*, belonging to the French *CNRS*, according to the specification provided by CNAO. The CNAO Beam Diagnostic group provided the detector actuators, the installation on the beam line, and their implementation in the control system.

* elisa.rojatti01@universitadipavia.it

The SFHs are usually placed out of the nominal beam trajectory not to perturb the therapeutic beam. They are moved onto the beam path through a pneumatic actuator only during the daily beam quality controls. The QPM can be used during patient treatments, since it is installed in front of the "dump", namely a tungsten block placed in the H sector along the extracted beam trajectory. The dump is needed to stop the beam at each machine cycle, during few milliseconds after the extraction, until an orbit bump is created by four fast magnets in order to send the beam towards the selected treatment room.

Detectors Description

The SFH and the QPM active area (Fig. 1) is made up of two orthogonal planes of Polystyrene scintillating fibers, 0.5 mm thick and 0.5 mm wide (*Kuraray SCF-78 type*), each other adjacent and aluminized all around their surface and at one end to avoid any light cross-talk.

Figure 1: SFH (left) and QPM (right) active area.

Both SFH planes are made up of 128 fibers ($64 \times 64\, mm^2$). The QPM horizontal and vertical planes are respectively made up of 34 and 90 fibers ($17 \times 45\, mm^2$). Fibers are installed under vacuum at a pressure of $10^{-6} - 10^{-8}\, mbar$: the detector outgassing is mainly due to the glue that fixes the fibers.

When crossing fibers, the beam particles release energy and produce an amount of photons proportional to particles number and energy. The generated light is guided and focused, through a viewport, onto a CCD chip (1344 × 1024 pixels) of a digital camera (*Hamamatsu-C8484-03G, Peltier cooled,12 bits*) which acquires and processes the signals. The maximum camera acquisition rate is 50 Hz.

Content from this work may be used under the terms of the CC BY 3.0 licence (© 2015). Any distribution of this work must maintain attribution to the author(s), title of the work, publisher, and DOI.

ISBN: 978-3-95450-168-7 doi:10.18429/JACoW-IPAC2015-MOPHA052

OPTIMIZATION OF ILC CRYOMODULE DESIGN USING EXPLOSION WELDING TECHNOLOGY

A.Basti, F.Bedeschi, P.Fabbricatore, INFN, Pisa/Genova, Italy
B.Sabirov, J.Budagov, G.Shirkov, Yu.Taran, JINR, Dubna, Russia
A.Bryzgalin, L.Dobrushin, S.Illarionov, E.Pekar, EWI, Kiev, Ukraine

Abstract

In the current ILC TDR design both the helium vessel shell and the connected pipes are made of expensive titanium (Ti), one of the few metals that can be welded to niobium (Nb) by the electron beam technique (EBW).

We describe work done by JINR/INFN collaboration on the construction and evaluation of transition elements, obtained by explosion welding, which could couple the niobium cavity to a stainless steel (SS) helium vessel. Several designs for these transitions have been produced and studied showing varying levels of reliability.

Based on this experience a new design, including a minimal titanium intermediate layer, has been built. Tests of resistance of the bond to extreme temperature shocks like EBW and exposure to cryogenic temperature are presented.

INTRODUCTION

Initial work on this subject was the development of a bimetallic transition element Ti+SS from the He-supply pipe to the He-vessel to be able to build this pipe and all other ancillary parts connect to it in SS (see Fig.1).

Explosion welding of two different metals is a well-known technique, but it is normally used only to weld flat surfaces, making the construction of cylindrical transitions rather cumbersome.

A key development was obtained in collaboration with the Russian Federal Nuclear Center Institute of Experimental Physics (RFNC-VNIIEF in Sarov) where a unique method for welding coaxial tubes [1] was demonstrated: two coaxial tubes of the same diameter and thickness, with an internal removable steel core, were connected by means of an external explosion around a SS collar (see Fig.2).

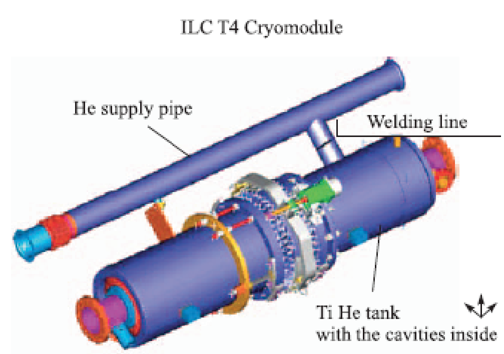

Figure 1: He-vessel connect to He-supply pipe.

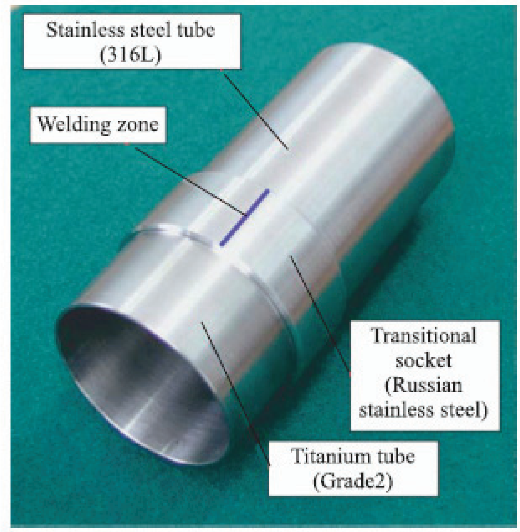

Figure 2: Ti+SS transition element.

Several samples were produced with this technique using various materials and dimensions. Finally ten samples matching the ILC cryomodule design were built and tested. The Ti+SS samples were subjected to a primary metallographic investigations of the welded joint including: macroanalysis, microanalysis, and measurement of microhardness [1]. The shear strength of the welded joint was also measured [1], the result turned out to be quite impressive: τ_{sh} about 250 MPa.

These samples were carefully leak-checked after several thermal cycles between room and liquid nitrogen temperature (77 K); no leaks were found [2,3,4,5]. They were also filled with helium at 6.5 atm and cooled to about 6 K in a cryo-cooler. The resistance of the joint after TIG welding close to it was also tested [6].

Finally the Ti+SS transitions were tested at Fermilab at the 2K temperature and under real Cryomodule conditions in the Fermilab's Horizontal Test System (HTS) and the A0 Vertical Test Dewar (A0VTD). No leaks were found also in this case [7,8,9,10].

The success obtained in explosion welding of bimetallic Ti+SS tubes led the collaboration to try a similar technique directly on Nb+SS tubes. This would allow the construction of a SS helium vessel using this transition element to connect to the cavity.

This new design would considerably facilitate the construction of the Cryomodule and, most of all, would substantially reduce the total cost of the accelerator.

Two schemes of making a transition element between the niobium cavity and the steel shell were studied: in the first the niobium tube is welded directly to the SS flange

Content from this work may be used under the terms of the CC BY 3.0 licence (© 2015). Any distribution of this work must maintain attribution to the author(s), title of the work, publisher, and DOI.

ISBN: 978-3-95450-168-7 doi:10.18429/JACoW-IPAC2015-MOPHA053

RADIATION MEASUREMENTS OF A MEDICAL PARTICLE ACCELERATOR THROUGH A PASSIVE RESONANT CAVITY

Alberto Leggieri[1,2], Franco di Paolo[1], Davide Passi[1],
Alessia Ciccotelli[2], Silvia De Stefano[2], Giuseppe Felici[2] and Filippo Marangoni[2]
[1]Università degli Studi di Roma "Tor Vergata", Dipartimento di Ingegneria Elettronica, Roma, Italy
[2]S.I.T. Sordina IORT Technologies S.p.A., Aprilia, Italy

Abstract

Dose measurements of a Medical Linear Accelerator (LINAC's) performed through a passive resonant cavity are shown in this paper. The cavity is coupled through a magnetic loop with a coaxial transmission line loaded on a microwave envelope detector. Output signal has been documented while receiving electron currents ranging from several values. This paper shows the complete equivalency, in terms of global performance, of the current revelation performed by exploiting the cavity-beam interaction principle with the classical technology, based on ionization chambers, without need of high voltage. The most important point is that the resonant cavity system, by measuring the beam current, gives a direct measurement of a physical observable quantity directly related with the dose deposed by the beam.

INTRODUCTION

Real time radiation measurement represents a fundamental aspect of medical Linear Accelerator (LINAC) development. This study was leaden by the need of a beam monitoring device for which several innovations have been proposed. In the medical LINAC field, strict regulations are imposed, mostly regarding the control of the emitted radiations delivered to the target [1], [2]. In this study the investigation have involved a medical mobile electron LINAC dedicated to intra operative radiation therapy (IORT). Actual dose monitoring systems are typically based ionization chambers and require high voltage biases [3], [4].

This study investigates on the possibility of measure dose emission through the power exchange of the beam current with a passive resonant cavity [5] placed at the output interface of the accelerator. Experimental evidence is presented showing the complete equivalency of the proposed system with the traditional technology, based on ionization chambers, however without need of high voltage. The major strength of the proposed system is represented by the direct relation between the deposed dose and beam current as physical observed quantity.

OPERATION OF MEASURING SYSTEM

The proposed radiation detector is based on the power exchange of the beam current with a passive resonant cavity [5] placed at the output interface of the accelerator.

LINAC beam current have a bunched time behavior and, as the bunches follow each other periodically in time, the spectral content of the current beam is a line at the accelerating frequency f and whole-number harmonics [4]. A simplified approach can be adopted by treating the bunched current as a square wave with an amplitude I_{beam} and duty cycle δ. The first harmonic would have an amplitude $I_1=2I_{beam}sin(\pi\delta)/\pi$. The LINAC considered in this study, operating at f =2998 MHz, can provide I_{beam}=1.11 mA, with I_1=0.66 mA. This harmonic content has been employed to induce oscillations in an opportune resonant cylindrical cavity operating in the TM_{010} mode at the accelerator normal mode frequency f.

Since the minimum energy of the beam is greater than 4 MeV, an opportune aluminum window (transparent to these energetic charges) is employed for allowing the beam crossing and entering the cavity. The window thickness is chosen to limit the surface scattering.

The beam current, exiting the LINAC, crosses the window and, centered on the axis, enters the cavity where image charges are induced on the walls exhibiting azimuthal symmetry [6]. While moving, they induce a wall current I_0 leading the cavity in resonance. An azimuthal magnetic induction field B_ϕ is generated in the cavity. A magnetic loop is placed inside the cavity volume and this field fluxes through the surface encircled by the loop, inducing a voltage V_p between the loop terminals. In order to maximize this flux, the surface enclosed by the loop is normal to the azimuthal direction.

In resonance, the cavity behaves as though its shunt impedance [6] while the loop is connected to a 50 Ω load through a coaxial line. In order to have the maximum transfer of available power, the loop shape and its distance from the axis of the cavity are chosen to have the right impedance transformation, matching the system.

For this reason it's of vital importance that the cavity shows a critical coupling, identifiable by a coupling factor k=1. This condition can be applied by employing the "detuned short position" technique [7].

The 50 Ω load closing the loop is the input port of a RF detector diode, at whose output port the envelope of V_p is

Content from this work may be used under the terms of the CC BY 3.0 licence (© 2015). Any distribution of this work must maintain attribution to the author(s), title of the work, publisher, and DOI.

ISBN: 978-3-95450-168-7 doi:10.18429/JACoW-IPAC2015-MOPHA054

INTERACTION POINT ORBIT FEEDBACK SYSTEM AT SuperKEKB

Y. Funakoshi, H. Fukuma, T. Kawamoto, M. Masuzawa, T. Oki, S. Uehara, H. Yamaoka
KEK, 1-1 Oho, Tsukuba, Ibaraki 305-0801, Japan
P. Bambade, D. E. Khechen, D. Jehanno, V. Kubytskyi, C. Rimbault, LAL, Orsay, France
S. D. Anderson, S. Gierman, M. Kosovsky, J. Seeman, C. M. Spencer, M. Sullivan, O. Turgut, U. Wienands, SLAC, Menlo Park, CA, USA

Abstract

In order to maintain an optimum beam collision condition in a double ring collider such as SuperKEKB it is essential to have an orbit feedback system at the interaction point (IP). We have designed such a system based on experiences at KEKB and PEP-II. For the vertical offset and crossing angle, we will rely on the system based on the beam orbit measurement similar to that used at KEKB. For the horizontal offset, however, we will utilize the dithering system which was successfully used at PEP-II. Some hardware devices have been already fabricated and others are in preparation. The present status of the development is reported.

INTRODUCTION

The design of the system has been done based on the experiences at KEKB [1]. In the following, we summarize differences between KEKB and SuperKEKB from the view point of the IP orbit feedback. Table 1 shows a comparison of the parameters related to the feedback. The symbols for the parameters in the table are those used commonly. A remarkable point with the parameters is that the horizontal beam-beam parameters of SuperKEKB are much smaller than those of KEKB. In SuperKEKB, we will adopt so-called "nano-beam scheme", where the horizontal beam sizes at IP are very small and the crossing angle is rather large to reduce the interaction region of the two beams drastically. In this scheme, we have to use the effective horizontal beam size shown in the table rather than the actual horizontal beam sizes in the calculation of the beam-beam parameters and the luminosity. With those small horizontal beam-beam parameters, we can not rely on the beam-beam deflection method for the orbit feedback at IP in the horizontal direction. Instead, we will adopt the dithering system for the horizontal orbit feedback which was used at PEP-II [2]. Another feature of the SuperKEKB parameters is much smaller vertical emittances (ε_y) than KEKB. Roughly speaking, the vertical orbit drift at the IP will be 3 or 4 times larger in units of the vertical beam sizes than the KEKB case. The vertical beta functions at the IP (β_y^*) are also small. With smaller IP beta functions, the orbit drift in units of the vertical beam sizes will be unchanged, since both beam sizes and the sizes of the drift are proportional to the square root of β_y^* assuming that the beta functions at source points of the orbit drifts are the same. However, the vertical beta functions at the final focus quadrupoles (QC1s) get larger with the smaller IP beta functions. Also considering a higher field gradient of QC1s, the sizes of the orbit vibrations due to the vibrations of QC1s are about the same as those at KEKB. Considering this situation and the smaller vertical emittances, the orbit changes due to the mechanical vibrations of the QC1s will be by more than one order of magnitude larger in units of the vertical beam sizes than those at KEKB. We have been carefully investigating the mechanical vibrations of the final doublets and making efforts to reduce the vibration amplitudes. In the following, we summarize those efforts and their expected effects to the luminosity.

Based on the KEKB data of the vibration magnitude of the final focus quadrupoles, the orbit motion at the IP could be 4 or 5 times larger than the vertical beam sizes in SuperKEKB. To overcome this problem, four countermeasures have been considered, *i.e.* using the coherency of vibrations of quadrupoles for electrons and positrons, modified magnet supports, additional damping for magnet vibrations and finally the orbit feedback. A modal analysis has been performed with the ANSYS code. Vertical oscillation frequencies due to the vibrations of the QC1s on the right side of IP (QC1RP and QC1LP) appear at around 25, 38 , 69 and 100 Hz. If we assume the coherency of the two magnets, the orbit differences of the two beams at the IP at the frequencies will be 18.6, 1.7, 8.3 and 3.1 nm in rms, respectively. The corresponding luminosity degradations are 4.6, 0.2, 0.3, 0.3 %, respectively. The luminosity loss due to the 25Hz oscillation is expected to be recovered by the orbit feedback. The luminosity loss due to the vibrations of QC1s on the left side is similar. In the calculation, the coherency of the two magnets for the electrons and positrons is very important. If there is no coherency, the orbit differences amount to a few times of the vertical beam sizes at the IP.

VERTICAL FEEDBACK

The orbit feedback in the vertical direction will be done with the same method as that for KEKB. Changes of closed orbits give the orbit offset at the IP and the crossing angle. The changes of the orbits are detected by using four BPMs at around the IP. A difference from KEKB is that a much faster feedback will be needed at SuperKEKB. As shown above, we need to suppress the orbit change at around 25Hz. The feedback system is composed of BPMs, a special wideband detector for the BPMs, a digital signal processor unit whose outputs are kicks of corrector magnets, a power supply controller, power supplies of the correctors and the corrector magnets.

Four BPMs for the feedback are installed on the IP side of the final focus quardupoles (QC1RE, QC1RP, QC1LE and

Content from this work may be used under the terms of the CC BY 3.0 licence (© 2015). Any distribution of this work must maintain attribution to the author(s), title of the work, publisher, and DOI.

ISBN: 978-3-95450-168-7 doi:10.18429/JACoW-IPAC2015-MOPHA056

STATUS OF LLRF CONTROL SYSTEM FOR SUPERKEKB COMMISSIONING

T. Kobayashi[#], K. Akai, K. Ebihara, A. Kabe, K. Nakanishi, M. Nishiwaki, J. Odagiri,
KEK, Tsukuba, Ibaraki, Japan
H. Deguchi, K. Hayashi, T. Iwaki, M. Ryoshi,
Mitsubishi Electric TOKKI System Corporation, Amagasaki, Hyogo, Japan

Abstract

Beam commissioning of the SuperKEKB will be started in JFY2015. A new LLRF control system, which is an FPGA-based digital RF feedback control system on the MicroTCA platform, has been developed for high current beam operation of the SuperKEKB. The mass production and installation of the new systems has been completed as scheduled. The new LLRF control systems are applied to nine RF stations (klystron driving units) among existing thirty stations.

As a new function, klystron phase lock loop was digitally implemented within the cavity FB control loop in the FPGA, and in the high power test it worked successfully to compensate for the klystron phase change. Beam loading was also simulated in the high power test by using an ARES cavity simulator, and then good performance in the cavity-voltage feedback control and the cavity tuning control was demonstrated to compensate the large beam loading for the SuperKEKB parameters.

INTRODUCTION

SuperKEKB is a new upgrade project, which is aiming at 40-times higher luminosity than the KEKB [1], accordingly it requires much lower-emittance and higher-current beam storage. The first commissioning of SuperKEKB (Phase-1) will start in JFY2015.

Accuracy and flexibility in accelerating field control are very essential for storage of high-current and high-quality beam without instability. Therefore, new low level RF (LLRF) control system, which is based on recent digital architecture, was developed for the SuperKEKB, and the good performance of the prototype was demonstrated in the high power test as reported in Ref. [2]. The existing analogue LLRF systems used for KEKB operation will be replaced by new ones, step by step. In the first commissioning of SuperKEKB, the new LLRF control systems are applied to nine LLRF stations among about thirty stations.

The accelerating frequency of the storage ring is about 508.9 MHz (CW operation). The regulation stability of 0.02% and 0.02º (rms) in the cavity amplitude and phase, respectively, were obtained in the high power test of the LLRF control system [2]; that sufficiently satisfies the requirements.

For the beam acceleration of the main ring (MR), both normal conducting cavities (NCC) and superconducting cavities (SCC) are used. The NCC, which is called ARES

#tetsuya.kobayashi@kek.jp

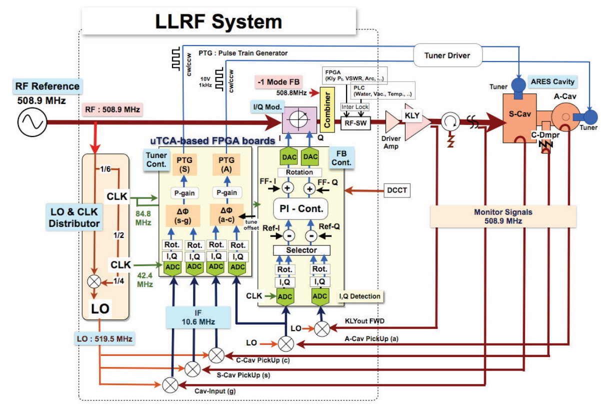

Figure 1: Block diagram for ARES cavity control.

[3], has a unique structure for the KEKB in order to avoid the coupled-bunch instability caused by the accelerating mod [4]. ARES is a three-cavity system: the accelerating (A-) cavity is coupled with a storage (S-) cavity via a coupling cavity.

A damping ring (DR) is newly being constructed at the injection linac for the positron emittance reduction. In the DR, the RF-frequency is the same as that of the main ring (MR), and three cavities, each of which is a HOM-damped single cell cavity (not an ARES type), are driven by one klystron for the acceleration. Thus another LLRF control system for the DR was also designed. It is almost the same as that of the MR, except the three-cavity vector sum control is required.

NEW LLRF SYSTEM FOR SUPERKEKB

Figure 1 shows a block diagram of cavity-voltage (Vc) feedback (FB) control and auto tuner control for the ARES cavity driving for the SuperKEKB. One klystron drives one cavity unit, so one LLRF control system corresponds to one cavity-unit control. The principal functions of this system are performed by five FPGA boards which work on MicroTCA platform as advanced

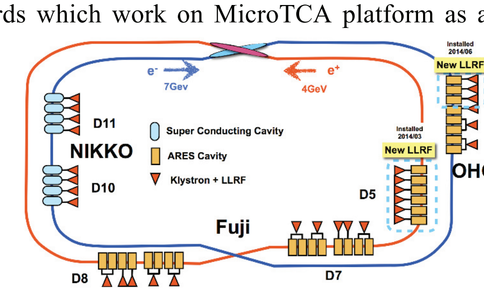

Figure 2: RF system layout for the Phase-1. Nine LLRF stations were replaced with the new ones.

Content from this work may be used under the terms of the CC BY 3.0 licence (© 2015). Any distribution of this work must maintain attribution to the author(s), title of the work, publisher, and DOI.

ISBN: 978-3-95450-168-7 doi:10.18429/JACoW-IPAC2015-MOPHA058

BEAM BASED GAIN CALIBRATION FOR BEAM POSITION MONITOR AT J-PARC MAIN RING

H. Kuboki, T. Toyama, J. Takano, and M. Tejima, KEK/J-PARC, Tsukuba, Ibaraki, Japan
S. Hatakeyama, Mitsubishi Electric System & Service Co., Ltd., Tsukuba, Ibaraki, Japan

Abstract

A new beam-based method to calibrate the gains of Beam Position Monitor (BPM) at J-PARC Main Ring has been developed using Total Least Square fitting (TLS). The usefulness of TLS method is evaluated by the simulation. The gains are analyzed from the data obtained with the beam mapping for low and high beam intensities, and are determined with the accuracy within ±0.8% for right electrode and ±0.6% for up and down electrode.

BEAM POSITION MONITOR AT J-PARC MAIN RING

Beam Position Monitor (BPM) is one of the essential elements in a synchrotron facility. Beam positions measured with the BPMs are used to correct the closed orbit distortion (COD).

We define the "gain" such as the proportionality coefficient between the signal detected at the ADC and the ideal signal with no error as shown in Eqs. (1) and (2). The signal strength from a BPM electrode varies depending on 1) transmission characteristics of a long cable, 2) processing circuit, and 3) contact resistance at the connected parts. These are the origin of the gain fluctuation to be corrected by Beam Based Gain Calibration (BBGC) [1]. A conventional BBGC method was applied to the BPMs installed at J-PARC Main Ring (MR), however, the gains have not been corrected adequately because of the difference of the electrode shape. Therefore, a new BBGC method should be established.

Figure 1 shows the schematic of a BPM used at MR. The BPM has four electrodes of left (L), right (R), up (U), and down (D). The signal from each electrode is transmitted to the processing circuit BPMC and converted to the digitized signals shown as V_L, V_R, V_U, and V_D. Signal strength from each electrode of the BPM is represented as following.

$$V_L = \lambda\left(1+\frac{x}{a}\right),\ V_R = \lambda g_R\left(1-\frac{x}{a}\right), \quad (1)$$

$$V_U = \lambda g_U\left(1+\frac{y}{a}\right),\ V_D = \lambda g_D\left(1-\frac{y}{a}\right), \quad (2)$$

where g_R, g_U, and g_D are defined as relative gains of R, U, D electrodes divided by the gain of L electrode ($g_L = 1.0$), x and y denote horizontal and vertical position of the beam, respectively, λ denotes the line density of the beam charge with the unit C/mm^2, and a represents the effective radius of the inner surface of the electrode from the BPM center. Removing x/a, y/a, and λ from Eqs (1) and (2), we can obtain the relation

$$-\frac{R}{g_R}+\frac{U}{g_U}+\frac{D}{g_D}=L, \quad (3)$$

where V_L, V_R, V_U, and V_D are replaced by L, R, U, and D, respectively, for simplification. If we have n-data sets of (L_i,R_i,U_i,D_i) $(i = 1,\cdots,n)$, n relations of Eq. (3) can be expressed using matrix form as

$$\underbrace{\begin{pmatrix} -R_1 & U_1 & D_1 \\ \vdots & \vdots & \vdots \\ -R_i & U_i & D_i \\ \vdots & \vdots & \vdots \\ -R_n & U_n & D_n \end{pmatrix}}_{\boldsymbol{X}} \underbrace{\begin{pmatrix} G_R \\ G_U \\ G_D \end{pmatrix}}_{\boldsymbol{G}} = \underbrace{\begin{pmatrix} L_1 \\ \vdots \\ L_i \\ \vdots \\ L_n \end{pmatrix}}_{\boldsymbol{L}}, \quad (4)$$

where $\boldsymbol{G} = (G_R, G_U, G_D)$ are defined as the inverse of the gains $(1/g_R,\ 1/g_U,\ 1/g_D)$. Equation (4) can be represented as $\boldsymbol{X}\cdot\boldsymbol{G} = \boldsymbol{L}$, where $\boldsymbol{X}$ and $\boldsymbol{L}$ denote $n\times 3$ matrix and n data of L_i $(i = 1,\cdots,n)$, respectively. Firstly, we calculate the solution $\boldsymbol{G}$ from Eq. (4). Then the gains (g_R,g_U,g_D) are obtained as the inverse of each element in $\boldsymbol{G}$.

The gains are changed by a different configuration of the circuit even with the same BPM. For example, the gain changes depending on a beam intensity because the circuit configurations have to be changed to accept various signal strengths generated by different beam intensities. Here, we show the results of BBGC for two different beam intensities in **RESULTS**.

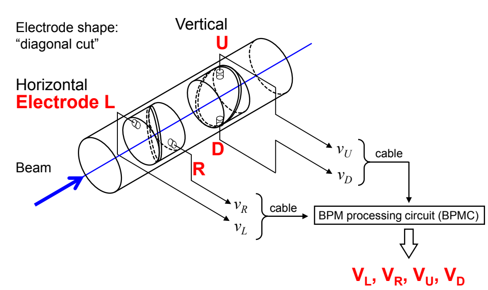

Figure 1: Diagonal-cut-type BPM at J-PARC MR.

SIMULATION

To solve Eq. (4), we have tested two methods: standard least squares fitting (LS) and total least squares fitting (TLS) [2]. We evaluated LS and TLS methods by a simulation as follows [1].

1. Gains are determined to be (g_L, g_R, g_U, g_D) = $(1.00, 1.01, 1.005, 0.975)$, which are defined as "True gain".

Content from this work may be used under the terms of the CC BY 3.0 licence (© 2015). Any distribution of this work must maintain attribution to the author(s), title of the work, publisher, and DOI.

ISBN: 978-3-95450-168-7 doi:10.18429/JACoW-IPAC2015-MOPHA059

CONTROL SYSTEM UPGRADE FOR SUPERKEKB INJECTOR LINAC

M. Satoh#, Y. Seimiya, F. Miyahara, K. Mikawa, T. Suwada, and K. Furukawa, KEK/ SOKENDAI, Tsukuba, Japan
T. Kudou, S. Kusano, Mitsubishi Electric System & Service Co., Ltd, Tsukuba, Japan
H. Saotome, M. Takagi, Kanto Information Service (KIS), Accelerator Group, Tsuchiura, Japan

Abstract

The KEKB project has successfully completed its decade operation in the June of 2010. SuperKEKB main ring is currently being constructed for aiming at the peak luminosity of 8 x 10^{35} $cm^{-2}s^{-1}$. The electron/positron injector linac upgrade is also going on for increasing the intensity of bunched charge with keeping the small emittance. The key upgrade issues are the construction of positron damping ring, a new positron capture system, and a low emittance photo-cathode rf electron source. The injector linac beam commissioning started in the October of 2013. The whole control system performance determines the beam operation efficiency of injector linac, and it eventually has a strong impact on the experimental results of physics. In this decade, the linac control system has gradually transferred from the in-house system to the Experimental Physics and Industrial Control System based one for increasing the availability of beam operation. In this paper, we present the detail of SuperKEKB injector linac control system.

INTRODUCTION

The linac beam control system is based on a standard client/server model with three levels. The original linac control system has been developed by using the in-house software libraries based on the remote procedure call (RPC). The client user interfaces have been designed by a command line interface and Tcl/Tk scripting language. Around a decade ago, the middle phase of KEKB operation, the linac control system has been upgraded to a new framework based-on the Experimental Physics and Industrial Control System (EPICS) [1] to improve the affinity between the linac and ring control systems. These improvements make it easy to analyze the correlations between the linac and ring parameters. Such analysis can help finding a source of injection rate deterioration. The new client user interfaces have been implemented by Python scripting language for the rapid software development. For the simultaneous top-up injection of KEB and PF rings, an event based timing system has been implemented to enable the pulse-to-pulse beam modulation [2].

CONTROL SYSTEM OVERVIEW

Server and Client Computer Environment

The linac control system is based on the server/client model. It is useful framework to integrate the different kinds of local controllers. In the beginning of KEB project, we used the six Compaq Alpha servers with the Tru64 UNIX operating system as the server computers. Two of them were connected to the RAID disk via SCSI bus interface, and they can work as the active/standby redundant NFS servers for the high availability operation. Since the Tru64 UNIX was obsoleted, they have been gradually replaced by the Linux-based machines. After some different types of high availability cluster system based on Linux were evaluated, eventually we made decision to use the Linux base system without cluster functionality. Instead of redundant system, the blade based server system was employed as the high reliability server systems. Currently, eleven Linux based blade servers are utilized as the server computers. Both of server and client side control software are running on the server machines. Currently, Linux distribution of CentOS 5.11 x86_64 are mainly used for the daily operation. CentOS 6.6 and 7 are also under test for the future utilization. The Tektronix X terminals and touch panel displays based on PC9801/DOS machines have been originally utilized as the operator terminals. These terminals were replaced by the Linux PC and Windows PC with the X server application software of ASTEC-X and Reflection X.

Network Environment

The network system is one of the most important infrastructures for the reliable accelerator control system. During the KEKB operation, Cisco Catalyst 4506 and 3750 were utilized as the core switches. Each of them were independently connected to 45 edge switches of Catalyst 2950 via optical fiber with 100 Mbps bandwidth. The two core switches worked as the active/standby redundant system. For the network connection between the edge switches and local controllers like programmable logic controllers (PLCs), the optical fiber is used for avoiding the noise generated by the klystron modulators.

Toward SuperKEKB, the core switch system was replaced by 6 of Cisco Catalyst 3750X. Each of them can work as the active/active redundant system based on the virtual switching system technology. We replaced also the edge switch by Catalyst 2960S, and the network connection between them was improved up to 1 Gbps bandwidth.

Local Controllers

For the injector linac control system, many kinds of different local controllers are utilized for the injector linac component control as listed in Table 1. The ladder PLCs control the magnet power supplies, vacuum pumps,

Corresponding author. *e*-mail address: masanori.satoh@kek.jp.

Content from this work may be used under the terms of the CC BY 3.0 licence (© 2015). Any distribution of this work must maintain attribution to the author(s), title of the work, publisher, and DOI.

ISBN: 978-3-95450-168-7 doi:10.18429/JACoW-IPAC2015-MOPHA060

FEASIBILITY STUDY ON MEASUREMENT AND CONTROL OF RELATIVE POSITIONING FOR NANO-BEAM COLLISION

H. Matsunaga#, H. Yoshioka, Takenaka Corp., Otsuka, Inzai 270-1395, Japan
Y. Ohsawa, R. Sugahara, M. Masuzawa, H. Yamaoka, KEK, Oho, Tsukuba 305-0801, Japan

Abstract

A key requirement of the SuperKEKB and future International Linear Collider projects is to measure and control the offset of very small beams with a precision of several nanometers at the interaction point. Using a relative positioning control introduces several technical problems because it is necessary to measure and control short-term vibration and long-term drift between the two distant points. In this paper, we offer a feasibility study for measuring and controlling nano-order relative position by using a laser interferometer and a piezoelectric stage.

INTRODUCTION

The SuperKEKB [1,2] is designed to improve peak luminosity to forty times that of KEKB luminosity and reduce the beam diameter to 60 nm. The beam diameter in the International Linear Collider will be 5 nm. To achieve these nano-beam collisions, it is essential to measure and control a relative offset between the electron and positron beams with a precision of several nanometers.

The electron and positron beam diameters are reduced by superconducting magnets located on both sides of the interaction point. Therefore, the most effective way is to measure and control the relative vertical beam offset at the installation points of superconducting magnets.

Many attempts have been performed to measure the microtremor at accelerator installation sites [3-6], however, those attempts have not been intended to measure relative offsets between two distant points. Kimura [7] proposed a method to measure a relative vertical offset via a water tube tiltmeter, but the method is not appropriate for measurement in the vibration region.

Yamashita [8,9] developed a mover system by using piezoelectric device. The mover can control the vibrations on a table with a precision of approximately 20 nm, however the mover is not designed to measure and control a relative offset between two distant points.

In this paper, we offer a feasibility study for measuring and controlling a nano-order relative position by using a laser interferometer and a piezoelectric stage.

MEASUREMENT ACCURACY OF THE LASER INTERFEROMETER

Experimental Systems

We adopted a laser interferometer (the laser system) of Keysight Technologies, Inc. The optical instruments are summarized in Table 1. The laser system can measure the relative displacement between a linear interferometer and a reflector with nano-order precision. We tested the measurement accuracy of the laser system in the frequency range 1‑100 Hz by using two shaking devices. Our experimental systems are shown in Figs. 1A and 1B.

#matsunaga.hiroki@takenaka.co.jp

Table 1: Optical Instruments

Laser head(C5517)	He-Ne laser: λ =633nm
Linear interferometer(10702A)	Resolution: λ /2
Reflector(10703A)	
Beam splitter(10701A)	15%-split

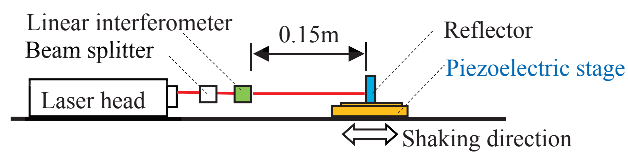

Figure 1A: Experimental system to verify accuracy using a piezoelectric stage.

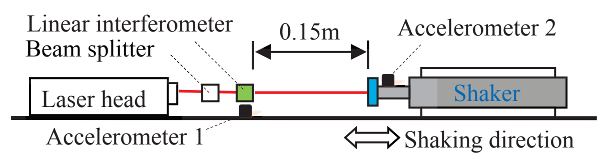

Figure 1B: Experimental system to verify accuracy using a shaker.

Table 2: Specifications of the Piezoelectric Stage

Stroke	200 μ m in XYZ directions
Capacitive type displacement sensor	Resolution of analogue output : 0.4 nm
Resolution in shaking	1 nm under closed-loop control

Figure 1A shows the shaking system by using a piezoelectric stage (the piezo stage) of PI-Japan Co. Ltd. Specifications of the piezo stage are summarized in Table 2. The piezo stage shakes with a precision of 1 nm in the frequency range 1‑10 Hz. The embedded capacitive-type displacement sensor has a resolution of 0.4 nm. We verify the measurement accuracy by comparing the obtained value with the output value of the capacitive sensor when shaking the reflector, as shown in Fig. 1A.

Figure 1B shows the shaking system with a low-frequency shaker of AR Brown Co. Ltd. Two servo-type accelerometers of Tokkyokiki Co. Ltd. are used to estimate the relative displacement by a dual integration

Content from this work may be used under the terms of the CC BY 3.0 licence (© 2015). Any distribution of this work must maintain attribution to the author(s), title of the work, publisher, and DOI.

ISBN: 978-3-95450-168-7 doi:10.18429/JACoW-IPAC2015-MOPTY001

DEVELOPMENT OF WIDEBAND BPM FOR PRECISE MEASUREMENT OF INTERNAL BUNCH MOTION

K. G. Nakamura, Kyoto University, Kyoto, Japan
T. Toyama, M. Okada, M. Tobiyama, Y.H. Chin, T. Obina, T. Koseki, KEK, Ibaraki, Japan
Y. Shobuda, JAEA, Ibaraki, Japan

Abstract

To suppress intra-bunch oscillations and to reduce particle losses, the intra-bunch feedback (IBFB) system has been developed in 2014 for the J-PARC Main Ring (MR). A new BPM was also installed to the MR for the IBFB system. This BPM has a sufficient frequency response and position sensitivity. (up to 1.5GHz within 15% fluctuation.) However, the performance needs to be further improved, particularly at high frequency, for more precise analysis of internal motions (e.g. due to electron clouds). We report the development of the BPM and precise measurement results of the BPM characteristics. We also show simulation studies of the digital equalizer which helps to reconstruct the beam shape from beam signals.

INTRODUCTION

The J-PARC is composed of three proton accelerators: the 400MeV linear accelerator (LINAC), the 3GeV Rapid Cycling Synchrotron (RCS), and the 30GeV Main Ring (MR) Synchrotron. At the J-PARC MR, transverse instabilities have been observed at the injection and during the acceleration. To suppress these instabilities, intra-bunch feedback system (IBFB) (Fig. 1) has been developed since 2014. It performs well in supressing instabilities and reducing beam losses [1].

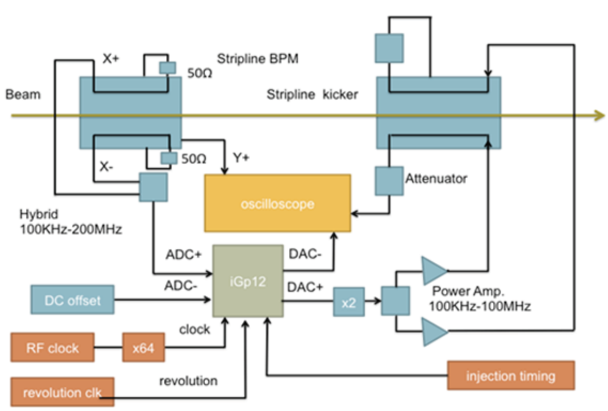

Figure 1: Schematic of the intra-bunch feedback system.

EXPONENTIAL TAPERED COUPLER

Exponential tapered couplers (ETC) [2] have been used for IBFB. They have a wider frequency response than a normal rectangular coupler. The details are described in Ref [1]. The ETC transfer function can be written as Eqs. (1) and (2). Measurement results agree with Eq. (1) within

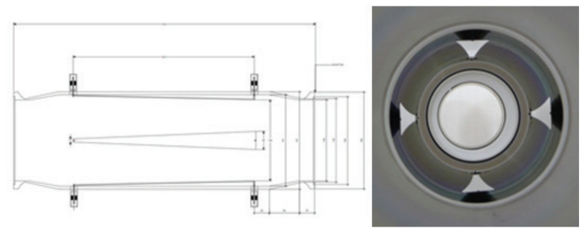

Figure 2: Side (left) and front (right) views of BPM.

15% fluctuation up to 1.5GHz (the blue line in Fig. 7). But a wider and flatter frequency response will be needed in future for more precise analysis of internal motions. In this paper, we report the development of the BPM to match measurement with theoretically designed response accurately.

$$|F(\omega)| = \frac{\frac{K\omega l}{c}}{\sqrt{a^2+\frac{4\omega^2 l^2}{c^2}}}\left(1+e^{-2a}-2e^{-a}\cos\frac{2\omega l}{c}\right)^{\frac{1}{2}} \tag{1}$$

$$Arg(F(\omega)) = \arctan\left(\frac{\frac{2\omega l}{c}\sin\frac{2\omega l}{c}+a(e^a-\cos\frac{2\omega l}{c})}{\frac{2\omega l}{c}(e^a-\cos\frac{2\omega l}{c})-a\sin\frac{2\omega l}{c}}\right) \tag{2}$$

NEW DESIGN OF BPM STRIPLINE

Impedance Matching

The fluctuation in the frequency response seems to be caused by the impedance mismatching in the BPM electrodes and some problems in the measurement method. The black line in Fig. 4 shows the impedance of electrodes measured by Time Domain Reflectometry (TDR). The two large peaks appear at the feed-through positions, and the fluctuation between them corresponds to impedance of the electrodes. The characteristic impedance of BPM is determined by the width and thickness of electrodes and their position. As the width is changed exponentially, the thickness or the distance from the chamber wall should be changed proportionally to the change in the width.

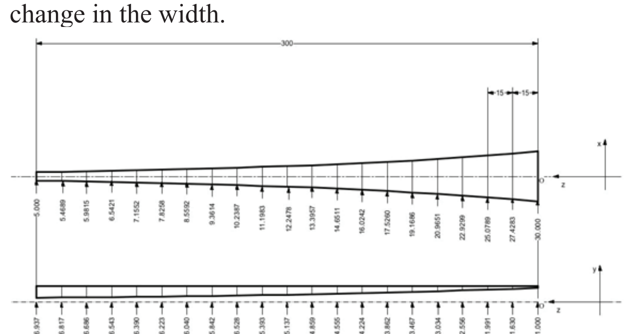

Figure 3: Design of new electrodes.

Content from this work may be used under the terms of the CC BY 3.0 licence (© 2015). Any distribution of this work must maintain attribution to the author(s), title of the work, publisher, and DOI.

6th International Particle Accelerator Conference IPAC2015, Richmond, VA, USA JACoW Publishing
ISBN: 978-3-95450-168-7 doi:10.18429/JACoW-IPAC2015-MOPTY002

Content from this work may be used under the terms of the CC BY 3.0 licence (© 2015). Any distribution of this work must maintain attribution to the author(s), title of the work, publisher, and DOI.

BUNCH LENGTH MEASUREMENT OF FEMTOSECOND ELECTRON BEAM BY MONITORING COHERENT TRANSITION RADIATION

Itta Nozawa[#], Masao Gohdo, Koichi Kan, Takafumi Kondoh, Astushi Ogata, Jinfeng Yang and Yoichi Yoshida
The Institute of Scientific and Industrial Research, Osaka University, Osaka, Japan

Abstract

Ultrashort electron bunches with durations of femtoseconds and attoseconds are essential for time-resolved measurements, including pulse radiolysis and ultrafast electron microscopy. However, generation of the ultrashort electron bunches is commonly difficult because of bunch length growth due to space charge effect, nonlinear momentum dispersion and so on. Several bunch length measurement methods for the ultrashort electron beams have also been considered so far, which have not been established yet. In this study, the femtosecond electron beams were generated using a laser photocathode radio-frequency gun linac and a magnetic bunch compressor. The bunch length measurement was carried out using a Michelson interferometer based on monitoring coherent transition radiation (CTR), which is characterized by square modulus of the Fourier transform of the longitudinal bunch distribution. Analyzing the experimentally obtained interferograms of CTR, the electron beams with the average duration of 5 fs were generated and measured successfully at the condition of bunch charge of 1 pC. Consideration of the longitudinal bunch shapes was also carried out using the Kramers-Kronig relation.

INTRODUCTION

Ultrashort electron bunches with pulse durations of femtoseconds and attoseconds are a key for applications of accelerator physics, for example, free electron lasers[1] and intense terahertz (THz) light sources[2]. Additionally, ultrashort electron bunches play an important role in time-resolved measurements such as pulse radiolysis[3] and ultrafast electron diffraction[4] because the time resolution of the measurements strongly depends on the bunch lengths of electron beams. On the other hand, much effort has been devoted to developing bunch length measurements of <100 fs electron bunches because of lack of time resolution of conventional longitudinal beam diagnostic methods including femtosecond streak cameras. Now, many researches of alternative measurement methods using coherent radiation (CR), electro-optic (EO) crystals, deflecting cavities have proceeded in order to evaluate bunch length of femtosecond electron bunches[5,6]. In this study, a bunch length measurement technique of the femtosecond electron bunches were investigated by monitoring coherent transition radiation (CTR) using a Michelson interferometer. The femtosecond electron bunches were generated by a photocathode-based linac with an arc-type magnetic bunch compressor[3,7]. As for the bunch length measurement monitoring CR, it is very important to detect broadband electromagnetic (EM) waves because the frequency range characterizes the time resolution of the bunch length measurement. Therefore, frequency range of the measurement system has been expanded by optimizing a beam splitter and a detector in the Michelson interferometer.

EXPERIMENTAL SETUP

Linac System for Generation of Ultrashort Electron Bunches

In this study, a laser photocathode radio frequency (RF) gun linac and an arc-type magnetic bunch compressor at the Institute of Scientific and Industrial Research (ISIR) in Osaka University were used for the generation of ultrashort electron bunches. Figure 1 shows the schematic diagram of the linac system[3,7].

This system is composed of a 1.6-cell S-band (2856 MHz) RF gun with a copper cathode, a 2-m-long S-band linear accelerating tube and a magnetic bunch compressor. In order to obtain electron beams with low emittances and short initial bunch lengths at the gun, a third harmonics of a Ti:Sapphire femtosecond laser (266 nm) was used for irradiating the copper cathode. Additionally, the charges of the electron bunches were suppressed to the picocoulomb-order to reduce bunch length growth due to the space charge effect. The electron bunches were accelerated to 4 MeV at the exit of the gun and 32 MeV at the exit of the accelerating tube. In the linear accelerating tube, an energy-phase correlation optimal for compression was also carried out for the magnetic compression. Finally, the electron bunches were

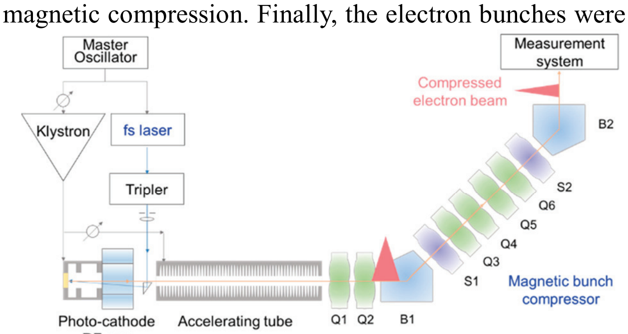

Figure 1: Schematic diagram of a laser photocathode RF electron gun linac and a magnetic bunch compressor. Q: quadrupole magnet; B: bending magnet; S: sextupole magnet.

#nozawa81@sanken.osaka-u.ac.jp

ISBN: 978-3-95450-168-7 doi:10.18429/JACoW-IPAC2015-MOPTY003

MEASUREMENT OF MOMENTUM SPREAD OF THE INJECTION BEAM WITH LONGITUDINAL TOMOGRAPHY METHOD IN THE J-PARC RCS

Masahiro Yoshimoto#, Hiroyuki Harada, Hideaki Hotchi, Pranab Kumar Saha, Fumihiko Tamura, Masanobu Yamamoto, Michikazu Kinsho
JAEA/J-PARC, Tokai-Mura, Naka-Gun, Ibaraki-Ken, JAPAN

Abstract

In the J-PARC RCS, the beam tuning toward the design output beam power of 1MW were started after the completing of the beam energy and beam current upgrades in the LINAC. One of the important issues to achieve the 1MW beam operation is the optimization of the injection beam. Due to the longitudinal beam tuning in the LINAC, we adopted the Longitudinal Tomography algorism to measure the momentum spread after the beam injection into the RCS. At first we confirmed the validity of our measurement tool developed with the Longitudinal Tomography algorism. And then longitudinal beam tuning with this tool were carried out.

INTRODUCTION

In order to observe two-dimensional (2D) beam distributions in the longitudinal phase space, the simple reconstruction tool had been developed with the Longitudinal Tomography (LT) algorithm for the 3-GeV rapid cycling synchrotron (RCS) at Japan Proton Accelerator Research Complex (J-PARC) [1]. Our reconstruction tool is adopted the Convolution Back-Projection (CBP) method [2] for the LT algorithms. This tool has some limitations to apply the beam measurement. However it is very simple enough to accelerate processing speed and achieve the on-line analysis. The reconstructed longitudinal 2D distribution has much useful information. It can diagnose not only the longitudinal beam dynamics in the RCS but also the longitudinal beam parameters from the LINAC.

In the J-PARC RCS, the beam tuning toward the design output beam power of 1MW were started after the completing of the beam energy and beam current upgrades in the LINAC. One of the important issues to achieve the 1MW beam operation is the optimization of the injection beam from the LINAC [3]. Due to the longitudinal tuning of the LINAC beam, the momentum spread (Δp/p) was measured with this reconstruction tool after the beam injection into the RCS.

MOMENTUM SPREAD MEASUREMENT WITH LONGITUDINAL TOMOGRAPHY

In order to apply the reconstruction tool with the simple LT algorism to the Δp/p measurement of the LINAC beam, there are some issues that we have to confirm, namely the reproducibility of the 2D distribution, the accuracy of the measurement quantity, and the expansion to the Acceleration mode. Thus our reconstruction tool has to be evaluated before the high power beam tuning.

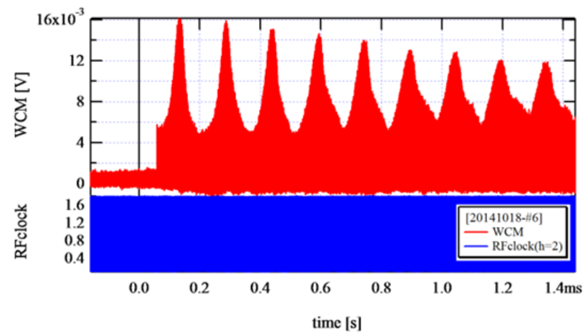

Figure 1: The typical beam bunch shape acquired by the WCM and the RF-clock generated by the LLRF.

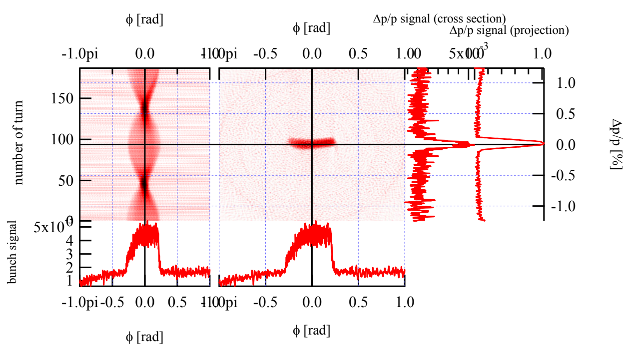

Figure 2: The reconstructed beam distribution in the longitudinal phase space with the CBP method.

Reconstruction Two-Dimensional Distribution in the Longitudinal Phase Space

The RCS adopted the multi-turn H^- charge-exchange injection scheme [4]. After the all bunched beams were injected, the longitudinal information of the LINAC beam was smeared out. Thus single intermediate bunched beam had to be injected and rotated in synchrotron phase-space. Figure 1 shows the typical measurement results of the circulating bunch signal by the WCM and the RF-clock signal generated by the low level RF (LLRF) system after the single intermediated bunched beam injection. A set of projected histograms for the Longitudinal Tomography can be obtained by cutting out from the WCM signal at the every rise timing of the RF clock. Figure 2 shows the results of the reconstruction. Left figures show the mountain plot during one synchrotron oscillation period and the first projected histogram. Right figure shows the reconstructed 2D distribution in the longitudinal phase

#E-mail address: yoshimoto.masahiro@jaea.go.jp

Content from this work may be used under the terms of the CC BY 3.0 licence (© 2015). Any distribution of this work must maintain attribution to the author(s), title of the work, publisher, and DOI.

ISBN: 978-3-95450-168-7 doi:10.18429/JACoW-IPAC2015-MOPTY004

WAKEFIELD MONITOR EXPERIMENTS WITH X-BAND ACCELERATING STRUCTURES

R. L. Lillestøl*, E. Adli, J. Pfingstner, Department of Physics, University of Oslo, Norway,
W. Farabolini, R. Corsini, S. Döbert, A. Grudiev, L. Malina, W. Wuench,
CERN, Geneva, Switzerland

Abstract

The accelerating structures for CLIC must be aligned with a precision of a few µm with respect to the beam trajectory in order to mitigate emittance growth due to transverse wake fields. We report on first results from wake field monitor tests in an X-band structure, with a probe beam at the CLIC Test Facility. The monitors are currently installed in the CLIC Two-Beam Module. In order to fully demonstrate the feasibility of using wakefield monitors for CLIC, the precision of the monitors must be verified using a probe beam while simultaneously filling the structure with high power rf used to drive the accelerating mode. We outline plans to perform such a demonstration in the CLIC Test Facility.

INTRODUCTION

In the Compact Linear Collider [1] (CLIC), wakefield monitors (WFMs) are indispensable for preserving the emittance in the main linac. Even with the tight mechanical alignment tolerances of 14 µm for the accelerating structures, the corresponding vertical emittance growth $\Delta\epsilon_y$ would be in the order of 200 %, which is clearly unacceptable. Therefore, the accelerating structures will be aligned to the beam with the help of wakefield monitors. To keep $\Delta\epsilon_y$ around 5 %, the alignment tolerance is 3.5 µm including systematic and random effects.

Wakefield monitors (WFMs) are used to measure the beam position based on transverse wakes from the passing bunches. In CLIC, it is foreseen to use TD26 accelerating structures in the main linac [1], which are tapered, damped travelling wave structures with a fundamental mode at 12 GHz. Each structure consists of 26 tapered cells, as well as two coupling cells. Four waveguides are connected to each cell and damp higher-order modes. For some of the accelerating structures, the waveguides of the first normal cells are extended for the WFMs. The internal geometry of such an accelerating structure is shown in Figure 1.

On the wide sides of each of these waveguides, an antenna is used to pick up a TM-like mode at 16.9 GHz [2]. In a similar way, an antenna at the short side of the waveguide picks up a TE-like mode at 27.3 GHz. Both these modes are dipole modes, where the amplitude has a linear dependency on the beam offset from the center of the structure. Since four waveguides are used around the cell, the beam offset in both transverse dimensions can be found.

* reidar.lunde.lillestol@cern.ch

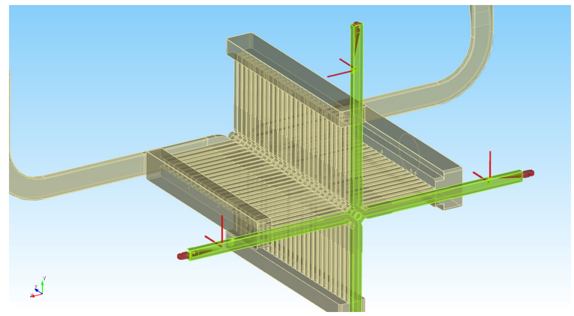

Figure 1: The internal geometry of a TD26 structure except for the first coupling cell. The WFM waveguides are shown in green and the pickup antennas in red.

The CLIC WFMs were first tested in the Two-Beam Test Stand [3, 4], which was formerly located in the same beam line as the present setup. By comparing two accelerating structures, these tests indicated a resolution of < 5µm for beam offsets of < 0.4mm.

WAKE FIELD TESTS AT THE CTF3

In the CLIC Test Facility 3 (CTF3) at CERN [5], a CLIC two-beam module (TBM) is presently installed in the Califes beamline. The CTF3 was built to demonstrate concepts and feasibilities related to CLIC, and Califes uses a probe beam representing the CLIC main beam. The TBM includes four accelerating structures, divided into two superstructures. For each superstructure, the second accelerating structure is equipped with WFMs, resulting in 8 signals for each of the two modes. The TBM also includes 2 Power Extraction and Transfer Structures (PETS), which provide about 90 MW of rf power at 12 GHz and feed the accelerating structures through a waveguide distribution network.

For each WFM signal, a bandpass filter is used to filter out unwanted modes. The signal is then read by a logarithmic detector and a digitizer. Since the time of the TBTS experiments, the mode frequencies are now different, since we now measure wakefields in the first normal cell instead of in the central cell. However, the readout electronics are still looking at the old mode frequencies, since the new bandpass filters have not yet been installed. Therefore, we measure signals at 18 ± 0.25 GHz and 24 ± 0.25 GHz instead of directly at the modes of 16.9 GHz and 27.3 GHz. Because of the low Q factors of the dipole modes, we still believe we pick up a part of the correct modes, but the signals are much weaker than they should be.

Content from this work may be used under the terms of the CC BY 3.0 licence (© 2015). Any distribution of this work must maintain attribution to the author(s), title of the work, publisher, and DOI.

ISBN: 978-3-95450-168-7 doi:10.18429/JACoW-IPAC2015-MOPTY006

STUDY ON THE INJECTION BEAM COMMISSIONING SOFTWARE FOR CSNS/RCS*

M.Y. Huang#, S. Wang, W.B. Liu, J. Qiu, L.S. Huang
[1] China Spallation Neutron Source, Institute of High Energy Physics, Chinese Academy of Sciences, Dongguan, China
[2] Dongguan Institute of Neutron Science, Dongguan, China

Abstract

The China Spallation Neutron Source (CSNS) accelerator uses H^- stripping and phase space painting method of filling large ring acceptance with the linac beam of small emittance. The beam commissioning software system is the key part of CSNS accelerator. The injection beam commissioning software for CSNS contains three parts currently: painting curve control, injection beam control and injection orbit correction. The injection beam control contains two subsections: single bunch beam calculation and LRBT beam control at the foil. The injection orbit correction also contains two subsections: injection orbit correction by the calculation and injection trim power control.

INTRODUCTION

CSNS is a high power proton accelerator-based facility [1]. The accelerator consists of an 80MeV H^- linac and a 1.6GeV Rapid Cycling Synchrotron (RCS) which accumulates an 80MeV injection beam, accelerates the beam to the designed energy of 1.6GeV and extracts the high energy beam to the target. Its beam power is 100kW and capable of upgrading to 500kW. The design goal of CSNS is to obtain the high intensity, high energy proton beam with a repetition rate of 25Hz for various scientific fields [2].

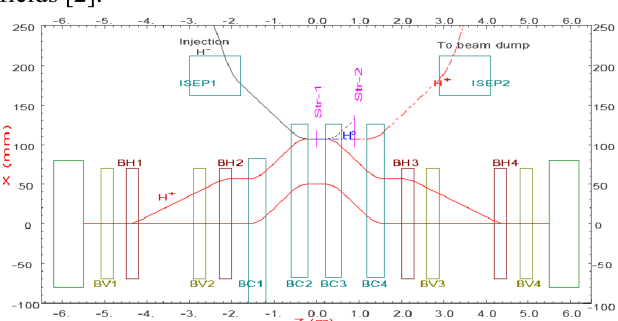

Figure 1: Layout of the RCS injection system.

For CSNS/RCS, a combination of the H^- stripping and the phase space painting method is used to accumulate a high intensity beam. Figure 1 shows the layout of the RCS injection system [3]. For the injection system, three kinds of orbit-bumps are prepared: a horizontal bump (BH1-BH4) for painting in x-x′ plane; a vertical bump (BV1-BV4) for painting in y-y′ plane; a horizontal bump (BC1-BC4) in the middle for an additional closed-orbit shift of 60mm [4].

The beam commissioning software which was programmed with the Java language plays a very important role in CSNS project, and it bases on the XAL application development environment which was developed initially by SNS laboratory [5]. The main application of this beam commissioning software system contains: device control, monitoring, online modeling and data analysis functions [6].

PAINTING CURVE CONTROL

In order to control the strong space charge effects which are the main causes of the beam losses in CSNS/RCS, the phase space painting method is used for injecting the beam of small emittance from the linac into the large ring acceptance. In general, there are two painting methods: correlated painting and anti-correlated painting. From our simulation results by using the code ORBIT [7], it can be found that the anti-correlated painting method may be more suitable for CSNS/RCS.

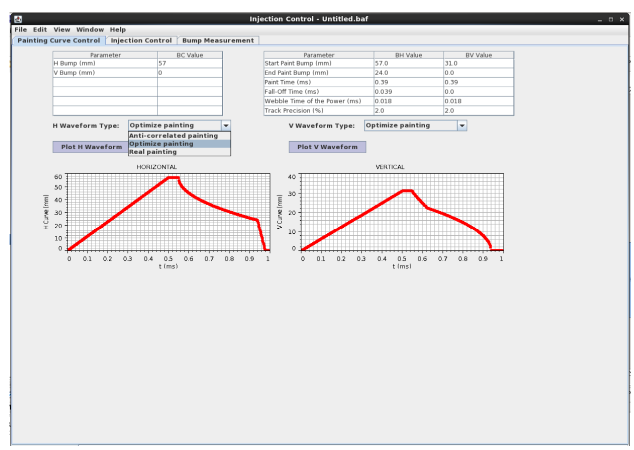

Figure 2: Injection painting curves control.

For the injection beam commissioning software of CSNS/RCS, there are three kinds of painting curves: ideal anti-correlated painting curve, optimize painting curve, and real painting curve. The optimized painting curve is obtained by the simulation and optimization of injection process. The real painting curve will be given by the accelerate operation and test. Figure 2 shows the control interface of the injection painting curves. It can be found that the painting curves can be called, displayed and saved.

*Work supported by National Natural Science Foundation of China (Project Nos. 11205185, 11175020 and 11175193)
#huangmy@ihep.ac.cn

Content from this work may be used under the terms of the CC BY 3.0 licence (© 2015). Any distribution of this work must maintain attribution to the author(s), title of the work, publisher, and DOI.

ISBN: 978-3-95450-168-7 doi:10.18429/JACoW-IPAC2015-MOPTY008

PRELIMINARY HARDWARE IMPLEMENTATION OF COMPENSATION MECHANISM OF SUPERCONDUCTING CAVITY FAILURE IN C-ADS LINAC

Z. Xue#, J. P. Dai, IHEP, Beijing,China
Y. Yang, L. X. Cheng, SINANO, Suzhou, China

Abstract

For the proton linear accelerators used in applications such as C-ADS, due to the nature of the operation, it is essential to have beam failures at the rate several orders of magnitude lower than usual performance of similar accelerators. In order to achieve this extremely high performance reliability requirement, in addition to hardware improvement, a failure tolerant design is mandatory. A compensation mechanism to cope with hardware failure, mainly RF failures of superconducting cavities, will be in place in order to maintain the high uptime, short recovery time and extremely low frequency of beam loss. The hardware implementation of the mechanism poses high challenges due to the extremely tight timing constraints, high logic complexity, and mostly important, high flexibility and short turnaround time due to varying operation contexts. We will explore the hardware implementation of the scheme using fast electronic devices and Field Programmable Gate Array (FPGA). In order to achieve the goals of short recovery time and flexibility in compensation algorithms, an advanced hardware design methodology including high-level synthesis will be used.

INTRODUCTION

The Chinese ADS (C-ADS) project is aimed to solve the nuclear waste problem and the resource problem for nuclear power plants in China. To C-ADS linac, which is a high power proton accelerator, unexpected beam trips may lead to the serious change of temperature and thermal stress in the reactor core, and eventually result in the permanent damage of facilities. Therefore, the extremely high reliability and availability for C-ADS linac was proposed [1, 2], as shown in Table 1.To reach such an ambitious goal, it is clear that reliability-oriented design practices need to be followed from the early design stage [3]. In particular: (1) a high degree of redundancy needs to be planned in critical areas. (2) “Strong design” is needed. (3) fault-tolerance capabilities have to be considered. This paper will focus on the concept of fault-tolerance, and present the preliminary hardware implementation of the compensation mechanism of the superconducting cavity failures in C-ADS linac.

Table 1: Specifications of C-ADS Proton Linac

Parameters	Design	
Particle	proton	
Energy	1.5	GeV
Current	10	mA
Beam Power	15	MW
RF Frequency	(162.5)/325/650	MHz
Duty Factor	100	%
Beam Loss	<1	%
Beam Trips/Year	<25000	1s<t≤10
	<2500	10s<t≤5min
	<25	t>5min

THE COMPENSATION MECHANISM

The compensation methods of superconducting cavity failures can be divided into global compensation method and local compensation one [3]. The global compensation means that all the cavities downstream of fault cavity attend the compensation, while the local compensation is related to the elements neighbouring the failing cavity. The global compensation has lower demand of the performance of each cavity, but it needs all cavities act at the same time, which means the RF control should be extremely accurate. By contrast, the local compensation has the advantage of involving a small number of elements, yet the performance margin of the elements must be larger.

The representative compensation work may be found on SNS, which adopts the global compensation. When the cavities fail, the machine will look up the database to find the data of compensation and then readjust the parameters of the working cavities. The whole process may take a few minutes, which is too long for C-ADS linac. In this paper, we tried another way to achieve the compensation by the hardware implementation of the scheme using fast electronic devices and Field Programmable Gate Array (FPGA). The preliminary compensation diagram of the injector I of C-ADS, which is a 10MeV proton linac, is shown in Fig.1.

xuezhou@ihep.ac.cn

Content from this work may be used under the terms of the CC BY 3.0 licence (© 2015). Any distribution of this work must maintain attribution to the author(s), title of the work, publisher, and DOI.

ISBN: 978-3-95450-168-7 doi:10.18429/JACoW-IPAC2015-MOPTY011

Content from this work may be used under the terms of the CC BY 3.0 licence (© 2015). Any distribution of this work must maintain attribution to the author(s), title of the work, publisher, and DOI.

OPERATION EXPERIENCE OF P-CARBON POLARIMETER IN RHIC*

H. Huang†, E.C. Aschenauer, G. Atoian, A. Bazilevsky, O. Eyser, D. Kalinkin, J. Kewisch, Y. Makdisi, S. Nemesure, A. Poblaguev, W.B. Schmidke, D. Steski G. Webb, K. Yip, A. Zelenski, BNL, Upton, New York, USA, I.G. Alekseev, D. Svirida, ITEP, Moscow, Russia

Abstract

The spin physics program in Relativistic Heavy Ion Collider (RHIC) requires fast polarimeter to monitor the polarization evolution on the ramp and during stores. Over past decade, the polarimeter has evolved greatly to improve its performance. These include dual chamber design, monitoring camera, Si detector selection (and orientation), target quality control, and target frame modification. The preamp boards have been modified to deal with the high rate problem, too. The ultra thin carbon target lifetime is a concern. Simulations have been carried out on the target interaction with beam. Modification has also been done on the frame design. Extra caution has been put on RF shielding to deal with the pickup noises from the nearby stochastic cooling kickers. This paper summarizes the recent operation performance of this delicate device.

INTRODUCTION

RHIC is the first and only polarized collider in the world. During the acceleration, there are possible polarization loss due to snake resonances. In addition, there are also gradual polarization loss during the typical 8 hours physics store. Therefore, fast polarization measurements are essential for the machine setup and physics programs [1]. The absolute polarization of RHIC beams are determined from polarized hydrogen jet [2]. However, the jet can only provide polarization with statistical error bars of 2-3% for a whole store. It is used to provide absolute beam polarization information for physics stores and to calibrate the p-Carbon polarimeter. The p-Carbon polarimeter provides the polarization decay during a store, the polarization profile information for experiments to use, and for possible polarization loss during acceleration.

The p-Carbon polarimeters in RHIC are based on elastic proton scattering with low momentum transfer and measurement of asymmetry in recoil carbon nuclei production [3]. This process has a large cross-section and sizable analyzing power of a few percents which has weak energy dependence in the 24-255 GeV energy range. A very thin (10 μg/cm^2, 5-10 μm wide) carbon ribbon target in the high intensity circulating beam produces high collision rate and a highly efficient DAQ system acquires up to 7×10^6 carbon events /sec. The details of the design and construction are described in Ref. [4]. A schematic of the chamber is shown in Fig. 1.

* Work performed under contract No. DE-AC02-98CH1-886 with the auspices of the DOE of United States, and with support of RIKEN(Japan).
† huanghai@bnl.gov

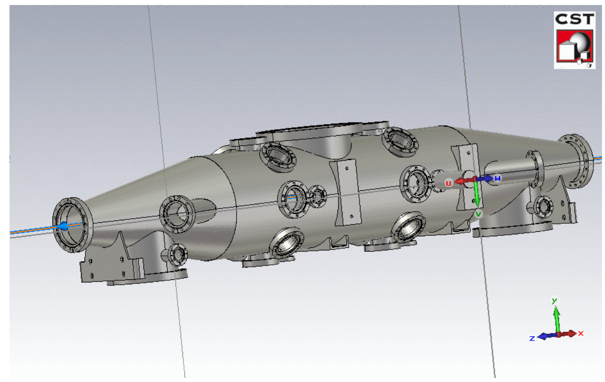

Figure 1: The 3D drawing of the polarimeter chamber. The taper structure (5:1) is to reduce the impedance impact on the overall RHIC ring impedance budget. The two view ports on both taper structure are used to monitor the target operation with remotely accessible cameras. The big view port on the top is for target installation and target motion monitor. Three cameras are mounted on these view ports to monitor the polarimeter target operation. There are two sets of six Si detectors ports surrounding the chamber on both sides of the big view port. There are six targets in both vertical and horizontal directions for each set.

TARGETS AND VACUUM CHAMBER

The use of thin target in polarimeter is essential to reduce multiple scattering for recoil carbon ions and also keep the event rate within the detectors and DAQ capabilities. Manufacturing of the ultra-thin carbon (amorphous graphite) targets requires high skill and is a time-consuming process [5]. To increase the yield of target production, the target thickness for last a few runs was at 10 μg/cm^2, instead of 5 μg/cm^2. The higher rate can be compensated by smaller Si detector strip size. As intensity increases over years, the target loss rate is higher. Cameras were installed before 2013 run. Camera videos show that the targets tails are glowing when crossing beam or even at park position, if it is near beam. About 2/3 of broken targets were broken at the tails instead of center where beam hits. This leads to hypothesis that the heat generated by the induced current on the target is the culprit [6]. The RF voltage is reduced during polarization measurement to prolong the target lifetime, as induced fields are weaker with longer bunch. Round shape fins are added this year based on the experiment test last year. The preliminary results show that the target lifetime is prolonged, even though the glowing light is not completely eliminated.

ISBN: 978-3-95450-168-7 doi:10.18429/JACoW-IPAC2015-MOPTY012

DESIGN AND TEST OF PROTOTYPE OF LLRF SYSTEM FOR KIPT NEUTRON SOURCE LINAC

X. Ma#, R. Liu, Y. Chi, G. Shu, IHEP, Beijing, China

Abstract

A 100 MeV/100 kW electron LINAC is being constructed by IHEP, China for the NSC KIPT Neutron Source project in Ukraine [1]. A LLRF system is required to produce the driver RF input of the klystron and maintain the accelerating phase and amplitude stability of the machine. The LLRF system consists of an RF reference distribution system, six identical control units, and the fast RF interlock module. The main part of control unit is the PXI-bus crate implemented with PXI9846 - 4 ADC digitizer board and ICS572 - high speed 2 ADC/2 DAC signal process board. An EPICS IOC based on WinDriver as the PCI device driver is developed and tested. Preliminary results show phase detect resolution of 0.03 degree (rms) of 2856MHz signal has been achieved.

INTRODUCTION

The 100MeV electron LINAC includes a triode-type gun, a 2856 MHz pre-buncher (PB), a 2856 MHz travelling wave buncher (B) and ten 2856 MHz travelling wave accelerating tubes (A0-A9). The layout of the LINAC is shown in Fig. 1. The pre-buncher, the buncher and the first accelerating tube are powered by one klystron. The second accelerating tube is powered by one single klystron to obtain a higher accelerating gradient. For the following accelerating tubes, each two are powered by one klystron. The Low-Level RF (LLRF) system is needed to control the phase and amplitude of each accelerating sections. The reference signal from master oscillator (MO) is distributed to each LLRF module by phase-stabilized coaxial cables.

REQUIREMENT ANALYSIS

In order to maintain the stability of the LINAC, the LLRF system must include the following requirements:

- The phase and amplitude stability of the accelerating field are ±2° and ±2% according the beam dynamic analysis [2]. The phase reference signal of each LLRF station must be stabilized.
- The LLRF system should generate drive waveform for the klystron and compensate the beam loading effect.
- The LLRF system should provide signal monitoring and some fast interlock functions such as loss of power protection and reverse power over-limit protection, etc.
- The LLRF system should provide the access point with the control system and the graphic user interface to the operators.

#maxp@ihep.ac.cn

SYSTEM DESIGN AND TEST

One typical control unit of the LLRF system is shown in Fig. 2. The hardware can be divided into two parts: the RF front-end module and the data acquisition (DAQ) module. The front-end module includes a frequency generator which provides the LO signal for the down-converters and up-converters as well as the Clock for the DAQ module. The DAQ module consists of three boards: ICS572F, PXI9846 and PXI3950, which are inserted in the same chassis with the PXI-bus connection.

The PXI9846 board from ADLINK has four 16-bit 40MSPS ADCs. It is used to digitize the down-converted IF signals of the forward/reverse signals of the klystrons and the accelerating tubes.

The ICS572F board from GE has two 14-bit 105 MSPS ADCs and two 14-bit 250 MSPS DACs. It is used to generate the drive signal of the klystron, detect the phase and amplitude of the pickup signal and implement PI and feed-forward control algorism in order to maintain the stability of the accelerating field.

The PXI3950 board from ADLINK is an embedded controller with an Intel x86 CPU and runs on the Windows XP 32-bit version operation system. The EPICS IOC which includes the device support of PXI9846 and ICS572F is built on this controller. The records that hold the waveforms of the signals and the control registers of the LLRF system are supported by these devices. So these records can be accessed by any Channel Access tools in EPICS through the Ethernet.

The version of EPICS base is R3.14.12.3 and the EPICS_HOST_ARCH is chose to be cygwin-x86.

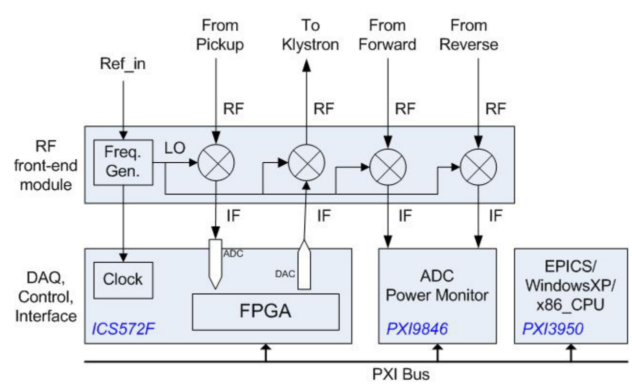

Figure 2: Structure of one LLRF control unit.

Data acquisition of PXI9846

There are two ways getting the samples through PXI9846 board: using task-oriented DAQPilot library or

Content from this work may be used under the terms of the CC BY 3.0 licence (© 2015). Any distribution of this work must maintain attribution to the author(s), title of the work, publisher, and DOI.

ISBN: 978-3-95450-168-7 doi:10.18429/JACoW-IPAC2015-MOPTY013

CONTROL SYSTEM FOR DC-SRF PHOTO-INJECTOR AT PEKING UNIVERSITY *

L. Feng†, L. Lin, F. Wang, J. Hao, S. Huang S. Quan, K. Liu, B. Zhang
Institute of Heavy Ion Physics, Peking University, Beijing 100871, China

Abstract

A control system has been designed and constructed to full-fill the operation requirement of the DC-SRF photo injector developed at Peking University. The system includes an analog laser phase lock system, FPGA based low level radio frequency (LLRF) control system, PLC based machine protection system, VME based magnet power control, and PC based EPICS IOC. All these systems were integrated to support the stable operation of the DC-SRF photo injector and has shown their robustness. The LLRF system was optimized and tuned for 2K CW/Pulse operation and the stability of amplitude and phase achieves 0.1% and 0.1° respectively.

INTRODUCTION

The DC-SRF [1] photo injector developed at Peking University was designed to generate high repetition rate electron beam in 3-5 MeV range. This injector combines a DC pierce gun and a 3.5-cell superconductor cavity which is capable to operate in both CW and pulse mode. Recently, we've completed the commissioning of the injector [2] and had conducted experiments such as THz coherent wiggler radiation [3] on the platform. The schematic layout of the platform is shown in Fig. 1 and the photo of beamline is shown in Fig. 2.

To make it easier to operate the injector, control of the driver laser, superconductor cavity, beam transport line and other auxiliary systems has to apply. And high level control application such as user interface, data archiver, system-wide interlock was also required.

An EPICS based control system was introduced for this purpose. The remote control of each subsystem was implemented by difference kinds of EPICS IOCs. Control System Studio (CSS) was chose as the OPI tool for its flexibility.

Along with the works on integrating the system, great efforts were also spent on dealing with various of instabilities observed during the experiments. These instabilities were mainly attributed to the phase jitter of laser and RF system. To reduce those instabilities, we've developed a digital Low Level Radio Frequency (LLRF) control system [4] and the laser phase lock system were improved to reduce the relative phase jitter.

SYSTEM DESIGN

The whole system can be divided into five subsystems: injector cryomodule, magnet power supply system, driver

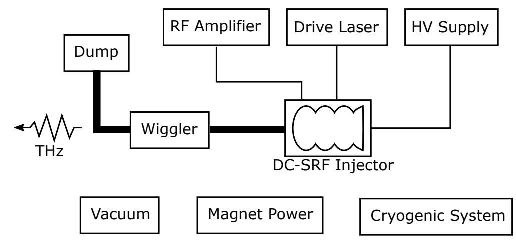

Figure 1: DC-SRF injector THz wiggler radiation experiment layout.

Figure 2: The DC-SRF injector and beamline.

laser system, RF control system, and other auxiliary systems such as cooling and vacuum system.

Injector Cryomodule Control

The DC-SRF injector cryomodule is one the main parts of the platform. Its primary function is to maintain 2 K conduction for the super conducting cavity. The cryogenic system that supplies LHe/LN for the cryomodule was constructed by Linde Inc. and Technical Institute of Physics and Chemistry, CAS. The cryogenic system was shipped with a standalone control system and operates independently. Other parts of the injector, however, need controls to ensure the proper operation of it. 16 temperature sensors were installed in the cryomodule. Two Cryocon Model-18 temperature monitors were used to measure those sensors. The measured values can then be transfered to a soft IOC through Ethernet. Because the Model-18 temperature monitor uses just plain text in their communication protocol, it is quite handy to interface them with Asyn/Stream Device module in the IOC.

Besides for the cryogenic system, a high voltage DC power supply is connected to the DC gun of the injector. The high voltage power supply has voltage control input, voltage read

* Work supported by Major State Basic Research Development Program of China (Grant No. 2011CB808302 and 2011CB808304)
† lwfeng@pku.edu.cn

Content from this work may be used under the terms of the CC BY 3.0 licence (© 2015). Any distribution of this work must maintain attribution to the author(s), title of the work, publisher, and DOI.

ISBN: 978-3-95450-168-7 doi:10.18429/JACoW-IPAC2015-MOPTY014

AN EXPERIMENTAL STUDY OF HIGHER-ORDER MODES EXCITED BY HIGH REPETITION RATE ELECTRON BEAM IN AN SRF CAVITY*

Yongfeng Gao, Liwen Feng, Jiankui Hao, Senlin Huang, Lin Lin, Xing Luo, Shengwen Quan, Fang Wang, Zhiwen Wang, Kexin Liu, Jia-er Chen
Institute of Heavy Ion Physics, School of Physics, Peking University, Beijing 100871, China

Abstract

Higher-order modes (HOMs) excited by electron beam traversing a superconducting rf (SRF) cavity contain lots of information and can be used for intra-cavity electron beam diagnostics. Unlike single bunch, multiple bunches would excite HOMs with a much complicated spectrum. In this paper, we present our recent research on HOMs excited by a high repetition rate electron beam in an SRF cavity. Especially, we focus on the integer multiple frequency peaks in the HOM spectrum, which are determined by the nearest eigen HOM peaks. The experiments were carried out on the DC-SRF photoinjector, which was operated at MHz repetition rate. The results agree well with theoretic analysis.

INTRODUCTION

Higher-order modes (HOMs) excited by electron beam travelling through a superconducting rf (SRF) cavity contain abundant information of the electron beam [1,2]. Lots of studies have been carried out for single electron bunch excited HOMs and the applications [2,3,4]. There are also some research on HOMs excited by multiple electron bunches [5,6], in which case, however, the characteristics of HOMs have not been well studied.

We recently studied HOMs excited by high repetition rate electron bunches, with the focus on HOM characteristics. Some preliminary experiments have been conducted on the DC-SRF photoinjector [7] at Peking University. In the following sections, we will first discuss the characteristics of HOMs excited by high repetition rate electron bunches. The HOM experiments on the DC-SRF photoinjector will then be introduced. Some preliminary test results with electron beam offset in the SRF cavity will also be presented.

HOM EXCITED BY HIGH REPETITION RATE ELECTRON BEAM

When high repetition rate electron bunches go through an SRF cavity, the excited HOMs may accumulate in the cavity, depending on the time interval between the bunches and the decay time of the modes. Considering a long train of electron bunches with the bunch charge of q, equally separated by T in time domain, the HOM voltage at the time t when the Nth bunch has passed through the cavity can be obtained using the superposition principle as [8]

$$\mathrm{V_N}(t) = \sum_{n=0}^{\mathrm{N}} V_q \cos[\omega_0(t-nT)]\, e^{-\frac{t-nT}{T_d}}, \qquad (1)$$

where V_q is the HOM voltage excited by a single bunch, ω_0 and $\mathrm{T_d}$ are the frequency and decay time of the mode, respectively.

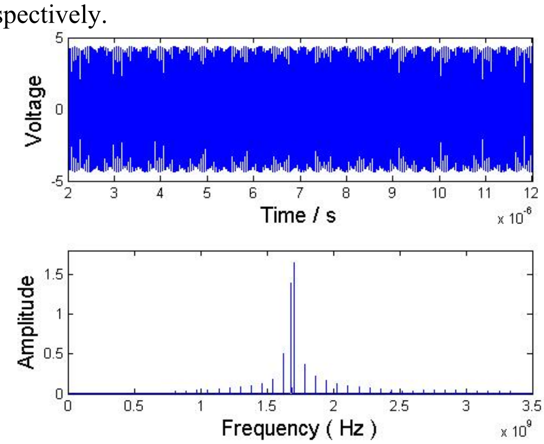

Figure 1: A typical waveform of HOM mode excited by a high repetition rate electron beam (upper) and its spectrum (lower). In the calculation, the repetition rate is assumed to be 81.25 MHz and the HOM frequency is assumed to be 1.685GHz.

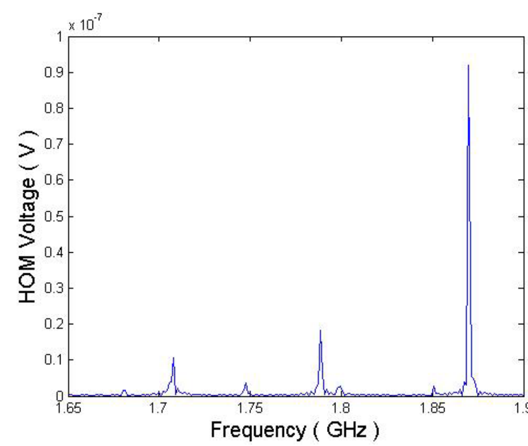

Figure 2: Simulated HOM spectrum, which is excited by a train of bunches at the repetition rate of 81.25MHz.

Figure 1 shows a typical waveform of HOM excited by a high repetition rate electron beam, calculated using Eq. (1), and its spectrum. It can be seen from the figure that the HOM spectrum is rather different to single bunch case [6]. Besides the peak at the HOM eigen frequency (referred to as eigen HOM peaks hereon), many other peaks can be observed at integer multiples of the bunch repetition frequency (referred to as IF peaks hereon).

*Work supported by National Natural Science Foundation of China (No. 11275014)

Content from this work may be used under the terms of the CC BY 3.0 licence (© 2015). Any distribution of this work must maintain attribution to the author(s), title of the work, publisher, and DOI.

ISBN: 978-3-95450-168-7 doi:10.18429/JACoW-IPAC2015-MOPTY015

BEAM COMPRESSION DYNAMICS AND ASSOCIATED MEASUREMENT METHODS IN SUPERCONDUCTING THz SOURCE

ZHOU Zheng, DU Yingchao, HUANG Wenhui
Department of Engineering Physics, Tsinghua University, Beijing 100084, PR China

Abstract

To ensure the quality of high brightness electron beams needed by the terahertz FEL facility at China academy of engineering physics(CAEP),which aims to obtain 100 to 300 terahertz light, a feed-back control system is required to monitor the amplitude and phase jittering by measuring beam arrival time as well as bunch length at the site of the beam position monitor(BPM).

In this paper, we make an idealized model of injector section and deduce analytic expressions of bunch arrival time and bunch length. In consideration of the space charge effect on bunch lengthening, bunch arrival time and bunch length as a function of DC gun voltage, buncher field amplitude and buncher phase is carefully calibrated by means of particle in cell (PIC) simulation. With the time and space resolution of the BPM, the control accuracy of phase is estimated to be 0.01 degree, while the amplitude is 0.04%.

INTRODUCTION

Owing to the challenge of advanced accelerator applications, the control accuracy of amplitude and phase is becoming stricter for control systems, under which circumstance emerges methods of beam-based feed-back control. Two representative examples are the fast feedback installed in Stanford Linear Collider(SLC) using BPM readings and fitted beams parameters to stabilize beams [1]; while a combination of RF and beam based feedback loops used at The Free Electron LASer at Hamburg(FLASH) has achieved regulation of ~10fs rms bunch arrival time jitter [2].

For the THz-FEL facility at CAEP [3], the main goal for the accelerator control systems is to achieve highly precise regulation of relative amplitude and absolute phase jitter below 0.01 % (rms) and 0.01 degrees (rms).

KINEMATIC MODEL WITHOUT SPACE CHARGE

In THz-FEL, the electron bunch has a length of ~30ps at the exit of the DC gun, and needs a bunching process through the downstream buncher to reach ~10ps length before entering the superconducting accelerating cavity. The BPM located close to the entrance of the accelerating cavity is used for beam position measurement. Here an ideal kinematic model without space charge is utilized to deduce analytical expressions of bunch arrival time and bunch length (compression ratio) at the site of BPM.

Arrival Time Jitter

In the FEL facility, the arrival time of electron bunch at the site of downstream BPM is effected by several factors, such as the voltage of the photocathode DC electron gun, the electric field amplitude of the buncher and working phase of the bucnher. When DC voltage, buncher amplitude and phase have a small perturbation, the consequent arrival time jitter can be decided by means of perturbation. As the perturbation of above mentioned factors is quite small compared to the set value, means of perturbation is used to find the linear relation between the arrival time and perturbation. Given parameters of the FEL facility, the linear relation between arrival time jitter and above-mentioned factors in shown by Equ. (1) to Equ. (3).

$$\Delta t\,(\mathrm{ps}) = -0.78\Delta V_0(kV)\ . \tag{1}$$

$$\Delta t\,(\mathrm{ps}) = -3.6\Delta\phi(\mathrm{deg})\ . \tag{2}$$

$$\Delta t\,(\mathrm{ps}) = 0\cdot\Delta V_b(kV)\ . \tag{3}$$

Here, V_0 is DC gun voltage, φ is the phase of the buncher, V_b is the gap voltage of buncher.

A Space Charge Tracking Algorithm (ASTRA) code is used to simulate the arrival time jitter versus DC gun voltage and phase of the buncher to check validity of the kinematic model. The result is shown in Fig. 1 ,Fig. 2 and Table 1.

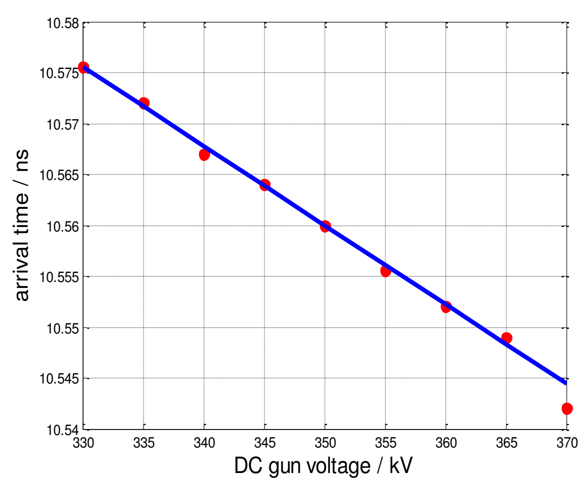

Figure 1: arrival time vs DC gun voltage.

Here, the red dot is the result of ASTRA simulation, while the blue line is theoretical result obtained from Equ. (1), and the same setting is used in following figures.

Content from this work may be used under the terms of the CC BY 3.0 licence (© 2015). Any distribution of this work must maintain attribution to the author(s), title of the work, publisher, and DOI.

ISBN: 978-3-95450-168-7 doi:10.18429/JACoW-IPAC2015-MOPTY016

STUDY OF DIAMOND DETECTOR APPLICATION AT THE FRONT END OF A HIGH INTENSITY HADRON ACCELERATOR*

Guangyi Ren, Yuxiong Li, Weimin Li#, Duohui He, National Synchrotron Radiation Laboratory, University of Science and Technology of China, HeFei, AnHui 230029 China
Ming Zeng, Department of Engineering Physics, Tsinghua University, Beijing, 100084, China

Abstract

Diamond detectors function as beam loss or luminosity monitors for high energy accelerators, such as LHC, Babar, etc. Because of regular detectors insufficient protection of the front end, diamond detectors owning significant characteristics, like time resolution in the nanosecond range, radiation hardness and negligible temperature dependence. Thus, diamond detectors have been becoming promising candidates for detecting BLMs of fully super-conducting hadron accelerator, such as C-ADS, FRIB. In this paper, the sensitivity of diamond detectors was simulated by Monte Carlo program FLUKA and GEAN4. Meanwhile, we tested the performance of a new prototype of CVD diamond detector, and compared it with Si-PIN and Bergoz detectors at the storage ring of the HLS II. The results of the diamond detector were consistent with other two detectors well. More evaluation of diamond detectors in low energy radiation field are ongoing.

INTRODUCTION

Beam loss monitors (BLMs) are common devices usedin hadron and lepton accelerators. Depending on accelerator specifies, BLMs could be just diagnostics or could play an essential role in the machine protection system (MPS). Beam loss control is one of the bottlenecks for beam power increasing for high intensity machine. Some new hadron accelerators, like the Chinese Accelerator-Driven System (C-ADS) and the Facility for Rare Isotope Beams (FRIB), are full superconducting accelerator[1][2]. The sc cavity is more sensitive to beam loss than roomtem perature accelerating section. Thus, it's necessary to provide a high level beam loss monitor system. A widely accepted rule of thumb is to limit the beam loss to 1 W/m to keep the radioactivation levels low enough for hands-on maintenance. As beam powers grow ever higher, the corresponding fraction of the allowable beam loss necessarily becomes smaller and thus more challenging.

There are some ordinary BLM detectors such as Bergoz in NSRL and ionization chamber in SNS[3]. The Bergoz detector is based on Si-PIN sensor, in many similar applications, the Si-PIN BLM detector encountered the radiation damage problem and had limited lifetime[4]. That's why the Si-PIN sensor is not enough for a high intensity accelerator. In SNS, The ionization chamber (IC) is the main detector type in the BLM system due to its simple design and immunity to radiation damage. The biggest problem is significant background from the X-ray radiation produced by the RF cavities. And it's not sensitive enough at lower energy. Thus, it's necessary to design new type BLM detector to meet the high intensity hadron accelerator at the low energy section.

* Work supported by XDA03000000.
#lwm@ustc.edu.cn

RADIATION FIELD SIMULATION

High Intensity Hadron Accelerator

Different from the room temperature accelerating section at the front-end of SNS or J-PARC, C-ADS or FRIB will accelerate the heavy ion by sc section from RFQ. In this paper, radiation field caused by beam loss of C-ADS injector will be fully discussed as a representative of new type accelerator.

Injector II, as a possible front-end of C-ADS linear accelerator, consisting of an ECR ion source, a 2.1 MeV room temperature RFQ and superconducting half wave resonator (HWR) cavities[5]. The sc accelerating section will stimulate the proton from 2.1MeV to 10 MeV. Figure 1 depicts the sc HWR cavity and the FLUKA simulation model. In the sc HWR cavity, the white structure is niobium cavity and the green one is titanium as insulation and support. Liquid helium fill the gap between niobium and titanium to keep low temperature.

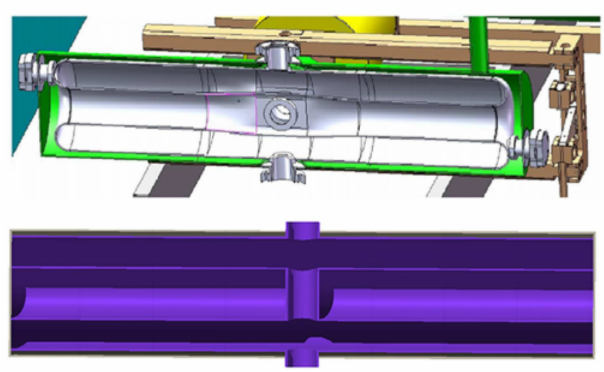

Figure 1: The upper one is the left view of HWR cavity and the lower one is the top view of FLUKA model.

Analyze of the Simulation

The secondary particles that hit the BLM detector may be electron, photon and neutron. Thay come from three mechanisms: prime proton loss, field emission and delayed process by activated materials. The sc accelerator

Content from this work may be used under the terms of the CC BY 3.0 licence (© 2015). Any distribution of this work must maintain attribution to the author(s), title of the work, publisher, and DOI.

ISBN: 978-3-95450-168-7 doi:10.18429/JACoW-IPAC2015-MOPTY019

PRECISE POSITION MEASUREMENT BY ANALYZING THE CORRELATION BETWEEN ELECTRODES OF A SINGLE BPM*

Zhichu Chen†, Longwei Lai, Yongbin Leng‡, Yingbing Yan
Shanghai Synchrotron Radiation Facility, Chinese Academy of Sciences, China
Shanghai Institute of Applied Physics, Chinese Academy of Sciences, China

Abstract

Beam position is one of the most important parameters in a particle accelerator. The more accurate and precise the measurement system is, the more features of the beam dynamics could be revealed. A method called model-independent analysis (MIA) takes advantage of multiple beam position monitors (BPM) on the storage ring to obtain the actual beam positions by removing the random noise of each BPM. Inspired by MIA, the original voltage waveforms obtained from the electrodes of a single BPM can also be decomposed to get the beam position information. This article discusses the results of the experiments and the evaluation of the performance of the BPM at the Shanghai Institute of Applied Physics.

INTRODUCTION

BPMs are commonly used in modern light sources. The calculations and the simulations of the electrodes have already been studied. Although the fabrications are mature, the individual differences in frequency response are inevitable. Nevertheless, the impedance matchings along the cables are difficult. Thus, the original signals from different electrodes are slight different, and these signals have been mixed with parts of their reflected ones. If we still use the traditional signal processing procedures, systematic errors will be introduced in the measurements.

The induced signal from the ith electrode can be written as:

$$V_i(t) = p_i(x) \cdot Q(t) * U_i(t), \tag{1}$$

where $p_i(x)$ is the position factor, $Q(t)$ is the bunch charge distribution factor and $U_i(t)$ is the impulse voltage response. Ideally, the responses $U_i(s)$'s are identical, so the linear approximation of a two-pickup BPM is

$$V_1 \simeq (1 + K_x \cdot x) \cdot K_q \cdot q \cdot U_0, \tag{2}$$
$$V_2 \simeq (1 - K_x \cdot x) \cdot K_q \cdot q \cdot U_0. \tag{3}$$

Thus, the position of the bunch is

$$x \simeq \frac{1}{K_x} \frac{V_1 - V_2}{V_1 + V_2}. \tag{4}$$

Including the response deviations and the random noises, the final signals are

$$V_1 \simeq (1 + K_x \cdot x) \cdot K_q \cdot q \cdot (U_0 + \Delta_1) + N_1, \tag{5}$$
$$V_2 \simeq (1 - K_x \cdot x) \cdot K_q \cdot q \cdot (U_0 + \Delta_2) + N_2. \tag{6}$$

The best linear approximation for the calculated position (higher order terms like $N_1 \cdot N_2$ or $\Delta_1 \cdot N_1$ have also been omitted after the Taylor expansion) will be

$$\begin{aligned}
&\frac{V_1 - V_2}{V_1 + V_2} \\
=&\frac{K_x x K_q q(2U_0 + \Delta_1 + \Delta_2) + K_q q(\Delta_1 - \Delta_2) + N_1 - N_2}{K_q q(2U_0 + \Delta_1 + \Delta_2) + K_x x K_q q(\Delta_1 - \Delta_2) + N_1 + N_2} \\
\simeq& K_x \cdot x \\
&- \frac{K_x^2 x^2 - 1}{2U_0 + \Delta_1 + \Delta_2} \cdot (\Delta_1 - \Delta_2) \\
&+ \frac{K_x \cdot x - 1}{K_q \cdot q \cdot (2U_0 + \Delta_1 + \Delta_2)} \cdot N_1 \\
&+ \frac{K_x \cdot x + 1}{K_q \cdot q \cdot (2U_0 + \Delta_1 + \Delta_2)} \cdot N_2.
\end{aligned} \tag{7}$$

The system resolution can only be improved by removing the last three terms of the r.h.s. of the above equation.

MODE SEPARATION

The area of the envelope of the signal is used in Equation (4) to minimize the influences of the random noise and the lag differences between cables. This method will improve the accuracy of the measurement, but the response differences between electrodes and the reflection in the cable are still there. Since these response deviations, signal reflections and random noises are linearly mixed into the final signal in Equations (5) and (6), a singular value decomposition (SVD) can potentially separate them as different modes. [1,2]

Rather than calculating the integrals of the envelopes of the raw ADC waveforms, We will create a waveform matrix and the SVD of the matrix will give several—as many as the number of electrodes—modes, some of which are, hopefully, unrelated to Δ_1, Δ_2, N_1 or N_2. The spatial vectors of the U_0-related mode(s) will be used to calculate the bunch position.

Since the signals are narrow-banded sine waves, there will be two principal components we're interested in: a $\sin \omega t$ mode and a $\cos \omega t$ mode. The rest modes can all be regarded

* Work supported by National Natural Science Foundation of China (No. 11305253)
† chenzhichu@sinap.ac.cn
‡ leng@sinap.ac.cn

Content from this work may be used under the terms of the CC BY 3.0 licence (© 2015). Any distribution of this work must maintain attribution to the author(s), title of the work, publisher, and DOI.

ISBN: 978-3-95450-168-7 doi:10.18429/JACoW-IPAC2015-MOPTY020

AN INTELLIGIENT TRIGGER ABNORMAL BEAM OPERATION MONITORING PROCESSOR AT THE SSRF*

L.W.Lai, Y.B.Leng#, Y.B.Yan, Z.C.Chen
SSRF, SINAP, Shanghai, China

Abstract

An intelligent trigger abnormal beam operation monitoring processor has been designed at the SSRF. By applying digital signal processing algorithms in FPGA, the processor keeps monitoring the beam operation status. It will output a trigger signal and store the turn-by-turn beam position data when abnormal events detected. The abnormal events include injection, beam loss, and abnormal disturbance. This ability makes the processor a powerful tool for abnormal operation causes analysing and machine study.

INTRODUCTION

SSRF beam current was increased from 220mA to 240mA at the end of 2013. Occasionally partial beam loss happened during the current upgrade period. BPM turn-by-turn data around the abnormal operation event is very useful to analyse the possible causes. SSRF has more than 140 Libera DBPM processors distributed around the 20 cells storage ring. Only when external interlock signal is received the DBPM to lock TBT data for analysis. Interlock signal is given only when beam lost completely or the beam orbit out of the preset range, partial beam loss is not included. This character makes Libera DBPM helpless for analysing the possible causes when partial beam loss happened. SSRF plans to increase the current to a higher level, final aim is 300mA. There is a very necessary to have an efficient tool for future current increasing.

SSRF storage ring runs at top-up mode since December 2012. To maintain the current at 240±2 mA, electrons are injected every 10 minutes. The injection disturbance introduced transverse oscillation gives opportunity to monitor the real-time tune value. Tune value is a very important indicator to evaluate the machine status. By applying FFT method on sampled BPM turn-by-turn data during injection, we can get tune value every 10 minutes.

Above applications require a specific DBPM with functions monitoring the ring status, when partial beam loss and injection are detected, it can intelligent triggered to store BPM turn-by-turn data automatically.

DBPM PROCESSOR

SSRF have developed a DBPM processor since 2007 [1, 2], the processor consists of two boards: a mezzanine board with four channels RF conditioning modules and ADCs, a carrier board with an ARM and a FPGA. Signals from four channel BPM pickups are fed into RF conditioning modules on the mezzanine board firstly. Then signals are filtered with band pass filter (Surface Acoustic Wave filter) to centralize in 500MHz with band width of 20MHz. Then the signals are maintained at an appropriate level with attenuators and amplifiers. After the conditioning, signals are sampled with ADCs (16bits, 117MHz) by means of undersampling theory. The digitized signal is processed with FPGA (Xilinx xc5vfx70t) on the carrier board. The implanted distributed control system (EPICS) on the ARM(s3c6410) made it an all-in-one instrument. Figure 1 is the architecture of DBPM processor, Figure 2 is the picture of the processor.

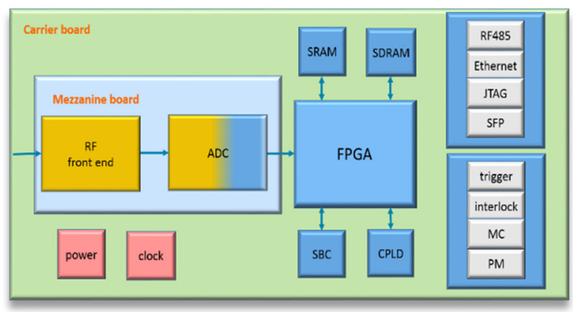

Figure 1: DBPM processor architecture.

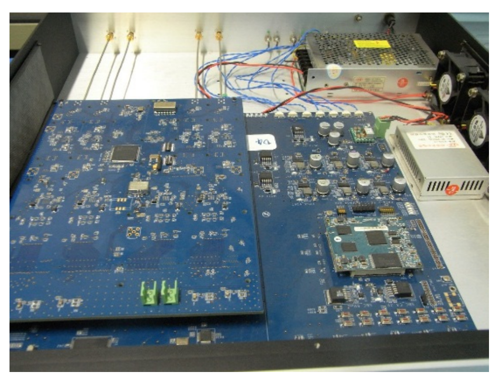

Figure 2: DBPM processor.

By applying FPGA, the DBPM provides different rate beam position data, including 694 kHz turn-by-turn (TBT) data, 50 kHz data, 10 kHz fast application (FA) data and 10 Hz slow acquisition (SA) data. The spatial resolution of TBT data is about one µm. The FPGA's powerful programmable ability enables us implement the abnormal beam operation monitoring function on the DBPM.

*Work supported by National Natural Science Foundation (No. 11305253, 11375255)
#lengyongbin@sinap.ac.cn

Content from this work may be used under the terms of the CC BY 3.0 licence (© 2015). Any distribution of this work must maintain attribution to the author(s), title of the work, publisher, and DOI.

ISBN: 978-3-95450-168-7 doi:10.18429/JACoW-IPAC2015-MOPTY021

MEASUREMENT OF CLOCK JITTER IN BEAM DIAGNOSTIC SYSTEM*

Yong Yang, Yongbin Leng#, Yingbing Yan
Shanghai Institute of Applied Physics (SINAP), CAS, Shanghai 201204, P. R. China

Abstract

Low clock jitter can improve the performance of beam diagnostic system. This paper presents a procedure for the direct measurement of low-level clock jitter. High resolution spectrum analyzer or broadband high sampling rate oscilloscope is not demanded by using this method. Simulation will be introduced.

INTRODUCTION

As the demand for high fidelity sampling of clock frequency in excess of 100MHz continues to increase in beam diagnostic system, the aperture uncertainty (jitter) of the system sampling clock itself is becoming the limiting factor of the achievable SNR of the whole signal-conditioning chain [1]. Numerous methodologies have been proposed and discussed, since jitter performance still is one of the most challenging issues in state-of-the-art sampled systems [2].

The most directed method is using broadband high sampling rate oscilloscope. However, to measure clock jitter less than 20ps, the sampling rate of oscillator must be more than 50Gsps where the effective number bits of the ADC in oscilloscope is more enough. Integrating the phase noise near the central frequency can also obtain the clock jitter if we have a high resolution spectrum analyzer. To measure low-level clock jitter, the dynamic range of spectrum analyzer will be not enough.

Another strategy to measure the clock jitter is through the SNR of the sampling system itself. The simplest and most widely adopted one infers the jitter value from the SNR measurements at high input frequency, where the random deviation σ_T of the occurrence of the sampling edge translates into a random voltage error $\sigma_{Vjitter}$ that dominates the noise deviation σ_V. The retro-fitting is usually accomplished according to the formula:

$$SNR = \frac{P_{in}}{\sigma_V^2} \approx \frac{P_{in}}{\sigma_{Vjitter}^2} = \frac{A_{IN}^2/2}{\sigma_T^2 \frac{(A_{IN}\omega_{IN})^2}{2}} \qquad (1)$$

as applied to a sinusoidal input of amplitude A_{IN} and angular frequency ω_{IN} ($= 2\pi f_{IN}$):

$$V_{IN}(t) = A_{IN}\sin(\omega_{IN} t) \qquad (2)$$

Previous methods of estimating the jitter from the ADC's SNR were hampered by the imperfect knowledge of the real values of thermal noise, random non-linearity contributions, and any additional noise effects entering Eq. (1). Determining a f_{IN} high enough for the formula to be applied was somewhat of an arbitrary process. At very high input frequencies lots of dynamic effects such as substrate noise, signal leakage, complex device behavior, and many more, affect the noise term of the equation thus making the jitter estimation harder.

This paper describes a precise yet easy method of measuring the jitter of a clock. The description of an innovative technique for the determination of the jitter in sampled-input systems is provided. The extraction of the period jitter from the SNR data collected on a 14b 105MSps ADC is then simulated.

CALCULATING JITTER THROUGH INPUT COHERENT SAMPLING

Coherent sampling (or locked-histogram) techniques have been successfully employed in the past in order to estimate clock jitter. However, this paper presents a parametric analysis of the correlation between the jitter and the phase of the input at which noise is measured. The main advantage of the proposed technique is that the measurements obtained from the clock under test are parametrically fitted to the true profile of the jitter in such a system, thus providing for a true numerical solution to the problem. In addition, since the results are fitted to the expected shape of the jitter vs. phase theoretical dependence, the clock jitter can be measured down to levels lower than the ones allowed by the noise floor of the converter.

Jitter Formula Derivation

The theoretical RMS voltage error $\sigma_{Vjitter}$ induced by the clock cycle jitter (defined as the standard deviation of the Gaussian distribution of the periods, σ_T) is calculated through the input slope via the formula:

$$\begin{aligned}\sigma_{Vjitter} &= \sigma_T \cdot \left|\frac{\partial V_{IN}(t)}{\partial t}\right| \\ &= \sigma_T \cdot A_{IN}\omega_{IN} \cdot \left|\cos(\omega_{IN} t)\right| \qquad (3)\end{aligned}$$

Equation (3) quantifies the well-known concept that when an ADC is sampling a sinusoidal input, the contribution of clock jitter is much more pronounced when the sampling instant coincides with the zero crossing of the input, and has very little impact on the output noise when the sampling instant coincides with the top or bottom of the input sinewave.

Figure.1 illustrates this concept: the Gaussian distributions shown on the right represent the histogram of the captured output samples of the ADC, in the two cases described.

*Work supported by National Nature Science Foundation of China(11375255)
#lengyongbin@sinap.ac.cn

Content from this work may be used under the terms of the CC BY 3.0 licence (© 2015). Any distribution of this work must maintain attribution to the author(s), title of the work, publisher, and DOI.

ISBN: 978-3-95450-168-7 doi:10.18429/JACoW-IPAC2015-MOPTY022

Content from this work may be used under the terms of the CC BY 3.0 licence (© 2015). Any distribution of this work must maintain attribution to the author(s), title of the work, publisher, and DOI.

BUNCH BY BUNCH DBPM PROCESSOR DEVELOPMENT AND PRELIMINARY EXPERIMENT IN SSRF*

Yongbin Leng#, Zhichu Chen, Longwei Lai, Yingbing Yan, Yong Yang, SSRF, Shanghai, China

Abstract

Digital BPM processor with turn-by-turn capability has been widely used in synchrotron radiation facilities over the world, which is proved to be very useful and powerful for daily operation and linear optics study but not good enough in the case of individual bunch information required. In order to sufficient individual bunch diagnostics requirements a development plan of the next generation DBPM processor with bunch-by-bunch capability has been initiated in SINAP since 2012. The whole development was divided into three steps: a concept processor based on digital oscilloscope IOC, an algorithm prototype processor based on commercial high speed ADC board, and a custom designed dedicated processor. The progress of this work and several preliminary beam experiments will be discussed in this paper.

INTRODUCTION

In order to improve the efficiency and quality of the light, the top-up mode was adopted at the SSRF since the end of 2012, which results more frequent beam injections (about one injection in ten minutes).[1] Since injection process involves a variety of equipments, parameters of all the equipments can not match perfectly with each other during the transient injection process. Any parameter mismatching will lead to a closed orbit distortion, which will leave a residual betatron oscillation after injection. For light source users, this disturbance must be as little as possible. An appropriate analysis and diagnosis tool is needed to provide basis for optimizing the parameters of related equipments.

The turn by turn position data and slow acquisition data acquired by normal DBPM processor can be used to observe the average effect of bunch train disturbance. The excitation current waveform mismatch between kickers and the alignment error of kickers can be studied by using these data. But the disturbance introduced by refilled bunch is hardly analysed using turn by turn data. In this case a new DBPM processor with bunch by bunch capability is required.

On the other hand realizing the measurements of the bunch by bunch position will also help study the beam impedance, coupling instability and nonlinear dynamics quantitatively, and can provide the accelerator physicists with an incredibly powerful machine study tool.

*Work supported by National Nature Science Foundation of China (11375255)

#lengyongbin@sinap.ac.cn

DEVELOPMENT OF BUNCH BY BUNCH DBPM PROCESSOR

The development was divided into three steps: a concept processor based on digital oscilloscope IOC, an algorithm prototype processor based on commercial high speed ADC board, and a custom designed dedicated processor.

Concept Prototype Based on Oscilloscope

A digital oscilloscope embedded EPICS IOC was developed in SSRF to do transverse position measurement at bunch-by-bunch rate.[2] The hardware setup si shown in Fig. 1. Broad band beam signals coupled from four button electrodes, passing through a BPF (central frequency 500MHz, BW 300MHz), are feed into four channels of scope directly. To satisfy bunch-by-bunch analyse requirement an high performance digital oscilloscope, practically Agilent DSO9064A (analogue BW 600MHz, real-time sampling rate 5GHz for 4 channels, and 100M samples per channel on-board buffer), is adopted. Beam signal will be recorded simultaneous at 5GHz sampling rate.

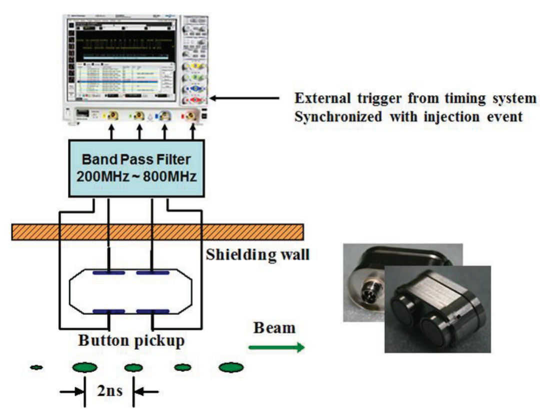

Figure 1: Hardware setup of the concept prototype of bunch-by-bunch processor.

If the sampling rate or its fraction is equal to machine RF frequency (synchronized sampling) the peak value of raw data can be used to calculate bunch charge and bunch position using Δ over Σ method directly. But for SSRF, RF frequency is usually varying between 499.654MHz and 499.674MHz depending on ground temperature. In this case using raw data will introduce a large sampling phase noise due to difference of RF and sampling frequency. A specific data processing method we called "virtual re-sampling" technique is employed to solve this problem. With correct sampling frequency and initial

ISBN: 978-3-95450-168-7 doi:10.18429/JACoW-IPAC2015-MOPTY023

BEAM DIAGNOSTIC OF THE LINAC FOR THE COMPACT HIGH-PERFORMANCE THz-FEL

T.N. Hu, B. Qin, P. Tan, K.F. Liu, Y.Q. Xiong, J. Yang, Q.S. Chen, W. Chen,
State Key Lab. of AEET, HUST, Wuhan 430074, China
Y.J. Pei#, Z.X. Tang, J. Liu, NSRL, USTC, Hefei 230029, China
Z.M. Wang, Chinagray, Hefei 230088, China

Abstract

With the aim to obtain short-pulse bunches with high peak current for a terahertz radiation source, an FEL-based LINAC is employed in HUST THz-FEL, and the LINAC consists of an EC-ITC RF gun, a disk-loaed waveguide structure with a constant gradient and collinear absorbing loads with focusing coils surrounded and so on. To achieve a balance between compactness and high performance, beam diagnostic system should be simple and high-precision. So that a cost-effective measurement scheme for the high-brightness beam extracted by the LINAC is needed. This paper will describe the beam line and beam diagnostic system of the LINAC in the HUST THz-FEL in detail and give corresponding assembly scheme. In addition, online monitor system is introduced.

BEAM LINE OF THE FEL-BASED LINAC

To achieve a balance of high performance and compact layout for a THz-FEL facility, HUST and USTC are cooperating to construct such a machine and perform corresponding experiment researches. And the facility is under commissioning right now. This facility is mainly composed of a novel EC-ITC RF gun, constant gradient travelling wave structure with a collinear absorbing load and an input coupler which makes the electric field be symmetry, and its focusing coil, beam diagnostics system, microwave power system, vacuum system, control system and so on[1]. The layout and main parameters of the LINAC are given by Fig. 1 and Table 1 respectively, and beam diagnostic equipments are sketched by Fig. 1 either.

Table 1: Main Specifications

Parameter	Unit	Value
Energy	MeV	4-15
Current	A	0.571(Macro pulse)
Width	us	1-5(Macro pulse)
	ps	1-10(Micro pulse)
Energy spread	%	0.2-0.5
Nor. emittance	mm mrad	<15
RF frequency	MHz	2856
Input power	MW	20

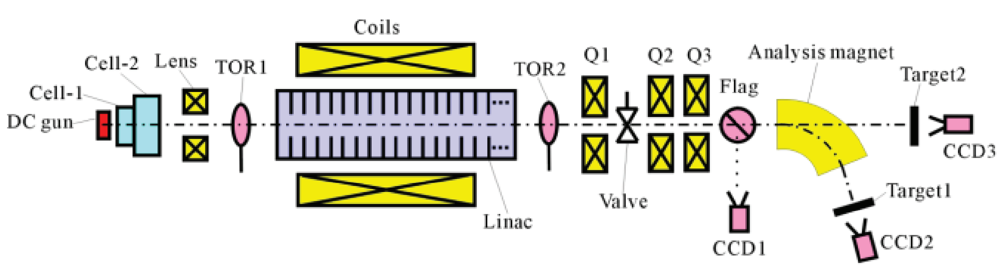

Figure 1: Layout of the HUST THz-FEL LINAC.

As the most important element, the EC-ITC RF gun plays a role of transfer DC beam to short bunches, and determines beam properties of the LINAC such as energy spread, transverse emittance, bunch length. In addition, by using velocity bunching of the standing-wave cavity, this type of gun can realize energy spread self-compensation, so that it helps to achieve the purpose of compressing the facility sizes.

Previous researches shown that, high quality bunches with ~0.3% energy spread, ~10mm mrad emittance, 201pC charge and ~2ps length can be generated by the EC-ITC RF gun[2,3]. However, in the process of dynamic calculations, a 5A DC beam are adopted as the input beam of the EC-ITC RF gun by means of parallel injection. In the actual situation, the DC electron gun has been designed to generate 4A DC beam, and it would be injected to the EC-ITC RF gun by negative angle. To press close to the actual situation, a 4A beam with negative angle is imitated, which can be shown by Fig. 2.

By adjusting power and phase parameters of two cells of the ITC cavities, the optimal results can be obtained. Dynamic results calculated by Parmela are shown in Fig. 3, meanwhile, detailed specifications of the bunches generated by EC-ITC RF gun with negative angle injection are listed in Table 2.

Content from this work may be used under the terms of the CC BY 3.0 licence (© 2015). Any distribution of this work must maintain attribution to the author(s), title of the work, publisher, and DOI.

ISBN: 978-3-95450-168-7 doi:10.18429/JACoW-IPAC2015-MOPTY025

HIGH-CURRENT RFQ DESIGN STUDY ON RAON

Jungbae Bahng, Eun-San Kim#, Kyungpook National University, Daegu 702-701, Korea
Bonghyuk Choi, IBS-RISP, Daejeon 305-811, Korea

Abstract

The Rare isotope Accelerator Of Newness (RAON) heavy ion accelerator has been designed for the Rare Isotope Science Project (RISP). RAON will produce 400 kW continuous wave (CW) heavy-ion beams, from proton beams to uranium beams, to support research in various scientific fields. The RAON system consists of an electron cyclotron resonance (ECR) ion source, low-energy beam transport systems (LEBTs), CW radio frequency quadrupole (RFQ) accelerators, a medium-energy beam transport (MEBT) system, and a superconducting linear accelerator (LINAC). We present the design study of the RFQ accelerator for deuteron beams with energies of 30 keV/u to 1.5 MeV/u and currents meeting the requirement of at least 15 mA at the target. We optimized the normal conducting CW RFQ accelerator, which has a high transmission and low longitudinal emittance. In this paper, we will present the design results of RFQ beam dynamics studies and their 2D and 3D EM analyses.

INTRODUCTION

The Rare isotope Accelerator Of Newness (RAON) heavy ion accelerator has been designed as a facility for the Rare Isotope Science Project (RISP). RAON will produce 400 kW continuous wave (CW) rare-isotope beams, from proton beams to uranium beams, using both the In-Flight Fragment (IF) and Isotope Separation On-Line (ISOL) systems, as shown in Fig. 1. For RISP to accomplish its objective, a high-intensity light-ion beam injector is required. An injector for a relatively light heavy-ion beam consists of a short low-energy beam transport (LEBT) system with two solenoids, radio frequency quadrupole (RFQ) accelerators, and a medium-energy beam transport (MEBT) system. The generated and accelerated ion beam from the high-intensity injector is then transferred to the main MEBT and accelerated by the main linear accelerator (LINAC). For use in the high-intensity injector system of RISP, we studied RFQ accelerators that are designed to accelerate high-intensity deuteron beams from 30 keV/u to 1.5 MeV/u. RFQ accelerators [1] are among the main components that can provide high-intensity beams by strong focusing, adiabatic bunching, and efficient acceleration. Since the main LINAC base frequency was chosen to be 81.25 MHz, we considered RFQ frequencies that are harmonics of this base frequency. To meet the requirement of at least a 15 mA current and achieve an economical structure, the RFQ frequency was chosen to be twice the base frequency, and the beam intensity was chosen to be 40 mA. In this paper, we focus on the beam dynamics and EM structure design of the RFQ.

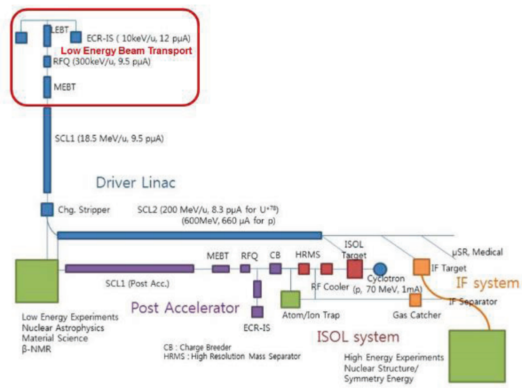

Figure 1: The layout of the RISP.

BEAM DYNAMICS DESIGN

The main RFQ design parameters are shown in Table 1.

Table 1: RAON RFQ Design Parameters

Particle (q/A)	D+ (1/2)
Frequency	162.5 MHz
I/O beam energy	30 keV/u → 1.5 MeV/u
Beam current	40 mA
Vane voltage	65~100 kV
Length	496 cm
Transmission rate	96.44 %
Tr. emittance	0.25 n.r. π mm-mrad
Max Surface Field	20.64MV/m (1.52 kilp.)

The goals of RISP high-intensity RFQ beam dynamics studies are to minimize the RFQ length, beam loss, and emittance growth. The basic objective regarding RFQs is to design beams with acceptable longitudinal bunching at the entrance of the LINAC. PARMTEQM [2] code, which was developed at Los Alamos National Laboratory, is used to generate RFQ parameters. In this study, we considered an RFQ operated at 162.5 MHz and a deuteron beam accelerated to 40 mA. We assumed that the RFQ had a low longitudinal emittance, thus avoiding transverse emittance growth, as well as a high transmission rate and short length. To optimize the RFQ design, we adopted a ramped vane voltage, slowly increased the modulation factor in the radial matching section, simultaneously

eskim1@knu.ac.kr

Content from this work may be used under the terms of the CC BY 3.0 licence (© 2015). Any distribution of this work must maintain attribution to the author(s), title of the work, publisher, and DOI.

ISBN: 978-3-95450-168-7 doi:10.18429/JACoW-IPAC2015-MOPTY028

Content from this work may be used under the terms of the CC BY 3.0 licence (© 2015). Any distribution of this work must maintain attribution to the author(s), title of the work, publisher, and DOI.

INTRODUCTION TO BINP HLS TO MEASURE VERTICAL CHANGES ON PAL-XFEL BUILDINGS AND GROUND*

Hyojin Choi†, Kwang Won Seo, Kyehwan Gil, Seung Hwan Kim, Heung-Sik Kang
Department of Accelerator, PAL-XFEL, Pohang, Korea

Abstract

PAL-XFEL is being installed and will be completed by December of 2015 so that users can be supported beginning in 2016. PAL-XFEL equipment should continuously maintain the bunch beam parameter. To this end, PAL-XFEL equipment has to be kept precisely aligned. As a part of the process for installing PAL-XFEL, a surface geodetic network and the installation of a tunnel measurement network inside buildings is in preparation; additionally, the fiducialization of major equipment is underway. After PAL-XFEL equipment is optimized and aligned, if the ground and buildings go through vertical changes during operation, misalignment of equipment's will cause errors in the electron beam trajectory, which will lead to changes to the beam parameter. For continuous and systemic measurement of vertical changes in buildings and to monitor ground subsidence (sinks) and uplift, the BINP Ultrasonic-type Hydrostatic Levelling System (HLS) is to be installed and operated in all sections of PAL-XFEL for linear accelerator, undulator and beam line. This study will introduce the operation principle, design concept and advantages (self-calibration) of BINP ULS Sensor, and will outline its installation plan and operation plan.

INTRODUCTION

During the construction of the Egypt Pyramids between 2600 and 2480 B.C., water was poured into an animal's gut in order to measure the hydrostatic level and strings were used to measure the wire position in the survey and alignment process. The Hydrostatic Levelling System (HLS) and Wire Position System (WPS) are still in use to format the horizontal axis in construction. The position of an object was measured by the human eye in the past, but these days it is measured by an electrical sensor and the data are analysed by computer - thanks to the advances in electronic equipment [1]. Recent advances in laser technology have made surveying an area of several tens of μm possible by using laser tracker [2]. But in cases where changes of the horizontal axis are measured continuously long-time, HLS and WPS, which are more precision (<1μm) then laser tracker, should be used.

HISTORY OF HLS USED ON THE ACCELERATOR

The HLS was developed by the Alignment and Geodesy (ALGE) group at the European Synchrotron Radiation Facility (ESRF) for long term monitoring and control of rapid realignment of the Storage Ring machine. The concept of the non-contact capacitive sensor developed at the ESRF for the monitoring of level differences in the ESRF storage ring has been considerably improved upon by the company FOGALE-Nanotech. ESRF announced the results of twelve years of experience in HLS operation and measurement [3]. Various types of HLS Sensors, including capacitive and ultrasonic sensors, have been developed and used. European Council for Nuclear Research (CERN) announced the results of the comprehensive testing of HLS Sensor and WPS Sensor in many forms [4]. The status and useful information about HLS and WPS used by many research institutes around the world is available at CLIC Pre-Alignment Workshop and International Workshop on Accelerator Alignment (IWAA).

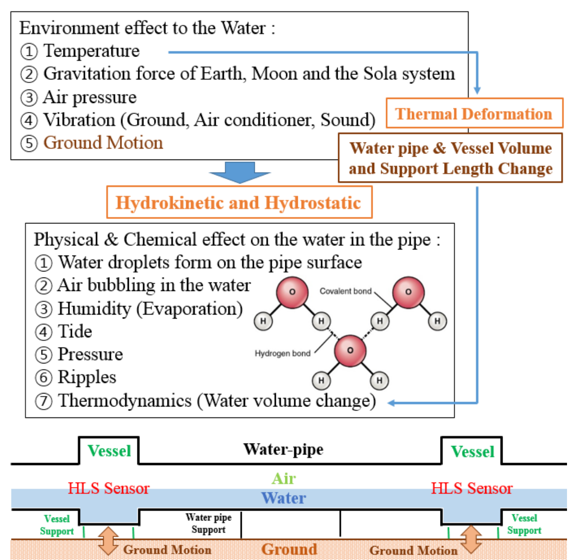

Figure 1: The surrounding environment influencing HLS.

HLS REFERENCE: WATER PIPE

The most important thing about HLS is the water pipe which provides the measurement reference. As shown in Figure 1, water within the water pipe should have good fluidity even with changes in the surrounding environment such as changes in temperature and pressure in order to maintain the constant level of water in the water pipe. It's the only way to calculate the floor deformation accurately using the measurement of all HLS Vessel floors. In terms of the fluid behaviour, after investigating studies about the way of calculating the water pipe diameter which is most appropriate for the length of full-filled and half-filled water pipes and the consequential stabilization time of water oscillation, the

*Work supported by Ministry of the Science, ICT and Future Planning
†choihyo@postech.ac.kr

ISBN: 978-3-95450-168-7 doi:10.18429/JACoW-IPAC2015-MOPTY030

CAPACITIVE LINEAR-CUT BEAM POSITION MONITOR DESIGN FOR ION SYNCHROTRON AT KHIMA PROJECT

Ji-Gwang Hwang *, Tae-Keun Yang, Seon Yeong Noh, Ga Ram Hahn, Won Taek Hwang, Chang Hyeuk Kim, Sang Hoon Nam
Korea Institute of Radiological and Medical Sciences, Seoul, Korea
Eun-San Kim
Kyungpook National University, Daegu, Korea

Abstract

The high precision beam position monitor is required to match and control the beam trajectory for the beam injection and closed orbit in synchrotron. It was also used for measuring the beta function, tune, and chromaticity. Since the bunch length at heavy ion synchrotron is relatively long, a few meters, a boxlike device with long plates of typically 20 cm is used to enhance the signal strength and to get a precise linear dependence with respect to the beam displacement. In this paper, we show the electromagnetic design of the electrode and surroundings to satisfy the resolution of 100 um, the criteria for mechanical aspect to satisfy the position accuracy of 200 um, and the measurement results of linearity by using the wire test bench.

INTRODUCTION

The the Korea Heavy Ion Medical Accelerator(KHIMA) project, a pproton and carbon therapy accelerator based on synchrotron, is currently under construction in Korea [1]. It can provide a low intensity proton and carbon beams with an energy in the range of 110 to 430 MeV/u for carbon beam and in the range of 60 to 230 MeV for proton which corresponds to the water equilibrium beam range of 3.0 to 27.0 g/cm^2 [2].

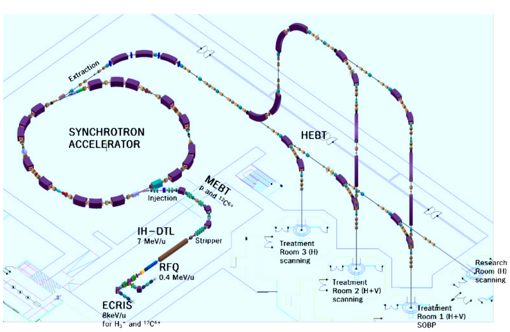

Figure 1: The layout of KHIMA accelerator.

The accelerator consists of the injector with RFQ and IH-DTL linacs, medium beam transport line, synchrotron, and high energy beam transport line. The high precision beam position monitor, which has a position resolution of $\sim$ 100 um, is required to match and control the beam trajectory for the closed orbit in synchrotron.

* hwang@kirams.re.kr

ELECTROMAGNETIC DESIGN

Since the beam intensity after the injection and capturing process in the synchrotron is low, $\sim 7.4^8$ particles for the carbon beams and $\sim 2.07 \times 10^{10}$ for the proton beams [3], the design of the beam position monitor which has the position resolution of 100 um and accuracy of 200 um is critical. The linear-cut beam position monitor was chosen to satisfy this requirements and it has the large linearity range [4]. The linear-cut beam position monitor consists of the two metal electrodes, the body for maintain the structure of the electrode, holders for combining the body with the vacuum chamber, and the vacuum chamber. The transverse and longitudinal dimension of the beam position monitor is limited because it would be installed inside the steering magnet. In order to increase the signal strength, the transverse dimension of the electrode was kept as large as possible within a limited chamber size. The 3D drawing of the designed beam position monitor is shown in Fig. 2.

Figure 2: 3D drawing of the beam position monitor.

Since the cross-talk between two electrodes determines mainly the position resolution of the beam position monitor, the distance between two electrodes is investigated to achieve lower cross-talk value that is shown in Fig. 3.

As shown in Fig. 3, the cross-talk is almost saturated when the distance between the electrodes is larger than 5 mm. Then the distance between the electrodes is determined to be 6 mm to achieve the cross-talk of less than -40 dB within an operation frequency of the beam position monitor from 0.48 MHz to 3 MHz.

The linearity of the beam position monitor is also calcu-

Content from this work may be used under the terms of the CC BY 3.0 licence (© 2015). Any distribution of this work must maintain attribution to the author(s), title of the work, publisher, and DOI.

ISBN: 978-3-95450-168-7 doi:10.18429/JACoW-IPAC2015-MOPTY033

FAST KICKER

V. Gambaryan, A. Starostenko, BINP SB RAS, Novosibirsk, Russia

Abstract

Pulsed deflecting magnet (kicker) project was worked out in BINP (Budker Institute of Nuclear Physics). The kicker design task is: impulsive force value is 1 mT*m, pulse edge is 5 ns, and impulse duration is about 200 ns. The unconventional approach to kicker design was offered. The possibility for set of cylinders using instead of plates using is considered. This approach allows us to reduce the effective plate surface. In this case, we can decrease effects related to induced charges and currents. In the result of modelling optimal construction was developed. It includes 6 cylinders (two sets in threes). Cylinders are 2 mm in cross-section. The magnet aperture is about 5 cm. Integral magnet length is about 1 meter. This length can be obtained by single magnet or by multiplied length of magnets array. Calculated field rise time (about 1.5 ns) satisfies the conditions. Induced current effect reducing idea was confirmed. For configuration with 3 cylinders pair (with cross section of 2 mm) induced current in one cylinder is about 10% and in the wall is about 40%. However for design with plates current is about 40% and 20% respectively. Obtained magnet construction allows controlling of high field homogeneity by changing currents magnitudes in cylinders. In general, we demonstrated the method of field optimization. On the basis of this work has been developed magnet design documentation. The magnet was made in BINP. At present is preparing the stand for magnetic measurements, launched works for the numerical simulation of beam dynamics in CST Studio. *Summary.* Optimal kicker design was obtained. Cylinders using idea was substantiated. Magnet was made.

THE KICKER CONCEPT DESIGN

The kicker design should accept several requirements. The first one is vacuum chamber and kicker symmetry axis coincidences. The second one is that central angel should be about 90˚. The optimisation parameter is magnetic field homogeneity in centrally located square area (2 cm x 2 cm).

GEOMETRY OPTIMIZATION

Computer simulation was carried out for kicker's parameters optimization. Calculations were realised in FEMM and Maxwell. The central angle, the cylinders number and diameter was optimized.

The Number of Cylinders

The initial geometry is shown in Fig. 1a. The cylinders with fixed diameters were placed in the vacuum chamber (with the radius of 7.5 cm) at a distance of 6 cm from its centre. The cylinders number arranges from 4 to 20. For comparison, geometry with plates was simulated (Fig. 1b). For simulating magnetic fields, the task formulated in harmonic analysis was solved on a frequency of 200 MHz. In this task cylinders are parallel connected to a current source. The impressed current in three left cylinders is +1kA, and in three right cylinders is –1kA.

Simulation results allow us to obtain the follow geometry characteristic: field homogeneity, mean value of magnetic field in the centre of the magnet, and magnet impedance.

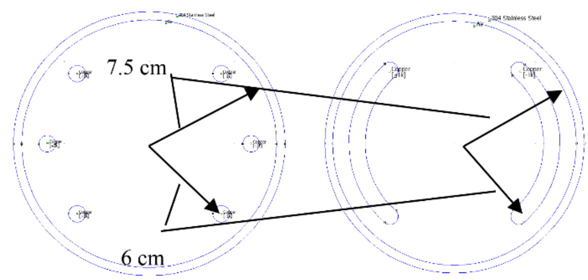

Figure 1: a). Geometry concept, b). Geometry with plates.

Field homogeneity is calculated according to Formula (1):

$$\delta B = \frac{B_{\max} - B_{\min}}{B_{\min}} \cdot 100\% , \quad (1)$$

where B_{max}, B_{min} – magnetic field maximum and minimum values, respectively, determined in centrally located square area (2 cm x 2 cm).

The field homogeneity dependence on the cylinders number is shown in Fig. 2. Here we can see that homogeneity with using 6 cylinders is equal 1%, and it does not dramatically change with the cylinders number increase. However, the increasing number of cylinders leads to a lot of technical problems associated with the vacuum feedthroughs. Thus, we should strive for the minimum number of cylinders.

The mean value of magnetic field is calculated under the same conditions as the field homogeneity. Calculation results are shown in Fig. 3. In this figure we can see that field mean value does not depend on the cylinders number.

Cylinder impedance is calculated according to energy method. To use this method two tasks were solved for the different number of cylinders. The first problem is harmonic magnetic problem. The second problem is electrostatic problem. Energies of magnetic and electric fields can be calculated according to formulas (2) and (3):

$$W_m = \frac{1}{2}\sum I_k \Psi_k , \quad (2)$$

$$W_e = U^2 C , \quad (3)$$

Content from this work may be used under the terms of the CC BY 3.0 licence (© 2015). Any distribution of this work must maintain attribution to the author(s), title of the work, publisher, and DOI.

ISBN: 978-3-95450-168-7 doi:10.18429/JACoW-IPAC2015-MOPTY034

DISTRIBUTED BEAM LOSS MONITOR BASED ON THE CHERENKOV EFFECT IN OPTICAL FIBER

Yu.I. Maltseva*, V.G. Prisekin, BINP SB RAS, Novosibirsk, Russia
F.A. Emanov, BINP SB RAS and NSU, Novosibirsk, Russia
A.V. Petrenko, BINP SB RAS, Novosibirsk, Russia; CERN, Geneva, Switzerland

Abstract

A distributed beam loss monitor based on the Cherenkov effect in optical fiber has been implemented for the VEPP-5 electron and positron linacs and the 510 MeV damping ring at the Budker INP. The monitor operation is based on detection of the Cherenkov radiation generated in optical fiber by means of relativistic particles created in electromagnetic shower after highly relativistic beam particles (electrons or positrons) hit the vacuum pipe. The main advantage of the distributed monitor compared to local ones is that a long optical fiber section can be used instead of a large number of local beam loss monitors. In our experiments the Cherenkov light was detected by photomultiplier tube (PMT). Timing of PMT signal gives the location of the beam loss. In the experiment with 20 m long optical fiber we achieved 3 m spatial resolution. To improve spatial resolution optimization and selection process of optical fiber and PMT are needed and according to our theoretical estimations 0.5 m spatial resolution can be achieved. We also suggest similar techniques for detection of electron (or positron) losses due to Touschek effect in storage rings.

INTRODUCTION

VEPP-5 Injection Complex [1] now is under commission and will supply BINP RAS colliders with electron and positron beams. The VEPP-5 Injection Complex consists of 270 MeV driving electron linac, 510 MeV positron linac and dumping ring. In order to control beam losses along beamline during the Complex commissioning and operation we proposed to use a distributed beam loss monitor based on the Cherenkov effect in optical fiber.

This type of beam loss monitor has been developed at several facilities such as FLASH (DESY), SPring-8 (RIKEN/JASRI), CLIC Test Facility (CERN) [2–4]. The monitor overview is given by T. Obina [5].

Compared with other distributed beam loss monitors such as long ionization chamber and scintillating fiber, optical fiber beam loss monitor (OFBLM) has the following advantages: fast response time (< 1 ns) which allows to detect multi-turn beam losses in a storage ring, near zero sensitivity to background signal (mainly gamma radiation) and synchrotron radiation, unlike scintillating fiber. Moreover, optical fiber is insensitive to magnetic field, but it is susceptible to radiation damage (except quartz fiber), which limits fiber lifetime. Another disadvantage of the OFBLM is an issue with its calibration.

* Yu.I.Maltseva@inp.nsk.su

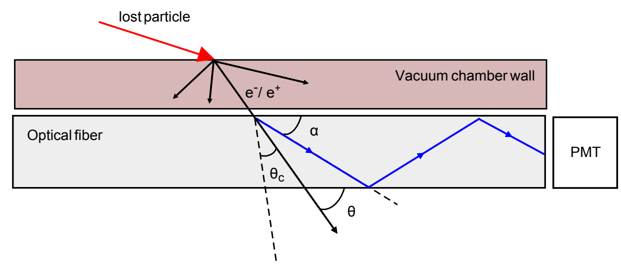

Figure 1: Scheme of beam loss monitor.

PRINCIPLE OF BEAM LOSS MONITOR

The basic idea behind the OFBLM is to detect a burst of the Cherenkov radiation (CR) generated in optical fiber by means of relativistic particles created in electromagnetic shower after highly relativistic beam particles (electrons or positrons) hit the vacuum pipe. Some of the Cherenkov photons propagate through the fiber and can be detected by PMT (Fig. 1). The following physical processes determine the beam loss detection principle of the OFBLM.

Cherenkov Radiation

The Cherenkov radiation is an electromagnetic radiation emitted in a cone around the moving charged particle with cone semi-angle θ_c:

$$\cos\theta_c(\lambda) = \frac{1}{\beta n(\lambda)} \tag{1}$$

where λ – radiation wavelength, β – particle velocity ($\beta = v/c$), n – medium refractive index. Neglecting refractive index dispersion, the number of the Cherenkov photons from a single electron or positron per unit photon energy per unit path length of the particle in a medium is given by:

$$\frac{dN}{d\lambda dx} = \frac{2\pi\alpha \sin^2\theta_c}{\lambda^2} \tag{2}$$

where α is the fine structure constant. According to eq. (2), the greater part of the Cherenkov photons is emitted in the UV range of the spectrum. For relativistic electron passing through plastic optical fiber (n = 1.492) the CR in visible spectrum (400 nm < λ < 700 nm) is generated with 30 photons per mm and emission semi-angle θ_c is about 48°.

Besides the CR, optical transition radiation can be detected by PMT. However, the number of optical transition radiation photons was estimated to be 10^4 times less than the number of the CR photons and thus can be neglected.

Content from this work may be used under the terms of the CC BY 3.0 licence (© 2015). Any distribution of this work must maintain attribution to the author(s), title of the work, publisher, and DOI.

ISBN: 978-3-95450-168-7 doi:10.18429/JACoW-IPAC2015-MOPTY036

RADIATION OF A BUNCH MOVING IN THE PRESENCE OF A BOUNDED PLANAR WIRE STRUCTURE*

Viktor V. Vorobev†, Andrey V. Tyukhtin‡, Sergey N. Galyamin, Aleksandra A. Grigoreva
St. Petersburg State University, St. Petersburg, 198504, Russia

Abstract

Three-dimensional [1, 2] and planar [3] periodic structures can be used for non-destructive diagnostics of charged particle bunches. Here we consider a semi-infinite planar structure comprised of thin conducting parallel wires. If the period of the structure is much less than the typical wavelength of the electromagnetic field, then the structure's influence can be described with help of the averaged boundary conditions [4]. We study radiation of a charged particle bunch with small transversal size and arbitrary longitudinal one in two cases: (i) the bunch moves orthogonally to the grid at some distance from the edge (Fig. 1) and (ii) it moves along the edge of the grid (Fig. 2). The problems are solved analytically. In both cases the bunch generates a surface wave which contains the information about the size of the bunch. The shape of the surface waves is similar to the radiation generated in the presence of 3D periodical wire structures [1], however planar structure is simpler for use in accelerating system. Some typical numerical results for bunches of various shapes are given.

PASSING BY THE GRID

Firstly we consider a bunch moving orthogonally to the semi-infinite wire grid at some distance from the edge (Fig. 1). It is assumed that the bunch has an infinitesimal transverse size and an arbitrary constant longitudinal charge distribution profile $\eta(\zeta)$. Current density has form

$$\rho_q(\vec{r}, t) = \delta(x + a_0)\,\delta(y)\,\eta(z - vt). \qquad (1)$$

We solve the problem in a long-wave approximation (i.e. $\lambda \gg a$). Such approximation allows us using averaged boundary condition (ABC) technique [4], which was applied for consideration of analogous problems earlier [3, 5]. The ABC are used to set electromagnetic boundary conditions in semi-plane $z = 0$, $x > 0$ (i.e. occupied by wires).

Thus, we get the problem of diffraction of the incident field of the bunch on the semi-infinite screen with specific boundary conditions. Then we use Wiener-Hopf technique [6] in order to acquire a strict analytical solution. The field of radiation has two parts: volume radiation and the surface wave. The spectral angular density of volume radiation in spherical coordinates system has the following form

$$w^v_\omega = \left(1 - \sin^2\theta\cos^2\varphi\right) cR^2 k_0^2 |A^v_{x\omega}|^2, \qquad (2)$$

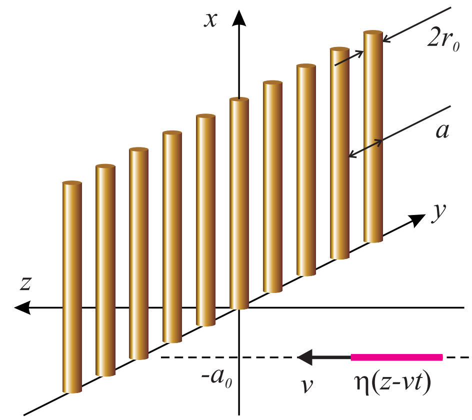

Figure 1: Bunch passing by the edge of a a grid structure.

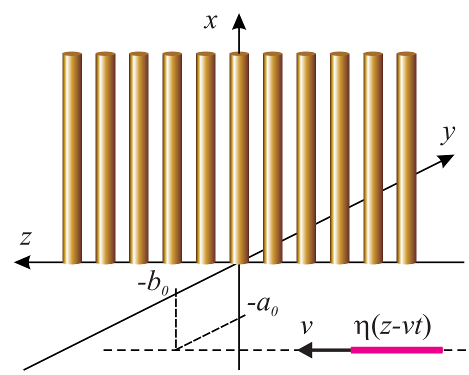

Figure 2: Bunch moving along the edge of a grid structure.

$$A^v_{x\omega} = \frac{\tilde{\eta}(\omega/v)}{\tilde{\kappa} c\beta} \frac{e^{ik_0R}}{R} \frac{\left(k_0 + \hat{k}_{x0}\right)^{-1}}{\tilde{G}_+\left(\hat{k}_{x0}, k_0\sin\theta\sin\varphi\right)} \times$$
$$\times \frac{\left(k_0\sin\theta\cos\varphi - \hat{k}_{x0}\right)^{-1}(1 - \sin\theta\cos\varphi)^{-1}}{\tilde{G}_-\left(k_0\sin\theta\cos\varphi, k_0\sin\theta\sin\varphi\right)}, \qquad (3)$$

$$\{x = R\sin\theta\cos\varphi,\ y = R\sin\theta\sin\varphi,\ z = R\cos\theta\},$$

where $k_0 = \omega/c$, $\hat{k}_{x0} = ik_0/\beta\sqrt{1 - \beta^2 + \beta^2\sin^2\theta\sin^2\varphi}$, $\tilde{\eta}(\xi)$ is a Fourier transform of bunch profile,

$$\tilde{G}_\pm\left(k_x, k_y\right) = \exp\left\{\ln\sqrt{\frac{\sin\sigma \pm \sin\tau}{1 \pm \sin\tau}} \pm \frac{1}{2\pi}\int_{\tau\pm\sigma\mp\pi}^{\tau\mp\sigma} \frac{t\,dt}{\sin t}\right\},$$

$$\tau = \arcsin\left(k_x / w_0(k_y)\right),\quad \sigma = \arccos\left(i / \left(\tilde{\kappa} w_0(k_y)\right)\right).$$

Here $-\pi < \operatorname{Re}\tau < \pi$, $\operatorname{sgn}\operatorname{Im}\tau = -\operatorname{sgn}\operatorname{Re}\tau$, $0 < \operatorname{Re}\sigma < \pi$, $w_0(k_y) = \sqrt{k_0^2 - k_y^2}$, $\tilde{\kappa} = \kappa/k_0 = \frac{a}{\pi}\ln\frac{a}{2\pi r_0}$.

* Work supported by grant of Russian Foundation for Basic Research (No.15-32-20985) and grant of President of Russian Federation (No.6765.2015.2).
† vorobjovvictor@gmail.com
‡ tyukhtin@bk.ru

Content from this work may be used under the terms of the CC BY 3.0 licence (© 2015). Any distribution of this work must maintain attribution to the author(s), title of the work, publisher, and DOI.

ISBN: 978-3-95450-168-7 doi:10.18429/JACoW-IPAC2015-MOPTY038

Content from this work may be used under the terms of the CC BY 3.0 licence (© 2015). Any distribution of this work must maintain attribution to the author(s), title of the work, publisher, and DOI.

NSLS-II DIGITAL RF CONTROLLER LOGIC AND APPLICATIONS*

B. Holub†, F. Gao, J. Kulpin, C. Marques, J. Oliva, J. Rose, N. Towne
NSLS-II, BNL, Upton, NY 11973 U.S.A.

Abstract

The National Synchrotron Light Source II (NSLS-II) accelerator consists of the Storage Ring, the Booster Ring and Linac along with their associated cavities. Given the number, types and variety of functions of these cavities, we sought to limit the logic development effort by reuse of parameterized code on one hardware platform. Currently there are six controllers installed in the NSLS-II system. There are two in the Storage ring, two in the Booster ring, one in the Linac and one in the Master Oscillator Distribution system.

INTRODUCTION

The NSLS-II accelerator consists of the Storage ring, the Booster ring and Linac along with their associated cavities. NSLS-II is committed to the use of digital RF controllers for controlling these cavities. The first generation of the digital RF controller was designed and built at Brookhaven National Laboratory (BNL) and successfully tested at the Canadian Light Source (CLS) [1]. Since that time a second generation controller was built that takes the original hardware, firmware and software and expands on their previous capabilities to make the controller versatile enough to be fielded into multiple NSLS-II subsystems (i.e., Storage ring, Booster ring, etc.). Some of the modifications made in the newest revision of the controller will be briefly described along with examples of its different uses and functions.

HARDWARE MODIFICATIONS

Figure 1 is the block diagram of the latest version of the controller showing its functionality. An explanation of the theory of operation will not be given in this paper as it has been written about in earlier publications [1], [2]. The main attributes of the hardware from the initial design are largely unchanged in this version but there are significant differences in terms of I/O and diagnostic capabilities. See Table 1 for a comparison of I/O capabilities between the original controller and the latest revision. As can be seen in Table 1 there is an increase in the number of opto-isolated and TTL inputs. The increase in inputs gives us the ability to handle more interlock triggers as well as more timing triggers going forward. Additionally, there is a small increase in the number of diagnostic LED indicators. In the latest version, the indicator LEDs are much more flexible because each is driven by a Field Programmable Gate Array (FPGA) pin instead of fixed signals external to the FPGA. Figure 2 illustrates the layout of the I/O on both the front and rear panels of the controller. The added extra I/O flexibility came at a cost, however, in that a second DAC output channel was eliminated, which was available in the original design. This channel was underutilized and was not imperative to the design. The seven channel slow ADC input circuit was scaled down to six channels. The slow DAC output circuit was removed to make room for an RS-232 channel that is used to control a tuner PLC.

Tuner Logic Addition

Tuner logic was developed in this latest revision to control the Storage ring cavity tuners. Located inside the FPGA, the tuner logic takes as its inputs the cavity field phase, the forward channel phase and a user supplied Phase Offset variable and computes an error signal for each tuner to act upon. This error signal is serialized, averaged and sent via the RS232 channel from the controller to the tuner PLC that then controls the tuner motors and moves them to drive that error signal to zero.

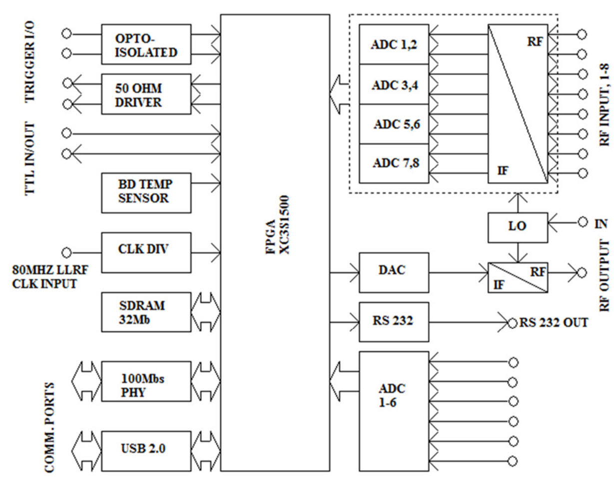

Figure 1: Functional diagram of the revised cavity field controller.

Table 1: Comparison of I/O

I/O Type	Original Rev	Latest Rev
OptoTrig-ins	2	4
TTL inputs	1	4
TTL outputs	3	4
F/P LEDs	6	7

*Work supported by the U.S. Department of Energy, Office of Science, Office of Basic Energy Sciences, under Contract No. DE-SC0012704
†bholub@bnl.gov

ISBN: 978-3-95450-168-7 doi:10.18429/JACoW-IPAC2015-MOPTY039

COMPACT SINGLE PASS BPM

M. Znidarcic, E. Janezic, M. Cargnelutti, Instrumentation Technologies, Solkan, Slovenia

Abstract

Monitoring and subsequent optimization of linacs and beam transfers requires specific instrumentation for beam position data acquisition and processing. Spark single pass BPM is the newly developed prototype intended for position and charge monitoring in classical single-multi bunch operation linacs and transfer lines. Flexibility of the instrument enables the installation on electron and proton single pass machines. The motivation, processing principles and first results are presented.

INTRODUCTION

In this paper we introduce a compact platform that aims to host a wide range of applications. First instruments built on this platform will be Spark EL and Spark HL (see Fig. 1). The instruments will be designed for processing of electron beams (Spark EL) and proton beams (Spark HL) in linear accelerators and beam transfers.

Figure 1: Libera Spark front/back panel.

A NEW PLATFORM

Looking at the beam instrumentation used to monitor and stabilize an accelerator, every device suits a specific role, but it is possible to identify some key components that are always present:

- RF front-end and analogue signal processing chains
- Internal communication buses
- Power supply unit
- Cooling system

In this new development, we take advantage of the latest advances in SoC technology to introduce a compact platform that combines a high level of hardware integration with our knowledge regarding reconfigurable analogue signal processing.

HW and SW Integration

Hardware and software are designed taking in account the balance between generality and optimization. It will be always possible to add specific features to customize it, opening at the same time the way for developing different applications, as shown in Fig. 2.

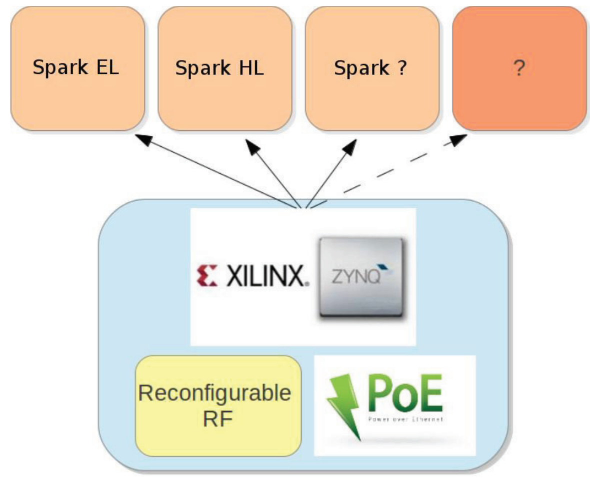

Figure 2: Platform concept based on SoC.

The core part is the SoC Xilinix Zynq 7020 [1] which combines the high-speed processing of the FPGA together with the flexibility of a CPU, all within the same chip. The inner communication between the two entities and the chance to share the same memory removes at the same time two of the biggest bottle-necks that still characterize separate-chip solutions:

- No communication protocols needed
- No data copy between FPGA and CPU.

The specifics of the analogue front-end will cover the user requirements. Integrations with specific band-pass filters, phase-locked-loop (PLL) and variable attenuators are possible if the application requires them. Fig. 2 shows an example of the HW architecture of a BPM application.

Low Power Instrument

SoC requires less power than a multiple-board solution. Furthermore proper selection of the RF components (amplifiers, analog-to-digital converters, etc.) reduces the amount of heat that the cooling system has to treat. This enables the way towards passive cooling with the integration of the heat sink in the crate. Consequently fans are no longer needed, and from the system point of view, the main advantages are:

- No moving parts means no maintenance required
- Fans-induced noise is no longer present on the signals
- Less space and less power required from the system.

With the low power requirement, precisely less than 15 Watt, the system can be powered over Ethernet according to the PoE standard IEEE802.3af. In the case of accelerator applications, if the unit is powered over Ethernet, it is possible to put it closer to the machine (e.g.

Content from this work may be used under the terms of the CC BY 3.0 licence (© 2015). Any distribution of this work must maintain attribution to the author(s), title of the work, publisher, and DOI.

ISBN: 978-3-95450-168-7 doi:10.18429/JACoW-IPAC2015-MOPTY040

HADRON BPM FOR THE FAIR PROJECT

M. Znidarcic, E. Janezic, P. Leban, Instrumentation Technologies, Solkan, Slovenia, K. Lang, GSI, Darmstadt, Germany

Abstract

The accelerators of the Facility for Anti-proton and Ion Research are designed to deliver stable and rare isotope beams covering a huge range of intensities and beam energies. FAIR will employ heavy ion synchrotrons for highest intensities, anti-proton and rare isotope production stations, high resolution separators and several storage rings where beam cooling can be applied. Instrumentation Technologies will develop and deliver a beam diagnostic system for SIS-100, HESR and CR rings. Furthermore the beam transfers will be equipped with the beam position diagnostics. The project is on schedule and the first instrument prototypes are already being under evaluation. This article discusses the new BPM electronics concept, the tests performed in the laboratory and the performance obtained.

INTRODUCTION

Almost ten years ago, twelve Libera BPMs were delivered to GSI. At that time the purpose was building the full diagnostic system for existing SIS-18 accelerator; Instrumentation Technologies provided the hardware with data storage while GSI built advanced Digital Signal Processing.

The UNILAC and the SIS 18-ring of the existing facility (blue) [1] will serve as injectors for the new facilities of the FAIR complex (red), such as the SIS-100 accelerator ring, the HESR storage ring and the various experimental areas (see Fig. 1).

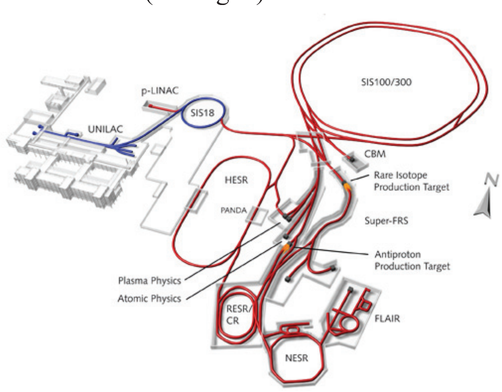

Figure 1: FAIR complex.

With FAIR project a new collaboration between GSI - FAIR and Instrumentation Technologies started. The driver for the new Hadron BPM is large SIS-100 synchrotron machine. Below are listed just some of starting points for building the new BPM system for FAIR project. A high accuracy in the order of 100 µm rms of beam position reading is required for the determination of the closed orbit, fast position readout in bunch-by-bunch manner is mandatory especially in cases when bunch manipulations will be performed, beam position data path has to be available for the closed-orbit feedback system etc.

Successful collaboration between GSI - FAIR and Instrumentation Technologies leaded to a detailed high level design. Excellent specifications and effective Instrumentation Technologies team, made it possible that in less than one year of hard work the first fully functional prototype of Libera Hadron instrument is available.

LIBERA HADRON

Libera Hadron system (see Fig. 2) is based on uTCA modular technologies with IPMI platform management. The system is therefore developed on multiple AMC modules, with each module covering different functionalities.

Figure 2: Libera Hadron.

The user can access the functions implemented in the Libera Hadron unit through a control system interface, called the Measurement and Control Interface (MCI). This interface was developed to facilitate the integration of Libera Hadron into the accelerator's control system software.

DATA PROCESSING

Libera Hadron has a capability of processing signals from shoe-box sensors or capacitive pickups, with various signal intensities, bunch repetition rates and bunch lengths [3]. Three stand alone algorithms are implemented for this purpose:

- Narrow Band analysis: Superheterodyne SDR receiver for processing bunch signals at extremely low bunch charges.
- Bunch-by-bunch for Shoe-box sensors: Bunch detection algorithm with baseline restorer for processing of unipolar signals.
- Bunch-by-bunch for capacitive sensors: Bunch detection algorithm for processing of bipolar pulses.

Libera Hadron provides four main data paths presented on Fig. 3 (raw ADC data, Bunch-by-bunch, Fast Acquisition and Slow Acquisition). Fast Acquisition data is available over SFP connector on the GDX module (optional).

Content from this work may be used under the terms of the CC BY 3.0 licence (© 2015). Any distribution of this work must maintain attribution to the author(s), title of the work, publisher, and DOI.

ISBN: 978-3-95450-168-7 doi:10.18429/JACoW-IPAC2015-MOPTY041

PROTOTYPE RESULTS WITH A COMPLETE BEAM LOSS MONITOR SYSTEM OPTIMIZED FOR SYNCHROTRON LIGHT SOURCES

Kees Bertus Scheidt, ESRF, Grenoble, France
Peter Leban, Instrumentation Technologies, Solkan, Slovenia

Abstract

Beam loss monitors in synchrotron light sources are finding an increasing utility in particular with the trend of numerous light sources pushing to lower emittances and thus higher intra-beam scattering, while operating in top-up injection modes and employing in-vacuum undulators in their rings. The development of an optimized electron BeamLoss Monitor aims at fulfilling, in one single system, all possible functionalities and applications like both the measurement of fast-time-resolved losses at injection and the possibility of ultra-sensitive detection of low & slow electron loss level variations. This optimized beam loss monitor system comprises both the acquisition electronics and up to four sensor head per unit. The sensor heads themselves, that can be configured for different sizes or volumes, are based on the detection of the electromagnetic shower resulting from an electron loss through the use of either Cherenkov radiator or gamma scintillator and a photomultiplier tube, all assembled in a single compact housing ready for installation.

DETECTION PRINCIPLE

The loss of a high energetic electron (i.e. its irreversible departure from the core of the beam) means that initially it will hit the vacuum chamber wall which then starts the creation of a so-called electro-magnetic shower: the initially created particles (electrons & positrons and γ-particles) will themselves create more particles but over a decreasing value of energy. The exact characteristics of this shower like the shape, length, number & type of particles, energy contents etc. depends much on the other obstacles (most often metallic) that the (developing) shower will encounter on its path: in a typical accelerator environment this series of obstacles comprises the vacuum chamber wall, vacuum flanges & pumps, magnet bodies, pipes, cables trays, girders, all kinds of supports and installed systems (valves, insertion devices, cavities) etc. This electro-magnetic shower is generally directed in a forward direction, i.e. in the same direction as that of the initially lost electron. However, each individual electron loss creates its own particular shower which can also have side or even back-scattered effects. Typical beam losses (in a unit of time) imply a significant number of electrons lost at the same location, and it is the sum of all these resulting showers that allows today to simulate and calculate a typical geometric distribution of that electro-magnetic shower (Figure 1).

This shower contains essentially two different types of particles that can be detected: particles with mass (electrons, positrons) and the γ-particles. Both types can be detected by the use of a suitable scintillator or radiator that converts the passage of such high energetic particle into a visible light photon. The detection of a mass-particle can be done with a specific radiator that converts its passage into so-called Cherenkov light, while for the detection of the γ-particles various optimized and highly efficient scintillator materials are available. The choice of the type of detector material depends on various considerations. In both cases, a visible photon is created that now needs itself to be detected, i.e. converted into an electrical signal and then to be recorded.

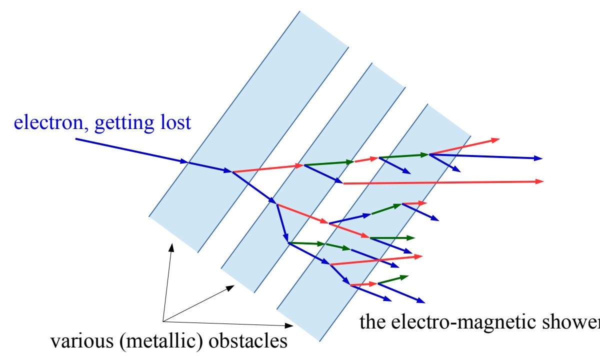

Figure 1: The electro magnetic shower.

The Photo-Multiplier Tube (PMT) will detect the visible light photon at its photo-cathode, and the emitted electron will be amplified inside this PMT and an electric current impulse will be created at its anode. And this anode's output signal will be transported over a cable to the electronics signal acquisition system. The PMT's photo-cathode is optically coupled to the scintillator (or radiator) via its input window. The size (area) of the photo-cathode and that of the scintillator (typically a cylindrical rod) are to be roughly matched so that a large part of the light generated inside this rod is effectively getting to the area of the photo-cathode. Typically diameters of 10 to 25 mm are of practical use.

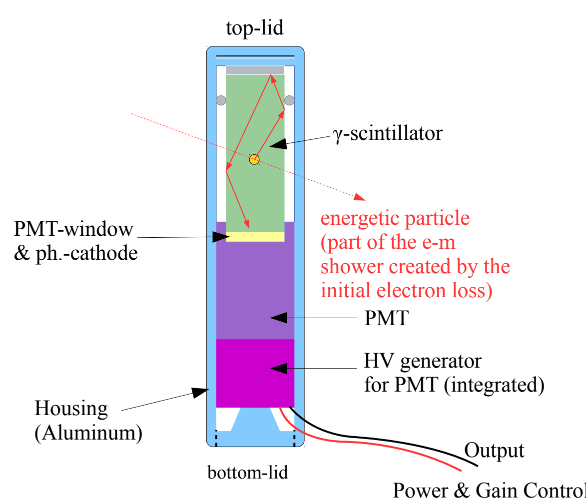

Figure 2: Scheme of the detector.

Content from this work may be used under the terms of the CC BY 3.0 licence (© 2015). Any distribution of this work must maintain attribution to the author(s), title of the work, publisher, and DOI.

ISBN: 978-3-95450-168-7 doi:10.18429/JACoW-IPAC2015-MOPTY042

Content from this work may be used under the terms of the CC BY 3.0 licence (© 2015). Any distribution of this work must maintain attribution to the author(s), title of the work, publisher, and DOI.

ALBA LLRF UPGRADES TO IMPROVE BEAM AVAILABILITY

A. Salom, F. Perez, B. Bravo, J. Marcos, CELLS, Barcelona, Spain

Abstract

ALBA is a 3GeV synchrotron light source located in Barcelona and operating with users since May 2012. The RF system of the SR is composed of six cavities, each one powered by combining the power of two 80 kW IOTs through a Cavity Combiner (CaCo). At present, there are several RF interlocks per week. The redundancy given by the six cavities makes possible the survival of the beam after one of these trips. In these cases, the cavity has to be recovered with the circulating beam. An auto-recovery process has been implemented in the digital LLRF system in order to recover the faulty RF plant with circulating beam. But these trips also create perturbations to the beam stability. In order to minimize the beam perturbations induced by these RF interlocks, an additional feed-forward loop has been implemented. The functionally, main parameters and test results of these new algorithms will be presented.

INTRODUCTION

The RF System of the ALBA SR has been designed to provide up to 3.6MV of accelerating voltage and to restore up to 540kW of power to the electron beam [1]. The main parameters of this system are summarized in Table 1.

Table 1: RF/LLRF Specifications of ALBA SR

Frequency	499.654	MHz
No of cavities	6	NC - HOM
RF Power (per cavity)	150	kW
RF Voltage (per cavity)	600	kV
Maximum Beam Current	400	mA
Nominal Beam Current	250	mA
Beam Losses per turn (U_0)	1.1	MeV
Synchrotron Frequency	5 - 9	kHz
Amplifiers type	IOT	
Main DSP of Digital LLRF	IQ mod/demodulation	
LLRF Amplitude stability	0.1	% rms
LLRF Phase stability	0.1	º rms

At present, there are several RF interlocks per week mainly due to internal arcs in the RF amplifiers. The redundancy of the RF system and the present operation of the SR at relatively low current (100mA) make possible the survival of the beam after one of these trips. An auto-recovery process has been implemented in the digital LLRF system in order to recover the faulty RF plant with circulating beam. However, when increasing the beam current in the SR, we have observed that the disturbances induced in the beam due to these RF trips can produce a partial or total beam dump. A feed-forward loop has been also implemented to compensate these perturbations and to increase the reliability of the RF systems

CAVITY AUTORECOVERY WITH BEAM

When there is a RF trip, the stopped cavity absorbs power to the circulating beam, since instants before the interlock that cavity was properly tuned. To avoid this situation, the LLRF detunes the cavity around 500kHz immediately after the interlock is detected. Besides this, the main feedback loops, amplitude and phase, get disabled and the LLRF Drive is set to a minimum level.

After clearing the interlock source, the operator sets the RF plant back into operation while the electron beam is still circulating in the SR. Then, the LLRF moves the plunger back to the position previous to the interlock detection, while keeping the LLRF drive to the minimum level and keeping the feed-back loops disabled. When the original position of the plunger is reached, the tuning loop gets enabled. In order to let the tuning loop adjust the resonance frequency of the cavity, the RF power provided by the amplifier should be high enough to overcome the beam loading effect of the circulating beam, but at the same time, it should be low enough to avoid triggering a reflected power interlock, since the cavity is completely detuned when the plant is set into operation.

After tuning the cavity, the amplitude and phase feed-back loops get enabled and the power is increased smoothly up to the nominal value set by the operator. It is important to notice that when the RF plant is set back to operation, there are no feed-back loops to adjust the phase of the cavity voltage with respect to the beam. In order to ensure the right synchronization between the LLRF drive in open loop and the phase of the beam, a digital phase shifter has been implemented at the output of the LLRF, which compensates any phase delay between the LLRF control output and the measured cavity voltage.

All the parameters for a proper cavity recovery are accessible via the LLRF control system: minimum power, detune frequency, phase delay, so that can be easily adjusted in case of changing the RF or beam conditions.

FEED-FORWARD LOOPS FOR RF TRIP COMPENSATION

Depending on the overvoltage factor of the RF and on the circulating beam current, the voltage disturbance caused by a cavity RF trip can be transparent or may cause a partial or total beam dump. The first step to compensate the perturbations caused by a RF trip is to proper characterize these disturbances.

ISBN: 978-3-95450-168-7 doi:10.18429/JACoW-IPAC2015-MOPTY043

UPDATE ON THE DEVELOPMENT OF THE NEW ELECTRONIC INSTRUMENTATION FOR THE LIPAc/IFMIF BEAM POSITION MONITORS*

Angel Guirao†, David Jimenez-Rey, Luis Miguel Martinez Fresno, Eduardo Molina Marinas, Joaquin Molla, Ivan Podadera, CIEMAT, Madrid, Spain
Ignacio Rivera, UCM/CIEMAT, Madrid, Spain

Abstract

Among all the LIPAc/IFMIF accelerator diagnostics instrumentation, the Beam Position Monitors (BPM's) are a cornerstone for its operation. An electronics system centered on self-calibration and extraction of beam phase information for Time-Of-Flight measurement is proposed for the twenty BPM stations distributed along the accelerator. The system under development is a fully digital instrumentation which incorporates automatic calibration of the monitors' signals and allows monitoring of both fundamental and second signal harmonics. The current state of the development and first experimental results of the system on the test bench will be presented.

INTRODUCTION

The team of the International Fusion Materials Irradiation Facility (IFMIF) prepares the installation and operation of the Linear Prototype Accelerator (LIPAc), which is currently under commissioning in Rokkasho, Japan [1]. An important non-interceptive beam instrumentation for the machine operation is provided by the BPMs diagnostic array system or stations, for beam commissioning and accelerator tuning and operation. It provides to the Central Control System (CCS) the variation of the beam centroid in the transverse plane (position) and the longitudinal plane (phase). A total of 20 BPM stations are distributed on the two transport lines –Medium Energy Beam Transport line (MEBT) and High Energy Beam Transport line (HEBT)-, plus the superconducting accelerating sections (SRF linac) and the essential locations defined by beam dynamic requirements in order to obtain an exhaustive feedback for steering and transporting the beam from the RFQ to the Beam Dump.

However the BPM stations located at the Diagnostics Plate will be committed to carrying out energy measurements inside HEBT as well, and not only beam position, as such information is crucial for the tuning of the cavities and a proper validation and characterization of the output beam in each beam commissioning stage. The energy is measured through phase measurement in order to extract the Time-Of-Flight (TOF) estimation for beam dynamics. In the previous years a series of evaluation on commercial options and a prototype for the electronics based on analog processing were evaluated [2] and the decision to undertake a custom design was promoted.

* This work has been funded by the Spanish Ministry of Economy and Competitiveness under the project FIS2013-40860-R and the Agreement as published in BOE, 16/01/2013, page 1988

† angel.guirao@ciemat.es

BEAM POSITION MONITOR ELECTRONICS

The current prototype for the electronic system is based on the CompactPCI (cPCI) architecture. The BPM system is integrated into the EPICS control system of the accelerator facility via Ethernet and the EPICS Channel Access, and the position and phase information is sent to the CCS updated at a rate of 2 Hz approximately. Likewise, it is required to make a database system based on EPICS Channel Access in order to save the most recent position and phase information at a rate of 0.5 Hz [3].

The BPMs requirements during the accelerator operation are summarized in Table 1.

Table 1: Main LIPAc BPM Parameters

Parameter	Value
Beam Parameters	
Beam energy	5 MeV..9 MeV
Beam current	90 mA..126 mA
RF pulse width	200 μs..CW
Duty cycle	0.1 %..100 %
Resolution and precision requirements	
Position resolution	10 μm
Position accuracy (ABS)	100 μm
Phase resolution	0.3 deg
Phase precision (ABS)	2 deg
Signal levels at the Front-End electronics input	
Max. input power	22 dBm
Required Input dynamic range	50 dB

General Layout

The full system is estimated to comprise of two cPCI racks [4], mounting a variety of boards as depicted in Fig. 1.

The current prototype, designed to demonstrate operation and provide service to the Medium Energy transport line (MEBT), sports the following hardware:

- A Central Processing Unit (CPU) running linux flavour CentOS as Operating System (OS) with kernel 2.6, integrated into the IFMIF control system via EPICS.
- Two Nutaq RF Digitizers [5] with 16 ADC channels of 14-bit with a sampling rate of 100 MHz with an

Content from this work may be used under the terms of the CC BY 3.0 licence (© 2015). Any distribution of this work must maintain attribution to the author(s), title of the work, publisher, and DOI.

ISBN: 978-3-95450-168-7 doi:10.18429/JACoW-IPAC2015-MOPTY044

MACHINE PROTECTION SYSTEMS AND THEIR IMPACT ON BEAM AVAILABILITY AND ACCELERATOR RELIABILITY

R. Andersson, A. Nordt, E. Bargalló, European Spallation Source, Lund, Sweden
E. Adli, University of Oslo, Norway

Abstract

Over the last decades, the complexity and performance levels of machine protection have developed. The level of reliability and availability analysis prior to operation differs between facilities, just as the pragmatic changes of the machine protection during operation. This paper studies the experience and development of machine protection for some of the state of the art proton and ion accelerators, and how it relates to reducing damage to and downtime of the machine. The findings are discussed and categorized, with emphasis on proton accelerators. The paper is concluded with some recommendations for a future high power linear proton accelerator.

INTRODUCTION

As the users of previous generations of research accelerators were mainly the actual developers, only the accelerator physicists themselves were concerned by the lack of protection. However, as the concept of user facilities was incorporated in the 70s, research in other fields became dependent on the accelerators performing as designed [1,2]. With this came higher demands on the machines to be more reliable and available [3]. However, even up to today, though the concepts of reliability and availability are targeted at an early stage, the main goal is still to push the beam parameters beyond existing limits. Once this goal is fulfilled, the machine reliability and beam availability receive more attention.

Because of the very high beam powers and energies in current and future accelerators [3–7], the risk of beam-induced damage is significant. In as little as a few microseconds, the energy from a deposited beam could lead to permanent damage or melting of the equipment [8]. For dealing with this, efficient protection systems need to be implemented together with appropriate monitoring. The beam interlock systems (BIS), receiving beam permit signals from the monitors, play a central role in these protection systems. The BIS creates an overall beam permit signal, which defines if beam operation will be continued or inhibited. For hazards not directly related to beam-induced damage, more sophisticated and flexible local protection systems could be implemented, which act between the monitors or sensors and the beam interlock system.

This paper looks into current state of the art proton and ion accelerator facilities and discusses their machine protection (MP) based on analysis prior to operation, pragmatic changes of the MP, and other measures of improvement.

RELIABILITY AND AVAILABILITY

Two figures to measure the performance of a system are reliability and availability, and this paper uses the following definitions [9].

Reliability is the probability of fulfilling the major design function (MDF) of the system, continuously and without interruptions, for a predefined period of time – for example one hour or one day. Mathematically, reliability is defined as $R(t) = e^{-\lambda t}$, where λ is the failure rate and t the predefined time period.

Availability is the probability to find the machine fulfilling its MDF, when it is claimed to be in operation. Mathematically, and after an extended period of operation (years), the availability can be calculated as $A(t) = 1 - MTBF/(MTBF + MDT)$, where $MTBF$ is mean time between failures and MDT is the mean downtime.

For user facilities especially, where the users are dependent on the accelerator operating as it should, those two figures of merit account to a large extent for the user satisfaction of the facility, and the aim for MP should be to have those numbers optimized.

STORAGE RINGS AND LINACS

The typical solution for MP to avoid beam-induced damage is to stop beam operation. Synchrotrons, such as the Large Hadron Collider (LHC), have the entire beam stored in its storage ring. The only option for protection in case of a hazardous fault is to extract and dump the beam, and then restart the injection and acceleration process [10]. This generally leads to low availability numbers, as much of the operational time is needed to inject and accelerate the beam up to nominal energy [11]. Therefore, the MP reliability has to be very high in order to avoid false dumping procedures.

Linacs, such as the superconducting linac at the Spallation Neutron Source (SNS), tend to aim for high average power, meaning a constant delivery of beam pulses without major interruptions. The advantage of such pulsed machines is, if an error occurs, the ability to 'skip' individual or groups of pulses or run in a degraded mode, e.g. at lower beam current or lower repetition rates. When the problem has been resolved, operation can continue as before. For this reason, high-power linacs tend to achieve higher beam availabilities than high-energy proton and ion storage rings. However, putting this simple idea into practice needs an advanced strategy for MP.

Comparing the two types of machines gives that storage rings tend to have a stronger connection between accelerator reliability and beam availability, due to the inevitable downtime associated with each beam dump.

Content from this work may be used under the terms of the CC BY 3.0 licence (© 2015). Any distribution of this work must maintain attribution to the author(s), title of the work, publisher, and DOI.

ISBN: 978-3-95450-168-7 doi:10.18429/JACoW-IPAC2015-MOPTY045

ESS RELIABILITY AND AVAILABILITY APPROACH

E. Bargalló, R. Andersson, A. Nordt, A. De Isusi, E. Pitcher, K.H. Andersen, ESS, Lund, Sweden

Abstract

Reliability and availability are key metrics for achieving the scientific vision of the European Spallation Source, ESS in Lund/Sweden. The approach taken to define the requirements and to analyze and improve these metrics is described in this contribution.

This paper describes the basis for ESS reliability and availability requirements. It describes where the requirements come from and how they are allocated among the subsystems. It puts the operation, users and the different subsystems' behavior in context, in order to provide a coherent framework to develop the RAMI* analyses for each ESS subsystem. The requirements shown here are not yet finalized and may change in the future; however, they are considered to be the base for the RAMI studies.

INTRODUCTION

ESS is a neutron source facility that will serve the scientific community by delivering spallation neutrons to a suite of scientific instruments where scientific users will be able to perform neutron scattering experiments. ESS will consist of a 5MW accelerator that accelerates protons to 2GeV, a rotating tungsten target where the spallation process takes place and the instruments where the users perform the experiments [1]. From a user perspective, the reliability and availability of the neutron beam and the neutron scattering instruments are key performance aspects of the ESS facility. High reliability and availability will ensure the execution of scientific experiments.

The methodology used to obtain the requirements considers not only the availability and reliability figures but also the specific needs extracted from user expectations of the neutron source in order to successfully perform their experiments. A top-down requirements allocation is being developed at the same time that bottom-up analyses are being undertaken. The experiments expected at ESS and their needs in terms of neutron beam performance (reliability, availability and quality) are described, as well as the tools used to analyze them. This contribution is the first step for these studies at ESS.

ESS RELIABILITY AND AVAILABILITY REQUIREMENTS

ESS requirements have been divided into Neutron Source and NSS (Neutron Scattering Systems) requirements. The Neutron Source includes all systems that contribute to the neutron beam production: Accelerator, Target, Integrated Controls System (ICS) and Site Infrastructure (SI) (only the conventional subsystems that could affect the neutron beam production). NSS include the Instrument Systems (including Guide Bunker & Monolith Shroud), Science Support Systems (SSS) and the part of SI that supplies to the NSS subsystems.

The work presented here is related to the neutron beam requirements.

Neutron Beam Needs for the Users

It was decided that the main goal for ESS is that "*At least 90% of the users should receive a neutron beam that will allow them to execute the full scope of their experiments*". Following this goal, the different kinds of experiments and their needs in order to execute their full scope were studied.

There will be two kinds of experiments: the kinetic and the integrated-flux experiments [2]. The kinetic experiments are expected to constitute about 10% of the total number of experiments that will be performed at ESS. For these experiments it is important to have a continuous beam for the duration of the measurement (an experiment is usually composed of several measurements). The duration is typically between a few seconds and several minutes. On the other hand, integrated-flux experiments (90% of the total number of experiments) are not affected by short beam interruptions; however, it is important for them to receive a high integrated neutron flux for the time allocated to them. The integrated neutron flux received by the experiments is directly related to the beam availability and the proton beam power. The duration of these experiments typically goes from one to seven days.

Neutron Beam Requirements to Satisfy the Users

Taking into account the specific needs for the experiments as well as the best practices and the operational flexibility, the following neutron beam requirements were extracted [3]:

Kinetic experiments: *"A reliability of at least 90% should be provided for the duration of the measurement. The measurement will be considered failed when the beam power is reduced to less than 50% of the scheduled power for more than 1/10th of the measurement length".*

Integrated-flux experiments: *"For the duration of the experiment at least 90% of the experiments should have at least 85% of beam availability and on average more than 80% of the scheduled beam power. The beam will be considered unavailable when its power is less than 50% of its scheduled power for more than one minute".*

These requirements were treated in order to obtain useful, traceable and consistent requirements that will be

* Reliability, Availability, Maintainability, Inspectability

Content from this work may be used under the terms of the CC BY 3.0 licence (© 2015). Any distribution of this work must maintain attribution to the author(s), title of the work, publisher, and DOI.

ISBN: 978-3-95450-168-7 doi:10.18429/JACoW-IPAC2015-MOPTY046

PERSONNEL SAFETY SYSTEMS FOR THE EUROPEAN SPALLATION SOURCE

S. L. Birch, A. Nordt, D. Paulic
European Spallation Source, ESS, Lund, Sweden

Abstract

Providing and assuring safe conditions for personnel is a key parameter required to operate the European Spallation Source (ESS).

The ESS will be responsible for developing all of the facility personnel safety related systems. All of these systems will be developed by the Integrated Control Systems Division (ICS) and all will be designed, manufactured, commissioned and operated in accordance with the IEC61508 standard, with regard to functional safety for Electrical/Electronic and Programmable Electronic (E/E/PE) safety related systems. This paper describes the ESS Personnel safety system's scope, strategy, initial design requirements, and methodology but also provides an update of the system design progress so far.

INTRODUCTION

In fall 2014 construction of the European Spallation Source (ESS) in Lund, Sweden started. The facility will comprise of a 2 GeV, 5 MW proton accelerator, a heavy metal tungsten target and 22 state of the art neutron instruments. The Integrated Control Systems (ICS) division will be responsible for the design, procurement, installation, commissioning and validation of all personnel safety systems at ESS.

PERSONNEL SAFETY SYSTEMS SCOPE

In late 2014 the overall scope of the ESS personnel safety systems was defined and 10 main systems were identified that are required to be commissioned, validated and operational for first beam of the European Spallation Source (ESS) facility in 2019. These systems are:

- The PSS for the on-site Cryogenic module test stand,
- The Accelerator Personnel Safety System,
- The Accelerator Radiation Monitoring System,
- The Accelerator Oxygen Depletion System,
- The Target Personnel Safety System,
- The Target Radiation Monitoring System,
- The Target Hot/Maintenance Cell Personnel Safety System,
- The Neutron Instrument LOKI Personnel Safety System,
- The Neutron Instrument NMX Personnel Safety System,
- The Neutron Instrument ODIN Personnel Safety System.

STANDARDS

IEC61508

As with many facilities within the accelerator research field, consensus has been that the international standard IEC61508-2010 [1] forms best practice for personnel safety systems. This has resulted in the wide adoption of this standard throughout many research facilities in the world. For it's personnel safety systems, ESS will implement the design, manufacture, commissioning, validation and operation in accordance with this standard. The IEC61508 lifecycle that ESS will follow is shown in Figure 1.

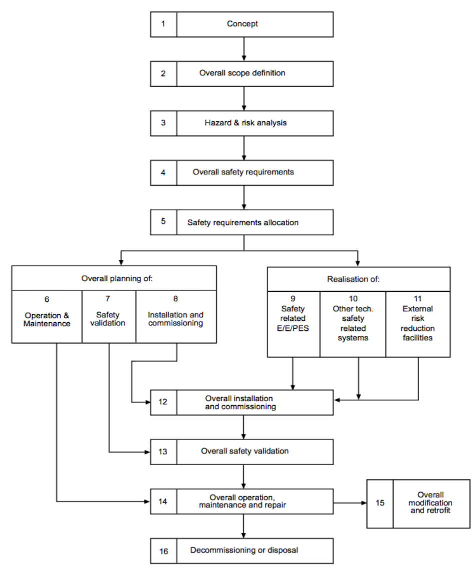

Figure 1: IEC61508 safety lifecycle.

Strålsäkerhetsmyndigheten (SSM) Swedish Radiation Authority

As part of the license application the SSM (the Swedish Radiation Authority) has requested that the ESS Personnel Safety Systems meet:

- SSM2014-127-1 [2]: "Review of application for licence for activity involving ionizing radiation" chapter 10 "review of control systems",
- SSMFS 2008-27 [3]: The Swedish Radiation Authority's "regulations concerning operations at accelerators and with sealed radiation sources".

It is important to point out that the ESS personnel safety systems primarily prevent both the public and workers

Content from this work may be used under the terms of the CC BY 3.0 licence (© 2015). Any distribution of this work must maintain attribution to the author(s), title of the work, publisher, and DOI.

ISBN: 978-3-95450-168-7 doi:10.18429/JACoW-IPAC2015-MOPTY047

ESS COLD LINAC BLM LOCATIONS DETERMINATION

M. Jarosz, A. Jansson, J.C. Kazantzidis, T. Shea, L.Tchelidze, European Spallation Source ESS, Lund, Sweden

Abstract

The linear accelerator of ESS will produce a 5 MW proton beam. Beam of this power must be strictly monitored by a specialized Beam Loss Monitoring (BLM) System to detect any abnormal losses and to ensure that operational losses do not lead to excessive activation. A long series of beam loss simulations was performed using MARS Monte Carlo code system in order to optimize the number and setting mounting locations of the detectors for best coverage, distinguishability and sensitivity. Simulations anticipated multiple possible beam loss scenarios resulting in different loss patterns. The results of energy deposition in air in the linac tunnel in multiple locations were analysed in several different ways. Incorporated methods varied from simple brute force approach to more sophisticated singular value decomposition based algorithms, all resulting in detector layout proposals. Locations selected for BLMs were evaluated for all methods.

INTRODUCTION

The linear accelerator of ESS will produce a 5 MW proton beam. Beam of this power must be strictly monitored by a specialized Beam Loss Monitoring (BLM) System to detect any abnormal losses and to ensure that operational losses do not exceed a limit of 1W/m [1]. CERN-type ionization chamber was chosen as the primary detector for the system [2]. The arrangements of the detectors along the whole machine still need to be fixed. This paper discusses the determination of the locations only in the cold linac.

SIMULATIONS

Different beam loss simulations were performed for four energies from ESS cold linac range, ranging from 220-2000MeV. For all of these energies 10 different possible locations along a pair cryomodule-quadrupole doublet were chosen (Fig. 1). At these locations three points on the beam pipe were treated as possible loss points. Losses were then simulated in MARS Monte Carlo code system [3] for 3 different angles relative to beam pipe wall: 1 mrad, 3 mrad and 1°.

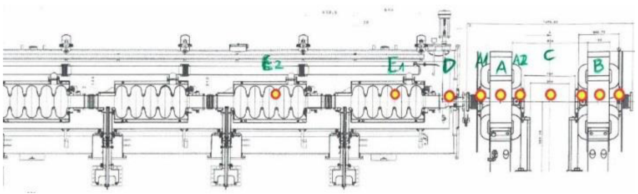

Figure 1: Loss point locations.

At the moment, the power deposited in air around a loss is used as primary indicator for suitable BLM locations as it is proportional to the BLM signal within certain limits. It can be therefore used as a good approximation for ionisation chamber response. For more accurate results, fluxes of various particles will be scored and converted into charge generated by the ionization chamber using the STRAM [4] tool described further in this paper.

MATRIX DESCRIPTION OF THE OPTIMIZATION PROBLEM

BLM's must be placed around the cryomodule-quad assemblies in the way that maximizes or at least optimizes three figures of merit: coverage, sensitivity and distinguishability of various losses. Evaluation in terms of distinguishability determines the number of beam loss scenarios possible to differentiate from each other judging by detector readings. Full coverage means reducing the number of cases which leave no traces in any of the detectors to zero and also equalising the sensitivity of the system to all loss points as much as possible. Maximizing sensitivity allows the detection of the smallest possible loss above noise level. Finally increasing resilience means minimising the loss of coverage due to failure of one or more detectors. This paper mostly focuses on maximization of coverage and distinguishability.

Let matrix M contain data on detector readings in all feasible locations. To make the situation realistic, one must select the number of monitors from the full list having in mind the optimization of coverage, sensitivity and distinguishability of losses. The problem could be described as:

$$d = M * l \tag{1}$$

where d is the vector (of length N_i – number of possible detectors) of detected losses in all possible detectors locations and l is the vector (of length N_j – number of simulated loss points) of losses at considered loss points. The set of loss point cases must be complete in order for the method to work. Excluding relevant loss points will lead to a bias in the result of monitor location selection. M therefore consists of N_j columns (different loss scenarios simulated) and N_i rows (different feasible detectors). At start the problem of finding l knowing d presented in eq. 1 is overdetermined with having more detectors then loss points, thus N_j is much smaller than N_i. By selecting a few monitor locations to place real detectors (reducing N_i to $n_i < N_j$) we introduce the underdetermination of the equation.

Decomposition of the matrix M produces the vector of its singular values. By checking its length one can judge what is the maximum number of loss scenarios that could be distinguished at all, using all feasible detectors. Using more detectors than this number doesn't increase the

Content from this work may be used under the terms of the CC BY 3.0 licence (© 2015). Any distribution of this work must maintain attribution to the author(s), title of the work, publisher, and DOI.

ISBN: 978-3-95450-168-7 doi:10.18429/JACoW-IPAC2015-MOPTY048

MACHINE PROTECTION STRATEGY FOR THE ESS

A. Nordt, T. Korhonen, T. Friedrich, C. Hilbes*, European Spallation Source ESS, Lund, Sweden
*ZHAW, Zurich University of Applied Sciences, Winterthur, Switzerland

Abstract

The ESS proton beam power of 125MW per pulse (5MW average) will be unprecedented and its uncontrolled release could lead to serious damage of equipment within a few microseconds only. To optimize the operational efficiency of the ESS facility allowing for very high beam availability with high reliability towards the end-users, accidents should be avoided and interruptions of beam operation have to be rare and limited to a short time.

Finding the right balance between efficient protection of equipment from damage and high beam availability is the key idea on which the ESS Machine Protection Strategy is being based on. Implementing and realizing the measures needed to provide the correct level of machine protection in case of a complex facility like the ESS, requires a systematic approach, which will be discussed in this paper. A method of how to derive machine protection relevant requirements and how to assure completeness of these will be outlined as well.

THE ROLE OF MACHINE PROTECTION AT THE ESS

ESS is facing high beam availability requirements and is largely relying on custom made, specialized, and expensive equipment for its operation. Damage to this equipment could cause long shutdown periods, inducing high financial losses and, as a main point, interfering with international scientific research programs relying on ESS operation and related beam production. Implementing a fit-for-purpose machine protection concept is one of the key challenges in order to mitigate these risks.

As a user facility for neutron science, overall availability of the ESS needs to be defined from a user point of view. Hence, it should be characterized by the average neutron production during a certain time period. Availability is interpreted as the average proportion of beam production time achieved during scheduled ESS research infrastructure operation time. In general, the availability characteristics of a system are determined by its reliability, maintainability and inspect-ability. The expected operational time between two consecutive corrective or preventive maintenance actions is defined as *mean time between maintenance* (MTBM). The time for diagnostics, corrective and preventive maintenance, logistics, cool down and restart times is defined as *mean down time* (MDT). Then, the operational availability can be described as:

$$\frac{MTBM}{MTBM + MDT}$$

High operational availability is thus achieved by increasing the mean time between maintenance while avoiding large mean down times. A detailed discussion in regard to varying user experiments is presented in [1].

The Machine or the Equipment Under Control (EUC)

In the context of ESS Machine Protection, the term “machine” or *equipment under control* (EUC) encompasses all elements in the Accelerator, Target Station and Neutron Science system segments - all being necessary for neutron beam production and its further use by the neutron science experiments. Figure 1 shows a simplified architectural view of the equipment under control (EUC) and the beam states.

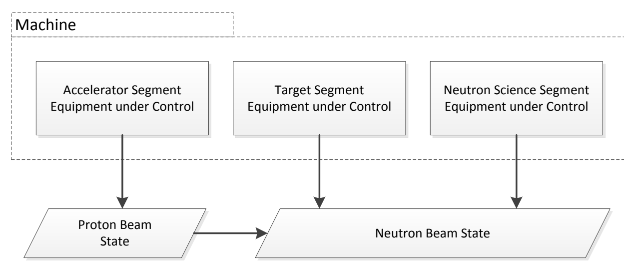

Figure 1: Simplified representation of the “machine”. Equipment under control from the accelerator segment controls the proton beam state. The neutron beam state is controlled by the Target and Neutron Science Segment EUC and is influenced by the proton beam.

Machine Protection Goals

The EUC is exposed to potential damage sources related to proton and neutron beam properties, related radiation, electrical power, vacuum, cooling, RF, etc. The severity of damage is defined with respect to neutron beam quality losses, quality loss duration and resource costs for the recovery of operational capabilities.

The goals for machine protection are defined as follows:

1. Machine protection shall, in that order, prevent and mitigate damage to the machine, be it beam induced or from any other source, in any operating condition and lifecycle phase, in accordance with beam and facility related availability requirements.
2. Machine protection shall protect the machine from unnecessary beam-induced activation having a potential to cause long-term damage to the machine or increase maintenance times, in accordance with beam and facility related availability requirements.

Machine protection is concerned with operational goals of the ESS, that means, enabling neutron science

Content from this work may be used under the terms of the CC BY 3.0 licence (© 2015). Any distribution of this work must maintain attribution to the author(s), title of the work, publisher, and DOI.

ISBN: 978-3-95450-168-7 doi:10.18429/JACoW-IPAC2015-MOPTY050

DESIGN, DEVELOPMENT AND IMPLEMENTATION OF A HIGHLY DEPENDABLE MAGNET POWERING INTERLOCK SYSTEM FOR ESS

M. Zaera-Sanz, A. Nordt, S. Birch, A. Monera, ESS, Lund, Sweden

Abstract

Approximately 350 resistive magnets and 350 power supplies (PS) will be installed in the 600 m long linear accelerator (LINAC) at the European Spallation Source, ESS, transporting the proton beam from the source to the target station. In order to protect this equipment from damage (e.g. due to overheating) and to take the appropriate actions required to minimise recovery time, a dedicated magnet powering interlock system is being designed. The magnet powering interlock system will safely switch off a PS upon the detection of an internal magnet or PS failure and inform the beam interlock system to inhibit further beam operation. The different failure modes and related mitigation techniques of magnets and their PS will be presented. Failures of the magnet cooling system can be detected for example by interlocking the opening of a thermo-switch or a flow-switch. To achieve the required level of dependability, an interlock system based on safety Programmable Logic Controller (PLC) technology, distributed safety PLC software programming tools, PROFINET fieldbus networking, and current loops for hardwired interlock signal exchanges, has been prototyped and will be discussed.

INTRODUCTION AND REQUIREMENTS

The scope of the magnet powering interlock system is to protect the magnet system from damage in case of a failure in the cooling or powering systems, and to take the appropriate action(s) to minimize time for recovery.

Due to the complexity and requirements of flexibility (not all the powering failures require a stop of beam operation), the magnet powering interlock provides local protection to the magnets and interfaces with the beam interlock system.

To protect the magnets from overheating, a set of normally closed thermoswitches are installed in the magnets and they open as soon as the temperature reaches the threshold level (typically 65ºC). A set of normally closed flow switches are also installed in the cooling system and they open when the threshold flow level is reached. Another possibility is the use of flow meters which involves measuring the actual cooling flow (typically water) and acting when this flow is below a threshold limit.

Following the reception of an overheating (notified by the thermoswitches or the flow sensors), the magnet powering interlock performs two actions: inform to the beam interlock system to stop beam operation, and switch off the corresponding power supply(ies) with a maximum delay of 1 second.

To avoid beam deflections, the above actions must follow a sequence, i.e., first stopping the beam and later switching off the power supply.

In case of a powering fault notified by the power supply to the magnet powering interlock system, the system must inform the beam interlock system in order to stop the beam operation. The power supply will be in this case automatically switched off by itself.

Figure 1 illustrates the systems involved in the execution of the protection functions and their dependencies upon each other.

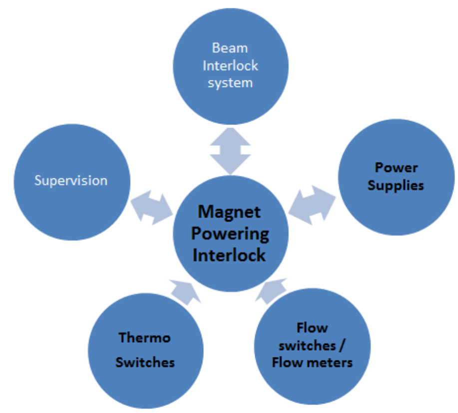

Figure 1: Relationship between the Magnet Powering Interlock system and other systems.

The magnet powering interlock system has to fulfil the following main requirements:

- Protect the magnets in the electrical circuits: in case of overheating, the necessary steps have to be taken to switch off power and stop beam operation.
- Protect the beam: the system should not generate beam stops if this is not strictly necessary. Faulty trigger signals leading to a stop of beam operation must be kept to a strict minimum in order to meet high beam availability requirements for ESS.
- Provide the evidence: in case of an overheating or a powering failure, the operator shall be notified about the root cause. The system must support the identification/diagnosis ability of the initial failure, also in case of multiple alarms (one initial failure that causes subsequent failures).
- Assist improving the operation: the diagnostics for failures should be easy. The status of the system must be clearly presented in the control room and should be transparent to the operator.

To fulfil the above requirements, the implementation of the magnet powering interlock prototype is based on PLC technology which makes use of hardwired current loops,

Content from this work may be used under the terms of the CC BY 3.0 licence (© 2015). Any distribution of this work must maintain attribution to the author(s), title of the work, publisher, and DOI.

ISBN: 978-3-95450-168-7 doi:10.18429/JACoW-IPAC2015-MOPTY052

EXPERIMENTAL AND SIMULATION STUDIES OF HYDRODYNAMIC TUNNELING OF ULTRA-RELATIVISTIC PROTONS*

F. Burkart#, R. Schmidt, D. Wollmann, M. Zerlauth, CERN, Geneva, Switzerland
N. Tahir, GSI, Darmstadt, Germany
A. Shutov, IPCP, Chernogolovka, Russia
A. Piriz, Universidad de Castilla - La Mancha, Ciudad Real, Spain

Abstract

The expected damage due to the release of the full LHC beam energy at a single aperture bottleneck has been studied. These studies have shown that the range of the 7 TeV LHC proton beam is significantly extended compared to that of a single proton due to hydrodynamic tunneling effect. For instance, it was evaluated that the protons and their showers will penetrate up to a length of 25 m in solid carbon compared to a static range of around 3 m. To check the validity of these simulations, beam-target heating experiments using the 440 GeV proton beam generated by the SPS were performed at the HiRadMat test facility at CERN [1]. Solid copper targets were facially irradiated by the beam and measurements confirmed hydrodynamic tunneling of the protons and their showers. Simulations have been done by running the energy deposition code FLUKA and the 2D hydrodynamic code, BIG2, iteratively. Very good agreement has been found between the simulations and the experimental results [2] providing confidence in the validity of the studies for the LHC. This paper presents the simulation studies, the results of a benchmarking experiment, and the detailed target investigations.

HYDRODYNAMIC TUNNELING

The theoretical investigations of the beam–target heating problem at LHC showed that the energy deposited by few ten proton bunches leads to strong heating that produces very high pressure in the beam heated region. This high pressure generates a radially outgoing shock wave that leads to a continuous density reduction at the target center. As a consequence, the protons of the subsequent bunches, and their hadronic showers, penetrate deeper into the target. Continuation of this process leads to a substantial increase in the range of the projectile particles and their hadronic shower. This phenomenon is called *hydrodynamic tunneling* of ultra-relativistic protons in solid targets. [2] It has a important implications on the machine protection design of every high stored beam energy accelerator.

EXPERIMENTAL SET-UP

Figure 1 shows the three targets used in the experiments before their installation in the HiRadMat facility. Each target comprises fifteen copper cylinders with a spacing of 1 cm in-between that allows for visual inspection of the target after the irradiation. Each cylinder has a radius of 4 cm and a length of 10 cm. The three assemblies of cylinders are enclosed in an aluminum housing that provides rigidity to the set-up and should prevent contamination of the facility. The front face of the first cylinder and the rear face of the last cylinder in the three target assemblies are covered with cylindrical aluminum caps. The experimental beam parameters were 440 GeV, a bunch intensity of 1.5E11 protons per bunch, bunch length of 0.5 ns and a bunch separation of 50 ns. Target 1 was irradiated with 144 bunches with a beam focal spot characterized by σ = 2 mm. Targets 2 and 3 were irradiated with 108 bunches and 144 bunches respectively, in both cases with a beam focal spot size characterized by σ = 0.2 mm.

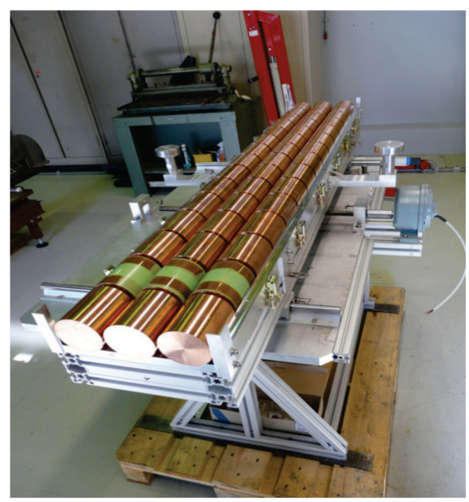

Figure 1: Target assembly.

EXPERIMENTAL RESULTS AND COMPARISON TO SIMULATIONS

The experiments were done in July 2012 and the target was opened after a cool-down period of about 10 months for a first visual inspection and the observations made at that time were published in [3,4] together with the theoretical interpretation [5]. This paper focus on the results for target 3. The results of the simulations are shown in Fig. 2. The temperature and the density along the target axis after the irradiation with 144 bunches are shown. It indicates a molten region for z = 0 - 2 cm, a

*Work sponsored by the Wolfgang Gentner Programme of the Federal Ministry of Education and Research. # florian.burkart@cern.ch

Content from this work may be used under the terms of the CC BY 3.0 licence (© 2015). Any distribution of this work must maintain attribution to the author(s), title of the work, publisher, and DOI.

ISBN: 978-3-95450-168-7 doi:10.18429/JACoW-IPAC2015-MOPTY053

ELECTROMAGNETIC DESIGN AND OPTIMIZATION OF DIRECTIVITY OF STRIPLINE BEAM POSITION MONITORS FOR THE HIGH LUMINOSITY LARGE HADRON COLLIDER

D. Draskovic, T. Lefevre, C. Boccard, R. Jones, M. Wendt, CERN, Geneva, Switzerland

Abstract

This paper presents the preliminary electromagnetic design of a stripline Beam Position Monitor (BPM) for the High Luminosity program of the Large Hadron Collider (HL-LHC) at CERN. The design is fitted into a new octagonal shielded Beam Screen for the low-beta triplets and is optimized for high directivity. It also includes internal Tungsten absorbers, required to reduce the energy deposition in the superconducting magnets. The achieved broadband directivity in wakefield solver simulations presents significant improvement over the directivity of the current stripline BPMs installed in the LHC.

INTRODUCTION

The High Luminosity upgrade for the Large Hadron Collider (HL-LHC) is scheduled to take place during the third long shutdown (LS3), when about 1.2 km of the present LHC ring will be modified. The upgrade aims at maximizing the integrated luminosity seen by the LHC experiments, with the aim of delivering 3000fb^{-1} by mid 2030 [1]. The main change will be the installation of completely new magnets for the focussing triplet in the two high luminosity collision points (ATLAS and CMS).

Seven stripline BPMs on each side of the interaction region in points 1 and 5 are currently foreseen to be installed, located in the magnet interconnect from quadrupoles Q1 to Q5. They should provide the means to control the orbit of the two beams at the interaction point (IP) with a high resolution and stability.

As the two counter-rotating LHC beams are in the same vacuum pipe throughout this whole region the BPMs need to be able to distinguish one beam from the other. The degree to which the measurement of one beam can be decoupled from the other in a common BPM is known as the directivity and its optimisation is the subject of this paper.

STRIPLINE BPM

A transmission line (stripline) couples to the transverse electromagnetic (TEM) field of the beam. Stripline BPMs can measure two beams travelling in opposite directions and ideally their upstream and downstream ports should only be sensitive to incoming particles from a given direction. The directivity of a stripline is defined as the ratio of signal power at the upstream port to that at the downstream port in response to a bunched beam particle distribution. The directional stripline BPMs currently installed in the LHC achieve a typical broadband directivity of ~20 dB [2].

To illustrate how directivity affects the accuracy of a stripline BPM, the positioning error of beam 1 in the presence of beam 2 was calculated for different beam positions and different beam intensities for the current LHC stripline BPM (BPMSX) and a BPM with improved directivity (27dB). The results are shown in Table 1. When the two beams have equal intensity and position, the error is null. However, in the LHC the beams are physically separated before the IP up to 20 mm and the error in this case can reach more than 3% of the scale factor (~half radius) assuming the current LHC stripline, but which can be three times better if the directivity is improved by a factor of 2.

Table 1: Positioning Error of Beam 1 as a Function of the Position of Beam 2 (in mm) for the New and Current LHC BPM

Error [%]	***x*=0 new**	***x*=10 new**	***x*=0 current**	***x*=10 current**	**Intensity Ratio I_2/I_1**
***y* = 0**	0	1.22	0	3.55	1
***y* = 5**	0.66	0.6	1.92	1.87	1
***y* = 10**	1.34	0	3.99	0	1
***y* = -10**	1.34	2.56	3.99	7.51	1
***y* = -10**	0.6	1.31	2.09	3.93	0.5
***y* = -10**	2.57	4.92	7.2	13.79	2

The errors are more dramatic when the beam intensities are unequal. A factor of 2 difference in intensities leads to an error of nearly 14% for the current design, which can be reduced down to 4% with improved directivity.

These errors only apply of course if the two beams actually cross in the BPM. Both for the current LHC and HL-LHC layouts the BPM locations are chosen so as to maximise the arrival time difference between the two beams to minimise the impact of this imperfect directivity. Nevertheless the influence of one beam on the other is still observed, in particular for BPMs which could not be ideally located.

This work is therefore focused on the design of a new stripline BPM, optimizing the directivity to provide the best possible accuracy.

Content from this work may be used under the terms of the CC BY 3.0 licence (© 2015). Any distribution of this work must maintain attribution to the author(s), title of the work, publisher, and DOI.

ISBN: 978-3-95450-168-7 doi:10.18429/JACoW-IPAC2015-MOPTY054

FIBRE MONITORING SYSTEM FOR THE BEAM PERMIT LOOPS AT THE LHC AND FUTURE EVOLUTION OF THE BEAM INTERLOCK SYSTEM

C. García-Argos, R. Denz, S. Gabourin, C. Martin,
B. Puccio, A. Siemko, CERN, Geneva, Switzerland

Abstract

The optical fibres that transmit the beam permit loop signals at the CERN accelerator complex are deployed along radiation areas. This may result in increased attenuation of the fibres, which reduces the power margin of the links. In addition, other events may cause the links not functioning properly and result in false dumps, reducing the availability of the accelerator chain and affecting physics data taking. In order to evaluate the state of the fibres, an out-of-band fibre monitoring system is proposed, working in parallel to the actual beam permit loops. The future beam interlock system to be deployed during LHC long shutdown 2 will implement online, real-time monitoring of the fibres, a feature the current system lacks. Commercial off-the-shelf components to implement the optical transceivers are proposed whenever possible instead of ad-hoc designs.

INTRODUCTION

The Beam Interlock System (BIS) [1] of the CERN accelerator chain is responsible for transmitting the beam permit along the Large Hadron Collider (LHC), the Super Proton Synchrotron (SPS), the transfer lines and the PS Booster.

The beam permit loop signals are two different square signals with frequencies 9.375 (loop A) and 8.375 MHz (loop B), sent in opposite directions. These beam permit loop signals are transmitted over single-mode optic fibre.

Figure 1 shows the topology of the beam permit loops at the LHC. There are two signals for each of the two beams, one transmitted clockwise and the other anti-clockwise.

There are seventeen Beam Interlock Controllers (BIC) in the LHC, two at each LHC point, named with the point number and side (left or right), and one at the CERN Control Centre (CCC), named CCR. The two generators of the beam permit signal, named CIBG, are installed in point 6, where the dump system is located.

In the SPS, there is a similar architecture, with one BIC per point, and two loops for one beam. Injection and extraction lines also have their own beam permit loops.

The controllers receive the users inputs, coming from the user systems. These inputs are connected with a logical AND inside the controller, resulting in the local permit at the BIC. If the local permit is true, then the BIC re-transmits the beam permit signal to the next BIC.

A total of 12 fibres are deployed at each controller: one for each incoming signal and one for each outgoing signal, for a total of eight active fibres. There are wo spare fibres to each of the neighbour controllers. The distance between controllers is varied, as short as a metre and as long as 6 kilometres.

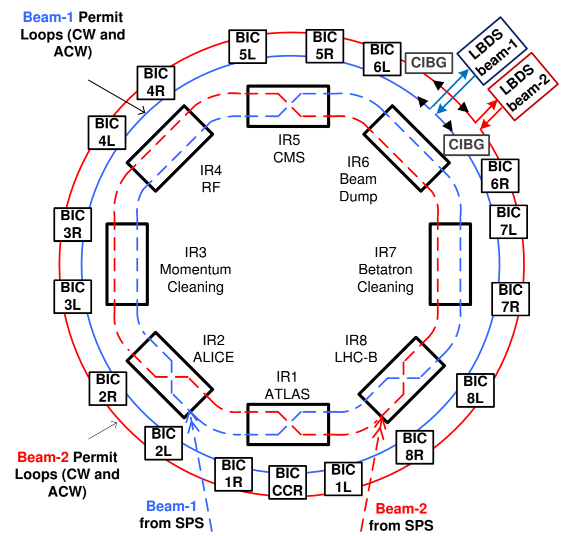

Figure 1: LHC beam permit loops.

OUT-OF-BAND FIBRE MONITORING

Motivation

The beam permit loops and the implementation of the optical links are described in [2]. The Controls Interlocks Beam Optical (CIBO) board designed at CERN uses an ELED single-mode transmitter and a PIN diode receiver to implement the optical transceiver for the beam permit signals.

The working wavelength of the loops is 1310 nm, and the receiver has a sensitive response in the range $(900, 1700)$ nm. The output power of the transmitter is typically between -25 and -15 dBm and the CIBO board is designed to deliver around -19 dBm.

The G.652 [3] type optical fibres have a maximum length of 6 km, with an initial worst case attenuation of 0.5 dB/km at 1310 nm. A number of false dumps have occurred that may have been caused by increased attenuation in the fibres, what drives the need for a monitoring system to evaluate their performance during operation.

Radiation can both create point defects in the silica and activate already existing defects, causing radiation induced

Content from this work may be used under the terms of the CC BY 3.0 licence (© 2015). Any distribution of this work must maintain attribution to the author(s), title of the work, publisher, and DOI.

ISBN: 978-3-95450-168-7 doi:10.18429/JACoW-IPAC2015-MOPTY055

BEAM LOSS MONITORING FOR RUN 2 OF THE LHC

M. Kalliokoski, B. Auchmann, B. Dehning, E. Effinger, J. Emery, V. Grishin, E.B. Holzer, S. Jackson, B. Kolad, E. Nebot Del Busto, O. Picha, C. Roderick, M. Sapinski, M. Sobieszek, F.S. Domingues Sousa, C. Zamantzas, CERN, Geneva, Switzerland

Abstract

The Beam Loss Monitoring (BLM) system of the LHC consists of over 3600 ionization chambers. The main task of the system is to prevent the superconducting magnets from quenching and protect the machine components from damage, as a result of critical beam losses. The BLM system therefore requests a beam abort when the measured dose in the chambers exceeds a threshold value. During Long Shutdown 1 (LS1) a series of modifications were made to the system. Based on the experience from Run 1 and from improved simulation models, all the threshold settings were revised, and modified where required. This was done to improve the machine safety at 7 TeV, and to reduce beam abort requests when neither a magnet quench nor damage to machine components is expected. In addition to the updates of the threshold values, about 800 monitors were relocated. This improves the response to unforeseen beam losses in the millisecond time scale due to micron size dust particles present in the vacuum chamber. This contribution will discuss all the changes made to the BLM system, with the reasoning behind them.

BEAM LOSS MONITORING SYSTEM

Energy deposition from beam losses can cause a quench of the superconducting LHC magnets or even lead to damage. The main protection against this is provided by the Beam Loss Monitoring (BLM) system. The BLM system consists of almost 4000 detectors spread around the LHC ring. The main detector type is an Ionization Chamber (IC), which are 50 cm long with an active volume of 1.5 l, filled with N_2 at 100 mbar overpressure. The detectors are parallel plate chambers with 61 circular aluminium electrodes of diameter of 7.5 cm, separated by a drift gap of 0.5 cm [1].

To cover the full dynamic range in locations with high losses, the ICs are installed in parallel to other less sensitive monitor types: Secondary Emission Monitors (SEM) or Little Ionization Chambers (LIC). Both are based on the same geometry as the ICs, but consist of only of three electrodes. The LICs have the same properties as the ICs but due to the reduced volume are 60 times less sensitive, while the SEMs operate in a 10^{-7} mbar vacuum and are 70,000 times less sensitive than the ICs.

For the start of Run 2, only the ICs are connected to the Beam Interlock System (BIS) [2] and able to give beam abort requests. The two other detector types are installed for monitoring purposes only.

NEW INSTALLATIONS

Relocation of Monitors

The operation of the LHC during Run 1 was affected by losses on the millisecond time scale. These losses are suspected to be provoked by dust particles falling into the beams, so-called Unidentified Falling Objects (UFOs) [3-4]. UFO events are seen as the most likely loss scenario in the LHC arcs during Run 2. Based on measurements performed with secondary particles generated by the beam wire scanner, it is calculated that the resulting signal of a UFO event at 7 TeV will be about 3 times higher than at 3.5 TeV [5].

To improve the response and the protection of the magnets against UFO losses, 816 ionization chambers were relocated from the quadrupole magnets (MQ) onto the intersection of the bending magnets (MB) in the arcs and dispersion suppressors (DS) of the LHC. Figure 1 shows how the existing BLMs were relocated. Figure 2 shows a monitor at the new location on top of a dipole-dipole interconnection. In this new location, the detectors monitor the losses from both beams.

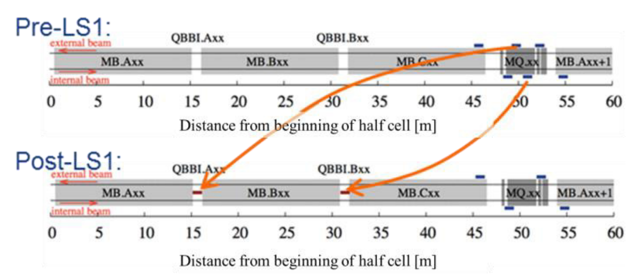

Figure 1: Relocation of beam loss monitors in the LHC arcs.

New Installations and Replacement of SEMs with LICs

SEMs are installed in parallel with the ICs to extend the dynamic range of the system towards higher dose rates to avoid saturation of the detector or electronics [6]. During Run 1 it was seen that in the events which surpassed the dynamic range of the ICs, the signal from the SEMs was still dominated by noise and no proper measurements could be made. Thus the SEMs were replaced with LICs in several locations. To further increase the dynamic range of the LICs, they are installed with RC filters connected. These filters reduce the peak amplitude for short losses, stretching the length of the signal by a factor depending on the values of the RC circuit.

Content from this work may be used under the terms of the CC BY 3.0 licence (© 2015). Any distribution of this work must maintain attribution to the author(s), title of the work, publisher, and DOI.

ISBN: 978-3-95450-168-7 doi:10.18429/JACoW-IPAC2015-MOPTY056

ELENA ORBIT AND SCHOTTKY MEASUREMENT SYSTEM

L. Søby, M. E. Angoletta, R. Marco-Hernandez, J. Molendijk, F. Pedersen, J. S. Quesada, CERN, Geneva, Switzerland; M. Bau, M. Ferrari, V. Ferrari, Brescia University, Italy

Abstract

A new Extra Low ENergy Antiproton ring (ELENA) is under construction at CERN to further decelerate the antiprotons from the existing Antiproton Decelerator (AD) to an energy of just 100 keV. This contribution will describe the beam position system foreseen for ELENA and how it can be adapted for Schottky measurements. The orbit system being developed is based on electrostatic shoebox beam position monitors fitted with Digital Down Converters (DDC). The main requirement is to measure complete orbits every 20ms with a resolution of 0.1mm for intensities in the range of 1-3E7 charges. The pick-up signals will, after amplification with a low noise charge amplifier, be down-mixed to baseband for position computation. In order to provide the longitudinal Schottky diagnostics of un-bunched beams, the 20 BPM sum signals will, after time of flight corrections, be added digitally to give an expected S/N increase of 13dB compared to using a single electrostatic pick-up.

INTRODUCTION

The Extra Low ENergy Antiproton ELENA ring [1] is a new synchrotron with a circumference of 30.4 m that will be commissioned at CERN in 2016. Table 1 provides a summary of ELENA's main parameters, while Fig. 1 gives a schematic view of the ELENA deceleration cycle which is expected to last some 20 seconds.

Table 1: ELENA Ring Main Parameters

Parameter	Injection	Extraction
Momentum, MeV/c	100	13.7
Kinetic Energy, MeV	5.3	0.1
Revolution frequency, MHz	1.06	0.145
Expected number of particles	$3\cdot 10^7$	$1.0\cdot 10^7$
Number of extracted bunches	4 (operationally)	
Extracted bunches length, m/ns	1.3/300	

The ELENA orbit measurement system will be based on 20 circular, electrostatic Beam Position Monitors (BPMs) made out of stainless steel and mounted inside quadrupoles and dipoles. After amplification of the signals by low noise amplifiers located very near to the BPMs, the difference and sum signals will be transported by ~50m cables to the rack where they will be digitized and processed.

In a second phase it is foreseen to use the same BPM sum signals for longitudinal Schottky measurements of un-bunched beams and intensity measurements for bunched beams.

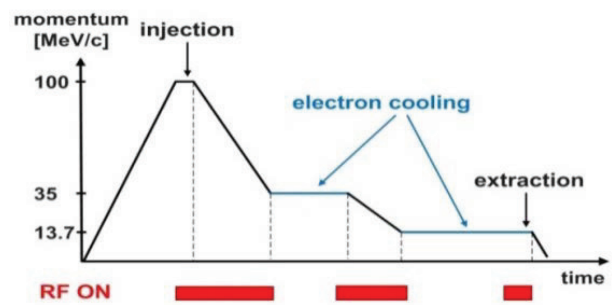

Figure 1: Schematic view of the ELENA cycle.

PICK-UP DESIGN

The proposed design is based on a stainless steel, 100 mm diameter vacuum tank containing two pairs of diagonally cut stainless steel electrodes, one for horizontal and one for vertical measurement. As can be seen in Fig. 2, no separate sum electrode is foreseen, with the sum signal generated by the addition of the electrode signals in the front-end amplifiers. Table 2 summarises the main parameters for the BPM system.

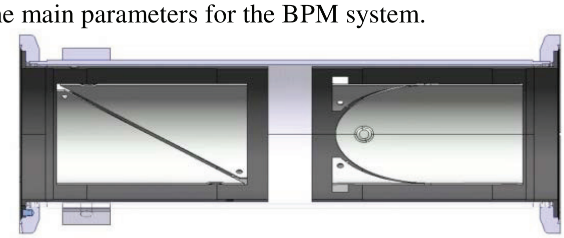

Figure 2: Cross section view of the ELENA Pick-up.

Table 2: Pick-up and Orbit Parameters

Parameter	Value
Resolution, mm	0.1
Accuracy, mm	0.3 – 0.5
Time resolution, ms	20
Electrode inner diameter, mm	66
Electrode length, mm	120
Electrode gap, mm	10
Electrode capacitance, pF	15
Bake out temperature, °C	250
Vacuum, Torr	3E-12

In order to use the BPM electrodes for Schottky measurements, it was necessary to optimize the design for high bandwidth and high sensitivity. To obtain a

Content from this work may be used under the terms of the CC BY 3.0 licence (© 2015). Any distribution of this work must maintain attribution to the author(s), title of the work, publisher, and DOI.

ISBN: 978-3-95450-168-7 doi:10.18429/JACoW-IPAC2015-MOPTY057

FEASIBILITY STUDY OF MONITORING THE POPULATION OF THE CERN-LHC ABORT GAP WITH DIAMOND BASED PARTICLE DETECTORS*

O. Stein, CERN, Geneva, Switzerland and University of Hamburg, Germany†
F. Burkart, B. Dehning, R. Schmidt, C. Buhl Sørensen, D. Wollmann, CERN, Geneva, Switzerland

Abstract

At the end of a physics fill and in case of a failure, the LHC beams must be extracted and transferred through a 750 m long line to the beam dump block. During the rise of the extraction kickers to their full strength a particle-free abort gap, with a length of 3 μs in the LHC filling pattern, is required to prevent beam losses that could lead to substantial quenching of magnets, with a risk of damage. Therefore the particle population in this abort gap, which is mainly due to un-bunched beam, is monitored. Above a certain threshold an active cleaning by excitation of betatron oscillations with the transverse feedback system is initiated. This paper describes a novel method of monitoring the abort gap population using diamond particle detectors for detecting the interactions of beam in the abort gap with neon gas, injected in the beam pipe. Two different layouts of the system and the expected interaction and detection rates are discussed.

IMPORTANCE OF THE ABORT GAP FOR THE LHC MACHINE PROTECTION

Due to the high stored energy in the LHC beams (362 MJ per beam at nominal energy) an uncontrolled, complete beam loss will cause serious damage in the accelerator components along the beamline. Therefore, in case of beam instabilities, machine failures or end-of-physics runs, the circulating beams have to be extracted and dumped in a controlled manner. For this purpose the dumping system, consisting of deflection magnets, the dump-line and the dump-block at the end, is installed separately for the two beams in point 6 of the LHC. This system is capable of dumping the beam safely without harming the machine.

In case of a beam abort the 15 kicker magnets (MKD) will be triggered to deflect the beam into the dump-line. The kicker magnets have a rise time of maximum 3 μs, the nominal bunch spacing in the LHC is 25 ns (50 ns). Bunches passing the kicker magnets whose fields are rising will experience a deflection smaller than it is needed for a proper extraction. These diverted bunches continue traveling on a wrong trajectory. This can result in beam losses which lead possibly to damage or quenches in the downstream magnets.

The LHC filling pattern contains a 3 μs long (ideally) particle-free gap, the so-called Abort Gap (AG), to ensure safe beam aborts. The extraction kicker magnets are synchronised to the abort gap to minimise the particle losses during the rise of these magnets.

Due to unbunched beam particles can accumulate in the abort gap. Therefore it is necessary to monitor the abort gap population continuously and if necessary induce countermeasures. One method to reduce the AG population is to excite the betatron oscillation of the particles in the gap with the LHC transverse damper system which are then lost on the collimators in point 7. This Abort gap Cleaning (AGC) method was used for abort gap cleaning, during Run 1.

Monitoring the Abort Gap Population

The main instrument to monitor the abort gap population at the LHC is the synchrotron radiation monitor (BSRA). This monitor detects the synchrotron light which is emitted when the particles pass the super conducting (sc) D3 magnet and the adjacent sc-undulator close to point 4. Due to mechanical problems in the BSRA setup the system was not always operational and no other redundant system existed to allow a continuous monitoring of the AG.

In case of a BSRA failure the AGC was switched on regularly which lead to shorter beam life time of the LHC beams.

Therefore, an additional system for monitoring the AG beside the BSRA would add a layer of redundancy.

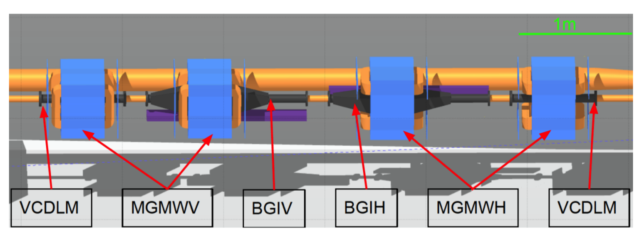

Figure 1: 3D-model of the BGI main components used for FLUKA simulations. VCDLM, 80 mm 316L drift tube. MGMW H/V, dipole. BGI H/V, vacuum chamber with BGI assembly. The second beam pipe can be seen in the background.

MONITORING THE ABORT GAP POPULATION WITH BEAM GAS INTERACTIONS

The beam gas ionisation monitors (BGI), one for each beams, are installed close to point 4 in the LHC. The original purpose of this device is to measure the transverse beam size [1].

* Work sponsored by the Wolfgang Gentner Programme of the Federal Ministry of Education and Research, Germany
† oliver.stein@cern.ch

Content from this work may be used under the terms of the CC BY 3.0 licence (© 2015). Any distribution of this work must maintain attribution to the author(s), title of the work, publisher, and DOI.

ISBN: 978-3-95450-168-7 doi:10.18429/JACoW-IPAC2015-MOPTY058

RESPONSE OF POLYCRYSTALLINE DIAMOND PARTICLE DETECTORS MEASURED WITH A HIGH INTENSITY ELECTRON BEAM *,†

O. Stein, CERN, Geneva, Switzerland and University of Hamburg, Germany ‡
F. Burkart, B. Dehning, R. Schmidt, C. Buhl Sørensen, D.Wollmann, CERN, Geneva, Switzerland
E. Griesmayer, CIVIDEC Instrumentation, Vienna, Austria

Abstract

Comprehensive understanding of beam losses in the CERN-LHC is required to ensure full machine protection and efficient operation. The existing BLM system using ionisation chambers is not adequate to resolve losses with a time resolution below some 10 μs. Ionisation chambers are also not adequate to measure very large transient losses, e.g. beam impacting on collimators. Diamond particle detectors with bunch-by-bunch resolution have therefore been used in LHC to measure fast particle losses with a time resolution down to a level of single bunches. Diamond detectors have also successfully been used for material damage studies in other facilities, e.g. HiRadMat at the CERN-SPS. To fully understand their potential, such detectors were characterised with an electron beam at the beam test facility in Frascati with bunch intensities from 10^3 to 10^9 electrons. The detector response and efficiency has been measured with a 50 Ω and a 1 Ω read-out system. This paper describes the experimental setup and the results of the experiment. In particular, the responses of three samples of 100 μm polycrystalline diamond detectors and two samples of 500 μm polycrystalline diamond detectors are presented.

DIAMOND BASED PARTICLE DETECTORS

During the experiments at the Beam Test Facility (BTF) in Frascati, Italy, the response function and the efficiencies of two diamond detectors (dBLM) types were measured. The first type (H-type) is a special detector which was developed for high intensity ranges. This detector type was used in the damage experiment in the HiRadMat facility at CERN in 2012 [2]. The second type (L-type) is used at the LHC for monitoring fast beam losses [3]. These two detectors types consist of polycrystalline diamond (pCVD) which differs in the size and quality of the active material, see tab.1.

During the experiments at the BTF, three H-type dBLMs (H1, H2, H3) and two L-type detectors (L1 and L2) were measured.

* Work sponsored by the Wolfgang Gentner Programme of the Federal Ministry of Education and Research, Germany
† Research supported by the High Luminosity LHC project
‡ oliver.stein@cern.ch

Table 1: Characteristics of the dBLMs used at the BTF experiments [4].

	H-type	L-type
Material	pCVD	pCVD
Area	round	square
	$r = 2.5$ mm	10×10 mm^2
Thickness	100 μm	500 μm
Nominal bias voltage	100 V	500 V
Company	Cividec	Cividec

BEAM PARAMETERS AND MEASUREMENT SETUP

The Beam Test Facility

The BTF is a beam line at the Daphne accelerator complex. In the used mode, a bunch of the primary electron beam of 500 MeV and an intensity of $\approx 10^9\ e^-$ was delivered into the experimental hall with a repetition rate of 1 – 2 Hz. The bunch length was in the order of 10 ns. The beam intensity was reduced by using scrapers in the beam line [1].

Experimental Setup

In the setup the dBLM detector was place in front of a reference detector. Both detectors were aligned on the beam axis. A collimator was placed between the two detectors to ensure that only electrons that passed through the dBLM are detected in the reference detector, see Fig.1.
The collimator consists of a 20 cm long hollow copper cylinder with an opening of the size of the active diamond crystal in the dBLM. The copper cylinder was followed by a lead cylinder for shielding Bremsstrahlung. The whole setup was shielded with lead to minimise the radiation levels in the experimental hall.
The signals of the dBLM and the icBLM were fed through 30 m long BNC-cables into a 50 Ω read-out system (scope, Agilent DSO 9254A).

The Reference Detector

For the measurements a standard LHC type ionisation chamber beam loss monitor (icBLM) was used as a reference detector. During the experiments the electron peak of the icBLM was measured which contains about 50 % of the whole charge. By applying a conversion factor to the

Content from this work may be used under the terms of the CC BY 3.0 licence (© 2015). Any distribution of this work must maintain attribution to the author(s), title of the work, publisher, and DOI.

ISBN: 978-3-95450-168-7 doi:10.18429/JACoW-IPAC2015-MOPTY059

FIRST OPERATIONAL EXPERIENCE OF DSL BASED ANALYSIS MODULES FOR LHC HARDWARE COMMISSIONING

C.Aguilera, M.Audrain, S.Boychenko, Z.Charifouilline, M.Dragu, R.Heil, M.Koza, K.Krol, J.C. Garnier, R.Orlandi, T.Ribeiro, S.Rowan, K.Stamos, M. Zerlauth, CERN, Geneva, Switzerland

Abstract

The superconducting magnet system of the Large Hadron Collider (LHC) has been fully re-commissioned ahead of the second run of physics production in 2015. More than 20,000 tests had to be performed and analysed to qualify around 1600 electrical circuits for operation at 6.5TeV. Automated analysis modules, defined directly by the various system experts in an English-like domain specific language (DSL), have been used successfully within the Accelerator Testing framework (AccTesting) during the latest re-commissioning campaign. For this, the experts define pass criteria for the powering tests, which are automatically verified, via assertion modules, in order for the test to pass. These modules currently analyse 4 test types executed for more than 1000 systems and even allowed experts to identify issues, which were missed by manual analysis during previous campaigns. This paper describes the first operational experience with such kind of analysis modules, as well as a follow-up analysis of the results compared with previous commissioning campaigns. The analysis looks at potential shortcomings of the framework and attempts to improve the dependability of automated analysis with regards to high current (>1kA) circuits of the LHC are outlined.

INTRODUCTION

The AccTesting framework has been developed at CERN with the aim of providing dependable tracking and execution of the more than 20,000 tests that have to be performed on the magnet powering circuits of the Large Hadron Collider (LHC) to qualify it for operation after long technical stops or maintenance interventions. The need for orchestration tools was already identified during the first commissioning phase of the LHC in 2007/2008. For this first commissioning phase, over 5000 tests were completed, using a set of rather heterogeneous tools for the definition, execution, tracking and analysis of the various powering tests [1].

In subsequent (re-)commissioning campaigns the number of tests to be executed steadily increased due to the increase in individual system tests in the commissioning program. The experience gained, however, allowed for considerable improvements in both, the automation of execution of powering cycles on the electrical circuits as well as the automation of analysis for transient data recordings produced during these different validation steps. In 2010, the tracking and execution of tests has been amalgamated into a single Java based framework, which has been used successfully during multiple campaigns ever since.

In an effort to further progress towards a coherent set of tools for the operation and expert crews of the LHC, the most recent campaign has seen the inclusion of a new analysis layer within the AccTesting framework, based on the use of a DSL.

DOMAIN SPECIFIC LANGUAGE FOR AUTOMATED ANALYSIS

The use of a domain specific language for data analysis bears many advantages that are outlined in [2] [3]. When investigating first operational experience with DSL based analysis modules, emphasis is given to assess the experience relative to the main design goals of the DSL, namely:

- Facilitating analysis tasks for equipment experts and automation crews
- Increasing system reliability through dependable automated analysis
- Increased performance and test efficiency due to the removal of manual analysis

Analysis Abstraction

With the introduction of the domain specific language, a considerable abstraction and decoupling of the analysis task from software and coding knowledge can be achieved. Specific knowledge about the analysis framework is not required. Software specialists provide access to the available data sources, configuration data as well as the implementation of analysis functionality by providing a set of assertions that can be executed on the recorded data. Equipment experts can focus on the implementation of the analysis modules by constructing algorithms to satisfy specific pass criteria out of the set of assertions. Figure 1 depicts two analysis modules, each consisting of 6-9 individual assertions that validate absolute values of measurements, exponential decays or second derivatives against well-defined thresholds.

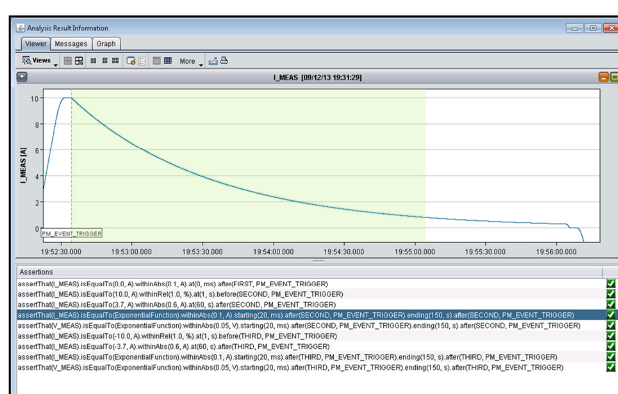

Content from this work may be used under the terms of the CC BY 3.0 licence (© 2015). Any distribution of this work must maintain attribution to the author(s), title of the work, publisher, and DOI.

ISBN: 978-3-95450-168-7 doi:10.18429/JACoW-IPAC2015-MOPTY060

Content from this work may be used under the terms of the CC BY 3.0 licence (© 2015). Any distribution of this work must maintain attribution to the author(s), title of the work, publisher, and DOI.

PULSE COMPRESSOR PHASE AND AMPLITUDE MODULATION BASED ON ITERATIVE LEARNING CONTROL*

Amin Rezaeizadeh†, Roger Kalt, Thomas Schilcher
Paul Scherrer Institut, Villigen, Switzerland
Roy S. Smith, Automatic Control Laboratory, ETH, Zürich, Switzerland

Abstract

This paper presents an alternative way to produce flat-topped RF pulses at the pulse compressor output. Flat-topped RF pulses are suitable for multi-bunch operation where it is often required that beams experience the same accelerating gradient. Moreover, the energy gain, in this case, is less sensitive to timing jitters. The proposed approach is based on Iterative Learning Control technique, which iteratively updates the input waveforms, in order to generate the desired output waveforms.

INTRODUCTION

The SwissFEL machine, currently being constructed at Paul Scherrer Institut, will provide a source of very bright and short X-ray pulses. The SwissFEL C-band (5.712 GHz) Linac consists of 26 Radio Frequency (RF) stations. Each station is composed of a single klystron feeding an RF pulse compressor and four accelerating structures. The pulse compressor designed for the SwissFEL is based on a single Barrel Open Cavity (BOC) which inherently has a high quality factor resulting in a significant energy storage capacity and a relatively long filling time [1]. In the original form of pulse compression, which is commonly referred to as the "phase jump" regime, the input phase flips by 180°, generating a reflected wave transient into the acceleration structure. This high power transient decays relatively slowly giving the RF structure time to build up an accelerating gradient higher than possible from the klystron alone. However, this RF pulse shape is not suitable for multi electron-bunch operation where it is often required that all electron bunches see the same amplitude and phase in the accelerating structure. More complicated operation modes are also possible by reversing the phase very slowly which is referred to as the "phase modulation". With a continuously modulated phase, the BOC output peak amplitude is lowered and flattened [2]. The SwissFEL RF drives operate in a pulsed mode at the rate of 100Hz, using normal conducting accelerating structures. The RF pulse length is of the order of 1-3μs and no digital RF feedback loop is run within a pulse. Iterative learning control (ILC) is a control technique for systems that operate in a repetitive manner [3]. In this method, the measured waveform or trajectory is compared to the desired one to give an error estimate, which is then used to update the inputs for the next run. Therefore, for our problem, i.e. controlling the pulse shape, an iterative approach is a good candidate. Previously in [4], a model-free ILC algorithm was employed

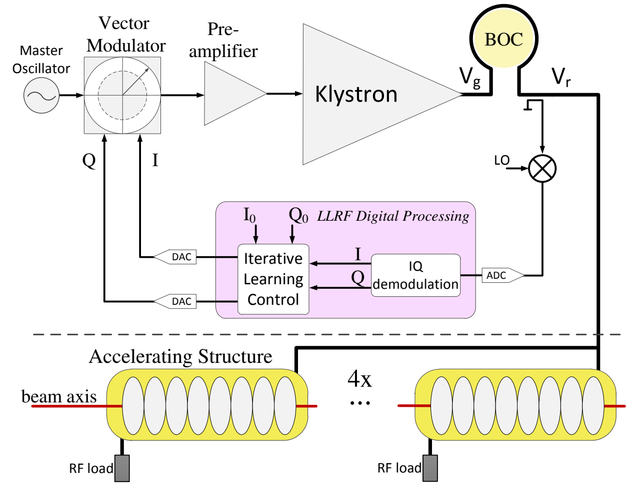

Figure 1: The simplified RF layout of a C-band RF station in the SwissFEL beamline.

to flatten the klystron RF pulse. In this paper, an ILC-based approach for producing flat-topped RF pulse is introduced, which modulates both input phase and amplitude waveforms. This method has been successfully applied on the RF pulse compressor at the SwissFEL Linac test facility.

SYSTEM DESCRIPTION

The layout of a C-band RF station is illustrated in Fig. 1. The RF signal source (5.7 GHz) is generated by a master oscillator. The discrete sequences of the in-phase, I, and quadrature, Q, components of the RF signal are fed into the vector modulator to be up-converted. Each sequence contains 2048 samples with sampling time of $T_s = 2.4$ ns. The RF signal drives the klystron and finally, the high power RF signal is split over four accelerating structures. The measured I and Q waveforms are used in the ILC controller to produce the next I and Q inputs to the Digital-to-Analog Converters (DAC). The control objective is to make flat amplitude and phase pulses at the output of the pulse compressor.

The Pulse Compressor Model

The relation between klystron and pulse compressor voltage is given by [2]

$$\alpha V_g = V_c + \tau \dot{V}_c, \tag{1}$$

where V_g and V_c are respectively the klystron and pulse compressor voltage phasors.

* Work supported by Paul Scherrer Institut.
† aminre@ee.ethz.ch

ISBN: 978-3-95450-168-7 doi:10.18429/JACoW-IPAC2015-MOPTY061

BEAM-BASED POWER DISTRIBUTION OVER MULTIPLE KLYSTRONS IN A LINEAR ACCELERATOR*

Amin Rezaeizadeh†, Roger Kalt, Thomas Schilcher
Paul Scherrer Institut, Villigen, Switzerland
Roy S. Smith, Automatic Control Laboratory, ETH, Zürich, Switzerland

Abstract

A linear accelerator including several klystron driver RF stations can be viewed as a single virtual RF station [1] with a certain accelerating RF voltage (in amplitude and phase). This paper develops an optimization scheme that, for a specified beam energy gain, determines the klystrons output powers and the modulators high voltages optimally. The algorithm employs the klystron nonlinear static characteristics curves to calculate the input RF amplitude of the drive chain.

INTRODUCTION

A linear accelerator (Linac) is composed of multiple Radio Frequency (RF) stations, delivering high power RF to feed the accelerating structures. If the high power is generated by klystrons, finding the appropriate operating points of the klystrons is a topic to be considered. In order to increase the RF stability as well as the efficiency, it is preferable to operate the klystron very close to its saturation limit. The saturating power depends on the high voltage of the klystron. Nonlinear characteristic curves of the klystron, make it not so straightforward to determine the high voltage and the input amplitude from a specified klystron output power. Figure 1 depicts the klystron output power versus the RF input amplitude and the voltage of the high voltage power supply (HVPS). Two contours of constant power are plotted to illustrate the problem. This issue has been previously addressed in [3] by introducing the concept of operating point determination (OPD). In this paper, we consider multiple klystrons, in which the operating points are determined according to the specified total energy gain. This leads us to the concept of beam-based multiple operating point determination (BM-OPD). In this scheme, an optimization procedure is developed which minimizes the high voltages of the klystrons, while keeping the total beam energy gain constant. Since the breakdown rate of the klystron is directly related to the high voltage level, the proposed optimization tends to reduce the probability of breakdowns. The approach is based on a convex optimization which uses the models of klystron characteristics and the energy gain of the RF stations. This method has been successfully tested at the SwissFEL injector test facility using three full-scale RF stations to simulate a Linac. The SwissFEL is currently being constructed at Paul Scherrer Institut [2]. The SwissFEL injector and the Linac RF drives operate in a pulsed mode at the rate of 100 Hz. There are 26 RF stations in the SwissFEL Linac. The proposed algorithm facilitates the RF setting with an automatic procedure for the specified energy gain of a Linac.

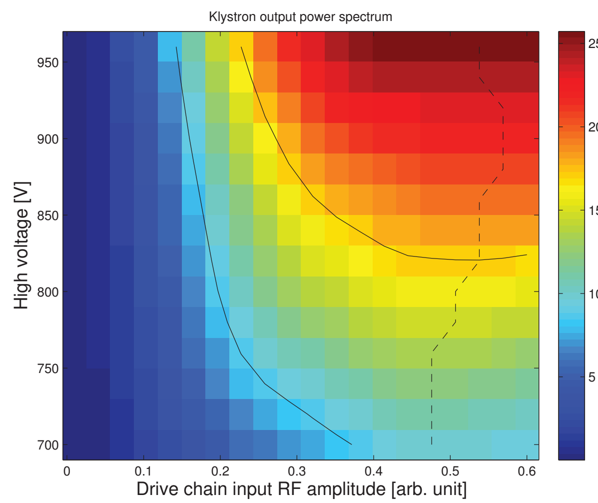

Figure 1: The klystron output power versus the RF input amplitude and the high voltage power supply setting. The curves (in black) denote the contours of constant output power. The dashed line indicates the saturating power. The klystron operating point should fall in the left side of the dashed line to avoid over-saturation.

OPTIMIZATION SCHEME

A Linac with multiple klystrons is often viewed as a single RF station with a certain energy gain. The energy gain can be tuned via each individual klystron RF amplitude as well as the high voltage. The way that the klystrons contribute to generate the desired total energy gain, is the main focus of this section. The distribution of the individual energy gain of the RF stations is done through an optimization problem. As a result, the RF power of each individual klystron is determined, which is then used as an input to the OPD, along with the predefined headroom to the saturation, to provide the assigned energy gain.

The optimization is meant to minimize the overall probability of breakdowns in klystrons, which usually occurs at higher high voltages. Throughout this study, we assume that the RF phases are set to zero, i.e. the “on-crest phase”.

We consider a Linac with M klystrons. The energy gain of each RF station, ΔE_i, is related linearly to the klystron output RF amplitude. That is,

$$\Delta E_i = \alpha_i y_i + \beta_i, \tag{1}$$

where y_i denotes the output amplitude of i-th klystron , and where β_i and α_i are constants. On the other hand, according

* Work supported by Paul Scherrer Institut.
† aminre@ee.ethz.ch

Content from this work may be used under the terms of the CC BY 3.0 licence (© 2015). Any distribution of this work must maintain attribution to the author(s), title of the work, publisher, and DOI.

ISBN: 978-3-95450-168-7 doi:10.18429/JACoW-IPAC2015-MOPTY062

THE ENERGY SAVING PROCESSES FOR UTILITY SYSTEM IN TPS

Chih-Sheng Chen, Wen-Shuo Chan, Yung-Chiang Chang, Yen-Ching Chung, Ching-Wei Hsu
Ching-Yuarn Liu, Zong-Da Tsai, Jui-Chi Chang
NSRRC, 101Hsin-Ann Road, Hsinchu Science Park, Hsinchu 30076, Taiwan

Abstract

There are more and more non-linear electronic equipments such as inverters using in facility nowadays. These non-linear electronic equipments let us achieve energy saving, but induce other electrical pollution to the whole power grid in contrast. How to take the advantages from these energy-saving equipments without electric pollutions should be well considered at the first step of the utility operation in TPS (Taiwan Photon Source). Meanwhile, for there will be lots of chance that TLS (Taiwan Light Source) and TPS will be operated at the same time, the electrical power consumption will increase with no doubt. Under the circumstances of limited budget, some energy saving processes for utility must be applied. According to the historical data, the utility consumes the majority of power consumption. Even a small portion of usage saved will be a respectable amount. Thanks to the connection pipe between two utility buildings, the realization of the energy saving processes at the first phase of TPS project becomes much easier.

INTRODUCTION

The accelerator is a sophisticated facility and sensitive to environmental changes. According to the research by J. C. Chang et al., the supplied air temperature and cooling water temperature are the critical factors to affect the beam orbit [1]. Once the temperature fluctuations of cooling water and air exceed 1 °C and 0.2 °C respectively, the stability of beam orbit will become worse. For this reason, a lot of efforts had been made to realize precise temperature control. On the other hand, precise temperature control prevents unnecessary energy lost. The later reason is getting more and more important when it comes to energy conservation. For air conditions, Z. D. Tsai et al. have made experiments applying the Run-Around Heat Recovery process to air handling unit [2]. From the results, the temperature fluctuation of outlet air could be minimized to ±0.05 °C, and the energy saving runs up to 30%. In this article, the benefit of connection pipe between chillers in TLS and TLS will be introduced. The TLS and TPS chilled water systems hence support to each other, and the reduction of power consumption is the additional profit while new chillers operating. The coefficient of performance (COP) of overall chilled water system goes up too.

After four years of engineering constructions, the first light of TPS shines on December 31, 2014. It encouraged every member in NSRRC, at the same time, it also means more and more energy is required to operate both TLS and TPS. Electrical power consumption is highly increased after the completion of civil construction of TPS. The number of contract power capacity has been increased from 3.5 MW in 2000 to 5.5 MW in 2015. The power bill in 2014 was also nearly three times more than in 2008. Figure 1 shows the monthly average fee in NSRRC from 2008 to 2014 [3]. Due to the rising bill and the limited budget, it is an urgent object to develop energy saving processes for utility group.

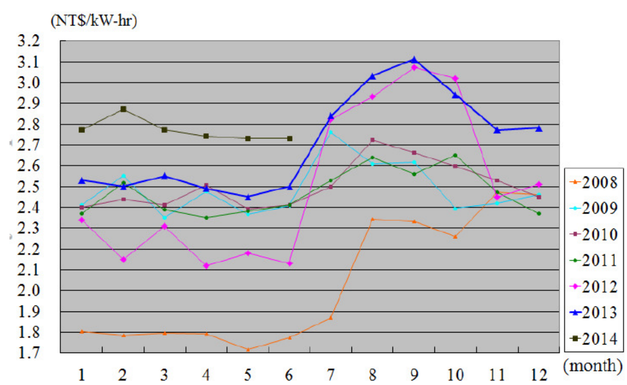

Figure 1: Monthly average fee from 2008 to 2014 in NSRRC.

RUN-AROUND HEAT RECOVERY PROCESS

Run-around heat recovery system is composed of ordinary air handling unit and two additional heat exchange coils. As shown in figure 2, these two additional heat exchange coils are used as pre-heating and pre-cooling coils separately.

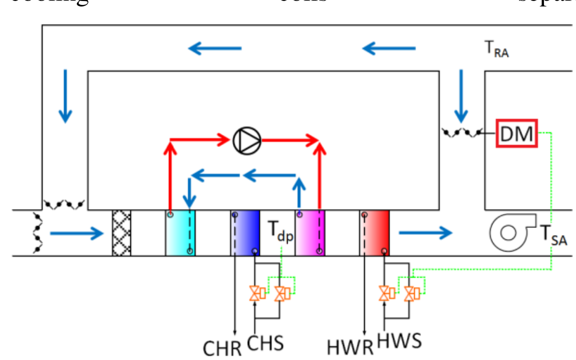

Figure 2: Control Diagram of High Precision Temperature Control System.

Counting from right side, the first coil is pre-cooling coil; the second one is cooling coil; the third and the

Content from this work may be used under the terms of the CC BY 3.0 licence (© 2015). Any distribution of this work must maintain attribution to the author(s), title of the work, publisher, and DOI.

ISBN: 978-3-95450-168-7 doi:10.18429/JACoW-IPAC2015-MOPTY063

THE FLEXIBLE CUSTOMIZED SUPERVISOR AND CONTROL SYSTEM FOR UTILITY IN TPS

Chih-Sheng Chen, Wen-Shuo Chan, Yung-Chiang Chang, Yen-Ching Chung, Ching-Wei Hsu, Ching-Yuarn Liu, Zong-Da Tsai, Jui-Chi Chang
NSRRC, 101Hsin-Ann Road, Hsinchu Science Park, Hsinchu 30076, Taiwan

Abstract

In order to maintain and operate a synchrotron radiation light source well requires quite a few efforts. All parts of the big machine, including vacuum system, all kinds of magnets, RF facility, cryogenic equipments, radiation security, optic devices and utility equipment must cooperate in harmony to provide high quality light. Any one of the above system contains lots of analog or digital signal transmission, not to mention the vast range of utility. Numbers of programmable automation controllers (PACs) are applied in utility system in TPS to ensure the utility operates normally. In addition to the high reliability and distribution, the flexible programmability of PAC is the most critical feature in this project. A well-designed program, Archive Viewer, provides a platform for showing these big data from all distributed systems. The architecture of the server system for utility is described in this paper as well.

INTRODUCTION

There are mainly three kinds of resources provided by the utility group in NSRRC. First, the de-ionized water (DIW) system offers cooling water to carry out waste heat generated by accelerator operation. The DIW system is composed of four subsystems in TLS and TPS respectively. The copper (Cu) DIW subsystem provides with cooling de-ionized water to take out exhaust heat while the magnet system and power supplies operate. The vacuum chambers in NSRRC are mostly made of aluminium; therefore, the aluminium (Al) subsystem is in charge of waste heat from the equipments of the vacuum group. The RF subsystem is for RF transmitters and cavities, and the Bl (beam line) and Bo (booster) subsystem is for the usage of all beam line devices. Second, the air system including air-condition system and compressed air system offers an environment with stable temperature and sufficient air pressure for pneumatic equipments running. The last part is the most critical, the reliable electric system ensures all electronics are working. All the three elements seem fundamental, however, an advanced facility like particle accelerator need a stably-operated and well-controlled utility system to realize. Referring to former studies of utility group in NSRRC, it is strongly proven that the stability of utility affects the operation of accelerator [1]. This article will focus on the water system and air system of TPS utility.

The temperature of DIW system is globally controlled within ± 0.1℃ in TLS due to former efforts [2]. With the experiences from TLS, the precise temperature control could be achieved by many local controllers. The specifications of TPS water subsystem are listed in Table 1. The capacities of cooling water, chilled water and hot water are larger than normal consumption. The over design capacity avoids unexpected heat load shock and ensures all systems work under the most suitable conditions.

Table 1: Specifications of Water Subsystems of TPS

	Temperature	Pressure	Capacity
Cu DIW	25 ± 0.1 °C	7.5 ± 0.1 kg	1659 GPM
Al DIW	25 ± 0.1 °C	7.5 ± 0.1 kg	380 GPM
RF DIW	25 ± 0.01 °C	7.5 ± 0.1 kg	1284 GPM
Booster DIW	25 ± 0.1 °C	7.5 ± 0.1 kg	1238 GPM
Cooling Tower	32 ± 0.5 °C	2.5 ± 0.1 kg	12000 RT
Chilled Water	7.0 ± 0.2 °C	2.5 ± 0.1 kg	8400 RT
Hot Water	50 ± 0.3 °C	2.5 ± 0.1 kg	1600 kW

CONTROL SYSTEMS OF TPS UTILITY

There are three typical controllers used in the utility system of TPS. They are Programmable Automation Controller (PAC), Direct Digital Control system (DDC) and Programmable Logic Controller. Direct digital control is an automated control by a computer, which is broadly used on HVAC (Heating, Ventilation and Air Conditioning) control systems based upon PLC technology. In the TPS project, DDC controllers are widely used in every AHU (Air Handling Unit) to achieve precise temperature control. Local controllers are responsible for the temperature steadiness of local area. Due to the diversity of air condition demands, there are quite a few typical models to satisfy all kinds of requirements.

The mathematical model had been established to find out the relationships between the beam orbit and the supplied air temperature [3]. The beam orbit stability will become worse once the fluctuation of environmental temperature exceeds 0.2℃. Based on this thesis, lots of efforts had been made to increase temperature steadiness during TLS. With the endeavours of TPS project, the fluctuation of supply air temperature is greatly reduced within ± 0.1℃. By means of PAC, the fluctuation could be minimized within ± 0.01℃ in laboratory. Owing to much more accurate sensors and high performance

Content from this work may be used under the terms of the CC BY 3.0 licence (© 2015). Any distribution of this work must maintain attribution to the author(s), title of the work, publisher, and DOI.

ISBN: 978-3-95450-168-7 doi:10.18429/JACoW-IPAC2015-MOPTY064

COMPENSATION STRATEGIES FOR RAMPING WAVEFORM OF TPS BOOSTER SYNCHROTRON MAIN POWER SUPPLIES

P. C. Chiu, C. Y. Wu, Jenny Chen, Y. S. Cheng, Demi Lee, B. S. Wang, K. B. Liu, K. H. Hu, K. T. Hsu
NSRRC, Hsinchu 30076, Taiwan

Abstract

Booster synchrotron for the Taiwan photon source project which is a 3 GeV synchrotron light source constructed at NSRRC had been commissioning successfully when the electron beam was accelerated to 3 GeV on December 16 2014. The booster is designed to ramp electron beams from 150 MeV to 3 GeV in 3 Hz therefore the large main power supplies have features of waveform play with trigger functionalities. However, due to the limited bandwidth of power supplies, different magnet loading will result in quite different phase lag for dipoles and four quadrupoles families and the relative err of input and output of dipole and quadrupoles would be quite different. To improve the relative error between the output readings and reference, several strategies are developed and will be summarized in this report.

INTRODUCTION

The TPS is a state-of-the-art synchrotron radiation facility featuring ultra-high photon brightness with extremely low emittance [1]. The 3 GeV stored electron beam with 5 mA was achieved and the first synchrotron light was observed in December 31. It consists of a 150 MeV electron Linac, a 3 GeV booster synchrotron, and a 3 GeV storage ring. The EPICS (Experimental Physics and Industrial Control System) was chosen for the TPS accelerator control.

The booster main power supplies are composed of one dipole power supply with maximum current 1200 Ampere and four family quadrupole power supplies with maximum current of 120/150 Ampere. At first, these power supplies supported external trigger and internal waveform generator for booster power supply ramping. However, the reproducibility of power supply itself was unsatisfactory at injection due to non-synchronize and asynchronous internal clock of power supply regulator and external trigger. Therefore, the original digital regulation loop was modified to analogue and control interface was also revised so that all of power supplies could be driven by synchronized current waveform reference with common clock source and trigger. It effectively improved the reproducibility more than 1/5 [2, 3].

Figure 1 shows the overall booster ring power supplies control interface. One dedicated EPICS IOC equipped with one CPU blade, one EVR fanout and ADC/DAC modules is built to serve synchronous control and monitor of main booster power supply. Serial to Ethernet adapter are used to interface with On/Off control and status monitor. Moreover, the DT8837 which has 24 bits ADC provide extra high more precision monitoring than ADC modules and also support the external clock for synchronization.

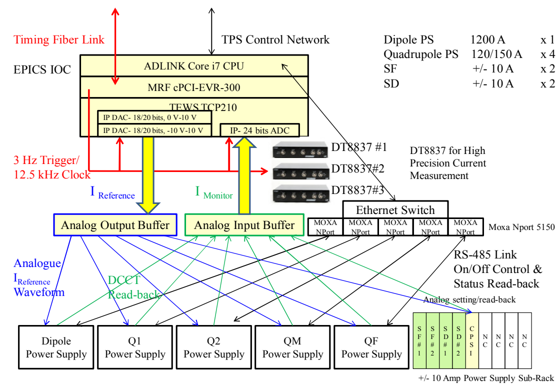

Figure 1: Control infrastructure of TPS booster ring power supplies.

POWER SUPPLY CHARACTERIZATION

Power supply for booster dipole and quadrupoles were contracted and delivered by Eaton. Figure 2 shows the step response of dipole and four quadrupole power supplies at first arrival. It exhibited quite different frequency response which would result in unacceptable tracking error difference between dipole and quadrupole power supplies at injection during ramping as Fig. 3. Adjusting loop gain of power supply analogue regulator by changing resistors could improve the difference but ineffective, imprecise and time-consuming. When one of power supply fails and the spared is necessary, the characterization of the spared would be required re-calibrated, this will cost much man-power and time. It will be quite a burden from maintenance points of view.

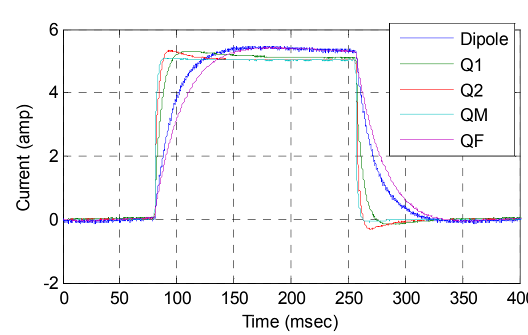

Figure 2: Step response of dipole and four quadrupole power supplies. Dipole and QF had slower response due to larger magnet loading.

Content from this work may be used under the terms of the CC BY 3.0 licence (© 2015). Any distribution of this work must maintain attribution to the author(s), title of the work, publisher, and DOI.

ISBN: 978-3-95450-168-7 doi:10.18429/JACoW-IPAC2015-MOPTY065

BEAM STABILITY OF THE TAIWAN LIGHT SOURCE STORAGE RING

Hung-Chiao Chen*, Hsin-Hui Chen, Szu-Jung Huang, Jar-An Li, Yao-Kwang Lin, Chang-Hor Kuo, Yung-Sen Cheng
National Synchrotron Radiation Research Center, 101 Hsin-Ann Road, Hsinchu Science Park, Hsinchu 30076, Taiwan, R.O.C.

Abstract

The Taiwan Light Source Storage Ring (SR) has been in operation since many years ago. Maintaining best stability of the electron beam is becoming the main challenge. This study endeavored to improve the electron beam stability and injection efficiency of The Taiwan Light Source Storage Ring (SR). Employing the artificial neural network (ANN)-constructed experiment design to analyze and optimize the storage ring betatron tunes .This report outlines the details of the beam stability and injection efficiency process experiment.

INTRODUCTION

Using the basic theory of response surface methodology (RSM), this study aimed to improve the electron beam stability and injection efficiency of the National Synchrotron Radiation Research Center (NSRRC) storage ring. Artificial neural network (ANN) design software, known as computer-aided formula engineering (CAFE) [1], was used to analyze and optimize the betatron tunes of the storage ring. We aimed to identify the main influential the betatron tunes of the storage ring and, through optimization, develop the betatron tunes of the storage ring adjustment program that best stability and maximizes injection efficiency of the electron beam.

DATA ANALYSIS

Artificial Neural Network

ANNs are construction methods for nonlinear models. Among which, back-propagation networks (BPNs) are currently the most representative and commonly applied of the ANN learning models [2, 3].

Beam Stability Analysis

After calculating the ANN model construction, we obtained the "train- and -test" error convergence curve, as shown in Fig. 1. The representative model construction was ideal because they appear to converge after approximately 1,500 computations.

chiao@nsrrc.org.tw

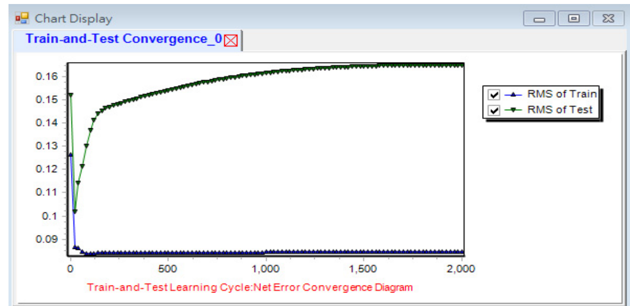

Figure 1: The "train- and -test " error convergence curve.

The "train- and -test" scatter plots for the training sample is shown in Fig. 2 respectively. The predictive ability of the representative model was also ideal [4].

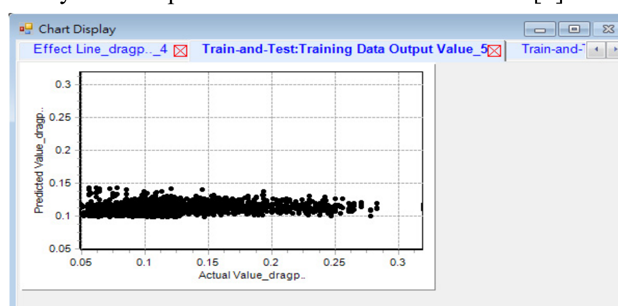

Figure 2: The "train- and -test " scatter plot of the training samples.

Analysis of the experimental results included sensitivity analysis and influence line analysis. Sensitivity analysis was conducted using weight value analysis graphs, and influence line analysis was conducted using a main effect diagram with status. The sensitivity analysis results revealed the significance of quality factors, as shown in Fig. 3. We found the betatron tune fy quality factor had the highest significance.

- The weight of the betatron tune fx was 0.015.
- The weight of the betatron tune fy was 0.061.

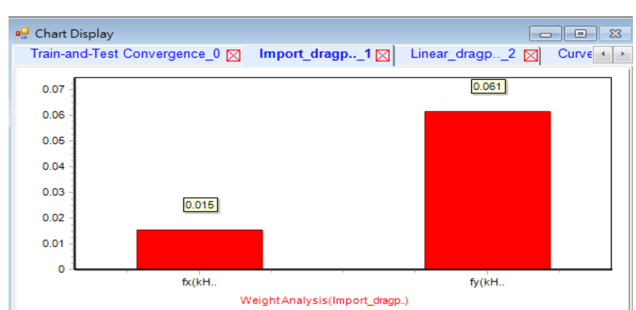

Figure 3: A bar graph of Y significance.

Content from this work may be used under the terms of the CC BY 3.0 licence (© 2015). Any distribution of this work must maintain attribution to the author(s), title of the work, publisher, and DOI.

ISBN: 978-3-95450-168-7 doi:10.18429/JACoW-IPAC2015-MOPTY069

CONTROL INTERFACE AND FUNCTIONALITY OF TPS BOOSTER POWER SUPPLY

C. Y. Wu, P. C. Chiu, Y. S. Cheng, C. Y. Liao, Jenny Chen, Demi Lee, C. H. Huang, K. H. Hu, K. T. Hsu
NSRRC, Hsinchu 30076, Taiwan

Abstract

The TPS booster is a synchrotron with injection energy at 150 MeV and extraction energy at 3 GeV in 3 Hz. Booster main power supplies consist of one dipole power supply with maximum current 1200 Ampere and four quadrupole family power supplies with maximum current of 120/150 Ampere. The small power supply for booster corrector and sextupole is a low noise switching power supply with +/- 10 Ampere current range. The TPS booster control environment is based on EPICS framework to support rich functionalities including power supply control, waveform management, operation supports, and so on. All power supplies support DC mode and 3 Hz ramping mode operation for TPS booster commissioning and operation. Efforts on control interface and functionality for TPS booster power supply will be summarizes.

INTRODUCTION

The TPS [1] is a latest generation of high brightness synchrotron light source which had completed phase I commissioning in March, 2015 [2-3]. It consists of a 150 MeV electron Linac, a 3 GeV booster synchrotron, and a 3 GeV storage ring. The EPICS (Experimental Physics and Industrial Control System) was chosen for the TPS accelerator control.

The control interfaces of TPS booster power supplies have two major categories: one is for the large main power supply which could provide current up to 1200 and 120/150 amperes and used for dipole magnets and quadrupole magnets respectively; the other is small power supply which supports +/- 10 Amperes current output and used for sextupole magnets and correctors. Table 1 summarizes the specifications of booster ring power supplies [4-5].

Table 1: TPS Booster Ring Power Supply Summary

Magnet	Type	Max Current	Number of PS	PS Vendor	Control Interface
Dipole	Unipolar	1200 A	1	Eaton[4]	RS485 & Analog interface
Quadrupole	Unipolar	120/150 A	4~5	Eaton	RS485 & Analog interface
Sextupole	Bipolar	± 10 A	4	ITRI [5]	Analog interface
Corrector	Bipolar	± 10 A	HC: 60 VC: 36	ITRI	CPSC (Ethernet)

All of these power supplies should have features of waveform play with external trigger functionalities to enable electron beams ramp from 150 MeV to 3 GeV in 3 Hz. The large power supply provides RS-485 control interface for ON/OFF and status reading and analog input for current setting. One dedicated EPICS IOC is used to serve its control and monitor. The small power supplies have 12 special designed corrector power supply controllers (CPSC) with embedded EPICS IOCs allocated at power supply rack for its control. The control environment of these power supplies will be summarized in this report. Fig. 1 shows the pictures of dipole and quadrupole power supply for booster synchrotron which had been installed in the site.

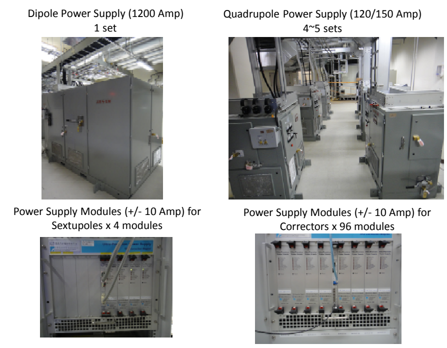

Figure 1: Large and small power supplies for the dipole, quadrupole, sextupole and correctors of TPS booster synchrotron respectively.

CONTROL INTERFACE OF BOOSTER MAIN POWER SUPPLY

The booster main power supplies are composed of one dipole power supply with maximum current 1200 Amperes and four family quadrupole power supplies with maximum current of 120/150 Amperes. These power supplies support analog input for power supply current setting (DC and AC). Serial to Ethernet adapter are used to interface between the booster main power supplies and EPICS IOC.

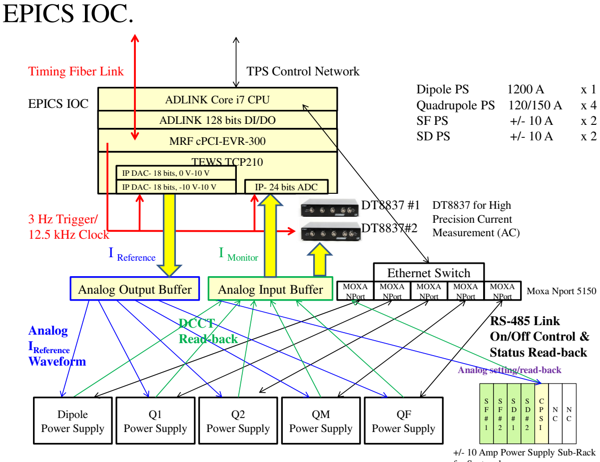

Figure 2: Control infrastructure of TPS booster ring dipole, quadrupole and sextupole power supplies.

Content from this work may be used under the terms of the CC BY 3.0 licence (© 2015). Any distribution of this work must maintain attribution to the author(s), title of the work, publisher, and DOI.

ISBN: 978-3-95450-168-7 doi:10.18429/JACoW-IPAC2015-MOPTY070

ONLINE RADFET READER FOR BEAM LOSS MONITORING SYSTEM

D. Lee, Y. S. Cheng, C. H. Huang, K. H. Hu, C. Y. Wu, J. Chen, K. T. Hsu
NSRRC, Hsinchu 30076, Taiwan

Abstract

To investigate the beam loss and its distribution during operation of synchrotron light sources at NSSRC, a sixteen-channel readout box is designed and implemented to read the threshold voltage of the RadFETs installed at the accelerator tunnel. To simplify the design, the reader plays a role of remote I/O for EPICS IOC. The IOC collects voltage from readers distributed in the accelerator to deduce the integrated dose and dose rate. User interface is shown in the control console for real-time display, and the archived data are processed off-line.

INTRODUCTION

The radiation-sensing field-effect transistor (RadFET) is a discrete p-channel metal-oxide-semiconductor field-effect transistor optimized for ionizing radiation [1]. The threshold voltage between the gate and source changes due to radiation-induced charges in the oxide layer when applying a constant drain current. The reader of the RadFETs acts by applying constant drain current and read the threshold periodically. The voltage is proportional to accumulated exposure dose, and the slop of the accumulated dose is dose rate. Many different designs are reported for high energy detector and accelerator systems [1,2,3] with various considerations. Some are with simple interfaces and some are with intelligence ones. For a synchrotron light source, the RadFET will be a useful device to detect beam loss caused by the various mechanisms. A simply and low cost reader designed and implemented for beam loss study will be summary in following paragraph.

OVERVIEW OF THE READER IMPLEMENTATION

In order to achieve the high-density installation of the RadFETs, the reader is designed to link up to sixteen RadFETs using unshielded-twisted-pair network cables with standard RJ-45 connector, as shown in Fig. 1. In the radiation exposure period, the gate voltage is zero-biased or apply specific positive bias to increase sensitivity. In the readout period, a constant specific current is applied to the drain of RadFET to measure the threshold voltage (V_{th}) of the reader. The readout period is one minute now and the threshold voltage is readout one by one through a 24-bit analog-to-digital convertor (ADC). The control processes are programmed in the input/output controller (IOC) of the experimental physics and industrial control system (EPICS) and PVs are published into the control network, shown in Fig. 2. An operation interface is designed to show the threshold voltage of each RadFET, accumulated dose, dose rate even dose rate distribution. The threshold voltage of each RadFET is recorded in the archive server for the further analysis.

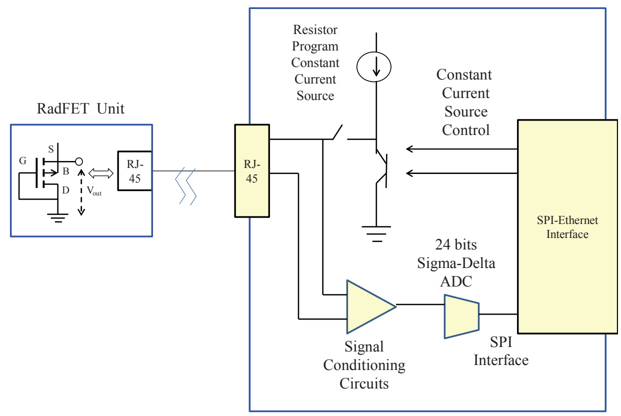

Figure 1: Simple schematic diagram of an individual RadFET reading hardware.

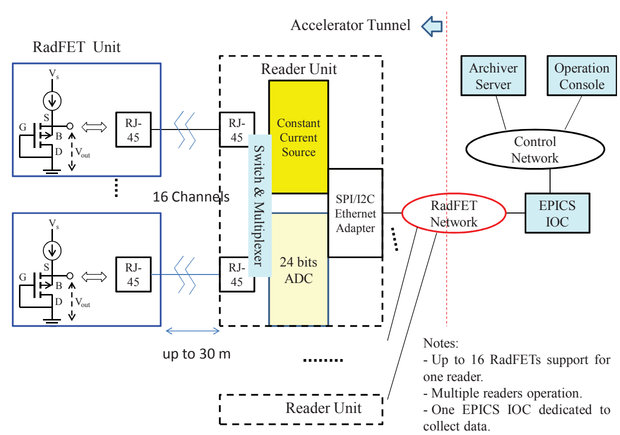

Figure 2: Block diagram of the RadFET readers system.

HARDWARE CONSIDERATION

Several issues have been identified during functionality discussion phase. To simplify software development cycle, it was decided that the reader just plays as roles of remote I/O units without local intelligence from viewpoints of control system. It needs not to do software programming at the reader side. To make easily cable to the data acquisition controller, the interface is Ethernet. Minimizing the interconnecting inside the reader is achieved by SPI interface to read threshold voltage of

Content from this work may be used under the terms of the CC BY 3.0 licence (© 2015). Any distribution of this work must maintain attribution to the author(s), title of the work, publisher, and DOI.

ISBN: 978-3-95450-168-7 doi:10.18429/JACoW-IPAC2015-MOPTY071

FPGA BASED GLOBAL ORBIT FEEDBACK IN THE TAIWAN LIGHT SOURCE

C. H. Kuo, P. C. Chiu, K. H. Hu, Demi Li, Y. S. Cheng, K. T. Hsu
NSRRC, Hsinchu 30076, Taiwan

Abstract

The global orbit feedback for the 1.5 GeV electron storage ring of TLS has been operated more than ten years. This system uses general processors to control feedback loop with 1 kHz rate. It is very important for various operation of storage ring now, but some hardware components could have been out of stock in the future. As a prototype, a FPGA based fast global orbit feedback at a 10 kHz data acquisition rate has been developed. A micro-TCA liked platform with FPGA board is used to implement control algorithm and acquire BPM data from Libera Brillance. The correction algorithm is written in VHDL and connected to power supply with AURORA digital links. The system architecture will be discussed in this report.

INTRODUCTION

Orbit feedback system operation of general processors is integrated with Libera Brilliance since 2008. The Brillance supports many beam position functions: slow position data acquisition, post mortem and tune measurement in the TLS. The group topology of Libera Brilliance to acquire fast data at 10 kHz rate has been under testing to verify long-term reliability and stability. The general processors are enough for orbit control. There are two reasons to migrate general processor to FPGA. One, single processor is hard to handle many individual PID control algorithm calculation; another is general cpu platform and operation system that couldn't be upgraded in the future. From maintenance points of view, keep control system of TLS and TPS to be same can reduce this cost. The grouping latency of Libera have been measured and tested that is satisfied for orbit feedback system. It is reliable. The new system is still following this structure. On the other hand, the corrector power supply control is also migrated to FPGA with rocket I/O interface from general cpu with VME bus. Integration of all of the new switching power supplies will be accomplished recently.

THE FPGA BASED FEEDBACK PLATFORM

Feedback System Overview

The TLS Fast Orbit Feedback Application runs in the micro-TCA liked chassis from commercial product. The BPM incoming data comes from the group of Libera Brilliance and is received through the SFP slot (GbE interface) in the GDX module [1]. The FOFB calculations and magnet output are implemented in the GDX module. Global orbit position is concentrated by a group of Libera Brilliance devices. Libera Grouping must be configured as per unit. The FOFB control algorithm runs in two same chassis of GDX, one for horizontal and one for vertical plane. Two Libera Brilliance devices from the group must be selected as master Liberas to output the global orbit position. The general overview is presented in Fig. 1.

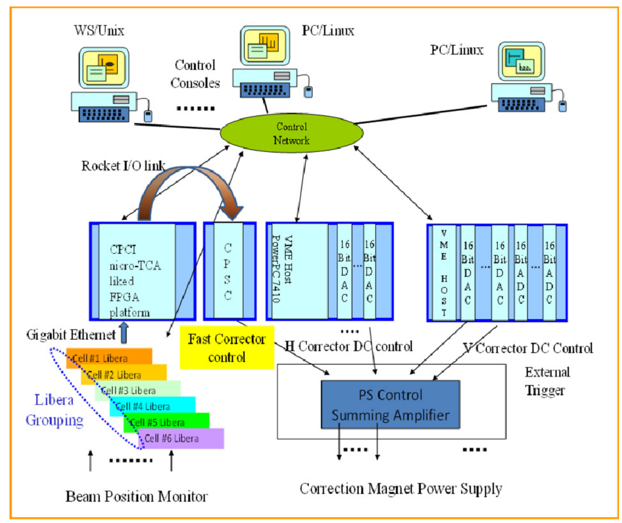

Figure 1: The overview system block diagram.

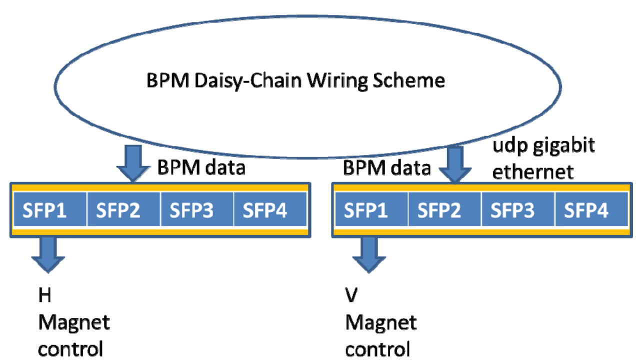

Figure 2: Feednack system is integrated by daisy-chain wiring bus of bpm with GDX module.

The global orbit data packet is received in the GDX of micro-TCA liked chassis, it is written to the circular buffer and it enters the FOFB calculation process which ends with DAC setting output on a SFP1 slot with AURORA 2.5 Gbps duplex protocol. It is then led to the Corrector Power Supply Controller Interface (CPSC) which provides analog output to corrector magnets [2]. The communication block diagram is shown in Fig. 2. The feedback platform photo is presented in Fig. 3.

Content from this work may be used under the terms of the CC BY 3.0 licence (© 2015). Any distribution of this work must maintain attribution to the author(s), title of the work, publisher, and DOI.

ISBN: 978-3-95450-168-7 doi:10.18429/JACoW-IPAC2015-MOPTY072

BEAM LOSS STUDY OF TLS USING RadFETs

C. H. Huang, S.H. Lee, Y.S. Cheng, K. H. Hu, C. Y. Wu, J. Chen, K. T. Hsu
NSRRC, Hsinchu 30076, Taiwan

Abstract

To realize the beam loss during the operation of Taiwan light source, P-type radiation-sensing field-effect transistors are setup around the storage ring. A sixteen-channel readout box is used to read the threshold voltage of the radiation-sensing field-effect transistors during irradiation. The beam loss distribution and mechanism at the injection period, decay mode and top up injection for routing operation will be studied in this report.

INTRODUCTION

The radiation-sensing field-effect transistor (RadFET) is a discrete p-channel metal-oxide-semiconductor field-effect transistor optimized for ionizing radiation [1]. Through detecting the voltage between the gate and source caused by the radiation-induced charges in the gate oxide during a forcing current, the radiation dose is obtained by a pre-recorded calibration curve.

For the last two decades, RadFETs have been found wide applications in the particle accelerator environment [2], space and clinical control. For a synchrotron light source such as Taiwan light source (TLS), the RadFET will be a useful device to detect beam loss due to the Touschek effect, the residual gas scattering, the intra-beam scattering and so on [3].

TLS is a synchrotron light source which equips with six-fold symmetry and three-bend achromatic (TBA) cells in storage ring. Its circumference is 120 m and the operating energy is 1.5 GeV. It equips with insertion devices including U50, U90, EPU56, W200, superconducting wavelength shifter (SWLS) and superconducting wiggler (SW60) in six 6-m long straight sections. Three identical superconducting wigglers (IASWR2, IASWR4, IASWR6) are installed in achromatic cells between the first and the second bending magnets of the second, fourth and sixth TBA cells.

RADFET READER SYSTEM

In order to achieve high density installation of the RadFETs, the reader is designed to link up to sixteen RadFETs with RJ-45 connectors and unshielded-twisted-pair network cables, as shown in Fig. 1. In the radiation exposure period, the gate voltage is zero-biased now or +5V for the positive-biased applications. In the readout period, a DC current with 12.5 μA is forcing into the gate for several seconds to obtain the threshold voltage (V_{th}) in the reader circuit configuration. The readout period is one minute now and the threshold voltage is readout one by one through a 24-bit analog-to-digital convertor (ADC). The control processes are programmed in the input / output controller (IOC) of the experimental physics and industrial control system (EPICS) and process variables (PVs) are published into the control network. An operation interface is designed to show the threshold voltage of RadFETs, accumulated dose, dose rate and dose rate distribution. The threshold voltage of RadFETs are recorded in the archive server for further analysis after the experiment [4].

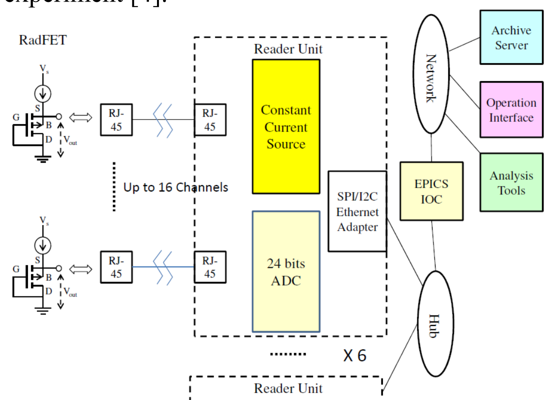

Figure 1: Block diagram of the RadFET readers' setup.

EXPERIMENTAL SETUP AND RESULTS

Six readers are setup below the girder of the second bending magnet in each cell of the storage ring to minimize the possible radiation damage, shown in Fig. 2(a). The uplink cables of six readers are connected to an Ethernet switch to form as a private network and then connect to the IOC in the equipment area of the TLS. In the first step, the two RadFETs are setup in the blue square position of Fig. 3 with one in the inside wall of the vacuum chamber shown in Fig. 2(b) and the other in the outside wall of the chamber in the storage ring.

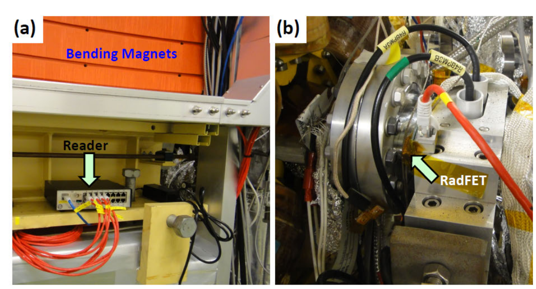

Figure 2: The setup of the (a) reader and (b) RadFET.

As the machine operates on the top-up mode, the detected radiation in the inside wall of the chamber is mostly larger than that in the outside wall, shown in Fig 4. That is because the beam loss caused by Touschek effect contributes into both sides but the beam loss caused by Bremsstrahlung only contributes to the inside wall. The detected dose rate is smaller than 0.3 Gy/hr except the

Content from this work may be used under the terms of the CC BY 3.0 licence (© 2015). Any distribution of this work must maintain attribution to the author(s), title of the work, publisher, and DOI.

ISBN: 978-3-95450-168-7 doi:10.18429/JACoW-IPAC2015-MOPTY073

COMMISSIONING OF BPM SYSTEM FOR TPS BOOSTER SYNCHROTRON

P. C. Chiu, K. H. Hu, C. H. Kuo, Y. S. Cheng, K. T. Hsu
NSRRC, Hsinchu 30076, Taiwan

Content from this work may be used under the terms of the CC BY 3.0 licence (© 2015). Any distribution of this work must maintain attribution to the author(s), title of the work, publisher, and DOI.

Abstract

Booster synchrotron for the Taiwan photon source (TPS) project which is a 3 GeV synchrotron light source constructed at NSRRC had ramped beam to 3 GeV successfully in December 16 2014 and later the stored beam in the storage ring had achieved 5 mA in December 31. The BPM electronics Libera Brilliance+ [1-2] are adopted for booster and storage ring of TPS. The provided BPM data is useful for beam commissioning where it can be used to measure beam position, rough beam intensity along the longitudinal position and also for tune measurement. This report summarizes the efforts on BPM measurement and related diagnostic tools during TPS booster commissioning.

INTRODUCTION

The TPS is a state-of-the-art synchrotron radiation facility featuring ultra-high photon brightness with extremely low emittance [3]. Civil constructions had been completed in early 2013. The TPS accelerator complex consists of a 150 MeV S-band linac, linac to booster transfer line (LTB), 0.15–3 GeV booster synchrotron, booster to storage ring transfer line (BTS), and 3 GeV storage ring. The booster has 6 FODO cells which include 7 BD dipoles with 1.6 m long and 2 BH dipoles with 0.8 m long in each cell. Its circumference is 496.8 meters and it is concentric with the storage ring in the same tunnel. At September 2014, booster BPM commissioning had committed with beam commissioning. After some hardware improvement such as power supply tuning, chamber and magnet re-alignment, demagnetization of chamber, kicker and septum improving and etc., booster had achieved beam ramped to 3 GeV at December 16 2014. Diagnostic system played a helpful rule to provided beam profile and information during booster commissioning. This report will focus on the booster BPM related environment, functionalities and measurement.

BOOSTER BPM FUNCTIONALITIES AND COMMISSIONING

The TPS booster ring has six cells where each cell is equipped with 10 BPMs which can be used to measure beam position and rough beam intensity along the longitudinal position. Fig. 1 shows the mechanical drawing of booster BPM which shapes 35x20 mm elliptical and button diameter 10.7 mm. The calibration factor Kx and Ky is 8.25 and 9.66 mm respectively.

The conceptual functional block diagram of the BPM electronics is shown in Fig. 2. It will provide several data type for different application. ADC and TBT data is acquired on demand by trigger; 10 Hz slow data is for DC average orbit and 10 kHz fast data could be applied for booster ramping orbit or fast orbit feedback application. It is also embedded with EPICS IOC for control, monitor and configuration. The timing AMC module would provide functionalities of synchronization, trigger, interlock and post-mortem. To support operation of the BPM electronics, functionalities like cold start, shutdown, housing, control system interface should meet the requirements. The delivered units also had been performed functionality and performance test to ensure compliance with this specification.

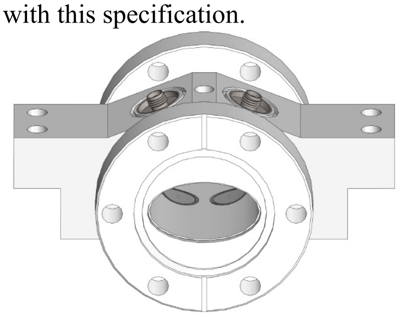

Figure 1: Button-type BPM for TPS Booster.

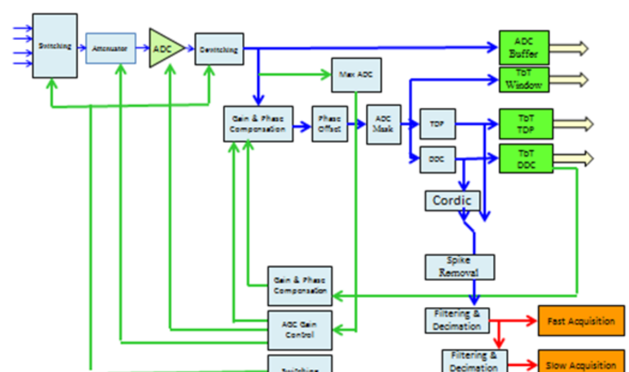

Figure 2: BPM platform functional block diagram.

At early September, the first turn of the booster beam had achieved soon after correctors steering. There are only few buttons of BPM found to have contact problems quickly by observing ADC data with extremely low count compared to other buttons. The real BPM calibration factor was agreed with the designed values by measuring and comparing the optical function of machine model.

BOOSTER BPM MEASUREMENT

For TPS booster BPM, there are 60 sets of phase-trimmed 0.240” form polyethylene coaxial cables connected between the buttons and BPM electronics. The gain variation of BPM electronics is less than 5%. The equal length of all cable sets will contribute the same

ISBN: 978-3-95450-168-7 doi:10.18429/JACoW-IPAC2015-MOPTY074

PRELIMINARY BEAM TEST OF SYNCHROTRON RADIATION MONITORING SYSTEM AT TAIWAN PHOTON SOURCE

C.Y. Liao#, C.Y. Wu, Y.S. Cheng, C.K. Kuan, J.Y. Chuang,
H.P. Hsueh, S.Y. Hsu, K.H. Hu, K.T. Hsu
NSRRC, Hsinchu 30076, Taiwan

Abstract

Taiwan Photon Source (TPS) is a third generation 3 GeV synchrotron light facility. The synchrotron radiation from a dipole can be used to observe the beam parameters. The synchrotron radiation monitor (SRM) systems were designed and implemented for the booster synchrotron and storage ring. The SRM for the booster synchrotron can serve to diagnose the energy ramping process. The beam size decreases when the energy increases was observed. In the storage ring, the streak camera was preferred to observe the beam behaviour of the consecutive bunches. The bunch length and longitudinal instability were observed. The preliminary beam test results are summarized in this report.

INTRODUCTION

The Taiwan Photon Source (TPS) is a state-of-the-art synchrotron radiation facility featuring ultra-high photon brightness with extremely low emittance. The TPS accelerator complex consists of a 150 MeV S-band linac, linac to booster transfer line (LTB), 0.15–3 GeV booster synchrotron, booster to storage ring transfer line (BTS), and 3 GeV storage ring. The storage ring has 24 DBA lattices cells with 6-fold symmetry configuration [1]. The TPS commissioning is separated into two phases. Phase I commissioning was done in the first quarter of 2015 with two Petra 5-cells cavities and without insertion devices. Phase II commissioning is scheduled to start in the third quarter of 2015 with two superconducting RF cavities and insertion devices.

The synchrotron radiation monitors are designed in the booster and storage ring of the TPS, which play an important role during the commissioning. The SRM for the booster synchrotron serves to characterize energy ramping process. In the storage ring, SRM can be used to measure the beam size, bunch length and beam behaviour, and fill pattern by X-ray pinhole camera, streak camera, and photon counting technique, respectively. The design overview and preliminary beam test results are presented in this paper.

SYSTEM DESIGN

Synchrotron Radiation Monitor for Booster

The SRM design of booster synchrotron was shown in Fig. 1. The light leads to the wall via a four-piece adjustable mirror, focusing through a lens (f = 1 m) and band-pass filter to GigE Vision camera. The camera trigger is synchronized with the machine cycle; change the delay time will change the energy point of observation. A 1-inch size CCD is used to quickly and easily to find a first-time beam spot. During the commissioning, a few times entering the tunnel is necessary to adjust the lens until the light beam is within the CCD's sensing area. This synchrotron light monitoring port was used for streak camera measurement for linac beam and booster stored beam also.

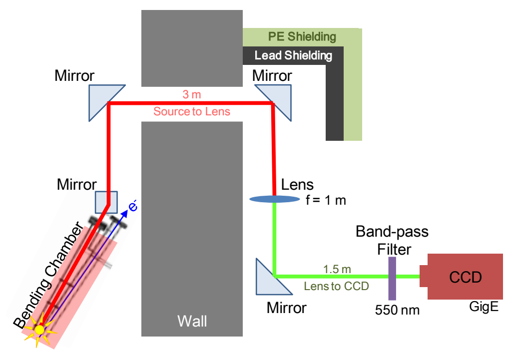

Figure 1: A side-view scheme of the synchrotron radiation monitor for the booster ring.

Diagnostics Beamline for Storage Ring

The photon diagnostics beamline for the TPS storage ring utilized visible light and X-ray of the synchrotron radiation which generated in a bending magnet. The photon diagnostics devices are summary in Table 1. The X-ray pinhole camera design as shown in Fig. 2, which is imaging the electron beam from bending magnet for the beam size and emittance measurements. They offer the required resolution and the dynamic range to measure the electron beam size accurately at all currents. The visible light of synchrotron radiation was design for streak camera, interferometer and fill pattern measurements, as shown in Fig. 3.

Table 1: The SRM Diagnostics Devices for Storage Ring

Monitor	Beam parameters
X-ray pinhole camera	Beam size and emittance
Fill pattern monitoring	Fill pattern and isolated bunch purity
Visible light interferometer	Alternative beam size
Visible light streak camera	Bunch length and behaviour

#liao.cy@nsrrc.org.tw

Content from this work may be used under the terms of the CC BY 3.0 licence (© 2015). Any distribution of this work must maintain attribution to the author(s), title of the work, publisher, and DOI.

ISBN: 978-3-95450-168-7 doi:10.18429/JACoW-IPAC2015-MOPTY075

Content from this work may be used under the terms of the CC BY 3.0 licence (© 2015). Any distribution of this work must maintain attribution to the author(s), title of the work, publisher, and DOI.

VIBRATION MEASUREMENT OF THE MAGNETS IN THE STORAGE RING OF TPS

C. H. Huang, P. C. Chiu, Demi Lee, C. Y. Liao, Y. S. Cheng, K. T. Hsu
NSRRC, Hsinchu 30076, Taiwan

Abstract

Taiwan photon source is a 3rd generation synchrotron light source which is in beam commissioning at NSRRC. Orbit stability within 100 nm range is essential for such a small emittance light source. Technical noise from the vacuum pumps, water flow, etc. will cause the vibration of quadrupoles and deleterious orbit stability. In order to investigate the magnitude of vibration in the magnets of the storage ring, the vibration spectra of the lattice quadruples; the coherence between the magnets, girders and ground will be systematic investigated in this report.

INTRODUCTION

Taiwan photon source (TPS) is a low emittance, third-generation light source in NSRRC. Its circumference is 518.4 m with 24 double-bend achromat (DBA) cells [1]. There are 6 long-straight sections and 18 standard-straight sections to accommodate insertion device. The vertical beam size at the centre of the standard cell of insertion devices straight is around 5 µm. This imposes a stringent requirement for the orbit stability. To obtain a high quality light source, the beam orbit motion needs to be controlled at least within 0.5 µm.

Ground vibration and the technical noise such as vacuum pumps and water flow will cause the magnet vibration and then leads to the distortion of the close orbit. The frequency of such vibration is much smaller than the revolution frequency of the electron beam so the vibration of the magnet can be treated as a constant displacement or beam offset [2]. The dominant effect is produced by the quadrupole and it introduces a kick angle (θ) to the beam: $\theta = eckyL/E$. k is the quadrupole strength; y is the beam offset to quadrupole center; L is the quadrupole length; E is the beam energy [3]. The closed orbit distortion (Δy_j) at j-th position caused by i-th quadrupole would be $\Delta y_j = \theta_i \sqrt{\beta_i \beta_j} \cos(\pi\nu - |\psi_j - \psi_i|)/(2\sin\pi\nu)$. Here β, ψ and ν are the beta function, phase and tune.

In this paper, we focus on vibration in the 240 quadrupoles of the storage ring. The vibration of devices and mechanical supports which may cause the magnets vibration will also be summary here. At last, the correlation between quadrupoles, girder and ground will also be studied.

PROBES AND DATA ACQUISITION SYSTEM

Low noise three-components seismometers, LE-3Dlite Mark II [4], with frequency range 1- 100 Hz is used in this study. The data acquisition unit (Data Translation DT8837), which is complied with LXI class C standard, provides Ethernet accesses via SCPI command to acquire data. Multiple DT8837s are synchronized by wired trigger bus (WTB) interface. To extend length limit of WTB cable, an in-house made small interface adapter from RJ-45 to Micro D is installed at the WTB connector of the DT8837 side. It allows unshielded twisted pair (UTP) cables to replace WTB cables and to send the trigger, sync and clock single from the timing system adapter to DT8837 more than 100 m. Coherent data acquisition can also be achieved by the aid of global timing system. A Matlab script can be running in the sever for the long-term measurement or in the laptop for the short-term measurement, shown in Fig. 1.

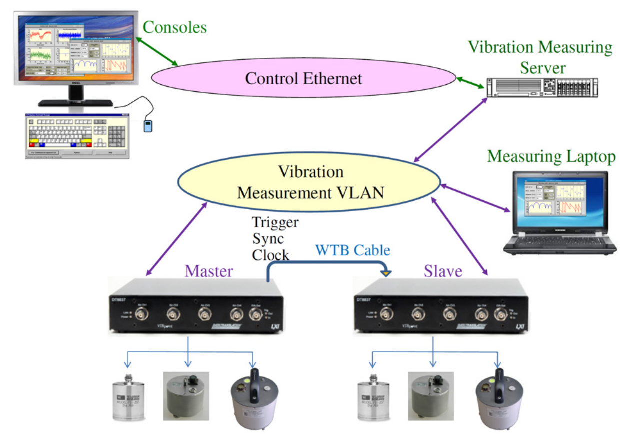

Figure 1: Configuration of vibration measuring system.

MESASURMENT RESULTS

Vibration of Quadrupoles and Dipoles

In the beginning of the commissioning of the storage ring, the vibration of quadruples and dipoles in all storage are measured to realize the relationship between vibration and beam motion. From the displacement spectra of magnets of the 21th cell as shown in Fig. 2 for example, there is a sharp resonance around 29 Hz. The maximum displacement amplitude is larger than 200 nm in vertical direction and 600 nm in horizontal direction within all the quadrupoles of the storage ring, shown in Fig. 3. This vibration frequency is caused by the turbo pumps. Although the turbo pumps do not directly contact to the magnets, the vacuum chambers which connect to turbo pumps are supported by the girders. Unfortunately, the vertical resonance frequency of the girder is around 30 Hz in which vibration would be magnified and translated into the magnets above the girder.

ISBN: 978-3-95450-168-7 doi:10.18429/JACoW-IPAC2015-MOPTY076

DEVELOPMENT OF EPICS APPLICATIONS FOR THE TAIWAN LIGHT SOURCE

Y. S. Cheng, Jenny Chen, C. Y. Liao, P. C. Chiu, C. H. Huang, K. T. Hsu
National Synchrotron Radiation Research Center, Hsinchu 30076, Taiwan

Abstract

The TLS (Taiwan Light Source) is a third generation of synchrotron light source, and it has been operated since 1993. The TLS control system is a proprietary design. It was performed minor upgrade several times to avoid obsolete of some system components and keep up-to-date during last two decades. The control system of the TPS project (Taiwan Photon Source) is based upon the EPICS framework. To save resources for TLS control system maintenance, adopt EPICS for newly developed and rejuvenated subsystems for some of the TLS control interfaces includes BPM system, insertion devices, bunch-by-bunch feedbacks, electronics instruments interface and so on. Some EPICS related applications have been developed, and EPICS graphical user interface is also operated at the TLS control consoles environment normally. Current system allowed two kinds of control environments working together. The efforts will be described at this report.

INTRODUCTION

The TLS is a third generation of synchrotron light source built at the National Synchrotron Radiation Research Center (NSRRC) site in Taiwan, and it has been operated since 1993. The TLS consists of a 50 MeV electron Linac, a 1.5 GeV booster synchrotron, and a storage ring with 360 mA top-up injection. The TLS Control system is a proprietary design [1]. Several minor upgrades had been performed to avoid obsolete during last two decades. It consists of console level workstations and VME based intelligent local controller (ILC) to interface with subsystems. Hardware and software on console level workstation change several times due to evolution of fast evolution of computer technology. PC running Linux is the current configuration. Due to the well design of the original control software structure, port to new platform without difficult.

The EPICS (Experimental Physics and Industrial Control System) is a set of open source software tools, libraries and applications developed collaboratively and used to create distributed soft real-time control systems for scientific instruments such as the particle accelerators and large scientific experiments [2]. Many particle accelerator facilities adopt EPICS framework for their control systems and gain good experiences. Many resources and supports are available as well as numerous applications for accelerator have been developed.

The EPICS toolkits were chosen as control system framework for the Taiwan Photon Sourece (TPS) of 3 GeV synchrotron light source [3]. The TPS control system with the EPICS mechanism has been integrated and commissioned. On the other hand, in order to adopt update technology and re-use expertise of manpower, the upgrade and maintenance for TLS control system adopts the EPICS as its framework. Moreover, some new installed subsystems runs EPICS control environment to reduce working load and use the same expertise of manpower.

In the TLS, the control console can continuously operate on the existing control system environment and develop additionally in the EPICS framework for the subsystem upgrade in the meanwhile.

Utilizing the EPICS channel access mechanism with the specific toolkits, the data can be accessed between the IOCs (Input Output Controller) and the clients. The various operation processes are developed and tested according to the various operation modes. The implementation of subsystems is introduced as followings.

EPICS ENVIRONMENT OF TLS CONTROL SYSTEM

To implement the EPICS support for some subsystems, the control environment of the IOC is set up with the specific EPICS base, modules and extensions at the Linux operation system. To control and monitor subsystems based on EPICS environment via Ethernet, the clients should be installed the specific EPICS base and the graphical operation toolkits, such as EDM (Extensible Display Manager) and MATLAB (channel access via the labCA module) for EPICS channel access.

Most of EPICS related files at control consoles are mounted from the file server by using the NFS service (Network File System) to simplify software version control. Various directories are created and saved into various versions of related files for various hosts and purposes. Various directories provide a mount point for hosts mounted according to various purposes. The directories include EPICS base, modules, extensions, saved data, temporary data and etc.

RUN EPICS IOC ON AN ILC OF TLS CONTROL SYSTEM

An EPICS IOC is activated on an ILC to support homogenous access from TLS console computers. TLS ILCs broadcast their dynamic data, DDB, at 10 Hz to simplify data transaction between consoles and ILCs; with SDB and database-access-library installed TLS console APs manipulate the signals efficiently. The TLS control system is an isolated system. To have the rich support of EPICS, the plans of two insertion devices control system upgrade had adopted the EPICS framework. To support access from existing TLS

Content from this work may be used under the terms of the CC BY 3.0 licence (© 2015). Any distribution of this work must maintain attribution to the author(s), title of the work, publisher, and DOI.

ISBN: 978-3-95450-168-7 doi:10.18429/JACoW-IPAC2015-MOPTY077

Content from this work may be used under the terms of the CC BY 3.0 licence (© 2015). Any distribution of this work must maintain attribution to the author(s), title of the work, publisher, and DOI.

CONTROL INTERFACE OF PULSE MAGNET POWER SUPPLY FOR TPS PROJECT

C. Y. Wu, Y. S. Cheng, C. S. Fann, Jenny Chen, C. Y. Liao, S. Y. Hsu,
Demi Lee, C. H. Huang, K. H. Hu, K.T. Hsu, K. K. Lin
National Synchrotron Radiation Research Center, Hsinchu 30076, Taiwan

Abstract

The TPS (Taiwan Photon Source) is low emittance 3 GeV synchrotron light source. The design and implementation of a pulse magnet power supply control system for beam injection and extraction were done. The EPICS embedded programmable logic controller (PLC) was applied to control pulse magnet power supply. The system comprises various input/output modules and a CPU module with built-in Ethernet interface. The control information (status of the power supply, ON, OFF, warn up, reset, reading/setting voltage, etc.) can be accessed remotely using EPICS client tools. The TPS timing system provide trigger signals for pulse magnet power supplies. The Ethernet-based oscilloscope is employed to observe current waveform of pulse magnet power supply with EPICS support. This paper describes control interface and operation GUI for the TPS pulse magnet power supply.

INTRODUCTION

The TPS [1] is a latest generation of high brightness synchrotron light source which has been under construction at the National Synchrotron Radiation Research Center (NSRRC) in Taiwan since February 2010. The civil construction works are finished in early 2014. The TPS pulse magnets consist of booster injection septum and kicker, booster extraction septums and kickers, storage ring injection septum and kickers, and storage ring diagnostic kickers (pingers). The pulse magnets installation and system integration were done soon after site available. The pulse magnets power supplies functionalities and performance were successfully verified with beam commissioning [2].

Table 1 lists main parameters of TPS kickers and septa pulse magnets. The EPICS IOC embedded PLC, F3RP61-2L IOC, was adopted for the pulse magnet power supply control. The F3RP61-2L IOC is compact, easy troubleshooting, and cost effective for pulse magnet power supply control. The pulse magnet power supply (pulser) requires small amount of I/O points, therefore, the F3RP61-2L IOC is more suitable compared with the applications of the TPS standard 6U CompactPCI platform with high I/O density.

The EPICS [3] was adopted as the TPS control system framework. A typical PLC in control environment is supervised by a remote IOC through serial link or Ethernet connections. It needs more work for developing both side of control software compared with using F3RP61-2L IOC. This report will summarize the pulse magnets power supplies related control environment, functionalities and measurement.

Table 1: Main Parameters of TPS Pulse Magnets

Magnet Type	Type	Operating Current (A)	Pulse Duration (μs)	Quantity
Booster Injection Kicker	PFN	~250	~1	1
Booster Extraction Kicker	PFN	~350	~1	2
Storage Ring Injection Kicker	Half-sine	~1100	~5	4
Storage Ring Pinger	Half-sine	-	~ 3	2
Booster Injection Septum	Half-sine	~2300	~400	1
Booster Extraction Septum	Half-sine	~10000	~400	2
Storage Ring Injection Septum	Half-sine	~10000	~400	2

SYSTEM CONFIGURATION

The control environment for TPS pulse magnets power supplies is shown in Fig. 1. The F3RP61-2L IOC is used to monitor status and control the pulse magnets power supplies. To support remote access of the current waveforms, oscilloscopes are managed by one dedicated EPICS IOC. To capture current transformer waveform of pulse magnets power supplies, the LAN extension for Instrumentation (LXI) or Ethernet-base oscilloscopes are connected to EPICS IOC via Ethernet interface.

Event based timing system is implemented to support commissioning and operation for the TPS [4-5]. The timing system is based on the events coming from event generator (EVG). EVG handles the accelerator synchronization and trigger the injection and the extraction pulse device. The timing IOC equipped with event receiver (EVR) will distribute trigger signal of the pulse magnets power supplies to synchronize the operation of the accelerator system. The TPS pulse magnets power supplies will be operated in 3 Hz repetition rate.

The I/O modules configuration of Yokogawa F3RP61-2L IOC is shown in Fig. 2. It includes power supply module, 16 bit digital input module, 16 bit digital output module, 8 channel analog input module (16 bit ADC) and 8 channel analog output module (16 bit DAC). The I/O modules are mastered by F3RP61-2L CPU module. The interlock function of pulse magnet power supply is handled by local hardware circuits. It uses relay and timer

ISBN: 978-3-95450-168-7 doi:10.18429/JACoW-IPAC2015-MOPTY079

THE INSTALLATION AND OPERATION OF TPS LASER PSD SYSTEM IN TPS STORAGE RING

M.L. Chen, P.S.D. Chuang, W.Y. Lai, H.C. Ho, K.H. Hsu, S.Y. Perng, H.S. Wang, C.J. Lin, D.G. Huang,T.C. Tseng, C.K. Kuan, J.R. Chen
NSRRC, Hsinchu, Taiwan

Abstract

24 sets of Laser PSD positioning system are parts of the TPS girder autoalignment system. Laser PSD positioning systems are installed in the straight section girders of TPS storage ring. The Laser PSD systems are assembled and calibrated in the Lab beforehand. The Laser and PSDs are assembled on girder and transported to TPS storage ring and Installed. During construction the system deviates from the normal position caused by variant temperature and external influence. For absolute position precision, another laser calibration system should be built to recalibrate the laser PSD system. This paper describes the installation of Laser PSD system in TPS storage ring and the status of the PSD system. A new absolute position calibration method for precision upgrade is also discussed.

INTRODUCTION

A precise auto-alignment scheme is developed to align and adjust the storage ring girders of Taiwan Photon Source (TPS). [1] Laser PSD system, part of auto-alignment scheme, is designed and developed to align two girders on both sides of the straight section. There are 6 sets of Laser PSD system for the 18m long straight section and 18 sets for 12m short straight section. To achieve high accuracy, a laser and position sensing device, PSD, with the accuracy of micrometer-scale has been designed and arranged for girder positioning [2-4].

The Laser PSD system is constructed by several main portions, including Laser, PSD, beam splitters and isolation tubes. The Laser with Gaussian distribution during working propagation distance, plays a role as a reference line of the girders of the straight-section, as shown in fig1.

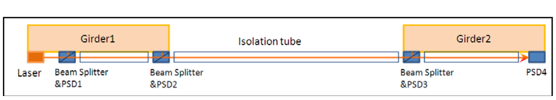

Figure 1: Architecture of Laser -PSD position system.

The PSD modules are adjusted and positioned within the error of micro-meter scale in advance. The PSD correction factors are calibrated. The absolute displacement accuracy of the Laser PSD system can be within 25 um by comparing with the Laser tracker. [5] After 24 sets of PSD system is assembled on girders in the lab, the girders system are transported to TPS storage ring and installed within the standard procedure for storage ring construction.

INSTALLATION OF LASER PSD SYSTEM IN TPS STORAGE RING

The Laser -PSD positioning system is constructed by several main portions, including Laser, PSD, beam splitters and isolation tubes. The Laser beam propagates in the isolation tubes, to prevent noise caused by temperature and flow of air due to the air conditioning system.

The first procedure of girder installation is to install the pedestals and positioning it in the tunnel. Followed by girders that are placed on the pedestals, and the isolating tube related fixtures which is positioned and assembled. The support of the isolation tube are adjusted and positioned in the straight section. The isolation tubes are connected and thermal insulation material are wrapped up around both sides of the tube to prevent air disturbance.

Figure 2: Laser potion and isolation tube of Laser -PSD system are assembled on the side of girder in lab. Then magnet girders are transported back and placed on pedestals in TPS tunnel.

Figure 3: The support of isolation tube are adjusted and positioned on the exact location of ground in the straight section of TPS storage ring.

Content from this work may be used under the terms of the CC BY 3.0 licence (© 2015). Any distribution of this work must maintain attribution to the author(s), title of the work, publisher, and DOI.

ISBN: 978-3-95450-168-7 doi:10.18429/JACoW-IPAC2015-MOPTY080

A MULTI-BAND SINGLE SHOT SPECTROMETER FOR OBSERVATION OF MM-WAVE BURSTS AT DIAMOND LIGHT SOURCE*

A. Finn†, P. Karataev, JAI at Royal Holloway University of London, Egham, UK
G. Rehm, Diamond Light Source, Oxfordshire, UK

Abstract

Micro-bunch instabilities (MBI) have been detected at many light sources across the world. The bursts produced as a result of this instability occur in the millimetre regime. More needs to be determined about the dynamics of MBI in order to confirm the simulations. Consequently, a single shot spectrometer has been created to investigate this instability at Diamond Light Source (DLS). Due to their low noise, ultra-fast response and excellent sensitivity, Schottky detector diodes make up this spectrometer. Currently, seven Schottky detectors are in place covering a range of 33-750 GHz. Unlike previous measurements carried out, each of the Schottky detectors has been characterised thus making the results obtained comparable to simulations. In this paper, we present the assessment of each Schottky detector in the spectrometer; the first results of the spectrometer's use in the beam and future plans for the spectrometer.

INTRODUCTION

Micro-bunching instabilities are common at many lights sources around the world [1–3]. They are known to limit the operation of the storage ring, as bursting can affect user experiments. As a result of this, light sources usually endeavour to avoid the conditions which result in these additional bursts. MBI produce coherent synchrotron radiation (CSR), bursts of CSR to be more precise. CSR from the whole bunch occurs when the wavelength of radiation exceeds the bunch length. CSR is also produced when structure in the longitudinal profile is of short length, and in this case the CSR can even enhance that structure further.

Since 2009, the Diamond storage ring is often operated in a dedicated low alpha mode [4], whereby the momentum compaction factor α is set to be between 17 and 70 times smaller than normal user mode. At DLS there are two varieties of low alpha modes to provide coherent radiation for THz/IR experiments and short-pulse radiation for pump-probe experiments. Due to the nature of the low alpha modes, i.e. the smaller bunch lengths, the MBI regularly occurs.

SCHOTTKY DETECTOR DIODES

Schottky Barrier Diodes (SBD) are best known for their fast response [5], low noise and excellent sensitivity. Operating at room temperature, SBDs are able to detect mm-waves and hence are often used as detectors within this wavelength range. The detector diodes that we have chosen are housed within waveguides and fed signal using horn antennas. A spectrometer has been designed using seven SBDs, with each detector covering a specific frequency band from 33-750 GHz. Table 1 shows the properties of the chosen SBDs.

* Work supported by Diamond Light Source, Oxfordshire, UK
† aiveen.finn.2013@live.rhul.ac.uk

Table 1: SBD Specifications

Detector Model	Stated Range	Sensitivity
DXP-22 [6]	33-50 GHz	1200 V/W
DXP-12 [6]	60-90 GHz	700 V/W
DET-08 [6]	90-140 GHz	600 V/W
WR5.1ZBD [7]	140-220 GHz	2000 V/W
WR3.4ZBD [7]	220-330 GHz	1500 V/W
WR2.2ZBD [7]	330-500 GHz	1250 V/W
WR1.5ZBD [7]	500-750 GHz	750 V/W

SPECTROMETER/DETECTOR ARRAY

DLS hosts a viewport which is dedicated to the investigation of CSR. The viewport transports the synchrotron radiation from bending magnet B06 to the viewport window. It is there that the detector array is placed on three motion stages for movement in x, y and z directions. The detector array is shown in Fig. 1 on its motion stages.

The plate shown (Fig. 1) is designed in such a way that all detectors are as close together as possible and observe as much signal as available. All horn antennas are at the same distance to the viewport to remove the risk of shadowing.

It is important for the cables between the detectors and the voltage amplifiers to be short. The input impedance of the amplifiers is high (10 kΩ), thus to accommodate a good signal-to-noise ratio around the revolution frequency, the cable capacitance must be low. In order to lower the capacitance, shorter cables were used, thus a plate housing the amplifiers was attached to the detector array allowing for minimal cable length. Following the voltage amplifiers the signals are carried out of the tunnel, where the signals are fed into a simultaneous 16-channel sampling digitiser.

DATA ANALYSIS

For a specified period of time, the data are captured with an external 5 Hz trigger. The data are then analysed in MATLAB. Due to limited bandwidth Ethernet, from the digitiser to the relevant computer for processing, it is impossible to continually stream data from the digitising unit to our computers for analysis, hence the snapshots of data being acquired. A digital down conversion (DDC) of the data is carried out, with the analysis locking in at the revolution frequency of the storage ring, (533.820 kHz). The information

Content from this work may be used under the terms of the CC BY 3.0 licence (© 2015). Any distribution of this work must maintain attribution to the author(s), title of the work, publisher, and DOI.

ISBN: 978-3-95450-168-7 doi:10.18429/JACoW-IPAC2015-MOPTY082

BEAM INSTRUMENTATION OF THE PXIE LEBT BEAM LINE *

R. D'Arcy†, B. Hanna, L. Prost, V. Scarpine, A. Shemyakin
Fermilab, Batavia, IL 60510, USA

Abstract

The PXIE accelerator [1] is the front-end test stand of the proposed Proton Improvement Plan (PIP-II) [2] initiative: a CW-compatible pulsed H- superconducting RF linac upgrade to Fermilab's injection system. The PXIE Ion Source and Low-Energy Beam Transport (LEBT) section are designed to create and transfer a 1-10 mA H^- beam, in either pulsed (0.001–16 ms) or DC mode, from the ion source through to the injection point of the RFQ. This paper discusses the range of diagnostic tools – Allison-type Emittance Scanner, Faraday Cup, Toroid, DCCT, electrically isolated diaphragms – involved in the commissioning of the beam line and preparation of the beam for injection into the RFQ.

PXIE LEBT DIAGNOSTICS REQUIREMENTS

The PXIE LEBT beam line, described in [3] and shown in Fig. 1, consists of a 30 keV H^- ion source, three solenoids with a pair of dipole correctors in each, a chopping system inserted between the last two solenoids, and a set of diagnostics combined with collimation systems.

Some of the peculiarities of the PXIE LEBT are related to the plan to commission PXIE first in a short-pulse mode and then to increase the pulse length, eventually operating in true DC mode. This will ultimately be accomplished with the LEBT chopper, capable of forming 0.001-16.6 ms pulses with a rise time of ~100 ns at a frequency of up to 60 Hz. For the tuning of the LEBT itself, and to decrease the load to the LEBT chopper absorber, the ion source has been equipped with a modulator that can pulse the extraction electrode, also at 60 Hz but with a rise time of ~1 μs. The chopper starts forming the final pulse length after the first ~ 1 ms of the modulator pulse, allowing the neutralisation near the ion source to reach a steady-state.

Correspondingly, diagnostics are required to provide information about the beam in two modes: DC and pulsed. In the latter, the control system provides separate time triggers for the diagnostics channels upstream of the chopper and remaining part of the LEBT. The initial nominal pulse length for PXIE commissioning is 5 μs, chosen as a compromise between the chances of damaging the SRF section and the need for reasonable measurement accuracy of downstream beam instrumentation.

The LEBT diagnostics can be divided into three groups: current monitors, apertures and scrapers, and the emittance scanner.

DIAGNOSTIC TOOLS

Current Monitors

The beam current can be measured by a DC Current Transformer (DCCT), an AC transformer (a.k.a. a toroid), and, at the commissioning stage, by the Faraday Cup (FC) at the end of the LEBT. Some indication of the beam current is also given by the ion source bias supply current but, because of a significant electron component at the ion source output, the latter may be up to 2 times higher.

The DCCT is installed downstream of the first solenoid and measures the beam current in DC or long-pulse (≥ 500 μs) modes. Its sensitivity to external magnetic fields requires a significant longitudinal space to ensure enough separation from both the first solenoid and a future bending magnet to be installed just downstream. Whilst the DCCT is currently the main tool used to measure the beam current the possibility of replacing it with a toroid during transition to the configuration with the bend is being discussed.

The LEBT toroid is installed downstream of the chopper. To measure the beam loss in the RFQ down to 1%, an identical toroid will be placed at the RFQ exit. A procedure to cross-calibrate both toroids with a relative accuracy at the 1% level is in development.

The Faraday Cup (FC) is a copper cylinder with an aperture radius, R, of 49.4 mm and a length, L, of 144.5 mm. By using the electrode in front of the FC (EID5) as a suppressor of secondary electrons it is shown that the capturing inefficiency is < 1%, in agreement with a simple estimation of $\sim 0.1 \times (L/R)^2$.

The resolution and bandwidth of the current monitors are shown in Tab. 1.

Isolated Electrodes and Scrapers

The PXIE LEBT beam line includes several Electrically Isolated Diaphragms (EIDs) (see Fig. 1), each biased with an individual +50 V floating power supply. The EIDs are copper, water-cooled tori with varying opening diameters depending on location (see Fig. 1 for sizes). Special circuitry allows measurement of the beam loss to an EID in DC and pulsed (> 1 μs) modes. In addition to beam control (physically scraping beam tails and altering neutralisation

Table 1: Parameters of the PXIE LEBT Current Monitors

	Resolution	Bandwidth
DCCT	< 10 μA	DC to 4 kHz
Toroid	< 10 μA	10 Hz to 4 MHz
Faraday Cup, Isolated Electrodes	< 5 μA	DC to 20 MHz

* Operated by Fermi Research Alliance, LLC, under Contract DE-AC02-07CH11359 with the U.S. DOE.
† rtpdarcy@fnal.gov

Content from this work may be used under the terms of the CC BY 3.0 licence (© 2015). Any distribution of this work must maintain attribution to the author(s), title of the work, publisher, and DOI.

6th International Particle Accelerator Conference IPAC2015, Richmond, VA, USA JACoW Publishing
ISBN: 978-3-95450-168-7 doi:10.18429/JACoW-IPAC2015-MOPTY083

PROGRESS TOWARDS ELECTRON-BEAM FEEDBACK AT THE NANOMETRE LEVEL AT THE ACCELERATOR TEST FACILITY (ATF2) AT KEK

N. Blaskovic Kraljevic, D. R. Bett, T. Bromwich, P. N. Burrows, G. B. Christian, M. R. Davis, C. Perry,
John Adams Institute, Oxford, UK

Abstract

Ultra-low latency beam-based digital feedbacks have been developed by the Feedback On Nanosecond Timescales (FONT) Group and tested at the Accelerator Test Facility (ATF2) at KEK in a programme aimed at beam stabilisation at the nanometre level at the ATF2 final focus. Three prototypes were tested: 1) A feedback system based on high-resolution stripline BPMs was used to stabilise the beam orbit in the beamline region c. 50m upstream of the final focus. 2) Information from this system was used in a feed-forward mode to stabilise the beam locally at the final focus. 3) A final-focus local feedback system utilising cavity BPMs was deployed. In all three cases the degree of beam stabilisation was observed in high-precision cavity BPMs at the ATF2 interaction point. Latest results are reported on stabilising the beam position to below 100 nanometres.

INTRODUCTION

A number of fast beam-based feedback systems are required at future single-pass beamlines such as the International Linear Collider (ILC) [1]. For example, at the interaction point (IP) a system operating on nanosecond timescales within each bunch train is required to compensate for residual vibration-induced jitter on the final-focus magnets by steering the electron and positron beams into collision. The deflection of the outgoing beam is measured by a beam position monitor (BPM) and a correcting kick applied to the incoming other beam. In addition, a pulse-to-pulse feedback system is envisaged for optimising the luminosity on timescales corresponding to 5 Hz.

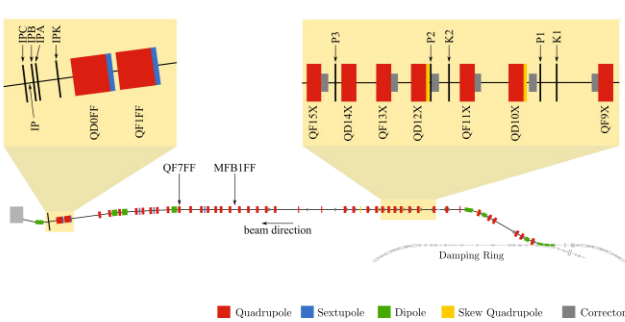

Figure 1: Layout [7] of the ATF extraction and final focus beamline with the FONT regions zoomed in.

The Feedback on Nanosecond Timescales (FONT) project has developed ILC prototype systems, incorporating digital feedback processors based on Field Programmable Gate Arrays (FPGAs), to provide feedback correction systems for sub-micron-level beam stabilisation at the KEK Accelerator Test Facility (ATF2) [2]. Previous results [3], [4] have demonstrated an upstream closed-loop feedback system that meets the ILC jitter correction and latency requirements. Furthermore, results demonstrating the propagation of the correction obtained using the upstream stripline BPM feedback system at ATF2 are reported in [5]. The ultimate aim is to attempt beam stabilisation at the nanometre-level at the ATF2 IP [6]. We report here the latest developments and beam testing results from the FONT project using a cavity BPM [7] to drive local feedback correction at the IP.

FONT5 SYSTEM DESIGN

An overview of the extraction and final focus beamlines at the ATF, showing the positions of the FONT5 system components in the IP region, is given in Fig. 1. The IP feedback system comprises a C-band cavity BPM (IPB) [7] and a short stripline kicker (IPK). The final focus magnets (QF1FF, QD0FF) can be used to steer the beam by introducing a position offset or to move the x and y beam waists longitudinally along the beamline. The offset of the QF7FF magnet can be used to change the pitch of the beam trajectory through the IP region.

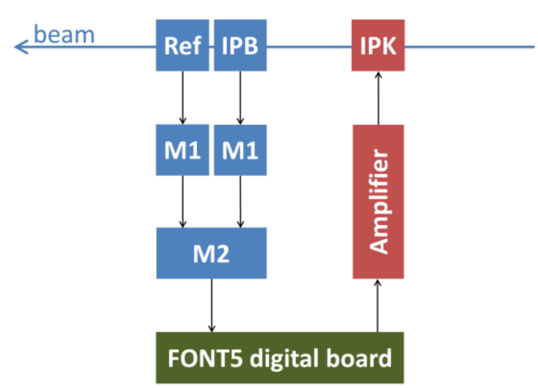

Figure 2: Schematic of IP feedback system showing the cavity BPM (IPB), reference cavity (Ref), first and second down-mixer stages (M1 and M2), FONT5 digital board, amplifier and kicker (IPK).

A schematic of the IP feedback system is given in Fig. 2. Determining the position of the beam at IPB requires both the dipole mode signal of IPB and the monopole mode signal of a reference cavity (Ref). The cavities were designed such that the y-port frequency of both signals is 6.426 GHz [8]. The signals are down-

Content from this work may be used under the terms of the CC BY 3.0 licence (© 2015). Any distribution of this work must maintain attribution to the author(s), title of the work, publisher, and DOI.

ISBN: 978-3-95450-168-7 doi:10.18429/JACoW-IPAC2015-MOPTY084

DESIGN, TESTING AND PERFORMANCE RESULTS OF A HIGH-RESOLUTION, BROAD-BAND, LOW-LATENCY STRIPLINE BEAM POSITION MONITOR SYSTEM

N. Blaskovic Kraljevic, D. R. Bett, T. Bromwich, P. N. Burrows, G. B. Christian, M. R. Davis, C. Perry,
John Adams Institute, Oxford, UK

Abstract

A high-resolution, low-latency beam position monitor (BPM) system has been developed for use in particle accelerators and beamlines that operate with trains of particle bunches with bunch separations as low as several tens of nanoseconds, such as future linear electron-positron colliders and free-electron lasers. The system was tested with electron beams in the extraction line of the Accelerator Test Facility at the High Energy Accelerator Research Organization (KEK) in Japan. The fast analogue front-end signal processor is based on a single-stage RF down-mixer. The processor latency is 15.6 +- 0.1 ns. A position resolution below 300 nm has been demonstrated for beam intensities of around 1 nC, with single-pass beam.

INTRODUCTION

A number of in-construction and proposed future particle accelerator designs feature trains of particle bunches with bunch-separation intervals in the ranges of nanoseconds to tens or hundreds of nanoseconds. For example, the International Linear Collider (ILC) design [1] calls for bunch trains comprising thousands of bunches separated in time by around 500 ns with a train repetition frequency of 5 Hz; the Compact Linear Collider (CLIC) design [2] specifies bunch trains comprising several hundred bunches separated in time by around 0.5 ns, with a train repetition frequency of 50 Hz. Free-electron lasers based on similar accelerating technologies as ILC and CLIC will have similar bunch-train time structures, such as the European XFEL [3], which will have a minimum bunch spacing of 200 ns and a repetition rate of 10 Hz. Beam control at such facilities calls for beam position monitors (BPMs) that can resolve bunches on an intra-train (ideally bunch-by-bunch) timescale, with submicron position resolution in single-pass mode. The design of such a BPM system is presented here.

FONT5 SYSTEM AT ATF2

The system was developed by the Feedback on Nanosecond Timescales (FONT) group [4] and it was deployed, commissioned and tested at the Accelerator Test Facility (ATF) [5] at KEK. The layout of the BPMs is shown in more detail in Fig. 1. The design goal for the FONT5 system is to stabilize the vertical beam position to the 1 µm level at the entrance to the final-focus system. This requires BPMs capable of resolving bunches separated in time by around 100 ns, and with a position resolution at the submicron level. For tests of the FONT5 system the ATF is operated in a mode whereby a train of two or three bunches is extracted from the damping ring and sent down the ATF2 beam line. The bunch separation is determined by the damping ring fill pattern and typically is chosen to be between 140 ns and either 154 ns (3-bunch mode) or 300 ns (2-bunch mode).

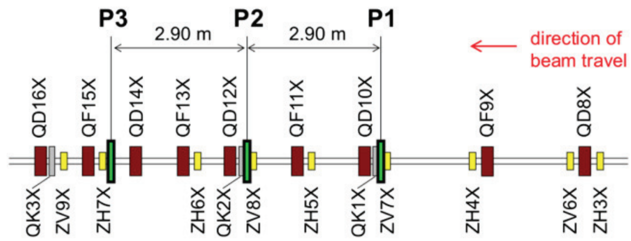

Figure 1: Layout of the FONT5 BPMs (P1, P2 and P3) in the ATF2 extraction line; quadrupole ("Q") and dipole corrector ('Z') magnets are indicated.

The FONT5 BPM system (Fig. 2) consists of three stripline BPMs (Fig. 3) each of which is instrumented with an analogue processor, and a custom multichannel digitizer. Stripline BPMs were used due to their inherently fast, broadband response and capability to resolve bunches with the required time resolution. In the FONT5 system, only the vertical plane of the BPMs is routinely instrumented.

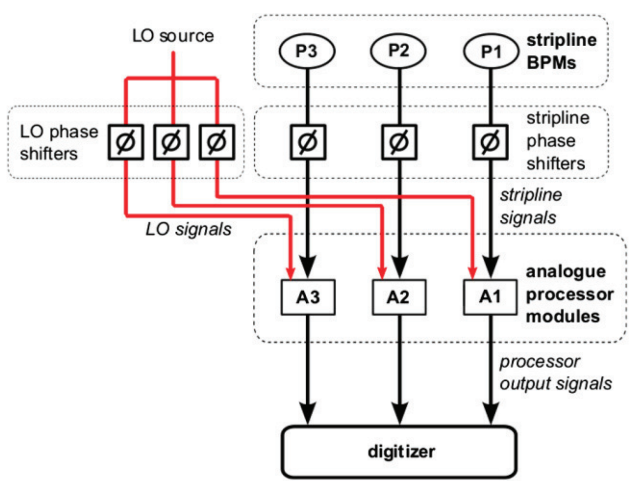

Figure 2: Schematic of the FONT5 BPM system. For each BPM, a phase shifter is used on one of the stripline signals to adjust the relative path lengths of the two input signals at the BPM processor, and another phase shifter is used to adjust the phase of the LO signal at each processor.

Content from this work may be used under the terms of the CC BY 3.0 licence (© 2015). Any distribution of this work must maintain attribution to the author(s), title of the work, publisher, and DOI.

ISBN: 978-3-95450-168-7 doi:10.18429/JACoW-IPAC2015-MOPWI001

FIRST RESULTS FROM BEAM TESTS OF THE CLIC DRIVE BEAM PHASE FEEDFORWARD PROTOTYPE AT CTF3*

J. Roberts, CERN, Geneva, Switzerland; JAI, Oxford, UK
A. Andersson, R. Corsini, P.K. Skowroński, CERN, Geneva, Switzerland
P.N. Burrows, G.B. Christian, C. Perry, JAI, Oxford University, UK
A. Ghigo, F. Marcellini, INFN/LNF Frascati, Italy

Abstract

In the CLIC two beam acceleration scheme 100 MV/m normal conducting cavities are fed with RF power extracted from a secondary high power but low energy drive beam. To ensure the efficiency and luminosity performance of CLIC the phase synchronisation between the high energy main beam and the drive beam must be maintained to within 0.2 degrees of 12 GHz. To reduce the drive beam phase jitter to this level a low-latency drive beam phase feedforward correction with bandwidth above 17.5 MHz is required. A prototype of this system has been installed at the CLIC test facility CTF3 to prove its feasibility, in particular the challenges of high bandwidth, high power and low latency hardware. The final commissioning and first results from operation of the complete phase feedforward system are presented here.

INTRODUCTION

The RF power used to accelerate the main beam in the proposed linear collider CLIC is extracted from a second 'drive beam'. To ensure the efficiency of this concept a drive beam 'phase feedforward' system is required to achieve a timing stability of 50 fs rms, or equivalently a phase stability (jitter) of 0.2 degrees of 12 GHz (the CLIC drive beam bunch spacing) [1–3]. This system poses a significant hardware challenge in terms of the bandwidth, resolution and latency of the components and therefore a prototype of the system has been designed, installed and commissioned at the CLIC test facility CTF3 at CERN. Phase feedforward is hereafter referred to as "PFF".

A schematic of the CTF3 PFF system is shown in Fig. 1. The phase is corrected utilising two kickers placed prior to the first and last dipole in the pre-existing chicane in the TL2 transfer line. By varying the voltage applied to the kickers the beam can be deflected onto longer or shorter paths through the chicane, thus inducing a phase shift. The goal is to demonstrate a 30 MHz bandwidth phase correction with a resolution of 0.2 degrees of 12 GHz. The required hardware consists of three precise phase monitors [4, 5] and two strip line kickers [5] designed and fabricated by INFN/LNF Frascati, and a kicker amplifier and digital processor [6] from the John Adams Institute at Oxford University. More detailed descriptions can be found in [7].

The latency of the PFF system, including cable lengths and the latency of each component, is below the 380 ns beam time of flight between the first monitor and the first kicker. This allows the same bunch that was originally measured to be corrected.

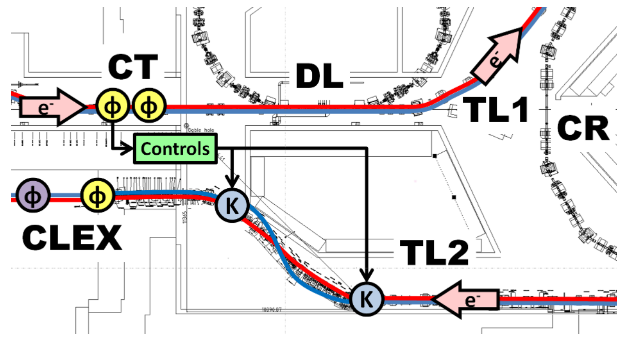

Figure 1: Simplified schematic of the PFF system. Red and blue lines depict orbits for bunches arriving late and early at the first phase monitor, ϕ, respectively. The trajectory through the TL2 chicane is changed using two kickers, K.

COMMISSIONING

The complete PFF system became available in October 2014. Previous results from commissioning of the optics and phase monitors are presented in [8].

The first prototype kicker amplifiers used for the tests presented here provide an output voltage of 340 V. They will be upgraded in stages over the course of 2015, ultimately providing the nominal voltage of 1.2 kV. Constant kick tests demonstrated that applying the maximal 340 V to the PFF kickers resulted in a phase shift of ±3.5°, thus verifying the functionality of the amplifiers, kickers and chicane optics (Fig. 2). The 30 ns rising and falling edges of the response to the kick correspond to 12 MHz amplifier bandwidth when rising from zero to maximum output. This is slew-rate limited and the bandwidth is expected to be 50 MHz for smaller variations.

The PFF algorithm on the digital processor varies the drive signal to the amplifier based on the upstream phase (measured in the CT line, see Fig. 1) in order to correct the downstream phase (after the correction chicane in CLEX) with 30 MHz bandwidth. Its performance was verified by observing the response in a BPM after the correction chicane whilst applying the PFF correction to one kicker at a time. Figure 3 proves that the applied kick has the same shape as the upstream phase.

During the commissioning it was apparent that the upstream phase jitter of up to 1° increased to as much as 4°

* Work supported by the European Commission under the FP7 Research Infrastructures project Eu-CARD, grant agreement no. 227579

Content from this work may be used under the terms of the CC BY 3.0 licence (© 2015). Any distribution of this work must maintain attribution to the author(s), title of the work, publisher, and DOI.

ISBN: 978-3-95450-168-7 doi:10.18429/JACoW-IPAC2015-MOPWI002

BUNCH LENGTH MEASUREMENTS USING SYNCHROTRON LIGHT MONITOR*

M.M. Ali, M.G. Tiefenback, Jefferson Lab, Newport News, VA 23606, USA

Abstract

Bunch length is measured at CEBAF using an invasive technique. The technique depends on applying an energy chirp for the electron bunch and imaging it through a dispersive region. Measurements are taken through Arc1 and Arc2 at CEBAF. The fundamental equations, procedure and recent results are given.

INTRODUCTION

CEBAF is a folded transfer line, with no natural stable bunch structure. Bunch length measurement and control are important for CEBAF because a too-long bunch would generate excessive energy spread, resulting in interrupted beam delivery due either to beam loss or failure to satisfy user requirements. Bunch length is commonly measured in the injector beam dump at up to 123 MeV using the "zero-phasing" method [1] before injection into the North Linac (NL). However, to mitigate periodic problems with control of bunch "tails," the beam undergoes a final magnetic compression in the injection chicane (four dipoles and nine quadrupoles) linking the injector and NL. After exiting the NL at up to 1.2 GeV, the beam follows the semi-circular arc 1A to its injection point into the South Linac (SL). Arc 2A returns the beam for reinjection into the NL. This cycle may be repeated for up to six passes through the NL, after which beam is delivered to Hall D (up to 12 GeV). The first two recirculation arcs incorporate high dispersion points at the central dipoles ($\eta_x \sim 5$ meters), enabling synchrotron radiation (SR) imaging to monitor energy stability and other beam properties. Bunch length measurement generally parallels that described in [2]. We discuss the relationship between measurement of bunch length and of transverse emittance and how we have used this approach to measure the steady-state bunch length for high-power CW beam.

To minimize the energy spread for users, the beam is accelerated at peak energy gain (on-crest). By altering the global ("gang") phase of a linac, the z-correlated energy spread may be increased. Off-crest acceleration increases the energy spread and the transverse beam size at the high dispersion monitor, enabling measurement of the bunch length. The early arcs of CEBAF are isochronous (M_{56}=0), so the longitudinal bunch structure is preserved. Shifting the linac phase by equal amounts of opposite polarity results in turn-by-turn compensation of the added energy spread while allowing observation in the 1A synchrotron light monitor (SLM). Under these conditions, bunch length measurement is possible at high CW beam current while maintaining lossless transport to the appropriate beam dump.

* Work supported by the U.S. Department of energy under U.S. DOE Contract No. DE-AC05-06OR23177

SLM ANALYSIS

We begin with a coordinate system (x,y,z,δ) following the beam, where (x,y) are transverse coordinates, z is the longitudinal coordinate, and δ is the relative deviation of a particle from the average bunch energy. We simplify by ignoring transverse momenta until we discuss initial state asymmetries below. When the beam is accelerated off-crest, a z-p_z correlation (often called a chirp) is induced. Longitudinal position is re-mapped into transverse position in regions with significant dispersion. With E_{inj} as the injector energy and E_{NL} as the linac energy gain,

$$E = E_{inj} + E_{NL}\cos(kz + \phi) \tag{1}$$

The linac energy gain is sinusoidal with k as the RF wave number, z as the longitudinal deviation from the bunch center at z=0, and ϕ is the phase shift of the accelerating RF. For short bunches and large ϕ, we consider kz < ϕ.

During off-crest acceleration, the average energy would decrease due to the cosine function. To keep the beam within the energy acceptance, the RF accelerating gradient is adjusted to hold beam energy constant.

$$E = E_{inj} + \frac{E_{NL}}{cos(\phi)}\cos(kz + \phi) \tag{2}$$

We re-write this to first order in kz as

$$E = E_{inj} + E_{NL} - E_{NL}kz\tan(\phi) \tag{3}$$

so that

$$\frac{E - \overline{E}}{\overline{E}} = \frac{-E_{NL}}{E_{inj} + E_{NL}}kz\tan\phi \tag{4}$$

where $\overline{E}$ is the average beam energy and is equal to (E_{inj} + E_{NL}). We take the initial beam to be sufficiently symmetric that the distribution function $F(x, y, z, \delta)$ is uncorrelated pairwise in x, z, and δ. The initial mean square energy spread and bunch length may be represented as

$$\langle z_0^2 \rangle = \int\int\int\int d\delta dz dx dy \quad z^2 \quad F \tag{5}$$

$$\langle \delta_0^2 \rangle = \int\int\int\int d\delta dz dx dy \quad \delta^2 \quad F \tag{6}$$

Adding a linear energy chirp shears the distribution in the δ-z plane in such a way that the altered distribution G may be written in terms of the initial function F evaluated at $\hat{\delta} = \delta - \lambda z$:

$$G(x, y, z, \delta) = F(x, y, z, \hat{\delta}) \tag{7}$$

$$\lambda = \frac{E_{NL}k\phi}{E_{inj} + E_{NL}} \tag{8}$$

Content from this work may be used under the terms of the CC BY 3.0 licence (© 2015). Any distribution of this work must maintain attribution to the author(s), title of the work, publisher, and DOI.

ISBN: 978-3-95450-168-7 doi:10.18429/JACoW-IPAC2015-MOPWI003

Content from this work may be used under the terms of the CC BY 3.0 licence (© 2015). Any distribution of this work must maintain attribution to the author(s), title of the work, publisher, and DOI.

LASERWIRE EMITTANCE SCANNER AT CERN LINAC4

K.O. Kruchinin*, G. Boorman, A. Bosco, S.M. Gibson, P. Karataev,
John Adams Institute at Royal Holloway, University of London, Egham, Surrey, TW20 0EX, UK
E. Bravin, T. Hofmann, U. Raich, F. Roncarolo, F. Zocca, CERN, Genewa, Switzerland
J. Pozimski, Imperial College, London, UK
A.P. Letchford, STFC/RAL/ASTeC, Chilton, Didcot, UK

Abstract

Linac 4 presently under construction at CERN is designed to replace the existing 50 MeV Linac 2 in the LHC injector chain and will accelerate the beam of high current negative hydrogen ions to 160 MeV. During the commissioning a laserwire emittance scanner has been installed allowing non-invasive measuring of the emittance at 3 MeV and 12 MeV setups. A relatively low power infrared fibre coupled laser was focused in the interaction region down to ~150 µm and collided with the ion beam neutralising negative ions. At each transverse laser position with respect to the ion beam the angular distribution of the neutral particle beamlets was recorded by scanning a diamond detector across the beamlet at a certain distance from the interaction point while the main beam of the H^- ions was deflected using the dipole magnet installed upstream the detector. Measuring the profile of the beamlet by scanning the laser across the beam allows to directly measure the transverse phase-space distribution and reconstruct the transverse beam emittance. In this report we will describe the analysis of the data collected during the 3 MeV and 12 MeV operation of the Linac 4. We will discuss the hardware status and future plans.

INTRODUCTION

The Linac 4 project located at CERN in Geneva, Switzerland was started in 2003 [1] and aims to build a 160 MeV H^- linear accelerator that will replace the existing proton Linac 2 as the injector to the Proton Synchrotron Booster (PSB). Injection of H^- instead of protons into the PSB would reduce the beam losses and provide more flexible operational conditions. At the end of commissioning the injection beam provided by Linac 4 is expected to double the brightness and intensity of the beam from the PSB. Linac 4 project is an essential step in the High Luminosity LHC upgrade required to future improvement of the CERN accelerator complex towards higher performance [2, 3]. Main parameters of the Linac 4 are presented in Table 1.

Table 1: Main Linac4 Parameters

Parameter	Value	Units
Overall Linac length	76.33	m
Output energy	160	MeV
Bunch frequency	352.2	MHz
Maximum repetition rate	2	Hz
Beam pulse length	400	µs
Max. beam duty cycle	0.08	%
Average pulse current	40	mA
Beam transverse emittance	0.4π	mm mrad
Beam power	5.1	kW

To successfully inject the beam from Linac 4 into PSB the transverse emittance at the machine top energy of 160 MeV has to be measured precisely. The conventional slit and grid beam diagnostics is precluded due to the excessive stopping range of a high energy H^- ions at 160 MeV in any possible slit material. Other methods, like the three - profile measurement, can be heavily affected by space charge effects and cannot handle the nominal Linac 4 pulse length of 400 µs. To overcome these problems a non-destructive method based on laserwire technology has been developed.

EXPERIMENTAL SETUP

In order to characterize the H^- ion beam at different stages of the LINAC4 commissioning a movable, temporary test bench has been used. After finishing the commissioning of the 3 MeV and 12 MeV stage the test bench was placed at the exit of the copper and first DTL section respectively. It was used to characterize the ion beam using various diagnostic tools such as beam current transformers, wire scanners, beam position monitors, bunch shape and halo monitors, a slit and grid emittance meter and a spectrometer line [4, 5].

The laserwire interaction is taking place inside the vacuum chamber that was initially designed to accommodate the movable graphite slit which is a part of the slit and grid emittance scanner [6]. The laser enters the vacuum chamber through a vacuum window, specially coated to reduce back reflections in the infrared range of wavelengths. After interaction the laser beam is dumped into one of the slit blades. Such location of the laserwire proved to be very useful because it allows to perform measurements using two different methods and cross-check the results.

The laserwire system consists of a remotely controlled pulsed laser mounted in a rack in the accelerator tunnel connected via an optical fibre to a laser delivery system which controls the size and position of the laser beam delivered to the interaction point (IP). A detection system was installed downstream of a dipole magnet to record the angular distribution of the neutralized particles from the H^- beam.

* konstantin.kruchinin.2012@live.rhul.ac.uk

ISBN: 978-3-95450-168-7 doi:10.18429/JACoW-IPAC2015-MOPWI004

Content from this work may be used under the terms of the CC BY 3.0 licence (© 2015). Any distribution of this work must maintain attribution to the author(s), title of the work, publisher, and DOI.

NOVEL SINGLE SHOT BUNCH LENGTH DIAGNOSTIC USING COHERENT DIFFRACTION RADIATION

R. Fiorito*, C. Welsch, H. Zhang, Cockcroft Institute, University of Liverpool, Daresbury, WA44AD, UK
A. Shkvarunets, IREAP, University of Maryland, College Park, MD, 20901, USA

Abstract

Current beam bunch length monitors that measure the spectral content of beam-associated coherent radiation to determine the longitudinal bunch form factor usually require wide bandwidth detection, Fourier transformation of spectral or interferometric data, phase retrieval algorithms and multiple beam pulses to obtain the bunch length. In this paper we discuss progress in the development of a novel single shot method that utilizes the frequency integrated angular distribution (AD) of coherent diffraction radiation (CDR) to measure the RMS bunch length directly. We also present simulation results that show how the AD changes with bunch length for two electron beam linacs, where we are planning to test this new method, our single shot measurement technique and plans for comparison to other bunch length monitors.

INTRODUCTION

Conventional RF accelerators as well as plasma wakefield accelerators have the ability to generate very short pulses of electrons (~10fs), and schemes are being developed to produce even shorter pulse lengths. A number of techniques have been developed to measure bunch length and even the longitudinal distribution of bunches down to ~10 fs in duration. These include Fourier transform interferometry, direct spectroscopy and various electro-optic techniques that sample either the Coulomb field of the bunch itself or the radiation field produced by the bunch interacting with a physical structure or an electromagnetic field. However, the experimental techniques required are usually complex and difficult to implement particularly for single shot measurements.

Frequently, measurement of the rms bunch length rather than the detailed longitudinal profile of the bunch is sufficient for tune up and accelerator monitoring. To meet this need we propose to develop a novel rms bunch length method that is noninvasive, easy to implement, simple to analyze, capable of bunch length measurements over a very wide range and has the potential for single-shot measurements.

BACKGROUND

For most cases of interest, the AD of the CDR can be calculated as the integrated spectral angular density of DR from single electron multiplied by the longitudinal form factor of the pulse:

$$\frac{dI^{CDR}_{bunch}}{d\Omega} \approx N_e^2 \int_{\Delta\omega} \frac{d^2 I_e^{DR}}{d\omega d\Omega} S_z(\sigma_z,\omega) d\omega \qquad (1)$$

The single electron spectral angular density, the first term of the integrand depends on the shape and size of the radiator as well as the frequency. This can be calculated for any size/shape radiator [1]. The second term of the integrand is the longitudinal bunch form factor, which is a function of the bunch length (σ_z). Assuming a model (e.g. a Gaussian) for the longitudinal bunch form factor and an appropriate frequency band, Eq. (1) can be integrated and fit to the measured AD data to produce the rms bunch length [1].

The method has been validated experimentally in a proof of principle experiment done at the Paul Scherrer Institute using repetitive picosecond electron beam pulses with energy E=100 MeV and a Golay cell to scan the angular distribution of the CDR in both the horizontal and vertical directions [2]. However, the measurement was time integrated, i.e. averaged over many repetitive macro-pulses and provided only 1D scans for the fit.

We propose to measure the entire AD projected onto the plane of an imaging detector to improve the accuracy of the measurement and to demonstrate single shot capability. The method will be tested at two accelerators with widely different bunch lengths and beam energies: the ALICE accelerator at Daresbury Laboratory and the FACET accelerator at SLAC.

EXPERIMENTS

ALICE

The beam parameters that are planned for our initial CDR AD imaging experiments on ALICE are: E=26 MeV, τ_{rms} = 0.7-1.3 ps, Q = 100 pC/micro-bunch, 1-4000 micro-bunches per macro-pulse and macro-pulse repetition rate f_{rep} = 10 Hz.

CDR will be created as each picosecond micro-bunch passes through a simple circular annular aperture inclined at 45^0 to the velocity of the electron beam. The CDR will emerge at 90^0, passing through a vacuum window and be imaged onto a pyroelectric array.

We have calculated the frequency integrated AD of CDR for an annular radiator (outer radius = 8mm and inner radius = 4mm) over the wavelength band 18-200 µm, which corresponds to a frequency band 0.15 - 2 THz, for different bunch lengths. In this band the longitudinal bunch form factor is most sensitive to changes in the bunch size. The results of our calculations are shown in Figure 1. The widths of the three distributions correspond to rms bunch widths: 0.7, 1.0 and 1.3 ps. The intensities are normalized to their respective peak values.

*ralph.fiorito@cockcroft.ac.uk

ISBN: 978-3-95450-168-7 doi:10.18429/JACoW-IPAC2015-MOPWI005

EMITTANCE AND OPTICS MEASUREMENTS ON THE VERSATILE ELECTRON LINEAR ACCELERATOR AT DARESBURY LABORATORY*

B.L. Militsyn, D.J. Scott, STFC/ASTeC, Daresbury, UK
S.D. Barrett, C. Topping, A. Wolski, University of Liverpool, Liverpool, UK

Abstract

The Versatile Electron Linear Accelerator (VELA) is a facility designed to provide a high quality electron beam for accelerator systems development, as well as industrial and scientific applications. Currently, the RF gun can deliver short (of order a few ps) bunches with charge in excess of 250 pC at up to 5.0 MeV/c beam momentum. Measurement of the beam emittance and optics in the section immediately following the gun is a key step in tuning both the gun and the downstream beamlines for optimum beam quality. We report the results of measurements (taking account of coupling and space charge) indicating normalised emittances of order 0.5 μm at low bunch charge.

INTRODUCTION: VELA LAYOUT

The injection beamline of VELA [1] (Fig. 1) comprises a 2.5 cell S-band photocathode gun with copper photocathode. The gun is driven with the third harmonic of a short (<76 fs rms) pulsed Ti:Sapphire laser with a typical pulse energy of 1 mJ. The size of the laser spot on the photocathode is typically below 0.5 mm. The gun is immersed in the magnetic field of a main gun solenoid which provides emittance compensation and focusing of the beam in the initial section of the injection line. A bucking coil located beside the gun zeroes the field on the photocathode. Further focusing is provided by four quadrupole magnets, each with a length of 0.1 m. These magnets are also used in the procedure for emittance measurement. Beam diagnostics include a wall current monitor for charge measurement, and three combined diagnostic stations containing YAG screens installed at 45° to the beam line. The emittance measurements presented in this paper are based on beam images observed on the YAG screens with high-sensitivity, high-resolution CCD cameras. Vertical and horizontal slits on YAG-02 and YAG-03 allow alternative methods for emittance characterization. A Transverse Deflecting Cavity (TDC) which is presently under commissioning will complete the diagnostic suite for 6D beam characterisation.

EMITTANCE AND OPTICS MEASUREMENTS WITH COUPLING

In general, the solenoid fields around the VELA gun (and especially any uncompensated magnetic field on the photocathode) will introduce coupling in the beam. Furthermore, space charge effects are expected to be significant, or even dominant, in many parameter regimes of interest for VELA. The techniques used for emittance and optics measurements therefore need to take into account both coupling and space charge. For the present, we assume that at low bunch charge (of order 10 pC) it is possible to include transverse space charge effects in a linear approximation: this will be discussed in more detail later.

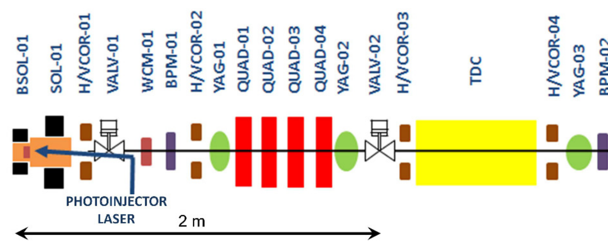

Figure 1: Layout of the VELA injection line.

Our goal is to determine the transverse emittances and Courant–Snyder parameters for the beam in the section of the VELA beam line immediately following the gun. Longitudinal effects will play some role, especially in the presence of space charge, and we plan to include the longitudinal dynamics in future work. For now, we assume that the relevant beam properties can be described by the 4×4 transverse covariance matrix Σ with elements $\Sigma_{ij} = \langle x_i x_j \rangle$, where x_i is an element of the phase-space vector $\vec{x} = (x, p_x, y, p_y)$ for a single particle, and the brackets $\langle\cdot\rangle$ indicate an average over all particles in the bunch. x and y are respectively the horizontal and vertical co-ordinates of a particle, and p_x and p_y the horizontal and vertical momenta scaled by a reference momentum P_0 (= 4.5 MeV/c in the present case). The eigenemittances are constant for a given beam under linear symplectic transport, and can be obtained from the covariance matrix Σ using the fact that the eigenvalues of ΣS are $\pm i\varepsilon_{\mathrm{I}}$ and $\pm i\varepsilon_{\mathrm{II}}$, where S is the 4×4 antisymmetric matrix with block diagonals:

$$S_2 = \begin{pmatrix} 0 & 1 \\ -1 & 0 \end{pmatrix}, \tag{1}$$

and ε_{I}, $\varepsilon_{\mathrm{II}}$ are the eigenemittances [2]. The Courant–Snyder parameters can be obtained from the eigenvectors of ΣS. To determine the eigenemittances and Courant–Snyder parameters at a given point in the beamline, we therefore need to determine the elements of the covariance matrix Σ at that point in the beamline. This can be done using quadrupole scans, as follows.

* Work supported by the Science and Technology Facilities Council, UK.

Content from this work may be used under the terms of the CC BY 3.0 licence (© 2015). Any distribution of this work must maintain attribution to the author(s), title of the work, publisher, and DOI.

ISBN: 978-3-95450-168-7 doi:10.18429/JACoW-IPAC2015-MOPWI006

DEVELOPMENT OF A SUPERSONIC GAS-JET MONITOR TO MEASURE BEAM PROFILE NON-DESTRUCTIVELY

H. Zhang[1,#], V. Tzoganis[1,2], A. Jeff[1,3], C. Welsch[1]
[1]Cockcroft Institute and university of Liverpool, Warrington, WA44AD UK
[2]RIKEN Nishina center, Japan
[3]CERN

Abstract

The measurement of the transverse beam profile is a great challenge for high intensity, high brightness and high power particle beams due to their destructive effects and thus non-destructive methods are desirable. Current non-destructive methods such as residual gas monitors and beam induced fluorescence monitors either requires a longer integration time or higher surrounding pressure to make a meaningful measurement. As a potentially improved technique, a supersonic gas-jet beam profile monitor has been developed by the QUASAR Group at the Cockcroft Institute, UK.

In this monitor, a 45 degree supersonic gas curtain is generated and interacts with beam when the beam crosses it. Ions generated by this process are then accelerated by an extraction electric field and finally collected by a Micro Channel Plate (MCP). Beam images are obtained via a phosphor screen and a CCD camera.

In this contribution, we briefly describe the working principles and present better beam profile measurement of a low energy electron beam using this monitor with newly installed pulsed valve.

INTRODUCTION

Beam profile monitoring is essential for any accelerator system in diagnosing the transverse property of particle beams. Many existing methods could be chosen based on the type, energy and lifetime of the specific particle beam as well as the system requirement such as vacuum condition and beam loss control. For an example, the beam diagnostic in the Ultra-low-energy Storage Ring (USR) [1] at GSI, in order to preserve a longer lifetime of the stored low energy antiproton beam, a vacuum condition of ~10^{-11} mbar is required. Meanwhile, considering the costly antiproton, a non-destructive method is preferred. These requirements basically limit the choice from the existing mature transverse diagnostics. Gas-based monitor, such as residual gas ionization monitor or fluorescent monitor, could be the potential candidate for USR project, because it reserves the vacuum condition quite well and disturbs the beam very little. However, a low ionization or fluorescent rate due to the low vacuum pressure requires a long integration time to obtain a meaningful profile and usually the measurement is in one dimension. In the USR case, the intrinsic integration time could be more than 100 ms which brings additional prerequisite for the primary beam stability. To reduce the integration time while keeping the non-destructive feature by using gas molecules, a novel 2-dimentional supersonic gas-jet ionization monitor is designed in Cockcroft Institute [2]. Previously, using the same principle, a magnetically focused oxygen molecular beam was implemented in HIMAC for fast heavy ion profile measurement [3] and a mechanically skimmed nitrogen beam in JPARC for the intense proton beam [4]. In this method, the localized gas intensity could increase by more than 5 orders of magnitude by the jet, which increases the ionization rate and thus shortens the integration time about the same order. Meanwhile, the vacuum is affected little due to the directionality of the supersonic gas-jet. In this paper, we will discuss the design and working condition of this monitor as well as recent results from an in-house low energy electron beam. Although the application is based on the USR due to its highly specialized requirement, this monitor could be generally used in any accelerators where the gas load is allowed.

WORKING PRINCIPLE AND TEST STAND

The schematic of the whole setup is shown in Fig. 1. The design is based on the Reaction Microscope [5]. To generate the supersonic gas flow, differential pumping technique is used in the nozzle chamber, the gas flow through a 30 um orifice from a high pressure area (few bar) to a low pressure area (about 10^{-1} to 10^{-2} mbar). With this large pressure difference, the gas will experience a free expansion process, and a supersonic flow will form inside a Mach disk. By placing the first conical skimmer (180 um in diameter) inside the Mach disk (less than 2 cm from the nozzle), we can guide a part of the supersonic flow into the following chambers to form a molecular flow and meanwhile avoid the effect from turbulence and other shock waves. An additional conical skimmer (400 um in diameter) is positioned 25 mm away from the first skimmer to further collimate the flow. In order to have a two dimensional measure of the primary beam profile, a third rectangular skimmer of 4*0.4 mm^2 is placed at 325 mm from the first skimmer before the interaction chamber under an angle of 45 degrees to create a screen-like jet. Detailed design and gas dynamics consideration including

#hao.zhang@cockcroft.ac.uk

Content from this work may be used under the terms of the CC BY 3.0 licence (© 2015). Any distribution of this work must maintain attribution to the author(s), title of the work, publisher, and DOI.

ISBN: 978-3-95450-168-7 doi:10.18429/JACoW-IPAC2015-MOPWI009

A MULTI-PINHOLE FARADAY CUP DEVICE FOR MEASUREMENT OF DISCRETE CHARGE DISTRIBUTION OF HEAVY AND LIGHT IONS*

Prabir K. Roy†, Stephen Taller, Ovidiu Toader, Fabian Naab, Shyam Dwaraknath, Gary S. Was
MIBL, NERS, University of Michigan, Ann Arbor, MI 48109, USA

Abstract

A new multi-pinhole Faraday cup (MPFC) device was designed, fabricated, and tested to measure ion beam uniformity, over a range of centimeters. There are 32 collectors within the device, and each of those is used as an individual Faraday cup to measure a fraction of the beam current. Experimental data show that the device is capable of measuring the charged particles distribution - which is either in the form of a raster scan, or a defocused beam.

INTRODUCTION

Materials degradation due to irradiation is a limiting factor in nuclear reactor lifetimes. Traditionally, materials have been irradiated in test reactors, such as the Fast Flux Test Facility (FFTF) or the BOR-60 fast nuclear reactor. Ion irradiations, using accelerated charged particles, to induce damage at high dose rates have been successful in emulating the microstructural features of materials irradiated in reactor [1, 2]. In ion irradiation experiments, a high energy beam is either raster scanned, in which the beam is scanned at high frequencies [3], or defocused, to distribute charge particles in a nearly uniform manner, over the material specimens. The measurement of the uniform distribution of particles over the sample surface is crucial to quantify the ion dose in these experiments. A Faraday cup, an optical system such as a scintillator and CCD camera, and a beam profile monitor (BPM) are typical devices used to measure distributions of charged particles in space. A Faraday cup measures the total current of a beam for the full aperture geometry of the instrument, resulting in a flux measurement for the cross sectional area of the cup without any additional spatial resolution. The photon conversion efficiency, and damage to the scintillator by the beam bombardment, limit the practicality of a scintillator based imaging system for assessing the spatial resolution over an extended period of time. A BPM has the ability to provide partial or discrete distribution of an integrated beam profile. The BPM measures the current from secondary electrons on a metal shell surrounding a rotating wire. The BPM, however, does not discriminate between ions and electrons, the latter of which can be problematic for assessing the full beam profile. To provide a better description of the beam density in spatial dimensions, we have designed a multi-pinhole Faraday cup (MPFC) device, to overcome some of the limitations of traditional measurement systems. This work serves to present the design and performance of this device under ion irradiation relevant conditions.

* Work supported by Michigan Ion Beam Laboratory users community
† pkroy@umich.edu

SCIENTIFIC AND TECHNICAL BASIS

In a typical Faraday cup, an electrode, or collector, is used to capture particles. As the Faraday cup measures the electric charge of a beam over time, electrons or ions from outside of the beam are undesirable. A suppressor electrode is used to reduce the entrance of any amount of unwanted particles. To make an effective Faraday cup, there are several guidelines to follow. These are: (1) Charged particles should not physically contact the suppressor. This allows for the suppressor to maintain constant electrical properties. (2) The collector should be relatively deep to minimize secondary electrons loss. (3) The voltage of the suppressor should be negative compared to the collector. (4) The collector may have its own voltage potential applied to minimize the entrance of secondary electrons from the vacuum, or to retain electrons those are generated from within the collector. A beam of scattered or stray particles can create secondary electrons from collisions with the walls of the vacuum system. A negative potential suppresses background electrons, but attracts ions. These low energy ions are rejected using a positive voltage on the collector. If the suppressor is touched by beam particles, especially with an intense or dense beam, the potential of the beam itself can alter the electron suppression. A measured beam current should not be sensitive to the bias voltages once the secondary electrons and plasma ions are properly suppressed [4]. If a Faraday cup functions ideally, the suppressor should not receive any beam current. Since the suppressor is capacitively coupled to the beam charge, a high beam density may result in a temporary spike in the suppressor current (if measured) when the beam strikes. The same scenario may true for a collector.

Based on these criteria, the MPFC was designed and fabricated. Figure 1(a) shows a computer rendering of the multi-pinhole Faraday cup. The device, when viewed at the most basic level, consists of a (1) front plate, (2) suppressor plate, and (3) 32 collectors to satisfy the desirable qualities of a Faraday cup. Table 1 shows parameters of the physical device. Figure 1(b) shows a WARP [5] code simulation to demonstrate equipotential lines and electrical force patterns between the grounded front plate, the suppressor plate held at -150V, and the collectors held at +90V.

The Tantalum front plate has 32 pinholes in line with the collectors to allow the beam to pass. Tantalum was selected because of its high melting temperature, to withstand beam heating, and for its low sputter yield. Because of the relative size of these pinholes to the full beam, the amount of particles passed to the collectors is much less than the number of primary particles. Using a geometric argument, a uniform, evenly distributed beam would have a percentage

Content from this work may be used under the terms of the CC BY 3.0 licence (© 2015). Any distribution of this work must maintain attribution to the author(s), title of the work, publisher, and DOI.

ISBN: 978-3-95450-168-7 doi:10.18429/JACoW-IPAC2015-MOPWI010

DESIGN AND DEVELOPMENT OF A BEAM STABILITY MECHANICAL MOTION SYSTEM DIAGNOSTIC FOR THE APS MBA UPGRADE*

R. Lill, B. Yang, G. Decker, N. Sereno
Advanced Photon Source, Argonne National Laboratory, Argonne, IL 60439 USA

Abstract

The Advanced Photon Source (APS) is currently in the conceptual design phase for the multi-bend achromat (MBA) lattice upgrade. In order to achieve long-term beam stability goals, a mechanical motion system (MMS) has been designed to monitor critical in-tunnel beam position monitoring devices. The mechanical motion generated from changes in chamber cooling water temperature, tunnel air temperature, beam current, and undulator gap position causes erroneous changes in beam position measurements causing drift in the x-ray beam position. The MMS has been prototyped and presently provides critical information on the vacuum chamber and beam position monitor (BPM) support systems. We report on the first results of the prototype system installed in the APS storage ring.

INTRODUCTION

In order to achieve the one micron long-term drift beam stability requirements seen in Table 1, all sources of mechanical motion of critical in-tunnel beam position monitoring devices must be carefully evaluated and appropriately addressed. Experiments conducted at the Advanced Photon Source (APS) clearly confirm that the thermal distortion of the vacuum chamber leads to movements of the BPMs up to 10 µm/˚C, or a 0.5 µm peak-peak for a cooling water temperature change of 0.05˚C peak-peak. This distortion is incompatible with the new beam stability requirements for the planned APS multi-bend achromat (MBA) upgrade. Research to quantify motion specifically for the APS accelerator tunnel and experiment hall floor has been ongoing for over five years [1].

The plan for the MBA upgrade is to use insertion device vacuum chambers (IDVCs) similar to what APS has installed today. Mechanical stability of BPM pickup electrodes mounted on these small-gap IDVCs potentially places a fundamental limitation on long-term x-ray beam stability for insertion device beamlines. The mechanical motion system (MMS) studies have opened a new window of understanding into how to measure and correct for these complex nonlinear mechanical movements with environmental changes. The MBA MMS design will monitor the position of the BPM in real time during user beam operations to compensate for the distortion of the insertion device vacuum chamber (IDVC).

* Work supported by U.S. Department of Energy, Office of Science, under Contract No. DE-AC02-06CH11357.

Table 1: MBA Beam Stability Requirements

Plane	AC rms Motion (0.01-1000 Hz)	Long-term Drift (100s-7 days)
Horizontal	1.7 µm 0.25 µrad	1.0 µm 0.6 µrad
Vertical	0.4 µm 0.17 µrad	1.0 µm 0.5 µrad

MMS SYSTEM OVERVIEW

One of the most critical locations for electron beam stability is at the insertion device points. The existing APS IDVC is extruded aluminum, shown in Fig. 1, with integrated beam position monitor electrode housings machined out at each end. The wall thickness of the completed chamber at the beam orbit position is 1 mm. The design uses a rigid strongback that limits deflection of the chamber under vacuum despite the thin wall. The IDVC beam position monitors (BPMs) provide the critical steering data necessary to maintain beam stability through the insertion device. The BPM button electrodes mounted in the machined platforms have a 4-mm diameter. There are two button electrodes mounted on a single miniature vacuum flange [2].

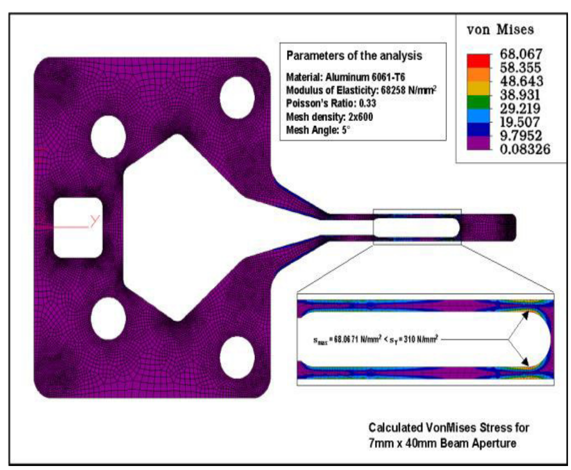

Figure 1: Existing storage ring IDVC cross section.

The rf and x-ray BPMs can be erroneously affected by changes in vacuum chamber cooling water temperature, tunnel air temperature, and beam current fluctuations. The block diagram shown in Fig. 2 illustrates the plan for instrumenting the MMS. Each ID location and grazing-incidence insertion device x-ray beam position monitor (GRID-XBPM) will be instrumented with capacitive detectors and hydrostatic detectors. The MMS is a real-time position monitoring system that measures the

Content from this work may be used under the terms of the CC BY 3.0 licence (© 2015). Any distribution of this work must maintain attribution to the author(s), title of the work, publisher, and DOI.

ISBN: 978-3-95450-168-7 doi:10.18429/JACoW-IPAC2015-MOPWI011

BEAM STABILITY R&D FOR THE APS MBA UPGRADE*

N. S. Sereno, N. Arnold, H. Bui, J. Carwardine, G. Decker, L. Emery, R. Farnsworth, R. Keane, F. Lenkszus, R. Lill, R. Lipa, S. Veseli S. Xu, and B. X. Yang
Argonne National Laboratory, Argonne, IL 60439, USA

Abstract

Beam diagnostics required for the APS Multi-bend acromat (MBA) are driven by ambitious beam stability requirements. The major AC stability challenge is to correct rms beam motion to 10% the rms beam size at the insertion device source points from 0.01 to 1000 Hz. The vertical plane represents the biggest challenge for AC stability, which is required to be 400 nm rms for a 4-micron vertical beam size. In addition to AC stability, long-term drift over a period of seven days is required to be 1 micron or less. Major diagnostics R&D components include improved rf beam position processing using commercially available FPGA-based BPM processors, new X-ray beam position monitors based on hard X-ray fluorescence from copper and Compton scattering off diamond, mechanical motion sensing and remediation to detect and correct long-term vacuum chamber drift, a new feedback system featuring a tenfold increase in sampling rate, and a several-fold increase in the number of fast correctors and BPMs in the feedback algorithm. Feedback system development represents a major effort, and we are pursuing development of a novel algorithm that integrates orbit correction for both slow and fast correctors down to DC simultaneously. Finally, a new data acquisition system (DAQ) is being developed to simultaneously acquire streaming data from all diagnostics as well as the feedback processors for commissioning and fault diagnosis. Results of studies and the design effort are reported.

INTRODUCTION

The small emittance of the Multi-bend acromat (MBA) lattice translates into much smaller beam dimensions in the horizontal plane at the insertion device (ID) source points compared to the present APS lattice [1]. Since beam centroid motion of an appreciable fraction of the beam size results in increased effective emittance for users, AC beam stability requirements for the MBA upgrade are defined as 10% of the minimum expected beam size at the insertion device (ID) source points over the band 0.01 - 1000 Hz. Furthermore, long-term drift from 100 seconds to a period of seven days is defined as an estimate of diffusive ground motion over the long term. Table 1 summarizes these requirements. Beam stability R&D for the MBA upgrade focuses on developing diagnostics and controls systems to meet or exceed these requirements.

* Work supported by the U.S. Department of Energy, Office of Science, Office of Basic Energy Sciences under Contract No. DE-AC02-06CH11357.

Table 1: MBA Upgrade Beam Stability Requirements

Plane	AC rms Motion (0.01-1000 Hz)		Long-term Drift (100 s - 7 Days)	
Horizontal	1.7 μm	0.25 μrad	1.0 μm	0.6 μrad
Vertical	0.4 μm	0.17 μrad	1.0 μm	0.5 μrad

MBA DIAGNOSTICS INTEGRATION

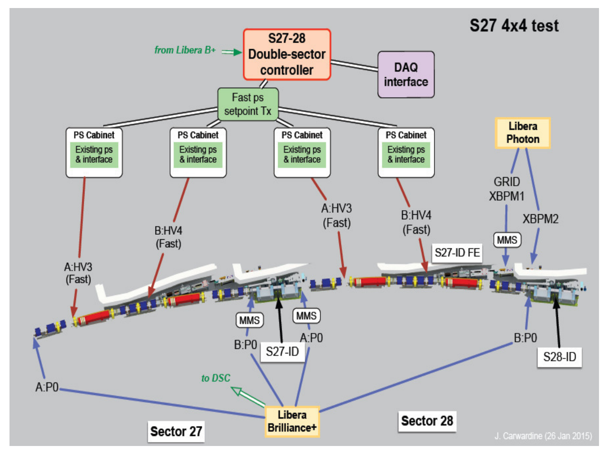

Figure 1: MBA diagnostics integrated R&D in APS storage ring sector 27. The P0 labels are ID BPMs and the HV labels are fast correctors.

Figure 1 shows the suite of diagnostics to be integrated and tested together as part of the MBA R&D plan. At the insertion device as well as the MBA arcs, we will use new commercial rf BPM electronics with a low noise floor. New high-power X-ray BPMs (called GRID for grazing-incidence insertion device) based on X-ray fluorescence off copper, and much less sensitive to background radiation coming from the ring multipoles, have been installed. A low power version of these X-ray BPMs based on Compton scattering off diamond is being developed for canted undulator beamlines. New hard X-ray intensity monitors will be installed to insure long-term reproduceability and relative flux calibration. A mechanical motion sensing system will be used to monitor position changes due to temperature, vibration, and ground motion at the ID rf BPMs as well as the X-ray BPMs. All these systems will be tied together using a distributed real-time orbit feedback system (RTFB) that will additionally take information from two pinhole cameras to correct coupling. The new RTFB system will include an increase of at least 15 in sampling rate (to 22 kHz) over the present system, increasing the closed-loop bandwidth to 1

Content from this work may be used under the terms of the CC BY 3.0 licence (© 2015). Any distribution of this work must maintain attribution to the author(s), title of the work, publisher, and DOI.

ISBN: 978-3-95450-168-7 doi:10.18429/JACoW-IPAC2015-MOPWI012

CONCEPTUAL DESIGN AND ANALYSIS OF A STORAGE RING BEAM POSITION MONITOR FOR THE APS UPGRADE*

B. Stillwell, R. Lill, R. Lindberg, M. O'Neill, B. Rocke, X. Sun, ANL, Argonne, IL 60439, USA
A. Blednykh, BNL, Upton, NY 11973, USA

Abstract

A conceptual design has been developed for a radio frequency (rf) pickup-type beam position monitor (BPM) for use in a multi-bend achromat (MBA) storage ring under consideration by the APS Upgrade project (APS-U) [1]. Beam feedback systems are expected to require fourteen rf BPMs per sector with exceptional sensitivity and mechanical stability. Simultaneously, BPM insertion length must be minimized to allow lattice designers the greatest freedom in selecting magnet lengths and locations. Envisioned is a conventional four probe arrangement integrated inside of a pair of rf-shielded bellows for mechanical isolation. Basic aspects of the design are presented along with the results of analyses which establish expected mechanical, electronic, and beam physics-related performance measures.

DESIGN OBJECTIVES

The ultimate goal of the BPM is to generate a set of electronic signals that precisely indicate the arrival time and lateral location of the passing particle beam. Perhaps the most challenging issue is maintaining adequate positional stability in the presence of synchrotron radiation heating of adjacent vacuum chambers, vibrational energy due to water cooling of vacuum chambers and magnets, and rf-induced heating of the BPM itself. The present guidance is that the BPMs should be vibrationally stable to an rms amplitude tolerance of 32 nm horizontally and 56 nm vertically at frequencies between 1 and 1000 Hz. BPM offset values will be established after storage ring systems have stabilized thermally under full-current operation, however the maximum acceptable aggregate of initial and thermally-driven misalignment prior to establishing the offsets has been found to be 500 µm. Once the offsets have been established, the contribution of long-term (thermal) drift to BPM reading error must be no more than 10 µm. Another limitation is available space. The presently envisioned magnet configuration provides a minimum of 125 mm to insert many of the BPMs at required locations.

INTERFACE CONSTRAINTS

There are many constraints that are imposed on the design to ensure that the BPM does not significantly compromise the performance of other technical systems. Foremost among these is that the BPM be compatible with the ultrahigh vacuum environment. Outgassing from internal surfaces must be limited so that average vacuum pressures across the sector can be maintained at a maximum of roughly 2 nTorr during operation. In addition, where BPMs are in close proximity with vacuum chambers coated with non-evaporable getter (NEG) material, the outgassing should not include species such as fluorine or chlorine that are known to cause permanent poisoning of the NEG material or be so excessive that the required thermal activation cannot be accomplished. The assembly should accommodate some degree of misalignment of the flanges on adjacent vacuum chambers. This flange misalignment has been estimated to be no more than 500 µm, a value which sums expected chamber fabrication and alignment tolerances. Also critical is that the BPM should not act to distort fields from the adjacent magnets and should not introduce unacceptable impedance effects on the particle beam. Finally, the BPM should tolerate the radiation environment, thermal-mechanical cycling, and ambient conditions for an expected machine lifetime of 20 years.

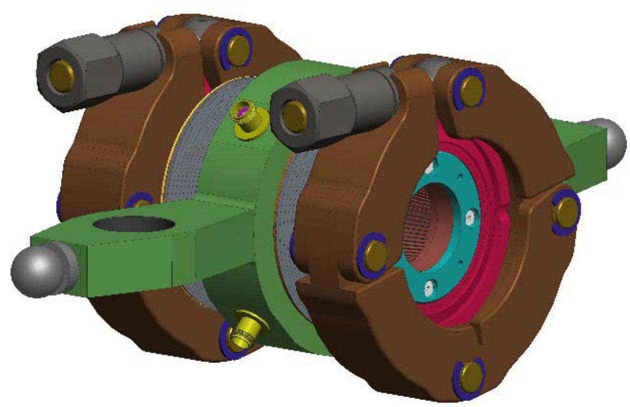

Figure 1: CAD model of BPM assembly.

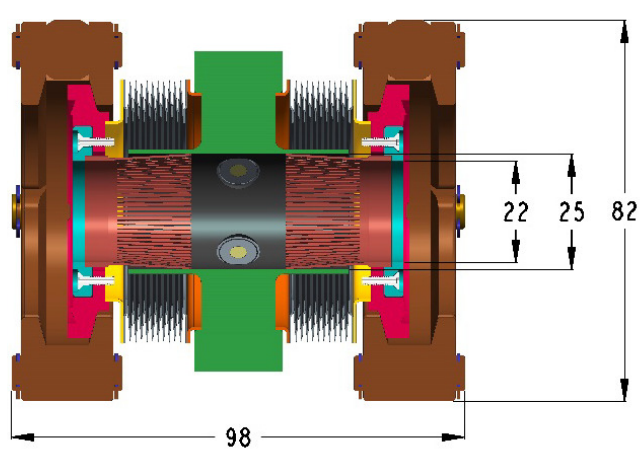

Figure 2: Cross section of BPM assembly.

* Work supported by U.S. Department of Energy, Office of Science, under Contract No. DE-AC02-06CH11357.

Content from this work may be used under the terms of the CC BY 3.0 licence (© 2015). Any distribution of this work must maintain attribution to the author(s), title of the work, publisher, and DOI.

ISBN: 978-3-95450-168-7 doi:10.18429/JACoW-IPAC2015-MOPWI013

CONTROL SYSTEM FOR THE LCLS II UNDULATOR PROTOTYPE*

Joseph Z. Xu[1], Nikita Strelnikov[1,2], Isaac Vasserman[1] and Richard Farnsworth[1]
[1]Advanced Photon Source, Argonne National Laboratory, Argonne, Illinois 60439, USA
[2]Budker Institute of Nuclear Physics, Novosibirsk 630090, Russia

Abstract

The Linac Coherent Light Source (LCLS) has been successfully operated for more than 6 years. In order to expand the capability and capacity of the LCLS, LCLS-II has been planned and funded by the Department of Energy. Advanced Photon Source (APS) at the Argonne National Lab is tasked with building the prototype of the LCLS-II undulator based on the concept of magnetic force dynamic compensation. The control system for the prototype is responsible for four motion and feedback channels with sub-micron level accuracy, eight load cells that monitor how the forces act on the system in real time, and multiple temperature sensors. A detailed description of the control system and its operation is reported.

INTRODUCTION

As the world's first x-ray free electron laser in operation, the LCLS facility at the Stanford Linear Accelerator Center (SLAC) has plans to be expanded in both capability and capacity to meet the needs of the scientific community. Different from the original fixed gap undulators, the LCLS-II will be equipped with adjustable gap undulators.

APS is to build a prototype of the LCLS-II undulator. The device is a 3-meter long adjustable gap undulator with a minimum gap of 7.0 mm and better than 10 micron tolerance [1]. Due to the magnetic force change in the scale of several thousands of kilograms in different gaps during operation, the magnetic force dynamic compensation scheme has been adopted [2].

The control system for the prototype is a windows based PXI system from National Instruments. It is capable of handling four motion axes, four absolute position feedbacks, eight load cell force sensors, and eight temperature sensors. Application software is LabVIEW based with field programmable gate array (FPGA) technology in monitoring the positions and the forces in real-time.

SYSTEM DESCRIPTION

The control system for the LCLS-II undulator prototype consists of a PXI crate with a windows based control card, an FPGA card, and a Digital Multimeter (DMM) card, all from National Instruments.

The peripherals of the system comprise the positioning control system and the positioning feedback system. The control system has four motors that drive the positioning systems. The motors are SmartMotor servomotors from the Animatics Corporation, with the motor control integrated in the back of each motor including an RS-232 serial interface. Each two motors drive one of the two ID strongbacks into the desired position to form the gap as needed. The motors are connected to the control card via an RS-232 serial interface. All four motors are connected in serial.

The position feedback system has four absolute digital linear encoders with Synchronous Serial Interface (SSI) from Fagor Automation. The resolution of the encoders is 0.1 micron. The maximum range of the encoders is 120 mm. The encoders are programmable. They are configured to 32 bits with non-grey code. The encoders are connected to the digital I/O interfaces of the FPGA card.

The forces acting on the actuators are monitored with eight load cells from Omega Engineering Inc. The load cells are bi-directional. They are powered by a voltage power supply that supplies a 10 volts dc excitation source. The voltage excitation power supply is from Agilent Technologies. The voltage is monitored by a DMM card. The analog outputs of the load cells are monitored by 16-bit analog-to-digital channels embedded in the FPGA card. The load cell signals are normalized by the excitation voltage to compensate the fluctuation of the excitation voltage. The precision of the force monitoring is about 0.2 lbs.

The temperatures are monitored with a web-enabled temperature measurement module equipped with eight RTD sensors. The module is from Omega Engineering Inc. It communicates with the control card via http protocol through a TCP/IP network. The precision of the temperature monitoring system is 0.1 degree Celsius. Figure 1 shows the schematic layout of the prototype device control system.

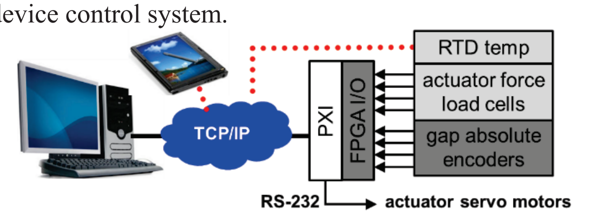

Figure 1: Schematic layout of the prototype device control system.

SOFTWARE

LabVIEW-based system software has been developed to coordinate the motion control and sensor data monitoring. The system can be accessed via the internet from anywhere, anytime through the facility's virtual

*Work supported by the U.S. Department of Energy, Office of Science, under Contract No. DE-AC02-06CH11357.

Content from this work may be used under the terms of the CC BY 3.0 licence (© 2015). Any distribution of this work must maintain attribution to the author(s), title of the work, publisher, and DOI.

ISBN: 978-3-95450-168-7 doi:10.18429/JACoW-IPAC2015-MOPWI014

DESIGN AND DEVELOPMENT FOR THE NEXT GENERATION X-RAY BEAM POSITION MONITOR SYSTEM AT THE APS*

B.X. Yang#, G. Decker, S. H. Lee, Y. Jaski, F. Westferro, N. Sereno, and M. Ramanathan
Advanced Photon Source, Argonne National Laboratory, Argonne, IL 60439, USA

Abstract

The planned Advanced Photon Source (APS) Upgrade will bring storage ring beam sizes down to several micrometers and require x-ray beam directional stability in 100 nrad range for undulator power exceeding 20 kW. The next generation x-ray beam position monitors (XBPMs) are designed to meet these requirements. We present commissioning data on the recently installed grazing-incidence insertion device x-ray beam position monitor (GRID-XBPM) based on Cu K-edge x-ray fluorescence from limiting absorbers of the front end for two inline undulators. It demonstrated a 30-fold improvement for signal-to-background ratio over existing photoemission-based XBPMs. Techniques and results for calibrating the XBPMs are also discussed.

INTRODUCTION

The planned APS Upgrade (APS-U) will dramatically reduce the electron beam size and divergence in the horizontal plane [1]. A major improvement in beam stability is required for APS users to benefit from this upgrade. Table 1 lists the stability goals, which are approximately 10% of the expected beam sizes. A new FPGA-based orbit feedback system and several new diagnostics are being developed to support this goal [2]. Among them, a new class of x-ray beam position monitors (XBPM) sensitive to only hard x-ray excitations is being developed. For the high heat load front end in the APS-U, two inline undulators will deliver up to 20 kW of x-ray power. We developed a grazing-incidence XBPM (GRID-XBPM) using the Cu K-edge x-ray fluorescence (XRF) from the front-end apertures to infer the undulator beam's core position [3]. A prototype test showed a significant reduction in bend magnet (BM) background [4]. Following this successful demonstration, two GRID-XBPMs were designed and constructed in the new front end and installed in 2014 [5]. In this work, we report the commissioning results of the first production XBPM and present its performance in a front end.

Table 1: MBA Upgrade Beam Stability Requirements

	AC rms Motion (0.01-1000 Hz)	Long-term Drift (100 s - 7 Days)
Horizontal	1.7 μm / 0.25 μrad	1.0 μm / 0.6 μrad
Vertical	0.4 μm / 0.17 μrad	1.0 μm / 0.5 μrad

BEND MAGNET BACKGROUND

In a previous test [5], the prototype XBPM was located downstream of a 4.5-mm front end exit aperture, with a 0.2 mrad horizontal acceptance angle. In the front end, however, the XBPM is located at 18.6 m from the source, downstream of a 10.6-mm aperture, with a 0.6-mrad horizontal acceptance angle. The increase in horizontal aperture is expected to increase BM background. Therefore, characterizing its impact became our first task. We measured the sum signal of all diodes / blades with the undulator gap fully open and then as a function of undulator gaps. Figure 1 shows the ratio of the undulator signal over the BM background for the best group of PIN diodes in the GRID-XBPM, along with those for installed APS photoemission XBPMs. We can see that the hard x-ray XBPM improves the signal-to-background ratio by 30 fold. To further reduce the impact of the BM background, we built three groups of PIN diodes into the GRID-XBPM. Not surprisingly, while the "best" group is most sensitive to the photons originated near the undulator axis, the "worst" group of PIN diodes is located furthest away from the undulator axis and is more sensitive to the BM background by a factor of eight. Subtracting a small fraction of the "worst" PIN signals from the "best" PIN signals will further reduce the impact of BM background by another factor of 5. This requires a special 6-channel XBPM electronics. In the remaining part of this work, however, we will continue with the conventional 4-channel electronics for presenting our commissioning experience.

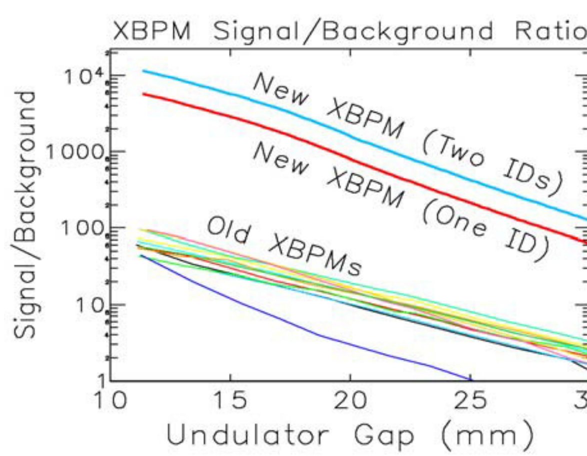

Figure 1: Ratio of undulator signal over BM background for the hard x-ray GRID-XBPM shows a 30-fold improvement over old style photoemission XBPMs.

* Work supported by the U.S. Department of Energy, Office of Science, under Contract No. DE-AC02-06CH11357.
# bxyang@aps.anl.gov

Content from this work may be used under the terms of the CC BY 3.0 licence (© 2015). Any distribution of this work must maintain attribution to the author(s), title of the work, publisher, and DOI.

ISBN: 978-3-95450-168-7 doi:10.18429/JACoW-IPAC2015-MOPWI015

Content from this work may be used under the terms of the CC BY 3.0 licence (© 2015). Any distribution of this work must maintain attribution to the author(s), title of the work, publisher, and DOI.

A LOW TIME-DISPERSION REFRACTIVE OPTICAL TRANSMISSION LINE FOR STREAK CAMERA MEASUREMENTS

J. G. Power[1#] and G. Ha[1,2]
[1]Argonne National Laboratory, Argonne, IL 60439, USA
[2]Department of Physics, POSTECH, Pohang, Gyeongbuk 790-784, KOREA

Abstract

Streak camera measurements of the electron bunch length are limited in resolution by several factors. These include: (1) the light source itself (e.g. OTR, Cherenkov, Synchrotron radiation), (2) dispersion from the refractive optical transport line (OTL) between the light source and the streak camera, and (3) the streak camera itself. The limiting resolution for pulses length of a few psec is caused by the OTL due to the very broad bandwidth of the light pulse (hundreds of nm). While an all-reflective OTL can eliminate dispersion, the system is complicated and expensive.

In this paper, we examine the time spread of the light pulse due to the dispersion in the lenses of the OTL. We present an analysis of the dispersion and benchmark it to measurements of the time dispersion for several different lens materials. Finally, we conclude with recommendations of the proper design of the refractive OTL to minimize the time dispersion while maximizing the signal.

STREAK CAMERA MEASURMENTS OF THE ELECTRON BUNCH LENGTH

Streak camera measurements of the electron (in general, charged particle) bunch length are well suited for the regime of greater than a few picoseconds. Our examples are based on a Hamamatsu [1] C1587 streak camera with a resolution of 2ps since this is the camera we own at the Argonne Wakefield Accelerator (AWA) Facility. Note that there exist streak cameras with significantly better resolution such as the Hamamatsu Fresca-200 with a resolution of 200 femtoseconds. In any case, the examples here can be extended to any particular case as long as one requires that the dispersion introduced by the optical transport line is less than one third of the minimum bunch length one desires to measure since this only introduces an error of less than ~5% ($\sqrt{1^2 + 0.33^2} = 1.05$).

A typical setup for the measurement of the electron bunch length is shown in Fig. 1. (1) The process begins when the electron bunch passes through the radiator (e.g. OTR) and generates a prompt, broadband, light pulse, of similar transverse and longitudinal profile to the electron bunch. (2) To avoid damage to the streak camera it is typically located far from the radiator and therefore the light pulse is often transported through a long, refractive, optical transport line (OTL) made up of a series of *glass* lenses [2]. Other solutions are possible, such as an all reflective OTL or to locate the streak camera near the radiator with adequate shielding, but we only consider the case of a long, refractive OTL in this paper. (For the remainder of the paper, we use the shorter phrase "OTL" to refer to "a long, refractive OTL".) The problem with the OTL is that light pulse length increases as it travels through the OTL due to the variation of the group velocity with frequency (a.k.a. group velocity dispersion) in the glass (pulse at bottom of Fig. 1). This means that by the time the light pulse arrives at the streak camera its length is significantly longer than the electron's bunch length. A bandwidth filter of ~10nm is typically used to reduce the lengthening to an acceptable level. (3) Finally, the light pulse arrives at the streak camera for measurement. Proper use of the streak camera is beyond the scope of the paper so we limit comments to bandwidth requirements of the streak camera since it has direct bearing on the subject of this paper. The bandwidth of the streak camera is determined by the input optics and the photocathode quantum efficiency. The AWA streak camera uses the N1643 streak tube with bandwidth of [200-850nm] and we used this for the examples in this paper.

REFRACTIVE AND GROUP INDEX

Dispersive media are characterized by a wavelength (or frequency) dependent susceptibility $\chi(\lambda)$, refractive index $n(\lambda)$, and group index $n_g(\lambda)$ [3]. The refractive index of

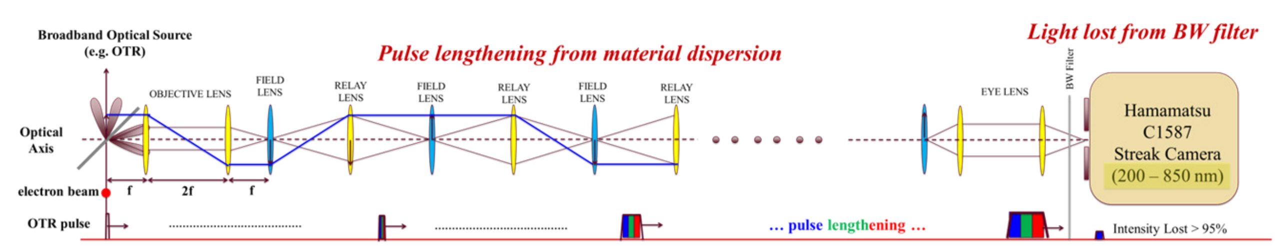

Figure 1: Setup for a Steak Camera based bunch length measurement.

#jp@anl.gov

ISBN: 978-3-95450-168-7 doi:10.18429/JACoW-IPAC2015-MOPWI016

DEVELOPMENT OF A VERSATILE BUNCH-LENGTH MONITOR FOR ELECTRON BEAMS AT ASTA*

A. H. Lumpkin#, R. Thurman-Keup, D. Crawford, D. Edstrom Jr., J. Ruan, and J. Santucci,
Fermi National Accelerator Laboratory, Batavia, IL 60510 USA

Abstract

We have installed a versatile bunch length monitor system at a location after the chicane in the ASTA beamline. Options for generating radiation from a metal screen and transporting coherent radiation to the Martin-Puplett Interferometer and optical transition radiation to a synchroscan streak camera are provided. There is also a chicane bypass line so this station can evaluate the uncompressed beam as well. The system will be used to characterize the bright beams of the photoinjector.

INTRODUCTION

The generation of bright electron beams at the Advanced Superconducting Test Accelerator ASTA/IOTA facility [1] at Fermilab has motivated implementation of a versatile bunch-length monitor located after the 4-dipole chicane bunch compressor for electron beam energies of 20-50 MeV and integrated charges in excess of 10 nC. The station includes both a Hamamatsu C5680 synchroscan streak camera and a Martin-Puplett interferometer (MPI). An Al-coated Si screen will be used to generate both optical transition radiation (OTR), coherent transition radiation (CTR), and coherent diffraction radiation (CDR) during the beam's interaction with the screen. A chicane bypass beamline will allow the measurement of the bunch length without the compression stage at the same downstream beamline location using OTR and the streak camera. The UV component of the drive laser has previously been characterized with a Gaussian fit sigma of 3.5 ps [2], and the uncompressed electron beam is usually expected to be similar to this value at low charge per micropulse. Elongation of the pulse to >15 ps at 250 pC per micropulse has been recently predicted [3]. In addition, OTR will be transported to the streak camera from the focal plane of the downstream spectrometer to provide an E-t distribution within the micropulse time scale. This application relies heavily on the synchronous sum of micropulses in order to obtain an image with adequate statistics. Commissioning of the system and initial results with beam will be presented.

EXPERIMENTAL ASPECTS

The high-power electron beams for the ASTA/IOTA facility [1] were generated in a photoinjector based on a UV drive laser and the L-band rf photocathode (PC) gun cavity. The system has a 3-MHz micropulse repetition rate with micropulse charges selectable from 2 pC to 3.2 nC by adjusting the UV laser intensity. The quantum efficiency of the Cs_2Te photocathode is 1-2 %, and the photoelectrons exit the gun at up to 5 MeV energy. After the rf gun there is a diagnostics station that includes an insertable profile screen, two rf BPMs, and an insertable Faraday cup to characterize the 4-5 MeV beam. The beam is captured in an L-band superconducting rf accelerator structure with 15-22 MV/m nominal gradient. This is followed by a beamline with a suite of diagnostics including rf BPMs, two toroids, a wall current monitor, a series of loss monitors, and 7 beam-profiling stations. Three of these are configured in the chicane, the bunch longitudinal profiling station, and in the focal plane of the electron spectrometer. A schematic of the beamline is shown in Fig. 1. There is a chicane bypass line which we employed in initial commissioning. Since the bunch length monitor is after the chicane, using the bypass line we can measure the bunch lengths without chicane based compression and then with chicane compression once it is commissioned.

The Bunch Length Monitors

The bunch length monitor architecture was intended to provide a central collection point for the various source points whose radiation is transported into the MPI box. As indicated in Fig. 2, the coherent and optical synchrotron radiation ((CSR) and (OSR), respectively) sources from two chicane dipoles, OTR, CTR, and CDR from the X121 station, and the OTR from the spectrometer focal plane are also available to the system as described previously [4]. However, for this initial commissioning period with no compression, we emphasize the streak camera implementation. The streak camera was located outside of the tunnel in a small enclosed optical table. This involves an ~15 m transport with eight mirrors. The mirror system is adjusted using alignment laser beams.

Readout from the streak camera is performed using a Prosilica 1.3 Mpixel GiG-E vision camera with a 2/3" CCD and with fiberoptic coupling from the tube phosphor. We had previously used both the online Java-based ImageTool and the offline MATLAB-based ImageTool processing programs [5,6] in the commissioning of the laser lab streak camera system. Initial measurements of the UV component indicated the bunch length Gaussian fit sigma to be ~ 4 ps, Unless noted otherwise, the streak camera's synchroscan unit was phase locked to the master oscillator, which operationally provides the rf sync for the linac, rf gun, and UV drive laser. We provided a description of the commissioning of the streak camera system and image acquisition tools and the application to the drive laser previously [7].

*Work supported under Contract No. DE-AC02-07CH11359 with the United States Department of Energy.
#lumpkin@fnal.gov

Content from this work may be used under the terms of the CC BY 3.0 licence (© 2015). Any distribution of this work must maintain attribution to the author(s), title of the work, publisher, and DOI.

ISBN: 978-3-95450-168-7 doi:10.18429/JACoW-IPAC2015-MOPWI017

BEAM EXTINCTION MONITORING IN THE Mu2e EXPERIMENT*

E.J. Prebys, P. Kasper, A. Gaponenko, Fermilab, Batavia, IL 60510, USA
L. Bartoszek, Bartoszek Engineering, Aurora, IL 60506, USA

Abstract

The Mu2e Experiment at Fermilab will search for the conversion of a muon to an electron in the field of an atomic nucleus with unprecedented sensitivity. The experiment requires a beam consisting of proton bunches of 250 ns FW, separated by 1.7 μsec, with no out-of-time protons at the 10^{-10} fractional level. The verification of this level of extinction is very challenging. The proposed technique uses a special purpose spectrometer that will observe particles scattered from the production target of the experiment. The acceptance will be limited such that there will be no saturation effects from the in-time beam. The precise level and profile of the out-of-time beam can then be built up statistically, by integrating over many bunches.

INTRODUCTION AND REQUIREMENTS

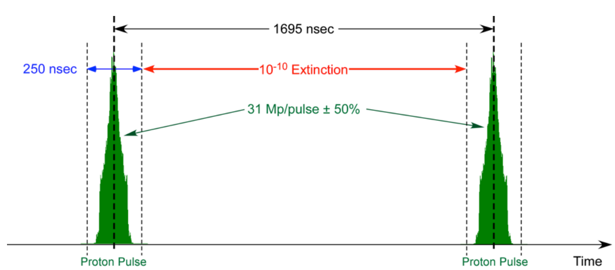

Figure 1: The proton bunch structure required by the Mu2e experiment.

The goal of the Mu2e experiment [1] is to search for the conversion into an electron of a muon that has been captured by a nucleus ($\mu N \rightarrow eN$). This manifestly violates the conservation of charged lepton flavor number, and its obvervation would therefore be an unambiguous indicator of physics beyond the Standard Model.

A key component of the experimental technique is the proton beam structure, which is illustrated in Figure 1. The primary beam consists of short (250 ns FW) proton bunches with 8 GeV kinetic energy, separated by approximately 1.7 μsec, which are used to produce pions, which subsequently decay to muons. To suppress backgrounds, it's vital that the interval between the bunches be free of protons at a level of at least 10^{-10} relative to the beam in the bunches. The technique used to achieve this level of extinction is described elsewhere [2]. It is achieved in two parts. The formation of the bunches in Fermilab Recycler and Delivery ring is expected to have extinction on the order of 10^{-5}. The remaining extinction will be accomplished in the primary beam line with a system of resonant dipoles and collimation, configured to allow only the in-time beam to be transmitted.

It is of course vital to verify that this level of extinction has been achieved, so the experiment has specified that a level of extinction of 10^{-10} or lower can be measured within a few hours of running at the nominal intensity.

* Work supported by the United States Department of Energy under Contract No. DE-AC02-07CH11359

TECHNIQUE

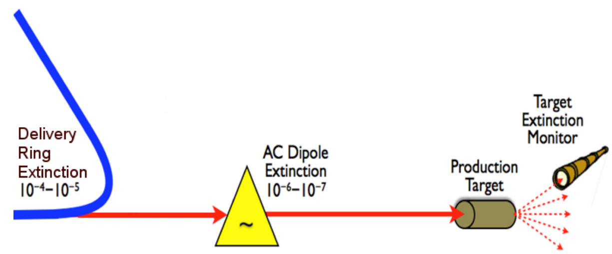

Figure 2: Concept for the statistical extinction monitoring technique.

Each bunch in the Mu2e experiment has roughly 3×10^7 protons, so our desired extinction level corresponds to less than one out-of-time proton every 300 bunches. Unfortunately, measuring single protons in the presence of such large bunches would require a dynamic range that is beyond state of the art for current beam instrumentation. We choose instead to focus on a statistical technique, as illustrated in Figure 2. The pion production target will be monitored by a dedicated spectrometer, the acceptance of which has been designed such that it will not be saturated by the particles observed from the in-time bunch. The spectrometer will then detect a small fraction of out-of-time particles, so that over many bunches, an accurate time profile can be integrated for both the in- and out-of-time protons. Over time, a measurement of the out-of-time beam can be made with increasing sensitivity, limited ultimately by the rate of fake background tracks.

It must be stressed that our aim is not to veto individual events occurring near out-of-time protons, but rather to verify that the total rate of such protons is below that which we have determined to be acceptable.

This technique is conceptually very similar to techniques that have been used for precision measurement of transverse beam halo [3].

DESIGN

The layout of the Mu2e pion production target is shown in Figure 3. Primary protons are incident on a Tungsten target that is within a superconducting solenoidal magnet. The experiment itself uses low momentum, backscattered

Content from this work may be used under the terms of the CC BY 3.0 licence (© 2015). Any distribution of this work must maintain attribution to the author(s), title of the work, publisher, and DOI.

ISBN: 978-3-95450-168-7 doi:10.18429/JACoW-IPAC2015-MOPWI018

NEW HADRON MONITOR BY USING A GAS-FILLED RF RESONATOR *

K. Yonehara†, A.Tollestrup, R.M. Zwaska, Fermilab, Batavia, IL 60510, USA
G. Flanagan, R.P. Johnson, Muons, Inc., IL 60510, USA
G. Fasce, CNI, Rome, I-00187, Italy

Abstract

A novel pressurized gas-filled RF-resonator beam monitor is proposed that will be simple and robust in high-radiation environments for intense neutrino beam facilities and neutron spallation sources. Charged particles passing through the resonator produce ionized plasma, which changes permittivity of the gas. Radiation sensitivity is adjustable using gas pressure and RF amplitude. The beam profile will be reconstructed by X, Y, and U hodoscopes using strip-shaped gas resonators.

INTRODUCTION

The Long Baseline Neutrino Facility (LBNF) is the flagship experiment at Fermilab. Hadron monitors play an important role to measure quality of the secondary charged particles and to precisely direct the beam to the neutrino detector located hundreds of kilometers away. An ionization chamber is a standard device to use as the hadron monitor in the NuMI beam line at Fermilab. Operational failure of the hadron monitor due to high radiation is the present issue. A custom hardline cable is used to bring the electrical connections across the body of the hadron monitor to each of its feedthroughs. Since these cables lie in the beam they are subject to radiation damage and possible signal pickup. To guard against both, the cables are designed with both polyimide and ceramic insulators around the conductor and enclosed in aluminum tubing [1]. These materials significantly improved the lifetime. However, the conventional hadron monitor still has a limited lifetime and the cabling structure is complicated. Especially, future hadron monitors must operate in even higher radiation environments. The LBNF beam line design beam power for the primary protons is > 2 MW, which is three times higher than the NuMI facility. There is no particle detector device currently working in such an extremely high radiation environment.

A gas-filled RF-resonator hadron monitor will be simple and radiation-robust in this environment. The gas-filled RF resonator has been originally developed for muon beam ionization cooling channels [2]. A conceptual drawing is shown in fig. 1. When the charged beam passes throughout the gas-filled resonator it produces a large amount of electron-ion pairs by interacting with gas. The permittivity in the resonator is changed proportional to the number of incident charged particles. The beam profile will be reconstructed by X, Y, and U hodoscopes using strip-shaped gas resonators.

* Work supported by Fermilab Research Alliance, LLC under Contract No. DE-AC02-07CH11359
† yonehara@fnal.gov

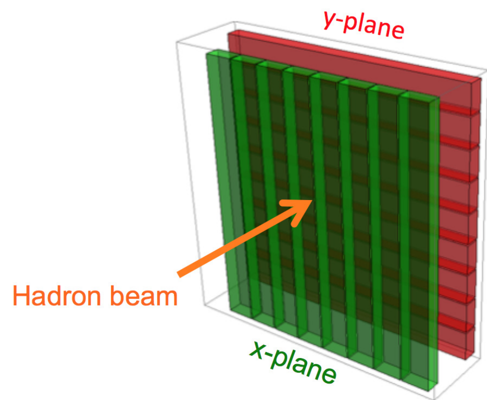

Figure 1: Schematic of the gas-filled RF hadron monitor.

PERMITTIVITY IN GAS-FILLED RF RESONATOR WITH PLASMA

The characteristic of permittivity is determined by electrons rather than ions since the ion mass is three orders of magnitude heavier than electron mass. We start our discussion from the equation of motion for a single electron in an RF field in gas,

$$m\ddot{\vec{r}} = -e\vec{E}e^{-i\omega_{RF}t} - m\nu\dot{\vec{r}}, \tag{1}$$

where ν is the collision frequency of the electron with gas molecules. The first term is acceleration of the electron by the external RF field while the second one is the frictional force caused by interactions with the gas. The electron motion is expected to be $r = r_0 e^{-i\omega t}$ where the position vector is assumed to be parallel to the electric field ($\vec{r} \| \vec{E}$). Putting this into eq. (1) results in

$$r_0 = -\frac{eE_0 e^{-i(\omega_{RF}-\omega)t}}{m(\omega^2+\nu^2)}\left(1 + i\frac{\nu}{\omega}\right). \tag{2}$$

The polarization of the gas plasma is given as

$$P = \frac{n_e e^2 E_0 e^{-i(\omega_{RF}-\omega)t}}{m(\omega^2+\nu^2)}\left(1 + i\frac{\nu}{\omega}\right) \equiv \varepsilon_0 \chi_e E(t), \tag{3}$$

where n_e is the total number of electrons in the resonator and χ_e is the susceptibility of the gas plasma. Assuming that ionization electrons are oscillating in phase with the RF electric field, i.e. $\omega = \omega_{RF}$, eq. (3) can be simplified, and the relative permittivity of gas plasma is derived as

$$\frac{\varepsilon}{\varepsilon_0} = 1 + \chi_e \simeq 1 + \frac{n_e e^2}{\varepsilon_0 m(\omega^2+\nu^2)}\left(1 + i\frac{\nu}{\omega_{RF}}\right). \tag{4}$$

This assumption is valid if the gas pressure is sufficient to cool electrons down to an equilibrium condition within one

Content from this work may be used under the terms of the CC BY 3.0 licence (© 2015). Any distribution of this work must maintain attribution to the author(s), title of the work, publisher, and DOI.

ISBN: 978-3-95450-168-7 doi:10.18429/JACoW-IPAC2015-MOPWI020
Content from this work may be used under the terms of the CC BY 3.0 licence (© 2015). Any distribution of this work must maintain attribution to the author(s), title of the work, publisher, and DOI.

DEVELOPMENT OF SIMPLE TRACKING LIBRARIES FOR ALS-U*

H. Nishimura#, D. Robin, K. Song, C. Steier, C. Sun, W. Wan
LBNL, Berkeley, CA 94720, USA

Abstract

A conceptual lattice design study of a new diffraction-limited light source requires complex and numerically intensive calculations due to increasing number of fitting parameters. This paper reports our ongoing effort of upgrading accelerator modeling and simulation libraries to carry out such design studies efficiently.

THE TRACY LIBRARIES

Tracy[1] is an accelerator modeling and simulation code developed as a part of the Advanced Light Source (ALS) conceptual design study[2] in late 1980's. The original version was written in Pascal, and its accelerator library was extracted and rewritten in C/C++ and later in C#.

The C/C++ version of the library was called Goemon, which is now Tracy++[3]. One of its applications is the use with multi-objective genetic algorithms (MOGA)[4] to optimize the existing ALS lattice[5], and the new lattice for a diffraction-limited light source called ALS-U[6] by using OpenMPI[7].

It is not common to use C# for scientific computing yet, however, the development effort of Tracy was moved to the C# version called Tracy#[8] a decade ago for better development efficiency and horizontal integrability than the C/C++ version but with some performance penalty at run time.

Taking the design study of ALS-U as an opportunity, the upgrade of these Tracy libraries have started. Cleaning up and simplifying the internal structures, they are upgraded to take benefit of the modern software and hardware technologies. These new version is called Tracy.Lite that comes in both C++ and C# versions.

TRACY.LITE

Goals

The goal is to create simpler, faster, and more reliable and flexible libraries than the Tracy++ and Tracy# combination. We do this first by limiting our scenario to the first phase of the conceptual lattice design studies where lattice errors are not considered but many parameter optimizations with multiple objectives and also straightforward scans are required. The modeling of realistic lattice errors is for the second phase.

Tracy.Lite supports multiple usage modes; a highly-parallelized batch execution mode for both MOGA and straightforward scan, and interactive mode using scripts.

*Work supported by the U.S. Department of Energy under Contract No. DE-AC02-05CH11231
H_Nishimura@lbl.gov

Based on our experience with Tracy++ and Tracy#, Tracy.Lite also has two implementations; Tracy.Lite++ in C++ and Tracy.Lite# in C#. Tracy.Lite++ is for the use on the HPC clusters and also on modern many-code CPUs. Tracy.Lite# is for the development efficiency, flexibility and the use from Python. By developing these two versions simltaneously, a better compatibility is established than the previous case.

Simplification

This is to make both design and implementation simple and concise to improve maintenance ability, development efficiency, execution speed and reliability.

The Element class models building blocks of the beam lines, such as drift spaces, various magnets, monitors and RF cavities. Tracy++ and Tracy# have the root class Element and its descendants which form a tree. This hierarchy has been removed and the single Element class supports all the Elements by distinguishing the types of building blocks by using the object attributes. This may look like a degeneration as a general Object-Oriented Programming practise, however, it makes external call from other programming languages, such as Python, much more transparent and feasible.

The lattice definition was done by using operation overloading effectively. As Tracy++ required complex memory management for it, Tracy.Lite++ uses generic containers as in Tracy# and Tracy.Lite#.

These effects are reflected in the library sizes as shown below.

Table 1: The Library Code Length in Lines

Library	Language	Core	ALS
Tracy++	C++	35K	6K
Tracy#	C#	22K	11K
Tracy.Lite++	C++	6K	2K
Tracy.Lite#	C#	5K	5K

Core is the body of the library not dedicated to ALS.
ALS is the model of various ALS lattice configurations.

Execution Speed

The speed up comes in the two directions; one is in a single thread mode by removing the hot spots where CPU time is wasted by using CPU profiling, and also simplifying the algorithms that are physically redundant in the ideal lattice design phase. The second is by multi-threading; Tracy.Lite++ uses OpenMP[9] and Tracy.Lite# uses Parallel.For[10] that is similar to OpenMP and a part of the .NET Framework.

ISBN: 978-3-95450-168-7 doi:10.18429/JACoW-IPAC2015-MOPWI021

THE LCLS-II LLRF SYSTEM[#]

L. Doolittle, G. Huang, A. Ratti, C. Serrano, LBNL, Berkeley, CA 94720, USA
R. Bachimanchi, C. Hovater*, JLAB, Newport News, VA 23696, USA
S. Babel, B. Hong, D. Van Winkle, SLAC, Stanford, CA 94309, USA
B. Chase, E. Cullerton, P. Varghese, FNAL, Batavia, IL 60510, USA

Abstract

The SLAC National Accelerator Laboratory is planning an upgrade (LCLS-II) to the Linear Coherent Light Source with a 4 GeV CW superconducting (SCRF) linac. The SCRF linac consists of 35 ILC style cryomodules (eight cavities each) for a total of 280 cavities. Expected cavity gradients are 16 MV/m with a loaded QL of ~ 4 x 10^7. The RF system will have 3.8 kW solid state amplifiers driving single cavities. To ensure optimum field stability a single source single cavity control system has been chosen. It consists of a precision four channel cavity receiver and two RF stations (Forward, Reflected and Drive signals) each controlling two cavities. In order to regulate the resonant frequency variations of the cavities due to He pressure, the tuning of each cavity is controlled by a Piezo actuator and a slow stepper motor. In addition the system (LLRF-amplifier-cavity) is being modeled and cavity microphonic testing has started. This paper describes the LLRF system under consideration.

INTRODUCTION

In the summer 2013 the LCLS-II project made the decision to build a superconducting electron linac in the first 10 sections of the SLAC tunnel. The new linac is using a TESLA-ILC 1.3 GHz style cryomodule similar to the ones being produced for the European X-FEL. The primary difference being that these cryomodules must support cw operation. The linac consists of an RF gun, buncher cavity, 35 eight cavity cryomodules and two eight cavity 3.9 GHz cryomodules for harmonic linearization. The linac will support cw beam currents up to 100 μA.

The 1.3 GHz cavities are optimized to support 16 MV/m gradients. The loaded Q is relatively high 4 x 10^7, implying a cavity bandwidth of 32 Hz. The Q_L can be adjusted through the coaxial coupler if further optimization is needed. Originally the project had chosen to power multiple cavities off of one large klystron using vector sum control. As the design progressed, the project made the decision to power and control each cavity individually. Therefore each cavity is powered by a 3.8 kW solid state amplifier (SSA). Microphonic detuning is expected to be a maximum of 10 Hz peak detuning (1.5 Hz rms.).

Cavity resonance control is provided by both a slow stepper motor and a fast piezo tuner. Care must be taken in operating both tuners because they are within the insulating vacuum of the cryomodule. For this reason the temperature of the stepper motor is continuously monitored. There are four redundant piezos for each cavity and they are configured to be driven two at a time. The cavity can have up to three of the piezos fail and still be operational.

Cavity field control is specified to be 0.01% and 0.01° for time periods faster than 1 Hz. For time slower than 1 Hz the accelerator must rely on beam based feedback to maintain the proper beam parameters (energy spread and shape). In addition the linac is segmented into four sections each with different beam-phase relationships. Figure 1 shows the linac and these segments. For these slower times phase and amplitude control is greatly relaxed to the 5-10% and 5-10° levels [1].

LLRF CONCEPTUAL DESIGN

The design is being developed collaboratively between LBNL, FNAL, SLAC and JLAB. The LLRF design builds upon recent design experiences at those laboratories [2, 3, 4]. Figure 2 shows a block diagram of the conceptual LLRF design. Not shown is the second RF station controlling the two other cavities. The layout is designed around the SLAC gallery to cryomodule foot print that the project has settled on; four SSA's/tunnel penetration. Given that footprint the LLRF system for each cryomodule is divided between two penetrations. Four cavities are powered and controlled for each penetration. LLRF control is split between a precision receiver chassis (PRC) which processes four cavity signals and the RF station that processes the forward and reverse power and provides the drive signal to the SSA. Each RF station controls two cavities. For economy and maintainability RF, IF and FPGA hardware are shared between the PRC and the RF stations.

This work was supported by the LCLS-II Project and the U.S. Department of Energy, Contract DE-AC02-76SF00515
* hovater@jlab.org

Content from this work may be used under the terms of the CC BY 3.0 licence (© 2015). Any distribution of this work must maintain attribution to the author(s), title of the work, publisher, and DOI.

ISBN: 978-3-95450-168-7 doi:10.18429/JACoW-IPAC2015-MOPWI022

Content from this work may be used under the terms of the CC BY 3.0 licence (© 2015). Any distribution of this work must maintain attribution to the author(s), title of the work, publisher, and DOI.

EXPERIMENTAL STUDY OF A TWO-COLOR STORAGE RING FEL *

J. Yan[1,†], Y. K. Wu[1], S. Mikhailov[1], H. Hao[1], V. Popov[1],
J. Li[2], J. Wu[3], N. A. Vinokurov[4] and S. Huang[5]
[1]DFELL/TUNL, and Department of Physics, Duke University, Durham, NC, USA
[2]NSRL, University of Science and Technology of China, Anhui, China
[3]SLAC National Accelerator Laboratory, Menlo Park, CA, USA
[4]Budker Institute of Nuclear Physics, Novosibirsk, Russia
[5]Institute of Heavy Ion Physics, Peking University, Beijing, China

Abstract

Multi-color Free-electron Lasers (FELs) have been developed on linac based FELs over the past two decades. On the storage ring, the optical klystron (OK) FEL in its early days was demonstrated to produce lasing at two adjacent wavelengths with their spectral separation limited by the bandwidth of single wiggler radiation. Here, we report a systematic experimental study on the two-color operation at the Duke FEL facility, the first experimental demonstration of a tunable two-color harmonic FEL operation of a storage ring based FEL. We demonstrate a simultaneous generation of two FEL wavelengths, one in infrared (IR) and the other in ultraviolet (UV) with a harmonic relationship. The experimental results show a good performance of the two-color FEL operation in terms of two-color wavelength tunability, power tunability and power stability.

INTRODUCTION

Since the theoretical prediction and the first experimental demonstration by John Madey in 1970s [1,2], free-electron lasers (FELs) have seen great development over the past few decades and have become increasingly attractive light sources to several scientific research fronts. A common FEL configuration requires an optical cavity to oscillate and amplify electron beam radiation and is thus called an oscillator FEL [3]. An oscillator FEL can be driven either by an electron storage ring or a linac. Oscillator FELs mainly operate in the spectral region from IR to UV. Since early 1990s, multi-color, especially two-color FEL operations have been frequently discussed and realized on several linac based FELs. The first two-color FEL operation was realized on CLIO [4], an oscillator FEL operating in the mid-infrared regime, where two FEL wavelengths were produced by the same electron beam and two undulators with different undulator strengths inside a single optical cavity. Two more linac based oscillator FELs reported their successful two-color operations later on [5,6]. Another FEL configuration, the so-called single-pass FEL, is mainly driven by linacs and do not use an optical cavity. In these FELs, FEL beam amplification is realized via the interaction between the electron beam and the radiation it emits [7,8] or an external laser [9,10] in a single pass. Single-pass FELs are the dominant coherent light sources in the vacuum UV (VUV) and x-ray regimes. Recently two-color operations have also been experimentally demonstrated on several single-pass FELs [11–15] in the short-wavelength spectral regions.

Unlike in a linac, an electron beam in a storage ring is recycled and participates in the FEL interaction repeatedly over many passes. Therefore, the physics challenges for the two-color operation of a storage-ring FEL include the control and management of two competing lasing processes and maintanance of simultaneous lasing at two wavelengths in multiple passes. In this article, we report a systematic experimental study on the two-color operation at the Duke FEL facility, the first experimental demonstration on the multi-color operation of a storage ring based FEL in both IR and UV, in which, a simultaneous generation of two FEL wavelengths (IR and UV) with a harmonic relationship has been realized. The experimental results illustrate a good performance of our two-color FEL operation in terms of two-color wavelength tunability, power tunability and power stability. In addition, the two-color FEL can serve as a photon source for the two-energy gamma-ray production via Compton backscattering at the High-Intensity γ-ray Source (HIGS) [16].

EXPERIMENTAL SETUP

The operation of the Duke FEL system can use a variety of wiggler configurations with four available electromagnetic wiggler magnets, two planar OK-4 wigglers and two helical OK-5 wigglers (see Fig. 1), which provides the possibility of operating two-color FEL using the same electron beam at a single beam energy. In the harmonic two-color FEL research, three wigglers as shown in Fig. 1 are powered up, including the upstream helical OK-5 wiggler (OK-5A) and two planar OK-4 wigglers (OK-4A and OK-4B) in the middle section. The downstream OK-5 wiggler (OK-5D) was disconnected. Upstream OK-5A wiggler is used to lase at the fundamental wavelength in IR, and two downstream OK-4 wigglers in the optical klystron configuration is tuned to lase at the second harmonic in UV. The lasing wavelengths are varied by changing the strength of the magnetic field in the OK-5 and OK-4 wigglers, respectively. Two bunchers, $B1$ between OK-5A and OK-4 wigglers and $B2$ sandwiched by two OK-4 wigglers, are used to provide fine tuning of the harmonic FEL lasing. The harmonic two-color FEL lasing is realized at the fundamental wavelength

* Work supported in part by the US DOE grant no. DE-FG02-97ER41033.
† junyan@fel.duke.edu, 1-919-660-2667.

ISBN: 978-3-95450-168-7 doi:10.18429/JACoW-IPAC2015-MOPWI023

DEVELOPMENT PLAN FOR PHYSICS APPLICATION SOFTWARE FOR FRIB DRIVER LINAC *

M. Ikegami, G. Shen, Facility for Rare Isotope Beams, Michigan State University, MI 48824, USA

Abstract

Facility for Rare Isotope Beams (FRIB) is a high-power heavy ion accelerator facility currently under construction at Michigan State University. We recently decided to adopt EPICS V4 for the architecture for commissioning application software development for FRIB linac. In this paper, we present our plan for the commissioning application development with its present status.

INTRODUCTION

Facility for Rare Isotope Beams (FRIB) is a high-power heavy ion accelerator facility currently under construction at Michigan State University under a cooperative agreement with the US DOE [1]. Its driver linac operates in CW mode and accelerates all stable ions to energies above 200 MeV/u with the beam power on target up to 400 kW. The linac has a folded layout as shown in Fig. 1, which consists of a front-end, three Linac Segments (LSs) connected with two Folding Segments (FSs), and Beam Delivery System (BDS) to deliver the accelerated beam to target. The linac is located in a tunnel underground with the exception of two ECR ion sources located on the ground level (not shown in Fig. 1). The beam is delivered to the linac tunnel through a vertical beam drop. LSs consist of two types of superconducting QWRs (Quarter Wave Resonators) with geometrical β of 0.041 and 0.085, and two types of superconducting HWRs (Half Wave Resonators) with geometrical β of 0.29 and 0.53. LS1, LS2, and LS3, respectively, have 14, 24, and 6 cryomodules. The total number of superconducting cavities is 332 including rebuncher cavities in FSs. The linac has four tuning beam dumps, BD FS-1a, BD FS-1b, BD FS-2, and BD BDS, as shown in Fig. 1.

FRIB driver linac is substantially larger both in scale and beam power than existing facilities of a similar kind, which poses significant challenges in realizing beam commissioning or initial tuning of operating parameters. Efficient commissioning is essential to minimize the risk of component damage by beam loss during the commissioning. Then, high level application software assisted by online model is essential to realize efficient commissioning. In addition, we expect frequent change of accelerated ion species to meet the request from users once user operation is started. Judging from the present operation cycle of coupled cyclotron facility in Michigan State University, we may change ion species once in a week or two. Then, swift retuning after switching ion species is essential to realize high beam availability. It will require physics application to support model based retuning. We present our plan to develop physics applications to serve these purposes in this paper while our present emphasis is put on those to support commissioning. We here define physics applications as high level application software for commissioning utilizing model. We also discuss our plan to develop software infrastructure to support those applications and their development in this paper. Our discussion here does not include simple OPIs (Operator Interfaces) to show and set values for PVs (Process Variables) which is supposed to support accelerator operation.

* Work supported by the U.S. Department of Energy Office of Science under Cooperative Agreement DE-SC0000661.

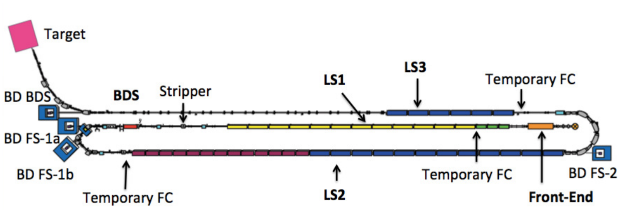

Figure 1: Schematic layout for FRIB driver linac.

ARCHITECTURE FOR PHYSICS APPLICATION SOFTWARE

While we have assumed OpenXAL [2] for the architecture for physics application software development, we recently decided to adopt EPICS V4 [3] for the architecture instead of OpenXAL. EPICS V4 has been rapidly developed to support recent commissioning of NSLS-II, and we can take advantage of the most up-to-date developments by adopting it. Its nobel design features include three-tier structure with middle layer services which enables efficient development of high level applications (See Fig. 2).

One of the advantages of OpenXAL is the integrated online model. However, OpenXAL model does not support features specific but essential to FRIB linac including multi-charge state acceleration, non-axial symmetric field of an RF cavity, etc. It necessitates significant extension of func-

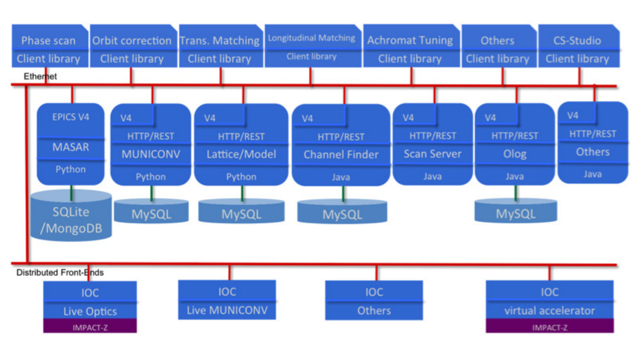

Figure 2: Planned architecture for FRIB physics application.

Content from this work may be used under the terms of the CC BY 3.0 licence (© 2015). Any distribution of this work must maintain attribution to the author(s), title of the work, publisher, and DOI.

6th International Particle Accelerator Conference IPAC2015, Richmond, VA, USA JACoW Publishing
ISBN: 978-3-95450-168-7 doi:10.18429/JACoW-IPAC2015-MOPWI024

Content from this work may be used under the terms of the CC BY 3.0 licence (© 2015). Any distribution of this work must maintain attribution to the author(s), title of the work, publisher, and DOI.

ACCELERATOR ONLINE SIMULATION PLATFORM*

P. Chu#, Y. Zhang, MSU, East Lansing, MI 48824, USA

Abstract

A platform for accelerator online beam simulation has been established for various accelerators. This modelling platform supports multiple simulation codes for different sections of the complex machine which cannot be properly modelled with a single online simulation tool. Model data for the platform is stored in a relational database which is designed to accommodate most simulation data. The stored data is accessible with physics intuitive data API (Application Programming Interface). Presently, the platform is supporting Open XAL, MAD-X and IMPACT simulation codes. In addition to the model data storage and access, tools such as data comparison and simple graphing capability are also included in the platform.

INTRODUCTION

Modern accelerators with high precision requirements often rely on good online model for their machine tuning. However, each machine is likely having its own unique physics simulation issues which requires different modelling tools to deal with. For example, some lower energy machines are sensitive to space charge effects which need a good space charge code, while higher energy machines can be calculated without space charge. This model dependent machine simulation usually requires customized software code for each simulation tool. On the other hand, a properly designed platform with minimal overhead can provide a universal solution for various machines. Such a platform has been developed and prototyped.

One relatively easy way to achieve a platform for various modelling tools is shown in Fig. 1 as centre piece of the physics application architecture. The key components in this approach for the online simulation platform are a data container which can accommodate model data for different modelling tools, a set of common data access APIs for the data container, and data adapters between the data container and various modelling codes. For this model platform implementation, the model data container is a relational database, as shown in the middle of Fig. 1, which will be described in the next section. Besides the database itself, it is necessary to provide a set of data access API instead of tedious SQL (Sequential Query Language) statements for querying the saved model data. For each modelling tool, the input data should be generated programmatically so the model run can be automated, while the model output data should be parsed and saved into the database via convenient API. These tools are the model data adapters which will be explained in details later.

Additionally, both offline and online model data can utilize the same platform. Open XAL [1] as a physics application framework provides the interface to the control systems. Even fitted empirical machine model can be included in this platform.

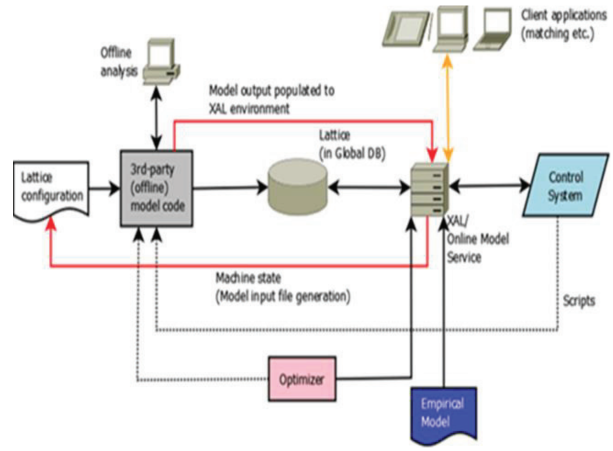

Figure 1: Online Model Platform schematic diagram.

MODEL DATABASE

The model database used for the data container is part of an accelerator database effort from the collaboration among FRIB, NSLS-II (National Synchrotron Light Source II) and ESS (European Spallation Source). The blue print for this database was from IRMIS-3 [2]. Originally there were two separate sub-schemas, one for lattice data including device settings and the other one for model run data. Because there is significant overlap between these two data areas, it is efficient to merge them into one schema to minimize data duplications. There are 20 tables in this database schema with a potential hook point to another part of the accelerator database, namely the Configuration Database which is for accelerator hardware data. The key feature for this database is to use "property name and value" pair to store most model data, i.e. the model parameter names are also part of data as opposed to the traditional way of defining the parameter names as database column labels. The detail of the Lattice and Model database tables can be found in the Lattice/Model Schema and API Release Note from the Open EPICS Model download area [3].

DATA ACCESS API

Besides the database itself, there is a set of data access APIs also developed as part of the Lattice and Model package. The software package is Java based which takes full advantage of the latest Object to Relational Mapping (ORM) technology, a mapping mechanism between

---

*Work supported by the U.S. Department of Energy Office of Science under Cooperative Agreement DE-SC0000661
#chu@nscl.msu.edu

ISBN: 978-3-95450-168-7 doi:10.18429/JACoW-IPAC2015-MOPWI025

PHASE AND AMPLITUDE TUNING ALGORITHMS FOR THE FRIB SUPERCONDUCTING CAVITIES *

Yan Zhang#, Paul Chu, Zhengqi He
FRIB, Michigan State University, East Lansing, MI 48824, USA

Abstract

FRIB driver linac will deliver all heavy ion beams up to uranium for beam energy above 200 MeV/u and maximum beam power on fragment target 400 kW for nuclear physics researches. Phase and amplitude tuning of all the FRIB superconducting cavities – 332 of them in the linac, are important to low power beam commissioning as well as high power operations. Because of relatively low beam energy and high acceleration gradient, the particle velocity changes significantly in the cavity RF gaps and the beam bunch structure cannot be preserved perfectly in the further downstream beam diagnostics, beam longitudinal tuning algorithms are studied for different types of FRIB cavities and for various beam energies, which include acceleration cavities as well as re-buncher cavities.

INTRODUCTION

The FRIB, Facility for Rare Isotope Beams, is currently under construction on the campus of MSU, Michigan State University. The project is funded by the US Department of Energy Office of Science, MSU, and the State of Michigan. The total budget of the project is about 730 million dollars, and it will be completed in 2022 [1].

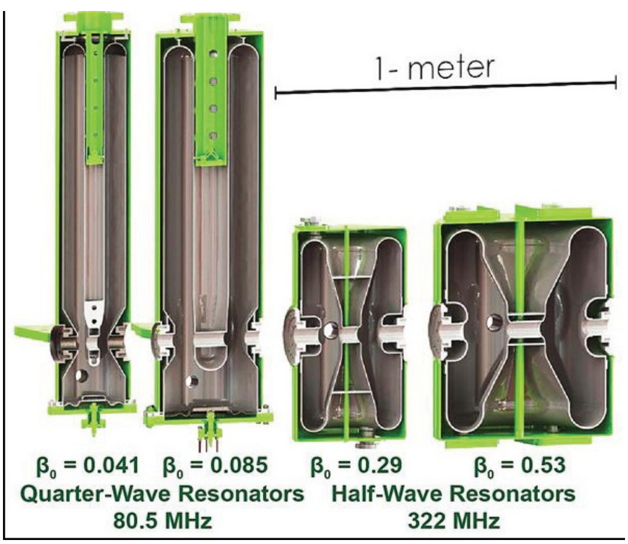

Figure 1: The FRIB cavities: beta 0.041 and 0.085 QWRs, 80.5 MHz; beta 0.29 and 0.53 HWRs, 322 MHz.

The FRIB driver linac is a state-of-the-art high power CW linac, and it includes 4 different types of SRF cavities as shown in Figure 1. Two types of quarter wave resonators (QWR) accelerate beams from 0.5 to 20 MeV/u, and then two types of half wave resonators (HWR) accelerate beams to above 200 MeV/u [2]. Because the acceleration gradient of the FRIB cavities goes up to 8 MV/m and the beam velocity increases from beta about 0.03 to 0.6 through the driver linac, the maximum velocity change in a single low beta cavity for a 2-pi phase scan can be above 10%, and the beam bunch structure may only survive a few meters downstream of the cryomodule, tuning of the cavity phase and amplitude is very difficult compare with that of a high energy linac. In this paper, SRF cavity phase and amplitude tuning algorithms are studied.

TUNING OF THE HWR CAVITY

In a RF linac for proton beam or heavy ion beams, Delta-T [3], and phase scan signature matching [4] techniques are widely applied to tune cavity phase and amplitude in which beam position/phase monitor (BPM) pairs are utilized to measure the absolute beam phase while scanning the cavity phase and amplitude; the synchronous phase as well as the acceleration gradient of the cavity can then be precisely determined by signature matching of the BPMs' time-of-flight (TOF) measurements against the RF cavity model. In this paper, we mainly focus on the applications of phase scan signature matching techniques.

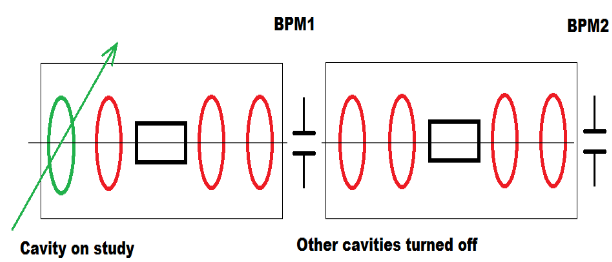

Figure 2: Schematic configuration of cavity phase scan

Figure 2 shows a schematic configuration of the cavity phase scan measurements. A pair of BPMs is downstream of the RF cavity on study, with all other cavities between the BPMs and the scanning cavity turned off, a 2-pi phase scan of the cavity is performed and the beam phase is recorded with the BPM pair. Because the beam current is low compare with that of a pulsed SRF linac such as the SNS, beam loading induced RF fields in the off cavities downstream may not significantly affect the measurements which is different to the SNS linac [5].

In the studies, IMPACT [6] is used for generation of the beam absolute phases exactly at the locations of the BPM pair. Then a thin-lens model of the RF cavity is applied:

* Work supported by the U.S. Department of Energy Office of Science under Cooperative Agreement DE-SC0000661
# zhangy@frib.msu.edu

Content from this work may be used under the terms of the CC BY 3.0 licence (© 2015). Any distribution of this work must maintain attribution to the author(s), title of the work, publisher, and DOI.

ISBN: 978-3-95450-168-7 doi:10.18429/JACoW-IPAC2015-MOPWI026

TRANSVERSE MATCHING OF HORIZONTAL-VERTICAL COUPLED BEAMS FOR THE FRIB LINAC *

Yan Zhang #, Paul Chu, Zhengqi He, Steve Lund, Dylan Maxwell
FRIB, Michigan State University, East Lansing, MI 48824, USA

Abstract

FRIB driver linac will deliver all heavy ion beams up to uranium with energy above 200 MeV/u and maximum beam power on fragment target 400 kW. Strong horizontal-vertical coupling exists in the linac since superconducting solenoids are installed to focus multi charge state beams. Further, the low beta SRF cavities have raised quadrupole field components, and the combined effects make beam transverse matching challenging. In this paper, we study transverse matching of horizontal-vertical coupled beams based on beam profile measurements with multiple wire scanners. Issues such as the initial beam conditions fit with coupling not unique, and errors of beam diagnostics and magnets introduce further complications are addressed. Nonetheless, the simulation studies show that satisfactory transverse matching can be achieved with proper tuning.

INTRODUCTION

The FRIB, Facility for Rare Isotope Beams, is currently under construction on the campus of MSU, Michigan State University. The project is funded by the US Department of Energy Office of Science, MSU, and the State of Michigan. The total budget of the project is about 730 million dollars, and it will be completed in 2022 [1].

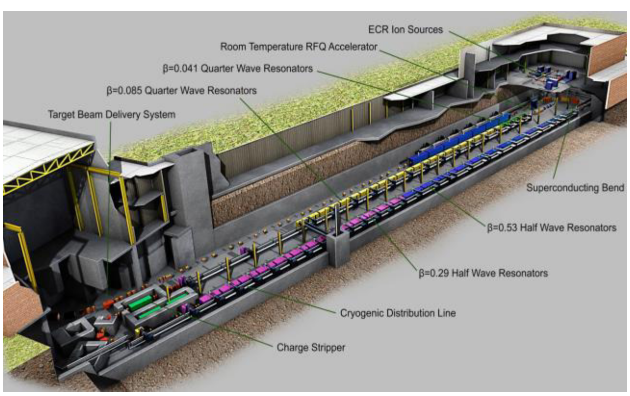

Figure 1: Layout of the FRIB driver linac.

The major accelerator system of the facility is a SRF continue-wave (CW) linac, the FRIB driver linac, which consists of a front end, three linac segments (LS), two 180° achromatic isochronous folding segments that connect the three LS, a liquid lithium charge stripper for more efficient accelerations of high power heavy ion beams, and a beam deliver system which transport the primary beams onto the fragment target for production of rare isotopes for nuclear physics research. The FRIB drive linac will be installed underground about 10 meters deep on the campus of MSU. Figure 1 shows the layout of the driver linac [2]. To reach the design beam power for the heaviest ions, multi charge beams are accelerated simultaneously in the linac: in the design, two charge states in LS1, and up to 5 charge states in LS2 and LS3. In the linac, superconducting solenoids are used for transverse beam focusing.

Because the injection beam is generated within a strong magnetic field from an ECR ion source [3], the beam distribution has strong correlation. Since generally beams emerging from ECR ion sources are not axisymmetric, the ion particles are born with x-y coupling. In addition, beam asymmetries further develop due to dispersions in bending magnets of the folded linac lattice. Even in the solenoid lattice of the straight linac segment, significant dipole and quadrupole components within the quarter wave resonators (QWRs) impact on the beam acceleration and transport, particularly at low energy, usually the beam is significantly deviated from axisymmetric [4]. Due to these effects, for transverse matching of the FRIB linac, we have to deal with a strongly coupled beam which is not axisymmetric.

PARAMTERS OF X-Y COUPLED BEAM

To describe a horizontal-vertical (x-y) coupled beam, second order moments of 4D beam matrix are applied:

$$\sigma = \begin{pmatrix} \langle \boldsymbol{xx} \rangle & \langle \boldsymbol{xx'} \rangle & \langle xy \rangle & \langle xy' \rangle \\ \langle \boldsymbol{xx'} \rangle & \langle \boldsymbol{x'x'} \rangle & \langle x'y \rangle & \langle x'y' \rangle \\ \langle xy \rangle & \langle x'y \rangle & \langle \boldsymbol{yy} \rangle & \langle \boldsymbol{yy'} \rangle \\ \langle xy' \rangle & \langle x'y' \rangle & \langle \boldsymbol{yy'} \rangle & \langle \boldsymbol{y'y'} \rangle \end{pmatrix} \tag{1}$$

Because of symmetry, there are 10 independent variables in the matrix. Two parameterizations are often utilized to deal with linear coupling: Edwards-Teng [5] and Ripken [6]. Implements of these two parameterizations can be found in, e.g. MAD-X [7] and Elegant [8]. Relationships between the two methods are analysed by Lebedev and Bogacz [9]. We use Ripken's parameterization method.

The 10 parameters chosen are: 4 alpha functions, 4 beta functions, and 2 emittances (β_{1x}, β_{1y}, β_{2x}, β_{2y}, α_{1x}, α_{1y}, α_{2x}, α_{2y}, ε_1, ε_2). Additionally, for beam envelop solution 2 phase advances (ν_1, ν_2) are needed [9]. The phase advances can be derived from these alpha and beta functions. Measurable beam rms sizes along x, y, and at 45° diagonal (d) are [9]:

$$\begin{aligned} \sigma_x &= \sqrt{\varepsilon_1\beta_{1x} + \varepsilon_2\beta_{2x}} \\ \sigma_y &= \sqrt{\varepsilon_1\beta_{1y} + \varepsilon_2\beta_{2y}} \\ \sigma_d &= \frac{\sqrt{\sigma_x{}^2 + \sigma_y{}^2 + 2\delta\cdot\sigma_x\sigma_y}}{\sqrt{2}} \end{aligned} \tag{2}$$

where, $\delta = \dfrac{\sqrt{\beta_{1x}\beta_{1y}}\,\varepsilon_1 \cos\nu_1 + \sqrt{\beta_{2x}\beta_{2y}}\,\varepsilon_2 \cos\nu_2}{\sigma_x\sigma_y}$

* Work supported by the U.S. Department of Energy Office of Science under Cooperative Agreement DE-SC0000661
# zhangy@frib.msu.edu

Content from this work may be used under the terms of the CC BY 3.0 licence (© 2015). Any distribution of this work must maintain attribution to the author(s), title of the work, publisher, and DOI.

ISBN: 978-3-95450-168-7 doi:10.18429/JACoW-IPAC2015-MOPWI027

Content from this work may be used under the terms of the CC BY 3.0 licence (© 2015). Any distribution of this work must maintain attribution to the author(s), title of the work, publisher, and DOI.

OPEN XAL CONTROL ROOM EXPERIENCE*

P. Chu#, D. Maxwell, Y. Zhang, MSU, East Lansing, MI 48824, USA
C.K. Allen, T. Pelaia, A.P. Shishlo, ORNL, Oak Ridge, TN 37831, USA

Abstract

This paper reports the control room experience, lessons learned, and quick deployment approach for the Open XAL application environment. Open XAL is a java-based framework for building high-level accelerator applications, it is a major revision of the XAL framework which was developed at the Spallation Neutron Source (SNS). Open XAL is site neutral and may be deployed at multiple accelerator facilities. Currently, Open XAL is installed at SNS and at the Re-Accelerator facility of Michigan State University. At SNS we are in the final process of replacing the old XAL environment with Open XAL; we describe the upgrade process and our accelerator operations experience using Open XAL. At Michigan State University (MSU), Open XAL has been tested during a cryomodule commissioning and results will be shown.

INTRODUCTION

The XAL [1] based applications have been successfully applied to SNS commissioning and early operation. Open XAL [2], on the other hand, is the updated version of XAL with international collaboration effort. Besides any common software practice, it is particularly important for software usability and customer satisfaction, especially for a new version of an already-successful software. Control room tests for Open XAL also can uncover issues which cannot be found with any offline tests. Unique challenges such as co-existence of operation for XAL and the new Open XAL applications are described below. New applications based on the Open XAL library are also demonstrated.

SNS CONTROL ROOM EXPERIENCE

Given that SNS is fully operational, it provides both challenges and opportunities for migrating from the mature XAL platform to the new Open XAL platform. The primary opportunity is to verify the code in a real operational environment while the primary risk is failure of the software affecting machine performance for production. To mitigate this risk as well as to facilitate software verification, we have chosen to deploy both XAL and Open XAL side by side which itself presents a challenge.

Following the summer of 2014 maintenance period, we have positioned Open XAL as the default accelerator physics toolset, and the old XAL code has been frozen and kept as a fallback and a benchmark source. All new applications and scripts are written against Open XAL.

*Work supported by the U.S. Department of Energy Office of Science under Cooperative Agreement DE-SC0000661 and DE-AC05-00OR22725
#chu@nscl.msu.edu

XAL and Open XAL Coexistence

Running Open XAL alongside of XAL presents several challenges due to requirements and incompatibilities. XAL was built to run against Java 6, while Open XAL was built against Java 7. Due to a performance issue discovered in Java 7, it is not feasible to run XAL under Java 7. To support Java 6 for XAL and Java 7 for Open XAL, separate launch environments for XAL and Open XAL were configured using BASH scripts.

Services presented a challenge since XAL uses XML-RPC and Open XAL uses JSON-RPC over WebSockets. Services and their associated clients must both be running on the same software platform (either XAL or Open XAL) to communicate with each other. A service such as the PV Logger which both logs continuously and on demand from a client creates a problem since both XAL and Open XAL clients must continue to work and be able to request the PV Logger to log on demand. To address this issue, the PV Logger service was modified to allow an optional on-demand-only mode. The Open XAL variant is configured to log both on demand and continuously (normal mode) while the XAL variant logs just on demand to support XAL client requests without generating duplicate logs.

Both XAL and Open XAL can read and write the same documents, but the accelerator optics input is different due to a new format for the online model configuration in Open XAL and ongoing device changes in Open XAL. Since it is common for documents to reference the associated accelerator optics, we needed to address this problem of a user opening a document referencing an XAL or Open XAL accelerator optics in an application running under the wrong platform. To address this issue, the Open XAL optics file includes a new version attribute which is set to 2.0 and the absence of this version or version 1.0 implies XAL. Both XAL and Open XAL code was modified to verify the accelerator optics version, alert the user and load the compatible optics file.

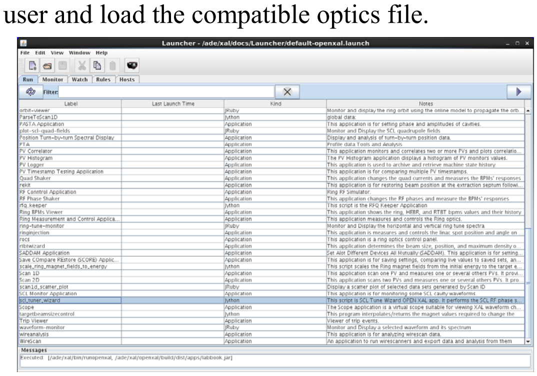

Figure 1: Open XAL Application Launcher.

With these changes XAL and Open XAL can coexist without issue and both versions can open documents

ISBN: 978-3-95450-168-7 doi:10.18429/JACoW-IPAC2015-MOPWI028

INITIAL EXPERIMENTAL RESULTS OF A MACHINE LEARNING-BASED TEMPERATURE CONTROL SYSTEM FOR AN RF GUN

A.L. Edelen#, S.G. Biedron, S.V. Milton, Colorado State University, Fort Collins, CO, USA
B.E. Chase, D.J. Crawford, N. Eddy, D. Edstrom Jr., E.R. Harms, J. Ruan, J.K. Santucci, Fermi National Accelerator Laboratory*, Batavia, IL, USA
P. Stabile, ADAM, Geneva, Switzerland

Abstract

Colorado State University (CSU) and Fermi National Accelerator Laboratory (Fermilab) have been developing a control system to regulate the resonant frequency of an RF electron gun. As part of this effort, we present initial test results for a benchmark temperature controller that combines a machine learning-based model and a predictive control algorithm. This is part of an on-going effort to develop adaptive, machine learning-based tools specifically to address control challenges found in particle accelerator systems.

INTRODUCTION

The electron gun at the advanced superconducting test accelerator [1-3] is a 1½ cell normal-conducting copper RF photoinjector operating at 1.3 GHz. It is water-cooled and shows a 23-kHz shift in resonant frequency per °C change in cavity temperature. Thus, establishing satisfactory control of the water temperature at the cavity entrance is the first step toward ensuring the gun is kept at the proper resonant frequency. Existing requirements state that this water temperature should be regulated to within ±0.02°C [2]. This regulation loop can then be nested within another control algorithm that determines what the water temperature needs to be in order to either a) directly minimize the detuning or b) achieve an operator-specified cavity temperature set point. As an intermediate result, this discussion considers the latter case. This also facilitates comparison with the existing controller.

Water System Overview

A simplified schematic of the water system is given in Fig. 1. A detailed description is given in Ref. [4]. The two controllable variables are 1) the flow control valve setting and 2) the heater power setting. For this particular system there are several control challenges:

- Due to water transport and thermal time constants, long time delays exist in the system responses (~10s from the valve to T02, ~30s from T02 to TIN, ~20s from TIN to TCAV, and ~60s from TOUT to T06).
- Without compensation, any change in the temperature of the water exiting the gun (either due to an increase in waste heat from the gun or a change in the temperature of the water entering the gun) will circulate back into the mixing chamber and have a secondary impact on the cavity temperature.
- There are fluctuations in the low conductivity water (LCW) supply temperature. While it is nominally regulated to within ±0.5°C, larger spikes can occur.

Due to the TCAV sensor location and the cavity geometry, the temperature recorded will be higher than the cavity wall temperature under RF power. Thus, for resonance control using operator-specified TCAV set points, it is important to note that the set point required to maintain the proper resonant frequency will increase with increasing average RF power.

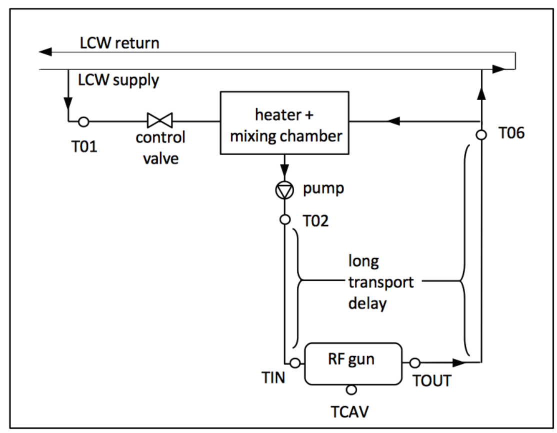

Figure 1: Layout of the water system and relevant instrumentation. T01, T02, TIN, TCAV, TOUT, and T06 are temperature sensors.

Existing Controller

Presently, the cavity temperature is being regulated by a feedforward/PI controller developed at Fermilab that adjusts the valve setting such that a TCAV set point is reached. An older version of the controller is described in [4], and a recent response to a 1-°C step change in the set point is shown in Fig. 2. This is under no RF power.

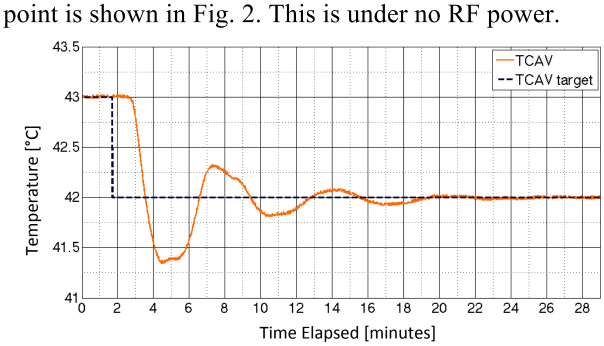

Figure 2: A 1-°C step change under the existing PI controller. The oscillations are due to water recirculation.

*Operated by Fermi Research Alliance, LLC under Contract No. De-AC02-07CH11359 with the United States Department of Energy.
#auralee.morin@colostate.edu

Content from this work may be used under the terms of the CC BY 3.0 licence (© 2015). Any distribution of this work must maintain attribution to the author(s), title of the work, publisher, and DOI.

ISBN: 978-3-95450-168-7 doi:10.18429/JACoW-IPAC2015-MOPWI029

ELECTRON BOMBARDMENT OF ZnTe EO BUNCH CHARGE DETECTOR FOR SIGNAL LIFETIME STUDIES IN RADIATION ENVIRONMENT

J. Williams, S. Biedron, S. Milton CSU, Fort Collins, CO 80523, USA
S. Benson, S. Zhang, JLab, Newport News, VA 23606, USA

Abstract

Electro-optic(EO) detection of bunch charge distribution utilizing the nonlinear Pockel's and Kerr effect of materials has been implemented at various facilities as a method of passive detection for beam preservation throughout characterization[1-12]. Most commonly, the inorganic II-VI material ZnTe is employed due to its strong Pockel's EO effect and relatively high temporal resolution (~90 fs)[2]. Despite early exploration of radiation damage on ZnTe in exploration of semi-conductor materials in the 1970's, full characterization of EO response over radiation exposure lifetime has yet to be performed. The following paper presents a technique for ZnTe crystal characterization studies throughout radiation exposure at various energies and dosages by analyzing the changes in index of refraction including bulk uniformity, and THz signal response changes.

INTRODUCTION

The development of non-invasive charge distribution detectors based on the electro-optic properties of materials has seen various implementations at electron accelerators [1-4], and particularly in free-electron laser facilities. Though there are various electro-optic detector arrangements that range in method of data encoding and measurement, the typical electro-optic bunch detector is arranged to measure the passing profile of the electric field of relativistic electron bunches by probing the polarization shift in the electro-optic material with a synched laser. This polarization shift arises out of the electro-optic effect induced in a particular material (e. g. ZnTe, GaP, DAST, etc) by the strong electric field of the passing bunches. These EO-materials have a high 1st order non-linear coefficient, resulting in an index of refraction anisotropy that is linearly proportional to the applied field.

In contrast to the previously referenced facilities which employ EO detectors, the JLab and CSU facilities operate at a higher average current. It is suspected that this higher average current environment may present a greater hazard to the crystals. Studies that look into damage induced by either the probing laser beam or radiation environment seen by the materials within the accelerator vacuum are limited [5] and thus so is a direct correlation between detector signal and crystalline lattice defects induced while in operation. In order to develop a thorough understanding of signal properties throughout an EO material's lifetime, studies of material lattice properties (index of refraction, electro-optic coefficient, etc) before and after bombardment by electrons of various energies and at varying doses is laid out in this paper.

METHODS

It is planned that a picture of the material properties throughout its lifetime within an accelerator environment can be simulated through exposure of the materials to electron beams of various energies (2-16 MeV) at varying doses. The exposed materials will be characterized before and after exposure using an assortment of optic analysis tools to get a thorough picture of the complex index of refraction, electro-optic coefficient, and any other perturbations of the original material properties. This information will help develop an accurate picture of material response throughout its lifetime and help to deconvolve signal error arising from defects within the material itself or other sources.

Exposure Procedure

Exposure is planned on an operational cancer therapy machine with available electron beam energies between 2-16 MeV and various dosing rates. The crystals will be placed at a proper distance and covered by a suitable amount of material to deposit the beams' energy at the desired location within the crystals.

As different defects may arise at different energies and intensities, a different crystal sample will be exposed for each electron beam energy. After each dosing, optical characterization of the materials will help paint a picture of material properties over lifetime within a radiation environment.

Material Characterization

Prior to exposing these materials, a complete picture of material optical properties will be assessed using an assortment of optical diagnostics. The complex index of refraction, its homogeneity throughout the material, absorption and luminescence spectra, and electro-optic response are to be measured using an ellipsometer, Mach-Zehnder interferometer, absorption and luminescence spectrometers, and a THz-kit, respectively. The purpose and data produced by the various devices is outlined below:

- ***Ellipsometer*** -Produces a map of the complex index of refraction for the materials over a range of wavelengths (200-2000nm). Both transmission and reflection geometries for both faces is planned. Changes in the complex index of refraction may be

Content from this work may be used under the terms of the CC BY 3.0 licence (© 2015). Any distribution of this work must maintain attribution to the author(s), title of the work, publisher, and DOI.

ISBN: 978-3-95450-168-7 doi:10.18429/JACoW-IPAC2015-MOPWI030

LOW EMITTANCE TUNING WITH A WITNESS BUNCH *

D. Rubin, R. Meller, J. Shanks
CLASSE, Ithaca, NY 14850

Abstract

Electron positron damping rings and colliders will require frequent tuning to maintain ultra-low vertical emittance. Emittance tuning begins with precision beam based measurement of lattice errors (orbit, transverse coupling, and dispersion) followed by compensation with corrector magnets. Traditional techniques for measuring lattice errors are incompatible with simultaneous operation of the storage ring as light source or damping ring. Dedicated machine time is required. The gated tune tracker (the device that drives the beam at the normal mode frequencies) and the bunch-by-bunch, turn-by-turn beam position monitor system developed at CESR are integrated to allow synchronous detection of phase. The system is capable of measuring lattice errors during routine operation. A single bunch at the end of a train of arbitrary length, is designated as the witness. The witness bunch alone is resonantly excited, and the phase and amplitude of the witness is measured at each of the 100 beam position monitors. Lattice errors are extracted from the measurements. Corrections are then applied. The emittance of all of the bunches in the train is measured and the effectiveness of the correction procedure demonstrated.

INTRODUCTION

Ultra-low vertical emittance is essential to achieve high luminosity in electron/positron colliders. In a linear collider, the sources of the low emittance beams are the damping rings. The vertical emittance specification for the International Linear Collider is 2pm-rad (at 5GeV) [1]. In circular colliders, the equilibrium emittance of the electron and positron storage rings likewise determines the luminosity. In SuperKEKB the vertical emittance target is 1.5pm-rad (7GeV) [2].

The principle source of vertical emittance in collider damping rings is misalignment of the guide field magnets. Transverse coupling is generated by tilted quadrupoles, and vertical dispersion by tilted dipoles and displaced quadrupoles. Low emittance tuning is the procedure to minimize the effects of the misalignments. The sources of dispersion and coupling are determined with beam based measurements. Corrector magnets are then deployed to compensate those sources. The emittance targets for both ILC and SuperKEKB have been achieved in storage rings (mostly light sources) with emittance tuning [3] [4].

Traditional emittance tuning procedures require dedicated machine time for the beam based measurements. Instrumentation has been developed at CESR for beam based measurements based on a single witness bunch, and thus allow continuous monitoring of coupling, betatron phase advance, dispersion, and orbit during normal operation. Lattice parameters are measured and corrector strengths adjusted without interruption. The witness bunch (perhaps the bunch at the end of a train) is resonantly excited at horizontal, vertical and, in principle, longitudinal normal mode frequencies, and the turn by turn position of the bunch measured at each of the 100 beam position monitors (BPMs) in the storage ring. The phase and amplitude of the response at the resonant frequencies characterizes the lattice functions.

BEAM BASED MEASUREMENT OF LATTICE PARAMETERS

The lattice properties are determined by measuring the linear mapping (transfer function) between BPMs. The mapping is extracted from measurements of a large number of non-degenerate trajectories. In the orbit response method (ORM) [5] [6], the distinct trajectories are generated by varying the strength of horizontal and vertical dipole correctors to create a matrix of position versus corrector. Typically there are many more measurements than BPMs and the system is overconstrained. The matrix is inverted by singular value decomposition to yield transfer functions. The ORM method is very powerful and can provide information about the calibration of the dipole correctors and beam position monitors as well as the linear transfer function from one BPM to the next. However, the measurements are incompatible with normal operation. Dedicated machine time is needed to make the orbit measurements. The measurements can be time consuming, as each steering must be varied sequentially and orbits collected at each step. Finally, the measurement time will scale with the circumference (or at least the number of beam position monitors and corrector magnets) of the ring.

In a storage ring equipped with BPMs capable of turn-by-turn position measurements, the set of non-degnerate trajectories can be collected much more quickly. A bunch can be excited simultaneously at the three normal mode tunes (horizontal, vertical, and longitudinal) by fast kickers, with width less than the minimum bunch spacing. (Two tune trackers are presently implemented in CESR, thus limiting simultaneous measurement to two of the three planes.) In CESR the bunch-by-bunch feedback kickers are used to drive the beam. As long as the betatron and synchrotron tunes are non integer, each turn will provide a distinct trajectory and each is recorded by the BPMs. The linear mapping between BPMs is extracted from the trajectory data as before. The signal noise is reduced by filtering the data at the normal mode tunes. In particular, an amplitude and phase is identified at each of the four BPM electrodes, for each of the

* Work supported by the National Science Foundation PHY-0734867 and PHY-1002467 and Department of Energy DE-FC02-08ER- 41538 and DE-SC0006505

Content from this work may be used under the terms of the CC BY 3.0 licence (© 2015). Any distribution of this work must maintain attribution to the author(s), title of the work, publisher, and DOI.

ISBN: 978-3-95450-168-7 doi:10.18429/JACoW-IPAC2015-MOPWI031

MICROWAVE MODELING FOR ELECTRON CLOUD DENSITY MEASUREMENTS AT CESRTA*

J.P. Sikora†, Y. Li, CLASSE, Ithaca, New York 14853 USA
S. De Santis, LBNL, Berkeley, California 94720 USA

Abstract

The electron cloud (EC) density in accelerator beam-pipe has been measured using resonant microwaves. The resonances are produced by changes in beam-pipe geometry that generate reflections and standing waves, with typical behavior being similar to a section of waveguide with shorted ends. The technique uses fact that the EC density will shift the resonant frequencies. In previous analysis, we have made the simplifying approximation that the standing waves are multiples of a half-wavelength and that the magnitude of the electric field is symmetric about the longitudinal center of the resonance. In this paper we show that some changes in beam-pipe geometry will result in asymmetric electric field magnitudes along the resonant length. When this is combined with an EC density that varies along this length, the magnitude of the frequency shift will be altered. We present our initial attempt to correct for this effect by modeling the existing beam-pipe using CST Microwave Studio® to obtain a more realistic electric field distribution. This correction is then applied to data taken with beam at several resonant frequencies. The measurements were made at the Cornell Electron Storage Ring (CESR), which has been reconfigured as a test accelerator (CESRTA) providing electron or positron beams ranging in energy from 2 to 5 GeV.

INTRODUCTION

The resonant microwave technique for measuring electron cloud (EC) density has been developed at Cornell over the past several years. Beam-pipe resonances are produced by microwave reflections – a common source being the longitudinal slots at the location of ion pumps, which interrupt the transverse currents of TE waves. The resonant response is obtained by coupling microwaves in/out of the beam-pipe using beam position monitor (BPM) buttons. The measurement technique uses the fact that the beam-pipe's natural frequency ω_0 will be shifted an amount $\Delta\omega$ by the presence of an electron cloud density n_e according to Eq. 1, where E_0 is the magnitude of the resonant electric field, e and m_e are the charge and mass of an electron, ε_0 is the vacuum permittivity and V the resonant volume.

$$\frac{\Delta\omega}{\omega_0} \approx \frac{e^2}{2\varepsilon_0 m_e \omega_0^2} \frac{\int_V n_e E_0^2 \, dV}{\int_V E_0^2 \, dV} \tag{1}$$

An outline of the technique is given in Ref. [1]. In that initial presentation, the simplifying assumption is made that the EC density n_e is uniform over the resonant volume. Equation 1 shows that under these conditions, the resonant field does not need to be known, since the integrals will cancel.

A model for the beam-pipe is a section of waveguide with its ends shorted. The resonant frequencies correspond to m half wavelengths with an envelope $E_0 sin[m\pi(z/L)]$, where m is an integer ≥ 1, z is the location along the beam-pipe and L is the length of the resonant section. This will have resonances at frequencies given by

$$f^2 = f_c^2 + (mc/2L)^2 \tag{2}$$

with f_c the waveguide cutoff frequency and c the speed of light. There is one location, 43E in CESR, where the measured response follows Eq. 2 reasonably well. At that location there is a set of BPM buttons between two ion pumps (with longitudinal slots) and no other changes in geometry. Using Eq. 2, the cutoff frequency f_c of the CESR aluminum beam-pipe extrusion was determined to be 1.8956 GHz. However elsewhere in the storage ring, the beam-pipe resonances do not match this series of frequencies very well. Figure 1 shows the physical layout at the location 15E in CESR, along with the beam-pipe response. The triangles at the top of the plot show the resonant frequencies expected based on the 1.8956 GHz cutoff frequency of the extrusion and the 2820 mm distance between the ion pumps. The larger dark triangle is the cutoff frequency f_c. Dotted lines on the plot connect the observed resonances with the frequencies expected with a shorted waveguide. The first resonance is well below the beam-pipe cutoff frequency.

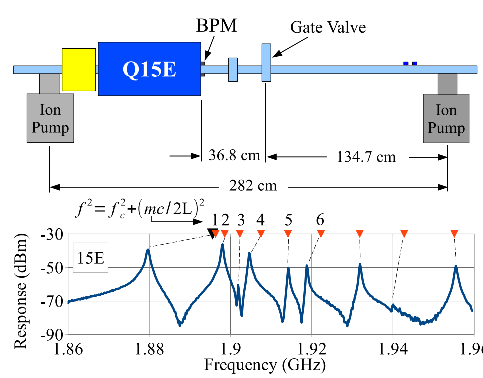

Figure 1: Sketch of the beam-pipe section at 15E along with its resonant response. Triangles show the predicted frequencies for a simple shorted waveguide. Dotted lines connect those frequencies with the measured response peaks.

* This work is supported by the US National Science Foundation PHY-0734867, PHY-1002467 and the US Department of Energy DE-FC02-08ER41538, DE-SC0006505.
† jps13@cornell.edu

Content from this work may be used under the terms of the CC BY 3.0 licence (© 2015). Any distribution of this work must maintain attribution to the author(s), title of the work, publisher, and DOI.

ISBN: 978-3-95450-168-7 doi:10.18429/JACoW-IPAC2015-MOPWI032

ANALYSIS OF PRIMARY STRIPPER FOILS AT SNS BY AN ELECTRON BEAM FOIL TEST STAND

E.P. Barrowclough, C.S. Feigerle, University of Tennessee, Knoxville, TN 37996, U.S.A.
C.F. Luck, L.L. Wilson, R.W. Shaw, M.A. Plum, Oak Ridge National Laboratory, Oak Ridge, TN 37831, U.S.A.

Abstract

Diamond foils are used at the Spallation Neutron Source (SNS) as the primary strippers of hydride ions. A nanocrystalline diamond film, typically 17 x 45 mm with an aerial density of 350 µg/cm^2, is deposited on a corrugated silicon substrate using plasma-assisted chemical vapor deposition. After growth, 30 mm of the silicon substrate is etched away, leaving a freestanding diamond foil with a silicon handle that can be inserted into SNS for operation. An electron beam test facility was constructed to study stripper foil degradation and impact on foil lifetime. The electron beam capabilities include: current up to 5 mA, 0.300 mm^2 focused spot size, and rastering in the x- and y-directions. A 30 keV and 1.6 mA/mm^2 electron beam deposits the same power density on a diamond foil as a 1.4 MW SNS beam. Rastering of the electron beam exposes a similar area of the foil as SNS beams. Experiments were conducted using the foil test stand to study: foil flutter and lifetime; effects of corrugation patterns, aerial densities, foil crystallite size (micro vs. nano), and boron doping; temperature distributions and film emissivity; and conversion rate of nanocrystalline diamond into graphite.

BACKGROUND

Diamond stripper foils have been developed at Oak Ridge National Laboratory (ORNL) for use within the SNS since 2003 [1-2]. The foils are grown on a semiconductor grade (100) silicon wafer using plasma-assisted chemical vapor deposition, and include nanocrystalline diamond, microcrystalline diamond, and occasionally boron-doped nanocrystalline diamond. The design size and aerial density of the foils have varied greatly over the years, with the current size and aerial density being a 17 mm x 45 mm and 350 µg/cm^2. This aerial density corresponds to a diamond film of approximately 1.0 µm thick. Once the foils are grown, 30 mm of the silicon substrate is chemically etched away to leave a free-standing portion of diamond at the bottom of the foil that is 17 mm x 30 mm and a silicon handle at the top that is 17 mm x 15 mm. A variety of lithography patterns are implemented on the silicon growth surface that transfers into the conformal to help give the needed rigidity and flatness when the silicon substrate is etched away. The growth and processing of these diamond foils has been optimized and routinely produces high quality stripper foils for use within the SNS.

The current status of SNS is providing researchers with a pulsed beam of 0.94 GeV, 1.0 to 1.4 MW, at a pulse rate and width of 60 Hz/975 µs. In the past few years, several obstacles have delayed the progress of SNS to provide a constant design value of 1.4 MW. These obstacles are the result of growing pains of a decade old machine. Some examples that SNS employees have faced in recent months include multiple mercury target failures; water contamination in various portions of the linac; multiple components that have either failed completely or have limited operation; issues with foil brackets; and the rare foil failure. Despite these issues, SNS employees have been able to successfully diagnosis and resolve these problems.

In order to further develop the foil program at ORNL and meet the growing needs of SNS, a team of researchers from ORNL, SNS, and the University of Tennessee (UTK) formed the Foil Development Team (FDT) in 2001. This group consists of both highly skilled technicians in foil growth and development, experts in chemical vapor deposition, and experts in accelerator physics. The mission of this group is to design and develop foils for use in the SNS to maintain current operating conditions of 1.0 to 1.4 MW, along with developing foils for future SNS upgrades to 2.0 and 3.0 MW. One aspect of this team that is of particular interest to this work is developing and characterizing a variety of foils to determine how well the foils will perform under SNS operating conditions. This includes the use of an electron beam test stand to help determine how foils will perform under various thermal loads experienced in the SNS.

FOIL TEST STAND

Since the SNS started full operation in 2006, it has been desirable to provide high reliability the various users coming from around the world. Therefore it was difficult to experiment with the different foil composition and types that were being developed, and it severely limited the foil development program. In 2009 the FDT deemed it necessary to develop a table top test stand that would allow a more adaptable approach to testing foil properties than what could be done during normal operation at SNS. This test stand would allow a variety of foils to be examined, along with determining the various properties that influence the success of a foil within the SNS. Since having an accelerated H$^-$ beam was not feasible as a table top source, a source was required that would both meet the size restriction but still apply the same thermal load that the foils experience actual operation. Therefore it was calculated that a 30 keV beam could apply a high enough current density to simulate the thermal load of the SNS. This device became known as the Electron Beam SNS

Content from this work may be used under the terms of the CC BY 3.0 licence (© 2015). Any distribution of this work must maintain attribution to the author(s), title of the work, publisher, and DOI.

ISBN: 978-3-95450-168-7 doi:10.18429/JACoW-IPAC2015-MOPWI033

Content from this work may be used under the terms of the CC BY 3.0 licence (© 2015). Any distribution of this work must maintain attribution to the author(s), title of the work, publisher, and DOI.

ADVANTAGES TO AN ONLINE MULTI-PARTICLE BEAM DYNAMICS MODEL FOR HIGH-POWER PROTON LINACS*

L.J. Rybarcyk#, X. Pang and S.A. Baily, LANL, Los Alamos, NM 87545, USA

Abstract

High-power proton linacs like the 800-MeV LANSCE accelerator typically use a physics-based approach and online single-particle and envelope beam dynamics models to establish nominal set points for operation. However, these models are not good enough to enable immediate transition to high-power operation. Instead, some amount of empirical adjustment is necessary to achieve stable, low beam-loss operation. At Los Alamos, we have been developing a new online model, which employs multi-particle beam dynamics, as a tool for providing more information and insight to the operations staff, especially during this transition to high-power operations. This presentation will discuss some of the advantages and benefits of using this type of tool in the tune-up and operation of a high-power proton linac.

INTRODUCTION

Examples of high-power proton linear accelerators (linacs) range from the relatively compact yet powerful LEDA CW RFQ that once demonstrated 670 kW of beam at 6.7 MeV [1] to a more extensive system like the SNS pulsed linac that has recently provided over 1.2 MW of beam at 940 MeV [2]. At present, the 800-MeV linac at the Los Alamos Neutron Science Center (LANSCE) operates at 120 Hz and provides proton and H^- beam macro-pulses, with a combined power of over 100 kW, to several target stations in support of basic and applied research. However, one thing that these and other high power linacs have in common is the need to minimize beam losses and the resultant deleterious effects on the structure and to the operation.

A physics-based tune-up approach is generally used to establish operational set points of beam-line devices in order to simultaneously produce beams with the desired characteristics and low loss. This approach utilizes online single-particle and beam-envelope models, e.g. [3-5], that enable the accelerator operations staff to set beam centroids and rms widths to their desired trajectories and matched sizes, respectively. However, at many high-power facilities, the model-based tuning is not the final solution. In addition, some amount of empirical loss-based tuning is required to achieve loss-levels necessary for sustained high-power operation [6].

It is this shortcoming with the existing approach that has motivated us to pursue a new online multi-particle beam dynamics model for our linac. A multi-particle model brings a higher level of realism and accuracy to the process and should begin to enable operations staff to reach a more complete tune-up solution as well as monitor on-going performance. Previously, multi-particle simulations were confined to offline analysis due to computational limitations. This new model [7], however, combines well-established beam dynamics algorithms and high-performance GPU technology in a workstation-class computer with access to the accelerator set points via the control system to provide rapid results of the actual linac operation to personnel 24/7. This new model can be operated in continuous mode, where the results are constantly being updated as machine variables are modified, or as a script-based tool to analyze measurement results or carry out beam simulations studies. In this paper we will explore some of the advantages of this new approach.

MODEL ADVANTAGES

A multi-particle beam dynamics model has several advantages over existing online single-particle and envelope models currently used on proton linacs. Some of these are features that machine designers have benefited from for years. First, the multi-particle model is not limited to simple beam representations but can utilize more realistic beam distributions. Secondly, important emittance growth mechanisms are included in the model. Thirdly, beam losses can now be included in evaluating machine settings. Fourthly, virtual measurements provide feedback on the effect of set-point adjustments and tuning. These benefits are discussed below.

Realistic Beam Distributions

The use of multi-particle distributions in modeling is especially advantageous in high-power proton linacs where transverse and longitudinal tails can contribute to beam losses. For example, at LANSCE each beam species is accelerated up to 750 keV using Cockcroft-Walton (C - W) technology. Following each C-W is a low-energy beam transport (LEBT) that contains a number of elements including quadrupole magnets and a single-gap 201.25-MHz buncher cavity. Just upstream of the 201.25-MHz drift-tube linac (DTL) the two beam species (H^+, H^-) are merged into a common LEBT that contains four matching quads and another identical buncher cavity. Since each C-W produces DC beam within a macropulse, the two RF cavities are used to prebunch these beams and increase the longitudinal capture in the DTL. This prebunching results in significant tails on the beam distributions. Shown in Fig. 1. are the simulated H^+ beam phase space distributions at the end of the LEBT. The input beam to the simulation is a combination of a transverse 4-D hypersphere, generated with Twiss

* Work supported by the United States Department of Energy, National Nuclear Security Agency, under contract DE-AC52-06NA25396.
#lrybarcyk@lanl.gov

ISBN: 978-3-95450-168-7 doi:10.18429/JACoW-IPAC2015-MOPWI034

ADAPTIVE ACCELERATOR TUNING *

Alexander Scheinker, LANL, Los Alamos, NM 87545, USA†

Abstract

A recently developed, model-independent feedback controller is presented, which is robust to measurement noise, and able to tune an arbitrary number of coupled parameters of an unknown system, simultaneously, based only on a user-defined cost function. Unlike genetic algorithms, which are a useful model-based tool for the optimization of a well known fixed system, the algorithm presented here is actually useful for implementation in hardware on actual machines as a feedback tuning and control loop, because it can compensate for the unknown time-varying disturbances/changes that all large machines experience. We present recent in-hardware experimental results obtained at the Los Alamos Neutron Science Center and at the Facility for Advanced Accelerator Tests (FACET), demonstrating the schemeÕs ability to simultaneously tune many parameters and its robustness to noise and system time-variation.

INTRODUCTION

Model-based schemes have been utilized for the design and optimization of particle accelerators, genetic algorithms (GA) in particular have become popular in recent years. When sufficient computer resources are available, lengthy GA searches have successfully found good starting points for machine designs by sampling a large parameter space. However, large complex machines are time-varying systems with time dependent, unpredictable disturbances and uncertainties including misalignments, thermal cycles, phase drifts, damage, and regions with limited beam measurements. Therefore, following a GA-based or any other model-based optimization approach, once an actual machine is constructed, many parameters have to be re-tuned, and re-tuned often as the system's characteristics drift with time.

When performing feedback on the beam or RF systems, there is a need for model-independent controllers which can handle the time-varying systems, especially for future accelerators such as MaRIE [1]. We present a model-independent feedback controller [2, 3], which is robust to measurement noise, and able to tune an arbitrary number of coupled parameters of an unknown system, simultaneously, based only on a user-defined cost function. The algorithm is especially useful for implementation in-hardware on actual machines as a feedback tuning and control loop, because it can compensate for the unknown time-varying disturbances/changes that all large machines experience.

OPTIMIZATION SCHEME

In an accelerator there are many important parameters

$$\mathbf{x}(t) = (x_1(t), \ldots, x_m(t)), \tag{1}$$

some of which are observable and others that can only be estimated or averaged, such as RMS beam width, various measures of emittance, beam current, etc... These evolve according to some complicated nonlinear, time-varying dynamics, such as

$$\frac{\partial \mathbf{x}(t)}{\partial t} = \mathbf{f}(\mathbf{x}(t), \mathbf{s}(t), \mathbf{p}(t), t), \tag{2}$$

where $\mathbf{f}(\mathbf{x}(t), \mathbf{s}(t), \mathbf{p}(t), t)$ is usually linearized or approximated in some other way so that the dynamics (2) can be numerically evaluated. In these dynamics there may be an arbitrary number of uncertain, uncontrollable, time-varying parameters

$$\mathbf{s}(t) = (s_1(t), \ldots, s_m(t)), \tag{3}$$

which include misaligned components, noise, disturbances, jitter, magnetic fields that depend on currents in an uncertain way due to hysteresis, and environmentally caused temperature variations which lead to phase drifts, to name a few, which makes the simulation of anything other than an estimate of of the actual system impossible. Also, there may be an arbitrary number of controlled parameters

$$\mathbf{p}(t) = (p_1(t), \ldots, p_n(t)), \tag{4}$$

including magnet current settings, phase and amplitude set points in RF systems, and control loop feedback gains, to name a few. The goal of the adaptive scheme presented here is the same as the goal of beam physicists and operators: the minimization of some chosen "cost" associated with accelerator performance such as the tuning of magnet and RF systems to minimize beam loss along the accelerator or to minimize the deviation of the final beam energy from a desired set point. The cost is some analytically unknown, but available for measurement function of the many controlled and uncontrolled parameters and states of the system, $C(\mathbf{x}(t), \mathbf{s}(t), \mathbf{p}(t), t)$. In practice, the actual cost, C, is rarely available for measurement, rather a noise-corrupted version $\hat{C} = C + n(t)$ is what arrives at the control system. The adaptive scheme is incredibly robust to random noise, the parameter tuning dynamics are

$$\frac{\partial p_i}{\partial t} = \sqrt{\alpha\omega_i} \sin\left(\omega_i t + k\left[\underbrace{C(\mathbf{x}, \mathbf{s}, \mathbf{p}, t) + n(t)}_{\hat{C}(\mathbf{x}, \mathbf{s}, \mathbf{p}, t)}\right]\right), \tag{5}$$

where $\omega_i \neq \omega_j$ for all $i \neq j$, which for large $\omega_i \gg 1$, results in average parameter dynamics

$$\dot{\bar{p}}_i = -\frac{k\alpha}{2}\frac{\partial C(\mathbf{x}, \mathbf{s}, \bar{\mathbf{p}}, t)}{\partial \bar{p}_i}, \tag{6}$$

a gradient descent which minimizes the *actual* C, not $\hat{C}$, as long as the noise is random, a result that is both mathematically proven and demonstrated in hardware [3, 5]. This

* This research was supported by Los Alamos National Laboratory.
† ascheink@lanl.gov

Content from this work may be used under the terms of the CC BY 3.0 licence (© 2015). Any distribution of this work must maintain attribution to the author(s), title of the work, publisher, and DOI.

ISBN: 978-3-95450-168-7 doi:10.18429/JACoW-IPAC2015-MOPWI035

Content from this work may be used under the terms of the CC BY 3.0 licence (© 2015). Any distribution of this work must maintain attribution to the author(s), title of the work, publisher, and DOI.

CHARACTERIZATION OF VISIBLE SYNCHROTRON RADIATION POLARIZATION AT SPEAR3*

Jeff Corbett and Andrew Kiss, SLAC National Accelerator Laboratory, Menlo Park, USA
Chunlei Li, East China University of Science and Technology, Shanghai, China
Mark Boland, Synchrotron Light Source Australia, Clayton, Australia

Abstract

Schwinger's equations predict the angular- and spectral distribution of synchrotron radiation across a wide band of the electromagnetic spectrum. Using a visible-light diagnostic beam line, it is possible to characterize the electric field polarization state as a function of vertical observation angle and compare with theory. Complications include accounting for σ- and π-mode transmission factors at mirror surfaces and precise alignment of the polarizing optics with the principle beam axes. The Stokes parameters are measured and beam polarization ellipse reported.

INTRODUCTION

Synchrotron radiation has both partially-coherent and fully polarized electromagnetic field properties, each used for a wide range of scientific research. With the advent of high-power, short-pulse free-electron lasers, applications depending on the spatial beam coherence are increasing at a rapid rate. Similarly elliptically polarized x-rays have become an increasingly powerful tool to study magnetic dichroism and chirality at both storage rings and FEL facilities. At SPEAR3, a visible-light diagnostic beam line originally constructed to study transverse and longitudinal electron beam dynamics has recently been used to study both the transverse spatial coherence [1] and polarization state of the beam [2].

The polarization state can be characterized by measuring beam power transmitted through linear polarizing elements oriented at systematic angles with respect to the beam axis. In this way is it possible to obtain 'slice' measurements of the beam polarization ellipse which can be combined to concisely express the beam polarization state in terms of the Stokes parameters [3,4]. Using the visible SR component, polarization measurements can be made with conventional optical elements in a relatively straightforward manner.

To cross-check the measurements it is also possible to calculate the Stokes parameters and corresponding beam polarization ellipse using Schwinger's equations for the SR field [5]. The 'classical' Schwinger equations express the electric field in terms of both radiation frequency and, conveniently, vertical observation angle. Hence it is possible to both measure and calculate the SR polarization state in the visible light regime as a function of vertical observation angle.

*Work sponsored by US Department of Energy Contract D E-AC03-76SF00515, Office of Basic Energy Sciences, China Scholarship Council and the Fulbright Scholarship Fund.
Corresponding author: corbett@slac.stanford.edu

SPEAR3 DIAGNOSTIC BEAM LINE

The visible-light diagnostic beam line at SPEAR3 contains a horizontal 'cold finger' to block the on-axis hard x-ray beam followed by a rhodium-coated mirror to horizontally reflect the SR light down the beam line [6]. The cold finger intercepts ±0.6 mrad of the beam at the midplane and the remaining beam line apertures have

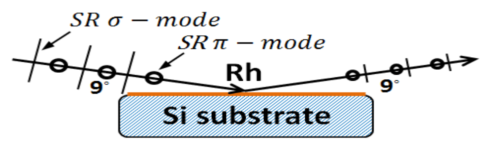

Figure 1: Visible light extraction mirror. Note *E*-field attenuation and relative phase shift upon reflection.

an acceptance of 3.5 mrad x 6 mrad. For measurements reported here only ±2.2 mrad was available in the vertical plane. As indicated in Fig. 1, the dipole-radiation SR beam hits the Rh mirror at a shallow angle of 9° causing attenuation and phase shift of the σ-mode (horizontal) and π-mode (vertical) visible light components.

For beam polarization measurements, we constructed a remote-controlled system with rotatable polarizer, 532nm bandpass filter (BP) and power meter all on a continuous-scan vertical stage [7]. An insertable quarter waveplate (QWP) shown in Fig. 2 is optically matched to the bandpass filter and used to determine beam helicity for Stokes parameter measurements [3, 4].

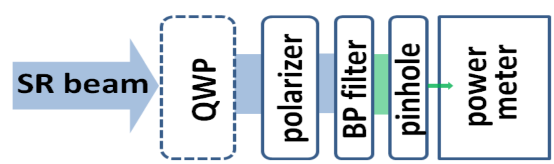

Figure 2: Stokes parameter measurement apparatus.

SR FIELD REPRESENTATION

The well-known Schwinger equations for synchrotron radiation express the SR radiation field in terms angular frequency ω and vertical emission angle $\psi^\dagger$ [5]

$$E_{x0} \triangleq \tilde{E}_\sigma(\omega,\psi) = C_0 K_{2/3}(\omega,\psi) \tag{1a}$$

$$E_{y0} \triangleq \tilde{E}_\pi(\omega,\psi) = C_0 \frac{-i\gamma\psi}{\sqrt{1+\gamma^2\psi^2}} K_{1/3}(\omega,\psi). \tag{1b}$$

where C_0 is a function of ω and ψ, γ is the electron beam Lorentz factor and K are modified Bessel functions.

†standard frequency and angle normalizations implied

ISBN: 978-3-95450-168-7 doi:10.18429/JACoW-IPAC2015-MOPWI036

INVESTIGATION OF CONTINUOUS SCAN METHODS FOR RAPID DATA ACQUISITION*

C. L. Li, East China University of Science and Technology, Shanghai 200237, China
A. M. Kiss#, SLAC National Accelerator Laboratory, Menlo Park, CA, 94025, USA
W. J. Zhang, University of Saskatchewan, Saskatoon S7N5A9, Canada

Abstract

It is common practice to perform spatially resolved X-ray data acquisition by automatically moving components to discrete locations and then measuring beam intensity with the system at rest. While effective, scanning in this manner can be time consuming, with motors needing to accelerate, move and decelerate at each location before recording data. Information between data points may be missed unless fine grid scans are performed, which accounts for a further increase of scan time. Recent advances in commercial hardware and software enables a continuous scan capability for a wide range of applications, which saves the start and end of step motors. To compare scanning performance, both step and continuous scan modes were examined using the SPEC command language with both commercial and in-house hardware. The advantages and limitations of each are discussed.

INTRODUCTION

Step scan data collection can be achieved by a motor moving with intermittent motion and the signal collected when the system is at rest. Several studies have been made with the step scan method to acquire data [1-4]. One advantage with this method is that high position precision can be achieved. It is also a direct and simple method to collect scan data. However, there are some disadvantages with the step scan method such as induced start/stop vibrations and an increase in data collection time.

Each data point during a step scan requires the detector to accelerate, move, and decelerate, causing vibrations. A settling time can be defined to allow vibrations to dampen but this will further increase the data collection time which is already increased by the need to start and stop the motors. For example, in a typical scan application a detector moves in angle from 0° to 60° with a step size of 0.01° so the data set contains 6,000 points. As acceleration and deceleration time is required to move the motor to each point, an extra 0.5 s must be allocated for each step of the scan [5]. An extra 3,000 s is therefore required to complete the scan. The extra time can be reduced if large step sizes are used during the experiment, but significant diffraction peaks may be missed. It is therefore desirable to minimize scan time while reducing vibrations in the system.

*Work supported by Department of Energy contract DE-AC02-76SF00515 and the China Scholarship Council.
andykiss@slac.stanford.edu

Continuous scanning on the other hand bypasses vibrational problems and reduces latency time. One technique that can benefit from a continuous scan is basic X-ray diffraction (XRD), often used to study the crystal structure of samples. A typical XRD experimental system is comprised of monochromatic X-rays, motion controller, a diffraction signal detector and a data processing system. The detector is moved along a path where the diffraction signal from the sample is distributed. The detector acquires an angle-dependent diffraction signal to analyse the electronic sample structure. In the past, several approaches to continuous scan measurements have been used for X-ray diffraction experiments [6-8].

This paper presents a new method for continuous scan measurements using SPEC as the command language with both commercial- and in-house motor controllers and detector read back electronics. The continuous scan mode is defined here as uninterrupted motor movement with continuous data acquisition. The motion of the detector can maintain a constant velocity or change velocity during the scan to account for changes in X-ray diffraction signal strength. As a result, vibrations in the system as well as total data acquisition time are reduced.

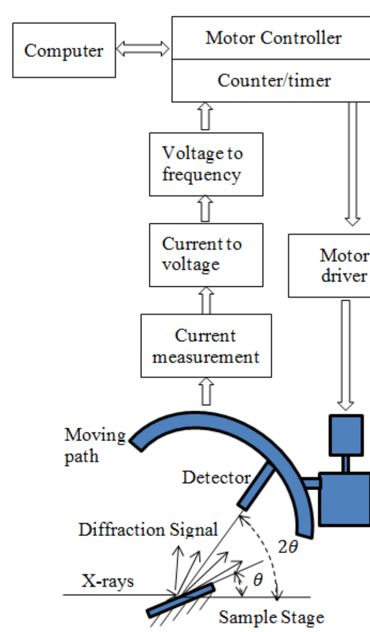

Figure 1: Schematic for the SSRL continuous scan XRD system.

Content from this work may be used under the terms of the CC BY 3.0 licence (© 2015). Any distribution of this work must maintain attribution to the author(s), title of the work, publisher, and DOI.

ISBN: 978-3-95450-168-7 doi:10.18429/JACoW-IPAC2015-MOPWI037

UPGRADE AND OPERATION OF THE DEMONSTRATION 4GS/SEC. INTRA-BUNCH INSTABILITY CONTROL SYSTEM FOR THE SPS *

J. E. Dusatko#, J. D. Fox, C. H. Rivetta, O. Turgut (SLAC National Accelerator Laboratory, Menlo Park, California USA), W. Höfle (CERN, Geneva Switzerland)

Content from this work may be used under the terms of the CC BY 3.0 licence (© 2015). Any distribution of this work must maintain attribution to the author(s), title of the work, publisher, and DOI.

Abstract

We present the expanded system implementation and operational experience details for the "Demo" technology platform commissioned at the SPS in January 2015. The system has been expanded during the LS1 shutdown with added features. The upgraded system has enhanced performance and more robust synchronization to the beam and accelerator timing system. Central to the new features are 1 GHz bandwidth kickers and RF amplifiers (including associated equalizers) which allow excitation and control of higher modes within the 2 ns bunch. We highlight the expanded features, and present their details.

BACKGROUND

Following the success of the initial run of the CERN LHC, the LHC injector complex is being upgraded to provide higher intensity and brightness beams to enable the discovery of new physics. As part of the LHC Injectors Upgrade (LIU) project, the entire injector chain from Linac4 to the SPS is being upgraded [1]. One performance limitation in the SPS is the formation of transverse vertical intra-bunch instabilities due to electron cloud instability (ECI) and transverse mode coupled bunch instability (TMCI) effects. These effects limit the intensity of the beam injected into the LHC.

A collaborative research and development project to mitigate these intra-bunch instabilities involving simulation and modelling [2], hardware development and measurement efforts has been undertaken. One outcome of this work has been the development of a feedback control demonstration system. This demonstration system has provided encouraging results [3] in Machine Development (MD) studies at the SPS, undertaken during LHC Run1, just prior to Long Shutdown 1. The next step in the evolution of the demonstrator system is the upgrade of several key components.

OVERVIEW OF SYSTEM

The feedback demonstrator or demo system [4] consists of multiple components as shown in the diagram of Figure 1. Items targeted for upgrades are indicated here as well. Vertical beam displacement is sensed using a stripline BPM pickup structure and the Δ output of a hybrid is filtered, equalized and amplified by the analog front end. The analog signal is then digitized by the feedback processor, which is essentially a reconfigurable high speed digital signal processor. Sampling at 4GSa/s the system takes 16 samples across a single 4ns SPS injection bunch. We treat these 16 samples or slices independently and process each with a separate 16-tap FIR filter inside the processor. The FIR coefficients are the same for each slice. The filtered data is translated back into the analog domain by a 4GSa/s DAC. The converted analog signal is presented to the analog back end where it is filtered, equalized, amplified and split before being sent to the power amplifiers and finally to the kicker structure which applies a corrective field to the beam.

Additional components include the frequency multiplier which generates the 2GHz sample clock (both edges are used, giving 4GHz effectively) from the 200MHz SPS RF reference. And the excitation system which allows us to generate a perturbation signal onto the beam for driven motion studies. Finally, a set of adjustable delay lines are required to provide phase alignment of the timing of the beam arrival with the sampling operation at the pickup and the application of correction and excitation signals with beam in the kicker.

WORK TO DATE

The demo system platform in being upgraded in two phases as described in [5], [6]. Phase 1 upgrades include mitigation of ADC spectral lines driven by noise pickup and ground loops inside the feedback processor chassis. Improvements in the timing and synchronization of the reference and sampling clocks; and the migration of the excitation function to inside the feedback processor, allowing feedback and excitation signals to be summed digitally. Phase one upgrades have been completed, while phase 2 work is now underway. These include the expansion of processing beyond one bunch to handle 16 bunches. As well as the addition of an orbit offset compensation mechanism to dynamically remove the beam orbit offset, which limits the overall dynamic range of the system. Beyond these, some additional features and improvements have been and are being made to the feedback processor. Central to the effectiveness of the feedback system are the RF power amplifiers and kicker structure, which are also being upgraded.

UPGRADES

Feedback Processor

The feedback processor was built to initially process a single SPS bunch at injection. The system is being expanded to handle multiple bunches with processing occurring is a parallel, pipelined manner. The ADC snapshot memory currently uses internal FPGA SRAM limiting capture lengths to 32000 turns. An upgrade

*Work supported by the U.S. Department of Energy under contract DE-AC02-76SF00515 and the US LHC Accelerator Research program (LARP)
#jedu@slac.stanford.edu

ISBN: 978-3-95450-168-7 doi:10.18429/JACoW-IPAC2015-MOPWI041

IDENTIFICATION OF INTRA-BUNCH TRANSVERSE DYNAMICS FOR MODEL BASED WIDEBAND FEEDBACK CONTROL AT CERN SUPER PROTON SYNCHROTRON*

O.Turgut†, C. Rivetta, J. Dusatko and J. D. Fox, SLAC, Menlo Park, CA 94305, USA
W, Hofle, CERN, Geneva, Switzerland

Abstract

Multi-input multi-output (MIMO) feedback design techniques can be helpful to stabilize intra-bunch transverse instabilities induced by electron-clouds or transverse mode couplings at the CERN Super Proton Synchrotron (SPS). These MIMO techniques require a reduced order model of intra-bunch dynamics. We estimate a linear reduced order MIMO models for transverse intra-bunch dynamics and use these models to design model based MIMO feedback controllers. The effort is motivated by the plans to increase currents in the SPS as part of the HL-LHC upgrade. Parameters of the reduced order models are estimated based on driven beam SPS measurements. We study different types of controllers. We test the model based designs using macro particle simulation codes (CMAD and HEADTAIL) and compare its performance with FIR filters tested during beam measurements of the feedback system in SPS machine development (MD) studies.

INTRODUCTION

Electron clouds and machine impedance can cause intra-bunch instabilities at the CERN Super Proton Synchrotron (SPS). The high current operation of the SPS for LHC injection requires mitigation of these problems. Modern control techniques can be used to stabilize the bunch. These techniques are powerful tools allowing us to evaluate and understand the performance and the limits of the system beforehand. Yet, they require reduced order models of intra-bunch dynamics to design optimal or robust controllers. System identification techniques can be used to get these required reduced order models.

The feedback system senses the vertical positions at multiple locations within the nanosecond-scale bunch. Control filters use these measurements to calculate correction signals and apply them back onto the bunch using the kicker as an actuator. A 4 Gs/Sec. digital feedback system has been developed to process the motion signals and generate the correction actions [1]. Due to the very fast intrinsic time requirement of the system, a parallel computation control filter architecture has been used developed.

In this paper, we show the use of system identification techniques to estimate parameters of linear models representing single bunch dynamics. We define the form of the reduced order model. We show an example of identification applied to data from SPS measurements. We use reduced order models to design model based controllers. We compare a model based IIR controller with an existing FIR filter for a specific case using nonlinear macro particle simulation codes.

REDUCED ORDER MODEL AND IDENTIFICATION

Any linear dynamical system can be represented in state space matrix form. A discrete time system sampled at every revolution period k with p inputs and q outputs is represented by

$$\begin{aligned} X_{k+1} &= AX_k + BU_k \\ Y_k &= CX_k \end{aligned} \tag{1}$$

where $U \in R^p$ is the control variable (external excitation), $Y \in R^q$ is the vertical displacement measurement, $A \in R^{n\times n}$ is the system matrix, $B \in R^{n\times p}$ is the input matrix, and $C \in R^{q\times n}$ is the output matrix. For a MIMO system, the model order n determines the complexity.

$$Y(z) = \left[D^{-1}(z)N(z)\right] U(z) \tag{2}$$

where [] represents the transfer function matrix ($\in R^{q\times p}$) for a system with p inputs and q outputs in z domain. $D(z)$ and $N(z)$ represent denominator and numerator of discrete time transfer function matrix between input-output couples.

$$\left[N_r \mid -D_r\right] \begin{bmatrix} U(k) \\ Y(k) \end{bmatrix} = 0 \tag{3}$$

Given the input $U(k)$ and output $Y(k)$ signals, the estimation of the transfer function coefficient matrices N_r and D_r is obtained by solving the last linear equation using time domain data. Assuming full observability of the system, we can represent our state space in discrete time observable canonical form. This enables us to represent the system with the minimum number of model parameters [2] [3] [4].

SPS Measurements - Bunch Dynamics Identification

Multiples MDs have been conducted at the CERN SPS ring driving the bunch with different excitations (open loop) and testing feedback controllers to stabilize the bunch dynamics (closed loop). Those measurements were conducted using a single bunch in the machine with intensities of about $1-2\times10^{11}$ protons at the injection energy, 26 GeV and Q26 lattice configuration.The driven tests with different excitation signals have been designed such that the kicking signal

* Work supported by the U.S. Department of Energy under contract DE-AC02-76SF00515 and the US LHC Accelerator Research program (LARP).
† oturgut@stanford.edu

Content from this work may be used under the terms of the CC BY 3.0 licence (© 2015). Any distribution of this work must maintain attribution to the author(s), title of the work, publisher, and DOI.

ISBN: 978-3-95450-168-7 doi:10.18429/JACoW-IPAC2015-MOPWI044

BEAMLINE INSERTIONS MANAGER AT JEFFERSON LAB *

M. Johnson†, Jefferson Lab, Newport News, VA, 23606

Abstract

The beam viewer system at Jefferson Lab provides operators and beam physicists with qualitative and quantitative information on the transverse electron beam properties. There are over 140 beam viewers installed on the 12GeV CEBAF accelerator. This paper describes an upgrade consisting of replacing the EPICS based system tasked with managing all viewers with a mixed system utilizing EPICS and high level software. Most devices, particularly the beam viewers, cannot be safely inserted into the beam line during high-current beam operations. Software is partly responsible for protecting the machine from untimely insertions. The multiplicity of beam-blocking and beam-vulnerable devices motivate us to try a data-driven approach.

The beamline insertions application components are centrally managed and configured through an object-oriented software framework created for this purpose. A rules-based engine tracks the configuration and status of every device, along with the beam status of the machine segment containing the device. The application uses this information to decide on which device actions are allowed at any given time.

VIEWER SYSTEM

CEBAF Operations at Jefferson Lab run continuously 24/7 to support a program of experimental physics and accelerator studies. Control system software supports this effort in part by providing operators with the tools needed to diagnose and resolve issues with accelerator hardware and instrumentation. The software system that controls the insertion and retraction of viewers and other devices, dubbed "Insertables", has been rewritten using object-oriented programming methods and deployed to give operators and support personnel the ability to diagnose and resolve problems at all hours.

This new software system provides better encapsulation, separating device configuration from device behavior. A comprehensive view of insertable beamline components makes it easier to find configuration anomalies, such as device channel assignments that do not follow established patterns. Device failures during off hours have been diagnosed using debug screens and resolved quickly. Overall, faster problem diagnosis and resolution has resulted in a reduction in down time caused by this type of component.

In the following sections, we describe the context, requirements, and techniques employed in implementing this system.

Figure 1: Beam Spot on Viewer

SOFTWARE REQUIREMENTS

The operation of the CEBAF accelerator at Jefferson Lab relies on a wide variety of devices which must be physically inserted into the beam line when needed. Beam viewers measure beam profile and provide information about transverse beam characteristics. Faraday cups measure beam intensity at several points around the accelerator. Insertable dumps provide device protection and control of beam transport to the experimental end stations. These devices and a variety of others are critical to the delivery of a precisely tuned electron beam.

To support this heterogeneous and frequently changing hardware configuration, the software system must:

- Provide a hardware-domain description of each device in a format useful to engineers
- Reduce the duty-cycle of the beam in response to a request to insert a vulnerable device
- Change device-protection strategy when accelerator zones change between active and inactive.
- Allow an inactive experimental end-station to work with viewers without interfering with an active experiment
- Respond to unauthorized device motion by protecting the machine
- Track device motion and find faults in behavior (broken switches, inactive actuators)

---

* Notice: This manuscript has been authored by Jefferson Science Associates, LLC under Contract No. DE-AC05-06OR23177 with the U.S. Department of Energy. The United States Government retains and the publisher, by accepting the article for publication, acknowledges that the United States Government retains a non- exclusive, paid-up, irrevocable, world-wide license to publish or reproduce the published form of this manuscript, or allow others to do so, for United States Government purposes.

† michaelj@jlab.org

Content from this work may be used under the terms of the CC BY 3.0 licence (© 2015). Any distribution of this work must maintain attribution to the author(s), title of the work, publisher, and DOI.

ISBN: 978-3-95450-168-7 doi:10.18429/JACoW-IPAC2015-MOPWI045

THE CEBAF ELEMENT DATABASE AND RELATED OPERATIONAL SOFTWARE*

T. Larrieu, M. Joyce, M. Keesee, C. Slominski, R. Slominski, D. Turner
JLAB, Newport News, VA 23606, USA

Abstract

The newly commissioned 12GeV CEBAF accelerator relies on a flexible, scalable and comprehensive database to define the accelerator. This database, coined the CED (CEBAF Element Database) delivers the configuration for CEBAF operational tools, including hardware checkout, the downloadable optics model, control screens, and much more. The presentation will describe the flexible design of the CEBAF Element Database (CED), its features and assorted use case examples.

BACKGROUND

The Jefferson Lab CEBAF accelerator is a superconducting recirculating linear accelerator capable of delivering continuous wave electron beams simultaneously to multiple experimental halls. Previously capable of delivering 6GeV, CEBAF recently underwent an extensive multi-year $338M upgrade project to double its energy capacity to 12GeV and add a fourth experimental hall (Fig. 1). The upgraded accelerator was commissioned successfully between November 2013 and May 2014. The CEBAF Element Database (CED) was an indispensable tool during the commissioning.

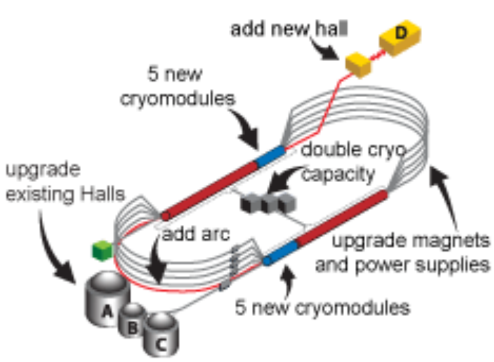

Figure 1: The CEBAF 12GeV Upgrade Project.

DATABASE DESIGN

The CED design is based upon a modified Entity-Attribute-Value with Classes and Relationships (EAV/CR) data model [1]. Whereas in a traditional schema adding support for new accelerator hardware would involve adding additional tables and columns to the database, the EAV/CR data model employed by the CED is introspective – defining a new class of accelerator hardware in the CED simply involves adding rows to the already-existing metadata "catalog" tables. Once defined in the catalog, existing software is fully capable of interacting with the new entities after discovering their properties from the metadata tables.

A major benefit of the EAV/CR data model is that its static schema is well suited to integration with Oracle Workspace Manager [2] to provide timestamp-based versioning of table rows, named save points, and multiple independent workspaces (akin to branches in a software version control system).

DATABASE IMPLEMENTATION

Layout

To optimize performance for the different use cases, the CED database instance is distributed among three database users/schemas as shown in Figure 2. The operational schema stores the current machine configuration and is optimized for performance. The historical schema provides efficient storage and access to (read-only) historical save points (snapshots). And the development schema is used to create workspace branches where data can be edited and prepared before being promoted to the operational schema.

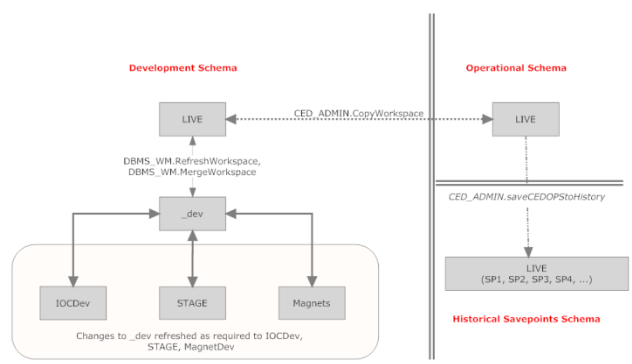

Figure 2: The CED three schema layout.

The details of the three schema layout are transparent to non-administrative users who need simply specify an optional workspace or savepoint name when interacting with the database.

Workspaces

As a rule, users do not directly edit data in the operational schema. Instead, updates are prepared in a development workspace and merged into OPS upon request. A database administrator receiving a merge request will audit the proposed changes for validity and then promote the changes to the operational schema. Administrators make use of a web-based management

* Notice: Authored by Jefferson Science Associates, LLC under U.S. DOE Contract No. DE-AC05-06OR23177. The U.S. Government retains a non-exclusive, paid-up, irrevocable, world-wide license to publish or reproduce this manuscript for U.S. Government purposes.

Content from this work may be used under the terms of the CC BY 3.0 licence (© 2015). Any distribution of this work must maintain attribution to the author(s), title of the work, publisher, and DOI.

ISBN: 978-3-95450-168-7 doi:10.18429/JACoW-IPAC2015-MOPWI046

eDT AND MODEL-BASED CONFIGURATION OF 12 GeV CEBAF *

D. Turner, Jefferson Lab, Newport News, VA 23606, USA

Abstract

This paper discusses model-driven setup of the Continuous Electron Beam Accelerator Facility (CEBAF) for the 12GeV era, focusing on the `elegant` Download Tool (`eDT`). `eDT` is a new operator tool that generates magnet design setpoints for various machine energies and pass configurations. `eDT` was developed as a tool to facilitate reducing machine configuration time and reproducibility by way of an accurate accelerator model.

MOTIVATION

An accurate accelerator model is critical for accelerator operations, as it enables comparisons of expected and observed beam behavior and helps identify root causes of discrepancy [1]. A well-modeled machine ensures predictability and reproducibility.

CEBAF supports a highly dynamic nuclear physics program. Energy and pass changes occur rather frequently. In an extreme case, we performed eleven pass changes and three energy changes in a one month period. Reducing tune time is crucial for such a program. An infrastructure of tools and procedures that systematically identify differences between the machine and the model will permit convergence which will lead to reductions in tune time, faster recovery from failures, and a better understanding of CEBAF 12GeV accelerator controls and dynamics.

`eDT` is a major component of the new infrastructure and operational paradigm supporting model-driven setup and operation of 12GeV CEBAF. `eDT` computes magnet design setpoints directly from the CEBAF model and applies them to the machine.

OVERVIEW OF CEBAF

CEBAF is a 5.5-pass, 12GeV continuous wave (CW) electron accelerator. It utilizes a photoinjector source capable of delivering greater than 85% spin polarization. CEBAF is comprised of two anti-parallel superconducting RF linacs connected by two sets of recirculation arcs. Jefferson Lab recently completed the upgrade of CEBAF from a 5-pass, 6GeV machine to 5.5-pass, 12GeV. See Fig. 1.

MACHINE SETUP DURING THE 6GeV ERA

Operators would initially configure the machine for a given energy and passes by using a software tool which scaled machine settings from previous configurations which were believed to be well-tuned. This usually didn't work without excessive tuning time as the machine was not modeled well and the magnet mapping was incomplete. The mode of operations would then be a cycle of tweaking, measuring, and tweaking again. Using these methods, pass and energy changes would take from several hours to several shifts.

During 6GeV, there was no central source for configuration control. Occasionally, hardware changes did not propagate to operator tools and screens. There was also no feedback into the model. The model was not updated to reflect operational experience.

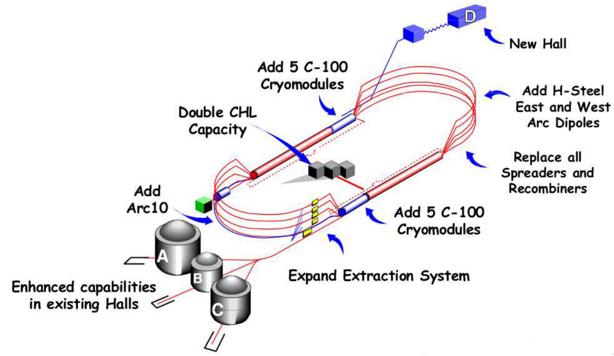

Figure 1: Scope of the 12GeV CEBAF upgrade.

MACHINE SETUP FOR 12GeV

To address the problems with configuring and modeling CEBAF, the CEBAF Modeling Team was formed to establish tools and procedures for model-driven configuration for 12GeV [1]. The Modeling team meets weekly while CEBAF is running, and semiweekly during scheduled maintenance periods.

The Modeling Team switched to `elegant` [2] to model CEBAF. `elegant` is a 6-D accelerator simulation code that does particle tracking, optimization, synchrotron radiation, scattering, and others. It is open-source code developed at the Advanced Photon Source (APS) at Argonne National Laboratory and it is actively maintained and continuously improved by both APS and the worldwide accelerator community. It has a large user base and it is more "industry standard" than the `OptiM` or `Art++` modeling tools previously used at CEBAF [6]. `elegant` is a command line tool that works well behind the scenes as an engine to drive operator tools. `elegant` is parallel capable for large scale simulations. `elegant` integrates well with the fully developed Self Describing Data Sets (`SDDS`) [3] toolset and infrastructure, making large scale data processing simpler [4], [5]. `elegant` also has better (and better tested) functionality to incorporate magnet errors which is an important part of reconciling online modeling with machine measurements [6].

* Notice: Authored by Jefferson Science Associates, LLC under U.S. DOE Contract No. DE-AC05-06OR23177. The U.S. Government retains a non-exclusive, paid-up, irrevocable, world-wide license to publish or reproduce this manuscript for U.S. Government purposes.

Content from this work may be used under the terms of the CC BY 3.0 licence (© 2015). Any distribution of this work must maintain attribution to the author(s), title of the work, publisher, and DOI.

ISBN: 978-3-95450-168-7 doi:10.18429/JACoW-IPAC2015-MOPWI047

ARCHITECTURAL IMPROVEMENTS AND NEW PROCESSING TOOLS FOR THE OPEN XAL ONLINE MODEL*

C.K. Allen, T.A. Pelaia II, ORNL, Oak Ridge, Tennessee 37831 USA
J. Freed, University of South Carolina, South Carolina 29208 USA

Abstract

The *online model* is the component of Open XAL providing accelerator modeling, simulation, and dynamic synchronization to live hardware. Significant architectural changes and feature additions have been recently made in two separate areas: 1) the managing and processing of simulation data, and 2) the modeling of RF cavities. Simulation data and data processing have been completely decoupled. A single class manages all simulation data while standard tools were developed for processing the simulation results. RF accelerating cavities are now modeled as composite structures where parameter and dynamics computations are distributed. The beam and hardware models both maintain their relative phase information, which allows for dynamic phase slip and elapsed time computation.

BACKGROUND

Open XAL is an open source development environment used for creating accelerator physics applications, scripts, and services [1]. The project has seen collaboration among SNS, CSNS, ESS, GANIL, TRIUMF and FRIB. Open XAL was born out of XAL, an application framework originally developed for the SNS in the early 2000s [2]. Open XAL is configurable for multi-site operation and the project facilitates multi-institutional development. It was initially released at the end of 2010 and is currently working toward its 6th milestone. For a status report on Open XAL see Pelaia [3]. For information on using Open XAL see the USPAS 2014 course *Control Room Accelerator Physics* material [4]. For material on the architecture of Open XAL see [5].

One significant component of Open XAL is the *online model*. This paper is concerned with two recent upgrades to the online model, data processing and the RF cavity model. For a perspective of these upgrades consider the overall architecture of online model; it is built according to the Element/Algorithm/Probe software architecture of Malitsky and Talman [6], which offers a robust implementation strategy for accelerator system modeling. Figure 1 is a UML diagram of the online model. A class,

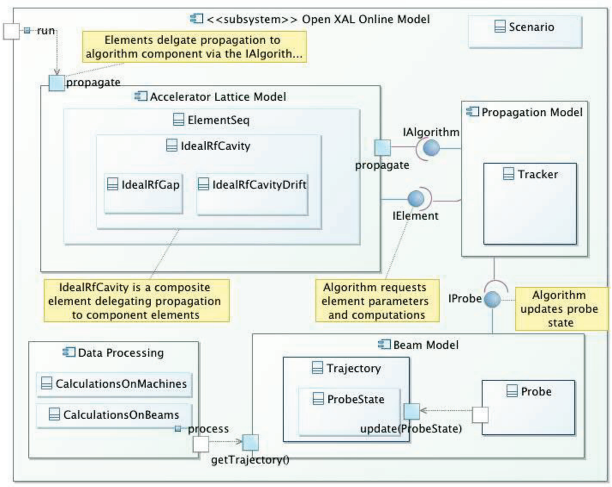

Figure 1: Open XAL online simulator architecture.

`Scenario`, encapsulates most of the online model and has the entry port `run()`. Also shown in the figure are four major components of the online model, the Accelerator Lattice, the Propagation Model, the Beam Model, and the Data Processing component; the three former components correspond to Element, Algorithm, and Probe, respectively, of Malitsky and Talman's architecture. The last component is not technically part of the online model. However, since it so closely ties to the model and it is a topic of the paper it is shown bound more tightly than implemented. The Accelerator Lattice represents hardware and computes hardware parameters. The Propagation Model component performs the dynamics interaction for hardware objects and the beam then updates the Beam Model with the results. The Beam Model represents some aspect of the particle beam, a single particle, the RMS envelopes, a transfer map, etc. The first topic of this paper, simulation data management and processing, is shared between the Beam Model and the Data Processing. The second topic, RF cavity modeling, is a part of the Accelerator Lattice component.

SIMULATION DATA AND ANALYSIS

The representation, storage, and analysis of online model simulation data are significantly improved. A new architecture for data handling was implemented which separates data maintenance and data analysis. This refactoring reduced code support by ten classes.

* This manuscript has been authored by UT-Battelle, LLC, under Contract No. DE-AC0500OR22725 with the U.S. Department of Energy. The United States Government retains and the publisher, by accepting the article for publication, acknowledges that the United States Government retains a non-exclusive, paid-up, irrevocable, world-wide license to publish or reproduce the published form of this manuscript, or allow others to do so, for the United States Government purposes. The Department of Energy will provide public access to these results of federally sponsored research in accordance with the DOE Public Access Plan (http://energy.gov/downloads/doe-public-access-plan).

Content from this work may be used under the terms of the CC BY 3.0 licence (© 2015). Any distribution of this work must maintain attribution to the author(s), title of the work, publisher, and DOI.

ISBN: 978-3-95450-168-7 doi:10.18429/JACoW-IPAC2015-MOPWI048

OPEN XAL BUILD SYSTEM*

T. Pelaia II#, ORNL, Oak Ridge, TN 37831, USA

Abstract

Open XAL is an accelerator physics software platform developed in collaboration among several facilities around the world. The build system is implemented through Apache Ant build files and features zero configuration simplicity based on directory patterns. These directory patterns allow for correctly building the Open XAL environment including the core and site specific applications, services, extensions, plugins and resources. Options are available for deployment and custom application packaging. This paper describes the Open XAL build rules, options and workflows.

INTRODUCTION

The Open XAL [1, 2] build system was designed from scratch to build multiple components with zero configuration while allowing for optional customization. Apache Ant was chosen as the build tool. Components include the core, extensions, plugins, services, applications and scripts. The final products are a single shared library plus the applications and services that depend on that shared library. Scripts don't require any build processing except to be copied for deployment. The goal of the build system is to provide zero configuration builds driven by convention.

BUILD REQUIREMENTS

Apache Ant [3] was chosen as the build tool since it is mature, commonly available, well supported and currently the standard build tool for Java. The version of Ant must be at version 1.9 or later to support all of the build commands and settings used in this project. Java J2SE 7 or later is required for compiling the current source code. The Open XAL project contains all the source code and libraries required to build the project.

ZERO CONFIGURATION

The Open XAL project delivers on the goal of building the entire project using a single command with zero configuration. Simply typing the command, "ant" in a terminal at the root of the project will build all executables. A second command, "ant install" can optionally be used for installing the executables in a deployment directory whose path can optionally be configured. Typing the command, "ant help" will display the list of all available build commands. Build files also exist throughout the project to allow builds at different levels of the tree. For example, one can build just a single application.

It is notable that zero configuration is true even when adding new components to the project. This is possible because the Open XAL build system is founded upon two principles: component separation and convention over configuration.

Component Separation

Component separation means that allowable dependencies between components are restricted. This separation facilitates efficient compilation and deployment and provides well defined dependency rules. Components are categorized as the core, plugins, extensions, services, applications and scripts.

The core consists of common foundation packages and has no compile time dependencies on any other components. Plugins provide runtime support for the core. For example, a plugin could provide a branded database driver that is required at runtime for the core's generic database tools. Extensions provide additional support packages to be shared among applications, scripts and services. Plugins and extensions can depend upon each other and on the core. Applications, scripts and services [4] are the end use executables and they may depend upon the core, extensions and plugins. Applications and services may also explicitly provide extensions. For example, a service provides an extension containing the public remote interface that clients will use to communicate with the service.

While not enforced, it is encouraged that any external library be wrapped so as to abstract functionality from the details of the external library. This allows for flexibility in replacing external libraries. Furthermore, it makes it easier to identify missing components since component packages follow an Open XAL naming convention whereas external library package names are not under our control.

Convention over Configuration

The build system uses convention over configuration to determine how to assemble and build components. The directory layout and naming convention determine how components are identified and how to package each component.

At the top level, component directories are appropriately named apps (for applications), core, extensions, plugins, scripts and services. A component bundle placed under any of these directories will be interpreted accordingly. Except as noted, a component

* This manuscript has been authored by UT-Battelle, LLC, under Contract No. DE-AC0500OR22725 with the U.S. Department of Energy. The United States Government retains and the publisher, by accepting the article for publication, acknowledges that the United States Government retains a non-exclusive, paid-up, irrevocable, world-wide license to publish or reproduce the published form of this manuscript, or allow others to do so, for the United States Government purposes. The Department of Energy will provide public access to these results of federally sponsored research in accordance with the DOE Public Access Plan (http://energy.gov/downloads/doe-public-access-plan).
# pelaiata@ornl.gov

Content from this work may be used under the terms of the CC BY 3.0 licence (© 2015). Any distribution of this work must maintain attribution to the author(s), title of the work, publisher, and DOI.

ISBN: 978-3-95450-168-7 doi:10.18429/JACoW-IPAC2015-MOPWI049

OPEN XAL SERVICES ARCHITECTURE*

T. Pelaia II#, ORNL, Oak Ridge, TN 37831, USA

Abstract

Open XAL is an accelerator physics software platform developed in collaboration among several facilities around the world. It includes a powerful new services extension that allows for natural remote procedure calls. The high level services interface is based upon custom implementations of modern standard protocols such as JSON-RPC and WebSockets. This choice of modern protocols allows for flexibility such as seamless communication with web clients free of plugins plus rich object type support. The JSON parser was designed for convenient data type transformations with easy extensibility, high performance and low memory overhead. The Open XAL services architecture features a simple application programming interface, high performance, memory efficiency and thread safety.

INTRODUCTION

Open XAL [1, 2] is a Java based platform for building accelerator physics software. The software products can be categorized as either application or standalone service. Here, an application refers to software with a user interface that is launched by an end user and runs until the user quits the application. A standalone service is software that runs perpetually unattended and has no user interface. Other client applications may communicate with a service for management or to display data from the service. Services are useful for monitoring, logging and certain calculations that are best suited to be offloaded from the client.

The Open XAL services framework is designed to provide a high level API to discover and communicate with services over standard protocols implemented internally. The communication protocols were chosen to allow for both thick application and thin web browser clients.

FEATURES

The services framework is designed to provide a high performance, low overhead remote communication mechanism that translates local Java calls into remote messages without having to provide stubs. Furthermore, it provides for dynamic registration and lookup which eliminates the need for configuring service addresses and allows services to be launched from any server on the local network rather than tied to one specific server. The implementation is thread safe and can process multiple concurrent calls.

PROTOCOLS

The services framework is built upon three standard protocols: multi-cast DNS, JSON-RPC [3] and WebSocket [4]. The multi-cast DNS protocol is implemented using the external JmDNS [5] library. The JSON-RPC and WebSocket protocols have been implemented directly in Open XAL. All three protocols are wrapped in the services framework so as to allow the public API to be independent of these internal protocols. Most of the interaction with the services framework is through the ServiceDirectory class and specifically the default singleton of this class known as the "default directory."

Multi-cast DNS

The open source JmDNS library provides the implementation of multi-cast DNS that is used in Open XAL. Multi-cast DNS allows for dynamic registration and lookup of services. A service is registered by name and type pair and are bound to the provided IP address and port. Clients can lookup services using the name and type pair and the IP addresses and ports of matching services are provided.

The services framework hides the details of the underlying JmDNS library. A service is simply registered using the default directory passing only the service name, a Java interface and the service provider implementing the Java interface. Internally, the fully qualified lowercase name of the Java interface is converted to a properly formatted multi-cast DNS type by replacing periods with underscores and appending "_tcp.local." to provide a unique type that conforms to the requirements.

JSON-RPC

A variant of JSON-RPC is the messaging protocol that is used to encode messages with JSON constructs. This protocol is hidden from the caller as method calls are automatically converted to the messaging protocol. Internally, a message request is encoded as a JSON [6] object (also known as a dictionary) using the "message," "params" and "id" keys. The message parameter consists of the service name followed by the method name separated by "#" such as "*MyService#doSomething*" for example. The params are an array of JSON encoded parameters to pass. The id parameter is an incremented integer that is used to uniquely identify the request.

A custom JSON implementation is used to efficiently encode and decode JSON to and from Java objects. This

* This manuscript has been authored by UT-Battelle, LLC, under Contract No. DE-AC0500OR22725 with the U.S. Department of Energy. The United States Government retains and the publisher, by accepting the article for publication, acknowledges that the United States Government retains a non-exclusive, paid-up, irrevocable, world-wide license to publish or reproduce the published form of this manuscript, or allow others to do so, for the United States Government purposes. The Department of Energy will provide public access to these results of federally sponsored research in accordance with the DOE Public Access Plan (http://energy.gov/downloads/doe-public-access-plan).
# pelaiata@ornl.gov

Content from this work may be used under the terms of the CC BY 3.0 licence (© 2015). Any distribution of this work must maintain attribution to the author(s), title of the work, publisher, and DOI.

ISBN: 978-3-95450-168-7 doi:10.18429/JACoW-IPAC2015-MOPWI050

Content from this work may be used under the terms of the CC BY 3.0 licence (© 2015). Any distribution of this work must maintain attribution to the author(s), title of the work, publisher, and DOI.

OPEN XAL STATUS REPORT 2015*

T. Pelaia II#, C.K. Allen, A. Shishlo, A. Zhukov, ORNL, Oak Ridge, TN 37831, USA
Y.C. Chao, C. Gong, F. Jones, R. Newhouse, TRIUMF, Vancouver, BC V6T 2A3, Canada
P. Chu, D. Maxwell, Y. Zhang, MSU, East Lansing, MI 48824, USA
R. Fearn, L. Fernandez, E. Laface, M. Munoz, ESS, Lund, Sweden
J. Freed, University of South Carolina, Columbia, SC 29208, USA
P. Gillette, P. Laurent, G. Normand, GANIL, CAEN 14076, France
H. Hale, University of Tennessee, Knoxville, TN, USA
Y. Li, CSNS, Dongguan Campus, Institue of High Energy Physics, Chinese Academy of Sciences, Dongguan 523803, China
I. List, M. Pavleski, Cosylab, Ljubljana, Slovenia
P. Scruggs, East Tennessee State University, Johnson City, TN, USA

Abstract

Open XAL is an accelerator physics software platform developed in collaboration among several facilities around the world. The Open XAL collaboration was formed in 2010 to port, improve and extend the successful XAL platform used at the Spallation Neutron Source for use in the broader accelerator community and to establish it as the standard platform for accelerator physics software. The site-independent core is complete, active applications have been ported, and now we are in the process of verification and transitioning to using Open XAL in production. This paper will present the current status and a roadmap for this project.

INTRODUCTION

Open XAL [1] is an open source accelerator physics software platform written in Java. The Open XAL project began in mid 2010 as a response to requests from the international accelerator physics community to adopt an open source accelerator physics platform based on XAL [2] from the Spallation Neutron Source (SNS) at Oak Ridge National Lab (ORNL) and establish a standard platform for accelerator physics software.

The goals of the project are to provide a common accelerator physics core to be developed in collaboration, provide a rapid development environment and to modernize the source code. Since the last status report [3], the development effort has shifted from porting code to verification, modernization and new functionality. The API has stabilized, and the project is production ready. This paper covers the collective contributions of the collaboration.

* This manuscript has been authored by UT-Battelle, LLC, under Contract No. DE-AC0500OR22725 with the U.S. Department of Energy. The United States Government retains and the publisher, by accepting the article for publication, acknowledges that the United States Government retains a non-exclusive, paid-up, irrevocable, world-wide license to publish or reproduce the published form of this manuscript, or allow others to do so, for the United States Government purposes. The Department of Energy will provide public access to these results of federally sponsored research in accordance with the DOE Public Access Plan (http://energy.gov/downloads/doe-public-access-plan).
# pelaiata@ornl.gov

SOFTWARE HIERARCHY

The software is grouped among the core, extensions, plugins, services, applications and scripts. The core consists of packages that include the accelerator object graph, the online model, abstract channel interface and general supporting tools such as common math libraries, archiving, messaging, database access and concurrency. This core is intended to be shared in common across all Open XAL distributions, and it has no compile time dependency on other components.

Extensions and plugins are components which may optionally depend on other extensions and plugins and the core. A plugin differs from an extension in that the core depends on a plugin being implemented (but not the actual implementation) whereas the core has no dependency on an extension. Plugins consist of controls channel access support and database adaptors. For example, the core specifies generic database tools, but a database adaptor plugin provides support for a specific database driver. Extensions include packages of general use in applications, scripts and services but not in the core. Examples of extensions include the application framework, service framework, lattice generation, fitting, scanning and widgets such as plotting tools.

Applications, scripts and services are executables and may depend upon the core, plugins and extensions. Applications and scripts are launched by users and have a user interface whereas services are headless and run perpetually in the background independent of user interaction. Applications differ from scripts in that applications are written in Java and are thus fully compiled prior to runtime versus scripts that may be written in a Java variant of Ruby or Python scripting languages and are not compiled prior to runtime.

A top level site directory contains optional site specific resources and configurations that take precedence over resources and configurations of the same name in the

ISBN: 978-3-95450-168-7 doi:10.18429/JACoW-IPAC2015-MOPWI052

RESPONSIVITY STUDY OF DIAMOND X-RAY MONITORS WITH nUNCD CONTACT

M. Gaowei [#], J.Smedley, Brookhaven National Laboratory, Upton, NY, 11973, USA
T. Zhou, E. Muller, Stony Brook University, Stony Brook, NY, 11794, USA
A. Sumant, Argonne National Laboratory, Argonne, IL, 60439, USA

Abstract

Nitrogen doped ultrananocrystalline diamond (nUNCD) grown on the surface of a CVD single crystal diamond is tested at various beamlines covering an x-ray photon energy range of 200eV to 28 keV. The nUNCD has much lower x-ray absorption than metal contacts and is designed to improve the performance of our device. The responsivity of nUNCD diamond x-ray detector is compared with the conventional platinum coated diamond x-ray beam position monitor and the results are presented in this paper.

INTRODUCTION

The ultrananocrystalline diamond (UNCD) thin films exhibit similar physical properties to single crystal diamond in the aspects of mechanical, thermal and resistance to radiation damage. Current UNCD thin films are prepared by microware plasma chemical vapor deposition (MPCVD) or hot filament chemical vapor deposition (HFCVD) with mixed H_2/CH_4 or Ar/CH_4 plasma chemistries. Nitrogen is introduced to UNCD thin film to improve its electrical conductivity to semi-metallic level, and therefore can be considered as a replacement of metal to function as an electrode in various applications like biomedical devices, biosensors, and in our case the x-ray monitors. [1, 2]

In this paper, a diamond device prepared with nitrogen doped ultrananocrystalline diamond (nUNCD) on both sides as electrodes is studied and results are compared with the device fabricated with traditional platinum contact.

EXPERIMENTAL

In order to improve the performance of the diamond x-ray monitor, nUNCD layers of 200 nm ~ 500 nm are grown on a 4 mm × 4 mm × 0.3 mm electronic grade ([N] ~ppb) single crystal CVD diamond as contact electrodes at Argonne National Laboratory (ANL).

X-ray white beam topography and birefringence images were recorded for this sample prior to device fabrication. X-ray topography was performed at Beamline X19C, National Synchrotron Light Source (NSLS) and birefringence images were taken using a polarized microscope. 2D current maps and calibrated responsivity vs photon energy of this diamond were collected at various beamlines in NSLS, covering a photon energy range of 0.2~28keV. Beamline U3C provides monochromatic beam of photon energy from 0.2~1 keV, while beamline X8A provides x-ray from 1~6.5 keV and beamline X15A from 6.5~28 keV, with an intensity ranged from 10^{-9}~10^{-6} W/mm^2. [3] Measurements at U3C are performed in a vacuum level of 10^{-7}torr and at X8A in a vacuum of 10^{-6} torr due to the high absorption rate of air for low energy photons, and is in air at X15A. Incident x-ray power is calibrated using silicon photodiodes at both U3C and X8A (with thickness of 25 µm and 52 µm respectively), while air-filled ionization chamber is used at X15A. Various biases in the saturated range of either DC level or in the form of square wave with adjustable magnitude, frequency and duty cycle, were applied on tested diamond plates to assure full collection of desired charge carriers (positive biases for hole collection and negative biases for electron collection).

RESULTS AND DISCUSSION

Figure 1 shows the compared results of the 2 imaging techniques. The nUNCD contact is completely transparent under the white beam at X19C (Fig.1a). The dark circled area in Fig.1b indicates the nUNCD contacts on both sides of the diamond. Prominent contrast of slip bands in diamond single crystal was observed in both topography and birefringence images.

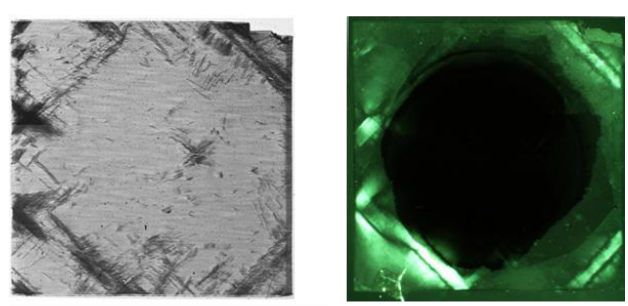

(a) (b)

Figure 1: (a) X-ray topography and (b) birefringence images of the nUNCD coated diamond.

2D current maps of this diamond are collected at various beamlines at different energies. The values of x-ray attenuation length of diamond (the depth into the diamond measured along the surface normal where the

*Work was supported by U.S. Department of Energy under grants KC0407-ALSJNT-I0013 and DE-FG02_08ER41547. Use of the National Synchrotron Light Source, Brookhaven National Laboratory, was supported by the U.S. Department of Energy, Office of Science, Office of Basic Energy Sciences, under Contract No. DE-AC02-98CH10886.
#mgaowei @bnl.gov

Content from this work may be used under the terms of the CC BY 3.0 licence (© 2015). Any distribution of this work must maintain attribution to the author(s), title of the work, publisher, and DOI.

ISBN: 978-3-95450-168-7 doi:10.18429/JACoW-IPAC2015-TUXB1
Content from this work may be used under the terms of the CC BY 3.0 licence (© 2015). Any distribution of this work must maintain attribution to the author(s), title of the work, publisher, and DOI.

FRANZ AND SMALL-SCALE ACCELERATOR-DRIVEN NEUTRON SOURCES

C. Wiesner*, S. Alzubaidi, M. Droba, M. Heilmann, O. Hinrichs, B. Klump, O. Meusel, D. Noll, O. Payir, H. Podlech, U. Ratzinger, R. Reifarth, A. Schempp, S. Schmidt, P. Schneider, M. Schwarz, W. Schweizer, K. Volk, C. Wagner, IAP, Goethe University, Frankfurt am Main, Germany

Abstract

This paper gives an overview of the opportunities and challenges of high-intensity, low-energy light-ion accelerators for neutron production. Applications of this technology range from the study of stellar nucleosynthesis and astrophysical phenomena to medical applications such as Boron neutron capture therapy (BNCT). The paper includes details of the FRANZ facility, under development at Frankfurt University.

INTRODUCTION

Applications of Neutron Beams

Neutrons are an important tool for probing the structure of matter. They are electrically neutral, but sensitive to the magnetic properties of the material, as well as for different isotopes, providing excellent opportunities for material sciences [1]. Their high penetration depth in material and their strong sensitivity for light elements facilitate neutron imaging techniques [2, 3].

Nuclear Astrophysics The investigation of neutron capture processes is especially relevant to provide a deeper understanding of stellar nucleosynthesis and astrophysical phenomena. About 50% of the element abundances beyond iron are produced via the slow neutron capture process or s-process. This process takes place mostly inside of asymptotic-giant-branch (AGB) stars. Here, the neutron temperature ranges from 8 keV to 90 keV. Therefore, a proper modeling of the stellar nucleosynthesis requires the knowledge of neutron capture cross-sections between 1 keV and 400 keV [4, p. 14].

BNCT There are increasing efforts to use neutron beams for cancer therapy. Presently, there are eight initiatives in the world to develop accelerator-based Boron Neutron Capture Therapy (BNCT) [5]. If boron-10 that has been selectively incorporated into the tumor tissue captures a neutron, it decays into short-ranging alpha particles and lithium-7 nuclei, which can efficiently destroy the cancer cells [6]. Epithermal neutrons of up to 10 keV are required to assure sufficiently high penetration depth into the tissue while still having a sufficiently high capture cross section.

Neutron Production

Since free neutrons are unstable, dedicated production setups are required. Traditionally, nuclear fission reactors have been used for neutron production. They provide a high average neutron (n) flux of typically up to 1×10^{15} n s^{-1}cm^{-2}. Recently, spallation neutron sources combine a comparable or even higher flux than reactors with a flexible time structure.

Complementary to these large-scale facilities, small-scale accelerator-driven neutron sources based on light ion beams at low energy can provide intense neutron beams with flexible time structure in the energy range from keV to MeV.

SMALL-SCALE ACCELERATOR-DRIVEN FACILITIES

Opportunities

Typical small-scale accelerator-driven neutron sources employ light ions at several MeV energy to generate neutrons via nuclear reactions as the ^{7}Li(p,n)^{7}Be, the ^{9}Be(p,n)^{9}B or the ^{9}Be(d,n)^{10}B reaction. For low proton energies, the ^{9}Be(p,n) reaction produces less (and higher-energetic) neutrons than the ^{7}Li(p,n) reaction [7]. However, the target material might be easier to handle.

The ^{7}Li(p,n)^{7}Be reaction as the most prolific reaction has a relatively low production threshold of 1.88 MeV. The resulting neutron energy lies in the keV to hundreds of keV range, depending on the primary proton energy. This includes the relevant energy spectrum for stellar nucleosynthesis as well as for BNCT application.

In contrast, reactors or spallation neutron sources provide neutrons in a wide energy spectrum, including much lower and much higher energetic neutrons. In a reactor, the fission neutrons, starting with several MeV energy, are typically moderated down to thermal energies. In spallation processes, some neutrons can reach energies up to the incident proton energy of hundreds of MeV, with the larger part having energies around 1 MeV to 10 MeV.

At small-scale facilities, the neutron energy spectrum can be further refined by adjusting the primary beam energy and the thickness of the production target [4, p. 23]. This allows to limit the neutron spectrum to the region of interest for the given application, reducing the background that is induced by higher energy neutrons and creating a neutron flux for the energy region of interest that is comparable to the flux in large-scale facilities.

This effect is increased for the ^{7}Li(p,n)^{7}Be reaction when proton energies just above the production threshold are employed. In this case, due to kinematic collimation, neutrons are only emitted in a forward cone with an opening angle of 120°, significantly increasing the neutron flux at the sample position [4].

* wiesner@iap.uni-frankfurt.de

ISBN: 978-3-95450-168-7 doi:10.18429/JACoW-IPAC2015-TUXB2

UPGRADE OF THE UNILAC FOR FAIR

L. Groening, S. Mickat, R. Brodhage, A. Adonin, X. Du, R. Hollinger, O.K. Kester, A. Orzhekhovskaya, B. Schlitt, G. Schreiber, H. Vormann, C. Xiao, GSI, Darmstadt, Germany
H. Hähnel, U. Ratzinger, A. Seibel, R. Tiede, Goethe University of Frankfurt, Frankfurt, Germany

Abstract

The UNIversal Linear Accelerator (UNILAC) at GSI serves as injector for all ion species from protons to uranium since four decades. Its 108 MHz Alvarez type DTL providing acceleration from 1.4 MeV/u to 11.4 MeV/u has suffered from material fatigue. The DTL will be replaced by a completely new section with almost same design parameters, i.e. pulsed current of up to 15 mA of $^{238}U^{28+}$ at 11.4 MeV/u. A dedicated source terminal & LEBT for operation with $^{238}U^{4+}$ is currently constructed. The uranium source needs to be upgraded in order to provide increased beam brilliances and for operation at 2.7 Hz. In parallel a 70 MeV / 70 mA proton linac based on H-mode cavities is under design and construction.

THE FAIR PROJECT

GSI is currently constructing the Facility for Ion and Antiproton Research (FAIR) [1]. It aims at provision of $2{\times}10^{11}$/s uranium ions at 1.5 GeV/u. Due to its high rigidity uranium imposes the highest challenges to the accelerator chain wrt fields and machine protection. Additionally, a total of $2{\times}10^{12}$/s cooled anti-protons are to be delivered. The complete accelerator chain is depicted in Fig. 1 and its more detailed description as well as its current status of design and construction is given in [2]. These proceedings are on the injector linacs of the facility. The existing UNIversal Linear ACcelerator UNILAC will provide all primary ions but protons. A dedicated proton linac is currently under design and construction. In order to deal with the FAIR requirements in the upcoming decades the UNILAC needs a considerable upgrade. These upgrade activities are described in the next section. Afterwards the proton linac is presented together with its current status wrt design, construction, and commissioning of components.

UPGRADE OF THE UNIVERSAL LINEAR ACCELERATOR UNILAC

The existing UNILAC (Fig. 2) serves as injector for FAIR together with the subsequent synchrotron SIS18. The UNILAC has three ion source terminals that can be operated in pulse-to-pulse switching mode at 50 Hz. One terminal is equipped with an ECR source providing highly charged ions. Another terminal houses a Penning source providing low intensity beams at intermediate charge states. The third terminal is dedicated to provision of intense beams of low-charged ions. It can be equipped with various source types as MUCIS and CHORDIS for light to intermediate-mass ions for instance. Intense heavy ion beams are produced in a MEVVA or VARIS source at 2.2 keV/u. Beams are bunched

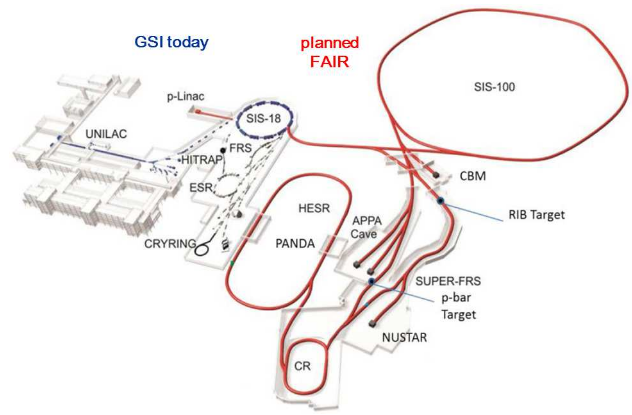

Figure 1: Facility for Anti proton and Ion Research (FAIR) to be built at GSI.

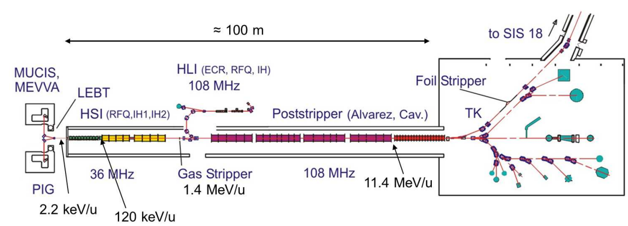

Figure 2: The UNIversal Linear ACcelerator (UNILAC) at GSI.

and pre-accelerated to 120 keV/u along a 9 m long RFQ operated at 36 MHz. Afterwards two IH-cavities provide for acceleration to 1.4 MeV/u. For uranium the highest particle numbers are obtained by using the charge state $^{238}U^{4+}$. After the IH-DTL the acceleration efficiency is increased by passing the beam through a gaseous stripper which delivers a mean charge state of $^{238}U^{28+}$ at its exit. This increase of charge state is at the expense of intrinsic particle loss as about 89% of the uranium ions are stripped to a charge state different from 28+. After dispersive selection of the desired charge state the beam is matched to the subsequent post stripper Alvarez DTL. The latter is operated at 108 MHz and comprises five tanks. Its exit beam energy is 11.4 MeV/u being the injection energy for the synchrotron SIS18. The UNILAC design parameters are listed in Table 1. The age of the UNILAC together with the requirement to provide reliable and intense beams for the upcoming FAIR era calls for a revision of the UNILAC. In the following the planned upgrade activities are illustrated.

Source, LEBT, MEBT, and RFQ

In order to provide the mean uranium intensity required for FAIR the source has to be operated with a repetition

Content from this work may be used under the terms of the CC BY 3.0 licence (© 2015). Any distribution of this work must maintain attribution to the author(s), title of the work, publisher, and DOI.

ISBN: 978-3-95450-168-7 doi:10.18429/JACoW-IPAC2015-TUXB3

700 kW MAIN INJECTOR OPERATIONS FOR NOνA AT FNAL *

P. Adamson†, Fermi National Accelerator Laboratory, Batavia, IL 60510, USA

Abstract

Following a successful career as an antiproton storage and cooling ring, the Fermilab Recycler was repurposed as a proton stacker as part of the NOνA project, in order to increase the maximum NuMI beam power from 400 kW to 700 kW. Using the Recycler to prepare beam for acceleration in the Main Injector, we have been able to increase the beam power delivered to NuMI to a sustained weekly average in excess of 400 kW and a best hourly average of 482.8 kW. I discuss the commissioning progress to date, and describe the remaining steps along the way to achieving the 700 kW design goal.

NOνA

The NOνA [1], [2] (NuMI Off-axis ν_e Appearance) long-baseline experiment in the Fermilab NuMI neutrino beam aims to make precision measurements of muon-neutrino survival and muon- to electron-neutrino oscillation for both neutrino and antineutrino beams traveling from Fermilab to a "Far Detector" 810 km away in Ash River, MN. It aims to address the outstanding questions in neutrino physics—whether the neutrino mass eigenstates have "normal" or "inverted" mass ordering (whether the dominant components of the electron neutrino are the lightest or the heaviest states); whether the mixing angle θ_{23} is maximal, or if it differs from 45°, whether it is larger or smaller; whether the CP symmetry is violated in the neutrino sector; and whether the three-flavor PMNS matrix is sufficient to explain neutrino oscillations, or if new physics is required.

In order to accomplish these goals, as well as building a massive (14 kT) Far Detector, the NOνA project [3] upgraded the beam power delivered to the NuMI facility from a nominal 400 kW to a nominal 700 kW.

BEAM DELIVERY TO NUMI

The NuMI beam begins as H^- ions accelerated to 400 MeV in a normal-conducting linac. On injection to the Booster, they pass through a stripping foil which converts the H^- to protons. The injected beam typically wraps the Booster circumference about 13 times to achieve a normal intensity of around 4×10^{12} protons per Booster batch. The booster is a 15 Hz resonant synchrotron, and accelerates protons to 8 GeV KE (8.9 GeV/c momentum). Not all 15 Hz cycles contain beam or rf voltage. An overview of the Fermilab accelerator complex is shown in figure 1.

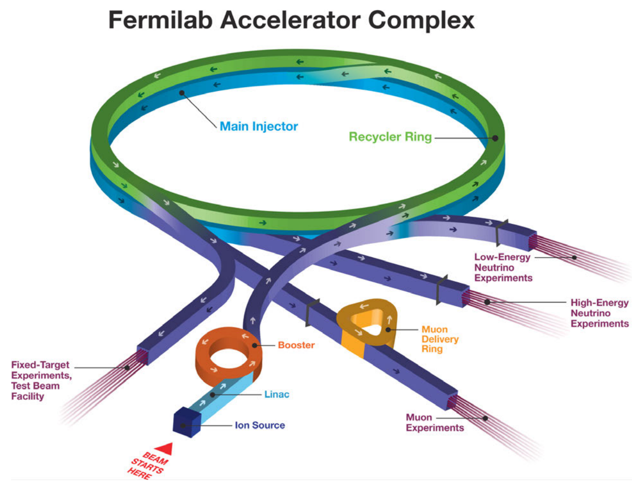

Figure 1: Fermilab accelerator complex in 2015.

In the Collider era, the Booster was injected into the Main Injector, and accelerated to 120 GeV/c. The Main Injector circumference is seven times that of Booster, allowing six Booster batches to fit around the machine once a gap to accommodate the rise time of the extraction and abort kickers has been left. Slip-stacking [4] was used to combine two Booster batches into one for five of these six batches. The need to provide two kicker gaps in order to share this beam between the antiproton source and the NuMI beamline precluded slip-stacking the final batch.

The NOνA upgrade moves the slip-stacking process from the Main Injector to the Recycler—an 8.9 GeV/c permanent magnet machine in the Main Injector tunnel no longer needed in its prior role as an antiproton storage and cooling ring. Separating the time-consuming accumulation of Booster batches at 8 GeV from the acceleration allows the Main Injector to continuously ramp up and down, while the Recycler accumulates and slip-stacks the beam for the next pulse. As shown in figure 2, for 12-batch slip-stacking, Recycler has begun preparing the next pulse before Main Injector has extracted the previous one.

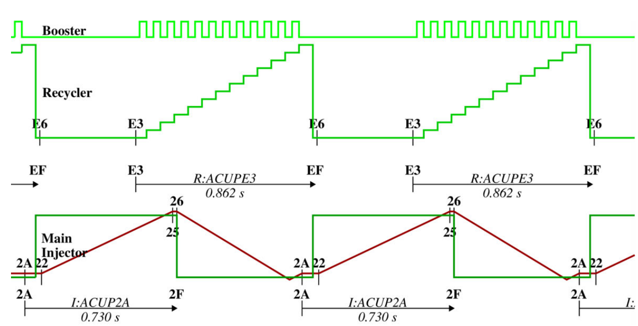

Figure 2: Relative timing of Booster, Recycler and Main Injector cycles for NOνA-era NuMI operation. Beam in each machine is shown in green, and Main Injector momentum in red. The start and end of cycle clock events for MI and Recycler are also shown.

* Operated by Fermi Research Alliance, LLC under Contract No. De-AC02-07CH11359 with the United States Department of Energy.
† pa@fnal.gov

Content from this work may be used under the terms of the CC BY 3.0 licence (© 2015). Any distribution of this work must maintain attribution to the author(s), title of the work, publisher, and DOI.

ISBN: 978-3-95450-168-7 doi:10.18429/JACoW-IPAC2015-TUYB1

PROGRESS OF SuperKEKB

T. Miura#, T. Abe, T. Adachi, K. Akai, M. Akemoto, A. Akiyama, D. Arakawa, Y. Arakida, Y. Arimoto, M. Arinaga, K. Ebihara, K. Egawa, A. Enomoto, J. W. Flanagan, S. Fukuda, H. Fukuma, Y. Funakoshi, K. Furukawa, T. Furuya, K. Hara, T. Higo, H. Hisamatsu, H. Honma, T. Honma, R. Ichimiya, N. Iida, H. Iinuma, H. Ikeda, M. Ikeda, T. Ishibashi, H. Ishii, M. Iwasaki, A. Kabe, T. Kageyama, H. Kaji, K. Kakihara, S. Kamada, T. Kamitani, S. Kanaeda, K. Kanazawa, H. Katagiri, S. Kato, S. Kazama, M. Kikuchi, T. Kobayashi, H. Koiso, Y. Kojima, M. Kurashina, K. Marutsuka, M. Masuzawa, S. Matsumoto, T. Matsumoto, H. Matsushita, S. Michizono, K. Mikawa, T. Mimashi, F. Miyahara, K. Mori, T. Mori, A. Morita, Y. Morita, H. Nakai, H. Nakajima, T. T. Nakamura, K. Nakanishi, K. Nakao, H. Nakayama, T. Natsui, M. Nishiwaki, J. Odagiri, Y. Ogawa, K. Ohmi, Y. Ohnishi, S. Ohsawa, Y. Ohsawa, N. Ohuchi, K. Oide, T. Oki, M. Ono, H. Sakai, Y. Sakamoto, S. Sasaki, M. Sato, M. Satoh, K. Shibata, T. Shidara, M. Shirai, A. Shirakawa, M. Suetake, Y. Suetsugu, R. Sugahara, H. Sugimoto, T. Suwada, S. Takasaki, T. Takatomi, T. Takenaka, Y. Takeuchi, M. Tanaka, M. Tawada, S. Terui, M. Tobiyama, N. Tokuda, K. Tsuchiya, X. Wang, K. Watanabe, H. Yamaoka, Y. Yano, K. Yokoyama, M. Yoshida, M. Yoshida, S. Yoshimoto, K. Yoshino, R. Zhang, D. Zhou, X. Zhou, Z. Zong, KEK, Ibaraki, Japan
D. Satoh, Tokyo Inst. of Technology, Tokyo, Japan

Abstract

SuperKEKB is designed based on the 'nano-beam scheme' with the target luminosity of 8×10^{35} cm^{-2}s^{-1}. The design of the interaction region (IR) with a very low β_y* at the interaction point (IP) is discussed. The status of the installation and the injector commissioning of SuperKEKB is reported.

INTRODUCTION

The previous project KEKB was an e−/e+ collider that is used for physics experiments mainly conducted at the Υ(4S) resonance. KEKB has the highest peak luminosity in the world, 2×10^{34} cm^{-2}s^{-1}. KEKB has been in operation until 2010. Afterward, upgrading of KEKB has been initiated toward SuperKEKB. The target luminosity is 8×10^{35} cm^{-2}s^{-1}, which is 40times higher than that of KEKB. The required integral luminosity is 50 ab^{-1}. For the upgrade, the KEKB tunnel is being reused, and the KEKB components are being reused as much as possible in SuperKEKB.

Luminosity mainly depends on three parameters: the beam currents (I), the beam-beam parameter (ξ_y), and the vertical beta function (β^*_y) at the interaction point (IP). For achieving 40 times higher luminosity than that of KEKB, the current I is doubled, the beam-beam parameter ξ_y is kept almost at the same level, and β^*_y is reduced to 1/20 of the KEKB value, based on the 'nano-beam scheme'. Table 1 shows the SuperKEKB machine parameters. As the nano-beam collision scheme, beams collide at a large crossing angle, 83 mrad. Thus, the length of the overlap region of the two beams at the IP is expressed as σ_x*/ϕ. For realization of the small β^*_y, low horizontal emittance ε_x and small β^*_x are necessary. The value of β^*_y at the SuperKEKB is 0.3 mm.

As part of an additional design concept, beam energies are changed. The LER energy is increased for longer Touschek lifetime and mitigation of emittance growth owing to the intra-beam scattering. In HER, as the energy is decreased, emittance becomes lower and synchrotron radiation (SR) power decreases. For the low SR power, the KEKB beam chamber can be reused.

Table 1: SuperKEKB Machine Parameters

Parameters	units	LER	HER
Beam energy	GeV	4	7.007
Half crossing angle ϕ	mrad	41.5	
Num. of bunches		2500	
H emittance ε_x	nm	3.2	4.6
Emittance ratio	%	0.27	0.25
Beta functions β^*_x/β^*_y	mm	32/0.27	25/0.30
Beam currents I	A	3.6	2.6
Beam-beam param.ξ_y		0.088	0.081
Bunch length	mm	6.0	5.0
H beam size σ_x*	µm	10	11
V beam size σ_y*	nm	48	62
Luminosity	cm^{-2}s^{-1}	8×10^{35}	

The estimated beam lifetimes for both rings are ~6 min, obtained without the consideration of without beam-beam effect. An effect of the beam-beam interaction to the beam lifetime and other beam-beam related issue are discussed elsewhere [1]. Therefore, high bunch charge

#takako.miura@kek.jp

Content from this work may be used under the terms of the CC BY 3.0 licence (© 2015). Any distribution of this work must maintain attribution to the author(s), title of the work, publisher, and DOI.

ISBN: 978-3-95450-168-7 doi:10.18429/JACoW-IPAC2015-TUYB2

Content from this work may be used under the terms of the CC BY 3.0 licence (© 2015). Any distribution of this work must maintain attribution to the author(s), title of the work, publisher, and DOI.

ACCELERATOR PHYSICS IN ERL BASED POLARIZED ELECTRON ION COLLIDER*

Yue Hao†, C-A Dept. Brookhaven National Laboratory, Upton, NY 11973, USA

Abstract

This talk will present the current accelerator physics challenges and solutions in designing ERL-based polarized electron-hadron colliders, and illustrate them with examples from eRHIC and LHeC designs. These challenges include multi-pass ERL design, highly HOM-damped SRF linacs, cost effective FFAG arcs, suppression of kink instability due to beam-beam effect, and control of ion accumulation and fast ion instabilities.

INTRODUCTION

Deep inelastic scattering already have taught us on the inner structure and dynamics inside nucleon. To get a much greater insight of the nucleon structure, including the distribution of the momentum, spin and flavor of the quarks and gluons, a high luminosity electron ion collider (EIC) is required.

In an EIC, the ion beam is accelerated to desired energy and stored in an synchrotron ring, while the electron accelerators has two options. An electron storage ring, together with its injector and booster, can be built and form a 'ring-ring' collision scheme with the ion ring. Alternatively, an energy recovery linac (ERL) can serve as electron accelerator, and form a 'linac-ring' scheme, or an ERL based EIC. In an ERL, the electron beam gain energy from the RF cavities (usually superconducting) with the accelerating phase. After the electron beam collides with the ion beam, it will be decelerated in the same RF cavity, with the decelerating phase which is ensured by the pass length of the electron beam. The energy is then used to accelerate the new electron bunches. This energy recovery process enables high collision rate, hence high luminosity. Therefore in an ERL based collider, the electron beam is always fresh, however, its energy is re-used.

There are several benefits of an ERL based EIC over a 'ring-ring' counterpart, which include:

- The beam-beam limit of the electron beam is removed due to a single collision for every electron bunch, which leads to an higher luminosity,
- The electron can be dumped at a much lower energy,
- The simpler synchronization of the electron beam with various ion energies.

Currently, there are two ERL based EIC proposed. One is the eRHIC [1] project in Brookhaven National Laboratory, the other is LHeC [2] in CERN. eRHIC uses the operating RHIC (Relativistic Heavy Ion Collider) to provide up to

Table 1: The Baseline Parameters of eRHIC and LHeC

Parameters	eRHIC		LHeC	
	e	p	e	p
Energy (GeV)	15.9	250	60	7000
Bunch spacing (ns)	106		25	
Intensity, 10^{11}	0.07	3.0	0.01	1.7
Current (mA)	10	415	6.4	860
rms norm. emit. (mm-mrad)	23	0.2	50	3.75
$\beta^*_{x/y}$ (cm)	5	5	12	10
rms bunch length (cm)	0.4	5	0.06	7.6
IP rms spot size (μm)	6.1		7.2	
Beam-beam parameter		4×10^{-3}		1×10^{-4}
Disruption parameter	36		6	
Polarization, %	80	70	90	None
Luminosity, 10^{33} cm^{-2}s^{-1}	4.9		1.3	

Table 2: ERL Parameters of eRHIC (15.9 GeV) and LHeC

Parameter	eRHIC	LHeC
# of pass	12	3
# of linac	1	2
energy gain per pass (GeV)	1.322	20
energy gain per linac (GeV)	1.322	10
SRF frequency (MHz)	422	721
Accelerating gradient (MV/m)	11	10
ERL recirculating pass	FFAG	Sep. pass

250 GeV proton and 100 GeV/n heavy ion and a new ERL electron accelerator to provide polarized electron beam from 1.3 GeV to 21.2 GeV. eRHIC will achieve 4×10^{33} cm^{-2}s^{-1} luminosity from collision of 250 GeV proton and 15.9 GeV electron beam. The LHeC use 7 TeV proton beam from the LHC and add an ERL to provide 60 GeV polarized electron beam, with the luminosity reaching 10^{33} cm^{-2}s^{-1}. Table 1 lists the baseline parameter of both ERL base EIC designs. For both designs, a multi-pass ERL scheme is adopted to save cost on the expensive Superconducting RF structure, i.e. the electron beam passes the linac with accelerating phase several times to accumulate energy before collision. eRHIC also adopts the non-scaling FFAG concept to avoid large number of ERL recirculating passes. Table 2 summarize the ERL parameters.

* Work supported by Brookhaven Science Associates, LLC under Contract No. DE-AC02-98CH10886 with the U.S. Department of Energy.
† yhao@bnl.gov

ISBN: 978-3-95450-168-7 doi:10.18429/JACoW-IPAC2015-TUYB3

Content from this work may be used under the terms of the CC BY 3.0 licence (© 2015). Any distribution of this work must maintain attribution to the author(s), title of the work, publisher, and DOI.

PROGRESS ON THE DESIGN OF THE POLARIZED MEDIUM-ENERGY ELECTRON ION COLLIDER AT JLAB*

F. Lin#, A. Bogacz, P. Brindza, A. Camsonne, E. Daly, Ya.S. Derbenev, D. Douglas, R. Ent, D. Gaskell, R. Geng, J. Grames, J. Guo, L. Harwood, A. Hutton, K. Jordan, A. Kimber, G. Krafft, R. Li, T. Michalski, V.S. Morozov, P. Nadel-Turonski, F. Pilat, M. Poelker, R. Rimmer, Y. Roblin, T. Satogata, M. Spata, R. Suleiman, A. Sy, C. Tennant, H. Wang, S. Wang, H. Zhang, Y. Zhang, Z. Zhao, Jefferson Lab, Newport News, VA, USA
P. N. Ostroumov, Argonne National Laboratory, Argonne, IL 60439 USA
D.P. Barber, Deutsches Elektronen-Synchrotron (DESY), 22607 Hamburg, Germany
Yu.M. Filatov, Moscow Inst. of Phys. and Tech., Dolgoprydny, and Joint Inst. for Nucl. Research, Dubna, Russia
S. Abeyratne, B. Erdelyi, Northern Illinois University, DeKalb, IL 50115 USA
A. Castilla, J. Delayen, C. Hyde, K. Park, Old Dominion University, Norfolk, VA 23529 USA
A. Kondratenko, M. Kondratenko, Sci. & Tech. Laboratory Zaryad, Novosibirsk, Russia
Y. Cai, Y.M. Nosochkov, M. Sullivan, M-H Wang, U. Wienands, SLAC National Accelerator Laboratory, Menlo Park, CA 94305 USA
J. Gerity, T. Mann, P. McIntyre, N.J. Pogue, A. Sattarov, Texas A&M University, College Station, TX, USA

Abstract

The Medium-energy Electron Ion Collider (MEIC) at JLab is designed to provide high luminosity and high polarization needed to reach new frontiers in the exploration of nuclear structure. The luminosity, exceeding 10^{33} cm^{-2}s^{-1} in a broad range of the center-of-mass (CM) energy and maximum luminosity above 10^{34} cm^{-2}s^{-1}, is achieved by high-rate collisions of short small-emittance low-charge bunches made possible by high-energy electron cooling of the ion beam and synchrotron radiation damping of the electron beam. The polarization of light ion species (p, d, ^{3}He) can be easily preserved and manipulated due to the unique figure-8 shape of the collider rings. A fully consistent set of parameters have been developed considering the balance of machine performance, required technical development and cost. This paper reports recent progress on the MEIC accelerator design including electron and ion complexes, integrated interaction region design, figure-8-ring-based electron and ion polarization schemes, RF/SRF systems and ERL-based high-energy electron cooling. Luminosity performance is also presented for the MEIC baseline design.

INTRODUCTION

The proposed MEIC at JLab is designed to meet the requirements of science program outlined in the EIC white paper [1]. The overall MEIC design strategies [2,3] towards achieving high luminosity and high polarization have not changed since 2006 but technical design aspects have evolved. In particular, the updates from the 2012 MEIC design report [3] are the results of an ongoing optimization process for performance, cost, technical risk and potential for phasing and future upgrades.

Main changes with respect to the design report in 2012 are given as follows [4].

- Ion and electron collider ring circumferences have been increased from 1.5 to 2.2 km.
- Electron collider ring is designed reusing PEP-II components (magnets, vacuum chambers, RF, etc.).
- Ion collider ring is designed based on super-ferric magnet technology.
- Only one single 8 GeV figure-8 shape booster is needed based on super-ferric magnets.

In this paper, we provide technical descriptions of the main subsystems on the baseline design and present the resulting luminosity performance.

MEIC BASELINE DESIGN

The MEIC is designed to be a traditional ring-ring collider. The central part of this facility is two figure-8 shape collider rings that are vertically stacked and housed in the same underground tunnel, as shown in Fig. 1. The figure-8 crossing angle is 81.7°, partitioning a collider ring into two arcs and two long straights. The ion beam executes a vertical excursion to the plane of electron ring for a horizontal crossing for electron-ion collisions. Two collider rings have nearly identical circumferences of approximately 2.2 km, and fit well in the Jefferson Lab site.

* Notice: Authored by Jefferson Science Associates, LLC under U.S. DOE Contract No. DE-AC05-06OR23177 and DE-AC02-06CH11357. The U.S. Government retains a non-exclusive, paid-up, irrevocable, world-wide license to publish or reproduce this manuscript for U.S. Government purposes.
# fanglei@jlab.org

ISBN: 978-3-95450-168-7 doi:10.18429/JACoW-IPAC2015-TUXC2

ENGINEERING CHALLENGES OF FUTURE LIGHT SOURCES

R.T. Neuenschwander*, L. Liu, S.R. Marques, A.R.D. Rodrigues, R.M. Seraphim, LNLS, Brazil

Abstract

We review some of the present engineering challenges associated with the design and construction of ultra-low emittance storage rings, the 4th generation storage rings (4GSR). The field is experiencing a growing interest since MAX-IV, followed by Sirius, started to build storage rings based on multi-bend-achromat (MBA) lattices. It was the recent progress in accelerator technology that allowed these facilities to base their designs on this kind of lattice. Although the challenges are starting to be overcome, many issues are still open and a lot of R&D is required until the 4GSR achieve optimal performance.

INTRODUCTION

Over the past few years an explosion of activities in the field of storage-ring based light sources has started, marking the beginning of a new generation in the history of storage rings, the fourth generation, where the electron beam emittance is reduced by at least an order of magnitude with respect to third generation machines, approaching the diffraction limit for multi-keV photons. The first audacious step was taken by the MAX-IV project in Sweden [1], a 3 GeV storage ring using a 7BA lattice that is based on quite a few new accelerator technological concepts. Following the path initiated by MAX-IV is the Sirius project in Brazil [2] with a 3 GeV 5BA lattice, similar emittance and circumference, but with its own set of particularities that reflects both a different user community and a different local industry condition. Both are green-field projects that are presently under construction. Other green-field projects that are being planned include BAPS in Beijing [3] and ILSF in Iran [4]. A big part of the recent activities in the field involve the plans of existing facilities in converting third generation machines into fourth generation ones. Some of these projects are well advanced, like ESRF [5], APS [6] and Spring-8 [7]; and others are at different conceptual stages, including ALS [8], Soleil [9], Diamond [10], SSRF [11], and others. Figure 1 shows a survey of emittances for some existing machines that are in operation for users, for machines under construction or in commissioning phase and for planned green-field or upgrade to existing machines.

The activity in the field can also be assessed by the great number of recent workshops [12-14] and special publications [15-16] on the subject.

The scaling laws in a storage ring that relate the emittance, the total number of dipoles, the beam energy and the ring circumference have been known for a long time. The first lattices based on MBA cells were proposed in the early 1990's [17], but their practical implementation had to wait for the technological advances that came about 20 years later. To understand the difficulties, we recall that the basic idea for emittance reduction using MBA lattices is that a large number of dipoles, and thus small deflection angle per dipole, allows the dispersion function to be kept focused to small values in the dipoles. The dispersion function plays an important role in determining the equilibrium emittance because it is directly related to the excitation of oscillations when a particle's energy is changed due to the emission of a photon. To keep the dispersion function small, strong focusing quadrupoles are needed between the dipoles. The strong quadrupoles and the small dispersion, in turn, require strong sextupoles to compensate for chromatic aberration effects. The strengths required have a big impact on the design of the magnets: the bore radius has to shrink and consequently the aperture available for the vacuum chambers is also reduced. The small vacuum chamber aperture has a big impact on the vacuum system because the conductance of the vacuum pipe is reduced (it scales as the cube of the pipe radius) and a new approach with distributed pumping is needed to keep the pressure low. Also the resistive wall impedance becomes an issue and may require a material with higher electrical conductivity for the chambers to minimize its effects.

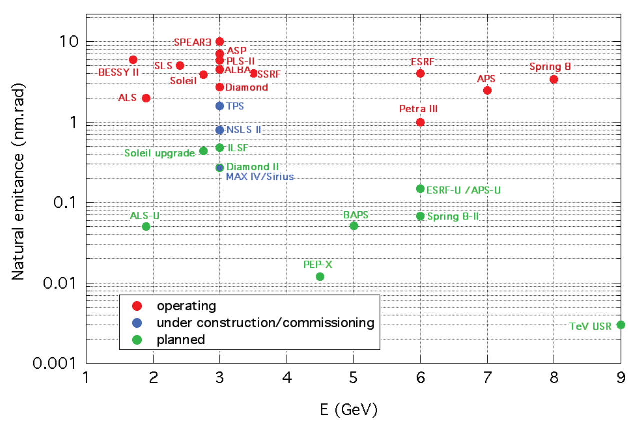

Figure 1: Survey of emittances versus energy for some existing machines that are in operation for users, for machines under construction or in commissioning phase and for some planned green-field or upgrade to existing machines.

The strong magnetic field gradients also imply high orbit amplification factors: the orbit amplitude becomes very sensitive to alignment errors of the magnets. The high amplification factors combined with the very small beam sizes impose stringent tolerance requirements for the magnets alignment and vibration amplitude, which translate into tight tolerances for the floor and girder vibrations. The high orbit stability requirement is also pushing the technology of beam diagnostics, fast feedback systems, special injection hardware to minimize

* regis.terenzi@lnls.br

Content from this work may be used under the terms of the CC BY 3.0 licence (© 2015). Any distribution of this work must maintain attribution to the author(s), title of the work, publisher, and DOI.

ISBN: 978-3-95450-168-7 doi:10.18429/JACoW-IPAC2015-TUXC3

COMMISSIONING OF THE TAIWAN PHOTON SOURCE

C. C. Kuo, J. Y. Chen, M. S. Chiu, P. J. Chou, Y. C. Liu, H. J. Tsai,
F. H. Tseng, K. T. Hsu, G. H. Luo and C. T. Chen
National Synchrotron Radiation Research Center, Hsinchu 30076, Taiwan

Abstract

The Taiwan Photon Source (TPS) is a 3-GeV third-generation synchrotron light source located in Hsinchu, Taiwan. After ground breaking on February 7, 2010 and five years of construction and hardware developments, commissioning of the beam began on December 12, 2014. The booster ring reached the design energy of 3 GeV on December 16. Beam transferred to the storage ring and first accumulation at 3 GeV produced the first synchrotron light on December 31. This report presents results and experience of the TPS commissioning.

INTRODUCTION

The 3-GeV TPS is located on the campus of NSRRC in Hsinchu Science Park together with the 1.5-GeV Taiwan Light Source (TLS) which has been in operation since 1993. To expand the capacity for research with synchrotron light and its capability at NSRRC, we initiated in 2004 a feasibility study for the construction of a medium energy and low emittance light source. Funding of the TPS project was approved in 2007 and a ground-breaking ceremony of TPS was held on February 7, 2010. The civil construction required about four years to complete. The installation of TPS accelerator components began in October 2013 when beneficial occupancy was available. Most installation work for the Linac and booster ring was completed by the end of July 2014. Permission for commissioning the TPS with beam was issued by the AEC on August 1. Tests of the system and improvements of the harware with beam have proceeded since then.

The 150-MeV beam from the Linac to the booster was available in mid August and tests of the booster power supplies conducted in parallel. Hardware optimizations were in progress like reducing the post-pulse residual field in the booster injection kicker or repair of a burned booster-dipole power supply due to overheating of the ground-current protection circuit-board during a full power ramping test.

At the beginning of September, a multi-turn circulating beam was observed in the booster ring. The beam survived up to 35 ms in mid September, but capture and storage of the beam did not succeed with the RF turned on. Attempts to correct orbit distortions within 4 mm still failed to capture beam. We found also that the corrector strengths required to get many turns were three times the simulated values. The beam pipes of the booster ring, made of stainless steel 304, have an elliptical shape, 35 mm (H) and 20 mm (V), and thickness of 0.7 mm. Distortion and misalignment of the pipes could be critical. Care was taken to realign the chambers and magnet positions. On November 12 it was recognized that the relative permeabilty (ranging from 1.2 to 2.0) of the pipes arising from the cold-drawn process of the pipe manufacture was too large. The magnetic fields of the combined-function dipoles (including quadrupole and sextupole gradients in dipole magnets) at 150 MeV could generate errors an order magnitude higher than tolerances. These chambers were taken apart and heat treated up to 1050 °C and then reinstalled within three weeks [1]. The relative permeability of the pipes after heat treatment was reduced to less than 1.01 [2].

Soon the beam survived 50 ms on December 11 and a beam was stored on December 12. Tests of the energy ramping began on December 15 and 3 GeV were reached the next day.

To prepare the extraction from the booster ring and its injection into the storage ring TPS was shut down from December 19 to 23. During this period, installation work and subsystem tests of the booster to storage ring transfer line (BTS) as well as the storage ring continued. The DC extraction septum operating at 3 GeV severely affected the booster capture at 150 MeV and ramping efficiency because of residual leakage field from the shielded septum chamber. Without further effort to shield the leakage field, we extracted a 1.5-GeV beam instead and injected it into the storage ring on December 26; the beam was stored the next day. After adding extra correctors nearby the DC extraction septum, extraction at 3 GeV became feasible on December 30 and an accumulated beam of up to 5 mA could be stored on December 31, 2014. The DC septum was replaced with an AC type in January, 2015.

Two 5-cell PETRA cavities were used to commission the storage ring in Phase I. The maximum stored current of 100 mA was achieved on March 26 after improvement of the RF feedback loop. Cleaning with synchrotron light (an accumulated beam dose up to 35 A.h before shutdown in April) could effectively improve the vacuum conditions for the commissioning in Phase II with superconducting RF (SRF) cavity modules.

During the commissioning period, the rules for radiation safety were strictly adhered to. In user mode the integrated dose should be less than 2 μSv per 4 h.

Before shutdown for the installation of the SRF and insertion devices (IDs) beginning in April, the hardware improvements, lattice characterization and system optimization etc. proceeded. Diagnostic and control systems played a major role during the commissioning stage [3,4,5]. We adopted middle-layer, high-level

Content from this work may be used under the terms of the CC BY 3.0 licence (© 2015). Any distribution of this work must maintain attribution to the author(s), title of the work, publisher, and DOI.

ISBN: 978-3-95450-168-7 doi:10.18429/JACoW-IPAC2015-TUYC2

MULTI-GeV PLASMA ACCELERATION RESULTS AT BELLA*

A. J. Gonsalves †, K. Nakamura, J. Daniels, H.-S. Mao, C. Benedetti, D. E. Mittelberger, E. Esarey, C. B. Schroeder, Cs. Tóth, J. van Tilborg, S. S. Bulanov, C. G. R. Geddes, and W. P. Leemans
Lawrence Berkeley National Laboratory, CA 94708, USA

Abstract

Stable multi-GeV electron beams were obtained in a laser plasma accelerator via precision control over capillary discharge plasma parameters and alignment. The plasma density was determined by measuring the group velocity of laser pulses propagated through the plasma channel. The channel depth was measured using laser centroid oscillations. Improved pointing control was achieved by accurate alignment of capillary angle and position. The pointing fluctuation was 0.6 mrad rms, which was comparable to the electron beam divergence. Simulations showed electron beams in reasonable agreement with experiment via strong self-focusing and injection into multiple plasma periods behind the laser pulse. These processes are strongly parameter dependent, reinforcing the need for precise plasma target control.

INTRODUCTION

Over the past decade laser plasma accelerators (LPAs) [1,2] have produced electron beams with energy $\gtrsim$ GeV using cm-scale plasmas [3–6], motivating their use for a wide range of light sources [7–12] and as a path towards a TeV-class linear collider [13,14]. For these and other applications it is important to reduce the laser pulse energy required to reach a given electron energy, since the size and cost of the LPA is dominated by the laser system. A preformed plasma channel can achieve this by mitigating diffraction of the laser beam and extending the acceleration length. In 2006, experiments with laser pulses of energy 2 J demonstrated the generation of electron beams with energy of 1 GeV using a preformed plasma channel [3]. Subsequently other experiments without preformed channels achieved electron beams with tails up to 1.45 GeV with laser energy a few times greater [4]. With the availability of petawatt class lasers, electrons were accelerated in non-preformed plasmas with energy up to 2-3 GeV using laser energy $\approx$ 100 J [5] and 25 J [6].

In this paper two electron acceleration experiments are presented. The first shows the generation of electron beams with energy up to 4.2 GeV using just 16 J of laser energy coupled to a preformed plasma channel [15]. As will be discussed, analysis of the beam parameters on input conditions was complicated by the electron beam angle fluctuation, and the limited angular acceptance of the magnetic spectrometer, which was between ±0.5 mrad and ±1.1 mrad, depending on electron beam energy and applied magnetic field. For the second experiment more accurate capillary alignment techniques were developed and the input laser pulses were spatially filtered to mitigate capillary damage. The electron beam pointing fluctuation was reduced to 0.6 mrad rms, which allowed for consistent observation of electron beams with full-width-half-maximum (FWHM) divergence < 1 mrad.

EXPERIMENTAL SETUP

In the experiments, laser pulses at a wavelength λ = 815 nm with bandwidth 40 nm were generated by the 1 Hz repetition rate Ti:sapphire-based BELLA (BErkeley Lab Laser Accelerator) petawatt laser [16]. The laser pulses were focused to a spot size of $w_0 = 52 \pm 2$ µm (Fig. 1) using an off-axis parabolic mirror with focal length of 13.5 m, where w_0 is defined as the radius at which the intensity decreased by $1/e^2$ of the peak value. The maximum total laser pulse energy delivered at the focal location was $\approx$ 16.6 J, as measured by a power meter inserted into the beam before the off-axis paraboloid. Typical pulse durations at optimum compression were $\tau_0 = 39 \pm 4$ fs (FWHM) as measured by a frequency resolved optical gating (FROG) system. The use of a deformable mirror and wavefront sensor enabled high focal spot quality (Strehl ratio 0.8 ± 0.1) and an associated normalized laser strength $a_0 \gtrsim 1.6$ for 16 J input energy, where $a_0 = 8.5 \times 10^{-10}\, \lambda\, [\mu\mathrm{m}] \sqrt{I_0 [\mathrm{W\,cm^{-2}}]}$ and I_0 is the peak intensity of the laser pulse.

The electron beam profile and position at 11.1 m from the exit of the plasma structure were measured using a calibrated phosphor screen imaged onto a CCD camera. The phosphor screen had field of view ±3 mrad, but only the center ±1 mrad of the electron beam passed through the hole in the optical wedge and power meter. Outside of this angle the electron beam passed through 46 mm of Aluminum and 81 mm of glass, which will approximately double the beam size on the phosphor screen for electron energy of 2 GeV and initial divergence 0.5 mrad. The electron beam energy and charge were measured using a 2.5 m-long magnetic spectrometer of design similar to the spectrometer used in Ref. [3].

As with previous experiments the laser was guided by a capillary discharge plasma channel [17–21] to maximize the electron energy gain [3,22]. In the present experiments the channel length was increased to 9 cm, and density lowered to between 6×10^{17} cm^{-3} and 11×10^{17} cm^{-3} to increase the acceleration length and electron beam energy. In addition the capillary diameter was increased to 500 µm to minimize damage from the increased laser pulse energy. The capillary discharge was operated with hydrogen using a current pulse of the form $I_{\max} \exp(1 - e^{-t/t_w} - t/t_w)$, where $I_{\max}$ = 250 A and t_w = 88 ns. The laser pulses arrived $\approx$ 30 ns after the peak of the current pulse. Two capillaries

* Work supported by DOE under DE-AC02-05CH11231 and DE-FG02-12ER41798
† ajgonsalves@lbl.gov

Content from this work may be used under the terms of the CC BY 3.0 licence (© 2015). Any distribution of this work must maintain attribution to the author(s), title of the work, publisher, and DOI.

ISBN: 978-3-95450-168-7 doi:10.18429/JACoW-IPAC2015-TUYC3

SCALING DOWN SYNCHRONOUS ACCELERATION: RECENT RESULTS, CURRENT STATUS, AND FUTURE PLANS OF A SUBRELATIVISTIC DIELECTRIC LASER ACCELERATION PROJECT*

J. McNeur†, M. Kozak, A. Li, N. Schoenenberger, A. Tafel, P. Hommelhoff
Friedrich-Alexander-University, Erlangen, Germany
Max-Planck-Institut für die Physik des Lichts, Erlangen, Germany

Abstract

The current status of subrelativistic acceleration via optical-scale Dielectric Laser Accelerators (DLAs), with an emphasis on those developed and tested at Friedrich-Alexander University in Erlangen, Germany, is reviewed. This promising field of accelerators has demonstrated proof-of-principle results in multiple energy regimes and current efforts are moving towards developing miniaturized standalone relativistic electron sources. The near-term experiments necessary to reach this goal are detailed.

INTRODUCTION

Dielectric laser accelerators (DLAs) aim to leverage commerically available near-infrared and optical lasers and the well-developed field of dielectric nanofabrication to accelerate charged particles with gradients approaching 10 GeV/m [1]. DLAs operate under the same principle of synchronous acceleration employed by numerous RF linear accelerators worldwide and first theorized by Wideroe in 1928 [2]. This principle was adapted towards laser-use via inverse Smith-Purcell radiation [3] and inverse Cherenkov radiation [4] in the 1960s and the idea of introducing dielectrics was conceived in the 1990s [5, 6]. The field gradients from commerically available lasers and the breakdown thresholds of candidate DLA materials allow DLAs to both scale down in size and scale up in field gradient in comparison to their RF brethren [7].

Recent experiments have demonstrated the principle of dielectric laser acceleration of both subrelativistic (30 keV [8] and 100 keV [9]) and relativistic (60 MeV [10]) electron beams. The demonstration of acceleration of 30 keV electrons in Erlangen is documented in detail here. The future directions of the Erlangen DLA project, aimed towards development of a miniaturized standalone relativistic electron source, are then outlined.

THE SINGLE GRATING DLA

The specific geometry used to accelerate 30 keV electrons is the 'single grating DLA', a fused silica phase mask with grating teeth of periodicity on the order of the incident laser wavelength. It has been designed, fabricated and tested. A cross-section of this fused silica grating mask along with the longitudinal electromagnetic fields (of the accelerating mode) excited when the grating is struck by an incident laser, is shown in Figure 1. Although Figure 1 displays the third harmonic field pattern excited by the incident laser, all harmonics of this fundamental mode are excited, each with a phase velocity of $\frac{c\lambda_p}{n\lambda}$ where c is the speed of light, λ_p is the periodicity of the single grating, n is the order of the harmonic, and λ is the central wavelength of the incident laser. As described above, synchronous acceleration occurs if and only if the phase velocity of one of the excited harmonics matches the velocity of electrons traversing the near-field profile above the grating (travelling from left to right in Figure 1).

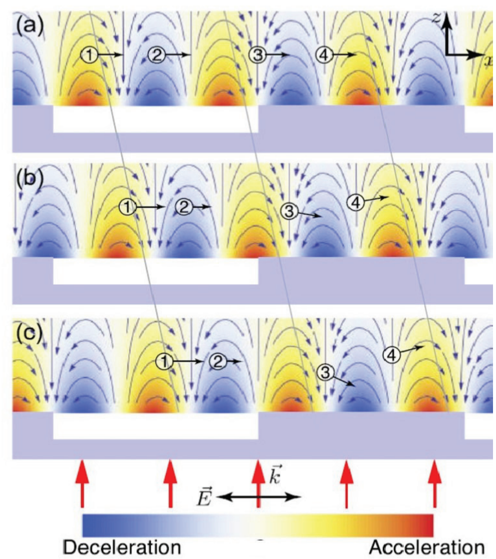

Figure 1: Three consecutive snapshots in time of the evolution of the third harmonic of the excited fields along with the evolution of four different injection phases corresponding to acceleration (1), deceleration (2) or deflection (3,4).

Two features of the field patterns in Figure 1 are of note (and described in more detail elsewhere [11]): 1) for an electron beam that samples all phases of the accelerating mode (such as the beam used in the experiment described below), half of the electron beam will see accelerating fields whereas half will see decelerating fields, and 2) only those electrons that are injected within the transverse evanescent decay length of the accelerating mode (within 200nm of the grating surface in the below experiment) will traverse fields of significant magnitude. The latter of these conditions then requires that the electron beam must be aligned to within 200nm of the grating surface. However, clipping of

* Work supported by ERC grant "NearFieldAtto"
† joshua.mcneur@fau.de

Content from this work may be used under the terms of the CC BY 3.0 licence (© 2015). Any distribution of this work must maintain attribution to the author(s), title of the work, publisher, and DOI.

ISBN: 978-3-95450-168-7 doi:10.18429/JACoW-IPAC2015-TUAB1

CORRECTION OF NONLINEAR COUPLING RESONANCES IN THE SPRING-8 STORAGE RING

M. Takao*, K. Soutome, K. Fukami and Y. Shimosaki
JASRI/SPring-8, Hyogo, Japan

INTRODUCTION

At recent light source rings, the top-up operation, in which the beam is injected during the user experiments, is widely used to make up the short lifetime and to keep the current constant. Since the beam is injected in the magnet array gap of the insertion device closing, it is important to protect the insertion devices from the electron irradiation.

The injection efficiency decreases as the vertical scraper closing as shown in Fig. 1. This implies that, although the injected beam initially oscillating in horizontal direction with a large amplitude, the vertical spread of the injecting bean is generated by a coupling resonance [1–3].

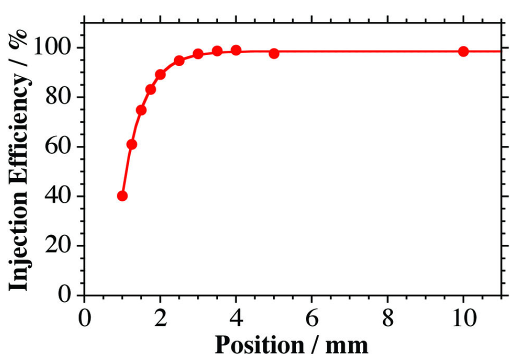

Figure 1: Injection Efficiency vs. Vertical Scraper position.

This is true for a particle scattered by Thouschek effect, i.e. the collision within a bunch. Figure 2 shows the typical dependence of the Touschek lifetime on the RF accelerating voltage. The electron scattered at the nonzero dispersion starts to oscillate in horizontal direction with an amplitude proportional to the momentum deviation. Although in low RF voltage the lifetime is limited by the longitudinal dynamics, it is dominated by the transverse dynamics in high RF voltage. Similar to the injection efficiency, the lifetime decreases as the vertical scraper closing, which implies that the coupling plays important role in beam loss mechanism [1–3].

At the spring-8 storage ring one of the insertion devices generates the strong coupling resonance, i.e. the skew octupole resonance, affecting the injection efficiency and the beam lifetime. Here we report the correction of the coupling resonance by using the skew octupole magnet. Furthermore, the simulation study for the improvement of the momentum acceptance by means of the skew sextupole magnet.

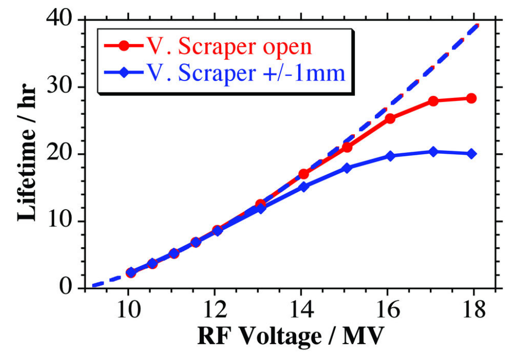

Figure 2: Lifetime vs. Vertical Scraper position.

COUPLING RESONANCE INDUCED BY AN INSERTION DEVICE

The insertion device ID07 of the SPring-8 is a special one composing of 8 figure-8 (4 horizontal and 4 vertical) undulators [4]. It is found that the vertical figure-8 undulator strongly excites the skew octupole coupling resonance so as to reduce the injection efficiency and the beam lifetime. Figure 3 shows the variation of the injection efficiency as the gap of ID07 closing under the condition of the vertical scraper gap 2mm. To emphasize the effect of the coupling resonance, we close the scraper to 2 mm. Since ID07 is out-vacuum undulator, the reduction is caused by the dynamical effect, i.e. the coupling resonance.

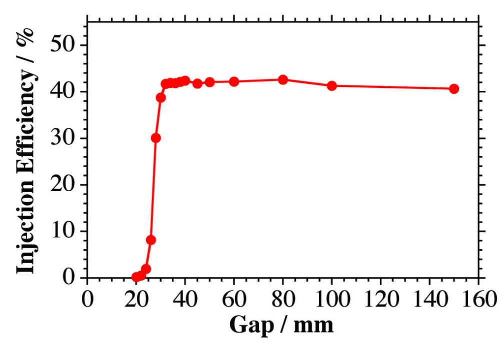

Figure 3: Injection Efficiency vs. ID07 gap.

To understand the dynamics, we measure the beam oscillation by using the turn-by-turn beam position monitor (BPM). We kick the stored single bunch beam to give a large amplitude like an injection beam by means of the bump magnet. Figures 4 show the beam oscillation with the initial amplitude 10 mm, which is a typical amplitude of the injection beam. The left (right) figure at the upper row shows the hor-

* takao@spring8.or.jp

Content from this work may be used under the terms of the CC BY 3.0 licence (© 2015). Any distribution of this work must maintain attribution to the author(s), title of the work, publisher, and DOI.

ISBN: 978-3-95450-168-7 doi:10.18429/JACoW-IPAC2015-TUAB2

Content from this work may be used under the terms of the CC BY 3.0 licence (© 2015). Any distribution of this work must maintain attribution to the author(s), title of the work, publisher, and DOI.

FIRST COLLECTIVE EFFECTS MEASUREMENTS IN NSLS-II WITH ID'S

A. Blednykh#, B. Bacha, G. Bassi, W. Cheng, J. Choi, Y. Hidaka, Y. Li, B. Podobedov, V. Smalyuk, T. Shaftan, T. Tanabe, G. Wang, F. Willeke, L.-H. Yu
BNL, NSLS-II, Upton, NY, 11973-5000, USA

Abstract

As another important milestone towards the final goal to store an average current of 500mA, the average current of 200mA, distributed within ~1000 bunches, was recently achieved in the NSLS-II storage ring after the installation of three Damping Wigglers and four In-Vacuum Undulators. First measurements of the collective effects and instability thresholds, both in single- and multi-bunch mode, are discussed.

INTRODUCTION

The new 3GeV NSLS-II storage ring is in operation with the first six beam-lines designed as a part of the project. The average current of 200mA within ~1000 bunches has been stored as another important milestone in intensity increasing with the final goal of 500mA. For the current lattice configuration with three damping wigglers (3DW's), two Elliptically Polarizing Undulators (EPU's) and four In-Vacuum Undulators (4IVU's) installed and one SC CESR-B 500MHz RF cavity with $V_{RF} = 1.78MV$ used for operation, the estimated RMS bunch duration at low current is $\sigma_s = 6mm$ with energy spread $\sigma_\varepsilon = 8.8 \times 10^{-4}$ (Bending Magnets (BM) + 3DW's). The RMS bunch duration, for the bare lattice with DW magnet gaps open, is $\sigma_s = 3.4mm$ with energy spread $\sigma_\varepsilon = 5 \times 10^{-4}$. Some key parameters for the collective effects beam studies are given in Table 1.

Table 1: NSLS-II Parameters for Collective Effects Studies

Energy, $E_0(GeV)$	3
Revolution period, $T_0(\mu s)$	2.6
Momentum compaction, α	3.7 x 10^{-4}
Energy loss, $U(keV)$	287 (BM) 674 (BM+3DW's)
RF voltage, $V_{RF}(MV)$	1.78
Synchrotron tune, ν_s	6.8 x 10^{-3}
Damping time, $\tau_x, \tau_s(ms)$	54, 27 (w/o DW's) 23, 11.5 (w 3DW's)
Energy spread, σ_ε	5 x 10^{-4} 8.8 x 10^{-4} (BM+3DW's)
Bunch duration, $\sigma_s(mm)$	3.4 (w/o DW's) 6 (w 3DW's) Ignoring bunch lengthen.

SINGLE BUNCH

The stabilizing effect of positive chromaticity on the single bunch threshold current has been studied for a lattice with 3DW's and 4IVU's magnet gap closed (beamline operations). The single bunch current is limited due to the vertical Transverse Mode Coupling Instability (TMCI). The measured bunch current threshold is $I_{th} = 0.95mA$ at zero chromaticity (Fig. 1a), $I_{th} = 3.2mA$ at chromaticity $\xi_{x/y} = +5/+5$ (Fig. 2a) and $I_{th} = 6mA$ at chromaticity $\xi_{x/y} = +7/+7$. There is no significant effect on increasing the accumulated Single Bunch (SB) current up to chromaticity $\xi_{x/y} = +5/+5$. The horizontal tune shifts as a function of SB current (Figs. 1b, 2b) indicates a stronger effect of the broad-band quadrupole impedance due to installed 4IVUs, to be compared with the results for a bare lattice (w/o ID's) presented in [1], where the horizontal tune shifts were independent of the SB current.

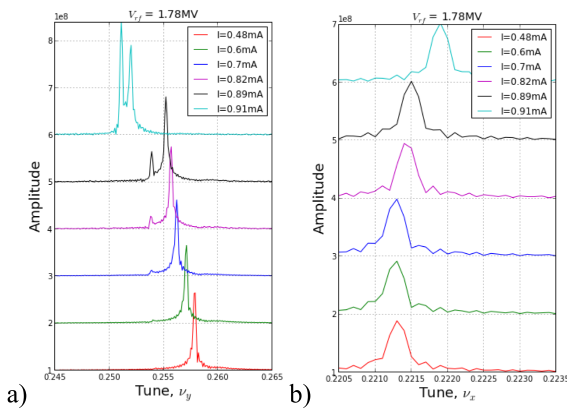

Figure 1: Chromaticity $\xi_{x/y} = 0/0$. All ID's gap closed.

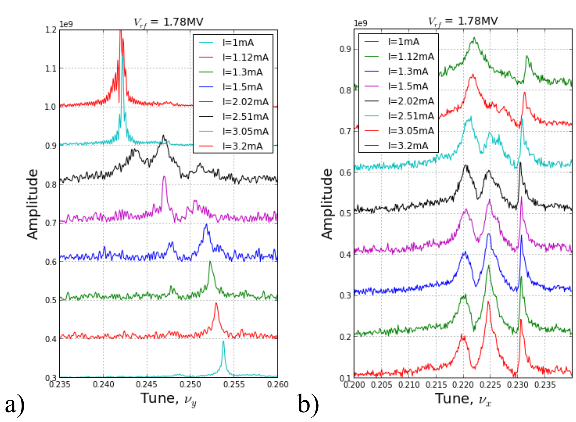

Figure 2: $\xi_{x/y} = +5/+5$. All ID's gap closed.

To adjust the linear chromaticity from zero to $+7/+7$, only the settings of the chromatic sextupoles have been changed. The injection efficiency was 50% at chromaticity $+7/+7$ without further lattice optimization. Betatron oscillations have been excited by kicking the bunch in both directions with horizontal and vertical pingers. The measured spectra (Figs. 1,2) from Turn-by-Turn (TbT) data are plotted with arbitrary offsets and

*Work supported by DOE contract DE-SC0012704.
#blednykh@bnl.gov

ISBN: 978-3-95450-168-7 doi:10.18429/JACoW-IPAC2015-TUAB3

CHROMATICITY EFFECTS FOR SPACE CHARGE DOMINATED BEAMS IN THE CERN PS BOOSTER

V. Forte*, CERN, Geneva, Switzerland - Université Blaise Pascal, Clermont-Ferrand, France
E. Benedetto, F. Schmidt, CERN, Geneva, Switzerland

Abstract

In view of the LHC Injectors Upgrade (LIU) project, an extensive campaign is on-going in the CERN PS Booster (PSB) to study collective effects for the future operation with the 160 MeV injection from Linac4. In operation, the machine is running with uncorrected natural chromaticity. This paper focuses on the study of the effects of chromaticity on losses and beam blow-up.

INTRODUCTION

The CERN PS Booster is the first synchrotron in the LHC accelerator chain. In the framework of the LIU project, a campaign of renovations takes place to host the new H$^-$ injection energy of 160 MeV from Linac4, instead of the present 50 MeV proton injection from Linac2 [1]. The main physical reason for this change is the large incoherent space charge (s.c.) tune spread that presently limits the brightness of the beams (especially for those meant for the LHC). Through the Linac4 it will be possible to tailor the transverse and longitudinal emittances in the PSB to fit the requirements of the high-luminosity future LHC beams [2]. The purpose of this paper is to investigate the effects of the chromaticity in this machine in combination with space charge. To date, the PSB is always operated with the uncorrected natural chromaticities of (ξ_x = -0.8, ξ_y = -1.6). The chromatic detuning can be modulated via one family of 16 normal chromatic sextupoles, distributed one per period along the machine. This limitation leads to a coupled control of the horizontal and vertical chromaticities, as shown in Fig. 1.

The interaction between chromaticity and space charge will be taken into account for negative chromaticities, to avoid the development of coherent instabilities, since the PSB is operating below transition. At an energy of 160 MeV PSB experiments close to two different resonances are being discussed to underline the correlation between the incoherent space charge tune spread and the chromatic one. The simulations are being performed with the PTC-ORBIT code [3]. Lastly, a prediction for future LHC operations is being attempted for different chromatic conditions.

SPACE CHARGE AND CHROMATICITY

The space charge field has a defocusing effect in both the horizontal and vertical plane, see e.g. [4]. Each particle feels a s.c. detuning, which depends on the line density (protons/m) and the size of the transverse amplitudes. In addition to that, the chromaticity also induces a detuning

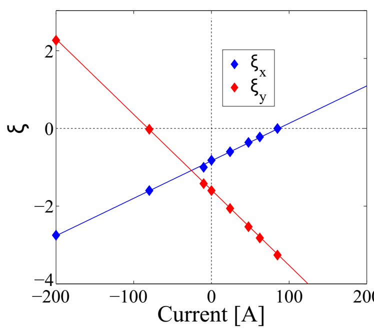

Figure 1: Measured vertical (red) and horizontal (blue) chromaticities vs. current [A] in the chromatic sextupoles.

which is proportional to the particle momentum offset Δp/p and the chromaticity ξ itself.

The particles in a bunch will in general feel both effects. Figure 2 shows the path of a particle with a large synchrotron amplitude, which goes from regions in which both the line density (s.c. component) and the momentum offset (chromatic component) are large, to the head or the tail of the bunch, in which the space charge tune shift is almost zero while the Δp/p can have a large excursion. In particular, one can consider three "branches" in its motion:

- AB - the space charge detuning is large. For positive Δp/p (and negative chromaticity, such as in the PSB) both effects are defocusing and they sum up;
- BC - in the vicinity of the bare tune, when the particle is sitting in the head or the tail of the bunch, the s.c. component is almost absent and the tune is moving on a line which slope depends on the ration between horizontal and vertical chromaticity;
- CD - the space charge component is large again, however for negative Δp/p, the chromatic detuning is positive, i.e. goes in the opposite direction with respect to the space charge one.

The orientation and the length of these three "branches" depends on the chromaticity value, on the synchrotron amplitude and on the particle actions in the horizontal and vertical plane, as explained in details in [5].

According to the chromatic working point, indeed, the entire tune footprint changes, as is shown in Fig. 3, and for the same bare tune it may or may not touch a given resonance line, e.g. the $3Q_y = 13$, in the case studied in this paper. Similarly to Fig. 2, Figure 4 analyses (in red) the different tune evolutions of particles performing large synchrotron oscillations, for different chromaticities: these particles are good candidates to be perturbed through the periodic resonance crossing mechanism [6].

* vincenzo.forte@cern.ch

Content from this work may be used under the terms of the CC BY 3.0 licence (© 2015). Any distribution of this work must maintain attribution to the author(s), title of the work, publisher, and DOI.

ISBN: 978-3-95450-168-7 doi:10.18429/JACoW-IPAC2015-TUBB1

CHARGE STRIPPER DEVELOPMENT FOR FRIB*

F. Marti#, P. Guetschow, FRIB, East Lansing, MI, USA
Y. Momozaki, J. A. Nolen, C. B. Reed, ANL, Argonne, IL 60439, USA
A. Hershcovitch, P. Thieberger, BNL, N.Y., USA

Abstract

The Facility for Rare Isotope Beams (FRIB) at Michigan State University is building a heavy ion linac to produce rare isotopes by the fragmentation method. The linac will accelerate ions up to U to energies above 200 MeV/u with beam powers up to 400 kW. At energies between 16 and 20 MeV/u the ions will be stripped to higher charge states to increase the energy gain downstream in the linac. The main challenges in the stripper design are due to the high power deposited by the ions in the stripping media (~ 30 MW/cm^3) and radiation damage if solids are used. For that reason self-recovering stripper media must be used. The baseline stripper choice is a high-velocity, thin film of liquid lithium with an alternative option of a helium gas stripper. We present in this paper the status of the R&D and construction of the final stripper. Extensive experimental work has been performed on both options.

INTRODUCTION

Michigan State University was charged by the Office of Science of the Department of Energy of the US to design and build the Facility for Rare Isotope Beams (FRIB) at the end of 2008. The facility is funded by the Office of Nuclear Physics with contributions and cost share from Michigan State University. The goal of the facility is the production of rare isotopes produced by the in-flight separation method. This method provides fast development time for any isotope and allows short lived isotopes to be available. The facility will provide fast, stopped and reaccelerated beams of secondary ions.

One of the main components of the facility is a driver linac capable of producing beams of ions from the low mass region up to U at energies above 200 MeV/u and with a total beam power on target of 400 kW [1]. The linac is folded in three segments running parallel to each other with two 180 degree bends in between. After the first segment linac and before the first bend a charge stripper is located to increase the Q/A of heavy ions by more than a factor two.

This paper describes the options considered for the charge stripper and the status of their design and construction.

CHARGE STRIPPER CHALLENGES

Traditional charge strippers in accelerators are designed utilizing thin films of solid materials, in many cases carbon [2]. The main difference between FRIB and accelerators that strip intense H^- beams is that even though the currents are lower in FRIB, the energy loss per ion per unit length is much higher for heavy ions than for protons (see Figure 1).

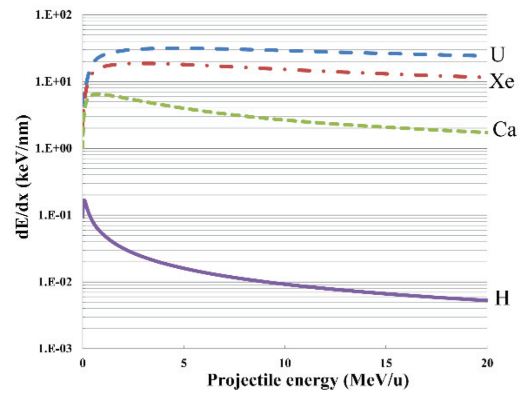

Figure 1: Comparison of the energy loss per unit length in carbon foils for some heavy ions and protons. A single U ion deposits three orders of magnitude higher power than a proton of the same velocity. Stripping energies at FRIB are between 16 and 20 MeV/u.

There appears to be a critical threshold in the linear energy deposition for the formation of tracks in graphite of the order of 7 keV/nm, with a track produced for every ion with energy above 18 keV/nm [3]. Heavy ions like Xe and U have a dE/dx higher than this threshold, while protons are much lower.

Besides the radiation damage, the thermal effects are also important. At the energies of the FRIB stripper the U beam would deposit about 30 MW/ cm^3 power densities in the carbon foil.

Given the above considerations we have looked at two options for the charge stripper, liquids and gases. Both can be made to survive the high power deposition and no lattice damage occurs.

OPTIONS

Liquid Lithium Stripper

A liquid lithium charge stripper was first proposed by J. A. Nolen [4] from Argonne National Laboratory (ANL). A fast moving film (~ 50 m/s) would be able to carry away the thermal energy deposited by the beam before reaching high temperatures (below boiling). Lithium has some very attractive properties when used as stripping media, it has a very low vapor pressure at the melting temperature (181 C and 1.5 10-9 Torr) compared with other potential liquids like mercury (2 mTorr at room temperature). It has a high boiling point (1342 C) and it

*Work supported by the U.S. Department of Energy Office of Science under Cooperative Agreement DE-SC0000661
#marti@frib.msu.edu

Content from this work may be used under the terms of the CC BY 3.0 licence (© 2015). Any distribution of this work must maintain attribution to the author(s), title of the work, publisher, and DOI.

ISBN: 978-3-95450-168-7 doi:10.18429/JACoW-IPAC2015-TUBB2

THE ACCELERATOR FACILITY OF THE FACILITY FOR ANTIPROTON AND ION RESEARCH

Oliver Kester#, Peter Spiller, Frank Becker, Oleksiy Dolinskyy, Lars Groening, Klaus Knie, Hartmut Reich-Sprenger, Wolfgang Vinzenz, Martin Winkler
GSI Helmholtzzentrum für Schwerionenforschung, Darmstadt, Germany
Dieter Prasuhn, Forschungszentrum Jülich, Germany

Abstract

The accelerators of the facility for Antiproton and Ion Research – FAIR are under construction. The very sophisticated system of accelerators is designed to produce stable and rare isotope beams with a significant variety of intensities and beam energies. FAIR will explore the intensity frontier of heavy ion accelerators and the ion and antiproton beams for the experiments will have highest beam quality for cutting edge physics to be conducted. The main driver accelerator of FAIR will be the SIS100 synchrotron. In order to produce rare isotope beams (RIB), which are several orders of magnitude more intense compared to beams provided by existing RIB facilities, a unique superconducting fragment separator is under construction. A system of storage rings will collect and cool secondary particles from the FAIR. As the construction of the FAIR accelerators and the procurement has started, an overview of the designs, procurements plans and infrastructure preparation can be provided.

INTRODUCTION

The FAIR facility in the Modularized Start Version (MSV) [1] will consist of six circular accelerators (SIS18, SIS100, CR, HESR, ESR and CRYRING), of two linear accelerators (p-Linac, UNILAC) and of about 1.5 kilometres of beam lines see Fig. 1. The existing GSI UNILAC-SIS18 accelerators will serve as injector to the FAIR SIS100 synchrotron. GSI is in charge of the SIS100, the HEBT, Super-FRS and the overall technical coordination of the FAIR accelerator complex. Many systems are constructed in consortia with international partners. The Research Centre Jülich will build the HESR - High Energy Storage Ring - for the research with high-energy antiprotons using the PANDA detector; BINP Novosibirsk takes care of the construction of the collector ring CR.

The driver accelerator of FAIR is the fast ramping, superconducting heavy ion synchrotron - SIS100 - that allows the acceleration of the most intense beams of stable elements from Protons (30 GeV) to Uranium (10 GeV/u) [2]. The FAIR driver accelerator will provide high energy/ high intensity proton and heavy ion beams to the various experimental stations. The CBM- Plasma- and Biomat-experiments are directly supplied with primary beams from the SIS100. Two target stations for the generation of secondary beams (pbar and RIBs) allow the conversion of primary ions into secondary particles.

#o.kester@gsi.de

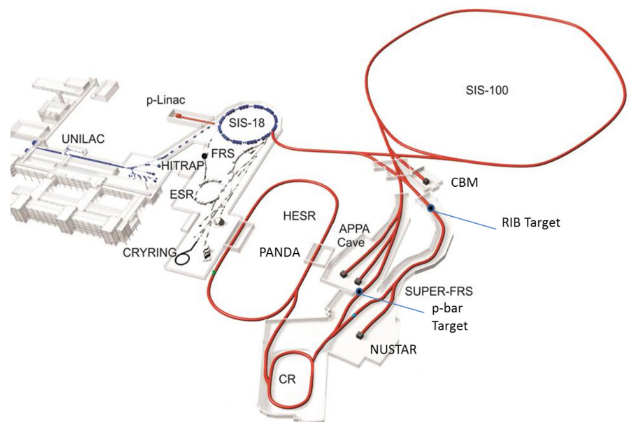

Figure 1: Overview of the GSI and the FAIR accelerator facility.

The Super-FRS will be the most powerful in-flight separator worldwide for exotic nuclei up to relativistic energies. Rare isotopes of all elements up to uranium can be produced and spatially separated within some hundred nanoseconds, thus very short-lived nuclei can be studied efficiently. The Super-FRS is a large-acceptance superconducting fragment separator with three branches serving different experimental systems. The accelerator facility is complemented by a system of storage rings. The main task of the collector ring (CR) is stochastic cooling of radioactive ions or antiproton beams from the production targets. In addition, this ring offers the possibility for mass measurements of short-lived ions, by operating in isochronous mode. The high-energy storage ring (HESR) is optimized for antiprotons of energy up to 14 GeV. This ring will operate with an internal target and associated detector set-up (PANDA).

OPERATION SCENARIOS

The main system parameter of the FAIR accelerators shown in Table 1, are the basis for the operation of the facility. The following typical operation scenarios of the FAIR accelerator facility are foreseen:

A) High intensity, high energy proton beams at energies up to 29 GeV: The proton linac injects protons into the SIS18 at 70 MeV beam energy, which will then be accelerated to 4 GeV in the SIS18. Merging of four proton bunches from SIS18 into a single bunch and subsequent compression into a 50 ns pulse for acceleration up to 29 GeV is accomplished in the SIS100. Thereby a single bunch of up $2*10^{13}$ protons will be delivered to the anti-

Content from this work may be used under the terms of the CC BY 3.0 licence (© 2015). Any distribution of this work must maintain attribution to the author(s), title of the work, publisher, and DOI.

ISBN: 978-3-95450-168-7 doi:10.18429/JACoW-IPAC2015-TUBB3

Content from this work may be used under the terms of the CC BY 3.0 licence (© 2015). Any distribution of this work must maintain attribution to the author(s), title of the work, publisher, and DOI.

RECENT PROGRESS OF J-PARC RCS BEAM COMMISSIONING - TOWARD REALIZING THE 1-MW OUTPUT BEAM POWER

Hideaki Hotchi for the J-PARC RCS beam commissioning group
J-PARC center, Japan Atomic Energy Agency, Tokai, Naka, Ibaraki, 319-1195 Japan

Abstract

J-PARC RCS is now in the final beam commissioning phase aiming for the design output beam power of 1 MW. This paper presents our approaches to beam loss issues that we faced on the process of the beam power ramp-up toward 1 MW.

INTRODUCTION

The J-PARC 3-GeV Rapid Cycling Synchrotron (RCS) is the world's highest class of high-power pulsed proton driver aiming at the output beam power of 1 MW [1]. The injector linac delivers a 400-MeV H^- beam to the RCS injection point, where it is multi-turn charge-exchange injected through a 350-μg/cm^2-thick HBC stripping foil over a period of 0.5 ms. RCS accelerates the injected protons up to 3 GeV with a repetition rate of 25 Hz, alternately providing the 3-GeV proton beam to the Material and Life Science Experimental Facility and to the 50-GeV Main Ring Synchrotron by switching the beam destination pulse by pulse.

Recently the hardware improvement of the injector linac has been completed, by which the injection energy was upgraded from 181 MeV to the design value of 400 MeV in 2013, and then, the injection peak current was upgraded from 30 mA to the design value of 50 mA in 2014. In October, 2014 after completing these series of injector linac upgrades, RCS started the final stage of beam commissioning aiming for the design output beam power of 1 MW. This paper presents our approaches to beam loss issues that we faced on the process of the beam power ramp-up toward 1 MW.

550-kW BEAM TEST CONDUCTED AFTER THE INJECTION ENERGY UPGRADE (RUN#54)

In April, 2014 (Run#54), RCS conducted a 550-kW high intensity beam test with the upgraded injection energy of 400 MeV, using a 0.5 ms-long injection pulse with a peak current of 24.6 mA and a chopper beam-on duty factor of 60%. In this beam test, the operating point was set at (6.45, 6.42), where systematic beam loss measurements were performed with various injection painting parameters, and compared with the old data taken with the lower injection energy of 181 MeV.

In order to minimize space-charge induced beam loss, RCS employs injection painting for both transverse and longitudinal phase spaces [2]. On the transverse plane, correlated painting with a painting emittance of 100π mm mrad (ε_{tp}) was applied in this beam test. On the other hand, for longitudinal painting [3,4], the momentum offset injection of 0.0, −0.1 and −0.2% (Δp/p) was tested in combination with superposing a 2nd harmonic rf with an amplitude of 80% (V_2/V_1) of the fundamental rf. As an additional control in longitudinal painting, the phase sweep of the 2nd harmonic rf was also employed during injection from −100 to 0 degrees (ϕ_2) relative to that of the fundamental rf.

Painting parameter ID

Parameter ID	ϵ_{tp} (π mm mrad)	V_2/V_1 (%)	ϕ_2 (degrees)	$\Delta p/p$ (%)
1	–	–	–	–
2	100	–	–	–
3	–	80	−100	–
4	–	80	−100	−0.1
5	–	80	−100	−0.2
6	100	80	−100	–
7	100	80	−100	−0.1
8	100	80	−100	−0.2

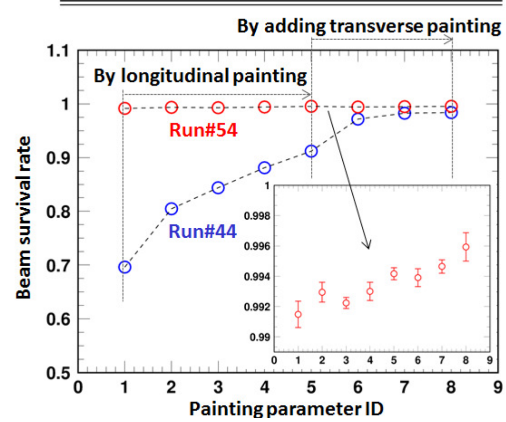

Figure 1: Beam survival rates measured with various combinations of transverse and longitudinal painting (IDs 1 to 8), where the red circles correspond to the data taken with the upgraded injection energy of 400 MeV with a beam intensity of 553 kW, while the blue ones are the old data taken with the lower injection energy of 181 MeV with a similar beam intensity of 539 kW.

Figure 1 shows the beam survival rates measured with various combinations of transverse and longitudinal painting (IDs 1 to 8). In this figure, the red circles correspond to the data taken in this beam test with a beam intensity of 553 kW (4.60×10^{13} ppp), while the blue ones are the old data (Run#44 in November, 2012) taken with the lower injection energy of 181 MeV with a similar beam intensity of 539 kW (4.49×10^{13} ppp). As shown by the blue circles, the larger parameter dependence was observed for the lower injection energy of 181 MeV, since the space-charge effect is more critical. In this case, 30%-big beam loss appeared with no painting. But, this beam loss was drastically decreased from ID 1 to ID 5 by longitudinal painting, and from ID 5 to ID 8 by adding

#hotchi.hideaki@jaea.go.jp

ISBN: 978-3-95450-168-7 doi:10.18429/JACoW-IPAC2015-TUAC1

BEAM INSTRUMENTATION AND DIAGNOSTICS FOR HIGH LUMINOSITY LHC

R. Jones, E. Bravin, B. Dehning, T. Lefevre, H. Schmickler, CERN, Geneva, Switzerland

Abstract

The extensive array of beam instrumentation with which the LHC is equipped, has played a major role in its commissioning, rapid intensity ramp-up and safe and reliable operation. High Luminosity LHC (HL-LHC) brings with it a number of new challenges in terms of instrumentation that will be discussed in this contribution.

INTRODUCTION

The following sections will describe the main beam instrumentation and diagnostic developments underway or foreseen as part of the High Luminosity Upgrade Project of the LHC, HL-LHC [1].

BEAM LOSS MEASUREMENT

Monitoring of beam losses is essential for the safe and reliable operation of the LHC. While the existing system [2] is believed to meet the needs of the HL-LHC for the arc regions, this will no longer be the case for monitors in the high luminosity interaction points, and for monitors located in high radiation areas.

Beam Loss Monitors for the Triplet Magnets

The HL-LHC high luminosity insertions region magnets will be subjected to an enhanced continuous radiation level due to the increase in collision debris resulting from the higher luminosity. With the presently installed configuration of ionisation chambers in this region, outside of the cryostats, the additional signal from any quench provoking accidental loss would be completely masked by that coming from collision debris.

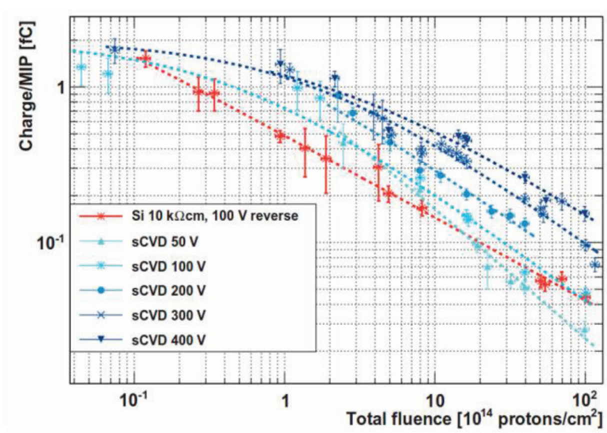

Figure 1: Charge collection efficiency for silicon and diamond detectors with increasing radiation fluence in a cryogenic environment.

The option of placing radiation detectors inside the cryostat of the triplet magnets as close as possible to the superconducting coils is therefore under study. The dose measured by such detectors would correspond more precisely to the dose deposited in the coils, which ultimately sets the quench level. Three detectors have been investigated as candidates for operation in a high radiation, cryogenic environment [3]: single crystal chemical vapour deposition (CVD) diamond; p+-n-n+ silicon wafers; liquid helium ionisation chambers.

Irradiation at cold up to several Mega-Gray showed a degradation of the charge collection efficiency by a factor of 15 in both CVD diamond and silicon (Fig. 1). The major downside of silicon compared to diamond at room temperature, its much higher leakage current when irradiated, is seen to disappear at liquid helium temperatures. Tests of detectors mounted inside the cryostats of existing LHC magnets are currently ongoing with the aim of gaining experience with the long term performance of such detectors under operational conditions.

Radiation Tolerant Beam Loss Monitor ASIC

The quench levels estimated for 7 TeV running are, for some detectors, very close to the noise level of the acquisition system. The noise is mainly determined by the length of cable required to bring the signal from the radiation hard detector to the less radiation tolerant front-end electronics. Development has started to implement this electronics in a radiation hard Application Specific Integrated Circuit (ASIC). This ASIC is still based on the current to frequency conversion used in the existing system, but packaged in a compact, radiation-tolerant form with an increased dynamic range (Fig. 2). The technique employed allows the digitisation of bipolar charge over a 120dB dynamic range (40fC - 42nC) with a 40µs integration time and an adjustable, temperature compensated conversion current reference [4].

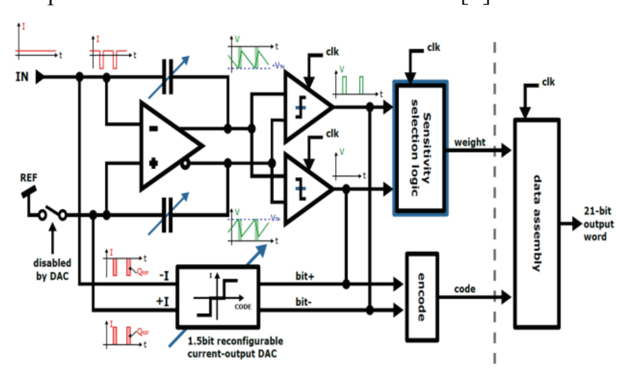

Figure 2: Schematic of the BLM ASIC implementation.

Total Ionizing Dose (TID) effects have been investigated using an X-ray beam with 20 keV peak energy. The characteristics of the device were measured

Content from this work may be used under the terms of the CC BY 3.0 licence (© 2015). Any distribution of this work must maintain attribution to the author(s), title of the work, publisher, and DOI.

ISBN: 978-3-95450-168-7 doi:10.18429/JACoW-IPAC2015-TUAC2

WIDEBAND VERTICAL INTRA-BUNCH FEEDBACK AT THE SPS - 2015 RESULTS AND PATH FORWARD*

J.D. Fox, J. Dusatko, C. Rivetta, O. Turgut,
Stanford Linear Accelerator Center Stanford, CA USA
W. Hofle, U. Wehrle CERN Geneva, Switzerland
S. De Santis LBL Berkeley, CA USA

Abstract

We present experimental measurements taken from CERN SPS machine development studies with a wideband intra-bunch feedback channel prototype. The demonstration system is a digital processing system with recently installed wideband kicker and amplifier components. This new hardware extends the bandwidth up to 1 GHz and allows driving and controlling multiple vertical transverse modes in the bunch. The studies are focused on driving the bunch with spectrally controlled signals to identify a reduced model of the bunch dynamics and testing model-based feedback controllers to stabilize the bunch dynamics. The measurements are structured to validate reduced MIMO models and macro-particle simulation codes, including the dynamics and limits of the feedback channel. Noise effects and uncertainties in the model are evaluated via SPS measurements to quantify the limits of control techniques applied to stabilize the intrabunch dynamics.

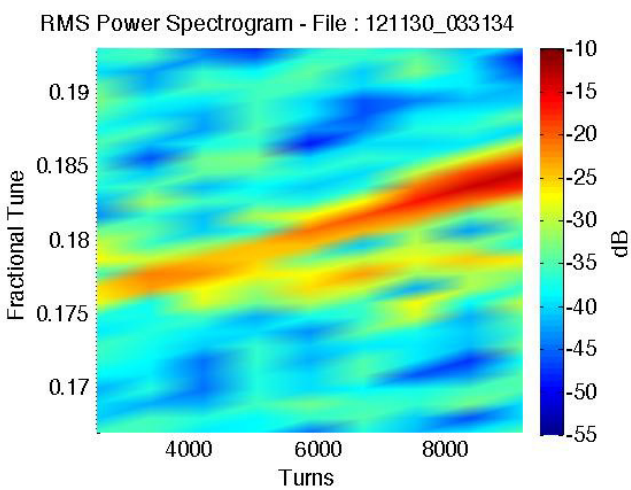

Figure 1: Open-loop vertical beam response chirp spectrogram measurement (no feedback). A 16 sample modulated excitation is driven by the kicker unto the SPS beam for 10,000 turns. The chirp excitation passes through the mode zero tune of 0.177 at turn 4000, and then the mode 1 upper synchrotron sideband at turn 8000 (Q20 lattice). The color code shows the amplitude of the motion for the detected signal.

* Work supported by the U.S. Department of Energy under contract # DE-AC02-76SF00515 and the US LHC Accelerator Research Program (LARP).

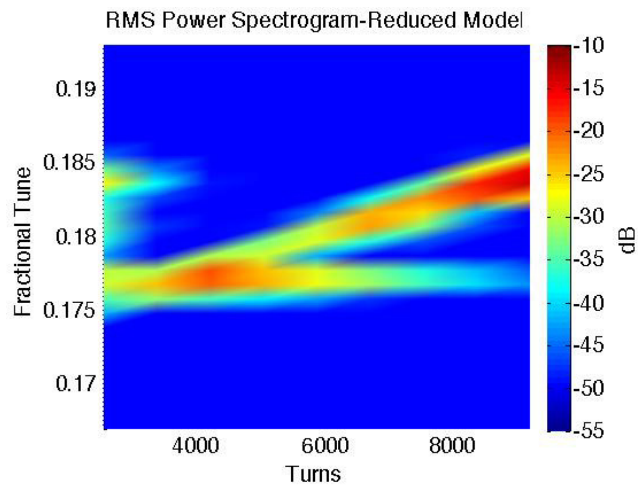

Figure 2: Beam motion spectogram response for the reduced beam model (same excitation as Figure 1). Comparing with the physical measurement we see very close agreement between the oscillation frequencies and the amplitudes of the excited motion.

EVALUATING THE UPGRADED SYSTEM PERFORMANCE

A single-bunch wideband digital feedback system was initially commissioned at the CERN SPS in November 2012[1]. The project is part of a larger LHC injector upgrade[2]. In 2014 during the shutdown interval this system has been expanded with installation of wideband kickers and associated RF amplifiers[3]. While the original bandwidth-limited system achieved control of mode zero and mode 1 unstable beams, we must explore the achieved performance of the wideband kickers, and understand necessary capabilities to control beam conditions anticipated in the HL operating scenario. Our goal in testing the demonstration system is to validate the performance as achieved, and using simulation tools predict behavior for high-current and HL upgraded injector conditions. We cannot expect the limited-function Demonstration System to have the capability of the final system, instead we want to confidently predict the behavior and margins of a more complex full-featured system. To do this, we need methods to simulate realistic future beam conditions interacting with possible feeback systems, and methods to compare the behavior of the Demonstration system and beam against simulations. In this near term we must study the system under a sub-set of HL beam conditions, and validate that our

Content from this work may be used under the terms of the CC BY 3.0 licence (© 2015). Any distribution of this work must maintain attribution to the author(s), title of the work, publisher, and DOI.

ISBN: 978-3-95450-168-7 doi:10.18429/JACoW-IPAC2015-TUAC3

Content from this work may be used under the terms of the CC BY 3.0 licence (© 2015). Any distribution of this work must maintain attribution to the author(s), title of the work, publisher, and DOI.

OPTIMIZATION OF BEAM LOSS MONITOR NETWORK FOR FAULT MODES*

Z. Liu#, D. Liu, S. Lidia, Z. He, Q. Zhao, FRIB, East Lansing, MI 48824, USA

Abstract

Beam Loss Monitoring (BLM) System is an essential part to protect accelerator from machine faults. Compared with the empirical or uniform BLM arrangement in most accelerators, our new optimization approach proposes a “minimum spatial distribution” for BLM network. In this distribution, BLMs shall be placed at a small set of “critical positions” that can detect all failure / FPS trigger-able events of each fault mode. In additional, to implement a more advanced function of fault diagnosis, BLM should also be placed at “discrimination points” for fault-induced loss pattern recognition. With examples of FRIB failure event simulations, the author demonstrates the proof of concept to locate these “critical positions” and “discrimination points” for the minimum spatial distribution of BLMs.

INTRODUCTION

As an essential part of Machine Protection System (MPS) input, the BLM system plays an important role to detect and diagnosis machine faults. This imposes categorized functional requirements for BLM system. For example, the fault detection requires BLM device to have fast response for big losses, while the fault diagnosis requires BLM device sensitive enough to diagnose issues with beam tuning/slow losses and able to differentiate between controlled and uncontrolled losses. These requirements determine the type and structure of BLM system, e.g., FRIB BLM system including fixed position Halo Monitor Ring, BCM and movable radiation detectors. In this paper, we are not going to discuss the structural determination of BLM system, instead, we will focus on the spatial optimization of a pre-assumed BLM system.

Our goal of spatial optimization for fault detection is to minimize the number of BLMs while still be able to detect all Fast Protection System (FPS) trigger-able failure events that generate significant losses. To achieve this, we need to quantify correlations between BLM locations for classes of events, so that at least one BLM at the “critical positions” can trigger FPS when a component-failure event induces significant losses. Section 2 introduces the methodology to find the ensemble of “critical points”, with the simulation example of single cavity failures.

Fault diagnosis, or loss pattern recognition, is a more advanced functional requirement for BLM network. It was typically determined empirically at most accelerators. To prepare for loss pattern recognition, we need to put detectors at “discrimination points” that can distinguish patterns. Section 3 shows how to identify discrimination points for a fault mode with the principal component analysis (PCA) [1] method.

CRITICAL POSITIONS

As the first goal of spatial optimization for BLM network, we are looking for a set of “critical positions”, where at least one BLM can trigger FPS when a failure event induces over-threshold losses.

Example Fault Mode Simulation

In order to demonstrate the methodology to find “critical positions”, we simulated loss distributions of single cavity quenching events. In the simulation, every accelerator element in the FRIB lattice was considered a loss point. In total there are 572 element/loss points in FRIB lattice. To simulate cavity failure event, we turned off one cavity’s voltage and phase completely, did particle tracking and simulated particle loss power with IMPACT [2]. By turning off the 332 accelerating and bunching cavities one by one, we got 241 loss distributions. The other 91 cavities are in the high energy part, where transverse emittance growth from longitudinal mismatch takes longer distance and therefore the failures do not necessarily generate losses.

Using the same terminology in Statistics, the loss positions are “variables” or “dimensions”, and the cavity failure are “observations”. The loss matrix for single-cavity-failure mode is therefore 572 variables × 241 observations.

Correlation Matrix

As we mentioned in the introduction, the “critical positions” are defined based on quantifying correlations between BLM locations, i.e. loss points, for classes of failure events. If a group of adjacent loss positions are highly correlated with each other in positive direction, they can be considered as a “localized loss area” and only one BLM needs to be placed there.

To quantify the “localized loss area”, we need to compute the correlation matrix $R_{n\times n}$ for matrix $X_{m\times n}$, whose element $R(i,j)$ is the correlation coefficient of i$^{\text{th}}$ column and j$^{\text{th}}$ column:

$$R(i,j) = \frac{Cov(X_i,X_j)}{\sigma(X_i)\cdot\sigma(X_j)}\,.$$

$cov(X_i,X_j)$ is the covariance of the i$^{\text{th}}$ and j$^{\text{th}}$ column/loss position, and $\sigma(X_i)$ is the standard deviation of i$^{\text{th}}$ column. In our case for beam loss monitoring, we

*This work is supported by the U.S. Department of Energy Office of Science under cooperative agreement DE-SC0000661.
#liuz@frib.msu.edu

ISBN: 978-3-95450-168-7 doi:10.18429/JACoW-IPAC2015-TUBC1

RECENT PROGRESS AND OPERATIONAL STATUS OF THE COMPACT ERL AT KEK

S. Sakanaka, M. Adachi, S. Adachi, T. Akagi, M. Akemoto, D. Arakawa, S. Araki, S. Asaoka, K. Enami, K. Endo, S. Fukuda, T. Furuya, K. Haga, K. Hara, K. Harada, T. Honda, Y. Honda, H. Honma, T. Honma, K. Hosoyama, K. Hozumi, A. Ishii, X. Jin, E. Kako, Y. Kamiya, H. Katagiri, H. Kawata, Y. Kobayashi, Y. Kojima, Y. Kondou, A. Kosuge, T. Kume, T. Matsumoto, H. Matsumura, H. Matsushita, S. Michizono, T. Miura, T. Miyajima, H. Miyauchi, S. Nagahashi, H. Nakai, H. Nakajima, N. Nakamura, K. Nakanishi, K. Nakao, K. Nigorikawa, T. Nogami, S. Noguchi, S. Nozawa, T. Obina, T. Ozaki, F. Qiu, H. Sagehashi, H. Sakai, S. Sasaki, K. Satoh, M. Satoh, T. Shidara, M. Shimada, K. Shinoe, T. Shioya, T. Shishido, M. Tadano, T. Tahara, T. Takahashi, R. Takai, H. Takaki, T. Takenaka, O. Tanaka, Y. Tanimoto, N. Terunuma, M. Tobiyama, K. Tsuchiya, T. Uchiyama, A. Ueda, K. Umemori, J. Urakawa, K. Watanabe, M. Yamamoto, Y. Yamamoto, Y. Yano, M. Yoshida,
High Energy Accelerator Research Organization (KEK), Tsukuba, Ibaraki 305-0801, Japan
R. Hajima, S. Matsuba, M. Mori, R. Nagai, N. Nishimori, M. Sawamura, T. Shizuma,
Japan Atomic Energy Agency (JAEA), Tokai, Naka, Ibaraki 319-1195, Japan
M. Kuriki, Y. Seimiya*, Hiroshima University, Higashihiroshima, Hiroshima 739-8530, Japan
E. Cenni*, SOKENDAI (the Graduate University for Advanced Studies), Tsukuba, Ibaraki, Japan
J.-G. Hwang*, Kyungpook National University, Daehakro, Bukgu, Daegu 702-701, Korea

Abstract

The Compact Energy Recovery Linac (cERL) is a superconducting test accelerator aimed at establishing technologies for the ERL-based future light source. After its construction during 2009 to 2013, the first CW beams of 20 MeV were successfully transported through the recirculation loop in February 2014. In the autumn of 2014, we installed a laser Compton scattering (LCS) system which can provide high-flux X-ray to a beamline. We report our progress in the cERL including recent advances in beam tuning, an increase in the beam current, and successful commissioning of the LCS system.

INTRODUCTION

Superconducting (SC) linacs can provide both low-emittance and high average-current electron beams that are very useful for producing ultra-brilliant X-rays [1] or for driving X-ray free-electron lasers in continuous wave (CW) operation [2]. In Japan, we have been conducting R&D effort for the ERL-based synchrotron light source [3]. To demonstrate critical technologies for the ERL-based light source, we constructed the Compact ERL (cERL). The principal parameters of cERL are given in Table 1.

Figure 1 shows the statistics of beam operation time (that is, the time while the beam was on) during FY2013-2014. The first CW beams of 20 MeV were successfully transported through the recirculation loop in February 2014 [4,5]. After the commissioning, various accelerator studies have been carried out. They include an establishment of start-up tuning, correction of beam optical functions, study on beam losses [6], and measurements of beam emittances in a recirculation loop. Some of the results of these studies are reported in the next section.

Table 1: Principal Parameters of the cERL

	Design	In operation
Beam energy	35 MeV	20 MeV
Injector energy	5 MeV	2.9 - 6 MeV
Normalized emittance	0.1 µm·rad@7.7 pC 1 µm·rad@77 pC	under study
Beam current	10 mA	80 µA

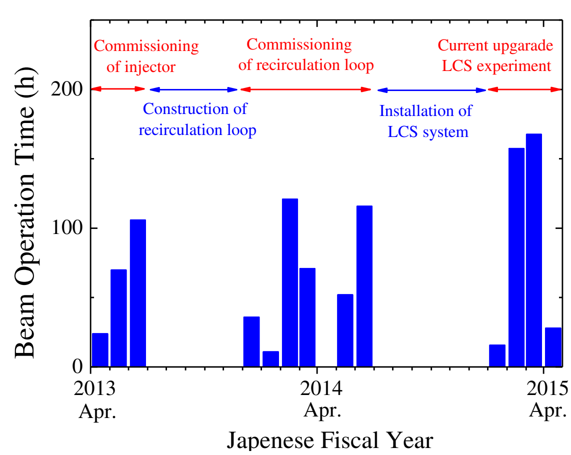

Figure 1: Statistics of beam operation time per month.

* On leave

Content from this work may be used under the terms of the CC BY 3.0 licence (© 2015). Any distribution of this work must maintain attribution to the author(s), title of the work, publisher, and DOI.

ISBN: 978-3-95450-168-7 doi:10.18429/JACoW-IPAC2015-TUBC2

MULTI-GHz PULSE-TRAIN X-BAND CAPABILITY FOR LASER COMPTON X-RAY AND γ-RAY SOURCES*

D. J. Gibson†, G. G. Anderson, S. G. Anderson, R. A. Marsh, M. J. Messerly, M. A. Prantil, C. P. J. Barty, LLNL, Livermore, CA 94550, USA

Abstract

A wide variety of light-source applications would benefit from increased average brightness, which generally corresponds to increasing average current in the driving accelerator. Presented is an accelerator architecture that is capable of producing hundreds of electron bunches, spaced as close together as every RF cycle, which provides the chance to increase current while maintaining beam quality. This system relies on an X-band photoinjector and a photoinjection drive laser that is driven by the same rf source to ensure synchronization, and an interaction laser system designed to match the duty cycle of the electron pulse train. Results of the photoinjector laser performance and initial experimental measurements of beam quality in accelerated bunch trains are presented, along with a discussion of the impact on the performance of tunable, narrow-bandwidth x-ray and γ-ray beams based on Compton-scattering.

INTRODUCTION

While some photonic applications, such as time resolved imaging, require a large number of photons in a short time (i.e. a high peak brightness), many applications (medical imaging, nuclear resonance fluorescence measurements, material assay, etc.) don't have such a stringent requirement and can benefit from increasing not only the peak brightness of the source, but also the average brightness.

In a Compton-scattering based source, a high intensity laser beam scatters of a high brightness electron beam and generates x-rays with an energy of

$$E_\gamma = \frac{2\gamma^2 (1 - \cos\varphi)}{1 + \gamma^2\theta^2} h\nu$$

ignoring recoil, where γ is the electron Lorentz factor, φ is the incidence angle between the electrons and photons, θ is the observation angle relative to the electron direction of travel, and ν is the laser frequency. Properly apertured, such a beam can provide a very narrow bandwidth, easily tunable x-ray or γ-ray source. The number of scattered x-rays depends on the overlap integral between the laser and electron beam and therefore is a function of electron and photon density. To increase the flux from an electron bunch, the options include: focusing the beam harder, which increases the angular spread and therefore broadens the bandwidth; increase the charge, which will increase the beam emittance, with a similar result on the spectrum; or increase the laser energy, which is limited by the introduction of nonlinear scattering effects with also broaden the beam bandwidth.

As has been discussed elsewhere [1], very little of the laser energy is used in the scattering process. Sending more electron bunches, rather than more electrons in a single bunch, can make efficient reuse of the unscattered laser photons. This is the motivation for putting electrons into every accelerating RF bucket, increasing in the average current of between 10x and 100x and resulting in a comparable increase in x-ray flux. Accomplishing this in practice requires a photoinjector-based accelerator architecture capable of pumping energy into the electrons without inter-bunch wakefield effects destroying the beam, a photoinjection laser system capable of generating precisely timed multi-GHz pulses to generate the electrons, and an interaction laser designed to interact with a train of pulses, rather than a single pulse.

DRIVE LASER

The architecture for a laser capable of generating a multiple-GHz pulse train is described in detail in Ref. [2]. The 11.424 GHz RF that drives the accelerator is frequency divided to 5.712 GHz and used to an electro-optic modulator. A 1040-nm cw laser pulse passes through the modulator and is carved into an 11.424 GHz pulse train. This pulse train then passes through a series of amplifiers and acousto-optic modulators, resulting in 50 ns bursts of pulses at a 28 kHz repetition rate with 150 mW of average power. This beam then passes through 300 m of single mode optical fiber, where self phase modulation generates bandwidth with a nearly linear chirp on the individual pulses. These chirped pulses then pass through a large-mode-area photonic crystal fiber and a small grating pair compressor, resulting in a laser with 5 μJ per micropulse, 500 micropulses per burst, and a 28 kHz burst rate.

To allow accelerator demonstration in parallel with laser development, an Amplitude Ti:Sapphire laser system is used in place of the multi-GHz system. Up to 20 mJ of uncompressed 780 nm laser light at 10 Hz is transported to the accelerator hall, where the pulses are compressed to 200 fs and frequency tripled to 260 nm. In order to generate multiple pulses, a hyper-Michelson pulse stacker [3] is used. Tests to date have been conducted with four pulses, but up to 16 can be generated with the exisiting system hardware. The beam is then apertured to provide a sharp radial edge, typically with a 0.5 mm diameter, but other diameter are available. The apertured beam is then relay imaged to the photoinjector cathode, providing typically 10 μJ per pulse in the UV.

* This work was performed under the auspices of the U.S. Department of Energy by Lawrence Livermore National Laboratory under Contract DE-AC52-07NA27344.

† gibson23@llnl.gov

Content from this work may be used under the terms of the CC BY 3.0 licence (© 2015). Any distribution of this work must maintain attribution to the author(s), title of the work, publisher, and DOI.

ISBN: 978-3-95450-168-7 doi:10.18429/JACoW-IPAC2015-TUBC3

Content from this work may be used under the terms of the CC BY 3.0 licence (© 2015). Any distribution of this work must maintain attribution to the author(s), title of the work, publisher, and DOI.

RECENT RESULTS FROM FEL SEEDING AT FLASH*

J. Bödewadt†, S. Ackermann, R. Aßmann, N. Ekanayake, B. Faatz, G. Feng, I. Hartl, R. Ivanov, T. Laarmann, J. Mueller, T. Tanikawa, DESY, Hamburg, Germany
Ph. Amstutz, A. Azima, M. Drescher, L. Lazzarino, C. Lechner, Th. Maltezopoulos, V. Miltchev, T. Plath, J. Roßbach, University of Hamburg, Germany
K. Hacker, S. Khan, R. Molo, DELTA, Dortmund, Germany

Abstract

The free-electron laser facility FLASH at DESY operates since several years in SASE mode, delivering high-intensity FEL pulses in the extreme ultraviolet and soft x-ray wavelength range for users. In order to get more control of the characteristics of the FEL pulses, external FEL seeding has proven to be a reliable method to do so. At FLASH, an experimental setup to test several different external seeding methods has been installed since 2010. After successful demonstration of direct seeding at 38 nm, the setup is now being operated in HGHG and later in EEHG mode. Furthermore, other studies on laser-induced effects on the electron beam dynamics have been performed. In this contribution, we give an overview of recent experimental results on FEL seeding at FLASH.

INTRODUCTION

Fully coherent radiation in the extreme ultra-violet (XUV), soft-, and hard X-ray spectral range is highly demanded for a variety of scientific fields. In combination with the demand for highest spectral brightness, this lead to the development of free-electron lasers (FEL) [1–4]. These devices have been operated for more than a decade using the principle of self-amplified spontaneous emission (SASE) [5, 6]. In this operation mode, the FEL radiation has a high degree of transverse coherence but it suffers from a poor longitudinal coherence due to the stochastic shot-noise, which is the startup source for the SASE amplification process. In contrast to that, an external seed source which initiates the FEL process allows to maintain the good coherence properties of the seed. Two different schemes for FEL seeding have been proposed and demonstrated in the past: Firstly those, which manipulate the electron bunch distribution such that a strong microbunching is created at the seed wavelength. The harmonic content of the density modulation is able to drive the FEL at high harmonics as in the high-gain harmonic generation (HGHG) [7] and the echo-enabled harmonic generation (EEHG) [8] operation modes. Secondly those, which initiate the FEL process directly at the target wavelength. Seed sources are either a high-harmonic generation (HHG) [9] source driven by conventional lasers (HHG seeding) [10] or a SASE FEL with a subsequent monochromator in so-called self-seeding schemes [11].

* Supported by the Federal Ministry of Education and Research of Germany under contract 05K13GU4 and 05K13PE3
† contact: joern.boedewadt@desy.de

The FEL facility in Hamburg, FLASH, at DESY is operated since 2005 as a user facility in SASE mode [1]. Since 2010, an experimental setup for seeding developments has been installed prior to the main SASE undulator of the FLASH1 [12]. At this setup, the direct HHG seeding at 38 nm was demonstrated in 2012 [13]. A limited contrast ratio as well as the fact that the hit rate of the external pulses with the electron bunches was dominated by the relative arrival time variations, which were in the order of the pulse durations, lead to the decision to set the focus of the seeding R&D at FLASH on HGHG and EEHG seeding [14, 15]. Other facilities have demonstrated self-seeding for photon energies above 700 eV [16, 17] and HGHG seeding for wavelength between 4 nm and 80 nm [18]. The EEHG principle has been demonstrated for wavelength down to ≈170 nm [19]. In the following, we will describe the current status of the FEL seeding developments at DESY.

EXPERIMENTAL SETUP

The Seeding Section in FLASH1

Figure 1 shows a schematic layout of the FLASH1 FEL beamline. An overview of the entire FLASH facility can be found in [20]. After the energy collimator, the seeding section starts with two short electro-magnetic wigglers (labeled MOD1 and MOD2) with 5 full periods [21] each followed by a magnetic chicane C1 and C2. Four variable-gap undulators with an effective length of 10 m act as the FEL radiators. The FEL pulses are guided to a photon diagnostics section using a mirror system. The chicane C3 steers the electron beam around the extraction mirrors. The following transverse deflecting structure (TDS) and a dispersive dump section allows to diagnose the longitudinal phase space distribution of the electron bunches.

The Seed Laser

The 266-nm seed pulses are generated by third-harmonic generation (THG) of near-infrared (NIR) Ti:sapphire laser pulses. The UV pulse energy at the interaction region with the electron bunch can be set up to 280 μJ, the Rayleigh length is about 1.4 m. The longitudinal position of the beam waist can be adjusted by changing the NIR focusing into the THG setup. To relax the tolerance of the transverse laser-electron overlap, the waist has been set about 1 m after the end of undulator MOD2. The seed beam position and size is measured before and after MOD2 using fluorescence screens.

ISBN: 978-3-95450-168-7 doi:10.18429/JACoW-IPAC2015-TUAD1

MAGNET DESIGN AND CONTROL OF FIELD QUALITY FOR TPS BOOSTER AND STORAGE RINGS

J. C. Jan#, C. Y. Kuo, C. H. Chang, H. H. Chen, Y. L. Chu, Y. T. Yu, F. Y. Lin, M. H. Huang, C. S. Yang, I. C. Sheng, C. S. Hwang, G. H. Luo, C. T. Chen, NSRRC, Hsinchu 30076, Taiwan

Content from this work may be used under the terms of the CC BY 3.0 licence (© 2015). Any distribution of this work must maintain attribution to the author(s), title of the work, publisher, and DOI.

Abstract

High quality magnets were designed, fabricated and installed in the Taiwan Photon Source (TPS). The lattice of the storage ring (SR) is based on a double-bend achromat (DBA) structure with an emittance 1.6 nm-rad and a small dispersion in the straight sections. A concentric booster ring (BR) is designed and constructed to share the same tunnel with the SR. The first synchrotron light from the TPS storage ring at 3 GeV was observed on Dec. 31, 2014. This accomplishment indicated that the precision of the profile and the field quality of the magnets as well as the alignment of the girders attained world class. The integral multipole components of the SR-quadrupole and SR-sextupole magnets conform to strict specifications. The maximum offset of the measured mechanical center in the magnets is better than ±0.01 mm after feet-shim. The offset of the magnetic center of the magnets is better than ±0.02 mm, as inspected with a rotating-coil method. The field quality of the BR-dipole and BR-quadrupole magnets were within design errors and proved in the beam commissioning. A study of relative permeability of the vacuum chamber was implemented during testing of the hardware of the booster ring. The magnetic field was distorted by the nonentity relative permeability of the vacuum pipes. This field distortion caused by the vacuum pipe is discussed in this paper.

INTRODUCTION

The Taiwan Photon Source (TPS) is a third-generation synchrotron light source, constructed at the National Synchrotron Radiation Research Center (NSRRC). To accommodate the constraints of the existing building, the magnets of the storage ring (SR) and the booster ring (BR) are constructed in the same tunnel, forming a concentric arrangement. The SR and the BR are composed of 48 SR-dipoles, 240 SR-quadrupoles, 168 SR-sextupoles, 54 BR-dipoles, 84 BR-quadrupoles and 24 BR-sextupole magnets. Buckley System Ltd. (New Zealand) was awarded the main contract to provide 641 magnets for the SR and the BR; Danfysik A/S (Denmark) constructed 255 magnets for transfer lines and corrector magnets. The preliminary magnetic design and engineering of the magnet system began in 2005 [1-3]; the TPS project was approved in 2007. A one-section prototype including 23 magnets was fabricated in 2011. The mass production of magnets was begun in 2012. In total, 641 magnets of the SR and BR were delivered by Oct. 2013. The hardware installation and integration of the accelerator including magnets, vacuum chambers, girders and diagnostic tools completed in mid-August, 2014. The system integration and improvement were completed on Dec. 12, 2014. The first synchrotron light at 3 GeV was observed with no correction applied on Dec. 31, 2014. The design, fabrication and correction of TPS magnets are presented in reports [2, 4-5].

#janjc@nsrrc.org.tw

MECHANICAL ERROR AND QUALITY OF THE MAGNETIC FIELD

The precise pole profile of a magnet is manufactured by either a Computer Numerical Control Machine (CNC) or a Wire Electrical Discharge Machine (WEDM). The SR-dipole and long SR-quadrupole magnets are machined with a CNC Machine because of the long yoke length; other magnets are machined by WEDM. Figures 1(a), (b), (c) and (d) display the sketches and labels of pole profile for SR-dipole, BR-dipole, SR-quadrupole and SR-sextupole magnets, respectively. The yoke length of SR-dipole, short SR-quadrupole, long SR-quadrupole, SR-sextupole, BR-dipole (BH/BD) and BR-quadrupole (pure) magnets are labelled as DL_1, SQL, LQL, SL, DL_2 and BQL, respectively. The bore diameter of the BR-quadrupole magnets is labelled as BQd.

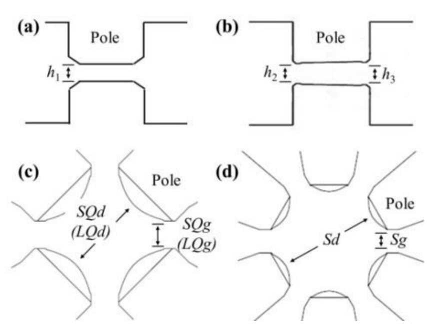

Figure 1: Pole profiles and labels of (a) SR-dipole, (b) BR-dipole, (c) short/long SR-quadrupole and (d) SR-sextupole magnets.

Table 1 lists the mechanical error (mean value±standard deviation) of the SR and BR magnets. The bore diameters of a long SR-quadrupole is counted without a yoke-shim [4]. The discrepancy between the designed and machined value of the bore diameter is better than 0.014 mm. The discrepancy between the designed and machined value of the pole gap of the SR magnet is better than 0.011 mm. The iron yokes of the SR and BR magnets are laminated with 1 and 0.5 mm of 50CS1300 silicon steel, respectively. The deviation of the laminated yoke length was controlled to be smaller than 0.15 % of the yoke length or one thickness of a lamination. The machining

ISBN: 978-3-95450-168-7 doi:10.18429/JACoW-IPAC2015-TUAD2

COMPARISON BETWEEN MEASURED AND COMPUTED TEMPERATURES OF THE INTERNAL HIGH ENERGY BEAM DUMP IN THE CERN SPS

G. Steele, F. Pasdeloup, R. Folch, V. Kain, I. V. Leitao, R. Losito, C. Maglioni,
A. Perillo-Marcone, F. Velotti, CERN, Geneva, Switzerland

Abstract

The SPS high energy internal dump (TIDVG) is designed to receive beam dumps from 102.2 to 450 GeV. The absorbing core is composed of 2.5 m graphite, followed by 1.0 m of aluminium, then 0.5 m of copper and 0.3 m of tungsten, all of which is surrounded by a water cooled copper jacket. An inspection during Long Shutdown 1 (LS1) revealed significant beam induced damage to the Al section of the dump block. Temperature sensors were installed to monitor the new dump replacing the damaged one. This paper summarises the correlation between the temperature measured as a function of the energy deposited and the corresponding temperatures computed in a numerical model combining FLUKA and ANSYS simulations. The goal of this study is the assessment of the thermal contact quality between the beam absorbing blocks and the copper jacket, by analysing the cooling times observed from the measurements and from the thermo-mechanical simulations. This paper presents an improved method to estimate the efficiency and long term reliability of the cooling of this type of design, with the view of optimising the performance of future dump versions.

INTRODUCTION

The Target Internal Dump Vertical Graphite (TIDVG) device is used as a high energy (102.2 to 450 GeV) dump for the SPS accelerator. It must withstand the entire range of beams accelerated in the SPS supercycle, including fixed target experiments and injection into the LHC (see Table 1).

Table 1: SPS Run 2 Beam Energies and Intensities

Name	E [GeV]	Bunch Int.	# of Bunches
LHC 25 ns	450	1.2e11	288
LHC 50 ns	450	1.2e11	144
Doublet	450	1.6e11	144
Fixed Target	400	9.52e9	4200

The waveforms of 2 vertical kickers combined with 3 horizontal sweepers in the SPS beam dump system make the whole beam be spread over a relatively large area on the front face of the absorbing core. Since year 2000 three devices have been installed: TIDVG 1 (2000 – 2004), TIDVG 2, (2006 – 2013), TIDVG 3 (installed in 2014). The composition of the three TIDVGs is broadly similar. TIDVG 1 and 2 consist of an absorbing core, encased in a copper jacket surrounded by iron shielding, both containing cooling pipes. The absorbing core is composed of 2.5 m of graphite, 1.0 m of aluminium, 0.5 m of copper and 0.3 m of tungsten. TIDVG3 has a slightly longer (2.7 m) graphite section and a slightly shorter (0.8 m) Al section, because it is the limiting component [1]. During LS1, an endoscopy of TIDVG2 showed significant damage to the Al core section. Energy deposition and thermo-mechanical studies indicated that it did not come from one powerful shot but more likely repetitive dumping of a high power beam. TIDVG2 needed to be replaced by TIDVG3, reusing the iron yoke.

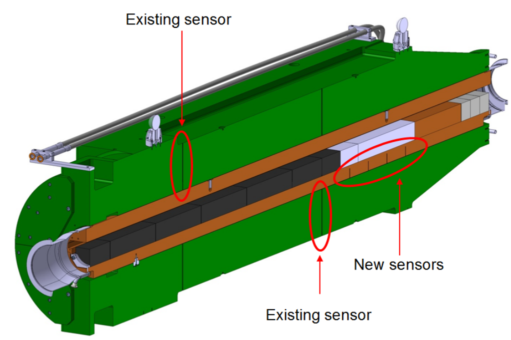

Figure 1: Position of existing and new temperature sensors in the yoke and copper jacket.

Four temperature sensors are installed in the yoke, positioned to give an indication of the temperature on the Cu jacket. Only 2 will be connected due to the number of available connections. Before installation 4 new sensors were inserted into the replacement Cu jacket, positioned to provide sufficient coverage as well as redundancy around the Al section (see Fig. 1). Finally, sensors were installed at the entrance and exit of one cooling circuits, in the Cu jacket.

The extent of the damage prompted several studies to determine the most likely time period when it occurred, and to develop an improved thermo-mechanical model. It serves as a post-mortem tool and to set operational limits for the TIDVG3 for future runs. This paper details the steps taken to improve and verify the simulation model.

SIMULATIONS

Energy Deposition Simulations

FLUKA [2, 3] simulations used a model of the TIDVG3 geometry, and particle density maps from tracking simulations as input (see Fig. 2). Energy density maps for each Run2 beam type are then used as input for the following thermo-mechanical studies. Fig. 3 shows the simulated peak energy deposition along the absorbing core of the TIDVG

Content from this work may be used under the terms of the CC BY 3.0 licence (© 2015). Any distribution of this work must maintain attribution to the author(s), title of the work, publisher, and DOI.

ISBN: 978-3-95450-168-7 doi:10.18429/JACoW-IPAC2015-TUAD3

LLRF COMMISSIONING OF THE EUROPEAN XFEL RF GUN AND ITS FIRST LINAC RF STATION

J. Branlard*, G. Ayvazyan, V. Ayvazyan, Ł. Butkowski, M. Grecki, M. Hoffmann, F. Ludwig, U. Mavrič, M. Omet, S. Pfeiffer, K. Przygoda, H. Schlarb, C. Schmidt, H. Weddig, B. Yang, DESY, Hamburg, Germany
S. Bou Habib, K. Czuba, M. Grzegrzółka, E. Janas, K. Oliwa, J. Piekarski, I. Rutkowski, R. Rybaniec, D. Sikora, W. Wierba, Ł. Zembala, M. Żukociński, ISE, Warszawa, Poland
W. Cichalewski, D. Makowski, A. Mielczarek, P. Perek, T. Poźniak, DMCS, Łódź, Poland
A. Piotrowski, Fast Logic, Łódź, Poland

Abstract

The European X-ray free electron laser (XFEL) at the Deutsches Elektronen-Synchrotron (DESY), Hamburg Germany is in its construction phase. Approximately a third of the super-conductive cryomodules have been produced and tested. The RF gun is installed since 2013; periods of commissioning are regularly scheduled between installation phases of the rest of the injector. The first linac, L1, consisting of 4 cryomodules powered by one 10 MW klystron is installed and being commissioned. This contribution reports on the installation and preparation work of the low-level radio frequency system (LLRF) to perform the commissioning of the XFEL first components. The commissioning plans, schedule and first results are presented.

INTRODUCTION

An overview of the low level radio frequency (LLRF) system for the European XFEL is given in [1], with a description of the system architecture and the functionality of its main components. Details about the Micro Telecommunication Architecture (MicroTCA.4)-based LLRF system are found in [2] while performance results evaluated in the FLASH accelerator at DESY are given in [3]. Last year, the first component of the XFEL accelerator, the RF gun, was installed in the injector building. A description of its LLRF and the first results of its commissioning are reported in [4]. This contribution reports on the next XFEL milestone, namely, the installation and commissioning of the first linac, corresponding to the first 4 cryomodules installed into the XFEL tunnel (XTL). Results observed with the first beam produced at the XFEL injector are also presented. Figure 1 gives a schematic layout of the accelerator sections of the XFEL (Ax), grouped into injector, linac 1, 2 and 3.

INSTALLATION

Tunnel Installation

All XFEL cryomodules first undergo a series of tests [5,6] performed in the accelerating module test facility (AMTF). The next step consists of installing the waveguide distribution

* julien.branlard@desy,de

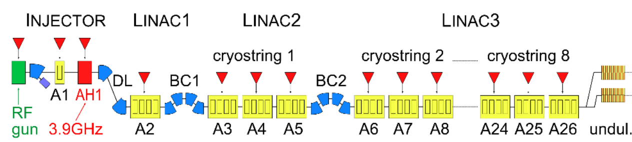

Figure 1: Layout of the XFEL linacs, separated by the dog leg (DL) and the two bunch compressors (BCs).

system, tailored according to each cavity's gradient performance [7]. The complete system (cryomodule + waveguide) is then mounted inside the tunnel, suspended to the ceiling, after which the string connection work can start. The intermodule welding connections are performed and the cryogenic feed- and end-cap at each end of the cryostring are installed. Vacuum connections are performed; the racks containing all electronics can then be placed underneath the modules.

Figure 2: Cryomodule transport into the XFEL tunnel.

The racks require individual water connection for their cooling units, connection to the mains and installation of the concrete radiation shielding, to the side and above the racks. The cabling work can then start (RF, Ethernet, interlock, vacuum, piezo, tuners, optical fiber etc...), from rack to rack and also between racks and cryomodule patch panels. The cabling work requires careful planning and sequential timing;

Content from this work may be used under the terms of the CC BY 3.0 licence (© 2015). Any distribution of this work must maintain attribution to the author(s), title of the work, publisher, and DOI.

ISBN: 978-3-95450-168-7 doi:10.18429/JACoW-IPAC2015-TUBD1

OPTICS MEASUREMENT AND CORRECTION DURING ACCELERATION WITH BETA-SQUEEZE IN RHIC*

C. Liu†, A. Marusic, M. Minty, Brookhaven National Laboratory, Upton, NY 11973, USA

Abstract

In the past, beam optics correction at RHIC has only taken place at injection and at final energy, with interpolation of corrections partially into the acceleration cycle. Recent measurements of the beam optics during acceleration and squeeze have evidenced significant beta-beats that, if corrected, could minimize undesirable emittance dilutions and maximize the spin polarization of polarized proton beams by avoiding the high-order multipole fields sampled by particles within the bunch. We recently demonstrated successful beam optics corrections during acceleration at RHIC. We verified conclusively the superior control of the beam realized via these corrections.

INTRODUCTION

It is desirable to minimize the machine optics (β-functions/phase advances) errors during beam acceleration to improve dynamic aperture for heavy ions and reduce depolarization resonance strengths for polarized proton program. However, it is not practical to pause at step-stones for optics measurement and correction in the simultaneous beam acceleration and beta-squeeze ramp. We demonstrated recently an on-the-fly beam optics measurement during beam acceleration and successfully implemented corrections which substantially suppressed beta-beats on the ramp in RHIC. The method of the measurement and correction is presented in the following sections.

BEAM OPTICS MEASUREMENT DURING BEAM ACCELERATION

Turn-by-turn measurements of the beam position with an applied excitation to the beam has been used at many accelerators to infer fundamental optical parameters such as the tune, the phase advance between BPMs, and with input from the accelerator model, the β-functions. Many different algorithms for data analysis have been successfully applied such as fitting in time domain [1], interpolated FFT technique in frequency domain [2, 3, 4] and statistical techniques (PCA, ICA) [5, 6] finding beam motions in a high dimension data. The interpolated FFT technique was adopted in this report to analyze the machine optics in RHIC.

The acquired turn-by-turn BPM data with the beam kicked by the tune meter kicker multiple times usually oscillates for less than 500 turns because of decoherence for a typical chromaticity setting (∼2 above transition, ∼-2 below transition). The application of interpolated FFT analysis on these BPM data yielded high precision tune, phase advances and β-functions measurement despite the limited data points acquired. This demonstration opens up the possibility of acquiring turn-by-turn BPM data with the tune meter on the ramp for optics measurement [7, 8].

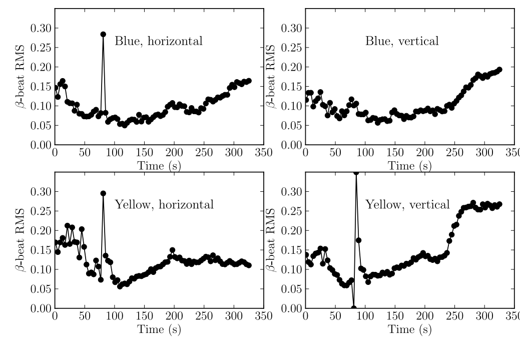

Figure 1: The measured beta-beats during beam acceleration (high energy Au-Au, 2014). Transition crossing occurs at $\sim$ 85 seconds after the start of acceleration.

Measurements of the beam optics were made reproducible by ensuring reproducible beam orbits and betatron tunes using the now standard beam feedback systems during acceleration. While orbit and tune feedback operate independently, the BPM measurements used by orbit feedback and the turn-by-turn BPM measurements share the same networks for data delivery. The timing of the delivery of beam position measurements for these two systems was therefore carefully staggered to avoid data corruption. Orbit feedback operated at its standard 1 Hz rate. We allowed 200 ms corresponding to an upper limit on the time to transmit all (4 planes from both accelerators) the average orbit BPM data well in excess of the 150 ms required based on previous measurements [9]. After delivery of the data for orbit feedback, the beam was excited in one plane followed a short time later by excitation in the other plane, where the spacing between applied excitations was set ($\sim$ 500 turns) to be longer than the decoherence time.

Since the volume of data being acquired is large, we present the deviation of the machine optics in the form of global beta-beat Root-Mean-Square (RMS) during beam acceleration. Figure 1 shows the RMS beta-beats at each time of optics measurement during beam acceleration for the Au-Au physics ramp in 2014.

* The work was performed under Contract No. DE-AC02-98CH10886 with the U.S. Department of Energy.
† Email: cliu1@bnl.gov

Content from this work may be used under the terms of the CC BY 3.0 licence (© 2015). Any distribution of this work must maintain attribution to the author(s), title of the work, publisher, and DOI.

ISBN: 978-3-95450-168-7 doi:10.18429/JACoW-IPAC2015-TUBD2

Content from this work may be used under the terms of the CC BY 3.0 licence (© 2015). Any distribution of this work must maintain attribution to the author(s), title of the work, publisher, and DOI.

FINAL COOLING FOR A HIGH-LUMINOSITY HIGH-ENERGY LEPTON COLLIDER

D. Neuffer, Fermilab, Batavia, IL 60532 USA
H. Sayed, BNL, Upton, NY, 11973 USA
T. Hart, D Summers, University of Mississippi, Oxford, MS 38655, USA

Abstract

The final cooling system for a high-energy high-luminosity lepton collider requires reduction of the transverse emittance ε_t by an order of magnitude to ~0.00003 m (rms, N), while allowing longitudinal emittance ε_L to increase to ~0.1m. In the present baseline approach, this is obtained by transverse cooling of low-energy muons within a sequence of high field solenoids with low-frequency rf systems. Recent studies of such systems are presented. Since the final cooling steps are mostly emittance exchange, a variant form of that final system can be obtained by a round to flat transform in x-y, with transverse slicing of the enlarged flat transverse dimension followed by longitudinal recombination of the sliced bunchlets. Other variants are discussed. More explicit emittance exchange can greatly reduce the cost of a final cooling system.

INTRODUCTION

The P5 report stated that "for e^+e^- colliders, the primary goals are improving the accelerating gradient and lowering the power consumptions."[1] Both of these goals are achieved by increasing the mass of the electrons to a level where multiturn acceleration to TeV's is possible, and radiation effects are small. Increasing the mass to 105.66 MeV changes TeV electrons from a radiation source and enables the possibility of multi TeV heavy electron (μ) colliders. Parameters for possible multiTeV Colliders are included in Table 1.

Table 1: High-energy Heavy-lepton Collider Parameters

Parameter	**Higgs (1/8TeV)**	**3TeV**	**6TeV**
Beam energy	0.063	1.5	3
Heavy $e^{-/+}$/ bunch	$2\ 10^{12}$	$2\ 10^{12}$	$2\ 10^{12}$
Circumference (m)	300	2767	6302
Tune	5.16/4.56	20.1/22.2	38.2/40.1
Compaction	0.08	-3E-4	-1.2E-3
Emittance (μ,N)	300	25	25
Collision β_t (cm)	3	0.5	0.25
Energy spread	0.003%	0.1%	0.1%
rep rate	30 Hz	12 Hz	6 Hz
Luminosity (10^{34}cm^{-2}s^{-1})	0.002	4	12

The multi-TeV scenarios require cooling the beam transversely to ε_t ~0.00003m (rms, N (normalized)) while allowing a longitudinal emittance of ε_L ~0.1m (rms, N).[2] The present 6-D cooling systems cool the muons to ~0.0003m transversely and ~0.001m longitudinally.[3] Thus the collider scenarios require a "final cooling" system that reduces ε_t by a factor of ~10 while allowing longitudinal emittance increase. We will discuss several approaches toward obtaining final cooling parameters.

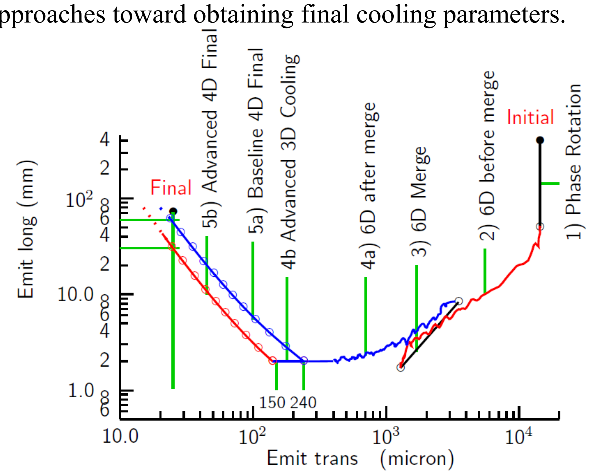

Figure 1: Progression of emittances throughout a collider cooling scenario.

BASELINE FINAL COOLING

A baseline approach to final cooling was developed by Palmer et al. This includes transverse ionization cooling of low-energy muons within high field solenoids, with lower energies and higher fields obtaining smaller ε_t .[4, 5] At low-energies, the variation of momentum loss with energy anti-damps the beam longitudinally, increasing ε_L. Figure 1 shows the progression of emittances throughout a collider cooling scenario, with the "final cooling" portion of that displayed as the lines with transverse emittance decrease and longitudinal emittance increase leading to final values at ε_t = 25μ and ε_L = ~30---60mm.

For final cooling, the beam momentum is reduced initially to 135 MeV/c and only transverse cooling is used. The final cooling system consists of ~a dozen stages. Each stage consist of a high-field small bore magnet with an H_2 absorber within the magnet, followed by an rf and drift system within lower-field to phase-rotate and reaccelerate the muons. From stage to stage, the muon beam energy is reduced (from 66 MeV toward

ISBN: 978-3-95450-168-7 doi:10.18429/JACoW-IPAC2015-TUBD3

EFFECTS OF ACCELERATING STRUCTURES ON ON-LINE DFS IN THE MAIN LINAC OF CLIC

J. Pfingstner[1,2,*], E. Adli[1], D. Schulte[2]
[1]University of Oslo, Oslo, Norway, [2]CERN, Geneva, Switzerland

Abstract

Long-term ground motion will create significant dispersion in the time-scale of hours in the main linac of CLIC. To preserve the emittance to an acceptable level, a dispersion correction with on-line dispersion-free steering (DFS) is inevitable. For this on-line technique, the dispersion has to be measured using beam energy variations of only about one per mil in order to not disturb the operation of the accelerator. For such small energy variations, the interaction of the particle beam and the accelerating structures creates large enough additional signals components in the measured dispersion to cause the dispersion correction to not work properly anymore. In this paper, the additional signals are described and their effect on the DFS algorithm is analysed. Finally, methods for the mitigation of the deteriorating signal components are presented and studied via simulations.

INTRODUCTION TO ON-LINE DFS

Linear colliders are very sensitive to element misalignments, due to their ultra-small beam emittances. These misalignments are not only of static nature, but change over time as a result of the impact of ground motion. For time scales below a few minutes, the ground motion induced luminosity loss can be mitigated with orbit feedback systems and mechanical magnet stabilisation systems [1]. Over longer time periods, however, it is not sufficient to correct only the beam orbit. Also the steadily increasing dispersion has to be addressed. For the CLIC main linac, e.g., this dispersion causes an emittance growth in the more critical vertical direction of $\Delta\epsilon_y = 0.75$ nm per hour. This simple empirical law has been found via simulation studies. It assumes ground motion according to the ATL law [2] with a constant A of 10^{-5} μm/s/m.

To avoid this emittance growth, a scheme has been proposed in which the dispersion is corrected during the accelerator operation in a transparent way (similar to an orbit feedback). This scheme, named online dispersion free steering (DFS), is based on the well-known DFS algorithm [3]. The DFS algorithm consists of two steps. Firstly, the dispersion $\eta(s)$, where s is the longitudinal position in the beam line, is determined via the beam orbit change $\Delta x(s)$ of two measurements $x_{E_0}(s)$ and $x_{(1+\delta)E_0}(s)$ due to a change in beam energy of δE_0, where E_0 is the nominal beam energy,

$$\eta(s) = \frac{\Delta x(s)}{\delta} = \frac{x_{(1+\delta)E_0}(s) - x_{E_0}(s)}{\delta}. \tag{1}$$

The dispersion $\eta(s)$ is then used to compute and apply quadrupole magnet misalignments $\theta(s)$ that cancel $\eta(s)$ in a least square sense. Additional constrains can be imposed in the computation of $\theta(s)$, to limit the amplitude of the correction and to not create too large beam orbit excursions [4]. In practice DFS is not applied in one step to the whole linac, but rather in a sequential fashion to overlapping subsection called bins (36 in the case of the CLIC main linac).

The basic form of DFS is intended to be used in the commissioning phase and during performance tuning campaigns. In these cases, large relative energy variations δ (5% to 10%) can be used, since the beams are not used for physics data taking. If DFS should be used on-line, however, only small δ in the order of 1 per mil are acceptable (energy acceptance of the beam delivery system). This results in small orbit variations $\Delta x(s)$, which reduces the measurement quality dramatically, due to the higher relative measurement noise of the beam position monitors (BPM). To recover the necessary measurement quality, an averaging method has been proposed and successfully tested in simulations [5].

Robustness studies have revealed, however, that the online DFS algorithm is sensitive to certain effects due to accelerating structures [6], namely wake fields and structure tilts. In this paper, the influence of these effects on the online DFS algorithm is analysed and modifications to the algorithm are proposed that recover the performance of the dispersion correction. These modifications are tested in simulations and the final emittance growths are reported.

EFFECTS DUE TO ACCELERATING CAVITIES

The sources of dispersion in a particle beam can be traced back to different types of dipole kicks. In linear accelerators without bending magnets, the main sources of dipole kicks are misaligned quadrupole magnets (feed-down effect). The purpose of the DFS algorithm is to cancel this dispersion, by adding new dispersion created by intentionally offsetting quadruple magnets. However, there are also other sources of dipole kicks in linear accelerators that create dispersion. These dipole kicks originate from accelerating structures, either because of imperfect alignment, e.g. tilts, or due to transverse wake fields. In the following, it will be shown that the dispersion due to dipole kicks from accelerating structures create undesirable signals in the dispersion measurement Eq. (1) that deteriorate the performance of the on-line DFS correction. Also strategies to suppress these unwanted signals are presented.

Deteriorating effects of transverse wake fields: An offset of the beam in an acceleration cavity creates transverse wake fields. These transverse wake fields are zero

* juergen.pfingstner@cern.ch

Content from this work may be used under the terms of the CC BY 3.0 licence (© 2015). Any distribution of this work must maintain attribution to the author(s), title of the work, publisher, and DOI.

ISBN: 978-3-95450-168-7 doi:10.18429/JACoW-IPAC2015-TUPWA001

MEASUREMENT OF THE INCOHERENT DEPTH OF FIELD EFFECT ON HORIZONTAL BEAM SIZE USING A SYNCHROTRON LIGHT INTERFEROMETER

M. J. Boland, AS, Clayton, Victoria, Australia
J. Corbett, SLAC, Menlo Park, CA, USA
T. Mitsuhashi, KEK, Tsukuba, Ibaraki, Japan

Abstract

The electron beam size as measured using synchrotron light in a circular accelerator is influenced by the incoherent depth of field effect. This effect comes about due to the instantaneous opening angle of the emitted synchrotron radiation (SR) and the acceptance angle of the SR light monitor beamline. Measurements were made using a visible light interferometer at the visible light beamlines in three circular accelerators at ATF, SPEAR3 and AS. The first order spatial coherence of the beam was measured and from that the horizontal beam size was calculated. The data is compared with a theory of synchrotron radiation with and without the horizontal incoherent field depth effect.

INTRODUCTION

The work in the paper covers in more detail the horizontal theory presented in Ref. [1]. If we accept the theory of the coherence of SR given in Ref. [2,3], then the highly relativistic motion of electrons in a storage ring results in temporal squeezing at the point of photon emission. From the observers frame of reference, this gives the appearance of a small cusp in the trajectory which – in the visible part of the spectrum – effectively forms a diffraction limited window from which the SR emerges. Each single electrons emits pencil of light having approximately the same opening angle in vertical and horizontal (precisely speaking the vertical distribution has π component so a small difference exists) which is then occupied by a single mode of 1 photon (or vacuum when photon number is zero). The opening angles of the pencils of light are $(\lambda/\rho)^{1/3}$ in both for vertical and horizontal.

The independent electrons in the bunch emit this pencil of light with a probability roughly proportional to the fine structure constant $\alpha = 1/137$. According to quantum physics, a fraction of a photon does not exist, leaving the situation that only one electron in every 137 electrons emits one single photon. The observed intensity downstream is the incoherent summation of these pencils of light. In an light source storage ring there are a lot of electrons in the bunch, so the SR is still very bright. One single photon mode in a pencil of light is coherent, so an interferogram created by a double slit interferometer must have a contrast of exactly 1 for many observations of individual photons emitted by single electrons. So, if this pencils of light illuminate a double slit downstream, as shown in Fig. 1, the following situations emerge in the horizontal case.

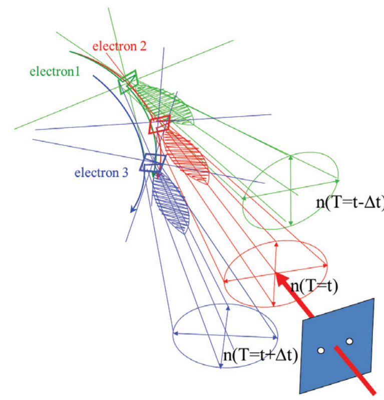

Figure 1: Photon emission from an electron beam in storage ring bending magnet.

Situation 1: beam upstream of tangent starts to illuminates slits.

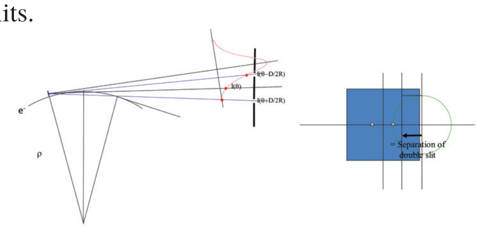

Situation 2: tangential beam evenly illuminates slits.

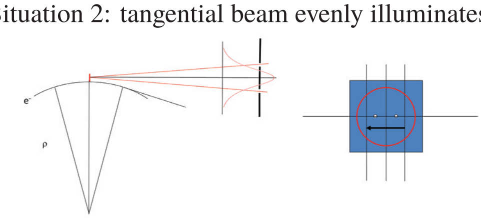

Situation 3: beam downstream of tangent last illumination of slits.

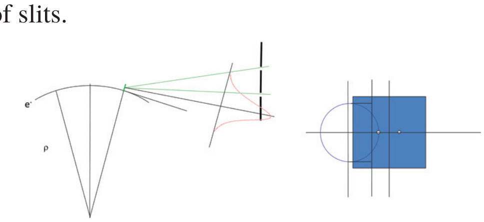

Figure 2: Horizontal sweeping of beam over double slits.

Situation 1 in following figure shown pencil of light start to illuminate the one of double slit, full noon illumination

Content from this work may be used under the terms of the CC BY 3.0 licence (© 2015). Any distribution of this work must maintain attribution to the author(s), title of the work, publisher, and DOI.

ISBN: 978-3-95450-168-7 doi:10.18429/JACoW-IPAC2015-TUPWA002

LAYOUT OPTIONS FOR THE AXXS INJECTOR AND XFEL

M. J. Boland, Y.-R. Tan and D. Zhu, AS, Clayton, Victoria, Australia

Abstract

A new injector is being planned for the Australian Synchrotron that is designed to feed both an upgraded storage ring and an XFEL. The desire to fit the AXXS project on the same site as the existing light source presents several layout difficulties. Several options are studied and simulations are performed to check the impact each choice has on the beam performance.

INTRODUCTION

The Australian X-Band X-Ray Source (AXXS) [1] is part of an effort to use the CLIC [2] x-band technology from CERN to develop a Free Electron Laser (FEL). A research and development collaboration has been formed [3] and a baseline design for the linac has emerged [4]. This paper explores some of the layout options that are specific to the Australian Synchrotron (AS) site in Melbourne, Australia. At this stage it will be attempted to fit the construction of an FEL to be co-located on the same site as the existing storage ring and to use the linac to inject into the new multi bend achromat (MBA) lattice that is being designed to replace the existing storage ring. Including the neighbouring car park on one side and an empty lot on the other side, there is 550 m of land available on the existing AS site (see Fig. 1).

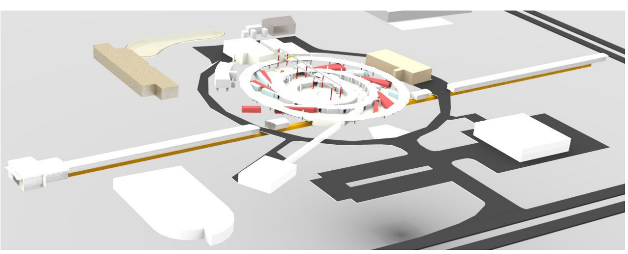

Figure 1: AS site with proposed AXXS FEL overlay.

As explained in Ref. [1], the first phase of any upgrade project is to fill out the remaining beamlines (marked in red on Fig. 1) on the existing storage ring, before replacing the storage ring with a new diffraction limited storage ring (DLSR) [5]. The AXXS linac can then replace the current injection system, necessary to inject into a DLSR which will have a very narrow magnet apertures – approximately 12.5 mm for the present DLSR designs [6] compared to 37.5 mm for the current AS ring [7].

STORAGE RING UPGRADE

The user community of over one thousand users per year is very satisfied with the operation of the current storage ring. There is high demand for beamtime and some beamlines are heavily oversubscribed – up to five times more beamtime is requested than can be provided. The first priority for the facility is to complete the build-out of the available space for beamlines, which amounts to five more insertion devices and several bending magnets. In parallel there is also a very active part of the x-ray user community in Australia who are doing research using FELs, spearheaded by the Centre for Advanced Molecular Imaging [8]. Both these factors in the Australian user community are driving the efforts on the AXXS project.

The first steps towards designing a new storage ring have been taken following the trend in MBA lattice designs [9], see for example the MAX IV facility currently being built [10]. The lattice functions for one cell are shown in Fig. 2 and the constraints that have been used are a) circumference remains 216 m to fit in the same tunnel and b) the beamline source points remain in the same location.

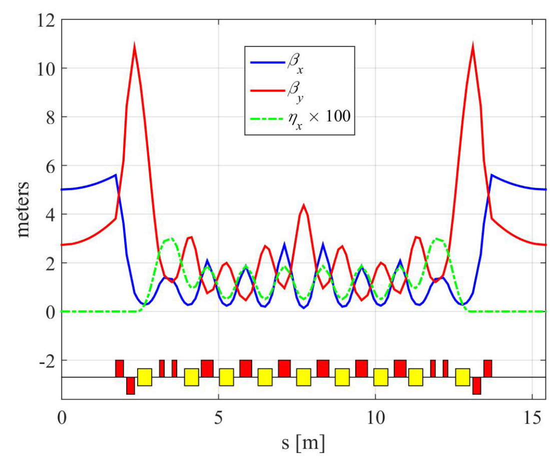

Figure 2: Lattice functions of AS MBA cell.

Some of the parameters for the MBA are listed in Table 1.

Table 1: Selected Machine Parameters for MBA Lattice Compared with Present DBA Lattice

Parameter	DBA	MBA
Beam Energy (GeV)	3.0134	3.0000
Beam Current (mA)	200.0000	200.0000
Horizontal Emittance (nm)	10.3488	0.2023
Vertical Emittance (nm)	0.1035	0.0607
Critical Photon E (keV)	8.1068	6.6371
Energy Spread (%)	0.1021	0.1047
Lin. Energy Acceptance (%)	2.1774	7.4462
α_c (10^{-3})	2.1115	0.1976
Bunch Length (ps)	23.0879	7.1781
Bunch Length (mm)	6.9218	2.1520
Horizontal Tune	13.2900	46.1038
Vertical Tune	5.2160	19.1729

Content from this work may be used under the terms of the CC BY 3.0 licence (© 2015). Any distribution of this work must maintain attribution to the author(s), title of the work, publisher, and DOI.

ISBN: 978-3-95450-168-7 doi:10.18429/JACoW-IPAC2015-TUPWA004

OPERATOR ROLES AT THE AUSTRALIAN SYNCHROTRON

Don McGilvery, Greg LeBlanc, Australian Synchrotron, Clayton, Australia

Abstract

The Accelerator Operators at the Australian Synchrotron undertake a wide variety of critical functions as part of their regular duties. In addition to normal Control Room duties, they play a major Role in Machine Physics, provide after hours support for Users on Beamlines and contribute extensively to the Controls and Database Development across the facility.

OPERATIONS AT THE AUSTRALIAN SYNCHROTRON

The Australian Synchrotron (AS) has been in User Beam Operation for 8 years. It comprises a 3GeV electron storage ring with a full energy injector. Top Up Operation commenced in 2013 and there are currently 10 beamlines. The yearly schedule includes 5000 hours of User Beam and 2000 hours of Machine Development and Physics.

Operator Rostering

Operators are rostered to cover 24 hours a day, 7 days per week. Two Operators are rostered on each shift and work a 12 hour 7 day on, 7 day off , 7 nights on 7 days off rotating roster. The Operators find this particular roster rotation works extremely well. It features minimal shift changes, every second weekend off and sufficient time to prepare for and recover from the night shifts. For 75% of the week the Operators are the only AS staff regularly on site and they play a key role in the delivery of great science.

Diversity of Tasks

Since commencing Top Up Operations and the provision of uninterruptible power to the Storage Ring, RF and the Conventional Facilities, minimal Operator intervention is required to maintain stored beam during User Operations.

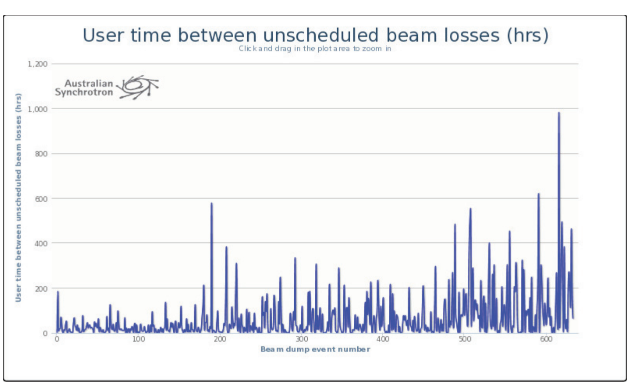

Figure 1: Reliability improvement of operation indicated by the increasing times between unscheduled beam trips.

The reliability of operation of the Australian Synchrotron (see Figure 1) is demonstrated by the recent delivery of 982 hours of User Beam without an unscheduled beam loss event. Some time is still required for dealing with minor trips, tuning, fault diagnosis and recovery but most Operator time is devoted to other activities and projects.

Operator Projects

Some of the Operator Projects include:

- The development of an Electronic Log Book
- Maintaining the Facility Statistics and KPI's.
- EPICS, Database and Web page maintenance
- Design and construction of a Tunnel Robot
- Development of Environmental Monitors
- Improvement to Beam Diagnostics
- Auto-tune Routines for the Accelerators

A key Role the Operators now undertake is to provide "After Hours Support" to Users on Beamlines.

After Hours Support for Users on Beamlines

Beamline Science staff provide support for Users between 8:00 and 18:00 Monday to Friday and are rostered on call weekends and until 22:00 each night. At other times the Operators provide the Ussr support. Furthermore any requests for on call User support is provided through the Control Room. This has been a very successful undertaking with the Operators now handling around 70 User support calls each month.

Operators have been formally trained on a number of beamlines and are able to apply their machine problem solving skills to assist with fault resolution and training on beamlines.

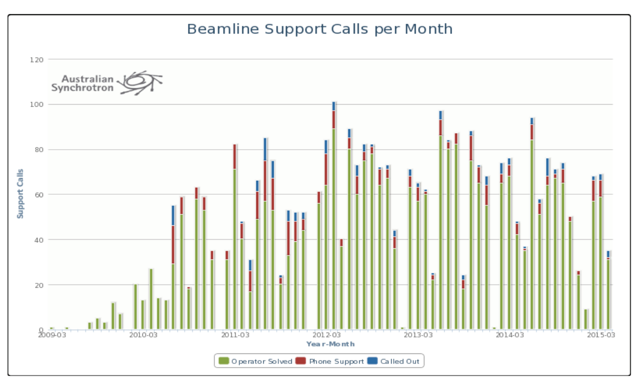

Figure 2: Graph showing the number of beamline support calls per month handled by the Operator.

It can be seen in Figure 2 that the number of support calls handled by the Operators grew over the first couple of

Content from this work may be used under the terms of the CC BY 3.0 licence (© 2015). Any distribution of this work must maintain attribution to the author(s), title of the work, publisher, and DOI.

ISBN: 978-3-95450-168-7 doi:10.18429/JACoW-IPAC2015-TUPWA005

COMPARISON OF BUNCH COMPRESSION SCHEMES FOR THE AXXS FEL

T. K. Charles, D. M. Paganin,
School of Physics and Astronomy, Monash University, Clayton, Australia
A. Aksoy, Ankara University, Golbasi / Ankara, Turkey
M. J. Boland, R. Dowd, Australian Synchrotron, Clayton, Australia
A. Latina, D. Schulte, CERN, Geneva, Switzerland

Abstract

Different types of electron bunch compression schemes are compared for the AXXS FEL design study. The main linac for the proposed machine is based on CLIC x-band structures. This choice leaves several options for the bunch compression schemes which impact the injection system RF band. Both harmonic linearization and phase modulation linearization are considered and their relative strengths and weaknesses compared. Simulations were performed to compare the performance of an s-band injector with a higher harmonic RF linearization to an entirely x-band injector and linearization scheme. One motivation for the study is to optimize the length of the AXXS machine, allowing the linac to fit onto the proposed site and also act as the injector to the existing storage ring at the Australian Synchrotron

AXXS

AXXS (Australian X-band X-ray Source) [1] is strategically planned to incorporate an upgrade of the current Australian Synchrotron storage ring and provide a new high brightness sub-Angstrom wavelength XFEL. The design includes a 6 GeV linac based around the CLIC x-band linac [2, 3].

PHASE MODULATION LINEARIZATION

In attempting to linearize the longitudinal phase space most FELs around the world employ harmonic linearization. When looking to design an all x-band linac, as is the case of AXXS, the high frequency accelerating structures preceding the first bunch compressor make harmonic linearization more difficult to achieve.

Phase modulation linearization is the term introduced in this paper to describe a new method of linearization. Through independently varying the phases of two cavities positioned before the first bunch compressor, 2nd order effects encountered through bunch compression can be minimized. These 2nd order effects refer to both the RF curvature impressed onto the beam during accelerating, plus the second order longitudinal dispersion, T_{566}, of the magnetic chicane.

Implementation of Phase Modulation Linearization is sketched in Fig. 1. To establish an energy chirp, the RF phase of the first section after the injector, ϕ_0, is chosen to be 70°. The two additional cavities required for Phase Modulation Linearization are shown as having the parameters V_1, ϕ_1, V_2 and ϕ_2.

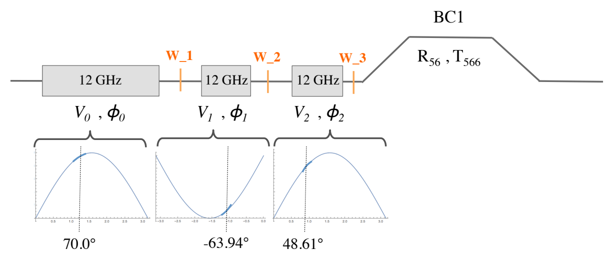

Figure 1: Layout of an x-band FEL accelerator design, up to end of first bunch compressor, which employs Phase Modulation Linearization. Included are markers showing location of longitudinal phase space plots in Fig. 3.

Analytical Approach

The beam energy after passing through the accelerating section leading up to the first bunch compressor is,

$$E_f = E_i + V_0 \cos(\phi_0 + k_x z_0) + V_1 \cos(\phi_1 + k_x z_0) + \ldots \\ + V_2 \cos(\phi_2 + k_x z_0), \quad (1)$$

where V_0, V_1, V_2, represent the RF voltages of the three sections shown in Fig. 1, and ϕ_0, ϕ_1, and ϕ_2, are the RF phases of these sections, where the RF phase is defined to be 90° at the crest of the RF acceleration, and over the interval $0 < \phi < 90°$ defines the negative slope of the RF curve (i.e. the head of the bunch is accelerated less than the tail). z_0 is the position of an electron with respect to the bunch center, and k_x is the wave number of the RF frequency.

The longitudinal position of any electron as it passes through the dispersive region of the chicane is,

$$z_f(\delta) = z_i + R_{56}\delta + T_{566}\delta^2 + U_{5666}\delta^3 + \ldots \quad (2)$$

Taking the Taylor series expansion of Eq. 1, calculating the relative energy deviation and then substituting the result into to the dispersion relation (Eq. 2), the final longitudinal position is,

$$z_f = z_0 + R_{56}(az_0 + bz_0^2) + T_{566}(az_0 + bz_0^2)^2 \\ + \text{higher order terms} \quad (3)$$

$$= z_0(1 + aR_{56}) + (bR_{56} + a^2T_{566})z_0^2 \\ + 2abT_{566}z_0^3 + b^2T_{566}z_0^4 + \text{higher order terms} \quad (4)$$

Content from this work may be used under the terms of the CC BY 3.0 licence (© 2015). Any distribution of this work must maintain attribution to the author(s), title of the work, publisher, and DOI.

ISBN: 978-3-95450-168-7 doi:10.18429/JACoW-IPAC2015-TUPWA006

SIRIUS ACCELERATORS STATUS REPORT

A.R.D. Rodrigues*, F. Arroyo, O.R. Bagnato, J.F. Citadini, R.H.A. Farias, J.G.R.S. Franco, L. Liu, S.R. Marques, R.T. Neuenschwander, C. Rodrigues, R.M. Seraphim, O.H.V. Silva, LNLS, Brazil

Abstract

Sirius is a 3 GeV synchrotron light source that is being built by the Brazilian Synchrotron Light Laboratory (LNLS). The electron storage ring is based on a modified 5BA cell to achieve a bare lattice emittance of 0.27 nm.rad in a 518 m circumference ring that contains 20 straight sections of alternating 6 and 7 meters in length. The 5BA cell accommodates a thin permanent magnet high field (2 T) dipole in the center of the middle bend producing hard X-ray radiation (ε_c=12 keV) with a modest contribution to the total energy loss.

In this paper we discuss the main achievements and issues for Sirius accelerators. Developments in beamlines are not discussed here.

INTRODUCTION

Over the last year the earthwork at the Sirius site was completed and the building foundation work has began just after the groundbreaking ceremony on Dec. 19, 2014. See Fig. 1. The project underwent an overall budget and schedule revision after the detailed engineering design of the building was concluded. Start of machine installations is now scheduled for the end of 2017.

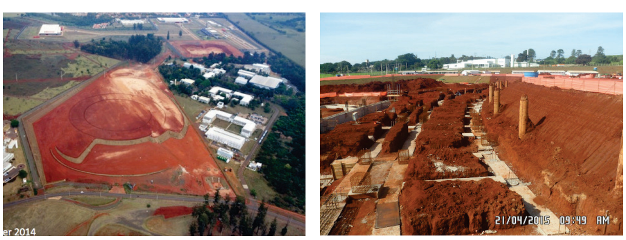

Figure 1: Aerial view taken in October 2014 of the Sirius site with earthwork completed (left) and construction of building foundation as of April 2015 (right).

The storage ring design optics has been upgraded to improve the matching in phase space between the electron beam and photon beam from insertion devices [1]. The main parameters for this new mode are summarized in Table 1. Most of the accelerator subsystems are in R&D and prototyping phase; a few are already under production, such as the booster magnets.

MAGNETIC LATTICE

A few modifications in the magnetic lattice have been implemented to optimize the design and fabrication of the magnets as well as to provide more space in the arc: the quadrupole lengths have been reduced, the slow orbit correctors and skew quadrupoles have been combined into the sextupoles, the different types of dipoles have been segmented into a rectangular unit block, and the horizontal and vertical fast orbit correctors have been combined to minimize the length of special vacuum chambers. The BPMs adjacent to the insertion straight sections have been moved closer to quadrupoles to optimize the beam-based alignment process and the BPM downstream the central dipole has been removed to avoid synchrotron radiation power. The optical properties for the new lattice are described in more detail in ref [1]. The injection straight section has also been optimized for injection with a pulsed multipole magnet. In this case, the conventional four kickers are not necessary and more space is available to optimize the pulsed magnet injection. A single kicker is kept for on-axis injection during commissioning.

Table 1: Sirius Storage Ring Main Parameters

Energy	3.0	GeV
Circumference	518.4	m
Horizontal emittance	0.19 - 0.27	nm.rad
Betatron tunes (H/V)	48.14 / 13.12	
Natural chromaticity (H/V)	-126.1 / -79.4	
Natural energy spread	0.076	%
Natural bunch length	2.3	mm

VACUUM SYSTEM

The vacuum system design for a standard storage ring sector is complete. Prototypes for bellows, BPMs, fast orbit correctors, multipoles and dipole vacuum chambers have been produced and prototypes for crotch absorbers and dipole chambers with narrow antechambers are under production. Pumping for Sirius will be based on NEG coating with in-house deposition. The NEG coating procedure has already been developed and optimized for most chamber geometries; even the 6 mm height narrow dipole antechamber already showed good activation results. For in-situ NEG activation a special 0.4 mm thick heating jacket has been developed by EXA-M. The jacket, which fits in the narrow gap between the vacuum chamber and the magnet poles, includes an external radiation shield to reduce heat transfer to the magnet. Further R&D work is being devoted to the optimization of crotch absorbers, bellows and BPMs.

The booster dipole vacuum chambers have been contracted to a local company (FCA Brasil).

* ricardo.rodrigues@lnls.br

Content from this work may be used under the terms of the CC BY 3.0 licence (© 2015). Any distribution of this work must maintain attribution to the author(s), title of the work, publisher, and DOI.

ISBN: 978-3-95450-168-7 doi:10.18429/JACoW-IPAC2015-TUPWA007

UPGRADED OPTICS FOR SIRIUS WITH IMPROVED MATCHING OF ELECTRON AND PHOTON BEAM EMITTANCES

L. Liu*, F. H. de Sá, N. Milas, A. H. C. Mukai, X. R. Resende, LNLS, Campinas, Brazil

Abstract

A new optics has been designed for Sirius with improved betatron function matching in the 6 meter-long low beta straight sections for insertion devices. Both horizontal and vertical betatron functions are set to 1.5 m in the center of the section, improving the matching of the electron and undulator photon beams. In addition, the horizontal beam stay clear has also been reduced allowing for small horizontal gap devices as well as the conventional small vertical gap ones. The new design optics has been optimized to the same previous performance regarding dynamic aperture and momentum acceptance.

INTRODUCTION

To take advantage of the unprecedented X-ray brightness from insertion device photon sources offered by the 4th generation storage rings, it is important to match the electron and photon beam phase space orientations. It is well known that the effective photon beam distribution in phase space is the convolution between the diffraction-limited radiation emittance and the transverse electron beam emittances [1]. When the electron beam emittance becomes comparable to the diffraction-limited photon emittance, the effective photon beam brightness is greatly affected by the mutual orientations of both beams in phase-space. Matching the orientations will maximize the photon beam brightness. To improve the matching conditions in Sirius, we have reduced the horizontal betatron function at the center of the low β_x straight sections (SSB) from 4 in the previous mode [2] to 1.5 m in the new mode.

This modification also results in a reduction of the horizontal beam-stay-clear (BSC) at the SSB sections, which opens the possibility for small horizontal gap insertion devices in addition to the conventional small vertical gap ones.

DESIGN OPTICS

The Sirius lattice has alternating high and low horizontal betatron function straight sections for insertion devices. A high β_x is desired at the injection straight section and at long or canted undulator sections; and a low β_x optimizes the brightness from short undulator sources. At the high β_x sections (SSA) a quadrupole doublet is used to match the optical functions whereas at the low β_x sections (SSB) a quadrupole triplet is used. The extra quadrupole at SSB reduces the straight section length from 7 to 6 meters.

We have recently upgraded the Sirius design optics to further improve the beam brightness from undulator sources installed in the center of the low beta sectors by reducing the horizontal betatron function from 4 to 1.5 m. This corresponds to the optimum matching for undulators of approximately 4.5 m in length, according to the relation $\beta_{opt} \approx L/\pi$. For Sirius, 2-m long undulators are planned for SSB sections. Although not perfectly matched for this case, an increase of 10 to 25% in brightness, depending on the photon energy, is expected.

The new optics can be implemented preserving the bare lattice emittance of 0.27 nm.rad and without requiring changes to magnets or power supplies. The reduction in horizontal beta leads to an increase in the horizontal tune by two integers while the vertical tune is reduced by one. The dynamic aperture and momentum acceptance for this new operation point in tune space have been optimized to the same values of the previous mode. As a result a similar beam lifetime of approximately 10 hours is achieved for 500 mA with third harmonic cavity, uniform filling, 1% emittance ratio and both chromaticities set to +1.5 to reduce resistive wall growth rates. The optimization process uses the tracking-based multi-objective genetic algorithm MOGA [3] to refine the initial solutions. The new optics has thus been adopted as the official design mode for Sirius.

Further modifications in the lattice have been implemented in connection with the detailed design of the magnets. In particular, the quadrupole lengths have been reduced, the slow orbit correctors and skew quadrupoles have been combined with the sextupoles, the different types of dipoles have been segmented into a rectangular unit block, and the horizontal and vertical fast orbit correctors have been combined to minimize the length of special vacuum chambers. The BPMs adjacent to the insertion straight sections have been moved closer to quadrupoles to optimize the beam-based alignment process and the BPM downstream the central dipole has been removed to avoid synchrotron radiation power. The reduction in quadrupole length and the option for combined sextupoles and orbit correctors opened up significant space in the lattice: the magnets share in the total circumference is reduced from 45% to 39%.

The new lattice configuration is shown in Figure 1 and the main parameters in Table 1. Figure 2 shows the lattice function modifications for the previous and the new design optics.

* liu@lnls.br

Content from this work may be used under the terms of the CC BY 3.0 licence (© 2015). Any distribution of this work must maintain attribution to the author(s), title of the work, publisher, and DOI.

ISBN: 978-3-95450-168-7 doi:10.18429/JACoW-IPAC2015-TUPWA008

Content from this work may be used under the terms of the CC BY 3.0 licence (© 2015). Any distribution of this work must maintain attribution to the author(s), title of the work, publisher, and DOI.

MIXING AND SPACE-CHARGE EFFECTS IN FREE-ELECTRON LASERS*

E. Peter#, A. Endler, F. B. Rizzato, UFRGS, Porto Alegre, Brazil
A. Serbeto, UFF, Niterói, Brazil

Abstract

This work aims to understand the single pass FEL dynamics with an initially cold beam, through a semi-analytical model, based in a group's previous works in beams [1, 2]. The central point of the model is the compressibility factor, which allows establishing the transition from Compton to Raman regimes. The model is useful also to perform analytical estimates of the elapsed time until the onset of mixing and the saturated amplitude of the radiation field. Semi-analytical and full simulations results are compared, showing a good agreement.

INTRODUCTION

Free-electron lasers are devices that efficiently convert the kinetic energy of a relativistic electron beam into the energy of electromagnetic radiation. An electromagnetic wave (called laser or radiation) copropagates with the electron beam, which passes through a static and periodic magnetic field generated by a wiggler. Due the presence of the laser and wiggler fields, the electrons lose velocity, giving their energy to the laser. This single pass FEL, with initially cold beam, in general, is well explored in literature, both in Compton and Raman regimes [3-5].

In a FEL, there is interaction between the electrons and the ponderomotive well (formed through the superposition of the wiggler and laser electromagnetic fields) and among themselves. The last interaction is called space-charge effect.

When the electric charge is small in the system, the ponderomotive well mainly drive the particle dynamics, and the particles are attracted to the bottom of the well. In this case, electric repulsion is weak, and the particles revolve as a whole around themselves in the particle phase-space. This regime is called Compton.

But, when the charge increases, the mixing process in the phase-space become different (Raman regime). Electric repulsion offers resistance against the ponderomotive well, and the process is similar to the case of magnetically focused charged beams [1,6].

The main target of this work is review the paper [7] using more adequate parameters to FEL operation, establishing a threshold between Compton and Raman regimes. We made it through a semi-analytical approach based on the compressibility factor, whose zeroes indicate the onset of mixing in phase-space. This semi-analytical model can provide an estimative of the time and the position in the ponderomotive well for the onset of mixing and the saturated amplitude of the radiation field.

*Work supported by CNPq and FAPERGS, Brazil, and by the US-AFOSR under the grant FA9550-09-1-0283.
#peterpeter@uol.com.br

PHYSICAL MODEL

A complete description of FEL dynamics must include laser, electron phase and energy evolutions and space-charge effects, which occurs due a longitudinal electric field. We start with the laser and wiggler (w) fields. They are described by the respective vector potentials (with $\hat{e} = (\hat{x} + i\,\hat{y})/\sqrt{2}$)

$$\frac{e}{mc^2}\vec{\mathcal{A}}_w(z) = a_w(e^{-i\,k_w z} + c.c.)\,\hat{e}\ , \qquad (1)$$

$$\frac{e}{mc^2}\vec{\mathcal{A}}(z) = -i\left[a(z)e^{i(k\,z-\omega\,t)} - c.c.\right]\hat{e}. \qquad (2)$$

The dimensionless laser amplitude $a(z)$ is a slowly varying function of z. As for the space-charge contribution, to satisfy the periodic boundary conditions, we consider a thin electron beam moving at the center of the pipe. An equivalent physical picture is of a beam propagating along the z axis with two grounded plates located at $y = \pm L/2$. Based on a sheet beam model [8], Poisson equation is solved, demanding 2π periodicity for the variable $\theta = k_p z - \omega t$, where $k_p = k + k_w$ is the ponderomotive wave number and θ is the particle phase in the ponderomotive potential. In the limit of large values of L, the electric field generated at θ by one particle of unitary charge located at θ' can be expressed as the following periodic saw-tooth function, which is the dimensionless Green's function for the electric field:

$$E_z{}^G(\theta,\theta') = sign(\theta-\theta')[\pi - Abs(\theta-\theta')]. \qquad (3)$$

Therefore, the total electric field at particle phase θ (where $\eta^2 = \omega_p{}^2/\omega^2$, and ω_p is the plasma frequency)

$$E_z(\theta\,) = \eta^2\langle E_z{}^G(\theta,\theta')\rangle. \qquad (4)$$

From Lorentz equation, we write (where $\gamma = [(1+|a_{TOT}|^2)/(1-v_z{}^2)]^{1/2}$ is the relativistic Lorentz factor and v_z is the longitudinal velocity):

$$\frac{d\gamma_j}{dz} = -\frac{a_w}{2\gamma_j}\left(ae^{i\theta_j} + c.c.\right) + v_{zj}v_pE_z(\theta_j). \qquad (5)$$

ISBN: 978-3-95450-168-7 doi:10.18429/JACoW-IPAC2015-TUPWA009

50 MeV ELECTRON LINAC WITH A RF GUN AND A THERMOIONIC CATHODE

A. Setty, A.S. Chauchat, D. Fasse, D. Jousse, P. Sirot Thales Communications & Security (TCS), 4 avenue des Louvresses 92 230 Gennevilliers, France

Abstract

The low energy part of our pre injectors is made up of a 90 kV DC thermoionic triode gun, followed by a 500 MHz sub harmonic pre buncher and a 3 GHz pre buncher. We propose a new design for a 50 MeV linac with a RF gun [1]. This study will compare the beam dynamics simulations for the new design and for our previous pre injectors.

RF CAVITY F – 3F

The RF gun F – 3F is integrated in a modulated cavity at sub harmonic frequencies 200 MHz and 600 MHz followed by a drift in order to bunch the beam.

The main difficulty is to adapt the cavity geometry in order to have exactly at harmonic 3: $F_3 = 3 \times F_0$.

Then, in order to be synchronised with the travelling wave section frequency we must obtain: $F_{3GHZ} = 15 \times F_0$.

The electrons emission is produced by a thermoionic cathode implemented inside the RF cavity

The feeding RF power is of 25 kW, the entry accelerating field, at the cathode position, is equal to 1.2 MV/m and the crest field is of 6.5 MV/m.

The grid is modulated at 200 MHz with a pulse length gate of 500 ps, i.e. a phase beam extension equal to 36 degrees. We can then choose the appropriate phase with respect to the RF cavity field.

GENERAL DESCRIPTION OF THE F/3F RF GUN 50 MeV LINAC

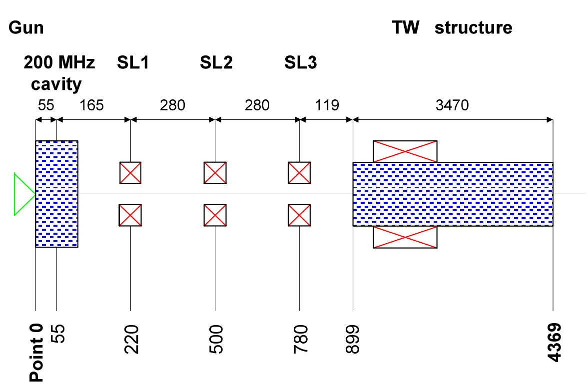

Figure 1: F/3F RF GUN 50 MeV linac (unit in mm).

Figure 1 shows a schematic layout of the F/3F RF gun 50 MeV linac. The subsystems are listed below:

- A RF gun with a thermoionic cathode.
- A 200 MHz/600 MHz cavity.
- Three focusing shielded lenses between the cavity and the accelerating structure.
- A travelling wave accelerating structure.
- A solenoid surrounding the beginning of the structure.

The total length is around 4.4 meters for 50 MeV beam energy. Our previous design for the BESSY II linac at the same energy had a total length of around 8 meters [2].

BEAM DYNAMICS SIMULATIONS

The Gun and the Cavity

The injection line from the gun to the accelerating structure includes the RF cavity with a 25 kW at 200 MHz and a 2.3 kW at 600 MHz.

The drift space between the cavity exit and the RF input of the section is around 900 mm long.

The radial focusing along the drift space is provided by 3 shielded lenses with respectively a magnetic field of 700, 400 and 450 Gauss.

At the cavity exit without space charge, the beam energy varies from 317 keV to 349 keV for a phase extension of 6 degrees at 200 MHz.

Figure 2 shows the phase-energy diagram at 200 MHz cavity exit. For a total charge of 240 pC, the energy varies from 274 keV to 354 keV, an energy spread of 80 keV, for a phase extension of 13 degrees at 200 MHz, i.e. 195 degrees at 3 GHz.

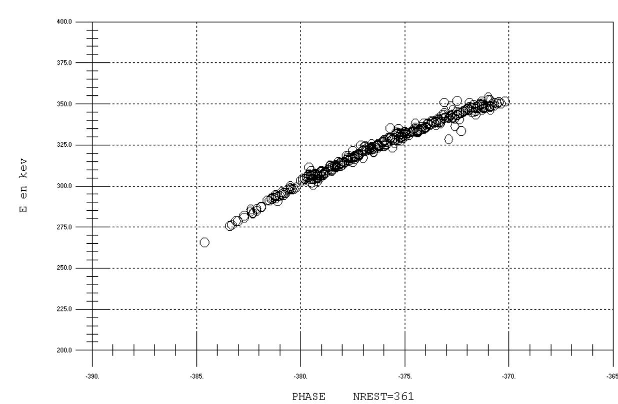

Figure 2: Phase-energy diagram at the cavity exit.

Figure 3 shows the phase-energy diagram at the accelerating structure entry after a drift space of 900 mm. For the phase extension, the same time scale was taken for figures 2 and 3.

After the drift, the phase extension was reduced from 195 degrees to 40 degrees for 91% of the gun charge.

The Accelerating Section

The main accelerating structure is identical to those made for the ALBA and BESSY II pre injectors [3].

Content from this work may be used under the terms of the CC BY 3.0 licence (© 2015). Any distribution of this work must maintain attribution to the author(s), title of the work, publisher, and DOI.

ISBN: 978-3-95450-168-7 doi:10.18429/JACoW-IPAC2015-TUPWA011

Content from this work may be used under the terms of the CC BY 3.0 licence (© 2015). Any distribution of this work must maintain attribution to the author(s), title of the work, publisher, and DOI.

PROGRESS ON THE LUNEX5 PROJECT

M. E. Couprie, C. Benabderrahmane, P. Berteaud, C. Bourassin-Bouchet, F. Bouvet, J. Bozek, F. Briquez, L. Cassinari, L. Chapuis, J. Daillant, J. Da Silva, Y. Dietrich, M. Diop, J. P. Duval, M. El Ajjouri, T. El Ajjouri, C. Herbeaux, N. Hubert, M. Khojoyan, M. Labat, P. Lebasque, N. Leclercq, A. Lestrade, A. Loulergue, P. Marchand, O. Marcouillé, J. L. Marlats, F. Marteau, C. Miron, P. Morin, A. Nadji, R. Nagaoka, F. Polack, F. Ribeiro, J. P. Ricaud, G. Sharma, P. Rommeluère, P. Roy, K. Tavakoli, M. Thomasset, M. Tilmont, S. Tripathi, M. Valléau, J. Vétéran, W. Yang, D. Zerbib, Synchrotron SOLEIL, France
S. Bielawski, C. Evain, C. Szwaj, PhLAM/ CERLA, Lille, France
E. Roussel, FERMI@ELETTRA, Sincrotrone Trieste, Basovizza, Italy
G. Lambert, V. Malka, A. Rousse, C. Thaury, Lab. d'Optique Appliquée, Palaiseau, France
G. Devanz, C. Madec, A. Mosnier, CEA/DSM/IRFU/SACM, Saclay, France
D. Garzella, B. Carré, CEA/DSM/IRAMIS/ LIDyL, Saclay, France
N. Delerue, Laboratoire de l'Accélérateur Linéaire, Orsay, France
X. Davoine, CEA/DAM/DIF, Bruyères-Le-Châtel, France
A. Dubois, J. Lüning, LCPMR, Paris-VI, France

Abstract

LUNEX5 (free electron Laser Using a New accelerator for the Exploitation of X-ray radiation of 5th generation) aims at investigating the production of short, intense, coherent Free Electron Laser (FEL) pulses in the 40-4 nm spectral range. It comprises a 400 MeV superconducting Linear Accelerator for high repetition rate operation (10 kHz), multi-FEL lines adapted for studies of advanced FEL schemes, a 0.4 - 1 GeV Laser Wake Field Accelerator (LWFA) for its qualification by a FEL application, a single undulator line enabling advanced seeding and pilot user applications. Different studies and R&D programs have been launched. A test experiment for the demonstration of 180 MeV LWFA based FEL amplification at 200 nm is under preparation, thanks to a proper electron beam manipulation. Specific hardware is also under development such as a cryo-ready 3 m long undulator of 15 mm period.

INTRODUCTION

Since the laser discovery [1] and the first FEL [2] in the infra-red in Stanford on MARK III, followed by the ACO FEL at Orsay [3] in the visible and harmonic generation [4] in the VUV, VUVX light sources are actively developed around the word [5-8]. After the early FEL times, France has remained quite active, with the Super-ACO FEL [9-11] and first user applications [12-14], collaborations on UVSOR [15] and ELETTRA [16]. Besides the CLIO infra-red FEL [17] moved from oscillator to single pass configuration, with a particular interest on seeding schemes (influence of the undulator helicity [18], pulse splitting [19], sidebands [20], seeding with high order harmonics in gas (HHG) [21-23]) and on the transverse properties [24].

The LUNEX5 [25-28] demonstrator (see Fig. 1) aims at exploring several directions for the production of short, intense, and coherent FEL pulses between 40 to 4 nm on the first, third and fifth harmonics.

A 400 MeV superconducting (SC) linac with 2-3 modified XFEL type cryomodules at 1.3 GHz (fed with solid state amplifiers) will enable a CW operation for high repetition rate and multiple users. The qualification of an elementary RF unit with SC cavity, low level RF and solid state amplifier for CW operation is under study. The electron bunch is compressed thanks to a dogleg with sextupoles, enabling phase space linearization and cancellation of the second order dispersion [28]. The gun will be either superconducting [29] or APEX type [30]. In addition, an LWFA [31] based FEL configuration will be explored, requiring a specific beam transfer line able to handle the divergence (1 mrad) and energy spread (1 %) [32-35].

The single FEL line with different cryo-ready undulator segments of 15 and 30 mm period will allow Echo Enable Harmonic Generation (echo) [36] and HHG seeding to be compared for further handling of the spectral and temporal properties. SC linac based FEL calculations anticipate more than 10^{11} photons/pulse and 10^{27}peak brightness on the fundamental wavelength. Two pilot user experiments in gas phase and condensed matter will qualify the FEL performance in the different cases.

After the completion of the LUNEX5 Conceptual design Report at the end of 2011 [25], complementary studies and R&D have been launched.

Figure 1: LUNEX5 sketch: cryomodules (yellow), LWFA laser hutch (grey), undulators (4 radiators and 2 echo modulators) (purple), pilot user experimental sections (green).

ISBN: 978-3-95450-168-7 doi:10.18429/JACoW-IPAC2015-TUPWA012

SOLEIL STATUS REPORT

A. Nadji, Y.-M. Abiven, N. Béchu, F. Bouvet, P. Brunelle, A. Buteau, L. Cassinari, , M.-E. Couprie, X. Delétoille, C. Herbeaux, N. Hubert, N. Jobert, M. Labat, J.-F. Lamarre, P. Lebasque, A. Lestrade, A. Loulergue, P. Marchand, O. Marcouillé, J.-L. Marlats, L. S. Nadolski, R. Nagaoka, P. Prigent, K. Tavakoli, M.-A. Tordeux, M. Valléau, Synchrotron SOLEIL, Gif-sur-Yvette, France

Abstract

The 2.75 GeV synchrotron light source SOLEIL (France) delivers photons to 27 beamlines and 2 new ones are under construction. The commissioning of the Femtoslicing operation mode involving two beamlines is in progress. The uniform filling pattern is now available to users with a 500 mA stored beam current. The operation of the two canted and long beamlines ANATOMIX and Nanoscopium both using in-vacuum insertion devices (IDs) as a photon source has been raising challenges still under investigation. Upgrades of crucial subsystem equipment like magnet power supplies, storage ring RF input power couplers, and solid state amplifiers are continuing. New user requests for beam stability are under upgrade consideration. Other projects for the storage ring are ongoing such as the design and construction of new insertion devices, new multipole injection kicker, localised small and round photon beam production, as well as R&D on 500 MHz solid-state amplifiers. In parallel first studies for a future upgrade of the machine have been progressing.

OPERATION

Today, 27 beamlines are opened to the users. The last two beamlines ANATOMIX and PUMA, currently under commissioning, will be available to the Users by 2016. Five electron beam filling patterns are routinely delivered during user operation in Top-up injection mode (see Table 1 and Figure 1).

Table 1: Five Different Filling Patterns for SOLEIL Users

Filling pattern	2014 user operation	Achieved ultimate performance
Uniform (416 bunches)	430 mA (one week at 490 mA)	500 mA
Hybrid (312 + 1 bunches)	425 + 5 mA	455 + 5 mA
8 bunches	90 mA	110 mA
1 bunch	16 mA	20 mA
Hybrid Low-Alpha (bunch length/bunch current)	4.7 ps RMS / 65 µA/ bunch	2.5 ps RMS / 10 µA/bunch

In 2014, 6370 hours of beam time have been scheduled shared in 1329 hours for Machine studies and 5041 hours for user operation. A total of 4963 hours were actually issued to the Users which correspond to an availability of the photon beam for the beamlines of 98.5 %.

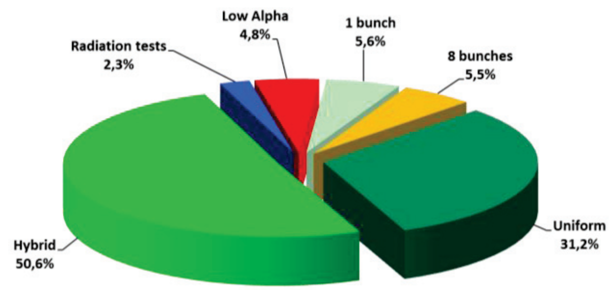

Figure 1: Time distribution of the five filling patterns delivered to Users during 2014.

Over the 35 scheduled weeks, the availability was above 99 % during 21 weeks during 5 of which it was at 100 %. In the very near future, the uniform user operation mode will be delivered with a current of 500 mA.

Operation in this mode has been tested successfully for one week at 490 mA in user operation. In addition, beam current in hybrid mode will be upgraded to 450 mA shortly. The distribution of multibunch mode beam time is different from last year [1]. The hybrid filling pattern is most common, closely followed by the uniform mode while the three other modes are almost at the same percentage as shown in Figure 1. Bunch purity is now maintained to a few 10^{-4} level over a full week thanks to the upgrade of the LINAC bunch cleaner.

As has been the case for the last two years, external electrical power drops are the main source of beam interruption. The main cause is the heavy work around the construction of a new university (Paris-Saclay) nearby SOLEIL. This problem represents 35 % of the beam time lost in 2014. The second main source of beam interruption (15 %) was human errors. Fault rates of equipment are reasonably low as can be seen in Figure 2. In particular, the fraction of lost time due to power supply dysfunctions or failures is drastically reduced compared to the previous years. The Mean Time Between Failures (MTBF) has reached a new record of 75 hours and the Mean Time To Recover (MTTR) has reached 1.09 hour.

Five feedbacks (FB) are simultaneously in operation (Slow Orbit FB, Fast Orbit FB, Transverse FB, Tune FB and Coupling FB). Top-up injection allows constant beam current intensity within ± 0.5 %. The long and short term photon beam position stability is reaching the desired performance. Using global orbit feedback systems, the long term position drift (8 h) is below 1 µm RMS and the short term (0.1 Hz – 1 kHz) vertical noise is below 300 nm RMS. Recently, a regularization of the singular values

Content from this work may be used under the terms of the CC BY 3.0 licence (© 2015). Any distribution of this work must maintain attribution to the author(s), title of the work, publisher, and DOI.

ISBN: 978-3-95450-168-7 doi:10.18429/JACoW-IPAC2015-TUPWA013

LINEAR AND NONLINEAR OPTIMIZATIONS FOR THE ESRF UPGRADE LATTICE

N. Carmignani, L. Farvacque, S. M. Liuzzo, B. Nash, T. Perron,
P. Raimondi, R. Versteegen, S. White, ESRF, Grenoble, France

Abstract

The ESRF storage ring will be replaced in 2020 by a new hybrid multi bend achromat lattice with 134 pm · rad equilibrium horizontal emittance. To determine the best working point, large scans of tunes and chromaticities have been performed, computing Touschek lifetime and dynamic aperture. From different working points, the multi-objective genetic algorithm NSGA-II has been used to optimize the nonlinear magnets values and some linear optics parameters. The analysis have been carried out on lattices with errors and corrections. The optimizations have produced lattices with longer lifetime and larger dynamic aperture for different working points with positive chromaticities.

INTRODUCTION

The ESRF upgrade storage ring will provide x-rays with a 40 times higher brilliance than the present machine, with 5 % coherence at 1 keV [1]. The optics functions of the hybrid multi bend achromat lattice cell are shown in figure 1. The 32-fold symmetry of the lattice is broken at the injection straight section, where the horizontal β function is increased to 18 m, to allow off-axis injection. Touschek lifetime and dynamic aperture are two crucial parameters for lattice design: the first for beam stability and limited losses around the ring [2], the second to increase injection efficiency. The reduced beam size of the upgrade lattice is detrimental for the Touschek lifetime: the scattering rate increases due to the higher bunch density. The dynamic aperture, even if larger in terms of beam size compared to the current machine, is only 10 mm with errors at the injection (8 mm is the minimum required).

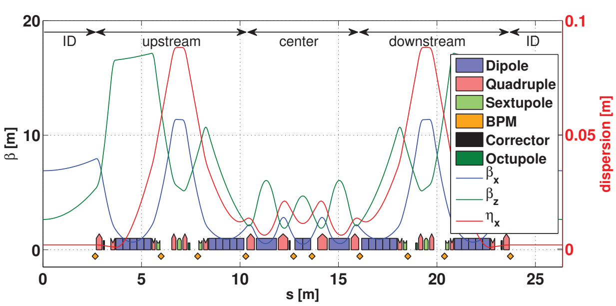

Figure 1: Twiss functions of the ESRF upgrade lattice.

This paper reports the various methods used to optimize the linear and non-linear optics in order to improve the Touschek lifetime and the dynamic aperture. A deterministic technique to partially cancel the effect of the injection cell symmetry breaking will also be addressed.

Simulations

Beam dynamics simulations are done with the Matlab Accelerator Toolbox (AT) [3] [4] [5] and they are designed to exploit the ESRF computer cluster (768, 2GHz cores).

The Touschek lifetime is computed with the Piwinski formula [6], assuming a current per bunch of 0.23 mA. The momentum acceptance computation is limited to four lattice cells, with a loss of only 5% in the accuracy compared to the computation with 32 cells.

Linear optics matching

The linear optics of the cell is obtained putting constraints on the following parameters: the β functions and the dispersion at the focusing sextupoles, in the straight sections and in the middle of the cell, the phase advances between the sextupoles and the total tune of the cell. The target values of this parameters are optimized to improve the properties of the lattice. Nevertheless these modifications have impact on the non-linear optics, demanding for an iterative process of optimization.

LATTICE OPTIMIZATIONS

Working point scan

To determine the optimal tune working point we vary the horizontal and vertical tune over various units and compute the Touschek lifetime and the dynamic aperture, as shown in figure 2.

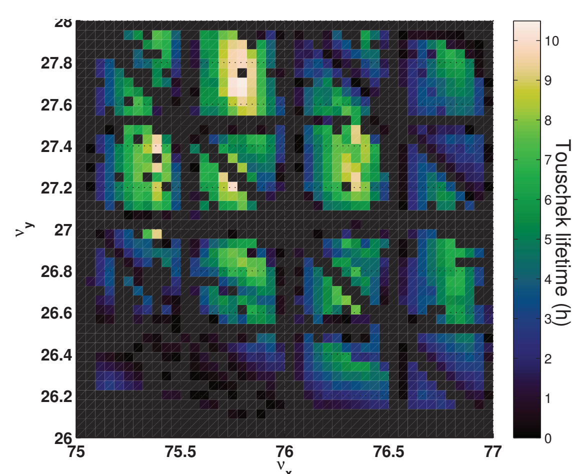

Figure 2: Touschek lifetime for different tunes values.

Keeping the same error seed for the whole scan, at each working point a complete commissioning-like procedure is performed: search for the closed orbit, corrections of orbit, linear optics and coupling [7]. The sextupoles are not

Content from this work may be used under the terms of the CC BY 3.0 licence (© 2015). Any distribution of this work must maintain attribution to the author(s), title of the work, publisher, and DOI.

ISBN: 978-3-95450-168-7 doi:10.18429/JACoW-IPAC2015-TUPWA014

INFLUENCE OF ERRORS ON THE ESRF UPGRADE LATTICE

S.M. Liuzzo, J.C. Biasci, N. Carmignani, L. Farvacque, G. Gatta, G. Le Bec, D. Martin, B. Nash, T. Perron, P. Raimondi, R. Versteegen, S. White, ESRF, Grenoble, France

Abstract

To determine the tolerable alignment and magnetic errors for the ESRF upgrade, we study their influence on Touschek lifetime and dynamic aperture. The correction of each set of errors studied is performed with a commissioning-like procedure, from the search for a closed orbit to the correction of resonance driving terms. Each kind of error is studied independently for each relevant family of magnets. The tolerable values deduced from the analysis are within the practical limits. The impact of the measured and simulated survey errors is also considered, defining the position of the currently installed lattice as the one of least impact for the realignment of X-ray beamlines.

INTRODUCTION

The ESRF Phase II Upgrade storage ring will replace the present light source in 2020, increasing the X-rays brilliance by a factor 40 providing 5% of coherence (at 1 keV) [1]. The chosen lattice for the upgrade is a Hybrid Multi Bend Achromat (HMBA) lattice, with theoretical equilibrium horizontal emittance of 134 pmrad. This lattice is depicted in Fig.1 and features a 32 fold symmetry. The symmetry is broken at the injection straight section to allow for higher beta-functions at the injection point. This insertion has effects on lifetime and dynamic aperture shown in [2]. The sextupoles are located in high dispersion and beta regions (dispersion bumps) and with an almost perfect -I transformation between the first three and last three sextupoles. This allows to cancel the second order sextupolar effects [3]. To enforce this condition in the limited space of the cell, two families of high gradient (91 T/m) focusing quadrupoles (QF6/8) are included together with combined function dipoles (DQ) [4]. To achieve these large fields a smaller bore radius is required and the vertical apertures in the central region of the lattice are reduced to 6.5 mm (10 mm in the rest of the cell). This small aperture and the phase space distortion between the sextupoles lead to strong error sensitivity in this region, mitigated by the smaller equilibrium beam size. To optimize the emittance of the lattice, the first and last two dipoles used in the cell have a longitudinal gradient (DL). In addition one family of octupoles is used to adjust the horizontal detuning with amplitude.

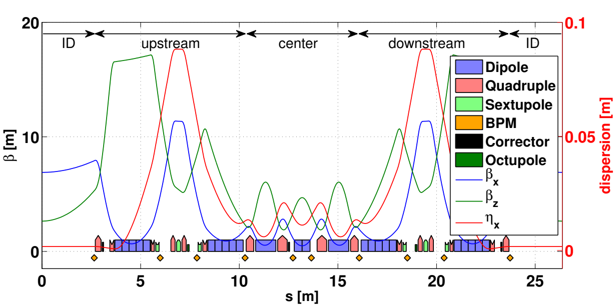

Figure 1: ESRF upgrade unit lattice cell (HMBA).

In this paper we look at the influence of alignment and field errors on lifetime, dynamic aperture and injection efficiency for all the magnets (version S28).

Errors Modeling

The coordinate system used in this document follows the trajectory of the reference orbit. The errors studied for dipoles, quadrupoles, sextupoles, octupoles and girders (support of magnet groups) are:

- transverse displacements Δx (radial) and Δy (vertical)
- longitudinal displacements Δs
- rotation about the beam direction $\Delta\psi$
- integral field errors $\frac{\Delta K_0}{K_0}$, $\frac{\Delta K_1}{K_1}$, $\frac{\Delta K_2}{K_2}$, $\frac{\Delta K_3}{K_3}$
- multipole errors (random and systematic)
- survey errors (random and systematic)

The DL dipoles and DQ dipoles are modeled in the lattice using several separated dipoles. The errors set in these magnets take in account this modeling choice and move the DLs and DQs slices as single magnets. Girder displacements are simulated by systematic movements of all magnets on the same girder. Beam position monitors (BPM) are displaced following the girders. Rotations of the dipoles are included as errors and do not affect the reference orbit.

Lattice Tuning and Correction

Simulations are done using the Accelerator Toolbox [5]. The errors are set for the desired magnet and the correction is performed with all the available correctors in the lattice: three dedicated correctors and six sextupoles with coils for horizontal and vertical steering and skew quadrupole correction. After the application of a procedure to find the closed orbit, the correction is performed following the techniques used in operation for the present accelerator: correction of tunes, orbit, normal and skew quadrupole resonance driving terms [6] and finally chromaticities. The procedure is iterated until convergence. Additional sextupole and octupole corrections are under investigation, together with many other algorithms, to be able to exploit all the available tuning knobs. The final parameters after correction are: rms orbits of ~ 100 µm, rms dispersion < 1 mm in the horizontal plane and ~ 200 µm in the vertical plane, < 1 % β-beating in both planes and the an emittance ratio of ~ 0.1 %. The required correctors strengths are within the power supply limits.

IMPACT OF ERRORS

The conditions to be achieved for a lattice with errors are:

- at least 8 mm of dynamic aperture towards the inner

Content from this work may be used under the terms of the CC BY 3.0 licence (© 2015). Any distribution of this work must maintain attribution to the author(s), title of the work, publisher, and DOI.

ISBN: 978-3-95450-168-7 doi:10.18429/JACoW-IPAC2015-TUPWA016

MODELING OF BEAM LOSSES AT ESRF

R. Versteegen*, P. Berkvens, N. Carmignani, J. Chavanne, L. Farvacque, S.M. Liuzzo, B. Nash, T. Perron, P. Raimondi, K.B. Scheidt, S. White, ESRF, Grenoble, France

Abstract

As the ESRF enters the second phase of its upgrade towards ultra low emittance, the knowledge of the beam loss pattern around the storage ring is needed for radiation safety calculations and for the new machine design optimisation. A model has been developed to simulate the Touschek scattering and the scattering of electrons on residual gas nuclei in view of producing a detailed loss map of the machine. Results of simulation for the ESRF are presented and compared with real beam measurements.

INTRODUCTION

Mapping of the electron beam losses in synchrotron light sources is needed as the beam parameters are pushed and the beam lifetime is reduced to optimise the machine performance for the users. It is necessary to anticipate the protection of various machine equipment and insertion devices from radiation damage. It is also requested from the radiation safety point of view to ensure easy access to the accelerator for maintenance. The tool developed to produce such a detailed description of beam losses, providing the electron loss locations as well as their transverse coordinates and energy when they reach the vacuum chamber aperture, is described in the first part of this paper. Simulations are then compared with experimental data taken on the ESRF storage ring. Finally, the experimental proof of principle of the foreseen collimation scheme for the machine upgrade is presented.

LOSSES FROM RANDOM PROCESSES

Three random interactions are simulated independently: elastic scattering within the bunches (Touschek losses), elastic and inelastic scattering between electrons and residual gas nuclei (Coulomb scattering and Bremsstrahlung).

Touschek losses

The Touschek effect is a large angle Coulomb scattering between two electrons inside a bunch. The transverse momentum is transferred to the longitudinal plane, which leads to the loss of one or both particles because of the limited energy acceptance of the machine [1].

The random particle generation has been developed in Matlab [2], within the Accelerator Toolbox (AT) [3]. In order to save computing resources, the lattice momentum acceptance $\Delta E/E$ is computed beforehand at each longitudinal step ds. Only particles out of the acceptance are generated and tracked to their loss point. Consequently all six coordinates are stored when the particles reach the aperture. The number of particles $N_{p,lost}$ to be generated over the full bunch population N_{tot} is calculated using the theoretical loss rate $1/\tau_T$ as implemented in AT (Piwinski formula [4]):

$$N_{p,lost}(s) = \frac{N_{tot}\mathrm{d}s}{\mathrm{c}}\frac{1}{\tau_T(s)} \tag{1}$$

The initial coordinates of the particles to track $[x\ x'\ y\ y'\ z\ \delta]_{1,2}$ are randomly generated using the 6D beam matrix depending on the position along the lattice and imposing $x_1 = x_2$, $y_1 = y_2$, $z_1 = z_2$. They are selected if the energy deviation resulting from the scattering process exceeds the momentum acceptance. The scattering angle χ and hence the longitudinal momentum kick $\pm\Delta\delta = \pm\gamma v/2|\cos\chi|$ for a colliding pair of electrons are computed according to the Møller differential cross section:

$$\frac{\mathrm{d}\sigma}{\mathrm{d}u} = \frac{8\pi \mathrm{r}_0^2}{(v/\mathrm{c})^4}\frac{u^2-2}{u^3} \tag{2}$$

with $u = \cos\chi$, $v = x_1' - x_2'$ is the relative velocity of the scattering electron pair (neglecting vertical contribution), and r_0 is the classical electron radius.

The random particle generation is repeated until $N_{p,lost}(s)$ is reached. The loss locations are recorded independently from the scattering points to get the full ring loss map.

Vacuum losses

Following the same philosophy as for Touschek losses, collisions of electrons and the residual gas nuclei are simulated randomly in order to accumulate the corresponding contribution to the beam lifetime [5]. Special care was taken to be able to define a varying pressure along the lattice, and to be able to modify the gas composition and pressure locally.

Bremsstrahlung The Bremsstrahlung process is described by the Beithe-Heitler differential cross section:

$$\frac{\mathrm{d}\sigma}{\mathrm{d}|\delta|} = \frac{4\mathrm{r}_0^2 Z^2}{137}\frac{1}{|\delta|}F(|\delta|) \tag{3}$$

with $F(\delta) = \left(\frac{4}{3}(1-|\delta|)+\delta^2\right)\ln\frac{183}{Z^{1/3}}$, Z being the atomic number of the scattering nucleus.

The negative side of the momentum acceptance δ_m is used to compute the number of particles to track by integrating the loss probability for $|\delta| > |\delta_m|$, summing over the gas composition (α_{ij} is the number of nucleus j per molecule i constituting the gas and p_i its partial pressure):

$$\frac{N_{p,lost}}{N_{tot}} = \frac{4\mathrm{r}_0^2\mathrm{d}s}{137}\left(\frac{4}{3}\ln\frac{1}{|\delta_m|}-\frac{5}{6}\right)\sum_j \mathrm{Z}_j^2\ln\frac{183}{\mathrm{Z}_j^{1/3}}\sum_i \alpha_{ij}\frac{\mathrm{p}_i}{\mathrm{kT}} \tag{4}$$

* reine.versteegen@esrf.fr

Content from this work may be used under the terms of the CC BY 3.0 licence (© 2015). Any distribution of this work must maintain attribution to the author(s), title of the work, publisher, and DOI.

ISBN: 978-3-95450-168-7 doi:10.18429/JACoW-IPAC2015-TUPWA017

COLLIMATION SCHEME FOR THE ESRF UPGRADE

R. Versteegen*, P. Berkvens, N. Carmignani, L. Farvacque, S.M. Liuzzo, B. Nash, T. Perron, P. Raimondi, S. White, ESRF, Grenoble, France

Abstract

The ultra low emittance foreseen for the ESRF Upgrade will translate into a limited Touschek lifetime, increasing substantially the loss rate around the ring compared to the present machine. Consequently it becomes crucial to know the distribution of electron beam losses to optimize the radiation shielding and to protect the insertion devices from radiation damage. Such loss maps of the storage ring can be produced thanks to the simulation of the Touschek scattering process along the lattice. It is shown that about 80 % of the beam losses can be collimated in a few chosen locations only, keeping the resulting lifetime reduction smaller than 10 %.

INTRODUCTION

The multi-bend achromat lattice of the ESRF upgrade will allow for a reduction of the horizontal emittance down to less than 150 pm.rad [1]. Assuming the same vacuum conditions as today, the beam losses will be dominated by the intra-beam Touschek scattering, implying a reduction of the lifetime by a factor ~ 3 compared to the present machine [2]. A detailed map of beam losses around the ring is necessary to protect the insertion devices and the various machine equipment from radiation damage, as well as to anticipate a proper shielding to guarantee a radiation free zone outside of the accelerator tunnel. For that purpose Touschek scattering has been simulated for the ESRF upgrade lattice using the simulation tool described in [3]. Concentrating most of the losses in a few locations only using scrapers would be highly desirable for radiation handling. The model and simulation results for the new lattice are introduced in the first part of this paper, before describing the collimation scheme. Detailed 6D coordinates of lost electrons on the machine physical aperture are available thanks to the tracking of scattered particles. As shown in the last part, these are valuable input for the collimators' shape optimization regarding the resulting radiation shower.

ESRF UPGRADE BEAM LOSSES

The ESRF upgrade lattice is made of thirty-two cells. The strict periodicity is broken first by the two non standard injection cells where the optics is optimised to allow off-axis injection, and second by the RF cavities, located in three distinct straight sections (cells 5, 7, 25). The physical aperture considered in the model is simplified to three regions plus the injection straight section (see Fig. 1). They correspond to the high betatron functions (β) regions on both sides of the regular cells, the central part with low β (a smaller bore radius is necessary for the high gradient quadrupoles), and the straight sections where the aperture is defined by the Insertion Devices (IDs). To figure the presence of in-vacuum undulators, some parts of the straight sections have a vertical aperture as small as ±3 mm. The main horizontal aperture restriction is at the septum location on the inside of the ring. The model contains either rectangular or elliptical aperture depending on the location.

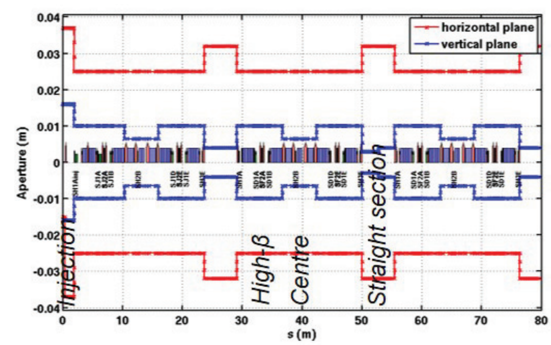

Figure 1: Physical aperture limits of the ESRF upgrade lattice cells. Dipoles, quadrupoles and sextupoles are figured by blue, magenta and green rectangles respectively.

The simulated Touschek loss map is shown in Fig. 2 for the lattice without errors, starting from the injection point. It assumes a vertical emittance of 5 pm.rad and 0.23 mA per bunch, leading to a Touschek lifetime of about 45 h. Each peak corresponds to a physical element of maximum 0.5 m length (including drift spaces).

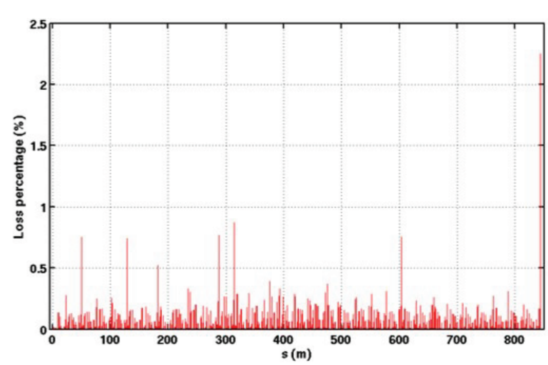

Figure 2: Touschek losses along the lattice without errors.

The highest peaks correspond to the in-vacuum IDs locations, except the last one at s ≈844 m corresponding to the septum blade. Apart from these specific locations arising because of a smaller physical aperture, the effect of the periodicity breaking of the lattice functions is not so strong thanks to the careful nonlinear optics matching [2]. In Fig. 3 the losses of all cells are stacked over one machine period,

* reine.versteegen@esrf.fr

Content from this work may be used under the terms of the CC BY 3.0 licence (© 2015). Any distribution of this work must maintain attribution to the author(s), title of the work, publisher, and DOI.

ISBN: 978-3-95450-168-7 doi:10.18429/JACoW-IPAC2015-TUPWA018

Content from this work may be used under the terms of the CC BY 3.0 licence (© 2015). Any distribution of this work must maintain attribution to the author(s), title of the work, publisher, and DOI.

PROGRESS REPORT OF THE BERLIN ENERGY RECOVERY PROJECT bERLinPro*

M. Abo-Bakr#, W. Anders, A. Burrill, A. Büchel, K. Bürkmann-Gehrlein, P. Echevarria, A. Frahm, H.-W. Glock, A. Jankowiak, C. Kalus, T. Kamps, G. Klemz, J. Knobloch, J. Kolbe, J. Kühn, O. Kugeler, B. Kuske, P. Kuske, A. Matveenko, A. Meseck, R. Müller, A. Neumann, N. Ohm, K. Ott, E. Panofski, F. Pflocksch, D. Pflückhahn, J. Rahn, J. Rudolph, M. Schmeißer, O. Schüler, J. Völker, Helmholtz-Zentrum Berlin, Berlin, Germany.

Abstract

The Helmholtz Zentrum Berlin is constructing the Energy Recovery Linac Project bERLinPro on its site in Berlin Adlershof. The project is intended to expand the required accelerator physics and technology knowledge mandatory for the design, construction and operation of future synchrotron light sources. The project goal is the generation of a high current (100 mA), high brilliance (normalized emittance below 1 mm mrad) cw electron beam at 2 ps rms bunch duration or below.

The planning phase of the project is completed and the design phase of most of the components is finished. Many of them have already been ordered. After some delay the construction of the building has started in February 2015. The status of the various subprojects as well as a summary of current and future activities will be given. Major project milestones and details of the project time line will be finally introduced.

INTRODUCTION

In 2008 the Helmholtz-Zentrum Berlin (HZB) submitted a proposal to build an ERL test facility to investigate its potential as accelerator technology for "Next Generation Multi User Synchrotron Light Sources". In October 2010 the Helmholtz Association approved the proposal, the official project started in the beginning of 2011.

The bERLinPro [1] layout as a single-pass ERL is shown in Fig. 2, together with the project's basic set of parameters. The 6.5 MeV bERLinPro injector consists of a 1.3 GHz, 1.4 cell SRF gun, followed by a booster module containing three 2-cell-cavities. The beam is merged into the main linac via a dogleg merger and accelerated by three 7-cell sc cavities to 50 MeV. Following recirculation via a racetrack, the decelerated beam is dumped in a 650 kW, 6.5 MeV beam dump. Space is provided in the return arc to install future experiments or insertion devices to demonstrate the potential of ERLs for user applications.

A staged installation of bERLinPro is planned, initially focused on the development and successful operation of a high current SRF gun. Depending on the availability of the 100 mA, full current Gun-2 in this first installation phase, called "banana", a medium to full current from the gun will be accelerated in the booster, characterized and optimized and finally sent to the dumpline. The maximum kinetic energy is 6.5 MeV, since the linac is not yet installed at this time. For the second "recirculation" stage the main linac and the recirculator will be installed and commissioned to demonstrate efficient energy recovery of the full current, 50 MeV beam.

In the next sections progress of the various subproject groups within the last 12 months will be presented together with an updated project time line.

PHOTOCATHODE R&D

As quantum efficiency, intrinsic emittance, temporal response and operational lifetime of the photocathode are key issues for the bERLinPro photoinjector a cathode preparation and characterization test lab has been established at HZB, where various kinds of cathodes can be produced and tested (see Fig. 1). A promising candidate to fulfil the requirements for an electron source is the bi-alkali antimonide CsK_2Sb [2]. An in-situ preparation and surface analysis system for CsK_2Sb photocathodes was commissioned at HZB since October 2014 and first samples have been very recently prepared with the sequential growth procedure. The lab operates two chambers: the preparation chamber, equipped with an effusion cell for Sb and with SAES alkali metal dispensers for K and Cs and the surface analysis chamber, equipped with a SPECS PHOIBOS 100 electron analyzer. An X-ray source for XPS and He ion source for LEIS are also attached to the analysis chamber, as well as an additional port for

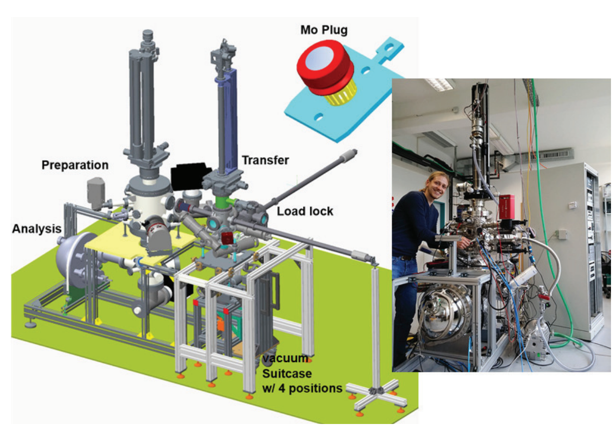

Figure 1: Drawing of the CsK2Sb-photocathode preparation and analysis system equipped with transfer chamber, load lock and vacuum suitcase for photocathode plug transport.

* Work supported by the German Bundesministerium für Bildung und Forschung, Land Berlin and grants of Helmholtz Association
# Michael.Abo-Bakr@helmholtz-berlin.de

ISBN: 978-3-95450-168-7 doi:10.18429/JACoW-IPAC2015-TUPWA019

Content from this work may be used under the terms of the CC BY 3.0 licence (© 2015). Any distribution of this work must maintain attribution to the author(s), title of the work, publisher, and DOI.

A CANTED DOUBLE UNDULATOR SYSTEM WITH A WIDE ENERGY RANGE FOR EMIL

J. Bahrdt, H.-J. Bäcker, W. Frentrup, C. Rethfeldt, M. Scheer, B. Schulz, S. Gottschlich
Helmholtz-Zentrum Berlin, Germany

Abstract

At BESSY II a canted double undulator system for the Energy Materials In-situ Laboratory EMIL is under construction. The energy regime is covered with two undulators, an APPLE II undulator for the soft and a cryogenic permanent magnet undulator CPMU-17 for the hard photons. The layout and the performance of the undulators are presented in detail. The minimum of the vertical betatron function is shifted to the center of the CPMU-17. The neighboring quadrupoles and an additional quadrupole between the undulators control the vertical betatron function. Prior to the undulator installation a testing chamber with four movable vertical scrapers has been implemented at the CPMU-17 location. Utilizing the scrapers the new asymmetric lattice optics will be tested and optimized.

INTRODUCTION

EMIL, the Energy Material in-situ Laboratory at BESSY II, is under construction. The facility offers the tools for in-situ and in-system X-ray analysis of materials and devices for photovoltaic applications and for (photo-) catalytic processes. Spectroscopic methods such as PES, PEEM, HAXPES, XES, XAS, XRF, XRD are well suited for the investigation of sample structures with arbitrary depth information between a few nanometer and the micrometer regime. The EMIL laboratory is described in detail in [1]. Two canted undulators deliver photons over a wide energy regime: An APPLE II undulator for soft X-rays (80 eV- 2.2 keV) and a planar CPMU for hard X-rays up to 8 keV. Two beamlines including a double crystal monochromator (hard photons) and a collimated plane grating monochromator with variable deflection angle (soft photons) distribute the light to various end stations. The short period small-gap undulator CPMU-17 will be operated in a mini-beta section to mitigate deleterious effects to the storage ring performance and to avoid beam scraping with the magnets.

MINI-BETA-SECTION

The implementation of short-period small-gap undulators into low energy storage rings requires specific lattice modifications to maintain the beam lifetime at the reduced vertical aperture. Small-gap undulators installed in dedicated mini-beta section are in operation at the NSLS X-ray ring for many years [2]. At BESSY II it was decided to shift the waist of the vertical betatron function to the center of the cryogenic undulator. Asymmetric detuning of the neighbouring quads and an additional quad between the undulators permit a minimum aperture of 5 mm. The lattice modification and the asymmetric re-wiring of the adjacent multipoles are described in detail in [3] [4]. The modified optics without the central quad was already tested with beam. Meanwhile, the central quad and a testing chamber at the location of the CPMU-17 are installed. The chamber is equipped with four vertical scrapers for the detection of the vertical aperture at two locations which gives information about the size and the gradient of the vertical betatron function. The undulators are canted by an angle of 2 mrad which is accomplished with an electromagnetic coil integrated into the central quad. Space for a replacement with permanent magnet 1-mrad-steerers at a later time is foreseen. The 1-mrad kicks are generated from the steerer coils integrated in the neighbouring sextupoles.

UE-48 APPLE II UNDULATOR

The UE-48 is an APPLE II undulator with full polarization control (see Fig. 3). The low photon energy device is designed to cover the range between 80 eV (including the Si L II/III-edge at 99eV) and 2.2 keV (including the Si-K- edge at 1839eV) with the harmonics 1-7. The parameters are listed in Table 1.

Table 1: Parameters of the UE-48

Period length	48 mm
Number of periods	29, symmetric endpoles
Minimum magnetic gap	15 mm nominal
Gap between mag. rows	0.8 mm
Operational modes	Elliptical, inclined, universal
Magnets	$Nd_2Fe_{14}B$, transversally pressed in a dye
A-magnet (long. magn.)	1.28 T / 1670 kA/m
B-magnet (vert. magn.)	1.33 T / 1275 kA/m
B_{eff} (hor. lin. / hel. / vert. lin. / inclined 45°)	0.791 T / 0.626 T / 0.535 T / 0.443 T

The magnets were sorted with respect to systematic production errors, glued to pairs (one A- and one B-magnet) and finally machined before magnetization. The pairs were magnetized in a 45° oriented magnetic field where the easy orientations of the individual magnets determined the individual block magnetization orientation. This procedure will be described in detail in a separate publication.

ISBN: 978-3-95450-168-7 doi:10.18429/JACoW-IPAC2015-TUPWA020

BNL ATF II BEAMLINES DESIGN *

M.Fedurin[#]*, Y. Jing, D. Stratakis, C. Swinson, BNL, Upton, NY, 11973, USA*

Abstract

The Brookhaven National Laboratory. Accelerator Test Facility (BNL ATF) is currently undergoing a major upgrade (ATF-II). Together with a new location and much improved facilities, the ATF will see an upgrade in its major capabilities: electron beam energy and quality and CO_2 laser power. The electron beam energy will be increased in stages, first to 100-150 MeV followed by a further increase to 500 MeV. Combined with the planned increase in CO_2 laser power (from 1-100 TW), the ATF-II will be a powerful tool for Advanced Accelerator research. A high-brightness electron beam, produced by a photocathode gun, will be accelerated and optionally delivered to multiple beamlines. Besides the energy range (up to a possible 500 MeV in the final stage) the electron beam can be tailored to each experiment with options such as: small transverse beam size (<10 um), short bunch length (<100 fsec) and, combined short and small bunch options. This report gives a detailed overview of the ATF-II capabilities and beamlines configuration.

UPGRADE TO ATF II

The Accelerator Test Facility was established over a quarter of a century ago [1]. For more than two decades it has served national and international accelerator scientists, through a proposal-driven, program committee reviewed process that makes beams available to a broad community of users from Academia, U.S. National Laboratories, Accelerator Facilities and Small Businesses. The ATF offers the state-of-the-art tools that are required by its user community, including sources of high-brightness electron beams and synchronized high-power laser beams [2]. While making these available for accelerator science R&D, the ATF continuously upgrades, reinvents and revamps these tools.

The current experiment program has e-beam only (Wake Field Acceleration in Quasi Non-linear Plasma and Dielectrics [3,4], THz radiation in dielectrics [5]),

Table 1: Projected Beam Parameters

Parameter	Expected Value
Energy	0-150 MeV
Maximum charge	3 nC
Normaliazed emittance	1 mm-mrad
Bunch current	100 A
Compressed bunch	1700 A
Compressed bunch length	10 fsec

combined laser and e-beam (Inverse FEL acceleration and X-ray generation from non-linear Inverse Compton Source [6,7]) and laser only experiments (Ion Acceleration [8]).

The ATF upgrade is focused on three principal components: electron accelerator, CO_2 laser, and experiment area. The plan for the CO_2 laser is to increase power from the present 1 TW to 100 TW and the experiment hall area will increase to seven times it's the size of that available at the current ATF. A detailed description of the electron accelerator upgrade will be discussed here, with specific focus on beamline configuration.

GENERAL BEAMLINE DESIGN

The ATF II electron accelerator will succeed the present ATF electron beam generation technology. The electron source will continue to be a photocathode electron gun (pioneered at the ATF). The fourth harmonic of an Nd:YAG laser, incident on a copper cathode, yields 5E-3 e^-/γ at the present ATF. This gives a high-brightness electron beam with peak current of 100 A and 1 μm

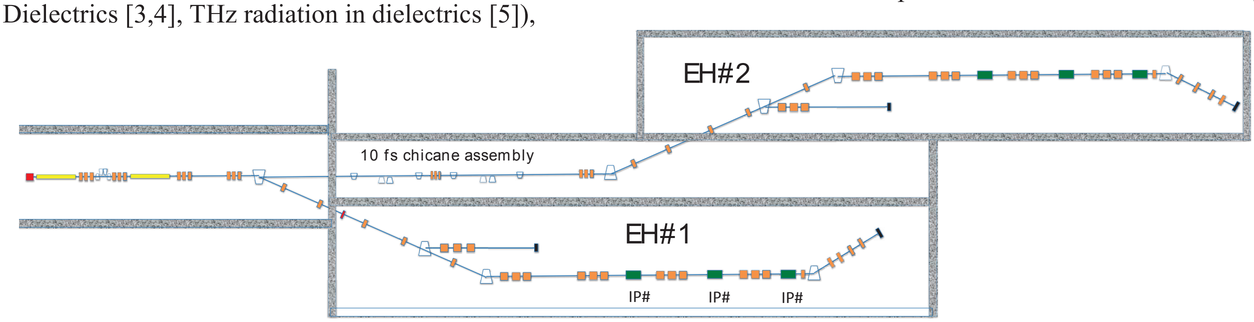

Figure 1: Schematic view of ATF II beamline configurations.

*Work supported by Brookhaven Science Associates, LLC under Contract No. DE-AC02-98CH10886 with the U.S. Department of Energy
e-mail: fedurin@bnl.gov

Content from this work may be used under the terms of the CC BY 3.0 licence (© 2015). Any distribution of this work must maintain attribution to the author(s), title of the work, publisher, and DOI.

ISBN: 978-3-95450-168-7 doi:10.18429/JACoW-IPAC2015-TUPWA021
Content from this work may be used under the terms of the CC BY 3.0 licence (© 2015). Any distribution of this work must maintain attribution to the author(s), title of the work, publisher, and DOI.

A NEW METHOD TO GENERATE ULTRASHORT AND COHERENT PULSES OF SHORT-WAVELENGTH SYNCHROTRON RADIATION*

S. Khan†, Center for Synchrotron Radiation (DELTA), TU Dortmund University, 44227 Dortmund, Germany

Abstract

A laser-based method to generate ultrashort pulses of synchrotron radiation in electron storage rings is coherent harmonic generation (CHG) using two undulators to produce coherent radiation at harmonics of the initial laser wavelength by microbunching. The bunching factor and thus the pulse intensity, however, decreases exponentially with increasing harmonic order. Echo-enabled harmonic generation (EEHG), proposed in 2009 as FEL seeding scheme, can be used to produce short synchrotron radiation pulses at higher harmonics, but requires three undulators in a straight section. In this paper, a less space-consuming method based on seeding with intensity-modulated laser pulses is introduced, which also has the potential of significant bunching factors at high harmonics.

INTRODUCTION

The advent of linac-based free-electron lasers (FELs) with extremely intense and ultrashort pulses in the femtosecond range has opened up new opportunities for time-resolved studies of ultrafast atomic phenomena. However, only four FELs with sub-visible wavelengths have yet been commissioned and they are essentially single-user facilities with 5-120 bunches (or bunch trains) per second [1–4]. On the other hand, synchrotron light sources based on electron storage rings serve many users simultaneously with a typical bunch rate of 500 MHz and very stable beams, but the pulse duration is 30-100 ps (FWHM). With more than 50 synchrotron light sources in operation worldwide [5], it is worthwhile to investigate methods to extend their capabilities towards shorter pulse duration and higher peak intensity.

In an electron storage ring, the synchrotron motion translates a natural energy spread of typically $\sigma_E \approx 10^{-3}E$ (rms) into a bunch length, depending on the radiofrequency (RF) voltage and momentum compaction factor $\alpha \approx (\Delta L/L)/(\Delta E/E)$. A strong reduction of α at the expense of bunch charge and beam emittance is used at several synchrotron light sources to shorten the bunches to a few picoseconds, see e.g. [6].

SHORT-PULSE GENERATION

Rather than shortening the bunches further, the femtosecond regime is more easily accessible by extracting synchrotron light from a short fraction, a "slice", of the bunch. A femtosecond laser pulse co-propagating with an electron bunch through an undulator (the "modulator") tuned to the laser wavelength causes a sinusoidal modulation of the electron energy within the bunch slice. Femtosecond laser pulses are typically generated by Ti:sapphire lasers at a wavelength of 800 nm (photon energy $E_\mathrm{P} = 1.55$ eV). With a pulse energy E_L in the mJ range ($\approx 10^{16}$ eV) and a pulse duration around $\sigma_\mathrm{L} \approx 20$ fs (rms), the modulation amplitude [7]

$$\Delta E \approx 0.2\,\sqrt{E_\mathrm{L} E_\mathrm{P}}\,\sqrt{M_\mathrm{U}/M_\mathrm{L}} \qquad (1)$$

will exceed the natural energy spread of the electron beam. The expression is valid as long as the number of undulator periods M_U is smaller than the number of optical cycles $M_\mathrm{L} = 2\sqrt{2\ln 2}\,c\,\sigma_\mathrm{L}/\lambda_\mathrm{L}$ per FWHM pulse length.

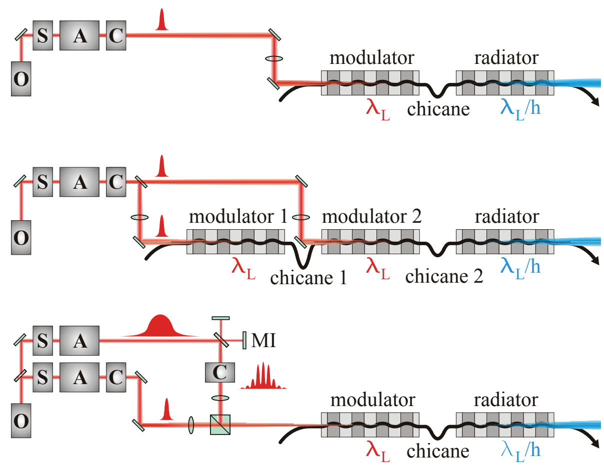

Figure 1: Top: Coherent harmonic generation (CHG) using a laser-induced electron energy modulation in an undulator ('modulator'), converted to a density modulation in a chicane and coherent radiation in a second undulator ('radiator'). Center: Echo-enabled harmonic generation (EEHG) based on laser-electron interaction in two modulators. Bottom: New method with laser-electron interaction at different times in the same modulator. Also shown: laser oscillator (O), stretcher (S), amplifier (A), compressor (C), and Michelson interferometer (MI).

One way to exploit the energy modulation in a second undulator (the "radiator") is to transversely displace the off-energy electrons in dipole magnets, providing a spatial separation between the short radiation component from the slice and the long component from the rest of the bunch [8–11]. Another method making use of the laser-induced energy modulation is known as coherent harmonic generation (CHG) [12–15], see Fig. 1 (top). Here, a density modulation (microbunching) is created by energy-dependent path length differences in a magnetic chicane, allowing to generate coherent radiation at harmonics of λ_L in the radiator. The

* Work supported by BMBF (contract 05K13PE3).
† shaukat.khan@tu-dortmund.de

ISBN: 978-3-95450-168-7 doi:10.18429/JACoW-IPAC2015-TUPWA022

Content from this work may be used under the terms of the CC BY 3.0 licence (© 2015). Any distribution of this work must maintain attribution to the author(s), title of the work, publisher, and DOI.

CHARACTERIZATION AND OPTIMIZATION OF ULTRASHORT AND COHERENT VUV PULSES AT THE DELTA STORAGE RING*

S. Khan†, F. H. Bahnsen, M. Bolsinger, S. Hilbrich, M. Höner, M. Huck, C. Mai,
A. Meyer auf der Heide, R. Molo, H. Rast, G. Shayeganrad, P. Ungelenk,
Center for Synchrotron Radiation (DELTA), TU Dortmund University, 44227 Dortmund, Germany
H. Huck, Deutsches Elektronen-Synchrotron Zeuthen, 15738 Zeuthen, Germany

Abstract

At DELTA, a 1.5-GeV synchrotron light source operated by the TU Dortmund University, a source for coherent and ultrashort vacuum-ultraviolet (VUV) and terahertz (THz) pulses is now in operation. The VUV source is based on a laser-induced energy modulation and coherent harmonic generation (CHG). A subsequently developing dip in the longitudinal electron distribution gives rise to coherent THz radiation. Recent results regarding the optimization of the laser-electron interaction and characterization of the CHG pulses are presented.

INTRODUCTION

Synchrotron radiation with short wavelengths is the standard tool to study the structure of matter on the atomic level. However, synchrotron radiation pulses with a duration of 30 to 100 ps (FWHM) are too long to study dynamic processes such as chemical reactions, phase transitions, fast magnetic changes, etc. which take place on the sub-picosecond scale. The femtosecond regime, on the other hand, has been made available by mode-locked lasers at near-visible wavelengths which are not suitable to probe inner atomic shells or to provide spatial resolution on the atomic scale.

The need for radiation with short wavelength *and* short pulse duration has prompted new developments such as the free-electron laser (FEL) providing extremely brilliant short-wavelength radiation with femtosecond pulse duration. To date, four linac-based FEL facilities at short wavelengths are in single-user operation (FLASH, LCLS, SACLA, and FERMI) while more than 50 synchrotron light sources worldwide [1] supply multiple beamlines simultaneously with brilliant and tunable radiation. It is therefore worthwhile to study methods which allow to generate shorter pulses at conventional synchrotron light sources.

SHORT-PULSE GENERATION

Some methods to generate sub-ps radiation pulses at storage rings are borrowed from FEL seeding schemes using a femtosecond laser pulse to modulate the energy of electrons within a short "slice" at the center of a long electron bunch. In a subsequent undulator, a short radiation pulse is emitted from the slice together with a long pulse from the rest of the bunch. Off-energy electrons are either transversely displaced in order to separate the short and long components of incoherent undulator radiation spatially ("femtoslicing" [2]) or a magnetic chicane may convert the energy modulation into a density modulation (microbunching) giving rise to a short pulse of coherent radiation at harmonics of the laser wavelength [3]. As long as the signal-to-background ratio

$$\frac{P_{\text{short}}}{P_{\text{long}}} = \frac{n_{\text{short}}^2\, b_h^2}{n_{\text{long}}} = f^2\, n_{\text{long}}\, b_h^2 \quad \text{with} \quad f \equiv \frac{n_{\text{short}}}{n_{\text{long}}} \qquad (1)$$

is tolerable, no geometric separation is required. Here, $f \approx 10^{-3}$ is the ratio between the number of electrons in the slice and in the bunch, and b_h is the bunching factor for harmonic number h. With $n_{\text{long}} = 10^{10}$, as an example, $b_h = 0.1$ would yield an excellent signal-to-background ratio of 10^2. This scheme is known as coherent harmonic generation (Fig. 1 a). Here, the bunching factor decreases with increasing harmonics as $b_h \sim \exp(-h^2)$. In contrast to that, echo-enabled harmonic generation (EEHG, Fig. 1 b) [4] involving a two-fold energy modulation is able to generate higher harmonics according to $b_h \sim h^{-1/3}$.

Further downstream along the storage ring, the energy-dependent electron path length leads to a dip in the longitudinal electron distribution giving rise to coherent THz radiation [5].

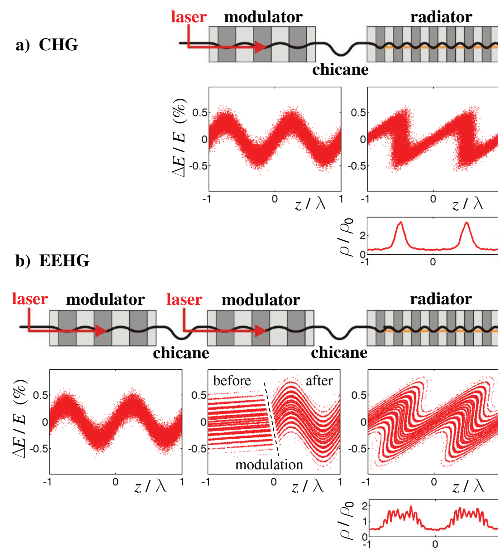

Figure 1: Short-pulse schemes a) CHG and b) EEHG with respective electron distributions in phase space (relative energy deviation $\Delta E/E$ versus longitudinal coordinate z in units of the laser wavelength λ) and electron density $\rho(z/\lambda)$.

* Work supported by BMBF (05K13PE3 and 05K13PEC), DFG (INST 212/236-1 FUGG) and the Land NRW.
† shaukat.khan@tu-dortmund.de

ISBN: 978-3-95450-168-7 doi:10.18429/JACoW-IPAC2015-TUPWA023

A STEP CLOSER TO THE CW HIGH BRILLIANT BEAM WITH THE ELBE SRF GUN-II

R. Xiang#, A. Arnold, P. Michel, P. Murcek, J. Teichert, HZDR, 01328 Dresden, Germany
P. Lu, H. Vennekate, TU Dresden & HZDR, 01328 Dresden, Germany

Abstract

In order to achieve the CW electron beam with a high average current up to 1 mA and a very low emittance of 1 µm, an improved superconducting photo-injector (SRF Gun-II) has been installed and commissioned at HZDR since 2014. This new gun replaces the first 3.5-cell SRF gun (SRF Gun-I) at the SC Linac ELBE. The RF performance of the niobium cavity has been evaluated, the beam parameters for low charge bunches have been measured, and the first beam has been guided into the ELBE beam line. The results agree with the simulation very well. The photocathode transfer system has been installed for the first high current beam test planned in 2015. However, the unexpected strong degradation on the cavity and also on the photocathode was found soon after the first photocathode exchange. In this contribution the results of the SRF Gun-II commissioning and the latest experiment will be presented in detail.

MOTIVATION

The development of top quality photocathode electron guns has become one of the key technologies for modern light sources and large collide facilities based on electron accelerators. There are several successful photo-gun types for various facility requirements [1], like DC guns, rf guns, SRF guns [2] and so on. The Rossendorf SRF Gun-I successfully operated for the radiation source ELBE at HZDR from 2007 to 2014. To achieve higher current and lower beam emittance, a new 3+1/2-cell niobium cavity with a superconducting solenoid and a new 13 MHz laser have been recently developed.

SRF GUN-I

The SRF Gun-I developed within a collaboration of the institutes HZB, DESY, MBI and HZDR has been operated for the supercondctung linac ELBE since 2007 [3] (Fig.1). With the Cs_2Te photocathode driven by a 13 MHz UV laser, the SRF gun produced beams up to 400 µA. The maximum energy of the electron beam reached 3.3 MeV, bunch charge 400 pC and transverse emittance was 3±1 mm mrad with 80 pC bunch charge. In April 2013 the first IR-FEL succeeded in ELBE driven by SRF Gun-I [4].

SRF Gun-I was at the same time a test bench for the SRF gun techniques, CW beam diagnostics and normal conducting photocathode materials:

- The principle concept of SRF cavity with normal conducting photocathode works practically well.
- There is no obvious degradation found in the cavity quality (Fig.2). E_{acc} reached 6.5 MV/m in CW mode, and 8 MV/m in pulsed mode, corresponding to peak field on axis E_{peak} 17.5 MV/m and 22 MV/m, respectively.

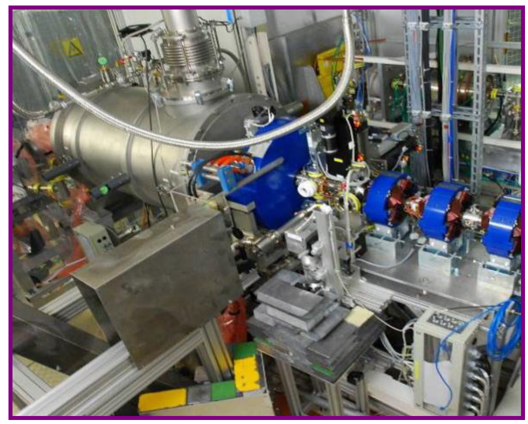

Figure 1: SRF gun-I with the diagnostic beam line.

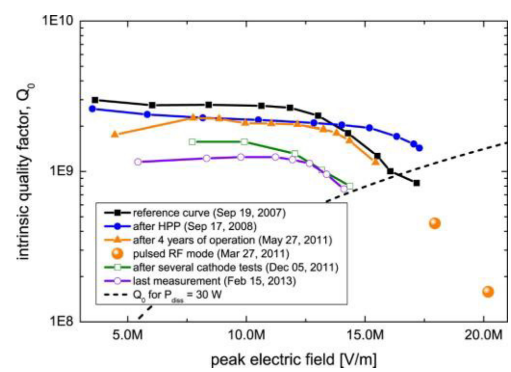

Figure 2: RF measurement result for SRF Gun-I shows that the cavity with cathode inside has the quality factor Q_0 as same as the virgin cavity

- Performance of Gun-I cavity is limited by strong field emission; half-cell is the weak point for the mechanical stability and Lorenz force detuning.
- Multipacting appears mostly in the photocathode area; bias voltage is able to suppress the multipacting.
- LN_2-cooled photocathode works in gun for a long life time; photocathode exchange can be performed in short time without cavity warming up; However, photocathode itself and the exchange process must be particle free.
- RF-focusing, solenoid compensation and proper laser shaping are helpful methods for the emittance compression, but a high acceleration gradient at

r.xiang@hzdr.de

Content from this work may be used under the terms of the CC BY 3.0 licence (© 2015). Any distribution of this work must maintain attribution to the author(s), title of the work, publisher, and DOI.

ISBN: 978-3-95450-168-7 doi:10.18429/JACoW-IPAC2015-TUPWA025

BEAM HEAT LOAD ANALYSIS WITH COLDDIAG: A COLD VACUUM CHAMBER FOR DIAGNOSTICS

R. Voutta *, S. Casalbuoni, S. Gerstl, A. W. Grau, T. Holubek, D. Saez de Jauregui, Karlsruhe Institute of Technology (KIT), Karlsruhe, Germany
R. Bartolini, M. P. Cox, E. C. Longhi, G. Rehm, J. C. Schouten, R. P. Walker, Diamond Light Source, Oxfordshire, England
M. Migliorati, B. Spataro, INFN/LNF, Frascati, Italy

Abstract

The knowledge of the heat intake from the electron beam is essential to design the cryogenic layout of superconducting insertion devices. With the aim of measuring the beam heat load to a cold bore and understanding the responsible mechanisms, a cold vacuum chamber for diagnostics (COLDDIAG) has been built. The instrumentation comprises temperature sensors, pressure gauges, mass spectrometers and retarding field analyzers, which allow to study the beam heat load and the influence of the cryosorbed gas layer. COLDDIAG was installed in the storage ring of the Diamond Light Source from September 2012 to August 2013. During this time measurements were performed for a wide range of machine conditions, employing the various measuring capabilities of the device. Here we report on the analysis of the measured beam heat load, pressure and gas content, as well as the low energy charged particle flux and spectrum as a function of the electron beam parameters.

INTRODUCTION

Superconducting insertion devices (IDs) can generate higher magnetic fields than permanent magnet IDs with the same gap and period length, increasing the photon flux and the brilliance. The cryogenic design of superconducting IDs requires the knowledge of the beam heat load to the cold vacuum chamber. Potential beam heat load sources are synchrotron radiation, geometric and resistive wall impedance, and electron and/or ion bombardment. To understand the discrepancies between the calculated predictions and the beam heat load observed in several devices [1–3], a cold vacuum chamber for beam heat load diagnostics (COLDDIAG) has been built [4]. After its installation in the Diamond Light Source (DLS) storage ring in September 2012, the beam heat load, pressure and gas content, and the low energy charged particle flux and spectrum have been measured during user operation and in dedicated machine physics sessions until August 2013. A subsequent offline calibration of the beam heat load measurements [5] has been performed in order to remove the contribution of the thermal transitions to the beam heat load from the measurements, which turned out to be about half of the total measured heat load. In the following we present some of the main results from the beam heat load analysis of the data taken with COLDDIAG at the DLS.

* robert.voutta@kit.edu

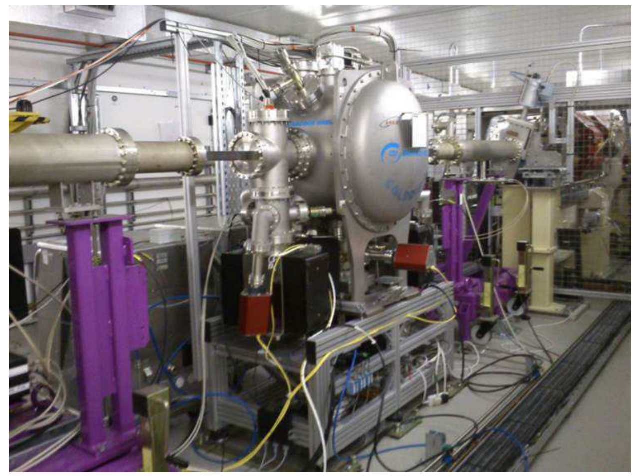
Figure 1: COLDDIAG installed in the DLS storage ring.

EXPERIMENTAL SETUP

COLDDIAG is composed of three sections, an upstream and downstream warm section and a cold section in between. The cold section is cooled down by a Sumitomo RDK-415D cryocooler to a base temperature of about 4 K. Each section is equipped with a diagnostic port, providing a retarding field analyser (RFA), a residual gas analyser (RGA) and a pressure gauge. Eight temperature sensors in each warm section and 24 temperature sensors in the cold section allow to record the temperature distribution along the beam tube (liner) and in the cold UHV chamber. The beam heat load is calibrated using 6 heaters attached to the liner, one in each warm section and four in the cold section. The heaters in the cold section can also be used to regulate the temperature of the cold liner to a specific temperature (usually 20 K) during operation. Two additional heaters, one at each thermal transition to the cold liner, were installed after the removal from the DLS in order to reproduce the temperatures at the thermal transitions during the measurements in an offline calibration. Figure 1 shows COLDDIAG installed in a straight section of the DLS storage ring.

BEAM HEAT LOAD

The beam heat load was measured during user operation and in various machine physics sessions, scanning a wide range of machine parameters. The measurements discussed here were performed with the liner at a fixed temperature

Content from this work may be used under the terms of the CC BY 3.0 licence (© 2015). Any distribution of this work must maintain attribution to the author(s), title of the work, publisher, and DOI.

ISBN: 978-3-95450-168-7 doi:10.18429/JACoW-IPAC2015-TUPWA026

SIMULATION OF OPTICAL TRANSPORT BEAMLINES FOR HIGH-QUALITY OPTICAL BEAMS FOR ACCELERATOR APPLICATIONS*

J. Bödewadt†, N. Ekanayake, DESY, Hamburg, Germany

Abstract

High-quality optical beams play already an important role in the field of particle accelerators which will most probably become even more prominent in the view of laser-driven particle accelerators. Nowadays, optical transport beamlines are needed for particle generation in photo injectors, for particle acceleration in laser-driven plasma wakefield accelerators, for particle beam diagnostics such as synchrotron radiation monitoring systems, or for particle manipulation schemes e.g. for external seeding of free-electron lasers. For the latter case, also the photon beam transport to the user end-stations requires dedicated optical beamlines. The utilized wavelengths range from the hard x-ray up to the far-infrared spectral range. Parameters such as surface quality, polarization effects, in- and out-of-vacuum damage thresholds, mechanical stability, dispersion effect, etc. need to be studied for the variety of applications. Here, we present the simulation results of the optical transport beamline for the seeding experiment at the free-electron laser FLASH and give a comparison to our measurement results.

INTRODUCTION

Designing optical systems for the application in particle accelerators needs to fulfill a variety of different demands. Especially the transport of high-quality laser beams for particle beam production or manipulation required detailed planning and quality control to achieve the desired properties. One example for the application of lasers in particle accelerators is the external seeding of free-electron lasers (FEL). The idea is to use the laser to manipulate the beam properties of an ultra-relativistic electron beam such that it efficiently generates very intense and fully coherent radiation pulses in the soft and hard x-ray spectral ranges. The interaction of the laser and the electron beam takes place in an undulator magnet which deflects the electron beam to an undulatory trajectory leading to a non-zero transverse velocity components. This, in turn, allows the interaction of the electrons with the electric field of the laser beam.

Seeding Experiment

Since 2010 an experimental setup for seeding has been installed at the FEL facility FLASH at DESY [1]. Initially installed for the investigation of direct FEL seeding [2] it also allows for the study of other schemes such as high-gain harmonic generation (HGHG) [3] or echo-enabled harmonic generation (EEHG) [4].

* Supported by the Accelerator R&D program grant no. E.56607
† contact: joern.boedewadt@desy.de

SEED LASER INJECTION SYSTEM

The seed laser utilized in the seeding experiments at FLASH is a commercial, solid-state, Ti:sapphire system based on the chirped-pulse amplification technique (CPA) and consists of a mode-locked oscillator and a flash-lamp-pumped amplifier system (regenerative and booster) [5]. The system is capable of generating ultrashort laser pulses up to 50 mJ with 60 fs (FWHM) duration at a 10-Hz-repetition rate and a center wavelength of 800 nm. In 2012, a new laser transport beamline has been installed to inject ultraviolet (UV) laser pulses at a wavelength of 266 nm [6]. The generation of the UV pulses is done by frequency tripling (THG) of near-infrared Ti:sapphire laser pulses. Currently, the THG setup is located in the accelerator tunnel and placed under vacuum as shown in Figure 1. After UV generation, four mirrors (labeled M1 to M4) are used to steer the UV beam onto the electron beam axis without any refocusing of the UV beam. The longitudinal focus position is controlled by the NIR focusing into the THG setup. A half-wave plate allows for polarization control and a 1-mm-thick crystalline quartz window (QW) divides the ultra-high machine vacuum from the vacuum of the THG setup.

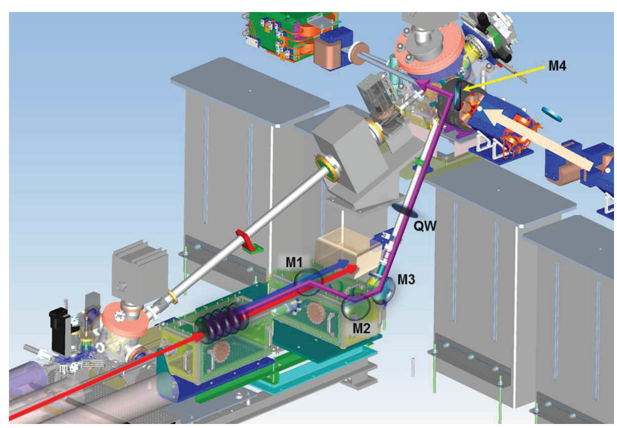

Figure 1: Seed laser injection setup. The NIR pulses arrive at the THG setup located in the accelerator tunnel inside high-vacuum chambers. The generated UV beam is steered with four mirrors onto the electron beam axis. The ultra-high vacuum of the machine is separated by a 1-mm-thick crystalline quartz window (QW).

Beam Polarization

For planar undulators, only the electric field component parallel to the deflection plane of the undulator couples to the electron beam. Therefore, the beam polarization of the

Content from this work may be used under the terms of the CC BY 3.0 licence (© 2015). Any distribution of this work must maintain attribution to the author(s), title of the work, publisher, and DOI.

ISBN: 978-3-95450-168-7 doi:10.18429/JACoW-IPAC2015-TUPWA028

SIMULATION RESULTS OF THE BEAM TRANSPORT OF ULTRA-SHORT ELECTRON BUNCHES IN EXISTING BEAM TRANSFER LINES TO SINBAD

U. Dorda, R. Assmann, K. Floettmann, B. Marchetti, Y. Nie, J. Zhu, DESY, Hamburg, Germany

Abstract

SINBAD, the upcoming accelerator R&D facility at DESY, will host multiple independent experiments on the production and acceleration of ultra-short bunches including plasma wakefield experiments. As a possible later upgrade the option to transport higher energy electrons (up to 800MeV) or positrons (up to 400MeV) from the existing DESY Linac II to the facility is studied. Though existing a possible connection using e.g. a part of the DESY synchrotron as a transfer line and a currently unused transfer-line, these machines were not designed for the desired longitudinal bunch compression and high peak current required by e.g. beam driven plasma wake-field experiments. Simulation results illustrate the modifications to the current layout that would have to be implemented and the corresponding achievable beam parameters.

INTRODUCTION

The SINBAD project [1] aims to set up a dedicated accelerator R&D facility in the former DORIS facility at DESY, Hamburg. This facility will contain multiple independent experiments in the context of advanced, compact acceleration concepts like plasma wake field (PWFA) or dielectric acceleration for ultrafast science. While there will be a dedicated linac for ultra-short bunches, it's energy will be limited to about 200 MeV. The aim of this study is to investigate if the existing Linac II can be used to accelerate electrons to 800 MeV and to subsequently transport them through existing beam lines to SINBAD. Provided that a sufficiently high beam current could be delivered, this would allow to perform e.g. beam driven plasma wake field experiments and FEL seeding studies. Additionally Linac II is capable of producing 400 MeV positrons which is only possible at very few facilities worldwide. While the maximal achievable positron beam current will not be too high, proof of principle experiments of acceleration in a PWFA could be performed as a first step of studying possible future PWFA-based high energy colliders.

Figure 1 shows the existing beam transport system from the electron gun to the SINBAD facility passing through Linac II, the "Positron Intensity Accumulator" (PIA) ring, the "L-weg", the DESY II synchrotron, the "R-Weg" and finally half of the former DORIS arc. As the lines up to including the DESY II, are used as injector chain to the Petra III synchrotron light source, it must be assumed that no significant modifications interfering with the standard operation can be implemented. On the other hand, the R-Weg and the final former DORIS arc serve no other purpose and are free to be modified. Initially it was studied if an existing, empty direct tunnel from the PIA ring to the R-Weg (see dotted line in Figure 1) could be used instead. This option had to be discarded as the dispersion created by the 90 degree dipole of PIA could no be closed and thus the subsequent long straight section would result in a very large linear momentum compaction factor R56 (the 56 element of the linear transfer matrix R). Furthermore, while the tunnel was originally foreseen for beam transport, by now constructional modifications imply that the radiation protection shielding is no longer sufficient.

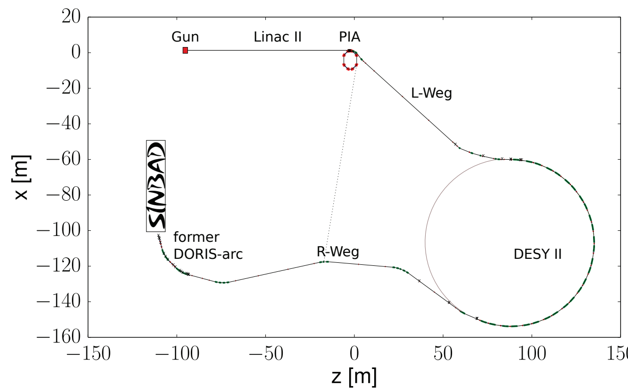

Figure 1: The geometric layout of the beam transport system from the electron gun of Linac II up to the SINBAD facility.

Using an unmodified PIA ring-optics and the corresponding section of the DESY ring-optics as transfer-line, the overall optics from the end of the Linac II to SINBAD would result in the very large R56-transfer matrix element (R56 > 150m). It is therefore obvious that significant changes must be implemented to be able to deliver bunches with a reasonable bunch length.

MODIFIED BEAM OPTICS

In a first step the optics of each part was optimized for a small linear momentum compaction (R56) and only then the second order elements (T566) were accounted for. The R56 element of a transfer line is (mainly) determined by the dispersion D in the dipoles and the dipole strength $1/\rho$ ($R56 \propto D \cdot \rho$). While the arrangement and properties of the dipoles is fixed by machine geometry, altering the beam optics allows to modify the dispersion function and thus the overall R56 element.

Gun & Linac

While the electrons at Linac II were until very recently extracted from an old DC-gun with a subsequent bunching cavity, an upgrade to add a second additional DC-gun has

Content from this work may be used under the terms of the CC BY 3.0 licence (© 2015). Any distribution of this work must maintain attribution to the author(s), title of the work, publisher, and DOI.

ISBN: 978-3-95450-168-7 doi:10.18429/JACoW-IPAC2015-TUPWA029

ARES: ACCELERATOR RESEARCH EXPERIMENT AT SINBAD

B. Marchetti, R. W. Assmann, C. Behrens, R. Brinkmann, U. Dorda, K. Floettmann, J. Grebenyuk, M. Huening, Y. Nie, H. Schlarb, J. Zhu, DESY, Hamburg, Germany

Abstract

ARES is a planned linear accelerator for R&D for production of ultra-short electron bunches. It will be hosted at the SINBAD facility, at DESY in Hamburg [1]. The goal of ARES is to produce low charge (0.2 - 50 pC), ultra-short (from few fs to sub-fs) bunches, with high arrival time stability (less than 10fs) for various applications, such as external injection for Laser Plasma Wake-Field acceleration [2]. The baseline layout of the accelerator foresees an S-band photo-injector which compresses low charge electron bunches via velocity bunching and accelerates them to 100 MeV energy. In the second stage, it is planned to install a third S-band accelerating cavity to reach 200 MeV as well as two X-band cavities: one for the linearization of the longitudinal phase space (subsequently allowing an improved bunch compression) and another one as a Transverse Deflecting Cavity (TDS) for longitudinal beam diagnostics. Moreover a magnetic bunch compressor is envisaged allowing to cut out the central slice of the beam [3] or hybrid bunch compression.

INTRODUCTION

Ultra-short electron bunches, having a RMS length below 1 fs, are of great interest for various applications. First of all they can be used for ultrafast science, for example to generate ultra-short radiation pulses or to run electron diffraction experiments. Moreover they are expected to allow superior performances when injected into novel compact accelerating structures (e.g. based on Plasma Wake-Fields Acceleration). Besides studying novel acceleration techniques aiming to produce high brightness short bunches, the ARD group at DESY is working on the design of a conventional RF accelerator that will be hosted at SINBAD (Short and INnovative Bunches and Accelerators at Desy). ARES (Accelerator Research Experiment at Sinbad) will allow the production of such ultra-short bunches and the direct experimental comparison of the performance achievable by using different compression techniques. At a later stage ARES will be used to inject ultra-short electron bunches into laser driven Plasma Wake-field Accelerator.

Limits for the Bunch Length Compression

The factors limiting the minimum bunch length in the field of linear accelerators are well known. The main limitation is the space charge repulsion among the electrons in the bunch. As the effect scales as γ^{-2} (with γ being the relativistic factor of the beam), it limits the maximum electron densities especially at low energies [4].

The next limitation is set by the sinusoidal shape of the RF fields or the non-linear space charge force causes non-linear distortions of the distribution of the electrons in the longitudinal phase space [5]. Also a magnetic chicane or a dogleg, when present, contains non-linear dispersion terms that increase the longitudinal emittance of the beam. Additionally, when the magnetic compression is considered, Coherent Synchrotron Radiation (CSR) further spoils the longitudinal emittance of the beam [6].

Finally the uncorrelated energy spread of the beam, which is related to the minimum achievable spot size of the laser at the photo-cathode plays also a minor role in the optimization [7].

At ARES we plan to accelerate electron bunches with very low charge (0.2 - 50 pC)[1] to moderate energy levels (100-200 MeV) and to compress them to fs and sub-fs bunch-duration.

The chosen energy range allows to relax the space charge limitation, that characterizes the low energy accelerators (3-5 MeV), while dealing with a considerably more compact and relatively simple accelerator than the high energy (>1 GeV) user facilities.

LAYOUT OF THE ACCELERATOR

The project is foreseen to be realized in several stages. In this paper we will refer to two main stages of the installations. A baseline layout will allow the production of ultra-short bunches thanks to the velocity bunching compression technique [8]. The upgraded layout will allow to compress the beam also with the slit method [3] and by using an hybrid velocity bunching scheme. The introduction of a linearizing cavity is also foreseen.

Baseline Layout

Table 1: Main Accelerator Parameters

Parameter	Baseline Layout	Upgraded Layout
Main RF Frequency	2998 MHz	2998 MHz
Rep. Rate	10 Hz	10 Hz
N. of bunches	1	1
Final e- energy	100 MeV	200 MeV
Bunch charge	0.2 pC - 50 pC	0.2 pC - 1nC
Arrival time stability	<50 fs	<10 fs

The baseline layout of ARES is represented in Fig. 1 while a summary of the main accelerator parameters is presented in Table 1. The electron bunch will be generated by photo-emission from a Cs2Te or metallic cathode embedded in a 1.5 cells, 2.998 GHz frequency, RF gun of the REGAE type [9]. An emittance compensating solenoid having about 0.3 T peak field is placed at the gun exit. The first accelerating

[1] Some of the experiments planned at a later stage in the SINBAD facility would benefit from the use of high charge electron bunches, therefore we plan to make possible the extraction up to ~ 1nC charge from a Cs2Te cathode.

Content from this work may be used under the terms of the CC BY 3.0 licence (© 2015). Any distribution of this work must maintain attribution to the author(s), title of the work, publisher, and DOI.

6th International Particle Accelerator Conference IPAC2015, Richmond, VA, USA JACoW Publishing
ISBN: 978-3-95450-168-7 doi:10.18429/JACoW-IPAC2015-TUPWA030

Content from this work may be used under the terms of the CC BY 3.0 licence (© 2015). Any distribution of this work must maintain attribution to the author(s), title of the work, publisher, and DOI.

COMPRESSION OF AN ELECTRON-BUNCH BY MEANS OF VELOCITY BUNCHING AT ARES

B. Marchetti, R. W. Assmann, U. Dorda, J. Grebenyuk, J. Zhu, DESY, Hamburg, Germany

Abstract

ARES is a planned linear accelerator for research and development in the field of production of ultra-short electron bunches. The goal of ARES is to produce low charge (0.2 - 50 pC), ultra-short (from few fs to sub-fs) bunches, with improved arrival time stability (less than 10 fs) for various applications, such as external injection for Laser Plasma Wake-Field acceleration. The ARES layout will allow to perform and compare different kind of conventional e-bunch compression techniques, such as pure velocity bunching, hybrid velocity bunching (i.e. velocity bunching plus magnetic compression) and pure magnetic compression with the slit insertion. This flexibility will allow to directly compare the different methods in terms of arrival time stability and local peak current. In this paper we present simulation results for the compression of an electron bunch with 0.5 pC charge. We compare the case of pure velocity bunching compression to the one of a hybrid compression using velocity bunching plus a magnetic compressor.

INTRODUCTION

Ultra-short electron bunches, having a RMS length below 1 fs, are of great interest for various applications. First of all they can be used for ultrafast science, for example to generate ultra-short radiation pulses or to run electron diffraction experiments. Moreover they are expected to allow superior performances when injected into novel compact accelerating structures (e.g. based on Plasma Wake-Fields Acceleration) [1]. Besides studying novel acceleration techniques aiming to produce high brightness short bunches, the ARD group at DESY is working on the design of a conventional RF accelerator that will be hosted at SINBAD (Short and INnovative Bunches and Accelerators at Desy) [2]. ARES (Accelerator Research Experiment at Sinbad) [3] will allow the production of such ultra-short bunches and at a later stage it will be used to inject ultra-short electron bunches into laser driven Plasma Wake-field Accelerator.

One of the characteristics of this accelerator is that it will allow the direct experimental comparison of the performance achievable by using different bunch length compression techniques. In this paper we will focus on the pure velocity bunching and hybrid compression techniques, while we refer the reader to references [4] and [5] for more information about the working points using the magnetic compression and the study of the arrival time stability of the beam.

SIMULATIONS

The elements of ARES which are relevant for the simulations presented in this paper are shown in Fig. 1. In particular we select 4 locations that will be important in the following plots:

- Z1, located at 12.9m and corresponding to the exit of the linac in the baseline layout;
- Z2, located at 18.3m and corresponding to the entrance of the section that matches the beam to the dogleg;
- Z3, located at 21.2m, i.e. the dogleg entrance;
- Z4, located at 30.2m, i.e. the dogleg exit.

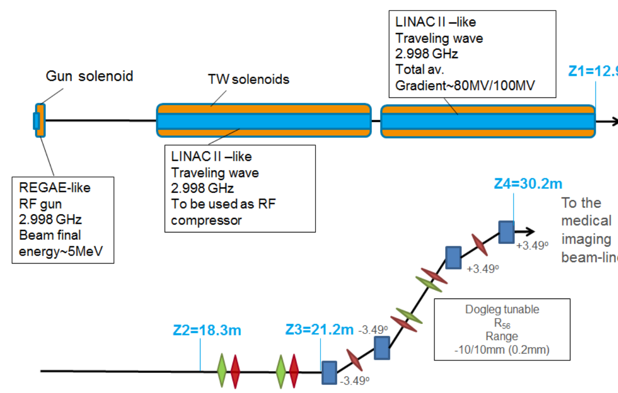

Figure 1: Elements of the ARES beam-line, which are relevant for the simulations described in this paper.

Pure Velocity Bunching

Injecting a not ultra relativistic electron bunch into a RF cavity close to the 0 phase of the electric field, where the head of the bunch sees a lower field amplitude than the tail, the beam is compressed because of the induced velocity chirp. Since the average velocity of the bunch is less than the velocity of the RF field, the first slips along the second, moving towards the crest. In this way it is possible to compress and accelerate an electron bunch at the same time.

In 2010 it has been firstly experimentally shown that it is possible to compress a beam with this technique while controlling the transverse emittance oscillations, through the so-called emittance compensation method [6].

The transverse dynamics of a beam accelerated along a constant focusing channel is described by the envelope equation [7]. Any mismatch between the space charge correlated forces and the external focusing leads to slice envelope oscillations that cause oscillations of the transverse normalized emittance. By properly matching the beam with the focusing channel surrounding the RF compressor it is possible to get close to the invariant envelope beam solution of the envelope equation, that minimizes the transverse emittance growth [8].

ISBN: 978-3-95450-168-7 doi:10.18429/JACoW-IPAC2015-TUPWA031

Content from this work may be used under the terms of the CC BY 3.0 licence (© 2015). Any distribution of this work must maintain attribution to the author(s), title of the work, publisher, and DOI.

COMPRESSION OF TRAIN OF BUNCHES WITH RAMPED INTENSITY PROFILE AT SPARC_LAB

B. Marchetti, DESY, Hamburg, Germany
E. Chiadroni, M. Ferrario, R. Pompili, INFN/LNF, Frascati, Italy
A. Bacci, INFN, Milano, Italy
A. Cianchi, Universitá Tor Vergata, Roma, Italy

Abstract

The production and acceleration of train of bunches with variable spacing in the ps/sub-ps range having ramped intensity profile are interesting to drive a plasma wave in the so-called resonant Plasma Wake-Fields Acceleration (r-PWFA) [1]. At *SPARC_LAB* trains having a constant intensity profile have been produced for the first time by using a shaped photo-cathode laser combined with the use of the velocity bunching compression technique [2–4]. If the sub-bunches have ramped intensity, i.e. they have different charge density, the space charge force affects differently the development of the longitudinal phase space of each one of them during the compression. In this paper we present preliminary simulations for the compression of a ramped train of bunches. The differences between the beam dynamics for a train of bunches having constant intensity profile and the ramped train are underlined. We discuss also the possibility of properly tuning the shaping of the photocathode laser to balance the space charge effect.

INTRODUCTION

Research and Development in the field of Plasma Wakefield Acceleration (PWFA) [5] spread worldwide in the last decades because of the promising results obtained by pioneering experiments such as Ref. [6, 7]. This technique foresees the generation of extremely high (~ GV/m) accelerating gradients having extremely short period (ps or sub-ps) thanks to the creation of a plasma wave in a gas excited by a laser pulse (Laser driven plasma Wake-Field Acceleration - LWFA) or by a particle beam (beam driven Plasma Wake-Field Acceleration).

The use of a train of bunches allows to overcome the main disadvantage of the beam driven acceleration with respect to the laser driven one, i.e. the necessity of a relatively big linac that accelerates the electrons driving the plasma wake-field. Indeed the accelerating field driven by the electron bunch can be increased by resonantly driving the wave through a modulation of the current of the driver.

The transformer ratio of the process is defined as the ratio of the maximum voltage that can be gained by a trailing particle to the voltage lost by a particle in the drive bunch. It can be maximized by using ramped bunch trains as a driver [8].

Nevertheless the beam dynamics of trains of pulses is extremely delicate and the tuning of one parameter (sub-bunch length, sub-bunch transverse emittance, relative spacing) at the entrance of the plasma chamber requires a re-adjustment of the train starting from the photo-cathode.

In this paper we show how it is possible to match a ramped comb driver beam at the exit of the linac by properly shaping the transverse spot size of the different sub-bunches. This method appears to be easy to implement in a realistic experimental setup.

SIMULATIONS

SPARC_LAB Layout

In Fig. 1 the layout of the *SPARC_LAB* facility is shown. The linear accelerator is constituted by a Sband RF gun of the SLAC/UCLA type followed by 3 Sband travelling wave cavities. At the end of the linac is foreseen to be placed a plasma chamber for a beam driven plasma experiment. After the gun there is a short space available for the installation of a linearizing cavity. This element is crucial for obtaining a periodic train spacing after the RF compression. In the following we will include an Xband linearizer located at this position.

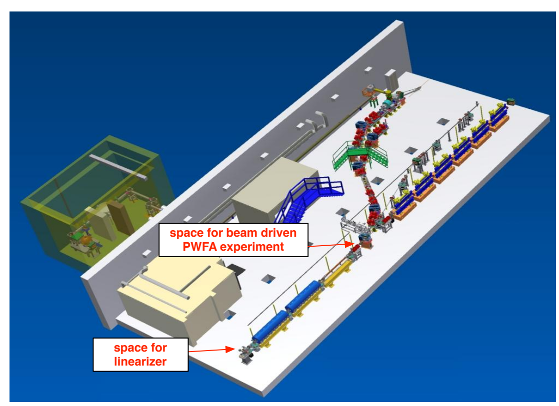

Figure 1: Layout of *SPARC_LAB*.

Compression of a Train of Bunches with Velocity Bunching

At *SPARC_LAB* train of bunches are realized by illuminating the photo-cathode with a longitudinally modulated laser [9–11] , the so-called comb pulse. In this configuration the electrons of each sub-bunch experience a large longitudinal space charge field with a linear correlation along the sub-bunch. The work done by the space charge force produces an energy modulation within the sub-bunch that can be transformed into a density modulation by an RF compressor.

ISBN: 978-3-95450-168-7 doi:10.18429/JACoW-IPAC2015-TUPWA032

PROGRESS IN THE INJECTOR UPGRADE OF THE LINAC II AT DESY

Y.C. Nie#, M. Hüning, C. Liebig, M. Schmitz, DESY, Hamburg, Germany

Abstract

A new injection system is under development for the LINAC II at DESY to improve the reliability of the machine and mitigate the radiological problem due to electron losses at energy of hundreds of MeV. It consists of a 100 kV triode DC gun, a 2.998 GHz pre-buncher, a novel 2.998 GHz hybrid buncher, and the dedicated beam transport and diagnostic elements. As the key components, the pre-buncher and the hybrid buncher realize a two-stage velocity bunching process including the ballistic bunching and the phase space rotation. Therefore, they produce a certain number of well-bunched 5 MeV micro-bunches from the input 2 ns-50 ns electron pulse for the downstream LINAC II. The overall upgrade plan, developments of the critical components, as well as the latest beam test results will be reported.

OVERALL INJECTOR UPGRADE

The layout of LINAC II at DESY and its injector upgrade are shown in Fig. 1 [1, 2]. LINAC II provides 450 MeV electrons for the light source PETRA III at the moment. Moreover, it has great potential to provide higher energy electron bunches (e.g. 800 MeV) for the Helmholtz distributed ARD facility SINBAD [3]. Within LINAC II, sections 1-3 are surrounded by solenoids with the maximum magnetic field of 0.08 T. The solenoid fields of sections 6 and 7 can reach 0.4 T in the case of positron operation. In addition, there are quadrupoles for the beam transport from the electron gun to PIA.

The new injector of LINAC II has been constructed and is being tested. Its main components are: an 100 kV DC triode gun that delivers 2-50 ns long electron pulses, a 2.998 GHz pre-buncher, a 2.998 GHz hybrid buncher consisting of both standing-wave (SW) and travelling-wave (TW) cells enclosed by a focusing solenoid, a dogleg that serves as an energy filter and delivers the electrons into the old gun beamline, 6 distributed quadrupoles, and a number of diagnostic instruments including 4 toroids, 6 beam position monitors and 4 fluorescent screens with 4 faraday cups inside. The old gun is kept as a reserved electron source. In a long term plan, it might be replaced with a photoinjector to produce ultra-short bunches. To make the coexistence of the two injectors possible, section 2 has been replaced by a beam transport line.

KEY COMPONENTS

For the injector, the critical problem is how to capture the non-relativistic electrons and bunch the ns long pulses into a certain number of micro bunches with high efficiency. Therefore, a two-stage Velocity Bunching (VB) strategy is employed. The first stage, i.e. the ballistic bunching is realized by the one-cell pre-buncher that operates at 90° ahead of the RF crest to introduce a primary velocity modulation. In the second stage, the phase space rotation [4] is used. It is an alternative to the magnetic compressor to provide high brightness ultra-short electron bunches that are required for FELs and some advanced accelerator concepts, such as the bunch-driven plasma wakefield accelerators. In our case, the hybrid buncher is used. The key issue is optimizing the injection phase and controlling the dephasing process that depends on the injection energy. If the injection energy is too low, the beam may transit across the RF crest, and then the de-bunching process occurs. To avoid this case, the one-cell SW section should have sufficient electric field to accelerate the incoming electrons rapidly.

In ASTRA [5] simulations, the wave phase of the hybrid buncher were optimized to make the output bunch length shortest. Here, the wave phase refers to the phase at the time $t = 0$ when the electrons start to be emitted at the cathode, denoted by Φ_0. Figure 2 shows the evolution of the bunch length σ_z versus the longitudinal position at different Φ_0. It can be seen that the optimal wave phase that gives the shortest bunch is -42°. When the bunch is compressed too fast, like in the case of Φ_0 = -60°, the different longitudinal slices can crossover each other, as a result, the bunch length increases again after reaching the minimum value. If the bunch is compressed too slowly, like in the case of Φ_0 = -20°, the bunching will be frozen before having reached the maximum compression due to the acceleration. In the case of Φ_0 = -42°, the bunch is compressed to the minimum length and then the longitudinal waist is frozen, since the beam velocity has become close enough to the RF phase velocity.

Figure 3 shows variations of the momentum gain rate dP_z/dz and the relativistic velocity $\beta = v/c$ along with the longitudinal position for the synchronous electron in the centre of one micro bunch, from the entrance of the pre-buncher to the exit of the hybrid buncher. It can be seen that the synchronous electron has been neither accelerated nor decelerated after the pre-buncher. In contrast, in the hybrid buncher, it is accelerated rapidly by the SW cell from β = 0.54 to 0.75, and to 0.995 at the end of the TW section. The evolution of the momentum gain in the TW section implies that the bunch undergoes a dephasing process while being both accelerated and bunched over the first several cells, and then becomes approaching the crest of the wave mainly for accelerating. Such a combination is ideal to produce well-bunched relativistic electron bunches for the downstream LINAC II. Note that the field distribution in the hybrid buncher is not ideally flat in reality. However, the residual field unflatness after tuning is acceptable in the viewpoint of the beam dynamics performance, as illustrated in [6, 7].

#yuancun.nie@desy.de

Content from this work may be used under the terms of the CC BY 3.0 licence (© 2015). Any distribution of this work must maintain attribution to the author(s), title of the work, publisher, and DOI.

ISBN: 978-3-95450-168-7 doi:10.18429/JACoW-IPAC2015-TUPWA033

STATUS OF THE SOFT X-RAY FREE ELECTRON LASER FLASH

Mathias Vogt, Bart Faatz, Josef Feldhaus, Katja Honkavaara, Siegfried Schreiber, Rolf Treusch,
DESY, Hamburg, Germany

Abstract

The superconducting free-electron laser FLASH at DESY routinely produces up to several thousand photon pulses per second with wavelengths in the soft X-ray and XUV regime and with energies up to 0.5 mJ per pulse. In 2014 the assembly of a second undulator beamline, FLASH2, was finished. Recommissioning of the FLASH linac and the original FLASH1 beamline was finished already end of 2013 and the commissioning of FLASH2 started in February 2014. Only a few weeks have been reserved for dedicated set up of FLASH2, and most of its commissioning has been performed parasitically during the FLASH1 user run. The first beam was extracted through the septum to the FLASH2 beamline on March 4th, 2014, and the first lasing of FLASH2 at a wavelength of about 40 nm was achieved on August 20th, while FLASH1 was lasing simultaneously with 250 bunches at 13.5 nm. We summarize here the status of the FLASH2 commissioning and the FLASH1 operation during its 5th user period.

INTRODUCTION

The soft X-ray SASE FEL FLASH [1–4] at DESY in Hamburg, Germany is driven by a normal conducting RF photo cathode gun (RF-gun) and a superconducting linac consisting of seven 1.3 GHz accelerating modules with eight TESLA-type 9-cell cavities each. The superconducting modules are capable of producing 800 μs long accelerating flat tops every 100 ms. The UV injector lasers [5] and the Cs_2Te photo cathode [6] are in their standard set up capable of producing 800 μs long pulse bursts of 800 pulses (1 MHz) at 10 Hz. FLASH is therefore ideal for an upgrade to share the long bunch trains between multiple beamlines and thus serve several FEL user experiments simultaneously at 10 Hz burst repetition rate. The accessible wavelength range produced by the FLASH1 undulator is 4.2 nm up to 52 nm. Every year FLASH attracts more users than could possibly be served with only one undulator beam line. A selection of publications based on science at FLASH can be found in [7]. In 2012 and 2013 a new second beam line, FLASH2 [8, 9], was built. Its commissioning started in February 2014. A detailed overview over the history of the FLASH facility can be found in [1]. A schematic layout of the facility with its common parts, i.e. RF-gun, first acceleration stages, two magnetic chicanes (“bunch compressors”), 3rd harmonic compression linearization and the main linac (four acceleration modules), the extraction switch yard and the two beam lines FLASH1 and FLASH2 is shown in Fig. 1. A more detailed description of the layout and a table of typical run parameters can be found in [2].

FLASH1 USER OPERATION AND HIGHLIGHTS OF STUDIES

In 2014 about 4200 h ($\approx$ 50% of the total year) were dedicated to user operation, roughly 3400 h ($\approx$ 40%) for machine development, photon beamline commissioning and general accelerator studies, and approximately 1200 h ($\approx$ 10%) for shutdown mantenance and commissioning. The overall down time over the ca. 7800 h of scheduled operation was $\approx$ 4.5%. Routinely, high SASE energies with up to several hundreds of μJ or alternatively short photon pulses (< 50 fs) were achieved for 10 to 4000 pulses per second. In April 2014 the RF coupler window of the RF-gun was changed because of a developing vacuum leak. The unavoidable reconditioning of the window affected the FEL operation in so far that the initial RF pulse duration did only allow for about 30 bunches per train over the first three weeks and that it took another month to reach 400 bunches [2]. Since June 2014 however, the RF-gun is running very stable with a gradient at the cathode of about 53 MeV/m (corresponds to about 4.8 MW of forward power) and 470 μs flat top.

Using a new third injector laser, capable of producing pulses of only about 1 ps duration, lasing was achieved in single spike mode, i.e. with 3 to 5 fs long photon pulses [10]. The group performing seeding experiments in the FLASH1 e^- beamline has recently achieved HGHG seeding around 38 nm with an energy contrast of about 1000 [11]. Although seeding experiments so far were all performed during dedicated studies, schemes for quasi-parasitic operation parallel to FLASH1 user operation are under preparation [12]. With the increased requirements on beam quality and reproducibility (e.g. for seeding and multi beamline operation) and given the fact that optics perturbations are known to exist in the FLASH injector, it became necessary to start a campaign on optics consolidation [13]. A progress report of the optics studies is given in [14]. Since autumn 2013 accelerator modules are regulated by a sophisticated MTCA.4 based LLRF system [15, 16]. The RF-gun was upgraded to the MTCA.4 in January 2015 [17, 18].

The 5th user period finished in the end of April 2015 and after a short shutdown in May the 6th user period will start in June 2015. The three week shutdown in May is dedicated to complete the radiation shielding in the area between the FLASH1 and FLASH2 tunnels, including survey and realignment of the undulator and photon beamlines.

FLASH2 COMMISSIONING & PARALLEL OPERATION OF TWO BEAMLINES

To preserve as much FLASH1 user time as possible, only very little dedicated FLASH2 commissioning time was allocated. First beam passed the septum on March 4th, 2014 and

Content from this work may be used under the terms of the CC BY 3.0 licence (© 2015). Any distribution of this work must maintain attribution to the author(s), title of the work, publisher, and DOI.

ISBN: 978-3-95450-168-7 doi:10.18429/JACoW-IPAC2015-TUPWA034

STATUS OF THE RECOMMISSIONING OF THE SYNCHROTRON LIGHT SOURCE PETRA III

R. Wanzenberg#, M. Bieler, M. Ebert, L. Fröhlich, J. Keil, J. Klute, G. Kube, G. K. Sahoo,
DESY, Hamburg, Germany

Abstract

At DESY the Synchrotron Light Source PETRA III has been extended in the North and East section of the storage ring to accommodate ten additional beamlines. The PETRA ring was converted into a dedicated synchrotron light source from 2007 to 2009. Regular user operation started in summer 2010 with a very low emittance of 1 nm at a beam energy of 6 GeV and a total beam current of 100 mA. All photon beamlines were installed in one octant of the storage ring. Nine straight sections facilitated the installation of insertion devices for 14 beam lines. Due to the high demand for additional beamlines the lattice of the ring was redesigned to accommodate 10 additional beamlines in the future. In an one year long shut-down two new experimental halls were built. The recommissioning of PETRA III started in February 2015. We are reporting the current status of the synchrotron light source including the performance of the subsystems.

PETRA III

PETRA was originally built as an electron – positron collider and was operated from 1978 to 1986 in this mode. From 1988 to 2007 PETRA was used as a preaccelerator for the HERA lepton hadron collider ring at DESY. After the end of the HERA collider physics program the PETRA ring was converted into a dedicated 3rd generation synchrotron radiation facility, called PETRA III [1]. Beam operation started in 2009 [2] and all 14 beamlines are operational since 2011. Due to the high demand for additional beamlines the lattice of the ring was redesigned to accommodate 10 additional beamlines in the framework of the PETRA III extension project [3, 4, 5]. User operation ended in February 2014 and the short user run of only four weeks can be considered as an extension to the long run period which started back in 2013. It was also the last user operation before a long shut down period of about one year which was started to implement the facility extension project.

General Layout of the PETRA III Extension

Two tunnel sections about 80 m long in the North and the East of the PETRA ring were completely reconstructed and new experimental halls were built to extend the PETRA III synchrotron light facility. In the future more light will be available for users at 10 new beamlines in addition to the already existing 14 beam lines in the Max von Laue experimental hall. The location of the new halls is shown in Fig.1. A detailed layout of the hall North of the PETRA extension is shown in Fig.2. The original plan to reuse the existing accelerator tunnel [3, 4] was not implemented since a new tunnel section is advantageous for the installation of the front end components of the beamlines. The decision to completely reconstruct the tunnel sections was one of the reasons to revise also the project schedule.

Figure 1: Layout of PETRA III. Two new halls in the North and East have been added.

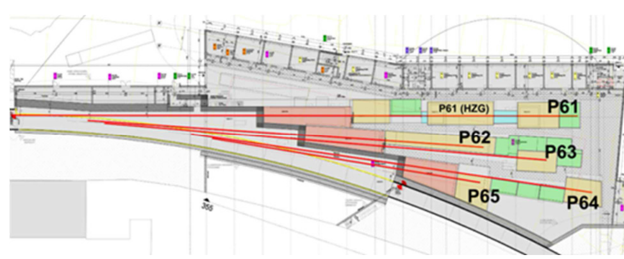

Figure 2: Hall North of the PETRA III extension.

Parameters and Optics

Four beamlines in the North and respectively in the East hall will be fed by four undulators that are installed in two canted DBA like cells that have replaced a part of the FODO lattice. Six 5.3 m long dipoles have been replaced with six shorter dipole magnets (1 m and 0.5 m long). The new lattice configuration is shown in Fig. 3 for the North extension [3,6]. A photo of the section is shown in Fig. 4.

#rainer.wanzenberg@desy.de

Content from this work may be used under the terms of the CC BY 3.0 licence (© 2015). Any distribution of this work must maintain attribution to the author(s), title of the work, publisher, and DOI.

ISBN: 978-3-95450-168-7 doi:10.18429/JACoW-IPAC2015-TUPWA035

Content from this work may be used under the terms of the CC BY 3.0 licence (© 2015). Any distribution of this work must maintain attribution to the author(s), title of the work, publisher, and DOI.

PROGRESS IN OPTICS STUDIES AT FLASH

J. Zemella, T. Hellert, M. Scholz, M. Vogt, DESY, Hamburg, Germany

Abstract

FLASH is the superconducting soft X-ray Free Electron Laser in Hamburg at DESY, Germany. Good control over the beam optics is a key aspect of the operation of a SASE FEL. In 2013 a second beam line, FLASH2, was assembled and the modifications necessary to feed the two beam lines were installed downstream of the FLASH linac. As reported before [1] we started a campaign of optics consolidation. We give an update on the progress of this effort and on results.

INRODUCTION

The superconducting soft X-ray Free Electron Laser in Hamburg (FLASH) [2] at DESY, Germany has recently been upgraded to operate two FEL beam lines, FLASH1 and FLASH2 [3], to potentially serve more users. For optimum FEL performance several several optical criteria have to be met. The most critical ones are the beam waists in the bunch compressors and at he septum of the switchyard (switching the e^- beam between FLASH1 and FLASH2) [4] and matching in the periodic solution of the in the FEL undulators of the two beam lines. In theory it suffices to match the space charge dominated beam from the RF photo cathode gun to the design optics of the linac to meet all the conditions at least for an uncompressed bunch. However it is a well known but not well understood fact that in FLASH the optics is strongly perturbed almost right after the matching point. A campaign of optics consolidation was started in 2013 and described in [1].

THEORY

This section is partial repetition of [1]. Our tools consist of a suite of shell scripts and c–programs utilizing a version of MAD8 which has been extended for linacs [5, 6] as optics engine. The actual machine optics is reconstructed by reading the magnet currents from the control system.

Orbit Response Matrix (ORM) Technique

In a linac the (i, j)-th element of the ORM is defined as the linearized response of a given coordinate (q_i) at the i-th monitor (BPM) to a kick θ_j from the j-th steerer

$$\Delta q_i = \left(\mathbf{R}_{i\leftarrow j}\right)_{q,p} \ \Delta\theta_j \tag{1}$$

where for the moment we neglect inter plane coupling, $\mathbf{R}_{i\leftarrow j}$ is the transport matrix from s_j to s_i [7], and $q, p = 1, 2$ for the horizontal and $q, p = 3, 4$ for the vertical phase plane. In a linac $\mathbf{R}_{i\leftarrow j} \equiv 0$ for $s_i < s_j$. The measured ORM contains calibration errors of both monitors (a_i) and steerers (b_j),

$$\mathbf{R}^{\text{meas}}_{i\leftarrow j} = a_i \, \mathbf{R}^{\text{machine}}_{i\leftarrow j}\{k_1^{(l)} : s_l \in (s_j, s_i)\} \, b_j \tag{2}$$

where the $k_1^{(l)}$ are the quadrupole strengths in-between steerer and monitor. Thus, before non–linear minimization can be applied to identify and/or correct focusing errors, robust estimates of the a_i's and b_j's have to be extracted from the ORM data while fulfilling suitable consistency constraints [8]. Many BPMs in FLASH have been calibrated in a beam based way, relying on the calibration of nearby upstream steerers. This introduces coupling between the a_i's and the b_i's ans is thus an additional complication

MEASUREMENTS

In this section the measurements are presented to investigate the optics perturbation we are expecting at the end of DBC2 section up to the end of ACC2 section. As mentioned before, this has been done by mainly using the ORM technique. Figure 2 shows the relative difference of the measured and theoretical orbit response from UBC2 to DBC3 section for design optics.

The orbit response is calculated by a linear fit to the BPM readings for five steerer kick strengths using the fit function implemented in gnuplot [9] weighted by the rms error of 10 BPM readings for each kick strength. The error for the slope is the error of the fit calculated by gnuplot. A python code performs the fit of the steerer calibrations and BPM gains. In this analysis the measurement data is fitted to the model data. The fit program performs a minimization of the error of the difference ORM weighted by the error of the orbit response using an iterative method based on SVD algorithm.

The ORM measurement in Fig. 2 is representative for a whole set of ORMs taken in the design optics with the injector matched for 0.3 nC. It shows a quite good correspondence between model and measurement up to BPM 11DBC2 for both planes. The fitted steerer calibrations are between 0.9 and 1.15 except H10ACC1 with 0.5. The fitted BPM gains between 0.9 and 1.4 except BPM 9ACC2 with 2.9 in x and 2.4 in y plane and 9ACC3 with 1.6 in x and 1.1 in y plane.

The calibration of BPM UBC2 (1.8 in x and 1.2 in y plane) is far off because it has been calibrated using a nearby steerer whose calibration if far off (H10ACC1). The steerers in UBC2 and DBC2 are of the same type so that in this analysis the mean of the fitted steerer calibrations is used because the steerer calibrations should be almost the same for all these steerers. Whenever the section over which the response was measured intersects with the stretch from approximately BPM 11DBC2 to the steerers in ACC2, the model does not fit the measurements. However the response of the two steerers ACC2 and ACC3 are in good agreement with the theoretical prediction. Thus it is clear that there must be a noticeable optics perturbation located in that section. So far this is not a new result and just reconfirms the findings of many others, e.g. [8]

We have a couple of candidates for causing the perturbation described above, see Fig. 2. Several of them are hidden

ISBN: 978-3-95450-168-7 doi:10.18429/JACoW-IPAC2015-TUPWA036

POSSIBILITY OF LONGITUDINAL BUNCH COMPRESSION IN PETRA III

I. Agapov *, European XFEL GmbH, Hamburg, Germany,
S. Tomin , NRC Kurchatov Institute, Moscow, Russia,
and European XFEL GmbH, Hamburg, Germany
R. Wanzenberg, DESY, Hamburg, Germany

Abstract

A scheme of short bunch production in storage rings using a longitudinally focusing insertion was presented in [1]. In this work we study the possibility of integrating such insertion into the PetraIII storage ring. In particular, we discuss possible optics solutions to integrate RF stations, chicane-type delay sections, and the undulators into existing ring geometry.

INTRODUCTION

A possibility of short bunch production in storage rings using compression followed by decompression was presented in [1]. There it was also shown that the scheme can be used to operate a high gain FEL in a low emittance storage ring such as Petra III [2]. At Petra III several straight sections are presently available, e.g. one of about 70 m length in the North-West (NW) section (see Fig. 1) The scheme is briefly introduced in first section. Possible solutions in terms of electron optics are discussed in the second section. As part of the compression and decompression, sections with variable R_{56} of opposite signs are required. While a slight modification of an arc provides a section with necessary positive R_{56}, the negative R_{56} requires larger modification to the optics. It turns out that designing such a section is rather challenging due to issues with emittance preservations. A short chicane with rather strong bending magnets could increase the equilibrium emittance significantly and installation of such a chicane for large negative R_{56} does not seem feasible. However, a modification to the scheme where both chicanes have positive R_{56} requires very minor changes to the present machine layout (apart from installing two RF sections) at the cost of slightly more complex longitudinal dynamics.

SCHEME

The scheme proposed in [1] is based on the observation that longitudinal focusing similar to the bunch compression in linac-based FELs could potentially be run in a storage ring. An RF section followed by a section with energy-dependent time delay acts as a 'compressor', and the mirror reflection of this setup acts as a 'decompressor'. The scheme is sketched in Fig. 2. With the peak bunch current thus increased by an order of magnitude and small emittance of a ring such as Petra III operation of a high gain ring FEL could be potentially possible for soft x-rays of energies below approx. 1-2 keV. The longitudinal phase space map for the insertion is

$$M = M_{RF2} \cdot M_{C2} \cdot M_{C1} \cdot M_{RF1} \quad (1)$$

where the magnetic section maps are given by matrices

$$M_{C1,C2} = \begin{pmatrix} 1 & R_{56}^{(1,2)} \\ 0 & 1 \end{pmatrix} \quad (2)$$

and the RF section maps are

$$M_{RF1,RF2} : \begin{pmatrix} t \\ p \end{pmatrix} \rightarrow \begin{pmatrix} t \\ p + V^{(1,2)} \sin(\omega_{RF} \cdot t) \end{pmatrix} \quad (3)$$

Here t and p are longitudinal coordinates usually measured in meters and relative energy units, R_{56} is the standard notation for dispersive time delay, $V^{(1,2)}$ are total RF voltages for the compressor and the decompressor, and ω_{RF}

Table 1: PETRA III beam parameters [2]

Parameter	High charge	Low charge
Beam energy	6 GeV	
Circumference	2304 m	
No. bunches	40	960
Emittance ε_x	$1.2 \cdot 10^{-9}$ m · rad	
Emittance ε_y	$1.2 \cdot 10^{-11}$ m · rad	
Energy spread	10^{-3} (6 MeV)	
Bunch charge	19 nC	0.8 nC
Bunch length	44 ps (rms)	
Peak current	170 A	7 A
Average current	100 mA	100 mA
Long. damping time	8 msec	
Transv. damping time	16 msec	

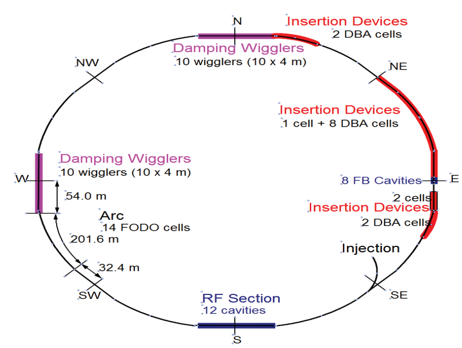

Figure 1: Present layout of Petra III

* ilya.agapov@xfel.eu

Content from this work may be used under the terms of the CC BY 3.0 licence (© 2015). Any distribution of this work must maintain attribution to the author(s), title of the work, publisher, and DOI.

ISBN: 978-3-95450-168-7 doi:10.18429/JACoW-IPAC2015-TUPWA037

STATISTICAL OPTIMIZATION OF FEL PERFORMANCE

I. Agapov *, G. Geloni, European XFEL GmbH, Hamburg, Germany
I. Zagorodnov, DESY, Hamburg, Germany

Abstract

Modern FEL facilities such as the European XFEL will serve a large number of users, thus understanding and optimizing their performance parameters such as the output power is important. In this work we describe the statistical approach to such optimization under assumption that the possibility of modelling is limited by uncertainties. We present experience of such statistical optimization of SASE radiation power for FLASH and discuss how the results of empirical tuning can be fed back into the model used in simulations.

INTRODUCTION

Experience shows that extensive tuning of an FEL may be required to reach design parameters. The main objective of the present study is to understand methods and design software tools for automatic tuning of FEL parameters. Since many uncertainties are present, we propose to perform such optimization based on empirical methods using very little model information. This roughly mimics what a human operator is doing, only taking advantage of more powerful and faster computations. The possibility of using the model enters into the design of the empirical method. We call such approach statistical. It is described in the first two sections of the paper, including its demonstration at FLASH. The second objective is to try to deduce the model parameters from the measurements so that more realistic calculations can be done. Such problem is typically ill-posed since there is usually much less diagnostics than the potential causes of deviation from design performance. We discuss a possible approach to such model inference in the last section, although its practical feasibility remains to be demonstrated. The statistical tuning software is part of the OCELOT framework ([1, 2]).

EMPIRICAL OPTIMIZATION AT FLASH

Optimization is implemented as an arbitrary sequence of optimization steps, each step maximizing the SASE pulse energy with a certain group of devices. A group of devices can be arbitrary, in practice such groups as all launch steerers, FODO quadrupoles, matching quadrupoles, steerers between undulators etc. are used. Optimization using a group of devices is usually performed with the simplex (Nelder-Mead) method, although other methods can be used too. The objective function used in maximization is proportional to the SASE pulse energy averaged over several bunch trains. Beam losses approaching the alarm threshold are penalized so that in practice the optimization algorithm always avoids beam losses. To better understand the performance of the optimizer response functions of SASE energy to the control parameters can be studied. Examples of such response functions for launch steerers and FODO quadrupoles are shown in Figs. 1 and 2. The scans are done such that starting from some average value the magnet current is first driven up, then down, and then up again. One can see a certain "hysteresis" effect, which is mostly due to the drift in the radiation power. Figure 3 shows such fluctuations when the machine is not interfered with apart from some feedbacks runnning. When present, this drift sets a limit to the optimizer performance. Figure 2 also shows the presence of quadrupole misalignment through the coupling of the quadrupole strength to the orbit, mostly in the vertical direction.

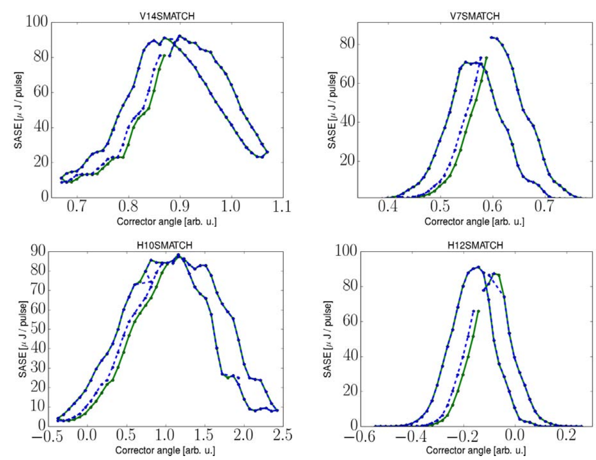

Figure 1: SASE response functions to launch steerers. Green is the set and blue is the read back values.

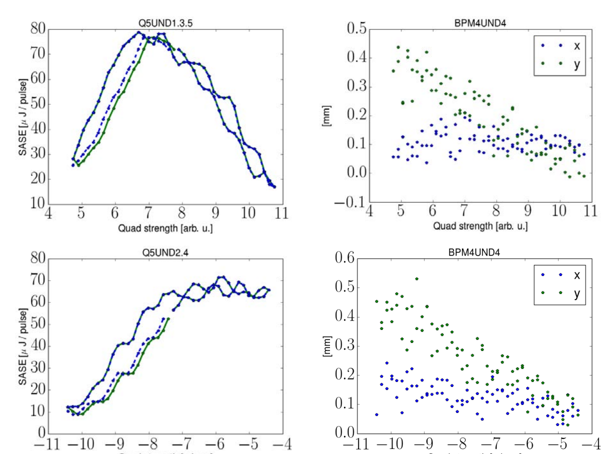

Figure 2: SASE and orbit response functions to FODO quadrupole strength.

* ilya.agapov@xfel.eu

Content from this work may be used under the terms of the CC BY 3.0 licence (© 2015). Any distribution of this work must maintain attribution to the author(s), title of the work, publisher, and DOI.

ISBN: 978-3-95450-168-7 doi:10.18429/JACoW-IPAC2015-TUPWA038

OPTICS COMPENSATION FOR VARIABLE-GAP UNDULATOR SYSTEMS AT FLASH

Ph. Amstutz*, C. Lechner, T. Plath, Universität Hamburg, Germany
S. Ackermann, J. Bödewadt, M. Vogt, DESY, Hamburg, Germany

Abstract

Variable-gap undulator systems are widely used in storage rings and linear accelerators to generate soft- and hard x-ray radiation for the photon science community. For cases where the effect of undulator focusing significantly changes the electron beam optics, a compensation is needed in order to keep the optics constant in other parts of the accelerator. Since 2010, the free-electron laser (FEL) facility FLASH is equipped with two undulator sections along the same electron beamline. The first undulator is a variable-gap system used for seeding experiments, the second undulator is a fixed-gap system which serves the user facility with FEL radiation. Varying the gap in the first undulator will change the beam optics such that the FEL process in the second undulator is dramatically disturbed. For the correction of the beam optics an analytical model is used to generate feed forward tables which allows to make part of the beamline indiscernible for the subsequent sections. The method makes use of the implicit function theorem and can be used for any perturbation of the beam optics. Here, we present the method and its implementation as well as measurements performed at FLASH.

INTRODUCTION

The super-conducting linear accelerator FLASH at DESY in Hamburg serves two parallel undulator beamlines, FLASH1 and FLASH2. While FLASH2 is currently being prepared for user operation, FLASH1 has been delivering soft x-ray photons for user experiments since 2005 [1]. As shown in Fig. 1, upstream of the FLASH1 main undulator an experimental setup for FEL seeding (sFLASH) is located. It features two electro-magnetic undulators as well as four variable-gap undulator modules and thus is the ideal testbench for the study of several different seeding schemes [2].

The focusing properties of the seeding undulators in the vertical plane will have an impact on the beam optics at the entrance of the main undulator. At lower beam energies this change can easily be in the order of several tens of percent and thus significantly decreases the FEL performance in the main undulator. Therefore, the disturbance introduced by the seeding radiators has to be corrected for by adjusting the strength parameters of quadrupole magnets in that section to match the optics in the main undulator again.

While most algorithms typically find a suitable correction by numerically solving minimization problems, we present an analytical method. It is based on the implicit function theorem (compare for instance [3]) and allows for the determination of correction parameters as a function of the introduced disturbance. Furthermore, we present measurements confirming the calculations.

THE METHOD

During these calculations the optics will be described employing transverse linear beam optics. We denote the 4×4 transformation matrix describing the effect of the entire section of the beamline as $M(\rho)$, where $\rho \in \mathbb{R}^n$ is a set of all the machine parameters which are needed to fully define the optics, e.g. strength parameters of quadrupole magnets and undulator gaps. We define two machine states ρ and ρ_0 to be equivalent if their matrices are identical

$$M(\rho) = M(\rho_0). \tag{1}$$

The goal of our calculations is to find the disturbed state ρ that is equivalent to the undisturbed case ρ_0 to keep the optical functions after the section constant. For this purpose we split ρ into the parameters that introduce the disturbance σ (here, undulator gaps) and the ones that are used for the correction τ. Under the assumption of uncoupled matrices, $M(\rho)$ consists of two 2×2 block matrices. Since the determinants of both block matrices have to equal unity, Eq. (1) can be reduced to 6 equations of the form

$$\Delta M_{i,j}(\rho, \rho_0) = M_{i,j}(\rho) - M_{i,j}(\rho_0) = 0. \tag{2}$$

By defining a C^1 function $B : \mathbb{R}^n \to \mathbb{R}^6$ to have these six matrix element differences for a given, constant ρ_0 as its components, the set of equations (2) can be written as

$$B(\sigma, \tau) = 0. \tag{3}$$

The implicit function theorem now assures the existence of a unique function $\tau(\sigma)$ around ρ_0, so that

$$B(\sigma, \tau(\sigma)) = 0, \tag{4}$$

if the Jacobian determinant $\det \mathbf{J}_B(\tau)|_{\rho_0} \neq 0$, which we at this point will assume to be true [3]. We see, that B and τ have to be of the same dimension for the correction function to be unique, meaning that the desired compensation can be achieved by adjusting six correction parameters. The derivative of this correction function can be obtained by analytical means from Eq. (4)

$$\frac{\mathrm{d}\tau(\sigma)}{\mathrm{d}\sigma} = -\left(\frac{\partial}{\partial\tau} B(\sigma, \tau(\sigma))\right)^{-1} \cdot \frac{\partial}{\partial\sigma} B(\sigma, \tau(\sigma)). \tag{5}$$

This defines a system of six coupled differential equations. Therefore, by solving this system the sought correction function $\tau(\sigma)$ can be obtained. Due to the complexity of the involved terms it will in general not be possible to find the solution analytically and a numerical approximation is needed.

* philipp.amstutz@desy.de

Content from this work may be used under the terms of the CC BY 3.0 licence (© 2015). Any distribution of this work must maintain attribution to the author(s), title of the work, publisher, and DOI.

ISBN: 978-3-95450-168-7 doi:10.18429/JACoW-IPAC2015-TUPWA039

TRANSVERSE GRADIENT UNDULATOR-BASED HIGH-GAIN-FELS — A PARAMETER STUDY

A. Bernhard*, E. Burkard, V. Afonso Rodríguez, C. Widmann, A.-S. Müller, KIT, Karlsruhe, Germany

Abstract

Transverse gradient undulators (TGU) have recently been discussed as sources for High Gain Free Electron Lasers (FEL) driven by electron beams with an elevated energy spread as for example generated in storage rings or wakefield accelerators. In this contribution we present the results of a parameter study based on the one-dimensional TGU-FEL theory making realistic assumptions on the key parameters achievable for the transverse gradient undulator. We show for which parameter areas LWFA-driven TGU-FELs are virtually technically feasible today and which technical improvements would be required to employ the concept for a laboratory-scale X-Ray FEL.

INTRODUCTION

Is a "table-top" high-gain X-ray free-electron laser driven by a laser wakefield accelerator employing a transverse gradient undulator scheme realistic?

Almost immediately after the experimental demonstration of laser wakefield acceleration (LWFA) of plasma electrons in the highly non-linear regime [1–3] the discussion started how this acceleration scheme could be used to realize compact free-electron lasers fitting into a normal laboratory and delivering laser-radiation in the X-ray regime [4–6] usable e.g. for advanced medical imaging techniques.

The main obstacle on the way to such an admittedly appealing scenario is the comparably large energy spread of the LWF-accelerated electrons (1 % to 10 %). Grüner et al. [6] pointed out that the unfavorable effect of the energy spread could be compensated by the high peak current of the short-bunched LWFA electrons. However, the assumptions the authors made on achievable LWFA beam- as well as undulator parameters have not proved realistic so far.

More recently more elaborated high-gain FEL schemes for electron sources with increased energy spread have been proposed that employ a special preparation of the electron beam phase space distribution by means of magnetic chicanes. Such schemes rely either on bunch decompression [7, 8] or on a transverse spectral dispersion matched to a transversely varying undulator field amplitude. These transverse-gradient undulator high-gain FEL schemes have been discussed both for self amplification of spontaneous emission (SASE) [9, 10] and high-gain harmonic generation (HGHG) [11] scenarios.

In our study we investigated the TGU-SASE case based on the 1-D theory described in [9, 10], searching for optimized and technically feasible TGU parameters for several sets of LWFA beam parameters, moving from beam properties that can be routinely achieved today to beam properties that have been achieved in individual cases to properties that would actually be required.

ACCESSIBLE PARAMETER SPACE

The TGU-FEL scheme implicates modifications of the 1D-FEL equation [10] through the introduction of a modified Pierce parameter

$$\rho_{\mathrm{TGU}} = \rho_{\mathrm{FEL}} \left(1 + \frac{\eta^2 \sigma_\delta^2}{\sigma_x^2}\right)^{-\frac{1}{6}} \tag{1}$$

and an effective energy spread

$$\sigma_{\delta,\mathrm{eff}} = \sigma_\delta \left(1 + \frac{\eta^2 \sigma_\delta^2}{\sigma_x^2}\right)^{-\frac{1}{2}}. \tag{2}$$

Here, ρ_{FEL} is the unmodified Pierce parameter, σ_δ the energy spread, σ_x the transverse beam size (approximated as constant in 1D-theory) and η the dispersion function which is presupposed to be matched to the TGU parameters through the relation

$$\eta = \frac{2 + K_0^2}{\alpha K_0^2}, \tag{3}$$

where K_0 is the undulator parameter at the transverse position for the central beam energy and $\alpha = \frac{1}{K_0} \left.\frac{\partial K}{\partial x}\right|_{x=0} =: \frac{1}{K_0}\alpha_K$ the relative transverse K-gradient, i.e. the linear approximation $K(x) = K_0(1+\alpha x)$ is assumed to be admissible.

The crucial parameters entering into the TGU-FEL equation are therefore the undulator period length λ_u, influencing both the unmodified Pierce parameter and the undulator parameter, the undulator flux density amplitude $\tilde{B}_0 = \tilde{B}(x = 0)$ and the transverse gradient α_K on the one hand, the transverse beam size σ_x on the other hand. In the following, we discuss our considerations on the accessible ranges for these parameters.

TGU Parameters

Technically, transverse gradient undulators are realized by a transverse variation of the undulator gap. Several possible TGU geometries have been discussed in [12, 13] particularly for superconducting TGUs. Among those the TGU geometry consisting of two cylindrically shaped halves provides the highest achievable transverse field gradients. Indeed we consider the statement adequate that the cylindrical superconducting TGU defines the upper limits of the technically achievable crucial TGU parameters for a given gap and period length [14].

To estimate these limits we use the analytic expressions for the field of a cylindrical TGU given in [12], combined with a 2D finite element calculation used to determine the optimum

* axel.bernhard@kit.edu

Content from this work may be used under the terms of the CC BY 3.0 licence (© 2015). Any distribution of this work must maintain attribution to the author(s), title of the work, publisher, and DOI.

ISBN: 978-3-95450-168-7 doi:10.18429/JACoW-IPAC2015-TUPWA042

Content from this work may be used under the terms of the CC BY 3.0 licence (© 2015). Any distribution of this work must maintain attribution to the author(s), title of the work, publisher, and DOI.

STATUS OF THE ACCELERATOR PHYSICS TEST FACILITY FLUTE

M.J. Nasse*, A. Bernhard, I. Birkel, A. Böhm, A. Borysenko, S. Hillenbrand, N. Hiller, S. Höninger, S. Marsching, A.-S. Müller, R. Rossmanith, R. Ruprecht, M. Schuh, M. Schwarz, B. Smit, S. Walther, M. Weber, P. Wesolowski, KIT, Karlsruhe, Germany
R.W. Assmann, M. Felber, K. Flöttmann, C. Gerth, M. Hoffmann, P. Peier, H. Schlarb, B. Steffen, DESY, Hamburg, Germany
R. Ischebeck, B. Keil, V. Schlott, L. Stingelin, PSI, Villigen, Switzerland

Abstract

A new compact versatile linear accelerator named FLUTE (Ferninfrarot Linac Und Test Experiment) is currently under construction at the Karlsruhe Institute of Technology (KIT). It will serve as an accelerator test facility and allow conducting a variety of accelerator physics studies. In addition, it will be used to generate intense, ultra-short THz pulses for photon science experiments. FLUTE consists of a ~7 MeV photo-injector gun, a ~41 MeV S-band linac and a D-shaped chicane to compress bunches to a few femtoseconds. This contribution presents an overview of the project status and the accompanying simulation studies.

INTRODUCTION

The objectives of the linear accelerator FLUTE, developed and being constructed at KIT in collaboration with PSI and DESY, range from studying space charge and coherent radiation induced effects to bunch compression studies and systematic comparison of simulation code results with measurements [1]. Furthermore, it will serve as a test bench for advanced diagnostics and instrumentation. The generated intense THz radiation will be used for various experiments for example to study the radiative impact on relevant biomedical tissue. The most important design parameters based on simulations are summarized in Table 1.

Table 1: Main FLUTE Parameters from Simulation

Parameter	**Value**	**Unit**
Final electron energy	~41	MeV
Electron bunch charge	~1–3000	pC
Final electron bunch length (RMS)	~1–300	fs
Pulse repetition rate	10	Hz
Energy / THz pulse	up to ~3	mJ
Power / THz pulse	up to ~5	GW

FLUTE LAYOUT

The design layout is depicted in Fig. 1 showing details of the planned diagnostics components. The main components are: the *electron gun*, pre-accelerating the electrons to an energy of ~7 MeV, including a focusing solenoid; the *low-energy diagnostics section* comprising two screens, beam position monitors (BPM), and an integrating current transformer (ICT) for determining the electron beam current, as well as a spectrometer with a quadrupole for energy measurements; the *linac* accelerating the electrons to an energy of ~41 MeV, followed by the *first high energy diagnostics section* including an electro-optical longitudinal profile monitor (EOM) for determination of the longitudinal bunch profile [2]; a quadrupole triplet, also located in this section to focus the beam appropriately in both transverse directions; the *bunch compressor* consisting of four dipole magnets [3] including some diagnostics in the dispersive section, directly followed by the *THz out-coupling optics*; the *final diagnostics section* including another EOM and a high-energy spectrometer; the Faraday cup used with radiation shielding as *electron dump*.

SIMULATION RESULTS

We use several software programs to optimize the layout of FLUTE. For low charges ASTRA [4] is employed for the entire machine. For charges above ~1 nC comparisons have shown that especially at the end of the chicane, where the electron bunches become very short, coherent synchrotron radiation (CSR) induced effects become dominant [5]. In these cases, CSRtrack [6] was employed in the chicane. For the calculation shown here ASTRA was used, whereas the generated THz spectra und pulse profiles were computed with in-house developed algorithms [7].

Electron Beam

To study the influence of the space between the gun cathode and the linac we performed a set of ASTRA simulation runs with different distances. For this comparison the relevant parameters like RF and laser phase, solenoid and quadrupole triplet focusing strength, chicane dipole fields, and laser spot size and length have been optimized for each case separately. Figures 2 and 3 show first results for a cathode–linac distance of 3 m. This distance allows enough space for the low-energy diagnostics components and later for a buncher cavity. Please note, that in this paper CSR-induced effects have not been studied. This is why we restrict ourselves here to a bunch charge of ≤100 pC where these effects are relatively small.

The transverse RMS beam size plotted in Fig. 2 for both 1 pC and 100 pC bunch charges show that the size after the gun, but before the linac can be kept below 1.4 mm. Furthermore, we reach a small bunch size of ≤105 µm at the end

* Michael.Nasse@kit.edu

ISBN: 978-3-95450-168-7 doi:10.18429/JACoW-IPAC2015-TUPWA043

NON-INTERFEROMETRIC SPECTRAL ANALYSIS OF SYNCHROTRON RADIATION IN THE THz REGIME AT ANKA

J. L. Steinmann*, M. Brosi, E. Bründermann, M. Caselle, E. Hertle, N. Hiller, B. Kehrer, A.-S. Müller, P. Schönfeldt, M. Schuh, P. Schütze, M. Schwarz, KIT, Karlsruhe, Germany
J. Hesler, Virginia Diodes Inc., Charlottesville, VA, USA

Abstract

Interferometry is the quasi-standard for spectral measurements in the THz- and IR-range. The frequency resolution, however, is limited by the travel range of the interferometer mirrors. Therefore, a resolution in the low megahertz range would require interferometer arms of about 100 m. As an alternative, heterodyne measurements provide a resolution in the Hertz range, an improvement of 6 orders of magnitude. Here we present measurements done at ANKA with a VDI WR3.4SAX, a mixer that can be tuned to frequencies from 220 GHz to 330 GHz and we show how the bunch filling pattern influences the amplitude of specific frequencies.

INTRODUCTION

The single particle synchrotron spectrum emitted by an electron in a bending magnet is broad-band and also continuous. In a storage ring where an electron bunch emits synchrotron radiation on every turn, the emitted electric field consists of equally spaced (T_0) series of short pulses. As an approximation we assume a Dirac delta function ($\delta(t)$) as bunch signal which leads to an infinite pulse train, known as Dirac comb or Shah distribution, that can be represented as a Fourier series [1]:

$$f(t) = \sum_{n=-\infty}^{\infty} \delta(t - nT_0) = \frac{1}{T_0} \sum_{n=-\infty}^{\infty} e^{j2\pi n \frac{t}{T_0}} \qquad (1)$$

The importance of this lies in the fact that the Shah distribution is its own Fourier transform which gives us a discretized spectrum

$$\mathcal{F}(\omega) = \omega_0 \sum_{p=-\infty}^{\infty} \delta(\omega - p\omega_0) \qquad (2)$$

The distance between the frequency combs is the revolution frequency ($\omega_0 = 2\pi f_0$, at ANKA: $f_0 = 2.71$ MHz). By having not only one bunch filled, but each RF-bucket (at ANKA: 184), amplified parts with harmonics of the accelerating radio frequency show up. This is because the buckets are not equally filled with electrons, but show some inhomogeneity as illustrated in Fig. 1.

The spectral components of a circulating electron beam have been described by Schott in 1912, long before synchrotrons were being thought of as light sources [2]. However, recent literature does not pay much attention to the spectral lines of synchrotron radiation, as they couldn't be resolved nor exploited by measurements [3, p. 807]. This has changed now.

* johannes.steinmann@kit.edu

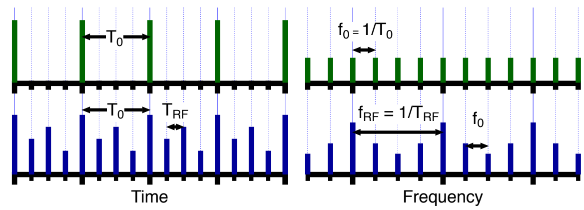

Figure 1: Theoretical spectrum of a series of short pulses as they happen in a storage ring. Each revolution the same pulse is seen, leading to a frequency comb spaced by the revolution frequency (top). By filling all buckets with (slightly) different bunch charges, we see the filling pattern modulated onto the frequency comb, showing extra amplification at the accelerating radio frequency (bottom).

The synchrotron radiation spectrum and the calculation of the frequencies are similar to the signal of a pick-up electrode. Also there, the short signal from the bunch is repeatedly coming by, creating a frequency comb whose analysis is a standard tool for longitudinal diagnostics in synchrotrons and therefore well studied [3, p. 627ff] [4, p. 165ff]. Taking the coherent synchrotron oscillation with frequency ω_s and amplitude $\hat{\tau}$ with bunch current $I = \frac{Ne\omega_0}{2\pi}$ and Gaussian bunch length σ_0 into account, we arrive at [5, p. 264ff]:

$$\mathcal{F}(\omega) = I \sum_{p,m=-\infty}^{\infty} j^{-m} J_m(p\omega_0\hat{\tau})\delta(\Omega) e^{\frac{-(p\omega_0\sigma_0)^2}{2}} \qquad (3)$$

$\Omega = \omega - p\omega_0 + m\omega_s$ leads to the known revolution harmonics. Additionally, every harmonic has satellites spaced by ω_s, where the m-th satellite has a spectral amplitude corresponding to the Bessel function of order m: $J_m(p\omega_0\hat{\tau})$. By having no coherent synchrotron oscillation ($\hat{\tau} = 0$), the satellites vanish. In a multi-bunch fill, due to non-uniform bunch currents, additional amplified harmonics of the bunch spacing appear.

The amplification of the frequencies corresponding to the repetition rate of the emitting particles is called superradiant and has been observed before [6]. Additionally its potential for spectroscopy has been shown recently [7, 8].

In this paper we present a method, how to deal with aliasing when analyzing heterodyne measurements, and how specific superradiant frequencies can be created by adjusting the filling of the bunch train.

MEASUREMENT SETUP

To increase the emitted THz radiation, ANKA is operated in the low-alpha mode, where the momentum com-

Content from this work may be used under the terms of the CC BY 3.0 licence (© 2015). Any distribution of this work must maintain attribution to the author(s), title of the work, publisher, and DOI.

ISBN: 978-3-95450-168-7 doi:10.18429/JACoW-IPAC2015-TUPWA044

Content from this work may be used under the terms of the CC BY 3.0 licence (© 2015). Any distribution of this work must maintain attribution to the author(s), title of the work, publisher, and DOI.

TEST ELECTRON SOURCE FOR INCREASED BRIGHTNESS EMISSION BY NEAR BAND GAP PHOTOEMISSION*

S. Friederich†, K. Aulenbacher
Institut für Kernphysik, Johannes Gutenberg-Universität Mainz, D-55128 Mainz, Germany

Abstract

A new photoemissive electron source is being built in order to make use of the reduction of ensemble temperature in near band gap photoemission. It will operate at up to 200 kV bias voltage with NEA GaAs photocathodes. High bunch charges will be investigated in pulsed mode with respect to the conservation of emittances at low energy excitations. High field gradients at the cathode surface will also allow further investigation of the field emission process of these photocathodes.

INTRODUCTION

The temperature of electron ensembles emitted from NEA photocathodes, e. g. GaAs(Cs:O), is reduced if the exciting photon energy approaches the band gap of the semiconductor [1]. This promises to increase the beam brightness $\propto 1/T$. We want to explore if it is possible to exploit this phenomenon for the production of high bunch charges, which may be relevant for applications such as ERL-based light sources. In order to achieve such bunches, a high gradient, high voltage source is needed to cope with the effects of space charge in a vacuum and also internal effects, for instance photovoltage [2]. A particular challenge is that the work function of the material is extremely low (≈ 1.4 eV) - at least if GaAs is chosen as a cathode. A variable field strength in the new source will allow to investigate field emission thresholds for these low work function cathodes.

In respect of that, a new photoemission electron source is under development at the institute for nuclear physics Mainz. The bias voltage will be up to 200 kV and the accelerating field strength will reach up to 5 MV/m. A more detailed view on the design and some simulations are discussed in the following.

SOURCE DESIGN

The design of the Small Thermalized Electron source At Mainz (STEAM) is based on the photoemission electron sources used at MAMI [3] and CEBAF at Jefferson Laboratory [4]. It is illustrated in Fig. 1.

As photoemissive material a p-doped gallium arsenide (GaAs) crystal held by a molybdenum carrier called the "puck" will be used. It is coated with a thin caesium and oxygen layer which forms the negative electron affinity (NEA). The work function is reduced to ≈ 1.4 eV allowing to achieve high quantum efficiencies at low excitation energies. On the other hand, the low work function may provoke field emission if the electric field gets too high.

Inverted Insulator

In order to get a compact source, the cathode electrode holding the photoemissive material is mounted on an R30 "inverted" insulator that points directly into the source chamber. It has three advantages compared to the old insulator tubes: Its size is smaller and allows a compact design, it offers less metallic surfaces that may lead to parasitic field emission and it is cheaper because it is used commercially in the X-ray industry.

Cathode Electrode Design

The cathode electrode is made of low-permeable stainless steel 1.4429 ESU. It is mounted vertically on the insulator and holds the photocathode with the NEA GaAs, which is kept in position due to gravitation.

After exceeding its lifetime, the photocathode needs to be refreshed and for the new preparation it needs to be extracted. Therefore, the source will operate in a load-lock operation: A second chamber for the photocathode preparation will be connected to the source chamber, not affecting its ultra-high vacuum.

Elevator Construction

To provide the mechanical movements needed for cathode exchange, an elevator construction is implemented into the cathode electrode design, see Fig. 2. A rack and pinion gear that is driven by a manipulator levitates the puck inside the cathode electrode so that it can be grabbed by a "fork" mounted on a second manipulator and transferred into the preparation chamber. Using copper in combination with titanium prevents galling and reduces attrition to a minimum [5]. This elevator construction will be tested under ultra-high vacuum conditions after a bake-out procedure at 250 °C at the end of 2015. The manipulator driving the elevator is retracted from the high voltage region during operation.

Anode Design

The shape of the anode is convex in order to keep the outer field strength at the cathode electrode side low while achieving a field strength at the photocathode surface of up to 5 MV/m at a distance of 37 mm between photocathode and anode (200 kV bias). These values were simulated and optimized using CST EM Studio [6] with respect to the goal of keeping the global absolute field strength below 8 MV/m, see Fig. 3. The anode is mounted on a potential-free tube and thereby allows to measure the lost beam and field emission currents emitted from the cathode electrode

* Work supported by Federal Ministry of Education and Research under the joint project "HOPE"
† frieders@kph.uni-mainz.de

ISBN: 978-3-95450-168-7 doi:10.18429/JACoW-IPAC2015-TUPWA045

FURTHER INVESTIGATIONS ON THE MESA INJECTOR*

R. Heine†, K. Aulenbacher, S. Friederich, C. Matejcek, F. Schlander
Institut für Kernphysik, Johannes Gutenberg-Universität Mainz, Mainz, Germany

Abstract

The MESA ERL (**M**ainz **E**nergy-recovering **S**uper-conducting **A**ccelerator) to be built at Mainz in the next years is a multi turn recirculating linac with beam currents of up to 10 mA. The dynamic range of the beam currents demanded by the experiments is of at least two orders of magnitude. This is a special challenge for the layout design of the injector. In this paper we present the current status of the design of the injector linac called MAMBO (**M**illi**AM**pere **BO**oster).

INTRODUCTION

MESA will be operated in two modes: the first is the external beam (EB) mode; there the beam is dumped after being used with the external fixed target experiment P2. The current required for P2 is 150 μA with polarised electrons at 155 MeV. The second mode is energy recovery (ER). The experiment served in this mode is an (pseudo) internal fixed target experiment named MAGIX. It demands an unpolarised beam of 1 mA at 105 MeV. In a later stage the ER-mode current shall be upgraded to 10 mA.

The concept of MAMBO was presented in [1]. MAMBO consists of a low energy beam transport (LEBT) section preparing a 100 keV beam with a chopper buncher system for capture in the first linac RF-section. The electrons are provided by a 100 keV DC photo gun that is driven by a pulsed laser. Although the laser pulses will last some 200 ps, delayed emission of electrons and dark currents make a chopper system necessary to cut off tails.

The electrons are accelerated by four room temperature RF-sections to 5 MeV. The frequency is determined by the SRF structures of the main linac, which are using TESLA technology at 1.3 GHz. The normal conducting structures are bi-periodic $\pi/2$ standing wave structures. The first section is a graded-β, the 2nd section has a constant $\beta < 1$ and the last two sections are $\beta = 1$. The geometry of the cells is derived from the MAMI injector [2].

BEAM DYNAMICS

The beam dynamics was simulated with PARMELA [3]. To receive more realistic results the space charge mesh was improved to allow for a changing bunch spacing due to energy gain. Especially inside a graded-β section the distance between bunches changes from cell to cell. This was modelled by using the `continue` command followed by a `scheff` line with altered mesh data. Further the number of particles was increased to 300,000 to allow for halo effects to become visible. Also now the 3D space charge functionality of PARMELA is used.

Table 1: Bunch Data at the Start of LEBT (i) and at the Exit of MAMBO (f)

		stage -1		stage - 2
I_b	[mA]	0.15	1	10
$\Delta\phi_i$(100%)	[°]	93.6	93.6	93.6
ΔT_i(100%)	[keV]	0.002	0.13	1.1
$\Delta\phi_f$ (RMS)	[°]	0.14	0.36	1.9
ΔT_f (RMS)	[keV]	0.85	2.2	5
$\Delta T_f/T$ (RMS)	$\times 10^{-4}$	1.7	4.4	10

While arranging focussing elements, now spacial constraints, e.g. positions of flanges, are considered leading to minor alteration in their positions.

The particle distribution now used for simulation has been extracted from CST Particle Studio [4] simulations of the photo source at a given bunch length (see Table 1). The phase spaces achieved with the linac configuration meet the design goals of MAMBO stage-1 ($\Delta\varphi \leq 3°$, $\Delta T/T = O(10^{-4})$) [1]. The parameters of stage-2 will not meet these goals, since space charge forces lead to an energy blow-up right from the gun. The energy spread achieved by MAMBO at 10 mA is 10^{-3}. The most demanding experiment P2 will be satisfied with the results for 150 μA, while MAGIX, which is asking for high currents, can cope with larger energy spread, so stage-2 parameters should be acceptable. This has to be investigated within the design of the main linac.

Space charge calculations also revealed that it is not possible to accelerate 10 mA inside the first RF-section without additional focussing applied over this section. Further an increase of the beam hole diameter in the iris seems to be advantageous.

RF-DESIGN

The MAMI structure has been scaled to 1.3 GHz and some modifications have been made to increase the coupling between cells, this will provide a better field flatness. Compared to the MAMI profile the coupling slots have been moved outside, this increases the area of the slots and therefore the coupling. To close the passband gap, the radius of the coupling cells was reduced. To allow for emittance blow up due to space charge the beam pipe diameter was increased on cost of ca. 10% of shunt impedance. The alterations of MAMBO structure compared to MAMI Ilac are visible in Fig. 1.

* Work supported by the German Federal Ministry of Education and Research and German Science Foundation under the Cluster of Excellence "PRISMA"
† rheine@uni-mainz.de

Content from this work may be used under the terms of the CC BY 3.0 licence (© 2015). Any distribution of this work must maintain attribution to the author(s), title of the work, publisher, and DOI.

ISBN: 978-3-95450-168-7 doi:10.18429/JACoW-IPAC2015-TUPWA046

Content from this work may be used under the terms of the CC BY 3.0 licence (© 2015). Any distribution of this work must maintain attribution to the author(s), title of the work, publisher, and DOI.

FACILITY UPGRADE AT PITZ AND FIRST OPERATION RESULTS

A. Oppelt #, P. Boonpornprasert, A. Donat, J. Good, M. Gross, H. Huck, I. Isaev, L. Jachmann, D. K. Kalantaryan, M. Khojoyan, G. Koss, G. Kourkafas, M. Krasilnikov, W. Köhler, O. Lishilin, D. Malyutin, J. Meissner, D. Melkumyan, M. Otevrel, M. Penno, B. Petrosyan, S. Philipp, M. Pohl, Y. Renier, T. Rublack, B. Schöneich, J. Schultze, F. Stephan, F.Tonisch, G. Trowitzsch, G. Vashchenko, R.Wenndorff, DESY, Zeuthen, Germany
M. Bakr, Assiut University, Assiut, Egypt
D. Richter, HZB, Berlin, Germany
G. Asova, INRNE, Sofia, Bulgaria
C. Hernandez-Garcia, JLab, Newport News, VA 23606, USA
G. Pathak, Hamburg University, Hamburg, Germany

Abstract

The Photo Injector Test facility at DESY, Zeuthen site (PITZ), develops, optimizes and characterizes high brightness electron sources for free electron lasers like FLASH and the European XFEL.

In the last year, the PITZ facility was significantly upgraded by the installation of a new normal conducting radio-frequency (RF) gun cavity with its new waveguide system for the RF feed, which should allow stable and reliable gun operation, as required for the European XFEL. Other relevant additions include beamline modifications for improving the electron beam transport through the PITZ accelerator and preparing the installation of a plasma cell. Furthermore, the laser hutch was re-arranged in order to house an additional, new photo cathode drive laser system which will produce 3D ellipsoidal laser pulses to further improve the electron beam quality.

This paper describes the facility upgrades and reports on the first operation experience with the new gun setup.

FACILITY UPGRADE GOALS

In the past, record low emittances at different charge levels were obtained at PITZ [1]. During the last two years, the PITZ facility was then mainly devoted to the preparation of RF guns for their later operation at FLASH and the European XFEL [2], with the main focus on operational stability, which is a critical issue for these user machines.

In view of improving both, beam quality and operation reliability, the PITZ facility was upgraded in summer 2014. The upgrade was realized under three main aspects: preparations for a new laser system for further improvement of the electron beam quality, installation of a new gun cavity together with its new RF feed system for improving the operational stability, and modifications of the PITZ beamline which will be described below.

3D ELLIPSOIDAL LASER SYSTEM

While the low beam emittances reported in [1] were obtained with a flat-top temporal laser profile, the overall brightness of a photo injector can be further improved by using an ideal electron bunch profile which, according to simulations, is ellipsoidal in space and time [3]. Due to the linearization of the space charge forces, homogeneous 3D ellipsoids are the best distributions for high brightness charged beam applications [4].

Quasi-3D ellipsoidal electron bunches can be produced by a laser system delivering 3D ellipsoidal laser pulses. For PITZ, such an advanced laser system was developed at the Institute of Applied Physics in Nizhny Novgorod, in the framework of a joint German-Russian research activity* [5]. Simulations have shown that this photo cathode laser system has the potential to significantly reduce the emittance of the electron bunches generated by the PITZ photo injector, and can also reduce the sensitivity on machine parameter changes [6], thus allowing more stable and reliable operation – key requirements for single-pass FELs like FLASH and the European XFEL.

The installation of the new laser system at PITZ required a major re-arrangement of the laser hutch, which already accommodated the flat-top photo cathode laser system used for a long time at PITZ. In late autumn 2014, the 3D laser system was installed in the re-arranged laser hutch. Meanwhile, first photo electrons have been produced with the 3D ellipsoidal laser system [5]. In the near future, comparative measurements with both photo cathode laser systems (3D ellipsoidal shape vs. cylindrical shape) are planned in terms of beam quality (emittance) and robustness against machine parameter changes (jitter).

BEAMLINE MODIFICATIONS

Extensive beam dynamics simulations have accompanied the development of the 3D ellipsoidal laser

anne.oppelt@desy.de
*Work supported by the German Federal Ministry of Education and Research (BMBF), project 05K10CHE “Development and experimental test of a laser system for producing quasi 3D ellipsoidal laser pulses”, Helmholtz Joint Research Groups, project HRJRG-400 and RFBR grant 13-02-91323.

ISBN: 978-3-95450-168-7 doi:10.18429/JACoW-IPAC2015-TUPWA047

Content from this work may be used under the terms of the CC BY 3.0 licence (© 2015). Any distribution of this work must maintain attribution to the author(s), title of the work, publisher, and DOI.

FIRST RESULTS ATTAINED WITH THE QUASI 3-D ELLIPSOIDAL PHOTO CATHODE LASER PULSE SYSTEM AT THE HIGH BRIGHTNESS PHOTO INJECTOR PITZ*

T. Rublack#, J. Good, M. Khojoyan, M. Krasilnikov, F. Stephan,
DESY Zeuthen, Zeuthen, Germany,
I. Hartl, S. Schreiber, DESY Hamburg, Hamburg, Germany,
A. Andrianov, E. Gacheva, E. Khazanov, S. Mironov,
A. Potemkin, V. V. Zelenogorskii, IAP/RAS, Nizhny Novgorod, Russia
E. Syresin, JINR, Dubna, Moscow Region, Russia

Abstract

A demand on modern high brightness photo injectors required for a successful operation of linac-based free electron lasers is the possibility to generate beams with minimized beam emittance. A major way to optimize this parameter is the operation of photo cathode laser systems generating shaped laser pulses. Up to now flat-top laser pulses have been used at PITZ to achieve this goal.

As a next step in the optimization of photo injectors operated in the space charge dominated regime, the implementation of a photo cathode laser system capable to produce quasi 3-D ellipsoidal laser pulses had been considered as a result of beam dynamics simulations. That show a significant improvement in electron beam emittance compared to conventional cylindrical pulses.

The Institute of Applied Physics (IAP RAS, Nizhny Novgorod, Russia) has developed such a photocathode laser system in collaboration with the Joint Institute of Nuclear Research (JINR, Dubna, Russia) and the Photo Injector Test facility at DESY, Zeuthen site (PITZ). The laser pulse shaping is realized using spatial light modulators. The laser system is capable of pulse train generation. Just recently the delivery of the laser system and the implementation of it into the existing laser beam line at PITZ were finished. First electrons generated by the new laser system have been generated shortly after that. Although emittance measurements have not performed yet, the work presented there is a first significant step towards experimental investigation of the advantages of quasi 3-D ellipsoidal photo cathode laser pulses.

In this contribution the overall setup, working principles and the actual progress of the development as well as first results of electron beam generation will be reported.

INTRODUCTION

Ultrafast spectroscopy in the range of a few femtoseconds or even shorter as an instrument to investigate the behaviour of very fast processes, e.g. thermal excitation of molecules, has become a very popular instrument in various scientific research fields.

Wavelengths in the XUV are necessary for a lot of these experiments [1]. Such beams can be provided by linac-based Free-Electron Lasers (FELs) such as the Free-electron LASer in Hamburg (FLASH) and the European X-ray Free-Electron Laser (European XFEL).

FELs like these two operate on the basis of the Self Amplified Spontaneous Emission (SASE) process [2], which requires an extremely high space charge density of the radiating electron bunches. Therefore, requirements such as high peak current, low energy spread, and small transverse emittance of the electron beam are inevitable. The latter property cannot be improved in the linac and thus the emittance must be minimized in the photo injector.

One of the main possibilities to achieve this requirement is the shaping of the photo cathode laser pulses. By utilizing spatial cylindrical laser pulses with a temporal flat-top instead of Gaussian profile, a significant reduction of the transverse emittance of space charge dominated beams can be achieved.

While at most FELs the Gaussian laser pulse profile is used as the standard, at PITZ a flat-top temporal profile is used by default. Using this shaped laser pulses measurements of the normalized transverse projected beam, emittance between 0.7 and 0.9 mm mrad for electron beams of 1 nC bunch charge have been obtained [3].

To improve this emittance value, simulations with different kinds of laser pulse shapes were performed. As a result it could be shown by several simulations that the next step towards further reduction of the emittance is the use of 3-D ellipsoidal photo cathode laser pulses [4,5].

Laser systems capable of generating such laser pulses for trains of microbunches are currently not available. Therefore, a prototype was developed, constructed and recently installed at PITZ.

BEAM DYNAMICS SIMULATIONS

Beam dynamics simulations have been used to study the influence of different laser beam shapes on the electron beam quality. Therefore, three different types of laser shapes were investigated: 1) spatially cylindrical

*Work supported by the German Federal Ministry of education and Research, project 05K10CHE "Development and experimental test of a laser system for producing quasi 3D ellipsoidal laser pulses", Helmholtz Joint Research Groups, project HRJRG-400 and RFBR grant 13-02-91323.
#Tino.Rublack@desy.de

ISBN: 978-3-95450-168-7 doi:10.18429/JACoW-IPAC2015-TUPWA048

RADIATIVE COOLED TARGET FOR THE ILC POLARIZED POSITRON SOURCE*

A. Ushakov,† University of Hamburg, Hamburg, Germany
F. Dietrich, S. Riemann, T. Rublack, DESY, Zeuthen, Germany,
P. Sievers, CERN, Switzerland

Abstract

The target for the polarized positron source of the future International Linear Collider (ILC) is designed as wheel of 1 m diameter spinning with 2000 revolutions per minute to distribute the heat load. The target system is placed in vacuum since exit windows would not stand the load. In the current ILC design, the positron target is assumed to be water-cooled. Here, as an alternative, radiative cooling of the target has been studied. The energy deposition in the target is the input for ANSYS simulations. They include the temperature evolution as well as the corresponding thermo-mechanical stress in the target components. A principal design is suggested for further consideration.

INTRODUCTION

The ILC will provide e^+e^- collisions in the energy range from 250 to 500 GeV, upgradeable to 1 TeV [1]. The positron beam – 3×10^{10} e^+/bunch, 1312 bunches/pulse (2625 for the high luminosity option) and 5 Hz repetition rate – will be produced using the e^- beam which passes a superconducting helical undulator up to 231 meters long to generate circularly polarized photons [2]. The polarized photons hit a Titanium-alloy target located 400 m downstream the undulator to produce polarized positrons [3]. Depending on the undulator parameters, a polarization of about 30% can be achieved for the positron beam which can be enhanced up to 50% using a photon collimator [4]. The corresponding intensity reduction of the positron beam has to be compensated by a longer undulator section.

The typical total average power deposited in the positron target is about 5 kW corresponding to 1.4 MW during the pulse. This power is deposited in the 0.4 radiation length thick Ti6Al4V target ($0.4\,X_0 = 1.48$ cm). In order to distribute the heat load of the photon beam, a target wheel of radius $r = 0.5$ m is proposed. It rotates with 2000 revolutions per minute (rpm) corresponding to a rim velocity of $v = 100$ m/s. The wheel rotates in vacuum since exit windows would not stand the load. Based on first results of running a target wheel prototype [5], it is expected that the proposed water cooling will be a challenge. An alternative could be cooling by thermal radiation: the heat deposited in the Ti alloy target diffuses to a radiator filling the inner part of the wheel. This radiator is rotated and radiates the heat to a stationary cooler. It is also located in the vacuum, opposite of the radiator, and it is water-cooled.

The energy loss calculated with FLUKA Monte Carlo code [6] for the parameter set 500 GeV (high luminosity) and a collimated photon beam with $r = 1$ mm which corresponds to 50% positron polarization. The photon beam hits the target rim with 2625 bunches in a train of 961 μs duration and 5 Hz repetition rate. A photon beam power of about 80 kW is required to achieve a positron beam with 50% polarization and a bunch charge of 3.2 nC. About 4 – 5 kW is deposited in the target. The instantaneous temperature rise per bunch train in the rotating target is roughly 120 K per bunch train since the heat load is distributed on the rotating wheel rim (almost 200 K for the high luminosity option). Only after about 7.4 seconds the beam hits the same place again. The heat dissipation in the target as well as stress and deformation in the target wheel system are calculated with ANSYS [7].

RADIATIVE COOLING

Following the Stefan-Boltzmann radiation law,

$$W = \sigma\epsilon AG(T^4 - T_{\mathrm{cool}}^4)\,, \tag{1}$$

where $\sigma = 5.67 \times 10^{-8}$ W m^{2}K^4 is the Stefan-Boltzmann constant, ϵ the effective surface emissivity, A the surface area and G a geometric form factor, a radiative area $A > 1.6\,\mathrm{m}^2$ is required to remove 5 kW from the positron target assuming $\epsilon = 0.8$, $T = 250\,°$C, $T_{\mathrm{cool}} = 20°$C, $G = 1$.

Temperature Distribution in a Simplified Model

The average energy deposition in the target is 5 kW, the precise value depends on the centre-of-mass energy and the luminosity. As a first ansatz a simple model is considered: The target wheel is a full disk of thickness 1.4 cm. The rim is made of Ti6Al4V and has an emissivity of $\epsilon = 0.25$; the radiative inner part is made of copper with $\epsilon_{\mathrm{radiator}} = 0.7$. The radiation of 5.125 kW is into the environment of $T_{\mathrm{cool}} = 22\,°$C. The resulting stationary radial temperature profile is shown in Fig. 1. The thermal conductivity in Ti alloy is substantially lower than in copper so that the temperature gradient is steep. To avoid temperatures in the target rim above the recommended limits for long-term operation, the contact between target and radiator must be designed accordingly.

* Work supported by the German Federal Ministry of Education and Research, Joint Research Project R&D Accelerator "Spin Optimization", contract number 19XL7Ic4
† andriy.ushakov@desy.de

Content from this work may be used under the terms of the CC BY 3.0 licence (© 2015). Any distribution of this work must maintain attribution to the author(s), title of the work, publisher, and DOI.

ISBN: 978-3-95450-168-7 doi:10.18429/JACoW-IPAC2015-TUPWA051

ELETTRA STATUS AND FUTURE PROSPECTS

E. Karantzoulis#, A. Carniel and S. Krecic, Elettra – Sincrotrone Trieste, Italy

Abstract

The operational status of the Italian 2.4/2.0 GeV third generation light source Elettra is presented together with possible future upgrades and a vision to its future.

INTRODUCTION

Located on the outskirts of Trieste, Elettra operates for users since 1994 being the first third generation light source for soft x-rays in Europe. During those 20 years many improvements were made in order to keep the machine updated and therefore competitive with the other more recent and modern light sources already designed to operate in top-up. Following the successful set in operation of the full energy injector in 2008, Elettra established top-up operations [1] in spring 2010, although not originally designed for it. Operating in top-up proved to be and still is very beneficial for the machine [2].

Except the above mentioned big upgrades other minor ones added to the smooth and reliable operation of Elettra as reported previously [3]. At the same time studies based on various upgrade scenarios that define the upgrade Phase I are performed. This phase includes plans for upgrading the energy from 2.4 to 2.5 GeV, the possibility of decreasing the emittance [3] (in the present paper the superconducting wiggler currently in operation is taken into consideration), coupling control [4] and mainly rearranging the space for a larger short straight section to be used for additional longer insertion devices.

ELETTRA STATUS

Elettra operates 24 hours/day, seven days a week delivering more than 5000 hours/year of synchrotron light from IR to soft x-rays to 28 beam lines of which 10 are served from dipoles while 2 are in construction/conditioning using light from a superconducting [5] 49 pole 64 mm period 3.5 T wiggler. Many types of insertion devices used such as planar, Figure 8, APPLE II, electromagnetic while one beam line uses a canted set of APPLE II type undulators. The machine consists of a 100 MeV linac a 2.5 GeV booster and a 2/2.4 GeV storage ring. At about 75% of user dedicated time Elettra operates at 2 GeV while for the remaining 25% at 2.4 GeV being the only facility to operate at two energies (both in top-up). The main operating modes are multibunch with a dark gap of 42 ns and hybrid (at 20% of the total user beam time) with a single bunch in the middle of the dark gap. The operating intensities are 310 mA at 2 GeV and 160 mA at 2.4 GeV with a 5 mA single bunch added when in hybrid mode.

In Figure 1, the net availability (blue) is shown during the 3 phases of operations of Elettra; in fact before 2008 the storage ring ramped in energy, whereas after 2008 operates with a full energy injector and since 2010 in top-up. The numbers clearly show that the availability is continuously improving.

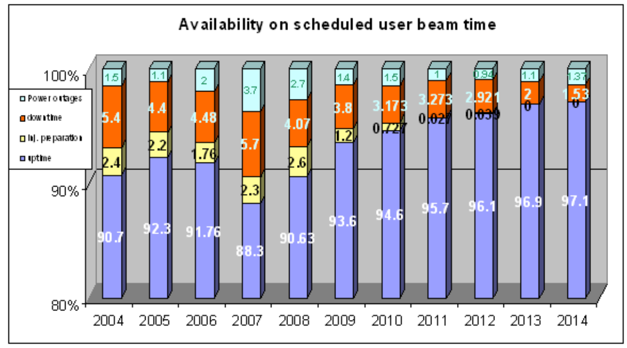

Figure 1: Availability of Elettra. The downtime is shown with red, with yellow the time lost for refilling and with light turquoise the time lost due to external electric power surges.

The downtime distribution amongst the subsystems of Elettra is shown in the next figure 2. As one can observe almost one third of the downtime is due to external electric power surges.

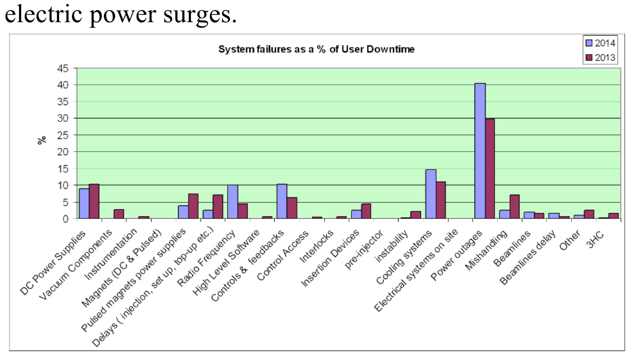

Figure 2: System failures as percent of user downtime for 2014 and 2013.

Another important number indicative of the reliability of a light source is the mean time between failures (MTBF).

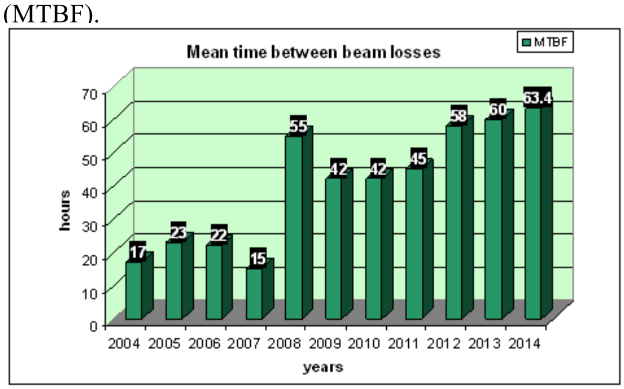

Figure 3: Mean time between beam failures.

#emanuel.karantzoulis@elettra.eu (2015)

Content from this work may be used under the terms of the CC BY 3.0 licence (© 2015). Any distribution of this work must maintain attribution to the author(s), title of the work, publisher, and DOI.

ISBN: 978-3-95450-168-7 doi:10.18429/JACoW-IPAC2015-TUPWA052

Content from this work may be used under the terms of the CC BY 3.0 licence (© 2015). Any distribution of this work must maintain attribution to the author(s), title of the work, publisher, and DOI.

ELETTRA 2.0 - THE NEXT MACHINE

E. Karantzoulis, Elettra – Sincrotrone Trieste, Italy

Abstract

A next generation light source (ULS) to replace Elettra, the third generation Italian light source is presented and discussed.

INTRODUCTION

Located on the outskirts of Trieste, Elettra operates for users since 1994 being the first third generation light source for soft x-rays in Europe. During those 20 years many improvements were made in order to keep the machine updated and competitive with the other more recent and modern light sources. Although Elettra will continue serving the scientific community for some more years, it was felt that the right time has come to prepare her successor and therefore studies were performed on this issue [1].

After the 4th generation light sources came to operation, it became evident that free electron lasers (FEL) cannot replace storage rings (SR) (therefore the term 4th generation is not reflecting the reality since each generation replaces the previous one) but rather are complementary. There are many reasons for that such as the SR high repetition rate and the fact SRs can serve a very large number of experiments whereas FELs serve only few (usually one).

SR light sources clearly cannot compete with FELs on the pulse length (ps against fs) at least at comparable intensities but there is a big margin of improvement on other beam characteristics. Already in the 90's people were speculating on diffraction limited light sources [2, 3] although the times were not yet ripe.

In general a ULS compared to a 3rd generation must have a much higher brilliance (at least one order of magnitude at low photon energies e.g. 1 keV) a high level of coherence in both planes (the 3rd generation has only high vertical coherence) smaller spot size and divergence, higher flux and variety of insertion devices.

Certainly all those beam properties, highly desirable for many experiments, have a great impact on the design and operability of those machines. Reducing the emittance by more than an order of magnitude may result in using higher gradients therefore higher chromaticities, smaller dynamic apertures and stronger non-linear effects. If on this one adds other requirements as for example installing the new machine in the same tunnel in replacement of the old one the degree of complication may increase exponentially.

REQUIREMENTS FOR ELETTRA 2.0

In a previous paper [1] an exhaustive analysis of emittances, beam sizes and free available space for realistic lattices from 4 to 9 bend achromats was made. How Elettra2.0 should be came by merging that analysis with the requirements of the users as expressed during a workshop on the Future of Elettra in April 2014 and summarized below:

- Energy 2 GeV
- Same building, same ring circumference (259-260m)
- Maintain the existing ID beam lines, same position
- Maintain the existing bending magnet beam lines
- Emittance reduction by more than 1 order of magnitude
- Electron horizontal beam size less than 60 um
- Intensity 400 mA, maintain the filling patterns as before (hybrid, single bunch etc.)
- Free space available for IDs not less than that of Elettra
- Use the existing injectors i.e. off-axis injection
- 6+6 months downtime for installation and commissioning

The above user requirements and the analysis made in [1] led us to adopt the 6-bend achromat as best solution.

ELETTRA 2.0 LATTICES

The 6-bend achromat optics, shown in Figure 1 (using OPA [4]), has an emittance of 0.25 nm-rad with WP (33.2, 9.3) and natural chromaticities (-63,-50). The corresponding horizontal beam size at the straight sections is 40 μm for the horizontal and 3 μm for the vertical one at 1% coupling (however higher coupling i.e. towards round beams to avoid resistive wall effects is preferable) and the divergence is 6 μrad. The dipoles have now a field of 0.8 T (compared with 1.2 T at 2 GeV of Elettra) and their maximum quadrupole component is 17 T/m (compared with 2.8 T/m in Elettra). The quadrupoles have a maximum gradient of 53 T/m (compared with 15 T/m in Elettra).

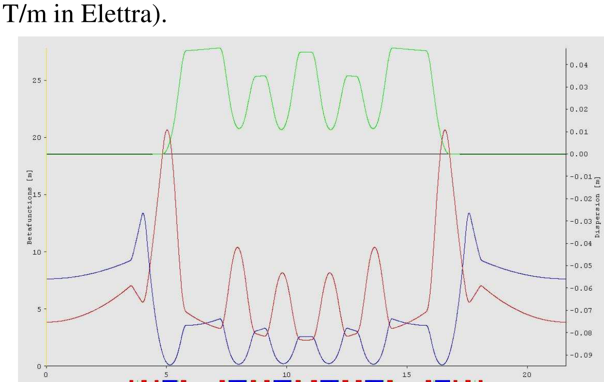

Figure 1: Elettra2.0 lattice 1.

The dispersion in the arcs is low (40 mm compared with 400 mm in Elettra) meaning that also the short straight sections (1.4 m long) situated in the arcs before the outer dipoles can be used for insertion devices with

emanuel.karantzoulis@elettra.eu (2015)

ISBN: 978-3-95450-168-7 doi:10.18429/JACoW-IPAC2015-TUPWA053

INFLUENCE OF A NON-UNIFORM LONGITUDINAL HEATING ON HIGH BRIGHTNESS ELECTRON BEAMS FOR FEL

E. Roussel*, E. Allaria, M. B. Danailov, G. De Ninno, S. Di Mitri, E. Ferrari, D. Gauthier, L. Giannessi, G. Penco, Elettra-Sincrotrone Trieste S.C.p.A., Basovizza, Italy

Abstract

Laser-heater systems are essential tools to control and optimize high-gain free electron lasers (FELs), working in the x-ray wavelength range. Indeed, these systems induce a controllable heating of the energy spread of the electron bunch. The heating allows in turn to suppress longitudinal microbunching instabilities limiting the FEL performance. In this communication, we show that a long-wavelength energy modulation of the electron beam induced by the laser heater can persist until the beam entrance in the undulators, affecting the FEL emission process. This non-uniform longitudinal heating can be exploited to investigate the electron-beam microbunching in the linac, as well as to control the FEL spectral properties. Here, we present experimental, analytical and numerical studies carried out at FERMI.

INTRODUCTION

In free electron lasers (FELs), relativistic electron bunches are used to produce intense light from the far infrared to the EUV and X-rays domain [1]. This fourth generation light-source requires electron beams of high quality with very low emittance and high peak current. The control of peak current is achieved by compressing the electron bunch through dispersive magnetic chicane along the accelerator. Many FELs have shown up a longitudinal instability growing up in these chicanes, called microbunching instability which leads to the formation of structures in the electron bunch longitudinal phase-space (in position and energy) [2]. This instability, typically driven by the coherent synchrotron radiation (CSR) and the longitudinal space charge (LSC) effect, increases the electron beam slice energy spread and can limit the FEL emission. The use of the so-called laser heater (LH) is a possible technique to control or even suppress the microbunching instability [3]. This enables to carefully adjust the slice energy spread of the electron beam.

Here we show that a modulated LH pulse can induce a controllable modulation of the slice energy spread of the electron beam, i.e. leading to a non-uniform longitudinal heating. This modulation can be sustained by the microbunching instability in the linac and so, can survive until the entrance of the electron beam in the undulators. This induced modulation allows us to investigate the microbunching instability along the accelerator. Moreover, the FERMI FEL [4, 5] is based on the high gain harmonic generation (HGHG) seeding scheme [6] and the interaction of this modulated electron beam with the seed laser can lead to the emission of multi-color FEL light.

* eleonore.roussel@elettra.eu

MODULATED LASER HEATER

The laser heater system process consists in a resonant laser-electron interaction in an undulator placed after the photoinjector [7] (Fig. 1). The FERMI LH system [8] consists of a short undulator in the middle of a chicane in which the electron beam interacts with a near infrared laser pulse. The electron beam and the laser pulse overlap both transversally and longitudinally. The modulated laser heater pulse is obtained using the chirped pulse beating technique [9]. In this technique, two copies of a chirped laser pulse interferes with one copy delayed with respect to the other. This leads to an output laser pulse with a quasi-sinusoidal modulation whose frequency is proportional to the delay. The main LH parameters are given in Table 1. The delay between the two LH pulses is equal to 28.2 ps which leads to a modulation at a beating wavelength of 32.6 μm (Fig. 2(b)).

Table 1: Main Laser Heater Parameters

Laser heater parameters	
Wavelength	780 nm
Bandwidth (FWHM)	8.4 nm
Pulse duration (FWHM)	12.9 ps
Energy	≤70 μJ
Delay between the 2 pulses	28.2 ps
Beating frequency (wavelength)	9.2 THz (32.6 μm)

NON-UNIFORM HEATING

We apply this modulated LH pulse on the electron beam. Using numerical simulations based on Genesis [10], we checked that a modulation of the energy spread is induced in the LH undulator and survives after the half-chicane of the LH section. The main parameters are given in Table 2. The average power of the laser heater used for the numerical simulation is low (below 1 MW). Indeed, the modulated region of the LH pulse is located in the tail of the main LH pulse (Fig. 2(b)) where the intensity of the LH is weak.

In Figure 3(a), one can see that at the exit of the LH undulator, the electron beam undergoes an energy modulation at the optical wavelength (here, 780 nm) but also an energy spread modulation at the beating wavelength of the LH pulse (here, 32.6 μm). However, the principle of the LH is to induce a controllable increase of the slice energy spread of the beam without modulation of the beam. In that purpose, the half-chicane of the LH is designed to smear out the modulation at 780 nm. By applying the transport matrix R corresponding to the half-chicane, we verified that the energy modulation is suppressed but the energy spread modulation is conserved

Content from this work may be used under the terms of the CC BY 3.0 licence (© 2015). Any distribution of this work must maintain attribution to the author(s), title of the work, publisher, and DOI.

ISBN: 978-3-95450-168-7 doi:10.18429/JACoW-IPAC2015-TUPWA054

THE FERMI SEEDED FEL FACILITY: OPERATIONAL EXPERIENCE AND FUTURE PERSPECTIVES

Michele Svandrlik#, Enrico Allaria, Laura Badano, Filippo Bencivenga, Carlo Callegari, Flavio Capotondi, Davide Castronovo, Paolo Cinquegrana, Marcello Coreno, Riccardo Cucini, Ivan Cudin, Miltcho B. Danailov, Gerardo D'Auria, Raffaele De Monte, Giovanni De Ninno, Paolo Delgiusto, Alexander Demidovich, Simone Di Mitri, Bruno Diviacco, Alessandro Fabris, Riccardo Fabris, William M. Fawley, Mario Ferianis, Eugenio Ferrari, Paola Finetti, Paolo Furlan Radivo, Giulio Gaio, David Gauthier, Federico Gelmetti, Luca Giannessi, Fatma Iazzourene, Maya Kiskinova, Stefano Krecic, Marco Lonza, Nicola Mahne, Claudio Masciovecchio, Massimo Milloch, Fulvio Parmigiani, Giuseppe Penco, Lorenzo Pivetta, Oksana Plekan, Mauro Predonzani, Emiliano Principi, Lorenzo Raimondi, Primoz Rebernik Ribic, Fabio Rossi, Eléonore Roussel, Luca Rumiz, Claudio Scafuri, Claudio Serpico, Paolo Sigalotti, Cristian Svetina, Mauro Trovò, Alessandro Vascotto, Marco Veronese, Roberto Visintini, Dino Zangrando, Marco Zangrando
Elettra, Trieste, Italy

Abstract

FERMI is the seeded FEL user facility in Trieste, Italy, producing photons from the VUV to the soft X-rays with a high degree of coherence and spectral stability. Both FEL lines, FEL-1 and FEL-2, are now available for users, down to the shortest wavelength of 4 nm. We will report on the completion of the commissioning of the high energy FEL line, FEL-2, and on the operational experience for users, in particular those requiring specific FEL configurations, like two-colour experiments. We will also give a perspective on the improvements and upgrades which have been triggered by our experience and are aiming to maintain as well as to constantly improve the performance of the facility for our user community.

INTRODUCTION

FERMI [1] has been operating for external users since December 2012, on the VUV to EUV FEL-1 line, covering photon energies between 12 eV and 62 eV [2]. High degree of longitudinal and transverse coherence, tunability, spectral stability with pulses close to the Fourier limit, very low time jitter synchronization to an optical pump laser are among the distinguishing features that make this facility very attractive for the scientific community. The capability of controlling the radiation polarization is another of the unique characteristics of FERMI; a characterization of the degree of polarization in various configurations has recently been reported in [3].

The EUV to soft X-rays photon energy range is covered by the FEL-2 line (62 eV to 310 eV). As a very important milestone, in September 2014 the energy per pulse reached the nominal expected intensity, 10 μJ at 4 nm, the shortest wavelength. The spectral quality and operability characteristics of FEL-2 are similar to those typical of FEL-1, even if an upgrade program has been started to guarantee the same robustness, reliability and flexibility that the user community experiences on FEL-1.

#michele.svandrlik@elettra.eu

Three beamlines, each equipped with an experimental station, are now opened for users: Diffraction and Projection Imaging (DiProI), Elastic and Inelastic Scattering TIMEX (EIS-TIMEX), Low Density Matter (LDM). Three more will be available for users in 2016.

FEL-2 COMMISSIONING RESULTS

In order to efficiently seed the electron beam at short wavelengths, FEL-2 is based on a double stage cascaded HGHG scheme. The external laser seeds the 1st stage that consists of a modulator and a two sections radiator; the photon pulse generated in the 1st stage seeds the 2nd stage, made by a second modulator and a six sections radiator. The magnetic chicane after the 1st stage delays the electron beam with respect to the photon pulse, to shift the seed generated in the 1st stage onto fresh electrons.

First lasing of FEL-2 was successfully demonstrated in October 2012 at 14.4 nm [4]. The performance of FEL-2 was then progressively optimized and extended to shorter wavelengths until in September 2014, finally, nominal operating conditions were attained at the lower edge of the wavelength range of FEL-2, namely 4.0 nm [5]. Main parameters for FEL-2 are listed in Table 1.

Table 1: FEL-2 Main Parameters

Parameter	**Value**
Beam Energy (GeV)	1.0 - 1.5
Peak Current (A)	700 - 800
Repetition Rate (Hz)	10 - 50
Wavelength range (nm)	20 - 4
Polarization	variable
Expected pulse length (fs)	< 100
Energy per pulse (μJ)	up to 100 (~10, 4 nm)
Typical rel. bandwidth % rms	~0.03 (~0.07, 4 nm)
Shot to shot stability % rms	~25% (~ 40%, 4 nm)

This result was achieved after an accurate machine optimization, by setting the peak bunch current to 700 A, the beam energy at 1.5 GeV, keeping the emittance around 1.5 mm mrad for a properly matched beam at the

Content from this work may be used under the terms of the CC BY 3.0 licence (© 2015). Any distribution of this work must maintain attribution to the author(s), title of the work, publisher, and DOI.

ISBN: 978-3-95450-168-7 doi:10.18429/JACoW-IPAC2015-TUPWA055

Content from this work may be used under the terms of the CC BY 3.0 licence (© 2015). Any distribution of this work must maintain attribution to the author(s), title of the work, publisher, and DOI.

DAΦNE GAMMA-RAY FACTORY

D. Alesini, S. Guiducci, C. Milardi, A. Variola, M. Zobov (INFN/LNF, Frascati, Rome, Italy);
I. Chaikovska, F. Zomer (LAL, Orsay, France)

Abstract

Gamma ray sources with high flux and spectral densities are the main requirements for new nuclear physics experiments to be performed in several worldwide laboratories with dedicated facilities. The paper is focalized on a proposal of experiment on γ photons production using Compton collisions between the DAΦNE electron beam and a high average power laser pulse, amplified in a Fabry-Pérot optical resonator. The calculations show that the resulting γ beam source has extremely interesting properties in terms of spectral density, energy spread and γ flux comparable (and even better) with the last generation γ sources. The energy of the γ beam depends on the adopted laser wavelength and can be tuned changing the energy of the electron ring. In particular we have analyzed the case of a γ factory tunable in the 2-9 MeV range. The main parameters of this new facility are presented and the perturbation on the transverse and longitudinal electron beam dynamics is discussed. A preliminary accelerator layout to allow experiments with the γ beam is presented with a first design of the accelerator optics.

INTRODUCTION

Many projects worldwide, based on Compton back-scattering between electron bunches and counter propagating laser pulses, are aimed to generate γ photons with high flux and high spectral densities [1-5].

For this purpose it is necessary both to increase the number of electron-photon collisions and to control the electron and laser beam qualities. In normal conducting photo-injectors [6] the maximum repetition rate of the collisions cannot exceed few kHz and also the bunch charge cannot overcome few hundred of pC to preserve good beam quality. On the other hand, due to the very good beam emittance, it is possible to strongly focalize the beam at the interaction point (IP). Then colliding lasers with a high energy per pulse and low repetition rate are required [3-4]. High flux and high spectral densities can be also obtained using storage ring and high rep. rate laser. The aim of the proposal [7] presented in this paper is to create such a source using the DAΦNE stored electron beam colliding with a laser beam amplified in a Fabry-Perot Cavity (FPC) similar to the one designed and fabricated at LAL Orsay, and used in the ATF experiment [8].

DAΦNE is an e+e- collider operating at the energy of Φ-resonance (1.02 GeV c.m.) [9]. Few machine parameters [10,11], are summarized in Table I. As discussed in the paper, the extremely high current storable in the electron ring and the achievable beam emittance, allow reaching excellent γ-beam qualities comparable (and even better) with those of the new generation sources. Moreover, with a proper choice of the machine parameters, the interval between two consecutive collisions of an electron with a photon can be much longer than the damping time of the machine and the beam dynamics is completely dominated by the dynamics of the electron ring without the laser.

Table I: DAΦNE Parameters

Energy	E [MeV]	510
Machine length	L [m]	97.6
Max. stored current	I_{MAX} [A]	2.5 (e- ring)
RF frequency	f_{RF} [MHz]	368.67
Max RF voltage	V_{RF_MAX}[kV]	250
Harmonic number	h_N	120
Min.bunch spacing	T_B[ns]	2.7 (=1/f_{RF})
Hor. emittance	ε_x [mm mrad]	0.250
Coupling	$coupl=\varepsilon_y/\varepsilon_x$ [%]	<0.5
Bunch length	σ_t [ps]	40-60
Energy spread	ΔE/E [%]	0.04-0.06
Long. Damp. time	τ_{damp} [ms]	17

COLLISION SCHEME AND RESULTS

Compton sources can be considered as electron-photon colliders. For a generic γ-source there are four important quantities that characterize the source: the total number of scattered photons per second over the 4π solid angle, the rms source bandwidth (BW), the number of photons per second in the bandwidth and the spectral density. These quantities can be calculated with simple formulas that can be found in [4,7,12-15].

A simple sketch of the interaction region is given in Fig. 1.

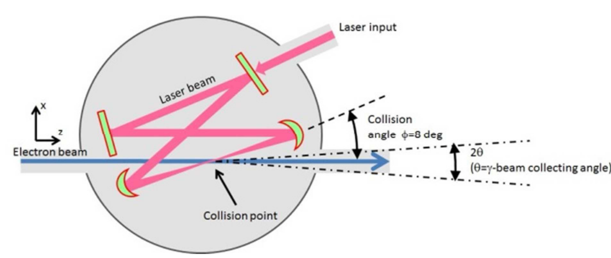

Figure 1: Simple sketch of the interaction region.

Since, in the DAΦNE ring, the coupling can be small (typically <1%) we have considered, at the IP, the case of a flat electron beam and a round laser beam with equal vertical dimensions. It is easy to demonstrate [7] that, to have an equal contribution of the electron beam emittance to the γ final energy spread in both horizontal and vertical planes, the ratio of the β-functions β_y/β_x at the IP has to be equal to the machine coupling. The results of the calculations are given in Fig. 2-3 where few important γ-source parameters have been plotted as a function of the

ISBN: 978-3-95450-168-7 doi:10.18429/JACoW-IPAC2015-TUPWA056

Content from this work may be used under the terms of the CC BY 3.0 licence (© 2015). Any distribution of this work must maintain attribution to the author(s), title of the work, publisher, and DOI.

NEW GUN IMPLEMENTATION AND PERFORMANCE OF THE DAΦNE LINAC

Bruno Buonomo, Luca Gennaro Foggetta, Graziano Piermarini, INFN/LNF, Frascati (Roma), Italy

Abstract

A new electron gun system has been developed for the DAΦNE LINAC, and put into operation since January 2014. Several elements of the system were upgraded, including a new grid pulser, an improved bias voltage system and a renewed cathode socket.

The new LINAC gun has now a wider range of parameters, i.e. the emission pulse length spans from 1.4 ns up to 40 ns, while the better control of the grid and bias voltage allows a maximum peak current of 5 A with a pulse repetition rate of 50 Hz. This paper describes the details of the pulser, the power supply, the socket, all the service components of the upgraded gun and its integration in the main LINAC control system. A report on the performance of the LINAC with the new gun will follow.

INTRODUCTION

The injector of the DAΦNE accelerator complex is an S band (2856 MHz) LINAC that alternately produces and accelerates the electron and positron beams up to the collider operation energy of 510 MeV. Before injection into the Main Rings the beams are stored into the Accumulator ring for phase space damping. The LINAC has been designed, built, and installed by TITAN BETA (USA); the system checking has been done jointly by TITAN BETA and LNF personnel, while the commissioning with both beams has been entirely performed by the LNF staff. The commissioning phase started on April 1996 and was concluded on February 1997.

Since November 2002 the LINAC also delivers beam to Beam Test Facility (BTF)[1] at a maximum repetition rate of 50 Hz: electrons with energy up to 750 MeV, with a typical current of 180 mA/pulse, or positrons with energy up to 510 MeV, with a typical current of 85 mA/pulse. The Beam Test Facility (BTF) is a beam transfer line optimized to produce single electrons and positrons mainly for high-energy detectors calibration in the energy range between 25 MeV and the maximum LINAC energy, and can provide beam in a very wide range of intensities, up to 10^{10} electrons/pulse.

LINAC GUN DESCRIPTION AND PARAMETERS

The electron source consists of a gridded electron gun with replaceable cathode, high voltage deck 150 kV power supply, isolation transformer and sufficient corona shielding to be processed up to full voltage in air.

The deck contains all the necessary electronics to operate the electron gun, and includes fiber optical links to the low level control chassis. Typical operation values are 6 A 120 kV in the positron mode, and 0.5 A 120 kV in the electron one. In normal operation (DAΦNE injection at 510 MeV) the gun is pulsed at 50 Hz with a rectangular waveform of 10 ns.

Up to this date, two different type of cathode grid assembly (HWEG-1227[2] and EIMAC Y796[3]) have been used to provide electron/positron beams during the DAΦNE LINAC operation. The difference between the two types is the size and current capabilities of the planar cathodes. The main specifications of the EIMAC Y796 installed in May 2010 are summarized in Table 1.

Table1: Cathode Grid Assembly Data Sheet

Conflat Size	3-3/8"
Grid-Cathode Spacing (DGK)	170 microns (cold)
Emission, typical	12 A @ Ec=100V
Cathode Area	2.0 cm²
Cathode Heater Voltage	6.0/7.5 V
Cathode Heater Current, typ.	5.8 A @ 6.0 V
Cathode Type	Planar Dispenser

UPGRADE OF ELECTRON GUN

In order to increase the efficiency of the DAΦNE LINAC, a complete upgrade of the electronic control chassis of the electron gun has been performed, starting in January 2014.

A new socket cathode has been installed to obtain the best electrical connection between the high voltage deck and cathode (see Figure 1).

Inside the isolated high voltage station, the old custom TITAN BETA electronics has been replaced, and the new gun electronics (grid pulser and multiple outputs DC Power Supply System) was installed (see Figure 2).

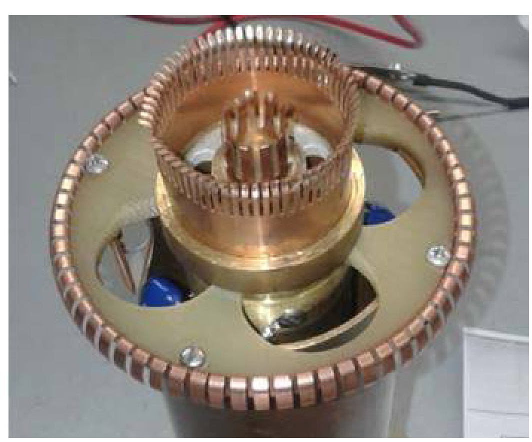

Figure 1: New cathode socket.

ISBN: 978-3-95450-168-7 doi:10.18429/JACoW-IPAC2015-TUPWA057

DAΦNE LINAC: BEAM DIAGNOSTICS AND OUTLINE OF THE LAST IMPROVEMENTS

Bruno Buonomo, Luca Gennaro Foggetta, INFN/LNF, Frascati (Rome), Italy

Abstract

The LINAC of the DAΦNE complex is in operation since 1996, both as injector of the e^+ e^- Φ-factory, and, since 2003, for the extraction of electron beam to the Beam Test Facility. In the last years, many improvements have been developed in different sub-systems of the LINAC, aiming at a wider, tuneable range of beam parameters, in particular the pulse time width and the pulse charge. A long term measurement campaign has been recently started to characterize the LINAC performance after that many sub-systems has been overhauled and improved, starting from RF power (i.e. klystron substitution, modulator renewal, RF driver layout, SLED tuning) as well as the timing system, magnets, cooling, vacuum, control system and energy/position diagnostics. This work reports the latest results on the optimization of the fully consolidated system.

LINAC DESCRIPTION

The electron-positron LINAC of the DAΦNE collider complex is a ~60 m long, S-band (2856 MHz) linear accelerator, and has been in operation since 1997. It includes a thermionic gun[1], four 45 MW SLEDed klystrons (Thales TH-2128C) and 15, 3 m long travelling-wave accelerating sections[2].

With reference to figure 1, it is possible to see that three of the klystrons have exactly the same configuration consisting of an evacuated rectangular waveguide network with three 3 dB splitters arranged in order to divide the klystron power into four equal parts, feeding each one an accelerating section. The fourth klystron has a different configuration: half the power is sent to the capture section (CS), the first section downstream the positron converter (PC), while the second half is equally divided between two branches feeding the accelerating section P1 the first one, the prebuncher, the buncher and the accelerating section E1 the second one.

All the 15 accelerating sections (E1-E5, CS, P1-P9) are of the same type: the well known 3 m long, 2/3 π travelling wave, constant gradient, SLAC design structures. In our configuration, with 45 MW coming out the klystron, the nominal accelerating component of the electric field is 24 MV/m in the CS and 18 MV/m in the remaining accelerating sections.

The phase adjustments between the sections are performed by means of low power 360° phase shifters upstream the RF amplifiers of each klystron, and by a high power 360° phase shifter that uncouples the CS from E1. The relative phasing between accelerating sections belonging to the same klystron network were regulated once and for all by properly adjusting the rectangular waveguides upstream the section inputs.

The above described configuration allows changing arbitrarily the phase of the CS with respect to E5, and this is an important feature in the positron mode of operation.

The four modulators are able to produce a pulse of 4.5 µs flat top with a repetition rate at 50 Hz, with a HV power supply with resonant circuit charging the pulse forming network (PFN), composed by 9 LC cells up to 50 kV, and a switching thyratron (type EEV CX2168).

The positron converter subsystem is based on the SLAC scheme. The conversion is obtained by interposing to the electron beam a metallic target and collecting the produced positrons by a flux concentrator jointly with DC solenoid magnets, generating a 5 T peak magnetic field. The system allows the choice of three different targets, with thickness varying around 2 radiation lengths, built with an alloy of 75% of tungsten and 25% of rhenium. A remotely controlled actuator permits to extract the target from the beam path during the electron mode of operation.

The focusing system is configured according to the requirements of the interested LINAC portion. An easy way to describe this system is to follow a particle beam from the gun to the LINAC end. The first coil that the beam finds is the bucking coil, used for reducing the presence of magnetic field in the gun cathode region, followed by a 'thin lens' with a solenoid driving the beam to the pre-buncher. The pre-buncher, buncher and the accelerating section E1 are immersed in a solenoidal field produced by 14 Helmholtz coils. A quadrupole doublet between E1 and E2 allows matching between the solenoidal focusing system with the FODO that transports the beam to the positron converter.

The FODO is composed by two quadrupoles per each of the four accelerating sections (E1-E4). A high gradient quadrupole triplet upstream the positron converter is used for focusing the beam into a 1 mm (RMS) radius spot on the converter target. The focusing system on the positron converter area and on the accelerating sections CS and P1 has been already described.

Downstream this part is placed the positron/electron separator which, in the positron mode, separates secondary positrons and electrons in 2 different paths and eliminates the electrons by means of a beam stopper. In the remaining part of the LINAC, from section P2 to P9, a FODO, composed by 26 quadrupoles with steps tapered according to the beam energy, completes the focusing scheme.

A network of vertical and horizontal correctors, in general a couple on each of the accelerating sections, is used for LINAC orbit correction.

Content from this work may be used under the terms of the CC BY 3.0 licence (© 2015). Any distribution of this work must maintain attribution to the author(s), title of the work, publisher, and DOI.

ISBN: 978-3-95450-168-7 doi:10.18429/JACoW-IPAC2015-TUPWA058

STUDY OF A C-BAND HARMONIC RF SYSTEM TO OPTIMIZE THE RF BUNCH COMPRESSION PROCESS OF THE SPARC BEAM

D.Alesini, M. Bellaveglia, M. Ferrario, A. Gallo, INFN LNF, Frascati, Italy
A. Bacci, M. Rossetti Conti, V. Petrillo, A.R. Rossi, L. Serafini, INFN sez. Milano, Milano, Italy
F. Cardelli, L. Piersanti, INFN sez. Roma1, Roma, Italy
B. Marchetti, DESY, Hamburg, Germany

Abstract

The SPARC linac at the INFN Frascati Labs is a high brilliance electron source with a wide scientific program including production of THz and Thomson backscattering radiation, FEL studies and plasma wave acceleration experiments. The linac is based on S-band RF and consists in an RF Gun followed by 3 accelerating structures, while an energy upgrade based on 2 C-band accelerating structures is ready to be implemented. Short bunches are ordinarily produced by using the linear RF bunch compression concept. A harmonic RF structure interposed between the Gun and the 1st accelerating structure can be used to optimize the RF compression by a longitudinal phase space pre-correction, allowing to reach shorter bunches, a much more uniform current distribution and in general to control better the whole compression process. Here we report the results of numerical studies on the SPARC bunch compression optimization through the use of a harmonic cavity, and the design of a C-band RF system to implement it. The proposed system consists in a multi-cell SW cavity powered by a moderate portion of the total RF power spilled from the C-band power plant already installed for the linac energy upgrade.

INTRODUCTION

The SPARC_LAB [1,2] linac at the INFN Frascati Lab produces high brightness electron beams by means of the Velocity Bunching (VB) [3], a technique that preserves the low emittance value shown by the beam at the photo-injector GUN exit [4,5,6].

In the last few years the worldwide interest in high brightness electron beams moved towards very low charge ($0.5 - 20\ pC$) ultra-short bunches. This interest is aimed at performing experiments like single spike X-ray Free Electron Laser (XFELs) [7,8], Plasma Wake Field Acceleration (PWFA) [9] and Laser Wake Field Acceleration (LWFA). To satisfy the request of ultra-short, high quality bunches, the VB process can be improved by adding a High Harmonic Cavity (HHC) to pre-correct the bunch Longitudinal Phase Space (LPS) to shorten and flatter the charge distribution. The HHC is also an additional tool to shape the beam in peculiar configurations, such as comb-like distributions [10].

The LPS pre-correction scheme in the Magnetic Bunch Compressors (MBCs) is already well known [11] and the nonlinear term in the beam LPS coming from the curvature (second-order term) of the accelerating RF can be fully compensated by a decelerating HHC. The required correction field to compensate the curvature of the main accelerating RF is given by:

$$V_h \cos\phi_h = -V_{acc} \cos\phi_{acc} / n^2 \quad (1)$$

where V_h, V_{acc} and ϕ_h, ϕ_{acc} are the amplitudes and phases of the harmonic and accelerating voltages respectively, and $n = f_h / f_{acc}$ is the harmonic number. According to Eq. 1 the larger the harmonic number, the lower the beam deceleration required for LPS linearization. At LCLS (SLAC's XFEL), a fourth harmonic of the S-band linac (2.856 GHz) is used, while at the European XFEL and FLASH (Germany) the third harmonic of the main L-band linac (1.3 GHz) is used.

The main difference between MBCs and VB pre-correction schemes is related to the space charge effects, that are negligible for MBCs while are a major issue for the VB that needs to be performed at quite low energies (4-7 MeV). The VB [3] is based on the slippage of not fully relativistic bunches on the accelerating RF wave towards the capture phase, and the bunch distribution in the LPS at the end of the process is affected not only by the RF curvature, but also by space charge effects that are damped by the energy increase but enhanced by compression. The final result is more a distortion than a simple curvature of the LPS, and cannot be easily compensated following the Eq. 1 as for the MBCs case. This difference is crucial; as a matter of fact the correction efficiency is no longer related to the harmonic order as in Eq. 1, but rather to the bunch deceleration before the injection into the first RF accelerating section downstream the Gun where VB takes place, as it is reported in the next paragraph.

SIMULATIONS

To better understand the LPS deformation due to Space Charge (SC) effects we started simulating an ideal VB compression case at SPARC using only the first two S-band accelerating cavities. We considered a large 1nC bunch charge to stress the SC effects, 10ps flat-top (no rise-time) laser pulse, at the cathode, with a uniform transverse profile of 1mm (R_{max}). The Gun was powered at 140 MV/m (6.5 MeV at the exit) and the two TW cavities respectively at 23 MV/m and 33 MV/m. The first

Content from this work may be used under the terms of the CC BY 3.0 licence (© 2015). Any distribution of this work must maintain attribution to the author(s), title of the work, publisher, and DOI.

ISBN: 978-3-95450-168-7 doi:10.18429/JACoW-IPAC2015-TUPWA059

Content from this work may be used under the terms of the CC BY 3.0 licence (© 2015). Any distribution of this work must maintain attribution to the author(s), title of the work, publisher, and DOI.

MODELING OF PHOTOEMISSION AND ELECTRON SPIN POLARIZATION FROM NEA GaAs PHOTOCATHODES*

O. Chubenko, A. Afanasev
The George Washington University, Washington, DC 20052, USA

Abstract

Many nuclear-physics and particle-physics scientific laboratories, including Thomas Jefferson National Accelerator Facility, Newport News, VA 23606 (Jefferson Lab) which studies parity violation and nucleon spin structure, require polarized electron sources. At present, photoemission from strained GaAs activated to negative electron affinity (NEA) is a main source of polarized electrons. Future experiments at advanced electron colliders will require highly efficient polarized electron beams, which sets new requirements for photocathodes in terms of high quantum efficiency (QE) ($\gg$ 1%) and spin polarization ($\approx$ 85%). Development of such materials includes modeling and design of photocathodes, material growth, fabrication of photocathodes, and photocathode testing. The purpose of the present work is to develop a semi-phenomenological model, which could predict photoemission and electron spin polarization from NEA GaAs photocathodes. Detailed Monte Carlo simulation and modeling of physical processes in photocathodes is important for optimization of their design in order to achieve high QE and reduce depolarization mechanisms. Electron-phonon interactions near the surface and influence of the presence of quantum heterostructures on the diffusion length are studied in depth. Simulation results will be compared to the experimental results obtained at Jefferson Lab and can be used to optimize the photocathode design and material growth, and thus develop high-polarization high-brightness electron source.

INTRODUCTION

For more than 50 years, photoemission from GaAs and GaAs-based photocathodes has been a main source of polarized electrons for many nuclear-physics and particle-physics facilities. Due to a large direct band gap ($E_g = 1.42eV$) and ability to achieve NEA levels (Fig. 1), GaAs can be used to emit polarized electrons efficiently. The efficiency of photocathodes is described by spin polarization, the degree to which the spin is aligned with a given direction, and QE, the ration of the number of emitted electrons to the number of incident photons.

Band model is used to describe optical transitions between valence and conduction bands (Fig. 2). Near the center of Brillouin zone (Γ point) transitions between s-type conduction band state ($l = 0$) and p-type valence band state ($l = 1$) are possible. Since $|l - s| \leq j \leq l + s$, conduction band state is doubly degenerate ($j = 1/2$; $m_j = -1/2, 1/2$). For the valence band we have a four-fold degenerate state ($j = 3/2$; $m_j = -3/2, -1/2, 1/2, 3/2$), which is separated from a doubly degenerate state ($j = 1/2$; $m_j = -1/2, 1/2$) by an energy distance $\Delta \approx 0.3eV$, spin-orbit splitting.

Taking into account four-hold degeneracy of the $j = 3/2$ state, an effective mass description of the valence band structure is commonly used. It is assumed that the valence band consists of two types of holes, the heavy holes ($m_j = \pm 3/2$) and light holes ($m_j = \pm 1/2$). So the valence band consists of three bands: heavy hole valence band, light hole valence band, and split-off valence band.

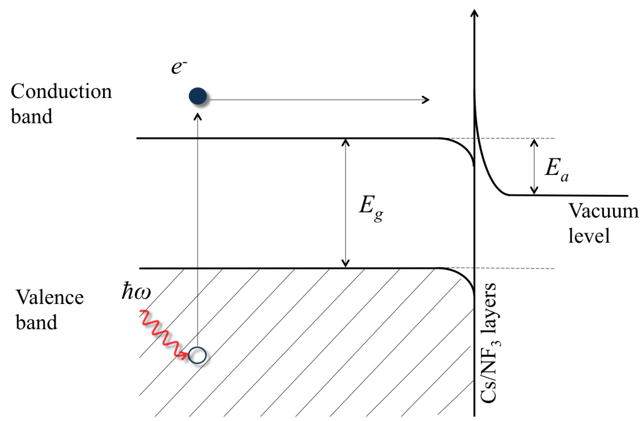

Figure 1: Photoemission from GaAs activated to NEA by putting layers of Cs and NF_3 on the surface of photocathode: photoexcitation of valence electrons into the conduction band; transport of electrons to the surface; emission of electrons into the vacuum.

When unstrained GaAs is illuminated by circularly polarized light (right-polarized, for example), two transitions from $P_{3/2}$ state are allowed, with three times as many electrons in one spin state as in the other spin state (Fig. 3). So theoretically, unstrained GaAs can provide maximum 50% polarization. But because of different depolarizing mechanisms, it is limited at about 35%.

To improve polarization, mechanical strain of GaAs crystals is used. GaAs is grown on a thick substrate, for example GaAsP, whose different lattice constant provides the crystal strain resulting in the valence band degeneracy remove. So excitation by the laser light of certain wavelength allows single transitions from the valence band states, theoretically giving 100% polarization (Fig. 4). But again, depolarizing effects decrease this value to 85%.

Alternating layers of strained GaAs form a Super Lattice (SL) structure (Fig. 5), which helps to improve both polarization and QE.

* Work supported by The George Washington University and Thomas Jefferson National Accelerator Facility

ISBN: 978-3-95450-168-7 doi:10.18429/JACoW-IPAC2015-TUPWA060

Content from this work may be used under the terms of the CC BY 3.0 licence (© 2015). Any distribution of this work must maintain attribution to the author(s), title of the work, publisher, and DOI.

DESIGN OF DIFFRACTION LIMITED LIGHT SOURCE RING WITH MULTI-BEND LATTICE ON A TORUS-KNOT

A. Miyamoto[1] and S. Sasaki[2]
1) Toshiba Corporation Power Systems Company
8, Shinsugita-cho, Isogo-ku, Yokohama, Japan
2) HSRC; Hiroshima Synchrotron Radiation Center, Hiroshima University
2-313 Kagamiyama, Higashi-Hiroshima, Japan

Abstract

We proposed a torus knot type synchrotron radiation ring in that the beam orbit does not close in one turn but closes after multiple turns around the ring. Currently, we are designing a new ring based on the shape of a (11, 3) torus knot for our future plan 'HiSOR-II.' This ring is mid-low energy light source ring with beam energy of 700 MeV.

Recently some light source rings are achieving very low emittance that reaches a diffraction limited light by adopting a multi-bend scheme to the arc section of the ring. It is not difficult for low-mid energy VUV-SX light source ring because the electron beam less than 10 nmrad can provide the diffraction limited light in the energy less than 10eV. However the multi-bend lattice has many families of the magnets, therefore it is not easy to decide the parameters of the lattice. Especially, it is difficult for the torus knot type SR ring because there is a lot of geometric limitation around the cross points of orbits. We present the details of the designing procedure and the specifications of the ultra-low emittance light source ring having innovatively odd shape.

INTRODUCTION

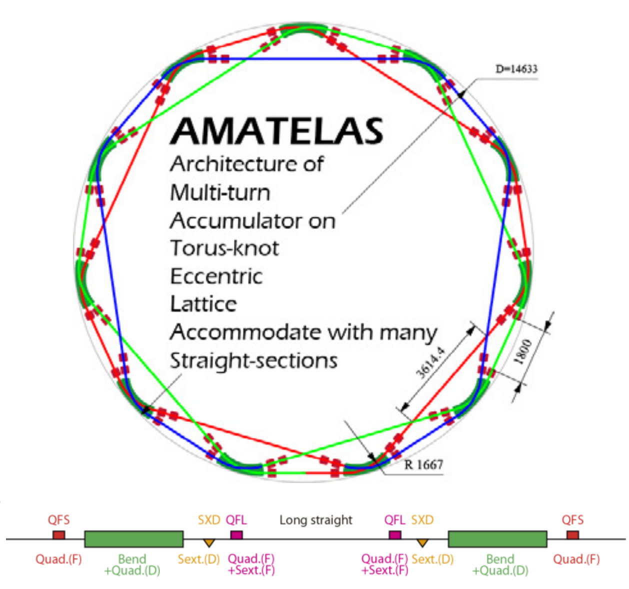

Figure 1: Schematic drawings of (11, 3) AMATELAS designed for HiSOR-II and the lattice of unit cell.

For small light source rings, it is very important to obtain a lot of straight sections in which we can install insertion devices, but it is difficult in reality because they are occupied by various magnets, RF systems or beam monitors. In this context we got a hint from the shape of the torus knot [1], and contrived the ring which had the orbit closed after multiple turns around the ring [2] and named it AMATELAS.

We are planning a new light source ring for our facility [3], therefore we are designing a new ring based on the shape of a (11, 3) torus knot for our future plan 'HiSOR-II' [4]. This ring has 11 long straight sections and we can place insertion devices efficiently by placing the elements such as quadrupole magnets near bending magnet, outside of the orbit crossing section. Furthermore, this ring has about 3 times longer closed orbit in comparison with the conventional ring, the diameter of this ring is as compact as 15 m, but its total orbit length is as long as 130 m. The (11, 3) AMATELAS designed for HiSOR-II storage ring [5] and the lattice of unit cell are shown in Figure 1, and beta or dispersion function of a unit cell is shown in Figure 2.

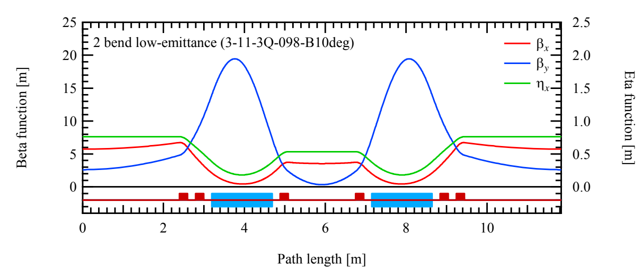

Figure 2: Optical function of (11, 3) AMATELAS for HiSOR-II storage ring.

ULTRA-LOW EMITTANCE RING WITH MULTI-BEND LATTICE

In late years, some compact light source ring achieved ultra-low emittance of several tens of nmrad. For VUV light sources, it means that it obtains the diffraction limited light to achieve such a low emittance beam. Generally, the beam emittance to obtain the diffraction limited light is given as the following.

$$\varepsilon \leq \frac{\lambda}{4\pi}$$

ISBN: 978-3-95450-168-7 doi:10.18429/JACoW-IPAC2015-TUPWA061

ANALYSES OF LIGHT'S ORBITAL ANGULAR MOMENTUM FROM HELICAL UNDULATOR HARMONICS*

S. Sasaki#, A. Miyamoto, Hiroshima Synchrotron Radiation Center, Hiroshima University, Kagamiyama, Higashi-Hiroshima, Japan
M. Hosaka, N. Yamamoto, Nagoya University Synchrotron Radiation Research Center, Chigusa-ku, Nagoya, Japan
T. Konomi, M. Katoh, UVSOR, Institute for Molecular Science, National Institutes of Nature Sciences, Okazaki, Japan

Abstract

Spiral interference patterns between two different harmonic radiations from two tandem-aligned helical undulators were observed by using a scanning fiber multi-channel spectrometer and a UV-CCD camera placed at the beamline of S1 straight section in UVSOR-III storage ring. By a series of measurements, various interference patterns such as single, double, and triple spirals were observed which concur with the theoretical predictions for every mode in the right or left circular polarization. The rotation of an interference pattern by rotating a polarizer was also observed.

INTRODUCTION

A photon beam propagating in the vacuum may carry a quantized orbital angular momentum (OAM) [1, 2]. Based on this fact, many applications in the visible wavelength regime to use light's OAM has been reported such as the manipulation of small particles [3-5], quantum entanglement [6], vector vortex coronagraph for astronomy [7], efficient mode conversion for OAM resolved spectroscopy [8], and so on. On the other hand in the shorter wavelength regime, there have been not many activities on this exotic property due to some difficulties to endow and control such a property. However, after the theoretical prediction that higher harmonic radiation from a helical undulator carries OAM was made [9, 10], this novel property attracts a great deal of attention because it may be used as a new probe for synchrotron radiation science that would be performed in a diffraction limited light source facility such as the MAX-IV, NSLS-II, or APS-II. Although the diffraction limited x-ray source does not yet exist, the first experimental evidence that the second harmonic radiation from a helical undulator carries OAM was presented by Bahrdt, *et al*. at BESSY II [11]. Successive systematic experiments have been done at the UVSOR-III. Here we present experimental results and analyses on OAM properties of undulator harmonic radiation.

EXPERIMENAL SETUP

The 750 MeV UVSOR-III is already a diffraction limited light source in the UV region. In this ring, a tandem-aligned double-APPLE undulator system similar to that in BESSY II is installed for FEL and coherent light source experiments. Using this set-up with a few reduced ring energies, we observed spiral interference patterns between two different harmonic radiations with a scanning fiber multi-channel spectrometer and a CCD camera placed at the end of BL1U Beamline. By these measurements, various interference patterns such as single, double, and triple spirals were observed which concur with the theoretical prediction for every mode in the right or left circular polarization. The rotation of an interference pattern by rotating a polarizer was also observed.

Table 1 shows the total emittance and corresponding diffraction limited wave length at each stored electron energy.

Table 1: Ring Parameters for Experiment

Ring Energy	Emittance	Diffraction Limit. Wave Length
750 MeV	17.5 nm-rad	220 nm (6 eV)
600 MeV	10.9 nm-rad	138 nm (9 eV)
500 MeV	7.6 nm-rad	100 nm (12 eV)
400 MeV	4.8 nm-rad	63 nm (20 eV)

The top view of undulator straight section of UVSOR-III ring is shown in Fig. 1.

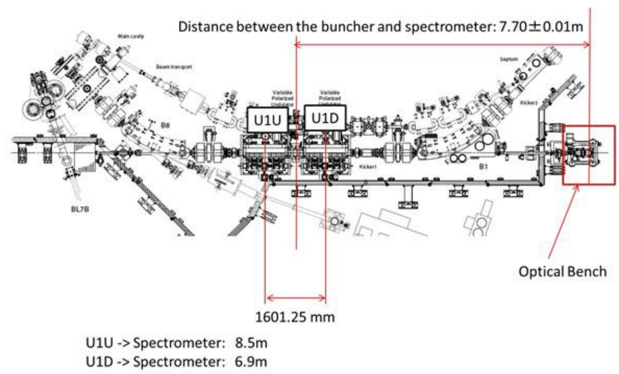

Figure 1: Top view of undulator straight section used for experiment.

Figure 2 shows a schematic view of experimental setup for the intensity distribution measurement with a

*Work supported by the Joint Studies Program (2013-) of the Institute for Molecular Science, and JSPS KAKENHI Grant #26390112.
#sasakis@hiroshima-u.ac.jp

Content from this work may be used under the terms of the CC BY 3.0 licence (© 2015). Any distribution of this work must maintain attribution to the author(s), title of the work, publisher, and DOI.

ISBN: 978-3-95450-168-7 doi:10.18429/JACoW-IPAC2015-TUPWA062

GaAs PHOTOCATHODE ACTIVATION WITH CsTe THIN FILM

Masao Kuriki[#1], Yuji Seimiya[#2], Kazuhide Uchida[#3], HU/AdSM, Higashi-Hiroshima, Japan
Shigeru Kashiwagi, Tohoku University, Sendai, Japan

Abstract

GaAs is an unique and advanced photocathode which can generate highly polarized and extremely low emittance electron beam. The photo-emission is possible up to 900nm wavelength. These advantages are due to NEA (Negative Electron Affinity) surface where the conduction band minimum is higher than the vacuum energy state. The NEA surface is artificially made with Cs-O/F evaporation on the cleaned GaAs surface, but the NEA surface is fragile, so that the emission is easily lost by poor vacuum environment and high emission density. NEA activation with any vital material is desirable. We found that the GaAs can be activated by CsTe thin film which is known as a vital photo-cathode material. The photo-electron emission spectrum extends up to 900 nm wavelength which corresponds to the band-gap energy of GaAs. The result strongly suggests that the surface becomes effectively NEA state by the CsTe thin film.

INTRODUCTION

GaAs is a III-V type semiconductor with 1.4 eV direct band gap energy at G point. Valence band electron states which have different angular momentum from -3/2 to 3/2 are degenerated. By employing circularly polarized laser light (+1 or -1 angular momentum) to excite these electron to the conduction band, one of the spin states (-1/2 or +1/2) is enhanced. By introducing special technique as strain and/or super-lattice to break the degeneration, only one spin state can be excited at the conduction band. To extract these spin-polarized electrons in the conduction band to the vacuum state, we need additional energy because the vacuum state is in higher energy state than that of the conduction band minimum in ordinal surface (PEA; Positive Electron Affinity). In contrast, NEA (Negative Electron Affinity) surface where the conduction band minimum energy is higher than that of the vacuum state, makes electron emission possible once they are excited to the conduction band. NEA surface is artificially made on p-type GaAs by adsorption Cs and O/F on the surface. Because the polarized electron excited to the conduction band is in the minimum, the emission is possible only with the NEA surface. NEA surface is however fragile, so it is easily damaged by a poor vacuum quality and particle bombardment. Therefore, the use of the NEA GaAs cathode is currently limited in a DC biased gun and it is not compatible to RF guns.

#1 mkuriki@hiroshima-u.ac.jp
#2 current affiliation is KEK, Japan.
#3 current affiliation is Cosy lab. inc.

If the NEA surface could be made on GaAs surface with a robust thin layer, it could be compatible with RF gun and use of the polarized electron beam would be widen. There was an UPS experiment suggesting that CsTe film on GaAs surface would be NEA[1]. The energy states evaluated from the experiment is shown in Fig. 1. The surface energy state of CsTe on GaAs was 3.1 eV lower than that of bare GaAs according to the experiment[1]. By assuming the work function of bare GaAs is 4.4 eV, the work function of CsTe on GaAs is expected to be 4.1 - 3.1 = 1.3 eV which is lower than the band-gap energy, 1.4 eV. This results strongly suggest that the surface is NEA, because Fermi level of p-GaAs is at the top of the valence band energy.

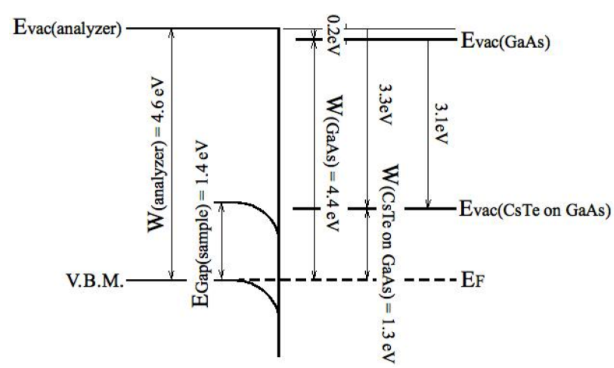

Figure 1: Energy states of CsTe film on GaAs surface. Reprinted from Ref. [1].

The surface state can be understood hetero-junction hypothesis where Fermi energy states for both materials are common. Because Fermi energy of p-GaAs is very close to the top of the valence band energy, the conduction band minimum of GaAs energy becomes higher if the work-function of the surface film f_s is lower than the band-gap energy of GaAs, E_{BG}. The condition for NEA surface is simply expressed as

$$E_{BG} - \varphi_s > 0. \quad (1)$$

In this article, we studied the photo-elelctron emission properties of CsTe-GaAs. Because Cs_2Te is known as one of reliable and robust photo-cathode material[2], NEA activation with CsTe thin film on GaAs could improve the robustness of NEA GaAs photo-cathode.

EXPERIMENT

The experiment was performed in extremely high quality vacuum environment. Zn doped GaAs wafer is placed in a vacuum chamber pumped by ion pump and NEG pump. Typical vacuum pressure during the experiment was $4.0 \times 10^{-9} \sim 2.0 \times 10^{-8}$ Pa. An evaporator

Content from this work may be used under the terms of the CC BY 3.0 licence (© 2015). Any distribution of this work must maintain attribution to the author(s), title of the work, publisher, and DOI.

ISBN: 978-3-95450-168-7 doi:10.18429/JACoW-IPAC2015-TUPWA063

Content from this work may be used under the terms of the CC BY 3.0 licence (© 2015). Any distribution of this work must maintain attribution to the author(s), title of the work, publisher, and DOI.

FEL ENHANCEMENT BY MICROBUNCH STRUCTURE MADE WITH PHASE SPACE ROTATION

M. Kuriki#, Yuji Seimiya##, HU/AdSM, Higashi-Hiroshima, Japan
R. Kato##, ISIR, Osaka U., Osaka, Japan
S. Chen, K. Ohmi, J. Urakawa, KEK, Ibaraki, Japan
S. Kashiwagi, Tohoku U., Sendai, Japan

Abstract

FEL is one of the ideal radiation source over the wide range of wavelength region with a high brightness and a high coherence. Many methods to improve FEL gain and quality have been proposed by introducing an active modulation on the bunch charge distribution. The transverse-longitudinal phase-space rotation is one of the promising method to realize the density modulation as the micro-bunch structure. Initially, a beam density modulation in the transverse direction made by mechanical slits, is properly transformed into the density modulation in the longitudinal direction by the phase-space rotation. The micro-bunch structure made with this method has a large tunability by changing the slit geometry, the beam line design, and the beam dynamics tuning. For FEL, energy chirp made by the emittance exchange should be properly corrected. Simulation results and possible applications are discussed.

INTRODUCTION

Laser light is currently widely used for not only to reveal the nature dynamics, but also various applications. Advantages of the laser light over ordinal light source are short duration and coherence. As nature of the laser light, it is almost fully coherent not only in spatial, but also in temporal. In the state of the art technology of the laser, a very short pulse in range of ps to fs is easily obtained by employing mode-lock technique. In various process observed in nature, e.g. electron, nuclear, atomic, and molecular dynamics are in the same range, i.e. from ps to fs. By using these coherence and the short duration, the laser light can be a powerful tool to study these objects. On the other hand, the available energy (wavelength) range by the laser is limited from IR to near-UV. There is a strong demand for tunable, coherent, and short pulse light source. Free Electron Laser (FEL) is one of the solution providing such light. FEL is firstly proposed by J. Madey and now several FEL in X-ray region are in operation[2][3] and construction[4]. SASE FEL is grown from a shot noise and therefore has a large fluctuation, less temporal coherence, and broaden specturm. Seeded FEL as HGHG[5], EEHG[6], etc. which introduce small power laser light to initiate the radiation process have been proposed to improve the FEL performance. More direct density modulation in the bunch intensity is possible by employing the phase-space rotation technique.

#mkuriki@hiroshima-u.ac.jp
##current affiliation is KEK, Japan.

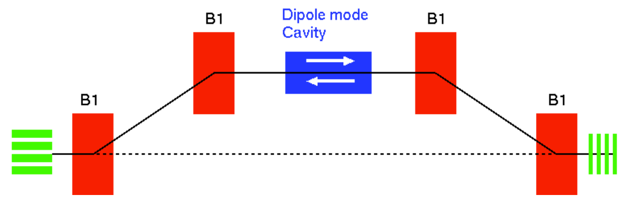

Figure 1: This is a schematic drawing of the beam line for x-z phase-space rotation which consists of one chicane and one dipole mode cavity. It converts the transversely modulated beam to the longitudinally modulated beam.

The schematic view of the beam-line to make the micro-bunch structure by the phase-space rotation is shown in Fig. 1. The beam-line consists from one chicane and one dipole mode RF cavity, such as TM_{110}. The transversely modulated beam generated by mechanical slits is converted to the longitudinally modulated beam. In general, temporal modulation such as micro-bunching can be produced by a photo-cathode with a temporal laser intensity modulation, or laser-beam interaction in undulator like the seeded FEL. It requires a state of the art of technology. On the other hand, the transverse spatial modulation can be made with the mechanical slits and ordinal beam optical components. It is therefore easily obtained. The x-z phase-space rotation give another way to produce the micro-bunching which is applicable for the seeded FEL.

The matrix representation of the beam line M_{EEX} (EEX section) is expressed as

$$M_{EEX} = M_D(\eta,\xi,L)\, M_C\, M_D(\eta,\xi,L)$$

$$= \begin{bmatrix} 0 & 0 & -L/\eta & \eta - L\xi/\eta \\ 0 & 0 & -1/\eta & -\xi/\eta \\ -\xi/\eta & \eta - L\xi/\eta & 0 & 0 \\ -1/\eta & \dfrac{-L}{\eta} & 0 & 0 \end{bmatrix} \quad (1),$$

where M_D and M_C are matrices for the dog-leg and the cavity, h is dispersion, x is momentum compaction, and L is the section length. The matrix is defined in x and z phase-space which is four dimensional in total. Here, the matching condition of the cavity strength parameter k and h given as

$$1 + \eta k = 0 \quad (2),$$

is assumed where k is defined as

ISBN: 978-3-95450-168-7 doi:10.18429/JACoW-IPAC2015-TUPWA064

STUDY OF INHERENT POTENTIAL FOR EMITTANCE REDUCTION AT THE SPRING-8 STORAGE RING

Yoshito Shimosaki #, JASRI / SPing-8, Hyogo, Japan

Abstract

A design study for an upgrade project of the SPring-8, the SPring-8-II, is in progress, which is a full-scale major lattice modification. Besides the design study for the SPring-8-II, an inherent potential of achieving much higher brilliance than that of the present SPring-8 has been explored for the general evaluation. In this paper, the evaluation of the inherent potential for the SPring-8, not for the SPring-8-II, in terms of increasing the brilliance is discussed.

INTRODUCTION

The SPring-8 storage ring is the third generation type synchrotron radiation facilities with the circumference of 1436 m in Hyogo, Japan. The basic super-period of the ring is 4, and one super-period consists of 9 unit cells, 2 matching cells and a long drift of 30 m (see Figure 1). The natural emittance for the user operation has been reduced from 6.4 nm.rad to 2.4 nm.rad, step by step [1, 2]. The present user-optics with 2.4 nm.rad was opened since 2013, which was optimized for the equilibrium emittance not to be changed drastically by the radiation excitation and the radiation damping due to insertion devices (IDs) in order to provide the stable photon-flux during the user-time [1, 2]. The top-up injection has been utilized to store the electrons of 99.5 mA with the beam energy of 7.976 GeV. The brilliant hard X-ray of the order of 10^{20} photons / sec / mm^2 / mrad^2 / 0.1 % B.W. has been provided.

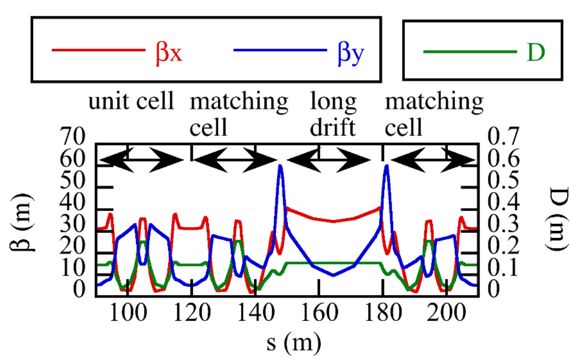

Figure 1: Lattice function of present user optics at the SPring-8 storage ring.

In order to advance promising science and to support industrial innovations, the design study for an upgrade project of the SPring-8, the SPring-8-II, is in progress [3]. In order to increase the brilliance, the electron emittance will be reduced by a multi-bend scheme [4] with a longitudinally varying dipole field [5], by a lower energy operation (6 GeV) than that of the present (8 GeV) and by utilizing a radiation damping by IDs.

Besides the design study for the future SPring-8-II, an inherent potential of achieving much higher brilliance than that of the present user optics has been explored for the SPring-8 storage ring, in order not only to provide brilliant photon beams for "current users" but also to verify a strategy of the lattice design for the SPring-8-II before switching the optics to the SPring-8-II in 2019-2020. Here, the double bend (DB) lattices have theoretically and experimentally been examined at 6 GeV and 8 GeV, and the mixture of both "DB optics" and "double bend achromat (DBA) optics with the damping wigglers" has theoretically been examined. In these designs, it is noted that magnet positions are unchanged and magnetic fields are optimized within the specifications. In this paper, the evaluation of the inherent potential for the SPring-8, not for the SPring-8-II, is presented.

OPTIMIZATION OF DB OPTICS

In general about an optics design, freedoms of the quadrupole and sextupole magnetic fields normalized by beam energy can be expanded by lowering beam energy even within the specifications of the power supplies. From this point of view, DB optics specialized particularly for increasing the brilliance, not the flux density, has been examined at 6 GeV (see Figure 2) in order to explore a potential of the SPring-8 storage ring [6].

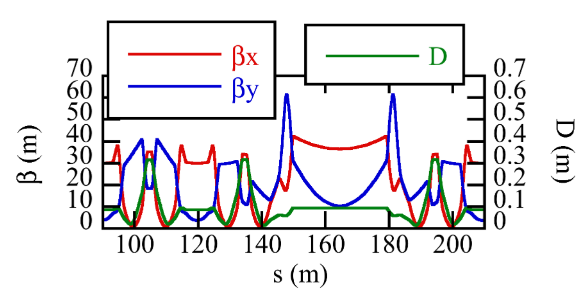

Figure 2: Lattice function of DB optics optimized for 6 GeV at the SPring-8 storage ring.

β_x, β_y and D at the ID positions in Figure 2 are optimized (1) to enhance the emittance damping by IDs, and (2) to decrease the effective photon emittance by matching between the 30 keV photon beam size and the electron beam size at the ID position. The effective photon emittance of 10 keV photon in Figure 2 (6 GeV)

#shimosaki@spring-8.or.jp

Content from this work may be used under the terms of the CC BY 3.0 licence (© 2015). Any distribution of this work must maintain attribution to the author(s), title of the work, publisher, and DOI.

ISBN: 978-3-95450-168-7 doi:10.18429/JACoW-IPAC2015-TUPWA065

Content from this work may be used under the terms of the CC BY 3.0 licence (© 2015). Any distribution of this work must maintain attribution to the author(s), title of the work, publisher, and DOI.

GENERATION OF MULTI-BUNCH BEAM WITH BEAM LOADING COMPENSATION BY USING RF AMPLITUDE MODULATION IN LASER UNDULATOR COMPACT X-RAY (LUCX)

M. Fukuda#, S. Araki, Y. Honda†, N. Terunuma†, J. Urakawa, KEK, Ibaraki, Japan
K. Sakaue, M. Washio, RISE, Tokyo, Japan

Abstract

We have been developing a compact X-ray source based on inverse Compton scattering (ICS) between an electron beam and a laser pulse stacked in an optical cavity at Laser Undulator Compact X-ray (LUCX) accelerator in KEK. The accelerator consists of a 3.6-cell photo-cathode rf-gun, a 12-cell standing wave accelerating structure and a 4-mirror planar optical cavity. Our aim is to obtain a clear X-ray image in a shorter period of times and the target flux of X-ray is $1.7\text{x}10^7$ photons/pulse with 10% bandwidth at present. To achieve this target, it is necessary to increase the intensity of an electron beam to 500 nC/pulse with 1000 bunches at 30 MeV. Presently, we have achieved the generation of 24 MeV beam with total charge of 600 nC in 1000 bunches with the bunch-by-bunch energy difference is within 1.3% peak to peak. The beam-loading has been compensated by injecting the beam before rf power has been filled (ΔT method) and by modulating the amplitude of the rf pulse. We report the results of the multi-bunch beam generation and acceleration in the LUCX accelerator.

INTRODUCTION

X-rays are applied to various area of application, such as medical application, biological science, material science etc. Synchrotron radiation which is generated by GeV order storage rings is commonly used as high brightness X-ray sources. However the rings are generally huge and expensive. On the other hand, an X-ray source based on ICS can be compact and inexpensive compared with its rings because this method can produce X-rays with the same energy by utilizing an electron beam with the lower energy by the rings about two orders of magnitude. However this method requires more development.

In order to develop a compact X-ray source based on ICS for X-ray imaging, we have constructed the LUCX accelerator at KEK. X-rays are generated by ICS between a multi-bunch electron beam with the energy of 24~40 MeV and a laser pulse with the wavelength of 1064 nm in this accelerator.

UPGRADE OF LUCX ACCELERATOR

X-ray imaging experiments have been started here since the autumn of 2011. We have succeeded to take the X-ray image of fish bone [1] so far. However, it took two hours to get this image due to low intensity of X-ray with 10^4 photons/pulse. Therefore we have upgraded this accelerator to increase the intensity of X-rays in 2012. A 3.6-cell rf-gun, a 12-cell booster and a 4-mirror planar optical cavity have been installed and commissioned. The X-ray generation and the X-ray imaging are already started after upgrade [2]. The number of bunches has been extended from 150 bunches to 1000 bunches now. Table 1 shows the present and the design parameters of an electron beam. The target intensity of X-rays is $1.7\text{x}10^7$ photons/pulse 10%b.w. at the energy of 15keV in this upgrade.

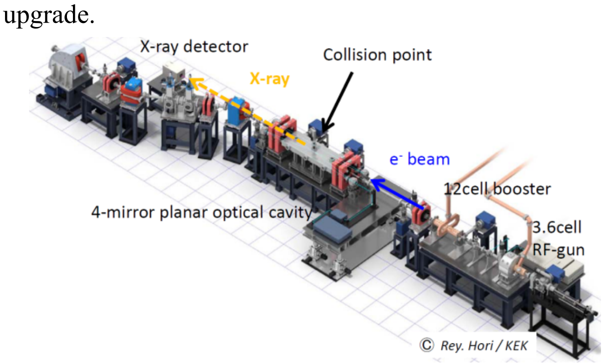

Figure 1: The beamline of the LUCX accelerator.

Table 1: Present and Design Parameters of Electron Beam

	Present	Design
Energy	24MeV	30MeV
Intensity	0.6nC/bunch	0.5nC/bunch
Number of bunch	1000	1000
Beam size (rms)	80μm x 50μm	33μm x 33μm
Pulse length(FWHM)	15ps	15ps

LUCX ACCELERATOR

The the LUCX accelerator is shown in Fig. 1. A 3.6-cell photo-cathode rf-gun generates an electron beam with the energy of 10 MeV and then the beam is accelerated to 30 MeV by a 12-cell booster. After that, the beam is collided with a laser pulse in a 4-mirror planar optical cavity and then X-rays are generated by ICS. The electron beam is separated from the X-ray by a bending magnet and then is dumped to the beam dump. The X-rays are extracted from a beamline through a Be window with the thickness of 300 μm and then detected by either a micro-channel plate (MCP) or an SOI imaging sensor [3].

#mfukuda@post.kek.jp
† Science of the Graduate University for Advanced Studies (SOKENDAI), Ibaraki, Japan

ISBN: 978-3-95450-168-7 doi:10.18429/JACoW-IPAC2015-TUPWA066

DEVELOPMENT OF A HIGH AVERAGE POWER LASER FOR HIGH BRIGHTNESS X-RAY SOURCE AND IMAGING AT cERL

A. Kosuge*, A. Akagi, Y. Honda†, S. Araki, J. Urakawa, T. Terunuma†, KEK, Oho, Tsukuba, Ibaraki
R. Nagai, T. Shizuma, M. Mori, R. Hajima, JAEA, Tokai, Naka, Ibaraki 319-1195 Japan

Abstract

High brightness X-rays via laser-Compton scattering (LCS) of laser photons stored in an optical cavity by a relativistic electron beam is useful for many scientific and industrial applications such as X-ray imaging. The construction of compact Energy Recovery Linac (cERL) is now in progress at KEK to generate low-emittance and high-current electron beams. In order to demonstrate the generation of high brightness LCS X-rays, it is necessary to develop a high average power injection laser and an optical four-mirror ring cavity with two concave mirrors which is used to produce a small spot laser beam inside the cavity. In this presentation, we will show the result of the development of the high average laser system, the LCS X-rays generation, and the X-ray imaging.

INTRODUCTION

There has been a growing interest in the laser-Compton scattering (LCS) light source. The LCS and a high average power laser with an optical cavity enables generation of monochromatic, bright and tuneable X-rays. Such a photon source is expected to bring breakthrough in fundamental researches [1], medical [2] and industrial applications [3].

The development of the Compact ERL (cERL) is ongoing at KEK to produce low emittance and high-current recirculating electron beams [4]. By combining advanced laser technology with the cERL, a high brightness LCS X-ray beam can be generated. In this paper, we will show the detailed properties of the high average laser used for the LCS X-ray generation at cERL. We will also show the results of the measurement of the LCS X-rays and the X-ray imaging.

PERFORMANCE OF THE SEED LASER SYSTEM AND THE OPTICAL CAVITY

In our experiments, we employ a commercial passively mode-locked diode pumped solid state laser system (ARGOS, Time Bandwidth Products (JDSU)). The oscillator operates at a repetition rate of f_{rep} = 162.5 MHz which has an integer relation with the fundamental RF of the cERL. This laser system delivers an average power of 45 W and pulse duration of 10 ps. The laser beam ejected from the laser system is passed through a mode matching telescope in order to match the laser beam to the cavity mode.

We employ a four-mirror cavity with two concave mirrors to produce a small spot laser beam inside a cavity. Since the LCS X-rays are generated by collision of laser photons and relativistic electrons, the laser beam is required to be well focused at the collision point where the spot size (rms) of the cERL electron beam at the experiment is about 13 - 130 μm (horizontal) and 20 - 25 μm (vertical).

The optical setup of our cavity locking laser system is shown in Fig. 1 (a). The optical cavity consists of two flat mirrors (M1 and M2) and two concave mirrors (M3 and M4). The radius of curvature of the concave mirrors which are manufactured by LMA (Laboratoire des Matériaux Avancés) is 420 mm and the reflectivity is about 99.999 %. The reflectivity of the flat mirror (M2) is 99.99 % and the input coupler mirror (M1) is 99.9 %.

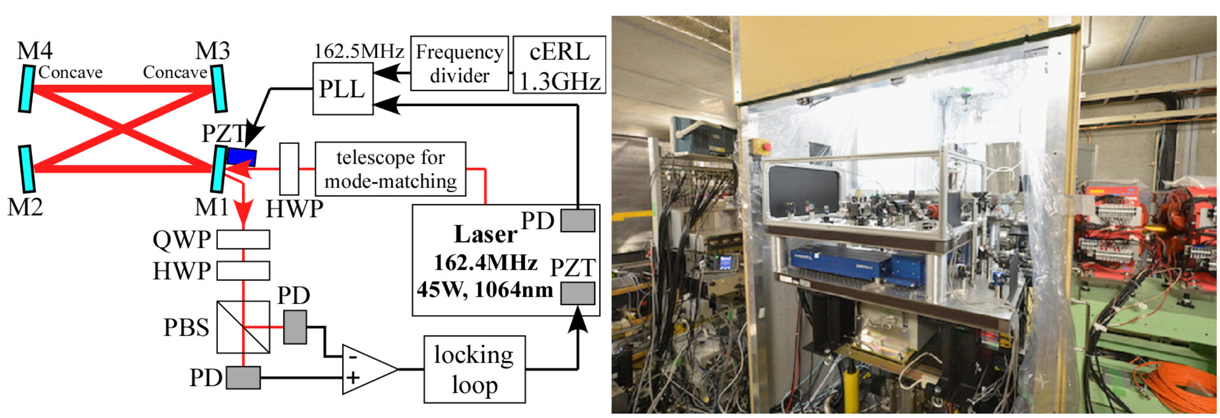

Figure 1: Schematic diagram of the optical cavity and a cavity locking loop configuration and the picture of the laser system and the optical cavity on the movable table in the cERL accelerator room.

* atsushi.kosuge@kek.jp
† Science of the Graduate University for Advanced Studies (SOKENDAI)

Content from this work may be used under the terms of the CC BY 3.0 licence (© 2015). Any distribution of this work must maintain attribution to the author(s), title of the work, publisher, and DOI.

ISBN: 978-3-95450-168-7 doi:10.18429/JACoW-IPAC2015-TUPWA067

STATUS OF HIGHER BUNCH CHARGE OPERATION IN COMPACT ERL

T. Miyajima*, Y. Honda, R. Takai, T. Obina, M. Shimada, K. Harada, M. Yamamoto, K. Umemori, H. Sakai, T. Miura, F. Qiu, N. Nakamura, S. Sakanaka
KEK, Tsukuba, Ibaraki 305-0801, Japan
N. Nishimori, R. Nagai, R. Hajima, JAEA, Tokai-mura, Ibaraki 319-1195, Japan
D. Lee, KNU, Daegu, 702-701, Korea

Abstract

In the KEK compact ERL (cERL), machine studies toward higher bunch charge operation is one of the most important issues. From January 2015 to April 2015, we carried out a higher bunch charge operation with an bunch charge of 0.5 pC for the experiment of laser compton scattering. After the study of space charge effect and optics tuning, we succeeded in the recirculation operation with the emittance, which was close to the design value. Moreover, a test operation in the injector section with the bunch charge of 7.7 pC was carried out as a preparation toward the recirculation operation with the average current of 10 mA.

INTRODUCTION

The compact ERL (cERL) is a test accelerator to demonstrate beam performance and high average current operation in an energy recovery linac. It consists of a photocathode DC gun, superconducting RF cavities, a recirculation loop, and a beam dump. The layout of the cERL is shown in Fig. 1. Since commissioning of the injector in April 2013, production and transportation of low-emittance beams have been demonstrated with several tens of fC where the space charge effect can be neglected. In the low bunch charge operation, an energy recovery operation through the recirculation loop with an average current of 6.5 μA was also demonstrated.

One of the most important issues in the cERL operation is to obtain low-emittance and short bunch, high-quality beams under the space charge effect. Since June 2013, we have been studying higher-charge operation with bunch charges of up to 7.7 pC which corresponds to a peak current of 10 mA [1]. To minimize emittance growth due to the space charge effect, we have been developing beam tuning methods.

From January 2015, we increased the maximum average current up to 100 μA [2], and carried out a higher bunch charge operation with the bunch charge of 0.5 pC for the experiment of laser compton scattering (LCS) [3,4]. In this operation, we have to control the space charge effect, because we can not neglect the effect in this bunch charge. Our goal for this operation is to achieve a recirculation without emittance growth. Moreover, we carried out a test operation in the injector section with the bunch charge of 7.7 pC to correct a numerical model for higher-charge and low energy beam. In this paper, we report optics design, tuning methods and our results from higher-charge operations of the injector and the recirculation loop.

* tsukasa@post.kek.jp

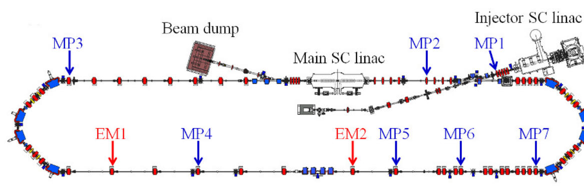

Figure 1: Layout of cERL. MP and EM indicate optics matching point and emittance measurement point, respectively.

RECIRCULATION OPERATION FOR LASER COMPTON SCATTERING

For the LCS operation, the higher bunch charge was required in order to increase the LCS signal power. However, the maximum bunch charge is limited to 77 fC for 1.3 GHz CW operation, in which the maximum average current reaches 100 μA, and it is not enough for the LCS operation. Then, we switched the repetition frequency of the gun excitation laser from 1.3 GHz to 162.5 MHz, and increased the bunch charge to 0.5 pC, in which the average current corresponded to 81μA.

Optics Design

The optics design strategy for the 0.5 pC operation is to use the same RF settings of the injector and main SC linac as the normal operation with several tens of fC to maintain the beam energy, and the same optics parameters at the exit of main SC linac in order to reduce tuning parameters. Under these conditions, we can quickly switch the operation mode from the normal mode to the higher-charge mode. For both operation modes, the beam kinetic energies at the gun, the injector and the main SC linac are 390 keV, 2.4 MeV and 19.4 MeV, respectively, and the distribution of the cathode excitation laser is a gaussian distribution with the rms length of 3 ps.

The optics for the higher-charge operation was designed by the following two steps. In the fist step, we adjusted the strengths of the two solenoid magnets in the injector section to satisfy a condition of emittance compensation. In the second step, based on these solenoid settings, we adjust quadrupole magnets between the injector and the main SC linac to satisfy a optics matching condition at the exit of the main SC linac for recirculation operation, whose values are β_x = 2.67 m, β_y = 2.12 m, α_x = −0.6 and α_y = −0.18. Figure 2 shows the design optics from the gun to the main SC linac for the 0.5 pC recirculation operation. At the exit of the main SC linac, the design horizontal and

Content from this work may be used under the terms of the CC BY 3.0 licence (© 2015). Any distribution of this work must maintain attribution to the author(s), title of the work, publisher, and DOI.

ISBN: 978-3-95450-168-7 doi:10.18429/JACoW-IPAC2015-TUPWA068

SIMULATION STUDY OF BEAM HALO AND LOSS FOR KEK COMPACT ERL

O. Tanaka#, N. Nakamura, M. Shimada, T. Miyajima, S. Sakanaka, High Energy Accelerator Research Organization (KEK), Oho 1-1, Tsukuba, Ibaraki 305-0801, Japan

Abstract

At the KEK Compact ERL (cERL) designed to operate at high-brilliance and high-current electron beams, the maximum averaged current was recorded at about 80 μA for the beam energy 20 MeV on April 2015 and should be increased up to 10 mA in a step-by-step manner in a few years. In order to increase the beam current by reducing the beam loss, we need to know the mechanism of the beam loss. For this purpose we investigate beam halo originated from characteristics and imperfections of an electron gun system, using the tracking code GPT (General Particle Tracer). The beam halo can be lost by the beam-pipe apertures and the collimators in the cERL beam line. In this paper, we will present the measurement and simulation results including the beam halo formation and the beam loss distribution along the beam line.

INTRODICTION

During the last cERL commissioning (January – April, 2015) a high repetition rate (162.5 MHz) electron beams of a 20 MeV energy were produced to test the Laser-Compton scattering (LCS) facility newly installed to the beam line [1] – [2]. Since the average current in the machine is significant (from some pA up to some μA), the beam halo management is extremely important topic for the successful operation.

The beam halo is known to be a collection of particles of any origin and behaviour which lies in the low density region of the beam distribution far away from the core [3]. The beam halo is a key parameter to be improved for any high intensity accelerator. Therefore, experimental measurements and analytical evaluation of the halo distribution are very important to understand the way to minimize the number of particles in the tail region of the beam distribution.

We assume the main reasons of the beam halo in cERL to be:

- Dark current from the gun and from accelerator cavities [4];
- Off-energy beam tails due to mis-steered beam;
- Scattering from residual gas, Touschek scattering [4];
- Beam line elements misalignment, kicks from the couplers, and so on.

The main goal of our research is to understand the beam halo formation processes and to obtain beam halo and corresponding beam loss distribution. Thus, we aim to minimize the radiation damage of the accelerator elements, to avoid emission of secondary electrons, to lower the irradiation outside the machine and nuclear activation of the transport channel, to prevent cavity's quenches, to suppress noise inside detectors, and to reduce the beam loss.

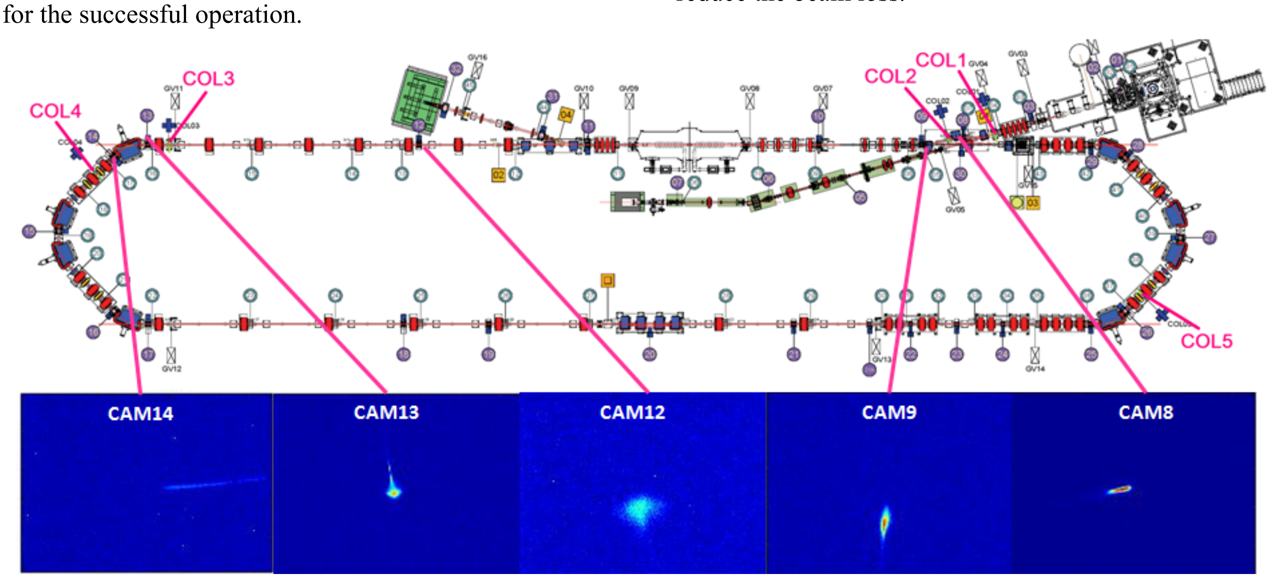

Figure 1: Layout of cERL. Collimators positions and tail profiles screen captures for laser phase +20 deg (42 ps tail).

*Work supported by the "Grant-in-Aid for Creative Scientific Research of JSPS (KAKENHI 15K04747)
#olga@post.kek.jp

Content from this work may be used under the terms of the CC BY 3.0 licence (© 2015). Any distribution of this work must maintain attribution to the author(s), title of the work, publisher, and DOI.

ISBN: 978-3-95450-168-7 doi:10.18429/JACoW-IPAC2015-TUPWA069

SIMULATION STUDY ON BUNCH COMPRESSION AND DECOMPRESSION FOR THE COMPACT ERL*

N. Nakamura, M. Shimada, T. Miyajima, K. Harada, O. A. Tanaka, S. Sakanaka,
High Energy Accelerator Research Organization (KEK), Tsukuba, Ibaraki, Japan

Abstract

We study bunch compression and decompression in the Compact Energy Recovery Linac (cERL) at KEK by using simulations to achieve an ultra-short bunch for generation of the THz coherent radiation planned for the near future. In this study, off-crest acceleration in the main superconducting linac and non-zero R_{56} optics in the two arc sections are used and sextupole magnets are introduced into the two arc sections for optimizing T_{566} of the arc sections. The results of the simulation study show that the bunch can be compressed to less than 50 fs and then almost decompressed to the initial bunch length.

INTRODUCTION

The commissioning of the entire cERL was started in December 2013 and the beam recirculation and energy recovery were achieved in February 2014[1]. In 2015, the maximum average current was recorded at about 80 μA and laser-Compton scattering X-rays was successfully generated[2]. In the next step, generation of THz coherent radiation is planned for 2015 - 2016.

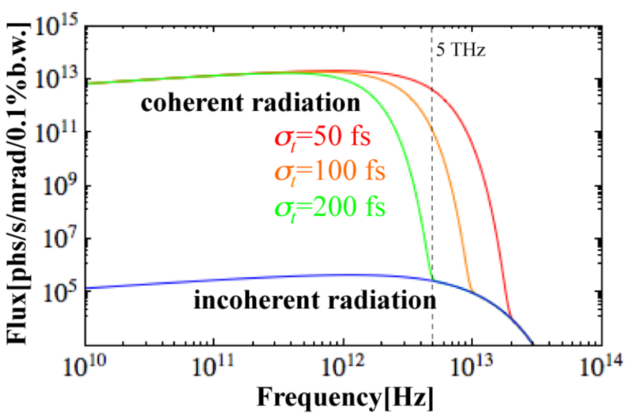

Figure 1: CSR spectra of the 20 MeV cERL for three different bunch lengths of 50, 100 and 200 fs, at the bunch charge of 7.7 pC and the bunch repetition frequency of 130 kHz.

The coherent synchrotron radiation (CSR) spectra generated at a bending magnet of the arc sections are calculated and shown in Fig. 1. An electron bunch less than 100 fs is required for providing intense THz-CSR up to 5 THz to users. We simulate bunch compression and decompression in the cERL by using a tracking code ELEGANT [3] to check the feasibility of generating such an ultra-short bunch. In the bunch compression and decompression simulation, sextupole magnets were added in the two arc sections for optimizing T_{566} of the arc sections. In this paper, we present the simulation results and requirements for the sextupole magnets including their field strengths, number and layout.

LINEAR OPTICS AND SEXTUPOLE MAGNETS OF ARC SECTIONS

Linear Optics

In the bunch compression and decompression scheme of the cERL, the bunch is accelerated off-crest in the main superconducting linac to have a correlation between the energy and longitudinal position and then the bunch length is compressed with a positive R_{56} optics of the 1st arc section. After the bunch compression, the bunch length is decompressed through the 2nd arc section with a negative R_{56} optics and then decelerated off-crest to compress the energy spread to the initial value before the beam enters the dump line. Figure 2 shows the linear optics with three different R_{56} values. The optics with R_{56}=0 is used in the normal operation and the optics with R_{56}=0.15 m and R_{56}=-0.06 m correspond to the 1st and 2nd arc sections in the bunch compression and decompression operation, respectively.

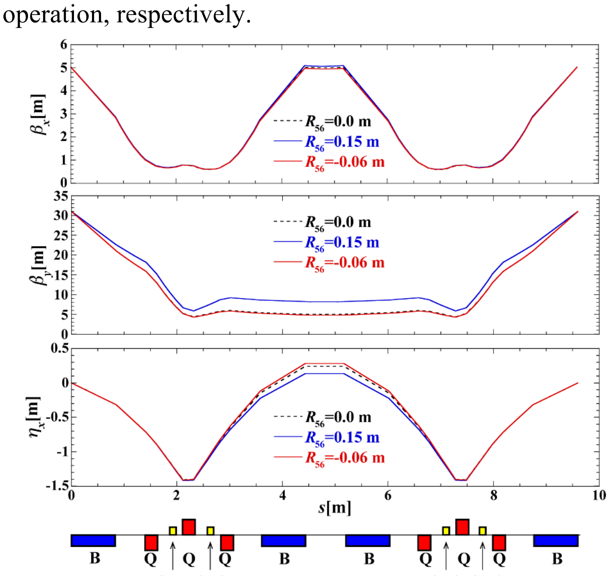

Figure 2: Horizontal and vertical betatron functions (β_x, β_y) and dispersion function (η_x) of the arc sections with three different R_{56} values of 0.0 m (black broken line), 0.15 m (blue solid line) and -0.06 m (red solid line). B, Q and SX1-4 indicate the bending, quadrupole and sextupole magnets, respectively.

*norio.nakamura@kek.jp

Content from this work may be used under the terms of the CC BY 3.0 licence (© 2015). Any distribution of this work must maintain attribution to the author(s), title of the work, publisher, and DOI.

ISBN: 978-3-95450-168-7 doi:10.18429/JACoW-IPAC2015-TUPWA070

CST SIMULATIONS OF THz CHERENKOV SMITH-PURCELL RADIATION FROM CORRUGATED CAPILLARY

K. Lekomtsev[#1,2], N. Terunuma and J. Urakawa, KEK[1], Tsukuba, Japan
A.A. Ponomarenko, A.A. Tishchenko, MEPhI[2], Moscow, Russia
P. Karataev, RHUL, Egham, UK

Abstract

Cherenkov Smith - Purcell radiation (SPR) from a corrugated channel in infinite dielectric material is simulated and compared with a theoretical investigation for such geometry. Dependencies of Cherenkov and SPR intensities on the corrugation depth and the internal radius of the channel are discussed. A corrugated capillary with partial metal coating is also considered in the simulations in order to obtain optimal values of the corrugation depth and the external radius of the capillary.

INTRODUCTION

Terahertz frequency range includes frequencies from 0.3 to 10 THz. This part of electromagnetic spectrum has a variety of potential applications ranging from fundamental, such as studies of physical systems dynamics, to security applications, such as screening of concealed materials [1,2]. Further advances in development of a linac based, tunable and narrow band coherent source of THz radiation are very important. Mechanisms of Cherenkov radiation and SPR may be used for generation of THz radiation via coherent emission [3, 4].

In this report we discuss a hybrid mechanism for generation of coherent THz radiation based on Cherenkov and SPR, produced when a short (100 fs) electron bunch travels through a corrugated channel in dielectric material. The radiation generated by the corrugated channel was simulated using CST (Computer Simulation Technology) Particle Studio (PS) and compared with the theoretical study developed for a corrugated channel in infinite material [5]. LUCX accelerator at High Energy Accelerator Research Organisation (KEK) has been upgraded by introducing a femtosecond Ti:Sapphire laser system and is currently able to generate short, tens to hundreds femtosecond duration electron bunches [6,7]. For a proposed experimental study at LUCX facility at KEK in Japan SPR will be generated in a dielectric capillary with partial metal coating acting as a radiation reflector; the radiation will leave the capillary through the outer boundaries, not covered by the reflector. This geometry allows for generation of narrow-band, coherent SPR in THz region; as well as for more efficient radiation generation, compared, for example, to a flat diffraction grating.

Theoretical Background

Theoretical calculations of the Cherenkov Smith – Purcell radiation from a corrugated channel in infinite dielectric are based on the method of polarization current density (see chapter 4 in [8]). Coulomb field of moving electrons polarizes the material and as a result each elementary volume of the material emits radiation. Electrons in the bunch are distributed with a Gaussian distribution. The polarization currents produce secondary electromagnetic field which then propagates through the material. The spectral - angular distribution of the radiation is given in [5]. The positions of the Cherenkov peak and the SPR peaks satisfy the following dispersion relation:

$$cos\theta = \frac{2\pi m}{kd} + \frac{1}{\beta\sqrt{\varepsilon(\omega)}}; \quad (1)$$

where θ is the polar angle depicted as Theta in Fig. 1; β is the charge speed in terms of the speed of light; k is the wave number in the dielectric; d is the groove period; and m is a diffraction order. The value of $m = 0$ corresponds to the Cherenkov peak, and the values of $m = \pm n; n = 1,2,3 \ldots$ correspond to the peaks of SPR.

SIMULATION GEOMETRY

The simulations are performed using CST PS Particle In Cell (PIC) solver [9]. The simulated geometries are shown in Fig. 1 and in Fig. 2. Figure 1 shows the geometry used for a comparison with the theory; the calculation domain is filled with dielectric in the radial direction, which in combination with open boundary conditions creates a quasi - infinite geometry. An electron bunch propagates through the channel producing Cherenkov and SPR at angles Theta satisfying the dispersion relation (1).

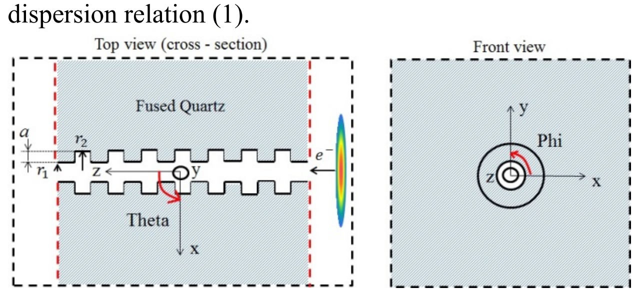

Figure 1: Geometry 1, quasi-infinite in r direction.

Figure 2 depicts the capillary with the reflector. The electron bunch travels with an offset in the capillary in order to generate Smith-Purcell radiation more efficiently. Both in Fig. 1 and Fig. 2 black dashed lines show non-reflective borders (open boundaries) in the calculation domain; and the red dashed lines show reflective borders. Values of the electric field are calculated at each

#konstlek@post.kek.jp

Content from this work may be used under the terms of the CC BY 3.0 licence (© 2015). Any distribution of this work must maintain attribution to the author(s), title of the work, publisher, and DOI.

ISBN: 978-3-95450-168-7 doi:10.18429/JACoW-IPAC2015-TUPWA071

IMPROVEMENTS OF THE LASER SYSTEM FOR RF-GUN AT SUPERKEKB INJECTOR

R. Zhang*, M. Yoshida, T. Natsui, X. Zhou, Y. Ogawa, KEK, Tsukuba, Japan

Abstract

According to the requirements of SuperKEKB project, the electron beams with a charge of 5 nC and a normalized emittance of 10 µm are expected to be generated at injector linac. In order to meet these demands, an Ytterbium laser system has been being built. For realizing the laser system operating under 25 Hz with double bunch or 50 Hz, improvements of laser system are being done. We obtained 3.0 nC bunch charge by use of Yb:YAG/Cu soldering composite to overcome thermal effect. This demonstration indicates that effective and excellent thermal management can be realized for high repetition laser operation. Cryogenic experiment is also introduced.

INTRODUCTION

Higher luminosity is required in SuperKEKB. The photocathode RF gun with strong electric focusing filed for high-current, low-emittance should be adopted in the injector linac. For generating electron beams with a charge of 5 nC and a normalized emittance of 10 µm in the photocathode RF gun, according to the simulation of emittance due to the space charge effect, the ultraviolet (UV) laser source with a pulse width of several tens of picoseconds (ps) is required [1]. Furthermore, for reducing the energy spread, the laser pulse should be reshaped to rectangle from Gaussian shape [2].

With the aim of achieving the demands on the laser source, a hybrid laser system which includes an ytterbium (Yb) ions doped fiber oscillator, Yb-doped fiber amplifier and thin disk Yb:YAG amplifiers. For 2 Hz repetition rate test, more than 1 mJ UV pulse energy was obtained. As a result, the electron beams with a charge of 5.6 nC were generated. When the laser system was upgrade to 25 Hz, 20 mJ fundamental laser pulse energy and 700 µJ UV pulse energy were obtained and 3.0 nC electron beams were gotten [1, 3].

For the repetition rate of electron beam, the 25 Hz with double bunches and 50 Hz are requested. In order to realize excellent thermal management under high repetition rate operation, the laser system has been being improved.

IMPROVEMENTS OF THE LASER SYSTEM

In the ref [4], 0.8 nC electron beams were obtained by using of Yb laser system. By reforming the laser system configuration, 3.0 nC electron beam was archived under 25 Hz operation.

Figure 1 shows the layout of Yb laser system. The seed laser pulse was generated by an Yb-doped fiber ring oscillator. An electro-optical fiber pulse picker is adopted for decreasing the repetition rate of seed laser to 10.38 MHz. Then laser is amplified by Yb fiber pre-amplifier and chirped to about 30 ps by a transmission grating stretcher. Subsequently, two stages of Yb doped large-mode-area polarizing double-clad photonic crystal fiber are selected as the first and main amplifier to get strong enough pulse energy [5]. Because thin disk laser possesses very favourable thermal management, this configuration is used to obtain the mJ-class pulse energy. A regenerative Yb:YAG thin disk regenerative amplifier and four stages multi-pass amplifiers are employed. UV pulse laser at 259 nm for photocathode is generated by using two frequency-doubling stages and then injected into RF gun.

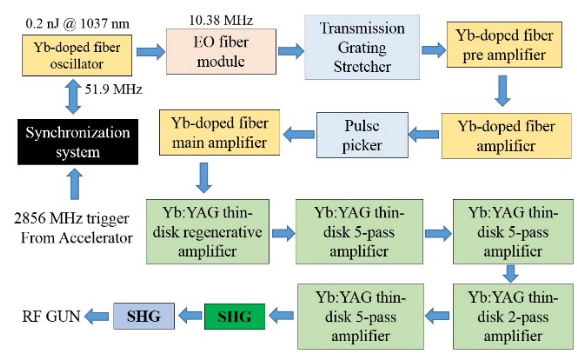

Figure 1: Layout of laser system.

Au-Sn soldering Yb:YAG/Cu Composite for Amplifier

The difficulty in controlling thermomechanical distortions has been one of the most important factors for preserving high beam quality and developing high average power solid-state lasers. By comparing with the 0.8 nC electron beams result we reported in the ref [4], 3.0 nC electron beams were gotten by using of Yb:YAG thin disk and copper plate composite. Waste heat generated in laser active disk can be removed to the copper plate effectively. Due to effective thermal removal in regenerative amplifier and multi-pass amplifiers, the amplified laser pulse became more stable and efficient.

Gold-tin (AuSn) was selected as soldering material for bonding Yb:YAG thin disk and copper plate. It possesses several advantages. Firstly, it has high thermal conductivity and low thermal expansion coefficient, as listed in Table 1. The thermal conductivity is high for AuSn comparing to that of indium-tin (InSn), this is very helpful for waste heat removal. Secondly, the deformation of AuSn is weak on heating because its thermal expansion

*rui.zhang@kek.jp

Content from this work may be used under the terms of the CC BY 3.0 licence (© 2015). Any distribution of this work must maintain attribution to the author(s), title of the work, publisher, and DOI.

ISBN: 978-3-95450-168-7 doi:10.18429/JACoW-IPAC2015-TUPWA072

COHERENT THOMSON SCATTERING RADIATION GENERATED BY USING PEHG

S. Chen, K. Ohmi, D. Zhou, KEK, 1-1 Oho, Tsukuba 305-0801, Japan
S. Huang, IHIP, Peking University, Beijing 100871, China

Abstract

The density modulation method of the newly proposed PEHG is used to generate ultra-short electron longitudinal structures for the bunch of a 100MeV ERL. Coherent Thomson scattering radiation in EUV range can be emitted by the scattering of such a modulated bunch with a long wavelength laser.

INTRODUCTION

Thomson scattering of an intense laser by relativistic electrons has thus drawn a considerable attention by its possibility of generating short wavelength radiations with relatively lower beam energy. In the recent years, several Thomson scattering light sources have been builted and some new methods of improving the performance of Thomson scattering light sources have been proposed. However, because of the bunch length is usually much longer than the radiation wavelength in these cases, the scattered radiation is mostly incoherent. In order to generate coherent Thomson scattering radiation, electron bunches with ultra-thin longitudinal structures, whose length is compariable or even shorter than the wavelength of scattered radiation, should be obtained first. In order to get such a ultra-thin longitudinal structure in electron bunches, several methods have been proposed previously [1, 2]. In this paper, we are referring a newly proposed bunch longitudinal density modulation method which is called Phase-merging Enhanced Harmonic Generation (PEHG) [3–5] to generate the ultra-thin bunch slices. By colliding with a long wavelength laser pulse generated by ERL beam, coherent and ultra-short pulse radiation is emitted through coherent Thomson scattering.

THOMSON SCATTERING

When a relativistic electron beam collides with an intense laser beam propagates along the inverse direction, the electrons start to oscillate driven by the Lorentz force of the laser electromagnetic field and generate intense and highly concentrated radiation along the direction of electrons propagate. This laser-electron collision process is so called Thomson scattering. The strength of the incident laser is described by the dimensionless vector potential, which can be expressed by the parameters of laser as

$$a_L = \frac{eE_L}{m_e c\omega_L} = 0.85 \times 10^{-9} \lambda_L[\mu m] I_0^{1/2}[W/cm^2] \quad (1)$$

where E_L, ω_L are the electrical field and the angular frequency of the incident laser. The radiation wavelength of Thomson scattering is quite similar to the undulator radiation thus it is also called *laser undulator radiation*. Considering the scenario of backscattering, the radiation wavelength is

$$\lambda_r = \frac{\lambda_L}{4\gamma^2}(1 + \frac{a_L^2}{2} + \gamma^2\theta^2) \quad (2)$$

where θ is the radiation angle and λ_L is the wavelength of the incident laser. Because of λ_L is usually much smaller than the traditional undulator period, one can generate radiation with similar wavelength but much smaller γ.

DENSITY MODULATION BY PEHG

Basic Principle of PEHG

PEHG was first proposed as an alternated harmonic generation method to the traditional HGHG [7, 8]. The performance of traditional HGHG method is restricted by the existence of initial energy spread of the electron bunch. As is shown in Eq. 3,

$$b_n = < e^{-in\theta_j} >= e^{-\frac{1}{2}n^2\sigma_\gamma^2(\frac{d\theta}{d\gamma})^2} J_n(n\Delta\gamma\frac{d\theta}{d\gamma}). \quad (3)$$

where $\frac{d\theta}{d\gamma} = 2\pi R_{56}/\lambda_s\gamma_0$, λ_s is the wavelength of seeding laser, γ_0 is the Lorentz factor of electron beam, σ_γ is the initial energy spread, $\Delta\gamma = \frac{k_s a_u F_B}{\gamma_0} a_s N_u \lambda_u$ with $F_B = J_0(\xi) - J_1(\xi)$ and $\xi = a_u^2/2/(1 + a_u^2/2)$, is the maximum energy modulation. The bunching factor drops exponentially with the harmonic increases due to the none-zero σ_γ in the exponential term. Because the bunching factor is the Fourier expansion of the longitudinal distribution, this also indicates the length of the longitudinal structure in the phase space is restricted.

In PEHG, the traditional modulator undulator is replaced by a *Transverse Gradient Undulator (TGU)* with transverse field gradient α and a dog-leg section is put in the front stream of the TGU to provide a dispersion η. The dog-leg acts a function of transverse-longitudinal coupling to establish a correlation between transverse position with energy. Then the electron bunch passes through the TGU and this correlation alternated to the correlation between electron energy and different undulator parameter. The principle equation inside the TGU is shown in Eq. (4) [3],

$$\frac{\gamma' - \gamma_0'}{\gamma - \gamma_0} = 1 - \frac{2\pi N_u \Delta\gamma}{\gamma_0}(\frac{\alpha\eta K_0{}^2}{K_0^2 + 2} - 1). \quad (4)$$

where γ_0' and γ' are the Lorentz factor of an reference electron and an arbitrary electron which have the same phase at the exit of the dog-leg; γ_0 and γ are the corresponding

Content from this work may be used under the terms of the CC BY 3.0 licence (© 2015). Any distribution of this work must maintain attribution to the author(s), title of the work, publisher, and DOI.

ISBN: 978-3-95450-168-7 doi:10.18429/JACoW-IPAC2015-TUPJE001

DESIGN OF WAVELENGTH TUNABLE COHERENT X-RAY SOURCE*

J. Hyun#, M. Yoshida, M. Satoh, SOKENDAI and KEK, Tsukuba, Japan
T. Sakai, Y. Hayakawa, T. Tanaka, K. Hayakawa, I. Sato, Nihon University, Funabashi, Japan
K. Endo, TOYAMA Co., Ltd., Kanagawa, Japan

Content from this work may be used under the terms of the CC BY 3.0 licence (© 2015). Any distribution of this work must maintain attribution to the author(s), title of the work, publisher, and DOI.

Abstract

KEK, Nihon University, and TOYAMA CO., Ltd. have been developing a thin-radiation shielded coherent X-ray source that can cover the X-ray energy range from 3 to 25 keV. The X-ray is the parametric X-ray radiation generated by the high energy electron beam passing through a single crystal. It has a feature that offers quasi-monochromaticity, directivity, and a large divergence angle for the incident beam. These suggest the possibility of application to medical treatments and diagnosis.

Furthermore, reduction of the radiation that is mainly generated at the beam dump will be achieved by the beam energy recovery system. This system consists of the accelerating structure, the decelerating structure, and the beam recovery transport system including four bending magnets. The RF structures are operated under low temperature of 20 K to get a high Q value in the rf recirculation system and a high energy conversion efficiency from the accelerated electron beam to the rf in the decelerating structure. Parametric X-ray radiation is generated from a single crystal that was bombarded with the electron beam accelerated up to 75 MeV. The electrons passing through the crystal is transported into a decelerating structure and then is decelerated to 3 MeV there. Quadrupole magnets are arranged to transport the achromatic beam except for in the arc sections. Simulations have been done on the beam transport, the parametric X-ray radiation intensity and the emittance growth.

INTRODUCTION

Nihon University, KEK, and TOYAMA Co., Ltd. have been developing a coherent X-ray source. This coherent X-ray means parametric X-ray radiation (PXR). This features quasi-monochromaticity, directivity and energy tunability by rotating the target crystal. A coherent X-ray is expected to be useful in a wide range of fields, for example crystal structure analysis, treatment of cancer and X-ray imaging. Nihon University group has been successful in providing PXR to users and has reported X-ray images using PXR in many papers [1, 2].

Most of the light source facilities provide synchrotron radiation to user's experiments as the X-ray sources. Due to the nature of this radiation with continuous spectrum, a monochromator is installed in the beam line to use the X-rays with a specific energy. On the other hand, the PXR X-rays are quasi-monochromatic, the energies of which are tunable with the rotation angle of the target crystal.

In the accelerator design, the decelerating structure has been employed for reducing unwanted radiation at the beam dump. The accelerating and decelerating structures are operated under the low temperature of 20 K in order to get a high efficiency of the energy conversion. Additionally, to get the coherent X-ray, the PXR generation system is used. Calculation and simulation have been carried out on the beam optics, the PXR intensity and the emittance growth. Figure 1 shows the layout of the coherent X-ray source based on the linear accelerator.

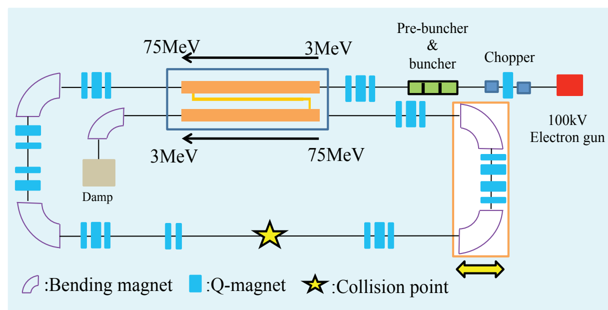

Figure 1: Layout of the coherent X-ray source based on linear accelerator.

PARAMETRIC X-RAY RADIATION

PXR is generated when relativistic charged particles pass through a crystal. This radiation can be interpreted that the virtual photon fields around the electrons are diffracted by the crystal planes. The features of PXR are beam coherence, large divergence angle with respect to the electron beam and PXR energy not affected by electron beam energy. Since the emitted X-rays satisfy the Bragg diffraction condition, the X-ray energy can be controlled by adjusting the angle between the incident beam and the specific crystal plane.

In this accelerator, the electron beam is accelerated to 75 MeV with a pulse duration of 2.5 μs and a repetition rate of 50 Hz. The average beam current is approximately 30 μA. Si or Diamond crystal will be used as the target because these crystals are heat-resistant. Furthermore, Si single crystals are readily available. The thickness of the target must be less than 0.2 mm to avoid too much emittance growth. Under this condition, the number of the PXR photons is expected to be about 10^{-9} photons/e^- [3].

#hyon@post.kek.jp

ISBN: 978-3-95450-168-7 doi:10.18429/JACoW-IPAC2015-TUPJE002

DEMONSTRATION OF HIGH-FLUX PHOTON GENERATION FROM AN ERL-BASED LASER COMPTON PHOTON SOURCE

R. Nagai*, R. Hajima, M. Mori, T. Shizuma,
JAEA, Tokai, Naka, Ibaraki 319-1195, Japan
T. Akagi, S. Araki, Y. Honda, A. Kosuge, N. Terunuma, J. Urakawa,
KEK, Oho, Tsukuba, Ibaraki 305-0801, Japan

Abstract

Accelerator and laser technologies required for laser Compton scattering (LCS) photon source based on an energy-recovery linac (ERL) have been developed at the Compact ERL (cERL) facility. A high-flux, energy tunable, and monochromatic photon source such as the ERL-based LCS photon source is necessary for nondestructive assay of nuclear materials. For the demonstration of the ERL-based LCS photon generation, a laser enhancement cavity was installed at the recirculation loop of the cERL. The electron beam energy, the laser wavelength, and the collision angle are 20 MeV, 1064 nm, and 18 deg., respectively. The calculated maximum energy of the LCS photons is about 7 keV. A silicon drift detector (SDD) with active area of 17 mm^2 placed 16.6 m from the collision point was used for observation of the LCS photons. As a result of the measurement, the flux on the detector, central energy, and energy width of the LCS photons were obtained as 1200 /s, 6.91 keV, and 81 eV, respectively.

INTRODUCTION

A high-flux and energy tunable photon generation based on laser Compton scattering (LCS) by an electron beam from an energy-recovery linac (ERL) is a key technology for a nondestructive assay (NDA) of nuclear materials. In order to generate such a photon beam, a small-emittance and high-current electron beam as well as a high-power laser are necessary. The ERL is an optimum apparatus to accelerate a high-quality electron beam [1]. The energy of LCS photons can be selected by changing the electron energy, laser wavelength, or collision angle between the electron and laser beams. Furthermore, the energy width of LCS photons can be narrowed by putting a small-diameter collimator which restricts the scattering angle.

Accelerator and laser technologies required for a high-flux LCS photon generation has been developed at the Compact ERL (cERL) facility. The cERL which is a test accelerator for ERL-based light sources has been constructed by collaborative team of High Energy Accelerator Research Organization (KEK), Japan Atomic Energy Agency (JAEA), other Japanese universities, and institutes [2]. In this paper, we present the first result of the LCS photon generation at the cERL.

* nagai.ryoji@jaea.go.jp

Table 1: Properties of the Electron Beam

Energy [MeV]	20
Bunch charge [pC]	0.36
Bunch length [ps, rms]	2
Spot size [μm, rms]	30
Emittance [mm mrad, rms]	0.4
Repetition Rate [MHz]	162.5

ELECTRON AND LASER BEAM PROPERTIES

The cERL consists of a photo cathode DC electron gun, a normal conducting buncher cavity, a superconducting injector linac, a three-dipole injection merger, a superconducting main linac, and a recirculating beam transport loop. The electron beam with bunch charge of 0.36 pC and bunch length of 3 ps was generated at repetition rate of 162.5 MHz by the photo cathode electron gun with acceleration voltage of 390 kV. The repetition rate of the electron beam pulse in cERL is originally 1300 MHz, but it was changed to 162.5 MHz which is same as the laser repetition for the demonstration of a LCS photon source. The generated beam was accelerated to 2.9 MeV by the injector linac before merging to the recirculation loop. Then, the electron beam was accelerated to 20 MeV by the main linac and was transported to the collision points with the laser beam. The electron beam was focused to rms size of 30 μm and was bunched to rms bunch length of 2 ps at the collision point. After the collision with the laser beam, the electron beam was injected again to the main linac with a deceleration RF phase. The recirculated beam was decelerated and fed back the energy to the superconducting RF cavity. This recovered RF energy was again used to accelerate subsequent electron beam. The properties of the electron beam at the collision point is summarized Table 1.

Since the cross-section of the Compton scattering is small, efficient recycling of laser photons is important to realize a high-flux LCS photon source. This efficient recycling can be achieved by introducing a laser enhancement cavity. The laser enhancement cavity is a high-finesse Fabry-Pérot optical cavity which stores laser pulses injected from an external mode-locked laser. In the LCS photon source, a 4-mirror cavity is employed to achieve high stability and small waist size [3]. As shown in Fig. 1, two sets of 4-mirror cavities are stacked in the same gimbals but are independently adjustable.

Content from this work may be used under the terms of the CC BY 3.0 licence (© 2015). Any distribution of this work must maintain attribution to the author(s), title of the work, publisher, and DOI.

ISBN: 978-3-95450-168-7 doi:10.18429/JACoW-IPAC2015-TUPJE003

QUASI-TRAVELING WAVE RF GUN AND BEAM COMMISSIONING FOR SUPERKEKB

Takuya Natsui#, Mitsuhiro Yoshida, Xiangyu Zhou, Yujiro Ogawa, KEK, Ibaraki, Japan

Abstract

We are developing a new RF gun for SuperKEKB. High charge low emittance electron and positron beams are required for SuperKEKB. We will generate 7.0 GeV electron beam at 5 nC 20 mm-mrad by J-linac. In this linac, a photo cathode S-band RF gun will be used as the electron beam source. For this reason, we are developing an advanced RF gun which has two side coupled standing wave field. We call it quasi-traveling wave side couple RF gun. This gun has a strong focusing field at the cathode and the acceleration field distribution also has a focusing effect. This RF gun has been installed KEK J-linac. Beam commissioning with the RF gun is in progress.

INTRODUCTION

The upgrade of KEKB to SuperKEKB is going on. Since high luminosity is required in SuperKEKB, improvement of beam emittance and charge is necessary. Table 1 is upgrade parameter of e- and e+ beam.

Table 1: e- and e+ Beam Parameters

	KEKB (e+/e-)	SuperKEKB (e+/e-)
charge [nC]	1 / 1	4 / 5
Emittance [mm-mrad]	2100 / 300	10 / 20

We are developing a photo cathode S-band RF gun for high charge (5 nC) low emittance (20 mm-mrad) beam generation. A thermionic cathode DC gun was used in KEKB. However it is difficult to make a low emittance beam with the DC gun. Thus RF gun must be installed to realize required electron beam parameter. However the standard on-axis coupled 1.5 cell RF gun is not suitable for this high charge beam, because standard gun is used up to about 1 nC by ordinary. If we obtain 5 nC in the gun, beam size will be too large. We have to consider both beam focus and emittance preservation. Thus it is necessary to make a focusing field against the space charge in the cavities. But in this on-axis coupling cavity, it is difficult to arrange the field freely on the axis. Since beam hole is also the coupling hole. Thus annular coupling is required.

We had tested Disk and Washer (DAW) type RF gun [1]. DAW cavity is an annular coupling cavity. Using this gun, we evaluated the cathode of two types LaB_6 or Ir_5Ce. As a result, we confirm that Ir_5Ce is suitable for photo cathode in terms of quantum efficiency and lifetime. In the DAW type RF gun study, we confirmed that electric field focusing technique is effective for high charge low emittance beam generation. However, focusing is still not enough in this gun, generated beam still has divergence angle. Since 5 nC is maximum output, this gun has no margin. In addition, beam energy is still low (3 MeV). Thus we have to consider the further emittance preservation in beam transport.

We are developing a new advanced RF gun. It has new acceleration scheme, we call it as a quasi-traveling wave. In this method, higher accelerating field and stronger focusing field are expected. It is very efficient acceleration method. This quasi traveling wave cavity is realized by using a two side couple cavities.

Annular coupled cavities as DAW or side coupled cavities are possible to make narrow acceleration gap. The narrow gap makes the focus field. Our DAW RF gun is using this focus field. Side coupled cavity also can be made the narrow gap. However, these cavities have a long drift space as Fig.1 (a) that shown normal side couple cavities. Due to the long drift space, the DAW RF gun generates beam with a divergence angle.

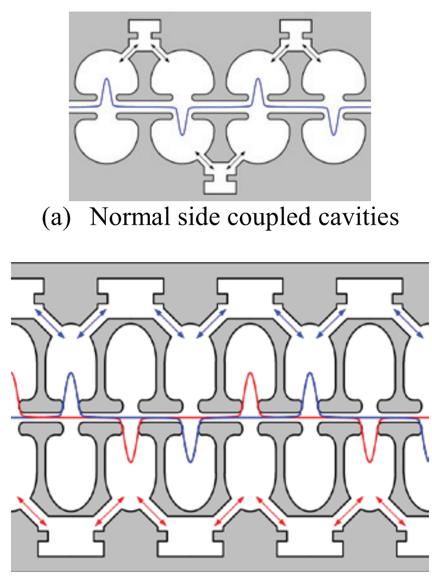

(a) Normal side coupled cavities

(b) Quasi traveling wave side coupled cavities

Figure 1: Structure of the quasi traveling wave cavity.

One solution is to use two standing wave cavities. If two side coupled cavities are arranged staggered, we obtain a double standing wave field as Fig.1 (b). These two standing wave side coupled cavities are independent electromagnetically. If we feed RF power with $\pi/2$ phase difference, acceleration field is similar to traveling wave to accelerated beam. Since two side coupled cavities are possible to place on the same axis, a quasi-traveling wave

#takuya.natsui@kek.jp

Content from this work may be used under the terms of the CC BY 3.0 licence (© 2015). Any distribution of this work must maintain attribution to the author(s), title of the work, publisher, and DOI.

ISBN: 978-3-95450-168-7 doi:10.18429/JACoW-IPAC2015-TUPJE004

NARROW BAND COHERENT EDGE RADIATION AT UVSOR-III

M. Hosaka, D. Oodake, N. Yamamoto ,Y. Takashima, Synchrotron Radiation Research Center, Nagoya University, Nagoya, Japan
H. Zen, Institute of Advanced Energy, Kyoto University, Uji, Japan
S. Bielawski, C. Szwaj, PhLAM, Villeneuve d'Ascq, France
T. Konomi, J. Yamazaki, M. Katoh, UVSOR, Institute for Molecular Science, Okazaki, Japan

Abstract

Edge radiation in the long wavelength region can be an interesting new light source because of its properties of highly collimation and radial polarization. Recently a dedicated beam-line for edge radiation was constructed at UVSOR-III. Coherent radiation from electron bunches after the interaction with the amplitude modulated laser was successfully observed at the beam-line. Intensity of the radiation as functions of the electron beam current and THz wavelength was measured. Spatial distribution of the radiation intensity was also measured. The pattern was not reproduced by a calculation.

INTRODUCTION

Coherent synchrotron radiation (CSR) in THz region can be produced from an electron bunch shorter than the radiation wavelength. Because of high radiation power, being proportional to the square of number of electrons in the bunch, CSR can be a new tool for various applications. However, in typical storage rings, electron bunch length is longer than THz wavelength. But they succeeded in producing CSR by shortening bunch length using special condition of storage rings called low-alpha operation [1]. Laser bunch slicing is another technique for producing CSR by creating mm or sub-mm dip structure in electron bunch [2]. In both cases, broad band CSR with wavelength longer than the bunch length or the dip structure is produced.

At UVSOR storage ring, we demonstrated that, by injecting amplitude modulated laser pulses into the ring, quasi-monochromatic and tuneable terahertz (THz) CSR can be produced [3]. In this method, periodic micro-density structure of THz scale was created on the electron bunch, as the result of the laser-electron interaction in an undulator. In the experiment, the radiation from a bending magnet where electrons are moving along a circular trajectory, is extracted. As a next step we planned to extract the radiation from edges of bending magnets, where electrons experience rapid change of the magnetic field. The radiation is called edge radiation and has distinctive features as compared to normal synchrotron radiation: highly collimation even in long wavelength region, annular radiation pattern and radial polarization [4]. Applying our technique of amplitude modulation laser, intense narrow band edge radiation is expected to be generated. Moreover, radially polarized light can be converted to Z-polarized one by using a high NA lens [5]. Novel new applications of the radiation, such as surface science and solid state physics are expected.

In this article, we describe a new beam-line for edge radiation and some preliminary results from the experiments to characterize narrow band coherent edge radiation.

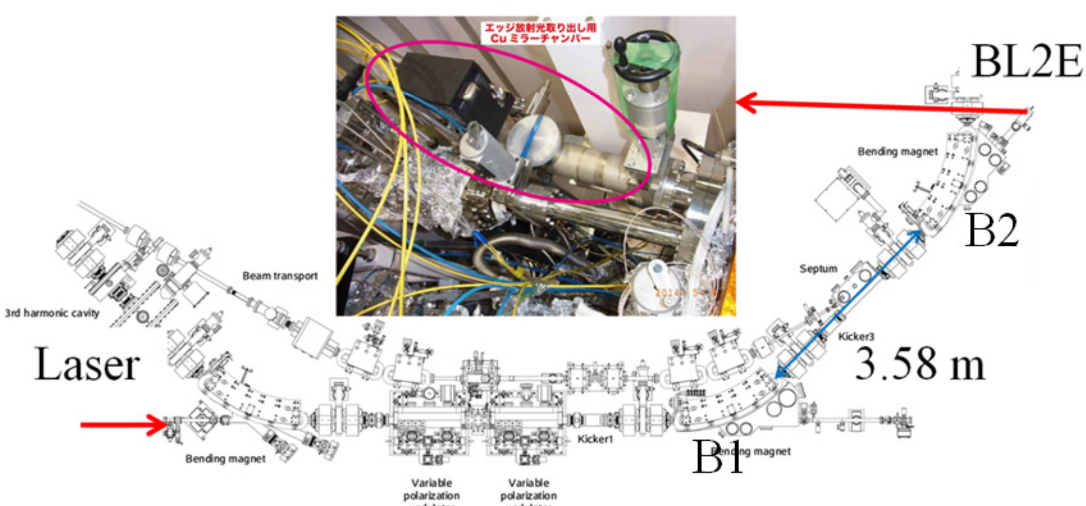

Figure 1: Drawing of UVSOR-III storage ring around undulator 1U [6] and a photograph of BL2E beam-line for detection of edge radiation.

Content from this work may be used under the terms of the CC BY 3.0 licence (© 2015). Any distribution of this work must maintain attribution to the author(s), title of the work, publisher, and DOI.

ISBN: 978-3-95450-168-7 doi:10.18429/JACoW-IPAC2015-TUPJE005

DEVELOPMENT OF PULSED MULTIPOLE MAGNET FOR AICHI SR STORAGE RING*

K. Ito#, M. Hosaka, A. Mano, T. Takano, Y. Takashima, Nagoya University, Nagoya, Japan
N. Yamamoto, KEK, Tsukuba, Japan
K. Hayashi, M. Katoh, UVSOR, Okazaki, Japan

Content from this work may be used under the terms of the CC BY 3.0 licence (© 2015). Any distribution of this work must maintain attribution to the author(s), title of the work, publisher, and DOI.

Abstract

We designed a Pulsed Multipole Magnet (PMM) for Aichi SR storage ring. The design goal is to suppress displacement of stored electron beams smaller than 10 percent of stored beam size. In our past research, we established a technique to compensate magnetic field error. At this time, we estimated effects of magnetic field generated by current leads and of electric field caused by potential differences in the coil. Then, we designed the configuration of current leads to minimize the perturbations to the stored beam. It is expected that the amplitude of electron beam would be suppressed to 4 percent horizontally and 0.08 percent vertically of the beam size.

INTRODUCTION

Aichi SR, a 1.2 GeV storage ring light source, is the newest synchrotron light source in Japan. The ring is equipped with four superconducting bending magnet, which can provide hard X-rays to more than 10 beam-lines. The storage ring has been operated with the top-up injection mode since the beginning of the users operation in 2013[1]. The parameters of Aichi SR storage ring are shown in Table 1. So far, the stability of 0.2% for the stored beam current is achieved. In the usual injection scheme, four pulsed kicker magnets create a bump orbit. At the beam-lines in this orbit, synchrotron radiation is lost due to momentary displacement of a stored beam orbit. Because Aichi-SR is relatively small, the local bump lies in about a half of the circumference and there exist many beam-lines. For those reasons, this problem is quite essential.

In order to solve it, we decided to introduce the PMM injection scheme, which enables beam injection without perturbing the stored beam [2,3,4,5]. However, in reality, a PMM didn't completely suppress perturbations to stored beams. The effect of quadrupole field was treated in [3] and the effect of dipole field error and its compensation method was discussed in [5]. In this work, we treat electric field generated by the conductors and magnetic field generated by current leads, which have not been considered in the previous studies, and design a PMM. Our design goal is suppressing the amplitude of the electron beam oscillation less than 10 percent of stored beam size.

Table 1: Parameters of Storage Ring

Electron Energy	1.2 GeV
Circumference	72 m
Current	>300 mA
Natural emittance	52 nm-rad
Betatron tune	(4.72, 3.18)
RF frequency	499.7 MHz
Harmonics number	120
(β_{x1}, β_{y1}) @superbend	(1.63, 3.99) m
(β_{x2}, β_{y2})@straight section	(29.9, 3.72) m
$(\sigma_{x1}, \sigma_{y1})$ @superbend	(0.328, 0.0909) mm
$(\sigma_{x2}, \sigma_{y2})$ @ straight section	(1.60, 0.0849) mm

ito.keiya@j.mbox.nagoya-u.ac.jp

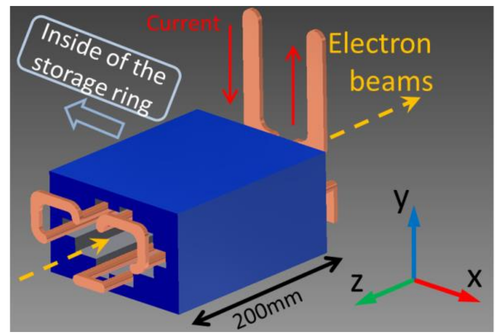

Figure 1: The appearance of the PMM of Aichi SR.

PULSED MULTIPOLE MAGNET

Figure 1 shows the appearance of the PMM of Aichi SR. It consists of a yoke and a single-turn coil. The yoke is painted blue in Fig. 1 and is made of laminated silicon steel. Its height, width and length are 120 mm, 180 mm and 200 mm, respectively. Electron beams pass through this yoke. The coil is painted orange and as a matter of convenience, we divide it to 3 parts. First, we call the part inside of the yoke "main coils." Second, we call the part outside of the yoke in the left side of Fig. 1 "upstream current leads" and similarly, call the opposite side "downstream current leads." Pulsed current runs through the coil to excite the magnetic field. Its waveform is a half-sine pulse whose width is 960 ns. Figure 2 shows the cross-section of the PMM with magnetic field lines. The current runs through 6 conductors in alternate directions and excites sextupole magnet field. Figure 3 shows the magnetic field distribution in the horizontal plane. The stored beam passing at the center is not affected by the magnetic field. On the other hand, the injected beam passing at 20 mm from the center is kicked and captured. The $B_y \cdot L$ component of the magnetic field has to be about 27 $\mathrm{mT} \cdot m$ at the injected beam orbit.

ISBN: 978-3-95450-168-7 doi:10.18429/JACoW-IPAC2015-TUPJE006

RECENT DEVELOPMENTS OF UVSOR-III*

M. Katoh#, H. Kenji, J. Yamazaki, UVSOR, Okazaki, Japan
M. Hosaka, Y. Takashima, Nagoya U., Nagoya, Japan
M. Adachi, T. Konomi, N. Yamamoto, KEK, Tsukuba, Japan

Abstract

A 750 MeV VUV synchrotron light source, UVSOR, has been operational since 1983. After the major upgrade in 2003 and in 2012, the machine UVSOR-III is now routinely operated with small emittance of 17 nm-rad and six undulators, as the beam current is kept at 300mA with top-up injection. New pulsed sextupole magnet for the beam injection has been under testing. New light source development station for FEL, CSR, CHG, LCG etc. was constructed is being developed. Reconstruction of the optical cavity for the resonator FEL has started.

INTRODUCTION

UVSOR was designed and built early in 1980's as a 2nd generation synchrotron light source in the vacuum ultraviolet range with emittance larger than 100 nm-rad and few insertion devices. The most recent parameters of UVSOR are shown in Table 1. The emittance is one of the smallest among the low energy synchrotron light sources below 1GeV. In addition, totally six undulators are operational in this small storage ring. The beam current is kept at 300mA with the top-up injection scheme. In this paper, we briefly review the upgrade history of UVSOR. Then, we describe recent status of the machine and some results from the recent researches and developments on light source technologies.

Table 1: Basic Parameters of UVSOR-III

Beam Energy	750 MeV
Circumference	53.2 m
Cell Structure	Extended DB
Emittance	17 nm-rad
Energy Spread	5.4E-4
Straight Sections for I.D.	4m x 4 1.5m x 2
Beam Current	300 mA (top-up)
Injector	15 MeV Linac 750MeV Synchrotron

30 YEARS OF UVSOR

In Dec. 2013, we celebrated the 30 year anniversary of the UVSOR Facility. The recent view of the storage ring is shown in Fig.1. In this section, we will give an overview of the history of the facility focussing on the accelerator upgrades.

Figure 1: Recent view of UVSOR-III storage ring.

UVSOR-I

We shall call the machine UVSOR-I, in the period from the first light in 1983 to the first major upgrade in 2003. It consisted of 4 DBA cells with four 3-m straight sections [1]. Its emittance was 120 - 160 nm-rad, depending on the operating betatron tunes. It has two undulators and a superconducting wiggler [2]. The operation energy of the storage ring was initially 600 MeV and was soon upgraded to 750 MeV. However, the energy of the injector remained at 600 MeV.

During this period, many beam-lines were constructed and commissioned. On the other hand, the basic performance of the storage ring was not changed drastically. The research on free electron laser started in 1980's. A new optical klystron of variable polarization was installed in 1990's [3] and the lasing in the deep UV range was demonstrated [4]. A study on the low-alpha operation was carried out [5]. The 3rd harmonic RF cavity was installed, which was effective to suppress the longitudinal instabilities and to improve the Touschek lifetime [6]. The accelerator control system was upgraded [7].

UVSOR-II

In 1990's, construction of 3rd generation synchrotron light sources started all around the world, and continued in 2000's. To meet the increasing demands for brighter

*Work partly supported by JSPS KAKENHI Grant Number 26286081, 23360043 and by MEXT/JST Quantum Beam Technology Program.
#mkatoh@ims.ac.jp

Content from this work may be used under the terms of the CC BY 3.0 licence (© 2015). Any distribution of this work must maintain attribution to the author(s), title of the work, publisher, and DOI.

ISBN: 978-3-95450-168-7 doi:10.18429/JACoW-IPAC2015-TUPJE007

MEASUREMENT OF TEMPORAL ELECTRIC FIELD OF ELECTRON BUNCH USING PHOTOCONDUCTIVE ANTENNA

K. Kan[#1], J. Yang, A. Ogata, T. Kondoh, M. Gohdo, I. Nozawa, T. Toigawa, Y. Yoshida[#2]
ISIR, Osaka University, Osaka 567-0047, Japan

Abstract

A temporal electric field profile, which is a radially polarized terahertz (THz) pulse from an electron bunch, was measured by a large-aperture photoconductive antenna (PCA) with micro-structured concentric electrodes for the detection of THz pulses. Photo-induced charge carriers were generated by irradiation of femtosecond laser pulses on semiconductor plane of the electrodes on the PCA. Time-domain measurement of coherent transition radiation (CTR) was conducted by the measurement of electric-field-induced current output from the PCA with sweeping the timing of the laser irradiation. The measurements on femtosecond electron bunches of 32 MeV and >80 pC will be reported.

INTRODUCTION

Short electron bunches with durations of picoseconds to femtoseconds are useful for generation of light in terahertz (THz) range [1] and time-resolved studies of ultrafast phenomena and reactions, including ultrafast electron diffraction (UED) [2] and pulse radiolysis [3,4,5]. Electro-optic sampling [6], which is one of detection techniques of THz light pulse, is used in diagnostics of electron bunches. In EO samplings, the birefringence of EO crystals is induced by the beam electric field, and laser polarization corresponding to the longitudinal electron beam profile is detected [7,8]. EO monitors based on the temporal decoding have revealed the Coulomb field of a root mean square (rms) width of 60 fs from femtosecond electron bunches [8]. Interferometers [9] have been also used for the detection of single mode or multimode THz pulses generated by electron bunches and slow-wave structures [10,11]. Coherent transition radiation (CTR), which is generated by electron bunches crossing a boundary between different media, has been measured by interferometers and grating-type spectrometers [12,13]. Photoconductive antennas (PCAs), which are composed of semi-insulating (SI) semiconductor with electrodes, are widely used for both generation and detection of THz pulses in THz time-domain spectroscopy [14,15,16,17,18]. PCAs could be good candidates for analyzing temporal electric field profiles of electron bunches due to the correlation between electric-field-induced current output and THz electric field strength [17]. Fabrication of a large-aperture PCA is expected to enhance both generation efficiency and detection sensitivity of THz pulses with designed polarization character. Enlarged aperture of PCA and concentric electrode configuration scheme in the present study utilizes the application of PCAs with enhanced sensitivity and radial polarization feature. The application of those PCAs on the detection of THz pulses from electron bunches will be a new methodology for beam diagnostics.

In this paper, analysis of the temporal electric field profile of CTR using a large-aperture PCA with micro-structured concentric electrodes is demonstrated. CTR was emitted by femtosecond electron bunches from a photocathode-based linac. The PCA enabled the detection of radially polarized THz pulses with adequate sensitivity according to the geometry of electrodes. Photo-induced charge carriers were generated by irradiation of a femtosecond laser on the PCA. Electric-field-induced current was obtained as THz electric field strength of CTR at the duration of the laser irradiation.

EXPERIMENTAL SETUP

Generation of Femtosecond Electron Beam

Femtosecond electron bunches were generated by the photocathode-based linac [13,19,20], which consists of a 1.6-cell S-band radio frequency (RF) gun with a copper cathode, a 2-m-long traveling-wave linac, and an arc-type magnetic bunch compressor as shown in Fig. 1. The photocathode of RF gun was excited by 4th harmonic (262 nm) of a picosecond laser with an energy of <180 μJ/pulse and a pulse width of 5 ps FWHM at 10 Hz. The electron bunches were accelerated in the gun and the linac using a 35-MW klystron. In the linac, the electron bunches were accelerated to 32 MeV at a linac phase of 100° for an optimal energy modulation of electron bunches [13]. The accelerated electron bunches were compressed to femtosecond by the magnetic bunch compressor, which was composed of bending magnets (B), quadrupole magnets (Q), and sextupole magnets (S). CTR was generated by the compressed femtosecond electron bunch.

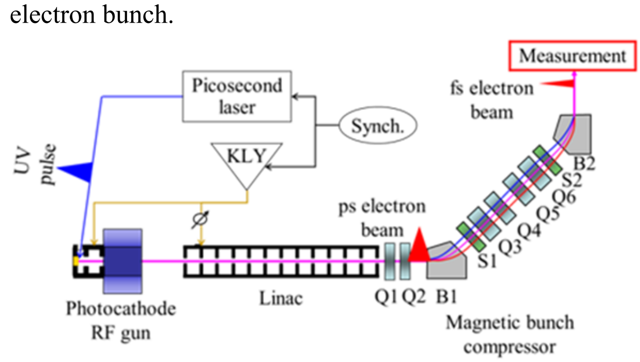

Figure 1: Diagram of photocathode-based linac.

#1: koichi81@sanken.osaka-u.ac.jp
#2: yoshida@sanken.osaka-u.ac.jp

Content from this work may be used under the terms of the CC BY 3.0 licence (© 2015). Any distribution of this work must maintain attribution to the author(s), title of the work, publisher, and DOI.

ISBN: 978-3-95450-168-7 doi:10.18429/JACoW-IPAC2015-TUPJE008

Content from this work may be used under the terms of the CC BY 3.0 licence (© 2015). Any distribution of this work must maintain attribution to the author(s), title of the work, publisher, and DOI.

RELOCATION AND IMPROVEMENT STATUS OF THE SCSS TEST ACCELERATOR TO PROVIDE DUAL FEL DRIVERS AT SACLA *

Yuji Otake #, on behalf of the members of XFEL research and development division,
RIKEN, Koto 1-1-1, Sayo-cho, Sayo-gun, Hyogo 679-5148, JAPAN

Abstract

To increase user experiment chances at SACLA, equipping a new beamline and an additional linac as a further FEL driver is effective. For these reasons, the SCSS test accelerator as the prototype of SACLA is reused, because of terminating its role. SCSS with an electron beam energy of 250 MeV generated an extreme ultraviolet laser with 50~60 nm. We relocated SCSS into the SACLA undulator hall and improved its performance. Three newly designed C-band acceleration-structures for the relocated SCSS accelerator with an acceleration gradient of 46 MeV/m at maximum boost an electron beam energy of up to 500 MeV. By FEL simulation, the EUV-FEL with 10~40 nm and 100 μJ are expected by the increased electron energy and 2 undulators with 5 m long each. By taking opportunity of the relocation, performance improvements of instruments, such as an inverter charger for the pulse-forming network (PFN) of a klystron modulator, were also done. The relocation work of the linac with several instrument developments finished in the summer of 2014 and rf conditioning for the units almost finished in the spring of 2015.

INTRODUCTION

Free-electron lasers (FEL) [1] generate fruitful science results [2] and already become important instruments for science. They have attractive features, such as wide wavelength tenability up to an X-ray region, compared with ordinal laser devices. However they are usually expensive, because of a single user machine being not like ring photon sources. In order to increase experiment chances for users, we had plans for constructing another new beamline BL-2, as well as the existing X-ray beamline BL-3, and an additional linac to drive a FEL in the existing beamline BL-1 of SACLA [3]. Light generated by this linac with a 450~500 MeV electron beam and the BL-1 covers lower wavelengths from 10 nm to 40 nm. This wavelength will be extended up to several nm by a future extension plan to increase a beam energy up to 1.4 GeV by adding 9 C-band acceleration units and 2 undulators. In order to realize the linac for the BL-1, we already had a very suitable machine that is the SCSS test accelerator. The roll of the test accelerator to check feasibility of the X-ray free-electron laser (XFEL) already terminated at that point. Therefore, we decided relocation of the test accelerator from the original place to the SACLA undulator hall. However, space for the relocation is not so wide. Furthermore we want to cover further shorter wavelength of the laser for the experiment users. For these reasons, a higher electron-beam energy by high-gradient acceleration was planned for the relocated test accelerator. We developed a 2π/3 mode qusi-constant gradient (CG) accelerating structure with a highly acceleration gradient of 45 ~ 47 MV/m, which is about 10 % bigger than the present SACLA's case. [4]

By taking opportunity of the relocation, performance improvements of instruments, such as an inverter charger for the pulse-forming network (PFN) of a klystron modulator at SACLA, were also done [4], since the performance, such as a trouble rate, of the inverter was not then perfect for us. Furthermore, individual device controllers using programmable logic controllers (PLC) and a low-level rf (LLRF) system for SCSS was different to those of SACLA. They should fit to the present control system for SACLA, because of easily building and easy maintenance. The rf phase and amplitude stability of the LLRF system for the test accelerator, as which temporal drift is over several pico-second, was not sufficient. Hence, we changed the controller and LLRF system from SCSS's one to the standard instruments for SACLA. [5] The permanent magnet-cell arrangement of the SCSS's undulator was different from that of SACLA. The magnetic period of the undulator was adjusted from 15 mm (K=1.5 at the maximum) to 18 mm (K=2.1 at the maximum). [5] Machine construction for this relocation now proceeds and almost finished. In this paper, the construction status of the relocated SCSS test accelerator, which is under high-power rf conditioning, and improvement status of the above-mentioned accelerator instruments are described.

CONSTRUCUTION AND INSTRUMENT IMPROVEMENTS STATUS

Accelerator Feature and Construction

In accordance with the plan to realize the linac mentioned above, the relocation of the SCSS test accelerator was started in 2013. The relocated accelerator is settled in the upstream of the BL-1 in the undulator hall, as shown in Fig. 1. Figure 2 depicts machine configurations before and after the relocation.

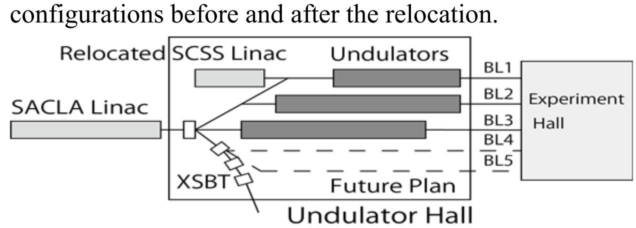

Figure 1: Place to install the relocated SCSS test accelerator (LINAC) in the undulator hall of SACLA.

#otaek@pring8.or.jp

ISBN: 978-3-95450-168-7 doi:10.18429/JACoW-IPAC2015-TUPJE009

STUDY ON FREQUENCY MULTIPLIER OF A PULSED LASER REPETITION USING AN OPTICAL CAVITY*

T. Kobayashi†, R. Suzuki, K. Sakaue, M. Washio,
Waseda University, Tokyo, Japan

Abstract

We have been studying a compact electron accelerator based on an S-band Cs-Te photo-cathode rf gun at Waseda University. The system is using S-band rf of 2856MHz. When a repetition of the electron bunch is integral multiple of rf, it enables a lot of electron bunch acceleration for the rf gun. The repetition of the electron bunch generated by a photo-cathode rf gun depends on the oscillating frequency of the pulsed mode-locked laser. We have been developing a mode-locked Yb-doped fiber laser based on Non-Linear Polarization Rotation (NLPR). However, its repetition is limited by the fiber length to produce NLPR. So we have started to develop the external optical cavity which is multiplier of a pulsed laser repetition. It would enable the rf gun to generate high-dose electron beam in a very short time. In this conference, we will report design of the external optical cavity to multiply the pulsed laser repetition, the experimental results of the frequency multiplying of a mode-locked Yb-doped fiber laser, and the future prospects.

INTRODUCTION

At Waseda University, a compact linear accelerator system, based on a 1.6 cell S-band Cs-Te photo-cathode rf electron gun, is applied for the various researches, such as laser Compton scattering (LCS) [1] and pulse radiolysis [2]. When a repetition of the electron bunch is integral multiple of rf, it enables a lot of electron bunch acceleration for the rf gun. The repetition of the electron bunch generated by a photo-cathode rf gun depends on the oscillating frequency of the pulsed mode-locked laser. The Yb-doped fiber laser studied as excitation pulsed laser for Cs-Te photo-cathode rf gun at Waseda University [3] has virtue of allowing high-power by Chirped Pulse Amplification (CPA), and its compactness. However it is necessary to make the repetition frequency higher in some way, because of the difficulty to get repetition rate more than about 100MHz. The repetition frequency is limited by the laser oscillation cavity length. Therefore, we have been developing an optical cavity to multiply frequency of the pulsed laser repetition.

*Work supported by Photon and Quantum Basic Research Coordinated Development Program from the Ministry of Education, Culture, Sports, Science and Technology, Japan.
†leli__o__1905@suou.waseda.jp

PRINCIPLE OF FREQUENCY MULTIPLIER USING AN OPTICAL CAVITY

In order to multiply the repetition frequency of pulsed laser by an optical cavity, there are roughly two conditions.

The first condition is that an optical cavity length matches with an integral multiple of laser half-wavelength. The condition is shown in Fig. 1.

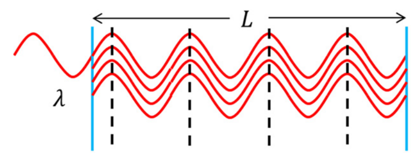

Figure 1: Schematic of storage condition of CW laser.

This is storage condition of continuous wave (CW) laser, and given by:

$$L = n\frac{\lambda}{2} \tag{1}$$

where L, λ, and n are the optical cavity length, laser wavelength and integer, respectively.

The second condition is that an optical cavity length matches with integer part of the laser's going around length. The condition is shown in Fig. 2.

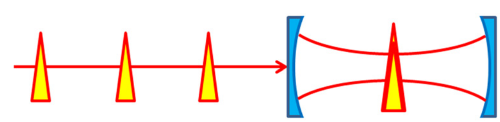

Figure 2: Schematic of overlapping of pulses.

This is overlapping of pulse, frequency multiplying, and given by:

$$L = \frac{L_{laser}}{m} = \frac{c}{mf_{rep}} \tag{2}$$

where L_{laser}, c, f_{rep}, and m are the laser oscillator cavity length, velocity of light, repetition frequency of pulsed laser and integer, respectively.

It is possible to achieve storage of pulsed laser and frequency multiplying of pulsed laser repetition by that consists of an optical cavity to satisfy the above conditions. The repetition frequency of pulsed laser passed this frequency multiplier is $f'_{rep} = mf_{rep}$ (Fig. 3).

Content from this work may be used under the terms of the CC BY 3.0 licence (© 2015). Any distribution of this work must maintain attribution to the author(s), title of the work, publisher, and DOI.

ISBN: 978-3-95450-168-7 doi:10.18429/JACoW-IPAC2015-TUPJE010

Content from this work may be used under the terms of the CC BY 3.0 licence (© 2015). Any distribution of this work must maintain attribution to the author(s), title of the work, publisher, and DOI.

STUDY OF Cs-Te PHOTOCATHODE FOR RF ELECTRON GUN*

Shuri Matsuzaki, Mariko Nishida, Kazuyuki Sakaue, Masakazu Washio,
Waseda University, Tokyo, Japan
Hokuto Iijima, Tokyo University of Science, Tokyo, Japan

Abstract

At Waseda University, we have been studying high quality electron beam with an rf electron gun. In recent accelerator study and application researches, high quality electron beam are strongly required. Photocathode is a key component to generate higher quality electron beam, thus we started to develop a Cs-Te photocathode as an electron source since 2007. Cs-Te photocathode shows high quantum efficiency (Q.E.) (~10 %) and has long life time (~several months). From 2013, we built a photocathode evaporation chamber and started photocathode study. In this study, our purpose is to clarify their property and to establish an ideal evaporation recipe. We succeeded in producing high quality Cs-Te photocathode, and electron beam generated by our Cs-Te photocathode shows high charge (4.6 nC/bunch) and high Q.E. (1.74 %) in our rf electron gun. Furthermore, we found a Q.E recovery after Cs deposition process and it causes higher Q.E. than usual due to, we believe, Cs deposition quantity or Cs deposition speed. Thus we are now surveying the optimum Cs evaporation parameters. In this conference, we will report a detail of our photocathode development system, the latest progress of optimization study of Cs-Te photocathode and future plans.

INTRODUCTION

At Waseda University, we have been studying high quality electron beam generation with photocathode rf gun and it was applied for several experiments, such as laser Compton scattering (LCS) [1] and pulse radiolysis [2]. In recent accelerator study and application researches, high quality and high charge electron beam are strongly required. Photocathode is a key component to generate high charge electron beam, thus we started to use a Cs-Te photocathode as an electron source since 2007 and built a photocathode evaporation chamber in 2013. Cs-Te photocathode is widely used because of its property of high quantum efficiency (Q.E.) (~10 %) with UV light and long life time (~several months). In this study, our purpose is to clarify their property and to establish an ideal evaporation recipe. We found a Q.E. recovery after Cs deposition process and started to research its mechanisms because it caused higher Q.E.. In our past study, we have already clarified that Te deposition seemed to not have relationship with it. Carrying out further study, we developed two new devices. The first device is a newly-designed evaporation source holder which enables us to measure Cs deposition quantity and Cs deposition rate. The second device is a substrate heating system. In this paper, we describe our results of optimization study of Cs-Te photocathode preparation by means of substrate temperature in the Cs deposition.

*Work supported by Cooperative and Supporting Program for Researches and Educations in Universities and NEDO(New Energy and Industrial Technology Development Organization.
#matsuzaki@akane.waseda.jp

EXPERIMENTAL EQUIPMENTS

Photocathode Evaporation Chamber

We built a photocathode evaporation chamber in 2013. Figure 1 shows the appearance of the chamber. It is required ultrahigh vacuum for preparing Cs-Te photocathode, therefore, the chamber is equipped several vacuum pumps. Its vacuum level can reach 6×10^{-8} Pa after chamber baking (~200 ℃, 24 h).
Since the chamber is independent from our rf gun, we adopted a load-lock system to transfer a photocathode without air exposure.

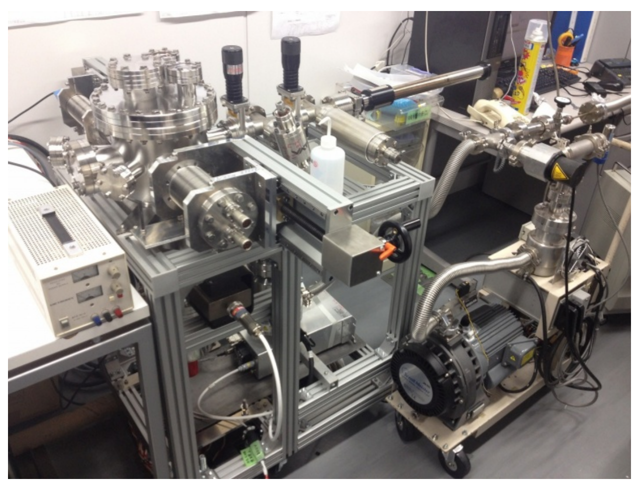

Figure 1: The appearance of the photocathode evaporation chamber.

Evaporation Source Holder

In order to make it possible to measure Cs deposition quantity and Cs deposition rate, we developed a newly-designed evaporation source holder shown in Fig. 2. It can be mounted four kinds of evaporation source (tellurium, antimony, cesium and potassium). Sb and K are in preparation for multi-alkali photocathode study in near future. As shown in Fig. 2, this Evaporation source holder is equipped two Cs dispensers. These dispensers

ISBN: 978-3-95450-168-7 doi:10.18429/JACoW-IPAC2015-TUPJE011

LASER-COMPTON SCATTERING X-RAY SOURCE BASED ON NORMAL CONDUCTING LINAC AND OPTICAL ENHANCEMENT CAVITY *

K. Sakaue†, WIAS, Waseda University, Tokyo, Japan
M. Washio, RISE, Waseda University, Tokyo, Japan
S. Araki, M. Fukuda, Y. Honda, N. Terunuma, J. Urakawa, KEK, Ibaraki, Japan

Abstract

We have been developing a compact X-ray source via laser-Compton scattering (LCS) at KEK-LUCX (Laser Undulator Compact X-ray source) facility. The LUCX system is based on S-band normal conducting linac with an energy of 30 MeV and optical enhancement cavity for photon target. As a photon target, we invented a burst mode laser pulse storage technique for a normal conducting linac, which enables to store the high power laser pulses at the timing of electron bunches. The peak storage power exceeds to more than 250 kW with 357 MHz repetition. Electron linac is under operation with multi-bunch mode, 1000 bunches/train with 600 pC charge in each bunches. We have succeeded to produce 1000 pulse/train LCS X-ray train. Combining high repetition rate electron linac and burst mode optical enhancement cavity, more than 10^9 ph./sec/10% b.w. flux would be possible. In this conference, the introduction of our test facility LUCX, recent experimental results, and future prospective including normal conducting LCS X-ray source will be presented.

INTRODUCTION

An X-ray generation method based on laser-electron Compton scatterings (LCS) is one feasible technique for a high brightness compact X-ray source. It utilizes a process in which energetic electrons scatter elastically a target laser photons, with an energy transfer from the electrons to the photons. The advantages of LCS are compactness thanks to its short undulation period by laser electric field[1], high brightness caused by the focused electrons and photons, and relatively large divergence angle due to small Lorentz factorγ. For instance, a 30 MeV electron beam with the laser wavelength of ~ 1 μm can produce 15 keV X-rays. This advantage has propelled worldwide laboratories to develop compact LCS X-ray sources with a brightness equivalent to the second generation light sources.

We have been developing a compact X-ray source based on an optical enhancement cavity operated with a burst amplifier[2] and a normal conducting pulsed linac. The pulse X-ray trains were already observed using a multi-bunch electron beam and an optical enhancement cavity[3]. Also, we have already tried to take X-ray images by LCS X-rays[4]. Recently, we have upgraded both accelerator system and enhancement cavity in order to increase the photon flux.

The paper describes the recent status of our accelerator and optical enhancement cavity, especially focused on the burst mode operation of enhancement cavity system, experimental results of LCS X-ray generation and feasibility study of our X-ray source extrapolating our recent results.

EXPERIMENTAL SETUP

In this section, we mention about our LUCX facility, based on normal conducting linac and optical enhancement cavity.

Multibunch Normal Conducting Linac

The LUCX facility is located inside the housing of the KEK Accelerator Test Facility (ATF). Firstly, we show the accelerator layout in Fig.1 The LUCX accelerator is an S-band, normal conducting rf linac operating with 12.5Hz pulsed electron beam. The electron bunches were produced by 3.6cell photo-cathode rf electron gun and accelerated up to 30MeV by 12cell standing wave booster linac. This linac can produce multibunch electron beam by irradiating the UV laser pulses with high repetition rate. Detail of multibunch beam handling is described in [5]. Successful approach of multibunch beam manipulation by rf amplitude/phase modulation allows us to produce 1000 electron bunch with 2.8ns bunch space on one rf pulse. The LCS interaction point is located at the center of optical enhancement cavity. The multibunch electron and optically enhanced laser pulses were interacted with each other inside the optical cavity. After interacting with laser, electron bunches are separated from the LCS X-ray by bending magnet and transported to the beam dump.

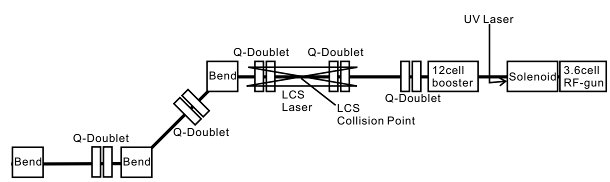

Figure 1: Facility layout of LUCX.

* Work supported by Photon and Quantum Basic Research Coordinated Development Program from the Ministry of Education, Culture, Sports, Science and Technology, Japan.
† kazuyuki.sakaue@aoni.waseda.jp

Content from this work may be used under the terms of the CC BY 3.0 licence (© 2015). Any distribution of this work must maintain attribution to the author(s), title of the work, publisher, and DOI.

ISBN: 978-3-95450-168-7 doi:10.18429/JACoW-IPAC2015-TUPJE012

Content from this work may be used under the terms of the CC BY 3.0 licence (© 2015). Any distribution of this work must maintain attribution to the author(s), title of the work, publisher, and DOI.

PRELIMINARY RESULT OF PHOTON COUNTING ACQUISITION SCHEME FOR LASER PUMP/ X-RAY PROBE EXPERIMENTS*

J. He[1], Y. Zhang[2], Z. H. Gao[2], Y. F. Zhou[2], Y. F. Sui[1],J. H. Yue[1], J. S. Cao[1], Y. Tao[2]
[1]Division for Accelerators, [2]Beijing Synchrotron Radiation Facility, Institute of High Energy Physics, Beijing 100049, China

Abstract

R&D project has been initiated for a proposed ultralow emittance (~50pm.rad) synchrotron light source built in Beijing. The R&D includes the development of high repetition rate laser pump/X-ray probe for ultrafast dynamics detection in future source. In a typical laser pump/X-ray probe measurement, the X-ray pulse follows a laser pulse in adjustable delay. We are interested in the difference between laser on and laser off at different delay, which will snapshot dynamic process. To capture this trivial difference, it requires the acquisition system to single out the signal from this special X-ray pulse at adequate S/N ratio. For the R&D of high repetition rate pump-probe, we have set up a prototype counting acquisition system based on NIM modular electronics, which was tested in Beijing Synchrotron Radiation Facility (BSRF). The laser will be synchronized with a camshaft bunch at 124 kHz, a tenth of the revolution frequency. Avalanche Photo Diode (APD) was used to detect the X-ray pulse from this camshaft bunch due to its nanosecond response. Before the laser is delivered, we mimic the 124 kHz laser- on signal. The signals from APD are separated by power dividers into two Constant Fraction Discriminator (CFD) input channels. The signal in laser-on/off channel is gated out using the 1.24MHz timing signal divided from 499.8 MHz RF signal, while the mimic laser-on signal gated out at 124 kHz. Multiplied by ten times, the mimic laser-on signal counts should be consistent with the laser-on+off counts, if our counting modular works well. We carried out this test at 1W1B wiggler beam line to measure the Fe fluorescence signal. The performance of our system is demonstrated in the good consistency between mimic laser on and laser on+off signals.

INTRODUCTION

Synchrotron radiation characterization technology is developed with the advancement of the accelerator technology. There is a first generations light source Beijing Electron Positron Collider (BEPC) II in Institute of High Energy Physics (IHEP). It can be operated in either of two modes: SR mode for the BSRF (Beijing Synchrotron Radiation Facility) and Colliding mode for BES III (Beijing Spectrometer III) [1]. A third generation light source High Energy Light Source (HEPS) is in a state of pre-research [2]. Table 1 shows the main parameters of BEPCII and HEPS. After the development of different steady state analysis methods, dynamic information study is developed in many synchrotron light sources [3-6], which are called time-resolved detections using a method of Pump-Probe. To use laser excitation (pump) samples and synchrotron light to detected (Probe) the samples. The goal of the experiment is to detect the trivial difference between the ground state and exiting state.

The light source will provide synchronous photons with a special time structure in these experiments, which is called mixed (Hybrid) model, bunches current and bunches gap are not the same. There will be a bunch or some bunches which called camshaft bunch, which have a larger gap and a bigger current than the normal one. In order to make X-rays synchronized with laser spatially and temporally, there are some preliminary study are done for HEPS on BEPCII [7,8].

Synchrotron-based laser pump/x-ray probe experiments on an ns or faster time scale have typically used ultrafast lasers suffering from the limitation of low repetition rates on the order of 1-10 kHz. This severely limits the data collection efficiency, since the x-ray bunches repeat at a much higher rate. This is particularly critical for XAFS experiments, which require very large S/N ratios (~ 10^4 or better) to extract useful EXAFS far above the absorption edge. In order to set up a high frequency laser ultrafast time-resolved beam line on the HEPS, some preliminary test results will be introduced in this article.

Table 1: Main Parameters of BEPCII and HEPS

Parameters	BEPCII Collide mode	BEPCII Synchrotron mode	HEPS [2]
Energy E_0 (GeV)	1~2.1	2.5	6
Circumference (m)	237.531	241.129	1296.14
RF frequency (Mhz)	499.8	499.8	499.8
Harmonic number	396	402	2000
Revolution frequency (Mhz)	1.264	1.243	0.2315
Revolution Period (ns)	792	804	4320

EXPERIMENT

As shown in the Table 1, the revolution period of the electron is 804 ns and the harmonic number is 402 for synchrotron mode. There are many normal bunches and a

*This work is supported by the NSFC under grant No.11305186.

ISBN: 978-3-95450-168-7 doi:10.18429/JACoW-IPAC2015-TUPJE013

LATTICE DESIGN OF LOW BETA FUNCTION AT INTERACTION POINT FOR TTX-II*

Tenghui Rui, Wenhui Huang
Accelerator Laboratory, Department of Engineering Physics,
Tsinghua University, Beijing 100084, China

Abstract

TTX-II is a storage ring being designed at Accelerator Laboratory in Tsinghua University as the second phase of Tsinghua Thomson scattering x-ray source (TTX), to increase the average photon flux generated. To achieve a small beta function at the interaction point, four pairs of quadrupole magnets, whose focusing strengths are optimized, are added to the baseline. The lattice design is presented in this work.

INTRODUCTION

For a storage ring dedicated to the generation of X-ray by means of Thomson scattering, the transverse beam sizes at the interaction point have great influence on machine performance. The number of scattered photon in a collision between electron beam and laser beam is determined by the beam luminosity and total cross section of Thomson scattering [1].

$$n_\gamma = L\sigma \tag{1}$$

In laboratory frame, the luminosity is described by Eq. 2 [1].

$$L = \frac{n_e n_l / 2\pi}{\sqrt{\sigma_{ye}^2 + \sigma_{yl}^2}\sqrt{\sigma_{xe}^2 + \sigma_{xl}^2 + (\sigma_{se}^2 + \sigma_{sl}^2)\tan^2(\frac{\varphi}{2})}} \tag{2}$$

where $\sigma_{x,y,se}$ and $\sigma_{x,y,sl}$ denote the horizontal, vertical and longitudinal sizes of electron and laser beams at interaction point, $n_{e,l}$ the particle numbers of electrons and photons. The collision plane is horizontal and φ is the collision angle between electron and photon beams.

The transverse beam sizes at a specific location in a storage ring is determined by beam emittance and optical functions.

$$\sigma_{xe} = \sqrt{\epsilon_x \beta_x + \eta_x^2 \delta_p^2} \tag{3}$$

$$\sigma_{ye} = \sqrt{\epsilon_y \beta_y} \tag{4}$$

where ϵ_x and ϵ_y are the horizontal and vertical emittances, δ_p the momentum spread of the electron beam, η_x the dispersion function at IP, and β_x and β_y the horizontal and vertical beta functions at IP.

To reduce the transverse beam sizes at IP, either the betatron function or the emittance should be minimized. In this work, the design of a mini-beta lattice is presented.

* Work supported by National Natural Science Foundation of China(NSFC)(10735050,11127507).

MINI-BETA LATTICE

The baseline design of TTX-II and the previous mini-beta lattice design are discussed in [2, 3]. To avoid element intersection and to match the ring revolution frequency with synchronizing system frequency(2856 MHz), the ring circumference has to be changed. Moreover, the layout of the magnets has to be rearranged because the stripline kicker strength is not sufficient enough for beam injection. The layout of the current design is shown in Fig. 1.

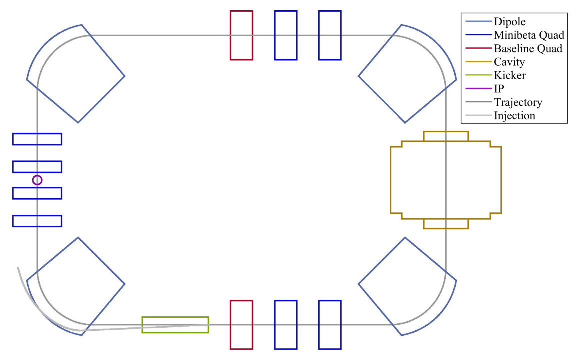

Figure 1: Layout of the mini-beta lattice.

Two pairs of quadrupoles are placed around the interaction point to provide strong focusing of the electron beam. Another two pairs of quadrupoles are placed in the straight sections between the baseline quadrupoles and bending magnets, to help adjust ring parameters such as working point and dispersion.

To find potential configurations for the lattice, all possible settings of quadrupole strengths are scanned and filtered by properties of interest such as betatron tunes and natural chromaticities. The time complexity of this algorithm depends exponentially on the number of variables, so the step size of scanning has to be large and we can only get a rough idea of what can be achieved with the current layout. For further optimization, genetic algorithm technique(GA) is exploited. To speed up convergence, the initial values of optimizing variables are chosen from the scan results. Then a population of possible settings are created and evolved by mimicking natural evolution process such as mutation, crossover and selection. The objective of GA is a function of lattice properties such as betatron tunes, beta functions and dispersion function at IP, natural chromaticities and momentum compaction factor. The program ELEGANT is used in the optimization process [4].

Figure 2 shows the optical functions of the optimized mini-beta lattice.

Content from this work may be used under the terms of the CC BY 3.0 licence (© 2015). Any distribution of this work must maintain attribution to the author(s), title of the work, publisher, and DOI.

ISBN: 978-3-95450-168-7 doi:10.18429/JACoW-IPAC2015-TUPJE014

Content from this work may be used under the terms of the CC BY 3.0 licence (© 2015). Any distribution of this work must maintain attribution to the author(s), title of the work, publisher, and DOI.

AN X-BAND LINAC WITH TUNABLE BEAM ENERGY*

Zhang Liang,[1,2,†] Shi Jiaru,[1,2] Wang Ping,[1,2] Zhang Zhe,[1,2] Du Yingchao,[1,2] Jin Qinxiu,[1,2] Tang Chuanxiang,[1,2] Chen Huaibi,[1,2] Han Yuansheng,[3] and Wang Chuanjing[3]
[1]Department of Engineering Physics, Tsinghua University, Beijing 100084, People's Republic Of China
[2]Key Laboratory of Particle &Radiation Imaging (Tsinghua University), Ministry of Education, Beijing, People's Republic Of China
Nuctech Company Limited, Beijing, People's Republic Of China

INTRODUCTION

X-ray system is widely used in medical diagnosis and treatment [1]. In the existing medical imaging systems, the energy lower than 500keV X-ray is normally generated by X-ray tube. And the energy higher than 2MeV X-ray is generally generated by low energy electron linacs, energy between 0.5MeV and 1.5MeV X-ray source remains almost a blank. In the energy range, the ability of the X-ray tube has almost reached the limit. With the improvement of energy, the cost of X-ray tube rapidly rises [2]. Recently, the research of energy adjustable linac is of high interest and various institutions around the world are focusing on this topic [3-6].

In x-ray imaging, appropriate x-ray energy is required for different substances to meet a better sensitivity. The energy varies from several hundreds of keV to several MeV. In the low energy end, x-ray tubes has been well developed. However, tubes with energy higher than 500keV is not easy to obtain. Linacs with energy at MeV levels are also adopted in the industrial for radiographic applications such as non-destructive test and cargo inspection.

An X-band linac has been developed to produce beam with energy from 0.5MeV and 1.5MeV. During the design process, some kinds of software such as PARMELA and SUPERFISH have been used for cell optimization and beam dynamics study. After fabrication by high-precision machines tools, we measured the frequencies and field distribution in the cold test. The results were similar to the precious simulations.

MAIN PRINCIPLE

The tube of the accelerator is separated into two sections which is different from single accelerating tube. By changing the amplitude and phase of the second linac section, it is possible to realize the change of energy continuously.

*Work supported by Tsinghua University Initiative Scientific Research Program No. 20131080112
†zhangliang13@mails.tsinghua.edu.cn

The principle of changing the beam energy is described as follows: The energy of the electron beam is correlate with the acceleration phase. If the accelerating tube is divided into two segments, the first section accelerates the electron energy to E_1, and the second section of the accelerating tube can accelerate the electrons to an Energy of E_2 while the phase is adjustable, so the final energy is (see Eq. 1):

$$E = E_1 + E_2 \cos\varphi . \tag{1}$$

Figure 1 shows the schematic diagram of the system configuration of the X-band linac. The RF power is supplied by one source, which is a magnetron in this design. The power is divided into two parts: one is fed into the first accelerating section directly; the other is fed into the second accelerating section through an attenuator and a phase shifter, which are used to change the amplitude and the phase of the second tube [7].

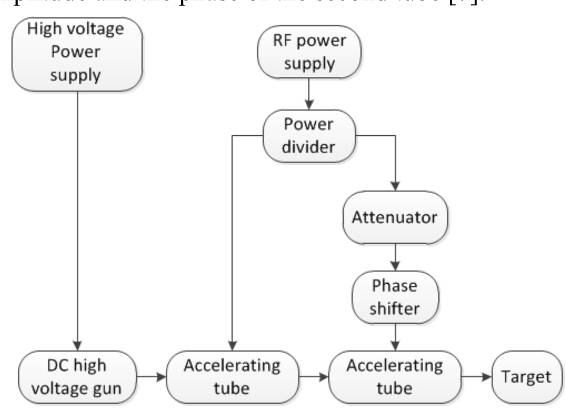

Figure 1: Schematic diagram of the linac system.

Since the electron beam energy is between 0.5MeV to 2MeV, the traditional industrial measurement method can not meet the needs of energy measurement accuracy.

During the measurement of electron beam energy, we can use current-thickness curvilinear to extrapolate the energy. Experiment results show that if we take aluminium as the absorbing material, we can get the database diagram about the current and the thickness of the aluminium plate. The simulation result is shown in Fig.2.

ISBN: 978-3-95450-168-7 doi:10.18429/JACoW-IPAC2015-TUPJE015

BETA FUNCTION MATCHING AND TUNE COMPENSATION FOR HLS-II INSERTION DEVICES*

Bing Li, Wei Xu, Ke Xuan, J.Y.Li†
National Synchrotron Radiation Laboratory,
University of Science and Technology of China, Hefei, Anhui 230029, China

Abstract

In order to increase its brightness and improve the performance, the Hefei Light Source (HLS) was completely renovated from 2010 to the end of 2014. The magnet lattice of the new storage ring consists of four double bend achromatic (DBA) cells. There are eight straight sections which can be used to install up to 6 insertion devices (IDs). Currently, five insertion devices have been installed in the storage ring. It is known that the dynamics of the electron beam motion in the storage ring would be influenced by the insertion device, depending on its physical properties. In order to keep high performance operation of the storage ring and make the insertion device transparent to the rest of the storage ring, a complex compensation scheme is developed to match the beta functions at both ends of a ID and perform transverse tune compensation. This scheme has been integrated into the EPICS based control system of the HLS-II. The result indicates that the scheme is very effective to compensate the impact of the insertion devices.

INTRODUCTION

The Hefei light source (HLS) at the National Synchrotron Radiation Laboratory (NSRL) was overhauled to increase its brightness and improve the performance. This major upgrade was started in 2010 and finished at the end of 2014. The new light source, named HLS-II, is comprised of an 800 MeV linac, a beam transfer line and an 800 MeV electron storage ring. Some critical parameters of the HLS-II storage ring are listed in Table 1.

Table 1: Main Parameters of the HLS-II Storage Ring [1]

Name	Value
Beam energy (MeV)	800
Circumference (m)	66.13
Magnet lattice	DBA
Beam emittance (nm·rad)	38
ν_x/ν_y	4.414/3.346
Number of IDs installed	5

Four fold double bend achromatic (DBA) cells are adopted as the magnet lattice of the HLS-II storage ring. The storage ring has two types of straight sections, four 4-meter long and four 2-meter long straight sections. One 4-meter long straight section is used to install the injection devices, and one 2-meter long straight section is used to hold the RF cavity. The rest straight sections can be used to install up to 6 insertion devices (IDs) . At present time, five insertion devices have been installed in the storage ring and providing strong narrow band synchrotron radiation for various user experiments. It is known that an insertion device would have strong impact on the optical parameters of the storage ring, depending on the physical properties of the insertion device. In order to keep high performance operation of the storage ring and make the insertion device transparent to other parts of the storage ring, a complex compensation scheme is developed to match the beta functions at both ends of the ID and perform compensation for the transverse tune. This scheme has been implemented in the EPICS based control system of the HLS-II storage ring. The impact of the IDs is automatically compensated by the control system according to the gap between the top and bottom magnetic poles.

As one example, this paper reports the compensation results of one of the HLS-II insertion devices. It first illustrates the fitting for the scheme, and then a beam based calibration of the scheme is reported. The tune shift and orbit distortion after the compensation are also presented in this paper.

* Work supported by the NSFC, fund code A050501.
† jingyili@ustc.edu.cn, 086-5521-63602100.

REVISIT OF THE COMPACT OF AN UNDULATOR ON THE STORAGE RING OPTICS

Considering a horizontal undulator, the magnetic field is given by [2]

$$B_y = B_0 \cosh k_w y \cos k_w z, \tag{1}$$

where $k_w = 2\pi/\lambda_w$ is the wave number of the undulator, B_0 is the peak value of the magnetic field. The vector potential of the undulator is

$$\vec{A_x} = -\frac{B_0}{k_w} \cosh k_w y \sin k_w z. \tag{2}$$

And the normalized vector potential is

$$\begin{aligned} a_x &= \frac{eA_x}{P_0} = -\frac{eB_0}{\gamma\beta mck_w} \cosh k_w y \sin k_w z \\ &= -\frac{K_w}{\gamma\beta} \cosh k_w y \sin k_w z, \end{aligned} \tag{3}$$

where $K_w = \frac{eB_0}{mck_w} = \frac{eB_0\lambda_w}{2\pi mc}$ is the undulator strength parameter.

In the undulator, the Hamiltonian for the electron motion is given by [2]

$$H \simeq \frac{(p_x - a_x)^2 + p_y^2}{2(1+\delta)}, \tag{4}$$

Content from this work may be used under the terms of the CC BY 3.0 licence (© 2015). Any distribution of this work must maintain attribution to the author(s), title of the work, publisher, and DOI.

ISBN: 978-3-95450-168-7 doi:10.18429/JACoW-IPAC2015-TUPJE016

COHERENT SYNCHROTRON RADIATION FIELD AND THE ENERGY LOSS IN A WAVY BEAM*

Derong Xu†, Hongliang Xu‡, USTC/NSRL, Hefei, Anhui, China

Abstract

The synchrotron radiation will be coherent when the wavelength of the radiation can be compared with the bunch length. There are two approaches to produce Coherent Synchrotron Radiation (CSR) on a storage ring. One is to compress the bunch length, the other one is to produce a wavy beam which has high spatial repetition along the longitudinal direction. The latter one can expand the radiation frequency range of a light source. However, CSR can bring nonlinear effect which brings in extra instability. The Liénard-Wiechert potentials in three-dimensional space may have very complicated forms. The most common way to investigate CSR is numerical method. This paper try to use a simple model to obtain energy loss of the electrons in theory.

PHYSICAL PICTURE

Assuming an electron moves along a fixed circular orbit of radius ρ with a constant speed $|\vec{\beta}| = \beta$. At the present moment, the electron locates at point P. We want to know the fields around point P. Radiation field in the orbit plane is discussed in [1]. To simplify the question, we assume the observation point A just above or below the trajectory. Thus, we get a two dimensional model. The field of point A is emitted at an earlier time when the electron located at point P'. The relations between P,P' and A are as shown in Fig. 1.

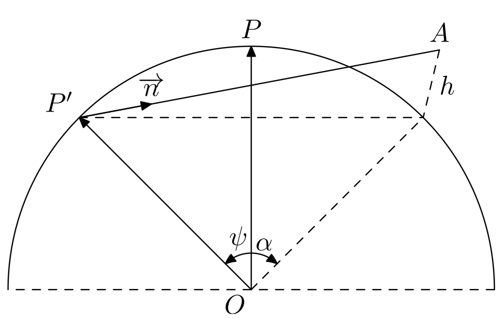

Figure 1: Diagram of the 2D model. ψ is the retarded angle, α is the azimuthal angle between P and P', h is the height of A relative to the orbit plane. Here $h > 0$ means the observation point A is above the orbit plane and $\alpha > 0$ means A is ahead of the electron present position P. ψ is always positive and $-\pi < \alpha < \pi$.

According to the geometric relationship, we can get the retarded equation:

$$\frac{\psi^2}{\beta^2} = (\frac{h}{\rho})^2 + 4\sin^2(\frac{\psi+\alpha}{2}). \tag{1}$$

The retarded equation is nonlinear, so it is generally not possible to obtain an exact answer. However, under some approximations, we can get some meaningful analytic solutions.

SOLUTION OF THE RETARDED EQUATION

Equation (1) shows that the retarded angle ψ depends on the electron's energy γ, the longitudinal azimuthal angle α and the height between the observation point to the orbit plane. In other words: from equation (1), we can get the numerical solution as shown in Fig. 2 and Fig. 3.

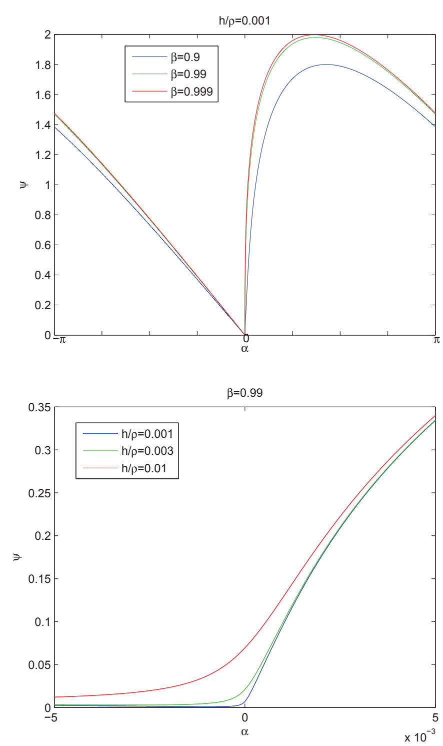

Figure 2: Retarded angle ψ as a function of α. The upper shows how ψ varies with the whole α when $h/\rho = 0.001$ for different β(or γ). And the lower shows small α when $\beta = 0.99$ for different h/ρ.

The conclusions are: (a)$\psi = \alpha_0$ when $\alpha = -\alpha_0$, here $\alpha_0 = h\beta/\rho$; (b)ψ is bounded; (c)ψ grows rapidly when $\alpha > 0$; (d)ψ is weakly related to γ when γ is large enough; (e)$(\psi + \alpha)/2 < 0$ when $\alpha < 0$ and vice verse.

* Supported by National Natural Science Foundation of China (11375176)
† xuderong@mail.ustc.edu.cn
‡ hlxu@ustc.edu.cn

Content from this work may be used under the terms of the CC BY 3.0 licence (© 2015). Any distribution of this work must maintain attribution to the author(s), title of the work, publisher, and DOI.

ISBN: 978-3-95450-168-7 doi:10.18429/JACoW-IPAC2015-TUPJE017

Content from this work may be used under the terms of the CC BY 3.0 licence (© 2015). Any distribution of this work must maintain attribution to the author(s), title of the work, publisher, and DOI.

THE GENERATION OF HIGHLY INTENSE THz RADIATION BASED ON SMITH-PURCELL RADIATION *

Yuanfang Xu†, Weiwei Li † ‡, Zhigang He §, Qika Jia, NSRL USTC, HeFei, AnHui 230039, China

Abstract

A photocathode RF gun can generate trains of THz sub-picosecond electron bunches by illuminating the cathode with trains of laser pulses. Let this electron bunches passes close to the surface of a lamellar grating, THz radiation will be emitted, which is the so-called Smith-Purcell Radiation (SPR). If the lamellar grating has a narrow groove, this radiation will be narrow band. By choosing suitable parameters, the SPR frequency can be resonant with the electron bunches frequency, and then generate highly intense, narrow band THz coherent radiation.

COHERENT SMITH-PURCELL RADIATION

When an electron beam passes close to the surface of a periodic structure (such as a metallic grating), radiation is emitted because of the interaction of the particles with the periodic structure, which is the so-called Smith-Purcell radiation (SPR)[1]. The intensity of radiation is proportional to the number of periods of the grating (N_g), hence it is strongly compared to other coherent radiation generation techniques such as synchrotron, transition and diffraction radiation.

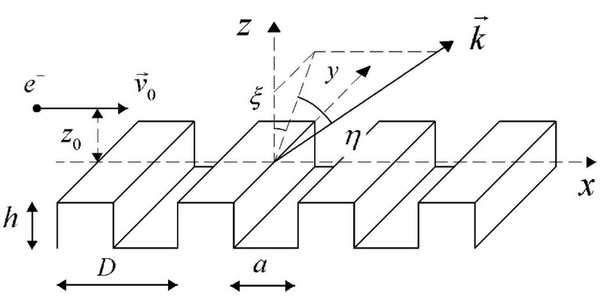

Figure 1: Definition of the geometry. The electron beam moves with constant reduced velocity $v_0 = \beta_0 c$ at a distance $z = z_0$ parallel to the grating surface in x-direction.

According to the theory of di Francia[2], the emission mechanism of SP radiation can be interpreted in analogy to the diffraction of light as the diffraction of the field of the electrons (virtual photons) which pass the grating at a distance z_0 away from its surface by the grating grooves. One characteristic signature of SPR is that it must fulfill the dispersion relation

$$\lambda = \frac{2\pi c}{\omega} = \frac{D}{|n|}\left(\frac{1}{\beta_0} - \sin\eta\right) = \frac{2\pi}{k_0}, \quad (1)$$

where λ is the wavelength of the radiation, n is the spectral order, β_0 is the ratio of the electron velocity to the speed of light c, D is the period of the grating, and k_0 is the wave number. For one electron, the radiated energy density per unit solid angle in direction (η, ξ) of the SPR of order n can be written as[2]

$$\frac{\mathrm{d}W_n}{\mathrm{d}\Omega} = \frac{Le^2}{2D^2\varepsilon_0}\frac{n^2\cos^2\eta\cos^2\xi}{(1/\beta_0 - \sin\eta)^3}|R_n|^2 \exp\left(\frac{-2z_0}{\lambda_e}\right), \quad (2)$$

Where $|R_n|^2$ is radiation factor, $L = N_g D$ is the total length of grating, N_g is the number of grating periods, η and ξ are the emission angles as introduced in Fig. 1, and λ_e is the so-called "evanescent wavelength". For N_e electrons in a bunch, coherent radiation is produced for wavelengths longer than the bunch length. The total energy density becomes

$$\left(\frac{dW_n}{d\Omega}\right)_{N_e} = \frac{dW_n}{d\Omega}(N_e S_{inc} + N_e(N_e - 1)S_{coh}^2), \quad (3)$$

where S_{inc} and S_{coh} are the incoherent and the coherent form factors, respectively.

RADIATION FACTOR: NARROW BAND SMITH-PURCELL RADIATION

To calculate the radiation energy, the key problem is to calculate the radiation factors. Van den Berg model[3, 4] is a rigorous solution under infinitely long and wide grating assumption. The radiated energy is calculated by solving two separated integral equations, each having a periodic Green's function, excited by the charge wake fields. Kesar and co-workers developed EFIE[5] and FDTD[6] model which extend Van den Berg's model for a finite grating size, and the two models agree well with each other. However they are more complex and need a much longer computation time. For the low relativistic elctron energies($\sim KeV$), Van den Berg's model ensures a reasonable agreement with experiments[7, 8]. The experiment at 15 MeV have demonstrated good agreement between measured power and the predictions of the EFIE model[9]. The simulated results at 18 MeV with 20 period length showed that in the plane (x,z), the angular radiation intensity per groove is greater than that of Van den Berg's model and their intensity shapes are close to each other[5]. As the number of periods increases, the simulated radiation intensity will be more and more close to that of Van den Berg's model[5, 6, 10].

*Supported by National Natural Science Foundation of China (No. 11205152 and No. 11375199) and Fundamental Research Funds for the Central Universities (No. WK2310000042 and No. WK2310000047).
†These authors contributed equally to this work
‡Now at INFN, Italy as a joint PhD student.
§Corresponding author, email: hezhg@ustc.edu.cn

ISBN: 978-3-95450-168-7 doi:10.18429/JACoW-IPAC2015-TUPJE018

ON-AXIS INJECTION SCHEME FOR ULTIMATE STORAGE RING WITH DOUBLE RF SYSTEMS

B. C. Jiang, Z. T. Zhao, S. Q. Tian, M. Z. Zhang, Q. L. Zhang,
Shanghai Institute of Applied Physics, Chinese Academy of Sciences, Shanghai 201800, China

Abstract

An on-axis injection scheme using double RF systems for an ultimate storage ring with very small dynamic aperture is proposed. By altering RF voltages, empty RF buckets can be created which will be used for on-axis injection. After bunches are injected, a reverse voltage altering process is performed and the injected bunches can be longitudinally dumped to the main buckets.

INTRODUCTION

A storage ring using "multi-bend achromat" (MBA) optics to reduce the natural emittance by one or two orders of magnitude down to current synchrotron light source storage rings has been proposed since 1995 [1]. After decades of efforts, this will become reality at MAX IV lab [2]. If the ring circumference is in the 1~2 kilometers range, the emittance of the electron beam will reach the photon diffraction-limited region for hard X-ray, an area that is of great interest to the synchrotron light community that could provide synchrotron radiation with high repetition rates and high brightness holding a large percentage of spatially coherent flux [3, 4]. A storage ring with these characteristics is called an "ultimate storage ring" (USR).

MBA optics employs much more numbers of bending magnets to decrease the bending angle θ of a single magnet and so reduce the natural emittance, which decreases as θ^3. Thus stronger quadrupoles are required to suppress the small dispersions created in the bending magnets, leading inevitably to the large negative native chromaticities in both transverse planes. In order to combat the head-tail instability and avoid large tune shifts of off-momentum particles, the chromaticities are usually corrected to slightly above zero, so strong chromatic sextuples are needed. These nonlinear elements will significantly reduce dynamic apertures presenting a great challenge for USR lattice design [5]. Many of the USR lattices which have been designed to date only provide horizontal dynamic apertures of around 2mm [6, 7, 8], leading to severe difficulties in injection.

One of the on-axis injection schemes, "swap-out injection", has been proposed [9], which uses a fast dipole kicker to inject fresh high charge beam onto the closed orbit while the stored beam is extracted. Swap-out scheme provides a baseline to inject the beam into the storage ring with a rather small dynamic aperture without major technical challenges. Recently, a novel longitudinal on-axis injection scheme was proposed in [10], in which a low frequency RF system is used, the bunch is injected at a phase with large deviation from the synchrotron phase and with energy slightly higher than the stored beam. Then the injected bunch damps to the synchrotron phase. For a storage ring with large energy acceptance this is a compact on-axis injection scheme without significant changing of the hardware.

In this paper, a possible approach for injecting beams into the USR, a new on-axis injection scheme is proposed. By altering the two RF voltages, empty RF buckets can be created which will be taken for on-axis injection. After bunches are injected, the voltage altering process will be reversed and the injected bunches can be longitudinally transferred to the main buckets (where the stored bunches are located). The energy oscillation of the injected bunches in this process can be controlled to less than 1%.

TWIN RF BUCKETS PRODUCTION

Assume that the storage ring has two RF systems, with the main RF system operating at 250MHz and the other one at the 2nd harmonic frequency 500MHz. The time dependence of the RF voltages are given by

$$V_m = \widehat{V_m}(st)cos(\omega_m t) \quad (1)$$

$$V_h = \widehat{V_h}(st)cos(2(\omega_m t - \varphi_s) - \pi/2), \quad (2)$$

$$\varphi_s = arccos(\frac{U_0}{\widehat{V_m}(0)}), \quad (3)$$

Where V_m, V_h are the voltage of the main and 2nd harmonic RF system respectively. The amplitudes of the RF voltages $\widehat{V_m}(st)$, $\widehat{V_h}(st)$ are modulated stepwise in a preset pattern. φ_s is the synchrotron phase of the main RF system, st denotes the modulating step, U_0 is the radiation energy loss per turn, and ω_m is the angular frequency of the main RF system.

If $\widehat{V_h}(st)$ is increased from near zero to its maximum value, while $\widehat{V_m}(st)$ is kept constant, one RF bucket will be split into two (twin) buckets as shown in Fig 1. As the stored bunches are located at synchrotron phases, they will be partitioned into two parts. In order to prevent the already stored bunches from being partitioned, a 'knot' as shown in Fig. 2 should be formed slightly before φ_s. The expression for the voltage of the second RF system should be modified to

$$V_h = \widehat{V_h}(st)cos(2(\omega_m t - \varphi_s) - \frac{\pi}{2} + \Delta\theta). \quad (4)$$

We call $\Delta\theta$ the synchrotron phase deviation and assume $\Delta\theta > 0$.

Figure 2 shows the detailed total voltage evolution process with $\Delta\theta > 0$. The stored bunch marked by the red dot will be pushed backward and the second empty RF

Content from this work may be used under the terms of the CC BY 3.0 licence (© 2015). Any distribution of this work must maintain attribution to the author(s), title of the work, publisher, and DOI.

ISBN: 978-3-95450-168-7 doi:10.18429/JACoW-IPAC2015-TUPJE019

OPERATING CASCADED HIGH-GAIN HARMONIC GENERATION WITH DOUBLE-PULSE ELECTRON BEAMS

Zhen Wang[1], Chao Feng[1], Qiang Gu[1], Lihua Yu[2,*], Zhentang Zhao[1,†]
[1]Shanghai Institute of Applied Physics, Chinese Academy of Sciences, Shanghai 201800, China
[2]National Synchrotron Light Source, Brookhaven National Laboratory, New York 11973, USA

Abstract

Cascading stages of high-gain harmonic generation (HGHG) is a promising candidate for the generation of fully coherent x-ray radiation. However, fluctuation of the output pulse energy is still a critical issue for a realistic facility with cascaded HGHG scheme. In this paper, we proposed using double-pulse electron beams to drive two stages cascaded HGHG, which will be helpful for increasing the stability of the output pulse energy against the arriving timing jitter in the second stage. Methods to generate the required double-pulse electron beams are introduced in the paper and three-dimensional simulations are carried out to show the significantly improvement of the FEL stability comparison with the standard cascaded HGHG by using this technique.

INTRODUCTION

Free electron lasers (FELs) hold great promise for the generation of coherent x-ray radiation with high brightness and ultra-fast time structures which will enable scientists in physics, chemistry, biology and medicine to study nature down to the molecular and atomic level at a time-scale that fits this resolution [1]. For nowadays, self-amplified spontaneous emission (SASE) FEL [2] is still the primary candidate for nanometer and sub-nanometer wavelength FEL generation. As the world's first hard x-ray FEL facilities, the Linac Coherent Light Source (LCLS) and the Spring-8 Angstrom Compact Free Electron Laser (SACLA) have demonstrated x-ray FEL technology in an impressive fashion [3-5]. However, SASE FEL suffers from the limited temporal coherence and large statistical fluctuations as the initial radiation starts from the electron beam shot noise.

To improve the FEL performance, frequency up-conversion schemes, such as high-gain harmonic generation (HGHG) [6,7], echo-enabled harmonic generation (EEHG) [8-10] and phase-merging enhanced harmonic generation (PEHG) [11,12], etc., have been proposed to manipulate the electron beam phase space with external coherent laser sources. In the standard HGHG, coherent micro-bunching is formed in the electron beam after energy modulation and density modulation. The output radiation, which inherits the properties of the seed laser, can have a high degree of temporal coherence and much stable central wavelength and output pulse energy compared to SASE. These properties of HGHG FEL have already been demonstrated in several single-stage HGHG experiments. However, the need to limit the growth of the energy spread prevents the possibility of reaching X-ray wavelength in a single-stage HGHG. To overcome this problem, cascading multiple stages of HGHG with 'fresh-bunch' technology have been proposed [13] and recently realized at FERMI for coherent soft X-ray generation at the wavelength of 20 to 4 nm [14-17]. The experimental results at FERMI show great output stability for the first stage HGHG but large pulse energy fluctuation up to 50-60% (FWHM) in the second stage [18], which may be a quite serious problem for FEL users. Such a critical energy fluctuation may primarily originates from the interplay of timing jitter between the relative arrival times of the electron beam and seed lasers, together with variations of the electron beam of properties along the longitudinal direction: for different shots, seed laser pulses in the modulator of the second stage will interact with parts of electron beam with quite different beam qualities.

In this paper, we propose using double-pulse electron beam to significantly improve the output stability of a two stages HGHG. The two pulses are separately used for producing of high harmonic radiation pulses in two stages. With the first bunch length much longer than the second one, the radiation pulse from the first stage can cover the whole bunch length in the second stage. Thus makes the power output much less sensitive to the small relative arrival timing jitter in the second stage. We first show the simulation results of a standard two stages HGHG. Then, we will introduce methods to generate two-pulse electron beams that fit the requirement. Summaries and conclusions are given in the last.

STANDARD CASCADED HGHG WITH A SINGLE-BUNCH ELECTRON BEAM

The Shanghai Soft x-ray FEL facility (SXFEL) is a test facility based on two-stage cascaded HGHG, as shown in Fig. 1. The linac of SXFEL consists of an injector, a laser heater system, a main accelerator (L1, L2 and L3) and two bunch compressors (BC1 and BC2). The electron beam is generated in a 1.6-cell S-band photocathode RF gun with initial bunch length of 8 ps, bunch change of around 500pC and peak current of 50A. Then the electron beam is boosted to 210MeV in L1 (S-band) and compressed by 5 times in the first bunch compressor (BC1). After that, the beam is boosted again to about 420MeV in L2 (S-band) and compressed twice further in the second bunch compressor (BC2). Finally, L3 (C-band) is used to future accelerate the electron beam to 840 MeV

*Email: lhyu@bnl.gov
†Email: zhaozhentang@sinap.ac.cn

Content from this work may be used under the terms of the CC BY 3.0 licence (© 2015). Any distribution of this work must maintain attribution to the author(s), title of the work, publisher, and DOI.

ISBN: 978-3-95450-168-7 doi:10.18429/JACoW-IPAC2015-TUPJE021

INTERACTION CHAMBER DESIGN FOR A SUB-MeV LASER-COMPTON GAMMA-RAY SOURCE

Hanghua Xu[#], Jianhui Chen, Gongtao Fan, Dong Wang, Hailong Wu, Benji Xu,
SINAP, Shanghai, China

Abstract

Previously, fixed angle Laser-Compton Scattering (LCS) experiments have been conducted at the terminal of the 100MeV LINAC of the Shanghai Institute of Applied Physics, using SINAP-I [1] and SINAP-II [2] facility. Sub-MeV energy continuously tunable laser-Compton light source device (SINAP-Ⅲ) is an updated facility that will allow the collision angle between the laser and electron beam continuously adjustable from 20° to 160°. This new feature will enable convenient control on the peak energy of the generated X/γ ray, especially when the energy of electrons cannot be momentarily adjusted, e.g. on the storage ring.

Keeping the electron beam and laser beam waist coincident at arbitrary angle is crucial for LCS gamma-ray production, an interaction chamber containing a rotatable bracket that holds a series of plane mirrors and convex lens is presented. This work is a summary of its design.

The simulation of photon production's variation caused by the system errors is performed using a MC code [3]. The accuracies of installation and adjustment of mirrors and lens are given according to the simulation results. The sizes of these optical devices are also optimized to make the chamber as compact as possible due to space limitation.

INTRODUCTION

In the past ten years, with the development of advanced accelerator and laser technology, the new X / γ-ray source based on Compton scattering obtain a rapid development and was rated as one of the most potential in the field of ultra- short pulse light sources. It uses high-power short-pulse laser beam with high brightness relativistic electron beam interaction, Compton scattering to produce high flux, short-pulse, quasi-monochromatic X/γ-rays. Currently, many research institutions such as LLNL [4], BNL [5], SLAC, IAC, MIT, Spring8, JAEA, INFN and ESRF are committed to the construction of the experimental device of LCS. The peak energy of produced X/γ-rays have wide applications in nuclear physics, medicine, energy, defence and industrial applications. The peak energy of the scattered X/γ-ray photon [2] is

$$E_x = E_L \frac{(1-\beta\cos\theta_L)}{1-\beta+\dfrac{E_L}{E_e}(1-\cos\theta_L)}$$

Where β is the electron velocity normalized to the speed of light, E_e and E_L are the energies of the incident electron and laser photon, and θ_L is the incident angle of the laser photon with respect to the direction of the incident electron beam. Traditionally, this value can only be varied by changing E_e (electron's energy) or E_L (the wave length of laser), which is inconvenient.

SINAP-III facility [6] is a sub-MeV gamma-ray source based on Laser Compton scattering. It is constructed on the branch line of SDUV-FEL [7]. The electrons and laser are both imported from the principle line into an interaction chamber. A specially designed laser transport system enables θ_L to be continuously changed from 20° to 160°, scattered photon energy E_x is thus continuously adjustable easily without changing E_e, E_L.

In this paper, we present the optical design of the interaction chamber and the study on the tolerance of mirrors.

LASER TRANSPORT SYSTEM

To achieve the continuously adjustability of the colliding angle of the electron beam and laser beam, a rotatable structure is designed.

Basic Structure

As shown in Fig.1, laser beam would propagate along the path from mirror No.6 to mirror No.0. The green lines in Fig. 1 is the maximum envelope of laser beam that these Optical elements' apertures can hold.

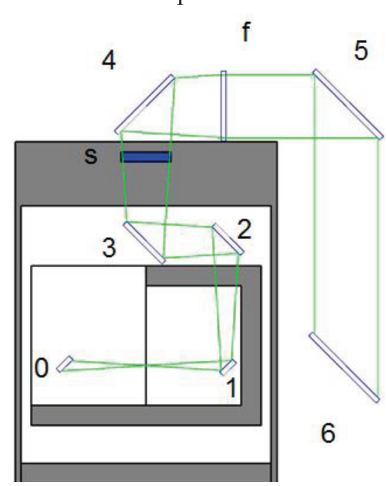

Figure 1: Basic optical structure (side view). The rectangles with number 0-6 represent plane mirrors, the rectangle referring to "f" is a convex lens, and the one with "s" is a transparent glass which covers the chamber.

#xuhanghua@sinap.ac.cn

Content from this work may be used under the terms of the CC BY 3.0 licence (© 2015). Any distribution of this work must maintain attribution to the author(s), title of the work, publisher, and DOI.

ISBN: 978-3-95450-168-7 doi:10.18429/JACoW-IPAC2015-TUPJE022

STUDY ON BEAM DYNAMICS OF A KNOT-APPLE UNDULATOR PROPOSED FOR SSRF

Q.L. Zhang, B.C. Jiang, S.Q. Tian, Q.G. Zhou, Z.T. Zhao
SINAP, Shanghai, 201800, P.R. China

Abstract

A new type of undulator, Knot-APPLE undulator, is proposed for SSRF as a solution to reduce the heat load of on-axis high harmonics without losing its capability of tuning synchrotron polarization. It will be applied for SSRF Photoemission Spectroscopy beamline (PES-beamline) in the near future. Impact of the undulator on the beam dynamics has been studied based on the 3D magnetic field model and kick map analysis. Linear optics can be retained by quadrupole compensation within two adjacent cells. Dynamical aperture (DA) shrinkage has been found in the tracking and optimized with sextupoles. An active correction scheme of current strips is studied to compensate the kick maps, and both the linear and nonlinear effects are suppressed.

INTRODUCTION

Shanghai Synchrotron Radiation Facility (SSRF) is an intermediate energy light source opened to users since 2009 [1]. There are 7 beamlines in operation, 5 of which are from insertion devices including IVUs, wigglers and EPU. Another 6 beamlines are under commissioning, including the 'dreamline' based on a double EPU, two canted beamlines from canted IVUs in one straight section, and some other beamlines from IVUs or bending magnets. In near future, a new type of undulator, Knot-APPLE undulator, will be equipped in SSRF storage ring for PES-beamline [2]. Main parameters of the existing IDs and Knot-APPLE in SSRF are listed in Table 1.

Table 1: Main Parameters of Existing IDs and Knot-APPLE in SSRF

	Type	λ_{ID}	L_{ID}	$B_{y,peak}$
H08U	EPU	10cm	4.2m	0.6T*
H09U58	EPU	5.8cm	4.9m	0.68T*
H09U148	EPU	14.8cm	4.7m	0.67T*
H13W	Wiggler	14cm	1.4m	1.94T
H14W	Wiggler	8cm	1.6m	1.2T
H15U	IVU	2.5cm	2m	0.94T
H17U	IVU	2.5cm	2m	0.94T
H18U	IVU	2.5cm	1.6m	1T
H19U1	IVU	2cm	1.6m	0.84T
H19U2	IVU	2cm	1.6m	0.84T
Knot-APPLE	EPU	20cm	4.4m	0.7T*

* For horizontal polarization mode

In this paper we will firstly give a brief introduction of Knot-APPLE undulator, and then estimate its effects on beam dynamics using kick map analysis. Quadrupole compensation is studied, and the linear optics could be retained. The nonlinear effect, which brings significant reduction of dynamical aperture, was optimized with sextupoles. Furthermore, an active correction scheme of current strips is also considered to compensate the kick maps, so as to suppress both the linear and nonlinear effects. The preliminary simulation gives us an encouraging result that the linear effect would be an order less and the dynamical aperture is tolerable for operation.

KNOT-APPLE UNDULATOR

Knot-APPLE combines the advantages of both the Knot and the APPLE type of structure in EPU fabrication, and could reduce the on-axis heat load without lose its ability to generate variable polarization [2]. With such a complicated structure, Knot-APPLE would significantly impact on beam dynamics. To estimate its effects, the 3D magnetic field model has been established, as shown in Fig. 1.

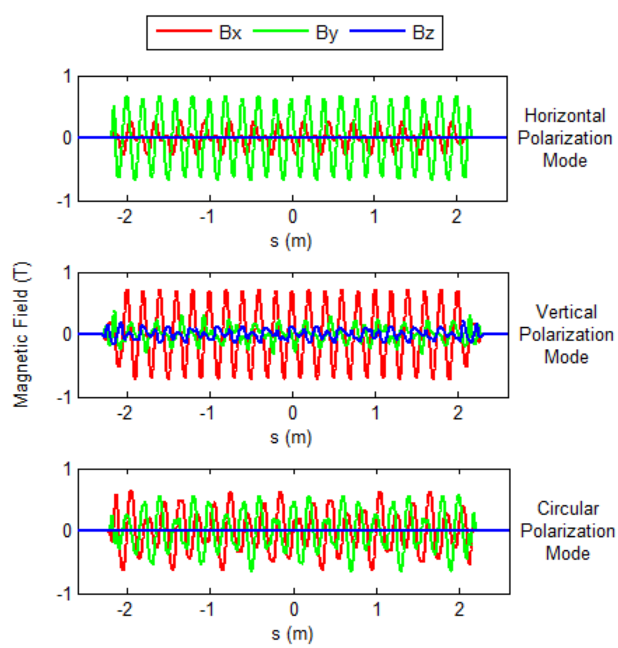

Figure 1: Magnetic field of the Knot-APPLE undulator at minimum gap.

Content from this work may be used under the terms of the CC BY 3.0 licence (© 2015). Any distribution of this work must maintain attribution to the author(s), title of the work, publisher, and DOI.

ISBN: 978-3-95450-168-7 doi:10.18429/JACoW-IPAC2015-TUPJE023

CONSIDERATION ON THE FUTURE MAJOR UPGRADES OF THE SSRF STORAGE RING

Z.T. Zhao, L.X. Yin, Y.B. Leng, B.C. Jiang, S.Q. Tian, M.Z. Zhang for the SSRF team
Shanghai Institute of Applied Physics, Shanghai 201800, P. R. China

Abstract

The SSRF storage ring began its user operation in 2009, currently it is operating at the energy of 3.5GeV, the natural emittance of 3.9 nm-rad and the beam current of 240 mA, serving for 13 beamlines with 9 IDs. Around 2020, there will be close to 40 operational beamlines at SSRF, which demand to further improve the performance of the existing storage ring, such as implementing the new lattice with superbends and installing 18 more new IDs. Looking for the future beyond Phase-II beamline project, a major upgrade towards a diffraction limited storage ring is under consideration. This paper presents the initial proposal on the ultimate storage ring upgrade for SSRF.

INTRODUCTION

The Shanghai Synchrotron Radiation Facility (SSRF) is a third generation light source, consisting of a 150 MeV electron linac, a full energy booster, a 3.5 GeV storage ring with circumference of 432m, and now 13 operational beamlines and 16 experimental stations. It started users' operation in May 2009 and already served more than 10000 users from all over China.

SSRF switched to top up operation [1] for routine user experiments in December 2012, its ring current had been gradually increased from 200mA to 240mA during the last 3 years. The major efforts for increasing the beam current is made on conditioning the superconducting RF cavity and suppressing beam instabilities. At present, the bunch filling pattern is shown in Fig. 1, four 125-bunch-trains separated by 55-empty-bucket gaps. While previous one is a uniform 550-bunch train, followed by a 170-empty-bucket gap. The main reason for such a filling pattern is to reduce the fast ion instability that is caused by high current and the newly installed undulators where the vacuum pressure is higher than the rest part of the ring.

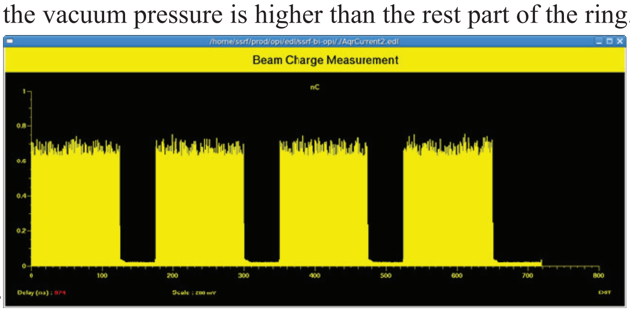

Figure 1: Bunch filling pattern of the SSRF storage ring.

Hybrid filling pattern has also been provided for users. A single bunch of 5 mA which is followed by a bunch train with current of 225 mA has been successfully run for the time resolution experiments. The time gap between single bunch and the bunch train is 110-empty-bucket gap as shown in Fig. 2.

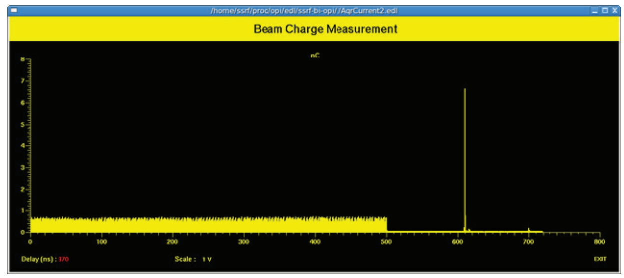

Figure 2: Hybrid bunch filling pattern in the storage ring.

The storage ring fast orbit feedback was successfully commissioned in 2013, and it has been implemented in users' operation since then. The system contains 60 fast correctors and 40 BPMs in each plane working at 10 kHz, controlling the orbit at the both end of straight sections [2]. The effective bandwidth is better than 100 Hz. The fast orbit feedback system works together with the slow orbit feedback system controlling the long term orbit stability to 0.26 μm and 0.25 μm (RMS) in horizontal and vertical planes respectively.

Over the past 3 years, five new insertion devices have been installed in the ring. Three of them are in vacuum undulators and two of which are dual canted with a canted angle 6 mrad. Another one is a double elliptical polarized undulator (DEPU) as shown in Fig. 3. The DEPU holds two undulators with period 58 mm and 148 mm respectively which can be shifted mechanically in horizontal plane to the electron beam orbit. The purpose of such a design is to provide soft X-rays with the photon energy from 20 eV to 2000 eV to one beamline. The additional one is a prototype of cryogenic permanent magnet undulator (CPMU) for performance evaluation. At present the phase error of this CPMU is under calibration and measurement through photon spectrum.

Figure 3: Twin EPU in the storage ring tunnel.

Content from this work may be used under the terms of the CC BY 3.0 licence (© 2015). Any distribution of this work must maintain attribution to the author(s), title of the work, publisher, and DOI.

ISBN: 978-3-95450-168-7 doi:10.18429/JACoW-IPAC2015-TUPJE032

UPDATES OF THE PAL-XFEL UNDULATOR PROGRAM

Dong Eon Kim, Moo-Hyun Cho, Young-Gyu Jung, Heung-Sik Kang, In Soo Ko,
Hong-Gi Lee, Sangbong Lee, Woul Woo Lee, Bong-Gi Oh, Ki-Hyeon Park, Hyung Suck Suh,
PAL, Pohang, KOREA
Suren Karabekyan, Joachim Pflueger, EU-XFEL, Hamburg, Germany

Abstract

Pohang Accelerator Laboratory (PAL) is developing a 0.1 nm SASE based FEL based on 10 GeV S-band linear accelerator named PAL-XFEL. At the first stage, PAL-XFEL needs two undulator lines for photon source. The hard X-ray undulator line requires 18 units of 5 m long hybrid-type conventional planar undulator and soft X-ray line requires 6 units of 5 m long hybrid type planar undulator with additional few EPUs for final polarization control. PAL is developing undulator magnetic structure based on EU-XFEL concepts. The key parameters are min pole gap of 8.3 mm, with period length 26 mm (HXU), 35 mm (SXU), and 5.0 m magnetic length. . In this report, the prototyping, and the development of pole tuning procedure, the impact of the background field error, and the effects of the girder bending on the optical phase error will be presented.

INTRODUCTION

The Pohang Accelerator Laboratory (PAL) has been developing SASE based light sources since 2011. The target wavelength is 0.1nm for hard X-ray SASE radiation, with 10 GeV class S-band linear accelerator. For soft X-ray SASE, 3.0 nm FEL radiation using 3.15 GeV electron beam is assumed. To achieve this target, a few key components like low emittance (0.5 μm) photo cathode RF gun, and EU-XFEL style out vacuum undulator system are being developed [1]. For undulator system, there will be 18 undulators for X-ray line and 6 planar undulators with additional two EPUs (Elliptically Polarized Undulator) are expected. The EPUs will be used for polarization control at the last stages of lasing. The major parameters of the X-ray FEL and undulator line is slightly changed recently and the updated parameters are shown in Table 1. A minor changes were the magnetic gap and period. The gap was changed from old 7.2mm to 8.3 mm resulting period change from 24.4 mm to 26.0 mm maintaining 0.1 nm SASE lasing at 10 GeV electron beam energy. The number of required units for soft X-ray SASE line is estimated to be 6 5 m long planar undulators with 2 additional EPUs. The major parameters of the HXU undulator system is summarized in Table 1. The parameters of the EPUs are under study now, and the magnetic pole gap is 10.0 mm with 44.0 mm magnetic period to match the resonance condition with the conventional hybrid undulator for soft X-ray undulator lines. The horizontal space between magnetic arrays are tuned to 4.0 mm to secure the transverse roll off of Keff within 0.50 mm to 5.0×10^{-4} at helical mode where Kx=Ky. At non-planar mode, Keff is defined by the usual formula $Keff^2 = Kx^2 + Ky^2$. A detailed design and quoting is going on and the final contract is expected to be early 2015.

Among the available five undulator lines in the undulator halls, only two undulator lines will be prepared during the construction period of year 2011-2105: a hard X-ray FEL line (HX1) with 18 undulators and a soft X-ray FEL line (SX1) with 8 undulators are anticipated. HX1 covers the wavelength range of λ=0.06 - 0.6 nm using a 4 to 10-GeV electron beam and uses linear polarization, variable gap, out-vacuum undulators. SX1 covers the wavelength of λ = 1.0 - 4.5 nm using a 3.15-GeV electron beam. In SX1, two EPUs (Elliptically Polarized Undulator) following six planar undulators will be used for polarization control at the last stages of lasing. An enough space is reserved in the undulator halls for the future upgrade to accommodate a total 29 undulators for HX1 and 16 undulators for SX1.

Table 1: Major Parameters of the HXU Undulator

Symbol	Unit	Nominal value
E	GeV	10.000
g	mm	8.30
λ_u	mm	26.0
L_{und}	5	5.0
λ_r	nm	0.100
B_{eff}	Tesla	0.8124
K		1.9727
Optical phase error	degree	Less than 7.0
Total number	EA	18

UNDULATOR SYSTEM

For the PAL-XFEL undulators, the EU-XFEL design and technology [2,3] was adopted and further developed. The EU-XFEL design is a well proven using standardization and optimization for mass serial production and was successfully used for the production of 91 undulators for the EU-XFEL

At PAL a full scale prototype undulator was built. It is based on the EU-XFEL concept with some modification reflecting different magnetic periods and pole gaps. In addition, precision tilt meters were attached to the girders to monitor the tilting and tapering of the undulator. Also the control systems are developed to be used in EPICs environment. A prototype is based on the old magnetic periods of 24.4mm and old magnetic gap of 7.2 mm had

Content from this work may be used under the terms of the CC BY 3.0 licence (© 2015). Any distribution of this work must maintain attribution to the author(s), title of the work, publisher, and DOI.

ISBN: 978-3-95450-168-7 doi:10.18429/JACoW-IPAC2015-TUPJE033

Content from this work may be used under the terms of the CC BY 3.0 licence (© 2015). Any distribution of this work must maintain attribution to the author(s), title of the work, publisher, and DOI.

A RESEARCH ON THE REVERSE TAPERING METHOD TO GAIN HIGH POWER POLARIZED PHOTON BEAM WITH FIXED WAVELENGTH

C. H. Shim, I. S. Ko, Pohang University of Science and Technology, Pohang 790-784, Korea
J. -H. Han, Y. W. Parc#, Pohang Accelerator Laboratory, Pohang 790-784, Korea

Abstract

Polarization of soft X-ray photon can be controlled with combination between planar undulators and helical ones. We need to give a reverse tapering to the planar undulators to make microbunching in the electron beam while the linearly polarized radiation power is depressed. In this case, however, resonance wavelengths in each planar undulator are different each other. Therefore, proper initial undulator parameter and tapering strength parameter have to be chosen to obtain high power polarized photon beam with fixed wavelength. In this research, method for deciding suitable reverse tapering is presented using simulation results of PAL-XFEL soft X-ray case with 10 GeV electron beam energy.

INTRODUCTION

In the soft X-ray regime, polarization control is essential for some experiments [1]. Applying the reverse tapering method to planar undulator section, the high degree of polarization of photon beam can be obtained by using only a couple of helical undulators, and this scheme is demonstrated at LCLS. [2,3].

Objective of undulator tapering is generally to obtain high radiation power by maintaining resonance condition according to decreasing electron beam energy [2]. In the reverse tapering case, however, resonance conditions in each planar undulator are different each other, so resonance wavelength is also changed along planar undulators. Therefore, appropriate initial undulator parameter and tapering strength parameter have to be selected to gain high power photon beam with fixed wavelength.

In this research, method for choosing suitable reverse tapering is presented using simulation results of PAL-XFEL soft X-ray case with 10 GeV electron beam energy. All simulations are performed as time-dependent model in GENESIS 1.3 using real beam properties [4].

THEORY

Reverse Tapering Method

In the reverse tapering method, undulator parameter a_w is increased along the undulator length as shown in Fig. 1 [2]. Bunching factor is growing while radiation power is quite suppressed compared with non-tapering case. Tapering strength parameter, β, is defined as

$$\beta = -\frac{\lambda_u}{4\pi\rho^2}\frac{a_w(0)}{1+a_w(0)^2}\frac{da_w}{dz}$$

where λ_u is period of undulator, ρ is FEL parameter,

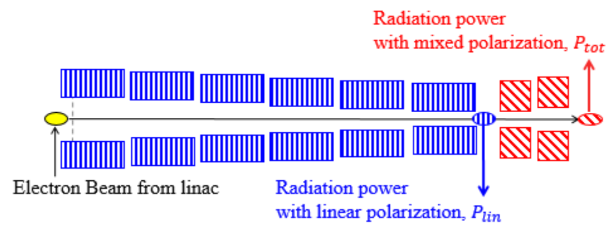

Figure 1: Schematic diagram for reverse tapering method. (Blue Box) Reverse tapered planar undulators (Red Box) Helical undulators.

$a_w(0)$ is initial undulator parameter and da_w/dz is derivative of undulator parameter along undulator length. When the reverse tapering method is applied, β is negative.

Polarization

Electric fields of linearly polarized radiation and circularly polarized radiation are given by the Eq. 1 [5].

$$\vec{E}_{lin} = E_{lin}\cos(kz - \omega t + \phi_{lin})\,\hat{x} \quad (1.a)$$

$$\vec{E}_{cir} = E_{cir}\cos(kz - \omega t + \phi_{cir})\,\hat{x} + E_{cir}\cos(kz - \omega t \pm \pi/2 + \phi_{cir})\,\hat{y} \quad (1.b)$$

The circularly polarized radiation is amplified at the same phase of linearly polarized radiation, so ϕ_{lin} is equal to ϕ_{cir}. Total electric field is given by the combination of two electric field equations and given by

$$\vec{E}_{tot} = \vec{E}_{lin} + \vec{E}_{cir} = (E_{lin} + E_{cir})\cos(kz - \omega t + \phi_{cir} - \theta)\,\hat{x} + E_{cir}\cos(kz - \omega t \pm \pi/2 + \phi_{cir})\,\hat{y} \quad (2)$$

The radiation power can be calculated from the electric field of radiation in Eq. 1 and Eq. 2 as follows [5]:

$$P_{lin} = E_{lin}^2 \quad (3.a)$$

$$P_{cir} = 2E_{cir}^2 \quad (3.b)$$

$$P_{tot} = (E_{lin} + E_{cir})^2 + E_{cir}^2 \quad (3.c)$$

In simulation, only P_{lin} and P_{tot} are obtained as shown in Fig. 1. So P_{cir} is calculated using relations above and it is induced as follows:

$$P_{cir} = P_{tot} - \sqrt{P_{lin}(2P_{tot} - P_{lin})} \quad (4)$$

Stokes parameter is also expressed in terms of P_{lin} and P_{tot} as given by Eq. 5 [5].

$$S_0 = (E_{lin} + E_{cir})^2 + E_{cir}^2 = P_{tot} \quad (5.a)$$

$$S_1 = (E_{lin} + E_{cir})^2 - E_{cir}^2 = \sqrt{P_{lin}(2P_{tot} - P_{lin})} \quad (5.b)$$

$$S_2 = 2(E_{lin} + E_{cir})E_{cir}\cos(\pi/2) = 0 \quad (5.c)$$

$$S_3 = 2(E_{lin} + E_{cir})E_{cir}\sin(\pi/2) = P_{tot} - P_{lin} \quad (5.d)$$

The fraction of circularly polarized radiation, $|S_3/S_0|$, is given by Eq. 6 [6].

$$\left|\frac{S_3}{S_0}\right| = \frac{P_{cir}+\sqrt{2P_{lin}P_{cir}}}{P_{lin}+P_{cir}+\sqrt{2P_{lin}P_{cir}}} = 1 - \frac{P_{lin}}{P_{tot}} \quad (6)$$

#young1@postech.ac.kr

ISBN: 978-3-95450-168-7 doi:10.18429/JACoW-IPAC2015-TUPJE034

A PRELIMINARY REPORT FROM LOUISIANA STATE UNIVERSITY CAMD STORAGE RING OPERATING WITH AN 11 POLE 7.5 TESLA WIGGLER

R. S. Amin, P. Jines, D. Launey, K. Morris, V. P. Suller, Y. Wang,
LSU CAMD, Baton Rouge, LA 70806 USA
N. Mezentsev, S. Khruschev, V. Lev, V. Shkaruba, V. Syrovatin, O. Tarasenko, V. Tsukanov, A. Volkov, A. Zorin,
BINP, Novosibirsk, Russia

Abstract
Louisiana State University installed a 7.5 T superconducting wiggler in May 2013 on the electron storage ring located at the Bennett Johnson, Sr. Center for Advanced Microstructures and Devices (CAMD). The wiggler's influence on betatron tunes and functions, orbit, lifetime, performance, and other relevant beam parameters are described. We further comment on device operations and modifications to ring operations that were necessary to provide light for both wiggler and dipole stations.

INTRODUCTION

Louisiana State University (LSU) operates the CAMD light source at the Center for Advanced Microstructures and Devices. This electron storage ring has been delivering synchrotron radiation (SR) regularly since 1992. The working energy of the storage ring is 1.3 GeV, and injection energy is approximately 180 MeV. CAMD has a circumference of 55.2 meters. There are 4 dispersion free straights and 8 dipoles operating at 1.48 Tesla. Each dipole chamber has two ports delivering SR with a critical photon energy of 1.6 keV. A 7 Tesla superconducting wavelength shifter installed in straight section 2 increased this critical photon wavelength to 7.95 keV for three x-ray beamlines. In 2007, a proposal was made to increase the amount of x-ray radiation being delivered to protein crystallography, x-ray absorption spectroscopy, and tomography experiment stations [1]. In May 2013, a 7.5 Tesla 11-pole multipole wiggler (MPW) with 4 additional fractional field poles was installed in CAMD's third straight section. This device has been delivering light routinely at 5.5 Tesla since October 2014.

The device was built by N. Mezentsev's group at Budker Institute for Nuclear Physics (BINP). Overall the layout is similar in design to SIBERIA-2's superconducting multipole wiggler. However, in terms of physical dimension and stored energy this device is the largest ever fabricated by BINP [2].

*Work supported by … NSF Grant Number: DMR-0923440
Louisiana State University

GENERAL MPW PARAMETERS

The CAMD MPW supplies 3 x-ray beamlines with a critical photon wavelength of 8.53 keV. The 11 main poles are used to generate SR While the two twin outer poles control trajectory by introducing ¼ and ¾ field. Basic parameters are listed in the Table 1.

Table 1: General Parameters

Parameter	Value
Poles	11 full; 2 ¾ field pole; 2 ¼ field pole
Peak Field	7.5 Tesla
Wiggler Pole Period	193.4 mm
Pole Gap	25.2 mm
Beam Aperture	15 mm by 80 mm
Physical Length (Magnet)	1594 mm
Field Energy Stored	≈ 850 kJ
Power Output at 7.5 T	7.38 kW at 100 mA
Superconducting Currents	205 A (central coils), 143 A (side coils)

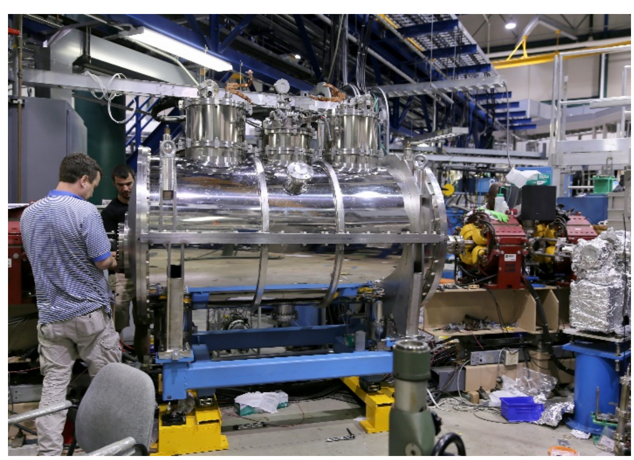

Figure 1: The MPW installed on the CAMD ring.

Content from this work may be used under the terms of the CC BY 3.0 licence (© 2015). Any distribution of this work must maintain attribution to the author(s), title of the work, publisher, and DOI.

ISBN: 978-3-95450-168-7 doi:10.18429/JACoW-IPAC2015-TUPJE035

Content from this work may be used under the terms of the CC BY 3.0 licence (© 2015). Any distribution of this work must maintain attribution to the author(s), title of the work, publisher, and DOI.

OPTIMIZATION OF TURN-BY-TURN MEASUREMENTS AT SOLEIL AND ALBA LIGHT SOURCES

M. Carlá, Z. Martí, G. Benedetti, Alba, Cerdanyola del Valles, Spain
L. Nadolski, Soleil, Saint Aubin, France

Abstract

Beam position monitor turn-by-turn measurements paves the way for fast storage ring lattice diagnostics. On the other hand turn by turn technique is by its very nature delicate, requiring an extensive system tuning and understanding. During last year several tests to retrieve linear model informations from turn by turn measurements have been carried out in collaboration between the synchrotron of Soleil and Alba. A routine to extract phase advance and betatron amplitude from turn by turn measurements has been developed. Moreover a first attempt to retrieve quadrupole errors from such observables has been done.

INTRODUCTION

To meet the required performance, modern synchrotron light sources demand a fine control over lattice parameters. Lattice assessment methods, usually employed used at Alba and Soleil, are based on slow orbit acquisition (i.e. LOCO [1–3].) The response of the beam orbit to a change of each dipole corrector is recorded and lattice parameters are then fitted to reproduce the experimental results. The robustness of such method resides in the precise but slow orbit change measurements that have to be repeated for a large number of correctors, until a response matrix is obtained. Turn-by-turn measurements represent a fast way to compare the behavior of the machine lattice with respect to the nominal model, resulting in a good candidate to implement rapid optics correction. To validate the capabilities of the turn-by-turn approach a measurement campaign has been launched in conjunction between the synchrotron of Soleil and Alba.

TURN-BY-TURN SETUP

In order to produce good observations of the transverse dynamics, the beam motion has to be excited coherently and kept coherent as long as possible. The excitation is produced by means of a magnetic pinger, with a characteristic pulse time shorter than the revolution period and a pulse profile as flat as possible [4, 5].

On the other hand the delicate coherent motion of electrons is easily washed out by second order effects jointly with the finite emittance of the beam. Especially the dependence of the transverse tunes on the kick amplitude and electrons energy (chromaticity). Such effect can be minimized by properly tuning the sextupoles in the ring [6].

Soleil

The Soleil storage ring is equipped with 122 beam position monitor (BPM) each of them connected to a Libera electron receiver. Even if such receiver system guarantees a high bandwidth, it is till not enought to discern the beam position sampled at successive turns. This phenomenon is commonly known as turn smearing. To cope with this inconvenience a post processing of the data is required, where the response function of the BPM to a single turn signal is deconvoluted from the recorded signal. The response function can be measured by injecting a short train of electron bunches in the ring and dumping it out after exactly one turn.

Alba

The Alba storage ring is equipped with 120 BPMs equipped with the Libera Brilliance receiver [7]. Such receiver can be reprogrammed with a non-standard firmware (MAF [8]), developed originally under request of ESRF, that is immune to the smearing effect. In MAF the turn mixing is avoided by substituting the narrow band infinite impulse response filter, that causes the smearing, with a finite impulse response filter obtained by means of a fixed time integration window. This different filter design requires a special setup procedure, where the integration window is synchronized with the train of bunches traveling in the ring. The synchronization was adjusted by scanning the delay of the window and looking for the maximum of the sum signal from the four BPM's buttons. The MAF design not only avoids the smearing effect but also ensures a lower noise, being the signal integrated only when the train of bunches transits through the BPM. The reduction of the integration time results thus in less noise entering the BPM's demodulation chain.

TURN-BY-TURN ANALYSIS

Turn-by-turn data have been analyzed using the interpolation approach described in [9], that ensures a very precise reconstruction of amplitude and phases information.

Lattice Jitter

In an ideal system without noise the tune signal measured by each BPM is expected to have the same frequency. The observed agreement between different BPM in the same shot is remarkable ($\sigma = 7.0{\times}10^{-7}$). On the other hand a shot to shot fluctuation of the tune frequency is evident($\sigma = 2.3 \times 10^{-4}$) even if small. A similar behavior, but of smaller entities, has been observed also at Soleil. No correlation between the tune fluctuation and the kick strength is observed, nor a simple trend in time of the tune variation. Most likely the source of such fluctuation resides in the residual line-ripple coming from quadrupoles power supplies. Figure 1 shows the tune jitter spectrum. Two main contributions, at 100 Hz and 300 Hz are clearly visible.

ISBN: 978-3-95450-168-7 doi:10.18429/JACoW-IPAC2015-TUPJE036

A NEW BENCH CONCEPT FOR MEASURING MAGNETIC FIELDS OF BIG CLOSED STRUCTURES

J. Campmany, F. Becheri, C. Colldelram, J. Marcos, V. Massana*, L. Ribó, J. Nicolás, CELLS-ALBA Synchrotron, 08290 Cerdanyola del Vallès, Barcelona, Catalonia, Spain

Abstract

The measurement of big closed magnetic structures is becoming a challenge of great interest. The main reason is the tendency towards building accelerators with high magnetic fields produced by small gap magnets, as well as the development of cryogenic or superconducting narrow-gap insertion devices. The usual approach, based on side-measurements made with a Hall probe mounted on the tip of a motorized arm mounted on a long granite bench is no more applicable to such closed structures. So, new concepts and approaches have been developed, mainly relying on complex devices that insert a Hall probe inside the magnetic structure maintaining the desired position by closed-loop controls. The main problem of these devices is that they are not general-purpose oriented: they need a special vacuum chamber, require a specific geometry of the magnetic structure, or do not provide 3D field-map measurements. We present in this paper a new bench that has been built at ALBA synchrotron that is simple, multi-purpose and can be a general solution for measuring big closed structures.

INTRODUCTION

The conceptual approach to design this new bench has been presented elsewhere [1],[2]. Basically, it consists in placing a very light Hall probe in the middle of a flexible belt that can be easily introduced inside a magnetic system. The edges of this belt are then attached to an external mechanical bench to position the Hall probe with a high degree of accuracy. Magnetic fieldmaps are recorded operating in on-the-fly mode: that is, acquiring the magnetic field values at the same time the Hall probe is moving along a path. The path is a set of straight lines oriented along the longitudinal direction (Z) that can be independently defined to scan any desired region.

For CELLS standardization reasons, we used step motors controlled via the Icepap motion driver system [3], developed by a collaboration participated by CELLS.

The main challenges that, if not solved, could have jeopardized the feasibility of this concept were:

- Vibrations of the flexible belt.
- Positioning Accuracy of the Hall probe.
- Synchronization between movement and acquisition.
- Alignment of Hall probe with respect to gravity.

The first challenge is related to the vibrational eigenvalues of the mechanical structure; the second to the straightness, linearity and flatness of the bench; the third to the real time control system; and the latter to the methodology used for measurements.

REQUIREMENTS

A general view of the bench is shown in Figure 1.

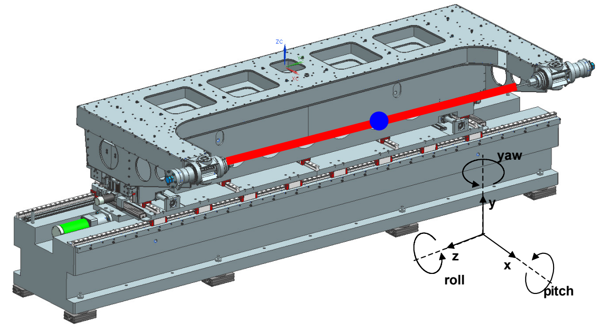

Figure 1: General view of the new Hall probe bench and reference system. Stretched belt is painted red, and Hall probe position is marked with a blue dot.

The specifications of the bench are shown in Table 1.

Table 1: Main Specifications

Magnitudes on top of Hall probe	Values
X positioning tolerance	$\pm 25\cdot 10^{-6}$ m
X stroke	0.2 m
Y positioning tolerance	$\pm 25\cdot 10^{-6}$ m
Y stroke	0.1 m
Z positioning tolerance	$\pm 10\cdot 10^{-6}$ m
Z stroke	1.2 m
Z positioning resolution	$10\cdot 10^{-6}$ m
Pith angle tolerance	$\pm 50\cdot 10^{-6}$ rad
Yaw angle tolerance	$\pm 100\cdot 10^{-6}$ rad
Roll angle tolerance	$\pm 50\cdot 10^{-6}$ rad
Eigenfrequency (Z direction)	> 50 Hz
On-the-fly velocity	$\sim 15\cdot 10^{-3}$ m/s

In order to fulfil the positioning and angular tolerances, the material for the bench basis is granite, and the linear guides and mechanical chain have been designed according to the usual high precision mechanics concepts.

Regarding vibrations, the key point is the fact that the Hall probe is placed on a stretched string, and therefore

Content from this work may be used under the terms of the CC BY 3.0 licence (© 2015). Any distribution of this work must maintain attribution to the author(s), title of the work, publisher, and DOI.

ISBN: 978-3-95450-168-7 doi:10.18429/JACoW-IPAC2015-TUPJE037

MAGNETIC MEASUREMENTS OF THE NSLS-II INSERTION DEVICES

M. Musardo#, D. Harder, C. A. Kitegi and T. Tanabe
National Synchrotron Light Source II, Brookhaven National Laboratory
Upton, New York 11973-5000, USA

Abstract

This paper presents the results and the recent progress in the magnetic measurements of the insertion devices (IDs) for the National Synchrotron Light Source-II (NSLS-II) at Brookhaven National Laboratory (BNL). A detailed analysis of the magnetic measurements is carried out for various IDs with particular attention at the influence of the magnetic field errors on the devices spectral performance. Several specific details of the measurements and the recent results from IDs commissioning are presented.

INTRODUCTION

The NSLS-II is a state-of-the-art electron storage ring of 3 GeV third generation light source at Brookhaven National Laboratory. NSLS-II has been designed and constructed to deliver photons with high average spectral brightness in the 2 keV to 10 keV energy range exceeding 10^{21} ph/s/0.1%bw/mm^2/mrad^2, and high spectral flux exceeding 10^{15} ph/s/0.1%bw. This performance requires the storage ring to support a very high-current electron beam (I = 500 mA) with a very small horizontal (down to 0.5 nm-rad) and vertical (8 pm-rad) emittance. [1].

NSLS-II will be able to accommodate more than 60 beam-lines in the final built-out for a wide-range of scientific programs, with future development of additional beam-lines through canted insertion devices and multiple hutches [2].

At the time of this report 13 insertion devices have been installed into the storage ring and are currently under commissioning and studies [3,4]. All these IDs were procured as a "turn-key" devices from main ID companies (Danfysik, HITACHI and Kyma).

They include 6 damping wigglers (DWs), utilized to achieve a low horizontal beam emittance and as broadband sources of very bright and high flux x-rays superior to conventional bend-magnet sources, 2 Apple-II type undulator with four movable arrays, for full polarization control and 5 In-Vacuum Undulator for hard X-Ray. The basic parameters characterizing the NSLS-II IDs installed so far are listed in Table 1.

MAGNETIC FIELD MEASUREMENTS

All insertion devices mentioned above underwent rigorous magnetic measurements before installation into the storage ring in order to validate the ID performance requirements and confirm the measurement data of vendors. Furthermore some IVUs went through magnetic retuning performed at BNL with vendor technicians in order to improve the magnetic field quality.

Table 1: NSLS-II Insertion Devices Installed

Cell ID	Beam line	Type	Length [mm]	Period [mm]	B_{PEAK} [Tesla]	Gap [mm]
23	CSX1 CSX2	Apple II	4.0 (2x2)	49.0	0.57 (C) 0.94 (V) 0.72 (H) 0.4 (45°)	11.5
10	IXS	IVU	3.0	22.0	0.78	7.4
3	HXN	IVU	3.0	20.0	1.03	5.2
11	CHX	IVU	3.0	20.0	1.03	5.2
5	SRX	IVU	1.5	21.0	0.9	6.2
19	FMX	IVU	1.5	21.0	0.9	6.2
28	XPD PDF	Hybrid PM	6.8 (2x3.4)	100	1.8	15
8	ISS	Hybrid PM	6.8 (2x3.4)	100	1.8	15
18	FXI	Hybrid PM	6.8 (2x3.4)	100	1.8	15

Magnetic Measurement Facility

The magnetic measurement system facility at BNL consists in a 3D Hall probe-mapping bench MMB-6500 for local magnetic field measurement and an Integrated Field Measurement System (IFMS) for first and second field integral measurement [5]. The IFMS is a versatile measurement system as it includes 3 different field integral measurement systems, a stretch wire system, a flipping coil system and a long board. The flipping coil has been used to measure IDs field integral.

A fully integrated SENIS 3-axis ultra-low noise probe, accurately recalibrated [6], is used as Hall sensor in order to measure three independent components of the magnetic field at single location. The Hall sensors arranged along longitudinal axis have a magnetic field sensitive volume of 150 *x* 1 *x* 150 µm, which allows very high-resolution measurements with a linearity error up to 2 T less of 0.15% and a good angular accuracy with an orthogonality error < 2°.

The full control of the measurement system is carried out using a LabView software. Recent developments have allowed the automation of ID gap/phase motions and

Work performed under the auspices of U.S. Department of Energy, under contract DE-SC0012704.
#musardo@bnl.gov

Content from this work may be used under the terms of the CC BY 3.0 licence (© 2015). Any distribution of this work must maintain attribution to the author(s), title of the work, publisher, and DOI.

ISBN: 978-3-95450-168-7 doi:10.18429/JACoW-IPAC2015-TUPJE038

IMPACT OF INSERTION DEVICES ON THE MAX IV STORAGE RINGS

S.C. Leemann*, H. Tarawneh, MAX IV Laboratory, Lund University, SE-22100 Lund, Sweden

Abstract

There will be multiple compensations employed for insertion devices in the MAX IV storage rings. Apart from well-known dipole corrections and previously detailed local and global linear optics matching, certain insertion devices in the MAX IV storage rings will also require nonlinear optics adjustments and/or skew quadrupole corrections. The goal of such corrections is ensuring sufficient dynamic aperture as well as low residual emittance coupling. This paper will present a few studies that rely on tracking through kick maps in order to quantify detrimental effects of insertion devices on dynamic aperture and vertical emittance, develop suitable countermeasures, and finally, verify restored storage ring performance.

INTRODUCTION

During the design phase of the MAX IV storage rings several example insertion devices (IDs) were used to develop compensation strategies [1–4]. This resulted in ID compensation schemes where the storage ring optics are matched in a two-stage process both locally and globally to each ID thus making the ID transparent to other users [3,4]. The first step is *local*: the beta functions of the achromats adjacent to the ID are matched to the ID by adjusting quadrupole gradients (implemented as a feedforward table depending on ID gap and phase settings). This is a rather fine adjustment because of the low beta functions in the ID straights. Nevertheless, a small phase advance leading to a tune shift for the entire ring results. This is then corrected in the second matching step: a *global* matching is carried out where quadrupole gradients around the ring are gently adjusted to restore the design working point (implemented in a feedback scheme relying on an online tune measurement). Ideally, the result of these two matching steps is that the ID becomes transparent to the rest of the ring. The beta functions in the sextupoles and octupoles are virtually unchanged and the working point is at its design value. Therefore, the chromatic and amplitude-dependent tune shifts (ADTSs) are restored to their design behavior thus replicating the tune footprint of the design lattice with its large dynamic aperture (DA) and good lifetime.

Already during the design process limits were set for acceptable multipole content in IDs [4] and used for ID specification. In the meantime, RADIA kick maps for the Phase I IDs [5] have been prepared so actual tracking studies can now be performed to verify the proposed compensation scheme leads to acceptable storage ring performance. The kick maps are inserted into the Tracy-3 lattice model and the optics matching is carried out (assuming that all first and second-order ID integrals have been canceled using dedicated dipole correctors at the IDs). The effect on optical functions, tune shifts, and coupling is then assessed and additional nonlinear and/or skew quadrupole matching requirements are derived where necessary. Performance of all optics adjustments combined is again verified using 6D tracking including imperfections (misalignments as well as field and multipole errors) [6] to determine overall resulting DA, lifetime, and coupling. Examples of such studies will be discussed in this paper. It should be pointed out, however, that several effects of IDs on the storage rings are not treated here: firstly, the effect of IDs on emittance, energy spread, bunch length, and lifetime can become severe in the ultralow-emittance lattice of the 3 GeV storage ring [7]; the effect of optics matching and choice of coupling on resulting brightness [8]; and finally, IDs can have many implications for collective behavior and instabilities; this is, however, also beyond the scope of this paper.

Optics Matching in the 3 GeV Storage Ring

In the 3 GeV storage ring local matching (cf. Fig. 1) is achieved by adjusting the quadrupole doublets (QFend/QDend) in the matching cells adjacent to the ID so the beam is over-focussed in the ID [1, 3]. This allows compensating the ID focusing without actually increasing the beam size in the ID. Global matching is then carried out by adjusting all QFend/QDend around the ring coherently by a small amount. Such corrections leave the optical functions in the unit cells virtually unchanged and the working point is exactly restored. Note that this matching does not involve excitation of the pole-face strips (PFSs) that are used to adjust the vertical focusing in the gradient dipoles.

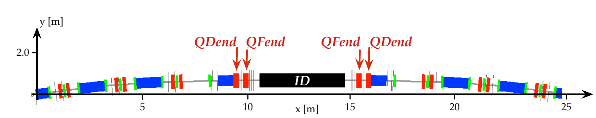

Figure 1: Schematic of an ID installed in a long straight section between two achromats of the 3 GeV storage ring. The two quadrupole families involved in the optics matching are indicated.

Furthermore, the 3 GeV storage ring lattice contains three octupole families that allow direct shaping of the ADTSs [9]. These can be used to counteract amplitude detuning that arises from strong IDs. Finally, all sextupoles and octupoles in the 3 GeV storage ring carry auxiliary coils that can be powered, among other ways, as a skew quadrupole. This opens the possibility for strong local coupling corrections around specific IDs.

Optics Matching in the 1.5 GeV Storage Ring

In the 1.5 GeV storage ring local matching (cf. Fig. 2) is achieved by adjusting the combined quadrupole/sextupole

* simon.leemann@maxlab.lu.se

Content from this work may be used under the terms of the CC BY 3.0 licence (© 2015). Any distribution of this work must maintain attribution to the author(s), title of the work, publisher, and DOI.

ISBN: 978-3-95450-168-7 doi:10.18429/JACoW-IPAC2015-TUPJE039

RECENT RESULTS ON THE PERFORMANCE OF Cs_3Sb PHOTOCATHODES IN THE PHIN RF-GUN

C. Hessler, E. Chevallay, S. Doebert, V. Fedosseev, I. Martini, M. Martyanov, CERN, Switzerland

Abstract

For the CLIC drive beam a photoinjector option is under study at CERN as an alternative to the thermionic electron gun in the CLIC baseline design. The CLIC drive beam requires a high bunch charge of 8.4 nC and 0.14 ms long trains with 2 ns bunch spacing, which is challenging for a photoinjector. In particular the required long and high intensity laser pulses cause a degradation of the beam quality during the frequency conversion process, which generates the ultra-violet laser beam needed for standard Cs_2Te photocathodes. To overcome this issue Cs_3Sb cathodes sensitive to green light have been studied at the high-charge PHIN photoinjector since a few years. In this paper recent measurements of fundamental properties of Cs_3Sb photocathodes such as quantum efficiency, cathode lifetime and dark current from summer 2014 will be presented, and compared with previous measurements and with the performance of Cs_2Te photocathodes.

INTRODUCTION

The Compact Linear Collider (CLIC) is a future e^+e^- collider, which is currently under study by a worldwide collaboration led by CERN [1]. It is based on a novel two-beam acceleration scheme, which requires a high peak and average current drive beam accelerator for generating 12 GHz RF power needed to accelerate the main beam. In the baseline design, the drive beam is foreseen to be produced by a thermionic electron gun and a sub-harmonic bunching system [2]. However, the bunching system generates parasitic satellite pulses, which get lost during the acceleration process. This can create radiation issues and will reduce the system power efficiency.

These limitations can be avoided if a photoinjector is used as a drive beam source and the required time structure for the CLIC beam combination scheme [1] is already produced on the laser side. Such a photoinjector option for the CLIC drive beam is currently under study at the high-charge photoinjector PHIN [3], which was originally developed and constructed to study its feasibility as drive beam source for the CLIC Test Facility 3 (CTF3). Practically satellite-free beam production with the required time structure has been demonstrated at PHIN [4].

However, the CLIC drive beam parameters are challenging for a photoinjector (Table 1) and efforts are on-going to improve the PHIN parameters towards CLIC requirements [5]. In particular the combination of 140 µs long trains, 8.4 nC bunch charge, 2 ns bunch spacing and 50 Hz macro-pulse repetition rate for CLIC is beyond the parameters of any existing photoinjector. This unique parameter set has a strong impact on the photocathode lifetime and also on the laser system: The required long and high-intensity laser pulses cause a degradation of the beam quality during the 4^{th} harmonics frequency conversion process, which generates the ultra-violet laser beam needed for standard Cs_2Te photocathodes. Since the 2^{nd} harmonics conversion process to produce green light is not affected by this problem, a potential solution is to use photocathodes sensitive to green light such as Cs_3Sb or K_2CsSb instead of Cs_2Te cathodes. For the CLIC photoinjector studies Cs_3Sb has been chosen because the existing production setup for Cs_2Te could be used, which made it possible to extensively profit from the experience gained with Cs_2Te. In this paper the latest results of the Cs_3Sb photocathode studies at PHIN will be presented. In parallel, R&D work on the surface characterization of photocathodes [6] and further development of the laser system are also on-going at CERN.

Table 1: PHIN and CLIC Design Parameters

Parameter	PHIN	CLIC
Charge / bunch (nC)	2.3	8.4
Train length (µs)	1.2	140
Bunch spacing (ns)	0.66	2.0
Bunch rep. rate (GHz)	1.5	0.5
Number of bunches	1800	70000
Macro pulse rep. rate (Hz)	5	50
Charge / train (µC)	4.1	590
Beam current / train (A)	3.4	4.2
Bunch length (ps)	10	10
Charge stability	<0.25%	<0.1%
Cathode lifetime (h) at QE > 3% (Cs_2Te) or QE > 0.5% (Cs_3Sb)	>50	>150
Norm. emittance (µm)	<25	<100

PHIN PHOTOINJECTOR

Layout

The PHIN photoinjector is installed at an off-line test stand at CTF3 (Fig. 1). It consists of a 2.5 cell RF cavity operated at 3 GHz and two solenoids, which provide the focusing of the electron beam. A test beam line is available with various diagnostic elements for beam measurements. The electron beam is produced by illuminating a Cs_2Te or Cs_3Sb photocathode with an ultra-

Content from this work may be used under the terms of the CC BY 3.0 licence (© 2015). Any distribution of this work must maintain attribution to the author(s), title of the work, publisher, and DOI.

ISBN: 978-3-95450-168-7 doi:10.18429/JACoW-IPAC2015-TUPJE040

SURFACE CHARACTERIZATION AT CERN OF PHOTOCATHODES FOR PHOTOINJECTOR APPLICATIONS

I. Martini, E. Chevallay, V. Fedosseev, C. Hessler, H. Neupert, V. Nistor, M. Taborelli, CERN, Geneva, Switzerland

Abstract

R&D on photocathodes takes place at CERN within the CLIC (Compact Linear Collider) project. Photocathodes are produced as thin films on Oxygen Free copper substrate using a co-deposition technique, and characterized in a dedicated laboratory with a DC photo-electron gun. A new UHV carrier vessel compatible with CERN's XPS (X-ray Photoelectron Spectroscopy) analysis equipment has been commissioned and is used to transport photocathodes from the production laboratory to perform a systematic study of different compounds used as photoemissive materials. In this paper photocathodes used in a RF photoinjector will be characterized and the correlation of their surface properties with their performance will be investigated.

INTRODUCTION

Within the CLIC (Compact Linear Collider) project, feasibility studies of a photoinjector option for the drive beam as an alternative to its baseline design using a thermionic electron gun [1] are on-going. This R&D program covers both the laser and the photocathode side. The main challenge for a drive-beam photoinjector is to achieve high bunch charges, long trains and high bunch repetition rates together with sufficiently long cathode lifetimes. Cs_2Te cathodes, sensitive to ultra-violet (UV) laser beam, produced at CERN showed good quantum efficiency and reasonable lifetime in the high-charge PHIN RF photoinjector [2]. However the CLIC design parameters are more demanding (Table 1). The available laser pulse energy in UV for 140 µs long pulse trains is currently limited due to a degradation of the beam quality during the 4th harmonics conversion process. Using green laser beam in combination with Cs_3Sb cathodes would overcome this limitation.

Both Cs_3Sb and Cs_2Te photocathodes were produced at CERN by co-deposition process and tested in the PHIN RF photoinjector (more detail in ref. [3]). In this paper the cathode surface composition is analysed through XPS technique and correlated to the cathode performance.

CATHODES PRODUCTION AND CHARACTERIZATION

In the CERN photoemission laboratory the cathodes are produced by co-deposition technique resulting in high Quantum Efficiency (max QE~20% for Cs_2Te, max QE~7% for Cs_3Sb) [4,5]. The different chemical elements (Cs, Te or Sb) are evaporated at the same time to mix together in the vapour phase before the deposition onto the OFE copper substrate.

Table 1: CLIC and PHIN Beam Parameters

Parameter	CLIC	PHIN
Charge/bunch (nC)	8.4	2.3 (nominal) 9.2 (achieved)
Bunch length (ps)	10	10
Bunch rep. rate (GHz)	0.5	1.5
Number of bunches	70000	1800
Train length (µs)	140	1.2
Charge/train (µC)	590	4.1
Macro pulse rep. rate (Hz)	50	5
Charge stability (%)	<0.1	<0.25
Beam current/train (A)	4.2	3.4
Cathode lifetime (h) at QE>3% (Cs_2Te), QE>0.5% (Cs_3Sb)	>150	>50

The cathodes are illuminated with a UV (or green for Cs_3Sb) laser beam during the deposition in order to measure the QE evolution and optimize the process accordingly. The deposited layer thicknesses vary between tens to hundreds of nm [5].

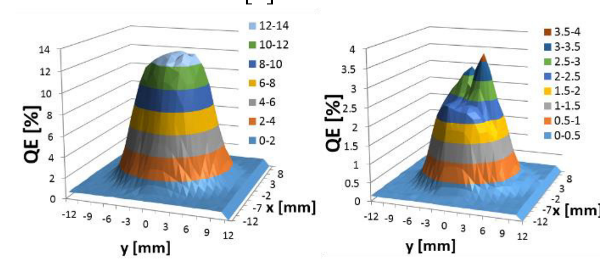

Figure 1: QE maps of Cathode #198 (Cs_2Te) as newly produced (left) and used in the RF photoinjector (right).

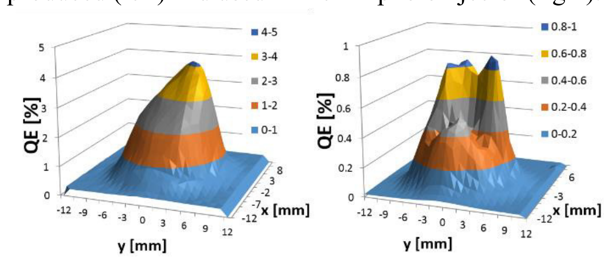

Figure 2: QE maps of Cathode #199 (Cs_3Sb) as newly produced (left) and used in the RF photoinjector (right).

The QE maps (see Fig. 1 and Fig. 2) are obtained in the photoemission laboratory scanning the cathode surface with a small spot size laser beam while the produced charge

Content from this work may be used under the terms of the CC BY 3.0 licence (© 2015). Any distribution of this work must maintain attribution to the author(s), title of the work, publisher, and DOI.

ISBN: 978-3-95450-168-7 doi:10.18429/JACoW-IPAC2015-TUPJE041

PROGRESS ON A COMPACT ACCELERATOR DESIGN FOR A COMPTON LIGHT SOURCE*

K. Deitrick[1†], J.R. Delayen[1,2], B.R.P. Gamage[1], G.A. Krafft[1,2], T. Satogata[1,2]
[1] Center for Accelerator Science, Old Dominion University, Norfolk VA, 23529, USA
[2] Thomas Jefferson National Accelerator Facility, Newport News VA, 23606, USA

Abstract

A compact Compton light source using an electron linear accelerator is in design at the Center for Accelerator Science at Old Dominion University and Jefferson Lab. We report on the current design, including beam properties through the entire system based on a full end-to-end simulation, compare current specifications to design goals, and target areas for improvement.

INTRODUCTION

Compton Light Source

At present, there is a high level of interest in an inverse Compton light source with a compact floor plan due to the wide variety of applications such a system could facilitate. To this end, a preliminary design was developed and presented, with the necessary electron beam and resulting x-ray beam properties shown in Table 1 [1].

Table 1: Electron Beam Parameters at Collision, Compton Source Parameters

Parameter	Value	Units
Energy	25	MeV
Bunch charge	10	pC
Repetition Rate	100	MHz
Average current	1	mA
Normalized $\epsilon_{\rm rms}$	0.1	mm-mrad
$\beta_{x,y}$	5	mm
FWHM bunch length	3.0 (0.9)	psec (mm)
RMS energy spread	7.5	keV
X-ray energy	Up to 12	keV
Photons/crossing	1.6×10^6	
Flux	1.6×10^{14}	photon/sec
Average brilliance	1.5×10^{15}	photons/(sec-mm^2-mrad^2-0.1% BW)

Simulation Tools

A number of accelerator codes were used to develop an end-to-end simulation. CST Microwave Studio© (CST) is an electromagnetic (EM) field solver [2]. SUPERFISH is also an EM field solver, provided the geometry is cylindrically symmetic, developed by Los Alamos [3]. The tracking through the accelerating section was performed by ASTRA (A Space-charge TRacking Algorithm), which tracks particles through user-defined external fields [4]. Space charge was taken into account throughout, and the image charge due to the cathode was included within the gun.

After emerging from the linac, the beam dynamics were calculated by `elegant` [5]. Translating the final bunch produced by ASTRA into the SDDS format required by `elegant` was done by a specific function provided within the package for that purpose.

ACCELERATION

Electron Gun

The electron gun is a 500 MHz superconducting RF (SRF) quarter-wave design, originally based on the shape proposed by Harris et al. [6]. The design is highly reentrant in order to mitigate the growth of the transverse normalized emittance due to space charge. In order to remove a surface tangential discontinuity near the cathode, the design was slightly altered. The RF properties of the altered design are presented in Table 2 [7].

Table 2: RF Properties of the 500 MHz Quarter Wave Electron gun at $E_{\rm acc} = 1$ MV/m

Parameter	Value	Units
Frequency of accelerating mode	499.3	MHz
λ/4	150	mm
Design β	0.95	
Stored energy	44	mJ
QR_s	83.5	Ω
R/Q	154	Ω
Peak electric surface field (E_P)	3.67	MV/m
Peak magnetic surface field (B_P)	6.64	mT
E_P/B_P	1.81	mT/(MV/m)

In order to study the beam dynamics of a bunch, the EM fields of the gun calculate by SUPERFISH were exported and translated into the format required by ASTRA. A 10 pC bunch consisting of 2000 electrons with a plateau longitudinal distribution of length 24 ps, σ_r of 0.5 mm, and negligible initial emittance or transverse momentum was generated and tracked by ASTRA through the gun. Both the space charge of the bunch and the mirror-image contribution of the cathode were included in this simulation. The properties of the beam after the exit of the gun (15 cm from

* Partially authored by Jefferson Science Associates, LLC under U.S. DOE contract NO. DE-AC05-6OR23177.
† kdeit001@odu.edu

Content from this work may be used under the terms of the CC BY 3.0 licence (© 2015). Any distribution of this work must maintain attribution to the author(s), title of the work, publisher, and DOI.

ISBN: 978-3-95450-168-7 doi:10.18429/JACoW-IPAC2015-TUPJE042

TRANSVERSE TUNES DETERMINATION FROM MIXED BPM DATA *

P. Zisopoulos, Y. Papaphilippou, F. Antoniou, CERN, Geneva, Switzerland
A. S. Müller, E. Hertle, ANKA, Karlsruhe, Germany

Abstract

Decoherence due to non-zero chromaticity and/or amplitude dependent tune-shift, but also damping mechanisms can affect the accurate tune determination by leaving a limited number of turns for frequency analysis of the turn by turn (TbT) position data. In order to by-pass these problems, Fourier analysis of mixed TbT data from all BPMs can be employed. The approach is applied in two different accelerators, a hadron collider as the LHC and a synchrotron light source as the ANKA storage ring. The impact in the accuracy of the method in the case of missing BPM data is also discussed.

INTRODUCTION

The most common technique for measuring the tune involves application of refined Fourier analysis on recorded beam position data. In the presence of decoherence, the available interval of turns for analysis is limited [1]. An alternative method exists [2], [3], which allows a very fast and accurate tune determination and consists of combining the data from all the BPMs and analysing them.
In this paper, this method is tested on TbT data from the ANKA electron storage ring and the Large Hadron Collider (LHC). The Numerical Analysis of Fundamental Frequencies (NAFF) [4] is employed for the frequency analysis. The analysis is repeated after lowering the noise levels of the TbT data with the Singular Value Decomposition (SVD) method [5] and comparisons are carried out.

DESCRIPTION OF THE METHOD

The method requires the mixing of the original TbT BPM data. More specifically, if the number of BPMs is M, and their TbT signal is of the form $x_M = [x_M[1]x_M[2]...x_M[N]]$, where N the number of turns, the data from all BPMs can be mixed together in the form $\tilde{x} = [x_1[1]x_2[1]...x_M[1]...x_1[N]...x_M[N]]$. In this way, the sampling rate becomes $\frac{1}{M}$ and the new tunes are scaled with respect to the old ones as $\tilde{Q} = \frac{Q}{M}$, where $\tilde{Q}$ and Q are the new and old measured tunes respectively. A one turn periodic error exists, due to the lack of BPM symmetry neither in the longitudinal position nor to the machine optics which introduces an extra frequency modulation without affecting the results. Rescaling the new frequencies $\tilde{Q}$ with M, can determine the integer and fractional part of the betatron tune.

* The research leading to these results has received funding from the European Commission under the FP7 Research Infrastructures project EuCARD-2, grant agreement no.312453

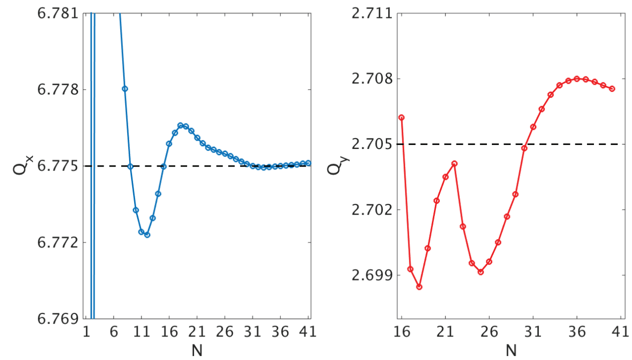

Figure 1: Tune measurements for ANKA. Horizontal tune is in the left column and the vertical tune in the right column. The black dashed line is the measurement produced from the ANKA tune-tracker.

MEASUREMENTS FOR ANKA

ANKA is a third generation light source which features a storage ring with a circumference of 110.4 m. Electron bunches are accelerated to a nominal energy of 2.5 GeV for the production of synchrotron radiation. Betatron oscillations are excited by using the injection kickers and the kick lasts for roughly 3 μs, i.e. 9 turns. Transverse beam position data are recorded from 35 BPMs for about 2000 turns. The ANKA tune-tracker [6] determines tunes of q_x=0.77 and q_y=0.70 for the horizontal and vertical plane respectively. The integer parts of the tunes are Q_x =6 for the horizontal plane and Q_y=2 for the vertical. The frequency analysis of the vertical TbT data shows strong transverse coupling in the frequency spectrum. This can be explained from the fact that the kick delivered to the bunches is horizontal.

In Fig. 1, results from tune measurements using the mixed TbT data method, are shown with respect to the number of turns. The method needs less than 10 turns to determine the horizontal tune and converge to a value within 40 turns. Regarding the vertical plane, this method needs 16 turns for the tune measurement due to the transverse coupling, while convergence is obtained in 37 to 45 turns. This is testified in the top plots of Fig. 2 where the absolute difference between consecutive tune values is presented as a function of the number of analysed turns. This difference becomes of the order of 10^{-4} within 25 turns for the horizontal plane and within 35 turns for the vertical plane. The trend of both curves is decreasing and oscillating with respect to the number of turns due to decoherence. The analysis is repeated after the original TbT data are decomposed in their singular modes and modes with not important information are eliminated. The amplitude modulation, due to the local beta functions, is removed with normalization of the data

Content from this work may be used under the terms of the CC BY 3.0 licence (© 2015). Any distribution of this work must maintain attribution to the author(s), title of the work, publisher, and DOI.

ISBN: 978-3-95450-168-7 doi:10.18429/JACoW-IPAC2015-TUPJE044

LOCAL ORBIT RESPONSE MATRIX MEASUREMENT AT SLS

Masamitsu Aiba and Michael Böge, PSI, Villigen, Switzerland

Abstract

The experimental determination of linear optics is essential to achieve a high performance ring accelerator. One of the methods, linear optics from closed orbits, is widely employed to correct linear optics. Due to the ring nature, a quadrupole error at a location of the ring affects the entire orbit response measurement data. The orbit response, however, can be localised to a certain region of the ring when an orbit feedback (or orbit correction) is applied to the rest of the ring. The quadrupole errors located in the region, where the feedback is acting, then have no impact, and the ring optics can be examined locally. An application of this technique to the Swiss light source is discussed.

INTRODUCTION

The experimental determination of linear optics is essential to achieve a high performance ring accelerator. One of the methods, linear optics from closed orbits (LOCO) [1], is widely employed to correct linear optics. The orbit response matrix (ORM) is entered into the LOCO algorithm as an observable. It is the difference of beam positions at the beam position monitors (BPMs) that are measured by changing the corrector excitation currents. Since ORM is determined by the lattice focusing, the ring optics can be corrected by minimising the deviation of ORM from the ideal, model ORM (ORM deviation).

We applied LOCO to the Swiss Light Source (SLS) storage ring [2] and found significant discrepancy in the result as discussed in the next section. This motivated us to develop a method to examine the ring optics locally, i.e. "local orbit response matrix" (LORM) measurement. We present first measurements and our findings.

LOCO AT SLS

The relevant parameters of the SLS storage ring are listed in Table 1 and the result of LOCO correction iteration is shown in Fig. 1.

Table 1: SLS Storage Ring Parameters

Parameter	Value	Unit
Circumference	288	m
Beam energy	2.4	GeV
Number of TBA cells	12	-
Betatron tunes (H/V)	20.43/8.74	-
Number of BPMs/correctors	73/73	-
Number of quadrupoles	177	-

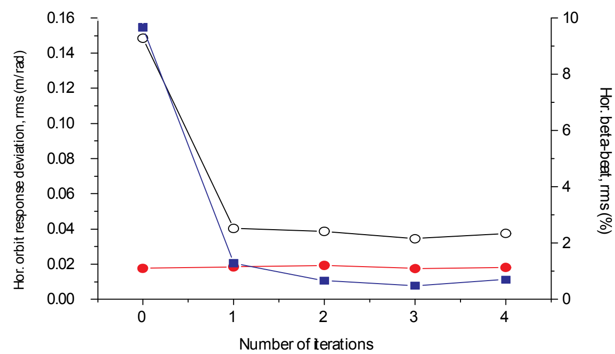

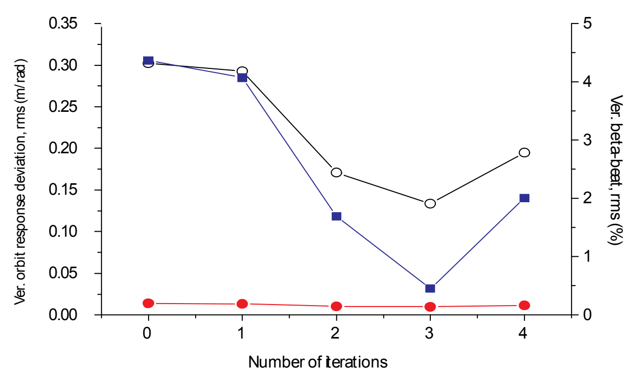

Figure 1: LOCO correction iteration result. The red curve is the ORM deviation after LOCO fit, and the black curve is the ORM deviation after another LOCO fit that excludes the quadrupole strengths from the fitting parameters. The ORM deviation is represented as single rms value over many ORM elements. The blue curve is the beta-beat found from LOCO fit. It is noted that the beta-beat is not found directly from LOCO measurement. Instead, it is inferred from the optics model by applying the quadrupole corrections found from the fit. The noise level (statistical error) of ORM measurement is 0.01 m/rad rms.

Figure 1 was obtained from LOCO optics correction iteration *with the machine*: we measure ORM, compute possible quadrupole corrections, vary the quadrupole excitation currents accordingly and measure again ORM. To compute the quadrupole corrections, the model ORM is fitted to the measured ORM by varying the quadrupole strengths, the corrector calibrations and the BPM calibrations. The coupling terms between the horizontal and vertical planes are not used in this study because the correction of beta functions is main concern. We apply singular value decomposition (SVD) for the fit with appropriate singular value cut (see Ref. [2] for detail).

The ORM deviation after the fit corresponds to the red curve in Fig. 1. We performed another fit at each iteration step with the corrector and BPM calibrations, excluding

Content from this work may be used under the terms of the CC BY 3.0 licence (© 2015). Any distribution of this work must maintain attribution to the author(s), title of the work, publisher, and DOI.

ISBN: 978-3-95450-168-7 doi:10.18429/JACoW-IPAC2015-TUPJE045

Content from this work may be used under the terms of the CC BY 3.0 licence (© 2015). Any distribution of this work must maintain attribution to the author(s), title of the work, publisher, and DOI.

ROUND BEAM OPERATION IN ELECTRON STORAGE RINGS AND GENERALISATION OF MOBIUS ACCELERATOR

Masamitsu Aiba, Michael Ehrlichman, and Andreas Streun, PSI, Villigen, Switzerland

Abstract

"Round beam" rather than a flat beam is preferable for a significant fraction of the beamline users in light sources. It is realised by equally distributing the natural emittance into the horizontal and vertical planes. There are a few approaches for the emittance distribution, and here we explore the so-called Mobius accelerator scheme, where a transverse (horizontal-vertical) emittance exchange results at each turn of beam revolution. The original proposal of Mobius accelerator was based on a set of five (or six) successive skew quadruples, requiring a dedicated long straight section. We generalise the Mobius accelerator to find other possible configurations. Applications to a light source storage ring lattice and a tracking result are also presented.

INTRODUCTION

A significant fraction of the beamline users at Swiss light source (SLS) prefer a "round beam" rather than a flat beam, and hence we study possible options in the context of a planned SLS upgrade, where the storage ring will be replaced with a very low emittance ring while utilising the existing building and injector complex [1]. For a small emittance beam, the emittance growth due to intra bunch scattering (IBS) can be significant, and thus a mitigation of the emittance growth is another motivation.

The coupling scheme is realised by equally distributing the natural emittance into the horizontal and vertical planes. There are a few approaches for the emittance equalisation. One method is to utilise a linear coupling resonance, where the horizontal and vertical emittances are exchanged over a period shorter than the radiation damping time. The other method that we explore in this study is the so-called Mobius accelerator [2].

GENERALISATION OF MOBIUS ACCELERATOR

The Mobius accelerator was originally proposed by Talman [2] and tested at CESR [3]. The transverse particle coordinates are interchanged at a location of the storage ring, and thus an immediate horizontal-vertical emittance exchange results at each turn of beam revolution. The synchrotron radiation induced emittance growth and damping is thus distributed equally among the two modes. The result is each mode has half the natural emittance. The coordinate interchange can be realised with five (or six) successive skew quadrupoles – Mobius insertion − as proposed in [2]. The requirements for the Mobius insertion are

- interchanging the transverse particle coordinates,
- and matching to the closed ring lattice parameters.

The Mobius insertion represented in a 4-by-4 transfer matrix is an off-diagonal block matrix,

$$\begin{bmatrix} 0 & D \\ D & 0 \end{bmatrix} \text{ with } D = \begin{bmatrix} 1 & L \\ 0 & 1 \end{bmatrix}. \tag{1}$$

The first requirement is obviously fulfilled with the above matrix. The second requirement is fulfilled when the lattice parameters (with skew quadrupoles turned off) are the same for the horizontal and vertical planes at both ends of the Mobius section and when the length L is adjusted to be the length of the Mobius insertion. It is straightforward to switch between the nominal operation mode (flat beam) to the round beam mode, simply turning on and off the skew quadrupoles.

It is of interest to explore possible configurations different from the above mentioned one not only for the Mobius accelerator but also for a coordinate interchange in a beam transport line. For example, a slice emittance measurement can be performed in both planes with a given transverse deflection cavity, which streaks the beam either in the horizontal or the vertical plane.

General Configuration

We assume arbitrary transfer matrices between skew quadrupoles to represent a general beam transport line:

$$(M_e)S_nR_nS_{n-1}R_{n-1}\cdots R_1S_1(M_s) \tag{2}$$

where S is the transfer matrix for skew quadrupole and R is an arbitrary uncoupled transfer matrix, which may include normal quadrupoles. The original configuration with five skew quadrupoles is also represented with the above notation with M being a drift matrix. The matrices M_e and M_s in parenthesis are discussed later.

Multiplying at the transfer matrix in a brute force manner generates many terms in the equations we need to solve. The equations are, however, significantly simplified using the normalised coordinates. The transfer matrix R in the normalised coordinate system is then simply a rotation matrix, and a thin skew quadrupole is represented as

$$\begin{bmatrix} 1 & 0 & 0 & 0 \\ 0 & 1 & -K & 0 \\ 0 & 0 & 1 & 0 \\ -K & 0 & 0 & 1 \end{bmatrix} \tag{3}$$

where K is the normalised skew quadrupole strength, k, multiplied by the length of the magnet, l, and the "effective" beta function,

$$K = \sqrt{\beta_x\beta_y}kl, \tag{4}$$

ISBN: 978-3-95450-168-7 doi:10.18429/JACoW-IPAC2015-TUPJE046

INVESTIGATION OF THE INJECTION SCHEME FOR SLS 2.0

A. Saa Hernandez* and M. Aiba, PSI, Villigen, Switzerland

Content from this work may be used under the terms of the CC BY 3.0 licence (© 2015). Any distribution of this work must maintain attribution to the author(s), title of the work, publisher, and DOI.

Abstract

SLS 2.0, an upgrade of the Swiss Light Source (SLS), aiming at a natural horizontal emittance in the range of 100 pm, is planned and under study. This will be achieved by replacing the current magnet lattice of the electron storage ring by a new multibend achromat magnet lattice, while reusing the injector chain and most of the existing infrastructures. The new low emittance ring will impose more restrictive constraints on injection due to a smaller machine aperture and a very compact lattice, dominated by non-linearities. We performed a study to find the optimum injection scheme for SLS 2.0 among the conventional and more advanced schemes; namely multipole kicker injection (off-axis and also on-axis matched to the off-momentum closed orbit) and longitudinal injection.

INTRODUCTION

SLS 2.0, a low emittance upgrade of the Swiss Light Source (SLS) is planned and under study [1]. This will be achieved by replacing the current lattice of the storage ring by a new multibend achromat lattice [2], while reusing the injector chain and most of the existing infrastructures. Various lattices are currently being developed in an iterative process. The latest stable lattice version released, named *ah04n*, provides a natural horizontal emittance of 183 pm·rad in a 288 m ring circumference. But this lattice, as most low emittance lattices, imposes restrictive constraints on injection due to a small machine aperture (10 mm inner beam pipe) and dynamic aperture (~8 mm for on-momentum particles and <5 mm for particles with a momentum deviation of ± 3%). Additionally, the lattice is very strong-focusing and is dominated by non-linearities as natural chromaticities of -163/-70 in units of 2π (horizontal/vertical) have to be corrected. We investigated different injection options aiming to fulfill the following soft (S) and hard (H) constraints:

- (H) top-up compatible.
- (H) compatible with the booster output parameters: horizontal (vertical) emittance of 7 (1) nm·rad, bunch length of 19 mm and momentum spread of 0.08%.
- (S) avoid the use of a kicker bump, in order to improve the photon beam stability.
- (S) transverse on-axis injection in order to relax the requirements on dynamic aperture. The option of a round beam, under consideration at this stage of the design, could only be implemented if injection is (quasi) on-axis.
- (S) compact layout, ideally compatible with the installation of other devices in the same straight section.

* angela.saa-hernandez@psi.ch

INJECTION SCHEMES FOR SLS 2.0

Different injection options for SLS 2.0 are briefly described. After their drawbacks are considered they are either discarded or further developed.

Conventional Injection

The conventional injection scheme, also used at SLS [3], employs a static septum and a dynamic magnetic chicane (or kicker bump). The bump rises to bring the closed orbit to the vicinity of the septum at the time of injection and falls within a few electron beam revolutions to prevent the injected bunch being lost at the septum. In this scheme, the injected bunch is transversely separate from the circulating bunches and performs large betatron oscillations before it is merged into the circulating beam due to synchrotron radiation damping.

We built an injection insertion into the lattice *ah04n* on the long (10 m) straight section where the present transfer line from the booster ends. The injection point (IP) remains located in the middle of the straight and the four dipole kickers are symmetrically positioned at both sides of the IP. Kicker deflections of 2.2 mrad would be needed to generate a bump of 7 mm amplitude. Assuming a bump half-sine time of 4 μs, the kickers would be active for 4 turns. If a septum thickness of 2.5 mm and a conservative clearance value of 2.5 mm are also assumed the beam could not be injected with a distance smaller than 7.5 mm of the bumped orbit. The resulting oscillations around the stored beam during the first turns would have amplitudes >10 mm, bigger than the physical and dynamic apertures and therefore not feasible. A horizontal beta function bump could also be created with the use of the matching sections at both sides of the straight, but the consequent break of lattice symmetry is not desired at this point of the design. Therefore this injection scheme is not our favourite option for SLS 2.0.

An on-axis version of this scheme was implemented in LEP [4] and has also been investigated. In this scheme the kickers are situated on a dispersive straight section and the bunch is injected on-axis, but with a momentum offset, onto the corresponding closed orbit. We rapidly discarded this option for SLS 2.0 since the required dispersion (7.5 mm / 3 % = 2.5 m) is not compatible to the low emittance lattice design.

ISBN: 978-3-95450-168-7 doi:10.18429/JACoW-IPAC2015-TUPJE047

Content from this work may be used under the terms of the CC BY 3.0 licence (© 2015). Any distribution of this work must maintain attribution to the author(s), title of the work, publisher, and DOI.

DESIGN STUDIES FOR AN UPGRADE OF THE SLS STORAGE RING

A. Streun, M. Aiba, M.Böge, M. Ehrlichman, Á. Saá Hernández, PSI, Villigen, Switzerland

Abstract

An upgrade of the Swiss Light Source (SLS) would replace the existing storage ring by a low aperture multibend achromat lattice providing an emittance of about 100–200 pm at 2.4 GeV, while maintaining the hall, the beam lines and the injector. Since emittance scales inversely cubically with the number of lattice cells, an SLS upgrade is challenged by the comparatively small ring circumference of only 288 m. A new concept for a compact low emittane lattice is based on longitudinal gradient bending magnets for emittance minimization and on anti-bends (i.e bends of opposite field polarity) to disentangle dispersion and horizontal beta function in order to provide the optimum matching to the longitudinal gradient bends while minimizing the contribution to chromaticity.

INTRODUCTION

The Swiss Light Source (SLS) is in user operation since 2001. The storage ring is a 12 triple bend achromat (TBA) lattice providing an equilibrium emittance of 5.0 nm at 2.4 GeV beam energy. SLS had to accommodate experiments covering a wide range of photon energies and polarizations, which resulted in a lattice layout with 3 different types of straights: 6 × 4 m, 3 × 7 m and 3 × 11.5 m. In 2005/06 the FEMTO insertion for laser-beam slicing and three 3 Tesla superbends were installed in order to provide sub-ps X-ray pulses and hard X-rays up to 45 keV. Today the SLS is fully equipped with 18 user beam lines and delivers about 5000 hours of user beam time per year at an availability of 97.3% (10 years average) [1].

In recent years, progress in technology and lattice design, mainly pioneered by the MAX IV project [2], introduced a generational change in the field of electron storage rings: multibend achromat (MBA) lattices based on the miniaturization of vacuum chambers and multipole magnets provide an increase of photon beam brightness by 1–2 orders of magnitude and a corresponding increase of spatial coherence. Thus, in a few years from now, the third generation lights sources may no longer be competitive with respect to most advanced experimental techniques like coherent imaging, ptychography, resonant inelastic X-ray scattering etc. So, like for many other facilities, an upgrade is considered for the SLS too. It is planned to replace the storage ring by a new one providing 100–200 pm emittance, while keeping the shielding walls, the beam line source points and the injector complex.

However, the circumference of the SLS is rather small compared to other machines, thus replacing the TBAs by MBAs alone will not provide the desired emittance: just scaling the lattice of MAX IV to the energy and size of SLS results in an emittance of about 1 nm, which would not justify a major upgrade. Also damping wigglers are precluded by lack of space.

A potential way out is based on a new type of lattice cell providing five times lower emittance, which will be presented in the next section. Design studies for an upgraded SLS based on this cell will be presented in the section after the next. The issues of dynamic aperture optimization, error sensitivity, injection schemes and possible round beam operation are treated elsewhere [3–6].

A NEW LOW EMITTANCE CELL

The Problem of the TME Cell

The minimum theoretical emittance (TME) ϵ^{TME} which can be provided by a gradient-free bending magnet of given deflection angle is well known [7], but a periodic and symmetric lattice cell which fulfills the matching conditions for the horizontal beta function $\beta_{xo}^{\mathrm{TME}}$ and the dispersion η_o^{TME} at the bend center, is of little practical use: the dispersion production of a bend is given by its curvature, $\eta'' = h = eB/p$, and acts like a defocusing force on the dispersion. Adjusting the horizontally focusing quadrupoles to match exactly the TME conditions for the dispersion *and* the beta function and finding a periodic solution, i.e. $\beta_x' = \eta' = 0$ a the cell ends, results in an over-focused beta-function and a very high horizontal betatron phase advance of 284.5°. The lattice cell thus needs a second focus in order to accommodate the excess betatron phase, so it becomes rather long and the optics is overstrained. As a consequence, only relaxed TME-cells are commonly used, where the cell phase advance is well below 180°, and the emittance is about a factor 3–6 larger than the TME. Defining dimensionless parameters

$$F = \epsilon/\epsilon^{\mathrm{TME}} \qquad b = \beta_{xo}/\beta_{xo}^{\mathrm{TME}} \qquad d = \eta_o/\eta_o^{\mathrm{TME}}$$

elliptic iso-emittance contours $F(b,d)$ are obtained as shown in Fig. 1 (left) [8].

Construction of a low emittance cell with unstrained optics proceeds by two steps:

1. disentangle beta function and dispersion using anti-bends,
2. minimize emittance using longitudinal gradient bends.

Anti-bends

Anti-bends (AB), i.e. bends of negative field forming a star-shaped rather than a polygonal lattice have been considered in the 1980s and 90s for isochronous rings or for enhanced radiation damping (“wiggler lattice”). The potential for emittance reduction had been noticed [9] but was never exploited.

ISBN: 978-3-95450-168-7 doi:10.18429/JACoW-IPAC2015-TUPJE048

Content from this work may be used under the terms of the CC BY 3.0 licence (© 2015). Any distribution of this work must maintain attribution to the author(s), title of the work, publisher, and DOI.

ORBIT CORRECTION AND STABILITY STUDIES FOR ULTRA-LOW EMITTANCE STORAGE RINGS

M. Böge, M. Aiba, A. Streun, PSI, Villigen, Switzerland

Abstract

Ultra-low emittance storage rings exhibit extremely strong focusing and sextupolar chromaticity corrections. The therefore mandatory excellent centering of the closed orbit in the small aperture magnets is a challenging task and necessitates a proper beam diagnostics and correction layout. Correction and stability studies for a possible ultra-low emittance upgrade of the Swiss Light Source [1] are presented.

LAYOUT FOR BEAM POSITION MONITORS AND DIPOLE CORRECTORS

In order to perform a proper optics and orbit correction of ultra-low emittance rings it is necessary to provide a proper sampling of the optical functions. Especially the horizontal beta function and the horizontal dispersion, which are strongly suppressed in the center of the bending magnets in order to achieve small horizontal emittance [2], need to be corrected close to their design values in order to achieve ultimate performance. The necessary information in the center of the bends can be provided by means of photon beam position monitors (photon BPMs) [3]. It does not necessarily need correction capability at the same location since orbit response matrix (ORM) based optics correction methods [4] and the correction of dispersion orbits by means of the RF frequency only need the orbit information at these locations. In this context it is important to note that the detection of dispersion related orbit deviations is strongly improved by providing orbit measurements at large and small horizontal dispersion values.

The correction of the non-dispersive closed orbit can be provided by correctors adjacent to the bending magnets. Furthermore horizontal dipole correctors would be inefficient due to the very small horizontal beta function (see Fig. 1 on the next page). Otherwise it is highly desirable to have pairs of horizontal and vertical dipole correctors adjacent to electron BPMs (RF BPMs) in order to allow for transparent localized corrections especially in the vicinity of insertion devices in the case of an ultra-low emittance light source. For a comprehensive review of orbit control techniques refer to [5].

For one of the presently favored layouts (Version AD05F) of the upgrade of the Swiss Light Source (SLS-2) [1] 192 RF BPMs and the same number of adjacent horizontal/vertical correctors have been chosen in order to provide the necessary orbit correction capability. For the measurement of the beam positions in the centers of the bending magnets five photon BPMs have been added in each of the twelve arcs which adds another 60 photon BPMs to the system. Figure 1 on the next page depicts one arc section of SLS-2 (Version AD05F) together with the optical functions and the additional photon BPMs (#1-#5). Figure 2 summarizes the photon and RF BPM layout with 20+64=84 BPMs for one 3rd of the ring corresponding to a horizontal and vertical phase advance of 13.14 and 3.585 respectively. The BPMs are shown as "+" with the value of the corresponding horizontal (blue), vertical (red) beta function and the horizontal dispersion (green).

SCHEME FOR ORBIT CORRECTION

In the SLS-2 case the orbit correction is carried out utilizing a Singular Value Decomposition (SVD) [6] based orbit correction algorithm, which "inverts" the (192+60)x192 non-square ORMs treating the horizontal and vertical plane independently and using all 192 eigenvalues, which becomes feasible due to a "good-natured" SVD eigenvalue spectrum, a proper Beam-Based Alignment (BBA) [7] of quadrupoles and adjacent BPMs (half the element-to-element error corresponding to 4μm assumed in simulation) and a low noise BPM [8] ($\approx$50 nm resolution corresponding to 19-bit resolution assuming $\pm$25 mm maximum orbit excursions) and correction system ($\approx$1 nrad resolution corresponding to 20-bit for maximum corrector strength of $\pm$1 mrad) [9].

LAYOUT OF MAGNET SUPPORTS

Common magnet supports (girders) are very important in order to reduce the element to element alignment error in low emittance storage rings like SLS [10, 11]. They allow to reach a small relative misalignment of adjacent magnets on a girder (8 μm assumed in the simulation for SLS-2) which are the main source of orbit distortions and coupling. A single magnet structure containing different magnetic elements [12] serves the same purpose but removes the possibility of aligning magnets within the structure. For SLS-2 the choice of the magnet structure has not yet been made. But this does not matter for the simulation since in both cases the magnet structures are realized as "correlated" misalignments. For the simulation 12 girders of $\approx$18 m length have been chosen which cover the 12 arcs. 25 μm of absolute and 10 μm of relative misalignment from one girder to the next have been allowed. These small errors have been chosen since the simulation does not contain first turn steering ("beam threading") in order to get a closed orbit within the aperture limitations for large errors. Furthermore it is assumed that the ring has been re-aligned during commissioning time based on beam and mechanical survey data [13–15].

ISBN: 978-3-95450-168-7 doi:10.18429/JACoW-IPAC2015-TUPJE049

TPS LINAC RELOCATION AND BEAM TEST OF THE LTB TRANSFER LINE

H.P. Chang#, C.L. Chen, C.S. Fann, K.L. Tsai, Y.S. Cheng, S.Y. Hsu, K.T. Hsu, A.Y. Chen, Y.C. Lin, J. Liu, and K.K. Lin
National Synchrotron Radiation Research Center, Hsinchu, Taiwan

Abstract

The Taiwan Photon Source (TPS) 150 MeV linac has been relocated from its 2011 test site to the TPS linac tunnel in 2014. After functional test of the linac hardware modules, the beam parameters were carefully examined at a 31-degree bend diagnostic beam line LTD (linac to beam dump) and compared with previous results. Then, the 150 MeV electron beam was delivered to the linac to booster transfer line (LTB) for beam commissioning. The beam optics matching at both the LTB entrance (i.e. linac exit) and the LTB exit (i.e. injection point of booster) was performed for injection optimization purpose. The LTB lattice setting was verified in the beam steering through LTD and LTB with the help of diagnostics tools such as beam profile monitors (SM) and beam position monitors (BPM). The overall performance of the linac and LTB will be described in this report.

INTRODUCTION

The goal of TPS linac relocation and beam test of the LTB is to meet the requirement of the TPS beam commissioning planned in 2014. Relocation of the TPS linac was well prepared in 2013 and initiated when the TPS linac tunnel was available for the linac installation in 2014. Beam test of the linac and LTB has been performed on time in August 2014 according to the beam test scenario set by the Taiwan Atomic Energy Council [1-3].

We summaries the milestone of the TPS linac relocation processes as followings:

- May 2011 ~ Nov 2013: The linac was under the routine operation after its acceptance. The main tasks were performed during this period includes: familiar with system operation, training platform for colleagues, trouble shooting and failure analysis, and preparation for relocation.
- Nov 2013 ~ Feb 2014: The preparation for relocation includes the cable labelling of power and signal cables, disassembly of acceleration sections and waveguides.
- Feb 2014 ~ May 2014: On-site installation of functional modules and their testing.
- Jun 2014 ~ Aug 2014: Linac rf processing, beam test of linac, LTD, and LTB.

The overall performance of the linac and LTB transfer line will be described in the following sections.

TPS LINAC RELOCATION

The 150 MeV TPS linac has been operating at its test site since the acceptance test in 2011 [4,5]. It was shut down and packaged for the relocation in November 2013 and then it was moved to the TPS linac tunnel in February 2014. Linac installation was finished in three months. It included the installation and functional test of each linac module such as electron gun, the magnets (solenoid, corrector, and quadrupole), modulators etc. The rf processing was then performed for the preparation of beam test. Figures 1 and 2 show the relocated TPS linac and power supplies at the TPS site.

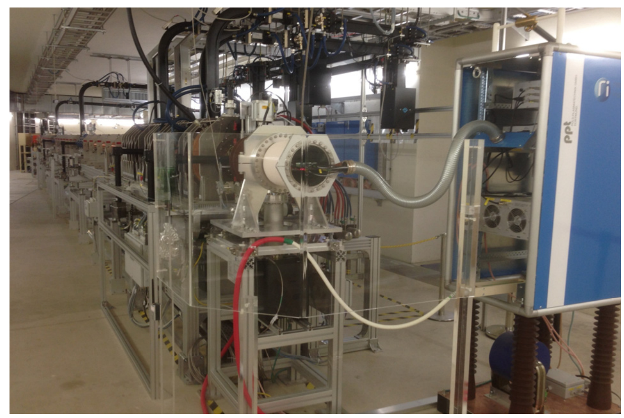

Figure 1: The linac installed in the TPS tunnel.

Figure 2: The power supply area of the TPS linac.

BEAM PARAMETERS MEASUREMENT

As illustrated in Figure 3, the 31-degree bend LTD is used as the linac diagnostic beam line [6]. Beam parameters at the exit were verified with profile monitoring, lattice manipulation and compare with the matching calculation.

The linac and LTB were ready for beam test in July 2014. On August 1, the Atomic Energy Council issued the permission of TPS radiation protection plan for beam commissioning. Beam test of linac and LTB was

#peace@nsrrc.org.tw

Content from this work may be used under the terms of the CC BY 3.0 licence (© 2015). Any distribution of this work must maintain attribution to the author(s), title of the work, publisher, and DOI.

ISBN: 978-3-95450-168-7 doi:10.18429/JACoW-IPAC2015-TUPJE050

DESIGN OF A RESONANT TRANSITION RADIATION SOURCE IN THE SOFT X-RAY RANGE

P. Wang, K. C. Leou, Department of Engineering and System Science, NTHU, Hsinchu, Taiwan
N.Y. Huang, W.K. Lau, A.P. Lee, NSRRC, Hsinchu, Taiwan

Abstract

Resonant transition radiation (RTR) can be generated from multi-layer structures when they are driven by relativistic electron beams. In consideration of using the NSRRC 90 MeV photoinjector as driver, we examined the feasibility of generating narrow-band soft x-rays from various multi-layer structures. Based on analytical theory, the expected angular-spectral distribution and photon yield of these radiators are calculated and compared.

INTRODUCTION

The feasibility of using multi-layer structures for generation of RTR in soft x-ray range is being investigated. We tentatively targeted the radiation energy of these structures centred at 2 keV and 620 eV. Radiation near this photon energy ranges found to be useful in research areas such as imaging of biomolecules, atom and molecular physics. The low-emittance NSRRC photoinjector system will be used to drive such RTR sources. In this system, the MeV electron beam from the laser driven photo-cathode rf gun are accelerated to its maximum energy of 90 MeV. The nominal parameters of the drive beam used in this study are listed in Table 1.

Table 1: Parameters of the Electron Beam Generated From the NSRRC Photoinjector

Beam energy	90 MeV
Emittance	0.8 mm-mrad
Bunch length	2.2 psec
Bunch Charge	100 pC

RESONANT TRANSITION RADIATION

The existence of transition radiation (TR) was predicted by Ginzburg and Frank in 1949[2]. For a charged particle traveling across the boundary between two media of different dielectric constants, the radiation fields can be calculated with classical electromagnetic theory. In the x-ray range, the dielectric constant can be described by Drude model adequately. The angular-spectral distribution of transition radiation from the boundary of two media being excited by a single electron at normal incidence is [3]:

$$\frac{d^2W_{TR}}{d\Omega d\omega} = \frac{e^2}{4\pi^2 c^3}\omega^2 \sin^2(Z_1 - Z_2)^2 \tag{1}$$

where

$$Z_{1(2)} = \frac{4c}{\omega[\gamma^{-2} + \theta^2 + (\omega_{p1(2)}^2/\omega^2)]} \tag{2}$$

$\omega_{p1(2)}$ is the plasma frequency of material 1 (or 2).

For an N-layer structure which is fabricated by interleaved stacking of material 1 with thickness l_1 and material 2 with thickness l_2, the angular-spectral distribution of RTR can be calculated from the following equation with the phase shift as well as absorption in materials are considered[3, 4]:

$$\left(\frac{d^2W_{TR}}{d\Omega d\omega}\right)_N = \left(\frac{d^2W_{TR}}{d\omega d\Omega}\right)F_1F_N \tag{3}$$

where the factor F_1 describes the inner-foil resonance such that

$$F_1 = 1 + \exp(-\sigma_1) - 2\exp(-\sigma_1/2)\cos(2\varphi_1) \tag{4}$$

and F_N describes the inter-foil resonance as

$$F_N = \frac{F_{Nn}}{F_{Nd}} \tag{5}$$

$$F_{Nn} = 1 + \exp(-N\sigma) - 2\exp(-N\sigma/2) \times \cos[N(2\varphi_1 + 2\varphi_2)]$$

$$F_{Nd} = 1 + \exp(-\sigma) - 2\exp(-\sigma/2) \times \cos(2\varphi_1 + 2\varphi_2)$$

where

$$\varphi_{1(2)} = l_{1(2)}/Z_{1(2)},$$

$$\sigma_{1(2)} = \mu_{1(2)}l_{1(2)},\ \ \sigma = \sigma_1 + \sigma_2.$$

$\mu_{1(2)}$ is the x-ray absorption coefficient of material 1(2).

From the equations of F_1 and F_N, the resonance conditions of RTR can be obtained.

$$\varphi_1 = (2n-1)\pi/2 \tag{6}$$

$$\varphi_1 + \varphi_2 = m\pi \tag{7}$$

Content from this work may be used under the terms of the CC BY 3.0 licence (© 2015). Any distribution of this work must maintain attribution to the author(s), title of the work, publisher, and DOI.

ISBN: 978-3-95450-168-7 doi:10.18429/JACoW-IPAC2015-TUPJE052

BUNCH COMPRESSION IN THE DRIVER LINAC FOR THE PROPOSED NSRRC VUV FEL

N.Y. Huang#, W.K. Lau, A.P. Lee, NSRRC, Hsinchu, Taiwan
A. Chao, K. Fang, M.H. Wang, J. Wu, SLAC, Menlo Park, CA 94025, USA

Abstract

A bunch compressor is designed for the S-band driver linac system of the proposed NSRRC VUV free electron laser (FEL). Instead of using a more conventional rf harmonic linearizer, one main feature of this compressor is to use electron linearization optics to correct the nonlinearity in the energy-time correlation of the electron bunch longitudinal phase space. The strategy of compressor design will be discussed by an analytical calculation and particle tracking simulation. The beam dynamics which include the collective instabilities such as the space charge effects, the wake fields and the coherent synchrotron radiation (CSR) effects are discussed.

INTRODUCTION

A photocathode rf gun driver linac system for a proposed FEL facility by making maximum use of existing hardware at National Synchrotron Radiation Research Center (NSRRC) is under study [1]. The baseline design is a fourth harmonic high gain harmonic generation (HGHG) FEL seeded by a 266 nm laser to generate VUV radiation at 66.5 nm. The layout of the proposed facility is shown in Fig. 1. The length of the accelerator system from the gun cathode to the exit of the last linac section is about 28 m and the length of the diagnostics and FEL stations is about 8 m. The whole facility tightly fits into the existing $38\text{m}\times5\text{m}$ tunnel.

Generally, the electron beam after the bunch compressor has the profile of a banana shape instead of a single straight line in the longitudinal phase space. The high order dispersion term of the bunch compressor and the high order energy chirp of the accelerating rf wave are the origin of these nonlinearities. These nonlinearities set the limitation of compression in bunch length and lead to undesirable current spikes in the compressed bunch. In order to control this nonlinear effect, usually a higher harmonic rf section is added at the upstream of the compressor. However, such a linac section together with its klystron system requires additional expense. In this study, a magnetic compressor with linearization optics by the introduction of quadrupole and sextupole magnets is applied instead [2, 3]. The setup of this injector system is considered to be much more cost-effective.

BUNCH COMPRESSOR WITH LINEARIZATION OPTICS

Assume the energy of injected electron is relativistic, there is no relative phase slippage between the rf field and the electron, the energy of an electron after rf acceleration in a traveling wave constant gradient accelerating structure can be expressed as

$$E_f(z) = E_{i0}(1+\delta_i) + eV_0\cos(\phi_0 - kz), \qquad (1)$$

where V_0, k, ϕ_0 are the accelerating peak voltage, the wave vector and the initial rf phase respectively, δ_i is the initial uncorrelated energy spread which is induced by rf and space charge effect in the gun, z is the particle's longitudinal position relative to the bunch center. In this report, we define the bunch head as the electron with large relative longitudinal position, i.e. with relative earlier arrival time. The relative energy spread after passing through an rf section is [3]

$$\delta(z) = \frac{E_f(z) - E_{f0}}{E_{f0}} = a\delta_i + h_1 z + h_2 z^2 + h_3 z^3 + \ldots, \qquad (2)$$

where $a = E_{i0}/E_{f0}$ is the adiabatic damping factor and

$$\begin{cases} h_1 = \dfrac{keV_0}{E_{f0}}\sin\phi_0, \ 1^{\text{st}} \text{ order energy chirp} \\ h_2 = -\dfrac{k^2 eV_0}{2E_{f0}}\cos\phi_0, \ 2^{\text{nd}} \text{ order chirp} \\ h_3 = -\dfrac{k^3 eV_0}{6E_{f0}}\sin\phi_0, \ 3^{\text{rd}} \text{ order chirp} \end{cases}. \qquad (3)$$

The signs of the 1st order and the 3rd energy chirp depend on the operation of initial rf phase. The 2nd order energy chirp is always negative if the initial phase is for electron acceleration. A negative first order energy chirp $h_1<0$ means the bunch tail has higher energy than the bunch head. The chirped beam is then sent to a dispersive region for bunch compression. The longitudinal position of an electron traversing the dispersive region is described as

$$z_f = z_i + R_{56}\delta + T_{566}\delta^2 + U_{5666}\delta^3 + \ldots, \qquad (4)$$

where R_{56}, T_{566} and U_{5666} are the first, second and third order longitudinal dispersion. Neglect the initial high order correlations of energy spread, the longitudinal position of an electron can be expressed by combining Eq.2 and Eq.4 as,

#huang.ny@nsrrc.org.tw

Content from this work may be used under the terms of the CC BY 3.0 licence (© 2015). Any distribution of this work must maintain attribution to the author(s), title of the work, publisher, and DOI.

ISBN: 978-3-95450-168-7 doi:10.18429/JACoW-IPAC2015-TUPJE053

HARDWARE IMPROVEMENTS AND BEAM COMMISSIONING OF THE BOOSTER RING IN TAIWAN PHOTON SOURCE

H. J. Tsai, J. Y. Chen, M. S. Chiu, P. C. Chiu, P. J. Chou, K. H. Hu, Y. C. Liu, F. H. Tseng, K. T. Hsu, C.C. Kuo, G. H. Luo and C. T. Chen
National Synchrotron Radiation Research Center, Hsinchu 30076, Taiwan

Abstract
Taiwan Photon Source (TPS), a low emittance 3-GeV third-generation synchrotron light source, began its hardware integration testing, safety checkout and beam commissioning on August 12, 2014 [1]. The booster ring and the storage ring share the same tunnel in a concentric fashion; the booster ring has circumference 496.8 m, the largest among light source facilities in operation. A combined-function FODO lattice is adopted for the booster ring with natural emittance 10 nm-rad. After hardware improvements were completed, the commissioning of the beam in the booster ring began on December 12 and attained the 3-GeV design energy on December 16.

INTRODUCTION

Because of constraints at the site, the TPS booster ring shares the same tunnel with the storage ring [2]. The circumference of the booster ring is 498.6 m, the largest booster ring of light source facilities in operation. To reduce the number of magnets, dipole magnets combined quadrupole and sextupole components were adopted, as in SLS and ALBA [3, 4]. The sizes of magnets and vacuum chambers are optimized to save space, construction cost and power consumption. The major parameters of the TPS booster are listed in Table 1. The imperfection issues in hardware integration and commissioning results are reported in this article.

Table 1: Major Parameters of the TPS Booster Ring

Booster parameters	
Circumference	496.8 m
Length of straight section	6.02 m
Harmonic number	828
RF frequency	499.654 MHz
Bending radius, ρ	12.223 m
Betatron tune , ν_x/ν_y	14.380/9.302
Natural chromaticity, $\xi_x/\ \xi_y$	-16.82/-13.24
Momentum compaction	0.0024735
Damping partition, $J_x/J_y/J_e$	1.81/1.00/1.19
Energy spread at 3 GeV	0.095174 %
Natural emittance at 3 GeV	10.32 nm rad
Damping time, $\tau_x/\tau_y/\tau_e$, at 3 GeV	9.4/16.9/14.2 ms
Damping time, $\tau_x/\tau_y/\tau_e$, at 150 MeV	75/136/115 s
Energy loss per turn at 3 GeV	586 keV
Rate of ramping repetition	3 Hz

HARDWARE IMPROVEMENTS

Most installation work in the booster ring was completed by the end of July, 2014. The 150-MeV beam from the Linac to the entrance of the booster ring was available in mid-August; field acceptance tests and tuning of power supplies for the booster magnets were concurrently conducted with beam commissioning due to very tight installation schedule. Beam-based testing of the hardware and improvement of the booster subsystem were in progress. Several hardware glitches were discovered; the solutions were implemented swiftly, for example, the repair of a burned power supply of a booster dipole magnet due to overheating in a protection circuit board while conducting a test with full power rating at high power, the reduction of flat-top field variation of injection kicker from ±2% to ±0.4% and the residual field of post-pulse from +5% to ±0.4% for injection kicker with ferrite load, etc.

At the beginning of September, having the first turn in the booster ring was easily obtained by beam steering; after optimization of transfer efficiency and minimized of the charge loss in the Linac and transfer line, a multi-turn circulating beam was observed; the beam survived up to 35 ms in mid September, but it did not show up capturing and beam storage. We tried to correct the distortions of the beam orbit within 4 mm and to scan the RF frequency, phase and gap voltage but without beam capture phenomena. At the same time, we found that the corrector strengths were about three times the simulated values including the misalignment and tolerance of magnet-field. The vacuum pipe, made of stainless steel (SUS304), has a small elliptic cross section, 35 mm x 20 mm, and thickness 0.7 mm in booster. At the initial stage of beam commissioning, dimension distortions and misalignments of the pipes were critical. More care was taken to realign the chambers' and the magnets' positions. The key setback that stalled the progress of testing the booster hardware was found on November 12. The pipes had a high relatively permeability (ranging from 1.2 to 2.0), which induced from cold-drawn during manufacture [5] without proper annealing process. These unqualified chambers were taken apart and treated in vacuum oven up to 1050 °C, and then re-installed within three weeks. The relative permeability of the pipes, after that treatment, was reduced to be within 1.01 [6].

Several issues were encountered that jeopardized the stability and injection efficiency of the beam; three major problems were encountered, which the booster launching condition deviated 2 mm from optimum because of a leakage field of the DC extraction septum in the horizontal plane, which a random injection kicker strength decreased about -2 % due to misfiring induced on

Content from this work may be used under the terms of the CC BY 3.0 licence (© 2015). Any distribution of this work must maintain attribution to the author(s), title of the work, publisher, and DOI.

ISBN: 978-3-95450-168-7 doi:10.18429/JACoW-IPAC2015-TUPJE054

Content from this work may be used under the terms of the CC BY 3.0 licence (© 2015). Any distribution of this work must maintain attribution to the author(s), title of the work, publisher, and DOI.

DEVELOPMENTS IN CLARA ACCELERATOR DESIGN AND SIMULATIONS

P. H. Williams*, D. Angal-Kalinin, A. D. Brynes, D. Dunning, J. K. Jones, J. W. McKenzie, B. L. Militsyn, B. D. Muratori & N. R. Thompson, ASTeC, Daresbury Laboratory, Warrington, Cheshire, UK
S. Spampinati, University of Liverpool & The Cockcroft Institute, Warrington, Cheshire, UK

Abstract

We present recent developments in the accelerator design of CLARA (Compact Linear Accelerator for Research and Applications), the proposed UK FEL test facility at Daresbury Laboratory. The layout changes include a dedicated collimator in CLARA front end to provide some control over the dark current, changes to low energy diagnostics section and modifications to FEL modules. The progress in the design simulations mainly focuses on a comparison of using ELEGANT and CSRTrack for the Variable Bunch Compressor and first considerations of requirement of laser heater for CLARA.

THE CLARA ACCELERATOR

CLARA is a proposed 250 MeV FEL test facility at Daresbury Laboratory [1]. The front end of CLARA incorporates an S-bend to transport the beam to presently operational VELA facility [2] and the gun for CLARA will share the same RF and drive laser infrastructure [3]. The changes to CLARA layout presented here since IPAC14 [4] include: a dedicated collimator in CLARA Front End to reduce the dark current from the injector, removal of Transverse Deflecting Cavity (TDC) from the low energy diagnostics section, inclusion of the post-linac diagnostics section with TDC and changes to the FEL modules. Preliminary investigations of requirements on laser heater and updates on simulations in magnetic chicane mode using CSRTrack [5] are presented. The Front End of CLARA will be installed later this year with first beam commissioning starting early 2016.

CHANGES TO ACCELERATOR LAYOUT

There have been a number of changes to the layout of the CLARA accelerator since 2014 (see Fig. 1). The reasons for each change have either been the gaining of operational experience on VELA, unforeseen engineering constraints or the enabling of additional capabilities. The front end has been finalised and components are either delivered or on order. This includes linac-1, a 2 m S-band structure capable of accelerating beam to ~55 MeV and its attendant klystron and modulator; beam transport elements towards linac 2, S-bend to the existing VELA beamline and spectrometer; BPMs and diagnostic stations including screens, slits, collimators and Faraday cups. After linac-2, space for a possible laser heater has been retained, the variable bunch compressor (VBC) layout has been finalised and magnets and other components are currently under engineering specification. To save space the transverse deflecting cavity (TDC) and diagnostics immediately following the VBC have been removed, leaving one TDC section immediately following linac-4, and one immediately following the FEL. The baseline machine simulations have been altered to take account of these changes.

COLLIMATION IN FRONT END

Although CLARA is a relatively low power machine (maximum average beam power of around 10 W [1]), and severe beam loss problems are not anticipated, collimation is included in the front end lattice to mitigate effects of dark current and beam halo. We propose to include a gun collimator similar to that in VELA where a 1mm thick tungsten plate with different hole sizes is used to collimate gun dark current [6]. In CLARA, the collimator will be included in the drive on the first YAG station, immediately upstream of the first linac. The collimator will utilise cylindrical hole diameters of 4, 6 and 9 mm.

In addition, we propose an additional collimator in the matching section between the first two linac modules, where the beam energy is tens of MeV. We envisage a similar arrangement to that used at FERMI where thick copper collimators are used, with tapering to reduce wakefields and a choice of several different apertures [7]. The engineering specifications of this collimator are being finalised.

* peter.williams@stfc.ac.uk

ISBN: 978-3-95450-168-7 doi:10.18429/JACoW-IPAC2015-TUPJE055

THE EVOLUTION OF THE TRANSVERSE ENERGY DISTRIBUTION OF ELECTRONS FROM A GaAs PHOTOCATHODE AS A FUNCTION OF ITS DEGRADATION STATE

L.B. Jones*, B.L. Militsyn, T.C.Q. Noakes
STFC Daresbury Laboratory, ASTeC & the Cockcroft Institute, Warrington WA4 4AD, UK
H.E. Scheibler, A.S. Terekhov
Institute of Semiconductor Physics (ISP), SB RAS, Novosibirsk 630090, Russia

Abstract

The brightness of a photoelectron injector is fundamentally limited by the mean longitudinal and transverse energy distributions of the photoelectrons emitted from its photocathode, and is increased significantly if the mean values of these quantities are reduced. To address this, ASTeC constructed a Transverse Energy Spread Spectrometer (TESS) [1] – an experimental facility designed to measure these transverse and longitudinal energy distributions which can be used for III-V semiconductor, alkali antimonide/telluride and metal photocathode research. We present measurements showing evolution of the transverse energy distribution of electrons from GaAs photocathodes as a function of their degradation state. Photocathodes were activated to negative electron affinity in our photocathode preparation facility (PPF) [2, 3] with quantum efficiency around 10.5 %. They were then transferred to TESS under XHV conditions, and progressively degraded through controlled exposure to oxygen. Data has been collected under photocathode illumination at 635 nm, and demonstrates a constant relationship between energy distribution and the level of electron affinity.

INTRODUCTION

The development of high–performance accelerator drivers for Free–Electron Laser facilities requires electron source technology which delivers a high–brightness electron beam for reasons that are well–documented [4]. Electron beam brightness in a linear accelerator is fundamentally limited by injector brightness, and this is itself limited by the source beam emittance or the *intrinsic emittance* of the cathode source. Electron beam brightness will be increased significantly by reducing the longitudinal and transverse energy spread in the emitted electrons, thereby creating a *cold beam*. To accomplish this goal, we must understand the mechanisms which define the intrinsic emittance whether these are related to the properties external to the photocathode such as surface roughness and preparation methods, or properties internal to the photocathode such as purity, doping level, crystal structure, band structure etc. Consequently, the study of photocathode physics and electron emission have become important areas for research by the worldwide accelerator community.

* lee.jones@stfc.ac.uk

TRANSVERSE ENERGY MEASUREMENT

To measure the transverse energy using TESS, a photocathode is illuminated with a tightly-focussed laser beam typically 100 μm FWHM in diameter at extremely low intensity, and its emission footprint recorded at some known distance from the photocathode surface. Assuming a vanishingly-small source size, and knowing the drift distance travelled by the photoelectrons, and the effective voltage through which they have been accelerated (defining their flight time), the transverse energy component required to generate the observed emission footprint can be determined.

On emission from a photocathode, the transverse energy of a photoelectron is a convolution of the component of the electron momentum parallel to the cathode surface immediately prior to emission and the effects of surface diffraction during the emission process. It is measurable as the beam emittance at some distance from the source, and data from the TESS place an upper limit on the mean transverse energy (MTE). Measurement of the angular distribution of photoelectrons from a surface is very difficult due to the necessity to work with extremely low–energy electrons which can be potentially mis–steered through exposure to stray electric and magnetic fields. Even the application of angle–resolved photoelectron spectroscopy to measure this angular distribution is challenging as the angular distribution is affected by the specific geometry of the vacuum chamber and experiment itself, so measurements will vary in each installation. In the case of GaAs, published work indicates that the emission cone is narrow with a half–angle of only 15 ° [5].

For GaAs photocathodes, the upper limit on transverse electron energy is determined primarily by three factors, these being the illumination wavelength, the level of electron affinity and the photocathode temperature. The profile of the measured transverse energy distribution curve (TEDC) itself depends on various elastic and inelastic electron scattering processes at the photocathode–vacuum interface, which are themselves dependent on a number of factors such as surface roughness, surface diffraction, material structure/crystallinity etc.

The TESS system provides the ability to measure this transverse energy, and to make direct comparisons between photocathodes which have been prepared in different ways or experienced different conditions during operation. This

Content from this work may be used under the terms of the CC BY 3.0 licence (© 2015). Any distribution of this work must maintain attribution to the author(s), title of the work, publisher, and DOI.

ISBN: 978-3-95450-168-7 doi:10.18429/JACoW-IPAC2015-TUPJE056

VELA MACHINE DEVELOPMENT AND BEAM CHARACTERISATION

D.J. Scott [#*], D. Angal-Kalinin[*], A. Brynes[*], F. Jackson[*], J.K. Jones[*], J.W. McKenzie[*], B.L. Militsyn[*], M.D. Roper[*], E. Snedden[*], T.C.Q. Noakes[*], A. Kalinin[*], B. Muratori[*], S. Mathisen[*], L.K.Rudge[*], M. Surnam,* R. Valizadeh[*], A.E. Wheelhouse[*], P.H. Williams[*], STFC ASTeC, Daresbury Laboratory, UK
S. Barrett, C.Topping [*], A. Wolski [*], University of Liverpool, UK
A. Lyapin, E. Yamakawa, Royal Holloway University of London, UK
Steve Syme, FMB-Oxford, UK

Abstract

Recent developments on the VELA (Versatile Electron Linear Accelerator) RF photo-injector at Daresbury Laboratory are presented. These are three-fold; commissioning/installation, characterising and providing beam to users. Measurements for characterising the dark current (DC), 4-D transverse emittance, lattice functions and photoinjector stability are presented. User beam set ups to provide beam for electron diffraction and Cavity Beam Position Monitor development are summarised.

INTRODUCTION

VELA is a facility designed to provide a high quality electron beam for accelerator systems development, industrial and scientific applications. It comprises of a 2.5 cell S-band photocathode gun with copper photocathode providing beam to experiments in the accelerator hall and 2 dedicated user areas. More information on the layout, design and early commissioning can be found in [1,2].

INSTALLATION & COMMISSIONING

As well as first commissioning of a second user area, Beam Area 2, in preparation for users in May 2015 a number of new devices were installed, including, a copper cathode, gun klystron, and transverse deflecting cavity (TDC).

New Gun Klystron

The RF power to the photo-injector gun is provided by a Thales TH2157 klystron, which is incorporated in a ScandiNova K2 klystron modulator. The modulator consists of a number of parallel solid state IGBT switching modules providing the primary voltage to a pulse step-up transformer which is capable of providing a 250 kV, 150 A flat top pulse of 0.5 – 3 µS at a pulse repetition rate between 1 – 400 Hz, with rate of rise for the pulse of between 150 – 215 kV/µs. The klystron is a 10 MW klystron operating at 2998.5 MHz, the original was a 10 year old klystron provided by Strathclyde University. During the first period of VELA commissioning it was noted that the electron beam momentum was low and did not align well with the measured RF cavity power. An investigation established that; the peak RF power capability was less than 10 MW and not all of the power entering the cavity was accelerating the beam. The new klystron provided an increase in momentum from ~4.9 to ~5.1 MeV/c. The power in the cavity is currently under investigation with further modelling work planned.

Cathode Replacement

The new cathode was diamond polished to a roughness of 100 nm, but this process has resulted in some peripheral diamond inclusions visible under SEM. Although not ideal, this cathode is now being used as the original cathode was not well polished and the effect of machining (i.e. turning) marks could clearly be seen in the downstream beam distribution, e.g. Fig. 1. Also, it was hoped that a smoother polished surface would reduce the DC, as described below.

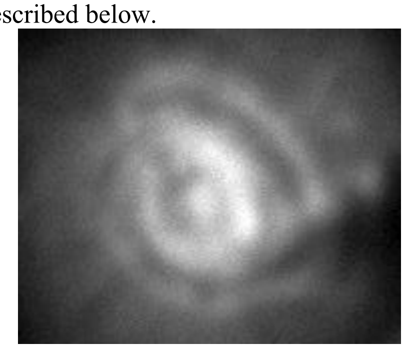

Figure 1: Beam image with rings attributed to machining marks on cathode.

Transverse Deflecting Cavity

The TDC, further explained in [3], is an S-band 9-cell copper cavity operating at 2998.5 MHz designed to provide a transverse kick of ~5 MV. Cold RF test characterisation has been performed and the cavity conditioned to 3.8 MW RF power at a repetition rate of 10 Hz and with a pulse width of 2.5 µs. Only a small number of vacuum events occurred during conditioning. An electron beam was then successfully transported through the TDC and first tests showed the expected behaviour: adjusting the TDC RF phase with constant RF amplitude moved the beam vertically on a downstream screen and increasing the RF gradient for a constant RF phase produced an increased vertical size of the beam image on the screen. Further characterisation of the TDC and electron bunch is planned for later in 2015.

#duncan.scott@stfc.ac.uk
*and the Cockcroft Institute, Daresbury Laboratory, UK

Content from this work may be used under the terms of the CC BY 3.0 licence (© 2015). Any distribution of this work must maintain attribution to the author(s), title of the work, publisher, and DOI.

ISBN: 978-3-95450-168-7 doi:10.18429/JACoW-IPAC2015-TUPJE057

Content from this work may be used under the terms of the CC BY 3.0 licence (© 2015). Any distribution of this work must maintain attribution to the author(s), title of the work, publisher, and DOI.

REALISTIC UNDULATORS FOR INTENSE GAMMA-RAY BEAMS AT FUTURE COLLIDERS*

A. Alrashdi[1,2,3†], I. Bailey[1,2], and D. Newton[2,4]
[1]Physics Department, Lancaster University, Lancaster, UK
[2]Cockcroft Institute, Daresbury Science and Innovation Campus, Warrington, UK
[3]King Abdulaziz City for Science and Technology, Riyadh, Kingdom of Saudi Arabia
[4]Department of Physics, University of Liverpool, Liverpool, UK

Abstract

The baseline designs for the ILC and CLIC require the production of an intense flux of gamma rays in their positron sources. In the case of CLIC the gamma rays are produced by a Compton backscattering source, but in this paper we concentrate on undulator-based sources as proposed for the ILC. We present the development of a simulation to generate a magnetic field map based on a Fourier analysis of any measured field map. We have used a field map measured from the ILC helical undulator prototype to calculate the typical distribution of field errors, and used them in our calculations to produce simulated field maps. We show that a loss of gamma ray intensity of $\sim$ 8% could be expected, compared to the ideal case. This leads to a similar drop in positron production which can be compensated for by increasing the undulator length.

INTRODUCTION

In the ILC, to achieve the required gamma-ray flux, a 150 GeV electron beam needs to pass through a long helical undulator (approximately 147 m) with a K of 0.93 and a peak field on-axis of 0.88 T successfully. This undulator nominally contains 84 modules of active length 1.7825 m. Dipole magnets may be used to correct the beam in between the modules to redirect the beam to the central axis. Errors in the undulator field can alter the flux, energy distribution and polarisation of the gamma rays. Below we demonstrate a technique to quantify the effect of these errors.

MAGNETIC FIELD MAP

Ideal Magnetic Field Map

Equations 1 and 2 describe the magnetic field inside an ideal helical undulator,

$$B_x = B_0 \sin \frac{2\pi z}{\lambda_u} \tag{1}$$

$$B_y = B_0 \cos \frac{2\pi z}{\lambda_u} \tag{2}$$

where B_0 is the field strength, z is the distance along the primary axis of the undulator, and λ_u is the period size.

* This research was funded in part by the STFC Cockcroft Institute Core grant no. ST/G008248/1.
† aalrashdi@kacst.edu.sa

Measured Magnetic Field Map

There were two field maps measured from the ILC prototype undulator modules using a Hall probe on-axis [1]. Imperfections in the magnet winding or deformation of the magnet 'former' lead to errors in the field. The magnet prototype field map was manipulated to add tapering for the first 2 and last 2 periods to ensure that the electron will stay close to the centre of the undulator if injected along the centre.

Simulated Magnetic Field Map

In order to produce a simulated magnetic field map based on a measured field map. We introduced errors in the magnetic field strength as well as in the period size over the length of the undulator along the z direction. This is discussed in more detail here [2]. The model used ensures the simulated map will not have a discontinuity. We compared the Discrete Fourier Transforms of the x-projections of the magnetic fields within the undulator for the measured data and simulated data to tune the model.

Our studies suggest that similar trajectories are obtained for particles travelling through the simulated field whether or not the errors in the y projection of the field are calculated independently of those in the x projection of the field. For this work we assumed that the errors in x and y have the same characteristic size and distribution.

TRACKING THE ELECTRON INSIDE THE UNDULATOR

Below we refer to three types of undulator data: ideal, measured, and simulated which we used as input to the HUSR simulation code [3,4]. In the ideal case, an electron will feel an average magnetic field strength of zero and will be transported through the undulator with a total deflection of zero as long as it is injected at an appropriate angle or tapering is used. The electron is injected on axis and the measured and simulated fields are manipulated to add tapering for the first 2 and last 2 periods. Fig 1 shows the position of the electron on the x and y axes. The radius of the helical trajectory has a standard deviation of 8×10^{-12} m reflecting the small numerical uncertainty in the simulation.

ISBN: 978-3-95450-168-7 doi:10.18429/JACoW-IPAC2015-TUPJE058

PREPARATION OF POLYCRYSTALLINE AND THIN FILM METAL PHOTOCATHODES FOR NORMAL CONDUCTING RF GUNS*

S. Mistry[#], M. Cropper, Department of Physics, Loughborough University, Loughborough, Leicestershire, LE11 3TU, UK;
R. Valizadeh, K.J. Middleman, A.N. Hannah, B.L. Militsyn and T.C.Q. Noakes, ASTeC, STFC Daresbury Laboratory, Sci-Tech Daresbury, Daresbury, Warrington, Cheshire, WA4 4AD,

Abstract

A comparison of quantum efficiency (QE) and work function (WF) measurements of polycrystalline and thin film metal photocathodes for use in normally conducting RF (NCRF) guns, similar to the S-band gun under development for the CLARA project at Daresbury, are reported. Cu and Nb thin films were grown on a Si substrate by magnetron sputtering and subsequently prepared by annealing and Ar ion sputtering. To determine the surface chemistry, X-ray photoelectron spectroscopy (XPS) was employed. QE measurements were enabled using a 265 nm UV LED. WF measurements were carried out using a Kelvin probe. Annealing the Cu thin film to 250°C yielded a QE of $1.2\cdot10^{-4}$; one order of magnitude higher than the QE for sputter cleaned and post annealed polycrystalline Cu. The optimum QE measurement for Nb thin film was $2.6\cdot10^{-4}$, which was found to be comparable to the results obtained for cleaned bulk Nb. Analysis of XPS data of these metals suggest surface composition and surface chemistry are main contributing factors to the QE and WF.

INTRODUCTION

Our interest in metal photocathodes stems from the installation of VELA (Versatile Electron Linear Accelerator) at Daresbury Laboratory (DL) [1]. As with many NCRF guns, VELA injector uses a metal photocathode for its fast response that allows for much shorter pulses, and it's relative insensitivity to the vacuum environment. VELA gun uses a Cu disk photocathode, integrated onto the back wall of the Cu cavity; this yields a QE of approximately 10^{-5}. Now the interest has turned to investigating alternative metals to Cu, with potentially better photocathode performance. The metal photocathodes will be installed in NCRF guns such as VELA and also high repetition rate guns for future 4th generation light sources test facility such as the Compact Linear Accelerator for Research and Applications (CLARA) [2], a proposed Free Electron Laser test facility, which will require a fast response time cathode with a reasonable QE.

A range of polycrystalline metals have already been investigated and several metals have been identified as yielding reasonable QE values (greater than 10^{-5}), namely Mg, Pb, Zr, Nb and Ti [3]. The next stage is to study the properties of these metals when deposited as thin films. The use of thin films could potentially evade problems of RF breakdown that commonly occur in adjoining metal disks to the Cu cavity [4].

This study will report a comparison of QE, work function and chemical composition of Cu and Nb thin films versus bulk metal cathodes.

EXPERIMENTAL PROCEDURE

Magnetron sputtering has been used to deposit metal thin films on Si(100) substrates; this is a preliminary experiment, and so for operational photocathodes an appropriate substrate material will be chosen. The Si substrates were cleaned and degreased in ultrasonic bath of acetone, IPA, methanol and then finally washed in deionised water. Nb and Cu were sputtered onto the Si substrate; Kr sputter gas was used at 3 mbar and the magnetron was operated at a DC power of 600 W.

As was the procedure for the polycrystalline cathodes, the thin films were then carefully inserted into a sample holder and then cleaned in an ultrasonic bath of acetone for 10 minutes before analysis.

An ESCALAB Mk II XPS instrument has been adapted for the purpose of preparing and analysing the cathode samples. For this experiment, surface analysis techniques were used to obtain measurements of QE, WF and surface chemical composition. The following measurements were carried out in the analysis chamber of the ESCALAB Mk II at a pressure of approximately 10^{-10} mbar.

A 265 nm LED with 12 nm bandwidth was used for excitation of the cathodes. The intensity of the LED was calibrated using a UV sensor. The resulting drain current from the cathode was measured using a pico-ammeter.

The KP Technology UHVKPm100 equipment installed in ESCALAB Mk II is used to create a potential difference between the cathode and the tip of the Kelvin probe, and thus infer a work function with a resolution of less than 3 meV.X-Ray Photoemission Spectra were measured Al Kα illumination and the emitted electrons energy analysed with a hemispherical analyser. The XPS system has an energy resolution of approximately 1.1 eV and a spatial resolution of 100 µm. This technique is used to qualitatively and quantitatively assess the cathode chemical composition.

* The work is part of EuCARD-2, partly funded by the European Commission, GA 312453.
# sonal.mistry@stfc.ac.uk

Content from this work may be used under the terms of the CC BY 3.0 licence (© 2015). Any distribution of this work must maintain attribution to the author(s), title of the work, publisher, and DOI.

ISBN: 978-3-95450-168-7 doi:10.18429/JACoW-IPAC2015-TUPJE059

Content from this work may be used under the terms of the CC BY 3.0 licence (© 2015). Any distribution of this work must maintain attribution to the author(s), title of the work, publisher, and DOI.

MODELING OF AN ELECTRON INJECTOR FOR THE AWAKE PROJECT

O. Mete*, G. Xia, †The University of Manchester, Manchester, UK
R. Apsimon, G. Burt, †Lancaster University, Lancaster, UK
S. Doebert, CERN, Geneva, Switzerland
R. Fiorito, C. Welsch, †The University of Liverpool, Liverpool, UK

Abstract

Particle-in-cell simulations were performed by using PARMELA to characterise an electron injector with a booster linac for the AWAKE project in order to provide the baseline specifications required by the plasma wakefield experiments. Tolerances and errors were investigated. A 3 GHz travelling wave structure designed by using CST code. Particles were tracked by using the field maps acquired from these electromagnetic simulations. These results are presented in comparison with the generic accelerating structure model within PARMELA.

INTRODUCTION

The AWAKE project is a proton driven plasma wakefield acceleration experiment by utilising the driver proton beam from CERN's SPS injector and a custom photo injector for the witness (trailing) electron beam [1, 2].

Figure 1 shows the layout of the injector consisting of an S-band standing wave RF gun (SW), previously used in CERN's PHIN photo injector [3], followed by laser optics to direct the laser onto the cathode. Beamline continues with beam current and position monitors and a pepper pot emittance measurement system suitable for a beam subject to space charge effects. A new S-band booster section (accelerating travelling wave structure, ATS) was designed by using CST suite [4] and introduced in the model to boost the beam energy to a region adjustable between 16 – 20 MeV. ATS is followed by a quadrupole triplet and a downstream screen to perform quadrupole scans for emittance measurement.

The tracking studies have been performed by using PARMELA [5]. For ATS the model provided by PARMELA and field maps extracted from CST were used and compared. Implementation of CST maps into PARMELA are discussed in the following sections.

BOOSTER LINAC

An S-band booster linac, ATS, was designed as a travelling wave structure with constant gradient of 15 MV/m through the entire structure (Fig.2) . It consists of 30 cells with 120° phase advance and varying radii matched to 1 μm precision. ATS was optimised for low reflection coefficient of about 2.5%. The multipole terms [7] due to transverse RF-kicks are 9.4241×10^{-7} mT, 7.8418×10^{-5} mT/m and 4.9×10^{-3} mT/m^2, respectively, from dipole to sextuple terms.

* oznur.mete@manchester.ac.uk
† and The Cockcroft Institute, Sci-Tech Daresbury, Warrington, UK

USING CST FIELD MAPS IN PARMELA

In order to use CST field maps in PARMELA tracking simulations, a MATLAB [6] script was prepared to format the standard CST field maps into the form required by PARMELA . The information that PARMELA requires on each line of a field map can be found in Table IV-2 from the program manual [5].

In PARMELA, two field maps must be provided for a travelling wave structure; one produced with Neumann boundary condition (cosine map) and the other with Dirichlet boundary condition (sine map). These fields which are shifted in phase by 90° are fed into PARMELA by using the TRWCFIELD command. A single TRWAVE line is used to represent the entire ATS including the bore tubes with lengths equal to a cell length at each end of ATS to account for the fringe fields.

BASELINE DESIGN

In order to maintain the balance between the emittance growth and the energy spread within ATS, a 10° off-crest phase was chosen for the baseline design by using the CST maps of the current design while the SW is optimised for the highest energy. In addition, the same beam dynamics conditions can be met with on-crest RF phase in the case of the PARMELA model for a travelling wave structure.

The space charge component of the emittance is compensated using the field produced by two solenoids located around the SW. Slightly different working points to satisfy the constant envelope condition were determined for the field distributions from PARMELA and CST models.

The beam dynamics specifications are presented in Table 1 in comparison with these two.

Table 1: Required specification and values produced with different models.

Parameter	Required	PARMELA Map	CST Map
E (MeV)	16	16	16
ΔE/E (%)	0.5	1.3	1.1
$\epsilon_{x,y}$ (mm mrad)	2	1.7,1.8	2.3, 2.5
$\beta_{x,y}$ (m)	5	4, 4	0.8, 0.8
$\alpha_{x,y}$	0	-0.2,-0.2	-1.4, -1.2

ISBN: 978-3-95450-168-7 doi:10.18429/JACoW-IPAC2015-TUPJE060

DEVELOPMENT OF ADVANCED FOURTH GENERATION LIGHT SOURCES FOR THE ACCELERATOR SCIENCE LABORATORY

T. Chanwattana[1], R. Bartolini[1,2], A. Seryi[1], E. Tsesmelis[3]
[1]John Adams Institute, University of Oxford, OX1 3RH, UK
[2]Diamond Light Source Ltd, Oxfordshire, OX11 0QX, UK and
[3]CERN, Geneva, Switzerland

Abstract

The John Adams Institute for Accelerator Science (JAI) has proposed the realisation of the Accelerator Science Laboratory (ASL) at the University of Oxford as a facility for the development of advanced compact light sources enabling accelerator science research and applications. The installation of a compact light source in the ASL is planned with two options for the accelerating technologies. Firstly, a conventional RF based accelerator is considered to be a driver for a short pulse THz coherent synchrotron radiation (CSR). The other option focusses on the radiation produced by a Laser Plasma Accelerator (LPA) advanced accelerator technique that will provide the possibility to shorten the length of the beamline. This paper presents results of the studies on beam dynamics for both options of compact light sources in the ASL.

INTRODUCTION

Compact advanced fourth generation light sources enable advanced research and experiments in a wide range of applications in small-scale facilities, especially at universities. The John Adams Institute for Accelerator Science (JAI) at the University of Oxford has been studying the possibility of establishing the Accelerator Science Laboratory (ASL) as an accelerator laboratory dedicated to advanced research with compact light sources. Many facilities worldwide aim to generate terahertz (THz) radiation, which is required in numerous scientific experiments and applications, such as imaging and spectroscopy of molecules, disease diagnostics and organism detection, electron beam diagnostics, safety non-destructive monitoring and weapons inspection. The THz radiation can be produced by various schemes, such as solid state oscillators, gas and quantum cascade lasers, coherent synchrotron radiation (CSR) and free electron lasers (FELs). Currently, the ASL aims at producing short pulse THz CSR from a dipole magnet with two options of acceleration technologies. The first option is based on the acceleration of electron beams with a conventional RF linac and shortening of the electron bunch length by a magnetic chicane bunch compression. The other is to utilize the electron beam with extremely short bunch length produced from laser plasma accelerator (LPA) in a bubble regime to produce the coherent radiation. This paper presents beam dynamics studies of the THz radiation source for the ASL in both options after [1] and the assessment of the achievable performance.

RF-DRIVEN RADIATION SOURCE

Beam Dynamics

A beamline of the THz radiation source based on the RF linac consists of a 1.6-cell S-band photocathode gun, an S-band cavity, an X-band harmonic cavity and a four-dipole magnetic chicane as shown in Fig.1. An electron beam emerges from a cathode in the RF gun. The S-band cavity accelerates the beam to reach the desired energy and employs the emittance compensation process to increase beam brightness. The X-band harmonic cavity is used for linearization of the beam longitudinal phase space, which offers better control of bunch length compression in the magnetic chicane. The synchrotron radiation is generated at the last dipole magnet of the chicane.

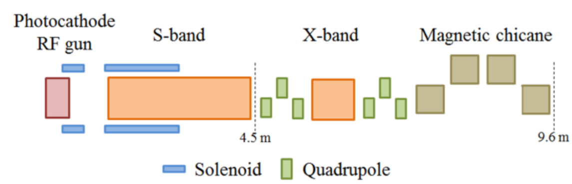

Figure 1: Layout of the RF-driven radiation source.

Beam dynamics of this RF-based radiation source has been studied with start-to-end (S2E) simulations starting from the beam at the photocathode gun to the generation of CSR. The simulation is separated into two parts: the injector, comprising the RF-gun and the S-band cavity and the second part comprising the X-band cavity, the bunch compressor and its matching section. Low bunch charge is considered in order to get short bunch length leading to our target to generate the short pulse THz radiation. Hence, the simulations were done based on two choices of bunch charge: 100 pC and 500 pC.

Injector

The first part of the S2E, from the photocathode gun to the end of the S-band cavity, was simulated with ASTRA [2] because of the dominance of the space charge effect on a low energy beam. RF frequency of both components is 2.856 GHz. A flat-top laser profile is considered in both 100 pC bunch and 500 pC bunch. After the gun, the electron beam is focussed by a solenoid to get the minimum beam waist at a position where the S-band cavity is located at in order to compensate emittance growth by using an appropriate accelerating gradient. The S-band cavity accelerates the beam to about 55 MeV and also operates off-crest in order to introduce a

Content from this work may be used under the terms of the CC BY 3.0 licence (© 2015). Any distribution of this work must maintain attribution to the author(s), title of the work, publisher, and DOI.

ISBN: 978-3-95450-168-7 doi:10.18429/JACoW-IPAC2015-TUPJE061

Content from this work may be used under the terms of the CC BY 3.0 licence (© 2015). Any distribution of this work must maintain attribution to the author(s), title of the work, publisher, and DOI.

INJECTION STUDIES FOR THE DIAMOND STORAGE RING

I.P.S. Martin, M. Apollonio, Diamond Light Source, Oxfordshire, U.K.
R. Bartolini, Diamond Light Source, Oxfordshire, U.K., and
John Adams Institute, University of Oxford, U.K.

Abstract

The Diamond storage ring will be upgraded during 2016 by replacing one of the existing double bend achromat (DBA) cells with a double-DBA (DDBA) cell [1]. It is anticipated that both the on and off momentum dynamic aperture will reduce as a result of this change. In order to prepare for this eventuality, injection into the Diamond storage ring has been recently studied in detail. In particular, the oscillation amplitude, angle and energy of the injected beam have been determined, along with the position of the stored beam with respect to the septum plate. Following these studies, the injected beam energy has been matched to the storage ring, and plans have been put in place to move the injection septum 4 mm closer to the stored beam centre line.

INTRODUCTION

The Diamond storage ring will be upgraded in August 2016 by replacing one of the existing DBA cells with a single DDBA cell [1]. The primary goal of this exercise is to increase the capacity for insertion device beamlines; however, the extensive design and engineering work involved also serves as a good basis from which to proceed towards a full low emittance upgrade of the entire storage ring [2].

When developing the upgrade lattice, the main focus has been on retaining the existing Twiss parameters at the ID source points, whilst at the same time minimising the impact of the upgrade on the lifetime and injection efficiency. At present it is anticipated the lifetime will drop by ~10% to 15%, with a similar drop in the injection efficiency [3]. A low-alpha lattice solution is also being developed in parallel to this work [4]. In this case the impact on the on- and off-momentum dynamic aperture is more dramatic, reducing the injection efficiency to close to zero (assuming the existing injection parameters).

In order to combat this reduction in injection efficiency, it has been proposed to reduce the separation between stored and injected beams from the existing 8.3 mm. This reduction could in principle be achieved by moving the stored beam closer to the septum plate by increasing the amplitude of the injection kicker magnets, or alternatively by applying a static orbit bump across the straight using the dipole corrector magnets embedded in the sextupoles. However, the preferred solution is to move the septum magnet from the existing position of -16 mm offset from the stored beam centre line to -12 mm offset. This has the advantage that the kicker magnets can then be run at a lower field (thereby reducing the disturbance to the stored beam during top-up injection cycles), and also allows for single-shot on-axis injection (forming part of the DDBA commissioning plan).

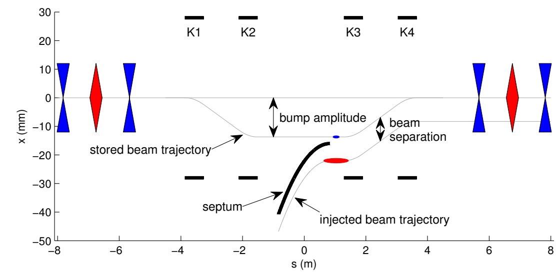

Figure 1: Injection schematic for the Diamond storage ring.

INJECTION SCHEME

Injection into the Diamond storage ring is carried out within a single long straight section. The scheme uses four pulsed kicker magnets to bump the stored beam towards the septum magnet, with the injected beam arriving at a nominal displacement of -8.3 mm from the stored beam. A schematic of the injection process is shown in Fig. 1, and the main parameters are given in Table 1.

The nominal beam separation was decided upon during the design phase after assuming highly pessimistic values for the stored and injected beam emittances, alignment tolerances on the septum plate and shot-to-shot variability in the injected beam trajectory. In principle, the separation could be reduced to the absolute minimum value of $3\sigma_{stored}$ + $3\sigma_{inj}$ + septum thickness = 5.8 mm. However, this would leave no contingency for trajectory or transient closed orbit errors due to non-closure of the kicker bump.

Table 1: Injection Parameters

Parameter	Value
Nom. injected beam size (1σ)	0.69 mm
Nom. stored beam size (1σ)	0.18 mm
Nom. septum displacement (inside edge)	-16 mm
Septum thickness	3.2 mm
Nom. bump amplitude	-13.7 mm
Max. bump amplitude	-18.8 mm
Nom. stored/injected beam sep.	8.3 mm
Storage ring revolution period	1.87 μs
Kicker pulse duration (half sine)	6 μs

MEASUREMENTS

In order to set a realistic limit on the minimum achievable stored and injected beam separation, studies have been made on the impact of various parameter changes. At the same time, investigations were carried out to identify potential detrimental effects resulting from the septum move.

ISBN: 978-3-95450-168-7 doi:10.18429/JACoW-IPAC2015-TUPJE062

FIRST TRANSPARENT REALIGNMENT TESTS AT THE DIAMOND STORAGE RING

M. Apollonio, P. Dudin, M. Hoesch, W. J. Hoffman, E. C. Longhi,
A. J. Rose, A. Thomson, Diamond Light Source, Oxfordshire, U.K.
R. Bartolini, Diamond Light Source, Oxfordshire, U.K. and John Adams Insitute, Oxford, U.K.

Abstract

The Transparent Realignment (TR) of the Diamond Storage Ring is a program of work to improve the mechanical alignment of the machine by carefully moving the magnet girders with a virtually zero impact on the associated beamlines. The girders can be moved by means of a 5-axis motion system under remote control via the EPICS toolkit from the Diamond Control Room. Currently three cells (three girders in each) have been equipped with a permanent protection system to prevent excessive deflection across each of the inter-girder vacuum bellows. The protection and motion systems are installed in the associated Control and Instrumentation Area (CIA). Full commissioning of the motion and protection systems have been completed. Results from the alignment test sessions are hereby reported.

INTRODUCTION

The realignment of a storage ring (SR) is key to reach low vertical emittances, down to few pm or even sub pm [1, 2]. Today the realignment or control of the alignment status of a machine is part of routine programmes in many facilities. At Diamond this request became more important after low coupling (C=0.3 %, ϵ_y = 8 pm rad) became the standard user mode in March 2013.

Care must be taken when correcting for mechanical misalignments, since moves can potentially impact on nearby insertion devices (IDs). The strategy to mitigate this effect has been devised and initially tested at the end of 2013. It consists in the careful use of orbit bumps (Golden Offsets, GO) at the primary BPMs facing an ID straight, that restore the orbit where it was prior to the alignment, as thoroughly described in [3]. In this paper we introduce the new remote control system, capable of moving three girders at a time, and show the results obtained in the realignment of straight-05. We focus on the effects of introducing GOs and subsequently remove them, with the beamline realigning to the new machine configuration. A view to future tests is presented at the end of the document.

SURVEY ASSISTED GIRDER ALIGNMENT (SAGA)

Choice of Cells to be Realigned

The horizontal and vertical planes are periodically surveyed at Diamond, as shown in [3, 4]. In the vertical plane figures are reported as levels of the girder edges respect to a best fit plane, interpolating all the monument levels as measured in a full survey campaign of SR. Figure 1 shows a snapshot of the vertical plane alignment as of June 2014, where variations as large as 600 μm are seen. In order to reduce the magnitude of the realignment moves a smooth curve was fitted to the monument positions whose period is about half of the SR length (561.6 m). The curve is a sine wave with a mildly variable amplitude, and the long wavelength ensures that a realignment to this baseline should be effective while keeping girder moves within few hundred microns. Figure 1 guides the choice of cells 4, 5 and 6 as parts of the lattice to be realigned, in an ideal continuation of the work previously done to align cell 3. The initial highly mis-aligned pattern in cells 4 and 5 (gray segments), has been brought to a more tamed configuration by April 2015, resulting in an overall aligned sequence from cell-3 to cell-5. As described later, this reduced the vertical corrector magnet (VCM) strength used to correct the orbit.

Survey is the primary source of information for the moves imparted to girders. Sometimes, however, the predicted change in corrector strength can be used as a guide to realignment, as indeed happened when realigning straight-05. realignment moves are monitored by the survey team, showing that imparted moves and survey data are in good agreement, with typical monument discrepancies of less than 15 μm.

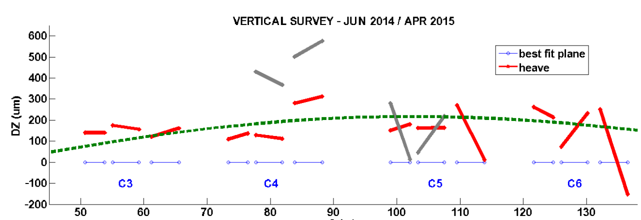

Figure 1: Vertical survey of the Diamond Storage Ring. The red segments join the monuments at girder edges, showing the present situation after the realignment of straight-05, while the gray ones show the state of the machine before it. The dashed green line is a fit to the 148 monument levels, which is used as realignment baseline (see text).

Girder Control

Until mid 2014 girders were individually moved by means of a stand-alone crate connecting a laptop hosting the software to control the 5-axis cam motors that perform a girder move in the corresponding degrees of freedom (sway, yaw, heave, pitch and roll about the s-axis of the girder).

A protection system of Linear Variable Differential Transformers (LVDT) was temporarily mounted to ensure that

Content from this work may be used under the terms of the CC BY 3.0 licence (© 2015). Any distribution of this work must maintain attribution to the author(s), title of the work, publisher, and DOI.

ISBN: 978-3-95450-168-7 doi:10.18429/JACoW-IPAC2015-TUPJE063

Content from this work may be used under the terms of the CC BY 3.0 licence (© 2015). Any distribution of this work must maintain attribution to the author(s), title of the work, publisher, and DOI.

HYBRID SEVEN-BEND-ACHROMAT LATTICE FOR THE ADVANCED PHOTON SOURCE UPGRADE*

M. Borland, V. Sajaev, Y. Sun, A. Xiao, ANL, Argonne, IL 60439, USA

Abstract

A hybrid seven-bend-achromat lattice has been designed for the APS upgrade. We describe the design goals, constraints, and methodology, including the choice of beam energy. Magnet strength and spacing is compatible with engineering designs for the magnets, diagnostics, and vacuum system. Dynamic acceptance and local momentum acceptance were simulated using realistic errors, then used to assess workable injection methods and predict beam lifetime. Predicted brightness is two to three orders of magnitude higher than the existing APS storage ring. Pointers are provided to other papers in this conference that cover subjects in more detail.

INTRODUCTION

The Advanced Photon Source [1] is a 7-GeV, 100-mA, 40-sector, 3^{rd} generation storage ring light source with a 1104-m circumference, providing beams to dozens of insertion device (ID) and bending magnet (BM) beamlines simultaneously. After more than 20 years of operation, a major upgrade of the lattice is under consideration. Since APS is an existing facility, a number of constraints must be imposed on any new lattice; these are described in [2].

The basic goal of the lattice design effort is to provide a much lower beam emittance and ultimately an enhancement of x-ray brightness by more than two orders of magnitude for x-rays above 20 keV. The approach is to use a multi-bend achromat (MBA) lattice [3–6], taking advantage of the E^2/M^3 scaling [7, 8] of the natural emittance ϵ_0 with the beam energy E and the number of dipoles per sector M.

After considering various concepts [9–11], it was determined that the ESRF-II "hybrid" concept [11] gave the lowest emittance by a factor of more than two. It also gave sextupoles that are three-to-four times weaker, leading to the adoption of this concept.

APS presently delivers 100 mA in 24 bunches about 75% of the time. For the upgrade, a total current of 200 mA with as few as 48 bunches is required, giving the same single-bunch current of 4.2 mA. The APS MBA lattice has a well-developed impedance model [12] that was used to predict single bunch current limits [13]. It shows that a chromaticity of +5 is needed in both planes to ensure the required single-bunch current.

Bunch-lengthening is important in order to preserve the emittance and improve the Touschek lifetime of low-emittance beams. The APS upgrade will incorporate a higher-harmonic cavity (HHC) for this purpose. Detailed studies of beam dynamics with the HHC have been performed [14, 15], leading to the conclusion that a bunch duration in excess of 50-ps rms is possible.

* Work supported by the U.S. Department of Energy, Office of Science, Office of Basic Energy Sciences, under Contract No. DE-AC02-06CH11357.

DESIGN METHODS

We started our design by scaling the ESRF-II lattice to the APS number of cells and the cell length. Through an iterative process, we developed a matching command file for `elegant` [16] that incorporated limitations from magnetic modeling as well as requirements for space between elements to accommodate vacuum and diagnostic components [17]. Owing to the large gradients and sextupole strengths coupled with the short magnet lengths, the equivalent hard-edge magnet strength limits are length-dependent; these limits are incorporated into the matching using fits to data from magnetic modeling [18]. In the early stages, the matching runs also included the overall ring geometry. The matching benefited from use of `Pelegant`'s parallel simplex optimizer [19, 20],

Wide-ranging tune scans were performed next. For each working point, we evaluated the dynamic acceptance (DA) and local momentum acceptance (LMA) using `Pelegant` for a nominal set of magnet errors assuming symmetrically-powered sextupoles. Multi-objective comparison of the results led to selection of a few promising regions, for which a multi-objective genetic algorithm (MOGA, similar to [21, 22]) was applied based on DA and Touschek lifetime [2, 23]. The algorithm was variously allowed to change the lattice linear optics and the sextupoles, with the sextupoles being given a two-sector translational symmetry (making for 12 sextupole families). Linear optics was varied both by high-level linear optics goals (e.g., tunes, maximum beta functions) and separately by direct variation of gradients; the latter seems more effective. Of the several regions explored, $\nu_x \approx 95.1$ and $\nu_y \approx 36.1$ yielded the best results. The lattice functions are shown in Fig. 1, while lattice properties are listed in Table 1.

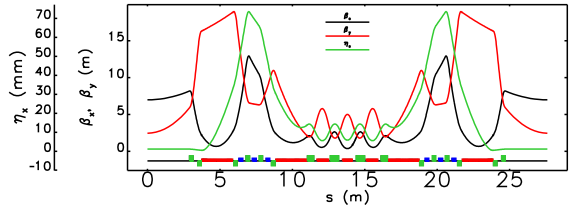

Figure 1: Lattice functions for the APS MBA lattice.

The DA, shown below, is small but suitable for on-axis swap-out injection [24–26]. An alternate lattice supporting accumulation is described in [27]. Figure 2 shows the

ISBN: 978-3-95450-168-7 doi:10.18429/JACoW-IPAC2015-TUPJE064

Content from this work may be used under the terms of the CC BY 3.0 licence (© 2015). Any distribution of this work must maintain attribution to the author(s), title of the work, publisher, and DOI.

CALIBRATION OF FAST FIBER-OPTIC BEAM LOSS MONITORS FOR THE ADVANCED PHOTON SOURCE STORAGE RING SUPERCONDUCTING UNDULATORS*

J. Dooling†, K. Harkay, Y. Ivanyushenkov, V. Sajaev, A. Xiao, ANL, Argonne, IL 60439, USA
A. Vella, University of Illinois, Urbana-Champaign, IL 61801 USA

Abstract

We report on the calibration and use of fast fiber-optic (FO) beam loss monitors (BLMs) in the Advanced Photon Source storage ring (SR). A superconducting undulator prototype (SCU0) has been operating in SR Sector 6 (“ID6”) since the beginning of CY2013, and another undulator SCU1 (a 1.1-m length undulator that is three times the length of SCU0) is scheduled for installation in Sector 1 (“ID1”) in 2015. The SCU0 main coil often quenches during beam dumps. MARS simulations have shown that relatively small beam loss (<1 nC) can lead to temperature excursions sufficient to cause quenching when the SCU0 windings are near critical current. To characterize local beam losses, high-purity fused-silica FO cables were installed in ID6 on the SCU0 chamber transitions and in ID1 where SCU1 will be installed. These BLMs aid in the search for operating modes that protect the SCU structures from beam-loss-induced quenching. In this paper, we describe the BLM calibration process that included deliberate beam dumps at locations of BLMs. We also compare beam dump events where SCU0 did and did not quench.

INTRODUCTION AND MOTIVATION

The Superconducting Undulator Prototype (SCU0) is the first operating SCU in the APS storage ring (SR) [1]. SCU0 is installed in ID6 and has been producing photons for users since early 2013. The success of SCU0 has promoted the construction of SCU1. The length of the undulator in SCU0 is 0.33 m; in SCU1, the undulator length is 1.075 m. Often during beam dumps caused by the Machine Protection System (MPS), SCU0 quenches. Quenching inconveniences the x-ray users and potentially leads to magnet damage.

Simulations with MARS [2] have shown that relatively small beam losses (< 1 nC) can lead to temperature excursions sufficient to cause quenching when the SCU windings are near critical current. An initial model simulated a 1-nC, point beam of 7-GeV electrons striking the top of the vacuum chamber at the upstream end of the SCU0 magnet. With the beam starting upstream at the center of the chamber, this required a vertical angle of 4.3 mrad. Though unrealistically large, this beam trajectory allows a preliminary estimate of temperature rise within the SCU0 magnet windings for a given charge loss. Temperature excursions in the first 5 mm of undulator above the chamber are presented in

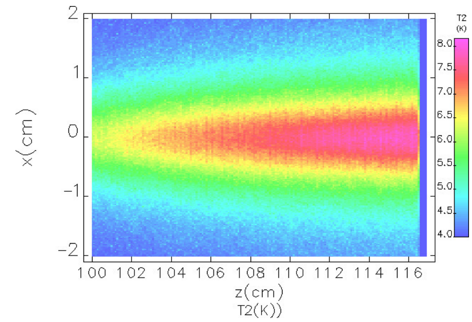

Figure 1: Temperature rise simulated in SCU0 after 1-nC of 7-GeV electrons strike the top of the vacuum chamber at the upstream end of the undulator (z=83 cm).

Figure 1 for an initial temperature of 4.2 K. Modeling with `elegant` [3] in other ID sectors shows that beam dumps deposit most of the beam on the upstream ID chamber transition section, making loss in the SCU0 undulator much more diffuse than indicated in Fig. 1. A temperature rise in excess of 1.9 K can lead to quenching at the SCU0 operating current of 500 A.

We present study and simulation results used to empirically calibrate the fast, fiber optic (FO) BLMs [4] installed in ID6. The calibration is then employed to evaluate losses recorded in ID6 caused by two separate beam dump events. In one case, the event did not lead to a quench of the SCU0 main coil, while in the other case, a quench did occur.

FIBER OPTIC BEAM LOSS MONITOR

Loss of primary, 7-GeV electrons leads to an electromagnetic (EM) shower composed of photons, electrons, and positrons. The high-purity, fused-silica fiber optic (FO) cable bundles are sensitive to all three of these EM shower components (in the case of photons, via pair production). Light is generated within the fibers via Čerenkov radiation as well as Optical Transition Radiation (OTR).

Experimental Description

Once light is generated within a fiber, the fiber provides a guide to an optical detector; in this case, Hamamatsu “subminiature” R7400 photomultiplier tubes (PMTs). Four fiber bundles are positioned in two pairs, one pair upstream of the SCU0 cryostat and the other downstream on the vacuum chamber transitions. The radiator ends of each bundle are placed parallel to the beam trajectory at the nominal beam centerline position; one bundle above and the other below

* Work supported by the U.S. Department of Energy, Office of Science, Office of Basic Energy Sciences, under Contract No. DE-AC02-06CH11357.
† dooling@aps.anl.gov

ISBN: 978-3-95450-168-7 doi:10.18429/JACoW-IPAC2015-TUPJE065

MULTI-BUNCH STABILITY ANALYSIS OF THE ADVANCED PHOTON SOURCE UPGRADE INCLUDING THE HIGHER-HARMONIC CAVITY*

L. Emery†, M. Borland, T. Berenc and R. Lindberg, ANL, Argonne, IL 60439, USA

Abstract

Multi-bunch stability simulations were done for the very-low-emittance hybrid seven-bend-achromat (H7BA) lattice proposed for the Advanced Photon Source (APS) upgrade. The simulations, performed using `elegant`, were meant to determine whether the long-term wakefields of the higher-order modes (HOMs) of the main 352-MHz cavities will produce an instability. The multi-particle simulations include the important effects of the Higher-Harmonic Cavity (HHC) and the longitudinal impedance of the new vacuum chamber. These realistic simulations show that the HHC provides additional damping in the form of the Landau damping. Still, the HOMs may likely produce a multi-bunch instability which can be cured with more effective HOM damping or a longitudinal feedback system.

INTRODUCTION

The present Advanced Photon Source (APS) ring has sufficient damping to suppress multi-bunch instabilities in the longitudinal and transverse planes. The APS Upgrade ring, with the Hybrid MBA optics [1], will have a larger current of 200 mA, somewhat smaller synchrotron radiation damping, and reduced longitudinal focusing. This will result in a higher tendency for (particularly) longitudinal multi-bunch oscillations generated from the wakefields of the higher-order mode resonances (HOMs) of the 352-MHz single-cell cavities of the APS ring. Even though only 12 of the original 16 cavities will be kept, the HOMs tend to act individually and any one or two of them may cause an instability.

Another difference from the present APS is the presence of a higher-harmonic cavity (HHC) [2], which stretches the bunch to reduce the IBS emittance growth and to make the lifetime longer [3]. The longitudinal dynamics are significantly changed with the HHC, which will provide some Landau damping to any longitudinal centroid oscillations.

To accurately include the HHC, which changes the potential well and makes the motion anharmonic, a tracking simulation must be done. Though we realize that reference [4] gives some analytical predictions, tracking is the most straightforward way to approach this problem (see for example [5]).

The HOM spectrum of each cavity was modeled by [6] from frequency-domain finite element code CST [7]. The ten lowest modes below the cut-off (1640 MHz) of the cavity beam pipe were selected. The spectrum is dominated by one strong HOM around 540 MHz, which has been damped by a factor of 8 in four of the cavities at APS. We assume that for the APS Upgrade all cavities will have this mode damped by the same amount. The other HOMs in the aggregate contribute about the same effect as this damped mode. The cavities were constructed differently from each other to systematically stagger the HOM frequency by at least 210 kHz (a little less than one revolution frequency). However, the frequencies of the individual HOMs are not known exactly and can change during operation. Thus we have a huge parameter space of possible HOM frequencies to explore, which requires a Monte Carlo approach.

We have done preliminary calculations of expected multi-bunch mode growth rates using a normal mode analysis [8], which assumes single-particle bunches and harmonic motion. This calculation method cannot include the effect of the HHC and impedance, which is a severe limitation. However, because the calculation is very fast, one can apply a large number of realizations of the possible 120 HOM frequencies (10 HOMs for each of the 12 cavities), and thereby obtain a cumulative distribution of expected growth rate.

In the section that follows we report on multi-particle tracking that fully includes the HHC and impedance. Here we perform calculations for far fewer HOM-spectrum scenarios.

Multi-bunch beam modes in the transverse plane are considered stable because of the coherent damping from the short-range transverse wake and the deliberately-chosen positive chromaticity. This stability is unaffected by the presence of the HHC. Results from a Monte Carlo calculation with dipole HOMs of randomized frequencies are given in Table 2.

PRELIMINARY MONTE CARLO CALCULATIONS

The stability of the modes were first examined by assuming that each bunch behaves as a point charge. Though we know this is an approximation, we can quickly perform Monte Carlo calculations of possible maximum growth rates and assess the need to make further calculations.

The main lattice parameters that control longitudinal growth rate are given in Table 1 and appear in the following equation for the maximum growth rate of a multi-bunch beam mode due to a single HOM resonance:

$$G = \frac{\alpha_c I_{\text{total}}}{2(E/e)\nu_s}(R_s f_{\text{HOM}}) \exp(-\omega^2\sigma_t^2), \quad (1)$$

where α_c is the momentum compaction, I_{total} is the stored current, E/e is the beam energy in eV units, ν_s is the synchrotron tune, R_s is the (circuit definition) shunt impedance of the monopole HOM, f_{HOM} is the frequency of the HOM

* Work supported by the U.S. Department of Energy, Office of Science, Office of Basic Energy Sciences, under Contract No. DE-AC02-06CH11357.
† lemery@anl.gov

Content from this work may be used under the terms of the CC BY 3.0 licence (© 2015). Any distribution of this work must maintain attribution to the author(s), title of the work, publisher, and DOI.

ISBN: 978-3-95450-168-7 doi:10.18429/JACoW-IPAC2015-TUPJE066

DEVELOPMENT OF AN ABORT KICKER AT APS TO MITIGATE BEAM LOSS-INDUCED QUENCHES OF THE SUPERCONDUCTING UNDULATOR*

Katherine C. Harkay#, Jeffrey C. Dooling, Yury Ivanyushenkov, Robert Laird, Frank R. Lenkszus, Cedric C. Putnam, Vadim Sajaev, Ju Wang, ANL, Argonne, IL 60439, USA

Abstract

The first superconducting undulator (SCU0) at the Advanced Photon Source (APS) has been delivering 80-100 keV photons for user science since January 2013. SCU0 often quenches during beam dumps triggered by the machine protection system (MPS). SCU0 typically recovers quickly after a quench, but SCU1, a second, longer device to be installed in 2015, may take longer to recover. We tested using injection kickers as an abort system to dump the beam away from SCU0 and the planned location of SCU1. An alternate trigger was tested that fires the kickers with MPS. We demonstrated that controlling the beam dump location with kickers can significantly reduce the beam losses at SCU0, as measured by fiber optic (FO) beam loss monitors (BLMs), and can also prevent a quench. A dedicated abort kicker system has been developed based on `elegant` simulations. A spare injection kicker was modified to produce the required waveform. Injection kicker tests, simulations, and the abort kicker design are described. Demonstration of this strategy in APS has implications for the APS Upgrade, where more SCUs are planned.

EXPERIMENTAL TESTS

A superconducting undulator, SCU0, installed in APS was found to quench 80% of the time during beam dumps triggered by MPS. Simulations and beam studies suggest that beam losses > 50 pC in a small coil volume deposit energy sufficient to raise the coil temperature above the NbTi critical temperature [1,2]. Quench recovery is typically fast enough to allow SCU0 to be operated once the beam is restored. The consequences of beam-induced quenches is potentially greater for the longer device, SCU1, since it may require longer recovery time.

FO BLMs [3] were installed in Sector 6 ("ID6") on the SCU0 vacuum chamber (warm) transitions to characterize the beam losses [2]. Horizontal injection kickers (IK) were used to test a beam abort system. The injector kicker pulse waveform is ~2 μs FWHM. In order to kick out a full turn, which is 3.68-μs long, two horizontal injection kickers were used as a pair, with the second kicker timing shifted by half a turn. We used IK1 (in Sector 38) and IK4 (in Sector 40) as a pair, and IK2 and IK3 (both in Sector 39) as another pair. The kickers were set to their maximum peak kicks of ~1.5 mrad and it was verified that the entire beam was lost. The studies were repeated for the nominal 102 mA stored in 24 and 324 uniformly-spaced bunches, two APS operating modes. In Table 1, the BLM integrated loss charge for an MPS trip is compared to that using the kickers. The results demonstrate that controlling the beam loss location with kickers can significantly reduce the beam losses at SCU0.

To test whether lower ID6 beam losses can prevent a quench, 102 mA were stored in 24 bunches and SCU0 was powered to a typical main coil current of 650 A. IK1 and IK4 were fired, dumping the entire beam, and SCU0 did not quench. In this case, the losses at SCU0 were below the BLM measurement threshold.

Table 1: Total Uncalibrated ID6 BLM Charge, Comparing MPS Beam Dumps with Injection Kickers

Dump type	24 bunches (nC)	324 bunches (nC)
MPS	444	480
IK1+IK4	1	6
IK2+IK3	30	44

BEAM ABORT SYSTEM

The present method of dumping the beam during an MPS trip is to interrupt the rf amplifier drive for 100 ms, which causes the beam to move towards the chamber wall as the rf field decays and the beam loses energy to synchrotron radiation. The beam is lost mostly on the smallest aperture, which is the ID4 vacuum chamber [4], but beam losses are also clearly observed at ID6 where SCU0 is installed. To control the loss location at the level required, a kicker will be employed to dump the beam away from ID chambers.

While the injection kicker tests were a successful proof of principle, the loss distribution is not ideal, in that beam is lost in ID1, the planned location of SCU1 (see Model validation). The beam abort system should limit losses at both SCU0 and SCU1. Also, injection kicker abort configurations are incompatible with top-up operation.

The new beam abort system will use a dedicated horizontal kicker in the Sector 36 rf straight section, that stays charged during user operation, and whose discharge is triggered by MPS. Should the abort kicker fail to fire, MPS would dump the beam as usual. Using a peak kick ≥ 1 mrad, the entire beam is lost on the chamber walls within a few turns. Beam losses are mainly on the thick septum chamber in the injection straight section [5].

*Work supported by U. S. Department of Energy, Office of Science, under Contract No. DE-AC02-06CH11357.
#harkay@aps.anl.gov

Content from this work may be used under the terms of the CC BY 3.0 licence (© 2015). Any distribution of this work must maintain attribution to the author(s), title of the work, publisher, and DOI.

ISBN: 978-3-95450-168-7 doi:10.18429/JACoW-IPAC2015-TUPJE067

STATUS OF THE APS UPGRADE PROJECT*

S. Henderson#
APS Upgrade Project, Argonne National Laboratory, Argonne, IL 60439, USA

Abstract

A concept for an upgrade to the Advanced Photon Source based on a multi-bend achromat lattice is being developed at Argonne National Laboratory. An MBA upgrade to the APS will reduce the horizontal emittance by a factor of ~50. Coupled with superconducting undulators, the APS-U brightness will be two to three orders of magnitude beyond that which is available today at the APS.

INTRODUCTION

There is world-wide interest [1] in constructing 4th generation synchrotron radiation facilities with greatly reduced emittance based on multi-bend achromat (MBA) lattices [2]. MBA lattices promise to reduce the achievable horizontal emittance in electron storage rings by large factors, due to the favourable scaling of emittance [3] with the number of dipole magnets.

$$\varepsilon_x \propto \frac{E^2}{N_d^3} \quad (1)$$

Argonne National laboratory is developing a concept for a MBA upgrade to the Advanced Photon Source based on a multi-bend achromat lattice. This concept is the centerpiece of the Advanced Photon Source Upgrade Project (APS-U), which includes in addition to an upgrade to the storage ring, new insertion devices, front-ends and a suite of new and upgraded beamlines and associated optics and detector improvements.

APS-U CONCEPT AND PERFORMANCE

A conceptual design of the APS-U Project has been developed. The concept includes the following elements:

- A new 6 GeV MBA high-brightness storage ring in the existing APS tunnel
- Doubling of the ring stored beam current to 200 mA
- New insertion devices optimized for brightness and flux at the reduced storage ring energy
- New and upgraded beamline front-end systems of a common design for maximum flexibility
- A suite of new and upgraded beamlines designed for best-in-class performance with the high-brightness source
- Optics and detector improvements for remaning beamlines to take full advantage of MBA source properties
- Improved electron and photon stability

Table 1 compares the APS Upgrade storage ring design and performance parameters to those of the APS in present operation. The APS-U MBA lattice (described in more detail in [4]) is a seven-bend design based on the ESRF hybrid lattice concept [5]. The beam energy is reduced from the present 7 GeV to 6 GeV in order to further reduce the horizontal emittance. The beam current will be twice that which is routinely operated today.

Two operating modes are envisioned. The first mode is optimized for the highest possible brightness, and includes 324 regularly spaced bunches of 0.6 mA per bunch in a “flat-beam” configuration with 10% emittance coupling. A second mode – the timing mode – is optimized for a smaller number of equally spaced bunches with higher bunch current of 4.2 mA in a round-beam configuration with full emittance coupling to achieve an acceptable Touschek beam lifetime. The high-brightness mode achieves a horizontal emittance of 68 pm-rad, which is a factor of approximately 50 times smaller than present operation.

The brightness at 8 keV is a factor of 80 larger than today; the brightness at 20 keV is a factor of 340 larger than today, and that at 80 keV is a factor of 380 larger than today. The available coherent flux is higher by the same factors. The single bunch brightness is a factor of 25 greater than that achieved today.

Since the beam energy is reduced, undulator periods should be reduced accordingly to maintain similar first harmonic energies. In addition, APS-U will incorporate a suite of superconducting undulators, building upon recent developments of the last several years [6]. Front-ends will be upgraded to incorporate the recent High Heat Load Front-end concept that has been developed and successfully deployed at APS [7].

An MBA lattice at the APS opens new capabilities that don’t exist today in coherence techniques with high energy x-rays. Beamline investments, through an open proposal process, will ensure international competiveness of the beamline suite at the time of project completion and beyond. Targeted improvements to beamline optics are also incorporated into the concept to ensure that beamlines are positioned to take advantage of the MBA source properties.

Beam stability requirements are quite stringent [8]. Electron and photon stability requirements impact the engineering design at every level.

APS-U CONCEPTUAL DESIGN

Lattice

The APS-U lattice [4] is designed to optimize hard x-ray brightness by minimizing horizontal emittance in a MBA lattice. The lattice is composed of 40 identical sectors, each of which contains seven bending magnets.

*Work supported by U.S. Dept. of Energy, Office of Science, under Contract No. DE-AC02-06CH11357.
#hendersons@anl.gov

Content from this work may be used under the terms of the CC BY 3.0 licence (© 2015). Any distribution of this work must maintain attribution to the author(s), title of the work, publisher, and DOI.

ISBN: 978-3-95450-168-7 doi:10.18429/JACoW-IPAC2015-TUPJE068

DEVELOPMENT AND PERFORMANCE OF 1.1-M LONG SUPERCONDUCTING UNDULATOR AT THE ADVANCED PHOTON SOURCE*

Y. Ivanyushenkov#, C. Doose, J. Fuerst, K. Harkay, Q. Hasse, M. Kasa, D. Skiadopoulos, E.M. Trakhtenberg, Y. Shiroyanagi, E. Gluskin, ANL, Argonne, IL 60439, USA

Abstract

Development of superconducting undulators continues at the Advanced Photon Source (APS). The second superconducting undulator, SCU1, has been built and prepared for installation in the storage ring at the APS. This undulator has a 1.1-m long superconducting magnet and utilizes an improved version of the cryostat of the first superconducting undulator, SCU0. The results of the cold test of the SCU1 are presented in this paper.

INTRODUCTION

Superconducting undulators outperform other undulator technologies in terms of undulator peak field for a given period length and magnetic gap. The higher undulator field lead to higher photon fluxes, especially at higher photon energies. The advantage of superconducting undulator technology has been confirmed at the APS by operational performance of the SCU0. This undulator with a 0.3-m long magnet generates higher photon flux above 80 keV than a 2.4-m long hybrid undulator [1]. The next logical step was to increase the length of the SCU magnet. Such a milestone has been achieved with SCU1 – the second superconducting undulator developed at the APS. This paper gives a short description of the SCU1 and presents the cold test results of the undulator in detail.

SCU1 PARAMETERS

Parameters of SCU1 are listed in Table 1. The period length of 18 mm was chosen to have continuous photon energy coverage above 40 keV. The length of the magnet is 1.1 m – more than 3 times the length of the SCU0 magnet.

Table 1: Main Design Parameters of SCU1

Parameter	Value
Cryostat length, m	2.06
Magnetic length, m	1.1
Undulator period, mm	18
Magnetic gap, mm	9.5
Beam vacuum chamber vertical aperture, mm	7.2
Undulator peak field, T	0.97
Undulator parameter, K	1.63
Photon energy at fundamental, keV	11.7-25

*Work supported by U.S. Department of Energy, Office of Science, under Contract No. DE-AC02-06CH11357.
#yury@aps.anl.gov

SCU1 DESIGN

Cryostat

The SCU1 uses a cryostat, which is an improved copy of the SCU0 cryostat [2]. Modifications include the addition of optical windows to the cryostat vacuum vessel that allow direct observation and measurement of the cold mass vertical position inside the cryostat. Also, several thermal links were added to improve cooling of the cold mass support frame. Kevlar strings that support the cold mass in the cryostat have been improved as well.

Magnet

The SCU1 magnet is continuously wound with a superconducting wire onto a low-carbon steel former, or a core (see Fig. 1). The winding scheme is different from the one used in the SCU0 magnet. Instead of first winding all odd grooves and then making a 180-degree turn and winding back all even grooves, the turn is now made after winding each groove. In the new core design, magnetic poles are left only on the face side of the core and the poles on the other sides are non-magnetic. Also, three liquid helium (LHe) channels in the SCU0 design are replaced with a larger diameter single channel in the SCU1 core. As a result of the design simplification, the cost of a 1.1-m SCU1 core is about the same as that of a 0.3-m long SCU0 core. It is worth highlighting that the SCU1 cores were fabricated to a very high level of precision. The measured groove dimensions were within 30 μm rms.

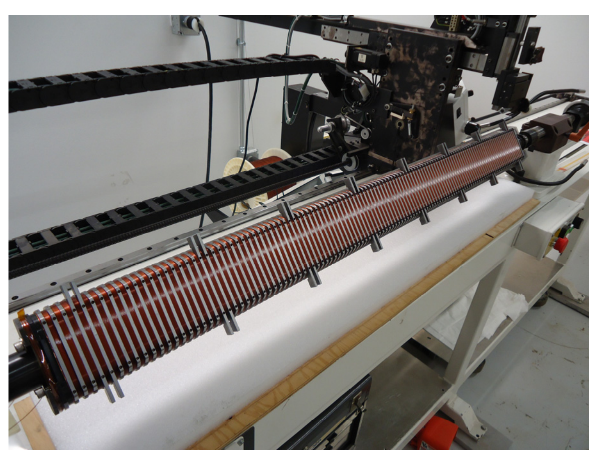

Figure 1: SCU1 magnet core on winding machine.

Similar to SCU0, a commercially available NbTi superconducting round wire is used in the SCU1 magnet, except a wire diameter of 0.6 mm is chosen instead of the 0.7 mm diameter used in the SCU0. The smaller wire size

Content from this work may be used under the terms of the CC BY 3.0 licence (© 2015). Any distribution of this work must maintain attribution to the author(s), title of the work, publisher, and DOI.

ISBN: 978-3-95450-168-7 doi:10.18429/JACoW-IPAC2015-TUPJE069

FAST INJECTION SYSTEM R&D FOR THE APS UPGRADE*

F. Lenkszus, A. Xiao, J. Carwardine, A. Cours, G. Decker, L. Morrison, X. Sun, J. Wang, F. Westferro, C.Y. Yao, ANL, Argonne, IL 60439, USA
A. Krasnykh, SLAC, Menlo Park, CA 94025 USA

Abstract

The MBA upgrade for the APS will operate with bunch swap out and vertical on-axis injection. The planned 324 bunch fill pattern places difficult demands on the injection and extraction kickers. The present concept uses dual stripline kickers driven by high voltage (HV) pulsers. Minimizing perturbation on adjacent bunches requires very fast rise and fall times with relatively narrow (< 20 ns), 15 kV pulses. To achieve these requirements, a multifaceted R&D program has been initiated. The R&D includes the HV pulser, stripline kicker and HV feedthrough. The requirements for injection and extraction, progress on prototype development, and results of our HV pulser investigations are discussed.

INTRODUCTION

The Advanced Photon Source (APS) storage ring will be upgraded to use a multiband achromat (MBA) lattice to provide enhanced hard x-ray brightness and coherent flux to beam-lines [1]. The MBA lattice will operate with bunch swap out and vertical on-axis injection. In this scheme, a target bunch will be extracted to a beam dump and the resulting empty RF bucket filled with a replacement bunch from the APS injectors. The planned 324 bunch fill pattern with its 11.4 nanosecond bunch spacing places very demanding requirements on the extraction and injection systems to minimize perturbations to the stored bunches immediately upstream and downstream of the target bunch. The extraction and injection sections will each consist of four dual blade small-aperture stripline kickers with each kicker driven by a fast dual output high voltage pulser. In addition, the injection section will include a Lambertson septum. Parameters for the injection/extraction sections are listed in Table 1.

To address these requirements, an R&D program is underway which includes the kickers, fast high voltage pulsers and high voltage feedthroughs.

KICKER

Swap-out injection will require pulsed deflecting kickers fast enough to select individual bunches spaced as closely as 11.4 ns without significantly disturbing neighboring bunches.

*Work supported by the U.S. Department of Energy, Office of Science, Office of Basic Energy Sciences, under Contract No. DE-AC02-06CH11357.

Table 1: Injection/Extraction Parameters

Key Parameters		
Total Kick Angle	2.88	mrad
Number of Kickers	4	
Kicker Strength	1	mrad/m
Length of Each Kicker	72	cm
Blade to Blade Voltage	30	kV
Vertical Aperture	9	mm
Minimum Bunch Spacing	11.4	ns
Maximum Residual kick to Stored Beam	< 2.5	% amplitude
Pulse Rise Time (10%-90%)	4.5	ns
Pulse Width (90%-90%)	5.9	ns
Pulse Fall Time (90%-10%)	4.5	ns

Physics

Impedance-matching plays an essential role in achieving maximum kicker strength, reducing local high voltage concentration, which can lead to breakdown, and minimizing beam impedances. The optimization strategy is to match the differential impedance as close as possible to a 50 ohm line impedance, while allowing some mismatch in the common mode impedance [2]. A "vaned" body geometry has been adopted to provide better common mode impedance matching, while "D" shaped blades are used to improve field uniformity within the good field region. Figure 1 shows the cross section of the kicker.

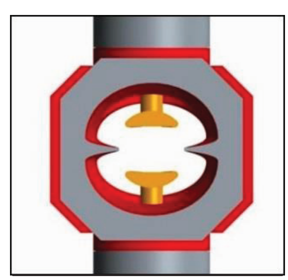

Figure 1: Kicker cross section.

The kicker has tapered end sections to better match the impedance to the feedthroughs. The design has been optimized by running a multi-objective optimization process with a 2D simulation program. A 3D simulation

Content from this work may be used under the terms of the CC BY 3.0 licence (© 2015). Any distribution of this work must maintain attribution to the author(s), title of the work, publisher, and DOI.

ISBN: 978-3-95450-168-7 doi:10.18429/JACoW-IPAC2015-TUPJE070

PRELIMINARY EXPERIMENTAL INVESTIGATION OF QUASI ACHROMAT SCHEME AT ADVANCED PHOTON SOURCE*

Yipeng Sun†, Hairong Shang, ANL, Argonne, IL 60439, USA

Abstract

Next generation storage rings require weaker dipole magnets and stronger quadrupole focusing to achieve very low emittance. To suppress the geometric and chromatic optics aberrations introduced by the strong sextupoles, achromat and quasi achromat schemes are applied in the lattice design to improve the beam dynamics performance. In this paper, some preliminary experimental investigation of the quasi achromat scheme at the Advanced Photon Source (APS) are presented. Three different operation lattices are compared on their beam dynamics performance. Although none of these operation lattices achieve ideal quasi achromat condition, they have certain relevant features. It is observed that fewer resonances are present in the nominal operation lattice which is most close to quasi achromat required conditions.

OVERVIEW

First-order and second-order achromats [1] have been applied in particle accelerators for a long time. The geometric and chromatic aberrations are eliminated by adopting integer betatron phase advance in certain beamlines. Similar third-order achromat design approaches were developed analytically and numerically [2] [3], where the concepts of repetitive identical cells and integer phase advance are used. For the next generation storage ring lattice designs, a third order geometric achromat is proposed with the assistance of harmonic sextupoles [4]. Quasi-achromat [5] is also proposed, which aims to minimize terms that are most relevant to the beam dynamics performance such as dynamic acceptance (DA) and lifetime. ESRF is proposing a hybrid multi-bend achromat (MBA) upgrade where the local cancellation scheme of $-I$ phase separation is employed [6]. Both quasi-achromat schemes and local cancellation schemes [6] are considered in the Advanced Photon Source (APS) MBA upgrade lattice design studies [5] [7].

In the lattice design studies, it is observed that fewer resonances are present in the achromat and quasi-achromat schemes. To investigate the beam dynamics performance of the achromat and quasi-achromat schemes, some preliminary experimental studies are performed at the APS storage ring. The APS storage ring is a third generation synchrotron-radiation light source, with a circumference of 1104 meters and an effective beam emittance of 3.13 nm. Three different operation lattices with different features have been compared. These lattices are the nominal lattice, hybrid lattice, and reduced horizontal beam size (RHB) operation lattice. For the APS storage ring nominal lattice, the linear optics in one of 40 identical sectors is shown in Fig. 1 where the starting and ending point are the insertion device (ID) center. The betatron phase advance is 0.905 in horizontal plane and 0.481 in vertical plane, which are close to the quasi-achromat condition [5]. In the horizontal plane, the total betatron phase advance is equal to integer every 10 repetitive cells. In the following sections, some experimental results are discussed. The bunch fill pattern is 24 bunches that are evenly distributed in the storage ring.

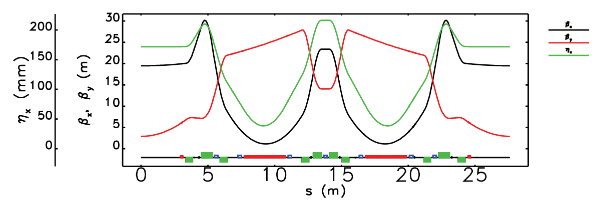

Figure 1: Twiss parameters in one arc section of APS storage ring. Green blocks represent quadrupoles, red blocks represent dipoles, and blue blocks represent sextupoles.

NOMINAL OPERATION LATTICE

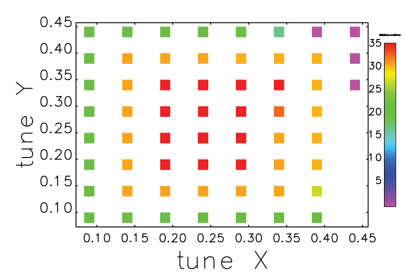

Figure 2: Stored beam current on ν_x-ν_y space during fractional tunes scan on nominal APS lattice.

The nominal APS operation lattice has 40 identical cells, with the optics in one such cell shown in Fig. 1. The standard operation mode of the APS storage ring has a total beam current of 102 mA, evenly distributed in 24 single bunches with top-up injection. Before the latest APS run, both the linear and nonlinear optics has a periodicity of 40. In the latest run, a smaller aperture ID vacuum chamber is installed at ID4, which has impact on injection efficiency and lifetime. It is noted that the minimum physical aperture of APS ring is located at ID4. The sextupoles in two sectors besides this ID chamber are optimized to manipulate the stored beam transverse phase space [8]. The nonlinear optics periodicity is slightly affected in these two sectors. The chromaticity is corrected to +2 in both horizontal and vertical planes. In Fig. 2 a stored beam current contour map

* Work supported by the U.S. Department of Energy, Office of Science, under Contract No. DE-AC02-06CH11357.
† yisun@aps.anl.gov

Content from this work may be used under the terms of the CC BY 3.0 licence (© 2015). Any distribution of this work must maintain attribution to the author(s), title of the work, publisher, and DOI.

ISBN: 978-3-95450-168-7 doi:10.18429/JACoW-IPAC2015-TUPJE071

ALTERNATE LATTICE DESIGN FOR ADVANCED PHOTON SOURCE MULTI-BEND ACHROMAT UPGRADE*

Yipeng Sun†, Michael Borland, ANL, Argonne, IL 60439, USA

Abstract

A 67-pm hybrid-seven-bend achromat (H7BA) lattice is proposed for a future Advanced Photon Source (APS) multi-bend-achromat (MBA) upgrade. This lattice requires use of a swap-out (on-axis) injection scheme. Alternate lattice design work has also been performed to achieve better beam dynamics performance than the nominal APS MBA lattice, in order to allow beam accumulation. One of such alternate H7BA lattice designs, which still targets a very low emittance of 76 pm, is discussed in this paper. With these lattices, existing APS injector complex can be employed without the requirement of a very high charge operation. Studies show that an emittance below 76 pm can be achieved with the employment of reverse bends in an alternate lattice. We discuss the predicted performance and requirements for these lattices and compare them to the nominal lattice.

OVERVIEW ON ALTERNATIVE LATTICE DEVELOPMENT

In the nominal lattice design [1] for the APS Multi-Bend Achromat (MBA) upgrade, the equilibrium emittance is pushed to the lowest achievable value employing reasonable magnet technology. To this end, seven dipole magnets with transverse or longitudinal gradients, plus strong quadrupole focusing are adopted in each arc cell. The associated strong nonlinearities make the dynamic acceptance not large enough for beam accumulation given the large injected beam size and allowing for a reasonable septum thickness. On-axis swap-out injection seems to be the only workable method for this lattice.

Lattice alternatives have been explored with relaxed goals for the emittance, which may achieve better beam dynamics performance than the nominal lattice, plus possibility for off-axis accumulation. Off-axis accumulation has several advantages. It requires minimal changes from existing systems (injectors, control, timing, etc.). It does not require new techniques as for the on-axis injection scheme (very fast kickers, high-charge-booster, beam dump, etc.). However, it may require better magnet quality, alignment precision, power supply stability, and beam trajectory/orbit control. It may also require additional octupoles and power supplies for these magnets, in order to achieve larger acceptance. Finally, using accumulation restricts the use of small horizontal gaps in IDs (insertion device).

Three different types of lattice structure, from five-bend achromat (5BA) to eight-bend achromat (8BA), were investigated and compared in terms of their requirements on the techinical systems and their beam dynamics performance:

- MAX-IV style: uniform TME cells [2]
- ESRF-II hybrid-lattice style: dispersion bump with -I separation [3]
- SIRIUS-inspired [4]: combination of MAX-IV and ESRF-II

Reverse dipole fields in focusing quadrupole magnets [5] are also considered and adopted in the lattice design. Of all these lattices investigated, a Hybrid-7BA lattice design appears to be the most promising in terms of allowing for the possibility of off-axis accumulation. This design is presented in some detail below. The general lattice design considerations and constraints are discussed in [1].

ALTERNATE H7BA LATTICE DESIGN

Magnets

To generate the dispersion bump more efficiently than uniform dipole magnets and achieve a smaller equilibrium emittance, two 6-section longitudinal gradient dipoles (LGD) are employed at both sides of the dispersion bump. A uniform dipole section length of 0.27 m is adopted. The maximum dipole field is 0.45 T in the LGDs, whereas it is 0.73 T in the central dipoles with transverse gradient. The maximum quadrupole gradient is 82 T/m. All the quadrupole magnets are within engineering design limits with more than a 10% margin, while all the sextupole magnets are within engineering design limits with more than a 20% margin. The maximum pole-tip fields are: 1 T for quadrupoles; 0.6 T for sextupoles; 0.3 T for octupoles. Similar to the nominal lattice design, a 3-pole-wiggler is placed in the center of each cell, to be used for bending magnet beamlines. In each cell, six focusing quadrupole magnets are integrated with reverse dipole fields—a feature not yet included in the nominal lattice—to further optimize the emittance and dispersion. The total number of magnets (dipoles, quadrupoles and sextupoles) is the same as used in the nominal lattice design.

Comparison with Nominal Lattice

Compared to the nominal lattice, the alternate H7BA lattice design has three potential advantages:

- Uniform-section-length dipole magnets are easier to produce and operate.
- Each cell has 2.5 meters of free space available for other accelerator components (e.g., injection kickers, skew quadrupoles, steering magnets, etc.).
- Four additional 0.32 m spaces are available to install ocutpoles near the dispersion peak in each cell.
- The ID straight length increased from 5.8 m to 6.1 m.

* Work supported by the U.S. Department of Energy, Office of Science, under Contract No. DE-AC02-06CH11357.
† yisun@aps.anl.gov

Content from this work may be used under the terms of the CC BY 3.0 licence (© 2015). Any distribution of this work must maintain attribution to the author(s), title of the work, publisher, and DOI.

ISBN: 978-3-95450-168-7 doi:10.18429/JACoW-IPAC2015-TUPJE072

ADVANCED PHOTON SOURCE INJECTION RELATED SIMULATION AND MEASUREMENT*

Yipeng Sun†, ANL, Argonne, IL 60439, USA

Abstract

Injection efficiency is one of the key factors in ensuring successful operation of storage ring light sources. In this paper, injection simulation and measurement studies at the Advanced Photon Source will be presented. The tracking simulations and measurements are compared in terms of the dynamic aperture and injection efficiency. Injection efficiency is also measured on the betatron tunes space and on different stored beam orbits.

OVERVIEW

This section introduces the basic concepts for the simulation and measurement studies discussed in the following sections, including: injection scheme, septum position, stored/injected beam separation, smaller measured ID4 physical aperture, definition of measured injection efficiency, etc..

The main ring at the Advanced Photon Source (APS) is a third-generation synchrotron radiation light source research facility. The circumference is 1104 meters and the beam effective emittance is 3.13 nm. The APS accelerator complex is composed of electron guns, linac, transport lines, a particle accumulator ring (PAR), a booster, and a storage ring. The electron beam is accelerated from 450 MeV to 7 GeV in the booster synchrotron over a half second. The electron beam is then injected into the 7 GeV storage ring through a booster-to-storage ring transport line (BTS). The linear optics in one of 40 sectors at APS storage ring is shown in Figure 1. A thick septum, a thin septum and four injection kickers (IK1, IK2, IK3, IK4) are employed in two sectors of the ring as the injection system. Injection efficiency into the storage ring is a key parameter to ensure successful operations of the light source.

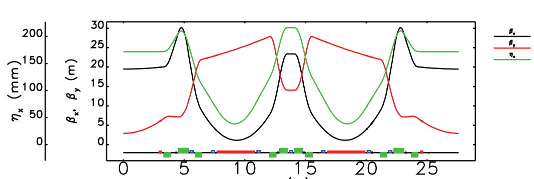

Figure 1: Twiss parameters in one arc section of APS storage ring. Green blocks represent quadrupoles, red blocks represent dipoles, and blue blocks represent sextupoles.

The closed injection bump is shown by the black curve in Fig. 2. The injection kickers are optimized for better injection efficiency and acceptable impact on the stored beam, as a result of which the injection ocsillation is shared between the stored and injected beams. Figure 2 shows trajectories of the stored (red curve) and injected (green curve) bunches using the non-closed bump. Beam separation between injected beam and stored beam closed orbit (without injection bump) at the septum location was set to 22 mm. For closed-bump injection, the stored bunch is not disturbed (black curve), but the oscillation of injected bunch is larger, shown by the blue curve in Fig. 2.

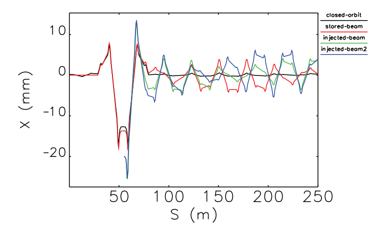

Figure 2: Beam trajectories for injection. Black: stored beam, closed bump. Blue: injected beam, closed bump. Red: stored beam, non-closed bump. Green: injected beam, non-closed bump. The septum magnet is at 56 m.

The position of the septum magnet with respect to the closed orbit of the stored beam was measured and is shown in Fig. 3. In Fig. 3 the electron beam lifetime (in minutes) is plotted in x-y space at the septum. It is observed that the septum is at x=-17 mm. Good agreement is achieved between two measurement methods, which are based on steering correctors, and BPM set points (plus orbit feedback) respectively. The measurement also agrees with the design.

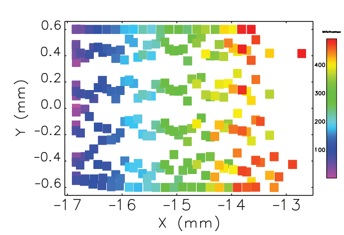

Figure 3: Beam-based measurement of the septum magnet position relative to stored beam. Color map showing the beam lifetime measured in minutes (5 to 500 minutes).

The minimum physical aperture of Advanced Photon Source is at ID4, which was ± 15 mm in x, and ± 2.5 mm in y. In the latest run, a smaller aperture vacuum chamber is installed at ID4. Beam-based physical aperture measurements show that ID4 now has a real aperture of roughly ± 13 mm in x, and ± 1.5 mm in y. Injection efficiency was

* Work supported by the U.S. Department of Energy, Office of Science, under Contract No. DE-AC02-06CH11357.
† yisun@aps.anl.gov

Content from this work may be used under the terms of the CC BY 3.0 licence (© 2015). Any distribution of this work must maintain attribution to the author(s), title of the work, publisher, and DOI.

ISBN: 978-3-95450-168-7 doi:10.18429/JACoW-IPAC2015-TUPJE073

RESULTS OF MAGNETIC MEASUREMENTS OF 2.8 m LONG VERTICALLY POLARIZING UNDULATOR WITH THE DYNAMIC COMPENSATION OF MAGNETIC FORCES*

Isaac Vasserman, Nikita Strelnikov, Emil Trakhtenberg, Joseph Xu, Efim Gluskin
ANL, Argonne, IL 60439, USA

Abstract

A novel undulator prototype with a horizontal magnetic field and dynamic compensation of magnetic forces has recently been developed at the Advanced Photon Source (APS) as a part of the LCLS-II R&D program. This undulator should meet stringent requirements for any LCLS-II insertion device. These requirements include limits on the field integrals and phase errors for all operational gaps, and the reproducibility and accuracy of the gap settings. Extensive mechanical testing has resulted in a performance that meets the requirements on the undulator gap setting. The magnetic tuning has been accomplished by applying a set of magnetic shims. As a result, the satisfactory performance of the undulator prototype has been demonstrated.

INTRODUCTION

The absolute majority of synchrotron radiation (SR) sources, including free electron lasers (FEL), utilize insertion devices (IDs) with a vertically oriented magnetic field. This preferential direction is the result of the strong asymmetry – the horizontal size is much larger than the vertical one – of the electron beam cross-section in the storage rings, which is the main source of synchrotron radiation. Although e-beam in FELs is quite symmetric in the transverse plane, ID designers have not taken real advantage of it thus far. This status quo could soon be changed because of recent advancements in the design of ultra-small emittance storage rings. Such machines promise to operate with round e-beams and execute on-axis injection. Therefore, the development of novel planar IDs with horizontal magnetic fields becomes a practical matter.

There are at least two major advantages of rotating ID geometry by 90 degrees. One is related to the rotation of the polarization plane of emitted radiation, which results in the transformation of monochromators and experimental set-ups to the "gravity neutral" systems. In many cases it would significantly simplify the construction and operation of these set-ups. The second advantage is also related to the "gravity neutral" design, but now applies to the undulator mechanical system. When such a design is combined with the magnetic force compensation system, the ID gap drive mechanism could become quite compact without sacrificing stringent requirements on the accuracy and reproducibility of the ID gap control.

Currently all FELs around the world utilize the traditional approach in the design of ID gap drive mechanisms, regardless of the type of IDs: out of vacuum, in-vacuum, APPLE-type, etc. These designs are loaded with very strong, often bulky beams that are able to withstand tremendous magnetic forces without noticeable distortions, and with very precise mechanical components that permit control of the ID magnetic gap value at a micron level. Typically the fabrication of such devices requires unique machine tools that can process several meter beams within a few microns of precision. Recently, after more than a decade of developments, European XFEL successfully constructed several dozen 5-m long IDs with a very sophisticated ID drive system that meets XFEL specifications [1]. SACLA XFEL in Japan has followed the design of in-vacuum IDs developed for the Spring-8 storage ring [2], and FERMI FEL in Trieste, Italy [3] is using APPLE-type IDs for its soft x-ray FEL. Newly built XFEL in Pohang, South Korea is adopting European XFEL ID design [4], and Swiss FEL follows SACLA's footsteps by choosing in-vacuum IDs [5].
The alternative ID design based on the "gravity neutral" concept with the dynamic compensation of magnetic forces has recently been developed at the APS.

First, a short prototype (847-mm-long) of an ID with the dynamic compensation of magnetic forces was designed, built and tested at the APS of the Argonne National Laboratory. The ID magnetic forces were compensated by the set of conical springs with exponential force change placed along the ID strong back [6]. Based on the magnetic measurements of the ID effective magnetic field (Beff), it has been demonstrated that the magnetic gaps within an operating range were controlled accurately and reproducibly within ± 1 micron. Successful tests of this ID prototype led to the design of a 2.8-m long device based on the same concept. Schematics of the 2.8-meter long prototype are shown in Fig. 1. There were load cells attached to the actuators to control the uncompensated force remaining due to preload and errors in matching the magnetic force and spring force.

*Work supported by the U.S. Department of Energy, Office of Science, under Contract No. DE-AC02-06CH11357.

Content from this work may be used under the terms of the CC BY 3.0 licence (© 2015). Any distribution of this work must maintain attribution to the author(s), title of the work, publisher, and DOI.

ISBN: 978-3-95450-168-7 doi:10.18429/JACoW-IPAC2015-TUPJE074

LCLS INJECTOR LASER MODULATION TO IMPROVE FEL OPERATION EFFICIENCY AND PERFORMANCE

S. Li*, D. Bohler, J. Corbett, A.S. Fisher, S. Gilevich, Z. Huang, A, Li, D. Ratner, J. Robinson, F. Zhou, SLAC, Menlo Park, CA 94025, USA
R. Fiorito, E. Montgomery, University of Maryland, College Park, MD 20742, USA
H. Zhang, Cockcroft Institute and University of Liverpool, Warrington, WA44AD, UK

Abstract

In the Linear Coherent Light Source (LCLS) at SLAC, the injector laser plays an important role as the source of the electron beam for the Free Electron Laser (FEL). The injector laser strikes a copper photocathode which emits photo-electrons due to photo-electric effect [1]. The emittance of the electron beam is highly related to the transverse shape of the injector laser. Currently the LCLS injector laser has hot spots that degrade the FEL performance. The goal of this project is to use adaptive optics to modulate the transverse shape of the injector laser, in order to produce a desired shape of electron beam. With a more controllable electron transverse profile, we can achieve lower emittance for the FEL, improve the FEL performance and operation reliability. We first present various options for adaptive optics and damage test results. Then we will discuss the shaping process with an iterative algorithm to achieve the desired shape, characterized by Zernike polynomial deconstruction.

INTRODUCTION

The injector laser of a Free Electron Laser (FEL) is a source to produce electron beams which are then accelerated to relativistic speed and generate coherent radiation in the undulator. At Linear Coherent Light Source (LCLS) at SLAC, the injector laser consists of a Ti:Sapphire laser system, producing 2 ps laser pulses at 760 nm wavelength. The infrared laser is then converted to ultraviolet wavelength (253 nm) via nonlinear process in a frequency tripler. The laser strikes a copper photocathode which emits photo-electrons due to the photo-electric effect [1].

Currently the LCLS injector laser has hot spots in its transverse profile. Figure 1 is a typical example of the transverse profile of the LCLS injector laser (left) and electron beam (right) near cathode. Non-uniformities in laser profile and cathode quantum efficiency lead to the non-uniformities in electron beam, which increase the electron beam emittance in the downstream linac and FEL. Lower emittance electron beam can enhance FEL performance. Other studies have shown certain types of laser transverse profile lead to lower electron emittance [2, 3]. Therefore, with adaptive optics, we can distinguish two major advantages. One is to remove non-uniformities in the electron beam, and the other is to shape the beam into an arbitrary profile [4].

In this paper, we present various options for the adaptive optics to modulate the injector laser, and show damage test results for these materials. We also discuss the shaping process with an iterative algorithm, in which Zernike polynomial reconstruction is used to characterize the transverse shape of the laser.

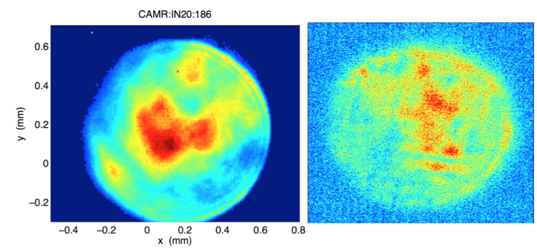

Figure 1: Example of LCLS injector laser transverse profile (left). Example of electron beam transverse profile (right).

ADAPTIVE OPTICS

There are various options for adaptive optics. We have considered Digital Micro-mirror Device (DMD), liquid crystal Spatial Light Modulator (SLM), and Deformable Mirror (DM). These materials have different properties and work in different wavelength ranges. In this section we will briefly describe how each device works and present damage test results.

Infrared (IR) Beam: DMD and SLM

The diagram of the damage test is shown in Fig. 2. The test was done at the HOLE laser lab at SLAC, with a laser identical to the LCLS injector laser. The laser is a 2 ps pulsed laser at 760 nm wavelength 120 Hz. The waveplate and polarizer allow us to tune the laser beam energy. The iris cuts the beam and is imaged through a lens onto the sample plane. The beam energy varies from 20 μJ to 1 mJ. At the image plane we replaced the camera with the sample and let the laser hit the chip at different spots for an exposure time up to 40 minutes. We gradually increased the beam energy and moved the sample across the surface until we saw visible damage on the pixels. Then we took the sample to the microscope lab and looked at the damage under microscope.

The Texas Instrument DLP7000 is a DMD made of an array of micro-mirrors. When powered on, each individual micro-mirror can deflect at ±12° angle. The shaping process is done by grouping individual micro-mirrors to macro-mirrors which consist of, for example, 5×5 micro-mirrors. For a certain macro-mirror, we can randomly turn off a number of micro-mirrors according to the ratio of cur-

* siqili@slac.stanford.edu

Content from this work may be used under the terms of the CC BY 3.0 licence (© 2015). Any distribution of this work must maintain attribution to the author(s), title of the work, publisher, and DOI.

ISBN: 978-3-95450-168-7 doi:10.18429/JACoW-IPAC2015-TUPJE075

SIMULATION STUDY OF INJECTION PERFORMANCE FOR THE ADVANCED PHOTON SOURCE UPGRADE*

A. Xiao†, V. Sajaev, ANL, Argonne, IL 60439, USA

Abstract

A vertical on-axis injection scheme has been proposed for the hybrid seven-bend-achromat (H7BA) [1] Advanced Photon Source upgrade (APSU) lattice. In order to evaluate the injection performance, various errors, such as injection beam jitter, optical mismatch and errors, and injection element errors have been investigated and their significance has been discovered. Injection efficiency is then simulated under different error levels. Based on these simulation results, specifications and an error-budget for individual systems have been defined.

INTRODUCTION

A hybrid seven-bend-achromat (H7BA) lattice has been designed for the APSU. It features a 67 pm natural emittance and its brightness exceeds today's APS by two to three orders of magnitude. Strong nonlinear effects associated with the design present a great challenge to the injection design. Based on investigations made for several different injection configurations, an on-axis single sector "swap-out" vertical injection scheme was adopted, and the injection performance was calculated including various machine errors.

The change of Courant-Snyder invariant $\Delta A_u = A_u - A_{u,0}$ is used to determine quantitatively which injection errors dominate, ($A_u = \gamma_u u^2 + 2\alpha_u uu' + \beta_u u'^2$, where u stands for x or y, γ_u, α_u and β_u are corresponding optical function at the injection point, $A_{u,0}$ is the value in ideal conditions). For an error that causes equivalent emittance increase, A_u stands for the equivalent emittance with errors; for an error that causes beam centroid motion, A_u is equivalent to the amplitude of the motion, as $\Delta u = \sqrt{\Delta A_u \beta_u}$.

This paper first describes the types of errors that were included in the injection study. It then gives calculated ΔA_u under various error levels, which are chosen based on our past operational experience and on assumptions about the new hardware systems. The range of ΔA_u is obtained by summarizing contributions from all types of errors, and the significance of each sub-system error is identified. The injection performance is studied by simulating injection efficiency at different ΔA_u levels. The specifications and an error-budget for individual systems are given based on the overall injection performance requirement. To validate the obtained specifications, a simulation that includes shot-to-shot variations of various parameters is done, and results are given at the end. The injection efficiency is simulated by 1000-turn tracking a bunch consisting of 2000 particles with a distribution corresponding to that of the booster. Synchrotron radiation, apertures, rf systems, etc. are included in tracking.

TYPE OF INJECTION ERRORS

Many imperfections could occur during injection:

Transverse Optical Function Mismatch

This is a systematic error. Because of the filamentation process after injection, a transversely mismatched injected bunch is equivalent to a matched bunch with emittance ellipse enclosing the entire mismatched bunch ellipse, as seen in Fig. 1. The emittance increase $\Delta A = A - A_0$ depends on the magnet strength errors in the booster to storage ring (BTS) transport line, and on how well the optical functions can be corrected.

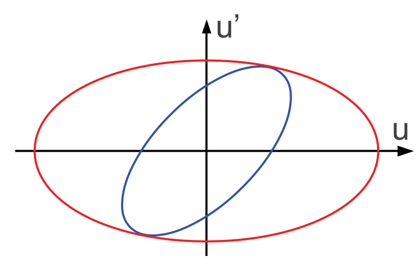

Figure 1: Optical function mismatch at the injection point. Blue - mismatched injected beam emittance A_0; red - equivalent injected beam emittance A.

To evaluate how ΔA varies versus the magnet strength error level, the current APS BTS line design, with an arbitrary matrix added at the end to match optical functions at the injection point, is used as the simulation model. Mismatched optical functions and associated ΔA are calculated at three magnet strength error levels: 1%, 2%, and 3%. 5000 uniformly distributed random cases are simulated for each error level, and the maximum of ΔA for all cases with beta function error of less than 5%, 10%, and 15% are calculated, see Fig. 2. Beta function error is used because this parameter is convenient to measure and correct in practice. From Fig. 2, it is seen that emittance increase depends strongly on the magnet strength error level, in a way that is not strongly reflected in the beta function error at the injection point. Based on our operational experience, three cases are chosen for the injection performance simulation studies: no optical errors; beta error level at 10% and magnet strength error level at 1%, which gives $\Delta Ax = 20$ nm and $\Delta Ay = 4$ nm; beta error level at 10% and strength error level at 2%, which gives $\Delta Ax = 40$ nm and $\Delta Ay = 8$ nm.

* Work supported by the U.S. Department of Energy, Office of Science, Office of Basic Energy Sciences, under Contract No. DE-AC02-06CH11357.
† xiaoam@aps.anl.gov

Content from this work may be used under the terms of the CC BY 3.0 licence (© 2015). Any distribution of this work must maintain attribution to the author(s), title of the work, publisher, and DOI.

ISBN: 978-3-95450-168-7 doi:10.18429/JACoW-IPAC2015-TUPJE076

DESIGN STUDY OF THE HIGHER HARMONIC CAVITY FOR ADVANCED PHOTON SOURCE UPGRADE*

S.H. Kim#, M.P. Kelly, P.N. Ostroumov, T. Berenc, G. Decker, J. Carwardine,
ANL, Argonne, IL 60439, USA

Abstract

A higher-harmonic cavity is planned for the proposed Advanced Photon Source (APS) multi-bend achromat (MBA) lattice to increase the bunch length, improve the Touschek lifetime and increase the single-bunch current limit. We have investigated a range of options including 3rd, 4th, and 5th harmonics of the main radio frequency (RF) system, as well as configurations with and without external RF power couplers. The current baseline is a single 4th harmonic superconducting cavity with adjustable RF couplers and a slow tuner which provide the flexibility to operate over a wide range of beam currents. The cavity is designed to provide 0.84 MV at 1408 MHz for the nominal 6 GeV, 200 mA electron beam, and 4.1 MV main RF voltage. In this paper, we discuss the harmonic cavity parameters based on analytical calculations of the equilibrium bunch distribution and make comparisons to other options.

INTRODUCTION

The APS at Argonne National Laboratory is planning an upgrade based on a MBA lattice for which the transverse emittance will be much smaller [1,2]. Beam dynamics studies show very small transverse beam sizes, ~10 µm rms in both the horizontal and vertical directions, which will result in more frequent Touschek scattering. To reduce the Touschek scattering probability a higher harmonic bunch lengthening RF system will be required and in this paper we will present how this improves the Touschek lifetime [1,2].

Physics parameters for the higher-harmonic cavity (HHC) have been derived from this study. Possible options for the HHC were as follows:

- Harmonic number, for example, 3rd, 4th, or 5th.
- Superconducting or normal conducting.
- Passive (driven only by beam) or active mode (including an external RF generator).
- In passive mode, with or without external RF power couplers.

As a baseline design we have chosen a 4th harmonic superconducting cavity operated in the passive mode with external RF power couplers terminated in matched loads. This was done based on analytical calculations of the equilibrium longitudinal bunch distribution for the combined RF voltage of the main and higher harmonic system. A unique feature of this design compared to that of other machines, such as ALS and ELETTRA [3,4], will be the use of adjustable RF power couplers. In combination with a frequency tuner, this permits adjustment of both the amplitude and phase of the harmonic voltage such that the cavity can be optimized for different beam currents even in the passive mode of operation.

In the following section, we will discuss the ‘optimum’ bunch lengthening condition, the harmonic number, the choice for superconducting technology, and operation at different beam currents. Non-optimum conditions will also be discussed. The detailed design of the HHC is presented in [5] and particle tracking simulations with the HHC are discussed in the [6].

HHC PARAMETERS

Optimum Bunch-Lengthening Condition

The longitudinal charge distribution in a bunch was analytically calculated from the potential well generated by the main and harmonic RF voltage. The combined RF voltage V seen by an electron at phase ϕ is represented by [3,7]

$$V(\phi) = V_m\{\sin(\phi + \phi_m) + k\sin(n\phi + \phi_h)\}, \quad (1)$$

where V_m is the main RF voltage, k is the ratio of the harmonic voltage to the main RF voltage, n is the harmonic RF number, ϕ_m is the phase of the main RF, ϕ_h is the phase of the harmonic voltage. The charge distribution, ρ, in equilibrium with radiation damping and quantum excitation can be represented by [3,8]

$$\rho(\phi) = \rho_0 \exp\left(\frac{-\Phi(\phi)}{\alpha_c^2\sigma_e^2}\right), \quad (2)$$

where ρ_0 is a normalization factor, α_c is the momentum compaction factor, σ_e: the relative RMS energy spread, and Φ is the potential defined by [3,7]

$$\Phi(\phi) = \frac{\alpha_p}{2\pi h E_s}\int_0^{\phi}\{eV(\phi') - U_0\}d\phi', \quad (3)$$

where E_s is the synchronous energy, h is the harmonic number of the main RF relative to the ring revolution frequency, and U_0 is the energy loss per turn. In this study, we use the following values: V_m = 4.1 MV, U_0= 2.24 MeV, h = 1296, α_c= 5.86×10^{-5}, σ_e=9.5×10^{-4}.

The ‘optimum’ condition for bunch lengthening is to cancel the slope of the main RF at the bunch center such that the potential well is flat around the bunch center. Under this condition, the first and second derivatives of $V(\phi)$ must vanish at the synchronous phase [3,7]. The

*Results in this report are derived from work performed at Argonne National Laboratory. Argonne is operated by UChicago Argonne, LLC, for the U.S. Department of Energy under contract DE-AC02-06CH11357.
#shkim121@anl.gov

Content from this work may be used under the terms of the CC BY 3.0 licence (© 2015). Any distribution of this work must maintain attribution to the author(s), title of the work, publisher, and DOI.

ISBN: 978-3-95450-168-7 doi:10.18429/JACoW-IPAC2015-TUPJE077

Content from this work may be used under the terms of the CC BY 3.0 licence (© 2015). Any distribution of this work must maintain attribution to the author(s), title of the work, publisher, and DOI.

INSTABILITY THRESHOLDS FOR THE ADVANCED PHOTON SOURCE MULTI-BEND ACHROMAT UPGRADE*

R. R. Lindberg, ANL, Argonne, IL 60439, USA, and A. Blednykh, BNL, Upton, NY 11973, USA

Abstract

An important operating mode for the multi-bend achromat (MBA) upgrade at the Advanced Photon Source (APS) calls for 200 mA average current divided evenly over 48 bunches. Ensuring that the desired 4.2 mA single bunch current can be stably stored requires a detailed understanding of the impedance in the MBA ring. We briefly discuss modeling sources of impedance using the electromagnetic codes `GdfidL` and `ECHO`, and how we then include both geometric and resistive wall wakefields using the tracking code `elegant` to predict collective instabilities. We first validate our procedures by comparing APS experimental measurements to tracking predictions using the APS storage ring impedance model. We then discuss the MBA impedance model, for which we find that a chromaticity of 5 units is sufficient to obtain the required 4.2 mA single bunch current. Finally, we mention certain design changes that may reduce the impedance and allow for a reduction in chromaticity.

INTRODUCTION

There are many potential sources of instabilities, but observations at high-energy storage rings such as the APS have shown that the dominant collective effects are typically due to impedances/wakefields. To be more specific, transverse wakefields give rise to transverse beam instabilities that ultimately limit the single-bunch current at the APS, while longitudinal wakefields predominantly lead to bunch lengthening (which usually eases operational requirements), an increase in energy spread (which is typically not too detrimental), and rf-heating of vacuum components (which can be problematic). Transverse impedances will continue to be the dominant driver of collective effects for the MBA. Hence, understanding and calculating the impedance is critical for accurate predictions of the single-bunch current limit. Here we describe our efforts to model wakefields and predict collective effects for the APS MBA Upgrade including the bunch-lengthening higher harmonic cavity (HHC).

IMPEDANCE MODEL AND SIMULATION

We have adapted to the MBA lattice the impedance model and tracking simulation methods that Y.-C. Chae developed for the APS over the past decade. This model has successfully reproduced various impedance-driven collective effects observed in the APS ring [1, 2]; extending it to the MBA was straightforward once the primary impedance sources were identified and analyzed. In this model, the effects of impedances/wakefields are represented by a single "impedance element" in the code `elegant` [3]. To reduce the distributed impedance from the entire ring to a localized perturbation, we first divide the impedance into its resistive wall and geometric components. We compute the resistive wall contribution using analytic formulas, and calculate the geometric impedance with numerical simulation codes. We list the various resistive wall and geometric impedance sources identified for the MBA storage ring in Table 1.

We use two codes to compute the geometric impedance. We compute the wakefields for components possessing axial symmetry using the 2D `ECHO` code [4], while structures that vary in 3D are analyzed with the commercial code `GdfidL` [5]. To balance numerical efficiency and accuracy, within these codes we model the (point particle) wakefields by the wake potential generated by a 1-mm long bunch, as this approximation has had good success in predicting the onset of various instabilities in the present APS. In addition, we have performed several numerical tests that use wake potentials derived from shorter electron bunches, and these have proven to give the same results in terms of the single-bunch current limit for the APS-U lattice.

The total transverse wake potential of the ring is found by weighting each contribution by its local beta-function and summing. For example, if we label each element by j and the vertical geometric beta-function at that element by $\beta_{y,j}$, the weighted geometric wakefield along y is

$$\langle \beta_y W_y^{\text{geo}} \rangle = \sum_{\text{elements } j} \beta_{y,j} W_{y,j}^{\text{geo}}. \tag{1}$$

An analogous expression holds for W_x, while the total longitudinal wakefield is the simple sum $\langle W_z^{\text{geo}} \rangle = \sum_j W_{z,j}^{\text{geo}}$.

The corresponding impedances are then computed via the discrete Fourier transform, and the "total impedance" is obtained by adding the geometric and resistive wall contributions. Finally, we use these impedances with the particle tracking code `elegant` as a single element by dividing by the lattice function $\beta_{x,y}$ at its chosen location.

We show how well our impedance model and tracking simulations can perform by comparing the predictions of the present APS impedance model to recent experiments in Fig. 1. The first two plots show that the APS impedance model does a very good job predicting the longitudinal behavior; the first plot compares the current-dependent bunch lengthening predicted by simulation (blue points) with a fit to experimental data in red, while the second panel shows reasonably good agreement for both the microwave instability threshhold at approximately 6-7 mA and the subsequent growth in energy spread as I_{bunch} increases. Finally, the last panel compares the predicted single bunch current stability threshhold with I_{limit} measured at the APS storage ring for various levels of the chromaticity ξ defined by

* Work supported by the U.S. Department of Energy, Office of Science, Office of Basic Energy Sciences, under Contract No. DE-AC02-06CH11357.

ISBN: 978-3-95450-168-7 doi:10.18429/JACoW-IPAC2015-TUPJE078

MODELING OF IMPEDANCE EFFECTS FOR THE APS-MBA UPGRADE*

R.R. Lindberg, ANL, Argonne, IL 60439, USA and A. Blednykh, BNL, Upton, NY 11973, USA

Abstract

Understanding the sources of impedance is critical to accelerator design, and only becomes more important as vacuum chambers become smaller and closer to the electron beam. The multibend achromat upgrade at the Advanced Photon Source (APS) requires small, 22-mm diameter vacuum chambers and even smaller (6 mm) gaps for the insertion devices, so that both rf heating and wakefield-driven transverse instabilities become important concerns. We discuss modeling the primary sources of geometric impedance using the electromagnetic finite difference codes GdfidL and ECHO, and how these codes are influencing vacuum and accelerator component design.

INTRODUCTION

The vacuum design of the planned multi-bend achromat (MBA) upgrade at the APS must consider many often competing factors. First, the pumping must be able to achieve an ultra-high ($\lesssim$ 1 nTorr) vacuum, which is accomplished using local ion pumps in tandem with distributed pumping provided by high surface sorption materials such as non-evaporative getter (NEG) coatings. Second, engineers must find a way to handle the high heat loads associated with synchrotron radiation, both to maintain component integrity and to limit photon-stimulated desorption of gas molecules from the chamber walls. Third, the chambers must be compatible with the magnet design, and permit efficient extraction of bending magnet and undulator radiation for science.

While there are other vacuum design considerations, this list is sufficient to show that the desires of vacuum engineers are typically in conflict with those of an accelerator physicist interested in minimizing beam related wakefields/impedances. These wakefields result from changes in vacuum chamber geometry, and can lead to damaging levels of rf-heating and/or intensity-dependent instabilities. Here, we discuss our efforts to model the geometric sources of impedance associated with the MBA, and how our results are informing vacuum design.

MBA IMPEDANCE MODEL

We analyze the geometric impedance of the MBA using three basic steps. First, we try to identify the primary sources of impedance associated with a particular vacuum design. Second, we use electromagnetic codes to numerically calculate the wakefields associated with each impedance element. Third, we assess the effects of the wakefields on rf heating and beam stability. The next few paragraphs will discuss each of these steps in more detail.

* Work supported by the U.S. Department of Energy, Office of Science, Office of Basic Energy Sciences, under Contract No. DE-AC02-06CH11357.

Table 1: Elements that contribute to the geometric impedance (BPM = beam position monitor).

Sector (×40)		Ring	
Element	**Num.**	**Element**	**Num.**
BPM	12	Inject. kicker	4
ID BPM	2	Extract. kicker	4
ID transition	1	Feedback	2
Bellow	14	Stripline	1
Flange gap	52	Aperture	2
Crotch abs.	2	Fund. cavity	12
In-line abs.	12	Rf transition	4
Gate valve	4	Harm. cavity	1

We identify potential sources of impedance by drawing heavily on our experience with the present APS impedance model [1], since this model has shown rather good agreement with experimentally measured collective effects at the APS storage ring. We have found that important sources of impedance include both those from large changes in geometry, such as the insertion device (ID) transitions and injection/extraction kickers, and from relatively small perturbations that occur many times in the ring, like the bellows and flange gaps. We list the elements that presently compose the MBA impedance model in Table 1.

We then numerically simulate each impedance element to extract the longitudinal and transverse wakefields. We employ the 2D ECHO code [2] to solve for wakefields in axially symmetric elements, which presently include the flange gaps and in-line photon absorbers. Structures without axial symmetry are analyzed using the 3D commercial code GdfidL [3]. ECHO directly outputs wakefields of a given multipole order (we require the $m = 0$ longitudinal and transverse dipole wakes), while we derive the transverse dipole, quadrupole, and monopole wakefields from GdfidL output after a small amount of post-processing.

Finally, we assess the effects of wakefields using a combination of analytic tools and tracking-based simulations. We apply analytic expressions such as the loss factor to obtain important information regarding the energy loss and potential rf-heating issues, and the tracking code elegant [4] to predict detailed information regarding the influence of collective effects on beam stability. Note that the numerically calculated wakefields are actually those excited by a Gaussian bunch of duration σ_b, which in turn yields an impedance whose high-frequency components are suppressed by a Gaussian filter of width $1/\sigma_b$. Several test cases have shown that the predicted collective effects are independent of σ_b provided $\sigma_b \leq 1$ mm, and we use the bunch length $\sigma_b = 1$ mm for all wakefield simulations. More details on the tracking results can be found in [5].

Content from this work may be used under the terms of the CC BY 3.0 licence (© 2015). Any distribution of this work must maintain attribution to the author(s), title of the work, publisher, and DOI.

ISBN: 978-3-95450-168-7 doi:10.18429/JACoW-IPAC2015-TUPJE079

Content from this work may be used under the terms of the CC BY 3.0 licence (© 2015). Any distribution of this work must maintain attribution to the author(s), title of the work, publisher, and DOI.

HIGH CHARGE DEVELOPMENT OF THE APS INJECTOR FOR AN MBA UPGRADE*

C.-Y. Yao#, N. Sereno, Ju Wang, M. Borland, Doug Horan, H. Shang, X. Sun, K. Harkay, R. Lindberg, J. Calvey, Advanced Photon Source,
Argonne National Laboratory, Argonne, IL 60439, USA

Abstract

The APS MBA (multi-bend achromat) upgrade storage ring will employ a "swap out" injection scheme and requires a single-bunch beam with up to 20 nC from the injector. The APS injector, which consists of a 375-MeV linac, a particle accumulator ring (PAR), and a 7-GeV synchrotron (Booster), was originally designed to provide up to 6 nC of beam charge. High charge injector study is part of the APS upgrade R&D that explores the capabilities and limitations of the injector through machine studies and simulations, and identifies necessary upgrades in order to meet the requirements of the MBA upgrade. In the past year we performed PAR and booster high charge studies, implemented new ramp correction of the booster ramp supplies, explored non-linear chromatic correction of the booster, etc. This report presents the results and findings.

INJECTOR TIMING

At 2 Hz operations we have achieved ~10 nC in the PAR. In order to achieve up to 20 nC beam charge the injector cycle must be extended to at least 1 s to accumulate enough Linac bunches, and to allow sufficient damping time. A prototype timing module that supports both 2Hz and 1Hz operations has been designed and is currently under hardware test.

NON-LINEAR RAMP FOR THE BOOSTER MAIN SUPPLIES

The Booster accelerates beam from 375-MeV injection energy to 7-GeV extraction energy in 224 ms. Damping time, bunch length and beam stability varies during this process. We mainly rely on chromatic correction and radiation damping to maintain beam stability.

Chromatic correction for the booster is complicated by the eddy current in the vacuum chamber due to ramping of the dipole field. The original sextupole strengths are designed to maintain a +1 chromaticity in both planes at extraction energy. This is inadequate for high charge beam. In order to provide higher chromatic correction at low beam energy we developed a new ramp correction programs that support non-linear ramps for the quadrupole and sextupole supplies. Figure 1 shows a non-linear ramp for the SD sextupole supply. This allows us to apply high chromatic correction during the first half of the ramp where the beam instability is stronger.

*Work supported by the U.S. Department of Energy, Office of Science, under Contract No. DE-AC02-06CH11357.
#cyao@aps.anl.gov

We are also considering upgrading the sextupole power supplies to higher current ratings to achieved a chromaticity of 6 to 7 in both planes in the full Booster cycle.

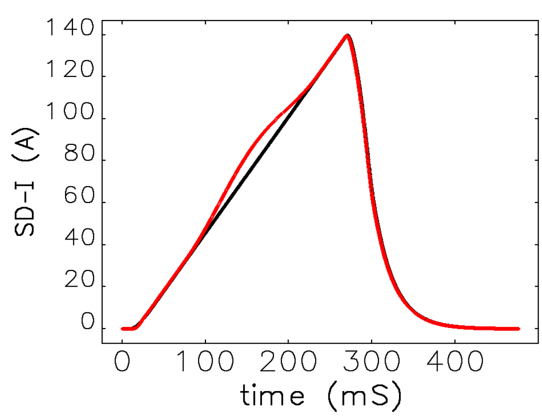

Figure 1: SD magnet new non-linear (Red) and original linear (Black) ramps.

NEW BPM AND CORRECTOR RAMP SYSTEM

A new Booster BPM system has been designed that utilizes a BSP-100 [1] module that was originally developed for APS storage ring. The new system will provide up to 10 average beam orbit readings along the 224 ms energy ramp.

A V344 arbitrary waveform generator (AWG) module and a V490 ADC module [2] are selected for the new corrector ramp control system.

The BPM system is under test and EPICS interface for a single V344 module has been tested. Full implementation is under way.

ANALYSIS OF BOOSTER CHAMBER IMPEDANCE

The Booster vacuum chamber is made of 316L stainless steel, and the associated longitudinal and transverse impedance was obtained using standard analytic formulas. In addition, Table 1 lists the vacuum components that represent the main contributions to the geometric impedance. The wakefields due to these elements were calculated using the 3D electromagnetic code GdfidL [3], with the exception of the rf cavities.

ISBN: 978-3-95450-168-7 doi:10.18429/JACoW-IPAC2015-TUPJE080

FIRST BEAM AND HIGH-GRADIENT CRYOMODULE COMMISSIONING RESULTS OF THE ADVANCED SUPERCONDUCTING TEST ACCELERATOR AT FERMILAB*

D.J. Crawford#, C. Baffes, D. Broemmelsiek, K. Carlson, B. Chase, E. Cullerton, J. Diamond, N. Eddy, D. Edstrom, E. Harms, A. Hocker, C. Joe, A. Klebaner, M. Kucera, J. Leibfritz, A. Lumpkin, J. Makara, S. Nagaitsev, O. Nezhevenko, D. Nicklaus, L. Nobrega, P. Piot, P. Prieto, J. Reid, J. Ruan, J. Santucci, W. Soyars, G. Stancari, D. Sun, R. Thurman-Keup, A. Valishev, A. Warner, S. Wesseln, Fermilab, Batavia, IL 60510, USA

Abstract

The advanced superconducting test accelerator at Fermilab has accelerated electrons to 20 MeV and, separately, the International Linear Collider (ILC) style 8-cavity cryomodule has achieved the ILC performance milestone of 31.5 MV/m per cavity. When fully completed, the accelerator will consist of a photoinjector, one ILC-type cryomodule, multiple accelerator R&D beamlines, and a downstream beamline to inject 300 MeV electrons into the Integrable Optics Test Accelerator (IOTA). We report on the results of first beam, the achievement of our cryomodule to ILC gradient specifications, and near-term future plans for the facility.

INTRODUCTION

A superconducting radio frequency (SRF) accelerator test facility is currently under construction at Fermilab. Once complete, the accelerator will consist of a photoinjector front-end, two superconducting booster cavities, a 50 MeV beamline, a beam acceleration section consisting of one ILC-type cryomodule, multiple downstream beamlines, the IOTA storage ring with various diagnostics to conduct beam tests, and a high-power beam dump. This paper describes the commissioning effort of the facility to date. [1]

Front-end

The front-end consists of a 1.5 cell normal conducting RF Gun resonating at 1.3 GHz with a peak accelerating gradient of up to 45 MV/m, a cesium telluride (Cs_2Te) cathode for photoelectron production, a 3 ps pulsed 263 nm ultra-violet (UV) laser delivery system, and a diagnostic area for measuring the charge and spot size of the photoelectron beam. [2] The UV laser system is tuneable from 1 to 3000 micro-bunches within a 1 ms bunch train at a maximum 5 Hz repetition rate. Two solenoid magnets, each capable of a peak field of 0.28 T at 500 A, surround the RF Gun cavity. The main solenoid provides the appropriate field for focusing the electron beam to the booster cavities. The bucking solenoid cancels the magnetic field from the main solenoid at the photocathode surface in order to minimize beam emittance.

Booster Cavities

There are 2 small cryomodules after the front-end known as Capture Cavity 1 (CC1) and Capture Cavity 2 (CC2). Each of these cryomodules contains one 9-cell L-band cavity operating at 1.3 GHz, driven by a 300 kW klystron, and capable of average accelerating gradients >22 MV/m. These cavities will also be used to “chirp” the beam, i.e. generate a time-momentum correlation, in preparation for bunch compression in the chicane. Downstream of these cavities is space allotted for a future SRF 3.9 GHz cavity intended to be used for bunch linearization during bunch compression. [3]

Currently, CC2 is installed and CC1 will be installed upstream of CC2 during summer 2015 and will allow for a maximum beam energy of 50 MeV.

50 MeV Beamline

After CC2, the electron beam enters the 50 MeV beamline. There is a quadrupole doublet to control the beam size for emittance measurements, a matching section into a chicane, a 4-dipole chicane for bunch compression (R56 = -0.18 m), and a matching section into a 22.5° vertically downward bending dipole. This dipole, upstream of the absorber, will serve as the low energy spectrometer. The 50 MeV beam absorber is capable of accepting up to 550 W of beam power. [3, 4]

The beamline also consists of 13 horizontal and vertical trim dipole magnets, 6 transverse profile monitors (TPM), 19 beam position monitors (BPM), 2 toroids, 2 wall current monitors (WCM), and 8 beam loss monitors connected to the Machine Protection System (MPS). Each TPM contains either a 100 µm thick cerium-doped yttrium aluminum garnet (YAG) screen or a 100 µm thick lutetium yttrium oxyorthosilicate (LYSO) screen. Each TPM also contains an optical transition radiation (OTR) foil of 25 µm or 1 µm thick, and a 1951 USAF optical resolution target for pixel and resolution calibration. The TPM in the chicane has a slit mask experiment installed in the OTR position.

Installation of the 50 MeV beamline was completed earlier this year. A schematic beamline is shown in Fig. 1.

* Operated by Fermi Research Alliance, LLC under Contract No. DE-AC02-07CH11359 with the United States Department of Energy.
# dcrawford@fnal.gov

Content from this work may be used under the terms of the CC BY 3.0 licence (© 2015). Any distribution of this work must maintain attribution to the author(s), title of the work, publisher, and DOI.

ISBN: 978-3-95450-168-7 doi:10.18429/JACoW-IPAC2015-TUPJE081

MODEL OF DARK CURRENT IN SRF LINAC

A. Sukhanov*, N. Solyak, A. Saini, I. Tropin, Fermilab†, Batavia, IL 60510, USA

Abstract

Currently, few linacs based on 9-cell TESLA-type SRF cavities are being designed or bult, including XEFL, LCLS-II and ILC. Dark current electron generated by field emission in SRF cavities can be captured and accelerated in the linac up to hundreds MeV before they removed by focusing magnets. Lost dark current electrons interact with the materials surrounding SRF cavities and magnets, produce electromagnetic showers and contribute to the radiation in the linac tunnel. In this paper we present a model of dark current in a linac based on TESLA cavities. We show preliminary results of the simulation applied to ILC main linac.

INTRODUCTION

In superconducting radio-frequency (SRF) cavities electrons can be emitted from the surface of the cavity in the region of the high electric field via field emission (FE). Emitted electrons are then may be captured in accelerating regime and contribute to the dark current (DC). Because of their broad angular, space and phase distribution, large fraction of dark current particles is lost downstream of the originating cavity, in subsequent cavities of the linac, focusing magnets and other beam line components. Lost particles may cause additional heat and RF loading on superconducting cavities. If lost electrons from DC have large enough energy, they produce electromagnetic showers of secondary particles which irradiate cables and electronic components inside the cryostat (cryo-module, CM) containing cavities. Radiation penetrating beyond CM walls may affect electronics in the linac tunnel and personnel and electronics in the service part of the tunnel. Thus, design of SRF linacs requires extensive investigation of DC radiation in order to protect accelerator components from radiation damage and optimize thickness and cost of the radiation shields. Some of the recent studies of DC in SRF linacs are listed in [1–4].

In this paper we describe a model of dark current in SRF linac. Our model combine tracking of electrons in RF field of cavities and magnetic field of focusing magnets with simulation of interactions of lost particles with the materials of the accelerator components.

MODEL

We use MARS package to simulate interaction of DC particles with the materials of linac components and surrounding infrastructure. In order to understand average and maximum radiation conditions and minimize time consuming MARS simulation, we separate our study into following steps:

- Losses inside individual cavity. Radiation from particles lost inside the same cavity where they were emitted. The normalized level of radiation is the same for each cavity in the linac.
- Losses from DC produced by a single cavity. We assume that only one cavity in a string of cavities between focusing magnets[1] contributes to DC. In a worst case emitting cavity is located next to the magnet. Survived DC electrons are accelerated through the string and lost in the next magnet.
- Losses from DC generated by all cavities.

In this paper we focus on steps 1 and 2 and leave step 3 for the future studies.

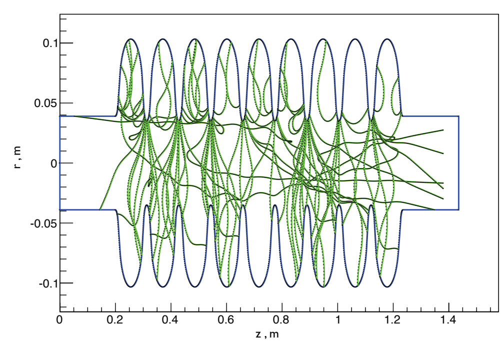

Figure 1: Trajectories of the FE electrons.

Field Emission Model

We use SuperLANS code to calculate RF field in the 9-cell TESLA-type cavity. Time dependence of the electric field is assumed to be $E \sim \cos(\omega t + \phi)$, where RF phase ϕ varies from 0 to 2π. Emitter locations are chosen randomly according to uniform distribution along the cavity surface from the entrance of the 1st cell to the exit of the 9th cell. Each emitted electron is assigned the weight calculated from Fowler-Nordheim model: $W_{FN}(E) = N_{FN}(\beta_{FN}E)^2 \exp(-B_{FN}\varphi^{3.2}/\beta_{FN}E)$, where $B_{FN} = 6.83 \cdot 10^3$, niobium work function $\varphi = 4.2$ eV, and field enhancement factor β has a typical value of 100. Normalization constant N_{FN} is selected such that $W_{FN}(E_{max}) = 1$, where maximum surface electric field in TESLA cavity is $E_{max} = 2E_{acc}$, and E_{acc} is accelerating field on the cavity axis[2]. For subsequent tracking and MARS simulation we select track with $W_{FN} > 0.01$.

* ais@fnal.gov
† Operated by Fermi Research Alliance, LLC under Contract No. De-AC02-07CH11359 with the United States Department of Energy.

[1] In ILC such a string contains 3 CM and 26 cavities, while in LCLS-II it is 1 CM and 8 cavities

[2] For ILC $E_{acc} = 31.5$ MV/m and $E_{max} = 63$ MV/m.

Content from this work may be used under the terms of the CC BY 3.0 licence (© 2015). Any distribution of this work must maintain attribution to the author(s), title of the work, publisher, and DOI.

6th International Particle Accelerator Conference IPAC2015, Richmond, VA, USA JACoW Publishing
ISBN: 978-3-95450-168-7 doi:10.18429/JACoW-IPAC2015-TUPJE084

DEVELOPMENT OF NONLINEAR INJECTION KICKER MAGNET FOR ALS ACCELERATOR*

Chris Pappas, David Robin, Christoph Steier, Changchun Sun, Charles Allen Swenson, Jin-Young Jung, Dennis Baum, LBNL, Berkeley, CA 94720 USA

Abstract

The ALS in now engaged in the construction of a new hard x-ray beam line and insertion device for protein crystallography. The scope of work entails the reconfiguration of ALS Sectors 1-3 to make room for the new insertion device. The project will require the melioration of the ALS injection system as well as the development of a longitudinal RF kicker. A key aspect of the injector work is the development and integration of a nonlinear injection kicker (NLK) magnet system to facilitate top off injection without noticeable motion of the beam. The technology will, in principal, ultimately allow the removal of the conventional bump injection magnets presently located in ALS Sector 1. The nonlinear injection concept has been explored at several other light sources [1]. We examine the beam dynamics and magnet design requirements to adapt this technology to the ALS lattice with its 1.9 GeV beam. The work will review the injection beam matching, tracking simulations, the electromagnetic design and tolerance analysis, and power supply design. The paper will also review the project plan for the integration of this technology into the ALS.

INTRODUCTION & NLK TECHNOLOGY

NLK technology offers the promise of a compact space efficient injection technology without the inclusion of injection bump magnets common to 3rd generation storage rings like the ALS. The technology is attractive for this reason. Other laboratories have build and tested prototypes of NLK designs with varying success [2,3], however none are presently now in use for a user facility. Soleil and MAXIV are working together on a modified BESSY design they plan to use at both facilities [4]. The reason NLKs have thus far not used for operations has been lower injection efficiency compared to conventional kicker approaches. The successful accelerator integration of the NLK requires the co-development of several key-supporting technologies such as: the optimization of the magnetic field shape to match the requirements for the injected and stored beams, a magnetic design and measurement technology that allows shim correction of field errors resultant from construction tolerances, and a reliable method for spatial fiducialization of the magnetic fields. The NLK technology under development at ALS employs a novel winding configuration resultant from a genetic algorithm to optimize injection efficiency. The windings symmetry is neither quadrupolar or sextupolar.

*This work was supported by Lawrence Berkeley National Laboratory under U.S. Department of Energy Contract No. DE-AC02-05CH11231.

REQUIREMENTS FOR ALS, DESIGN METHODOLOGY & OPTIMIZATION

The ALS requirements have evolved from the concept developed at BESSY and is presently in development at Soleil. These concepts position eight magnet buses at 45° from the axis. The inner buses are driven with current in one direction and the outer buses with current of the opposite polarity. A BESSY type magnet geometry, flux lines, and the normalized y component of the **B** field are shown in Figure 1. The ideal magnet has the advantage of zero field, and dB/dx on axis, however is not an optimal field shape for injection into the ALS due to the 275 nm beam emittance of the ALS injection booster.

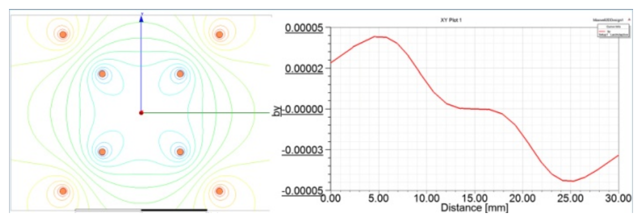

Figure 1: Modified BESSY magnet flux and **B**y.

From tracking simulations it became clear that the shape of the field in a BESSY type magnet is not optimal for injection into the ALS. In particular, a profile that has a wider zero field region near the axis, rises more steeply to the peak, and then decays more slowly would improve the injection efficiency. An exploration of the wire symmetries using analytic solutions for the magnetic fields indicated that the field could be flattened in the region of the injected beam while maintaining the field requirements for the stored beam. The resultant wire geometry could be called a double diamond configuration as illustrated in Figure 2. Another aspect of the design study entailed a tolerance analysis of both winding configurations. The resultant magnetic field errors in the stored beam region were comparable for either winding configuration indicating the validity of the approach.

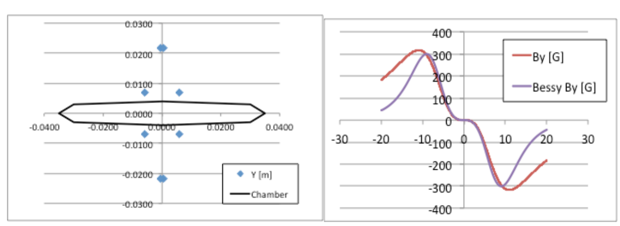

Figure 2: ALS NLK winding configuration and comparative plot of **B**y for the ALS and X wire configurations.

Content from this work may be used under the terms of the CC BY 3.0 licence (© 2015). Any distribution of this work must maintain attribution to the author(s), title of the work, publisher, and DOI.

ISBN: 978-3-95450-168-7 doi:10.18429/JACoW-IPAC2015-TUPMA001

PROGRESS OF THE R&D TOWARDS A DIFFRACTION LIMITED UPGRADE OF THE ADVANCED LIGHT SOURCE*

C. Steier†, A. Anders, D. Arbelaez, J. Byrd, K. Chow, R. Duarte, J. Jung, T. Luo, A. Madur, H. Nishimura, J. Osborn, C. Pappas, L. Reginato, D. Robin, F. Sannibale, S. De Santis, R. Schlueter, C. Sun, C. Swenson, W. Waldron, E. Wallen, W. Wan, LBNL, Berkeley, CA 94720, USA

Abstract

Improvements in brightness and coherent flux of about two orders of magnitude over operational storage ring based light sources are possible using multi bend achromat lattice designs [1]. These improvements can be implemented as upgrades of existing facilities, like the proposed upgrade of the Advanced Light Source, making use of the existing infrastructure, thereby reducing cost and time needed to reach full scientific productivity on a large number of beamlines. An R&D program funded by internal laboratory funds was started at LBNL to further develop the technologies necessary for diffraction-limited storage rings (DLSR). It initially involves five areas, and focuses on the specific needs of soft x-ray facilities: vacuum system/NEG coating of small chambers, injection/pulsed magnets, RF systems/bunch lengthening, magnets/radiation production with advanced radiation devices, and beam physics design optimization. Some hardware prototypes have been built. The work will expand in the future to demonstrate necessary key technologies at the subsystem level or in beam tests and include new areas like photon beamline optics.

INTRODUCTION

To achieve diffraction-limited performance throughout the soft x-ray (SXR) range, the ALS-U proposal pushes the limit of accelerator design beyond the level of the first examples of multi bend achromat (MBA) light sources currently under construction. Because ALS-U is a smaller and lower energy machine than all other proposed MBA machines or upgrades, with a resulting larger effect of intrabeam scattering (IBS), it requires design solutions different from those being pursued for the higher energy projects [2]. Therefore an R&D program funded by laboratory directed research and development funds (LDRD) was started in early FY14 at LBNL with the goal of reducing the technical risks of a soft x-ray diffraction limited storage ring and to optimize the possible performance of an eventual upgrade proposal.

Similar to the approach elsewhere, we have chosen a multi-bend achromat lattice, in our case with nine bends (9BA), and retained twelve arcs as in the existing ALS [3] (see Figure 1). No damping wigglers are foreseen and round beams will be used. Lattice optimization is ongoing, including optimization of the nonlinear dynamics wih genetic algorithms, similar to past work for the ALS brightness upgrade [4].

* This work was supported by the Laboratory Directed Research and Development Program of Lawrence Berkeley National Laboratory under U.S. Department of Energy Contract No. DE-AC02-05CH11231.
† CSteier@lbl.gov

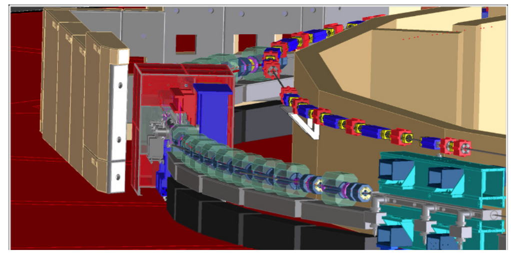

Figure 1: Model of ALS-U storage ring, accumulator and existing undulators in the ALS tunnel.

Including the effects of IBS, harmonic cavities, as well as insertion devices, the baseline lattice provides equal emittances of about 50 pm at 500 mA in both planes, yielding straight section beamsizes of around 10 μm. The electron beam ellipse is matched well to the diffraction ellipse leading to excellent brightness performance for soft x-rays (see Figure 2).

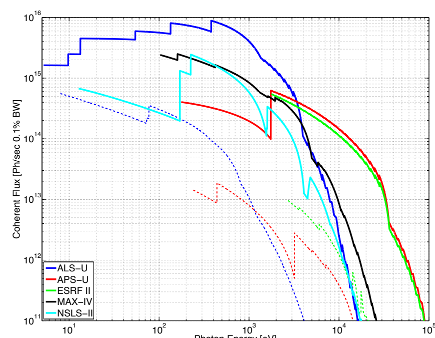

Figure 2: Coherent flux envelopes for ALS-U (blue) and several other facilities and upgrades. Dashed lines indicate pre-upgrade performance of facilities in operations now.

R&D PROGRAM

The R&D program at LBNL towards soft x-ray diffraction limited light sources initially involved five areas: Vacuum system/NEG coating of small chambers, Injection/pulsed magnets, RF systems/bunch lengthening, magnets/radiation production with advanced radiation devices, and Beam Physics optimization of the overall upgrade proposal. Several hardware protoypes have been built and the work includes demonstration of necessary key technologies at the subsystem level or in beam test. The program was recently expanded to include new areas, like photon beamline optics. It concentrates on the areas with the highest technical risk,

Content from this work may be used under the terms of the CC BY 3.0 licence (© 2015). Any distribution of this work must maintain attribution to the author(s), title of the work, publisher, and DOI.

ISBN: 978-3-95450-168-7 doi:10.18429/JACoW-IPAC2015-TUPMA003

MICROBUNCHING PHENOMENA IN LCLS-II *

M. Venturini†, J. Qiang, C. Papadopoulos
LBNL, Berkeley, CA 94720 USA
Y. Ding, P. Emma, Z. Huang, G. Marcus, A. Marinelli, Y. Nosochkov, T. Raubenheimer, L. Wang, M. Woodley
SLAC, Menlo Park, CA 94025 USA

Abstract

The microbunching instability has long been recognized as a potential limiting factor to the performance of X-ray FELs. It is of particular relevance in LCLS-II [1] due, in part, to a layout that includes a long bypass beamline between the Linac and the undulators. Here we focus on two aspects of the instability that highlight the importance of 3D effects.

ANOMALOUS HEATING

'Trickle' Heating

The Laser Heater (LH) is the established method to control the microbunching instability, exploiting the microbunching sensitivity to energy-spread induced mixing. In LCLS-II the LH is located at the exit of the injector at about 100 MeV beam energy; it consists of a 0.54 m undulator placed in the middle of a weak 4-dipole chicane and a $\lambda_L = 1030$ nm laser system. Concerns about the 'trickle' heating effect, discovered during LCLS commissioning [2], motivated the high-resolution numerical studies with the code IMPACT [3] presented here. Trickle heating is an echo-like phenomenon, in which the E/z micro-correlations generated by the laser/electrons interaction in a finite-dispersion region induce z/x correlations on the same micro-scale downstream of the LH (while the E/z micro-correlations are eventually washed out by the finite transverse emittance). The z/x correlations appear at relatively well localized points along the lattice separated by π phase advance in the horizontal betatron motion. The associated longitudinal space-charge forces modify the electron energy resulting into anomalous heating, which is undesirable, as it may compromise accurate control of the heater operation. To speed up the numerical calculations without sacrificing accuracy, we simulate a flat-top bunchlet meant to model a short section of the bunch core (but long enough to span many laser wavelengths). For the $Q = 100$ pC bunches discussed here the peak current in the core is $I_{\rm pk} \simeq 14$ A. For high fidelity simulations, the particle charge is the same as that of a physical electron (this is the case for the results of all the simulations presented in this paper). We track the bunchlet with initial gaussian energy density and σ_{E0} slice rms energy spread, starting from the exit of the injector, a few meters upstream of the LH chicane; σ_{E0} from high brightness injectors is not known very well but is expect to be on the order of 1-2 keV, including IBS effects: in our simulations we exercised a range of values. The action of the laser on the beam is modeled as a point-like interaction inducing a sinusoidal energy modulation and occurring in the middle of the physical undulator. The electron dynamics through the undulator itself is modeled as that of a drift (IMPACT has the capability to track the electrons through the undulator and laser-pulse fields, but it is time consuming and unnecessary for our purposes here). The bunch is followed through the LH chicane and a 50-m long collimation section to the entrance of the first Linac section (L1). An example of bunchlet longitudinal phase space is shown in Fig. 1, left picture. The prominent energy chirp, due to longitudinal space charge in the short bunchlet, is removed in the analysis before determining the energy spread distribution shown in the right picture. For comparison, the density observed at the exit of the LH chi-

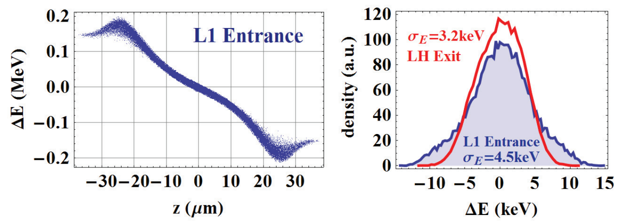

Figure 1: Longitudinal phase-space (left) of bunchlet at entrance of L1 and energy density in the core (right, blue curve). For comparison, the red curve on the right figure is the energy density at exit of the LH chicane;$\sigma_{E0} = 2$ keV.

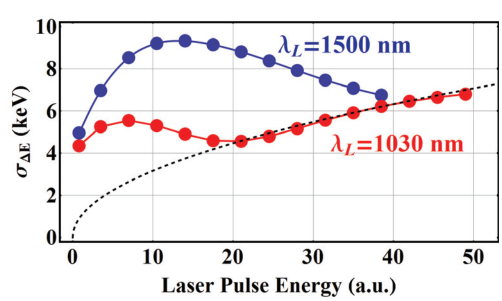

Figure 2: Energy spread at the entrance of L1 (two choices of laser wavelengths) showing evidence of the 'trickle' heating effect; $\sigma_E = 0.1$ keV. The dashed line is the nominal heating in the absence of collective effects.

* Work supported by DOE, in part under Contract No. DE-AC02-05CH11231 and through the LCLS-II project.
† mventurini@lbl.gov

Content from this work may be used under the terms of the CC BY 3.0 licence (© 2015). Any distribution of this work must maintain attribution to the author(s), title of the work, publisher, and DOI.

ISBN: 978-3-95450-168-7 doi:10.18429/JACoW-IPAC2015-TUPMA004

SYNTHESIS OF ULTRA-THIN SINGLE CRYSTAL MgO/Ag/MgO MULTILAYER FOR CONTROLLED PHOTOCATHODE EMISSIVE PROPERTIES

Daniel Velázquez, Rachel Seibert, Zikri Yusof, Jeff Terry, Linda Spentzouris
IIT Physics Department, Chicago, IL, 60616, USA

Content from this work may be used under the terms of the CC BY 3.0 licence (© 2015). Any distribution of this work must maintain attribution to the author(s), title of the work, publisher, and DOI.

Abstract

Photocathode emission properties are critical for electron beam applications such as photoinjectors for free electron lasers (FEL) and energy recovery Linacs (ERL). We investigate whether emission properties of photocathodes can be manipulated through the engineering of the surface electronic structure. The multilayers described here have been predicted to have emission properties in correlation with the film thickness. This paper describes how ultra-thin multilayered MgO/Ag/MgO films in the crystallographic orientations (001) and (111) multilayers were synthesized and characterized. Preliminary results of work function measurements are provided.

Films were grown by pulsed laser deposition at 130 °C for the (001) orientation and 210 °C for the (111) orientation at a background pressure of ~ 5×10-9 Torr. Epitaxial growth was monitored in-situ using reflection high-energy electron diffraction, which showed single crystal island growth for each stage of the multilayer formation. Photoelectron spectroscopy was used to track the chemical state transition from Ag to MgO during the deposition of successive layers. The Kelvin probe technique was used to measure the change in contact potential difference, and thus work function, for various MgO layer thicknesses in comparison with bare single crystal Ag(001)and Ag(111) thin films. The work function was observed to reduce with increasing thickness of MgO from 0 to 4 monolayers as much as 0.89 eV and 0.72 eV for the (001) and (111) orientations, respectively. Photoelectron spectra near the Fermi level revealed electron density shifts toward zero binding energy for the multilayered surfaces with respect to the clean Ag surfaces.

INTRODUCTION

Much of the development of photocathode materials has been aimed to the growth of photoemissive thin films with low work function (WF), and high quantum efficiency (QE) [1]. It has been shown, in some cases, that metal-insulator junctions can lead can lead to the modification of the WF for coverages of a few monolayers of metal oxides on metallic substrates, both theoretically and experimentally [2-5]. Reduction of WF and increase of QE can be achieved simultaneously by coating metal surfaces with Cs or CsBr [6,7]. Cs ion implantation on Cu, Ag and Au has also been shown to also reduce the WF and increase QE while still retaining the robustness of a metal, nonetheless, sacrificing the crystalline quality of the substrate [8]. However, the production of electron beams suitable for new photoinjector technologies in many instances requires low emittance beams from the cathode itself [2]. Therefore, the cathode intrinsic emittance plays an increasingly important role in new electron beam source designs [1].

A theoretical model by Nemeth et al. [2] describes the density functional theory (DFT) simulation of a multilayered structure MgO/Ag(001)/MgO in the configuration of 4 monolayers of Ag(001) flanked by n monolayers (ML) of MgO, where n is a small integer. This model indicates that it is possible to reduce the emittance of a photoemitted electron beam as the surface band structure exhibits a narrowing the density of states near the Γ-point neighboring the Fermi level when the thickness n of the MgO layers is 2 or 3 monolayers. In addition, this and other similar model [3] predict a work function drop of 1 eV to 1.5 eV from that of a bare Ag(001) surface. Measurements using atomic and Kelvin probe force microscopies (AFM and KPFM) show that even the deposition of MgO on a Ag(001) single crystal substrate produces a work function drop of 1.1 eV (1 ML) and 1.4 eV (2 ML) from the work function of the silver substrate, for 1 and 2 monolayers respectively [4,5].

More recently, an effort to quantify the effect on the emittance of 4 monolayers of MgO deposited on a Ag(001) substrate was carried out by Droubay et al. [9] who used Angle Resolved Photoelectron Spectroscopy (ARPES) to show that there was an enhancement of the photoemission intensity at the Γ-point near the Fermi level for the MgO coated Ag(001) in comparison with the uncoated Ag(001) substrate. Nonetheless, the ARPES spectrum for the MgO coated surface also exhibited the presence of sharp side bands near the Brillouin Zone boundaries which had the effect of increasing the total intrinsic emittance to 0.97 μm/mm from 0.47 μm/mm for the bare Ag(001) surface.

In this paper we present test results of multilayered MgO/Ag/MgO films as photoemitters. These multilayers were synthesized by Pulsed Laser Deposition (PLD) and characterized by Reflection High-Energy Electron Diffraction (RHEED) and Photoelectron Spectroscopy (PES) to show the formation of the crystalline and chemical structure of the multilayered films. It was found that there was a gradual decrease of the relative work function for MgO coated Ag surfaces in the (001) and (111) crystallographic orientations with respect to that of uncoated surfaces as the thickness of the flanking layers increased.

ISBN: 978-3-95450-168-7 doi:10.18429/JACoW-IPAC2015-TUPMA007
Content from this work may be used under the terms of the CC BY 3.0 licence (© 2015). Any distribution of this work must maintain attribution to the author(s), title of the work, publisher, and DOI.

NUMERICAL INVESTIGATION OF A CASCADED LONGITUDINAL SPACE-CHARGE AMPLIFIER AT THE FERMILAB'S ADVANCED SUPERCONDUCTING TEST ACCELERATOR *

A. Halavanau[1], P. Piot[1,2]
[1] Department of Physics and Northern Illinois Center for Accelerator & Detector Development, Northern Illinois University, DeKalb, IL 60115, USA
[2] Accelerator Physics Center, Fermi National Accelerator Laboratory, Batavia, IL 60510, USA

Abstract

In a cascaded longitudinal space-charge amplifier (LSCA), initial density noise in a relativistic e-beam is amplified via the interplay of longitudinal space charge forces and properly located dispersive sections. This type of amplification process was shown to potentially result in large final density modulations [1] compatible with the production of broadband electromagnetic radiation. The technique was recently demonstrated in the optical domain [2]. In this paper we investigate, via numerical simulations, the performances of a cascaded LSCA beamline at the Fermilab's Advanced Superconducting Test Accelerator (ASTA). We especially explore the properties of the produced broadband radiation. Our studies have been conducted with a grid-less three-dimensional space-charge algorithm.

INTRODUCTION

Longitudinal space-charge driven microbunching instabilities arising in bunch compressors (BC) were predicted and observed over the last decade [3–5] . It was recently proposed to employ this microbunching instability mechanism to form attosecond structures in a bunch for the subsequent generation of intense broadband radiation pulses [2, 6]. The experimental setup that enables the generation of space-charge-induced modulation is relatively simple: it consists of focusing sections (e.g. FODO cells) where energy modulations due to the space-charge impedance arise, interspaced with bunch compression chicaness. The BCs convert the incoming energy modulation into a density modulation. Several of these (FODO+BC) modules are cascaded so to result in a large final density modulation. Such a modulated beam can be then used to generate coherent radiation at the wavelengths comparable to the modulation period. The purpose of this paper is to explore the possible use of this scheme at the Advance Superconducting Test Accelerator (ASTA) currently under commissioning at Fermilab.

SPACE-CHARGE EFFECTS IN LSCA

When transverse and longitudinal space-charge forces are approximately equal, or longitudinal space-charge force begins to dominate, the particle dynamics within the bunch becomes complicated [7] and microbunching process can be affected by transverse instabilities to a large extent. As transverse space-charge forces are suppressed by a factor of $1/\gamma^2$, one has to operate at sufficiently large γ to decrease the contribution from transverse space-charge effects. That fact justifies the use of the high energy beamlines (> 300 MeV) (such as ones planned at ASTA facility). Our studies show that the LSCA process is still possible at lower energies, but it requires wider beam sizes to reduce the contribution from the transverse space-charge fields.

The estimated gain per one chicane in LSCA is proportional to space-charge impedance $Z(k,r)$ [8]:

$$G = Ck|R_{56}|\frac{I}{\gamma I_A}\frac{4\pi L_d|Z(k,r)|}{Z_0}e^{-\frac{1}{2}C^2k^2R_{56}^2\sigma_\delta^2}, \quad (1)$$

where R_{56} is the BC longitudinal dispersion, $I_A = 17$ kA is the Alfvèn current, L_d is the drift length, σ_δ is the rms fractional energy spread, $C \equiv \langle z\delta\rangle/\sigma_z$ is the chirp, and $Z_0 \equiv 120\pi$ is the free-space impedance.

The exponential term in Eq. 1 induces a high-frequency cut-off of the modulation. Note, that after traveling through a BC, the modulation wavelength will be shortened by a compression factor $(1 + R_{56}C)$. The impedance $Z(k,r)$ is partially determined by the properties of the wakefields inside the BC [8]. Later on, the LSC impedance was shown to mainly cause the effect [1, 6]. The on-axis LSC impedance is given by [9]

$$Z(k) = -i\frac{Z_0}{\pi\gamma\sigma}\frac{\xi_\sigma}{4}e^{\xi_\sigma^2/2}\mathrm{Ei}(-\frac{\xi_\sigma^2}{2}), \quad (2)$$

and has a maximum at modulations with wave numbers around $k = \gamma/\sigma_\perp$, where $\sigma_\perp$ is the rms transverse beam size. Thus, by tuning of the betatron function, transverse emittance, beam energy, and compressor parameters, one has some flexibility in selecting the final modulation wavelength.

To characterize the current (density) modulations one can introduce the bunching factor

$$b(\omega) = \frac{1}{N}\Big|\sum_n \exp(-i\omega t_n)\Big|, \quad (3)$$

where t_n is the temporal coordinate of the n-th macroparticle and N is the total number of particles. The electromagnetic radiation emitted by a bunch of electrons is of the form $\frac{dW}{d\omega d\Omega} = [N + N(N-1)b(\omega)^2]\frac{dW}{d\omega d\Omega}|_1$, where $\frac{dW}{d\omega d\Omega}|_1$ represents the single-electron radiation spectral fluence associated to the considered electromagnetic process.

* This work was supported by the US Department of Energy under contract DE-SC0011831 with Northern Illinois University.

ISBN: 978-3-95450-168-7 doi:10.18429/JACoW-IPAC2015-TUPMA008

NUMERICAL STUDY OF THREE DIMENSIONAL EFFECTS IN LONGITUDINAL SPACE-CHARGE IMPEDANCE*

A. Halavanau[1], P. Piot[1,2]
[1] Department of Physics and Northern Illinois Center for Accelerator & Detector Development, Northern Illinois University, DeKalb, IL 60115, USA
[2] Accelerator Physics Center, Fermi National Accelerator Laboratory, Batavia, IL 60510, USA

Abstract

Longitudinal space-charge (LSC) effects are generally considered as detrimental in free-electron lasers as they can seed instabilities. Such "microbunching instabilities" were recently shown to be potentially useful to support the generation of broadband coherent radiation pulses [1,2]. Therefore there has been an increasing interest in devising accelerator beamlines capable of sustaining this LSC instability as a mechanism to produce a coherent light source. To date most of these studies have been carried out with a one-dimensional impedance model for the LSC. In this paper we use a N-body "Barnes-Hut" algorithm [3] to simulate the 3D space charge force in the beam combined with ELEGANT [4] and explore the limitation of the 1D model often used.

INTRODUCTION

Space-charge forces are essential to account for in realistic beam dynamics simulations. The nature of these forces lies in particle-to-particle Coulomb interaction. However, the numerical complexity of the problem grows as $O(N^2)$, where N is the number of particles. Therefore, it is not possible to exactly compute all space-charge contributions. Several approximation techniques can be used: mean-field on a grid approximation [5], space-charge impedance [6], analytical sub-beams or ensembles model [7]. All of those methods reduce the problem's complexity via some approximations which ultimately limits the maximum attainable spatial resolution.

Space-charge problem is very similar to the well-known N-body problem in celestial mechanics. One of the most effective algorithms for the gravitational N-body problem is the so called "tree" or Barnes-Hut (BH) algorithm [3], which scales as $O(N \log N)$. In this paper we present the results obtained using a modified version of the program available at [8]. Such a code was successfully employed to simulate early beam dynamics in photocathode [9]. Other more efficient algorithm have been recently developed [10, 11] and will be eventually used in further refinement of our work.

METHOD & VALIDATION

For the studies presented in this paper and our cascaded space charge amplifier study [17], we used the BH algorithm as an external script within the ELEGANT simulations. At a user-specified axial locations along the accelerator beam line, space charge kicks were applied. The distribution at the defined locations was saved and Lorentz transformation to the bunch rest frame was applied. The BH algorithm was used to obtain the 3D electrostatic field $\mathbf{E}'$. This field was then transformed in the laboratory frame and the obtained electromagnetic fields $(\mathbf{E}, \mathbf{B})$ were used to compute the Lorentz force on each of the macroparticles composing the beam. We used an impulse approximation so that only the momentum was altered by the space charge force. The distribution then was finally passed back to ELEGANT and tracked up to the next space-charge kick where the above process repeated. The main assumption in our calculations was that there was no magnetic field in the rest frame. This assumption although not strictly valid, was shown to hold for the beam with low energy spread typically produced in photoinjectors [12]. We henceforth refer to the combination of the BH algorithm with ELEGANT as "ELEGANT-BH".

To validate our simulations we both rely on analytical results and simulations carried out with the ASTRA program [5]. We first consider a 3D homogeneous ellipsoidal bunch with electric field linearly dependent on the position within the charge distribution as [13]

$$E_u(u) = \frac{C}{\gamma^2}\frac{(1-f)u}{r_u(r_x+r_y)r_z}, \text{ and } E_z(z) = \frac{Cf}{r_x r_y r_z}z, \quad (1)$$

where $C \equiv 3Q/(4\pi\epsilon_0)$, $u \in [x, y]$, $r_{x,y,z}$ are the ellipsoid semiaxes, $f \approx \sqrt{r_x r_y}/3\gamma r_z$ and Q is the bunch charge. The simulated fields are in excellent agreement with the field given by Eq. 1 as shown on Fig. 1. To assess longer-term

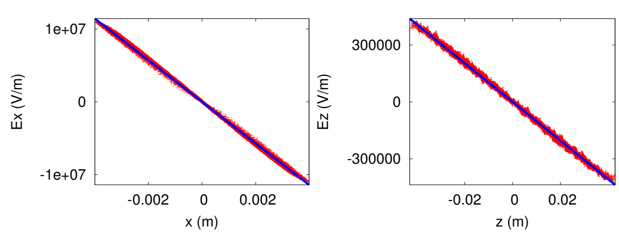

Figure 1: Transverse (left) and longitudinal (right) electric field experienced by the macropaticle simulated with ELEGANT-BH (symbols) and obtained from Eq. 1 (lines).

tracking, we compared the evolution of the beam envelope over a drift space. For a stationary uniform beam the transverse envelope evolution is governed by [14]

$$a''_{x,y} - \frac{\varepsilon^2_{rx,ry}}{a^3_{x,y}} - \frac{K}{2(a_{x,y}+a_{y,x})} = 0, \quad (2)$$

* This work was supported by the US Department of Energy under contract DE-SC0011831 with Northern Illinois University.

Content from this work may be used under the terms of the CC BY 3.0 licence (© 2015). Any distribution of this work must maintain attribution to the author(s), title of the work, publisher, and DOI.

ISBN: 978-3-95450-168-7 doi:10.18429/JACoW-IPAC2015-TUPMA010

DEVELOPMENT OF A FIELD-EMISISON TYPE S-BAND RF-GUN SYSTEM FOR HIGH BRIGHTNESS ELECTRON SOURCE APPLICATIONS

Y. M. Shin[1,2], A. Green[1], N. Barov[3]
[1]Department of Physics, Northern Illinois University, Dekalb, IL 60115, USA
[2]Accelerator Physics Center (APC), FNAL, Batavia, IL 60510, USA
[3]Far-Tech Inc., San Diego, CA 92121, USA

Abstract

Electron beams emitted from a cold cathode are thermally stable and mono-energetic with a small phase-space volume. We have been developing a field-emission type RF-gun system for high brightness electron source applications, including electron scattering/diffraction and tunable coherent X-ray/THz generation. The system consists of a single-gap gun-cavity and an S-band klystron/modulator capable of powering the gun with up to 5.5 MW peak (PRR = 1 Hz, duration = 2.5 μs). The designed gun built with the symmetrised side-couplers has surface field on the cathode ranging 50 – 100 MV/m with 1.3 – 1.7 MW klystron-power and 1.2 field ratio (HFSS). ASTRA simulations also indicate that the gun produces the beam with transverse emittances of less than 1 mm-mrad with 10 – 20 pC bunch charge at 500 keV beam energy. Under the gun operating condition, particle tracking/PIC simulations (CST) show that a single-tip CNT field-emitter produces short pulsed bunches (~ 1/10 RF-cycle) with small emittance (≤ 0.01 mm-mrad) and high peak current density (≥ 10,000 kA/cm^2). After the gun is fully installed and commissioned, a CNT-tip cathode will be tested with RF-field emission.

INTRODUCTION

Beam brightness cannot be improved, but only spoiled along the downstream accelerator. Therefore, high quantum efficiency (QE) and low intrinsic emittance, plus long lifetime, are very necessary for injector-type electron sources. The beam emitters of the electron sources are required to have a high QE and uniform emission at the longest possible wavelength with fast response time (< 100 ps). Emittance can be diluted by space charge expansion seeded by non-uniform electron emission. In order to minimize intrinsic emittance, cathode surfaces should preferably be atomically flat within a few nanometers of peak-to-peak variation. Furthermore, operating lifetime of more than 1 year with a reasonable vacuum level of 10^{-10} Torr range and easy, reliable cathode cleaning or rejuvenation/re-activation is strongly preferred.

Linac-based coherent radiation sources need bright electron beams, but injectors comprised of conventional DC-guns and RF-bunchers for longitudinal pulse compression have inherent limitations in reducing transverse and longitudinal emittance. While thermionic and photo-cathodes have been most widely employed with injectors for accelerator machines, certainly there are some practical limits in applying them to a compact, high brightness electron source [1–4].

Usually, field emitters have been studied for the applications of long pulse operation. The main advantages of field emission are that it simply generates pulsed beam and that the beams emitted under the emitters have low transverse emittance. Normally, the thermionic cathodes and field emitters are tolerant of poor vacuum and they have a long operating lifetime. However, the beam from the electron sources usually has long a bunch length (> 100 ps) and large longitudinal emittance with a lack of beam-profile control. Although high beam currents could be created and accelerated by an electron gun with field-emitters, it is difficult to find stable and reproducible operating conditions. Recently, various cathode materials have been extensively developed for vacuum microelectronic applications [5]. While actual RF devices like field-emitter tube amplifiers are still based on tip arrays of refractory metals, cathodes with nano-crystalline diamond materials would be preferred, if the field emitters have sufficient uniformity and high current stability.

CNT-TIP FIELD-EMITTER CATHODE

Flat panel display technology with commercial interest has stimulated research on the fabrication and characterization of nanostructured materials for field emission applications. However, it turned out that low cost fabrication over large areas is very challenging, particularly for applications demanding large emission currents requiring robust emitter materials. It was found that CNTs are quite suitable for the application as they are low-cost, robust, nano-structured material [6]. Previously, field emission of CNT cathodes was demonstrated with multi-walled carbon nanotubes (MWNTs) as well as single-walled carbon nanotubes (SWNTs) [7]. Carbon nanotubes have several advantages over other field-emitting materials. In contrast to commonly used emitters such as tungsten, a nanotube is not a metal, but a structure built by covalent bonds. The activation energy for surface migration of the emitter atoms is thus much larger than for a tungsten electron source. Therefore, the tip can withstand extremely strong fields (several V/nm). Depending on the exact arrangement of the carbon atoms, the cylinders are semiconducting or metallic conductors and the tubes can be closed or open at one or both ends. Furthermore, when compared with other film field emitters such as diamond or amorphous carbon structures, CNTs show a high aspect ratio, a small radius of

Content from this work may be used under the terms of the CC BY 3.0 licence (© 2015). Any distribution of this work must maintain attribution to the author(s), title of the work, publisher, and DOI.

ISBN: 978-3-95450-168-7 doi:10.18429/JACoW-IPAC2015-TUPMA012

DEVELOPING AN IMPROVED PULSED MODE OPERATION FOR DUKE STORAGE RING BASED FEL*

S.F. Mikhailov#, H. Hao, V.G. Popov, Y.K. Wu
FEL Laboratory/TUNL, and Dept. of Physics, Duke University, Durham, NC 27708, USA

Abstract

The Duke FEL and High Intensity Gamma-ray Source (HIGS) facility is operated with an e-beam from 0.24 to 1.2 GeV and a photon beam from 190 to 1060 nm. Currently, the energy range of the gamma-ray beam is from 1 MeV to about 100 MeV, with the maximum total gamma-ray flux about 3E10 gammas per second around 10 MeV. The FEL is typically operated in quasi-CW mode. Some HIGS user experiments can benefit tremendously from a pulsed mode of FEL operation. For that purpose, a fast steering magnet was developed years ago [1] to modulate the FEL gain. This allows a build-up of a high peak power FEL pulse from a well-damped electron beam. However, the use of this gain modulator at low e-beam energies can dramatically limit e-beam current due to beam instability and poor injection. It also suffers from the problem of a significantly reduced e-beam lifetime. To overcome these shortcomings, we developed and successfully tested an RF frequency modulation technique to pulse the FEL beam. In this paper, we will describe this development, and report our preliminary results of this improved pulsed FEL operation.

DUKE FEL/HIγS FACILITY

The Duke storage ring is designed as a dedicated FEL driver and a host of several FEL wigglers in a thirty-four meter long FEL straight section. The main parameters of the Duke accelerators and FEL's are listed in Table 1.

A planar optical-klystron FEL, the OK-4 FEL, consists of two planar wigglers sandwiching a buncher magnet.

Table 1: Parameters of Duke Accelerators and FELs

Accelerators	Storage ring	Booster injector
Operation energy [GeV]	0.24-1.2	0.16-1.2
Maximum current [mA]	125	15
Circumference [m]	107.46	31.902
Revolution frequency [MHz]	2.79	9.397
RF frequency [MHz]	178.55	
FELs	OK-4	OK-5
Polarization	Horizont.	Circular
No. of wigglers	2	4
No. of regular periods	33	30
Wiggler periods [cm]	10	12
Maximum peak field [kG]	5.36	3.17
Maximum K_w	5.00	3.53
Maximum current [kA]	3.0	3.5
FEL wavelength [nm]	190 - 1064	

* Supported in part by US DoE grant DE-FG02-971ER41033.
# smikhail@fel.duke.edu

A circular optical-klystron FEL employs up four OK-5 helical wigglers, two of them in the middle of the straight section are switchable with two planer OK-4 wigglers. In 2005, operating with two OK-4 and two OK-5 wigglers simultaneously, we demonstrated lasing of the world's first distributed optical klystron FEL, the DOK-1 FEL, with a record FEL gain for storage ring based FELs [2].

DEVELOPMENT OF RF FREQUENCY SWITCH (Q-SWITCH)

Typically, in all the wiggler configurations and polarizations, the Duke FEL is operated in a quasi CW mode. For some user experiments, a pulsed FEL may become exceptionally beneficial. This allows users to additionally reduce the noise background by two to three orders of magnitude using time discrimination synchronized with FEL macro-pulses. To enable a pulsed mode of FEL operation, a fast steering magnet (so called FEL gain modulator) was developed [1]. It decouples the e-beam from the FEL beam in the interaction region for most of time, but periodically allows a brief overlap of the electron and FEL beams. This enables a pulsed mode of FEL operation with a high peak power in the FEL macro-pulses. The low-energy regime is the most commonly demanded for the nuclear physics experiments using a pulsed beam. The production of gamma ray beams of high intensity requires also high beam currents.

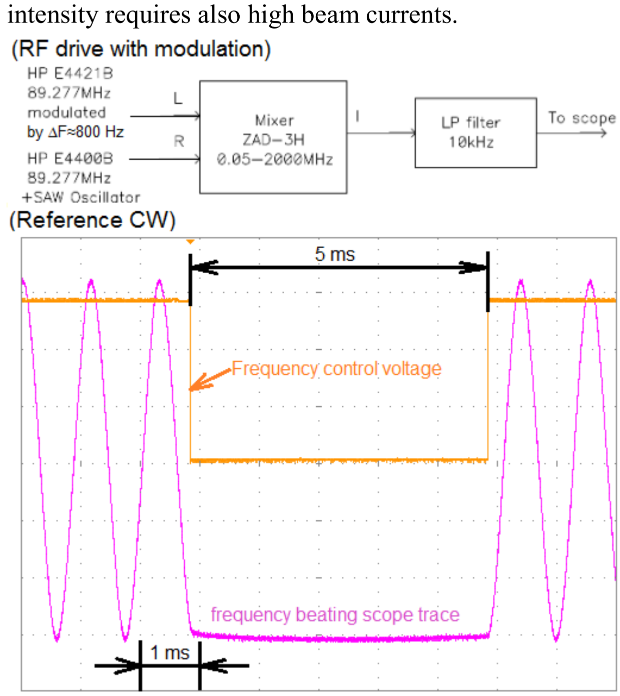

Figure 1: Fast switch of the RF frequency as demonstrated by the transition in time of the beating between the RF drive signal and a CW reference signal.

Content from this work may be used under the terms of the CC BY 3.0 licence (© 2015). Any distribution of this work must maintain attribution to the author(s), title of the work, publisher, and DOI.

ISBN: 978-3-95450-168-7 doi:10.18429/JACoW-IPAC2015-TUPMA014

EXTENDING OK5 WIGGLER OPERATIONAL LIMIT AT DUKE FEL/HIGS FACILITY*

Patrick Walter Wallace#, Mark Emamian, Hao Hao, Stepan F. Mikhailov, Victor Popov, Ying K. Wu
FEL/Duke University, Durham, North Carolina
Jingyi Li
FEL/Duke University, Durham, North Carolina; USTC/NSRL, Hefei, Anhui

Abstract

Since 2007 the HIGS facility has been operated to produce both linearly and circularly polarized gamma-ray beams using two FELs, the planar OK-4 FEL and helical OK-5 FEL. Presently, with the OK-5 FEL operating at 192 nm, we can produce circularly-polarized gamma-ray beams between 1 and 100 MeV for user applications. Gamma-ray production between 80 and 100 MeV required an extension of the OK-5 wiggler operation beyond the designed current limit of 3.0 kA. In 2009, we upgraded cooling and machine protection systems to successfully extend OK-5 operation to 3.5 kA. To realize HIGS gamma-ray operation beyond 100 MeV and ultimately toward 150 MeV (the pion-threshold energy), with various limitations of the VUV mirror technology, the OK-5 wigglers will need to be operated at an even higher current, between 3.6 and 4.0 kA. In this paper we present our technical solution to further extend the operation range of the OK-5 wigglers, and report our preliminary results with high-current wiggler operation.

BACKGROUND

Need for Higher Wiggler Current

The energy of gamma-rays produced in the Duke Free Electron Laser (FEL) depends on the FEL lasing wavelength, the energy of the stored electron beam, and the magnetic field strength of the wiggler magnets [1]. The maximum gamma energy at the High Intensity Gamma Source (HIGS) currently available for users is 100 MeV, using 190 nm FEL mirrors and operating with 1.05 GeV electrons and a current of 3.5 kA in the OK-5 wigglers. There are important experiments which need higher energy gammas (eg. proton spin polarizability), up to 110–120 MeV. Having no expectation in the short-term of obtaining robust and highly reflective mirrors for shorter wavelengths, nor of a significant increase of the electron beam energy in the storage ring, we need to identify ways to operate the wigglers at higher currents.

The main design and operational parameters of the OK-5 wigglers are given in Table 1.

Table 1: Parameters for OK-5 Wigglers

Polarization	Circular
No. of wigglers	4
No. of regular periods	30
Wiggler period [cm]	12
Maximum current [kA]	3.5
Maximum magnetic field [kG]	3.17
Maximum K_w	3.53
FEL wavelength [nm]	190 - 1064

Figure 1: T-Rex power supplies at Duke FEL.

2009 Upgrade

Prior to 2009, operating the wigglers at the design maximum of 3.0 kA, and using the shortest wavelength of conventional mirrors (240 nm), the maximum gamma energy was limited to 60 MeV. Raising the wiggler current up to 3.6 kA, gamma energies of 70 MeV would be achievable. Testing showed that operation above 3.0 kA tripped the magnet over-temperature switches (65 °C Klixons), and a new set was installed (90 °C). Next, we found that long-term operation above 3.5 kA increased the resistance of the magnet coils and connecting bus bars enough that the TRANSREX (T-Rex) power supply (see Figure 1) reached the maximum output voltage limit (about 100 V) when driving two wigglers in series, which limited wiggler current to 3.5 kA. The final steps of the upgrade were to add water flow switches to the cooling water return flows as protection against sudden loss of water flow, and to install new, faster response-time

* Supported in part by US DoE grant DE-FG02- 97ER41033.
# patwalla@fel.duke.edu

Content from this work may be used under the terms of the CC BY 3.0 licence (© 2015). Any distribution of this work must maintain attribution to the author(s), title of the work, publisher, and DOI.

ISBN: 978-3-95450-168-7 doi:10.18429/JACoW-IPAC2015-TUPMA016

Content from this work may be used under the terms of the CC BY 3.0 licence (© 2015). Any distribution of this work must maintain attribution to the author(s), title of the work, publisher, and DOI.

LIGHT SOURCE AND ACCELERATOR PHYSICS RESEARCH PROGRAM AT DUKE UNIVERSITY*

Y.K. Wu†
FEL Laboratory, Triangle Universities Nuclear Laboratory and Department of Physics, Duke University, Durham, NC 27708-0319, USA

Abstract

The light source and accelerator physics research program at Duke Free-Electron Laser Laboratory (DFELL), Triangle Universities Nuclear Laboratory, is focused on the development of the storage ring based free-electron lasers (FELs), and an FEL driven state-of-the-art Compton gamma-ray source, the High Intensity Gamma-ray Source (HIGS). With a maximum total flux about 3×10^{10} γ/s and a spectral flux of more than 10^3 γ/s/eV around 10 MeV, the HIGS is the world's most intense Compton gamma-ray source. Operated in the energy range from 1 to 100 MeV, the HIGS is a premier Compton gamma-ray facility in the world for a variety of nuclear physics research programs, both fundamental and applied. In this paper, we will describe our ongoing accelerator physics and light source development program in the areas of the storage ring magnetic optics characterization and compensation, FEL physics, and development of gamma-ray beams in the higher energy range (100 to 158 MeV).

INTRODUCTION

The primary light sources at the Duke Free-Electron Laser Laboratory (DFELL), Triangle Universities Nuclear Laboratory (TUNL), are storage ring based free-electron lasers (FELs) [1] and the FEL driven High Intensity Gamma-ray Source (HIGS) [2]. At the DFELL, we operate three accelerators: (1) a 0.16 – 0.27 GeV linac pre-injector; (2) a 0.16 – 1.2 GeV full-energy, top-off booster injector; and (3) a 0.24 – 1.2 GeV electron storage ring. The Duke storage ring is a dedicated host for an oscillator FEL with several wiggler configurations. This FEL is the photon beam driver for the world's most intense Compton gamma-ray source, the HIGS which produces intense gamma-ray beams from 1 to 100 MeV with a maximum total flux about 3×10^{10} γ/s and a maximum spectral flux of more than 10^3 γ/s/eV around 10 MeV. The Compton gamma-ray beam at the HIGS is highly polarized (linear or circular), and has an excellent energy resolution. Since 2008, the accelerator facility has been operated mainly as the Compton gamma-ray source facility for routine user research in the area of nuclear physics and nuclear astrophysics. The layout of the accelerator facility is shown in Figure 1 and a list of key parameters of the Duke booster injector and storage ring are summarized in Table 1.

* Work supported in part by the US DOE grant no. DE-FG02-97ER41033.
† wu@fel.duke.edu, 1-919-660-2654.

Table 1: Parameters for the Duke booster injector and storage ring. The storage ring FELs can be operated using two different sets of wigglers with the wiggler switchyard.

Parameter	Value
Booster Synchrotron	(Main Injector)
Circumference [m]	31.902
RF frequency [MHz]	178.55
Number of RF buckets	19
Injection energy [GeV]	0.16 – 0.27
Extraction energy [GeV]	0.16 – 1.2
Storage Ring	
Operation energy	0.24 – 1.2 GeV
Circumference	107.46 m
RF frequency	178.55 MHz
Number of RF buckets	64
Max beam currents	
One-bunch (FEL)	95 mA ($\geq$ 0.6 GeV)
Two-bunch (HIGS)	~ 125 mA ($\geq$ 0.5 GeV)
Multi-bunch (60)	> 300 mA ($\geq$ 0.5 GeV)
Duke FELs	(Wiggler Switchyard)
Linear and circular pol.	Two planar OK-4 wigglers
	plus two helical OK-5 wigglers
Circular polarization	Four helical OK-5 wigglers

STORAGE RING LATTICE CHARACTERIZATION

Since 2013, we have devoted substantial time and effort to characterizing and compensating the magnetic optics of the Duke storage ring in order to optimize its operation. One of major challenges in this area stems from the use of all combined function quadru-sextupoles in the arcs in order to minimize the cross-talk between adjacent magnets of different types in the very compact arc lattice [3]. These magnets are standard quadrupoles but are powered by two different currents in the inner and outer coils. Consequently, the magnetic centers are separated from the geometric centers typically by more than 2 mm. The actual beam orbit in each magnet is not unknown in advance, and is subject to the change of the settings of quadrupole and sextupole components. In addition, the BPMs in the arc are instrumented relative to the geometric center of the quadru-sextupoles, making them much less reliable/accurate monitors for beam orbit measurements and lattice calibration.

Collectively, these issues present some significant difficulty to use the LOCO method [4] to calibrate the Duke storage ring lattice. Therefore, we worked to develop a direct beta-function measurement technique using the global tune changes caused by varying the strength of a quadrupole

ISBN: 978-3-95450-168-7 doi:10.18429/JACoW-IPAC2015-TUPMA017

PULSED-WIRE MEASUREMENTS FOR INSERTION DEVICES

D'Audney, S. Stellingwerff, S.G. Biedron, S.V. Milton
Colorado State University, Fort Collins, CO, 80521 USA

Abstract

The performance of a Free-Electron Laser (FEL) depends in part on the integrity of the magnetic field in the undulator. Correcting magnetic field imperfections within the undulator is important for optimal FEL gain. Thus, the magnetic field must be properly mapped. A pulsed wire method is a quality method to achieve this when a traditional Hall device cannot be used. The pulsed-wire method works by sending a square current pulse through the wire, which will induce an interaction with the magnetic field due to the Lorentz force. This force causes the wire to be displaced, and this displacement travels along the wire in both directions as an acoustic wave. Measurement of the displacement in the wire over time using a motion detector yields the first or second integrals of the magnetic field. Dispersive effects in the wire are corrected using algorithms resulting in higher accuracy results. Once the fields are known, magnetic shims can be placed where any corrections are needed.

INTRODUCTION

The performance of a Free-Electron Laser (FEL) depends in part on the quality of the magnetic field in the undulator. The magnetic field on the axis of the undulator is transverse and sinusoidally varying due to the periodic sequence of dipoles. The length of these periods, and the electron beam energy, determine the wavelength of the radiation that will be generated. When a relativistic electron bunch from the particle accelerator is injected into the undulator, the static magnetic fields create transverse oscillations in the particles' trajectory. These oscillations cause the electrons to emit energy. The ideal trajectory of a relativistic electron bunch inserted along the axis is sinusoidal in the plane of oscillation. Phase errors are produced when the path of the electron is not the ideal sinusoidal trajectory, due to imperfections in the magnetic field. The dipole magnets should compensate each other to limit phase errors and diminish the divergence of the electron bunch to the optical beam. In the case of an FEL, phase errors in the electron trajectory lead to a reduction in electron beam bunching. This effect causes a reduction in the energy transfer from the e-beam to the optical field and hence, reduces FEL gain [1,2]. Thus, the magnetic field must be mapped and tuned to a level acceptable to efficient FEL operation. A pulsed-wire method can be used to determine the profile of the magnetic field.

Traditionally, the fields within these devices have been measured with high accuracy using a Gauss meter or Hall probe; however, with the advent of more complex and superconducting undulators these types of probe systems may not always be a viable option. Topographies such as narrow undulator gaps or cryogenic environments in superconducting undulators restrict measurement access. A pulsed wire method is an attractive option to map the magnetic field in a noninvasive manner [3-5]. In our particular case, the undulator has large metal spacers to keep the undulator gap steady. These spacers make it a solid candidate for a pulsed wire experiment.

The pulsed-wire method described here overcomes several effects that have previously limited the method's accuracy in characterizing the magnetic field in an undulator. The principal component of this technique is a thin current-carrying wire, specifically a 75-um Copper Beryllium wire which is used to simulate both the velocity and trajectory of a charged particle within the undulator. The Lorentz force acting upon the current within the wire causes movement in the wire, and this force is proportional to the local magnetic field acting on it. The resultant motion then propagates as a wave along the length of the wire. The displacement of the wire is measured by an optical detector and then processed using MATLAB algorithms. A schematic of a basic pulsed-wire method is shown in Fig. 1. To establish an absolute value for the pulsed-wire measurements being done, a characterized reference magnetic field is required. This field is applied along the wire external to the undulator fields and used to calibrate the measured undulator fields.

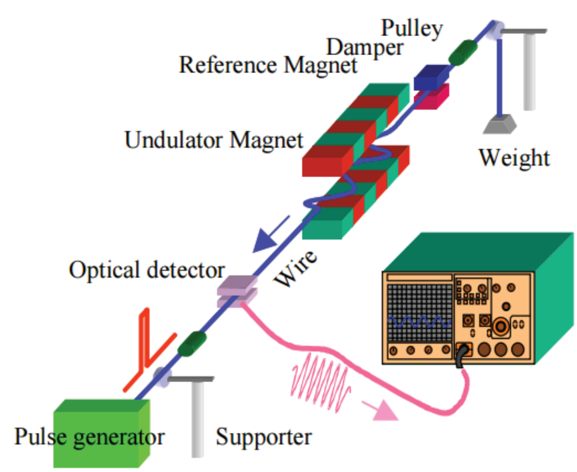

Figure 1: Simplified pulsed wire setup [6].

In the past, dispersive and finite pulse width effects within the wire have had undesirable consequences on the measured field profile. Recently developed algorithms compensate for these effects and increase the accuracy of the measurements [6]. Magnet imperfections can be easily corrected by using small magnetic shims once the field is characterized [2, 7].

Content from this work may be used under the terms of the CC BY 3.0 licence (© 2015). Any distribution of this work must maintain attribution to the author(s), title of the work, publisher, and DOI.

ISBN: 978-3-95450-168-7 doi:10.18429/JACoW-IPAC2015-TUPMA018

Content from this work may be used under the terms of the CC BY 3.0 licence (© 2015). Any distribution of this work must maintain attribution to the author(s), title of the work, publisher, and DOI.

AN IMPROVED ANALYTIC MODEL OF ELECTRON BACK-BOMBARDMENT IN THERMIONIC-CATHODE RF GUNS

J. P. Edelen#, S. G. Biedron, J. R. Harris, S.V. Milton, Colorado State University, Fort Collins, CO
J. W. Lewellen, LANL, Los Alamos, NM

Abstract

This paper describes work done at Colorado State University to improve upon the recent theory developed to predict the back-bombardment power in single-cell thermionic-cathode electron guns. The previous theory used a square-wave approximation of the time varying field to solve for the total kinetic energy deposited on the cathode due to the back-bombarded electrons. In addition the transit time factor was added as a correction to compensate for the non-sinusoidal field. By solving for the back-bombardment power using a sinusoidal field, the transit time factor can be removed and therefore a better overall model is produced. These alterations continue to accurately predict how back-bombardment varies as a function of the gun parameters and provides improvement when compared to the existing theory.

INTRODUCTION

Recent work has successfully developed a first principles model that accurately predicts the back-bombardment power for single-cell thermionic-cathode electron guns as a function of the design parameters, Equation 1 [1]:

$$P_{ave} = \frac{3E_0 I c^2}{4\alpha^2 f v_{eff}} TK \qquad (1)$$

Here E_0 is the peak RF field in the gap, α is the RF wavelength normalized to the gap length ($\alpha = \lambda_{rf}/L_{gap}$), f is the RF frequency, I is the average beam current, v_{eff} is the effective velocity of electrons in the gap defined by Equation 2, T is the transit time factor defined by Equation 3, and K is the field normalization factor defined by Equation 4.

$$v_{eff} = c\sqrt{1 - \left(1 + \frac{qE_0\lambda}{2m_0c^2\alpha}\right)^{-2}} \qquad (2)$$

$$T = \frac{\sin(\pi c/\alpha v_{eff})}{\pi c/(\alpha v_{eff})} \qquad (3)$$

$$K = \frac{\int_0^{L_{gap}} E(z)dz}{E_0\lambda/\alpha} \qquad (4)$$

In the previous work we used a square wave in order to reveal exact solutions to the equations of motion and solve for the back-bombardment power. Follow-on studies indicated that a sinusoidal field could also be used to solve for the back-bombardment power, contingent on the constant velocity principle used in the previous work.

This paper presents a modification to the theory that utilizes a sinusoidal time varying field, which makes for a better a-priori model and allows for the omission of the transit time factor from the back-bombardment power equation. We begin with an overview of the modification to the theory and compare these results with both the previous model and the numerical solutions to the relativistic equations of motion. The new model is then compared with simulations performed using SPIFFE [2]. Finally we provide a quantitative comparison between the new model and the existing model over a wide range of parameters.

ADDITION OF A SINUSOIDAL FIELD TO THE BACK-BOMBARDMENT MODEL

To solve for the back-bombardment power, the effective kinetic energy as a function of the electron emission time is calculated using Equation 5.

$$K_{eff}(t_0) = v_{eff}\int_{t_0}^{t_0+t_{transit}} E_0\sin(\omega t)dt \qquad (5)$$

Here $t_{transit}$ is the particle transit time. The particle transit time is different for particles that exit the gun and those that are back-bombarded. For particles that exit the gun the transit time is $t_{transit}^{fw} = \lambda/(\alpha v_{eff})$. For particles that are back-bombarded the transit time is a function of the emission time given by $t_{transit}^{bb}(t_0) = 4(\tau/2 - t_0)$ [1]. Solving Equation 5 for both the output case and the back-bombardment case, gives the effective kinetic energy of all the particles as a function of their emission time (Green line in Figure 1). This was compared with the result of numerically integrating the relativistic equations of motion of the same representative geometry, which gives the blue line in Figure 1. Additionally the model derived in previous work by using a square wave field is given in black.

This shows that there is still a fairly poor agreement for the output beam, however the new model is much better than the previous model. However, when computing the back-bombardment power only the area under the curve to the right of the discontinuity is of interest. Inspection of both the blue and green curve shows that this is indeed a reasonable approximation.

jedelen@engr.colostate.edu

ISBN: 978-3-95450-168-7 doi:10.18429/JACoW-IPAC2015-TUPMA019

SIMULATION AND ANALYSIS OF LASER/ELECTRON BEAM INTERACTION FOR USE AS A FREE ELECTRON LASER

J.A. Einstein#, S.G. Biedron, S.V. Milton, H.P.Freund,
Colorado State University, Fort Collins, CO 80525, USA
G. Dattoli, ENEA – Divisione Fisica Applicata Centra Rierche Frascati, Roma, Italy

Abstract

Through the use of simulation tools and theoretical analysis techniques, the Free Electron Laser process is investigated for a wiggler that is generated by an ultrafast laser system. The development and availability of such systems allows for novel FEL designs due to the high peak power of such lasers. Even though such high powers are possible, difficulties arise due to inhomogeneity in the laser pulse. This project looks at simulation results for a system with a realistic laser pulse profile and looks in to the pulse-shape effects on various system parameters. Models are presented for the expected behavior with important parameters noted, as well as highlighting possible difficulties that might occur experimentally. While head-on interaction has been proven experimentally for the short wavelength regime [1], we believe that using a co-propagating laser can provide benefits that have currently been untested. This experimental setup is outlined in Lawler, J et al [2], and we are currently simulating how the use of an ultrashort laser pulse as an electromagnetic wiggler will affect characteristics of the output radiation.

INTRODUCTION

Free electron lasers (FELs) are a highly tunable, flexible light source, with significant opportunities to act as high power, low wavelength sources for industry and research. An FEL relies upon a highly periodic, alternating field to take advantage of electron motion to generate light. Current undulator designs require the use of strong magnets or electro magnets to generate a strong enough field, and often need to be quite long to obtain the desired level of coherence in the output light.

Several new undulator designs have been proposed and tested, including a microwave undulator [3], and several designs have been proposed for optical undulators of various design [4], [5], and a co-propagating optical design [2].

Recent advances in the peak energies possible with ultrafast laser sources and in beam shaping and control allow for the use of optical pulses as an undulator. This allows for a significant decrease in the required length of an undulator and allows for the use of lower electron beam energies while still generating low-wavelength light. The miniaturization of the system leads to several advantages, not the least of which is a significant decrease in cost. In addition, the use of a laser pulse as the undulator allows for the use of COTS components for the transport and shaping optics.

Joshua.Einstein@colostate.edu

This paper presents results of a simulation of the proposal from Lawler, et al, in reference [2], modified by the use of an ultrafast laser. This design uses a co-propagating, sheared laser pulse to generate an undulator-like field.

Proposed Experimental Setup

The experimental design is based on transporting an ultrashort pulse through a series of optical components to shear the wave fronts in to a uniform, undulator-like design. Several methods have been considered for how to shear a laser pulse, with various benefits for each depending on the qualities of the incoming laser pulse.

We propose a system using an ultrashort pulse that is sheared using a blazed grating with necessary correction optics and diagnostics. A schematic of the interaction can be seen in figure (1). Several proposals have been made for perpendicular illumination of the beamline, and integrating some of those ideas with ours will be beneficial [6].

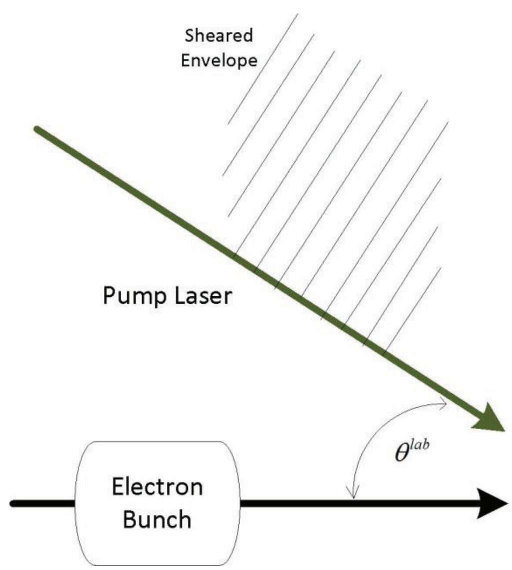

Figure 1: Beam interaction schematic.

Simulation Setup

Two simulation codes were used for simulating the undulator section of the proposed design. ONEDFEL is a 1D, non-time-averaging code, and MEDUSA is a full 3D simulation code [6]. In order to approximate the envelope of an ultrafast pulse, the already built-in feature of undulator tapering was used. This function used a sin2 envelope instead of a Gaussian, but is valid for simulating the effect of such a variable field undulator.

Content from this work may be used under the terms of the CC BY 3.0 licence (© 2015). Any distribution of this work must maintain attribution to the author(s), title of the work, publisher, and DOI.

ISBN: 978-3-95450-168-7 doi:10.18429/JACoW-IPAC2015-TUPMA020

Content from this work may be used under the terms of the CC BY 3.0 licence (© 2015). Any distribution of this work must maintain attribution to the author(s), title of the work, publisher, and DOI.

PEPPo: USING A POLARIZED ELECTRON BEAM TO PRODUCE POLARIZED POSITRONS

A. Adeyemi*, Hampton University, Hampton, VA, USA
on behalf of the PEPPo Collaboration

Abstract

An experiment demonstrating a new method for producing polarized positrons has been performed at the CEBAF accelerator at Jefferson Laboratory. The PEPPo (Polarized Electrons for Polarized Positrons) concept relies on the production of polarized e^+/e^- pairs originating from the bremsstrahlung radiation of a longitudinally polarized electron beam interacting within a 1.0 mm tungsten pair-production target. This paper describes preliminary results of measurements using an 8.2 MeV/*c* electron beam with polarization 84% to generate positrons in the range of 3.1 to 6.2 MeV/*c* with polarization as high as ~80%.

INTRODUCTION

Polarized positrons are a powerful probe for the investigation of numerous physics phenomena. At thermal energies, polarized positrons may be used to study spintronic properties of materials [1]. Accelerated to GeV energies, the comparison between polarized electron and positron scattering cross-sections tests the precision of the electromagnetic interaction for the investigation of nucleon and nuclear structure [2]. At TeV energies, polarized positrons are essential for testing the Standard Model in the context of the International Linear Collider (ILC) [3].

Polarized positrons are produced in radioactive beta-decay [4], or by man-made methods such as the Sokolov-Ternov self-polarization of unpolarized positrons in a storage ring [5] or resulting from pair-production following the irradiation of nuclei with circularly polarized gamma rays. For the latter method, circularly polarized gamma rays can be produced via Compton back-scattering [6] or using a helical undulator [7]. Both techniques produced positrons with a high degree of positron spin-polarization and demonstrated the potential for high yield. However, both methods require very high electron beam energies 10-100 GeV and elaborate technologies.

In this work, we demonstrate a new technique for the production of polarized positrons, and with very low beam energy ~10 MeV. The idea, suggested in the late 1990's in the context of the ILC [8, 9], relies on the production of circularly-polarized gamma rays by the bremsstrahlung produced using polarized electrons; these photons then create polarized positrons via pair-production on nuclei. By demonstrating the technique at low energy, we avoid issues associated with high power targets and activation, illustrating the applicability of this technique to the design of future polarized positron sources, whether at similar or much higher energy where yield may be significantly increased.

* adeyemi@jlab.org

EXPERIMENT

The PEPPo experiment [10] was installed at the Jefferson Lab CEBAF injector where a highly spin-polarized 84% electron beam with energies up to 10 MeV could be provided. The electron beam could be delivered for characterization to either a Mott scattering electron polarimeter or a precision electron spectrometer; alternatively it could be sent to the PEPPo apparatus (see Fig. 1) which included: the e^+/e^- production target, a quarter-wave solenoid to collect positions within a large divergence angle, a combined-function spectrometer to select and focus discrete positron momenta slices, a pair of coincidence positron annihilation detectors, and a second solenoid to transport and focus positrons through an 8 mil Al window to the PEPPo polarimeter.

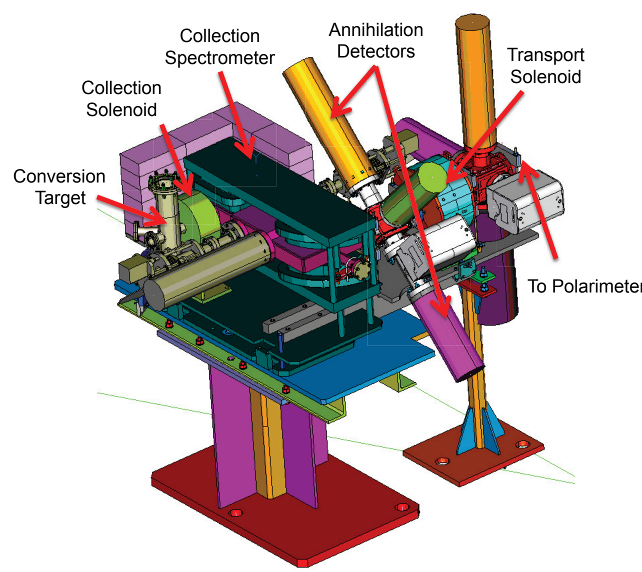

Figure 1: Vacuum beam line includes the insertable production target, a solenoid to collect e^+, a double-bend spectrometer to define the momentum acceptance, a positron annihilation detector, and a second solenoid to transport e^+ to an exit vacuum window in front of the polarimeter.

PEPPO POLARIMETER

The PEPPo polarimeter (see Fig. 2) is a Compton transmission type polarimeter that relies on the bremsstrahlung spectrum produced by longitudinally polarized positrons (or electrons) having small energy and angular distributions interacting with a reconversion target at the entrance of the polarimeter. The polarimeter takes advantage of the differential cross section for the Compton scattering of circularly polarized bremsstrahlung photons with a longitudinally polarized electron target (P_T) [11]. The measurement of the

ISBN: 978-3-95450-168-7 doi:10.18429/JACoW-IPAC2015-TUPMA021

OPTIMIZATION OF AN IMPROVED SASE (iSASE) FEL*

L. Gupta†, Cornell University, CLASSE, Ithaca NY 14853, USA
K. Fang, J. Wu, SLAC National Accelerator Lab, Menlo Park CA, 94025, USA

Abstract

In order to improve free electron laser technology for the future LCLS II at SLAC, a new strategy for creating radiation with increased temporal coherence is under development. The improved Self-Amplified Spontaneous Emission (iSASE) FEL utilizes phase shifters which allow for the spontaneously emitted radiation to interact with and stimulate more electrons to radiate coherently. Five phase shifters were simulated, with 34 normal-conducting undulators and focusing-defocusing quadrupoles as an LCLS II FEL lattice using the FEL software Genesis 1.3. Two general schemes, one providing a total phase shift of arbitrary distribution, the other providing a sequential or distributed phase shift, were simulated and optimized using a simulated annealing algorithm. The results suggest that the phase shifters must provide a total shift comparable to the bunch length, and the shifts must be distributed with one large shift, followed by smaller shifts.

INTRODUCTION

A new frontier in fundamental science research, with applications in biological, material, and various other physical sciences, is the use of free electron lasers, or FELs. Only a few FELs exist at various particle accelerator facilities around the world, including the Linear Coherent Light Source (LCLS) at SLAC, and new designs are being developed for use in conjunction with improved accelerators. Specifically, the LCLS II at SLAC will use superconducting technology that could produce brighter hard x-ray FELs than is currently possible at existing FEL facilities. Currently, the LCLS FEL has been able to produce hard x-rays that allow for angstrom resolution imaging [1]. However, the bandwidth of the current LCLS FEL is large relative to that of a transform limited laser. As there is need for highly coherent FEL radiation, FELs must be improved to provide such radiation to users.

Improved SASE (iSASE)

A new strategy for constructing FELs is the improved Self-Amplified Spontaneous-Emission (iSASE) undulator, which can overcome the limitations of a SASE FEL [2, 3]. The key disadvantage that must be overcome in the SASE FEL is the limited slippage that occurs; therefore increasing the slippage would increase the temporal coherence of the emitted radiation. The slippage is artificially increased in the iSASE FEL by adding phase shifters, that increase the path travelled by the electron bunch [2]. By increasing the path length of the electron bunch, the radiation, which is not affected by the phase shifter, continues on a straight trajectory and is able to “catch-up" to the head of the electron bunch. Due to this improvement, the randomly emitted radiation is able to stimulate further coherent radiation from the entire bunch, which increases the overall temporal coherence of the FEL radiation [2, 3]

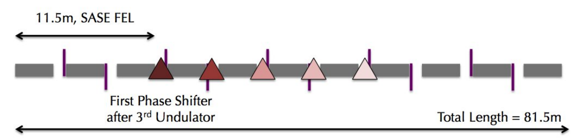

Figure 1: The base-lattice layout for the simulated FEL; the first phase shifter was placed after the third undulator, with focusing and defocusing quadrupoles maintaining the beam optics through the FEL.

The iSASE FEL has only been in development at SLAC for a short period of time, yet has already been shown to work as the theory predicts in both simulations and experimentally [2]. Because the initial simulations show that the iSASE FEL could produce coherent radiation, the next step in the design process is to optimize the chicanes within the undulator system. The program Genesis 1.3, with improvements made for the current simulation requirements, can be used to simulate an iSASE FEL and return information about the radiation that would be generated in such an FEL undulator system [2–4]. In order to design an efficient and effective iSASE FEL, the chicane lengths and positions within the FEL must be optimized such that the temporal coherence and the brightness of the radiation are maximized, and the radiation bandwidth is minimized. The integration of an optimized iSASE FEL with the LCLS II at SLAC could therefore be a significant development in FEL technology.

SIMULATION SET-UP

In order to optimize the phase shifter strengths for an LCLS II type, normal conducting FEL, a lattice the following lattice was set-up. First, the base-lattice was created with 34 undulators and 33 quadrupoles set up in a focusing-defocusing layout, over the 81.5 m long FEL.The lattice also included five phase shifters, the first of which was placed after the third undulator (three gain lengths), creating essentially a short SASE FEL with known slippage length, l_{slip}. Each phase shifter consists of four bending magnets, and is 40 cm long. A general schematic is shown in Fig. 1. Once the lattice was constructed, the focusing and defocusing strengths for the lattice were calculated and the beta functions for the beam were simulated in Tao, the tool for accelerator optics, which runs using Bmad (charged particle simulation subroutine library). Once the beta function

* Supported by US DOE FWP- 2013-SLAC-100164 and DOE SULI.
† lg344@cornell.edu

Content from this work may be used under the terms of the CC BY 3.0 licence (© 2015). Any distribution of this work must maintain attribution to the author(s), title of the work, publisher, and DOI.

ISBN: 978-3-95450-168-7 doi:10.18429/JACoW-IPAC2015-TUPMA022

CESR UPGRADE AS A HIGH-ENERGY, HIGH-BRIGHTNESS X-RAY LIGHT SOURCE*

J. Shanks†, D.L.Rubin, CLASSE, Ithaca, NY 14853, USA

Abstract

The Cornell Electron Storage Ring (CESR) operates most of the year as the Cornell High Energy Synchrotron Source (CHESS). CESR was originally designed and operated as an electron/positron collider, circulating high-emittance beams in order to maximize luminosity. Beam lines were developed to extract x-rays from both electron and positron beams. The two beams share a common vacuum chamber, and are electrostatically separated to avoid collisions. The requirement to store counter-rotating beams significantly constrains the storage ring optics, limiting emittance and, beam current, and bunch distributions. The proposed upgrade eliminates two-beam operation in favor of a single optimized on-axis beam. Several new undulator-based beam lines are planned. The horizontal emittance is reduced in steps, first from 90 nm to 20 nm at 5.3 GeV, and then in a ring-wide upgrade to as low as 300 pm at 6 GeV. The low-emittance optics are based on multi-bend achromats with combined function bends. The details of the optics, apertures, and magnet parameters are presented.

INTRODUCTION

The Cornell Electron Storage Ring (CESR) is a 768-meter e^+/e^- storage ring, with operating energies 1.8–5.3 GeV. Originally developed to operate parasitically while CESR collided electrons and positrons for high energy physics [1,2], CHESS takes advantage of the counter-rotating beams, with seven lines illuminated by light from the positron beam and four from the electron beam. With the conclusion of the particle physics program in 2008, CESR continued to circulate both species of particles, in order to feed the existing CHESS beam lines.

Maintenance of two-beam operation places a long list of constraints on the optics [3,4], including minimum achievable emittance, and injection efficiency. Top-off injection is limited to a single species as the single synchrotron injector is shared by both electrons and positrons.

Here, a proposal is outlined that optimizes performance with a single beam, and that can accommodate additional insertion devices. All CHESS beam lines would be reconfigured to accept an undulator source, and all beam lines would be oriented in the same direction. The same sextant where the beam lines are located is also the source of a disproportionate fraction of the total emittance. Reconfiguration of the lattice in this sextant with double-bend achromat (DBA) cells thus allows re-orientation of the beam lines as well as a substantial reduction of the horizontal emittance.

* Work supported by National Science Foundation grant DMR-1332208
† js583@cornell.edu

PROPOSED UPGRADE

CESR presently uses a FODO-style lattice, with a long straight section for the former CLEO detector. The strong dipoles required for bending into the CLEO straight presently contribute $\approx 60\%$ of the radiation integral I_5, and thus dominate the horizontal emittance.

The proposed upgrade replaces one sextant of the lattice centered at the CLEO straight with six double-bend achromat (DBA) cells. Between each DBA there will be a four-meter zero-dispersion straight for insertion devices. Figure 1 demonstrates how the new layout will remove the CLEO detector straight, following the arc of the ring more continuously. The change in CESR will mandate removing part or all of the CLEO detector that remains in the experimental hall.

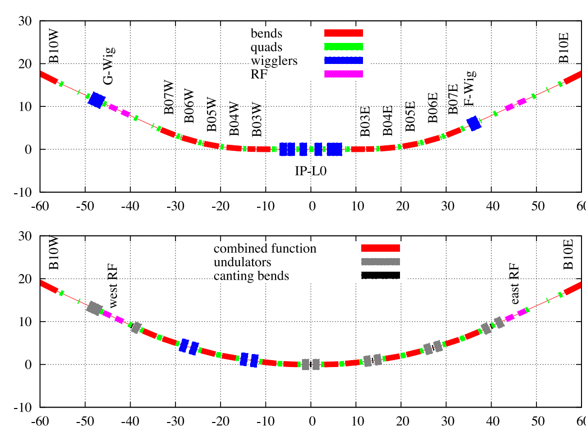

Figure 1: Top: existing user area layout. Bottom: proposed change to user area, removing the CLEO detector straight. All counter-clockwise beam lines will be replaced with clockwise-facing lines, and all beam lines will utilize undulator sources.

Twiss parameters are shown for one DBA cell in Fig. 2, and for the entire ring in Fig. 3. Magnet parameters for one DBA cell are shown in Table 1. Dipoles in the DBA cells will be combined-function dipole-quadrupoles, contrasting with the fixed-purpose dipoles presently installed throughout CESR. Two of the three quadrupoles in each DBA will reuse existing magnet stock. As with the rest of CESR, all quadrupoles in the upgraded region will be independently powered in order to retain flexibility in the optics.

An unusual feature of the proposed lattice is a lack of sextupoles in the DBA sextant. CESR does not presently have sextupoles through this sextant, relying on sextupoles in the remaining 5/6 of the ring to compensate chromaticity and nonlinear dynamics. Dynamic aperture is $> 20\sigma$ of the stored beam.

Content from this work may be used under the terms of the CC BY 3.0 licence (© 2015). Any distribution of this work must maintain attribution to the author(s), title of the work, publisher, and DOI.

ISBN: 978-3-95450-168-7 doi:10.18429/JACoW-IPAC2015-TUPMA023

TWO-DIMENSIONAL CALCULATION OF CHANNELING RADIATION SPECTRUM FOR HIGH-BRIGHTNESS HARD X-RAY PRODUCTION

Wade D. Rush, Jack J. Shi
Department of Physics & Astronomy, The University of Kansas, Lawrence, KS 66045, USA

Abstract

The channeling radiation spectrum is calculated without using the one-dimensional approximation in the planar channeling radiation model or the single-string approximation in the axial channeling radiation model. The obtained spectrum of the two-dimensional channeling radiation is significantly different from those previously calculated with the approximations. The calculation presented here is of the channeling radiation experiments conducted at Fermilab Advanced Superconducting Test Accelerator (ASTA) photoinjector with electron beam energies of 20 to 50 MeV and a diamond target. The computational method developed in this work can be applied to general cases of different crystals and beams with different energy and emittances.

INTRODUCTION

High-energy channeling radiation is produced by a relativistic electron beam interacting with a crystal lattice when the beam channels through the crystal. When an ultra-relativistic electron enters a crystal, the electron will channel through the crystal lattice if its incident angle relative to a specific lattice direction is sufficiently small [1]. A high-intensity ultra-relativistic electron beam could produce high-brightness hard X-rays due to the perturbation of the transverse motion of beam electrons in the crystal. To study this channeling radiation theoretically and numerically, the interaction between the lattice ions and beam electrons has previously been modelled with two different approximations. In the planar channeling approximation [2–4], the radiation from beam electrons is calculated approximately using the Bloch wave function of the electrons solved in a one-dimensional transverse space. In the axial channeling model [2, 5], on the other hand, a single-string approximation of the lattice potential results in a rotational symmetry in the two-dimensional transverse space that greatly simplifies the computational complexity of the original problem of two-dimensional energy bands calculation. Even though these approximations have been justified by the fact that the most relevant energy states for the channeling radiation are those deeply bound states, it is not clear what the conditions are for the validity of the approximations, especially for the case of high-brightness electron beams. In this paper, the channeling radiation spectrum is calculated numerically by solving the Bloch wave function in the two-dimensional transverse space without using the planar or axial channeling approximations. This study is for the upcoming channeling radiation experiments on Fermilab ASTA facility with a 20 to 50 MeV electron beam incident on a diamond lattice along the [-110] lattice direction [6, 7]. In this study, we used a 14.6 MeV electron beam with rms emittance of 0.1 μm in the both transverse directions and the beta functions at the crystal are 4.0 m in the both directions.

LATTICE INTERACTIONAL POTENTIAL IN TRANSVERSE PLANE

When a relativistic beam electron channels through a crystal, the ions of the crystal lattice interact with the electron and affect the motion of the electron. The change of the electron motion results in the emission of photons. Since the longitudinal motion of the electron is ultra-relativistic, the interaction from the ions is too weak to have any effect on the longitudinal motion. The transverse motion of the electron is non-relativistic and the interaction from the ions could have a significant effect on the motion. For the transverse motion, in this study, the interaction potential $V(x, y)$ in the transverse plane is obtained by averaging the lattice potential $V_{cell}(\vec{r})$ in three-dimensional space along the longitudinal direction, where $V_{cell}(\vec{r})$ is the interaction potential of the ions in one unit cell and calculated by using Doyle-Turners formula based on a fitting to the electron scattering factor of the crystal [8]. Due to the periodicity of the lattice in the transverse plane, $V(x, y)$ can be written as a Fourier expansion with the reciprocal lattice vectors projected to the transverse plane. For a beam channeling along the [-110] direction of diamond lattice, the x and y axis of the transverse plane can be chosen to be along the [110] and [001] direction, respectively, and the reciprocal lattice constants of the transverse plane are $b_1 = 2\sqrt{2}\pi/a$ and $b_2 = 2\pi/a$ for the two directions, where a is diamond lattice constant. The interaction potential for the transverse motion of beam electrons can then be written as

$$V(x, y) = \sum_{k_1, k_2=-\infty}^{\infty} V_{k_1,k_2}\, e^{i(k_1 b_1 x + k_2 b_2 y)} \tag{1}$$

where the expansion coefficients V_{k_1,k_2} are calculated using the formulas given in [5] and the summations of k_1 and k_2 need to be truncated at $\pm k_{max}$ for a numerical solution of the Schrödinger equation of the beam electron in the lattice. In this study, it was found that the convergence of the truncation occurs at $k_{max} = 20$ as the change of $V(x, y)$ due to the additional terms of $k_{max} > 20$ is negligible. Figure 1 plots $V(x, y)$ in a unit cell and shows that the interaction potential in the transverse plane does not have a rotational symmetry of the potential used in the axial channeling approximation. The asymmetry of $V(x, y)$ between the x and y direction is because the two-dimensional lattice in the transverse plane becomes rectanglar as $b_1 \neq b_2$, which results from the projection of the cubic diamond lattice to the transverse plane.

Content from this work may be used under the terms of the CC BY 3.0 licence (© 2015). Any distribution of this work must maintain attribution to the author(s), title of the work, publisher, and DOI.

ISBN: 978-3-95450-168-7 doi:10.18429/JACoW-IPAC2015-TUPMA025

X-BAND RF PHOTOINJECTOR FOR LASER COMPTON X-RAY AND GAMMA-RAY SOURCES*

R.A. Marsh†, G.G. Anderson, S.G. Anderson, D.J. Gibson, C.P.J. Barty
Lawrence Livermore National Laboratory, Livermore, CA 94550, USA

Abstract

Extremely bright narrow bandwidth gamma-ray sources are expanding the application of accelerator technology and light sources in new directions. An X-band test station has been commissioned at LLNL to develop multi-bunch electron beams. This multi-bunch mode will have stringent requirements for the electron bunch properties including low emittance and energy spread, but across multiple bunches. The test station is a unique facility featuring a 200 MV/m 5.59 cell X-band photogun powered by a SLAC XL4 klystron driven by a Scandinova solid-state modulator. This paper focuses on its current status including the generation and initial characterization of first electron beam. Design and installation of the inverse-Compton scattering interaction region and upgrade paths will be discussed along with future applications.

INTRODUCTION

Accelerator-based x-ray and gamma-ray sources are expanding rapidly, with several large facilities in construction both in Japan and in Europe [1, 2]. LLNL has a successful history utilizing gamma-rays generated by a linac-driven, laser-based Compton scattering gamma-ray source [3, 4, 5, 6]. Next generation advancements in linac-based x-ray and gamma-ray production require increasing the average flux of gamma-rays at a specific energy (that is, $N/eV/sec$ at the energy of interest). One way to accomplish this is to increase the effective repetition rate by operating the RF photoinjector in a multi-bunch mode, accelerating multiple electron bunches per RF macro-pulse. This multi-bunch mode will have stringent requirements for the electron bunch properties including low emittance and energy spread, but across multiple bunches. An X-band test station has been built and commissioned at LLNL to develop multi-bunch electron beams and generate x-rays. This paper summarizes progress and describes the current status and future direction of the project.

Building on the design work for a 250 MeV gamma-ray source, and leveraging hardware and engineering done for the VELOCIRAPTOR X-band accelerator [7], LLNL established an X-band test station for laser-Compton research and development. The current test station parameters are summarized in Table 1. Beam dynamics are summarized in Fig. 1 for a 100 pC bunch generated in the Mark 1 X-band RF gun and accelerated by a single T53 traveling wave accelerating section. The goals of establishing the test station have been a demonstration of X-band technology for laser-Compton applications and pushing the state-of-the-art with novel interaction concepts. The current goals of the test station efforts are first x-ray demonstration, initial x-ray application experiments, electron beam optimization, demonstration of multiple electron bunches spaced as close as every RF bucket, and upgraded controls systems. Success has been achieved on all of these fronts, with preliminary results reported in this paper and [8].

Table 1: Test Station Parameters

Charge	25–250 pC
Bunch Duration	2 ps
Bunch Rise/Fall	<250 fs
Normalized Emittance	<1 mm mrad
Gun Energy	7 MeV
Cathode Field	180–200 MV/m
Coupling β	1.7
Section Gradient	~70 MV/m
Final Energy	30 MeV

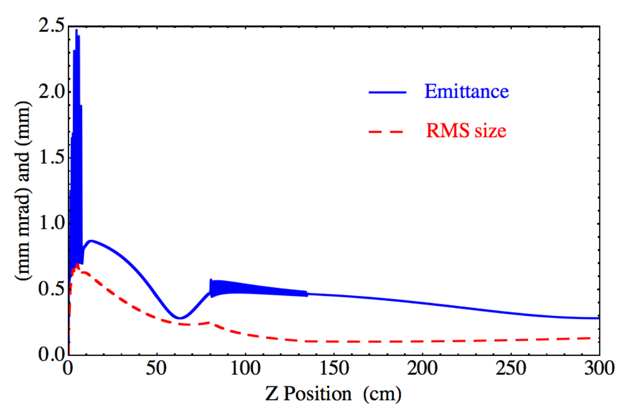

Figure 1: PARMELA beam dynamics simulation for a bunch charge of 100 pC.

TEST STATION

The accelerator is built around a state-of-the-art X-band RF photoinjector [9]. RF power is provided by a 50 MW 11.424 GHz SLAC built XL4 klystron powered by a solid-state Scandinova modulator. The high voltage modulator

* This work performed under the auspices of the U.S. Department of Energy by Lawrence Livermore National Laboratory under Contract DE-AC52-07NA27344
† marsh19@llnl.gov

Content from this work may be used under the terms of the CC BY 3.0 licence (© 2015). Any distribution of this work must maintain attribution to the author(s), title of the work, publisher, and DOI.

ISBN: 978-3-95450-168-7 doi:10.18429/JACoW-IPAC2015-TUPMA026

STATUS OF THE MARIE X-FEL ACCELERATOR DESIGN*

J.W. Lewellen#, K.A. Bishofberger, B.E. Carlsten, L.D. Duffy, F.L. Krawczyk, Q.R. Marksteiner, D.C. Nguyen, S.J. Russell, R.L. Sheffield, N. Yampolsky, LANL, NM 87545, USA

Abstract

The Matter-Radiation Interactions in Extremes (MaRIE) facility is intended to probe and control the time-dependent properties of materials under extreme conditions [1]. At its core, the "MaRIE 1.0" X-FEL is being designed to deliver pulse trains of ~10^{10} 42 keV photons, with a minimum bunch spacing of 2.4 ns, enabling time-dependent studies particularly of mesoscale phenomena. The X-FEL accelerator is also intended to deliver a series of 2 nC electron bunches to enable electron radiography concurrently with the X-ray pulse train, so as to provide multi-probe capability to MaRIE.

In 2014, the reference design for the MaRIE X-FEL 12 GeV driver linac was changed from an S-band normal-conducting to an L-band superconducting linac to accommodate pulse trains up to 100 µs in duration. This paper does not present a complete solution for the MaRIE linac design; rather it describes our current reference design, achieved parameters, areas of concern and paths towards mitigation of identified issues.

REQUIRED PERFORMANCE

The MaRIE X-FEL is intended to generate coherent 42 kV X-ray photons using a 12 GeV electron beam. This places tight constraints on the electron beam slice emittance and energy spread. Table 1 lists the some of the major performance requirements for the MaRIE linac.

REFERENCE DESIGN

Design Overview

The MaRIE linac is a 12 GeV, superconducting electron linear accelerator based on the use of ILC-type cryomodules. The general layout is shown in Figure 1. The majority of the linac consists of ILC-type cryomodules [2] containing 1.3 GHz TESLA-type 9-cell cavities. The 3.9 GHz (3^{rd}-harmonic) modules [3] are located before the bunch compressors to provide for linearization of the longitudinal bunch profile prior to compression. Dual-chicane bunch compressors are located at 250 MeV and 1 GeV. Following the end of the linac the beam passes through an energy droop corrector [4], the beam switchyard (incorporating smooth-pipe dechirpers) and finally the undulators, with space reserved for in-situ diagnostics in each section.

Table 1: Major Performance Goals for the MaRIE Linac

Parameter	Units	Value
Beam energy	GeV	12
Linac frequency	GHz	1.3
Cavity gradient	MV/m	31.5
Max. macropulse duration	µs	100
Bunches / macropulse		10 – 100
Bunch charge, XFEL	nC	0.1 nominal 0.2 max
Bunch charge, eRad	nC	2
Intrabunch energy spread		$\leq 1\cdot10^{-4}$
Slice energy spread		$\leq 1.5\cdot10^{-4}$
RMS slice emittance	µm	≤ 0.2

Beam Source

The design assumes an 0.2 µm rms normalized transverse emittance at the undulator entrance, placing stringent performance requirements on the photoinjector. The MaRIE photoinjector is based on a modified PITZ design: a 1.6-cell normal-conducting structure resonant at 1.3 GHz, with a coaxial RF feed to promote field symmetry. The PITZ gun has obtained a normalized emittance of 0.2 µm at 100 pC [5] so its demonstrated performance represents a good starting point for the MaRIE injector.

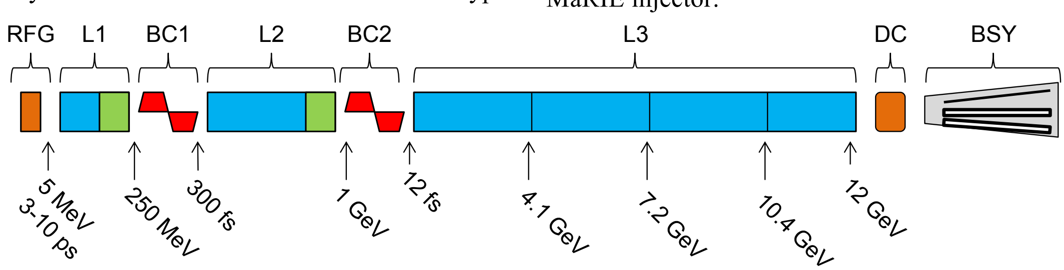

Figure 1: Schematic layout of the MaRIE linac. Room-temperature structures are copper-colored; 1.3 GHz superconducting in blue; 3.9 GHz superconducting in green. RFG is the photoinjector; L1-L3 are the three major sections of the MaRIE superconducting linac; BC1 and BC2 are the first and second dual-chicane bunch compressors; DC is the energy droop corrector; and BSY is the beam switchyard region.

The MaRIE gun design uses a redesigned solenoid with the axial magnetic field peak much closer to the cathode [6]. A very small laser spot is required to avoid

*Work supported by the MaRIE program at Los Alamos National Laboratory, under contract DE-AC52-06NA25396
jwlewellen@lanl.gov

Content from this work may be used under the terms of the CC BY 3.0 licence (© 2015). Any distribution of this work must maintain attribution to the author(s), title of the work, publisher, and DOI.

ISBN: 978-3-95450-168-7 doi:10.18429/JACoW-IPAC2015-TUPMA028

FEASIBILITY STUDY FOR AN X-RAY FEL OSCILLATOR AT THE LCLS-II*

T. J. Maxwell#, J. Arthur, Y. Ding, W. M. Fawley, J. Frisch, J. Hastings, Z. Huang, J. Krzywinski, G. Marcus, SLAC, Menlo Park, CA 94025, USA
K.-J. Kim, R. R. Lindberg, D. Shu, Y. Shvyd'ko, S. Stoupin, ANL, Argonne, IL 60439, USA

Abstract

We show that a free-electron laser oscillator generating X-ray pulses with hard X-ray wavelengths of order 0.1 nm is feasible using the presently proposed FEL-quality electron beam within the space of existing LCLS-II infrastructure when combined with a low-loss X-ray crystal cavity. In an oscillator configuration driven by the 4 GeV energy electron beam lasing at the fifth harmonic, output x-ray bandwidths as small as a few meV are possible. The delivered average spectral flux is at least two orders of magnitude greater than present synchrotron-based sources with highly stable, coherent pulses of duration 1 ps or less for applications in Mössbauer spectroscopy and inelastic x-ray scattering.

INTRODUCTION

Contemporary light sources based on the X-ray free electron laser such as the LCLS [1] and SACLA [2] utilizing self-amplified spontaneous emission (SASE) are now in operation delivering previously unrealizable per-pulse X-ray brightness enhanced over synchrotrons due to the partial longitudinal coherence and full transverse coherence from the high-gain X-ray amplification of ultra-short pulses. However, due to the stochastic nature of the SASE process, the production of stable, fully coherent X-ray pulses remains a challenge for accelerator-based light source facilities world-wide. Hard X-ray self-seeding (HXRSS) demonstrated improved longitudinal coherence and spectral brightness [3] by reducing the X-ray bandwidth mid-amplification to concentrate downstream gain into a narrower spectrum. While this has led to a 2- to 5-fold increase in brightness, HXRSS still relies on the SASE seed, not reaching full, stable longitudinal coherence.

Since the advent of proposed high-rep rate, superconducting FEL linac drivers such as that of the LCLS-II [4], new potential solutions emerge. In this Manuscript, we revisit one scheme based on the continuous recirculation of X-rays to be used for seeding subsequent shots: the low-gain X-ray FEL oscillator (XFELO) [5]. In an XFELO, a low-loss X-ray cavity is wrapped around the FEL undulator, as in an optical FEL oscillator. Where the beam rep rate is equal to the round-trip time of the cavity and the single-pass, low-gain power increase exceeds the round-trip power loss (to initiate start up), the intra-cavity power builds exponentially over many passes, saturating as the single-pass gain comes to equilibrium with the loss. We consider whether a device satisfying these starting requirements is feasible for an LCLS II-type beam, and with what basic considerations.

LAYOUT

Constructing a low-loss X-ray cavity on a scale sufficient to contain an FEL undulator presents difficult challenges. As a best candidate, we suppose an XFELO geometry using high-reflectivity diamond crystal mirrors in a near-backscattering Bragg geometry [6]. To allow for central energy tunability, we adopt the proposal of [7], as illustrated in Figure 1. The electron beam is injected magnetically into the undulator. Four symmetrically arranged Bragg crystals are used to recirculate the hard X-ray output, with two (or two sets of) compound refractive lenses (CRLs) providing cavity focusing. The first crystal following the undulator would be made thin to allow a 4% out coupling of useful radiation.

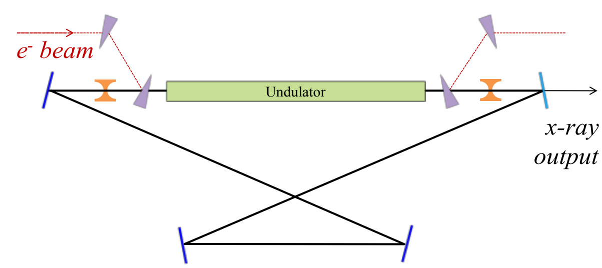

Figure 1: XFELO four crystal, two CRL cavity geometry

The baseline LCLS-II calls for a 4 GeV electron beam energy with variable gap undulators to allow X-ray generation from 0.25 – 5 keV. As the XFELO operates in low-gain, we consider a fifth harmonic XFELO [8] to allow operation well within the hard X-ray regime above 8 keV. At the LCLS-II repetition rate of 0.929 MHz, a round-trip cavity length of 323 m would be required. With the primary restriction of beam rate presumed to be the average beam power on the MW-class primary beam dumps of the ~1 MHz beam at 4 GeV and 100 pC per bunch, we consider doubling the beam rate to 1.86 MHz at a reduced 50 pC per bunch so that the cavity length may be shortened to 161 m.

Under these assumptions, several photon energies are achievable using diamond crystals. In particular, 14.4 keV of the C* (337) reflection, 9.13 keV with C* (333), and

* Work supported under US Department of Energy contract DE-AC02-76SF00515.
# tmaxwell@slac.stanford.edu

Content from this work may be used under the terms of the CC BY 3.0 licence (© 2015). Any distribution of this work must maintain attribution to the author(s), title of the work, publisher, and DOI.

6th International Particle Accelerator Conference IPAC2015, Richmond, VA, USA JACoW Publishing
ISBN: 978-3-95450-168-7 doi:10.18429/JACoW-IPAC2015-TUPMA030

NARROWBAND CONTINUOUSLY TUNABLE RADIATION IN THE 5 TO 10 TERAHERTZ RANGE BY INVERSE COMPTON SCATTERING*

Z.R. Wu, K. Fang, M.-H. Wang, J.H. Wu,
SLAC National Accelerator Lab, Menlo Park, CA 94555, USA

Abstract

5 to 10 THz has recently become the frontier of THz radiation sources development, pushed by the growing interests of spectroscopy and pump-probe material study in this frequency range. This spectrum “Gap” lies in between the several THz range covered by Electro-Optical crystal based THz generation, and the tens of THz range covered by the difference frequency generation method. The state-of-the-art EO crystal THz source using tilted pulse front technique has been able to reach ~ 100 MV/m peak field strength, large enough to be used in an inverse Compton scattering process to push these low energy photons to shorter wavelengths of the desired 5-10 THz range. The required electron beam energy is within 1~2 MeV, therefore a compact footprint of the whole system. The process would occur coherently granted the electron beam is bunched to a fraction of the radiation wavelengths (several microns). A system operating at KHz or even MHz repetition rate is possible given the low electron energy and thus low RF acceleration gradient required. This work will explore the scheme with design parameters and simulation results.

INTRODUCTION

Terahertz has been a frequency range of a plethora of molecular spectral features and dynamic characteristics, yet lack of strong sources to probe or drive the samples under study. Both transient pulses of extraordinary peak electric field strength and multi-cycle narrowband radiation of high brightness and frequency tunability are very much desired, preferably at high repetition rate for the purpose of ultrafast dynamics study. Despite of recent rapid growth on THz light sources, high-brightness tunable narrowband radiations are still rare to none on the chart, both in the low-frequency (1-5 THz) range and in the high-frequency (5-10 THz) range [1]. This type of sources are particularly interesting because of their peak power thus exceptional peak field strength to drive nonlinear effects or absorptive samples, meanwhile narrowband oscillation to exclusively excite specific vibrational or rotational modes of molecules. From the state-of-the-art terahertz source map shown in Fig. 1, the most promising source that currently covers the 5-10 THz range is the quantum cascade laser (QCL). However, it could barely reach 100 mWatt average output power level at 10 THz and needs to be operated at LHe cryogenic temperatures. Continuous-wave operation of QCL also implies low peak power.

This paper intends to propose a narrowband, continuously tunable, high peak power source in the 5-10 THz range, based on inverse Compton scattering process (ICS). Low-frequency seed light can be obtained via tabletop laser based THz generation, which is then scattered by electrons to high frequencies into the targeted 5-10 THz range. In order to enhance the electron/photon interaction, the pulse front of THz seed light can be tilted and its transverse mode modulated to a uniform profile rather than Gaussian distribution. The final radiation achieved is ultra-bright due to its small bandwidth and high peak power, and its central frequency can be continuously tuned by altering electron energy or scattering angle.

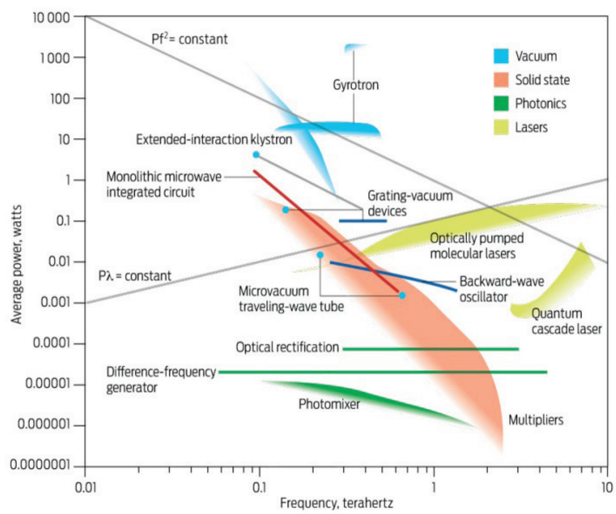

Figure 1: A radiation sources map in the 0.01 to 10 THz range. The power-frequency slope of Pf^2= constant is expected for RF based devices to develop into higher THz frequencies, whereas the power-wavelength line of $P\lambda$= constant is expected for commercial laser based sources. Courtesy of Carter M. Armstrong, IEEE SPECTRUM, Aug. 17, 2012, illustrated by George Retseck.

PHOTON YIELD ESTIMATION

Recent developments in high power near-Infrared laser have enabled delivery of high pulse energy THz transients from a tabletop system, based on optical rectification process in nonlinear EO crystals [2]. Groups at SLAC laser department have demonstrated generation of THz pulses of about 2 ps long and ~50 uJ energy, using a room-temperature $LiNbO_3$ EO crystal pumped by 800 nm laser of 3 mJ pulse energy at 1 kHz repetition rate. Liquid

*Work supported by U.S. Department of Energy under Grants DE-AC02-76SF00515, DE-FG02-13ER41970 and by DARPA Grant N66001-11-1-4199.
#wzr@slac.stanford.edu

Content from this work may be used under the terms of the CC BY 3.0 licence (© 2015). Any distribution of this work must maintain attribution to the author(s), title of the work, publisher, and DOI.

ISBN: 978-3-95450-168-7 doi:10.18429/JACoW-IPAC2015-TUPMA031

Content from this work may be used under the terms of the CC BY 3.0 licence (© 2015). Any distribution of this work must maintain attribution to the author(s), title of the work, publisher, and DOI.

DISPERSIVE PROPERTY OF THE PULSE FRONT TILT OF A SHORT PULSE OPTICAL UNDULATOR*

M-H. Wang†, J. Wu, and Z. Wu, SLAC, Menlo Park, CA 94040, USA
J. Liang, Department of Biomedical Engineering, Washington University in St. Louis, St. Louis, MO 63130, USA

Abstract

A short pulse laser can be used as an optical undulator to achieve a high-gain and high-brightness X-ray free electron laser (FEL) [1]. To extend the interaction duration of electron and laser field, the electron and laser will propagate toward each other with an small angle. In addition, to maintain the FEL lasing resonant condition, the laser pulse shape need be flattened and the pulse front will be titled. Due to the short pulse duration, the laser pulse has a broad bandwidth. In this paper, we will first describe the method of generalized Gaussian beam propagation using ray matrix. By applying the Gaussian beam ray matrix, we can study the dispersive property after the pulse front of the short laser is tilted. The results of the optics design for the proposal of SLAC Compton scattering FEL are shown as an example in this paper.

INTRODUCTION

With rapid progress in generating table-top terawatt laser pulse and fiber optics, the optical undulator can provide effective magnetic field B_u on the order of kilo-Tesla, which can provide strong enough effective undulator strength K for lasing. To fulfil an optical undulator for FEL, the interaction range of electron and laser pulse should be with 10-20 FEL gain length, and the equivalent undulator strength K should be kept constant for a given radiation γ. In order to increase the electron and laser pulse interaction range, the laser and electron need to co-propagate synchronously.

It is known that the angular dispersion (AD) will generate pulse front tilt (PFT). Gratings are ideal for this purpose as they can introduce large linear angular chirps. Nevertheless, besides the PFT, AD will also increase spatial dispersion (SD). As the pulse propagates, different frequency in the pulse becomes increasingly separated from each other. AD will also introduce negative group-delay dispersion (GDD). Both SD and GDD will lead temporal broadening of the laser and degrade the performance of the optical undulator in FEL. Therefore it is important to investigate the dispersive property before the PFT laser is sent to interact with an electron bunch.

The geometrical optics uses ray transfer matrix (also called ABCD matrix) to trace the light ray path through space and optical devices. Take one dimension ray trace for example:

$$\begin{pmatrix} x \\ \theta \end{pmatrix}_{out} = \begin{pmatrix} A & B \\ C & D \end{pmatrix}_n \cdots \begin{pmatrix} A & B \\ C & D \end{pmatrix}_1 \begin{pmatrix} x \\ \theta \end{pmatrix}_{in} \quad (1)$$

where x is position, θ is the slope and matrices 1 to n represent different optical components or spaces. The radius of curvature of the ray is $q = \frac{x}{\theta}$. The ABCD law for the radius of curvature is:

$$q_{out} = \frac{Aq_{in}+B}{Cq_{in}+D} \quad (2)$$

It is easy to extend the ray transfer matrix to two dimensions. Where A, B, C, and D become 2 by 2 matrices.

The ABCD matrix could be extended to "ray-pulse" matrices which takes account of dispersive effects in both spatial coordinates (as in the usual paraxial ABCD matrix approach) and in the temporal domain [2]. These matrices could be applied to write a space-time integral analogous to a generalized Huygens integral. By using both ray-pulse matrices and the propagation laws for Gaussian ray pulses which are space and time varying, the conventional results for Gaussian beams through various optical components could be derived. In this paper, we will first describe the method of generalized Gaussian beam propagation using ray matrix. By applying this method, we will investigate the dispersive properties of the optics design for the proposal of SLAC Compton scattering FEL.

GENERALIZED GAUSSIAN BEAM PROPAGATION USING RAY MATRIX

A short pulse laser is a finite size Gaussian beam. The electric field of the laser propagating along the z-axis in (x, ω) space can be expressed as:

$$E(x,\omega) = E_0 \exp\left(-\frac{\omega^2\tau_0^2}{4}\right)\exp\left(-i\frac{k_0x^2}{2q}\right) \quad (3)$$

where k_0 is the nominal wave-number, ω is the offset from the centre angular frequency, τ_0 is the pulse length and q is the complex q parameter of a Gaussian beam:

$$\frac{1}{q(z)} = \frac{1}{z+iZ_R} = \frac{1}{R(z)} - i\frac{\lambda_0}{\pi W^2(z)} \quad (4)$$

where Z_R is the Rayleigh range, $R(z)$ is the radius of curvature of the wave front, λ_0 the nominal wave length and $w(z)$ is the spot size $w(z) = w_0\sqrt{1+(\frac{z}{z_R})^2}$ with w_0 being the waist size.

A comprehensive matrix method for propagating Gaussian ultrashort pulses with Gaussian spatial profiles having spatio-temporal couplings was given by Kostenbauder [2]. The ray-pulse matrix for an optical system that introduces couplings can be written as [3]:

* Work supported by the US DOE No. DE-AC02-76SF00515.
† mhwang@slac.stanford.edu

ISBN: 978-3-95450-168-7 doi:10.18429/JACoW-IPAC2015-TUPMA033

A BUNCH COMPRESSION METHOD FOR FREE ELECTRON LASERS THAT AVOIDS PARASITIC COMPRESSIONS *

S.V. Benson#, D.R. Douglas, C.D. Tennant, F.G. Wilson,
Jefferson National Accelerator Facility, Newport News, VA 23606, USA
D. C. Nguyen, Los Alamos National Laboratory Los Alamos NM 87545 USA

Abstract

Virtually all existing high energy (>few MeV) linac-driven FELs compress the electron bunch length through the use of off-crest acceleration on the rising side of the RF waveform followed by transport through a magnetic chicane. This approach has at least three flaws: 1) it is difficult to correct aberrations- particularly RF curvature, 2) rising side acceleration exacerbates space charge-induced distortion of the longitudinal phase space, and 3) all achromatic "negative compaction" compressors create parasitic compression during the final compression process, increasing the CSR-induced emittance growth.

One can avoid these deficiencies by using acceleration on the falling side of the RF waveform and a compressor with M_{56}>0. This approach offers multiple advantages: 1) It is readily achieved in beam lines supporting simple schemes for aberration compensation, 2) Longitudinal space charge (LSC)-induced phase space distortion tends, on the falling side of the RF waveform, to enhance the chirp, and 3) Compressors with M_{56}>0 can be configured to avoid spurious over-compression.

We will discuss this bunch compression scheme in detail and give results of a successful beam test in April 2012 using the JLab UV Demo FEL.

INTRODUCTION

To preserve electron beam brightness in a linac based accelerator used as an FEL driver it is necessary to produce a long, low peak current bunch in the injector, accelerate off crest in the accelerator, and then bunch in a bunch compressor. Brightness preservation is difficult due to the effects of LSC, coherent synchrotron radiation (CSR), and RF curvature. The canonical method for compression is to accelerate on the rising side of crest and compress in a chicane, which requires use of negative momentum compaction. It is possible however to reverse this and accelerate on the falling side of crest and compress in a bend with positive momentum compaction. When used in an energy recovering linac (ERL), this option has many advantages.

COMPRESSION OPTIONS

We describe here a low-energy compression method, which is a parallel-to-point longitudinal map. At higher beam energies, one usually wants to have a two-stage compression. Though this example describes the low energy procedure, the same ideas described below may still apply to the final compression of a high-energy system.

Negative Momentum Compaction Compressor

In most linear accelerators the simplest method of achieving a non-zero momentum compaction is to use a magnetic chicane. This is illustrated in Fig. 1. The beam is accelerated on the rising portion of the RF waveform, leading to the higher energy electrons being in the rear of the bunch. A transport system with negative momentum compaction then compresses the bunch. Note that the second order momentum compaction (T_{566}) is non-zero positive in a chicane, and is thus the wrong sign to correct for the RF curvature in the electron bunch. RF curvature is generally handled using harmonic RF, which is used to create a nearly linear voltage versus time and to additionally compensate for the T_{566} of the chicane.

Longitudinal space charge tends to accelerate the head of the bunch and decelerate the tail. This reduces the energy spread of the bunch, which is helpful in matching the energy spread to the acceptance of the FEL. In some cases however, it can produce second or third order curvature in the distribution, which decreases the peak current after the compressor unless it can be compensated using the harmonic RF and transport settings.

Similarly, CSR can produce curvature that can cancel part of the RF curvature on the bunch. If too large, however, it can produce a monoenergetic segment in the longitudinal phase space. This part of the bunch cannot be compressed due to the lack of any time-energy correlation. This is shown schematically in Fig. 2.

The emittance growth due to CSR can be large in a negative momentum compaction bending system because the compaction in a single dipole is always positive. This means that the momentum compaction of the transport upstream of the last dipole must be more negative than is required to simply bunch the beam. The beam is, for example, over-bunched in the earlier magnets of a chicane, and then slightly debunched to the optimum length in the last dipole. There is thus a parasitic compression that is inherent in a chicane compressor.

* This work was supported by U.S. DOE Contract No. DE-AC05-84-ER40150, the Air Force Office of Scientific Research, DOE Basic Energy Sciences
#felman@jlab.org

Content from this work may be used under the terms of the CC BY 3.0 licence (© 2015). Any distribution of this work must maintain attribution to the author(s), title of the work, publisher, and DOI.

ISBN: 978-3-95450-168-7 doi:10.18429/JACoW-IPAC2015-TUPMA034

CONTROL OF SYNCHROTRON RADIATION EFFECTS DURING RECIRCULATION WITH BUNCH COMPRESSION*

D.R. Douglas#, S.V. Benson, R. Li, Y. Roblin, C.D. Tennant, Thomas Jefferson National Accelerator Facility, Newport News, VA 23606, USA,
G.A. Krafft, B. Terzic, Old Dominion University, Norfolk, VA, 23529, USA
C.-Y. Tsai, Virginia Polytechnic Institute and State University, Blacksburg, VA, 24061, USA

Abstract

Studies of beam quality during recirculation [1] have been extended to an arc providing bunch compression with positive momentum compaction [2]. It controls both incoherent and coherent synchrotron radiation (ISR and CSR) using methods including optics balance [3] and generates little microbunching gain. We detail the dynamical basis for the design, discuss the design process, give an example, and provide simulations of ISR and CSR effects. Reference will be made to a complete analysis of microbunching effects [4].

METHODS FOR CSR/ISR CONTROL

Recirculation and energy recovery are established means of cost-performance optimization. Their use for FEL drivers can be challenging because of the impact of CSR on beam quality, and the desirability of limiting machine size and complexity. Here, we describe a method providing bunch length compression and recirculation in a modest footprint (~10 m diameter at ~1 GeV) while limiting beam quality degradation due to CSR. The method is scalable to higher energy (by increasing bend radius and machine diameter).

"Conventional" Compressor Design

A FODO-based recirculation arc can be used as a compressor; as $M_{56}>0$, an incident bunch with an appropriate energy chirp will be compressed with advantages discussed elsewhere [5]. When employed as a means of final bunch compression, the impact of CSR is however dramatic and detrimental. Using a simple 1-D CSR model in DIMAD [6], we studied compression of a 150 pC, 0.5 μm-rad normalized emittance beam to ~70 fsec x 0.1% δp/p while bending through 180° at 0.71 GeV in an arc comprising eight quarter-integer FODO cells with bend radius of 2 m. The beam emittance increases as a consequence of phase space redistribution driven by the CSR interaction, but effects can be mitigated as follows:

1. Chromatically correct the lattice and compensate lattice and CSR-induced curvature in the longitudinal phase space, *i.e.*, set T_{566}. Here, this is assumed to have been done in upstream transport so as to allow compression of small relative momentum spreads while avoiding use of strong nonlinearities. We model it with a quadratic phase-energy correlation in the incoming beam (a T_{655} term).
2. Introduce lattice perturbations to suppress linear x-δp/p and x'-δp/p correlations in the beam by introducing perturbative dispersion trims.
3. Trim chromatic corrections to suppress CSR-induced nonlinear phase space distortions [7].
4. Optimize the betatron match by varying beam input parameters to minimize output emittance.

After optimization, the output emittance was ~2 mm-mrad, representing a factor of four growth in the input.

The cause of the phase space redistribution is clear: as the bunch compresses, energy modulation across the bunch due to CSR increase dramatically. As a result, the compensation described by Di Mitri et al. [8] breaks down despite the presence of desirable betatron phase and amplitude relationships inherent to the achromat. Small shifts introduced when the bunch is long are inadequate to offset the larger shifts induced when the bunch is short.

Excitation-Modulated Compressor Design

Breakdown in emittance compensation can be mitigated by redistribution of bending along the beamline and optimization as described above. The method is simple: increase the angle of bending in initial FODO cells – thereby enhancing the impact of CSR early in the beam line while the bunch is long – and decrease the bending angle in the final FODO cells, reducing the effect of CSR while the bunch is short. Initial simulation of such an excitation-modulated system shows immediate benefit. An optimized linearly declining bend (using dipoles of 40°, 35°, 30°,… 10°, 5°) presented less emittance degradation than a conventional arc. Guided by the concepts of optics balance [9] and magnifying achromats [10] (in both, upstream and downstream perturbations are balanced by the choice of the intervening lattice optics), we added a dispersion generator to provide additional control of the beam and lattice, and manually adjusted the bending pattern to minimize output emittance. Care in selection of bend angles further reduced emittance dilution; choice of bend radius managed ISR effects.

As in the conventional arc, the degraded output phase space presented correlated distortions that could be compensated by perturbing the beam line optics as described above, limiting growth of normalized emittance from 0.5 to 1 μm-rad, a factor of two lower than in the

* This material is based upon work supported by the U.S. Department of Energy, Office of Science, Office of Nuclear Physics under contract DE-AC05-06OR23177.
#douglas@jlab.org

Content from this work may be used under the terms of the CC BY 3.0 licence (© 2015). Any distribution of this work must maintain attribution to the author(s), title of the work, publisher, and DOI.

ISBN: 978-3-95450-168-7 doi:10.18429/JACoW-IPAC2015-TUPMA035

CONTROL OF SYNCHROTRON RADIATION EFFECTS DURING RECIRCULATION*

D.R. Douglas#, S.V. Benson, A. Hofler, R. Kazimi, R. Li, Y. Roblin, C.D. Tennant, Thomas Jefferson National Accelerator Facility, Newport News, VA 23606, USA,
G.A. Krafft, B. Terzic, Old Dominion University, Norfolk, VA, 23529, USA,
C.-Y. Tsai, Virginia Polytechnic Institute and State University, Blacksburg, VA, 24061, USA

Abstract

We use results by Di Mitri et al. [1] as the basis of a method for suppression of synchrotron-radiation-driven beam quality degradation during recirculation.

Use of second-order achromatic superperiodic recirculation transport based on individually isochronous and achromatic superperiods of low-quantum-excitation lattices is found to provide control of both emittance degradation from coherent synchrotron radiation (CSR) and microbunching instability (μBI) gain. Use of such low excitation lattices and choice of sufficiently large bend radius also insures incoherent synchrotron radiation (ISR) driven effects are well-managed.

METHODS FOR CSR/ISR CONTROL

Di Mitri *et* al. have derived conditions under which CSR-induced emittance growth can be suppressed during transport through bending systems [1]. We apply these conditions using a simple methodology to generate a design for a recirculation transport line giving little emittance growth even at high bunch charges, and exhibiting low microbunching instability gain.

The method (described in more detail elsewhere [2]) is as follows: utilize superperiodic recirculation transport phased as in a second-order achromat, with individually isochronous and achromatic superperiods. Each superperiod is to be based on low-quantum-excitation structures of familiar types, such as three-bend achromats (TBA), Chasman-Green (two-bend) achromats, or theoretical-minimum-emittance cells (TME). Modulation of focusing, choice of betatron phase advance, dispersion modulation, or other means is then used to make individual superperiods achromatic and isochronous. Use of low excitation lattices and sufficiently large bend radius then insures ISR effects are well-managed.

Choice of rational period tune with overall second-order achromatic structure – coupled with individual period isochronicity – then insures that the conditions for the suppression of CSR-driven emittance growth as described in [1] are met. This was observed in earlier studies [3], but in addition to the control of CSR-induced emittance degradation we have found that this also suppresses microbunching instability gain over a broad range of parameter space [4].

* This material is based upon work supported by the U.S. Department of Energy, Office of Science, Office of Nuclear Physics under contract DE-AC05-06OR23177.
#douglas@jlab.org

The suppression of microbunching gain appears to relate to limits placed on modulation of momentum compaction by the use of periodically isochronous transport. As will be seen from the examples below, the gain is very low for a periodically isochronous arc with small compaction modulations and modest R_{51}, R_{52}, and R_{56}, while similar, but aperiodic, structures with large compaction oscillations have high gain.

Control of ISR

As noted above, ISR control can be provided by use of an appropriate combination of a low-quantum-excitation transport lattice architecture and adequately large dipole bending radii [5].

APPLICATION OF DESIGN METHODOLOGY

Nearly all requirements for CSR suppression in a recirculator are met by the original design concept for the CEBAF arcs [6]. Control can be enhanced by adding provisions for small bend-plane beam envelope in the dipoles and provision for control of terms such as T_{566} (though this is in principle possible with only minor modification of the "stock" CEBAF transport system [7]).

We have thus generated a slightly modified version of the CEBAF arc transport line, based on TME focusing cells [8]. When four cells – each with 90^o betatron tune – are concatenated, an achromatic (to second order) but nonisochronous superperiod results (Figure 1).

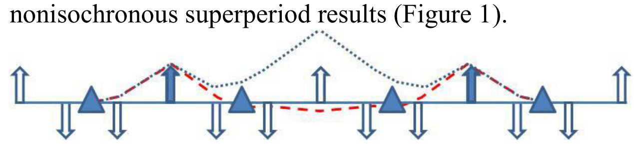

Figure 1: TME-cell-based superperiod structure for recirculation arc concept design. Natural dispersion of second order achromat – dotted blue line; modulated dispersion of isochronous linear achromat – dashed red.

By increasing the strength of the highlighted quadrupoles (which have 180^o betatron phase separation), the dispersion can be driven down in the inner dipoles, the tunes split, and a linearly achromatic, isochronous superperiod obtained. As with CEBAF, optimization using all quad families then allows choice of tune, matched envelopes, enforced achromaticity, and selection of momentum compaction. Choice of rational superperiod tune and corresponding multiplicity then gives – with appropriate sextupole correction – a second-order

Content from this work may be used under the terms of the CC BY 3.0 licence (© 2015). Any distribution of this work must maintain attribution to the author(s), title of the work, publisher, and DOI.

ISBN: 978-3-95450-168-7 doi:10.18429/JACoW-IPAC2015-TUPMA036

Content from this work may be used under the terms of the CC BY 3.0 licence (© 2015). Any distribution of this work must maintain attribution to the author(s), title of the work, publisher, and DOI.

FIRST e$^-$/ γ COMMISSIONING RESULTS FOR THE GLUEX EXPERIMENT/HALL D AT CEBAF*

M. McCaughan†, T. Satogata, Y. Roblin, J. Benesch
Thomas Jefferson National Acceleration Facility (TJNAF), Newport News, VA 23606, USA

Abstract

Experimental Hall D, with flagship experiment GlueX, was constructed as part of the 12 GeV CEBAF upgrade. A new magnetically extracted electron beam line was installed to support this hall. Bremsstrahlung photons from retractable radiators, are delivered to the experiment through a series of collimators following a long drift to allow for beam convergence. Coherent Bremsstrahlung generated by interaction with a diamond radiator will achieve a nominal 40% linear polarization and photon energies between 8.5 and 9 GeV from 12.1 GeV electrons, which are then tagged or diverted to a medium power 60kW electron dump. The expected photon flux is 10^7-10^8 Hz. This paper discusses the experimental line design, commissioning experience gained since first beam in spring 2014, and the present results of beam commissioning by the experiment.

HALL DESIGN AND CONSTRAINTS

Design constraints in the layout of Hall D included a project requirement that the Hall be 100m from the road, thus resulting in an 8 degree pitch in the ramp relative to the North Linac elevation. [1] Space constraints for optical elements resulted in a sensitivity to the input envelope and an inability to null leakage vertical dispersion at the bottom of the ramp. This provides for interesting tuning idiosyncrasies including nulling horizontal and minimizing vertical dispersion to the 5C00 retractable dump, envelope matching with the dispersion leakage, and correcting any leakage at the top of the ramp using the dipole string and pairs of quadrupoles on the ramp. The electron dump has a safety limit of the lower of 60 kW or 5 uA with an administrative limit of 3 uA imposed by the Hall at any energy. Design Twiss parameters are shown in Fig. 1.

GlueX is the flagship experiment of the new experimental Hall D, its goal being to provide critical data needed to quantitatively understand quark and gluon confinement in quantum chromodynamics (QCD). GlueX uses the photo-production of exotic hybrid and light mesons via the coherent bremsstrahlung technique to produce a linearly polarized photon beam of up to 9 GeV, as these mesons explicitly manifest gluonic degrees of freedom in the confinement regime, and thus of great interest to study. [2]

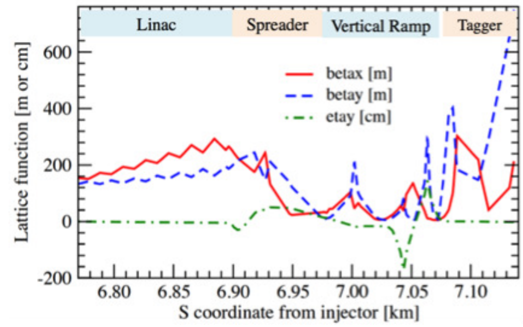

Figure 1: Twiss Parameters in Hall D.

ENGINEERING RUN I (SPRING 2014)

A number of 12 GeV project goals were accomplished during this run, most notably delivering beam of at least 2nA at above 10 GeV to both the 5C00 retractable dump as well as the tagger dump through the 12 GeV capable beam line at 5.5 passes. Emittance measurements & differential orbit data was taken throughout the machine for summer analysis. The analysed data was later fed into the model via body gradient error correction, synchrotron light losses, etc. Spring saw first beam through vast portions of the upgraded accelerator (passes 4+) with first beam in arc 10 on 2 May 14. Sixth pass beam was then sent through the North Linac, threaded through the B-spreader, arriving for the first time at the 5C00 dump at 3:53 on 3 May14, after which orbits & path length were optimized. [3] Numerous differential orbit measurements were conducted for later analysis & testing on the two new synchrotron light monitors was performed.

Following the setup of CEBAF at a familiar energy (6.1 GeV) so as to not stress RF/magnets while treading first beam through the reassembled machine, the total energy was scaled to 10.5 GeV. Scaling went less than ideally & the machine had to be setup again from first principles at the higher energy resulting in a delay of several days. Beam returned to the 5C00 dump at 2:53 on 7 May 2015 with ~80% transmission. Path length, dispersion corrections, & envelope matching in the machine later improved transmission. Differential orbit data was collected to characterize the problems, localizing them to parts of the spreaders & recombiners, where they were then minimized with orbit & optics changes. In preparation to send beam to the Tagger dump a set point based on the Tosca model was found (8.21 MG*cm), & a compromise set point of 8 MG*cm selected to start with to account for synchrotron light losses. After continued improvements to orbit, optics, & path length beam returned to the 5C00 dump at 20:24 7 May 14.

* Notice: Authored by Jefferson Science Associates, LLC under U.S. DOE Contract No. DE-AC05-06OR23177. The U.S. Government retains a non-exclusive, paid-up, irrevocable, world-wide license to publish or reproduce this manuscript for U.S. Government purposes.
†michaelm@jlab.org

ISBN: 978-3-95450-168-7 doi:10.18429/JACoW-IPAC2015-TUPMA037

Content from this work may be used under the terms of the CC BY 3.0 licence (© 2015). Any distribution of this work must maintain attribution to the author(s), title of the work, publisher, and DOI.

COMMISSIONING OF THE 123 MeV INJECTOR FOR 12 GeV CEBAF*

Y. Wang, A. Hofler and R. Kazimi, Jefferson Lab, Newport News, VA 23606, USA

Abstract

The upgrade of CEBAF to 12GeV included modifications to the injector portion of the accelerator. These changes included the doubling of the injection energy and relocation of the final transport elements to accommodate changes in the CEBAF recirculation arcs. This paper will describe the design changes and the modelling of the new 12GeV CEBAF injector. Stray magnetic fields have been a known issue for 6 GeV CEBAF injector, the results of modelling the new 12GeV injector and the resulting changes implemented to mitigate this issue are describe in this paper. The results of beam commissioning of the injector are also presented.

BRIEF HISTORY

The Continuous Electron Beam Accelerator Facility (CEBAF) at Jefferson Lab was originally designed in the mid-1980s to provide 4 GeV of continuous electron beam. In 2009 the beam energy was successfully raised to 6 GeV after refurbishment of ten 25 MeV capable (C25) cryomodules, and the injector energy was raised from 45 MeV to 67.5 MeV. The injector and other sections of the beamline had the capacity to support 6 GeV operations; therefore, no hardware upgrades were needed for the injector.

As the CEBAF scientific program progressed, in the late-1990s the laboratory and the user community developed a scientific case that demanded a higher energy – the 12 GeV upgrade of CEBAF [1]. Upgrading CEBAF to 12 GeV will enable the generation and study of exotic meson states, contributing to a better understanding of the confinement and the forces within the nuclei. An extended period of 12 GeV installation started in May 2012, and the beam-based commissioning started in October 2013.

HARDWARE CHANGES [2]

There are two major changes in the injector (shown in Fig.1and Fig. 2). The first change is to replace the second full C25 cryomodule just upstream of the injection chicane with a 100 MeV capable one (C100). To meet the energy requirement of the 12 GeV CEBAF and maintain the 0.11284 energy ratio between the injector and the linacs, the injector energy was increased from 67.5 MeV to 123 MeV. In the 6 GeV injector, the beam energy started at 130 keV at the gun increasing to ~500 keV after the capture RF element and ~6 MeV at the exit of the 2-cavity SRF booster. The final injector beam energy (up to 67.5 MeV) was reached after transport through two full C25 type cryomodules. The energy required for the 12 GeV injector is 123 MeV, well beyond the capability of two C25 crymodules. Changing the second cryomodule to C100 provided the extra needed energy gain [3]. C100's maximum achieved energy gain during cryomodule commissioning was 115 MeV satisfying 12 GeV operations with sufficient headroom.

The second change stems from the interference with the new high energy beam recirculation transport arc for the 12 GeV upgrade (at the same elevation). Several injector elements were moved to provide enough physical clearance. The injector full energy spectrometer dipole and diagnostic dump line were shifted upstream by 4.57 m. The bending angle of the spectrometer line was changed for a better physical fit between beamline elements. The start of the injector chicane was moved upstream by 20.51 m. The spacing between the 5-quad matching section in the dispersion free line is shortened due to this change.

With the increased energy, several beam transport and corrector magnets were improved or added. The number of trim magnet girders in the chicane region was increased from 7 to 9 to provide good flexibility for alternative optics that can vary the M_{56} compression in the chicane. Each girder has a beam position monitor (BPM), a horizontal corrector, a vertical corrector, and a quad. Both the spectrometer dipole magnet and the power supply remained unchanged but operate at a higher current, but the power supplies for the four chicane dipoles were upgraded from 10 A to 12 A to match the increased beam momentum. Four of the five matching quads were upgraded from QD type to QB type to provide stronger focusing power. Ten correctors were upgraded from AT type to DB and DJ type to have more steering strength (shown in Table 1).

Table 1: Magnet types and their strength

Type	Quad Strength (Gauss)	Dipole Strength (G-cm)
QD	3250	
QB	14143	
AT		328
DB		926
DJ		981
BT		2826

Beam diagnostics were added. Two viewers and two beam wire scanners were added to the matching section to speed up the optics matching process. A BPM was, also, added to have two BPMs to establish the proper trajectory

* Notice: Authored by Jefferson Science Associates, LLC under U.S. DOE Contract No. DE-AC05-06OR23177. The U.S. Government retains a non-exclusive, paid-up, irrevocable, world-wide license to publish or reproduce this manuscript for U.S. Government purposes.

ISBN: 978-3-95450-168-7 doi:10.18429/JACoW-IPAC2015-TUPMA038

OBSERVATION OF SIGNIFICANT QUANTUM EFFICIENCY ENHANCEMENT FROM A POLARIZED PHOTOCATHODE WITH DISTRIBUTED BRAG REFLECTOR*

S. Zhang#, M. L. Stutzman, and M. Poelker, Jefferson Lab, Newport News, Virginia, USA
Y. Chen, and Aaron Moy, SVT Associates, Inc., Eden Prairie, Minnesota, USA

Abstract

Polarized photocathodes with higher Quantum efficiency (QE) would help to reduce the technological challenge associated with producing polarized beams at milliampere levels, because less laser light would be required, which simplifies photocathode cooling requirements. And for a given amount of available laser power, higher QE would extend the photogun operating lifetime. The distributed Bragg reflector (DBR) concept was proposed to enhance the QE of strained-superlattice photocathodes by increasing the absorption of the incident photons using a Fabry-Perot cavity formed between the front surface of the photocathode and the substrate that includes a DBR, without compromising electron polarization. Here we present recent results showing QE enhancement of a GaAs/GaAsP strained-superlattice photocathode made with a DBR structure. Typically, a GaAs/GaAsP strained-superlattice photocathode without DBR provides a QE of 1%, at a laser wavelength corresponding to peak polarization. In comparison, the GaAs/GaAsP strained-superlattice photocathodes with DBR exhibited an enhancement of over 2 when the incident laser wavelength was tuned to meet the resonant condition for the Fabry-Perot resonator.

INTRODUCTION

The nuclear physics research at Jefferson Lab requires high energy and high current polarized electron beams that originated from a low energy polarized electron source. Superior quality photocathodes producing both high QE and electron polarization are key to critical elements to guarantee the successful implementation of the existing physics programs and are also of vital importance in satisfying the demand of future machines such as the medium-energy electron-ion colliders (MEIC) [1] currently under intensive study. Although polarization over 85% has been achieved, the QE is still relatively low, usually ~ 1%. In this report, we present the characterization and study of a new type of strained-superlatice photocathode designed to significantly improve the QE while still maintaining high electron polarization.

As shown in Fig. 1(a), usually the incident laser beam makes only a single pass through the active layer of a standard GaAsP/GaAs photocathode structure, with most of the laser energy deposited in the substrate, leading to unwanted cathode heating. For high current applications where the laser power can reach Watt-levels, this may serve to evaporate the cesium from the surface and reduce the QE [2].

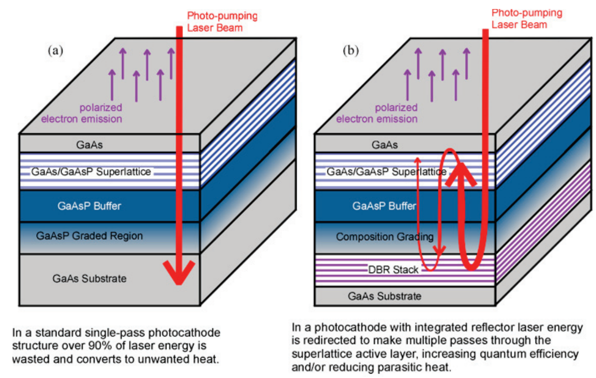

Figure 1: Illustration of (a) a standard strained-superlattice photocathode with a single-pass laser beam, and (b) the photocathode combined with a DBR mirror for confining the unabsorbed laser beam within the active layer.

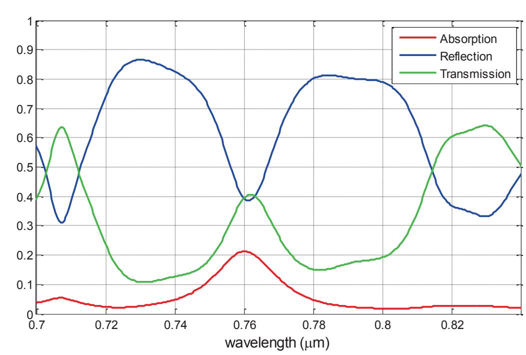

Figure 2: Calculation of absorption, reflectivity and transmission of a photocathode with DBR structure.

To overcome this issue, a new structure was proposed [3] by combining the device active layer with a semiconductor-based mirror structure as illustrated in Fig. 1(b), where a Fabry-Perot (FP) cavity around the active layer is formed using a distributed Bragg reflector (DBR) as a bottom mirror and surface-to-vacuum reflection as the top mirror (Fig. 1b). Such an optical configuration allows effectively confinement of the laser beam inside the active layer region and therefore increases the amount of light absorbed by the photocathode without increasing the pump laser power. A calculation of absorption, reflectivity and transmission of a DBR photocathode at

*Authored by Jefferson Science Associates, LLC under U.S. DOE Contract No. DE-AC05-06OR23177. The U.S. Government retains a non-exclusive, paid-up, irrevocable, world-wide license to publish or reproduce this manuscript for U.S. Government purposes.
shukui@jlab.org

Content from this work may be used under the terms of the CC BY 3.0 licence (© 2015). Any distribution of this work must maintain attribution to the author(s), title of the work, publisher, and DOI.

ISBN: 978-3-95450-168-7 doi:10.18429/JACoW-IPAC2015-TUPMA041

Content from this work may be used under the terms of the CC BY 3.0 licence (© 2015). Any distribution of this work must maintain attribution to the author(s), title of the work, publisher, and DOI.

ON THE CHARACTERIZATION OF A CCR SOURCE*

A. V. Smirnov#, RadiaBeam Technologies Inc., Santa Monica, CA 90404, USA

Abstract

Peak and spectral brightness of a resonant long-range wakefield extractor are evaluated. It is shown that the brightness is dominated by beam density within the slow wave structure and antenna gain of the outcoupling. Far field radiation patterns and brightness of circular and high-aspect-ratio planar radiators are compared. A possibility to approach the diffraction limited brightness is demonstrated. Role of group velocity in designing of the Cherenkov source is emphasized. The approach can be applied for design and characterization of various structure-dominated sources (e.g., wakefield extractors with gratings or dielectrics, or FEL-Cherenkov combined sources) radiating into a free space using an antenna (from microwave to far infra-red regions). The high group velocity structures can be also effective as energy dechirpers and for diagnostics of microbunched relativistic electron beams.

INTRODUCTION

For generation of a relatively narrow bandwidth mm-sub-mm wave radiation resonant Cherenkov radiation can be an attractive alternative to undulator radiation due to the exceptional compactness of the radiator and capability to operate at lower energies. Such a coherent Cherenkov radiation (CCR) source is usually supplied by an antenna and employs a circular [1] or planar configuration [2,3]. Most of FIR FEL sources do not employ radiating structure and operate in a diffraction limited mode due to attainability of low emittance electron beams (namely, with geometric emittance lower than the emittance of diffraction limited photon beam $\lambda/2\pi$).

An attempt is made to pave an engineering path for characterization of structure-dominated sources employing radiators (or extractors). The sources comprising an antenna are not limited by CCR mechanism but may also include undulator with fast or slow-wave structure (e.g., mm-wave Bragg resonator and waveguide), or Cherenkov-FEM combined sources [4]. .

ANTENNA GAIN AND BRIGHTNESS

Unlike unbounded FEL and undulator the radiation pattern from a structure-dominated source is formed by an antenna, whereas the beam serves only as a launcher for the structure. It is convenient to express the power density S and brightness B via the modal antenna directivity D_n or gain G_n [5] assuming nearly normal orientation of the detector with respect to the incident rays:

$$S=\frac{dP_{ff}}{dA}=\frac{1}{4\pi R_d^2}\sum_n G_nP_n,\quad B=\frac{d^2P_{ff}}{dAd\Omega}\approx\frac{1}{4\pi A_A}\sum_n G_nP_n,\qquad(1)$$

where R_d is the distance between the source and the detector (object), $R_d>>W_A$, W_A is the maximum antenna dimension, $R_d>>W_A^2/\lambda$, A_A is the antenna aperture area, $G_n=(1-|\Gamma_n|^2)\eta_nD_n$, $D_n=4\pi P_{ff}^{-1}dP_{ff}/d\Omega$, P_{ff} is the modal power of far-field radiation, $d\Omega$ and dA are the infinitesimal small solid angle and area, and P_n is the modal power on the transition from the slow-wave structure to the antenna having return loss Γ_n and modal efficiency η_n.

The modal energy and power radiated at the structure exit can be calculated analytically [6,7]. For a single microbunch and single mode operation the peak brightness can be calculated as follows:

$$B_{1b}=\frac{G_n}{4\pi A_A}\frac{\omega}{4}\frac{r}{Q}|v_{gr}|\cdot\left(\frac{q\Phi}{1-\beta_{gr}/\beta}\frac{1-\exp(-\alpha L)}{\alpha L}\right)^2,\qquad(2)$$

where $\omega=2\pi f$ is the circular frequency of the resonant Cherenkov radiation $\omega=h(\omega)v$, $h(\omega)$ is the wavenumber defined by the structure dispersion, q is the bunch charge, L is the structure length, $r=E_z^2/(dP/dz)$ is the shunt impedance, $\beta=v/c$, $v_{gr}=\beta_{gr}c$, is the group velocity, Q is the Q-factor, $Q|\beta-\beta_{gr}|>>1$, $\alpha=\pi f/Qv_{gr}$ is the attenuation, and $\Phi=\exp(-(\omega\sigma_t)^2/2)$ is the formfactor for a Gaussian bunch having r.m.s. duration σ_t.

For a long ($t>t_f=L/v_{gr}$) train of coherent microbunches with interval T_b less than the drain time $T_d=L(v_{gr}^{-1}-v^{-1})$ the brightness can be calculated as follows:

$$B_{train}=\frac{G_n}{4\pi A_A}\frac{\omega}{4}\frac{r}{Q}\frac{1}{|v_{gr}|}\left|I\Phi L\frac{1-e^{-\alpha L(1+ia_s)}}{\alpha L(1+ia_s)}\right|^2,\qquad(3)$$

where I the beam current within the train, $a_s=2Q(f/f_b-1)/(1-v_{gr}/v)$ is the generalized detuning, and $f_b=1/T_b$ is the frequency of the microbunched train (or its resonant sub-harmonic).

The spectrum FWHM of the radiation induced by a single microbunch is determined by the inversed radiation pulse length which is equal to the drain time. Therefore the peak spectral brightness for that case is evaluated as:

$$\frac{\Delta B_{1b\_Peak}}{\Delta f}\approx\frac{G_n}{4\pi A_A}\frac{\omega}{4}\frac{r}{Q}\frac{L}{1-\beta_{gr}/\beta}\cdot\left(q\Phi\frac{1-\exp(-\alpha L)}{\alpha L}\right)^2.\qquad(4)$$

For a long (~steady state) coherent train of microbunches the spectral brightness is proportional to the train duration $>t_f$ at $T_b^2<<T_d^2$ and neglecting jitter within the train. In transient mode (i.e. for pulse lengths comparable to the t_f) the spectral brightness under these conditions can be estimated as product of (3) and the filling time t_f.

For some applications an averaged brightness can be more important rather than the peak brightness. For the "single bunch" mode of radiation the averaged brightness

*Work supported by US DoE Contract DE- SC-FOA-0000760
#asmirnov@radiabeam.com.

ISBN: 978-3-95450-168-7 doi:10.18429/JACoW-IPAC2015-TUPMA042

THz RADIATION GENERATION IN A MULTIMODE WAKEFIELD STRUCTURE*

S. Antipov#, C. Jing, S. Baryshev, and A. Kanareykin, Euclid Techlabs LLC, Solon, OH 44139
D. Wang, W. Gai, A. Zholents, Argonne National Laboratory, Argonne, IL 60439
M. Fedurin, Brookhaven National Accelerator Laboratory, Upton, NY 11973

Abstract

A number of methods for producing sub-picosecond beam microbunching have been developed in recent years. A train of these bunches is capable of generating THz radiation via multiple mechanisms like transition, Cherenkov and undulator radiation. We utilize a bunch train with tunable spacing to selectively excite high order $TM_{0,n}$ modes in a multimode structure. In this paper we present experimental results obtained at the Accelerator Test Facility of Brookhaven National Laboratory.

INTRODUCTION

THz radiation production is of great interest in science and industry. There are many approaches to the development of THz sources [1], for example laser driven THz emitters, solid state oscillators (high frequency diodes), quantum cascade laser-based and electron beam driven. In this paper we present a THz source based on wakefield excitation by an electron beam. When electron beam passes through a slow-wave structure (power extractor) it decelerates due to emitting Cherenkov radiation (wakefield). The power extractor can be designed to be tunable and operate at THz frequencies. In this case the beam will generate THz radiation. It is important, however, that the beam spectrum has THz frequency content; a DC current will not be able to excite THz radiation.

In the past decade, many approaches have been investigated to generate THz micro bunches that include: bunch generation from a photoinjector with micro laser pulses produced by birefringent crystals [2]; bunch train with a picosecond separation using an emittance exchanger combined with transverse beam masking and other similar techniques [3, 4]; some bunch compression techniques [5, 6] and a two-step approach based on beam self-wake energy modulation followed by a compression in chicane [7, 8].

Once the bunch train with sub-picosecond spacing (and hence a THz frequency content) had been generated it can be used to generate THz radiation by various mechanisms: transition, Cherenkov, undulator and Smith Purcell radiation. In this paper we report on experimental results of high order mode generation in a multimode dielectric loaded wakefield structure by a sub-picosecond bunch train. In Figure 1 a spectrum of TM_{0n} modes is presented on the left. On the right a spectrum of the bunch train is shown in blue. In a multimode structure bunch train will excite modes that belong to its spectrum hence selecting only one or two modes. This paper is a continuation and improvement of our work reported earlier [9].

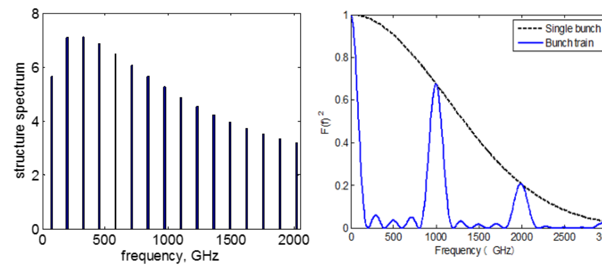

Figure 1: Left: Cherenkov spectrum of the multi-mode wakefield structure. Right: Formfactor of single bunch and bunch train.

EXPERIMENT

The experiment using a tunable bunchtrain was performed at the Accelerator Test Facility at Brookhaven National Laboratory. Figure 2 shows the general experimental layout.

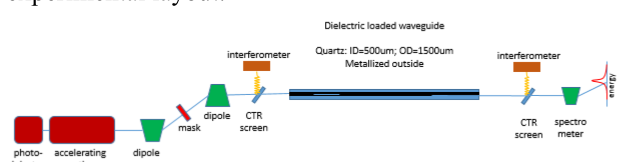

Figure 2: Experiment setup at ATF beamline.

For this experiment, the electron bunch was accelerated off-crest in the linac (to introduce an energy chirp, linear correlation between energy and longitudinal position of the particle) to 60 MeV and sent through a "dogleg" type magnetic achromat with two identical dipole magnets. A beam collimator mask was placed at the high dispersion point between the dipoles where the beam transverse size was dominated by the chirp induced in the linac. Therefore the transverse pattern introduced by the mask appeared in the longitudinal charge density distribution after the achromat. The image of the beam taken directly after the mask and shown in Figure 3 (top) represents the longitudinal beam distribution after the dog leg. The actual distance between these beamlets appearing in the longitudinal direction after the dogleg was measured by the interferometer equipped with a helium-cooled bolometer that received the coherent transition radiation (CTR) signal emitted by the beamlets passing through a thin foil. From these measurements the distance between beamlets was determined and the phosphor screen image after the mask was calibrated. This measurement is

*Work supported by the Department of Energy SBIR program under Contract #DE-SC0009571.
#s.antipov@euclidtechlabs.com

Content from this work may be used under the terms of the CC BY 3.0 licence (© 2015). Any distribution of this work must maintain attribution to the author(s), title of the work, publisher, and DOI.

ISBN: 978-3-95450-168-7 doi:10.18429/JACoW-IPAC2015-TUPMA043

Content from this work may be used under the terms of the CC BY 3.0 licence (© 2015). Any distribution of this work must maintain attribution to the author(s), title of the work, publisher, and DOI.

EXPERIMENTAL TEST OF SEMICONDUCTOR DECHIRPER*

S. Antipov#, C. Jing, S. Baryshev, and A. Kanareykin, Euclid Techlabs LLC, Solon, OH, 44139, USA
S. Stoupin, W. Gai, A. Zholents, Argonne National Laboratory, Argonne, IL, 60439, USA
S. Baturin, LETI, Saint-Petersburg, Russia
M. Fedurin, C. Swinson, Brookhaven National Accelerator Laboratory, Upton, NY, 11973, USA

Abstract

We report the observation of de-chirping of a linearly chirped (in energy) electron bunch by its passage through a 4 inch long rectangular waveguide loaded with two silicon bars 0.25 inch thick and 0.5 inch wide. Silicon being a semiconductor has a conductivity that allows it to drain the charge fast in case if some electrons get intercepted by the dechirper. At the same time the conductivity is low enough for the skin depth to be large (on the order of 1 cm) making the silicon loaded waveguide a slow wave structure supporting wakefields that dechirp the beam.

INTRODUCTION

The free electron laser (FEL) is considered to be the main candidate for a short wavelength (UV to X-ray), short pulse (femto- to attosecond) light source. Demands on the electron beam needed to drive this class of FELs have become more and more challenging, including high repetition rate (~ MHz), high peak current (a few kA), and low emittance (sub-micron normalized emittance) [1].

Short pulses (subpicosecond) are central to many of the next generation light source initiatives that are typical of modern linear accelerators. At the same time, at the output of the last compressor the electron beam will be left with a small chirp to compensate for wakefield effects through the rest of the accelerating stages [2, 3]. Although relatively small, this energy spread needs to be compensated using a specially designed device. The use of a Cherenkov dielectric wakefield compensation scheme ("silencer") to correct the correlated energy distribution (chirp) of a short, low emittance electron bunch was originally suggested in references [4, 5]. This technology using an adjustable dielectric compensating structure can be applied to a soft X-ray FEL SRF linac. We study dielectric loaded accelerating structures as chirp compensating devices. The first dielectric loaded dechirper was demonstrated at Accelerator Test Facility (ATF) of Brookhaven [6]. At the same time a standard iris-loaded structure was proposed as a dechirper for NGLS [8]. We demonstrated a tunable (via aperture size) planar chirp compensating structure that can accommodate various scenarios for beam chirp at the accelerator facility recently [8]. In this paper we present experimental results from Accelerator Test Facility (ATF) of Brookhaven National Laboratory (BNL) where a tunable semiconductor-based dechirper was tested.

*Work supported by the Department of Energy SBIR program under Contract #DE-SC0006299.
#s.antipov@euclidtechlabs.com

TUNABLE CHIRP CORRECTOR

Short bunches with high peak currents in the kA range are desirable for applications like FEL. They are obtained by compression of the energy-chirped beam in a chicane. Compressed beam after chicane carries residual chirp – energy variation along the beam. For successful lasing of the FEL this chirp has to be removed. A passive device, dechirper, was suggested to remove this residual chirp [4, 5]. Nearly every new FEL project entertains the idea of using dechirper for chirp correction.

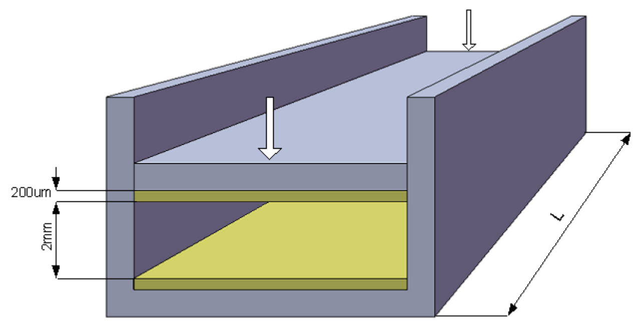

Figure 1: Conceptual design of a tunable dielectric loaded rectangular chirp corrector.

Figure 1 shows a photo and a schematic of a *tunable* dechirper. It is a dielectric loaded waveguide. Alternatively it can be corrugate wall waveguide. High current electron beam passing through such structure generates wakefield (cherenkov radiation). Spectrum of such wakefield is shown on Figure 2. Most importantly there is a wake inside the beam itself: the head decelerates the tail (Figure 3).

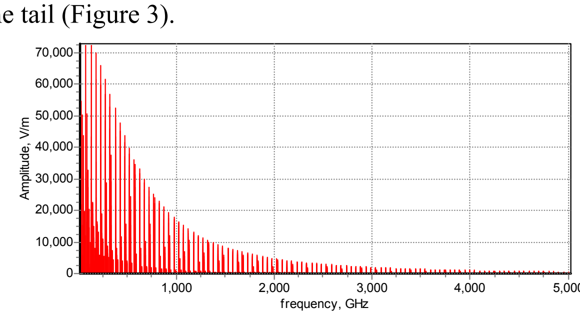

Figure 2: Spectrum of modes excited by the σz = 10 micron gaussian beam (equivalent to the rising edge of the quasi-rectangular beam) inside the 1 mm thick alumina plates, 600 micron gap structure.

ISBN: 978-3-95450-168-7 doi:10.18429/JACoW-IPAC2015-TUPMA047

MULTIPACTING-FREE QUARTER-WAVELENGTH CHOKE JOINT DESIGN FOR BNL SRF *

Wencan Xu[#,1], S. Belomestnykh[1,2], I. Ben-Zvi[1,2], C. Liaw[1], K. Smith[1], R. Than[1], J. Tuozzolo[1], E. Wang[1], D. Weiss[1], A. Zaltsman[1]

[1)] Collider-Accelerator Department, Brookhaven National Lab, Upton, NY 11973, USA
[2)] Physics & Astronomy Department, Stony Brook University, Stony Brook, NY 11794, USA

Abstract

The BNL SRF gun cavity operated well in CW mode up to 2 MV. However, its performance suffered due to multipacting in the quarter-wavelength choke joint. A new multipacting-free cathode stalk was designed and conditioned. This paper describes RF and thermal design of the new cathode stalk and its conditioning results.

INTRODUCTION

The 704 MHz half-cell SRF gun was designed to provide up to 350 mA, 2 MV electron beams for ERL [1] at BNL, which is a R&D project for future RHIC projects: eRHIC [2], Coherent-Electron-Cooling [3], and Low Energy RHIC Electron Cooler [4]. Without a cathode stalk insertion, the SRF gun cavity reached the design voltage of 2 MV in CW mode in horizontal tests. However, strong multipacting in the quarter-wavelength choke-joint occurred during commissioning with a copper cathode stalk. Multipacting in the choke-joint was later understood with simulations [5]. While the beam commissioning was carried out with this cathode stalk and successfully generated first beam in November 2014 [6], a multipacting-free choke joint has been designed, tested and showed that it is truly multipacting-free. This paper discusses multipacting issues observed in the old cathode stalk, and then presents the multipacting-free choke-joint design and test results.

MULTIPACTING IN THE SRF GUN

Figure 1 shows the SRF gun cryomodule. The 704 MHz half-cell SRF cavity is the core part of the module. A quarter-wavelength choke-joint cathode is used to support photo-cathode. A pair of opposing fundamental power couplers (FPCs) is used to deliver up to 1 MW of RF power in CW mode. A high temperature superconducting solenoid (HTSS) is employed to compensate space charge. A room-temperature ferrite HOM damper with ceramic break is used to damp HOM power. Without a cathode stalk insert, the gun cavity was successfully commissioned and reached the design goal of 2 MV in CW mode. However, strong multipacting occurred during commissioning with a copper cathode stalk insert. Figure 2 shows signals during the cathode stalk conditioning, when strong multipacting was observed. The reflected power could be as low as 50% of the forward power when multipacting is active. The main reason for multipacting was distortion of grooves due to BCP and high SEY in the stainless steel area. After spending some time conditioning mutipacting (to suppress it), we were able to operate the gun at 1.9 MV with 18% duty factor. We used this cathode stalk for beam commissioning in pulse mode, while a new multipacting-free cathode stalk was designed.

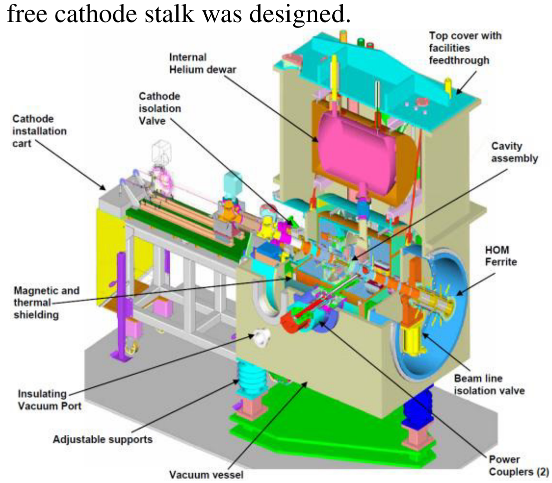

Figure 1: ERL SRF gun cryo-module.

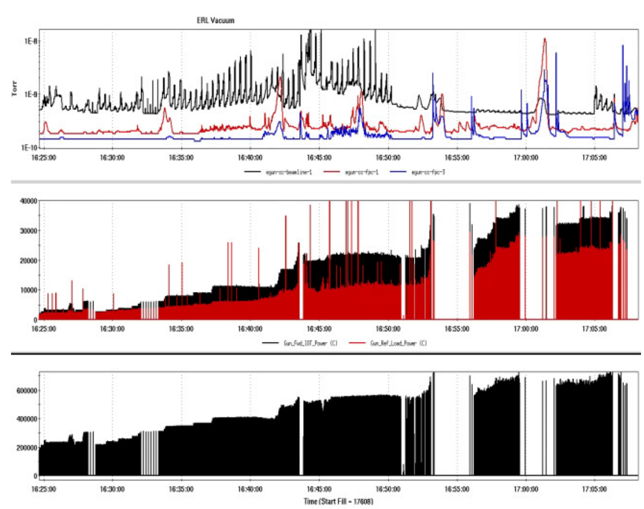

Figure 2: Signature of strong multipacting in the cathode stalk: vacuum behavior (above); reflected and forward power difference due to multipacting (middle); cavity voltage (bottom).

* This work is supported by Brookhaven Science Associates, LLC under Contract No. DE-AC02-98CH10886 with the U.S. DOE.
#wxu@bnl.gov

Content from this work may be used under the terms of the CC BY 3.0 licence (© 2015). Any distribution of this work must maintain attribution to the author(s), title of the work, publisher, and DOI.

ISBN: 978-3-95450-168-7 doi:10.18429/JACoW-IPAC2015-TUPMA048

Content from this work may be used under the terms of the CC BY 3.0 licence (© 2015). Any distribution of this work must maintain attribution to the author(s), title of the work, publisher, and DOI.

EXPERIMENTAL AND SIMULATIONAL RESULT OF MULTIPACTORS IN 112 MHz QWR INJECTOR

T. Xin[#,1,2], I. Ben-Zvi[1,2], S. Belomestnykh[1,2], J. C. Brutus[1], J. Skaritka[1], Q. Wu[1], B. Xiao[1]
[1]Brookhaven National Laboratory, Upton, NY 11973
[2]Stony Brook University, Stony Brook, NY 11794

Abstract

The first RF commissioning of 112 MHz QWR superconducting electron gun was done in late 2014. The coaxial Fundamental Power Coupler (FPC) and Cathode Stalk (stalk) were installed and tested for the first time. During this experiment, we observed several multipacting barriers at different gun voltage levels. The simulation work was done within the same range. The comparison between the experimental observation and the simulational results are presented in this paper. The observations during the test are consisted with the simulation predictions. We were able to overcome most of the multipacting barriers and reach 1.8 MV gun voltage under pulsed mode after several round of conditioning processes.

INTRODUCTION

The CeC PoP system is being installed in the Relativistic Heavy Ion Collider (RHIC) at Brookhaven National Laboratory [1]. The commissioning of 112 MHz QWR superconducting electron injector with the beam pipe coaxial fundamental power coupler (FPC) and choke joint cathode stalk was done in late 2014 and continued into early 2015. During the test we observed mainly three bands of multipacting barriers which correspond to the resonators located in cavity, FPC and cathode stalk, respectively. The observed multipactors consistent with the previously simulated results given by Track3P package.

EXPERIMENT SETUP

The general layout of experiment is showed in Figure 1. The cryomodule of 112 MHz QWR gun was connected with RHIC main Helium loop via a Quiet Helium Source and working at 4.3 K.

Beam pipe coaxial FPC can transmit up to 2 kW RF power and establish 2 MV gun voltage in the cavity. The inner conductor of the FPC is water cooled and the surface of the FPC is gold plated in order to reduce emissivity. The location of the FPC tip was designed to be adjustable within a ±2 cm range for the sake of coupling tuning [2].

The half wavelength cathode stalk was also install for the commissioning. The stalk was designed to create a choke joint between the cathode plane and the cavity nose cone. Special impedance mismatching is utilized so that the RF loss on the surface of the stalk is minimized. The surface of stalk is also gold plated to reduce the static thermal load to the cryosystem.

The design parameters of the injector are shown in Table 1. The cavity is designed to run at 112 MHz in CW mode. The energy gain of electron is 2 MeV and repetition rate is 78 kHz. During this experiment we didn't use the multi-alkali cathode but a dummy molybdenum puck as the placeholder to provide correct RF boundary condition.

Table 1: Design Parameters of the 112 MHz Electron Injector

Parameters	Value
Frequency	112 MHz
Charge per Bunch	1~3 nC
Repetition Rate	78 kHz
Acceleration Voltage	1~2 MV
Cavity Q_0	1.8e8
R/Q	122 Ω

Experimental Results

Several multipacting barriers were observed during the commissioning of the injector. We've already seen the 50 kV barrier in the previous experiment with this cavity [3]. The new structures in this experiment are the FPC and cathode stalk. Both of them are coaxial structures hence are vulnerable to multipacting. As the matter of fact, we observed three most persistent barriers while ramping up the cavity voltage. The first one was found near 50 kV, which we knew is located in the cavity. The second and third relatively strong barriers were encountered when gap voltage was in the range of 100 kV to 200 kV and 600 kV to 800 kV respectively. Since the field strength in the FPC gap is much stronger than that of the cathode stalk, we believe the former multipactor is located in the FPC and the latter one in the cathode stalk. This expectation is further confirmed by simulation results given by the SLAC Track3P package and will be discussed in more detail in the next section.

After several rounds of conditioning, most of the multipacting barriers were overcame and the cavity can now reach 1.8 MV gun voltage in pulsed mode and 1.3 MV in CW mode. The CW mode voltage is limited by field emission. Further condition process is undergoing.

* This work was carried out at Brookhaven Science Associates, LLC under Contracts No. DE-AC02-98CH10886 and at Stony Brook University under grant DE-SC0005713 with the U.S. DOE.
#txin@bnl.gov

ISBN: 978-3-95450-168-7 doi:10.18429/JACoW-IPAC2015-TUPMA049

FIRST BEAM COMMISSIONING AT BNL ERL SRF GUN*

Wencan Xu[#,1], Z. Altinbas[1], S. Belomestnykh[1,2], I. Ben-Zvi[1,2],S. Deonarine[1], L. DeSanto[1], D. Gassner[1], R. C. Gupta[1],H. Hahn[1], L. Hammons[1], Chung Ho[1], J. Jamilkowski[1], P. Kankiya[1], D. Kayran[1], R. Kellerman[1], N. Laloudakis[1], R. Lambiase[1], C. Liaw[1], V. Litvinenko[1,2], G. Mahler[1], L. Masi[1], G. McIntyre[1], T. Miller[1], D. Phillips[1], V. Ptitsyn[1], T. Seda[1], B. Sheehy[1], K. Smith[1], T. Rao[1], A. Steszyn[1], T. Tallerico[1], R. Than[1], J. Tuozzolo[1], E. Wang[1], D. Weiss[1], M. Wilinski[1], A. Zaltsman[1]

[1)] Collider-Accelerator Department, Brookhaven National Lab, Upton, NY 11973, USA
[2)] Physics & Astronomy Department, Stony Brook University, Stony Brook, NY 11794, USA

Abstract

The 704 MHz SRF gun successfully generated the first photoemission beam in November of 2014. The configurations of the test and the sub-systems are described. The latest results of SRF commissioning, including the cavity performance, cathode QE measurements, beam current/energy measurements, are presented in the paper.

INTRODUCTION

The R&D ERL [1] at BNL is an electron accelerator designed for high average current, up to 350 mA. It serves as a test bed for future RHIC projects, such as eRHIC [2], Coherent-Electron-Cooling [3], and Low Energy RHIC Electron Cooler [4]. The 704 MHz half-cell SRF gun is designed to provide 0.5 A, 2 MeV electron beam. Commissioning of the SRF gun is being carried out in stages: without a cathode stalk (finished in early 2013), with a copper cathode stalk (finished in fall of 2013), and beam commissioning (started in mid-2014) [5, 6, 7]. The 704 MHz half-cell SRF gun has successfully generated electron beams in November of 2014. This paper discusses the first beam test results.

BEAM COMMISSIONING LAYOUT

Following the step-by-step commissioning plan, the first beam commissioning of the SRF gun was done with a straight beam line ending up at a faraday cup, instead of going through a Zig-Zag, a merging scheme for the high- and low-energy beams consisting of dipole magnets bending in the vertical plane designed to minimize emittance growth [8]. The beam line configuration is shown in Figure 1. The Cs_3Sb photocathode [6, 7] was deposited on the cathode stalk with copper substrate (a new cathode stalk will use Ta substrate) in the cathode deposition system located outside the ERL blockhouse. Then, the cathode stalk was moved to the ERL blockhouse inside a cathode transport cart and inserted into the SRF gun. A load-locked system is used for the connection between the SRF gun and the cathode transport cart. Following the 704 MHz half-cell SRF cavity, there is a high temperature superconducting solenoid (HTSS), a room-temperature HOM absorber (Now, instead of the absorber, a room temperature solenoid was installed there for better beam quality), a laser cross, an Integrated Current transformer (ICT), a Beam Position Monitor (BPM), a vertical and horizontal beam corrector, a beam halo monitor, a pepper pot beam emittance measurement, a beam profile monitor and a Faraday cup. The dipole magnet for bending electron beams to the Zig-Zag is locked out for the first beam tests.

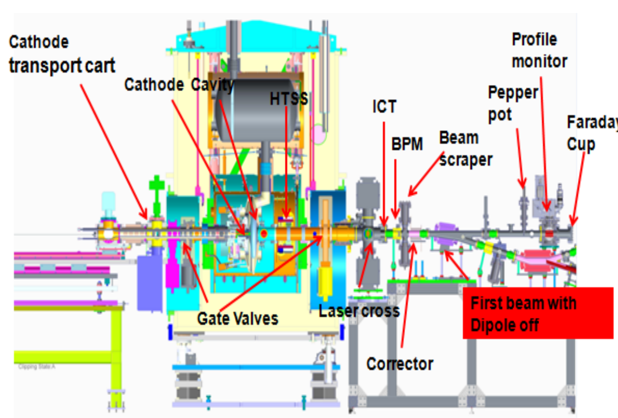

Figure 1: First beam commissioning configuration.

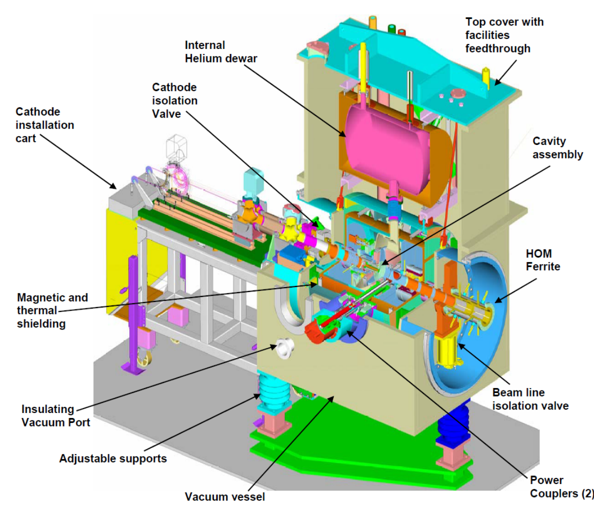

Figure 2: SRF gun cryomodule.

* This work is supported by Brookhaven Science Associates, LLC under Contract No. DE-AC02-98CH10886 with the U.S. DOE.
#wxu@bnl.gov

Content from this work may be used under the terms of the CC BY 3.0 licence (© 2015). Any distribution of this work must maintain attribution to the author(s), title of the work, publisher, and DOI.

ISBN: 978-3-95450-168-7 doi:10.18429/JACoW-IPAC2015-TUPMA050

Content from this work may be used under the terms of the CC BY 3.0 licence (© 2015). Any distribution of this work must maintain attribution to the author(s), title of the work, publisher, and DOI.

NSLS-II INJECTOR COMMISSIONING AND INITIAL OPERATION*

B. Bacha, G. Bassi, J. Bengtsson, A. Blednykh, E. Blum , S. Buda, W. Cheng, J. Choi, J. Cuppolo, R. D'Alsace, M. Davidsaver, J. DeLong, L. Doom, D. Durfee, R. Fliller, M. Fulkerson, G. Ganetis, F. Gao, C. Gardner, W. Guo, R. Heese, Y. Hidaka, Y. Hu, M. Johanson, B. Kosciuk, S. Kowalski, S. Kramer, S. Krinsky, Y. Li, W. Louie, M. Maggipinto, P. Marino, J. Mead, G. Oliva, D. Padrazo, K. Pedersen, B. Podobedov, R. Rainer, J. Rose, M. Santana, S. Seletskiy, T. Shaftan, O. Singh, P. Singh, V. Smalyuk, R. Smith, T. Summers, J. Tagger, Y. Tian, W. Wahl, G. Wang, G. Weiner, F. Willeke, L. Yang, X. Yang, E. Zeitler, E. Zitvogel, P. Zuhoski, National Synchrotron Light Source II, Brookhaven National Laboratory, Upton, NY 11793, USA
A. Akimov, P. Cheblakov, I. Churkin, A. Derbenev, S. Gurov, V. Kiselev, A. Korepanov, S. Sinyatkin, A. Zhuravlev, Budker Institute of Nuclear Physics, Novosibirsk, Russia

Abstract

The injector for the National Synchrotron Light Source II (NSLS-II) storage ring consists of a 3 GeV booster synchrotron and a 200 MeV S-band linac. The linac was designed to produce either a single bunch with a charge of 0.5 nC of electrons or a train of bunches up to 300 ns long containing a total charge of 15 nC. The booster was designed to accelerate up to 15 nC each cycle in a train of bunches up to 300 ns long. Linac commissioning was completed in April 2012. Booster commissioning was started in November 2013 and completed in March 2014. All of the significant design goals were satisfied including beam emittance, energy spread, and transport efficiency. While the maximum booster charge accelerated was only 10 nC this has proven to be more than sufficient for storage ring commissioning and operation. The injector has operated reliably during storage ring operation since then. Results will be presented showing measurements of linac and booster operating parameters achieved during commissioning and initial operation. Operating experience and reliability during the first year of NSLS-II operation will be discussed.

INTRODUCTION

The NSLS-II is a third generation electron storage ring at Brookhaven National Laboratory [1]. It was commissioned in 2014 and began user operations in February, 2015. The NSLS-II injector consists of a 3 GeV booster synchrotron, a 200 MeV S-band linac, the associated transport lines, and the storage ring injection straight (Fig. 1). The linac is capable of producing either a single bunch of up to 0.5 nC of charge or a train of bunches up to 300 nS long containing a total charge of 15 nC. The linac was commissioned in 2012 and met all of its design specifications with one exception: only 11 nC was accelerated in multibunch mode instead of the 15 nC specified [2]. Since then up to 13 nC has been accelerated within the specified 0.5% energy spread.

The 3 GeV booster is a 158.4 m circumference synchrotron developed jointly by Brookhaven National Laboratory (BNL) and the Budker Institute of Nuclear Physics (BINP) [3, 4]. Danfysik developed the dipole power supplies as a subcontractor on the booster project. The booster has a four-fold symmetric design lattice using combined function magnets to create a FODO-like lattice in each quadrant with matching quadrupole triplets at both ends of each quadrant [5]. The RF system uses a 7 cell PETRA type 500 MHz cavity. The booster operates at a 1 Hz repetition rate but was designed to be upgraded to 2 Hz. Booster commissioning was completed in March 2014 and has delivered electrons to the NSLS-II storage ring since then.

The storage ring injection straight contains 4 half-sine 8.5 mrad kicker magnets. Each kicker is excited by an IGBT pulser with 10 series stages of 20 parallel IGBTs per stage. The kicker magnets and pulsers were built at BNL. The kickers produce a 5.4 μsec pulse which is slightly longer than twice the 2.6 μsec revolution time of the storage ring. This has not been a problem so far but the pulse width can easily be reduced by using smaller pulse capacitors. The system was designed to pulse at 10 kV but only 7.9 kV is required for operation. Amplitude stability σ<0.015% was demonstrated over 24 hours of operation in the pulsed magnet laboratory in a non temperature controlled environment.

An out-of-vacuum, 150 μsec, 100 mrad septum from Danfysik is used for storage ring injection. The system has demonstrated an amplitude stability <0.1%, time jitter <10 ns, and leakage field <8 μT-m.

BOOSTER COMMISSIONING RESULTS

Booster commissioning was started in late November 2013 and completed by March 2014. All major design goals for the booster were met except that the maximum charge accelerated in multibunch mode (MBM) was only 10 nC compared to a design goal of 15 nC. Since <3 nC per cycle from the booster has been required for the first year of storage ring commissioning and operation it was decided not to spend additional time increasing the

*This manuscript has been authored by Brookhaven Science Associates, LLC under Contract No. DE-SC0012704 with the U.S. Department of Energy.
#blum@bnl.gov

ISBN: 978-3-95450-168-7 doi:10.18429/JACoW-IPAC2015-TUPMA052

NSLS-II RADIO FREQUENCY SYSTEMS *

J. Rose†, F. Gao, A. Goel, B. Holub, J. Kulpin, C. Marques, M. Yeddulla
NSLS-II, BNL, Upton, NY 11973, USA

Abstract

The National Synchrotron Light Source II is a 3 GeV X-ray user facility commissioned in 2014. The NSLS-II RF system consists of the master oscillator, digital low level RF controllers, linac, booster and storage ring RF sub-systems, as well as a supporting cryogenic system. Here we will report on RF commissioning and early operation experience of the system.

INTRODUCTION

The NSLS-II radio frequency system was designed as a whole from the master oscillator, its distribution to subsystems, from digital field controllers to high power amplifiers driving normal and superconducting cavities. The RF drives the grid of the planar triode in the DC electron gun creating the electrons that are bunched and accelerate to 200 MeV in the 2.998 GHz linac, are captured and accelerated in the 499.68 MHz bucket of the booster RF and accelerated to 3 GeV. The 3 GeV electrons extracted from the booster are injected into the RF buckets of the superconducting cavities in the storage ring where they are accumulated up to 500 mA. This paper describes these systems.

MASTER OSCILLATOR

The master oscillator is the reference frequency for the RF systems as well as the master clock for the timing system. Because it is the ultimate source of amplitude and phase noise imposed on the beam through the RF cavity field, specifications from x-ray beam line requirements were derived [1]. These are given in Table 1.

Table 1: Longitudinal Beam Stability Requirements

	Phase Jitter Δθ [°]	**Momentum Jitter Δp/p [%]**
Timing-dependent experiments	0.14	0.005
Vertical divergence (from momentum jitter)	2.4	0.09
10% increase in σ_s due to filamentation	1.8	0.065
Vertical centroid jitter	0.82	0.03

In order to meet the demands of timing experiments we took the timing dependent experiments requirements of 0.14 degrees phase jitter and 0.005 % momentum jitter as the requirement for the RF system. The master oscillator must contribute no more than a fraction of this. We chose an Agilent E8257D synthesized signal generator with low phase noise options. Frequency agility is required for a number of applications, including measurement of chromaticity, measurement of dispersion and compensation of orbit length due to wavelength shifters. Of these, chromaticity measurements are the most demanding. With the parameters of the NSLS II baseline design ($\alpha = 3.68\ 10^{-4}$, $\gamma = 5871$, $f_{rf} = 500$ MHz) and the assumption that the tune change $\Delta\nu_{x,y}$ should be at least 3 times the tune spread $\sigma\ \nu_{x,y}$ to get good resolution for the tune measurement when measuring small chromaticity's down to $\xi_{x,y} = 0.1$, and an educated guess for the tune spread of $5.\ 10^{-3}$ in both transverse planes, we obtain $\Delta f_{rf} = -\ \alpha\ 3\sigma\ \nu_{x,y}\ f_{rf} / 0.1 \approx \pm 29$ kHz

The generator allows for software commanded phase continuous frequency modulation which will be used for the above measurements as well as in a slow frequency or "radial" loop to make corrections for small changes in electron beam orbit caused by seasonal or diurnal temperature variations in ring circumference. The MO output is amplified and split to be distributed to the storage ring RF cavity field controllers, injector RF systems, the timing system, a streak camera and the bunch by bunch feedback system.

DIGITAL CAVITY FIELD CONTROLLER

The starting point for the NSLS-II cavity field controller was the architecture of the SNS controller designed by Doolittle et al [2]. This architecture utilizes up/down conversion from RF to the 50 MHz IF frequency using LO and AD/DA clocks derived from the Master Oscillator frequency, which is also the synchrotron ring RF frequency. New hardware was designed [3] for the NSLS-II RF frequency of 499.68 MHz. The most significant improvement was in the development of new firmware to provide new capability necessary for the operation of a synchrotron. Given the number, types and variety of cavities that they are to control, modular FPGA code and conditional compilation was used. For example, instantiation of feedback, interlock components and ramp generators are conditional depending on the needs of the RF system towards which the build is targeted.

Storage Ring Compilation

The Storage Ring compilation contains the feedback logic with set-point generation and feedback gain control. It also contains a ramp down block which when triggered by an external interlock ramps the fixed field set point to zero in a 1ms timescale. This prevents tripping the transmitter on reverse power as would happen should the RF drop out in microseconds.

* Work supported by DOE contract DE-SC0012704
† rose@bnl.gov l.gov

Content from this work may be used under the terms of the CC BY 3.0 licence (© 2015). Any distribution of this work must maintain attribution to the author(s), title of the work, publisher, and DOI.

ISBN: 978-3-95450-168-7 doi:10.18429/JACoW-IPAC2015-TUPMA053

EXPERIENCE WITH FIRST TURNS COMMISSIONING IN NSLS-II STORAGE RING

S. Seletskiy#, G. Bassi, J. Bengtsson, A. Blednykh, E. Blum, W. Cheng, J. Choi, R. Fliller, W. Guo, R. Heese, Y. Hidaka, S. Kramer, Y. Li, B. Podobedov, T. Shaftan, G. Wang, F. Willeke, L. Yang, X. Yang, BNL, Upton, NY 11973, USA

Abstract

In this paper we describe our experience with commissioning of the first turns in the NSLS-II storage ring. We discuss the problems that we encountered and show how applying a dedicated first turns commissioning software allowed us to diagnose and resolve these problems.

INTRODUCTION

The first phase of the NSLS-II Storage Ring (SR) commissioning [1-3] took place in the spring of 2014. As a result of the first phase the routine injection efficiency of better than 90% was achieved. The beam was successfully accumulated up to 25 mA. One of the main challenges in establishing the beam in the SR was obtaining first few turns.

Below we describe our experience with obtaining first few turns and eventually a spiralling beam in the NSLS-II Storage Ring.

SR DESCRIPTION

The 3 GeV Storage Ring [4] consists of 15 short straight (low-β) and 15 long straight (high-β) sections. It contains 30 double bend achromats (DBA). The SR lattice is shown in Fig. 1.

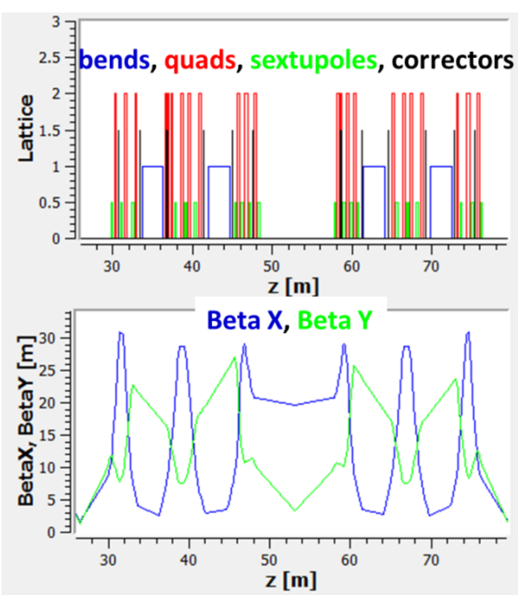

Figure 1: NSLS-II Storage Ring lattice.

Injection into the SR is performed with the aid of the DC and pulsed injection septa and four fast kickers forming a closed bump [5]. The injected beam exits the pulsed septum parallel to and with -24.5 mm displacement from the central axis of the injection straight section. In design injection scheme the stored beam is moved in the injection region towards the injected beam and returned back on axis at the exit of the fourth kicker. The injected beam has residual betatron oscillations of about 10 mm at the exit of injection section. Schematic of injection section (IS) is shown in Fig 2.

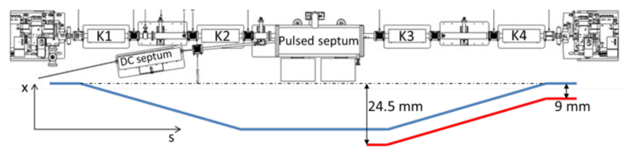

Figure 2: SR injection section and designed injection scheme (red colour represents injected beam, blue colour represents stored beam).

FIRST TURNS AND ON-AXIS INJECTION

The initial SR lattice was set to the design values. All SR sextupoles were set to zero current for the first turn commissioning. For the safety reasons the beam charge during initial commissioning was kept below 1 nC and injection rate was 0.3 Hz.

We decided to perform initial injection in the SR on axis, i.e. to minimize the betatron oscillations of injected beam. To achieve on-axis injection we applied horizontal -11 mm DC bump, which was created with the aid of regular beam trajectory correctors, on top of the AC bump in the injection straight. An example of such symmetric DC bump is shown in Fig. 3.

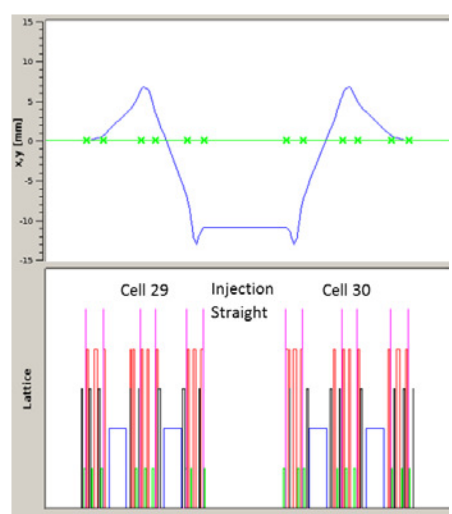

Figure 3: Horizontal DC bump in injection straight section.

#seletskiy@bnl.gov

Content from this work may be used under the terms of the CC BY 3.0 licence (© 2015). Any distribution of this work must maintain attribution to the author(s), title of the work, publisher, and DOI.

ISBN: 978-3-95450-168-7 doi:10.18429/JACoW-IPAC2015-TUPMA054

HIGH LEVEL APPLICATION FOR FIRST TURNS COMMISSIONING IN NSLS-II STORAGE RING

S. Seletskiy#, A. Blednykh, J. Choi, Y. Hidaka, B. Podobedov, G. Shen, L. Yang
BNL, Upton, NY 11973, USA

Abstract

The typical problems occurring during commissioning of the first turns in the storage rings include shorted coils or reversed polarity of the magnets, cross-cabling of magnet power supplies and reversed polarity of BPMs. In this paper we describe a dedicated high level control application, which was created and utilized for commissioning of the first turns in the NSLS-II storage ring.

INTRODUCTION

Years of experience in commissioning of storage rings (SR) show that obtaining first few turns commonly is one of the main challenges in establishing the beam in the SR. A typical storage ring is a complicated system consisting of hundreds (if not thousands) of devices. While it has been a routine practice to perform thorough integration tests prior to attempting the first injection into the ring, various hardware problems during SR commissioning with the beam are nonetheless rather common. Such problems usually hinder obtaining the first turns in the SR and result in significant loss of time.

Examples of the problems faced by various synchrotron facilities during commissioning the first turns in the storage rings include magnets with reverse polarities [1,2], cross-cabling of magnet power supplies [1], shorted magnet coil [3], obstruction of physical aperture in the SR [2,3], wrong polarity of beam position monitors (BPMs) [2] and mismatch between pulsed magnets waveforms [4,5].

Below we describe dedicated First Turn Analysis (FTA) software that was created with the goal of quickly finding possible problems described above. The FTA was successfully used for commissioning of the first turns in NSLS-II storage ring and proved to be a valuable tool [6].

GENERAL IDEA

The general idea of the First Turns Analysis tool was inspired by OPTIM [7]. Our goal is to combine interactive simulations of beam trajectory with live online measurements of beam position monitors. By interactive simulations we mean that when any parameter of the accelerator model is changed in the interactive GUI the user immediately sees the updated results on respective plots.

By updating the model simultaneously with the settings of the actual magnets and by plotting together the resulting beam trajectories predicted by the model and the live BPM readings one can obtain a rather powerful tool for analysis of the beam dynamics. Indeed, from comparing the simulated and the real trajectories one can easily deduce the source of their digression. The wrong polarity of the magnets can be quickly detected from trajectory response to the change in magnet settings. The same is true for cross-cabled magnets. As for the shorted magnet coils, the comparison of simulated and real differential trajectories shall be enough for their detection.

The beauty of this approach is that it does not require any additional off-line analysis. Any accelerator physicist equipped with such software shall be able to quickly pin-point the origin of the problem.

CODE DEVELOPMENT

As many other NSLS-II software applications [8] our code is written in Python [9]. For communications with the BPMs and magnet power supplies we rely on APHLA [10] – Python middle layer developed specifically for NSLS-II.

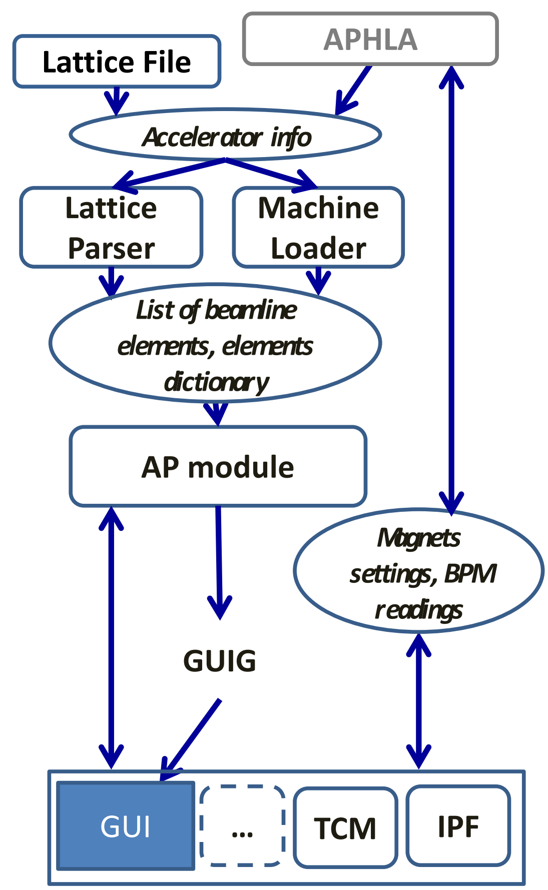

Figure 1: General overview of the FTA software architecture.

We took a modular approach to the design of the FTA code. Its most important modules include: the Accelerator

#seletskiy@bnl.gov

Content from this work may be used under the terms of the CC BY 3.0 licence (© 2015). Any distribution of this work must maintain attribution to the author(s), title of the work, publisher, and DOI.

ISBN: 978-3-95450-168-7 doi:10.18429/JACoW-IPAC2015-TUPMA055

Content from this work may be used under the terms of the CC BY 3.0 licence (© 2015). Any distribution of this work must maintain attribution to the author(s), title of the work, publisher, and DOI.

ANALYSIS OF POSSIBLE BEAM LOSSES IN THE NSLS II STORAGE RING

Y. Li, S. Seletskiy#, W. Guo, R. Fliller, S. Kramer, B. Podobedov, T. Shaftan, B. Wahl, F. Willeke, BNL, Upton, NY 11973, USA

Abstract

The NSLS-II accelerators are installed within radiation shielding walls that are designed to attenuate the radiation generated from an assumed beam loss power to a level of <0.5mrem/h at the outer surface of the bulk shield walls. Any operational losses greater than specified level are expected to be addressed by installing supplemental shielding near the loss point in order to attenuate the radiation outside the shield wall to the design level. In this paper we report the analysis of the electron beam missteering in the NSLS-II Storage Ring for the determination of supplementary shielding.

INTRODUCTION

The missteering (caused by operator's mistake or by a magnet failure) of the electron beam freshly injected into NSLS-II Storage Ring (SR) [1] can result in unacceptable radiation levels on experimental floor. Design of respective radiation protection shielding [2] relies on detailed analysis of physically possible steering errors. In this paper the potential angles and offsets of the missteered beam are calculated by implementing the cascaded parameter scan (CPS) [3]. This method was originally developed for the top-off safety analysis, was realized in a parallel python code and benchmarked with other top-off safety simulators developed in SLAC and LBNL. The results of the studies were double-checked with independent simulations using simplified magnets fields profiles and a smaller number of tracked beam particles (explained below). The detailed description of the analysis results is given in [4].

SR DESCRIPTION

Figure 1 schematically shows the lattice of NSLS-II Storage Ring. The SR lattice contains 30 double bend achromats (DBA). There are 15 short straight (low-β) and 15 long straight (high-β) sections.

The storage ring is designed to accept 3GeV electron bunches from the Booster. An interlock in the Booster to Storage Ring transport line [7] constrains the injected beam energy within a window of 2 - 3.15GeV.

Our analysis is based on particle tracking, which is performed by solving a set of ordinary differential equations describing electron motion in magnetic field. The magnets field profiles are obtained from their 3D models. To simplify the calculation while keeping the adequate accuracy [5, 6] we use 1D transverse profiles for quadrupoles and sextupoles and 2D profile for dipoles in the horizontal middle plane. Figure 2 shows magnetic fields used in the simulations.

The dipole power supply current and voltage are interlocked within 2% window. Each dipole has a back-leg winding, which can contribute ≤ 3% field variation. The total possible dipole field range scanned was chosen as ±5% around its nominal setting.

The range for the other SR magnets was set by the maximum current of their power supplies and their possible magnetic fields, as listed in [4].

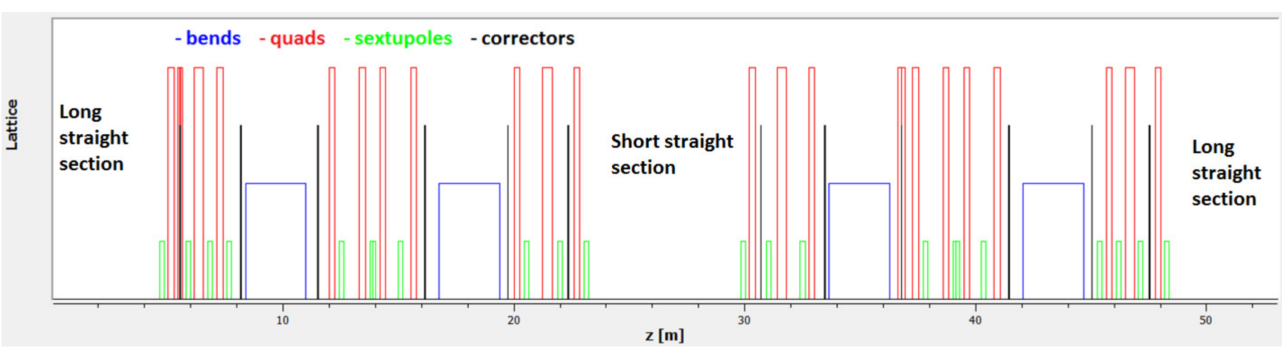

Figure 1: NSLS-II SR lattice.

BEAM STEERING ANALYSIS

The CPS utilizes the following beam tracking algorithm. We start with the phase space of beam trajectories defined by the geometric acceptance of the long straight section. Such phase space area covers all possible incident beam trajectories.

Next, we track trajectories within the phase space through the first beamline element varying its field and the beam energy over their full range. We record each beam trajectory's coordinates in phase space after it passes the magnet and find the maximum angle and position of trajectories not intercepted by the magnet yoke. Then we discard the trajectories that were lost on the vacuum chamber and the surviving trajectories define a phase space volume. This phase space was used to

#seletskiy@bnl.gov

6th International Particle Accelerator Conference IPAC2015, Richmond, VA, USA JACoW Publishing
ISBN: 978-3-95450-168-7 doi:10.18429/JACoW-IPAC2015-TUPMA056

ANALYSIS OF POSSIBLE BEAM LOSSES IN THE NSLS II BSR TRANSFER LINE

S. Seletskiy#, R. Fliller, W. Guo, S. Kramer, Y. Li, B. Podobedov, T. Shaftan, B. Wahl, F. Willeke,
BNL, Upton, NY 11973, USA

Abstract

The NSLS-II accelerators are installed within 0.8 – 1 m thick radiation shielding walls. The safety considerations require attenuating the radiation generated from possible electron beam losses to a level of <0.5mrem/h at the outer surface of the bulk shield walls. Any operational losses greater than specified level shall be addressed by installing supplemental shielding near the loss point. In this paper we discuss simulation studies that identified potential beam loss locations. Results of these studies were used for identification of imposed radiation risks and for specification of the supplemental shielding design necessary to mitigate those risks.

INTRODUCTION

The NSLS-II accelerator complex [1] consists of 200 MeV linac, the Booster accelerating beam to 3 GeV, the 3 GeV Storage Ring (SR) and the two transfer beamlines – Linac to Booster transfer line and Booster to Storage Ring (BSR) transfer line. Missteering of the e-beam that can be caused by operator's mistake or by magnet failure can result in unacceptable radiation levels on experimental floor. Design of personnel radiation protection shielding [2] at NSLS-II relies on detailed analysis of physically possible steering errors in various parts of accelerator. In this paper we describe such analysis for the Booster to Storage Ring transfer line. An inventorial description of the beam steering considerations in the BSR and of their effect on radiation safety can be found in [3].

BEAMLINE DESCRIPTION

Below we consider three beamlines (Fig. 1): the Booster extraction section (ES), the Booster to Storage Ring transfer line phase 1 (BSR-P1) and the BSR transfer line phase 2 (BSR-P2).

The Booster ES consists of four slow bumps forming local closed 4-bump BU1, BU2, BU3 and BU4, four fast kickers K1, K2, K3 and K4, pulsed septum magnet SP1 and a DC septum magnet SP2. These magnets are utilized for the extraction of the beam from the Booster into the BSR line. All four bumps (B1-4) are powered in series. Pairs of kickers K1-2 and K3-4 are powered in series as well.

The BSR-P1 line consists of five quadrupoles (Q1, Q2, Q3, Q1BD and Q2BD) and one bending magnet (B1). These magnets transport beam to the beam dump when bending magnet B2 is turned off.

The BSR-P2 includes Q1-Q3 and B1 as well as quadrupoles Q4-Q14 and bends B2-B4. These magnets transport beam to the Storage Ring. Injection into the Storage Ring is performed with SP3 and IS, which are the DC and pulsed SR injection septa respectively. The SR injection region is analysed for in [4, 5].

Detailed description of each of the BTS beamlines elements is given in [3].

BEAM STEERING ANALYSIS IN ES

Although the ES magnets are supposed to be used only at extraction energy of 3 GeV technically they can fire at any point of Booster ramp. Since these magnets are powered in series there are three scenarios to consider: either kickers K1 and K2 fire, or K3 and K4 fire, or four bumps BU1-4 fire. With the approach to the analysis described farther in this paper and under provision that bumps BU2-4 are treated independently from bump BU1 (see below) the three described scenarios cover all possible local beam losses that can happen under any feasible ES settings.

a.)

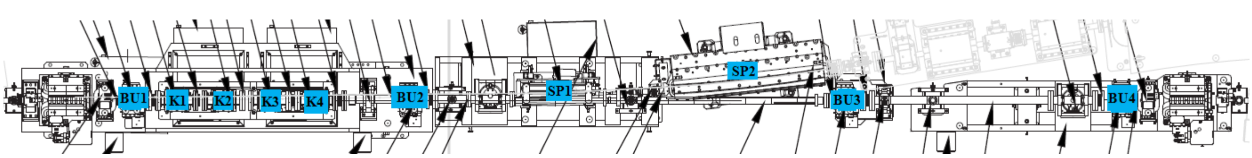

b.)

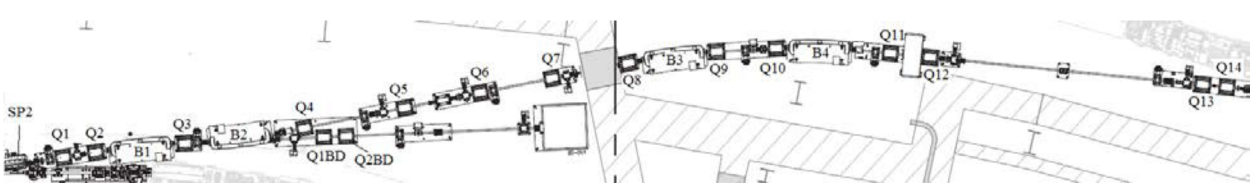

Figure 1: The Booster extraction section (a) and the Booster to storage ring transfer lines phase 1 and phase 2 (b).

#seletskiy@bnl.gov

Content from this work may be used under the terms of the CC BY 3.0 licence (© 2015). Any distribution of this work must maintain attribution to the author(s), title of the work, publisher, and DOI.

ISBN: 978-3-95450-168-7 doi:10.18429/JACoW-IPAC2015-TUPMA057

Content from this work may be used under the terms of the CC BY 3.0 licence (© 2015). Any distribution of this work must maintain attribution to the author(s), title of the work, publisher, and DOI.

COMMISSIONING OF ACTIVE INTERLOCK SYSTEM FOR NSLS II STORAGE RING

S. Seletskiy#, C. Amundsen, J. Choi, J. De Long, K. Ha, C. Hetzel, H. Hseuh, Y. Hu, P. Ilinski, S. Kramer, Y. Li, M. Maggipinto, J. Mead, D. Padrazo, T. Shaftan, G. Shen, O. Singh, R. Smith, W. Wahl, G. Wang, F. Willeke, L. Yang, BNL, Upton, NY 11973, USA

Abstract

The NSLS-II storage ring is protected from possible damage from insertion devices (IDs) synchrotron radiation by a dedicated active interlock system (AIS). It monitors electron beam position and angle and triggers beam dump if beam orbit exceeds the boundaries of pre-calculated active interlock envelope. In this paper we describe functional details of the AIS and discuss our experience with commissioning of the AIS for the first eight IDs installed in the storage ring.

INTRODUCTION

The final phase of the NSLS-II Storage Ring (SR) commissioning [1-3] took place in the fall of 2014. This phase included commissioning of first eight insertion devices (three damping wigglers (DW), one elliptically polarized and four planar in-vacuum undulators) and raising stored beam current to 50 mA. The final SR commissioning phase also included commissioning of the six beamlines (two of three DWs do not have beamlines) and of respective beamline frontends (FE).

One of the most important tasks for this phase was commissioning of the ID active interlock (AI), which protects the SR and the FEs components from possible damage from ID synchrotron radiation (IDSR).

There is another part of the AIS, which protects the SR from bending magnets synchrotron radiation. This part of the system is not discussed in this paper.

Below we describe our experience with the AI commissioning.

AIS DESCRIPTION

The active interlock is designed [4] to continuously monitor beam orbit in IDs and to drop the beam in case it exits predefined AI envelope (AIE) [5]. Typical AIE is an xx' or yy' phase space rectangle of +/-0.5 mm and +/-0.25 mrad. Fig. 1 schematically shows signals that the AI is monitoring for each ID.

The AIS calculates beam angle and deflection at the center of the drift between two neighbouring beam position monitors (BPMs) [6] from respective BPMs readings (10 kHz data). The beam current readings are obtained from the storage ring DCCT. In case of canted IDs the current of the canting magnets, which create a local bump on the beam orbit, are monitored by the AI as well.

The statuses of the bending magnet photon shutter (BMPS) and the frontend photon shutter, a.k.a. ID photon shutter (IDPS), are also monitored by the AI.

When the e-beam is not interlocked the BMPS and the IDPS protect the FE and the beamline from bending magnet synchrotron radiation and from IDSR respectively.

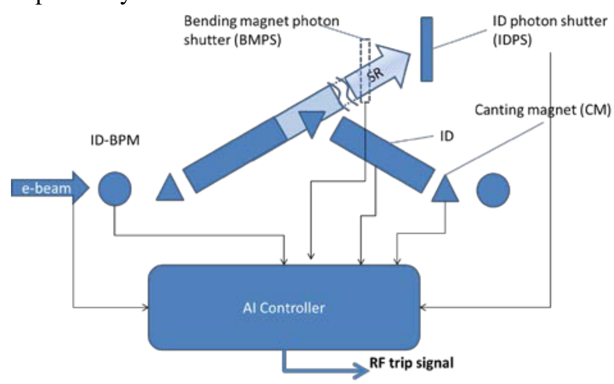

Figure 1: Schematic of signals from various hardware to the AIS. Here we show the canted IDs for the purpose of generality.

The overall structure of active interlock system is schematically shown in Fig. 2.

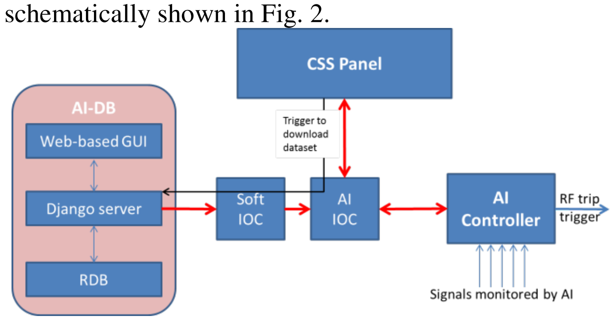

Figure 2: Schematics of the Active Interlock System.

The main functional block of the AIS is the AI controller (AIC). It performs the monitoring of various hardware signals and "makes a decision" on whether the beam shall be dumped. The beam dump is realized by tripping low level RF. The FPGA was chosen for AIC to minimize the response time of the AIS.

The information about AIE for each ID and about respective BPMs is downloaded to the AIC from the AI database (AI-DB). The AI-DB runs on Django server [7] with underlying MySQL relational database and a web-based GUI.

The GUI for the AIS is realized in Control System Studio (CSS) [8] as a standard CSS panel.

The logic of the AIC is shown in Fig. 3.

The logic gates encircled by the green line are responsible for engaging the active interlock. It is getting engaged either when the beam current is above 0.2 mA

#seletskiy@bnl.gov

ISBN: 978-3-95450-168-7 doi:10.18429/JACoW-IPAC2015-TUPHA003

SPUTTER GROWTH OF ALKALI ANTIMONIDE PHOTOCATHODES: AN IN OPERANDO MATERIALS ANALYSIS*

J. Smedley[#], M. Gaowei, J. Sinsheimer, K. Attenkofer, J. Walsh, Brookhaven National Laboratory, Upton, NY, 11973, USA
S. Schubert, J. Wong, H. Padmore, Lawrence Berkeley National Laboratory, Berkeley, CA, 94720, USA
J. Kuhn, Helmholtz-Zentrum Berlin, Berlin, 12489, Germany
E. Muller, Z. Ding, Stony Brook University, Stony Brook, NY, 11794, USA
H. Frisch, University of Chicago, Chicago, IL, 60637, USA
H. B. Bhandari, H. Lingertat, V. Wang, O. Ovechkina, V. V. Nagarkar, Radiation Monitoring Devices, Watertown, MA, 02472, USA

Abstract

Alkali antimonide photocathodes are a strong contender for the cathode of choice for next-generation photon sources such as LCLS II or the XFEL. These materials have already found extensive use in photodetectors and image intensifiers. However, only recently have modern synchrotron techniques enabled a systematic study of the formation chemistry of these materials. Such analysis has led to the understanding that these materials are inherently rough when grown through traditional sequential deposition; this roughness has a detrimental impact on the intrinsic emittance of the emitted beam.

Sputter deposition may provide a path to achieving a far smoother photocathode, while maintaining reasonable quantum efficiency. We report on the creation and vacuum transport of a K_2CsSb sputter target, and its use to create an ultra-smooth (sub nm roughness) cathode with a 2% quantum efficiency at 532 nm.

ROUGHNESS AND EMITTANCE

The Alkali Antimonides are a class of materials (I_3V semiconductors) often used as photocathodes, both in detectors [1] and accelerators [2]. Many of these compounds are capable of achieving a quantum efficiency (QE) of several percent for green light, making them attractive for high average current accelerator applications. The typical sequential deposition process used to form these materials results in a cathode which is very rough (25 nm RMS for a 50 nm thick cathode, with a 100 nm spatial period) [3]. This results in an undesirable field dependence of the intrinsic emittance [4,5]; an emission field of 6 MV/m is sufficient to double the intrinsic emittance of a K_2CsSb cathode illuminated with green light (the expected value should be 0.5 µm/mm [6]). Assuming a simple sinusoidal modulation of the surface height, the field-induced emittance growth can be shown to be given by Eq. (1)

$$\varepsilon_{rough} = \sigma_{x,y}\sqrt{\frac{\pi^2 a^2}{2m_0 c^2 \lambda} Ee} \tag{1}$$

where a is the amplitude, λ is the wavelength of the surface height modulation, σ is the rms beam size and E is the field gradient. Figure 1 shows the effect of roughness using this model for an amplitude of 25 nm and a surface wavelength of 100 nm. These values are typical for a sequential thermal deposition process. We can see that at fields that are relevant to high gradient photo-guns, there would be a drastic increase in emittance. We can also use this same model to detemine the amplitude necessary so that we can achieve room temperature kT defined emittance (0.225 microns / mm rms). We assume that the wavelength of the sinusoidal modulation is always 4 times the amplitude, as often observed in thin film growth. For a field of 20 MV/m, we find that a roughness amplitude of less than 1 nm is required. This is close to the roughness of super-polished etched Silicon,

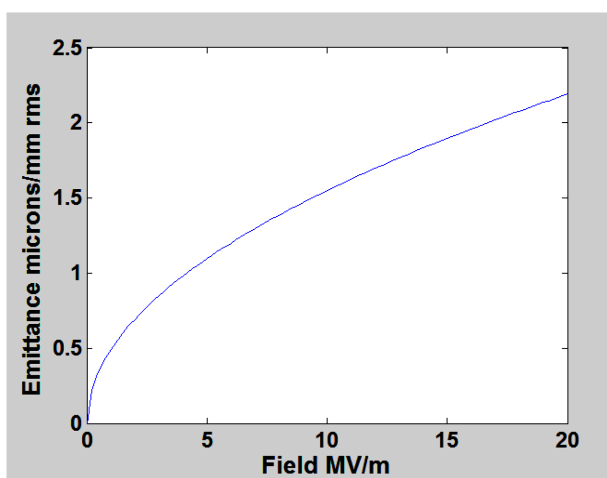

Figure 1: Dependence of emittance on field, for a sinusoidal modulation of the surface with an amplitude of 25 nm and a period of 100 nm.

*Work supported by U.S. DoE, under KC0407-ALSJNT-I0013 and SBIR grant # DE-SC0009540. NSLS was supported by DOE DE-AC02-98CH10886, CHESS is supported by NSF & NIH/NIGMS via NSF DMR-1332208
#smedley @bnl.gov

Content from this work may be used under the terms of the CC BY 3.0 licence (© 2015). Any distribution of this work must maintain attribution to the author(s), title of the work, publisher, and DOI.

ISBN: 978-3-95450-168-7 doi:10.18429/JACoW-IPAC2015-TUPHA004

Content from this work may be used under the terms of the CC BY 3.0 licence (© 2015). Any distribution of this work must maintain attribution to the author(s), title of the work, publisher, and DOI.

NSLS-II STORAGE RING INJECTION OPTIMIZATION*

G.M. Wang#, T. Shaftan, E. Blum, W.X. Cheng, J. Choi, Y. Li, S. Seletskiy, Y. Tian, L. Yang, L.H. Yu, BNL, Upton, NY, 11973, U.S.A

Abstract

The National Synchrotron Light Source II (NSLS-II) is a state of the art 3 GeV third generation light source at Brookhaven National Laboratory. The SR is designed to work in top-off injection mode. The injection straight includes a septum and four fast kicker magnets with independent amplitude and timing control. The beam injection is designed as 9.5 mm off-axis in x plane and on-axis injection in y plane. To capture the injected beam within the SR acceptance for high injection efficiency, it requires 6-D phase space match. Besides that, the fast kickers formed local bump is also required to be locally to minimize the injected beam extra betatron oscillation and keep the stored beam disturbance within the specification, 10 % beam size to minimize the injection transient. This paper will present our injection commissioning experience.

INTRODUCTION

The National Synchrotron Light Source II (NSLS-II) is a 3 GeV, ultra-small emittance (H: 1 nm-rad and V: 8 pm-rad), high brightness third generation light source [1].

The Storage Ring phase I commissioning started in Mar. 2014 and finished in one and a half months later to achieve 25 mA stored beam current with >90% injection efficiency.

The designed beam injection is 9.5 mm horizontal off-axis injection and vertical on axis injection. The commissioning strategy is to circulate beam first by doing on-axis injection [2] with sextupoles and RF off, then get the stored beam with sextupoles and RF on and finally move to nominal off-axis injection [3] to accumulate high beam current with good injection efficiency. In this paper, we describe our experience.

SR INJECTION OVERVIEW

The NSLS II storage ring injection system is located in one 9.3 m long straight section. As shown in Fig. 1, it consists of four kickers, a DC septum and a pulsed septum for beam injection. The four kicker magnets, producing a closed bump in x plane for stored beam, are placed symmetrically in the straight section. Their bending angles are the same but in different bend direction. The stored beam gets the maximum bump amplitude at the middle of injection straight line. There are one injection straight flag, 4 BPMs and two neutron beam loss monitor are dedicated for injection related beam monitor and study. BPMs P1 and P4 are centered on the SR stored beam orbit, P2 is shifted by X = -5.8 mm off center and P3 is shifted by X = -15 mm from SR stored beam center. These four BPMs are inside the local fast bump and can be used for the bump amplitude study. 180 BPMs along the ring were used for the bump leakage study.

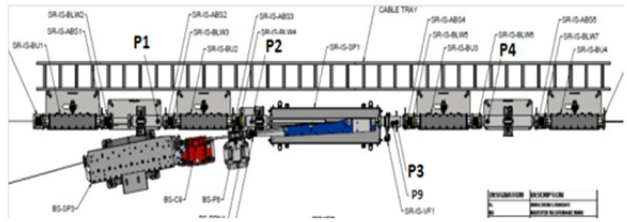

Figure 1: Top view of the SR injection straight section.

When the injected beam arrives, kickers K1 and K2 kick the stored beam towards the septum knife by 15 mm. The stored beam and the injected beam merge at the exit of the AC septum. Kickers K3 and K4 will kick both beam, so that the stored beam returns to its designed orbit, and the injected beam is off-axis oscillation. These kickers angle are 7.5 mrad with 5.2 μs kicker pulse length, two times long of storage ring revolution. The stored beam bump amplitude is 15 mm. The injected beam and stored beam relative position at the exit of septum is shown in Fig. 2. The designed stored beam equilibrium orbit is 17.5 mm away from septum knife with 2.5 mm safe region away from septum knife. At the end of bump, injection beam is 9.5 mm away from stored beam close orbit, which requires ~11 mm SR acceptance, comparing with the SR designed acceptance 15 mm [4].

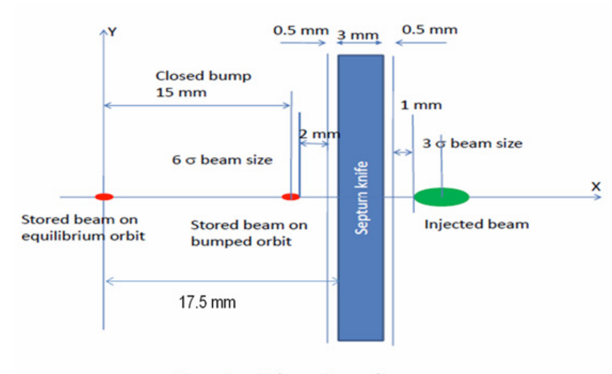

Figure 2: Injected beam and stored beam relative position at the exit of septum.

FAST KICKERS STUDY

Each kicker has independent voltage and timing control. The kicker voltage to the kick strength conversion is not very precise from the lab measurement. The timing delay is separated into two control parts. One is for four kickers' common delay relative to the injection time, and the other is for each kicker precise delay to compensate the cable length or beam arrival time difference. The initial timing trigger for all kickers is

#gwang@bnl.gov

ISBN: 978-3-95450-168-7 doi:10.18429/JACoW-IPAC2015-TUPHA005

TOOLS FOR NSLS II COMMISSIONING

G.M. Wang#, T. Shaftan, G. Bassi, A. Blednykh, W.X. Cheng, J. Choi, M. Davidsaver, L. Dalesio, J. De Long, K. Ha, Y. Hidaka, Y. Hu, Y. Li, D. Padrazo, S. Seletskiy, G. Shen, K. Shroff, O. Singh, T. Summers, Y. Tian, H. Xu, L. Yang, X. Yang, F. Willeke
BNL, Upton, NY, 11973, U.S.A

Abstract

The National Synchrotron Light Source II (NSLS-II) is a state of the art 3 GeV third generation light source at Brookhaven National Laboratory. As many facilities worldwide, NSLS II uses the EPICS control system to monitor and control all accelerator hardware. Control system studio (CSS) is used for simple tasks such as monitoring, display, setting of PVs. browsing the historical data, et. al. For more complex accelerator physics applications, a collection of scripts are mainly written in Python and part from Matlab during commissioning. With the close collaboration and fully support from control group, more and more CSS features were developed for operation convenience and several high level applications are interfaced with users in CSS panels for daily use based on softiocs. This paper will present the tools that we have been used.

INTRODUCTION

The National Synchrotron Light Source II (NSLS-II) is a 3 GeV, ultra-small emittance (1 nm-rad), high brightness third generation light source [1]. The storage ring commissioning started in Mar. 2014 and took ~ two months and reached the key performance parameters (goal: 25 mA), 50 mA with superconducting RF cavity in July 2014 [2,3]. Since Feb. 2015, it started to provide the user operation for phase I project beam lines.

As many other facilities [4,5], NSLS II chose the Experimental Physics and Industrial Control System (EPICS) as its control system to monitor and control the accelerator hardware. It interfaces to the accelerator instruments and devices (such as Power supply, digitizer, and motor) with IOC (Input Output Controllers). Channel Access is used as the interface to the machine process variables (PVs).

The typical control applications include two types, simple monitor/control device and complex accelerator physics application for studies and machine optimization (measurements, data analyses and applying correction). Mainly, we use cothread to access the process variables (PVs) in Python script for complex accelerator physics applications and the CSS (BOY) [6] panel for simple tasks such as monitoring, displaying and setting of the machine Process Variables (PVs). The PVs history can be saved from data archive system. Besides, MATLAB is also available for programming and EDM panels are also used. All source codes including panel configurations are controlled and managed by mercurial version in the control system.

To keep the beam commissioning time efficient, various tools were developed for data displaying, collecting and processing. Besides machine status and physics applications, we also developed the daily used operation tools [7], such as save/compare/restore tool, data archive and browsing, alarm and warning monitor, elog, eticket, channel finder service and applications.

In this paper, we'll present our commissioning tools experience.

MACHINE STATUS APPLICATION

All of the monitor and control panels are created with software tools in Control System Studio (CSS), which is an Eclipse-based collection of tools to monitor and operate large scale control systems. The interface allows the operators to edit the desired ramp/soak profiles and provides the option to use predefined recipes.

The NSLS-II operation panels [8] include the user panels and the expert panels. They display the device status and parameters (setpoint and readback) and show the device performance. A user panel shows only information that user is required, such as the magnet current setpoint, readback or fault status. The expert panel shows all the information that expert can fully control the device or diagnose the device, such as power supply operation mode, fault details.

HIGH LEVEL APPLICATION

Besides the devices status and control, we also develop high level applications to realize the accelerator physics application tools. It is to translate the raw/processed data from PV to the "physics" parameters, such as from beam size reading to beam emittance or orbit measurement and correction.

An extensive set of libraries and scripts [9] have also been written in Python for more dynamic and physics related study. A high level physics applications (HLAs) library, which maps flat EPICS process variables (PVs) to object oriented accelerator components, was developed. This mapping is dynamical and configurable from channel finder service (CFS). CFS associates PVs with properties and tags. HLAs library constructs an accelerator structure based on PVs properties and tags and make them with the search feature and group manipulatable. This makes high level application user more convenient, such as operation type of elements (BPMs, correctors) or individual element based on their name pattern, position… HLAs library also wraps the unit conversion functions between physics unit and hardware unit.

#gwang@bnl.gov

Content from this work may be used under the terms of the CC BY 3.0 licence (© 2015). Any distribution of this work must maintain attribution to the author(s), title of the work, publisher, and DOI.

ISBN: 978-3-95450-168-7 doi:10.18429/JACoW-IPAC2015-TUPHA006

NSLS-II STORAGE RING INSERTION DEVICE AND FRONT-END COMMISSIONING

G. Wang#, T. Shaftan, C. Amundsen, G. Bassi, J. Bengtsson, A. Blednykh, E. Blum, W. Cheng, J. Choi, O. Chubar, T. Corwin, M. Davidsaver, L. Doom, W. Guo, D. Harder, P. He, Y. Hidaka, Y. Hu, P. Ilinski, C. Kitegi, S. Kramer, Y. Li, M. Musardo, D. Padrazo, B. Podobedov, K. Qian, R. Rainer, J. Rank, S. Seletskiy, S. Sharma, O. Singh, V. Smaluk, R. Smith, T. Summers, T. Tanabe, F. Willeke, L. Yang, X. Yang, L. Yu, BNL, Upton, NY 11973, USA

Abstract

The National Synchrotron Light Source II (NSLS-II) is a state of the art 3 GeV third generation light source at Brookhaven National Laboratory. During spring/ summer of 2014, the storage ring was commissioned up to 50 mA without insertion devices. In the fall of 2014, we began commissioning of the project beamlines, which included seven insertion devices on six ID ports. Beamlines IXS, HXN, CSX-1, CSX-2, CHX, SRX, and XPD-1 consist of elliptically polarized undulator (EPU), damping wigglers (DW) and in-vacuum undulators (IVU) covering from VUV to hard x-ray range. In this paper, experience with commissioning and operation is discussed. We focus on reaching ring storage ring performance with IDs, including injection, design emittance, compensation of orbit distortions caused by ID residual field, source point stability, beam alignment and tools for control, monitoring and protection of the ring chambers from ID radiation.

INTRODUCTION

The National Synchrotron Light Source II (NSLS-II) is a 3 GeV, ultra-small emittance (1 nm-rad), high brightness (>10^{21} photons s^{-1} mm^{-2} $mrad^{-2}(0.1\%BW)^{-1}$) third generation light source [1]. It can support 60~80 beamlines stemming from insertion devices, three pole wiggles and bending magnets. The storage ring (SR) commissioning took about two months and reached and exceeded key performance parameters (KPP were 25 mA at 3 GeV of the beam energy) with superconducting RF cavity during July 2014 [2-4]. Once the start-up goals were accomplished we moved to phase-I insertion devices commissioning. The insertion device (ID) and their front end (FE) commissioning commenced in Oct., 2014 and took about 2 months for all the project IDs so that the beamline commissioning with the beam began in Dec. 2014. Since then all installed IDs operate routinely supplying light for the NSLS-II users at the level of 50 mA of circulating current.

NSLS-II design is based on 30 cells of double-bend-achromat lattice, including 15 long straight sections (9.3 m) and 15 short straight sections (6.6 m). The IDs [5] location and their main parameters are listed in Table 1.

In this paper we describe the results of the ID commissioning including compensation of their effects on closed orbit, perturbation of linear optics, optimization of emittance and injection efficiency, as well as the ID source point alignment along the front-ends, testing of equipment protection system and reaching high beam stability.

Table 1: NSLS II Phase I IDs Main Parameters

Beam Line	Type	L [m]	λ [mm]	K_{max}	Gap [mm]
CSX1/ CSX2	EPU49	4	49	2.6 (heli) 4.3 (Lin) 3.2 (vlin) 1.8 (45d)	11.5
IXS	IVU22	3	22	1.52	7.4
HXN	IVU20	3	20	1.83	5.2
CHX	IVU20	3	20	1.83	5.2
SRX	IVU21	1.5	21	1.79	6.4
XPD/ PDF	DW100	6.8	100	~16.5	15.0

ID COMMISSIONING

Changing ID gaps affects stored beam closed orbit, perturbs linear optics (inducing tune shift and beta beat), reduces injection efficiency. All project IDs were commissioned in several steps: 1) aligning beam orbit in an ID with the stored beam in low current, (along with the ID elevation adjustment if available); 2) measuring ID field integrals and minimizing related orbit distortions by setting fields in the ID trim coils (usually the latter took several iterations so to reach residual distortions on the ~μm level; 3) collect correction ID coil currents into a single lookup table and interpolate the measured values for a range of gaps; 4) measure the optics distortion at different gaps and correct them distortion by comparing with the ideal model; 5) assess and optimize ID impact on the injection efficiency.

Close Orbit Perturbation and Compensation

The ID impact on the beam dynamics in the first order comes from the non-zero 1st and 2nd residual magnetic field integrals. These integrals introduce local orbit position and angle shifts and lead to closed orbit distortion. This effect is local and is compensated by the ID trim coils, installed on both ID ends.

The closed orbit change as a function of the ID gap is on the order of 20 μm rms for the IVUs, 40 μm rms for the EPU and 150 μm rms for DWs. After the first iteration, the rms value of residual orbit is corrected to <5 μm. After a few iterations, the final residual orbit rms value is under 2 μm.

#gwang@bnl.gov

Content from this work may be used under the terms of the CC BY 3.0 licence (© 2015). Any distribution of this work must maintain attribution to the author(s), title of the work, publisher, and DOI.

ISBN: 978-3-95450-168-7 doi:10.18429/JACoW-IPAC2015-TUPHA007

NSLS II BOOSTER EXTENDED INTEGRATION TEST*

G.M. Wang#, T. Shaftan, B. Bacha, A. Blednykh, E. Blum, W.X. Cheng, J. Choi, M. Davidsaver, J. De Long, L. Dalesio, R. Fliller, G. Ganetis, W. Guo, K. Ha, Y. Hu, W. Louie, G. Shen, O. Singh, V. Smaluk, Y. Tian, L. Yang, X. Yang, F. Willeke
BNL, Upton, NY, 11973, U.S.A
P. Cheblakov, A. Derbenev, A. Erokhin, S. Karnaev, S. Sinyatkin
BINP, Novosibirsk, Russia

Abstract

The National Synchrotron Light Source II (NSLS-II) is a state of the art 3 GeV third generation light source at Brookhaven National Laboratory. While the installation activities in the booster-synchrotron are nearly completed and waiting for the authorization to start the booster commissioning, the injector and accelerator physics group have engaged into the Integrated Testing phase. We did the booster commissioning with simulated beam signals, called extended integrated testing (EIT) to prepare for the booster ring commissioning. It is to make sure the device function along with utilities, timing system and control system, to calibrate diagnostics system, debug High Level Applications, test and optimize all the operation screens to reduce the potential problems during booster commissioning with beam.

INTRODUCTION

The NSLS-II [1] is a state of the art 3 GeV third generation synchrotron light source at Brookhaven National Laboratory. The injection system consists of a 200 MeV linac, a booster ring 3 GeV, transport lines and the storage ring injection straight. The linac commissioning was in April 2012. The booster commissioning [2] includes Linac to Booster transport line, Booster and Booster to dump transport line. But the start of the booster commissioning was moved towards later in the project schedule due to increase in the scope of the booster ARR review and uncertainty.

To make the beam commissioning smooth and efficient, a new phase of booster commissioning was introduced, Extended Integration Test (EIT) [3]. In this phase we will model the beam-induced signals through the EPICS controls and test and optimize all engineering screens and High-Level applications and safety systems with the actual hardware controls and operating subsystems but only with simulated beam signals without the real beam present in the machines. This phase is likely to reduce the time of the booster and transport line (TL) commissioning with the beam, train the commissioning team and reduce safety concerns related to the commissioning and operations.

In this paper, we report our experience with booster extended integrated testing.

*This manuscript has been authored by Brookhaven Science Associates, LLC under Contract No. DE-AC02-98CH10886 with the U.S. Department of Energy.
#gwang@bnl.gov

EXTENDED INTEGRATION TEST

Extended Integrated Testing is carried out to exercise the beam commissioning without beam.

The EIT objectives are following through the commissioning sequence:

1) Passing the beam through transport lines.
2) Matching the beam emittance with the accelerator acceptance.
3) Observation and correction of the beam trajectory at the first turn closing.
4) Beam optimization during injection and RF capture.
5) Accelerating beam along the energy ramp.
6) Extracting beam.
7) Measuring the extracted beam parameters in the diagnostics transport line.

It provided the environment to test applications for routine beam parameters measurement and correction. Meanwhile, real time alarms and interlock signals was also engaged in the operation system and this trained operators on commissioning and operations of the live machine safely.

The hardware operates as in the actual commissioning, including power supplies, vacuum, diagnostics and RF systems. Equipment Protect System and Personal Protection System will be tested during the unit and integrated testing stages.

The beam signals for the non-existing beam are simulated and generated by a computer program, ELEGANT [4]. Then they are transported by the same data channel as the real beam signal would travel. In this process, we test and optimize all the operation screens, high level applications by subsystem with the actual hardware controls. This function is realized by setting the diagnostics related PVs to the simulation mode. These diagnostic devices require reconfiguration of the EPICS records: Booster beam diagnostics (36 BPMs, 1 DCCT, 1 FCT, 6 Beam flags, 2 SR monitors, 1 Tune measurement system), LTB part II diagnostics (3 BPMs, 4 Beam flags, 1 FCT), BSR TL part I diagnostics (4 Beam flags, 4 BPMs, 1 ICT, 1 FCT and 1 Faraday cup). 'Beam' signals include closed orbit readings, turn by turn data from BPMs system, beam intensity signals, beam image signals and so on. The unknown imperfections of the booster alignment are included in the model as well. The hardware real readback including power supplies, RF and timing systems, are feed into Elegant Model and controlled by high level applications.

Content from this work may be used under the terms of the CC BY 3.0 licence (© 2015). Any distribution of this work must maintain attribution to the author(s), title of the work, publisher, and DOI.

ISBN: 978-3-95450-168-7 doi:10.18429/JACoW-IPAC2015-TUPHA008

NSLS-II INJECTOR HIGH LEVEL APPLICATION TOOLS*

G.M. Wang#, T. Shaftan, E. Blum, R. Fliller, Y. Hu, X. Yang
BNL, Upton, NY, 11973, U.S.A

Abstract

The National Synchrotron Light Source II (NSLS-II) is a state of the art 3 GeV third generation light source at Brookhaven National Laboratory. The injection system consists of a 200 MeV linac, a 3 GeV booster synchrotron and transfer lines in connection of linac, booster and storage ring. The transfer lines, designed and built from BNL, are equipped with sufficient diagnostics to commission to characterize the beam parameters from linac and booster. In the paper, we summarized the high level applications tools, beam emittance, energy and energy spread measurement, developed during the injector commissioning.

INTRODUCTION

The NSLS-II [1] is a state of the art 3 GeV third generation synchrotron light source at Brookhaven National Laboratory. It consists of a 200 MeV linac, a booster ring accelerating beam from 200 MeV to 3 GeV, a 3 GeV Storage ring and transport lines in between them. Both transfer lines are equipped with sufficient diagnostics to commission along with linac/booster and characterize their beam parameters.

As many other facilities [2,3], NSLS II chose the Experimental Physics and Industrial Control System (EPICS) as its control system to monitor and control the accelerator hardware. It interfaces to the accelerator instruments and devices (such as Power supply, digitizer, and motor) with IOC (Input Output Controllers). Channel Access is used as the interface to the machine process variables (PVs).

The typical operation applications include two types, simple monitor/control device and complex accelerator physics application for studies and machine optimization (measurements, data analyses and applying correction). Mainly, we use cothread to access the process variables (PVs) in Python script for complex accelerator physics applications and the CSS (BOY) [4] panel for simple tasks such as monitoring, displaying and setting of the machine Process Variables (PVs). Besides, MATLAB is also available as an alternative tool and EDM panels are used for Linac control system from the linac vendor Research Instruments, GmbH. All source codes including panel configurations are controlled and managed by mercurial version in the control system.

Both Python and CSS are new environment for accelerator control. Python has a lot of libraries and strong support from scientific computing community. It has very powerful functions for scientific calculation and logic control. CSS has simple feature to display/control PVs with simultaneous data sharing environment, but with a lot of new features for operations convenience, such as create olog entry, data browser to view history, et.al, which benefits the strong support from control group. So NSLS II all the related commissioning and operation tools are developed from scratch. In fact, a lot of highly operation demanding high level applications were developed based on soft IOCs and combined python and CSS advantages together with powerful calculation and convenient display interface.

To keep the beam commissioning time efficient, we did the the subsystem integration test and extended integration test [5]. In this paper, we'll present main applications for injector commissioning and operation.

MACHINE STATUS APPLICATION

All of the monitor and control panels are created with software tools in Control System Studio [6] (CSS), which is an Eclipse-based collection of tools to monitor and operate large scale control systems. The interface allows the operators to edit the desired ramp/soak profiles and provides the option to use predefined recipes.

The NSLS-II operation panels [7] include the user panels and the expert panels. They display the device status and parameters (setpoint and readback) and show the device performance. A user panel shows only information that user is required, such as the magnet current setpoint and readback. The expert panel shows all the information that expert can fully control the device or diagnose the device, such as power supply operation mode and magnet temperature.

Figure 1 shows one example for BR current monitor, include the FCT output for each turn current and number of bunches, the DCCT beam current along ramping, which average many turns data signal.

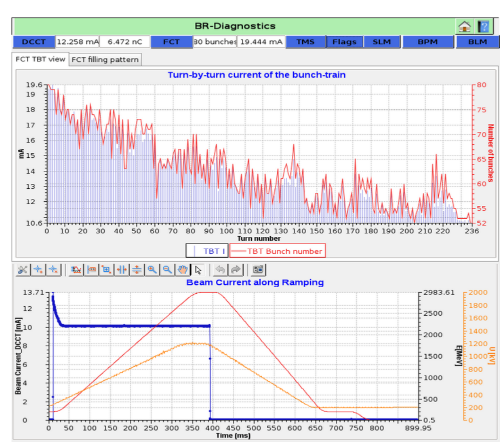

Figure 1: Booster ring current monitor along ramping.

* This manuscript has been authored by Brookhaven Science Associates, LLC under Contract No. DE-AC02-98CH10886 with the U.S. Department of Energy.
#gwang@bnl.gov

Content from this work may be used under the terms of the CC BY 3.0 licence (© 2015). Any distribution of this work must maintain attribution to the author(s), title of the work, publisher, and DOI.

ISBN: 978-3-95450-168-7 doi:10.18429/JACoW-IPAC2015-TUPHA009

NSLS-II STORAGE RING COUPLING MEASUREMENT AND CORRECTION*

G. Wang#, L. Yu, Y. Li, T. Shaftan, L. Yang, BNL, Upton, NY 11973, USA

Abstract

The National Synchrotron Light Source II (NSLS-II) is a state of the art 3 GeV third generation light source at Brookhaven National Laboratory. To achieve the goal, 8 pm level vertical beam emittance, the coupling due to the misalignment in quads and vertical beam offset in sextuples must be corrected. Traditional method, based on response matrix, such as LOCO, is wildly used measure and corrects the coupling. In this paper, we present a new method to measure and correct the coupling with BPMs TBT data from fast kickers or pingers excited betatron oscillation. Besides the TBT data, other method, is also used to characterize the coupling.

INTRODUCTION

The National Synchrotron Light Source II (NSLS-II) is a 3 GeV third generation light source [1,2] with ultra-low horizontal emittance (1 nm-rad). In the vertical plane, the designed emittance is < 8 pm-rad, reaching the x-ray diffraction limit. They are very critical to increase NSLS II brightness $>10^{21}$ photons s^{-1} mm^{-2} $mrad^{-2}(0.1\%BW)^{-1}$ and affect beam lifetime.

The vertical plane emittance main contributions are the betatron coupling and vertical dispersion [3]. The linear coupling comes from the misalignment (rolling) of quadrupoles and the vertical orbit displacement through sextupoles induced skew quadrupole effect. The vertical dispersion comes from the coupling contribution (such as all coupling errors from quads roll, sextuples offsets, main dipole magnets pitch, skew quadrupoles at locations with non-zero horizontal dispersion) and non-coupling contribution (such as vertical offset in quadrupoles induced dipole kick).

The common method to assess the linear coupling is to measure the minimum tune separation [4] between two coupling modes. Experimentally, the minimum tune separation is measured by tuning quadrupoles to bring horizontal and vertical tunes as close as possible. Another common way used in storage ring to assess the coupling to fit orbit respond matrix non-zero off-diagonal elements with LOCO [5] algorithm to identify coupling source and the needed corrector strength. There are other ways to observe the coupling effect, such as the vertical beam size, beam lifetime and horizontal excitation betatron oscillation effect on vertical residual betatron oscillation.

In this paper, a new method is discussed to measure and correct the betatron coupling with BPMs TBT data from fast kickers or pingers excited betatron oscillation. As the turn by turn data cannot reflect the vertical dispersion effect, the coupling correction is separated into two steps. First, the vertical dispersion is corrected with dispersive skew quadrupoles. Then the coupling is corrected with the non-dispersive skew quadrupoles from turn by turn data. This order cannot change, as dispersive skew quadrupoles affect both dispersion and coupling, but non-dispersive skew quadrupoles only affect betatron coupling.

One big advantage of this method is that this method only takes seconds to excite the beam, collect the data and apply the correction.

VERTICAL RESIDUAL BETATRON OSCILLATION MINIMIZING

If beam is excited by one injection kicker (horizontal plane only, with negligible vertical component), with initial offset $\vec{x}_0 = [0, \Delta x', 0, 0]^T$ at the location of the kicker, and it will do the betatron oscillation in the following turns. Ignoring the radiation damping, the subsequent BPM readings for next several turns are written as

$$\vec{x}_n = R^n \vec{x}_0$$

where n is the turn index and R is the storage ring's one-turn transport matrix. $\vec{x}_n = [x, x', y, y']^T$ includes BPMs reading in horizontal and vertical plane. We measure the dependence of the vertical residual oscillation on the skew quadrupoles currents, and write it as a matrix

$$M_{n,ij} = \frac{\Delta y_{i,n}}{\Delta I_j}$$

where ΔI_j is the current change of the j^{th} skew quadrupole, $\Delta y_{i,n}$ is the i^{th} BPM's n^{th} $(n \geq 1)$ turn y readings.

Thus the needed skew quadrupoles strengths for coupling correction can be obtained by solving the following linear equations

$$y_{i,n} = M_{n,ij} I_j.$$

The minimum number of turn-by-turn data should cover a full betatron oscillation. Usually several iterations are needed to let the solution to converge.

EXPERIMENTAL RESULT

NSLS II is designed as 30 cell double-bend-achromatic lattice, 15 super periods. In order to control the vertical beam size, each cell is designed to have a skew quadrupole. In the odd numbered cells, they are located in

* This manuscript has been authored by Brookhaven Science Associates, LLC under Contract No. DE-AC02-98CH10886 with the U.S. Department of Energy.
#gwang@bnl.gov

Content from this work may be used under the terms of the CC BY 3.0 licence (© 2015). Any distribution of this work must maintain attribution to the author(s), title of the work, publisher, and DOI.

ISBN: 978-3-95450-168-7 doi:10.18429/JACoW-IPAC2015-TUPHA010

Content from this work may be used under the terms of the CC BY 3.0 licence (© 2015). Any distribution of this work must maintain attribution to the author(s), title of the work, publisher, and DOI.

DESIGN OF THE NSLS-II TOP-OFF SAFETY SYSTEM*

R. P. Fliller III#, L. Doom, G. Ganetis, C. Hetzel, P.K. Job, Y. Li, T. Shaftan, S. Sharma, O. Singh, G-M. Wang, Z. Xia. Brookhaven National Laboratory, Upton, NY, 11973, USA

Abstract

The NSLS-II accelerators finished commissioning in the fall of 2014, with beamline commissioning underway. Part of the design for the NSLS-II is to operate in top off mode. The Top Off Safety System (TOSS) is presently being installed. In this report we discuss the Top Off Safety System design and implementation, along with the necessary tracking results and radiological calculations.

INTRODUCTION

All modern synchrotron light sources are built to operate in a mode of quasi-continuous injection known as top off injection [1-3]. This mode of operation allows for more stable operation by keeping the beam current constant, and hence the thermal load on beamline optics constant. However, this mode of operation presents a unique safety hazard, that is, injection into the storage ring with the photon shutters open. This may allow the possibility of freshly injected electron beam to pass through a beamline front end into the first optics enclosure and cause unacceptably large radiological dose on the experimental floor. A properly designed safety system is required to prevent this from occurring.

The design of the Top Off Safety System (TOSS) for the NSLS-II is the culmination of many years of work.[4-6]. In this paper, we report on the requirements and design of the various interlocks of the TOSS. We discuss the various interlocks and apertures required for safe top off and the maximum credible incident in the event of an errant injected bunch.

HAZARD ANALYSIS

The tracking which was performed to specify the interlocks for top off safety is discussed in various places. [4,5,7]. In brief, a safe point is specified in the beamline front ends and the goal of the tracking is to ensure that no injected electrons can go beyond the safe point. For reasons of computational expediency, the decision was made to track positrons backward from the safe point into the nearest straight section of the storage ring. Particles which can be tracked to the nearest storage ring straight section denote unsafe trajectories. Certain apertures in the storage ring and front end, along with a set of interlocks are specified eliminate all unsafe trajectories. The interlocks will be the same for all front ends, and the apertures will be specified on a per front end case. Common designs of the front ends simplify the specification of apertures, with similar apertures called out for multiple beamlines.

Figure 1 shows a typical analysis. Tracking starts at the right of the figure and attempts to find all trajectories which can propagate through all of the apertures to the left. The red lines show the envelope of trajectories. The various magnets are shown by the colored boxes. The dipole magnet deflects the trajectories into the vacuum chamber for all possibilities allowed by the interlocks and aperture misalignments. Because no trajectories propagate to the left and therefore this beamline is safe.

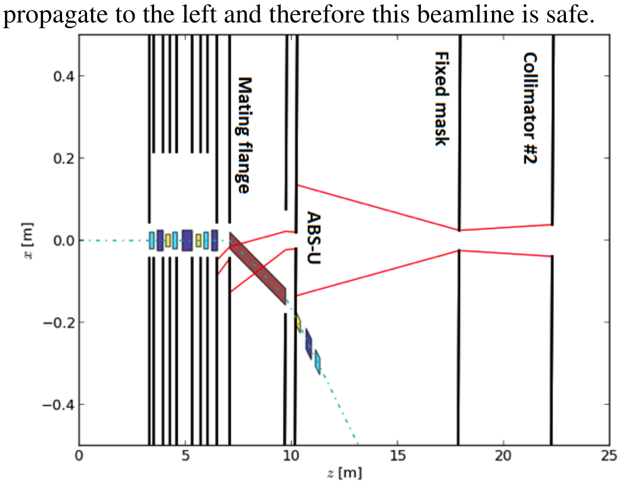

Figure 1: Example of particle tracking for SRX beamline. Tracking starts at Collimator #2 on the right and attempts to get to the storage ring straight on the left. The red lines denote the envelope of trajectories. No trajectories pass to the straight, therefore these are safe.

The tracking calculations do not assume the presence of stored beam in the ring. Neglecting this allows the calculations to find unlikely scenarios where injected beam may escape the ring, but may be incompatible with stored beam. The interlocks and apertures render all trajectories safe. Including a stored beam interlock removes the possibility of many of these scenarios, making the possibility of injected beam escaping down a front end to the safe point even more unlikely.

When x-rays are being delivered to a beamline during top-off, the safety shutters are in theopen position and the first optical enclosure (FOE) will be secured with no access to the personnel. The primary radiological safety concern for the top-off injection is where injected electrons are conveyed through the front-end and strike the safe point, which is closest to the ratchet wall collimator.

The radiological calculations use the front end with the largest apertures to date, which is the SRX beamline. The dose rate during top off operation was calculated for

* This manuscript has been authored by Brookhaven Science Associates, LLC under Contract No. DE-SC0012704 with the U.S. Department of Energy.
#rfliller@bnl.gov

ISBN: 978-3-95450-168-7 doi:10.18429/JACoW-IPAC2015-TUPHA012

LOCO APPLICATION TO NSLS2 STORAGE RING DISPERSION AND BETA BEATING CORRECTION

Xi Yang†, BNL, Upton, NY 11973, USA

Xiaobiao Huang, and James A. Safranek, SLAC, Menlo Park, CA 94303, USA

Abstract

During the short run in early July, 2014, we made changes to the setup of Matlab Linear Optics from Closed Orbits (LOCO) for NSLS-II and applied it successfully to the linear optics correction. The Matlab middle layer (MML) setup was also verified with Input-Output tests for all quadrupole families. The LOCO setup was further tested with an intentional quadrupole error. After the successful LOCO correction, the RMS beta beating was reduced from the initial value of 5.5% to 1.9% in x, and 5.6% to 1.0% in y. The RMS horizontal dispersion error was reduced from 21 mm to 6 mm. It is critical to keep the same closed orbit for LOCO correction. Because some correctors were nearly saturated at the time, closed orbit couldn't be controlled for additional iterations. We expect LOCO to achieve better optics correction after the orbit control is improved.

INTRODUCTION

LOCO has been a powerful beam-based diagnostics and optics control method for storage rings and synchrotrons worldwide ever since it was established at NSLS by J. Safranek [1]. This method measures the orbit response matrix and optionally the dispersion function of the machine. The data are then fitted to a lattice model by adjusting parameters such as quadrupole and skew quadrupole strengths in the model, BPM gains and rolls, corrector gains and rolls of the measurement system. Any abnormality of the machine that affects the machine optics can then be identified. The resulting lattice model is equivalent to the real machine lattice as seen by the BPMs. Since there are more than five BPMs per betatron period in NSLS2 storage ring, the model is a very accurate representation of the real machine. According to the fitting result, one can correct the machine lattice to the design lattice by changing the quadrupole and skew quadrupole strengths. LOCO is so important that it is routinely performed at many electron storage rings to guarantee machine performance, especially after the Matlab-based LOCO code [2] became available. The Matlab version includes a user-friendly interface, with many useful fitting and analysis options.

MATLAB LOCO CODE IMPROVEMENT

Full Jacobian (J) calculation takes four hours for NSLS2 storage ring compared to five minutes linear J in a standard laptop. Besides, J doesn't change significantly when the solution is close to the global minimum. Therefore, a selection between calculating a new or reusing an existing J at every LOCO iteration has been implemented in "loco.m". The standard size of J for NSLS2 storage ring (SR) is ~130k·2k. Singular Value Decomposing (SVD) JTJ (~2k·2k) instead of J for all fitting methods is implemented to speed up the SVD calculation. Using the Optimized weights for all fit parameters minimizes the changes of quadrupole gradients while at the same keeping the good fitting result. Reducing quadrupole families and grouping neighbouring quadrupoles in the fitting are introduced to cure the degeneracy problem caused by the coupling between fit parameters. Five families, QL1, QL2, QH1, QH2, and QM2, instead of all eight families, QL1, QL2, QL3, QH1, QH2, QH3, QM1, and QM2, are used in the LOCO fitting. Also, two QM2 quadrupoles at the same cell are grouped together. All these new features have been tested before updating the relevant codes.

CRITICAL ISSUES BEING EXAMINED

The following lists the most important steps that one has to check before LOCO application:

1. LOCO connection to machine

   Matlab middle layer (MML) mapping between hardware and channel access in the control system has been examined for all the quadrupoles, sextupoles, correctors, and BPMs. They are in good agreement.

   MatLab codes that generate LOCO files and implement optics correction have been checked and no error is found.
2. Quadrupole saturation

   $\Delta K/K = \Delta I/I$ is not accurate. As an example of QM2 quadrupoles, at the operational current ~140A, K/I=1.2·$\Delta K/\Delta I$, as shown in Figure 1.

   Our solutions are: iterate several times; use unit conversion, amp2k.m and k2amp.m, based on measured magnet excitation curves in MML for ΔI [3].
3. Quadrupole hysteresis

   Cycle magnets after optics corrections are applied.
4. BPMs not reproducible

   Use constant current and filling pattern
5. Orbit control

   The tolerance on orbit reproducibility has to be well understood and setup properly.

† xiyang@bnl.gov

Content from this work may be used under the terms of the CC BY 3.0 licence (© 2015). Any distribution of this work must maintain attribution to the author(s), title of the work, publisher, and DOI.

ISBN: 978-3-95450-168-7 doi:10.18429/JACoW-IPAC2015-TUPHA013

SKEW-QUAD PARAMETRIC-RESONANCE IONIZATION COOLING: THEORY AND MODELING*

A. Afanasev#, George Washington University, Washington, DC 20052, USA
Y. Derbenev, V.S. Morozov, A. Sy, Jefferson Lab, Newport News, VA 23606, USA
R.P. Johnson, Muons, Inc., Batavia, IL, USA

Abstract

Muon beam ionization cooling is a key component for the next generation of high-luminosity muon colliders. To reach adequately high luminosity without excessively large muon intensities, it was proposed previously to combine ionization cooling with techniques using a parametric resonance (PIC). Practical implementation of PIC proposal is a subject of this report. We show that an addition of skew quadrupoles to a planar PIC channel gives enough flexibility in the design to avoid unwanted resonances, while meeting the requirements of radially-periodic beam focusing at ionization-cooling plates, large dynamic aperture and an oscillating dispersion needed for aberration corrections. Theoretical arguments are corroborated with models and a detailed numerical analysis, providing step-by-step guidance for the design of Skew-quad PIC (SPIC) beamline.

INTRODUCTION

Experiments at energy-frontier colliders require high luminosities, of order 10^{34} cm^{-2} sec^{-1} or more, in order to obtain reasonable rates for events having point-like cross sections. High luminosities require intense beams, small transverse emittances, and a small beta function at the collision point. For muon colliders, high beam intensities and small emittances are difficult and expensive to achieve because muons are produced diffusely and must be cooled drastically within their short lifetimes. Ionization cooling is a major first step toward providing adequate luminosity without large muon intensities, and its 6D-implementation with a helical cooling channel was described in Ref. [1]. Further reduction of emittances requires anomalously large magnetic fields in ionization-cooling channels, but the use of parametric resonance allows relaxing this requirement, while providing significant beam cooling effects [2].

PIC CONCEPT

In the PIC technique the resonant approach to particle focusing can achieve equilibrium transverse emittances that are at least an order of magnitude smaller than in conventional ionization cooling. The main principle is similar to half-integer parametric resonant extraction from a synchrotron, except for targeting different variables of the phase space [2]. Briefly speaking, parametric resonance provides focusing of the muon beam at periodic locations down the beamline; the beam angular spread is naturally maximized at these locations, therefore unw anted angular smearing (or "heating") due to multiple Coulomb scattering in ionization-cooling plates has the least effect.

While the concept of PIC has been around for a few years, its practical implementation faced several difficulties that were addressed by an Epicyclic PIC proposal [3] and proposed epicyclic twin-helix magnetic structure [4]. The latter uses a superposition of two opposite-helicity equal-period equal-strength helical dipole harmonics and a straight normal quadrupole. Here we propose and develop a technique that will help to avoid (integer) resonances in such a system that requires periodic focusing, making the important step toward its engineering design.

COUPLING RESONANCE IN PIC

Our proposal is based on inducing a linear betatron coupling resonance in PIC transport line between the horizontal (x) and vertical (y) planes. Previously developed (and described in Ref. [4]) twin-helix magnetic system is supplemented with skew quads that generate coupling between horizontal and vertical betatron motion.

Let us consider the effect of such coupling, first in a simplified model. The equations for coupled betatron oscillations are

$$x_b'' + k_x^2 x_b + g y_b = 0$$
$$y_b'' + k_y^2 y_b + g x_b = 0$$

where $k_x^2 = K^2 - n$, $k_y^2 = n$, with K^2 and n denoting the curvature function and quad strength, respectively. Coupling g is provided by 45^o-skewed quadrupoles.

In the case of constant coefficients, the above system has an analytic solution described by superposition of two normal-mode oscillations with wave vectors $k_{1,2}^2 = \frac{1}{2}(k_x^2 + k_y^2 \pm \sqrt{(k_x^2 - k_y^2)^2 + 4g^2})$.

$$x_b(s) = C_1 \cos(k_1 s) + C_1' \sin(k_1 s) + G \cdot (C_2\, cos(k_2 s) + C_2'\, sin(k_2 s))$$
$$y_b(s) = -G \cdot (C_1 \cos(k_1 s) + C_1' \sin(k_1 s)) + C_2\, cos(k_2 s) + C_2'\, sin(k_2 s),$$

where $G = (k_2^2 - k_y^2)/g = -(k_1^2 - k_x^2)/g$, and s is the path length along the reference trajectory. The constants are obtained from initial conditions at s=0:

*Work supported in part by DOE STTR Grants DE-SC0005589 and DE-SC0007634, and and DOE Contract No. DE-AC05-06OR23177
#E-mail: afanas@gwu.edu

Content from this work may be used under the terms of the CC BY 3.0 licence (© 2015). Any distribution of this work must maintain attribution to the author(s), title of the work, publisher, and DOI.

ISBN: 978-3-95450-168-7 doi:10.18429/JACoW-IPAC2015-TUPTY001

Content from this work may be used under the terms of the CC BY 3.0 licence (© 2015). Any distribution of this work must maintain attribution to the author(s), title of the work, publisher, and DOI.

INTERACTION REGION FOR A 100 TeV PROTON-PROTON COLLIDER

R. Martin*, CERN, Geneva, Switzerland and Humboldt University Berlin, Germany
R. Tomás, CERN, Geneva, Switzerland
B. Dalena, CEA/IRFU, Gif-sur-Yvette, France

Abstract

As part of its post-LHC high energy physics program, CERN is conducting a study for a new proton-proton collider, FCC-hh, running at center-of-mass energies of up to 100 TeV, pushing the energy frontier of fundamental physics to a new limit. At a circumference of 80-100 km, this machine is planned to use the same tunnel as FCC-ee, a proposed 90-350 GeV high luminosity electron-positron collider. This paper presents the design progress and technical challenges for the interaction region of FCC-hh.

INTRODUCTION

FCC-hh aims to provide proton collisions almost one order of magnitude higher than the Large Hadron Collider (LHC), posing a great challenge for the interaction region optics.

The current lattice for the interaction region is shown in Fig. 1. Each side of the Interaction Point (IP) consists of a final triplet, a beam separation section and a matching section, followed by the dispersion suppressor (not pictured here). For the dispersion suppressor (DS), two options are currently considered: a half bend DS and an LHC-like DS. The decision for one DS design will be based on optics considerations as well as a cost optimum in terms of dipole filling factor and number of independently powered quadrupoles.

Table 1: Parameters for the FCC-hh Interaction Region (IR) [1]

	Baseline	Ultimate
Beam energy [TeV]	50	
IR length [m]	1400	
Number of IPs	2 + 2	
Luminosity [10^{34}cm^{-2}s^{-1}]	5	20
IP β function β^* [m]	1.1	0.3
Normalized emittance [μm]	2.2	

Final Triplet

In a first approach, the LHC interaction region design was scaled up by a factor of $(50/7)^{1/3} \approx 2$, resulting in an L^* of 46 m. This early design showed a large radiation load from the debris at the IP. As a solution, the longer triplet design of HL-LHC [2] was adapted. To mitigate the radiation dose further, the quadrupoles were lengthened by an additional ≈ 30 %, giving a length of 20 m for Q1 and Q3 and 17.5 m for Q2a/b . At the same time, L^* was reduced to 36 m in order to keep the maximum β function at the same level [3]. With a coil aperture of 100 mm and a shielding thickness

* roman.martin@cern.ch

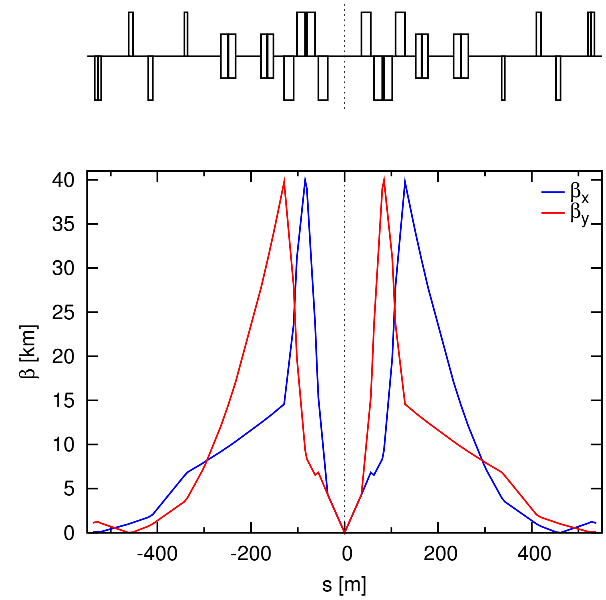

Figure 1: FCC-hh interaction region design with $\beta^* = 0.3$ m and $L^* = 36$ m.

of 15 mm, the radiation dose for this triplet is acceptable (Fig. 2).

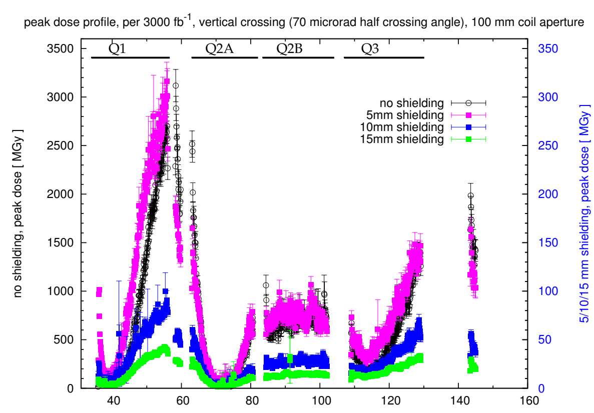

Figure 2: Radiation dose in the triplet magnets from physics debris with (right scale) and without (left scale) shielding. For 15 mm shielding and the shown integrated luminosity of 3000 fb^{-1}, the dose looks acceptable [4].

Beam Separation

As in the LHC layout, the two beams are colliding under a small crossing angle introduced by orbit correctors. Both beams pass the same final triplet and are separated and re-

ISBN: 978-3-95450-168-7 doi:10.18429/JACoW-IPAC2015-TUPTY003

STUDY OF THE DYNAMIC RESPONSE OF CLIC ACCELERATING STRUCTURES

E. Daskalaki, NTUA, Athens, Greece
V. Rude, ESGT-CNAM, Le Mans, France
A. Vamvakas, M. Duquenne, H. Mainaud-Durand, S. Doebert, CERN, Geneva, Switzerland

Abstract

CLIC is a linear electron-positron collider, 48 km long, consisting of more than 20000 repetitive modules. The target beam size of 1 nm dictates very tight alignment tolerances for the accelerating structures (AS). In order to assess the effect of short-term RF power interruptions (breakdowns or failure modes) on the alignment, the dynamic behaviour of the AS was investigated on the prototype two-beam module. On a dedicated experimental setup, the thermal and mechanical time constant (TC) was monitored as a function of ambient temperature, water flow and power. The experimental results showed that the thermal TC ranged between 4 and 11 minutes and presented strong correlation with the cooling water flow. These results were in very good agreement with the theoretical expectations. The displacement dynamics were found to be comparable with the thermal ones. The study indicates that temperature measurement, which is a fast and easy process, can be used as an indicator of the AS displacement. Moreover, it is shown than the transient response can be efficiently controlled through appropriate regulation of the cooling water flow.

INTRODUCTION

CLIC [1] is a multi-TeV normal conducting electron-positron collider foreseen to be constructed in two 21-km long linacs comprising more than 20000 repetitive modules. The principle of CLIC lies on the concept of two beams, a high-energy Main Beam (MB) and a low-energy, high-intensity Drive Beam (DB). The MB is accelerated in the Accelerating Structures (AS) by the RF power produced from the Power Extraction and Transfer Structures (PETS) of the DB. The alignment tolerances of CLIC are very tight due to the low target beam size of 1 nm. All components must be pre-aligned without beam with an accuracy of 10 µm. Alignment can be affected by the power dissipation on the components estimated to be 7 kW per module during normal operation.

A prototype two-beam module has been assembled in order to study the thermo-mechanical behavior of CLIC components [2]. In the module, the power is applied by electrical heaters, while ambient conditions and cooling can be regulated. Until now, temperature and alignment have been extensively studied during steady-state under different operating conditions [3]-[5]. However, in order to assess the effect of short-term power interruptions, e.g. during a failure mode, the study of transient response is important.

In this paper, the dynamic thermo-mechanical response of the CLIC AS is investigated as a function of the main operation conditions of CLIC, i.e. the water flow, ambient temperature and dissipated power. The correlation of the thermal and mechanical response is evaluated as well as the agreement of the experimental results to theoretical expectations.

THEORETICAL ANALYSIS

When the AS is powered-up, the power of the heater (P_h) is assumed to be distributed among the AS material (P_{cu}), the water (P_{water}) and the air (P_{air}):

$$P_h = P_{cu} + P_{water} + P_{air} \tag{1}$$

The time response of each power component is described as follows [6]:

$$P_{cu}(t) = m_{cu} c_{p,cu} \frac{dT_{cu}(t)}{dt} \tag{2}$$

$$P_{water}(t) = \dot{m}_w c_{p,w} \left[T_w(t) - T_w(0) \right] \tag{3}$$

$$P_{air}(t) = hA_{cu} \left[T_{cu}(t) - T_\infty \right] \tag{4}$$

where $c_{p,x}$ the heat capacity, m_{cu} the AS mass, A_{cu} the AS surface, $\dot{m}_w$ the water mass flow, h the heat transfer coefficient, and T_∞, T_{cu} and T_w the ambient, AS and outlet water temperatures respectively. Combining Eq. 1-4, the temperature response of the AS is described by a first order differential equation with the following analytic solution:

$$T_{cu}(t) = T_{ss} - ce^{-t/\tau} \tag{5}$$

where T_{ss} is the steady-state AS temperature, c is a constant and τ is the time constant (TC) given by:

$$\tau = \frac{m_{cu} c_{p,cu}}{\dot{m}_w c_{p,w} + hA_{cu}} \tag{6}$$

The TC describes the speed of a first-order system's response to a step input and equals the time to reach the 62.3% of its steady-state. A similar approach can be followed for the AS power-down.

Based on the theoretical analysis, the TC depends on the material and geometry (mass and surface) of AS and is inversely proportional to the water flow.

Content from this work may be used under the terms of the CC BY 3.0 licence (© 2015). Any distribution of this work must maintain attribution to the author(s), title of the work, publisher, and DOI.

ISBN: 978-3-95450-168-7 doi:10.18429/JACoW-IPAC2015-TUPTY004

Content from this work may be used under the terms of the CC BY 3.0 licence (© 2015). Any distribution of this work must maintain attribution to the author(s), title of the work, publisher, and DOI.

TRACKING SIMULATION FOR BEAM LOSS STUDIES WITH APPLICATION TO FCC

M. Boscolo, INFN-LNF, Frascati, Italy; H. Burkhardt, CERN, Geneva, Switzerland

Abstract

We present first results on FCC-ee beam losses using a tracking simulation tool originally developed and successfully applied to Flavor Factories designs.

After a brief description of the tool, we discuss first results obtained for FCC-ee at top energy, both for the Touschek effect and radiative Bhabha scattering.

INTRODUCTION

CERN recently launched in a worldwide collaboration the new study for a design of a “Future Circular Collider” FCC with a circumference of about 100 km to be built in the CERN area; the target is a hadron collider (FCC-hh) at centre-of-mass energies close to 100 TeV with possible intermediate step of a e^+e^- collider (FCC-ee) in the centre-of-mass energy range of 90 – 400 GeV [1].

One of the challenges for FCC is to reach very high luminosities in combination with low or at least acceptable backgrounds and radiation levels in the interaction regions. To reach this goal, the interaction region design needs to cope with both the machine and detector constraints in a balanced machine detector interface (MDI) design. This is obtained by studies that include the simulation of the accelerator-related detector backgrounds, which can be divided in two main sources: losses of beam particles (the main focus of this paper) and synchrotron radiation [2]. Particle effects that cause beam losses can be generated either by single beam effects, mainly Touschek and beam-gas scattering all around the ring, or by beamstrahlung, radiative Bhabha, e^+e^- pairs production, referred to as *IP backgrounds*. At FCC all these effects need dedicated studies.

The timeline of the FCC design study aims for CDRs to be ready by the end of 2018. In the present stage the lattice design and beam parameters are evolving; the beam loss rates are expected to vary accordingly. We present here the tools that will be used to perform these studies for all the optics and at the different energies, together with the first results.

TOOL FOR MDI SIMULATIONS

To perform the tracking simulations of beam losses for the Machine Detector Interface studies we have started from the tool developed for the Flavor Factories [3], with the plan to adapt and upgrade it to the requirements of FCC. This is an on-going work and first results are presented here. We started to evaluate the Touschek and radiative Bhabha processes for the current optics.

The work can be subdivided in two different steps:

- read the machine lattice description and generate the twiss and aperture files;
- track the beam particles with the proper Monte Carlo depending on the effect under investigation.

MACHINE LATTICE

The starting point of the studies is the machine lattice layout in the form of the MAD-X input files [4]. As a first step, we run the MAD-X program to produce the twiss tfs file which contains the magnetic lattice description.

The beam loss estimates presented in the following sections have been obtained for the currently proposed lattices [5-6]. Parameters relevant for these studies are listed in Table 1.

Table 1: FCC-ee Parameters Relevant for Beam Losses Estimate

parameter	unit	
Beam Energy	GeV	175
Total length	km	100
Particles/bunch	10^{11}	4
Energy Spread	10^{-3}	2.6
Emittance x/ y	nm / pm	2.1 / 4.3
β_x^* / β_y^*	m	0.5 / 0.001
Emittance x/ y	nm / pm	2.1 / 4.3

The horizontal and vertical physical apertures are defined by means of an external file. As a start, we have assumed here a constant physical aperture of 2 cm and 4 mm in the horizontal and vertical planes, respectively. More reliable predictions will be possible when the apertures in the machine and in particular in the IP region have been defined. Our main focus here is on the discussion of the methods and trends, rather than on lifetime and loss rate numbers that may still change a lot.

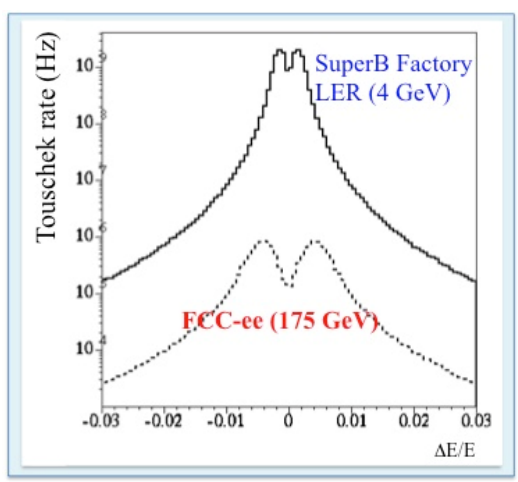

Figure 1: Rate of Touschek particles for FCC-ee (dotted line) compared to SuperB LER (black line).

ISBN: 978-3-95450-168-7 doi:10.18429/JACoW-IPAC2015-TUPTY006

STUDY OF ELECTRON CLOUD INSTABILITIES IN FCC-hh

K. Ohmi, KEK, Tsukuba, Japan
L. Mether, D. Schulte, F. Zimmermann, CERN, Geneva, Switzerland

Abstract

Electron cloud effects are serious issue for LHC and future hadron colliders, FCC-hh. Electron cloud causes coherent instabilities due to collective motion between beam and electrons. Electron cloud also causes incoherent emittance growth due to nonlinear force of beam-cloud electron force. We discuss the fast head-tail instability and the emittance growth in FCC-hh.

INTRODUCTION

The future circular hadron collider FCC-hh has been designed as 50 TeV×50TeV proton collider with 100 km circumference. The relativistic gamma factor (γ=53,000) is higher than those of many electron storage- ring light sources. The wave lengths of the emitted photons are in the X-ray region, which is comparable with those as light sources. Electrons are produced by the photons which hit the surface of the beam screen inside the cryostat.

Electrons are attracted and accelerated by the beam force. Electrons accumulated in the beam chamber may contribute an additional heat load to the cryostat, and cause beam instabilities and emittance growth. In this paper we focus on the beam instabilities and emittance growth caused by the electron cloud.

THRESHOLD ELECTRON DENSITY OF FAST HEAD-TAIL INSTABILITY

Electrons oscillate in the field of the proton beam. The oscillation frequency near the beam centre is given by

$$\omega_e = \sqrt{\frac{\lambda_p r_e c^2}{\sigma_y(\sigma_x+\sigma_y)}} \tag{1}$$

where λ_p and $\sigma_{x(y)}$ are the line density of the proton bunch and its transverse beam size, respectively. r_e is the classical electron radius.

Electron cloud induces a short range wake force with the frequency of Eq. (1). Threshold of electron density is determined by a balance of the strength of the wake field and Landau damping due to the slippage (synchrotron motion). The threshold density is given by [1,2]

$$\rho_{e,th} = \frac{2\gamma\nu_s\omega_e\sigma_z/c}{\sqrt{3}KQr_0\beta L} \tag{2}$$

K characterizes how many electrons contribute to the instability and Q is the quality factor of the wake field. We use $K=\omega_e\sigma_z/c$ and the empirical formula $Q=\min(\omega_e\sigma_z/c,7)$. Table 1 shows parameters for FCC-hh and the corresponding electron threshold density. The tune shift induced by an electron cloud at the threshold density is also included in the table.

Table 1: Parameter List for FCC-hh.

		inj	top
Energy	E(TeV)	3.3	50
Bunch population	N_p (10^{10})	10	10
Emittance	ε (nm)	0.625	0.0413
Averaged beta	β (m)	200	200
Bunch length	σ_z (m)	0.08	0.08
Synchrotron tune	ν_s	0.0019	0.0019
Electron freq.	$\omega_e/2\pi$	3.56GHz	14 GHz
Electron osc.	$\omega_e\sigma_z/c$	5.97	23
Threshold density	$\rho_{e,th}$	4.4×10^{10}	5.7×10^{11}
Tune shift at thr.	$\Delta\nu_{th}$	0.00039	0.00033

SYNCHROTRON RADIATION AND PHOTO-ELECTRON EMISSION

Charge particles passing through a bending magnet emit photons in the form of synchrotron radiation. The number of photons emitted by a particle per metre is expressed as

$$N_\gamma = \frac{5\alpha}{2\sqrt{3}}\frac{\gamma}{\rho_{Bend}} \tag{3}$$

For FCC-hh, with ρ_{bend}=11.3 km, the number is 0.035/p.m (per proton metre) at 50 TeV and 0.0023/p.m at injection energy of 3.3 TeV. The critical energy

$$E_c = \frac{3\hbar c}{2}\frac{\gamma^3}{\rho_{Bend}} \tag{4}$$

is 3.96 keV at 50 TeV (1.1 eV at 3.3 TeV). The quantum efficiency of photoelectron emission is 0.2-0.3 for shallow angle of photon incidence. Most of the photons hit the outside wall of the screen. Some part of the reflected photons hit a wide area of wall. The number of electrons produced by a bunch passage per metre is 10^9 (50 TeV) - 10^8 (3.3 TeV). Considering the chamber cross section 10 cm^2, the density resulting from the photoelectrons of a single bunch, $\rho_e=10^{12}$ - 10^{11} m^{-3}, already is higher than the instability threshold. Electron production can be suppressed by several kinds of surface

#ohmi@post.kek.jp

Content from this work may be used under the terms of the CC BY 3.0 licence (© 2015). Any distribution of this work must maintain attribution to the author(s), title of the work, publisher, and DOI.

ISBN: 978-3-95450-168-7 doi:10.18429/JACoW-IPAC2015-TUPTY007

STUDY OF BEAM-BEAM EFFECTS IN FCC-he

K. Ohmi, KEK, Tsukuba, Japan
F. Zimmermann, CERN, Geneva, Switzerland

Abstract

Beam-beam effects of the ring-ring scheme of FCC-he and LHeC are being studied using weak-strong simulations. The beam-beam tune shift of the electron beam is one order larger than that of proton beam. The study of the electron motion under the beam-beam interaction is the main subject. Luminosity and equilibrium beam size and beam lifetime are analysed.

INTRODUCTION

Proton (hadron)-electron collision is one of the operation modes of FCC. Either an ERL or a storage ring is considered for the electron beam accelerator. In this paper we focus on the storage ring, i.e. the so-called ring-ring scheme. The electron beam collides with proton beam with energy E=50 TeV. The shape of the FCC proton beam is close to round, with equal emittances in both transverse planes. The electron beam should have the same beam size at the collision point. The emittance of the proton beam is very small, ε=0.04 nm. β^*_{xy}=0.4/0.1 m for the proton beam gives the IP beam size σ_{xy}=4/2 μm. On the other hand, the rms bunch length of the proton beam is very long, i.e. 8 cm, to be compared with only 1-2 mm for the electron beam. To optimally match the beam sizes at IP, the choice of the electron-beam emittance and β^*_{xy} is multi-faceted. Strong hourglass effect appears for β^*_{xy} squeezed to values smaller than the proton bunch length. The allowed synchrotron-radiation power of 50 MW limits the total bunch intensity of electron beam. The beam-beam tune shift of proton beam is rather small, while that of electron beam tends to be large. We can choose either $\beta^*_{xy}\sim\sigma_z$ or $\beta^*_{xy} \ll \sigma_z$. The study of the beam-beam interaction for large beam-beam tune shifts in a weak-strong model is the main subject of this paper.

Table 1: Parameter List of FCC-he [1]

	Electron		Proton
Energy [GeV]	60	120	50000
Bunches/beam	10600	1360	10600
Bunch intensity	9.4×10^{10}	6×10^{10}	1×10^{11}
Bunch length [cm]	0.15	0.12	8
Emittance [nm]	1.9	0.94	0.04/0.02
$\beta^*_{x/y}$ [mm]	8/4	17/8.5	400/200
beam-beam ξ	0.13	0.13	0.022
L [10^{34}cm^{-2}s^{-1}]	6.2	0.7	

BEAM-BEAM SIMULATION METHOD

We are using weak-strong simulations in which the proton beam is represented by a fixed Gaussian distribution of macro-particles, that is, the proton and electron beams are regarded as the strong and weak beams, respectively.

The proton beam (bunch) is sliced into 100-200 pieces longitudinally. The number of pieces required depends on the ratio of σ_z/β_y. The electro-magnetic field of a proton beam traveling at the speed of light is formed in the plane perpendicular to the traveling direction. The electro-magnetic field of each slice depends on the charge in a slice of thickness dz and on the distribution (Gaussian in x-y plane). The motion of the weak beam particles is modelled by applying kicks corresponding to the integrated effect of the electro-magnetic field per slice followed by drifts between slices. The kick, which a charged particle with a deviation of (x,y) from the center of the distribution experiences, is expressed using Bassetti-Erskine formula [2]. The beam size $\sigma_{xy}(s)$ where electron particle (z) collides with a proton slice (z_i) depends on the collision point s: $s=(z-z_i)/2$. $\sigma_{xy}(s)$ is determined by the beta function variation near the IP. A longitudinal kick is applied to guarantee the symplecticity [3]. The beamstrahlung is also taken into account [4, 5].

LUMINOSITY SIMULATION FOR FCC-he AND LHeC

Simulations are performed using 10,000 macro-particles for the luminosity calculation [5]. The collision range of two beams with bunch length σ_{zp} (protons) and σ_{ze} (electrons) is $s \approx \pm(\sigma_{z,p}+\sigma_{z,e}) \approx \pm\sigma_{z,p}$. The ratio between proton bunch length and electron IP beta function β_{ye} is σ_{zp}/β_{ye}~10 at 120 GeV or 20 at 60 GeV. The area s~β_{ye} is divided into 10 steps to ensure a good convergence of the simulation. The total number of bunch slices (z_i) is chosen 100 (120 GeV) and 200 (60 GeV). The simulations are performed over 2,000 and 20,000 turns for 120 and 60 GeV, respectively. These simulation periods correspond to 2000/144=14 times, or 20,000/1,152=17 times, the radiation damping time, respectively. The transverse tune is chosen as (ν_x, ν_y)=(0.54,0.61), which has been found to be the best working point for FCC-ee [6]. The synchrotron tune is chosen as 0.025.

Luminosity and beam sizes of the electron beam are evaluated turn by turn. Figure 1 shows the evolution of luminosity. The luminosity drops very quickly in collisions for both 120 GeV and 60 GeV e^-, much below the design values of 7×10^{33} and 6.2×10^{34} cm^{-2}s^{-1}, respectively.

Content from this work may be used under the terms of the CC BY 3.0 licence (© 2015). Any distribution of this work must maintain attribution to the author(s), title of the work, publisher, and DOI.

ISBN: 978-3-95450-168-7 doi:10.18429/JACoW-IPAC2015-TUPTY008

COMMISSIONING STATUS AND PLAN OF SUPERKEKB INJECTOR LINAC

M. Satoh#, M. Akemoto, Y. Arakida, D. Arakawa, N. Iida, H. Iwase, A. Enomoto, Y. Enomoto, S. Fukuda, Y. Funakoshi, K. Furukawa, T. Higo, H. Honma, M. Ikeda, K. Kakihara, S. Kazama, H. Katagiri, T. Kamitani, H. Kaji, M. Kikuchi, M. Kurashina, H. Koiso, H. Matsushita, S. Matsumoto, T. Matsumoto, S. Michizono, K. Mikawa, T. Mimashi, T. Miura, F. Miyahara, T. Mori, A. Morita, H. Nakajima, K. Nakao, T. Natsui, Y. Ohnishi, S. Ohsawa, Y. Ogawa, Y. Seimiya, T. Shidara, A. Shirakawa, M. Suetake, H. Sugimoto, T. Suwada, T. Takenaka, M. Tanaka, M. Tawada, Y. Yano, K. Yokoyama, M. Yoshida, R. Zhang, X. Zhou, KEK/ SOKENDAI, Tsukuba, Japan
D. Satoh, TITECH, Tokyo, Japan

Abstract

The SuperKEKB main ring is currently being constructed for aiming at the peak luminosity of 8 x 10^{35} $cm^{-2}s^{-1}$. The electron/positron injector linac upgrade is also going on for increasing the intensity of bunch charge with keeping the small emittance. The key upgrade issues are the construction of positron damping ring, a new positron capture system, and a low emittance photo-cathode rf electron source. The injector linac beam commissioning started in the October of 2013. In this paper, we report the present status and future plan of SuperKEKB injector commissioning.

INTRODUCTION

The KEKB project has successfully completed its decade operation in the June of 2010. During the KEKB operation, the injector linac provided the different flavors of electron and positron beams to four independent storage rings; KEKB e-, e+, PF, and PF-AR rings. The linac beam is injected into each storage ring in every time interval of 20 ms since the linac parameters of timing and low level rf phase can be arbitrary controlled up to 50 Hz for the simultaneous top-up injection of three rings except PF-AR. For the simultaneous top-up injection, an event based timing control system has been implemented to the injector linac control system in the October of 2008 [1]. The achievement of simultaneous top-up injection made a strong impact on the triumph of KEKB project. It improve the KEKB and PF stored current stabilities up to 0.05% and 0.01%, respectively.

Figure 1 and Table 1 show the layout and the main parameters of SuperKEKB injector linac, respectively. Toward SuperKEKB project [2], the main issue is the high bunch charge transportation with keeping small emittance. For increasing the positron intensity, the flux concentrator and 10 large aperture S-band accelerating structures have been successfully manufactured and installed into the beam line [3, 4]. As a low emittance and high intensity electron source, we have designed and installed a photo-cathode rf gun cavity based on a noble new scheme in the summer of 2013 [5]. For the new rf gun system, a new laser system has been also built for aiming at the temporal modulation to obtain the longitudinal square shape beam which can help to reduce the energy spread [6, 7].

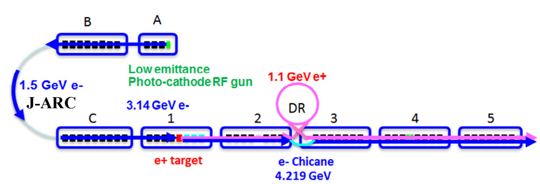

Figure 1: Layout of SuperKEKB injector linac.

Table 1: Main Parameters of SuperKEKB Injector Linac

	KEKB		SuperKEKB	
	e-	e+	e-	e+
Beam energy (GeV)	8	3.5	7	4
Bunch charge (nC)	1	1 (10*)	5	4 (10*)
Normalized vertical emittance (mm·mrad)	100	2100	20	20
Normalized horizontal emittance (mm·mrad)	100	2100	50	100
Energy spread (%)	0.05	0.125	0.08	0.07
Bunch length (mm)	1.3	2.6	1.3	0.7
# of bunch with interval of 96 ns	2			
Maximum beam repetition (Hz)	50			

*: Primary electron beam for positron production.

BEAM COMMISSIONING

Overview

The beam commissioning started in the October of 2013. At the beginning phase of beam commissioning, we mainly devoted the tuning of rf gun laser system for aiming at the high intensity bunch charge generation.

Corresponding author. *e*-mail address: masanori.satoh@kek.jp.

Content from this work may be used under the terms of the CC BY 3.0 licence (© 2015). Any distribution of this work must maintain attribution to the author(s), title of the work, publisher, and DOI.

ISBN: 978-3-95450-168-7 doi:10.18429/JACoW-IPAC2015-TUPTY010

THE LUMINOSITY REDUCTION WITH HOURGLASS EFFECT AND CROSSING ANGLE IN AN E-P COLLIDER

Yuemei Peng*, Key Laboratory of Particle Acceleration Physics and Technology, Institute of High Energy Physics, Chinese Academy of Sciences, Beijing, China
Yuhong Zhang, Thomas Jefferson National Accelerator Facility, Newport News, Virginia, USA

Abstract

This paper derived the luminosity reduction caused by crossing angle and hourglass effect in an asymmetric collision. Here, we gave the general expressions of the geometrical reduction factor of luminosity for the asymmetric case caused by crossing angle and hourglass effect, for tri-Gaussian bunches colliding. We also gave it simple expression in some special cases to recover the earlier results, such as the formulas for only hour-glass effect exist and only crossing angle exist. The expressions used in e-p collider are also analysed in detail.

INTRODUCTION

An electron-ion colliders CehC based on CepC-SppC have been envisioned in China for reaching new frontiers of high energy and nuclear physics. In order to have larger collision frequency, bunch spacing is very small in the *CehC* design. This will cause the problem of parasitic collisions: bunches may interact with each other not only at the interaction point (IP) but also at points around the IP, which can be avoided by collision with a crossing angle. The proton beam have much longer bunch length than the electron beam, though both of them have the bunch length comparable to the betatron function at the interaction point, the hourglass effect is still can't neglected.

There had been several expressions of collision luminosity, which treat collision with the head-on collision of asymmetric beams with hourglass effect [1, 2], angled collision of round beams with hourglass effect [3], the angled collision of symmetric beams with hourglass effect [4] and asymmetric angled collision with hourglass effect [5]. Here, the word symmetric or asymmetric is concerned with the beam sizes of colliding beams but not the beam energies.

This paper uses the integral method to give a more general expression of the geometrical reduction factor of luminosity for asymmetric tri-Gaussian bunches angled collision with hourglass effect.

LUMINOSITY FOR ANGLED COLLISION WITH HOURGLASS EFFECT

Consider two bunches of particles with densities $\rho_1(x,y,s,t)$ and $\rho_2(x,y,s,t)$, the number of particles is N_1 and N_2, all particles are assumed to move with the common velocity $\vec{v}_1$ and $\vec{v}_2$. Then, the colliding luminosity is given by the overlap integral both in time and in space [6]

$$L = N_1 N_2 N_b f_{rev} K \int \iiint_{-\infty}^{+\infty} \rho_1 \rho_2 \, \mathrm{dxdydsdt} \,. \qquad (1)$$

Where, f_{rev} is the revolution frequency, K is the kinematic factor, which is expressed as

$$\mathrm{K} = \sqrt{(\vec{v}_1 - \vec{v}_2)^2 - (\vec{v}_1 \times \vec{v}_2)^2 / c^2} \,. \qquad (2)$$

x, y, s are the coordinates in the lab frame. However, the distribution functions are assumed Gaussian distributions only in the commoving frame, namely,

$$\rho_1(x_1, y_1, s_1, t) = \rho_{1x}(x_1)\rho_{1y}(y_1)\rho_{1s}(s_1 - ct)$$

$$\rho_2(x_2, y_2, s_2, t) = \rho_{2x}(x_2)\rho_{2y}(y_2)\rho_{2s}(s_2 - ct)$$

Here,

$$\rho_{iz}(u) = \frac{1}{\sigma_{iz}\sqrt{2\pi}} exp\left(-\frac{u^2}{2\sigma_{iz}{}^2}\right) \quad i = 1,2, \quad z = x, y, \qquad (3)$$

$$\rho_{is}(s - s_0) = \frac{1}{\sigma_{is}\sqrt{2\pi}} \exp\left(-\frac{(s-s_0)^2}{2\sigma_{is}{}^2}\right), \quad i = 1,2, \qquad (4)$$

$$\sigma_{iz} = \sigma_{iz}^* \sqrt{1 + \frac{s_i{}^2}{\beta_{iz}^{*\,2}}} \,. \quad i = 1,2, \qquad z = x, y, \qquad (5)$$

If there is a crossing angle $\emptyset$ in horizontal (x, s)-plane in the collider, we need to transform the co-moving frame coordinates to the lab frame coordinates, shown in figure 1.

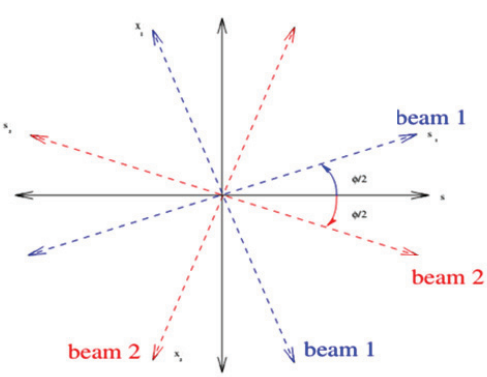

Figure1: Coordinates transformation.

$$\begin{cases} x_1 = x \cdot cos\frac{\emptyset}{2} - s \cdot sin\frac{\emptyset}{2}, s_1 = s \cdot cos\frac{\emptyset}{2} + x \cdot sin\frac{\emptyset}{2} \\ x_2 = -x \cdot cos\frac{\emptyset}{2} - s \cdot sin\frac{\emptyset}{2}, s_2 = -s \cdot cos\frac{\emptyset}{2} + x \cdot sin\frac{\emptyset}{2} \end{cases} \qquad (6)$$

*pengym@ihep.ac.cn

Content from this work may be used under the terms of the CC BY 3.0 licence (© 2015). Any distribution of this work must maintain attribution to the author(s), title of the work, publisher, and DOI.

ISBN: 978-3-95450-168-7 doi:10.18429/JACoW-IPAC2015-TUPTY011

A PRELIMINARY DESIGN OF THE CEPC INTERACTION REGION*

Y.W. Wang#, S. Bai, H.P. Geng, T.J. Bian, X.H. Cui, D. Wang, J. Gao, Y.S. Zhu
IHEP, CAS, Beijing, 100049, PRC

Abstract

CEPC (Circular Electron and Positron Collider) is a circular Higgs Factory with optimized energy 240 GeV. In order to achieve luminosity as high as $2 \times 10^{34} \mathrm{cm}^{-2}\mathrm{s}^{-1}$, CEPC calls for a small vertical beta function at IP ($\beta_y^* = 1.2$ mm) which was provided by the final focus of the interaction region. In this paper, a preliminary design of the CEPC interaction region was presented. The optimization of dynamic aperture with interaction region insertion and the machine detector interface was discussed as well.

INTRODUCTION

CEPC (Circular Electron and Positron Collider) is a circular Higgs Factory with optimized energy 240 GeV [1]. In order to achieve luminosity as high as $2 \times 10^{34} \mathrm{cm}^{-2}\mathrm{s}^{-1}$, CEPC calls for a small vertical beta function at the interaction point (IP) ($\beta_y^* = 1.2$ mm) which was provided by the final focus of the interaction region. In this paper, a preliminary design of the CEPC interaction region (IR) was presented. The optimization of dynamic aperture with IR insertion and the machine detector interface was discussed as well. Table 1 shows the key parameters of the interaction region.

Table 1: Key Parameters of the Interaction Region [1]

Parameters	Unit	Value
Distance from QD0 to IP [$L*$]	m	1.5
Number of IP [N_{IP}]	-	2
Beam energy [E]	GeV	120
Emittance [$\varepsilon_x/\varepsilon_y$]	m • rad	6.12E-09 / 1.84E-11
Beta function at IP [β_x^*/β_y^*]	mm	800 / 1.2
Bunch length total [$\sigma_{z,tot}$]	mm	2.88
Energy spread total [$\sigma_{\delta,tot}$]	%	0.177
Luminosity / IP [L]	$\mathrm{cm}^2\mathrm{s}^{-1}$	2.04E+34

The IR of CEPC has been designed with the following requirements:

- Provide small beam sizes at the IP.
- The large chromaticity generated by final doublet (FD) must be compensated locally in order to achieve a large momentum acceptance of 2% for the whole ring.
- The solenoid field from the detector compensated to minimize its perturbation on the beam motion .
- The sizes of the accelerator equipment inserted into the detector should be constrained to provide the largest possible angular acceptance for the detector.
- The beam-induced background should be acceptable for the detector.

*Work Supported by National Natural Science Foundation of China (11175192) and the CAS Centre for Excellence in Particle Physics (CCEPP).
#wangyw@ihep.ac.gov

INTERACTION REGION

Optics Design

In order to achieve very high luminosity, CEPC calls for a small vertical beta function at IP ($\beta_y^* = 1.2$ mm). The small β_y^* require the final quadrupole as close to the IP as possible in order to minimize the chromaticity and keep the beta function lowest possible at the final quadrupole, as shown in Eq. 1. ξ_y is the vertical chromaticity generated in the final quadrupole QD0, β_y is the vertical beta function at QD0 and L^* is the distance from the IP to QD0. To facilitate the design of final focus, we choose $L^* = 1.5$ m.

$$\xi_y \simeq \frac{L^*}{\beta_y^*}, \beta_y \simeq \frac{L^{*2}}{\beta_y^*} \tag{1}$$

The chromaticity correction scheme of final focus (FF) had been well developed for the linear collider programs from 1980s, such as SLC, NLC, FFTB [2-4], and adopted by the circular collider programs such as SuperB [5] and SuperKEKB [6]. CEPC also adopt a FF optics similar to the linear colliders'. Unlike the single pass feature in a linear collider, the final focus design of a circular collider has to fix many specific issues.

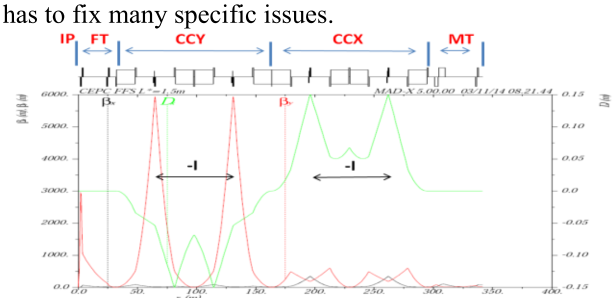

Figure 1: Lattice functions of the final focus.

The final focus system is a telescopic transfer line, starting from IP, which includes: a final telescopic transformer (FT), chromaticity correction section on the vertical plane (CCY), chromaticity correction section on the horizontal plane (CCX) and matching telescopic transformer (MT), see Fig. 1.

Content from this work may be used under the terms of the CC BY 3.0 licence (© 2015). Any distribution of this work must maintain attribution to the author(s), title of the work, publisher, and DOI.

ISBN: 978-3-95450-168-7 doi:10.18429/JACoW-IPAC2015-TUPTY012

ORBIT CORRECTION IN CEPC*

S. Bai#, H.P. Geng, J. Gao, IHEP, Beijing, China

Abstract

With the discovery of the higgs boson at around 125GeV, a circular higgs factory design with high luminosity (L ~ 10^{34} $cm^{-2}s^{-1}$) is becoming more popular in the accelerator world. The CEPC project in China is one of them. To reduce the cost, pretzel scheme was considered in CEPC orbit design. The presence of every kind of errors and misalignments will destroy the pretzel orbit. In this paper, we correct the distorted pretzel orbit in the CEPC main ring using the dipole correctors and beam position monitors. The pretzel orbit was recovered and the maximum corrector strengths are got.

INTRODUCTION

With the discovery of a Higgs boson at about 125 GeV, the world high-energy physics community is investigating the feasibility of a Higgs Factory, a complement to the LHC for studying the Higgs [1]. There are two ideas now in the world to design a future higgs factory, a linear 125 × 125 GeV e^+e^- collider and a circular 125 GeV e^+e^- collider. From the accelerator point of view, the circular 125 GeV e^+e^- collider, due to its low budget and mature technology, is becoming the preferred choice to the accelerator group in China. To reduce the cost, only one tunnel may be digged. In this case, e+ and e- bunches will be travelled in the same tunnel and separated by several electrostatic sperators. This is so called the “pretzel” scheme [2] which has already been demonstrated in LEP. The position of the pretzel closed orbit in CEPC main ring is affected by the field errors and the alignment errors in the magnets. The orbit errors are mainly due to displaced quadrupoles. Deviations of the beam orbit from the ideal positions can be detected by the beam position monitors (BPM) located near each quadrupole. The closed orbit errors as measured by these monitors can be corrected by a series of dipole correctors near each quadrupole.

In this paper, the field errors and alignment errors of the magnets are first specified. The distorted closed orbit is then calculated and corrected by the approximately distributed dipole correctors. The maximum strengths of correctors are got for manufacture.

THEORY

The orbit correction vector $\overrightarrow{\Delta_c}$ at all the monitors is related to the beam bump $\vec{\theta}$ at all the correctors by [3]:

$$\overrightarrow{\Delta_c} = T\vec{\theta} \tag{1}$$

Where T is a m x n matrix with m the number of monitors and n the number of correctors; the elements of T are

$$T_{ij} = \frac{\sqrt{\beta_i \beta_j}}{2\sin \pi\nu} \cos \nu(\pm\pi + \phi_i - \phi_j) \tag{2}$$

Where ν is the betatron wave number, β is the betatron function; ν φ is the betatron phase. The plus sign in front of π is used for the case of $\varphi_i < \varphi_j$ and the minus sign for $\varphi_i > \varphi_j$. The orbit deviation is given by:

$$\overrightarrow{\Delta} = \overrightarrow{\Delta_0} + \overrightarrow{\Delta_c} \tag{3}$$

Where $\overrightarrow{\Delta_0}$ is the orbit deviation measured before correction. The sum of the squares of the orbit deviation

$$S = \sum_{i=1}^{n} (\Delta_{0i} + \Delta_{ci})^2 \tag{4}$$

We wish to find the vector $\overrightarrow{\theta_n}$ which minimizes the value of S, i.e., $\partial S / \partial \theta_n = 0$ for n=l, 2, ... N.

IMPERFECTIONS IN THE MAGNETS

The CEPC machine imperfections mainly consist of the field errors and misalignment errors of every kinds of magnets, bending magnets, quadrupoles and sextupoles. The largest contributions to the orbit distortions come from the misalignment of the quadrupoles. We choose the imperfections setting similar to LEP [4]:

Table 1: LEP Magnet Error Parameters

	Dipole	Quadrupole
<y> mm	0.2	0.1
<x> mm	0.3	0.1
<tilt> mrad	0.1	0.1
<△B/B> rms values	5e-4	
<△K/K> rms values		5e-4

THE DISTORTED PRETZEL ORBIT WITH ALL ERRORS

With all the field and misalignment errors of the magnets given in the above table 1, which are distributed in Gaussian and cut at three sigma, the horizontal and vertical orbit deviation at all the BPMs before orbit correction, are shown in figure 1 and figure 2:

*Work supported by the National Natural Science Foundation of China (NSFC, Project 11175192) and in part by the CAS Center for Excellence in Particle Physics (CCEPP).
#baisha@ihep.ac.cn

Content from this work may be used under the terms of the CC BY 3.0 licence (© 2015). Any distribution of this work must maintain attribution to the author(s), title of the work, publisher, and DOI.

ISBN: 978-3-95450-168-7 doi:10.18429/JACoW-IPAC2015-TUPTY015

STUDY ON THE TRANSVERSE PAINTING DURING THE INJECTION PROCESS FOR CSNS/RCS*

M.Y. Huang#, S. Wang, N. Huang, J. Qiu, S.Y. Xu, L.S. Huang
1：China Spallation Neutron Source, Institute of High Energy Physics, Chinese Academy of Sciences, Dongguan, China
2：Dongguan Institute of Neutron Science, Dongguan, China

Abstract

For the China Spallation Neutron Source (CSNS), a combination of the H^- stripping and phase space painting method is used to accumulate a high intensity beam in the Rapid Cycling Synchrotron (RCS). In this paper, firstly, the injection processes with different painting ranges and different painting methods were studied. With the codes ORBIT and MATLAB, the particle distribution and painting image were obtained. Then, the reasonable painting range which is suitable for the aperture size and magnet gap can be selected. Since the real field uniformity of BH3 and BV3 is not completely in conformity with the design requirement, the painting method and painting range also need to be selected to reduce the effects of bad field uniformity.

INTRODUCTION

CSNS is a high power proton accelerator-based facility [1]. The accelerator consists of an 80MeV H^- linac which is upgradable to 250MeV and a 1.6GeV RCS with a repetition rate of 25Hz which accumulates an 80MeV injection beam, accelerates the beam to the designed energy of 1.6GeV and extracts the high energy beam to the target. The design goal of beam power for CSNS is 100kW and capable of upgrading to 500kW [2].

For the high intensity proton accelerators, the injection with H^- stripping is actually a practical method. In order to reduce the beam losses in CSNS/RCS, the phase space painting method is used for injecting the beam of small emittance from the linac into the large ring acceptance [3].

Due to the aperture size at the BH3/BV3 position becomes smaller and the real field uniformity of BH3/BV3 in some place is greater than the design requirement, the reasonable painting range and painting method for CSNS/RCS need to be studied and chosen again [4].

PAINTING RANGE AND PARTICLE DISTRIBUTION

For CSNS/RCS, the previous aperture size at the BH3/BV3 position during the injection region was 163mm. However, due to the space at the BH3/BV3 position was so narrow, the aperture size was changed to smaller (150mm). Because of this, the transverse painting range, the painting method and the particle motion distribution during the injection process need to be studied again in detail.

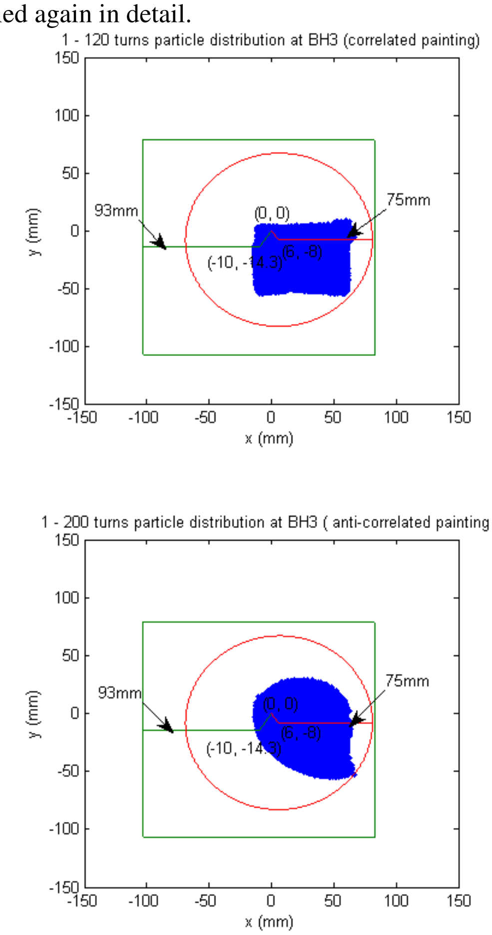

Figure 1: The particle distribution of all the 200 turns at the BH3 position for correlated painting and anti-correlated painting, respectively.

With the code ORBIT [5], the injection processes with different painting methods and painting ranges can be simulated. The painting image and particle distribution of each turn can be obtained. Then, using the code MATLAB, the particle distribution data of each turn can be analyzed and the data of all the 200 turns can be combined together. Then, it can be estimated that whether the aperture size and the magnet gap of BH3/BV3 will be suitable for the particle motion of all the 200 turns. Therefore, the reasonable painting range and painting method can be obtained.

*Work supported by National Natural Science Foundation of China (Project Nos. 11205185, 11175020 and 11175193)
#huangmy@ihep.ac.cn

Content from this work may be used under the terms of the CC BY 3.0 licence (© 2015). Any distribution of this work must maintain attribution to the author(s), title of the work, publisher, and DOI.

ISBN: 978-3-95450-168-7 doi:10.18429/JACoW-IPAC2015-TUPTY016

STUDY OF BACKGROUND AND MDI DESIGN FOR CEPC*

T.Yue, Q.Qin, Key Laboratory of Partical Acceleration Physics and Technology, IHEP, Beijing, China

Abstract

CEPC (circular electron positron collider) is a high energy electron positron collider proposed by IHEP, which is designed to provide e^+e^- collisions at the centre-of-mass energy of 240 GeV and deliver a peak luminosity greater than $1\times10^{34}cm^{-2}s^{-1}$ at each interaction point. The super high energy brings many challenges in machine design, especially in the control of background and protection of detectors. We describe the preliminary research result about background and MDI design.

INTRODUCTION

CEPC is short for circular electron positron collider with 120 GeV beam energy. Now we have just finished the Pre-CDR of it. Based on the lattice and IR design released now, we have made some preliminary research on background and MDI design. The research will be updated with the future lattice design.

MAIN PARAMETERS AND IR DESIGN

The main machine parameters are list in Table1.

Table 1: The Main Parameters of CEPC

Parameter		Unit
Beam energy [E]	120	GeV
Circumference [C]	54.752	Km
Luminosity [L]	2.04E+34	cm-2s-1
Number of IP [NIP]	2	
Bunch number [nB]	50	
betax at IP	0.0012	m
betay at IP	0.8	m

In general, the sensitive region for the detectors is within several meters from IP. For CEPC, we just concern about the region within ±4meters from IP. The layout of IR and MDI design are illustrated in Figure 1. There are four quadrupole magnets in this region, two of them designed for focusing and others for defocusing.

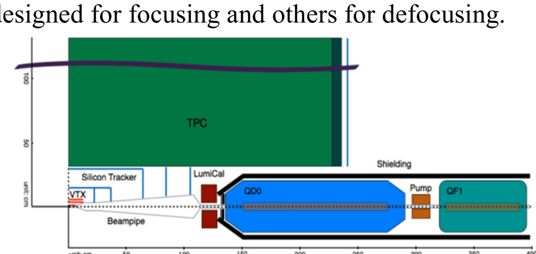

Figure 1: Layout of the MDI of CEPC.

The beam background of CEPC consists of synchrotron radiation background and lost particles background. The synchrotron radiation background has two sources, from the last bending magnets and from the quadrupole magnets in the final focus region. As for the lost particles background, there are many background source for CEPC, but the main source are beamstrahlung and radiative bhabha scattering.

SR BACKGROUND

When the beam passes through the last bending magnets upstream the IP, its orbit will be bended by the magnetic field with a SR fan emitted along the orbit direction. This SR fan will scan the IR region and may make damages on the detectors. In addition, for the beam size effect in horizontal and vertical plane, the particles in the edge of the beam will see the magnetic field of quadrupole magnets because of the displacement. Then it will also emit a SR fan and this SR also need to be analyzed.

The energy spectrum of the SR photons can be characterised by the critical energy [1], which can be calculated by the following formula.

$$E_c = \frac{3}{2}\hbar c\gamma^3 / \rho \tag{1}$$

For the last bending magnets upstream the IP, the bending radius of it is about 3780m,. Substitute it into the formula 1 with a 120GeV energy, we can get the critical energy of the photons from the last bending magnets is about 938KeV. As a comparison, the SR spectrum in LEP at 45.6GeV is less than 100GeV [2]. As for the SR photons from quadrupole magnets, we can still calculate the critical energy as the formula 1 with a new definited bending radius.

$$(1/\rho)_{quad} = kr^*\sqrt{\varepsilon_x\beta_x + \varepsilon_y\beta_y} \tag{2}$$

where the term with a square root symbol is the radial RMS beam size. The critical energy of the SR photons from quadrupole magnet is proportion to the beam size. If we assume a 12 times RMS beam size, the corresponding critical energy is about 23MeV which is pretty high.

In order to estimate the photons distribution and power distribution of SR in the IR, We use a code provided by Mike Sullivan to simulate the synchrotron radiation background, the simulation result is showed in Figure 2.

Content from this work may be used under the terms of the CC BY 3.0 licence (© 2015). Any distribution of this work must maintain attribution to the author(s), title of the work, publisher, and DOI.

ISBN: 978-3-95450-168-7 doi:10.18429/JACoW-IPAC2015-TUPTY017

ION POLARIZATION CONTROL IN THE MPD AND SPD DETECTORS OF THE NICA COLLIDER

A.D. Kovalenko, A.V. Butenko, V.D. Kekelidze, V.A. Mikhaylov, JINR, Dubna, Russia
A.M. Kondratenko, M.A. Kondratenko, STL "Zaryad", Novosibirsk, Russia
Yu.N. Filatov, MIPT, Moscow, Russia

Abstract

Two solenoid Siberian snakes are placed in the opposite collider's straight sections are used to control deuteron's and proton's polarization in the NICA collider. Solenoid snakes substantially reconstruct beam's orbital motion. The change of the polarization direction in the vertical plane of MPD and SPD detectors occurs due to insertion of polarization control (PC) solenoids in the magnetic lattice of the collider. The solenoids rotating particle's spin by small angels practically do not influence on the beam's orbital motion parameters. The dynamic of the polarization vector as function of the orbit length for cases of longitudinal and vertical polarization in the MPD and SPD detectors are presented.

SPIN TRANSPARANCY MODE IN NICA

NICA project at JINR is aimed at the experiments with polarized protons and deuterons at both SPD and MPD detectors over beam momentum range from 2 to 13.5 GeV/c [1, 2]. To control efficiently polarization of protons and deuterons as well it was proposed to use the collider in, so called, "spin transparency" mode, which is realized if two identical solenoid Siberian Snakes are placed in the opposite straight sections of the collider (Fig. 1) [3].

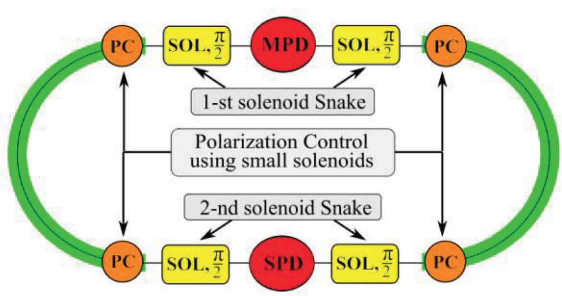

Figure 1: The polarization control scheme of protons and deuterons in the NICA collider.

The Snakes are divided symmetrically onto two parts by MPD and SPD setups. The transparency mode means that the influence of the fields generated by the two Snakes and the collider's arcs doesn't change the spin direction from turn to turn, i.e. the magnetic system is transparent for the spin. The NICA collider with two Snakes becomes similar to the figure-8 collider project at JLAB [4]. The field integrals of half solenoid Snake for protons and deuterons at maximum momentum are equal to 12.5 T·m and 40 T·m respectively.

BEAM POLARIZATION MANIPULATION IN SPD AND MPD DETECTORS

The unique feature of a spin transparency accelerator is the possibility to obtain any particle polarization using small magnetic field integrals [3]. The proton and deuteron polarization in the NICA collider ring can be efficiently controlled by weak solenoids. Any angle between the polarization and the beam direction lying in the vertical plane of SPD (MPD) detector can be obtained by introducing polarization control (PC) insertions. Each PC insertion is based on two weak solenoids separated by arc's dipoles. A symmetric scheme of polarization control with two PC insertions located at the both sides of the SPD (MPD) detector is presented in Fig. 2.

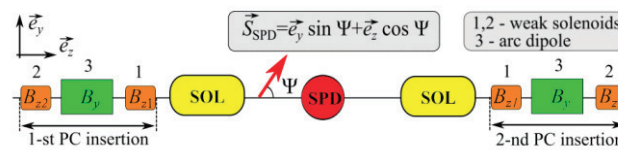

Figure 2: Polarization control by means of weak (PC) solenoids in SPD (MPD) detector.

The spin tune ν induced by PC insertions should exceed substantially the strength of $\nu = 0$ spin resonance. The strength is determined by the beam's emittances and by misalignments and manufacturing imperfections of the collider's magnetic system elements. Spin tune values are estimated to $\nu_p = 0.01$ and $\nu_d = 0.003$ for proton and deuteron case respectively.

A scheme of the snake's solenoids and weak PC solenoids positions is presented in Fig. 3. The eight snake's solenoids of 5.5 m long each are marked with yellow. The ten PC solenoids of 0.4 m long each are marked with orange. The snake solenoid fields are equal to 2.3 T for protons and 7.3 T for deuteron at the maximum momentum.

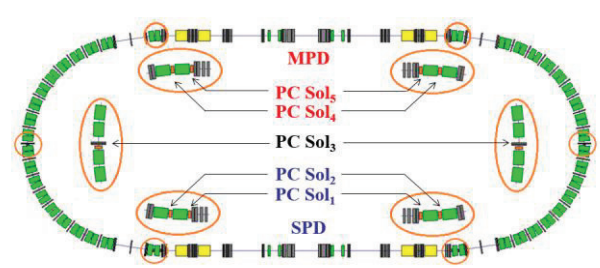

Figure 3: Placement of PC solenoids in NICA collider.

Content from this work may be used under the terms of the CC BY 3.0 licence (© 2015). Any distribution of this work must maintain attribution to the author(s), title of the work, publisher, and DOI.

ISBN: 978-3-95450-168-7 doi:10.18429/JACoW-IPAC2015-TUPTY018
Content from this work may be used under the terms of the CC BY 3.0 licence (© 2015). Any distribution of this work must maintain attribution to the author(s), title of the work, publisher, and DOI.

INTERACTION REGION FOR CRAB WAIST SCHEME OF THE FUTURE ELECTRON-POSITRON COLLIDER (CERN)*

A. Bogomyagkov†, E. Levichev
BINP, Novosibirsk 630090, Russia

Abstract

Design study in CERN of the accelerator that would fit 80-100 km tunnel called Future Circular Colliders (FCC) includes high-luminosity e^+e^- collider (FCC-ee) with center-of-mass energy from 90 to 350 GeV to study Higgs boson properties and perform precise measurements at the electroweak scale [1–3]. Crab waist interaction region provides collisions with luminosity higher than 2×10^{36} $cm^{-2}sec^{-1}$ at beam energy of 45 GeV. The small values of the beta functions at the interaction point and distant final focus lenses are the reasons for high nonlinear chromaticity limiting energy acceptance of the whole ring. The paper describes interaction region for crab waist collision scheme in the FCC-ee, principles of tuning the chromaticity correction section in order to provide large energy acceptance.

INTRODUCTION

One of the limiting factors of high energy e^+e^- collider (FCC-ee) is beamstrahlung [4–6], which limits the beam life time. Consideration of this effect by different authors gave several sets of parameters to achieve high luminosity and feasible beam lifetime. The first one is based on head-on collisions [7], the second is relying on crab waist collision scheme [6, 8] with crossing angle $2\theta = 30$ mrad. Both sets implement the same values of beta functions at the interaction point (IP): $\beta_x^* = 0.5$ m, $\beta_y^* = 0.001$ m and require energy acceptance of the ring more than ±2% to provide feasible beam life time. Advantages of the crab waist set are higher luminosity (7.5 times at 45 GeV) and crossing angle that provides natural separation of the bunches. The list of parameters relevant to present work is in Table1.

Lattice of the interaction region (IR) should satisfy several requirements:

1. since successor to FCC-ee is proton accelerator, the IR tunnel should be straight;
2. small values of IP beta functions produce large chromaticity, which should be compensated as locally as possible in order to minimize excitation of nonlinear chromaticity;
3. synchrotron radiation power loss should be significantly smaller than in the arcs;
4. synchrotron radiation at high energy will produce flux of high energy gamma quanta, therefore the lattice should minimize detector background;
5. small beta functions at IP enhance effects of nonlinear dynamics, decreasing dynamic aperture and energy acceptance of the ring, therefore the lattice should be optimized to provide large dynamic aperture and energy acceptance.

Table 1: Relevant Parameters for Crab Waist IR [6]

	Z	W	H	tt
Energy [GeV]	45	80	120	175
Perimeter [km]	100			
Crossing angle [mrad]	30			
Particles per bunch [10^{11}]	1	4	4.7	4
Number of bunches	29791	739	127	33
Energy spread [10^{-3}]	1.1	2.1	2.4	2.6
Emittance hor. [nm]	0.14	0.44	1	2.1
Emittance ver. [pm]	1	2	2	4.3
β_x^*/β_y^* [m]	0.5 / 0.001			
Luminosity / IP [10^{34} $cm^{-2}s^{-1}$]	212	36	9	1.3
Energy loss / turn [GeV]	0.03	0.3	1.7	7.7

FINAL FOCUS QUADRUPOLES

The minimum distance from IP to the face of the first quadrupole is chosen to be $L^* = 2$ m which at the present moment looks like a good compromise between beam dynamics [9] and detector constraints. Having the minimum distance the maximum reliably achievable gradient defines the quadrupole length. In the present study we demanded the quadrupole strength to be lower than 100 T/m, which is a very relaxed condition. Particles trajectories from IP through the FF doublet are on Figure 1 together with lines at several angles representing detector blind spot and rectangles for bare apertures of the quadrupoles. Quadrupole parameters length, gradient and radius of aperture at $E = 175$ Gev are presented in Table 2. The distance between bare apertures for the first quadrupoles is 3.5 cm, for the second pair the distance is 14.2 cm.

LATTICE

The IR lattice should provide desired values of optical functions at IP and compensate geometrical and chromatic aberrations which define dynamic aperture (DA) and energy acceptance of the ring. The optics of IR consists of sev-

* Work is supported by the Ministry of Education and Science of the Russian Federation
† A.V.Bogomyagkov@inp.nsk.su

ISBN: 978-3-95450-168-7 doi:10.18429/JACoW-IPAC2015-TUPTY019

REALISTIC BEAM HALO MODEL STUDY IN THE EXTRACTION LINE OF ATF2

N. Fuster-Martínez, IFIC (CSIC-UV)*,Valencia, Spain
A. Faus-Golfe, IFIC (CSIC-UV) and LAL, Université Paris-Sud, Orsay, France
P. Bambade, S. Liu, S. Wallon, LAL,Université Paris-Sud, Orsay, France
G. White, E. Marin, SLAC†, USA
K. Kubo, N. Terunuma, T. Okugi, T. Tauchi, KEK and SOKENDAI, Japan

Abstract

The understanding and control of the transverse beam halo distributions is an important issue to reduce sources of background noise in Future Linear Colliders (FLC) and specifically at ATF2. A realistic model of the beam halo in the old extraction line of the ATF damping ring was obtained in 2005, based on wire scanner measurements. Recently, new measurements were done in the new extraction line of ATF2, using both wire scanners, in 2013, and Optical Transition Radiation monitors (OTR), in 2014. The beam halo propagation through the ATF2 beamline by means of tracking simulations has been investigated using as input a purely Gaussian and uniform beam halo model.

INTRODUCTION

ATF2 [1] is a scaled down version of the Final Focus System (FFS) of the FLC with the two main goals of obtaining a vertical beam spot size at the virtual Interaction Point (IP) of 37 nm and to stabilize the beam at the nanometer level. For the beam size measurement at the IP a novel technique is used based on a laser interferometer beam size monitor (Shintake monitor). The beam halo consists of tails extending far beyond the Gaussian core of the beam that could be intercepted by the beam pipe creating undesired photonic background. In FLC, such particle losses would be unacceptable and could have devastating effects on the experiments. In ATF2, halo hitting on the beam pipe after the IP can generate a large amount of background limiting the Shintake monitor performance. Therefore, it is of great importance to understand the beam halo distribution and to control the background that could be generated by it. In order to investigate the beam halo distribution in ATF2 measurements were done in 2013 in the EXT line and post-IP with the wire scanners following the procedure done in 2005 in the old ATF2 beamline [2]. Complementary, in 2014, measurements were taken with the multi-OTRs system which is located close to the EXT line wire scanners. All the data has been analyzed and a summary of the measurements done in the EXT line is presented on this paper. In addition to these measurements, by the end of 2014 a Diamond Sensor (DS) has been installed in the Post-IP line of ATF2 in order to perform dedicated beam halo measurements [3, 4].

* Work supported by IDC-20101074, FPA2013-47883-C2-1-P and ANR-11-IDEX-0003-02
† Work supported by the US Department of Energy contract DE-AC02-76SF00515

BEAM HALO MEASUREMENTS IN THE EXT LINE OF ATF2

The ATF2 beamline is divided in three sections: the Extraction Line (EXT) with the diagnostics and matching sections, the Final Focus System (FFS) and the Post-IP line with some diagnostics and the dump. In Fig. 1 the location of the different devices being used to investigate the beam halo and background in the ATF2 beam line are depicted. In the EXT line we find the wire scanners and the OTR system and in the post-IP line we have one wire scanner and the recently installed DS.

Wire Scanners Beam Halo Measurements

At ATF2 five wire scanners are used to measure the beam size at different locations. In our experiment the wire scanner named MW2X located in the EXT line was used. A Cherenkov detector and a Photomultiplier (PMT) at around 26 m downstream of MW2X is installed to detect the bremsstrahlung photons generated by the wire scanners when scanning the beam. A different set of beam halo measurements were performed in April, June and December 2013 using MW2X in the EXT line. During these runs the beam energy was 1.3 GeV and the beam intensity was between 5-7 10^9 electrons. The optics configuration used was ten times the nominal β_x^* and the nominal β_y^* at the IP $(10\beta_x^* \times 1\beta_y^*)$. The beam halo scans have been performed with different PMT voltages in order to increase the sensitivity of the wire scanner. Then, the data was normalized to the lowest voltage and left and right scans have been combined because the beam halo observed in the EXT line is symmetric. The data combined is fitted to a power function of the number of sigmas following the analysis done in [2]:

$$\rho_{V,H}/N = (A/N)X^{-b} \tag{1}$$

where $\rho_{V,H}$ is the vertical and horizontal beam halo density respectively, N is the total number of particles, A, b are constants, and X is the number of sigmas.

In Fig. 2 it is shown all the data taken in 2013 with MW2X wire scanner corresponding to the vertical (top) and horizontal (bottom) beam halo distribution. The resulting fit for all the combined data is the following:

$$\begin{aligned} \rho_V/N &= (9 \pm 4)X^{-(7.3\pm0.3)} \quad 3 < X < 5 \\ \rho_V/N &= (0.001 \pm 0.001)X^{-(1.5\pm0.3)} \quad X > 5 \end{aligned} \tag{2}$$

Content from this work may be used under the terms of the CC BY 3.0 licence (© 2015). Any distribution of this work must maintain attribution to the author(s), title of the work, publisher, and DOI.

ISBN: 978-3-95450-168-7 doi:10.18429/JACoW-IPAC2015-TUPTY020

BUILDING A LUMINOSITY MODEL FOR THE LHC AND HL-LHC *

F. Antoniou, G. Arduini, Y. Papaphilippou, G. Papotti, CERN, Geneva, Switzerland

Abstract

One key objective of the High Luminosity LHC Upgrade is to determine a set of beam parameters and the hardware configuration that will enable the LHC to reach a peak luminosity of 5×10^{34} cm^{-2} s^{-1} and ultimately 7.5×10^{34} cm^{-2} s^{-1} with leveling, allowing an integrated luminosity of 250-300 fb^{-1} per year. In order to determine the integrated performance, it is important to develop a realistic model of the luminosity evolution during a physics fill. In this paper, different mechanisms affecting luminosity lifetime in the LHC are discussed and a luminosity model is presented. The model is bench-marked with data from LHC Run I.

INTRODUCTION

The performance of a collider is best described by the luminosity (integrated over time), which, in general, is given by [1]:

$$\mathcal{L}(t) = \frac{n_b f_{\text{rev}} N_1(t) N_2(t)}{2\pi\sigma_x(t)\sigma_y(t)} H\left(\sigma_s(t), \beta^*\right) F_{\text{geom}}(\sigma_s(t), \beta^*),$$

where n_b the number of colliding bunches, f_{rev} the revolution period, $N_{1,2}$ the number of particles per bunch for each beam, $\sigma_{x,y}$ the rms horizontal and vertical beam sizes at the collision point, β^* the beta function at collision (assuming round optics) and σ_s the rms bunch length. Due to the crossing angle at collision ϕ and the fact that the beta function varies rapidly around the interaction point (IP), a geometric $F_{\text{geom}}(\sigma_s, \beta^*)$, and the hourglass effect reduction factor $H(\sigma_s, \beta^*)$ should be considered.

In 2012, LHC ran at a top energy of 4 TeV and was filled with 50 ns spaced bunches. During collisions different mechanisms arise, causing emittance blow up and/or current losses, leading to luminosity decay in time. In the case of LHC, a simple exponential fit with a constant lifetime over time, cannot describe the luminosity decay. It is thus of paramount importance of identifying and understanding the different complex and interleaved mechanisms leading to luminosity degradation, building finally a model which is essential for optimizing the machine performance and for making accurate predictions for the future of the collider. Such a model can be implemented in an on-line tool for following the luminosity behavior of each LHC fill.

There were several studies concerning the LHC luminosity lifetime [2–8], mainly based on semi-empirical laws through statistical analysis of the LHC run I data. Although luminosity is a macroscopic indicator of global collider performance, the observed bunch-by-bunch (bbb) variations in the transverse and longitudinal emittances and in current, impacts its evolution and finally the integrated luminosity

* Research supported by EU FP7 HiLumi LHC - Grant Agreement 284404

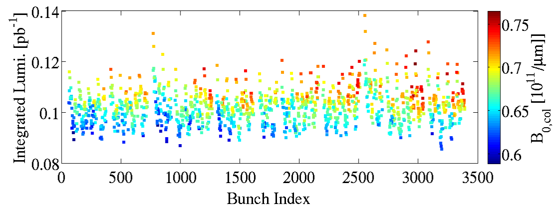

Figure 1: Bunch-by-bunch integrated luminosity for fill3232 from LHC Run I data, color-coded with the initial brightness at collisions.

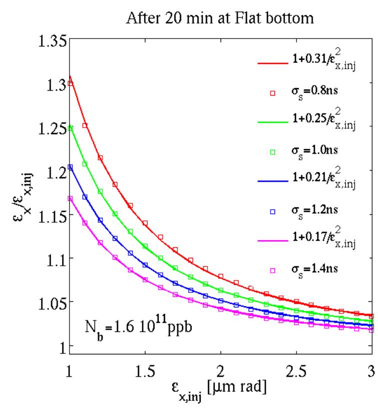

Figure 2: Parameterization of the IBS effect after 20 min at FB with the injected transverse emittance, for different input bunch lengths and for a bunch current of 1.6×10^{11} *ppb*.

per fill. This is clearly shown in Fig. 1, where the bbb integrated luminosity is color-coded with the ratio of the bunch current over transverse emittance (assuming round beams), or initial brightness, at the beginning of collisions for fill 3232. An accurate model should be able thus to represent the contribution of each bunch to luminosity. In this paper, different mechanisms affecting luminosity lifetime in the LHC are discussed and the status of a LHC luminosity model, taking into account the bbb variations, is presented.

EMITTANCE EVOLUTION

The emittance evolution of the beams in the LHC during the flat bottom (FB), the ramp and the first part of the flat top (FT) (before the squeeze) is dominated by the intra-beam scattering (IBS) effect [9]. During the squeeze and while the beams are brought to collision, the situation becomes more complicated, as during the LHC run I certain bunches were becoming unstable causing emittance blow up and losses [10]. During collisions a combination of effects including burn-off, IBS, beam-beam, noise, etc., cause emittance blow up and current losses [3].

Based on the assumption that IBS is the dominant effect during FB, scaling laws can be derived by using sim-

Content from this work may be used under the terms of the CC BY 3.0 licence (© 2015). Any distribution of this work must maintain attribution to the author(s), title of the work, publisher, and DOI.

ISBN: 978-3-95450-168-7 doi:10.18429/JACoW-IPAC2015-TUPTY022

Content from this work may be used under the terms of the CC BY 3.0 licence (© 2015). Any distribution of this work must maintain attribution to the author(s), title of the work, publisher, and DOI.

ALTERNATIVE OPTICS DESIGN OF THE CLIC DAMPING RINGS WITH VARIABLE DIPOLE BENDS AND HIGH-FIELD WIGGLERS

S. Papadopoulou, F. Antoniou, Y. Papaphilippou, CERN, Geneva, Switzerland

Abstract

The CLIC Damping Rings baseline design aims to reach an ultra-low horizontal normalised emittance of 500 nm-rad at 2.86 GeV, based on the combined effect of TME arc cells and high-field super-conducting damping wigglers, while keeping the ring as compact as possible. In this paper, an alternative design is described, based on TME cells with longitudinally variable bends and an optimized Nb_3Sn high-field wiggler. The impact of these changes on ring optics parameters and the associated optimisation steps are detailed taking into account the dominant effect of intrabeam scattering.

LAYOUT AND DESIGN REQUIREMENTS

The CLIC Damping rings (DRs) have to accommodate a 2.86 GeV beam and should damp it down to normalized horizontal and vertical emittances of 500 nm-rad and 5 nm-rad respectively. The longitudinal normalised emittance should be kept below 6 keV·m. The requirements for ultra-low emittances in all three planes give rise to a series of collective effects [1], with intrabeam scattering (IBS) being the dominant one.

The DRs' layout consists of a racetrack with two arcs and two long straight sections (LSS). The arcs are composed by theoretical minimum emittance (TME) cells and the LSS by FODO cells filled with damping wigglers. Space is also reserved for RF cavities, injection and extraction equipment [2]. The lattice functions between the arcs and the straight sections are matched from the dispersion suppressors and beta matching sections.

In this paper, an alternative design using longitudinally variable bends in the arc TME cells and an optimized high-field wiggler in the FODO cells is proposed. Through this approach, it is possible to achieve the desired output parameters and at the same time decrease the ring's circumference.

LONGITUDINALLY VARIABLE BENDS

Longitudinally variable dipoles, whose magnetic field varies along their length, can provide lower horizontal emittances than a uniform dipole of the same bending angle [3,4]. Actually in order to achieve that, the bending radius ρ_x of a variable bend should have an evolution similar to the one of the uniform dipole's dispersion invariant $\mathcal{H}(s)$ [5–9]: maximum magnetic field should be applied at their center, and it should be decreasing towards the edge of the dipole.

Two examples of variable bends are presented in this paper, they are described by the bending radii forming a step (green line) and a trapezium shape (blue line), as shown in Fig. 1. They are characterised by two lengths L_1 and L_2 with different bending radii ρ_1 and ρ_2. The evolution of the

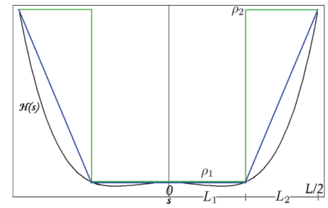

Figure 1: The evolution of the dispersion invariant $\mathcal{H}(s)$ along the uniform dipole (black line) and the bending radius evolution along the variable bends- coloured with green for the step and with blue for the trapezium profile.

bending radius ρ_{st} and ρ_{tr}, for the step and the trapezium profile, respectively, are:

$$\rho_{st}(s)= \begin{cases} \rho_1, & 0<s<L_1 \\ \rho_2, & L_1<s<L_1+L_2 \end{cases}$$

$$\rho_{tr}(s)= \begin{cases} \rho_1, & 0<s<L_1 \\ \rho_1+\dfrac{(L_1-s)(\rho_1-\rho_2)}{L_2}, & L_1<s<L_1+L_2 \end{cases}$$

The emittance reduction factor $F_{TME} = \epsilon_{TME_{uni}}/\epsilon_{TME_{var}}$ is the ratio of the absolute minimum emittances of a uniform with respect to a variable field dipole, and its parametric behaviour can be obtained using analytical expressions for the TME cells [9]. For this study, it is useful to define the lengths and bending radii ratios as $\lambda = L_1/L_2$ and $\rho = \rho_1/\rho_2$, respectively. In Fig. 2, the F_{TME} is parametrized with ρ and λ with the restriction of $\lambda > 0.1$, for the step (left) and the trapezium (right) profile. The areas where F_{TME} is high are blue-colored, while red-colored are the

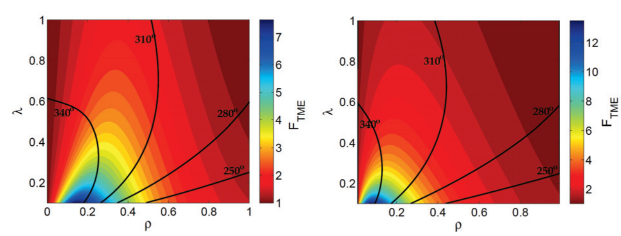

Figure 2: The parametrization of the emittance reduction factor F_{TME} with ρ and λ for the step (left) and the trapezium (right) profile. The black contour lines correspond to different values of the horizontal phase advance.

areas where the reduction is insignificant. For both profiles the highest possible reductions are localized in the limits where $\lambda \to 0.1$. The reductions achieved for the trapezium profile are higher than the ones for the step profile [7]. In the case of non uniform dipoles, even for the TME optics conditions, the horizontal phase advance μ_x always depends on ρ and λ. It is clear that remarkable reductions are reached for phase advances lower than the unique phase advance of the uniform dipole's TME ($\mu_x = 284.5°$). This

ISBN: 978-3-95450-168-7 doi:10.18429/JACoW-IPAC2015-TUPTY023

Content from this work may be used under the terms of the CC BY 3.0 licence (© 2015). Any distribution of this work must maintain attribution to the author(s), title of the work, publisher, and DOI.

LESSONS LEARNED FROM THE FIRST LONG SHUTDOWN OF THE LHC AND ITS INJECTOR CHAIN

K. Foraz, M. Barberan, M. Bernardini, J. Coupard, N. Gilbert, D. Hay, S. Mataguez, D. McFarlane, E. Vergara, CERN, Geneva, Switzerland

Abstract

The First Long Shutdown (LS1) of the LHC and its Injector chain, which started in February 2013, was completed by the first quarter 2015. A huge number of activities have been performed; this paper reviews the process of the coordination of LS1 from the preparatory phase to the testing phase. The preparatory phase is a very important process: an accurate view of what is to be done, and what can be done is essential. But reality is always different, the differences between what was planned and what was done will be described. The paper will recall the coordination, reporting and decisional processes, highlighting points of success and points to be improved in terms of general coordination, in-situ coordination, safety coordination, logistics and resource management.

INTRODUCTION

After a long shutdown lasting two years (LS1), the Large Hadron Collider (LHC) and the whole accelerator chain are now running, and the physics in LHC at an energy of 13TeV will start as early as June 2015. The restart of the LHC marked the completion of a very challenging, intense and enriching period, the LS1.

As defined by the directorate of CERN the LS1 aims to perform all activities needed for a safe and reliable operation of the accelerator complex at nominal energy, taking into account essential rules: safety first, quality second and schedule third.

ORGANISATION

The LS1 started in February 2013, and the preparatory phase last two years. Since the beginning, the project leader, F. Bordry, has been nominated, and the project structure has been built. The LS1 Committee has been created, as the steering committee, concerned with all technical and organisational aspects of the LS1 for the CERN accelerator complex. [1]

Several sub-projects structures have been created, with specific activities and scopes. In the LHC machine the major projects were the Superconducting Magnets and Circuits Consolidation (SMACC) and the Radiation to Electronics (R2E); these projects reported directly to the LS1 committee, and ad hoc project structures have been established. In the Injectors (PSBooster, PS, SPS) several projects have also been performed, and the project leaders reported directly to their Group leaders, who reported the overall progress to the LS1 committee; in these cases, no specific structures have been implemented. Concerning the maintenance activities, for the whole accelerator complex, they were under the responsibility of the Group leaders.

Follow Up

In the LHC machine, specific indicators have been implemented to follow up the major projects as SMACC (Figure 1) and R2E; the maintenance and other activities were followed by the LS1-LHC dashboard, which gave the overall overview of the progress of all the activities in the LHC machine [2]. In the Injectors, one progress curve per injector has been created, to follow up the progress of projects and maintenance activities.

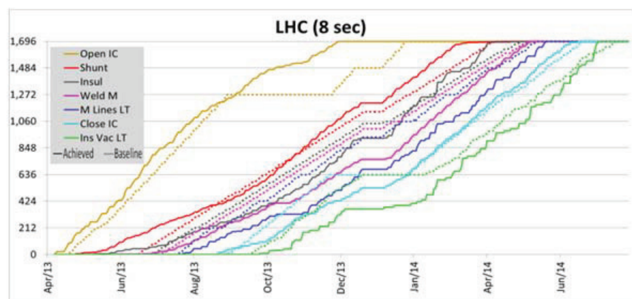

Figure 1: – LS1-SMACC Dashboard.

For each machine, LHC, SPS, PS and PSBooster a technical coordinator has been appointed. The technical coordination is part of the EN-MEF Group, and the main role is to manage activities in the short and medium term. The technical coordinators chair weekly coordination meetings following up the progress of activities and the main milestones, reviewing safety aspects and issues, and gathering all the stakeholders. The technical coordinators were following the Quality Assurance Process ensuring that 3D integration studies were kept up to date, Engineering Change Requests (ECR) are edited, and their follow-up is correctly implemented. Moreover from time to time, they provided ad hoc support to equipment groups in order to ensure a smooth progress.

Baseline Versus Reality

In the accelerator complex, the Long Shutdown 1 roadmap included (Figure 2):

- A preliminary test phase in order to detect existing faults,
- A preparatory phase including lock-out,
- The work phase,
- The recovery of operational conditions,
- The hardware tests.

ISBN: 978-3-95450-168-7 doi:10.18429/JACoW-IPAC2015-TUPTY024

UPDATED SIMULATION STUDIES OF DAMAGE LIMIT OF LHC TERTIARY COLLIMATORS*

E. Quaranta†, A. Bertarelli, R. Bruce, F. Carra, F. Cerutti, P. Gradassi, A. Lechner, S. Redaelli, E. Skordis, CERN, Geneva, Switzerland

Abstract

The tertiary collimators (TCTs) in the LHC, installed in front of the experiments, in standard operation intercept fractions of 10^{-3} halo particles. However, they risk to be hit by high-intensity primary beams in case of asynchronous beam dump. TCT damage thresholds were initially inferred from results of destructive tests on a TCT jaw, supported by numerical simulations, assuming simplified impact scenarios with one single bunch hitting the jaw with a given impact parameter. In this paper, more realistic failure conditions, including a train of bunches and taking into account the full collimation hierarchy, are used to derive updated damage limits. The results are used to update the margins in the collimation hierarchy and could thus potentially have an influence on the LHC performance.

INTRODUCTION

During the first run in 2010-2013, the Large Hadron Collider (LHC) [1] was successfully operated at energies up to 4 TeV and at stored energies of 146 MJ with proton beams [2]. In 2015, the operation will resume after a long shutdown at an energy of 6.5 TeV, with the aim of achieving 7 TeV in the future. Further upgrades of luminosity are foreseen within the High-Luminosity LHC (HL-LHC) project, by increasing the beam intensity, reducing the beam emittance and decreasing β^* at the Interaction Points (IPs).

Given the destructive potential of such energetic beams, a multi-stage collimation system [3] must ensure efficient beam halo cleaning, prevent the superconducting magnets quench and protect the machine in case of beam failures. The investigation of the consequences of the LHC beam impacts in case of single turn beam losses on the tertiary collimators, which are made of a tungsten heavy alloy (Inermet180) and not robust enough to intercept large beam intensities, close to the IPs is fundamental to ensure machine protection and has also consequences on the luminosity performance [3, 4].

The LHC filling scheme has a gap of about 3 μs without beam, to allow the 15 extraction kicker magnets (MKDs) to rise up to full field during a standard beam dump. Nevertheless, faults could lead to an asynchronous beam dump, where the MKDs trigger is not synchronised with the abort gap. The worst scenario is represented by the spontaneous misfiring of one kicker module, followed by the re-triggerig of all the others, the so-called *single module pre-firing* [5]: due to the slowest rising time up to the total kicker field that is required for the extraction of the beam in Point 6 (IP6), several bunches may receive an intermediate kick and be sent directly to sensitive equipment, as machine aperture and non-robust collimators. During the operation at low β*, the next aperture bottleneck downstream of the dump protections in IR6 might be the TCTs at the interaction points [6]. It is therefore important to understand safe limits for the present TCTs, which have their active parts made of Inermet180.

In the past, first damage estimates for tungsten collimators were calculated through advanced simulations [7]. One single bunch with variable intensity impacting the TCT jaw at a fixed impact parameter was considered. The distribution of the energy density deposited by the protons provided inputs for complex wave propagation calculations to reproduce the dynamic responses in the impacted structure of the collimator. These thresholds have been updated in light of recent beam tests at the CERN HiRadMat facility [8, 9].

A new simulation setup is now available that introduces an initial step of particle tracking simulations to study a more realistic scenario of failure and impacts on the TCTs. After introducing the improved simulation chain used for this study, on overview of the most relevant scenarios for the LHC will be given, followed by simulation setup for the case of tertiary collimators hit by protons scattered out from IR6 collimators (for this reason labelled as "secondary protons" from now on, to be distinguished from particles hitting directly the TCT, called instead "primary protons") in the nominal 7 TeV optics for Beam 2. To conclude, results and new damage limits will be presented for this case.

THE SIMULATION CHAIN

Particle Tracking with SixTrack

Particle tracking simulations were performed using a modified version of the SixTrack collimator routine [10–12]. A single MKD module pre-fire was simulated for a train of LHC protons at 7 TeV with the full collimation system in place. The real 25 ns beam time structure was considered accounting for bunch spacing between consecutive impacts: each of them receives a different kick angle according to the rising of the kicker field. Thus, fractions of several bunches will impact on the TCT jaw.

SixTrack simulations were done for a perfect machine, without errors on optics, apertures and collimators. Possible errors are accounted for by scanning TCT positions around their nominal settings, down to apertures of IR6 protection devices. Only the TCT settings in the low-β* insertions IR1 and IR5 were modified, since these would be the most exposed locations in case of a dump failure of Beam 1 and Beam 2, respectively. The coordinates of the particles in SixTrack that experience inelastic interaction inside the TCTs provide inputs for full shower simulations.

* Research supported by EU FP7 HiLumi LHC (Grant agree. 284404)
† elena.quaranta@cern.ch

Content from this work may be used under the terms of the CC BY 3.0 licence (© 2015). Any distribution of this work must maintain attribution to the author(s), title of the work, publisher, and DOI.

ISBN: 978-3-95450-168-7 doi:10.18429/JACoW-IPAC2015-TUPTY025

BETATRON CLEANING FOR HEAVY ION BEAMS WITH IR7 DISPERSION SUPPRESSOR COLLIMATORS *

P. D. Hermes†, CERN, Geneva, Switzerland and University of Münster, Germany
R. Bruce, J. M. Jowett and S. Redaelli, CERN, Geneva, Switzerland

Abstract

The betatron collimators in IR7 constitute the backbone of the collimation system of the LHC. A fraction of the secondary halo protons or heavy-ion fragments, scattered out of the primary collimator, is not captured by the secondary collimators but hits cold magnets in the IR7 dispersion suppressor (DS) where the dispersion starts to increase.

A possible approach to reduce these losses is based on the installation of additional collimators in the DS region. In this paper, simulations of the cleaning efficiency for Pb^{82+} ions are used to evaluate the effect of the additional collimators. The results indicate a significant improvement of the heavy-ion cleaning efficiency.

INTRODUCTION

The CERN Large Hadron Collider (LHC) [1] is a proton and heavy-ion collider designed for an unprecedented energy of 7 Z TeV (with Z indicating the charge multiplicity). The envisaged High Luminosity (HL) LHC upgrade is aiming to increase the total stored proton beam energy from the present design value of 362 MJ to 700 MJ [2]. Also the LHC heavy-ion programme aims to deliver more luminosity to the experiments by an increase of the number of stored $^{208}Pb^{82+}$ ions [3].

A multi-stage collimation system [1, 4] is installed to provide adequate protection of the superconducting magnets and avoid quenches. The primary (TCP) and secondary (TCS) collimators, as well as the shower absorbers (TCLA) are installed in the two collimation insertions IR3 (momentum cleaning) and IR7 (betatron cleaning), while tertiary collimators (TCT) protect the superconducting triplet magnets of the experimental insertions. For both, proton and heavy-ion operation, the most critical locations of beam cleaning losses are the dispersion suppressor (DS) magnets of IR7. Protons which were subject to single diffractive scattering in the TCPs and heavy-ions having undergone fragmentation processes to isotopes with different magnetic rigidities are likely to be absorbed in this region where the dispersion increases. The heavy-ion collimation inefficiency in this region was measured and simulated to be two orders of magnitudes worse than with protons. This could become a limiting factor for the reachable luminosity, in spite of the much smaller heavy-ion beam intensities [5, 6].

The cleaning performance of the collimation system is quantified by the number of lost nucleons $N_{\mathrm{loc}}(s) = \sum_i n_i(s) A_i$ (with n_i being the number of lost nuclei of the isotope i and A_i the mass number) at the position s over the distance Δs normalized by the total number of losses at the collimators N_{tot}, the so called local cleaning inefficiency $\eta(s)$, given by [7]

$$\eta(s) = \frac{N_{\mathrm{loc}}(s)}{N_{\mathrm{tot}}\,\Delta s}. \tag{1}$$

With regard to the envisaged increase of the stored proton beam energy, the installation of additional collimators (called TCLD) is discussed at the DS regions of IR7. Simulations for protons predict a significant improvement of the cleaning efficiency with these collimators [8–10].

In this article, we study the simulated cleaning efficiency of the collimation system for a beam of $^{208}Pb^{82+}$ ions for the three cases: no TCLD, one TCLD in cell 8 (TCLD8) and two TCLDs installed in the cells 8 and 10.

SIMULATION METHOD

The proposed layout of the collimation system with the TCLD collimators as well as the collimator settings and beam properties are presented in detail in [9]. The concept is based on the replacement of two 8.33 T dipole magnets [1] in the cells 8 and 10 (at distances of 292.4 m and 371.9 m from IP7) of the IR7 DS by two shorter and stronger dipole magnets respectively [11]. The freed space is used for the installation of the TCLDs.

In proton operation, a large fraction of the particles interacting with the TCP are scattered into the secondary collimators and absorbers or hits the TCP again on a subsequent turn, making the collimation system very efficient. With heavy-ion beams, numerous ions are fragmented into isotopes with different magnetic rigidities while their angular deviations are mostly not sufficient to be intercepted by the TCS. In consequence, the local cleaning inefficiency in the DS is much more critical in the heavy-ion case than in the proton case. For many of the incoming ions, the collimation system acts effectively like a single-stage system with the primary collimators only.

SixTrack [12, 13] is a program designed for multi-turn proton tracking in storage rings. It provides an integrated environment for symplectic tracking based on a thin-lens model of the accelerator lattice together with a Monte-Carlo module to simulate proton-matter interactions in the collimators [14]. The particle loss positions in the aperture are computed by comparing the simulated particle tracks with a detailed model of the machine aperture. Losses in the collimators are identified if protons undergo inelastic interactions (except single-diffractive scattering) with the material.

* Work supported by the German Wolfgang Gentner Programme of the Bundesministerium für Bildung und Forschung. Research supported by FP7 HiLumi LHC – Grant agreement 284404.
† phermes@cern.ch

Content from this work may be used under the terms of the CC BY 3.0 licence (© 2015). Any distribution of this work must maintain attribution to the author(s), title of the work, publisher, and DOI.

ISBN: 978-3-95450-168-7 doi:10.18429/JACoW-IPAC2015-TUPTY027

SIXTRACK SIMULATIONS OF BEAM CLEANING DURING HIGH-BETA OPERATION IN THE LHC

R. Bruce*, CERN, Geneva, Switzerland

Abstract

The 1000 m high-beta run in the LHC provided very clean conditions for observing experimental backgrounds. In ATLAS, a much higher background was observed for Beam 2 than for Beam 1, suspected to be caused by upstream showers from beam losses on collimators or aperture. However, no local beam losses were observed in the vicinity. This paper presents SixTrack simulations of the beam cleaning during the high-beta run. The results demonstrate that, for the special optics and collimator settings used, the highest loss location in IR1 is at the TAS absorber just in front of the ATLAS detector, where no beam loss monitor is installed. Furthermore, the highest losses are seen in Beam 2. The results could thus provide a possible explanation of the ATLAS observations, although detailed shower calculations would be needed for a quantitative comparison.

INTRODUCTION

The schematic layout of the the CERN Large Hadron Collider (LHC) [1] is shown in Fig. 1. It has two counter-rotating beams (B1 and B2) and consists of 8 arcs and 8 straight insertion regions (IRs). At the end of its first proton physics run, in 2012, the LHC collided 4 TeV beams using an optical β-function β^* =60 cm at the high-luminosity experiments ATLAS [2] and CMS [3]. This value was optimized to be as low as possible [4], for highest luminosity, in order to increase the rate of rare events.

Downstream of ATLAS and CMS, the forward physics experiments ALFA [2] and TOTEM [5] are installed, which are specialized at measuring the proton-proton cross section from elastic scattering. In order to accurately measure the scattering angles of outgoing protons, TOTEM and ALFA require a minimum angular divergence at the interaction point (IP). So instead of the small β^* used in the high-luminosity runs, which imply a large angular divergence at the IP, these experiments benefit from a very large β^*.

Therefore, short special physics runs were performed with a particular high-β optics, where the largest value used was β^* =1 km during LHC fill 3216 on October 24 in 2012 [6]. This run was carried out at low intensity for machine protection reasons and used special collimator settings. The primary collimators (TCP) in the betatron cleaning insertion IR7 [7] were used to scrape down the beam to about 2 σ [8] (σ is defined as the local beam size calculated using the standardized normalized emittance of 3.5 μm and the ideal β-function) and then retracted by about 0.5 σ. This removed the beam halo in the scraping range and allowed to minimize the background at the forward-physics experiments. Other scrapings were performed using the TCP in the momentum cleaning insertion IR3, to remove the off-momentum tails. Cycles of TCP scraping and subsequent retraction had to be repeated several time, after a re-population of beam tails that reached the TCP cut.

* roderik.bruce@cern.ch

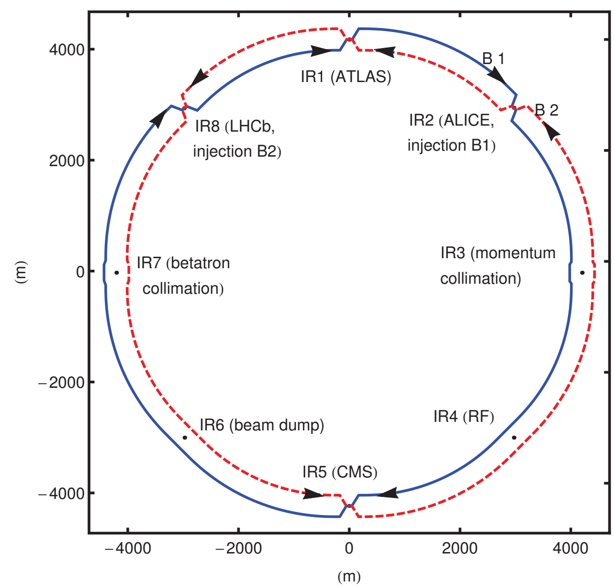

Figure 1: The schematic layout of the LHC (the separation of the two rings is exaggerated). The two beams are brought into collision at the four experiments ATLAS, ALICE, CMS and LHCb. Figure taken from Ref. [9].

BACKGROUND IN HIGH-β RUN

Beam-halo induced background occurs in the LHC experiments when halo protons initially hit a TCPs and then scatter back into the beam to an oscillating orbit, which leads to a final loss position on collimators or the machine aperture close to the experiments [10]. The unwanted background signals are caused by secondary shower particles that enter the detectors.

ATLAS and CMS were acquiring data during the high-β run. The low intensity and low luminosity provided very clean conditions to observe beam-halo induced background, since, during the scraping by the collimators, this was by far the dominating beam loss process. However, some intriguing observations were made by ATLAS [11]. A clear increase of background was observed in the counter-clockwise rotating B2 in strong correlation to beam scraping in IR3. This background was much stronger than what was observed in B1 and when the beam was scraped in IR7. Furthermore, during the IR3 scraping, no beam loss monitors (BLMs) close to ATLAS indicated local losses, that could be the origin of the observed background.

Content from this work may be used under the terms of the CC BY 3.0 licence (© 2015). Any distribution of this work must maintain attribution to the author(s), title of the work, publisher, and DOI.

ISBN: 978-3-95450-168-7 doi:10.18429/JACoW-IPAC2015-TUPTY028

Content from this work may be used under the terms of the CC BY 3.0 licence (© 2015). Any distribution of this work must maintain attribution to the author(s), title of the work, publisher, and DOI.

COLLIMATOR LAYOUTS FOR HL-LHC IN THE EXPERIMENTAL INSERTIONS*

R. Bruce†, F. Cerutti, L.S. Esposito, J.M. Jowett, A. Lechner, E. Quaranta, S. Redaelli, M. Schaumann, E. Skordis, G. Eleanor Steele, CERN, Geneva, Switzerland
H. Garcia Morales, R. Kwee-Hinzmann, Royal Holloway, University of London, Surrey, UK

Abstract

This paper presents the layout of collimators for HL-LHC in the experimental insertions. On the incoming beam, we propose to install additional tertiary collimators to protect potential new aperture bottlenecks in cells 4 and 5, which in addition reduce the experimental background. For the outgoing beam, the layout of the present LHC with three physics debris absorbers gives sufficient protection for high-luminosity proton operation. However, collisional processes for heavy ions cause localized beam losses with the potential to quench magnets. To alleviate these losses, an installation of dispersion suppressor collimators is proposed.

INTRODUCTION

It is planned to upgrade the CERN Large Hadron Collider (LHC) [1] to the High-Luminosity LHC (HL-LHC) [2, 3] after about 10 years of operation. The main goal of the upgrade is to achieve an integrated proton luminosity of about 3000 fb^{-1} over a decade at each of the high-luminosity experiments ATLAS and CMS. For this goal, it is needed to operate with a yearly luminosity production that is more than an order of magnitude higher than in the first LHC run [4]. This can be made possible by using beams with higher intensity and lower emittance, as well as smaller β-functions (15 cm, to be compared with the nominal 55 cm) at the interaction points (IPs).

In its nominal proton configuration, the LHC operates with beams at an unprecedented energy of 7 TeV with a total stored beam energy of about 362 MJ per beam. The two beams are guided by superconducting magnets, which risk to quench if just a tiny fraction of the full beam is lost locally. In order to protect the cold magnets, a multi-stage collimation system has been installed [1, 5, 6]. The collimators are mainly installed in the insertion regions (IRs) called IR3 (momentum cleaning) and IR7 (betatron cleaning). However, there are also collimators installed around the IPs: Tertiary collimators (TCTs) provide local protection on the incoming beam, and physics debris absorbers (TCLs) are installed on the outgoing beam to intercept collision products.

The HL-LHC poses new challenges for the collimation system. The total stored energy will increase to about 700 MJ per beam (2.2×10^{11} protons per bunch), and the higher luminosity causes a higher rate of collision debris. Furthermore, major upgrades and layout changes are foreseen in the experimental IRs. As an example, the layout around ATLAS, in IR1, is shown in Fig. 1 for both the first LHC run in 2010–2013 (Run 1) and for HL-LHC. Most notably, in order to allow a very small $\beta^* = 15$ cm, new large-aperture inner triplet quadrupoles will be installed, and the novel ATS optics scheme [7] will be deployed. The layout at CMS, in IR5, is identical.

Apart from protons, the LHC operates also a shorter period every year with heavy ions (mainly Pb^{82+}). Physical processes in the collisions, specific to heavy ions, create secondary beams with altered magnetic rigidity that are lost in very localized spots, where they risk to quench magnets [8, 9]. This could become critical in HL-LHC with an upgraded heavy-ion luminosity.

It is crucial to ensure that the HL-LHC is well protected by its collimation system during both proton and heavy-ion operation. This article investigates the local protection around the experiments and the need for upgrades. The global performance of the IR3 and IR7 beam cleaning system is discussed elsewhere [10, 11].

INCOMING BEAM

In the present LHC, a pair of TCTs (called TCT4), consisting of one horizontal and one vertical collimator, is installed in cell 4 on the incoming beam in front of each experiment. They should protect the local aperture bottlenecks that arise in the triplets in cells 1–3, when β^* is squeezed to small values, from both unavoidable losses during regular operation and accidental losses during beam failures, in particular asynchronous beam dumps. They should also decrease the experimental background [12]. All these aspects have to be verified for HL-LHC.

In HL-LHC, with $\beta^* = 15$ cm using ATS optics [7, 13], the critical aperture bottlenecks to be protected are no longer necessarily only in the triplet [14], which will be replaced to have a significantly larger aperture. The β-functions upstream of the TCT4 will also be significantly larger than in the nominal configuration, which could potentially introduce new bottlenecks, in particular in cells 4–5. If significant losses would be expected there, additional protection should be considered. This can be achieved by the installation of an additional pair of TCTs in cell 5, called TCT5, which should protect cells 4–5.

To assess the need of local protection in the experimental IRs in case of asynchronous beam dumps, we use SixTrack [15, 16] to simulate the losses around the LHC with the same method as in Refs. [17, 18]. We use the HL-LHC lattice version 1.0 [19] with baseline collimator settings [20]. Initial studies without any TCTs in the experimental IRs

* Research supported by EU FP7 HiLumi LHC – Grant agreement 284404
† roderik.bruce@cern.ch

ISBN: 978-3-95450-168-7 doi:10.18429/JACoW-IPAC2015-TUPTY029

Content from this work may be used under the terms of the CC BY 3.0 licence (© 2015). Any distribution of this work must maintain attribution to the author(s), title of the work, publisher, and DOI.

COLLIMATION CLEANING AT THE LHC WITH ADVANCED SECONDARY COLLIMATOR MATERIALS*

E. Quaranta†, R. Bruce, A. Mereghetti, S. Redaelli, A. Rossi
CERN, Geneva, Switzerland

Abstract

The LHC collimation system must ensure efficient beam halo cleaning in all machine conditions. The first run in 2010-2013 showed that the LHC performance may be limited by collimator material-related concerns, such as the contribution from the present carbon-based secondary collimators to the machine impedance and, consequently, to the beam instability. Novel materials based on composites are currently under development for the next generation of LHC collimators to address these limitations. Particle tracking simulations of collimation efficiency were performed using the Sixtrack code and a material database updated to model these composites. In this paper, the simulation results will be presented with the aim of studying the effect of the advanced collimators on the LHC beam cleaning.

INTRODUCTION

The collimation system of the CERN Large Hadron Collider (LHC) is designed to efficiently absorb high energy beam losses and assure machine protection [1, 2]. Its multi-stage architecture is based on primary and secondary collimators (TCPs and TCSGs, respectively), made of a carbon-fiber-carbon composite (CFC). This choice has been made to guarantee good thermal stability and high robustness against beam induced losses for the collimators with the jaws the closest to the beam. Tungsten-based tertiary collimators (TCTs) and absorbers with higher particle stopping potential are instead devoted to protect the LHC experimental regions and reduce the background to experiments, at the expense of robustness against beam losses.

Since the first design of the present system [2], non-metallic collimators largely contribute to the impedance of the whole machine [3], mainly because of the low electrical conductivity of the CFC. The impedance is an electromagnetic concern of paramount importance in particular for the High Luminosity (HL) upgrade of the LHC [4], which aims at doubling the bunch intensity and at reducing the beam emittance.

Consequently, an intense R&D program has started at CERN to explore novel materials for new collimator jaws which could possibly replace some of the present CFC ones. The idea is to combine the excellent thermal properties of graphite or diamond with those of metals and metal-based ceramics of high mechanical strength and, above all, good electrical conductivity. The most promising materials identified so far are Molybdenum Carbide - Graphite (MoGr) composite and Copper-Diamond (CuCD) composite [5].

The effect of novel composite materials on the cleaning performance of the LHC collimation system must be investigated and the results used to complete the picture of the collimator material specifications. Therefore, a palette of materials is implemented in the tools used for LHC halo cleaning simulations. The first outcomes of the study are presented in this paper.

IMPLEMENTATION OF NEW MATERIALS IN SIXTRACK

The particle tracking code Sixtrack with collimation features [6–8] was upgraded to implement new composite materials. This setup is used as state-of-the-art simulation tool for collimation studies at the LHC. When energetic particles interact with matter, as for the LHC proton beams with the collimator material, scattering mechanisms occur. These mechanisms are reproduced in SixTrack by a Monte-Carlo code deriving from the K2 scattering routine [9], which has been also recently reviewed and improved [10].

Four composite materials, some of them already used in present collimators and others of interest for future collimation upgrades, have been added to the existing material database in SixTrack: MoGr and CuCD as alternatives to CFC for primary and secondary collimators; Inermet180, a tungsten heavy alloy used in the jaws of tertiary collimators and absorbers; Glidcop, a copper-based composite.

The routine treats mono-element materials. Thus, composite materials are dealt with by calculating off-line "effective" input parameters starting from material composition, as discussed below. The most important ones are listed in Table 1, along with the composition. For comparison, the same table lists CFC, already coded in SixTrack as pure carbon.

The atomic number Z and atomic weight A of each compound material was derived as average weighted on the atomic fraction of their components

$$p = \sum_i at_i \cdot p_i, \tag{1}$$

where p is the property of the compound to be computed, p_i are the values of the property, extracted from the Particle Data Group database [11], for the i-th element present in the material and at_i the atomic content of each element in the composite.

While traversing a medium and interacting with the electromagnetic field of the target atoms, a charged particle may lose energy by ionization according to the Bethe-Bloch

* Research supported by EU FP7 HiLumi LHC (Grant agree. 284404) and EuCARD-2 (Grant agree. 312453)
† elena.quaranta@cern.ch

ISBN: 978-3-95450-168-7 doi:10.18429/JACoW-IPAC2015-TUPTY031

TOOLS FOR FLEXIBLE OPTIMISATION OF IR DESIGNS WITH APPLICATION TO FCC

H. Burkhardt, CERN, Geneva, Switzerland
Manuela Boscolo, INFN-Frascati, Italy

Abstract

The interaction regions of future high-luminosity colliders require well balanced designs, which provide both for a very high luminosity and at the same time keep backgrounds and radiation at tolerable levels. We describe a set of flexible tools, targeted at providing a first evaluation of losses in the interaction region as part of the design studies, and their application to FCC.

INTRODUCTION

Studies on "Future Circular Colliders" FCC with emphasis on a hadron collider at centre-of-mass energies of the order of 100 TeV and as possible intermediate step an e^+e^- collider for the 90 to 400 GeV energy centre-of-mass energy range, to be installed in a new 80 to 100 km long tunnel, were recently launched by CERN in worldwide global collaboration [1].

Combining the requirements for very high luminosity at high beam energies with the need for low or at least tolerable background and radiation levels to the experiments at the interaction regions will be particularly challenging and require a well balanced machine detector interface design and optimization.

The FCC studies are currently in an early design stage. In this phase, the machine description can be expected to change frequently, and detailed aperture and material information will not always be available.

TOOL SET FOR MACHINE DETECTOR INTERFACE SIMULATIONS

We have started to develop a tool set "MDISim" for **M**achine **D**etector Interface **SIM**ulations. MDISim can be subdivided in three different steps.

1. Read machine lattice description, generate twiss, survey and geometry files
2. Visualization of the geometry and analytic estimates including calculation of synchrotron radiation
3. Detailed simulation of the passage of particles through materials

We use and combine the existing standard tools, MAD-X [2], ROOT [3] and GEANT4 [4]. We will now describe the steps in more details.

1 – MACHINE LATTICE

The basis and starting point for the studies is the magnetic lattice machine description in the form of MAD-X input files. In the first step, we run the MAD-X program using "MDISim" default twiss and survey selections and attributes, to produce detailed twiss and survey tfs-files for the magnetic lattice and accelerator geometry description. R-matrix or sector map information can optionally be selected for output in the twiss file to enable tracking by mapping in the second step. Running MAD-X to generate the twiss and survey files is very fast. It takes less than 10 seconds to generate the files for a 100 km machine with 50 000 elements. The two files contain tables with all relevant information element by element, as required as input for the second step.

The global parameters relevant for the whole machine like the beam energy, particle type and number of particles are provided in the header of the twiss table. The twiss file uses local *Courant Snyder* coordinates s, x, y where s is the position along the circumference and x, y the horizontal and vertical distance from the design orbit. The transverse coordinates (x, y) can be increased using a scalefactor. The survey file specifies the element positions x, y, z in a global Euclidian coordinate system.

2 – VISUALIZATION OF THE GEOMETRY AND ANALYTIC ESTIMATES

The second step starts by reading and merging the twiss and survey files generated by MAD-X. Both local "Courant Snyder" as well as global Euclidian coordinates (with transverse Euclidian coordinates renamed to $x2$, $y2$) are now available at the end of each element. In addition translation from local to global coordinates and vice versa is made available by linear transformation (shift plus rotation) for any arbitrary position. This makes it straightforward to add tracks from beam loss simulations [5] or magnetic lattice tracking, given in local coordinates, to the geometry display which uses Euclidian coordinates.

For the second step we use ROOT, linked to our MDISim library package which deals with tfs-file reading and merging, ROOT geometry generation and analytic estimates.

The graphics capabilities (zoom, rotation, selection or deselection of components) of ROOT with EVE and OpenGL are used to display the geometry [6] as shown in Fig. 1.

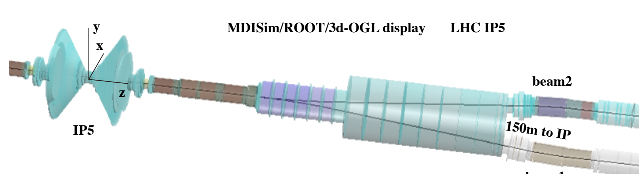

Figure 1: Display of the LHC IP5 geometry. Transverse (x,y) dimensions were increased by a factor of 100.

The program is designed to already start to work with only a minimum amount of information required. Any section

Content from this work may be used under the terms of the CC BY 3.0 licence (© 2015). Any distribution of this work must maintain attribution to the author(s), title of the work, publisher, and DOI.

ISBN: 978-3-95450-168-7 doi:10.18429/JACoW-IPAC2015-TUPTY032

STUDY OF MUON BACKGROUNDS IN THE CLIC BEAM DELIVERY SYSTEM

H. Burkhardt, L.Gatignon, A. Latina, D. Schulte, R. Tomas, CERN, Geneva, Switzerland
B. Pilicer *, E.Pilicer, I. Tapan, Uludag University, Bursa, Turkey

Abstract

We describe the detailed modelling of muon background generation and absorption in the CLIC beam delivery system. The majority of the background muons originates in the first stages of halo collimation. We also discuss options to use magnetised cylindrical iron shields to reduce the muon background flux reaching the detector region.

INTRODUCTION

For the Compact Linear Collider (CLIC) project, high energy beam will be transported to the interaction region (IR) by the Beam Delivery System (BDS) [1]. The BDS is 2796 m long and consists of four sections which are diagnostics, energy and betatron collimation and final focus, respectively. The betatron collimation section has horizontal and vertical spoilers ($\sim 1\,X_0$) and absorbers ($\sim 20\,X_0$) to remove halo particles. The interaction of the halo particles with the spoilers and absorbers produces secondary particles including muons. Most of the secondary particles will be absorbed rather locally. High energy muons are not stopped by the absorbers and may reach the experimental detectors at the interaction point. Here we study how the background muon flux to the detector can be reduced using cylindrical magnetized shielding blocks of 5 m or $\sim 300\,X_0$ length. The main processes for muon production are gamma conversion into muon pairs (Bethe-Heitler process, $\gamma e^- \rightarrow \mu^+\mu^-e^-$) and annihilation of positrons with atomic electrons into muon pairs ($e^+e^- \rightarrow \mu^+\mu^-$). For the study described here we use the BDS of the CDR, and include the process of e^+e^- annihilation into hadrons ($e^+e^- \rightarrow$ hadrons) as an additional source for background muons [2]. The description of an earlier study can be found in [3].

MUON PRODUCTION PROCESSES

We use Geant4 (version Geant4.10.01) for the simulation of the interaction of the beam particles and secondary particles with the material in the beam line [4, 5]. The cross sections for the electromagnetic processes which are at the origin of muon production are shown in Fig. 1 as a function of the incoming beam energy, up to 1.5 TeV (maximum beam energy for CLIC).

The kinetic energy of atomic electrons in matter is very small compared to the beam energies considered here. In a very good approximation, we are dealing with the annihilation of high energy positrons with electrons at rest. The

* Research supported by 2214 International Doctoral Research Fellowship Programme TUBITAK.

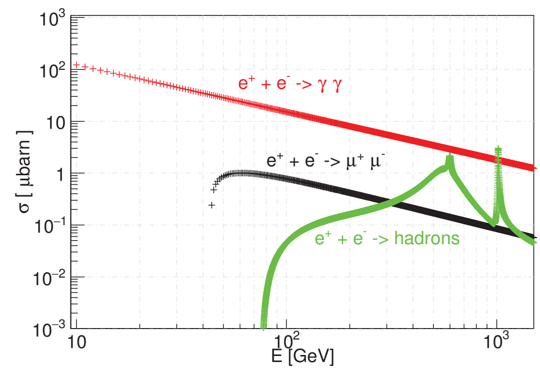

Figure 1: Cross sections for annihilation into two gammas (red markers), $\mu^+\mu^-$ (black markers) and hadrons (green markers) in laboratory frame energy.

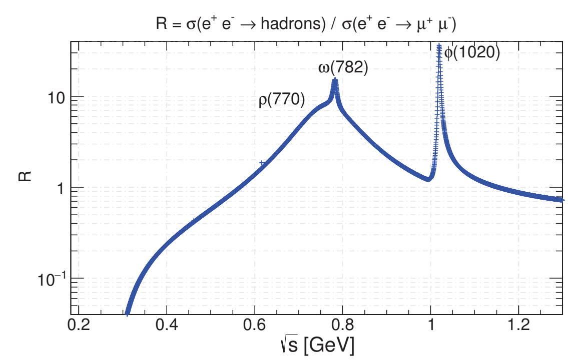

Figure 2: Ratio R = $\sigma_{e^+e^-\rightarrow hadrons}/\sigma_{e^+e^-\rightarrow\mu^+\mu^-}$ as function of the center of mass energy frame.

relevant centre of mass energy for the annihilation of high energy positrons of energy $E_{\rm beam}$ with electron of mass m_e at rest is $\sqrt{2 \cdot m_e \cdot E_{beam}}$, or 1.24 GeV at 1.5 TeV beam energy [2]. The ratio R of hadron to muon cross sections for the relevant centre-of-mass energy range is shown in Fig. 2. The peaks in the cross section for annihilation to hadrons correspond to the masses of vector resonances. The first two peaks visible at around 600 GeV beam energy correspond to $\rho(770)$ and $\omega(782)$. The peak around 1 TeV beam energy corresponds to the $\phi(1020)$. At these beam energies, the muon production by collimation of high energy positrons will be increased compared to muon background by electron collimation.

The hadrons produced in e^+e^- annihilation at these energies are : K^+K^-, K_SK_L, $\pi^+\pi^-$, $\pi^+\pi^-\pi^0$, $\pi^0\gamma$, $\eta\gamma$. The charged pions, kaons and the K_L are relatively long lived and will only rarely produce background muons by hadron decay. High energy photons produced in the decay of the

Content from this work may be used under the terms of the CC BY 3.0 licence (© 2015). Any distribution of this work must maintain attribution to the author(s), title of the work, publisher, and DOI.

ISBN: 978-3-95450-168-7 doi:10.18429/JACoW-IPAC2015-TUPTY033

CIVIL ENGINEERING OPTIMISATION TOOL FOR THE STUDY OF CERN'S FUTURE CIRCULAR COLLIDERS

C. Cook, B. Goddard, P. Lebrun, J. Osborne, Y. Robert, CERN, Switzerland
C. Sturzaker, M. Sykes, Y. Loo, ARUP, UK
J. Brasser, R. Trunk, AMBERG, Switzerland

Abstract

The feasibility of Future Circular Colliders (FCC), possible successors to the Large Hadron Collider (LHC), is currently under investigation at CERN. This paper describes how CERN's civil engineering team are utilising an interactive tool containing a 3D geological model of the Geneva basin. This tool will be used to investigate the optimal position of the proposed 80 km-100 km perimeter tunnel. The benefits of using digital modelling during the feasibility stage are discussed and some early results of the process are presented.

INTRODUCTION

A five year international design study at CERN to investigate the feasibility of 'Future Circular Colliders' (FCC), potential successors to the Large Hadron Collider (LHC), began with a kick-off meeting held in Geneva in February 2014. The emphasis of the study is on a hadron collider with a centre-of-mass energy of the order of 100 TeV in a new 80 km – 100 km tunnel as a long-term goal. The design study includes a 90-350 GeV lepton collider, seen as a potential intermediate step. A lepton-hadron collider option is also being examined.

By the end of its construction in 2008, civil engineering accounted for around one third of the consolidated project cost of the LHC. Therefore, significant importance is placed on the civil engineering design when investigating the feasibility of the FCC. The earliest stages of any construction project offer the most opportunity for maximising quality and reducing total project costs. With this in mind, CERN is working in partnership with world leading engineering consultancies to utilise the latest methods and technology in order to ensure the best possible outcome from the first stages of design.

This paper describes the use of an interactive tool containing a 3D geological model of the Geneva basin. The Tunnel Optimisation Tool (TOT) is being used to assess the feasibility of the designs of the FCC study currently under study and their orientation with respect to the geology, terrain, surface constraints, their connection to the LHC and other siting considerations.

STUDY SCOPE

The Leman Basin, which contains the LHC, is surrounded by natural formations creating sensible boundaries for the FCC study area. Previous experience from the construction of CERN's previous particle colliders, LEP and LHC, has shown that the properties of the Leman Basin sedimentary rock, known as 'molasse', provide good conditions for tunnelling. During the excavation of the tunnel for CERN's Large Electron-Positron (LEP) collider, significant problems were caused by water ingress from the limestone formations in the Jura mountain range which lies to the west of Geneva.

For this reason, one of the primary aims when positioning the FCC tunnel is to maximise the fraction of the tunnel length in the molasse rock and minimise that in the limestone. Another primary concern is to orientate the tunnel in a way that limits the depth around its perimeter, therefore minimising the total depth of the shafts. These two primary concerns lead to natural boundaries in the form of the Jura range to the northwest, the Vuache mountain to the southwest and the Pre-Alps to the southeast and east. A boundary is placed in the north due to the increasing depth of Lake Geneva in the northerly direction.

THE DIGITAL APPROACH

The very first stages of a construction project offer the highest opportunity for overall reduction of cost, schedule and environmental impact (Fig. 1). A digital approach to the FCC feasibility study has enabled the CERN civil engineering team to extract the maximum value from the large amount of available data relating to the terrain, geology, hydrology, environment and built-environment of the Geneva basin, including man-made hazards such as geothermal boreholes. Locating the optimal position for any given design of the FCC tunnel requires all elements of this data to be analysed simultaneously.

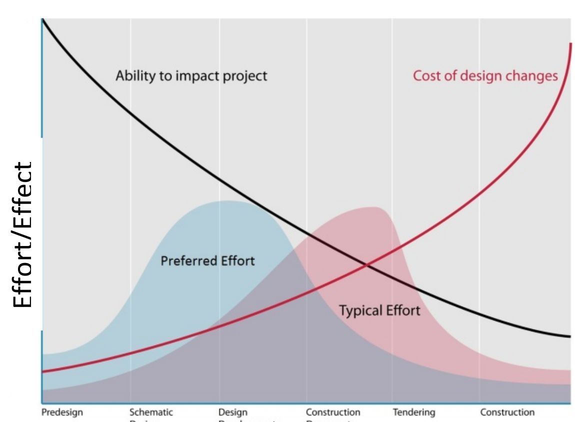

Figure 1: Macleamy's Curve (2004) from the Construction Users Roundtable

Content from this work may be used under the terms of the CC BY 3.0 licence (© 2015). Any distribution of this work must maintain attribution to the author(s), title of the work, publisher, and DOI.

ISBN: 978-3-95450-168-7 doi:10.18429/JACoW-IPAC2015-TUPTY035

Content from this work may be used under the terms of the CC BY 3.0 licence (© 2015). Any distribution of this work must maintain attribution to the author(s), title of the work, publisher, and DOI.

BEAM DYNAMICS REQUIREMENTS FOR THE POWERING SCHEME OF THE HL-LHC TRIPLET*

M. Fitterer, R. De Maria, S. Fartoukh, M. Giovannozzi, CERN, Geneva, Switzerland

Abstract

For the HL-LHC, β^* values as small as 15 cm are envisaged as baseline scenario for the high luminosity insertions IR1 and IR5, thus leading to an increase of the maximum β-functions in the inner triplet (IT). The larger beta-functions in the IT result in a higher sensitivity of the beam to any linear or non-linear, static or dynamic, field imperfections in the IT region. In this paper, we summarize accordingly the tolerances of the triplet power supplies in terms of current ripple, stability and reproducibility. Both the baseline IT powering scheme and other alternative schemes will be presented, the later reducing the tune shift caused by a current modulation and thus weakening its possible impact on the long term stability.

INTRODUCTION

A modulation in the current of a power supply in general results in a change of the magnetic field which in turn causes a modulation of the normalized quadrupole strength. Possible effects of this modulation on the linear optics are β-beat, orbit deviations and a tune modulation, where the expected tune shift is given by the well known formula:

$$\Delta Q = \frac{1}{4\pi} \oint \beta(s) \Delta k(s) ds \tag{1}$$

with $\Delta k(s)$ being the modulation of the normalized quadrupole strength due to the modulation of the current by the power converter (PC) itself. As shown in [1] the β-beat and orbit deviation are small in case of the IT PCs in IR1 and IR5, while the effect on the tune is non-negligible. In addition, the modulation of the tune can also have an effect on the non-linear beam dynamics [2, 3] and has been experimentally demonstrated at several machines (e.g. at the SPS and HERA [4–7]), where the modulation resulted in a reduction of the beam life time and increased losses. In order to avoid a performance degradation due to the effect of a modulation of the PC current, an extensive beam dynamics study has been launched with the aim to specify the required tolerances. A short summary of this study is given in this paper.

MODEL OF THE IT POWER CONVERTERS

The first step in the specification of the tolerances of the IT PCs from a beam dynamics point of view, is to translate the voltage and current specification of the PC into a modulation of the normalized quadrupole strength. For the IT PCs two regimes are in general distinguished:

- **current-control:** for low frequencies (< 0.1 Hz) the current of the PC is directly controlled and the modulation of the quadrupole strength can be seen as random noise in the < 0.1 Hz range.
- **voltage-control:** due to the different components of a PC and the power grid itself, certain frequencies are present in the current spectrum, in general referred to as "ripple frequencies". The tolerances for the different frequencies are usually given in terms of voltage.

As the magnetic field scales linearly with the current, the normalized quadrupole strength is given by:

$$k(f) = T_{\mathrm{Itok}}(f) \times I_{\mathrm{PC}}(f) \tag{2}$$

in case of a direct control of the current.

To translate the voltage modulation in a modulation of the normalized quadrupole strength, the following model has been applied:

$$k(f) = T_{\mathrm{Itok}}(f) \times T_{\mathrm{VtoI,load}}(f) \times V_{\mathrm{PC}}(f) \tag{3}$$

where T_{Itok} is the transfer function from the PC current to the normalized quadrupole strength, which is assumed to be constant, $T_{\mathrm{VtoI,load}}(f)$ is the transfer function of the circuit seen by the PC and $V_{\mathrm{PC}}(f)$ is the voltage modulation. The circuit of the super-conducting IT magnets seen by the PC ($T_{\mathrm{VtoI,load}}(f)$) can in general be represented by an RL circuit. This implies that the higher the magnet inductance of the circuit, the stronger the attenuation of the modulation of the current and thus normalized quadrupole strength. In this model the effect of the cold bore, absorbers and beam screen is not included due to which an additional frequency dependent attenuation is expected.

IT POWERING SCHEMES

For the HL-LHC IT three different powering schemes are considered at the moment, which are illustrated in Fig. 1. The scheme "Baseline" is the current baseline powering scheme [8, 9], and the schemes "Q1Q2Q3" and "Q1Q2a-Q2bQ3" are alternative powering schemes under consideration. As will be shown later, the scheme Q1Q2a-Q2bQ3 features the smallest tune shift in the current-control regime and the scheme Q1Q2Q3 in the voltage-control regime due to its large inductance ($L_{\mathrm{tot}} = L_{\mathrm{Q1}} + L_{\mathrm{Q2}} + L_{\mathrm{Q3}}$). The magnet inductance and resistance used for the calculation of the normalized quadrupole strength with Eqn. 3 are summarized in Table 1.

* The HiLumi LHC Design Study is included in the High Luminosity LHC project and is partly funded by the European Commission within the Framework Programme 7 Capacities Specific Programme, Grant Agreement 284404.

ISBN: 978-3-95450-168-7 doi:10.18429/JACoW-IPAC2015-TUPTY036

Content from this work may be used under the terms of the CC BY 3.0 licence (© 2015). Any distribution of this work must maintain attribution to the author(s), title of the work, publisher, and DOI.

CROSSING SCHEME AND ORBIT CORRECTION IN IR1/5 FOR HL-LHC*

M. Fitterer, R. De Maria, S. Fartoukh, M. Giovannozzi, CERN, Geneva, Switzerland

Abstract

In this paper we review the orbit correction strategy and crossing scheme adjustment for the HL-LHC orbit correctors in IR1/5 in view of the new optics and layout version HLLHCV1.1. The main objectives are to optimize the crossing scheme, in particular to reduce the strength of the orbit correctors at D2, and to validate the strength specifications of the several orbit corrector magnets involved, including a budget reserved for the correction of the orbit distortions from various sources.

INTRODUCTION

One of the objectives in view of the preparation of the new HL-LHC layout version HLLHCV1.1 [1,2] compared to HLLHCV1.0 [2], was the review of the necessary orbit corrector strength based on [3,4] and investigation of a possible reduction of the strength of the correctors at D2 (MCBRD) and at Q3 (MCBX3). Such a reduction is based on the reuse of the Q4 quadrupole of the nominal LHC as a new Q5 for the HL-LHC. Thanks to the two additional orbit correctors at Q5 (Fig. 1), it is then possible to extend the crossing scheme until Q5 inclusive and reduce the corrector strength.

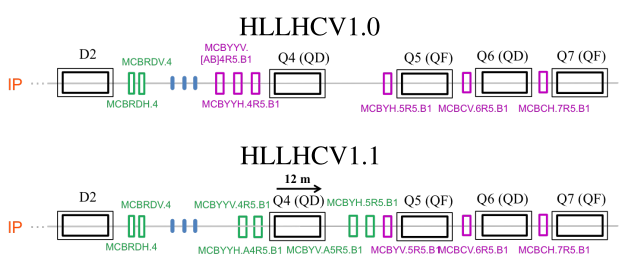

Figure 1: Schematic layout of the orbit correctors in IR1/5 in the D2 to Q7 region (longitudinal positions are not to scale). Representatively, IR5 Beam 1 right of the IP is shown. Orbit correctors used (additionally) for the crossing scheme are indicated in green and orbit correctors only used for orbit correction in pink. For Beam 2 the plane of correction is inverted for the orbit correctors at Q4, Q5 and Q6 due to the change of polarity of the quadrupoles for the other beam.

The orbit correctors in IR1 and IR5 in general have to provide sufficient strength for coping with the following aspects:

1. crossing and separation schemes,
2. beam based alignment of crab cavities,
3. luminosity and Van der Meer scans,
4. correction of inner triplet (IT) misalignment and feed-down from transfer function errors,
5. correction of closed orbit distortions generated by the arc imperfections.

The corrector strength for crossing and separation, luminosity and Van der Meer scans, and correction of IT errors depends only on the IT strength and the chosen crossing angle and separation. During the pre-squeeze the IT strength increases from injection to pre-squeezed optics and stays constant during the telescopic squeeze [5] and for all squeezed optics (round and flat). In most cases the studies are therefore only conducted for the injection optics at 7 TeV with $\beta^* = 6$ m, and for round collision optics marking the two "corner" cases during the pre-squeeze, where the round collision optics configuration has been chosen as reference for all squeezed optics. The results for the other squeezed optics can be then obtained by linear scaling with the crossing angle and separation, if changed. All optics parameters are summarized in Table 1.

Table 1: Optics parameters for layout HLLHCV1.1 and HLLHCV1.0."xing" is the half crossing angle and "sep" is the half separation. "round" and "flat" optics are squeezed collision optics. The optics parameters for injection (inj) are given after the ramp at 7 TeV.

	$\beta^*_{x/y}$ [m]	xing [μrad]	sep [mm]
pre-squeeze	0.44/0.44	±295	±0.75
round	0.15/0.15	±295	±0.75
flat	0.30/0.075	±275	
inj (7 TeV)	6.0/6.0	±295	±0.75

In this paper we only give a short summary of the main results, explicitly points 1, 2 and 4. Further details can be found in [6].

CORRECTION OF TRIPLET MISALIGNMENT AND FEED-DOWN FROM TRANSFER FUNCTION ERRORS

In order to asses the required corrector strength for misalignment and transfer function errors of the IT, Monte Carlo simulations using MAD-X have been conducted. For all simulations 10 000 seeds have been used. As a worst case scenario uniformly distributed errors have been assumed using the following reference values:

- ±0.5 mm transverse alignment errors,
- ±10 mm longitudinal alignment errors,
- $\pm 2 \times 10^{-3}$ relative gradient errors.

All results can be scaled linearly as the transverse alignment and relative quadrupole gradient errors both scale linearly

* The HiLumi LHC Design Study is included in the High Luminosity LHC project and is partly funded by the European Commission within the Framework Programme 7 Capacities Specific Programme, Grant Agreement 284404.

ISBN: 978-3-95450-168-7 doi:10.18429/JACoW-IPAC2015-TUPTY037

HLLHCV1.1: OPTICS VERSION FOR THE HL-LHC UPGRADE*

R. De Maria, S. Fartoukh, M. Fitterer, CERN, Geneva, Switzerland

Abstract

The optics and layout of the HL-LHC are evolving as the new hardware is being studied and integrated, any additional requirements from the experiments detailed, and other constraints of different nature clarified. Here we present the changes of version 1.1 of the optics and layout with respect to the previous version 1.0, which include the current hardware choices and an outlook on the main resulting optics limitations and the possible future evolutions of the layout.

INTRODUCTION

The High-Luminosity LHC project (HL-LHC) [1] relies on a reduction of β^* at the interaction points (IP) of the ATLAS and CMS experiments, IP1 and IP5 respectively. Larger aperture magnets [2] are foreseen to be compatible with the increased beam size in the interaction region (IR) and crab cavities [3] to compensate for the geometric reduction factor introduced by the crossing angle. The achromatic telescopic squeeze scheme (ATS) [4] is foreseen to preserve optics flexibility and guarantee the correction of the chromatic aberrations when reducing β^*, at the cost of extending the optics transitions to the arcs and neighbouring insertions and of increasing the beam size in the arcs. The new scheme also requires a stronger quadrupole in IR6 and will benefit from an additional sextupole in the arcs around the IR1,5.

This paper presents the latest baseline layout and optics models of the HL-LHC, labelled HLLHCV1.1, which is an evolution of HLLHCV1.0 and previous layouts [5]. We will also give an outlook of the future evolution of the layout based on recent developments from hardware studies.

LAYOUT

The HL-LHC layout is based on the nominal LHC with changes in particular in the straight sections of IR1 and IR5. A summary of the layout changes with respect to the LHC is given in Table 1. Figure 1 shows a sketch of the layout for the right part to IR5 (the left part is symmetric with respect to the IP and the layout of IR1 is identical to the IR5 layout). The main changes from HLLHCV1.0 to the HLLHCV1.1 are:

- updated triplets and interconnection lengths,
- change of position of the Q4 magnets,
- one additional cavity module (4 instead of 3) per side, beam and per IR,
- a different hardware for Q5 (MQY at 1.9 K) in IR1 and IR5 instead of a new MQYL (longer MQY) type,
- a different hardware for Q5 in IR6 (an additional MQY, thus two MQYs, instead of a new MQYL type magnet),
- revised orbit corrector layout in the D2-Q4 area [6].

* The HiLumi LHC Design Study is included in the HL-LHC project and is partly funded by the European Commission within the Framework Programme 7 Capacities Specific Programme, Grant Agreement 284404.

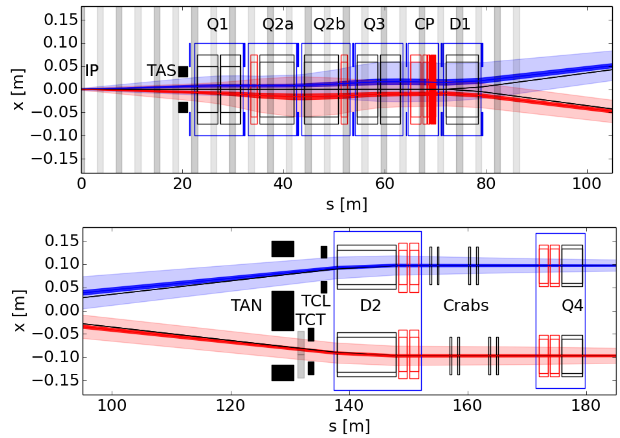

Figure 1: Sketch of the Layout on the Right Side of IP1 and IP5 from the IP to D1 (top) and from D1 to Q4 (bottom). Dark blue and red area show the 2σ beam envelops of Beam 1 and Beam 2. Light blue and red areas show the 12 σ beam envelops with imperfections (20% beta beating and 2 mm orbit error). On the top plot, gray bands highlight the location of the parasitic encounters for 25 ns bunch spacing and small blue boxes the BPMs.

The Q4 has been moved towards the arc in order to reduce the required voltage of the crab cavities and with the additional benefit of more available space for the additional crab cavity module and other equipment to be installed in the crab cavity region. Furthermore, the crab cavity modules are arranged in a different layout: two staggered pairs to optimize the required deflecting voltage regardless of the crossing plane. In HLLHCV1.0 the crossing and separation scheme bumps were closed just before the crab cavities with the orbit corrector at D2 (MCBRD), in order to minimize the orbit at the location of the crab cavities, however leading to a large strength of the MCBRD orbit correctors. In HLLHCV1.1 a considerable reduction has be achieved by sharing the strength needed for the crossing scheme bump between the orbit corrector at Q4 and the MCBRD at D2 at the cost of a non-zero residual orbit at the location of the crab cavities [6]. HL-LHC optics needs stronger Q5s in IR1/IR5/IR6 than those of LHC and for IR1/IR5 also with larger aperture. For Q5 HLLHCV1.1 adopts less expensive solutions as compared to the new magnet type (MQYL) proposed in HLLHCV1.0. In IR1/IR5 the existing MQM is replaced with the current Q4 (MQY) fitted to be cooled at 1.9 K to reach 200 T/m. Another alternative would have been to use a double MQYY as Q5 in IR1/IR5 to give more strength in Q5 (used mainly for large β optics) and more aperture that could be used in alternative optics schemes [7]. In IR6 doubling the existing MQY brings enough strength for the ATS squeeze optics.

Content from this work may be used under the terms of the CC BY 3.0 licence (© 2015). Any distribution of this work must maintain attribution to the author(s), title of the work, publisher, and DOI.

ISBN: 978-3-95450-168-7 doi:10.18429/JACoW-IPAC2015-TUPTY038
Content from this work may be used under the terms of the CC BY 3.0 licence (© 2015). Any distribution of this work must maintain attribution to the author(s), title of the work, publisher, and DOI.

BPM TOLERANCES FOR HL-LHC ORBIT CORRECTION IN THE INNER TRIPLET AREA*

M. Fitterer, R. De Maria, CERN, Geneva, Switzerland

Abstract

For the HL-LHC beam spot sizes as small as 7 mum are considered for the high luminosity insertions IR1 and IR5. In addition, the luminosity has to be levelled over several hours by changing beta* resulting in constant changes of the optics and thus orbit changes. The small beam size and the continuous optics changes in general make the alignment of the beams at the IP challenging. In order to avoid continuous luminosity scans for the alignment of the beams at the IP, the orbit correction has to rely on the readings of the BPMs in the IT region. In this paper we review the requirements on resolution and accuracy of the BPMs and compare different options for the placement of the BPMs in the IT region.

INTRODUCTION

The aim of the simulations presented in this paper is the definition of the precision and ranking of the BPMs in IR1/5 in terms of their efficiency. Explicitly the following points have to be specified:

- **the precision needed for a sufficient fill to fill reproducibility**: The minimum precision is defined by the precision required to find collisions at the beginning of a fill, while optimally the BPM precision should allow to find 1% of the luminosity at the beginning of the fill using only the BPMs and without the aid of luminosity scans.
- **the precision needed during one fill:** Assuming that the BPMs are recalibrated at the beginning of the fill, the BPM precision needs to be sufficiently good to keep the beams in collision without loss of luminosity, explicitly keeping the luminosity loss smaller than 1%.

ORBIT CORRECTION IN THE NOMINAL AND HL-LHC

Orbit Correction in the Nominal LHC

In the current LHC the orbit is corrected for each beam individually using a SVD and limiting the number of eigenvalue [1] . Explicitly a global orbit correction is performed and no individual correction of interaction regions (IRs). In all IRs, three BPMs per side and per beam are installed in the inner triplet area, which are however not used in standard operation at the moment. From experience in the LHC, BPMs closest to the IP are in gernal best for the correction of the orbit at the IP and a correction is usually still possible with 2 out of 3 BPMs.

* The HiLumi LHC Design Study is included in the High Luminosity LHC project and is partly funded by the European Commission within the Framework Programme 7 Capacities Specific Programme, Grant Agreement 284404.

Furthermore, around 10 μm of orbit drift at the IP are observed from fill to fill and around 100 μm during a period of several months [2]. The behaviour of the drifts also suggests a ground motion like behavior with the orbit deviation mainly originating from the misalignment of quadrupoles.

The general strategy for the LHC orbit correction is:

1. correct to the golden orbit of the previous fill at the end of the squeeze
2. conduct a lumiscan to optimize luminosity. The obtained orbit then redefines the "golden orbit"
3. orbit correction to the golden orbit defined by the initial lumiscan. The BPMs at the IT are explicitly not included in the correction.
4. in case of a relevant drop in luminosity, additional lumiscans are conducted

Orbit Correction in the HL-LHC

Between the nominal LHC and the HL-LHC differences and similarities exist in respect of the orbit correction. As the experiments can not accept the peak luminosity delivered by the HL-LHC, β^*-leveling over several hours is foreseen in order to reach the maximum integrated luminosity. A change in β^* entails a change of the optics which in turn results in a change of the orbit. In view of the orbit correction, two cases should be distinguished for the β^*-leveling:

- leveling using the pre-squeezed optics, for which the magnet strength in IR1/5 is changed for the squeeze of the same. This is the case for $\beta^* > 0.44$ m.
- leveling using the squeezed optics, for which the magnet strength in IR1/5 stays constant but instead the strength in the adjacent IRs is changed (IR2/8 and IR4/6). This is the case for $\beta^* < 0.44$ m.

Using the squeezed optics for the β^*-leveling might be preferred in view of the orbit correction as IR1/5 stay unchanged. This case would be similar to the nominal LHC, assuming that the orbit at the entrance and exit of IR1/5 can be controlled sufficiently well.

The orbit deviations in mm due to ground motion are expected to be similar for the HL-LHC as for the LHC. The reason is that the machine stays unchanged except for the IT and the integrated quadrupole strength of the nominal and the HL-LHC triplet is approximately the same, and thus the same orbit deviation in terms of mm are expected. However, the HL-LHC envisages smaller beam spot sizes than the LHC making the luminosity more sensitive to small orbit deviations.

The general orbit correction strategy for the HL-LHC could be:

ISBN: 978-3-95450-168-7 doi:10.18429/JACoW-IPAC2015-TUPTY039

LHC TRANSFER LINES AND INJECTION TESTS FOR RUN 2

C. Bracco, J.L. Abelleira, R. Alemany-Fernandez, M.J. Barnes, W. Bartmann, E. Carlier, L. Drøsdal, M.A. Fraser, K. Fuchsberger, B. Goddard, J. Jentzsch, V. Kain, N. Magnin, M. Meddahi, J.S. Schmidt, L.S. Stoel, J. Uythoven, F. M. Velotti, J. Wenninger, CERN, Geneva, Switzerland

Abstract

The Transfer Lines for both rings of the LHC were successfully recommissioned with beam in preparation for the start-up of Run 2. This paper presents an overview of the Transfer Line and Sector Tests performed to bring the LHC back into operation after a two-year period of shut-down for consolidation and upgrade. The tests enabled debugging of critical software and hardware systems and validated changes made to the transfer and injection systems. The beam-based measurements carried out to validate the optics and machine configuration are summarised along with the hardware systems.

INTRODUCTION

A combination of bumpers, fast kickers (MKE) and DC electromagnetic septa (MST and MSE) is installed in two SPS Long Straight Sections (LSS6 for Beam 1 and LSS4 for Beam 2) to extract the 450 GeV proton and ion beams towards the LHC [1]. The beams are then transported along two ~3 km long Transfer Lines (TL: TI 2 and TI 8) to the LHC. A system of collimators (TCDIs) is installed at the end of each TL to protect the LHC aperture from large amplitude oscillations due to failures occurring upstream in the line or during SPS extraction.

The injection into the LHC [2] is performed in two Insertion Regions (IR2 and IR8) towards a series of five Lambertson type septum magnets (MSI). Four kicker magnets (MKI) deflect the beam onto the LHC orbit.

The LHC injection system is particularly critical due to the use of high voltage fast (900 ns rise time) kickers and the relative likelihood of failure scenarios (i.e. erratic firing, flashovers, etc). A passive absorber (TDI) is installed at 90° phase advance from the injection kicker to protect the LHC aperture in case of kicker misfiring. The TDI is also used to stop the beam during injection setup.

Accurate hardware checks are performed during the machine check-out period following long shutdowns and/or relevant modifications. Tests with beam are also required to fully validate the systems and insure the correct functionality of each equipment. For this purpose TL and Sector Tests were carried out before the startup of the second LHC Run (in November 2014 and March 2015 respectively). A summary of the performed checks and of the most relevant outcomes are presented.

LS1 ACTIVITIES

The CERN accelerator complex underwent a long period of consolidation works in view of the second LHC run and operation at 6.5 TeV. Among others, upgrades were performed on the SPS extraction, TL and LHC injection systems. In the following only the activities directly related to the TL and Sector Test measurements are mentioned.

The quadrupole magnets of the SPS ring, TI 2 and TI 8 were re-aligned.

A clean and steady injection into the LHC strongly depends on the stability of the beam trajectory in the TLs. A reference trajectory, which allows to minimise the injection oscillations into the LHC, has to be defined. A periodic re-steering of the lines is then necessary to compensate for the long term drifts which are induced by variations of the SPS orbit. Current ripples at the MSE Power Converter (PC) were identified as the major source of shot-to-shot variations in the horizontal trajectory of both TLs [3]. Already during Run 1 several mitigation measures were put in place (recabling and new configuration of the PC output filters) and the ripple was reduced from 20 A (2011) down to 4 A (2012). Further upgrades were applied during LS1.

On top of the shot-to-shot variations, a bunch-by-bunch pattern could be observed which sampled the MKE waveform. During LS1 the last unserigraphed MKE in LSS4 was replaced with a serigraphed magnet to lower the impedance. Moreover, adjustments were applied to two of the Pulse Forming Networks (PFNs) to try to flatten the MKE waveform.

A number of consolidations were applied to the MKIs in order to reduced the ferrite yoke heating and the flashover rate [4]. The ceramic chambers were equipped with a full complement of screen conductors and a modified external metal cylinder at the capacitively coupled end. This required a full validation of the high voltage performance of the MKI magnets.

TL TEST

The TL test consisted in extracting both Beam 1 and Beam 2 from the SPS and transporting them until the absorber blocks (TED) located at the end of TI2 and TI8 respectively. This exercise was performed using pilot bunches of ~5×10^9 protons.

SPS Extraction

In preparation for the TL test, SPS extraction setup and aperture measurements were carried out on October 21st 2014. The defined settings for the bumpers, kickers and septa were compared with the theoretical values and those used in 2012; they were well consistent and the beam could be successfully extracted.

A scan of the aperture at the septa was accomplished by scaling the amplitude of the extraction bump with the MKE on (extraction channel) and off (circulating beam aperture).

Content from this work may be used under the terms of the CC BY 3.0 licence (© 2015). Any distribution of this work must maintain attribution to the author(s), title of the work, publisher, and DOI.

ISBN: 978-3-95450-168-7 doi:10.18429/JACoW-IPAC2015-TUPTY040

COMPARISON OF BEAM SIZES AT THE COLLIMATOR LOCATIONS FROM MEASURED OPTICS AND BEAM-BASED COLLIMATOR ALIGNMENT AT THE LHC

G. Valentino*, R. Bruce, A. Langner, S. Redaelli, R. Tomás
CERN, Geneva, Switzerland

Abstract

At the Large Hadron Collider (LHC), the collimation hierarchy is defined in units of the betatron beam size using the sizes at each collimator location. The beam size at a given collimator can be inferred from the gap measurement during beam-based alignment campaigns, when the collimator touches a reference beam halo defined with the primary collimators. On the other hand, the beta functions at each collimator are also measured as a part of the standard LHC optics validation. This paper presents a comparison of the beam size measurements at the collimator locations applying these two techniques for different machine configurations. This work aims at determining which is the most reliable method for setting the collimator gaps at the LHC.

INTRODUCTION

The LHC accelerates two counter-rotating beams to a nominal energy of 7 TeV, corresponding to 362 MJ of stored energy per beam. An uncontrolled beam loss of only 7.6×10^6 p s^{-1}m^{-1} in a superconducting magnet can induce enough heating to cause a quench. In Run 1, a multi-stage system composed of 43 collimators per beam was operated to protect the LHC against losses of circulating beam [1]. Each collimator is composed of two jaws which need to be positioned equidistant from the beam, based on the beam centre and beam size at the collimator location. The upstream and downstream corners of each jaw can be moved independently by dedicated stepper motors. Most of the LHC collimators are located in Insertion Region (IR) 3 and IR 7 to clean particles with large momentum and betatron offsets, respectively. The IR7 horizontal aperture is shown in Fig. 1. The collimators are installed in the horizontal, vertical and skew planes to ensure the best coverage of the transverse phase space.

COLLIMATOR ALIGNMENT

The beam center and the beam size at each collimator are measured during a commissioning period at the start of the run. These values are measured for four machine modes: injection, flat top, squeezed separated, and colliding beams, and are used to calculate the operational jaw settings for the whole run. Thanks to the reproducibility of the beam orbit, one set up per machine mode per year has proven to be sufficient for now. Alignments are repeated if the machine configuration (e.g. β^*, crossing angle) is changed.

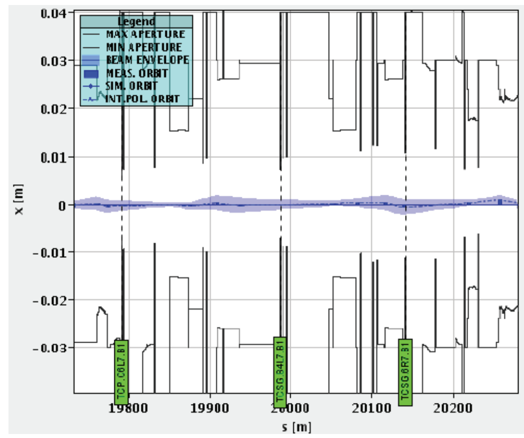

Figure 1: The IR7 horizontal aperture and beam orbit, with the envelope denoting the 1-σ beam size. The green text boxes show names of a few IR7 horizontal collimators.

Each collimator is set up using a four-step procedure [2]. The jaw of a reference collimator, taken to be the IR7 primary collimator (TCP) in the same plane as the collimator to be aligned, is first moved in steps of 5 μm (top energy) or 20 μm (injection energy). A feedback loop is used to stop the movement when the beam losses from a downstream Beam Loss Monitor (BLM) exceed a pre-defined threshold [3] (step 1). The opposite jaw is then aligned to the beam. After the reference cut in the halo is established, the i^{th} collimator i can be aligned (step 2). The reference collimator is re-aligned to the beam to account for halo depletion during the previous alignment (step 3). Finally, the collimator is retracted to the hierarchy positions (step 4).

At the start of the horizontal collimator alignment, the momentum halo is cut using the primary collimator in the high-dispersion region in IR3. This ensures that the halo intercepted by the other collimators is dominated by the betatron contribution, and has proved to give more stable and reliable results [6] for the beam centres. The inferred beam size at the collimator i is expressed in terms of the jaw half gap and the reference cut in units of σ, n_1:

$$\sigma_i^{\text{inf}} = \frac{x_i^{\text{L}} - x_i^{\text{R}}}{n_1^{k-1} + n_1^k} \quad (1)$$

where x_i^{L} and x_i^{R} are the left and right aligned jaw positions, and k is an index for the number of reference collimator alignments. The half-gap opening n_1 in units of σ for the two reference collimator alignments is calculated

* gianluca.valentino@cern.ch

Content from this work may be used under the terms of the CC BY 3.0 licence (© 2015). Any distribution of this work must maintain attribution to the author(s), title of the work, publisher, and DOI.

ISBN: 978-3-95450-168-7 doi:10.18429/JACoW-IPAC2015-TUPTY042

NON-LINEAR COUPLING STUDIES IN THE LHC

T. Persson, E. H. Maclean, R. Tomás, CERN, Geneva, Switzerland
Y. I. Levinsen, ESS, Lund, Sweden

Abstract

The amplitude detuning has been observed to decrease significantly as the horizontal and vertical tunes approach each other. This effect is potentially harmful since it could cause a loss of Landau damping, hence giving rise to instabilities. The measured tune split $(Q_x - Q_y)$ versus amplitude is several times bigger than what can be explained with linear coupling. In this paper we present studies performed to identify the dominant sources of the non-linear coupling observed in the Large Hadron Collider (LHC).

INTRODUCTION

Linear transverse coupling has been studied thoroughly in a large number of accelerators. In light sources it plays an important role for the equilibrium emittance and it has been demonstrated to enhance other resonances [1, 2]. In the Large Hadron Collider (LHC) the control of the coupling is also of importance for a reliable tune feedback. The approach to correct the coupling in the LHC has been to first correct the strong local sources during commissioning [3] and then use two orthogonal knobs to correct the observed drifts of the global coupling [4]. The two knobs are designed to correct the real and the imaginary part of the C^- respectively. The absolute value of the $|C^-|$ is, in the linear theory, equal to the $\Delta Q_{\min}$ which is the closest approach of the transverse tunes [5]. A lot of progress in the control of the linear coupling was made during Run I of the LHC. The improvements included a better understanding of the resonance driving terms relation to the $|C^-|$, as well as improved data filtering and a tool to measure and correct the coupling based on the injection oscillations [6, 7].

The off-momentum dependence of the coupling, also known as the chromatic coupling was studied and a successful correction was demonstrated in [8]. These efforts have resulted in a good understanding and control of the linear and the off-momentum coupling in the LHC. In this article we discuss studies to identify sources of an observed amplitude dependence of the transverse coupling.

EXPERIMENTAL OBSERVATIONS

Particles with different amplitude will be focused differently in sextupoles but since the focusing is also dependent on the phase the effect almost cancels out. Octupoles magnets on the other hand introduce a bigger amplitude dependence of the tunes. This is of importance to reduce collective effect instabilities in the LHC. The behavior of this detuning is dependent on the powering of the octupoles but is also influenced by other resonances in the tune diagram.

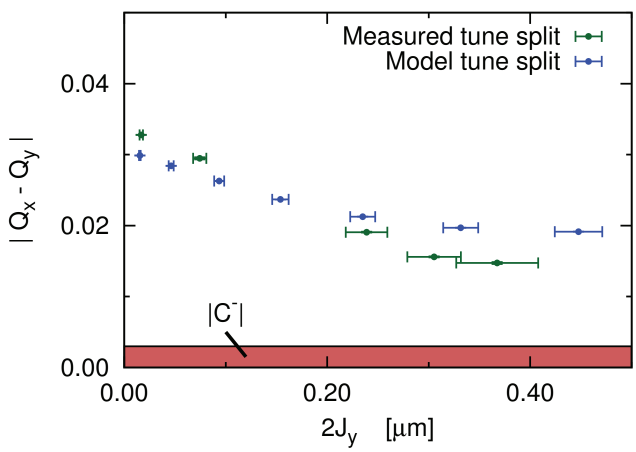

Figure 1: The tune split as a function of the action from the measured data as well as from the simulation based on the nonlinear model of the LHC. The linear $|C^-|$ was measured during the study and is indicated by the red area.

The naive expectation is that in a situation with coupling the detuning would be similar to the situation without coupling far away from the $|C^-|$ and only close to the stopband change the behaviour. During Non-linear dynamics studies in 2012 it was observed that this was not the case [9]. When large vertical kicks were applied to the beam the tunes did not approach each other as much as one would expect from the amplitude detuning. Instead the tune split seemed to saturate at a distance 4 times larger than the linear $|C^-|$. During the measurement the action was also measured and the large increase of the horizontal action for vertical kicks could not be explained by means of linear coupling. These observations gave rise to the interpretation of an amplitude dependent $|C^-|$. This feature was also well reproduced in the non-linear model of the LHC as seen in Fig. 1. The non-linear model of the LHC contains the best available knowledge about the errors in magnets as well as misalignment. The simulation was performed using tracking and the linear coupling was matched to the measured values. The magnitude of the kicks were also reproduced in the simulation.

IDENTIFICATION OF SOURCES

The non-linear model of the LHC contains many sources of non-linear errors and misalignment. In order to determine which type of sources were needed to cause an am-

Content from this work may be used under the terms of the CC BY 3.0 licence (© 2015). Any distribution of this work must maintain attribution to the author(s), title of the work, publisher, and DOI.

ISBN: 978-3-95450-168-7 doi:10.18429/JACoW-IPAC2015-TUPTY043

ANALYSIS OF INTENSITY-DEPENDENT EFFECTS ON LHC TRANSVERSE TUNES AT INJECTION ENERGY

T. Persson, R. De Maria, M. Giovannozzi, R. Tomás, CERN, Geneva, Switzerland
Y. Wei, IHEP, Beijing, China

Abstract

The LHC Run I has provided a huge amount of data that can be used to deepen the understanding of the beam behaviour. In this paper the focus is on the analysis of transverse tunes at injection energy to detect signs of intensity-dependent effects. BPM data, recording the injection oscillations of the operational beams during the ring-filling phase, have been analysed in detail to enable extracting useful information about the tune shift vs. injected beam intensity. The data processing and the results are discussed in detail, including also possible implications for future operation.

INTRODUCTION

During the first years of LHC operation [1] a gold mine of observations and beam measurements has been collected. Among the several aspects of beam dynamics that can be probed thanks to these data, the evolution of the transverse tunes along the cycle are of particular interest [2]. The tune variation is mainly governed by the magnetic fields and any time-variation of the quadrupolar fields is impacting on the tune stability, which, in turns, might affect the accelerator's performance. Moreover, comparison of the measured tune evolution against the known features of the magnetic model can lead to improvements to the predictivity of the model in view of, e.g., defining a feedforward correction to ease the feedback system.

The data taken during normal operation have already highlighted a good agreement with the prediction of the magnetic model. However, a clear sign of intensity-dependent effects has been observed [2]. Such an effect is visible in the tune evolution during the filling process at injection in the LHC. The standard data analysis applied in Ref. [2] could not provide any quantitative estimate of the tune shift as a function of beam intensity. This effect had been quantified in Ref. [3] based on a number of assumptions for the estimate of the so-called Laslett coefficients [4, 5] (see also Refs. [6–8] for additional detail on this topic). Also in the case of the tune variation with intensity, a feedforward approach could be taken to devise a compensation strategy. Clearly, one should also asses whether this effect could impact the beam dynamics and the beam quality, and a quantitative evaluation of the phenomenon is the first step in this process.

In this paper an improved analysis of the data collected during the operational LHC fills, mainly during the 2012 physics run, is presented. It allows deriving the measured tune shift as a function of intensity. The delicate and interesting topic of comparing the theoretical estimate with observations is left aside for the time being.

MEASUREMENT METHODS

The LHC Base-Band-Tune, BBQ [9], is the most sensitive instrument for tune measurement and provides reliable measurements for single bunches or when the LHC transverse damper (ADT) is not active. For the case of circulating bunch trains, the signal level drops below the noise lines corresponding to 50 Hz harmonics and the noise introduced by the ADT, thus preventing any reliable measurement (see Fig. 1). BBQ data are logged continuously in the form of turn-by-turn data, post-processed spectra, and estimated tune values. Continuous turn-by-turn data are only available for limited periods of time.

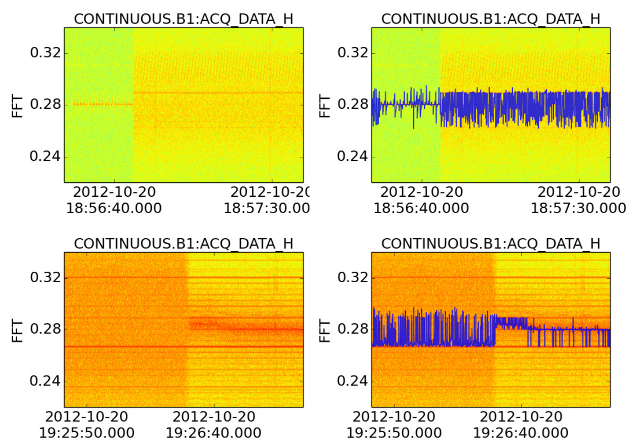

Figure 1: Horizontal BBQ spectra as a function of time (right) with superimposed estimated tune values (blue lines) during the injection process. In the top-left plot the horizontal (0.28) and vertical tunes (0.31) can be recognized when only a pilot bunch is present. However, as soon as other bunches are injected and the ADT activated the noise exceeds the signal level and the estimated tunes are extremely noisy. The bottom figures show the transition when the ADT is switched off, revealing again the tune signature. In fact, the estimated tune values become more reliable, although still occasionally lock on noise lines.

The LHC ADT [10] uses special BPMs and electronics to provide sensitive bunch-by-bunch, turn-by-turn beam position measurements. The 4 BPMs are installed in the insertion region (IR) 4 in the quadrupoles Q7 and Q9 for both beams and transverse planes. Raw data are not logged systematically, as only the 2000 turns of the first injected bunch are available in the logging database. An example of the information available from these BPMs is shown in Fig. 2, where typical injection oscillation signals are shown. A fit with an exponentially decaying sinusoid shows an excellent

Content from this work may be used under the terms of the CC BY 3.0 licence (© 2015). Any distribution of this work must maintain attribution to the author(s), title of the work, publisher, and DOI.

6th International Particle Accelerator Conference IPAC2015, Richmond, VA, USA JACoW Publishing
ISBN: 978-3-95450-168-7 doi:10.18429/JACoW-IPAC2015-TUPTY045

INTERACTIONS BETWEEN MACROPARTICLES AND HIGH-ENERGY PROTON BEAMS

S. Rowan*, A. Apollonio, B. Auchmann, A. Lechner, O. Picha, W. Riegler, H. Schindler, R. Schmidt, F. Zimmermann, CERN, Geneva, Switzerland

Abstract

A known threat to the availability of the LHC is the interaction of macroparticles (dust particles) with the LHC proton beam. At the foreseen beam energy of 6.5 TeV during Run 2, quench margins in the superconducting magnets will be 2-3 times less, and beam losses due such interactions may result in magnet quenches. The study introduces an improved numerical model for such interactions, as well as Monte-Carlo simulations that give the probability of such events resulting in a beam-dump during Run 2.

INTRODUCTION

The phenomenon of UFOs (Unidentified Falling Objects), i.e., interactions of falling macroparticles (dust particles) with the proton beam, is well documented [1, 2]. Similar effects are known from other, mostly electron and anti-proton machines [3, 4, 5]. The LHC is the first proton machine where this phenomenon can be found. Figure 1 shows observations of UFO rates during the LHCs Run 1 with beam energies up to 4 TeV. With up to 13 UFOs per hour during a 25-ns bunch-spacing test run, falling macroparticles were estimated to become a significant threat to the availability of the LHC when operating at 6.5 TeV [6]. Such interactions produce particle showers that deposit energy in the adjacent superconducting magnets, possibly leading to magnet quenches. The current strategy to mitigate the effects this phenomenon is to detect the beam-losses with beam-loss monitors, and to trigger a preventative beam dump as soon as a threshold is exceeded.

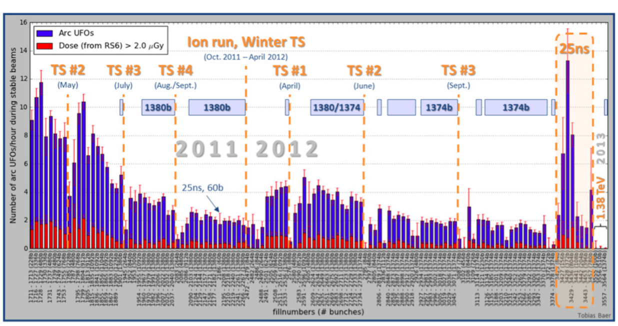

Figure 1: Number of arc UFOs per hour during stable beams in 2011 and 2012. Courtesy T. Baer.

There have been a number of detailed particle-shower simulations and beam-loss experiments to improve the understanding of such quench events [7, 8]. In order to estimate the true extent of the threat and to study relevant mitigation strategies, a numerical model of such macroparticle-to-beam interactions has been constructed, progressing on previous works [9, 10]. The simulated proton-loss rate was translated into signals in the beam-loss monitors (BLMs) based on the above particle-shower simulations. With this model, Monte-Carlo simulations have been carried out to reproduce measured data from 2012, and to extrapolate to Run 2 operating conditions.

NUMERICAL MODEL

A typical interaction between a macroparticle and the high-energy proton beam interaction - commonly referred to as a UFO event, is described as follows:

- A macroparticle (dust) falls from the beam screen or vacuum chamber.
- The macroparticle is ionized by elastic collisions with the proton beam releasing free electrons.
- Inelastic collisions result in particle showers recorded by BLMs, and potential quenches.
- The macroparticle is repelled by the beam's electric field.

Equation of Motion

The macroparticle's acceleration $\ddot{\vec{r}}$, with $\vec{r}$ the transverse position vector, is determined by gravity and by the force exerted by the electric field of the beam $\vec{E}$ on the macroparticle charge Qe,

$$\ddot{\vec{r}}(x, y, t) = \frac{Q(t)e}{m}\vec{E}(x, y) + \vec{g}, \tag{1}$$

with e the electron charge, m the macroparticle mass, g the gravitational constant, and $\vec{E}$ modeled by the Bassetti-Erskine formula [11] with recommendations for numerical stability from [12]. The total beam charge per unit length is given by $N_\mathrm{p}e/C$, with C the LHC circumference and N_p the total number of protons in the beam.

Macroparticle Charge Rate

Elastic interactions with the macroparticle lead to ionization. As a result, the charge rate, $\dot{Q}$, determines the beam's electric field influence. The charging formula, which is related to the Bethe-Bloch formula, is derived from the distribution N_e of knock-on electrons found in [13] with appropriate approximations,

$$\frac{\partial^2 N_\mathrm{e}}{\partial T \partial z} \approx 2\pi r_\mathrm{e}^2 m_\mathrm{e} c_0^2 n \frac{1}{T^2}. \tag{2}$$

* scott.rowan@cern.ch, s.rowan.1@researach.gla.ac.uk, with CERN, Switzerland, and The University of Glasgow, United Kingdom

Content from this work may be used under the terms of the CC BY 3.0 licence (© 2015). Any distribution of this work must maintain attribution to the author(s), title of the work, publisher, and DOI.

ISBN: 978-3-95450-168-7 doi:10.18429/JACoW-IPAC2015-TUPTY046

IMPACT OF BEAM LOSSES IN THE LHC COLLIMATION REGIONS

E. Skordis*, R. Bruce, F. Cerutti, A. Ferrari, P. G. Ortega, P. D. Hermes,
A. Lechner, A. Mereghetti, S. Redaelli, V. Vlachoudis
CERN, Geneva, Switzerland

Abstract

The upgrade of the LHC energy and brightness, from the 2015 restart at close to design energy until the HL-LHC era with considerable hardware development and layout renewal, poses tight challenges in terms of machine protection. The collimation insertions and especially the one dedicated to betatron cleaning (IR7), where most of the beam halo is intercepted to spare from losses the cold sectors of the ring, will be subject to a significant increase of radiation load, whose leakage to the nearby dispersion suppressors must be kept sustainable. The past LHC run, while displaying a remarkable performance of the collimation system, offered the opportunity for a demanding benchmarking of the complex simulation chain describing the beam losses and the macroscopic effects of the induced particle showers, this way strengthening the confidence in the reliability of its predictions. This paper discusses the adopted calculation strategy and its evolution options, showing the accuracy achieved with respect to Beam Loss Monitor measurements in controlled loss scenarios. Expectations at design energy, including lifetime considerations concerning critical elements, will also be presented.

INTRODUCTION

The design stored energy of the Large Hadron Collider (LHC) [1] of about 362 MJ per beam is capable of causing catastrophic damage to the machine. However, even a very small fraction of that can induce both quenches of the superconducting (SC) magnets as well as material damage. Consequently, the inevitable proton losses have to be adequately intercepted before touching the machine aperture.

The collimation system installed in the LHC [2, 3] proved to be capable of sustaining up to 1MW of impacting protons for 1 s [4, 5] and protecting the machine from damage and quench. However the collimators themselves are not designed to absorb the entirety of the energy of the halo protons but rather divert it to an area with less sensitive equipment. The most exposed area is the insertion region (IR) 7 [6], where 3 different kinds of collimators, primaries (TCP), secondaries (TCSG) and active absorbers (TCLA), hierarchically extract the beam halo particles and absorb part of the primary, secondary and tertiary shower. The rest of the energy is deposited in the other LHC elements and eventually in the tunnel walls. A tiny but potentially harmful fraction leaves the IR7 straight section and reaches the dispersion suppressor (DS) where the SC magnets are installed.

To be able to make accurate predictions of the collimation performance in future running scenarios, and ensure that magnets are sufficiently protected, it is crucial to have a reliable and well-benchmarked simulation chain. Sixtrack [7, 8] and FLUKA [9-11] are the two simulation tools used for the tracking of the protons and the calculation of the secondary particle shower development and its effects, respectively. In order to validate the predictions, Beam Loss Monitor (BLM) signals are also simulated and compared against measurements for well-defined scenarios such as the collimation quench test in 2013 [2]. The goal of this paper is to present the updated results of the energy deposition calculations for the IR7 and the BLM benchmark with the most recent developments in the simulation procedure.

SIMULATION CHAIN

Tracking of Protons around the LHC Ring

The first necessary step of the simulation chain is to track the halo protons around the ring and create a map of proton hits in the collimators. The tracking is done using Sixtrack, a six-dimensional phase space multi-turn tracking code that uses thin-lens element-by-element tracking through the magnetic lattice.

Together with a detailed aperture model, Sixtrack has been using its own built-in Monte Carlo code to deal with interactions, other than nuclear inelastic events, between beam particles and collimator jaw material. In this way a distribution of inelastic interactions in the LHC collimators is produced as initial condition for FLUKA [12]. Nowadays, the development of the Sixtrack-FLUKA active coupling [13] takes advantage of the specialized and highly benchmarked interaction models of FLUKA as well as of the detailed geometrical models of the collimator devices to describe all kinds of interactions in a consistent way, improving the simulation accuracy.

Particle Shower Simulations

As a second step, the general purpose particle physics Monte Carlo code FLUKA is used in order to calculate the values of interest (e.g. thermal load in critical elements, power density in the SC coils, dose in the warm magnets, BLM signals etc.) from the particle showers initiated by protons interacting with the collimators. All the relevant elements in the IR7, including collimators, magnets, BLMs, device supports, cables, tunnel walls, etc. are modelled in detail and then accurately assembled by the LineBuilder [14] to create a geometry of several hundreds of meters (Fig. 1).

*eleftherios.skordis@cern.ch

Content from this work may be used under the terms of the CC BY 3.0 licence (© 2015). Any distribution of this work must maintain attribution to the author(s), title of the work, publisher, and DOI.

ISBN: 978-3-95450-168-7 doi:10.18429/JACoW-IPAC2015-TUPTY047

Content from this work may be used under the terms of the CC BY 3.0 licence (© 2015). Any distribution of this work must maintain attribution to the author(s), title of the work, publisher, and DOI.

ERL WITH NON-SCALING FIXED FIELD ALTERNATING GRADIENT LATTICE FOR eRHIC*

Dejan Trbojevic, J. Scott Berg, Stephen Brooks, Yue Hao, Vladimir N. Litvinenko, Chuyu Liu, Francois Meot, Michiko Minty, Vadim Ptitsyn, Thomas Roser, Peter Thieberger, Nicholaos Tsoupas, Brookhaven National Laboratory, Upton, Long Island, New York, USA

Abstract

The proposed eRHIC electron-hadron collider uses a "non-scaling FFAG" (NS-FFAG) lattice to recirculate 16 turns of different energy through just two beam lines located in the RHIC tunnel. This paper presents lattices for these two FFAGs that are optimised for low magnet field and to minimise total synchrotron radiation across the energy range. The higher number of recirculations in the FFAG allows a shorter linac (1.322GeV) to be used, drastically reducing cost, while still achieving a 21.2 GeV maximum energy to collide with one of the existing RHIC hadron rings at up to 250GeV. eRHIC uses many cost-saving measures in addition to the FFAG: the linac operates in energy recovery mode, so the beams also decelerate via the same FFAG loops and energy is recovered from the interacted beam. All magnets will be constructed from NdFeB permanent magnet material, meaning chillers and large magnet power supplies are not needed. This paper also describes a small prototype ERL-FFAG accelerator that will test all of these technologies in combination to reduce technical risk for eRHIC.

INTRODUCTION

A possible future Electron Ion Collider (EIC) at Brookhaven National Laboratory will be placed in the existing tunnel of the superconducting Relativistic Heavy Ion Collider (RHIC→eRHIC) [1-5]. This is a design for the additional electron accelerator to provide polarized electrons with an energy range from 5 to 21 GeV. Electrons will collide with existing polarized protons or ^{3}He, or with other heavy ions from deuterons to Uranium.

The existing RHIC has been producing fascinating results so far with extraordinary performance above any expectations. RHIC represents a complicated chain of many accelerators, starting with the Electron Ion Beam Source (EBIS) with Radio Frequency Quadrupole (RFQ) and the polarized proton source (development of polarized ^{3}He has already started). It is the only collider in the world with the ability to collide unequal species and polarized protons. RHIC was the first to measure the formation of a "perfect liquid" consisting of quark gluon plasma (QGP). This system of accelerators and one of the two superconducting rings in RHIC will be reused in the future EIC while electrons will be provided by a new accelerator. Electron acceleration comes from a single superconducting linac with an energy gain of 1.322 GeV, accelerator design for producing electrons with energies up to 21.2 GeV is based on up to 16 passes through the linac with energy recovery (ERL). After polarized electrons are accelerated to the top energy (eRHIC has 15.9 or 21.2 GeV modes) and collided with the polarized protons or ions, their energy is recovered in the same linac. There are the same number of decelerating passes through the linac as accelerating passes, but at negative voltage (180° phase) so the energy is recovered. They reach the initial injection energy during the last pass. The "blue" hadron ring is shown schematically above the two electron beam lines (upper left corner in Fig. 1). Orbit offsets in the NS-FFAG electron rings are shown in Fig. 2. The hadron Interaction Region (IR) magnets are shown at the bottom of Fig. 1 with electrons and ions

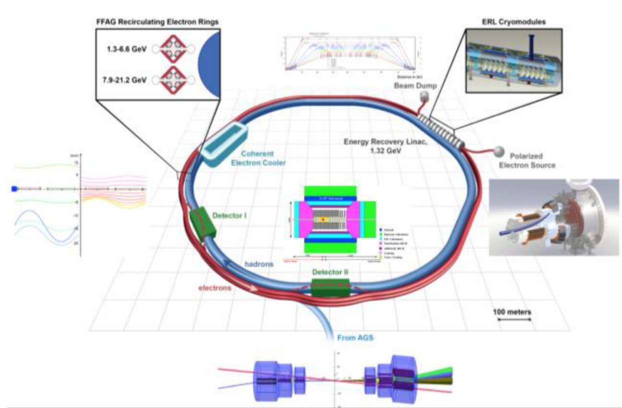

Figure 1: Layout of eRHIC: Existing "blue" superconducting hadron ring (centre); Two electron NS-FFAG beam lines (top left, with beam orbits on left); Polarized electron Gatling gun (right); Combiners and separators (top centre); Interaction region schematic (bottom) at the 6 o'clock point; and the superconducting linac (top right).

A MICROSCOPE FOR GLUONS

An EIC will be used to study the "spin puzzle" to determine quark and gluon contributions to the total proton spin, including the spatial distribution of quarks and gluons inside nuclei – a "microscope for gluons".

eRHIC Parameters

The new EIC collider eRHIC should achieve very high luminosities of the order of 10^{34} due to the expected small emittance of both electron and proton/ion beams. A new coherent electron cooling scheme is proposed for the

* Work performed under Contract Number DE-AC02-98CH10886 with the auspices of the US Department of Energy

ISBN: 978-3-95450-168-7 doi:10.18429/JACoW-IPAC2015-TUPTY048

CHANGES TO THE TRANSFER LINE COLLIMATION SYSTEM FOR THE HIGH-LUMINOSITY LHC BEAMS

V. Kain, O. Aberle, C. Bracco, M. Fraser, F. Galleazzi, E. Gianfelice-Wendt, A. Kosmicki, F. Maciariello, M. Meddahi, F.-X. Nuiry, G. Steele, F. Velotti, CERN, Geneva, Switzerland

Abstract

The current LHC transfer line collimation system will not be able to provide enough protection for the high brightness beams in the high-luminosity LHC era. The new collimation system will have to attenuate more and be more robust than its predecessor. The active jaw length of the new transfer line collimators will therefore be 2.1 m instead of currently 1.2 m. The transfer line optics will have to be adjusted for the new collimator locations and larger beta functions at the collimators for absorber robustness reasons. In this paper the new design of the transfer line collimation system will be presented with its implications on transfer line optics and powering, maintainability, protection of transfer line magnets in case of beam loss on a collimator and protection of the LHC aperture.

INTRODUCTION

The transfer line collimators in the SPS-to-LHC transfer lines have been designed to attenuate and be robust enough for ultimate LHC intensity at 450 GeV. After the high luminosity upgrade the LHC will require beams from injectors with a brightness much increased with respect to the nominal or even ultimate LHC intensities.These parameters will only be achievable after substantial upgrades in the LHC injectors themselves [1]. The beam characteristics after the LHC Injector Upgrade (LIU) and the LHC ultimate beam which are relevant for the discussion in this paper are summarized in Table 1.

Table 1: LIU beam parameters in the SPS at 450 GeV [1]. BCMS stands for the beam production scheme "Batch Compression, Bunch Merging and Splitting"

	$p^+/bunch$	ε	$N_{bunches}$
Ultimate	1.7×10^{11}	$3.5\ \mu m$	288
Standard LIU	2.3×10^{11}	$2.1\ \mu m$	288
BCMS LIU	2.0×10^{11}	$1.3\ \mu m$	288

The impact of 450 GeV LIU beams on a collimator will create high energy deposition within a few microseconds and hence very high dynamic loads. The jaws will have to be made of materials of high shock resistance. Highest shock resistance can be found in carbon based materials with densities of 1.4 g/cm^3 to 1.8 g/cm^3. As the damage potential for equipment scales with brightness, the new collimators will have to provide roughly a factor 3 more attenuation to arrive at the same protection level as the current collimation system. The collimator jaws will therefore have to become 2.1 m long instead of the 1.2 m. The material choice will be detailed below.

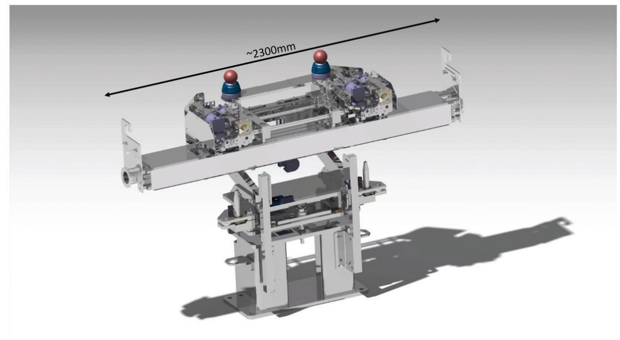

Figure 1: First version of 3D design of LIU transfer line collimator.

In the following the solution for the LIU transfer line collimators (TCDIs) and the remaining uncertainties on the design choice will be presented. The required modifications of the TI 8 optics will also be summarized and the implications on the protection of the LHC at injection discussed. A detailed functional specification of the LIU SPS-to-LHC transfer line collimation system can be found in [2].

CONCEPTUAL DESIGN OF THE LIU SPS-TO-LHC TRANSFER LINE COLLIMATORS

The design of the LIU TCDIs is based on the existing collimators installed in TI 2 and TI 8 [3]. The main difference is the requirement for longer jaws. A first version of the 3D design is shown in Fig. 1. The tolerances for jaw movement range, setting and alignment are also compatible with those originally specified. The allowed surface roughness will however be ± 100 μm instead of currently ± 50 μm.

Another difference might be the jaw material. Currently Steinemann R4550 Graphite is used. The peak energy deposition seen in the jaw varies as a function of the impact parameter, with larger values seen as the impact parameter increases. The increase in peak energy deposition and, correspondingly, temperature is not reflected in the thermomechanical stresses seen in the material, which are worst in the case of a 1 σ impact parameter. The results of the simulations with BCMS beam impacting a TCDI jaw at 1 σ, for both Steinemann R4550 Graphite (density1.83 g/cm^3) and 3D carbon-carbon (density 1.7 g/cm^3) jaw materials, are summarized in Table 2. For each material a different equivalent stress criterion was used [4]. The relevant robustness criterion for graphite is the Mohr-Coulomb criterion

Content from this work may be used under the terms of the CC BY 3.0 licence (© 2015). Any distribution of this work must maintain attribution to the author(s), title of the work, publisher, and DOI.

ISBN: 978-3-95450-168-7 doi:10.18429/JACoW-IPAC2015-TUPTY049

Content from this work may be used under the terms of the CC BY 3.0 licence (© 2015). Any distribution of this work must maintain attribution to the author(s), title of the work, publisher, and DOI.

PROTECTION OF SUPERCONDUCTING MAGNETS IN CASE OF ACCIDENTAL BEAM LOSSES DURING HL-LHC INJECTION*

A. Lechner†, M.J. Barnes, C. Bracco, B. Goddard, F. L. Maciariello, A. Perillo Marcone, N.V. Shetty, G. Steele, J. Uythoven, F.M. Velotti, CERN, Geneva, Switzerland

Abstract

The LHC injection regions accommodate a system of beam-intercepting devices which protect superconducting magnets and other accelerator components in case of missteered injected beam or accidentally kicked stored beam, e.g. due to injection kicker or timing malfunctions. The brightness and intensity increase required by the High Luminosity (HL) upgrade of the LHC necessitates a redesign of some devices to improve their robustness and to reduce the leakage of secondary particle showers to downstream magnets. In this paper, we review possible failure scenarios and we quantify the energy deposition in superconducting coils by means of FLUKA shower calculations. Conceptual design studies for the new protection system are presented, with the main focus on the primary injection protection absorber (TDI) and the adjacent mask (TCDD).

INTRODUCTION

The transfer lines from the SPS join the LHC in the ALICE and LHCb experimental insertions (IR2 and IR8) where four kicker magnets (MKIs) apply the final vertical deflection (0.85 mrad) on injected bunch trains [1]. To protect machine components in case of MKI malfunctions and timing errors, the injection regions accommodate a system of beam-intercepting devices and masks. The main element of the protection system is the TDI, a movable two-sided absorber installed at a phase advance of 75–95° from the MKIs. The TDI is located between a pair of superconducting dipoles (D1 and D2), which reduce the beam separation and bring the counter-rotating beams onto colliding orbits. In case of beam impact on the TDI, the single-bore D1 downstream of the TDI is the most exposed magnet and is protected by a mask (TCDD) which intercepts secondary particle showers leaking from the TDI. The TDI and TCDD are complemented by further collimators and masks downstream in the insertion regions, which provide some additional protection in case of phase errors.

The High Luminosity (HL) upgrade of the LHC requires an increase of the bunch intensity at LHC injection from 1.15×10^{11}/1.7×10^{11} (nominal/ultimate LHC) to 2.3×10^{11} protons. Together with a smaller beam emittance, this yields a significantly higher brightness than existing injection protection devices were designed for. These beam parameters not only pose a challenge for the robustness of absorber materials, but put new demands on the protection of superconducting magnets, particularly the D1 magnet.

* Research supported by the High Luminosity LHC project
† Anton.Lechner@cern.ch

Following a review of possible failure scenarios, this paper evaluates the protection provided by the existing TDI and TCDD and proposes potential solutions to reduce the energy density in the D1 coils. Other relevant aspects related to the upgrade of LHC injection protection devices, particularly the material robustness, are presented in another paper [2].

FAILURE SCENARIOS

In order to sufficiently protect the LHC during injection but also allow for some operational margin, the TDI jaws are maintained at a half gap of $6.8\sigma_n$ [3], where σ_n corresponds to the nominal LHC emittance (ε_n=3.5 μm·rad). With a β-function of ~43 m, this yields a jaw opening of approximately 7.6 mm. It is assumed that the same settings can be retained for HL-LHC operation since no significant optics changes are foreseen in the injection regions. A malfunction of the MKIs can affect either the injected or stored beam, but also both beams in the same event for specific kicker timing errors. As can be seen in the Table 1, different failure modes can affect a maximum of either 159 or 288 bunches (plus some bunches which are swept) and can give rise to different kick strengths, which in turn lead to different impact positions on the TDI jaws.

In case no kick is applied to the injected bunch train or in case circulating bunches are deflected with 100% of the MKI kick strength (timing error), beams typically impact on the TDI some 30–35 mm from the absorber block edge. The energy deposition in downstream magnets is however significantly higher if bunches impact close to the edge or if they graze along the jaws since secondary particle showers can escape through the TDI gap. Such events occur if the injected beam is deflected by approximately 90% or 110% (impact on the upper or lower jaw, respectively), or if the

Table 1: Overview of possible injection failure scenarios. Combination of different failures are not considered. The expected kick strength is expressed as a percent fraction of the nominal kick strength. Swept bunches are not included in the table.

Failure case	Bunches	Kick strength
Charging failure	288 (inj.)	99–101%
Main switch erratic	159 (inj. or circ.)	≤100%
Main switch missing	288 (inj.)	75%
Magnet breakdown	≤288 (inj.)	75–125%
Timing error	≤288 (inj.)	0%
	≤288 (circ.)	100%

ISBN: 978-3-95450-168-7 doi:10.18429/JACoW-IPAC2015-TUPTY050

CONSIDERATIONS FOR THE BEAM DUMP SYSTEM OF A 100 TeV CENTRE-OF-MASS FCC HH COLLIDER

T. Kramer, M.G. Atanasov, M.J. Barnes, W. Bartmann, J. Borburgh, E. Carlier, F. Cerutti, L. Ducimetière, B. Goddard, A. Lechner, R. Losito, G.E. Steele, L.S. Stoel, J. Uythoven, F. Velotti, CERN, Geneva, Switzerland

Abstract

A 100 TeV centre-of-mass energy frontier proton collider in a new tunnel of 80–100 km circumference is a central part of CERN's Future Circular Colliders (FCC) design study. One of the major challenges for such a machine will be the beam dump system, which for each ring will have to reliably abort proton beams with stored energies in the range of 8 Gigajoule, more than an order of magnitude higher than planned for HL-LHC. The transverse proton beam energy densities are even more extreme, a factor of 100 above that of the presently operating LHC. The requirements for the beam dump subsystems are outlined, and the present technological limitations described. First concepts for the beam dump system are described and the feasibility discussed, highlighting in particular the areas in which major technological progress will be needed. The potential implications on the overall machine and other key subsystems are described, including constraints on filling patterns, interlocking, beam intercepting devices and insertion design.

INTRODUCTION

CERN is leading an international collaboration for the conceptual design of colliders housed in a new tunnel of 80-100 km circumference in the Geneva region. In the frame work of the FCC-hh collider study [1] a major challenge will be the safe disposal of the up to 8 GJ beams. The extraction system must function with extreme reliability during beam presence, from 1st injection up to extraction with top level beam energy, to minimize the risk of severe damage to the machine. The dumping action must be synchronized with a particle free abort gap and the magnetic field of the extraction and dilution elements must closely track the beam energy. Asynchronous emergency dump action, allowed in the LHC, needs to be avoided as far as possible as it would be a major issue for the protection devices. The beam rigidity is more than seven times higher than in the LHC: this, together with machine protection considerations imposes ambitious hardware parameters. In addition the stored beam energy itself presents a serious challenge for the interception and dump devices. An overview of the relevant FCC-hh parameters is given in Table 1. Three different extraction concepts are being studied [2] and are further outlined in this paper together with the main extraction system elements.

Table 1: FCC-hh Parameters [2]

Beam parameter	Unit	Injection	Extraction
Kinetic Energy	TeV	3.3	50
Beta/Gamma		~1/3518	~1/53290
Revolution time	µs	~333	~333
Magnetic rigidity	T·km	11.0	166.8
Emittances (transv.)	µm	2.2	2.2
Stored beam energy	GJ	0.65	8.5

EXTRACTION CONCEPTS

All extraction concepts assume a fast extraction scheme, with one dedicated dump system per beam, which extracts the beam in a single turn towards an external dump block. Therefore fast kickers, strong septa and dilution kickers are needed. Other versions of these designs with special insertion magnet concepts, e.g. quadrupoles which allow for beam passage through the cryostat, are under consideration and would require lower strengths for the kickers and/or septa. The abort gap for all versions is assumed to be 3 µs.

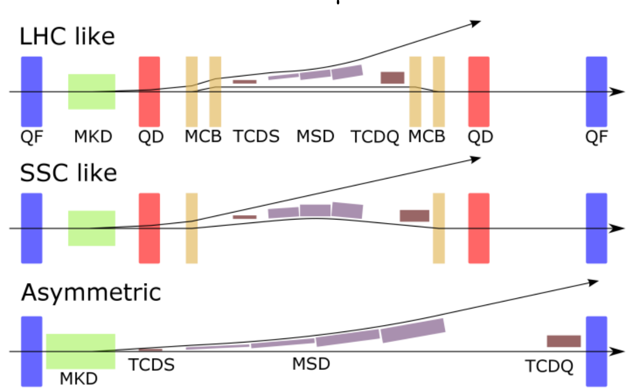

Figure 1: Preliminary insertion concepts.

LHC Scaled / LHC Like Concept

The LHC beam dump system (LBDS) [3] has been reviewed and scaled to the FCC energies as a first approach. This design uses a kicker (MKD, Fig. 1) and septum (MSD) placed around a quadrupole (QD), to enhance the kick. For the first purely scaled system hardware parameters were not advantageous hence in a "LHC like" version the optics were tuned and an

Content from this work may be used under the terms of the CC BY 3.0 licence (© 2015). Any distribution of this work must maintain attribution to the author(s), title of the work, publisher, and DOI.

ISBN: 978-3-95450-168-7 doi:10.18429/JACoW-IPAC2015-TUPTY051

Content from this work may be used under the terms of the CC BY 3.0 licence (© 2015). Any distribution of this work must maintain attribution to the author(s), title of the work, publisher, and DOI.

INJECTION PROTECTION UPGRADE FOR THE HL-LHC

J.Uythoven, N.Biancacci, C.Bracco, L.Gentini, B.Goddard, A.Lechner, F.L.Maciariello, A.Perillo Marcone, N.Shetty, G.Steele, B.Salvant, F.Velotti, CERN, Geneva, Switzerland,
O.Frasciello, M.Zobov, INFN/LNF, Frascati, Italy

Abstract

The injector complex of the LHC is undergoing important changes in the light of the LIU project to provide brighter beams to the LHC. For this reason and as part of the High Luminosity LHC project the injection protection system of the LHC will be upgraded in the Long Shutdown 2 (2018 - 2019) to be able to protect downstream elements against injection failures with the high brightness, high intensity HL-LHC beams. The upgraded LHC injection protection system will consist of a segmented injection protection absorber TDIS and auxiliary collimators and masks. The layout modifications are described, and the machine element protection and absorber jaw robustness studies are presented for the new systems.

INTRODUCTION

The injection protection system of the LHC is being upgraded as part of the HL-LHC project [1]. The upgrade of the injector complex to prepare the higher intensity proton beam for the HL-LHC is taking place under the LIU project [2] and is foreseen to be finished in the LHC Long Shutdown 2 (2018 – 2019). This means that also the upgrade of the injection protection system as described in this paper should be finished by 2019.

The LHC injection protection system consists of a number of absorbers, part of them movable, to intercept the beam in case of failures of the LHC injection kicker magnets. The different elements are described in [3]. The different kicker failure modes and the TCDD absorber protecting the D1 separation dipole are described in [4].

INJECTION ABSORBER TDIS

Absorber Material Considerations

The injection absorber TDIS is the primary protection of the LHC against injection failures and must be able to withstand the impact of a full injection train consisting of 288 bunches in the case of injection kicker (MKI) failures [3]. Different candidate materials for the absorber blocks are presently being considered, including different grades of boron nitride, graphite and carbon-reinforced-carbon, all having a low density, a low coefficient of thermal expansion, a high strength and a low Young's modulus. Graphite R4550 (SGL) is so far the preferred candidate, as is it seems to be a good compromise in terms of availability of shapes, machinability, costs and performance.

To study the energy deposition and stress wave propagation in the absorber blocks during beam impact, simulation studies based on FLUKA [5, 6] and ANSYS [7] were carried out. Table 1 shows the obtained Mohr-Coulomb Safety factor for Graphite R4550 for different HL-LHC beam parameters. The results correspond to the worst case scenario, where 288 bunches impact close to the jaw edge. The Mohr-Coulomb Safety factor, which is explained in detail in [3], must be greater than 1 in order to guarantee the absorber survival. As can be seen in the table, this is just the case for Standard HL-LHC beam parameters, while in the case of the smaller BCMS type beams and a bunch intensity of 2.0e11 protons, the number of injected bunches will need to be reduced to 240 bunches per injection.

It should be noted that the material limits used for this analysis are rather conservative. Currently a test bench is under preparation to expose blocks of the above candidate materials to proton beams with equivalent brightness in order to observe their behaviour (HiRadMat experiment to be carried out at CERN in 2016).

Table 1: HL-LHC Beam Parameters at Injection with Resulting Mohr-Coulomb (MC) Safety Factor for TDIS Jaw Made of Graphite R4550

Beam	Emit, x,y [μm]	Nb [p/bunch]	# bunches	MC Safety Factor
Standard	2.0	2.3e11	288	1.01
BCMS	1.3	2.0e11	288	0.90
BCMS	1.3	2.0e11	240	1.43

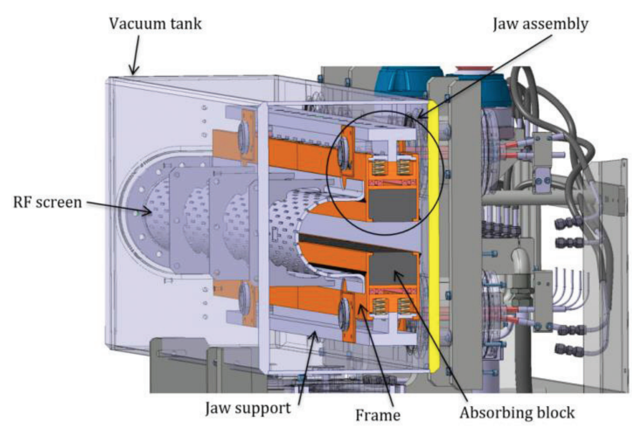

Figure 1: Preliminary design of one TDIS module.

Design Considerations

The preliminary TDIS design consists of three modules of equal length, containing different absorber materials. The first two modules consist of low-Z absorber blocks for which the above mentioned Graphite R4550 is assumed. The third module consists of higher Z materials.

ISBN: 978-3-95450-168-7 doi:10.18429/JACoW-IPAC2015-TUPTY052

Content from this work may be used under the terms of the CC BY 3.0 licence (© 2015). Any distribution of this work must maintain attribution to the author(s), title of the work, publisher, and DOI.

NEW METHOD FOR VALIDATION OF APERTURE MARGINS IN THE LHC TRIPLET*

V. Chetvertkova, R. Schmidt, F. Velotti, D. Wollmann, CERN, Geneva, Switzerland

Abstract

Safety of LHC equipment including superconducting magnets depends not only on the proper functioning of the systems for machine protection, but also on the accurate adjustment of the protective devices such as collimators. In case of a failure of the extraction kicker magnets, which are part of the beam dumping system, it is important to ensure protection of the superconducting triplet magnets from missteered beam. The magnets are located to the right of Interaction Point 5 (IP5) and are protected by one set of collimators in the beam dumping insertion in IR6 and another set close to the triplet magnets. In this paper, a new method for verification of the correct collimator position with respect to the aperture is presented. It comprises the application of an extended orbit bump with identical trajectory as the beam trajectory after a deflection by the beam dump kickers. By further increasing the bump amplitude and successively moving in/out the collimators in the region of interest, the accurate positioning of the collimators can be validated. The effectiveness of the method for LHC IP5 and IP1 and both beams is discussed.

INTRODUCTION

Missteered beams could put in danger accelerator equipment by creating losses at unexpected locations, which could lead to quenches of the superconducting components or damage of the exposed parts in case of larger beam losses. One of the reasons for missteered beam in the LHC is the firing of all the 15 modules of the extraction kicker (MKD) non-synchronously with the abort gap [1]. In this case individual bunches will experience a kick of lower amplitude then needed to direct the beam into the beam dump channel. Missteered bunches should be intercepted by the TCDQ-TCSG assembly [2]. If this fails, the TCT collimators should intercept the beam. Figure 1 presents the collimators between the MKD and the triplet (MQX) as seen by Beam 2. However, if these collimators are not properly aligned other equipment will be in danger, depending on the optics, i.e. phase advance from the MKD. Asynchronous dumps are expected to occur at least once per year.

Such missteered clockwise (Beam 1) and counter-clockwise (Beam 2) beams might be harmful for the triplets in the interaction points IP1 and IP5, respectively. Checking the aperture margins is of particular relevance when operating with the collision optics and the ATS (Achromatic Telescopic Squeeze) beam optics [3], because in these cases the respective triplets will be the aperture bottlenecks if the collimators are not set properly.

* Work supported by COFUND grant PCOFUND-GA-2010-267194

For this reason it is crucial to assure the proper settings of collimators around the triplets that are also at risk in case of asynchronous beam dumps together with a wrong setting of other protection devices. This paper suggests an alternative method of checking the aperture margins of the collimators and the triplets.

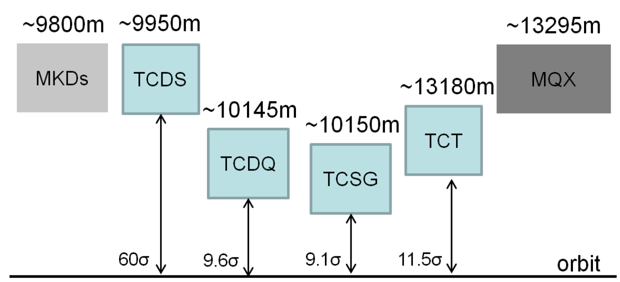

Figure 1: Scheme of collimators between the MKD and the MQX at IP5 [4] for Beam 2 (the zero of the coordinate system is at IP1). The longitudinal location of the component is shown (above) together with the retraction (below, expressed in beam σ-units) from the reference orbit.

METHOD

The proposed aperture-validation method is based on the fact that the beam trajectory of missteered beam can be reproduced by creating a 4-corrector orbit bump. The present study is devoted to the validation of the aperture margins around the MQX; therefore the global orbit bump is established around it. For beam 2, the bump starts before the MKD and closes after the IP5. Figure 2 shows a comparison of a trajectory of missteered beam and an orbit bump, corresponding to 1 µrad deflection angle at the MKD, calculated with ATS optics. The maximum of the orbit bump in both collision and ATS optics is observed in the triplet, for injection optics this is not the case.

The experimental measurements could be performed in two different ways: (1) by moving out the collimators, (2) by moving them in. For both approaches it is important to know the beam size, e.g. to cut the tails of the beam using primary collimators (TCP) in Sector 7.

The former approach starts with moving in the collimators to the initial positions. When increasing the amplitude of the bump one will start seeing losses by the Beam Loss Monitors (BLMs) at the TCDQ and the TCSG since their offsets from the centre of the vacuum chamber (in beam-σ units) are smaller than for the TCT. Knowing the beam size and the amplitude of the orbit bump (deflection angle at the MKD) it is possible to evaluate the offset of the collimators once the losses are registered. Before proceeding with the measurements of the aperture

ISBN: 978-3-95450-168-7 doi:10.18429/JACoW-IPAC2015-TUPTY053

ROADMAP TOWARDS HIGH ACCELERATOR AVAILABILITY FOR THE CERN HL-LHC ERA

A. Apollonio, M. Brugger, L. Rossi, R. Schmidt, B. Todd, D. Wollmann, M. Zerlauth, CERN, Geneva, Switzerland

Abstract

High Luminosity-LHC is the future upgrade of the LHC that aims at delivering an integrated luminosity of 3000 fb-1 over about 10 years of operation, starting from 2025. Significant modifications [1] will be implemented to accelerator systems, including new superconducting magnets, crab cavities, superconducting links, new collimators and absorbers based on advanced materials and design and additional cryo-plants. Due to the limit imposed by the number of simultaneous events at the experiments (pile-up) on peak luminosity, the latter will be levelled to $5*10^{34}$ $cm^{-2}s^{-1}$. The target integrated luminosity can only be achieved with a significant increase of the total available time for beam collisions compared to the 2012 LHC run, despite a beam current that is planned to double the nominal 0.58 A. Therefore one of the key figures of merit to take into account for system upgrades and new designs is their impact on the accelerator availability. In this paper the main factors affecting LHC availability will be discussed and predictions on the impact of future system upgrades on integrated luminosity presented. Requirements in terms of the maximum allowed number of dumps for the main contributing systems to LHC unavailability will be derived.

INTRODUCTION

High availability is becoming one of the key requirements for many accelerator facilities in the world. In the past only few categories of accelerators were considered as availability-critical. These are typically user-oriented facilities like synchrotron light sources and medical accelerators. Nowadays the challenging objectives on new projects around the world impose to consider availability as a fundamental requirement from early project and design stages. HL-LHC is the first particle collider with a defined integrated luminosity target [1]. HL-LHC aims at producing 250-300 fb^{-1} per year, for a total of 3000 fb^{-1} over about 10 years of operation. For ultimate parameters, the project is aiming at 400 fb^{-1} per year.

The considered baseline for the yearly LHC run time for physics production is 160 days. This implies an average integrated luminosity production of 1.9 fb^{-1} per day. For comparison, the total integrated luminosity produced by the LHC in 2011 was 5 fb^{-1}. Such increase of luminosity production has strong implications on availability requirements. Figure 1 shows that considering 2012 LHC availability and nominal HL-LHC parameters, a yearly production of 200 fb^{-1} could be achieved [2, 3]. Availability is expressed in the chart as a function of two quantities, the so-called *machine failure rate* and the *average fault time*. The *machine failure rate* indicates the fraction of premature beam aborts (i.e. beam dumps) which are initiated by machine protection systems upon the detection of any system failure. In 2012 the machine failure rate amounted to 70 %. Every time the beams were dumped, an average of 5.5 h – the so-called turnaround time - was required before colliding beams could be re-established. The *average fault time* measures the time spent to recover operating conditions after a fault occurs. In [3] it was shown that the fault time ranges from few minutes to many hours, depending on the fault and system root cause.

Improving these figures is mandatory to achieve the challenging goals of integrated luminosity of the HL-LHC project. The plot shows that an improvement of about 50 % of the average fault time, combined with a reduction of about 20 % of the machine failure rate will be required. This has strong implications on the system designs.

In this paper the main limitations to LHC availability will be discussed, based on the experience with the first LHC run (2010-2012). A strategy to identify individual system requirements in view of the HL-LHC era will be presented.

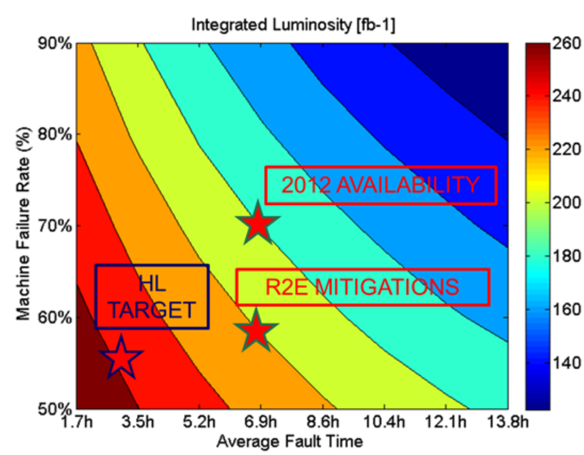

Figure 1: Fault time classification from 2012 observations.

LIMITING FACTORS FOR HL-LHC AVAILABILITY

The first LHC run allowed identifying possible availability bottlenecks for future LHC runs. Several system failure modes and effects were identified as critical for operation. Considering HL-LHC operation requires extrapolating the current knowledge to new operating conditions, i.e. increased energy and beam intensity and reduced operational margins for all systems. LHC run 2 (2015-2018) will represent an important

Content from this work may be used under the terms of the CC BY 3.0 licence (© 2015). Any distribution of this work must maintain attribution to the author(s), title of the work, publisher, and DOI.

ISBN: 978-3-95450-168-7 doi:10.18429/JACoW-IPAC2015-TUPTY054

RF DESIGN OF THE CLIC STRUCTURE PROTOTYPE OPTIMIZED FOR MANUFACTURING FROM TWO HALVES

Hao Zha, Alexej Grudiev, CERN, Geneva, Switzerland
Valery Dolgashev, SLAC, Menlo Park, CA 94025, United States

Abstract

We present the RF design of a 12GHz Compact Linear Collider (CLIC) main linac accelerating structure prototype. The structure is made from two longitudinally symmetric halves. The main manufacturing process of each half is precision milling. The structure uses the same iris dimensions as the CLIC-G structure [1] but the cell shape is optimized for milling. The geometry is optimized to reduce the surface electric and magnetic fields and the modified Poynting vector. This design can potentially reduce fabrication cost.

INTRODUCTION

Accelerating structures are usually manufactured by precision turning of individual cells, andcombined with precision milling for complex parts such as rf power couplers. These multiple parts are brazed into a complete structure. An alternative approach is the use of precision milling to cut cells into metal blocks that comprise either halves or quarters of the complete structure [2, 3].

In this paper we describean accelerating structure milled out of two halves and brazedtogether. One of the main motivations for this work is to study the high gradient performance of accelerating structures made with novel manufacturing methods. We found experimentally [4,5] that metal surfaces that are in metal-to-metal contact but not bonded or brazed have poor high power performance. We also have experimental evidence that small gaps (under 1 mm) were damaged even in setups where there were no currents flowing through the gaps (see damage of the disk rim in Fig. 6 of [6]).

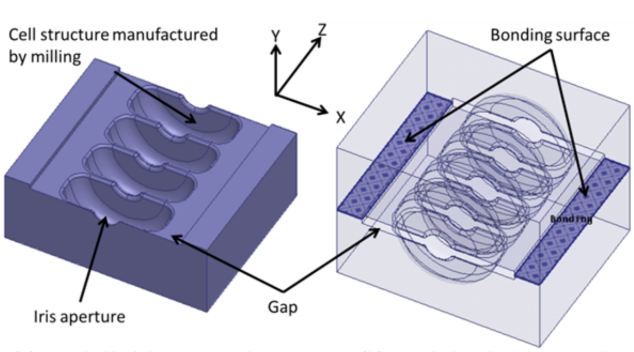

Figure 1: Manufacturing accelerating structure by milling on two halves of copper plate (HFSS model [7]).

Thus we introduced the 1 mm gap between the two halves of the structure to avoid un-brazed metal-to-metal contacts (shown in Fig.1). The gap is in cut-off at the working frequency to minimize fields leaking toward brazed surfaces and it is thus reducing the effect of imperfections of brazing fillets on rf performance. We note that a similar approach could be used to reduce trapping of long-range wakefields in the structure [4].

The full tapered structureincludes 24 regular travelling wave cells and 2 matching cells. It works at 11.994GHz with $2\pi/3$ mode. Each regular cell uses the same iris dimensions as the CLIC-G structure [8]. The structure uses a so called waveguide coupler, with matching transitions to standard WR-90 waveguides. The geometry is optimized to simplify the machining process, as well as to reduce the maximum surface electric and magnetic fields andthe local modified Poynting vector(*Sc*) [9].We used the commercial finite element code HFSS [7]for the simulations.

RF OPTIMIZATION OF SINGLE CELL GEOMETRY

One quarter of the cell prototype of the HFSS model is shown in Fig. 2. The flatbed besides the cell represents the gap between two halves. This single cell model will be used to optimize of the geometry.

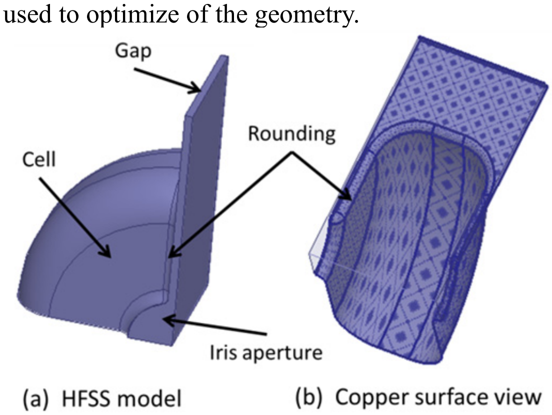

Figure 2: Initial geometry before the optimization.

The gap design changes the boundary condition in the cell and consequently affectsthe surface field. Figure 3 shows the comparison of our new structure with the regular un-damped middle cell of CLIC-G (T24). Wenote that the larger gap will significantly increase the maximum surface field and *Sc*.We use 1mm gap as compromise between increasing surface fields and degrading high power performance due to small gap (Fig. 6 in [6]).

Content from this work may be used under the terms of the CC BY 3.0 licence (© 2015). Any distribution of this work must maintain attribution to the author(s), title of the work, publisher, and DOI.

ISBN: 978-3-95450-168-7 doi:10.18429/JACoW-IPAC2015-TUPTY055

Content from this work may be used under the terms of the CC BY 3.0 licence (© 2015). Any distribution of this work must maintain attribution to the author(s), title of the work, publisher, and DOI.

OPTIMIZATION OF THE RF DESIGN OF THE CLIC MAIN LINAC ACCELERATING STRUCTURE

Hao Zha, Alexej Grudiev, CERN, Geneva, Switzerland

Abstract

We present a new optimized design of the accelerating structure for the main linac of CLIC (Compact Linear Collider). The new structure has lower surface magnetic fields and larger wall rounding compared to the baseline design described in the CLIC Concept Design Report (CDR). This new design should reach higher accelerating gradients and has a reduced manufacturing cost. The details of the RF design procedure and the obtained results are presented in this paper.

INTRODUCTION

The baseline design of the Compact Linear Collider main linac is called 'CLIC-G', which was described in the CLIC Conceptual Design Report (CDR) [1]. In recent few years, a lot of work related to this design was carried out. High power tests on the prototype structure with beam loading were made to understand the high-gradient limits [2]. A beam-based wakefield measurement verified the suppression of the long-range transverse wakefield of this design [3]. Mechanical design and manufacturing cost assessment of CLIC-G structures were studied [4]. It resulted that further improvement of the CLIC-G design is possible. RF and wakefield studies were carried out and a new optimized design to CLIC-G with lower pulse temperature rise and reduced manufacturing cost was presented.

RF DESIGN

A single cell of the CLIC-G structure is shown in Fig. 1. Four waveguides terminated with RF loads suppress the transverse wakefields. The waveguide geometry enhances the surface magnetic field and results in a higher surface pulse temperature rise, which is the likely explanation of higher break-down rate of the CLIC-G structure than the corresponding un-damped structure operating at the same gradient [5]. Gaps located between the cavities and waveguides are so-called waveguide openings. The widths of the openings are smaller than the waveguide width, in order to reduce the maximum magnetic field. Smaller opening however reduce the coupling of higher order modes (HOMs) from cavities to the RF loads. Thus the waveguide openings play an important role in balancing high power performance and wakefield suppression. The profile edge of the wall geometry in the cavity contains a straight line plus two quarter elliptical arcs and has been optimized to minimize the surface field. Rounding (0.5 mm) is used along the bottom edge to fit the machining.

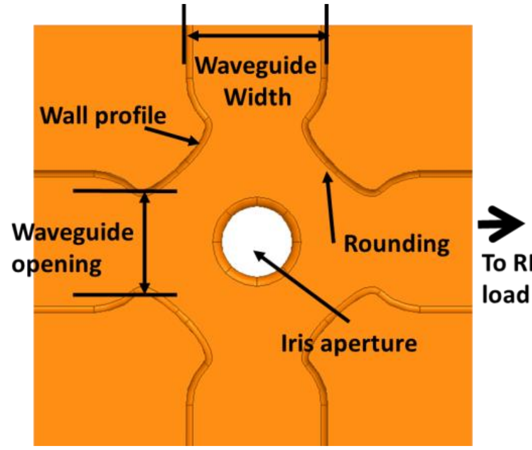

Figure 1: Geometry of a single CLIC-G cell.

The radii of the iris aperture in the CLIC-G design are from 3.15 mm to 2.35 mm. The average value and tapering of the iris aperture was determined by the global optimization considering the performance and the total cost [6]. The iris profiles have been optimized to minimize the surface electric field and the modified Poynting vector *Sc* [7]. This iris geometry is already well designed and will not be changed in this work. The cell geometry optimization is thus concentrated on the wall profile, waveguide geometry and the rounding.

Wall Profile

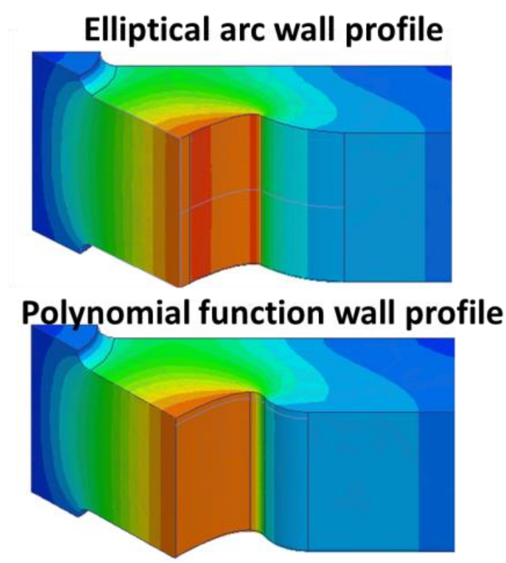

Figure 2: Comparison between elliptical and polynomial wall shape (figures were from HFSS simulations on 1/8 of the middle cell).

ISBN: 978-3-95450-168-7 doi:10.18429/JACoW-IPAC2015-TUPTY056

BEAM-BASED MEASUREMENTS OF LONG RANGE TRANSVERSE WAKEFIELDS IN CLIC MAIN LINAC ACCELERATING STRUCTURE

Hao Zha, Andrea Latina, Alexej Grudiev, Walter Wuensch, Daniel Schulte, Anastasiya Solodko, CERN, Geneva, Switzerland
Giovanni De Michele, Ecole Polytechnique Fédérale de Lausanne, Lausanne, Switzerland and Paul Scherrer Institut, Villigen PSI, Switzerland
Erik Adli, University Of Oslo, Oslo, Norway
Nate Lipkowitz, Gerald S. Yocky, SLAC National Laboratory, Menlo Park, California, USA

Abstract

The baseline design of CLIC (Compact Linear Collider) uses X-band accelerating structures in the main linacs. Every accelerating structure cell has four waveguides, terminated with individual RF loads, to damp the unwanted long-range transverse wakefields in order to maintain beam stability in multi-bunch operation. In order to experimentally verify the calculated suppression of wakefields, a prototype structure has been built and installed in FACET test facility at SLAC. The results of the measurements of the wakefields in the prototype structure, by means of positron and electron bunches, are presented.

INTRODUCTION

The main linac of the Compact Linear Collider (CLIC) uses X-band normal conducting structures operating at an accelerating gradient of 100MV/m [1]. In order to increase luminosity and minimize power consumption, multiple bunch trains are accelerated in each RF pulse. The multi-bunch trains however introduce a demanding beam stability issue because transverse misalignments between the beam and the rf structures result in the excitation of long-range transverse wakefields, which kick transversely the following bunches. Beam dynamics calculations indicate that a transverse wakefield kick of a bunch on the following bunch must be suppressed to less than 6.6 V/pC/m/mm, in order to maintain the beam stability in the main linac [2].

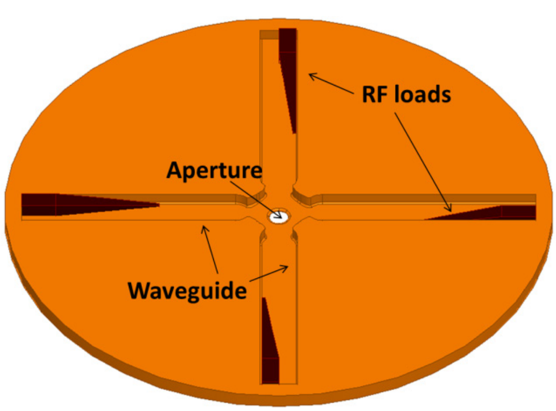

Figure 1: Geometry of single CLIC-G cell.

Figure 1 shows geometry of one CLIC accelerating structure disk. This geometry was well designed for both the high power performance and the wakefield suppression [3]. Given the availability of both electron and positron bunches simultaneously, the time-domain long-range wakefields of X-band structure could be measured at the FACET facility in SLAC National Accelerator Laboratory [4]. Figure 2 shows the measurement setup: NRTL (North -Ring-To-Linac) and SRTL (South-Ring-To-Linac) are independent beam lines and provide relativistic electron and positron bunches respectively. Both beam lines merge at LINAC02, where the test structure is located. The positron beam (drive bunch) was set to travel the test structure with a transverse offset to excite a transverse wakefield; the following electron bunch (witness bunch) is deflected by this wakefield.

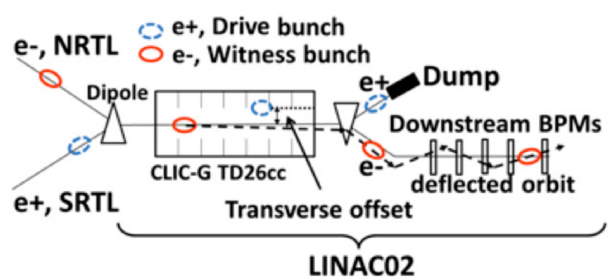

Figure 2: Layout of the experiment.

Downstream of the structure a dipole magnet splits the trajectories of the witness and drive bunches: the positron bunch is dumped, and the wakefield is inferred from the deflection of the electron orbit as measured by the downstream beam positron monitors (BPMs). Similar experiments have previously been performed at the FACET facility [5-7] and at the AWA facility in Argonne National Laboratory [8].

A dedicated prototype structure was built to carry out this experiment. The geometry of such prototype was the one of the CLIC 3 TeV baseline accelerating structure: the so-called CLIC-G TD26cc design, which contains 26 regular cells and compact input and output power couplers [3]. The structure cells were made of aluminium disks clamping together with long bolts. This simplified construction is acceptable for this experiment since the loaded Q of the dipole mode is very low, of the order of 10. The damping waveguides were terminated by silicon

Content from this work may be used under the terms of the CC BY 3.0 licence (© 2015). Any distribution of this work must maintain attribution to the author(s), title of the work, publisher, and DOI.

ISBN: 978-3-95450-168-7 doi:10.18429/JACoW-IPAC2015-TUPTY057

SCENARIOS FOR CIRCULAR GAMMA-GAMMA HIGGS FACTORIES

R. Aleksan, CEA Saclay, Paris, France; A. Apyan, Northwestern U., Evanston, USA
Y. Papaphilippou, F. Zimmermann, CERN, Geneva, Switzerland

Abstract

The Higgs boson can be produced directly in gamma-gamma collisions generated by laser Compton back scattering off 80-90 GeV electron or positron beams. We discuss options for realizing a gamma-gamma Higgs factory using a high-energy circular e+e- collider, and/or its top-up injector ring, and compare the parameters and advantages of such a facility, including the expected performance, with those for a Higgs factory based on a recirculating linac, such as SAPPHiRE.

MOTIVATION

Even if no new unexpected finding is unveiled by the coming LHC Run 2, the evidence for non-baryonic dark matter, the cosmological baryon-antibaryon asymmetry and non-zero neutrino masses call for physics beyond the Standard Model. New particle accelerators are necessary to explore this physics. At present two design studies are underway for large accelerator complexes, i.e. the global Future Circular Collider (FCC) study [1] and the Chinese CepC/SppC [2]. In this paper we explore the possibility to realize a $\gamma\gamma$ collider Higgs factory based on the infrastructure of a future circular lepton collider, considering the example of the FCC-ee. A $\gamma\gamma$ Higgs factory can be realized by back-scattering two counter-propagating focused 80-90 GeV electron bunches off a laser pulse some ~1 mm before the e^-e^- collision point so that the backscattered γ's collide with a small spot size.

PRINCIPLE

In case the FCC-ee is used as the basis for such a $\gamma\gamma$ collider, the necessary electron bunches can be extracted from the two rings of the FCC-ee collider, one of which would need to have a magnet polarity opposite to the one required for its (e+) operation in the e+e^- collision mode. For the $\gamma\gamma$ option, we consider only e- beams since the luminosity will crucially depend on the rate at which the particle beams can be produced and accelerated. Generating a sufficient rate of positrons would be challenging. At a beam energy of 80-90 GeV about 4000 bunches per beam can be stored in the two collider rings, with a bunch intensity corresponding to ~100 MW of synchrotron radiation in total. After injection an initial synchrotron-radiation damping period of about 1000 turns (about two transverse amplitude damping times) is granted to establish the equilibrium emittances. Then one bunch per turn is extracted and collided in a dedicated bypass $\gamma\gamma$ interaction line with a bunch taken from the other beam; see Fig. 1.

Since the FCC-ee design features a single booster injector [3,4], which, in this application, would also need to switch polarity for injecting into one or the other ring, we can consider a cycle pattern, where one ring is half empty when the injection for the second ring takes place. The cycle is illustrated in Fig. 2, for a booster period of 1 s, and a booster-field ramp rate close to 500 G/s (corresponding to ~170 GeV/s, comparable to the SPS energy-ramp rate for the CNGS beam). For this cycle, the maximum total synchrotron radiation power in the two collider rings is only 3/4 of the amount one would expect when filling both rings completely.

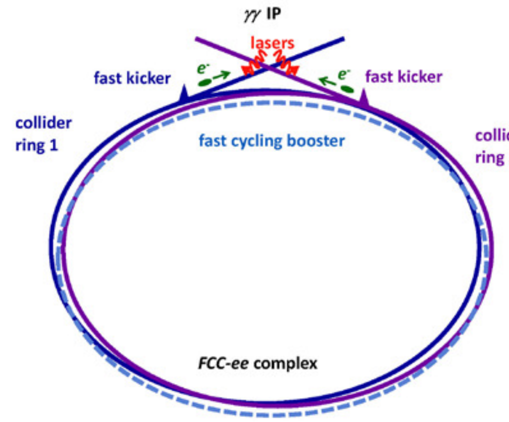

Figure 1: Schematic $\gamma\gamma$ collider based on filling the two FCC-ee collider rings with e^- bunches and extracting one bunch per beam and per turn into a dedicated $\gamma\gamma$ line.

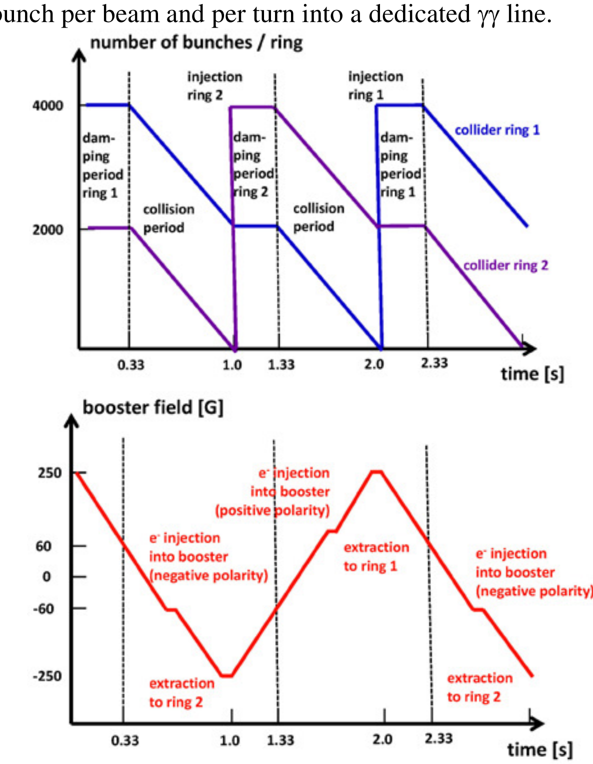

Figure 2: Cycle pattern for the two collider rings (top) and for the fast cycling booster (bottom). The injection energy is taken to be 20 GeV.

Content from this work may be used under the terms of the CC BY 3.0 licence (© 2015). Any distribution of this work must maintain attribution to the author(s), title of the work, publisher, and DOI.

ISBN: 978-3-95450-168-7 doi:10.18429/JACoW-IPAC2015-TUPTY058

Content from this work may be used under the terms of the CC BY 3.0 licence (© 2015). Any distribution of this work must maintain attribution to the author(s), title of the work, publisher, and DOI.

MITIGATING PERFORMANCE LIMITATIONS OF SINGLE BEAM-PIPE CIRCULAR e^+e^- COLLIDERS

M. Koratzinos, University of Geneva, Switzerland and F. Zimmermann, CERN, Geneva, Switzerland.

Abstract

Renewed interest in circular e^+e^- colliders has spurred designs of single beam-pipe machines, like the CEPC in China, and double beam pipe ones, such as the FCC-ee effort at CERN. Single beam-pipe designs profit from lower costs but are limited by the number of bunches that can be accommodated in the machine. We analyse these performance limitations and propose a solution that can accommodate O(1000) bunches while keeping more than 90% of the ring with a single beam pipe.

SINGLE BEAM-PIPE LIMITATION

The CEPC collider [1] is a single beam-pipe e^+e^- collider with the main emphasis on 120 GeV per beam running with possible running at 45 and 80 GeV. Bunch separation is ensured by a pretzel scheme and the maximum number of bunches is limited to 50. This very small number of bunches for a modern Higgs factory introduces luminosity limitations at 120 GeV, and severe limitations at any eventual 45 GeV running.

A machine of the size of CEPC at 120 GeV ought to be designed to be operating at the beam-beam limit and not reach the beamstrahlung limit first. The best way to reach this goal is by keeping the bunch charge low and emittances as small as possible. A large momentum acceptance also helps. Another way (and the route chosen for the CEPC) is to keep the bunches as long as possible, but this gives rise to lower instability thresholds as well as to geometric luminosity loss. According to our calculations and with reasonable assumptions for the length of the FODO cell and phase advance, we arrive at an optimal number of bunches of around 120 at 120 GeV [2]. The accommodation of this number of bunches with the pretzel scheme would be more demanding.

For an eventual running at 45 GeV the limit of 50 bunches would be inadequate, as hundreds of bunches would be needed to explore the full potential of the machine [2].

THE 'BOWTIE' DESIGN

Without changing the basic design philosophy of the project, where the single-beam pipe approach was chosen to minimise cost, we can envisage an approach that preserves the low cost of the single beam pipe and at the same time accommodates hundreds of bunches without the use of a pretzel scheme. This approach is illustrated in Figure **1**. All arcs contain a single beam pipe but the straight sections where the experiments are located are increased in length and after the RF section a series of electrostatic separators splits the two beams sufficiently far apart transversely so that separate beam pipes and magnetic elements can be used to manipulate the electron and positron beams individually, and without any parasitic collisions. The length of the electrostatic separator section would be around 100 m on both sides of the straight section. Since now the beams travel in separate beam pipes, great flexibility about the choice of collision angle is ensured. The FCC-ee is pursuing a crab waist approach which gives excellent performance at low energies and where the crossing angle is 30 mrad.

Assuming a total length of the double beam pipe to be 2×2000m, and assuming that bunches within a train can be separated longitudinally by as little as 2 m (7 ns) then 2×1000 bunches for each species can be accommodated in the machine.

The ratio of single to double beam pipe would be ~4/52 or about 8%. Note that the cost increase would be much smaller than the above figure and actually the cost per luminosity unit would be greatly improved.

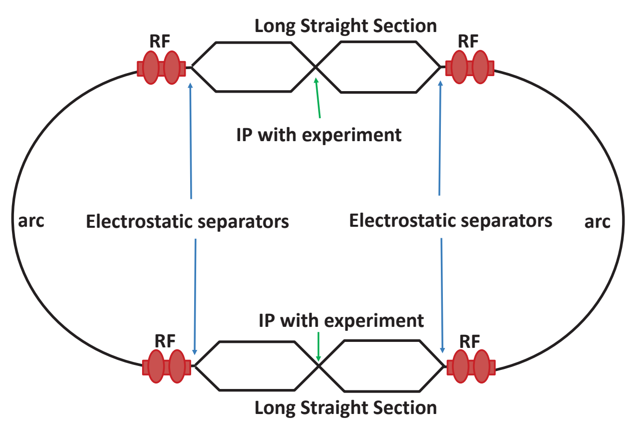

Figure 1: Schematic of the 'bowtie' idea (not to scale).

ELECTROSTATIC SEPARATORS

For illustration purposes we have chosen the LEP electrostatic separators [3]. These were 4 m long, 11 cm wide and the maximum operating voltage was 220 kV. Each separator produced a maximum deflection of 145 μrad at 55 GeV. These separators were not without problems: aspects that need to be looked at include possible impedance issues in view of the awkward shape of the separators and reliability issues due to sparking provoked by synchrotron radiation.

Using 12 of these LEP separators (48 m total length) operated at maximum voltage would provide a separation of 20 mm ×2 to the two beams after a distance of 50 m, and a further drift space of 50 m would increase the beam

ISBN: 978-3-95450-168-7 doi:10.18429/JACoW-IPAC2015-TUPTY059

Content from this work may be used under the terms of the CC BY 3.0 licence (© 2015). Any distribution of this work must maintain attribution to the author(s), title of the work, publisher, and DOI.

FIRST CONSIDERATIONS ON BEAM OPTICS AND LATTICE DESIGN FOR THE FUTURE ELECTRON-POSITRON COLLIDER FCC-ee

B. Haerer, B. J. Holzer, F. Zimmermann CERN, Geneva, Switzerland
A. Bogomyagkov, BINP, Novosibirsk, Russia

Abstract

Following the recommendations of the European Strategy Group for High Energy Physics, CERN launched the Future Circular Collider Study (FCC) to investigate the feasibility of a new large circular collider for high energy physics research. This paper presents the constraints on the design of the lattice and optics of the lepton collider version of FCC, that has to be optimised for four different beam energies and parameter sets. Special emphasis is put on the need for a highly flexible magnet lattice in order to achieve the required beam emittances for the four energies and on the layout of the interaction region that will have to combine an advanced mini-beta concept, an effective beam separation scheme and a local chromaticity control to optimise the momentum acceptance and dynamic aperture of the ring.

INTRODUCTION

The lepton collider part of the FCC study is based on racetrack geometry with a circumference of about 100 km and foresees the design of an electron-positron collider, running at four different centre-of-mass energies to allow precision measurements at the Z resonance, at the energy with maximum Higgs production rate, as well as above the WW and t-tbar thresholds [1]. For each energy the beam parameters depend crucially on the synchrotron light emission and the lattice has to be optimised to provide the emittance target values that are summarised together with the general beam parameters in the parameter list of Table 1. The general layout of the machine is shown in Figure 1.

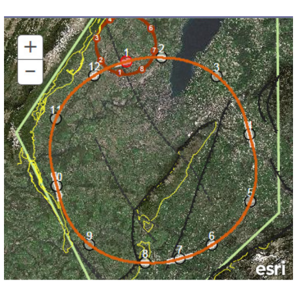

Figure 1: Geometry of the FCC storage ring.

MAIN PARAMETRES

The general parameters [2] have been optimised for each beam energy and are determined by the overall synchrotron radiation load that can be accepted in the design. In general, for all operation energies the same global synchrotron radiation limit of P_γ =50 MW has been assumed, leading e.g. to a considerable higher number of stored bunches at the lowest operation energy and to a large variation of beam emittances over the complete energy range of the machine.

Table 1: FCC-ee Parameters at Four Different Beam Energies

	Z	W	H	t
Beam Energy (GeV)	45.5	80	120	175
Current (mA)	1450	152	30	6.6
Bunch population 10^{11}	1.8	0.7	0.46	1.4
Bunch number	16700	4490	1360	98
Hor. Emittance (nm)	29	3.3	0.94	2
Vert. Emittance (pm)	60	7	1.9	2
β_x function at IP(m)	0.5	0.5	0.5	1
β_y function at IP(mm)	1	1	1	1

General Layout of the Lattice Cells

The design of the basic cell follows the usual rules for particle beams that are determined by synchrotron radiation aspects. The basic cell that has been chosen for 175 GeV operation is shown in Figure 2. It combines four dipole magnets and two main quadrupoles in a 50 m long FODO cell.

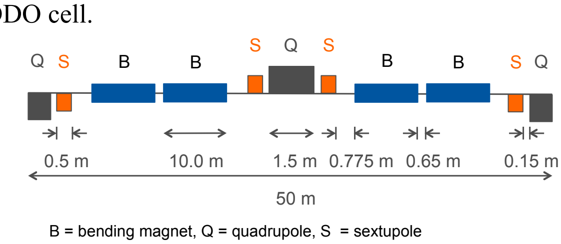

Figure 2: FODO cell chosen for the arc design. The cell parameters are optimised for maximum dipole fill factor and design emittance.

Applying the usual scaling laws for the beam emittance of lepton rings, the dispersion and the arc beta function,

$$\varepsilon = \left(\frac{\delta p}{p}\right)^2 \left(\gamma D^2 + 2\alpha D D' + \beta D'^2\right) \qquad (1)$$

$$\hat{D} = \frac{\ell^2}{\rho} * \frac{\left(1 + \frac{1}{2}\sin\frac{\psi_{cell}}{2}\right)}{\sin^2\frac{\psi_{cell}}{2}}$$

ISBN: 978-3-95450-168-7 doi:10.18429/JACoW-IPAC2015-TUPTY060

THE FCC-ee STUDY: PROGRESS AND CHALLENGES

M. Koratzinos, University of Geneva, Switzerland
S. Aumon, C. Cook, A. Doblhammer, B. Haerer, B. Holzer, R. Tomas, F. Zimmermann, CERN, Geneva, Switzerland
U. Wienands, SLAC, USA; L. Medina, Universidad de Guanajuato, Leon, Mexico
M. Boscolo, INFN Laboratori Nazionali di Frascati, Italy; A. Bogomyagkov, D. Shatilov and E. Levichev, BINP, Novosibirsk, Russia

Abstract

The FCC (Future Circular Collider) study represents a vision for the next large project in high energy physics, comprising an 80–100 km tunnel that can house a future 100TeV hadron collider. The study also includes a high luminosity e^+e^- collider operating in the centre-of-mass energy range of 90–350 GeV as a possible intermediate step, the FCC-ee. The FCC-ee aims at definitive electro-weak precision measurements of the Z, W, H and top particles, and search for rare phenomena. Although FCC-ee is based on known technology, the goal performance in luminosity and energy calibration make it quite challenging. During 2014 the study went through an exploration phase. The study has now entered its second year and the aim is to produce a conceptual design report during the next three to four years. We here report on progress since the last IPAC conference.

INTRODUCTION

The discovery of the Higgs boson with a mass of around 125 GeV has recently revived interest in circular colliders [1]. The FCC-ee study reported here was kicked off in February 2014. It is an ambitious project that aims to perform physics studies in a variety of different beam energies, the main ones being 45 GeV for precision studies of the Z boson, 80 GeV for precision studies of the W, 120 GeV for the Higgs and 175 GeV for the top quark. Other beam energies might also be needed (notably a monochromatic run at 63 GeV is being investigated). Running at different energies requires different machine configurations and parameter sets have already been published [2] to serve as a baseline. For instance, the 45 GeV running is characterised by high beam current (1.5 A) putting stringent requirements to the power couplers of the RF system. On the other hand, the 175GeV running is characterised by the need for very low emittances to mitigate the beamstrahlung problem and relatively high total RF voltage (12 GV). High momentum acceptance is also needed for high energy running (175 GeV and to a lesser extend 120 GeV), also to mitigate the beamstrahlung effects. The parameter set already published is expected to evolve as more performant solutions are being engineered. The largest potential improvement is the development of the 'crab waist' interaction region scheme, where a large crossing angle (30 mrad) and crab sextuples allow for beam-beam parameters much larger than with the head-on baseline scheme, resulting in much higher luminosity at the Z running and modest gains all the way up to the Higgs running. The past year was explicitly intended to be an exploratory phase without the aim for convergence on a specific solution. Nevertheless, work in a number of areas has resulted in multitude of papers submitted for presentation at IPAC15, which this contribution aims to summarise.

CIVIL ENGINEERING

The civil engineering team at CERN are investigating the feasibility of an 80 km – 100 km tunnel in the Geneva basin to house the FCC machines [3]. Like any civil engineering feasibility study for a large-scale project, one of the major challenges is the management and manipulation of an enormous amount of spatial data. A feasibility study is an inherently iterative process as new data comes to light and parameters of the study evolve.

The traditional approach therefore requires significant resources in terms of time and man-power. However, to more effectively and efficiently conduct the study, CERN is employing the use of a specially designed interactive tool, containing a 3D geological model of the Geneva basin. The Tunnel Optimisation Tool (TOT) has been developed and is based on commercially available Geographical Information System (GIS) software.

A tunnel design is uploaded to TOT and positioned within the geology of the Geneva basin. The tool then outputs key information for a given setup including the geology intersected by the tunnel, the shaft depths, interaction with the built-environment, including buildings and geothermal boreholes and interaction with the environment including environmentally protected areas.

Another challenge for the study has been making a quantitative comparison between different solutions. Given the high number of variables and multiple objectives for optimisation (minimise shaft depths, minimise tunnel length in limestone, minimise length and slope of injection tunnels from the LHC, etc.), some form of detailed analysis is required. Comparison also needs to not only be made between two positions of the same tunnel but also between two tunnels of different circumference.

A list of factors related to the cost/risk of construction of each element of the FCC project (tunnel, shafts and caverns) have been compiled which are based on engineering experience of tunnelling projects. The data from TOT is extracted and multiplied by the relevant factor, giving a total cost/risk value to any given solution.

An alternative method of analysis is also under investigation. This is the use of an optimisation algorithm,

Content from this work may be used under the terms of the CC BY 3.0 licence (© 2015). Any distribution of this work must maintain attribution to the author(s), title of the work, publisher, and DOI.

ISBN: 978-3-95450-168-7 doi:10.18429/JACoW-IPAC2015-TUPTY061

COMBINED OPERATION AND STAGING FOR THE FCC-ee COLLIDER*

M. Benedikt†, B. Holzer, E. Jensen, R. Tomas, J. Wenninger, F. Zimmermann, CERN, Geneva Switzerland; A. Bogomyagkov, E. Levichev, D. Shatilov, BINP, Novosibirsk, Russia
U. Wienands, SLAC, USA; K. Ohmi, K. Oide, KEK, Tsukuba, Japan

Abstract

FCC-ee is a proposed high-energy electron positron circular collider that might initially occupy the 100-km FCC tunnel which would eventually house the 100 TeV FCC-hh hadron collider. The parameter range for the e^+e^- collider is large, operating at c.m. energies from 90 GeV (Z-pole) to 350 GeV ($t\bar{t}$ production) with beam currents ranging between 1.5 A and 7 mA, at fixed synchrotron radiation power of 50 MW per beam, and the radiative energy loss varying from about 30 MeV/turn to 7500 MeV/turn. This presents challenges for the radiofrequency (rf) system due to the varying rf voltage requirements and beam loading conditions. In this paper we present a possible gradual evolution of the FCC-ee complex by step-wise expansion, and possibly reconfiguration, of the superconducting rf system and of the optics. The performance attainable at each step is discussed, along with possible advantages and drawbacks.

PHYSICS GOALS AND ENERGIES

The highest priority of a potential future e^+e^- collider in the 100-km FCC tunnel is Higgs production at a centre-of-mass energy of about 240 GeV corresponding to the peak rate of $e^+e^- \to ZH$ events. The second FCC-ee priority is running on the Z pole (91 GeV c.m.) with exceptionally high luminosity in order to generate 10^{12}–10^{13} Z's over a couple of years. Further FCC-ee collision energies will be at the $t\bar{t}$ threshold ($\sim$ 350 GeV c.m.), at the WW threshold, and possibly, with energy monochromatization, on the $e^+e^- \to H$ resonance ($\sim$125 GeV). The baseline physics program assumes no longitudinal polarization. However, scaling from LEP experience, some transverse polarization of non-colliding bunches is expected at the Z and up to the WW threshold, which can be used for precise calibration of the beam energy.

PARAMETERS AND OPERATION MODES

The number of FCC-ee interaction points (IPs) could be 2 or 4. A model used to describe the performance of LEP [1] suggests that with two collision points the maximum beam-beam tune shift and the luminosity per IP could be about 40% higher than with four collision points. However, the collision conditions for many of the FCC-ee scenarios are rather different from those at LEP. Preliminary weak-strong simulations for FCC-ee indicate a weaker dependence on the number of IPs, i.e. only a 10–20% gain in the maximum beam-beam tune shift at 240 GeV c.m. with 2 instead of 4 IPs [2] and even less (or no) gain at 91 GeV c.m. However, our further discussion assumes two IPs.

For constant synchrotron radiation power, e.g. 50 MW per beam, at lower beam energy the beam current increases as the inverse fourth power of energy. The much higher beam current at lower energy implies a correspondingly increased number of bunches.

Indeed, the requirements on the rf system differ substantially at low and high energies. On the Z pole the beam current is about 1.5 A, but the energy loss per turn only some 30 MeV and the rf voltage required is moderate. The cavity impedance is a concern for this mode of operation [3]. In consequence, the smallest number of cavities which can still provide 2×50 MW to the beams would be desired. Conversely, when running at the ZH peak or at the $t\bar{t}$ threshold the beam current is much lower, 30 or 7 mA, but the energy loss per turn amounts to 1.7 or 7.6 GeV, respectively, calling for a total rf voltage of up to 11 GV. Because of the lower beam current and higher beam energy, the cavity impedance is less of a concern here. Therefore, a staging where cavity modules are installed in steps appears natural.

The geometric emittance from the arcs scales as $\theta_b^3\gamma^2$ [4], where θ_b denotes the bending angle per arc cell and γ the Lorentz factor. The natural emittance decrease at lower energy can be counteracted by choosing longer optical cells in the arcs. The baseline parameter set of FCC-ee [5] assumes a 50-m arc FODO cell length, required for ZH and $t\bar{t}$ running, a 100 m cell length for the WW threshold and a 300-m cell length at the Z pole [6]. The increased cell length at lower energies allows for the geometric emittance to stay roughly constant or even to increase, at similar bunch charge, in order for the beam-beam tune shift to remain at, or below, the expected energy-dependent limit [1].

If the cell length is held constant, equal to 50 m, at the lower beam energies the emittance shrinks substantially. In this case the beam-beam tune shifts can still be kept under control, however, with the help of a large crossing angle, complemented by crab-waist sextupoles. In such a crab-waist scenario, the luminosity at the Z pole is about an order of magnitude higher than for the baseline [7]. The low-emittance crab-waist running implies extremely small vertical emittance values. Table 1 compares some example parameters (based on analytical calculations, and not fully optimized) for the proposed schemes at two beam energies.

It may be possible to further reduce the rf voltage, much

* This work was supported in part by the European Commission under the FP7 Capacities project EuCARD-2, grant agreement 312453.
† michael.benedikt@cern.ch

Content from this work may be used under the terms of the CC BY 3.0 licence (© 2015). Any distribution of this work must maintain attribution to the author(s), title of the work, publisher, and DOI.

ISBN: 978-3-95450-168-7 doi:10.18429/JACoW-IPAC2015-TUPTY062

FCC-hh HADRON COLLIDER — PARAMETER SCENARIOS AND STAGING OPTIONS*

M. Benedikt†, B. Goddard, D. Schulte, F. Zimmermann, CERN, Geneva, Switzerland;
M.J. Syphers, MSU, East Lansing, U.S.A.

Abstract

FCC-hh is a proposed future energy-frontier hadron collider, based on dipole magnets with a field around 16 T installed in a new tunnel with a circumference of about 100 km, which would provide proton collisions at a centre-of-mass energy of 100 TeV, as well as heavy-ion collisions at the equivalent energy. The FCC-hh should deliver a high integrated proton-proton luminosity at the level of several 100 fb^{-1} per year, or more. The challenges for operating FCC-hh with high beam current and at high luminosity include the heat load from synchrotron radiation in a cold environment, the radiation from collision debris around the interaction region, and machine protection. In this paper, starting from the FCC-hh design baseline parameters we explore different approaches for increasing the integrated luminosity, and discuss the impact of key individual parameters, such as the turnaround time. We also present some injector considerations and options for early hadron-collider operation.

BASELINE PARAMETERS

The FCC hadron collider FCC-hh will provide pp collisions at a centre-of-mass energy of 100 TeV using 16-T Nb_3Sn magnets in a tunnel of about 100 km circumference (FCC-hh baseline) [1, 2, 3, 4].

The FCC design beam current of 0.5 A is about equal to the LHC design and obtained with 10^{11} protons per bunch at a bunch spacing of 25 ns. An alternative parameter set with a reduced bunch spacing of 5 ns and correspondingly scaled charge and emittance will also be explored.

Scaling the interaction region from the LHC design, the free distance from the interaction point (IP) is increased, from 23 m to more than 40 m, and the IP beta function is doubled, to $\beta^*_{x,y} = 1.1$ m. With these parameters the FCC baseline luminosity becomes 5×10^{34} cm^{-2}s^{-1}, equal to the luminosity of the High-Luminosity LHC (though with more energetic collision debris), and, as for the HL-LHC, the integrated luminosity per year is about 250 fb^{-1}, assuming 180 days per year scheduled for physics operation, and an availability of 70%.

PHYSICS GOALS

The key physics goals of the FCC are the complete exploration of the Higgs boson and a significant extension, via direct and indirect probes, of the search for physics phenomena beyond the Standard Model [5]. The baseline FCC-hh integrated-luminosity goal of 3 ab^{-1} translates into a discovery reach of about 32 TeV for Standard-Model like couplings. Raising the luminosity by a factor of 10 increases the discovery reach only by about 20% in energy. The higher luminosity leads to much increased event rates, and better statistics, at low masses, and would, for example, allow measuring the Higgs self coupling to better than 5%. Synthesizing the discussions from several theory workshops, an ultimate integrated luminosity goal of 10–20 ab^{-1} for the FCC-hh seems well justified [5].

INCREASING INTEGRATED LUMINOSITY

The FCC-hh luminosity can be increased in a number of ways. First, the IP beta function may be reduced. An advanced interaction-region (IR) optics is already being developed, which can reach $\beta^*_{x,y} = 30$ cm [6], yielding almost a factor 4 gain in peak luminosity. Second, the beam-beam limit of $\Delta Q_{\rm tot} = 0.01$ assumed in the baseline, appears conservative as the LHC and the Tevatron have routinely been running with two times larger values, and as more than three times higher tune shifts have been obtained in LHC beam experiments without any noticeable impact on beam lifetime or emittance growth [7]. Much stronger radiation damping at the FCC-hh (transverse emittance damping time of 1 h) might further boost the achievable beam-beam tune shift if the effect of the radiation damping is similar to the one found on lepton colliders [8]. In addition, head-on beam-beam compensation by electron lenses, recently demonstrated at RHIC [9], is likely to support even higher tune shifts. For all the above reasons we consider the possibility of a total beam-beam tune shift as high as $\Delta Q_{\rm tot} = 0.03$ (sum of two IPs). Third, we assume that the initial turnaround time t_{ta} (the period from the end of one physics fill to the start of the next physics collisions) can be reduced from 5 hours in the baseline to 4 h, after a couple of years of beam operation.

Based on the above considerations we envisage two operational phases of the FCC-hh. “Phase 1” corresponds to the baseline with a peak luminosity of 5×10^{34} cm^{-2}s^{-1} and an average luminosity production of 250 fb^{-1} per year. “Phase 2” achieves about a factor 6 higher peak luminosity of $\sim 3 \times 10^{35}$ cm^{-2}s^{-1} and produces more than 1000

* This work was supported in part by the European Commission under the FP7 Capacities project EuCARD-2, grant agreement 312453, and HORIZON 2020 project EuroCirCol, grant agreement 654305.
† michael.benedikt@cern.ch

Content from this work may be used under the terms of the CC BY 3.0 licence (© 2015). Any distribution of this work must maintain attribution to the author(s), title of the work, publisher, and DOI.

ISBN: 978-3-95450-168-7 doi:10.18429/JACoW-IPAC2015-TUPTY063

FCC-ee: ENERGY CALIBRATION

M. Koratzinos, A. Blondel, University of Geneva, Geneva, Switzerland; E. Gianfelice-Wendt, Fermilab[1], Batavia IL, USA; F. Zimmermann, CERN, Geneva, Switzerland.

Abstract

The FCC-ee aims to improve on electroweak precision measurements, with goals of 100 keV on the Z mass and width, and a fraction of MeV on the W mass. Compared to LEP, this implies a much improved knowledge of the centre-of-mass energy when operating at the Z peak and WW threshold. This can be achieved by making systematic use of resonant depolarization. A number of issues have been identified, due in particular to the long polarization times. However the smaller emittance and energy spread of FCC-ee with respect to LEP should help achieve a much improved performance.

INTRODUCTION

Accurate energy determination is a fundamental ingredient of precise electroweak measurements. In the case of LEP1 the centre of mass energy at and around the Z peak was known with an accuracy of around 2×10^{-5}. The exact contribution of the energy error to the mass and the width of the Z are presented in [1].

The proposed circular collider FCC-ee [2] is capable of delivering statistics a factor ~10^5 larger than LEP at the Z and WW energies, therefore there is a need not only to achieve similar performance as far as energy determination is concerned, but to do significantly better.

The beam energy of large storage rings continuously changes due to internal and extraneous causes. This evolution can be modelled, but energy changes are many orders of magnitude larger than the instantaneous accuracy of a depolarization measurement. For example, small changes in the diameter of the ring due to elastic deformations of the earth's crust (due to, for instance, tidal forces) can have a big effect on the energy of the electrons and positrons. This is due to the small momentum compaction factor α_c which relates changes in energy to changes in the orbit length of a storage ring:

$$\frac{\Delta E}{E} = -\frac{1}{\alpha_c}\frac{\Delta L}{L} \tag{1}$$

where L is the orbit length. Table 1 shows changes in energy for a $4\cdot10^{-8}$ circumference change (typical for tide-induced changes) for LEP and FCC-ee.

The many other effects that contribute to energy changes are discussed in [3]. None of them has a very fast changing component, so monitoring the energy every ~10 minutes would ensure a negligible extrapolation error.

The RF configuration can give rise to different energies at the IPs and for electrons and positrons, as can the slightly different orbit for the separated rings, therefore both species should be measured, something that was not done at LEP.

Table 1: Change in energy of a 45GeV beam for a circumference change of $\mathbf{4\cdot10^{-8}}$

Storage ring	Circumference (km)	α_c	ΔE (MeV)
LEP	27	$2\cdot10^{-4}$	9
FCC-ee	100	$5\cdot10^{-6}$	360

The only method that can provide the accuracy needed is the so-called resonant depolarization technique [3], each measurement of which has an instantaneous accuracy of O(10^{-6}). It is based on the fact that the spin of an electron in a storage ring (in a perfectly planar machine and in the absence of solenoids) will precess $a\gamma$ times for one revolution in the storage ring, where a is the anomalous magnetic moment and γ the Lorenz factor of the electron and therefore the spin tune ν is

$$\nu = a\gamma = \frac{aE}{mc^2} = \frac{E[MeV]}{440.6486(1)[MeV]} \tag{2}$$

Deviations from the above formula are small and are discussed in [4] and [5]where they were found negligible for LEP, but should be revised in view of the much improved precision aimed at the FCC-ee.

The average of all spin vectors in a bunch is defined as the polarization vector $\vec{P}$. Therefore the average energy of a bunch can be computed by selectively depolarizing a bunch of electrons or positrons which have been polarized to an adequate level and measuring the frequency at which this depolarization occurs. Beam polarization is usually measured by laser polarimeters which exploit the spin dependence of the Compton scattering cross section. The accuracy with which the instantaneous average energy of the bunch is computed using this method is O(100KeV) – a value much smaller than the beam energy spread.

TRANSVERSE POLARIZATION

Electron and positron beams in a storage ring naturally polarize due to the Sokolov-Ternov effect [6]. For the purposes of energy calibration, important figures of merit are the asymptotic value of polarization that can be reached and the time constant of polarization build-up.

The maximum achievable polarization value is given by the theory as

$$P_{max} = \frac{8}{5\sqrt{3}} \cong 0.924 \tag{3}$$

[1] Operated by Fermi Research Alliance, LLC under Contract No. DE-AC02-07CH11359 with the United States Department of Energy

Content from this work may be used under the terms of the CC BY 3.0 licence (© 2015). Any distribution of this work must maintain attribution to the author(s), title of the work, publisher, and DOI.

ISBN: 978-3-95450-168-7 doi:10.18429/JACoW-IPAC2015-TUPTY066

BEAM CLEANING IN EXPERIMENTAL IRS IN HL-LHC FOR THE INCOMING BEAM*

H.Garcia-Morales†, Royal Holloway University of London, United Kingdom
R. Bruce, S. Redaelli, CERN, Geneva, Switzerland

Abstract

The HL-LHC will store 675 MJ of energy per beam, about 300 MJ more than the nominal LHC. Due to the increase in stored energy and a different interaction region (IR) optics layout, the collimation system for the incoming beam must be revisited in order to avoid dangerous losses that could cause quenches or machine damage. This paper studies the effectiveness of the current LHC collimation system in intercepting cleaning losses close to the experiments in the HL-LHC. The study reveals that additional tertiary collimators would be beneficial in order to protect not only the final focusing triplets but also the two quadrupoles further upstream.

INTRODUCTION AND MOTIVATION

The optics of the HL-LHC [1] is based on the Achromatic Telescope Squeezing (ATS) scheme [2]. This scheme allows to push the LHC nominal β^* to about 15 cm at IP1 and IP5. The reduction of β^* implies an increase of the β-function at the Final Triplet (FT) region, as well as in the matching section. In addition, the bunch charge and consequently the stored energy in the beam is aimed to increase by almost a factor 2. Therefore, it is foreseen to replace the FT and the quadrupoles Q4 and Q5 by new magnets with larger apertures. Nevertheless, the available normalized aperture is tight, which might expose these magnets to beam losses that could potentially cause quenches. Therefore, the collimation system must be revisited in order to ensure acceptable loss levels.

MACHINE CONDITIONS

The betatron cleaning insertion allows to limit the transverse extension of the beam halo by "cleaning" particles with large betatron amplitudes. The momentum cleaning system catches the longitudinal losses induced by off-momentum particles. The whole system provides a multistage cleaning [3,4] with primary collimators closest to the beam, followed by secondary collimators. Special attention must be put in the Interaction Regions (IRs) in order to avoid high levels of beam background deposited in the detector and possible quenches and damages in the FT due to the aperture bottleneck. For that reason, additional tertiary collimators (TCTs) are introduced just upstream of the FT.

The collimation performance is assessed in simulations using SixTrack [5, 6] and quantified in terms of the local cleaning inefficiency η, defined as the ratio of the local losses N_{loc} over a distance Δs to the total losses on collimators N_{tot} [7],

$$\eta = \frac{N_{\mathrm{loc}}}{N_{\mathrm{tot}}\Delta s} \tag{1}$$

Table 1: Nominal TCT Openings at Different IRs.

	IR1	IR2	IR5	IR8
$n_{\mathrm{TCT}}[\sigma]$	8.3	30	8.3	30

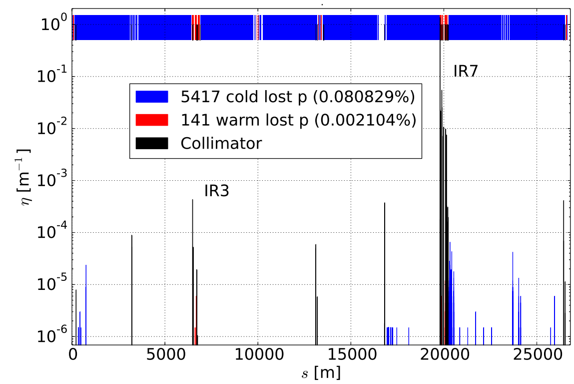

Figure 1: Example of a loss map representing the losses along the ring for Beam1 considering nominal apertures and Tertiary collimators in their nominal setting (8.3σ). Black lines represent losses in collimators, blue lines losses in cold regions and red lines are losses in warm regions.

In Fig. 1 the loss map for the HL-LHC version 1 optics and $\beta^* = 15$ cm for beam 1 and horizontal halo (initial losses on horizontal TCP), as simulated with SixTrack, is shown under nominal collimator configuration. The betatron (IR7) and momentum cleaning (IR3) insertions are clearly identified with large black spikes representing losses in collimators. Blue and red spikes represent losses in cold and warm regions respectively.

QUADRUPOLE APERTURE SCAN

The FT aperture represents a key parameter in the upgrade of the LHC optics towards the HL-LHC. In order to evaluate the beam losses, we have performed simulations using SixTrack where magnet aperture has been reduced as an effective approach to take into account several sources of errors. Pessimistic conditions of the machine such as alignment, orbit and optics errors can be seen as an effective aperture reduction.

The magnet aperture in IR1 and IR5 have been scanned individually for different magnets of the FT as well as Q4

* Research supported by EU FP7 HiLumi LHC Grant agreement 284404
† hector.garcia.morales@cern.ch

Content from this work may be used under the terms of the CC BY 3.0 licence (© 2015). Any distribution of this work must maintain attribution to the author(s), title of the work, publisher, and DOI.

ISBN: 978-3-95450-168-7 doi:10.18429/JACoW-IPAC2015-TUPTY067

Content from this work may be used under the terms of the CC BY 3.0 licence (© 2015). Any distribution of this work must maintain attribution to the author(s), title of the work, publisher, and DOI.

BEAM INDUCED BACKGROUND SIMULATION STUDIES AT IR1 WITH NEW HIGH LUMINOSITY LHC LAYOUT*

R. Kwee-Hinzmann†, S. M. Gibson, John Adams Institute at Royal Holloway
University of London, Egham, UK
R. Bruce, F. Cerutti, L.S. Esposito, A. Lechner, CERN, Geneva, Switzerland

Abstract

In the High Luminosity LHC (HL-LHC), the collimation system will be upgraded in the high-luminosity experimental regions. Additional protection is planned for the Q4 and Q5 magnets that are located further upstream of the tertiary collimators that protect the inner triplet magnets. We evaluate the effect of this proposed collimation layout for the incoming beam 1 on machine-induced background in the experimental area of IR1 (ATLAS). The main scenario is the round optics with β^* of 15 cm, but a flat scenario is also briefly discussed.

INTRODUCTION

The High Luminosity (HL) LHC is a major upgrade project to produce in total 3000 fb^{-1} integrated luminosity for each, ATLAS and CMS, starting installation around 2023 [1]. In particular, the upgrade plans affect the experimental insertion regions (IR) IR1 and IR5, housing ATLAS and CMS respectively, to reach higher luminosities. The optics have been re-designed (ATS – achromatic telescopic squeeze – optics [2]) and require e.g. larger-aperture magnets for squeezing the optics to 15 cm in the horizontal and vertical plane at the high-luminosity interaction points (IPs) 1 and 5 in order to achieve the luminosity goal. New possible aperture bottlenecks arise due to HL-LHC layout changes, and the quadrupoles Q5 and Q4 may no longer be sufficiently protected, see also Fig. 1. To address this, the collimation system [3, 4] will be upgraded in the experimental IRs. While these upgrades are in detailed in [5], the focus of this paper is on upgrade plans for the incoming beam. The new layout forsees to place in cell 5 a vertical and horizontal tertiary collimator (TCT5s for TCTH.5 and TCTV.5). As they are further away from the exisiting horizontal and vertical collimators (TCT4s that are TCTH.4 and TCTV.4), as illustrated in Fig. 1, they could help reducing beam-induced halo background. This paper presents a first estimate of the reduction based on simulations.

BEAM HALO BACKGROUND

Beam particles in the accelerator oscillate around an ideal orbit but diffuse out the beam core due to various beam dynamics effects (e.g. particle-particle scattering within a bunch, interactions between colliding bunches, scattering with residual gas-molecules) forming the *beam halo* and unavoidable losses. The task of the collimation system is to

* Research supported by FP7 HiLumi LHC–Grant agreement 284404
† Regina.Kwee@rhul.ac.uk

Table 1: HL half-gap collimator settings. Only the so-called 2σ-retracted settings are used in this paper. Full and updated settings can be found in [6].

collimators	nominal settings [σ]	2σ-retracted settings [σ]
TCP3	12 (now 15)	15
TCSG3	15.6 (now 18)	18
TCP7	6	5.7
TCSG7	7	7.7
TCT IR1/5	8.3	10.5

safely remove these halo particles in two dedicated insertion regions, IR7 for betatron and IR3 for momentum cleaning [3, 4]. Tertiary collimators (TCTs) in IR1 and IR5 complement the IR7/3 collimators and are installed to protect the inner triplet magnets. Halo protons leaking from IR7/3, should mostly be stopped by the TCTs. While interacting with the collimator material, they produce particle showers that contribute to the machine-induced halo background. This background source is considered in the following.

BEAM HALO SIMULATION SETUP

The simulation is performed in two parts, analogue to [7]. First, a tracking code, SixTrack [8], is used to track halo proton distributions customised by the user through a magnetic field lattice, see also [9]. The beam halo is usually simulated in horizontal (h) and vertical (v) distributions. When a collimator is hit, a built-in, recently updated Monte-Carlo model [10] decides on the physics process. Protons continue in the lattice until they dissociate in an inelastic interaction with the collimator material or (in a post-processing step) are lost on the aperture. As a result, loss locations around the ring can be identified and protons lost on the TCTs serve in second step as an initial distribution in FLUKA [11, 12].

Two cases were simulated, TCT4s only and TCT4s + TCT5s, to quantify the effect of the TCT5s for incoming beam 1 (B1). Inelastic interactions are forced in FLUKA at locations given by SixTrack on the TCT4s and (when included) TCT5s which generate a particle flux towards the experiment. All shower particles are recorded at the machine-detector interface plane at 22.6 m from the IP.

HL-LHC SIMULATION SCENARIOS

We assume the nominal HL-LHC scenario with 2.2×10^{11} protons per bunch, 2736 bunches per beam, 25 ns bunch spacing and a beam energy of 7 TeV. For the study of colli-

ISBN: 978-3-95450-168-7 doi:10.18429/JACoW-IPAC2015-TUPTY069

SIMULATION OF HOLLOW ELECTRON LENSES AS LHC BEAM HALO REDUCERS USING MERLIN*

H. Rafique†, R. J. Barlow, University of Huddersfield, Huddersfield, UK
R. Appleby, S. Tygier, University of Manchester, Manchester, UK
R. Bruce, S. Redaelli, CERN, Geneva, Switzerland

Abstract

The Large Hadron Collider (LHC) and its High Luminosity (HL) upgrade foresee unprecedented stored beam energies of up to 700 MJ. The collimation system is responsible for cleaning the beam halo and is vital for successful machine operation. Hollow electron lenses (HELs) are being considered for the LHC, based on Tevatron designs and operational experience [1], for active halo control. HELs can be used as soft scraper devices, and may operate close to the beam core without undergoing damage [2]. We use the Merlin C++ accelerator libraries [3] to implement a HEL and examine the effect on the beam halo for various test scenarios.

INTRODUCTION

HELs are novel devices which generate and control a hollow beam of electrons through an accelerator beam pipe. By directing the accelerator beam through the HEL beam, one may achieve various effects via the electromagnetic interaction. At the Tevatron, electron lenses (ELs) have been used for beam beam compensation (solid electron beam) [4], removal of beam from the abort gap (solid electron beam) [5], and halo scraping (hollow electron beam) [2].

It was originally proposed [6] that ELs could be used for tune spreading, satellite bunch removal, and halo scraping in the LHC. When combined with a multi-stage collimation scheme such as that in the LHC, HELs become an enhancer, increasing the diffusion, and the impact parameter of halo particles hitting the primaries [7].

The benefits of a HEL in a collimation scheme are numerous; firstly the electron beam is well controlled, and has many operation modes that may enhance the collimation of halo particles. The HEL beam can intercept the machine beam at a greater insertion (lower σ) than a solid scraper, as there is no heat load to manage, and no effect on machine impedance. The HEL can be switched on and off whereas a solid scraper would need to be inserted, and though both require alignment setup, the HEL may be used on a turn by turn, or even bunch by bunch basis. This means that the HEL can be used to deplete the halo, so that beam losses are minimised in the case of a rapid orbit jitter or crab cavity failure in HL-LHC.

MERLIN HEL MODEL

Merlin makes a number of assumptions when modelling the HEL:

- Fringe fields are ignored.
- Multipole field components created by e^- beam asymmetries are ignored.
- The e^- beam is azimuthally symmetric.
- Edge effects from the HEL beam are ignored (transverse area of interest ≈ few mm, longitudinal ≈ few m).
- Only the active part of the HEL is considered (toroids and solenoids are ignored).
- The HEL is run such that the electrons travel in the same direction as the proton beam, so that the HEL kick given to a machine particle is focussing.

Implementation

For a HEL of length L, with electron beam current I, the kick for a particle at a transverse displacement r, neglecting the electron radial profile is given by Eq. 1 [8].

$$\theta_{max}(r) = \frac{1}{4\pi\epsilon_0 c^2} \frac{2LI(1+\beta_e\beta_p)}{(B\rho)_p\beta_e\beta_p} \frac{1}{r} \tag{1}$$

where β_e and β_p are the Lorentz β of the HEL electron beam, and machine proton beam respectively, and $(B\rho)_p$ is the proton beam rigidity.

Including the electron radial profile, the kick may be reduced, for example for a perfect HEL profile (uniform between R_{min} and R_{max} and axially symmetric) it is given by Eq. 2 [8].

$$\theta_{kick} = \begin{cases} 0, & r < R_{min} \\ \frac{r^2-R^2_{min}}{R^2_{max}-R^2_{min}}\theta_{max}, & R_{min} < r < R_{max} \\ \theta_{max}, & r > R_{max} \end{cases} \tag{2}$$

Merlin contains both this perfect profile and a more realistic radial profile, based on the parameterisation of the measured beam profile [9]. The kicks for both profiles are shown in Fig. 1. R_{min} and R_{max} were set to 4 and 6.8 σ respectively.

In practice integration of a HEL into the LHC is non-trivial . The HEL is a superconducting device and therefore needs access to the LHC's high pressure He supply. As the HEL operates on one LHC beam, space between the two beam lines is required. Two candidate locations have been identified as RB-44 and RB-46, both in IR4, either side of the RF insertion [10]. Using Merlin, a HEL was implemented into the LHC lattice at RB-46. The optics parameters are shown in Table 1.

Operation Modes

The Merlin HollowElectronLensProcess offers 4 operation modes, similar to the HEL model in SixTrack [11].

* Research supported by FP7 HiLumi LHC (Grant agreement 284404)
† haroon.rafique@hud.ac.uk

Content from this work may be used under the terms of the CC BY 3.0 licence (© 2015). Any distribution of this work must maintain attribution to the author(s), title of the work, publisher, and DOI.

ISBN: 978-3-95450-168-7 doi:10.18429/JACoW-IPAC2015-TUPTY070

STRONG-STRONG SIMULATIONS OF β^*-LEVELLING FOR FLAT AND ROUND BEAMS

M. Crouch, University of Manchester and The Cockcroft Institute, U.K.
B. D. Muratori, ASTeC, STFC Daresbury Laboratory and The Cockcroft Institute, U.K.
R. B. Appleby, University of Manchester and The Cockcroft Institute, U.K.

Abstract

Simulations of β^* luminosity levelling using the strong-strong beam-beam code *COMBI* are undertaken. Simulations for both flat and round beam profiles are discussed and analysed with respect to the coherent spectra. It is shown that bunches with a round beam profile will have a beam-beam parameter that is independent of β^* over the levelling steps. Flat bunches however will have a beam-beam parameter that is dependent on β^* over the levelling steps since the beam aspect ratio will change. This will change the tune of the π-mode as the β^* is levelled, which could lead to a resonance crossing.

INTRODUCTION

The High Luminosity Large Hadron Collider (HL-LHC) upgrade will allow the LHC to reach ever higher luminosities. However an increase in luminosity will lead to higher "pile up" in the machine detectors. To prevent higher "pile up" in the machine detectors luminosity levelling has been suggested, which will hold the luminosity constant over the duration of a physics run. There are a number of suggested methods of levelling the luminosity, although β^*-levelling at IP1 and IP5 (Interaction Point) in combination with offset levelling at IP8 are the baseline methods of luminosity levelling [1]. Levelling by reducing the β^* as the luminosity decays exponentially will hold the longitudinal vertex density constant throughout the process for head on collisions. This is required by the detectors.

Flat beams have been proposed as an alternate method of operation if crab cavities are not installed in the HL-LHC. Flat beams will provide a low β-function at the IP, allowing higher luminosities to be reached.

In this paper, results from luminosity levelling using a 4D strong-strong beam-beam code are discussed and analysed for the case of β^*-levelling without offset using the Soft Gaussian approximation. Here a constant bunch intensity is assumed, resulting in a luminosity increase as the β-function at the IP changes.

LEVELLING MATRIX

Since the action of changing the β-function at the IP is an adiabatic process, the emittance in both planes should be conserved before and after the levelling step. To describe this within the code, a levelling matrix is applied such that as the spatial component of the particle phase space is reduced, the momentum of the particle phase space is increased. This can be derived by considering the phase space ellipse and the particle spatial and momentum components. The initial particle position and momentum can be expressed as a function of the β^* before and after the levelling step. The beams are focused in the transverse spatial components, which is given by

$$\frac{u_1}{u_2} = \sqrt{\frac{\beta^*_{1,u}}{\beta^*_{2,u}}} \tag{1}$$

where $u = x, y$ and the subscripts 1, 2 indicate before and after the levelling step. Likewise in the transverse momentum plane, the particles undergo a defocusing given by

$$\frac{p_{u,1}}{p_{u,2}} = \sqrt{\frac{\beta^*_{2,u}}{\beta^*_{1,u}}}. \tag{2}$$

The levelling map can be expressed as a matrix and is given by

$$\begin{pmatrix} u_2 \\ p_{u,2} \end{pmatrix} = \begin{pmatrix} \sqrt{\frac{\beta^*_{2,u}}{\beta^*_{1,u}}} & 0 \\ 0 & \sqrt{\frac{\beta^*_{1,u}}{\beta^*_{2,u}}} \end{pmatrix} \begin{pmatrix} u_1 \\ p_{u,1} \end{pmatrix}. \tag{3}$$

This matrix is applied between the levelling steps in both the horizontal and vertical plane to ensure that the emittance is conserved.

In this article, flat and round beam profiles were investigated to determine any possible emittance growth that may arise due to the levelling process. Only head on collisions at a single IP were simulated, although multiple IP collisions are undergoing investigation. Introducing an asymmetry between planes such that $\beta^*_x \neq \beta^*_y$ allows the flat beam option to be studied for the simple case of a single head on collision per turn at one IP. The β-function at the IP was reduced every $500K$ turns (approximately 44 seconds in the machine). The β-function at the IP for the round beam was reduced in steps of,

$$\beta^*_{x,y} = 0.60\ m \rightarrow 0.40\ m \rightarrow 0.20\ m \rightarrow 0.15\ m,$$

The β^* for the flat beam profile was reduced only in the vertical plane, in steps of,

$$\beta^*_y = 0.60\ m \rightarrow 0.40\ m \rightarrow 0.20\ m \rightarrow 0.10\ m \rightarrow 0.075\ m,$$

while the β-function at the IP in the horizontal plane is held constant at $\beta^*_x = 0.3$ m. Note that in these simulations, the bunch intensity is assumed to be held constant at $n_b = 2.2 \times 10^{11}$ protons per bunch. This provides a worse case scenario in terms of the beam-beam interaction. The starting parameters for the simulations are given by the HL-LHC parameters in Table 1,

Content from this work may be used under the terms of the CC BY 3.0 licence (© 2015). Any distribution of this work must maintain attribution to the author(s), title of the work, publisher, and DOI.

ISBN: 978-3-95450-168-7 doi:10.18429/JACoW-IPAC2015-TUPTY072

A NEW ILC POSITRON SOURCE TARGET SYSTEM USING SLIDING CONTACT COOLING*

Wei Gai#, Darrell Scott Doran, Robert Erck, George Fenske, Victor Guarino, Wanming Liu
ANL, Argonne, IL 60439, USA

Abstract

The R&D of the baseline positron source target for ILC is still ongoing after TDR due to the uncertainty of rotating vacuum seal and water cooling system of the fast spinning target wheel. Different institutes around the globe have proposed different approaches to tackle this issue. A spinning target wheel system with sliding contact cooling has been proposed by ANL. The proposed system eliminated the needs of rotating vacuum seal by using magnet bearings and vacuum compatible motor driven solid spinning wheel target. The energy deposited from positron production process is taken away via sliding cooling pads sliding against the spinning wheel.

INTRODUCTION

The ILC baseline positron source [1] is a helical undulator based positron source which produces 2×10^{10} positrons per bunch at the IP with the nominal ILC bunch structure and pulse repetition rate. It is designed with a 50% overhead and can deliver up to 3×10^{10} at injection into the 0.075 mrad transverse dynamic apertures of the damping ring. The main electron linac beam has an energy that varies between 100 and 250 GeV and passes through ~150m of helical undulator, with a 1.15 cm period and a K value of 0.92. At 150 GeV, the first harmonic cut-off of the photon drive beam is 10.1 MeV and the beam power is ~63 kW. Approximately 4.4 kW of this power is deposited in the target in ~1mm rms spot. A windowless moving target is required to handle the high beam power and heat deposition.

The ILC baseline positron production target [1] is a rotating titanium alloy wheel. The target wheels sit in a vacuum enclosure at 10^{-8} Torr (needed for NC RF operation), which requires vacuum seals for access to the vacuum chamber. The rotating shaft penetrates the enclosure using one vacuum pass-through. The R&D of target remains on-going. Even though the vacuum specification of the rotating vacuum seal has been demonstrated, its lifetime and reliability still requires further R&D. Many alternative target schemes have been discussed by collaborating researchers around the globe. The simplest one have been discussed is to use differential pumping to replace the rotating vacuum seal and keep the current configuration of water cooling from inside the target wheel. This scheme could eliminate the possible failure of the vacuum but still have the potential mechanical problem associated the water cooling channels inside the target wheel. To further address the ILC positron source target issue, DESY group proposed a radiation cooling scheme [2] and ANL group proposed a discrete target system [3].

The discrete target system adopted the concept of EM rail gun to eliminated the mechanical motion coupler of any kind between inside and outside of vacuum and thus eliminated the potential life time and reliability problem of the current ILC target system. But it needs a larger scale of changing to the current ILC positron source layouts which is not preferred.

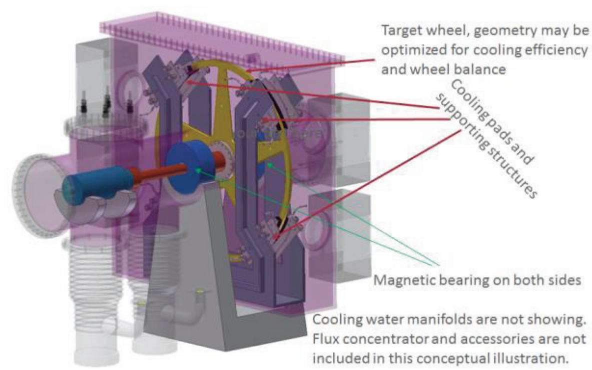

Figure 1: Conceptual illustration.

The original problem with the spinning wheel target is introduced as a result of water cooling from inside of the spinning target wheel. If we were not trying to cool the target from inside the spinning wheel, we won't need the rotational water union and thus eliminate the potential premature failure of the target system. The DESY group is working on the radiation cooling scheme. As a backup plan, we are looking into the sliding contact cooling scheme. The details of this sliding contact cooling scheme for ILC undulator based positron source are presented here in this paper.

GENERAL CONSIDERATIONS

As illustrated in Fig. 1, instead of cooling the target with water flow inside the target wheel, we use spring loaded cooling pads sliding against the target wheel and taking away the energy deposited in target resulting from positron production. Inside the cooling pads are cooling channels with cooling liquid flowing constantly. Since

The submitted manuscript has been created by UChicago Argonne, LLC, Operator of Argonne National Laboratory ("Argonne"). Argonne, a U.S. Department of Energy Office of Science laboratory, is operated under Contract No. DE-AC02-06CH11357. The U.S. Government retains for itself, and others acting on its behalf, a paid-up nonexclusive, irrevocable worldwide license in said article to reproduce, prepare derivative works, distribute copies to the public, and perform publicly and display publicly, by or on behalf of the Government.

*Work supported by DOE
#wg @anl.gov

Content from this work may be used under the terms of the CC BY 3.0 licence (© 2015). Any distribution of this work must maintain attribution to the author(s), title of the work, publisher, and DOI.

ISBN: 978-3-95450-168-7 doi:10.18429/JACoW-IPAC2015-TUPTY073

AN ALTERNATIVE HIGH LUMINOSITY LHC WITH FLAT OPTICS AND LONG-RANGE BEAM-BEAM COMPENSATION *

Stéphane Fartoukh, CERN, Geneva, Switzerland, Alexander Valishev, FNAL, Batavia, IL, USA, Dmitry Shatilov, BINP, Novosibirsk, Russia

Abstract

In the baseline scenario of the High-Luminosity LHC (HL-LHC), the geometric loss of luminosity in the two high luminosity experiments due to collisions with a large crossing angle is recovered by tilting the bunches in the interaction region with the use of crab cavities. A possible backup scenario would rely on a reduced crossing angle together with flat optics (with different horizontal and vertical β^* values) for the preservation of luminosity performance. However, the reduction of crossing angle coupled with the flat optics significantly enhances the strength of long-range beam-beam interactions. This paper discusses the possibility to mitigate the long-range beam-beam effects by current bearing wire compensators (or e-lens). We develop a new HL-LHC parameter list and analyze it in terms of integrated luminosity performance as compared to the baseline. Further, we evaluate the operational scenarios using numerical simulations of single-particle dynamics with beam-beam effects.

INTRODUCTION

The HL-LHC is being designed to deliver an integrated luminosity of at least 250 fb^{-1}/year in each of the two high-luminosity LHC experiments, ATLAS and CMS [1, 2]. The ambitious performance target for ATLAS and CMS cannot be met without pushing to the extreme both the optics, namely β^* [3], and the beam parameters at the exit of the LHC injector chain [4]. It relies as well on a number of key innovative and challenging technologies, such as: (i) new larger aperture superconducting magnets in order to preserve the transverse acceptance of the two high-luminosity insertions at low β^*, and (ii) crab cavities, which are high-frequency RF transverse deflectors creating quasi head-on collisions at the interaction point (IP) despite of the crossing angle, hence preserving the luminosity gain with $1/\beta^*$. The instantaneous luminosity is however limited by several factors, in particular by the total number of interactions per bunch crossing (pile up) and its line density, which can rapidly degrade the quality of the data collected for the physics analysis. In this respect, the HL-LHC relies on a levelled luminosity not exceeding 5×10^{34} cm^{-2}s^{-1} for a 25 ns bunch spacing (about 2750 bunches per beam), and corresponding to about 140 pile up (PU) events on average per bunch crossing with a peak line density of 1.25 event/mm. This is achieved through the use of challenging

* Research supported by DOE via the US-LARP program and by EU FP7 HiLumi LHC - Grant Agreement 284404

Table 1: Baseline Parameters of the HL-LHC Using Crab Cavities, Compared to Two Alternative Scenarios With Long-Range Beam-Beam Compensator.

Parameters	Baseline	Alt. 1	Alt. 2
Energy [TeV]	7		
Bunch spacing [ns]	25		
Number of collisions at IP1,5	2736		
Particles/bunch [10^{11}]	2.2		
Norm. emittance [μm]	2.5		
Bunch length [cm]	7.50	10.0	
β_x^*/β_y^* [cm] from start to end of levelling	68/68 $\rightarrow$ 15/15	47/47 $\rightarrow$40/10	112/28 $\rightarrow$40/10
Crossing angle [μrad]	590 (12.5 σ)	280 (9.7 σ)	
Levelled luminosity [10^{34}cm^{-2}s^{-1}]	5.0		
Virtual luminosity [10^{34} cm^{-2}s^{-1}]	19.6	10.5	
Levelling time [h]	8.3	5.2	
Pile up [events /crossing]	138		
Peak PU density [mm^{-1}]	1.25	1.31	
Luminous region (r.m.s.) [cm]	4.4	4.3	
Integrated luminosity [fb^{-1}] in 8 h $\rightarrow$ 10 h	1.44 $\rightarrow$1.75	1.34 $\rightarrow$ 1.55	

luminosity levelling techniques, presently via a gradual reduction of β^* in order to compensate for the proton burn off during the physics store. In order to sustain such a high luminosity over a typical period of 8-10 hours, the beam parameters, in particular the total beam current, shall correspond to a so-called virtual luminosity, which would be of the order of 2×10^{35} cm^{-2}s^{-1} should all the other parameters, for instance β^*, be pushed to the limit at the beginning of the levelling process. The aim of this paper is to propose an alternative set of parameters and scenarios in terms of optics and hardware needed, which stays competitive with the present HL-LHC baseline both in terms of physics data quantity (integrated performance) and data quality (pile up density).

PERFORMANCE REACH OF ALTERNATIVE SCENARIOS IN COMPARISON WITH THE BASELINE

The baseline parameters of the HL-LHC (25 ns version [5]) and two alternative scenarios are listed in Tab. 1. The list includes key values, such as the virtual luminosity (taking into account the hour-glass effect and the RF curvature

Content from this work may be used under the terms of the CC BY 3.0 licence (© 2015). Any distribution of this work must maintain attribution to the author(s), title of the work, publisher, and DOI.

ISBN: 978-3-95450-168-7 doi:10.18429/JACoW-IPAC2015-TUPTY074

MUON BEAM EMITTANCE EVOLUTION IN THE HELICAL IONIZATION COOLING CHANNEL FOR BRIGHT MUON SOURCES *

K. Yonehara†, C. Yoshikawa, Fermilab, Batavia, IL 60510, USA
Ya.S. Derbenev, A. Sy, JLab, Newport News, VA, USA
C. Ankenbrandt, R.P. Johnson, S.A. Kahn, Muons, Inc., Batavia, IL 60510, USA
B. Freemire, IIT, Chicago, IL, USA
M. Chung, UNIST, Ulsan 689-798, Korea

Abstract

Characteristic of a helical lattice for six dimensional muon ionization cooling will be presented to utilize for a bright muon source. The beta function and the dispersion in the lattice are tunable by adjusting the helical magnetic component. As a result, the cooling decrements and the equilibrium beam emittance in transverse and longitudinal phase spaces are flexible. A helical magnetic component can be adjusted by changing the geometry of helical solenoid magnets. Manipulating a cooling path is an important capability in a bright muon source to serve a high quality muon beam for various muon beam applications.

INTRODUCTION

A bright muon source is an ultimate tool to realize precise measurements in high-energy particle experiments. Muons are a true elementary particle, hence background events in $\mu^+\mu^-$ collisions are significantly less complicated than hadron colliders. Since muons are 200 times heavier than electrons they can be accelerated to a multi-TeV energy without any synchrotron-radiation losses. Beamstrahrung is negligible in high energy $\mu^+\mu^-$ collisions, hence the energy spread in a multi-TeV muon collider is significantly narrower than that in electron-positron collisions. The s-channel Higgs boson production rate in $\mu^+\mu^-$ collisions is 40,000 times larger than in electron-positron colliders ($\sigma_{Higgs} \propto m^2_{l^+l^-}$). Thus, a muon collider Higgs factory is the only machine that can directly measure the mass width of Higgs bosons. Besides, a high energy muon storage ring provides an intense monochromatic neutrino beam.

Since muons are a tertiary particle the initial muon beam temperature after pion decays is too hot to admit the beam into the conventional accelerator complex. The beam should be cooled down to adequate temperature for a muon accelerator complex within a muon life time. To achieve fast cooling, a helical muon six-dimensional (6D) phase space ionization Cooling Channel (HCC) is proposed. Theoretically, the 6D beam volume can be reduced 10^6 in a 300 m-long HCC. It consists of a high-pressure H_2 gas-filled helical RF system which is incorporated into a helical magnet. Gas in the RF cavities acts as not only an ionization cooling matter but also buffering dark currents to achieve high RF gradients in multi-Tesla fields. The helical magnetic component is generated by using a helical solenoid coil. Since the HCC lattice is a continuous structure there is no betatron resonance. It realizes a huge momentum acceptance.

The helical solenoid coil is flexible to tune the beta function and the dispersion by adjusting the geometry of coil and adding the correction magnet [1]. The lattice parameters are the key to manipulate the cooling decrements and the equilibrium emittance in transverse and longitudinal phase spaces. We demonstrate the theoretical predictions for the phase space mapping to design the cooling path and a numerical evaluation at the specific cooling condition for conceptual design of the HCC.

FLEXIBILITY OF HCC

The HCC linear theory in a homogeneous cooling matter was derived by Derbenev and Johnson [2]. The theory was confirmed by comparing with various numerical results [3–5]. Figures 1 and 2 show the validation of HCC theory. We used G4Beamline in the simulation effort [6]. H_2 gas pressure is 160 atm at room temperature and 20 60μm-thick-Be RF windows per meter are equally distributed on the beam path. According to the theory, the transverse betatron

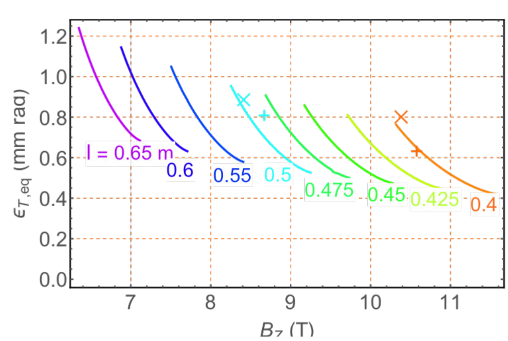

Figure 1: Prediction (a solid line) and the numerical result (a cross mark) of the transverse equilibrium emittance. Values in the plot represents the helical period, λ.

function, $\hat{\beta}_T$ is characterized by the helical period, λ and the solenoidal field strength, B_z, i.e. $\hat{\beta}_T$ is lower in shorter λ and/or stronger B_z. Therefore, lower equilibrium ε_T is made at shorter λ and/or stronger B_z and vice versa. On the other hand, the longitudinal betatron function, $\hat{\beta}_L$ is characterized by a momentum slip factor, η which is given by the dispersion, D. According to the theory, D becomes closer to the energy transition, i.e. $\eta \sim 0$ (isochronous) in stronger

* Work supported by Fermilab Research Alliance, LLC under Contract No. DE-AC02-07CH11359 and DOE STTR grant DE-SC0007634
† yonehara@fnal.gov

Content from this work may be used under the terms of the CC BY 3.0 licence (© 2015). Any distribution of this work must maintain attribution to the author(s), title of the work, publisher, and DOI.

ISBN: 978-3-95450-168-7 doi:10.18429/JACoW-IPAC2015-TUPTY076
Content from this work may be used under the terms of the CC BY 3.0 licence (© 2015). Any distribution of this work must maintain attribution to the author(s), title of the work, publisher, and DOI.

BEAM-BEAM SIMULATION OF CRAB CAVITY WHITE NOISE FOR LHC UPGRADE*

J. Qiang#, LBNL, Berkeley, CA94720, U.S.A.
J. Barranco, T. Pieloni, CERN, Geneva, Switzerland
K. Ohmi, KEK, Tsukuba, 305-0801, Japan

Abstract

High luminosity LHC upgrade will improve the luminosity of the current LHC operation by an order of magnitude. Crab cavity as a critical component for compensating luminosity loss from large crossing angle collision and also providing luminosity leveling for the LHC upgrade is being actively pursued. In this paper, we will report on the study of potential effects of the crab cavity white noise errors on the beam luminosity lifetime based on strong-strong beam-beam simulations.

INTRODUCTION

The High Luminosity (HL) LHC upgrade [1], aims at a tenfold increase (3000 fb^{-1}) of the integrated luminosity by 2035 as compared to its initial goal (300 fb^{-1}). This will be achieved by an increase of the instantaneous luminosity by almost an order of magnitude and therefore we expect the beam to beam electromagnetic interactions (i.e. beam-beam effects) to become stronger. It is important to evaluate the potential impact of these effects on the beam quality (e.g. emittance) in the high luminosity upgrade. In the HL-LHC upgrade, crab cavities (CCs) are proposed to compensate for geometric luminosity loss due to the crossing angle operation in collision which will lead to a 70% loss of luminosity. On the other hand, crab cavities may also have a detrimental impact on the beam quality due to imperfections. Phase noise errors in the CCs lead to a fluctuation of the bunch centroid position at the interaction point, which causes emittance growth. Amplitude errors in the CCs cause bunch size fluctuations and emittance growth. Simulations were carried out to assess the implication of the phase errors for the LHC parameters [2, 3, 4]. New development in the HL LHC design parameters and the improvement of the simulation tool to include a transverse damper model [5] demands new simulations. In this paper we present the simulation results to study the effects of crab cavity phase and voltage white noise errors on the peak luminosity of colliding beams.

COMPUTATIONAL SETUP

All simulations presented in this study were done using a strong-strong collision model implemented in the code BeamBeam3D [6]. In order to reduce numerically induced emittance growth, and to gain computation speed, the fields were computed assuming a Gaussian particle distribution, instead of a self-consistent approach. This assumption is justified by the fact that the initial Gaussian particle distribution does not change significantly in a short period of time under stable conditions. In order to keep the residual noise level low, one million macroparticles were used. The particle distribution in the longitudinal direction was divided into 8 slices. Two collisions per turn, corresponding to the interaction points (IPs) 1 and 5 in the LHC, were simulated. The crossing plane was horizontal in one IP5 (CMS experiment) and vertical in the other IP (ATLAS experiment). Linear transfer maps, calculated using the working point tunes, were employed to transfer the beam between collisions. The crab cavities are located 90 degrees phase advance from each IP. To model the beam transport through the crab cavity, we have assumed a thin lens approximation where the transfer map in the *x*-*z* plane is given by

$$\begin{aligned} x^{n+1} &= x^n \\ P_x^{n+1} &= P_x^n + \frac{qV}{E_s}\sin(\omega z^n / c + \phi) \\ z^{n+1} &= z^n \\ \delta E^{n+1} &= \delta E^n + \frac{qV}{E_s}\cos(\omega z^n / c + \phi) x^n \end{aligned} \quad (1)$$

where V is the voltage of the crab cavity, E_s is the particle energy, ϕ is the phase of the cavity, and ω is the angular frequency of the cavity. A similar transfer map with x replaced by y is used in the y-z plane.

The damper model uses a Hilbert-notch filter and two pick-ups per beam and plane, as the actual system in LHC does [7]. The correction kick at turn n due to one pick-up is given by

$$\Delta X' \propto g \sum_m H_m(\varphi_H) \times (X_{n-d+1-m} - X_{n-d-m}), \quad (2)$$

where H_m are the coefficients of the Hilbert filter and φ_H is the phase that needs to be determined as a function of the tune and damper gain g, and d is the delay of the damper in the units of turns. The actual kick is the superposition of two terms associated with different pick-ups. In the simulation, the damper's gain was set to 0.05 at each pickup. Noise is inserted to match the measurement [5]. The detailed physical parameters used in the simulations are given in Table 1 [8].

EFFECTS OF CRAB CAVITY PHASE WHITE NOISE ERROR

Under ideal conditions, the crab cavity will compensate the crossing angle collision completely and there is no

*Work supported by the Director of the Office of Science of the US Department of Energy under Contract no. DEAC02-05CH11231 and by the FP7 HiLumi LHC http://hilumilhc.web.cern.ch
#jqiang@lbl.gov

ISBN: 978-3-95450-168-7 doi:10.18429/JACoW-IPAC2015-TUPTY077

Content from this work may be used under the terms of the CC BY 3.0 licence (© 2015). Any distribution of this work must maintain attribution to the author(s), title of the work, publisher, and DOI.

STRONG-STRONG BEAM-BEAM SIMULATION OF BUNCH LENGTH SPLITTING AT THE LHC*

J. Qiang#, S. Paret, LBNL, Berkeley, CA 94720 USA
T. Pieloni, CERN, Geneva, Switzerland
K. Ohmi, KEK, Tsukuba, 305-0801, Japan

Abstract

Longitudinal bunch length splitting was observed for some LHC beams. In this paper, we will report on the study of the observation using strong-strong beam-beam simulations. We explore a variety of factors including initial momentum deviation, collision crossing angle, synchrotron tune, chromaticity, working points and bunch intensity that contribute to the beam particle loss and the bunch length splitting, and try to understand the underlying mechanism of the observed phenomena.

INTRODUCTION

LHC has made important scientific discovery since its beginning of operation. In some runs of 2012, it was observed that two colliding beams starting with similar longitudinal bunch length split up after some time due to selective transverse emittance blow-up that occurs at the end of the squeeze beam mode [1]. A study based on weak-strong simulation was reported last year [2]. In this paper, we have carried out strong-strong beam-beam simulations to understand the underlying mechanism that drives the bunch length splitting given the initial unequal transverse emittances of the two colliding beams [3].

COMPUTATIONAL SETUP

All simulations presented in this study were done using a strong-strong collision model implemented in the code BeamBeam3D [4]. In order to reduce numerically induced emittance growth, and to gain computation speed, the beam-beam fields were computed assuming a Gaussian particle distribution, instead of a self-consistent approach. This assumption is justified by the fact that the initial Gaussian particle distribution does not change significantly in a short period of time under stable conditions. One million macroparticles were used for each beam. The particle distribution along the longitudinal direction was divided into 8 slices. Two collisions per turn, corresponding to the Interaction Points (IPs) 1 and 5 in the LHC, were simulated. The crossing plane was horizontal at one IP and vertical at the other IP. Linear transfer maps, calculated using the working point tunes, were employed to transfer the beams between collisions. The damper model uses a Hilbert-notch filter and two pick-ups per beam and plane, as the actual system in LHC does [5]. The actual kick is the superposition of two terms associated with different pick-ups. An artificial 4 sigma aperture is assumed in the simulation to enhance the transverse particle losses from nonlinear beam-beam effects coming from the head-on and long range encounters in the LHC real configuration. This limit in aperture seems also a good choice since it is compatible with the expected dynamical aperture in the LHC during these observations [3]. The detailed physical parameters used in the simulations are given in Table 1.

*Work supported by the Director of the Office of Science of the US Department of Energy under Contract no. DEAC02-05CH11231 and by the FP7 HiLumi LHC http://hilumilhc.web.cern.ch
#jqiang@lbl.gov

Table 1: Physical Parameters used in the Simulations

Parameter	Value
N_p	1.5×10^{11}
$\varepsilon_{nb1}, \varepsilon_{nb2}$ / μm	2.5/3.5
β^* / m	0.6
σ / μm	18.8/22.2
σ_z / cm	9.74
Q_x	64.31
Q_y	59.32
Q_z	0.0019
θ / mrad	0.29
g_1, g_2	0.05/0.05
Damper noise	on
Collisions / turn	1 hor., 1 ver.

SIMULATION RESULTS

Using the above computational set-up, we carried out strong-strong simulations. Figure 1 shows the longitudinal rms bunch length evolution of two colliding beams with a machine chromaticity 15 and relative momentum deviation 0.0165%. The two beams starting with the same longitudinal bunch length split up after some time. Beam 1 is the beam with smaller emittance 2.5 mm, while beam 2 is the one with larger transverse emittance 3.5 mm. Due to the difference in emittance, beam 2 will experience different beam-beam effects from beam 1. The core of the beam 2 will see strong nonlinear beam-beam effects from the beam 1, while the core of the beam 1 will see mostly linear beam-beam effects from the core of the beam 2.

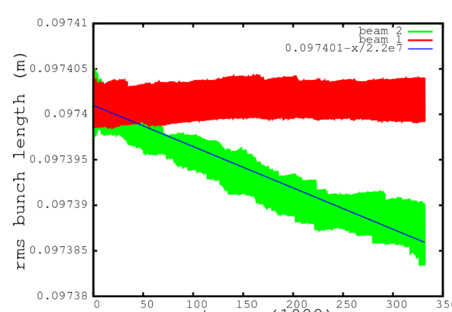

Figure 1: Longitudinal rms bunch length evolution of two colliding beams.

ISBN: 978-3-95450-168-7 doi:10.18429/JACoW-IPAC2015-TUPTY078

Content from this work may be used under the terms of the CC BY 3.0 licence (© 2015). Any distribution of this work must maintain attribution to the author(s), title of the work, publisher, and DOI.

FIXED-ENERGY COOLING AND STACKING FOR AN ELECTRON ION COLLIDER*

S. Assadi, J. Gerity#, P. McIntyre, and A. Sattarov
Texas A&M University, College Station, TX 77845 USA

Abstract

The proposed designs for polarized-beam electron-ion colliders require cooling of the ion beam to achieve and sustain high luminosity. One attractive approach is to make a fixed-energy storage ring in which ions are continuously cooled and stacked during a collider store, then transferred to the collider and accelerated for a new store when the luminosity decreases. An example design is reported for a 6 GeV/u superferric storage ring for this purpose, and for a d.c. electron cooling system in which electron space charge is fully neutralized so that high-current magnetized e-cooling can be used to best advantage.

EIC DESIGNS

High-energy collisions of polarized beams of electrons and ions provide the possibility of extending the study of the spin structure and dynamics in nuclear matter to clarify the spin dynamics of quarks and gluons in nuclei [1]. Those studies require highly polarized beams of electrons and ions, colliding in an asymmetric pair of storage rings.

Several designs have been proposed for the purpose: eRHIC [2], in which polarized electrons from a recirculating electron linac (ERL) are collided with polarized ions in one ring of RHIC; MEIC [3], in which highly polarized beams of electrons and ions are collided in a pair of rings configured as a figure 8 lattice to naturally preserve high polarization; ENC [4], in which polarized beams are colliding in a pair of circular rings.

All such colliders share a common challenge: to accumulate a filling of intense ion bunches with high polarization so that they are ready for injection to the ion ring of the collider whenever the present store loses either luminosity or polarization.

Accumulation of intense beams of polarized ions requires a matching of particle flow between the low-energy stage and the high-energy stage of acceleration. The line current density in a bunch is limited at low energy by the space charge tune shift [5]

$$\Delta\nu_{SC} = \frac{NBIr_i\beta_y}{\pi\nu\beta^2\gamma^3\sigma_y(\sigma_x+\sigma_y)}$$

and by intrabeam scattering (IBS) [6]

$$\Gamma_{IBS} = \frac{N_b r_i^2 c}{64\pi^2\beta^3\gamma^2\epsilon_x\epsilon_y\sigma_p\sigma_s} L_C I$$

where N = total number of particles in a bunch, R = ring radius, B = ratio of peak to average current in bunches, $L_C \sim 20$ = Coulomb logarithm, I = amplification factor from image currents on the beam tube, $r_i = Z^2e^2/Am_pc^2$, a = r.m.s. beam radius, $\mathcal{E}_x, \mathcal{E}_y$ = invariant emittances, σ_p = fractional energy spread, and σ_s = bunch length.

Particle flow through the acceleration sequence must accommodate the strong energy dependence of Γ_{IBS} and $\Delta\nu_{\mathrm{SC}}$. It would not be possible to accelerate at low energy the line charge density that could be sustained in collision at high energy. Maximum bunch charge and minimum emittance are attained if ion bunches are accelerated to an intermediate (relativistic) energy and cooled using d.c. electron cooling. The same e-cooling can be used to accumulate repeated cycles of ion production to build bunch intensity to the limits imposed by Γ_{IBS} and $\Delta\nu_{\mathrm{SC}}$ at that energy. The cold stack is then available whenever the luminosity or polarization declines in a store.

This approach was used with great success in the Fermilab Recycler [7]. The choice of optimum energy for cooling and stacking is a balance: as energy increases the sustainable bunch line intensity increases, but also the maximal longitudinal drag force $F_\parallel$ and transverse damping rate $\Gamma_\perp$ from electron cooling decreases. These quantities in the co-moving frame come directly from the plasma physics of non-equilibrium relaxation between plasmas of electrons and ions [8]:

$$\Gamma_\perp^* = \frac{8\sqrt{2\pi}Z^2r_er_ic\mathcal{L}}{3}n_e^*\left(\frac{kT_e}{m_ec^2}+\frac{kT_i}{m_ic^2}\right)^{-3/2}$$

$$F_\parallel^* = 2\pi Z^2r_e^2m_ec^2n_e^*\mathcal{L}\left(\frac{c}{\Delta_\parallel^*}\right)^2,$$

where $\mathcal{L}$ is the Coulomb logarithm over the accessible range of impact parameters, and n_e^* is the electron density and T_e and T_i are the electron and ion temperatures in the co-moving frame.

The lab-frame quantities are γ-boosted appropriately:

$$\Gamma_\perp = \eta\Gamma_\perp^*/\gamma^2 \qquad F_\parallel = \eta F_\parallel^*/\gamma$$

where η is the fraction of the cooling ring circumference in which electron cooling is happening.

For the example of the MEIC design for ion acceleration, the approximate optimum choice of ion kinetic energy for cooling is ~6 GeV/u. The cooling ring design and the electron cooling discussion below pertain to that MEIC Ion Ring.

* This work supported by the George and Cynthia Mitchell Foundation.
# jgerity@tamu.edu

ISBN: 978-3-95450-168-7 doi:10.18429/JACoW-IPAC2015-TUPTY079

Content from this work may be used under the terms of the CC BY 3.0 licence (© 2015). Any distribution of this work must maintain attribution to the author(s), title of the work, publisher, and DOI.

INITIAL MODELING OF ELECTRON CLOUD BUILDUP IN THE FINAL-FOCUS QUADRUPOLE MAGNETS OF THE SUPERKEKB POSITRON RING

J. A. Crittenden, CLASSE*, Cornell University, Ithaca, NY 14850, USA

Abstract

We present modeling results for electron cloud buildup in the final-focus quadrupole magnet nearest the interaction point in the SuperKEKB positron storage ring. The calculations employ as input recently obtained estimates of synchrotron radiation absorption rates on the vacuum chamber wall including the effect of photon scattering. While the effect both adds to and subtracts from photoelectron production at the points in the ring where unscattered photons strike the wall, it also produces cloud in the other regions. Results for beam-pipe-averaged and beam-averaged cloud densities are presented, as are estimates for the contribution to the fractional vertical coherent tune shift. The effect of the strong magnetic fields is studied and the dependence on the vacuum chamber surface secondary yield characteristics is considered. Cloud buildup is modeled with a 2D particle-in-cell macroparticle tracking code validated using recent measurements of electron trapping in a quadrupole magnet at the Cornell Electron Storage Ring Test Accelerator.

INTRODUCTION

The SuperKEKB e+e- collider is scheduled to begin operation in 2016. It will provide measurements of the decays of bound states of B quarks with unprecedented statistical precision. High luminosity operation depends on the strong field gradient region provided by the superconducting final-focus quadrupole magnets within 2 m of the interaction point (IP), with beta function values reaching as high 3000 m. Tune shifts near the interaction region have been calculated to be the dominant contribution to the total tune shift around the ring [1, 2]. These calculations did not include contributions from the final-focus quadrupole magnets. Recently, calculations of the synchrotron radiation distribution around the 4 GeV SuperKEKB positron ring including the effects of photon scattering on the walls of the vacuum chamber have become available [3]. The results show substantial rates of absorption in the final-focus quadrupoles, comparable to the highest rates in the arcs of the ring. In addition, the first measurements of electron trapping in a high-energy positron storage ring have been obtained recently in the context of the Cornell Electron Storage Ring Test Accelerator (CesrTA) program [4], allowing validation of an electron cloud buildup model for an ambient quadrupole magnetic field. The model successfully reproduced the trapping fraction when parameters were tuned to the signals observed in a time-resolving electron detector. Here we report on the initial application of this model for the case of cloud buildup in the upstream final-focus quadrupole nearest the IP in the SuperKEKB positron storage ring.

* Work supported by the US National Science Foundation contracts PHY-0734867, PHY-1002467, the U.S. Department of Energy contract DE-FC02-08ER41538 and the Japan/US Cooperation Program

SUPERKEKB FINAL-FOCUS QUADRUPOLE MAGNETS

The final-focus quadrupole magnet nearest the IP in the positron ring, designated QC1RP, is 334 mm long and its center is located 935 mm from the IP. It operates at a field gradient of 68.74 T/m [5]. Superposed on this high-gradient quadrupole field is a non-uniform longitudinal field from the BELLE-II solenoid compensation magnets, as shown in Fig. 1 [6]. The longitudinal component of this field varies from about 1 T to approximately 2.5 T over the 334-mm length of the QC1RP magnet. For the purpose of the model described here, the solenoid compensation field has been assumed to be 2 T, rotated around the vertical axis by half the crossing angle, i.e. $\frac{83}{2}$ mrad, relative to the axis of the quadrupole field. Copper and TiN-coated surfaces are under consideration for the cylindrical, 21-mm-inner-diameter vacuum chamber.

PHOTON TRACKING AND CLOUD BUILDUP MODELING

The results from the X-ray photon scattering and tracking code which are used as input to the electron cloud buildup modeling in the QC1RP magnet [3] are shown in Fig. 2. Together with the overall photon absorption rate, the azimuthal distribution of absorbed photons (Fig. 2a)) is an important consideration for cloud development in a magnetic field, since cloud electrons are guided by the field lines, emphasizing the contribution of those produced on field lines near the beam which intersect the vacuum chamber wall. Figure 2b) shows the photon absorption rate to

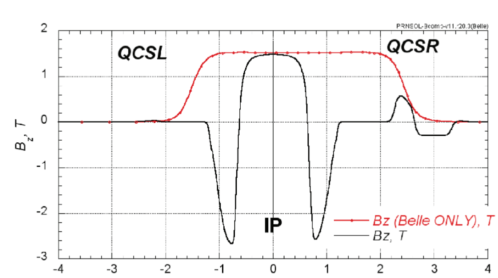

Figure 1: Longitudinal magnetic field component from the BELLE-II solenoid alone (red) and including the compensation field (black).

ISBN: 978-3-95450-168-7 doi:10.18429/JACoW-IPAC2015-TUPTY080

SYNCHROTRON RADIATION ANALYSIS OF THE SUPERKEKB POSITRON STORAGE RING

J.A. Crittenden and D.C. Sagan
CLASSE*, Cornell University, Ithaca, NY 14850, USA
T. Ishibashi and Y. Suetsugu
High Energy Accelerator Research Organization (KEK), 1-1 Oho, Tsukuba, Ibaraki 305-0801, Japan

Abstract

We report on modeling results for synchrotron radiation absorption in the SuperKEKB positron storage ring vacuum chamber including the effects of photon scattering on the interior walls. A detailed model of the geometry of the inner vacuum chamber profile has been developed and used as input to a photon tracking code. Particular emphasis is placed on the photon absorption rates in the electron-positron interaction region.

INTRODUCTION

The SuperKEKB e+e- collider will provide high-precision measurements of the production and decay of bound states of B quarks in the interactions of 4-GeV positrons with 7 GeV electrons. Commissioning is scheduled to begin in 2016. The design of the vacuum system [1] incorporates a variety of countermeasures to limit electron cloud buildup in the positron ring. The Cornell Electron Storage Ring Test Accelerator (CesrTA) program [2], in operation since 2008, has provided a wealth of information on the efficacy of such mitigation techniques via extensive measurements and model development which has also been used in the design of the International Linear Collider positron damping ring. [3, 4]. Here we report on results from a detailed modeling study of synchrotron radiation photon scattering and absorption on the interior surfaces of the vacuum chamber in the positron ring. In general, the effect of photon scattering on the walls of the vacuum chamber both adds and subtracts to the photon absorption rate (and therefore photoelectron production) at any point in the ring. However, such calculations can result in significant incident photon rates in regions where no synchrotron radiation strikes the wall directly.

VACUUM CHAMBER MODEL

Standard beam pipes in the positron storage ring have a circular beam channel and two rectangular antechambers on either side, as shown in Fig. 1. Synchrotron radiation photons irradiate the outer wall of the antechamber on the outside of the ring. The diameter of the beam channel and the half width at the horizontal axis are 90 mm and 110 mm, respectively. Strip-type non-evaporable getters (NEG) pumps are installed in the antechamber on the inside

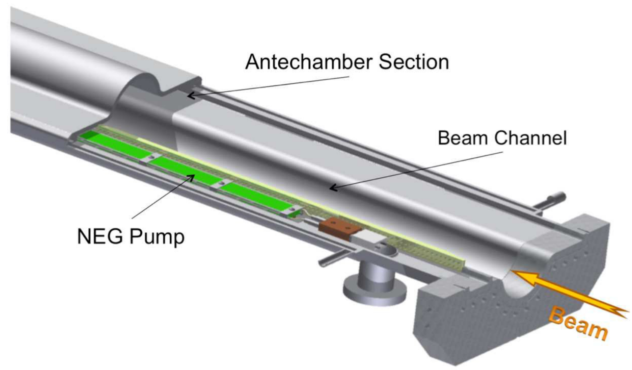

Figure 1: Schematic drawing of a beam pipe in arc sections of the positron storage ring.

of the ring. The pump channel is connected to the beam channel through a screen. A cross section of the standard beam pipe in the vacuum chamber model for the present calculations is shown in Fig. 2. The screens for the NEG pumps are defined as photon-absorbing walls in the model. In the wiggler sections, the photons strike both sides of the beam pipe, so both antechambers are used as channels for photon absorption. The rear walls of the antechambers are roughened to reduce scattering [1]; here we assume them to be totally absorptive. Circular beam pipes have been adopted in the interaction region (IR). The diameters vary in a staircase pattern from 80 mm at the entrance of the final focusing magnets (QCs) to 21 mm at the interaction point (IP). The beam pipes in the QCs on one side of the IP are

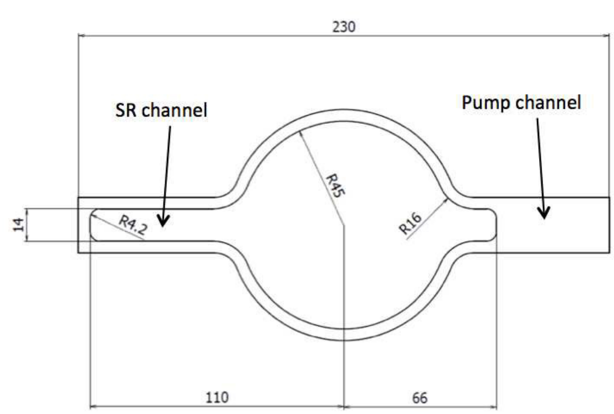

Figure 2: Cross section of the vacuum chamber model in the arc sections.

* Work supported by the US National Science Foundation contracts PHY-0734867, PHY-1002467, the U.S. Department of Energy contract DE-FC02-08ER41538 and the Japan/US Cooperation Program

Content from this work may be used under the terms of the CC BY 3.0 licence (© 2015). Any distribution of this work must maintain attribution to the author(s), title of the work, publisher, and DOI.

ISBN: 978-3-95450-168-7 doi:10.18429/JACoW-IPAC2015-TUPTY081

Content from this work may be used under the terms of the CC BY 3.0 licence (© 2015). Any distribution of this work must maintain attribution to the author(s), title of the work, publisher, and DOI.

DESIGN OF A 6 TeV MUON COLLIDER*

M-H. Wang†, Y. Nosochkov, Y. Cai, SLAC, Menlo Park, CA 94025, USA
M. Palmer, FNAL, Batavia, IL 60510, USA

Abstract

A design of a muon collider ring with the center of mass energy of 6 TeV is presented. The ring circumference is about 6.3 km, and the β functions at collision point are 1 cm in both planes. The ring linear optics, the non-linear chromaticity correction scheme in the Interaction Region (IR), and the additional non-linear field orthogonal knobs are described. The IR magnet specifications are based on the maximum pole tip field of 20 T in dipoles and 15 T in quadrupoles. The results of the beam dynamics optimization for maximum dynamic aperture are presented.

INTRODUCTION

A muon collider is one of the potential candidates for a future energy frontier colliding machine. Considering requirements on energy, luminosity and wall power in operation, the preferred choice of the center of mass muon beam energy appears to be near 6 TeV [1]. In order to obtain peak luminosity of $\geq 10^{34}$ $cm^{-2}s^{-1}$ in the TeV range, a number of demanding requirements to the collider optics should be satisfied [2]. These include a low beta function (β^*) at the Interaction Point (IP), small circumference for high revolution frequency, large dynamic aperture, and low momentum compaction factor for a short bunch length ($\sigma_z<\beta^*$). The requirements are arising from a short muon lifetime and relatively large values of transverse emittance and momentum spread that can be realistically achieved with ionization cooling. They also come from the limitations on the maximum magnetic fields as well as the necessity to protect superconducting (SC) magnets and collider detectors from muon decay products. Another complication is the "hot spots" of radiation which can be induced by neutrinos from muon decay in straight sections [3]. As a result, straight sections without bending field must be very short. More detailed discussion of these requirements can be found in Ref. [2].

LINEAR OPTICS

For a 6 TeV muon collider ring, achieving a short circumference and strong focusing in the IR requires rather high magnetic field. In this design, we chose the circumference of ≈6.3 km (approximately the size of the Tevatron) and the maximum pole-tip field of 20 T in dipoles and 15 T in quadrupoles. We expect that future advances in SC magnet design will make achieving such a strong field possible. The designed ring lattice has a two-fold symmetry (periodicity) and consists of two identical IRs and two arcs.

* Work supported by the US DOE No. DE-AC02-76SF00515 and HEP.
† mhwang@slac.stanford.edu

Interaction Region

The Interaction Region is the most challenging part of a high luminosity collider due to the extremely high beta functions in the final focusing (FF) quadrupoles generating large non-linear chromaticity as well as creating high sensitivity to magnet errors. The designed optics of one half of the IR of the 6 TeV machine is shown in Fig. 1, where the IP is on the left-hand side with β^* = 1 cm in x and y planes. The IP is followed by a 6 m free space and a FF quadrupole doublet where vertical beta function reaches an extremely high value of 134 km. The remaining part of the IR is made of FODO-like lattice where most of the space between the quadrupoles is filled with dipole magnets to avoid hot spots of neutrino radiation. Due to the high beta functions, the FF quadrupoles generate very large non-linear chromaticity resulting in a non-linear chromatic tune shift and large energy dependent perturbation of beta functions. These effects must be locally compensated to avoid a severe degradation of the ring momentum acceptance.

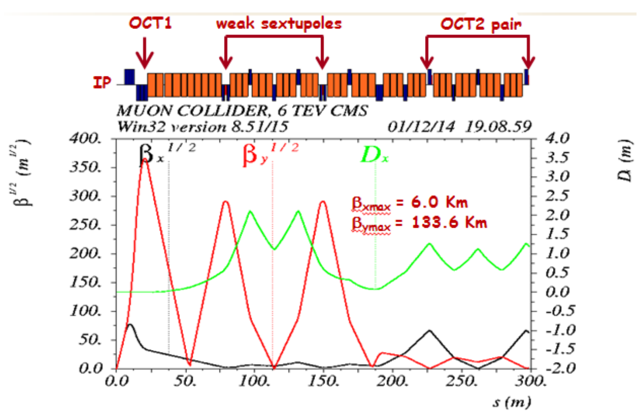

Figure 1: Linear optics of one half of the IR starting from IP. Two –I sextupole pairs (y and x) are placed at large β_y and β_x peaks for local correction of the FF quadrupole non-linear chromaticity. Positions of weak sextupoles and octupoles for additional non-linear correction are also shown.

The designed IR chromaticity correction scheme is based on two (x and y) non-interleaved pairs of sextupoles on each side of the IP, where the sextupoles in each pair are separated by –I transformation for cancellation of the 2nd order sextupole geometric (amplitude dependent) aberrations. The sextupoles are placed near the high beta peaks (x and y) to maximize their effective strengths. This correction scheme will be discussed in more detail later. At each end of the IR there is a dispersion suppressor FODO section followed by a ~40 m of non-dispersive

ISBN: 978-3-95450-168-7 doi:10.18429/JACoW-IPAC2015-TUPTY082

SCANNING SYNCHRONIZATION OF COLLIDING BUNCHES FOR MEIC PROJECT*

#Y. Derbenev, V. Popov, Jefferson Lab, Newport News, VA, USA
G. Kazakevich, Euclid TechLabs LLC, Cleveland, OH, USA
Yu. Chernousov, Institute of Chemical Kinetics and Combustion, Novosibirsk, Russia

Abstract

Synchronization of colliding beams is one of the major issues of an electron-ion collider (EIC) design because of sensitivity of ion revolution frequency to beam energy. A conventional solution for this trouble is insertion of movable bent chicanes in the arcs space. In our report we consider a method to provide space coincidence of encountering bunches of the crab-crossing orbits in the Interaction Region (IR) while repetition rates of two beams do not coincide. The method utilizes pair of fast kickers realizing a bypass for the electron bunches as the way to equalize positions of the colliding bunches at the Interaction Point (IP). A dipole-mode warm or SRF cavities fed by the magnetron transmitters are used as fast kickers, allowing a broad-band phase and amplitude control. The proposed *scanning synchronization* method implies stabilization of luminosity at a maximum via a feedback loop. This synchronization method is evaluated as perspective for the Medium Energy Electron-Ion collider (MEIC) project of JLab with its very high bunch repetition rate.

INTRODUCTION

In the MEIC's [1] medium ion energy range, maintaining a constant ion revolution frequency (given by the revolution frequency of electrons) with energy is troubled by a non-negligible change of the reference orbit in magnets. The earlier proposed baseline way of solving this problem is twofold. Firstly, at certain discrete energies corresponding to different harmonic numbers of the ion collider ring, synchronization of collisions is restored. The energy values are fairly closely spaced below at $\gamma \ll \sqrt{2q}$, where γ is ion Lorentz-factor, and q is number of bunches on the ion orbit. The correspondent maximum energy is about 36 GeV/u due to the very short bunch spacing of about 40 cm in MEIC, which may provide enough options for heavy ions with energies of only up to 40 GeV/u. However, there is a big energy gap from 36 to 100 GeV for protons. Covering the gaps between the harmonic energies is the second part of the synchronization problem. A number of different approaches to this issue have been proposed. Conceptually the simplest one is to adjust the ion ring circumference within the range of plus or minus a half of the 748.5 MHz RF wave length, i.e. by ±20 cm, using path-length movable chicanes as it is shown in Fig. 1, [2].

*Authored by Jefferson Science Associates, LLC under U.S. DOE Contracts No. DE-AC05-06OR23177 and DE-AC02-06CH11357.
#derbenev@jlab.org

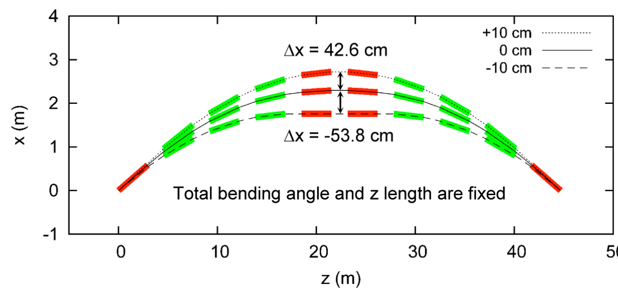

Figure 1: Schematic of an arc path-length chicane with movable magnets.

SCANNINNG SYNCHRONIZATION DYNAMIC CONCEPT

We consider a possibility of synchronization of the electron-ion colliding beams avoiding change of the orbit circumference. Instead, we consider a scheme of the cross-colliding beams with collision point moved periodically by a small scanning the beam directions in real time. For very most of the e-i bunch pairs, this scanning compensates for time delay of ion arrival at the nominal (central) Interaction Point (IP). The direction tilt of bunches is produced by RF deflecting resonators with varying amplitude and/or phase of the RF voltage, Fig. 2.

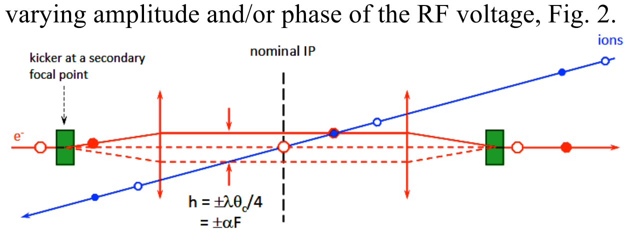

Figure 2: Schematics of the RF controlled bypass of e-beam for e-i synchronization by moving the collision point in real time.

The RF kicker is supposed to provide transverse variation of bunch trajectories in the Interaction Region (IR) in range of: $h = \pm \lambda\theta/4 = \pm\alpha F$.

Here: λ=40 cm is bunch spacing, θ =50 mr is crossing angle, α is kick angle produced by the maximum RF voltage amplitude, and F is focal distance of the IR focusing magnet block. At F =4 m we obtain h =5 mm, and required maximum kick α =1.25 mr. Maximum longitudinal deviation of the collision point will be 10 cm. Note that, in case that shift of the *collision point* (CP) is shared equally with the ion beam, the bypass parameters for each of two beams are reduced by a factor of 2, together with the similar reduction of the CP deviation.

Content from this work may be used under the terms of the CC BY 3.0 licence (© 2015). Any distribution of this work must maintain attribution to the author(s), title of the work, publisher, and DOI.

ISBN: 978-3-95450-168-7 doi:10.18429/JACoW-IPAC2015-TUPTY083

Content from this work may be used under the terms of the CC BY 3.0 licence (© 2015). Any distribution of this work must maintain attribution to the author(s), title of the work, publisher, and DOI.

CONCEPTUAL MEIC ELECTRON RING INJECTION SCHEME USING CEBAF AS A FULL ENERGY INJECTOR*

Jiquan Guo#, Fanglei Lin, Robert Rimmer, Haipeng Wang, Shaoheng Wang, Yuhong Zhang, JLAB, Newport News, VA 23606, USA

Abstract

The Medium-energy Electron-Ion Collider (MEIC) proposed by Jefferson Lab is planning to use the newly upgraded 12 GeV CEBAF 1497 MHz SRF CW recirculating linac as a full-energy injector for the electron collider ring. The electron collider ring is proposed to reuse the 476MHz PEP-II RF system to achieve high installed voltage and high beam power. The MEIC electron injection requires 3-10 (or 12) GeV beam in 3-4μs long bunch trains with low duty factor and high peak current, resulting in strong transient beam loading for the CEBAF. In this paper, we propose an injection scheme that can match the two systems' frequencies with acceptable injection time, and also address the transient beam loading issue in CEBAF. The scheme is compatible with future upgrade to 952.6 MHz SRF system in the electron ring.

INTRODUCTION

The MEIC proposed by JLab is a high luminosity electron-ion collider with 3 to 10 GeV electrons and 20 to 100 GeV protons (or up to 40 GeV per nucleon for heavy ions), with the possibility to upgrade to higher energy [1, 2]. The nominal beam current in the electron ring is 3 A, but the current is also limited by synchrotron radiation power at high energy, and by RF cavity impedance induced coupled bunch instability at low energy [3]. The newly upgraded 12 GeV CEBAF linac is chosen as the full energy injector for the electron ring. It's also natural to consider reusing the high power RF system of the recently retired PEP-II in MEIC's electron ring, since PEP-II was designed for similar beam current and system RF power [4]. Although PEP-II and CEBAF have different RF frequencies, we note that 7/22 (very close to 1/π by incident) of the CEBAF linac's 1497 MHz frequency is 476.3 MHz, which is within the operational range of PEP-II's 476 MHz RF system.

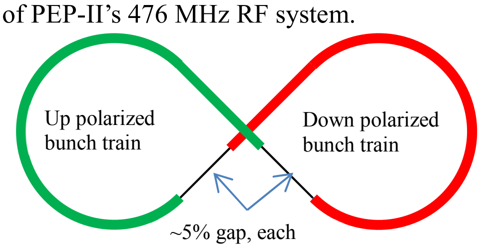

Figure 1: Bunch trains in the MEIC figure-8 ring

In the baseline design, each of the MEIC collider rings will provide two bunch trains with opposite spin polarization in the same ring, with two gaps of ~5% circumference in between, as shown in Fig. 1. The gaps result from the injection kickers' rise/fall time, and will also serve for the purposes of ion clearing etc. Under the full current operation, every bucket in the bunch train will be filled. In case the current is far below the beam-beam limit due to other limiting factors such as synchrotron radiation power, the bunch rep-rate may be reduced to a fraction of the RF frequency for higher luminosity.

Currently the harmonic number of the electron ring is set at 3416, with a circumference of around 2150 m and the revolution time of 7.17 μs.

THE ELECTRON INJECTION SCHEME

The electron ring will use transverse phase space injection. For each kicker cycle, a polarized bunch train with the length of ~45% collider ring circumference (3.23 μs) will be injected into the 1st half ring, followed by another oppositely polarized bunch train filling the 2nd half of the ring. The electron ring's transverse damping time τ_d ranges from 6 to 376 ms, depending on the beam energy and the use of damping wigglers. About $2\tau_d$ is needed to damp the injected beam before the next injection into the same half ring.

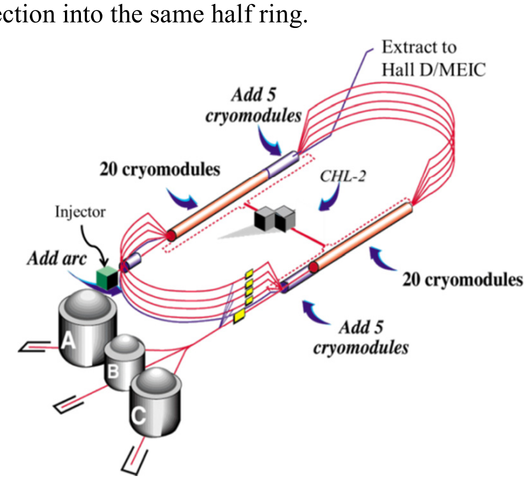

Figure 2: CEBAF after 12 GeV upgrade

Maximizing the Pulsed Bunch Train Current in CEBAF

To achieve a reasonable injection time, we need to maximize the pulsed beam current generated from CEBAF. As shown in Fig. 2, the beam in CEBAF can be accelerated during the 6 passes in the north linac and 5 passes in the south linac, before it's extracted to Hall D or MEIC. The CEBAF is capable of delivering CW extracted beam with ~1 MW beam power, nominally limited by the beam dump's CW power rating, but also limited by the system's total RF power. The beam current circulating in the linacs is usually 5-6 times of the

* Authored by Jefferson Science Associates, LLC under U.S. DOE Contract No. DE-AC05-06OR23177
#jguo@jlab.org

ISBN: 978-3-95450-168-7 doi:10.18429/JACoW-IPAC2015-TUPTY084

UPDATE ON THE MEIC ELECTRON COLLIDER RING DESIGN*

F. Lin#, Ya.S. Derbenev, L. Harwood, A. Hutton, V.S. Morozov, F. Pilat, Y. Zhang, Jefferson Lab, Newport News, VA, USA
Y. Cai, Y.M. Nosochkov, M. Sullivan, M-H Wang, U. Wienands, SLAC, Menlo Park, CA, USA

Abstract

The electron collider ring of the Medium-energy Electron-Ion Collider (MEIC) at Jefferson Lab is designed to accumulate and store a high-current polarized electron beam for collisions with an ion beam. We consider a design of the electron collider ring based on reusing PEP-II components, such as magnets, power supplies, vacuum system, etc. This has the potential to significantly reduce the cost and engineering effort needed to bring the project to fruition. This paper reports on an electron ring optics design considering the balance of PEP-II hardware parameters (such as dipole sagitta, magnet field strengths and acceptable synchrotron radiation power) and electron beam quality in terms of equilibrium emittances.

INTRODUCTION

The electron complex of the MEIC is designed to meet the physics requirements for the project [1]. These include a beam energy range of 3 to 10 GeV, a beam current of 3 A up to an energy above 6 GeV, a short bunch length (approximately 1 cm) and small transverse emittance over a wide energy range to support the luminosity requirement, and a longitudinal polarization of 70% or above at collision points with a reasonably long lifetime. In addition, the linear density of synchrotron radiation power is less than 10 kW/m and the total power less than 10 MW.

The CEBAF 5.5 pass SRF recirculating linac serves as a full energy injector to the MEIC electron collider ring. No further upgrade is needed beyond the current CEBAF 12 GeV upgrade in terms of beam current and polarization (> 85%). In the MEIC baseline design, the PEP-II 476 MHz RF system will be reused in the electron collider ring [2]. To synchronize the RF bucket between CEBAF whose RF frequency is 1497 MHz and the electron collider, we note that 7/22 of the CEBAF linac frequency is 476.3 MHz. This frequency is well within the operational range of the PEP-II 476 MHz cavities and klystrons. Details of the injection concept is discussed in these proceedings [3].

After the last recirculation in the CEBAF, the beam is sent to a transfer line after the north linac [4]. The transfer line between the linac and the MEIC electron collider ring is made of FODO cells with 120° of phase advance using the PEP-II Low Energy Ring (LER) dipoles and quadrupoles. The strengths of dipoles and quadrupoles are well within their specifications. There are a number of reasons to choose a phase advance of 120°. First, it keeps the quadrupole gradients low enough so that the PEP-II LER quadrupoles can be reused. Second, it is compatible with a missing dipole scheme for dispersion suppression. Third, such phase advance insures that there is no significant emittance growth due to synchrotron radiation during the transport of electron beam from the CEBAF to the MEIC electron collider ring. The length of the entire transfer ling is approximately 333 m.

The electron and ion collider rings of the MEIC are designed to follow the same footprint and share the same underground tunnel. The electron ring determines the overall geometry that the ion ring follows with the exception of the region around the IP due to the 50 mrad crossing angle. The dimension of the electron ring should be able to accommodate all machine components. This paper presents the electron collider ring optics design using the PEP-II High Energy Ring (HER) magnets.

ELECTRON COLLIDER RING DESIGN

The MEIC electron collider ring is designed as a FODO lattice in both arcs and straights, using the majority of PEP-II dipoles and quadrupoles within the limit of their strengths [5]. Particular machine blocks, such as spin rotators, interaction regions and RF sections etc., are designed as modules using new dipoles and quadrupoles, inserted and matched into the base line lattice.

Each arc has 34 normal FODO cells and 8 matching cells (4 in each end of the arc). The normal FODO cell is 15.2 m long and filled with two 5.4 m long PEP-II dipoles and two 0.56 m long PEP-II arc quadrupoles. Each quadrupole is followed by a PEP-II sextupole for chromatic compensation in the arcs. Though the dipole field strength of 0.3 T at 10 GeV in the MEIC is higher than the 0.27 T shown in [5], PEP-II dipoles can reach 0.363 T because they were originally designed for the PEP 18 GeV electron beam. For the MEIC application, each dipole has a 3.3 cm sagitta based on a bending angle of 2.8°. This sagitta is 1.1 cm larger than the PEP-II dipole sagitta of 2.2 cm, but it is still within the dipole good field region of 5 cm. The matching cell has the same length and magnets of the normal FODO cell, except that the quadrupoles are adjusted to match the optics between the normal FODO cell and the Universal Spin Rotator (USR). The spin rotator is designed with interleaved solenoids and dipoles, and quadrupoles in between for the optics, to rotate the electron polarization between the vertical (in arcs) and longitudinal (at IP) direction from 3 to 12 GeV [6]. Note that the spin rotator does not change the design orbit over the entire range of electron beam energies. The transverse orbital coupling induced by the longitudinal

* Notice: Authored by Jefferson Science Associates, LLC under U.S. DOE Contract No. DE-AC05-06OR23177 and DE-AC02-06CH11357. Work also supported by the U.S. DOE Contract No. DE-AC02-76SF00515. The U.S. Government retains a non-exclusive, paid-up, irrevocable, world-wide license to publish or reproduce this manuscript for U.S. Government purposes.
# fanglei@jlab.org

Content from this work may be used under the terms of the CC BY 3.0 licence (© 2015). Any distribution of this work must maintain attribution to the author(s), title of the work, publisher, and DOI.

ISBN: 978-3-95450-168-7 doi:10.18429/JACoW-IPAC2015-TUPWI001

TURNKEY SYSTEMS COST OPTIMIZATION BY ITERATIVE DESIGN OF MAGNETS AND POWER SUPPLIES

M. Cavellier, W. Beeckman, J.D. Holzmann, F. Forest, SIGMAPHI, Vannes, France

Abstract

For more than 30 years, Sigmaphi has been manufacturing magnets and power supplies. Its teams are now able to supply a complete particle beamline, from beam optics calculation to on-site installation and alignment. These combined skills allow design optimization for turnkey systems in order to reduce their purchasing and running costs. A common though widespread in scientific community is that savings are possible by making the complete (and optimized) design of a magnet before asking an industrial company to manufacture it. At first glance, only looking at the design cost, it may be true. But in most cases, considering the complete system and running costs, this hypothesis is false. Based on the average cost breakdown between material and workmanship in a magnet and the related power supply, it is highlighted how an iterative design can reduce the total cost of the system. Two examples of successful iterative designs are presented: a tunable kicker magnet with its pulser, and a 70 meters beamline designed, manufactured and installed by Sigmaphi.

INTRODUCTION

A common though widespread in scientific and accelerator's engineering community is that savings are possible by making the complete (and optimized) design of a magnet before asking an industrial company to manufacture it. At first glance, only looking at magnet costs, this may be true. But in most cases, considering the complete system and running costs, this hypothesis is false. Power supplies are the first "victims" of magnets size optimization, and the consequences on running costs can be dramatic.

The best practice is to adapt magnet design to standard power supplies, and mutualize magnets design as much as possible through what we call here "iterative design".

An example of successful iterative design is presented here.

GUIDELINE FOR ITERATIVE DESIGN

The entry point for designing a cost-adapted solution is functional needs. The one who designed his magnet without considering the task of his colleague from power supply can be sure that his system will not be optimized.

The main steps for iterative and cost-optimized design are:

- Beam optics.
- Magnets design, which give main parameters: bore or gap, effective length, field or gradient.
- Electrical parameters of magnets, through coils design.
- Determining if a standard "on-shelf" power supply is close to what is required. If not, all the possibilities must be explored to change coils and magnet design to fit standard power supply, keeping in mind the objective of using the device with the lowest power.
- Verifying that power consumption is lower than the initial target. If not, a new iteration starting from one of the stages above is necessary.
- In case of a beam line where several pairs of magnet/power supply are to be designed, check if there are possibilities to group magnet design: same bore diameter/length to use same coils, even if magnet is used at 70 or 80% of its full capacity.

  Of course, this last step is strongly limited by the space constrains you may have.

EXAMPLE

An example of successful iterative design led by Sigmaphi is given here. Sigmaphi was in charge of designing, manufacturing, installing and aligning a 70m beam line for JINR in Dubna, Russia: Acculina-2. Beam optics responsibility was held by JINR, but teams from both sides worked together to adapt it in order to reduce significantly running costs.

For this beam line, the necessary quantities of magnets are presented in Table 1, and part of the layout in Fig. 1.

Starting from the initial specification, seven iterations were necessary to come up with an optimized design of both magnets and power supplies.

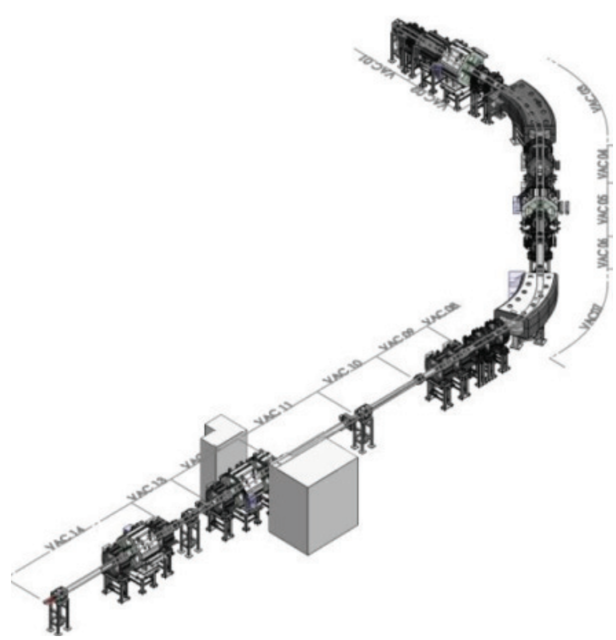

Figure 1: Partial layout of Acculina-2 beam line.

Content from this work may be used under the terms of the CC BY 3.0 licence (© 2015). Any distribution of this work must maintain attribution to the author(s), title of the work, publisher, and DOI.

ISBN: 978-3-95450-168-7 doi:10.18429/JACoW-IPAC2015-TUPWI003

PROTON BEAM APPLICATIONS FOR SILICON BULK MICROMACHINING

P. Nenzi, G. Bazzano, F. Marracino, L. Picardi, C. Ronsivalle, V. Surrenti, M. Vadrucci, ENEA C.R. Frascati, Frascati, Italy
C. Snels, M. Tucci, ENEA Casaccia, Roma, Italy
F. Ambrosini, M. Balucani, A. Klysko, DIET - University «La Sapienza», Roma

Abstract

We have investigated the effects of deep hydrogen implantation into *n*- and *p*-type silicon wafers ((100) oriented, with resistivity in the 1-20 Ω·cm range). Deep implantation has been achieved using the Hitachi-AccSys PL-7 RF LINAC set for 3.0 MeV beam energy, degraded to 1.8 MeV. Hydrogen has been implanted 30 µm below the wafer surface with an implant dose (fluence) >5x10^{15} cm^{-2}. Samples were partly covered by a metal mask during implant. Porous silicon has been formed on the exposed samples to study the effect of hydrogen irradiation. We have found that porous silicon formation is inhibited in the irradiated areas on *p*-type silicon and promoted on the *n*-type one.

INTRODUCTION*

Ion implantation into semiconductors is one of the key industrial applications of particle accelerators. Figure 1 shows the most common implantation energies, doses, and chemical species, employed in the semiconductor industry.

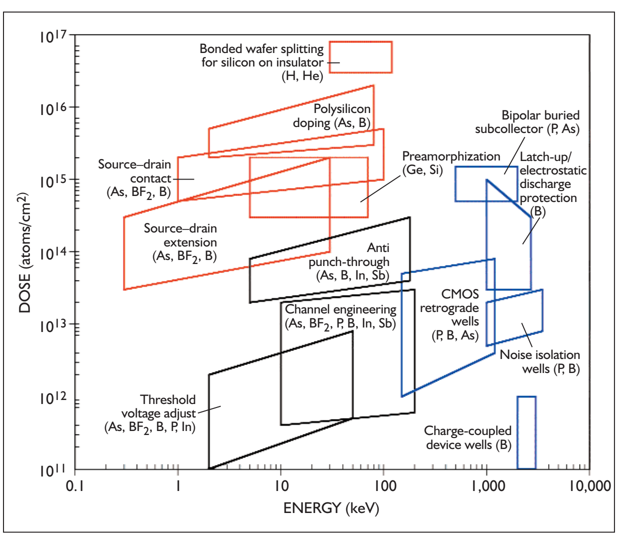

Figure 1: Process and dose application space for semiconductor industry. Hydrogen implantation has been used mainly for the manufacturing of SOI wafers where doses in excess of 5x10^{16} are required.

* Work supported by the TOP-IMPLART project funded by Regione Lazio.

Hydrogen implantation has been historically relegated to the manufacturing of SOI (Silicon-On-Insulator) wafers [1, 2] and, more recently, in the bulk micromachining of silicon in conjunction with the formation of porous silicon [3, 4].

CEA LETI has commercially exploited hydrogen implantation since 1994 [2] for the production of SOI wafers. The technique, known with the name "smart cut", uses protons (H$^+$ ions) to create lattice defects in correspondence of the stopping range. In this technology, 150 keV protons are used, corresponding to an implantation peak at 1.25 µm below the surface. A layer with dopant concentration of 10^{16} cm^{-3} has been achieved with implant dose (fluence) higher than 5x10^{16} cm^{-2}.

When the above concentration is reached it is possible to thermally trigger the coalescence of the defects to create "bubbles" in the silicon crystal and cleave the wafer along a plane parallel to its surface in a position corresponding to the stopping range.

Silicon micromachining technologies, based on hydrogen irradiation, follows the discovery that, irradiated areas cannot be converted into porous silicon [3]. The starting material was *n*- and *p*-type silicon 0.015-0.020 Ω·cm and 0.010-0.020 Ω·cm, respectively, and the proton energy was 2 MeV. The authors attributed that behavior to the defects induced by the proton beam in the silicon crystal. A more recent explanation of this phenomenon has been given in [5], in which the authors attribute the suppression of porous silicon formation to defect induced by the beam to *holes* transport through the lattice (porous silicon formation requires continuous *holes* supply). They simulated hole current of an irradiated structure into silicon using a commercial finite elements code (COMSOL) solving the Poisson's and continuity equation (in two dimensions) at different biases and verified their results experimentally.

In such technologies, porous silicon is used as sacrificial material, due to its etching selectivity with respect to silicon (up to 1x10^5:1, for potassium hydroxide (KOH) etch). In such technologies [4], silicon is patterned with a focused proton beam, e.g. Nuclear Microprobe [6], (essentially an high energy Focused Ion Beam) with a spot size of 200 nm to locally induce defects into the silicon lattice. Protons (or He ions) with energies in the range 0.25 MeV to 2 MeV at fluencies between 5x10^{14} cm^{-2} to 5x10^{15} cm^{-2} are employed. Complex three-dimensional structures can be realized with such technologies [7].

Content from this work may be used under the terms of the CC BY 3.0 licence (© 2015). Any distribution of this work must maintain attribution to the author(s), title of the work, publisher, and DOI.

ISBN: 978-3-95450-168-7 doi:10.18429/JACoW-IPAC2015-TUPWI004

STATUS OF THE TOP-IMPLART PROTON LINAC

P. Nenzi, A. Ampollini, G. Bazzano, F. Marracino, L. Picardi, C. Ronsivalle,
V. Surrenti, M. Vadrucci, ENEA C.R. Frascati, Frascati, Italy
C. Snels, ENEA Casaccia, Roma, Italy
F. Ambrosini, DIET - University «La Sapienza», Roma, Italy

Abstract

In this work we present the latest update on the construction of the TOP-IMPLART proton LINAC at the ENEA C.R. Frascati Accelerators Laboratory. TOP-IMPLART is a 150 MeV proton accelerator for protontherapy applications funded by Regione Lazio (Italy). We have successfully commissioned the first 3GHz LINAC structure reaching the energy of 11.6 MeV (from 7 MeV), demonstrating the first proton acceleration in a SCDTL structures at this energy. The second SCDTL LINAC has been tuned and brazed and in delivery to the installation site, the third one is under construction.

INTRODUCTION

The TOP-IMPLART (Intensity Modulated Proton Linear Accelerator for RadioTherapy) accelerator [1-3] is a proton LINAC designed for medical applications (i.e. cancer treatment). This project, funded by the local government (Regione Lazio), is a joint venture of three Italian research institutions: ENEA, ISS, and IRE-IFO (the end-user). The accelerator, when completed, will deliver a proton beam with energy variable in the 85 MeV to 150MeV range (with a planned upgrade to 230 MeV, not yet funded). The funded TOP-IMPLART accelerator consists of three sections, an injector (up to 7 MeV), a medium energy section (7 MeV to 35 MeV), and a high-energy section (35 MeV to 150 MeV). The injector is a commercial LINAC, the PL-7 designed by Hitachi-AccSys, operating at 425 MHz with 100 µs wide pulses and a pulse repetition frequency (PRF) of 100 Hz (maximum). The rest of the accelerator operates at 2997.92 MHz with a pulse width of 4 µs. The medium energy section consists of four SCDTL (Side Coupled Drift Tube LINAC), an ENEA patented design, driven by a single 10MW klystron tube. The high-energy section of consists of 12 CCL structures driven by four 10MW klystron tubes.

The injector section is connected to the first SCTDL structure by a LEBT (Low Energy Beam Transfer Line) consisting of a first quadrupole doublet followed by a deflecting magnet and a second quadrupole doublet. The LEBT is meant to focus the beam to fit the SCDTL pipe that has 4 mm diameter, whereas the injector pipe is 35mm diameter. The deflecting magnet is used to deliver the proton beam to a vertical beam-line used in radiobiology experiments [4-6].

The operating frequencies of the injector and of the other LINACs are not in harmonic relation and phase synchronization between the two is not achievable. Phase synchronization strategy of the medium- and high-energy sections is presented in [7].

The task under completion is the construction of the medium energy section (from 7MeV to 35 MeV). The first structure has been successfully installed and commissioned and the second one is undergoing the final brazing before delivery to the installation site. The actual layout of the TOP-IMPLART accelerator is shown in Fig. 1.

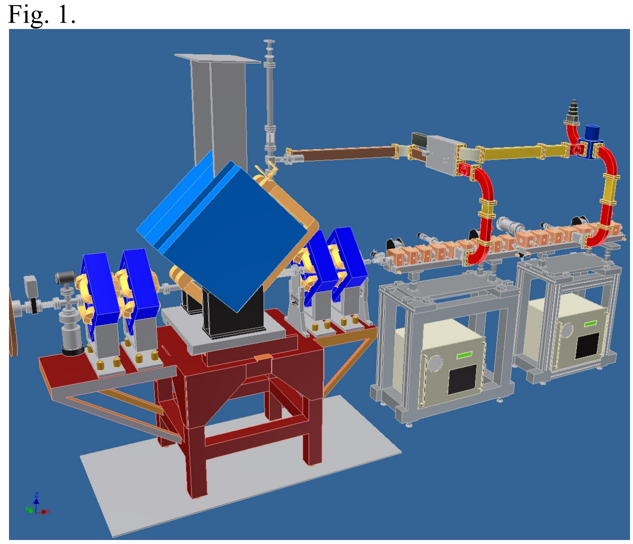

Figure 1: Layout of the TOP-IMPLART accelerator with the LEBT (left) and the first two SCDTL structures each one on his own table. The RF driving line is shown.

Each SCDTL structure is installed onto an independent table onto thermally isolated posts and is heated to the working temperature by a chiller unit placed under the structure itself. The RF driving line consists of a power splitter with adjustable split-ratio. Moreover, a waveguide switch is installed in the second structure branch, to dump RF power to a load when the second structure is used in transport mode only (for the 11.6 MeV beam).

SCDTL-1 OPERATION

The first SCDTL (referred as SCDTL-1) structure is in operation (Fig. 2). SCDTL-1 (1.1 m long) is composed of 9 DTL tanks with 4 side coupled cells per tank; in the intertank space PMQs (Permanent Magnet Quadrupoles) with gradient values around 197 T/m are placed. The structure is equipped with its own chiller that keeps temperature stable within 0.2 °C around 42 °C in such a way that the resonant frequency is exactly 2997.92 MHz. A motorized mechanical tuner can regulate the frequency

Content from this work may be used under the terms of the CC BY 3.0 licence (© 2015). Any distribution of this work must maintain attribution to the author(s), title of the work, publisher, and DOI.

ISBN: 978-3-95450-168-7 doi:10.18429/JACoW-IPAC2015-TUPWI005

PROTON IRRADIATIONS OF MICRO-TOM RED HAIRY ROOTS TO MIMIC SPACE CONDITIONS

M. Vadrucci, G. Bazzano, L. Picardi, P. Nenzi, C. Ronsivalle, V. Surrenti,
ENEA Radiation Sources Laboratory, Research Center Frascati, Rome, Italy
E. Benvenuto, A. Desiderio, S. Massa, C. Snels, M.E. Villani,
ENEA, Biotechnology Laboratory, Research Center Casaccia, Rome, Italy
F. Ambrosini, Sapienza University of Roma - DIET, Rome, Italy

Abstract

The purpose of the BIOxTREME project, launched by ENEA (Italian National Agency for New Technologies, Energy and Sustainable Economic Development) and funded by ASI (Italian Space Agency), is to formulate new biological drugs having a stimulant activity on the immune system, finalizing the production for a "ready to use" resource in Bioregenerative Life Support Systems (BLSSs) for space missions intended for long-term duration, in deep space, and with multiple crews.

One of the project tasks is to study the effects of physical insults on plants, trying to simulate cosmic environment on the production platforms exposing biological material to ionizing radiation, static magnetic fields and microgravity.

In order to examine the biological effects, to test plant radio-resistance and to build dose-response curves we carried out proton irradiations of anthocyanin rich (red) "hairy roots" derived from the tomato cultivar Micro-Tom with different proton energies for several doses with the TOP-IMPLART accelerator at the ENEA Frascati Research center.

The biological samples were placed in a holder specially made in a movable real-time monitoring chamber calibrated in dose. The fluence-homogeneity measurements over the sample and the calibration of the monitoring system were performed using GafChromic EBT3 films, placed in air in the same position as the biological samples to be irradiated. The present paper describes the experimental set-up and reports the preliminary results.

THE BIOXTREME PROGRAM

Plants can be considered as natural 'bioreactors' for the production of bioactive molecules (e.g. amino acids, vitamins, pigments, antioxidants, complex carbohydrates, proteins, etc.) and biotechnological drugs also including adjuvants or immuno-stimulating molecules.

An important field of interest is the farming of plants in extreme conditions such as those found in the aerospace environment: the prospect of breeding plants in the Space is an essential requirement for long-duration exploratory-class manned missions because they would provide an important physical support as a resource ready for use in Bioregenerative Life Support Systems (BLSS).

The International Space Station and its crew in Space are subjected to galactic cosmic rays (GCR) and solar particle events (SPE). The GCR spectrum is composed primarily of high-energy protons and atomic nuclei, namely about 87% high energy protons, 12% alpha-particles and 1% heavier ions up to iron (HZE) instead SPE consist of low to medium energy protons and alpha-particles. Numerous Space flight and ground-based experiments have been performed to study the biological effects of cosmic radiation on humans in the perspective of manned space missions.

In 2014 ASI has funded the ENEA-project BIOxTREME (BIO-plant factories for the formulation of bioactive molecules endowed with microbicidal, immunostimulating and antioxidant activity, for life in extreme conditions) which aims to formulate new drugs for the astronauts involved in long-term space missions. One of the key features of these drugs is that they have to induce stimulating activity on the immune system through the optimization of the production of natural antioxidants present in plants [1].

The BIOxTREME project is devoted to simulate cosmic conditions exposing plant samples in proton beams, gamma rays, static magnetic fields and microgravity. One of the experimental objectives of the Biotechnology Laboratory at ENEA is the study of alterations in the normal physiology of the living plants in such extreme conditions by profiling biological effects according to "SYSTEM BIOLOGY" technologies, such as proteomics.

In the framework of this program, irradiation of red Micro-Tomato (Micro-Tom) "hairy roots" was carried out with low energy proton beams extracted from the TOP (Oncological Therapy with Protons)-IMPLART (Intensity Modulated Proton Linear Accelerator for RadioTherapy) linear accelerator in operation at ENEA Radiation Sources Laboratory [2].

MICRO-TOM 'RED' "HAIRY ROOTS"

Micro-Tom has been considered the best choice for use in BLSS during human spaceflights. It is a Tomato cultivar (*Solanum lycopersicum*) originally created for ornamental purposes [3] and further widely used as a model species in several studies that defined in detail of the genetic and physiological makeup of this plant. The dwarf phenotype (plant height= 15 cm approx.) is undoubtedly an advantage for growing in small spaces. The miniaturization was obtained by introducing three recessive mutations in the genetic background of tomato

Content from this work may be used under the terms of the CC BY 3.0 licence (© 2015). Any distribution of this work must maintain attribution to the author(s), title of the work, publisher, and DOI.

ISBN: 978-3-95450-168-7 doi:10.18429/JACoW-IPAC2015-TUPWI006

HOW KNOWLEDGE AND TECHNOLOGICAL TRANSFER CAN DEVELOP INTO AN INDUSTRIAL REALITY: KYMA SRL CASE HISTORY

Raffaella Geometrante, Kyma S.r.l., Trieste, Italy
Mauro Zambelli, Kyma S.r.l., Trieste, Italy

Abstract

Kyma was established in 2007 as a spin-off company of Elettra-Sincrotrone Trieste, to design, realize and install all the 18 undulators of FERMI, the seeded FEL, at the time being built at the Elettra lab in Trieste, Italy. For Kyma establishment, Elettra-Sincrotrone Trieste formally transferred to the new company know-how and references relevant to Insertion Devices and, by a Knowledge Transfer monetarily evaluated, could participate to Kyma capital owning the 51% of the shares. In few years, Kyma became a well-known organization in the light source community. After more than forty Insertion Devices and sixty phase shifters designed and manufactured, Kyma is now recognized as a qualified partner for design and development of this kind of equipment. Some examples of Kyma industrial achievements in developing skills, knowledge, technologies methods of manufacturing transferred by Universities and Institution, will be presented. An example out of many: the joint effort between Kyma and Cornell University right now leading to the development of a new perspective into the ID world, i.e. the CHESS Compact Undulators (CCU).

ORIGIN AND STRUCTURE OF THE COMPANY

Kyma was established in August 2007 by Elettra - Sincrotrone Trieste S.C.p.A. (ST), with the primary purpose to design, realize and install the undulators for the FERMI@Elettra project, namely the new Free-Electron Laser, at the time being built at the ST site in Basovizza, Trieste, Italy.

The origin of Kyma relies on the 20-years experience of ST on the development, testing, installation and operation of insertion devices.

At the moment of the launch of the FERMI project a question about the possibility to start a spin-off company, fully devoted to the insertion devices design and manufacturing, was posed.

After a feasibility study during the year 2006 a European tender was launched to find possible suppliers of mechanical, magnetic and control subsystems for the realization of eighteen undulators for the FERMI@Elettra project.

In the tender a clause was included that the proponent(s) had to supply the undulators not directly, but through a new company to be set up together with Elettra - Sincrotrone Trieste.

The tender procedure was completed in spring 2007 and the new company was formally established in August of the same year.

Kyma is located in the Sincrotrone Trieste site in Basovizza, Trieste, an aerial view of which is shown in figure 1, where the FERMI@Elettra facility can be seen in the forefront.

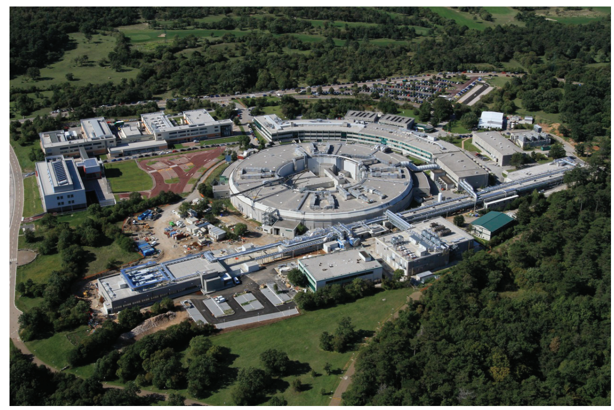

Figure 1: The Elettra site with the FERMI@Elettra Free-Electron Laser facility in the forefront.

Know-how and References

At the moment of the establishment of Kyma Srl, Elettra - Sincrotrone Trieste formally transferred to the new company all the know-how and the references relevant to insertion devices.

In fact the capital of the company was formed by 51% of shares as intangible assets supplied by Elettra - Sincrotrone Trieste and 49% of liquid capital supplied by the partners.

As a consequence of this approach, all the references of Elettra - Sincrotrone Trieste on insertion devices are now formally owned by Kyma Srl.

In this way, more than twenty years experience in design, assembling, characterization and operation of insertion devices at Elettra - Sincrotrone Trieste, meets now the manufacturing capabilities of the industrial partners, to build up a world-class company for insertion devices realization (see Fig. 2).

Content from this work may be used under the terms of the CC BY 3.0 licence (© 2015). Any distribution of this work must maintain attribution to the author(s), title of the work, publisher, and DOI.

ISBN: 978-3-95450-168-7 doi:10.18429/JACoW-IPAC2015-TUPWI007

Content from this work may be used under the terms of the CC BY 3.0 licence (© 2015). Any distribution of this work must maintain attribution to the author(s), title of the work, publisher, and DOI.

ALGORITHM OF RECONSTRUCTING PARTICLE DISTRIBUTION IN N-DIMENSIONAL PHASE SPACE FROM PROFILE IN BEAM TRANSPORT

T. Aoki#, Research & Development Group, Hitachi, Ltd., Hitachi, Japan

Abstract

A new method of reconstructing particle distribution from measured profile in beam transport is proposed. In this method, particle distribution in arbitrary dimensional phase space can be reconstructed from profiles in transport system. The particle distribution is obtained by solving a following equation: $I=D\rho$, where I is a counted number of particles at a single channel of the profile monitor, D is a matrix representing relation between I and ρ, and ρ is number of particles included in a single n-dimensional voxel of phase space at start point of the beam transport. We succeeded formulation of matrix D from transportation matrix of the beam transport R, and discovered that D is formulated as piecewise-polynomials of elements of R. We show details of the formulation of D and results of simulations of reconstruction of particle distribution in phase space by this method.

INTRODUCTION

Purpose of this study is to propose a new method of reconstructing particle distribution in phase space. In particle beam therapy, it is demanded to deliver a narrow beam to isocenter in order to realize conformal irradiation. To realize the narrow beam size at isocenter, a tuning of high energy beam transport (HEBT) system and measurement of beam is important. Conventionally, Quadrupole scan method [1] is applied for measurement in HEBT system. Quadrupole scan method is effective when particle distribution in phase space is Gaussian, and we can measure emittance ε, twiss parameters α and β. However, the particle distribution is not Gaussian, it is required that not only measurement of these parameters but also particle distribution in phase space is required. Because the beam energy is larger than 70MeV/u in HEBT, the slit scan method is not applicable for the measurement. Therefore we adopt the new method that improved phase space tomography method [2]. By this phase space tomography method, transverse phase space (x, x') and (y, y') distribution. However in beam tuning in particle therapy, the information about dispersion is need. In this study, we propose the new method which realizes a measurement of particle distribution in arbitrary dimensional phase space.

THEORY

Let $\rho(\boldsymbol{x}; z)$ be the distribution of the particle in phase space at the beam line position z. The phase space coordinates $\boldsymbol{x}$ are (x, x', y, y', s, δ). x and y are spatial transvers displacements from design orbit. δ is momentum displacement $\Delta p/p$. s is longitudinal displacement from beam centroid. x' and y' are dx/dz and dy/dz respectively. To obtain the distribution at specified point z_0 in HEBT, we measure the number of particles in small voxel of phase space from measured profile in HEBT. We define ρ_i as number of particles in ith voxel in phase space, I_{x_j} as number of particles counted in the jth channel of profile monitor at $x=x_j$. Assuming the distribution in the single voxel is flat, a relation of ρ_i and I_{x_j} become

$$I_{x_j} = \sum_{k=1}^{n} \int_{x_j-\frac{w}{2}}^{x_j+\frac{w}{2}} \phi_k(x) \cdot \rho_k \mathrm{d}x \tag{1}$$

where w is width of profile monitor channel, and $\phi_k(x)$ is projected volume of kth phase space voxel on x-axis. Assembling this relation, we get a equation

$$\boldsymbol{I} \stackrel{\text{def}}{=} \begin{pmatrix} I_1 \\ \vdots \\ I_m \end{pmatrix} = \boldsymbol{D} \begin{pmatrix} \rho_1 \\ \vdots \\ \rho_k \end{pmatrix} \stackrel{\text{def}}{=} \boldsymbol{D\rho} \tag{2}$$

where $\boldsymbol{D}$ is defined as

$$\boldsymbol{D} = \left(d_{ij}\right)_{\substack{1\le i\le k \\ 1\le j\le m}} \tag{3}$$

and

$$d_{ij} = \int_{x_j-\frac{w}{2}}^{x_j+\frac{w}{2}} \phi_i(x) \mathrm{d}x. \tag{4}$$

Therefore, we can obtain the particle distribution ρ by solving the eq.(2). To solve the eq.(2), it is required that the formula for projected volume $\phi_i(x)$ and enough number of measurement of profiles.

Derivation formula for Projected Volume

We derive the formula for projected volume of a N-dimensional parallelepiped constructed by N vectors $\boldsymbol{a}_1$, $\boldsymbol{a}_2$... $\boldsymbol{a}_N$. in this section. At first, In the case of N=1, it is clear that

$$\phi^{(1)}(x) = \frac{1}{c_1} \mathrm{rect}\left(\frac{x - x_\mathrm{c}}{c_1 a_1}\right) \tag{5}$$

where c_1 is a cosine of the angle between $\boldsymbol{a}_1$ and x-coordinate, a_1 a length of $\boldsymbol{a}_1$, x_c is a x-coordinate of centroid of the voxel, and rect(x) is the rectangular function defined as

$$\mathrm{rect}(x) \stackrel{\text{def}}{=} \begin{cases} 0, \text{if } |x| < \frac{1}{2} \\ 1, \text{if } |x| \ge \frac{1}{2} \end{cases} \tag{6}$$

Figure1 shows this situation. The 1 dimensional voxel is a segment of line in phase space. So, the projected volume is a rectangular function.

#takamichi.aoki.my@hitachi.com

ISBN: 978-3-95450-168-7 doi:10.18429/JACoW-IPAC2015-TUPWI008

RF GUN BASED ULTRAFAST ELECTRON MICROSCOPY*

J. Yang#, K. Kan, T. Kondoh, Y. Yoshida, ISIR, Osaka Universiry, Osaka, Japan
J. Urakawa, KEK, Tsukuba, Japan

Abstract

Ultrafast electron microscopy (UEM) would be a powerful tool for the direct visualization of structural dynamic processes in matter. The resolutions of the observation on femtosecond time scales over sub-nanometer (even atomic) spatial dimensions have long been a goal in science. To achieve such resolutions, we have designed and constructed a femtosecond time-resolved relativistic-energy electron microscopy using a photocathode radio-frequency (RF) electron gun (RF based UEM). The RF gun has successfully generated a high-brightness electron beam with bunch length of 100 fs and emittance of near 0.2 mm-mrad, which are essential beam parameters for the achievement of nm-fs space-time resolution in the microscopy. Both the static measurements of both relativistic-energy electron diffraction and image have been succeeded. In this presentation, the activities on RF based UEM are introduced. The requirements and limitations of the beam parameters are reviewed. The concept and design of RF based UEM are reported. Finally, some demonstrations of the relativistic-energy UEM images are reported.

INTRODUCTION

Transmission electron microscopy (TEM) is a powerful tool to observe directly the image from specimen with high spatial resolution. When coupled with time resolution, it, which also called ultrafast electron microscopy (UEM), would be the strongest tool for the study of ultrafast dynamics in materials. Currently, the UEM with the time-spatial resolution of nanosecond and nanometer has been achieved in conventional TEM through the use of photo-activated electron source driven by a nanosecond laser in the non-space-charge-limited regime with ns-long pulse length. A large number of important phenomena, i.e. phase transformations, melting, re-solidification, nucleation and growth of damage in nanosecond time region, have been investigated. To achieve a high time resolution overcoming the space-charge limitation, we have proposed and designed a femtosecond time-resolved relativistic-energy electron microscopy using a photocathode radio-frequency (RF) electron gun. In 2009 [1,2], we have developed a RF gun to generate a low-emittance femtosecond-bunch electron beam: 100 fs and 0.1 mm-mrad, which are essential for the achievement of nm-fs space-time resolution in future. In 2010, we constructed successfully an instrument of ultrafast relativistic-energy electron diffraction (UED) using the RF gun [3-5]. The time resolution of 100 fs has been achieved. In 2012, a first prototype of RF gun based relativistic-energy TEM (which is called *rf-UEM*) has been constructed at Osaka University [6,7]. The resolutions of 1 nm and 100 fs in spatial and temporal respectively will be challenged. In 2014, a new RF gun with the highest repetition rate of 1 kHz was designed and produced to generate a further low-emittance and low-energy-spread electron beam in *rf-UEM*. Both the static measurements of relativistic-energy electron diffraction and image have been succeeded in the prototype. In this poster, the activities on UED and UEM are introduced. The concept and design of the new RF gun and the prototype of RF gun based relativistic-energy electron microscopy are reported. The beam dynamics and challenges in femtosecond RF gun will be discussed. Finally, some demonstrations of the relativistic-energy TEM images, the single-shot and time-resolved UED measurements are reported.

* Work supported by a Basic Research (A) (Grant No. 26246026) of Grant-in-Aid for Scientific Research from MEXT, Japan.
#yang@sanken.osaka-u.ac.jp

1 kHz NORMAL CONDUCTING RF GUN

To achieve the aim resolutions of 1 nm and 100 fs in spatial and temporal, an electron source in *rf-UEM* has to be able to generate a low emittance and low energy spread beam, such as 0.1 mm-mrad for the normalized emittance and 10^{-4} or 10^{-5} for the energy spread. In addition, low dark current and ultrahigh stabilities on charge and energy are also required. For these reasons, we have designed and fabricated a new structure RF gun with following optimum considerations and improvements:

- New shapes of the structures in both the RF cavity wall and the iris between the half cell and the full cell are designed near to the ideal contour to reduce the nonlinear electric fields. A large aperture of the iris was used to reduce the electric field on the cavity surface and to reduce both the transverse emittance and energy spread.
- The conventional laser injection ports in the half cell were removed for good field symmetry. A new insertion function of the photocathode in the cathode plate was designed. It will be used to develop a transmission photocathode to generate a further low thermal emittance beam from the RF gun.
- New wall-structural turners were designed in the half and full cells to adjust precisely the field balance.
- The field emission due to the strong electric field between the cathode plate and the half-cell cavity is the biggest problem in old type RF gun. In the new RF gun, the cathode plate was blazed on the half-cell cavity without the use of the helicon flex vacuum shield. The dark current from the new gun was greatly suppressed to <0.01 pC/pulse. The

Content from this work may be used under the terms of the CC BY 3.0 licence (© 2015). Any distribution of this work must maintain attribution to the author(s), title of the work, publisher, and DOI.

ISBN: 978-3-95450-168-7 doi:10.18429/JACoW-IPAC2015-TUPWI009

DEVELOPMENT OF UN-DESTRUCTIVE INSPECTION SYSTEM FOR LARGE CONCRETE INFRASTRUCTURE BY USING ACCELERATOR BASED COMPACT NEUTRON SOURCE*

A. Taketani[1#], Y. Seki[1], H. Ohta[1], T. Hashiguchi[1], S. Yanagimachi[1], Y. Otake[1], Y. Yamagata[1], Y.Ikeda[1], H. Baba[1], [1]RIKEN, Wako, 351-0198, Japan
S. Wang[1,2], Q. Jia[2,1], G. Hu[2,1], [2]XI'AN Jiaotong university, Xi'an, 710049, China
K. Hirota[3,1], [3]Nagoya university, Nagoya, 464-8601, Japan
S. Tanaka[4], [4]IPNS, KEK, 305-0801, Japan
K. Kino[5], [5]Hokkaido university, Sapporo, 060-0808, Japan

Abstract

Aged large concrete structure, such as highways, bridges and boating docks, need to be inspected by un-destructive method in order to determine whether maintenance or rebuild. If maintenance work is appropriate, diagnosis will be needed. We have been developing un-destructive inspection system by using fast neutron which can penetrate thick concrete. Fast neutron detector is developed with plastic scintillator and semiconductor photon sensors. It can identify 16mmϕ steel rod through 300mm thick concrete. After prototyping detector experiments, new large area detector are designed and build.

INTRODUCTION

In Japan, many bridges were built in 1960 to 1970's, when Japanese economy had been expanded rapidly. So they will become end of life in next a few decades. However society will not able to rebuild all of them by budget limitation. It is urgent needs to develop and establish a method to investigate with un-destructive way.

Thirty nine percent of the bridges of Japan, which are longer than 15m, are built by pre-stressed concrete (PC) construction method [1]. It is combination of high tensile strength of steel and concrete's great compressive strength. Solid duct is inserted in the concrete structure. Steel rods or wires are put in the duct with pre-tension. Then the duct is filled by the concrete. However it has been known that techniques in 60's and 70's could not guarantee the duct was filled without void. Rain water can penetrate into voids in the duct through cracks in the concrete structure and make corrosions on the steel. Hence the steel rods or wires degrade their strength. As result, the structure may fall down. Thus it is important to investigate gap in the concrete and size of the steel rods or wires. The typical size of the duct is about 3cm diameter. Therefore our target is 3cm imaging resolution.

Fast Neutron

The absorption cross section of fast neutron, which energy is around 1MeV, is order of 1 barn (10^{-24}cm^2) against to major elements of concrete, oxygen, aluminium and silicon [2]. For X-ray case, it is order of 1000 barn [3]. Neutron has much higher penetration power for concrete structure. It is suitable to obtain transmission image.

Needs to Develop

The requirements, which are needed to establish fast neutron imaging system, are (1) transportable neutron source, (2) 2D fast neutron detector, and (3) image processing which can reconstruct as 3D view of the inside of concrete structure. Fig.1 shows final goal of the project. A neutron source is mounted on an automobile with a target station. Fast neutron is emitted to downward. Thus bridge floor is exposed to the fast neutron. Transmitted neutrons are detected underneath of the bridge by 2D fast neutron detector, which is attached to a swing arm.

By the Japanese law of concerning the prevention from the hazards due to radiation and others [4], it is allowed to operate transportable accelerator with less than 4MeV out of doors for un-destructive inspection of bridges.

Figure 1: Transportable neutron source and 2D fast neutron detector.

In this paper, we report about a prototype of 2D fast neutron detector, which was tested with accelerator-based compact neutron source.

Because the detector will be used out of doors, stable operation with mechanical movement, temperature and humidity excursion, and low power consumption are required. By the above technical reasons, combination of plastic scintillator and semiconductor photon sensor is chosen.

#taketani@riken.jp

Content from this work may be used under the terms of the CC BY 3.0 licence (© 2015). Any distribution of this work must maintain attribution to the author(s), title of the work, publisher, and DOI.

ISBN: 978-3-95450-168-7 doi:10.18429/JACoW-IPAC2015-TUPWI010

DEVELOPMENT OF A PULSE RADIOLYSIS SYSTEM BY ULTRA-FAST SUPER CONTINUUM PROBE LIGHT AT WASEDA UNIVERSITY*

Y. Ito†, Y. Soeta, Y. Hosaka, K. Sakaue, M. Washio, Waseda University, Tokyo, Japan

Abstract

We have been studying the pulse radiolysis using photo-cathode rf gun at Waseda Univ. Pulse radiolysis is one of the powerful methods to trace early chemical reactions by ionizing radiation. In pulse radiolysis, the probe light absorption, which produced by active species formed by electron beam of rf gun, is measured at each wavelength and made possible to trace reactions. Therefore, we have used the super continuum (SC) light for the probe light. The SC light has a broad spectrum and is generated by nonlinear optical effect caused by injecting picosecond laser to photonic crystal fiber (PCF). However, the resulting SC light was unstable because its peak intensity was not enough. We need to use a femtosecond pulsed laser which is expected to be stronger peak intensity than a picosecond laser. We have developed a mode-locked Yb-doped fiber laser based on Non-Linear Polarization Rotation as a femtosecond pulsed laser and the chirped pulse amplification system which will be able to amplify the femtosecond pulse. In this conference, we will report the performance of the SC light using this fiber laser system, recent results of pulse radiolysis experiments and the future plans.

INTRODUCTION

The photo-cathode rf gun has been developed at Waseda University, and pulse radiolysis has been studied as application of electron beam obtained by photo -cathode rf gun. In pulse radiolysis, the probe light absorption, which produced by active species formed by electron beam of rf gun, is measured at each wavelength and made possible to trace reactions. When we measure the lifetime of the target transient active species, temporal resolution of pulse radiolysis is determined mainly by the pulse width of electron beam and probe light. Probe light is required to be pulsed light with high intensity, good stability and broad spectrum. On these backgrounds, we have started to study SC light based on PCF for the probe light.

SUPER CONTINUUM (SC) LIGHT WITH PHOTONIC CRYSTAL FIBRT (PCF)

The SC light with PCF is a new technique of pulsed white light generation. Figure 1 (left) shows the cross-sectional micrograph of PCF. PCF is the optical fiber which is made of silica glass and clad has many micro air holes. The refractive index difference between core and clad become higher by these holes. It can realize the small core area of PCF and contributes to enhance the nonlinear optical effect. The SC light has a broad spectrum and is generated by nonlinear optical effect caused by the high peak intensity of pulsed laser in PCF. The spectrum of SC light previously generated by picosecond pulsed laser (4ps) is shown in Fig. 1 (right). It is clear that the SC light has enough spectral bandwidth, however, the resulting SC light was unstable because the peak intensity was not enough. Thus we started to use a femtosecond pulsed laser which is expected to be stronger peak intensity than a picosecond laser. We have developed a mode-locked Yb-doped fiber laser based on Non-Linear Polarization Rotation as a femtosecond pulsed laser. [1]

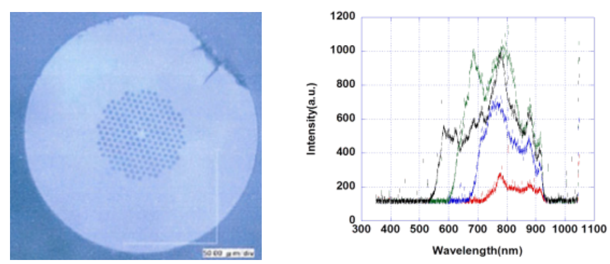

Figure 1: Cross-sectional micrograph of PCF (left) and the spectrum of SC (right).

Yb-DOPED FIBER

We have developed a fiber laser oscillator for injecting to PCF based on Yb-doped fiber as gain medium. Yb is one of the rare-earth elements and Yb-doped fiber is a fiber which is doped $Yb^{3+}$to the core. The energy level of Yb^{3+} has a simple structure compared with Er^{3+}, Nd^{3+}, and it is possible to ignore the excited state absorption, therefore excitation efficiency of Yb^{3+} is higher than the others. Yb-doped fibers make exceptional sources in the 1.0 – 1.1 μm wavelength range because of an excellent power conversion efficiency of over 80% and a broad tunability over several tens of nanometers. [2]

NONLINEAR POLARIZATION ROTATION (NPR)

Using Nonlinear Polarization Rotation as mode-locking method, we generate a pulsed laser. The NPR is one of the passive mode-locking methods. Figure 2 shows a mechanism of NPR mode-locking. In the fiber, a nonlinear optical effect tends to occur because a laser peak power becomes higher to the long interaction length and small core diameter of the fiber. In the passive mode-locked fiber laser, NPR with polarizer is commonly employed as a saturable absorber. When injecting linear polarized light to the fiber, phase difference is generated by difference of polarization intensity and a linear

* Work supported by NEDO (New Energy and Industrial Technology Development Organization).
# y-ito-0102-4758@fuji.waseda.jp

Content from this work may be used under the terms of the CC BY 3.0 licence (© 2015). Any distribution of this work must maintain attribution to the author(s), title of the work, publisher, and DOI.

ISBN: 978-3-95450-168-7 doi:10.18429/JACoW-IPAC2015-TUPWI014

Content from this work may be used under the terms of the CC BY 3.0 licence (© 2015). Any distribution of this work must maintain attribution to the author(s), title of the work, publisher, and DOI.

DESIGN OF A SUPERCONDUCTING GANTRY FOR PROTONS

Cristian Bontoiu*, Jose Sanchez-Segovia, FABIS, Spain
Rafael Berjillos, Javier Perez Bermejo, TTI, Spain
Ismael Martel, Univ. of Huelva, Spain

Abstract

The last decade brought much interest in proton therapy within the medical and accelerator communities. Using normal conducting technology, the high-energy beams required can be handled only with large and heavy magnets which causes prohibitive costs. While lattice design work on a superconducting gantry has been carried out for a decade [1] there is yet no practical implementation. The University of Huelva in collaboration with the Andalusian Foundation for Health Research (FABIS) is currently involved in developing and assembling a prototype for a compact superconducting proton gantry [2]. Magnet design and performance is described along with beam dynamics results for the main gantry arcs and for the final spot scanning system using realistic magnetic field maps thoroughly.

INTRODUCTION

The gantry should operate within as much as possible of the medically relevant energy range 100 MeV to 250 MeV delivering proton bunches of about 1 mm rms transverse size with a beam divergence within 2 mrad. Due to space limitations its optical lattice can be made of combined-function magnets which both bend and focus the beam. Tumour scanning in depth involves change of the beam energy which is quicker than the jumps of current intensity allowed by the superconducting magnets and therefore the lattice must hold beams of variable energies at fixed field. The current lattice is composed of 36 magnets installed on two arcs of 2.5 m radius as shown in Fig. 1.

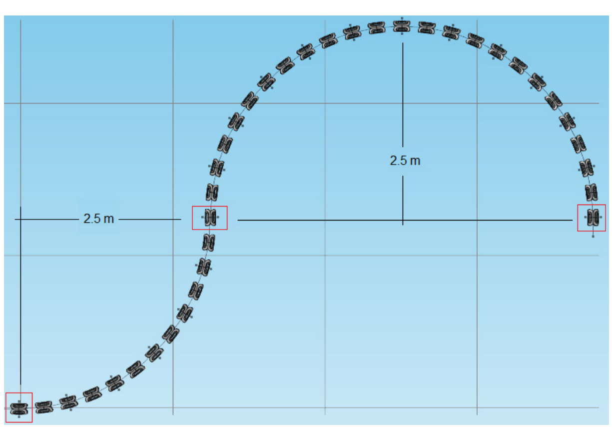

Figure 1: A lattice made of 36 combined-function magnets with the bending radius of 2.5 m.

MAGNET DESIGN

Successful operation of SC magnets in large scale projects like the LHC, has motivated and inspired the development of a simplified version of combined-function magnets using bent cos-θ dipole and quadrupole coils. They consists of one layer of quadrupole coils installed on the top of one layer of dipole coils, both layers spanning about 3.5° axially. Numerical modelling has been achieved in Comsol [3] resulting in three-dimensional magnetic field maps overlapped, scaled and used for particle tracking studies.

Dipole Coils

The dipole coils have been designed using three 1 cm thick coil blocks whose azimuthal distribution minimizes the b_3, b_5, b_7, b_9, b_{11} multipoles as described in [4]. A view is shown in Fig. 2 with the inner radius set at 5 cm.

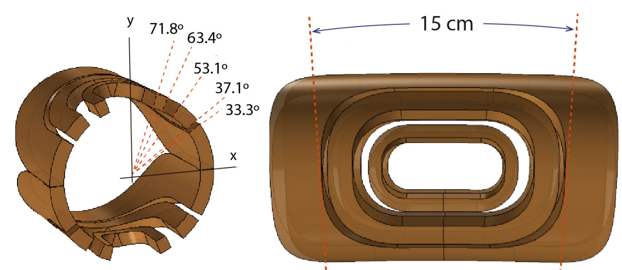

Figure 2: Three-dimensional layout of the SC dipole coils.

The dipole magnetic field is highly homogeneous, as it can be seen across the transverse cross-section in Fig. 3. A current density of about 350 A/mm^2 is required to handle proton beams of 250 MeV.

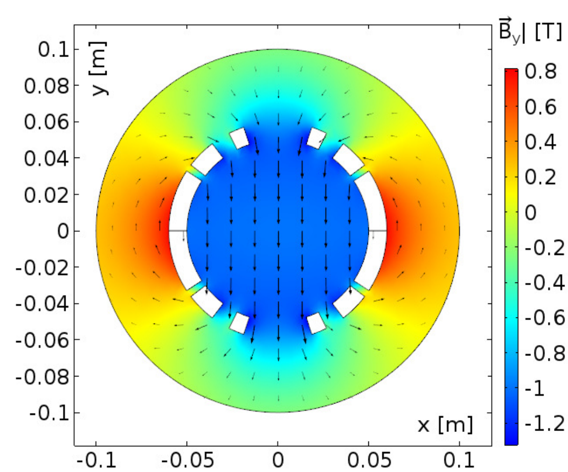

Figure 3: Dipole magnetic field distribution within the transverse cross-section plane.

* cbontoiu@gmail.com

ISBN: 978-3-95450-168-7 doi:10.18429/JACoW-IPAC2015-TUPWI015

EXPERIENCE ON SERIAL PRODUCTION OF THE QUADRUPOLE MOVERS WITH SUBMICROMETRIC REPEATABILITY FOR THE EUROPEAN XFEL*

J.Munilla#, J.Calero, L.García-Tabarés, A.Guirao, J.L.Gutiérrez, T.Martínez, E.Molina Marinas, F.Toral, C.Vázquez, CIEMAT, 28040, Spain
C. Martins, E. Ramiro, F. Ramiro, RAMEM, 28027, Spain
J.A. Gorrotxategi, B.Junkera, M.Tarragual, A.Urzainki, HTS/ZEHATZ, 20850, Spain

Abstract

CIEMAT is in charge of the design and manufacturing of the quadrupole movers with submicrometric repeatability for the XFEL.EU intersections. Prototyping of these precision devices was successful but manufacturing them in a serial production scheme (101 units) implies some changes at design, fabrication procedures and quality controls. This paper will present some of the main problems and solutions adopted to transform a prototype made at a research facility into a serial production at a conventional industrial company. Also, it describes the inspection and tests, the quality controls and reporting procedures. All the devices have been validated and recepted. This paper describes the adopted procedure and the performance of the serial units.

INTRODUCTION

Quadrupole Movers (QM) for the European XFEL [1] will be installed in the intersections between each pair of undulators. CIEMAT is fully responsible for the conceptual and engineering designs. 95 units are part of the Spanish in-kind contribution and 6 additional units were ordered by DESY.

During the research and development stage, three prototypes have been built from 2009 to 2012 [2]. In the last one, some design changes have been included to optimize serialized production and reduce costs at industry. XFEL-EU has given final acceptance on the prototype and technical specification for serial production in 2012. The production of the QMs has been split in two bunches to reduce risks, in special with the tight schedule. CIEMAT allocated two contracts for half of the serial production each one in 2013. Spanish companies RAMEM and HTS/ZEHATZ were awarded with the contracts.

FUNCTIONAL REQUIREMENTS

The complete list of parameters of the XFEL quadrupole movers has been published elsewhere [2]. Submicrometric repeatability for movements in 2 axes (horizontal and vertical) is the most challenging one. The vertical load to withstand is 75 kg, while small lateral forces are admissible (about 10 N).

In order to achieve a compact design, a wedged configuration was chosen for the vertical movement. Both axes include a high precision linear actuator and a closed-loop control system fed by two LVDT sensors. Precision adjustable limit switches and hard stops are needed to maximize quadrupole travel length without interference with the beam pipe.

All the QMs adjustments must be measured and reported. This information will allow parametric control and calibration for the intersection control system. Moreover, all the QMs should be interchangeable apart of these parameters.

QUALITY AND DOCUMENTATION REQUIREMENTS

The main objective of the quality assurance system is to guarantee the achievement of the technical specifications. Both manufacturers have created and maintained a quality management system (QMS) according to UNE-EN ISO 9001 and UNE-EN-9100 standards.

Also, to ensure quality and integrity of units from first manufacture steps to final reception at XFEL facilities, CIEMAT has designed a procedure based on three reports for each unit:

1. Manufacture Report includes materials and components certificates and metrology reports in order to ensure traceability. It is intended for internal use to prevent malfunctions or potential problems before assembling and testing.
2. Validation Report includes final repeatability test results, adjusting parameters and the verification of accomplishment for all specifications before delivery. This is uploaded to XFEL.EU document management system (EDMS) for future references. This report is made by manufacturer.
3. Reception Reports include additional verifications and tests after delivery. This report is done by CIEMAT as cross-check and it is also uploaded to EDMS. Any possible deviation or problem during transportation can be detected.

In addition to documentation explained above, special procedures have been stablished:

- An accessible code is permanently engraved onto each part in an area that does not affect its operation or the engineering tolerances. At the same time, it

*This work is partially supported by the Spanish Ministry of Science and Innovation under SEI Resolution on 17-September-2009 and Project ref. AIC10-A-000524
#javier.munilla@ciemat.es

Content from this work may be used under the terms of the CC BY 3.0 licence (© 2015). Any distribution of this work must maintain attribution to the author(s), title of the work, publisher, and DOI.

ISBN: 978-3-95450-168-7 doi:10.18429/JACoW-IPAC2015-TUPWI016

GANTRY 3: FURTHER DEVELOPMENT OF THE PSI PROSCAN PROTON THERAPY FACILITY

A. Koschik*, C. Bula, J. Duppich, A. Gerbershagen, M. Grossmann, J.M. Schippers, J. Welte
PSI, Paul Scherrer Institut, 5232 Villigen, Switzerland

Abstract

PSI and its Center for Proton Therapy (CPT) is extending its research capabilities in the field of proton therapy and pencil beam scanning technology. Gantry 3 will be an additional treatment room at the PROSCAN facility at PSI, Villigen, Switzerland. It will feature a 360° scanning Gantry delivered by Varian Medical Systems. The Gantry design is based on Varian technology, which will be combined with advanced PSI active scanning technology.

The further development of fast energy switching as well as precise spot and continuous line scanning irradiation modes are main research topics at the PROSCAN facility. A major challenge with Gantry 3 is the link of the existing PSI PROSCAN system with the Varian ProBeam system, while retaining the system integrity and high performance level. Additionally, Gantry 3 will be installed and commissioned while keeping the other treatment rooms (Gantry 1, Gantry 2, Optis 2) in full operation.

The current development and project status is presented.

INTRODUCTION

PSI has a long-standing successful history in the development and application of irradiation technologies for treatment of cancer. With the inauguration of Gantry 1 in 1996 [1], PSI has pioneered the irradiation technique using actively scanned pencil proton beams. In 2007 the world's first 250 MeV superconducting cyclotron for proton therapy COMET was installed at PSI's PROSCAN facility [2].

Spot scanning, the proton-dose delivery technique developed at PSI is being further developed for fast re-painting and precise spot scanning on Gantry 2 [3] which is treating patients since 2013. The Optis 2 irradiation room allowing for accurate treatments of eye melanoma using passive scattering technology complements the PROSCAN facility.

PSI takes a further step by extending the research and treatment capabilities with an additional Gantry treatment room sponsored by the Swiss Canton of Zurich. Gantry 3 is realized in collaboration with Varian Medical Systems (VMS), which continues the fruitful research collaboration with Varian that has led to the development of the superconducting cyclotron COMET.

The main goal of the Gantry 3 project is to realize an additional scanning Gantry by 2016 with performance and capabilities comparable to PSI Gantry 2.

Figure 1 shows the layout of the PROSCAN facility with the cyclotron and the beam lines delivering the proton beam to the treatment areas Gantry 1, Gantry 2, Optis 2 and the new area Gantry 3. The new Gantry 3 will be installed behind a newly built extension of the existing fixed beam line for experiments.

PROSCAN BEAMLINE

Extracted beams from COMET are focused on a degrader, which can decrease the energy of the proton beams to the patient to any value in the range of 70 − 230 MeV. The degrader is followed by collimators and an energy selection system to obtain a well-defined beam emittance (max.30π mm mrad), and a maximum beam momentum spread of ±1.0%.

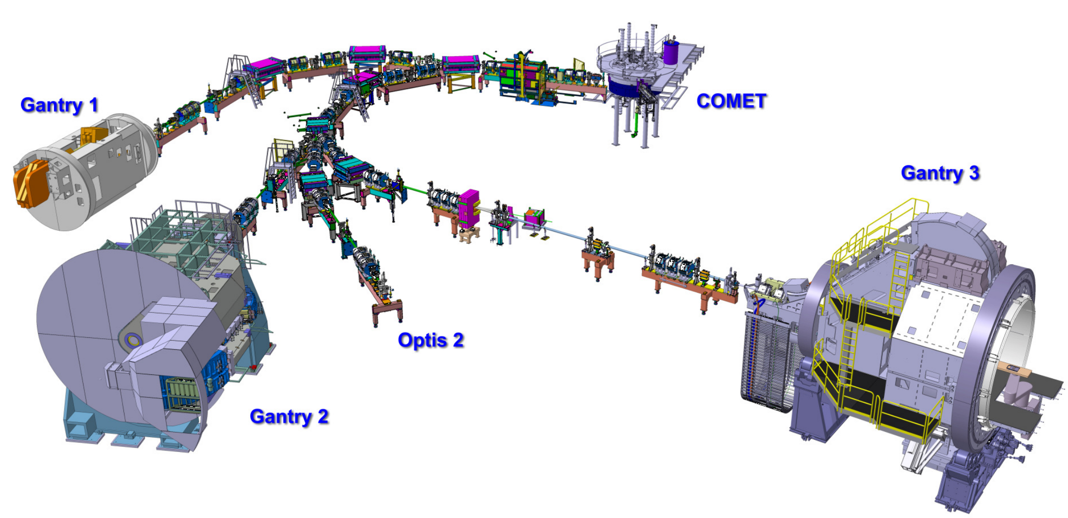

Figure 1: Layout of the PROSCAN facility beam lines including the new Gantry 3 area.

* alexander.koschik@psi.ch

Content from this work may be used under the terms of the CC BY 3.0 licence (© 2015). Any distribution of this work must maintain attribution to the author(s), title of the work, publisher, and DOI.

ISBN: 978-3-95450-168-7 doi:10.18429/JACoW-IPAC2015-TUPWI017

Content from this work may be used under the terms of the CC BY 3.0 licence (© 2015). Any distribution of this work must maintain attribution to the author(s), title of the work, publisher, and DOI.

SINGLE-SHOT MULTI-MeV ULTRAFAST ELECTRON DIFFRACTION ON VELA AT DARESBURY LABORATORY

L.K. Rudge, S. Mathisen, P. Aden, R.J. Cash, J.A. Clarke, D.M.P. Holland, J.W. McKenzie, M.D. Roper, T.C.Q. Noakes, J. Jones, A. Kalinin, B.L. Militsyn, B.D. Muratori, D. Scott, F. Jackson, P. Williams, Y. Saveliev, D. Angal-Kalinin, M. Surman#, STFC ASTeC, Daresbury Laboratory, Daresbury, UK.
D.A. Wann, P.D. Lane, Dept. of Chemistry, University of York, York, UK.
J.G. Underwood, Dept. of Physics and Astronomy, UCL, London, UK.

Abstract

Accelerator-based Ultrafast Electron Diffraction (UED) is a technique for studying both static structure and sub-100 fs dynamic structural changes on the atomic scale. In this paper we present the first electron diffraction results, obtained in 2014, on the Versatile Electron Linear Accelerator (VELA) at Daresbury Laboratory. Diffraction patterns were observed with much less than 1 pC transported to the detection screen. Single-shot and multi-shot accumulated diffraction data are presented from single crystal and polycrystalline samples. Apertures of different sizes placed directly in front of the sample offer some control over the contamination due to dark current, but also reduce the charge contributing to the diffraction pattern. We discuss future developments for electron diffraction on VELA, including further beam optimisation, the measurement of bunch length with a newly installed Transverse Deflecting Cavity (TDC), and the plans for pump-probe studies.

INTRODUCTION

Structural science, particularly structural biology, is a major driver in the development of new light sources. However, many important materials such as membrane proteins and protein complexes cannot be crystalised into sufficiently large crystals for use in conventional X-ray diffraction arrangements and moreover, are often damaged by the beam before the data collection can be completed. A new approach is to use X-ray Free-Electron Lasers (FELs) to produce ultra-high intensity sub-100 fs X-ray pulses to allow single shot diffraction data to be recorded before the sample deteriorates, that is, the data collection is faster than the radiation damage. This approach is being pursued at SACLA [1] and LCLS [2]; for example LCLS have recently successfully carried out X-ray diffraction imaging of a giant Mimivirus [3].

Structural evolution on a time-scale comparable to that of the making and breaking of chemical bonds can also be studied with these high intensity X-ray FELs. Recently, ultrafast resonant soft X-ray diffraction experiments at LCLS allowed the optically stimulated changes of charge-density wave correlations in $YBa_2Cu_3O_{6.6}$ to be followed [4].

An attractive alternative approach to using X-ray FELs to study structural changes is ultrafast electron diffraction. Achieving the femtosecond time resolution needed to observe dynamic changes in molecules requires the use of multi-MeV electrons to reduce space charge effects that lengthen the bunch.

Electrons offer several advantages over X-rays for diffraction studies:

(1) Electrons have a Coulombic interaction with both the electrons and the nuclei of the target atom whilst X-rays only scatter from the electrons. Electrons thus have a scattering cross-section which is 4-6 orders of magnitude larger than that of X-rays.

(2) Electrons have a lower ratio of inelastic to elastic scattering cross-sections than do X-rays.

(3) Electrons deposit a lower energy into the target during inelastic collisions than do X-rays [5-7].

The net result is that electrons deposit three orders of magnitude less energy per useful scattering event than do X-rays, thereby reducing the damage done to the sample. While it is frequently argued that a 10 fs X-ray pulse will “beat” Coulomb explosion of the molecule, this may not be the case as the electron density from which X-rays are scattered is being disrupted on much faster (attosecond) timescales. In contrast, electrons scatter from the nuclei and so are much less susceptible to damage mechanisms which remove electron density. Ultrafast electron diffraction also has notable cost advantages over FELs for diffraction experiments since much smaller scale accelerators, such as VELA [8], can be used.

UED ON VELA

A description of the electron diffraction system on VELA has been presented elsewhere [9] where it was shown that, although sub-100 fs 1 pC bunches can be generated at the gun, the bunch length increases as the beam propagates along the accelerator. A schematic of the accelerator is shown in Fig. 1. For the electron diffraction experiments described in this article, VELA was operated at 4 MeV/c. Seven quadrupole magnets, located between the gun and the sample chamber, are used to shape the electron beam. The beam can be imaged on YAG screens at several places along the accelerator, including the sample position.

mark.surman@stfc.ac.uk

ISBN: 978-3-95450-168-7 doi:10.18429/JACoW-IPAC2015-TUPWI019

NEUTRON SHIELDING OPTIMIZATION STUDIES

Adriana Bungau, Roger Barlow, University of Huddersfield, Huddersfield, UK
Michael Shaevitz, Columbia University, New York, USA
Jose Alonso, Larry Bartoszek, Janet Conrad, MIT, Cambridge, Massachusetts, USA

Content from this work may be used under the terms of the CC BY 3.0 licence (© 2015). Any distribution of this work must maintain attribution to the author(s), title of the work, publisher, and DOI.

Abstract

The IsoDAR sterile-neutrino search calls for a high neutron flux from a 60 MeV proton beam striking a beryllium target, that flood a sleeve of highly-enriched ^{7}Li, the beta-decay of the resulting ^{8}Li giving the desired neutrinos for the very-short-baseline experiment. The target is placed very close to an existing large neutrino detector; all such existing or planned detectors are deep underground, in low-background environments. It is necessary to design a shielding enclosure to prevent neutrons from causing unacceptable activation of the environment. GEANT4 is being used to study neutron attenuation, and optimising the layers of shielding material to minimize thickness. Materials being studied include iron and two new types of concrete developed by Jefferson Laboratory, one very light with shredded plastic aggregate, the other with high quantities of boron. Initial studies indicate that a total shielding thickness of 1.5 meters produces the required attenuation factor, further studies may allow decrease in thickness. Minimising it will reduce the amount of cavity excavation needed to house the target system in confined underground spaces.

ISODAR EXPERIMENT

IsoDAR (Isotopes-Decay-At-Rest) is a novel, high intensity source of electron antineutrinos which aims for searches for physics beyond standard model [1]. The goal is to produce 1.29×10^{23} electron antineutrinos per year with a mean energy of 6.4 MeV. IsoDAR consists of an ion source, a cyclotron accelerating the protons to 60 MeV which impinge on a Be target placed next to a kiloton-scale scintillator detector [2]. The requirement of the accelerator is to deliver 10 mA proton beam at 60 MeV on the target. The solution to provide such a high current is to accelerate 5 mA beam of H_2^+ ions using the DAEDALUS injector cyclotron as a driver. As a results of the inelastic interactions of low energy protons or deuterons with the Be target ^{8}Li isotopes are produced which then decay producing electron antineutrinos. Apart from the ^{8}Li isotopes produced in the target, additional ^{8}Li is produced in the surrounding materials by secondary neutrons. Electron antineutrinos are detected by the inverse-beta decay (IBD) process in a detector and a possible choice for detector is KAMLAND in the Kamioka mine in Japan.

The IsoDAR target (Fig. 1) consists of a hollow cylinder of beryllium with the target proper being a 1.7 cm thick end face of the cylinder. The target thickness is calculated to optimise the production of neutrons and minimise heat deposited in the beryllium. The beam is spread over the 20 cm diameter face of the target by a wobbler magnet that decreases the peak power density deposited on the target. The secondary neutrons produced in the target are moderated in the cooling water before entering the sleeve where they are captured on ^{7}Li to produce ^{8}Li. The purity of the ^{7}Li in the FLiBe sleeve is 99.995%. The sleeve is surrounded by a graphite reflector to reflect the neutrons back into the sleeve.

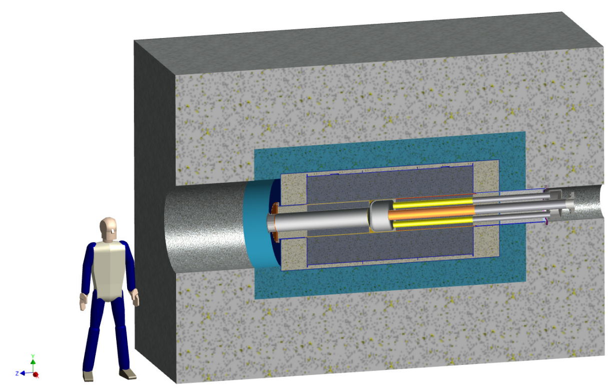

Figure 1: The IsoDAR target system and shielding. The target is a hollow centered cylinder surrounded by the FLiBe sleeve and a graphite reflector and cooled with water. The shielding in the current design consists of steel (shown in blue) and boron rich concrete (grey). A space for wobbler magnets is left in front of the target.

SHIELDING

The proposed site for the IsoDAR target is the KAMLAND control room which has the dimensions $3.5 \times 28 \times 2.25$ m. This space must contain the target assembly and the graphite reflector surrounding the sleeve while the remaining space (≈50 cm) will be used for neutron shielding. Preliminary calculations indicate that the space for neutron shielding will need to be enlarged particularly in the vertical direction. Techniques for rock removal must be discussed as blasting is not allowed.

Our collaborators from KAMLAND and RIKEN gave us valuable guidelines in establishing the requirements of the shielding and radiation protection. In this respect the rock activation due to artificially produced radionuclides must

ISBN: 978-3-95450-168-7 doi:10.18429/JACoW-IPAC2015-TUPWI021

PROGRESS ON A 30 - 350 MeV NORMAL-CONDUCTING SCALING FFAG FOR PROTON THERAPY*

J.M. Garland†, R.B. Appleby‡, H. Owen and S. Tygier
University of Manchester, Manchester, M13 9PL, United Kingdom, and
The Cockcroft Institute, Warrington, WA4 4AD, United Kingdom

Abstract

We present our progress on a new design for a 30 - 350 MeV scaling FFAG for proton therapy and tomography - NORMA (NOrmal-conducting Racetrack Medical Accelerator) which allows the realisation of proton computed tomography (pCT) and utilises normal conducting magnets in both a circular and racetrack configuration which are designed using advanced optimisation algorithms developed in PyZgoubi. The ring and racetrack configurations have average circumferences of around 60 and 70 m respectively, peak magnetic fields of < 1.8 T, average orbit excursions < 50 cm and dynamic aperture calculations of > 50 mm.mrad using a novel technique. The racetrack design has a total magnet-free straight length of 4.9 m at two opposing points, designed to ease injection and extraction systems.

INTRODUCTION

The treatment of cancer using proton therapy is widely regarded as having many advantages over conventional therapies due to the more localised dose deposition in the tumour, realisable as a characteristic Bragg peak at a depth determined by the incident proton energy; around 70 - 250 MeV for human tissue treatment [1–3]. Fast, effective treatment of a tumour volume requires precise and rapid energy variation and transverse beam scanning for effective use of treatment time and localisation of dose so as to limit surrounding healthy tissue damage. Furthermore, the technique of proton computed tomography (pCT) is highly desirable clinically due to the ability to obtain real-time diagnostics on the treatment of the tumour; however pCT requires a proton energy of around 350 MeV, not currently attainable from current proton therapy centres or designs.

An FFAG (Fixed-Field Alternating-Gradient) accelerator [4] is a good choice of machine which meets these requirements as protons may be accelerated up to 350 MeV with pulse-to-pulse energy variation up to 1 kHz and variable energy extraction. The 70 - 250 MeV proton (and carbon ion), non-scaling FFAG PAMELA (Particle Accelerator for MEdicaL Applications) [5] is capable of the desired treatment regime but not pCT in the proton ring, and has potentially complicated and expensive superconducting magnets [6]. Previous studies [7] showed the possibility of inserting magnet-free straights into a ring while maintaining a suitable DA and optics. We are designing a 30 - 350 MeV scaling, proton FFAG with normal conducting magnets which has a conventional ring and a racetrack configuration to ease injection and extraction. Although our second design has only magnet-free drifts inserted, we still refer to it as a racetrack to distinguish it form the circular design. The ring design has a circumference of around 60 m and a dynamic aperture (DA) of > 60 mm.mrad, the racetrack has a circumference of around 70 m, with two 4.9 m magnet-free straight sections and a DA of > 50 mm.mrad. Both designs will have orbit shifts over the energy range of < 50 cm with peak magnetic fields <1.8 T, but relatively large sized magnets; 0.5 m aperture, 1.0 m length. However, scaling FFAGs with similar sized magnets have been constructed and successfully operated [8–10].

NORMA RING

An FDF (focusing - defocusing - focusing) triplet is being used and optimised in the NORMA design with scaling, sector-type magnets where the field in each magnet in the radial direction is defined by

$$B(r) = B_0 \left(\frac{r}{r_0}\right)^k , \qquad (1)$$

where B_0 is the magnetic field at the reference radius r_0 and k is the field index. A schematic diagram of the cell is shown in Fig. 1 where the geometric parameters are indicated. The number of cells, geometry within each cell, magnetic field strengths of the F and D magnets and the field index were optimised using specific algorithms which we developed using PyZgoubi for the optimisation of NORMA [11, 12]; some initial analytical analysis was also used in this process.

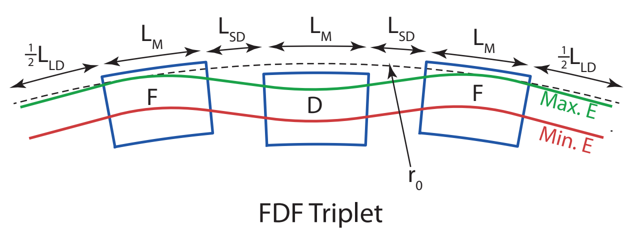

Figure 1: Geometry of the FDF triplet cell used in NORMA showing the sector-type magnets in blue, the minimum and maximum energy orbits (30 and 350 MeV) in red and green respectively and the reference radius r_0 as a dashed black line. For optimising the geometry, the free parameters were selected as the cell length L_{cell}=$2L_{LD}$+$3L_M$+$2L_{SD}$, the triplet length L_{trip}=$3L_M$+$2L_{SD}$, and the packing factor α=L_{trip} / L_{cell}.

* Work supported by STFC Grant No. ST/K002503/1
† james.garland@manchester.ac.uk
‡ robert.appleby@manchester.ac.uk

Content from this work may be used under the terms of the CC BY 3.0 licence (© 2015). Any distribution of this work must maintain attribution to the author(s), title of the work, publisher, and DOI.

ISBN: 978-3-95450-168-7 doi:10.18429/JACoW-IPAC2015-TUPWI022

GEM*STAR ACCELERATOR-DRIVEN SUBCRITICAL SYSTEM FOR IMPROVED SAFETY, WASTE MANAGEMENT, AND PLUTONIUM DISPOSITION

Robert Abrams†, Mary Anne Clare Cummings, Gene Flanagan,
Rolland Paul Johnson, Thomas J. Roberts, Muons, Inc, Illinois, USA
Charles Bowman, ADNA, Los Alamos, New Mexico, USA
Bruce Vogelaar, Virginia Polytechnic Institute and State University, Virginia, USA

Abstract

Operation of high-power SRF particle accelerators at two US National Laboratories allows us to consider a less-expensive nuclear reactor that operates without the need for a critical core, fuel enrichment, or reprocessing. A multipurpose reactor design that takes advantage of this new accelerator capability includes an internal spallation neutron target and high-temperature molten-salt fuel with continuous purging of volatile radioactive fission products. The reactor contains less than a critical mass and almost a million times fewer volatile radioactive fission products than conventional reactors like those at Fukushima. We describe GEM*STAR[1], a reactor that, without redesign, will burn spent nuclear fuel, natural uranium, thorium, or surplus weapons material. A first application is to burn 34 tonnes of excess weapons grade plutonium as an important step in nuclear disarmament under the 2000 Plutonium Management and Disposition Agreement[2]. The process heat generated by this W-Pu can be used for the Fischer-Tropsch conversion of natural gas and renewable carbon into 42 billion gallons of low-CO_2-footprint, drop-in, synthetic diesel fuel for the DOD.

GEM*STAR SYSTEM

The main elements of the GEM*STAR system are a particle accelerator and associated beam transport, the GEM*STAR reactor, and the ancillary facilities for utilizing the heat output for electricity generation and/or chemical processes. A block diagram of the elements is shown in Fig. 1.

*The GEM*STAR Reactor*

The heart of the GEM*STAR system is the reactor [1, 2], which consists of a graphite core matrix of tubular elements through which molten salt containing the fuel mixture circulates. As illustrated schematically in Fig. 2, pumps drive the molten salt down the periphery, up around the holding tank, and up through the graphite tubes, which act as the moderator, and back to the periphery. The molten salt level is maintained by an overflow pipe that returns the excess molten salt to the holding tank. A helium gas flow above the salt level is used to purge the volatile products from the reactor core. The accelerator beam strikes a target in the reactor to produce neutrons to control the fission rate in the reactor and maintain sub-critical operation.

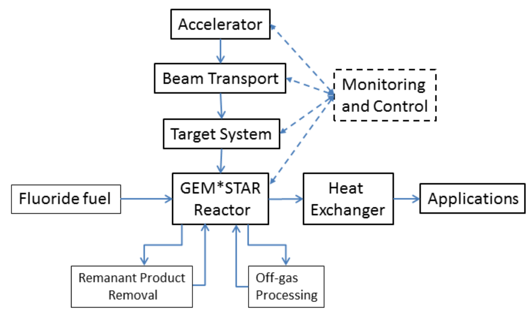

Figure 1: Block diagram showing major elements of the GEM*STAR system.

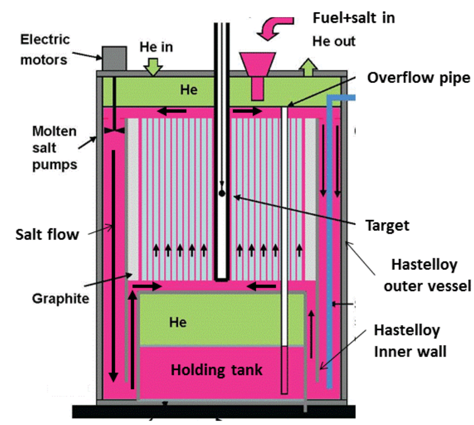

Figure 2: Cross-sectional view of GEM*STAR reactor.

The molten salt mixture is shown in magenta. Helium gas is shown in green. Secondary flow loop tubes, shown in blue, carry process heat from the core to an external heat exchanger for use by the applications. LiF salt, mixed with fluorides of plutonium, natural uranium, and thorium can be used as fuel mixtures, as well as spent nuclear fuel rods and surplus weapons material. The fuel preparation does not require MOX processing and encapsulation. Since the number of neutrons generated is independent of any particular fission chain reaction, a variety of fissile or fertile materials can be handled with one reactor design. The reactor operates in a subcritical mode, at $k_{eff} \approx 0.98$.

---
†boba247@muonsinc.com
1 Charles D. Bowman, R. Bruce Vogelaar, et al., Handbook of Nuclear Engineering, Springer Science+Business Media LLC (2010).
2 http://www.state.gov/r/pa/prs/ps/2010/04/140097.htm

© Content from this work may be used under the terms of the CC BY 3.0 licence (© 2015). Any distribution of this work must maintain attribution to the author(s), title of the work, publisher, and DOI.

ISBN: 978-3-95450-168-7 doi:10.18429/JACoW-IPAC2015-TUPWI026

A MONOCHROMATIC GAMMA SOURCE WITHOUT NEUTRONS*

R.W. Garnett#, S.S. Kurennoy, L.J. Rybarcyk, and T.N. Taddeucci, LANL, Los Alamos, NM 87545

Abstract

High-energy gamma rays can be efficiently produced using the direct excitation of the 15.1-MeV level in ^{12}C via the (*p*, *p*') reaction with the threshold energy of 16.38 MeV. The threshold for neutron production via ^{12}C (*p*, *n*) is 19.66 MeV, so there is an energy window of 3.28 MeV where the 15.1-MeV photons can be produced without any direct neutrons. Thick-target yield estimates indicate that just below the neutron production threshold, the photon output is about twice that of the more well-known ^{11}B (*d*, *n*) reaction requiring 4-MeV deuterons, with the expected 15.1-MeV photon flux to be approximately $1x10^{11}$ $s^{-1}sr^{-1}$ per 1 mA of 19.6-MeV proton current on a carbon target. A compact pulsed proton accelerator capable of 10-mA or greater peak currents to drive such a gamma source will be presented. The accelerator concept is based on a 4-rod RFQ followed by compact H-mode structures with PMQ focusing.

INTRODUCTION

Conventional bremsstrahlung-based interrogation of special nuclear materials in cargo is not very efficient because its gamma energy spectrum is dominated by low-energy photons. On the contrary, 15-MeV photons are well matched to the peak of the photo-fission cross section for uranium. Such gamma rays can be efficiently produced using direct excitation of the 15.1-MeV level in the ^{12}C via (*p*, *p*') reaction that has the threshold energy of 16.38 MeV [1]. The threshold of neutron production via ^{12}C (*p*, *n*) is 19.66 MeV, so there is a window of 3.28 MeV where the 15.1-MeV photons can be produced without any direct neutrons. The thick-target yield estimates in [1] indicate that just below the neutron production threshold, the 15.1-MeV photon output is about twice that in the ^{11}B (*d*, *n*) reaction with 4-MeV deuterons (See Fig. 1).

For the latter, we estimated the 15.1-MeV photon flux as $5 \cdot 10^{10}$ $s^{-1}sr^{-1}$ per 1 mA of deuteron current [2]. Therefore, we expect a 15.1-MeV photon flux of $1 \cdot 10^{11}$ $s^{-1}sr^{-1}$ per 1 mA of 19.6-MeV protons on a carbon target – much higher than with conventional sources, and without the neutron background. Having such a monochromatic source of high-energy photons significantly reduces the total dose required for SNM interrogation in cargo. The detection efficiency also increases due to eliminated neutron background and shorter pulses.

ACCELERATOR SYSTEM

To implement the above promising approach, we need a compact system that accelerates protons with peak currents of 10s mA to 19.6 MeV. Based on our previous results [2, 3], one attractive option is a compact pulsed accelerator that consists of an RFQ followed by H-mode structures with PMQ focusing (H-PMQ). For preliminary estimates, we use results [3] where replacing the 201.25-MHz LANSCE drift-tube linac (DTL) by much more efficient H-PMQ accelerator structures [4] of the same frequency was studied. A 750-keV RFQ (~2 m) is followed by two inter-digital H-PMQ (IH-PMQ) tanks with the accelerating gradient 2.5 MV/m to bring protons to 5.4 MeV [3]. After that we switch to cross-bar H-PMQ structures (CH-PMQ); likely, three CH-PMQ tanks will be needed to accelerate protons to 19.6 MeV. The total accelerator length is estimated to be ~12 m, but can be reduced by increasing the gradient. The transverse size will be well within 1-m diameter. With peak currents below 50 mA, the highest values in designs [2, 3], the required maximum peak RF power should be less than 2.5 MW. The system is illustrated in Fig. 2 and looks feasible.

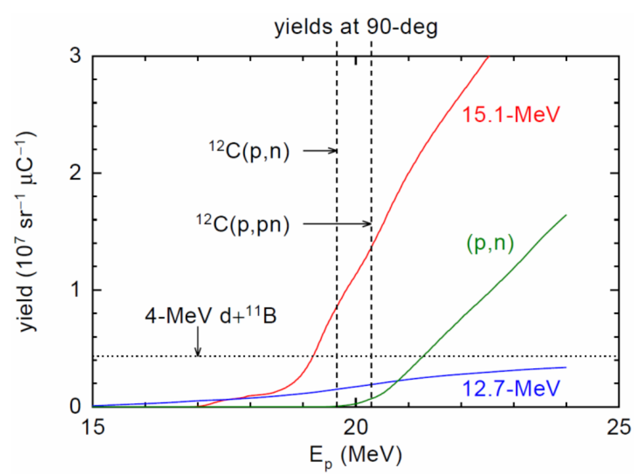

Figure 1: Thick-target yields for p+^{12}C photon and neutron production reactions.

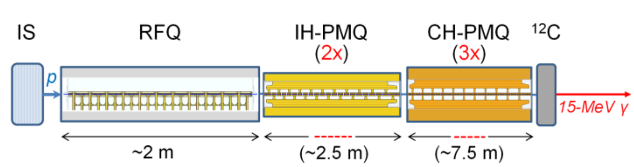

Figure 2: Accelerator scheme.

Ion Source and RFQ

Proton ion sources (IS) providing peak currents of 10s mA at duty factors up to 10-20% are readily available [5]. The IS will be connected to the RFQ entrance by a short electrostatic, low-energy beam transfer line (LEBT). The LEBT can also serve as the beam switch with on-off times ~50 ns as in the SNS front end. The 750-keV RFQ can be of either 4-vane or 4-rod type. Based on our recent

* Work supported by the United States Department of Energy, National Nuclear Security Agency, under contract DE-AC52-06NA25396.
# rgarnett@lanl.gov

Content from this work may be used under the terms of the CC BY 3.0 licence (© 2015). Any distribution of this work must maintain attribution to the author(s), title of the work, publisher, and DOI.

ISBN: 978-3-95450-168-7 doi:10.18429/JACoW-IPAC2015-TUPWI027

RADIOGRAPHY CAPABILITIES FOR MATTER-RADIATION INTERACTIONS IN EXTREMES*

P. L. Walstrom#, R. W. Garnett, R. L. Barber, J. A. O'Toole, T. S. Gomez, C. A. Chapman, H. R. Salazar, Los Alamos National Laboratory, Los Alamos, New Mexico 87545

Abstract

The Matter-Radiation Interactions in Extremes (MaRIE) experimental facility [1] will be used to discover and design the advanced materials needed to meet 21st century national security and energy security challenges. This new facility will provide the new tools scientists need to develop next-generation materials that will perform predictably and on-demand for currently unattainable lifetimes in extreme environments. The MaRIE facility is based on upgrades to the existing LANSCE 800-MeV proton linac and a new 12-GeV electron linac and associated X-ray FEL to provide simultaneous multiple probe beams, and new experimental areas. In addition to the high-energy photon probe beam, both electron and proton radiography capabilities will be available at the MaRIE facility. Recently, detailed radiography system studies have been performed to develop conceptual layouts of high-magnification electron and proton radiography systems that can meet the experimental requirements for the expected first experiments to be performed at the facility. A description of the radiography systems, their performance requirements, and a proposed facility layout are presented.

FACILITY MISSION

The mission need is to provide qualification, certification, and assessment of materials in the nuclear deterrent stockpile. Material interfaces, defects, and microstructure between the scales of atomic structure and the engineering continuum (the so-called mesoscale) determine time-dependent properties, from shock response to manufacturing processes to aging. Test samples will be synthesised and characterized at the mesoscale, and their dynamic behavior in time-dependent extreme conditions characterized by use of both imaging and diffractive scattering with multiple probes at multiple spatial and time scales.

FACILITY OVERVIEW

The MaRIE facility (see Fig. 1) will be built on the TA-53 site at LANL and will make use of the existing 800-MeV proton linac. New facility components include a 12-GeV electron linac, 42-keV X-ray FEL/undulator, X-ray, electron, and proton beam lines, new experimental halls, and materials fabrication/characterization facilities. X-ray, electron, and proton beams intersect in multibeam radiography areas or hutches (see Fig. 2).

*Work supported by US Department of Energy, Office of National Nuclear Security Administration. Contract No. DE-AC52-06NA25396.
walstrom@lanl.gov

12-GeV Superconducting Electron Linac

The choice of a superconducting (SC) linac was driven by the requirement of having up to 30 microbunches over a time window of up to 100 μs, which rules out high-gradient normal-conducting structures [2]. The SC linac will use the same basic 1.3-GHz cavities as planned for the European XFEL and LCLS-II. The design assumes a cavity accelerating gradient of 31.5 MV/m. The total length of the linac is 750 m, which gives it an average (real-estate) gradient of 16 MV/m.

Undulator

The undulator is a hybrid permanent magnet type with an on-axis field of 0.7 T and a period of 1.86 cm. The total undulator length is 138 m. There are 28 undulator segments and 16 FODO periods, each with a length of 8.6 m. Two of the FODO periods contain chicanes and monochromators for seeding.

FEL Undulator and X-Ray Beam Transport

In the initial stage of the facility, a single undulator/FEL will be used to produce a bright, coherent X-ray beam of up to 42 keV energy with a photon flux in excess of 2×10^{10} photons in each 30-fs pulse. Silicon kinoform lenses are used to expand the x-ray beam. Bragg scattering from crystals is used to deflect the X-ray beam at small angles of up to 5 degrees into multiple X-ray beamlines. Another set of kinoform lenses, labelled "objectives", then focus the expanded X-ray beam onto the targets with different focused spot radii, depending on the experimental requirements.

12-GeV Electron and 800-MeV Proton Radiography Systems

Proton radiography (pRad) is a mature technology, with systems operating in the USA, Germany, and Russia. Electron radiography (eRad) in the GeV range is under development [3], with proof-of-principle experiments planned for the summer of 2015 at SLAC. Both eRad and pRad have the same basic system components, but the physics of beam interaction with objects differs: ionization energy loss and multiple Coulomb scattering (MCS) are nearly the same for both eRad and pRad, but bremsstrahlung energy loss is important in eRad and negligible for pRad, and nuclear scattering is important for pRad but small for eRad. Bremsstrahlung energy loss limits 12-GeV eRad of high-Z materials (U, Pu, etc.) to thicknesses of a few millimeters or less. Object thicknesses in 800-MeV pRad are limited by MCS, dE/dx energy loss, and second-order lens chromatic aberrations. Both techniques use matching illuminating beams, point-

Content from this work may be used under the terms of the CC BY 3.0 licence (© 2015). Any distribution of this work must maintain attribution to the author(s), title of the work, publisher, and DOI.

ISBN: 978-3-95450-168-7 doi:10.18429/JACoW-IPAC2015-TUPWI028

VARYING AMPLITUDE RASTER PATTERN FOR HIGH POWER ISOTOPE PRODUCTION TARGETS*

J. Kolski†, J. Audia, H. Bach, Y. Batygin, J. Bradley, M. Connors, J.W. Engle, E. Espinoza, E. Figueroa, M. Hall, M. Martinez, M. Nortier, D. Reass, W. Roybal, H. Watkins,
LANL, Los Alamos, NM, 87545, USA

Abstract

The Isotope Production Facility (IPF) at LANSCE [1, 2] produces medical radionuclides strontium-82 and germanium-68 by bombarding rubidium chloride and gallium metal targets respectively with a 100 MeV proton beam, 230 μA average current. Rastering the proton beam is necessary to distribute beam power deposited as heat in the target and allow for higher average beam current for isotope production. We currently use a single circle raster pattern with constant amplitude and frequency. In this paper, we demonstrate two different varying amplitude raster patterns (concentric circle and spiral) to achieve uniform target coverage and expose more target volume to beam heating. In this proof-of-principle experiment, we compare beam spot uniformity measured by irradiating films and foils for both raster patterns.

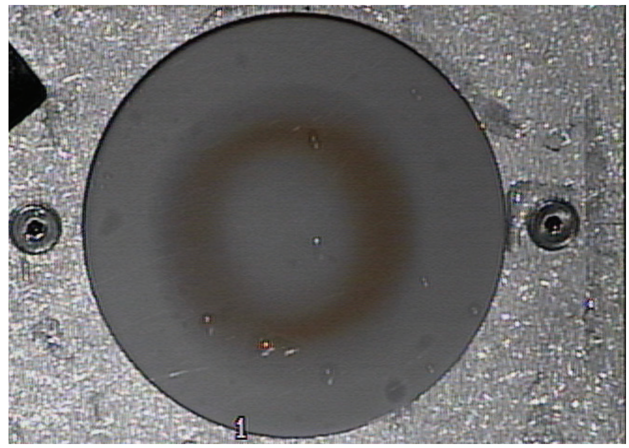

Figure 1: Beam spot at the IPF target with the single circle production raster pattern measured by film irradiation.

INTRODUCTION

A horizontal and a vertical steering magnet perform the beam rastering for IPF [3]. The steering magnets are modulated by the same frequency generator with maximum bandwidth 5 kHz. Steering magnet amplitude can be controlled separately via digital controllers. During typical production, IPF receives 625 μs long macropulses, yielding with the raster frequency ~3 raster revolutions per macropulse.

The current single circle production raster pattern with typical 15 mm radius results in the beam spot at the IPF target shown in Fig. 1. All beam heat is deposited in the thin ring and little beam hits the target center. The goal of this proof-of-principle investigation is to demonstrate that with minor modifications to existing equipment, an amplitude varying raster pattern (concentric circle or spiral) can "fill in" the target center, distributing the beam heating over more target volume, and yielding uniform target coverage.

RASTER PATTERNS

We demonstrate two different amplitude varying raster patterns: concentric circle and spiral [4, 5]. Both methods have a square root amplitude and sinusoidal frequency dependence with time, Fig. 2.

$$\begin{pmatrix} R_x \\ R_y \end{pmatrix} = A(t) \times \Phi(t) \sim \sqrt{t} \times \begin{cases} \cos(2\pi f t + \phi) \\ \sin(2\pi f t + \phi) \end{cases} \quad (1)$$

In the concentric circle method, the raster amplitude is constant for each macropulse. The amplitude changes in between macropulses, executing the square root dependence with more larger radii circles and fewer smaller radii circles. The uniform beam spot is achieved in several macropulses. Due to equipment protection considerations, we do not execute the pattern in order of radii size. Instead, we "mix up" the radii as observed in Fig. 2. In this paper, we study a concentric circle pattern with 100 different radii.

In the spiral case, the square root amplitude dependence is executed during each macropulse by spending more time at larger radii and less time at smaller radii. A macropulse-to-macropulse phase shift due to the raster frequency and the 120 Hz machine repetition rate rotates the spiral to give the uniform beam spot on target after several macropulses. Care was taken to ensure that the raster frequency was not a multiple of the 120 Hz machine repetition rate, as this would yield a zero degree macropulse-to-macropulse phase shift.

SET UP AND MEASUREMENT

We set up for this experiment with a 5 Hz repetition rate to IPF in order to achieve ~10 μA average current (for equipment protection reasons) using the production peak current, 3.4 mA. After each raster pattern was loaded into the controller, we inserted a measurement stack into the IPF target position. The measurement stack held a 0.5 mm thick polyethylene film and a 1 mm thick titanium foil. We simultaneously irradiated both film and foil with 100 macropulses of rastered beam. The plastic film image was captured with

* Work supported in part by United States Department of Energy under contracts DE-AC52-06NA25396 and DE-AC52-06NA253996. LA-UR 15-23007
† Electronic address: jkolski@lanl.gov

Content from this work may be used under the terms of the CC BY 3.0 licence (© 2015). Any distribution of this work must maintain attribution to the author(s), title of the work, publisher, and DOI.

ISBN: 978-3-95450-168-7 doi:10.18429/JACoW-IPAC2015-TUPWI029

BASELINE SCHEME FOR POLARIZATION PRESERVATION AND CONTROL IN THE MEIC ION COMPLEX*

Ya.S. Derbenev, F. Lin, V.S. Morozov, Y. Zhang, JLab, Newport News, Virginia
A.M. Kondratenko, M.A. Kondratenko, Science and Technique Laboratory Zaryad, Novosibirsk
Yu.N. Filatov, MIPT, Dolgoprudny, Moscow Region

Abstract

The scheme for preservation and control of the ion polarization in the Medium-energy Electron-Ion Collider (MEIC) has been under active development in recent years. The figure-8 configuration of the ion rings provides a unique capability to control the polarization of any ion species including deuterons by means of "weak" solenoids rotating the particle spins by small angles. Insertion of "weak" solenoids into the magnetic lattices of the booster and collider rings solves the problem of polarization preservation during acceleration of the ion beam. Universal 3D spin rotators designed on the basis of "weak" solenoids allow one to obtain any polarization orientation at an interaction point of MEIC. This paper presents the baseline scheme for polarization preservation and control in the MEIC ion complex.

INTRODUCTION

Colliders "Transparent to the Spin"

Colliders with a figure-8 topology are natural representatives of colliders "transparent to the spin". In such colliders, effect on the spin of one arc is compensated by the other arc. Thus, effect of "strong" arc fields on the spin is reduced to zero. Any spin direction repeats after a particle turn, i.e. the collider has no preferred spin direction. This means that the particles are in the region of a zero-integer spin resonance and the spin tune is zero $\nu=0$.

Colliders transparent to the spin offer a unique opportunity to efficiently control the ion polarization using small magnetic field integrals. In such a collider, any small perturbation has a strong effect on the beam polarization. To stabilize the spin direction, one must introduce additional fields into the collider's lattice, which "shift" the spin tune by a small value ($\nu << 1$) and set the necessary orientation of the polarization. "Weak" fields have essentially no effect on the beam's orbital characteristics. What especially stands out is the possibility of using weak solenoids, which do not impact the closed orbit at all. In the collider's energy range of up to 100 GeV, the field integrals of these solenoids are approximately two orders of magnitude lower than the field integrals of the spin rotators with strong fields. There is no problem with changing the fields of such solenoids during adjustment of the beam polarization direction. It becomes possible to reverse the spin in less than a second allowing for polarized beam experiments at a new precision level.

Strength of the Zero-integer Spin Resonance

The required weak field integrals are limited by the strength of the zero-integer spin resonance w_0: $\nu >> w_0$. The resonance strength is the value of the average spin field, which is determined by deviation of the trajectory from the ideal design orbit. The resonance strength consists of two parts: a coherent part arising due to additional dipole and longitudinal fields on a trajectory deviating from the design orbit and an incoherent part associated with the ions' betatron and synchrotron oscillations (beam emittances). The coherent part of the spin field is determined by linear effects and lies in the orbital plane. The incoherent part of the spin field is not present to first order in orbit deviations due to the non-resonant nature of the oscillations about the closed orbit. The coherent part of the spin field providing the main contribution to the resonance strength can be compensated by a pair of solenoids, which can be used to set any orientation and magnitude of the spin field in the collider's plane. Compensation of the coherent part of the resonance strength allows one to greatly reduce the field integrals of the control solenoids. The technique for compensation of integer resonance harmonics is well known and has been successfully utilized, for example, at the AGS [1]. Thus, figure-8 colliders allow one to take polarized beam experiments to a conceptually higher precision level.

Let us demonstrate the main advantages of spin-transparent figure-8 colliders by applying this concept to the tasks of polarization preservation and spin manipulation during experiments in the ion complex of MEIC.

ION POLARIZATION IN THE MEIC ACCELERATOR COMPLEX

In the new design, the MEIC ion complex (see Fig. 1) consists of sources for polarized light ions and non-polarized light to heavy ions, a 280 MeV pulsed SRF ion linac, an 8 GeV booster, and a medium-energy collider ring [2]. The ion collider ring is stacked vertically above the electron collider ring, and takes a vertical excursion to the plane of the electron ring for a horizontal crossing. Two interaction points of the electron and ion beams lie in the plane of the electron ring.

* Authored by Jefferson Science Associates, LLC under U.S. DOE Contracts No. DE-AC05-06OR23177 and DE-AC02-06CH11357. The U.S. Government retains a non-exclusive, paid-up, irrevocable, world-wide license to publish or reproduce this manuscript for U.S. Government purposes.

Content from this work may be used under the terms of the CC BY 3.0 licence (© 2015). Any distribution of this work must maintain attribution to the author(s), title of the work, publisher, and DOI.

ISBN: 978-3-95450-168-7 doi:10.18429/JACoW-IPAC2015-TUPWI030

NUMERICAL CALCULATION OF THE ION POLARIZATION IN MEIC*

Ya.S. Derbenev, F. Lin, V.S. Morozov, Y. Zhang, JLab, Newport News, VA 23606, USA
A.M. Kondratenko, M.A. Kondratenko, Sci. & Tech. Laboratory Zaryad, Novosibirsk, Russia
Yu.N. Filatov , MIPT, Dolgoprudny, Moscow Region, Russia

Abstract

Ion polarization in the Medium-energy Electron-Ion Collider (MEIC) is controlled by means of universal 3D spin rotators designed on the basis of "weak" solenoids. We use numerical calculations to demonstrate that the 3D rotators have negligible effect on the orbital properties of the ring. We present calculations of the polarization dynamics along the collider's orbit for both longitudinal and transverse polarization directions at a beam interaction point. We calculate the degree of depolarization due to the longitudinal and transverse beam emittances in case when the zero-integer spin resonance is compensated.

INTRODUCTION

Jefferson Lab presently considers an updated scheme of the MEIC electron-ion collider project with the main changes related to a switch to 3 T super-ferric magnets and an increase of the collider ring circumference to ~2.2 km [1]. The ion collider ring retains a figure-8 shape, remains transparent to the spin and, as before, allows for an efficient control of polarization of any ion species by "small" solenoids rotating the particle spins by small angles. The main element of the polarization control system is a universal 3D spin rotator designed using "weak" solenoids [2]. Below we present numerical calculations demonstrating operability of the 3D rotator in the new lattice of the MEIC ion collider ring.

3D SPIN ROTATOR IN MEIC COLLIDER

A universal 3D spin rotator consists of three modules for control of the n_x, n_y, and n_z polarization components (see Fig. 1) [2, 3].

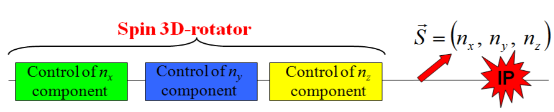

Figure 1: 3D spin rotator schematic.

Figure 2 shows the module for control of the radial polarization component n_x, which consists of two pairs of opposite-field solenoids and three vertical-field dipoles producing a fixed orbit bump. The control module for the vertical polarization component n_y is the same as that for the radial component except that the vertical-field dipoles are replaced with radial-field ones. To keep the orbit bumps fixed, the fields of the vertical- and radial-field dipoles must be ramped proportionally to the beam momentum. The module for control of the longitudinal polarization component n_z consists of a single weak solenoid.

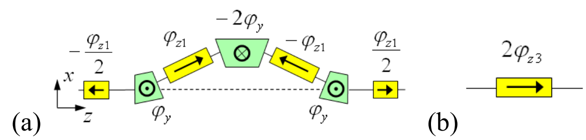

Figure 2: Modules for control of the radial n_x (a) and longitudinal n_z (b) polarization components.

Figure 3 shows schematically placement of the radial (green) and vertical (blue) dipoles as well as of the weak control solenoids (yellow) between the lattice magnets (black) of a collider's straight.

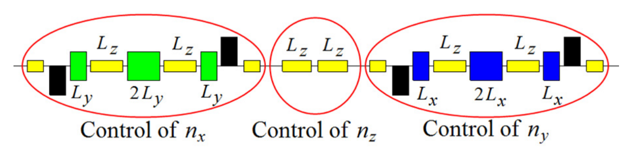

Figure 3: Placement of the 3D spin rotator elements.

The dipole and solenoid lengths are $L_x = L_y = 0.6$ m and $L_z = 2$ m, respectively. In the modules for control of the transverse polarization components, the dipoles produce a fixed orbit bump of ~18 mm in the whole momentum range. The maximum dipole field is 3 T while the field of the control solenoids does not exceed 2 T. This allows one to set the spin tune to $\nu_p = 0.01$ for protons and $\nu_d = 10^{-4}$ for deuterons and also to stabilize any polarization direction at any location in the collider during an experiment essentially with no perturbation to the collider's orbital properties.

EFFECT OF 3D SPIN ROTATOR ON THE ORBITAL BEAM PARAMETERS IN MEIC

Effect of the 3D spin rotator is calculated for multiple reversals of the beam polarization in the vertical plane (yz) of the detector during an experiment (spin flipping). Figures 4 and 5 show graphs of the solenoid fields in the n_y and n_z modules of the 3D rotator versus the angle Ψ between the spin and the beam direction for deuterons and protons. Superconducting pulsed solenoid field of 2 T can be ramped in about 1 second [4].

* Authored by Jefferson Science Associates, LLC under U.S. DOE Contracts No. DE-AC05-06OR23177 and DE-AC02-06CH11357.
The U.S. Government retains a non-exclusive, paid-up, irrevocable, world-wide license to publish or reproduce this manuscript for U.S. Government purposes.

Content from this work may be used under the terms of the CC BY 3.0 licence (© 2015). Any distribution of this work must maintain attribution to the author(s), title of the work, publisher, and DOI.

ISBN: 978-3-95450-168-7 doi:10.18429/JACoW-IPAC2015-TUPWI031

STATUS OF THE MEIC ION COLLIDER RING DESIGN*

V.S. Morozov#, Ya.S. Derbenev, L. Harwood, A. Hutton, F. Lin, F. Pilat, Y. Zhang,
Jefferson Lab, Newport News, VA 23606, USA
Y. Cai, Y.M. Nosochkov, M. Sullivan, M-H Wang, U. Wienands,
SLAC, Menlo Park, CA 94025, USA
J. Gerity, T. Mann, P. McIntyre, N.J. Pogue, A. Sattarov,
Texas A&M University, College Station, TX 77843, USA

Abstract

We present an update on the design of the ion collider ring of the Medium-energy Electron-Ion Collider (MEIC) [1] proposed by Jefferson Lab. The design is based on the use of super-ferric magnets. It provides the necessary momentum range of 8 to 100 GeV/*c* for protons and ions, matches the electron collider ring design using PEP-II components, fits readily on the JLab site, offers a straightforward path for a future full-energy upgrade by replacing the magnets with higher-field ones in the same tunnel, and is more cost effective than using presently available current-dominated super-conducting magnets. We describe complete ion collider optics including an independently-designed modular detector region.

DESIGN OVERVIEW

The ion collider ring accelerates protons and ions from 8 to up to 100 GeV/*c* and is designed to provide luminosity above 10^{33} cm^{-2}s^{-1} in the momentum range from 20 to 100 GeV/*c*. The overall layout of the ion collider ring indicating the main components is shown in Fig. 1. The ring consists of two 261.7° arcs connected by two straight sections intersecting at an 81.7° angle. The ion collider ring's geometry is determined by the electron collider ring [2,3]. The ion arcs are composed mainly of FODO cells. The last few dipoles at either end of each arc are arranged to match the geometry of the ion collider ring. One of the straights houses an interaction region and is shaped to make a 50 mrad crossing angle with the electron beam at the interaction point. The second straight is mostly filled with FODO, however, retaining the capability of inserting a second interaction region. The overall ion ring circumference is 2153.89 m. The main building blocks of the ring are described below.

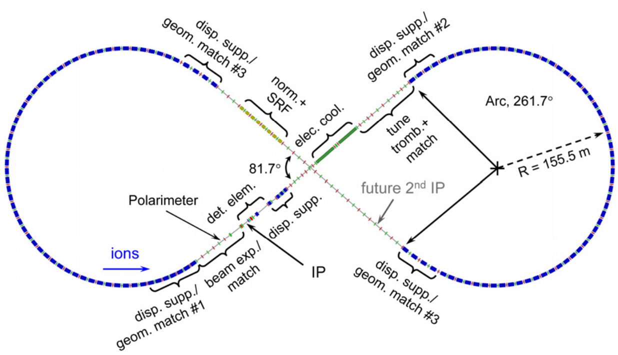

Figure 1: Layout and main components of the ion collider ring.

*Authored by Jefferson Science Associates, LLC under U.S. DOE Contracts No. DE-AC05-06OR23177 and DE-AC02-06CH11357. The U.S. Government retains a non-exclusive, paid-up, irrevocable, world-wide license to publish or reproduce this manuscript for U.S. Government purposes. Work supported in part by the US DOE Contract No. DE-AC02-76SF00515.

#morozov@jlab.org

ARCS

The main building block of the ion arcs is a FODO cell shown in Fig. 2. It has been designed considering a balance of geometric, engineering and beam dynamical aspects. It has the same average bending radius as the electron arc. The ion FODO cell length is chosen at 22.8 m to be 1.5 times that of the electron FODO cell. Such a size allows for use of super-ferric magnets [4] up to a proton momentum of about 100 GeV/*c*. Each 8 m long dipole has a maximum field of about 3.06 T and bends the beam by about 4.2° with a bending radius of about 109.1 m.

The required magnet apertures are determined using a sum of a ±10 rms beam size at injection (including betatron and dispersive contributions), a ±1 cm closed orbit allowance, and, in case of dipoles, a plus or minus a half of the orbit arc's sagitta. To make the dipole horizontal aperture size more manageable, each dipole is implemented as two 4 m long straight pieces reducing the

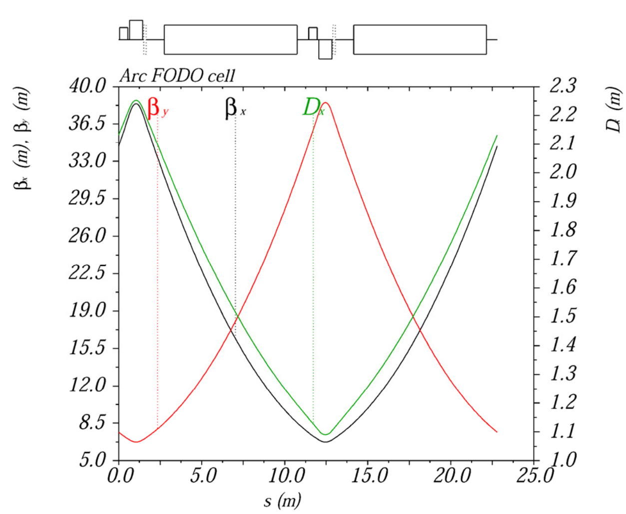

Figure 2: Ion arc FODO optics.

Content from this work may be used under the terms of the CC BY 3.0 licence (© 2015). Any distribution of this work must maintain attribution to the author(s), title of the work, publisher, and DOI.

ISBN: 978-3-95450-168-7 doi:10.18429/JACoW-IPAC2015-TUPWI032

PROGRESS ON OPTIMIZATION OF THE NONLINEAR BEAM DYNAMICS IN THE MEIC COLLIDER RINGS*

Y. Nosochkov†, Y. Cai, M. Sullivan, M-H. Wang, U. Wienands, SLAC, Menlo Park, CA, USA
V.S. Morozov, Ya.S. Derbenev, F. Lin, F. Pilat, Y. Zhang, Jefferson Lab, Newport News, VA, USA

Abstract

One of the key design features of the Medium-energy Electron-Ion Collider (MEIC) proposed by Jefferson Lab is a small beta function at the interaction point (IP) allowing one to achieve a high luminosity of up to 10^{34} cm^{-2}s^{-1}. The required strong beam focusing unavoidably causes large chromatic effects such as chromatic tune spread and beam smear at the IP, which need to be compensated. This paper reports recent progress in our development of a chromaticity correction scheme for the ion ring including optimization of dynamic aperture and momentum acceptance.

INTRODUCTION

Design of the Medium-energy Electron-Ion Collider (MEIC) [1] at Jefferson Lab is aimed at reaching high luminosity of up to 10^{34} cm^{-2}s^{-1}. The latter requires a small beam size and, therefore, small beta function (β^*) at the interaction point (IP). As a result, beta functions in the nearest to IP final focusing quadrupoles (FFQ) become very large ($\propto 1/\beta^*$) making the FFQ the main source of chromaticity in the ring. Since the FFQ linear chromaticity (i.e. first order tune shift with momentum deviation $\delta_p = \Delta p/p$) is straightforward to cancel with conventional two-family sextupoles in the ring arcs, the main concern is the large non-linear chromaticity. The latter is driven by a large perturbation of momentum dependent beta function created by the FFQ chromatic kick. This perturbation could lead to a strong non-linear momentum dependence of tune and the β^*. The increased tune spread could excite stronger effects of betatron resonances on dynamic aperture, thus limiting the momentum acceptance; and the IP chromatic beam smear would increase the effective beam size resulting in a lower luminosity. To compensate the FFQ non-linear chromaticity, a dedicated correction system is required. This paper presents a study of two correction options for the ion ring including the results of dynamic aperture optimization.

LATTICE

The MEIC ring circumference has been recently increased to $\simeq 2.2$ km [1]. This allows the re-use of the PEP-II High Energy Ring [2] components in the electron ring and the use of super-ferric magnets [3] in the ion ring. The two rings are stacked vertically in the same tunnel and have a

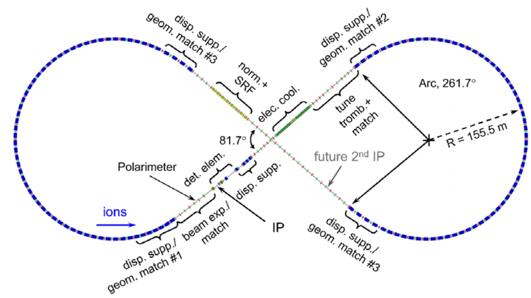

Figure 1: Top view layout of the ion ring.

figure-8 layout, as shown in Fig. 1, which optimizes preservation of the ion polarization [4]. The design collision beam energies are: 3-10 GeV for electrons, 20-100 GeV for protons, and up to 40 GeV per nucleon for ions. Each ring consists of two 90° FODO arcs and two long straight sections. One straight contains the interaction region (IR), a polarimeter, a cooling section and tune trombone, while the other FODO straight houses accelerating cavities and can be upgraded to a second IR in the future. The beams collide at 50 mrad horizontal angle at the IP.

The ion ring lattice (before chromaticity correction adjustment) is shown in Fig. 2, where the machine natural chromaticity is $\xi_{x,y} = [-101.1, -111.6]$. The two FODO arcs are the only dispersive regions suitable for the chromaticity correcting sextupoles. The IR optics is shown in Fig. 3, where $\beta^*_{x,y} = 10 \times 2$ cm corresponding to the IP rms beam size of $\sigma^*_{x,y} = 18 \times 3.6$ μm for 100 GeV protons. Due to the detector requirements, the IR optics is made asymmetric with 7 m free space downstream of IP versus 3.6 m on the upstream side. This results in a factor of 3 higher beta functions in the downstream FFQ leading to stronger chromatic perturbation. The downstream side also includes a detector spectrometer optics with a second focal point which further increases the IR chromatic asymmetry.

CHROMATICITY CORRECTION

As pointed out, the large non-linear chromaticity generated by the FFQs requires a dedicated correction. Due to the $\simeq \pi$ phase advance between the upstream and downstream FFQs their chromatic contributions add up. If not locally cancelled, the chromatic beta perturbation would propagate around the ring giving rise to large non-linear momentum dependence of the tune. A conventional solution is to use local sextupoles generating a chromatic beta wave opposite to the one from FFQ, so they cancel each other. A separate local correction is needed on each side of IP in order to avoid the IP chromatic beam smear. Desired conditions at

* Authored by Jefferson Science Associates, LLC under US DOE Contract No. DE-AC05-06OR23177 and DE-AC02-06CH11357. The US Government retains a non-exclusive, paid-up, irrevocable, world-wide license to publish or reproduce this manuscript for US Government purposes. Work supported by the US DOE Contract DE-AC02-76SF00515.
† yuri@slac.stanford.edu

Content from this work may be used under the terms of the CC BY 3.0 licence (© 2015). Any distribution of this work must maintain attribution to the author(s), title of the work, publisher, and DOI.

ISBN: 978-3-95450-168-7 doi:10.18429/JACoW-IPAC2015-TUPWI033

MATCHING INTO THE HELICAL BUNCH COALESCING CHANNEL FOR A HIGH LUMINOSITY MUON COLLIDER

A. Sy#, Y. Derbenev, V.S. Morozov, Jefferson Lab, Newport News, VA 23606, U.S.A.
C. Ankenbrandt, R. P. Johnson, Muons, Inc., Batavia, IL 60510, U.S.A.
D. Neuffer, K. Yonehara, C. Yoshikawa, Fermilab, Batavia, IL 60510, U.S.A.

Abstract

For high luminosity in a muon collider, muon bunches that have been cooled in the six-dimensional helical cooling channel (HCC) must be merged into a single bunch and further cooled in preparation for acceleration and transport to the collider ring. The helical bunch coalescing channel provides the most natural match from helical upstream and downstream subsystems. This work focuses on the matching from the exit of the multiple bunch HCC into the start of the helical bunch coalescing channel. The simulated helical matching section simultaneously matches the helical spatial period λ in addition to providing the necessary acceleration for efficient bunch coalescing. Previous studies assumed that the acceleration of muon bunches from p=209.15 MeV/c to 286.816 MeV/c and matching of λ from 0.5 m to 1.0 m could be accomplished with zero particle losses and zero emittance growth in the individual bunches. This study demonstrates nonzero values for both particle loss and emittance growth, and provides considerations for reducing these adverse effects to best preserve high luminosity.

INTRODUCTION

A high luminosity muon collider requires fast cooling of muons by six orders of magnitude in phase space to obtain short, intense bunches. This six-dimensional cooling is envisioned to be achieved in two stages: initial multi-bunch cooling of trains of small bunches, and single bunch cooling of a larger density bunch in preparation for the final cooling towards collision densities. The transition between multi-bunch cooling and single bunch cooling requires an intermediate bunch recombination process with minimal beam loss.

The Helical Cooling Channel (HCC) [1-4] has been proposed as a means to achieve the six-dimensional cooling of both multiple bunches of muons and single bunches of muons. The HCC allows for continuous emittance exchange for efficient cooling, with longitudinal momentum restored through RF acceleration. In this cooling scheme, muons traverse a series of helical channels, with successive sections utilizing smaller helical spatial period λ and higher RF frequency as the muon emittances are reduced. Bunch recombination to a large single bunch necessitates a return to a larger λ and corresponding lower RF frequency, and the single bunch cooling then proceeds in a similar manner, through helical channels with successively smaller λ and higher RF frequency. A helical bunch coalescing channel provides the most natural match from the upstream multi-bunch HCC to the downstream single bunch HCC and has been explored extensively [5-7] as part of the general HCC design. The helical bunch coalescing channel uses varying RF frequencies to induce an energy-time correlation in the muon bunch train. This energy-time correlation imparts relative velocities to individual bunches such that all bunches in the bunch train align in time at the end of a short drift section and can be captured into a single RF bucket. Previous studies of the helical bunch coalescing channel demonstrated particle transmission of over 90% with an RF fill factor as low as 25%, with room for optimization, but used lower RF frequencies that are no longer relevant to the system. The previous studies also excluded transition sections necessary to match the muon bunches from the exit of the upstream multi-bunch HCC to the entrance of the helical bunch coalescing channel. This work addresses the transition section required to match the muon bunches from λ = 0.5 to 1.0 m and total momentum p=209.15 MeV/c to 286.816 MeV/c in preparation for bunch merging in the helical bunch coalescing channel previously explored.

#amysy@jlab.org

TRANSITIONING TO THE HELICAL BUNCH COALESCING CHANNEL

Muons exit the upstream multi-bunch HCC with λ = 0.5 m, RF frequency of 650 MHz, and total momentum on the reference orbit of 209.15 MeV/c. This bunch coalescing method has been found to be more efficient at higher muon momentum [6]; these most recent studies assumed that the acceleration of muons to 286.816 MeV/c could be accomplished with zero emittance growth and zero beam loss. The bunch coalescing channel described in [6] also utilizes λ = 1.0 m and RF frequency of 200 MHz. This parameter mismatch necessitates a transition section to evaluate the emittance growth and particle losses induced by the matching section and to allow for an end-to-end simulation of the complete six-dimensional cooling channel. The most efficient transition section will simultaneously accelerate muons while adiabatically increasing λ. We note that the previous bunch coalescing channel was simulated using RF frequency of 200 MHz, and the bunch merge performance is expected to scale with higher RF frequency.

SIMULATION GEOMETRY

The transition section to the helical bunch coalescing channel was simulated using G4Beamline/GEANT4 [8]. RF cavities of length 5 cm were used throughout the transition section, with 60 μm thick beryllium windows

Content from this work may be used under the terms of the CC BY 3.0 licence (© 2015). Any distribution of this work must maintain attribution to the author(s), title of the work, publisher, and DOI.

ISBN: 978-3-95450-168-7 doi:10.18429/JACoW-IPAC2015-TUPWI034

Content from this work may be used under the terms of the CC BY 3.0 licence (© 2015). Any distribution of this work must maintain attribution to the author(s), title of the work, publisher, and DOI.

CAPTURE, ACCELERATION AND BUNCHING RF SYSTEMS FOR THE MEIC BOOSTER AND STORAGE RINGS*

S. Wang#, J. Guo, F. Lin, V. Morozov, R. Rimmer, H. Wang, Y. Zhang
Jefferson Lab, Newport News, VA 23606, USA

Abstract

The Medium-energy Electron Ion Collider (MEIC), proposed by Jefferson Lab, consists of a series of accelerators. The electron collider ring accepts electrons from CEBAF at energies from 3 to 12 GeV. Protons and ions are delivered to a booster and captured in a long bunch before being ramped and transferred to the ion collider ring. The ion collider ring accelerates a small number of long ion bunches to colliding energy before they are re-bunched into a high frequency train of very short bunches for colliding. Two sets of low frequency RF systems are needed for the long ion bunch energy ramping in the booster and ion collider ring. Another two sets of high frequency RF cavities are needed for re-bunching in the ion collider ring and compensating synchrotron radiation energy loss in the electron collider ring. The requirements from energy ramping, ion beam bunching, electron beam energy compensation, collective effects, beam loading and feedback capability, RF power capability, etc. are presented. The preliminary designs of these RF systems are presented. Concepts for the baseline cavity and RF station configurations are described, as well as some options that may allow more flexible injection and acceleration schemes.

INTRODUCTION

For the ion accelerator complex, one major change from earlier design is that only one booster exists between the source-linac system and ion collider ring [1]. In this booster, ions are captured and form a single long bunch, accumulated to the required bunch charge, and then ramped, to 8 GeV(H^+)/3.2 GeV/u(lead ion) and cooled, before being transferred to the ion collider ring. In the ion collider ring, nine long bunches are formed before being ramped to collision energy. At collision energy, the long bunches are debunched and rebunched in to 476 MHz buckets before collision with the electron bunches.

For the electron collider ring, it accepts bunch trains from CEBAF. The RF system needs to provide synchrotron radiation energy compensation and bunch longitudinal formation at different collision energies with high enough beam current, and stable operation.

CAPTURE AND RAMPING RF CAVITIES IN BOOSTER AND ION COLLIDER RING

In the ion source-linac system, ion bunch trains are accelerated to 285 MeV (proton) or 114 MeV/u (lead ions) before being delivered to the booster. Like other rapid cycling synchrotrons, the micro bunches from the linac will be accumulated in the booster ring, captured by the potential well produced by the RF field. The 8 GeV booster ring is designed to utilize multi-turn injection with combined longitudinal and transverse painting and charge exchange mechanism.

At low energy, space charge effect is the most important effect that limits the maximum available total charge in each ramping cycle. That is why a long bunch is needed in the booster in order to lower the space charge density.

During the energy ramping process in both booster and collider rings the beta of ions varies so the RF frequency needs to be variable to keep up with the revolution frequency. So, we need choose the inductance-loaded RF cavities as the ramping cavities. Because the ramping rate is limited by the super-ferric bending magnets [2], the total gap voltage needed for ramping is not high, as shown in Table 1. We chose ferrite-loaded cavities for the design for the lower cost. In the design, we assumed a linear ramping process. Design data for the ramping cavities in booster and collider ring are shown in Table 2.

Table 1: Summary of Ramping Cavity Configuration

	Booster	Collider
Circumference (m)	238.88	2149.9
Harmonic Number	1	9
Gaps per Cavity	2	
Cavity Number	2	7
Cavity Length (m)	2.2	
Total Cavity Length (m)	4.4	15.4
Ferrite Toroid Inner Radius (m)	0.25	
Ferrite Toroid Outer Radius (m)	0.5	
Ferrite Stack Length (m)	1	
Maximum Gap Voltage (kV)	10	

Table 2: Summary of Ramping Cavity RF Parameters

	Booster		Collider	
	H^+	$^{208}Pb^{67+}$	H^+	$^{208}Pb^{67+}$
Energy(GeV/u)	0.285 ~ 8	0.114 ~ 3.2	8 ~ 100	3.2 ~ 40
RF Frequency (MHz)	0.817 ~1.274	0.571 ~ 1.22	1.248 ~1.255	1.223 ~ 1.25
Ramping Time (Sec)	0.404	0.57	12.0	12.2
Vgap (kV)	8.0	5.75	7.9	7.9
Beam Power (kW)	8.0	1.85	27.5	10.8

* Notice: Authored by Jefferson Science Associates, LLC under U.S. DOE Contract No. DE-AC05-06OR23177 and DE-AC02-06CH11357. The U.S. Government retains a non-exclusive, paid-up, irrevocable, world-wide license to publish or reproduce this manuscript for U.S. Government purposes.
# wang@jlab.org

ISBN: 978-3-95450-168-7 doi:10.18429/JACoW-IPAC2015-TUPWI035

MEIC PROTON BEAM FORMATION WITH A LOW ENERGY LINAC[#]

Yuhong Zhang*, Thomas Jefferson National Accelerator Facility, Newport News, VA USA

Abstract

The MIEC proton and ion beams are generated, accumulated, accelerated and cooled in a new green-field ion injector complex designed specifically to support its high luminosity goal. This injector consists of sources, a linac and a small booster ring. In this paper we explore feasibility of a short ion linac that injects low energy protons and ions into the booster ring.

INTRODUCTION

A polarized medium-energy electron-ion collider, MEIC, has been envisioned as a future facility at JLab beyond the 12 GeV CEBAF program [1,2]. This future collider is designed to deliver high performance including high luminosities and high polarization of both electron and light ion beams. Its luminosity concept [3] is based on a high bunch repetition rate, up to 476 MHz, which enables small emittance, short bunch length, and very strong final focusing.

The MEIC proton and ion beams are generated in a new ion injector in a green field. Recently, great efforts were made to optimize the injector design for achieving better performance and for lowering the cost. The first major change of the design is elimination of a large booster ring (3 to 20 GeV) by allowing the beams being injected directly into the collider ring from the small booster [4]. The proton extraction energy from the booster is raised to 7.9 GeV, therefore greatly easing the space charge bottleneck when the beam is injected into a full size ring (the large booster has a same circumference as the collider ring). The second major change is a proposed reduction of the linac energy by nearly 60%, leading to a large reduction of the ion linac cost. Lowering the linac energy, however, has serious impact on the process of ion beam formation, therefore, the injection scheme must be reformulated to accommodate lower injection energies and to alleviate the much stronger space charge effect. This paper reports a recent study of this topic.

MEIC ION INJECTOR

The MEIC ion injector is designed with the following major components [2]: polarized ion sources (for H^-/D^- and ^3He) and non-polarized ion sources (up to lead); a pulsed linac made of a warm front end and SRF cavities; and a single booster ring (up to 7.9 GeV). The booster ring also includes a DC electron cooler for assisting accumulation of ions and, as a part of a multi-step cooling scheme [5,6], for the initial stage of emittance reduction of all ion beams. Such DC cooling is very efficient at low energies thus it greatly improves the overall cooling rate.

Like all hadron facilities, it is a long process to form and accelerate an ion beam for collisions with an electron beam in MEIC. This process can be outlined below:

1. Eject the used beam from the collider ring, cycle the magnets;
2. Accumulate protons strip-injected from the linac to the booster ring;
3. Ramp energy to 2 GeV (the DC cooling energy);
4. Perform DC electron cooling;
5. Ramp to 7.9 GeV (the booster ejection energy);
6. Transfer the beam into the collider ring; cycle the booster ring magnets;
7. Repeat step 2 to 6 to fill the collider ring, perform electron cooling during stacking;
8. Ramp to the collision energy (20 to 100 GeV)
9. Perform bunch splitting to reach high bunch repetition rate while continuing electron cooling;
10. Resume *e-p* collisions.

Figure 1 below illustrates this beam formation process. The number of injection cycles from the booster to the collider ring depends on the linac energy. Formation of heavy ion beams in MEIC follows a similar process except it requires more injections from the booster ring.

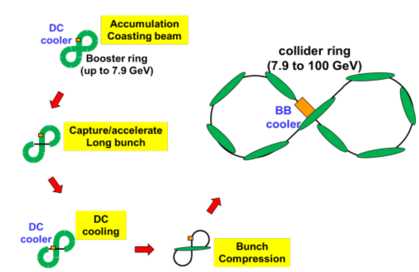

Figure 1: An illustration of the MEIC ion beam formation process. It requires multiple transfers of accumulated long bunches from the booster to the collider ring. The beam intensity is limited by the magnet apertures and the space charge effect at injection of the booster.

The MEIC ion linac is designed to accelerate protons to 285 MeV and (partially stripped) ions such as $^{208}Pb^{67+}$ to 100 MeV per nucleon [1,2,7]. Presently, we are exploring feasibility of replacing this SRF linac by a cost-effective pulsed warm RF linac (as first suggested by this author), the conceptual development is underway [8]. Alternately, lowering the linac energy could also achieve a substantial cost reduction for MEIC. One approach is installing only the warm front end and the first section of the SRF linac for the present MEIC baseline. As a result, the proton energy from the linac is 120 MeV and the lead ion energy is about 40 MeV per nucleon [7]. It is planed that extra space will be reserved for the remaining part of the SRF linac as an option of future MEIC luminosity upgrade.

INJECTION SCHEME WITH A LOW ION LINAC ENERGY

It is understood that intensity of an accumulated hadron beam in a booster ring is primarily limited by the magnet

The work is authored by Jefferson Science Associates, LLC under U.S. DOE Contract No. DE-AC05-06OR23177.
* yzhang@jlab.org

Content from this work may be used under the terms of the CC BY 3.0 licence (© 2015). Any distribution of this work must maintain attribution to the author(s), title of the work, publisher, and DOI.

ISBN: 978-3-95450-168-7 doi:10.18429/JACoW-IPAC2015-TUPWI037

Content from this work may be used under the terms of the CC BY 3.0 licence (© 2015). Any distribution of this work must maintain attribution to the author(s), title of the work, publisher, and DOI.

ELECTRON COOLING STUDY FOR MEIC*

H. Zhang#, D. Douglas, Ya Derbenev, Y. Zhang, Jefferson Lab, Newport News, VA 23606, USA

Abstract

Electron cooling of the ion beams is one critical R&D to achieve high luminosities in JLab's MEIC proposal. In the present MEIC design, a multi-staged cooling scheme is adapted, which includes DC electron cooling in the booster ring and bunched beam electron cooling in the collider ring at both the injection energy and the collision energy. We explored the feasibility of using both magnetized and non-magnetized electron beam for cooling, and concluded that a magnetized electron beam is necessary. Electron cooling simulation results for the newly updated MEIC design is also presented.

INTRODUCTION

The medium energy electron ion collider (MEIC) proposed by JLab can deliver a luminosity above 10^{34} $\mathrm{cm}^{-2}\mathrm{s}^{-1}$ at a center-of-mass energy up to 65 GeV. It offers an electron energy up to 10 GeV, a proton energy up to 100 GeV, and corresponding energies per nucleon for heavy ions with the same magnetic rigidity [1]. Cooling of proton and ion beams is essential for reduction of beam emittance, suppressing the intra-beam scattering (IBS) effect thus achieving the high luminosity. The conventional electron cooling technique is chosen and a multi-stage cooing strategy has been developed.

Figure 1 shows the schematic layout of the MEIC ion complex, including a DC cooler in the booster and a bunched beam cooler in the collider ring. Since the electron cooling time is in proportion to the energy and the 6D emittance of the ion beam, it is preferred to begin the process of cooling the ion beam to the desired emittance at the lower energy. In addition, it is necessary to apply cooling during collision to maintain the emittance, otherwise the strong IBS effect will lead to a quick increase of the ion beam emittance and the luminosity will collapse. The cooling scheme for the proton beam includes the following three stages: (1) DC cooling for 2 GeV proton beam in the booster, (2) bunched beam cooling for proton beam at the injection energy (8 GeV) in the collider ring, and (3) bunched beam cooling for proton beam at the collision energy in the collider ring.

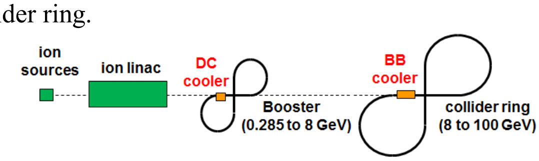

Figure 1: MEIC ion complex layout.

The technology of DC cooling is mature. A magnetized DC cooler with similar performance required by MEIC has been successfully built and commissioned at the COSY facility at Juelich [2]. The cooling by a bunched electron beam is beyond the state-of-art. The MEIC bunched beam cooler is composed of two 30 meter long cooling sections and an ERL circulator ring, which allows to repeatedly use the electron bunch tens of times. In the following we will discuss the necessity of using magnetized electron beam in the bunched beam cooler and present some simulation results.

MATCHING OF BETATRON FUNCTION IN SOLENOID

The transfer matrix of a solenoid can be written as

$$M=\begin{pmatrix} C^2 & SC/k & SC & S^2/k \\ -kSC & C^2 & -kS^2 & SC \\ -SC & -S^2/k & C^2 & SC/k \\ kS^2 & -SC & -kSC & C^2 \end{pmatrix},$$

where $k=B_0/(2B\rho)$, B_0 is the magnetic field inside the solenoid, $B\rho$ is the magnetic rigidity of the reference particle moving along the central trajectory, $C=\cos kL$, $S=\sin kL$, and L is the effective length of the solenoid [3]. Assuming the incoming beam is round with no correlation in the transverse directions, the Σ matrix of the incoming beam can be written as

$$\Sigma_i=\begin{pmatrix} \sigma_{11} & \sigma_{12} & 0 & 0 \\ \sigma_{12} & \sigma_{22} & 0 & 0 \\ 0 & 0 & \sigma_{11} & \sigma_{12} \\ 0 & 0 & \sigma_{12} & \sigma_{22} \end{pmatrix}.$$

At the exit of the solenoid, we have

$$\Sigma_f=M\Sigma_i M^T=\begin{pmatrix} \Sigma_{xf} & 0 \\ 0 & \Sigma_{yf} \end{pmatrix},$$

where M^T is the transpose of M, $\Sigma_{xf}=\Sigma_{yf}=\Sigma$ and component-wisely

$$\Sigma_{11}=C^2\sigma_{11}+\frac{2CS}{k}\sigma_{12}+\frac{S^2}{k^2}\sigma_{22},$$
$$\Sigma_{12}=\Sigma_{21}=-kSC\sigma_{11}+(C^2-S^2)\sigma_{12}+\frac{SC}{k}\sigma_{22},$$
$$\Sigma_{22}=k^2S^2\sigma_{11}-2kCS\sigma_{12}+C^2\sigma_{22}.$$

To keep the transverse bunch size constant inside the solenoid, we need to have constant β function, which means $\beta(s)=\beta$ and $\alpha(s)=0$ for $0\le s\le L$. Thus we have $\sigma_{12}=0$ and $\sigma_{22}=\varepsilon/\beta=\sigma_{11}/\beta^2$ in the solenoid. Since the transverse bunch size does not change, we have

$$\sigma_{11}=C^2\sigma_{11}+\frac{2CS}{k}\sigma_{12}+\frac{S^2}{k^2}\sigma_{22}=C^2\sigma_{11}+\frac{S^2}{k^2\beta^2}\sigma_{11}.$$

So that

$$\beta=\frac{1}{|k|}=\frac{2B\rho}{B_0}=\frac{2p}{qB_0}, \qquad (1)$$

where p, and q are momentum and the charge number of the particle. Eq. (1) is the matching condition for the transverse β function in a solenoid.

The Larmor frequency of a charged particle inside a solenoid is $\omega=Bq/\gamma m_0$, where m_0 is the mass of the

*Work supported the U.S. Department of Energy, Office of Nuclear Physics, under Contract No. DE-AC05-06OR23177 and No. DE-AC02-06CH11357.
#hezhang@jlab.org

ISBN: 978-3-95450-168-7 doi:10.18429/JACoW-IPAC2015-TUPWI038

A HIGH ENERGY *e-p/A* COLLIDER BASED ON *CepC-SppC**

Yuhong Zhang#, Thomas Jefferson National Accelerator Facility, Newport News, Virginia, USA
Yuimei Peng, Institute of High Energy Physics, Chinese Academy of Science, Beijing, China

Abstract

Construction of *CepC* and *SppC*, the proposed future energy frontier circular *e+e-* and *pp* colliders in China, provides an opportunity to realize *e-p* or *e-A* collisions in a CM energy range up to 4.1 TeV. This paper presents a preliminary conceptual design of this *e-p/A* collider. The design parameters and anticipated luminosities will be given. We also discuss staging approaches to realize this collider with a low cost and at an earlier time.

INTRODUCTION

Recently, a circular *e+e-* collider (*CepC*) with a 240 GeV CM energy as a Higgs factory has been proposed at Institute of High Energy Physics (IHEP) in China. Its envisioned upgrade, a *pp* collider (*SppC*), will be built for the next energy frontier to reach 70 TeV CM energy [1]. Based on *CepC-SppC*, a multi-TeV electron-proton/ion collider, *CepC-SppC e-p/A collider* (code named *SehC* in this paper), will provide a probe (through ultra deep inelastic scatterings) that can reach unprecedentedly deep inner structure of the matters. Luminosity of the *e-p* collisions can reach middle of 10^{33}/cm^2/s [1].

DESIGN CONSIDERATIONS

An assumption of this design study is that there will be no major upgrade of *CepC* and *SppC* for realizing the *e-p/A* collisions. Thus, the *e-p/A* performance will be determined primarily by the beams that the envisioned *e+e-* and *pp* colliders could provide. The design will follow the *CepC-SppC* operational limit such as the maximum beam energies and currents, the synchrotron radiation (SR) power budget. The design will also observe limits on the parameters due to collective effects such as beam-beam interactions. However, within these limits, beam parameters such as the bunch repetition rate, bunch charges, emittance aspect ratio or crossing angles, can be altered for achieving an optimized performance.

CepC and *SppC* are two very different colliders in terms of parameters of the colliding beams. The *CepC* electron beam has 50 bunches due to a single-ring design while the *SppC* proton or ion beam has a large number of bunches varying from 3000 to 6000. This fact plus an extremely asymmetry of beam emittance aspect ratios effectively exclude the option of simultaneous operations of *e+e-* and *e-p/A* collisions in the *CepC-SppC* complex. Without this constraint, the electron beam is no longer limited to 50 bunches, it can be increased to match the bunch numbers of a proton beam from *SppC*.

Selection of the final focusing parameters for the *e-p/A* collisions is driven by the interaction region (IR) design considerations. For example, the beam spot sizes should be matched at an interaction point (IP) in order to alleviate the beam-beam effect. Nevertheless, the *CepC* lepton beam is extremely flat (the aspect ratio is as high as 333) while the *SppC* proton beam is basically round. Matching of these two beams requires very large vertical beta-star for the electron beam thus blows-up the beam-beam parameters. The operational scenario that the *e-p/A* and *e+e-* collisions will not be run simultaneously provides the opportunity to change the electron beam to a round one by utilizing the transverse optics coupling.

In the *SppC* energy regime, the synchrotron radiation and its effect on the proton or ion beam are no longer negligible. The damping time of a proton or heavy ion beam is similar or even shorter than the time of beam store. As a consequence, the proton or ion beam emittance will approach to an equilibrium value (in a balance of radiation damping and quantum excitation, and intra-beam scatterings) during the beam store. This will affect the peak luminosity as well as the integration of luminosity over one store of the beam.

The *e-p/A collider* based on *CepC-SppC* is a highly asymmetric one with an energy ratio up to 292, a highest value compared to all other *e-p/A* colliders ever been constructed or studied. The simple kinematics shows the reactant particles from collisions will go dominantly in the forward direction of the proton or ion beam. Therefore, it is expected that the forward detection of particles with extremely small scattering angles will be a critical requirement of the detector. Designing an IR to support such extreme forward detections is challenging and will require thorough studies. At the moment, as a straw-man design, we will adopt the similar final focusing parameters (beta-star β^*) of the *CepC* and *SppC* colliders respectively.

Lastly, the science programs utilizing deep inelastic scatterings as a probe usually demand experimental data collected over an energy scan. This requires the *e-p/A* collider design to be optimized over a broad energy range for both electron and proton/ion beams. In this paper, we present design parameters at a representative energy point, namely, 120 GeV electron energy and 35 TeV proton energy, the highest energies that *CepC* and *SppC* could provide. Luminosities at three other electron energies corresponding to *Z, W* and *T* processes are also given.

e-p COLLISION PARAMETERS

Table 1 below presents the nominal design parameters for the *CepC-SppC e-p* collisions. There will be only one beam in the *CepC* ring, thus the electron beam current can be doubled to 33.8 mA while still under the operational limit of 100 MW total SR power. The electron beam could have thousand bunches to match the bunch pattern

*This material is based upon work supported by the U.S. Department of Energy, Office of Science, Office of Nuclear Physics under contract DE-AC05-06OR23177.
yzhang@jlabl.org

Content from this work may be used under the terms of the CC BY 3.0 licence (© 2015). Any distribution of this work must maintain attribution to the author(s), title of the work, publisher, and DOI.

ISBN: 978-3-95450-168-7 doi:10.18429/JACoW-IPAC2015-TUPWI039

MODELING CRABBING DYNAMICS IN AN ELECTRON-ION COLLIDER*

A. Castilla[1,2,3†], V. S. Morozov[2], T. Satogata[1,2], J. R. Delayen[1,2]
[1]Center for Accelerator Science, Old Dominion University, Norfolk, VA 23529, USA
[2]Thomas Jefferson National Accelerator Facility, Newport News, VA 23606, USA
[3]Universidad de Guanajuato (DCI-UG), Departamento de Fisica, Leon, Gto. 37150, Mexico

Abstract

A local crabbing scheme requires $\pi/2$ (mod π) horizontal betatron phase advances from an interaction point to the crab cavities on each side of it. However, realistic phase advances generated by sets of quadrupoles or Final Focusing Blocks (FFB), between the crab cavities located in the expanded beam regions and the IP differ slightly from $\pi/2$. To understand the effect of crabbing on the beam dynamics in this case, a simple model of the optics of the Medium Energy Electron-Ion Collider (MEIC), including local crabbing, was developed using linear matrices and studied over multiple turns (1000 passes) of both electron and proton bunches. This model was applied to determine linear-order dynamical effects of the synchro-betatron coupling induced by crabbing.

INTRODUCTION

It is a common practice to use linear models when initially designing and studying machine lattices. Then, special care needs to be taken when looking into non-linear effects in a ring (for example), to avoid higher order resonances that may rise undesirable dynamic conditions for the machine operations (i. e. beam filamentation, beam breakup, etc). Due to the high luminosity requirements imposed on the MEIC [1], stable beam operation while using crossing angle correctors [2] is of a major importance. In the present work we have reduced the entire electron and proton storage rings 6D dynamics to a simple linear map representation [3], excluding the interaction region (IR) (see Fig. 1).

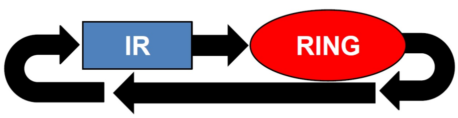

Figure 1: Conceptual sketch of the interaction region (blue) connected on its extremes by a linear map of the ring (red).

Similarly, a simplified model of a symmetric IR using linear elements in the thin lens approximation [4], such as *horizontal crab kickers*, *FFBs*, and *drifts*, was implemented for both electron and proton bunches (see Fig. 2 (a)). A more realistic layout of the current MEIC interaction region is described in Fig. 2 (b). We performed analytical calculations for the propagation of 6D Gaussian bunch distributions

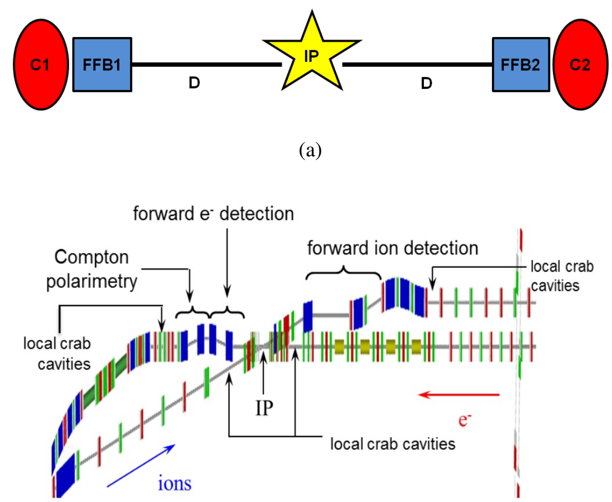

(b)

Figure 2: Schematic of the symmetric IR showing the 1st and 2nd crab cavity locations in red (C1 and C2 respectively), the FFBs in blue, the connecting drifts, and the IP in yellow (a). Layout of the current MEIC IR (b).

through the system for a 1000 passes as a first step to study the linear effects on the beams due to implementation of zero-length linear crabbing kicks to account for a 50 mrad total crossing angle. The parameters for the used Gaussian distributions are listed in Table 1.

Table 1: Parameters Used for the Particle's Distributions

Parameter	Electrons	Protons	Units
Energy	5	60	GeV
Number of particles	10^5	10^5	–
$\epsilon_{N,x}$	54	0.35	μm
$\epsilon_{N,y}$	11	0.07	μm
$\sigma_{\Delta p/p}$	7.1	3.0	$\times 10^{-4}$
σ_z	0.75	1	cm

RELATIVE PHASE ADVANCE

The relative phase advance ($\Delta\psi_{x,12}$) constriction for the crab cavitites, in a local scheme, states that the bunch should complete an integer number of betatron half oscillations between the crab cavity locations (corresponding to C1 and

* Authored by Jefferson Science Associates, LLC under U.S. DOE Contract No. DE-AC05-06OR23177.
† acastill@jlab.org

Content from this work may be used under the terms of the CC BY 3.0 licence (© 2015). Any distribution of this work must maintain attribution to the author(s), title of the work, publisher, and DOI.

ISBN: 978-3-95450-168-7 doi:10.18429/JACoW-IPAC2015-TUPWI040

END-TO-END SIMULATION OF BUNCH MERGING FOR A MUON COLLIDER

Yu Bao, Gail Hanson, University of California, Riverside, Department of Physics and Astronomy
Robert B. Palmer, Diktys Stratakis, BNL, Upton, Long Island, NY, USA

Abstract

Muon accelerator beams are commonly produced indirectly through pion decay by interaction of a charged particle beam with a target. Efficient muon capture requires the muons to be first phase-rotated by rf cavities into a train of 21 bunches with much reduced energy spread. Since luminosity is proportional to the square of the number of muons per bunch, it is crucial for a Muon Collider to use relatively few bunches with many muons per bunch. In this paper we will describe a bunch merging scheme that should achieve this goal. We present for the first time a complete end-to-end simulation of a 6D bunch merger for a Muon Collider. The 21 bunches arising from the phase-rotator, after some initial cooling, are merged in longitudinal phase space into seven bunches, which then go through seven paths with different lengths and reach the final collecting "funnel" at the same time. The final single bunch has a transverse and a longitudinal emittance that matches well with the subsequent 6D rectilinear cooling scheme.

INTRODUCTION

A high luminosity Muon Collider requires intense single muon bunches. A full scheme of a Muon Collider has been designed by the Muon Accelerator Program (MAP). In this scheme the muons are produced by a high power proton beam hitting on a target, and then they are captured and phase-rotated [1] into 21 bunches. The large initial emittance is reduced by ionization cooling, and for a high luminosity collider, the bunches need to be merged into one of each sign.

The merge concept was outlined in previous studies with preliminary simulations [2]. In this paper, we present an updated design with an end-to-end simulation using G4Beamline [3].

MERGE SCHEME

Figure 1 shows the bunch merge scheme. The incoming beam consists of 21 bunches from the output of the initial cooling channel. Each bunch has a transverse emittance (ϵ_T) of 1.3 mm and a longitudinal emittance (ϵ_L) of 1.7 mm. The 21 bunches are first merged longitudinally into seven bunches, by using radio frequency (rf) cavities with a series of rf harmonics. Then the seven bunches are transversely merged into one bunch. A kicker magnet kicks the seven bunches into seven "trombones" [4] (Only two trombones are shown in Fig. 1). Each trombone has a different arc length so that seven bunches arrive at the collecting section at the same time. A "funnel" [4] is designed to get the seven bunches close to each other to form a single bunch. In the

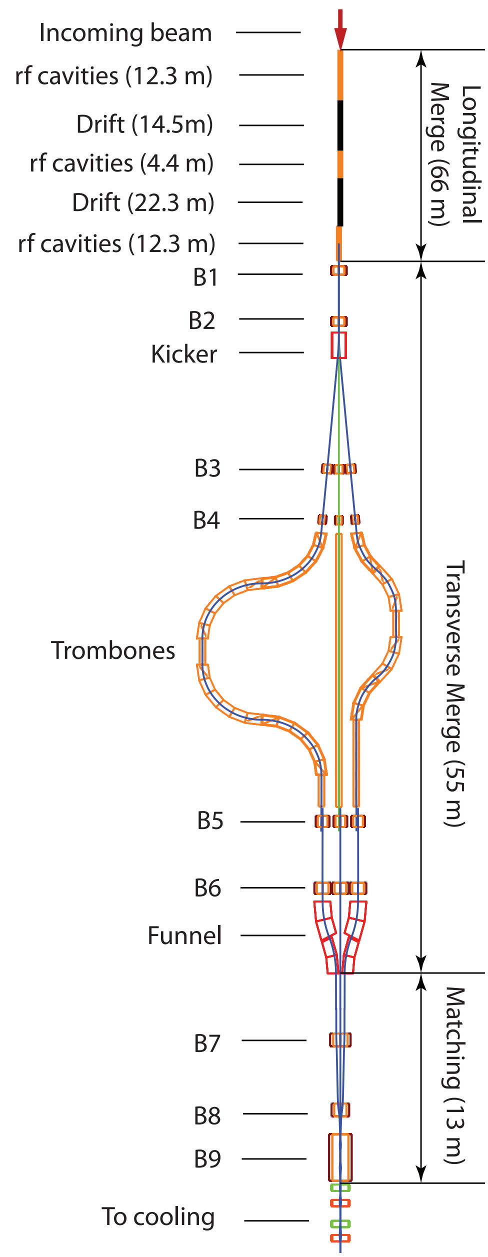

Figure 1: Merge Scheme. B1 - B9 are solenoid magnets for beam matching.

end a matching section with three solenoids will match the bunch into the post-merge cooling channel.

Longitudinal Merge

The longitudinal merge uses the rf cavities with frequencies from 108 MHz to 1950 MHz to phase-rotate the bunches

Content from this work may be used under the terms of the CC BY 3.0 licence (© 2015). Any distribution of this work must maintain attribution to the author(s), title of the work, publisher, and DOI.

ISBN: 978-3-95450-168-7 doi:10.18429/JACoW-IPAC2015-TUPWI042

INITIAL RESULTS FROM STREAKED LOW-ENERGY ULTRA-FAST ELECTRON DIFFRACTION SYSTEM

J.J. Hartzell#, R. Agustsson, L. Faillace, A. Smirnov, S. Boucher,
RadiaBeam Technologies, Santa Monica, CA 90404, USA
P. Musumeci, E. Threlkeld, UCLA, Los Angeles, CA 90095, USA

Abstract

RadiaBeam, in collaboration with UCLA, is developing an inexpensive, low-energy, ultra-fast, streaked electron diffraction (S-UED) system which allows one to reconstruct a single ultrafast event with a single pulse of electrons using and RF deflector. The high-frequency (GHz), high voltage, phase-locked RF field in the deflector enables temporal resolution of atomic events as fine as sub-100 fs. In this paper, we present an overview of the system being developed and the initial experimental results. We also discuss the challenges based on our design of a UED system that incorporates a novel, high-resolution dielectric-loaded RF deflector and a solid-state X-band amplifier.

INTRODUCTION

Time resolved observation of atomic motion is one of the frontiers of modern science, and advancements in this area will greatly improve our understanding of many basic sciences. One technique under active development in this area is ultrafast electron diffraction (UED). UED has already been used to study solid state phase transitions [1], gas phase reactions [2], strongly coupled systems [3] and surface dynamics [4]. To improve the resolution of their UED measurements, researchers need shorter electron bunches and methods increase temporal resolution on the detected electrons. By placing an RF deflecting cavity immediately after a sample, the time-dependant, diffracted electron beam can be "streaked," transforming the temporal evolution of the diffraction pattern from the sample into a transverse image [5]. In this project, we are developing a complete S-UED system based on a dielectric loaded RF deflector and a novel solid-state power amplifier (SSPA), see Fig. 1. The system also includes the requisite electron gun, laser, magnetic optics, and imaging components.

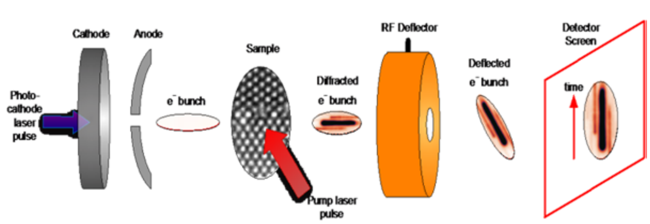

Figure 1: Overview of UED system, from photo-cathode emission on (left), through the sample, then deflector, and finally the streaked image (right).

*Work supported by DOE grant #: DE-SC0006274
#Hartzell@RadiaBeam.com

HARDWARE

The UED system was assembled in the Pegasus Lab at the University of California, Los Angeles. The beam line was initially installed and commissioned during fabrication of the dielectric deflector. During this time we conditioned the gun to its operating voltage and worked through the alignment procedure for the magnetic optics. The diagnostics were also tested during this time and the results were compared to earlier simulations. The important components of the system are described in further detail below.

Electron Gun

The 100 kV gun shown in Figure 2 was purchased from a Dutch company, AccTech. The HV conditioning and initial photo-beam measurements were carried out without insertion of the radio-frequency deflector in the beam-line to make the initial alignment process less difficult. Although the purchased version of the DC gun is not operable under ultra-high vacuum due to the use of elastomer O-rings, it is appropriate for our UED application which only requires vacuum of 10^{-6} Torr.

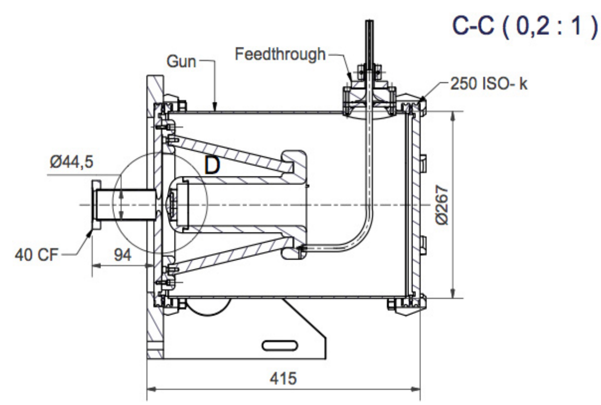

Figure 2: 100 kV electron gun employing a copper photo-cathode purchased from AccTech.

Dielectric Loaded Deflector

The deflector design was performed using the 3D code HFSS. We eventually decided to pursue a dielectric loaded structure since it saved us time and resulted in a device that was easier to manufacture than an all-copper version for such low charge. At the same time, RadiaBeam wanted to develop a medium-power (few hundred watts) RF power source using solid-state devices, and the two technologies were good compliments to each other. Figure 3 shows a 3D model of our 6 cm long

Content from this work may be used under the terms of the CC BY 3.0 licence (© 2015). Any distribution of this work must maintain attribution to the author(s), title of the work, publisher, and DOI.

ISBN: 978-3-95450-168-7 doi:10.18429/JACoW-IPAC2015-TUPWI043

CHROMATIC EFFECTS IN LONG PERIODIC TRANSPORT CHANNELS

Vladimir N. Litvinenko, Yue Hao and Yichao Jing
Department of Physics and Astronomy, Stony Brook University, Stony Brook, NY 11794, USA
Collider-Accelerator Department, Brookhaven National Laboratory, Upton, NY 11973, USA

Abstract

Long periodic transport channels are frequently used in accelerator complexes and suggested for using in high-energy ERLs for electron-hadron colliders. Without proper chromaticity compensation, such transport channels exhibit high sensitivity to the random orbit errors causing significant emittance growth. Such emittance growth can come from both the correlated and the uncorrelated energy spread. In this paper we present results of our theoretical and numerical studies of such effects and develop a criteria for acceptable chromaticity in such channels.

INTRODUCTION

The subject of emittance growth resulting from non-compensated chromaticity in single pass linac focusing systems was exhaustively studied in the era of linear colliders decades ago. Some of the classical treatment can be found in [1-4] and references therein. Effects described in these papers are fully applicable to energy recovery linacs with non-compensated chromaticity, e.g. a case presented in my paper [5] where it was suggested to use a strongly chromatic lattices to improve the beam's stability in energy-recovery linacs (ERLs), or as proposed for an ERL with FFAG arcs [6]. Recently we realized, that, naturally, such lattices would exhibit a very high sensitivity to orbital errors – the effect described in details in ref. [1-4]. Such errors could, in turn, significantly increase the beam's emittance. These emittance increase can be either stationary or time-dependent – the later is determined if beam orbit is stable or is time dependent.

In this paper we briefly review a simple case when the orbit errors are random. We also use orbit correction approach described in [1-3], and applied to a long chromatic arcs, to define sensitivity to beam-position measurement (BPM) errors.

Finally, we would like to note that there is a continuing effort of finding a robust solution for chromatic FFAG arcs (which operates beams with multiple energies) using various orbit corrections scheme to avoid beam emittance growth [7].

ORBIT DISTORTION IN CROMATIC LATTICE

Let's consider a simple uncoupled motion on a arc (or straight beam-line, then $K_o=0$) comprised of periodic cells with $K_{x,y,o}(s+P)=K_{x,y,o}(s)$:

$$x''+\frac{K_x(s)}{1+\delta}x=K_o(s)-\frac{eB_y(s)}{p_oc(1+\delta)}-\frac{e\delta B_y(s)}{p_oc(1+\delta)};$$

$$y''+\frac{K_y(s)}{1+\delta}y=+\frac{e\delta B_x(s)}{p_oc(1+\delta)};\ K_o(s)\equiv\frac{1}{\rho(s)}.$$

where $\delta B_{x,y}(s)$ are field errors and $\delta=\dfrac{E-E_o}{E_o}$ is the relative energy deviation from the reference (design) energy. It is well known that within the stability range of the periodic cell, one can find periodic reference orbit

$$K_o(s+C)=K_o(s);\ B_y(s+C)=B_y(s)$$

$$\eta^\delta+\frac{K_x(s)}{1+\delta}\eta^\delta=K_o(s)-\frac{eB_y(s)}{p_oc(1+\delta)};\ \eta^\delta(s+C)=\eta^\delta(s)$$

and Courant-Snyder function fully describing transverse oscillation about the reference orbit (here we use y-direction as example):

$$\mathrm{w}_y^\delta(s+C)=\mathrm{w}_y^\delta(s+C);\ \beta_y^\delta=\left(\mathrm{w}_y^\delta\right)^2;$$

$$y=a_y\cdot\mathrm{w}_y^\delta(s)\cdot\cos\left(\psi_y^\delta(s)+\varphi_y\right);\ \frac{d\psi_y^\delta}{ds}=\frac{1}{\beta_y^\delta(s)};$$

$$y'=\begin{Bmatrix} a_y\cdot\mathrm{w}_y'^\delta(s)\cdot\cos\left(\psi_y^\delta(s)+\varphi_y\right)\\ -\dfrac{a_y}{\mathrm{w}_y^\delta(s)}\cdot\sin\left(\psi_y^\delta(s)+\varphi_y\right)\end{Bmatrix}.$$

There is well known expression for the orbit distortions caused by an arbitrary field errors. Here we rewrite it with emphasis on the energy dependence:

$$\delta y_\delta(s)=\mathrm{w}_y^\delta(s)\int_0^s\sin\left(\psi_y^\delta(s)-\psi_y^\delta(s_1)\right)\mathrm{w}_y^\delta(s_1)\frac{e\delta B_x(s_1)}{p_oc(1+\delta)}ds_1;$$

$$\delta y'_\delta(s)=\int_0^s\begin{Bmatrix}\mathrm{w}_y'^\delta(s)\sin\left(\psi_y^\delta(s)-\psi_y^\delta(s_1)\right)+\\ \dfrac{1}{\mathrm{w}_y^\delta(s)}\cos\left(\psi_y^\delta(s)-\psi_y^\delta(s_1)\right)\end{Bmatrix}\mathrm{w}_y^\delta(s_1)\frac{e\delta B_x(s_1)}{p_oc(1+\delta)}ds_1$$

which indicative of the resulting orbit dependence on particle's energy and lattice chromaticity. Naturally, similar treatment is applicable to horizontal motion:

$$\mathrm{w}_x^\delta(s+C)=\mathrm{w}_x^\delta(s+C)$$

$$x=\eta^\delta(s)+a_x\cdot\mathrm{w}_x^\delta(s)\cdot\cos\left(\psi_x^\delta(s)+\varphi_x\right)+\delta x_\delta(s)$$

$$\beta_x^\delta=\left(\mathrm{w}_x^\delta\right)^2;\frac{d\psi_x^\delta}{ds}=\frac{1}{\beta_x^\delta(s)};$$

$$\delta x_\delta(s)=-\mathrm{w}_x^\delta(s)\int_0^s\sin\left(\psi_x^\delta(s)-\psi_x^\delta(s_1)\right)\mathrm{w}_x^\delta(s_1)\frac{e\delta B_y(s_1)}{p_oc(1+\delta)}ds_1.$$

Further in the paper we will use index z both to x and y. To estimate effect of chromaticity and orbit distortions on the beam emittance

Content from this work may be used under the terms of the CC BY 3.0 licence (© 2015). Any distribution of this work must maintain attribution to the author(s), title of the work, publisher, and DOI.

ISBN: 978-3-95450-168-7 doi:10.18429/JACoW-IPAC2015-TUPWI044

FINAL MUON EMITTANCE EXCHANGE IN VACUUM FOR A COLLIDER*

Don Summers†, John Acosta, Lucien Cremaldi, Terry Hart, Sandra Oliveros,
Lalith Perera, Wanwei Wu, University of Mississippi - Oxford, University, MS 38677, USA
David Neuffer, Fermilab, Batavia, IL 60510, USA

Abstract

We outline a plan for final muon ionization cooling with quadrupole doublets focusing onto short absorbers followed by emittance exchange in vacuum to achieve the small transverse beam sizes needed by a muon collider. A flat muon beam with a series of quadrupole doublet half cells appears to provide the strong focusing required for final cooling. Each quadrupole doublet has a low β region occupied by a dense, low Z absorber. After final cooling, normalized xyz emittances of (0.071, 0.141, 2.4) mm-rad are exchanged into (0.025, 0.025, 70) mm-rad. Thin electrostatic septa efficiently slice the bunch into 17 parts. The 17 bunches are interleaved into a 3.7 meter long train with RF deflector cavities. Snap bunch coalescence combines the muon bunch train longitudinally in a 21 GeV ring in 55 μs, one quarter of a synchrotron oscillation period. A linear long wavelength RF bucket gives each bunch a different energy causing the bunches to drift until they merge into one bunch and can be captured in a short wavelength RF bucket with a 13% muon decay loss and a packing fraction as high as 87%.

INTRODUCTION

Due to s-channel production, a muon collider [1] may be ideal for the examination of H/A Higgs scalars which could be at the 1.5 TeV/c^2 mass scale and are required in supersymmetric models [2]. But what is the status of muon cooling? As noted in Table 1, more than five orders of magnitude of muon cooling have been shown in two simulated designs [3, 4] but not quite the six orders of magnitude needed for a high luminosity muon collider. Also as can be seen in Table 1, some of the longitudinal cooling needs to be exchanged for lower transverse emittance.

A long solenoid [5] with a 14 Tesla magnetic field and a 200 MeV/c muon beam gives a betatron function of $\beta_\perp = 2p/[3.0B] = 2(200\,\text{MeV/c})/[3.0\,(14\,\text{T})] = 9.5\,\text{cm}$ and works with high pressure or liquid hydrogen absorber. The short 14 T solenoids in the final stage of the Rectilinear Cooling Channel [4] give $\beta^* = 3.1$ cm in a region of limited length, which is filled with lithium hydride absorber. To get to the lower betatron values of about 1 cm needed by a muon collider for final cooling, quadrupole doublet cells are explored herein. Table 2 gives transverse equilibrium emittances for a number of low Z materials, particularly those with high densities.

* Work supported by NSF Award 0969770
† summers@phy.olemiss.edu

Table 1: Helical and Rectilinear Cooling Channel normalized 6D emittances from simulations and the emittance needed for a muon collider. The channels cool by over five orders of magnitude and need less than a factor of 10 more for a collider. The 21 bunches present after initial phase rotation are also merged into one bunch during cooling.

	ϵ_x (mm)	ϵ_y (mm)	ϵ_z (mm)	ϵ_{6D} (mm^3)
Initial Emittance [4]	48.6	48.6	17.0	40,200
Helical Cooling [3]	0.523	0.523	1.54	0.421
Rectlinear Cooling [4]	0.28	0.28	1.57	0.123
Muon Collider [1]	0.025	0.025	70	0.044

Table 2: Muon equilibrium emittance at 200 MeV/c (β = v/c = 0.88) for hydrogen, lithium hydride, beryllium, boron carbide, diamond, and beryllium oxide absorbers, [6–8]. $\epsilon_\perp = \beta^* E_s^2/(2g_x\,\beta\, m_\mu c^2 (dE/ds) L_R)$, where β^* twiss is 1 cm, E_s is 13.6 MeV, the transverse damping partition number g_x is one with parallel absorber faces, $m_\mu c^2$ is 105.7 MeV, and L_R is radiation length.

Material	Density g/cm^3	L_R cm	dE/ds MeV/cm	$\epsilon_\perp$ (mm - rad) (equilibrium)
H_2 gas	0.000084	750,000	0.00037	0.036
Li H	0.82	97	1.73	0.059
Be	1.85	35.3	3.24	0.087
B_4C	2.52	19.9	4.57	0.109
Diamond	3.52	12.1	6.70	0.123
Be O	3.01	13.7	5.51	0.132

QUADRUPOLE DOUBLET COOLING

Following Feher and Strait [9] and their paper including the LHC final focus quadrupole triplet design in 1996 with a β^* of 50 cm, we look into a short quadrupole doublet for final muon cooling with a β^* of 1 cm. Focal lengths in x and y differ in the doublet. The outer two LHC quadrupoles are focusing in the first transverse dimension and defocusing in the second transverse dimension. The inner double length quadrupole is focusing in the second transverse dimension and defocusing in the first transverse dimension. The relation between β functions, focal length (L_f), and beam size is

$$\beta^* \beta_{\max} = b\, L_f^2 \quad \text{and} \quad \sigma_x = \sqrt{\epsilon_x \beta_x/(\beta\gamma)} \qquad (1)$$

where b is a fudge factor equal to 1.65 for the LHC. Thus a lower β^* leads to a larger $\beta_{\max}$ and larger bore quadrupoles.

Content from this work may be used under the terms of the CC BY 3.0 licence (© 2015). Any distribution of this work must maintain attribution to the author(s), title of the work, publisher, and DOI.

ISBN: 978-3-95450-168-7 doi:10.18429/JACoW-IPAC2015-TUPWI045

Content from this work may be used under the terms of the CC BY 3.0 licence (© 2015). Any distribution of this work must maintain attribution to the author(s), title of the work, publisher, and DOI.

CONSEQUENCES OF BOUNDS ON LONGITUDINAL EMITTANCE GROWTH FOR THE DESIGN OF RECIRCULATING LINEAR ACCELERATORS

J. Scott Berg, BNL*, Upton, NY 11973, USA

Abstract

Recirculating linear accelerators (RLAs) are a cost-effective method for the acceleration of muons for a muon collider in energy ranges from a couple GeV to a few 10s of GeV. Muon beams generally have longitudinal emittances that are large for the RF frequency that is used, and it is important to limit the growth of that longitudinal emittance. This has particular consequences for the arc design of the RLAs. I estimate the longitudinal emittance growth in an RLA arising from the RF nonlinearity. Given an emittance growth limitation and other design parameters, one can then compute the maximum momentum compaction in the arcs. I describe how to obtain an approximate arc design satisfying these requirements based on the deisgn in [1]. Longitudinal dynamics also determine the energy spread in the beam, and this has consequences on the transverse phase advance in the linac. This in turn has consequences for the arc design due to the need to match beta functions. I combine these considerations to discuss design parameters for the acceleration of muons for a collider in an RLA from 5 to 63 GeV.

INTRODUCTION

For the muon accelerator scenario described in [2], they envision an RLA accelerating from 5 to 63 GeV, which would accelerate beams for two stages of a Higgs factory, and would be reused for a higher energy collider with a substantially larger emittance. Important machine parameters are given in Tables 1 and 2. Details of the rationale for many of these parameters can be found in [3].

An RLA allows rapid acceleration while making multiple passes through a linac by having a beam splitter at the ends of the linac and arcs for each energy that return the beam to the linac. Having large numbers of arcs at the splitter can become a problem, particularly for large beam emittances and small energy spacings. A "dogbone" RLA geometry helps address this [4]. Bogacz [1] has described a technique to design the "droplet" arcs for this lattice; I will adopt that basic technique here.

I first discuss a generic technique to obtain a droplet arc design according to Bogacz' concept, and obtain from that an approximation to the time of flight dependence on energy in the arc. I then compute an approximation to the longitudinal emittance growth which depends on that time of flight parameter. I finally put these together to determine parameters for the RLA that will meet the requirements.

* This manuscript has been authored by employees of Brookhaven Science Associates, LLC under Contract No. DE-SC0012704 with the U.S. Department of Energy. The United States Government retains a non-exclusive, paid-up, irrevocable, world-wide license to publish or reproduce the published form of this manuscript, or allow others to do so, for United States Government purposes.

Table 1: Beam and Machine Parameters [2]. The left two columns are for a Higgs factory, the rightmost column for a higher energy collider.

Particles per bunch ($\times 10^{12}$)	2	4	2
Longitudinal emittance (mm)	1.0	1.5	70
Transverse emittance (μm)	400	200	25
Initial total energy (GeV)	5	5	5
Final total energy (GeV)	63	63	63
Maximum emittance growth (%)		10	
Maximum decay loss (%)		11.0	
Physical aperture (σ)		4.5	

Table 2: Assumed Cavity Parameters

Frequency (MHz)	325	650
Gradient (MV/m)	20	25
Maximum cells per cavity	4	5
Maximum cavity passes	9	3
Additional length at each end (cells)	1.5	

DROPLET ARC

The structure of a droplet arc is described in Table 3 and shown in Fig. 1. From the linac to the middle, the sections consist of

- Dispersion matching cells from the linac to the arc
- Outward bending cells

Table 3: Droplet Arc Structure

Cells	Bend Angle	Cell Length
2	$-\theta_m/2$	L_m
n_o	$-\theta$	L
2	0	L
n_i	θ	L
2	0	L
n_o	$-\theta$	L
2	$-\theta_m/2$	L_m

ISBN: 978-3-95450-168-7 doi:10.18429/JACoW-IPAC2015-TUPWI047

TARGET AND ORBIT FEEDBACK SIMULATIONS OF A muSR BEAMLINE AT BNL*

W. W. MacKay†, 25 Rhododendron Circle, Asheville, 28805
M. Blaskiewicz‡, W. Fischer, and P. Pile, BNL, Upton, NY 11972

Abstract

Well-polarized positive surface muons are a tool to measure the magnetic properties of materials since the precession rate of the spin can be determined from the observation of the positron directions when the muons decay. The use of the AGS complex at BNL has been explored for a muSR facility previously. Here we report simulations of a beamline with a target inside a solenoidal field, and of an orbit feedback system with single muon beam positioning monitors based on technology available today.

INTRODUCTION

Muon spin rotation, relaxation and resonance (μSR) is a powerful technique for studying local magnetic fields in samples. When a positive pion decays at rest into a positive muon, the muon has a kinetic energy of 4.119 MeV (momentum 29.792 MeV/c) and its spin is opposite to its direction (negative helicity). If the pion decays near the surface of a target the resulting muons lose little energy, and the result is a beam of muons with a narrow energy distribution and almost 100% polarization. When these positive muons are implanted in matter with a magnetic field the muons precess at a rate proportional to the local field. When the muon decays the positron momentum is preferentially along the direction of the muon spin.

In this paper, we present improvements of our previous design for a surface muon beam line at BNL [1, 2] including optimization of the target and muon capture. Also we discuss the efficacy of a possible orbit feedback section to increase the density of the muon beam for experiments.

A beam of protons with kinetic energy 1.5 GeV will be extracted from the AGS (see Fig. 1) and focused onto a thin 0.5 mm wide target. An average intensity of 10^{14} proton/s with a normalized rms emittance of 8π μm is quite achievable from the AGS. Detailed parameters of the AGS and injector chain for μSR were presented previously [1].

The tracking code G4BEAMLINE [3] has been used for most simulations of the beam line in this paper.

MUON TARGET AND CAPTURE

Pions which are produced and stop in the target will decay yielding muons which may exit the target if they are within 0.7 mm of the surface of the graphite target (see Fig. 2). Pions stopped any deeper in the target will produce muons which stop and decay inside the target leading to higher backgrounds and heating of the target and nearby beam-line elements. By making a long, horizontally thin target with the proton beam running down the length and having a waist focused at the center of the target, we can get surface muons from pions stopped near the surface with a minimum of background and heating. Fig. 3 shows a 200 mm long, 0.5 mm target, 50 mm high graphite target with a beam (noninteracting in the figure) having a $\sigma_h^* = 0.25$ mm waist. For 10^{14} protons/s simulations yield about 15×10^9 μ^+/s 0.2 mm from the target's surface. Four times as many positrons are produced, but most are outside the momentum acceptance of the beam line.

To capture the muon beam, we use a decreasing field from four solenoids placed around the target as shown in Fig. 4. A scan of the capture efficiency versus the field of the upstream solenoid (−1) shown in Fig. 5 demonstrates that capture is more efficient with a negative slope to the axial field around the target. This is reminiscent of Adiabatic Matching Devices [6] used in positron linacs. Fig. 6 shows the momentum distributions of μ^+ and e^+ at the exit of the solenoid 3.

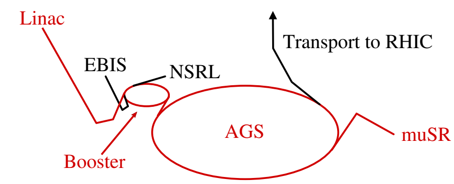

Figure 1: Schematic of the AGS complex with sections to be used for μSR shown in red.

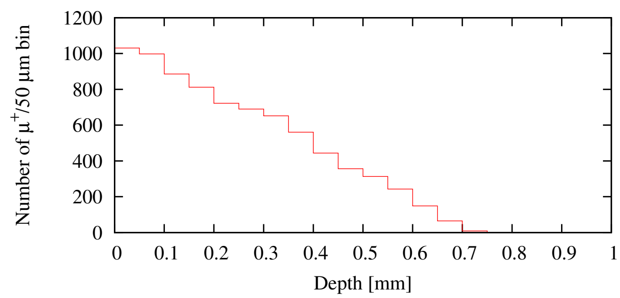

Figure 2: Number of μ^+ exiting the target from a uniform distribution of rest π^+ placed inside a thick block of graphite. No μ^+ come from a depth greater than 0.7 mm.

Figure 3: Top view of target and proton beam. The proton beam is focused onto the middle of the narrow graphite $200 \times 50 \times 0.5$ mm ($l \times h \times w$) target.

* Work supported by U.S. DOE under contract No DE-AC02-98CH10886 with the U.S. Department of Energy.
† wwmackay@charter.net
‡ blaskiewicz@bnl.gov

Content from this work may be used under the terms of the CC BY 3.0 licence (© 2015). Any distribution of this work must maintain attribution to the author(s), title of the work, publisher, and DOI.

ISBN: 978-3-95450-168-7 doi:10.18429/JACoW-IPAC2015-TUPWI048

EXPERIMENTAL DEMONSTRATION OF INTERACTION REGION BEAM WAIST POSITION KNOB FOR LUMINOSITY LEVELING*

Yue Hao†, Yun Luo, Aljosa Marusic, Guillaume Robert-Demolaize, BNL, Upton, NY 11973, USA
Mei Bai, Forschungszentrum Jülich GmbH (FZJ) Institut für Kernphysik, Germany
Zhe Duan, Institute of High Energy Physics, Beijing, China
Xiaozhe Shen, SLAC, Menlo Park, CA 94025

Abstract

In this paper, we report the experimental implementation of the model-dependent control of the interaction region beam waist position (s^* knob) at Relativistic Heavy Ion Collider (RHIC). The s^* adjustment provides an alternative way of controlling the luminosity and is only known method to control the luminosity and reduce the pinch effect of the future eRHIC. In this paper, we will first demonstrate the effectiveness of the s^* knob in luminosity controlling and its application in the future electron ion collider, eRHIC, followed by the detail experimental demonstration of such knob in RHIC.

GEOMETRIC REDUCTION OF LUMINOSITY

In collider operation, it is sometimes useful to control (lower) the luminosity for one detector without affecting others. There are many methods to control the luminosity for one specific interaction point (IP), for instance, introducing offsets between two colliding beams or increasing the waist beta function of both beams at IP. It is straightforward that adjusting the location of the beta waist (s^*) can achieve the same goal.

The luminosity at one IP can be calculated from the following integral

$$L = N_1 N_2 f \int \rho_1 (x, y, s + s_0)\, \rho_2 (x, y, s - s_0)\, dxdydsds_0 \tag{1}$$

where N_1, N_2 ,ρ_1 and ρ_2 are the bunch intensities and 3-D normalized distribution functions of two colliding beam respectively, f is the bunch repetition rate. $s = (z_1 + z_2)/2$ and $s_0 = ct = (z_1 - z_2)/2$ correspond to the collision location and time of two beam slices at z_1 and z_2. We assume both beams has Gaussian distribution in all three dimensions:

$$\rho_{1/2} = \frac{1}{(2\pi)^{\frac{3}{2}} \sigma_{x,1/2}\sigma_{y,1/2}\sigma_{s,1/2}} \times \exp\left[-\frac{x^2}{2\sigma^2_{x,1/2}(s)} - \frac{y^2}{2\sigma^2_{y,1/2}(s)} - \frac{z^2}{2\sigma^2_{z,1/2}}\right] \tag{2}$$

where subscripts 1 and 2 represents two colliding beams and σ_x, σ_y and σ_z are the rms beam sizes. Including hourglass effect and the shifted s^*, the two transverse beam sizes are function of the longitudinal position:

$$\sigma_{x/y,1/2}(s) = \sigma^*_{x/y,1/2}\left(1 + \frac{\left(s - s^*_{x/y,1/2}\right)^2}{\beta^{*2}_{x/y,1/2}}\right) \tag{3}$$

where $\sigma^{*2} = \beta^*\epsilon$, β^* is the beta star located at beta waist position s^*, ϵ is the beam emittance.

The luminosity integral (Eq. 1) can be evaluated by integrate the transverse coordinates and the normalized time s_0, and reads:

$$L = \frac{N_1 N_2 f}{2\pi\sqrt{\sigma^2_{x,1} + \sigma^2_{x,2}}\sqrt{\sigma^2_{y,1} + \sigma^2_{y,2}}} G = L_0 G$$

where L_0 is the luminosity with zero length, and G is the geometric factor that reflects the reduction of hourglass effect and shifted s^*. G has the following integration form:

$$G = \int \frac{e^{-u^2} du/\sqrt{\pi}}{\sqrt{1 + \frac{(u-u^*_{x,1})^2}{t^2_{x,1}} + \frac{(u-u^*_{x,2})^2}{t^2_{x,2}}}\sqrt{1 + \frac{(u-u^*_{y,1})^2}{t^2_{y,1}} + \frac{(u-u^*_{y,2})^2}{t^2_{y,2}}}} \tag{4}$$

with

$$t^2_{x/y,1/2} = \frac{2\beta^*_{x/y,1/2}\left(\sigma^{*2}_{x/y,1} + \sigma^{*2}_{x/y,2}\right)}{\epsilon_{x/y,1/2}\left(\sigma^2_{z,1} + \sigma^2_{z,2}\right)}$$

and the scaled beta waist position s^* reads,

$$u_{x/y,1/2} = \frac{\sqrt{2} s^*_{x/y,1/2}}{\sqrt{\sigma^2_{z,1} + \sigma^2_{z,2}}}$$

where ϵ is the rms emittance. In the RHIC and its future upgrade eRHIC, both beam are designed to be round with matched rms beam size at the waist position, $\sigma^{*2}_{x/y,1/2} = \sigma_r$. The expression for $t_{x/y,1/2}$ reduces to $t_{x/y,1/2} = 2\beta^*_{x/y,1/2}/\sqrt{\sigma^2_{z,1} + \sigma^2_{z,2}}$.

USE s^* AS LUMINOSITY CONTROL KNOB

We propose to control the luminosity of one collision point by moving the waist position $s^*_{x/y}$ of one of the colliding beam. Taking RHIC beam parameter as an example, we will demonstrate the effectiveness of this method. RHIC has round beam and identical design parameters for two

* Work supported by Brookhaven Science Associates, LLC under Contract No. DE-AC02-98CH10886 with the U.S. Department of Energy.
† yhao@bnl.gov

Content from this work may be used under the terms of the CC BY 3.0 licence (© 2015). Any distribution of this work must maintain attribution to the author(s), title of the work, publisher, and DOI.

ISBN: 978-3-95450-168-7 doi:10.18429/JACoW-IPAC2015-TUPWI049

POLARIZED PROTON BEAM FOR eRHIC*

H. Huang†, F. Meot, V. Ptitsyn, T. Roser, BNL, Upton, NY 11973, USA

Abstract

RHIC has provided polarized proton collisions from 31 GeV to 255 GeV in past decade. To preserve polarization through numerous depolarizing resonances over the whole accelerator chain, harmonic orbit correction, partial snakes, horizontal tune jump system and full snakes have been used. In addition, close attentions have been paid to betatron tune control, orbit control and beam line alignment. The polarization of 60% at 255 GeV has been delivered to experiments with 1.8×10^{11} bunch intensity. For the eRHIC era, the beam brightness has to be maintained to reach the desired luminosity. Since we only have one hadron ring in the eRHIC era, existing spin rotator and snakes can be converted to six snake configuration for one hadron ring. With properly arranged six snakes in RHIC and additional reduction of emittance growth in AGS, the polarization can reach 70% at 250 GeV. This paper summarizes the effort and plan to reach high polarization with small emittance for eRHIC.

INTRODUCTION

The parameters for eRHIC proton beam is 70% polarization with 3×10^{11}/bunch and 0.2 πmm-mrad normalized emittance [1]. This emittance is at store and is expected to be cooled down by coherent electron cooling(CeC) [2]. On the ramp, the emittance will be larger as delivered by AGS. The resonance strength associated with the larger emittance will be stronger. This paper will discuss how the 70% polarization can be achieved based on current status of RHIC polarized proton operation and possible snake configuration changes.

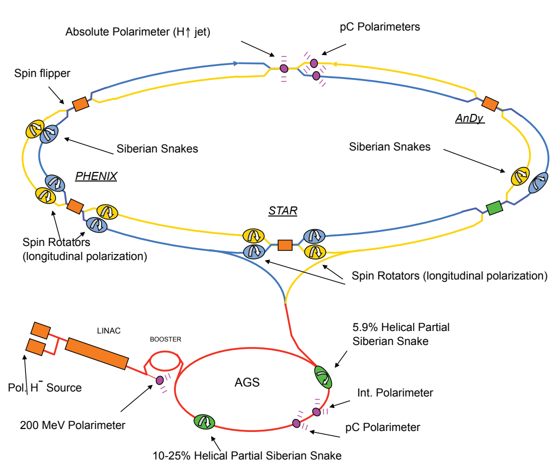

Figure 1: Layout of RHIC complex.

The current proton acceleration chain is shown in Fig. 1. High intensity and high polarization H^- is produced from the polarized proton source. The H^- beam polarization is measured at the end of 200 MeV linac as 80-82%. The beam is then strip-injected into AGS Booster. The Booster vertical tune is set high so that $0 + \nu_y$ intrinsic resonance is avoided. Two imperfection resonances are corrected by orbit harmonic correction. In the AGS, two partial Siberian snakes separated by 1/3 of the ring are used to overcome the imperfection and vertical intrinsic resonances [3]. The vertical tune on the energy ramp is mostly above 8.98, so that it is in the spin tune gap and away from the high order snake resonances. To avoid the horizontal intrinsic resonances driven by the partial snakes, a pair of pulsed quadrupoles are employed to jump cross the many weak horizontal intrinsic resonances on the ramp [4]. Two full Siberian snakes are used in each of the two RHIC rings to maintain polarization [5]. The betatron tune, coupling and orbit feedback on the energy ramp are also crucial for polarization preservation.

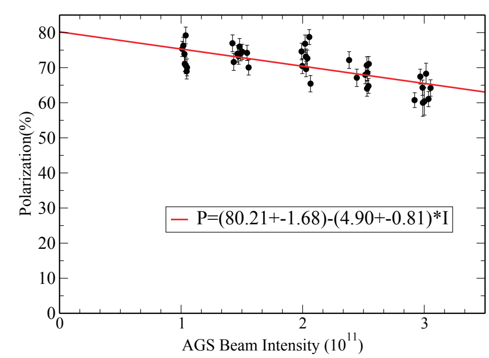

Figure 2: AGS polarization at extraction as function of bunch intensity. The polarized proton source can deliver intensity of 9×10^{11} at the Booster input. Booster scraping (both horizontal and vertical) is used to reduce the beam emittance for AGS injection. The intensity in this figure is changed by varying the Booster scraping level.

The polarization measured at the AGS extraction is shown in Fig. 2 as function of beam intensity. The intensity was reduced by Booster scraping. The polarization dependence on intensity is really dependence on emittance. As higher intensity is always associated with larger emittance, and consequently stronger depolarizing resonance resonance strength, lower polarization is expected for higher intensity. As shown in Fig. 2, the polarization at 3×10^{11} is about 65%. The AGS Ionization Profile Monitor(IPM) can measure beam emittance but the measured beam size is affected by space charge force. To mitigate the effect, the RF is turned off at flattop. The emittance reported by IPM with RF off is plotted in Fig.3. Since there is pos-

* Work performed under contract No. DE-AC02-98CH1-886 with the auspices of the DOE of United States, and with support of RIKEN(Japan).
† huanghai@bnl.gov

Content from this work may be used under the terms of the CC BY 3.0 licence (© 2015). Any distribution of this work must maintain attribution to the author(s), title of the work, publisher, and DOI.

ISBN: 978-3-95450-168-7 doi:10.18429/JACoW-IPAC2015-TUPWI050

OPTICS CORRECTION FOR THE MULTI-PASS FFAG ERL MACHINE eRHIC*

C. Liu†, S. Brooks, V. Litvinenko, M. Minty, V. Ptitsyn, D. Trbojevic, BNL, Upton, NY 11973, USA

Abstract

Gradient errors in the multi-pass Fixed Field Alternating Gradient (FFAG) Energy Recovery Linac (ERL) machine, eRHIC, distort the beam orbit and therefore cause emittance increase. The localization and correction of gradient errors are essential for an effective orbit correction and emittance preservation. In this report, the methodology and simulation of optics correction for the multi-pass FFAG ERL machine eRHIC will be presented.

INTRODUCTION

Electron Relativistic Heavy Ion collider (eRHIC) is a new research tool proposed to be built at the existing RHIC facility. The design of the electron machine provides a cost-effective upgrade of RHIC for collision of electron beam with the full array of RHIC hadron beams [1]. Two circular electron accelerators with FFAG lattice are designed to be placed in RHIC tunnel to provide electron beams with top energy at 15.9 and 21.2 GeV [2]. The electron beam will be accelerated from 1.3 GeV to the top energies and energy recovered after collisions. The accelerating passes and decelerating passes in each machine go through the same vacuum chamber thanks to the small dispersion values. The beta functions of each energy differ from each other.

The deviation of the gradient from design will distort beam trajectories and the optical functions. Even though the orbit distortion can be fixed by dipole correctors, the distortion of optical functions will be detrimental for the effectiveness of orbit correction. Therefore, it would be desirable to be able to disentangle dipole errors and quadrupole errors and correct them independently. We adopted the orbit response method (ORM) [3], which has been widely applied for circular rings, and extend it for the multi-pass FFAG case to locate and correct quadrupole errors in eRHIC FFAG machines.

PROPERTIES OF THE LINEAR NON-SCALING FFAG LATTICE

In the eRHIC FFAG design, the magnets are pure focusing and defocusing quadrupoles shifted horizontally relative to a circular orbit. The field experienced by the beam is $G*x$, G is the magnet gradient, x is the horizontal beam position relative to the magnet center. The orbits of beams with different energies are plotted in Fig. 1, with respect to the circular orbit. The energy deviations are calculated with

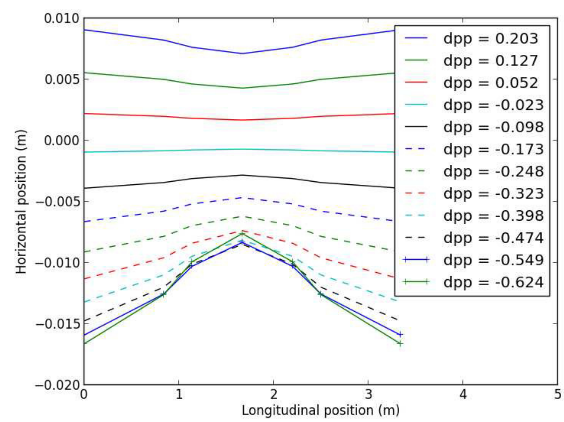

Figure 1: The orbits for beams with different energies in a single FODO cell of the FFAG lattice.

respect to 17.6 GeV. The overall horizontal offsets between beams is ∼25 mm. The beams can therefore fit in the same beam pipe. The close-together beam orbits present a challenge for beam position measurement for individual beams [4].

The beta functions in both planes are plotted in Fig. 2 and 3 for beams with different energies. The responses in terms of beam position changes are expected to be different for beams with different energies.

OPTICS CORRECTION ALGORITHM

In linear FFAG, orbit response deviation depends only on gradient errors linearly. Orbit response deviation from the model can be measured by varying dipole correctors

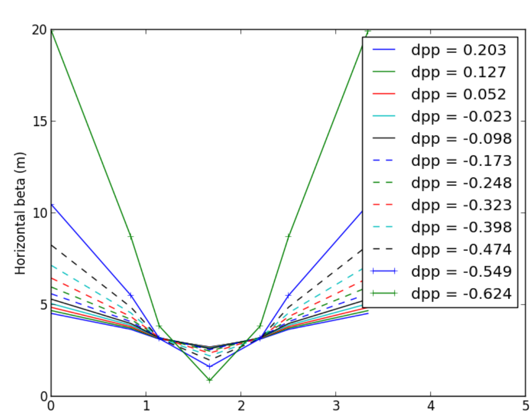

Figure 2: The horizontal beta functions for beams with different energies in a single FODO cell of the FFAG lattice.

* The work was performed under Contract No DE-AC02-98CH10886 with the U.S. Department of Energy.
† cliu1@bnl.gov

Content from this work may be used under the terms of the CC BY 3.0 licence (© 2015). Any distribution of this work must maintain attribution to the author(s), title of the work, publisher, and DOI.

ISBN: 978-3-95450-168-7 doi:10.18429/JACoW-IPAC2015-TUPWI051

STUDY OF ORBIT CORRECTION FOR eRHIC FFAG DESIGN*

C. Liu†, Y. Hao, V. Litvinenko, F. Meot, M. Minty, V. Ptitsyn, D. Trbojevic
BNL, Upton, NY 11973, USA

Abstract

The unique feature of the orbits in the eRHIC Fixed Field Alternating Gradient (FFAG) design is that multiple accelerating and decelerating bunches pass through the same magnets with different horizontal offsets. Therefore, it is critical for the eRHIC FFAG to correct multiple orbits in the same vacuum pipe for better spin transmission and alignment of colliding beams. In this report, the effects on orbits from multiple error sources will be studied. The orbit correction method will be described and results will be presented.

INTRODUCTION

Electron accelerators based on FFAG lattice are designed to be placed in the existing Relativistic Heavy Ion Collider (RHIC) tunnel for collision of electron and heavy ion beams [1]. The advantages of the FFAG lattice are in two aspects: the magnets are at fixed fields and there is strong focusing in the transverse planes. A machine with such lattice accepts beams over a large energy range. The dispersion function is very small ($\sim cm$) so that orbits of beams with different energies stay in the same vacuum pipe with small horizontal offsets. The orbits will be distorted differently if either the magnets are misaligned or there are magnet gradient errors. The misalignment and gradient errors in a FFAG lattice need therefore to be compensated locally to restore all the orbits to the design values. Dipole and quadrupole trims will be placed at each and every magnet center to correct the said errors. Considering the large number of magnets in the rings, a global correction scheme must detect local errors quickly and precisely. Furthermore, enough beam position monitors (BPMs) for beam position measurement is also critical to locate the errors effectively.

The lattice design has evolved much in the past year with optimization of linac size and synchrotron radiation [2, 3]. The orbit correction simulation will be presented in this paper is based on a single FFAG ring design, which accelerates electron beam from 1.9 to 10 GeV and decelerates the beam back to 1.9 GeV via energy recovery. The injected beam will be accelerated before entering the FFAG arc. Therefore, there are 9 accelerating beam passes and 8 decelerating passes through the FFAG arcs. As the beam gets accelerated, the betatron tune per FFAG cell changes from ∼0.44 to ∼0.1 in the horizontal plane and ∼0.3 to ∼0.04 in the vertical plane discretely [1].

* The work was performed under Contract No. DE-AC02-98CH10886 with the U.S. Department of Energy.
† cliu1@bnl.gov

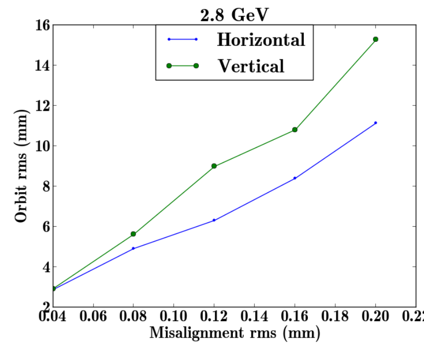

Figure 1: RMS of beam orbit distortion in eRHIC FFAG in both planes due to magnet misalignment errors, for the beam in the first pass with energy 2.8 GeV.

The measurement of beam positions is challenging for continuous bunch train with $\sim ns$ spacing between bunches. A gap in the electron beam bunch train, which coincides with the abort gap in RHIC, is necessary for ion clearing purpose. A diagnostic bunch will be put in the gap for routine monitoring of the beam positions continuously [4].

ORBIT DISTORTION DUE TO MISALIGNMENT AND GRADIENT ERROR

In the eRHIC FFAG design, the magnets are pure focusing and defocusing quadrupoles shifted horizontally in position relative to a circular orbit. The field experienced by the beam is $G * x$, G is the magnet gradient, x is the horizontal beam position relative to the magnet center.

The orbit distortion due to misalignment of magnets was studied in simulation. The orbit deviation root-mean-square (rms) in two planes for beam at $2.8GeV$ is shown in Fig. 1 for a range of misalignment rms. The same orbit distortion due to misalignment erros were studied for the other 8 beam passes. The magnification factors, the ratio between orbit rms and misalignment rms, are compared for all passes. The magnification factor decreases with beam rigidity as expected in the horizontal plane, however not in the vertical plane. Analytical calculation of the magnification factor ($\propto \frac{\sqrt{\beta_1\beta_2}}{\nu\gamma}$, β_1, β_2 are the betatron functions at the magnets and BPMs, ν is the tune per cell, γ is the Lorentz factor) confirmed the count-intuitive behavior in the vertical plane, shown in Fig. 2.

The orbit distortion due to magnet gradient errors was studied in simulation as well. The orbit rms in the horizontal plane only for beam at 2.8 GeV is shown in Fig.3 for a

Content from this work may be used under the terms of the CC BY 3.0 licence (© 2015). Any distribution of this work must maintain attribution to the author(s), title of the work, publisher, and DOI.

ISBN: 978-3-95450-168-7 doi:10.18429/JACoW-IPAC2015-TUPWI052

END-TO-END 9-D POLARIZED BUNCH TRANSPORT IN eRHIC ENERGY-RECOVERY RECIRCULATOR, SOME ASPECTS

F. Méot, S. Brooks, V. Ptitsyn, D. Trbojevic, N. Tsoupas
Collider-Accelerator Department, BNL, Upton, NY 11973, USA

Abstract

This paper is a brief overview of some of the numerous beam and spin dynamics investigations undertaken in the framework of the design of the FFAG based electron energy recovery re-circulator ring of the eRHIC electron-ion collider project.

INTRODUCTION

A Fixed Field Alternating Gradient (FFAG) doublet-cell version of the energy recovery recirculator of the eRHIC electron-ion collider is being investigated [1]. A pair of such FFAG rings placed along RHIC recirculate the electron beam through a 1.322 GeV linac (ERL), from respectively 1.3 to 6.6 GeV (5 beams) and 7.9 to 21.2 GeV (11 beams), and back down to injection energy. A spreader and a combiner are placed at the linac ends for proper orbit and 6-D matching, including time-of-flight adjustment.

FFAG LATTICE

The second, 11 beam, 21.2 GeV ring is considered in this discussion since it produces the major SR induced particle and spin dynamics perturbations. The cell is shown in Fig. 1, there are 138 such cells in each one of the 6 eRHIC arcs. The 6 long straight sections (LSS) use that very cell, with quadrupole axes aligned. In the twelve, 17-cell, dispersion suppressors (DS) the quadrupole axes slowly shift from their distance in the arc, to zero at the LSS.

Fig. 2 shows the transverse excursion and magnetic field along orbits across the arc cell. Fig. 3 shows the energy dependence of the deviation angle and curvature radius in the two quadrupoles, and the energy dependent tunes and chromaticities.

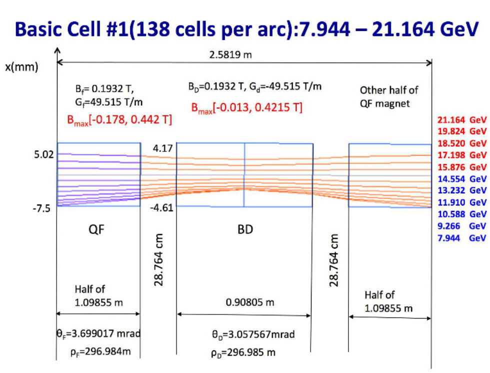

Figure 1: Arc cell in the 7.944-21.16 GeV recirculating ring.

The y-precession of the spin over the six 138-cell arcs amounts to $6 \times 138 \times a\gamma\theta_{\text{cell}} = a\gamma \times (2\pi - 0.688734)$ rad (with the difference to $a\gamma \times 2\pi$ corresponding to the contribution of the 12 DS), *i.e.*, from 18 precessions at 7.944 GeV to 48 at 21.164 GeV. ($a = 0.00116$ is the electron anomalous magnetic factor, γ the Lorentz relativistic factor).

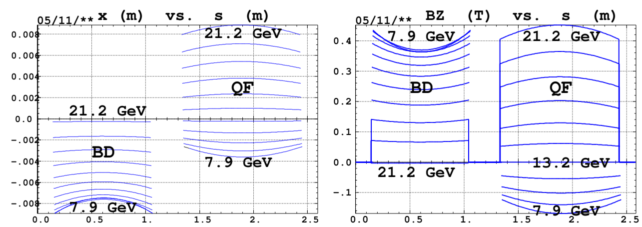

Figure 2: Transverse excursion in the quadrupole frame (hence artefact of trajectory discontinuity) (left) and hard-edged magnetic field (right), along the 11 orbits across the arc FFAG cell.

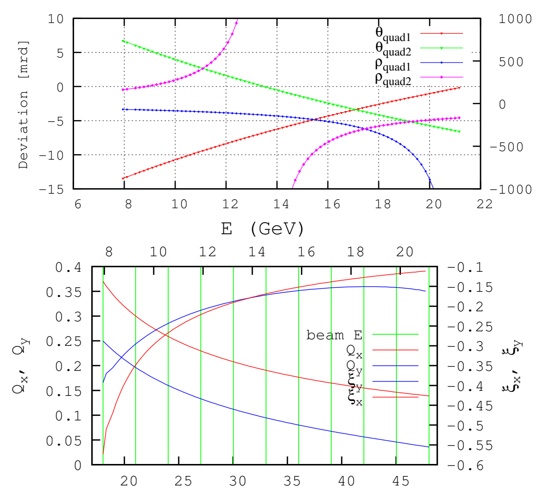

Figure 3: Top : energy dependence of deviation and curvature radius in arc cell quads. Bottom : cell tunes and chromaticities; the vertical bars materialize the 11 design energies.

SYNCHROTRON RADIATION

The SR induced energy loss relative to the the bunch centroid and the energy spread write, respectively

$$\frac{\overline{\Delta E}}{E_{\text{ref}}} = 1.9 \times 10^{-15}\,\frac{\gamma^3 \Delta\theta}{\rho},\ \frac{\sigma_E}{E_{\text{ref}}} = 3.8 \times 10^{-14}\,\frac{\gamma^{\frac{5}{2}}\sqrt{\Delta\theta}}{\rho} \tag{1}$$

with $\Delta\theta$ the arc length and $1/\rho$ the curvature, assumed constant. Taking for average radius, in the QF (focusing quad) and BD (defocusing quad) magnets respectively, $\rho_{\text{BD}} \approx \frac{s_{\text{BD}}}{\Delta\theta_{\text{BD}}}$, $\rho_{\text{QF}} \approx \frac{s_{\text{QF}}}{\Delta\theta_{\text{QF}}}$ (with s_{BD} and s_{QF} the arc lengths) and considering in addition, with l_{BD}, l_{QF} the magnet lengths, $s_{\text{BD}} \approx l_{\text{BD}}$, $s_{\text{QF}} \approx l_{\text{QF}}$, then one gets,

Content from this work may be used under the terms of the CC BY 3.0 licence (© 2015). Any distribution of this work must maintain attribution to the author(s), title of the work, publisher, and DOI.

ISBN: 978-3-95450-168-7 doi:10.18429/JACoW-IPAC2015-TUPWI053

POLARIZATION SIMULATIONS IN THE RHIC RUN 15 LATTICE *

F. Méot, H. Huang, Y. Luo, V. Ranjbar, G. Robert-Demolaize, S. White
Collider-Accelerator Department, BNL, Upton, NY 11973, USA

Abstract

RHIC polarized proton Run 15 uses a new acceleration ramp optics, compared to RHIC Run 13 and earlier runs, in relation with electron-lens beam-beam compensation developments [1, 2]. The new optics induces different strengths in the depolarizing snake resonance sequence, from injection to top energy. As a consequence, polarization transport along the new ramp has been investigated, based on spin tracking simulations. Sample results are reported and discussed.

SIMULATED OPTICS

Main parameters of the *simplified* RHIC polarized proton optics considered for these simulations are given in Tab. 1, "Run 13" stands for the earlier optics, "Run 15" stands for the new one with betatron functions as displayed in Fig. 1. Tracking outcomes will be given for both cases,

Table 1: Optical Parameters in the Simulations

		Run 13	Run 15
Orbit length	m	3833.8452	
γ_{tr}		23	23.5
Q_x		28.685	29.68
Q_y		29.673	30.67
Q'_x		1	2.3
Q'_y		1	2.2
RHIC rings' snake 1 and snake 2 :			
Spin rotation (deg.)		180, 180	
Axis angles (deg.)		+45, −45	

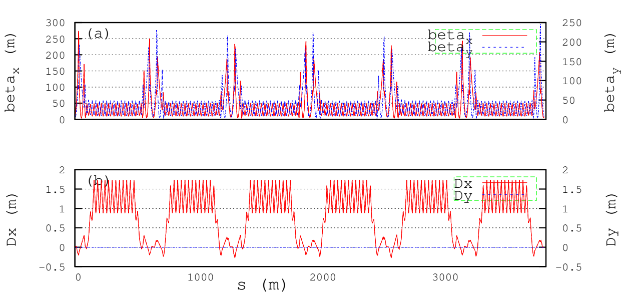

Figure 1: Betatron functions (maintained constant) in the ramp simulation, case of the new optics.

for comparison. In the simulations, optical functions are maintained unchanged over the all ramp from injection, E=23.8 GeV, to collision, E=100 GeV (total energy). The $E \approx 33$ GeV optics is taken in the "Run 15" case, the location of the strongest intrinsic depolarizing resonance, $G\gamma = 93 - Q_y$. Higher energy optics was used in the "Run 13" case, however the intrinsic reonance strengths do not change much, in spite of the varying optics, during the ramp. The resonance sequence so obtained in the 23-100 GeV range is displayed in Fig. 2, Tab. 2 gives the strengths of the strongest ones.

RESONANCE STRENGTHS

Intrinsic resonance strengths for the old and for the new optics are displayed in Fig. 2. They have been computed in the thin-lens approximation, namely,

$$\frac{J_n^{\pm}}{\sqrt{\epsilon_y/\pi}} = \frac{1+\gamma G}{4\pi}\Sigma_k \left\{ \begin{array}{l} \cos(\gamma G\alpha_k \pm \psi_{y,k})+ \\ i\,\sin(\gamma G\alpha_k \pm \psi_{y,k}) \end{array} \right\} (KL)_k \sqrt{\beta_{y,k}} \tag{1}$$

where the sum extends over the lattice quadrupoles

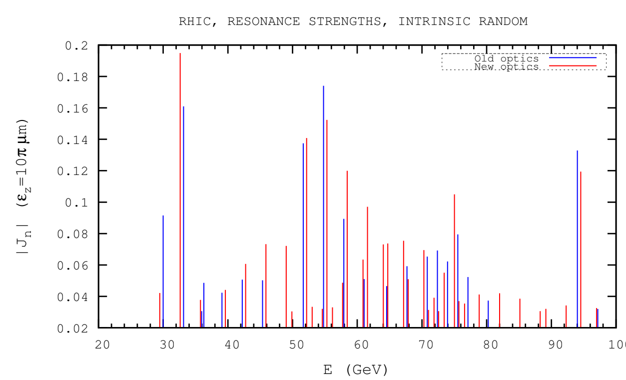

Figure 2: Resonance strengths in the simulation of the old and new optics.

Table 2: Strongest Resonances in the old and in the new Optics. Respectively, $Q_y = 29.673$ and $Q_y = 30.67$.

$n \pm Q_y$	E (GeV)	$\lvert J_n(\epsilon_{y,\text{norm.}} = 10\,\pi\mu\text{m})\rvert$ Old optics	New optics
93 - Q_y	~33	0.161	0.195
69 + Q_y	~52	0.137	0.141
75 + Q_y	~55	0.174	0.152
174 - Q_y	~75	0.080	0.105
150 + Q_y	~94	0.133	0.120

(counter-rotating beam orbits are vertically separated at the

* Work supported by Brookhaven Science Associates, LLC under Contract No. DE-AC02-98CH10886 with the U.S. Department of Energy.

Content from this work may be used under the terms of the CC BY 3.0 licence (© 2015). Any distribution of this work must maintain attribution to the author(s), title of the work, publisher, and DOI.

ISBN: 978-3-95450-168-7 doi:10.18429/JACoW-IPAC2015-TUPWI054

9-D POLARIZED PROTON TRANSPORT IN THE MEIC "FIGURE-8" COLLIDER RING - FIRST STEPS*

F. Méot, Collider-Accelerator Department, BNL, Upton, NY 11973, USA
V.S. Morozov, JLab, Newport News, VA 23606, USA

Abstract

Spin tracking studies in the MEIC figure-8 collider ion ring are presented, based on a very preliminary design of the lattice. They provide numerical illustrations of some of the aspects of the figure-8 concept, including spin-rotator based spin control, and lay out the path towards a complete spin tracking simulation of a figure-8 ring.

INTRODUCTION

Figure 1 and Table 1 summarize the characteristics and nominal parameters of the figure-8 ring, the optical functions are shown in Fig. 2 and Fig. 3. Details can be found in [1].

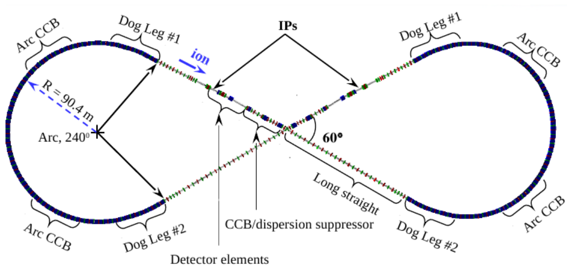

Figure 1: MEIC collider ion ring.

Table 1: Parameters of the 60 GeV MEIC Figure 8 Collider Proton Ring

circumference	m	1415.3
energy	GeV	60
polarization goal	%	>70
H/V emittances	$\pi\mu$m	0.35 / 0.07
H/V β^*	cm	10 / 2
max. β_x / β_y	m	2301 / 2450
H/V tunes		25.79 / 26.27
H/V chromas, natural		-224 / -233
momentum compaction	10^{-3}	5.76
transition γ		13.18

SPIN TRACKING

The present studies were done using a very preliminary design of the lattice, however not optimized for the spin dynamics and in particular not including the system intended for polarization control in MEIC. They can be viewed as simplified numerical illustrations of some of the aspects of the figure-8 concept, while laying out the path towards a complete spin tracking simulation.

The ray-tracing code Zgoubi is used in these studies [2].

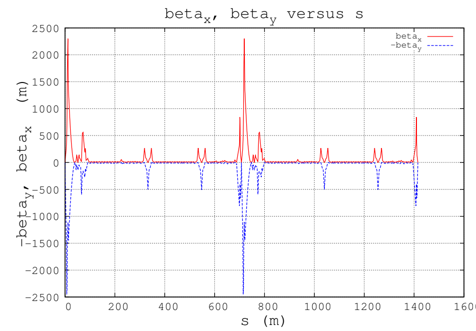

Figure 2: Betatron functions, horizontal and vertical.

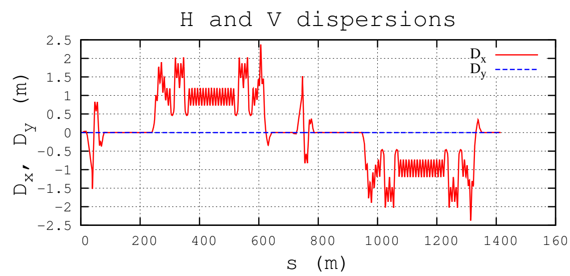

Figure 3: Dispersion functions, horizontal and vertical.

Particle with Zero Initial Coordinates

We start by tracking three particles with zero initial coordinates and with, respectively, fully longitudinal ($S_x^i = 1$), radial ($S_y^i = 1$), vertical ($S_z^i = 1$), initial spin orientation, for 200,000 turns through an ideal lattice containing no imperfections.

Figure 4-left shows the non-zero spin components of the three particles every 100 turns versus the turn number : the longitudinal spin component S_x of an initial $S_x^i = 1$ particle, the radial spin component S_y of a $S_y^i = 1$ particle, and the vertical spin component S_z of a $S_z^i = 1$ particle, all feature the same quasi-constant, quasi-unitary value vs. the turn number, as expected in a figure-8 ring. This validates the applicability of Zgoubi to this kind of study and demonstrates that it has the necessary numerical precision at least at the level of the chosen number of turns.

Effect of the Betatron Oscillations on Spin

We next launch three particles from one of the MEIC interaction points (IPs), with all three different initial spin orientations as earlier, and with initial horizontal and vertical

* Work supported by Brookhaven Science Associates, LLC under Contract No. DE-AC02-98CH10886 with the U.S. Department of Energy. Authored in part by Jefferson Science Associates, LLC under U.S. DOE Contract No. DE-AC05-06OR23177 and DE-AC02-06CH11357. U.S. Government retains a license to publish or reproduce this manuscript for U.S. Government purposes.

Content from this work may be used under the terms of the CC BY 3.0 licence (© 2015). Any distribution of this work must maintain attribution to the author(s), title of the work, publisher, and DOI.

ISBN: 978-3-95450-168-7 doi:10.18429/JACoW-IPAC2015-TUPWI055

CHROMATIC EFFECTS AND ORBIT CORRECTION IN eRHIC ARCS

F. Méot, C. Liu
Collider-Accelerator Department, BNL, Upton, NY 11973, USA

Content from this work may be used under the terms of the CC BY 3.0 licence (© 2015). Any distribution of this work must maintain attribution to the author(s), title of the work, publisher, and DOI.

Abstract

This paper gives a brief overview of some aspects of the beam dynamics effects induced by the natural chromaticity in the eRHIC FFAG lattice.

INTRODUCTION

A Fixed Field Alternating Gradient (FFAG) doublet-cell version of the energy recovery recirculator of the eRHIC electron-ion collider is being investigated [1, 2, 3]. A pair of such FFAG rings placed along RHIC recirculate the electron beam through a 1.322 GeV linac (ERL), from respectively 1.3 to 6.6 GeV (5 beams) and 7.9 to 21.2 GeV (11 beams), and back down to injection energy. A spreader and a combiner are placed at the linac ends for proper orbit and 6-D matching.

SIMULATION CONDITIONS

The second, 11 beam, 21.2 GeV ring is considered in this discussion for convenience. The cell is shown in Fig. 1, there are 138 such cells in each one of the 6 eRHIC arcs. The 6 long straight sections (LSS) use that very cell, with quadrupole axes aligned. In the twelve, 17-cell, dispersion suppressors (DS) the quadrupole axes slowly shift from their distance in the arc, to zero at the LSS, in a reputedly "adiabatic" manner (details can be found in [3]).

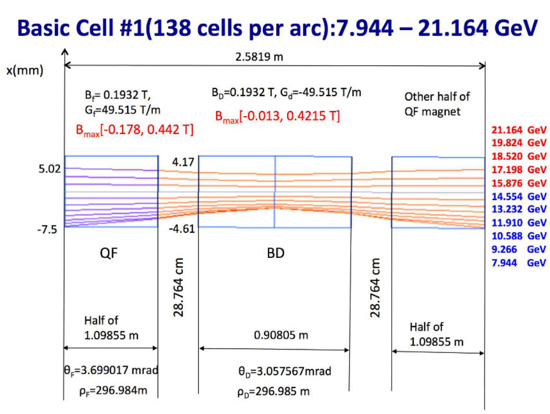

Figure 1: Arc cell in the 7.944-21.16 GeV eRHIC ERL ring [4].

Energy dependent cell tunes and chromaticities are displayed in Fig. 2. Additional details concerning the lattice and beam dynamics can be found in [5].

A complete ring is considered in the simulations discussed in the following,

$$6 \times \left[\frac{1}{2}\mathrm{LSS} - \mathrm{DS} - \mathrm{ARC} - \mathrm{DS} - \frac{1}{2}\mathrm{LSS}\right] + \mathrm{Linac}$$

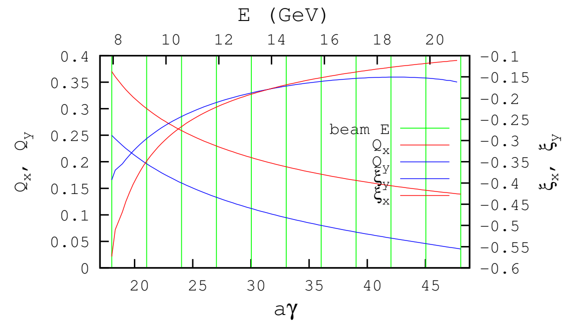

Figure 2: Energy dependence of cell tunes and chromaticities; the vertical bars materialize the 11 design energies.

The origin of the ring (the location where the bunches are injected) is taken in the middle of the LSS since the reference orbit is zero there, whatever the energy.

SR energy loss is roughly compensated at the linac : the actual energy gain is 1.322 GeV + half the energy loss at the previous pass + half the energy loss at the next pass. In particular the starting energy is 7.944 GeV + half the energy loss at pass #1.

EMITTANCE GROWTH

Due to the large chromaticity (Fig. 2), any beam misalignment results in its phase extent in phase space, following $\Delta\phi = 2\pi\xi\delta E/E$. SR for instance is an intrinsic cause since it introduces both energy spread and beam shift [5]. This SR effect is small however com-

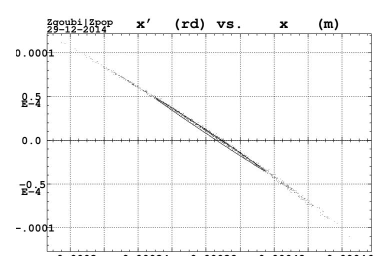

Figure 3: SR induced horizontal phase space portrait, for an initially zero 6-D emittance bunch, as acquired after an 11 GeV pass in the eRHIC ring.

pared to nominal beam emittances, it is illustrated in Fig. 3 which shows the phase-space portrait acquired by a bunch launched with zero emittances and energy spread, after a single 11 GeV pass in the eRHIC ring, assuming a very small beam misalignment in the DS regions (in the sub-millimeter range, as induced by a "lack of adiabaticity" of the adiabatic DS). Note that here we introduce a measure

ISBN: 978-3-95450-168-7 doi:10.18429/JACoW-IPAC2015-TUPWI059

INFLUENCE OF PLASMA LOADING IN A HYBRID MUON COOLING CHANNEL *

B. Freemire†, Illinois Institute of Technology, Chicago, IL 60563, USA
D. Stratakis, Brookhaven National Laboratory, Upton, NY 11973, USA
K. Yonehara, Fermi National Accelerator Laboratory, Batavia, IL 60510, USA

Abstract

In a hybrid 6D cooling channel, cooling is accomplished by reducing the beam momentum through ionization energy loss in wedge absorbers and replenishing the momentum loss in the longitudinal direction with gas-filled rf cavities. While the gas acts as a buffer to prevent rf breakdown, gas ionization also occurs as the beam passes through the pressurized cavity. The resulting plasma may gain substantial energy from the rf electric field which it can transfer via collisions to the gas, an effect known as plasma loading. In this paper, we investigate the influence of plasma loading on the cooling performance of a rectilinear hybrid channel. With the aid of numerical simulations we examine the sensitivity in cooling performance and plasma loading to key parameters such as the rf gradient and gas pressure.

INTRODUCTION

A key challenge on producing intense muon beams is that they are created in a diffuse phase-space. As a result, the volume of the 6-Dimensional (6D) phase-space must be rapidly reduced via ionization cooling [1]. To reduce the transverse emittance, the beam is strongly focused with high magnetic fields and subsequently sent through an absorber material to reduce its overall momentum. Longitudinal emittance reduction is achieved by using wedge shaped absorbers and generating dispersion such that particles with higher energy pass through more material. In the aforementioned scheme, the cavities are filled with gas in order to prevent rf breakdown facilitated by multi-Tesla magnetic fields. Recently, a multi-stage tapered rectilinear channel capable for reducing the 6D emittance by at least five orders of magnitude has been designed and simulated [2, 3]. In that scheme the assumed gas pressure was 34 atm at room temperature.

An important issue in high-pressure gas filled cavities is rf power loading due to beam-induced plasma. Incident beam particles interact with dense hydrogen gas and cause significant amounts of ionization. Due to the high frequency of collisions with neutrals, electrons reach equilibrium within the picosecond time scale and move by the instantaneous external electric field. These charged particles, mainly electrons, absorb power from the electromagnetic field in the cavity. Thus subsequent beam bunches will experience a reduced electric field. This external field drop effect is reinforced by repetitive beam inflow. An experiment performed at the MuCool Test Area at Fermilab studied the formation of plasma created by a proton beam and its evolution over the course of many 805 MHz rf cycles [4]. In this paper, we investigate the influence of plasma loading on the cooling performance of a rectilinear hybrid channel.

* Work supported by Brookhaven Science Associates, LLC under Contract No. DE-SC0012704 with U.S Department of Energy
† freeben@hawk.iit.edu

COOLING MUON BUNCHES

The cooling scheme we consider starts with the post-phase-rotation beam [5] that yields bunch trains of muons from which we use only 21 (see Fig. 1).

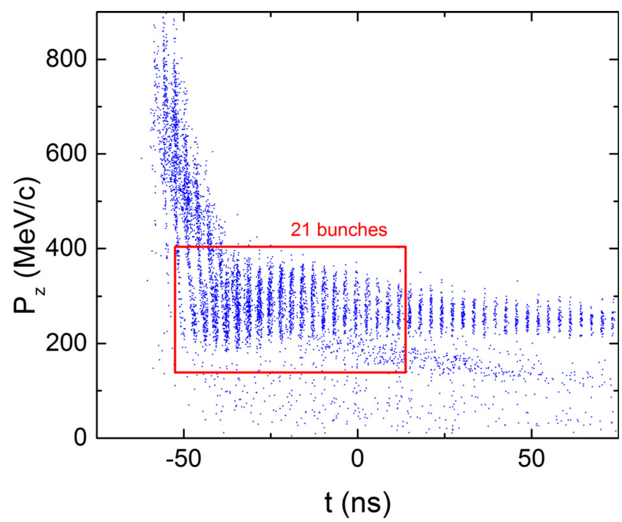

Figure 1: Longitudinal phase-space at the cooler entrance.

We consider a four-stage (A1-A4) tapered channel where each stage consists of a sequence of identical cells and the main lattice parameters are summarized in Tables 1 and 2. In all simulations the cavities are filled with gas at pressures of 34 or 100 atm at room temperature. The performance of the channel was simulated with the ICOOL code. The optimum performance for each pressure was found by using the conventional algorithm "Nelder-Mead" by scanning the rf phase, rf gradient, reference momentum, absorber length and wedge angle with the goal to maximize the beam luminosity within a given stage.

Table 1: Lattice Parameters for 34 atm

Stage	A1	A2	A3	A4
rf Freq. (MHz)	325	325	650	650
rf E (MV/m)	28.33	23.44	28.53	32.52
rf Phase (deg)	13.50	15.36	20.55	16.40
rf Length (m)	0.255	0.250	0.135	0.135

Content from this work may be used under the terms of the CC BY 3.0 licence (© 2015). Any distribution of this work must maintain attribution to the author(s), title of the work, publisher, and DOI.

ISBN: 978-3-95450-168-7 doi:10.18429/JACoW-IPAC2015-TUPWI060

Content from this work may be used under the terms of the CC BY 3.0 licence (© 2015). Any distribution of this work must maintain attribution to the author(s), title of the work, publisher, and DOI.

RHIC POLARIZED PROTON-PROTON OPERATION AT 100 GeV IN RUN 15*

V. Schoefer†, E.C. Aschenauer, G.Atoian, M.Blaskiewicz, K.A.Brown, D.Bruno, R.Connolly, T.D'Ottavio, K.A.Drees, Y.Dutheil, W.Fischer, C.J.Gardner, X.Gu, T.Hayes, H.Huang, J.S.Laster, C.Liu, Y.Luo, Y.Makdisi, G.Marr, A.Marusic, F.Meot, K.Mernick, R.Michnoff, M.Minty, C.Montag, J.Morris, G.Narayan, S.Nemesure, P.Pile, A.Poblaguev, V.Ranjbar, G.Robert-Demolaize, T.Roser, W.B.Schmidke, F.Severino, T.Shrey, K.Smith, D.Steski, S.Tepikian, D.Trbojevic, N.Tsoupas, J.Tuozzolo, G.Wang, S.White, K.Yip, A.Zaltsman, A.Zelenski, K.Zeno, S.Y.Zhang, BNL, Upton, Long Island, New York, USA

Abstract

The first part of RHIC Run 15 consisted of ten weeks of polarized proton on proton collisions at a beam energy of 100 GeV at two interaction points. In this paper we discuss several of the upgrades to the collider complex that allowed for improved performance. The largest effort consisted in commissioning of the electron lenses, one in each ring, which are designed to compensate one of the two beam-beam interactions experienced by the proton bunches. The e-lenses raise the per bunch intensity at which luminosity becomes beam-beam limited. A new lattice was designed to create the phase advances necessary for a beam-beam compensation with the e-lens, which also has an improved off-momentum dynamic aperture relative to previous runs. In order to take advantage of the new, higher intensity limit without suffering intensity driven emittance deterioration, other features were commissioned including a continuous transverse bunch-by-bunch damper in RHIC and a double harmonic RF cature scheme in the Booster. Other high intensity protections include improvements to the abort system and the installation of masks to intercept beam lost due to abort kicker pre-fires.

INTRODUCTION

RHIC provided polarized proton ($\vec{p}$) collisions at a beam energy of 100 GeV for ten weeks during the FY15 physics run. RHIC has a pair of spin rotators in each ring at each colliding IP that allow for collisions with an arbitrary stable spin direction at the point of collision. The run is divided here into three periods. The stable spin direction at the PHENIX experiment was kept vertical for all three periods (no spin rotation at PHENIX). The stable spin direction at STAR was oreiented longitudinally, vertically and then longitudinally again for each respective period. Figure 1 summarizes the performance relative to previous runs.

LATTICE

In order for the electron lenses to provide beam-beam compensation without exciting additional resonances, the betatron phase advances between the lenses and the proton-proton interaction need to be compensated needs to be a multiple of π. An early iteration of a lattice that met this phase advance requirement was tested (without an electron lens) in Run 13 at 255 GeV [1]. The Run 13 experience indicated that careful control of the 2/3 betatron resonance driving terms is important to preserving the transverse emittance and the beam lifetimes even at injection energy. For Run 15 a new lattice was developed [2]. The new lattice has a phase advance of π between the electron lens location and the proton-proton collision point at PHENIX. In addition, the lattice has 90 degrees betatron phase advance per cell, which produces passive compensation of the 2/3 resonance driving terms from the lattice sextupoles. Attaining the 90 degrees phase advance per FODO cell requires increasing the integer part of the tunes in each plane by 1 unit, a change from $(Q_x, Q_y) = (28.690, 29.685)$ to $(29.690, 30.685)$. The final β^* at the two proton-proton collision points is 0.85 m.

The β function at the point of each proton-electron collision is kept as large as possible (15 m) in order to prevent electron lens-driven transverse mode coupling instabilities [3].

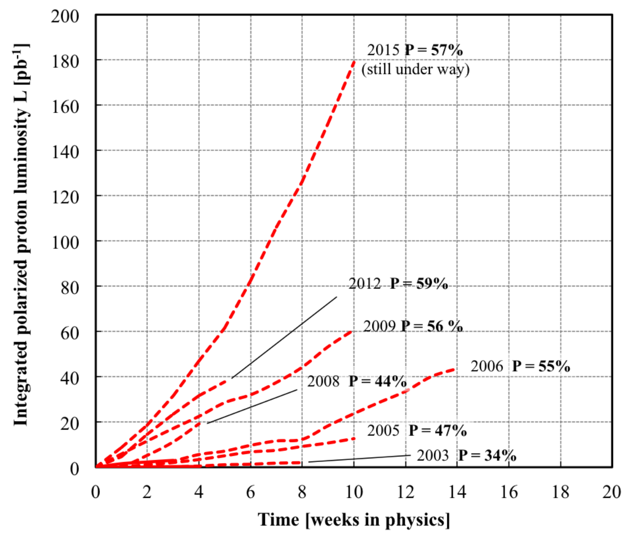

Figure 1: Integrated luminosity and polarization for all RHIC 100 GeV polarized proton runs.

* Work supported by Brookhaven Science Associates, LLC under Contract No. DE-AC02-98CH10886 with the U.S. Department of Energy
† schoefer@bnl.gov

ISBN: 978-3-95450-168-7 doi:10.18429/JACoW-IPAC2015-WEXB1

COHERENT SYNCHROTRON RADIATION IN ENERGY RECOVERY LINACS

C. C. Hall, S. G. Biedron, A. L. Edelen, S. V. Milton
Colorado State University, Fort Collins, Colorado 80523, USA
S. Benson, D. Douglas, R. Li, C. D. Tennant
Thomas Jefferson National Accelerator Laboratory, Newport News, Virginia 23606, USA
B. E. Carlsten
Los Alamos National Laboratory, Los Alamos, New Mexico 87545, USA

Abstract

Collective beam effects, including coherent synchrotron radiation (CSR), have been studied on free-electron lasers (FELs). Here we will discuss a particular case of the CSR effects, that in energy-recovery linacs (ERLs). Special consideration is given to these machines because of their high average beam power and the architecture of the machine for energy recovery forces extreme bends. A recent study conducted on the JLab IR FEL looked at how CSR impacts both average energy and the energy spectrum of the beam. Such studies are important, both broadly, to the understanding of CSR and more specifically for a number of proposed ERL projects. A few proposed examples include the MEIC bunched beam cooler ERL design and ERL FELs for potential lithography purposes that would operate in the EUV range.

INTRODUCTION

The damaging effects of coherent synchrotron radiation (CSR) have been an area of intense research for free-electron lasers (FELs). For the very short bunches required in many FELs the very intense CSR can cause a host of problems, such as, increasing emittance and the slice energy spread, as well as, giving rise to the microbunching instability [1–4]. For energy recovery linacs (ERLs) CSR can be especially troubling due to the design of these machines. In order to recover the stored power in the beam it must be brought back through the linac. This necessitates the use of arcs composed of many dipole magnets where there is the potential for a great deal of CSR generation. ERLs could also face additional issues [5] due to very high currents that are often used in such machines, from 10 mA up to 100 mA in proposed machines. CSR remains a difficult computational problem to model due to the scaling with number of particles N as N^2 [6]. To model CSR in most accelerator simulations a 1-D model is employed that projects the transverse bunch distribution onto a line [7]. Thus far this model has shown great success in comparison with experiments [8, 9]. Since the 1-D CSR model has been so effective there is still some question as to at what point it becomes unreliable. Various 2-D and 3-D models of CSR have been developed, but to date analysis of most experiments with the 1-D model has been sufficient [10–12]. As CSR continues to be a topic of ongoing interest within the FEL community it is important to continue to perform machine studies to help better characterize its affects and to improve theory and simulation. In the first part of this paper we give an overview of a recent experiment performed on the Jefferson Lab ERL FEL driver studying CSR [13] and describe some of the key lessons learned. The second part reviews some ongoing accelerator projects for which CSR and other collective effects instabilities may be a key concern.

JLAB EXPERIMENT DESCRIPTION

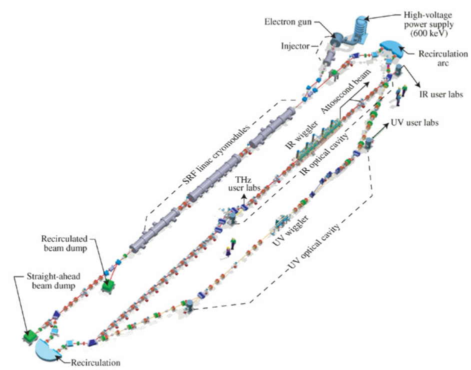

Figure 1: Layout of the JLab FEL. The IR wiggler line was used in the experiment described here.

The JLab ERL IR FEL driver [14] (Fig. 1) consists of an SRF linac that was used to accelerate the 9-MeV beam from the injector up to 135 MeV. The beam passes through the first recirculation arc which is used to provide first and second order longitudinal phase space control through the use of quadrupole and sextupole magnets placed in dispersive regions of the arc. By tuning the quadrupoles it is possible to easily manipulate the total momentum compaction (R_{56}) of the machine. Final compression of the bunch is normally performed in a standard four-dipole chicane immediately before the wiggler. This chicane also provides separation between the FEL optical components and electron beam. After passage through the wiggler (not active during the experiment) the beam passes through a THz suppression chicane [15] which serves to decompress the bunch slightly before it reaches the second recirculation arc. This decompression helps to alleviate heating on the downstream FEL optics due to CSR production in the leading dipole of the second arc. In the second arc the beam again undergoes more

Content from this work may be used under the terms of the CC BY 3.0 licence (© 2015). Any distribution of this work must maintain attribution to the author(s), title of the work, publisher, and DOI.

ISBN: 978-3-95450-168-7 doi:10.18429/JACoW-IPAC2015-WEXB2

Content from this work may be used under the terms of the CC BY 3.0 licence (© 2015). Any distribution of this work must maintain attribution to the author(s), title of the work, publisher, and DOI.

MEASUREMENT AND SIMULATION OF ELECTRON CLOUD INDUCED EMITTANCE GROWTH AT CESRTA

L Pentecost, Colgate University, Hamilton NY USA
K. G. Sonnad, J. Flanagan, K. Ohmi KEK, Tsukuba, Japan
L. Bartnik, M. Billing, M. Forster, G. Dugan CLASSE, Cornell University, NY USA
R. Holtzapple, K McArdle, M. Miller, S. Tucker Cal Poly, San Luis Obispo, CA, USA
M.T.F. Pivi, MedAustron Wiener Neustadt, Austria

Abstract

This paper presents recent observations obtained on the study of electron cloud induced instabilities and emittance growth on positron beams at the Cornell Electron-Positron Storage Ring Test Acceleartor (CesrTA), and the simulation of these phenomena under similar beam conditions using the program CMAD. Results show that the transition to large bunch oscillations ocurrs at similar electron cloud densities in experiments as well as simulations. Beam size measurements were carried out using an x-ray beam size monitor (xBSM). The spectrum of the motion of the bunches were recorded using beam position monitors. The experiment consisted of using a train of positron bunches to generate the electron cloud, and observation of a “witness bunch" at different positions behind the train. Motion of the bunches in the train were controlled using feedback, thus suppressing multi-bunch effects. This experimental set up was suitable for comparison with simulations because the simulations were carried out only to study single bunch effects.

INTRODUCTION

The CesrTA program consists of using the Cornell Electron-Positron Storage Ring as a test facility to study physics associated with linear collider damping rings [1]. One of the activities of the program was the study of the response of the positron beams to electron clouds under different conditions. This paper reports the results of experiments carried out in April 2014, along with simulations performed under similar conditions. Table 1 gives the conditions under which experiments were performed.

Table 1: CesrTA Parameters

Parameter	Value
Energy	2.085 GeV
Horizontal Emittance	2.6 nm
Vertical Emittance	20 pm
Bunch Length	10.8 mm
Bunch Spacing	14 ns
Momentum Compaction	6.8e-3
Revolution Frequency	390.1 kHz
Horizontal Tune	0.58
Vertical Tune	0.62
Synchrotron Tune	0.055

Earlier simulation studies using the program CMAD [3] were performed for CesrTA Ref [6], that showed several qualitative features also observed in the experiments. Since then, the CMAD program has undergone various improvements that has enabled better comparisons with simulations. At the same time, the method of observation underwent a change, which made it more suitable for comparison with simulations. The so called "witness bunch"(WB) method of observation consists of using a train of positrons to generate the electron cloud. The sole purpose of the train is to generate the cloud rather than for studying its response to electron clouds. The transverse motion of the bunches in the train was always well suppressed with the help of feedback. This helps eliminate multi-bunch effects. The witness bunch was placed at varying positions behind the train, and the behavior of this bunch alone was observed under different conditions. It should be noted that the witness bunches used for different measurements never existed. That is, when the observation of one of them was completed, the bunch was removed and replaced by the next one under a different condition. The instrumentation associated with performing this swap of bunches is given in Ref [7]. One of the conditions that was varied was the position of the WB behind the train, which is equivalent to varying cloud density encountered by the bunch. Other experiments on varying the chromaticity, witness bunch charge, emittance etc were attempted but the data obtained was insufficient and it was clear that a more exhaustive study is necessary to study these effects.

TUNE SHIFT ANALYSIS

The spectrum of the witness bunch was obtained by gating BPM signal from a single bunch and feeding the signal to a spectrum analyzer. The details of the instrumentation is given in [9]. These measurements provide information on tunes that are most prominent in the motion of the bunch. Figure 1 shows plots of the fractional tune vs signal amplitude, of the first bunch in the train and the witness bunch. It is assumed that the first bunch does not encounter any cloud, and thus the tune shift of the witness bunch with respect to the corresponding first bunch in the train is the electron cloud induced tune shift. These results shown had a current of 0.5mA in all the bunches (train + witness). The figure shows the tune shifts of witness bunches at positions 74 and 47, behind the 45 bunch train. The spacing between the WB and the end of the train may be computed by (WB position − no of bunches in train) × bunch-spacing. Thus WB at 47

ISBN: 978-3-95450-168-7 doi:10.18429/JACoW-IPAC2015-WEXB3

Content from this work may be used under the terms of the CC BY 3.0 licence (© 2015). Any distribution of this work must maintain attribution to the author(s), title of the work, publisher, and DOI.

REALIZATION OF PSEUDO SINGLE BUNCH OPERATION WITH ADJUSTABLE FREQUENCY*

C. Sun†, D. S. Robin, C. Steier, G. Portmann
Lawrence Berkeley National Laboratory, Berkeley, CA 94706, USA

Abstract

We present the concept and results of pseudo-single-bunch (PSB) operation—a new operational mode at the Advanced Light Source (ALS)—that can greatly expand the capabilities of synchrotron light sources to carry out dynamics and time-of-flight experiments. In PSB operation, a single electron bunch is displaced transversely from the other electron bunches using a short-pulse, high-repetition-rate kicker magnet. Experiments that require light emitted only from a single bunch can stop the light emitted from the other bunches using a collimator. Other beam lines will only see a small reduction in flux due to the displaced bunch. As a result, PSB allows to run timing experiments during the multibunch operation. Furthermore, the time spacing of PSB pulses can be adjusted from milliseconds to microseconds with a novel "kick-and-cancel" scheme, which can significantly alleviate complications of using high-power choppers and substantially reduce the rate of sample damage.

INTRODUCTION

A major limitation of synchrotron light sources is the ability to easily serve two classes of experiments simultaneously, namely, brightness or flux limited experiments and timing experiments. High brightness experiments require filling most of the rf buckets with electrons, thus maximizing the total current while minimizing the current per bunch. In such a multibunch filling pattern, the bunch spacing is typically only a few nanoseconds between electron bunches. On the other hand, timing experiments require longer timeing between x-ray pulses. For example, in the case of laser-pump x-ray-probe timing experiments, it is desirable to have only one x-ray pulse per laser pulse. Since such lasers operate between kHz and MHz rates, this implies a distance between pulses of ms to μs.

At the Advanced Light Source (ALS) facility, we have been exploring a new mode of operation that we call "pseudo-single-bunch" (PSB) operation, the goal of which is to allow high-flux and timing experiments to run simultaneously [1–4]. The idea behind PSB operation is to use a high-repetition (MHz)-rate, short-pulse (<100 ns) kicker [5] to vertically displace a single "camshaft" bunch relative to the bunch train. Experiments that require light emitted only from a single bunch can block the light emitted from the other bunches using a collimator with only light from the camshaft bunch reaching the experiment. The PSB timing could be at the orbital period (656 ns) or longer, depending upon how frequently the bunch is displaced.

Here we discuss the results of our studies on the PSB operational mode, especially the novel "kick-and-cancel" (KAC) scheme that can deliver a single pulse with adjustable frequency [3]. A similar idea was previously suggested [6], but to our knowledge this is the first time that it has been realized.

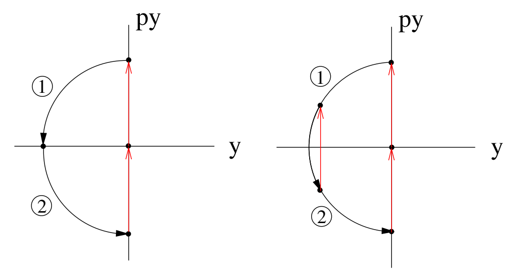

Figure 1: Illustration of the KAC scheme in the phase space at tunes 0.25 and 0.333.

KICK-AND-CANCEL (KAC) SCHEME

Working Principle

The idea of the KAC scheme is that by adjusting the ring tune and the PSB kick pattern, the camshaft bunch can first be displaced to a different orbit and then kicked back to its original one within a few turns. This KAC process can be repeated at will to create a PSB pulse with an adjustable repetition rate.

The KAC scheme can be easily understood using a normalized phase space diagram as shown in Fig. 1. In this plot, two schemes are illustrated at tune $\nu_y = 0.25$ and $\nu_y = 0.333$. For example, at tune $\nu_y = 0.25$, the camshaft bunch is first displaced to a different vertical orbit and then proceeds two turns. At the end of the second turn, the bunch has the same vertical offset but the inverse angle to the one after the first kick. At this time, if another identical kick is applied, the bunch will be put back to its original orbit. Similarly, at $\nu_y = 0.333$, three kicks and three orbital tunrs are required in order to restore the displaced orbit.

After the beam orbit is restored to the original orbit, we can wait any time of period (KAC period N) and then repeat this kick and cancel process, thus creating single-bunch pulses with adjustable repetition rates.

* Work supported by the Director Office of Science of the U.S. Department of Energy under Contract No. DE-AC02-05CH11231
† ccsun@lbl.gov

ISBN: 978-3-95450-168-7 doi:10.18429/JACoW-IPAC2015-WEYB1

Content from this work may be used under the terms of the CC BY 3.0 licence (© 2015). Any distribution of this work must maintain attribution to the author(s), title of the work, publisher, and DOI.

BENCHMARKING AND APPLICATION OF SPACE CHARGE CODES FOR RINGS

Shinji Machida*, STFC/RAL/ASTeC, Didcot, United Kingdom

Abstract

This presentation should present an overview of efforts for benchmarking and application of space charge codes for rings. After briefly recalling the historical background of the simulation efforts of space charge effects in rings, we will overview the present benchmarking efforts against experimental results.

INTRODUCTION

Benchmarking of a code in the accelerator community is usually referred to as an effort to confirm validity of a code by comparing the prediction of a code 1) with measured data, 2) with theory based on the same physics and 3) with other similar codes. In this paper, we will discuss why the benchmarking of space charge codes is important and still a challenge now.

Space charge codes using macro particles# consisting of two parts. The first part is to update macro particle coordinates as a result of space charge effects integrated in each small time step. The second part is to advance macro particle coordinates in the same time period, which is entirely determined by the external lattice elements. Separation of the two parts and alternative evaluation of them are thought to be essential in order to take into account local details of the beam envelope and the *s*-dependent space charge potential, where *s* is the direction of the beam travel. If the beam emittance in transverse and longitudinal directions evolves, the space charge potential is updated so that the calculation is self-consistent. Although the second part, which is free from space charge, can be easily symplectic, that is the essential feature for long term tracking, evaluating space charge effects is susceptible to any kinds of modelling details. It is possible that the symplectic condition is violated if we employ the Particle in Cell (PIC) method (see below) to obtain a non-smooth space charge potential. Ref. [1] further discusses the conditions of symplectic time evolution when using PIC.

The idea of evaluating the space charge potential using macro particles came from plasma physics [2]. A brute force way of calculating the space charge potential is to sum up the binary interaction among the whole macro particle ensemble (Particle Particle or PP method), but it is not efficient from the computational point. A more practical approach is to divide the configuration space using a grid and then allocate macro particles to and calculate the Coulomb potential at each grid point. This is called the Particle Mesh method or the Particle in Cell (PIC) method [3].

Whether the PP or the PIC method is employed, the number of macro particles is much less than reality, several orders of magnitude less, e.g. 10^6 macro particles to represent 10^{12} real particles, and that may introduce non-physical effects. One of them is the numerical intrabeam scattering, which causes continuous emittance blow up [4].

A different approach is to fix the space charge potential at the beginning and keep it unchanged during the tracking. This is not a self-consistent calculation. However, when the space charge effects are a small perturbation, the change of charge distribution and therefore the change of the space charge potential are negligible and the dynamics is mainly determined by the external lattice elements. In fact, space charge effects in rings are relatively small because the periodic structure excites resonances and tune is allowed only a small shift, e.g., a few per cent change in terms of tune shift, so that the approximation is well justified. The advantage is that it is free from the numerical noise which the PIC method cannot avoid and can make the whole tracking exactly symplectic. On the other hand, some kind of instabilities, such as envelope instabilities due to space charge cannot be modelled [5].

One day in the not too distance future, the same number of macro particles as real particles in rings may be tracked in simulation with space charge effects once computational power has progressed significantly. Space charge codes at present, however, have to use some approximation, often drastic one as we mention later, and the validation of codes are essential.

In this paper, we will briefly review the benchmarking efforts of space charge codes in the past. We will then overview the present activities in detail. It is interesting to see that each period places different emphasis on the benchmarking because of the accelerator projects at that time, available computational resource and theoretical understanding. We would like to note that there was a similar review paper 10 years ago [6].

BACKGROUND

In the accelerator community, the first time when a space charge simulation code for rings was used was probably in the 80s. Although space charge codes for linacs had existed earlier, codes for rings were not easy to write because the number of calculation steps was much larger so it demanded heavy computational power.

There was the demand to preserve transverse rms emittance in high energy hadron colliders and avoid luminosity deterioration. There was also the need to minimise beam loss in high intensity hadron accelerators and so allow hand-on maintenance. It was the time when Superconducting Super Collider (SSC) in the US and KAON Factory in Canada were proposed. People knew

*shinji.machida@stfc.ac.uk

#Numerical Vlasov solver is another way for space charge codes without macro particles, but we do not discuss it here.

ISBN: 978-3-95450-168-7 doi:10.18429/JACoW-IPAC2015-WEYB2
Content from this work may be used under the terms of the CC BY 3.0 licence (© 2015). Any distribution of this work must maintain attribution to the author(s), title of the work, publisher, and DOI.

BEAM DYNAMICS IN A HIGH FREQUENCY RFQ

A.M. Lombardi, V. A. Dimov, M. Garlasche', A. Grudiev, S. Mathot, E. Montesinos, S. Myers, M. Timmins, M. Vretenar, CERN, Geneva, Switzerland

Abstract

CERN is constructing a 750 MHz Radio Frequency Quadrupole (RFQ) which can accelerate a proton beam to 5 MeV in a length of 2 m. The beam dynamics strategic parameters have been chosen to make this RFQ a good candidate for the injector of a medical facility operating at frequency of 3 GHz . Minimising beam losses above 1 MeV, containing the RF power losses and opening the road to industrialisation have been the guidelines for an unconventional RFQ design. In this paper, the optimisation efforts, the structure design and the expected beam qualities will be detailed. The status of the construction as well as the potential for further developments will be presented.

INTRODUCTION

The office for medical application, created by the CERN director general in 2013 with the aim for CERN to become established as an important facilitator of medical physics in Europe, has -amongst others-the task of developing on-going accelerator, detector and information technologies in ways that will benefit medicine. In this framework the office has responded to the needs of several linac-based hadron-therapy projects and has created a study group for a high frequency RFQ with the aim of capitalising on the recent developments around the RFQ for the LINAC4 project, which was successfully commissioned in 2013.

Linac based proton-therapy facilities are the new generation in the field of hadron therapy machines, the main advantage with respect to the established PIMMS [1] design - being the possibility of fast energy variation (pulse-to-pulse). Typical linac-based facilities [2,3] include high-frequency, high-gradient structures resonating at the frequency of 3 GHz, equipped with Permanent Magnet Quadrupoles. Typically about 20m of accelerator are sufficient to bring the energy from 10 to 250 MeV, including a medium velocity structure up to 40 MeV and a high velocity structure up to 250 MeV. The effectiveness of accelerating non-relativistic protons with 3GHz has been demonstrated from the energy of 11 MeV [4]. It is believed that effective use from energies as low as 5 MeV is feasible. Below 5 MeV the use of 3GHz is excluded and a solution must be found for the missing link.

A HIGH FREQUENCY RFQ

The starting parameters for the RFQ design are reported in Table1. These are the working parameters used to define the layout and will be discussed in the following.

Table 1: RFQ and Source Specifications

Parameter	Value
RF Frequency	Subhar of 3GHz
Input energy	>30keV
Output Energy	5 MeV
Output Pulse Current	30 μA
Repetition frequency	200 Hz
Pulse duration	20 μsec
Transverse Emittance (100%,normalized)	0.4 (π mm-mrad)
Bunch length	±20 deg at 3 GHz
Energy spread	±35 keV
Length	Less than 2.5m

The combination of parameters as detailed in the table above calls for an unconventional RFQ design, as both the longitudinal and the transverse acceptance at 5MeV are factors smaller than the values currently obtained at this energy. Although the design of the source is outside the scope of this paper, we considered the source when defining the RFQ layout and we made sure that the challenges (emittance, extraction energy and current) were balanced between the source and the RFQ.

General Layout

In this paragraph we describe the fundamental choices that brought to the definition of the RFQ, the first one being the frequency. The choices as described here are motivated for the specific use of this RFQ in a proton therapy facility; they are not universal choices, as will be detailed in the last paragraph of this paper where other uses are proposed. The frequencies of 600, 750MHz and 1 GHz were considered: the higher the frequency the easier the frequency jump at 5 MeV but also the higher the technological jump from existing RFQs. From a purely beam-dynamics point of view the use of a higher frequency is certainly an advantage. We then compared 600 and 750 MHz on the basis of power losses consideration. The capacitance per unit length is a very weak function of the frequency, much more dependent on the ratio between the transverse radius of curvature and the average radius (ρ/r0). We can therefore assume that the capacitance is the same and we know from [5] that the power losses per meter scale like the V^2 $f^{3/2}$ where V is the vane voltage and f the frequency. For the same vane voltage the 750 MHz RFQ would use 1.4 times more power per meter, but we found out that the overall length of the RFQ would compensate for this disadvantage, and finally for the same vane voltage and same output energy the total power would be approximately the same. As the

ISBN: 978-3-95450-168-7 doi:10.18429/JACoW-IPAC2015-WEYB3

INTERPLAY OF BEAM-BEAM, LATTICE NONLINEARITY, AND SPACE CHARGE EFFECTS IN THE SuperKEKB COLLIDER

D. Zhou*, H. Koiso, A. Morita, K. Ohmi, Y. Ohnishi, K. Oide, H. Sugimoto
KEK, 1-1 Oho, Tsukuba, Ibaraki 305-0801, Japan
Y. Zhang, IHEP, Beijing, China

Abstract

The SuperKEKB B-factory adopts nanobeam scheme for the collision, which consists of large crossing angle and very small vertical beta function at the interaction point. Simulations have revealed that the luminosity of SuperKEKB will be very sensitive to perturbations from various sources. This paper discusses various beam dynamics issues involved in the SuperKEKB collider, including beam-beam, lattice nonlinearity, and space charge effects, as well as their interplay and planned mitigations.

INTRODUCTION

The SuperKEKB is designed with the strategy of so-called nanobeam scheme, which was originally proposed by P. Raimondi for SuperB [1]. The electron and positron beams collide with a horizontal crossing angle of $\theta = 83$ mrad. The horizontal emittances are $\epsilon_{x+} = 3.2$ nm and $\epsilon_{x-} = 4.6$ nm, taking into account the intra-beam scattering effects. The beam sizes at the IP are $\sigma_{x+} = 10.1\,\mu$m and $\sigma_{x-} = 10.7\,\mu$m. The overlap area of the two beams is $\Delta s = 2\sigma_x/\theta \approx 0.25$ mm, which is about 1/20 of the nominal bunch length. Another feature of SuperKEKB is the small vertical beta function at IP, which is squeezed to be $\beta^*_{y+} = 0.27$ mm and $\beta^*_{y-} = 0.3$ mm, comparable to the overlap area Δs. The vertical emittances are assumed to be $\epsilon_{y+} = 8.64$ pm and $\epsilon_{y-} = 12.9$ pm, taking into account various intensity-dependent and -independent effects. Comparing with its predecessor, the emittances of SupkerKEKB rings are about 1/5 and 1/20, and the beta functions are about 1/40 and 1/50 of those of KEKB rings in the horizontal and vertical directions, respectively.

Since the KEKB rings, as reviewed in Refs. [2–4], have experienced many beam dynamics issues which affected the luminosity performance, it is expected that the luminosity performance of SuperKEKB will be even more sensitive to various imperfections or perturbations, such as machine errors, lattice nonlinearity, intra-beam scattering, beam-beam interaction, space charge, impedance-driven instabilities, etc. Regarding to the beam dynamics issues associated to the electron-positron colliders, there are reviews in Refs. [5–7]. The progress of next generation B-factory projects have been reviewed in Refs. [8–10], and in Ref. [11] especially the most recent status of SuperKEKB. This paper is dedicated to discussing a few beam dynamics issues which might set challenges for the future commissioning of the SuperKEKB. For more information of beam dynamics issues at SuperKEKB, such as intra-beam scattering, electron cloud effects, impedance effects, optics optimization, etc., the interested readers are directed to Refs. [12–16].

* dmzhou@post.kek.jp

BEAM DYNAMICS ISSUES

This section gives a brief overview of some important beam dynamics issues in SuperKEKB. Since most of these issues appear to be more prominent in the low energy ring (LER), we mainly use the LER for illustrations rather than the high energy ring (HER) in the following discussions.

Beam-beam Interaction

It is well accepted that the ‘sweet spot’ in the tune space for achieving highest luminosity at an electron-positron collider usually locates at an area close to half integer. To search for the best working point in the tune space, luminosity scans are performed for both LER and HER, with the fractional tunes in the range of [0.5, 0.75] and the beam currents set to design values. The tune scan results of luminosity using a weak-strong model for the LER and HER are demonstrated in Fig. 1 with scaled colours, and Fig. 2 show the relevant scans of vertical rms beam sizes. It is seen that the strong synchro-betatron resonances of $2\nu_x - N\nu_s = Integer$ exist in the nanobeam scheme. This is due to the large crossing angle chosen for the purpose of mitigating hourglass effects. Furthermore, the resonances of $\nu_x + 2\nu_y + N\nu_s = Integer$, $2\nu_y - \nu_s = Integer$, and $\nu_x - \nu_y - \nu_s = Integer$ also restrict the choice of working point. The working points have to be kept far enough from these strong resonances. In general, the luminosity is very sensitive to the vertical beam size. With higher beam energy, the electron beam in HER is more robust than the positron beam in LER with respect to the beam-beam driven synchro-betatron resonances. At present, both the main rings of the SuperKEKB are optimized with fractional tunes of [0.53, 0.57]. The working point is selected from islands isolated by the beam-beam resonance lines. But notice that the island areas might shrink when the lattice nonlinearity and machine errors strengthen those resoances [13].

Lattice Nonlinearity

For SuperKEKB, most of the unavoidable lattice nonlinearity is attributed to the interaction region resulting from the extremely small beta functions at IP and low emittances. For examples, the nonlinear terms from the drift space near IP, so called kinematic terms, and the Maxwellian fringe fields of final focus (FF) superconducting quadrupoles will become very important. The dynamic aperture (DA) lim-

Content from this work may be used under the terms of the CC BY 3.0 licence (© 2015). Any distribution of this work must maintain attribution to the author(s), title of the work, publisher, and DOI.

ISBN: 978-3-95450-168-7 doi:10.18429/JACoW-IPAC2015-WEXC1

Content from this work may be used under the terms of the CC BY 3.0 licence (© 2015). Any distribution of this work must maintain attribution to the author(s), title of the work, publisher, and DOI.

MACHINE AND PERSONNEL PROTECTION FOR HIGH POWER HADRON LINACS

M. Ikegami Facility for Rare Isotope Beams, Michigan State University, MI 48824, USA

Abstract

Machine and personnel safety are increasingly important for high power hadron linacs as involved beam power increases. Design requirements and characteristic features of machine protection system and personnel protection system are reviewed for operating and proposed high power hadron linacs, such as J-PARC, SNS, FRIB, ESS, and IFMIF.

INTRODUCTION

Demand for high power hadron linacs has been increasing for various applications in recent years, which include driver for spallation neutron source, irradiation of material for fusion reactor development, and physics experiments utilizing intense secondary beams. A number of high power hadron linacs are currently under operating, construction, or planning around the world to meet this demand. Prospect for future application for an accelerator driven subcritical reactor or transmutation of nuclear waste has further motivated the pursuit of higher beam power.

Seeking higher beam power, the personnel and machine safety become increasing important as a risk of catastrophic failure has also been increased. PPS (Personnel Protection System) and MPS (Machine Protection System) are key systems to protect personnel and machine safety for accelerators. In this paper, we review design requirements and characteristic features for PPS and MPS for operating and proposed high power hadron linacs. Among a number of high power hadron linacs, we take the following five projects in this paper, namely, FRIB (Facility for Rare Isotope Beams), J-PARC (Japan Proton Accelerator Research Complex), SNS (Spallation Neutron Source), ESS (European Spallation Source), and IFMIF (International Fusion Material Irradiation Facility). For IFMIF, the linac for IFMIF/EVEDA (Engineering Validation and Engineering Design Activities) is also discussed. As summarized in Table 1, the average beam power level we discuss in this paper ranges from a few hundred kW to a several MW.

PERSONNEL PROTECTION SYSTEM

Challenges in PPS specific to high power hadron linacs are mostly related to radiation hazard mitigation. As the involved beam power is high, it can cause radiation hazard both with prompt and induced radiation.

Prompt Radiation During Normal Operation

For prompt radiation during normal operation, it is usual to control the radiation level at accessible area by shielding assuming certain amount of chronic beam loss. For example, shielding for the linac tunnel of FRIB is designed to keep the expected radiation dose rate at accessible area below 1 μSV/h assuming uniform beam loss of 1 W/m for the beam line. The goal of 1 μSv/h is deduced from the internal yearly dose limit (or ALARA goal) for radiation workers in FRIB and assumption for possible occupying hours per year. As shielding design involves radiation transport calculation, some margin is added in FRIB for its ambiguity. The beam loss assumption of 1 W/m comes from the empirical hands-on maintenance limit for proton accelerators, and we assume that we won't operate for long term with tolerating the beam loss exceeding this level. Radiation monitors connected to PPS are placed in accessible areas to monitor the radiation level, and they inhibit the beam if the radiation dose rate exceeds the assumed level. The linac itself could be operated with higher beam loss than 1 W/m, but the radiation monitor system guarantees that the radiation dose rate from chronic beam loss does not exceed the expected level. Although the dose rate limit for accessible area and assumed beam loss may be different for each facility, they share the basic strategy in their shielding design. As the dose limit is defined as an average over a period of time usually longer than one hour, fast response is not required for radiation monitor in this context.

Prompt Radiation at an Abnormal Event

However, the situation can be very different at a fault event where the dose rate can be higher by orders of magnitudes than that in normal operation. We here consider two kinds of faults. One is the worst case beam loss event where full power beam is lost at a single point. The other is beam delivery to unintended area.

Single point beam loss For the former, detailed fault analysis with radiation transport calculation is indispensable to design appropriate protection. In the case of FRIB, the most vulnerable locations to this hazard in the linac building is in the front-end area due to its unique linac layout (See Fig. 1). In FRIB, ion sources are located at the surface level and the beam is led to linac tunnel through a vertical drop. Then, the accelerated beam comes back to the vicinity of the vertical drop due to its folded layout. The dose rate around the vertical drop can be very high if we have a full power single point beam loss of the accelerated beam in the vicinity of the vertical drop. Radiation transport calculation shows that the dose rate could reach a few tens of mSv/h at the surface of the shielding block (See Fig. 2) [1]. Systematic analysis reveals that we have significant radiation dose rate only in the vicinity of four large openings in the linac building, which enables us to focus on protection around those limited areas. Our tentative internal goal for integrated dose at a single abnormal

ISBN: 978-3-95450-168-7 doi:10.18429/JACoW-IPAC2015-WEXC2

ADVANCES IN PROTON LINAC ONLINE MODELING*

Xiaoying Pang†
Los Alamos National Laboratory, Los Alamos, NM, 87545, USA

Abstract

This paper will review current online modeling tools used for proton linacs and then focus on a new approach that marries multi-particle beam dynamics with modern GPU technology to provide pseudo real-time beam information in a control room setting. Benefits to be discussed will include fast turnaround, accurate beam quality prediction, cost efficiency, test bed for new control and operation scheme development and operator training.

INTRODUCTION

Accelerator online modeling codes are indispensable tools in proton linac control rooms. At their hearts are the online beam dynamics simulators. These simulators are developed to have direct access to real machine parameters and to be able to provide fast predictions of various beam quantities. Together with some optimization tools, they can guide accelerator operators to tune up and troubleshoot the linac systems efficiently. Existing online simulators for proton linacs are mostly developed based on the envelope model which represents a r.m.s. equivalent beam as an ellipse in phase space and uses a linear representation of the space charge force. While the envelope model enables fast response and good accuracy for beam matching and steering in most cases, it lacks the capability to simulate using real beam distributions and study a range of real-world scenarios where the beam is not a nicely formed ellipsoid or the beam intensity is high enough so that a more accurate representation of the space charge force is needed. For high power beam operations, there will be less room for operational error, therefore a more accurate multi-particle online simulator is needed to provide more realistic beam information and tuning guidance.

In the following sections, we will first review the existing online modeling tools and briefly discuss the need for a multi-particle simulator for high power beam operations. Then we will introduce the high performance simulator (HPSim) that we have been developing. Details about the design, performance and its applications will be presented.

EXISTING ONLINE MODELING TOOLS

The list of tools presented here is by no means exhaustive, but they can be considered representative of what have been used in proton linac control rooms worldwide.

* Work supported by U.S. DOE, NNSA under contract DE-AC52-06NA25396
† xpang@lanl.gov

TRACE2D/3D

TRACE2D and TRACE3D [1] are well-established envelope based simulation codes initially developed at LANL. TRACE2D represents a beam using phase space ellipses in the two transverse planes, while the TRACE3D has the additional capability of simulating the longitudinal beam dynamics by assuming a 3D ellipsoidal beam shape. In both cases, the beam is a r.m.s. equivalent representation and it is described as a sigma matrix whose elements are related to the Twiss or Courant-Snyder parameters. Since they only track beam through the beamline elements represented as R-matrices and only consider the linear part of the space charge force, TRACE2D/3D simulations can be very fast, which makes them perfect for accelerator online modeling. In fact, the TRACE2D is still used in the proton linac control room at the Los Alamos Neutron Science Center (LANSCE). The physics algorithms of TRACE2D/3D have been used in the development of other online modeling tools and they have been widely used to benchmark against other similar codes.

XAL Online Model

XAL is a Java development framework for accelerator applications [2]. It was first developed and tested at the Spallation Neutron Source (SNS) and has been widely adopted by several accelerator sites, not limited to proton accelerator facilities. The online modeling tools [3] of XAL can simulate not only linacs but also storage rings. It comes with a suite of tools [4] that can be very useful in accelerator tuning, i.e. PASTA [5] for warm linac RF setpoint tuning, SLACS for superconducting cavity [6] RF setpoint tuning and tools for orbit corrections, etc. Like TRACE3D, the XAL online model tracks a beam in the 6D phase space based on the envelope model and uses the linear space charge approximation.

ESS Linac Simulator

More recently, a new online beam dynamics simulator is being developed at the European Spallation Source (ESS) [7–9]. It is also an envelope model based simulator. In order to be able to simulate the 5MW beam correctly, better treatment of the RF transformation and nonlinear space charge effect have been implemented [8]. However, the nonlinear space charge effect is calculated by assuming the beam distribution is Gaussian within the 3D ellipsoid.

HIGH PERFORMANCE ONLINE MULTI-PARTICLE SIMULATOR

The common theme of the existing online simulators for proton linacs is that they are all based upon the envelope

Content from this work may be used under the terms of the CC BY 3.0 licence (© 2015). Any distribution of this work must maintain attribution to the author(s), title of the work, publisher, and DOI.

ISBN: 978-3-95450-168-7 doi:10.18429/JACoW-IPAC2015-WEXC3

IMPROVING THE ENERGY EFFICIENCY OF ACCELERATOR FACILITIES*

M. Seidel, PSI, Villigen, Switzerland
E. Jensen, European Organization for Nuclear Research (CERN), Switzerland
R. Gehring, Karlsruhe Institute of Technology (KIT), Germany
J. Stadlmann, P. Spiller, GSI Helmholtzzentrum für Schwerionenforschung GmbH (GSI), Germany
T. Parker, European Spallation Source (ESS), Lund, Sweden

Abstract

New particle accelerator based research facilities tend to be much more productive, but often in coincidence with higher energy consumption. The total energy consumption of mankind is steeply rising and this is mainly caused by quickly developing countries. Some European countries decided to terminate nuclear power generation and to switch to sustainable energy production. Also the CO2 problem gives rise to new approaches for energy production and in all strategies the efficiency of utilization of electrical energy plays an important role. For the public acceptance of particle accelerator projects it is thus very important to optimize them for best utilization of electrical energy and to show these efforts to funding bodies and to the public. Within the European accelerator development program Eucard-2 [1] we organise a network EnEfficient [2] that aims at improving the energy efficiency of accelerators. In this paper we give some background information on the political situation, we describe the power flow in accelerator facilities and we give examples for developments of efficient accelerator systems, such as magnets, RF generation, heat recovery and energy management.

ENERGY – THE POLITICAL SITUATION

Over the history of mankind the consumption of energy shows a steep growth with the industrial revolution. Especially in the last few decades the growth is dramatic and many people see this development critically. Massive burning of fossil energy carriers causes high CO_2 emission, one of the causes for global warming and climate change. Nuclear power has other problems and is disputed. But even if one believes in technical advances, the development shown in Fig. 1 looks unhealthy and one might suspect that the growth rate cannot stay intact for long. The mentioned problems have caused a higher awareness on energy related issues around the world. Especially in Europe some countries try to change their energy generation schemes away from coal and nuclear power, in favour of sustainable energy production like wind and solar. In all strategies a high efficiency of electrical power utilization is of utmost importance. When a new research facility is proposed, its energy consumption is thus a critical aspect for the successful public and political acceptance. Statistical information on existing accelerator facilities can be found in [3]. In those countries with a larger fraction of renewable energies we observe also a technical impact of new energy strategies. While coal and nuclear power plants provide continuous base power, wind and sun are strongly fluctuating. Already today, spot market prices of energy vary by an order of magnitude. In extreme cases prices go even negative, when additional consumers are needed to avoid a breakdown of the grid. Energy storage systems could solve this problem. At present only limited technical solutions exist, which allow storing significant amounts of energy. As a result we observe fluctuations in availability of cheap electrical energy.

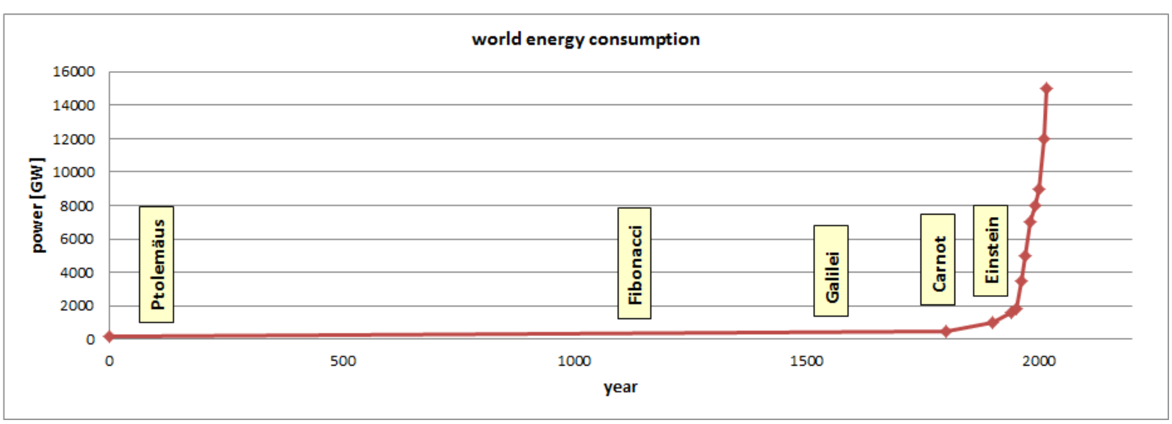

Figure 1: The world energy consumption shows a steep increase in the last 100 years. (Data before 1800 is estimated by scaling consumption in proportion to world population.)

* EuCARD² is co-funded by the partners and the European Commission under Capacities 7th Framework Programme, Grant Agreement 312453

Content from this work may be used under the terms of the CC BY 3.0 licence (© 2015). Any distribution of this work must maintain attribution to the author(s), title of the work, publisher, and DOI.

ISBN: 978-3-95450-168-7 doi:10.18429/JACoW-IPAC2015-WEYC1

TECHNICAL CHALLENGES OF THE LCLS-II CW X-RAY FEL*

T.O. Raubenheimer# for the LCLS-II Collaboration, SLAC, Menlo Park, CA 94025, USA

Abstract

The LCLS-II will be a CW X-ray FEL upgrade to the existing LCLS X-ray FEL at the SLAC National Accelerator Laboratory (SLAC). This paper will describe the overall layout and describe the technical challenges that the upgrade project faces.

INTRODUCTION

The LCLS-II is an X-ray Free-Electron Laser (FEL) which will upgrade the LCLS FEL at SLAC. The LCLS-II is designed to deliver photons between 200 eV and 5 keV at repetition rates as high as 1 MHz (929 kHz) using a superconducting RF linac (SCRF) linac while still providing pulses at short wavelengths and high X-ray pulse energy over the photon range of 1 to 25 keV using the existing 120 Hz copper RF (CuRF) LCLS linac.

The LCLS-II project is being constructed by a collaboration of US laboratories consisting of Argonne National Lab. (ANL), Cornell University (CU), Fermilab (FNAL), Jefferson Lab. (JLab), Lawrence Berkeley National Lab. (LBNL), and SLAC. In addition, the project has substantial assistance from the EuXFEL project as well as the other international laboratories focused on SCRF development and XFEL's.

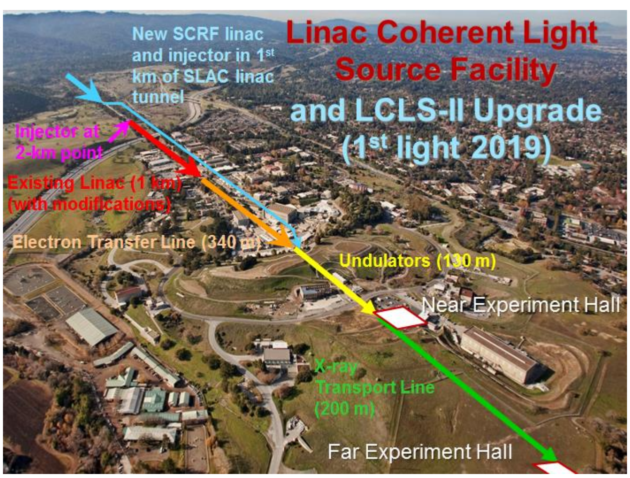

Figure 1: Schematic of the LCLS facility with the LCLS-II SCRF upgrade shown in blue.

The SCRF linac will be installed in the first third (1 km) of the SLAC linac tunnel and a bypass line will bring the high rate beam around the middle third of the existing linac and the existing LCLS CuRF linac as illustrated in Figure 1. Beams from both the CuRF and the SCRF linac will be transported to the existing LCLS Undulator Hall where, to cover the full photon-energy range, the existing LCLS fixed gap undulator will be removed and the facility will install two variable-strength (gap-tunable) undulators, one dedicated to the production of Soft X-rays (SXR Undulator) from 0.2 – 1.3 keV and one dedicated to production of Hard X-rays (HXR Undulator) from 1.0 – 25.0 keV. The facility will also allow the possibility of generating near transform-limited pulses using self-seeding as well as downstream monochromators.

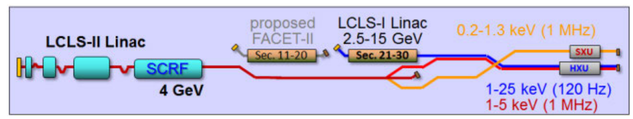

Figure 2: Schematic layout of the LCLS-II project.

As illustrated in Figure 2, the facility is constructed to either deliver high-rate beam from the SCRF linac to both the SXR and HXR undulators, or to deliver the high-rate beam to the SXR undulator and deliver beam from the existing copper CuRF linac at 120 Hz to the HXR undulator.

The LCLS-II will have the high peak brightness capability and flexibility of LCLS while also having the ability to provide MHz rate beams from a CW SCRF linac. The operating regimes are:

1. Soft X-ray photons from SASE and self-seeding between 0.2 and 1.3 keV at MHz rates, with an average X-ray power in excess of 20 Watts;
2. Hard X-ray photons from SASE between 1.0 and 5.0 keV at MHz rates with an average X-ray power in excess of 20 Watts and with the possibility of a future upgrade to self-seeding operation at energies between 1 and 4 keV;
3. Hard X-ray photons with SASE between 1 and 25 keV and self-seeding between 4 keV and 13 keV at 120 Hz, with mJ-class pulses and performance comparable to or exceeding that of LCLS.

Bunches from the SCRF linac will be directed to either the HXR or SXR with a high rate magnetic kicker that will allow independent control of the beam rate being delivered to either undulator. The SCRF linac will be intrinsically more stable than the LCLS linac and the energy stability of the electron beams is specified to be <0.01% rms which >10x more stable than that from the CuRF linac. The timing stability in the initial implementation of LCLS-II is specified to be better than 20 fs rms and is expected to be less than 10 fs rms. It is expected that the stability of the SCRF beams will be

* Work supported by DOE Contract: DE-AC02-76-SF00515
# torr@stanford.edu

Content from this work may be used under the terms of the CC BY 3.0 licence (© 2015). Any distribution of this work must maintain attribution to the author(s), title of the work, publisher, and DOI.

ISBN: 978-3-95450-168-7 doi:10.18429/JACoW-IPAC2015-WEYC2

STATUS OF THE PAL-XFEL CONSTRUCTION*

H. S. Kang, K.-W Kim, I. S. Ko, PAL, Pohang, Kyungbuk, Korea

Abstract

The PAL-XFEL, a 0.1-nm hard X-ray FEL facility consisting of a 10-GeV S-band linac, is being constructed in Pohang, South Korea. Its building construction was completed at the end of 2014. The installation of the 10-GeV linac started in January 2015 will be completed by the end of 2015 together with undulators and beam lines. The commissioning will get started in January 2016 aiming for the first lasing of hard X-ray FEL. We will report the current status, construction progress, and commissioning plans for the PAL XFEL project, including major subsystem preparations.

INTORDUCTION

The Pohang Accelerator Laboratory (PAL), Pohang, South Korea, is developing a 0.1 nm SASE based FEL, named PAL-XFEL, for high power, short pulse X-ray coherent photon sources. It is adjacent to the existing 3-rd generation light source, PLS-II, which was upgraded to a 3-GeV/400-mA/6-nm facility in 2010 (see Fig. 1). The PAL-XFEL project was started from 2011 with the five-year total budget of 400 MUSD, its building construction completed by the end of 2014, and successively the installation of linac, undulator, and beam line follows and will be completed by the end of 2015. The FEL commissioning will get started in early 2016.

The PAL-XFEL includes a 10-GeV S-band normal conducting linac, which is 700 m long and consists of a photocathode RF gun, 174 S-band accelerating structures with 50 klystron/modulators, one X-band RF system for linearization, and three bunch compressors (see Table 1). Beyond the 10-GeV linac, a 250-m long hard x-ray undulator hall follows. An experimental hall, which is 60-meters long and 16-meters wide, is located at the end of the facility. The total length of the building is 1,110 meters.

The PAL-XFEL linac is divided into four acceleration sections (L1, L2, L3, and L4), three bunch compressors (BC1, BC2, BC3), and a dogleg transport line to undulators as shown in Fig. 2 [1]. The L1 section consists of two RF units each of which is comprised with one klystron and two S-band structures, while L2 has 10, L3 has 4, and L4 has 27 RF units each of which has one klystron, four accelerating structures, and one energy doublers. A laser heater to mitigate micro-bunching instability is placed right after the injector, and an X-band cavity placed right before the BC1.

Among the available five undulator lines in the undulator halls, only two undulator lines will be prepared during the construction period of Year 2011-2105: a hard X-ray FEL line (HX1) and a soft X-ray FEL line (SX1) as shown in Fig. 2. HX1 covers the wavelength of λ=0.06 - 0.6 nm using a 4 to 10-GeV electron beam, and uses linear polarization, variable gap, out-vacuum undulators. SX1 covers the wavelength of λ = 1.0 - 4.5 nm using a 3.15-GeV electron beam.

Figure 1: Picture of construction site taken in January 2015.

Table 1: Parameters of PAL-XFEL

Linac	
FEL radiation wavelength	0.1 nm
Electron energy	10 GeV
Slice emittance	0.5 mm-mrad
Beam charge	0.2 nC
Peak current at undulator	3.0 kA
Pulse repetition rate	60 Hz
Electron source	Photo-cathode RF-gun
Linac structure	S-band normal conducting
Undulator	
Type	out-vacuum, variable gap
Length	5 m
Undulator period	2.6 cm
Undulator min. gap	8.3 mm
Vacuum chamber dimension	6.7 x 13.4 mm

To achieve the beam energy stability of below 0.02% and the arrival time jitter of 20fs for the PAL-XFEL, the linac RF parameters should be as stable as 0.03 degrees for the RF phase and 0.02% for the RF amplitude for S-band RF systems, and 0.1 degree / 0.04% for the X-band linearizer RF system. The pulse-to-pulse klystron RF stability is determined by the klystron beam voltage

Content from this work may be used under the terms of the CC BY 3.0 licence (© 2015). Any distribution of this work must maintain attribution to the author(s), title of the work, publisher, and DOI.

ISBN: 978-3-95450-168-7 doi:10.18429/JACoW-IPAC2015-WEYC3

COMMISSIONING AND OPERATION OF THE ARIEL ELECTRON LINAC AT TRIUMF*†

M.Marchetto, F. Ames, Z. Ang, R.A. Baartman, I. Bylinskii, Y.C. Chao, D. Dale, K. Fong, R. Iranmanesh, F. Jones, D. Kaltchev, J. Kavarskas, P. Kolb, S.R. Koscielniak, A. Koveshnikov, M. Laverty, R.E. Laxdal, Y. Ma, L. Merminga, N. Muller, R. Nagimov, R. Nussbaumer, T. Planche, M. Rowe, S. Saminathan,V.A. Verzilov, Z. Yao, Q. Zheng,V. Zvyagintsev
TRIUMF, Vancouver, Canada

Abstract

ARIEL is the new TRIUMF facility for production of radioactive ion beams that will enable the delivery of three simultaneous RIB beams to the ISAC experimental stations. Two additional target stations will produce beams by using either a 50 kW proton or from 500 kW electrons via photo-fission. The electron beam driver is going to be a 50 MeV 10 mA CW superconducting electron linac. The first stage of the e-linac installation is completed and commissioning is underway. The paper will present the e-linac design characteristics, installation, commissioning strategy and current results.

INTRODUCTION

The ISAC (Isotope Separation and ACceleration) facility at TRIUMF produces rare isotope beams (RIB) using the ISOL (Isotope Separation On Lina) method. ISAC uses the TRIUMF cyclotron as driver to accelerate protons at 500 MeV up to 100 μA of current. This is presently the highest power (up to 50 kW of beam power) driver beam for an ISOL facility. It allows to produce the most intense RIB of certain species like ^{11}Li for which yield of $2.2 \cdot 10^4$ s^{-1} has been achieved. The current limitation of ISAC is that only a single RIB is available for fifteen experimental stations distributed in three areas: low, medium and high energy [1].

The ARIEL project [2] is meant to triple the RIB availability by delivering three simultaneous beams. The project consists of augmenting the present proton driver beam from the cyclotron and associated ISAC target stations with the addition of a new electron linac (e-linac) driver and a second proton beam driver from the cyclotron and associated two new target stations and low energy RIB delivery systems as illustrated in Fig. 1. The new e-linac is going to deliver 50 MeV electrons up to 10 mA for a maximum beam power on target of 0.5 MW.

A first stage of the ARIEL installation including a 30 MeV portion of the e-Linac and electron beamlines plus new ARIEL building and infrastructure is now nearing completion. The second phase encompassing the upgrade of the e-Linac to full energy, new target stations new proton beam line and low energy RIB beam lines is now under fund request adjudication.

* Funded under a contribution agreement with NRC (National Research Council Canada)
† Capital funding from CFI (Canada Foundation for Innovation)

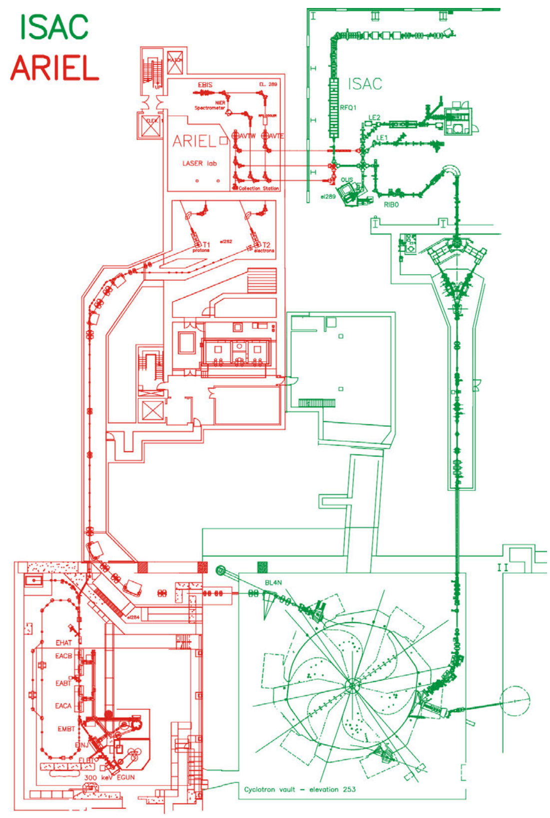

Figure 1: ISAC (green) and ARIEL (red) facilities at TRIUMF.

Accelerated electrons can be used to generate RIBs via the photo-fission process [3]. The electrons are slowed either in the target material itself or in an upstream converter material to generate bremsstrahlung radiation that produce fissions in the actinide target material. The fission production resonance is centered near an incident photon energy of 15 MeV such that the production yield saturates around an electron energy of 50 MeV. Figure 2 shows yield production comparing 10 μA, 500 MeV protons on a 25 g/cm^2 UCx target and 10 mA, 50 MeV electrons on a Hg converter and 15 g/cm^2 UCx target. The two production methods are complementary. Electrons produce more neutron rich isotopes with less isobaric contamination. A beam current of 10 mA at 50 MeV is required to produce the goal rates of 10^{13} fissions/sec in an actinide target of sufficient density. This sets the operating boundary envelope for the completed electron linac. The electron linac is housed in a pre-existing shielded former

Content from this work may be used under the terms of the CC BY 3.0 licence (© 2015). Any distribution of this work must maintain attribution to the author(s), title of the work, publisher, and DOI.

ISBN: 978-3-95450-168-7 doi:10.18429/JACoW-IPAC2015-WEAB1

Content from this work may be used under the terms of the CC BY 3.0 licence (© 2015). Any distribution of this work must maintain attribution to the author(s), title of the work, publisher, and DOI.

COMPENSATING TUNE SPREAD INDUCED BY SPACE CHARGE IN BUNCHED BEAMS

Vladimir N. Litvinenko and Gang Wang
Department of Physics and Astronomy, Stony Brook University, Stony Brook, NY 11794, USA
Collider-Accelerator Department, Brookhaven National Laboratory, Upton, NY 11973, USA

Abstract

The effects of space charge play a significant role in modern-day accelerators, frequently constraining the beam parameters attainable in an accelerator or in an accelerator chain. They also can limit the luminosity of hadron colliders operating either at low energies or with sub-TeV high-brightness hadron beams. The latter is applied for strongly cooled proton and ion beams in eRHIC – the proposed future electron-ion collider at Brookhaven National Laboratory. Using an appropriate electron beam would compensate both the tune shift and the tune spread in the hadron beam in a coasting beam. But these methods cannot compensate space charge tune spread in a bunched hadron beam. In this paper we propose and evaluate a novel idea of using a co-propagating electron bunch with miss-matched longitudinal velocity to compensate the space charge induced tune-shift and tune spread.

INTRODUCTION

The paper is motivated by developing a high-energy high-luminosity electron-ion collider at Brookhaven National Laboratory called eRHIC [1] with a very short (5 cm RMS) and strongly cooled proton and ion beams with normalized transverse emittances of 0.2 mm·mrad.

Space-charge effects have been known in accelerator physics for a half of the century. There is an extensive literature [2-23] describing the effects of space charge. A nonlinear space-charge force induces an irreducible transverse tune-spread, i.e. the tune dependence on both the hadron's longitudinal position inside the bunch, z, and the amplitude of the transverse oscillations.

It is well known that space-charge effects fall as a high power of the beam's relativistic factor:

$$\Delta Q_{sc} \approx -\frac{Z^2 r_p}{A}\frac{N_o}{4\pi\beta_h^2\gamma^3\varepsilon}\frac{C}{\sqrt{2\pi}\sigma_z} \qquad (1)$$

where C is the ring's circumference, Z is the charge, and A is the atomic number of the hadron (e.g., an ion, for proton $Z=A=1$), $r_p = e^2/m_p c^2$ is the classical radius of the proton, $\gamma^2 = 1/(1-\beta^2)$ is the relativistic factor of hadron beam, N_o is number of hadrons in the bunch with an RMS bunch length of σ_z, and ε is the beam's transverse emittance.

Naturally, the maximum tune shift is experienced by the particles in the center of the beam, while the particles with large amplitude of oscillations experience a smaller value of the tune shift. The overall tune-spread is determined by its value for the center particles.

We are presenting here a strongly compressed version of our studies. Detailed description is published in full-size (24-page long) article [24].

For a round beam with equal emittances, the transverse tune shifts depend on particle's location inside the bunch as follows:

$$\delta Q_{x,y} = \delta Q_{sc}(z)\cdot f_{x,y};$$

$$\delta Q_{sc}(z) = -\frac{C}{4\pi\varepsilon}\frac{1}{\beta^2\gamma^3}\frac{Z^2 r_p}{A}\cdot\frac{N_o}{\sqrt{2\pi}\sigma_z}\cdot e^{-\frac{z^2}{2\sigma_z^2}}; \quad (2)$$

$$f_x = \left\langle \frac{2}{1+\sqrt{\beta_y/\beta_x}} \right\rangle; f_y = \left\langle \frac{2}{1+\sqrt{\beta_x/\beta_y}} \right\rangle.$$

Since the longitudinal motion of hadrons usually is very slow (e.g. $Q_s << Q_{x,y}$), the tune of the particle depends not only on the amplitudes (actions) of the transverse oscillations, but also on their longitudinal the location within the bunch.

One practically important feature of the space-charge effects is a very strong dependence on the relativistic factor, γ: $\delta Q_{sc} \propto \gamma^{-3}/(1-\gamma^{-2})$. While the power one of γ naturally comes from the increasing rigidity of the beam, the γ^{-2} comes from the effective cancelling of the forces from the electric and magnetic fields induced by the beam

$$\vec{F}_\perp = eZ\left(\vec{E}_\perp + \beta_o\left[\hat{z}\times\vec{B}_\perp\right]\right) \equiv \frac{eZ\cdot\vec{E}_\perp}{\gamma^2}. \qquad (3)$$

Several practical schemes were suggested for space-charge tune shift and tune spread compensation by colliding an electron beam with hadron beam (e.g., an electron lens), or employing an electron column induced in a residual gas [25-29]. The tune shift given by the colliding beam does not suffer from γ_h^{-2} cancelation: for round electron beam having RMS size of σ_e and the interaction length of L, the tune shift is given by the following:

$$\delta Q_{x,yel} = \frac{Z}{A\beta_h\gamma_h}\frac{r_p}{4\pi\sigma_e^2}\cdot\frac{I_e}{ec\beta_e}\left(1+\beta_e^2\right)\cdot L\left\langle\beta_{x,y}\right\rangle; (4)$$

where $\beta_e = v_e/c$ is the normalized velocity and of the electron beam.

ISBN: 978-3-95450-168-7 doi:10.18429/JACoW-IPAC2015-WEAB2

BEAM AND SPIN DYNAMICS FOR STORAGE RING BASED EDM SEARCH*

A. Lehrach[#] on behalf of the JEDI Collaboration
Institut für Kernphysik, Forschungszentrum Jülich, 52425 Jülich, Germany
III. Physikalisches Institut B, RWTH Aachen University, 52074 Aachen, Germany
JARA-FAME (Forces and Matter Experiments)

Abstract

Full spin-tracking simulations of the entire experiment are absolutely crucial to explore the feasibility of the planned storage ring EDM (Electric Dipole Moment) experiments and to investigate systematic limitations. For a detailed study during the storage and build-up of the EDM signal, one needs to track a large sample of particles for billions of turns. In addition, benchmarking experiments have to be performed to check and to further improve the simulation tools.

INTRODUCTION

Permanent EDMs of fundamental particles violate both time invariance *T* and parity *P*. Assuming the *CPT* theorem this implies *CP* violation. The Standard Model (SM) predicts non-vanishing EDMs. Their magnitudes, however, are expected to be unobservably small with current experimental techniques. The discovery of a non-zero EDM would be a signal for new physics and could explain the matter-antimatter asymmetry observed in our Universe. Different approaches to measure EDMs of charged particles are pursued at Brookhaven National Laboratory (BNL) [1] and Forschungszentrum Jülich [2] with an ultimate goal to reach a sensitivity of 10^{-29} e·cm in a dedicated storage ring. The Jülich-based JEDI Collaboration (Jülich Electric Dipole moments Investigations) has been formed to exploit and demonstrate the feasibility of such a measurement and to perform the necessary R&D work towards the design of a dedicated storage ring [3]. As a first step R&D work at COSY is pursued. Subsequently, an EDM measurement of a charged particle will be performed at COSY with limited sensitivity. On a longer time scale, the design and construction of a dedicated storage ring will be carried out.

EXPERIMENTAL METHOD

The principle of every EDM measurement (e.g., neutral and charged particles, atoms, molecules) is the interaction of the particles' electric dipole moment with an electric field. In the center-of-mass system of a particle electric dipole moments $\vec{d}$ couple to the electric fields, whereas magnetic dipole moments $\vec{\mu}$ (MDM) couple to magnetic fields.

The spin precession in the presence of both electric and magnetic fields is given by:

$$\frac{d\vec{S}}{dt} = \vec{d} \times \vec{E}^* + \vec{\mu} \times \vec{B}^*. \qquad (1)$$

$\vec{E}^*$ and $\vec{B}^*$ denote the electric and magnetic fields in the rest frame of a particles. In case of moving particles in a circular accelerator or storage ring, the spin motion is covered by the Thomas-BMT equation and its extension for EDM:

$$\frac{d\vec{S}}{dt} = \vec{S} \times (\vec{\Omega}_{\mathrm{MDM}} + \vec{\Omega}_{\mathrm{EDM}}),$$

$$\vec{\Omega}_{\mathrm{MDM}} = \frac{q}{m}\left[G\vec{B} - \frac{\gamma G}{\gamma+1}\vec{\beta}(\vec{\beta}\cdot\vec{B}) - \left(G - \frac{1}{\gamma^2-1}\right)\frac{\vec{\beta}\times\vec{E}}{c}\right],$$

$$\vec{\Omega}_{\mathrm{EDM}} = \frac{\eta q}{2mc}\left[\vec{E} - \frac{\gamma}{\gamma+1}\vec{\beta}(\vec{\beta}\cdot\vec{E}) + c\vec{\beta}\times\vec{B}\right]. \qquad (2)$$

$\vec{S}$ in this equation denotes the spin vector in the particle rest frame in units of $\hbar$, t the time in the laboratory system. β and γ are the relativistic Lorentz factors, q and m the charge and the mass of the particle, respectively. $\vec{E}$ and $\vec{B}$ denote the electric and magnetic fields in the laboratory system. Two angular frequencies $\vec{\Omega}_{\mathrm{MDM}}$ and $\vec{\Omega}_{\mathrm{MDM}}$ are defined with respect to the momentum vector. The gyromagnetic anomaly $G=(g-2)/2$ with the Landé g-factor and η are dimensionless and related to the magnetic and electric dipole moments of the particle as follows:

$$\vec{\mu} = 2(G+1)\frac{q\hbar}{2m}\vec{S}, \vec{d} = \eta\frac{q\hbar}{2mc}\vec{S}. \qquad (3)$$

In a planar storage ring the spin precession in the horizontal plane is governed by the MDM. If an EDM exists, the spin vector will experience an additional torque. The resulting vertical spin component, proportional to the size of the EDM, will be measured by scattering the particles of the stored beam at an internal target and analyzing the azimuthal distribution of the scattered particles. A coherent buildup of the vertical polarization only takes place within the time the spins of the particle ensemble stays aligned. Since the spin tune is a function of the betatron and synchrotron amplitudes of the particles in the six-dimensional phase space, spin decoherence is caused by beam emittance and momentum

*Work supported by BMBF International Cooperation (Grant Number RUS 11/043) and Jülich-Aachen Research Alliance JARA-FAME.
#a.lehrach@fz-juelich.de

Content from this work may be used under the terms of the CC BY 3.0 licence (© 2015). Any distribution of this work must maintain attribution to the author(s), title of the work, publisher, and DOI.

ISBN: 978-3-95450-168-7 doi:10.18429/JACoW-IPAC2015-WEAB3

Content from this work may be used under the terms of the CC BY 3.0 licence (© 2015). Any distribution of this work must maintain attribution to the author(s), title of the work, publisher, and DOI.

INTRA-BEAM SCATTERING EFFECTS IN ELENA*

J. Resta-López, J. R. Hunt, C. P. Welsch,
Cockcroft Institute and The University of Liverpool, UK

Abstract

Intra-Beam Scattering (IBS) is one of the main limiting processes for the performance of low energy ion storage rings, such as the Extra Low ENergy Antiproton ring (ELENA) that is being constructed at CERN. IBS effects limit the achievable equilibrium 6D beam phase space volume during the cooling process, as well as the stored beam intensity. In this contribution we analyse the IBS effects on the beam dynamics of the ELENA ring in detail. Numerical simulations using the codes BETACOOL and MAD-X have been performed to compute the beam life time and the equilibrium phase space parameters with electron cooling in the presence of IBS.

INTRODUCTION

ELENA [1] is a small synchrotron equipped with an electron cooler, which is currently being constructed at CERN to further decelerate antiprotons from the Antiproton Decelerator (AD) [2] from 5.3 MeV to 100 keV kinetic energy with a beam population of $\sim 10^7$ cooled antiprotons. Electron cooling will be used to counteract the emittance and the momentum spread blow-up caused by the deceleration process. This will increase the intensity of antiprotons delivered to the antihydrogen experiments at the AD by one to two orders of magnitude.

The ELENA cycle is schematically shown in Fig. 1. There are two cooling plateaus: the first cooling plateau lasts approximately 8 s at 35 MeV/c momentum, and the second one is applied for 2 s at 13.7 MeV/c. In both cases the cooling is applied to a coasting beam. A third cooling at 13.7 MeV/c will be applied to bunched beams prior to extraction.

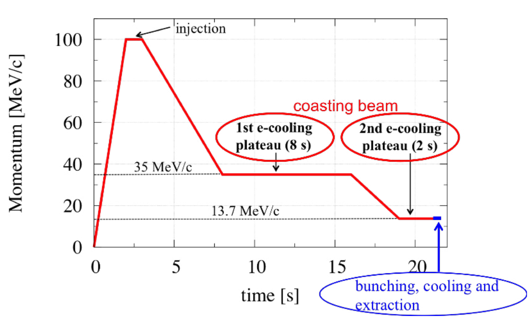

Figure 1: ELENA cycle.

A particular challenge for low energy ion storage rings, such as ELENA, is the question of achievable beam life time and stability. To address this question, we are investigating the long-term beam dynamics in ELENA considering different effects limiting the achievable phase space volume obtained under electron cooling. Among these effects, IBS and rest gas scattering are important sources of beam heating.

For ELENA with the nominal vacuum pressure $P = 3 \times 10^{-12}$ Torr, it has been estimated that the effect of rest gas scattering would be practically negligible with respect to IBS [3, 4]. Therefore, in this paper we focus mainly on the study of the IBS effects.

IBS can be defined as a beam heating effect produced by multiple small-angle Coulomb scatterings of charged particles within the accelerator beam itself. It causes an exchange of energy between the transverse and longitudinal degree of freedom, thus leading to the growth of the beam phase space dimensions. The theory of IBS is extensively described in the literature, e.g. [5–8], and many of these IBS models are implemented in the simulation code BETACOOL [9,10]. This code allows us to calculate the evolution of beam distributions in the transverse and longitudinal phase space under the action of cooling and different scattering effects, and has been successfully benchmarked against experimental data, see e.g. [11].

IBS becomes stronger when the phase space volume of the beam is reduced by cooling, thus limiting the achievable final emittances, which are determined by an equilibrium state between IBS and cooling. In the next sections we investigate the beam evolution for the two ELENA cooling plateaus in the presence of IBS.

BEAM EVOLUTION

Beam dynamics simulations are performed using the code BETACOOL [9, 10], using the nominal beam parameters and electron cooling parameters adopted from [1,12] and the ELENA ring lattice with working point $Q_x \simeq 2.3$, $Q_y \simeq 1.3$ [13] in MAD-X format [14].

The simulations are based on a Monte-Carlo method (model beam algorithm of BETACOOL), with the following conditions: 1000 modelled macroparticles; electron cooling considering a cylindrical uniform electron beam distribution with transverse temperature $k_B T_{e\perp} = 0.01$ eV and longitudinal temperature $k_B T_{e\parallel} = 0.001$ eV; the cooling friction force is computed using the Parkhomchuk's model for a magnetised electron distribution [15]; rest gas and IBS effects are also included. For the IBS, the Martini model [7] is used. More details can be found in [4].

First Cooling Plateau

Let us consider first initial Gaussian distributions with relatively large rms transverse emittances and momentum

* Work supported by the EU under Grant Agreement 624854 and the STFC Cockcroft Institute core Grant No. ST/G008248/1.

ISBN: 978-3-95450-168-7 doi:10.18429/JACoW-IPAC2015-WEBB1

PLANS FOR DEPLOYMENT OF HOLLOW ELECTRON LENSES AT THE LHC FOR ENHANCED BEAM COLLIMATION*

S. Redaelli, A. Bertarelli, R. Bruce, D. Perini, A. Rossi, B. Salvachua, CERN, Geneva, Switzerland
G. Stancari, A. Valishev, FNAL, Batavia, IL, USA

Abstract

Hollow electron lenses are considered as a possible means to improve the LHC beam collimation system, providing active control of halo diffusion rates and suppressing the population of transverse halos. After a very successful experience at the Tevatron, a conceptual design of a hollow e-lens optimized for the LHC was produced. Recent further studies have led to a mature preliminary technical design. In this paper, possible scenarios for the deployment of this technology at the LHC are elaborated in the context of the scheduled LHC long shutdowns until the full implementation of the HL-LHC upgrade in 2023. Possible setups of electron beam test stands at CERN and synergies with other relevant electron beam programmes are also discussed.

INTRODUCTION

The Large Hadron Collider (LHC) [1] at the European Organization for Nuclear Research (CERN) is designed to collide 7 TeV proton beams each of an unprecedented stored energy of 362 MJ. Its High-Luminosity (HL-LHC) upgrade project [2] aims at doubling the beam current while reducing by more than 30 % the beam emittance. Proton and ion beam halo cleaning in a superconducting accelerator poses obvious concerns. Even if the LHC Run I operation in 2010-2013 was successful, as stored energies up to 150 MJ were handled without accidental quenches [3,4], uncertainties apply to the extrapolations to higher energies. Various means to improve the LHC collimation performance are therefore under investigation.

Hollow electron beams can boost the performance of a collimation system through an active control of halo particles' diffusion speed and tail population. A low-energy, hollow electron beam that runs co-axially to the circulating hadron beam, over a few meters, can act on the halo particles at transverse amplitudes below that of the primary collimators, as shown in Fig. 1, without perturbing the beam core. The present multi-stage collimation system must remain in place to safely dispose of the halo particles that are resonantly driven unstable by the electron beam, possibly modulated in intensity, at smooth and tunable loss rates.

The cleaning performance of the LHC betatron collimation system has been the subject of a recent project review [5]. The Run I experience was acknowledged as very promising in view of operations at higher energy. The control of beam losses was recognized as a critical concern for future LHC upgrades. In this paper, the motivation for studying hollow e-lenses for the LHC are reviewed and the status of the present lens design for the LHC, derived from the conceptual design report in [6], is presented. In the conclusions, different plans for the possible timeline for deployment into the LHC are discussed.

* Research supported by FP7 HiLumi LHC, Grant Agreement 284404 and by the US DOE through the US-LARP program. Fermilab is operated by Fermi Research Alliance, LLC under Contract DE-AC02-07CH11359 with the US DOE.

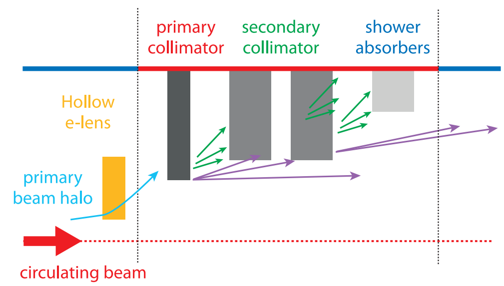

Figure 1: Scheme illustrating the conceptual integration of a hollow elens in the present collimation system hierarchy.

MOTIVATION

In 2012, the primary collimator gaps of the betatron cleaning system were as small as 2.1 mm, i.e. 4.3 betatron σ for an emittance of 3.5 μm. These settings in mm intentionally equaled the nominal settings at 7 TeV: experience could be gained operating the LHC with the tightest betatron cut. Figure 2 [7] shows the distributions of minimum lifetime recorded in high intensity fills in 2012 and compares it with what was recorded in 2011, when collimators were set at larger gaps of 5.7 σ. One can see that the beam lifetime was significantly reduced, with minimum lifetime values regularly dropping well below 1 h, whereas very few cases with lifetimes below 4 h were observed in 2011. Although extrapolations are not straightforward as the geometrical emittance will be smaller at 7 TeV, we consider the 2012 experience more representative, as also stressed in [5]. Note that beam tails at the LHC are over populated compared to nominal Gaussian distributions as they fill the entire primary collimator gaps [8]. Particularly critical are the squeeze, when the closed orbit varies in the time scale of seconds, and the preparation of squeezed beams for collisions ("adjust" mode) [7].

As an example, at 4 TeV a lifetime of 0.2 h led to peak loss rates up to 200 kW. The collimation system limit before risking plastic deformation of the jaw is 500 kW. For the 7 TeV HL-LHC, losses could reach 1 MW if similar lifetime drops were observed. So, even if upgraded cleaning performance [9] were sufficient to avoid quenches in regular operation, beam losses should be kept under control in order to avoid potential damage to the collimators.

Content from this work may be used under the terms of the CC BY 3.0 licence (© 2015). Any distribution of this work must maintain attribution to the author(s), title of the work, publisher, and DOI.

ISBN: 978-3-95450-168-7 doi:10.18429/JACoW-IPAC2015-WEBB2

Content from this work may be used under the terms of the CC BY 3.0 licence (© 2015). Any distribution of this work must maintain attribution to the author(s), title of the work, publisher, and DOI.

FIRST CONSIDERATIONS ON BEAM OPTICS AND LATTICE DESIGN FOR THE FUTURE HADRON-HADRON COLLIDER FCC-HH

B. Dalena, A. Chance, J. Payet, CEA, IRFU, SACM, F-91191 Gif-Sur-Yvette
R. Alemany, B. Holzer and D. Schulte, CERN

Abstract

The main emphasis of the Future Circular Collider study is the design of a 100 TeV proton-proton collider in a new tunnel of about 100 km circumference. This paper presents the first optics design of the future hadron collider (FCC-hh). The basic layout follows a quasi-circular geometry "quasi racetrack" with 8 arcs and 8 straight sections, four of which designed as interaction points. Assuming 16 T dipole magnets, a first version of the ring geometry and magnet lattice is presented, including the optics of the foreseen high luminosity regions and of the other straight sections dedicated to the installation of injection/extraction lines, beam dump etc., and an arc structure with optimized dipole fill factor to reach the target center-of-mass energy of 100 TeV.

INTRODUCTION

Following the recommendations of the European Strategy Group, an integrated design study for accelerator projects in a global context, with emphasis on proton-proton and electron-positron high-energy frontier machines has been undertaken. The Future Circular Collider study FCC is investigating three possible storage rings options, housed in a tunnel of roughly 100 km circumference: an e^+e^- collider (FCC-ee), a hadron-hadron collider (FCC-hh), and an electron-hadron (FCC-eh) option. In order to reach the extreme high energy of the FCC-hh collider an *R&D* program on dipole magnets started with the aim of producing a field as high as 16 T. In the following we present the first considerations for the FCC-hh beam optics, taking into account the main machine parameters given in [1] as well as the geological and magnets constraints.

Layout of the FCC-hh Ring

Recently, the layout of the FCC-hh ring has converged to a "quasi racetrack" shape with 2 high luminosity interaction points (IPs) and 2 other with lower luminosity. The high luminosity operation IPs are located in Long Straight Sections LSS-PA-EXP and LSS-PG-EXP. Correspondingly, the lower luminosity IPs are located in LSS-PF[PH]-EXP (shown in Fig. 1). Two more LSS (LSS-PL[PB]-INJ) are dedicated to injection and two Extended Straight Section (ESS) are used for collimation and extraction [2]. The optics of the interaction regions are assumed to be anti-symmetric with respect to their centers. Moreover, the quadrupole is focusing at the beginning of all the long straight section and it is defocusing at the end. Four short arcs (SAR) and four long arcs (LAR) complete the layout, shown in grey and in black in Fig. 1, respectively. A first version of the optics can be found in [4]. The problem we want to handle is to compute the different parameters of the main quadrupoles and dipoles to fit with the layout and to match the arcs cells to the insertions regions. At the same time we want to explore the sensitivity of the overall lattice to these parameters.

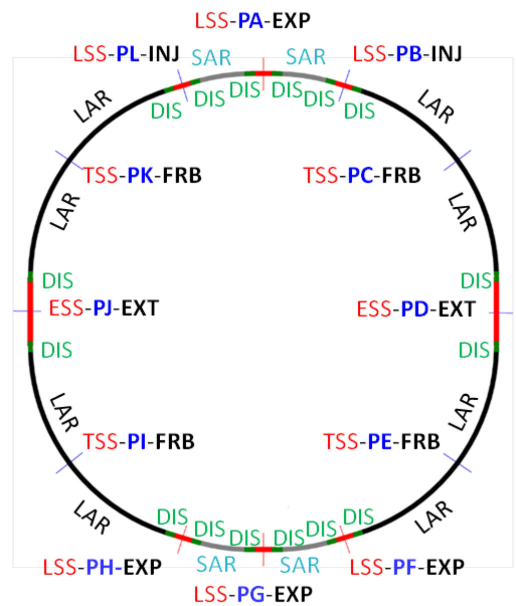

Figure 1: Layout of the FCC-hh ring.

FIRST ORDER OPTICS AND INTEGRATION WITH THE STRAIGHT SECTIONS

Some parameters of the optics are considered as fixed and other as advised. The parameters we have considered as fixed for the optimization of the baseline lattice are reported in Table 1.

Table 1: Input Parameters for the Optimization of the FCC-hh Arc Cells

Parameter	Value
center-of-mass energy	100 TeV
total ring length	100.12 km
LSS and ESS length	1.4 and 4.2 km
dipole magnetic length	14.3 m
dipole-dipole separation	1.36 m
magnet aperture radius	25 mm
sextupole magnetic length	0.5 m
quadrupole-sextupole separation	1.0 m
cell phase advance H/V	90 °

ISBN: 978-3-95450-168-7 doi:10.18429/JACoW-IPAC2015-WEBB3

LATTICE AND ITS RELATED BEAM DYNAMICS ISSUES IN THE CEPC STORAGE RING*

H. Geng#, G. Xu, Y. Zhang, Q. Qin, S. Bai, Y. Wang, D. Wang, Y. Peng, T. Yue, Z. Duan
Institute of High Energy Physics, Beijing, China

Abstract

CEPC was proposed as an electron and positron collider ring with a circumference of 50-100km to study the Higgs boson. Since the proposal was made, the lattice design for CEPC has been carried out and a preliminary conceptual design report has been written at the end of 2014. In this paper, we will describe the philosophy and results of our lattice design. The procedure of dynamic aperture optimization will be shown. A specific issue for CEPC, the pretzel orbit, which has been found distorting the linear lattice for a considerable amount, will be examined. The ways that we are trying to correct the pretzel orbit effect and the results will be shown.

INTRODUCTION

On 4th July, CERN announced that both the ATLAS and CMS experiments had discovered a new Higgs-like boson[1-3]. Since then, many proposals had been made to build a new collider to study this new particle in detail. The linear and circular electron and positron are considered to be the most feasible one. At the end of the year 2012, the candidates of a Higgs factory, their pros and cons were compared in detail at the ICFA workshop[4,5]. It was also at this workshop, the concept of CEPC and SPPC was raised[6].

CEPC (Circular Electron and Positron Collider) was proposed as an electron and positron collider ring with a circumference of 50-100km to study the Higgs boson. The lattice design for CEPC has been carried out since the end of 2013. In about one year time, a preliminary conceptual design report has been written at the end of 2014. In this paper, we will describe the philosophy and results of our lattice design. A specific issue for CEPC, the pretzel orbit, which has been found distorting the linear lattice for a considerable amount, will be examined. The ways that we are trying to correct the pretzel orbit effect and the result will be shown. We will also discuss the saw tooth effect on the linear lattice and dynamic aperture of the ring.

LINEAR LATTICE

The layout of the ring is shown in Fig. 1. The circumference of the ring is 54km with 8 arcs and 8 straight sections. There are four IPs in the ring, IP1 and IP3 will be used for CEPC, while IP2 and IP4 will be used for SPPC. The RF sections are distributed in each straight section. At each straight section, the RF cavities will be symmetrically placed at the two ends of the section.

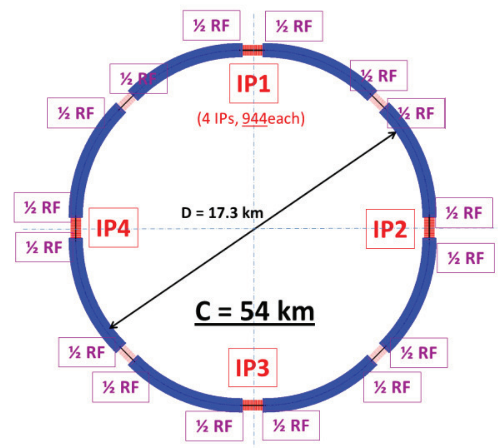

Figure 1: Layout of the CEPC storage ring.

The lattice for CEPC ring has been chosen to use the standard FODO cells with 60 degrees phase advances in both transverse planes. The FODO cell structure is chosen to have a maximum filling factor. The 60 degrees phase advance is chosen to have a relatively large beam emittance, so that a relatively longer beamstrahlung beam lifetime.

A standard FODO cell with 60 degrees phase advance is shown in Fig.2. The length of each bend is 19.6m, the length of each quadrupole is 2.0m. There is one sextupole, with a length of 0.4 m, next to each quadrupole for chromatic corrections. The distance between the sectupole and the adjacent magnet is 0.3 m, while the distance between each quadrupole and the adjacent bending magnet is 1.0 m. The total length of each cell is 47.2 m.

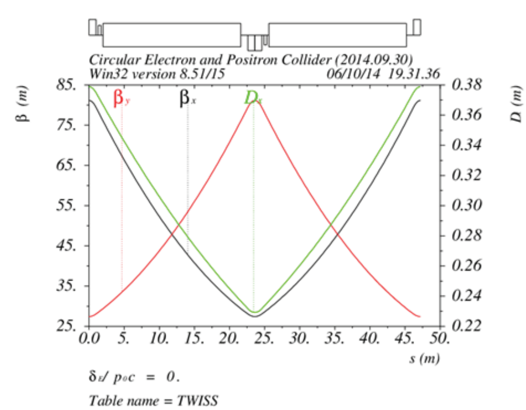

Figure 2: Beta functions and dispersion function of a standard FODO cell with 60/60 degrees phase advance in CEPC ring.

*Work supported by National Natural Science Foundation of China, Grant No. 11405188 and the Innovation Foundation of the Institute of High Energy Physics.
#genghp@ihep.ac.cn

Content from this work may be used under the terms of the CC BY 3.0 licence (© 2015). Any distribution of this work must maintain attribution to the author(s), title of the work, publisher, and DOI.

ISBN: 978-3-95450-168-7 doi:10.18429/JACoW-IPAC2015-WEAD1

COMMISSIONING AND RECENT EXPERIMENTAL RESULTS AT THE ARGONNE WAKEFIELD ACCELERATOR FACILITY (AWA)*

M.E. Conde#, D.S. Doran, W. Gai, W. Liu, J.G. Power, C. Whiteford, E. Wisniewski, ANL, Argonne, IL 60439, USA
S. Antipov, C. Jing, J. Qiu, Euclid Techlabs LLC, Solon, OH 44139, USA
J. Shao, D. Wang, Tsinghua University, Beijing, China
G. Ha, Department of Physics, POSTECH, Pohang, Gyeongbuk 790-784, Korea

Abstract

The commissioning of the upgraded AWA facility has been recently completed. The L-band electron gun has been fully commissioned and has been successfully operated with its Cesium Telluride photocathode at a gradient of 80 MV/m. Single bunches of up to 100 nC, and bunch trains of up to 32 bunches with a maximum total charge in the trains of 600 nC have been generated. Six pi-mode accelerating cavities bring the beam energy to 70 MeV. Initial measurements of the beam parameters have been performed. This intense beam has been used to drive wakefields in several structures, including a 26 GHz dielectric loaded power extractor, an 11.7 GHz photonic-band-gap metallic structure (PBG), and an 11.7 GHz metallic iris loaded power extractor. A second beamline provides electron bunches to probe the wakefields generated by the intense drive beam. A recent experiment has demonstrated acceleration (and deceleration) of the witness beam, in the so-called two-beam-accelerator scheme, with accelerating gradients over 40 MV/m.

AWA FACILITY

The main mission of the Argonne Wakefield Accelerator Facility (AWA) is to develop technology for future accelerator facilities. The AWA facility has been used to study and develop new types of accelerating structures based on electron beam driven wakefields. In order to carry out these studies, the facility employs a photocathode RF gun capable of generating electron beams with high bunch charges and short bunch lengths. This high intensity beam is used to excite wakefields in the structures under investigation, thus being referred to as the Drive Beam. There is a second electron beam that is used to probe the wakefields generated by the Drive Beam, and it is referred to as the Witness Beam.

The facility is also used to investigate the generation and propagation of high brightness electron beams, and to develop novel electron beam diagnostics. More recently, the facility has attracted interest from the broader scientific community, and collaborations on a wider range of topics have been fostered by the DOE-HEP stewardship initiative.

The AWA high intensity drive beam is generated by a photocathode RF gun, operating at 1.3 GHz. This one-and-a-half cell gun typically runs with 12 MW of input power, which generates an 80 MV/m electric field on its Cesium Telluride photocathode surface. Six seven-cell standing-wave π mode accelerating structures increase the energy of the beam produced by the drive gun from 8 MeV to 70 MeV.

The charge of the drive electron bunches can be easily varied from 0.1 to 100 nC, by varying the energy of the laser pulse incident on the photocathode. The high quantum efficiency of the Cs_2Te photocathode – routinely made in house and reaching over 15% QE – makes it possible to generate high charge bunches with laser pulses of relatively low energy. Thus, the laser pulse can be split into a sequence of laser pulses separated in time by one RF period, and this laser pulse train can be used to generate an electron bunch train.

The AWA laser system consists of a Spectra Physics Tsunami oscillator followed by a Spitfire regenerative amplifier and two Ti:Sapphire amplifiers (TSA 50). It produces 1.5 mJ pulses at 248 nm, with a pulse length of 2 to 8 ps FWHM and a repetition rate of up to 10 pps. A final KrF Excimer amplifier is optionally used to increase the energy per pulse to 15 mJ.

The Drive and the Witness beamlines propagate in opposite directions, and come to a common area designated beamline switchyard, where each beamline can branch out into a few beamlines and where experiments are conducted. The beamline switchyard allows wakefield experiments to be performed using either the collinear configuration, in which the drive and witness bunches travel along the same structure, or the two-beam-accelerator configuration, in which RF power is transferred from the drive beam decelerating structure to the witness beam accelerating structure, by means of a waveguide.

COMMISSIONING

The Drive beamline has been commissioned to an energy of 69 MeV, however, after a few weeks of operation, the RF window installed on one of the accelerating cavities showed signs of multipacting at full RF power. Mostly likely this was caused by some defect in the Titanium Nitride coating applied to the ceramic surface of the RF window. A couple of spare RF windows are in hand, and the defective window will be replaced soon. For now, operation of the Drive beamline has continued, but using a slightly reduced RF power level at the mentioned accelerating cavity. As a consequence, the

*Work supported by by the U.S. Department of Energy under contract No. DE-AC02-06CH11357.
#conde@anl.gov

Content from this work may be used under the terms of the CC BY 3.0 licence (© 2015). Any distribution of this work must maintain attribution to the author(s), title of the work, publisher, and DOI.

ISBN: 978-3-95450-168-7 doi:10.18429/JACoW-IPAC2015-WEAD2

EXPERIMENTAL RESULTS OF CARBON NANOTUBE CATHODES INSIDE RF ENVIRONMENT

L. Faillace[#], S.M. Boucher, J. Hartzell, A. Murokh, RadiaBeam Technologies, Santa Monica, CA 90404, USA
J.C.T. Thangaraj, FermiLab, Batavia, IL 60510, USA
D. Mihalcea, H. Panuganti, Northern Illinois University, DeKalb, IL 60115, USA
P. Piot, FermiLab, Batavia, IL 60510 and Northern Illinois University, DeKalb, IL 60115, USA

Abstract

Carbon Nano Tubes (CNT's) as field-emitters have been investigated for more than two decades and can produce relatively low emittance electron beams for a given cathode size. Unlike thermionic cathodes, CNT cathodes are able to produce electrons at room temperature and relatively low electric field (a few MV/m). In collaboration with FermiLab, we have recently tested CNT cathodes both with DC and RF fields. We observed a beam current close to 1A with a ~1cm^2 CNT cathode inside an L-band RF gun. Steady operation was obtained up to 650 mA and the measured current vs. surface field plot showed perfect agreement with the Fowler-Nordheim distribution.

INTRODUCTION

High-brightness electron beams are required for a number of applications, from advanced accelerators to 4th generation light sources. However, the current technology for producing such beams requires an expensive, complicated laser system to drive a photocathode in an RF gun. Furthermore, this technology is difficult to extend to very high duty cycles, as is necessary for superconducting accelerators.

Carbon nanotubes (CNTs) have been investigated [1] for more than two decades as field-emitters and can produce relatively low emittance electron beams [2] for a given cathode size, without a need of the laser. Unlike thermionic cathodes, CNT cathodes are able to produce electrons at room temperature and relatively low applied electric fields (a few MV/m). Nevertheless, they have historically either produced low currents and are prone to damage. Moreover, they are difficult to gate with conventional techniques and therefore are unable to produce short pulses.

RadiaBeam has recently tested CNT cathodes both with DC and RF fields. We have observed beam currents up to about 1A (averaged over macropulse) with a CNT cathode inside an S-band RF gun. Steady operation was observed up to 650 mA and the measured current versus surface field plot showed good agreement with the Fowler-Nordheim distribution [3, 4] (see Figure 1).

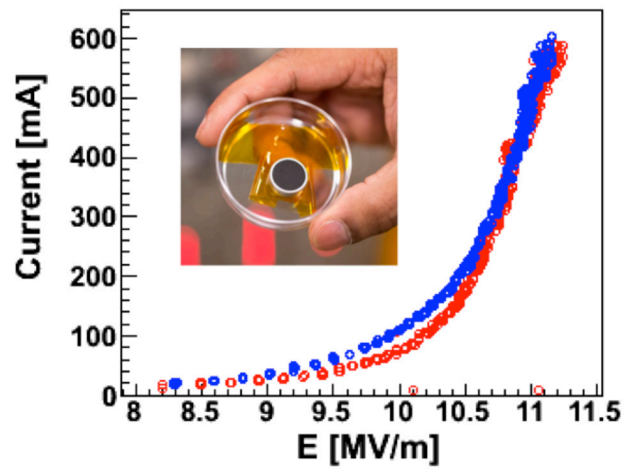

Figure 1: I-E curves. The measurements were performed with solenoids off (red) and solenoids on (blue).

DC TESTS AT RADIABEAM

Various CNT cathode samples were optimized and characterized at RadiaBeam. The cathode design as well as the whole high-voltage (HV) pulsed DC test setup were carried out according to the load-lock system for cathode insertion inside the 1.3 GHz RF gun already functioning at the HBESL facility. Eventually, two cathodes, a smaller and a bigger sample, were tested inside RF environment at Fermilab showing promising results for future applications.

Workflow

The workflow diagram that was followed for all operations is shown in Figure 2. The fabrication and cleaning of the cathode substrates were performed in-house. The CNT deposition processes, electrophoretic deposition (EPD) and chemical vapor deposition (CVD), were carried out at the California Nano-Systems Institute CNSI (UCLA) by our collaborators as well as Xintek (for the two samples used in FermiLab experiment). We then performed HV pulsed DC tests at RadiaBeam. The final RF testing took place at HBESL-FermiLab.

*Work supported by DOE grant # DE-SC0004459
#faillace@radiabeam.com

Content from this work may be used under the terms of the CC BY 3.0 licence (© 2015). Any distribution of this work must maintain attribution to the author(s), title of the work, publisher, and DOI.

ISBN: 978-3-95450-168-7 doi:10.18429/JACoW-IPAC2015-WEAD3

QUANTUM EFFICIENCY IMPROVEMENT OF POLARIZED ELECTRON SOURCE USING STRAIN COMPENSATED SUPER LATTICE PHOTOCATHODE

N. Yamamoto*, X.G. Jin, M. Yamamoto, KEK, Tsukuba, Japan
T. Miyauchi, A. Mano, M. Hosaka, Y. Takashima, Nagoya University, Aichi, Japan
Y. Takeda, Adavancd Science and Technology Foundation, Aichi, Japan

Abstract

In order to improve the quantum efficiency (QE) of the NEA-GaAs based polarized electron source. GaAs/GaAsP strain-compensated superlattice (SL) samples with thickness up to 720 nm were fabricated and a electron spin polarization (ESP) of 92 % and QE of 1.6 % were achieved at the pump laser energy of 1.59 eV for an 196nm-thickness sample. Furthermore, as results of the spin-resolved analyses, a slightly degradation of the crystalline quality for thicker thickness samples were indicated, however the effect for the beam performance was negligible up to the thickness of 720 nm. Then it is confirmed that the ESP is limited by the spin relaxation effect during electron transport in the semiconductor for the thicker thickness strain-compensated SLs.

INTRODUCTION

The GaAs-type semiconductor photocathode (PC) with a negative electron affinity (NEA) surface is used as a conventionally polarized electron source (PES). Recently, highly polarized electron beams produced by the NEA-GaAs PCs have been widely applied as a source for electron microscopes, such as a low energy electron microscopy (SPLEEM) [1] and a transmission electron microscopy (Spin-TEM) [2]. For applications in future high energy accelerators, generation of highly polarized and intense electron beam is an important technology. The International Linear Collider (ILC) requires a electron beam with > 80% electron spin polarization (ESP) and a bunch charge of 4.8 nC at the exit of the gun [3]. For the electron-ion collider at BNL, same polarization and an average current of 50 mA are required [4].

To answer these needs of future high energy accelerators, we have developed the polarized electron source for more than twenty years, and the GaAs/GaAsP strained superlattice (SL) PC was developed and demonstrated the ESP of around 90% and the quantum efficiency (QE) of 0.5% by using reflected type [5] and transmission type [6] PCs. As the NEA-type PCs have an intrinsic advantage for the beam emittance [7], high brightness beam with high ESP could be obtained [8]. However, the beam brightness is limited practically by the lack of QE value. Furthermore, to realize high intense beam required by future high energy accelerators, the QE improvement becomes important.

Recently, we have developed the strain-compensated SL PCs [9]. In the strained SL structure of conventional strained SL PCs, increasing SL layer thickness causes strain accumulation, resulting in the introduction of defects. Then the crystalline quality becomes worse and the SL thickness is limited. To overcome this problem, the use of a strain-compensated SL has been proposed. In such a structure, an opposing strain is introduced in the barrier layers to offset the strain in the quantum well layers so that no critical thickness limitation exists on the overall thickness of the SL structure and high crystalline quality is expected.

To demonstrate this effect of the strain-compensated SL PC, GaAs/GaAsP strain-compensated SL PCs have been developed and PC samples with the SL thickness from 96 to 720 nm were fabricated on the AlGaAsP buffer layer. Furthermore, in the measurements, the ESP of 92 % and the QE of 1.6 % were achieved by using the 192 nm sample [10].

In this paper, we reported the details of the GaAs/GaAsP strain-compensated SL PCs and discussed the thickness dependence of the crystalline parameter, such as an energy gap, a band width and a band split value between heavy hole and light hole bands at the valence-band maximum.

Table 1: Design Parameters of PC samples

Parameter	value
Band gap energy	1.54 eV
Cond. band Minimum width	29 meV
Heavy hole (HH) band Width	< 1 meV
Light hole (LH) band Width	29 meV
Band Split between HH and LH	75 meV

DESIGN OF STRAIN-COMPENSATED SL

GaAs/GaAsP strain-compensated SL samples were fabricated using a low-pressure metal organic vapor phase epitaxy (MOVPE) system with a vertical cold-wall quartz reactor. The 12-, 24-, 36-, 60- and 90-pair $GaAs/GaAs_{0.62}P_{0.38}$ strain-compensated SL layers were grown with on a 500-nm thick $Al_{0.1}Ga_{0.9}As_{0.81}P_{0.19}$ buffer layer and GaP substrate. The thickness of the each SL layer was 4 nm.

In the above configuration, the designed SL parameters could be calculated and shown in Table 1. The band gap energy is set to be 1.54 eV and lower than that of the buffer and substrate materials. Then the pump laser could be also irradiated the SL layers from the substrate side (transmission PC). The band width of heavy hole (HH) and Light hole (LH) minibands at the valence-band maximum are less than 1 meV and are 29 meV, respectively. The band split value between

* naoto.yamamoto@kek.jp

Content from this work may be used under the terms of the CC BY 3.0 licence (© 2015). Any distribution of this work must maintain attribution to the author(s), title of the work, publisher, and DOI.

ISBN: 978-3-95450-168-7 doi:10.18429/JACoW-IPAC2015-WEBD1

12 GeV CEBAF TRANSVERSE EMITTANCE EVOLUTION*

T. Satogata, Y, Roblin, M. Tiefenback, and D. Turner
Jefferson Lab, Newport News, VA 23606, USA

Abstract

We present commissioning results of measurements of beam phase space evolution of the newly commissioned 12 GeV CEBAF accelerator. These measurements range over two orders of magnitude in energy for a non-equilibrium beam, from near the photocathode to the diamond bremsstrahlung target for the GlueX experiment. We also compare these measurements to modeled beam evolution, and emittance growth expectations driven by synchrotron radiation.

INTRODUCTION

The Jefferson Lab CEBAF (Continuous Electron Beam Accelerator Facility) has been upgraded to double the peak beam energy from 6 GeV to 12 GeV [1]. The 12 GeV upgrade included the addition of 10 new "C100" cryomodules (each supplying 4x the gradient of original CEBAF cryomodules), a central helium liquefier upgrade, upgraded recirculation arcs, and the addition of a new 12 GeV experimental hall, Hall D. Beam [2] and RF [3] commissioning activities have been ongoing since 2013, including optics tuning and characterization of beam parameters for the new facility.

The upgrade parameters of relevance are shown in Table 1. Though the requirements of emittance and energy spread appear to loosen between 6 GeV and 12 GeV, the 12 GeV parameters are dominated by synchrotron-radiation (SR) driven emittance growth in higher energy recirculation arcs as discussed in the remainder of this paper.

Table 1: CEBAF 6 GeV to 12 GeV Parameters

	6 GeV Operations	12 GeV Design
Emittance at max energy (geometric rms): horiz, vert	(1, 1) nm-rad	(10, 2) nm-rad
Energy spread at max energy (rms)	$2.5\text{x}10^{-5}$	Halls A-C: $5\text{x}10^{-4}$ Hall D: $5\text{x}10^{-3}$

CEBAF 12 GEV OPTICS

Theory

For a relativistic electron beam traversing a 180-degree multi-cell bend of bend radius ρ, the rms geometric (unnormalized) emittance growth and energy spread due to SR are given by [4,5]:

$$\Delta\epsilon \approx 2 \times 10^{-27} \left(\frac{\gamma^5}{\rho[\mathrm{m}]^{\,2}}\right) \langle\mathcal{H}\rangle \quad (1)$$

$$\sigma_{\mathrm{E}}^2 \approx 1.2 \times 10^{-33}\ \mathrm{GeV}^2 \left(\frac{\gamma^7}{\rho[m]^{\,2}}\right) \quad (2)$$

where the traditional curly-H function is used.

The CEBAF tunnel geometry and dipole packing fraction preclude mitigation of SR-driven emittance and energy spread growth by increasing the bend radius. However, SR-driven emittance growth can be controlled in CEBAF by reducing curly-H in high-γ arcs, similar to standard practice in current-generation synchrotron light sources. This approach was taken in the original CEBAF design to meet 6 GeV program goals [6] but was more aggressively pursued in the 12 GeV era.

Other smaller sources of emittance growth in a recirculating linac such as CEBAF are transverse nonlinearities and coupling of longitudinal RF nonlinearity to transverse motion. Magnet measurements performed during the 12 GeV upgrade indicated that transverse nonlinear fields are acceptably small. Longitudinal nonlinearities are carefully managed with bunch compression in an injection chicane with tunable M_{56}, and monitoring of linac RF cresting.

CEBAF Optics Modifications

The recirculating linac design of CEBAF requires that each separate arc is matched to each linac through separate vertical beam spreader and recombiner sections. The spreader sections also include a dispersion-free matching straight to enable arc-by-arc transverse beam envelope matching using wire scanners and matching quadrupole scans. Matching performed in these regions, and in injector matching sections, provided emittances shown in later sections of this paper.

The arcs were originally configured as achromatic, isochronous, imaging, and FODO transport systems to minimize beam size while transporting beams transparently from spreaders to recombiners. For 12 GeV commissioning, the optics were modified to double-bend achromat (DBA) cells in arcs 6-10, providing a 30-40% reduction in curly-H and projected emittance growth. An example of DBA optics for the highest energy arc (arc 10) is shown in Figure 1.

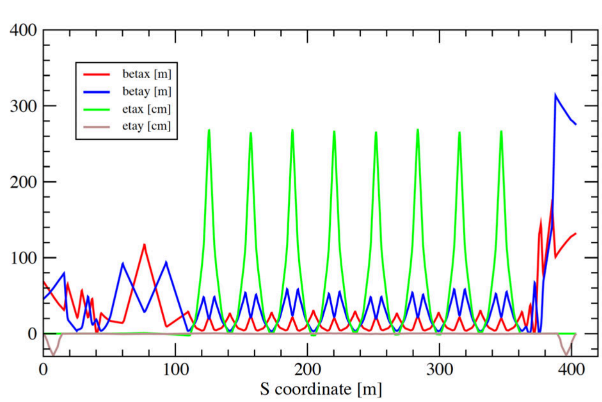

Figure 1: Arc 10 DBA optics for CEBAF SR-driven emittance growth reduction.

Content from this work may be used under the terms of the CC BY 3.0 licence (© 2015). Any distribution of this work must maintain attribution to the author(s), title of the work, publisher, and DOI.

ISBN: 978-3-95450-168-7 doi:10.18429/JACoW-IPAC2015-WEBD2

Content from this work may be used under the terms of the CC BY 3.0 licence (© 2015). Any distribution of this work must maintain attribution to the author(s), title of the work, publisher, and DOI.

SURVEY OF COMMISSIONING OF RECENT STORAGE RING LIGHT SOURCES*

M. Borland, ANL, Argonne, IL 60439, USA
Riccardo Bartolini, Ian Martin DLS, Oxfordshire, UK
Les Dallin, Canadian Light Source, Saskatchewan, Canada
Francis Perez, CELLS-ALBA Synchrotron, Cerdanyola del Valles, Spain
Peter Kuske, Roland Mueller, HZB, Berlin, Germany
Laurent Stanislas Nadolski, SOLEIL, Gif-sur-Yvette, France
James A. Safranek, SLAC, Menlo Park, California, USA
Seunghwan Shin, PAL, Pohang, South Korea
Zhao Zhentang, SINAP, Shanghai, China

Abstract

The Advanced Photon Source and other existing storage ring light sources are contemplating replacing an operating storage ring with a multi-bend achromat lattice [1–6]. Existing light sources have large user communities who are greatly inconvenienced by extended shutdowns. Hence, there will be a premium placed on rapid commissioning of the new lattice. To better understand the possibilities, we undertook a survey of recent commissioning experiences at third-generation light sources. We present a summary of that survey here.

INTRODUCTION

APS, ESRF, and other existing synchrotron light source facilities are contemplating replacing their operating storage rings. Users and funding agencies insist that "dark time" is minimized. APS, for example, is targeting 12 months for removal, installation, and commissioning of a new multi-bend achromat replacement ring. Of this 12 month period, only three months are set aside for commissioning. Other facilities are facing similarly demanding constraints.

As a result, we need to determine how realistic such short commissioning intervals are. We also need to determine what factors are most likely to prevent successful commissioning in such a short time, and what steps can be taken to ensure rapid commissioning. Toward this end, we surveyed recently-commissioned light sources to understand their experience, where "recently-commissioned" was defined as within the last 10-15 years.

The survey questions were created at APS by M. Borland, L. Emery, J. Kerby, and A. Zholents. In the interest of brevity, the questions are paraphrased below. Responses directed at the survey questions were received from seven facilities, namely, ALBA, BESSY-II, DLS, PLS-II, SOLEIL, SSRF, and SPEAR3. Information was also provided by CLS. The co-authors of this paper responded to the survey for their respective facilities.

* Work supported in part by the U.S. Department of Energy, Office of Science, Office of Basic Energy Sciences, under Contract No. DE-AC02-06CH11357.

A potential source of confusion is that commissioning may mean different things to different people. As part of the survey, we suggested the following definition: commissioning begins when beam is first injected into the ring. It ends when the ring is capable of supporting meaningful beamline commissioning, which generally requires several conditions

1. The ring can routinely store a significant fraction of the planned initial operating current for periods of 8 hours or more.
2. The lattice and emittance are essentially at the initial design configuration and values.
3. The lifetime is workable.
4. The orbit and beam stability are workable.
5. One or more ready-to-use insertion devices are installed and available.

Respondents to the survey generally agreed with this definition. In some cases, delivery of beam to "friendly users" was considered the endpoint.

QUESTIONS AND ANSWERS

Question: How was the commissioning schedule developed? This question was intended to ask about the process for developing the commissioning schedule, but wasn't very clear and was misunderstood by several respondents. Common themes in answers included: Basing the schedule on experience at other facilities; e.g., PLS-II followed the SPEAR3 example of 6 month replacement followed by 6 month commissioning. In some cases, requirements were driven by the user community. Also mentioned were: extensive discussions among commissioning team, creation of a list of major milestones, and definition of a phased commissioning approach.

What was the scheduled duration of commissioning and how was it structured? Scheduled duration ranged between 4 and 12 months, with 6 months being the most common response (five). Other responses (one each) included 3 months, 9 months, and 12 months. Hence, in terms of planning, the 3 month commissioning period contemplated by APS is a factor of two shorter than typically contemplated.

ISBN: 978-3-95450-168-7 doi:10.18429/JACoW-IPAC2015-WEBD3

RECENT DEVELOPMENTS ON SUPERCONDUCTING UNDULATORS AT ANKA

S. Casalbuoni*, A. Cecilia, S. Gerstl, N. Glamann, A. Grau, T. Holubek, C. Meuter, D. Saez de Jauregui, R. Voutta, ANKA, Karlsruhe Institute of Technology, Karlsruhe, Germany
C. Boffo, Th. Gerhard, M. Turenne, W. Walter, Babcock Noell GmbH, Würzburg, Germany

Abstract

A research and development program on superconducting undulators (SCUs) is ongoing at the ANKA (ANgstrom source KArlsruhe) synchrotron at KIT. This technology is of interest to improve the spectral characteristics of the emitted photons in third and fourth generation light sources. We present here the results obtained within the ongoing collaboration with the industrial partner Babcock Noell GmbH (BNG) on NbTi conduction cooled planar devices. Investigations on the application of alternative superconductors as well as a summary of the achievements reached to precisely characterize the magnetic field properties of SCUs and to measure the beam heat load to a cold bore are also described.

INTRODUCTION

ANKA (ANgstrom source KArlsruhe) and Babcock Noell GmbH (BNG) are pursuing a research and development program aiming to developing superconducting undulators (SCUs). The collaboration is focused on conduction cooled SCUs, with coils wound using NbTi wire, and with a movable vacuum gap.

The first milestone reached within the collaboration is the successful development and operation of a full scale (1.5 m long coils) superconducting undulator with 100.5 full periods of 15 mm (SCU15) in the ANKA storage ring. The spectral characterization is being performed at the IMAGE beamline. This full scale device demonstrates for the first time that superconducting undulators generate, while in operation in a storage ring, a higher magnetic field with respect to permanent magnet undulators including cryogenic cooled ones manufactured using the best material (PrFeB) available nowadays.

As a next step the collaboration is developing SCU20, a device with 20 mm period length for the NANO beamline at ANKA. Undulator mockup coils with 20 mm period length and 300 mm long have been designed, manufactured and tested.

In the first part of this contribution we focus on the performance of the SCU15 during the first months of operation in the ANKA storage ring. In the second section, we report on the 300 mm long mockup with 20 mm period length and its calculated spectral performance inferred from the measured magnetic field. The final section describes the tools and instruments not commercially available, under development at ANKA and necessary for the development of SCUs. These instruments are needed for precise magnetic field measurements and for measuring and possibly understanding the beam heat load to a cold bore.

* sara.casalbuoni@kit.edu

SCU15

ANKA and BNG designed, manufactured and tested a superconducting undulator with 15 mm period length and 100.5 full periods.

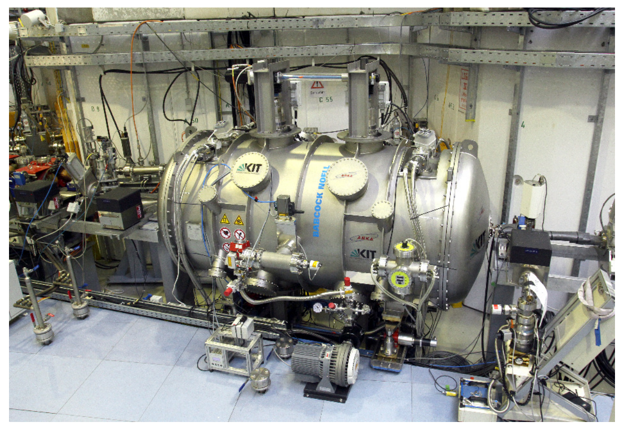

Figure 1: SCU15 installed in the ANKA storage ring.

The SCU15 has been assembled and successfully tested at BNG in summer 2014. The tests performed at BNG have been successfully repeated after transport at ANKA out of the ring. The test procedure included the cooldown, excitation, vacuum measurements and warm up of the system. Cooldown and warm up times of approximately 7 and 4 days, respectively, were achieved. The SCU15 was installed in the storage ring during the December 2014 shutdown and has been in operation with beam since the beginning of 2015 (see Fig.1).

One of the biggest challenges of the project was the development of the beam chamber (liner) which, together with the requirement for an UHV radiation-hard environment and low resistive losses [1], must open from 7 to 15 mm in operation at 10 K. Opening the vacuum gap to 15 mm is needed in the ANKA storage ring during electron beam injection and energy ramping. A movable gap might be appealing for other light sources during commissioning and/or operation, even if all other projects developing superconducting undulators in other facilities concentrate on fixed gap devices [2]. To be competitive with cryogenic permanent magnet undulators (CPMUs), high magnetic fields on axis are required; thus the coils of SCUs should be as close as possible to the beam axis, which can only be achieved by minimizing the distance between the liner and the coils. The SCU15 has

Content from this work may be used under the terms of the CC BY 3.0 licence (© 2015). Any distribution of this work must maintain attribution to the author(s), title of the work, publisher, and DOI.

ISBN: 978-3-95450-168-7 doi:10.18429/JACoW-IPAC2015-WEPWA001

ELECTRON BEAM TRANSFER LINE FOR DEMONSTRATION OF LASER PLASMA BASED FREE ELECTRON LASER AMPLIFICATION

A. Loulergue, M. Labat, C. Evain, M. Khojoyan, W. Yang, M. E. Couprie
Synchrotron SOLEIL, Saint-Aubin, France, PhLAM/CERCLA, Villeneuve d'Ascq, France

Abstract

One direction towards compact Free Electron Lasers (FEL) is to replace the conventional linac by a laser plasma driven beam, provided proper electron beam manipulation to handle the value of the energy spread and of the divergence is done. Applying seeding techniques enables also to reduce the required undulator length. The rapidly developing LWFA are already able to generate synchrotron radiation. With an electron divergence of typically 1 mrad and an energy spread of the order of 1 %, an adequate beam manipulation through the transport to the undulator is needed for FEL amplification. A test experiment for the demonstration of FEL amplification with a LWFA is under preparation in the frame of the COXINEL ERC contract. A specific design of electron beam transfer line following different steps with strong focusing variable strength permanent magnet quadrupoles, an energy de-mixing chicane with conventional dipoles and second set of quadrupoles for further dedicated focusing in the undulator has been investigated. Beam transfer simulations and expected FEL power in the XUV will be presented.

INTRODUCTION

FEL based fourth generation light sources [1-2] presently offer femtosecond tunable radiation in the X–ray domain. Besides the preparation of additional FEL light sources for users around the world, new schemes are also under investigation. In view of the fifth generation light sources [3] several approaches are considered. One direction goes towards the improvement of FEL performance in a wide spectral range and with versatile properties and flexibility for users. Another one aims at reducing the size either by exploring further seeding and / or by replacing the conventional linear accelerator by a compact alternative one. Indeed, the rapidly developing Laser WakeField Accelerator (LWFA) [4-5] are now able to generate synchrotron radiation. With an electron divergence of typically 1 mrad and an energy spread of the order of few percent, an adequate beam manipulation through the transport to the undulator is required for FEL amplification. Different strategies have been proposed, such as a decompression chicane [6], a transverse gradient undulator [7] and lastly a dedicated chromatic matching [8-9]. The studies presented here take place in the context of the LUNEX5 (free electron Laser Using a New accelerator for the Exploitation of X-ray radiation of 5th generation) [10] collaboration, aiming at investigating the production of short, intense, coherent pulses in the 40-4 nm spectral range with a 400 MeV superconducting linac and a LWFA both connected to a single FEL for advanced seeding configurations. The LWFA has first to be qualified by the FEL application. In this frame, beam transfer simulation of longitudinal and transverse manipulation of a LWFA electron beam showing that theoretical amplification is possible, a test experiment is under preparation, with the support of different grants.

BEAM MANIPULATION

The electron different trajectories through the refocusing stage, according to their energy, span the trace phase space distribution adding the chromatic emittance. From phase space geometry, the initial divergence drastically increases this effect. The slice energy sorting of the chicane will then transfer the chromatic emittance into mismatch from slice to slice along the undulator and spoil the FEL process efficiency. Up to second order, a general quadrupole transfer using the usual TRANSPORT notation limited to the horizontal plane is given by:

$$\begin{pmatrix} x \\ xp \end{pmatrix} = \left[\begin{pmatrix} r_{11} & r_{12}=0 \\ r_{21} & r_{22} \end{pmatrix} + \delta \begin{pmatrix} r_{116} & r_{126} \\ r_{216} & r_{226}=0 \end{pmatrix} \right] \begin{pmatrix} x_0 \\ xp_0 \end{pmatrix}$$

with (x xp) the position-angle coordinates and δ the energy deviation. In addition, cancelling the chromatic term r_{226}, the 3 rms associated image momenta according to their relative energy deviation are approximated by:

$$\sigma_x^2(\delta) = r_{11}^2 \sigma_0^2 + r_{126}^2 \sigma_{xp0}^2 \delta^2$$
$$\sigma_{xxp}(\delta) = r_{126} \sigma_{xp0} \delta / r_{11}$$
$$\sigma_{xp}^2(\delta) = \sigma_{xp0}^2 / r_{11}^2$$

with the $(\sigma_{x0}\ \sigma_{xp0})$ initial rms beam size and divergence. The energy slice geometrical emittance are given by $\epsilon_0 = \sigma_{x0}\ \sigma_{xp0}$ and the total geometrical emittance integrated over the energy deviation, is given by:

$$\epsilon_t^2 = \epsilon_0^2 + \epsilon_{chrom}^2 = \epsilon_0^2 + \left(\frac{r_{126}}{r_{11}} \sigma_{xp0}^2 \sigma_\delta\right)^2$$

The second term of the right hand side is the chromatic emittance that is drastically enhanced by the initial divergence to the square.

Content from this work may be used under the terms of the CC BY 3.0 licence (© 2015). Any distribution of this work must maintain attribution to the author(s), title of the work, publisher, and DOI.

ISBN: 978-3-95450-168-7 doi:10.18429/JACoW-IPAC2015-WEPWA003

SIMULATIONS OF ELECTRON-PROTON BEAM INTERACTION BEFORE PLASMA IN THE AWAKE EXPERIMENT

U. Dorda, R. Assmann, J. Grebenyuk, DESY, Hamburg, Germany
C. Bracco, A. Petrenko, J. Schmidt, CERN, Geneva, Switzerland

Abstract

The on-axis injection of electron bunches in the proton-driven plasma wake at the AWAKE experiment at CERN implies co-propagation of a low-energy electron beam with the long high-energy proton beam in a common beam pipe over several meters upstream of the plasma chamber. The possible effects of the proton-induced wakefields on the electron bunch phase space in the common beam pipe region may have crucial implications for subsequent electron trapping and acceleration in plasma. We present the PIC simulations with CST Studio as well as direct-beam-beam interaction simulations of the tentative common beam pipe setup and the two beam co-propagating in it.

INTRODUCTION

The AWAKE experiment is a proof-of-principle experiment that aims to utilize the 400 GeV proton beam from the SPS to drive a plasma-wake allowing to accelerate electrons from a few MeV to the GeV scale within a single plasma stage of a few meter length [1]. For this purpose a low-energy electron beam is bent onto the high-energy proton beam trajectory a few meters upstream of the plasma chamber (Figure 1) [2]. This paper reports on studies performed on the effect (wake fields and direct beam-beam interaction) of the proton beam on the electron beam over these few meters of common vacuum chamber. In this section, the common beam pipe is circular with a default diameter of d = 60 mm up to 1 m before the start of the plasma chamber where it's diameter is reduced to d = 40 mm (Assumed thickness: 2 mm, conductivity: 7.7E6 S/m). This common section is equipped with several quadrupoles allowing to focus the electron beam at the plasma entrance, corrector magnets and beam diagnostic devices [3]. In the foreseen

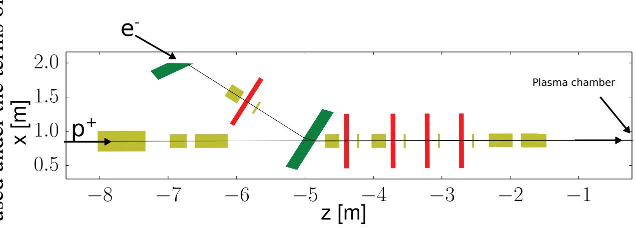

Figure 1: Sketch of the layout upstream of the plasma chamber where the high energy proton and low energy electron beam co-propagate (green: dipoles, red: quadrupoles, yellow: orbit correctors & beam diagnostic devices).

default operation scenario, the arrival of the two beams is adjusted to position the short electron beam slightly behind the center of the significantly longer proton bunch. To be on the safe side and to anticipate experimental modifications, a centered electron beam sampling the maximal direct beam-beam force was assumed. Table 1 and Figure 2 list/illustrate the proton and electron beam parameters and optics in this common section.

Table 1: Beam Parameters of the Proton and Electron Beam

Parameter	Protons	Electrons
Energy [GeV]	400	0.016
Nr of particles	3E11	1.2E9
$\epsilon_{n,xy}$ [π mm mrad]	3.5	2.0
Bunch length [1σ, mm]	120	1.2
Momentum spread [10^{-3}]	2.0	5.0
β_x [m]	7.0	1.02
β_y [m]	7.0	5.39

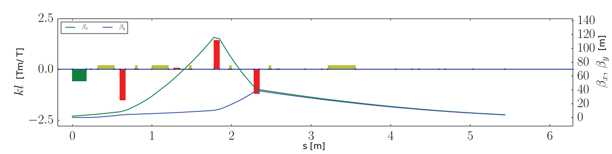

Figure 2: Electron beam optics along the common beam section. The $\beta_{x,y}$ of the proton beam is almost constant at $\approx 7m$.

WAKE FIELD STUDIES WITH CST

The "Particle In Cell" (PIC) - solver of "CST Particle Studio 2014" was used to simulate the interaction between the two beams including wake-fields taking a mock-up geometry of the vacuum chamber into account. The 6D-initial particle distributions (25000 macro-particles electrons, 50000 macro-particle protons) were externally created and imported using the "CST-particle interfaces" feature. In order to reduce the computational effort, the proton beam was cut right after the electron beam. As the two beams are launched at separate locations, the perturbations due to the non-self-consistent initialization are no issue. The fields of the magnets (dipoles and quadrupoles) were imported into CST based on ideal, hard edge models. Due to the large size of the model, special attention had to be put on the choice of mesh-parameters, where a valid compromise between computational feasibility and physical correctness had to be found. While a suitable trade-off could be found to represent the longer distance effects of the wake-fields including the interaction with the vacuum chamber, a separate code based on analytical field-formulas had to be written to study the direct beam-beam interaction at low amplitudes (see next

Content from this work may be used under the terms of the CC BY 3.0 licence (© 2015). Any distribution of this work must maintain attribution to the author(s), title of the work, publisher, and DOI.

ISBN: 978-3-95450-168-7 doi:10.18429/JACoW-IPAC2015-WEPWA005

SIMULATIONS STUDY FOR SELF-MODULATION EXPERIMENT AT PITZ

G. Pathak*, F. Grüner, A. Martinez de la Ossa, Universität Hamburg, 22761 Hamburg, Germany
T. Mehrling, J. Osterhoff, DESY, Hamburg 22607, Germany
M. Groß, F. Stephan, DESY, Zeuthen 15738, Germany
C. Benedetti, C. B. Schroeder, LBNL, Berkeley, CA 94720, USA

Abstract

Self-modulation (SM) of proton beams in plasma has recently gained interest in context with the PWFA experiment proposed by the AWAKE collaboration at CERN. Instrumental for that experiment is the SM of a proton beam to generate bunchlets for resonant wave excitation and efficient acceleration. A fundamental understanding of the underlying physics is vital, and hence an independent experiment has been set up at the beamline of the Photo Injector Test facility at DESY, Zeuthen site (PITZ), to study the SM of electron beams in a plasma.

In this contribution we present simulation results of SM experiments at PITZ using the particle-in-cell code HiPACE. The simulation study is crucial to optimize the beam and plasma parameters for the experiment. Of particular interest is the energy modulation imprinted onto the beam by means of the generated wakefields in the plasma. With the support of simulations, the observation of this information in the experiment can be used to deduce key properties of the accelerating electric fields, such as their magnitude and their phase velocity, both of significant importance for the design of self-modulated plasma-based acceleration experiments.

INTRODUCTION

Plasma wakefield acceleration was proposed as an alternative of conventional acceleration methods due to the large accelerating fields [1]. Accelerating wakefields in excess of 50 GeV/m have been achieved in $85cm$ long plasma using a 42 GeV drive electron beam [2]. However, different stages would be required for further acceleration of electrons owing to limited drive beam energy.

Recently, it has been proposed to use short and high energetic proton beams to drive a plasma wave so as to accelerate electron beams to the TeV-energy scale in a single plasma stage [3], rather than in multiple stages, as required with electron drivers. In order to excite large amplitude plasma waves in such a scheme, the driver bunch length (L^{beam}) needs to be shorter than the plasma wavelength (λ_p). However, available proton bunches from the Super Proton Synchrotron at CERN are very long (~12 cm) in comparison with the foreseen plasma wavelength for this experiment (λ_p ~1 mm). The AWAKE experiment thus relies on the fact that a long proton bunch ($L^{beam} > \lambda_p$) is self-modulated during its propagation in the plasma, thereby being split into a train of ultra-short sub-bunches with a length on the order of λ_p, so that the plasma wave is resonantly excited [4]. The self-modulation is a result of transverse two-stream instability, occurring through the coupling of the transverse wakefield with the beam radius evolution. When a long bunch with the beam length $L^{beam} > \lambda_p$ and transverse size σ_r enters the plasma, it is radially modulated by the periodic focusing forces, and the beam density modulation ($n_b \propto \sigma_r^2$) provides feedback for the instability to grow. Consequently, this instability self modulates the long beam into ultra short bunches at the plasma wavelength scale, which resonantly drive the plasma wake. The instability is convective and grows both along the bunch (ζ) and along the plasma (z) as illustrated by the number of e-folding growths for a flat-top bunch, [4]:

$$N_{e-folding} \cong \frac{3^{3/2}}{4}\left(\nu\frac{n_{b0}m_e}{n_p M_b \gamma}\right)^{1/3}(k_p\zeta)^{1/3}(k_p z)^{2/3} \quad (1)$$

Where ω_p is the plasma frequency, $k_p = c/\omega_p$, $\nu \approx 1 - \frac{(k_p\sigma_{r0})^2}{6}$, σ_{r0} the initial bunch radius, n_{b0} the initial beam density, M_b the bunch particle mass.

The study of the self-modulation of electron beams from the Photo Injector Test Facility at DESY, Zeuthen site (PITZ) offers a unique possibility to demonstrate and optimize the self-modulation instability experimentally and to gain insight into the underlying physics of the involved processes [5]. Self-modulation in PITZ electron beam has been already shown with OSIRIS simulations [6]. The particular interest of this experiment is to see a significant modulation of the beam energy spectrum, which will be resolvable in the experiment. In the following section, results from numerical studies, aiming at the optimization of the PITZ beam and plasma parameters, are presented. Simulations on the self-modulation instability are performed using the particle-in-cell code HiPACE [7]. This code provides the possibility to import beams from the particle tracking code ASTRA [8].

SIMULATION PARAMETERS

A particle tracking code, ASTRA is used to track the beam from the RF photo-electron gun to the entrance of the plasma, $6.2m$ downstream [8]. The average energy of the bunch is $E = 22MeV$ with energy spread of $\Delta E/E = 0.1\%$. The simulation uses a moving window ($8.4mm \times 1.7mm \times 1.7mm$) that propagates at the speed of light (c), with resolution of $k_p\Delta z = 0.025$ and $k_p\Delta y = k_p\Delta x = 0.04$. Table 1 shows the beam and plasma parameters for different conditions that are used to study the self-modulations.

* gaurav.pathak@desy.de

Content from this work may be used under the terms of the CC BY 3.0 licence (© 2015). Any distribution of this work must maintain attribution to the author(s), title of the work, publisher, and DOI.

ISBN: 978-3-95450-168-7 doi:10.18429/JACoW-IPAC2015-WEPWA006

LASER PROPAGATION EFFECTS DURING PHOTOIONIZATION OF METER SCALE RUBIDIUM VAPOR SOURCE

J. Moody, F. Batsch, A. Joulaei, E. Öz, P. Muggli, Max Planck Institute for Physics, Munich, Germany
N. Berti, J. Kasparian, University of Geneva, Switzerland

Abstract

The baseline AWAKE experiment requires a 10 meter long plasma source with a density of 10^{15} cm^{-3} and a density uniformity of 0.2%. To produce this plasma, a temperature stabilized rubidium vapor source is photoionized by a terawatt peak power laser pulse. In this paper we describe the laser pulse evolution within the plasma source including the dispersive, diffractive, and photoionization effects on the laser pulse. These calculations will be experimentally investigated in a meter long heat pipe oven using scaled laser parameters.

INTRODUCTION

The AWAKE project is a proof of principle proton driven plasma wakefield electron accelerator experiment [1, 2], that scheduled to begin initial experiments at CERN in 2016. The experiment employs a 400 GeV proton beam from the Super Proton Synchrotron (SPS) that propagates through a 10 meter plasma to produce GeV/m wakefields via the mechanism of the self modulation instability [3–5]. The second phase of the AWAKE experiment, scheduled to begin in 2017, relies on SMI to accelerate a 15 MeV electron beam from a photoinjector and single RF booster. The electrons are injected on the axis of the proton beam 100 plasma periods behind the laser pulse that ionizes the rubidium and creates the plasma. For controlled injection of the electron beam to occur, the plasma wakefields must have a stable, well defined phase up to the longitudinal injection position, placing a requirement of 0.2% density uniformity on the plasma source.

The plasma is produced from a 10^{15}cm^{-3} rubidium vapor source. A 10 meter heat exchanger cell is being developed and built by Grant Instruments Ltd. [6]. The density of the rubidium vapor in the cell is well defined by the temperature of the device. A detailed description of the device, including density vs. temperature curves is given by E. Öz and P. Muggli [7]. The requirement of < 0.2% density stability over the device in the baseline design of the experiment is met by achieving the same level of temperature stability over the 10 meter device. Lastly, to create the plasma, the rubidium is photoionized by a 4 TW peak power laser pulse via field ionization described by Keldysh [8]. Because we are operating in a low Keldysh parameter regime in which the intensity is high and frequency low, the ionization time is much less than the laser pulse length and occurs at a laser threshold intensity of 2 TW/cm^2.

Rubidium was chosen over other Alkali metals due to it's low ionization energy of 4.2 eV and the relative technical simplicity of its use including producing the baseline vapor density at 200 degrees C and it being a solid at room temperature. The laser used to ionize the rubidium vapor was purchased from Amplitude Technologies [9]. This laser is uses and Erbium doped fiber oscillator with a central wavelength of 780 nm with a bandwidth of approximately 10 nm. The laser system is a chirped pulse amplification system that stretches the ~100 fs pulse to ~ 100 ps, amplifies it to a maximum value of 600 mJ, then recompresses the laser pulse so that it has a peak power of 4 TW at a maximum energy of 450 mJ per pulse.

To understand the laser pulse propagation we are conducting rubidium ionization experiments on a 1 m heat pipe oven and the laser to be used for the CERN experiment at Max Planck Institute for Physics (MPP). A comparative table of parameters for both the AWAKE experiment and the MPP scaled investigation are shown in Table 1.

Table 1: AWAKE and MPP Phase B Parameters

Parameter	AWAKE	MPP Phase B
Laser Pulse Energy	450 mJ	100 mJ
Rayleigh Range	5 m	35 cm
Rubidium Vapor Length	10 m	1 m

This paper describes the laser pulse propagation studies currently ongoing at MPP investigating the evolution of the pulse as it ionizes meter length scale Rubidium vapor.

DESCRIPTION OF MPP EXPERIMENT

The experiment at MPP is broken into two phases. Phase A is the study of the quasi-linear effects of the laser passing through cm scale rubidium at the baseline density of 10^{15}cm^{-3}. This length scale was chosen because the variation in the index of refraction across the bandwidth of the laser due to anomalous dispersion, $\delta n/n$ is on the order of 10^{-4}. With a wave number on the order of 10^6 m^{-1}, we expect order unit phase change across the bandwidth of the laser pulse at cm scales.

For this experiment we used a small rubidium cell with a length of 3.5 cm. This cell was heated to 200 degrees C and the density was measured using the "hook method" technique [10, 11], which employs a white light Mach-Zehnder interferometer and high resolution spectrometer. The separation of the first large distortions of the interference fringes near the D2 resonance line for rubidium acts as a diagnostic for the vapor density. An image of the cell can be seen on the left in Fig. 1.

Upon verification of the rubidium vapor density for a given temperature, 400 μJ laser pulses were propagated through

Content from this work may be used under the terms of the CC BY 3.0 licence (© 2015). Any distribution of this work must maintain attribution to the author(s), title of the work, publisher, and DOI.

ISBN: 978-3-95450-168-7 doi:10.18429/JACoW-IPAC2015-WEPWA007

THE AWAKE, PROTON-DRIVEN PLASMA WAKEFIELD EXPERIMENT AT CERN

P. Muggli*, Max Planck Institute for Physics, Munich, Germany
for the AWAKE Collaboration

Abstract

We briefly describe the current status of the AWAKE experiment in terms of physics and experimental program.

INTRODUCTION

Plasma wakefield acceleration has made remarkable progress since it was proposed [1] and plasma wakefields were first observed [2]. In particular, very large accelerating gradient ($\sim 50\,GeV/m$) and energy gain ($\sim 42\,GeV$) where measured in a meter-scale plasma [3]. A witness electron bunch was accelerated with a narrow energy spread ($\sim$ %) and a significant energy transfer efficiency ($\sim$ 30%) [4].

The AWAKE experiment at CERN [5] aims at exploring the possibility of using a proton (p^+) bunch to drive large amplitude wakefields ($\sim\ GV/m$) in plasmas. Proton bunches are interesting because they carry large amounts for energy (kilojoules). It was shown in numerical simulations that a single LHC p^+ bunch could potentially be used to accelerate electrons to TeV scale energies, in a single plasma stage with GeV/m accelerating gradient [6].

The large momentum p^+ bunches ($\sim 400\,GeV/c$ at SPS and $\sim 7\,TeV/c$ at LHC) are long ($\sigma_z \cong 10-12\,cm$). In order to reach $\sim\ GV/m$ accelerating fields, the plasma density n_{e0} needs to be in the $10^{14}-10^{15}\,cm^{-3}$ range since their amplitude is on the order of $E_{WB} = m_e c\omega_{pe}/e$. Here $\omega_{pe} = \left(n_{e0}e^2/\epsilon_0 m_e\right)^{1/2}$ is the plasma electron (angular) frequency. At these electron plasma densities the plasma wave or wakefields wavelength ($\lambda_{pe} = 2\pi c/\omega_{pe}$) is on the order of $1\,mm$. A relativistic charged particle bunch traveling in a plasma with wakefields period much shorter than its length ($\lambda_{pe} \ll \sigma_z$) is subject to the self-modulation instability (SMI) [7].

The SMI is a transverse instability that arises from the interplay between transverse components of the plasma wakefields locally increasing (decreasing) the bunch density through focusing (defocusing), and the wakefields being driven stronger (weaker) by regions of larger (smaller) bunch density. The modulation period is $\cong \lambda_{pe}$ and the modulated bunch resonantly drives the plasma wakefields. In order to avoid another transverse instability, the current filamentation instability (CFI) [8], the bunch must be focused near the entrance of the plasma to a transverse size σ_r smaller than the cold plasma collisionless skin depth c/ω_{pe}: $\sigma_r \leq 168\,\mu m$ for n_{e0} up to $10^{15}\,cm^{-3}$.

The occurrence of the SMI can be detected by characterizing the structure of the p^+ when exiting the plasma, the corresponding plasma density modulation and the wakefields this density modulation supports through the acceleration of externally injected electrons.

Experiments will start in late 2016 with the first goal of observing and characterizing the SMI of the p^+ bunch, including seeding of the SMI, in a single, $10\,m$-long plasma. Experiments scheduled for mid 2017 will focus on the external injection of electrons into the wakefields. Acceleration from $\sim 20\,MeV$ to over $1\,GeV$ is expected. Later experiments will use two plasmas, the first one for seeding and SMI development, and the second one for acceleration. The second one can be very long thanks to the high energy of the p^+ bunch that is thus able to drive wakefields over many tens of meters [9].

PROTON BUNCH

In the AWAKE experiment, the $\sim 400\,GeV/c$, $\sigma_z \cong 12\,cm$ SPS bunch with $1-3\times10^{11}$ p^+ is focused to $\sigma_r \cong 200\,\mu m$ near the entrance of the plasma. The p^+ bunch has a low normalized emittance, $3.5\,mm-mrad$ and a small relative momentum spread of 0.35%. Its focused beta function is $\cong 5\,m$, half the plasma length.

PLASMA SOURCE

The plasma source consists of a rubidium (Rb) vapor ionized by a short ($\cong 100\,fs$) and intense laser pulse [10]. Rubidium was chosen because it has a low ionization potential ($4.177\,eV$) for its first electron and a relatively large one for the second ($27.28\,eV$). Since the appearance intensity for ionizations scales with the fourth power of the laser intensity [11], only about $1.3\times10^{11}\,W/cm^2$ are necessary to free the first electron, while a 1984 times larger intensity is required to ionize the second one. Note that in this case the p^+ beam impact or field ionization fraction is very small. Rubidium also has a relatively large ion mass, which makes the experiment less sensitive to ion motion [12]. This is important since the useful wakefields span many plasma wavelengths behind the ionizing laser pulse and the start of the wakefields. The Rb vapor with density $n_0 = 10^{14}-10^{15}\,cm^{-3}$ is created in an oil heat-exchanger and can accommodate either a very uniform constant density that may be necessary for external injection [13] or a (linear) density gradient. The density is reached at oil and vapor temperatures between 150 and 200^o C. The vapor column is $40\,mm$ in diameter and $\cong 10\,m$-long. The vapor density is measured using the hook method [14].

Since field-ionization is a threshold process, the plasma density and its uniformity are equal to those of the Rb vapor. At the densities considered here, the plasma radius needs to be everywhere at least one millimeter ($\geq c/\omega_{pe}$). Sim-

* muggli@mpp.mpg.de

Content from this work may be used under the terms of the CC BY 3.0 licence (© 2015). Any distribution of this work must maintain attribution to the author(s), title of the work, publisher, and DOI.

ISBN: 978-3-95450-168-7 doi:10.18429/JACoW-IPAC2015-WEPWA008

MEASURING THE SELF-MODULATION INSTABILITY OF ELECTRON AND POSITRON BUNCHES IN PLASMAS*

P. Muggli†, O. Reimann
Max Planck Institute for Physics, Munich, Germany
L.D. Amorim, N.C. Lopes, L.O. Silva, J.M. Vieira
Instituto Superior Tecnico, Lisbon
J. Allen, S.J. Gessner, M. Hogan, S.Z. Green, M.D. Litos, B.D. O'Shea, V. Yakimenko
SLAC, Menlo Park, California, USA
G. Andonian, C. Joshi, K. Marsh, W. Mori, N. Vafaei-Najafabadi, O. Williams
UCLA, Los Angeles, USA
E. Adli, C. A. Lindstrom, V. B. Olsen
University of Oslo, Norway

Abstract

We briefly describe some of the features of the E209 experiment at SLAC-FACET. The experiment aims at studying the physics of the self-modulation instability of long electron and positron bunches in dense plasmas. Encouraging initial results were obtained so far. Further experiments will take place soon.

INTRODUCTION

The E209 experiment at SLAC-FACET uses the well instrumented PWFA facility to study the self-modulation instability (SMI) of long charged particle bunches in m-long, dense plasmas [1]. In this context, bunches are considered as long when their duration is many periods of the electron plasma wave ($\tau \gg 2\pi/\omega_{pe} \sim n_{e0}^{-1/2}$) or their length many wavelengths of the wave ($L \gg \lambda_{pe} \sim n_{e0}^{-1/2}$). Here n_{e0} is the plasma electron density, $\omega_{pe} = \left(n_{e0}e^2/\epsilon_0 m_e\right)^{1/2}$ is the electron (angular) plasma frequency and $\lambda_{pe} = 2\pi c/\omega_{pe}$. In the FACET case the electron (e^-) or positron (e^+) bunch can be between 1.0 and 1.5 mm and the plasma density in the 10^{16} to 10^{18} cm^{-3} range ($335 \geq \lambda_{pe} \geq 34$ µm). This means that the particle bunch can be the equivalent of a few tens of plasma wavelengths long.

The SMI develops because of the positive feedback between the transverse wakefields alternating from focusing to defocusing over a plasma wavelength and the bunch density increasing/decreasing as a result. Transverse bunch slices of larger/lower density drive stronger/weaker wakefields, closing the feedback loop. The instability typically grows and saturates over a few ($5-10$) centimeters with the E209 beam and plasma parameters. The resulting periodic modulation of the bunch density due to the radial change can then resonantly drive wakefields over long plasma distances.

SMI OCCURRENCE

The occurrence of the SMI has (at least) three observable effects on the bunch.

1. The driving of wakefields leads to energy loss (and gain) by the drive bunch particles. This can in principle be measured at FACET with the imaging magnetic spectrometer that has an energy resolution on the order of 0.4% of the incoming particles energy, or better than 100 MeV around the 20 GeV bunch energy [2].
2. The transverse profile of the bunch is modified by the SMI occurrence when observed downstream of the plasma. At that location and without plasma the bunch has typically transverse Gaussian profiles with different rms sizes due to the different emittances in the horizontal and vertical planes ($\epsilon_{Nx,y} = 50, 5$ mm-mrad). When the SMI occurs the transverse profile is expected to have a focused core surrounded by a halo consisting of the defocused particles. This situation has already been observed with e^+ bunches approximately λ_{pe}-long. In this case the halo originates from the non-linear nature of the focusing fields [3]. This is observed by imaging onto a CCD camera the backward optical transition radiation (OTR) emitted by the bunch when traversing a thin titanium foil placed at 45^o with respect to the beam axis. Note that because the OTR wavelength (400-800 nm) is much shorter that the characteristic longitudinal and transverse size of the bunch, this radiation is emitted incoherently.
3. The coherent transition radiation (CTR) emitted by the bunch when traversing another thin titanium foil carries information about the bunch density modulation. Since the modulation is periodic with period $\cong \lambda_{pe}$, the wavelength spectrum of the radiation should exhibit a peak at $\cong \lambda_{pe}$. The spectrum of the radiation can be obtained using Fourier transform infrared (FTIR) spectroscopy. The CTR is sent through an interferometer and the interferometer signal recorded as a function of the delay or path length difference (PLD) between the two arms of the interferometer. The interferometer signal is then Fourier transformed and one can show that

* Work at SLAC is supported by DOE contract DE-AC02- 76SF00515. The authors would like to acknowledge the contributions of J. Yocky and N. Lipkowitz. No useful beam would be available for E209 without them.
† muggli@mpp.mpg.de

Content from this work may be used under the terms of the CC BY 3.0 licence (© 2015). Any distribution of this work must maintain attribution to the author(s), title of the work, publisher, and DOI.

ISBN: 978-3-95450-168-7 doi:10.18429/JACoW-IPAC2015-WEPWA010

A HIGH INTENSITY PROTON SOURCE FOR THE EUROPEAN SPALLATION SOURCE FACILITY

Luigi Celona, Luciano Allegra, Lucio Andò, Antonio Caruso, Giuseppe Castro, Francesco Chines, Giuseppe Gallo, Santo Gammino, Alberto Longhitano, Salvatore Marletta, David Mascali, Lorenzo Neri, S. Passarello, INFN/LNS, Catania, Italy
Giuseppe Torrisi, INFN/LNS, Catania; Università Mediterranea di Reggio Calabria, Reggio Calabria, Italy

Abstract

Along the last 25 years, INFN-LNS has gained a relevant role in R&D of plasma-based ion sources. The laboratory is currently involved in the construction of the Proton Source and Low Energy Beam Transport (LEBT) line for the European Spallation Source. ESS – based on a 2.0 GeV, 62.5 mA proton accelerator for neutron production – will be a fundamental instrument for research and applications. The proton source is required to produce at least 74 mA proton beam at 2.25 π.mm.mrad emittance (99% normalized), 2.86 ms pulse duration, 14 Hz repetition rate. We will illustrate the design of the source, the ongoing study of the radio frequency to plasma coupling, the result of a parametric study of the extraction system, the final layout of the LEBT – based on beam transport studies and the chopper strategy – and the first steps of the devices installation at the INFN-LNS test-bench site.

INJECTOR FOR THE ESS ACCELERATOR

The source named Proton Source for ESS (PS-ESS) (see Figure 1) was designed with a flexible magnetic system and a compact tetrode extraction system with the goal to minimize the emittance and the time needed for the maintenance operations. The ESS injector design has taken advantage of recent theoretical updates together with the new plasma diagnostics tools developed at INFN-LNS. The proton beam requirements is of 74 mA. The ability to reduce the current up to 6 mA with a precision of 2 mA, without changing the proton source conditions is reached with a six blade iris housed in the LEBT. The beam stability during the normal operations (in terms of current and emittance) shall be within ±3.5% from pulse to pulse variation and ±2% of the beam current averaged over a period of 50 us. This requirement is considered fundamental by the beam physics group, for the high energy RF cavities. The pulse duration is 2.86 ms with 14 Hz repetition rate. The requirements for the proton source and the LEBT are summarized in the Table 1. A detailed study of the beam transport in regime of space charge compensation was done and experimentally verified [1]. A chopper was designed to speed up the beam pulse rise and fall time. The final aim is to achieve a reliability better than 95% for the whole accelerator, thus meaning that the source reliability is expected to be greater than 99%.

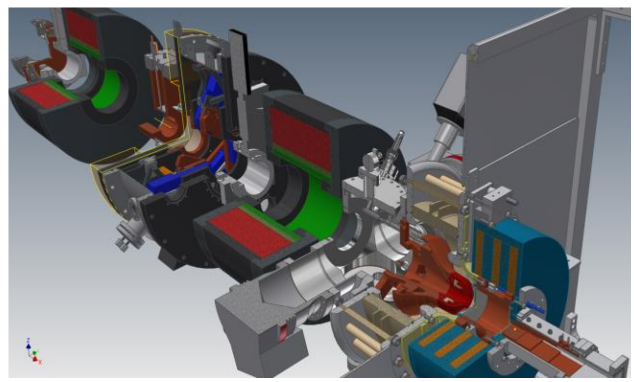

Figure 1: 3D rendering of the PS-ESS with the LEBT.

Table 1: PS-ESS Requirements

Parameters	Value
Proton current range	60-74 mA
Proton fraction	>80%
Current stability (50us averaged)	±2%
Pulse to pulse variation	±3.5%
Beam energy	70-80 ±0.1 keV
Repetition rate	1-14 Hz
Pulse length	5-2880 ±1 us
Current reduced using iris	2-74 ±1 mA
Restart after vacuum break	<32h
Restart after cold start	<16h
Emittance (99% normalized)	<2.25 π.mm.mrad
Twiss parameter α	1.02 ±20%
Twiss parameter β	.11 ±10%
Beam pulse rise and fall time	<20 us
LEBT pressure	<6e-5 mbar

PLASMA AND BEAM MODELLING

The INFN-LNS group fixed a challenging milestone for the simulation of the entire process underlying ion-beam generation. The plasma studies were performed by developing different plasma diagnostics and own code plasma modelling and to simulate the dynamics of space charge compensation (SCC), both in stationary and transient regimes. The new PIC code includes also

Content from this work may be used under the terms of the CC BY 3.0 licence (© 2015). Any distribution of this work must maintain attribution to the author(s), title of the work, publisher, and DOI.

ISBN: 978-3-95450-168-7 doi:10.18429/JACoW-IPAC2015-WEPWA012

Content from this work may be used under the terms of the CC BY 3.0 licence (© 2015). Any distribution of this work must maintain attribution to the author(s), title of the work, publisher, and DOI.

DESIGN OF A MICROWAVE FREQUENCY SWEEP INTERFEROMETER FOR PLASMA DENSITY MEASUREMENTS IN ECR ION SOURCES*

G. Torrisi, INFN-LNS, Catania, Italy; Università Mediterranea di Reggio Calabria, Reggio Calabria, Italy
R. Agnello, G. Castro, L. Celona, V. Finocchiaro, S. Gammino,
D. Mascali, L. Neri, S. Passarello, INFN-LNS, Catania, Italy
G. Sorbello, University of Catania, Catania, Italy; INFN-LNS, Catania, Italy
T. Isernia, Università Mediterranea di Reggio Calabria, Reggio Calabria, Italy

Abstract

Electron Cyclotron Resonance Ion Sources (ECRIS) are among the candidates to support the growing request of intense beams of multicharged ions. Their further development is related to the availability of new diagnostic tools, nowadays consisting of few types only of devices designed on purpose for such compact machines. Microwave Interferometry is a non-invasive method for plasma diagnostics and represents the best candidate for the whole plasma density measurements. Interferometry in ECR Ion Sources is a challenging task due to their compact size. The typical density range of ECR plasmas ranging from 10^{11} to about 10^{12} cm^{-3}, causes the probing beam wavelength to be in the order of few centimetres which is comparable to the chamber radius. The paper describes the design of a new microwave interferometer based on the so-called "frequency sweep" method: the density is here derived by the frequency shift of a beating signal obtained during the fast sweep of both probing and reference microwave signals; inner cavity multipaths contributions can thereby be suppressed by cleaning the spurious frequencies from the beating signal spectrum.

INTRODUCTION AND MOTIVATION

The development of microwave diagnostics is a fruitful strategy because microwaves crossing the plasma are sensitive to the entire energetic spectrum of the plasma, allowing global evaluation of the average density. In the classical scheme of a microwave Mach-Zender type interferometry, a microwave signal at frequency larger than any cutoff/resonance frequency of the plasma under investigation is splitted into two different branches: the first one is launched into the plasma, the second one is used as reference signal, propagating into a waveguide of calibrated length, as shown in Fig. 1.

The basic idea [1] is that the density can be determined from phase shift which explicitly depends on the natural plasma oscillation ω_p, i.e. the electron density, as depicted by the mathematical relation below:

$$\Delta\phi = \int_0^L \frac{\omega}{c}\left[1-\left(1-\frac{\omega_p^2}{\omega^2}\right)^{1/2}\right] dl \tag{1}$$

* Work supported by the 5^{th} National Commission of INFN (VESPRI Experiment)

where L is the plasma length along which the integral is calculated, c the speed of light, ω the probing microwave pulsation, $\omega_p^2 = \frac{n_e e^2}{m_e \epsilon_0}$ the plasma oscillation, and the other quantities are the standard fundamental physical constants. In ECRIS the measurement is greatly complicated by the mechanical constraints, which limit considerably the ratio L/λ, where L is the characteristic length of the plasma chamber, and λ is the wavelength.

In our experimental setup, typical of all ECRIS setup, the direction of the electromagnetic wave vector $\vec{k}$ is along the magnetostatic confinement field $\vec{B}_0$, then the dispersion relation of the magnetized plasma has two solutions: right-hand (R) and left-hand (L) circularly polarized waves, with the following propagation constants:

$$k_R = \frac{\omega}{c}\sqrt{1-\frac{\omega_p^2}{\omega(\omega-\omega_g)}} \tag{2}$$

$$k_L = \frac{\omega}{c}\sqrt{1-\frac{\omega_p^2}{\omega(\omega+\omega_g)}} \tag{3}$$

where $\omega_g = eB_0/m_e$ is the electron cyclotron frequency and we can assume that the collision frequency is much smaller than the microwave frequency. Without loss of generality we choose a cartesian reference system so that the z axis is parallel to $\vec{B}_0$ and to the yz plane containing the propagation constant vector $\vec{k}$ directed along $\vec{B}_0$. In this configuration the electric field vectors associated to R and L waves can be written as:

$$\vec{E}_R = (\hat{x} - i\hat{y})e^{ik_R z} \tag{4a}$$

$$\vec{E}_L = (\hat{x} + i\hat{y})e^{ik_L z} \tag{4b}$$

The sum of the two waves provides the composed wave $\vec{E}_t = \vec{E}_R + \vec{E}_L$ having the following effective constant of propagation:

$$k_{eff} = (k_R + k_L)/2$$

So, the phase shift due to the presence of the plasma is:

$$\Delta\phi = \int_0^L (k_0 - k_{eff})dL \tag{5}$$

where $k_0 = \frac{\omega}{c}$ is the free space propagation constant.

Figure 1 highlights the conceptual layout of an interferometer setup applied to small-size plasma chambers like in case

ISBN: 978-3-95450-168-7 doi:10.18429/JACoW-IPAC2015-WEPWA013

A TRANSPORT BEAMLINE SOLUTION FOR LASER-DRIVEN PROTON BEAMS

A. Tramontana (a,b) *, G. A. P. Cirrone (a), G. Cuttone (a), G. Candiano(a),
M. Costa(a), G. Gallo(a), R. Leanza(a,b), M. Maggiore (c), R. Manna(a),
V. Marchese(a), G. Milluzzo(a,b), G. Petringa(a), D. Rizzo(a), F. Romano (a),
S. Salamone(a), F. Schillaci (a),V. Scuderi (a,d)
(a) INFN-LNS, Catania, Italy
(b) University of Catania, Catania, Italy
(c)INFN-LNL, Legnaro (PD), Italy
(d)) Institute of Physics of the ASCR, Prague, Czech Republic

Abstract

Laser-target interaction represents a very promising field in several potential applications, from nuclear physics to medicine. On the other hand optically accelerated particle beams are characterized by some extreme features, often not suitable for several applications, as an high peak current, a poor shot-to-shot reproducibility and a wide energy and angular distribution. Therefore many efforts are currently ongoing for the development of specific beam transport devices in order to obtain controlled and reproducible output beams. In this framework, this work want to report about a transport beamline solution dedicated to laser-driven beams and made of two main sections: a quadrupole-focusing device and an energy selector system. A test beam-line consisting of prototypes has been realised at INFN-LNS (National Institute of Physics-South National Laboratories, Ct, I) and partially tested with conventional accelerated proton beams. Moreover, some of these prototypes have been already tested with laser-driven beams.
Several simulations have been also performed using the Geant4 Monte Carlo toolkit, in order to best exploit the beamline potentiality. Preliminary simulations of a transported beamline to select 5 MeV and 24 MeV proton beams are here reported.

INTRODUCTION

Nowadays, the interest in particle acceleration from ultra intense lasers is strongly growing, thanks to the huge number of potential applications and to the possibility to investigate new physics regimes and phenomena. In particular, it is becoming evident that, in the next future, laser-driven acceleration could represent a different and perhaps more effective alternative as respects to the actual conventional particle accelerators. It could bring to more compact and less expensive acceleration systems and, consequently, to a larger spread of radiation beams around the word [1]. Such reasons are stimulating the interest of many physicists for the improvement and the optimisation of the interaction regimes as well as of the overall quality of these new kinds of beams. Beyond the improvement at the laser-target interaction level, many efforts are spent for the development of specific beam transport devices. Interesting options with microlens, magnetic chicanes, quadrupoles, solenoids and radio frequency cavities are reported in literature [2], however for all these approaches, there are different crucial parameters, as the acceptance angle of the transport system that, considering the wide input divergence, limits the number of output particles. In this framework, this paper reports about a Monte Carlo study of a transport beamline solution for laser-accelerated proton beams.

* tramontana@lns.infn.it

TRANSPORT BEAMLINE

Ions accelerated by laser-matter interaction are characterized by high intensities, multiple species and charge states, wide energy spectrum and large energy-dependent angular distribution. Therefore, in order to make these non-conventional beams suitable for multidisciplinary applications, mainly in terms of reproducible and controlled output features, the design of specific transport elements seems to be mandatory. Bearing in mind these purposes, a transport beamline prototype has been designed and already realized at INFN-LNS. It consists of two main elements: a collecting-focusing sector and an energy selector system (ESS). Both elements have been separately tested with conventional protons up to 12 MeV, delivered by the TANDEM system of INFN-LNS and INFN-LNL. The ESS has been also tested with non-conventional beams at the Queens' University of Belfast, where the TARANIS laser system is installed [3]. Results will be reported elsewhere.
As regarding the quadrupole system, it should be able to collect, focus and pre-select in angle and energy the accelerated particles (fig. 1).

It is composed of four remotely controlled permanent quadrupoles with magnetic field gradients of 110T/m and 114T/m, 20mm bore and with lengths of 40 and 80mm, respectively [4]. This system allows to cover a wide energy operational range, from 0 up to 30MeV.
The final beam energy refinement is then obtained by means of the second transport device.

It is mainly composed of a central slit and four permanent dipoles with alternating polarity. Thanks to the magnetic field of the first two dipoles, particles with different energies are spatially separated on the radial plane. Then the central

Content from this work may be used under the terms of the CC BY 3.0 licence (© 2015). Any distribution of this work must maintain attribution to the author(s), title of the work, publisher, and DOI.

ISBN: 978-3-95450-168-7 doi:10.18429/JACoW-IPAC2015-WEPWA014

LOW TEMPERATURE PROPERTIES OF 20 K COOLED TEST CAVITY FOR C-BAND 2.6-CELL PHOTOCATHODE RF GUN*

T. Tanaka#, M. Inagaki, K. Nakao, K. Nogami, T. Sakai, LEBRA, Nihon University, Funabashi, Japan
T. Shintomi†, ARISH, Nihon University, Tokyo, Japan
M. Fukuda, T. Takatomi, J. Urakawa, M. Yoshida, KEK, Tsukuba, Japan
D. Satoh, Tokyo Institute of Technology, Tokyo, Japan

Abstract

In order to examine the basic properties of a cryogenic C-band photocathode RF gun cavity, a 2.6-cell π-mode test cavity was fabricated in KEK. The temperature dependence of the resonant frequency and the Q-value in the cavity were measured ranging from room temperature to 21 K. The increase in the resonant frequency by the cavity cooling from 296.65 K to 21 K has been 188 kHz greater than the one estimated from the linear expansion coefficients for OFHC copper material. The unloaded Q-value of 64650 at 21 K has been in agreement with the result of the SUPERFISH calculation carried out by assuming the surface resistance of the copper material to be 3.54×10^{-3} Ω at 5712 MHz on the basis of the theory of the anomalous skin effect.

INTRODUCTION

A cryogenic C-band 2.6-cell photocathode RF gun, which operates at 20 K, is under development at Nihon University for the future possibility of use in a compact linac-driven X-ray source at KEK [1]. The cavity material is 6N8 high purity copper with the residual resistance ratio (RRR) higher than 3000, which is considered effective to suppress the RF power loss in the cavity wall significantly at low temperatures. The operating frequency of the RF gun cavity is 5712 MHz. The main specifications of the gun are listed in Table 1 [2]. In order to investigate the low-temperature properties of the cavity, a 2.6-cell π-mode test cavity was fabricated in KEK with ultra-precision machining and diffusion bonding techniques. Since it was intended to examine the effect of the high purity copper material on the low-power RF properties at 20 K, the cavity consisted of only axis-symmetric components as shown in Fig. 1 [2]. Thus, the two-dimensional code POISSON-SUPERFISH [3] was used for the design calculation of the cavity.

Table 1: Specifications for the 2.6-Cell 20 K Cryogenic Photocathode RF Gun [2]

RF frequency	5712	MHz
Source peak RF power	4	MW
Q_0	> 60000 @20 K > 11000 @298 K	
Shunt impedance	~ 550 @20 K ~ 100 @298 K	MΩ/m
Coupling coefficient	20	
Cavity length	68.2	mm
RF pulse duration	2	μs
RF pulse repetition rate	50	Hz
Maximum wall RF loss	0.73	MW
Output beam energy	3	MeV
RF duty factor	0.01	%
Maximum beam charge	0.5	nC/bunch
Laser pulse repetition rate	357	MHz
Laser pulse length	10-20	ps
Maximum beam energy	3.5	MeV

In the measurements at room temperature, the resonant frequency converted to 23.5 °C in vacuum was approximately 300 kHz lower than the designed value. The unloaded Q-value and the shunt impedance deduced from the field distribution measurement have shown good agreement with the SUPERFISH simulation [2,4].

In this paper the RF properties of the cavity measured at around 20 K are reported and compared with the predicted values from the SUPERFISH simulation and the NIST data for the linear expansion coefficients of OFHC copper [5].

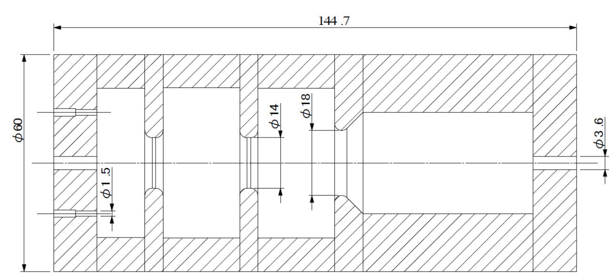

Figure 1: Cross-sectional view of the test cavity. The RF power is fed into the cavity through an antenna inserted into either hole in the left-side end plate.

EXPERIMENTAL SETUP

The experiment has been carried out using a cryogenic cooling system in KEK. The cooling system consists of a cylindrical vacuum chamber and a refrigerator unit (Daikin Industries V108C5L) installed on the top of the chamber. The test cavity has been mounted on a copper base plate with a cylindrical surface having the same radius as the outer side wall of the cavity. The base plate has been attached to the cold head of the refrigerator through a copper fitting plate and a copper block as shown in Fig. 2. Silicon thermal grease has been applied to both sides of the base plate to improve the thermal conductance between the cavity and the fitting plate. The cavity temperature has been monitored by semiconductor temperature sensors

*Work supported by the Photon and Quantum Basic Research Coordinated Development Program of the Japanese Ministry of Education, Culture, Sports, Science, and Technology (MEXT).
†Present affiliation: KEK, Tsukuba, Japan.
#tanaka@lebra.nihon-u.ac.jp

Content from this work may be used under the terms of the CC BY 3.0 licence (© 2015). Any distribution of this work must maintain attribution to the author(s), title of the work, publisher, and DOI.

ISBN: 978-3-95450-168-7 doi:10.18429/JACoW-IPAC2015-WEPWA015

RF INPUT COUPLER FOR 20 K COOLED C-BAND 2.6-CELL PHOTOCATHODE RF GUN*

T. Tanaka#, M. Inagaki, K. Nakao, K. Nogami, T. Sakai, LEBRA, Nihon University, Funabashi, Japan
T. Shintomi†, ARISH, Nihon University, Tokyo, Japan
M. Fukuda, T. Takatomi, J. Urakawa, M. Yoshida, KEK, Tsukuba, Japan
D. Satoh, Tokyo Institute of Technology, Tokyo, Japan

Abstract

Based on the low-power and low-temperature RF properties of the basic 2.6-cell cavity, a new cavity with the RF input coupler was fabricated in KEK. The coupler consists of a cylindrical waveguide and a mode converter from rectangular TE_{10} to cylindrical TM_{01} mode with both the elements having been located on the accelerating cavity central axis. The structure and the dimensions of the coupler have been designed using the 3-D simulation code CST Studio. The 2.6-cell structure has been modified from the previous test cavity. The RF properties of the cylindrical part of the cavity, measured without the mode converter before finishing, were in good agreement with the result of the CST Studio calculation. However, the behaviours of the $|S_{11}|$ and the field distributions in the completed cavity have to be investigated further because of possible non-axisymmetric field in the cylindrical waveguide.

INTRODUCTION

For the future use in the compact linac-driven X-ray source at KEK [1], a cryo-cooled C-band cavity for a photocathode RF gun has been under development. The RF properties measured on the basic 2.6-cell test cavity have shown that the π-mode accelerating frequency and the unloaded Q-value at around 20 K were well predicted from the room-temperature properties [2-4]. As the next stage of the development, a new cavity equipped with an input coupler has been designed. In the new design, a coaxial coupler which had originally been assumed was not employed because of possible difficulties in the cooling of the thin central electrode. Instead, a cylindrical coupler has been designed, which consists of a cylindrical waveguide and a mode converter that converts the rectangular TE_{10} mode to the cylindrical TM_{01} mode with both of them located on the accelerating cavity central axis. The basic design of the accelerating cells has not been greatly changed from that in the first test cavity. However, the design of the third disk located next to the coupling structure, has been changed so that it has the same shape as the other disks.

The cavity has been designed using the simulation codes SUPERFISH [5] and CST Studio [6]. SUPERFISH has been used primarily for the calculation of the resonant frequency of the cylindrical parts, while the 3-D code CST Studio has been necessary for the calculation of the RF properties of the whole structure including the coupler.

The low-power test cavity was fabricated in KEK with ultra-precision machining. The results of the design simulations and the RF property measurements at room temperature are presented in this paper.

DESIGN AND SIMULATIONS

Choice of Cylindrical Coupler

From the specification of the 20-K cryo-cooled photocathode RF gun cavity, the coupling coefficient of the RF input coupler has been required to be as large as about 20 [2]. The coupler was not included in the basic 2.6-cell test cavity, just the RF cutoff cylinder being reserved temporarily as a part of the outer wall of a coaxial coupler. For a high power operation of the cavity, an efficient heat removal structure is required of the thin inner electrode of the coaxial coupler, which seems difficult to realize in the C-band low-temperature cavity.

In order to avoid the heat removal problem with the coaxial coupler, a cylindrical coupler that was employed in an X-band photocathode RF gun [7] has been designed. The cylindrical coupler has the same advantage with a coaxial coupler that, though modifications are required in the method of the cavity cooling, it is possible to locate a focusing device such as a solenoid coil centered at any position on the cavity axis.

The cross-sectional view of the cavity for the low-power test is shown in Fig. 1. In the fabrication of the cavity, high purity 6N8 copper was used for the accelerating cells and the neighboring long portion of the cylindrical waveguide.

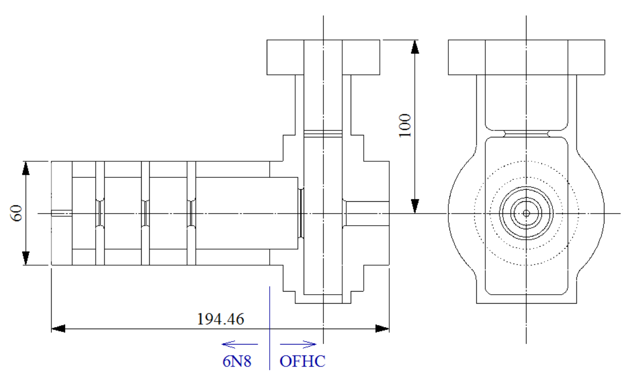

Figure 1: Cross-sectional view of the low power test cavity with the cylindrical input coupler. The hole in the left-side end plate is for the bead-pull measurement of the field.

*Work supported by the Photon and Quantum Basic Research Coordinated Development Program of the Japanese Ministry of Education, Culture, Sports, Science, and Technology (MEXT).
†Present affiliation: KEK, Tsukuba, Japan.
tanaka@lebra.nihon-u.ac.jp

Content from this work may be used under the terms of the CC BY 3.0 licence (© 2015). Any distribution of this work must maintain attribution to the author(s), title of the work, publisher, and DOI.

ISBN: 978-3-95450-168-7 doi:10.18429/JACoW-IPAC2015-WEPWA016
Content from this work may be used under the terms of the CC BY 3.0 licence (© 2015). Any distribution of this work must maintain attribution to the author(s), title of the work, publisher, and DOI.

CSKSB PHOTOCATHODE R&D WITH HIGH QUANTUM EFFICIENCY AND LONG LIFETIME

Y. Seimiya*†, M. Kuriki, A. Yokota, R. Kaku, HU/AdSM, Higashi-Hiroshima, Japan,
T. Konomi†, Inst. Molecular Sci., Aichi, Japan, M. Yamamoto, T. Miyajima, KEK, Tsukuba, Japan.

Abstract

Advanced electron linear accelerator such as Energy Recovery Linac and Free Electron Laser needs high brightness electron source. Photocathode is suitable for the high brightness requirement because some of them has low emittance and high quantum efficiency. In the photocathode, CsKSb multi-alkali photocathode has excellent features: high quantum efficiency, long lifetime, and driven by visible light, for example green laser. Therefore, the multi-alkali photocathode is considered to be one of the best candidates for the high brightness electron source of the advanced electron accelerator. We report developments of our evaporation system and results of quantum efficiency and lifetime measurement in Hiroshima University. Multi-alkali surface analyzation has being measured by ultra-violet photoemission spectroscopy to study conditions between the multi-alkali performances and the surface condition in Institute Molecular Science. We also report the status of the progress abort the study.

INTRODUCTION

Photocathode can generate a low emittance and short pulse beam by conditioning the spot size and pulse length of a laser, comparing to thermal cathode. The photocathode is essential device for high brightness electron source in advanced electron Linac such as Energy Recovery Linac (ERL) [1] or Free Electron Laser (FEL). For example, ERL requires high average current electron beam in range of 10~100mA and low emittance down to 0.1 mm.mrad.

Generally, a laser with shot wave length has lower power than that with long wave length. Multi-alkali cathode has high Quantum Efficiency (QE) about 10% and long lifetime with green laser. Green laser can be obtained easily as second harmonics of 1μm solid state laser, such as Nd:YAG or Yb:YAG. Therefore, the multi-alkali photocathode is considered to be one of the best candidates for the high brightness electron source of the advanced electron accelerator. According to a study by Cornell University, 1/e lifetime of the cathode is estimated as 30 hours with 60mA extracted current [2]. We examined the cathode performances, such as QE and the cathode lifetime, in Hiroshima University. Multi-alkali surface analyzation has also being measured by ultra-violet photoemission spectroscopy to study conditions between the multi-alkali performances and the surface condition in Institute Molecular Science (IMS). In our evaporation system, antimony(Sb), potassium(K), and cesium(Cs) are evaporated one by one in an extremely high vacuum condition, typically 4×10^{-9}Pa as a base pressure.

EVAPORATION SYSTEM

In Hiroshima University, evaporation system for multi-alkali cathode study was originally constructed. The schematic layout in the evaporation chamber is shown in Fig. 1. The multi-alkali cathode is made by the evaporation system, and its properties and performances are measured. We can extract the photo-current by a laser irradiating a substrate through a view port and QE and the cathode lifetime are measured. To monitor evaporation thickness for each materials, a quartz thickness monitor is implemented in the system. Additionally, the cathode substrate and the thickness monitor are placed symmetrically around the evaporation source to measure the thickness simultaneously during the evaporation. The evaporation source is also designed to generate the vapor symmetrically. A ceramic heater mounted behind the substrate and the substrate temperature is monitored and controlled by a thermo-coupler. For the simultaneous measurement of QE and thickness, the laser light illuminates the substrate diagonally in order to avoid interference between laser light and the substrate. The substrate made by 30mm×30mm SUS304 is used. QE map on the substrate can be obtained by scanning the laser irradiation area on the substrate with moving stage mounted on mirror. This QE mapping is performed by a green laser first, and performed by a blue laser second. The mapping is done every two hours. It takes 12 minutes to get these both QE map and laser irradiate a special point we chose during the other time of the interval, two hours. Blue laser which has about 2.3mW power and 405nm wave length and green laser which has about 0.45mW power and 532nm wave length on the substrate are used in our experiment.

Ultra-high vacuum is required during multi-alkali cathode evaporation and charge extracting from the substrate. Ion pump and NEG pump are used. Base vacuum pressure is about $10^{-8} \sim 10^{-7}$Pa during evaporation.

RESULTS

Cathode Evaporation Experiment

CsKSb cathode is made by Sb, K, and Cs evaporation in this order on the substrate. The typical process is following:

1. The substrate is heated to 600°C for heat cleaning. After that, it is cooled down and held temperature around 100°C.
2. Sb is evaporated up to a determined thickness.
3. K is evaporated up to a scheduled thickness.
4. Cs is evaporated until QE is saturated.

* yuji.seimiya@kek.jp
† KEK from April 2015

ISBN: 978-3-95450-168-7 doi:10.18429/JACoW-IPAC2015-WEPWA017

AN OPTIMIZATION OF ILC POSITRON SOURCE FOR ELECTRON-DRIVEN SCHEME

Y. Seimiya*, M. Kuriki, T. Takahashi, M. Urano, HU/AdSM, Higashi-Hiroshima
T. Okugi, T. Omori, M. Satoh, J. Urakawa, KEK, Tsukuba, S. Kashiwagi, Tohoku U., Sendai

Abstract

International Linear Collider is a future accelerator to find new physics behind the electroweak symmetry breaking by precise measurements of Higgs sector, Top quark, and so on. ILC has capacities to reveal new phenomena beyond Standard model, such as Supersymmetry particles and dark matters. In current design of positron source, undulator scheme is adapted as a baseline. In the scheme, positrons are generated from gamma rays through pair-creation process in Ti-alloy target. Generations of the gamma rays by the undulator radiation requires more than 130 GeV electrons. Therefore, a system demonstration of the scheme is practically difficult prior to the real construction. Consequently, it is desirable to prepare a technical backup of this undulator scheme. We study an optimization of positron source based on the conventional electron-driven scheme for ILC. In this scheme, positron beam is generated by several GeV electron beam impinging on W-Re target. Although heavy heat load and destruction of the target is a potential problem, it can be relaxed by stretching the effective pulse length to 60 ms instead of 1 ms, by a dedicated electron linac for the positron production. In this report, a start-to-end simulation of the electron-driven ILC positron source is performed. Beam-loading effect caused by multi-bunch acceleration in the standing wave RF cavity is also considered.

INTRODUCTION

International Linear Collider (ILC) is an electron and positron collider, which has a total length of 33 km ,with a center-of-mass energy of 500 GeV (first phase). ILC Technical Design Report was published in 2013 [1]. In the report, positrons are generated by undulator scheme as the baseline. In a helical undulator, polarized electron beam radiates gamma rays. The gamma rays are irradiated on a Ti (titanium) alloy target, and they are converted to polarized positrons through the pair-creation process. To obtain an enough amount of positrons, the gamma ray energy has to be more than 10 MeV, which requires a 150 GeV driving electron beam with a 10 mm undulator period. Therefore, the high-energy electron beam are shared by the gamma ray generation in the undulator and the collision with the positron. This undulator scheme has never been in operation for an accelerator, and it is difficult to demonstrate the system practically prior to the construction because more than 100 GeV electron beam is necessary as the positron driver. Therefore, a backup is desirable to reduce unknown technical risks.

The strongest candidate of the positron source as a backup is the conventional electron-driven scheme. In this conventional scheme, a several-GeV electron beam impinges on a heavy metal target. Gamma rays by Bremsstrahlung process are converted to positrons through the pair creation. In this scheme, the positrons cannot be polarized even if electron beam is polarized. According to the SLC experiments, the peak energy deposition density (PEDD) in the target should be less than 35 J/g [2–4] to avoid any damage to the target. The electron-driven positron source for the ILC was designed in Ref. [5]. In this design, a dedicated electron linac is assumed and the positron is generated in 63 ms out of 199ms which is ILC pulse interval for the collision. The generated positrons are stored on DR (Damping Ring) in 136 ms for the damping and sent to the main linac for the collision in the last 1ms. By the stretching of the beam pulse, the heat load on the target can be reduced by a factor 60. The electron-driven positron source for ILC can be accommodated in the tunnel designed for the undulator positron source, because the tunnel is wide enough. The compatibility of both schemes is one of the hottest topic in LCC (Linear Collider Collaboration). [6].

Our aim is to show that an enough number of positrons are obtained in DR acceptance by keeping PEDD less than 35 J/g under realistic parameters. By studying the yield as a function of various conditions, the design has been optimized [7]. In addition, effects caused by multi-bunch acceleration (beam-loading) and its compensation are considered in this report.

POSITRON SOURCE STRUCTURE AND REQUIREMENT

Electron-driven positron source consists of an electron driver linac, a positron production target, an AMD for transverse momentum suppression, a positron injector linac up to about 200 MeV, a chicane to remove positrons with a large momentum deviation and electrons, a positron booster up to 5.0 GeV, and an Energy Compression System (ECS) section as shown in Fig. 1. DR stored once the generated positron for the damping and the damped beam is sent to the main linac. The transverse DR acceptance (dynamic aperture) is $\gamma A_x + \gamma A_y < 0.07$ m, where γ is the Lorenz factor, and A_x and A_y are action values in the horizontal (x) and vertical (y) directions, respectively. The longitudinal acceptance is expressed as

$$\left(\frac{z}{0.035}\right)^2 + \left(\frac{\delta}{0.0075}\right)^2 < 1, \qquad (1)$$

* yuji.seimiya@kek.jp, KEK from April 2015

Content from this work may be used under the terms of the CC BY 3.0 licence (© 2015). Any distribution of this work must maintain attribution to the author(s), title of the work, publisher, and DOI.

ISBN: 978-3-95450-168-7 doi:10.18429/JACoW-IPAC2015-WEPWA018

RE-ACCELERATION OF ULTRA COLD MUON IN J-PARC MLF*

M. Yoshida#, F. Naito, KEK, Tsukuba, Ibaraki, Japan
S. Artikova, Y. Kondo, JAEA/J-PARC, Tokai-mura, Ibaraki, Japan
N. Hayashizaki, Tokyo Institute of Technology, Japan
Y. Iwashita, Kyoto University, Uji, Kyoto, Japan
K. Torikai, Gunma University, Maebashi, Gunma, Japan

Abstract

The ultra cold muon beam by two-photon laser resonant ionization of muonium atoms is unique way to obtain very low emittance muon beam. Its muon source is a surface muon from the muon target in MLF where one percent proton beam from J-PARC RCS is reacted. In close collaboration with the Muon Science Establishment (MUSE) at Material and Life science experimental Facility (MLF) of the Japan Proton Accelerator Research Complex (J-PARC), we are developing the reacceleration system of the ultra cold muon beam. Its optimum accelerating structure is similar to a proton accelerator in low beta part and an electron accelerator in high beta part.

Further the muon bunch is only two bunch corresponding to the bunch structure of the J-PARC RCS. Thus we are testing the dielectric transmission line accelerator based on the photoconductive switch as the alternative acceleration method..

ULTRA COLD MUON IN J-PARC MLF

The surface muon of 4 MeV from proton target is once stopped at the muon target. The muonium is thermally emitted from the target and excited by the VUV laser. The ultra cold muon generated by this method has very low emittance and become the unique probe to the material science and the elementary particle physics.

Figure 1 shows the layout of the MUSE at MLF of J-PARC. The re-acceleration of the ultra cold muon is planned to install for two lines called as U-line and H-line of total four extraction lines.

The H-line will be used for some elementary particle physics experiments including the g-2 experiment which requires 200 MeV muon beam. The U-line is used for the material science. The muon microscopy with the muon re-acceleration is planned to install at U1B area.

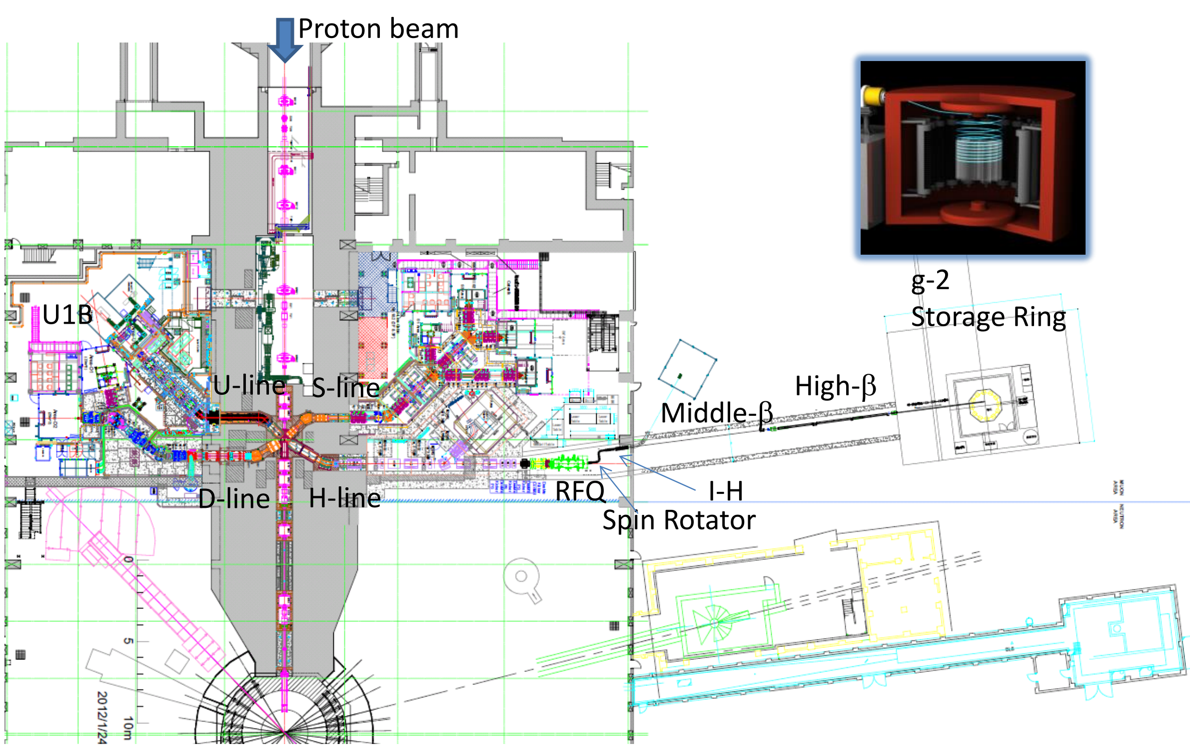

Figure 1: Layout of MUSE at MLF of J-PARC.

*Work supported by … JSPS KAKENHI Grant Number 26108718
#mitsuhiro.yoshida@kek.jp

Content from this work may be used under the terms of the CC BY 3.0 licence (© 2015). Any distribution of this work must maintain attribution to the author(s), title of the work, publisher, and DOI.

ISBN: 978-3-95450-168-7 doi:10.18429/JACoW-IPAC2015-WEPWA019

DEVELOPMENT OF ACCELERATOR-DRIVEN COMPACT NEUTRON SOURCES

K. Hirota*, G. Ichikawa, M. Kitaguchi, Y. Kiyanagi, H. M. Shimizu,
K. Tsuchida, A. Uritani, K. Watanabe and JCANS Collaboration,
Nagoya University, Nagoya, 464-8602, Japan

Abstract

Compact neutron sources are good tools for neutron scientist. In this paper we will present the current situation of compact accelerator-driven neutron source and the status of the facility of Nagoya University.

INTRODUCTION

Neutron is a very good probe to investigate inner structure of materials. The large neutron facilities like J-PARC MLF and SNS were constructed in decade, and ESS facility are start to construct. These large facilities are very good tools to study in academic field. However, the opportunity to use is very low, many neutron scientists use this facilities once or several a year. The beam time is less than 10 days in many case science many scientists want to use these powerful machine. The scientists require more neutron beam to study physics, chemistry and engineering.

One of the solution to solve this situation is constructing Compact Accelerator-driven Neutron Source(CANS). The CANS has some merit comparing with large neutron facilities. The constructing cost is lower than larger facilities. The opportunity to use neutron beam is so frequently. All devices from accelerator to detectors are able to handle by ourselves, that is very good for student education. The amount of radiation is smaller than that of the large-scale facilities. Unfortunately the emitted total neutron is much lower than large facilities and it is not suitable for the measurement of statistics-dominant. We can use these CANS for BNCT(Boron Neutron Capture therapy), neutron imaging, device development and so on. In this paper we will present the current situation of CANS and the status of the facility of Nagoya University.

l Q–“¡ p l ZQl Q¡ ; “ap l

There are some methods for generating neutrons. In general, the emitted neutron flux has following relation,

$$NeutronFlux = I_{beam} \times Eff_n \times Eff_{Mod} \quad (1)$$
$$I_{beam} = I_{peak} \times (Duty) \quad (2)$$

where, I_{beam} is an intensity of accelerated beam, Eff_n, and Eff_{Mod} are efficiency of neutron emission and moderation, I_{peak} is a peak current of accelerated beam, duty denotes duty cycle of accelerator.

Fission reaction is using at research reactor, and spallation reaction is using at large neutron facilities like J-PARC, SNS, and ISIS. These two methods have good neutron emission efficiency. Photonuclear reaction and low energy proton (or deuteron) reaction are using at compact neutron sources. The other neutron emission methods are fusion reaction and radioisotope. These two methods are lower neutron flux than the other methods in the laboratory use.

In CANS, neutron emission efficiency is not so high and neutron flux is lower than that of large facilities. In order to compensate the neutron flux, these reactions require the incident beam intensity. One solution is increase duty ratio by using cyclotron or electro static accelerator. However, it is not suitable for the case of pulse imaging method, which need neutron TOF(time of flight) information. In this case, we have to try to increase the peak current by using linear accelerator. In these way, we have to select the suitable acceleration beam properties.

The incident beam energy is also important for CANS. High incident beam energy increasing the accelerator and radiation shield size, and also increase the construction cost. On the other side, the low energy beam decrease the neutron emission efficiency. The relation between incident beam energy and neutron emission is written in elsewhere [1]. The selection of beam energy and target should be carried out carefully. In less than 2 MeV region, the deuteron beam is only useful for CANS. But the moderation efficiency in eq. (1) is not so good because of the emitted neutron average energy is more than one MeV. In 2 - 5MeV region, proton beam and Li target is suitable for CANS, however Li target is difficult to use, and second solution is Be target [2]. In more than 5 MeV region, Be target is suitable [3].

NUANS

Nagoya University Accelerator-driven Neutron Source (NUANS) is constructing at Nagoya, Japan. The aim of this neutron source is the evaluation test machine about Li target for BNCT. In general, the total neutron emission needs 10^{13} n/sec for BNCT use. We are planning to achieve this number by using high duty machine, DC beam accelerator. An electrostatic accelerator, dynamitron and an ECR ion source are using for the incident proton beam injector. The proton beam energy and DC beam current are 2.8 MeV and 15 mA, respectively. The accelerator is doing the final test at production factory and shipping within few month.

The Li target and epi-thermal moderator are also important components for neutron source. We select the emboss structured target [4] and MgF_2 neutron moderator for NUANS.

* hirota@phi.phys.nagoya-u.ac.jp

Content from this work may be used under the terms of the CC BY 3.0 licence (© 2015). Any distribution of this work must maintain attribution to the author(s), title of the work, publisher, and DOI.

ISBN: 978-3-95450-168-7 doi:10.18429/JACoW-IPAC2015-WEPWA021

A NEW DC MUON BEAM LINE AT RCNP, OSAKA UNIVERSITY

Yuki Matsumoto, Akira Sato, Yoshitaka Kuno, Hideyuki Sakamoto,
Yasunori Kohno, Yu Nakazawa, Osaka University, Osaka, Japan
Masaharu Ieiri, Michifumi Minakawa, KEK, Tsukuba, Japan
Hiroshi Ueda, Yoshitaka Kawashima, Keiji Takahisa, Kichiji Hatanaka,
Mitsuhiro Fukuda, Shunpei Morinobu, Osaka University RCNP, Osaka, Japan

Abstract

A new DC muon beam line has been constructed at RCNP, Osaka University. The MuSIC, which has the highest muon production efficiency using superconducting solenoidal magnets, has successfully demonstrated to provide a 3 x 10^8 [μ+/s/μA]. In 2014, the solenoidal magnets of the MuSIC were extended by a new beam line with normal conducting magnets. The new beamline consists of beam slits, quadrupole magnets, bending magnets and a DC separator. This new beamline is designed for muon experiments such as μSR experiments and muonic X-ray measurements. To study the performance of the beams provided by the beamline , a beam test was done in December 2014 and February 2015. In this paper, a detail design of MuSIC including the new beamline and result of the beam test are written.

INTRODUCTION

The MuSIC is a high intensity muon beam facility at RCNP, Osaka University (Figure 1). The proton beam is provided by the RCNP's ring cyclotron. The proton beam power is 400 W. The MuSIC achieves a muon yield of 10^8 [μ+/s/μA]. Compared with that, the the Paul Sherrer Institute (PSI) achieve a same muon yield with 1.3 MW proton beam. This shows that the muon production efficiency of the MuSIC is over 1000 times higher than that of PSI. The MuSIC has two features.

Pion Capture System

The pion capture system is a system involves a pion capture solenoid and a 36∘ curved transport solenoid. Protons enter the pion capture solenoid and hit a graphite target. Pions produced from protons are captured by a magnetic field of the pion capture solenoid and the 36∘ curved transport solenoid transport these pions. Pions decay to muons while transported.

MuSIC M1 Beam Line

MuSIC M1 Beam Line has SLITs(SL), Staring Magnets(STH), Quadrupole Magnets(QM), Bending Magnets(BM) and a DC separator(SR). Particles transported by the 36° curved transport solenoid enter the MuSIC M1 Beam Line. While passing through the beam line, focused muons with uniform momentum are taken out.

PION CAPTURE SYSTEM

The construction of the pion capture system was completed in 2009. In 2010 measurement proved that the Mu-

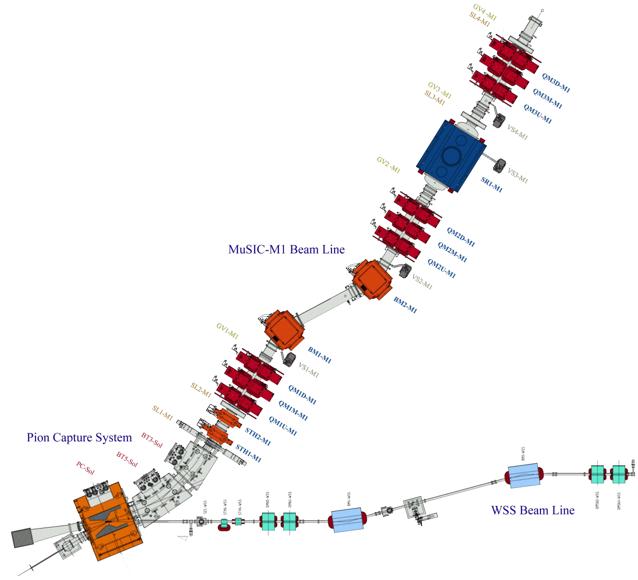

Figure 1: Layout of MuSIC.

SIC achieves about 10^8 [μ/s/μA] muon production efficiency. This is 1000 times higher than that of PSI and TRIUMF. The details are described in this section.

Features

A special structure of the pion capture system is enable the MuSIC to achieve a high muon production efficiency. In the case of the conventional muon beam facility, the neutron facility uses same proton beam line. So the structure of muon beam facility should be like Figure 2 (left. The target is thin and the pion capture solenoid is set beside the target. In contrast, the MuSIC can use full proton beam. Figure 2 (right) shows the structure of the MuSIC pion capture system. A 200 mm thick graphite target stops the protons, so a large mount of pions are produced. Pions are captured by the pion capture solenoid surrounding the graphite target over a large solid angle. It makes pion production and capture efficiency higher. Pions captured by the pion capture solenoid are transported by the 36° curved transport solenoid and decay to muons. A 2 T solenoid magnet and a 0.04 T dipole magnet select muon charge and momentum. Thus the MuSIC obtains a high muon production efficiency.

G4beamline

G4beamline is a simulator based on Geant4 [1]. The MuSIC structure from the graphite target to the 36° curved transport solenoid were described by G4beamline. 392 MeV

Content from this work may be used under the terms of the CC BY 3.0 licence (© 2015). Any distribution of this work must maintain attribution to the author(s), title of the work, publisher, and DOI.

ISBN: 978-3-95450-168-7 doi:10.18429/JACoW-IPAC2015-WEPWA023

DEVELOPMENT OF MUON LINAC FOR THE MUON G-2/EDM EXPERIMENT AT J-PARC

M. Otani, T. Mibe, Y. Fukao, N. Saito, M. Yoshida, KEK, Oho, Tsukuba, 305-0801, Japan
R. Kitamura, U. Tokyo, Tokyo, Japan
Y. Kondo, JAEA, Tokai, Naka, Ibaraki, 319-1195, Japan
Y. Iwashita, Kyoto University, Uji, Kyoto, Japan
for the E34 collaboration

Abstract

Muon acceleration is beyond our experiences. It enables us to measure the muon anomalous magnetic moment with an accuracy of 0.1 ppm and search for electric dipole moment with a sensitivity of $10^{-21}\mathrm{e}\cdot\mathrm{cm}$ to explore beyond Standard Model of elementary particle physics. We are developing a linac dedicated to the muon acceleration and planning to try the muon acceleration by utilizing slow negative muonium production. This paper described status of these developments.

INTRODUCTION

Though the discovery of Higgs at LHC completed the particles predicted in Standard Model (SM) of elementary particle physics, some observations such as dark matter existence indicate new physics beyond SM at some energy scale or interaction scale. One of the clues for new physics is anomaly of the muon anomalous magnetic moment $(g-2)_\mu$; There is a $\sim 3\ \sigma$ discrepancy between the SM prediction and the experimental value measured by E821 with a precision of 0.54 ppm [1]. Measurement with higher precision (0.1 ppm) is necessary to confirm this anomaly.

It should be also mentioned that measurements up to now rely on the technique of the magic momentum. Because the muon beam generated from the secondary pions in flight has large emittance, focusing with electric field in addition to the magnetic field is necessary in storage ring. The anomalous spin precision vector of muon is written by

$$\vec{\omega} = -\frac{e}{m}\left[a_\mu\vec{B} - (a_\mu - \frac{1}{\gamma^2-1})\frac{\vec{\beta}\times\vec{E}}{c} + \frac{\eta}{2}(\vec{\beta}\times\vec{B} + \frac{\vec{E}}{c})\right] \quad (1)$$

where e is elementary charge, m is muon mass, a_μ is anomalous magnetic moment, γ is the Lorentz Factor, β is the ratio of particle velocity to the speed of light c, and η is electric dipole moment. The second term depending on the electric field is eliminated when the muon momentum is 3.094 GeV/c, so called magic momentum. Measurement with a new method should be surveyed for verification of the $(g-2)_\mu$ anomaly.

The muon electric dipole moment (EDM) is also sensitive to new physics because it is strongly suppressed in SM (10^{-38} e·cm), and violates CP symmetry assuming the CPT theorem. In addition to that, there is a possibility that anomaly of $(g-2)_\mu$ can be explained by finite EDM with an order of 10^{-20} e·cm [2], whereas current direct limit is 1.9×10^{-19} e·cm [3].

The E34 experiment [4] aims to measure $(g-2)_\mu$ with a precision of 0.1 ppm and search for EDM with a sensitivity to 10^{-21} e·cm by utilizing high intensity proton beam at J-PARC and newly developed novel technique of the ultra-cold muon beam. Figure 1 shows the experimental setup. The experiment utilizes the proton beam from the 3 GeV Synchrotron ring to Materials and Life Science facility (MLF). The proton beam is injected to the graphite target. The generated surface muons are extracted to one of the muon beamline of H-line. Surface muons stop in the muonium (μ^+e^-, Mu) production target of the silica aerogel and then form thermal muoniums. The paired electron in the muonium is knocked out by laser and thermal muon (3 keV/c) is generated. Then the muon is accelerated up to 300 MeV/c and injected to the storage ring supplying 3 T. The decay positron is detected by the silicon strip tracker and the spin precession frequency is obtained from variation of counting rate of the decay positron.

Thanks to the ultra-cold beam ($\sigma_{pT}/p = 10^{-5}$) where p_T is the transverse momentum of the beam particles, the electric focusing is not necessary anymore. Eq. 1 becomes

$$\vec{\omega} = -\frac{e}{m}\left[a_\mu\vec{B} + \frac{\eta}{2}(\vec{\beta}\times\vec{B})\right] \quad (2)$$

Because the anomalous magnetic moment and EDM are perpendicular each other, these can be measured simultaneously.

One of the milestones for the experiment is verification of the muon acceleration from thermal energy to 212 MeV, which is the first case in the world. This paper describes status of developments of the muon accelerator and the first experimental verification of the muon acceleration. Other developments can be found elsewhere [5–7].

DEVELOPMENTS FOR THE MUON LINEAR ACCELERATOR

To suppress muon loss in the acceleration, the muon should be accelerated in a sufficiently short period. To realize the fast acceleration, a linac dedicated to the muon is being developed. Since velocity (β) of a muon largely varies during acceleration, several types of RF cavities should be adopted to realize sufficiently effective acceleration along with β. Three types of cavities are adopted: inter-digital H-mode (IH) for low β (< 0.27), disk and washer (DAW) for middle β ($0.27 < \beta < 0.7$), and disk loaded structure for high β ($0.7 < \beta$) section.

Content from this work may be used under the terms of the CC BY 3.0 licence (© 2015). Any distribution of this work must maintain attribution to the author(s), title of the work, publisher, and DOI.

ISBN: 978-3-95450-168-7 doi:10.18429/JACoW-IPAC2015-WEPWA024

DEVELOPMENT OF A C-BAND RF GUN WITH A CONIFEROUS-TREE-TYPE CARBON NANOSTRUCTURE FIELD EMISSION CATHODE*

Y. Taira, H. Kato, R. Kuroda, H. Toyokawa, AIST, Tsukuba, Japan

Abstract

Recently, coniferous formed carbon nano-structure (CCNS) as a field emission cold cathode has been developed. Tips of it have a nanometer-size tubular structure that becomes thicker on the substrate side. Owing to this configuration, the CCNS is considered to be more stable in high electric fields than carbon nanotubes. Characteristic of the field emission of the CCNS under an electrostatic field was revealed in the previous study. We have developed a C-band RF gun to reveal characteristic for a RF field. An important quantity for the field emission cathode which is called field enhancement factor was measured as 894 ± 54 by applying the electric field from 20 to 30 MV/m. This value is lower than that obtained by an electrostatic field up to 7.4 MV/m. Reduction of the enhancement factor was due to the destruction of tips of the CCNS by a high electric field.

INTRODUCTION

We have fabricated a C-band RF gun which used a field emission cathode of coniferous-tree-type carbon nano-structure (CCNS) cathode. Aim of it is a development of a tabletop size high-energy x-ray source and a terahertz radiation source.

If a wavelength of emitted radiation is longer than a bunch length of an electron beam, each radiation is coherently enhanced. Terahertz radiation is coherently enhanced by using the sub-picosecond electron beam. Electrons are emitted only in the restricted phase by the field emission. This characteristic is suitable for the generation of the short pulsed electron beam. Generation of the short pulsed electron beam in the range from sub-picosecond to picosecond is usually achieved by a photocathode and a short-pulsed laser system. If the picosecond electron beam can be generated via a field emission, it contributes to a miniaturization of the equipment.

We use the CCNS as a field emission cathode. Appearance of the CCNS cathode is shown in Fig. 1. The CCNS is deposited on a stainless steel substrate with the diameter of 6 mm by plasma-enhanced chemical vapor deposition. A detailed method is described in Ref. [1]. The CCNS has a following structure, which a graphene sheet composed of carbon has a coniferous form, and the tip has a nanometer-size tubular structure that becomes thicker on the substrate side [1]. A lot of studies concerning the field emission characteristics of carbon nanotubes (CNT) are carried out. CNT is a uniform diameter from the substrate side to the tip. On the other hand, the CCNS has the similar tip shape as CNT and becomes thicker towards the substrate side. Owing to this structure, the CCNS is considered to be more stable in high electric fields than CNT. In the previous study using the electrostatic field, it was found that a field emission current was 1.6 mA at the electric field of 7.4 MV/m, current density was 200 mA/cm^2, and field enhancement factor was 1562 [1]. In this proceedings, we report the first measurement of the field emission properties of the CCNS under the RF field.

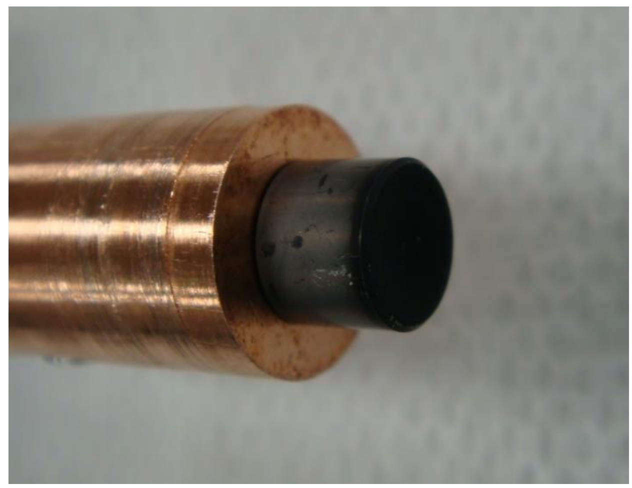

Figure 1: Appearance of CCNS cathode. The diameter of the CCNS is 6 mm.

C-BAND RF GUN

Appearance of the C-band RF gun is shown in Fig. 2. The detailed structure is described in Ref. [2]. This C-band RF gun is a single cell cavity, which the radius and length are 21.6 mm and 16.1 mm, respectively. RF power is inputted from a magnetron (New Japan Radio Co., Ltd. M1602). A four-port circulator, a directional coupler, and a pressurization window are connected between the magnetron and the C-band RF gun. Forward and reflected

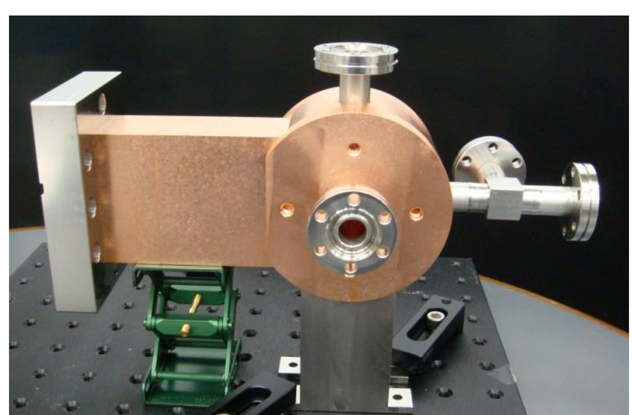

Figure 2: Appearance of the C-band RF gun.

Content from this work may be used under the terms of the CC BY 3.0 licence (© 2015). Any distribution of this work must maintain attribution to the author(s), title of the work, publisher, and DOI.

ISBN: 978-3-95450-168-7 doi:10.18429/JACoW-IPAC2015-WEPWA025

Content from this work may be used under the terms of the CC BY 3.0 licence (© 2015). Any distribution of this work must maintain attribution to the author(s), title of the work, publisher, and DOI.

RF ACCELERATION OF IONS PRODUCED BY SHORT PULSE LASER

Y. Fuwa*†, Y. Iwashita, H. Tongu,
S. Inoue, M. Hashida, S. Sakabe, Kyoto University, Uji, Kyoto, Japan
M. Okamura, BNL, Upton, NY 11973, USA
A. Yamazaki, Nagoya University, Nagoya, Aichi, Japan

Abstract

An laser ion source which produces bunched ion beam is proposed to enhance an acceleration efficiency of ion accelerator front end with RFQ linac. To demonstrate a production of an initially bunched ion beam, H_2 gas was ionized by short pulse laser in an RF electric field. As a result, ions captured by the RF field were observed by an ion probe.

INTRODUCTION

RFQ (Radio Frequency Quadrupole) linac [1] has been the essential component of ion accelerator front ends for tens of years[2]. Since ordinary ion sources provide DC (unbunched) ion beam, the function of RFQ includes not only acceleration and radial focusing but also adiabatic bunching. Therefore, conventional RFQ consists of three or four sections; radial matching section, (shaper section), bunching section, and accelerating section[3]. At the bunching section, the beam is bunched adiabatically by longitudinal RF electric field. However, satisfying the adiabatic condition, the vane modulation and synchronous phase rise gradually to the values for accelerating section. Therefore, bunching section takes lengthy part of RFQ tank, where the longitudinal field contribute almost only for bunching and not for acceleration. Hence the accelerating efficiency along the entire RFQ tank decreases.

If the beam is already bunched at the entrance of RFQ, bunching section is not needed and beam can be accelerated along the whole part of RFQ tank. Then, the accelerating efficiency of RFQ can be improved. For production of such a bunched beam, laser plasma induced by short pulse laser has promising potential. The ions in the plasma produced by short pulse laser are supposed to have also short pulse structure. If the bunch of the short pulse ions can be captured by RF bucket at the laser interaction region before an expansion of plasma, the production of short pulse bunch can be achieved and direct injection of the bunched ion beam into RFQ can be realized. The schematic image of the front end with direct injection of bunched ions into RFQ is shown in Fig.1. This scheme is similar to the RF gun, while the electrons are replaced with the ions.

In this paper, an experiment to demonstrate the capturing of laser-induced ions in RF bucket is described.

EXPERIMENT

To demonstrate the capturing of ions produced with a short pulse laser by RF electric field, H_2 gas was irradiated

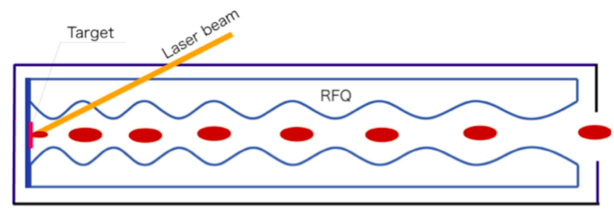

Figure 1: Schematic image of RFQ with initially-bunched ion beams.

by short pulse laser in an accelerating gap of an RF resonator and the accelerated charged particle was detected by a probe electrode. The layout of experimental equipments is shown in Fig.2. In this section, the component used in this experiment is described. The experiments were performed in a vacuum chamber with a pressure of 0.02 Pa.

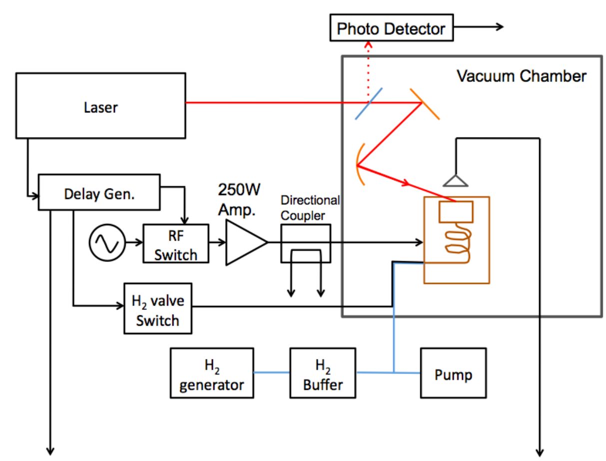

Figure 2: Image of Experimental Layout.

Laser

The experiment was performed with a terawatt 40-fs Ti:sapphire laser system in Institute for Chemical Research, Kyoto University. A laser pulse energy was tuned between 30 μJ and 100 μJ and a repetition rate of laser pulse was up to 5 Hz. The laser pulse was focused to a spot with 11 μm diameter by an off-axis parabolic mirror. The laser power density at the interacting point is $10^{14} \sim 10^{15}$ W/cm^2. The Rayleigh length of laser at interacting point is nearly 1 mm.

RF Resonator

To generate the longitudinal RF electric field, RF resonator was prepared. The frequency of the resonator is chosen as 53.3MHz, so that the ions with heavy masses com-

* Research Fellow of Japan Society for the Promotion of Science
† fuwa@kyticr.kuicr.kyoto-u.ac.jp

ISBN: 978-3-95450-168-7 doi:10.18429/JACoW-IPAC2015-WEPWA026

LOADING OF A PLASMA-WAKEFIELD ACCELERATOR SECTION DRIVEN BY A SELF-MODULATED PROTON BUNCH

V. K. Berglyd Olsen*, E. Adli, University of Oslo, Norway
P. Muggli, Max Planck Institute for Physics, Munich, Germany
L. D. Amorim, J. M. Vieira, Instituto Superior Technico, Lisbon, Portugal

Abstract

We investigate beam loading of a plasma wake driven by a self-modulated proton beam using particle-in-cell simulations for phase III of the AWAKE project. We address the case of injection after the proton beam has already experienced self-modulation in a previous plasma. Optimal parameters for the injected electron bunch in terms of initial beam energy and beam charge density are investigated and evaluated in terms of witness bunch energy and energy spread. An approximate modulated proton beam is emulated in order to reduce computation time in these simulations.

INTRODUCTION

The AWAKE experiment [1] is a proof-of-principle demonstration of acceleration of an electron bunch to the TeV energy range in a single plasma section, using a proton bunch driver [2].

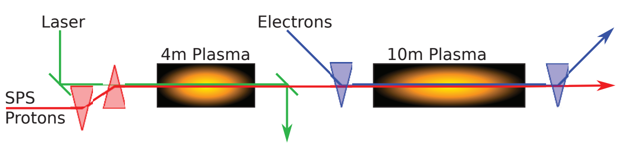

Figure 1: Simplified set-up of AWAKE Phase III. A long proton bunch experiences the SMI in a short plasma cell. The electron bunch is injected before the second plasma cell.

The AWAKE experiment proposes using a proton driver at 400 GeV, delivered by the SPS. The experiment is currently under construction at CERN, scheduled to start in late 2016. The SPS proton bunch is too long to generate a sufficiently strong wakefield [3]. A usable drive bunch needs to be close to the plasma wavelength λ_p in length; however, producing a short enough proton bunch is technically difficult.

The plasma wavelength and frequency are given by

$$\lambda_p = \frac{2\pi c}{\omega_p}, \quad \omega_p = \sqrt{\frac{N_p e^2}{m_e \varepsilon_0}}, \tag{1}$$

where N_p is the plasma electron density, e is the elementary charge, m_e is the electron mass and ε_0 is the vacuum permittivity.

A proton bunch with $\sigma_{z,0} k_p \gg 1$, where $\sigma_{z,0}$ is the initial length of the bunch, will under certain conditions develop a self-modulation instability (SMI) when it travels through a plasma [4]. The proton bunch will then develop into a train of micro bunches with a period on the order of λ_p.

In phase I of the AWAKE experiment the SMI of the proton bunch will be studied. In phase II, the proton wake will be studied using a long, externally injected electron bunch that will sample all phases of the wake. In phase III, acceleration of a short bunch in the wake of an already self-modulated proton beam will be studied, as illustrated in Fig. 1. In this paper we study the beam quality of a short electron bunch accelerated by an SMI proton wake in preparation for phase III of AWAKE.

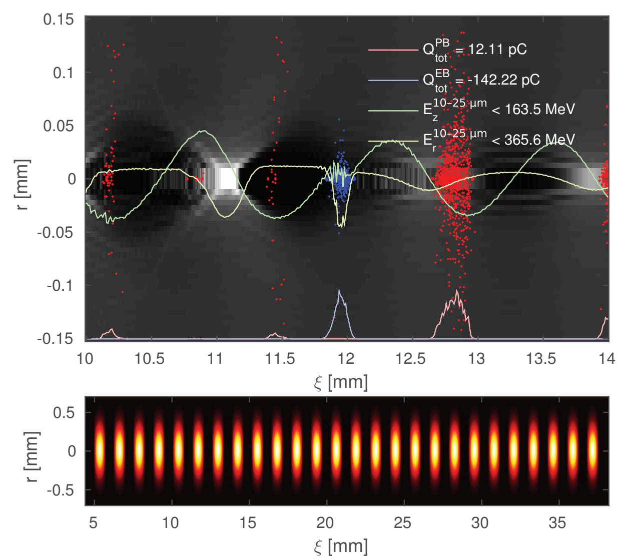

Figure 2: **Top:** An example showing the structure of the plasma electrons (grey) with a projection of the proton beam (red) and the electron bunch (blue) density on the bottom. The E_z (green) and E_r (yellow) fields have been overlayed on the plot. Shown is also a sample of electron (blue) and proton (red) macro particles. **Bottom:** An example of a pre-modulated proton drive beam at $t = 0$ plotted in terms of charge density.

SIMULATION SET-UP

All simulations in this paper have been performed using OSIRIS, a three-dimensional, relativistic, particle-in-cell code for modelling plasma based accelerators [5].

The parameter scans presented have all been run on a small scale test case with a shorter proton drive beam than AWAKE specifications. We simulate here only the second plasma stage in Fig. 1, assuming a pre-modulated proton beam profile with charge density function

$$\rho_{p^+}(\xi) = A\left[\frac{1}{2\sqrt{2}} + \cos\left(k_p\xi - \mu_1\right)\right] e^{-r^2/2\sigma_r}, \tag{2}$$

* v.k.b.olsen@fys.uio.no

Content from this work may be used under the terms of the CC BY 3.0 licence (© 2015). Any distribution of this work must maintain attribution to the author(s), title of the work, publisher, and DOI.

ISBN: 978-3-95450-168-7 doi:10.18429/JACoW-IPAC2015-WEPWA027

GAS FLOW INFLUENCE ON NEGATIVE HYDROGEN ION GENERATION WITHIN THE MICROWAVE-DRIVEN NEGATIVE ION SOURCE*

Shixiang Peng#, Yuan Xu, Zhang Tao, Haitao Ren, Jingfeng Zhang, Jie Zhao, Zhiyu Guo and Jia'er Chen,
SKLNPT & IHIP, School of Physics, Peking University, Beijing 100871, China
Ailin Zhang, School of Physics, UCAS, Beijing 100049, China

Abstract

H^- ion was generated through two processes within a volume Cs- free source. The density of molecule hydrogen gas will impact on the electron temperature within the primary discharge chamber that will influence the population of vibrational excited H_2^*. Within the extraction region, the interaction between molecule hydrogen and H^- ion will is cause the dissociation of negative ion. To better understand the gas flow influence on H^- ion generation within a volume negative ion source, a new Cs-free volume microwave-driven H- source body with two gas inlets was developed at Peking University (PKU). Experiment on gas flow and gas pressure distribution within the plasma chamber was carried out with this source body. In the meantime a two dimensional (2D) model for gas flow was developed. Details will be presented in this paper.

INTRODUCTION

The 2.45 GHz electron cyclotron resonance (ECR) ion source has been developed at many labs.[1, 2] This kind of ion source is widely used mainly for high current single charge state positive ions (H^+, D^+, He^+, O^+ etc.) generation which shows great performances in high stability, high reliability, easy maintenance and long lifetime. Recently, reliable negative hydrogen ion sources are also demanded in many high current facilities because H^- ion has significant advantages in beam transmission or injection into synchrotron. [3] H^- ion source is a kind of ion source which needs a lot of theoretical and experimental work. Among all kinds of H^- ion source, Penning ion source and the volume ion source operating with Cs are regarded as promising candidates, also ECR source is promising to generate H^-.[4] Since 2012, a 2.45 GHz microwave-driven H^- ion source without using Cs was designed at PKU. This ion source was intended to generate more than 10 mA H^- for the injector of SPRESA facility in China at the beginning. [5, 6]. Recently, a 35 mA H^- beam with 10% duty factor and a 16.5mA CW H^- beam at 35 keV have been produced with this source. However, just like Prof. Horst Klein said at 20 ICFA Workshop summary, "The ion sources, and especially the H^- sources, are still somewhat a black magic". [4] Many factors, such as electron density and temperature, molecule hydrogen gas distribution, etc., will influence the generation of H- ions [7]. To better understand the processes within a volume H- source, a series of experiments were carried out on the impaction of gas distribution. A 2D simulation was performance to study the pressure distribution with different inlets. More simulated and experimental results will be reported in this paper.

*Work supported by NSFC NO.11305004, 11175009 and 91126004.
#sxpeng@pku.edu.cn.

EXPERIMENT SETUP

Experiment was done on a compact permanent magnets 2.45 GHz microwave- driven Cs- free volume H^- source developed at PKU. The Schematic diagram is plotted in Fig.1. Its outside dimension is Φ116 mm×124 mm. Detail was described in Ref. 8. 2.45 GHz microwave is feed into discharge chamber through three-layer Al_2O_3 microwave window to heat the electrons confined by ECR resonance magnetic field.

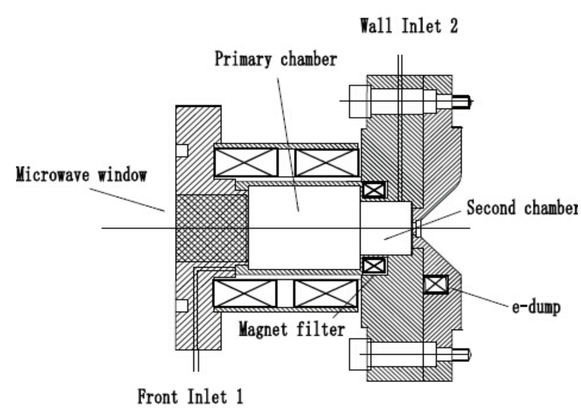

Figure 1: Schematic diagram of microwave-driven negative ion source.

As mention in Ref. 9, two processes will happen within this volume source. First, energetic electrons that heated by microwave will impact with hydrogen molecular to generate amount of vibrationally excited H_2^* in the primary discharge chamber. Then, H_2^* will interact with slow electrons in the second chamber to produce H^- ions. A magnetic filter field, which has a high diffusion constant only for slow electrons (<1 eV), is applied between primary and second discharge chamber to lower the electron temperature in the second chamber and prevent fragile H^- ions from being destructed by fast electrons.

The measurements in Ref. 10 & 11 show that T_e will decrease with operation pressure increasing in ECR ion source because the energy transfer between fast electrons and other particles will be enhanced with higher pressure which means high particle density in the chamber. Therefore, it is important to keep a relative higher pressure in the ion source especially in the second

Content from this work may be used under the terms of the CC BY 3.0 licence (© 2015). Any distribution of this work must maintain attribution to the author(s), title of the work, publisher, and DOI.

ISBN: 978-3-95450-168-7 doi:10.18429/JACoW-IPAC2015-WEPWA028

NUMERICAL SIMULATION ON EMITTANCE GROWTH CAUSED BY ROUGHNESS OF A METALLIC PHOTOCATHODE

Z. Zhang, C. Tang*, Tsinghua University, Beijing 100084, China

Abstract

The roughness of a photocathode could lead to an additional uncorrelated divergence of the emitted electrons and therefore to an increased thermal emittance. The randomness of the real-life photocathode surface makes it unrealistic to perform typical beam dynamics simulation to study the roughness emittance growth. We develope a numerical simulation code based on the point spread function (PSF) and an estimated form of electric field distribution on an arbitrary gently undulating surface to deal with the problem. The simulation result shows that the emittance growth factor is 1.04, which is much smaller than expected (1.5 ~ 2).

INTRODUCTION

Photocathodes are widely integrated in large particle sources. The quantum efficiency (QE) and intrinsic emittance determine the quality of the photocathode. D. Dowell gives formulas [1] to predict the QE and thermal emittance of a metallic smooth surface photocathode by using a simplified three-step model [2]:

$$\mathrm{QE}(\omega) \approx \frac{1-R(\omega)}{1+\dfrac{\lambda_{\mathrm{opt}}}{\lambda_{e-e}(\omega)}} \frac{(\hbar\omega-\phi_{\mathrm{eff}})^2}{8\phi_{\mathrm{eff}}(E_F+\phi_{\mathrm{eff}})}$$

$$\varepsilon_{n,x} = \sigma_x\sqrt{\frac{\hbar\omega-\phi_{\mathrm{eff}}}{3mc^2}}$$

Formula for QE agrees well with the experiments, while the emittance measured by some labs appeared to be two times larger than predicted [3,4]. It's widely believed that the differ between the experiment and analysis is caused by surface roughness of the photocathode.

Typical beam dynamics simulations require the electric field distribution in the simulation region as well as the initial particle samples. However it's hard to acquire on an arbitrary photocathode surface due to the computer memory and CPU limitation.

In this paper, we developed a numerical simulation code based on the point spread function (PSF) and an estimated form of electric field distribution on an arbitrary gently undulating surface to deal with the issues.

PRINCIPLES OF THE SIMULATION

Generation of the Initial Particle Samples

The keypoint of initial samples generation is how one include the emission angle diffusion introduced by the surface roughness, which is also known as "slope effect" [5,6]. This can be done in at least two ways:

1. Employ the similar three-step model as discussed in [1] and use the Monte Carlo method. Considering the emission process as shown in Fig. 1. One photon injected into a gentle slope on the bulk metal photocathode, travelling a distance of s along $-z$ direction, then absorbed by an electron of energy E, went towards surface with a direction angle (θ', ϕ') relative to the normal of the slope (the slope angle is θ) without scattering and finally escaped from the surface.

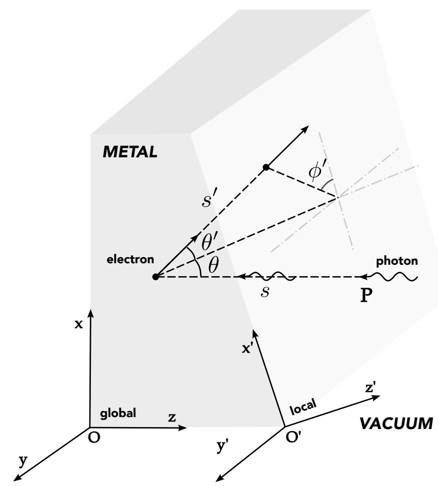

Figure 1: The schematic plot for the bulk photoemission on a part of a rough metallic cathode. The definitions of coordinates and variables are labeled in the plot.

The idea is to generate $s \sim \mathrm{Exp}(\lambda)$, $E \sim U(E_{\mathrm{F}}-\hbar\omega, E_{\mathrm{F}})$, $\theta' \sim U(0,\pi/2)$, $\phi' \sim U(0,2\pi)$, where $1/\lambda = 1/\lambda_{\mathrm{opt}} + 1/\bar{\lambda}_{\mathrm{e\text{-}e}}$, then apply the filter condition $(E+\hbar\omega)\cos^2\theta' \geq \phi_{\mathrm{eff}}$ to eliminate samples that cannot escape. All definitions of the parameters above are in consistence with [1]. However the sampling efficiency of this simple method is very low due to the fact that the QE of metal is usually $\sim 10^{-4}$.

2. Employ the point spread function (PSF) of the photocathode. In general, the PSF describes the response of an imaging system to a point source or point object. For photocathode, the PSF describes the response of a photocathode to a point laser source. With the PSF of photocathode, one could generate the samples without large loss (to be specified, our sampling pass rate is around 1/6, which will be explained later), therefore we choose the second sampling method.

The generalized momentum PSF For typical photoemission on metallic cathode, it's safe to ignore the dependence between electron momentum distribution and incident

* tang.xuh@tsinghua.edu.cn

Content from this work may be used under the terms of the CC BY 3.0 licence (© 2015). Any distribution of this work must maintain attribution to the author(s), title of the work, publisher, and DOI.

ISBN: 978-3-95450-168-7 doi:10.18429/JACoW-IPAC2015-WEPWA031

A COMPACT MULTIPLY CHARGED ION SOURCE FOR HADRONTHERAPY FACILITY

L. Celona[#], L. Andò, G. Castro, F. Chines, S. Gammino, O. Leonardi, D. Mascali, L. Neri, D. Nicolosi, F. Noto, F. Romano, INFN/LNS, Catania, Italy
G. Ciavola, CNAO Foundation, Milan; INFN/LNS, Catania, Italy
G. Torrisi, INFN/LNS, Catania; Universitá Mediterranea di Reggio Calabria, Reggio Calabria, Italy

Abstract

The ion sources for accelerators devoted to medical applications must provide intense ion beams, with high reproducibility, stability and brightness. AISHa (Advanced Ion Source for Hadrontherapy) is a compact ECRIS whose hybrid magnetic system consists of a permanent Halbach-type hexapole magnet and a set of independently energized superconducting coils. These coils will be enclosed in a compact cryostat with two cryocoolers for LHe-free operation. The microwave injection system has been designed for maximizing the beam quality through a fine frequency tuning within the 17.3-18.4 GHz band which is possible by using an innovative variable frequency klystron. The introduction of an integrated oven will allow the production of metal ions beams with relatively high intensity for light ions. “Accel-decel” extraction system will be used. The LEBT line will consist of a solenoid and a 90° dipole for ions selection. Two diagnostic boxes, made of Faraday cups, beam wires and slits, will allow the characterization the beam. Moreover, a system of scintillating screens and CCD cameras, placed after the solenoid will allow the investigation of the Frequency Tuning Effect (FTE) on the source performances.

INTRODUCTION

The AISHa ion source has been designed by taking into account the typical requirements of hospital-based facilities, where the minimization of the mean time between failures (MTBF) is a key point together with the maintenance operations which should be fast and easy. Therefore, a so called 3rd generation ECR ion source is not suitable, being quite complex for unskilled operators.

The new AISHa source is designed to be an intermediate step between the 2nd generation ECRIS, unable to provide the requested current and/or brightness and the 3rd generation ECRIS, too complex and expensive. It is intended to be a multipurpose device, operating at 18 GHz, in order to achieve higher plasma densities. It should provide enough versatility for future needs of the hadrontherapy, including the ability to run at larger microwave power to produce different species and highly charged ion beams and to be upgraded to higher frequency than 18 GHz. These demands implies also the simplification of all ancillary systems including an oven for metallic ion beams, which permits the production of new beam for hadrontherapy and for other applications. The source characteristics are described in Table 1.

The AISHa source is funded within the framework of the program of Sicilian Government named PO FESR 2007-2013 and a pool of Sicilian SME is associated with INFN for this project. The source is potentially interesting for any hadrontheraphy center using heavy ions.

Table 1: AISHa Source Characteristics

Parameters	Dimension
Radial Field (max)	1.3 T
Axial Field (INJ/MID/EXTR)	2.6 T /0.4 T / 1.7 T
Operating Frequency	18 GHz (TFH)
Operating Power	1.5 kW (1.5 kW)
Extraction Voltage (max)	40 kV
Chamber diameter / length	ø= 92 mm / 357 mm
Warm bore diameter / thickness	274.00 mm / 22 mm
Weight	600 Kg

MECHANICAL DESIGN

The plasma chamber will be stainless steel made and it is designed to operate at a maximum power rate of 2 kW by using a multi-channel water-cooling system. The insulation will be adapted to 40 kV operation by means of a 20 mm thick Glass Fiber/Carbon Fiber tube surrounding the hexapole, keeping superconducting magnets and yoke at ground potential. The movable extraction system will permit to adapt the AISHa source to other facilities (e.g. the high voltage platform for INFN-LNL).

A new type of DC-break has been designed to permit reliable operation up to 50 kV.

The layout of the source is shown in Fig. 1.

In the development of this new source some mechanical improvements have been introduced, in particular for the hexapole containment chamber and for the plasma chamber.

#celona@lns.infn.it

Content from this work may be used under the terms of the CC BY 3.0 licence (© 2015). Any distribution of this work must maintain attribution to the author(s), title of the work, publisher, and DOI.

ISBN: 978-3-95450-168-7 doi:10.18429/JACoW-IPAC2015-WEPWA032

Content from this work may be used under the terms of the CC BY 3.0 licence (© 2015). Any distribution of this work must maintain attribution to the author(s), title of the work, publisher, and DOI.

CsK_2Sb GROWTH STUDIES, TOWARDS HIGH QUANTUM EFFICIENCY AND SMOOTH SURFACES*

S. Schubert, H. Padmore, J. Wong, LBNL, Berkeley, CA 94720, USA
Z. Ding, M. Gaowei, E. Muller, J. Sinsheimer, J. Smedley, BNL, Upton, NY 11973, USA
J. Xie, ANL, Lemont, IL 60439, USA
J. Kuehn, HZB, Berlin, Germany

Abstract

The properties of CsK_2Sb, make this material an ideal candidate as photocathode for electron injector use. Producing photocathodes with quantum efficiencies of 5 % and greater at 532 nm poses no challenge, nevertheless the traditional growth mechanisms, which are based on a sequential deposition of Antimony, Potassium and Cesium at a range of temperatures up to 150°C yield a rough surface with a rms roughness in the range of 25 nm, determined by AFM [1]. Surface roughness in this region impacts the emittance. Whereas thermal sequential deposition gives a roughness on the order of the film thickness, for high gradient accelerators, we need a roughness on the order of 1 nm in order to preserve low emittance.

Studies are performed to optimize roughness. Various growth procedures are exploited and the resulting samples' surface roughness compared.

INTRODUCTION

Within the last years multi-alkali-antimonides have been a targeted material for use as photocathode for high brightness, high repetition rate and low emittance injector applications.

Their high quantum efficiency (q.e.) in the visible region and fast response time make alkali-antimonies prime candidates. The group of interest includes K_3Sb, Cs_3Sb and a number of multi-alkali antimonide materials like CsK_2Sb and $(Cs)Na_2KSb$, which exhibit q.e. of >5% at 532 nm wavelength.

These materials have been used in photomultiplier tubes for several decades [2], but little is known about the detailed chemistry of these materials during synthesis. Therefore adapting this technology and transfer it into production of reproducible and reliable photocathodes for the use in photoinjectors are still ongoing.

In an effort to understand the growth procedure and reaction mechanism and finally it's influence on the photocathode behavior, in-situ growth measurements are undertaken.

Nondestructive X-ray measurements are utilized to analyze the growth and morphology of alkali-antimonies. A number of experimental techniques are being used simultaneously. Information about film thickness, roughness, crystallinity and composition are being recorded and complimented by photocurrent (phc) measurements during deposition and spectral response measurements after growth. This paper will give a short comparative analysis on tested growth methods and their resulting surface roughnesses as determined by X-ray reflectivity (XRR) for CsK_2Sb photocathodes.

* Work supported by by U.S. DoE, under KC0407-ALSJNT-I0013, and the German BMBF, Helmholtz-Association and Land Berlin. NSLS was supported by DOE DE-AC02-98CH10886, CHESS is supported by NSF & NIH/NIGMS via NSF DMR-1332208.

EXPERIMENTAL

Wide angle X-ray diffraction (WAXD), X-ray scattering measurements and X-ray fluorescence (XRF) are performed in-situ during growth. After growth measurements include spectral response curves in the range from 200 - 800 nm and X-ray diffraction (XRD) measurement to verify crystallinity and composition of the crystalline phases.

Experiments are carried out at the Cornell High Energy Synchrotron Source (CHESS) at beam line G3, measurements are conducted at photon energies in the range of 9.8 keV to 11.26 keV. Two Pilatus 100K detectors are used to record the X-ray data. A Vortex-detector is positioned approx. 18 cm from the sample recording the fluorescence data. The active range of the detector starts at 2.5 keV, allowing for a reasonable detection of the K signal at 3.3 keV.

The materials are grown in a UHV system with a base pressure of $2{\cdot}10^{-10}$Torr or below. Water and Oxygen partial pressures are in the low 10^{-12} Torr range.

Sb is deposited from PtSb beads and Alkali metals from Alvatec or SAES getter sources. The deposition rate is held around 0.2 Å/s.

The photocurrent is monitored during the growth, a bias voltage of 20 V is applied and using a 5 mW green laser to illuminate the sample.

Further information about the setup can be found elsewhere [3].

The roughness and thickness data presented here are determined by Parratt's recursion, after extracting the XRR intensity from the raw images [4].

Si(100) and MgO(001) are used as substrates. The Si substrates are cleaned in aceton, followed by isopropyl-alcohol and as a last step dipped in HF and stored in DI water until transferred to the UHV system, which could take 10 min - 2 days.

MgO substrates were dipped in DI water. Both materials are blown dry with Nitrogen prior to mounting in the UHV chamber. Then the substrates are heated to 500°C for 1- 5h, after which they are cooled down to the respected deposition temperature.

During deposition the substrate is usually held at 100°C.

ISBN: 978-3-95450-168-7 doi:10.18429/JACoW-IPAC2015-WEPWA033

CHARACTERIZATION OF LASER-PLASMA ACCELERATED ELECTRON BEAM FOR A COMPACT STORAGE RING*

Seong Hee Park#, Yong-Ho Cha, Young Uk Jeong, Jeongsang Jo, Ha Na Kim, Kyung Nam Kim, Kitae Lee, Woojae Ryu, Jae Sung Shinn, Nikolay Vinokurov[1,2], [1]KAERI, Daejon, Korea, [2]BINP SB RAS, Novosibirsk, Russia

Abstract

A compact radiation source can be utilized by an electron beam from a Laser-plasma acceleration combined with localized shielding in a small laboratory. The stability of synchrotron radiation in wavelength and power depends on the shot-to-shot jitters of the energy and charge of an electron beam, which is strongly influenced by the plasma density of target and the jitters of a laser beam. With the 30 TW fs laser in KAERI, the optimization for generating the electron beam have done using the different shape of gas nozzle. We also present the pointing stability of the laser-accelerated electron beams.

INTRODUCTIONS

Laser-plasma electron acceleration has been attracted for high energy injectors, synchrotron radiation, XFEL, and so on, for a decade. The energy of laser-accelerated electrons is recorded over 4.2 GeV[1] and the energy spread is down to 1%. It is dramatically rapid developments in quality of electron beam generated by laser plasma interaction since the success of quasi-monochromatic electron beam generation in early 2000s. The more stable operation and/or the better quality of electron beams have been developed, the more diverse applications has been suggested and studied.

As like the conventional electron accelerators, there are many applications using it. The property of ultrashort pulse and compactness in radiation shielding can be strong advantages of newly developed applications. We can also consider it as an injector for storage ring such as an ultimate storage ring, which is recently under development to reduce the emittance. In aspect of compactness, we can develop as radiation sources using tens of TW laser system. Tens of TW laser system can be used for the generation of tens to hundreds of MeV electron beams, by either reducing the laser intensity or increasing the interaction length with plasma. We may use simple gas target, capillary discharge plasma, or possibly laser evaporated plasma using metal target.

Usage of metal target has been suggested for a compact storage ring using Laser-accelerated electron beam [2], in order to keep high vacuum inside storage ring. With gas targets, the injector should be separated by thin window to keep high vacuum inside the storage ring. However, laser induced plasma will generate small amount of plasma enough for laser acceleration, even in few mm long plasma density. Under the WCI Program, KERI and KAERI are developing the Laser-induced electron acceleration using the solid target.

To utilize Laser-accelerated electron beam as an injector, more detail studies for reliability are required. The pointing jitter of electron beam is recently done with KAERI 30TW laser system using the gas target. Optimization study of electron beam generation depending on laser and plasma density can apply to the case of solid target except exponentially decreasing plasma density along the vertical direction.

EXPERIMENTAL SET-UP

A 30 TW Ti:sapphire laser system at KAERI has been developed to utilize for laser-induced particle accelerations. Using total pumping energy of 4 J from two 2nd harmonic Nd:YAG lasers, the energy of 1.1 J is achieved with three staged amplifiers. The limitation of laser energy is mainly due to the limited size of gratings presently installed. New set of gratings including the compression chamber should be required to increase the laser power. After compression, the energy at target chamber is 60% of 1.1 J with pulse duration of 25 fs, yielding a 25-TW peak power.

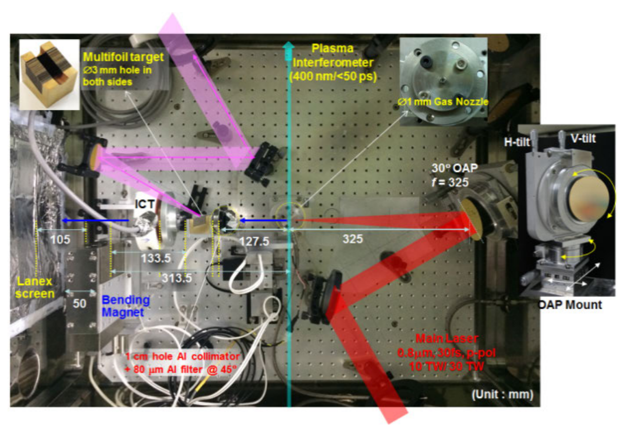

Figure 1: Layout of Experimental set-up

The laser beam was focused on a helium gas jet target using an off-axis parabola (OAP) mirror with a focal length of 326 mm. To vary the size of focal spot and the Rayleigh range, an iris is placed at the entrance to the target chamber and the laser pulse passing through the iris

*Work supported by the World Class Institute(WCI) Program of the National Research Foundation of Korea (NRF) funded by the Ministry of Science, ICT and Future Planning. (NRF Grant Number: WCI 2011-001)
#shpark@kaeri.re.kr

Content from this work may be used under the terms of the CC BY 3.0 licence (© 2015). Any distribution of this work must maintain attribution to the author(s), title of the work, publisher, and DOI.

ISBN: 978-3-95450-168-7 doi:10.18429/JACoW-IPAC2015-WEPWA034

HIGH-CHARGE-SHORT-BUNCH OPERATION POSSIBILITY AT ARGONNE WAKEFIELD ACCELERATOR FACILITY

Gwanghui Ha, Moohyun Cho, Won Namkung, POSTECH, Pohang, Gyeongbuk 790-784, KOREA
Wei Gai, Kwang-Je Kim, John Gorham Power, Argonne National Laboratory, Argonne, IL 60439, USA

Abstract

The Argonne Wakefield Accelerator (AWA) drive RF photoinjector linac was designed to generate a 75 MeV high charge bunch train of up to 100 nC per bunch. Recently we installed a double dog-leg type emittance exchange beam line and studies are now underway of two options to use a part of this beamline for the bunch compression. In one option, we introduce a chicane and in the other we use a single dog-leg. Simulations have been carried out to find the minimum bunch length for a range of charges (1- 40 nC) and the emittance growth due to coherent synchrotron radiation. We present GPT simulation results to show the high-charge-short-bunch operation possibilities at the AWA facility.

DOWNSTREAM BEAM LINE OF ARGONNE WAKEFIELD ACCELERATOR

The Argonne Wakefield Accelerator (AWA) has two main beam lines that are used to generate a drive beam and a witness beam for the demonstration of two beam acceleration (TBA) [1]. The drive linac consists of an L-band photocathode gun followed by six RF accelerating cavities to generate a 75 MeV beam. The main experimental beamline exits a straight from the dirve linac into two device under test areas with a spectrometer at the end. Recently, we installed a double dog-leg emittance exchange (EEX) beam line that has two identical dog-legs [2].

We are comparing two options for adding a magnetic bunch compressor to the AWA facility (Fig. 1): a chicane vs a dog-leg compressor. The first option, the chicane, adds a dipole to the straight ahead beamline while the second option, the dog-leg compressor, uses the first dog-leg of the EEX beamline. In the rest of paper, we present the results of the bunch compression achieved and the corresponding emittance growth for these beamlines

BUNCH COMPRESSION AND EMITTANCE GROWTH

A strong bunch compression is predominantly limited by the emittance growth in both the chicane and the single dog-leg (path “A” and path “B” in Fig. 1). Our GPT simulations include a 3D space-charge routine [3] and 1D CSR routine [4]. Table 1 shows the parameters of the EEX beam line and the incoming beam parameters at the AWA. The incoming beam energy was varied while the linac phase was changed to control the longitudinal chirp. We simulated incoming charges of {1, 5, 10, 20, 30 and 40 nC} with the gun launch phase set to 50 deg (maximum energy) and a fixed laser pulse length of 8 ps FWHM. These are the nominal operation parameters for the AWA drive gun.

Table 1: Beam Line Specification

Beam line parameters	**Value**	**Unit**
Bending angle	20	deg
Drift length in the dog-leg	2.0	m
Drift length between two dog-leg	1.5	m
η (dispersion of dog-leg)	0.9	m
ξ (momentum compaction of dog-leg)	0.3	m
Incoming beam parameters	**Value**	**Unit**
Maximum beam energy	75	MeV
Charge	0.1-100	nC
Bunch length	0.3-2.0	mm

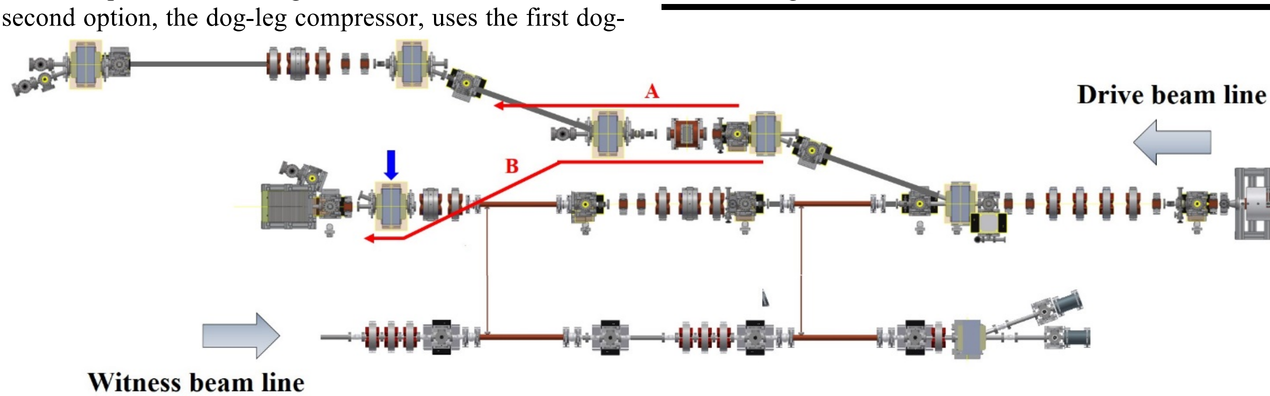

Figure 1: The downstream beam line configuration of the AWA. The dipole magnet indicated by the blue arrow is added for the chicane.

Content from this work may be used under the terms of the CC BY 3.0 licence (© 2015). Any distribution of this work must maintain attribution to the author(s), title of the work, publisher, and DOI.

ISBN: 978-3-95450-168-7 doi:10.18429/JACoW-IPAC2015-WEPWA035

INITIAL EEX-BASED BUNCH SHAPING EXPERIMENTAL RESULTS AT THE ARGONNE WAKEFIELD ACCELERATOR FACILITY

Gwanghui Ha, Moohyun Cho, and Won Namkung,
POSTECH, Pohang, Gyeongbuk 790-784, KOREA
Manoel Conde, Darrell Scott Doran, Wei Gai, Kwang-Je Kim, Wanming Liu, John Gorham Power, Yin-E Sun, Charles Whiteford, Eric Edson Wisniewski, and Alexander Zholents
Argonne National Laboratory, Argonne, IL 60439, USA
Chunguang Jing, Euclid TechLabs, Solon, Ohio 44139, USA
Philippe Regis-Guy Piot, Fermi National Accelerator Laboratory, Batavia, IL 60510, USA

Abstract

A program is under development at Argonne National Laboratory to use an emittance exchange (EEX) beamline to perform longitudinal bunch shaping (LBS). The double dog-leg EEX beamline was recently installed at the Argonne Wakefield Accelerator (AWA) and the goals of the proof-of-principle experiment are to demonstrate LBS and characterize its deformations from the ideal shape due to higher-order and collective effects. The LBS beamline at the AWA consists of insert-able transverse masks mounted on an actuator and four quadrupoles (to manipulate the transverse phase space) before the EEX beamline, which consists of two identical dog-legs and a deflecting cavity. The mask and input beam parameters are varied during the experiment to explore the shaping capability and clarify the deformation sources and their mitigation. Progress on the commissioning of the LBS beamline, initial experimental data and benchmarks to GPT [1] simulations will be presented.

EMITTANCE EXCHANGE BEAMLINE AT ARGONNE WAKEFIELD ACCELERATOR FACILITY

The emittance exchange (EEX) is an attractive tool to manipulate the phase space because of its unique characteristics [2]. In the EEX beam line, the entire longitudinal beam properties at the downstream are governed only by the upstream transverse properties. This characteristic can be applied to generate an arbitrary current profile for many applications [3]. The Argonne Wakefield Accelerator (AWA) is planning to demonstrate longitudinal bunch shaping (LBS) using EEX [4,5]. The EEX beam line was installed at the downstream of the AWA drive beam line last year and experiments have started this year. The EEX experiment at the AWA will take place in three stages: (1) EEX demonstration, (2) LBS demonstration, and (3) deformation study. Recently, we successfully finished the stage (1) and we present the experiment results here.

There are several different varieties of EEX beam lines [2,6,7], and the AWA installed the double dog-leg EEX beam line for the initial study. This beam line consists of four rectangular dipole magnets which make two identical dog-legs and one transverse deflecting cavity (TDC) as shown in Fig. 1. The linear transport matrix for the beam coordinate $X = [x, x', z, \delta]$ with $1 + \kappa\eta = 0$ condition is

$$R = \begin{bmatrix} 0 & L_c/3 & \kappa L_s & \eta + \kappa\xi L_s \\ 0 & 0 & \kappa & \kappa\xi \\ \kappa\xi & \eta + \kappa\xi L_s & L_c\kappa^2\xi/6 & L_c^2\kappa^2\xi^2/6 \\ \kappa & \kappa\xi L_s & L_c\kappa^2/6 & L_c\kappa^2\xi/6 \end{bmatrix}, \quad (1)$$

where L_s is $L + L_{bc} + L_c/3$, L is $(2L_b\cos\alpha + L_{bb})/\cos^2\alpha$, η is $(2L_b\cos^2\alpha - 2L_b\cos\alpha - L_{bb}\sin^2\alpha)/(\sin\alpha\cos^2\alpha)$, ξ is $(L_{bb}\sin^3\alpha + 2L_b\sin\alpha - 2\alpha L_b\cos^2\alpha)/(\sin\alpha\cos^2\alpha)$, α is the bending angle, L_b is the length of the dipole magnet, L_{bb} is the distance between dipoles, L_{bc} is the distance between the dipole and the TDC. L_c is the length of the TDC, and $\kappa\,(=\frac{eV}{E}\frac{2\pi}{\lambda})$ is the deflecting cavity kick strength [4,8].

The beam line parameters (Table 1) were chosen to simultaneously insure compatibility with the existing AWA facility and satisfy EEX requirements. The dispersion created by the dog-leg was large enough for the TDC [8]. The charge of the bunch at the entrance of the exchanger was set to 5 nC such that the charge after

Table 1: Beam Line and Input Beam Parameters used in the EEX Experiment

Beam line parameters	**Value**	**Unit**
Bending angle	20	deg
Dipole-to-Dipole distance	2.0	m
Dipole-to-TDC distance	0.5	m
η (dispersion of dog-leg)	0.9	m
ξ (momentum compaction of dog-leg)	0.3	m
κ (TDC kick strength)	-1.1	m^{-1}
Input beam parameters	**Value**	**Unit**
Beam energy	46.5	MeV
Charge before mask	5	nC
Charge after mask	~1	nC
Beam size at EY1	5	mm
Transverse emittance	25	μm
Bunch length	1	mm
Energy spread	0.5	%

#homehe@postech.ac.kr

Content from this work may be used under the terms of the CC BY 3.0 licence (© 2015). Any distribution of this work must maintain attribution to the author(s), title of the work, publisher, and DOI.

ISBN: 978-3-95450-168-7 doi:10.18429/JACoW-IPAC2015-WEPWA037

BEAM-DRIVEN TERAHERTZ SOURCE BASED ON OPEN ENDED WAVEGUIDE WITH A DIELECTRIC LAYER: RIGOROUS APPROACH*

Sergey N. Galyamin†, Andrey V. Tyukhtin, Aleksandra A. Grigoreva, Viktor V. Vorobev
St. Petersburg State University, Physical Faculty, St. Petersburg, 198504, Russia

Abstract

Terahertz frequency radiation (0.1-10 THz) is a promising tool for a number of scientific and practical applications. One promising scheme to obtain powerful and efficient THz emission is usage of beam-driven dielectric loaded structures [1]. Recently we have considered the problem where the microbunched ultrarelativistic charge exits the open end of a cylindrical waveguide with a dielectric layer and produces THz waves in a form of Cherenkov radiation [2]. To investigate the applicability of utilized approximations, we analyze here the case of orthogonal end of a waveguide with continuous filling. However, presented rigorous approach can be generalized for waveguide with vacuum channel. We use the combination of Wiener-Hopf technique and tailoring technique. The infinite linear system for magnitudes of reflected waveguide modes is obtained and solved numerically. We present typical field distributions over the aperture and typical radiation patterns in the Fraunhofer zone.

THEORY AND ANALYTICAL RESULTS

Convenient rigorous method for investigation of radiation from open-ended plane dielectrically loaded waveguides has been developed several decades ago [3]. Here we generalize this approach for the case of cylindrical geometry. At the current stage, we consider in detail the case of continuous filling, which is relatively simple. In the sequel, we plan to apply the developed technique for layered waveguide.

Consider a semi-infinite cylindrical waveguide with radius a filled with a dielectric ($\varepsilon > 1$) (Fig. 1). We suppose that single TM_{0l} waveguide mode incidents the orthogonal open end (cylindrical frame ρ, φ, z is used):

$$\left\{ H_{\omega\varphi}^{(i)}, E_{\omega\rho}^{(i)} \right\} = \left\{ 1, k_{zl} c (\omega\varepsilon)^{-1} \right\} J_1(\rho j_{0l}/a) e^{i k_{zl} z}, \quad (1)$$

$$E_{\omega z}^{(i)} = N J_0(\rho j_{0l}/a) e^{i k_{zl} z}, \quad N = ic(\omega\varepsilon)^{-1} j_{0l}/a, \quad (2)$$

where $J_0(j_{0l}) = 0$, $k_{zl} = \sqrt{k_0^2 \varepsilon - j_{0l}^2 a^{-2}}$, $\operatorname{Im} k_{zl} > 0$, $k_0 = \omega/c$. The reflected field in the area $z < 0$, $\sqrt{x^2+y^2} = \rho < a$ is decomposed into a series of waveguide modes propagating in opposite direction:

$$E_{\omega z}^{(r)} = \sum\nolimits_{m=1}^{\infty} N_m J_0(\rho j_{0m}/a) e^{-i k_{zm} z}, \quad (3)$$

where N_m are unknown "reflection coefficients" that should be determined. The vacuum area is divided into two subareas (1) and (2) (see Fig. 1), where the field is described by Helmholtz equation:

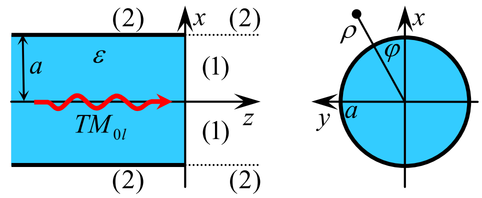

Figure 1: Geometry of the problem.

$$\left(\partial^2/\partial z^2 + \partial^2/\partial\rho^2 + \rho^{-1}\partial/\partial\rho + k_0^2 \right) E_{\omega z}^{(1,2)} = 0. \quad (4)$$

We introduce functions $\Psi_{\pm}(\rho,\alpha)$ (hereafter subscripts $\pm$ mean that function is holomorphic and have no zeros for $\operatorname{Im}\alpha > 0$ and $\operatorname{Im}\alpha < 0$, correspondingly):

$$\Psi_{+}^{(1,2)}(\rho,\alpha) = (2\pi)^{-1} \int_0^{\infty} dz E_{\omega z}^{(1,2)}(\rho,z) e^{i\alpha z}, \quad (5)$$

$$\Psi_{-}^{(2)}(\rho,\alpha) = (2\pi)^{-1} \int_{-\infty}^{0} dz E_{\omega z}^{(2)}(\rho,z) e^{i\alpha z}. \quad (6)$$

From (4) we obtain

$$\left(\frac{\partial^2}{\partial\rho^2} + \frac{1}{\rho}\frac{\partial}{\partial\rho} + \kappa^2 \right) \left\{ \begin{matrix} \Psi_{+}^{(1)} \\ \Psi_{-}^{(2)} + \Psi_{+}^{(2)} \end{matrix} \right\} = \left\{ \begin{matrix} F^{(1)} \\ 0 \end{matrix} \right\}, \quad (7)$$

$$F^{(1)} = (2\pi)^{-1} \partial E_{\omega z}^{(1)}/\partial z \Big|_{z=+0} - (2\pi)^{-1} i\alpha E_{\omega z}^{(1)} \Big|_{z=+0}, \quad (8)$$

where $\kappa = \sqrt{k_0^2 - \alpha^2}$, $\operatorname{Im}\kappa > 0$. Function $F^{(1)}$ is determined using continuity of $\partial E_{\omega\rho}/\partial\rho \sim \partial E_{\omega z}/\partial z$ and jump of $E_{\omega z}$ at $z = 0$, in the issue we obtain:

$$\Psi_{+}^{(1)} = C_1 J_0(\rho\kappa) + \Psi_p^{(1)}, \quad \Psi_{-}^{(2)} + \Psi_{+}^{(2)} = C_2 H_0^{(1)}(\rho\kappa), \quad (9)$$

$$\Psi_p^{(1)}(\rho,\alpha) = \frac{i}{2\pi} \left[\frac{k_{zl} - \alpha\varepsilon}{\kappa^2 - j_{0l}^2 a^{-2}} J_0\left(\frac{\rho j_{0l}}{a}\right) - \sum_{m=1}^{\infty} N_m \frac{k_{zm} + \alpha\varepsilon}{\kappa^2 - j_{0m}^2 a^{-2}} J_0\left(\frac{\rho j_{0m}}{a}\right) \right], \quad (10)$$

where $C_{1,2}$ are unknown coefficients. Utilizing $E_{\omega z} = 0$ for $\rho = a$, $z < 0$ and continuity of $E_{\omega z}$ and $\partial E_{\omega z}/\partial\rho \sim (\partial^2/\partial z^2 + k_0^2) H_{\omega\varphi}$ for $\rho = a$, $z > 0$, we obtain the following relation

$$\frac{\partial \Psi_{+}^{(2)}(a,\alpha)}{\partial a} = \frac{-\kappa J_1(a\kappa)}{J_0(a\kappa)} \Psi_{+}^{(2)}(a,\alpha) + \frac{\partial \Psi_p^{(1)}(a,\alpha)}{\partial a} \quad (11)$$

and Wiener-Hopf equation for $\Psi_{+}^{(2)}(a,\alpha)$:

*Work supported by the Grant of the President of Russian Federation (No. 6765.2015.2) and the Grant from Russian Foundation for Basic Research (No. 15-32-20985, 15-02-03913).
† s.galyamin@spbu.ru

Content from this work may be used under the terms of the CC BY 3.0 licence (© 2015). Any distribution of this work must maintain attribution to the author(s), title of the work, publisher, and DOI.

ISBN: 978-3-95450-168-7 doi:10.18429/JACoW-IPAC2015-WEPWA038

MODE TRANSFORMATION IN WAVEGUIDE WITH TRANSVERSAL BOUNDARY BETWEEN VACUUM AND PARTIALLY DIELECTRIC AREA*

A.A. Grigoreva †, A.V. Tyukhtin ‡, T.Yu. Alekhina, S.N. Galyamin,
Saint-Petersburg State University, Physical Faculty, Russia

Abstract

We consider the mode transformation in a circular waveguide with a transversal boundary between a vacuum part and a part with a cylindrical dielectric layer and a vacuum channel. It is assumed that an incident mode can be both propagating and evanescent. Analysis is carried out with the using the mode decomposition technique. Numerical algorithm for calculating the mode transformation at an arbitrary channel radius is also developed. Typical dependences for the reflection and transmission coefficients on the channel radius are presented and discussed.

INTRODUCTION

We study the electromagnetic field in a circular waveguide which consists of two semi infinite parts: one of them has a cylindrical dielectric layer and a vacuum channel, and the other does not have any filling. Such a problem is of interest, for example, for new perspective method of generation of terahertz radiation from an electron bunch in a dielectric loaded structure [1–3]. It is important to consider the field of the bunch flying into the vacuum part of the waveguide. Earlier this problem was considered for the case when the vacuum channel is absent [4, 5]. It is obvious that the principal modifications in the reflected and transmitted fields take place in the presence of the vacuum channel due to the effect of the mode transformation.

Another sample is the wakefield acceleration technique in the dielectric waveguide structures [6, 7]. The generation of the wakefield occurs at some distance after a driver flying into the dielectric part of waveguide. Analysis of process of the wakefield formation is essential for this application. This process is also interesting as well for development of the method of measurement of particle energy with applying the dielectric loaded waveguide [8, 9].

These examples show that both of the problem, when the bunch enters into the partially dielectric area, and the problem, when the bunch flies out of this, are of interest for applications. Such problems can be analyzed by means of an expansion of the incident field into a series of waveguide modes. Here we consider the case of a single incident mode. Note that such a problem statement is conventional in the waveguide theory and has an essential independent importance.

* Work supported by Russian Foundation for Basic Research (grant 15-02-03913) and grant of President of Russian Federation (6765.2015.2)
† aleksandra.a.grigoreva@gmail.com
‡ tyukhtin@bk.ru

THE CASE OF THE MODE FALLING FROM THE VACUUM PART

First, we assume that the left part of the waveguide ($z < 0$) is filled up with a medium having permittivity ε_c and permeability μ_c. The right part of the waveguide consists of a channel and a dielectric layer described by ε_c, μ_c and ε_d, μ_d respectively (Fig. 1). Initially we assume that media are dissipative that is Im $\varepsilon_{c,d} > 0$ for positive frequencies (these values will be tended to zero at numerical calculations). Both of the media are isotropic, homogeneous and nondispersive. We suppose that the z-axis coincides with the waveguide axis, and the transversal boundary is placed at $z = 0$. The incident field is one of the TM_{0i} mode which can be both propagating and evanescent.

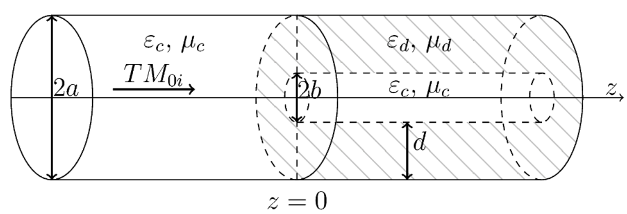

Figure 1: The problem geometry in the case of the mode falling from the vacuum part.

The solution is carried out by cross-linking method. This method presupposes that reflected and transmitted fields are presented as a series of eigenmodes. In order to obtain the equation for the excitation coefficients of the modes of reflected and transmitted fields, we use the continuity conditions for the tangential components of the field at the transversal boundary. After some transformation we obtain a system containing an infinite number of linear algebraic equations. For calculations, we consider the system of finite size. It is possible because the most of the modes are evanescent and they exponentially decrease with the distance from the boarder.

In general case, this matrix system is analytically unsolvable. However, in two dedicated cases (a narrow channel, $b \ll a$, and a thin dielectric layer, $d = (a - b) \ll a$) some approximate results can be obtained.

A Narrow Channel

The approximation for eigenvalues in the dielectric waveguide with a narrow channel ($b \ll a$) can be obtained using the iteration technique. One can see that eigenvalues don't have linear terms. In a similar way, the system of

Content from this work may be used under the terms of the CC BY 3.0 licence (© 2015). Any distribution of this work must maintain attribution to the author(s), title of the work, publisher, and DOI.

ISBN: 978-3-95450-168-7 doi:10.18429/JACoW-IPAC2015-WEPWA039

Content from this work may be used under the terms of the CC BY 3.0 licence (© 2015). Any distribution of this work must maintain attribution to the author(s), title of the work, publisher, and DOI.

THE AWAKE ELECTRON PRIMARY BEAM LINE

J. S. Schmidt, J. Bauche, B. Biskup*, C. Bracco, E. Bravin, S. Doebert, M. A. Fraser, B. Goddard, E. Gschwendtner, L. K. Jensen, O. R. Jones, S. Mazzoni, M. Meddahi, A. Petrenko, F. M. Velotti, A. Vorozhtsov, CERN, Geneva, Switzerland, P. Muggli, MPI, Munich, Germany, U. Dorda, DESY, Hamburg, Germany, L. Merminga, V. A. Verzilov, TRIUMF, Vancouver, Canada

Abstract

The AWAKE project at CERN is planned to study proton driven plasma wakefield acceleration. The proton beam from the SPS will be used in order to drive wakefields in a 10 m long Rubidium plasma cell. In the first phase of this experiment, scheduled in 2016, the self-modulation of the proton beam in the plasma will be studied in detail, while in the second phase an external electron beam will be injected into the plasma wakefield to probe the acceleration process. The installation of AWAKE in the former CNGS experimental area and the required optics flexibility define the tight boundary conditions to be fulfilled by the electron beam line design. The transport of low energy (10-20 MeV) bunches of $1.25{\cdot}10^9$ electrons and the synchronous copropagation with much higher intensity proton bunches ($3{\cdot}10^{11}$) determines several technological and operational challenges for the magnets and the beam diagnostics. The current status of the electron line layout and the associated equipment are presented in this paper.

INTRODUCTION

The AWAKE project at CERN will be the first experiment world wide to test plasma wakefield acceleration using a high energy (400 GeV) proton drive beam [1]. The first phase in 2016 will be focused on the study of the self-modulation instability of the drive bunch as described in [2]. In the second phase of the AWAKE project in 2017 the plasma wakefields will be probed with an externally injected electron beam.

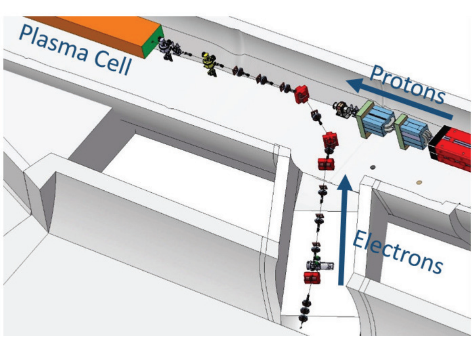

Figure 1: View of the AWAKE electron transfer line.

First studies on the electron transfer line have been presented in [3]. The bunch of $1.2{\cdot}10^9$ electrons will be produced by the PHIN electron gun, which will be recuperated from the CTF3 facility [4] with an output momentum of 5 MeV/c and accelerated to 10-20 MeV/c by a linac booster. The source will be located in a room adjacent to the proton gallery. From there the electron beam will be raised to the height of the proton line, where the two beams will be merged in a common beam line and injected into the plasma following the "on-axis" concept [3]. The general layout of the transfer line is shown in Fig. 1. The baseline parameters of the injected electron beam are summarized in Table 1. With these parameters, the capture efficiency of the electrons in the wakefields has been studied in [5].

Table 1: Electron Beam Parameters

Parameter	Value
Momentum [MeV/c]	10 - 20
Electrons/bunch	$1.2{\cdot}10^9$
Rep. rate [Hz]	10
Bunch length (z) [ps (mm)]	4 (1.2)
Relative momentum spread $\Delta p/p$ [%]	0.5
Emittance (r.m.s. norm.) [mm mrad]	2

ELECTRON BEAM LINE LAYOUT

Following the accelerator of the electron gun, a quadrupole triplet will match the beam into the transfer line. This 15 m long line will consist of three parts. After the matching triplet, two dipoles with a deflection angle of ±18° form an achromatic dog-leg to raise the beam by 1.16 m up to the level of the proton line with a slope of 20%. At this level two horizontal dipoles of ~32° bend the beam towards the proton line. The merging dipole is tilted by 3.2° to match the electron beam axis with the proton one, which has a slope 5.66% in the CNGS tunnel. The final part is the common beam line where the electrons and the protons share the same vacuum chamber and the electrons are focused by an independently powered quadrupole triplet to be captured in the plasma wakefield.

In total eleven quadrupoles will be distributed along the line to control the beta function and the dispersion of the beam. Their evolution along the transfer line is shown in Fig. 2 for the horizontal (x) and vertical (y) plane. The dispersion in y cannot be closed due to the general slope of the proton line and the plasma cell, but still crosses zero at the focal point. With this optics the experimental requirements are fulfilled with a 1σ bunch size at the nominal focal point of 228.1 μm in x and 226.04 μm in y as shown in Table 2.

* and Czech Technical University, Prague, Czech Republic.

ISBN: 978-3-95450-168-7 doi:10.18429/JACoW-IPAC2015-WEPWA040

GENERATION AND RADIATION OF PHz RING-LIKE ELECTRON-PULSE TRAIN

Fu-Han Chao [2], Chia-Hsiang Chen [1,3], Yen-Chieh Huang [1,2], Ping J. Chou[2,3]

[1]Institute of Photonics Technologies/Department of Electrical Engineering, National Tsing Hua University, Hsinchu 30013, Taiwan

[2]Department of Physics, National Tsing Hua University, Hsinchu 30013, Taiwan

[3]National Synchrotron Radiation Research Center, Hsinchu 30076, Taiwan

Abstract

In this paper, we propose a multi-ring structured photocathode to emit a set of longitudinally packed electron rings with a bunching frequency of 1 PHz during particle acceleration. We also present in this paper the beam dynamics and radiation of the structured electron-pulse train.

INTRODUCTION

In an electron radiation device, the constructive interference of the radiation fields from a periodic electron-pulse train [1] can rapidly increase the spectral radiation power at the fundamental or harmonics of the pulse frequency.

To generate radiation in the EUV or X-ray spectrum, the required pulse frequency of the electron beam should be few tens or even few hundreds of PHz. The repetition rate of electron pulses generated from an ordinary RF photoinjector is usually at 10-100 Hz, which is far below that for efficient EUV or X-ray radiation.

In this paper, we propose a technique to generate a PHz ring-like electron-pulse train from an RF photoinjector with a structured photocathode. Our study using the ASTRA simulation code confirms that a PHz 3-D electron-pulse train can be generated from a photoinjector with an excellent bunching factor [1].

In this paper, we also study the interference of the radiation fields of a 3-D structured electron-pulse train.

BUNCH DISTORTION DURING ACCELERATION

Since the acceleration fields in the RF cavities of a photoinjector or a Linac are radially dependent [2], the transit time of an electron in an accelerator is dependent on its radial position in the accelerator. We have investigated the evolution of ultra-short electron bunches in an RF photoinjector by using the particle tracking codes, PARMELA and ASTRA, and found that the different transit time of the electrons can distort the electron bunch during acceleration [3]. When the space charge effects are insignificant, the transit time of the electron is only influenced by its radial position in the cavity. A delta-function like layer of electrons in the longitudinal direction allows us to exploit the impulse response of the accelerator system for bunch distortion during particle acceleration. Fig. 1(a) shows a delta-function input beam of an RF photoinjector and Fig. 1(b) shows the impulse response at the injector exit simulated by PARMELA, where r is the radial position and $\Delta\phi$ is the acceleration phase of the electron. To plot Fig. 1, the peak acceleration field in the 1.6 cell, S-band photoinjector is 80MeV/m.

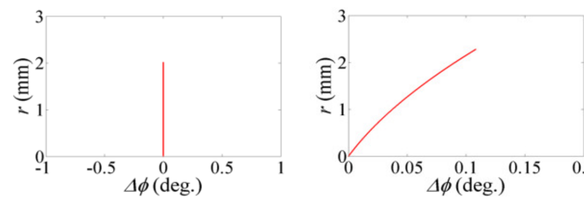

(a) (b)

Figure 1: $r-\Delta\phi$ electron distributions of a delta-function like electron bunch (a) at the cathode and (b) at the exit of a typical S-band photoinjector. Results obtained from simulation in PARMELA.

GENERATION AND ACCELERATION OF PHz RING-LIKE ELECTRON-PULSE TRAIN

The impulse response of the accelerator reveals a transverse-to-longitudinal relation of the accelerated electron bunch. With a specified transverse-to-longitudinal relation of particles for an accelerator, it is possible to modulate the longitudinal density of an accelerated electron beam by properly modulating the transverse electron density at the cathode. To reduce the azimuthal bunch distortion resulting from the space charge force, we implement a cylindrically symmetric transverse density modulation for the electrons at cathode. A multi-ring structure can be used for generating such a symmetrically distributed electron bunch, as shown in Fig. 2(a). The transverse bunch profile consists of a set of concentric particle rings laid in the plane of the cathode, as shown in Fig. 2(b). After being accelerated by the radially dependent RF field, the electron rings with different radiuses are separated and become an electron-pulse train in the longitudinal direction, as shown in Fig. 2(c). The longitudinal distances between the accelerated electron rings are affected by the initial radius of and the total charge in each electron ring.

The flux of electrons emitted at the cathode depends on the driver laser power and the material of the cathode. Fabricating a series of concentric metal rings on a dielectric coated cathode or vice versa is a way to spatially modulate the electron density and generate ring-like electron micro-bunches. Such a multi-ring-structured cathode, as shown in Fig. 2(a), can be manufactured by electron beam lithographic patterning. It is possible to

Content from this work may be used under the terms of the CC BY 3.0 licence (© 2015). Any distribution of this work must maintain attribution to the author(s), title of the work, publisher, and DOI.

ISBN: 978-3-95450-168-7 doi:10.18429/JACoW-IPAC2015-WEPWA041

Content from this work may be used under the terms of the CC BY 3.0 licence (© 2015). Any distribution of this work must maintain attribution to the author(s), title of the work, publisher, and DOI.

PLANS FOR A LINEAR PAUL TRAP AT RUTHERFORD APPLETON LABORATORY

D.J. Kelliher*, S. Machida, C. Plostinar, C.R. Prior,
STFC Rutherford Appleton Laboratory, ASTeC
S.L. Sheehy,
JAI, Oxford & STFC Rutherford Appleton Laboratory, ASTeC

Abstract

For over a decade, Linear Paul Traps (LPT) have been used in the study of accelerator beam dynamics. LPT studies exploit the similarity of the Hamiltonian with that of a beam in a quadrupole channel while having advantages in the flexibility of parameter choice, compactness and low cost. In collaboration with Hiroshima University, LPT research planned at STFC Rutherford Appleton Laboratory (RAL) in the UK aims to investigate a range of topics including resonance crossing, halo formation, long-term stability studies and space charge effects. Initially, a conventional quadrupole-based LPT will be built at RAL and used for a variety of experiments. In parallel, a design for a more advanced LPT that incorporates higher order multipoles will be pursued and later constructed. This multipole trap will allow non-linear lattice elements to be simulated and so broaden considerably the range of experiments that can be conducted. These will include the investigation of resonance crossing in non-linear lattices, a more detailed study of halo formation and the effect of detuning with amplitude. In this paper we report on progress made in the project to date and future plans.

INTRODUCTION

In a linear Paul trap an rf electric field confines a non-neutral plasma transversely. The quadrupole symmetry of the electrodes focus and defocus the plasma in analogy with a bunch in a FODO channel. Longitudinally the plasma is trapped in a potential well created by applying DC voltages to end cap electrodes. The secular frequency of the plasma, equivalent to the cell tune in an accelerator, can be adjusted by varying either the frequency or voltage applied to the rf electrodes. Following a period of plasma confinement in which an experiment is performed, the plasma is extracted by lowering one of the DC voltages and sent to an external diagnostic.

For over a decade LPTs have been used in the study of accelerator beam dynamics both at Hiroshima University, Japan [1], [2] and at Princeton University, USA [3], [4]. At RAL, plans are advanced for the construction of an LPT based on the S-POD device at Hiroshima. As in S-POD, the device will consist of segmented cylindrical rod electrodes and the plasma (typically Argon) will be ionised in-situ using an electron gun. Diagnostics will include a Faraday cup to measure the total number of ions and an MCP (Multi Channel Plate) screen imaged with a CCD camera (Fig.1).

Although initially a linear quadrupole trap will be constructed, the design should allow for the possibility of installing additional electrodes at a later date in order to add an octopole component. This would allow an investigation of halo formation in which the octopole term plays an important role [5]. It would also facilitate a study of detuning with amplitude during resonance crossing and when on-resonance in an extension of earlier work [6]. A more extensive list of proposed experiments can be found in ref. [7].

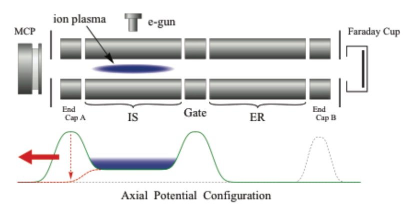

Figure 1: Schematic of S-POD showing the five segments used to create two trapping regions (IS: ion source region, ER: experimental region), and below, the potential well established by the DC voltages. As indicated by the arrows, by lowering the voltage applied to one set of end cap electrodes, the plasma moves towards an external diagnostic. The trap is about 20 cm in length and is operated at 1 MHz. Image courtesy of H. Okamoto and his group.

QUADRUPOLE TRAP DESIGN

Basic Design Parameters

The potential in the transverse plane in a LPT with quadrupole symmetry is given by

$$\Phi(x,y,t) = (U - V_0\cos(ft))\left(\frac{x^2 - y^2}{2r_0^2}\right) \tag{1}$$

where U is the DC potential applied to the end cap electrodes, V_0 is the rf voltage of frequency f and r_0 is the trap radius (i.e the radius that inscribes the trap electrodes). Making the following transformations

$$a_x = a_y = \frac{4qU}{mr_0^2 f^2}$$
$$q_x = -q_y = \frac{2qV_0}{mr_0^2 f^2}$$
$$\xi = ft/2$$

* David.Kelliher@stfc.ac.uk

ISBN: 978-3-95450-168-7 doi:10.18429/JACoW-IPAC2015-WEPWA043

Content from this work may be used under the terms of the CC BY 3.0 licence (© 2015). Any distribution of this work must maintain attribution to the author(s), title of the work, publisher, and DOI.

PROGRESS ON THE DESIGN OF THE RACETRACK FFAG DECAY RING FOR NUSTORM

J.-B. Lagrange*, J. Pasternak, Imperial College London, UK
R. B. Appleby, J. M. Garland, H. Owen, S. Tygier,
Cockcroft Institute and Manchester University, UK
Y. Mori, Kyoto University, Japan

Abstract

The neutrino beam produced from muons decaying in a storage ring would be an ideal tool for precise neutrino cross section measurements and search for sterile neutrinos due to its precisely known flavour content and spectrum. In the proposed nuSTORM facility pions would be directly injected into a storage ring, where circulating muon beam would be captured. The racetrack FFAG (Fixed Field Alternating Gradient) option for nuSTORM decay ring offers a very good performance due to a large dynamic and momentum acceptance. Machine parameters, linear optics design, beam dynamics and injection system for nuSTORM FFAG ring are discussed in this paper.

INTRODUCTION

Using a muon decay to produce a neutrino beam with a defined spectrum and flux composition is a well-established idea. This concept was developed into the Neutrino Factory facility proposal, which was then addressed in several dedicated research and development studies culminating in the International Design Study for the Neutrino Factory (IDS-NF) [1]. The Neutrino Factory consists of a high power proton driver, the output of which is directed towards a pion production target; a decay channel, where the muon beam is formed; the muon front end, where the beam is prepared for the acceleration and the muon accelerator to boost the energy to the required value. The muon beam is then injected into the decay ring, one of the straight sections pointing towards near and far detectors and producing ν beams for both interaction and oscillation physics. Although it has been shown that such a facility will be superior in its discovery potential with respect to a conventional neutrino beam facility based on pion decay, it requires the construction of many new accelerator components, which do not exist at present.

In order to allow for the start of neutrino physics experiments based on muon decay using conventional accelerator technology, the neutrinos from STORed Muon beam (nuSTORM) project was proposed [2]. In nuSTORM high energy pions produced at the target are directly injected into the ring after passing through a short transfer line equipped with a chicane to select charge of the beam. Once in the ring, decaying pions will form the muon beam. A fraction of the muon beam with energy lower than the injected parent pions will be stored in the ring and a fraction with similar or larger energy will be extracted with a mirror system of the injection at the end of the long straight section to avoid activation in the arc. They may also be used for accelerator research and development studies for future muon accelerators.

As the flux intensity is one of key elements for a successful neutrino experiment, it is proposed to push the momentum acceptance of the ring to ±8% or even ±16%. Although the design based on the standard accelerator lattice with separated function magnets has been proposed [3], the design based on scaling FFAG lattice is being developed in parallel. The scaling FFAG technology allows to have zero chromaticity with large dynamical acceptance, which enables large momentum spread of the beam with low losses by avoiding the dangerous resonances. This paper describes the update of the racetrack FFAG (RFFAG) ring design for nuSTORM.

RING DESIGN

Triplet Cell in the Straight Section

The RFFAG ring design consists of long straight sections pointing towards neutrino detectors, where the majority of the pions will decay into muons and along which the neutrino beam will be formed firstly from the pion decay and secondly from the muon decay. Both signals can be separated by the detector timing information. The ring contains also compact arcs in order to achieve a large neutrino beam production efficiency minimizing the size of the ring and the associated cost. An RFFAG design was proposed previously [4], but further study of neutrino production from pion decays presented interest in long baseline scenarios. This scenario is incompatible with any scallop of the beam in the production straight. In the previous design, the long straight part of the ring was made of doublet cells, where the beam had a scallop of ±12 mrad for more than 90% of the production straight. This solution can thus no longer be used if long baseline scenario are to be considered. Doublet cells were used in order to minimize the magnet packing factor to limit the cost, and to limit the betatron function beating in the arc. However, a careful choice of straight FFAG triplet can be used to have a similar betatron function beating in the arc, while keeping a low packing factor. A triplet with long drift space has the advantage to allow the beam to be guided without any scallop for most of the production straight, giving possibility to long baseline studies.

* j.lagrange@imperial.ac.uk

ISBN: 978-3-95450-168-7 doi:10.18429/JACoW-IPAC2015-WEPWA044

THE ALIGNMENT OF THE MICE TRACKER DETECTORS*

M. A. Uchida†, Imperial College London, UK
for the MICE collaboration

Abstract

The Muon Ionization Cooling experiment (MICE) has been designed to demonstrate the reduction of the phase-space volume (cooling) occupied by a muon beam using the ionization-cooling technique. This demonstration will be an important step in establishing the feasibility of muon accelerators for particle physics. The emittance of the beam will be measured before and after the cooling cell using a solenoidal spectrometer. Each spectrometer will be instrumented with a high-precision scintillating-fibre tracking detector (Tracker). The Trackers will be immersed in a uniform magnetic field of 4 T and will measure the normalised emittance reduction with a precision of 0.1%. A thorough knowledge of the alignment of the Trackers is essential for this accuracy to be achieved. The Trackers are aligned: mechanically inside the spectrometer solenoids, with respect to the MICE experimental hall, to one another, and to the magnetic and beam axes. These methods are described here.

INTRODUCTION

The Muon Ionization Cooling Experiment (MICE), in preparation at the Rutherford Appleton Laboratory in the UK, aims to demonstrate ionization cooling for the first time. Ionization cooling is the process of reducing the beam emittance (phase space) while maintaining the longitudinal momentum of the beam. Muons are produced with a large emittance, which must be condensed before acceleration. Muon beams are produced at the front end of a Neutrino Factory (NF) [1] with an emittance of 15–20 mm.rad, which must be reduced to 2–5 mm.rad. A Muon Collider [2] requires further cooling, reducing the emittance to 0.4 mm.rad in the transverse plane, and 1 mm.rad in the longitudinal plane. Due to the short muon lifetime, synchrotron radiation and stochastic cooling techniques are unsuitable for muon beams, and hence ionization cooling is the only process that can efficiently reduce the emittance of a muon beam within its lifetime.

The MICE experiment shown in Figure 1 will pass a muon beam through a low-Z material (absorber), where the muons lose both longitudinal and transverse momentum through ionization energy loss. A proportion of the lost longitudinal momentum is then restored using accelerating RF cavities that follow the absorber. Along with this cooling, however, there is a heating effect produced as a result of multiple scattering through the system, therefore, the net cooling is a balance between these two effects. This is described in Eq. 1, where the first term on the right hand side represents the cooling effect and the second term the heating effect:

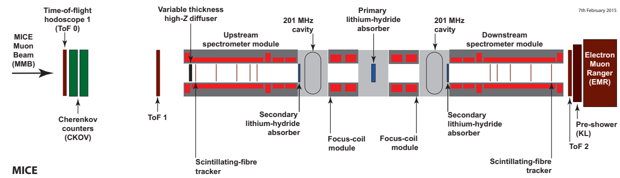

Figure 1: Schematic of the International Muon ionization Cooling Experiment (MICE), with the beam entering from the left.

$$\frac{d\epsilon_n}{ds} \sim -\frac{1}{\beta^2}\left\langle\frac{dE_\mu}{ds}\right\rangle\frac{\epsilon_n}{E_\mu} + \frac{1}{\beta^3}\frac{\beta_\perp(0.014\text{GeV})^2}{2E_\mu m_\mu L_R} \quad (1)$$

$\frac{d\epsilon_n}{ds}$ is the rate of change of normalised-emittance within the absorber; β, E_μ and m_μ the ratio of the muon velocity to the speed of light, muon energy, and mass respectively; $\beta_\perp$ is the lattice betatron function at the absorber; and L_R is the radiation length of the absorber material.

MICE aims to reduce the normalised emittance of the muon beam by a few percent and to measure the reduction with a precision of 0.1%. To do this each muon will be measured individually by an upstream and downstream high precision scintillating fibre tracking detector (Tracker). The Trackers are contained within super-conducting spectrometer solenoids (SSs) which produce a uniform 4 T field. The muon beamline has been commissioned and the beams produced have been shown by direct measurement with MICE particle detectors to be adequate for cooling measurements. The beam was experimentally studied paying particular attention to the rate, particle composition and emittance; the Trackers are built, fully tested, installed and are undergoing commissioning and calibration. MICE is surrounded by a partial return yoke (PRY) so as to minimise any stray magnetic field from the experiment.

MICE Step IV, shown in Figure 2 will begin data taking this year [3]. It will test the full system but without RF cavities to re-accelerate the beam (and will have only one absorber). Step IV can reduce normalised beam emittance but it will not restore longitudinal momentum and so it will not allow for a demonstration of sustainable cooling.

The final stage (see Figure 1), the Demonstration of Ionization Cooling will include the RF cavities and additional absorber modules and its construction is scheduled for completion in 2017.

* Work supported by the (UK) Science and Technology Facilities Council and the (US) Dept. of Energy and National Science Foundation
† m.a.uchida@imperial.ac.uk

Content from this work may be used under the terms of the CC BY 3.0 licence (© 2015). Any distribution of this work must maintain attribution to the author(s), title of the work, publisher, and DOI.

ISBN: 978-3-95450-168-7 doi:10.18429/JACoW-IPAC2015-WEPWA045

DEVELOPMENT OF A SPECTROMETER FOR PROTON DRIVEN PLASMA WAKEFIELD ACCELERATED ELECTRONS AT AWAKE

L. Deacon, S. Jolly, F. Keeble, M. Wing*, UCL, London, United Kingdom
B. Biskup†, E. Bravin, A. Petrenko, CERN, Geneva, Switzerland

Abstract

The AWAKE experiment is to be constructed at the CERN Neutrinos to Gran Sasso facility (CNGS). This will be the first experiment to demonstrate proton-driven plasma wakefield acceleration. The 400 GeV proton beam from the CERN SPS will excite a wakefield in a plasma cell several meters in length. To observe the plasma wakefield, electrons of 10–20 MeV will be injected into the wakefield following the head of the proton beam. Simulations indicate that electrons will be accelerated to GeV energies by the plasma wakefield. The AWAKE spectrometer is intended to measure both the peak energy and energy spread of these accelerated electrons. Improvements to the baseline design are presented, with an alternative dipole magnet and quadrupole focussing, with the resulting energy resolution calculated for various scenarios. The signal to background ratio due to the interaction of the SPS protons with upstream beam line components is calculated, and CCD camera location, shielding and light transport are considered.

INTRODUCTION

Proton bunches are the most promising drivers of wakefields to accelerate electrons to the TeV energy scale in a single stage. An experimental program at CERN — the AWAKE experiment [1, 2] — has been launched to study in detail the important physical processes and to demonstrate proton-driven plasma wakefield acceleration.

AWAKE will be the first proton-driven plasma wakefield experiment world-wide and will be installed in the CERN Neutrinos to Gran Sasso facility [3]. An electron witness beam will be injected into the plasma to observe the effects of the proton-driven plasma wakefield: plasma simulations indicate electrons will be accelerated to GeV energies [4]. In order to measure the energy spectrum of the witness electrons, a magnetic spectrometer will be installed downstream of the exit of the plasma cell. The design of the spectrometer was outlined in [5]. This paper will present the updated spectrometer design along with estimated energy resolution for various quadrupole and magnet settings.

SPECTROMETER DESIGN

Dipole Magnet

As a change to the previous design [6], a smaller, lighter and more efficient C-shaped magnet (HB4) was considered as an alternative to the window-shaped dipole (MBPS). The energy measurement uncertainties were also compared (see

* and DESY, Hamburg, Germany and University of Hamburg, Germany
† and Czech Technical University, Prague, Czech Republic

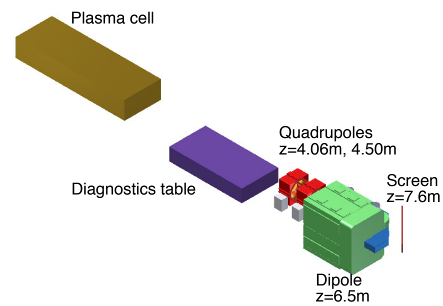

Figure 1: A 3D CAD image of the spectrometer system annotated with distances along the z direction from the exit of the plasma cell to the magnetic centres of magnets, and the centre of the scintillator screen.

Resolution below). It was finally decided to change the design and to use magnet HB4 instead of MBPS since HB4 has sufficient field strength and field width (see Table 1), and similar resolution to MBPS.

Table 1: Comparison Between Window-shaped Dipole MBPS and C-shaped Dipole HB4 [7].

Dipole	MBPS	HB4
Weight	15 t	8.5 t
Power consumption	60 kW	24 kW cycled
Integrated field	1.9 Tm	1.6 T cycled
Max. mag. field	1.65 T	1.5 T cycled
Hor. aper.	52 cm	32 cm
Vert. aper.	11 cm	8 cm
Iron length	1 m	1 m

Field maps and measurements Field measurements have been carried out [7] on the HB4 field at the magnetic centre and the integrated field has been measured along a line parallel to the z-axis running through the magnetic centre. Three dimensional field maps [8] calculated using the OPERA simulation software at various field strengths show agreement with the measurements to within 2-3% (Table 2), with fields calculated for 100 A, 170 A, 540 A and 650 A.

The measurable energy range can be set by changing the magnet current. The simulation results giving the currents and corresponding ranges are shown in Table 3. The magnet current can, of course, be set to intermediate values.

Content from this work may be used under the terms of the CC BY 3.0 licence (© 2015). Any distribution of this work must maintain attribution to the author(s), title of the work, publisher, and DOI.

ISBN: 978-3-95450-168-7 doi:10.18429/JACoW-IPAC2015-WEPWA046

TIME DOMAIN SIMULATIONS OF DETUNED ACCELERATING CAVITIES FOR TWO BEAM APPLICATIONS

L.R. Carver*, R.M. Jones, School of Physics and Astronomy, University of Manchester & The Cockcroft Institute of Science and Technology, Daresbury, UK

Abstract

A multi-harmonic accelerating cavity that has its fundamental and harmonic mode frequency detuned away from the bunch repetition frequency could provide the basis for a beam driven wakefield accelerator with high transformer ratios. The excitation of multiple harmonic eigenmodes will allow high gradients to be achieved without encouraging the onset of rf breakdown or pulsed surface heating. This accelerating cavity will be introduced, and time domain simulations verifying the theory will be shown.

INTRODUCTION

Cavities that have their fundamental accelerating mode frequency detuned away from the bunch repetition frequency could form the basis of a high gradient collinear two beam accelerator structure with high transformer ratios [1]. The field that is excited by the high current drive beam undergoes a phase shift that arises from the detuning, and the cavity can be designed such that the drive bunches are being decelerated by the steady state field. High transformer ratios can be achieved by interleaving the drive beam with a low current test beam, such that the test bunches are being accelerated as they traverse the cavity chain. A cavity of this design would remove the need for the Power Extraction Transfer System (PETS) found in the CLIC design [2].

A multi-harmonic cavity that operates at high gradients could act as an alternative cavity design for CLIC. Cavities of this type have unconventional surface electric and magnetic field profiles that can potentially lower the surface field emission and/or pulsed surface heating without compromising the accelerating gradient [3]. Two particular phenomena found in multi-harmonic cavities provide the main motivation for their use: (a) the anode-cathode effect, which can be found in an asymmetric multi-harmonic cavity that relies on fields pointing into one wall (cathode-like) to be significantly smaller than fields pointing away (anode-like) from the same wall. This effect will raise the work function barrier to supress field and secondary emission, and (b) a reduction in the surface heating by lowering the average $H_{||}^2$ along the surface.

Both of these concepts can be combined to give a cavity that is capable of operating at high gradients with reduced damage from pulsed surface heating, while maintaining high transformer ratios and collinear acceleration. This paper will verify some of the fundamental principles introduced here by time domain simulations. First, the transformer ratio and the surface fields will be verified for a single mode cavity. Then a third harmonic cavity structure will be introduced and similar comparisons presented that show the pulsed surface heating reduction.

* Lee.Carver@manchester.ac.uk

SINGLE MODE SIMULATIONS

A three cell π-mode standing wave cavity was designed with a fundamental frequency of 11.7292 GHz and the conductivity of the cavity walls was adjusted to give a quality factor of 500. The field in the cavity is excited by a traversing high current drive bunch, but the field undergoes a phase shift given by [4]

$$\tan\phi = -2Q\delta \tag{1}$$

where Q is the cavity quality factor, $\delta = (f_c - f_d)/f_c$ is the magnitude of the detuning, f_c is the cavity frequency and f_d is the drive bunch repetition frequency. For test bunch offsets of $t = \pi/2$, it emerges that $T = -2Q\delta$. Therefore, when exciting this cavity with a train of bunches with repetition frequency $f_d = 11.9942$ GHz, there is an anticipated transformer ratio $T = 22.59$. It can be shown that when considering the test bunch excited field, the transformer ratio is given by [1]

$$T = \frac{\varsigma - 2Q\delta}{1 + 2Q\delta\varsigma}, \tag{2}$$

where ς is the modified current ratio given by $\varsigma = \Theta_T I_T/\Theta_D I_D$ where $\Theta_{T,D}$ is the transit time factor and $I_{T,D}$ are the currents of the drive and test bunches respectively [5]. Here, both bunches traversing the cavity have $\beta \approx 1$. The cavity was excited by a train of 1 pC bunches with $\sigma_z = 4$ mm using ACE3P [6]. A bunch repetition frequency of 5.9971 GHz was employed (CLIC rf frequency, every other bucket filled) such that a Gaussian distribution of width $5\sigma_z$ did not result in any overlapping in the tails. Field monitors were placed along the cavity axis, and the bunch train continually excited fields in the cavity until steady state was reached. The steady state surface fields were then extracted.

To calculate the transformer ratio of a specific mode, only the fields from that mode should be considered. Therefore, a frequency filter was applied to the E_z field from each field monitor, such that the higher orer modes were excluded. The transformer ratio was calculated by determining the time offset of the drive bunches through the steady state field. The definition $T = \frac{\Delta W_T}{\Delta W_D}$ was used, where $\Delta W_{T,D}$ refers to the energy gained by a test bunch and the energy lost by the drive bunch respectively. The cavity Q and f_c were determined from the E_z profile from the probe at the center of the middle cell. The arrival time of each drive bunch at this probe was calculated and the field that the drive bunch

Content from this work may be used under the terms of the CC BY 3.0 licence (© 2015). Any distribution of this work must maintain attribution to the author(s), title of the work, publisher, and DOI.

ISBN: 978-3-95450-168-7 doi:10.18429/JACoW-IPAC2015-WEPWA047

EMITTANCE GROWTH IN A PLASMA WAKEFIELD ACCELERATOR

O. Mete*, K. Hanahoe, G. Xia, The University of Manchester, Manchester, UK
The Cockcroft Institute, Sci-Tech Daresbury, Warrington, UK
M. Labiche, Nuclear Physics Group, STFC Daresbury Laboratory, Sci-Tech Daresbury, Warrington, UK

Abstract

The interaction of the witness beam with the surrounding plasma particles and wakefields was studied. The implications of the elastic scattering process on beam emittance and, emittance evolution under the focusing and acceleration provided by plasma wakefields were discussed. Simulations results from GEANT4 are presented in this paper.

INTRODUCTION

The next generation of particle physics colliders will need to supplement pp collisions with e^+e^- and ep collisions to deliver precision and to address QCD research needs. Generally each successor collider should push the limits of the energy frontier further.

Plasma accelerators have made tremendous progress in the last few decades since the inception of the idea from Tajima and Dawson [1]. Nowadays, laser wakefield accelerators (LWFA) can achieve MeV-GeV level, electrons through millimetre to centimetre plasma cells [2–6]. Electron beam driven plasma wakefield acceleration (PWFA) has demonstrated energy doubling for an ultra relativistic 42 GeV electron beam in a metre long plasma structure [7]. The accelerating gradients measured in these experiments can be in the range of 10-100 GeV/m, which are 3-4 orders of magnitude larger than that in today's conventional RF-based particle accelerators.

Towards the realisation of a collider scheme based on plasma wakefield acceleration, challenges and issues must be explored.

EMITTANCE GROWTH DUE TO COULOMB SCATTERING

Under the conditions where a beam travels in the vacuum with a constant acceleration, emittance decreases with increasing energy according to the conservation of the area in the phase space given by Louville's theorem. This phenomenon is known as adiabatic damping. However, if the particles in the beam encounter a medium of gas or plasma, emittance diffusion occurs through scattering and competes against the adiabatic damping as suggested in Eq.1 [8];

$$\Delta\epsilon = \frac{F}{2\gamma\prime}\left[\sqrt{\gamma_f} - \sqrt{\gamma_i}\right], \qquad (1)$$

where $\gamma\prime$ is the rate of change of the acceleration, γ_f and γ_i are the final and initial beam energies, respectively. F is written as,

$$F = 2\pi r_e^2 n\left[\frac{-\pi\sigma_0^2 mc^2}{\lambda_p eE_{z0}cos(\phi)}\right]^{1/2} ln\left(\frac{\lambda_D}{R}\right), \qquad (2)$$

where r_e is the classical electron radius, m is the mass of the electron; n is the number of scattering centres, σ_0 is the initial beam size interacting with the scattering medium. The constant accelerating field is given as $E_{z0}sin(\phi)$.

Minimum and maximum scattering angles are determined through uncertainty in the momentum of the incident particle, p, (Eq.3) and the impact parameter, b.

$$\theta = \frac{\Delta p}{p}, \qquad (3)$$

the quantum mechanical limit $\Delta p\, b \geq \hbar$ applies resulting in Eq.4, where $\hbar$ is the reduced Planck constant,

$$\theta_{min,\,max} = \frac{\hbar}{p\, b_{max,min}}. \qquad (4)$$

The maximum impact parameter, b_{max}, comes from the shielding effect of the atomic electrons for a linear plasma wakefield. In a fully ionised plasma this will correspond to the Debye length, shown in Eq.5, where ϵ_0 is the electric permitivity of vacuum, k_B is the Boltzmann constant, T_e is the temperature of the plasma electrons, n_e is the number of electrons in the plasma and e is the charge of an electron:

$$\lambda_D = \sqrt{\frac{\epsilon_0 k_B T_e}{n_e e^2}}. \qquad (5)$$

The Debye length is the distance over which the potential of the nucleus is reduced to $1/e$ of its maximum value within a plasma due to the screening effect of the surrounding plasma electrons. For the nonlinear (bubble or blow-out) regime, where number density of the drive bunch is larger than the plasma, the maximum impact factor corresponds to the radius of the ion cavity [9].

The minimum impact parameter can be related to the effective Coulomb radius of the nucleus, R. The extrema of the scattering angle can be rewritten as in Eq.6.

$$\theta_{min} = \frac{\hbar}{p\lambda_D},\ \theta_{max} = \frac{\hbar}{pR} \qquad (6)$$

MONTE CARLO SIMULATIONS

The above theory can be examined by comparing it with the results from a Monte Carlo code which can simulate the particle-matter interactions such as GEANT4 [10, 11]. A particular scenario was simulated where an electron beam with given parameters, under constant acceleration and focusing, travels through a defined gas column undergoing only elastic Coulomb scattering. An example wake field of a 250 MeV proton drive beam is shown in Fig.1 within the simulation window of a few plasma periods. This result from

* oznur.mete@manchester.ac.uk

Content from this work may be used under the terms of the CC BY 3.0 licence (© 2015). Any distribution of this work must maintain attribution to the author(s), title of the work, publisher, and DOI.

ISBN: 978-3-95450-168-7 doi:10.18429/JACoW-IPAC2015-WEPWA048

DESIGN STUDIES AND COMMISSIONING PLANS FOR PARS EXPERIMENTAL PROGRAM

O. Mete*, K. Hanahoe, G. Xia, The University of Manchester, Manchester, UK and
The Cockcroft Institute, Sci-Tech Daresbury, Warrington, UK
M. Dover, M. Wigram, J. Wright, J. Zhang,The University of Manchester, Manchester, UK
J. Smith, Tech-X UK Ltd, Sci-Tech Daresbury, Warrington, UK

Content from this work may be used under the terms of the CC BY 3.0 licence (© 2015). Any distribution of this work must maintain attribution to the author(s), title of the work, publisher, and DOI.

Abstract

PARS (Plasma Acceleration Research Station) is an electron beam driven plasma wakefield acceleration test stand proposed for VELA/CLARA facility in Daresbury Laboratory. In order to optimise various operational configurations, 2D numerical studies were performed by using VSIM for a range of parameters such as bunch length, radius, plasma density and positioning of the bunches with respect to each other for the two-beam acceleration scheme. In this paper, some of these numerical studies and considered measurement methods are presented.

INTRODUCTION

PARS experimental station is planned on the soon-to-be-built VELA/CLARA beam line in the Daresbury Laboratories as shown in Fig. 1 [1,2]. PARS will receive an 250 MeV electron beam with a flexible parameter range. This will allow the station to conduct wide range systematic studies on electron driven plasma wakefield acceleration. Program aims to explore single and two-beam operation. The former aims to study maximum achievable accelerating gradient and head-to-tail acceleration with a single electron bunch. Whereas the latter aims to demonstrate the acceleration of a witness or trailing bunch. Numerical studies reported in this paper were performed by using VSim [3].

SINGLE BUNCH ACCELERATION

The maximum achievable accelerating gradient was studied for different bunch length and radius values between 30 − 75 μm and 20 − 100 μm, respectively, considering a 250 MeV electron bunch with a charge of 250 pC. Higher wakefields of 1 − 3 GV/m for a tightly focused drive beam (20μm), and 200 − 300 MV/m for more realistic beam sizes are possible within the bunch length range between 30 − 75 μm (Fig. 2). The achieved field gradient is proportional to the plasma density and after a certain density it scales inversely proportional to the squared bunch length as predicted by the linear theory Eq. 1,

$$E = 240(MV/m)\left(\frac{N}{4\times 10^{10}}\right)\left(\frac{0.6}{\sigma_z(mm)}\right)^2 \qquad (1)$$

* oznur.mete@manchester.ac.uk

where N is the density of background plasma electrons and σ_z is the bunch length. A realistic case of 50 μm bunch length and 100 μm bunch radius which yields 300 MV/m gradient for single bunch propagated 4.5 mm at a plasma density of $5\times 10^{21}\ m^{-3}$ was selected for further studies in this paper.

TWO-BUNCH ACCELERATION

A two-beam scenario was simulated using the baseline case detailed above. A second bunch of same sizes but with a certain fraction of the drive bunch charge was initially placed half a plasma wavelength ($\lambda_p/2$) behind the centre of the driver bunch. The maximum energy gain and the minimum energy spread of the trailing bunch was found to occur between ($\lambda_p/2 - 40$) μm and ($\lambda_p/2 - 20$) μm behind the driver bunch as shown in Fig. 3. The initial two beam configuration shown in Fig. 4(a) was tracked along a 0.5 m long plasma column. Figure4(b) shows the beam profiles evolved after 0.45 m reaching an energy of 315 MeV with a 10% energy spread. Energy spread control is under study through beam loading and bunch profile manipulation. A “fish-bone” structure starts forming in the driver bunch and both bunches are transversely focused where there is no significant bunch length change. 2D field distribution for the two-beam case is given in Fig. 5 with accelerating blue region and decelerating red region. Plasma wakefields consist of co-existing transverse and longitudinal fields as they are induced due to the motion of the plasma electrons in both directions. The transverse field accompanying the above longitudinal field is shown in Fig. 6(a) as a 2D intensity map. The transverse fields generally have a comparable field strength to the longitudinal fields (Fig. 6(b)) and they might act as focusing fields depending on the phase of the trailing bunch.

BEAM LOADING WITH TWO BUNCHES

It has been observed that in the presence of a second bunch the resulting field in the region is modified by the self electromagnetic field of this bunch. This phenomena is similar to the “beam loading” in the RF cavities. The position of the second beam can be adjusted so that the beam loading effect can be used, in favour of the scheme, in a way to reduce the energy spread on the second bunch by adjusting the field gradient across it. Such a scan was performed by moving the trailing bunch around its initial location at $\lambda_p/2$. Effect of the beam loading on controlling the energy

ISBN: 978-3-95450-168-7 doi:10.18429/JACoW-IPAC2015-WEPWA049

LOW ENERGY BEAM TRACKING UNDER SCATTERING FOR A COLD ELECTRON SOURCE IN MANCHESTER

R.B. Appleby*†, W. Bertsche§, M. Harvey¶, M. Jones, B. Kyle, O. Mete†, A. Murray¶, G. Xia†,
The University of Manchester, Manchester, M13 9PL, United Kingdom

Abstract

High quality electron beams, with high spatial and temporal resolution, have an important use in electron diffraction experiments to probe and study the constituents of matter. A cold electron source is being developed based on electron ionisation from an atom cloud trapped by using AC magneto-optical methods in the University of Manchester. The technique will produce bunches of electrons well suited for high precision and single shot electron diffraction. In this paper issues of modelling at low energies for this state of art electron source with very low energy spread are presented, with a focus on newly developed tools to model the scattering in the meshes used to support the extraction electric fields. The dependence on emittance growth on mesh wire thickness is studied.

INTRODUCTION

Electron diffraction experiments are an integral part of many fields of research, including crystallography, spectroscopy and investigations into chemical bonding. As these fields progress, there is an ever-increasing need for electron beams with better spatial and temporal resolution, requiring investigation into novel methods of increasing beam quality. The AC-MOT, currently being developed at Manchester, promises to deliver low-emittance and low temperature beams through the cooling of the electron source using magneto-optical trapping [1, 2]. It offers advantages over conventional magneto-optical trapping techniques through the AC magnetic field, such that there are no residual fields due to eddy currents persisting after the trapping cycle has ended. As such, the trajectories of electrons extracted from the AC-MOT are unaffected by stray external fields resulting in a more reliable electron source with potentially higher beam quality. We present in this paper newly developed tools to study particle transport and scattering in the Manchester-Cockcroft Institute experiment and show results of simulations conducted to model the extraction process from the AC-MOT. In this work several codes have been employed, namely CST [3], for modelling the experimental region and calculating the electric fields used for electron extraction; General Particle Tracer [4], for simulation of particle trajectories in drift spaces; and Geant4 [5, 6], for determining emittance growth due to scattering. Note that some preliminary calculations have been performed with FLUKA [7] but are not described in this paper. We outline an assessment of the extraction configuration which is being built and make the first look at the impact of mesh scattering on the transported electrons.

* Corresponding author, Robert.Appleby@manchester.ac.uk. † The Cockcroft Institute of Accelerator Science and Technology. § European Organisation for Nuclear Research, CERN. ¶ The University of Manchester - Photon Science Institute.

EXTRACTION REGION LAYOUT

The atoms in the MOT are ionised and the electrons are extracted using a series of electrostatic electrodes towards the diagnostic section (or later an electron diffraction experiment or injection into a FEL). A full description of the AC-MOT in this experiment can be found in [1]. After passing through the grounded MOT field coils, the electrons pass through three electrodes connected to 5 kV power supplies, which provide the extraction fields. An electrode is constructed of a stainless steel ring covered with a fine mesh, designed to support the fields but allow electron transmission. The three electrodes are followed by the Microchannel Plate (MCP) detector, with its front plate biased at 200 V. The electrode arrangement is shown in Fig. 1.

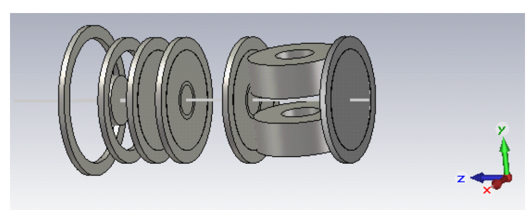

Figure 1: The layout of the extraction region, showing the extraction electrodes.

The need to accelerate and extract the electrons before the bunch is rapidly expanded by space-charge forces means the extraction voltages need to be high. The MOT coils are grounded and the voltage plates are positioned to provide a strong electric field over the MOT region and subsequent transport of the electrons towards the MCP is performed in a drift region delimited by the first and second electrodes, both held at 5 kV. A third plate very close to the second plate is held at 2 kV and provides a retarding electric field to slow the electrons down in a short time before the MCP to provide optimum MCP efficiency. The fast extraction configuration gives a strong field across the MOT, resulting in a larger energy spread than the penetrating field configuration described in [2]. Figure 2 shows the voltages applied to the plates and the resulting potential, computed using the electrostatic modelling tools of CST-Microwave Studio [3].

Content from this work may be used under the terms of the CC BY 3.0 licence (© 2015). Any distribution of this work must maintain attribution to the author(s), title of the work, publisher, and DOI.

ISBN: 978-3-95450-168-7 doi:10.18429/JACoW-IPAC2015-WEPWA051

Content from this work may be used under the terms of the CC BY 3.0 licence (© 2015). Any distribution of this work must maintain attribution to the author(s), title of the work, publisher, and DOI.

INVESTIGATIONS INTO DIELECTRIC LASER-DRIVEN ACCELERATORS USING THE CST AND VSIM SIMULATION CODES*

Y. Wei#, C.P. Welsch, Cockcroft Institute and University of Liverpool, UK
G. Xia, O. Mete, K. Hanahoe, Cockcroft Institute and University of Manchester, UK
J.D.A. Smith, Tech-X UK Ltd, Sci-Tech Daresbury, Warrington, UK

Abstract

Dielectric laser-driven accelerators (DLAs) based on gratings structures have received a lot of interests due to its high acceleration gradient up to GV/m and mature lithographic techniques for fabrication. This paper presents detailed numerical studies into the acceleration of relativistic and non-relativistic electrons in double gratings silica structures. The optimization of these structures with regards to maximum acceleration efficiency for different spatial harmonics is discussed. Simulations were carried out using the commercial CST and VSim simulation codes and results from both codes are shown in comparison.

INTRODUCTION

Dielectric laser-driven accelerators (DLA) have good potential to become a strong candidate for future electron accelerators. Due to a higher damage threshold than metals, these dielectric microstructures can support accelerating fields higher than what can be achieved in conventional accelerators. This can increase the acceleration gradients up to GV/m. An experiment has successfully demonstrated acceleration of relativistic electrons with an accelerating gradient of 250 MV/m in a fused silica double grating structure [1] and the acceleration of non-relativistic 28 keV electrons with a gradient of 25 MeV/m in a single grating structure was also observed [2].

This paper investigates dielectric laser-driven acceleration of electrons in a double grating structure exploiting the different spatial harmonics excited by the diffraction of the incident laser. The double grating structure was originally proposed by Plettner [3] and is shown in Figure 1. Each grating pillar adds a phase shift with respect to the adjacent vacuum space, which produces a longitudinally periodic oscillating electric field in the centre of the vacuum channel. Optimization studies into these structures by parameter variation studies have already been performed with the aim to increase the acceleration efficiency for highly relativistic electrons [4,5]. Here, we consider also the non-relativistic case where electrons are injected at an energy of 25 keV, corresponding to β=0.3, where β=v/c, v the electron velocity and c the speed of light. Different spatial harmonics were considered using the CST [6] and VSim [7] simulation codes to identify the optimum acceleration efficiency and comparing simulation results.

*This work is supported by the EU under Grant Agreement 289191 and the STFC Cockcroft Institute core grant No.ST/G008248/1.
#yelong.wei@cockcroft.ac.uk

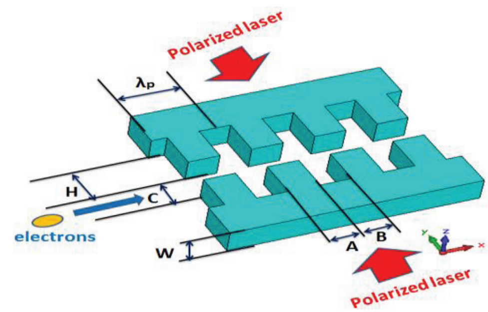

Figure 1. Schematics of a dielectric grating structure.

ACCELERATION OF HIGHLY RELATIVISTIC ELECTRONS

When a double grating structure is driven by two TM polarized laser beams from opposite sides, the diffraction of the incident laser at the grating excites different spatial harmonics which can all be used in principle to accelerate the electrons, see Figure 2.

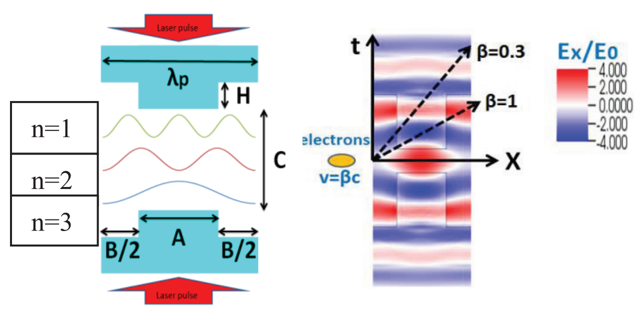

Figure 2. Illustration of the first, second and third spatial harmonics for the case that one grating period is illuminated by laser from two sides.

In the simulations an incoming plane wave with a wavelength of λ_0=1,550 nm was used to excite the grating structure from two sides. Silica (SiO_2, refractive index n=1.528) was chosen as grating material due to its good properties in terms of transparency and field damage threshold. Figure 3 shows the acceleration efficiency for different structure parameters for a grating period of λ_p = 1,550 nm. With an increase of the vacuum channel width C, the acceleration efficiency η gradually decreases, as can be seen in Figure 3(a). Figure 3(b) shows that the maximum acceleration efficiency can be achieved when the pillar height H=0.87λ_p. For further optimization the pillar ratio A/λ_p was varied and Figure 3(c) shows the resulting optimum acceleration efficiency of 0.25 and 0.26 as computed by VSim and CST, respectively.

ISBN: 978-3-95450-168-7 doi:10.18429/JACoW-IPAC2015-WEPWA052

RF CONDITIONING OF THE PHOTO-CATHODE RF GUN AT THE ADVANCED PHOTON SOURCE – NWA RF MEASUREMENTS*

T.L. Smith, N. DiMonte, A. Nassiri, Y. Sun, A. Zholents
ANL, Argonne, IL 60439, USA

Abstract

A new S-band photo-cathode (PC) gun was recently installed and RF conditioned at the Advanced Photon Source (APS) Injector Test-stand (ITS) at Argonne National Lab (ANL). The APS PC gun is a LCLS type gun fabricated at SLAC [1]. The PC gun was delivered to the APS in October 2013 and installed in the APS ITS in December 2013. At ANL, we developed a new method of fast detection and mitigation of the gun's internal arcs during the RF conditioning process to protect the gun from arc damage and to RF condition more efficiently. Here, we report the results of RF measurements for the PC gun and an Auto-Restart method for high power RF conditioning.

INTRODUCTION

RF measurements performed on the gun at the APS before installation confirmed the measurements made at SLAC before the gun was shipped to ANL. After the gun was fully RF conditioned and photo-electron beam commissioned in the ITS, the gun was baked to improve vacuum and then installed into the APS linac tunnel in August 2014 (Figure 1).

During the PC gun conditioning at the APS, three different protection systems were used to disable RF in order to prevent gun damage that could be caused by sustained or continuous arcing: 1) vacuum pressure interlock, 2) reflected RF power interlock, and 3) arc detector interlock. Arcing is a common phenomenon during RF conditioning and typically it is not required to disable the RF on every single random arc, however, it is prudent to disable the RF on all sustained arcs. A new Auto-Restart method has been developed that limits the number of arcs associated with the PC gun, which is interlocked to both the RF reflected power (~4µs trip) and the arc detector (~3µs trip) systems. During Auto-Restart, both protective systems will shut off RF to the gun every time there is a reflected power or an arc detected. The Auto-Restart scripts will turn the RF back on automatically in < 20ms if it is a single-arc event and not a sustained arc. With the APS linac operating at a maximum of 30 Hz repetition rate, the RF will turn back on easily before the next RF pulse. The Auto-Restart system is "fail-safe" in that if the Auto-Restart script would quit working, both protective circuits are hard-wire interlocked and the RF would trip off at the next arc event and will remain off.

* Work supported by U.S. Department of Energy, Office of Science, under Contract No. DE-AC02-06CH11357

PC GUN OVERVIEW AND MEASUREMENT RESULTS

The photo-cathode RF gun and its magnets are identical to the LCLS gun system. The 1.6 cell S-band RF gun has dual RF feeds to mitigate the dipole field [1]. The basic requirements from the RF gun design include ~15MHz mode separation between the zero and π modes, 120 MV/m accelerating gradient on axis, and a cavity quality factor Q0 > 11500 [2]. The gun and focusing magnets are critical in order to generate high-brightness beams. After gun conditioning in the ITS, the gun and the solenoid assembly were baked for five days at 150ºC in order to improve the gun base pressure. The PC gun and its beam line components were installed in the APS linac tunnel in August 2014 after completion of the bake. The vacuum conditions of the PC gun after linac installation are gun cathode cell (cold cathode gauge) = 7 x 10^{-9} Torr and gun waveguide = 2 x 10^{-10} Torr.

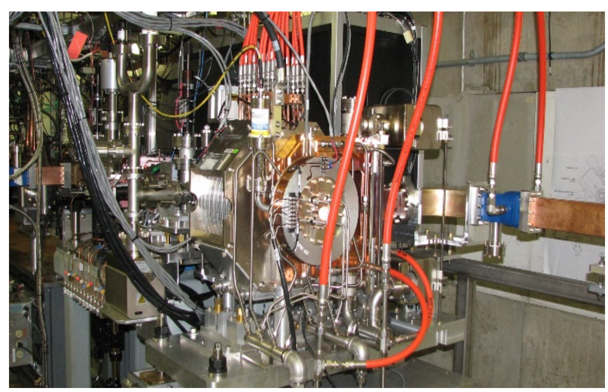

Figure 1: PC Gun Installed in the APS Linac Tunnel.

Initial network analyzer measurements were completed at SLAC, including bead drop measurements. Upon receiving the gun at the APS, RF measurements were performed using a closed water system to control the gun temperature such that the π-mode frequency was set to 2856.0 MHz. Resonant frequencies of the zero and π modes, quality factors, and coupling coefficients were made using a network analyzer. The gun body temperature was varied by ± 4ºC and the above measurements were repeated.

Unloaded Q, External Q and Loaded Q were measured using the Impedance Method [3]. To characterize the PC gun before installation, the following measurements were performed (see Table 1).

Content from this work may be used under the terms of the CC BY 3.0 licence (© 2015). Any distribution of this work must maintain attribution to the author(s), title of the work, publisher, and DOI.

ISBN: 978-3-95450-168-7 doi:10.18429/JACoW-IPAC2015-WEPWA053

FIRST ACCELERATION IN A RESONANT OPTICAL-SCALE LASER-POWERED STRUCTURE

R. B. Yoder, Goucher College, Dept. of Physics & Astronomy, Baltimore, MD 21204 USA
G. Travish, J. McNeur, E. Sozer, K. S. Hazra, B. Matthews
UCLA, Los Angeles, CA 90095, USA
R. J. England, Z. Wu, SLAC, Menlo Park, CA 94025, USA
E. Peralta, K. Soong, Stanford University, Dept. of Applied Physics, Stanford, CA 94305 USA

Abstract

The Micro-Accelerator Platform (MAP), an optical-scale dielectric laser accelerator (DLA) based on a planar resonant structure that was developed at UCLA, has been tested experimentally. Successful acceleration was observed after a series of experimental runs at SLAC's NLCTA facility, in which the input laser power was well below the predicted breakdown limit. Though acceleration gradients were modest (<50 MeV/m), these are the first proof-of-principle results for a resonant DLA structure. We present more detailed results and some implications for future work.

INTRODUCTION

Dielectric Laser Accelerators (DLAs) have the potential to operate with high (~GV/m) acceleration gradients, and represent a path toward extremely compact colliders and industrial accelerator technology [1]. DLA devices are optical-scale microstructures that can be fabricated on wafers via methods developed for the microchip industry, and powered using fiber lasers, which afford very high repetition rates in compact packages. These devices are naturally suited to a novel length and time scale, producing sub-fs, sub-μm and sub-pC bunches at MHz repetition rates.

Experimentally, advanced accelerators are at the proof-of-principle stage [2], with performance metrics including total energy gain, maximum acceleration gradient, and peak field strength. We report here on a series of experimental tests of the Micro-Accelerator Platform (MAP), a resonant DLA based on a slab-symmetric structure. As a resonant (rather than near-field) device, the MAP is distinct from other DLAs [1].

STRUCTURE AND FABRICATION

Theoretical analysis and many fabrication details of the MAP have been described in previous work [3,4]. In brief, the MAP is a slab-symmetric (planar) resonant structure constructed from a pair of partial Bragg reflectors (DBRs), which surround an accelerating gap. Laser power is coupled into the structure through a transmissive diffraction grating placed atop one of the surfaces, which serves to enforce a synchronous accelerating mode within the gap.

Potential dielectric materials used for fabrication are limited to a small class of oxides having high breakdown thresholds, high transparency, and good uniformity. The MAP is constructed on a fused silica substrate, with the DBRs made from alternating layers of hafnia and zirconia for maximum contrast. The MAP structures as built measured 1.0 ± 0.1 mm in length and 1.00 ± 0.01 mm in thickness, with a transverse area of 3.3 mm, comprising 1250 optical periods.

An error tolerance budget was established via simulation, tracking mode quality and resonant frequency shift. The main tolerance constraint is not the mode quality itself, but the need to maintain the resonant frequency within 25 THz. The most restrictive tolerances, on the boundary layers in the Bragg reflectors, are on the order of ±1 nm; and are at state-of-the-art, for many processes.

In practice, dozens to hundreds of half-structures were fabricated at once, diced, then bonded in pairs. Each structure was checked for quality both visually and optically. We note that bonding the structure halves, and determining the exact gap height, are significant technological challenges.

Content from this work may be used under the terms of the CC BY 3.0 licence (© 2015). Any distribution of this work must maintain attribution to the author(s), title of the work, publisher, and DOI.

ISBN: 978-3-95450-168-7 doi:10.18429/JACoW-IPAC2015-WEPWA055

PROTON INJECTION INTO THE FERMILAB INTEGRABLE OPTICS TEST ACCELERATOR (IOTA)*

E.J. Prebys, S. Antipov, H. Piekarz, A. Valishev, Fermilab, Batavia, IL 60510, USA

Abstract

The Integrable Optics Test Accelerator (IOTA) is an experimental synchrotron being built at Fermilab to test the concept of non-linear "integrable optics". These optics are based on a lattice including non-linear elements that satisfies particular conditions on the Hamiltonian. The resulting particle motion is predicted to be stable but without a unique tune. The system is therefore insensitive to resonant instabilities and can in principle store very intense beams, with space charge tune shifts larger than those which are possible in conventional linear synchrotrons. The ring will initially be tested with pencil electron beams, but this poster describes the ultimate plan to install a 2.5 MeV RFQ to inject protons, which will produce tune shifts on the order of unity. Technical details will be presented, as well as simulations of protons in the ring.

INTRODUCTION

Table 1: HINS Parameters for IOTA

Parameter	Value	Unit
Particle type	proton	-
Kinetic Energy	2.5	MeV
Momentum	68.5	MeV/c
β	.073	-
Rigidity	.23	T-m
RF structure	325	MHz
Current	8	mA
Circumference	39.97	m
Total Protons	9.1×10^{10}	-
RMS Emittance (un-normalized)	4	π-mm-mrad
Tune shift	-.51$\times B$	-
Pulse rate	<1	Hz
Pulse length	1.77	μsec

All particle optics to date have been based on linear magnetic systems of quadrupoles and dipoles. Higher order multipoles are treated perturbatively, and generally lead to instabilities if they are large enough. It has long been known that very specific conditions can produce stable orbits in non-linear magnetic systems [1] [2]; however, it was not until fairly recently that specific magnetic lattices were proposed that satisfy these conditions [3]. Such systems have stable orbits, but not unique tunes. They are therefore extremely insensitive to harmonic instabilities, thereby allowing the storage of beams with intensitities beyond those which would otherwise be limited by space charge tune shift.

* Work supported by the United States Department of Energy under Contract No. DE-AC02-07CH11359

The Integrable Optics Test Accelerator (IOTA) at Fermilab is being built to test this concept, and is described in detail elsewhere [4]. Initial tests will use a 150 MeV electron beam from the Advanced Superconducting Test Acceleratator (ASTA) facility at Fermilab [6]. By varying initial conditions, this electron beam can be used to probe the optical space of the ring; however, since the space charge effects on the electron beam will be negligible, it will not serve as a direct test of the inherent stability.

As a next step, we therefore plan to reuse the 2.5 MeV RFQ, which was built for Fermilab's High Intensity Neutrino Source (HINS) program [5]. This RFQ became available when the lab chose to focus instead on a CW ion source for its high intensity program.

DESIGN

IOTA

Figure 1 shows the IOTA ring. The ring is essentially an ordinary lattice with two straight sections to accommodate the non-linear elements for the proposed optical tests. A straight section is also provided for optical stochastic cooling tests, which are separate from the non-linear optics program.

Initial tests of the IOTA ring will use the 150 MeV electron beam from the ASTA test facility. This facility was built primarily to test 1.3 GHz cryomodules, of the sort that could be used for a linear electron collider. It is also used to support an electon-based R&D program. In the figure, the elecron beam is seen entering from the upper left. A system of dipoles can selectively direct the electron beam to the IOTA ring, a beam dump, or potentially other electron experiments.

Because space charge is not an issue for an electron beam of this energy, the non-linear optics will be probed by varying the initial position and trajectory of the beam and observing the orbit.

HINS RFQ

The High Intensity Neutrino Source (HINS) program began as R&D to develop the front end of an 8 GeV proton linac, which was being considered as an upgrade the the Fermilab accelerator complex (the so-called "Project X") [7]. To this end, a 2.5 MeV RFQ was built, with the goal of producing a beam up to several mA, with a duty factor of 1%. This was followed by a bunching cavity and a series of spoke resonators, with the goal of ultimately accelerating the beam to 10 MeV.

The source consists of a 50 kV filament proton source, capable of delivering 8 mA. The RFQ itself is a four vane

Content from this work may be used under the terms of the CC BY 3.0 licence (© 2015). Any distribution of this work must maintain attribution to the author(s), title of the work, publisher, and DOI.

ISBN: 978-3-95450-168-7 doi:10.18429/JACoW-IPAC2015-WEPWA056

Content from this work may be used under the terms of the CC BY 3.0 licence (© 2015). Any distribution of this work must maintain attribution to the author(s), title of the work, publisher, and DOI.

THE SINUOUS TARGET

R. Zwaska, FNAL, Batavia, IL 60510, USA

Abstract

We report on the concept for a target material comprised of a multitude of interlaced wires of small dimension. This target material concept is primarily directed at high-power neutrino targets where the thermal shock is large due to small beam sizes and short durations; it also has applications to other high-power targets, particularly where the energy deposition is great or a high surface area is preferred. This approach ameliorates the problem of thermal shock by engineering a material with high strength on the micro-scale, but a very low modulus of elasticity on the meso-scale. The low modulus of elasticity is achieved by constructing the material of spring-like wire segments much smaller than the beam dimension. The intrinsic bends of the wires will allow them to absorb the strain of thermal shock with minimal stress. Furthermore, the interlaced nature of the wires provides containment of any segment that might become loose. We will discuss the progress on studies of analogue materials and fabrication techniques for sinuous target materials.

INTRODUCTION

We propose to generate a new, engineered material for use in high-power accelerator targets. This material will be composed of a multitude of interlaced wires, or rills, of small dimension. The rills will be made of a thermal-shock resistant material, but will not be subject to stress accumulation due to their small size. The intrinsic bends of the wires will allow them to absorb the strain of thermal shock with minimal stress. The solid bulk of this material will have a dramatically reduced modulus of elasticity than the bare material, greatly improving its resistance to thermal shock. Furthermore, the interlaced nature of the wires provides containment of any segment that might become loose.

This material could accommodate dramatically higher beam powers without breaking itself to pieces because it is strong on the micro-scale, but resilient and flexible on the meso-scale. The challenges will be fabricating this material and devising a cooling scheme.

BACKGROUND

A high-power target is an integral part of a neutrino beam, muon beam, and areas outside HEP such as neutron and rare isotope sources. The target rests in the center of the entire facility; it is within the target that the majority of the transformation occurs from an intense proton (or other species) beam produced by the accelerator, to a beam of unstable or rare particles suitable for experimentation. The target is a singular item, being small on the scale of other beam components. Yet, it bears the brunt of thermal, mechanical, and radiation effects [1].

Intense beam facilities operate targets at the edge of their capability [2]. Frequently, the intensity of a facility is limited by the target, or compromises are made in efficiency to make the target more survivable. Extending the capability of targets is central to building the next generations of all these facilities.

The key novelty of the sinuous approach is to engineer a material's properties to make it more survivable. We capitalize on a counter-intuitive fact: a stronger material is often inferior as a target material.

The actual factor we are interested in is the stiffness of the material which often goes hand-in-hand with strength. Particularly, we are concerned with a material's modulus of elasticity (or bulk or Young's modulus). This factor is crucial as it is what causes material to break under the influence of beam (short of melting). As a beam passes through the material, its energy deposition is thermalized producing a very rapid temperature rise correlated to the spatial intensity of the beam. The beam necessarily has a non-uniform profile, leading to uneven heating of the material. The material will attempt to expand at a local level in response to the heat, but cooler areas will resist this change. The difference in expansions must be equalized through the application of stress to compress or expand the material. That stress, S, is directly correlated to the length difference to be corrected (strain, ϵ) and the bulk modulus, K: $S = K \times \epsilon$. If this stress exceeds the yield strength of the material, it will start to fail. This is a predominant design requirement for targets and other significant mechanical components. Figures of merit have been designed using these and other parameters to evaluate the suitability of various target materials [3].

Unfortunately, for most materials strength is directly proportional to the bulk modulus: a strong material will be stiff. We desire a material with high intrinsic strength on the micro-scale, but very flexible: having a low bulk modulus. The most straightforward way to achieve this is to make the material into a spring. Then, to build a bulk, these springs can be overlaid and combined to build up a material that is nearly uniform on the meso-scale of the proton beam. The temperature-induced strain on this material will be negligible to its ability to expand, and strains will be non-existent.

There are further advantages of the small scale of the primary material. The cross-section will be so small that the heating will be uniform on the length scales of the material, so it will simply expand uniformly at the micro-scale. Stress waves will be inhibited as they also depend on non-uniform heating and propagation through a bulk: any waves would simply travel along the wires. The material can also be made more resistant to radiation damage effects as the lattice dislocations in a material attempt to migrate through the bulk until reaching a grain boundary, and further to the exterior of the material. As this material will be much smaller, the

ISBN: 978-3-95450-168-7 doi:10.18429/JACoW-IPAC2015-WEPWA057

DESIGN CONCEPTS FOR MUON-BASED ACCELERATORS

R. D. Ryne, LBNL, Berkeley CA 94720 USA
J. S. Berg, H. G. Kirk, R. B. Palmer, D. Stratakis, BNL, Long Island NY USA
Y. Alexahin, A. Bross, K. Gollwitzer, N. V. Mokhov, D. Neuffer, M. A. Palmer, K. Yonehara, FNAL, IL
P. Snopok, IIT, Chicago IL USA
A. Bogacz, JLab, Newport News, VA 23606, USA
T. J. Roberts, Muons Inc., Chicago IL USA
J.-P. Delahaye, SLAC, Menlo Park CA USA

Abstract

Muon-based accelerators have the potential to enable facilities at both the Intensity and the Energy Frontiers. Muon storage rings can serve as high precision neutrino sources, and a muon collider is an ideal technology for a TeV or multi-TeV collider. Progress in muon accelerator designs has advanced steadily in recent years. In regard to 6D muon cooling, detailed and realistic designs now exist that provide more than 5 order-of-magnitude emittance reduction. Furthermore, detector performance studies indicate that with suitable pixelation and timing resolution, backgrounds in the collider detectors can be significantly reduced thus enabling high quality physics results. Thanks to these and other advances in design & simulation of muon systems, technology development, and systems demonstrations, muon storage-ring-based neutrino sources and a muon collider appear more feasible than ever before. A muon collider is now arguably among the most compelling approaches to a multi-TeV lepton collider. This paper summarizes the current status of design concepts for muon-based accelerators for neutrino factories and a muon collider.

INTRODUCTION

It has been more than 3 decades since muon colliders and muon storage rings were proposed [1-3]. Interest in muon colliders increased significantly following the observation that ionization cooling could be used to rapidly cool muon beams. Several workshops were held in the 1980s and 1990s, and in 1997 the Muon Collider Collaboration was formed, which later became the Neutrino Factory and Muon Collider Collaboration (NFMCC). By the late 1990's muon collider and neutrino factory design efforts were well-established worldwide. In 2007 the International Design Study for a Neutrino Factory (IDS-NF) was initiated. In 2011, muon R&D in the United States was consolidated into a single entity, the Muon Accelerator Program (MAP) [4].

The purpose of MAP is to perform R&D in muon accelerator technologies and to perform design & simulation to demonstrate the *feasibility* of concepts for neutrino factories and muon colliders. In the short time that MAP has existed there have been many accomplishments that have significantly changed our understanding of technology limits and design concepts for muon accelerators.

Particularly noteworthy is the situation regarding RF breakdown in magnetic fields, as is needed in ionization cooling systems. At the time MAP was initiated there was significant concern that RF cavities could not operate at sufficiently high magnetic fields while maintaining high gradients. Under MAP this phenomena has been understood and several solutions demonstrated. Careful cavity design has been shown to limit gradient loss with increasing magnetic field. Beryllium has been shown to have almost no damage due to breakdown compared with copper. Experiments at the Fermilab MuCool Test Area (MTA) have demonstrated that using cavities filled with high-pressure gas can prevent this breakdown, and that this is a viable technology for muon cooling systems [5].

Under MAP design studies have been carried out hand-in-hand with technology R&D, because for the designs to be credible they need to take account of technology limits. Though MAP has not involved detailed engineering studies, the designs studies have been performed with an awareness of gradient limits, space requirements for hardware, etc.

At this conference, more than 60 papers have been submitted on muon accelerator designs and technologies. Very many of these were submitted by MAP researchers. The following highlights some key accomplishments under MAP in design concepts for muon-based accelerators for neutrino factories and muon colliders.

DESIGN OVERVIEW

The MAP design & simulation effort included neutrino factories (short baseline and long baseline) and muon colliders. The Muon Accelerator Staging Study (MASS) developed a staged approach that bridged the Intensity Frontier and the Energy Frontier [6,7]. An important aspect is that each stage is both a facility for doing physics and an R&D facility for the next stage.

The staging begins with nuSTORM [8], a short-baseline neutrino facility that could be built with existing technology. Experiments done at nuSTORM could settle the sterile neutrino debate, and could provide precise neutrino cross-section measurements needed for long-baseline experiments like DUNE. In nuSTORM, pions would be injected into a decay ring with long straights where they would decay into muons that would be stored, and whose decays would produce a precision neutrino beam. The remaining non-decayed pion beam would be directed at a beam dump that would provide beam to an R&D platform on muon cooling.

Content from this work may be used under the terms of the CC BY 3.0 licence (© 2015). Any distribution of this work must maintain attribution to the author(s), title of the work, publisher, and DOI.

ISBN: 978-3-95450-168-7 doi:10.18429/JACoW-IPAC2015-WEPWA059

RF PLASMA-BASED ION SOURCE MODELING ON UNSTRUCTURED MESHES *

S. A. Veitzer†, Tech-X Corporation, Boulder, CO, 80303 USA
K. R.C. Beckwith, Tech-X Corporation, Boulder, CO, 80303 USA
M. Kundrapu, Tech-X Corporation, Boulder, CO, 80303 USA

Abstract

Ion source performance for accelerators and industrial applications can be improved through detailed numerical modeling and simulation. There are a number of technical complexities with developing robust models, including a natural separation of important time scales (rf, electron and ion motion), inclusion of plasma chemistry, and surface effects such as secondary electron emission and sputtering. Due to these computational requirements, it is typically difficult to simulate ion sources with PIC codes.

An alternative is to use fluid-based codes coupled with electromagnetics in order to model ion sources. These types of models can simulate plasma evolution and rf-driven flows while maintaining good performance. We show here recent results on modeling the H- ion source for the Spallation Neutron Source (SNS) at Oak Ridge National Laboratory (ORNL) using the fluid plasma modeling code USim. We present new meshing capabilities for generating and parallelizing unstructured computational meshes that have increased our parallel code performance and enabled us to model inductively coupled plasmas for long periods of operation.

ION SOURCE MODELING CHALLENGES

Ion sources are used in a large variety of research and industrial applications, including front-end uses for particle accelerators. A large class of sources produce ions through inductive coupling of rf energy with a plasma. For example, the internal antenna H- source currently in use, and the next-generation external antenna source at the Spallation Neutron Source (SNS) are both inductively coupled sources.

Accurate numerical models of ion sources can provide insights into techniques for both predicting source performance, as well as optimizing design features and understanding failure mechanisms and failure mitigation. However, in these kinds of systems there are typically physical processes that are operating on different spatial and temporal scales, which makes developing models that are both accurate and can be executed in a reasonable amount of time difficult. For instance, to explicitly capture the physics of plasma motion, a model must resolve the Debye length of the plasma over device lengths of many tens of cm, and resolve rf frequencies of tens of MHz over many hundreds or thousands of rf periods. In addition, ion motions are thousands of times slower than electron motions due to mass differences. The result is that numerical models require solving coupled equations on large physical domains with a very large number of computational cells, short time steps, and long duration simulations.

Due to the computational requirements, it is typically not possible to execute straight-forward explicit Particle-In-Cell (PIC) models for ion sources. Alternatively, models that ease time step restrictions over PIC models, such as fully implicit PIC models for both fields and particles (e.g. divergence-preserving ADI methods), some electrostatic methods, and fluid models that do not explicitly resolve electron motions, such as various magnetohydrodynamic (MHD) models can give results that are accurate and computationally efficient.

For PIC and fluid models, plasma and particle motions and electromagnetic and hydrodynamic fields are solved for on a computational grid, or mesh, that covers the domain of the simulation. Algorithms to efficiently solve these equations have been developed over the last 50 years and this continues to be an active area of research. Algorithms for solvers differ depending on the kind of mesh that is being used. For instance, on a structured mesh such as a uniform Cartesian mesh, one may employ the Yee algorithm in a Finite Difference Time Domain solver to compute electromagnetic fields to 2^{nd}-order accuracy. However, on an unstructured mesh, where mesh elements are comprised of tetrahedrons and hexahedrons, finite element or finite volume solvers are needed to gain 2^{nd}-order accuracy. Parallel computing, in the form of domain decomposition, is required to be able to model ion sources using any of the types of models described above. This is because in order to resolve the smallest physical processes, models can consist of meshes that have tens of millions of computational cells or more, meaning that the memory required to perform the computations are too large to fit into memory on a single computer, even with multiple cores. Parallel computation on large domain-decomposed meshes can provide sufficient performance in time-domain codes. Coupling distributed parallelism with reduced physical models that do not explicitly follow electron motions make it possible to simulate inductively coupled ion sources accurately while still being computationally efficient enough to perform long timescale simulations in a reasonable amount of wall-clock time.

* This work was performed under the auspices of the Department of Energy, Office of Basic Energy Sciences Award #DE-SC0009585. This research used resources of the National Energy Research Scientific Computing Center, a DOE Office of Science User Facility supported by the Office of Science of the U.S. Department of Energy under Contract No. DE-AC02-05CH11231.
† veitzer@txcorp.com

Content from this work may be used under the terms of the CC BY 3.0 licence (© 2015). Any distribution of this work must maintain attribution to the author(s), title of the work, publisher, and DOI.

ISBN: 978-3-95450-168-7 doi:10.18429/JACoW-IPAC2015-WEPWA060

INTERACTION OF A VOLUMETRIC METAMATERIAL STRUCTURE WITH AN ELECTRON BEAM

X. Lu, M. A. Shapiro, R. J. Temkin, MIT, Cambridge, MA 02139, USA

Abstract

A volumetric metallic metamaterial structure with a cubic unit cell is introduced. The unit cells can naturally fill all of space without additional substrates or waveguides. The structure can support a negative longitudinal electric mode that can couple to an electron beam. The dispersion characteristics of the unit cell are modeled by the effective medium theory with spatial dispersion. The theory also predicts the correct resonant frequencies of the emitted radiation excited by an electron beam traversing the structure. In the wakefield simulations, a backward radiation pattern is observed. The proposed metamaterial can be applied to beam diagnostics and wakefield acceleration.

INTRODUCTION

Metamaterials (MTMs) generally refer to subwavelength structures engineered to have exotic electromagnetic features. The resonator type [1] and the transmission line type [2] structures are developed as the negative refractive index MTMs for applications in electromagnetic cloaking, antenna design and microstrip lines, etc. However, the interaction of the MTMs with an electron beam is a new area of research and differs from the study of passive microwave devices where the planar MTM design is often adopted. The planar unit cells, like the split ring resonators, require supporting dielectric substrates, which will suffer from breakdown in the face of high power. Besides, electromagnetic fields are concentrated on the planar plates, so when an electron beam needs to be arranged in the structure, a reasonable spacing must be preserved between the beam and the planar structure, and the decreased field intensity at the beam location restricts the achievement of a large coupling impedance. These difficulties call for the design of a real 3D MTM unit cell. It should fill the space automatically, so we can study the fields in a bulk structure stimulated by the electron beam in a clean environment without the complexity arising from additional substrates or supporting parts.

In this paper, we will present the design of such a 3D MTM unit cell design. We will also introduce an analytical modeling technique, the effective medium theory with spatial dispersion. Radiation features and a possible application for wakefield acceleration will also be discussed.

DESIGN AND CHARACTERIZATION OF THE UNIT CELL

The unit cell is an all-metal coupled-cavity cubic crystal with beam holes and coupling slots. The structure design is shown in Fig. 1. The design frequency is 17 GHz, and the coupling slots through which the electromagnetic waves are coupled is about one tenth of the wavelength in size.

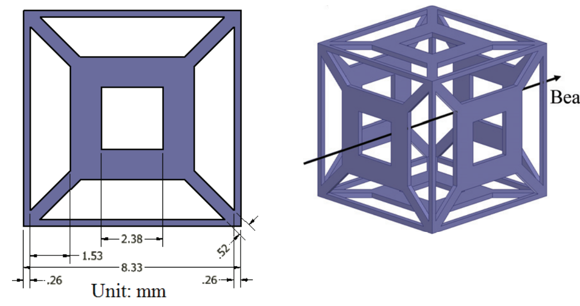

(a) (b)

Figure 1: Unit cell geometry. (a) Face view. The thickness of each face is 0.26mm. (b) 3D view. In later sections we will put an electron beam on the axis.

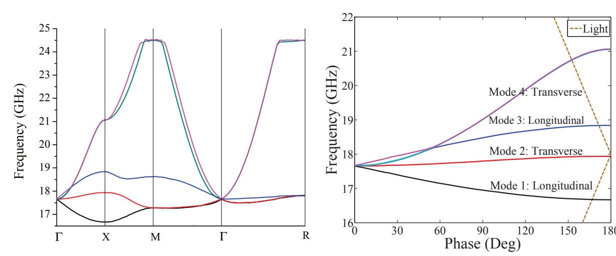

(a) (b)

Figure 2: Brillouin diagram of the unit cell. (a) Different regions in the first Brillouin zone. (b) $\Gamma - X$ region dispersion showing intersection with the light line.

We use both numerical simulation and analytical modeling to study the dispersion relations of the unit cell.

Numerical Simulation

The HFSS Eigenmode Solver is used to calculate the dispersion curves in the first Brillouin zone, as shown in Fig. 2. The high symmetry points for a simple cubic lattice are $\Gamma(0,0,0)$, $X(\pi/p,0,0)$, $M(\pi/p,\pi/p,0)$ and $R(\pi/p,\pi/p,\pi/p)$, where p is the period of the unit cell. We design the geometry to have a balanced structure with all the modes having the same cut-off frequency at the Γ point.

In the $\Gamma - X$ region, there are four modes. Among them, Mode 1 and Mode 3 are longitudinal, so they will couple strongly to an electron beam; Mode 2 and Mode 4 are transverse. The synchronized frequencies of the light line and the longitudinal modes are 16.7 GHz and 18.8 GHz, and the phase advance per cell is near 180°. Mode 1 can couple to the electron beam better than Mode 3, since in one unit cell Mode 1 has a field in the same direction, while Mode 3 has it in the opposite directions, as illustrated in Fig. 3.

Content from this work may be used under the terms of the CC BY 3.0 licence (© 2015). Any distribution of this work must maintain attribution to the author(s), title of the work, publisher, and DOI.

ISBN: 978-3-95450-168-7 doi:10.18429/JACoW-IPAC2015-WEPWA061

HIGH-GRADIENT TESTING OF METALLIC PHOTONIC BAND-GAP (PBG) AND DISC-LOADED WAVEGUIDE (DLWG) STRUCTURES AT 17 GHz*

B. J. Munroe†, J. X. Zhang, M. A. Shapiro, R. J. Temkin, MIT PSFC, Cambridge, MA 02139, USA

Abstract

Photonic Band-gap (PBG) structures continue to be a promising area of research for future accelerator structures. Previous experiments at 11 GHz have demonstrated that PBG structures can operate at high gradient and low breakdown probability, provided that pulsed heating is controlled. A metallic single-cell standing-wave PBG structure has been tested at 17 GHz at MIT to investigate how breakdown probability scales with frequency in these structures. A single-cell standing-wave disc-loaded waveguide (DLWG) was also tested at MIT as a reference structure. The PBG structure achieved greater than 90 MV/m gradient at 100 ns pulse length and a breakdown probability of 1.1×10^{-1} /pulse/m. The DLWG structure achieved 90 MV/m gradient at 100 ns pulse length and a breakdown probability of 1.2×10^{-1} /pulse/m, the same as the PBG structure within experimental error. These tests were conducted at the MIT structure test stand, and represent the first long-pulse breakdown testing of accelerator structures above X-Band.

INTRODUCTION

Photonic band-gap (PBG) structures, which use a lattice of metallic or dielectric rods to confine an accelerator mode while damping higher-order modes (HOMs), are a topic of ongoing experimental and theoretical work [1–5]. Previous experimental work has demonstrated successful acceleration using a traveling-wave PBG structure [1] as well as suppression of wakefields [4, 6]. More recent work by MIT and SLAC National Accelerator Lab has shown that metallic PBG structures can operate at high gradient and low breakdown probability, achieving gradients of greater than 100 MV/m with a breakdown probability of less than 10^{-3} per pulse per meter of structure [5].

In order to compare breakdown performance as a function of frequency, two standing wave high-gradient structures have been designed and fabricated for breakdown testing at 17 GHz at MIT. A round-rod PBG structure (MIT-PBG), for direct comparison to the PBG-R structure tested at 11 GHz, and a disc-loaded waveguide structure (MIT-DLWG), to serve as a reference for structure performance at 17 GHz, have been tested. The PBG and DLWG designs are electrically very similar to the structures tested at SLAC, although the mechanical designs of both structures are modified to use a clamped, as opposed to brazed, assembly. Each structure consists of one coupling cell on each side of central high-gradient cell; power is provided axially in the TM_{01}-mode through a mode launcher provided by SLAC National Accelerator Lab. A model of the PBG structure tested at MIT is shown in Fig. 1; the DLWG structure differs only in the center cell pieces. The details of the structure design can be found in [7].

* This work supported by the DOE, Office of High Energy Physics, Grant No. DE-SC0010075
† brian.j.munroe@gmail.com, now at Schlumberger-Doll Research Center, Cambridge, MA 02139, USA

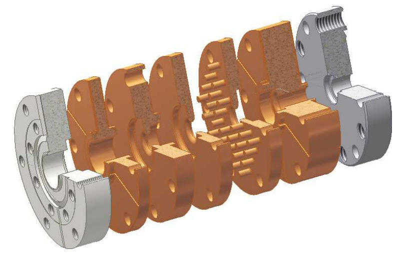

Figure 1: Expanded three quarter section view of the solid model of the 17 GHz PBG structure, showing two coupling cells and central PBG cell. Power is coupled in from the left.

EXPERIMENTAL SETUP

The standing-wave structure test stand at MIT is powered by a 25 MW traveling-wave relativistic klystron designed by Haimson Research Corporation (HRC) and coupled to the test stand through a 4.4 dB hybrid, also from HRC. The test stand is instrumented with incident and reflected power detection via a directional coupler, current monitors both upstream and downstream to detect dark current and breakdown electrons, and an optical diagnostic to look for light emission during breakdowns. In addition to these dedicated diagnostics the pressure in the chamber, which is vacuum-isolated from the rest of the rf system, can be monitored using the chamber ion pump.

The incident and reflected rf power signals are detected using Hewlett Packard HP 8473B low-barrier Schottky diodes coupled into at LeCroy LT264M oscilloscope. The diode traces are recorded by the associated computer system and used to calculate the gradient and peak surface temperature rise in the structure, which are calibrated using HFSS simulations and vector network analyzer measurements. The upstream and downstream current monitors are both composed of copper plates isolated from the body of the mode launcher and structure, respectively. The current monitor signals are used both to monitor the dark current during normal operation and to detect breakdown events. Breakdowns to be detected as a binary signal; if the current monitor signal goes off-scale, then a breakdown is determined to have occurred.

Content from this work may be used under the terms of the CC BY 3.0 licence (© 2015). Any distribution of this work must maintain attribution to the author(s), title of the work, publisher, and DOI.

ISBN: 978-3-95450-168-7 doi:10.18429/JACoW-IPAC2015-WEPWA062

Content from this work may be used under the terms of the CC BY 3.0 licence (© 2015). Any distribution of this work must maintain attribution to the author(s), title of the work, publisher, and DOI.

DESIGN AND HIGH-POWER TESTING OF A HYBRID PHOTONIC BAND-GAP (PBG) ACCELERATOR STRUCTURE AT 17 GHz*

JieXi Zhang†, Alan M. Cook, Brian J. Munroe, Michael A. Shapiro, Richard J. Temkin, Haoran Xu,
MIT PSFC, Cambridge, MA 02139, USA

Abstract

An overmoded hybrid Photonic Band Gap (HPBG) structure used as an accelerator cavity has been theoretically designed and high power tested at 17.1 GHz. The HPBG structure consists of a triangular lattice of dielectric (sapphire) and metallic (copper) rods. Due to the frequency selectivity, the hybrid PBG cavity can be operated in a TM_{02} mode. The maximum surface fields are on the triple point of the innermost row of the sapphire rods. The relatively high value of the surface fields resulted in a high breakdown rate (BDR) at a low gradient in the HPBG structure. Breakdown damage on the triple point edge and the metallization of copper onto the sapphire surface have been observed in the post-testing images. An improved HPBG design, that reduces the peak fields, has been developed. It will be built and tested in an effort to improve the HPBG performance.

INTRODUCTION

A periodic photonic structure, whose dispersion relation has photonic band gaps (PBG), can be applied to accelerators due to its frequency selectivity [1]. A traveling-wave (TW) multi-cell metallic PBG structure has demonstrated successful acceleration of electrons with a gradient of 35 MV/m [2]. Standing-wave (SW) metallic PBG (MPBG) structures have been studied with high power to investigate the breakdown rate at both SLAC and MIT [3–6].

A dielectric PBG structure has been theoretically studied [7]. A sapphire rod structure was previously built and cold tested but not tested at high power [8]. A hybrid PBG structure using both dielectric (sapphire) and metallic (copper) rods to form the triangular lattice array for an accelerator cavity was presented by this author [9]. The dielectric band gap map was calculated using HFSS. Since the dielectric band gap map has no cut off frequency, an overmoded operation with the TM_{02} mode confined in a defect cavity can be chosen by adjusting the lattice ratio a/b, where a is the radius of the dielectric rod and b is the lattice constant. This helps in the design of the geometry for a high frequency of 17 GHz. The defect is formed by removing the first four rows of sapphire rods. Metallic rods are added on the outermost row to increase the reflection, thus increasing the quality factor Q of the accelerating mode. Different rod patterns can be arranged by removing rods to increase the azimuthal uniformity of the TM_{02} mode and damp the higher-order-modes (HOMs). Cold test showing a single resonance at the right frequency has demonstrated the overmoded excitation.

* Work supported by the U.S. Department of Energy, Office of High Energy Physics, DE-SC0010075.
† zhangjx@mit.edu

In this paper, the design and the results of the high power testing of our first HPBG structure will be described. Post-test images will show some damage on both the dielectric and the metallic materials. An improved HPBG design to reduce the peak surface fields will be discussed.

EXPERIMENTAL DESIGN

To conveniently and comparably test the high power properties of a specific cavity, SLAC has developed a procedure of testing a single-cell, Standing-Wave cavity with two side cavities to concentrate the high field in the central test cavity [10]. The PBG structures tested at MIT follow the same design concept with a clamped assembly and scaled dimensions to match the resonant frequency of 17.14 GHz of the Haimson Research Corporation (HRC) klystron. Figure 1 shows the 3D model of the HPBG structure used in the SW test stand. A mode launcher is used to convert the rectangular waveguide mode to the input fundamental TM_{01} mode. The c-axis of each sapphire rod is aligned parallel to the longitudinal axis of the accelerator cavity. The birefringence of the sapphire gives a permittivity $\varepsilon_r = [9.398, 9.398, 11.587]$. The lattice parameters are a rod radius $a = 1.58$ mm and a rod spacing $b = 4.48$ mm. The length of the sapphire rods is 11.68 mm. Rods are inserted into copper plates with an insertion depth $d = 3$ mm. Fillets with a radius of $R_{fil} = 2.25$ mm are added on the triple point (the point where sapphire, copper and vacuum meet) of the six innermost rods to reduce the strong surface fields. The radius of the coupling iris is adjusted to obtain a critical coupling. The symmetry of the structure and the TM_{02} mode allows the simulation of the entire 360-degree structure with a 30-degree wedge. The final simulation result of S_{11} is shown in Figure 2. The resonant frequency f_0 and the quality factor Q_L are listed in Table 1. To compare, Figure 2 and Table 1 show results

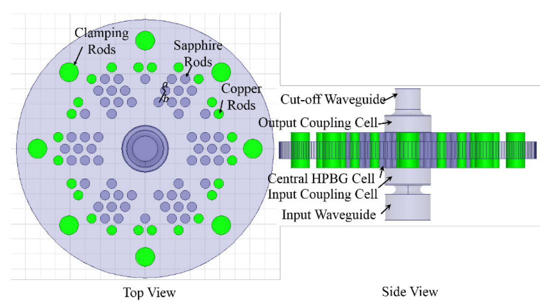

Figure 1: The SW model of the HPBG structure in the 3D simulation. Sapphire rods are shown in dark purple and metal rods in green.

ISBN: 978-3-95450-168-7 doi:10.18429/JACoW-IPAC2015-WEPWA063

BEAM-PLASMA EFFECTS IN MUON IONIZATION COOLING LATTICES*

J. Ellison, P. Snopok, Illinois Institute of Technology, Chicago, IL 60616, USA

Abstract

New computational tools are essential for accurate modeling and simulation of the next generation of muon based accelerator experiments. One of the crucial physics processes specific to muon accelerators that has not yet been implemented in any current simulation code is beam induced plasma effect in liquid, solid, and gaseous absorbers. We report here on the progress of developing the required simulation tools and applying them to study the properties of plasma and its effects on the beam in muon ionization cooling channels.

INTRODUCTION

Though muon accelerator simulation codes have been steadily improving over the years, there is still much room for improvement. Many single-particle processes and collective effects in vacuum and matter, such as space charge, beam-beam effects, plasma effects from ionized electrons and ions, etc. have not been studied thoroughly or implemented. In order to ensure proper accuracy of simulations, these effects have to be either deemed negligible or taken into account.

Ionization cooling is a method by which the overall emittance of a muon beam can be reduced. A beam is sent through a material, losing momentum as they ionize electrons, and reducing its overall emittance. By reaccelerating the beam through RF cavities, the longitudinal momentum is restored and any lost energy is regained (Fig. 1).

Muons will ionize material as they travel through absorbers. This can generate a plasma, and it is the interaction of the muon beam with the generated plasma that is studied here. Beam-plasma interaction is not taken into account currently in a majority of muon accelerator simulation codes. This can be needed when simulating ionization cooling and high-pressure gas-filled RF (HPRF) cavities.

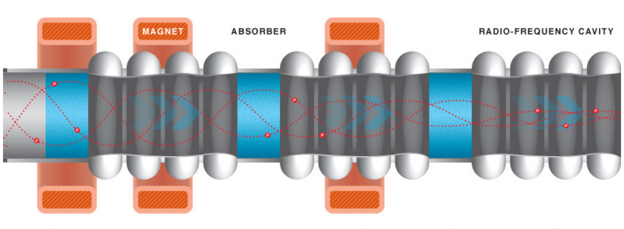

Figure 1: A diagram of ionization cooling. In each cell, absorbers reduce the transverse and longitudinal momentum of the muon beam, and RF cavities reaccelerate in the longitudinal direction only, reducing the overall emittance of the beam.

* Work supported by the U.S. Department of Energy.

The plasma effects have been studied by plasma physicists, but has not been studied extensively from a beam physics point of view. The plasma has been shown to not disrupt the beam or make it blow up [1]. For ionization cooling purposes, beam-plasma effects may have a large impact on the cooling rates for both charges of muon. Essentially, the head of a bunch sees a material with different properties than the tail of the bunch. Ionization rates vary from material to material so the effects may be more prominent in some materials than others.

QUALITATIVE SIMULATIONS

After several simulation packages were considered, the one found to best suit our needs was WARP [2]. WARP is an extensively developed particle in cell (PIC) simulation code designed to simulate charged particle beams with high space-charge intensity. A dense Gaussian beam of muons ($N = 10^{12}$, $p = 200$ MeV/c) was sent through a solenoidal magnetic field ($B = 5.46$ T) and Hydrogen gas (180 atm) with ionization and space-charge effects turned on only (scattering and straggling were not implemented).

The first simulation was without ionization effects turned on in order to have a baseline reference case. The second simulation added a plasma at each simulation step in the form of a thin cylinder of the beam radius containing the total number of plasma electrons (and ions) that were calculated to be created each step. The third simulation used a built-in ionization module of WARP that, given a cross section and density, would place an electron-ion pair at their creation point.

The number of secondaries generated in a single step can be calculated from the Bethe Equation [3] and is given by the following equation:

$$N_s = \left\langle \frac{dE}{dx} \right\rangle \frac{\rho}{W_i} \times d_s, \tag{1}$$

where N_s is the number of particles generated per step, d_s is the step length, $\left\langle \frac{dE}{dx} \right\rangle$ is the mean rate of energy loss by the muons, W_i is the average energy to produce an ion pair, and ρ is the mass density of the medium.

The cross section (σ) for a single particle in the beam is given by

$$R = nv\sigma, \tag{2}$$

where R is the rate of the reaction, v is the velocity of the beam, n is the number density of target particles. That leads to the cross section formula

$$\sigma = \left\langle \frac{dE}{dx} \right\rangle \frac{1}{W_i} \frac{\rho}{\rho_n}, \tag{3}$$

where ρ is the mass density of the absorber and ρ_n is the atomic density of the absorber.

Content from this work may be used under the terms of the CC BY 3.0 licence (© 2015). Any distribution of this work must maintain attribution to the author(s), title of the work, publisher, and DOI.

ISBN: 978-3-95450-168-7 doi:10.18429/JACoW-IPAC2015-WEPWA064

IONIZATION COOLING CHANNELS IN COSY INFINITY

B. Loseth, M. Berz, Michigan State University, East Lansing, MI 48824, USA
P. Snopok, Illinois Institute of Technology, Chicago, IL 60616, USA

Content from this work may be used under the terms of the CC BY 3.0 licence (© 2015). Any distribution of this work must maintain attribution to the author(s), title of the work, publisher, and DOI.

Abstract

Ionization cooling is a method to reduce the emittance of a beam through the use of absorbers, rf cavities, and strong solenoids for focusing, arranged into a condensed lattice. By tuning lattice parameters, it is possible to construct a staged cooling channel in which the beam emittance is always considerably greater than the minimum value. In the late stages of the cooling channel, space charge effects can become a significant obstacle to further emittance reduction once the beam becomes sufficiently condensed. A method has been implemented in COSY Infinity, a beam dynamics simulation and analysis code, which efficiently and accurately calculates the self-fields of all particles on each other based on a variant of the Fast Multipole Method (FMM). In this paper, we present simulations of a muon ionization cooling channel performed in COSY, utilizing the FMM, benchmarked against G4beamline, a standard code for muon beam analysis, in order to investigate the significance of space charge effects.

OVERVIEW OF IONIZATION COOLING

In the area of high energy colliders, using leptons has a significant advantage over hadrons due to hadron collisions being inefficient and complicated by secondary quark interactions. A muon collider could be used for high energy studies of lepton collisions without the limitations on energy due to synchrotron radiation. The muon beam is produced by sending protons through a target, producing pions which in turn decay into muons with a large momentum spread. In order to be accelerated, the six-dimensional (6D) phase space volume of the muon beam must be reduced for injection into a storage ring. Ionization cooling is currently the only feasible method for cooling the beam within a muon lifetime of 2.2 μs. In order for a full 6D ionization cooling experiment to be constructed, a baseline lattice design has to be studied and selected based on detailed simulations [1].

Emittance Reduction

For the reduction of transverse emittance, the beam is strongly focused with magnetic fields and subsequently passed through an absorber material to reduce overall momentum. The beam's longitudinal momentum is restored in RF cavities which results in a net reduction in transverse emittance. The change in the transverse emittance is described by:

$$\frac{d\varepsilon_n}{ds} = -\frac{1}{\beta^2}\frac{dE_\mu}{ds}\frac{\varepsilon_n}{E_\mu} + \frac{1}{\beta^3}\frac{\beta_T E_s^2}{2E_\mu m_\mu c^2 L_R},$$

$$\varepsilon_{n,min} = \frac{\beta_T E_s^2}{2\beta m_\mu c^2 L_R \left|\frac{dE_\mu}{ds}\right|},$$

where ε_n is the normalized transverse emittance, c is the speed of light, and $\beta = v/c$, E_μ, m_μ are the muon velocity, energy, and mass. The transverse betatron function within the absorber is β_T, dE_μ/ds is the energy loss per unit length in the absorber, L_R is the radiation length of the absorber material, and E_s is the characteristic scattering energy. The top equation describes the effects of cooling (first term) and heating (second term), and when the cooling rate equals the heating rate, we can find the minimum normalized transverse (or equilibrium) emittance ($\varepsilon_{n,min}$) for a given absorber material and focusing field.

To maximize cooling, materials with low Z and large radiation length (such as LH_2, LiH) are used in order to minimize multiple scattering. A high gradient RF field and high absorber density, the combination of which determines the energy loss per unit length dE_μ/ds, are used along with solenoids arranged such that there is strong focusing at absorbers, thus small β_T. Cooling typically occurs around a muon momentum of 200 MeV/c, where the curvature of the Bethe-Bloch function (to determine absorber dE_μ/ds) is favorable. The cooling channel is tapered into stages in order to vary the solenoid focusing, RF frequency and gradient, and geometry such that the minimum normalized emittance decreases with the beam [2–4].

The longitudinal momentum spread is reduced using the concept of emittance exchange. This process involves applying a magnetic field to create dispersion in the beam at wedge shaped absorbers, such that particles with higher energy pass through more material than those with lower energy, resulting in an overall reduction in the energy spread of the beam. The cooling process is essentially a transfer of emittance from the longitudinal to transverse direction combined with transverse ionization cooling for emittance reduction in all six dimensions.

SPACE CHARGE

One of the challenges presented in muon cooing channels is that as the size of the beam is reduced, Coulomb repulsion in the beam limits further emittance reduction. To investigate the effect of space charge, a method has been implemented in COSY INFINITY [5] to achieve efficient and accurate calculation of the interparticle Coulomb forces based on variants of the Fast Multipole Method (FMM). This method divides an arbitrary charge distribution into small boxes with a hierarchical structure. It then computes the multipole expansions and local expansions of charges far from the observer to achieve a computational efficiency that scales with the number of particles, N, and computational errors scaling with a high power of the expansion order. The FMM algorithm is especially suited for beam dynamics sim-

ISBN: 978-3-95450-168-7 doi:10.18429/JACoW-IPAC2015-WEPWA066

THE ADVANCEMENT OF COOLING ABSORBERS IN COSY INFINITY*

J. Kunz, P. Snopok†, Illinois Institute of Technology, Chicago, IL 60616, USA
M. Berz, K. Makino, Michigan State University, East Lansing, MI 48824, USA

Abstract

COSY Infinity is an arbitrary-order beam dynamics simulation and analysis code. It can determine high-order transfer maps of combinations of particle optical elements of arbitrary field configurations. For precision modeling, design, and optimization of next-generation muon beam facilities, its features make it a very attractive code. New features are being developed for inclusion in COSY to follow the distribution of charged particles through matter. To study in detail some of the properties of muons passing through material, the transfer map approach alone is not sufficient. The interplay of beam optics and atomic processes must be studied by a hybrid transfer map–Monte-Carlo approach in which transfer map methods describe the average behavior of the particles in the accelerator channel including energy loss, and Monte-Carlo methods are used to provide small corrections to the predictions of the transfer map accounting for the stochastic nature of scattering and straggling of particles. The advantage of the new approach is that it is very efficient in that the vast majority of the dynamics is represented by fast application of the high-order transfer map of an entire element and accumulated stochastic effects as well as possible particle decay. The gains in speed are expected to simplify the optimization of muon cooling channels which are usually very computationally demanding due to the need to repeatedly run large numbers of particles through large numbers of configurations. Progress on the development of the required algorithms is reported.

INTRODUCTION

Muons are tertiary production particles (protons → pions → muons) and high-intensity collection requires a large initial phase space volume. The resultant spray of muons must be amassed, focused, and accelerated well within the muon lifetime (2.2 μs in the rest frame). The only technique fast enough to reduce the beam size within the muon lifetime is ionization cooling. When muons traverse a material, both the longitudinal and transverse momentum components shrink due to ionization. The energy is then restored in the longitudinal direction only, leading to an overall reduction in the transverse beam size (cooling). In order to achieve cooling in the longitudinal direction, emittance exchange is used, usually involving wedge-shaped absorbers. For some applications such as a high-energy high-luminosity muon collider, cooling needs to be very aggressive: six-dimensional emittance reduction over six orders of magnitude is required to reach design goals.

* Work supported by the U.S. Department of Energy.

† psnopok@iit.edu

In order to carefully simulate the effect of the absorbers on the beam, one needs to take into account both deterministic and stochastic effects in the ionization energy loss. The deterministic effects in the form of the Bethe-Bloch formula with various theoretical and experimental corrections fit well into the transfer map methods approach, where the effect of the lattice on the particles is evaluated first by producing the so-called transfer map, and then is applied to a given initial distribution of particles. The arbitrary-order simulation code COSY Infinity [1] is a key representative of transfer map codes. COSY was chosen because of its built-in optomization tools, speed, its ability to produce high-order transfer maps, and its ability to control individual aberrations.

However, to take into account stochastic effects the transfer map paradigm needs to be augmented by implementing the corrections from stochastic effects directly into the fabric of COSY. Some of the fundamental ideas of the process were presented in [2] in application to quadrupole cooling channels, but the approximations used were fairly basic. In this work, a more rigorous theoretical approach is presented along with the resulting valiation.

STOCHASTIC PROCESSES

The stochastic processes of interest are straggling (fluctuation about a mean energy loss), angular scattering, transverse position corrections, and time-of-flight corrections (corresponding to the longitudinal position correction). The general outline to simulate these four beam properties will be discussed and benchmarked against two other beamline simulation codes, ICOOL [3] and G4Beamline [4], and (in the case of angular scattering) against experimental data [5]. The simulation followed the beam properties cited in [5], which were a pencil beam with an iinitial momentum of 172 MeV/c through 109 mm of liquid hydrogen (LH) with cylindrical geometry. The step sizes for ICOOL and G4Beamline were chosen to be a modest 1 mm in order to ensure a quality simulation. The step size for COSY was chosen as the entire cell (109 mm), since its algorithms are largely insensitive to step sizes, as will be shown later.

Straggling (Figure 1)

As the momentum range of interest is 50–400 MeV/c through low-Z materials, only ionization effects contribute to the mean energy loss. As such, Landau theory accurately describes the energy loss spectra, having the form [6]

$$f(\lambda) = \frac{1}{\xi} \cdot \frac{1}{2\pi i} \int_{c+i\infty}^{c-i\infty} \exp(x \ln x + \lambda x) dx,$$

where $\xi \propto Z\rho L/\beta^2 A$, and $\lambda \propto dE/\xi - \beta^2 - \ln\xi$. Here, Z, A, and ρ are the material parameters of charge, atomic mass,

Content from this work may be used under the terms of the CC BY 3.0 licence (© 2015). Any distribution of this work must maintain attribution to the author(s), title of the work, publisher, and DOI.

ISBN: 978-3-95450-168-7 doi:10.18429/JACoW-IPAC2015-WEPWA067

ACOUSTIC BREAKDOWN LOCALIZATION IN RF CAVITIES*

P. Lane, P. Snopok,† Y. Torun, Illinois Institute of Technology, Chicago, IL 60616, USA
E. Behnke, I. Levine, Indiana University South Bend, South Bend, IN 46634, USA
D. Peterson, Fermilab, Batavia, IL 60510, USA

Abstract

Current designs for muon cooling channels require high-gradient RF cavities to be placed in solenoidal magnetic fields in order to contain muons with large transverse emittances. It has been found that doing so reduces the threshold at which RF cavity breakdown occurs. To aid the effort to study RF cavity breakdown in magnetic fields it would be helpful to have a diagnostic tool which can detect breakdown and localize the source of the breakdown inside the cavity. We report here on acoustic simulations and comparisons with experimental acoustic data of breakdown from several RF cavities. Included in this analysis are our most recent results from attempting to localize breakdown using these data.

INTRODUCTION

Muon beams are desired for use in future particle physics experiments. Muon colliders could compliment hadron machines like the LHC without the need for prohibitively long accelerators that are proposed for electron-positron machines such as the ILC or CLIC. Neutrino physics would also benefit from having a neutrino factory which generates a neutrino beam from the decay of muons.

The main challenge with using muons for colliders and neutrino factories is creating tight muon beams. Muons are created from the decay of pions which themselves come from proton collisions with fixed targets. The resultant spray of muons must be collected, focused, and accelerated well within the muon lifetime (2.2 μs in the rest frame). The only feasible method that has been conceived for reducing the beam size prior to accelerating it is ionization cooling [1].

Ionization cooling uses low-Z materials as energy absorbers to reduce the overall momentum of muons. The muons are then subjected to electric fields which accelerate them only along the beam axis. To corral the muons as they are cooled transversely, strong solenoidal magnetic fields are used [1]. Unfortunately it has been found that the maximum accelerating gradient a cavity can produce without breaking down is significantly reduced in the presence of strong magnetic fields [2].

In order to improve the performance of accelerating cavities in strong magnetic fields, it would be useful to have a diagnostic tool that would indicate where breakdown sparks are occurring without having to shutdown the experiment and open the cavity to inspect damage. Acoustic data has been collected on the Muon Ionization Cooling Experiment's (MICE) 201.25 MHz RF cavity and the Modular Cavity at the MuCool Test Area (MTA) at Fermilab. We have demonstrated the feasibility of acoustic localization of breakdown spark sources with other cavities, and we present here experimental and simulation results as well as our path forward towards the goal of acoustic localization of breakdown.

* Work supported by U.S. Department of Energy
† psnopok@iit.edu

EXPERIMENTAL SETUP

The experimental setup for the MICE 201.25 MHz cavity at the MuCool Test Area (MTA) at Fermilab was previously described in detail [3]. Additional details on previous cavity setups was also previously presented [4]. Since then we have instrumented a newly built, cylindrical cavity, the Modular Cavity, with 10 passive, piezoelectric microphones. These microphones are nearly identical to those on the MICE cavity, with the main difference being added strain relief for the cable where it attaches to the microhpone housing. Four are placed on each end plate. The remaining two were placed on the underside of the waveguide. An additional variable gain amplifier box was installed in the MTA experiment hall for these new microphones. Connections to our DAQ system were simplified by the existance of enough spare capacity that no rearrangement of MICE cavity connections was necessary. Finally, our LabVIEW software has been rewritten for stability and to be easily configurable for multiple cavity setups.

EXPERIMENTAL RESULTS

MICE Cavity

The MICE cavity was run at the end of last year in no magnetic field. The signals are characterized by large spikes at the beginning that correspond with the RF pulse followed by oscillations that have an amplitude less than a volt (Fig. 1). This is true for both spark and non-spark signals, making it difficult to tell the difference on visual inspection between the two. Given that our experience with previous cavities shows a much larger response from spark than from normal RF pulse noise (referred to as the RF hammer), it was thought that the microphones might have been ruined during the cavity bakeout in preparation for evacuation. After the Fall running completed the Cu end plates on the MICE cavity were removed along with the 12 microphones attached to them (leaving 12 on the main body at a constant radius of 41 *cm*). We took the opportunity to test the microphones again by tapping on the cavity with a makeshift hammer that triggers the DAQ on contact with the cavity's conductive surface. All but two microphones were behaving normally. Since this cavity dissipates much more energy than previous cavities it was assumed that the acoustics in general would be much louder. We have put considerably more effort towards

Content from this work may be used under the terms of the CC BY 3.0 licence (© 2015). Any distribution of this work must maintain attribution to the author(s), title of the work, publisher, and DOI.

ISBN: 978-3-95450-168-7 doi:10.18429/JACoW-IPAC2015-WEPWA068

SIMULATION OF LASER PULSE DRIVEN TERAHERTZ GENERATION IN INHOMOGENEOUS PLASMAS*

Chenlong Miao#, IREAP, University of Maryland, College Park 20740, USA
John P. Palastro, Naval Research Laboratory, Washington DC 20375, USA
Thomas M. Antonsen, IREAP, University of Maryland, College Park 20740, USA

Abstract

Intense, short laser pulses propagating through inhomogeneous plasma can ponderomotively drive THz radiation. Here we consider a transition radiation mechanism (TRM) for THz generation as a laser pulse crosses a plasma boundary. Full format PIC simulations and theoretical analysis are conducted demonstrating that TRM results in low frequency, broad band, coherent THz radiation. The effect of a density ramp is also considered and shown to enhance the radiated energy.

INTRODUCTION

Electromagnetic terahertz radiation (THz) spans frequencies from 300 GHz to 20 THz. A wide variety of THz applications [1] include spectroscopy, remote detection, and medical and biological imaging. Intense THz pulses can be generated at large scale accelerator facilities via synchrotron or transition radiation, but the size and cost of such facilities are prohibitive for widespread use. This motivates the development of small-scale table top terahertz sources.

Existing small-scale terahertz sources are based on laser-solid interaction and are limited to μJ/pulse levels [2]. This has led to the consideration of laser-plasma based THz generation schemes. Examples include the transition radiation of a laser accelerated electron beam passing from plasma to vacuum producing energies in excess of 100 μJ/pulse [3], and radiation produced during two-color laser pulses gas ionization[4]. Here, with a combination of theory and simulation, we investigate a mechanism of ponderomotively driven THz radiation, which offers the possibility of high conversion of optical pulse energy to THz.

The mechanism occurs as a laser pulse crosses a plasma boundary [5] and is analogous to transition radiation emitted by charged particle beams. The THz radiation resulting from this transition radiation mechanism (TRM) is characterized by conical emission and a broad spectrum with the maximum frequency occurring near the plasma frequency [6].

The THz generation mechanism is simulated using the full format PIC simulation TurboWAVE [7], with the goal of increasing the conversion of optical energy to THz radiation. A range of laser pulse and plasma parameters is considered. We conduct the simulations in the lab frame with a finite sized plasma target illuminated by a laser pulse incident from the left, as shown in Fig. 1 for the case of a sharp boundary, uniform plasma. To investigate the power radiated from the plasma, we calculate the Poynting flux through the prescribed surfaces outside the plasma region. These represent the forward, backward and lateral radiation from the plasma.

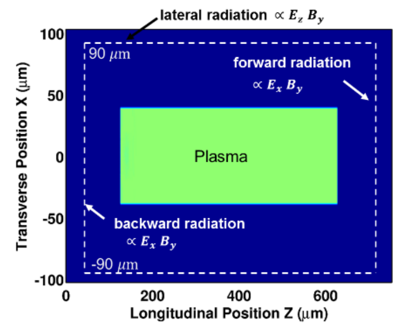

Figure 1: Diagnostic box outside the plasma channel. The Poynting flux through each surface is calculated.

TRANSITION RADIATION MECHANISM

We first consider a uniform plasma with sharp step boundaries as illustrated in Fig. 2. The plasma is 500 μm long and 90 μm wide with a density of $n = 2.8\times10^{18}\,cm^{-3}$. When the laser pulse crosses the vacuum-plasma boundary, it drives ponderomotive currents that produce radiation with frequencies near the plasma frequency.

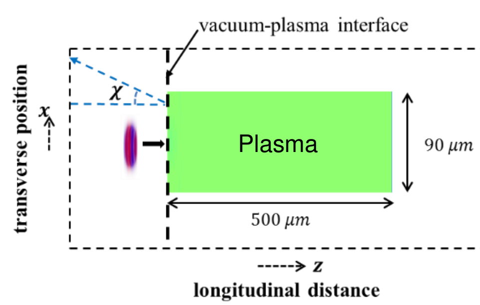

Figure 2: Diagram of simulation set up for transition radiation at the vacuum plasma boundary.

Following Ref. 5, a formula can be derived for the radiated energy per unit frequency (ω) and length (recall the simulations have 2D planar symmetry) across the left diagnostic boundary shown in Fig. 2.

$$\frac{dW_L}{d\omega} = \frac{L}{|\omega|}\frac{\omega_{p0}^2}{\omega_0^2}\frac{k_p^2}{\pi^{3/2}}\frac{a_0^2}{4}U_L\int_0^1 dy\,\frac{y^2\sqrt{1-y^2}\times\exp\left[-\frac{\omega^2}{2c^2}\left(L^2+R_L^2\left(1-y^2\right)\right)\right]}{\left|\varepsilon(\omega)\,y+\sqrt{y^2-\omega_{p0}^2/\omega^2}\right|^2}\,. \quad (1)$$

*Work supported by DOE
#clmiao@umd.edu

Content from this work may be used under the terms of the CC BY 3.0 licence (© 2015). Any distribution of this work must maintain attribution to the author(s), title of the work, publisher, and DOI.

ISBN: 978-3-95450-168-7 doi:10.18429/JACoW-IPAC2015-WEPWA070

Content from this work may be used under the terms of the CC BY 3.0 licence (© 2015). Any distribution of this work must maintain attribution to the author(s), title of the work, publisher, and DOI.

CONSIDERATIONS FOR AN EFFICIENT TERAHERTZ-DRIVEN ELECTRON GUN *

F. Lemery[1], P. Piot[1,2]
[1] Department of Physics and Northern Illinois Center for Accelerator & Detector Development, Northern Illinois University DeKalb, IL 60115, USA
[2] Accelerator Physics Center, Fermi National Accelerator Laboratory, Batavia, IL 60510, USA

Abstract

We investigate a dispersion-controlled-acceleration scheme of low-energy electrons to mitigate phase slipping using a tapered dielectric lined waveguide (DLW). Our approach matches the velocity of an electron being accelerated in a slab-symmetric structure in a constant electric field. We also present first experimental results of a THz pulse propagating in a slab-symmetric DLW.

INTRODUCTION

Although conventional electron sources are often used to investigate the performance of advanced acceleration concepts [1], their adaptation to serve as an injector for an optimized advanced accelerator remains challenging. Instead several groups have developed short-pulse electron sources, e.g., based on dielectric grating [2], free-space THz streaking [3, 4], or the proposed optically driven dielectric-waveguide sources [5]. Unfortunately, electron sources using an optical wave are typically limited in the charge they can produce since space charge is predominant at low energy and needs to be mitigated. For instance at $\lambda_{acc} = 800$ nm, a typical bunch length of a few nm would be required which would result in peak current, $Qc/(2\pi\lambda_{acc} \geq 6$ kA for a 1 pC bunch charge (here c is the light velocity). Alternatively, using a THz pulse with λ_{acc}=100 μm would result in a peak current on the order of 50 A (taking $\sigma_z \simeq 10^{-2}\lambda_{acc} \simeq 1$ μm). The latter value is consistent with values typically achieved in conventional photoinjectors, see Ref. [6] for example. Likewise, the trade-off between electron bunch length and charge could enable the production of higher charge (up to 100 pC) in exchange for longer bunches.

Recently, the development of efficient (2%) laser-based THz sources (300 GHz) has opened the path to the development of THz-driven linacs [7–10]. In this scheme, a radially-polarized THz pulse is co-propagated with an electron bunch in a dielectric-lined waveguide (DLW) with optimized geometry; THz pulses with mJ energies can support accelerating fields on the order of GV/m. The THz-pulse is also matched to the structure thereby mitigating possible excitation of spurious modes (e.g. dipole modes often excited in beam-driven schemes dielectric-wakefield acceleration [11]. This technique would work well at relativistic energies as the electron has a velocity close to the phase velocity of the THz pulse and the particle-wave slippage is negligible over the considered interaction lengths. In contrast, using a THz pulse to accelerate an electron bunch from rest, as recently demonstrated for the free-space case in Ref. [10], is prone to large phase-slippage effects that significantly alter the maximum energy achievable.

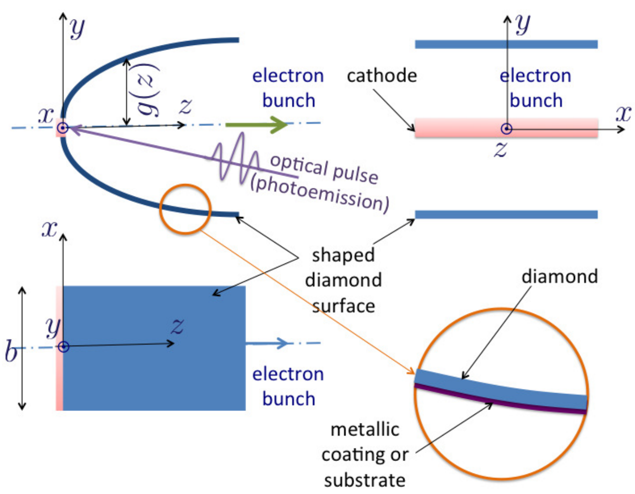

Figure 1: Section, top view and side view (respectively on top, bottom left and top right) of the proposed "THz gun" electron source.

This paper presents some preliminary considerations toward the development of a THz-driven electron source with some attempt to keep phase-slippage effects under control. A conceptual schematic of this low-energy electron source, henceforth dubbed "THz-gun", appears in Fig. 1: two thin dielectric surfaces deposited on a metallic substrate (or free-standing with metalized outer surfaces) are faced to each other.

DISPERSION-CONTROLLED ACCELERATION

The rate of phase slippage between an electromagnetic travelling wave with axial field $E_z(z,t) = E_0 \sin(\omega t - kz + \psi_0)$ (where ω and k are respectively the wave's frequency and wavector) and a particle with Lorentz factor γ is given by $d\psi/dz = \alpha k \sin(\psi)$ where $\psi = \psi(z,t) \equiv \omega t - kz + \psi_0$ (with ψ_0 being the injection phase), and $\alpha \equiv eE_0/(kmc^2)$ is

* Work supported by the by the Defense Threat Reduction Agency (DTRA), Basic Research Award # HDTRA1-10-1-0051, to Northern Illinois University. The work of P. P. is partially supported by the US DOE contract DE-AC02-07CH11359 to the Fermi research alliance LLC. F. L. was partially supported by a dissertation-completion award from the Graduate School of Northern Illinois University.

ISBN: 978-3-95450-168-7 doi:10.18429/JACoW-IPAC2015-WEPWA071

A COMPACT X-RAY SOURCE BASED ON A LOW-ENERGY BEAM-DRIVEN WAKEFIELD ACCELERATOR*

F. Lemery[1], D. Mihalcea[1], K. Chouffani[2] and P. Piot[1,3]
[1] Department of Physics, Northern Illinois Center for Accelerator & Detector Development, Northern Illinois University DeKalb, IL 60115, USA
[2] Idaho Accelerator Center, Pocatello, ID 83201, USA
[3] Accelerator Physics Center, Fermi National Accelerator Laboratory, Batavia, IL 60510, USA

Abstract

Accelerator-based X-ray sources have led to many scientific discoveries. Yet, their limited availability in large national laboratory settings due to the required infrastructure is a major limitation to their disseminations to a larger user community. In this contribution we explore the use of a low-energy electron beam produced out of a photoinjector coupled to a pair of dielectric structure to produce a higher energy (10-20 MeV) beam via a beam-driven acceleration scheme. The accelerated beam can then be used to produce X-rays via inverse Compton scattering.

INTRODUCTION

Modern accelerator-based X-ray sources have led to a wave of scientific advancements in various fields. Their inception relies primarily on energetic electrons which are manipulated to radiate either via undulators or inverse Compton scattering (ICS). In both radiation mechanisms the photon energy $O(\gamma^2)$, therefore an increase in the beam energy is significant. Recently, compact X-ray sources based on X-band RF technology has been proposed [1]. Likewise an X-ray source utilizing laser-plasma wakefield accelerator have been demonstrated [2]. Finally, most recently the possible use of a THz pulse to accelerate electron bunches have been put forward [3] and tested [4]. These solutions, although appealing, are either costly (X-band technology) and/or require the use of high-power lasers currently operating at low repetition rates.

A possible alternative to increase the beam energy is to rely on collinear beam driven acceleration using high-impedance media such as dielectric lined waveguides (DLW) – for dielectric-wakefield acceleration (DWFA) – or plasmas – for wakefield acceleration (PWFA). In collinear beam-driven schemes, a "drive" bunch is used to drive the wakefield in the medium while a properly delayed "witness" bunch at the proper phase is accelerated. The longitudinal wakefield produced by the drive bunch is given by

$$E(z) = \int_{-\infty}^{z} G(z-\zeta)S(\zeta)d\zeta, \quad (1)$$

where $G(z-\zeta) = 2\kappa\cos(k\zeta)$ is the longitudinal Green's function, κ the loss factor, and $k = \frac{2\pi}{\lambda}$ with λ being the wavelength of the mode supported by the medium. Additionally, in a DLW the maximum field strength generally scales as $E_+ \propto \Lambda(z)a^{-2}$ where a is the inner radius of the DLW and $\Lambda(z)$ is the longitudinal charge density. An essential figure of merit associated to beam-driven acceleration is the transformer ratio $\mathcal{R} = |E_+^{(m)}/E_-^{(m)}|$ where the superscript "m" refers to the maximum amplitude of the accelerating (E_+) or decelerating field (E_-), which describes the efficiency of the energy transfer of the drive bunch to the wake.

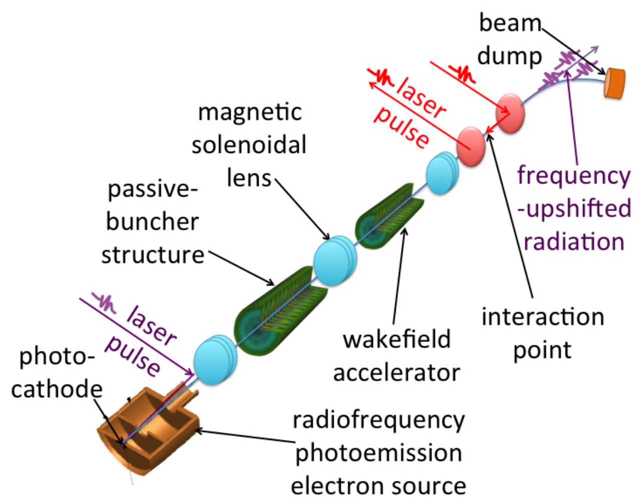

Figure 1: Overview of the compact source scheme: a photoinjected electron bunch passes through a series of DLWs for cascaded acceleration,the resulting high energy electrons are used with a laser to generate inverse Compton scattering.

Two practical challenges emerge for beam-driven acceleration at low energy. First, the geometric emittance associated to a low-energy photoinjected electron bunch sets an upper limit on the inner radius a and length L of the DLW structure. Second, the scheme relies on the production of a high-peak-current electron bunch along with the formation of a witness bunch.

To address some of these challenges, we propose an accelerator setup diagrammed in Fig. 1 based on a "cascaded acceleration" scheme. A high-quality electron bunch is produced in an RF gun and focused into a DLW structure (DLW1). The structure passively bunches the beam which

* This work is supported by US DOE contracts DE-AC02-07CH11359 to the Fermi research alliance LLC and DE-NA0001738 to Idaho Accelerator Center. F.L. is partially supported by the Dissertation-Completion Award from the Graduate School of Northern Illinois University.

Content from this work may be used under the terms of the CC BY 3.0 licence (© 2015). Any distribution of this work must maintain attribution to the author(s), title of the work, publisher, and DOI.

ISBN: 978-3-95450-168-7 doi:10.18429/JACoW-IPAC2015-WEPWA072

Content from this work may be used under the terms of the CC BY 3.0 licence (© 2015). Any distribution of this work must maintain attribution to the author(s), title of the work, publisher, and DOI.

FEASIBILITY OF CONTINUOUSLY FOCUSED TeV/m CHANNELING ACCELERATION WITH CNT-CHANNEL*

Y. M. Shin, Department of Physics, Northern Illinois University, Dekalb, IL 60115, USA and Accelerator Physics Center (APC), FNAL, Batavia, IL 60510, USA
A. Lumpkin, Accelerator Physics Center (APC), FNAL, Batavia, IL 60510, USA
R. M. Thurman-Keup, Accelerator Physics Center (APC), FNAL, Batavia, IL 60510, USA
V. Shiltsev, Accelerator Physics Center (APC), FNAL, Batavia, IL 60510, USA

Abstract

Atomic channels in crystals are known to consist of 10 – 100 V/Å potential barriers capable of guiding and collimating a high energy beam and continuously focused acceleration with exceptionally high gradients (TeV/m). However, channels in natural crystals are only angstrom-size and physically vulnerable to high energy interactions. Carbon-based nano-crystals such as carbon-nanotubes (CNTs) and graphenes have a large degree of dimensional flexibility and thermo-mechanical strength, which could be suitable for channeling acceleration of MW beams. Nano-channels of the synthetic crystals can accept a few orders of magnitude larger phase-space volume of channeled particles with much higher thermal tolerance than natural crystals. Our particle-in-cell simulations with 100 μm long effective CNT model indicated that a beam-driven self-acceleration produces 1 – 2 % net energy gain in the quasi-linear regime (off-resonance beam-plasma coupling, $n_p = 1000\ n_b$) with ASTA 50 MeV injector beam parameters. This paper presents current status of CNT-channeling acceleration experiment planned at the Advanced Superconducting Test Accelerator (ASTA) in Fermilab.

INTRODUCTION

Shock waves in an ionized plasma media, excited by relativistic particles, have been of great interest on account of their promise to offer extremely high acceleration gradients of G (max. gradient) = $m_e c\omega_p/e \approx 96 \times n_0^{1/2}$ [V/m], where $\omega_p = (4\pi n_p e^2/m_e)^{1/2}$ is the electron plasma frequency and n_p is the ambient plasma density of [cm^{-3}], m_e and e are the electron mass and charge, respectively, and c is the speed of light in vacuum. However, a practically obtainable plasma density (n_p) in ionized gas is limited to below ~ 10^{24} m^{-3}, which in principle corresponds to wakefields up to ~ 100 GV/m [1, 2], and it is realistically very difficult to create a stable gas plasma with a charge density beyond this limit. Metallic crystals are the naturally existing dense plasma media completely full with a large number of conduction electrons available for the wakefield interactions. The density of charge carriers (conduction electrons) in solids $n_0 = \sim 10^{26} – 10^{29}$ m^{-3} is significantly higher than what was considered above in gaseous plasma, and correspondingly the wakefield strength of conduction electrons in solids, if excited, can possibly reach 10 TV/m in principle.

The channels between atomic lattices or lattice planes aligned in a crystal orientation of natural crystals like silicon or germanium are sparse spaces with relatively low electron densities. Charged particles, injected into a crystal orientation of a mono-crystalline (homogeneous and isotropic) target material, undergo much lower nucleus and electron scatterings. The idea of accelerating charged particles in solids along major crystallographic directions was suggested by several scientists such as Pisen Chen, Robert Noble, Richard Carrigan, and Toshiki Tajima in the 1980's and 1990's [3–6] for the possible advantage that periodically aligned electrostatic potentials in crystal lattices are capable of providing a channeling effect [7–9] in combination with low emittance determined by an Ångström-scale aperture of the atomic "tubes". The basic concepts of atomic accelerator with short pulse driving sources like high power lasers or ultra-short bunches have been considered theoretically. However, the idea has never been demonstrated by experiment or simulation due to the extremely tight interaction condition of the Angstrom-size atomic channels in natural crystals and the complexity of electron dynamics in solid-plasma.

NANOTUBES FOR CHANNELING

Carbon nanotubes (CNTs) are a synthetic nanostructure, which is a roll of a graphene sheet, and its tube diameter can be easily increased up to sub-micron by optimizing fabrication processes (chemical vapor deposition, CVD). For channeling applications of high power beams, carbon nanostructures have various advantages over crystals [10]. Particles are normally de-channeled when the transverse forces are larger than the maximal electric field acting on channeled particles from crystal atoms, which is described by the critical angle. The dechanneling rate is significantly reduced and the beam acceptance is increased by the large size of the channels, e.g., a 100 nm wide CNT channel has larger acceptance than a silicon channel by three orders of magnitude. If the channel size is increased from angstroms to nanometers, the maximally reachable acceleration gradient would be lowered from ~ 100 TeV/m to ~ 1 TeV/m due to the decrease of effective plasma charge density. However, the nanotube channels still provide sufficiently large transverse and longitudinal fields in the range of TV/m. For the crystal channels in angstrom scale, the lattice dissociation time of atomic

* Work supported by the DOE contract No.DEAC02-07CH11359 to the Fermi Research Alliance LLC.

ISBN: 978-3-95450-168-7 doi:10.18429/JACoW-IPAC2015-WEPJE001

Content from this work may be used under the terms of the CC BY 3.0 licence (© 2015). Any distribution of this work must maintain attribution to the author(s), title of the work, publisher, and DOI.

OPTIMAL POSITRON-BEAM EXCITED PLASMA WAKEFIELDS IN HOLLOW AND ION-WAKE CHANNELS

Aakash A. Sahai *, Thomas C. Katsouleas
Dept of Electrical Engineering, Duke University, Durham, NC, 27708 USA

Abstract

A positron-beam interacting with the plasma electrons drives radial suck-in, in contrast to an electron-beam driven blow-out in the over-dense regime, $n_b > n_0$. In a homogeneous plasma, the electrons are radially sucked-in from all the different radii. The electrons collapsing from different radii do not simultaneously compress on-axis driving weak fields. A hollow-channel allows electrons from its channel-radius to collapse simultaneously exciting coherent fields [1]. We analyze the optimal channel radius. Additionally, the low ion density in the hollow allows a larger region with focusing phase. We have shown the formation of an ion-wake channel behind a blow-out electron bubble-wake. Here we explore positron acceleration in the over-dense regime comparing an optimal hollow-plasma channel to the ion-wake channel [2]. The condition for optimal hollow-channel radius is also compared. We also address the effects of a non-ideal ion-wake channel on positron-beam excited fields.

INTRODUCTION

Acceleration of positron beams is a major challenge for developing a collider using plasma-based acceleration techniques. Hollow-channel plasma is required for a collider-level plasma-based positron acceleration [1]. However, no analysis has been done to study the scaling laws of the hollow-channel properties based upon the positron beam properties. Similarly, the preparation of hollow-channels with properties suited for positron acceleration is still an ongoing research. In this paper we present a preliminary analysis of the scaling laws and application of the ion-wake channel for positron-beam driven wakefield acceleration. The ion-wake channel is a cylindrical soliton left behind in the plasma by a bubble wake train [2]. Studies of processes behind the plasma acceleration structures also helps in our understanding of the repetition-rate of the plasma colliders [4].

Positron beam interacts with a homogeneous plasma (density, n_0) unlike an ultrashort electron beam (peak density, n_{be}, radius, r_{be}). The plasma electrons see the repulsive force of the electron beam space-charge and are blown-out radially, $\frac{\mathrm{d}^2}{\mathrm{d}\xi^2}r = \frac{1}{r}\frac{1}{2\pi\beta_b^2}\frac{n_{be}(\xi)}{n_0}\pi\left(\frac{r_{be}(\xi)}{c/\omega_{pe}}\right)^2$ (at a fixed $\xi = c\beta_b t - z$, where $\omega_{pe} = \sqrt{\frac{4\pi n_0 e^2}{m_e}}$ and $\frac{c}{\omega_{pe}}$ is the plasma skin-depth). We look for radial plasma-electron dynamics at time t, just behind the current location of the drive-beam propagating at $c\beta_b$. This is done using an appropriate coordinate ξ such that the current longitudinal beam location is $c\beta_b t$ and $c\beta_b t - z$ is longitudinally behind the beam. The electrons coherently collapse back to the axis under the influence of the plasma ion restoring force; executing cylindrical plasma oscillations and driving a large on-axis longitudinal wakefield. The regions where the electrons are in the blow-out phase, unshielded plasma ions are left behind; quite conveniently exciting the focussing-phase of the transverse fields for an electron beam.

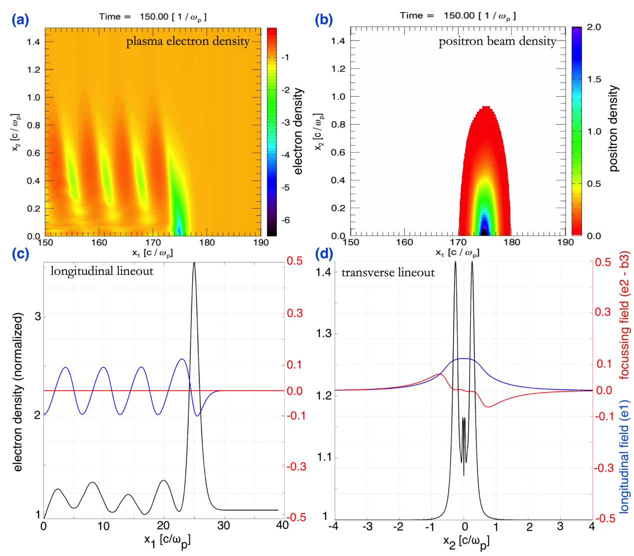

Figure 1: Positron-beam driven wakefields in a homogeneous plasma (a) electron density in 2D cylindrical space at $t = 150\omega_{pe}^{-1}$ (b) positron-beam in 2D cylindrical space (c) on-axis longitudinal (x_1) line-out: electron density (black), longitudinal field (blue), focussing field (red) (d) transverse (x_2) line-out at the peak longitudinal field.

The space-charge of an ultrashort positron beam (n_{bp}, r_{bp}), on the contrary, sucks in the plasma electrons and they collapse to the axis, $\frac{\mathrm{d}^2}{\mathrm{d}\xi^2}r = -\frac{1}{r}\frac{1}{2\pi\beta_b^2}\frac{n_{bp}(\xi)}{n_0}\pi\left(\frac{r_{bp}(\xi)}{c/\omega_{pe}}\right)^2$. However, there are 2 major problems with the suck-in wakefields in a homogeneous plasma. (i) The plasma electrons are sucked-in from different radii; with the radially closer ones experiencing a larger force and radially farther ones a smaller force (it is interesting to contrast this with an electron beam interacting with the plasma electrons). So, the collapse to the axis is not coherent and different rings of electrons arrive at different times. Due to the lack of optimal on-axis electron compression the wakefields are weak (note the on-axis compression in Fig. 1(a)). (ii) When the sucked-in electrons execute radial oscillations, the regions where the electrons are not in the on-axis compression phase has excess unshielded ions. The regions with ions are de-focussing for positrons (positrons to be accelerated are aligned to be

* aakash.sahai@gmail.com

ISBN: 978-3-95450-168-7 doi:10.18429/JACoW-IPAC2015-WEPJE002

PHOTOINJECTOR IMPROVEMENT AND CONTROL BY SURFACE ACOUSTIC WAVES*

A. Afanasev[1,2], C. Korman[2], R.P. Johnson[1]
[1]Muons, Inc., Batavia, IL, USA
[2]The George Washington University, Washington, DC, USA

Abstract

A new technique is being developed to enhance the efficiency of photocathodes used for electron sources in order to improve emission capabilities of electron sources, such as bunch charge and average current. The proposed technique is based on the use of surface acoustical waves (SAW) generated on the piezoelectric surface of a GaAs photocathode. The generation of SAW on piezoelectric substrates is known to produce strong piezoelectric fields that propagate on the surface of the material. These fields can significantly suppress recombination effects and result in enhanced quantum efficiency of photoemission. Experimental measurements of photoemission quantum efficiency are planned on semiconductors used as photocathode materials (e.g., GaAs) in presence of SAW with varied parameters. The experimental results will be used as input for physics modeling that will provide a basis for the design of operational SAW-enhanced photocathodes. The improved quantum efficiency and parameter control expected from the use of SAW will be useful for electron sources in particle accelerators as well as for commercialization in other fields, such as electron microscopy.

MOTIVATION

An experiment [1] reported strikingly long lifetimes of photo-excited electrons in a GaAs sample in the presence of piezoelectric fields induced by SAW. In this experiment, electrons and holes were photo-generated by a 5 µm diameter laser spot and were transported towards a semi-transparent metal strip, at which electron–hole recombination was induced by screening out SAW. The key observation relevant for potential applications for polarized electron sources is that spin polarization of the electrons during transport was preserved, at a distance of hundreds of microns. An observed increase of electron diffusion length with minimized de-polarization effects is an important motivation for our study. The advantages provided by the use of piezoelectric fields are not only limited to applications of SAW. Realization of piezoelectric fields in nano-scale devices has recently led to the development of the entire field of *piezotronics* and *piezophototronics* [2] that results from three-way coupling of piezoelectricity, photonic excitation, and semiconductor transport, leading to enhanced performance of photovoltaic cells and photon detectors.

Work supported by DOE STTR Grant DE-SC0006256 and Muons, Inc.
*E-mail: afanas@gwu.edu

It is our main objective to demonstrate the effects of piezoelectric fields, via SAW application, on photocathode performance. To the best of our knowledge, such an effect was never demonstrated before.

GENERATION OF SAW

SAW are presently a basis of a well-established technology used in multiple applications, primarily in SAW devices associated with electronic circuits. The telecommunications industry is probably the largest consumer of SAW devices, with an estimated 3 billion acoustic wave filters used per year [3]. In most applications SAW are generated (and detected) using a piezoelectric effect, namely, conversion of electrical energy into mechanical energy and vice versa. This is accomplished through the use of Interdigital Transducers (IDT) placed on a piezoelectric substrate, as shown in Fig. 1. An AC voltage, typically with frequencies up to 1 GHz, is applied to the IDT, resulting in one or more SAW propagating with the speed of sound v_{SAW}. The spacing λ of the structure on the IDT defines the wave number of each of the SAW, $k=2\pi/\lambda$. SAW are deformations of the crystal lattice that produce a periodic modulation of the electric charge and potential in piezoelectric semiconductors, such as GaAs (Fig.1).

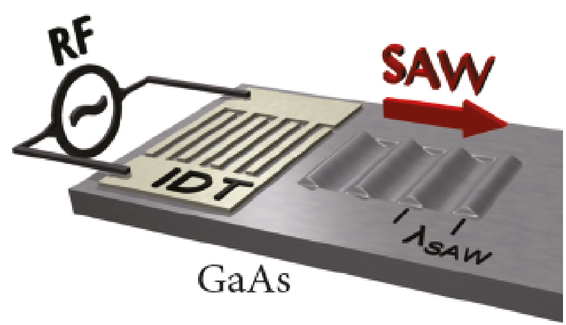

Figure 1: Generation of SAW on a piezoelectric substrate with an interdigital transducer (IDT) powered by an RF-source.

Typical values of the parameters related to experiments of interest [1,4] are frequency f = 840 MHz, wavelength λsaw = 3.4 µm, and speed $v_{SAW} \approx 3$ km/s. More formally, SAW are acoustic phonons with a linear dispersion relation between energy and wave vector, and their eigenmodes are described by the theory of elasticity. For a homogeneous medium, the three bulk elastic

Content from this work may be used under the terms of the CC BY 3.0 licence (© 2015). Any distribution of this work must maintain attribution to the author(s), title of the work, publisher, and DOI.

ISBN: 978-3-95450-168-7 doi:10.18429/JACoW-IPAC2015-WEPJE006

DIELECTRIC WAKEFIELD ACCELERATOR EXPERIMENTS AT ATF*

D. Shchegolkov#, E. Simakov, LANL, Los Alamos, NM 87545, USA
S. Antipov, Euclid TechLabs, Bolingbrook, IL 60440, USA
M. Fedurin, BNL, Upton, NY 11973, USA

Abstract

Dielectric wakefield acceleration (DWA) presents us with means to achieve the accelerating gradient high above the limits of conventional accelerators. In a typical DWA scheme a higher energy lower charge main bunch is accelerated in the wakefield produced by a preceding lower energy higher charge drive bunch inside of a hollow metal-encapsulated dielectric tube. To make use of as much energy of the drive bunch as possible, it is highly important that all parts of it decelerate uniformly. Close to uniform drive bunch deceleration can be achieved if its current is properly shaped.

At Accelerator Test Facility (ATF) at BNL we shaped the current of a chirped electron beam with an adjustable mask placed inside of the highly dispersive region in the magnetic dogleg. We passed the shaped beam current through a quartz tube and observed the beam particles' energy modulation at the tube's output with a spectrometer. By tuning the mask we were able to control the beam energy modulation and thus the wakefield profile in the tube.

INTRODUCTION

Dielectric wakefield accelerators are formed by one or several coaxial dielectric layers surrounded by metal cladding (Fig. 1). Wakefields in dielectric structures may reach gradients on the order of 10 GV/m [1] with 100 MV/m demonstrated in multiple experiments. They also have the remarkable property that the wakefield's axial electric field is transversely uniform due to the fact that the relativistic drive beam and the subsequent wakefield travel very nearly at the speed of light. As we noticed previously [2, 3], these unique properties may allow the use of DWAs as high gradient high brightness accelerators for X-ray free electron lasers.

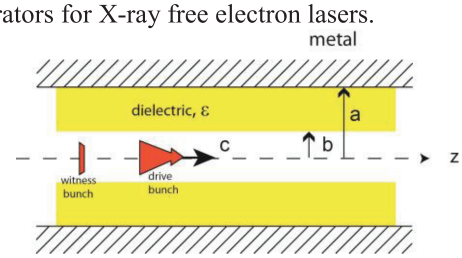

Figure 1: Schematic of the DWA.

An important parameter of each accelerator is its energy transfer efficiency. In case of the DWA it has to do with the transformer ratio (TR), which is the ratio of the accelerating field acting on the main bunch to the maximum deceleration field inside of the drive bunch. For the same accelerating gradient higher TR wakefield will ensure longer use of the drive bunch due to its smaller and more uniform deceleration. For any finite length longitudinally symmetric bunch the TR can never exceed 2 [4]. An enhanced TR can be achieved with a ramped beam or a ramp-profiled bunch train [4]. Recently a double triangular (DT) beam current was proposed [5]:

$$I(t) = \begin{cases} I_0 \cdot f \cdot t, & 0 \le t < \dfrac{1}{4f}; \\ I_0 \cdot \left(f \cdot t - \dfrac{1}{2\pi} \right), & \dfrac{1}{4f} \le t < T. \end{cases}$$

In the above formula, f is the frequency of a single mode accelerator, T – the total bunch duration, t – time, I_0 – a constant with units of current. In a single mode approximation the DT current produces strictly uniform deceleration of the drive bunch except for its very beginning part (Fig. 2). In reality, due to the finite thickness of the dielectric tube, more than one mode is exited; as a result, the TR is generally reduced (Fig. 2). For very long DT drive bunches the TR becomes proportional to the bunch length expressed in wavelengths of the induced wakefield radiation and thus the TR can be made very large.

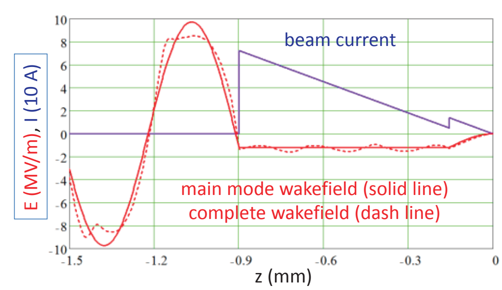

Figure 2: DT current and its wakefield in the tube chosen for the experiment: a=550 μm, b=400 μm, ε=3.8.

Even though the DT bunch has no steep rising edges, it is still difficult to produce with all the features in subpicosecond scale required for the accelerator operation at 300 GHz or higher frequencies.

At ATF we used an indirect method of current modulation employing a transverse DT beam mask [6]. The mask was made adjustable to compensate for beam parameters which were hard to control. An energy chirped beam was shaped with the mask, passed through a metal encapsulated quartz tube and visualized on a spectrometer. We tuned the mask and observed the beam energy change on the spectrometer. The idea of the experiment was that if the beam has a right DT shape then its picture on the spectrometer incurs minimum changes

*Work supported by the Department of Energy Laboratory Directed Research and Development program at LANL.
D_Shcheg@LANL.gov

Content from this work may be used under the terms of the CC BY 3.0 licence (© 2015). Any distribution of this work must maintain attribution to the author(s), title of the work, publisher, and DOI.

ISBN: 978-3-95450-168-7 doi:10.18429/JACoW-IPAC2015-WEPJE007

SIMULATION STUDIES OF BBU SUPPRESSION METHODS AND ACCEPTABLE TOLERANCES IN DIELECTRIC WAKEFIELD ACCELERATORS*

D. Shchegolkov#, E. Simakov, LANL, Los Alamos, NM 87545, USA
A. Zholents, ANL, Argonne, IL 60439, USA

Abstract

The advantage of dielectric wakefield accelerators (DWAs) is the ability to achieve accelerating gradients well above the limits of conventional accelerators. However DWAs will also produce high transverse wakefields if the beam propagates off-center, which grow even faster than the accelerating gradient when the width of the beam channel is decreased. It is highly important to suppress single beam breakup (BBU) instability in order for the beam to propagate long enough so that a reasonable amount of energy (e.g., 80%) from the drive bunch is extracted. In addition bending of the dielectric channel has a similar effect to off-center steering of the beam with the required tolerances on the channel straightness typically in a few micron range. For both rectangular and circular dielectric lined waveguides we use a FODO lattice with a tapered strength for suppression of BBU. We impose initial energy chirp on the drive beam to make use of the BNS damping. We change rectangular waveguide orientation by 90 degrees with a small step to make use of the quadrupole wakefield focusing. These and other techniques and tolerance requirements are discussed and simulation results are presented in this paper.

INTRODUCTION

Accelerating gradients as high as several GV/m have been demonstrated in short dielectric tubes fed by electron beams [1]. However, when it comes to staging, a problem of high transverse wakefields arises. Narrowing of the dielectric tube results in higher accelerating gradient which is generally in inverse proportion to the tube radius squared. However the transverse wakefields grow even faster in inverse proportion to the tube radius cubed [2]. Consequently smaller tube size causes premature BBU that will lower the accelerator efficiency and the maximum achievable energy due to the beam loss. More efficient use of the drive bunch can be obtained if the BBU instability is effectively suppressed.

SIMULATIONS IN ELEGANT

DWA modelling was performed in Elegant to study ideas and configurations for their effectiveness in fighting BBU [3]. Even though Elegant [4] is considered as a primarily transfer matrix type of an accelerator code, it has all the necessary capabilities to fully account for different particle energies in beamline elements (including quadrupole magnets) with momentum kicks. This is especially important as the drive and the witness bunches in the DWA may have different particle energies by as much as several orders. We implemented both longitudinal and transverse wakefields (dipole and quadrupole) in Elegant by supplying their Green's functions as a table of time dependent values in a separate input file.

BUNCH SHAPES FOR HIGH TRANSFORMER RATIO

To achieve high efficiency in a DWA a drive bunch with a ramped current which creates a high transformer ratio wakefield (HTRW) has to be used [5]. The wake of a ramped bunch has a uniform decelerating field acting on the whole drive bunch except only for a small part of it at the beginning, where the field is lower. It was suggested to use a specific double triangular (DT) current to excite the HTRW [6, 7]. Any HTRW is also associated with near linear growth of the transverse deflection force towards the tail of the drive bunch, which in turn linearly increases with the beam offset from the tube's axis. It makes the tail of the drive bunch most susceptible to the BBU. The main longitudinal and dipole wakefield modes have close frequencies, but their Green's functions are 90° out of phase with the longitudinal gradient reaching the peak value right behind the drive charge and the transverse gradient reaching its peak value a quarter wavelength downstream.

BBU SUPPRESSION

The well-established way to confine the charged particle beam is to use a FODO lattice consisting of magnetic quadrupoles of alternating polarity. The period of the FODO lattice has to be much smaller than the typical length of instability's growth. At the same time, smaller periods require higher magnetic gradient to provide adequate focusing. If quadrupoles are too strong, there is an overfocusing. So the quadrupoles need to be strong enough to have pronounced focusing effect, but not too strong to cause instability. As the drive beam loses energy the magnetic strength of the FODO lattice needs to be tapered to keep it optimal for the particles in the tail of the drive bunch which are most susceptible to the BBU (Fig. 1).

The FODO suppression of the BBU instability is not very efficiency as is. The reason for that is that once the beam has an off-center shift, it will oscillate in the FODO

*Work supported by the Department of Energy Laboratory Directed Research and Development program at LANL.
D_Shcheg@LANL.gov

Content from this work may be used under the terms of the CC BY 3.0 licence (© 2015). Any distribution of this work must maintain attribution to the author(s), title of the work, publisher, and DOI.

ISBN: 978-3-95450-168-7 doi:10.18429/JACoW-IPAC2015-WEPJE008

EXPERIMENTAL STUDY OF WAKEFIELDS IN AN X-BAND PHOTONIC BAND GAP ACCELERATING STRUCTURE*

Evgenya I. Simakov#, Sergey Arsenyev, Cynthia Buechler, Randall L. Edwards, and William Romero, Los Alamos National Laboratory, Los Alamos, NM 87545, USA
Manoel Conde, Gwanhui Ha, John Power, and Eric Wisniewski, Argonne National Laboratory, Argonne, IL 60439, USA
Chunguan Jing, Euclid Techlabs, LLC, Solon, OH 44139, USA

Abstract

We designed an experiment to conduct a detailed investigation of higher order mode spectrum in a room-temperature traveling-wave photonic band gap (PBG) accelerating structure at 11.7 GHz. It has been long recognized that PBG structures have great potential in reducing long-range wakefields in accelerators. The first ever demonstration of acceleration in room-temperature PBG structures was conducted at MIT in 2005. Since then, the importance of that device has been recognized by many research institutions. However, the full experimental characterization of the wakefield spectrum in a beam test has not been performed to date. The Argonne Wakefield Accelerator (AWA) test facility at the Argonne National Laboratory represents a perfect site where this evaluation could be conducted with a single high charge electron bunch and with a train of bunches. Here we describe fabrication and tuning of PBG cells, the final cold-test of the traveling-wave accelerating structure, and the results of the beam testing at AWA.

INTRODUCTION

The next generation of linear colliders with multi-hundred GeV to TeV beam energies pushes the frontiers of the current beam physics and technology with the goal of obtaining high luminosity of the beam and avoiding bunch to bunch beam breakup. Thus, the accelerating cavities for the future linear colliders must be selective with respect to the operating mode, and higher order mode (HOM) wakefields that affect the quality of the beam must be suppressed. Photonic Band Gap [1] (PBG) cavities have the unique potential to filter out HOM power and greatly reduce wakefields. A PBG structure or simply, photonic crystal, represents a periodic lattice of macroscopic components (e.g., rods), metallic, dielectric or both. For accelerator applications, two-dimensional PBG resonators based on arrays of metal rods are commonly employed. The first ever demonstration of acceleration in a PBG resonator was conducted at Massachusetts Institute of Technology (MIT) in 2005 [2]. Since then, the importance of PBG structures for accelerators has been recognized by many research institutions worldwide.

Two attempts to experimentally study wakefields in PBG accelerators were conducted to date, but were incomplete [3,4]. At this point, the full experimental characterization of the wakefield spectrum in a traveling-wave PBG accelerator is overdue.

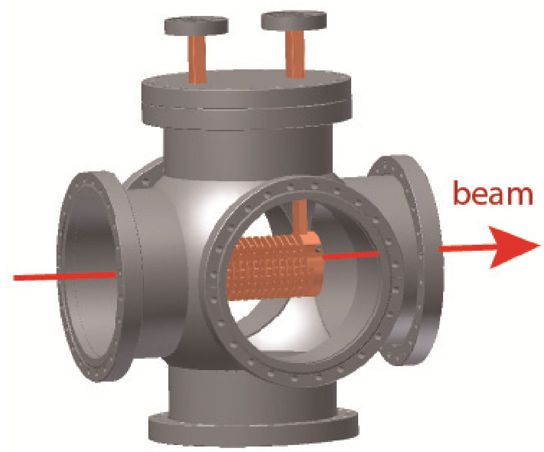

Figure 1: A 16-cell traveling-wave PBG accelerator structure with two waveguide couplers installed in a vacuum chamber for the wakefield tests.

DOE HEP funded a project at Los Alamos National Laboratory (LANL) to conduct the experimental characterization of the wakefield spectrum of a traveling-wave PBG accelerator structure. We put together an 11.7 GHz $2\pi/3$-mode accelerating structure of 16 PBG cells, installed it at the Argonne Wakefield Accelerator (AWA), passed an electron beam through the structure (as shown in Figure 1) and recorded the full traveling-wave (TW) wakefield spectrum.

DESIGN OF 11.7 GHz TW PBG ACCELERATOR

We designed a 16-cell traveling-wave $2\pi/3$-mode PBG accelerator structure with characteristics similar to the 6-cell MIT PBG structure [2]. The PBG accelerator was designed at the frequency of 11.7 GHz, which is 9 times the frequency of the AWA (1.3 GHz). The exact dimensions and the accelerator characteristics of the structure are summarized in Table 1.

*Work is supported by the U.S. Department of Energy (DOE) Office of Science Early Career Research Program.
#smirnova@lanl.gov

Content from this work may be used under the terms of the CC BY 3.0 licence (© 2015). Any distribution of this work must maintain attribution to the author(s), title of the work, publisher, and DOI.

6th International Particle Accelerator Conference IPAC2015, Richmond, VA, USA JACoW Publishing
ISBN: 978-3-95450-168-7 doi:10.18429/JACoW-IPAC2015-WEPJE010

Content from this work may be used under the terms of the CC BY 3.0 licence (© 2015). Any distribution of this work must maintain attribution to the author(s), title of the work, publisher, and DOI.

PARTICLE PRODUCTION OF A GRAPHITE TARGET SYSTEM FOR THE INTENSITY FRONTIER*

X. Ding,† UCLA, Los Angeles, CA 90095, USA
H.G. Kirk, Brookhaven National Laboratory, Upton, NY 11973, USA
K.T. McDonald, Princeton University, Princeton, NJ 08544, USA

Abstract

A solid graphite target system is considered for an intense muon and/or neutrino source in support of physics at the intensity frontier. We previously optimized the geometric parameters of the beam and target to maximize particle production at low energies by incoming protons with kinetic energy of 6.75 GeV and an rms geometric emittance of 5 mm-mrad using the MARS15(2014) code. In this study, we ran MARS15 with ROOT-based geometry and also considered a mercury-jet target as an upgrade option. The optimization was extended to focused proton beams with transverse emittances from 5 to 50 mm-mrad, showing that the particle production decreases slowly with increasing emittance. We also studied beam-dump configurations to suppress the rate of undesirable high-energy secondary particles in the beam.

INTRODUCTION

Neutrino-physics and muon-physics at the intensity frontier require the greatest possible beam intensities of neutrinos and muons. The target scenario for the present study is to use a 6.75-GeV proton driver with beam power of 1 MW [1] interacting with a graphite target in the so-called 20to2T5m4PDL target system configuration, as shown in Fig. 1.

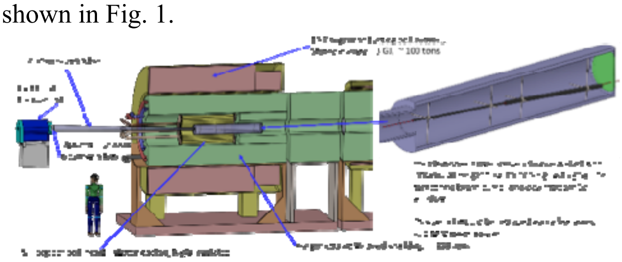

Figure 1: Layout of the 20to2T5m4PDL Target System configuration.

Figure 2 shows that the axial magnetic field for configuration 20to2T5m4PDL tapers adiabatically over 5 m from 20 T around the target to 2 T in the rest of Front End [2]. The inner radius of superconducting coils (SC) in the region surrounding the graphite target is 120 cm to permit sufficient internal tungsten shielding for a 10-year operational lifetime of the SC coils against radiation damage [3]. The first 50 m of the magnetic channel of the Front End is sketched in Fig. 3.

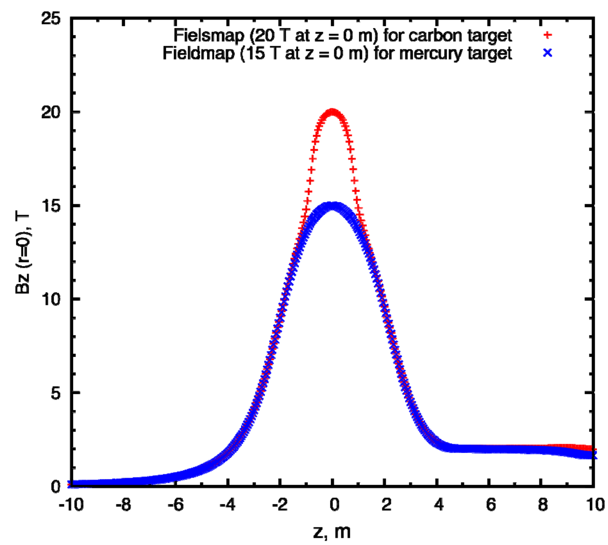

Figure 2: Axial magnetic field of the 20to2T5m4PDL (red dots) and 15to2T5m4PDL (blue dots) Front-End channels. The center of the target is at $z = 0$.

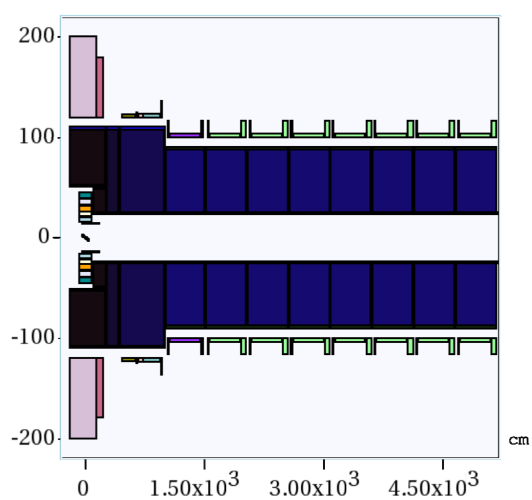

Figure 3: Schematic of the 20to2T5m4PDL Target System configuration, for $-2 < z < 50$ m.

The graphite-target, and graphite-beam-dump, rods are inside a double-walled stainless-steel containment vessel, with downstream Be windows, shown at the right of Fig. 1. These rods are radiation cooled, and the containment vessel is cooled by He-gas flow between its double walls. The outer cylinder extends over $-46 < z < 170$ cm, with outer radius $r = 15$ cm. The inner cylinder extends over $-45 < z < 169$ cm, with inner radius $r = 14$ cm. The

*Work supported in part by US DOE Contract NO. DE-AC02-98CH110886.
†xding@bnl.gov

ISBN: 978-3-95450-168-7 doi:10.18429/JACoW-IPAC2015-WEPJE011

HIGH RELIABILITY, LONG LIFETIME, CONTINUOUS WAVE H- ION SOURCE

Preston J. Barrows, University of Wisconsin - Madison, WI 53706, USA
Gabriel E. Becerra, Phoenix Nuclear Labs LLC, WI 53713, USA

Abstract

Phoenix Nuclear Labs (PNL) is developing a high-current, long-lifetime negative hydrogen (H-) ion source in partnership with Fermilab as part of an ion beam injector for future Intensity Frontier particle accelerators. In this application, continuous output with long lifetime and high reliability and efficiency are critical. Existing ion sources at Fermilab rely on plasma-facing electrodes and are limited to lifetimes of a few hundred hours, while requiring relatively high gas loads on downstream components. PNL's H- ion source uses an electrodeless microwave plasma generator which has been extensively developed in PNL's positive ion source systems, demonstrating 1000+ hours of operation and >99

INTRODUCTION

Ion sources are critical for a wide range of applications including basic science research, medical applications, and semiconductor production. In many cases, the performance and reliability of very large, complex, and expensive systems is limited by the performance and reliability of the ion source, which often represents a relatively small part of the total system in terms of size and cost. Thus, advances in ion source technologies can lead to drastic improvements in system performance relatively quickly. However, ion sources are complex devices that often suffer from reliability issues when pushed to high currents, as is often demanded by the rest of the system.

Lifetime and reliability issues can be troublesome for ion sources, and this can be especially true for negative hydrogen (H-) sources. Nonetheless, negative ion sources are still commonly used across a broad range of applications due to the fact that, for many applications, downstream system components require negative rather than positive ions. In this project, a new type of ion source that can produce high DC current output (up to 15 mA) and has a long lifetime (up to several months) has been designed. It is understood that the near term DoE need for such a source is to serve as an ion beam injector into future Intensity Frontier particle accelerators that are under development at Fermi National Lab and other DoE labs.

Intensity Frontier accelerators are next generation basic science research accelerators which include GeV-scale linacs able to operate at higher current levels than have ever been achieved at this energy level.

The leading H- ion source candidate that is currently under consideration by the Fermilab design team has a lifetime of a few hundred hours. This lifetime decreases further when operated at full power (15 mA). Furthermore, the source has high power requirements (15 kW) and high gas load

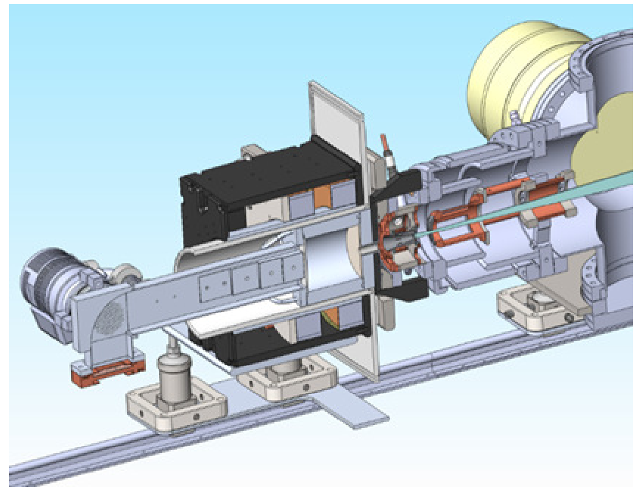

Figure 1: Cross-sectional view of negative ion source beamline.

(18-20 SCCM) on the downstream vacuum components. Though ion sources are cheap on the scale of large research accelerators, if a more reliable H- source is not developed the results of the entire project could be in jeopardy.

In this project, a modified 2.45 GHz microwave proton source has been evaluated as a generator of atomic hydrogen that will be used for surface production of H- ions. A cesiated surface converter is located between the proton source and the H- extraction region. In the extraction region, electrostatic lenses produce a low energy H- ion beam. Diagnostics developed in this work monitor neutral atomic hydrogen particle energy and flux, along with electron temperature and density near the extractor. A design for H- beam formation in a reduced plasma density environment has been developed. It is particularly important to reduce high temperature electron density in the converter region. Thus, the two ion source chambers (neutral production and H- conversion) are separated by a tunable magnetic dipole field.

DESCRIPTION

Phoenix Nuclear Labs (PNL) has developed a design for a negative hydrogen ion source. The device is driven by a plasma chamber that produces energetic electrons, positive hydrogen ions, and neutral hydrogen atoms. The particles generated by the plasma are filtered by a transverse magnetic field, which preferentially removes energetic electrons while allowing fast neutrals to pass. These neutrals are directed to a surface converter and produce the desired negative hydrogen ions, which are then extracted into a low energy beam using

Content from this work may be used under the terms of the CC BY 3.0 licence (© 2015). Any distribution of this work must maintain attribution to the author(s), title of the work, publisher, and DOI.

ISBN: 978-3-95450-168-7 doi:10.18429/JACoW-IPAC2015-WEPJE012

DESIGN AND OPTIMISATION OF DIELECTRIC LASER DEFLECTING STRUCTURES*

K. P. Wootton†, R. J. England, I. V. Makasyuk, Z. Wu, SLAC National Accelerator Laboratory, 2575 Sand Hill Rd, Menlo Park, CA 94025, USA
A. Tafel, Friedrich-Alexander Universitaet Erlangen-Nuernberg, Schlossplatz 4, 91054 Erlangen, Germany
R. L. Byer, E. A. Peralta, Stanford University, 450 Serra Mall, Stanford, CA 94305, USA

Abstract

Recent experimental demonstrations of dielectric laser-driven accelerator structures offer a path to the miniaturisation of accelerators. In order to accelerate particles to higher energies using a staged sequence of accelerating structures, integrating compatible micrometre-scale transverse deflecting structures into these accelerators is necessary. Using simulations, the present work outlines the design and optimisation of a fused-silica laser-driven grating deflecting structure for relativistic electron beams. Implications for device fabrication and experiments are outlined.

INTRODUCTION

The design of conventional particle accelerators is motivated by the Lorentz force, with magnetic fields for the efficient deflection of high energy particles. However, the possibility of transverse electric field gradient of the order 1 GV m^{-1} bypasses the need for magnetic fields for deflecting beams, and opens new options and length scales for accelerator design.

Recent experimental demonstrations of dielectric laser acceleration with electric fields exceeding 300 MeV m^{-1} are presented in Refs. [1–3]. Using ultrafast laser pulses of the order of 100 fs, this can be extended to electric field gradients of 1 GV m^{-1} [4].

The present work outlines electromagnetic simulations of a laser-driven dielectric deflecting structure. An experiment is proposed to demonstrate laser-driven dielectric deflecting structures with relativistic electron beams in a compact undulator.

THEORY

The theory of dielectric grating deflecting structures for relativistic electron beams is described in the previous work of Plettner, et al. [5–7]. Several key parameters can be used to compare dielectric accelerators of differing geometry. The accelerating gradient, denoted by G_0 is given by [8],

$$G_0 = \frac{q}{\lambda} \int_0^{\lambda} E_z[z(t), t] dz, \tag{1}$$

where q is the particle charge, λ is the laser wavelength, and the electric field E_z represents the electric field in the direction of travel of the electron. Similarly, a deflecting field can be denoted by D_0, defined by,

$$D_0 = \frac{q}{\lambda} \int_0^{\lambda} \left[\Big(E_x[z(t), t] - cB_y[z(t), t] \Big)^2 + \Big(E_y[z(t), t] + cB_x[z(t), t] \Big)^2 \right]^{\frac{1}{2}} dz, \tag{2}$$

where the electric and magnetic fields of the laser are decomposed into the directions x and y of Fig. 1.

The purpose of the dielectric grating structure is to generate periodic, local oscillations to the incident the electric field. The amplitude of the electric field therefore varies within the structure, with the maximum electric field anywhere in the structure defined as E_{max}. The maximum electric field in the structure determines the maximum incident electric field that the structure will sustain without damage.

One can define the field enhancement factor of a structure as $\eta = E_{\mathrm{max}}/E_0$ [9]. Hence, the acceleration factor f_A (denoted by Plettner, et al. as the damage factor [8]) is given by,

$$f_A = \frac{G_0}{E_{\mathrm{max}}}, \tag{3}$$

and the deflection factor by [9]

$$f_D = \frac{D_0}{E_{\mathrm{max}}}. \tag{4}$$

Given a material with a known damage threshold electric field E_{dam}, the structure accelerating and deflecting fields can be scaled based upon the incident electric field E_0.

STRUCTURE AND LASER

The geometry of the structure simulated in the present work is presented in Fig. 1 below. The structure coordinates are defined in rectangular Cartesian coordinates, with the electron beam propagating in the z direction. The grating is rotated at an angle α about the y axis.

The structure is assumed to be illuminated by a single plane wave source of wavelength λ, propagating with wavevector k in the $-y$ direction, linear polarisation axis perpendicular to the grating and incident electric field E_0. Assuming a relativistic electron beam ($v \approx c$), the grating period in the direction of the electron beam trajectory should satisfy $\lambda_p = \lambda \cos\alpha$ [5].

At the photon wavelength of interest $\lambda = 800$ nm, the index of refraction of fused silica is approximately $n = 1.5$, and the relative permittivity $\varepsilon_r = n^2 = 2.25$ [10].

* This work was supported by the U.S. Department of Energy under Grants DE-AC02-76SF00515, and DE-FG02-13ER41970.
† wootton@slac.stanford.edu

Content from this work may be used under the terms of the CC BY 3.0 licence (© 2015). Any distribution of this work must maintain attribution to the author(s), title of the work, publisher, and DOI.

ISBN: 978-3-95450-168-7 doi:10.18429/JACoW-IPAC2015-WEPJE013

Content from this work may be used under the terms of the CC BY 3.0 licence (© 2015). Any distribution of this work must maintain attribution to the author(s), title of the work, publisher, and DOI.

A NEW ACCELERATING MODE IN A SILICON WOODPILE STRUCTURE AND ITS HIGH-EFFICIENCY POWER COUPLER DESIGN*

Z.R. Wu#, C.H. Lee, C.K. Ng, K.P. Wootton, R.J. England
SLAC National Accelerator Lab, Menlo Park, CA 94555, USA

Abstract

Silicon woodpile photonic crystals provide a base structure that can be used to build a three-dimensional dielectric waveguide system for high-gradient laser-driven acceleration. A new woodpile waveguide design that hosts a phase synchronous, centrally confined accelerating mode with ideal Gaussian transverse profile is proposed. Comparing with previously discovered silicon woodpile accelerating modes, this mode shows advantages in better beam loading and higher achievable acceleration gradient. Several travelling-wave coupler design schemes developed for multi-cell RF cavity accelerators are adapted to the woodpile accelerator coupler design based on this new accelerating mode. A forward-wave-coupled, highly efficient silicon woodpile accelerator is achieved. Simulation shows high efficiency of over 70% of the drive laser power coupled to this fundamental woodpile accelerating mode, with less than 15% backward wave excitation. The estimated acceleration gradient, when the coupler structure is driven at the damage threshold fluence of silicon at its operating 1.506 um wavelength, can reach roughly 185 MV/m.

INTRODUCTION

Laser driven dielectric photonic bandgap (PBG) accelerating structures have drawn great interest due to the potential ~ GeV/m accelerating gradient and mature high-power, high-efficiency lasers as driving sources [1-3]. The Woodpile structure in particular provides three dimensional EM field confinement and manipulation, and has been shown to exhibit TM-like modes in the defect waveguide to support electron acceleration [4, 5]. Individual rods in the structure discretize the spatial dielectric distribution; therefore offer required degrees of freedom for mode control and building various coupling and focusing elements. The structure, if made of silicon, could potentially be well suited into standard photolithography process, and fabricated on a single wafer as an on-chip accelerator.

The woodpile structure is an arrangement of high-index dielectric scatters in a low-index background material (e.g. air), following a "woodpile" formation. The schematic in Fig. 1 Inset shows a woodpile accelerating waveguide design first proposed in [4]. The base lattice consists of rectangular silicon rods stacked layer-by-layer, whose collective scattering of light exhibits a three-dimensional photonic band gap. The structure possesses mirror symmetry about the XZ plane, permitting a symmetric monopole mode for acceleration. This mode is confined to the open and roughly rectangular channel, as marked by the red break line in Fig. 1 Inset, and it propagates in the z direction. The accelerator waveguide channel is $7h$ tall and $3a$-w wide along its two transverse directions, with definition of dimensions w, h, and a illustrated in the figure. Speed-of-light synchronous TM-like mode is present with this waveguide channel design. An integrated on-chip WPS accelerator is conceptually visualized in Fig. 1. An input laser pulse is split into different branches of silicon-on-insulator (SOI) waveguides, represented by solid black channels in the layout, to power multiple stages of woodpile accelerators (meshed cells in the layout). The SOI waveguides are basically silicon slabs sitting atop lower-refractive-index materials, which confine laser light mostly within the silicon by total internal reflection. Control of the flow of the laser power can be realized via splitters and couplers built upon these SOI waveguides [5]. Electrons traversing through the accelerator channel in the WPS waveguide get a kick at each accelerating cell by the laser field, and accelerate. Each accelerator stage contains a woodpile waveguide loop cavity in order to recycle the laser energy and enhance optical-to-beam efficiency, as the rectangular loops in the layout illustrate.

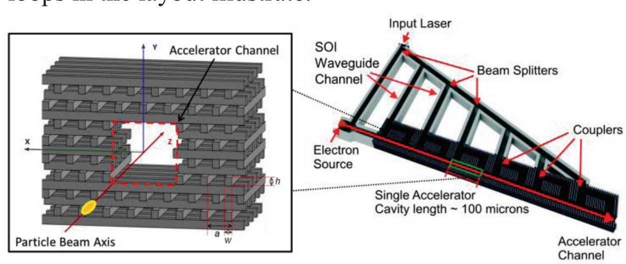

Figure 1: Conceptual schematic of an on-chip woodpile accelerator consisting of multiple accelerator cavities. Inset: Layout of a woodpile accelerator waveguide section supporting speed-of-light accelerating mode. Courtesy of Christopher McGuinness and Benjamin Cowan [4, 6].

A NEW ACCELERATING MODE

Several Accelerating waveguide designs based on silicon woodpile structure have been proposed before [4, 6]. By adjusting the waveguide aperture size and details at the interface between silicon and the channel wall, modal profile as well as phase/group velocities of the accelerating modes can be fine-tuned [6]. As an example, plotted in Fig. 2, Left is a propagating TM-mode with large longitudinal electric field component for

*Work supported by U.S. Department of Energy under Grants DE-AC02-76SF00515, DE-FG02-13ER41970 and by DARPA Grant N66001-11-1-4199.
#wzr@slac.stanford.edu

ISBN: 978-3-95450-168-7 doi:10.18429/JACoW-IPAC2015-WEPJE015

MUON TRACKING STUDIES IN A SKEW PARAMETRIC RESONANCE IONIZATION COOLING CHANNEL

A. Sy[#], Y. Derbenev, V.S. Morozov, Jefferson Lab, Newport News, VA 23606, U.S.A.
A. Afanasev, George Washington University, Washington, DC 20052, U.S.A.
R. P. Johnson, Muons, Inc., Batavia, IL 60510, U.S.A.

Abstract

Skew Parametric-resonance Ionization Cooling (SPIC) is an extension of the Parametric-resonance Ionization Cooling (PIC) framework that has previously been explored as the final 6D cooling stage of a high-luminosity muon collider. The addition of skew quadrupoles to the PIC magnetic focusing channel induces coupled dynamic behavior of the beam that is radially periodic. The periodicity of the radial motion allows for the avoidance of unwanted resonances in the horizontal and vertical transverse planes, while still providing periodic locations at which ionization cooling components can be implemented. A first practical implementation of the magnetic field components required in the SPIC channel is modeled in MADX. Dynamic features of the coupled correlated optics with and without induced parametric resonance are presented and discussed.

INTRODUCTION

The limit on the minimum achievable emittance in muon ionization cooling comes from the equilibrium between the cooling process and multiple Coulomb scattering in the absorber material. The concept of Parametric-resonance Ionization Cooling (PIC) is to push this limit by an order of magnitude in each transverse dimension by focusing the muon beam very strongly in both planes at thin absorber plates. This creates a large angular spread of the beam at the absorber locations, which is then cooled to its equilibrium value resulting in greatly reduced transverse emittances. Achieving adequately strong focusing using conventional magnetic optics would require unrealistically strong magnetic fields. Instead, PIC relies on a resonant process to provide the necessary focusing. A parametric resonance is induced in a cooling channel, causing focusing of the beam with the period of the channel's free oscillations. To attain simultaneous focusing in both planes at regular locations, the horizontal and vertical betatron oscillation periods must be commensurate with each other and with the channel's period. A magnetic channel possessing such optical properties, called a Twin helix channel, has been successfully developed and simulated [1].

Another important condition necessary for implementation of PIC is compensation of the beam smear from one focal point to another, to a degree where it is small compared to the focused beam size. Since the angular spread at the focal point is on the order of 100 mrad rms while the beam size is a fraction of a mm, this can be quite challenging. To mitigate this problem, the Twin helix channel was designed using continuous helical fields eliminating fringe-field effects. Significant progress has been made on compensation of aberrations using helical multipole fields [1]. However, multipole fields in combination with correlated optics introduce another serious problem, namely, non-linear resonances causing loss of dynamical stability.

To illustrate this problem, consider the Hamiltonian term of a continuous harmonically-varying octupole field $H_{oct} = n_{oct}\,(6x^2y^2 - x^4 - y^4)/4$ where $n_{oct} \sim \cos(2\pi mz/L)$ is the normalized octupole strength, m is an integer, z is the longitudinal coordinate, L is the channel period length, $x \sim \cos(2\pi\nu_x z/L)$ and $y \sim \cos(2\pi\nu_y z/L)$ are the horizontal and vertical transverse betatron coordinates, respectively, and ν_x and ν_y are the horizontal and vertical betatron tunes, respectively. Multiple octupole harmonics are needed in a cooling channel to compensate spherical aberrations. However, as can be clearly seen from the Hamiltonian, with our choice of betatron tunes of $\nu_x = 0.25$ and $\nu_y = 0.5$, any octupole harmonic m causes resonances in both planes. Dispersion further complicates the resonance structure. Selecting different betatron tunes does not help; as long as the betatron periods are integer multiples of the channel period as required by PIC, multipole fields will tend to cause non-linear resonance. This makes it difficult to find a set of multipoles sufficient for aberration compensation that does not cause beam instabilities.

To overcome this problem, we developed the concept of Skew PIC (SPIC). We introduce coupling in a cooling channel in such a way that the point to point focusing needed for PIC is preserved but the canonical betatron tunes are shifted from their resonant values, i.e. the canonical phase advances in the two planes are shifted from $m\pi$ values. A simple way to think of it is that the beam is azimuthally rotated between consecutive focal points. This moves the dispersion and betatron motion away from non-linear resonances. It also offers a number of other benefits: (a) it allows for control of the dispersion size for chromatic compensation; (b) it reduces the dimensionality of the aberration compensation problem to just the radial dimension and therefore reduces the number of required compensating multipoles; (c) it equates the parametric resonance rates in the two planes, and therefore only one resonance harmonic is needed; (d) it equates the two cooling decrements in the two transverse dimensions. In this paper, we present a design of a SPIC channel and first results of dynamics studies in this channel.

[#]amysy@jlab.org

Content from this work may be used under the terms of the CC BY 3.0 licence (© 2015). Any distribution of this work must maintain attribution to the author(s), title of the work, publisher, and DOI.

ISBN: 978-3-95450-168-7 doi:10.18429/JACoW-IPAC2015-WEPJE016

Content from this work may be used under the terms of the CC BY 3.0 licence (© 2015). Any distribution of this work must maintain attribution to the author(s), title of the work, publisher, and DOI.

INTENSE MUON BEAMS FROM THE CSNS SPALLATION TARGET

Yu Bao*, Gail Hanson,
Dept. of Physics and Astronomy, University of California, Riverside, CA, USA

Abstract

Intense muon beams are useful for a wide range of physics experiments. Currently most of the muon beams are produced by protons hitting thin targets sitting upstream of spallation neutron targets. The intensity of the muons is greatly limited by the small thickness of the muon targets, which are intended to have minimum impact on the proton beams. When the majority of the proton beam hits the spallation target, a large number of pions/muons are produced. After being captured in a solenoidal magnetic field, a high intensity muon beam can be produced. In this paper we take the Chinese Spallation Neutron Source (CSNS) target as an example and investigate the production of high intensity muon beams. Two possibilities are presented in this paper: an upstream collection of surface muons and a downstream collection of pions which is followed by a decay and compress channel to obtain a high intensity muon beam. Simulations show both methods can reach high intensities which could significantly increase the statistics of many experiments.

INTRODUCTION

When protons hitting spallation targets, a large number of pions are produced along with the neutrons. Such pions can be collected to produce high intensity muon beams in decay channels. Such muon beams can be injected into storage rings for neutrino studies. They can also be used for rare-decay researches if their energies are reduced by rf cavities. When the pions decay on the surface of the target, a highly polarized, mono-energy muon beam can be produced, which is called "surface muon". Such surface muon beams can be used for the next generation μSR applications, muonium spectroscopy, as well as searches for muon rare decays.

In this paper we investigate the production of pions and muons on the Chinese Spallation Neutron Source (CSNS) target [1]. In order to have minimum impact on the neutron production, we outline two possible ways of collecting the pions and muons: collecting surface muons from upstream of the target and collecting pions from downstream of the target. We present the collecting efficiency depending on various solenoidal magnet settings. Simulation results show that with reasonable settings the collecting efficiency for the surface muons and the pions can reach $1.3 \times 10^{-5} \mu^+/proton$ and $5 \times 10^{-3} \pi^+/proton$ respectively. Based on the 500 kW proton driver with an energy of 1.6 GeV, a surface muon beam of $6.5 \times 10^{10} \mu^+/s$ and a pion beam of $2.5 \times 10^{13} \pi^+/s$ can be reached at the end of the collecting solenoid. Such a surface muon intensity is on the same level as the planned HiMB project [2] at Paul Scherrer Institute (PSI).

* baoyubaoyu@gmail.com

For the collected pions downstream, we implement the front end [3] concept of the Neutrino Factory/Muon Collider to compress the momentum spread, and then decelerate the muons from pion decay to low energy so that they can be used for various experiments. Preliminary simulations based on G4beamline show a muon rate of $2 \times 10^{12} \mu^+/s$ can be reached with muon momentum lower than 75 MeV/c. Such an intense muon beam can significantly increase the statistics of many muon experiments such as Mu2e [4], Mu3e [2], etc.

COLLECTING SCHEME

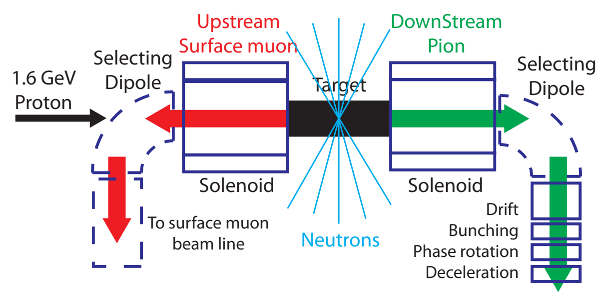

Figure 1: Scheme of collecting the surface muons upstream of the target and collecting the pions downstream.

Figure 1 shows the collecting scheme. The proton source has an rms size of 80 mm × 30 mm on the target. The geometry of the tungsten target is 170 mm in width, 70 mm in height and 570 mm in length. We put collecting solenoids upstream and downstream to focus the muons and pions that are produced in the target. In this way we minimize the influence on the neutron beams. Selecting dipoles can be implemented to guide the beams to further beam lines. In this paper we focus on the collecting efficiency of various settings of the collecting solenoids and implement the front end concept of the Neutrino Factory/Muon Collider to compress the muon momentum spread.

SURFACE MUONS

Figure 2 shows the momentum distribution of the surface muons on the upstream surface of the target. The spectrum has a peak at 28 MeV/c with a sharp cut at high momentum, representing the muons that decay right on the surface of the target. The stopped pions that decay inside but close to the surface of the target produce the muons with lower momentum. The higher momenta muons are produced by the pions that decay in flight. The production efficiency of the surface muons (p < 30 MeV/c) is $3.6 \times 10^{-5} \mu^+/proton$ on the target surface.

ISBN: 978-3-95450-168-7 doi:10.18429/JACoW-IPAC2015-WEPJE019

SIMULATIONS OF FIELD-EMISSION ELECTRON BEAMS FROM CNT CATHODES IN RF PHOTOINJECTORS

D. Mihalcea, Northern Illinois University, DeKalb, IL 60115, USA
L. Faillace, Radiabeam Technologies LLC, Santa Monica, CA 90404, USA
H. Panuganti, Northern Illinois University, DeKalb, IL 60115, USA
J. C. T. Thangaraj, Fermilab, Batavia, IL 60510, USA
P. Piot, Northern Illinois University, DeKalb, IL 60115, USA and Fermilab, Batavia, IL 60510, USA

Abstract

Average field emission currents of up to 700 mA were produced by Carbon Nano Tube (CNT) cathodes in a 1.3 GHz RF gun at Fermilab High Brightness Electron Source Lab. (HBESL). The CNT cathodes were manufactured at Xintek and tested under DC conditions at RadiaBeam. The electron beam intensity as well as the other beam properties are directly related to the time-dependent electric field at the cathode and the geometry of the RF gun. This report focuses on simulations of the electron beam generated through field-emission and the results are compared with experimental measurements. These simulations were performed with the time-dependent Particle In Cell (PIC) code WARP.

INTRODUCTION

To increase the power of the Free Electron Laser (FEL) to megawatt-level the injectors must be upgraded such that they could provide ampere level of average electron beam current [1]. Alternatively, low beam charge (picocoulomb-level) and extremely low emittance (10^{-10} m) are desirable to build compact ultra high brightness X-ray sources [2, 3].

Cathodes with deposited Field-Emitters (FE's) were extensively studied during the last decade and are proven to have some obvious advantages compared with the more standard photoemission or thermoionic cathodes. First of all there is no need for additional expensive components to extract the electrons from cathode: lasers (photoemission) and heating systems (thermoionic). In the case of FE's the electrons are extracted by an external electric field through quantum tunneling. The local electric field E at the surface of the FE is typically much larger than the applied electric field E_a by a factor β (enhancement factor) dependant on FE geometry. The current density of the electron beam is given by Fowler-Nordheim (FN) formula: $j = aE^2 exp\left(-\frac{b}{E}\right)$ where constants $a = \frac{1.42\times10^{-6}}{\Phi} exp\left(\frac{10.4}{\sqrt{\Phi}}\right)$ and $b = -6.56 \times 10^{-9}\Phi^{3/2}$ depend on cathode material through the work function Φ (in units of eV) [4] and E ($= \beta E_a$) is the external electric field at the surface of the FE.

Large effective emitting area combined with large enhancement factor are key elements to design efficient FE cathodes. In the recent years Carbon Nano Tubes (CNT's) proved to be promising FE candidates. CNT's are cylindrical single-wall or multi-wall nanostructures which can be deposited on the surface of a metallic cathode. They have extremely low electrical resistivity and are very robust at high temperature. Due to small diameter (1-50 nm) and high aspect ratio ($\sim$ 1000) the enhancement factor is high (typically several hundreds).

To maintain the simplicity of the injector it is desirable that the external applied electric field produced by the standard RF system, needed anyway to further accelerate the beam, is enough to produce the desired beam intensity. In this contribution we show that cathodes deposited with multi-wall randomly oriented CNT's can produce ampere-level beam currents when they are simply exposed to the fields inside a standard RF gun.

EXPERIMENTAL SETUP

The testing of the CNT FE cathodes was carried out at Fermilab High Brightness Electron Source Lab (HBESL) and described in [5]. The schematic top-view of the injector relevant components is shown in Fig. 1. The main component of this injector (normally used as a photoinjector) consists of a 1.5-cell resonant RF gun operated at 1.3 GHz. The RF power is provided by a 2 MW klystron in macropulses with adjustable duration and 0.5 Hz repetition rate. The typical macropulse duration for these experiments was chosen at 40 μs to compromise between achieving maximum charge in he bunch train and avoiding any significant energy depletion inside the gun due to beam loading. The peak field at the cathode can reach about 35 MV/m.

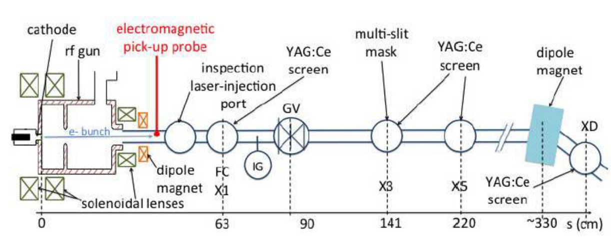

Figure 1: Simplified schematic top-view layout of HBESL injector.

The RF gun is embedded in the external magnetic field created by three solenoids to control the transverse size of the electron beam and to partially compensate the emittance growth. The beam current is measured with a Fara-

Content from this work may be used under the terms of the CC BY 3.0 licence (© 2015). Any distribution of this work must maintain attribution to the author(s), title of the work, publisher, and DOI.

ISBN: 978-3-95450-168-7 doi:10.18429/JACoW-IPAC2015-WEPJE020

Content from this work may be used under the terms of the CC BY 3.0 licence (© 2015). Any distribution of this work must maintain attribution to the author(s), title of the work, publisher, and DOI.

THE TWO BEAM ACCELERATION STAGING EXPERIMENT AT ARGONNE WAKEFIELD ACCELERATOR FACILITY*

C. Jing#, S. Antipov, J. Qiu, and A. Kanareykin, Euclid Techlabs LLC, Solon, OH 44139, USA
J.G. Power, M. Conde, W. Liu, E. Wisniewski, G. Ha, D. Wang, J. Shao, S. Doran, and W. Gai, ANL, Argonne, IL 60439, USA
J. Shi, Tsinghua University, Beijing, China

Abstract

Staging, defined as the accelerated bunch in a wakefield accelerator continues to gain energy from sequential drive bunches, is one of the most critical technologies, yet be demonstrated, required to achieve high energy. Using the Two Beam Acceleration (TBA) beamline at Argonne Wakefield Accelerator (AWA) facility, we will perform a staging experiment using two X-band TBA units. The experiment is planned to conduct in steps. We report on the most recent progress.

STAGING EXPERIMENT AT AWA

Linear colliders based on two-beam wakefield acceleration have a modular design [1]. A fundamental requirement of two beam wakefield acceleration that has yet to be demonstrated is the staging of sequential accelerating modules. For a successful staging demonstration two key issues need to be addressed: drive beam separation and the timing between wakefields from different stages and the accelerated (witness) beam.

In many approaches a fast deflector is required to direct beams from a drive bunch train into separate power extractor units feeding sequential accelerating stages for a witness beam. In the case of an L-band driver at the AWA the drive beam spacing is 50 ns. Stripline kickers or RF deflecting cavities can be used as fast deflectors on this time scale. We propose to use a standard strip line kicker for this proposal.

Another important issue for a staging demonstration is ability to synchronize the witness beam with the wakes generated in different stages. The solution considered up to now has been to bend the drive beam, which raised questions about the energy loss and beam degradation caused by coherent synchrotron radiation. Here we propose a new design based on the time delay of RF pulses in different stages with respect to the witness beam. This approach eliminates the need to bend a high charge beam 180 degrees. For the design of the RF delay line one has to consider two factors: line length and attenuation.

Demonstration of wakefield acceleration staging is the next big step towards validation of the approach as a whole. It proves that wakefield acceleration is indeed possible in a modular way. Once staging is demonstrated one can achieve TeV energies by stacking these modules. This approach allows for length reduction of the accelerator, as wakefield acceleration yields a high gradient operation in a short pulse mode.

Technical Approach

Most of wakefield collider concepts relied on bending the drive beams out of the drive train into the power extractor units to catch the appropriate phase of the witness beam. We are trying to avoid the need for a 180° arc in the drive beamline because coherent synchrotron radiation and its effects on the drive beam become a concern. Figure 1 shows a two beam acceleration concept with an RF delay substituting for the 180° bend. There are two types of staging when relevant to this concept.

- Each module is driven by its own drive beam or a drive bunch train. Separate modules need to be synchronized to accelerate the main beam (Figure 1); this process is called inter-module staging. Spacing between the drive beams, L_b, relates to the geometrical spacing between modules, L ($L_b=2L$) for synchronization to occur. A fast kicker is used to direct the drive beam to its respective module.
- There are numbers of power extractor – accelerator pairs inside a single module. This is done to extract as much energy out of the drive beam as possible. These units also have to be synchronized representing an intra-module staging. In our design the drive beam enters the last (from the main (witness, accelerated) beam point of view) power extractor (the m^{th}) in each module. The generated rf is transported through a longer rf waveguide which provides a delay time t_{dm}. The delay time of the rf transport line in the $(m\text{-}1)^{th}$ TBA pair is $t_{d(m-1)}$. At the exit of the power extractor #1, drive beam is dumped after exhausting most of its energy. At the moment when the rf from the 1st power extractor fills the 1st accelerating structure, the main beam is launched. Because the rf filling time for each accelerating structure is the same, if we assume the rf delay of the transport line in the first TBA pair t_{d1}=0, then $t_{d2}=2L_s/c$, $t_{dm}=2\times(m\text{-}1)\times L_s/c$, where m is the number of structures in each module and L_s is the length of a single structure. Besides the timing in RF delay lines between separate power extractors we need to address the issue of possible RF losses.

Experimental Plan

As the first step towards demonstration of complete staging, a simplified staging experiment was proposed, which includes one power extractor–accelerator pair for

*Work supported by US DoE SBIR Grant #DE-SC00011299.
#jingchg@anl.gov

ISBN: 978-3-95450-168-7 doi:10.18429/JACoW-IPAC2015-WEPJE021

FABRICATION AND DEMONSTRATION OF A SILICON BURIED GRATING ACCELERATOR

A. Ceballos, R. L. Byer, K. J. Leedle, E. Peralta, O. Solgaard, K. Soong
Stanford University, Stanford, California, USA
R. J. England, I. Makasyuk, K. P. Wootton, Z. Wu
SLAC, Menlo Park, California, USA
A. Hanuka
Technion, Haifa, Israel
A. Tafel
Friedrich-Alexander Universitaet Erlangen-Nuernberg, Erlangen, Germany

Abstract

Using optical electromagnetic fields in dielectric microstructures, we can realize higher-energy accelerator systems in a more compact, low-cost form than the current state-of-the-art. Dielectric, laser-driven accelerators (DLA) have recently been demonstrated using fused silica structures to achieve about an order-of-magnitude increase in accelerating gradient over conventional RF structures. We leverage higher damage thresholds of silicon over metals and extensive micromachining capability to fabricate structures capable of electron acceleration. Our monolithic structure, the buried grating, consists of a grating formed on either side of a long channel via a deep reactive ion etch (DRIE). The grating imposes a phase profile on an incoming laser pulse such that an electron experiences a net change in energy over the course of each optical cycle. This results in acceleration (or deceleration) as electrons travel down the channel. We have designed and fabricated such structures and begun testing at the SLAC National Accelerator Laboratory. We report on the progress toward demonstration of acceleration in these structures driven at 2 um wavelength.

INTRODUCTION

Dielectric laser-driven accelerators (DLA) hold promise as an advanced accelerator technology capable of reducing system size and cost. Dielectric materials can have significantly higher damage thresholds at optical wavelengths than metals, allowing for the generation of close to 100 times greater acceleration gradients, in the GV/m range [1]. This, combined with the smaller structure, matched to optical wavelengths at the micron or submicron scale, in principle can drive the miniaturization of accelerator systems. By leveraging decades of photolithography and micromachining technology development, these types of structures can be produced on a large scale for relatively small cost. Driving with commercially available lasers rather that klystrons compounds these size and cost benefits.

Several dielectric accelerator structures have been proposed [2–5], but the grating accelerator [6] is the most successfully demonstrated to date. Subrelativistic electrons have been accelerated in fused silica and silicon Smith-Purcell gratings [7, 8] and relativistic electron acceleration has been demonstrated in a fused silica dual grating structure [9]. A silicon grating-based structure for the acceleration of relativisitic electrons, the buried grating, has also been proposed [10].

Grating DLAs use a laser incident normal to an electron beam with the field polarized in the direction of electron motion. The phase front of the laser is modulated by the grating and then incident on the electron beam travels through vacuum near the grating. This modulated phase breaks the temporal symmetry of a planar wavefront and results in a net acceleration or deceleration, depending on the position of the electron along a grating period. Short-pulse lasers are used to achieve high peak fields in the structure, and therefore high accelerating gradients.

Here we present the progress made toward demonstration of the silicon buried grating structure proposed in [10].

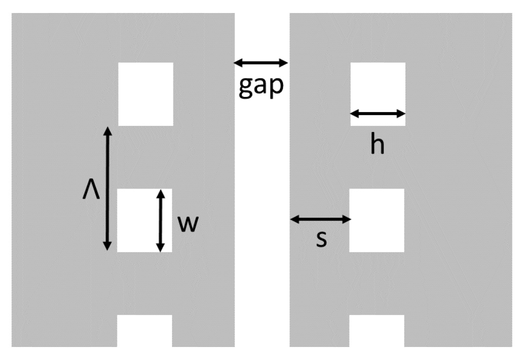

Figure 1: Illustration of parameters used in the design and simulation of buried grating structures.

DESIGN AND FABRICATION

Like previously demonstrated grating DLAs, the buried grating consists a phase grating adjacent to a vacuum region. The grating period is chosen such that the longitudinal component of the field (in the direction of electron travel) always produces an acceleration force. For phase matching the alternating acceleration field, we want the electron to traverse one grating period in one optical cycle, leading to the condition on the grating period of

$$\Lambda = \beta\lambda \tag{1}$$

Content from this work may be used under the terms of the CC BY 3.0 licence (© 2015). Any distribution of this work must maintain attribution to the author(s), title of the work, publisher, and DOI.

ISBN: 978-3-95450-168-7 doi:10.18429/JACoW-IPAC2015-WEPJE023

Content from this work may be used under the terms of the CC BY 3.0 licence (© 2015). Any distribution of this work must maintain attribution to the author(s), title of the work, publisher, and DOI.

CATHODE PERFORMANCE DURING TWO BEAM OPERATION OF THE HIGH CURRENT HIGH POLARIZATION ELECTRON GUN FOR eRHIC*

O. Rahman†, I. Ben-Zvi, C. Degen, D.M. Gassner, R. Lambiase,A. Pikin, T. Rao, B. Sheehy, J. Skaritka, E. Wang, BNL, Upton, NY 11973, USA J. Pietz, M. Ackeret, Transfer Engineering and Manufacturing, Inc, Fremont, CA 94539, USA
C. Yeckel, R. Miller, E. Dobrin, K. Thompson, Stangenes Industries, Palo Alto, CA 94303,USA

Abstract

Two electron beams from two activated bulk GaAs photocathodes were successfully combined during the recent beam test of the High Current High Polarization Electron gun for eRHIC. The beam test took place in Stangenes Industries in Palo Alto, CA, where the cathodes were placed in diagonally opposite locations inside the high voltage shroud.

No significant cross talking between the cathodes were found for the pertinent vacuum and low average current operation, which is very promising towards combining multiple beams for higher average current. This paper describes the cathode preparation, transport and cathode performance in the gun for the combining test, including the QE and lifetimes of the photocathodes at various steps of the experiment.

INTRODUCTION

The future Electron Ion Collider requires a high average current high polarization electron source. The average current requirement is 50 mA whereas the maximum average current demonstrated at other polarized electron sources is 4 mA. One very promising idea to obtain the high average current requirement is to combine multiple electron beams on to one axis by using a rotating magnetic field [1]. The key assumption in this proposal is that the operation of one cathode does not affect the lifetime of another cathode in the same vicinity. Therefore, based on the idea of combining multiple beams, a specialized DC electron gun has been designed at Brookhaven National Lab.

EXPERIMENTAL SETUP

For the low current proof of principle test in CA, the gun set up was simplified and is shown in figure 1. The major simplification being the absence of "Depressed collector" [2]. A Faraday cup, biased to 500 V, replaced the Depressed collector. The main goal of this test was to generate low current electron beams from two activated bulk GaAs situated radially opposite ends of the high voltage shroud. The maximum current from the cathodes were limited by a 2.88 G Ω current limiting resistor in series with the gun and a hard HV barrier at approximately 14 KV. Since two cathodes were to be operated at a very low repetition rate, the combiner magnet was essentially in a switch on-off mode. [3]

* Work supported by Brookhaven Science Associates, LLC under contract no. DE-AC02-98CH10886 with US DOE
† orahman@bnl.gov

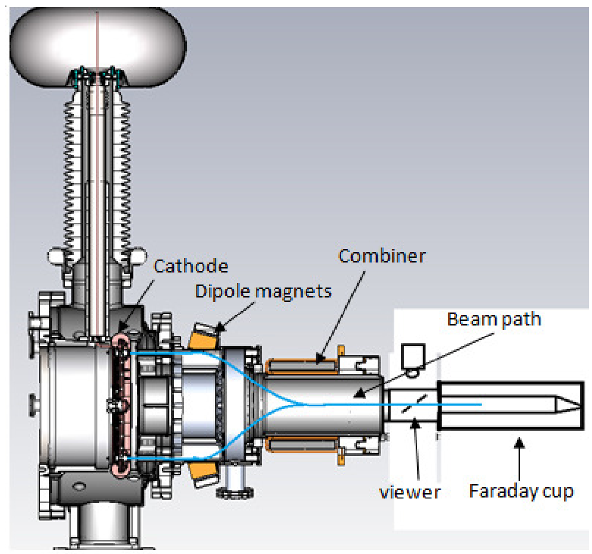

Figure 1: Schematic diagram of the gun.

Cathode Preparation Chamber and Transfer Line

The cathode preparation chamber and it's performance was described in the proceedings of PAC'13 [4]. In order to transport activated GaAs from the cathode preparation chamber to the gun, a transport line in between the gun and preparation chamber was installed. A custom made magnetic manipulator, manufactured by Transfer Engineering and Manufacturing, Freemont, CA [5], was attached to the other side of the preparation chamber.

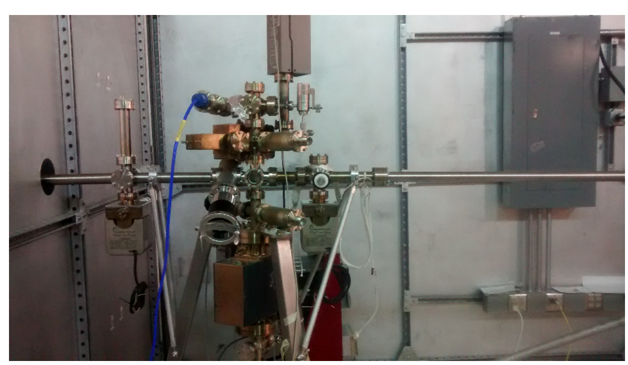

Figure 2: The transfer line, cathode preparation chamber and long manipulator, as shown from left to right.

In between the long manipulator and the preparation chamber, the placeholder cross was attached. This cross included

ISBN: 978-3-95450-168-7 doi:10.18429/JACoW-IPAC2015-WEPJE024

PROGRESS ON THE STUDY OF DIRECT LASER ELECTRON ACCELERATION IN DENSITY-MODULATED PLASMA WAVEGUIDES *

M.-W. Lin, B. W. Morgan, and I. Jovanovic†, Department of Mechanical and Nuclear Engineering, The Pennsylvania State University, University Park, PA 16802, U.S.A.
C.-Y. Hsieh, Y.-L. Liu, and S.-H. Chen, Department of Physics, National Central University, Jhongli 32001, Taiwan

Abstract

Direct laser acceleration of electrons can be achieved by utilizing the axial field of a guided, radially polarized laser pulse in a density-modulated plasma waveguide. When a short fs electron bunch is injected together with the drive laser pulse, our particle-in-cell simulations show that the electrostatic field, arising from plasma electrons perturbed by the laser ponderomotive force, increases the transverse divergence of the bunch electrons. Simulations are performed to study the method in which a precursor electron bunch is introduced prior to the main accelerated bunch. The precursor induces a focusing electrostatic field in the background plasma, which can considerably reduce the transverse expansion of the accelerated electrons. Based on the ignitor-heater scheme, density-modulated plasma waveguides are produced in experiments with high-Z gas targets and used to test the guiding of laser pulses. Supersonic gas jet nozzles for producing gas targets are simulated, designed, and then fabricated via additive manufacturing. Surface quality of the nozzles is evaluated via computed tomography.

INTRODUCTION

By guiding a radially polarized laser pulse in a density-modulated plasma waveguide, a large axial acceleration gradient on the order of tens of GV/m can be produced and used for direct laser acceleration (DLA) of electrons over an extended distance [1, 2]. The plasma waveguide extends the acceleration distance and the density modulation provides the quasi-phase matching (QPM) condition to improve the DLA efficiency. However, in addition to interacting with the laser fields, the injected bunch electrons also experience the nonlinear laser ponderomotive force and the electrostatic force from the resulting density variation of the background plasma electrons. The donut-shaped ponderomotive force of a radially polarized pulse pushes the plasma electrons to concentrate at the axis, which produces a transverse electrostatic force that can significantly defocus the electrons of a fs bunch after DLA [3].

In this study, we simulated the DLA scheme in which an additional precursor electron bunch is injected at a proper time prior to the main accelerated electron bunch. The precursor induces a focusing electrostatic field in the background plasma that can be used to considerably reduce the final transverse expansion of the accelerated electron bunch [4]. An all-optical method was experimentally implemented to produce density-modulated plasma channels with Ar gas target, which can be applied to realize the QPM of DLA. Next, micrometer-scale supersonic gas jet nozzles were designed and simulated for generating uniform gas density profiles needed for plasma waveguide production. Additive manufacturing techniques were applied to produce the nozzles.

DLA WITH A PRECURSOR

We carried out 3-D PIC simulations of DLA by the simulation framework VORPAL. Figure 1(a)-(c) summarizes the definition for the laser pulse for driving DLA and the 2.1-mm long plasma waveguide composed of alternating waveguide and neutral hydrogen sections that provide the necessary QPM condition. The waveguide sections have

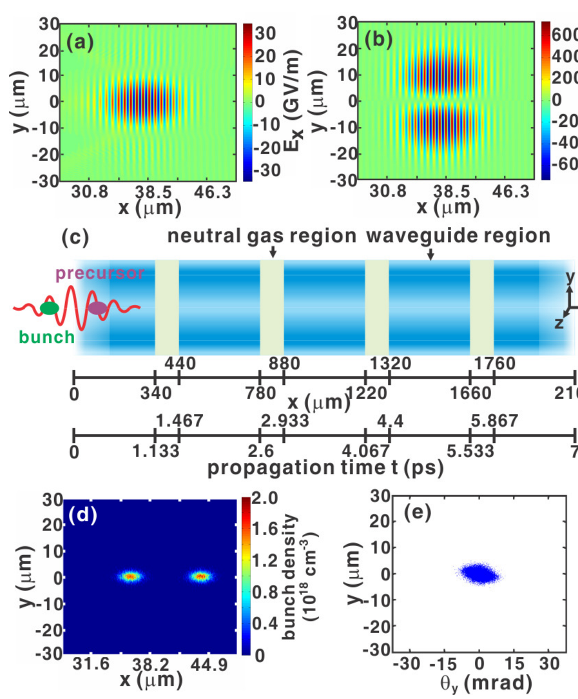

Figure 1: Snapshots of (a) longitudinal E_x and (b) transverse E_y electric fields of a 20-fs, 0.5-TW, radially polarized laser pulse pulse with a diameter of 15 μm; (b) illustration of a density-modulated plasma waveguide; (d) 2-D density distribution of the 6-fs, 40-MeV electron bunch and precursor injected in the simulation; (e) the trace space distribution for the bunch electrons shown in (d).

* Work supported by the United States Defense Threat Reduction Agency and the Ministry of Science and Technology in Taiwan.
† ijovanovic@psu.edu

Content from this work may be used under the terms of the CC BY 3.0 licence (© 2015). Any distribution of this work must maintain attribution to the author(s), title of the work, publisher, and DOI.

ISBN: 978-3-95450-168-7 doi:10.18429/JACoW-IPAC2015-WEPJE025

Content from this work may be used under the terms of the CC BY 3.0 licence (© 2015). Any distribution of this work must maintain attribution to the author(s), title of the work, publisher, and DOI.

PHASE SPACE DENSITY AS A MEASURE OF COOLING PERFORMANCE FOR THE INTERNATIONAL MUON IONIZATION COOLING EXPERIMENT

J. Scott Berg, BNL*, Upton, NY 11973, USA

Abstract

The International Muon Ionization Cooling Experiment (MICE) [1] is an experiment to demonstrate ionization cooling of a muon beam in a beamline that shares characteristics with one that might be used for a muon collider or neutrino factory. I describe a way to quantify cooling performance by examining the phase space density of muons, and determining how much that density increases. This contrasts with the more common methods that rely on the covariance matrix and compute emittances from that. I discuss why a direct measure of phase space density might be preferable to a covariance matrix method. I apply this technique to an early proposal for the MICE final step beamline. I discuss how matching impacts the measured performance.

INTRODUCTION

The analysis of the MICE particle trajectories must provide a numerical measure of the cooling performance, and must ensure that this performance measure is unbiased. To provide an example of a potential difficulty, I first examine two possible measures of cooling performance; the first is an increase in the phase space density

$$N_f \epsilon_{6i}/(N_i \epsilon_{6f}) \tag{1}$$

where the i subscripts refer to the initial distribution, the f subscripts to the final distribution, N refers to the number of particles, and ϵ_6 refers to the 6-D phase space emittance, defined to be the square root of the determinant of the 6-D second moment matrix. A different measure could be the luminosity increase:

$$N_f^2\sqrt{\epsilon_{6i}}/(N_i^2\sqrt{\epsilon_{6f}}) \tag{2}$$

This is generally a stronger condition than the increase in phase space density, but may be a more appropriate measure for a muon collider as it measures the eventual increase luminosity one might expect (though there are arguments for a different contribution from the longitudinal emittance).

I use an early version [2] of the MICE final step lattice. The design parameters are given in Tables 1–3. There are two 201.25 MHz cavities with a gradient of 16 MV/m, a length of 434.62 mm, centered at ±281.81 mm. The beam distribution will always be launched from −4050 mm and analyzed at +4050 mm. The beam has a total momentum of 200 MeV/c, and I only consider transverse dimensions. Simulations are performed using ICOOL [3].

To illustrate the potential difficulties I perform a simple simulation: I launch a beam with a Gaussian distribution in transverse phase space, matched to the 4.14565 T solenoid field at the launch point, including its angular momentum, with a given normalized emittance. I then compute the normalized emittance at the end using

$$\sqrt{\sigma_{xx}\sigma_{p_xp_x}\sigma_{yy}\sigma_{p_yp_y}} - \sigma_{xp_x}\sigma_{yp_y} - L^2/4 \tag{3}$$
$$L = \sigma_{xp_y} - \sigma_{yp_x} \tag{4}$$

where σ_{ij} are the corresponding elements of the second order moment matrix. I then use Eq. (1) to compute the increase in phase space density. Figures 1 and 2 show the results. Whether one sees cooling or not depends on the choice of the initial emittance, and there is no clear reason to choose one emittance over another. For small emittances,

Table 1: Solenoid coil geometry and currents [2] used in my simulations. Only the upstream half of the coils are listed; the downstream half is reflected about longitudinal position 0 and has opposite currents.

Long. Center (mm)	Length (mm)	Inner Radius (mm)	Outer Radius (mm)	Current (A/mm^2)
−4800.00	110.60	258.0	325.8	135.18
−4050.00	1314.30	258.0	280.1	152.44
−3300.00	110.60	258.0	318.9	127.37
−2900.00	199.50	258.0	288.9	113.12
−2461.00	201.30	258.0	304.2	123.04
−1202.75	213.30	267.0	361.8	40.00
−797.25	213.30	267.0	361.8	40.00

Table 2: Apertures [2] used in my simulation. Only the apertures upstream of the center are listed; the downstream apertures are identical.

Center (mm)	Length (mm)	Radius (mm)
−3592	2664	200
−1000	844	210
0	65	600

* This manuscript has been authored by employees of Brookhaven Science Associates, LLC under Contract No. DE-SC0012704 with the U.S. Department of Energy. The United States Government retains a non-exclusive, paid-up, irrevocable, world-wide license to publish or reproduce the published form of this manuscript, or allow others to do so, for United States Government purposes.

ISBN: 978-3-95450-168-7 doi:10.18429/JACoW-IPAC2015-WEPJE026

CONCEPTUAL DESIGN OF A QUADRUPOLE MAGNET FOR eRHIC*

H. Witte†, J. S. Berg, Brookhaven National Laboratory, Upton, NY, USA

Abstract

eRHIC is a proposed upgrade to the existing Relativistic Heavy Ion Collider (RHIC) hadron facility at Brookhaven National Laboratory, which would allow collisions of up to 21 GeV polarized electrons with a variety of species from the existing RHIC accelerator.

eRHIC employs an Energy Recovery Linac (ERL) and an FFAG lattice for the arcs. The arcs require open-midplane quadrupole magnets of up to 30 T/m gradient of good field quality.

In this paper we explore initial quadrupole magnet design concepts based on permanent magnetic material which allow to modify the gradient during operation.

INTRODUCTION

To discover and understand the emergent phenomena of Quantum Chromodynamics the eRHIC facility is presently being designed. eRHIC adds an electron accelerator to the existing proton accelerator called RHIC (Relativistic Heavy Ion Collider). eRHIC would be an unprecedented facility for Nuclear Physics to study QCD; it is planned to collide unpolarized and 80% polarized electrons (6.6–15.9 GeV) with up to 70% polarized protons (25-250 GeV). The center of mass energy range is 30–145 GeV.

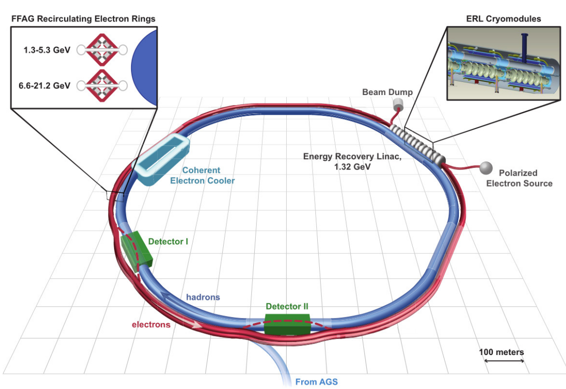

Figure 1: The layout of the eRHIC accelerator.

It was decided to employ the fixed-field alternating gradient (FFAG) accelerator concept for eRHIC. It is planned to add two FFAG rings to the RHIC tunnel for up to 16 beams. The targeted luminosity is $> 10^{33}$ cm^{-2} s^{-1}; plans exist to increase the hadron beam intensity, which would increase the luminosity to $> 10^{34}$ cm^{-2} s^{-1}. Collisions with Au and He are also planned. Figure 1 shows an overview of the facility.

* Work supported by Brookhaven Science Associates, LLC under Contract No. DE-AC02-98CH10886 with the U.S. Department of Energy.
† hwitte@bnl.gov

MAGNET REQUIREMENTS AND CONCEPT

The FFAG lattice requires quadrupole magnets with a gradient strength of up to 28 T/m in a good field region of ±17 mm. The required gradient quality is 1×10^{-3}. In addition to this the poles are not allowed to penetrate the area around the midplane. The open-midplane (±7 mm) is required because of synchrotron radiation.

One design choice is to use permanent magnets. This is possible as the magnets are not required to sweep. The use of permanent magnets allows to dispense with expensive power supplies in the RHIC tunnel, which also greatly simplifies cabling.

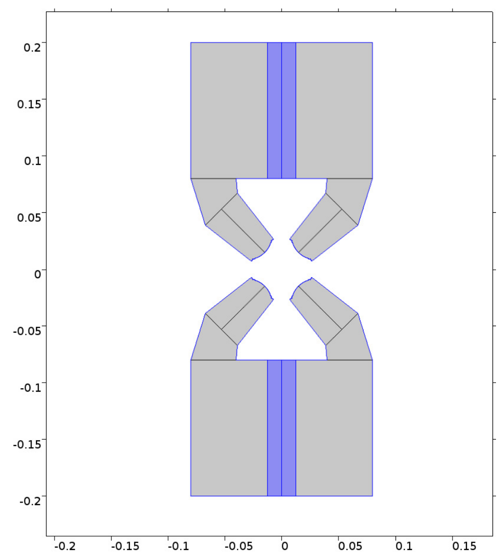

Figure 2: Magnet geometry. The permanent magnetic material is shown in blue.

We envisage NdFeB permanent magnetic material with a remanent magnetic field of about 1.1 T for this design. NdFeB is sufficiently radiation hard provided the grade chosen is relatively low. Studies are underway to demonstrate this.

The geometry of the permanent magnetic material is chosen so that the operating point of the permanent magnet is close to the energetic maximum. Figure 2 shows the general geometry of the quadrupole; the permanent magnets are shown in blue. The total cross-sectional area of the permanent magnets is 60 cm^2 and the height of each block about 12 cm.

The starting point for the initial design of the quadrupole are Tanabe's equations for quadrupoles [1]. The equations below are used to obtain approximate coordinates for the

Content from this work may be used under the terms of the CC BY 3.0 licence (© 2015). Any distribution of this work must maintain attribution to the author(s), title of the work, publisher, and DOI.

ISBN: 978-3-95450-168-7 doi:10.18429/JACoW-IPAC2015-WEPJE027

Content from this work may be used under the terms of the CC BY 3.0 licence (© 2015). Any distribution of this work must maintain attribution to the author(s), title of the work, publisher, and DOI.

PARTIAL RETURN YOKE FOR MICE STEP IV AND FINAL STEP*

H. Witte†, S. Plate, J. S. Berg, Brookhaven National Laboratory, Upton, NY, USA
J. Tarrant, STFC Rutherford Appleton Laboratory, Didcot, UK
A. Bross, Fermilab, Batavia, IL, USA

Abstract

This paper reports on the progress of the design and construction of a retro-fitted return yoke for the international Muon Ionization Cooling Experiment (MICE). MICE is a proof-of-principle experiment aiming to demonstrate ionization cooling experimentally.

In earlier studies we outlined how a partial return yoke can be used to mitigate stray magnetic field in the experimental hall; we report on the progress of the construction of the partial return yoke for MICE Step IV.

We also discuss an extension of the Partial Return Yoke for the final step of MICE; we show simulation results of the expected performance.

INTRODUCTION

Ionization cooling has been discussed for a long time for applications where particles need to be accelerated quickly. Ionization cooling so far has never been demonstrated experimentally; MICE is an experiment which is presently constructed at the Rutherford Appleton laboratory in the UK to demonstrate this for the first time [1].

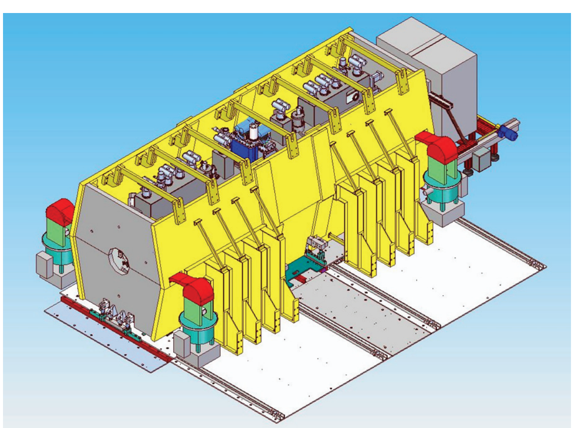

Figure 1: The MICE Partial Return Yoke.

At the time of writing MICE Step IV is under construction, which consists of 12 superconducting solenoids. Recently it was discovered that the MICE solenoids produce a substantial stray magnetic field, which can be problematic for equipment in the MICE hall.

To mitigate this risk the concept of the so-called Partial Return Yoke (PRY) was developed. The MICE PRY is a retro-fitted return yoke, which partially encloses MICE. Figure 1 shows the PRY surrounding the MICE solenoids in Step IV configuration.

In earlier papers we have described the concept, the expected shielding performance and the engineering [2–4]. This paper reports on the progress of construction, which includes magnetic testing of the low-carbon steel for the yoke and required adjustments of the MICE coil currents. The paper concludes with a concept of the extension of the PRY for the final step of MICE.

MATERIAL

For the MICE PRY a low carbon steel (C content $< 0.010\%$) was chosen because of the high saturation value in combination with a high relative magnetic permeability. The design of the PRY was carried out with magnetization curves supplied by the manufacturer. About 60 metric tons of 10 cm thick plate material was obtained; from each heat samples were taken.

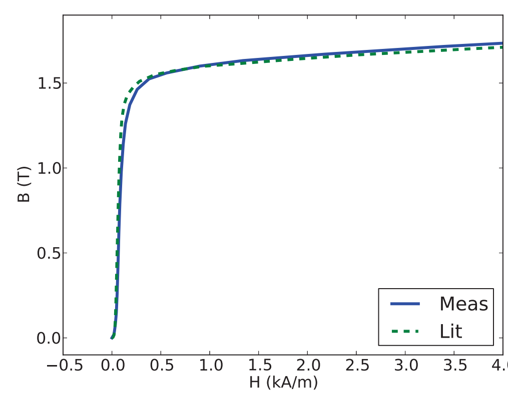

Figure 2: Comparison of the measured and literature magnetization curves of the MICE PRY low carbon steel.

The magnetization curves of the samples were measured by a commercial supplier; it was found that very little difference was observed between the different heats. Figure 2 shows the measured data in comparison to the initially used literature values and Fig. 3 the calculated relative magnetic permeability. As shown in the figures, there is a small variation of the material properties at small magnetic fields. At the operating point of the MICE PRY, which is indicated by the dashed line in Fig. 3, the measured permeability agrees well with the expected value. Simulations show that the differences in material properties lead to a change of the stray magnetic field in the MICE hall by about 1 Gauss (0.1 mT).

* Work supported by Brookhaven Science Associates, LLC under Contract No. DE-AC02-98CH10886 with the U.S. Department of Energy.
† hwitte@bnl.gov

ISBN: 978-3-95450-168-7 doi:10.18429/JACoW-IPAC2015-WEPJE033

THE PROGRESS OF FUNNELLING GUN HIGH VOLTAGE CONDITION AND BEAM TEST

E. Wang#, I. Ben-Zvi, D.M. Gassner, R. Lambiase, W. Meng, O. Rahman, A. Pikin, T. Rao, B. Sheehy, J. Skaritka ,BNL, Upton, NY 11973, USA

J. Pietz, M. Ackeret, Transfer Engineering and Manufacturing, Inc, Fremont, CA 94539, USA

C. Yeckel, R. Miller, E. Dobrin, K. Thompson, Stangenes Industries, Palo Alto, CA 94303,USA

Abstract

A prototype of a high average current polarized electron funneling gun as an eRHIC injector has been built at BNL. The gun was assembled and tested at Stangenes Incorporated. Two beams were generated from two GaAs photocathodes and combined by a switched combiner field. We observed the combined beams on a YAG crystal and measured the photocurrent by a Faraday cup. The gun has been shipped to Stony Brook University and is being tested there. In this paper we will describe the major components of the gun and recent beam test results. High voltage conditioning is discussed as well.

INTRODUCTION

In order to construct a future electron ion collider with high luminosity, a high average current and high bunch charge polarized electron source is under R&D at Brookhaven National Laboratory. Currently, the highest average current of polarized electron source was 4 mA achieved at JLab. The cathode lifetime is limited by ion back bombardment. To obtain average current of 50 mA and increase the lifetime, enlarging the photocathode emission area is a straight forward method. However, there are technical difficulties to get uniform photoemission and polarization from large superlattice GaAs photocathode. Uniform electrical field on the large cathode is another challenge as well. Alternatively, we developed a DC gun with multiple cathodes. Funneling the multiple electron bunches generated from several photocathodes to a single common axis could increase the total average current and single-cathode-lifetime. Here, we have to assume the individual cathode performance will not be affected by the rest of cathodes. The first step of the R&D program is proof of this principle.

The gun and beam parameters for eRHIC were described in reference [1]. To carry out the proof of principle test in a short time, we simplified the gun setup and started test with lower current to meet radiation limits. Our first gun conditioning and beam combining test was carried out at Stangenes Industries. Two beams were emitted from two cathodes positioned radially opposite to each other and combined by a switched combiner magnet. Beam current, cathode QE and lifetime was measured.

* Work supported by Brookhaven Science Associates, LLC under Contract No. DE-AC02-98CH10886 with the U.S. Department of Energy.
# wange@bnl.gov

GUN SETUP

The detailed gun design with beam optics was described earlier [2]. The depressed collector was replaced by a faraday cup which placed at the end of the beam line. It was biased to 500V to eliminate the secondary electron and back-scattering electrons. A pico-ammeter was connected in series to the Faraday cup. A fixed YAG crystal monitor was placed between the combiner magnet and Faraday cup for monitoring the beam profile and beam position. The YAG crystal has a hole at the centre which allows the beam pass through and reaches the Faraday cup. Figure 1 is the schematic layout of funnelling gun in this first beam test.

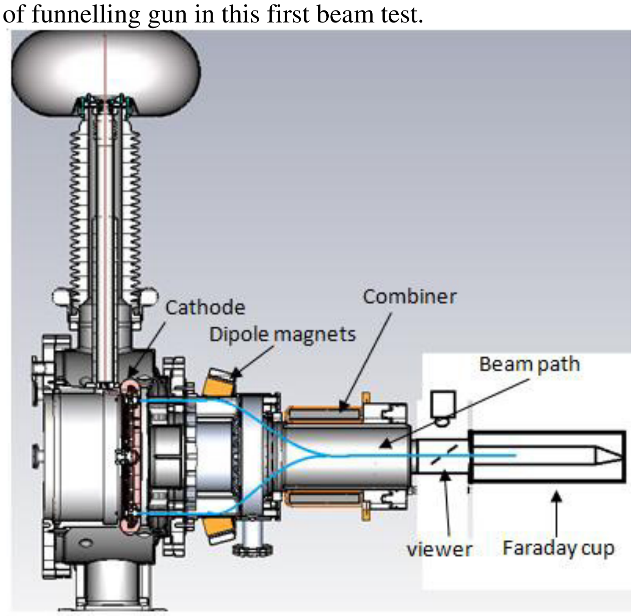

Figure 1: The schematic layout of the funnelling gun with beam measurement instruments

Two dipole magnets and combiner magnets were placed downstream of anode. The combiner was designed to have 20 coils with Sine distribution of the current. In our first beam test, it was simplified to six pairs of coils with constant current and driven by single power supply. Figure 2 shows the field distribution of measured magnetic field compared with the designed ideal field.

Content from this work may be used under the terms of the CC BY 3.0 licence (© 2015). Any distribution of this work must maintain attribution to the author(s), title of the work, publisher, and DOI.

ISBN: 978-3-95450-168-7 doi:10.18429/JACoW-IPAC2015-WEPMA001

PROPESED LINAC UPGRRADE WITH A SLED CAVITY AT THE AUSTRALIAN SYNCHROTRON, SLSA

Karl Zingre, Greg LeBlanc, Mark Atkinson, Brad Mountford, Rohan Dowd, SLSA, Clayton, Australia
Christoph Hollwich, SPINNER, Westerham, Germany

Content from this work may be used under the terms of the CC BY 3.0 licence (© 2015). Any distribution of this work must maintain attribution to the author(s), title of the work, publisher, and DOI.

Abstract

The Australian Synchrotron Light Source has been operating successfully since 2007 and in top-up mode since 2012, while additionally being gradually upgraded to reach a beam availability exceeding 99 %. Considering the ageing of the equipment, effort is required in order to maintain the reliability at this level. The proposed upgrade of the linac with a SLED cavity has been chosen to mitigate the risks of single point of failure and lack of spare parts. The linac is normally fed from two independent klystrons to reach 100 MeV beam energy, and can be operated in single (SBM) or multi-bunch mode (MBM). The SLED cavity upgrade will allow remote selection of single klystron operation in SBM and possibly limited MBM without degradation of beam energy and reduce down time in case of a klystron failure. The proposal for the SLED cavity upgrade is shown and the linac designs are detailed.

INTRODUCTION

The injector comprises a 100 MeV linac and a 3 GeV booster to enable full energy beam injection into the storage ring. The injector was upgraded later from decay to top-up mode operation to keep the storage ring at 200 mA current. Top-up has been continually running since then with an MBM injection of 0.5 mA every few minutes compared to a reinjection every 12 hours in decay mode.

Alongside top-up came the need to improve reliability and mean down time for the entire facility. Improvements on the injector were more cost effective to target mean down time due to the increase in wear on the system, single point of failure and the limited lifespan of devices such as the electron tubes. Improvements on the linac were necessary with two klystrons required for operation, and a failure could take weeks, depending on missing critical spare parts. The waveguide radio frequency (RF) distribution system for the linac was modified in the first stage in 2010, to test single klystron operation to power the whole linac; albeit at a reduced final beam energy. Booster injection was successful, but booster ramping remained unsolved as a lack of control in fine field adjustments at low energy levels from below 100 MeV. The increase in klystron trips operating at higher power levels was also not satisfactory. The next stage is to add a SLED cavity to overcome the current deficiencies. This paper will outline the proposed upgrade and benefits.

LINAC OVERVIEW

General Specifications

The 100 MeV 3 GHz linac structure is made of a 90 keV thermionic electron gun (GUN), a 500 MHz subharmonic prebuncher unit (SPB), preliminimary buncher (PBU), final buncher (FBU), and two 5 m accelerating structures. The structures are powered by two 35 MW pulsed klystrons supplied from a pulse forming network (PFN). The low level electronics include two pulsed 400W S band amplifiers to drive the klystrons, and two 500W UHF amplifiers for the GUN and SPB. The linac is based on the SLS/DLS design and was delivered by Research Instruments, formerly ACCEL, the modulators subcontracted to PPT-Ampegon, and the waveguide to SPINNER. The linac overview is shown in Figure 1, a summary of the general specifications listed in Table 1 and more details referenced to [1].

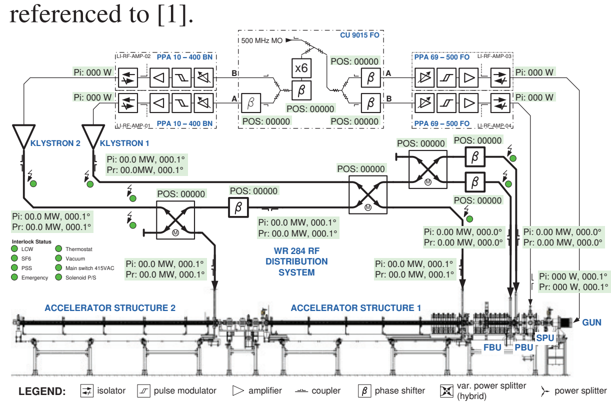

Figure 1: Linac overview.

Table 1: Linac Specifications

Quantity	Specification
Beam Energy	100 MeV
RF Frequency	2.997 GHz
Repetition rate	1 Hz
RMS Emittance	50 π mm mrad
Single/Multi-bunch pulse length	2/150 ns
Single/Multi-bunch pulse charge	> 0.5/4 nC

RF Distribution

The RF power from the two klystrons is transmitted and distributed across the SF6 pressurised WR284 waveguide distribution system. The first klystron feeds power to the PBU, FBU and first accelerating structure, with two successive variable power dividers used to distribute the correct amount of power to each section. The second klystron feeds the power to the second

ISBN: 978-3-95450-168-7 doi:10.18429/JACoW-IPAC2015-WEPMA002

THE BEAM CHOPPER POWER CONVERTER FOR MEDAUSTRON: SAFETY BY DESIGN AND DEVELOPMENT

T. Stadlbauer, R. Filippini, X. German, F. Osmic, P. Urschütz
EBG MedAustron, Wr. Neustadt, Austria
M.J. Barnes, T. Kramer, CERN, Geneva, Switzerland
M. Beerwald, U. Dirksen, Poynting GmbH, Dortmund, Germany

Abstract

MedAustron is the Austrian centre for hadron therapy and non-clinical research. The beam chopper system is an essential component for patient safety in specific hazardous situations as well as for beam delivery from the synchrotron to the irradiation rooms. This paper presents the results from the development phase and the commissioning of the MedAustron beam chopper system. Details will be given on the design, the risk management, the test and the verification of the chopper power converter (PKC).

SYSTEM DESCRIPTION

System Architecture

The beam chopper system is shown in Fig 1. It consists of one PKC, four kicker magnets (MKC [1], [2]) connected in series and a dump block, located in the high energy beam transfer line (HEBT).

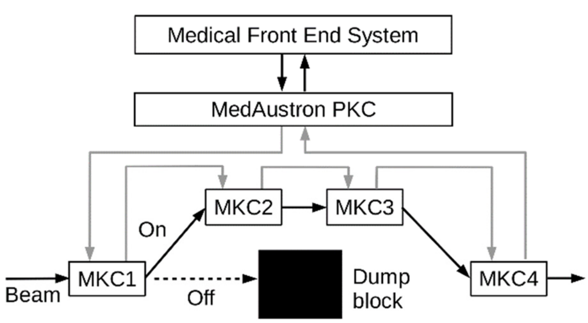

Figure 1: Schematic of the HEBT beam chopper system.

Functioning Principles

The beam chopper in the MedAustron Particle Therapy Accelerator (MAPTA) allows switching the beam in the irradiation room on and off. It performs two functions: 1) it contributes to deliver the beam into the irradiation rooms and 2) protects the patient from specific hazardous scenarios in case of faults. The system is designed to switch off the beam in less than 250 µs (Fig. 2), both in nominal and single fault condition. The beam chopper receives the set points, which are contained in the treatment file, from the accelerator control system (ACS) and is triggered by the Medical Front End (MF) system. If the chopper is switched on, the beam passes from the synchrotron through the chopper chicane in the HEBT to the irradiation room where the patient is treated. In case of detected faults in MAPTA, the chopper is commanded to switch off the beam; the safe state for the patient.

Nominal current	100 A – 630 A
Magnet maximum B-field	136 mT
Maximum output voltage (pulsed)	1500 V
Voltage (DC)	60 V
Repetition rate (max.)	20 Hz
Rise and fall time (max.)	250 µs
Dimension in mm	800 x 800 x 2000
Weight	700 kg

Figure 2: System parameters of PKC SVM-630A manufactured by Poynting GmbH.

REALISATION AND DEVELOPMENT

Design Requirements Specification

The design requirement document was the reference for the beam chopper development, in addition to the quality targets, the test concepts, the applicable standards and the time plan. The specification of the design requirements was structured in order to facilitate the generation of test cases. The preliminary design report, including prototype test, was followed by the definitive design report which concluded the development phase at Poynting GmbH.

Risk Management

The risk assessment of the PKC was carried out according to the MedAustron risk management guidelines in agreement with the EN ISO 14971 standard [3]. The following points were addressed: 1) identification of hazards and categories at risk, 2) compliance with applicable safety standards and 3) risk assessment and evaluation. The hazards analysis identified the situations at risk for the patient during irradiation and for the personnel during service. The risk assessment and evaluation for the PKC was performed by a failure mode, effects and criticality analysis (FMECA) according to IEC 60812 [4]. The FMECA considered the design of the PKC in three stages. The first stage was the preliminary design where the conceptual design was examined; the second stage was the definitive design and the third stage the as-built design. The close collaboration of all involved

Content from this work may be used under the terms of the CC BY 3.0 licence (© 2015). Any distribution of this work must maintain attribution to the author(s), title of the work, publisher, and DOI.

ISBN: 978-3-95450-168-7 doi:10.18429/JACoW-IPAC2015-WEPMA003

VACUUM SYSTEM DESIGN FOR THE SIRIUS STORAGE RING

R.M. Seraphim, O.R. Bagnato, R.O. Ferraz, H.G. Filho, G.R. Gomes, M. Nardin, R.F. Oliveira, B. M. Ramos, T.M. Rocha, A.R.D. Rodrigues, M.B. Silva, LNLS, Campinas, Brazil

Abstract

Sirius is a 3 GeV 4th generation light source under construction by the Brazilian Synchrotron Light Laboratory (LNLS). Sirius will have a low emittance storage ring, 0.28 nm.rad, based on 20 cells of a highly compact lattice – 5 bend achromat (5BA). This lattice concept leaves very little space for components and therefore requires narrow vacuum chambers with tight mechanical tolerances. Most of the storage ring vacuum chambers will be made of oxygen-free silver bearing (OFS) copper and have a circular cross section with inner diameter of 24 mm and a wall thickness of 1 mm. Unused synchrotron radiation will be distributed along the water cooled walls of the chambers. Due to the small conductance of the chambers, vacuum pumping will be based on distributed concept and then non-evaporable getter (NEG) coating will be extensively used, with more than 95% of the chambers being coated. In this paper, we present an overview of the storage ring vacuum system and the fabrication approach for some components.

INTRODUCTION

In order to reduce the horizontal emittance to sub-nm.rad value, the Sirius storage ring will be based on a 5-bend achromat (5BA) lattice [1], with a circumference of 518 m comprising 20 achromat cells, 10 straight sections of 7 m and 10 straight sections of 6 m.

The compact lattice of the storage ring leaves very little space for components and therefore requires narrow vacuum chambers. For this reason, the storage ring will base vacuum pumping mainly on NEG coatings.

The vacuum chambers will be made of OFS copper. The high electrical conductivity of this material minimizes the impact on the machine's impedance, while its thermal conductivity makes it a suitable choice to absorb unused synchrotron radiation. Also, OFS copper has good resistance to softening at the NEG activation temperature of 200°C.

LNLS NEG COATING FACILITY

Since all the vacuum chambers will have small vacuum conductance, on account of their narrow cross section, NEG coatings will be extensively used. The host lab of Sirius, LNLS, has signed a license agreement with CERN to develop the coating technology in Brazil. Moreover, LNLS has designed and built its own NEG coating facility to produce the vacuum chambers (Fig. 1). The current facility allows LNLS to produce coatings according to standards determined by CERN – offering the ability to coat vacuum chambers up to 3.2 m long and 450 mm in diameter.

Figure 1: NEG coating facility at LNLS.

THE STORAGE RING VACUUM SYSTEM

One achromat cell of the storage ring vacuum system is illustrated in Fig. 2. Each cell comprises 18 chambers, 2 crotch absorbers with radiation extraction ports and 1 pumping chamber to install an additional ion pump.

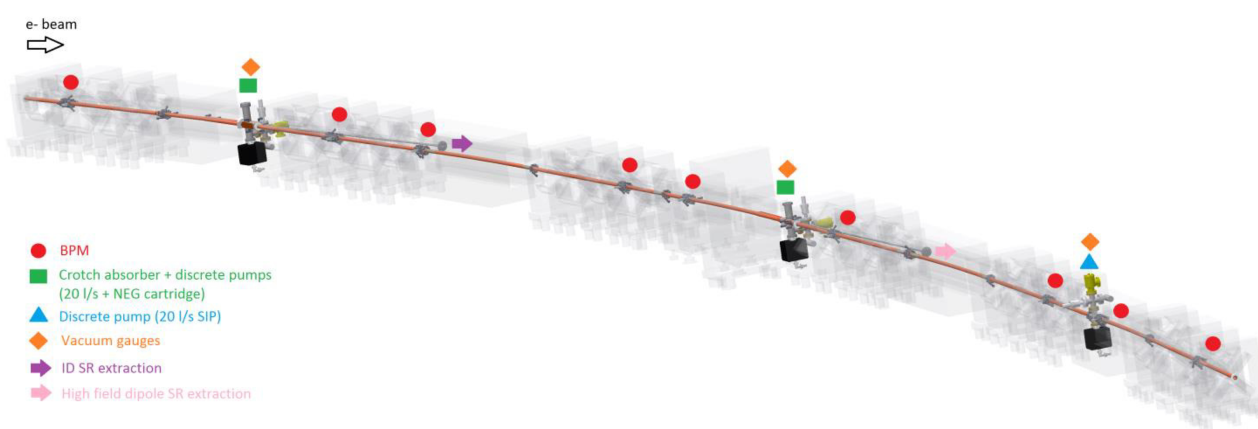

Figure 2: Vacuum system layout for one achromat cell.

Content from this work may be used under the terms of the CC BY 3.0 licence (© 2015). Any distribution of this work must maintain attribution to the author(s), title of the work, publisher, and DOI.

ISBN: 978-3-95450-168-7 doi:10.18429/JACoW-IPAC2015-WEPMA004

A 250 Hz AC SCAN MAGNET FOR HIGH-POWER RADIOISOTOPE PRODUCTION AND BNCT APPLICATIONS*

M.P. Dehnel, D.E. Potkins, T.M. Stewart, A. Kilbourne-Quirk, S. Tranfo, J. Chu, C. Hollinger
D-Pace, Inc., Nelson, BC, Canada
C. Philpott, Buckley Systems Ltd, Auckland, New Zealand

Abstract

This paper describes the proto-type magnet measurement results for a compact (212 mm effective length) yet large gap (97 mm) ambient air-cooled laminated AC scan magnet. A large aperture is essential for machine safety in radioisotope production, and Boron Neutron Capture Therapy (BNCT) applications with steady-state beam power up to 50 kW [1]. Rose shim and Purcell filter techniques are examined for improved transverse field flatness. The measured magnetic field and frequency response curves through a range from (250 Gauss, 70 Hertz) to (25 Gauss, 250 Hertz) are given for the case of an air-gap, SS316 beampipe, and SS316 bellows. Measured transverse and longitudinal magnetic field curves are also given. A model of the frequency response of the magnet was created and validated against measured data. The model simplifies power supply selection and maps effects of system natural frequency on the magnetic field. Tests were conducted with and without a resistor in parallel with the magnet coils. Lastly, an algorithm for a flat-topped square raster scanned beam intensity distribution is given.

FIELD MEASUREMENTS & IMPROVEMENTS

D-Pace has developed an AC Scan Magnet for high-power (tens of kW) single-pass beamlines for radioisotope production and BNCT applications. For these applications a short device is required (350 mm insertion length, and 212 mm magnetic effective length) with a large gap (97 mm), so excess space is provided transverse to beams up to 40 mm in diameter to provide clearance between the beam extents and the beam pipe. For high power beams, a small percentage of beamspill would melt beam pipe walls in a catastrophic manner. A good-field region transverse to the beam is achieved with our nominal design where the field is flat to within ±1% within ±20 mm of the beam axis, refer to Figure 1.

Modelling of Rose shims and Purcell filters with Infolytica's Gemini code, as illustrated in Figure 2, resulted in a magnetic field flat to within ±0.25% within ±20 mm of the beam axis. The modelling of several shim and filter designs were undertaken, and the results shown here were the best achieved for a 97 mm gap.

Figures 3 & 4 illustrate the measurement of the magnetic field for the case of (a) an air-gap, (b) 1.6 mm wall SS316 beam tube, and (c) 0.4 mm wall SS316 formed bellows. These measurements were undertaken to determine any degradation to magnetic field resulting from eddy currents in the SS316 tube or bellows material.

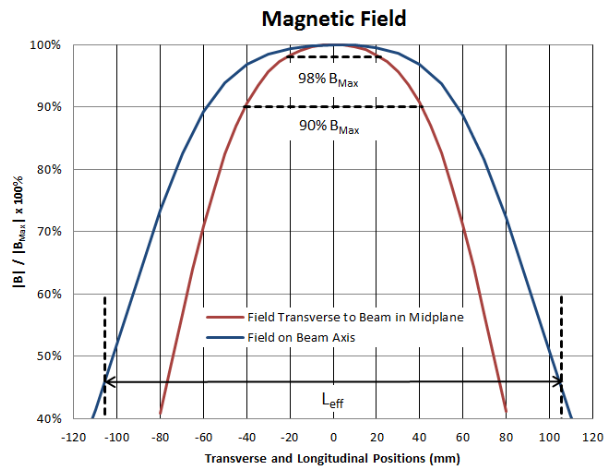

Figure 1: Measured normalized magnetic field transverse to the beam axis, and along the beam axis.

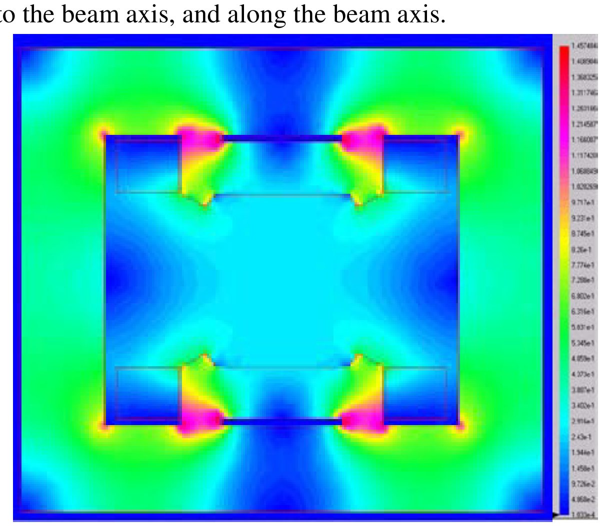

Figure 2: Magnetic field in Tesla. Each Rose shim is a triangle with base 20 mm in horizontal plane and height 8 mm at a point ¾ along the base. Each Purcell filter is an absence of C1010 material, centred at the pole base, 4 mm in height by 72 mm in width.

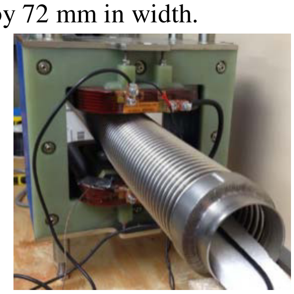

Figure 3: AC Scan Magnet Field Measurements.

Content from this work may be used under the terms of the CC BY 3.0 licence (© 2015). Any distribution of this work must maintain attribution to the author(s), title of the work, publisher, and DOI.

ISBN: 978-3-95450-168-7 doi:10.18429/JACoW-IPAC2015-WEPMA005

PARTICULARITIES OF THE ARIEL E-LINAC CRYOGENIC SYSTEM

I. Bylinskii, G. Hodgson, D. Kishi, S. Koscielniak, A. Koveshnikov, R. Laxdal, R. Nagimov, D. Yosifov, TRIUMF, Vancouver, Canada

Abstract

The Advanced Rare IsotopE Laboratory (ARIEL) is a major expansion of the Isotope Separation and Acceleration (ISAC) facility at TRIUMF [1]. A key part of the ARIEL project is a 10 mA 50 MeV continuous-wave superconducting radiofrequency (SRF) electron linear accelerator (e-linac). The 1.3 GHz SRF cavities are cooled by liquid helium (LHe) at 2 K [2]. The 4 K-2 K LHe transition is achieved onboard of each cryomodule by the cryoinsert containing counterflow heat exchanger augmented with JT-valve [3]. Air Liquide LHe cryoplant provides 4 K LHe to cryomodules. After successful commissioning of the cryoplant, 2 K sub-atmospheric (SA) system and cryomodules, the ultimate integration test confirmed stable operation of two cryomodules comprising two 9-cell SRF cavities. Particularities of this cryogenic system include conservative design of the oil removal system, original design heat exchanger in the SA pumping system, hermetic SA pumps, inline full SA flow purifier, multipurpose recovery/purification compressor, modular LHe distribution system, top-loaded design cryomodules, and overall radiation resistant design. The paper presents details of these features as well as integration tests results.

INTRODUCTION

The TRIUMF ten year plan (2010-2020) seeks to triple the laboratory nuclear physics scientific output by the additional of two new rare isotope beam (RIB) sources. These sources will supply the three existing experimental areas at the ISAC research facility which presently shares a single "driver" proton beam line (BL2A) for RIB production - resulting in under-utilization of experimental potential. The plan foresees a 50 MeV and 10 mA e-linac. Its major components are a 300 keV electron gun, 10 MeV injector cryomodule (ICM) with one 9-cell Nb elliptical cavity, and two 20 MeV accelerator cryomodules (ACM) each containing two 9-cell Nb elliptical cavities. The cavity frequency (1.3 GHz), type (9-cell elliptical), and operating temperature (2 K) have been chosen to benefit from the two decades of development, at the TESLA Test Facility.

For both budgetary and resource allocation reasons the e-linac project is planned in two phases. The first stage, ARIEL phase-I, includes two cryomodules (ICM and ACM #1). A third cryomodule will be added in ARIEL phase-II. The architecture of the ARIEL cryogenic system is shown in Figure 1.

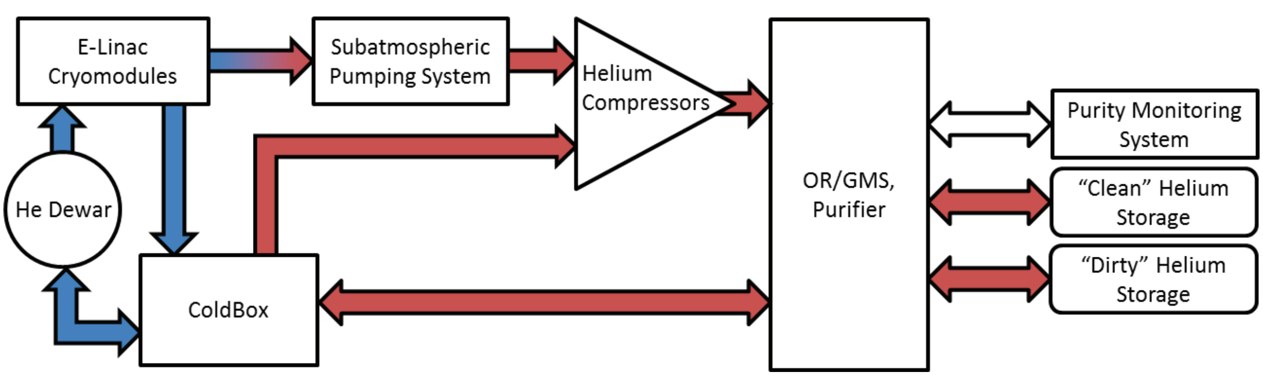

Figure 1: Architecture of the e-linac cryogenic system.

COMPRESSION AND GAS HANDLING

Compression Station

The compression station contains two Kaeser oil-flooded screw-type compressors (Figure 2). The main compression unit (Kaeser FSD571SFC) has 112 g/s capacity at the nominal discharge pressure of 14.5 bar(a). In addition, a smaller air-cooled recovery/purification compressor is installed. This unit (Kaeser CSD85) provides 15 g/s flow rate and is used for a dual purpose. In the event of a power failure the compressor uses power from an emergency power generator to recover all helium boil-off. During regular operation, this same compressor handles the entire throughput of the sub-atmospheric pumps when cryomodules are at full RF load. This helium flow can then be cleaned of impurities by passing through the purifier. This compressor is equipped with dedicated oil-removal and gas management system (OR/GMS). Additionally, this compressor will be used as a purification compressor, moving helium inventory through the purifier from the 'dirty' storage tank (to be installed as a part of ARIEL phase-II upgrade) to the 'clean' storage tank.

Oil Removal and Purification Systems

Oil removal system shall remove any oil vapors or oil aerosol particles from the process gas. The size of the

Content from this work may be used under the terms of the CC BY 3.0 licence (© 2015). Any distribution of this work must maintain attribution to the author(s), title of the work, publisher, and DOI.

ISBN: 978-3-95450-168-7 doi:10.18429/JACoW-IPAC2015-WEPMA007

EXPERIMENTAL STUDY OF MULTIPACTOR SUPPRESSION IN DIELECTRIC MATERIALS

M. EL Khaldi, W. Kaabi
LAL, ORSAY, France

Abstract

A novel coaxial resonator to investigate two-surface multipactor discharges on metal and dielectric surfaces in the gap region under vacuum conditions (~10^{-8} mbar) has been developed and tested. The resonator is ~ 100 mm in length with an outer diameter of ~ 60 mm (internal dimensions). A pulsed RF source delivers up to 30 W average power over a wide frequency range 650-900 MHz to the RF resonator. The incident and reflected RF signals are monitored by calibrated RF diodes. An electron probe provides temporal measurements of the multipacting electron current with respect to the RF pulses. In this paper we compare and contrast the results from the RF power tests of the alumina (97.6% Al_2O_3) and quartz samples without a coating, "the non-coated samples" and the Alumina and quartz samples with a TiN coating in order to evaluate a home made sputtered titanium nitride (TiN) thin layers as a Multipactor suppressor. The effectiveness of this method is presented and discussed in the paper.

INTRODUCTION

A multipactor discharge is a phenomenon in which electrons impact one or more material surfaces in resonance with an alternating electric field [1]. Two main conditions must be met in order to develop a multipactor discharge between two material surfaces. First, electrons traversing the gap must impact the electrode near the time the E-field reverses the direction. Second, electrons must impact the surface with enough energy to create electron multiplication by secondary emission, i.e. δ (E) $\geq$1. The discharge is sustained by the population of electrons that remain in phase with the RF electric field. Because the discharge is sustained by secondary electrons, multipactor discharges typically occur under vacuum conditions.

Multipactor discharges are considered detrimental to RF systems in most applications. The discharges can cause vacuum window failure, limit the delivery of RF power, detune resonant cavities, damage high power RF sources, and cause a local pressure rise due to the desorption of surface gases [2]. As mentioned, multipactor (MP) is often an undesirable phenomenon, and avoidance can be critical in the operation of certain systems, it can be avoided in several ways. A general cure against multipacting is to avoid the resonant conditions by either a proper choice of the geometry of the device [3, 4] or by coating the critical areas with a material with a lower secondary yield [5,6]. This way the effect of multipacting can be significantly reduced, but very often the MP phenomenon cannot be removed. Titanium nitride (TiN) coating is used as a proven anti-multipacting coating for dielectric-loaded accelerating (DLA) structures, and RF vacuum windows. Several experimental investigations have been performed at DESY and LAL-Orsay, aimed at reducing secondary electron emission and multipactor effects by TiN layers generation on dielectric or metal surfaces [7, 8].

We propose here an experiment facility for investigating two-surface multipactor discharges on dielectric and metal surfaces. The compact apparatus consists of a RF coaxial resonator in a high vacuum system (~ 10^{-8} mbar). The RF resonator is ~ 100 mm in length with an outer diameter of ~ 60 mm (internal dimensions), powered with a pulsed RF source delivering up to 30W average power. These experiments were successful in identifying multipacting and allowed us the evaluation of a homemade sputtered titanium nitride (TiN) thin layers as a Multipactor suppressor.

TiN COATING TECHNOLOGY

The presence of a dielectric window on a high power RF line has in fact a strong influence on the multipactor phenomenon, a resonant electron discharge that is strongly limiting for the RF components performances. The most important method to reduce the multipactor is to decrease the secondary emission yield of the dielectric window and the dielectric-loaded accelerating structures (DLA). Due to its low secondary electron emission coefficient, TiN thin film is used as a multipactor suppressor coating on RF ceramic coupler windows. For this purpose, a reactive DC magnetron sputtering bench has been developed at LAL-Orsay with the collaboration of the consortium Ferrara Ricerche-Italie in the frame of CARE program (Figure 1).

Within the sputtering process gas ions out of a plasma are accelerated towards a target consisting of the material to be deposited. Material is detached ('sputtered') from the target and afterwards deposited on a substrate in the vicinity. The process is realized in a closed recipient, which is pumped down to a vacuum base pressure ~ 10^{-8} mbar before deposition starts (Figure 1).

In the both sides of vacuum chamber, the machine is equipped with a 10 inch titanium disc target of high quality (grade2, minimum 99.7 % Ti). Two rotary magnet packs are placed just behind the targets to increase plasma density at their surface, and thus improve sputtering yield. Two power supplies are used to fix both target bias. A special rotating sample holder was designed to allow uniform deposition on the samples made of different materials and had different sizes and shapes. The machine allows also the RF etching of the substrate, a pretreatment step in order to remove particle contamination, as it is not possible to clean a ceramic (alumina) with solvent due to

Content from this work may be used under the terms of the CC BY 3.0 licence (© 2015). Any distribution of this work must maintain attribution to the author(s), title of the work, publisher, and DOI.

ISBN: 978-3-95450-168-7 doi:10.18429/JACoW-IPAC2015-WEPMA008

RF DESIGN OF A HIGH GRADIENT S-BAND TRAVELLING WAVE ACCELERATING STRUCTURE FOR THOMX LINAC

M. EL Khaldi, L. Garolfi
LAL, ORSAY, France

Abstract

There is growing demand from the industrial and research communities for high gradient, compact RF accelerating structures. The Thomx high gradient structure (HGS) is travelling wave (TW), quasi constant gradient section and will operate at 2998.55 MHz (30°C in vacuum) in the 2**π**/3 mode. The optimization of the cell shape (Electromagnetic design) has been carried out with the codes HFSS and CST MWS, in order to improve the main RF characteristics of the cavity such as shunt impedance, accelerating gradient, group velocity, modified Poynting vector, surface fields, etc. Prototypes with a reduced number of cells have been designed. For an input power of about 20 MW, EM simulation results show that an average accelerating gradient of 28MV/m is achieved which corresponds to a peak accelerating gradient of 35 MV/m, a peak surface gradient of 44 MV/m and peak modified Poynting vector S_{cmax} of 0.24 MW/mm^2.

INTRODUCTION

ThomX is a Compton source project in the range of the hard X rays (45/90 keV). The machine is composed of a 50-70 MeV injector Linac and a storage ring where an electron bunch collides with a laser pulse accumulated in a Fabry-Perot resonator. The final goal is to provide an X-rays average flux of $10^{11}/10^{13}$ ph/s. The emitted flux will be characterized by a dedicated X-ray line. Different users are partners in the ThomX project [1], especially in the area of medical science and cultural heritage. Their main goal will be the transfer of all the experimental techniques developed on big synchrotron rings to these more compact and flexible machines. The ThomX project has recently been funded and will be located on the Orsay University campus.

The beam will be generated by a 2.5 cells standing wave RF gun and accelerated with a conventional LIL-type structure with an operating peak accelerating gradient around 20 MV/m during the first commissioning phase. The Thomx injector linac energy will be upgraded from 50 MeV to more than 70 MeV by replacing a low gradient S-band TW section with a short high gradient S-band one.

A LAL-PMB collaboration on high gradient S-band structure research has been established in order to push the performance envelope of RF structures towards higher accelerating gradients. The program foresees the design, prototyping and high power testing of a high gradient compact S-band accelerating structure. The Thomx high gradient structure (HGS) is travelling wave, quasi constant gradient section and will operate at 2998.55 MHz (30°C in vacuum) in the 2**π**/3 mode. The section consists of five constant impedance (CI) landings with 16 identical cells plus four transition cells between the landings, in which the iris diameter decreases by 0.175 mm from one cell to another.

Before the construction of the final high gradient structure, prototypes with a reduced number of cells will be realized. The goals of these prototypes are to improve the machining of the cells and the brazing process.

The electromagnetic design of the prototypes has been performed with the codes CST MWS and HFSS. The choice of a single cell shape derives from an optimization aiming to maximize RF efficiency and minimize surface fields and modified Poynting vector at very high accelerating gradients. Such gradients can be achieved utilizing shape optimized elliptical irises, surface finish, appropriate materials and specialized fabrication procedures developed for high gradient structures.

DESIGN OPTIMIZATION AND ELECTROMAGNETIC SIMULATIONS

Traditionally, the surface electric field was long considered to be the main quantity which limits accelerating gradient because of its direct role in field emission [2]. There is clear evidence however, in data from both CLIC and NLC [3, 4] which covers structures with a wide range of RF parameters, that a simple constant surface field limit is insufficient to predict the performances of the different structures. Recently, new quantities such as the averaged power flow through the cell by the iris aperture circumference P/C [5] and the peak modified Poynting vector $S_c = \mathrm{Re}\{S\} + \mathrm{Im}\{S\}/6$ [6] have been considered to be responsible for high gradient limits.

During the design phase, the optimization of the main RF properties for the accelerating cavities (shunt impedance, accelerating gradient, group velocity, modified Poynting vector, surface fields, etc.) was carried out, by using the 3D simulation codes HFSS and CST MWS. A scan over several parameters has been performed in order to find the best combination of geometrical parameters in term of high gradient operations performance and reduced power consumption. In order to have a quantitative approach, it has been decided to find the cell geometry which minimizes the quantity η:

$$\eta \equiv \frac{P}{<E_a>^2}\cdot\frac{S_c}{<E_a>^2} = \frac{v_g}{\omega}\cdot\frac{S_c/<E_a>^2}{r/Q} \qquad (1)$$

This corresponds to having simultaneously the minimum power consumption and the minimum risk of breakdown (based on the S_c model) for a given accelerating field.

Content from this work may be used under the terms of the CC BY 3.0 licence (© 2015). Any distribution of this work must maintain attribution to the author(s), title of the work, publisher, and DOI.

ISBN: 978-3-95450-168-7 doi:10.18429/JACoW-IPAC2015-WEPMA009

3 GHz SINGLE CELL CAVITY OPTIMIZATION DESIGN

L. Garolfi*, M. El Khaldi, LAL, Orsay, France
N. Faure, PMB-ALCEN, Peynier, France

Abstract

In order to develop a high gradient S-band electron accelerating structure, an optimized travelling wave (TW) single-cell cavity operating at the frequency of 3 GHz with $2\pi/3$ phase advance, is proposed. Starting from the well-known accelerating cells design developed by the Laboratoire de l'Accélérateur Linéaire (LAL) and the Stanford Linear Accelerator Centre (SLAC), for linear accelerators; it is possible to improve the main RF parameters, such as quality factor, shunt impedance, enhancement factor and group velocity, by choosing a suitable shape of the inner surface [1]. Even though surface electric field is being considered as the only main quantity limiting the accelerating gradient; the importance of power flow and the modified Poynting vector [2], has been highlighted from high-gradient experimental data [3]. In this context, the new field quantity (S_c) is derived from a model describing the RF breakdown trigger phenomenon wherein field emission currents from potential breakdown sites produce local pulsed heating. In particular, the modified Poynting vector takes into account both active and reactive power flow travelling along the structure. The main results presented in this paper have been carried out with the 3D electromagnetic simulation codes: High Frequency Structural Simulator solver (HFSS) and CST MICROWAVE STUDIO (CST MWS).

INTRODUCTION

ThomX is a Compton backscattering compact light source project, aiming to produce an intense flux of monochromatic X rays (40 – 90 keV) resulting from collisions between laser pulses and relativistic electron bunches. The machine consists of a 50 – 70 MeV Linac injector and a storage ring. A demonstrator was recently funded and is going to be built in the Orsay University campus. The Linac injector is composed of a RF gun and one accelerating section able to boost the energy of particles. For the first stage of the machine commissioning, a "LIL"-type accelerating section is foreseen to be lent by the SOLEIL Laboratory, as a partner of the project. This section was developed by LAL-Orsay for the pre-injector of the Large Electron Positron Collider (LEP) at CERN. In order to reach a final energy of 50 MeV, the energy gain in the section must be 45 MeV. However, the accelerator should reach higher energies in order to produce X-rays beyond 50 keV [4]. Since the maximum targeted X-ray energy is 90 keV, the Linac design should allow beam energy of 70 MeV. A LAL-PMB collaboration on high gradient S-band structure research has been established in order to advance together in this field.

* garolfi@lal.in2p3.fr

The ThomX high gradient structure is a TW quasi-constant gradient section and will operate at 2998.55 MHz (30 °C in vacuum) in the $2\pi/3$ mode. It will be fabricated by PMB in order to increase the ThomX Linac energy up to 70 MeV, with an available input power of about 20 MW. The final structure will be made of 94 accelerating cells and 2 coupling cells.

RF DESIGN OPTIMIZATION

The accelerating gradient is limited by RF breakdown in normal conducting TW structures and it has been observed to depend on many parameters including surface electric field, pulse length, power flow and group velocity [5].

For a long time, the surface electric field was considered to be the main quantity which limits accelerating gradient because of its direct role in field emission while the magnetic field was considered to be unimportant. However, as more experimental data had been taken into account, it was clear that the maximum surface electric field could not serve as an ultimate constraint in the RF design, because of its large variation in different structures. New ideas about the ratio from the input power flow to the minimum iris circumference P/C as a better constraint to be used in RF design, appeared since 2006. Although the P/C parameter fits a large fraction of experimental data, deviations were observed from geometries scaled to different frequencies.

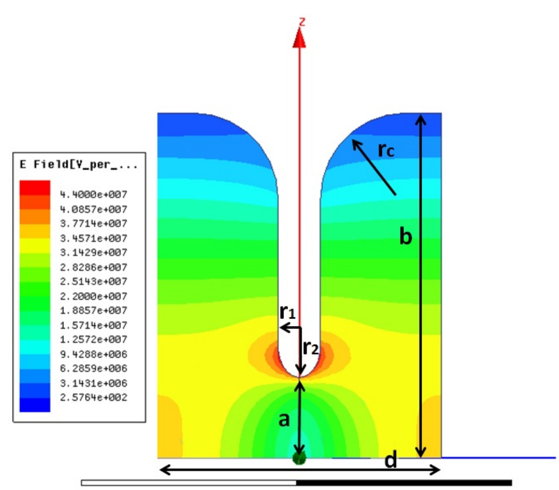

Figure 1: 2D section and electric field distribution of the half single cell.

A new model, is still based on the local complex power flow S (Poynting vector), but it also considers both a real and imaginary part of it, representing a combination of local electric and magnetic fields which sets a limit to achievable gradient.

Content from this work may be used under the terms of the CC BY 3.0 licence (© 2015). Any distribution of this work must maintain attribution to the author(s), title of the work, publisher, and DOI.

ISBN: 978-3-95450-168-7 doi:10.18429/JACoW-IPAC2015-WEPMA010

FIRST TEST RESULTS OF THE BERLINPRO 2-CELL BOOSTER CAVITIES

A. Burrill#, W. Anders, A. Frahm, J. Knobloch, A. Neumann, Helmholtz-Zentrum Berlin, Berlin Germany
G. Ciovati, W. Clemens, P. Kneisel, L. Turlington, Jefferson Laboratory, Newport News, VA, USA

Abstract

The bERLinPro Energy Recovery Linac (ERL) is currently being built at Helmholtz-Zentrum Berlin in order to study the physics of operating a high current, 100 mA, 50 MeV ERL utilizing all SRF cavity technology. This machine will utilize three unique SRF cryomodules for the photoinjector, booster and linac cryomodules respectively. The focus of this paper will be on the cavities contained within the booster cryomodule. Here there will be three 2-cell SRF cavities, based on the original design by Cornell University, but optimized to meet the needs of the project. All of the cavity fabrication, processing and testing was carried out at Jefferson Laboratory where 4 cavities were produced and the 3 cavities with the best RF performance will be fitted with helium vessels for installation in the cryomodule. This paper will report on the test results of the cavities as measured in the vertical testing dewar at JLab after fabrication and again after outfitting with the helium vessels.

INTRODUCTION

Helmholtz-Zentrum Berlin (HZB) is building a high average current, 100 mA, Energy Recovery Linac (ERL) at the site in Adlershof, Berlin Germany. The machine is designed using all superconducting RF accelerating cavities in order to demonstrate that the operation of such a machine is possible and to allow for a study of the physics of its operation.[1, 2] The 100 mA average current will be recirculated in a single pass at an energy of 50 MeV in continuous wave (c.w.) operation as shown in figure 1. The ERL is made up of a 1.4 cell SRF photoinjector cryomodule, fitted with a normal conducting multi-alkali (CsK_2Sb) photocathode, a 3 cavity booster cryomodule, the focus of this paper, and a 3 cavity linac cryomodule. More information on the photoinjector can be found in references 3 & 4.[3, 4] The booster cryomodule is designed to accelerate the 2 MeV beam from the photoinjector to 6 MeV for insertion into the recirculation arc and the linac cryomodule. Here the beam will be further accelerated to 50 MeV to make a single pass around the machine and then decelerated to 6 MeV and sent to the beam dump.

The ERL is designed to operate in a number of different modes to fully explore the operational parameter space associated with the recirculation of a high current, low emittance 5 MW beam. In many of these operating modes there is very strong beam loading for the photoinjector and booster cavities which places stringent demands on the fundamental power couplers, a topic which has been expanded upon in other publications and will not be covered here. In short, for the 100 mA operation the photoinjector and the accelerating booster

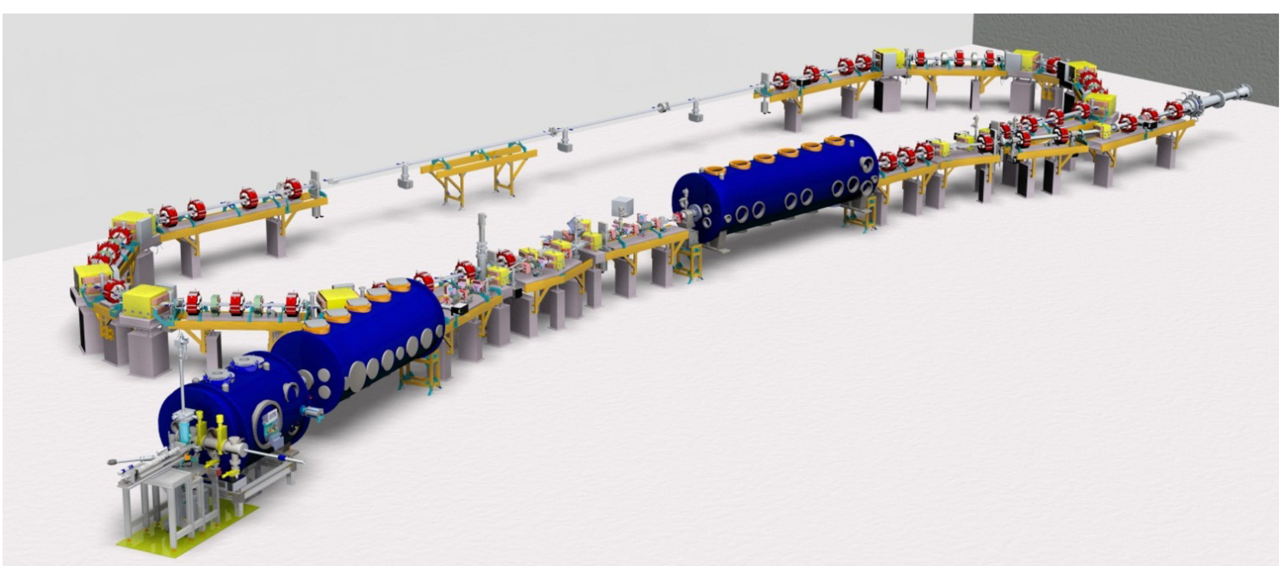

Figure 1: The bERLinPro Energy Recovery Linac machine layout.

#aburrill@helmholtz-berlin.de

Content from this work may be used under the terms of the CC BY 3.0 licence (© 2015). Any distribution of this work must maintain attribution to the author(s), title of the work, publisher, and DOI.

ISBN: 978-3-95450-168-7 doi:10.18429/JACoW-IPAC2015-WEPMA011

FIRST HORIZONTAL TEST RESULTS OF THE HZB SRF PHOTOINJECTOR FOR bERLinPro

A. Burrill♦, W. Anders, A. Frahm, J. Knobloch, A. Neumann, Helmholtz-Zentrum Berlin, Berlin, Germany
G. Ciovati, W. Clemens, P. Kneisel, L. Turlington, JLAB, Newport News, VA, USA

Abstract

The bERLinPro project, a small superconducting RF (SRF) c.w. energy recovery linac (ERL) is being built at Helmholtz-Zentrum Berlin in order to develop the technology required for operation of a high current, 100 mA, 50 MeV ERL. The electron source for the accelerator is a 1.4 cell SRF photoinjector fitted with a multi-alkali photocathode. As part of the HZB photoinjector development program three different SRF photoinjectors will be fabricated and tested. The photoinjector described herein is the second cavity that has been fabricated, and the first photoinjector designed for use with a multi-alkali photocathode. The photoinjector has been built and tested at JLab and subsequently shipped to HZB for testing in the horizontal test cryostat HoBiCaT prior to installation in the photoinjector cryomodule. This cryomodule will be used to measure the photocathode operation in a dedicated experiment called GunLab, the precursor to installation in the bERLinPro hall. This paper will report on the final results of the cavity installed in the helium vessel in the vertical testing dewar at Jefferson Lab as well as the first horizontal test in HoBiCaT.

INTRODUCTION

Helmholtz-Zentrum Berlin (HZB) has set out on a program to build a superconducting RF (SRF), high average current, Energy Recovery Linac (ERL) designed to operate at an electron beam energy of 50 MeV with 100 mA average current.[1] The ERL is designed to study the physics of the operation of a high current ERL in a number of different modes. This includes operation with bunch charges ranging from a few pC to 77 pC and repetition rates that range from low repetition rate burst modes up to c.w. operation at 1.3 GHz. This wide range of operating conditions will place great demands on many of the components of the ERL, and will certainly test the limits of the SRF photoinjector.[2]

In order to help mitigate the risks associated with operation of the SRF photoinjector HZB has set out on a multi-cavity photoinjector R&D program.[3] Four different SRF photoinjectors will be built and tested in order to gain experience with different aspects of the photoinjector operation. The first two photoinjectors in the development program were designed to utilize a lead photocathode and the results of these tests can be found in references 4-7.[4-7] The first photoinjector suitable for bERLinPro, called Gun 1.0, has been fabricated by Jefferson Lab and the preliminary data reported on previously.[8] This cavity is designed to utilize an independently cooled cathode stalk which will allow for the installation of a high quantum efficiency multi-alkali, CsK_2Sb, photocathode, suitable for generation of a 100 mA electron beam. In this paper we will report on the helium vessel welding and final test results in the JLab VTA as well as the first horizontal test results obtained at HZB in the HoBiCaT horizontal test cryostat.

HELIUM VESSEL WELDING AND FINAL VERTICAL TEST RESULTS

Following the cavity fabrication at JLab the cavity was processed and tested a number of times in an attempt to achieve the required operating gradient and quality factor for bERLinPro. Due to the new cavity design and the fact that this cavity was the first article produced, several challenges were encountered and the performance after 8 vertical tests was less than desired.[8] Due to schedule constraints the decision was made to attach the helium vessel to the cavity to progress the program. The titanium helium vessel was electron beam welded to the cavity while the cavity was kept under the static vacuum to avoid contamination of the inside of the cavity during the welding process. A photograph of the cavity following the helium vessel welding is shown in figure 1, with the cut-away of the cavity inside shown in figure 2.

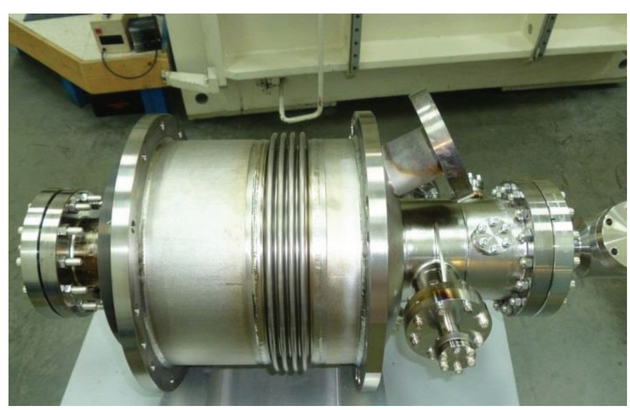

Figure 1: The SRF photoinjector for bERLinPro.

After the helium vessel welding and leak checking was complet the field flatness and frequency of the cavity were measured and found to be in very good agreement with the estimated values expected after the welding. The

♦andrew.burrill@helmholtz-berlin.de

Content from this work may be used under the terms of the CC BY 3.0 licence (© 2015). Any distribution of this work must maintain attribution to the author(s), title of the work, publisher, and DOI.

ISBN: 978-3-95450-168-7 doi:10.18429/JACoW-IPAC2015-WEPMA012

HIGH-Q CAVITY OPERATION: STUDY ON THE THERMOELECTRICALLY INDUCED CONTRIBUTION TO RF SURFACE RESISTANCE

J.M. Vogt, A. Neumann, J. Knobloch, O. Kugeler, A. Velez, Helmholtz-Zentrum Berlin, Germany

Abstract

We present a study concerning the operation of a superconducting RF cavity (non-doped niobium) in horizontal testing with the focus on understanding the thermoelectrically induced contribution to the surface resistance. Starting in 2009, we suggested a means of reducing the residual resistance by warming up a cavity after initial cooldown to about 20 K and cooling it down again [1]. In subsequent studies we used this technique to manipulate the residual resistance by more than a factor of 2 [2]. We postulated that thermocurrents during cooldown generate additional trapped magnetic flux that impacts the cavity quality factor. Since several questions remained open, we present here a more extensive study including measurement of two additional passband modes of the 9-cell cavity that confirms the effect. We also discuss simulations that substantiate the claim. While the layout of the cavity LHe tank system is cylindrically symmetric, we show that the temperature dependence of the material parameters result in a non-symmetric current distribution. Hence a significant amount of magnetic flux can be generated at the RF surface resulting in an increased surface resistance [3].

SETUP

A fully equipped TESLA-type cavity welded into a titanium tank and with a TTF-3 input coupler installed was mounted horizontally inside the HoBiCaT [4] cryostat. The TESLA-type cavity reported on here received a heavy BCP (about 150 µm) prior to a 2 h bakeout at 800°C (no N_2 anneal). A light BCP etch followed the heat treatment. Before the helium tank was welded onto the cavity a quality factor of about $2 \cdot 10^{10}$ in the π mode at 2K was measured in a vertical test which corresponds to a residual resistance R_{res} of 1.2 nΩ if one assumes that the BCS resistance R_{BCS} did not change between vertical and horizontal test (fitting parameters for R_{BCS} in horizontal test are listed below).

The cavity was equipped with Cernox sensors on the helium vessel head and beam pipes near the Nb-Ti joints. Furthermore two heaters were attached, one on each beam pipe. The setup including the helium supply is sketched in Figure 1.

HoBiCaT can cool the cavity with different schemes. The cryoplant fills the helium via the filling line at the bottom left and/or the 2-phase-pipe from the top right. As discussed below, we used three different cooling schemes: The initial cooldown, the thermal cycle and the parked cooldown.

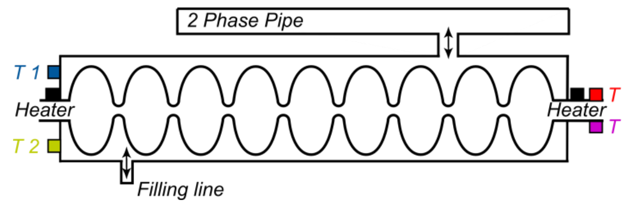

Figure 1: TESLA cavity in the LHe tank and equipped with four Cernox sensors and two heaters. The tank can be filled via the filling line and via the two phase pipe.

During the initial cooldown (whose temperature profile is shown in Figure 2a), the cavity is filled mainly via the filling line which creates a temperature gradient from its left to its right and from bottom to top. For a subsequent thermal cycle (Figure 2b), the cavity was filled via the 2-phase-pipe while the heaters were used to create a temperature difference between the cavity ends if desired. The targeted difference could be adjusted by varying the heater power. Values chosen were typical of those encountered during normal cooldowns. The "parked cooldown" (Figure 2c) from room temperature combines properties of both the initial cooldown and the thermal cycle. The cooling procedure of the initial cooldown was adapted to stop well before the sc phase transition. The cryoplant was balanced to maintain a constant temperature for 48 h. The set point was first set to 30K and then continuously lowered to 14K during this period. After all temperature sensors were clearly in equilibrium the set point was further lowered towards 1.8K and the cavity tank system transitioned with a small $\Delta T < 10$ K into the sc state.

THERMOELECTRIC EFFECT IN THE CAVITY HELIUM TANK SYSTEM

With the described setup, we investigated the hypothesis that thermoelectrically induced currents and their associated magnetic flux is responsible for the change of R_s upon thermal cycling. In the horizontal setup, the system is fabricated of two materials: Niobium (cavity) and titanium (helium tank) which create bimetal junctions. If a temperature difference is applied along the system (from left to right), a current is driven along the cavity and back through the tank. The additional temperature difference from bottom to top breaks the cylindrical symmetry of the system because the dc resistance of Nb and Ti is temperature dependent. Thus, even though mechanically the system is symmetric, the current is not and a magnetic field can be generated at the RF surface and get trapped during sc phase transition.

Content from this work may be used under the terms of the CC BY 3.0 licence (© 2015). Any distribution of this work must maintain attribution to the author(s), title of the work, publisher, and DOI.

ISBN: 978-3-95450-168-7 doi:10.18429/JACoW-IPAC2015-WEPMA013

HOM DAMPING OPTIMIZATION DESIGN STUDIES FOR BESSY VSR CAVITIES

A.Vélez, H.W. Glock, J.Knobloch, A.Neumann, Helmholtz-Zentrum Berlin, 12489 Berlin, Germany

Abstract

The BESSY VSR project is a future upgrade of the 3rd generation BESSY II light source. By using the same "standard" user optics, simultaneously long (ca. 15ps) and short (ca. 1.5ps) bunches will be stored. Thus, SRF higher harmonic cavities of the fundamental 500 MHz at two frequencies need to be installed in the BESSY II storage ring. This work describes the optimization studies for the waveguide-based HOM dampers and the adjustable fundamental power coupler for the 1.5 GHz first SRF cavity prototype.

INTRODUCTION

Simultaneous operation of long and short pulses by BESSY VSR represents a very attractive upgrade of the conventional storage ring operation concept. As described in [1] the addition to the 500MHz signal of two higher harmonics cavities and operating at zero crossing will lead to the desired combination of compressed and long bunches. Therefore 4 new SRF cavities (2x1.5 GHz and 2x1.75 GHz) need to be designed. These cavities will operate in CW at high field levels (E_{acc} =20 MV/m). The combination of these factors with high beam current (I_b=300mA) makes the cavity design a challenging goal since stable operation must be ensured [2]. Thus special attention must be paid to the damping of high order modes (HOMs) excited by the beam that may otherwise cause coupled bunch instabilities (CBIs) [3]. In order to avoid possible CBIs a stability condition is established imposing HOM impedances to be below feedback threshold both for longitudinal and transverse modes (5e4Ω-1e7Ω/m)[4]. This paper shows the current status of the design for the first 1.5 GHz cavity with special attention devoted to the optimization of the waveguide-based HOM damping technique [5,6]. To this end, EM calculations have been performed with both Ansoft HFSS and CST Microwave Studio [7,8] in order to compute the HOM-damped cavity spectrum

WAVEGUIDE HOM-DAMPING (WG-D)

The proved efficiency of WG-D absorbers [5] offers the capability to handle high power while offering very high damping levels. In addition the WG-D close distance to the cavity shows a better performance when propagating possible trapped modes as compared to beam-pipe ferrite absorbing solutions. The present designed WG-D end-groups consist on a 2 Y-shape beam-pipe section loaded with 3 equally spaced waveguides (120°). Both input and output WG-D are shifted 60° in order to cover for different mode polarisations. The length of the waveguides is set to 400 mm ensuring enough isolation for the fundamental TM_{010} π-mode (Q_{ext}=5e10) while reducing the risk of dust contamination.

Damping Studies

In order to avoid CBIs the limit on the feedback threshold forces the model to push the limits of the damping technique. As it is well known TM modes more often present higher R/Q*Q values and therefore represent the highest risk when dealing with CBIs. However a few TE modes with impedances in the order of the present threshold limit can be found due to band superposition effects and asymmetries (with coax coupler) [4]. Therefore the damping system must be optimized in a way that both TE and TM modes can be propagated.

Two main approaches are used on the damping optimization for the cavity prototype: extended WG (HZB.x.b) and enlarged beam-pipe (HZB.2.x).

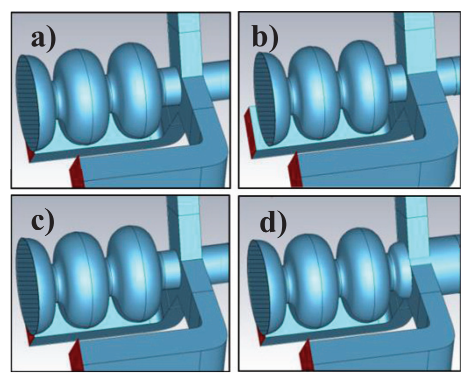

Figure 1: Layout of the two techniques applied on the optimization of the Y-shape waveguide absorbers. Extended WG-D (a~b). Enlarged beam-pipe (c~d).

In the first one, the beam-pipe diameter is equal to the iris (71mm) but the height (H) of the waveguide is increased from 50mm (HZB1a) to 60 mm (HZB1b). Therefore the propagated waveguide TE-like modes benefit from a lower cut-off (i.e f_c TE_{01}=2.50GHz) and are allowed to propagated through the WG-D. This effect is depicted in Fig 2 for the TE_{111}, TE_{011} and TE_{211} modes. However, in contrast to the enlarged beam-pipe, this approach is not as effective when damping most of the TM modes. On the other hand the enlarged beam-pipe approach benefits from the beam-pipe cut-off reduction due to the increase of its diameter (71mm~110mm). Therefore the beam-pipe cut-off for the first propagated mode is reduced to 1.65 GHz offering a great

Content from this work may be used under the terms of the CC BY 3.0 licence (© 2015). Any distribution of this work must maintain attribution to the author(s), title of the work, publisher, and DOI.

ISBN: 978-3-95450-168-7 doi:10.18429/JACoW-IPAC2015-WEPMA014

DEVELOPMENT OF NEW MICROCONTROLLER BASED POWER SUPPLY CONTROL UNITS AT ELSA

D. Proft*, T. Perlitius and W. Hillert, ELSA, Bonn, Germany

Abstract

At the electron stretcher facility ELSA electrons are accelerated with a high ramping speed of 6 GeV/s. This leads to strong requirements on the main magnets power supplies. In particular, any synchronization errors directly result in beam tune shifts and, at worst, beam loss.

The existing thirty years old control units are now being replaced by new in-house developed versatile microcontroller based ones. These allow the application of arbitrary ramp patterns and actual value acquisition in realtime. With an ethernet interface the ramp patterns can be uploaded directly to the power supplies. The flexible design also allows usage of the module to control other power supplies, e.g. those of the orbit correction magnets.

This presentation will give details on the developed hardware design and the performance of the modules compared to the existing ones.

POWER SUPPLIES AT ELSA

ELSA is a three-stage accelerator consisting of an injector with a 20 MeV LINAC, a 1.2 GeV booster synchrotron and a so-called *stretcher ring* for post acceleration to 3.2 GeV.

One acceleration cycle is typically 6 s long. Electrons from the injector stage are accumulated in the stretcher ring at 1.2 GeV and afterwards the beam energy is increased to a maximum of 3.2 GeV within 333 ms. This yields to a ramping speed of 6 GeV/s. A typical ELSA cycle is shown in Fig. 1.

Precise timing on the energy ramp imposes high requirements on the power supplies of the main magnets. The high ramp speed corresponds to a field change of 1.8 T/s of the main dipoles and thus a change in the supplied current of 5.2 kA/s. For the other magnets, e.g. quadrupoles, the slope is lower but still in the order of 1 kA/s.

In total there are six power supplies for the main magnets[1] manufactured by HOLEC . They require an analog set point value in the range from 0 V to 10 V being proportional to the desired current as well as digital signals for slow control of the device. At the moment these are provided by 30 years old in-house developed interface cards, so-called *MACS* CPUs, which are connected to VME CPUs via HDLC and finally via ethernet to the control system.

To avoid tracking errors on the ramp all interfaces are triggered by a common hardware *ramp start* trigger.

As a vital component of the accelerator these old MACS systems are now being replaced by a new microcontroller based solution. Goals for the new design are the change

* proft@physik.uni-bonn.de

[1] dipoles, 2 quadrupole families, 2 sextupole families and extraction sextupoles

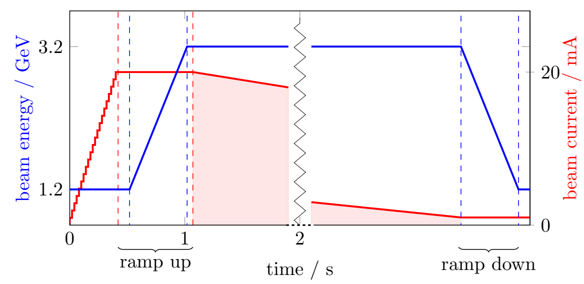

Figure 1: ELSA operation cycle consisting of accumulation, ramp up, extraction and ramp down phase.

from equidistant pre-sampled ramp patterns $I(t)$ to piecewise linear approximated ones and the ability to split the whole cycle timing into a ramp-up and ramp-down part (see Fig. 1) required for the new timing system [1].

Secondarily the new control units can be used for the corrector magnet power supplies as well [2], thus allowing to steer all magnets the same way. It also reduces tracking errors between the main magnets and the correctors on the energy ramp.

In total there are 54 corrector magnets each equipped with its own power supply. The interface is basically the same as for the main magnets except that the analog voltage is bipolar (±8 V) and the maximum current for the corrector magnets is ±8 A. Due to the high number of required power supplies it was decided to steer 4 power supplies mounted into one rack from one control unit.

HARDWARE DESIGN

Design goal for the new control units is, that all magnet power supplies can be operated with a uniform hardware module. A corresponding block diagram is shown in Fig. 2. A specialized daughter board is used to interface the different power supply's back plane connectors.

Crucial elements of the new control unit are two microcontrollers manufactured by *Atmel*. One, an *AT32UC3A1256* model is used for communication and other low priority tasks. With an attached *ethernet PHY*[2] the controller can be integrated into the existing networking infrastructure for configuration purposes and communication. Digital outputs and inputs are used for slow control of the attached power supply.

The other controller, an *ATXMEGA128A1U*, is used for real time tasks such as the output of DAC data on a regular time basis. A connected oscillator with 16 MHz and an accuracy of 30 ppm supplies the controller with a clock signal. The clock frequency is internally doubled using an

[2] Integrated circuit for the physical interface to the network.

Content from this work may be used under the terms of the CC BY 3.0 licence (© 2015). Any distribution of this work must maintain attribution to the author(s), title of the work, publisher, and DOI.

ISBN: 978-3-95450-168-7 doi:10.18429/JACoW-IPAC2015-WEPMA015

Content from this work may be used under the terms of the CC BY 3.0 licence (© 2015). Any distribution of this work must maintain attribution to the author(s), title of the work, publisher, and DOI.

WATER-COOLED THIN WALLED BEAM PIPES OF THE FAST RAMPING STORAGE RING ELSA

P. Hänisch*, B. Neff, W. Hillert - ELSA, Bonn University, Germany

Abstract

At the Electron Stretcher Facility ELSA of Bonn University thin walled beam pipes are in use to reduce eddy current loss to a minimum. The operation of the accelerator places high demands on the beam pipes like static stress because of the inner vacuum and additional one-sided thermal stress caused by synchrotron radiation. A first generation of thin walled beam pipes had been developed and manufactured during the construction of the stretcher ring in 1985. These pipes were successfully in operating stage the following ten years. The beam pipes had a wall thickness of 0.3 mm, a length of 3 m, and a bending radius of ca. 10.5 m. Special pipes with a sideway branch for synchrotron radiation experiments have been manufactured in the same assembly dimension. In the course of an intensity upgrade, a second generation of beam pipes has been developed in 1995. To reduce the thermal stress caused by the synchrotron radiation an internal water cooling was mounted. In this contribution the design and manufacturing principles of the thin walled beam pipes with water cooling are presented.

INTRODUCTION

The Electron Stretcher Accelerator ELSA [1] is a three-stage accelerator omprising two linacs, a booster synchrotron and a fast ramping pulse stretcher ring ($2\,\mathrm{T\,s^{-1}}$). To provide the fast ramping abilities of the stretcher ring it is essential to minimize the eddy current loss in the dipole gap. Since suitable radiation resistant non-conducting curved beam pipes are extremely difficult to manufacture this is most effectively achieved by building the vacuum chambers from stainless steel and reducing their wall thickness to a minimum. This reduction is mostly limited by the static stability of the beam pipe, the manufacturing possibilities, and the costs. First thin walled beam pipes had been constructed in 1985 and were in use from 1987 to 1995 when they have been replaced by a water-cooled version to enable an intensity upgrade at ELSA. The recent assembly of a new beam pipe by the university's workshops gave reason to rework the manufacturing process, especially those of beam pipes with a sideway branch and inner water cooling.

DIPOLE STANDARD BEAM PIPE

Setting up the Oval Shape of the Beam Pipe

Feedstock for all thin walled beam pipes at ELSA are round, welded pipes made of stainless steel with a wall thickness of 0.3 mm. This source material is as well used for the production of hydraulic formed vacuum bellows or metal bellow couplings. To form the round pipe into its oval shape it is pulled over a dedicated core at its full length of approx. 3 m. The core carries stainless steel balls which are positioned in wedge profile to expand the tube sideways. In contrast to cold-drawing or pultrusion the pipe is only bent and not stretched. Therefore, the circumference of the pipe remains constant throughout the entire processing operation and the required force can be performed by hand (see Fig. 1).

* haenisch@physik.uni-bonn.de

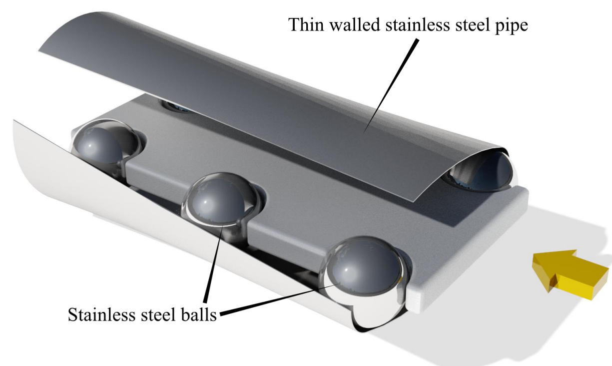

Figure 1: Schematic representation of the bending process to form the round feedstock into the required oval shape.

Mounting of the Reinforcing Ribs

In order to avoid further deformation caused by the ambient pressure on the evacuated oval pipe, it must be strengthened by additional reinforcing ribs. The design of the ribs is mostly influenced by their thickness, their maximum tolerable outer dimensions, and the distance between two adjacent ribs. Since the inner contour is determined by the oval shaped pipe and the height is limited by the size of the dipole gap, a careful minimization of the required amount of material resulted in a distance of ribs of 24 mm and a thickness of 1 mm. With an effective length of 3072 mm of each beam pipe, a considerably large number of in total 122 ribs are needed per pipe, taking into account the slightly different design of the beam pipe ends. To lower the production costs, the ribs were cut out of a stainless steel sheet using a water jet. The burr at the cut edges could be removed easily by vibratory grinding. This procedure turned out to be essential for later installation on the pipes since, in case of improper pre-treatment, burrs as well as any swarf clinging to the cut edges would cut deep marks in the thin walled pipe and could in worst case cause destruction of the entire pipe.

When mounting the ribs on the beam pipe, the pipe is fixed in a support structure to prevent it from crippling and to guide the ribs during their installation. Before mounting, fabrication tolerances of the inner rib contour have to be carefully controlled and, if necessary, adjusted. This turned out to be mandatory because only a tight fitting of the ribs

ISBN: 978-3-95450-168-7 doi:10.18429/JACoW-IPAC2015-WEPMA016

A NEW RF STATION FOR THE ELSA STRETCHER RING*

Manuel Schedler, Andreas Dieckmann, Philipp Hänisch, Wolfgang Hillert
ELSA, University of Bonn, Germany

Abstract

At the Electron Stretcher Facility ELSA of Bonn University, an increase of the maximum stored beam current from 20 mA to 200 mA is planned. The storage ring operates applying a fast energy ramp of 6 GeV/s from 1.2 GeV to 3.2 GeV and afterwards a slow extraction over a few seconds to the hadron physics experiments. The beam current is mainly limited due to missing RF power at highest energies in order to compensate for synchrotron radiation losses.

The current stretcher ring's RF station is based on a single 200 kW klystron driving two 5-cell PETRA type cavities. To achieve the desired beam current at maximum energy two additional 7-cell PETRA type cavities, drivin by a second klystron, will be installed. With this upgrade, sufficient beam lifetime for slow beam extraction will be provided and thus ensure an adequate duty cycle of the external beam current. The general setup of the new RF station as well as the changes in operation when switching from one to two stations will be presented.

THE ELECTRON STRETCHER ACCELERATOR – ELSA

ELSA is a three-stage electron accelerator. One of the two linear accelerators is used to inject an electron beam of 20 MeV into a booster synchrotron to gain an energy of typically 1.2 GeV. The beam can be accumulated and stored in the 164.4 m long stretcher ring, accelerated to a maximum energy of 3.2 GeV and, finally, slowly extracted to the hadron physics experiments using resonance extraction methods [1]. Figure 1 gives an overview of the ELSA facility including injector chain, stretcher ring and user experiments. The main operating parameters of the accelerator are summarized in Table 1.

On the fast energy ramp of typically 6 GeV/s in the stretcher ring fast changing beamloading effects lead to fast changing cavity voltages and phases. Figure 2 shows a typical post-acceleration cycle of the stretcher ring. To compensate for synchrotron radiation losses even at highest beam energies and intensities a new RF station is required. In addition, this station will allow to maintain the required overvoltage factor and lifetimes which of course have to be significantly greater than the extraction time of a few seconds to deliver a high quality and high intensity electron beam to the hadron physics experiments.

* Work supported by the DFG within the SFB/TR 16

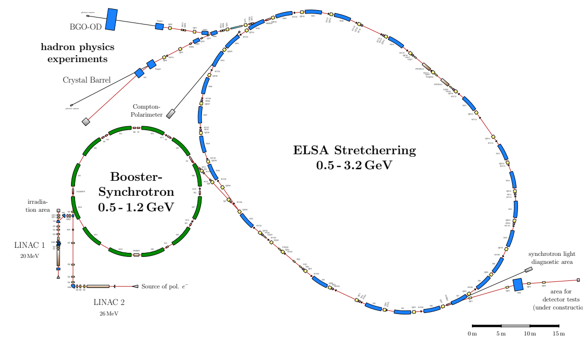

Figure 1: The Electron-Stretcher-Accelerator Facility ELSA

Table 1: Main Operating Parameters of the ELSA Stretcher Ring

Parameter	Value
Length	164.4 m
RF	499.669 MHz
Bunch spacing	2 ns
Harmonic number h	274
Filled buckets	274
Revolution frequency f_{rev}	1.8236 MHz
Beam energy E	1.2 GeV to 3.2 GeV
Beam current	20 mA to 200 mA
Ramping speed	$\leq$ 6 GeV/s
Injection rate	50 Hz
Momentum compaction factor α_c	0.0601

OVERVIEW AND SETUP OF THE NEW RF STATION

General Setup

The new RF station is based on two 7-cell PETRA type normal conducting RF cavities with a shunt impedance of 23 MΩ driven by a single klystron amplifier. The RF frequency is about 500 MHz as for the existing RF station. A magic T is used to split the amplified high power RF signal into two equivalent components in a WR1800 waveguide

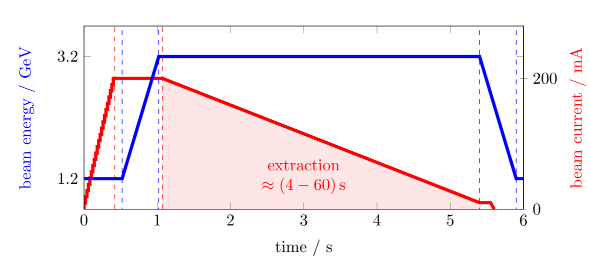

Figure 2: Post-acceleration mode of the ELSA stretcher ring.

Content from this work may be used under the terms of the CC BY 3.0 licence (© 2015). Any distribution of this work must maintain attribution to the author(s), title of the work, publisher, and DOI.

ISBN: 978-3-95450-168-7 doi:10.18429/JACoW-IPAC2015-WEPMA017

Content from this work may be used under the terms of the CC BY 3.0 licence (© 2015). Any distribution of this work must maintain attribution to the author(s), title of the work, publisher, and DOI.

ALVAREZ DTL CAVITY DESIGN FOR THE UNILAC UPGRADE

X. Du[1], A. Seibel[1,2], S. Mickat[1], L. Groening[1]
[1]GSI, Darmstadt, Germany; [2]Goethe-University, Frankfurt, Germany

Abstract

The 108.4 MHz drift tube linac (DTL) accelerator for GSI's UNLAC upgrade project is in its initial design stage using CST-MWS code. Optimization criteria for cavity design are effective shunt impedance (ZTT), transit-time factor, and electrical breakdown limit. In geometrical optimization we have aimed at increase of the energy gain in each RF gap of the DTL cells by maximizing ZTT per peak surface field with special designed tube profile. Multi-pacting probability is evaluated for one gap of typical single cell. For the beta profile design, a code based on VBA macros of CST is developed to perform cell by cell design with pre-optimized 3D tube structures. With this code several beta profile designs are presented and compared for the balance of power consumption, ZTT, tank length, and breakdown possibility of the complete cavity. The stability of the field has been taken into account and for this the crossed stem arrangement is assessed.

This paper gives a short introduction of the method, presents some important results. Possible countermeasures are discussed.

INTRODUCTION

At the existing DTL of the UNILAC five Alvarez cavities accelerate ions with an A/q of up to 8.5 from 1.4 MeV/u to 11.4 MeV/u over a total cavity length of 60 m [1]. The cavities operate at 108.4 MHz and at an rf-duty cycles of up to 30%[1].

The UNILAC upgrade intends to replace the existing Alvarez DTL with a newly designed DTL with same total length and output energy but with re-optimized shunt impedance and increased field stability. The existing Alvarez cavity tank I consists of 62 cells with tank diameter of 2 m, tube outer diameter of 200 mm, and tank length of 12 m. The designs and optimization of the new Alvarez cavities are based on the general parameters of the existing cavities.

DRIFT TUBE SHAPE DESIGN

The drift tube shape is designed to maximize the effective shunt impedance and to keep the peak electric surface field as low as possible [2]. A simplified single cell model is used for simulations with CST-microwave studio and static EM studio. The tube shape with a constant-radius corner and flat face with an angle is used at the beginning. The auto optimization tool in CST changes all parameters of the tube to obtain the best results. The parameters involved in the optimization are bore radius, drift tube face angle, drift tube corner radius, drift tube inner nose radius, drift tube outer nose radius, and drift tube flat length. But the field distribution on this tube always has a dominant maximum at certain area of the corner.

The new designed drift tube is built by a spline curve with a changing local curvature that is adjusted according to the desired surface field distribution.

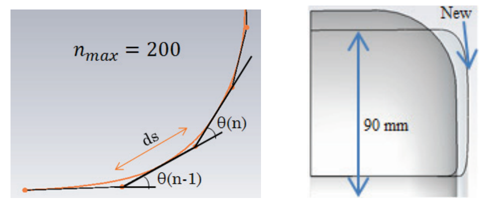

Figure 1: Spline for new tube shape design.

As shown in Fig. 1, the profile of the tube is made from steps of splines. The relationship between field distribution and curve is represented by

$$\theta(n) \xrightarrow{\text{yields}} \left.\frac{\partial^2 E_{surf}}{\partial l^2}\right|_{l=n*ds} \tag{1}$$

After the simulations, the surface field E_{surf} on the tube is evaluated. The angles of θ_n is reduced if the local field distribution is to be raised or θ_n is to be increased if the field is to be lowered. The sum of angles must be 180° such that the curve connects the inner radius to the outer radius.

With this new tube shape the surface field is uniformly distributed on the surface of the drift tube as shown in Fig. 2, keeping the maximum E_{surf} the same, while the ZTT is increased by about 12%. The tube shape is the same for all cells in one cavity for the convenience of fabrication, without discount its advantage on surface field distribution.

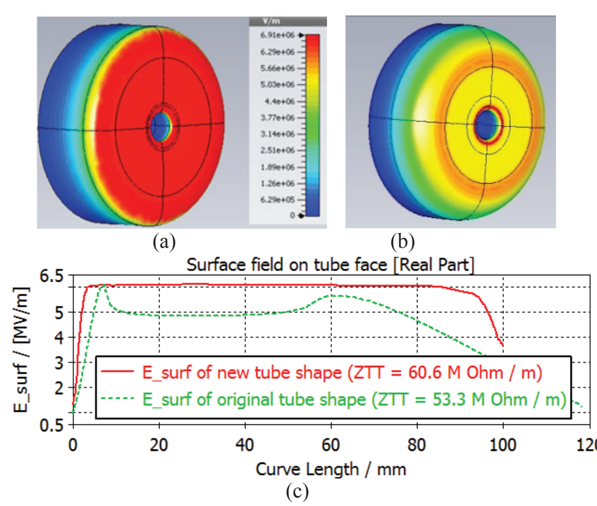

Figure 2: The surface field distribution (c) on the new tube shape (a) and on the original tube shape (b).

ISBN: 978-3-95450-168-7 doi:10.18429/JACoW-IPAC2015-WEPMA018

STATUS OF THE RING RF SYSTEMS FOR FAIR*

M. Frey, R. Balß, C. Christoph, O. Disser, G. Fleischmann, U. Hartel, P. Hülsmann, S. Jatta, A. Klaus, H.G. König, U. Laier, D.E.M. Lens, D. Mondry, K.-P. Ningel, H. Richter, S. Schäfer, C. Thielmann, T. Winnefeld, B. Zipfel, GSI, Darmstadt, Germany
K. Groß, TU Darmstadt, Darmstadt, Germany
H. Klingbeil, GSI and TU Darmstadt, Darmstadt, Germany

Abstract

For the FAIR (Facility for Antiproton and Ion Research) synchrotron SIS100 and the storage ring CR (Collector Ring), different RF cavity systems are currently being realized. In addition to the standard RF bucket generation and acceleration, these ring RF systems also allow more complex beam manipulations such as barrier bucket operation or bunch rotation in phase space. Depending on their purpose, the cavities are either loaded with ferrite material or with MA (Magnetic Alloy) ring cores. Independent of the type of cavity, a complete cavity system consists of the cavity itself, a tetrode-based power amplifier, a solid-state pre-amplifier, a supply unit including PLC (Programmable Logic Control), and an RF control system (so-called LLRF, low level RF system). In this contribution, the different systems are described, and their current status is presented.

SIS100 RF SYSTEMS

SIS100 will be the main synchrotron of the FAIR facility [1, 2]. This chapter is dedicated to the SIS100 RF systems. The mentioned RF voltages are the total peak voltages per cavity experienced by the beam.

SIS100 Accelerating System (SIS100 ACC)

The main accelerating system in SIS100, which works at harmonic number h=10, consists of 14 ferrite-loaded cavities whose parameters are shown in Table 1. The system is optimized for fast ramping and for a variety of operating modes.

Table 1: SIS100 Accelerating System (parameters for one cavity)

Parameter	Value
Frequency range	1.1-3.2 MHz
Maximum RF voltage	20 kV
Duty cycle	CW
RF power amplifier	Tetrode RS2054, single-ended
Installation length	3.0 m

For this system, the tendering process under the leadership of the FAIR GmbH* has successfully been completed. A consortium consisting of RI Research Instruments GmbH and Ampegon AG will deliver the overall system consisting of cavity, power amplifier, and power supply unit including PLC. Most parts of the LLRF system will consist of standardized GSI components. The technical design of the cavity is similar to the existing SIS18 ferrite cavities. Water cooling of the ferrite material is realized by cooling disks in-between the ring cores. A first sketch of the cavity in conceptual design phase is shown in Fig. 1.

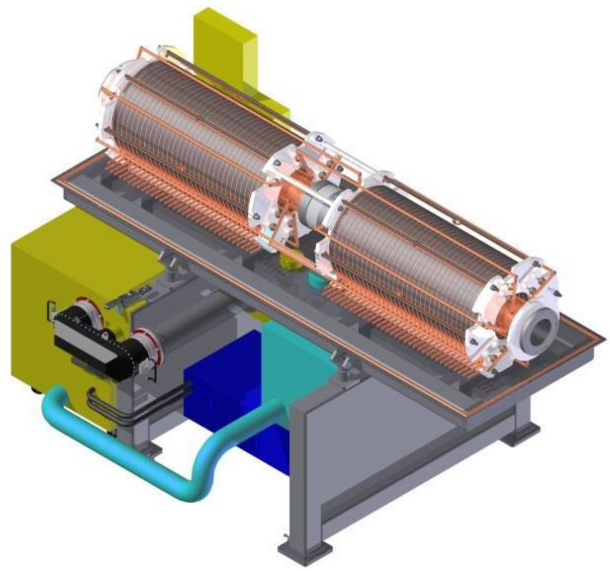

Figure 1: Conceptual design draft of SIS100 ACC cavity (image: RI Research Instruments GmbH).

In the first design phase, a specification for the ferrite ring material was agreed with the manufacturer after several ring core samples have been tested. The CDR (Conceptual Design Report) has been completed recently, the FoS (First of Series) will be delivered to GSI in 2016.

SIS100 Barrier Bucket System (SIS100 BB)

The barrier bucket system for SIS100 consists of two cavities loaded with magnetic alloy (MA) ring cores whose parameters are shown in Table 2. Each of the two cavities will create a single-sine pulse which can be shifted in time. Therefore, the beam can be captured between the two barriers (in the typical operating scenario, 8 of the 10 buckets generated by the SIS100 ACC system will be filled, and these 8 bunches will be combined to a long sausage-like bunch), and it will be pre-compressed by means of moving barriers in order to prepare the beam for final bunch rotation with the SIS100 BC system described below.

*Work supported by GSI Helmholtzzentrum für Schwerionenforschung GmbH & Facility for Antiproton and Ion Research in Europe GmbH (FAIR)

Content from this work may be used under the terms of the CC BY 3.0 licence (© 2015). Any distribution of this work must maintain attribution to the author(s), title of the work, publisher, and DOI.

ISBN: 978-3-95450-168-7 doi:10.18429/JACoW-IPAC2015-WEPMA019

Content from this work may be used under the terms of the CC BY 3.0 licence (© 2015). Any distribution of this work must maintain attribution to the author(s), title of the work, publisher, and DOI.

STATUS OF THE SUPER-FRS MAGNET DEVLOPMENT FOR FAIR

H. Müller, H. Leibrock, M. Winkler, P. Schnizer, E. Fischer, GSI, Darmstadt, Germany
L. Quettier, J.-E. Munoz-Garcia, Irfu, CEA, Saclay, France
L. Serio, CERN, Geneva, Switzerland

Abstract

The Super-FRS is a two-stage in-flight separator to be built next to the site of GSI, Darmstadt, Germany, as part of FAIR (Facility for Anti-proton and Ion Research). Its purpose is to create and separate rare isotope beams and to enable the mass measurement also for very short lived nuclei. Due to its three branches a wide variety of experiments can be carried out in the frame of the NUSTAR collaboration. Due to the large acceptance needed, the magnets of the Super-FRS have to have a large aperture and therefore only a superconducting solution is feasible. A superferric design with superconducting coils was chosen in which the magnetic field is shaped by an iron yoke. This paper presents the actual design status of the dipole and multipole magnets as well as the status of the development of the dedicated test facility at CERN.

INTRODUCTION

The Super-FRS is a new two-stage in-flight separator. It will be built as part of the future Facility for Antiproton and Ion Research (FAIR) in Darmstadt, Germany [1]. Due to its three branches (high-energy branch, low-energy branch, and ring branch) a wide variety of experiments will be possible [2,3]. The large acceptance required and the DC operation of the magnets led to a superconducting solution. Only the very first magnets after the target have to be built as normal conducting magnets with special radiation resistant conductor, due to the high radiation levels.

From protons to uranium all sorts of ions can be accelerated in the Super-FRS up to energies of about 1.5 GeV/u and with beam intensities of 10^{12}/s.

The general layout of the Super-FRS magnets is shown in Fig.1. Overall the Super-FRS consists out of 24 dipole magnets and 31 multiplets (containing 80 quadrupoles, 41 sextupoles, 14 steerers, and 46 octupoles).

Additional superconducting magnets are needed for the Energy Buncher in the low energy branch. These magnets are an Indian in-kind contribution to FAIR and are not treated within this paper.

MAGNET DESIGN

The magnets of Super-FRS have several common design features. Firstly, they are of so called superferric type (with the exception of the small correction magnets steerer and octupole which are made as surface coils). The magnetic field is shaped by the magnetic iron as for normal conducting magnets, but the coils of the magnet are wound with superconductors.

Secondly, the magnets have to be self-protected, i.e. they have to survive a quench without any damage even in case the quench protection system fails. Nevertheless dump resistors are foreseen for machine operation to extract as much energy as possible. The requirement of self-protected magnets leads to the use of superconductors with a high Cu/SC ratio (>9 in case of the dipoles, ~3.5 for quadrupoles and sextupoles).

Each of the magnets is powered individually and has its own pair of leads. To limit the size of the current leads and warm power cables the maximum current of the magnets have to stay below 300 A. This leads to coils wound of insulated wires rather than a cable.

The cooling of the magnets will be done by a pool boiling Helium bath. The design pressure of the Helium containers is set to 20 bars to avoid helium losses in case of quench and to be able to operate the cryogenic facility of FAIR with one common pressure.

An additional requirement is a warm beam pipe.

Despite of being operated in DC mode three consecutive triangular cycles up to maximum current with a ramp up time of 120 sec have to be possible in between the different operation cycles. This cycling is necessary to always have reproducible field conditions independent from the previous setting.

The beam height in Super-FRS is at 2 m the height of the cryogenic supply was fixed to 3.3 m over ground.

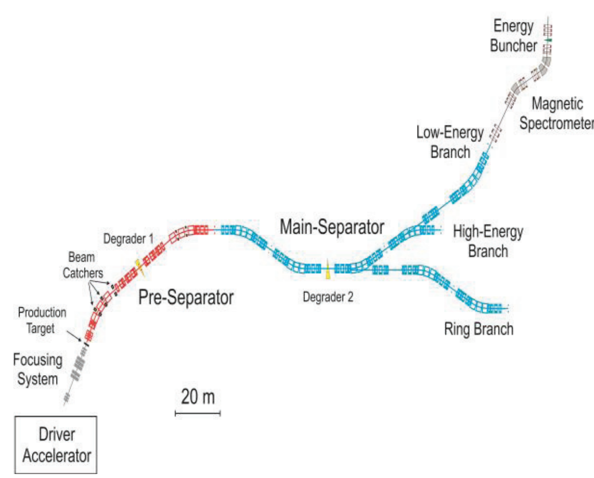

Figure 1: Magnetic Layout of Super-FRS.

ISBN: 978-3-95450-168-7 doi:10.18429/JACoW-IPAC2015-WEPMA020

SIS100 DIPOLE FIELD HARMONICS AND DYNAMIC APERTURE CALCULATIONS

C. Omet, E. Fischer, G. Franchetti, V. Kornilov, A. Mierau, C. Roux, D. Schäfer, P. Schnizer, S. Sorge, P. Spiller, K. Sugita
GSI, Darmstadt, Germany

Abstract

During the acceptance test of the First of Series (FoS) SIS100 superferric dipole magnet, detailed field measurements have been done. The harmonic coefficients have been extracted from these and dynamic aperture simulations have been done which are presented here. Furthermore, geometric precision measurement tools for the magnet have been developed to track down the field errors to geometric errors. Finally, mitigation actions have been taken to reduce these errors during manufacturing to ensure the design beam survival rate in SIS100.

SIS100 FOS DIPOLE PERFORMANCE

The SIS100 dipole magnet is a 3 m long super-ferric, curved magnet, see Fig. 1. It is the end of a successful development [1–4] and the first magnet with a high current coil made from Nuclotron cable and cooled by forced-flow 4.5 K two-phase He. It has a maximum field of 1.9 T and will be used at a very high ramp rate of up to 4 T/s in FAIR's driver synchrotron, SIS100. The gap size is 143 mm × 68 mm.

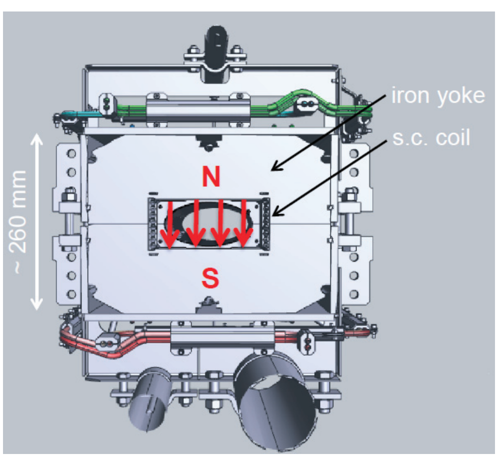

Figure 1: Cross section of the SIS100 dipole.

The First of Series (FoS) SIS100 dipole was delivered 2013 [5, 6] and has been thoroughly tested both at warm and cold conditions in the prototype test facility at GSI. Tests included electrical, geometrical, thermal checks and finally quench training and magnetic field measurements. The nominal current of 13.1 kA has been exceeded already after the second quench; even after several (8) thermal cycles, the magnet did not show a de-training behavior. AC losses at maximum ramp rate and triangular cycle have been measured to be 51 W, which is ≈30% below the calculated value and gives extra margin for the cryogenic plant of FAIR.

Beam stability during the 1 s long bunch-to-bucket injection from SIS18 into SIS100 has to be ensured. This poses a restriction onto the maximum allowable field errors of the magnets. For the dipoles, at injection field of 0.27 T (I = 1.5 kA), the good field region is 115 x 60 mm^2, where a field homogeneity of $\Delta B/B_0 \leq \pm 6 \times 10^{-4}$ is tolerated by design. Furthermore, it is important to have stable beams during middle to high energies at an up to 10 s long slow extraction plateau from SIS100 to the experiments, too.

Field Harmonics

The measurement campaign of the SIS100 dipole was based on the methods described in [7–10]. The following measurement systems were used:

- a single stretched wire system,
- a hall probe system,
- and a rotating coil probe system with transverse translated fields.

The last method allows deriving harmonics up to the 7$^{\text{th}}$ order reliably [6]. These measured data has been cross checked with a hall probe mapper and was proven to match. The analysis of these results, recalculated to a reference radius of 40 mm is shown in Fig. 2. Not allowed harmonics are larger than the allowed ones, which was somehow surprising and lead to detailed investigations of the magnet. In particular, the skew quadrupole is large.

To be useful for beam dynamics calculations, the harmonics have been re-calculated to be a valid expansion around the reference orbit, not the rotating coil probe axis.

Geometry Measurements

As for the magnet's super-ferric design, its magnetic field is dominated by the yoke's gap geometry. To track down the measured field errors to their probable root causes, the yoke geometry was measured very precisely. Therefore, special mechanical and capacitive measurement devices have been developed which are able to measure the gap height and width with a precision of ±10 µm in both warm and cold conditions. The measurements have been calibrated and cross checked with laser tracker measurements and found to be consistent.

The results of the gap height measurements along the magnet axis are shown in Fig. 3. The gap height is nonuniform along the magnet by ≈200 µm; the gap height between left and right side (parallelism) differs by ≈80 µm. As it will

Content from this work may be used under the terms of the CC BY 3.0 licence (© 2015). Any distribution of this work must maintain attribution to the author(s), title of the work, publisher, and DOI.

ISBN: 978-3-95450-168-7 doi:10.18429/JACoW-IPAC2015-WEPMA021

EFFICIENT PULSED QUADRUPOLE *

I. Petzenhauser#, U. Blell, P. Spiller, GSI, Darmstadt, Germany
C. Tenholt, IAP, Goethe-University, Frankfurt, Germany

Abstract

In order to raise the focusing gradient in case of bunched beam lines, a pulsed quadrupole was designed. The transfer channels between synchrotrons as well as the final focusing for the target line are possible applications. The quadrupole is running in a pulsed mode, which means an immense saving of energy by avoiding standby operation. Still the high gradients demand high currents. Hence a circuit had to be developed which is able to recover a significant amount of the pulsing energy for following shots. The basic design of the electrical circuit of the quadrupole is introduced. Furthermore more energy efficient circuits are presented and the limits of adaptability are considered.

ELECTRICAL CIRCUIT

As described in detail before, a pulsed quadrupole lens was designed [1] and a prototype was built (cf. Fig. 3) to prove the feasibility of the design. While the final system is supposed to handle currents up to 400 kA, the first prototype setup should operate at ~ 30 kA.

Its electrical circuit design is sketched in Fig.1. In this prototype, a 450 µF capacitor was charged to a voltage of 4700 V and discharged, producing a current pulse of ~ 33 kA and a pulse duration (FWHM) of ~ 60 µs (cf. Fig. 2).

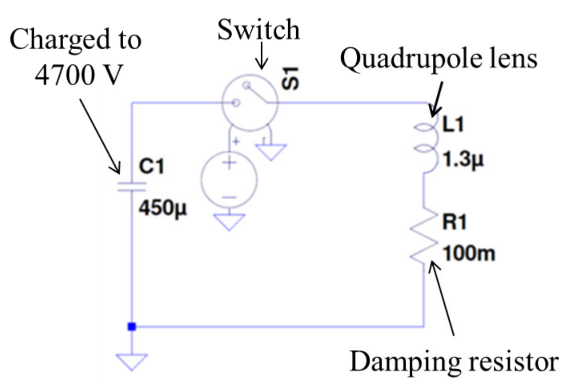

Figure 1: LTSpice[2] model of the electrical circuit of the prototype. The circuit is nearly critically damped to avoid oscillations.

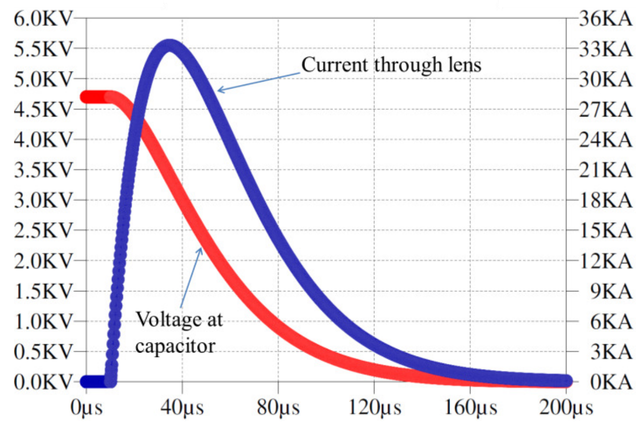

Figure 2: Pulsed current and voltage (Result of simulation in Fig. 1).

The electrical circuit presented in Fig. 1 is not suitable for a system with currents much higher than the 30 kA aimed for in this setup. Due to the damping resistance R1, a quite high voltage is required to realize high currents. For 400 kA operation, nearly 60 kV would be required. Also power dissipation (~ 16 GW at peak current) in the resistor and its cooling would be a serious issue, especially at higher repetition rates. Additionally, at 400 kA, the voltage drop across the 100 mΩ resistor would be 40 kV. Alternative electrical circuits will be discussed below. For the test circuit presented here, the resistance was a very simple possibility to damp the current critically and prevent a ringing discharge which would harm the capacitors lifetime. Due to the low repetition rate (1 shot in ~ 4 minutes) and the lower power input, cooling of the resistance was not an issue.

PROTOTYPE

To test the applicability of the design presented in [1], a prototype was built. The setup can be seen in Fig. 3. The upper part above the rectangular rack is the quadrupole lens itself. In the center of the lens is the vacuum tube. Inside the lens, this tube is made from alumina. The tube is positioned ~ 2 m above ground. Below the quadrupole lens, the pulsed power unit, i.e. capacitor, switch and damping resistor, is situated. It can be seen in more detail in Fig. 4. During operation, the rack is enclosed to prevent accidental contact with high voltage.

*Work supported by EuCARD-2-WP03-EnEfficient. EuCARD-2 is co-funded by the partners and the European Commission under Capacities 7th Framework Programme, Grant Agreement 312453
i.petzenhauser@gsi.de

Content from this work may be used under the terms of the CC BY 3.0 licence (© 2015). Any distribution of this work must maintain attribution to the author(s), title of the work, publisher, and DOI.

ISBN: 978-3-95450-168-7 doi:10.18429/JACoW-IPAC2015-WEPMA022

Content from this work may be used under the terms of the CC BY 3.0 licence (© 2015). Any distribution of this work must maintain attribution to the author(s), title of the work, publisher, and DOI.

PROGRESS OF THE KLYSTRON AND CAVITY TEST STAND FOR THE FAIR PROTON LINAC

A. Schnase[#], E. Plechov, J. Salvatore, G. Schreiber, W. Vinzenz, GSI, Darmstadt, Germany
C. Joly, J. Lesrel, IPN Orsay, CNRS-IN2P3 Université Paris Sud, France

Abstract

In collaboration between the FAIR project, GSI, and CNRS, the IPNO lab provided the high power RF components for a cavity and klystron test stand [1]. For initial operation of the 3 MW Thales TH2181 klystron at 325.224 MHz we received a high voltage modulator from CERN Linac 4 as a loan. Here we report, how we integrated the combination of klystron, high voltage modulator, and auxiliaries to accumulate operating experience. Klystron RF operation started on a water cooled load, soon the circulator will be included and then the prototype CH cavity in the radiation shielded area will be powered. The 45 kW amplifiers for the 3 buncher structures of the FAIR proton Linac were checked at the test stand, and the results are presented here.

TRANSISTOR AMPLIFIER TEST

In autumn 2014 three 45 kW transistor amplifiers for the 3 (re-)bunchers of the Proton Linac were delivered. The alignment of the amplifiers and the RF output was improved for easier installation by replacing the standard rollers with a version that is additionally equipped with adjustable feet as shown in the bottom of Fig 1.

Figure 1: One of the 45 kW amplifiers.

We confirmed the function of the inrush-current limiter and were able to replace the 125 A mains fuses with 63 A types. This allowed us to use a 3 phase standard CEE plug, which simplifies changing of the test setup. The firmware was adjusted to the expected pulsed modes. In operation, we need a repetition rate of 4 Hz; with some margin the amplifier should work at 5 Hz and actually the amplifier can handle repetition rates of 10 Hz and higher. The required pulse length is 0.2 ms. For testing, we used 0.4 ms long pulses. Such pulse pattern is shown in Fig. 2. The amplifier bias (yellow trace) is activated 1 ms before the RF is applied. The falling edge of the green trace triggers the power measurement. The light blue trace shows the RF output.

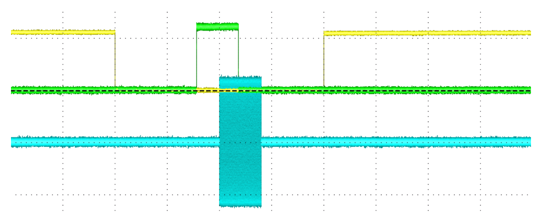

Figure 2: Amplifier test pulse pattern (0.5 ms/div).

Initial tests were conducted with a 50 Ω air cooled load at the amplifier output. The required 45 kW pulsed power was confirmed. The delay from RF-OFF command to RF-OFF was measured as less than 400 ns. From University of Frankfurt we received a compact 325 MHz test cavity structure to conduct site acceptance tests of these amplifiers under pulsed conditions driving a resonant load. This cavity was temporarily installed in a shielded area as shown in Fig. 3.

Figure 3: 325 MHz test cavity structure on support.

When discharges appear in the cavity, some power is reflected back to the amplifier. Thus we have to test the amplifier behavior not only for normal operation as shown in Fig. 4, but also for cavity conditioning.

[#] A.Schnase@gsi.de

ISBN: 978-3-95450-168-7 doi:10.18429/JACoW-IPAC2015-WEPMA023

ADVANCED MULTIPOLES AND APPROPRIATED MEASUREMENT TOOLS FOR FIELD CHARACTERIZATION OF SIS100 MAGNETS

Pierre Schnizer, Anna Mierau, Anke Gottsmann, Florian Kaether, Harald G. Weiss
Egbert Fischer, GSI, Darmstadt, Germany
Bernhard Schnizer, TU-Graz, Graz, Austria

Abstract

The heavy ion synchrotron SIS100 utilises fast ramped superconducting magnets. Describing and measuring these magnets requires advanced multipoles next to well adapted measurement techniques. We cover briefly the required theory adapted to the measurements, show which designs were available and which decisions had to be taken for measuring curved superconducting magnets. The series of SIS100 dipole magnets is going to be produced. These magnets will be measured at GSI. We present the foreseen field measurement procedure, outline the currently ongoing tests and give our calibration strategy.

INTRODUCTION

The heavy ion synchrotron SIS100 utilises fast ramped superconducting magnets [1, 2]; in particular as the vacuum chambers' inner surface is used as adsorption pump and thus has to be cold [3, 4].

These requirements led to a curved dipole with minimised aperture. The field provided within the aperture gap has to be fully understood so that today one can already forecast if the magnet's field quality will support the project targets of the high current machine.

The development of the advanced multipoles [5–7] allows describing the field within the curved beam path and the elliptic cross section of the vacuum chamber.

The required measurement devices were prepared in parallel adapted to the theoretical limitations.

THEORY

The standard description of the magnetic field for accelerator magnets is given by

$$B_y + \mathrm{i}B_x = \mathbf{B}(\mathbf{z}) = \sum_{n=1}^{\infty} \mathbf{C_n} \left(\frac{\mathbf{z}}{R_{Ref}}\right)^{n-1} \tag{1}$$

with $\mathbf{B}$ the 2D magnetic field and $\mathbf{C_n}$ the coefficient n, $z = x + \mathrm{i}y$ and R_{Ref} the reference radius. For elliptic apertures elliptic coordinates are adapted to the geometry. These coordinates (e.g. [8]) are given by

$$x + \mathrm{i}y = \mathbf{z} = e \cosh(\mathbf{w}) = e \cosh(\eta + \mathrm{i}\psi), \tag{2}$$

with x and y the Cartesian 2D coordinates, and $e = \sqrt{a^2 - b^2}$ the ellipse eccentricity. Then the field is given by

$$\mathbf{B}(\mathbf{w}) = \frac{\mathbf{E}_0}{2} + \sum_{m=1}^{\infty} \mathbf{E}_m \frac{\cosh(m\mathbf{w})}{\cosh(m\eta_0)}, \tag{3}$$

with $\mathbf{E}_m$ the elliptic coefficients and $\eta_0 = \tanh^{-1}(b/a)$.

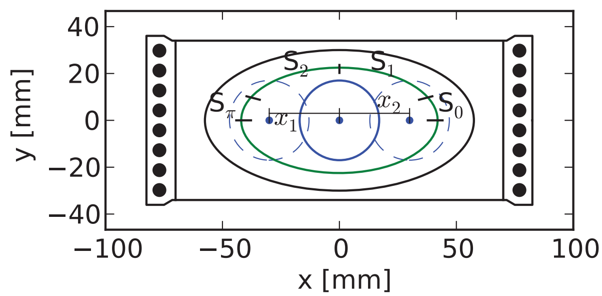

Figure 1: Rotating coil probe positions for measuring elliptic multipole coefficients. The beam aperture is indicated by a black ellipse. The green ellipse indicates the ellipse used currently in reconstruction. The blue circles indicate the area covered by the coil probe. S_0, S_1, S_2, S_π indicate the different parts where the coil probe is used. x_1 gives the offset of the coil probe measurement from the centre to the left side while x_2 gives the offset of the coil probe form the measurement to the right side. The magnet turns are indicated by the black filled circles and its inner aperture by a line.

Deduction of Equations for Error Analysis

The elliptic multipoles are derived from measurements from different positions (see Fig. 2) [5]. The coefficients $\mathbf{E_m}$ are obtained using the Fourier cosine transform

$$\mathbf{E}_m = \frac{2}{\pi} \int_0^{\pi} \mathbf{B}(\eta_0 + \mathrm{i}\psi) \cos([m]\psi)\, \mathrm{d}\psi, \tag{4}$$

with $\mathbf{B}$ the magnetic field along the ellipse, ψ the angle along the ellipse. The reconstruction is split in three parts for each coil, which finally add up to six parts as the parts which intermix have to be taken into account.

The coefficients were calculated numerically as given in [5]. An equivalent analytic expression is given below which allows deriving the influence of measurement errors.

All three coil probes will measure the same field described by some coefficients $\mathbf{C_n}$. While the coefficients obtained by the central coil probe are the $\mathbf{C_n}$, the ones obtained by the translated ones are given by

$$\mathbf{C}'_\mathbf{n} = \left[\mathcal{L}\binom{n-1}{k-1}\left(\frac{\mathbf{d_z}}{R_{Ref}}\right)^{n-k}\right]\mathbf{C_k}. \tag{5}$$

$\mathcal{L}$ indicates that this expression is an upper triangular matrix. This expression represents the so called "feed-down effect". On these set of harmonics ($\mathbf{C}^{\mathrm{r}\prime}_n$ for the coil on the right, $\mathbf{C}^{\mathrm{c}\prime}_n$

Content from this work may be used under the terms of the CC BY 3.0 licence (© 2015). Any distribution of this work must maintain attribution to the author(s), title of the work, publisher, and DOI.

ISBN: 978-3-95450-168-7 doi:10.18429/JACoW-IPAC2015-WEPMA024

SYSTEM DESIGN FOR A DETERMINISTIC BUNCH-TO-BUCKET TRANSFER*

T. Ferrand#,TEMF, Technische Universität Darmstadt, Darmstadt, Germany
J. Bai, IAP, Goethe Universität, Frankfurt am Main, Germany

Abstract

A deterministic bunch to bucket transfer system is currently under development in the frame of the FAIR project at GSI. To achieve our accuracy and stability requirements, a set of hardware modules will be implemented. These hardware modules are expected to provide values such as the relative phase advance between the RF systems of both, the source and the target synchrotron according to an external timing system. These values are exchanged via optical fibers between different supply rooms, and the considered RF signals are re-synthesized locally. These re-synthesized signals are synchronized to enable a precise phase advance control between the synchrotrons' RF systems. The first step of the development consists in modeling the actual DDS and DSP-based LLRF environment of the SIS18 under Ptolemy-II. Measurements on real devices will be performed concurrently to the simulation. We expect to use this simulation to refine our timing expectations regarding the synchronization process and the inter-module communication protocols and design the synchronization function, which will be implemented on the hardware modules.

INTRODUCTION

As it is foreseen in the frame of the construction of the Facility for Antiproton and Ion Research (FAIR) at GSI Helmholtzzentrum für Schwerionenforschung GmbH [1], the existing SIS18 is used as a pre-accelerator for the new acceleration chain. To fulfill this task, a Bunch-to-Bucket transfer procedure is being investigated.

The SIS18 is a separated functions synchrotron designed to accelerate a variety of ions from protons to uranium with different mass over charge ratios. Two ferrite-loaded cavities in combination with three MA-loaded cavities bring the beam to the transfer flattop. The transfer is performed at harmonic number 2 (see Table 1).

Table 1: List of Beam Parameters for SIS18 at the Flattop for Uranium $^{238}U^{28+}$.

Parameters	Value
Bending field B_0	1.73 T
Magnetic Rigidity $B_0\rho_0$	18 Tm
RF frequency f_0	1.56 MHz
Circumference of the reference orbit L_0	216.72 m

*Work supported by GSI
#ferrand@temf.tu-darmstadt.de

The future SIS100 will have a maximum magnetic rigidity of 100 Tm for a reference orbit five times larger than the reference orbit of the SIS18. Injections will be performed on harmonic number 10, so that under the transfer conditions the relative bunch repartition in the SIS18 and in the SIS100 is periodical and its revolution frequency is the frequency of the SIS100 at harmonic number 1.

Independently from the applied method and from the conditions relative to the design of the different accelerators, which compose the acceleration chain, the procedure, which we refer to as synchronization consists in controlling the relative phase advance between RF signals of the SIS18 and the corresponding reference signals derived from the SIS100 RF system. The described synchronization procedure is required to ensure the capture of the bunches composing the beam extracted from the SIS18 by the RF field generated by the 14 ferrite-loaded cavities of the SIS100.

SYSTEM DESIGN

Beam Dynamics During the Synchronization

According to the circumference ratio of their reference orbits, the measured relative phase advance between corresponding RF signals of the SIS18 with respect to the SIS100 is constant. Modifying the bending field value at the transfer flattop in the SIS18 results in steering the beam on a so-called synchronization orbit, which introduces a linear variation of the relative phase advance between the corresponding RF signals of the SIS18 resp. the SIS100. According to the main synchronization scenario under development for FAIR the beam is extracted from its synchronization orbit, imposing a maximum relative radial steering during the synchronization procedure shown in Eq.1.

$$\frac{\Delta L}{L_0}=2.4\cdot 10^{-4} \qquad (1)$$

The energy matching between the two RF fields, is ensured for this maximum radial steering by modifying the bending field accordingly. The maximum frequency offset resulting from these modifications is $\Delta f = -360$ Hz.

The synchronization requirements are fulfilled periodically according to the beating frequency Δf. The transfer can be triggered within a transfer window defined by the maximum phase error expectation of ± 0.5°

Content from this work may be used under the terms of the CC BY 3.0 licence (© 2015). Any distribution of this work must maintain attribution to the author(s), title of the work, publisher, and DOI.

ISBN: 978-3-95450-168-7 doi:10.18429/JACoW-IPAC2015-WEPMA026

HIGHER ORDER MODE PROPAGATION AND DAMPING STUDIES ON AXISYMMETRIC SUPERCONDUCTING MULTICELL RF-RESONATORS*

B.D. Isbarn†, B. Riemann, M. Sommer, T. Weis
TU Dortmund University (DELTA), Center for Synchrotron Radiation, Dortmund, Germany

Abstract

Higher order mode (HOM) propagation and damping is a major concern in feasibility studies regarding the upcoming upgrade of BESSY II, named BESSY-VSR, which involves the utilization of superconducting multicell RF-resonators in a storage ring while maintaining a reasonably high beam current typical for third generation synchrotron radiation facilities. In addition to the computation of typical figures of merit, we focus on studies of the mode propagation in axisymmetric structures. Due to the focus on axisymmetric studies we are able to use 2D codes to investigate in eigenmodes with substantialy higher frequencies than usually considered with full 3D codes in parametric studies. In this work we present preliminary studies involving mode propagation in superconducting elliptical multicell cavities.

INTRODUCTION

The upcoming BESSY II upgrade BESSY-VSR aims to provide both short and long electron bunch lengths simultaneously [1], this can be achieved through a modulation of the rf-frequency. In order to fullfill the space restrictions and field requirements the use of superconducting multicell rf-cavities is inevitable. Due to the vast intrinsic quality factors of superconducting cavities and the high beam currents of typical third generation synchrotron radiation facilities, proper higher order mode damping techniques must be implemented. A major concern for designing appropriate damping techniques is the mode propagation resp. the power flow in beam direction. We already investigated the mode propagation of a single cell spline cavity [2] using Floquet periodic boundary conditions in an earlier work [3]. To incorporate evanescent coupling and the mode propagation of normal modes we took this approach one step further and investigated in the mode propagation of a multicell cavity with varying beam tube lengths attached to the end of the multicell structure. In the following we are using the nomenclature of [4] to refer to the modes corresponding to the single cell cavity as *cavity modes* and to the modes emerging from the coupling of the single cell cavitiy into an array of cavities as *normal modes*.

NUMERICAL STUDIES

All numerical studies were performed on the 2D axisymmetric eigenvalue problem with COMSOL Multiphysics 5.0 [5]. The base cell design consisted of elliptical shaped cavities as displayed in Fig. 1 with the geometry parameters

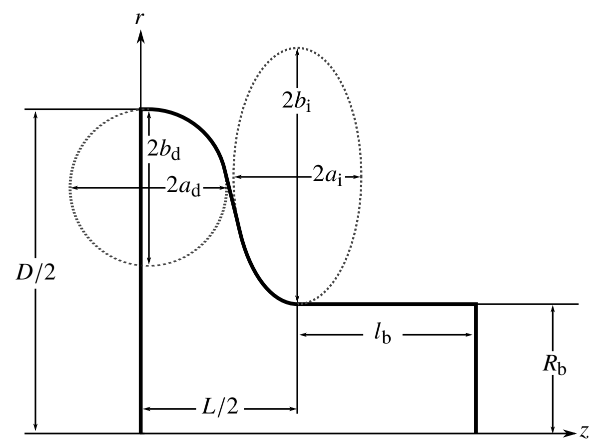

Figure 1: Geometry parameters of an elliptical cavity.

of the HZB layout [6]. These base cells were concatenated to form an array of 5 equally shaped cavities with beam tubes of length l_b attached to its ends. By restricting our scope of observation to equally shaped cells, without applying any end-cell tuning respectively optimization, we could increase the performance and therefore the observable parameter space.

Simulation Setup

In order to observe mode propagation we applied Floquet periodic boundary conditions at the ends of the attached beam tubes

$$\boldsymbol{E}_\mathrm{dst} = \boldsymbol{E}_\mathrm{src} e^{-i\boldsymbol{k}_z\cdot(\boldsymbol{r}_\mathrm{dst}-\boldsymbol{r}_\mathrm{src})}$$
$$\boldsymbol{H}_\mathrm{dst} = \boldsymbol{H}_\mathrm{src} e^{-i\boldsymbol{k}_z\cdot(\boldsymbol{r}_\mathrm{dst}-\boldsymbol{r}_\mathrm{src})}\ ,$$

where $\boldsymbol{E}_\mathrm{dst/src}$ and $\boldsymbol{H}_\mathrm{dst/src}$ represents the electric and magnetic field at the leftmost respectively rightmost port, and the wave vector $\boldsymbol{k}_z$ can be expressed as a function of the phase advance ψ and the overall length of the structure L_s

$$\boldsymbol{k}_z = \frac{\psi}{L_\mathrm{s}}\hat{z}\ .$$

All other boundaries were set to be perfect electric conductors (PEC) leading to loss-free solutions with real eigenvalues. We used the external quality factor as a figure of merit for the mode propagation, in analogy to the usual definition of the quality factor [4], described by

$$Q_\mathrm{ext} = \frac{\omega_0 U}{P_z} = \frac{\omega_0 \iiint_V \frac{1}{2}\varepsilon_0 \left|\boldsymbol{E}\right|^2 \mathrm{d}V}{\iint_A \rho_z \,\mathrm{d}A}\ .$$

* Work supported by the BMBF under contract no. 05K13PEB
† benjamin.isbarn@tu-dortmund.de

Content from this work may be used under the terms of the CC BY 3.0 licence (© 2015). Any distribution of this work must maintain attribution to the author(s), title of the work, publisher, and DOI.

ISBN: 978-3-95450-168-7 doi:10.18429/JACoW-IPAC2015-WEPMA027

FIRST CHARACTERIZATION OF A SUPERCONDUCTING UNDULATOR MOCKUP WITH THE CASPER II MAGNETIC MEASUREMENT SYSTEM

S. Gerstl#, S. Casalbuoni, N. Glamann, A. Grau, T. Holubek, D. Saez de Jauregui, R. Voutta, ANKA Synchrotron Radiation Facility, Karlsruhe Institute of Technology, Karlsruhe, Germany
C. Boffo, T. Gerhard, M. Turenne, W. Walter, Babcock Noell GmbH, Würzburg, Germany

Abstract

Superconducting insertion devices (IDs) can reach, for the same gap and period length a higher field strength compared to permanent magnet IDs. Their performance depends strongly on the magnetic field quality. While the magnetic measurements technology of permanent magnet based IDs made significant progress during the last years, for superconducting IDs similar major developments are necessary. As a part of our R&D program for superconducting insertion devices at the ANKA synchrotron radiation facility a measurement setup for conduction cooled superconducting coils with a maximum length of 2 m was built and commissioned. In the CASPER II (Characterization Setup for Phase Error Reduction) facility (see Fig. 1) the magnet coils can be trained and tested for maximum current and field quality, including the local field distribution as well as the first and second field integrals. In this paper we shortly describe the CASPER II setup and focus on the capability of this measurement device by presenting the results of a superconducting undulator mockup with a period length of 20mm.

INTRODUCTION

The performance of insertion devices (IDs) depends strongly on their magnetic field quality. It is of fundamental importance to characterize magnetic field properties of IDs accurately before installation in synchrotron light sources. While for permanent magnet IDs, commercially measuring systems exists, for the characterization of superconducting IDs they are not available. ANKA and Babcock Noell GmbH are pursuing an R&D program aiming to develop superconducting undulators (SCUs) for third and fourth generation light sources [1]. The SCUs developed and under development with BNG make use of NbTi superconducting wire and are conduction cooled. In order to characterize the magnetic field properties of these conduction cooled SCUs, the CASPER II facility has been developed at ANKA [2, 3].

The CASPER II facility is a horizontal test stand where up to 2 m long superconducting coils can be measured. The setup is cryogen free. The coils under test are put on an aluminium table in a high vacuum environment and surrounded by a shell-like structure of different temperature shields. Cooling is provided by four 2 stage cryocoolers from Sumitomo with a total cooling power of 5.5 W. An additional one stage cooler from Oerlikon is connected to the 80 K shield. In total eight 500 A current leads are installed to provide power to the main magnet and its correction coils.

For magnet training two switchable bipolar 1500 A power supplies from Bruker in conjunction with an in house designed quench detection system (built by the Institute for Data Processing and Electronics at the KIT) and a fast data acquisition system from National Instruments is available.

Figure 1: Picture of the CASPER II measurement system.

The local magnetic field perpendicular to the beam axis is measured by using 3 Hall probes, which are placed next to each other on a brass sledge. The Hall probes are placed at different horizontal positions in order to characterize a good field region of ± 10 mm. The sledge is guided by very precisely machined rails through the magnet and stepwise moved along the beam axis. To determine the position of the sledge a laser interferometer with a submircometer resolution is used. Further details can be found in Ref. [3].

For assessment of the vertical and horizontal first and second field integrals a piezo stage driven stretched wire setup is installed.

The full control and readout of the measurement system is programmed with LabView.

In this contribution we describe the CASPER II facility and its capabilities by presenting the results of the magnetic characterization of a 300 mm long prototype of the SCU20, a superconducting undulator with a period length of 20 mm under development within the collaboration between ANKA and BNG for use at the NANO beamline. An overview of the main features of the design is given in Ref. [4].

stefan.gerstl@kit.edu

Content from this work may be used under the terms of the CC BY 3.0 licence (© 2015). Any distribution of this work must maintain attribution to the author(s), title of the work, publisher, and DOI.

ISBN: 978-3-95450-168-7 doi:10.18429/JACoW-IPAC2015-WEPMA029

DESIGN OF A NORMAL CONDUCTING CAVITY FOR ARRIVAL TIME STABILIZATION AT FLASH*

M. Fakhari†, K. Floettmann, S. Pfeiffer, H. Schlarb, DESY, Hamburg, Germany
J. Rossbach, Uni HH, Hamburg, Germany

Abstract

It has been shown, that beam-based feedback loops stabilize the bunch arrival time in the femtoseconds range. However, further minimizing the bunch arrival time jitter requires a faster actuator that is a normal conducting cavity with higher bandwidth compared to narrow-band superconducting cavities. We present the design of a 4-cell normal conducting cavity that is going to be used in a fast beam-based feedback at free-electron laser FLASH at Hamburg. The input power will be injected to the cavity via a loop coupler from the side of the first cell. The operating frequency of the designed cavity is about 3 GHz with an adjustable bandwidth. The long range longitudinal wakefield calculation results are reported to investigate the cavity performance for multi-beam operation up to 3 MHz bunch repetition rate. The results declare that the influence of the long range wakefield on the arrival time jitter is less than 1 fs.

INTRODUCTION

The Free-Electron Laser FLASH at Hamburg provides short laser pulses to study the dynamics of molecular and chemical reaction on an atomic level. To generate the ultra short wavelength laser pulses, a high-quality electron beam is accelerated in superconducting cavities to an energy of 1.25 GeV and then sent through long magnetic undulators. The short wavelength laser light is used e.g. to study the temporal dynamics of matter typically carried out in a pump-probe arrangement, where atoms or molecules are excited by an external ultra-short pulse optical laser while their reactions are visualized using the FEL light. To achieve the required femtosecond resolution a precise regulation of bunch arrival time within a train of electron bunches is mandatory. For FEL users, it is therefore essential that the arrival time of the individual radiation pulses have a stability with a precision of a few femtoseconds only. Three superconducting accelerating modules, ACC1, ACC39 and ACC23, are being used to adjust the arrival time of the bunches [1]. However, since these modules are narrow bandwidth caused by their high quality factor, it takes a non-negligible time to stabilize the arrival time. Furthermore the final arrival time has a jitter of ± 150 fs peak to peak. Further minimizing the bunch arrival time jitter requires faster actuator, e.g. a normal conducting cavity with higher bandwidth compared to the narrow-band superconducting cavities. A normal conducting cavity is thus designed for this purpose. This cavity is going to be installed at FLASH main linac as shown in Fig. 1. Concerning the space limitation in FLASH a side coupling to this cavity is required. Since the input power of the cavity is less than 1kW it seems to be most efficient if the input power could be coupled to the cavity via a loop antenna instead of a waveguide coupler. In addition to space limits, it is more convenient to adjust the coupling constant by engaging the loop couplers. Besides, since the power supply is a solid sate amplifier with a coaxial cable as the output it would be easier to connect its output directly to a feedthrough instead of using a coaxial to waveguide converter. In this paper the designing process and the simulation results for the designed cavity are presented. The long range wakefield in the designed cavity has also been investigated to make sure that the desired arrival time resolution is achievable.

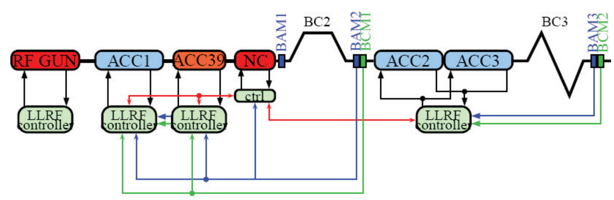

Figure 1: Place of installation of the NC cavity at FLASH

DESIGNING PROCESS

In order to design the fast feedback cavity, the arrival time deviation $\Delta t_A \approx \pm 150$ fs (peak-peak) needs to be corrected. This requires an energy correction of:

$$\Delta E = \frac{\Delta t_A \cdot c}{-R_{56}} \cdot E \approx \pm 37.5 \text{ keV} \tag{1}$$

where c is the speed of the light in free space, R_{56} is the bunch compressor parameter which is -0.18 m at FLASH-BC2, and the electron energy E is about 150 MeV. To achieve the required energy correction an accelerating voltage of $V_{acc} = \Delta E/e \approx 37.5$ kV is needed. Furthermore, a half bandwidth of 400 - 500 kHz is expected in order to make the cavity fast enough. The designed cavity is formed from four coupled pillbox cavities and has four fundamental TM_{010} normal modes which are named as 0-Mode, $\frac{\pi}{3}$-mode, $\frac{2\pi}{3}$-mode, and π-mode. These names are based on the phase shifts between adjacent cells. The operating mode is the π-mode with the frequency of 2998 MHz. After designing the cells of the cavity the most important part is to design its input coupler. By changing the coupling constant one can change the external quality factor and subsequently the bandwidth of the cavity. However, by changing the coupling constant the accelerating voltage also varies. For a cavity

* Work supported by the European Commission under the EuCARD-2 FP7 Research Infrastructures grant agreement no. 312453
† moein.fakhari@desy.de

Content from this work may be used under the terms of the CC BY 3.0 licence (© 2015). Any distribution of this work must maintain attribution to the author(s), title of the work, publisher, and DOI.

ISBN: 978-3-95450-168-7 doi:10.18429/JACoW-IPAC2015-WEPMA030

DESIGN AND CHARACTERIZATION OF PERMANENT MAGNETIC SOLENOIDS FOR REGAE

M. Hachmann, K. Floettmann, F. Mayet, DESY, Hamburg, Germany
T. Gehrke, DKFZ, Heidelberg, Germany

Abstract

REGAE is a small electron linear accelerator at DESY. In order to focus short and low charged electron bunches down to a few μm permanent magnetic solenoids were designed, assembled and field measurements were done.
Due to a shortage of space close to the operation area an in-vacuum solution has been chosen. Furthermore a two-ring design made of wedges has been preferred in terms of beam dynamic issues. To keep the field quality of a piecewise built magnet still high a sorting algorithm for the wedge arrangement has been developed and used for the construction of the magnets. The magnetic field of these solenoids has been measured with high precision and has been compared to the simulated magnetic field.

INTRODUCTION

The Relativistic Electron Gun for Atomic Exploration (REGAE) is a small 5 MeV linear accelerator at DESY in Hamburg, which produces short, low emittance electron bunches. It originally was meant for temporal resolving electron diffraction experiments [1]. But two further experiments are currently planned at REGAE. First, an external injection experiment for Laser Wakefield Acceleration (LWA) [2] will be performed in the framework of the LAOLA collaboration (LAboratory fOr Laser- and beam-driven plasma Acceleration). This experiment will provide a method for the reconstruction of the electric field distribution within a linear plasma wakefield. Second one is an extension of the original experiment. A time resolving high energy Transmission Electron Microscope (TEM) will be set up.
Both experiments require strong focusing magnets inside the new target chamber at REGAE. Permanent magnetic solenoids (PMSs) can provide the needed focusing strength due to their enormous surface current density, while having compact dimensions at the same time. Since short and strong solenoids, as required for REGAE, exhibit a distinct non-linearity, the induced emittance growth is relatively large and has to be minimized as far as possible. Furthermore, the focusing strength is not adjustable and 3D in-vacuum movers are required for positioning the magnets. Due to the chosen movers a weight limitation for the magnets reveals as an additional requirement. Overcoming these difficulties PMSs are an interesting alternative when a low energy beam has to be strongly focused.

DESIGN

A strong focusing is needed to generate a small transverse beam size for the external injection experiment and for a large magnification in the transmission electron microscope.

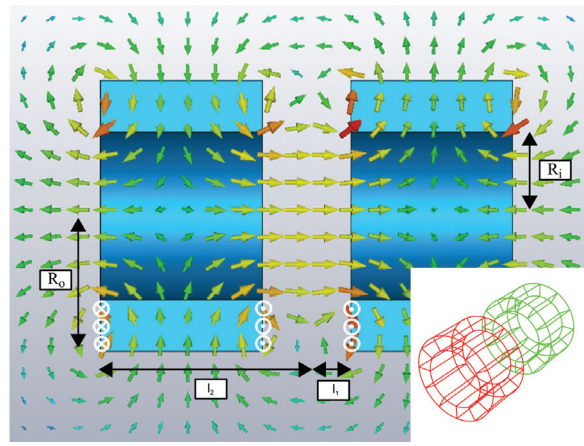

Figure 1: CST simulation of two radially magnetized rings (blue) and the conceptional wedge-based design.

This is achieved by the presented PMS design [3]. A second demand is a small emittance growth induced by the PMS. The investigations of different designs have shown that the induced emittance growth for two radially magnetized rings is considerably smaller than for an axially magnetized ring, if a weight limitation has to be applied. In the particular case at REGAE, a reduction of the emittance growth by 65% is feasible. Mimicking the magnetic field of the single axially magnetized ring with two radially magnetized rings allows for a larger influence on the field shape since a third free parameter, the distance $d = 2\,l_1$ between both rings, is introduced. The PMS dimensions (in mm) depicted in Fig. 1 are as follows $R_o = 25.4$, $R_i = 17$, $l_1 = 7.8$ and $l_2 = 44.8$ while the weight is just 0.628 kg. The focal length for a 5 MeV electron beam is ~ 0.2 m. For technical reasons radially magnetized rings need to be assembled from wedges. The imperfections of the wedges call for a sorting algorithm in order to preserve the field quality.

FIELD DESCRIPTION AND SORTING ALGORITHM

Field Model

Due to the necessity of a model which describes the resulting field of 24 wedges we developed a simple model: each wedge is described by current loops covering the surface (Fig. 2 **b**)), where each loop can be divided into four straight parts. The magnetic field can be calculated by means of *Biot-Savart's law* for a straight wire. The magnetization **M** of a wedge is defined by the direction and its magnitude which were measured by the manufacturer and can be translated into a tilt of the current loops or a variation of the current,

Content from this work may be used under the terms of the CC BY 3.0 licence (© 2015). Any distribution of this work must maintain attribution to the author(s), title of the work, publisher, and DOI.

ISBN: 978-3-95450-168-7 doi:10.18429/JACoW-IPAC2015-WEPMA031

Content from this work may be used under the terms of the CC BY 3.0 licence (© 2015). Any distribution of this work must maintain attribution to the author(s), title of the work, publisher, and DOI.

TIMING JITTER STUDIES FOR SUB-FS ELECTRON BUNCH GENERATION AT SINBAD

J. Zhu[#1,2], R. Assmann[1], U. Dorda[1], J. Grebenyuk[1], B. Marchetti[1]

[1] Deutsches Elektronen-Synchrotron, DESY, Hamburg, Germany
[2] Universität Hamburg, Hamburg, Germany

Abstract

Generation of ultra-short electron bunches with a few femtoseconds arrival-time jitter is the major challenge in plasma acceleration with external injection. Meanwhile, peak current stability is also one of the crucial factors for user experiments when the electron bunch is used for free-electron laser (FEL) generation. ARES (Accelerator Research Experiment at SINBAD) will consist of a compact S-band normal-conducting photo-injector providing ultra-short electron bunches of 100 MeV. We present bunch arrival-time jitter studies for two different compression schemes, velocity bunching and magnetic compression with a slit, at ARES with start-to-end simulations. Contributions from various jitter sources are quantified.

INTRODUCTION

External injection of electron bunches into laser-driven wakefield acceleration (LWFA) allows precise manipulation of the phasespace of the electron bunches and thereby provides possibilities to optimise the following acceleration and transport inside the plasma. However, the requirement on the synchronization of the electron bunch to the drive laser is rather stringent [1]. SINBAD (Short Innovative Bunches and Accelerators at DESY) is a proposed dedicated accelerator research and development facility [2]. One of the baseline experiments at SINBAD is LWFA with electron bunches generated by ARES (Accelerator Research Experiment at Sinbad) [3], which will allow the production of ultra-short bunches by velocity bunching (VB) [4] or by magnetic bunch compression (BC) with a slit [5].

In LWFA experiments, considering the general case that the cathode laser and the drive laser are different, the total timing jitter between the electron bunch and the drive laser is given by

$$\sigma_{t_{total}} \approx \sqrt{\sigma_{t_b}^2 + \sigma_{t_o}^2 + \sigma_{t_a}^2}\ , \quad (1)$$

where σ_{t_b} is the bunch arrival-time jitter (ATJ) relative to the reference, σ_{t_o} is the contribution from synchronization of the drive-laser oscillator and σ_{t_a} is the jitter of the drive-laser amplifier. The aim of this study is to quantify the term σ_{t_b} in equation (1) with different compression schemes at ARES and to identify the major jitter sources.

ANALYTICAL MODEL OF ATJ WITH MAGNETIC COMPRESSION

Considering a general case of a linac consisting of a gun and a couple of cavities powered by a single klystron, the ATJ of the electron bunch downstream of the chicane is well-known as [6]:

$$\sigma_{t_b} \approx \sqrt{\frac{R_{56}^2}{c^2}\left(\sigma_{\delta_V}^2 + \frac{h^2}{k_{rf}^2}\sigma_\phi^2 + \sigma_{\delta_B}^2\right) + \frac{\sigma_{t_0}^2}{C^2}}\ , \quad (2)$$

where R_{56} is the longitudinal dispersion of the chicane, c is the velocity of light, h is the chirp of the bunch, k_{rf} is the rf wave number, $C=1/(1+hR_{56})$ is the compression factor and σ_{δ_V}, σ_ϕ, σ_{δ_B} and σ_{t_0} are the cavity voltage jitter, the cavity phase jitter, the magnetic field jitter of the chicane and the ATJ at the gun exit respectively. However, in order to directly compress the pulse duration of the electron bunch generated at a photo-injector to sub-fs with only one compression stage, a sub-mm wide slit will be placed in the middle of the chicane at ARES. Since the slit only allows electrons with certain energies to go through, the energy jitter upstream of the chicane will almost *not* be converted into the ATJ downstream of the chicane. In this case, the bunch arrival time downstream of the chicane is given by

$$t_b \approx t_0 + t_c + \frac{s}{c}, \quad (3)$$

where t_0 is the arrival time of the bunch at the gun exit, t_c is the timing offset of the "collimated" bunch relative to the centroid of the whole bunch at the entrance of the chicane and s is the path length of the "collimated" bunch in the chicane. In this case, one can derive that the ATJ downstream of the chicane is given by

$$\sigma_{t_b} \approx \sqrt{\left(\frac{1}{hc}\right)^2 \sigma_{\delta_V}^2 + \left(\frac{1}{ck_{rf}}\right)^2 \sigma_\phi^2 + \left(\frac{R_{56}}{c}\right)^2 \sigma_{\delta_B}^2}\ . \quad (4)$$

It is obvious that equation (2) and (4) are the same in the case of full compression ($1+hR_{56}\approx 0$). Note that the ATJ at the gun exit will anyhow be fully compressed regardless of the compression factor in the case with a slit. In the meanwhile, however, the cavity phase jitter will be totally converted into the ATJ downstream of the chicane.

At ARES, two identical S-band travelling-wave structures (TWS) will be powered by their individual klystrons. In this case, one can prove that the minimum ATJ will be achieved when both TWSs are operated with the same voltage and phase, and is given by

$$\sigma_{t_b,\min} \approx \sqrt{\left(\frac{R_{56}}{c}\right)^2 \left(\sigma_{\delta_B}^2 + \frac{1}{2}\sigma_{\delta_V}^2\right) + \frac{1}{2}\left(\frac{1}{ck_{rf}}\right)^2 \sigma_\phi^2}\ . \quad (5)$$

ISBN: 978-3-95450-168-7 doi:10.18429/JACoW-IPAC2015-WEPMA033

UTILIZING GAS FILLED CAVITIES FOR THE GENERATION OF AN INTENSE MUON SOURCE*

Diktys Stratakis#, Brookhaven National Laboratory, Upton NY, USA
David V. Neuffer, Fermi National Accelerator Laboratory, Batavia IL, USA

Abstract

A key requirement for designing intense muon sources is operating rf cavities in multi-tesla magnetic fields. Recently, a proof-of-principle experiment demonstrated that an rf cavity filed with high pressure hydrogen gas could meet this goal. In this study, rigorous simulation is used to design and evaluate the performance of an intense muon source with gas filled cavities. We present a new lattice design and compare our results with conventional schemes. We detail the influence of gas pressure on the muon production rate.

INTRODUCTION

The relative immunity of muons to synchrotron radiation due to their large rest mass suggests that they may be used in place of electrons for fundamental high-energy physics research [1] as well as for various industrial and medical applications. However, the short lifetime of muons (2.2 μs in the rest frame) makes a muon beam very challenging technologically. Muons can be produced indirectly through pion decay by interaction of a multi-GeV, high-power (1-4 MW) proton beam with a stationary target. The muon yield is fractionally small, with large angle and energy dispersion. In this paper the production of pions, their decay into muons and the survival of muons during transport is studied.

MUON CAPTURE CHALLENGES

A key requirement in producing an intense muon source is that the phase space-volume of the produced beams must match the acceptance criteria of the downstream accelerators. This demands a front-end channel (the part of the facility between the target and the first linear accelerator) for manipulating the beam in transverse and longitudinal phase-space [2]. For the latter, a series of rf cavities form the resulting muon beam into strings of bunches with different energies, and then align them into nearly equal central energies by phase-rotating the beam. To reduce the volume of transverse phase-space, the bunches pass through a cooling channel, which reduces the beam's emittance using ionization cooling. The cooling channel consists of absorbers, which lower the transverse and longitudinal momentum of beam particles, and rf cavities, which restore the particle's longitudinal momentum, inside a magnetic channel. A common feature of the front-end lattices is that it requires the rf cavities to operate within strong magnetic fields that focus the muons.

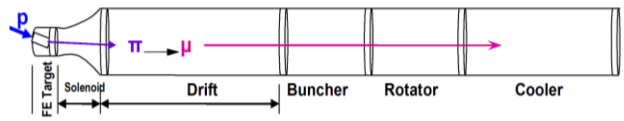

Figure 1: Schematic of the muon capture channel.

There are challenges in operating rf cavities in magnetic fields [3]. For instance, typical rf gradients in the cooling channel are 20-25 MV/m, while the magnetic field is near 2 T. Experimental and numerical studies indicated that this configuration enhances the possibility of rf breakdown. The use of rf cavities filled with high pressure hydrogen gas was proposed to overcome this difficulty. The gas not only provides the necessary momentum loss as a cooling material but also increases the breakdown gradient of the cavity. Experiments [4] have demonstrated that a breakdown gradient of 65.5 MV/m could be achieved in a 3 T magnetic field with 70 atm hydrogen gas. Here we investigate a muon capture channel which utilizes gas filled cavities and compare it's performance against the conventional vacuum channel. We examine the performance for two different pressures: One at 34 atm and one at 100 atm, both at room temperature.

SYSTEM OVERVIEW

As shown in Fig. 1, a 1 MW proton driver produces bunches with 6.75 GeV in energy. The beam is directed onto a carbon (C) target enclosed in a 20 T solenoid. The pions created are captured as they transverse a ~5 m long, tapered superconducting solenoidal magnet system, where the field profile drops adiabatically from 20 T to 2.0 T. This is followed by a drift section with a constant 2.0 T field, where the pions decay into muons, and the beam develops a time-energy correlation with a high-energy "head" and a low-energy "tail". Then the beam is bunched into a string of bunches in a "buncher" followed by "phi-E" rotator section that aligns the muon bunches to nearly equal energies (matched at 325 MHz spacing) and then cooled in 325 MHz cooling channel with LiH absorbers.

In the buncher the frequency declines along its length from cavity to cavity, starting from 490 MHz at the entrance and dropping to 365 MHz at the exit. The rf gradient gradually increases from 0 to 15 MV/m using the relation $15z/L_B$, where L_B is the buncher length. In the cooling channel the frequency further decreases from 364 to 326 MHz but the gradient remains fixed at 20 MV/m.

*This manuscript has been authored by employees of Brookhaven Science Associates, LLC under Contract No. DE-SC0012704 with the U.S. Department of Energy. In addition, it was operated by Fermi Research Alliance, LLC under Contract No. DEAC02- 07CH11359 with the United States Department of Energy.
#diktys@bnl.gov

Content from this work may be used under the terms of the CC BY 3.0 licence (© 2015). Any distribution of this work must maintain attribution to the author(s), title of the work, publisher, and DOI.

ISBN: 978-3-95450-168-7 doi:10.18429/JACoW-IPAC2015-WEPMA034

Content from this work may be used under the terms of the CC BY 3.0 licence (© 2015). Any distribution of this work must maintain attribution to the author(s), title of the work, publisher, and DOI.

BAKEOUT CONCEPT FOR THE HESR AT FAIR

Heinz Jagdfeld, Norbert Bongers, Patrick Chaumet, Frank Martin Esser,
Frank Jordan, Franz Klehr, Georg Langenberg, Ulrich Pabst, Larisa Semke
Forschungszentrum Juelich, Germany

Abstract

Forschungszentrum Juelich has taken the leadership of a consortium being responsible for the design of the High-Energy Storage Ring (HESR) going to be part of the FAIR project on the GSI campus in Darmstadt in Germany. The HESR is designed for antiprotons but can be used for heavy ion experiments as well. Therefore the vacuum is expected to be 10^-10 mbar or better. To achieve this also in the curved sections where 44 bent dipole magnets with a length of around 4.5 m will be installed, NEG coated dipole chambers will be used to reach the needed pumping speed and capacity. For activation of the NEG-material a bakeout system is required. The bakeout concept including the layout of the control system and the systematization of the heater packages for all components of the vacuum system are presented. Also the special design of the heater jackets inside the dipole will be shown where the geometrical parameters are very critical and space is very limited. The results of the simulation of temperature distribution in the dipole iron are compared to temperature measurements carried out at a testbench with different layouts of the heater jackets. The final design of the dipole heater jackets will be illustrated.

DESIGN DATA OF THE VACUUM SYSTEM OF THE HESR

The High-Energy Storage Ring for Antiprotons and Heavy Ions (HESR) will have a circumference of approx. 575 m and will therefore be the second largest accelerator ring in the FAIR facility. The low-loss, undisturbed acceleration, deceleration, and storage of the antiprotons and heavy ions in the synchrotron is only possible under UHV conditions at an average residual gas pressure below 1×10^{-10} mbar, or preferably 1×10^{-12} mbar for heavy ions, and at a very low magnetic permeability of the vacuum components.

The required operating pressure can only be reached if all vacuum components are manufactured in accordance with the dedicated specifications for the UHV system. As a result, special requirements apply to the materials used and their processing.

In detail the HESR will consist of 22 vacuum sections (incl. 2 for E-Cooler, 1 for PANDA), all separated with all-metal slide valves (max. section length 45 m). In the two arcs a bakeout system and a pumping system including NEG coated chambers inside the dipoles will be installed.

For roughing at least 6 mobile pumping stations with oil-free fore pumps are foreseen.

Every section contains at least two pirani and two penning test points and one mass spectroscopy. The design data of the HESR are listed below in Table 1.

Table 1: Design Data of the HESR@FAIR

Feature	Value /Description
circumference	575 m
radius arc	r = 49,5 m
length straights	l = 132 m
nb. dipoles	44 (l = 4.2 m), 50 Tm
nb. quadrupoles	84 (l = 0.6 m)
nb. sextupoles	60 (l = 0.3 m)
experiments	SPARC, PANDA, …
cooling systems	electron cooling 2-4 resp. 8 MeV stochastic cooling 2-4 resp. 6 GHz
dipole chambers	bended with radius of 29.43 m, 8.18°, length 4.40 m, NEG coated
spec. vacuum chambers	2 for inj. kicker, 7 for stoch. cooling
av. pressure range	1×10^{-9} - 1×10^{-12} mbar at RT
beam pipe	DN93x2 mm, AISI 316LN with low hydrogen content and low permeability, electropolished
nb. pumping bodies	approx. 180, four ports each, with rf-mesh inside
nb. pumping station roughing	approx. 6 – 8, mobile design
nb. vacuum pumps	approx. 540 (IZ, TSP and NEG)
nb. slide valves	22 (24), all metal with rf-mesh
nb. high speed shutter	4

BAKEOUT CONCEPT OF THE HESR

In the curved sections 44 bent dipole magnets with a length of around 4.4 m will be installed. NEG coated dipole chambers will be used to reach the needed pumping speed and capacity (see Fig. 1).

For activation of the NEG-material a bakeout system must be installed. The bakeout concept including the layout of the control system and the systematization of the heater packages for all components of the vacuum system is shown in Fig. 2 and 3. The heater jackets for all components in the curved sections - the straight sections will not be NEG-coated and do not need a bakeout system – were combined to repetitive elements. The bakeout concept with the sequence and duration of the heating procedure as well as the switch on and off points of the vacuum pumps are shown below. The bakeout process starts with heating up the non-NEG-coated components to

ISBN: 978-3-95450-168-7 doi:10.18429/JACoW-IPAC2015-WEPMA035

LOW- AND HIGH-BETA SRF ELLIPTICAL CAVITY STIFFENING

E. Zaplatin, Forschungszentrum Juelich, Germany,
A. Kanareykin, Euclid TechLabs, Ohio, U.S.A,
V. Yakovlev, FNAL, Geneva, IL, U.S.A

Abstract

Elliptical SRF cavities are the main accelerating structures in many accelerators worldwide. Different types of external loads on the resonator walls predetermine the main working conditions of the SC cavities. The most important of them are very high electromagnetic fields that result in strong Lorentz forces and the pressure on cavity walls from the helium tank that also deforms the cavity shape. Also mechanical eigen resonances of cavities are the main source of the microphonics. To withstand any kind of external loads on the resonator walls different schemes of the cavity stiffening were applied.

In the paper we report the basic investigations of the cavity stiffening using FNAL 650 MHz beta=0.92 and 0.61 as an example. The single-cell investigation results were used as the reference to develop the ultimate scheme of the helium vessel structure to ensure the best resonator stability.

PRESSURE RESPONSE OF MID-CELL

The first step of a superconducting elliptical cavity RF design is made as a trade-off in the optimization of the cell shape between the region of high electric field and the region of high magnetic field. In practice, the cavity performance may be limited not only by the RF characteristics, but also by detuning due to the Lorentz force, bath pressure fluctuations, or microphonics. Lorentz force detuning (LFD) is of concern primarily for pulsed accelerators such as the proposed Proton Improvement Plan-II (PIP-II) at Fermilab [1]. Hence, the strategy of cavity design should include the integrated simulations of RF and mechanical properties.

For the high energy sections of SC accelerators the well-studied multiple-cell elliptic cavities are optimal. An initial investigation should be provided on middle-cell geometries. Usually the simulations are made with the cell-to-cell junction constrained by symmetry. The goal for these calculations was to understand the behaviour and trends under different stiffening options.

The response of the cavity to a pressure differential is calculated with vacuum inside the resonator and ambient pressure outside. The pressure differential changes the cavity shape and shifts the RF frequency of the accelerating mode. Inward deformation near the iris (the region of high electric field) increases the capacitance and hence reduces the frequency. Inward deformation near the equator (high magnetic field region) reduces the inductance and hence increases the frequency. Thus the effects tend to cancel one another. Although the equator region is generally more rigid than the iris region, the volume change near the equator is larger due to the larger radius.

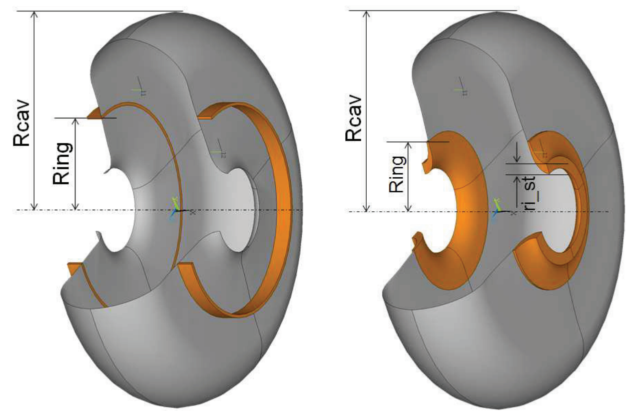

Figure 1: Elliptical mid-cell geometry (β= 0.61) with ring and iris stiffening options.

A stiffening ring position and a shape of the iris thickness can be used to change the frequency shift (Fig. 1) [2]. On the other hand the ring position also affects the Lorentz force detuning [3]. But differing from the pressure differential case the Lorentz forces at the dome region are directed outward the cavity volume. That's why the choice of the ring position is the trade-off between these two effects since their optimizations result in the different ring positions. For the pulsed accelerators like TeSLA the ring was placed to minimize primary the Lorentz force detuning (Fig. 2).

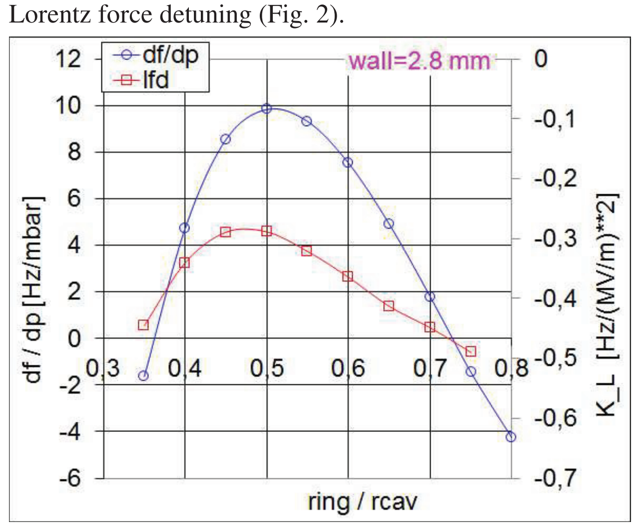

Figure 2: TeSLA mid-cell mechanical properties.

Content from this work may be used under the terms of the CC BY 3.0 licence (© 2015). Any distribution of this work must maintain attribution to the author(s), title of the work, publisher, and DOI.

ISBN: 978-3-95450-168-7 doi:10.18429/JACoW-IPAC2015-WEPMA036

Content from this work may be used under the terms of the CC BY 3.0 licence (© 2015). Any distribution of this work must maintain attribution to the author(s), title of the work, publisher, and DOI.

DOUBLE-CELL NOTCH FILTER FOR SRF GUN INVESTIGATIONS

E. Zaplatin, Forschungszentrum Juelich, Germany
A. Kanareykin, Euclid TechLabs, Ohio, USA
J. Knobloch, A. Neumann, Helmholtz-Zentrum Berlin, Germany
V. Yakovlev, FNAL, Geneva, IL, USA

Abstract

Some projects of SRF guns apply the design where the cathode can be easily and quickly removed. One of the disadvantages of this design is the RF power leakage from the accelerating gun cavity cells to the cathode housing that result in the excessive cathode heating. To minimize the RF power leak different kinds of choke filters are used to protect the cathode structure. These choke filters represent resonant circuits with zero input impedance and installed at the entrance of the cathode structure that shunt the cathode housing.

Still, since the choke filter frequency shift under working conditions is bigger than its bandwidth a filter tuning during assembly only in the warm stage seems insufficient and requires also fine-tuning during operation.

To eliminate the problems of the choke filter fine-tuning and hence ensure its stability during operation, a combination of the resonance choke elements can be implemented. In the paper we demonstrate advantages of the double-cell notch filter using B*ERL*inPro SRF gun cavity as an example with its simple design modifications.

CHOKE CELL GAP SIZE

First development of the SRF gun with choke-cell filter was done at FZDR [1]. The choke cell represents a cavity cell of a special shape surrounding the cathode and preventing the RF power from leaking out of the cavity. In this manner it works as a bandpass filter. The operation of the choke-cell is the same like quarter wave choke with similar S_{21}-parameter distribution [2]. An advantage of choke-cell is better possibilities for the cleaning and less probable and less stable multipactor discharge in the choke-cell. For the choke-cell structure the tuning procedure is simpler to compare with coaxial chokes and can be realized with well-developed SRF cell tuners. In HZDR and HZB [3] projects the SRF gun cavity frequency tuning is designed for the choke cell, half-cell and TESLA cells (Fig. 1). Since the half-cell and TESLA cells differ in their mechanical properties it was decided to use two separate tuning systems.

Still, caused by the narrow cathode channel and a small choke-cell gap chosen in HZDR and HZB projects, the standard buffered chemical polishing (BFP) and the high pressure rinsing (HPR) are not effective for the choke cell. This resulted in the lower quality of the surface treatment, which in its turn results in the higher probability of the electron resonance discharge (multipactor – MP), a high residual resistance and the residual impurities penetration into accelerating cells.

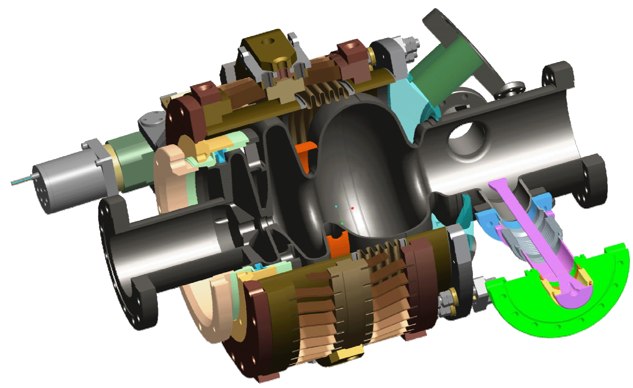

Figure 1: HZB 1.4.cell SRF gun.

To overcome the cleaning issue, the calculations have been provided to investigate the structure parameters on the choke-cell gap size. The simulation model that included half-cell, choke-cell and cathode coaxial transmission line was built using HZB SRF gun geometry (Fig. 2). The choke-cell gap size was varied from 6 mm (HZB project value) to 30 mm (full choke cell length) during simulations.

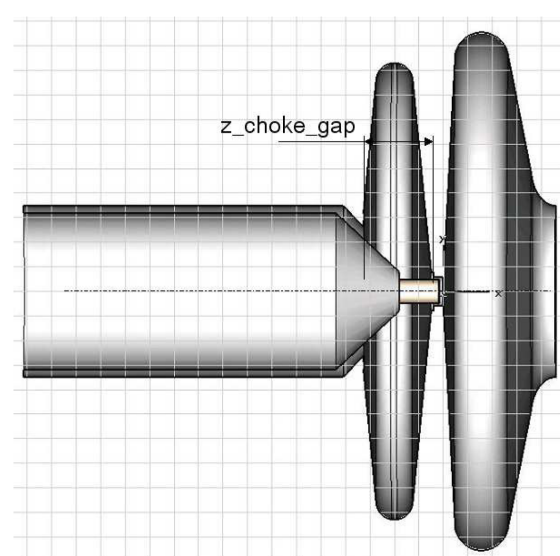

Figure 2: Choke-cell gap investigation simulation model.

ISBN: 978-3-95450-168-7 doi:10.18429/JACoW-IPAC2015-WEPMA037

MANUFACTURING AND FIRST TEST RESULTS OF EUCLID SRF CONICAL HALF-WAVE RESONATOR*

E. Zaplatin, Forschungszentrum Juelich, Germany
C. H. Boulware, T. L. Grimm, A. R. Rogacki, Niowave, Inc, Lansing, MI, USA
A. Kanareykin, Euclid TechLabs, Ohio, USA
V. Yakovlev, FNAL, Geneva, IL, USA

Abstract

Euclid TechLabs has developed a superconducting conical Half-Wave Resonator (162.5 MHz β=v/c=0.11) for the high-intensity proton accelerator complex proposed at Fermi National Accelerator Laboratory. The main objective of this project is to provide a resonator design with high mechanical stability based on an idea of the balancing cavity frequency shifts caused by external loads. A unique cavity side-tuning option has been successfully implemented. Niowave, Inc. proposed a complete cavity production procedure including preparation of technical drawings, manufacturing, processing steps and resonator high-gradient tests. During manufacturing a series of cavity and helium vessel modifications to simplify their fabrication were proposed. Following standard buffered chemical polish surface treatment and high-pressure rinse, a vertical test was carried out at Niowave's facilities.

Here we present the status of the project and the first high-gradient results.

INTRODUCTION

The conical Half-Wave Resonator (cHWR) design was reported earlier elsewhere [1-4]. The cavity RF parameters are shown in Table 1. A photo of the niobium cavity prototype being leak checked is shown in Fig. 1.

The main objective of the project was the conceptual design of the cHWR with its liquid helium vessel, minimizing the sensitivity of the resonant frequency to fluctuations in helium pressure.

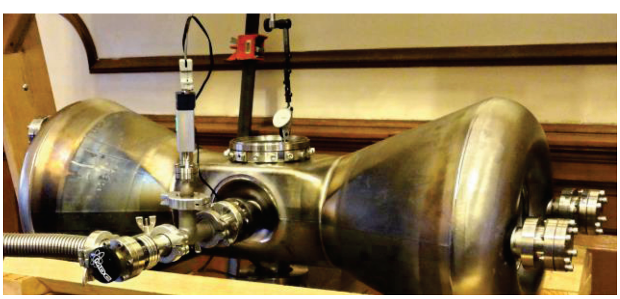

Figure 1: Modified cHWR with leak check setup.

Table 1: Conical HWR Parameters

frequency	MHz	162.5
β = v/c		0.11
R_aperture	mm	18
βλ	mm	202.94
R_cavity **)	mm	90
G	Ohm	36.36
R/Q	Ohm	119
E_{pk} / E_{acc} *)		5.1
B_{pk} / E_{acc} *)	mT/MV/m	7.1
B_{pk} / E_{pk}	mT/MV/m	1.39
tune	kHz/mm	-87
*) $L_{eff} = N_{gaps} * \beta\lambda/2$, where N_{gaps}=2 – number of gaps		
**) Cavity radius in center		

To use the outer conductor walls for cavity tuning deformations effectively, the central part of cHWR is made asymmetric with a planar surface on one side. This planar surface is used for tuning by deformation (Fig. 2).

The central resonator section optimization was made without compromising the cavity performance. The tuner ring is installed around the bellow (Fig. 2) connecting cavity and helium vessel tuning plates and provides compensation of the cavity tuning wall external pressure deformation (Fig. 3).

The side tuning procedure results in tune sensitivity up to 80 kHz/mm with acceptable stresses 350 MPa/mm and tuning pressure less than 1 kN/mm. There is nearly no dependence on the resonator frequency slow tuning.

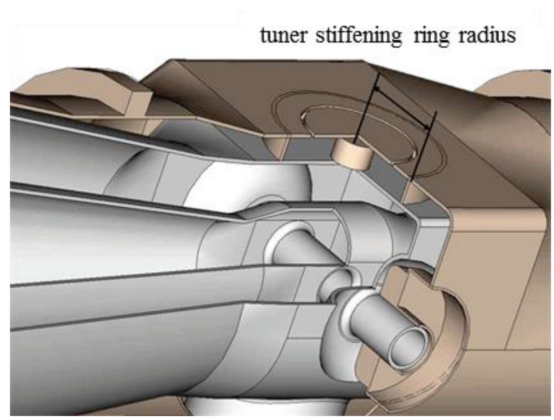

Figure 2: cHWR simulation model central part.

*Work supported by the DOE SBIR Program, contract # DE-SC0006302

Content from this work may be used under the terms of the CC BY 3.0 licence (© 2015). Any distribution of this work must maintain attribution to the author(s), title of the work, publisher, and DOI.

ISBN: 978-3-95450-168-7 doi:10.18429/JACoW-IPAC2015-WEPMA038

COMPACT IN-VACUUM QUADRUPOLES FOR A BEAM TRANSPORT SYSTEM AT A LASER WAKEFIELD ACCELERATOR*

A. Bernhard†, V. Afonso Rodriguez, J. Senger, W. Werner, C. Widmann, A.-S. Müller,
KIT, Karlsruhe, Germany

Abstract

For the transport and matching of electrons generated by a Laser Wakefield Accelerator (LWFA) a beam transport system with strong focusing magnets and a compact design is required. For the realization of such a beam transport system at the LWFA in Jena, Germany, two small series of inexpensive, modular quadrupoles were designed and built. The quadrupoles are iron-dominated electromagnets in order to keep the transport system adaptable to different energies and target parameters. To achieve the required field strength it was necessary to choose a small magnetic aperture. Therefore the magnets were designed for in-vacuum use with water-cooled coils. In this contribution the design, the realization and first field measurements of these quadrupoles are presented.

INTRODUCTION

Capturing, transporting and matching electron beams generated by Laser Wakefield Accelerators (LWFA) is a major challenge due to their significant energy spread, intrinsic divergence and pointing variance. To approach this problem experimentally one would certainly like to proceed step by step, each step involving a limited number of focusing and correcting magnets adapted to the respective experimental strategy. Such an approach, different from the situation at classical accelerators, calls for inexpensive, easy to build and easy to modify magnets providing maximal experimental flexibility.

Since the magnets, as explicated in more detail in the following section, have to be strong, compact, and adjustable to a not exactly predictable beam axis, the conventional concept of feeding a vacuum-beam pipe through the magnet gaps is discarded. Instead, the magnets should be capable of being operated in vacuum (10^{-5} mbar). At the same time it should be possible to tune the magnets on-line or to switch them off completely. Accordingly, in-vacuum electromagnets are the technology of choice.

Following these lines we designed, built and tested a set of electromagnetic in-vacuum quadrupoles and employed them in our first experimental step realizing a linear beam optics at the LWFA in Jena [1]. The basic design strategies applied can easily be transferred to higher-order multipole magnets for further experimental steps.

DESIGN REQUIREMENTS

Two small series of in-vacuum quadrupoles were realized. The magnetic and geometric design parameters for the two series are summarized in Table 1. The values for series *QG* result from an optimization with respect to the following geometric requirements and restrictions: On the one hand the large initial divergence of the beam in both transverse planes requires that the first magnets (either a doublet or a triplet) are placed as close as possible to the source and to each other. As a first approximation the focal length $f = (kl)^{-1}$ should be of the same order as the distance from the source. Here, $k = \frac{e}{p} g$ is the focusing strength, l the yoke length, g the field gradient and $\frac{e}{p}$ the beam stiffness, which is for our design beam energy of $E_0 = 120\,\mathrm{MeV}$ $\frac{e}{p} = 2.4\,\mathrm{T}^{-1}\,\mathrm{m}^{-1}$. At the same time the source-to-magnet center distance and the center-to-center distance between neighbouring magnets sets an upper limit to the full magnet length (including coils). To accommodate, on the other hand, a spectrally dispersed beam with a total dispersive beam splitting of ~ 4 mm, we chose an inscribed gap radius of 11 mm. Given this gap radius, the first estimations yielded 125 mm for the focal and 140 mm for the overall magnet length and 60 mm to 100 mm magnetic length as reasonable values. We note that for these parameters the thin lens approximation our estimation started off, is only valid in a heuristic sense.

The same basic consideration also applies to the series *QK*, however, these magnets are foreseen to be replaced by combined function quadrupole-sextupole magnets in a later experimental step. Consequently, following our design strategy of inexpensive and easy to modify magnets, the coils for series *QK* have already been designed and built for these magnets and therefore feature a sextupole geometry and a lower number of turns per coil.

Correspondingly the magnet coils for both series are laid out for being operated with standard laboratory power supplies and wound with a standard copper wire without internal cooling channel.

Table 1: Design Parameters for Two Small Series of Quadrupoles

Series	QG	QK
yoke diameter [mm]	210	203
magn. length [mm]	80	80
gap radius [mm]	11	11
turns/coil	465	412
max. operation current [A]	6	6
max. design field gradient [T/m]	39	30

* This work is partially funded by the German Federal Ministry for Education and Research under contract no. 05K10VK2 and 05K10SJ2.
† axel.bernhard@kit.edu

Content from this work may be used under the terms of the CC BY 3.0 licence (© 2015). Any distribution of this work must maintain attribution to the author(s), title of the work, publisher, and DOI.

ISBN: 978-3-95450-168-7 doi:10.18429/JACoW-IPAC2015-WEPMA040

MAGNET STUDIES FOR THE ACCELERATOR FLUTE AT KIT

S. Hillenbrand, A. Bernhard, M. J. Nasse, A.-S. Mueller, R. Rossmanith, R. Ruprecht, M. Sauter, S. Schott, M. Schuh, S. Schulz, M. Weber, P. Wesolowski, C. Widmann
KIT, Karlsruhe, Germany

Abstract

At KIT (Karlsruhe Institute of Technology) we are currently constructing the compact linear accelerator FLUTE (Ferninfrarot Linac Und Test Experiment). This 41 MeV machine is aimed at accelerator physics and synchrotron radiation research, using ultra-short electron bunches. The electrons are generated at a photo-cathode using picosecond long UV laser pulses. A magnetic chicane is used to compress the bunches longitudinally to a few femtoseconds [1,2].

This contribution describes both the magnet design, in particular the optimization of the chicane dipoles based on finite element method (FEM) simulations, as well as the implementation of a magnet measurement system.

INTRODUCTION

Many important questions from solid state physics to biological applications demand an analysis within a wide spectral range from THz to IR. These wavelengths are difficult to cover with high intensity using ring-based light sources. However, if the bunch length is comparable to or smaller than the desired wavelength, the electrons start to emit coherently, yielding a significant increase in flux [3].

To study bunch compression down to the fs-range, to study the influence on the generation of CSR (coherent synchrotron radiation), and to further the development of related diagnostics, a linac-based test accelerator named FLUTE (Ferninfrarot Linac Und Test Experiment) is currently under construction at KIT. The planned top-level parameters are listed in Table 1. For more information about FLUTE and the planned experiments, please refer to [1, 2] and the references therein.

Table 1: FLUTE Design Parameters

Linac Energy	41 MeV
Repetition Rate	10 Hz
Bunch Charge	1 pC - 3 nC
Pulse length	1 fs - 300 fs

To achieve the desired flexibility for experiments and the strong compression, a D-type bunch compressor is foreseen, cf. Fig. 1. As a detailed analysis of the future experiments depends on a precise description of the magnetic lattice used, OPERA [4] finite element simulations have been carried out for the chicane dipoles [5]. Particular emphasis has been put on the comparison of the calculated fringe fields with the analytical treatment used in the ASTRA [6] tracking code; and the calculation of the expected multipole components. The results are presented in the following section.

To measure the real field distribution of said magnets a measurement system featuring both a 3D Hall-probe and a stretched-wire set-up has been installed [7]. It is described in detail in the subsequent section.

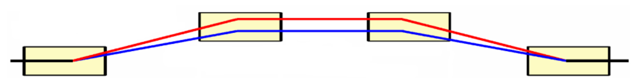

Figure 1: Schematic of a D-type bunch compressor. Particles with higher energy (blue) receive a smaller deflection in the dipole magnets (i.e. travel along a shorter path) than particles with a lower energy (red). For the correct initial energy distribution along the bunch, a bunch length compression can be achieved.

DIPOLE MAGNET DESIGN

Design Considerations

To allow maximal flexibility for future beam dynamics studies, the dipole magnets have to cover a large parameter range regarding beam energy and deflection angle, as listed in detail in Table 2. Two basic options are considered: a compact C-type and a wider, mechanically more stable H-type dipole magnet, cf. Fig. 2.

Table 2: Magnet Design Parameters

Electron beam energy	40 - 50 MeV
Deflection angle	0 - 15°
Magnetic field	0 - 120 mT
Magnet length	200 mm
Pole distance	45 mm
Transverse good field region C-type	76 mm
Transverse good field region H-type	240 mm

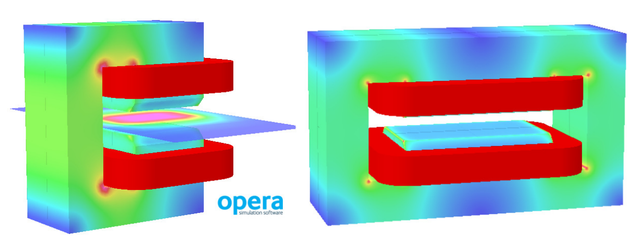

Figure 2: Possible C-type (left) and H-type (right) dipole magnet designs. The magnetic field strength within the magnet is indicated by colour map. For the C-type magnet, the magnetic field on axis is also illustrated

For the C-type magnets investigated, the transverse good field region (i.e. the area where the on-axis field does not

Content from this work may be used under the terms of the CC BY 3.0 licence (© 2015). Any distribution of this work must maintain attribution to the author(s), title of the work, publisher, and DOI.

ISBN: 978-3-95450-168-7 doi:10.18429/JACoW-IPAC2015-WEPMA041

rx Z^¿£¡ VJ¡»pj pN–gQ£ Vp¡ “^Qj ;al ‰ ENERGY-RECOVERING SUPERCONDUCTING ACCELERATOR MESA*

F. Schlander†, K. Aulenbacher, R. Heine, D. Simon, T. Stengler
Institut für Kernphysik, Johannes Gutenberg-Universität Mainz, D-55099 Mainz, Germany

Abstract

The Mainz Energy-recovering Superconducting Accelerator MESA requires superconducting RF systems that provide sufficient energy gain of 50 MeV per turn to an electron beam. The order of two Rossendorf-type cryomodules, containing two 9-cell 1.3 GHz XFEL-like cavities each, has been placed. Besides an overview of the adaptations required for the multipass and high current beam operation of the cryomodules, details about challenges regarding the installation of the cryomodules on the premises of the Institut für Kernphysik at Universität Mainz are given.

INTRODUCTION

Superconducting Radio Frequency (SRF) is a key technology for the Mainz Energy-recovering Superconducting Accelerator MESA. The both-sided SRF main linac will provide an energy gain of 50 MeV per turn, hence 12.5 MeV per cavity, as the cryomodule of choice is the Rossendorf-type cryomodule [1] containing two 9-cell TESLA/XFEL-type cavities. The complex structure of cryomodules containing the niobium cavities and its exterior parts require adaptions to each indiviual use. So the Rossendorf-type modules will undergo modifications as described in the following section. Further on the installation of the cryomodules at their dedicated spot in the MESA caverns requires detailed planning as construction work is needed. The plans for the installation will be presented in the subsequent section, followed by an outlook.

ROSSENDORF-TYPE CRYOMODULES

The Rossendorf-type cryomodules are well-characterised and in use at HZDR for more than a decade. A picture of one of the installed modules is shown in Fig. 1. Since then smaller adaptations have been applied to the design for easier assembly and better performance by the manufacturer Research Instruments GmbH [2]. These include an improvement of the liquid nitrogen shield and the use of niobium cavities undergoing the European XFEL preparation process [3].

For the purposes of MESA some additional changes will be applied. The Higher Order Mode (HOM) couplers will contain sapphire feedthroughs, improving the thermal conductivity and thus push the thermal breakdown of the superconducting HOM coupler antenna tip to a higher performance level.

* Work supported by the German Federal Ministery of Education and Research (BMBF) and German Research Foundation (DFG) under the Cluster of Excellence "PRISMA"
† schland@uni-mainz.de

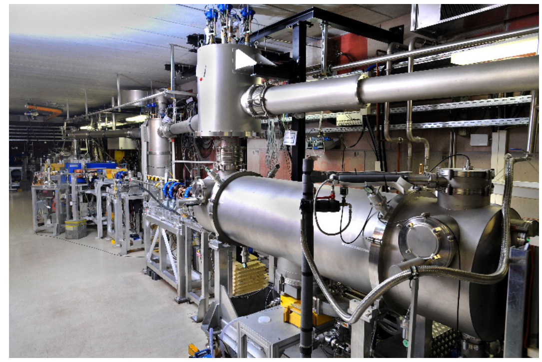

Figure 1: ELBE cryomodule (©Frank Bierstedt).

Due to the small bandwidth of the superconducting RF cavities, microphonics will be an issue for the energy recovery operation mode of MESA. To keep the frequency of the cavities under control, even for fast frequency changes, the tuner requires piezo technology which is not included in the standard Rossendorf type tuner and has to be replaced. Following from the tuner change, some redesign of the cavities' helium vessel is required. Besides the adaptations of the cryomodule, the coldboxes for the 4 K/2 K liquid helium (LHe) production including control system will also be provided, therefore only a $T = 4$ K LHe liquefier and the subatmospheric pumping units have to be provided by the institute.

SPACE CONSTRAINTS

In contrast to other projects, the facilities for MESA are already available, as they have been in use for a former experimental setup at the MAMI [4] accelerator. As these buildings are about 10 metres underground, the space foreseen is strictly limited, causing challenges in placing the lattice and all accelerator subsystems [5]. Special issues have to be faced for the cryomodules, as the current lattice places the cryomodules partially in apertures of the approx. 3 metres thick walls between the two accelerator halls MESA A/B. The front view sketch of the apertures and simplified insertions are shown in Fig. 2.

While the cryomodules itself fit into the apertures, the electric connections and the piping for the coolants will be an issue. The waveguides required for the RF supply reduce the space available for maintenance work and obstruct the passage to the end of the cryomodule which is located in the walls' aperture. Due to static reasons, a pedestal is required which will create a dead end, see Fig. 3.

In addition the cabling for RF and temperature diagnostics also hinders the transit, as the shearing forces applied might

Content from this work may be used under the terms of the CC BY 3.0 licence (© 2015). Any distribution of this work must maintain attribution to the author(s), title of the work, publisher, and DOI.

ISBN: 978-3-95450-168-7 doi:10.18429/JACoW-IPAC2015-WEPMA042

EXPERIENCE AND DEVELOPMENTS ON THE S-BAND RF POWER SYSTEM OF THE FERMI LINAC

A. Fabris#, P. Delgiusto, F. Pribaz, N. Sodomaco, R. Umer, L. Veljak, Elettra, Trieste, Italy

Abstract

The S-band linac of FERMI, the seeded Free Electron Laser (FEL) located at the Elettra laboratory in Trieste, operates on a 24/7 basis accumulating more than 6000 hours of operation per year. The performance and operability requirements of a user facility pose stringent specifications on reliability and availability on all the systems of the machine and in particular on the RF power plants. This paper provides a review and discusses the operational experience with the S-band power plants, klystrons and modulators, operating at S-band in FERMI. Based on the satisfactory results and following return of experience, upgrades of the existing power plants are being implemented in the continuous effort of extending the operability and availability of the systems. A description of these activities and an overview of the other developments under consideration on the RF power plants are also provided.

INTRODUCTION

FERMI, the Italian seeded FEL located in Trieste, consists of two FEL lines, FEL-1 and FEL-2, covering the wavelength range between 20 and 100 nm and between 4 and 20 nm respectively. Both the two FEL lines are now open to external users [1]. The accelerator is based on a 1.5 GeV S-band linac. Fourteen 3 GHz 45 MW peak RF plants are installed to power sixteen accelerating structures, the RF gun and the three RF deflectors. Two more accelerating structures will be added at beginning of 2016 [2]. An additional power plant is installed to provide a hot-spare backup solution for the first two. This power plant is also used as a test bench for R&D purposes.

POWER PLANTS DESCRIPTION

RF power requirements for the plants are typically around 33 MW peak, with the exception of the plant that powers the gun and the low energy deflector where the needs are around 21 MW. Each power plant is composed of a 45 MW klystron and modulator. All plants are designed to operate at 50 Hz pulse repetition rate [3]. Figure 1 shows one of the RF plants.

All klystrons are TH2132A from Thales. This tube can provide up to 45 MW in pulsed mode, 4.5 µs at 100 Hz. Typical peak beam cathode voltage and current for maximum output are 310 kV and 350 A.

All modulators are line PFN type and were assembled by local companies under FERMI design. The main parameters are summarised in Table 1. The high voltage power supply is a 50 kV, 2 A capacitor charging power supply from FuG with a specified pulse-to-pulse repetition accuracy better then 100 ppm at 50 Hz. The switching element is a thyratron (CX1536X) from E2V.

#alessandro.fabris@elettra.eu

Figure 1: One of the FERMI S-band plants.

Table 1: Modulator Parameters

Parameter	Value
Maximum operating voltage	320 kV
Maximum delivered current	350 A
Repetition frequency	50 Hz
RF pulse width	4.5 µs
Risetime/falltime	< 2 µs
Pulse flatness	< ± 1 %

OPERATIONS AND STATISTICS

The RF plants are in operation continuously on a 24 hours 7/7 basis for about 6500 operating hours per year. The uptime of the entire S-band system for year 2014 has been 93 %. This comprises as well the downtime due to the other parts of the RF system such as waveguides and accelerating structures. The main sources of downtime are klystron arc discharges that amount to roughly 70 % of the total number of faults. These faults are power dependent and are randomly distributed, although three plants show a much higher arc rate.

Mean lifetime of the klystrons in operation is 32,000 hours. This value is presently assumed for spare parts management. It must be noted that this statistics is evolving and we have the two oldest klystrons that have exceeded 70,000 hours of operation. However, now these have been installed in the less demanding plants in terms of RF output. Typical failure mechanism is a too high arc rate at the operating voltage, which eventually prevents reaching or maintaining the target klystron beam parameters. Klystrons operation is continuously monitored. High voltage conditioning and heater curve

Content from this work may be used under the terms of the CC BY 3.0 licence (© 2015). Any distribution of this work must maintain attribution to the author(s), title of the work, publisher, and DOI.

ISBN: 978-3-95450-168-7 doi:10.18429/JACoW-IPAC2015-WEPMA043

FIVE YEARS OF OPERATIONS FOR THE MAGNET POWER SUPPLIES OF FERMI

R. Visintini, Elettra Sincrotrone Trieste, Trieste, Italy

Abstract

FERMI, the FEL light source in Trieste, Italy, started its regular operation with external users in 2011. The construction of the facility began in 2008 and the commissioning of the complete system – LINAC, Undulators' chains (FEL-1 and FEL-2), photon front-end – started in 2010. On December 13, 2010 the first lasing occurred. From the Photo-injector to the electron Main Beam Dump (MBD), there are more than 400 magnets and coils, including those mounted on the accelerating sections of the LINAC and on the Undulators. With few exceptions, each magnet power supply energizes a single magnet/coil: there are about 400 magnet power supplies spanning from few tens of watt up to 42 kW. The power supplies types range from custom-made ones, to COTS (Commercial Off The Shelf), to in-house design (these accounting to 88% of the total). Almost all magnet power supplies are in use since mid-2010. During 5 years of operations, the reliability of the magnet power supplies proved to be extremely high: the downtime of FERMI operations due to magnet power supplies is very low.

INTRODUCTION

FERMI is the FEL source in operation for external users since 2011 [1] in the Elettra Research Center, in Trieste (Italy). FERMI is located extremely close to Elettra Storage Ring (SR) building: great care in planning and special low-vibration techniques were adopted not to interfere with the Users' activities on the Elettra's beamlines. FERMI is the long straight construction close to the circular Elettra SR building in Fig. 1.

Figure 1: Aerial view of FERMI and Elettra.

The civil works, carried out in about 4 years, ended in September 2010 but co-occupancy allowed the installation of the machine in parallel with the construction of the buildings and plants [2]. The commissioning started in September 2009 with the photoinjector and gun, and completed – excluding the experimental beamlines – in late 2010. The first seeded X-Ray lasing occurred on December 13, 2010 [3].

MAGNETS AND POWER SUPPLIES

The first magnet power supplies energized the gun solenoids and the injector spectrometer, starting in 2009. During 2010, about 400 more power supplies (PS) enter into operation on air- and iron-core magnets.

Design Strategies

In designing the magnet-PS combinations, we had multiple goals:

- Optimize the number of different PS for energizing the various types of magnets required by the particle physics design, taking in account the re-use of some magnets from the former LINAC to SR Transfer Line (TL) of Elettra.
- Standardize as much as possible the interface to the remote control and interlock (MPS – Machine Protection System).
- Make accurate estimations of the "contemporary factors", to define the actual power absorbed from the mains.
- Make realistic estimations of the dissipated power for the correct dimensioning of the HVAC (Heating Ventilation Air Conditioning) and water plants.

We achieved these goals through a close collaboration among the particle physics experts and the designers of the magnets, the PS, the control system, and the conventional plants. More details can be find in [4].

Power Supplies Types

The about 400 magnets and coils of FERMI belong to 37 different types, and, with few exceptions, they are individually energized. Following the optimization, the number of different PS types is 17: custom made, commercial ones (COTS – Commercial Off The Shelf) while the majority derives from an in-house design [5], as shown in Table 1.

Table 1: Types of Power Supplies

Type	# of Types	# of PS	Output [V/A]
Custom	2	4	25 – 55 / 750
COTS	12	31	15 -100 / 60 – 500
In-House	3	370	±12 - ±20 / ±5 - ±20
TOTAL	17	405	

Content from this work may be used under the terms of the CC BY 3.0 licence (© 2015). Any distribution of this work must maintain attribution to the author(s), title of the work, publisher, and DOI.

ISBN: 978-3-95450-168-7 doi:10.18429/JACoW-IPAC2015-WEPMA044

25 Hz SUB-MJ YTTERBIUM LASER SOURCE OF RF GUN FOR SUPERKEKB

X. Zhou#, T. Natsui, M. Yoshida, R. Zhang, Y. Ogawa, KEK, Tsukuba, JAPAN

Abstract

The electron beams with a charge of more than 5 nC and a normalized emittance of less than 10 μm are expected to be generated in the photocathode RF gun at the injector linac of SuperKEKB. An ytterbium (Yb)-doped fiber and Yb:YAG thin-disk hybrid laser system with a center wavelength of 259 nm and a pulse width of 20 ps is developed to obtain high peak energy pulses. As the result, more than 3 nC and 1 nC electron were generated in repetition of 25 Hz with single-bunch and double-bunch respectively.

INTRODUCTION

For injector linac of SuperKEKB project, more than 5 nC electron beams with double-bunch is expected to be generated in the photocathode RF gun. To high-current, low-emittance beams generation, the laser source with 1 mJ pulse energy, center wavelength of 259 nm and a pulse width of 20 ps are needed [1]. Especially, the broadband wavelength is required for the pulse shaping control. Therefore, a Ytterbium (Yb)-doped hybrid laser system, include an Yb-doped fiber oscillator, Yb-doped fiber amplifiers and thin-disk Yb:YAG amplifiers is developed.

For the repetition rate of electrum beam, the optional of 2 Hz, 5 Hz, 25 Hz and 50 Hz with single or double bunch were requested. Although, more than 5 nC electron with single-bunch has been generated in the 2 Hz and 5 Hz [2], when the repetition rate increases to 25 Hz, the condition of the laser amplifier system such as the thermal lens effect is changed seriously. To correspond to 25 Hz repetition rate, the laser was reformed.

LASER SYSTEM OF 25 HZ

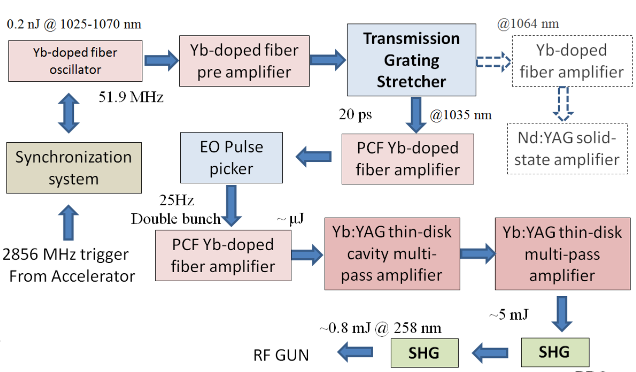

Figure 1: Layout of Laser system.

A schematic diagram of the laser setup is shown in Fig.1. The seed pulse with the pulse energy of 0.2 ns and spectrum of 1025-1070 nm was generated by an Yb-doped fiber ring oscillator. The pulse repetition is 51.9 MHz, synchronized with 2856 MHz trigger from accelerator. After an Yb fiber pre amplifier, the pulse was chirped to ~20 ps by a transmission grating stretcher with a spectral mask. An Yb-doped large-mode-area polarizing double-clad photonic crystal fiber was employed to the first amplification stage. Then, the pulse repetition rate of 25 Hz, double bunch was separated with two Electro-optic (EO) modulators. To increase the pulse energy, another Yb-doped LMA PCF was used. So the pulse was amplified to μJ-level, which was strong enough to be amplified by Yb:YAG thin-disk stage. To obtain the mJ-class pulse energy, several multi-pass amplifier stages were employed. Deep UV pulses for the photocathode are generated by using two frequency-doubling stages. High pulse energy and good stability were obtained. Finally, the pulses were injected into RF gun.

Backup of Yb Fiber Oscillator

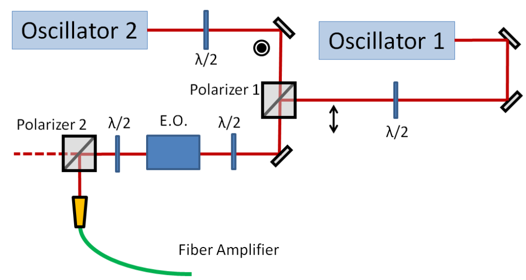

Figure 2: Selection of Oscillator.

The seed pulse was generated by a passive mode-locked oscillator with the pulse energy of 0.2 nJ at the repetition rate of 51.9 MHz (10.38*5 MHz). The spectral bandwidth is ~50 nm, from 1025 to 1070 nm. A piezoelectric transducer (PZT) is used to control the cavity length to lock the repletion rate with the 2856 MHz trigger from accelerator by a synchronization system. The mode-locked operation was stable for several months with good pulse quality and stability.

Because the oscillator is the most important part of all system, another backup oscillator was employed. As the fig.2, the two oscillators are set with cross polarizations that combine by polarizer 1. Then the EO modulator is used to change the polarization of the beams between the polarizer 1 and polarizer 2. The reflect beam of the seed pulses at polarizer 2 was chosen by the EO voltage control.

Upgrade of Yb Fiber Amplifier stages

In the fiber amplifier stages, the improvement is focus on the increase of the pulse quality. Two types amplifier was set up. For low power amplification, Yb fiber with the core diameter 4 μm same as the oscillator was used.

Content from this work may be used under the terms of the CC BY 3.0 licence (© 2015). Any distribution of this work must maintain attribution to the author(s), title of the work, publisher, and DOI.

ISBN: 978-3-95450-168-7 doi:10.18429/JACoW-IPAC2015-WEPMA045

ENERGY DEPOSITION AND DPA IN THE SUPERCONDUCTING LINKS FOR THE HILUMI LHC PROJECT AT THE LHC INTERACTION POINTS*

A. Bignami, F. Broggi#, C. Santini[1] INFN/LASA, Segrate, Italy, [1]and Politecnico di Milano, Italy
A. Ballarino, F. Cerutti, L. S. Esposito, CERN, Geneva, Switzerland

Abstract

In the framework of the upgrade of the LHC machine, the powering of the LHC magnets foresees the removal of the power converters and distribution feedboxes from the tunnel and its location at the surface[1]. The Magnesium Diboride (MgB_2) connecting lines in the tunnel will be exposed to the debris from 7+7 TeV p-p interaction. The Superconducting (SC) Links will arrive from the surface to the tunnel near the separation dipole, at about 80 m from the Interaction Point at IP1 and IP5. The Connection Box (where the cables of the SC Links are connected to the NbTi bus bar) will be close to the beam pipe.

The debris and its effect on the MgB_2 SC links in the connection box (energy deposition and displacement per atom) are presented. The effect of thermal neutrons on the Boron consumption and the contribution of the lithium nucleus and the alpha particle on the DPA are evaluated. The results are normalized to an integrated luminosity of 3000 fb^{-1}, value that represents the LHC High Luminosity lifetime. The dose delivered to the SC Links is found to be below the damage limit. Further studies are necessary to correlate the induced displacement per atom to the superconducting properties.

INTRODUCTION

In the framework of the High Luminosity LHC project MgB_2 superconducting links delivering up to 150 kA to the magnets are being developed at CERN[1]. The links will be exposed to the radiation field of the cascades generated by the debris from the Interaction Point (IP).

The dose and DPA in the Superconducting Links (SCL) closer to the beam pipe are evaluated using a Monte Carlo code. The consumption of ^{10}B by the neutron capture reactions is considered.

THE HILUMI LHC PROJECT AND THE COLD POWERING TASK

The Large Hadron Collider (LHC) will remain the most powerful accelerator in the world for at least the next two decades. Its full exploitation is the highest priority of the European Strategy for particle physics.

To extend its discovery potential, LHC will undergo a major upgrade in the 2020s. The objective is to increase its peak luminosity (and thus collision rate) by a factor five beyond its design value and the integrated luminosity by a factor ten. The novel machine configuration, the High Luminosity LHC, will rely on a number of key innovative technologies representing exceptional technological challenges. These include among others: cutting-edge 11-12 tesla superconducting magnets; very compact with ultra-precise phase control superconducting cavities for beam rotation; new technology for beam collimation; and long high-current superconducting lines (hereafter called "links").

In the present LHC configuration, the electrical feeding of the about 1700 LHC superconducting (SC) circuits requires the transfer of more than 3 MA of current from the power converters to the magnets. Now this is done via conventional copper cables for the room temperature path between power converters and current leads, High Temperature Superconductors (HTS) or resistive currents leads for the transfer to the 4.5 K liquid helium bath.

Nb-Ti bus-bars operated in liquid helium at 4.5 K or in superfluid helium at 1.9 K provide the connection to the SC magnets. In the present LHC configuration, power converters and current leads are both located in underground areas, the first mainly in alcoves, adjacent to the machine tunnel, and the second in dedicated cryostats that are near the LHC interaction points and in line with the SC magnets.

All equipment in the tunnel is exposed to significant levels of radiation. In Fig. 1 the dose in the tunnel, normalized at 3000 fb^{-1} is shown. It is a horizontal projection and the Connection Module (CM) is behind the beam line. The CM red colour is just to evidence it and it is not related with the dose, whose level is about the same as in D1.

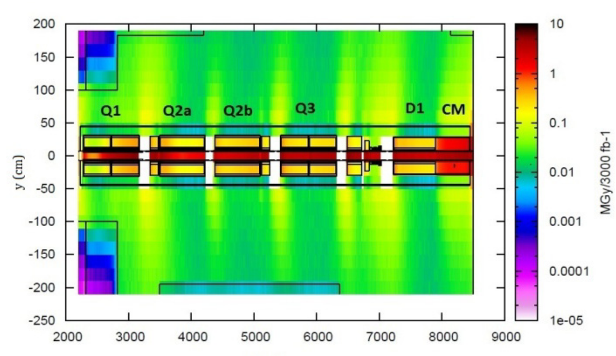

Figure 1: Dose in the insertion region of the tunnel (see text for detail) . The SCL and CM will be at about z=80 m from the IP.

For HL-LHC, the transmission of the current to the magnets is performed via SC links containing tens of cables feeding different circuits and transferring all

*The work is part of HiLumi LHC Design Study, partly funded by the European Commission, GA 284404, and included in the High Luminosity LHC project
#francesco.broggi@mi.infn.it

Content from this work may be used under the terms of the CC BY 3.0 licence (© 2015). Any distribution of this work must maintain attribution to the author(s), title of the work, publisher, and DOI.

ISBN: 978-3-95450-168-7 doi:10.18429/JACoW-IPAC2015-WEPMA046

STUDIES ON INNOVATIVE PRODUCTION METHODS OF HOM COUPLER FOR SRF 9-CELL CAVITY

K. Nohara*, N. Kawabata, K. Miyajima, M. Shinohara,
Shinohara Press Service Co. Ltd. (SPS), Funabashi, Chiba, Japan
H. Hayano, S. Kato, T. Saeki, A. Yamamoto, M. Yamanaka
High Energy Accelerator Research Organization (KEK), Tsukuba, Ibaraki, Japan

Abstract

Pure Nb for SRF cavity bears hard workability. In addition, HOM coupler composed of cup (outer conductor) and antenna (inner conductor), a primary device of end group components, is complicated in the shape, implying much harder formability. That is why current production methods so far show serious issues in cost-effectiveness and mass-productivity. The authors have created advanced press forming methods of HOM cup and HOM antenna aiming to solve the above issues, almost resulting in satisfied quality, cost and productivity. The innovative procedures are described, remaining a bit problems to be sorted out, and further R&D works are still ongoing.

INTRODUCTION AND TARGET

HOM coupler attached at both ends of cavity is one of indispensable devices to eliminate high order mode radio wave generated during the operation of machines to prevent lowering of accelerating voltage.

HOM coupler in Fig. 1 shows a cylindrical cup of an extremely tall body to diameter with protrusion on the flat bottom and off-center perforation followed by burring plus oblong hole on the side wall, and also an antenna demonstrating kind of unique view with a thick body, sharp corner and a large void. They are subject to EBW for assembling of HOM coupler.

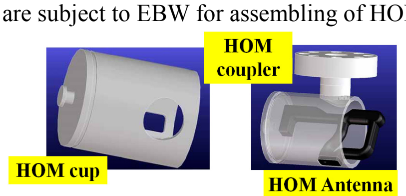

Figure 1: Schematic view of HOM coupler with cup and antenna.

From the shape and size of components, effective production methods sound quite difficult in parallel with making use of hard workable pure Nb. Now, several production methods have been implemented. However, there might be serious issues of cost-effectiveness and mass-productivity in particular.

Our final target is to invent advanced sheet plastic press-forming methods for HOM coupler i.e. HOM cup and HOM antenna aiming at realizing its satisfied function, prominent mass-productivity and drastic cost-effectiveness [1][2].

HARD WORKABLE PURE NB MATERIAL

There are close relation between material and forming, even more in tough workable pure Nb. Then, pure Nb annealed sheet (t2.8) was subject to uni-axial tension test together with commercial pure Fe sheet (t1.0) to examine both materials related to "sheet press forming" that should be most desirable due to applying plastic deformation which could make the shortest production time and extensive cost reduction available.

The diagram showing relations between applied force and displacement reveals large total elongation (λ_t) in Nb. However, the notable point is that λ_t is expressed as follows,

$$\lambda_t = \lambda_u + \lambda_\ell \qquad (1)$$

where indicated are uniform and local elongation each. It should be noted that λ_u and λ_ℓ correspond to plastic stable region (basically free from necking) and plastic unstable region (necking generation due to stress concentration), respectively. And the test results show the following relations,

$$\lambda_t(\mathrm{Nb}) > \lambda_t(\mathrm{Fe})\ ;\ \lambda_u(\mathrm{Nb}) < \lambda_u(\mathrm{Fe})\ ;\ \lambda_\ell(\mathrm{Nb}) > \lambda_\ell(\mathrm{Fe}) \qquad (2)$$

As the "ductility" is roughly equivalent to λ_u in case of press forming to avoid fracture in unstable plastic deformation, the experimental result (equation (2)) is important, namely Nb is hard workable compared with Fe. Adding, the last term of equation (2) gives rather an advantage to Nb when burring is applied. The following Ludwick's relation was proved [3],

$$\sigma = \varepsilon^n \qquad (3)$$

where σ and ε are true stress and true strain, and n is called work hardening coefficient showing hardenability of metals and alloys.

For the purpose of the conversion from the current methods to the whole plastic press forming, mechanical properties from pure Nb tensile test, and additionally observed data of Lankford's plastic strain ratio, r, at RT (Fig. 2 ; closely related to press drawability) together with popular pure Fe are useful. Further, we propose a new parametric index, ζ, which is defined and shown below using r, $\bar{r}$ (averaged r value in different directions) and Δr (indicating anisotropy of the material) [4],

$$r \equiv | r_w / r_t |, \qquad (4)$$

$$\bar{r} = \{ (r_o + r_{90}) + 2\, r_{45} \} / 4,\ \ \Delta r = \{ (r_o + r_{90}) / 2 \} - r_{45} \qquad (5)$$

$$\zeta \equiv \Delta r / \bar{r} \qquad (6)$$

where pure Nb is featured by much smaller n and ζ than pure Fe in addition to small ε_u and s_u (ultimate tensile strength). The facts are unfavorable and tough to accomplish the target [5][6].

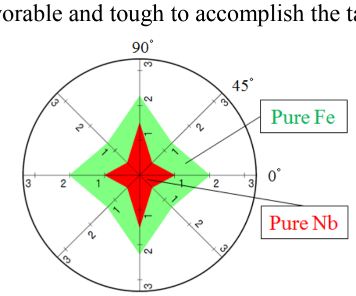

Figure 2: Plastic strain ratio, r , in different directions.

NEW PRESS DRAWING OF HOM CUP

One of points for the realization of a single process ultra-deep drawing is to strengthen the weak position of cylindrical body

* noharakh@tbn.t-com.ne.jp

Content from this work may be used under the terms of the CC BY 3.0 licence (© 2015). Any distribution of this work must maintain attribution to the author(s), title of the work, publisher, and DOI.

ISBN: 978-3-95450-168-7 doi:10.18429/JACoW-IPAC2015-WEPMA047

MHI'S PRODUCTION ACTIVITIES OF ACCELERATOR COMPONENTS

N. Shigeoka#, S. Miura, Mitsubishi Heavy Industries, Ltd., Mihara, Hiroshima, Japan

Abstract

Mitsubishi Heavy Industries (MHI) is manufacturing various types of accelerator components. As examples of recent production activities result of a mass-production of S-band accelerating structure for PAL-XFEL and a status of series production of C-band waveguide network for SwissFEL will be reported in this paper.

INTRODUCTION

Mitsubishi Heavy Industries (MHI) has started manufacturing of accelerator components such as accelerating structures in 1960s. For example, in a field of normal conducting accelerator, in recent years, MHI had handled mass production of C-band choke-mode accelerating structures and SLED for Riken SACLA, production of DTL, SDTL (Separated DTL), ACS (Annular Coupled Structure) for JAEA/KEK J-PARC [1]. In latest years, MHI manufactured over 120 S-band accelerating structures for PAL-XFEL project [2-4] and shipment has completed in March 2015. In addition, MHI has accepted order of C-band waveguide for SwissFEL project [5] in June 2014. One set of prototype waveguide has been already delivered to PSI in December 2014 and series production is in progress now.

S-BAND ACCELERATING STRUCTURES FOR PAL-XFEL

Mass-production of the S-band 3 m long accelerating structure [6-7] started in June 2012 and finished at March 2015. Totally 120 structures has been delivered to PAL. Appearance of the structure is shown in Figure 1 and main parameters are shown in Table 1.

Result of LLRF measurement after tuning shown in Figure 2. It shows excellent performance of production.

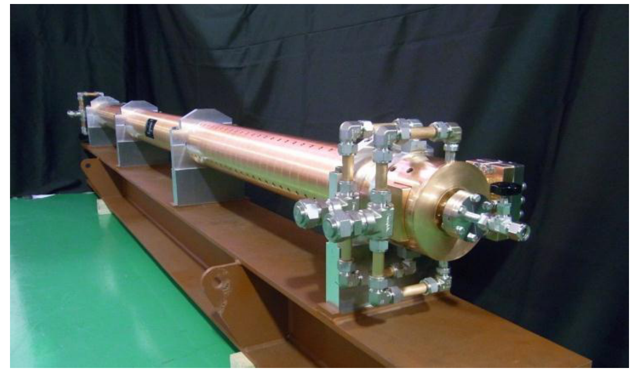

Figure 1: Appearance of the S-band accelerating structure for PAL-XFEL.

Table 1: Main Parameters of the S-band Accelerating Structure for PAL-XFEL

Item	Value
Operating frequency	2856 MHz
Accelerating type	C. G.
Phase shift per cavity	$2\pi/3$
Unloaded Q	13,000
Attenuation constant	0.56
Input / Output VSWR	< 1.05
Phase error	< +/- 2.5 degree
Number of cells	82 + 2 coupler cells
Filling time	0.84 μs
Length	3 m
Coupler type	Quasi-symmetrical

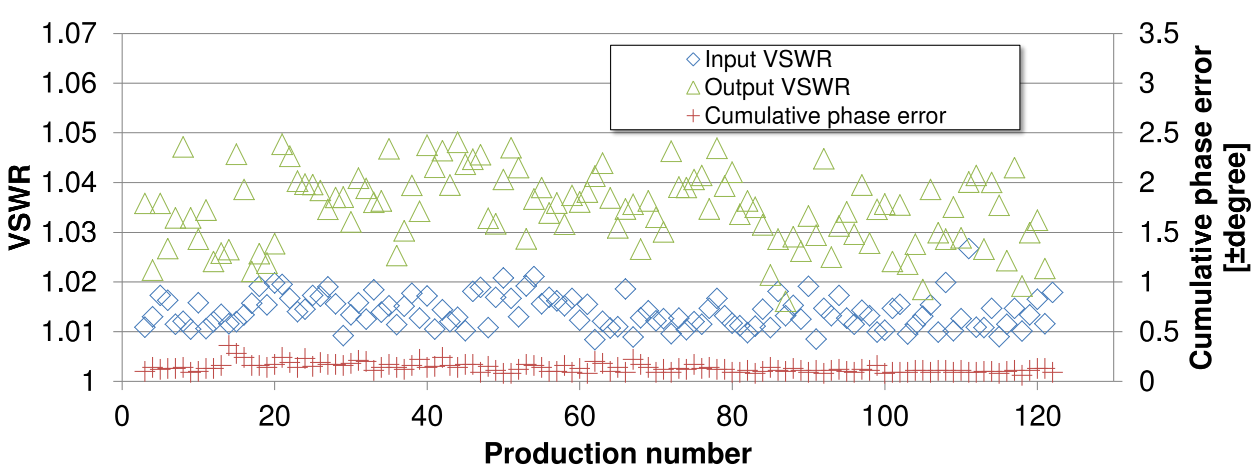

Figure 2: Input / Output VSWR and cumulative phase error of 120 S-band structure for PAL-XFEL after tuning.

#nobuyuki_shigeoka@mhi.co.jp

Content from this work may be used under the terms of the CC BY 3.0 licence (© 2015). Any distribution of this work must maintain attribution to the author(s), title of the work, publisher, and DOI.

ISBN: 978-3-95450-168-7 doi:10.18429/JACoW-IPAC2015-WEPMA048

DEVELOPMENT FOR MASS PRODUCTION OF SUPERCONDUCTING CAVITY BY MHI

T.Yanagisawa#, H.Hara, K.Kanaoka, K.Okihira, K.Sennyu, Mitsubishi Heavy Industries, Ltd., Mihara, Hiroshima, Japan

Abstract

MHI's activities for superconducting accelerator are reported. MHI has supplied several 9-cell cavities for STF (R&D of ILC project at KEK) and have been considering production method for stable quality, cost reduction and mass production. Furthermore MHI had produced another shape cavities and cryomodules for several R&D projects. These activities are reported in detail.

INTRODUCTION

Mitsubishi Heavy Industries (MHI) has supplied a 1.3GHz superconducting cavity for the STF project (STF is a project at KEK to build and operate a test linac with high-gradient superconducting cavities, as a prototype of the main linac systems for ILC.) for several years [1] [2]. The cavities from MHI-12 to MHI-30 reached Eacc= 33.9MV/m on average. This average Eacc approaches the ILC target, 35MV/m. (see Table 1 and Figure 1) And we have developed new techniques for improvement of productivity and for cost reduction for ILC.

On the other hand, MHI has supplied other shape cavities and the cryomodules for KEK's superconducting projects including STF [3]. (see Figure 2) The details of cavity manufacturing techniques and cryomodule for STF are described below.

Table 1: Cavity Production List

Project	Customer	Production year	Cell-number	Quantity	Remarks
STF	KEK	2005-2015	9	30	MHI-1 to MHI-30
ERL		2009-2010	2	3	For injector of KEK c-ERL project
		2010-2011	9	2	For main ring of KEK c-ERL project
		2013-2014	1.5	1	For Superconducting RF electron gun of ERL R&D
ILC R&D	MHI	2009	9	1	[MHI-A] Deep drawing for HOM cup LBW for stiffener and flange
		2010	2	1	[MHI-B] Seamless dumbbell, Auto buffing
		2012	9	1	[MHI-C] LBW for baseplate Welding all equator line in succession
		2014	9	1	[MHI-D] Nb Gr-2 flange Welding all equator line in succession(4 cavities/1 batch)

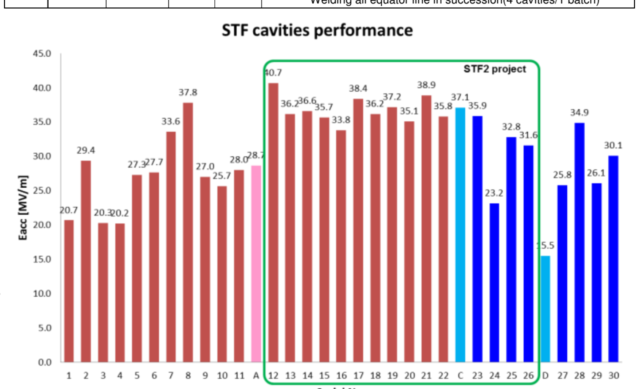

Figure 1: Performance of STF cavities.

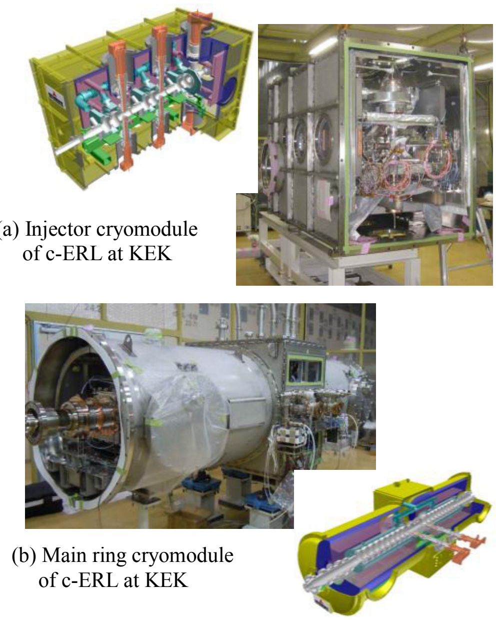

(a) Injector cryomodule of c-ERL at KEK

(b) Main ring cryomodule of c-ERL at KEK

Figure 2: Cryomodules for c-ERL at KEK.

MANUFACTURING TECHNIQUES OF CAVITY

Nb Gr-2 Flange

The flanges of Cavity are generally made by Nb-Ti alloy because of the welding quality with niobium and the hardness for vacuum seal. MHI has developed to use the Niobium for cavity flanges. (see Figure 3) This way causes the reduction of number of parts and number of welding.

MHI tested three kind of niobium made by Heraeus.

- ASTM Gr-2 Nb with surface hardening treatment
- ASTM Gr-2 Nb (No treatment)
- RRR300 Nb with surface hardening treatment

After the annealing same as cavity and the thermal cycle test using liquid Nitrogen, three material flanges passed the helium leakage test. From point of view of commercial availability, ASTEM Gr-2 Nb (No treatment) was adopted.

MHI has fabricated R&D cavity (MHI-D) using niobium flanges. During vertical test at 2K, there is no leak from niobium flanges. The Eacc (π-mode) of MHI-D was 15.5 MV/m, however the Max Eacc of each cell reached 36.6 MV/m by another mode measurement. MHI confirmed that the niobium flange can be applicable to the superconducting cavities.

Content from this work may be used under the terms of the CC BY 3.0 licence (© 2015). Any distribution of this work must maintain attribution to the author(s), title of the work, publisher, and DOI.

ISBN: 978-3-95450-168-7 doi:10.18429/JACoW-IPAC2015-WEPMA049

DEVELOPMENT OF THE CERAMIC CHAMBER INTEGRATED PULSED MAGNET FITTING FOR A NARROW GAP

C. Mitsuda*, T. Honiden, S. Sasaki, and N. Kumagai JASRI/SPring-8, Hyogo 679-5198, Japan
A. Sasagawa, KYOCERA Co. Ltd., Higashiomi-city, Shiga 529-1595, Japan
T. Nakanishi, SPring-8 Service Co. Ltd. (SES), Hyogo 678-1205, Japan

Abstract

We are pushing forward the development of a pulsed magnet that has a combined structure of magnet coils with a ceramic vacuum chamber, aiming to realize a small gap. The structure we are developing is that single turn air-coils are implanted along the longitudinal axis in the cylindrical ceramic chamber wall with thickness of 5 mm. The ceramic wall works for separating the vacuum from the atmosphere, as well as holding the coil structures mechanically and the electrical insulation of coils. We achieved the continuous operation over 200 days, without any failure, of current-excitation with 20 kV/7.7 kA pulse with 4 μsec width and repetition of 1Hz, using the dipole type prototype with the bore radius of 30 mm and the magnetic length of 0.3 m in 2013, while maintaining the vacuum pressure less than 10^{-6} Pa.

MERITS OF NARROW GAP MAGNET

The performances which are required in common to all pulsed magnet system are fast, strong, and high repeating pulsed magnetic field characteristics. In order to achieve these performances, there are two approaches. First one is developing a high power and high repetition pulsed power supply. Second one is reducing the power supply load as low as possible. The load reduction is an important issue. Because, if we try to achieve these performances without decreasing the load, the power supply system will have a large body size, consequently, need a huge installation space and give a restriction to the installation place of the system.

One of the best solutions to lower the power supply load is reduce the magnet pole gap. The kick angle is determined by the magnetic filed strength and field length. By the increased magnetic field with reducing the pole gap, the field length becomes shorter while keeping the kick angle the same. As a result, the coil inductance, hence the pulsed power supply load, become small. The low coil inductance is effective to achieve short pulse width and high repetition rate, in addition, to make the power supply small. The compact magnet and small power supply give the flexibility for setting position in an accelerator, making the kick efficiency optimum with the appropriate beta function value position.

Compact pulsed magnet with a narrow gap will fit to the future light source ring like generating diffraction limit synchrotron radiation [1]. Because the storage ring chamber size will be reduced in order to match the ultra low beam emittance and there is no enough space to install the pulsed magnet due to a large number of optical magnets. Additionally, it also will fit to small size storage rings that will require narrow installation spaces for these kinds of devices involving the injection kickers and correction kickers, and that have short revolution period requiring shorter pulse width.

* mitsuda@spring8.or.jp

CERAMIC CHAMBER INTEGRATION DESIGN AND THE ADVANTAGE

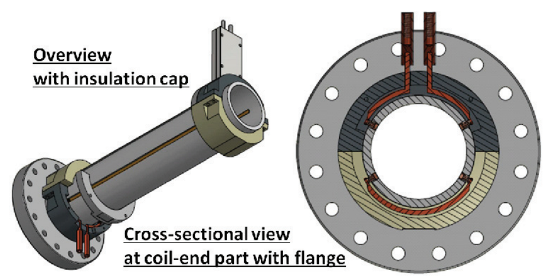

Figure 1: Design of dipole type CCIPM for the fabrication.

In an ordinary pulsed magnet, a ceramic chamber is used as a beam duct to reduce the eddy current effect for a pulsed magnetic field. Usually, the iron- or ferrite-core is set up outside of the ceramic chamber so that its magnetic poles sandwich the ceramic chamber. In this case, the distance(=magnet gap) between a magnetic pole and the beam is decided by the ceramic chamber bore radius, chamber thickness and clearance between the chamber and the pole. It is impossible to close the gap to the beam less than this restriction. On the other hand, in an air-coil type pulsed magnet, the coil is set up on the surface of the ceramic chamber so that its poles hold a ceramic chamber, or inside of the ceramic chamber like a strip-line kicker with complex supports. In the former case, the magnet gap is restricted by the ceramic chamber size. In the latter case, the complex support and coils cause an impedance unmatching of the beam wall current and increasing the chamber diameter to include the complex structures inside the chamber. To improve these insufficient aspects simultaneously, a ceramic chamber integrated type pulsed magnet was figured out.

The structure we are developing is that single turn air-coils are implanted along the longitudinal axis in the cylindrical ceramic chamber wall with thickness of 5 mm. For a dipole type magnet, four metallic bars (=coil) are totally implanted and one of bars is connected with another bars so that one pair of bars makes a coil. Implanting hole completely penetrates the chamber wall and is blocked up with the metallic bars. Figure 1 shows cross-sectional view of

Content from this work may be used under the terms of the CC BY 3.0 licence (© 2015). Any distribution of this work must maintain attribution to the author(s), title of the work, publisher, and DOI.

ISBN: 978-3-95450-168-7 doi:10.18429/JACoW-IPAC2015-WEPMA050

PERMANENT DIPOLE MAGNET R&D FOR SPring-8-II

T. Taniuchi#, T. Aoki, K. Fukami, S. Takano, T. Watanabe, JASRI/SPring-8, Hyogo, Japan

Abstract

Permanent magnets are promising components for future light sources in point of small electric power consumption, compactness and so on. We have proposed a variable-field permanent dipole magnet and demonstrated its performance. Following the result, a prototype magnet with a longitudinal field gradient and a magnetic shunt circuit was designed. The longitudinal field gradient dipole enables a lower beam emittance and a magnetic shunt circuit improves a temperature stability of the magnetic field strength. In this paper, simulation results for this magnet are presented. The interference with magnetic fields of neighboring magnets was also investigated.

INTRODUCTION

SPring-8-II is an upgrade project of SPring-8 and a very-low emittance storage ring with a high-packing-factor lattice has been studied [1]. As a dipole magnet system of the SPring-8-II, we plan to adopt permanent dipole magnets. Permanent magnets have advantages over electromagnets in terms of electric power consumption, stability and reliability because no power supply and no cooling system are necessary.

The proposed five-bend lattice of SPring-8-II is composed of a normal bending magnet (NB) at the center of the cell and four other bending magnets with longitudinal field gradient (LGB) as shown in Fig. 1.

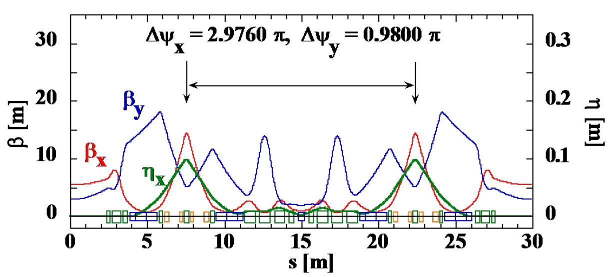

Figure 1: A unit cell of the 5-bend achromat optics for SPring-8-II.

LGB is divided into three segments and the strength of each segment is optimized to achieve a half of the emittance value with a conventional homogeneous dipole field. The major specifications of bending magnets are listed in Table 1.

We started R&D for permanent magnet dipole in 2013 and fabricated a sector magnet to verify fundamental performances [2]. Following this study, we have started a more specific design of LGB including an optimization of outer plates, magnetic shunts, field distributions, mechanical structures and so on.

#ihcuinat@spring8.or.jp

Table 1: Major specifications of permanent bending magnets.

Magnetic field [T] NB / 2 types of LGB	0.953 / 0.166, 0.296, 0.582 0.221, 0.395, 0.775
Effective length [m] NB / LGB	0.42 / 0.7, 0.7, 0.35
Gap [mm]	25
GFR [mm]	±12
Field error	5 x 10^{-4}

LONGITUDINAL GRADIENT BEND WITH OUTER PLATE

It is required to adjust magnetic field strength within a tolerable range after the fabrication, and possibly to change it in a relatively large range when the operating energy of an accelerator needs to be changed. In order to satisfy these requirements, we proposed a variable-field magnet with outer plates where the flux is intentionally leaked so that the magnetic field that beam experiences can be adjusted by moving the outer plates [2].

A configuration of LGB is shown in Fig. 2. Three outer plates are located above and below the main circuit where magnetic fluxes are leaked. A magnetic field strength of three magnets can be adjusted independently by changing the distance between the outer plate and the main circuit.

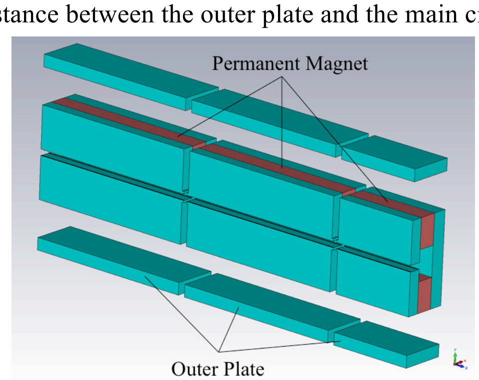

Figure 2: Longitudinal gradient bend with outer plates.

Fig. 3 shows a simulated longitudinal distribution of the magnetic field strength in an LGB for outer plate positions of 0 and 100 mm, respectively. We used CST STUDIO [3] for the magnetic field simulation. The magnetic field can be decreased below 30 percent of maximum strength at the closest position of the outer plate. A size, and a horizontal position of the outer plate will be optimized considering a tunable range and position sensitivity for the magnetic field. Alternative configurations have also been discussed such that

Content from this work may be used under the terms of the CC BY 3.0 licence (© 2015). Any distribution of this work must maintain attribution to the author(s), title of the work, publisher, and DOI.

ISBN: 978-3-95450-168-7 doi:10.18429/JACoW-IPAC2015-WEPMA051

Content from this work may be used under the terms of the CC BY 3.0 licence (© 2015). Any distribution of this work must maintain attribution to the author(s), title of the work, publisher, and DOI.

SUPERCONDUCTING SOLENOID PACKAGE PROTOTYPING FOR FRIB SRF LINAC*

K. Hosoyama#, K. Akai, S. Yamaguchi, KEK, Tsukuba, Japan
E. Burkhardt, K. Saito, Y. Yamazaki, FRIB, East Lansing, MI 48824, USA

Abstract

The solenoid package is consisted of a beam focusing superconducting 8 T 25 cm long solenoid coil wound by two graded NbTi SC wires and two racetrack shape X, Y-steering diploe beam corrector coils. All these coils were wound by "dry" winding. The solenoid coil was cold tested in the vertical cryostat and could reach to the design value of 8.9 T (99.5 A) without training. The full solenoid package was cold tested, including simultaneous excitation tests of all three coils, in the vertical cryostat successfully.

INTRODUCTION

KEK has more than 20 years long experience of design, fabrication, and cold test of small size 7T superconducting NbTi solenoid coils. We can utilize the existing coil winding machine and also the cryogenic facility for its cold test in KEK. A superconducting solenoid package prototyping for FRIB SRF Linac was designed, fabricated and cold tested at KEK under KEK/MSU collaboration program. The "dry" winding was used for the solenoid coil and racetrack shape steering coil winding, instead of using "wet" winding which is usually used for this size of solenoid coils. The "dry" winding has been developed and to date used for the fabrication of the small size solenoid coil in KEK.

REQUIREMENT

The required magnetic field of the solenoid package for FRIB are is 8 T with nominal operation current smaller than 100A. The operation temperature is 4.5 K and its temperature margin is +0.5 K. Inner diameter of the cold bore is larger than 4.0 cm and the solenoid coil length is 25 cm. The integrated magnetic dipole field strength for the steering coil is 0.03 Tm or larger at an operating current of 50 A. The field uniformity must be within 5% for both X and Y steering dipoles.

Table 1: Main Parameters of Coil and SC Wire

		Inner coil	Outer coil
Length	[mm]	250	250
Inner diameter	[mm]	54.25	86.25
Outer diameter	[mm]	86.5	131
Turns per layer		311	355
Layers		22	34
Dia. of bare SC wire	[mm]	0.80	0.65
Dia. of insulated SC wire	[mm]	0.75	0.70
Copper / SC		1.3	2.4
Filament diameter	[μm]	18	35
SC wire vender		Furukawa	Hitachi

*Work supported by the U.S. Department of Energy Office of Science under Cooperative Agreement DE-SC0000661.
kenji.hosoyama@kek.jp

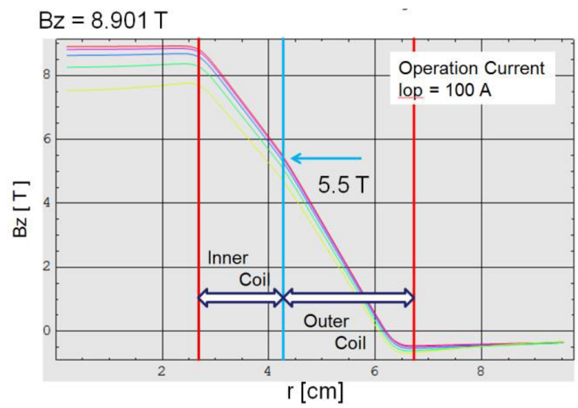

Figure 1: Magnetic Bz profile for the solenoid coil.

DESIGN OF 8T 25CM SOLENOID COIL

The main parameters of the solenoid and SC wires for inner and outer coils are summarized in Table 1. Figure 1 shows calculated Bz field profiles along radial direction for at z = 0 cm, 3 cm, 5 cm, 7 cm, 9 cm from the centre. The field uniformity inside the coil bore is very good due to the coil length is large compare to the coil inner diameter, and the field enhancement factor Bmax / B_0 is 1.0032. The self-inductance of this coil is 8.0 H.

Figure 2 shows the load line of the designed solenoid coil and critical curves (Ic) at 4.2 K and 4.5 K of the SC wire for the inner coil. The solenoid magnetic field Bz at the centre of coil reaches almost 9T at 4.2 K and 8.6 T at nominal operation temperature 4.5K over the required specification value 8T for FRIB. The solenoid has a temperature margin of 0.4 – 0.5 K

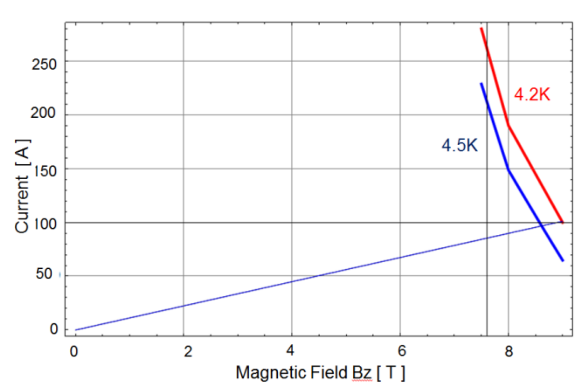

Figure 2: Load line of the solenoid coil with Ic curves.

ISBN: 978-3-95450-168-7 doi:10.18429/JACoW-IPAC2015-WEPMA052

LOW LEVEL RF SYSTEMS FOR J-PARC LINAC 50-mA OPERATION

Z. Fang, K. Futatsukawa, Y. Fukui, T. Kobayashi, S. Michizono, KEK, Japan
S. Shinozaki, E. Chishiro, F. Sato, JAEA, Japan

Abstract

In the summer of 2014, lots of improvements were carried out at the J-PARC proton linac, including the ion source, the Radio Frequency Quadrupole linac (RFQ), and the medium-energy beam-transport line from the RFQ to the Drift Tube Linac (DTL) called as MEBT1. Firstly, the output beam current of the ion source was upgraded from 30 to 50 mA. Then the former 30-mA RFQ with two RF power input ports was also replaced by a newly developed 50-mA RFQ with one input port. Furthermore for the MEBT1, a new chopper cavity was developed to replace the former one, and the RF power of the solid state amplifiers for the RF cavities at the MEBT1 were upgraded; from 10 to 30 kW for both of the Buncher-1 and Buncher-2 cavities, and from 30 to 120 kW for the chopper cavity. Finally, the old scraper used as chopped-beam dump after the chopper cavity was also replaced by a new dump system using two scrapers; A new function of separating the chopped beam automatically to the two scrapers was developed by modifying the FPAG control program in the low level control systems. After those improvements, in the September 2014 the J-PARC linac was successfully upgraded for 50-mA beam operation. The details of the improvements, especially for the low level RF systems, will be reported in this paper.

INTRODUCTION

The 400-MeV proton linear accelerator at the Japan Proton Accelerator Research Complex (J-PARC) consists of 324-MHz low-β and 972-MHz high-β accelerator sections, and the J-PARC linac is operated at a repetition rate of 25 Hz with a beam pulse width of 500 μs. From October 2006 to May 2013, only the 324-MHz low-β accelerator section was in operation with beam energy of 181 MeV. In the summer of 2013, the J-PARC linac was upgraded by installing the 972-MHz high-β accelerator section, and the proton beam was successfully accelerated to 400 MeV in January 2014. Then in the summer of 2014, the upgrade of the front end of the J-PARC linac, including the ion source, RFQ, and MEBT1, were successfully carried out for the 50-mA beam operation. An outline of the RF systems and RF cavities of the upgraded J-PARC 400-MeV linac is given in Fig. 1. In the 324-MHz low-β section, there are 23 RF stations, including one RFQ, two bunchers, one chopper, three DTLs (Drift Tube Linacs), and 16 SDTLs (Separated DTLs). In the 972-MHz high-β section, there are 25 RF stations. At each station, there is one ACS (Annular Coupled Structure) cavity. Among the 25 ACS cavities, there are 2 bunchers, 21 acceleration cavities, and 2 debunchers. Therefore, for the 400-MeV J-PARC linac, there are 48 RF stations and 64 cavities in total. The length of the J-PARC linac is approximately 300 m.

UPGRADED RFQ RF SYSTEM

In the summer of 2014, the RFQ was upgraded for the 50-mA beam operation. In the former 30-mA RFQ, called as RFQ-I, there were two RF power input ports. The RF power from the klystron was divided by a high-power hybrid divider, and forwarded to the two input ports of the RFQ-I through two waveguide systems. The RFQ-I was replaced by a newly developed 50-mA RFQ, called as RFQ-III. For the RFQ-III, there is only one input port. Thus, the hybrid divider in the waveguide systems will not be used, and it was removed in the summer of 2014 for the upgraded RFQ RF system, as shown in Fig. 2. The RF power from the klystron will be directly forwarded to the RFQ cavity.

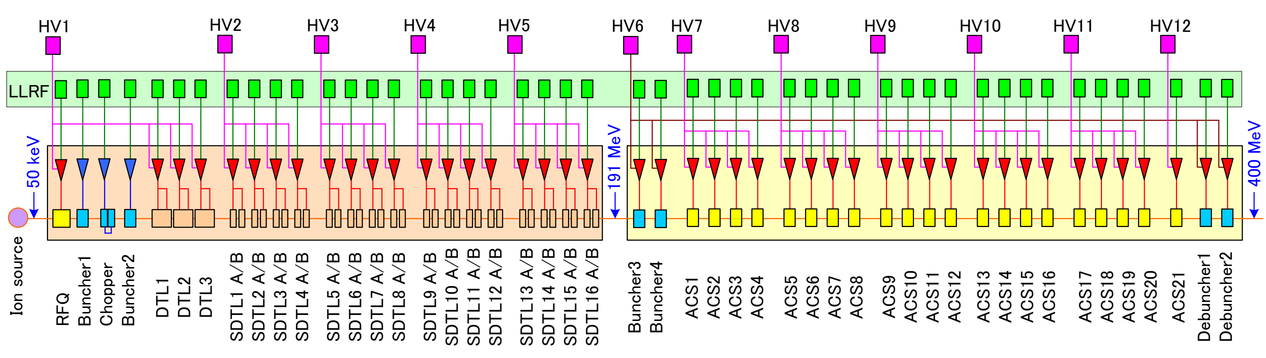

Figure 1: Outline of RF systems and RF cavities of the upgraded J-PARC 400-MeV linac.

Content from this work may be used under the terms of the CC BY 3.0 licence (© 2015). Any distribution of this work must maintain attribution to the author(s), title of the work, publisher, and DOI.

ISBN: 978-3-95450-168-7 doi:10.18429/JACoW-IPAC2015-WEPMA053

Content from this work may be used under the terms of the CC BY 3.0 licence (© 2015). Any distribution of this work must maintain attribution to the author(s), title of the work, publisher, and DOI.

MULTIPACTOR SIMULATIONS IN 325 MHz SUPERCONDUCTING SPOKE CAVITY FOR AN ELECTRON ACCELERATOR*

T. Kubo†, T. Saeki, KEK, High Energy Accelerator Research Organization, Tsukuba, Ibaraki, Japan
E. Cenni, Y. Iwashita, H. Tongu, Kyoto University, Uji, Kyoto, Japan
R. Hajima, M. Sawamura, Japan Atomic Energy Agency, JAEA, Tokai, Ibaraki, Japan

Abstract

To realize a compact industrial-use X-ray source with the laser-Compton scattering, a 325MHz superconducting spoke cavity for an electron accelerator operated at 4K is under development. Design-optimizations of the first prototype cavity were finished. Multipactor simulations were carried out as parts of optimization efforts. In this paper, procedures of multipactor simulations by using CST studio suite are briefly introduced. Then results of simulations and analyses to extract an optimum geometry are presented. A relation between a cavity geometry and an intensity of multipactor is also commented.

INTRODUCTION

In order to realize an industrial-use laser-Compton scattering compact X-ray source [1, 2], a superconducting cavity for electron acceleration is currently under development [3, 4]. We adopted a 325 MHz superconducting spoke cavity. The spoke cavity [5] has a small diameter around half the wavelength, namely, half a diameter of the elliptic cavity, and make it possible to reduce RF frequency, f_{RF}, with keeping its compactness. By setting $f_{\mathrm{RF}} = 325\,\mathrm{MHz}$, Bardeen-Cooper-Schrieffer (BCS) resistance ($\propto f_{\mathrm{RF}}^2$) is significantly reduced, and a cavity dissipation at 4 K nearly equals to that of 1.3 GHz elliptic cavity at 2 K.

The genetic algorithm (GA) known as a method of multi-objective optimization was used to design a spoke cavity by Sawamura et al [3, 4]. Cavities with minimized $E_{\mathrm{pk}}/E_{\mathrm{acc}}$ and $B_{\mathrm{pk}}/E_{\mathrm{acc}}$ were generated, from which geometries that maximize the achievable E_{acc} were extracted, where E_{acc}, E_{pk} and B_{pk} are the accelerating field, the peak electric-field and the peak magnetic-field, respectively. There are still degrees of freedom in the detailed design: corner radii of the end-plate and the spoke-base, and so on. Fig. 1 shows examples of geometries optimized by GA, which have similar RF characteristics, but each has different corner radius of the end-plate.

In order to finalize the detailed design, we carried out MP simulations of cavities optimized by GA and extract a model that may suppress a risk of MP as small as possible [6, 7]. In this paper, procedures and results of MP simulations are briefly summarized. Relations between cavity geometries and averaged secondary electron emission yield are also commented.

* The work is supported by Photon and Quantum Basic Research Coordinated Development Program from the Ministry of Education, Culture, Sports, Science and Technology, Japan.
† kubotaka@post.kek.jp

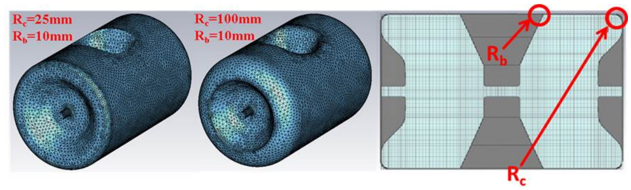

Figure 1: Examples of optimized cavity geometries. Both have optimized geometry and similar RF characteristics, but a detailed design (i.e., a corner radius of the end-plate in this example) is different from each other.

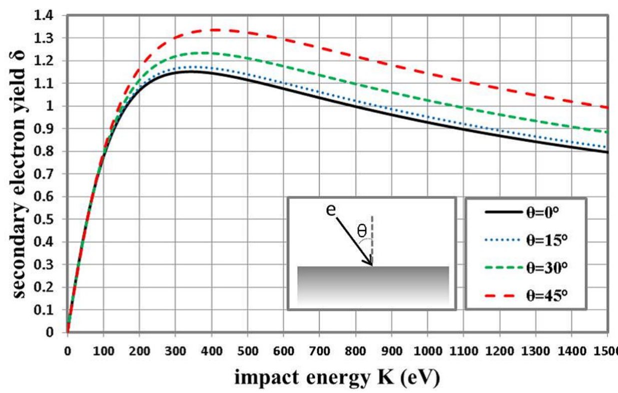

Figure 2: Furman model SEY as functions of impact energy. Each curve corresponds to an impact angle.

SIMULATION PROCEDURE

MP simulations were carried out by using CST studio suite. The procedure is as follows [7, 8, 9].

1. Calculate the electromagnetic-field distribution by using CST MW studio (MWS) Eigenmode solver.
2. Set secondary emission yield (SEY) of a cavity material on CST Particle Studio (PS) (see Fig. 2).
3. Put primary electron sources on a cavity surface. Set a number of primary electrons and their energies $O(10^3)$ and several eV, respectively.
4. Import the electromagnetic-field distribution obtained by MWS, and simulate electron-dynamics by using PS TRK solver (see Fig. 3).

The above procedure is repeated with sweeping E_{acc} and changing models.

In the step 2, we adopted the Furman model [10], in which an SEY is given as a function of the impact energy

ISBN: 978-3-95450-168-7 doi:10.18429/JACoW-IPAC2015-WEPMA054

A DISTURBANCE-OBSERVER-BASED CONTROLLER FOR LLRF SYSTEMS

F. Qiu[#], D. Arakawa, Y. Honda, H. Katagiri, T. Matsumoto, S. Michizono, T. Miura, T. Obina, KEK, Tsukuba, Ibaraki 305-0801, Japan
S. B.Wibowo, Sokendai, the Graduate University for Advanced Studies, Tsukuba, Japan

Abstract

Digital low-level radio frequency (LLRFs) systems have been developed and evaluated in the compact energy recovery linac (cERL) at KEK. The required RF stabilities are 0.1% rms in amplitude and 0.1° rms in phase. These requirements are satisfied by applying digital LLRF systems. To further enhance the control system and make it robust to disturbances such as large power supply (PS) ripples and high-intensity beams, we have designed and developed a disturbance observer (DOB)-based control method. This method utilizes the RF system model, which can be acquired using modern system identification methods. Experiments show that the proposed DOB-based controller is more effective in the presence of high disturbances compared with the conventional proportional and integral (PI) controller. In this paper, we present the preliminary results based on the experiments with DOB-based controller.

INTRODUCTION

At KEK, a 3 GeV energy recover linac (ERL) light source is proposed. For the demonstration, a compact ERL (cERL) was constructed as a prototype machine for the 3-GeV ERL project [1,2]. The cERL, which is a 1.3 GHz superconducting (SC) project, consists of an injector part and a recirculating loop part. Three two-cell cavities, called Inj. 1, Inj. 2, and Inj. 3, were installed in the injector, and two main nine-cell cavities were installed in the recirculating loop. To fulfill the required beam quality, the RF field fluctuations should be maintained at less than 0.1% (in amplitude) and 0.1° (in phase) in the cERL. Field programmable gate array (FPGA)-based digital low-level ratio frequency (LLRF) systems were developed to implement the RF field control [3].

In the LLRF systems of the cERL, disturbance signals such as 50-Hz microphonics and 300 Hz high-voltage power supply (HVPS) ripples will severely limit the performance of the LLRF systems [3]. Furthermore, during beam commissioning, the beam loading can be seen as another disturbance. In principle, these disturbance signals can be rejected or suppressed by applying high proportional and integral (PI) gains in the feedback (FB) control; however, the PI gains are limited by the loop delay. In the cERL, during the beam commissioning, we found that the PI gain is not sufficient in the presence of large disturbances. In view of this situation, we present a disturbance observer (DOB)-based approach that aims to control an LLRF system subject to large disturbances [4-5].

#qiufeng@post.kek.jp

In this paper, we first introduce the LLRF system in the cERL, and then describe the principle, design, and implementation of this DOB-based approach. Finally, preliminary results are used to compare the proposed DOB control and the previous PI control in the cERL beam commissioning.

LLRF SYSTEM

A simplified block diagram of the cERL LLRF system is shown in Fig. 1. The 1.3-GHz cavity probe signal is down-converted to a 10-MHz intermediate frequency (IF) signal. The IF signals are sampled at 80 MHz by 16-bit ADCs and then fed into the FPGA. The baseband and quadrature (I/Q) components are extracted from the IF signal with a non-IQ method. In the next stage, the I/Q signals are compared with their set values, and the errors are calculated. The errors are regulated with a PI controller and then added with a feedforward (FF) table. Finally, the combined signal is fed into the I/Q modulator via the 16-bit DACs to regenerate the 1.3-GHz RF signal. This regulated RF signal will be used to drive the high-power source, which drives the cavities [6,7].

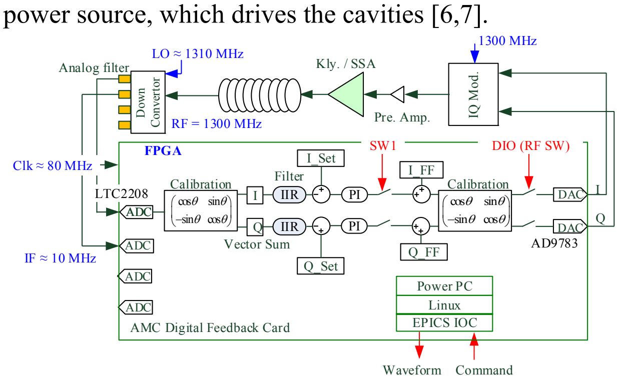

Figure 1: Schematic of the LLRF system in the cERL.

DOB CONTROL

The basic idea of DOB control is shown in Fig. 2(a) [4-5]. Here, $G_p(s)$ and $G_n(s)$ represent the transfer function of the actual plant (e.g., cavities and RF devices) and the nominal mathematical model. Signals d and d_e represent the real disturbance and the disturbance estimate, respectively. Signal *FF* represents the FF table output.

From Fig. 2(a), it is clear that the disturbance estimate d_e can be expressed by

$$d_e = (\varepsilon + d) G_p(s) G_n^{-1}(s) - \varepsilon . \qquad (1)$$

Content from this work may be used under the terms of the CC BY 3.0 licence (© 2015). Any distribution of this work must maintain attribution to the author(s), title of the work, publisher, and DOI.

ISBN: 978-3-95450-168-7 doi:10.18429/JACoW-IPAC2015-WEPMA055

THE MAGNET AND POWER SUPPLY SYSTEM FOR THE COMPACT-ERL*

Kentaro Harada#, Tatsuya Kume, Shinya Nagahashi, Norio Nakamura,
Shogo Sakanaka, Akira Ueda, KEK, Ibaraki, Japan

Abstract

The recirculation loop of the cERL (compact Energy Recovery LINAC) was constructed in 2013. In this paper, we show the magnet and the power supply system for the recirculation loop of the cERL. The recirculation loop consists of the eight main bending magnets at the arc section, sixty quadrupole magnets and ten small bending magnets for the three chicanes of the injection, extraction and circumference adjuster. The four power supplies are used for the chicane bending magnets, sixty for the quadrupoles, forty-eight for the horizontal correctors, and thirty-three for the vertical correctors. The EPICS (Experimental Physics and Industrial Control System) was adopted to control these power supplies.

INTRODUCTION

The cERL (compact Energy Recovery LINAC[1-3]) consists of the injector, merger, recirculation loop, extraction chicane, and the beam dump. The photocathode electron gun generates the electron beam. The beam goes to the recirculation loop after the acceleration by the injector cavities through the merger chicane. The main linac cavities accelerates the beam to about 20 MeV. After the recirculation loop, the main linac decelerate the beam to about 3 MeV. Finally the beam dump catches the "used" beam after the extraction chicane. In this paper, we show the magnet and power supply system of the cERL.

MAGNETS

The layouts of the magnets of the cERL are show in Fig. 1. For the magnet names in the figure, "B.."s are the bending magnets, "Q.." quadrupole magnets. "ZH.."s are the horizontal correctors and "ZV.." the vertical correctors. The all correctors at the recirculation path are the correction coils of the bending and quadrupole magnets. The four sextupoles for the bunch compression and restoration will be installed at the arc section in this summer of 2015. The parameters are shown in Table 1.

Bending Magnets

The bending angle of the main bending magnet at the arc sections (BMIF and BMIR in Fig. 1) are 45 degree. The parameters are shown in Table 1. The eight sector type magnets are connected to one power supply. The path of the magnetic power cable was fixed in order to avoid the large solenoidal loop. The picture of the magnet is shown in Fig. 2(a).

The magnetic core consists of the lamination of the silicon steel. The edge of the magnetic core was cut in order to form the sector shape after the lamination. The magnetic cables of 200 mm^2 cross section was used for the full energy operation of 245 MeV (800 A). With 20 MeV operation, the magnetic current is about 50 A and the capacity of the present power supply is 100 A/40 V. All bending magnets have the correction coils of fifty turns for the horizontal corrector. The hollow conductor was used for the main coil in order to 800 A operation. However, no water cooling was required for present 20 MeV operation.

The two ready-made bipolar power supplies of ±10 A/±40 V were used for the five small bending magnets of the merger chicane (Fig. 3(a)); the one connected to BMAG3-5 and the other BMAG1-2. (For the beam operation, the unipolar type power supplies were sufficient.) For the recirculation beam, the turn numbers of the coils of BMAG3-5 are adjusted to achieve the local bump orbit. For the injection beam, the edge angle of BMAG2 is fixed to eliminate the dispersion function at the entrance of the recirculation loop. The correction coils of these magnets are used for the precise adjustment of the

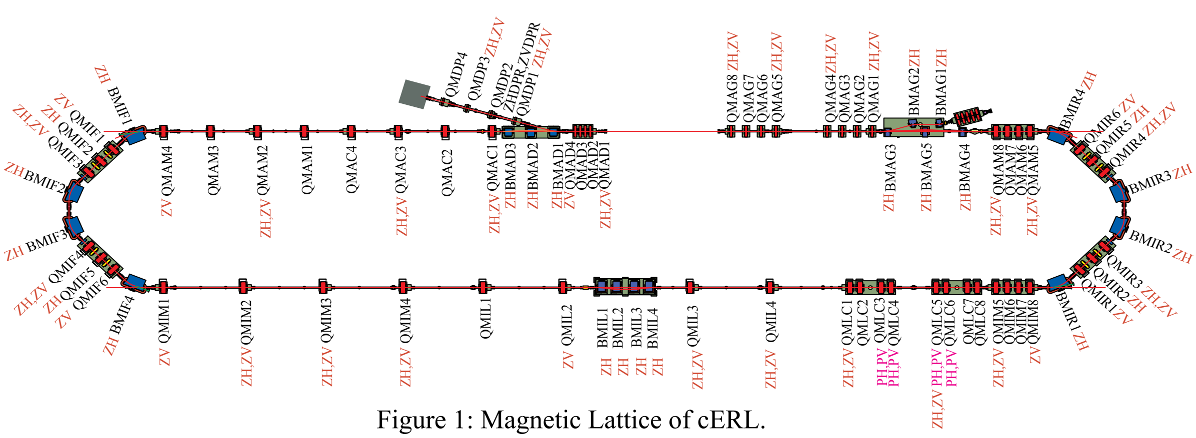

Figure 1: Magnetic Lattice of cERL.

*Work supported by "A government (MEXT) subsidy for strengthening nuclear security" of Japan.

#kentaro.harada@kek.jp

Content from this work may be used under the terms of the CC BY 3.0 licence (© 2015). Any distribution of this work must maintain attribution to the author(s), title of the work, publisher, and DOI.

ISBN: 978-3-95450-168-7 doi:10.18429/JACoW-IPAC2015-WEPMA056

DEVELOPMENT OF SUPERCONDUCTING SPOKE CAVITIES FOR LASER COMPTON SCATTERED X-RAY SOURCES

R. Hajima#, M. Sawamura, JAEA, Tokai, Ibaraki 3191195 Japan
T. Kubo, T. Saeki, KEK, Tsukuba, Ibaraki 3050801 Japan
E. Cenni, Y. Iwashita, H. Tongu, Kyoto University, Uji, Kyoto 6110011 Japan

Abstract

A 5-year research program on the development of superconducting spoke cavities for electron accelerators has been funded by MEXT, Japan since 2013. The purpose of our program is establishing design and fabrication processes of superconducting spoke cavity optimized for compact X-ray sources based on laser Compton scattering. The spoke cavity is expected to realize a compact industrial-use X-ray source with a reasonable cost and easy operation. We have chosen a cavity frequency at 325 MHz due to possible operation at 4 K and carried out cavity shape optimization in terms of electromagnetic and mechanical properties. Production of press-forming dies is also in progress. In this paper, we present overview and up-to-date status of the research program.

INTRODUCTION

Laser Compton scattered (LCS) X-ray sources are now widely explored as an important application of advanced accelerators, since they can produce high-brightness energy-tunable X-ray beams with a compact footprint [1,2]. Such LCS X-ray sources can be realized with any type of electron accelerator: RF linacs, racetrack microtrons, storage rings, and energy-recovery linacs.

A photon flux from LCS sources is proportional to the frequency and density of electron and laser beams at the collision. Spectral brightness is proportional to electron beam brightness. Thus, electron beams of high-average current and small emittance are preferable for high-flux and high-brightness LCS sources. In this sense, we consider the energy-recovery linac is suitable for LCS sources.

A 5-year research program has been established to develop fundamental technologies for a compact high-brightness LCS X-ray source. In the research program, we are developing superconducting spoke cavities for future LCS X-ray sources.

Spoke cavity was originally invented for acceleration of protons and ions (v/c<1), but it can also be applied to electron accelerators (v/c=1) with minor modification of cavity shape [3,4]. We suggest the spoke cavity realizes a compact industrial-use X-ray source with a reasonable cost and easy operation because of the following reasons: (1) with the same cavity radius, the resonant frequency of spoke cavities is almost half of elliptical cavities. As a result, 4-K operation becomes a practical solution by choosing a resonant frequency below 500 MHz. (2) Spoke cavities have small microphonic detuning thanks to their mechanical stiffness and unique electromagnetic property, the resonant frequency depending mainly on the spoke length. This small frequency fluctuation contributes to the reduction of RF source capacity for ERL operation. (3) the spoke cavities accommodate power couplers and HOM couplers at the side region, thus the multiple spoke cavities can be installed with a better packing factor than elliptical cavities that require couplers on the beam pipe. (4) cell coupling of spoke cavity is stronger than that of elliptical cavity. With the strong cell coupling, we can easily adjust the field flatness along a multi-cell (multi-spoke) structure.

In this paper, we describe the status of spoke cavity development program in Japan.

PROPOSED X-RAY SOURCE

The proposed X-ray source is based on an ERL and a laser enhancement cavity similar to the LCS source recently demonstrated at the Compact ERL (cERL) [5]. As seen in Table 1, the targeting goal of the project is to realize the collision of megawatt-class electron and laser beams for a high-flux and high-brightness X-rays. Average brightness expected in the LCS source is comparable to 10-keV X-rays from a bending magnet at KEK-PF (2.5 GeV, 400 mA). The X-ray flux and brightness are reduced by duty factor, if we operate the LCS source at a burst mode (1 ms x 10 Hz for example) for saving the machine construction and running cost.

Table 1: Parameters of the Proposed X-Ray Source

E-bean			
Energy / current	25 MeV / 30 mA	Norm. emittance	1 mm-mrad
Laser			
Wave-length	1 μm	Stored power	1 MW
LCS			
Repetition	325 MHz	Flux (100%BW)	1×10^{14} ph/s
Collision spot	20 μm (rms)	Average Brightness	3×10^{14} (c.u.)
X-ray	10 keV		

hajima.ryoichi@jaea.go.jp

Content from this work may be used under the terms of the CC BY 3.0 licence (© 2015). Any distribution of this work must maintain attribution to the author(s), title of the work, publisher, and DOI.

ISBN: 978-3-95450-168-7 doi:10.18429/JACoW-IPAC2015-WEPMA057

DEVELOPMENT OF HTS MAGNETS

Kichiji Hatanaka*, Mitsuhiro Fukuda, Keita Kamakura, Hiroshi Ueda,
Tetsuhiko Yorita, Takane Saito, Yuusuke Yasuda
Research Center for Nuclear Physics, Osaka University, 10-1 Mihogaoka, Ibaraki, Osaka, 567-0047
Takeo Kawaguchi
KT-Science, 1470-1-803, Fujie, Akashi, Hyogo, 673-0044

Abstract

We have been developing magnets utilizing high-temperature superconducting (HTS) wires for this decade. We built three model magnets, a mirror coil for an ECR ion source, a set of coils for a scanning magnet and a super-ferric dipole magnet to generate magnetic field of 3 T. They were excited with AC/pulse currents as well as DC currents. Recently we fabricated a cylindrical magnet for a practical use which polarizes ultracold neutrons (UCN). The field strength at the center is higher than 3.5 T which is required to fully polarize 210 neV neutrons. The magnet was used to polarized UCN generated by the RCNP-KEK superthermal UCN source. One dipole magnet is under fabrication, which is used as a switching magnet after the RCNP ring cyclotron and is planned to be excited by pulse currents. It becomes possible to deliver beams to two experimental halls by time sharing.

INTRODUCTION

High-temperature superconductor (HTS) materials were discovered in 1986 [1] for the first time. Significant efforts have been continued for the development of new and improved conductor materials [2] and it became possible to manufacture relatively long HTS wires of the first generation [3]. Today, many researches are ongoing to establish a reliable production process of the second generation HTS wires and their applications. Although many prototype devices using HTS wires have been developed, so far these applications have been rather limited in accelerators and beam line facilities [4].

At the Research Center for Nuclear Physics (RCNP) of Osaka University, we have investigated the performance of HTS wires applied for magnets excited by alternating current (AC) as well as direct current (DC) for ten years. We have fabricated four types of magnets. They are a cylindrical magnet [5], a scanning magnet with race-track shape coils [6], a super-ferric dipole magnet [7] and a solenoid like magnet consisting of double pan cakes [8]. The coil of the dipole magnet has a negative curvature and the magnet successfully generated the field higher than 3 T at operating temperature of 20 K. First three magnets are toy models, but the last one is actually used to polarize ultracold neutron (UCN). Based on the successful application, we are now constructing a HTS switching magnet to make a time sharing of beams from the RCNP ring cyclotron. We selected a commercially available first-generation HTS wire supplied by Sumitom Electric Industries, Ltd [9].

*hatanaka@rcnp.osaka-u.ac.jp

Designs and preliminary results of performance tests of fabricated magnets are summarized in this paper.

SCANNING MAGNET

A two-dimensional scanning magnet was fabricated to model a compact beam scanning system. The size of the irradiation field is 200 mm by 200 mm for 230 MeV protons at the distance of 1.25 m from the magnet center. The required magnetic field length is 0.185Tm. The scanning magnet consists of two sets of two racetrack-type coils. Each coil is built by stacking three double pancakes. The design parameters are summarized in Table 1. Figure 1 shows a photograph of one coil.

Table 1: Design Parameters of the HTS Scanning Magnet

Coils	Iner size	B_x: 150mm x 300mm.
		B_y: 150mm x 380mm
	Separation	70mm
	Maximum Field	0.6T
	# of tturns	420 x 2 for each B_x and B_y
	Winding	3 Double pancakes/coil
	Inductance/coil	B_x: 75mH, B_y: 92mH
	Temperature	20K
	Rated current	200A
Cryostat	Cooling power	45W at 20K, 53W at 80K

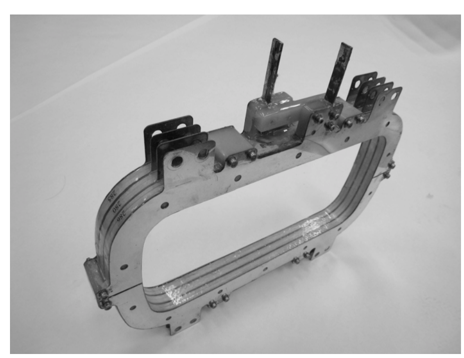

Figure 1: Single assembled B_x coil

Two sets of single-stage GM (Gifford-McMahon) refrigerators were used to cool the coils and the thermal shields. The critical current (Ic) of the HTS conductor depends on the operating temperature and the magnetic field at its surface. From the numerical estimation of the

Content from this work may be used under the terms of the CC BY 3.0 licence (© 2015). Any distribution of this work must maintain attribution to the author(s), title of the work, publisher, and DOI.

ISBN: 978-3-95450-168-7 doi:10.18429/JACoW-IPAC2015-WEPMA058

Content from this work may be used under the terms of the CC BY 3.0 licence (© 2015). Any distribution of this work must maintain attribution to the author(s), title of the work, publisher, and DOI.

NEW INJECTION BUMP POWER SUPPLY OF THE J-PARC RCS*

T. Takayanagi#, N. Hayashi, T. Ueno, K. Horino, K.Okabe, K. Kinsho, J-PARC, Japan
JAEA, Tokai-Mura, Naka-Gun, Ibaraki-Ken, Japan
Y. Irie, KEK, Ibaraki-Ken, Japan

Abstract

The new injection bump power supply for the shift bump (SB) magnet of the beam injection sub-systems at the J-PARC (Japan Proton Accelerator Research Complex) [1] 3-GeV RCS (Rapid Cycling Synchrotron) [2] has been developed and manufactured. The power capacity of the new power supply was more than doubled with the injection beam energy upgrading of the LIANC (Linear Accelerator) from 181 MeV to 400 MeV [3]. Furthermore, the low ripple noise on the output current was required to prevent the resonance of the RF shield loop at the ceramic duct with the excitation magnetic field [4]. The power supply newly adopted a capacitor commutation method to form the trapezoid waveform pattern (bump waveform). This paper reports characteristic about the new power supply.

INTRODUCTION

The new power supply for the injection SB-magnet, which is one of the beam injection sub-systems of the 3-GeV RCS in the J-PARC, has been developed and manufactured with the injection beam energy upgrading of the LINAC from 181 MeV to 400 MeV. The power supply capacity increases about twice the 181 MeV specifications. The previous SB power supply adapted the IGBT (Insulated Gated Bipolar Transistor) chopping system of the main circuit, which produces the continuous current ripple noise due to the switching [5]. However, the ripple noise on the output current had been resonated with the RF shield loop on the ceramics duct in the SB-magnet, resulting in a forced beam oscillation at the injection stage [4]. The circuit configuration of the new power supply has been changed to the capacitor commutation method using the charging and discharging circuits. This system forms the trapezoid waveform pattern (bump waveform) at 25 Hz repetition with only three times switching per pulse. Therefore, the current ripple noise caused by the switching was reduced considerably.

The SB power supply is comprised of the 16 banks in parallel. The 1 bank includes 12 rise-fall units (Rf-unit) and 2 flat-top units (Ft-unit), which produces an output current of 2 kA and an output voltage of 12 kV. So the maximum output current and output voltage are 32 kA and 12 kV, respectively. By controlling the capacitor voltage and the gate timing of the changeover switch in each unit individually, the power supply can produce an arbitrary waveform which has different rise-fall time and flat-top time duration with high accuracy. The RCS provides a high intensity beam for the MLF (Material and Life Science Experimental Facility) and MR (50-GeV Main Ring) in a time-sharing mode. The bump system changes the output current to meet the demand of different painting areas for the MLF and MR beams [6]. This paper summarizes the design and the experimental results of the new power supply.

*tomohiro.takayanagi@j-parc.jp

OVER VIEW OF THE POWER SUPPLY

Basic Circuit

The power supply is comprised of two kinds of unit. One is the Rf-unit that produces the peak voltage controlling the rise-fall time of the bump waveform. Another is the Ft-unit that maintains the flatness and duration at the flat-top. The basic circuit of the two units is the same, whose schematic view is shown in Fig. 1. The DC charger charges the main electrolytic capacitor C and the switching device of the IGBT defines each operation mode, which is the powering, regeneration and free-wheeling. The model of the bump waveform and the relationship between each unit and each operation mode are shown in Fig. 2 and Table 1. The peak current is determined by setting each DC charger parameter for the charging voltage of the capacitor and the duration of the rise-fall and flat-top is determined by the switching in a predetermined timing of each operation mode.

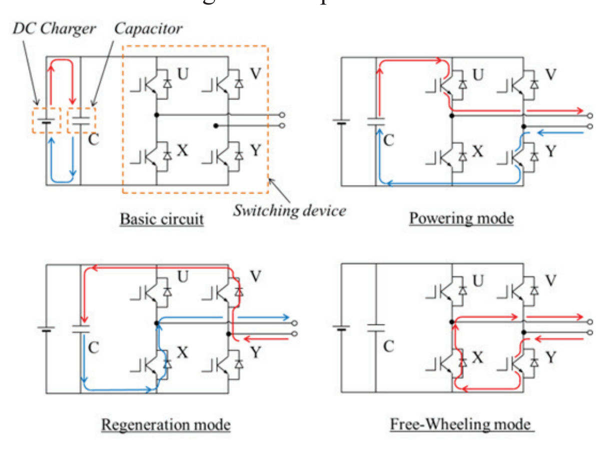

Figure 1: Base circuit of the unit.

Power Supply Construction

The schematic view of the 1 bank is shown in Fig. 3. The 1 bank is comprised of 12 Rf-units and 2 Ft-units, where all units are connected in series with the midpoint earth. The Rf-unit has two chopper stages connected in series. The capacitor unit is composed by 8 capacitors of 24 mF and the composite capacitance is 48 mF per one DC charger. The Ft-unit has two chopper stages with different charging voltages in order to change the output

ISBN: 978-3-95450-168-7 doi:10.18429/JACoW-IPAC2015-WEPMA059

DEGASSING OF KICKER MAGNET BY IN-SITU BAKE-OUT METHOD

J. Kamiya[#], N. Ogiwara, Y. Hikichi, M. Kinsho
JAEA/J-PARC, Shirakata Shirane 2-4, Tokai, Naka, Ibaraki, Japan
N. Miki, T. Yanagibashi
NAT, Muramatsu 3129-45, Tokai, Naka, Ibaraki, Japan

Abstract

New method of in-situ degassing of the kicker magnet in the beam line has been developed. The heater and heat shielding panels are installed in the vacuum chamber in this method. The heater was designed considering the maintainability. The graphite was selected as the heater and the high melting point metals were used as the reflectors just near the heater. The thermal analysis and the temperature measurement with the designed heater was performed. The ideal temperature distribution for the degassing of the kicker magnet was obtained. The outgassing of the graphite during rising the temperature was measured. The result showed that the outgassing was extremely suppressed by the first heating. This means the outgassing of the graphite heater was negligible as long as it is used in the beam line without exposure to the air.

INTRODUCTION

The usual way to reduce outgassing from a device in vacuum is to heat up a whole vacuum chamber containing the device. However, the situation, where this method can be applied, is limited due to the heat expansion of the chamber. Especially in accelerators, where the vacuum chambers are connected with nearby beam pipes, this normal bake-out method may not be applied. If a heat source and heat shields are appropriately installed inside the chamber, heat flux is directed to the device. Therefore the device can be baked out without raising the temperature of the vacuum chamber.

One candidate for such bake-out method to be applied is kicker magnets in J-PARC 3GeV synchrotron (RCS), which are installed in large vacuum chambers. The role of the kicker magnets is to extract an accelerated 3 GeV proton beam to a downstream beam transport line [1]. The voltage of 30 kV is applied from the power supply to the magnets in order to generate the magnetic field whose rise time is about 300 ns. The kicker magnets are installed in vacuum to prevent the discharge by such high voltage. The kicker magnet mainly consists of Ni-Zn ferrite cores, aluminium electrode plates. The total outgassing rate of the materials is large due to the large surface area. Therefore it is very important to develop a degassing method for the kicker magnets in the beam line because the vacuum quality may become poor after repeated exposures to air for the maintenances. The main outgassing component is water vapour [2]. Therefore the bake-out temperature should be above 100 °C, which is the typical desorption temperature of water vapour from the general surface. In the RCS beam line, 3 and 5 kicker magnets are located in vacuum chambers, whose length is 3 and 5 m, respectively. It is undesirable to use a normal baking method like baking the vacuum chamber of the kicker magnets because the large heat expansion of the vacuum chamber, which will be ~5 mm with a temperature rise of 100 ^{o}C for a chamber of 5 m length, will break nearby equipment such as alumina ceramics pipes. By applying the bake-out method, which is mentioned at the beginning of this chapter, only the kicker magnet is heated without raising the temperature of the vacuum chamber. So far, we performed the operability assessment of the new degassing method by the calculation with a simple model and the principal experiments using the R&D kicker magnet, which have the same structure as the production kicker magnets in RCS [3]. As a result, the ferrite cores were heated up above 100 °C while keeping the temperature rise of the vacuum chamber less than 20 °C. One of the technical issues was the design of the heater, which has a good maintainability. In this report, first, we will show the design and concept of the newly developed heater. Next, the temperature distribution of the kicker magnet and the vacuum chamber using the new heater is also presented. Finally, the vacuum characteristic of the heater material is reported.

DESIGN OF THE HEATER

Any heater is possible to be damaged eventually. Thus the exchange of the heater should be easily performed. The vacuum chambers for the kicker magnets in the RCS beam line has ports with flanges under each kicker magnets. The heater was designed to be inserted from the port. Therefore, the size of the heater should be less than the inner diameter of the port (ϕ 130 mm). In the previous calculation, it was known that about 1000 W is needed for the heater to rise the temperature of ferrite sufficiently above 100 °C [3]. When the 1000 W is supplied to the heater with about 100 mm diameter, the heater temperature would be more than 1000 °C. We selected graphite as the heater material, which meets such requirement. The physical properties of the selected graphite are summarized in Table 1. In addition to the suitable electrical resistivity, the high mechanical strength is the reason of choice. Figure 1 shows the appearance of the heater. The design was performed with checking the temperature distribution of the heater by the thermal analysis. In the analysis, about the heat transfer from the each material surface, the radiation was taken account for the vacuum side, while the natural convection was considered for the atmospheric side, The result of the thermal analysis when 1000 W was supplied to the

[#]junichiro.kamiya@j-parc.jp

Content from this work may be used under the terms of the CC BY 3.0 licence (© 2015). Any distribution of this work must maintain attribution to the author(s), title of the work, publisher, and DOI.

ISBN: 978-3-95450-168-7 doi:10.18429/JACoW-IPAC2015-WEPMA060

THE DEVELOPMENT OF CAVITY FREQUENCY TRACKING TYPE RF CONTROL SYSTEM FOR SRF-TEM

N. Higashi*, The University of Tokyo, Tokyo, Japan
M. Kuriki, HU/AdSM, Higashi-Hiroshima, Japan
S. Yamashita, ICEPP, Tokyo, Japan
A. Enomoto, Y. Funahashi, T. Furuya, X. Jin, Y. Kamiya, S. Michizono
M. Nishiwaki, H. Sakai, M. Sawabe, K. Ueno, M. Yamamoto, KEK, Ibaraki, Japan

Abstract

Superconducting accelerating cavities used in high-energy accelerators can generate high electric fields of several 10 MV/m by supplying radio frequency waves (RF) with frequencies matched with resonant frequencies of the cavities. Generally, frequencies of input RFs are fixed, and resonant frequencies of cavities that are fluctuated by Lorentz force detuning and Microphonics are corrected by feedbacks of cavity frequency tuners and input RF power. Now, we aim to develop the cavity frequency tracking type RF control system where the frequency of input RF is not fixed and consistently modulated to match the varying resonant frequency of the cavity. In KEK (Tsukuba, Japan), we are developing SRF-TEM that is a new type of transmission electron microscope using special-shaped superconducting cavity. By applying our new RF control system to the SRF-TEM, it is expected to obtain stable accelerating fields so that we can acquire good spatial resolution. In this presentation, we will explain the required stabilities of accelerating fields for SRF-TEM and the feasibility of SRF-TEM in the case of applying the cavity frequency tracking type RF control system.

WHAT IS SRF-TEM?

In material science, biology and other science regions, electron microscopes (EMs) are often used to observe sub-nanometer world. There are two kinds of EMs; transmission EMs (TEMs) and Scanning EMs (SEMs). TEMs are more suitable when insides of specimens are targets of studies. Past TEMs use electrostatic acceleration to give kinetic energy to electron beams. Therefore there has been a limit of accelerating energy because of discharge problems. The highest voltage of TEM is 3 MV which has been achieved in Osaka Univ. in Japan [1]. Now we are developing a new type of TEM called SRF-TEM, which applies high energy accelerator technologies; SRF cavities and photo-cathode DC electron gun. It will overcome the limit of accelerating energy so that thicker specimens could be observed. It will help to study the materials, for example, high temperature superconducting matters and magnetic materials and so on. SRF-TEM has other advantages; downsizing facilities, micro-second temporal resolution, less damages to biological samples and the potential for world's best spatial resolution.

* higashi@icepp.s.u-tokyo.ac.jp

CHROMATIC ABERRATION AND SPATIAL RESOLUTION OF TEMS

We could acquire higher energy than 3 MeV for TEMs easily employing RF acceleration with a superconducting cavity. However there is a problem to consider in advance of practical development; degradation of spatial resolution due to increase of chromatic aberration. Spatial resolution of TEMs is determined by following three factors; diffraction aberration, spherical aberration and chromatic aberration. Chromatic aberration occurs due to an energy spread ΔE of an electron beam so that focal lengths of beams are different. A conventional TEMs has low energy dispersion of $O(10^{-6})$. However RF acceleration of our SRF-TEM makes it larger by its sinusoidal electric fields. Therefore the chromatic aberration mainly determines the spatial resolution of SRF-TEM. Figure 1 shows the relation between the energy dispersion and the spatial resolution of our prototype SRF-TEM which accelerating energy is 300 kV. Note that the declination of the spatial resolution is saturated below 1.0×10^{-5} in the energy dispersion. This is because the chromatic aberration r_c is determined by

$$r_c = \alpha C_c \sqrt{\left(\frac{\Delta E}{E}\right)^2 + 4\left(\frac{\Delta J}{J}\right)^2} \tag{1}$$

,where α is the maximum angle of incident beam into the objective lens, C_c is the chromatic aberration constant, $\Delta J/J$ is the current stability of objective lens, which is 1.0×10^{-5} so that even if the energy dispersion is lowered

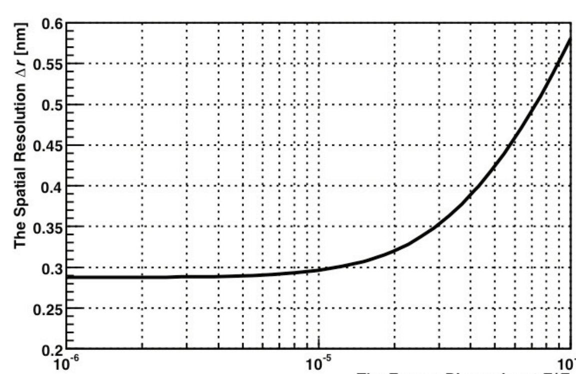

Figure 1: The relation of energy dispersion and the spatial resolution.

Content from this work may be used under the terms of the CC BY 3.0 licence (© 2015). Any distribution of this work must maintain attribution to the author(s), title of the work, publisher, and DOI.

ISBN: 978-3-95450-168-7 doi:10.18429/JACoW-IPAC2015-WEPMN003

THE MAGNETIC MEASUREMENT FOR LOW MAGNETIC FIELD STABILITY OF DIPOLE MAGNET FOR CEPC*

#Z.Zhang, F.Chen, B.Yin, H.Geng
Institute of High Energy Physics, CAS, Beijing 100049, China

Abstract

The CEPC (Circular Electron Positron Collider) project is in the pre-research stage. When the beam energy of booster is 120GeV, the magnetic field of deflection magnet is 640 G. In order to save funds for scientific research, we are ready to select the injection energy for 6 GeV, this corresponds to a magnetic field about 32 Gs. In such a low magnetic field, the effects of earth's magnetic field and ambient temperature variations cannot be ignored. In this paper, first written the collection procedures for magnetic field value and ambient temperature values by Labview software, then used a one-dimensional probe to measure the background magnetic field for three directions (Bx, By, Bz) and the value of the ambient temperature values, the time of data collection for each direction are more than 24 hours (every minute collecting a set of values). Finally, plus the different currents (3A, 6A.. 15A) to the dipole magnet, the time of measured and the data collected by over 24 hours. Based on the results of the analysis of large amounts of data, summarized and analyzed the effect of Earth's magnetic field and ambient temperature for dipole magnet in a low magnetic field.

INTRODUCTION

The Circular Electron Positron Collider (CEPC) is a long-term collider project, which will be divided into two phases. The first phase will construct a circular electron-positron collider in a tunnel with a circumference of 50 – 70 km, and detectors installed at two interaction points. The machine is expected to collide electron and positron beams at the center-of-mass energy of 240 – 250 GeV, with an instantaneous luminosity of 2×1034 $cm^{-2} s^{-1}$. The baseline design considers a single ring in a 50/70 km tunnel and electron/positron beams following a pretzelled orbit in the ring[1]. The accelerator parameters have been calculated and shown in Table 1.

Table 1: The Accelerator Parameters

Accelerator Parameters			
Beam energy[E](Gev)	120	**Lorentz factor[γ]**	234834.66
Circum Ference [C](km)	53.6	**Revolution period[T0](s)**	1.79×10^{-4}
SR power/ beam[P](MW)	50	**Magnetic rigidity[Bp](T*m)**	400.27
Bending radius[ρ](m)	6094	**Momrntum compaction factor[αp]**	4.15×10^{-5}

*Work supported by IHEP
#zhangz@ihep.ac.cn

When the beam energy of booster is 120GeV, the magnetic field of deflection magnet is 640 G. In order to save funds for scientific research, we are ready to select the injection energy for 6 GeV, this corresponds to a magnetic field about 32 Gs. In such a low magnetic field, the effects of earth's magnetic field and ambient temperature variations cannot be ignored.

According to the physical requirements of this experiment, first, a new program of measurement has been written by Labview software.Second, the preparation for hardware, the device of measurement and collimation. The device about measurement includes the Hall-probe measurement facility, the power supply and the dipole magnet; the device of collimation includes theodolite, level and collimation target.

THE DESCRIPTION OF PROGRAM

The Tesla meter is via RS-232 serial port to communicate with the computer. The main program consists of several parts, the serial port is defined, write, read, close, data acquisition (temperature and magnetic field values).The main structure of the program is the while loop and conditional structures.The the front panel of the program is shown in Fig. 1.

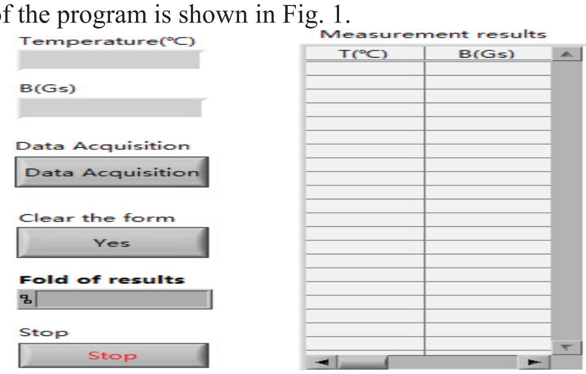

Figure 1: The front panel of the program.

THE DESCRIPTION OF HALL-PROBE MEASUREMENT FACILITY

The Hall-Probe measurement facility is a 3-axises mot ion bench. The movement of 3-axises(x, y and z) can be o perated by computer. The positioning accuracy of x, y and z axis is ±0.001mm and the positioning repeatability accu racy is ±0.01mm. In addition, this machine can be also us ed to adjust the rotation and pitch adjustment probe ensur e that the probe can measure the magnetic field perpendic ular to enter the area of the magnet, so that the total is a fi ve-dimentional adjustment system. The Teslameter and H all probe are produced by Group3 Led. The sensitive of th e MPT-141 Hall Probe is 1×0.5(mm).

Content from this work may be used under the terms of the CC BY 3.0 licence (© 2015). Any distribution of this work must maintain attribution to the author(s), title of the work, publisher, and DOI.

ISBN: 978-3-95450-168-7 doi:10.18429/JACoW-IPAC2015-WEPMN004

PROGRESS ON THE CSNS POWER SUPPLY SYSTEM

Xin Qi, Institute of High Energy Physics, Chinese Academy of Sciences
P.O. Box 918, Beijing, 100049, China

Abstract

The 1.6 GeV proton synchrotron proposed in the CSNS Project is a 25 Hz rapid-cycling synchrotron (RCS) with injection energy of 80 MeV. Beam power is aimed to 100 kW at 1.6 GeV. The power supply system consists of seven subsystems. Those power supplies have three operation modes: DC mode, AC plus DC mode and programmable pulse mode. This paper will introduce the Power Supply System status in recent years.

INTRODUCTION

The CSNS is designed to accelerate proton beam pulses to 1.6 GeV at 25 Hz repetition rate, striking a solid metal target to produce spallation neutrons. The accelerator provides a beam power of 100 kW on the target in the first phase. It will be upgraded to 500 kW beam power at the same repetition rate and same output energy in the second phase. This project has started construction in September 2011, and plans to complete the first phase in March 2018.

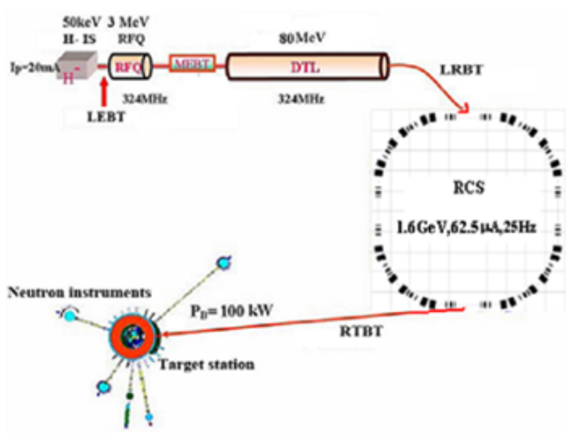

Figure 1: The structure diagram of CSNS.

Figure 1 shows the structure diagram of the CSNS. An ion source produces a peak current of 25 mA H- beam. RFQ linac bunches and accelerates it to 3 MeV. DTL linac raises the beam energy to 80 MeV. After H- beam is converted to proton beam via a stripping foil, RCS accumulates and accelerates the proton beam to 1.6 GeV before extracting it to the target. The Power Supply System consists of the LEBT, MEBT, DTL, LRBT, injection and extraction system, RCS and RTBT Power Supplies. All of them are Digital Power supply. Figure 2 shows the Digital Power Control Module (DPSCM), which is specially designed for CSNS. There is only one FPGA fulfilling the fully-digital control, and the design principle of system on a programmable chip (SOPC) has been implemented [1].

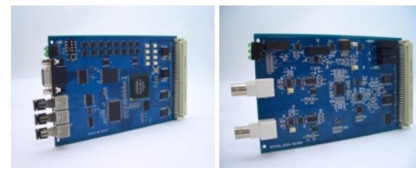

Figure 2: The DPSCM for CSNS Power Supply.

Table 1: Technical Specifications of DC PS

Number(sets)	239
Output Current(A)	10~1700
Output Voltage(V)	5~220
Output Power(Kw)	0.1~73
Stability(24 hours)	100ppm/500ppm
Ripple	≤ 0.01%

DC MAGNET POWER SUPPLY

Table 1 shows the technical specifications of CSNS DC magnet PS. Depending on the power level, this kind of PS has different topology. For the power less than 10 kW, the topology uses the DC/DC half-bridge or full-bridge switch PS; for the power less than 100 kW, the topology uses the Chopper.

In the past year, most of them have completed the production, testing and installation. Now the PS for LEBT and MEBT has worked for beam commissioning.

POWER SUPPLIES FOR RCS

In order to avoid drawing a large reactive power from the a.c. lines, the "White Circuit" type resonant network was adopted widely as the structure of the magnet power supply system of the rapid cycle synchrotron. There are two kinds of resonance configurations: the parallel resonance (PR) and the series resonance (SR) [2]. Usually, dipole magnets adopt the PR network because of the huge power variation and quadrupole magnets adopt the SR network. Considering the convenient machine repair and the controllability of magnet current, all magnets will adopt the SR network in the CSNS Project.

There are totally 24 dipole magnets and 48 quadrupole magnets, which consist of six families. Each magnet is connected in series to the others of its type, and is excited independently by the power supply system.

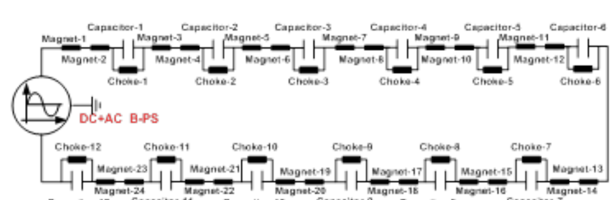

Figure 3: Resonant network of the RCS Dipole PS.

Content from this work may be used under the terms of the CC BY 3.0 licence (© 2015). Any distribution of this work must maintain attribution to the author(s), title of the work, publisher, and DOI.

ISBN: 978-3-95450-168-7 doi:10.18429/JACoW-IPAC2015-WEPMN007

RESEARCH DEVELOPMENT OF HIGN PRECISION INSTALLATION AND ALIGNMENT SYSTEM FOR HEPS*

Lei Wu#, Chunhua Li, Xiaolong Wang, Suying Chen, Haijing Wang, Huamin Qu
IHEP, Beijing, China

Abstract

High Energy Photon Source (HEPS) is a proposed 6 GeV third generation light source with high brightness and ultra-low emittance. Because the measurement error of the traditional optical survey method in the girder and magnet installation can't meet the tight alignment tolerance, the installation and alignment will not only rely on laser tracker and some other optical survey instruments. So HEPS is developing the research of high precision installation and alignment system which is consists of the design of auto-tuning girder based on beam alignment and research of vibrating wire alignment system based on magnetic measurement. This paper introduces the research development of installation and alignment system in storage ring of HEPS.

INTRODUCTION

HEPS will be a 5 GeV, 1296 meters circumference third generation synchrotron radiation facility with ultra emittance and extremely high brightness. The emittance will be better than 0.1nm·rad. The storage ring is a 48 cell 7BA lattice. Fig.1 is one of 48 typical cells. In order to install the magnets easily, the adjacent quadrupole magnets, sextupole magnets and the corrector will use a common multipole support girder. Blue block represents quadrupole magnets and green block represents sextupole magnets. The multipole support girder is designed 3.8 meters [1]

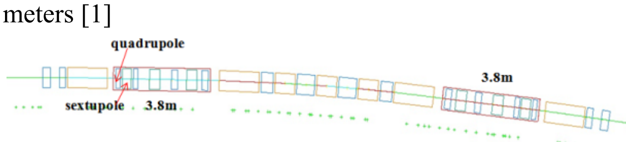

Figure 1: One of 48 typical cells.

Table 1: HEPS Alignment Tolerance

Tolerances	Magnet to Magnet	Girder to Girder
Horizontal	±0.03mm	±0.05mm
Vertical	±0.03mm	±0.05mm
Beam direction	±0.5mm	±0.5mm
Roll angle	±0.2mrad	±0.2mrad

*Work supported by HEPS project
#wulei@ihep.ac.cn

Table 1 shows the alignment tolerance in HEPS. It is difficult to achieve the required accuracy using the traditional optical survey. So vibrating wire alignment technique is considered to meet the tolerance ±0.03mm between magnet to magnet on a multipole girder. And auto-tuning girder can help to achieve the tolerance ±0.05mm between girder to girder.

AUTO-TUNING GIRDER

All girders in the storage ring will automatically adjust when the accelerator is running by monitoring the beams. The natural frequency of the auto-tuning girder should better than 30Hz. And the dynamic state of the auto-tuning girder must be stable. The high precision auto-tuning girder is based on the cam mover mechanism. The similar scheme has been used in Swiss Light Source [2], Taiwan Photon Source [3] and in some other facilities. The eccentric circle cam mover had demonstrated good resolution and good performance in the facilities which have used motorized adjusting mechanism. The design parameters of the auto-tuning girder for HEPS are in Table 2.

Table 2: Design Parameter of Auto-tuning Girder

Design parameter	Design value
Girder size(L×W)	3.8m×0.8m
Cam load	2.5t
Cam eccentric offset	7mm
Cam adjust range	X (-8.7mm~9.4mm) Y (-11.8mm~10.4mm)

Fig.2 is the schematic distribution of the girder supports and the location of the cam mover mechanisms. This eight girder supports distribute along the girder and form four groups of groove mounted mutually perpendicular. This can make full use of the adjust range of this 8 cam mover mechanisms.

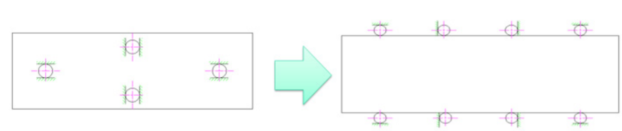

Figure 2: Distribution of girder supports and cam mover mechanisms.

In the storage ring, adjust the position of the girder is by adjusting the origin position of coordinate system. The adjustment process is divided into two steps. Firstly,

Content from this work may be used under the terms of the CC BY 3.0 licence (© 2015). Any distribution of this work must maintain attribution to the author(s), title of the work, publisher, and DOI.

ISBN: 978-3-95450-168-7 doi:10.18429/JACoW-IPAC2015-WEPMN008

MATERAL TEST OF PROTON BEAM WINDOW FOR CSNS

Haijing Wang#, Donghui Zhu, Huamin Qu, Ling Kang, Lei Wu
IHEP, Beijing, China

Abstract

The proton beam window (PBW) is one of the key devices of China Spallation Neutron Source (CSNS). Material selection of PBW is of particular importance. A5083-O was chosen in the previous work, and recently the material tests are done. The tests show the material has good microstructure, physical and mechanical performance. Creep lifetime is analyzed based on the creep test. All the experiments show the selected material is qualified.

INTRODUCTION

The PBW is one of the key devices of CSNS. It is located at the boundary of transport line and target, separating the high vacuum in the accelerator and helium atmosphere in the Helium Vessel. The material selection of the window is important. The heat dissipation, mechanical properties, scattering effect on proton beam, lifetime and so on should be considered. A single-double layered PBW was proposed for CSNS with the beam power of 100 kW in our previous work. A5083-O was chosen as the PBW material mainly for its low effect on beam, and allowable thermal and mechanical properties [1].

As the window is important to the CSNS project, the material should be tested before the window manufactured. The PBW suffers thermal increase because of the energy deposition. And under the comprehensive effects of temperature, boundary fixation, pressure from helium and cooling water and so on, there will be stress and deformation of the window. Generally, the creep temperature of materials is about 30-50% of melting temperature [2]. The working temperature of the window is 73 °C, about the 40% of the melting temperature, then the creep effect should be verified. The material tests contain chemical components, microstructure, physical properties, tensile experiments and creep experiments.

CHEMICAL COMPONENTS

Chemical components are tested by optical emission spectrometric analysis method. There are three samples from different locations and plates. Compared with the standards of GB/T 7999-2007, the materials are all up to standard.

MICROSTRUCTURE

The microstructure is inspected by metalloscope. The results show that the material microstructure is fiber texture. The procedure should be hot rolling and then homogenizing annealing. The plates are annealed completely, and have no defects such as slag inclusion, air hole or loosen. Figure 1 presents the microstructure.

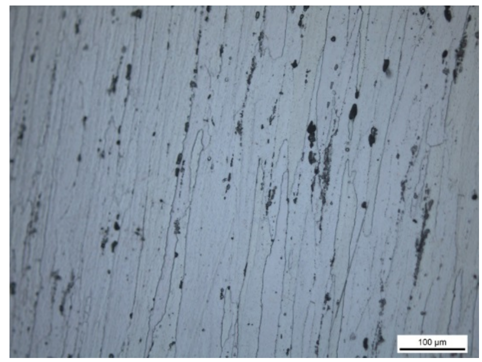

Figure 1: Microstructure (200×).

PHYSICAL PROPERTIES

The physical properties tested conclude density, coefficient of thermal conductivity, coefficient of thermal expansion, Poisson's ratio, modulus of elasticity and heat capacity, of which the results are showed in Table 1. All these items are tested from three samples from different locations and plates. And the results are the average values of each items separately. All these parameters will affect the thermal and structural conditions of the window, and are necessary for finite element analysis by ANSYS.

Table 1: Results of Physical Properties

Item	Results
Density ($g \cdot cm^{-3}$)	2.66
Coefficient of thermal conductivity ($W \cdot (m \cdot °C)^{-1}$)	119.7
Coefficient of thermal expansion ($10^{-6} \cdot °C^{-1}$)	24.2
Poisson's ratio	0.32
Modulus of elasticity (GPa)	70.3
Heat capacity ($J \cdot (kg \cdot °C)^{-1}$)	901

TENSILE PROPERTIES

The tensile properties should be estimated to make sure the window can work normally. There are two types of tensile experiments, at room temperature and high temperature separately.

#wanghaijing@ihep.ac.cn

Content from this work may be used under the terms of the CC BY 3.0 licence (© 2015). Any distribution of this work must maintain attribution to the author(s), title of the work, publisher, and DOI.

ISBN: 978-3-95450-168-7 doi:10.18429/JACoW-IPAC2015-WEPMN009

DESIGN AND THERMAL ANALYSIS OF ADS BEAM STOP

Minxian Li, Jianli Wang, Lei Wu, IHEP, Beijing, China

Abstract

ADS beam stop is an important device which required for the commissioning and accelerator tests of Accelerator Driven Sub-critical System (ADS), it is used to stop the beam which power is about 100kW and consume energy of the beam. This paper will present a triangular prism structure of the ADS beam stop, its mechanical design is described in detail, and there are numerous grooves and ribs in the cooling plates which is the core component of the beam stop. The thermal analysis is performed and its result proves that the triangular prism structure meet the design requirement.

INTRODUCTION

The China Accelerator Driven Sub-critical System(C-ADS) program is an important strategic research for solving nuclear waste and nuclear fuel problems. The Institute of High Energy Physics (IHEP) is responsible for Injector I which based on 325MHz RFQ and spoke cavities [1]. The driven accelerator works with an average beam current of 10mA. The ADS beam stop is an important terminal device of accelerator which used to stop the beam and consume energy of the beam, as no target is planned for the accelerated beam, so the ADS beam stop is required for the commissioning and accelerator tests. Table 1 Shows some design parameters of ADS beam stop.

Table 1: Design Parameters of ADS Beam Stop

Item	Result
Beam power	100kW
Beam current	10mA
Beam energy	10MeV
Beam diameter	200mm
Design water pressure	10kg/cm^2
Water velocity	2m/s
Water temperature	20°C
Vacuum pressure	6.67×10^6 MPa
Vacuum leak rate	2.67×10^3 MPa· m^3/s

MECHANICAL DESIGN

Material and Structure Choice

As the temperature, thermal gradients, and stress field in the beam stop material are directly dependant on the power density profile [2], therefore, it is an effective means by reducing the power density. The reduction of this power density is achieved by defocusing the beam to increase its size and by using a very low incidence angle in the beam stop thus maximizing the material surface area hit by the beam [3]. So the beam, which has a circular cross profile, is expanded to diameter 200mm at the beam stop entrance. In addition, use a smaller angle in order to increase the material surface area hit by the beam is another mean to reduce the power density. The Oxygen-free Copper (OFC) is chosen for the main material of the core component because of its thermal properties and activation criteria.

The triangular prism structure is used for the beam stop (Figure 1), the material surface area hit by the beam is changed with the angle of the two OFC plates, the angle of the two OFC plates should be properly chosen, avoiding large angle, which would produce high power density, and too small angle, which would increase the overall length of the beam stop. Besides, this structure is more convenient for processing.

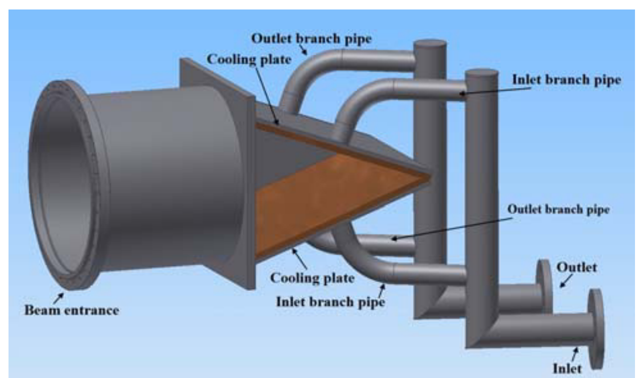

Figure 1: The structure of the ADS beam stop.

Cooling System

Due to the heat flux (or the power density) is very high, water is chosen as coolant of the cooling system. There are a number of long grooves (Figure 2&3) and ribs in the back of the OFC plates which opposite to the beam hit surface. The cooling water flow through the long groove from one side to another side, in this process, the heat exchange is performed and the heat is taken away by cooling water. The coolant channel geometry is chosen to provide adequate velocity in the high power density zone, avoiding high values, which would produce vibrations and material erosion, and too low values, which would not provide enough heat transfer [3]. Therefore, as a matter of past experience and calculation, the cooling water enters at a high velocity (2m/s), and the water pressure is 10kg/cm2.

Content from this work may be used under the terms of the CC BY 3.0 licence (© 2015). Any distribution of this work must maintain attribution to the author(s), title of the work, publisher, and DOI.

ISBN: 978-3-95450-168-7 doi:10.18429/JACoW-IPAC2015-WEPMN010

ANALYSIS OF THE ELECTROMAGNETIC FIELD IN THE COUPLER OF NORMAL TEMPERATURE TRAVELLING-WAVE ACCELERATING TUBE

X. He#, M. Hou, G. Shu, Key Laboratory of Particle Acceleration Physics and Technology, Institute of High Energy Physics, Chinese Academy of Science, Beijing, China

Abstract

With the developed requirement of the beam quality in modern accelerators, rapid development of all kinds of accelerating structures with different frequencies and materials have been achieved. However, the normal temperature travelling-wave (TW) accelerating structures which are widely used in Free Electron Laser (FEL) are still indispensable. For reducing the beam emittance, it is very important to optimize the symmetry of the high-order electromagnetic field in the coupler of such accelerating structures. In this paper, the symmetry of the electromagnetic field in TW accelerator couplers using different coupling mechanisms was analysed. A lot of design optimization as well as the result analysis work has been done for the three kinds of commonly used waveguide-coupled TW accelerating structures: single-feed electrical-coupling, dual-feed electrical-coupling using magic tee in feeding waveguide and dual-feed magnetic-coupling using J-type feeding waveguide. Finally, basing on lots of simulation results and the performances during the fabrication, measurement and RF conditioning of these three kinds of structures, the J-type racetrack coupler type is regarded as the best choice.

INTRODUCTION

The SLAC-type normal temperature travelling-wave accelerating structure is widely used in the large high-energy electron linear accelerators all over the world. The rotational-symmetrical cylindrical cavity or the racetrack cavity is usually used as the input coupler for this kind of accelerating structure. The rotational symmetry of the cylindrical cavity is affected by the introduction of the coupling hole of the cavity, which results in an asymmetry of the electromagnetic field within the envelope of the beam and then degrades the beam quality by increasing the beam emittance. By using the dual-feed accelerating structure instead of the single-feed, the symmetry of the electromagnetic field of the cylindrical cavity is improved, however, along the vertical direction of the two symmetrical coupling holes in the dual-feed cylindrical cavity, the symmetry is still affected. For further improving the symmetry of the electromagnetic field within the envelope of the beam, the racetrack cavity is adopted by elongating the cylindrical cavity along the vertical direction of the two coupling holes.

The research work concerning the improvement of the symmetry of electromagnetic field in the racetrack cavity comparing to the cylindrical cavity has been done in some articles [1]. However, all of them are focused only on one of the coupling mechanism, or only on the symmetry of electrical field. On the basis of considering several kinds of coupling mechanisms, the comprehensive analysis and compare work for the symmetry of electromagnetic field between the cylindrical and racetrack cavity has been done and some inferences has been given here.

STRUCTURE OF THE COUPLING CAVITIES

For better analysing the improvement of the symmetry of electromagnetic field in the racetrack cavity, three commonly used coupling mechanisms (numbered as coupling mechanism 1 to 3 in sequence) are chosen: the single-feed electrical-coupling (central frequency 2998 MHz), the dual-feed electrical-coupling using magic tee in feeding waveguide (central frequency 2856 MHz) and the dual-feed magnetic-coupling using J-type feeding waveguide (central frequency 2856 MHz). The structures of them are shown in Fig. 1a and the difference between the racetrack cavity and the cylindrical cavity is shown in Fig. 1b.

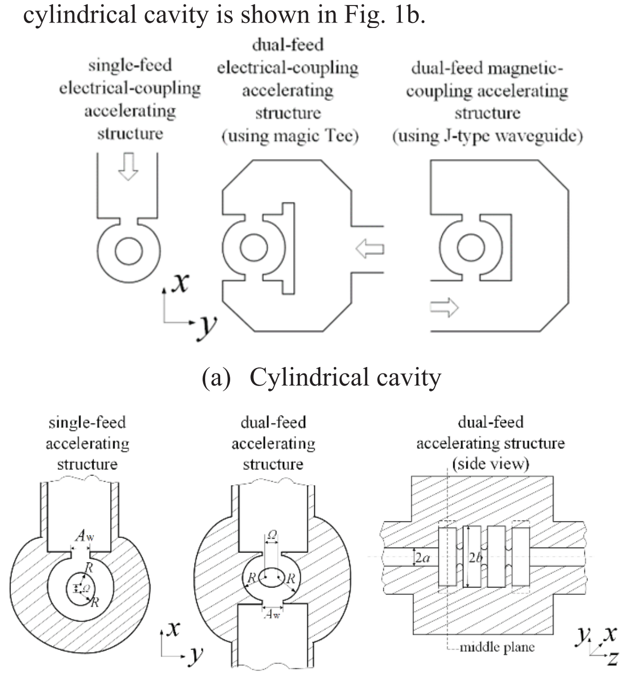

(a) Cylindrical cavity

(b) Racetrack cavity

Figure 1: Structure diagram of the input cavities.

An eccentric circle structure is adopted in coupling mechanism 1 (Fig. 1b) to compensate the asymmetry of electromagnetic field resulted from the introduction of the single coupling hole. The centre of the eccentric

hexiang@ihep.ac.cn

Content from this work may be used under the terms of the CC BY 3.0 licence (© 2015). Any distribution of this work must maintain attribution to the author(s), title of the work, publisher, and DOI.

ISBN: 978-3-95450-168-7 doi:10.18429/JACoW-IPAC2015-WEPMN011

RF MODULATION STUDIES ON THE S BAND PULSE COMPRESSOR

G. Shu[#], F. Zhao, S. Pei, Key Laboratory of Particle Acceleration Physics and Technology, Institue of High Energy Physics, Chinese Academy of Science, Beijing, China

Abstract

An S band SLED-type pulse compressor has been manufactured by IHEP to challenge the 100 MW maximum input power, which means the peak power around the coupling irises is about 500 MW at the phase reversal time. In order to deal with the breakdown problem, the dual side-wall coupling irises model was used. To further improve the reliability at very high power, RF phase modulation (PM) with flat-top output is considered. By using the CST Microwave Studio (MWS) transient solver, a new method was developed to simulate the time response of the pulse compressor. In addition, the theoretical and experimental results of the PM theory are also presented in this paper.

INTRODUCTION

The SLED-type pulse compressors play an important role in the linear accelerators to increase the efficiency of the klystron RF power. An S band SLED-type pulse compressor has been manufactured by IHEP to challenge 100 MW input peak power. At just one compressed pulse time (usually equal to the filling time of the travelling wave accelerating structure) from the incident RF pulse end, the incoming pulse phase is reversed 180^{o} by the PSK (phase shift keying) switcher, the output peak power will reach 500 MW. The extreme high power leads to the sparking phenomena around the SLED coupling irises and the first several accelerating cells.

A significant reduction of the electric fields near the irises had been achieved by adopting dual side-wall coupling irises model. High power test results show that the maximum input power can reach 85 MW. To further improve the high power reliability, the amplitude modulation (AM) and phase modulation (PM) of the SLED was considered to obtain the flat-top output. For AM, the input power is slowly increased to compensate the damped radiation power of the storage cavities during the pulse compressed interval. Due to the non-linear input/output characteristics of the klystron at high power, AM can't be implemented in the saturation regime [1]. For PM, the incoming RF pulse phase can be manipulated with a constant amplitude, thus the PM is a more feasible option.

THEORY AND SIMULATIONS

Figure 1 shows the equivalent circuit model of the SLED. The energy storage cavity can be regarded as an oscillating circuit. The voltage source refers to the RF generator.

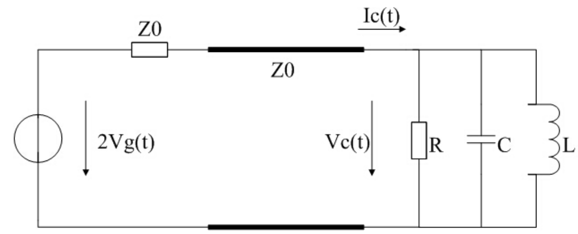

Figure 1: Equivalent circuit model of the SLED.

According to the Kirchhoff's law, the following differential equation can be obtained (dots mean derivatives with respect to time) [2][3].

$$\mathrm{Vr} + \tau\dot{\mathrm{Vr}} = \Gamma\mathrm{Vg} - \tau\dot{\mathrm{Vg}}, \quad (1)$$

where Vg is the equivalent complex voltage of the SLED input while Vr is the output. $\tau = 2Q_l/\omega_c$ is the filling time of the storage cavity, Q_l and ω_c are the loaded Q and the resonant angular frequency. Γ is the reflection coefficient and can be defined as $(\beta-1)/(\beta+1)$ with β the coupling factor.

The RF power is fed into the SLED at time t_0, the input has a phase jump with a step φ_0 (generally much less than 180^{o}) at time t_1, then the phase is increased continuously until the RF pulse ends at t_2. The phase modulation based upon the differential Eq. (1) is carried out during $t_1 \leq t < t_2$, then a compressed pulse with constant amplitude can be acquired.

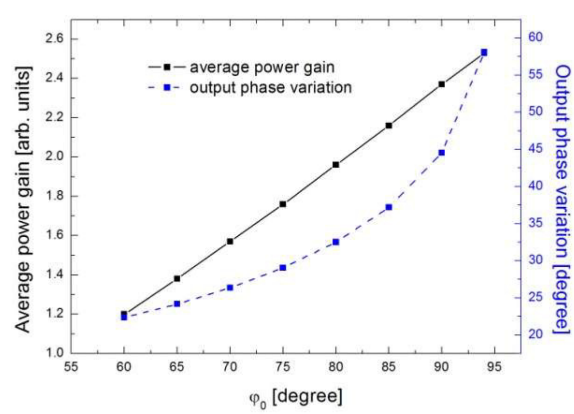

Figure 2: Dependence of the average power gain and the output phase variation on the phase jump step φ_0.

Figure 2 shows the dependence of the average power gain and the output phase variation on the phase jump step φ_0. The average power gain is proportional to φ_0, while the output phase variation increases with φ_0 as well. For the time duration $t_1 \leq t < t_2$, the output phase experiences a large variation. As we all know, the

#shug@ihep.ac.cn

Content from this work may be used under the terms of the CC BY 3.0 licence (© 2015). Any distribution of this work must maintain attribution to the author(s), title of the work, publisher, and DOI.

ISBN: 978-3-95450-168-7 doi:10.18429/JACoW-IPAC2015-WEPMN012

Content from this work may be used under the terms of the CC BY 3.0 licence (© 2015). Any distribution of this work must maintain attribution to the author(s), title of the work, publisher, and DOI.

CATHODE STALK OPTIMIZATION FOR A 325 MHz SUPERCONDUCTING QWR ELECTRON GUN*

P.L Fan†, F Zhu, S.W Quan, L Lin, Y.M Li, K.X Liu
Institute of Heavy Ion Physics, Peking University, Beijing 100871, China

Abstract

The structure of cathode stalk is very important for the performance of a superconducting QWR (Quarter Wave Resonator) electron gun. With improper design, RF power dissipation on the surface of cathode stalk and its surrounding tube can lead to a serious decrease of quality factor for superconducting QWR injector. We present here an optimized design of the cathode stalk for the 325 MHz superconducting QWR gun and special considerations are taken to minimize the power dissipation. The details of microwave simulation, beam dynamic simulation of the cavity with cathode stalks in different length, diameter and position are presented in this paper.

INTRODUCTION

An appropriate source is very important for the success of the proposed energy recovery linac (ERL) and high average power free-electron lasers (FELs). The superconducting radio frequency (SRF) electron guns offer great promise of very bright beams for use in electron injectors. QWR is compact at low RF frequency compared to elliptical cavity and its long wavelength allows to produce long electron bunches for which space charge effects can be minimized. Because of these potential benefits, projects of QWR electron gun have been developed at Naval Postgraduate School (NPS) [1], the University of Wisconsin [2] and Brookhaven National Laboratory (BNL) [3]. A 325MHz QWR electron gun has also been proposed at Peking University for obtaining higher beam current than the present DC-SRF gun.

One of the main problems of the SRF injectors is that a cathode inserted into the superconducting gun cavity causes worse performance of the SRF cavity. Usually we use a cantilevered stalk, not shorted directly to the cavity, to support the cathode in the desired position. This design has a singular flaw that the cathode stalk becomes an RF transmission line allowing RF energy to flow down it as a coaxial waveguide. As we know, any RF power pulled from the cavity degrades gun performance. This problem has been predicted in the Rossendorf gun [4] and Brookhaven SRF gun [5]. Both of them were designed to incorporate an RF choke to prevent the RF power flowing down the cathode stalk. The DC-SRF [6] gun in Peking University also offers an effective way to solve this problem, which combining a Pierce gun with a superconducting cavity. As to the QWR gun, its reentrant structure determines that a choke filter or a Pierce gun is not a good choice. So the design of the cathode stalk in QWRs is very important, the test in NPS shows that the quality factor of cavity with cathode stalk can be an order of magnitude smaller than that of the virgin cavity. We do some research on the design of the cathode stalk aiming to reduce the RF power dissipation on the cathode stalk on the basic of the 325MHz QWR electron gun.

* Work supported by National Basic Research Project (No. 011CB808302)
† fanpeiliang@163.com

325 MHz QWR ELECTRON GUN

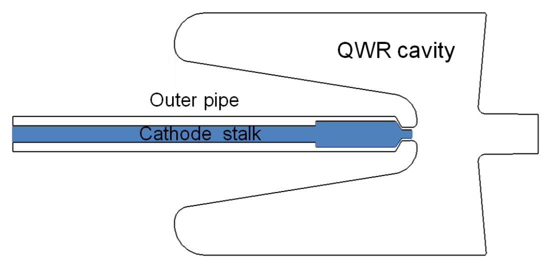

Figure 1: The schematic of 325MHz QWR cavity and the cantilevered cathode stalk.

The 325MHz QWR gun cavity design is given in reference [7], the simulation of the electromagnetic field of the QWR cavity was carried out with the Superfish code [8]. When the average accelerating electric field E_{acc}=20 MV/m, the stored energy of the cavity U=4.67 J and the cavity's intrinsic quality factor Q_0=1.536 $\times 10^9$ (T=4 K), the dissipated power in the cavity walls is given by

$$P_c = \frac{\omega_0 U}{Q_0} = 6.2\,\mathrm{W} \tag{1}$$

Here, we defined the RF power dissipation on the cathode surface and the outer pipe inner surface as P_d, that is

$$P_d = \frac{R_s}{2}\int_{A_1+A_2} H^2 da \tag{2}$$

Here, Rs is the surface resistance. We choose copper as the material of stalk because of its lower resistivity. A_1 and A_2 are the area of the cathode stalk surface and the area of the outer pipe inner surface, respectively. The QWR cavity and the cantilevered cathode stalk are shown in Figure 1.We define the quality factor which considering the RF power dissipation on the cathode surface and the surrounding tube inner surface as $Q_0^{'}$, which is defined as

$$Q_0^{'} = \frac{\omega_0 U}{P_c + P_d} \tag{3}$$

THE CATHODE STALK

Just like the input coupler, the cathode stalk and the outer pipe form a RF transmission line. We consider the case

ISBN: 978-3-95450-168-7 doi:10.18429/JACoW-IPAC2015-WEPMN013

Content from this work may be used under the terms of the CC BY 3.0 licence (© 2015). Any distribution of this work must maintain attribution to the author(s), title of the work, publisher, and DOI.

DEVELOPMENT OF DC-SRF INJECTOR AT PEKING UNIVERSITY*

Jiankui Hao, Shenwen Quan, Lin Lin, Liwen Feng, Fang Wang, Feng Zhu, Senlin Huang, Zhiwen Wang, Xiaodong Wen, Peiliang Fan, Kexin Liu#, Huamu Xie, Kui Zhao, Jiaer Chen
Institute of Heavy Ion Physics & State Key Laboratory of Nuclear Physics and Technology, Peking University, Beijing, China

Abstract

DC-SRF electron injector, which combines a DC Pierce gun and a 3.5-cell 1.3 GHz superconducting cavity in a cryomodule, has been developed at Peking University. Based on the improvements of beam line, LLRF system and 2K cryogenic system, stable operation of the DC-SRF injector has been carried out recently. Electron beams with 3.4 MeV energy and the currents of ~1mA in a macro-pulse mode was obtained. As the first application of this DC-SRF injector, THz radiation produced with a 10 period undulator was also detected. The description of the experiment process and results will be presented in this paper.

INTRODUCTION

To obtain electron beams with high average current and low emittance, superconducting radiofrequency (SRF) photocathode guns, which combine the high brightness of normal conducting RF photocathode guns with the advantage of CW operation of superconducting RF cavities, have been developed in many laboratories worldwide [1, 2]. For HZDR SRF photoinjector, the SRF cavity is a 3.5-cell TESLA type cavity and there is a center hole on the back wall of the half-cell for Cs_2Te photocathode installation, which is in normal conducting. An attached choke filter made of pure niobium was designed to protect RF power leak towards the cathode support system from a vacuum gap between the cavity and the photocathode [3]. This SRF injector has been in operation since 2008[4] and was used for FEL operation recently [5]. A 704 MHz half-cell cavity SRF gun with a double quarter wave choke joint cathode insert was constructed at BNL and K2CsSb was chosen as cathode material [6]. The RF conditioning has been carried out [7] and the beam test is underway.

DC-SRF injector was first proposed by Peking University in 2001 [8]. It combines a DC Pierce gun and a superconducting cavity. The feasibility of DC-SRF injector was demonstrated by the prototype injector with a 1.5-cell TESLA type superconducting cavity in 2004 [9]. An upgraded DC-SRF injector with a 3.5-cell large grain niobium cavity was then designed and constructed [10]. Conditioning of the DC-SRF photoinjector has been started since the 2K cryogenic system has been in operation in 2011 [11]. Based on a series of improvements on drive laser, photocathode, low level RF (LLRF) control system and beam diagnostic devices, electron beam with a current of mA level has been obtained at long-term stable operation. In this paper, the improvements, beam experiments and results of the DC-SRF photoinjector are described.

*Work supported by Major State Basic Research Development Program of China (Grant No. 2011CB808302 and 2011CB808304)
#Email: kxliu@pku.edu.cn

DC-SRF INJECTOR

Figure 1 shows the schematic view of the upgraded DC-SRF photoinjector. The cryomodule consists of the DC pierce gun, 3.5-cell superconducting cavity, helium vessel, liquid nitrogen shield, input power coupler, tuner and auxiliary systems.

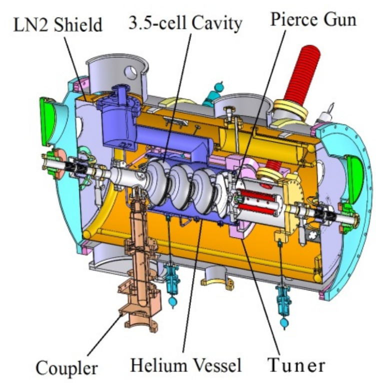

Figure 1: Schematic view of the DC-SRF photoinjector.

The designed DC voltage of Pierce gun is 90 kV. The surface electric field on the cathode is almost 5 MV/m and the peak electric field is lower than 13 MV/m. Simulations show that the electron beam experiences a focusing force when it leaves the cathode and is defocused around the anode [10]. The anode, which is also a part of the 3.5-cell cavity, is made of single crystal niobium in order to avoid the effect of the welding seam on the DC field distribution. The 3.5-cell large grain niobium superconducting cavity comprises three TESLA type cells and a special designed half-cell. The accelerating gradient of the cavity reaches 23.5 MV/m and the intrinsic quality factor Q_0 is higher than 1.2×10^{10} in vertical test [10]. The simulation shows that space charge effect of the electron beam is still remarkable due to the relatively low energy gained from the DC voltage. The gap between the Pierce gun and the 3.5-cell cavity should be as short as possible to prevent the beam from diverging too much due to space charge effect before it enters the high field area in the cavity. On the other hand, the RF field and DC static field infiltrating into each other should be suppressed. The length of connecting beam pipe between the DC anode and the half-cell of the cavity is 17 mm. The magnet field shielding of the DC-SRF injector is provided by the vacuum vessel, which is made of high pure iron plate with the thickness of 12 mm. The residual magnetic field in the

ISBN: 978-3-95450-168-7 doi:10.18429/JACoW-IPAC2015-WEPMN014
Content from this work may be used under the terms of the CC BY 3.0 licence (© 2015). Any distribution of this work must maintain attribution to the author(s), title of the work, publisher, and DOI.

A C-BAND DEFLECTING CAVITY DESIGN FOR HIGH-PRECISION BUNCH LENGTH MEASUREMENT*

Xiaopeng Jiang[a,b,#], Jiaru Shi[a,b], Ping Wang[a,b], Huaibi Chen[a,b]
[a] Department of Engineering Physics, Tsinghua University, Beijing 100084, PR China
[b] Key Laboratory of Particle and Radiation Imaging of Ministry of Education , Tsinghua University, Beijing 100084, PR China

Abstract

A standing wave RF deflecting structure has been designed as a tool for high-precision bunch length measurement. This 3-cell deflecting cavity is designed to operate at a frequency of 5.712GHz. In this paper, the RF design and thermal analysis of the deflecting cavity are introduced. We study the electromagnetic field distribution inside the cavity. The coupler design is also discussed. And the beam dynamics simulation is shown.

INTRODUCTION

RF deflecting cavities have been widely used in the characterization of the longitudinal and transverse phase space in ultra-short electron beams [1]. Recently an ultrafast electron source with femtosecond-level is used for diffraction and imaging system [2]. The main parameters of the bunch are given below (Table 1). A C-band deflecting cavity is designed for high-precision measurement of the bunch length.

Table 1: Beam Parameters

Parameters	Value
Electron beam energy (MeV)	2
Transverse beam size (mm)	0.5
Longitudinal beam size(fs)	20

In the second section of the paper, the design of the deflector is discussed including the structure design, electromagnetic field characterization, beam dynamics and the coupler design. Thermal simulation calculated by CST is shown in the third part.

RF DEFLECTOR DESIGN

The required transverse deflecting voltage V_T=1MV can be, achieved by both traveling wave (TW) and standing wave (SW) structures [1]. In our case, we choose a 3-cell SW structure operated at a frequency of 5.712GHz. The 3D-model draw by CST is shown in Figure 1.

Model Design

The main part of the model is composed of several cylinders. The radius of the cell is determined by both the frequency and flatness of the magnet field [3]. The working mode is TM_{110} mode and π-mode. Length of the middle cell is given by [3]:

$$l = \frac{\lambda}{2} = \frac{\pi c}{\omega_0}. \tag{1}$$

where λ and ω_0 are the wavelength and angular frequency of the microwave, c is the speed of light, l is the length of the middle cell which include half of the gap between middle cell and end cell each side. Meanwhile, the length of the end cell is determined by beam dynamics which is discussed later in this paper.

In order to make sure the polarization direction not changed while two cell coupled, two end cells are slotted on the edges which are perpendicular to the direction we put the coupler.

According to the discussion above, the dimensions of the cavity is shown in table 2.

Table 2: Dimensions of the RF Cavity

Dimensions	Value(mm)
Radius of middle cell	30.85
Length of middle cell	21.49
Radius of end cells	30.61
Length of end cells	10.93
Gap between cells	4.76
Radius of beam pipe	8
Radius of slots	3.5

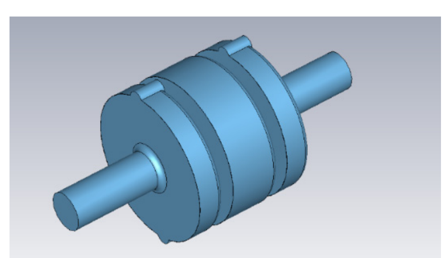

Figure 1: 3D-design of the deflector.

*Work supported by NSFC 11375098 and 11327902
#jxp14@mails.tsinghua.edu.cn

ISBN: 978-3-95450-168-7 doi:10.18429/JACoW-IPAC2015-WEPMN015

DARK CURRENT IMAGING EXPERIMENT IN AN L-BAND RF GUN

J.H. Shao[1,2,*], S. Antipov[2,3], S.V. Baryshev[2,3], H.B. Chen[1], M.E. Conde[2], D.S. Doran[2], W. Gai[2], C. Jing[2,3,#], W. Liu[2], J.G. Power[2], J.Q. Qiu[2,3], J.R. Shi[1], D. Wang[1,2], F.Y. Wang[4], C. Whiteford[2], E. Wisniewski[2], and L.L. Xiao[4]

[1]Tsinghua University, Beijing 100084, China
[2]Argonne National Laboratory, Lemont, IL 60439, USA
[3]Euclid Techlabs LLC, Solon, OH 44139, USA
[4]SLAC National Accelerator Laboratory, Menlo Park, CA 94025, USA

Abstract

The localized high electric field enhancement or low work function is the trigger for strong field emission, which however has yet been well experimentally studied. Using an L-band photocathode gun test stand at Argonne Wakefield Accelerator Facility (AWA), we've constructed an imaging beam line to observe field emission current from predefined emitters on cathode. Preliminary experiment results are present. Future plan is discussed.

INTRODUCTION

Field emission (a.k.a. dark current) plays an important role in development of high gradient rf devices [1]. Elimination of sharp edges and achievement of smooth surface finishing in fabrication to alleviate the field emission is a standard practice to avoid rf breakdowns in operation of high gradient accelerating structures. Field emission has been well explained by the Fowler-Nordheim formula with quantum mechanism [1, 2], which is governed by three independent parameters, the local field enhancement factor β, the emitter area Ae, and the work function φ.

Strong field emission observed in high gradient devices is dominated by emitters with high β or low φ [1, 3]. Previous dc studies by field emission scanning microscopy (FESM) [4] and tunnelling atomic force microscopy (TUNA) [5] have revealed different types of emitters, such as particulates, surface protrusion, grooves with trapped contaminants, grain boundary, etc. However, to the best of the authors' knowledge, no systematic study to exactly locate emitters in rf devices has been carried out yet.

Locating field emitters in rf devices might help understand the fundamental mechanism of field emission. Moreover, if the rf breakdown spot can be identified simultaneously, it will also help reveal the relationship between field emission and breakdown.

IMAGING PRINCIPLE

The gun used in this study is a 1.3 GHz L-band single cell photocathode gun with mountable cathode [6]. With 2 MW input power, the electric field on the flat cathode (noted as $E_{cathode}$) can reach 70~100 MV/m depending on the cathode position.

* jshao@anl.gov
# jingchg@anl.gov

A modified version of ASTRA code [7] is used to simulate the emission from the cathode as well as to track their movement to the downstream of the beam line. Due to the difficulties of accurately obtaining initial conditions, we've simulated the worst possible scenario (less constraint) of field emission on the cathode surface. In the simulation, we've assumed that 1) the initial kinetic energy of dark current is constant, 7 eV (Fermi energy of Cu), which is the maximum value of the real energy distribution [8]; 2) the emission angle follows uniform distribution over the entire 360° range; 3) the temporal structure of the emitted current is approximated by Gaussian distribution [9]; 4) space charge and mirror effect are not included; 5) $E_{cathode}$ is 100 MV/m and β is 80; 6) the radius of emitter is 0.

Dark current can be emitted over 180° rf phase, resulting a wide energy spread and complicated beam dynamics. Although there is a sharp peak with the highest energy gain, the rms energy spread is ~300 keV as illustrated in Fig. 1. The trajectory of electrons emitted from the same position but different phases will be completely different, causing blurred images at downstream after acceleration by the gun, as shown in Fig. 2(a) and (b).

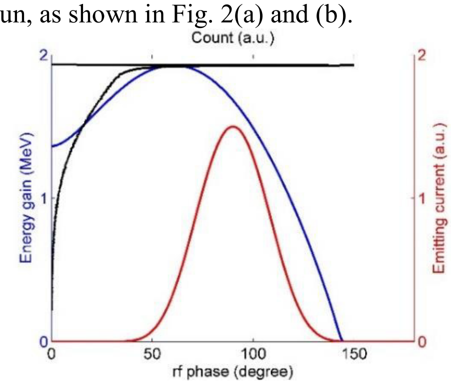

Figure 1: Energy gain (blue) and emitting current (red) at different rf phases and energy distribution (black).

To form a clear image, a straight-forward idea is to select electrons only from narrow phase band (or with narrow energy spread) and block others as shown in Fig. 2(c). This can be achieved by a solenoid (noted as the imaging solenoid) whose focusing depends on beam energy (thin lens approximation [10]):

$$\frac{1}{f} = \left(\frac{q}{2mc\beta\gamma}\right)^2 \int_l B^2 dz \qquad (1)$$

where f is the focusing length; m, q, cβ, and γ are mass, charge, speed and Lorentz factor of the particle; B and l

Content from this work may be used under the terms of the CC BY 3.0 licence (© 2015). Any distribution of this work must maintain attribution to the author(s), title of the work, publisher, and DOI.

ISBN: 978-3-95450-168-7 doi:10.18429/JACoW-IPAC2015-WEPMN016

Content from this work may be used under the terms of the CC BY 3.0 licence (© 2015). Any distribution of this work must maintain attribution to the author(s), title of the work, publisher, and DOI.

OBSERVATION OF DARK CURRENT DEPENDENCE ON STORED ENERGY IN AN L-BAND RF GUN*

J.H. Shao[1,2,#], S. Antipov[2,3], S.V. Baryshev[2,3], H.B. Chen[1], M.E. Conde[2], D.S. Doran[2], W. Gai[2], C. Jing[2,3], W. Liu[2], J.G. Power[2], J.Q. Qiu[2,3], J.R. Shi[1], D. Wang[1,2], F.Y. Wang[4,+], C. Whiteford[2], E. Wisniewski[2], and L.L. Xiao[4]
[1] Tsinghua University, Beijing 100084, China
[2] Argonne National Laboratory, Lemont, IL 60439, USA
[3] Euclid Techlabs LLC, Solon, OH 44139, USA
[4] SLAC National Accelerator Laboratory, Menlo Park, CA 94025, USA

Abstract

A pin cathode has been used to study the influence of stored energy on field emission in an L-band rf gun. The stored energy was tuned by adjusting the recess of the cathode in order to obtain the same electric field on the cathode tip. At same electric field, we have observed very strong correlation of dark current with stored energy, where five times enhancement of dark current was obtained with the stored energy increased by three fold. Beam dynamics study reveals that the correlation is not from the beam transmission. We'll present the experiment results as well the possible mechanisms about the phenomena.

INTRODUCTION

Field emission (i.e. dark current) plays an important role in high gradient rf devices. Generally, it's very harmful and can cause rf breakdown. It needs to be suppressed to achieve high gradient accelerating structures [1]. Dark current has been well explained by the Fowler-Nordheim formula with quantum mechanism [1, 2], which is governed by three independent parameters, the local field enhancement factor β, the emitter area Ae, and the work function φ. When φ is taken as its nominal value, β and Ae are usually inconsistent with surface analysis [3]. Moreover, they have a very large diversity from different accelerators with similar peak electric field but different frequency, group velocity and so on [1]. This might imply that the field emission might not be a completely local phenomenon, which could also relate with global parameters of a system.

Recent study in which two pins were attached to a WR90 waveguide has revealed that rf breakdown depends strongly on the net rf power flow through the waveguide [4]. As dark current is highly related to rf breakdown, we are motivated to exam its dependence on the net power flow or stored energy in a standing wave cavity. In this paper, dark current dependence on input power/ stored energy is studied with a standing wave rf photocathode gun with mountable cathode.

* Work support by the U.S. Department of Energy Early Career Research Program under contract code LAB 11-572
# jshao@anl.gov
+ fywang@slac.stanford.edu

EXPERIMENTAL SETUP

The experiment has been carried out on an L-band photocathode gun test stand at Argonne Wakefield Accelerator Facility (AWA), illustrated in Fig. 1. The forward and reflected rf power, and the field of the gun are monitored. A Faraday cup right at the exit of the gun measures the field emission current. Besides, a dark current imaging system is located downstream to index dark current emitters, which consists of a solenoid, a collimator, trim magnets, and YAG screens [5, 6].

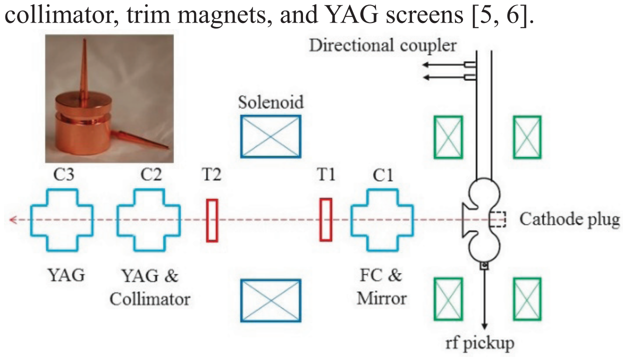

Figure 1: Layout of the L-band test stand. Inset: pin cathodes designed and fabricated in SLAC.

Pin cathodes are used to maintain the highest field in the gun to govern the field emission in the experiment. The field on the tip is at least four times higher than any other place of the gun. The copper pin cathode is 0.8 inch long with a R0.02 inch hemisphere tip as shown in inset of Fig.1.

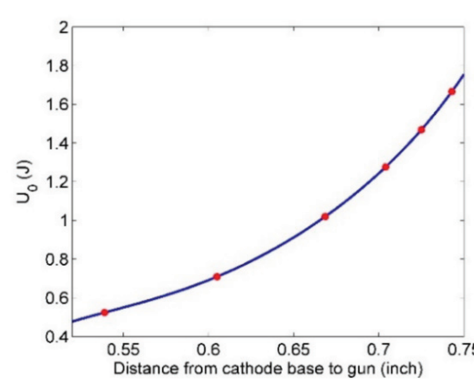

Figure 2: The stored energy at peak field of 625 MV/m vs the cathode positions from simulation, where the red points corresponds the different test sets.

ISBN: 978-3-95450-168-7 doi:10.18429/JACoW-IPAC2015-WEPMN017

HIGH POWER RF RADIATION AT W-BAND BASED ON WAKEFIELDS EXCITED BY INTENSE ELECTRON BEAM

D. Wang[1, 2], S. Antipov[1, 3], M. Conde[1], S. Doran[1], W. Gai[1], G. Ha[1], C. Jing[1, 3]
W. Liu[1] J. Power[1], J. Qiu[1, 3], C.Tang[2], E.Wisniewski[1]
[1] Argonne National Laboratory, IL, 60439, USA
[2] Tsinghua University, Beijing, 100084, China
[3] Euclid Tech. labs LLC, IL, 60439, USA

Abstract

We report the experiment design and preliminary results on high power RF generation at W-band based on coherent wakefields from the metallic periodic structure of 91 GHz PETS (power extraction and transfer structure), excited by intense electron beam at the Argonne Wakefield Accelerator (AWA) facility. The recently output RF power is 0.7 MW, with 67 MeV, 1.4 nC single electron beam going through the structure. The RF pulse length is 3.4 ns. We measure the energy loss of electron beam as reference to the RF generation, which agrees well with the simulation results. Next run is to increase the output RF power with higher charge and to excite coherent wakefields with electron bunch train. The output RF peak power is expected to be ~100 MW and the electrical field gradient can reach up to 400 MV/m, with RF pulse duration adjustable from few ns to 30 ns when excited with 5~10 nC charge in a single bunch and up to 32 sub bunches in total.

INTRODUCTION

High power and high frequency RF generation benefits high energy and compact accelerator, and is also important for high gradient and breakdown study [1].

We use a copper periodic structure with wakefields frequency of 91 GHz as a PETS (power extraction and transfer structure) to transfer energy of ultra-relativistic electron beam into the RF radiation. Preliminary experiment has been conducted at the Argonne Wakefield Accelerator (AWA) drive beam line. Experimental results demonstrate the mean energy loss is 1.6 MeV of the 1.4 nC electron single bunch, corresponding to RF power generation of 0.66 MW.

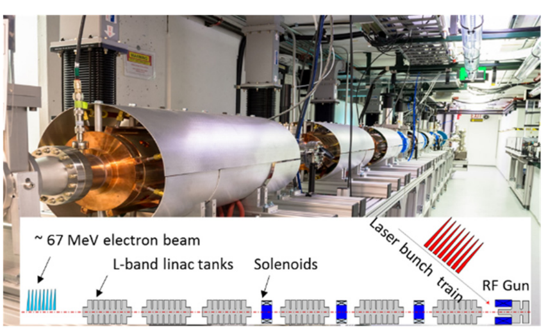

Figure 1: Layout of AWA drive beam line.

Since wakefields will be enhanced coherently when excited by bunch train with proper bunch spacing. We design the experiment aimed at 100 MW level RF generation at 91 GHz for the next run based on intense 1.3 GHz electron bunch train at AWA, with 5~10 nC charge in single bunch and up to 32 sub bunches in total.

The upgraded AWA drive beam line consists of a 1.3 GHz RF photocathode gun and 6 RF cavities [2], which has the capability to generate intense charged electron beam of 67 MeV, with picosecond RMS bunch length. AWA is designed to work at two modes of operation. In single-bunch mode, a high charge (up to 100 nC) bunch is generated. While in bunch-train mode, a laser bunch train illuminates the high current photocathode to generate an electron beam distributed up to 32 sub-bunches, with 1.3 GHz (769 ps) spacing. The electron bunch train will deliver up to ~ 1000 nC total charge. The layout of AWA is shown in Fig. 1.

ANALYSIS OF WAKEFIELD EXCITED BY BUNCH TRAIN

Two copper plates with periodic grooves make up the W-band structure, which is similar to Valery Dolgashev's 100 GHz structure [3]. We design two couplers on both end of the structure for bench test purpose and getting RF band pass. As shown in Fig. 2. We can choose the frequency by adjusting the gap between the two plates, when the gap 2a = 0.94 mm, the phase velocity is matched to the particle velocity at 91 GHz, thus wakefields interacts strongly with the on-axis bunch. The dimensions of the periodic groove in x/y/z direction are all about 1 mm, the total length of the structure L is 12.3 cm. The relative group velocity $\beta_g = \frac{v_g}{c} = 0.1$ and the loss factor is $\kappa_L = 13.3 MV/m/nC$.

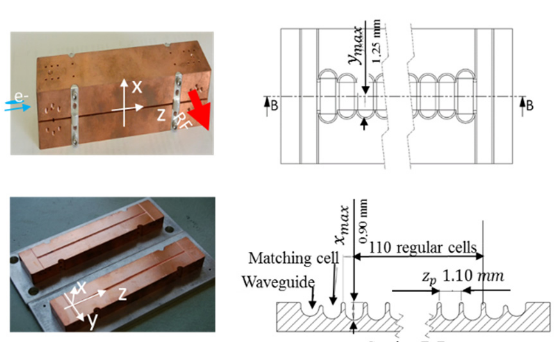

Figure 2: Sketch of W-band wakefield structure.

Content from this work may be used under the terms of the CC BY 3.0 licence (© 2015). Any distribution of this work must maintain attribution to the author(s), title of the work, publisher, and DOI.

ISBN: 978-3-95450-168-7 doi:10.18429/JACoW-IPAC2015-WEPMN018

MEASUREMENT OF CELL-CELL COUPLING COEFFICIENT IN PHOTOCATHODE RF GUN*

WANG Ping[a,b#], SHI Jiaru[a,b], GAO Qiang[a,b], ZHANG Liang[a,b], CHEN Huaibi[a,b]
[a] Department of Engineering Physics, Tsinghua University, Beijing 100084, PR China
[b] Key Laboratory of Particle and Radiation Imaging of Ministry of Education , Tsinghua University, Beijing 100084, PR China

Abstract

A photocathode RF gun is being developed in Tsinghua University. We measure the single cell frequency and the cell-cell coupling coefficient by a detuning method with high accuracy. This note presents the principle of the method and several examples.

INTRODUCTION

The 1.6 cell photocathode S-band gun has been used as the electron sources with high beam quality for many years. A lot of scientific research programs benefit from this type of photocathode RF gun, such as the compact x-ray source in Tsinghua University [1] and the LCLS in SLAC [2].

The achievement of a photocathode RF gun with good performance needs careful measurements and tunings of the RF cavities. However as is known the half cell of a photocathode RF gun makes the measurements of the RF properties difficult because of the cathode with no beam pipe. We can measure the full cell frequency by detuning the half cell. But if we want to obtain the frequency with high accuracy we have to detune the half cell by a large amount, which risk damaging the surface of the cathode [3]. The cell-cell coupling coefficient in photocathode RF gun is another very important parameter which influence the frequencies of both 0-mode and π-mode as well as the field balance [4]. Ref [4] give a full description of the tuning procedure for a photocathode gun, which can be used to calculate the cell-cell coupling coefficient with no approximation. However we have to measure the frequencies of the 0-mode and the π-mode, the quality factors and shunt impedances of the full cell and the half cell and the field balance for eventually calculating the cell-cell coupling coefficient.

In this paper we introduce a simple method to measure the frequencies of the full cell and the half cell and the cell-cell coupling coefficient. Only a small extra metal stick is used to detune the half-cell by a small amount. We start from the equivalent RLC circuit of the RF gun. Then we design a simplified model to show how we measure the RF gun.

BASICS OF MEASUREMENT

We can analysis an RF structure by the method of equivalent RLC circuit. The equivalent RLC circuit of the RF gun is shown in the Fig. 1. The two cells are coupled by the equivalent capacitor C. The two cells of the RF gun is different from each other. So they have different equivalent capacitors and Inductors.

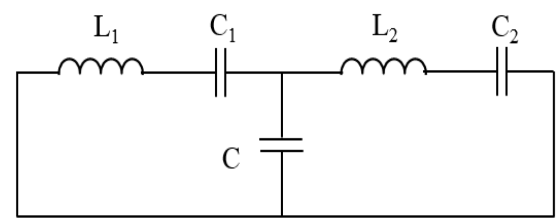

Figure 1: The equivalent RLC circuit.

We can easily obtain the relationship of the frequencies with cell-cell coupling coefficient [3]:

$$\frac{\left(f^2\right)^2}{f_h^2 \cdot f_f^2} - \left(\frac{1}{f_h^2} + \frac{1}{f_f^2}\right) \cdot f^2 + 1 - \frac{k^2}{4} = 0 \quad (1)$$

Here f is the frequency of the operating mode. The f_h and the f_f are the resonant frequencies of the half cell and the full cell. The solutions of equation (1) are the frequencies of the 0-mode and the π-mode. We can get:

$$f_0^2 + f_\pi^2 = f_h^2 + f_f^2 = x \quad (2)$$

$$f_0^2 \cdot f_\pi^2 = \left(1 - \frac{k^2}{4}\right) \cdot f_h^2 \cdot f_f^2 = y \quad (3)$$

We define two new variables x and y here. During the experiment we use a small metal stick to detune the half-cell through a laser port. So we change the frequency of the half cell while keeping the frequency of the full cell unchanged. The relationship between x and y are given:

$$y = \left(1 - \frac{k^2}{4}\right) \cdot f_f^2 \cdot x - \left(1 - \frac{k^2}{4}\right) \cdot f_f^4 = ax - b \quad (4)$$

Both of the variable x and y vary with the amount of the detuning and they have a simple linear relationship. We can easily obtain the slope and intercept of the straight

*Work supported by Tsinghua University Initiative Scientific Research Program No. 20131080112
#ping-wang13@mails.tsinghua.edu.cn

Content from this work may be used under the terms of the CC BY 3.0 licence (© 2015). Any distribution of this work must maintain attribution to the author(s), title of the work, publisher, and DOI.

ISBN: 978-3-95450-168-7 doi:10.18429/JACoW-IPAC2015-WEPMN019

CALORIMETRIC POWER MEASUREMENTS IN X-BAND HIGH POWER RF

Xiaowei Wu*[1,2], Nuria Catalan-Lasheras[3], Benjamin Jack Woolley[3], Walter Wuensch[3], Huaibi Chen[1,2], and Liang Zhang[1,2]
[1]Department of Engineer Physics, Tsinghua University, Beijing 100084, P.R.China
[2]Key Laboratory of Particle & Radiation Imaging (Tsinghua University), Ministry of Education, Beijing 100084, P.R.China
[3]CERN, Geneva, Switzerland

Abstract

With the aim to test prototype accelerating structures for CLIC at high-gradient, new klystron-based, X-band high power test stands are being built at CERN. These tests stands are referred to as Xboxes with Xbox1 and Xbox2 being already operational. Stainless steel loads are placed in the end of the Xbox-1 system to absorb the remaining power which comes out of the accelerating structure. Power information is important and needs to be measured precisely. A new power measuring method based on calorimetry is proposed independent from RF measurements subject to frequent calibration. The principles of the method and simulations are presented and the results of actual experimentation are used to validate the method. The results show calorimetric measurement is feasible method and have a good precision at this power level.

INTRODUCTION

X-boxes are X-band klystron-based high power test stands at CERN. They provide a peak power on the 50~100 MW range which generates a field gradient of about 100 MV/m in the prototype structures for the CLIC project [1]. The flexible and instrumented test stands provide important data for fundamental high-gradient studies including not only initial energy version of CLIC study but also X-band based XFEL linacs and medical linacs [2]. Xbox-1 has now been operated for over two years with the goal of conditioning and operating CLIC prototype accelerating structures. The preliminary results can be found in [3].

Stainless steel RF loads are placed in the end of Xbox-1 to absorb the remaining power which comes out of the testing structures. Power information is important for the data processing in operation and needs to be measured precisely. In order to achieve this goal, a new power measuring method based on calorimetry is proposed independent from RF measurements subject to frequent calibration.

This report describes the concept and principles of the calorimetric power measuring method. Simulation works and experimental set-up are also presented. The calorimetric power measuring experiment was done during the new CPI klystron's commissioning in Xbox-1 in 2014. The experimental results are used to validate the method and show that calorimetric measurement is a feasible method with good precision at this power level.

*wuxw12@mails.tsinghua.edu.cn

CONCEPT OF CALORIMETRIC POWER MEASUREMENT

The RF power coming out of the accelerating structures in Xbox-1 is fed into stainless steel RF loads. RF power was transformed into heat energy which will be taken away by the water cooling system in the load. In ideal situation, the RF input power should be equal as the heat energy taken away by the cooling water. The heat energy can be expressed as follows:

$$P = c \cdot \dot{m} \cdot \Delta T \, . \qquad (1)$$

P is the heat power absorbed by the cooling water. c is the specific heat capacity of water. $\dot{m}$ is the total mass flow rate of the water cooling system. ΔT is the temperature difference between input flow and output flow. The quantities $\dot{m}$ and ΔT can be measured by flowmeters which are attached to the water cooling system of the RF load. We can obtain input RF power by measuring these parameters in experiment and calculating heat power by the formula above. In order to avoid heat dissipation into ambient environment and improve measurement's accuracy, the loads are covered by heat insulation jackets.

SIMULATION OF THE LOAD

Before carrying out the experimental study of calorimetric power measurement, simulations of the RF load are needed for knowing electromagnetic and thermal properties of the system.

Basic Information of the Load

The stainless steel RF load used in Xbox-1 is double-band SS430 dry RF load, as shown in Fig. 1. The load is designed to be working at frequencies of 11.994 GHz and 11.424 GHz respectively [4]. It is made of magnetic stainless steel SS430 and consists of five functional parts which are shown in Fig. 2.

Content from this work may be used under the terms of the CC BY 3.0 licence (© 2015). Any distribution of this work must maintain attribution to the author(s), title of the work, publisher, and DOI.

ISBN: 978-3-95450-168-7 doi:10.18429/JACoW-IPAC2015-WEPMN021

Content from this work may be used under the terms of the CC BY 3.0 licence (© 2015). Any distribution of this work must maintain attribution to the author(s), title of the work, publisher, and DOI.

DESIGN AND RESEARCH OF SECONDARY ELECTRON EMISSION TEST EQUIPMENT WITH LOW ELECTRON ENERGY*

Yanhui Xu, Jie Wang, Bo Zhang, Le Fan, Xiangtao Pei, Yuanzhi Hong, Wei Wei, Yong Wang#,
National Synchrotron Radiation Laboratory, University of Science and Technology of China,
HeFei, AnHui 230029 China

Abstract

In particle accelerators, the secondary electrons resulting from the interaction between particles and vacuum chamber have a great impact on beam quality. Especially for positron, proton and heavy ion accelerators, massive electrons lead to electron cloud, which affects the stability, energy, emittance and beam life adversely. We have studied the secondary electron emission (SEE) of metal used for accelerators. A secondary electron emission measurement system with low electron energy has been designed and used to measure the SEE yield of metal and non-evaporable getter materials. With the equipment, we have obtained the characteristic of the SEE yield of stainless steel and oxygen free copper (OFC).

INTRODUCTION

The research of secondary electron emission has attracted great interest over the past many years [1-10]. In accelerator area, obtaining high quality beam is a main target. Under bombardment of massive particles, surface of vacuum chamber excites the secondary electrons, which affects beam quality, like stability, energy, emittance and beam life. For the reason above, measuring the secondary electron yield (SEY) of different materials is extremely critical and important. Finally, we intend to find low SEY materials used for accelerators.

Nowadays, most research institutes have measured SEY by reforming expensive SEM (scanning electron microscope) and AES (Auger Electron Spectroscopy) apparatus [2]. So we decided to design an independent secondary electron emission measurement equipment with low electron energy.

In this article, the basis for the design and some test of secondary electron emission measurement system with low electron energy was introduced.

TESTING PRINCIPLES

The secondary electron yield measurement principle is shown in Fig.1. I_p is the incident current, which causes the secondary electron emission from the surface material and I_s is the secondary electron current intensity. I_p and I_s are in opposite direction and I_t is the current flowing through the sample and is the sum of I_s and I_p. The secondary electron yield (σ) is the ratio of the secondary electron current and incident current. If I_p and I_t have been measured, we can obtain SEY value by the following formula:

$$\sigma = 1 - I_t / I_p \quad (1).$$

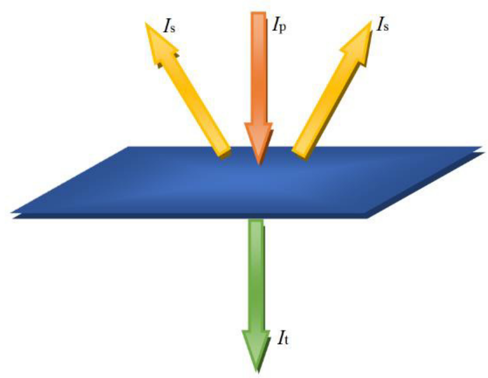

Figure 1: The SEY measurement principle.

There are two common methods of measurement: RP (Retarding Potential) method and ZR (Zero Retard) method. RP method can only measure vertical incident electron, because the electric field of sample bias in the case of oblique incidence will change the direction of the incident electron motion, so some incident electrons will not get to the sample surface. The sample is grounded with the method of ZR, and the bias voltage of the electron gun falls from zero to -300 V where the space charge effect appears, which is the main disadvantage of this method. In this mode, the incident current is changed with the increase of accelerating voltage, so both I_p and I_t need to be measured and recorded, then SEY value can be calculated by formula(1).

In further research, incident current I_p can be measured by a Faraday cup, which can reduce the irradiation time of the electron gun to the sample surface, so the charge accumulation of the sample surface will be less and the result accuracy will be improved. The schematic diagram of the Faraday cup is shown in Fig.2. Elastic scattering electrons from the surface will scatter to test indoor wall and produce secondary electrons, and these secondary electrons will cause a certain extent error to the measurement of I_s if reaching the sample surface. In order to eliminate this impact, some negative bias is applied on the samples.

* Work supported by the National Nature Science Foundation of China under Grant Nos.11475166.
#ywang@ustc.edu.cn

ISBN: 978-3-95450-168-7 doi:10.18429/JACoW-IPAC2015-WEPMN022

OPTIMIZATION DESIGN OF Ti CATHODE IN CERAMIC PIPE FILM COATING BASED ON THE SIMULATION RESULTS OF CST*

Jie Wang, Yanhui Xu, Bo Zhang, Wei Wei, Le Fan, Xiangtao Pei, Yuanzhi Hong, Yong Wang#,
National Synchrotron Radiation Laboratory，University of Science and Technology of China, HeFei, AnHui 230029, China

Abstract

The injection chamber at Hefei Light Source II (HLS II) consists of four ceramic vacuum chambers whose inner surface were coated with TiN thin film. The cross section of ceramic pipes is special racetrack structure. In order to improve the uniformity of the film, the structure of the cathode Ti plate needed to be optimized. In this article, CST PARTICLE STUDIO™ software had been used to simulate the influence of different target structure on discharge electric field distribution and electrons trajectories. Furthermore, the reliability of the simulation were analysed compared with the experimental results. Also, we put forward the optimization design of Ti cathode structure which could satisfy the requirement of uniformity of the thin film.

INTRODUCTION

TiN thin film causes great interest because of its low secondary electron yield (SEY), good electrical conductivity, stability of performance, ability to block hydrogen permeation, etc. [1-3]. TiN film deposition methods include DC magnetron sputtering, DC sputtering, hollow cathode discharge ion plating (HCD-IP) [4], RF sputtering et al. In general, the substrates are mainly flat plates, stainless steel cylindrical pipe [5], and ceramic vacuum chamber [6]. However, for some irregular type ducts, such as the racetrack type (Fig. 1) ceramic chamber in accelerators, the shape of the ceramic pipe will induce new and considerable technological difficulties for the uniformity of TiN coating which is important for vacuum performance and beam stability in the pipe.

Ceramic vacuum chamber is the key equipment of the electron storage ring injection system which was made of 99.9% pure alumina. The electrons injection chamber at Hefei Light Source II (HLS II) consists of four ceramic vacuum chambers whose inner surface are coated with thin conductive metal film, and the length of each vacuum chamber was 350 mm. Typically TiN or Ti are chosen while the sheet resistance of the film should be 0.3-0.8 Ω/sq. It was an extremely valuable research that how to get uniform TiN film which has high quality and meets the requirements of the physical design of the storage ring, such as mitigating the electron cloud instability [7]. This article mainly focuses on optimization design of Ti cathode in ceramic pipe which based on the simulation results of CST.

* Work supported by the National Nature Science Foundation of China under Grant Nos.11075157.
# ywang@ustc.edu.cn

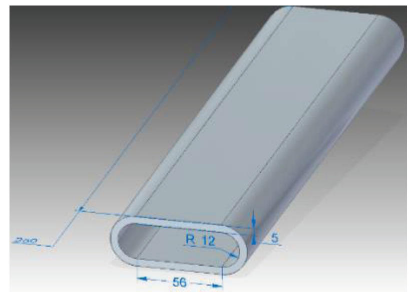

Figure1: A diagram of a ceramic vacuum pipe.

APPARATUS AND METHODS

Coating System

The TiN films are deposited onto the interior wall of ceramic vacuum pipe which is shown in Fig. 1, using DC magnetron sputtering method. The deposition system which is shown in Fig. 2 consists of observation window, 300 l/s turbo molecular pump, DC power supply, vacuum gauge, vacuum chamber and gas flow control system. Argon gas and nitrogen are introduced into the sputtering system through an adjustable leak valve. The typical sputtering parameters are: ~ -600 V cathode voltage, 5×10^{-1} torr gas pressure, 2:1 nitrogen and argon gas flow ratio, 200 Gauss magnetic field strength and 0.5 A sputtering current.

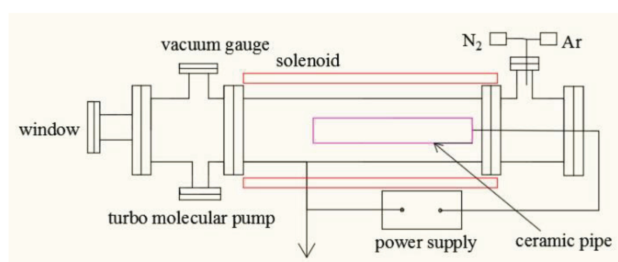

Figure 2: Schematic diagram of DC sputtering coating system.

TiN Coatings

Thickness was measured by use of a Sirion 200 Schottky field scanning electron microscope (SEM). Fig. 3 shows the cross-sectional and surface SEM morphology of specimen TiN film. It can be seen that the TiN film has a columnar structure which are mostly perpendicular to the film surface.

Content from this work may be used under the terms of the CC BY 3.0 licence (© 2015). Any distribution of this work must maintain attribution to the author(s), title of the work, publisher, and DOI.

ISBN: 978-3-95450-168-7 doi:10.18429/JACoW-IPAC2015-WEPMN023

VACUUM SYSTEM OF THE STORAGE RING OF HLS-II

Yong Wang#, Xiangtao Pei, Wei Wei, Bo Zhang, Le Fan, Yuanzhi Hong, Jie Wang, National Synchrotron Radiation Laboratory，University of Science and Technology of China, HeFei, AnHui 230029 China

Abstract

HLS storage-ring has been operated for more than twenty-five years. In 2014 we began to upgrade the machine, which is called HLS-II. The emittance is reduced to 40 nmrad, five insertion devices are added and the injection energy increases to 800MeV. Now the machine commissioning has already been completed. The typical life time is 300 mins at 300mA, 800MeV. The average pressure of static and dynamic vacuum are below 2×10-8 Pa and 1.2×10-7 Pa respectively. The design, installation and commissioning of the vacuum system of the storage ring are detailedly stated in this paper.

INTRODUCTION

The 800MeV electron storage ring of the National Synchrotron Radiation Laboratory (NSRL) is a dedicated VUV and soft X-ray synchrotron radiation light source. The construction of NSRL facility began on November, 1983 and was completed in 1989. HLS comprises of 200 MeV injector, 800 MeV storage ring, 12 beamlines and 15 experimental stations by 2010. In order to supply synchrotron light with higher brightness and stability to the users, the upgrading project of HLS has been carried out during 2010-2014. The main changes of the new HLS (HLS-II) include: The energy of the injector increases to 800 MeV, so the electrons can be injected to the storage ring with full energy. The lattice of the storage ring was changed from TBA to DBA. The beam emittance decreased to 40 nmrad. A group of multifunctional sextuple magnets are employed and thus the long and short straight section are both lengthened. Five insertion devices were installed in the storage ring.

A VACUUM SYSTEM OF STORAGE

The storage ring's circumference is 63.66 meters. The main vacuum pipes are made of 316LN stainless steel by welding. The section is octagonal as shown in Fig. 1. To reduce surface degassing and magnetic permeability induced by welding, the chambers are baked at 900 °C in the vacuum furnace. After this treatment, vacuum chambers of the total leak rate, outgassing rate and magnetic permeability are below 2×10^{-8} Pa L/s , 2×10^{-11} Pa L/s cm^2 and 1.02 respectively, which meet the design requirements. Considering the convenience of installing, commissioning and maintenance, 3 RF-shielded all-metal gate valves are used to separate the storage ring into three cells. 20 UHV gauges are distributed in the storage ring to monitor the vacuum and also for interlock protection system.

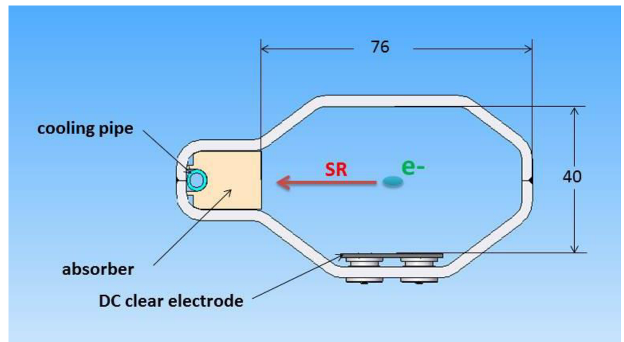

Figure 1: The section of the main vacuum pipe.

Because of the low electron energy, the deflection angle of the dipole magnet is relatively large, so the synchrotron light can hardly be absorbed by a lumped photon absorber. To ensure thermal stability of the vacuum pipes and reduce photon stimulated desorption, water-cooled absorbers made of oxygen-free copper which can protect the inner surface of the dipole magnet pipe from being hit by the synchrotron light, are arranged in the pipes along the beam direction and near the light outlet, as shown in Fig. 2. The absorbers in the pipes also act as supports and simplify the design of vacuum pipes.

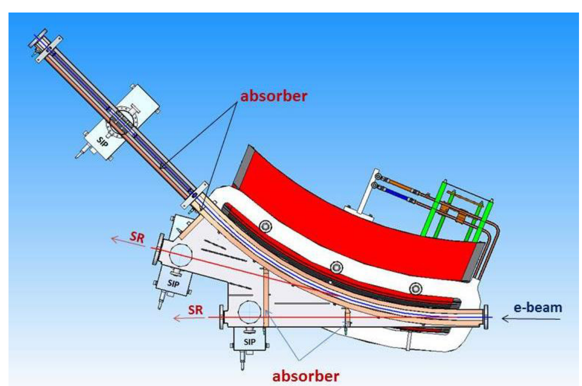

Figure 2: A standard segment of the storage ring.

18 RF-Shielded bellows are adopted to eliminate the machining and installing errors, deformation induced by temperature difference, and for the smooth transition of chambers with different sections. The bellows are machined by welding with high stability. Considering the smooth transition of chambers and high frequency contact resistance, the RF shield is achieved by using shield fingers. Shield fingers (Cu-Be) which bridge the gap between neighbouring flanges inside the welding bellows.

#ywang@ustc.edu.cn

Content from this work may be used under the terms of the CC BY 3.0 licence (© 2015). Any distribution of this work must maintain attribution to the author(s), title of the work, publisher, and DOI.

ISBN: 978-3-95450-168-7 doi:10.18429/JACoW-IPAC2015-WEPMN024

Content from this work may be used under the terms of the CC BY 3.0 licence (© 2015). Any distribution of this work must maintain attribution to the author(s), title of the work, publisher, and DOI.

EXPLORATION OF MULTI-FOLD SYMMETRY ELEMENT-LOADED SUPERCONDUCTING RADIO FREQUENCY STRUCTURE FOR RELIABLE ACCELERATION OF LOW- & MEDIUM-BETA ION SPECIES

Shichun Huang[#, 1,2], R.L. Geng[3]
[1] IMP, CAS, Lanzhou 730000, China
[2] UCAS, Beijing 100049, China
[3] JLAB, Newport News, VA 23606, USA

Abstract

Reliable acceleration of low- to medium-beta proton or heavy ion species is needed for future high current superconducting radio frequency (SRF) accelerators. Due to the high-*Q* nature of an SRF resonator, it is sensitive to many factors such as electron loading (from either the accelerated beam or from parasitic field emitted electrons), mechanical vibration, and liquid helium bath pressure fluctuation etc. To increase the stability against those factors, a mechanically strong and stable RF structure is desirable. Guided by this consideration, multi-fold symmetry element-loaded SRF structures (MFSEL), cylindrical tanks with multiple (n>=3) rod-shaped radial elements, are being explored. The top goal of its optimization is to improve mechanical stability. A natural consequence of this structure is a lowered ratio of the peak surface electromagnetic field to the acceleration gradient as compared to the traditional spoke cavity. A disadvantage of this new structure is an increased size for a fixed resonant frequency and optimal beta. This paper describes the optimization of the electro-magnetic (EM) design and preliminary mechanical analysis for such structures.

INTRODUCTION

SRF acceleration has become an enabling technology and many SRF accelerators are under construction or proposed world-wide for research in fundamental sciences and applications of society importance. TEM-type cavity structures, such as Quarter Wave Resonator (QWR), Half Wave Resonator (HWR) and spoke cavities [1] are usually chosen for accelerating protons or heavy ion species at low and medium beta (beta=v/c). Future heavy ion colliders such as MEIC [2], HIAF [3] are examples of proposed heavy ion machines that require SRF acceleration. A particular accelerating structure has its advantages and disadvantages over others in terms of mechanical (such as susceptibility to environmental vibrations and liquid helium pressure fluctuations), RF (such as peak surface electric and magnetic fields), and cryogenics (such as dynamic heat load). The consideration of high stability and high performance drives this present effort of exploring a mechanically strong and stable RF structure. For MFSEL structures, cylindrical tanks with multiple (n>=3) rod-shaped radial elements (see Fig. 1) were investigated as a starting point. The 3D computer simulation codes CST MWS and ANSYS were used to study electromagnetic and mechanical parameters, respectively. This paper provides the preliminary results of these types of structures.

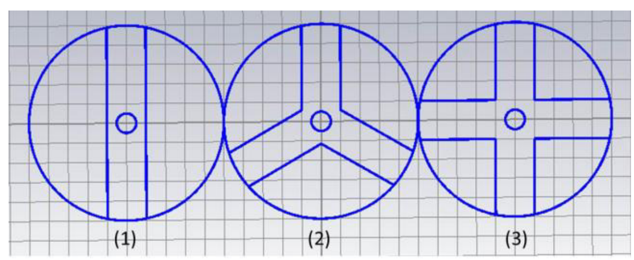

Figure 1:The general schematic of single-spoke structure (1) and MFSEL structure; three-fold (2) and four-fold (3).

EM DESIGN

The EM design of a multi(n=3,4)-fold symmetry element-loaded structure is to be compared with a baseline structure designed for high intensity proton acceleration in the framework of accelerator-driven system efforts at IMP [4] The baseline structure is a single spoke cavity with a beta = 0.32 and a frequency of 325 MHz. The MFSEL was originally proposed for muon acceleration [5]. More recently, similar structures were studied [6]. Figure 2 shows the side-cut view of a three-fold (TFSEL) symmetry element-loaded RF structure, with geometric dimensions as used in the numerical optimization. The geometric dimensions of the four-fold (FFSEL) symmetry element-loaded RF structure are similar to that of the TFSEL structure.

* Work supported by DOE. Authored by Jefferson Science Associates, LLC under U.S. DOE Contract No. DE-AC05-06OR23177. The U.S. Government retains a non-exclusive, paid-up, irrevocable, world-wide license to publish or reproduce this manuscript for U.S. Government purposes.
#hshch@jlab.org

ISBN: 978-3-95450-168-7 doi:10.18429/JACoW-IPAC2015-WEPMN025

HARMONIC RESONANT KICKER DESIGN FOR THE MEIC ELECTRON CIRCULAR COOLER RING*

Y. Huang#, IMP, CAS, Lanzhou 730000, China & UCAS, Beijing 100049, China
H. Wang, R.A. Rimmer, S. Wang, JLab, Newport News, VA 23606, USA

Abstract

Bunched-beam electron cooling of the high-energy ion beam emittance may be a crucial technology for the proposed Medium energy Electron Ion Collider (MEIC) to achieve its design luminosity. A critical component is a fast kicker system in the Circular Ring (CR) that periodically switches electron bunches in and out of the ring from and to the driver Energy Recovery Linac (ERL). Compared to a conventional strip-line type kicker, a quarter wave resonator (QWR) based deflecting structure has a much higher shunt impedance and so requires much less RF power. The cavity has been designed to resonate simultaneously at many harmonic modes that are integer multiples of the fundamental mode. In this way the resulting waveform will kick only a subset of the circulating bunches. In this paper, analytical shunt impedance optimization, the electromagnetic simulations of this type of cavity, as well as tuner and coupler concept designs to produce 5 odd and 5 even harmonics of 47.63MHz will be presented, in order to kick every 10^{th} bunch in a 476.3 MHz bunch train.

INTRODUCTION

Cooling of ion beams is critical in delivering high luminosities for the proposed MEIC [1].The present MEIC design utilizes a scheme of multi-stage cooling. In the booster, a DC cooler is used to assist accumulation of injected positive ions and reduce the beam emittance at the low energy. In the ion collider ring, an electron cooler utilizing high energy bunched beam will be responsible for cooling the medium energy ions to suppress intra-beam scattering (IBS) and maintain emittance during collisions. Two critical accelerator technologies in the bunched beam electron cooler are an ERL and a circulator ring (CR) to reduce the current and power of the cooling electron beam from the source and linac. As illustrated by the schematic drawing in Fig. 1, electron bunches are accelerated in an SRF linac, and then kicked into a closed ring that includes part of the ion collider storage ring. In this ring, electron bunches will be merged with the ions, and continuously cool the ion bunches in a long cooling channel, and then return to the linac for energy recovery after 25turns in the CR. In the present MEIC baseline design, the collision frequency is 476.3MHz, thus the repetition frequency of the electron bunches is 476.3MHz in CR and 19.052MHz in the ERL. A critical component in this scheme is a fast kicker system in the CR that periodically switches electron bunches in and out of the ring from and to the driver ERL. When the electron bunches are kicked into the CR (476.3MHz), every bunch in the ERL (19.052MHz) is kicked; when kicked out, every 25^{th} bunch is kicked and other 24 bunches are, ideally, undisturbed. The electron energy is 55MeV, assuming the kick angle is 0.001 rad, thus the kick voltage needed would be 55 kV. In the first R&D design, we just consider kicking every 10^{th} bunch in order to simplify the problem. The kick voltage pulse and bunch distance scheme is shown in Fig. 2 (red).

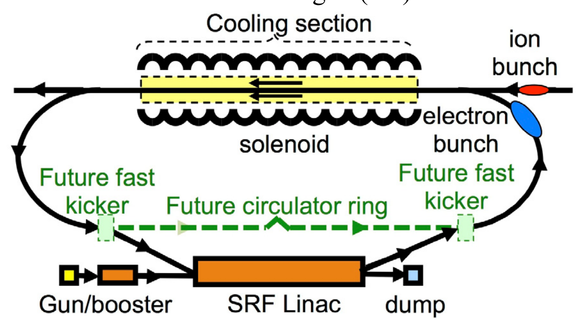

Figure 1: A schematic drawing of a bunched beam cooler based on an ERL, with bypass circulator ring connection in green.

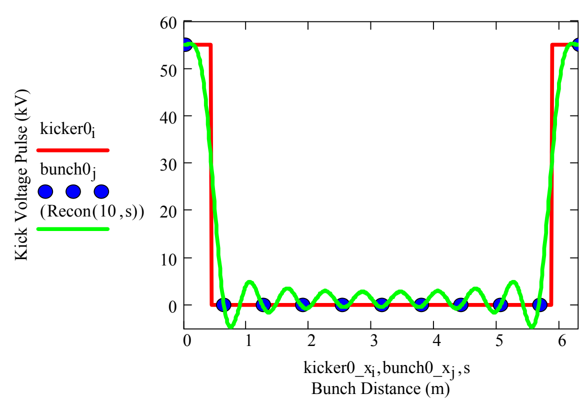

Figure 2: Ideal kicker voltage pulse (red) and bunch train scheme (blue) to kick every 10^{th} bunch, and the reconstructed kicker pulse with the first 10 harmonic modes (green).

GENERATION OF KICK VOLTAGE WITH FINITE HARMONIC MODES

The periodical kick voltage pulse can be described mathematically as a Fourier series expansion in compact trigonometric form [2]:

$$V_t = V_0 + \sum_{n=1}^{\infty} V_n \cos(n\omega_0 t + \varphi_n) \qquad (1)$$

Where V_t is the total kick voltage, the constant term V_0 represents a DC offset, ω_0 is bunch repetition frequency

*Work supported by Jefferson Science Associates, LLC under U.S.DOE Contract No. DE-AC05-06OR23177
#yulu@jlab.org

Content from this work may be used under the terms of the CC BY 3.0 licence (© 2015). Any distribution of this work must maintain attribution to the author(s), title of the work, publisher, and DOI.

ISBN: 978-3-95450-168-7 doi:10.18429/JACoW-IPAC2015-WEPMN026

DEVELOPMENT OF NON-RESONANT PERTURBING METHOD FOR TUNING TRAVELING WAVE DEFLECTING STRUCTURES

Jianhao Tan, Dechun Tong, Qiang Gu, Wencheng Fang, Zhentang Zhao*, SINAP, CAS, China

Abstract

For traveling wave accelerating structures, the tuning method assisted by bead pull technique based on non-resonant perturbation field distribution measurement has been widely applied. The method is also suitable for deflecting structures, but some key considerations of the field components of HEM11 mode and the selection of bead are discussed. A cage type of perturbing object has been made and applied on non-resonant perturbation measurements. The measurements on an S-band traveling wave deflecting structure are presented.

INTRODUCTION

Non-resonant perturbing method has been widely used on accelerating structure for field distribution measurement and guiding tuning procedure. For the purpose of tuning deflecting structure, non-resonant perturbing technology has been developed and applied for field distribution measurement in deflecting structure. As described in ref [1], non-perturbation method, which make the field measurement procedure fast, especially for long-period structure, and it uses direct measurements of the field distribution in the structure. For measurement and tuning travelling wave deflecting structure, the bead pull measurement based on non-resonant perturbation theory has been developed and will be applied.

NON-RESONANT PERTURBATION THEORY

According to the non-resonant perturbation theory [2], the reflection coefficients are measured at the input port of the structure in the absence of the perturbation object and in its presence. When the perturbing bead moves along a line from input port to output port, the magnitude and phase distribution of the electromagnetic field could be collected, which could be applied to get the information for tuning of the structure after the post-processing.

In non-resonant perturbation theory, the reflection coefficient and the field distribution in the structure have the relationship as follows:

$$2P_i(\Gamma_p - \Gamma_a) = -j\omega(k_e E_a^2 - k_m H_a^2) \tag{1}$$

Where Γ_p and Γ_a are the reflection coefficients in the input port in the presence and absence of the perturbing object, respectively. Ea and Ha are the complex vectors of the electric and magnetic field at the position of the bead in the structure, respectively. It is well known that, for traveling wave accelerating structure, the TM01 mode is used for beam acceleration, and the electric field EZ is the unique field component on axis. Then Eq. 1 becomes scalar equation, name as Eq. 2

$$\Delta S_{11} = S_{11p} - S_{11a} = \frac{-j\omega k_e}{P_i} E_z^2 = K_{ez} E_z^2 \tag{2}$$

Where ΔS_{11p} and ΔS_{11a} are reflection coefficients in the presence and absence of perturbation object, respectively, acquired from the NetWork Analyzer. $E_Z(z)$ is the electric field on axis, as the perturbing object goes through the structure along z, it is obvious that the amplitude of E_Z is proportional to the square root of the amplitude of ΔS_{11}, and the phase of E_Z is the half of the phase of ΔS_{11}, the information of measuring for tuning is collected.

For a deflecting structure, the operating mode is HEM11, which is a hybrid of TE11 and TM11 mode [3], and the field components have been calculated in [4]. Then Eq. 1 becomes a complicated equation, named as Eq. 3

$$\Delta S_{11} = \textstyle\sum_{i=x,y,z} (K_{ei} E_i^2 - K_{mi} H_i^2) \tag{3}$$

Where E_i and H_i are electric and magnetic field in different directions, respectively, K_i is defined as form factor of perturbing object. Further consideration, Eq. 3 can be expressed as,

$$\begin{aligned}\Delta S_{11} = \sum &[(K_{ei}|E_i^2|\cos 2\varphi_i + j|E_i^2|\sin 2\varphi_i) \\ &- (K_{mi}|H_i^2| + j|H_i^2|\sin 2\varphi_i)]\end{aligned} \tag{4}$$

Where φ_i and Ψ_i are the phase of electric and magnetic field. Eq. 4 indicate that, it is a multi-element complex equation, becomes difficult and complicated for measuring and guiding tuning multi-cell deflecting structure. A fast and reliable method for measurement is desperately needed.

In the travelling wave structure, the magnitude of E_Y and H_X nearly homogeneous on the axis cell by cell, but the positions of E_Y and H_X at their maximum are iris center and cavity center, respectively. For other four field components, except E_Z exist in coupler cavity, the distribution of E_Z, E_X, H_Y, and H_Z could be ignored in the structure on axis. Figure 1 shows the magnitude and phase distribution of E_Y and H_X along z. The magnitude and phase distribution in Figure 1(b) and (c), comparing with schematic drawing of structure in Figure 1(a), indicate that the electric field E_Y has maximum magnitude and flat phase shift in the iris center, on the contrary, H_X in the cavity center.

* zhaozhentang@sinap.ac.cn

Content from this work may be used under the terms of the CC BY 3.0 licence (© 2015). Any distribution of this work must maintain attribution to the author(s), title of the work, publisher, and DOI.

ISBN: 978-3-95450-168-7 doi:10.18429/JACoW-IPAC2015-WEPMN028

PRELIMINARY MECHANICAL DESIGN OF CERAMIC PIPE FILM COATING EQUIPMENT AT HEFEI LIGHT SOURCE II *

Jie Wang†, Yanhui Xu, Bo Zhang, Wei Wei, Le Fan, Xiangtao Pei, Yuanzhi Hong, Yong Wang#,
National Synchrotron Radiation Laboratory， University of Science and Technology of China, HeFei, AnHui 230029 China
Jiadong Lu†, School of Automation, Northwestern Polytechnical University, Xi'an, Shanxi 710072 China

Abstract

Ceramic vacuum chambers are important components of the injection chamber at Hefei Light Source II (HLS II). The length of each Ceramic vacuum chamber is 350 mm and their inner surface is coated with TiN thin film whose properties are low secondary electron yield (SEY), good electrical conductivity, stability of performance, ability to block hydrogen permeation. Considering that the cross section of Ceramic pipe is racetrack structure, Ti plate was chose as the cathode to improve TiN thin film deposition rate. Meanwhile, the authors designed a motor drive magnetron sputtering film coating equipment to obtain uniform TiN film.

INTRODUCTION

Ten years ago, ceramic chambers and ferrite kicker magnets were developed in HLS injection system and the inner surface of the ceramic chambers was coated with 0.1 ohm/square metallic Mo layers to meet the requirements of both the penetration of pulse magnetic field and small beam coupling impedance [1]. Now TiN or Ti are chosen as the metal coating material of the ceramic vacuum chamber in HLS II [2-6]. Furthermore, for the purpose of improvement of the deformation and uniformity of the thickness, Ling-Hui Wu et al. designed and fabricated a ceramic chamber using Ti films [7]. However, for some irregular type ducts, such as the racetrack type (Fig. 1) ceramic chamber in accelerators, the shape of the ceramic pipe will induce new and considerable technological difficulties for the uniformity of TiN coating which is important for the vacuum and beam stability in the pipes of storage ring.

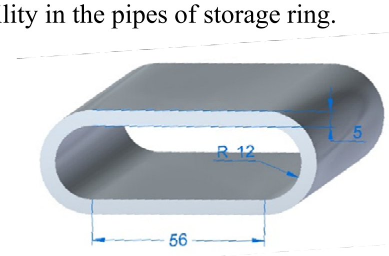

Figure1: A diagram of a ceramic vacuum pipe.

* Work supported by the National Nature Science Foundation of China under Grant Nos.11075157.
†These authors contributed equally to this work. They are co-first author.
#ywang@ustc.edu.cn

APPARATUS AND METHODS

Coating System

The TiN films are deposited onto the interior wall of ceramic vacuum pipe which is described in Fig. 1. The cross-section of shaped ceramic vacuum chambers in the system is a special type of racetrack with a small aperture. The schematic diagram of DC magnetron sputtering coating system which mainly consisted of vacuum gauge, solenoid, cathode, gas flow control system, power supply, 300 l/s turbo molecular pump and ceramic pipe, was shown in Fig. 2.

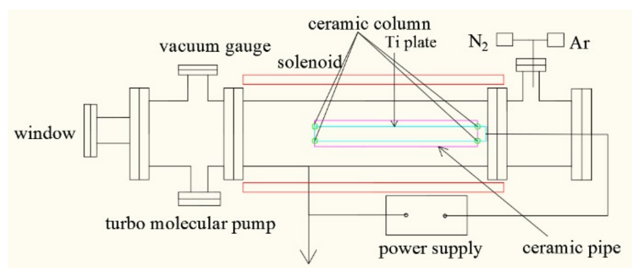

Figure 2: Schematic diagram of DC magnetron sputtering coating system.

The Uniformity of TiN Film and Electric Field Distribution

The electrostatic solver of CST software was used to simulate the electric field distribution in the case of ceramic pillars as cathode brace, during glow discharge. In this simulation, the voltage of the cathode plate and ceramic pillars was -680 V and 0 V respectively. In Fig. 3, the location of green arrow is the position of the ceramic pillars. According to the scale on the right side of Fig. 3, the electric displacement vector on the position of four ceramic pillars is two times higher than that on both ends of Ti cathode plate and also higher than other parts of the ceramic pipe. The electric field distortion caused that film thickness near the ceramic pillars is greater than the one on other parts, which also can be seen from Fig. 4. Therefore, the results of the simulation basically matched experimental results.

Content from this work may be used under the terms of the CC BY 3.0 licence (© 2015). Any distribution of this work must maintain attribution to the author(s), title of the work, publisher, and DOI.

ISBN: 978-3-95450-168-7 doi:10.18429/JACoW-IPAC2015-WEPMN030

TESTING PROCEDURES FOR FAST FREQUENCY TUNERS OF XFEL CAVITIES

K. Przygoda#, J. Branlard, O. Hensler, H. Schlarb, C. Schmidt, DESY, Hamburg, Germany
K. Kasprzak, IFJ-PAN, Cracov, Poland
W. Cichalewski, T. Pozniak, DMCS, Lodz, Poland

Abstract

The XFEL accelerator will be equipped with 100 accelerating modules. Each accelerating module will host 8 superconducting cavities. Every single cavity will be equipped with a mechanical tuner. Coarse tuning will be supported by a step motor. A fine tuning will be handled by double piezoelectric elements installed inside a single mechanical support, providing actuator and sensor functionality or redundancy. Before the main linac installation, all its subcomponents need to be tested and verified. The AMTF (Accelerator Module Test Facility) has been built at DESY to test all XFEL cryomodules. In total 1600 piezos need to be tested. Test procedures for fast frequency tuners have been developed to check their basic performance in cryogenic conditions (tuning range, acting and sensing abilities). High level applications have been first developed and next adopted to perform fully automated tests including report generation and data base storage. After the successful completion of the acceptance tests, the cryomodules will be prepared for tunnel installation.

INTRODUCTION

The 36 accelerating modules equipped with 1.3 GHz superconducting (SC) resonant cavities have been delivered to DESY since February 2014. The 26 (including 3 pre-series) cryomodules have been tested using AMTF test stand. The AMTF test stand has been equipped with 3 independent RF stations supported by cryogenic subcomponents, RF waveguide distributions and RF sources. The each RF station has been installed with LLRF control system based on MTCA.4 technology [1].

The pre-series and a few of first regular series of XFEL modules have been fully tested with both piezo tuners installed per single cavity including: DC scans, LFD compensation and microphonics measurement. The rest of the tests of regular XFEL 1.3 GHz modules have been reduced mainly due to time limitation (e.g. to train operators, limited space at storage buffer, sharing resources with 3 GHz modules) and technical problems (broken couplers, RF source problems, cabling issues).

The piezo DC scans have been proposed for checking not only the typical tuning range foreseen for the Saclay II model of the piezo tuner but also locating piezo looseness (mechanical mistake during piezo assembly), shorts on the cables and inside connectors or mistakes in cabling pinout (reversed piezo polarity). The acceptance criterion for piezo tuning range has been agreed to not be less than 850 Hz of cavity absolute static detuning value.

Lorentz force detuning (LFD) compensation can play crucial role not only for regular operation at high RF gradient conditions (above 30 MV/m) but also to evaluate the quench limit conditions for each cavity per accelerating module [2]. The actuator functionality of supporting piezo elements applied for each cavity has been checked. The LFD factor has been measured for each cavity for both middle (between 10 and 15 MV/m) and high gradient (between 19 and 30 MV/m) operating conditions. The acceptance test threshold has been initially set to be below 10 Hz of static and dynamic detuning values and next relaxed due to time constraints foreseen for the tests (less than 50 Hz).

The sensor functionality of each piezo element has been evaluated to study the main sources of the mechanical vibrations that can additionally modulate resonance frequency of the cavity. The dominated frequency component for all tested cavities has been located at 50 Hz (see Fig. 1).

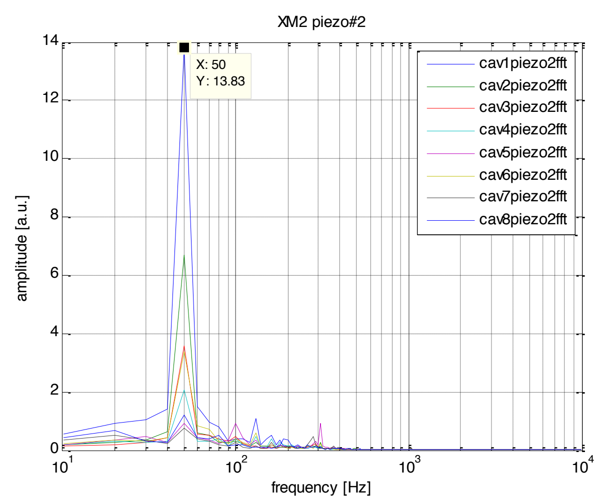

Figure 1: Microphonics measurement at XM-2 module.

Due to limited time the test procedure has been excluded from the regular tests.

LLRF CONTROL

The single RF station at AMTF has been installed together with LLRF control system designed according to MTCA.4 standard. The LLRF control system has been packed inside 9U, 12-slot crate equipped with cooling units, redundant power supply (PS), MTCA Carrier Hub (MCH), CPU and HDD, Advanced Mezzanine Card backplane (AMCB). In addition, the crate is equipped

#konrad.przygoda@desy.de

Content from this work may be used under the terms of the CC BY 3.0 licence (© 2015). Any distribution of this work must maintain attribution to the author(s), title of the work, publisher, and DOI.

ISBN: 978-3-95450-168-7 doi:10.18429/JACoW-IPAC2015-WEPMN031

AUTOMATED QUENCH LIMIT TEST PROCEDURE FOR SERIAL PRODUCTION OF XFEL RF CAVITIES

Karol Kasprzak, Daniel Konwisorz, Krzysztof Krzysik, Szymon Myalski, Jacek Swierblewski, Katarzyna Turaj, Mateusz Wiencek, Agnieszka Zwozniak, IFJ PAN, Krakow, Poland
Denis Kostin, Konrad Przygoda, DESY, Hamburg, Germany

Abstract

In the Accelerator Module Test Facility (AMTF) at DESY in Hamburg RF cavities and accelerating cryomodules are tested for the European X-ray Free Electron Laser (XFEL). Measurements are done by team of physicists, engineers and technicians from The Henryk Niewodniczanski Institute of Nuclear Physics Polish Academy of Sciences in Krakow, Poland, as a part of Polish in-kind contribution to XFEL. The testing procedures providing information about maximum available gradient and heat loads measurement are performed for the high gradients (up to 31MV/m). During these tests the cavity deformation caused by the Lorentz force is compensated by piezo (fast) tuners. For this purpose automated high level software was developed. This paper describes a method used to tune automatically the cavities during the RF tests. It was validated with the XFEL cryomodules. This improvement was implemented into the testing software and it is successfully used for testing of serial production cavities.

INTRODUCTION

In the Accelerator Module Test Facility (AMTF) at DESY in Hamburg serial-production accelerating cryomodules for the European X-ray Free Electron Laser (XFEL) are tested. Currently (status 28 April 2015) 28 out of 101 modules have been tested. The two vital acceptance measurements for them are called: flat top and heat loads [1, 2].

From RF point of view, during these measurements, it is critical to automatically regulate RF fields inside the cavities. It is essential for the time schedule as well as for the precision of the measurement. This is done by the high level feedback controller that regulates step (slow) motor and piezo actuators. The software is written in LabVIEW (see Fig. 1) . It was validated and successfully used for cryomodules testing.

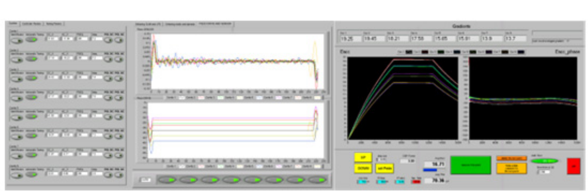

Figure 1: The controller software (left) and test software (right) during the heat loads measurement of the cryomodule XM33.

TESTING PROCEDURE

Flat Top Measurement

The aim of the flat top measurement is to obtain the following cavity parameters:

a) gradient when field emission is started – is visible on the X-ray detectors
b) (if possible) gradient when radiation starts exceeding 10^{-2} mGy/min
c) the maximum gradient (0.5 MV/m less than the quench, measured up to 31 MV/m)
d) power measured for the maximum gradient

31 MV/m is the gradient equivalent to maximum power for the single cavity, which will be available in the XFEL tunnel with respect to the planned klystron power (10 MW), losses in the waveguide system and power distribution. Single klystron will supply 4 cryomodules (in sum 32 cavities).

Also during this measurement the operating gradient is obtained as the minimum value from:

a) gradient when radiation starts exceeding 10^{-2} mGy/min
b) the maximum gradient
c) gradient when temperature measured on the input power coupler rises rapidly
d) gradient when input power coupler vacuum rises rapidly

Heat Loads Measurement

The aim of the heat loads measurement is to evaluate thermal loads during normal XFEL cryomodule operation. From the RF point of view, this procedure is done by changing power distribution in the waveguides. Values saved during flat top measurement are used as reference. As a result the cavities gradients used during heat loads measurement are limited by:

- operating gradient taken from the flat top measurement or
- 23.6 MV/m (XFEL goal gradient)

Furthermore, the waveguide power distribution during the AMTF measurements is paired, which means that the same power is set to the neighboring cavities. This determines the chosen gradient as the weakest from the cavity pair (1-2, 3-4, 5-6, 7-8).

Content from this work may be used under the terms of the CC BY 3.0 licence (© 2015). Any distribution of this work must maintain attribution to the author(s), title of the work, publisher, and DOI.

ISBN: 978-3-95450-168-7 doi:10.18429/JACoW-IPAC2015-WEPMN032

MICROPHONIC DISTURBANCES PREDICTION AND COMPENSATION IN PULSED SUPERCONDUCTING ACCELERATORS

R. Rybaniec*, L.J. Opalski, ISE WUT, Warsaw, Poland
V. Ayvazyan, L. Butkowski, S. Pfeiffer, K. Przygoda, H. Schlarb, Ch. Schmidt
DESY, Hamburg, Germany

Abstract

Accelerators are affected by the cavities detuning variation caused by external mechanical disturbances (microphonics). The paper presents microphonics estimation and prediction methods applicable for superconducting accelerators operating in pulsed mode. A mathematical model is built using the estimates of detuning during previous RF pulses. The model can be used for predictions of disturbances for the future time step and setup of the fast tuners accordingly. The proposed method was successfully verified with measurements conducted at the FLASH linac.

INTRODUCTION

Located at DESY, FLASH and currently constructed XFEL [1] are examples of the Linear Particle Accelerators (linacs) built using superconducting technology. Those linacs operate in pulsed mode regime. Because of the high operating gradients reaching up to 40 MV/m, during the pulse, RF cavities are detuned by the magnetic field pressure phenomena. In a RF cavity, electromagnetic field induces surface current and surface charges on the wall of the cavity. Interaction of the surface currents with a standing wave inside cavity generates a pressure, which mechanically deforms the cavity and as a consequence detunes it from the nominal frequency. In the literature it is known as Lorentz force detuning (LFD).

Another source of the detuning is caused by external mechanical forces acting on the RF cavities called microphonics. In opposite to the Lorentz force detuning, microphonics are generally not synchronized to the RF operation. Some sources of the microphonics are the helium plant, ground motions and man made machinery [2]. Pulsed mode operation at FLASH consists of the approx. 1.3 ms RF pulses with a repetition rate of 10 Hz. Time during the RF pulse is insufficient to measure the microphonic disturbance and compensate for it during the same pulse.

Due to a very high quality factor of superconducting cavities, detuning decreases the power transferred from the RF system. This reduces the RF system efficiency and also makes controlling stability of the accelerating gradient more difficult. In a situation where a high power amplifier is shared between many cavities, accelerating field control becomes more complicated, because detuning affects each cavity separately.

Conceptually (Fig. 1) it is possible to compensate for microphonics by predicting its level based on the information

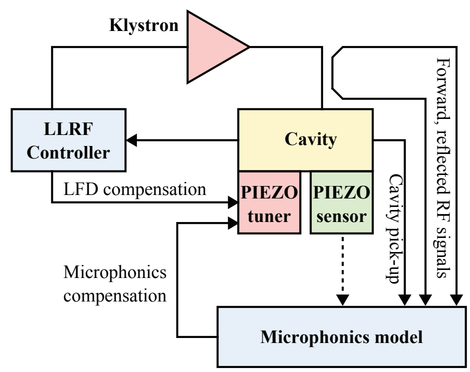

Figure 1: Block diagram of the proposed microphonics compensation method for a linac operating in pulsed mode.

from previous pulses. To enable this, a microphonics model has to be build during an operation of a facility. Possible information sources are RF signals during the pulse and (optionally) piezo sensors output in the time between the pulses. Piezo actuator can be used for fast tuning of the cavity based on the knowledge from the model, in the similar way as it is used for Lorentz force detuning compensation. This could decrease the amount of microphonic disturbances affecting the cavity.

In the paper a first implementation of this concept is evaluated. In the first attempt a simple auto-regressive (AR) model for the microphonics is used. Disturbances are estimated using the detuning computed from the RF signals. The method was validated with the open-loop measurements at the FLASH linac. First results show potential reduction of the detuning caused by microphonic disturbances in the accelerators operating in a pulsed mode.

MICROPHONIC DISTURBANCES ESTIMATION AND PREDICTION

During an operation of the facility, detuning of SRF cavities can be computed [3] using RF signals. This is accomplished with the first order cavity model [4]:

$$\frac{d\mathbf{V_c}}{dt} + (\omega_{1/2} - j\Delta\omega)\mathbf{V_c} = K_g \cdot \mathbf{V_g},$$

where $\mathbf{V_c}$ - cavity pick-up signal, $\omega_{1/2}$ - half-bandwidth of the cavity, $\Delta\omega$ - detuning and $K_g \cdot \mathbf{V_g}$ - is the calibrated generator voltage, calculated from the forward and reflected power signals. After separation of the real (I) and imaginary (Q) parts of the complex numbers, detuning can be

* radoslaw.rybaniec@desy.de

Content from this work may be used under the terms of the CC BY 3.0 licence (© 2015). Any distribution of this work must maintain attribution to the author(s), title of the work, publisher, and DOI.

ISBN: 978-3-95450-168-7 doi:10.18429/JACoW-IPAC2015-WEPMN033

THE FABRICATION OF PROTOTYPE NORMAL CONDUCTING REBUNCHER FOR THE MEBT IN RISP

Hye-Jin Kim*, Myung Ook Hyun, Bum-Sik Park
RISP, Institute of Basic Science, Daejeon, Korea

Abstract

The Medium Energy Beam Transport (MEBT) system of RAON consists of several quadrupole magnets for controlling the transverse beam parameter at the entrance of the low energy linac, three normal-conducting (NC) re-bunchers to match the longitudinal beam ellipse into the acceptance of the low energy linac and several diagnostic devices. The NC QWR re-buncher, which has a frequency of 81.25 MHz, a geometric beta factor of 0.032, and an effective length of 24 cm, has been fabricated and tested to demonstrate the frequency tuning by using slug tuner, power transmission and reflection with low input power, and pulsed high power transmission with cooling channels. In this presentation, we show the design and fabrication criteria for the high power, ~ 10 kW, re-buncher and its test results.

INTRODUCTION

The Medium Energy Beam Transport(MEBT) line system, which is located between the RFQ and the SCL, requires matching of the optical parameters in the transverse plane and removal of the unaccelerated ion beams from the RFQ. It also includes beam diagnostic devices to measure and control the beam quality and Twiss parameter at the entrance of the linac during a beam operation [1,2]. In our designed MEBT line, three normal-conducting re-bunchers with 81.25 MHz (β_g = 0.032) quarter wave resonators (QWRs) and eight room-temperature quadrupole magnets were chosen for the beam bunching, beam transport and matching. Strip-line beam position monitors, current monitors, a bunch length monitor, beam collimators and steering magnets are also installed in the MEBT line. The designed MEBT line can accept and control the transverse and the longitudinal distributions of several beams such as the 500 keV/u ^{238}U beam, the 500 keV proton beam, and the 500 keV/u ^{18}Ar beam [3].

ELECTROMAGNETIC AND MECHANICAL DESIGN

Two gap normal conducting 81.25 MHz quarter wave resonators (QWRs) were chosen to provide enough electric field for matching of the longitudinal phase space distribution from the RFQ into the linac [4]. The gap distance of the cavity is 5.9 cm that is consistent with the velocity of the ion beam. Based on the particle tracking simulation, the requirement of the peak electric field on the beam axis is about 3 MV/m to control the longitudinal phase space distribution and to remove the un-accelerated beams [5].

* hjkim87@ibs.re.kr

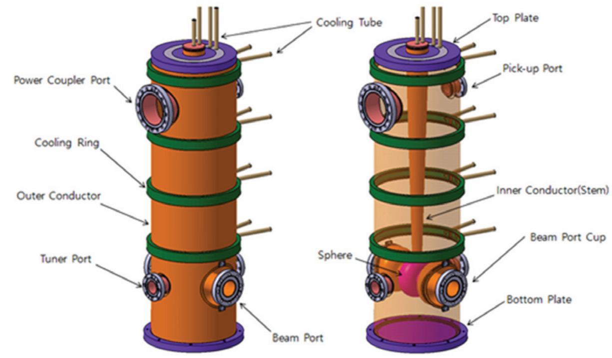

Figure 1: Drawing of the QWR cavity in MEBT of RAON.

As shown in Fig. 1, the bore radius of the beam pipe of the QWR cavity is 5 cm to minimize the uncontrolled beam loss. It was limited by the shunt impedance for getting a high acceleration field. The internal structure, such as shape of the stem, center sphere, and beam port, is optimized to decrease the surface electric field which strongly related with the heat loss from the QWR cavity. The electromagnetic design of the cavity is performed by using code CST-MWS and the electric field along the beam axis is shown in Fig. 2 [6].

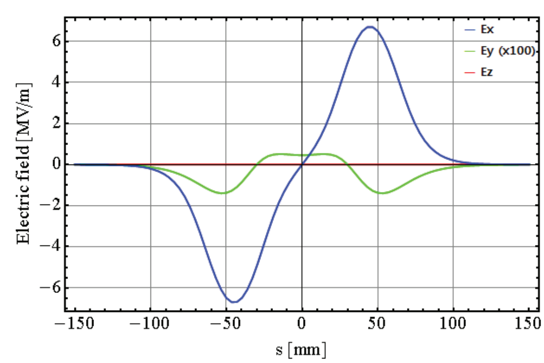

Figure 2: Electric field profile along the beam axis.

It has the electric field component on the vertical direction which can cause the orbit steering due to the structural asymmetry of the QWR cavity. The field strength, however, is small enough to ignore the orbit displacement at the entrance of the linac. It was confirmed by the tracking simulation.

The cooling of the QWR cavity is most significant factor for the mechanical design of the high power normal-conducting structure since the almost power, ~ 10 kW, is converted as the heat on the surface of the QWR cavity. The drawing for the cooling channels is shown in Fig. 3.

In order to suppress the heat up to 15 kW since the calculated power loss was to be about 10 kW for the electric field of 3 MV/m on the beam axis, the QWR cavity was produced

Content from this work may be used under the terms of the CC BY 3.0 licence (© 2015). Any distribution of this work must maintain attribution to the author(s), title of the work, publisher, and DOI.

ISBN: 978-3-95450-168-7 doi:10.18429/JACoW-IPAC2015-WEPMN034

ELECTRON EMISSION FROM SURFACE ROUGHNESS ON CAVITY IN LOW TEMPERATURE*

Heetae Kim[1], Yong Sik Chang[2], Gunn-Tae Park[1], Hyuk Jin Cha[1], Suk Choi[1], Wookang Kim[1,#]
[1]Rare Isotope Science Project, Institute for Basic Science, Daejeon 305-811, Republic of Korea
[2]Department of e-Business, Hanshin University, Osan, Kyungki 447-791, Republic of Korea

Abstract

Electron emission phenomenon from surface roughness on cavity is investigated. The distribution of the electric field from the surface roughness can be obtained on cavity surface. The field emission is calculated from the electric field distribution. The generalized electron emission from electric field and temperature effect is also calculated on the surface roughness of the cavity.

INTRODUCTION

When a body is heated, it generates thermal radiation. Blackbody radiation is used to measure the temperature of the heated body for all range of temperature. Size effect of thermal radiation [1-3] and the effective temperature for non-uniform temperature distribution were investigated [4-6]. Ionization efficiency of helium gas was investigated as a function of pressure and applied voltage with the use of a tungsten tip [7]. Unified theory of field and thermionic emission was constructed with a free electron gas model [8]. Properties of the thermal radiation from arbitrary fractional dimension were investigated [9]. Sheet resistance of graphene grown on different surface roughness of Cu films was measured [10].

In this research, we show total electron emission which includes electric field effect, temperature effect, and surface roughness effect on cavity. General electron emission is introduced and electron emission can be limited with a resistor. Effect of surface roughness causes the increased fractional dimension and focused electric field. Total electron emission can be calculated from thermionic and field emission.

GENERAL ELECTRON EMISSION

Electrons can be generated from heating, electric field, and UV light. Electron current density from thermionic emission, field emission and UV light can be expressed as

$$J = J_{therm} + J_{field} + J_{UV} \ , \tag{1}$$

where J_{therm}, J_{field} and J_{UV} represent the current density of thermionic emission, field emission, and UV, respectively.

Electrons come out of the metal when they get enough thermal energy to overcome the work function. The current density of thermionic emission is

$$J_{therm} = \frac{4\pi mek_B^{\ 2}}{h^3} T^2 e^{-\Phi_w / k_B T} \ , \tag{2}$$

where Φ_w is the work function, h is the Planck constant, m is the electron mass and k_B is the Boltzmann constant. Electrons make thermionic emission when they have higher energy than work function.

Electrons come out of the metal to which strong electric field is applied. Electron current density of field emission for zero-temperature approximation is

$$J_{field} = \frac{e}{2\pi h} \frac{\sqrt{E_F}}{(\Phi_w + E_F)\sqrt{\Phi_w}} F^2 e^{-4k\Phi_w^{\ 3/2}/3F} \ , \tag{3}$$

where $k = \sqrt{\frac{8\pi^2 m}{h^2}}$ is electron wave number and F is the electric field. This is the well-known Fowler-Nordheim equation.

LIMITATION OF ELECTRON EMISSION

Electron emission can be limited by applying a

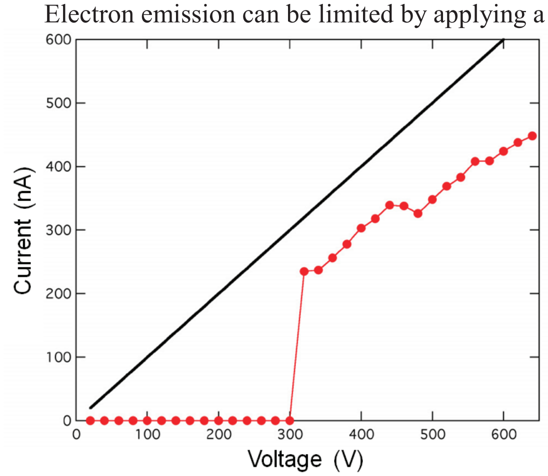

Figure 1: Current measurement is shown as a function of applied voltage.

resistor. The resistor having 1 G ohm is connected to carbon nanotubes. Carbon nanotubes are connected with an electrode by using epoxy. Electron collector is made of copper and the chamber is being pumped. Fig. 1 shows the electron current as a function of applied voltage. The

* This work was supported by the Rare Isotope Science Project of Institute for Basic Science funded by the Ministry of Science, ICT and Future Planning (MSIP) and the National Research Foundation (NRF) of the Republic of Korea under Contract 2013M7A1A1075764. This work was also supported by Hanshin University Research Grant.
# kwko11045@ibs.re.kr

Content from this work may be used under the terms of the CC BY 3.0 licence (© 2015). Any distribution of this work must maintain attribution to the author(s), title of the work, publisher, and DOI.

ISBN: 978-3-95450-168-7 doi:10.18429/JACoW-IPAC2015-WEPMN035

Content from this work may be used under the terms of the CC BY 3.0 licence (© 2015). Any distribution of this work must maintain attribution to the author(s), title of the work, publisher, and DOI.

QWR AND HWR CRYOMODULES FOR HEAVY ION ACCELERATOR RAON *

W.K. Kim, M.K. Lee, Y. K. Kim, G. T. Park, H.J. Cha, H.J. Kim, H. Kim#
Rare Isotope Science Project, Institute for Basic Science, Daejeon 305-811, Republic of Korea

Abstract

The accelerator called RAON has five kinds of cryomodules such as QWR, HWR1, HWR2, SSR1 and SSR2. The QWR and HWR1 cryomodules are designed and fabricated. The cryomodules will be operated at 2 K and 4 K in order to operate the superconducting cavities. The static heat load of the system was analytically computed for each configuration. The functional requirement of the cryomodules and the static heat load measurement of the QWR and HWR1 cryomodules are presented in this research.

INTRODUCTION

The accelerator called RAON which accelerates beam to 200 MeV/u has five kinds of cryomodules such as QWR, HWR1, HWR2, SSR1 and SSR2. The cryomodule of QWR and HWR1 cryomodules are designed and fabricated. The cryomodules will be operated with liquid helium of 2 K and 4 K in order to operate the superconducting cavities. Liquid helium above 2.172 K is normal fluid and liquid helium below 2.172 K is called superfluid. Superfluid properties of liquid helium are well-known and properties of superfluid fog were intensively investigated [1-4]. Blackbody radiation is changed due to size effect [5, 6]. The effective temperature for non-uniform temperature distribution was studied [7-9] and the thermal radiation from arbitrary fractional dimension was investigated [10]. The main role of the cryomodules is to minimize heat leak and heat generation, to supply cryogenic fluid and to align beam through superconducting cavities. The static heat load of the system was analytically computed for each configuration.

In this research, we show the fabrication design and static heat load measurement for QWR and HWR1 cryomodules.

CRYOMODULES

The cryomodule has Mu-metal magnetic shield to reduce earth's magnetic field by less than 10 mG. The crymododule consists of thermal shield of 40 K, intercepts and strong-back made of invar to align the cavity. The SCL11 section accelerates beam from 0.5 to 2.7 MeV/u. Table 1 shows the summary of SCL1 cryomodules for RAON. QWR cryomodule has one cavity, HWR1 has two cavities and HWR2 has four cavities. The length of QWR cryomodule is 450 mm, that of HWR1 cryomodule is 1,400 mm and that of HWR2 cryomodule is 2,720 mm. The SCL11 consists of 22 quarter wave resonators and SCL12 consists of 32 half wave resonators.

Table 1: Summary of SCL1 Cryomodules for RAON

SCL	Cavity	No. of cavity in CM	No. of CM	CM length (mm)
SCL11	QWR	1	22	450
SCL12	HWR	2	13	1,400
		4	19	2,720

Functional requirements of cryomodule are shown in Table 2. Cavity alignment is mainly changed by pumping chambers and cool-down process. Air pressure outside of cryomodule and thermal contraction due to cool-down process make alignment change. The alignment requirement is important for beam dynamics. Vacuum of cavity and chamber is required to reduce the heat load in cryomodule operation.

Table 2: Functional Requirements of Cryomodule

Note	Conditions	Requirement
Cavity alignment	X, Y	±0.25 mm
	Z	± 0.5 mm
	Tilt	± 0.1 °
Vacuum	Chamber	~10^{-5} torr
Vacuum	Cavity	~10^{-7} torr
System pressure rating	Reservoir 4.5 K pipe 40 K pipe	4 bar 20 bar 20 bar

EXPERIMENT

The main roles of cryomodules are to maintain operating condition of superconducting cavities and to keep alignment of beam line. High vacuum and thermal insulation are required for the cryomodules to maintain the operating temperature of superconducting cavities. A detailed conceptual design is performed to fabricate cryomodules. The stiffness of the strong back is designed sufficiently to make device alignment to remain within

* This work was supported by the Rare Isotope Science Project of Institute for Basic Science funded by the Ministry of Science, ICT and Future Planning (MSIP) and the National Research Foundation (NRF) of the Republic of Korea under Contract 2013M7A1A1075764.
# kim_ht7@yahoo.com

ISBN: 978-3-95450-168-7 doi:10.18429/JACoW-IPAC2015-WEPMN036

DESIGN STUDY ON A HIGH POWER RF AMPLIFIER FOR THE RFQ *

M.H. Chun†, K.H. Park, I.H. Yu, Y.S. Lee[1], D.S. Kim[2], M.H. Seo[2], Y.J. Moon[2], J.W. Ok[3], M.S. Won[3], J. Hong[3], B.S. Lee[3] and J. Bahng[4]
Pohang Accelerator Laboratory, Pohang, 790-834, Korea
[1]SKKU, Suwon, Korea, [2]Dawonsys, Siheung, Korea
[3]Korea Basic Science Institute, Busan, Korea
[4]Kyungpook National University, Daegu, Korea

Abstract

The RF amplifier of 100 kW (CW) at 165MHz has been studied for a Radio Frequency Quadruple (RFQ). The RFQ as a linear accelerator will be used for low energy beam section of KBSI accelerator system in order to accelerate and focus the ion beam up to 500keV/u [1]. An RF amplifier is composed of a drive, an intermediate, and a final amplifier stage with power supplies. The intermediate amplifier (IPA) of 5 kW is designed with solid state amplifier modules, and the final amplifier is designed with a tetrode tube. The high voltage power supply for the tetrode provides the fine regulation of 15 kV at 10 A. The RF amplifier is operated by program logic controller (PLC) with interlocks, and a low level RF control for RFQ accelerator. This paper describes the present design study on the 100 kW RF amplifier.

INTRODUCTION

The RF amplifier of 100 kW is composed of a Final Power Amplifier (FPA) of a tetrode TH781, IPA of 5kW with SSPA and a PLC control system. Main component of FPA is a tetrode amplifier: Thales tube TH781 and a resonant input/output cavity TH18781E [2].

Figure 1 shows the block diagram of high power RF amplifier including 6-1/8" coaxial transmission lines such as circulator, loads, directional coupler, and an RFQ.

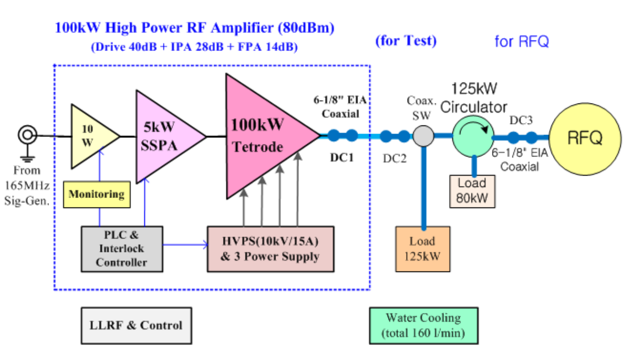

Figure 1: block diagram of RF amplifier for RFQ.

Main power supply is for the anode of 10 kV/15 A to get 100 kW RF output. The others are grids and heater power supplies. The PLC controls the amplifier including power supplies and manages interlocks. Table 1 shows design parameters of the amplifier.

Table 1: Design Parameter of Amplifier for RFQ

Specification	Value	Details
Frequency	165 MHz	Synthesizer
Bandwidth	± 0.8 MHz	-1 dBc
Amp. Stability	< ± 0.2 %	Close loop
Phase Stability	< ± 0.2 degree	Close loop
Operating mode	Continuous	or Pulse mode
Transmission Lines	6-1/8" EIA w/ Circulator	100 kW CW 150 kW peak
Interlock time	less than 2 us	fast, wired

FINAL AMPLIFIER

The final amplifying stage is based on the TH781 tetrode fabricated by Thales. The 100 kW/165 MHz amplifier with vacuum tube has advantages for high power up to 300 kW and cheaper than SSPAs. TH781 is only a tetrode for high power application at 165MHz and has been tested to other projects of IHEP, LANL and IFMIF (International Fusion Materials Irradiation Facility) [3][4][5]. Some power supplies including a high voltage anode supply are needed for operating the tetrode. Table 2 shows specification of power supplies and option items for the FPA of 100 kW RF output.

Table 2: Power supplies and accessories of FPA

Items	Specification	Details
Anode P/S	10kV / 15A	controlled
Screen Grid P/S	1200V / 0.7A	< ± 0.1 %
Control Grid P/S	-350V / 0.9A	< ± 0.1 %
Filament P/S	10V / 375A	DC or AC
Resonant Cavity	Input / Output	TH 18781E
HV Filter	< -50dBc	Option
Radiation Shielding	X-ray <5μsv/h RF <0.1mW/cm^2	Option

*Work supported by Korea Basic Science Institute in Korea.
† mhchun@postech.ac.kr

Content from this work may be used under the terms of the CC BY 3.0 licence (© 2015). Any distribution of this work must maintain attribution to the author(s), title of the work, publisher, and DOI.

ISBN: 978-3-95450-168-7 doi:10.18429/JACoW-IPAC2015-WEPMN037

Content from this work may be used under the terms of the CC BY 3.0 licence (© 2015). Any distribution of this work must maintain attribution to the author(s), title of the work, publisher, and DOI.

HIGH POWER KLYSTRON AMPLIFIERS FOR THE PLS AND PLS-II STORAGE RING *

M.H. Chun†, I.H. Yu. Y. Joo, I.S. Park, Y. Sohn and H.J. Park
Pohang Accelerator Laboratory (PAL), Pohang, 790-834, Korea

Abstract

The RF system of the Pohang Light Source-II (PLS-II) storage ring is operating at the 3.0 GeV/340 mA with three superconducting RF (SRF) cavities. PLS-II RF system was upgraded to 3.0 GeV/400 mA(max.) beam storage from 2.5 GeV/ 200mA of PLS. Each high power RF (HPRF) station is composed of a 300 kW klystron with power supplies, transmission components including a 350 kW circulator and load, and water cooling system. The klystrons are generally operated as a RF power source with high gain amplification for RF system of light sources. This paper describes the present operation status of 300 kW klystron amplifier and experiences of the former PLS 75 kW klystron amplifiers as well as RF system.

INTRODUCTION

The PLS-II machine of 3.0GeV is the upgraded third synchrotron light source from PLS of 2.5GeV. PLS-II has a full energy Linac and a storage ring. The PLS RF system was five independent RF stations. Each station was consisted of a modified 75kW klystron amplifier, a circulator, a single-cell normal conducting RF cavity with precise controlled water cooling system, all connected by 6-1/8" coaxial transmission lines and analogue type low level RF system [1][2]. But the upgraded PLS-II RF system in 2015 is operating for beam current of 340mA with three superconducting RF cavities supplied RF power through WR1800 waveguides from three 300kW klystron amplifiers with high voltage power supplies, and digital type LLRF control system [3]. Figure 1 shows the block diagram of PLS-II RF system with 300kW klystron amplifiers.

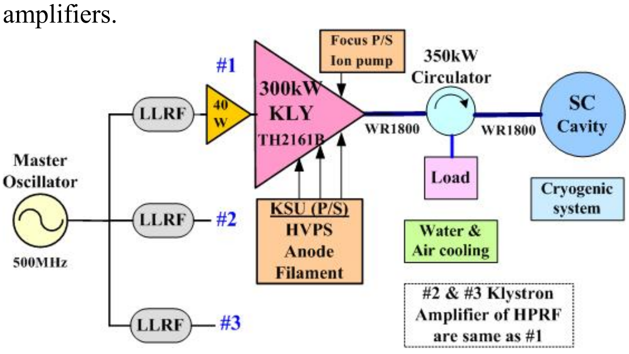

Figure 1: Klystron Amplifier at PLS-II RF system.

Also table 1 shows comparison of main parameters for PLS and PLS-II storage ring.

Table 1: Comparison of PLS and PLS-II

Specification	PLS(~2010)	PLS-II(2015)
Energy/Current	2.5GeV/200mA	3.0GeV/400mA
Emittance	18.9 nm-rad	5.8 nm-rad
Circumference	280.56 m	281.82 m
Total RF Power	200 kW	480 kW
RF Frequency	500.082MHz	499.964MHz
RF Power Sources	75kWx5	300kWx3
RF Voltage/Cavity	1.6MV, 4 NC	4.8MV, 3 SC

KLYSTRONS AS RF SOURCES

Klystrons have been used as RF sources for almost particle accelerators because of high power capacity and efficiency. Three 300kW high power klystron amplifiers are operating for PLS-II and some 60~75kW klystrons were used for PLS RF system. The TH2161B klystrons are operating some light sources such as SLS, IHEP, CLS, SSRF, TPS and NSLS-II storage rings. Table 2 shows comparison of klystron parameters: TH2161B of 300kW for PLS-II and K3773BCD of 75kW for PLS storage ring RF system [4].

Table 2: Comparison of CW Klystrons

Specification	TH2161B	K3773BCD
Frequency (B/W)	500MHz(2MHz)	470~860MHz (7MHz)
RF output (CW)	310 kW(max)	75 kW(max)
Beam V/I (peak)	54kV/9.5A	26.5kV/6.3A
Gain/Efficiency	40dB / 60%	35dB / 45%
μ-Perveance	1.62	2.00
Cavities	5 Integrated	4 External
Maker	Thales (France)	EEV (UK)

K3773BCD klystron was originally manufactured for UHF-TV transmitter application, and to be modified to CW operation for light sources. Similar UHF-TV klystrons of K3672BCD and K3775BCD are still operating at Elettra and Bessy-II [5].

*Work supported by Ministry of Science, ICT and Future Planning in Korea.
† mhchun@postech.ac.kr

ISBN: 978-3-95450-168-7 doi:10.18429/JACoW-IPAC2015-WEPMN039

RF ACCELERATING VOLTAGE OF PLS-II SUPERCONDUCTING RF SYSTEM FOR STABLE TOP-UP OPERATION WITH BEAM CURRENT OF 400 mA

Youngdo Joo#, Myung-Hwan Chun, In Soo Park, In-Ha Yu, Taekyun Ha, Ilmoon Hwang, Byung-Joon Lee, Younguk Sohn
Accelerator Division, Pohang Accelerator Laboratory, POSTECH, Pohang, Gyeongbuk, Korea

Abstract

During the beam store test up to 400 mA in the storage ring, it was observed that the vacuum pressure around the RF window of the superconducting cavity rapidly increases over the interlock level limiting the availability of the maximum beam current storing. We investigated the cause of the window vacuum pressure increment by studying the changes in the electric field distribution at the superconducting cavity and waveguide according to the beam current. An equivalent physical modeling was developed using a finite -difference time domain (FDTD) simulation and it revealed that the electric field amplitude at the RF window is exponentially increased as the beam current increases, thus this high electric field amplitude causes a RF breakdown at the RF window.

INTRODUCTION

As the RF accelerating voltage increases, the energy acceptance increases, as a result, the injection efficiency becomes higher. However, the energy acceptance of 2.5% is already sufficient for the injection efficiency of the PLS-II SR [1,2]. Therefore, the effect of the RF accelerating voltage higher than 3.6 MV on the injection efficiency is saturated. The Touschek lifetime keeps increasing until the RF accelerating voltage reaches about 3.6 MV, but it gets lower for the RF accelerating voltage higher than 3.6 MV. The longitudinal bunch length becomes shorter as the RF accelerating voltage increases as shown in Fig. 1(a). The shorter bunch can cause the problem of ion instability due to the short bunch interacting more strongly with the impedance of the vacuum chamber, enhancing outgassing in some local points. For an instance, the loss factor of the SC cavity taper section in the PLS-II SR is calculated and shown in Fig. 1(b). When the RF accelerating voltage increases from 3.6 MV to 5.0 MV, the beam bunch length is reduced by 17.5% and the loss factor is enlarged by 26.4%. This enlarged loss factor means that more power loss due to the wake-field occurs at the taper section increasing the surface temperature and vacuum pressure. . Therefore, it is recommended that the total RF accelerating voltage be kept at around 3.6 MV.

#ydjoo77@postech.ac.kr

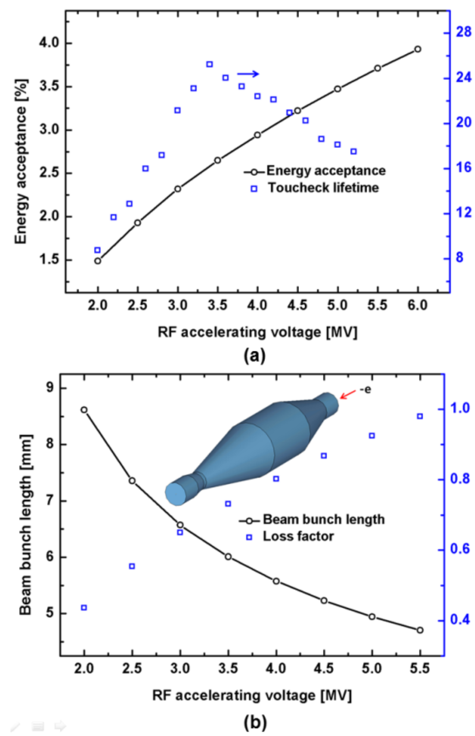

Figure 1: (a) Calculated energy acceptance and Touschek lifetime and (b) the beam bunch length and the loss factor of the PLS-II SC taper section. The three-dimensional modeling of the SC taper section is shown in the inset.

BEAM STORING MACHINE STUDY

The measured forward power, reflect power and window vacuum pressure from Fig. 2(a) are plotted to the beam current domain and shown in Fig. 2 together with the calculated beam power, forward power and reflect power of SC2 with the RF accelerating voltage of 1.2 MV. The calculated and measured powers are well matched until the beam current reaches 235 mA. However, the measured powers become unstable and show difference from calculated powers when the current is higher than 235 mA. Both the forward power and the reflect power are larger than those calculated. That means that the coupling ratio of the cavity is changed. When the beam current is dumped, it reaches 259 mA due to the window vacuum high interlock. The unpredictable changes in the coupling ratio and the rapid increment of window vacuum pressure strongly suggest that the changes in the electric field distribution must be examined at and around the ceramic window in the beam current domain.

Content from this work may be used under the terms of the CC BY 3.0 licence (© 2015). Any distribution of this work must maintain attribution to the author(s), title of the work, publisher, and DOI.

ISBN: 978-3-95450-168-7 doi:10.18429/JACoW-IPAC2015-WEPMN041

TECHNICAL OVERVIEW OF BUNCH COMPRESSOR SYSTEM FOR PAL XFEL

H.G. Lee, D.H. Na, S.B. Lee, B.G. Oh, Y.J. Seo, H.S. Suh, Y.G. Jung, D.E. Kim, K.H. Park, H.S. Kang, K.W. Kim
Pohang Accelerator Laboratory, POSTECH, Korea

Abstract

Pohang Accelerator Laboratory(PAL) is developing a SASE X-ray Free Electron Laser based on 10 GeV linear accelerator. Bunch compressor (BC) systems are developed to be used for the linear accelerator tunnel. It consists of three(BC1, BC2, BC3_H) hard X-ray line and one(BC3_S) soft X-ray line. BC systems are composed of four dipole magnets, three quadrupole magnet, BPM and collimator. The support system is based on an asymmetric four-dipole magnet chicane in which asymmetry and variable R_{56}. can be optimized. This flexibility is achieved by allowing the middle two dipole magnets to move transversely. In this paper, we describe the design of the stages used for precise movement of the bunch compressor magnets and associated diagnostics components.

INTRODUCTION

A bunch compressor support system has been fabricated and tested for the PAL XFEL. The machine of the PAL XFEL consists of four main sections: the linear accelerator, the hard x-ray undulator hall, the soft x-ray undulator hall and the experimental area. The accelerator, schematically shown in Figure 1, comprises the gun, the laser heater, four accelerating sections groups (L1–L4), four bunch compressors (BC1, BC2, BC3_H and BC3_S) and the spreader. The physics design of the magnetic bunch compressor is based on an asymmetric four-dipole chicane configuration [1]. The BC purpose is to reduce the electron bunch length, thus increasing the peak current, taking advantage of the beam correlated energy spread. Due to the accelerating process, there is an inherent longitudinal energy spread in the electron bunch. Passing through four bending magnets chicane, the path length is energy dependent and the electron bunch is compressed. At each bend, the electron bunch head delays with respect to the tail. Mounting high homogeneity magnetic field dipoles and having diagnostic devices centre on the beam at each chicane position are the main advantages of the movable chicane.

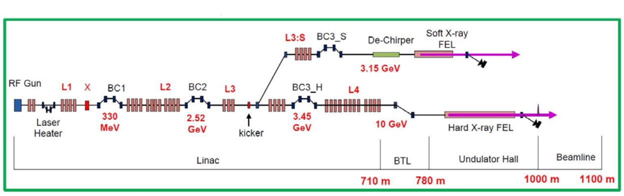

Figure 1: The schematic layout of the 3-BC lattice.

BUNCH COMPRESSOR OVERVIEW

The BC support system, shown in Figure 2 and Table 1, consist of four dipole magnets (DM), two tweak quadrupole magnets and a skew quadrupole magnet, two corrector magnets, BPM, collimator, screen and CSR monitor. The position of such diagnostic devices remains fixed with respect to the central dipoles.

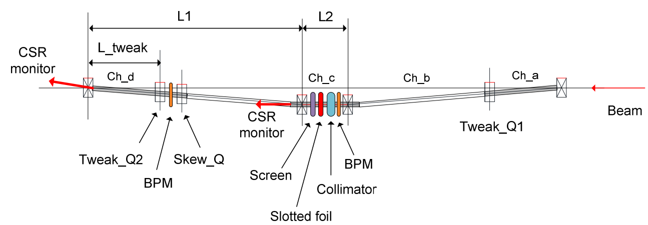

Figure 2: Layout of the BC support system.

Table 1: Major Parameters of the BC Support System

	BC1	BC2	BC3_H	BC3_S
Dipole angle , deg	4.9	3.0	1.7	1.7
Dipole length , m	0.2	0.7	0.7	0.7
L1 , m	4.4845	7.1905	7.597	6.397
L2 , m	1.2	1.8	1.8	1.8
L_tweak , m	1.146	1.3483	2.349	1.349
Aperture diameter of Tweak Quad, mm	44 (Q11)	44 (Q11)	44 (Q11)	44 (Q11)

The support systems of BC are composed of two fixed support and a moving support. The two central dipoles are mounted on a moving support that can have up to 627.0 mm motion orthogonal to the beam axis. A servo motor provides movement to the central stage and a linear encoder controls its exact position. The position accuracy of dipoles is within 50 μm.

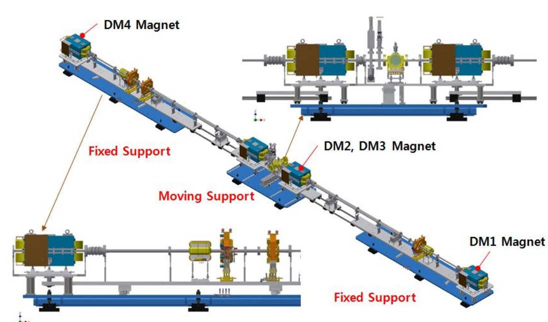

Figure 3: 3D modelling of BC support system.

Content from this work may be used under the terms of the CC BY 3.0 licence (© 2015). Any distribution of this work must maintain attribution to the author(s), title of the work, publisher, and DOI.

ISBN: 978-3-95450-168-7 doi:10.18429/JACoW-IPAC2015-WEPMN042

400 mA BEAM STORE WITH SUPERCONDUCTING RF CAVITIES AT PLS-II*

Younguk Sohn#, Myung-Hwan Chun, Taekyun Ha, Mansu Hong, Youngdo Joo, Heung-Sik Kang, Hyung-Gyun Kim, Kyung Ryul Kim, Tae-Yeon Lee, Chong-Do Park, Hong-Jib Park, In Soo Park, Seunghwan Shin, In-Ha Yu, Jong Cheol Yun, PAL, Pohang, Korea

Abstract

Three superconducting RF cavities were commissioned with electron beam in way of one by one during the last 3 years, and now PLS-II is in user service on the way of beam current to 400mA, the target of PLS-II. The cavities and cryomodules were prepared with SRF standard technology and procedures, then vertical test, windows conditioning, cryogenic test in each cryomodule, horizontal power test, conditioning, and commissioning without and with beam at PLS-II tunnel by collaboration with industries. All the cavities showed stable performances as good as not-observing any RF instability from cavities, couplers and windows up to 400 mA beam store, but observing several cavity quenches and minor vacuum bursts by abrupt power with control and human errors. The initial beam current for user run were recorded as 150 mA with one cavity, 280 mA with two cavities and 320 mA with three cavities. The 400 mA beam was also achieved with two cavities by decay mode and also with three cavities by top-up mode. The stabilities of RF amplitude and phase are good enough not to induce beam instabilities.

INTRODUCTION

The PLS-II of which is the upgraded light source from former PLS is mainly to increase the number of ID beamlines by changing magnet arrangement from double bend achromat lattice (DBA) to triple bend achromat lattice (TBA) [1], so that 20 ID beamlines are afforded at PLS-II. Also the upgrade machine is to provide higher brightness of photon beam, order of two through increasing electron beam energy and stored beam current, as 3 GeV and 400 mA, respectively.

The RF system of PLS-II should be high capacity of RF power and free from cavity higher mode (HOM) instabilities. The RF system must compensate the energy loss as much as 1024 keV and 200 keV from 24 bending magnets and 20 insertion devices, respectively. So the RF system must afford to provide 550 kW RF power properly for additional broad band loss from the SR structures and no coupled bunch instabilities (CBI) should be shown to 400 mA beam current by installing HOM free cavities. A superconducting RF (SRF) system is chosen to meet such a requirement, described above.

The baseline design [2] is a three-independent RF station, of which each RF cavity has its own power amplifier, transmission system, and a LLRF. With 3 SRF cavities, the design Vacc and forward RF power per each cavity are lower than their specification, which has been contributed to reduce cavity abnormality and to increase the lifetime of ceramic window and also of high power amplifier.

The 3 SRF stations were installed one by one during last 4 years as first 3 normal conducting cavities in 2011 and they were replaced with one SC cavity, then two more SC cavities during following two years. It is strategy to make time for operator to be familiar to SRF system, meanwhile for machine to be conditioned gradually by low synchrotron energy. Even though these consideration, we suffered from a lot of troubles such as vacuum bursts at RF window, cavity quenches from bad RF power control resulted to violent He evaporation and He refrigerator trip by poor protection and many human error by LLRF in the first 3 months. The trial and errors during beginning 3 months contributed to the performance normalization. First of all, we improved the listed trouble makers such as LLRF, interlock system between RF source and cavities, electric power control of He refrigerator. Also, we setup maintenance procedures as cavity partial warmup and pulse conditioning cavity and window before start of every user-run.

Then, the beam current with two SC cavities by top-up mode in 2013 was 120 mA at beginning of user run to 280 mA at last run. During the machine study, 400 mA beam current was touched during several ten minute, but it couldn't go on due to vacuum burst. Also we tried to increase beam current with one more SC cavity installation in 2014. Even with frequent partial warmup and pulse conditioning, the window vacuum burst still one of trouble for high beam current. It was overcome with deep study of relationship between RF forward power, reflected power and window dissipation heat [3]. With these result, stable 400 mA beam current with top-up mode was achieved during 2 hours in machine study.

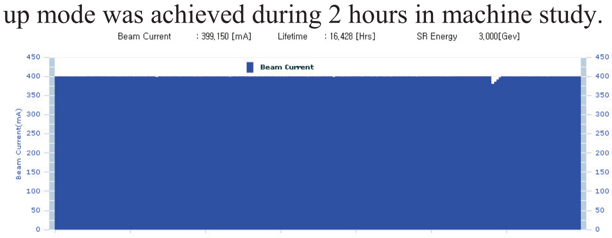

Figure 1 : Achievement of 400 mA top-up mode.

In 2nd half year of user run, beam current increased in run by run, 300 mA, 320 mA and 350 mA. At 350 mA operation, we couldn't provide stable user beam due to the vacuum interlock from the in-vacuum undulators.

*Work supported by the Minister of Science, ICT and Future Planning
younguk@postech.edu

Content from this work may be used under the terms of the CC BY 3.0 licence (© 2015). Any distribution of this work must maintain attribution to the author(s), title of the work, publisher, and DOI.

ISBN: 978-3-95450-168-7 doi:10.18429/JACoW-IPAC2015-WEPMN043

Content from this work may be used under the terms of the CC BY 3.0 licence (© 2015). Any distribution of this work must maintain attribution to the author(s), title of the work, publisher, and DOI.

THE RF STABILITY OF PLS-II STORAGE RING RF SYSTEM

I.H. Yu, Y.D. Joo, Y. Sohn, M.H. Chun, I.S. Park, H.J. Park, M.H. Chung, H.G. Kim, H.S. Kang, Pohang Accelerator Laboratory, Pohang, Korea
Y.S. Lee, Department of Energy Science, Sungkyunkwan University, Suwon, Korea

Abstract

The RF system for the Pohang Light Source (PLS) storage ring was greatly upgraded for PLS-II project of 400 mA, 3.0 GeV from 200 mA, 2.5 GeV. Three superconducting RF cavities with each 300 kW maximum klystron amplifier were commissioned with electron beam in way of one by one during the last 3 years for beam current of 400 mA to until March 2014. The RF system is designed to provide stable beam through precise RF phase and amplitude requirements to be less than 0.3% in amplitude and 0.3° in phase deviations. This paper describes the RF system configuration, design details and test results.

INTRODUCTION

The final quantitative goal of PLS-II is a top-up user-service operation with beam current of 400 mA to be completed by the end of 2014. The RF accelerating voltage of PLS-II RF system was set to 4.8 MV(1.6 MV/cavity), which was estimated using the maximum available beam current that works as a function of RF voltage, and the top-up operation test with the beam current of 400 mA was successfully carried out. The PLS-II has increased the beam energy from 2.5 GeV to 3 GeV; the number of IDs has been increased by a factor of two (20 IDs); and the beam current has been increased from 190 mA to 400 mA. The beam emittance has been reduced to below 10 nm while retaining the existing PLS tunnel as well as the existing injection system [1].

The radio-frequency (RF) system of the electron SR for the light source generates a sufficient RF accelerating voltage and transfers RF power to the electron beam to compensate for the beam energy loss due to synchrotron radiation from the bending magnets and IDs. Three superconducting RF systems are installed in the PLS-II storage ring.

The schematic diagram of a RF station in PLS-II storage ring is shown in Fig. 1. The PLS-II RF system consists of five major components: (1) low level RF control system(LLRF) with EPIC IOC, (2) a continuous wave (CW) klystron with a rated output power of 300 kW at the frequency of about 500 MHz, (3) a 300 kW circulator which isolates the klystron to protect the klystron form reflection power from cavity, (4) a 300 kW water cooling ferrite load which terminates the RF power by converting the RF power to thermal loss at the ferrite panel, and (5) a CESR-B type cryomodule produced by RI (former ACCEL).

The RF power generated by klystron is incident to the superconducting cavity (SC) through WR1800 waveguide, the ceramic RF vacuum window and the RF coupler to build a RF field at the SC RF cavity. The LLRF system gets the amplitude and phase information of the RF field from the signal at the cavity RF pickup and keeps the RF field stable by controlling the amplitude and phase of forward power in the presence of various external noises such as beam loading effect, mechanical vibrations, changes in the electrical length of the waveguide between the klystron and the cavity, and the pressure fluctuation in the Liquid He vessel [2].

Each cavity consists of a cell elliptical type. The cavities are tuned to 500MHz, and individually controlled by a mechanical stepper motor with tuner. Each cavity is powered and controlled by a single klystron and LLRF system. The klystrons produce 300 kW Maximum. The RF controls use a traditional heterodyne scheme and digital down conversion at an intermediate frequency (50 MHz). Each cavity field and resonance control PI algorithm is contained in two FPGAs. One FPGA is in the field control chassis (FCC manufactured by JLAB RF Group), controlling a single cavity. The resonance control chassis contains the other and controls three cavities simultaneously. Controls and interfaces for the most of RF system devices are provided through EPICS [3].

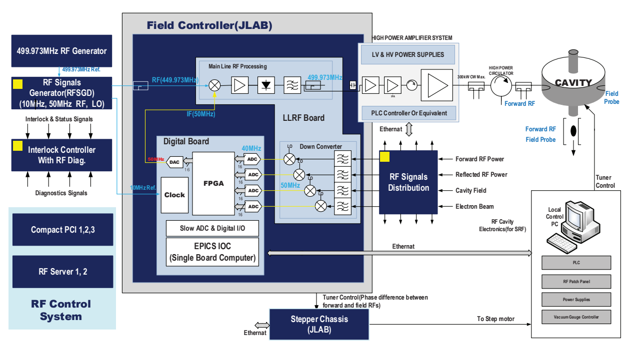

Figure 1: The schematic diagram of the RF station for PLS-II Storage Ring.

RF SIGNALS MEASUREMENT & FEEDBAK CONTROL HARDWARE

Each cavity is controlled by a single LLRF system, called here FCC. an FCC contains five fast ADC channels (receivers), although one receiver channel has no heterodyning frontend in order to direct sample 10 MHz external clock reference. All RF signals, once down-converted and digitized, are processed in an FPGA. The FCC requires an external 20 dBm LO (450 MHz) and external 3 dBm clock reference (10 MHz). The clock system has a programmable digital PLL and can work with different references as well as produce assorted sampling frequencies. A fast DAC channel produce 50

ISBN: 978-3-95450-168-7 doi:10.18429/JACoW-IPAC2015-WEPMN045

IOT USE AS A POWER SOURCE FOR A LINEAR ACCELERATING STRUCTURE

E. Savin, S. Matsievskiy, N. Sobenin, I. Sokolov, NRNU MEPhI, Moscow, Russia
A. Zavadtsev, LLC « Nano Invest », Moscow, Russia

Abstract

Nowadays the interest of using compact and high efficiency power sources called Inductive Output Tubes (IOT) [1] for feeding accelerating structures with the required pulsed power around 1MW is increasing. In this article results of the beam dynamics and geometry calculations for the L-band IOT S-band IOT and accelerator-generator hybrid module are presented. Different concepts of the cavity have been proposed, but the most efficient has been chosen. The layout of the generator cell with biperiodic buncher cells has been investigated. The hybrid structure composed from the generator cell and the compact SW accelerating section is proposed.

THE GOAL

The goal of the research is to find optimal geometry of the generator cells, output and injection systems for different types of the linear accelerators.

L-BAND PROTON LINEAR ACCELERATOR HYBRID STRUCTURE

Accelerating section consists from washers-diaphragms accelerating structure working on TH_{020} mode at 991 MHz frequency [2]. The idea is to create TH_{020} cavity designed for the same purpose as a klystron output cavity with six beam tubes (Fig. 1). Together with accelerating section they create the hybrid structure working on quasi $\pi/2$ mode [3] where connecting waveguide is a coupling cavity (Fig. 2).

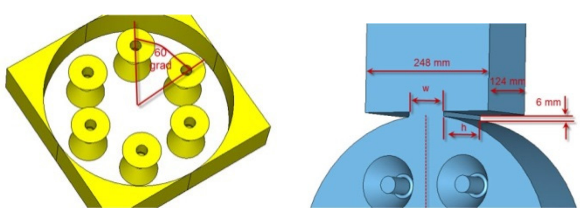

Figure 1: Generator cell geometry.

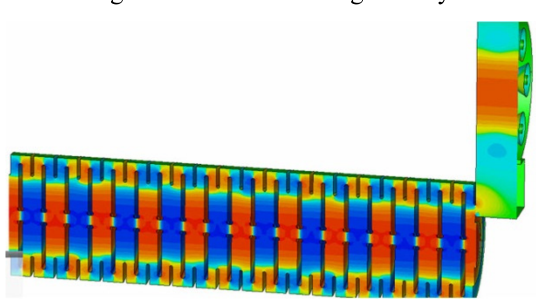

Figure 2: Generator-accelerator hybrid structure.

IOT DESIGN

Next geometries are designed on 2856 MHz working frequency regarding for the uncovered researches for the S-band IOTs. Geometry parameters were varied to achieve maximum output power [4] from the generator cell while inputting there six 5A (pulse) modulated electron beams (Fig. 3).

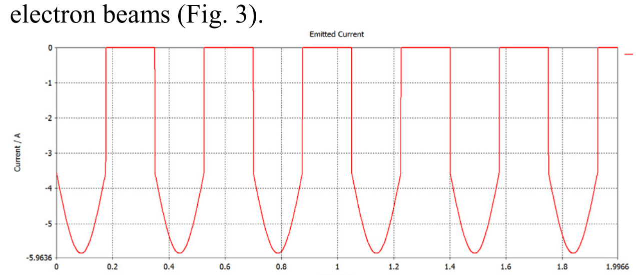

Figure 3: Emitted current from the one cathode.

TH_{020} Pillbox Cavity

TH_{020} wave type consists from two electric field maximums – one in the middle of the cavity and other one (radial) on the perimeter, thus we can put beam pipes in this maximum (Fig. 4).

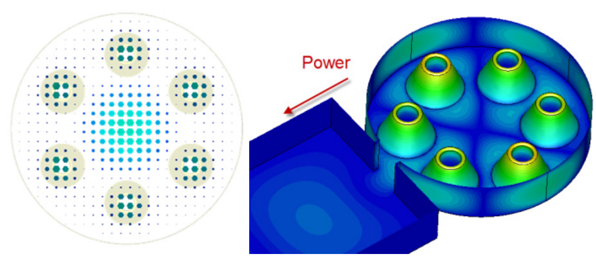

Figure 4: TH_{020} wave in resonator and the power output waveguide.

Maximum power level was reached by varying the beam gap and over coupling between generator cell and the output design by changing the window width w (Fig. 5). In every geometry variations the operating frequency was tuned to 2856 to match with injected beam frequency.

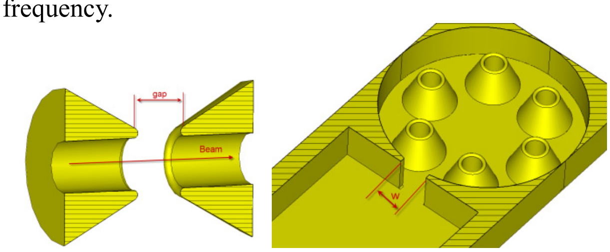

Figure 5: Generator parameters to adjust.

© Content from this work may be used under the terms of the CC BY 3.0 licence (© 2015). Any distribution of this work must maintain attribution to the author(s), title of the work, publisher, and DOI.

ISBN: 978-3-95450-168-7 doi:10.18429/JACoW-IPAC2015-WEPMN046

COMPASSION OF HIGHER ORDER MODES DAMPING TECHNIQUES FOR SUPERCONDUCTING 9-CELL STRUCTURE

Ya.V. Shashkov, N.P. Sobenin, A.Mitrofanov, National Research Nuclear University MEPhI (Moscow Engineering Physics Institute), Moscow, Russia
V. Zvyagintsev, TRIUMF, Canada's National Laboratory for Particle and Nuclear Physics, Vancouver, BC, Canada

Abstract

Modern types of accelerators, such as Energy recovery linacs, require low values of higher order modes (HOM) Q_{ext}. In accelerators with high current HOM could lead to high losses for the modes excitation, beam instability and beam break up. HOM couplers and waveguides are often used in such structures for HOM damping. Unfortunately they could lead to a violation of the axial symmetry of the accelerating field and negatively affect the beam emittance. Also these devices are subject for multipactor discharge and could be difficult in maintaining and fabrication. In this paper we examine several ways of HOM damping with ridged, fluted and corrugated drift tubes which are devoid of the above-mentioned drawbacks. The influence of the parameters of the drift tube on the HOM damping and on the parameters of the fundamental wave were analyzed.

INITIAL DESIGN

As a reference point for simulations 9-cell 1300 MHz superconducting accelerating cavity (Fig. 1a) [1] was analyzed. In order to estimate efficiency of HOM damping in such structure electrodynamic characteristics (EDC) [2] were calculated for the structure without couplers but with ideal load boundary conditions on at the end of drift tubes. EDC of operating mode presented in Table 1.

In order to estimate HOM frequency range dispersion characteristics (Fig. 1b) for TM_{010} modes and HOMs were plotted. The most dangerous HOMs for the structure are dipole modes TE_{111}, TM_{110}; quadrupole modes TE_{211} and TM_{210} and monopole mode TM_{011}. Line $\beta_{phase} = 1$ is also presented on the graph. Intersection points of dispersion characteristics with $\beta\text{-}_{phase} = 1$ line (synchronous point) represent modes with the highest interaction between particles and modes and requires additional attention. External Q-factor Q_{ext} and shunt impedance R_{sh} for HOMs and operational mode presented on the Fig 2 and 3. Q_{ext} values were calculated in CST Microwave Studio [3].

Comparison of the results with similar structures [4] showed that Q_{ext} for operating mode is nearly the same, for dipole modes it is three orders higher, 4-5 orders higher for quadrupole modes and for 2nd monopole HOM its two times higher.

Work is supported by Ministry of Education and Science grant 3.245.2014/r

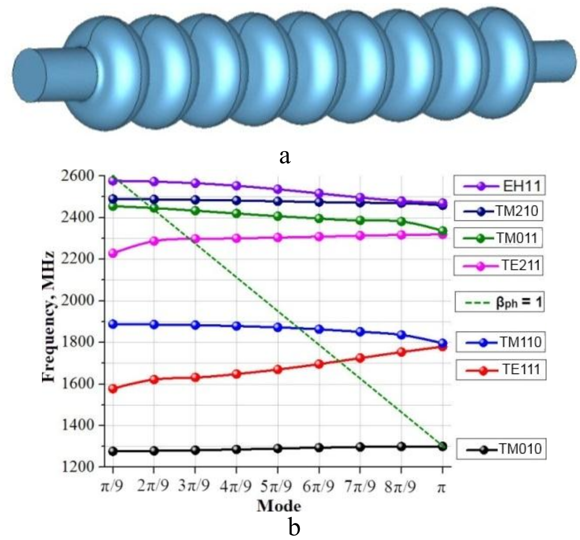

Figure. 1.Genearal view (a), dispersion characteristics (b), for 9-cell cavity with cylindrical beam pipes

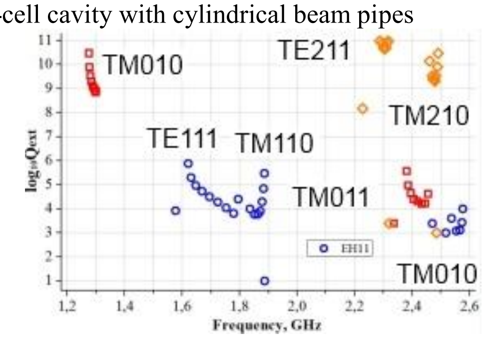

Figure. 2. Q_{ext} for 9-cell cavity with cylindrical beam pipes

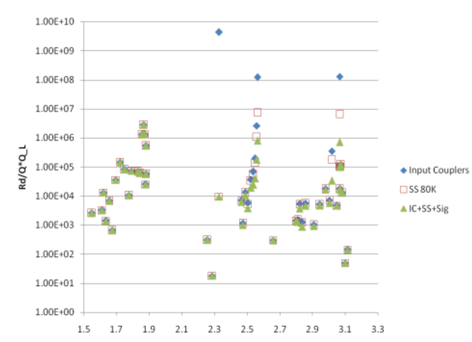

Figure. 3. R_{sh} (d) for 9-cell cavity with cylindrical beam pipes. Diamond - loaded just with input couplers, square - loaded in addition with stainless steel damping rings, triangle - stainless steel damping ring on coupler side and Sigradur damping ring on tuner side [1]

Content from this work may be used under the terms of the CC BY 3.0 licence (© 2015). Any distribution of this work must maintain attribution to the author(s), title of the work, publisher, and DOI.

ISBN: 978-3-95450-168-7 doi:10.18429/JACoW-IPAC2015-WEPMN047

SUPPRESSION OF HIGHER ORDER MODES IN AN ARRAY OF CAVITIES USING WAVEGUIDES*

Ya.V. Shashkov, N.P. Sobenin, NRNU MEPhI, Moscow, Russia
M.M. Zobov, LNF-INFN, Frascati (Rome), Italy

Abstract

In the frameworks of the High Luminosity LHC upgrade program an application of additional harmonic cavities operating at multiplies of the main RF system frequency of 400 MHz is currently under discussion. A structure consisting of two 800 MHz single cell superconducting cavities with grooved beam pipes coupled by drift tubes has been suggested for implementation. However, it is desirable to increase the number of single cells installed in one cryomodule in order to decrease the number of transitions between "warm" and "cold" parts of the collider vacuum chamber. Unfortunately it can lead to the appearance of higher order modes (HOM) trapped between the cavities. In order to solve this problem the methods of HOM damping with rectangular waveguides connected to the drift tubes were investigated and compared. In this paper we describe the results obtained for arrays of 2, 4 and 8 cavities.

INTRODUCTION

The Large Hadron Collider luminosity upgrade (HL-LHC) [1] project considers a possible implementation of harmonic cavities in addition to the main accelerating cavities working at 400 MHz to increase or to shorten bunches. In order to achieve the desired results a combination of the existing main RF cavities and harmonic cavities operating at 800 MHz is being studied. One of the main goals of the design of cavity is to fulfill strict HOM damping requirements. Several techniques for HOM damping such as beam pipe grooves, fluted beam pipes, ridged beam pipes etc. have been suggested, investigated and compared.

It is desirable to combine more cavities in a single cryostat in order to avoid multiple transitions between cryogenic and "warm" areas. However, connecting several cavities in a chain can create parasitic HOM that may affect the stability of circulating beams and lead to excessive power loss. The methods of HOM damping with rectangular and ridged waveguides attached to the beam pipes, usage of fluted and ridged beam pipes, as well as combinations of these methods have been considered and compared in order to solve this problem.

*Work is supported by Ministry of Education and Science grant 3.245.2014/г и and by the EU FP7 HiLumi LHC - Grant Agreement 284404.

SINGLE CELL

An initial design of the harmonic cavity was obtained by scaling (reducing) all the sizes of the LHC accelerating cavity operating at 400 MHz by a factor of 2 (Fig. 1) [2]. HOM damping is carried out with four couplers: two dipole and two broadband couplers. Unfortunately those couplers have some drawbacks including: violation of the cylindrical symmetry of the electromagnetic field in the structure which gives rise to the transverse component of the electric field (kick-factor), the complexity of the installation of robust power coupler on the same pipe with HOM couplers and possibility of multipacting discharges. That's why several alternatives HOM damping techniques have been investigated (Fig 2-4) [3].

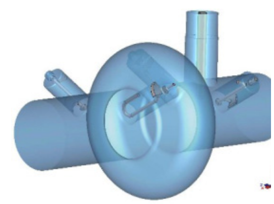

Figure 1: Accelerating cavity.

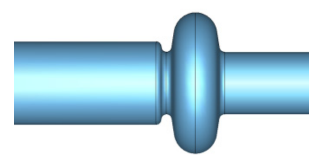

Figure 2: Cavity with grooved beam pipes.

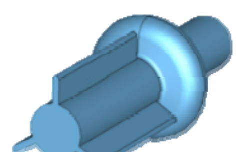

Figure 3: Structure with 3 flutes.

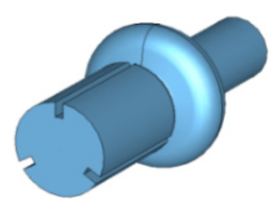

Figure 4: Structure with ridged beam pipe.

The frequency of dipole HOMs lies below the cut-off frequency of the TE_{11} wave and therefore cannot propagate along the drift tube in the structure shown in Fig. 1. The main feature of structures from Fig. 2-4 is that the HOMs frequencies become lower than the beam pipe cut-off frequency which allows [4] providing damping with a load placed in the drift tube outside the cryomodule. The results of wakefield simulations conducted with ABCI code [5] and CST [6] has clearly demonstrated that in these structures we managed to obtain a truly "single mode" cavity. We should not expect multibunch instabilities since the wake field decays completely at the distance of 15-25 m that corresponds to the actual bunch separation of 50 ns in LHC. The results obtained for single cell structures with grooved, fluted and ridged beam pipes are similar. In all the structures Q_{ext} are below 100 for all HOMs (except for a few modes

Content from this work may be used under the terms of the CC BY 3.0 licence (© 2015). Any distribution of this work must maintain attribution to the author(s), title of the work, publisher, and DOI.

ISBN: 978-3-95450-168-7 doi:10.18429/JACoW-IPAC2015-WEPMN049

CALIBRATION OF THE ACCELERATION VOLTAGE OF SIX NORMAL CONDUCTING CAVITIES AT ALBA

B. Bravo, A.Salom, J. Ocampo, U.Iriso, J.Marcos, P.Solans, F. Pérez, CELLS, Cerdanyola del Vallès

Abstract

ALBA is a 3GeVsynchrotron light source located in Barcelona and operating with users since May 2012.The ALBA storage ring uses six room temperature cavities; each one fed by combining two 80kW IOTs amplifiers at 499.654 MHz.

An accurate calibration of the RF voltage is required for the right adjustment of the RF phase with respect the beam. In addition, since the ALBA the ring accommodates several RF cavities, these may not be optimally phased with respect to each other, complicating the calculation of the total RF voltage. In this paper, the steps to calibrate the accelerating voltage of the SR will be presented and different methodologies to cross-check these calibrations.

INTRODUCTION

ALBA is a 3 GeV, 400 mA, 3rd generation Synchrotron Light Source in Cerdanyola, Barcelona, Spain, operating with users since May 2012.

The RF System, formed out of six RF plants, provides up to 3.6 MV of effective voltage and restores up to 540 kW of power to the electron beam. A cavity combiner add the power of two 80 kW IOTs to produce the more than 150 kW needed for each DAMPY cavity, a normal conducting HOM damped cavity developed by BESSY and based in the EU design cavity [1].

The total RF voltage seen by the beam depends on the relative RF phase between cavities which means that it is important to properly adjust RF field phase of each cavity with respect to the beam. To optimize the performance of the system, the RF voltage and phase of each cavity is controlled independently via a digital low level RF (DLLRF) [2].

OPERATION WITH SEVERAL RF CAVITIES

When several cavities are in operation the net accelerating voltage per turn is:

$$V_{acc} = \left|\overline{V_{cav,1}}\right| \sin(\phi_{s,1}) + \left|\overline{V_{cav,2}}\right| \sin(\phi_{s,2}) + \ldots, \quad (1)$$

where $\phi_{s,i}$ is the RF phase respect to the beam of each cavity.

The total effective voltage can be represented as the vector sum of the cavity voltage of each RF station:

$$\overline{V_{eff}} = \overline{V_{cav,1}} + \overline{V_{cav,2}} + \overline{V_{cav,3}} + \ldots \quad (2)$$

If the RF phase of the cavities with respect the beam is not the same the $\left|\overline{V_{eff}}\right|$ is reduced, as shown in figure 1 and 2.

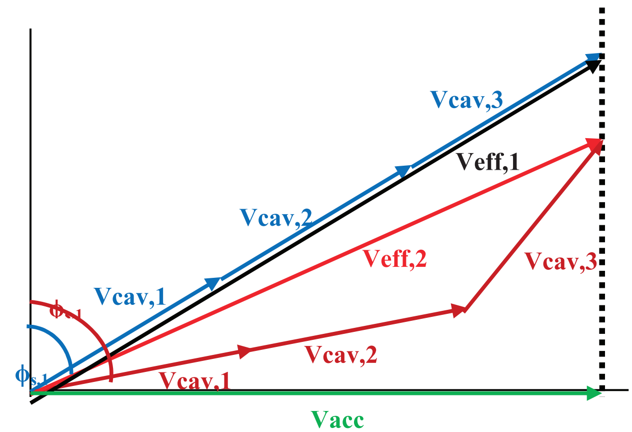

Figure 1: The effective voltage, Veff,1, is the sum vector of three cavity voltage in phase and Veff,2 is the sum when two cavities are in phase and one not $\phi_{s,1} = \phi_{s,2} \neq \phi_{s,3}$.

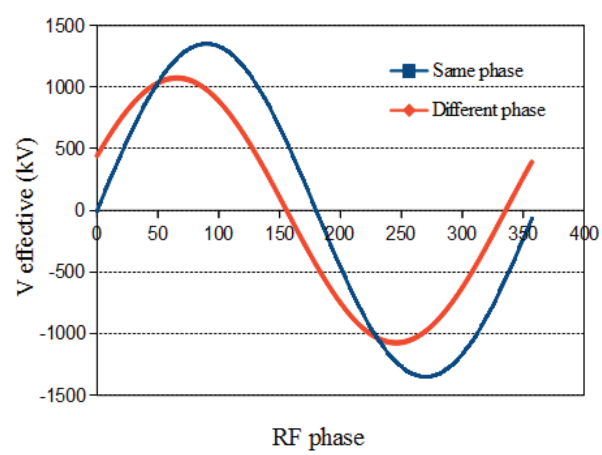

Figure 2: $\overline{V_{eff}}$ when RF phases between the three cavities are the same and when $\phi_1 = \phi_2 \neq \phi_3 = \phi_1 + 80$.

RF CALIBRATIONS

Forward and Reflected Power

RF power in the transmission lines is measured by means of directional couplers, device that couples a small amount of the power flowing through the line, in a given direction, towards one port.

Content from this work may be used under the terms of the CC BY 3.0 licence (© 2015). Any distribution of this work must maintain attribution to the author(s), title of the work, publisher, and DOI.

ISBN: 978-3-95450-168-7 doi:10.18429/JACoW-IPAC2015-WEPMN050

A PINGER MAGNET SYSTEM FOR THE ALBA SYNCHROTRON LIGHT SOURCE

M. Pont, N. Ayala, G. Benedetti, M. Carla, Z. Marti, R. Nuñez
ALBA-CELLS, 08290 Cerdanyola del Vallès, Spain

Abstract

A pinger magnet system consisting of two short kickers, one for each transversal plane, has been recently commissioned at the ALBA Synchrotron Light Source. The kickers excite large betatron oscillations on the electron beam in order to probe the linear and non-linear beam dynamics regime together with the turn by turn capabilities of the BPMs. The kickers are mounted around a single Ti coated ceramic vacuum chamber, have a length of 0.3 m each and provide a half sine pulse with an approximate pulse length of 1.5 us at an amplitude of 1.60 mrad in the horizontal plane and 1.15 mrad in the vertical plane. The pulser unit is based on solid state technology. This report summarises the steps followed from its design until its installation, electric and magnetic characterisation in the laboratory, and the first results with beam.

INTRODUCTION

To probe the non-linear regime of beam dynamics, a pair of pinger magnets have been designed, built in house and installed in the ALBA storage ring.

A single electron train will be kicked transversally by means of the pinger magnets, resulting in the excitation of betatron oscillations around the reference orbit. If the kick is strong enough the oscillations can reach the boundary of the non-linear region where the magnetic fields of the optics exhibits strong non-linearities.

The evolution of the dynamics of the electron train is then sampled; turn after turn, by beam position monitors (BPM). The pulse width must be such that the electron beam is kicked only once, all through the dynamic range of the pinger magnets. Beam dynamic results from the first studies performed with the pinger magnets are reported also in this conference [1,2] and the analysis of the impedance change due to the installation of the pinger magnets has also been evaluated [3].

MAGNETS SPECIFICATIONS

The maximum kick to be provided by the pinger magnets to the electron beam was specified as 1.60 mrad in the horizontal plane and 1.15 mrad in the vertical plane by the Beam Dynamics group. Under these kicks the dynamic aperture can be probed up to the physical limits of the vacuum chamber. The pinger magnets have been installed in a short straight section where the beta functions are 9.17 m and 5.14 m in the horizontal and vertical plane respectively. The pulse width is required to be smaller than twice the revolution time (896 ns) and the goal was to stay below 1.5 us for the whole range.

DESIGN OF THE MAGNETS

The design of the magnets is based on a window shaped magnet made with ferrites, CMD5055, from Ceramic Magnetic Ltd and a single turn coil. The main magnets parameters are presented in Table 1.

Table 1 Main Magnets Parameters

Parameter	Units	HOR	VER
Gap	mm	38	94
Ferrite length	mm	300	300
Max kick	mrad	1.60	1.15
Max field	T	0.053	0.038
Intensity	A	1614	2869
L_{magnet}	uH	1.00	0.16

The magnets have been installed around an existing ceramic chamber with inner dimensions 24x80 mm and a length of 780 mm, as shown in Figure 1.

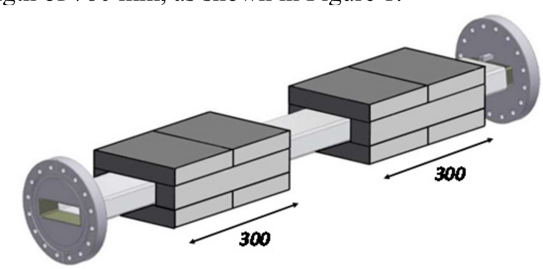

Figure 1: Installation of the magnets around the ceramic vacuum tube. Ferrite length in mm.

The chamber has a 0.4 μm Ti coating, which allows the circulation of the image current and it is thin enough not to generate significant eddy currents which might distort the magnetic pulse [4]. This ceramic chamber is the same that has been used for the ALBA storage ring injection kickers. Figure 2 shows the cross section of both magnets.

Magnetic simulations have been performed with OPERA-2d to ensure that the ferrites do not saturate. A field homogeneity of $\pm 5\cdot 10^{-4}$ has been achieved over ±25 mm. Figure 3 shows the magnetic field lines as obtained with OPERA-2d [5].

Content from this work may be used under the terms of the CC BY 3.0 licence (© 2015). Any distribution of this work must maintain attribution to the author(s), title of the work, publisher, and DOI.

ISBN: 978-3-95450-168-7 doi:10.18429/JACoW-IPAC2015-WEPMN051

DESIGN OF A SUPERCONDUCTING GANTRY CRYOSTAT

Cristian Bontoiu*, Jose Sanchez-Segovia, FABIS, Spain
Rafael Berjillos, Javier Perez Bermejo, TTI, Spain
Ismael Martel, Univ. of Huelva, Spain

Abstract

The University of Huelva in collaboration with the Andalusian Foundation for Health Research (FABIS) [1] and the TTI Company [2] is currently involved in developing and assembling a prototype for a compact superconducting proton gantry with the goal to generate a business case within the narrow niche of hadron therapy. While main beam characteristics are reported in [3], this article presents the current status of the engineering design for the cryostat and beam steering system. An account for the mechanical deformations due to magnetic forces and weight is also presented.

INTRODUCTION

Beam dynamics studies have shown that protons of 175 MeV±20% kinetic energy can be handled and delivered at the target using a simple gantry made of two arcs of radius 2.5 m with 90° and 180° respectively, as shown in Fig. 1.

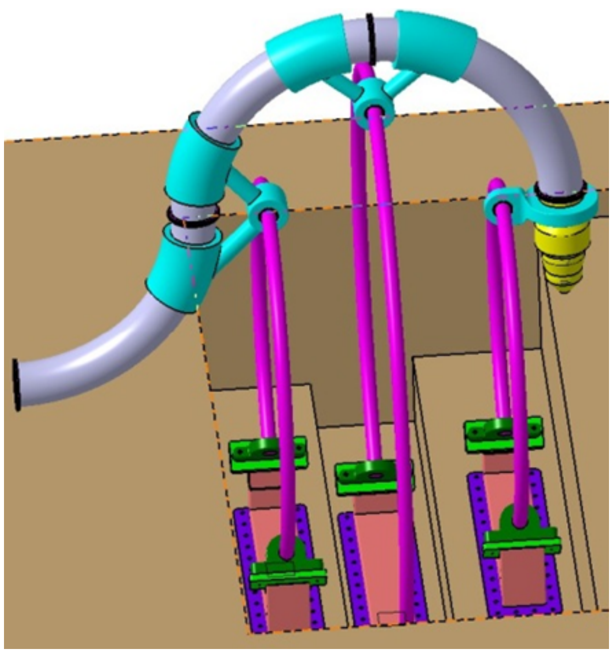

Figure 1: Overview of the gantry and its beam steering system installed on three support rings.

Within a preliminary design carried out in Catia [4] the gantry is installed on three rings which both take the load and constrain its motion within the plane defined by the isocentre. The main problems to be addressed for the cryostat are:

- mechanical support which cam minimize the deformations and stress due to the mass of the cryostat, coolant and magnets;
- rotation mechanism to enable a 270° excursion around the isocentre;
- technical solution for the junction between the rotating gantry arm and the fixed accelerator line to enable transfer of coolant and vacuum pumping;
- design of the support collars for the SC coils;

* cbontoiu@gmail.com

ASSEMBLY

The SC cryostat accommodates 36 combined-function magnets made of one one-layer quadrupole coils assembled on the top of one-layer dipole coils, their collars (clamps) and special channels for the coolant and vacuum insulation. In a simplified view as shown by Fig. 2 the cold liquid helium enters at 4 K through a coaxial pipe and fills the channel near the collars at hydrostatic pressure.

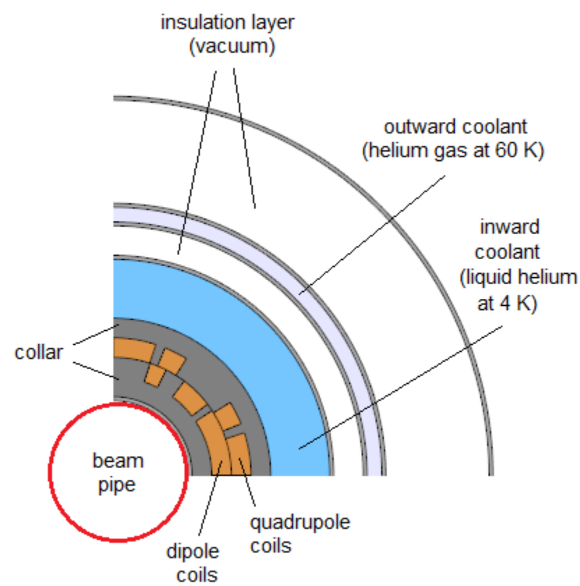

Figure 2: Sketch of the transverse layers to be considered for cryogenic cooling of the gantry.

As the SC coils trigger phase transition of helium from liquid to gas, bubbles accumulate at the highest point of the cryostat from where they can pass into a return coaxial channel through valves. These valves are distributed around the cryostat circumference and open synchronized with its motion only if they are at the highest altitude within some error margin. With rising vapour pressure the gas is pushed towards a larger coaxial port installed at the junction between the beam line and the gantry. There is a layer of vacuum between the liquid and gas helium layers and another one surrounding them in order to reduce heat transfer. Technical implementation of these ideas can be seen in Fig. 3 with the main components:

© Content from this work may be used under the terms of the CC BY 3.0 licence (© 2015). Any distribution of this work must maintain attribution to the author(s), title of the work, publisher, and DOI.

ISBN: 978-3-95450-168-7 doi:10.18429/JACoW-IPAC2015-WEPMN052

A NEW RF LABORATORY FOR DEVELOPING ACCELERATOR CAVITIES AT THE UNIVERSITY OF HUELVA

I. Martel, D. Gordo-Yáñez, A. K. Orduz, C. Bontiu, J. Dueñas, J. Sanchez-Segovia
University of Huelva, E-21071, Huelva, Spain

Abstract

The University of Huelva is presently involved in R&D projects for developing RF accelerator cavities. Two types of cavities are presently under design, a prototype of room temperature RFQ injector and a quarter-wave resonator for high intensity heavy-ion linear accelerators. The laboratory is equipped with dedicated test-bench for RF measurements, which includes high-power RF generators, network analyzer, amplifiers and power meters. A clean room is also available having a dedicated space for high-precision mechanical metrology and cavity mounting, together with a vertical cryostat for superconducting cavity test.

INTRODUCTION

Heavy-ion accelerators are the cornerstones of nuclear physics research. As our knowledge of subatomic degrees of freedom has increased during the last decade, new physics phenomena have emerged that require the construction of high intensity heavy-ion beams, with heavy-ion beam intensities of several milliamps on target.

A number of facilities are presently in construction around the world (ESS-Sweden, FRIB-USA, SPIRAL2-France) with will be soon operating and recognized as leading international research infrastructures. The need of high intensity beams demands however an important technological effort in developing high field RF accelerating cavities.

The main interest of implementation of a Radio-Frequency RF Laboratory at University of Huelva is to test the performance of RF cavity prototypes, allowing for improving the electromagnetic and thermo-mechanical design, mainly focused on heavy ion accelerators.

RF LABORATORY

The RF laboratory is complementary to a cryostat system foreseen for testing superconducting cavities. Main equipment of the lab is listed below:

- Agilent CX N9000A spectrum analyzer.
- Agilent 53181A, Frequency counter
- Rhode and Swartz Network analyzer 9k-6GHz
- 3 kW power-amplifier from DB-Elettronica
- Analog RF signal generator MXG N5181AEP from Keysight Technologies.

Figure 1: Bead pull system and cold model of RFQ in aluminium.

The lab is also equipped with a remotely operated beam pull system for field measurements (Fig. 1). The clean room is close to the test cryostat where superconducting cavities can be tested at T=4.5ºK. The space dedicated to the clean room has been prepared for assembly and testing of both particle detector systems and RF cavity systems. Total surface is of 50 m^2, divided in three main areas (Fig. 2):

- An over-pressurized area for entry of personnel and equipments of 20 m^2 (SAS).
- An ISO8 area of 30 m^2 containing a metrology system for quality control of mechanical elements.
- An ISO5 area of 4 m^2 has been prepared for special system assembly and manipulation.

The associated auxiliary equipment has been installed in a separate area of 18 m^2 close by the research complex.

First RF Tests

First activity of the lab has been dedicated to build and test a cold model (aluminium) of a RFQ cavity with design goal of 75.25 MHz, a representative working frequency of superconducting heavy-ion linacs. We have chosen an octagonal shaped cavity of 500 mm length (see Fig. 1), where four-vanes can be fixed using screws to the

Content from this work may be used under the terms of the CC BY 3.0 licence (© 2015). Any distribution of this work must maintain attribution to the author(s), title of the work, publisher, and DOI.

ISBN: 978-3-95450-168-7 doi:10.18429/JACoW-IPAC2015-WEPMN055
Content from this work may be used under the terms of the CC BY 3.0 licence (© 2015). Any distribution of this work must maintain attribution to the author(s), title of the work, publisher, and DOI.

RAMI OPTIMIZATION-ORIENTED DESIGN FOR THE LIPAC RF POWER SYSTEM

M. Weber, D. Regidor, C. de la Morena, P. Mendez, J.M. Arroyo, I. Kirpitchev, J. Molla, A. Ibarra
Centro de Investigaciones Energéticas, Medioambientales y Tecnológicas, CIEMAT, Madrid, Spain

Abstract

The Linear IFMIF Prototype Accelerator (LIPAc) is currently under construction in Rokkasho (Japan). LIPAc will generate a continuous wave (CW) 9 MeV deuteron beam at 125 mA. It will serve to validate the final IFMIF accelerator concept and technologies. The radiofrequency (RF) power system is being integrated by CIEMAT (Spain) in collaboration with its partner companies and European institutes. LIPAc RF Power System design has been performed aiming high reliability, high availability and easy maintainability to address one of the most important requirements for IFMIF. The target of LIPAc tests is to validate the technologies and designs for the final phase of IFMIF. Several improvements in reliability, availability and maintainability have been implemented in the LIPAc RF Power System. These improvements are based on both, new technologies and new maintenance philosophy. The results of their first tests are shown in this paper.

INTRODUCTION

IFMIF will irradiate fusion structural materials under similar energy spectrum to the Fusion Neutron energy spectrum in order to test them under inner fusion reactor conditions. The data obtained from IFMIF are required for the building of the future DEMOnstration Fusion Reactor. Any delay in the IFMIF Program would directly delay the Fusion Program and the commercial application of Nuclear Fusion Energy.

Achieving the required dpa on the materials pivots on two parameters: deuteron current at the accelerator and irradiation time. Since IFMIF deuteron current is foreseen to be the maximum reasonably achievable (125mA per accelerator), the only way to speed up the program is by increasing the availability.

The RF Power System is the main active system of the accelerator. It is one of the largest systems and shares interfaces with most of the Accelerator Systems. Consequently, its availability highly impacts on the IFMIF's overall availability. An EFDA Report on technological options for the IFMIF RF Power System [1] was presented in 2007, assessing the use of solid state power amplifiers instead of tetrode based amplifiers. This report concluded that in the near future it would be advisable to develop a solid state alternative for the IFMIF amplifiers to take advantage of the inherent solid state availability characteristics. However, this technology was not ready for the LIPAc project due to the still low power MOSFET technology available in 2007.

Taking that into account, the first IFMIF RAMI (Reliability, Availability, Maintainability and Inspectability) studies [2] proposed a new availability target for the RF Power System for improving overall IFMIF availability: it should reach 98.2%. Two strategies have been followed for this purpose:

1. Improvements in the tetrode based LIPAc RF System.
2. Improvements in the solid state technology for a better performance and tighter fitting to this application.

LIPAc was then considered as a validating test bench for new proposals and new technologies devoted to improve the RF Power System availability.

AVAILABILITY FACTORS

All the developed improvements have been proposed following a RAMI optimization-oriented methodology. It consists of the continuous and iterated interaction between designers and RAMI engineers aiming at an enhanced availability. Since maximum operation time is defined by the characteristics of the critical components of the beam line, the RF Power System availability can be directly related to MDT (Mean Down Time). Two are the main MDT factors in which RF Power System can be improved:

1. MTBF (Mean Time Between Failures), which is mainly related to the reliability of the system.
2. MTTR (Mean Time To Repair), which is mainly related to the maintainability of the system.

THE LIPAC TETRODE BASED RF MODULE

Due to the high number of RF power chains at IFMIF (104), their high power levels (<220 kW each) and the high number of components required by the tetrode technology, the IFMIF RF power system reference design would have shown an unacceptable availability from the IFMIF's point of view.

An innovative solution was proposed in order to improve the availability: The RF Module [3]. This is a structure containing two complete RF chains, as shown in Fig. 1. All the components of both RF chains (except the HVPS) are on board. This daring design was developed by CIEMAT and its partner companies INDRA SISTEMAS and SEVEN SOLUTIONS. The full power tests of the amplifier demonstrated its capabilities, exceeding the foreseen. The achieved gain after the fine tuning is 25.4dB showing very high anode efficiency (73% at final amplifier). With 230kW CW RF output, the

ISBN: 978-3-95450-168-7 doi:10.18429/JACoW-IPAC2015-WEPMN056

HIGH POWER TESTING OF THE FIRST RE-BUNCHER CAVITY FOR LIPAC*

F. Toral#, C. de la Morena, D. Gavela, I. Podadera, D. Regidor, M. Weber, CIEMAT, Madrid
B. Bravo, R. Fos, J.R. Ocampo, F. Pérez, A. Salom, P. Solans, CELLS, Cerdanyola del Vallès

Abstract

Two re-buncher cavities will be installed at the Medium Energy Beam Transport (MEBT) of the LIPAc accelerator, presently being built at Rokkasho (Japan). They are IH-type cavities with 5 gaps and will provide an effective voltage of 350 kV at 175 MHz for deuterons at 5 MeV. The first prototype has been designed at CIEMAT and built by the Spanish industry. The high power tests and RF conditioning have been successfully performed at the ALBA/CELLS RF laboratory. A solid state power amplifier, which has been developed by CIEMAT and its partner companies at Spain for the LIPAc RF System, has been used for the tests. The cavity has shown a performance according to calculations, regarding the dissipated power, peak temperatures and coupling factor. RF conditioning was started with a duty cycle of 3%, which was increased gradually till continuous wave (CW), which is the nominal working mode in LIPAc.

INTRODUCTION

Two re-buncher cavities will be installed in the MEBT line [1], as part of the Spanish contribution to LIPAc. Electromagnetic and mechanical simulations led to a design based on a 5-gap IH-type cavity providing a 350 kV effective voltage at 175 MHz [2]. The first of the two cavities has been manufactured and tested with low power [3]. Last step to validate this cavity is the high power test.

EXPERIMENTAL SETUP

The high power test of the re-buncher prototype was performed at CELLS RF laboratory. It is equipped with a bunker with a useful surface about 15 m^2. Ancillary equipment (cooling, power, instrumentation) is available to ease the test of different cavity configurations.

Two vacuum pumps (one ionic and one turbomolecular) were installed at the CF160 ports on both sides of the cavity. A cold cathode gauge was installed at the beam pipe port, to measure the vacuum level as close as possible to the region with higher electric field, that is, the drift tubes. It was connected through a 100 mm long pipe to avoid the influence of the RF fields. A RGA analyser was installed at the other beam pipe port. An arc detector was also present (Fig. 1).

Six PT100 sensors were located at the expected hottest spots at the cavity, according to FEM simulations: one on each endplate, in front of the nearest stem; on the input coupler; two at the top part of the main body and the last one at the bottom, close to the central stems base.

The mechanical performance of the tuners was checked: position of limit switches and movement accuracy were within specifications. One tuner is manual and its initial position was set to get the nominal resonant frequency when the motorized one is at midpoint. The automatic tuner was powered using the ALBA standard driver for step motors, which also manages the limit switches.

The cooling was designed with a pressure drop of 2.3 bar for a flow of 31 l/min: four parallel channels, two with 12 l/min and other two with 3.5 l/min. However, a pressure drop of 3.8 bar was measured for a flow of 27.8 l/min, likely due to underestimated pressure drops at the cross section steps and elbows. The valves present in each parallel channel were used to balance the pressure drops accordingly. This regime was kept during the conditioning and shown to be enough.

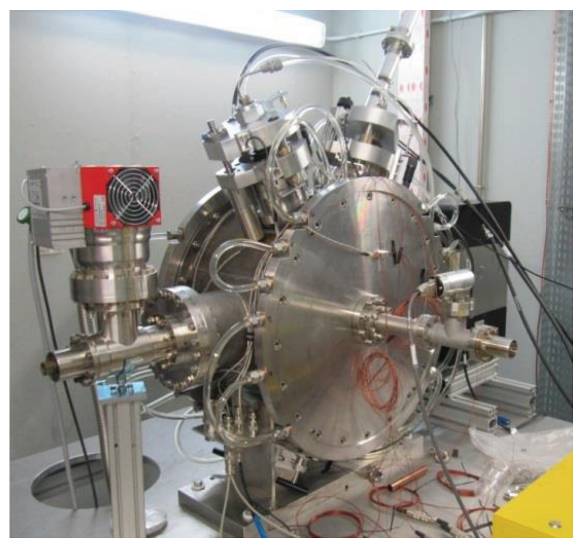

Figure 1: Test bench.

A solid state power amplifier (SSPA) [4] manufactured by BTESA (Spain) under CIEMAT specifications was used for the conditioning. It consists of ten parallel modules, each able to provide up to 2 kW. The low level RF system developed by CELLS/CIEMAT was used for the conditioning test bench, because all the local interlocks were already integrated: vacuum gauge, arc detector, reflected power, SSPA, temperatures, cooling flow, tuner limit switches and others. The enhanced low level RF system to be used in LIPAC has been developed by CIEMAT in collaboration with SevenSolutions (Spain).

*Work partially supported by Spanish Ministry of Economy and Competitiveness under projects AIC-A-2011-0654 and agreement published in BOE, 16/01/2013, page 1988
#fernando.toral@ciemat.es

Content from this work may be used under the terms of the CC BY 3.0 licence (© 2015). Any distribution of this work must maintain attribution to the author(s), title of the work, publisher, and DOI.

ISBN: 978-3-95450-168-7 doi:10.18429/JACoW-IPAC2015-WEPMN057

CALCULATION AND DESIGN OF A RF CAVITY FOR A NOVEL COMPACT SUPERCONDUCTING CYCLOTRON FOR RADIOISOTOPE PRODUCTION (AMIT)*

D. Gavela#, J. Calero, L. García-Tabarés, A. Guirao, D. Obradors-Campos, C. Oliver, J.M. Pérez Morales, I. Podadera, F. Toral, CIEMAT, Madrid, Spain

Abstract

The AMIT (Advanced Molecular Imaging Techniques) cyclotron will be a 8.5 MeV, 10 μA, CW, H^- accelerator for the purpose of radioisotope production. It includes a superconducting, weak focusing, 4 T magnet, which allows for a small extraction radius and a compact design. The RF cavity design has to deal with challenging requirements: high electric fields created by the required accelerating voltage (60 kV), a narrow aperture of the magnet leading to high capacitances and thermal losses, and a requirement for a small overall size of the cavity. A quarter wave resonator with one dee (two acceleration gaps) design was chosen. Calculations with numerical codes such as HFSS and ANSYS have been performed to compute the main RF parameters and the stresses and deformations of the cavity due to the power losses and vacuum operation. Finally, the fluid dynamics of the cooling circuits have been carefully studied.

INTRODUCTION

Positron-emission tomography (PET) is a broadly used technique around the world for biomedical human imaging. Therefore, there is a high and increasing demand for positron emitter isotopes. The most effective PET isotopes (like ^{11}C or ^{18}F) have a short half-life (20 min and 2 h, respectively). Low energy cyclotrons (below 15 MeV) are the most widely used devices for their production. There is a growing interest in developing compact, light and cheap cyclotrons, capable of running at a small facility and producing the isotopes close to the patient, reducing the transport inconveniences and the loss of activity of the isotopes.

Spanish AMIT collaboration aims at producing a compact cyclotron for production of ^{11}C and ^{18}F isotopes. It will accelerate 10 μA of H^- ions to 8.5 MeV. It includes a superconducting, weak focusing, 4 T magnet.

CONCEPTUAL DESIGN

Table 1 summarizes the technical specifications of the cavity. Since AMIT cyclotron is of classical type, the magnet air gap has uniform height. Its RF cavity configuration is based on the typical 180 degree dee, at the end of a quarter wave coaxial resonator. The weak focusing limits the number of particle turns before the beam is lost. This imposes, for the required final energy, a minimum of 60 kV per gap, according beam dynamics simulations [1].

Other configurations have been studied trying to reduce RF power losses. That dissipation is due to the currents necessary to charge the capacitance between the dee and the vacuum chamber wall. A 90 degree dee features half the capacitance, that is, half of the charging currents, one quarter of the initial power losses. However, the nominal frequency should be doubled, which would yield the same original power losses for the same gap voltage. Furthermore, the phase shift is doubled, so the gap voltage should be increased to reach the same output beam energy according with beam dynamics simulations, resulting in additional RF power losses.

Two 90 degree dees do not allow decreasing the gap voltage and consequently the power losses, because the phase shift is doubled with the frequency, arising similar problems than the single 90 degree dee configuration. Furthermore, this layout is hardly compatible with the space necessary for the instrumentation and beam extraction [2].

Table 1: Cavity Technical Specifications

Frequency	60 MHz
Gap voltage	60 kV
Magnet air gap	74 x 280 mm
Maximum beam extraction radius	115 mm
Maximum beam axial excursion	± 6 mm
Tuning range	± 140 kHz

The aim is to keep the peak electric field below 1.5 times Kilpatrick criterion, that is, below 14.2 MV/m, at all the parts except the puller. The peak temperature shall be below 60ºC to keep moderate thermal emission of electrons and increase of copper resistivity due to heating.

ELECTROMAGNETIC CALCULATIONS

Ansys (including the high frequency electromagnetic package HFSS), has been used to perform the RF simulations [3]. Firstly, a static electric model was used to optimize the central region geometry. Eigenmode HFSS analysis was performed afterwards to achieve the resonance and to get the field maps. Finally, both input power coupler and pickup probe were designed using the HFSS DrivenModal analysis.

*Work partially funded by CDTI and the Spanish Ministry of Economy and Competitiveness, under the subprogram CENIT, project AMIT, reference CEN-20101014
#daniel.gavela@ciemat.es

Content from this work may be used under the terms of the CC BY 3.0 licence (© 2015). Any distribution of this work must maintain attribution to the author(s), title of the work, publisher, and DOI.

ISBN: 978-3-95450-168-7 doi:10.18429/JACoW-IPAC2015-WEPMN058

Content from this work may be used under the terms of the CC BY 3.0 licence (© 2015). Any distribution of this work must maintain attribution to the author(s), title of the work, publisher, and DOI.

TRANSVERSE IMPEDANCE MEASUREMENTS AND DC BREAKDOWN TESTS ON THE FIRST STRIPLINE KICKER PROTOTYPE FOR THE CLIC DAMPING RINGS*

C. Belver-Aguilar, IFIC (CSIC-UV), Valencia, Spain
A. Faus-Golfe, IFIC (CSIC-UV) and LAL, Université Paris-Sud, Orsay, France
F. Toral, CIEMAT, Madrid, Spain
M.J. Barnes, H. Day, CERN, Geneva, Switzerland

Abstract

A first stripline kicker prototype for beam extraction from the CLIC Damping Rings (DRs) has been designed at IFIC and CIEMAT, with excellent field homogeneity, good power transmission and low beam coupling impedance. The prototype has been built by the company Trinos Vacuum Projects, and laboratory tests and measurements have been carried out at CERN to characterize, without beam, the electromagnetic response of the striplines. In this paper, we present the measurements of the transverse beam coupling impedance, using the coaxial wire method, and a comparison with simulations. Furthermore, results of DC breakdown tests, using High Voltage (HV) power supplies, are also reported.

TRANSVERSE BEAM COUPLING IMPEDANCE MEASUREMENTS

Measurements in the laboratory, without beam, are important to characterize the electromagnetic response of the striplines, and compare the results of the measurements with the electromagnetic simulations. The measurements carried out in this first prototype have been the following: (1) power reflection through the striplines, (2) longitudinal beam coupling impedance, and (3) transverse beam coupling impedance. In addition, DC breakdown tests have been carried out. In this paper, results for the transverse beam coupling impedance, as well as for the DC breakdown tests will be presented.

For transverse beam coupling measurements, two techniques are commonly used: (1) the two wire method, or (2) the moving single wire method [1,2]. The two wire method consists of inserting two wires in the striplines aperture, and driving them with opposite phase RF waves. With this method, the dipolar component of the transverse impedance is calculated, whereas with the moving single wire method the total transverse impedance (dipolar and quadrupolar components) is measured. The setup for the two measurements is shown in Fig. 1. The results of these measurements have been compared with CST Particle Studio (PS) [3] simulation results for the dipolar and the total transverse beam coupling impedance.

* Work supported by IDC-20101074, FPA2013-47883-C2-P and ANR-11-IDEX-0003-02

Two Wire Method

The dipolar component of the transverse impedance of the striplines has been measured by producing a dipolar field with two wires, of 0.5 mm diameter each, driven with opposite phases by using two hybrids. To have a measurable effect, the wire spacing should be significantly smaller than the aperture, due to the fact that the dipolar field created only interacts with the fringe fields and, therefore, the effects are small: a wire spacing of about a third of the aperture appears to be a good compromise [1]. In our case, for an aperture of 20 mm a wire spacing of 7 mm has been chosen. In order to match the two wire line impedance to the impedance of the Network Analyzer, the hybrids and the loads, a matching resistor at the ends of each wire has been used. To calculate the resistance value of each matching resistor, the following equation has been used:

$$R_S = Z_{line}/2 - Z_0 \tag{1}$$

where Z_{line} is the differential-mode line impedance and $Z_0 = 50\,\Omega$. The differential-mode line impedance for two wires with opposite polarity is given by:

$$Z_{line} = \frac{120}{\sqrt{\epsilon_r}}\text{acosh}\frac{\Delta}{d} \tag{2}$$

where ϵ_r is the relative permittivity of the medium between the wires ($\epsilon_r = 1$ here), d is the wire diameter and Δ is the wire spacing. In our case, using Eq. (2), the calculated value of Z_{line} is 399.7 Ω: low-inductance (carbon film) single series resistors of 160 Ω have been used for the matching network. The transmission parameter S_{21} has been measured with the Network Analyzer, and from this measurement the longitudinal impedance $Z_{||}$ can be estimated by using the formula [1]:

$$Z_{||} = -2Z_{line}\,ln(S_{21}) \tag{3}$$

Then the dipolar component of the transverse impedance has been found from the following equation:

$$Z_{\perp,dip} = \frac{cZ_{||}}{2\pi f\Delta^2} \tag{4}$$

where c is the speed of light, and f is the frequency at which the S_{21} parameter is measured. Results for the dipolar horizontal and vertical impedance are shown in Fig. 2, when terminating the electrodes with the "ideal" 50 Ω resistors from

ISBN: 978-3-95450-168-7 doi:10.18429/JACoW-IPAC2015-WEPMN059

Content from this work may be used under the terms of the CC BY 3.0 licence (© 2015). Any distribution of this work must maintain attribution to the author(s), title of the work, publisher, and DOI.

DESIGN STUDY AND CONSTRUCTION OF A TRANSVERSE BEAM HALO COLLIMATION SYSTEM FOR ATF2

N. Fuster-Martínez, IFIC (CSIC-UV)*, Valencia, Spain
A. Faus-Golfe, IFIC (CSIC-UV) and LAL, Université Paris-Sud, Orsay, France
P. Bambade, S. Liu, S. Wallon, LAL, Université Paris-Sud, Orsay, France
F. Toral, I. Podadera, CIEMAT, Madrid, Spain
K. Kubo, N. Terunuma, T. Okugi, T. Tauchi, KEK and SOKENDAI, Japan

Abstract

The feasibility and efficiency of a transverse beam halo collimation system for reducing the background in the ATF2 beamline has been studied in simulations. In this paper the design and construction of a retractable transverse beam halo collimator device is presented. The wakefield induced-impact of a realistic mechanical prototype has been studied with CST PS, as well as the wakefield beam dynamics impact by using the tracking code PLACET.

INTRODUCTION

ATF2 is a Beam Delivery System (BDS) built after the ATF Damping Ring (DR) providing a scaled-down version of the Future Linear Collider (FLC) Final Focus System (FFS) [1]. The two main goals of ATF2 are to obtain a vertical beam spot size at the virtual IP of 37 nm and to stabilize the beam at the nanometer level. The control and reduction of the beam halo that could be intercepted in the beam pipe producing undesired background is a crucial aspect for FLC and ATF2. A beam halo collimation system in ATF2 will play an essential role in the reduction of the background noise that could limit the performance of key diagnostic devices around the final focal point (IP), especially the Shintake Monitor (IPBSM) used for measuring the nanometer level vertical beam sizes and the recently installed Diamond Sensor (DS) in the post-IP beamline to investigate the beam halo distribution [2, 3]. A first feasibility study was done and reported in [4]. From these studies a vertical collimator system has been considered as the first priority. In this paper we present a first 3D mechanical design as well as a transverse wakefield study for the realistic 3D prototype by using the 3D electromagnetic solver CST PS [5]. Also the wakefield impact on the orbit and beam size has been evaluated by using the tracking code PLACET [6].

DETAILED 3D MECHANICAL DESIGN

A detailed version of the 3D mechanical design based on the optimized geometrical parameters reported in [4] and previous experiences in [7–10] is shown in Fig.1. The collimator jaws will be made of Copper (Cu) and the rest of the components including the transition part will be made of Stainless Steel (SS) because of stiffness and assembly considerations.

* Work supported by IDC-20101074, FPA2013-47883-C2-1-P and ANR-11-IDEX-0003-02

The seal of the rectangular chamber will be made with indium wires and other seals will be Cu seals for DN40CF flanges. An important part of the collimation device will be the retractable movable system with a expected precision of $\pm 10\mu m$. Two step by step EMMS-ST-42-S-...-G2 motors will be used to move independently the two rectangular vertical tapered jaws. In Fig.1 (right) a more detailed picture of the movers and slides is shown. The collimator is under construction and it will be installed at ATF2 in the 2015 fall run.

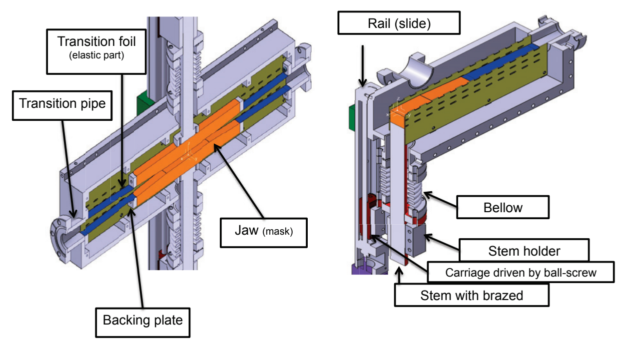

Figure 1: Detailed 3D mechanical design.

WAKEFIELD IMPACT STUDY: CST PS NUMERICAL SIMULATIONS

In this section we present a wakefield impact study of a realistic rectangular vertical tapered halo collimator structure based on the 3D mechanical design of Fig.1. The collimator system will add an impedance on the beamline that could perturb the beam stability, therefore it is important to minimize the wakefields and to demonstrate that the impact on the beam can be tolerated in terms of beam stability. The model simulated with CST PS is shown in Fig.2. The 3D model is divided in 3 millions of hexahedral mesh cells. The electromagnetic fields are exited by a gaussian bunch of 7 mm bunch length, 1 pC bunch charge and 1 mm offset in the vertical plane. The frequency up to which the fields will be taken into account for the wake potential calculation was set to 20 GHz. The main volume of the model is set to vacuum and it is surrounded by perfectly conducting material. The jaws are made of Cu and the material of the transition foil has been studied. Simulations have been made with SS and Aluminium (Al) transition foils. The resulting wakepotential can be seen in Fig.3. The impact of the material on this component of the collimator is small therefore SS has been

ISBN: 978-3-95450-168-7 doi:10.18429/JACoW-IPAC2015-WEPMN061

ESS PLC CONTROLS STRATEGY

D. Piso, S.L. Birch, A. Nordt, T. Gahl, P. Arnold, J. Weisend II, T. Korhonen
European Spallation Source, Lund, Sweden

Abstract

The European Spallation Source ESS AB is an accelerator-driven neutron spallation source. The Integrated Controls System (ICS) division is responsible for providing controls and monitoring for all parts of the machine (accelerator, target, neutron scattering systems and conventional facilities). Also, Accelerator Division, Target Division and other parts of the organisation will be deploying PLC Automation Systems. A large number of applications have been identified across all the facility where PLCs will be used: cryogenics, vacuum, water-cooling and fluid systems, power systems, and safety & protection systems. This work describes the different activities put in place and the strategy followed at ESS regarding PLC technologies. This strategy consists not only of the standardisation of a PLC vendor but also testing activities, generation of documentation and standardisation of other aspects (for instance, regarding installation). The documentation about PLC controls integration and standardisation and the approach to insert PLCs in the different controls workflows are described. Finally, the results of different tests (PLC timing correlation) are shown.

HARDWARE STRATEGY

The ICS division has deployed a hardware strategy based on the different types of applications expected in the ESS project. At the same time, a compromise is needed in order to keep the number of the different used technologies to a minimum, which ensures maintainability from a long term point of view. According, to this premises ICS has standardised three different types of technologies:

- **Fast, real-time signal processing**. In this category fall those cases that need state-of-the-art technology, a range of acquisition in MHz or GHz sampling rates, and FPGA-based processing in many occasions is included. For this type of applications ESS has decided to use the microTCA platform [1]. Currently, ICS is working in all the processes needed after the platform selection (firmware, software, operational procedures). This also, involves the selection of other technologies and standards like FMC (FPGA Mezzanine Card).

- **Middle-range I/O**. This segment is designated to fill the gap between the fast real-time I/O described above and the traditional industrial I/O solutions. In this segment, real-time requirements have still to be met but the requirements for data processing and transfer are less stringent. The ESS standard platform for this range of tasks is the EtherCAT [2] standard that uses regular Ethernet wiring but has a specialised protocol that enables tight time synchronization (kHz range I/O).

- **Industrial I/O**. Most of the systems that do not require tight synchronisation with the ESS accelerator cycles (14 Hz) are best served by programmable logic controllers (PLCs). PLCs will be considered when the built-in logic ensures safe operation of the device under control even if the connection to the upper layer (EPICS) is broken. Cooling systems, vacuum control, (slow) interlocks, etc., are typical examples of areas where PLC is an appropriate choice.

USE CASES

A large number of applications have been identified across all parts of the facility where PLCs will be used: cryogenics, vacuum, water-cooling, fluid and power systems, building management, safety and protection systems. They have common characteristics in terms of relatively long response for their control systems (tens to hundreds of miliseconds), standard industrial sensors and actuators, etc.

- **Cryogenic Systems**. ESS will own a number of cryogenic systems. The cooling power will be produced in 3 different cryoplants (Accelerator Cryoplant, Test Stand & Instruments Cryoplant and Target Moderator Cryoplant). A Cryogenic Distribution System will connect the cryoplants to the Accelerator, Target and Cryomodule Test Stand. The most important characteristics of these control systems (regarding PLCs) is that regulation-using PIDs will be needed. The I/O needed will be based on analog and digital acquisition. The protocols Profibus PA, Profibus DP and Profinet CBA, defined in the standard IEC 61784-1 will be extensively used, as the I/O needs to be highly distributed. Communication processors with serial interfaces may be also needed.

- **Vacuum Systems**. Vacuum Controls involve the handling of different types of signals, at different scanning rates and a great part of them at a suitable range for PLCs (<1Khz). Reading analog and digital signals from different gauges, controlling vacuum equipment with analog and digital signals (eg. mass flow controllers and gate valves) are the main use cases. In term of logic, PLCs will be mainly used for interlocks and maybe for implement states diagrams in order to control equipment.

- **Water-Cooling and Fluid Systems**. These are also typically industrial systems where the most frequent signals are analog I/O, digital I/O, PT100 temperature sensors and fieldbuses to distribute this periphery. From the logic point of view interlocking and regulation could be the major applications. Fluid Systems. Specialty

Content from this work may be used under the terms of the CC BY 3.0 licence (© 2015). Any distribution of this work must maintain attribution to the author(s), title of the work, publisher, and DOI.

ISBN: 978-3-95450-168-7 doi:10.18429/JACoW-IPAC2015-WEPMN062

MAX IV 3 GeV STORAGE RING MAGNET BLOCK PRODUCTION SERIES MEASUREMENT RESULTS

M. Johansson*, L-J. Lindgren, M. Sjöström, P. F. Tavares, MAX IV Laboratory, Lund, Sweden

Abstract

The magnet design of the MAX IV 3 GeV storage ring replaces the conventional support girder + discrete magnets scheme of previous third-generation synchrotron radiation light sources with a compact (Ø25 mm aperture) integrated design having several consecutive magnet elements precision-machined out of a common solid iron block. The production series of 140 integrated magnet block units, which was totally outsourced to industry, was completed mid-2014. This article presents mechanical and magnetic field measurement results of the full production series.

INTRODUCTION

The MAX IV synchrotron radiation facility [1], consisting of two storage rings, 3 GeV and 1.5 GeV, and a full energy linac, is currently being installed/commissioned in Lund, Sweden. The 3 GeV storage ring [2] has a multibend achromat (MBA) lattice, consisting of 20 achromats, each consisting of 7 cells, with a circumference of 528 m. The integrated magnet design concept of the 3 GeV ring has each lattice cell realized as one "magnet block", consisting of several consecutive magnet elements in a common solid iron yoke (see Fig. 1), so that the whole lattice consists of 140 such magnet block units. A detailed presentation of this magnet design has been given previously in [3].

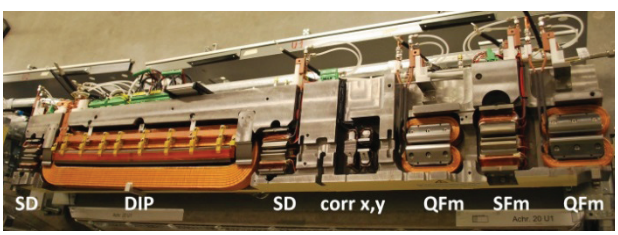

Figure 1: U1 magnet block bottom half.

There are 7 magnet block types per achromat (see Fig. 2). M1 and M2, 2.3 m long, are mirror identical. U1 and U2, 2.4 m long, are identical and U4/U5 are mirror identical to U1/U2. U3, 3.4 m long, has similar layout to the other U, but symmetric around its own midpoint.

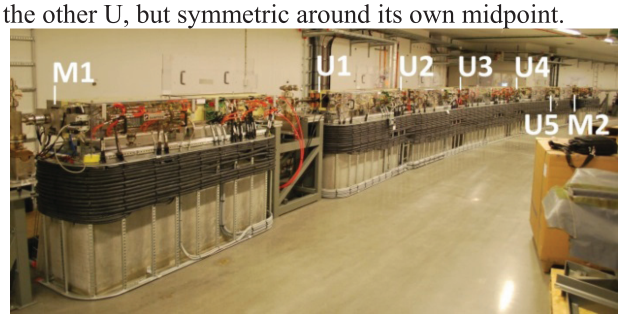

Figure 2: Achromat 04 in the 3 GeV ring, fully assembled.

*martin.johansson@maxlab.lu.se

Mechanical Design Concept

The main structural parts of the magnet blocks are the yoke bottom and yoke top blocks (Fig. 3), which are each machined from a single block of iron[1].

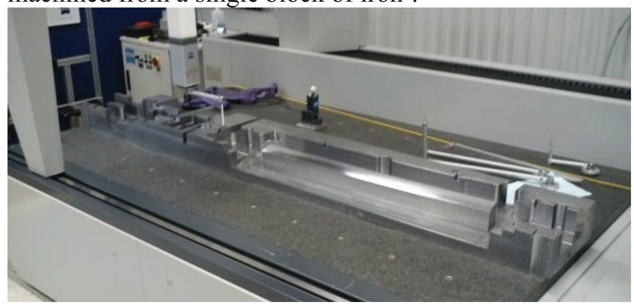

Figure 3: U4/U5 yoke bottom half undergoing 3D mechanical measurement.

The pole surface of the dipole is machined directly out of the block, whereas the quad and corr. pole tips are dismountable, to allow coil installation. Sextu- and octu-poles are designed as complete magnet halves, which are mounted in the yoke blocks (see Fig. 1). Mechanical tolerances for the different categories of function critical surfaces in the yoke bottom/top blocks are:

- Vertical mating planes for quad pole tips and sextupole/octupole yoke halves: distance to midplane ±0.02 mm.
- Sideways guiding slots for quad pole tips and sextupole/octupole yoke halves: distance to sideways ref. surfaces[2] ±0.02 mm.
- Midplane: flatness[3] tolerance 0.04 mm.
- Dipole: surface shape[4] tolerance 0.04 mm.

And tolerances for the other critical yoke parts are:

- Quad pole pieces: surface shape tolerance 0.02 mm
- Sextupole/octupole yoke halves with poles assembled: surface shape tolerance 0.04 mm.

Procurement

The production of the magnet blocks was outsourced as build to print-contracts, based on a technical spec. and full set of drawings [4] provided by MAX-lab, with suppliers being responsible for mechanical tolerances, and for performing field measurements according to MAX-lab instructions, and MAX-lab being responsible for the field measurement results. The contracts for the magnet blocks production were awarded in the fall of 2011, to two

[1] "ARMCO Pure Iron grade 4", C < 0.01%.

[2] Two outer corners on the yoke block together with the midplane define the mechanical reference frame in which all the tolerances are evaluated

[3] The mechanical tolerance called "flatness" is defined as peak-to-peak deviation between measured data points and a best fit-plane.

[4] The mechanical tolerance called "surface shape" is defined as the twice the amplitude of the largest deviation within the tolerance zone, ie 0.04 mm means ±0.02 mm.

Content from this work may be used under the terms of the CC BY 3.0 licence (© 2015). Any distribution of this work must maintain attribution to the author(s), title of the work, publisher, and DOI.

ISBN: 978-3-95450-168-7 doi:10.18429/JACoW-IPAC2015-WEPMN065

PROGRESS AT THE FREIA LABORATORY

M. Olvegård, A. K. Bhattacharyya, D. Dancila, T. Ekelöf, J. Eriksson, K. Fransson, K. Gajewski, V. Goryashko, L. Hermansson, M. Holz, M. Jacewicz, M. Jobs, Å. Jönsson, H. Li, T. Lofnes, H. Nicander, R. Ruber, A. Rydberg, R. Santiago Kern, R. Wedberg, V. Ziemann, Uppsala University, Sweden, R. Yogi, ESS, Lund, Sweden

Abstract

The FREIA Facility for Research Instrumentation and Accelerator Development at Uppsala University, Sweden, has reached the stage where the testing of superconducting cavities for the European Spallation Source (ESS) is starting. The new helium liquefaction plant has been commissioned and now supplies a custom-made, versatile horizontal cryostat, HNOSS, with liquid helium at up to 140 l/h. The cryostat has been designed and built to house up to two accelerating cavities, or, later on, other superconducting equipment such as magnets or crab cavities. A prototype cavity for the spoke section of the ESS linac will arrive mid 2015 for high-power testing in the horizontal cryostat. Two tetrode-based commercial RF power stations will deliver 400 kW peak power each, at 352 MHz, to the cavity through an RF distribution line developed at FREIA. In addition, significant progress has been made with in-house development of solid state amplifier modules and power combiners for future use in particle accelerators. We report here on these and other ongoing activities at the FREIA laboratory.

INTRODUCTION

The European Spallation Source (ESS) [1] is under construction in Lund, Sweden. Once completed it will deliver spallation neutrons to a large number of experiments with users from various disciplines interested in the fundamental atomic and molecular properties of materials. As any major accelerator complex, ESS strives to keep the power consumption to a minimum, which motivated the use of a superconducting linac. This linac provides an intense 5 MW proton beam of 2 GeV energy, in 2.86 ms long pulses with 14 Hz repetition rate to the ESS target.

The first superconducting section of the linac uses double-spoke cavities designed and tested at low power at Institut de Physique Nucléaire d'Orsay (IPNO), France. FREIA is charged with designing and testing RF generation and distribution systems for ESS and to test the double-spoke cavities at nominal power. One or several prototype cavities, equipped with a input power coupler and a cold tuning system, are expected mid 2015. The high-power tests require feeding the cavity with 3.5 ms long 352 MHz RF pulses of 400 kW power. It also includes cooling the cavity to, and keeping it at, 2 K. To this end, FREIA has a high capacity helium liquefaction plant and a tailor-made horizontal cryostat, which can serve two superconducting cavities simultaneously.

In parallel with the ESS study, FREIA hosts research programs such as the development of solid-state amplifiers for accelerator applications, the design of a combined compact THz/X-ray source, and studies within the ESS neutrino super-beam project. This paper gives a status overview of the FREIA laboratory, reporting on progress in infrastructure subsystems and on its main activities.

THE FREIA LABORATORY

The FREIA laboratory was inaugurated in June 2013 and is now nearly full of state-of-the-art equipment for accelerator research and development. The view of the 1000 m^2 hall, displayed in Fig. 1(a), is dominated by three radiation bunkers built with an iron pre-loaded concrete material (magnetite) to shield people and environment from the potential X-rays emitted during operation with high-power RF. The main bunker contains the superconducting RF (SRF) equipment for the spoke cavity and cryomodule tests for ESS. A smaller bunker has been pre-assigned to tests of high-gradient, high-frequency copper accelerating structures, either for the Compact Linear Collider or for possible future free electron lasers, or medical accelerators. Another small bunker will house a neutron source for research and educational activities in applied nuclear physics.

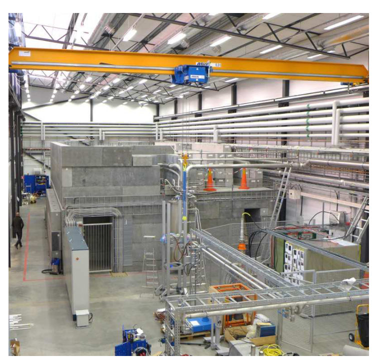

(a) FREIA

(b) HNOSS

Figure 1: The FREIA laboratory (a) and the horizontal cryostat HNOSS installed in the main bunker (b).

Helium Liquefaction Plant

The heart of the laboratory is the helium liquefaction and recovery plant. The liquefier L140 was acquired from Linde Kryotechnik AG and commissioned in March 2014.

Content from this work may be used under the terms of the CC BY 3.0 licence (© 2015). Any distribution of this work must maintain attribution to the author(s), title of the work, publisher, and DOI.

ISBN: 978-3-95450-168-7 doi:10.18429/JACoW-IPAC2015-WEPMN066

Content from this work may be used under the terms of the CC BY 3.0 licence (© 2015). Any distribution of this work must maintain attribution to the author(s), title of the work, publisher, and DOI.

HALL PROBE MEASUREMENTS OF 80 UNIT CELL MAGNETS FOR THE MAX-IV STORAGE RING

A. Ahl, Scanditronix Magnet, Vislanda, Sweden

Abstract

80 unit cell magnet segments have been manufactured by Scanditronix Magnet for the 3 GeV storage ring at MAX-IV in Lund, Sweden. All of the magnets have been approved by Max-lab after a large field measuring campaign using both a high precision Hall probe bench, as well as a new rotating coil system. Each unit cell magnet consists of one dipole, two quadrupole, three sextupole and one vertical and one horizontal corrector magnets. The Hall probe bench was used to measure the dipole magnet (with combined dipole and quadrupole component) as well as the quadrupole magnets. This paper will focus on the Hall probe measurements performed on the dipole magnets from the perspective of a manufacturer. E.g. the repeatability of the measurements and the relation between field performance and mechanical tolerances will be analysed.

MAX-IV

MAX-IV aims to be the new centre for synchrotron light in Sweden, and will be the replacement of the smaller MAX-II and MAX-III storage rings. The accelerator complex will consist of a linac and two storage rings (see Fig. 1), with the larger one having a circumference of 528 m and electron energy of 3 GeV. The concept is similar to that of the MAX-III accelerator, focusing on a compact magnet design, with combined function magnets. Also with separate magnetic elements built into the same iron block. This keeps the overall dimensions of the magnets down, as well as simplifies the alignment of the magnets [1].

The entire 3 GeV storage ring contains 20 achromats, with each achromat consisting of two matching cells and five unit cells. The cells contain one dipole magnet each which gives the storage ring the advantages of a multi-bend achromat lattice, which lowers the electron beam emittance. It also has the benefits of increasing the energy acceptance, as well as improves the dynamic aperture [2].

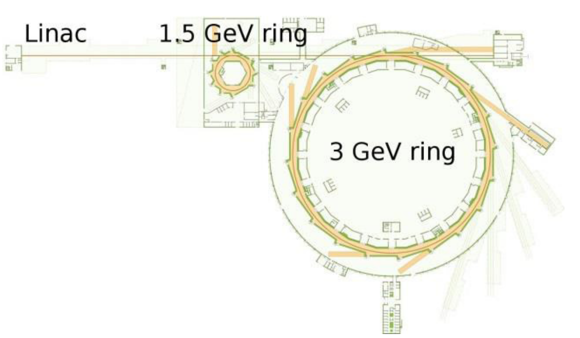

Figure 1: An overview of the MAX-IV accelerator complex. Courtesy of MAX IV Laboratory.

Scanditronix has produced four of the five unit cell families (U1, U2, U4 and U5) as seen in Fig. 2. The magnets contained in the U1 and U5 cells are identical, and U2 and U4 as well, the only difference is that the cells are mirrored versions of each other. However, all four families contain the same dipole magnet.

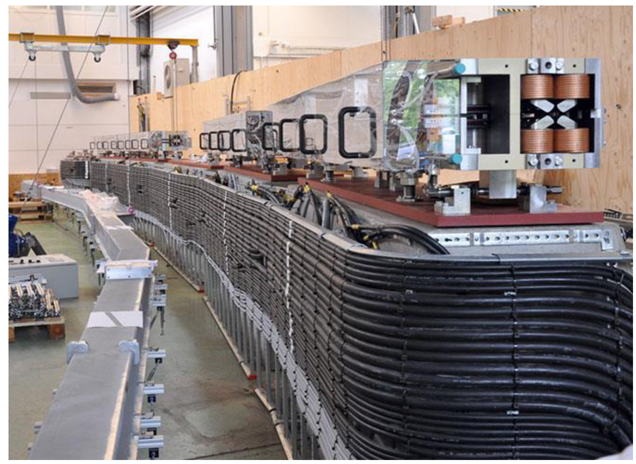

Figure 2: Image of one achromat (mock-up). Courtesy of MAX IV Laboratory.

Scanditronix Magnet selected two subcontractors for the machining of the iron blocks to keep the tight time schedule for the project. One company produced the U1 and U2 segments, and the other produced the U4 and U5 segments. It is seen from the results of the field measurements that there are no significant difference between the magnets machined at the two subcontractors.

HALL PROBE BENCH

Scanditronix Magnet acquired a new state-of-the-art Hall probe mapping bench (see Fig. 3) to meet the high precision in measurements that was required by Max-lab. This is located in a temperature controlled room where the magnets were stored until correct measuring temperature was achieved. The base of the measurement system is a 3D coordinate measuring machine (CMM) of portal type from Hexagon Metrology. This is built on a flat table of solid granite, to ensure a horizontal placement of the magnets, as well as a good resistance against vibrations.

The CMM has been equipped with a Hall probe and teslameter from Group3, with an absolute accuracy of ±0.01% of reading ±0.006% of range [3].

The CMM has a volumetric measuring range of 3000x1200x1000 mm, and an accuracy of about 5 µm per

ISBN: 978-3-95450-168-7 doi:10.18429/JACoW-IPAC2015-WEPMN067

UPGRADE OF THE TCDQ DILUTERS FOR THE LHC BEAM DUMP SYSTEM

M. G. Atanasov, W. Bartmann, J. Borburgh, C. Boucly, C. Bracco, L. Gentini, B. Moles, W. Weterings, CERN, Geneva, Switzerland

Abstract

The TCDQ diluters are installed as part of the LHC beam dump system to protect the Q4 quadrupole and other downstream elements during a beam dump that is not synchronised with the abort gap, or in case of erratic firing of the extraction kickers. These diluter elements installed during Run 1 were compatible with beam up to 60 % of the nominal intensity, which was insufficient for the second run of the LHC. This paper describes the requirements for the upgrade done during the First Long Shutdown (LS1), to make the TCDQ compatible with the full 7 TeV LHC beam at intensities that are required for the future runs of the machine. Subsequently the mechanical design changes, implementation and commissioning of the TCDQ are reported.

INTRODUCTION

The need to upgrade the single jaw moveable diluter elements Target Collimator Dump Quadrupole (TCDQ) was already apparent during the first run of the LHC. Whereas the initial design was sufficient for operating at the lower intensity adopted for the first physics run of the machine, simulations have shown that the system would not survive the impact of the LHC beam at ultimate intensity and beyond [1]. The proposed upgrade required the absorber material to be changed from 1.77 g/m^3 graphite to a sandwich of lower density carbon fibre-reinforced carbon (C/C) and graphite, and the total absorber length to be increased from 6 to 9 m [2]. The displacement system would also have to accommodate for a ±1 mrad radial displacement with respect to the longitudinal centre of the diluter [3] [4].

CONSTRUCTION OF THE ABSORBER

The upgrade of the diluter required the dismantling of the four tanks from the tunnel and the two spares for the replacement of the graphite absorber blocks with the C/C and graphite sandwich, and the refurbishment of the cooling circuit fittings. The old graphite blocks have been removed and stored in a radioactive storage bunker. The estimated dose rate during the dismantling was 1 µSv/h at 10 cm.

Absorber Blocks

The new absorber blocks measure 250 mm in length and 72 mm in height. The width is 40 mm for the C/C and 35 mm for the graphite. The C/C blocks of densities 1.4 and 1.75 g/m^3 are produced from carbon fibre preforms (or pre-pregs) using the Rapid Chemical Vapour Infiltration (R-CVI) technique. The first axis of maximum strength is the vertical *y* axis as seen by the beam. The fibre orientation in adjacent layers is 0º/90º/0º/90º. The graphite is of type R4550 with a density of 1.8 g/m^3. Figure 1 shows one of the C/C blocks during the quality assurance.

Figure 1: C/C absorber block.

In order to condition the new blocks for the Ultra-High Vacuum (UHV) of the LHC both material types were pre-cleaned with small amounts of alcohol and acetone. The final cleaning was done by CO_2 jet blasting. To reduce the outgassing rates, the blocks were subsequently heat-treated under vacuum in two two-hour stages at 600 ºC and 1000 ºC with several stabilization plateaux. Beam impedance considerations require the face of the C/C blocks adjacent to the beam to be copper coated by means of magnetron sputtering with a first layer of titanium providing better adherence for the 5 µm layer of copper. Furthermore as the figure shows the blocks at the extremities of each vacuum tank are tapered for a smooth transition between the racetrack endplate and the interior of the absorber structure.

Vacuum

After assembly the vacuum tanks were baked-out in an oven at 300 ºC for 24 hours with a temperature ramp of 13 ºC/h and a stabilization plateau at 150 ºC and subsequently aligned in a clean room. The tanks are equipped with heating jackets for bake-out in the LHC tunnel during commissioning of the vacuum sectors. The vacuum levels achieved during the validation in the assembly and test lab were in the order of $1{\cdot}10^{-10}$ mbar. The newly constructed spares are reaching the 10^{-11} mbar

Content from this work may be used under the terms of the CC BY 3.0 licence (© 2015). Any distribution of this work must maintain attribution to the author(s), title of the work, publisher, and DOI.

ISBN: 978-3-95450-168-7 doi:10.18429/JACoW-IPAC2015-WEPMN068

UPGRADE OF THE CERN SPS EXTRACTION PROTECTION ELEMENTS TPS

J. Borburgh, B. Balhan, M. Barnes, C. Baud, M. Fraser, V. Kain, F. Maciariello, G. Steele, F. Velotti, CERN, Geneva, Switzerland

Abstract

In 2006 the protection devices upstream of the septa in both extraction channels of the CERN SPS to the LHC were installed. Since then, new beam parameters have been proposed for the SPS beam towards the LHC in the framework of the LIU project. The mechanical parameters and assumptions on which these protection devices presently have been based, need validation before the new upgraded versions can be designed and constructed. The paper describes the design assumptions for the present protection device and the testing program for the TPSG4 at HiRadMat to validate them. Finally the requirements and the options to upgrade both extraction protection elements in the SPS are described.

INTRODUCTION

Extraction protection elements (TPSGs) are installed upstream of the magnetic septa in the SPS extraction channels towards the LHC. In Long Straight Section 4 (LSS4), the TPSG4 is installed upstream of 6 thick (MSE) septa, while in LSS6 the TPSG6 is installed just upstream of 2 thin (MST) septa. The first TPSG4 was installed in 2003, while the TPSG6 was installed in 2007 [1]. They protect the magnetic septa against mis-steered beams. This case should remain rare and the current of the extraction bumpers is interlocked to reduce the risk of a full impact. The case of an asynchronous firing of the kicker would result in a sweep of the beam over the diluter and the septa.

In case of full impact the TPSGs will dilute the beam such that the energy deposition and the subsequent temperature rise in the downstream MST septa conductors will stay at tolerable levels. In particular, the energy deposition in the cooling water of the septum conductor is critical, as it provokes shock waves in the cooling water circuit, which may lead leaking water to the beam vacuum.

ACTUAL DESIGN

The present devices were designed for direct impact of the full, so called LHC ultimate, LHC beam. The aim on the device was to properly protect the downstream septa, while surviving itself the impact sufficiently to avoid an exchange. Following updated calculations [2] more robust designs were proposed and built, making use of then state of the art 2D Carbon Reinforced Carbon (CfC). The TPSG4 was modified and the highly stressed graphite was partly replaced by CfC to cope with the dynamic mechanical stresses. With respect to the earlier version the TPSG4 was lengthened up to 3100 mm to compensate for the lower density of the CfC with respect to graphite. The design assumed impact centred around on a septum conductor cooling tube as on the initial calculations [3,4]. For the final design of the TPSG6 the CfC was also used to replace part of the graphite. The final absorbing sandwich is indicated in Table 1.

The graphite and CfC parts of the diluters themselves would sustain a full impact, while the Von Mises stress levels would exceed the maximum values permitted for the metallic blocks at the exit of the diluters. Since this stress level would only be exceeded in a small volume, it was deemed acceptable.

Table 1: TPSG Diluting Structure

	TPSG4	TPSG6
Graphite (CZ5) [m]	0.5	
Carbon reinforced Carbon [m]	1.7	1.75
Graphite (CZ5) [m]	0.3	0.85
Titanium (TiAl6V4) [m]	0.3	0.3
Inconel (Inco 718) [m]	0.3	0.6
Total dilution length [m]	3.1	3.5

The protection requirements for each TPSG (Table 2) are based upon the assumptions that the coil can withstand the same dynamic pressure as the coils are statically tested during construction. The maximum permissible pressure rise is obtained by reducing the pressure of the cooling circuit in operation in the SPS tunnel (25 bar) from the static test pressure. The maximum permissible copper temperature rise is determined by the space available in the yoke for the increase in length of the coil from the normal operating temperature. Finally the maximum water temperature rise in the cooling channels was determined from the permissible pressure rise using the ELSE code [2, 4].

TESTS AT HIRADMAT

To validate the diluter design assumptions, tests were prepared which took place at HiRadMat in 2012. The tests' aim was two-fold: to validate the design assumptions to protect the septa and to validate the assumption exceeding the maximum Von Mises stresses locally in the metallic blocks of the diluter is acceptable. A spare MSE and TPSG4 were made available for this test.

Content from this work may be used under the terms of the CC BY 3.0 licence (© 2015). Any distribution of this work must maintain attribution to the author(s), title of the work, publisher, and DOI.

ISBN: 978-3-95450-168-7 doi:10.18429/JACoW-IPAC2015-WEPMN070

MEASUREMENT TECHNIQUES AND APPLICATION OF COMBINED PARALLEL/ORTHOGONAL MAGNETIC BIAS ON A FERRITE TUNED RESONATOR IN LOW FREQUENCY RANGE (3-10 MHz)

G. Favia, CERN, Geneva, Switzerland; University of Rome "La Sapienza", Roma, Italy
F. Caspers, M. Morvillo, C. Rossi, C. Vollinger, CERN, Geneva, Switzerland

Abstract

We present several measurement methods for evaluation of magnetic properties of magnetically biased and non-biased ferrite samples in a coaxial test fixture. One important aspect is the crosscheck of results obtained by using different and independent measurement and evaluation methods. Since a rather high DC bias current has to be applied, a dedicated network was designed that allows the passage of up to 50 A DC without degradation of the RF performance. With a combination of calibration methods and a compensating topology with two identical sample holders, a good performance was achieved. In this context, magnetic material parameters for about 10 different types of ferrite were obtained. The orthogonal magnetic bias was added by placing the entire test fixture into a large toroidal coil. Thus, the bias field can be supplied independently from, and in addition to the classical parallel bias. An optimal combination between the two biasing fields was found, resulting in a reduction of magnetic losses up to 50 % on certain ferrites. We show that the mixed magnetization, normally used for garnets only, is beneficial also for other types of ferrites.

INTRODUCTION

Ferrite materials are used in the accelerator field as the core of the resonators for cavity frequency tuning purposes. The application of the ferrite however results in an increase of the losses and the inductance, since ferrite materials are characterized by their complex permeability μ_r that is expressed by: $\mu_r = \mu' - j\mu''$, where μ' contains information about the inductance and μ'' represents the magnetic losses. When exposed to a magnetic orthogonal or parallel bias field, one can observe a reduction of the ferrite permeability. Since the resonant frequency varies with the relative permeability as $1/\sqrt{\mu_r}$, it is therefore possible to tune a resonator by applying an external field. An accurate characterisation of the ferrites properties is essential since the choice of the ferrite has to take into account the range of the required frequency as well as the tolerated losses.
There exist many standard methods for μ-evaluation on ferrites, but we have to adapt one of them for the sample and core size in our applications. Indeed, we need to measure ferrite complex permeability and its dependence on external bias field for several reasons: datasheet information insufficient for our requirements, identification of unknown ferrite samples, study of the different behaviour of the samples caused by the magnetic remanence and characterization of special production ferrites.

OVERVIEW OF THE MEASUREMENT TECHNIQUES

The measurement test set consists of a coaxial line with one shorted end partially or completely filled with one or more toroidal shaped samples, placed at the shorted end. Ferrite samples of different shapes and materials have been characterized; that resulted in most of the cases in re-designing the sample holders to allow the implementation of the needed connections and a better fitting of the ferrite under test within the structure. Moreover, as will be described in the following, the measurements of the ferrite parameters were carried out with and without a magnetic bias field.

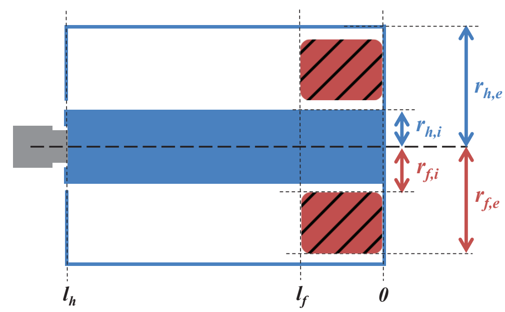

Figure 1: Schematic drawing of the experimental setup. The metallic holder (blue) houses a toroidal shaped ferrite (red) and features a connector (grey) used for S_{11} measurements.

Unbiased Measurements Technique

The permeability of the ferrite samples is evaluated from reflection coefficient measurements, performed with a Vector Network Analyzer (VNA). All measurements were performed using OSM (Open-Short-Matched) one-port calibration at the end of the test cable.
The S_{11} parameter calculated at the short end is obtained by normalizing the measured reflection coefficient of the sample holder filled by the ferrite sample $S_{11_{filled}}$ to the one of the empty sample holder $S_{11_{empty}}$:

$$S_{11} = \frac{S_{11_{filled}}}{S_{11_{empty}}}. \quad (1)$$

The input impedance of the ferrite under test, Z_f, is a complex number and is determined by:

$$Z_f = Z_0 \frac{1 + S_{11}}{1 - S_{11}} \quad (2)$$

with $Z_0 = 50\ \Omega$ being the characteristic impedance of the VNA. A first approach to evaluate the ferrite permeability

Content from this work may be used under the terms of the CC BY 3.0 licence (© 2015). Any distribution of this work must maintain attribution to the author(s), title of the work, publisher, and DOI.

ISBN: 978-3-95450-168-7 doi:10.18429/JACoW-IPAC2015-WEPMN071

Content from this work may be used under the terms of the CC BY 3.0 licence (© 2015). Any distribution of this work must maintain attribution to the author(s), title of the work, publisher, and DOI.

ENHANCED DIAGNOSTIC SYSTEMS FOR THE SUPERVISION OF THE SUPERCONDUCTING CIRCUITS OF THE LHC

R. Denz, Z. Charifoulline, K. Dahlerup-Petersen, A. Siemko, J. Steckert, CERN, Geneva, Switzerland

Abstract

Being an integral part of the protection system for the superconducting circuits of the LHC, the data acquisition systems used for the circuit supervision underwent a substantial upgrade during the first long shutdown of the LHC (LS1). The sampling rates and resolution of most of the acquired signals increased significantly. Newly added measurements channels like for the supervision of the quench heater circuits of the LHC main dipoles allow identifying specific fault states. All LHC main circuits are meanwhile equipped with earth voltage feelers allowing monitoring the electrical insulation strength, especially during the fast discharges. The protection system for the bus-bar splices is now capable to operate in different modes. By this measure, it is possible fulfilling the requirements for different specific tests like the warm bus-bar measurements and current stabilizer continuity measurements (CSCM) without field interventions.

INTRODUCTION

The protection system for the superconducting circuits of the LHC (QPS) covers 544 circuits with nominal current ratings from 100 A to 11870 A [1]. A total of 2516 data acquisition systems (DAQ) ensure the supervision of the protection system and diagnostics of the superconducting circuits. These systems communicate through field-bus links with the LHC accelerator control system.

Table 1: Circuits covered by the protection system

Circuit type	Quantity	DAQ systems
Main bends and quads	24	2124
Inner triplets	8	8
Insertion region magnets	94	68
Corrector magnet circuits	418	316
Total	**544**	**2516**

While status flags provide information on the state of the protection equipment and its readiness for operation, the majority of recorded analog signals serve for diagnostic purposes.

Based on the experience gained within the LHC operation so far and taking into account requests by equipment specialists, the data acquisition systems have been submitted to a major upgrade during LS1. The enhanced supervision capabilities, e.g. for the quench heater circuits, allow performing more detailed diagnostics of the superconducting circuits and facilitating the event analysis by automatic tools and equipment specialists. During the LHC hardware commissioning campaign in 2014/2015, magnet experts made already extensive use of the enhanced capabilities, e.g. for the analysis of 179 primary quench events recorded during main dipole powering tests [2].

QPS SUPERVISION UPGRADE

The various layers of the QPS supervision underwent a substantial revision, necessary to integrate new equipment, signals and commands. At this occasion, also the sampling rates and resolution of many analog signals have been revised and increased.

QPS Signals

The QPS DAQ transmits about 130000 signals, to the LHC accelerator control system with sampling rates of 0.1, 5 and 10 Samples/sec, when in normal operation mode. Depending on the signal type sampling rates during post mortem events, e.g. a magnet quench can be significantly higher.

Table 2: Signals produced by the QPS DAQ

Circuit type	Analog	Status flags	Total
Main bends and quads	26228	56388	82616
Inner triplets	200	248	448
Insertion region magnets	1408	4044	5452
Corrector magnet circuits	4088	17112	21200
Generic controller signals			22548
Total	**31924**	**77792**	**132264**

Field-bus Network

The QPS field-bus network, based on the WorldFIP™ standard, has been extended during LS1 by changing the network configuration and adding new segments and repeaters. This measure allowed reducing the number of individual clients per field-bus segment and almost doubling the transmission capacity of the physical layer of the QPS field-bus (see table 3). As a result, the time required for the transmission of the significantly larger post mortem data blocks is still within reasonable limits (~10 min). It is noteworthy that this time is independent of the number of simultaneously recorded events. The sampling rate for the majority of QPS analog signals

ISBN: 978-3-95450-168-7 doi:10.18429/JACoW-IPAC2015-WEPMN072

STATUS AND PLANNED EXPERIMENTS OF THE HIRADMAT PULSED BEAM MATERIAL TEST FACILITY AT CERN SPS*

Nikolaos Charitonidis, Ilias Efthymiopoulos, Adrian Fabich#, Malika Meddahi
CERN, Geneva, Switzerland
Eliana Gianfelice-Wendt, Fermilab, Batavia, Illinois, USA

Abstract

HiRadMat (High Irradiation to Materials) is a facility at CERN designed to provide high-intensity pulsed beams to an irradiation area where material samples as well as accelerator component assemblies (e.g. vacuum windows, shock tests on high power targets, collimators) can be tested. The beam parameters (SPS 440 GeV protons with a pulse energy of up to 3.4 MJ, or alternatively lead/argon ions at the proton equivalent energy) can be tuned to match the needs of each experiment. It is a test area designed to perform single pulse experiments to evaluate the effect of high-intensity pulsed beams on materials in a dedicated environment, excluding long-time irradiation studies. The facility is designed for a maximum number of 10^{16} protons per year, in order to limit the activation of the irradiated samples to acceptable levels for human intervention. This paper will demonstrate the possibilities for research using this facility and go through examples of upcoming experiments scheduled in the beam period 2015/2016.

INTRODUCTION

In the new era of high-brightness accelerators, the power of the circulating beam can be destructive during its interaction with the machine equipment (collimators, magnets, beam dumps). To avoid any possibly destructive incident that will compromise the operation of the accelerator, it is preferred that an experimental verification of the beam interaction with the equipment and materials is performed beforehand. Apart from the accelerator design itself, in the targetry applications, where a high-energy beam impinges on a target material for producing secondary particles, as is the case of Neutrino Beam facilities [1] or Muon Collider, where the flux of secondary particles requires a MW or even multi-MW power of the primary beam, the need of experimentally verifying the behaviour of the target material is imperative. HiRadMat (High Radiation to Materials) is a unique facility providing a pulsed, high-energy beam, available for tests in a controlled and safe way.

EXPERIMENTS IN HIRADMAT

The facility was commissioned in 2011. During 2012-2013, nine experiments were approved by the facility's scientific and technical boards and completed the data taking successfully [2]. Those experiments covered a broad spectrum of research topics, from a fully assembled LHC collimator and a SPS magnet septum, to high-power targetry investigating the effect of the proton beam on a tungsten powder target.

Depending on the scientific scope of each experiment online and/or offline (post -irradiation) analysis was used. Although rather challenging, online measurements are very interesting as they provide information on the dynamics of the beam impact. The main systems used for online measurements covered the following techniques: Doppler-laser-vibrometry measuring instantaneous deformations (up to 24 m/s at 2.5 MHz sampling), a fast camera (few kHz frame rate) for optical observations, accelerometers to measure the propagation of shock waves, temperature and acoustic measurements, and pressure gauges. The challenge in online instrumentation comes from the radiation field in the cavern that prohibits any installation of active electronics nearby unless specifically designed.

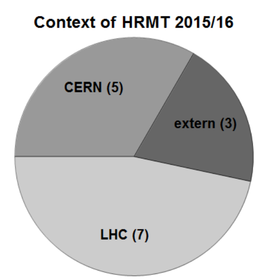

Figure 1: The context of the approved experiments for the beam period 2015-2016.

Following the start-up of the CERN accelerators after the LS1, for the period 2015-2016, fifteen experiments have already submitted their requests for beam time in the facility. The context of the experiments is shown in Fig. 1: seven experiments are directly related to accelerator operation for LHC (e.g. collimator materials), five have a general CERN oriented context (e.g. target development for the AD facility), and 3 experiments are proposed from international collaborations external to CERN (high-power targetry, optical microphones as beam loss monitor and testing the strength limits of beryllium windows for vacuum applications). For 2015, seven of these experiments are approved and scheduled. The current schedule of the experiments along with the cumulative proton budget can be seen in Fig 2.

* EuCARD-2 is co-funded by the partners and the European Commission under Capacities 7th Framework Programme, Grant Agreement 312453.
# adrian.fabich@cern.ch

Content from this work may be used under the terms of the CC BY 3.0 licence (© 2015). Any distribution of this work must maintain attribution to the author(s), title of the work, publisher, and DOI.

6th International Particle Accelerator Conference IPAC2015, Richmond, VA, USA JACoW Publishing
ISBN: 978-3-95450-168-7 doi:10.18429/JACoW-IPAC2015-WEPHA002

ELECTROMAGNETIC CHARACTERIZATION OF NEG PROPERTIES ABOVE 200 GHz FOR THE CLIC DAMPING RINGS

E. Koukovini-Platia*, G. Iadarola, G. Rumolo, C. Zannini, CERN, Geneva, Switzerland

Abstract

Non-Evaporable Getter (NEG) will be used in the CLIC Electron Damping Rings (EDR) to suppress fast beam ion instabilities due to its effective pumping ability. The electromagnetic (EM) characterization of the NEG properties up to high frequencies is required for the correct impedance modeling of the Damping Ring (DR) components. The properties are determined using WR-3.4 and WR-1.5 rectangular waveguides, based on a combination of experimental measurements of the complex transmission coefficient S_{21} with a Vector Network Analyzer (VNA) and CST 3D EM simulations, for the frequency ranges of 220-330 GHz and 500-750 GHz. The results obtained from NEG-coated Aluminum (Al) waveguides are presented in this paper.

METHOD

The impedance modeling of the DR chambers must include the contribution from coating materials applied for ultra-low vacuum pressure. This advocates for the correct characterization of this impedance in a high frequency range. The short DRs bunch length of 1.8 mm rms, translates into a frequency spectrum up to hundreds of GHz, therefore the characterization of NEG is necessary up to those frequencies.

The proposed method requires the use of a rectangular waveguide connected to a VNA and the 3D CST [1] simulation of the exact geometry waveguide. The waveguide is a 2-port network that can be described by means of the S-parameters as a function of frequency. The transmission coefficient S_{21}, from the scattering matrix, is related to the waveguide's attenuation, which depends on the effective conductivity.

The exact geometry waveguide can be simulated with CST and S_{21} is calculated assuming a certain conductivity of the coating material. However, assuming that conductivity is the unknown, several simulations can be done sweeping this parameter. Intersecting the measured data with the CST simulation, the conductivity that matches the measured losses is extracted at a specific frequency. By repeating the intersection over the whole frequency range of interest, the conductivity can be extracted as a function of frequency.

The method has been successfully benchmarked with known materials like copper and stainless steel and was used to characterize NEG at frequencies between 10 and 11 GHz [2].

MEASUREMENTS AT 220-330 GHz

Four rectangular waveguides, of type WR3.4, were used for measurements between 220 and 330 GHz. The waveguides were purchased from Virginia Diodes (VDI) [3] and are produced in 2-split blocks made of Al with a thin gold plating (see Figure 1).

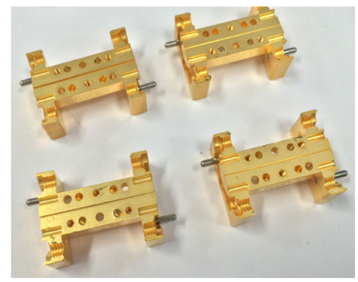

Figure 1: WR3.4 and WR1.5 waveguides from VDI made of Al with thin gold plating, with 25 mm length.

The waveguides were coated at CERN by magnetron sputtering, targeting at 3 μm NEG thickness. In Figure 2, the transmission S-parameters are plotted for the four waveguides (labeled as 1, 5-12, 5-15 and 5-16) as a function of frequency. In the same figure, the simulated S_{21} from CST is shown, assuming DC conductivity of NEG equal to 0.57×10^6 S/m and a uniform profile of 3 μm thickness.

The DC value was extracted from resistance measurements on NEG-coated glass samples with known coating thickness. From the measurements, the DC conductivity of NEG was scattered between 0.5×10^6 S/m and 0.7×10^6 S/m with an uncertainty of 15%. A factor of 1.5-2 difference with older measured values of the DC conductivity (1×10^6 S/m) is observed. This is attributed to the different coating setup used, and consequently due to the different cathode used for the NEG deposition.

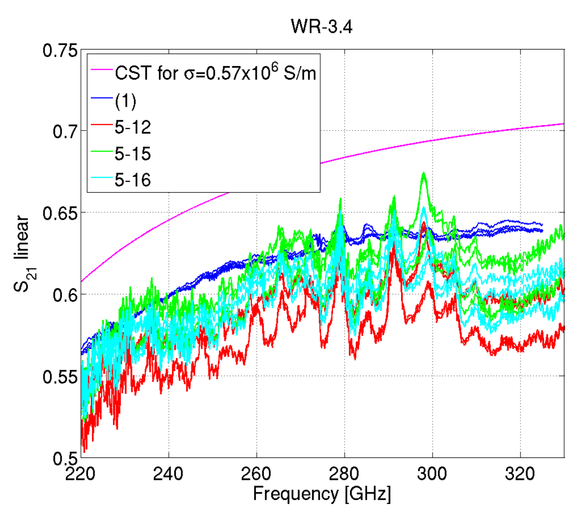

Figure 2: S_{21} comparison between CST (magenta) and measurements using the four WR3.4 waveguides.

---
* also affiliated at EPFL

Content from this work may be used under the terms of the CC BY 3.0 licence (© 2015). Any distribution of this work must maintain attribution to the author(s), title of the work, publisher, and DOI.

6th International Particle Accelerator Conference IPAC2015, Richmond, VA, USA JACoW Publishing
ISBN: 978-3-95450-168-7 doi:10.18429/JACoW-IPAC2015-WEPHA003

Content from this work may be used under the terms of the CC BY 3.0 licence (© 2015). Any distribution of this work must maintain attribution to the author(s), title of the work, publisher, and DOI.

MEASUREMENT OF NEG COATING PERFORMANCE VARIATION IN THE LHC AFTER THE FIRST LONG SHUTDOWN

V. Bencini, G. Bregliozzi, V. Baglin, C. Yin Vallgren, R. Kersevan, P. Chiggiato
CERN, Geneva, Switzerland

Abstract

During the Long Shutdown 1 (LS1) of the Large Hadron Collider, 90% of the Non-Evaporable Getter (NEG) coated beam pipes in the Long Straight Sections (LSS) were vented to undertake the planned upgrade and consolidation programmes. After each intervention, an additional bake-out and NEG activation were performed to reach the vacuum requirements. An analysis of the coating performance variation after the additional activation cycle has been carried out by using ultimate pressure and pressure build-up measurements. In addition, laboratory measurements have been carried out to mimic the LHC coated beam pipe behaviour. The experimental data have been compared with calculation obtained by Molflow+.

INTRODUCTION

In February 2013, after three years of productive data collection, the LHC operation stopped for a 2-year-long shutdown (LS1) aiming at consolidating and upgrading the collider for 13 TeV centre-of-mass energy collisions.

During this period, all LHC arcs were warmed up to room temperature (RT) to allow the consolidation of the magnet bus-bars located at each magnet interconnects and, in parallel, a re-commissioning of the room temperature LSS [1].

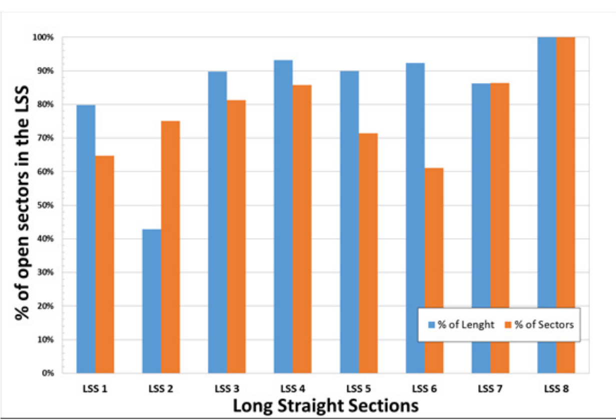

Figure 1: Percentage of open sectors during LS1.

The total length of the 8 LSS is 5.8 km which represents 14 % of the LHC ring length. By design, the LSS room temperature vacuum system is baked. About 85% of its surface is coated with 1-µm thick TiZrV film which provides most of the pumping speed once activated. During LS1, 148 room temperature vacuum sectors (about 5.1 Km) were opened and re-commissioned [1].

Figure 1 shows the percentage of the vacuum sectors that were opened during LS1 in the 8 different LSS; most of the sectors were vented. Afterwards, those sectors were baked and the NEG coating was activated.

Figure 2 shows the number of venting/activation cycles undergone by the vacuum sectors since their installation. About 80% of the NEG coated chambers had already been vented at least once before LS1. Possible detrimental effects on the vacuum performance of multiple venting/activation cycles were studied.

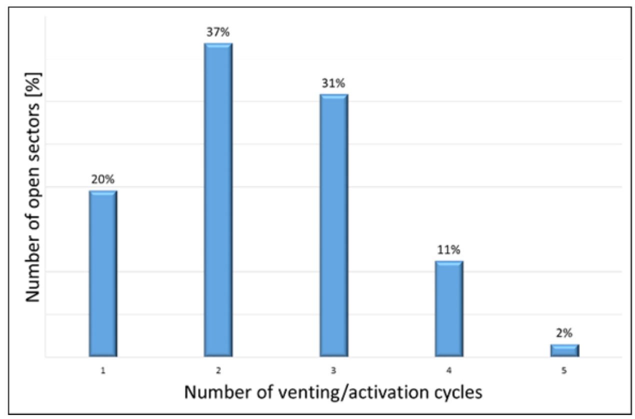

Figure 2: Distribution of baked sectors after LS1.

PRESSURE DISTRIBUTION ANALYSIS

As a first step, the study focused on the ultimate pressure values measured in the LSS. All data were collected one month after the end of the NEG activation. All NEG activations were always performed at 230°C and lasted 20 to 24h.

The distributions (see Fig. 3) of the measured values after each cycle were then plotted in order to identify possible trends. For each distribution, a curve fitting was added and the statistical central values were indicated by arrows. A clear decreasing trend of the pressures after each venting / activation cycle can be seen. The statistical central value decreases by a factor 0.7 after each venting/activation cycle as calculated by linear regression. This behaviour is the result of the combination of two different phenomena described in [2]: in one hand, the decrease of the outgassing rate of the Bayard-Alpert gauges and of the stainless steel module and, on the other hand, the decrease of the pumping speed, i.e. the sticking probability, of the NEG coating after each cycle. The latter was measured in a dedicated experimental set-up.

ISBN: 978-3-95450-168-7 doi:10.18429/JACoW-IPAC2015-WEPHA004

PRESENT QUALITY ASSURANCE FOR THE LHC BEAM VACUUM SYSTEM AND ITS FUTURE IMPROVEMENT

J. Sestak ,V. Baglin, G. Bregliozzi, P. Chiggiato
CERN, Geneva, Switzerland

Abstract

During the Long Shutdown 1 (LS1), the LHC beam vacuum system was upgraded to minimize dynamic vacuum effects like stimulated desorption and beam-induced electron multipacting. A quality assurance plan was mandatory due to the demanding vacuum performance and the limited access to the equipment during the following operation period. Laboratory assessment tests and underground interventions were performed following well-defined and approved procedures. All vacuum related activities were documented and written reports stored in dedicated databases. Quality controls were performed to find mechanical, cabling and equipment functionality non-conformities. Possible issues were identified, classified and tracked in a non-conformity database for future corrective actions. This contribution give an overview of the quality assurance policy followed during the LS1 and the non-conformities reported after quality control. Possible future improvements are also discussed.

INTRODUCTION

The LHC beam vacuum system [1] has several interfaces with other LHC systems. Its performance and reliability are one of the key-factors for successful operation of the accelerator. Because of the limited access for maintenance during operation, any unsuspected issue can bring significant time delay and additional cost. Due to these requirements, a quality management was implemented as an important part of LHC beam vacuum upgrade during the LS1 period.

LHC BEAM VACUUM SYSTEM AND LS1 UPRGADE

The LHC beam vacuum system consists of beam pipes at cryogenic temperature in the superconducting magnets, mainly in the arcs (ARC), and the long straight sections (LSS) operating to the greatest extent at room temperature. The ARC beam vacuum represents 86% of the total 27 km and is divided into 8 arcs operating on 1.9 K at an operational pressure lower than 10^{-6} Pa.

The LSS beam vacuum represents the remaining 14% of the storage ring circumference and accommodates the 4 main LHC experiments. The LSS include in total 174 vacuum sectors operating at room temperature together with 84 cryogenics sectors, stand-alone magnets (SAM) and inner triplets, operating at 4.5 K and 1.9K, respectively. Ultrahigh vacuum in the LSS is achieved using NEG coated chambers, NEG cartridges and ion sputtering pumps. Common pressure in the LSS after NEG activation is lower than10^{-9} Pa.

LS1 Beam Vacuum System Upgrade

During the LS1 upgrade (2013 – 2015) [2] both ARC and LSS were vented to air in order to integrate engineering changes. The LHC beam vacuum system was upgraded from the point of view of safety, performance, and reliability to meet RUN 2 requirements with 13 TeV collisions in the centre of mass.

For the ARC beam vacuum the following activities were held:

- Installation of Plug-In-Modules (PIM) half-shell protection.
- Installation of rupture disc at all quadrupole magnets.
- Installation of penning gauges to selected quadrupole magnets.
- Repair of non-conform PIM.

For the LSS the following activities were conducted:

- Repair of RF bridges in 96 warm modules.
- Exchange of solenoids by NEG coated RF bridges.
- Installation of additional 400 l/s NEG cartridges.
- Installation of NEG cartridges at SAM cryogenics sectors.
- Installation of modified ion-pumps with integrated NEG cartridges.
- Installation of vacuum and NEG pilot sectors.
- Upgrade of the experimental areas in order to improve the vacuum performance and reduce background.
- Re-commissioning due to activities on other systems (collimation, injection, instrumentation etc.).

LHC QUALITY ASSURANCE PLAN

The LHC Quality Assurance Plan (QAP) [3] was introduced during the LHC project phase in order to implement a Total Quality Management System, based on defect prevention and continuous process improvement. Using the quality assurance guidelines [4], QAP defines a whole product lifecycle including data management systems CERN EDMS (Data Management System) and CERN MTF (Manufacturing and Testing Folder).

LHC QAP for the Beam Vacuum System

During the LS1, all LHC arcs and the 148 room temperature vacuum sectors were vented and re-commissioned. In parallel with the underground activities,

Content from this work may be used under the terms of the CC BY 3.0 licence (© 2015). Any distribution of this work must maintain attribution to the author(s), title of the work, publisher, and DOI.

ISBN: 978-3-95450-168-7 doi:10.18429/JACoW-IPAC2015-WEPHA005

CHARACTERIZATION OF THE RF FINGERS CONTACT FORCE FOR THE LHC WARM VACUUM BELLOW MODULES

C. Blanch Gutiérrez, V. Baglin, G. Bregliozzi, R. Kersevan, P. Chiggiato
CERN, Geneva, Switzerland

Abstract

Along the 27 Km of LHC beam pipe, various types of vacuum bellow modules are needed to compensate the mechanical misalignments of the vacuum chambers during installation and to absorb their thermal expansion during the bake-out. In order to reduce the beam impedance during operation with beams these modules are equipped with RF bridges to carry the image current. They are usually made out of a copper tube insert at one side and Cu-Be RF fingers at the other end of the module. A spring is used to keep the contact between the RF fingers and the tube insert. The geometry and the choice of this spring become critical to ensure a good electrical contact.

In this paper, a description of the test bench used to measure the contact force together with the procedure applied and the measurements performed are given. A summary of the maximum radial and axial offsets between the RF fingers and the insert tube while keeping a good electrical contact is presented.

INTRODUCTION

In the LHC vacuum system almost 200 different types of warm vacuum modules are installed, making a total number of more than 1800 units. With different length, diameter and/or inner aperture, each type of module, by means of the RF transition inside, must ensure a good electrical continuity between the adjacent chambers. This electrical continuity is provided by the RF fingers and the tube insert which make a proper path, without geometrical discontinuities, for the image current when the beam is circulating through, avoiding large local impedances and electrical breakdown [1].

The electrical contact between the RF fingers and the tube insert depends on the geometry of both parts as well as on a spring, which assures the force to keep the contact [2] [3].

In order to qualify this electrical contact a test bench was implemented to measure the contact force between the RF fingers and the tube insert. Two different non-standard RF inserts types, one circular and one hippodrome geometry have been firstly tested and a bunch of tests are foreseen to characterize the rest of RF inserts installed currently in the LHC vacuum system.

THE TEST BENCH DESCRIPTION

Mechanical Set Up

The test bench used (Fig. 1) is made with three manual translational stages which allow the movement in the three axes. In one side of the test bench the RF fingers are fixed while in the other side the tube insert is attached.

With this set up, three degrees of freedom are allowed between both components of the RF bridge, being possible to set offsets positions in the three axes within a ± 0.5 mm precision.

The transition tube is wrapped with Kapton tape in order to insulate its electrical contact with all the RF fingers except one of them in which the contact force will be measured.

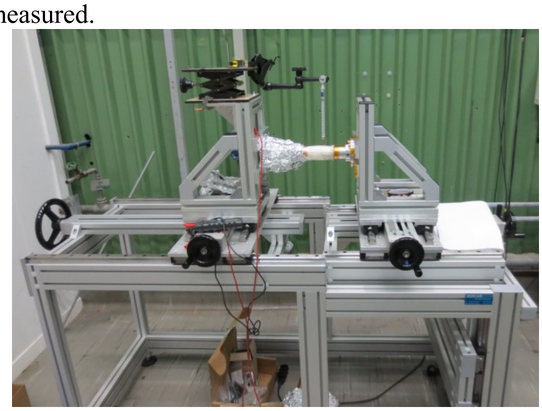

Figure 1: Test bench.

Above this finger a dynamometer attached to a mobile platform is placed. This dynamometer can measure in a range from 0 to 50g with a precision of 0.5g.

Electrical Set Up

The electrical set up consists in a Keithley multimeter connected in 4-wires measurement resistance mode (Fig. 2), to measure the contact resistance between the RF finger and the transition tube.

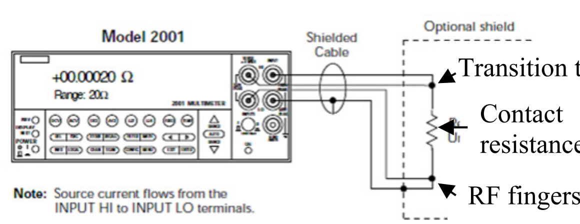

Figure 2: Electrical connection.

A different electrical set up was tested, applying 1 A constant current from the transition tube to the RF fingers, and measuring the voltage drop between them. Since $R=\Delta V/I$ and $I=1$ A, the voltage drop measured was equal to the resistance. However, since no difference or resolution improvement was observed with this second method, the first method was chosen for all the tests.

Content from this work may be used under the terms of the CC BY 3.0 licence (© 2015). Any distribution of this work must maintain attribution to the author(s), title of the work, publisher, and DOI.

ISBN: 978-3-95450-168-7 doi:10.18429/JACoW-IPAC2015-WEPHA006

RECOMMISSIONING OF THE COLDEX EXPERIMENT AT CERN

R. Salemme, V. Baglin, F. Bellorini, G. Bregliozzi, K. Brodzinski, P. Chiggiato, P. Costa Pinto, P. Gomes, A. Gutierrez, V. Inglese, B. Jenninger, E. Michel, M. Pezzetti, B. Rio, A. Sapountzis, R. Kersevan, CERN, Geneva, Switzerland

Abstract

COLDEX (COLD bore EXperiment), installed in the Super Proton Synchrotron (SPS) at CERN, is a test vacuum sector used in 2001-2004 to validate the Large Hadron Collider (LHC) cryogenic vacuum system with LHC type proton beams. In the framework of the R&D for the High Luminosity upgrade of the LHC (HL-LHC), COLDEX has been re-commissioned in 2014. The objective is the validation of the performance of amorphous carbon (a-C) coating at cryogenic temperature with LHC type beams. The existing COLDEX Cu beam screen has been therefore dismounted and carbon coated, while a complete overhaul of the vacuum, cryogenic and control systems has been carried out. This contribution describes the phases of re-commissioning, reviews the current experimental set-up and gives an overview of the possible measurements with COLDEX, in view of its HL-LHC experimental program.

INTRODUCTION

COLDEX is an experimental test vacuum sector that mimics the cold bore and beam screen cryogenic vacuum system adopted in the LHC cryomagnets. Originally designed to measure synchrotron radiation induced gas desorption [1], COLDEX was installed in SPS in 2001 to evaluate the impact of electron-cloud effects onto cryogenic vacuum systems [2].

During LHC Run 1, significant heal load due to beam induced electron cloud was observed on the beam screen of the Inner quadrupole Triplets. Extrapolation of these observations to the High Luminosity upgrade of the LHC (HL-LHC) predicts an intolerable increase of the dissipated heat load to the cryogenic system due to electron cloud build-up [3]. In order to reduce it, a-C coating is a potential candidate to mitigate the electron cloud effects due to its low Secondary Emission Yield (SEY) achieved at room temperature [4]. For HL-LHC purpose, this proposed base-line must be validated at cryogenic temperature with LHC type beams. For these reasons, COLDEX was re-commissioned and upgraded with a-C coated beam screen in 2014. A review of its scientific objectives is available in [5].

VACUUM SYSTEM

The COLDEX cryostat has been recovered from 2004. It houses a ~2.2 m long OFE copper beam screen (BS) inserted in a 316LN stainless steel cold bore (CB). The inner diameter (ID) of the CB is 113 mm. The BS is a circular, ID 67 mm, extruded pipe (Figure 1). It is perforated by two rows of 7.5x2 mm elongated holes (slots) which gives a transparency of 1% to the CB. The slots are shielded on their back with baffles capable to intercept straight electron paths to the CB. The BS is equipped with two 0.1 mm thin copper coated cold-to-warm transitions (CWTs) at its extremities. RF continuity is assured with RF fingers. The final adaptations to the upstream and downstream ID 100 mm chambers are tapered with conical apertures of 45°. Total pressure is measured at these two warm locations, *i.e.* upstream and downstream the BS, via calibrated Bayard-Alpert (VGI) hot cathode and Penning (VGHB) cold cathode ionization gauges.

Figure 1: Picture of the a-C coated beam screen during re-installation on February 2014.

A room temperature chimney faces a circular, ID 35 mm, vacuum port derived at the centre of the BS. At its top, a BA gauge is installed. This gauge allows monitoring the gas pressure in the BS which may be affected by electron stimulated desorption during electron cloud bombardment.

Two calibrated quadrupole mass spectrometers (RGA) are mounted on the BS chimney top and on the downstream chamber to perform analyses of the residual gas species in the cryogenic and room temperature parts, respectively. In the downstream warm chamber, a gas injection system, consisting in a bakeable 3.1 litres gas reservoir equipped with capacitance pressure gauges and connected to the vacuum system via variable leak valve, is fitted. This system is used to perform studies of gas transmission along the BS and pre-condensation of gas species onto the cold surface of the BS.

In order to give direct indication of electrons activity, two electrodes are employed. The chimney circular, Ø18 mm, electrode faces the BS aperture to the chimney

Content from this work may be used under the terms of the CC BY 3.0 licence (© 2015). Any distribution of this work must maintain attribution to the author(s), title of the work, publisher, and DOI.

ISBN: 978-3-95450-168-7 doi:10.18429/JACoW-IPAC2015-WEPHA007

AMORPHOUS CARBON COATINGS AT CRYOGENIC TEMPERATURES WITH LHC TYPE BEAMS: FIRST RESULTS WITH THE COLDEX EXPERIMENT

R. Salemme, V. Baglin, G. Bregliozzi, P. Chiggiato, R. Kersevan, CERN, Geneva, Switzerland

Abstract

Extrapolations of the Large Hadron Collider (LHC) Run 1 observations to the High Luminosity upgrade (HL-LHC) beam parameters predict intolerable increase of heat load on the beam screens of the Inner Triplets due to electron cloud. Amorphous carbon (a-C) coating of the beam screen surface is proposed to reduce electron cloud build-up, thereby minimising its dissipated power. In order to validate this baseline, COLDEX (COLD bore EXperiment) has been re-commissioned. Such experiment mimics the performance of the LHC cold bore and beam screen cryogenic vacuum system in the Super Proton Synchrotron (SPS). The main objectives of the study is the performance qualification of a-C coatings with LHC type beams while operating the beam screen in the 10 K to 60 K temperature range and the cold bore below 4.5 K. This paper reviews the status of COLDEX and the results obtained during its first experimental runs.

INTRODUCTION

During the Large Hadron Collider Run 1, considerable heat load (~200W) due to electron cloud was observed on the Inner Triplets (IT) beam screens during operation with 25 ns bunch spaced beams of nominal intensity. Extrapolations of these observations to the High Luminosity upgrade (HL-LHC) beam parameters predict an intolerable increase of heat load due to electron cloud build-up [1]. The increase of heat load is expected to be accompanied by increase of background to the LHC experiments. In order to mitigate the electron cloud build-up and, in turn, limit the heat load to an amount compatible with the IT cryogenics cooling capacity, the current baseline is to lower the IT beam screen surface Secondary Electron Yield (SEY) by amorphous carbon (a-C) thin film coating. Previous studies have shown that such a coating provides reliably low, as-received, SEY (typically <1.1 at room temperature) suitable in un-bakeable vacuum systems [2].

Successful mitigation of the electron cloud build-up with a-C coatings has been demonstrated in some SPS room temperature (RT) vacuum chambers with LHC type beams [2]. In order to further validate the HL-LHC baseline at cryogenic temperature, the COLDEX experiment has been re-commissioned in 2014. COLDEX is an experimental cryostat installed on a field-free by-pass of the SPS Long Straight Section (LSS) 4 which mimics the LHC cold bore and beam screen cryogenic vacuum system. A detailed description of the re-commissioning phases performed in 2014 and the current experimental setup is available in [3]. The main goal is the performance qualification of a-C coatings with LHC type beams while operating the beam screen in two temperature windows: the 5 to 20 K range, currently adopted for LHC and suitable for HL-LHC Inner Triplets, and the 40 to 60 K range under study for HL-LHC matching sections.

The experimental setup is conceived to study the beam induced multipacting in a LHC type cryogenic vacuum system as a function of the BS temperature (and, depending on it, of the presence of adsorbed gas species on its surface) and the circulating beam parameters (bunch intensity and spacing, total circulating intensity, at injection and flat-top energy). During a run, total pressure is measured along the vacuum system, *i.e.* in the RT upstream and downstream sections and in the cryogenic BS atmosphere. The dynamic pressure rise due to electron cloud is monitored with respect to the different circulating beams, and the conditioning obtained by beam dose is observed. The gas composition is followed-up constantly in both cryogenic and warm parts by residual gas analysers. In case of gas desorption, the primary and recycling desorption yields of the system can be estimated. The heat load dissipated by electron cloud onto the BS surface is measured as well as the electrons activity. Through benchmarking with available electron cloud build-up codes, the SEY of the surface can be deduced. The effects of adsorbed gas on the BS surface at cryogenic temperature is reproduced in dedicate runs by gas injections.

RESULTS DURING RUN 1

COLDEX first experimental run with a-C coating took place during the first SPS Scrubbing Run in November 2014. In a 7-day period, the accumulated beam dose exceeds 4 A·h. Two BS temperatures have been chosen: first 50 K, then 5 to 10 K. The CB was constantly kept at 4.5 K. At this temperature, the CB is capable of condensing all gas species (except He, which is only adsorbed up to 10^{14} He/cm^2), with a pumping speed fixed by the 1% transparency to the BS. One to four batches of 72 bunches, 25 ns bunch spaced, up to $1.3 \cdot 10^{11}$ proton per bunch (ppb), passed into COLDEX, mainly at 26 GeV/c, but also with energy ramp to 450 GeV/c. Hybrid (5+20 ns) bunch spaced doublet beams circulated as well, up to 4 batches and with a maximum intensity of $1.4 \cdot 10^{11}$ proton per doublet (ppd), equally split. Figure 1 shows the pressure evolution during the run along the COLDEX sector as well as the temperature range kept on the BS.

Significant pressure rises (up to ~$5 \cdot 10^{7}$ mbar, green and yellow curves) correlated to the beam circulation were observed upstream and downstream the COLDEX BS due to electron stimulated desorption. These parts are made of

Content from this work may be used under the terms of the CC BY 3.0 licence (© 2015). Any distribution of this work must maintain attribution to the author(s), title of the work, publisher, and DOI.

ISBN: 978-3-95450-168-7 doi:10.18429/JACoW-IPAC2015-WEPHA009

PROPAGATION OF RADIOACTIVE CONTAMINANTS ALONG THE ISOLDE BEAMLINE

M. Maietta, G. Vandoni, M. Ady, A. Dorsival, R. Kersevan, CERN, Geneva, Switzerland
A. Gottberg, TRIUMF, Vancouver, Canada

Abstract

Several Radioactive Ion Beam (RIB) facilities are in construction worldwide or undergoing upgrade. To ensure safe management of radioactive contamination, RIB vacuum systems are completely hermetical, with collection and storage of the effluents before controlled release. The layout of new RIB vacuum systems would be designed more efficiently with a better knowledge of the contaminant's propagation along the machine. At CERN, an experimental analysis of the propagation of radioactive species along the beam-line of ISOLDE was carried out during the last beam-run. The Monte-Carlo code Molflow+ was then used to interpret the results. We observe that radioactive rare gases are the major source of contaminant propagation. Propagation times of the order of some seconds were calculated and benchmarked with measurements for ^{6}He performed on beta scintillators on-line. The blocking effect of magnet separators and beam optics elements was partially confirmed.

INTRODUCTION

Since the first production of a radioactive ion beam (RIB) at the Niels-Bohr Institute in 1951 and the first ISOLDE facility in 1967 at CERN, RIB facilities have flourished worldwide, fostering nuclear research with exotic nuclei production. Several new projects [1], including an intensity upgrade of ISOLDE are bound to see the light of day in the coming years.

ISOLDE [2] produces RIBs by irradiation of a thick target with the pulsed 1.4GeV, 2μA average current proton beam from the PS Booster accelerator. Exotic nuclei generated by the collision diffuse and effuse through a tiny transfer line to the ion source, where ~10% of them are selectively ionized. Isotope separation is then achieved in either of two on-line separators. The General Purpose Separator (GPS) consists of a 70° bending magnet and an electrostatic switchyard, allowing selection of three mass separated beams. The High Resolution Separator (HRS) consists of two (90° and 60°) bending magnets plus focussing-defocussing and correction electrostatic multi-poles. The HRS is followed by a Radio Frequency Quadrupole Cooler and Buncher. The two separator lines converge into a common beam distribution system at the main switchyard, conveying high purity isotope beams to several experimental stations.

Most of the nuclei produced in the target are not ionized [3]; the volatile species diffuse via the transfer line across the ion source and through the beam-line. These are believed to be the cause of the contamination of the vacuum of RIB machines. To avoid contaminants dispersion along the beam-line, vacuum is achieved by turbomolecular pumps, connected via a totally hermetical common backing manifold to a set of primary pumps [4]. These convey the effluent gases to a gas storage system, which confines radioactive gas for controlled decay before release to the atmosphere via the nuclear ventilation system. By this scheme, all vacuum effluents from target to experimental beam-lines flow together into a common storage, thus mixing highly contaminated with less contaminated gas.

In order to gain knowledge on the distribution of neutral contaminants along the beam-line, we have sampled contamination with filters installed along the vacuum system, which were then analysed by gamma spectroscopy. In parallel, we have carried out a Monte-Carlo simulation of the diffusion of rare gases from the target along the beam-line. This article presents the approach and preliminary results obtained on the GPS branch of Isolde.

SAMPLING OF RADIOACTIVE SPECIES

Hybrid filters were installed at the exhaust of each turbomolecular pump during the machine shutdown. They consist in two filtering disks, one of 150μm thickness in hydrophilic mixed cellulose ester with 3 μm pores, the other one in carbon impregnated cotton fibre, clamped together by two stainless steel nets and installed in the thickness of a ISO-KF standard o-ring supporting ring. The turbomolecular pumps being isolated both at the inlet and at the outlet by valves, installation did not require venting of the beam-line nor of the backing manifold. The filters were kept in place for 4 months, seeing 9 different targets and more than 30 beams. The 3 filters installed on the turbomolecular pumps of the GPS branch were then removed after a 40h beam stop and analysed within 7 days in gamma spectroscopy with a high-purity Germanium detector. Pump GPS21 is installed upstream of the separator magnet and switchyard, while GPS22 and GPS23 are both installed at the same longitudinal coordinate right downstream of it. Radioactive species appearing in the 3 filters and relative activity are presented in Figure 1.

All species, besides ^{194}Au, are long-lived isotopes, of half-lives of the order of days. The gold isotope ^{194}Au is progeny of the very long-lived ^{194}Hg, in secular equilibrium. With the exception of the antimony isotopes, all species are issued from rare gas parents (radon, xenon and krypton) or from mercury (^{185}Os). Indeed, the specific

Content from this work may be used under the terms of the CC BY 3.0 licence (© 2015). Any distribution of this work must maintain attribution to the author(s), title of the work, publisher, and DOI.

ISBN: 978-3-95450-168-7 doi:10.18429/JACoW-IPAC2015-WEPHA010

THE VACUUM SYSTEM OF THE EXTRA-LOW ENERGY ANTIPROTON DECELERATOR ELENA AT CERN

R. Kersevan, CERN, Geneva, Switzerland

Abstract

The Extra Low Energy Antiproton ring (ELENA) is a CERN project aiming at constructing a 30 m circumference synchrotron which will take antiprotons extracted at 5.3 MeV from the Antiproton Decelerator (AD), and further decelerate them down to 100 keV [1].

The ring will be equipped with two electrostatic (ES) pulsed extraction deflectors which will allow to deliver the low-energy, cooled antiproton beams to a number of experimental beamlines [2]. The total length of these transfer lines, equipped with ES optical elements is of the order of 100 m. From the vacuum point of view, machine physics issues related to rest-gas scattering and intra-beam scattering mandate a very low average pressure limit, calculated to be 4.0E-12 mbar [3,4]. The very compact ring and the beam-instrumentation installed on it, with many components placed inside of the vacuum system, and lack of space to install lumped pumps, has pushed us to design a pumping system based primarily on non-evaporable getter (NEG) coatings, and few lumped integrated NEG-ion pumps.

The vacuum requirements for the transfer lines are a bit more relaxed, in the 1.0E-10 mbar range, but still require state-of-the-art solutions in order to reduce the potentially large outgassing of the many electrodes, insulators, metal connections used for the ES components installed inside the vacuum system. NEG-coating and integrated NEG-ion pumps will therefore be used here too.

The entire vacuum system of ELENA, with the exception of a short, initial part of the injection line coming from the AD machine, has been specified to be bakeable at 250 ºC.

MACHINE PHYSICS ISSUES AND VACUUM REQUIREMENTS

The low-energy of the antiproton beams, and the length of the deceleration and cooling cycles, mandate a very low average pressure along the ring, 4.0E-12 mbar [1,3-4]. This is not an unprecedented vacuum requirement at CERN, since the LEIR ring has, in the past, required the design of a vacuum system capable of reaching similar performances [5].

OVERVIEW OF THE MACHINE AND TRANSFER LINES

In the following, the naming conventions adopted for the ELENA project will be used, for brevity:

- LNI: injection line from AD;
- LNR: ELENA ring;
- LNExx: transfer lines (total of 9 sections/segments);
- LNS: H^+/H^- commissioning source

Figure 1 shows a bird's eye view of LNI, LNR, LNExx, and LNS. Figure 2 shows a busy intersection of vacuum lines, LNI, LNE, and LNS.

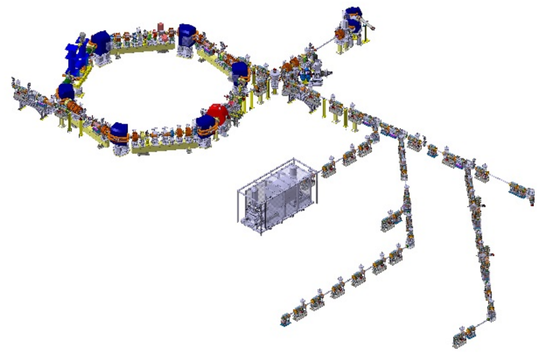

Figure 1: view of the whole ELENA complex, accelerators and beamlines.

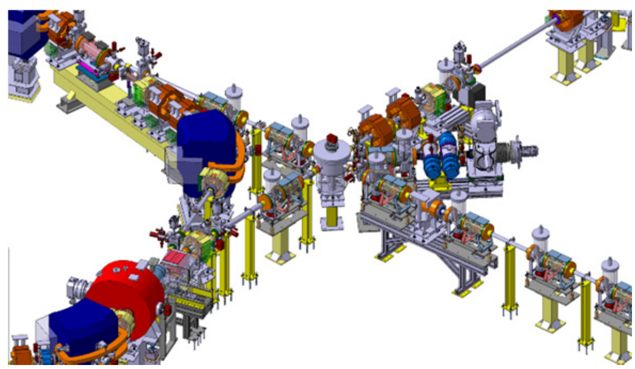

Figure 2: a busy crossing; the ion-switch (IS) chamber is in the middle, with its 5 connections to, clockwise from the 2-hour position: LNI from AD, LNS, LNE03, LNI going into LNR, and LNE00 coming out of the ring.

VACUUM CHAMBER MATERIALS AND FLANGES

Materials

The very low energy of the antiproton beam after the deceleration and cooling cycles mandate the choice of a very low magnetic permeability material. The choice has fallen on austenitic stainless steel, 316 LN grade, 3D-forged for all parts machined from blocks, and for flanges.

Flanges

The already mentioned lack of space longitudinally along the ring has pushed us to choose a conical ConFlat flange design, with collars instead of the usual holes. This is a solution which is already employed and validated at CERN on several machines since a long time, both for un-

Content from this work may be used under the terms of the CC BY 3.0 licence (© 2015). Any distribution of this work must maintain attribution to the author(s), title of the work, publisher, and DOI.

ISBN: 978-3-95450-168-7 doi:10.18429/JACoW-IPAC2015-WEPHA011

PHOTODESORPTION AND ELECTRON YIELD MEASUREMENTS OF THIN FILM COATINGS FOR FUTURE ACCELERATORS

M. Ady, P. Chiggiato, R. Kersevan, CERN, Geneva, Switzerland
Y. Tanimoto, T. Honda, KEK, Tsukuba, Japan

Abstract

The performance of future accelerators could be limited by electron cloud phenomena and high photodesorption yields. For such a reason, the study of secondary electron and photodesorption yields of vacuum materials is essential. The eradication or mitigation of both secondary electron and molecule desorption could strongly reduce the beam scrubbing time and increase the availability of nominal beams for experiments.

Surface modifications with the desired characteristics can be achieved by thin-film coatings, in particular made of amorphous carbon and non-evaporable getters (NEG).

In the framework of a new collaboration, CERN's vacuum group has manufactured several vacuum chambers with a geometry similar to the beam pipe of future accelerators, and has applied different coatings on each of them. The samples were then irradiated at KEK's Photon Factory (PF) with synchrotron radiation of 4 keV critical energy during several days, allowing the measurement of the photodesorption yield as a function of the photon dose.

This paper presents the experiment and briefly summarizes the preliminary photodesorption and photoelectron yield data of different coatings. The results can be used for future machine design with similar conditions, such as the FCC-hh.

INTRODUCTION

When designing future accelerators, synchrotron radiation (SR) must be taken into account not only for its thermal effects, but also because the induced electron cloud and high photon stimulated desorption (PSD) reduce the beam's lifetime. One way to mitigate these phenomena is the application of different types of thin film coatings.

To measure their efficiency, a collaboration has been set up between CERN's vacuum group and KEK: the goal was to characterize the effectiveness of NEG and amorphous carbon coatings, and the effect of activation and vacuum firing. CERN has therefore manufactured six vacuum chambers, each conditioned and coated differently, then these chambers were installed in one of the PF's experimental hutches in Tsukuba, Japan and data was collected during a two-month test campaign.

SAMPLES

The 1200 mm long, 61 mm internal diameter vacuum chambers are manufactured of 316L type stainless steel, with three 35 mm ports opened by mechanical extrusion and subsequent welding. All ports use standard ConFlat flanges, one rotatable (machine side) and four fixed.

The three ports are connected to DN40 CF vacuum feedthroughs with a pin on the vacuum side - these pins hold bent stainless steel disc-shaped electrodes. A screw fixing system allows precise height and orientation adjustment to ensure that the discs follow the tube profile, while leaving a 1 mm gap allowing to use them as electrodes kept at high voltage.

The tube is closed from one side by a DN63 blank flange with a 4 mm injection tube drilled from its side: this allows gas injection during the experiment. The other side is open. All chamber components were cleaned following standard CERN chemical degreasing procedure, and fasteners and small parts, such as screws were cleaned with ultrasound in an ethanol solution. Following this basic treatment, each sample was conditioned and coated differently. Table 1 summarizes the treatment and coating types.

Table 1: Treatment Types and Experiment Durations for the Six Vacuum Chambers

Sample	Treatment and coating	Experiment duration (days)
1	Reference stainless steel sample basic treatment only	10
2	Stainless steel sample vacuum fired	7
3	TiZrV NEG coating not activated	6
4	TiZrV NEG coating, activated prior to the experiment	6
5	TiZrV NEG coating vacuum fired, activated	7
6	Amorphous carbon coating vacuum fired	11

Samples 2, 5 and 6 were vacuum fired at 950 °C for 2 hours to liberate the H_2 gas stored in the bulk. Once ready, all samples were transported to Japan filled with nitrogen for protection of the inner surface.

EXPERIMENTAL SETUP

We performed our experiment in PF's BL-21 hutch. The beam current, SR critical energy and the incidence angle are chosen to correspond with future machine designs, such as the FCC-hh (4028 eV critical energy, 490 mA beam, 30.7 W/m SR power [1]): the SR in our setup is originating from a 0.9634 T dipole magnet 13 m upstream, with critical

Content from this work may be used under the terms of the CC BY 3.0 licence (© 2015). Any distribution of this work must maintain attribution to the author(s), title of the work, publisher, and DOI.

ISBN: 978-3-95450-168-7 doi:10.18429/JACoW-IPAC2015-WEPHA012

SYNCHROTRON RADIATION DISTRIBUTION AND RELATED OUTGASSING AND PRESSURE PROFILES FOR THE HL-LHC FINAL FOCUS MAGNETS*

R. Kersevan, CERN, Geneva, Switzerland

Abstract

The HL-LHC upgrade consists of many different subprojects. One of the most important ones is the installation of very large gradient inner triplet (IT) magnets, comprising 4 long superconducting (SC) quadrupoles, and a new superconducting D1 hosting a corrector package in the same cryostat. D2 is also a newly conceived SC magnet, and provision is made for 4x crab-cavities on each of the two separate beam lines, between D2 and Q4.

The HL-LHC final focus area, from Q4 to the interaction point, has been modelled based on the latest vacuum chamber geometry and orbits. The synchrotron radiation (SR) fans are computed using the Monte Carlo code SYNRAD+ [1]. The angular and energy dependence of the reflectivity of the copper surfaces is considered, as well as a representative surface roughness. Once the SR distributions are computed, they are converted into outgassing profiles by using conversion curves found in literature. The test-particle Monte Carlo code Molflow+ is then used [2] to compute the related gas density distribution. Warm areas are supposed to be NEG-coated, in order to reduce SR-induced desorption and the generation of secondary electrons. The calculation is repeated for 3 different conditioning times, corresponding to 1, 10, and 100 days at full nominal current of 1 A. It is shown that the resultant gas densities are always below the limit dictated by the ATLAS and CMS detectors' background and by the beam-gas scattering lifetime τ in the machine (τ >100 h). The SR ray-tracing calculations are carried out in the short-dipole approximation, i.e. no provision is made for edge radiation.

GEOMETRICAL ASSUMPTIONS

The latest geometry for the octagonal beam screen with tungsten-based shielding has been considered [3]. For the recombination chamber between D1 and TAN a "Y" chamber is assumed, with a common part for the two beams modelled as a 230 mm internal diameter (ID) round pipe splitting into two 80 mm ID separate chambers for the two beams. This "Y" chamber is supposed to be at room temperature, and NEG-coated, as presently done in the LHC. Since the exact geometry of the cold and warm beam-position monitors (BPMs) has not been finalized yet, they have been modelled as circular cylindrical objects connected to the neighbouring chambers via small-angle tapers. The cylindrical surface where the BPM electrodes are supposed to be located has a slightly bigger radius, so as to recess the electrodes and prevent them from being hit by direct SR coming from the triplet area magnets. A similar model has been assumed for the RF contact fingers of the sliding joints placed in the inter-connects between the different cryostats and/or room-temperature vacuum chambers.

SYNCHROTRON RADIATION RAY-TRACING

The orbits for round beams at collision on the right side of IR1/IR5 have been considered [4]. It is against these orbits that the ray-tracing code SYNRAD+ has been checked prior to generating the detailed 3D model of the internal part of the perforated beam-screen (BS) and vacuum chambers. To this aim, the corresponding twiss file has been used, setting the initial point of each trajectory segment and the corresponding angles in SYNRAD+ to the same values as in the orbit file. For clarity, the case of the vertical crossing in IR1 has been chosen. Figure 1 shows the 8 different orbit segments in Q1, Q2a, Q2b, Q3, D1 and D2 (where Q1 and Q3 are in effect 2 shorter quadrupoles sitting inside the same cryostat, while Q2a and Q2b have separated cryostats with additional corrector packages). Initially the complete SR fan is collected separately for the outgoing B1 beam and incoming B2 beam on two large planar rectangular facets which allow us to calculate the global SR photon flux, power, and spectra, see Fig. 1. It has been decided to set a low-energy photon cut-off value of 4 eV, since neither molecular desorption nor photo-electron production is expected to be generated by photons having energies lower than this value. The MC code automatically calculates the fraction f of photons generated within the 4-500 eV energy interval. The critical energy for the SC magnets D1 and D2 is equal to 29.4 eV and 23.6 eV respectively, while the critical energy of the 4 SC triplet magnets depends on the distance between the orbit and the magnetic centre of the particular magnet. The fraction f is, 0.116, 0.152, 0.229, 0.237, 0.187, 0.171, for Q1a, Q1b, Q2a, Q2b, Q3a, and Q3b, respectively. This shows that only a small fraction of the photon flux calculated analytically is actually a potential source of molecules or photo-electrons, and that using the analytic formula which gives the number of photons emitted per unit length of trajectory largely over-estimates the flux and the related photo-desorption and photo-electron production.

The beam size at each point of the orbit is calculated by taking into account the beam emittance, horizontal and vertical beta function, and dispersion as per standard formulae. Figure 1 shows in blue the cloud of source points of the SR rays traced. The local angle of emission is obtained by combining the natural SR divergence and

* Research supported by the High Luminosity LHC project

Content from this work may be used under the terms of the CC BY 3.0 licence (© 2015). Any distribution of this work must maintain attribution to the author(s), title of the work, publisher, and DOI.

ISBN: 978-3-95450-168-7 doi:10.18429/JACoW-IPAC2015-WEPHA013

THE ASSEMBLY EXPERIENCE OF THE FIRST CRYO-MODULE FOR HIE-ISOLDE AT CERN

Y. Leclercq#, G. Barlow, J-A. Bousquet, A. Chrul, P. Demarest, J-B. Deschamps, J-C. Gayde, M. Gourragne, A. Harrison, G. Kautzmann, D. Mergelkuhl, V. Parma, J-A. Ferreira-Somoza, M. Struik, M. Therasse, L. Williams, CERN, Geneva, Switzerland,
J. Dequaire, Intitek, Lyon, France

Abstract

The HIE ISOLDE project aims at increasing the energy of the radioactive ion beams of the existing REX ISOLDE facility from the present 3 MeV/u up to 10 MeV/u for an A/q up to 4.5 [1]. The upgrade includes the installation of a superconducting linac in successive phases, and ultimately comprising two low-β and four high-β cryo-modules. The first phase involves the assembly installation and test of two high-β cryo-modules, each housing five high-β superconducting cavities and one superconducting solenoid, aligned within tight tolerances. Following design and procurement of cryo-module components for 2 units, the first unit is now being assembled at CERN, in a dedicated facility including class100 (ISO5) clean rooms equipped with specific tooling. The assembly is foreseen to be complete and the cryo-module delivered to the beam-line in May 2015. In this paper, we present the assembly of the first unit, including the methodology, special tools, assembly procedures and quality assurance aspects. We report on the experience from this first assembly, including tests results, and present prospects for the next-coming cryo-module assemblies.

INTRODUCTION

The decision to implement a major upgrade [2] of the energy and intensity of the existing ISOLDE and REX-ISOLDE radioactive ion beam facilities at CERN requires the replacement of most of the existing ISOLDE post-acceleration equipment by a superconducting linac based on quarter-wave RF cavities housed together with superconducting solenoids in a series of four high-β and two low-β cryo-modules. The design and component procurement phases of the project complete for 2 high-β cryo-modules, CERN is now engaged for the first time in the assembly of cryo-modules, featuring a common insulation and beam vacuum, requiring, to preserve RF cavity performance, the installation of a purpose built ISO5 quality clean room and associated infrastructure. The assembly of the first high-β cryo-module started in late August 2014 and now at end April 2015 is completed. Although in all respects it is clearly a prototype, this first unit is destined for installation onto the HIE-ISOLDE beam-line in May 2015 and will there be subjected to full functional testing.

THE CRYOMODULE ASSEMBLY

The complete high-β cryo-module assembly is shown in Fig.1. The components and sub-assemblies comprising the cryo-module their specific characteristics and expected performance are detailed in [3].

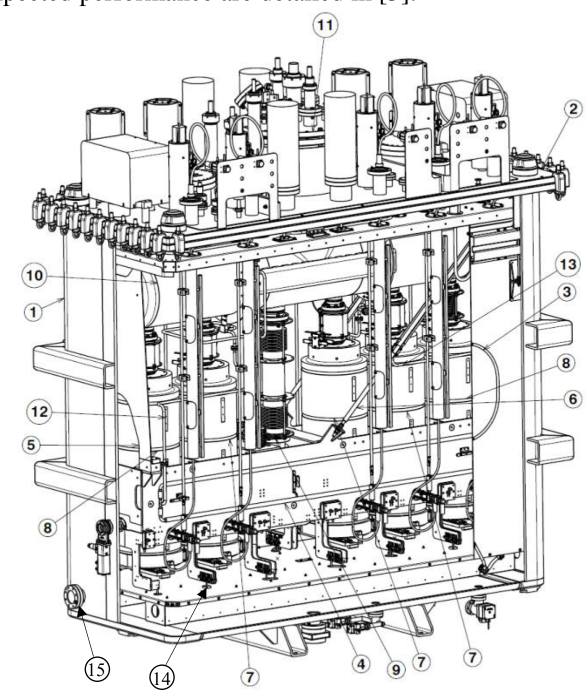

Figure 1: The complete HIE-ISOLDE high-β cryo-module; 1 Vacuum vessel lower box, 2 Vacuum vessel top plate assembly, 3 Thermal shield lower box, 4 Support frame, 5 Suspension end plate, 6 Tie-rod, 7 Inboard cavity, 8 Outboard cavity, 9 Down tube to solenoid, 10 Helium vessel, 11 Chimney assembly, 12 Support frame cooling supply, 13 Support frame cooling return, 14 Mathilde targets, 15 Mathilde viewport.

A vertical assembly, suspended from the mobile frame (see Figure 3) and essentially built from top downwards is implemented. The complete cryo-module assembly process has been separated into 20 sub-assembly stages, in a sequence imposed by the cryo-module design and by the tooling characteristics and featuring the installation of the RF cavities at the latest possible stage in order to minimize the risk of their contamination.

Content from this work may be used under the terms of the CC BY 3.0 licence (© 2015). Any distribution of this work must maintain attribution to the author(s), title of the work, publisher, and DOI.

ISBN: 978-3-95450-168-7 doi:10.18429/JACoW-IPAC2015-WEPHA015

Content from this work may be used under the terms of the CC BY 3.0 licence (© 2015). Any distribution of this work must maintain attribution to the author(s), title of the work, publisher, and DOI.

BEAM TESTS USING A WIDE BAND RF SYSTEM PROTOTYPE IN THE CERN PS BOOSTER

M.M. Paoluzzi, M.E. Angoletta, A.J. Findlay, M. Haase, M. Jaussi, A. Jones, J. Molendijk, J. Sanchez Quesada
CERN, Geneva, Switzerland

Abstract

In the framework of the LHC Injectors Upgrade project (LIU) and in view of a complete replacement of the existing CERN PS Booster (PSB) RF systems, a small scale, wide band prototype cavity was installed in 2012 in the machine. Following the encouraging tests done using this limited set up, an almost full scale, RF system prototype has been built and installed in the PSB during the Long Shutdown 1 (LS1). This modular, Finemet® loaded system covers the band 0.5 ÷ 4 MHz corresponding to the *h=1* and *h=2* frequency ranges. It uses solid-state power stages and includes fast RF feedback for beam loading compensation. New dedicated digital low level electronics have been implemented for all loops required for beam acceleration and interfaces with the general PSB control system. It allows using the new equipment at the fundamental and/or second harmonic of the beam revolution frequency as well as operating it in parallel with the existing RF systems. This paper describes the low level and power sections of the project and reports about the achieved results and experience built up so far.

INTRODUCTION AND SYSTEM DESCRIPTION

With the program under implementation in the frame of the LIU project [1, 2] and the coming into operation of the Linac4, the PSB extraction energy will rise to 2 GeV and the beam intensity to 2E13 ppb (nominal) or even 2.5E13 ppb (absolute maximum). This brings the beam peak current to ~32 A (half sine approximation) and the fundamental, second harmonic and DC components to 13 A, 8.5 A and 7.2 A respectively. Among other parameters, the ability of the machine to digest the highest intensities depends on the current and power available from the RF systems. To cope with this more demanding situation the performance of the PSB RF systems must be substantially improved. This can be achieved replacing the existing narrowband, tuned RF systems covering the *h=1* (C02 RF system) and *h=2* (C04 RF system) frequency ranges with cavities based on the wideband frequency characteristics of Finemet® magnetic alloy (MA) [3]. Full exploitation of the wideband characteristics suggests using a cellular configuration in which an accelerating gap is surrounded by a MA core on each side [4, 5], is driven by a solid-state amplifier and produces a fraction of the total accelerating voltage. 12 cells can be fitted in the space presently used by each C02 and C04 cavity for a total 8 kV per section. As three straight sections are presently occupied by these systems, the total maximum voltage can either be kept to 16 kV using two straight sections only or increased to 24 kV. The wide band response allowing multi harmonic operation, flexible adjustment of the *h=1* and *h=2* voltage components is possible and only limited by the total maximum voltage. However, installing wideband cavities in the PSB rings introduces longitudinal impedance covering many revolution frequency harmonics and special care must be taken for compensating the beam-loading. A fast RF feedback loop takes partial care of this and additional measures are implemented in the low level electronics.

Figure 1: 10-cell prototype MA cavity in PSB Ring 4.

To validate the choice of these deep and complex changes the prototype system installed in 2012 was upgraded during LS1 to 10 cells for a total of 7 kV. The experience gained with the 2012 amplifier prototypes allowed designing and producing a new generation of power stages. All weaknesses shown by the previous version were corrected. In particular mitigation of the of radiation effects on the solid-state devices is obtained by

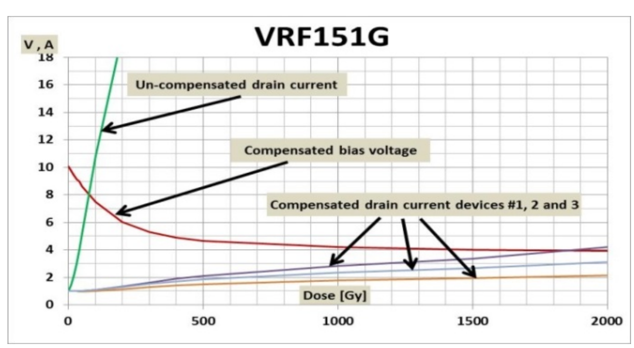

Figure 2: Mitigation of radiation effects on VRF151G RF Mosfet. The compensated device drain current variation vs. integrated dose is greatly reduced.

ISBN: 978-3-95450-168-7 doi:10.18429/JACoW-IPAC2015-WEPHA016

EXPERIMENTAL SETUPS TO DETERMINE THE DAMAGE LIMIT OF SUPERCONDUCTING MAGNETS FOR INSTANTANEOUS BEAM LOSSES

V. Raginel, B. Auchmann, R. Schmidt, D. Schoerling, A. Verweij, D. Wollmann
CERN-TE, 1211 Geneva 23, Switzerland

Abstract

The damage mechanisms of superconducting magnets due to the direct impact of high intensity particle beams are not well understood. Obvious candidates for upper bounds on the damage limit are overheating of insulation, and melting of the conductor. Lower bounds are obtained by the limits of elasticity in the conductor, taking into account dynamic effects (elastic stress waves). The plastic regime in between these two bounds will lead to differential thermal stress between the superconductor and stabilizer, which may lead to a permanent degradation of the magnet. An improved understanding of these mechanisms is required especially in view of the planned increase in brightness of the beams injected into the LHC [1] and of the future High Luminosity-LHC [2] and Future Circular Collider (FCC).

In this paper the plans for room temperature damage tests on critical parts of superconducting magnets and the strategy to test their damage levels at 4.3 K in the HiRadMat facility at CERN [3], using a 440 GeV proton beam generated by the Super Proton Synchrotron (SPS), is presented. Moreover the status of numerical simulations using FLUKA and multi-physics FEM code (ANSYS) to assess the different effect and the irradiation of the proposed experimental setup in preparation of the test is shown.

INTRODUCTION

Losses of the LHC beam can happen at very different time scales, the most critical are so-called ultrafast losses, less than 270 μs (~3 LHC turns). Protection against such losses depends on passive devices intercepting lost particles. The interaction between the LHC beam and these passive devices generates particle showers which can be intercepted by the downstream elements such as superconducting magnets causing quenches or in the worst case damage.

At several occasions the passive devices for injection protection demonstrated their efficiency: due to failures of the injection kickers the injected beam was partially intercepted by the injection absorbers thus preventing damage. However, one event is not understood, which lead to the damage of small corrector magnets. During LHC Run 1, three small corrector circuits in the LHC inner triplet left of IP2 (IT.L2) have been found open after a failure during injection. Several magnets including the main quadrupole magnet where these correctors are mounted on the front face quenched during this event [4].

In this paper the thermo-mechanical effects due to the interaction between high energetic particles and matter are described. Then potential damage of critical parts of a superconducting magnet and their consequences for the magnet are discussed. The roadmap to perform damage tests with and without proton beam is presented. A preliminary experimental setup for a test of superconducting coils and cable samples at 4.3 K at CERN HiRadMat facility with a 440 GeV proton beam is shown. Finally it is explained how the thermo-mechanical effect of beam impact on the proposed experimental setup will be assessed with numerical simulations.

THERMO-MECHANICAL EFFECTS

The absorption of intense high-energy proton pulses of several micro-seconds duration causes a considerable temperature increase of the same rise-time inside the intercepted material. During this short period, thermal expansion of the irradiated material is partly prevented by its mass inertia. This gives rise to dynamic stresses propagating through the material [5].

With increasing energy deposition in a material, dynamic stresses pass from the elastic, to the plastic and ultimately to the shock wave domain. No damage occurs if the material stays in the elastic domain but shock waves will lead to severe damage in the affected components.

For cryogenic copper, which is major part of superconducting cables, the limit of the elastic regime is reached with an energy deposition of < 50 J/cm3. For metal-based materials, like superconducting cables, it can be shown that shock waves do not appear before melting [6]. The energy deposition to melt copper is ~6 kJ/cm^3 [7]. It is not understood if energy deposition in the plastic regime between 50 J/cm^3 and 6 kJ/cm^3 will cause damage to NbTi filaments or a degradation of the polyimide tape insulation and therefore cause a permanent loss of performance of the magnet.

IDENTIFIED CRITICAL PARTS OF MAGNET

Superconducting cable, insulation, quench heater, copper wedges and end spacers were identified as the critical parts of the superconducting magnets of the LHC.

The LHC superconducting cables are classical Rutherford cables made out of NbTi/Cu wires (see Fig. 1). The breaking of some NbTi filaments due to high dynamic stresses could lead to a reduction of the critical current.

As shown in Fig. 2, cables are insulated with several layers of polyimide tapes. Damage on the insulation due to high temperature could cause a short circuit either to ground – fatal for the magnet – or inter-turn short – leading

Content from this work may be used under the terms of the CC BY 3.0 licence (© 2015). Any distribution of this work must maintain attribution to the author(s), title of the work, publisher, and DOI.

ISBN: 978-3-95450-168-7 doi:10.18429/JACoW-IPAC2015-WEPHA017

QUALIFICATION OF THE BYPASS CONTINUITY OF THE MAIN DIPOLE MAGNET CIRCUITS OF THE LHC

S. Rowan*, B. Auchmann, K. Brodzinski, Z. Charifoulline, B. Panev, F. Rodriguez-Mateos, I. Romera, R. Schmidt, A. Siemko, J. Steckert, H. Thiesen, A. Verweij, G. Willering, CERN, Geneva, Switzerland.
H. Pfeffer, FNAL, Batavia, IL 60150, U.S.A.

Abstract

The copper-stabilizer continuity measurement (CSCM) was devised in order to attain complete electrical qualification of all busbar joints, lyres, and the magnet bypass connections in the 13 kA circuits of the LHC. A CSCM is carried out at ∼20 K, i.e., just above the critical temperature, with resistive magnets. The circuit is then subject to an incremental series of controlled powering cycles, ultimately mimicking the decay from nominal current in the event of a magnet quench. A type test to prove the validity of such a procedure was carried out with success in April 2013, leading to the scheduling of a CSCM on all main dipole circuits up to and including 11.1 kA, i.e., the current equivalent of 6.5 TeV operation. This paper details the procedure, with respect to the type test, as well as the results and analyses of the LHC-wide qualification campaign.

INTRODUCTION

Following the 2008 incident [1], thorough investigation found that this was as a result of discontinuities in the superconducting busbar-joints' copper stabilizer - depicted in Fig. 1. To prevent such an event happening again, the LHC was operated at 3.5-4 TeV for the duration of Run 1. To allow for operation of up to nominal energy, it was decided that, during Long Shutdown 1 (LS 1), every interconnect (over 10,000) was to be repaired and consolidated with each splice having an electrical shunt applied, Fig. 2 [2].

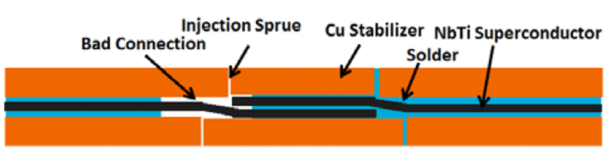

Figure 1: Depiction of a typical main dipole splice showing both good (right side) and bad (left side) continuity.

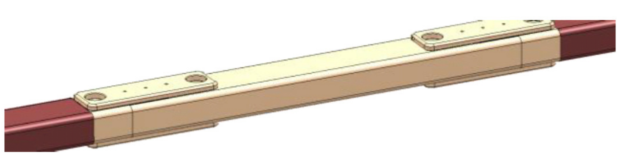

Figure 2: Illustration of the splice consolidation shunts, as applied, to reduce overall connection resistance and prevent adverse consequences from quenches in these locations [2].

LS 1 electrical quality control (ELQC) measurements at warm, ∼300 K, found that 5.9 % of all splices exceeded the acceptance criteria [3]. Furthermore, abnormally high resistances were found in the magnet bypasses, $> 200\ \mu\Omega$ (accepted maximum being $15.5\ \mu\Omega$) [4], as well as other types of soldered/welded connections [5]. Even though all discovered defects were consolidated, due to the foreseen quench training, with over 100 quenches predicted [6], an LHC-wide copper-stabilizer continuity measurement (CSCM) was carried out on all the main dipole circuits to guarantee that no defects were missed during LS 1 ELQC and that all aspects of all circuits are intact, in particular, the lyres, as they contain welded connections, but were not systematically checked during LS 1.

CSCM TEST PROCEDURE

The principle of a CSCM is to have the current bypass the magnets by operating at ∼20 K - just above the critical temperature, making the magnets resistive. Fig. 3 shows the expected current flowing through the magnet bypass along a main dipole circuit. To provide sufficient voltage to account for this, two 6.5 kA/200 V sub-converters had to be connected in series, normally connecting in parallel. The result, however, is that tests require a short period of over-current. The test also required protection system (PS) board modifications to monitor both the voltage across all busbar segments from the magnet voltage taps, "BS board A", and the voltage across the busbar segments as well as the adjacent diode leads connections, at the diode voltage taps, "BS board B". The difference of the two (B − A) gives the voltage across the bypass diode leads, which encompasses six contacts. The BS boards allowed for V, $\mathrm{d}V/\mathrm{d}t$ and $\mathrm{d}^2V/\mathrm{d}t^2$ thresholds to be set, ensuring detection and protection against any thermal runaways, by turning off the power converter (PC) (0.03 s decay constant due to the atypical inductance during a CSCM of only 3 mH, compared to 15.7 H during normal operation). Other, "DS", boards allowed for the monitoring of the voltage directly across the diodes.

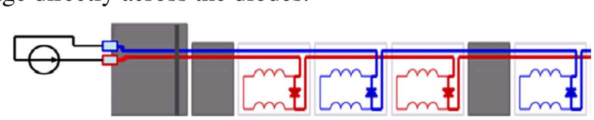

Figure 3: Depiction of the current flow during a typical CSCM test on a main dipole circuit. Note that all current flows through the bypass diodes instead of the magnets.

CSCM TYPE TEST IN LHC SECTOR 23

In April 2013, a CSCM type test was carried out [7]. Being prior to the splice consolidation campaign, thermal run-

* scott.rowan@cern.ch, s.rowan.1@researach.gla.ac.uk, with CERN, Switzerland, and The University of Glasgow, United Kingdom

Content from this work may be used under the terms of the CC BY 3.0 licence (© 2015). Any distribution of this work must maintain attribution to the author(s), title of the work, publisher, and DOI.

ISBN: 978-3-95450-168-7 doi:10.18429/JACoW-IPAC2015-WEPHA019

DEVELOPMENT AND PRODUCTION OF NON EVAPORABLE GETTER COATINGS FOR THE VACUUM CHAMBERS OF THE 3 GeV STORAGE RING OF MAX IV

P. Costa Pinto*, B. Bartova, B. Holliger, S.D. Marques dos Santos, V. Nistor, A. Sapountzis, M. Taborelli, I. Wevers, CERN, Geneva, Switzerland
J. Ahlbäck, E. Al Dmour, M. Grabski, C. Pasquino, MAX IV Laboratory, Lund University, Sweden

Abstract

MAX IV is presently under construction at Lund, Sweden, and the first beam for the production of synchrotron radiation is expected to circulate in 2016. The whole set of 3 GeV ring beam pipes is coated with Ti-Zr-V Non Evaporable Getter (NEG) thin film in order to fulfil the average pressure requirement of 1×10^{-9} mbar, despite the compact magnet layout and the large aspect ratio of the vacuum chambers. In this work, we present the optimizations of the coating process performed at CERN to coat different geometries and mechanical assembling used for the MAX IV vacuum chambers; the morphology of the thin films is analysed by Scanning Electron Microscopy; the composition and thickness is measured by Energy Dispersive X-ray analysis; the activation of the NEG thin film is monitored by X-ray Photoemission Spectroscopy; the vacuum performance of the coated beam pipes is evaluated by the measurement of hydrogen sticking coefficient. The results of the coating production characterization for the 84 units coated at CERN are presented.

INTRODUCTION

The 3 GeV storage ring of the MAX IV photon facility has a circumference of 528 m and includes 20 achromats with 19 straight sections devoted to insertion devices. The ring is characterized by ultra-low emittance obtained by applying a multi-bend achromat (MBA) magnet concept. Compact magnet design, (bore of 25 mm), and limited space between consecutive magnets poses drastic limitations on the vacuum system. To integrate the vacuum system with the magnets, the majority of the vacuum chambers were designed as 22 mm inner diameter, 1 mm thick copper tube. In order to ensure ultra-high vacuum conditions in the ring, the conductance limited chambers are coated with Non-Evaporable Getter (NEG) by DC magnetron sputtering [1]. To adapt the existing technology to coat the specific beam pipes of the 3 GeV ring, CERN and MAX IV Laboratory have set a collaboration. Currently, the majority of the chambers are manufactured and are being coated at three different facilities, including CERN where chambers with uncommon geometries are treated.

COATING PRODUCTION

All chambers were fabricated by FMB-Berlin. VC01, VC02A and VC02B are made of OFS copper while the VC02L is in 316LN stainless steel. The surface treatment was done at the fabricant following CERN standards [2], with the only exception of the copper tubes used in the construction of the VC01 type. For this case, the tubes were previously etched at CERN in a solution of ammonium persulphate in order to remove the outmost 80 µm of the surface (damaged skin) and passivated with a sulpho-chromic acid bath.

The VC01 is composed of three bent sections for a total deviation of 1.5°, a total length of 2.55 m and a circular aperture of 22 mm (Figure 1 a). In the bent sections, alumina spacers were used to ensure the centring of the cathode, which is made of 3 intertwisted elemental wires, each one of 1 mm diameter, of Ti, Zr and V). Each coating run lasted four days and two chambers were coated per run.

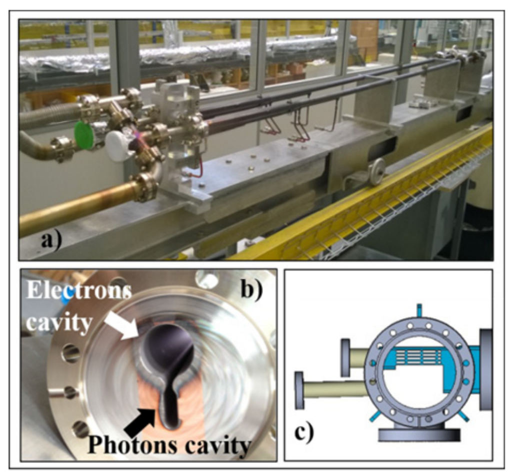

Figure 1: a) VC01 chambers on the coating support; b) photon and electron cavities for VC02B chamber (similar to VC02A); c) top view of the VC02L, with the inner grid.

The VC02A and VC02B are composed of two cavities, for the electron and extracted photon beams, respectively (Figure 1 b). They have a total length of 300 mm and 435 mm, respectively. The aperture of the electron cavity is the same for both, i.e. 22 mm, and the apertures of the photon cavities are tapered from 5 mm × 11 mm to 6 mm × 22 mm for VC02A and from 6 mm × 22 mm to 7 mm × 34 mm for VC02B. Electron cavities are coated using a cathode made of 1 mm elemental wires and presented no particular difficulty. Coating the photon cavities was the main challenge for this type of chambers. The cathodes were made from 3 intertwisted elemental wires with a

*Pedro.costa.pinto@cern.ch

Content from this work may be used under the terms of the CC BY 3.0 licence (© 2015). Any distribution of this work must maintain attribution to the author(s), title of the work, publisher, and DOI.

ISBN: 978-3-95450-168-7 doi:10.18429/JACoW-IPAC2015-WEPHA020

TITANIUM COATING OF CERAMICS FOR ACCELERATOR APPLICATIONS

Wilhelmus Vollenberg, Pedro Costa Pinto, Benjamin Holliger, Antonios Sapountzis, Mauro Taborelli, CERN, Geneva, Switzerland

Abstract

Titanium thin films can be deposited on ceramics, in particular alumina, without adherence problems. Even after air exposure their secondary electron yield is low compared to alumina and can be further reduced by conditioning or beam scrubbing. In addition, depending on the film thickness, titanium provides different surface resistances that fulfil requirements of ceramics in particle accelerators. Titanium thin films (MOhm range) are used to suppress electron multipacting and evacuate charges from ceramic surfaces. Thicker films (5-25 Ohm range) are applied to lower the surface resistance so that the beam impedance is reduced. In this contribution, we present the results of a development aimed at coating 2-meter long alumina vacuum chambers with a uniform surface resistivity by a dedicated DC magnetron sputtering configuration.

INTRODUCTION

Ceramic windows are frequently used for transmitting Radio-Frequency (RF) power, while maintaining the separation between vacuum and atmospheric pressure. However, the electrically insulating materials used for the ceramic windows have a high Secondary Electron Yield (SEY), far above the typical value for air exposed metal surfaces, and can lead to multipacting. Part of the power of the RF is dissipated in the multipacting electrons reducing efficiency. In addition the electrons impinging on the walls can generate local heating, which in turn can lead to cracking due to thermal stresses [1]. In general lowering the SEY can be achieved by appropriate thin film coatings [2, 3]. For instance Non-Evaporable Getters (NEG) are an ideal candidate in an Ultra High Vacuum (UHV) environment, provided a baked-out to at least at 180 ºC is possible (in addition, NEG thin films also pump most of the gas species present in UHV systems). On unbaked ceramics thin titanium films have proved their effectiveness also from the point of view of adhesion [4] and carbon coatings could be envisaged [3] as a solution in the future. In the case of RF windows the functional performance depends crucially on the correct electrical resistivity of the coating. Therefore in-situ resistance measurement during the thin film deposition process is systematically applied as a control method.

Ceramic vacuum chambers are also widely used for fast pulsed magnets, in order to avoid eddy current issues. Resistive titanium films are deposited inside these chambers to reduce the wall impedance perceived by the particle beam. In this case, as well, the surface resistance is measured during the coating process and after venting to air. Since the range of resistivity is tuned by the thickness in the following two examples we present the so called “ultrathin” and “thin” titanium films.

TITANIUM “ULTRATHIN” FILMS

RF ceramic Al_2O_3 windows are coated by DC sputtering in a dedicated coating set-up. Ceramics are degreased and vacuum fired (2 hours at 800 ºC under vacuum) prior to coating. A central titanium cathode is used in a cylindrical configuration to coat uniformly the inner surface of the ceramic window (Fig. 1). Prior to coating the system was pumped down to $3x10^{-7}$ mbar, without a bake-out. The coating takes 5 – 10 minutes at a plasma power of 50 W and Ar pressure of $4x10^{-2}$ mbar. The overall resistance (R_{total}) is measured in situ during the coating process between the top and bottom metallic collars of the ceramic assembly. Special attention should be given to enable an appropriate electrical contact between the collar and the titanium thin film during the process.

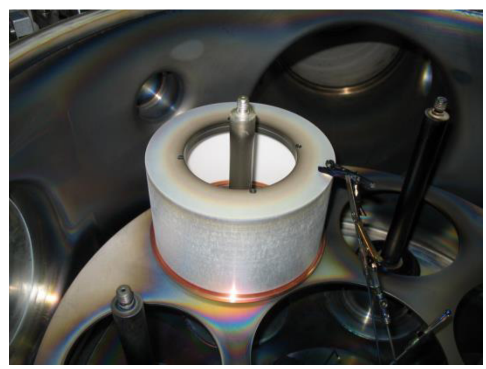

Figure 1: Cylindrical coating configuration for high resistivity coating of RF ceramic windows.

The square resistance (R□), which is a shape independent quantity characterising the coating, can be calculated from R_{total} and the given geometry of the ceramic assembly (by multiplying times the length and dividing by the width of the rectangular developed surface). RF windows are generally coated with R□ =10-20 MOhm, as measured in vacuum before venting. This is an empirically established value. By assuming the specific resistivity of bulk titanium this value would imply a thickness in the order of 10^{-4} nm, which is not physical. In reality the coating probably forms clusters leading to a percolation path for the transport. As a consequence of the air exposure after coating, the R□ increases to GOhm range values. Measurements on the resulting titanium coated Al_2O_3 samples show a SEY reduction from 7 (for uncoated alumina) to 2 [6]. These values refer to samples that were transported in air from the coating system to the SEY measurement system.

Content from this work may be used under the terms of the CC BY 3.0 licence (© 2015). Any distribution of this work must maintain attribution to the author(s), title of the work, publisher, and DOI.

ISBN: 978-3-95450-168-7 doi:10.18429/JACoW-IPAC2015-WEPHA021

STATUS OF HIE-ISOLDE SC LINAC UPGRADE

A. Sublet#, L. Alberty, K. Artoos, S. Calatroni, O. Capatina, M. A. Fraser, N. Jecklin, Y. Kadi, P. Maesen, G. Rosaz, K.-M. Schirm, M. Taborelli, M. Therasse, W. Venturini Delsolaro, P. Zhang, CERN, Geneva, Switzerland

Abstract

The HIE-ISOLDE upgrade project at CERN [1] aims at increasing the energy of radioactive beams from 3MeV/u up to 10 MeV/u with mass-to-charge ratio in the range 2.5-4.5. The objective is obtained by replacing part of the existing normal conducting Linac with superconducting Nb/Cu cavities. The new accelerator requires the production of 32 superconducting cavities in three phases: 10 high-beta cavities for phase 1 (2016), 10 high-beta cavities for phase 2 (2017) and possibly 12 low-beta cavities for phase 3 (2020). Half of the phase 1 production is completed with 5 quarter-wave superconducting cavities ready to be installed in the first cryomodule. The status of the cavity production and the RF performance are presented. The optimal Linac working configuration to minimize cryogenic load and maximize accelerating gradient is discussed.

INTRODUCTION

The superconducting post accelerator for the HIE-ISOLDE project [1] entered gradually the construction phase in 2013 after an R/D stage which had taken off in 2009 with the formal approval by CERN. The schedule of the project foresees to deliver beams up to 4.2 MeV/u for the heaviest species in autumn 2015 with a single high-beta cryomodule of 5 cavities. A second cryomodule will then be installed during 2016 bringing the beam energy up to 5.5 MeV/u for all the radionuclides available at ISOLDE. This will complete phase 1, making Coulomb excitation studies possible up to mass-to-charge ratio (A/q) = 4.5.

The cryomodules house five superconducting high-beta Quarter Wave Resonators (QWR) based on Nb/Cu technology [2-4], and a superconducting solenoid for beam focusing.

The QWR are installed in a common vacuum cryostat, i.e. the beam vacuum and the thermal insulation vacuum are connected. They are designed to work at 4.5 K at the resonant frequency of 101.28 MHz, and with a maximum power dissipation of 10 W at 6 MV/m.

This article presents the performance of the cavities and their assembly in first cryomodule.

COATING, TUNING AND TESTING

Production Scheme and Coating

The first cryomodule cavities production started end of 2013 and finished end of 2014: 5 cavities and a spare unit have been coated. The prototype and series QWR nomenclature chosen is QPX.Y and QSX.Y respectively, with X the cavity serial number and Y the Nb coating process number [5]. The copper substrates were manufactured at CERN for the two first prototypes (QP2 and QP3), the substrates for the series were manufactured by industry (QS1, QS2, QS3 and QS4) [6].

The coating process is based on DC-bias diode sputtering, the hardware setup (UHV chamber, Nb cathode, DC power supplies, etc.) and the process have been kept identical (production steps, coating recipe, etc.) for all the cavities produced as described in details in [7], except for QP2 substrate, which has seen an additional annealing prior to coating. Over the one year production period, a total of 7 coatings have been made on these 6 substrates: one cavity has been coated twice due to bad initial RF performances (QP3.2), one has been rejected due to bad initial RF performances (QS2.1) and has been stripped and re-coated (QS2.2) in February 2015. It will be used in the second cryomodule. Typically a period of about two months is necessary [8] from the copper substrate reception at CERN in order to obtain a coated cavity and verify its RF performance.

Cavity Tuning

To match the Linac frequency of 101.28 MHz at 4.5 K under vacuum the QWR must be tuned. This process is done in two distinct steps [9, 10] that take into account and compensate:

1. the frequency shifts (about 400 kHz) induced by: the manufacturing deviations, the chemical polishing, the Nb coating, the thermal contraction at the operation temperature
2. the cumulated frequency uncertainties (~10 kHz).

The first step addresses the frequency shifts, it consists of a pre-tuning of the cavity after reception at room temperature and before coating by trimming it to a determined “tip-gap” length [9, 10]. This length is calculated depending on the foreseen duration and number of chemical polishing (SUBU) [11] to which the substrate will be submitted. The chemical polishing is used to eliminate surface defects (inclusions, spatter, etc.) from the as received substrate. The cavity frequency shift has a linear dependence to the SUBU duration and typically a 26.5 +/- 3 kHz frequency shift was observed after the initial 40 minutes SUBU. The SUBU process might reveal additional defects that must be either mechanically or chemically polished again, thus introducing a further frequency shift. The stripping of one cavity and the new coating process (including SUBU) will also induce a frequency shift.

The second step addresses the frequency uncertainties within an active tuning range of about 40 kHz at 4.5 K.

#alban.sublet@cern.ch

Content from this work may be used under the terms of the CC BY 3.0 licence (© 2015). Any distribution of this work must maintain attribution to the author(s), title of the work, publisher, and DOI.

ISBN: 978-3-95450-168-7 doi:10.18429/JACoW-IPAC2015-WEPHA022

CHARACTERIZATION OF NB COATING IN HIE-ISOLDE QWR SUPERCONDUCTING ACCELERATING CAVITIES BY MEANS OF SEM-FIB AND TEM

B. Bártová#, S. Calatroni, A. Sublet, M. Taborelli, CERN, Geneva, Switzerland
A.B. Aebersold, D.T.L. Alexander, M. Cantoni, EPFL, Lausanne, Switzerland

Abstract

The Quarter Wave Resonators (QWR) high-β cavities (0.3 m diameter and 0.9 m height) are made from OFE 3D-forged copper and are coated by DC-bias diode sputtering with a thin superconducting layer of niobium. The Nb film thickness, morphology, purity and quality are critical parameters for RF performances of the cavity. They have been investigated in a detailed material study.

INTRODUCTION

In the frame of the High Intensity and Energy (HIE) ISOLDE project [1], the niobium coating of high beta superconducting quarter-wave resonators (QWRs) has entered series production. The first cryomodule is upon to be finalized [2], however development activities continue to improve the understanding and optimization of the sputtering setup and process. One major focus is the thin film characterization and its relation with the functionality of the layer. This paper presents the results of the microscopic approach to characterize the Nb layer of the cavity coating baseline process.

EXPERIMENT

A dummy copper cavity (Q4) [3] has been designed as a sample holder to characterize the niobium layer. Samples supports are 35 mm long, 10 mm wide and 1 mm thick copper plates. Samples are identified by their position in internal (i) or external (e) conductor and their distance from the bottom to the top of the cavity. Top band (TB) sample placed over the weld on the top of the cavity was observed as well.

The applied DC-bias sputtering baseline parameters are: 0.2 mbar Ar pressure, 8 kW powered Nb cathode, -80 V biased cavity, and a substrate temperature rising from 300°C up to 630°C (below the bake out temperature of 650°C) on the inner conductor during a coating step. The whole coating process lasts 4 days and is done in 14 steps of 25’ coating + 5h35’ cool down to 300°C each, leading to a net coating time of 6h.

The film morphology, its thickness and quality from the selected places along the cavity’s inner and outer conductors were studied by dual beam high-resolution field emission Scanning Electron Microscope (SEM) with Focused Ion Beam (FIB).

Transmission Electron Microscopy (TEM) observation were performed together with Energy Dispersive Spectroscopy (EDS) measurements and orientation and phase mapping with a spatial resolution of 2-3 nm. TEM lamella sample from top part of the cavity was prepared to study chemical composition, structure and grain orientation of coating grains.

X-ray florescence measurements (XRF) were performed to cross check the coating thickness.

CROSS-SECTION IMAGING

A standard sample preparation of the cross-section consists of 4 steps on a selected area of interest [4, 5]: (i) a deposition of protective layer (in our case carbon of 1.5 µm thickness) onto the sample surface in order to protect it from the ion beam damage during further milling, (ii) the removal of the material by sputtering using the staircase-like pattern with high Ga^+ beam current to form the large trench, (iii) reduction of the beam current and milling to reduce redeposition of sputtered material onto the sample surface, (iv) imaging of the final surface using either secondary or back-scattered electrons or secondary ions depending on the goal of the study. All SEM images presented in this paper were acquired using in-column secondary electron detector and low accelerating voltage in order to visualize grain structure at different places in the cavity and possible presence of porosity.

The niobium layer thickness, its structure and the presence of porosity

The coating thickness was measured by two techniques – XRF and from the cross-section images after the FIB preparation. It is evident from Table 1 that the inner conductor coatings i4 and i7 are much thicker comparing with the same positions on external conductor e2 and e7. The measurements by FIB shows higher values than by XRF.

Table 1: Comparison of Coating Thicknesses Characterized by FIB and XRF Techniques

Thickness [µm]	FIB	XRF
i4	7.25	6.68
i7	5.74	5.41
i9	2.66	2.21
e2	1.79	1.64
e7	2.27	2.07
e9	2.53	2.16
TBi	2.78	2.50

#barbora.m.bartova@gmail.com

Content from this work may be used under the terms of the CC BY 3.0 licence (© 2015). Any distribution of this work must maintain attribution to the author(s), title of the work, publisher, and DOI.

ISBN: 978-3-95450-168-7 doi:10.18429/JACoW-IPAC2015-WEPHA023

FERRITE-TUNER DEVELOPMENT FOR 80 MHz SINGLE-CELL RF-CAVITY USING ORTHOGONALLY BIASED GARNETS

C. Vollinger, F. Caspers, CERN, Geneva, Switzerland

Abstract

In the frame of the LHC Injector Upgrade program involving the existing 80 MHz cavities in the CERN PS accelerator, an orthogonally biased ferrite tuner is foreseen to complement the current motor-driven piston tuner. This ferrite tuner shall provide the possibility of a fast frequency shift of about 200 kHz on the fundamental mode, to allow a fast switching between proton and ion frequencies. In order to avoid water cooling and related issues, the challenge was to bring magnetic losses in the tuner to a minimum such that a forced air cooling scheme will be sufficient. The tuner was first designed with simulation tools, a prototype was built and low-power RF testing was performed on the tuner-cavity combination to evaluate tuning range, bandwidth, and stability. These tests were carried out on a single-cell copper RF cavity mock-up with a resonance frequency of 88 MHz, where the ferrite tuner is connected via a tuning loop and the perpendicular magnetic bias for the ferrite tuner is provided by a DC bias supply. Simulations and test data will be presented.

INTRODUCTION

For the acceleration of protons and ions, the CERN PS accelerator makes use of three single-cell RF-cavities with a resonance frequency of 80 MHz [1]. These existing cavities are currently equipped with piston tuners for frequency shifts to allow the acceleration of protons and ions. We developed a ferrite tuner with the intention to complement the motor-driven piston tuner and to provide a fast frequency shift of about 200 kHz on the fundamental mode. Consequently, we aimed for a design that provides a maximum frequency range that should be reached with a minimum change of biasing field while keeping the ferrite material sufficiently magnetized such that the material stays entirely in the low loss state during operation.

TUNER DESIGN

The tuner consists of a coaxial structure terminated with a shortened plug. The space between inner and outer conductor is partly filled with the low-loss tuneable ferrite garnet G-510 [2] and the tuner is inserted into a toroidal coil set-up that provides orthogonally magnetic biasing fields, i.e. the bias field is oriented perpendicular to the magnetic RF-field. The actual tuning is achieved by making use of the fact that the relative permeability of ferrites can be changed if a magnetic bias field (static or slowly varying) is applied to the material. In a first step, a design was carried out by means of simulations in HFSS. Figure 1 (left) shows a sketch of the ferrite-filled tuner with the biasing coils connected in series, and the HFSS model including the coupling loop that indicates the connecting plane to the cavity (right). It should be noted that the simulations have been carried out on the geometry of the 80 MHz cavity, for which also the final tuner design is intended.

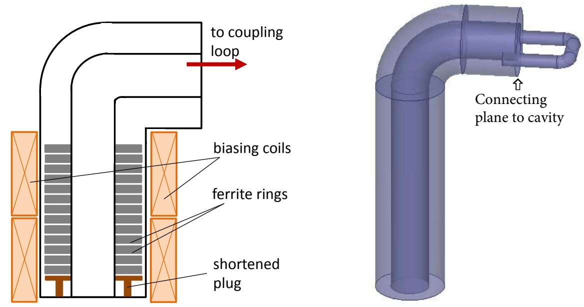

Figure 1: Left: Sketch of coaxial ferrite-filled tuner with bias coils; Right: HFSS model of tuner with coupling loop.

Due to availability, however, measurements were carried out on an 88 MHz mock-up cavity structure. Figure 2 shows a picture of the set-up with which a tuning range of ± 100 kHz around the resonant frequency f_{res} is pursued.

Figure 2: Picture of the mock-up 88 MHz cavity used for testing of the tuning-concept with the fast ferrite tuner.

The tuner design was constrained by a fixed ferrite ring size in order to make use of rings being available from a former application, and one of the existing access ports to the cavity had to be used due to local space restrictions. As a consequence, the tuner's coupling strength is limited due to its location, however, as we could show from our

Content from this work may be used under the terms of the CC BY 3.0 licence (© 2015). Any distribution of this work must maintain attribution to the author(s), title of the work, publisher, and DOI.

ISBN: 978-3-95450-168-7 doi:10.18429/JACoW-IPAC2015-WEPHA024

PRELIMINARY DESIGN OF A PERPENDICULAR BIASED FERRITE LOADED ACCELERATING CAVITY

J. Eberhardt, CERN, Geneva, Switzerland; TU Darmstadt, Darmstadt, Germany
F. Caspers, C. Vollinger, CERN, Geneva, Switzerland

Abstract

A ferrite loaded accelerating cavity with a frequency sweep of 18 to 40 MHz is studied for a possible upgrade of the CERN accelerator complex. The resonance frequency of a ferrite loaded cavity shifts by applying an external magnetic bias field to the ferrite material by means of changing the relative permeability. We present the electromagnetic design of such a cavity with a special emphasis on the modeling of the nonlinear, anisotropic and dispersive characteristics of the ferrite's relative permeability above magnetic saturation. For experimental crosscheck, a ferrite loaded resonant test setup was built which provides results for the material performance in a magnetic bias field. A comparison of numerical simulations and experimental measurements is shown and calculations are benchmarked by measurement data. Based on this study a preliminary design of a ferrite loaded accelerating cavity is described.

INTRODUCTION

The characteristics of ferrite loaded accelerating cavities are dominated by the properties of the ferrite material. During the development process it is essential to know the electromagnetic properties of the filling material. A measurement setup is described to investigate a possible resonance frequency swift, to measure the quality factor and to characterize the relative permeability of the ferrite material exposed to a perpendicular magnetic bias field. Moreover we model the measurement setup in an electromagnetic field simulation program and compare the results with the measurements. Based on this, we investigate an electromagnetic design of an accelerating cavity with a frequency sweep of 18 to 40 MHz.

FERRITE LOADED TEST SETUP

For the accelerating cavity, toroidal cores of the ferrite G-510 of 350 mm OD and 200 mm ID consisting of five segments were the largest size currently available by Trans-Tech Inc. [1]. The five segments were glued on top of an 3.3 mm thick *Al 995* toroidal carrier disc with the two component epoxy glue *Stycast 2850 FT*. *Al 995* provides high thermal conductivity of 29.3 W/m.K, a small dielectric loss factor of $\tan\delta_e = 2.9 \cdot 10^{-4}$ at 10 MHz and tight fabrication tolerances. Up to now, the large rings were only investigated in two resonant test setups with different purposes [2]. First, it was shown that doubling the resonance frequency of a measurement cavity is possible by changing a perpendicular magnetic bias field. But the frequency range achieved was well above the desired 18 to 40 MHz and a radiating open gap degraded the measured Q. Second, it was pointed out with another ferrite loaded resonant cavity that high quality factors of up to 5000 can be obtained, but the ferrite shift was limited due to a ferrite filling factor of ca. 25%. A dedicated test setup was developed to investigate the ferrite rings with two different measurement methods. A resonant measurement method is used to investigate the resonance frequency sweep dependent on the magnetic bias field and to measure the corresponding quality factor within the frequency range of interest. With the second method, a 1-port reflection measurement, we measured the complex permeability spectra, similar to the measurement setup presented in [3].

Resonant Measurement

The measurement cavity consists of a main cell, a top cover and a piston all made out of aluminum, see Fig. 1. A capacitive load of up to 1900 pF can be achieved by placing a 0.1 mm Teflon foil between top cover and the piston which reduces the resonance frequency of the empty cavity to 44.7 MHz.

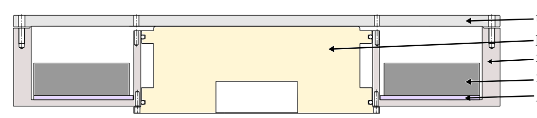

Figure 1: Resonant measurement setup.

The measurement setup is placed within the aperture of an H-dipole to apply a magnetic bias field which is perpendicular to the RF magnetic field. We could not detect resonances for magnetic bias fields below 35 mT, since in that range the losses of the ferrite material are rather high. With increasing magnetic bias field from 35 to 300 mT the resonance frequency shifts from 18.8 to 43.7 MHz due to the decreasing relative permeability of the ferrite, which is shown in Fig. 2.

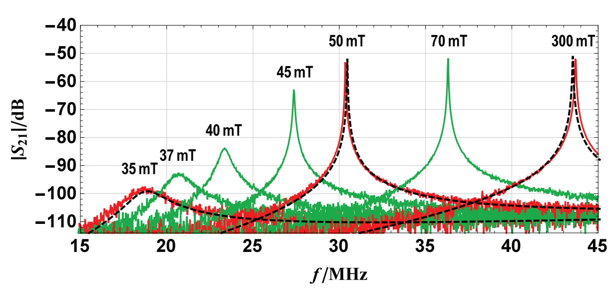

Figure 2: Measurement results (solid traces) of resonant ferrite filled setup in comparison with driven modal simulation results (dashed traces).

The unloaded quality factor can be measured via the 3 dB bandwidth of the transmission signal as a weakly coupling

Content from this work may be used under the terms of the CC BY 3.0 licence (© 2015). Any distribution of this work must maintain attribution to the author(s), title of the work, publisher, and DOI.

ISBN: 978-3-95450-168-7 doi:10.18429/JACoW-IPAC2015-WEPHA025

DESIGN OF A VARIABLE X-BAND RF POWER SPLITTER

Hao Zha, Igor Syratchev, Dmitry Gudkov, Alexej Grudiev, CERN, Geneva, Switzerland

Abstract

The design of the variable high RF power X-Band splitter is presented. The RF power division ratio is adjusted by mechanically changing the position of a special RF short circuit piston. The piston is mounted on a step-motor providing the precise linear movement. Throughout the design, special measures were taken to reduce the maximum electric field on the copper surface, as well as to maximise the frequency bandwidth of the device.

INTRODUCTION

High RF power X-band test stands for testing the normal conducting CLIC accelerating structures are now in operation at CERN. In general, these tests require a precise adjustment of the driving RF power level [1]. The RF splitter with arbitrary division ratio will be used to meet this need without changing the RF power provided by RF source itself. The RF splitter is a three port device, where one output port is connected to the DUT (Device Under Test) itself and the other is connected to the matched RF load, which absorbs the excessive RF power. The division of RF power between the two is adjusted by mechanically changing the position of a special RF short circuit piston (see Fig. 5 in [2]). The piston is an RF contact free device and is mounted to a step-motor providing the precise movement. Thus a continuous adjustment of the RF power is achieved.

PRINCIPLE OF OPERATION

The schematic of the splitter RF circuit is shown in Fig. 1. For the known parameters s_{ij} in the scattering matrix (1), the output power in each port y_n can be calculated using equation (2). Parameter ρ in equations (1 and 2) is the reflection from the RF short circuit piston.

The output power in the ports y_1, y_2 and y_3 depends on the RF phase of the reflection ρ. By controlling the position of the RF short circuit piston, this phase can be changed, thus the output power at ports 2 and 3 can be adjusted. In order to minimize the overall reflection, the RF splitter should be matched, thus y_1 should be equal to zero. Consequently s_{11} and s_{14} should be equal to zero as well, but not s_{41}, otherwise y_2 and y_3 will be de-coupled. This condition ($s_{14} \neq s_{41}$) breaks the symmetry of the RF circuit and makes matching of the device impossible.

$$\begin{pmatrix} y_1 \\ y_2 \\ y_3 \\ y_4 \end{pmatrix} = \begin{pmatrix} s_{11} & s_{12} & s_{13} & s_{14} \\ s_{21} & s_{22} & s_{23} & s_{24} \\ s_{31} & s_{32} & s_{33} & s_{34} \\ s_{41} & s_{42} & s_{43} & s_{44} \end{pmatrix} \begin{pmatrix} 1 \\ 0 \\ 0 \\ \rho y_4 \end{pmatrix} \quad (1)$$

$$\begin{pmatrix} y_1 \\ y_2 \\ y_3 \end{pmatrix} = \begin{pmatrix} s_{11} \\ s_{21} \\ s_{31} \end{pmatrix} + \begin{pmatrix} s_{14} \\ s_{24} \\ s_{34} \end{pmatrix} \frac{\rho s_{41}}{1-\rho s_{44}} \quad (2)$$

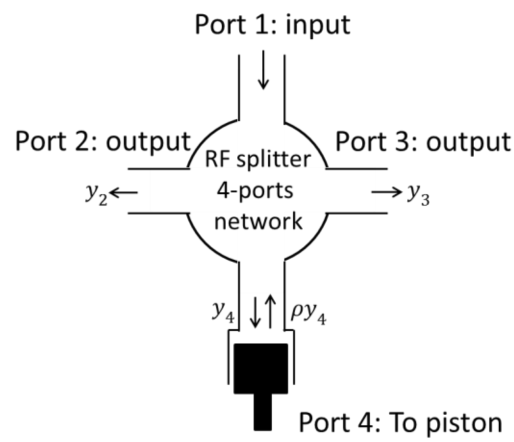

Figure 1: The 4 port network proposal for RF splitter.

The way to approach matching is to have a 5-port network where two ports are connected to the piston. It can be proven that a solution for the symmetric network exists in this case. A schematic of such a 5-port network is shown in Fig. 2. It uses 3 symmetric RF splitters to split the input port to 4 output branches. Each of the symmetric RF splitters is designed in a way that every port sees the combined impedance of the two others. The distance between the first and second symmetric RF splitter is a quarter-wavelength. According to transmission line theory, the total impedance seen by the input port is $\frac{1}{Z_2+Z_4} + \frac{1}{Z_3+Z_5}$, where Z_i is the impedance of each port by itself. As shown in Fig. 2, port 2 and 3 are output ports, thus $Z_2 = Z_3 = 1$. The RF short circuit pistons bring reactance, so that the values of Z_5 and Z_4 are purely imaginary. The input port will be matched if $Z_5 * Z_4 = 1$. That can be achieved by having 180 phase difference in reflection between the two short circuit pistons. The power division ratio is now determined only by the reflection phase of the pistons and can be varied from 0 to 1. This network design is very compact and has a broad frequency bandwidth. However, two synchronised short circuit pistons are needed, thus a certain complication of the mechanical design is unavoidable.

Content from this work may be used under the terms of the CC BY 3.0 licence (© 2015). Any distribution of this work must maintain attribution to the author(s), title of the work, publisher, and DOI.

ISBN: 978-3-95450-168-7 doi:10.18429/JACoW-IPAC2015-WEPHA027

SOLID STATE AMPLIFIER DEVELOPMENT FOR THE SWISS LIGHT SOURCE*

M. Gaspar†, T. Garvey, Paul Scherrer Institut, Villigen, Switzerland

Abstract

The Paul Scherrer Institute (PSI) currently operates a klystron amplifier on the booster ring of the Swiss Light Source (SLS). In order to have an optional RF source for the booster cavity, we have been developing a compact 500 MHz 65kW solid state RF amplifier. An important goal in this development is the optimization of efficiency at any given operating point. In order to achieve this, each RF module has been equipped with its own DC power supply (PS Controller), providing sufficient intelligence to adjust the drain and bias voltages in a fully independent and automatic way. With this technique it is possible to maximize the overall efficiency at any given RF output power. Considerable effort has been made in order to obtain extensive measurements from each individual module with the aim of investigating the behaviour of such a large number of combined arrays. We will discuss the amplifier design and present the results of measurements.

THE CONSTRUCTED 65 kW POWER AMPLIFIER SYSTEM

INTRODUCTION

Since the introduction of solid-state amplifiers on the synchrotron light source SOLEIL there has been considerable interest in use of such devices at other light source laboratories [1]. A modest R&D effort was started at the Paul Scherrer Institute (PSI) in order to develop this technology at 500 MHz resulting in a 4.5 kW prototype [2,3]. More recently, supported by the Swiss Commission of Technology and Innovation, we have developed a 65 kW amplifier described in this paper. This technology has been transferred to AMPEGON AG, our industrial partner for this project, for industrialization and commercialisation.

DESIGN DESCRIPTION

A large variety of tests were performed to evaluate the 65 kW amplifier system described here. Long duration tests were done with the amplifier delivering output powers of, 60 kW, 64 kW, and 68 kW. The system performed in an extremely stable fashion under all conditions.

Figure 1 shows a block diagram of the system. In this configuration all the 108 output amplifier stages, those that contribute to the system output power, are placed in parallel and are all combined by a large high power combining structure [4].

Figure 2 shows the conceptual design of the proposed system. In the middle, one sees the high power combiner tree, a fundamental component of existing high power distributed amplifiers based on solid-state technology. The RF amplifier modules and the PS Controllers are mounted around the combiner tree on 2 meter tall aluminium bars which are water cooled.

Figure 3 shows the constructed high power solid-state amplifier system. The amplifier itself is placed to the right. It is composed of six 2 m long cooling bars. Each cooling bar supports 18 RF amplifier modules on one side and 18 PS Controllers on the other side.

The RF output of the amplifier system is connected to a 100 kW water cooled load through a 3 m long high power EIA $6\frac{1}{8}$ coaxial transmission line, seen at the top. The water cooled load is placed at the left of the amplifier, and behind the rack.

The 19" rack to the left houses part of the components required to connect the amplifier to the mains, other components for monitoring and communication purposes and the pre-amplifiers with their power supplies. The amplifier system is connected to the rack at the top through a cable support.

The complete amplifier system weighs approximately 900 kg.

MEASUREMENT RESULTS

Figure 4 shows a typical output power scan, P_{out} and Efficiency vs. P_{in}. A complete power scan such as shown in Fig. 4 may take a full day to be done because of the time required for the measurements of the calibrated water cooled load to stabilize.

Figure 5 shows a frequency scan, P_{out} and Efficiency vs. P_{in} realized with a fixed power supply value, V_{dd} = 48 V, and for two different output power levels, P_{out} = 20 kW, a low efficiency operation, and P_{out} = 50 kW, a high efficiency operation. Assuming a good trade-off between gain and efficiency, a bandwidth better than 20 MHz at P_{out} = 50 kW is available with an efficiency better than 45%. At lower output power, as P_{out} =20 kW, the efficiency reduction is not an issue any more, thus much wider bandwidths are available.

The graph of Fig. 6 shows the quite high quality of the output frequency spectrum. This illustrates the noise near the carrier. Measurements over a wider span show that the second harmonic is present at -45 dBc and the third harmonic is absent, probably due to the limitations of the transistor to generate it.

The amplifier system was operated at full reflection, with a short circuit applied at the output, for about 15 minutes at

* We acknowledge the financial support of the Swiss Commission for Technology and Innovation under grant number 13192.1 PFFLM-IW.
† marcos.gaspar@psi.ch

Content from this work may be used under the terms of the CC BY 3.0 licence (© 2015). Any distribution of this work must maintain attribution to the author(s), title of the work, publisher, and DOI.

ISBN: 978-3-95450-168-7 doi:10.18429/JACoW-IPAC2015-WEPHA028

POWER SAVING STATUS AT NSRRC

J.C. Chang, W.S. Chan, T.S Ueng, Z.D. Tsai, Y.C. Lin, C.Y. Liu, Y.C. Chung, Y.F. Chiu, C.W. Hsu, Y.C. Chang, and K.C. Kuo
National Synchrotron Radiation Research Center (NSRRC), Hsinchu 30076, Taiwan

Abstract

National Synchrotron Radiation Research Center (NSRRC), Taiwan has completed the construction of the civil and utility system engineering of the Taiwan Photon Source (TPS) in 2014. On the last day of 2014, the Taiwan Photon Source (TPS) has delivered its first synchrotron light with 1mA stored beam current. The machine is in commission currently. The power consumption of TPS was about 5MW then. The ultimate power consumption of the TPS is estimated about 12.5MW. To cope with increasing power requirement in the near future, we have been conducting several power saving schemes, which include adjustment of supply air temperature according to the atmosphere enthalpy, replacement of old air conditioning unit (AHU), power consumption control by the operation of chillers, power factor improvement, and reduction of power consumption during long shutdown.

INTRODUCTION

NSRRC has been conducted several major projects, such as installation of superconducting rf cavities and magnets, construction of extension buildings in the Taiwan Light Source (TLS) for years. Besides, the TPS project has been in commission process. Those projects have been greatly increased the electrical power consumption. Currently, the contract power capacities of the Taiwan Light Source (TLS) and the TPS with the Taiwan Power Company (TPC) are 5.5MW and 7.5MW, respectively.

As the price of petroleum increased, the power bill had also been raised three times since 2008. The power bill of per kW-hr was increased about 35%, 40%, and 10% in 2008, June 2012, and Oct. 2013, respectively. Fig. 1 shows monthly average power bill per kW-hr of TLS from 2011 to 2015.

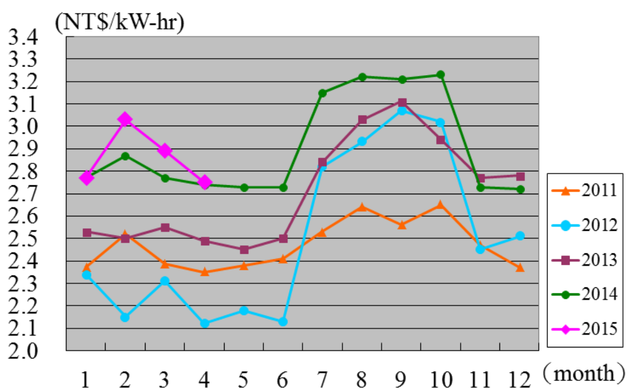

Figure 1: Monthly average power bill per kW-hr in NSRRC from 2011 to 2015.

To cope with fast growth of the power consumption and power bill, NSRRC has been conducting a series of power saving schemes since 2006 [1]. Those power saving schemes include optimization of chiller operation, power consumption control, improvement of temperature and humidity control, electrical power factor improvement, lighting system improvement, and application of heat pumps. We keep conducting those schemes and create some new ones, including modified run-around coil AHU, change of power bill calculation mode, and promotion of power saving. Some major schemes are described as follows.

CHILLED WATER PIPES CONNECTION BETWEEN TPS AND TLS

There are three utility buildings in NSRRC. The Utility Building I was constructed for the TLS 23 years ago. There are three chillers, each with 320 RT in capacity installed inside. Utility Building II was construction for the cryogenics and superconductivity systems 13 years ago. There are two 600 RT chillers and two 450 RT chillers installed inside. We had ever connected chilled water pipes between Utility Buildings I and II. It saved about 70 kW.

The civil construction Utility Building III for the TPS had been completed in Dec. 2012. Three chillers, each with 1,400 RT in capacity, had been installed inside. We had connected supplied and return chilled water pipes, each with 10 inch in diameter, between the second and the third Utility Buildings in 2013.

Figure 2 shows the chilled water piping system in the Utility Building II. The blue lines are the pipes connected between Utility Building I and II. The green lines are the pipes connected between Utility Building II and III.

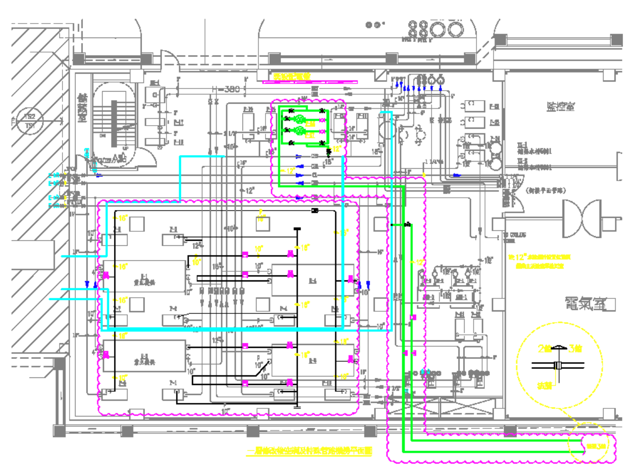

Figure 2: Chilled water piping in the Utility Building II.

Content from this work may be used under the terms of the CC BY 3.0 licence (© 2015). Any distribution of this work must maintain attribution to the author(s), title of the work, publisher, and DOI.

ISBN: 978-3-95450-168-7 doi:10.18429/JACoW-IPAC2015-WEPHA029

OPERATION OF BOTH UTILITY SYSTEMS OF TPS AND TLS AT NSRRC

J.C. Chang, T.S. Ueng, Z.D. Tsai, Y.C. Lin, W.S. Chan, C.Y. Liu, Y.C. Chung, Y.F. Chiu, C.S. Chen, Y.C. Chang, K.C. Kuo, Y.H. Liu
National Synchrotron Radiation Research Center (NSRRC), Hsinchu 30076, Taiwan

Abstract

The construction of the utility system for the 3.0 GeV Taiwan Photon Source (TPS) was started in the end of 2009. The utility building for the TPS ring had been completed in the end of 2014. The final acceptance test and improvement had also been completed in the end of 2014. The TPS is in commission and TLS is still in operation. Within limited manpower and budget, it is challenge to operate both utility systems stable and reliable. We provide good quality of electrical power, cooling water and precision air temperature. Power saving is also an important issue. The utility system presented in this paper includes the electrical power, cooling water, air conditioning, compressed air, and firefighting systems.

INTRODUCTION

Utility system is the infrastructure of a facility. It is also one of critical subsystem of an accelerator. Therefore, a good utility system can provide not only stable and precision electrical power, cooling water and air temperature for the beam operation, but also a safety, comfortable and working environment for all personnel. Besides, power saving becomes another important issue for the environment. There are more requirements for the utility system than ever.

After 22-year operation of TLS, TPS has been constructed and in the phase of commissioning. Based on the operation experience of TLS utility system and utility system design of other advanced accelerators, the utility system of TPS had been designed and constructed [1].

Considering the efficiency of operating TLS and the TPS, the TPS is constructed adjacent to TLS on the NSRRC campus. Some areas of TPS and TLS are even overlapped. Figure 1 shows the bird view of TPS, TLS and three Utility Buildings. The existing Research building is enclosed by the TPS storage ring building.

There are three utility buildings providing utility system for TLS and TPS. Utility Building I was constructed with TLS storage ring building in 1992. Utility Building II was constructed for the Cryogenics and superconducting systems in 2002. Main utility equipment of the TLS is installed in Utility Buildings I and II. Utility building III, especially for the TPS, is designed near the existing two utility buildings, as shown in Fig. 1.

There are two utility trenches from the Utility Building I and the Utility Building II respectively connecting to the TLS ring for the piping system and electrical power transmission. Likewise, there is a trench connecting the Utility Building III and TPS.

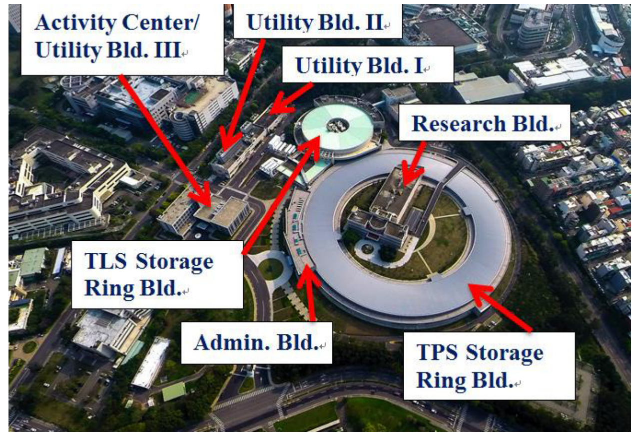

Figure 1: Bird view of TPS, TLS and three Utility Buildings.

MAN POWER OF UTILITY SYSTEM

When the TLS was constructed, there was an Engineering Division in charge of the civil and utility system construction and maintenance. Most members of the engineering division were engineers and technicians. As accelerator technique developed, the requirements of precision and stability of utility system were much higher than ever. The Engineering Division was reorganized under the Instrumentation Development Division as the Utility Group and recruited scientist members in 1996.

We had made many efforts on studying utility effects on beam quality and upgrading utility system since 1998. [2] Our monitoring and control system was first set up in 1999. The first SCADA (supervisory control and data acquisition) of electrical power system was built in 2003.

For the civil construction of TPS, there was a civil management group formed in 2006. As the civil construction was completed, the utility and civil management groups were merged as the utility and civil group in 2015. The man power of each subsystem is listed in Table 1.

Table 1: Man Power of Utility and Civil Group

Subsystem	Scientist	Engineer	Technician
Electrical Power		2	1
Water	1	1	1
Air Conditioning		2	1
Grounding/ EMI	1	1	
Civil		1	1
Others	1	1	
Total	3	8	4

Content from this work may be used under the terms of the CC BY 3.0 licence (© 2015). Any distribution of this work must maintain attribution to the author(s), title of the work, publisher, and DOI.

ISBN: 978-3-95450-168-7 doi:10.18429/JACoW-IPAC2015-WEPHA030

EMI MEASUREMENT FOR TPS BOOSTER KICKER AND SEPTUM SYSTEMS*

Yung-Hui Liu#, Chin-Shen Chen, June-Rong Chen, Wen-Shuo Chan,
NSRRC, 101Hsin-Ann Road, Hsinchu Science Park, 30076, Taiwan

Abstract

The purpose of this paper is to estimate the conducted and radiated Electromagnetic Interference (EMI) for subsystems in the TPS booster ring. A LISN (Line Impedance Stabilizing Network) system with a wide frequency range was conducted to measure the EMI spectrum of pulsed magnet system. The radiated EMI was tested by magnetic field probe, which the measurement frequency range is 100 kHz ~ 3 GHz. A stray current was tested by wide frequency current transformer in order to measure the conducted current for kicker and septum systems. According to the experiment results, the stray current could flow through the other subsystems or booster chamber, and it might be affected the stability of booster operation. Therefore reducing and eliminating the interference of EM waves will be a very important issue. The EMI prevention scheme will be continued.

INTRODUCTION

According to the experience of synchrotron operation, Electromagnetic Compatibility (EMC) is one affected factor for beam stability [1]. Electromagnetic Interference (EMI) also be an issue of TLS because of the limited space and top-up mode operation [2]. For TPS project, top-up mode injection will also be the basic operation mode in the future. Therefore, injection magnets will produce conducted and radiated EMI similar to TLS existing condition [3]. In order to eliminating and reducing interference between injection sections, a good EMI design should be implement in the beginning. Firstly, a good impedance match between pulsed power supply and magnet (load) should be notice carefully. Reducing EMI level by using appropriate EMI filters from power source could also reduce conducted EMI [4]. Secondly, the grounding scheme will design based on the TLS experience. Every kicker will have exclusive grounding bus directly connect to grounding networks. The spray current will also collect by several routs in order to increasing efficiency. Finally, the EMI enclosure is proved effective and will implement to kicker magnet and its pulser. All three steps are the total solutions to reduce conducted and radiated EMI of TPS pulsed magnets.

TPS PULSED MAGNETS LOCATIONS

The pulsed magnets in TPS are divided into 3 parts, shown as Fig. 1. The first part is booster injection section; there are one booster injection septum and one kicker included. The booster injection magnets guide the electron beam from LINAC to booster ring. After increasing the electron beam energy from 150 MeV to 3.0 GeV, the electron beam extract to the second part - booster extraction section. There are 2 booster extraction kickers and two septa in booster extraction section. Passing by the BTS (booster to storage ring) section, the electron beam is inject to the storage ring by 4 kickers and two septa (2 AC septum).

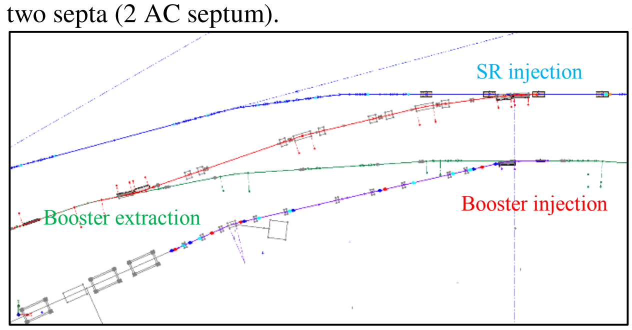

Figure 1: TPS pulsed magnets position.

GROUNDING SCHEME

According to TLS experience, the grounding scheme of TPS injection section as shown in Fig. 2. Every pulsed magnet will have exclusive grounding bus directly connect to TPS grounding networks. Because of the pulser and pulsed magnet are placed in different location, the grounding routes are connected separately for conduct stray current independently. Thus, paths of spray currents have no interchange between other subsystems.

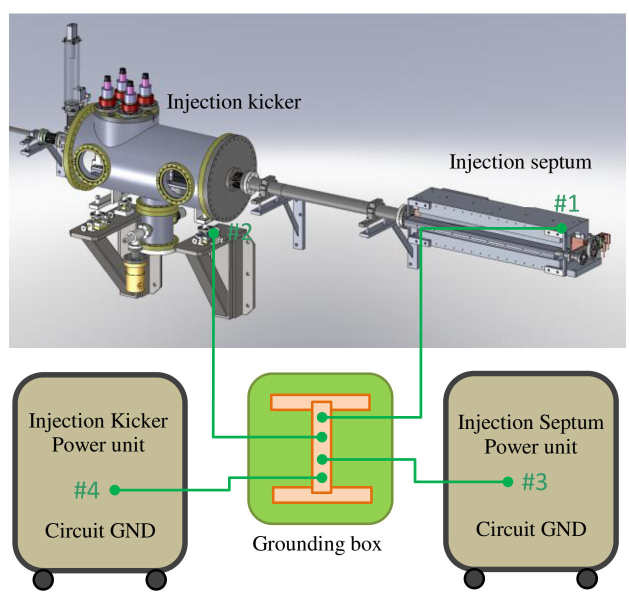

Figure 2: TPS injection pulsed magnets grounding scheme.

*Work supported by National Synchrotron Radiation Research Center
iris@nerrc.org.tw

Content from this work may be used under the terms of the CC BY 3.0 licence (© 2015). Any distribution of this work must maintain attribution to the author(s), title of the work, publisher, and DOI.

ISBN: 978-3-95450-168-7 doi:10.18429/JACoW-IPAC2015-WEPHA032

STUDY ON THE LN2 CONSUMPTION OF THE BEAMLINE LN2 TRANSFER SYSTEM FOR TPS PROJECT

H. C. Li, F. Z. Hsiao, H. H. Tsai, T. F. Lin, W. S. Chiou, S. H. Chang, W. R. Liao and W. S. Chan,
National Synchrotron Radiation Research Center, Hsinchu, 30076, Taiwan

Abstract

One system to transfer liquid nitrogen (LN_2) will be installed at TPS in 2015 for beamline. This system includes two transfer lines (length 600 m), eight keep-full devices and 26 branch lines with 26 control valves for 24 straight sections of beam lines. The required consumption of LN_2 for each beam line is 30 L/h. An archive system was developed to monitor and to calculate the consumption of LN_2 for each beam line. This consumption was calculated based on the pressure difference and the flow coefficient (K_v) of the control valve. This paper presents the configuration of the LN_2 supply system at NSRRC and a test bench of the calculation of LN_2 consumption. A simple test result is presented and discussed.

INTRODUCTION

A helium-cryogenic system with refrigeration (450 W) began its operation from 2003. The liquid-nitrogen (LN_2) supply system entered service at the same time. Figure 1 is the current status of the LN_2 supply system at NSRRC. The LN_2 supply system was finished for Taiwan Light Source (TLS) in 2009. The LN_2 transfer system for the Taiwan Photo Source (TPS) project began its installation and commissioning in 2013.

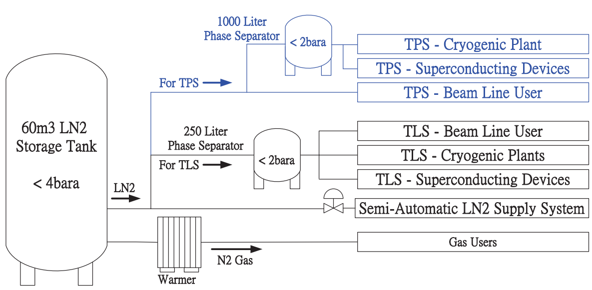

Figure 1: Configuration of the LN_2 supply system at NSRRC.

LN_2 Supply System at NSRRC

One LN_2 storage tank (60 m^3) replaced the original one (20 m^3) in 2009. In total, the LN_2 flows through a vacuum-shielded LN_2 transfer line (length > 300 m) and one phase separator (250 L) to users at TLS [1]. The TLS users comprised of two liquid-helium (LHe) refrigerators (450 W) [2], one superconducting RF cavity, five superconducting magnets, two beam-line laboratories, and one semi-automatic LN_2 supply system. A line (length > 300 m) for gaseous nitrogen (GN_2) used to purge or to clean the machine or experimental samples also existed inside the LN_2 system.

We installed a vacuum-shielded LN_2 transfer line (150 m), one phase separator (1000 L) and one helium refrigeration system (700 W) [3] in 2013. We finished the commissioning of a multi-channel line (LHe/GHe/LN_2 /GN_2) for four TPS superconducting RF cavities in 2015 April. The total length is more than 130 m. We began to install two vacuum-shielded LN_2 transfer lines (length 600 m) with 26 control valves used in TPS beam-line laboratories in 2015 April. Figure 3 shows the configuration of the LN_2 transfer system of NSRRC.

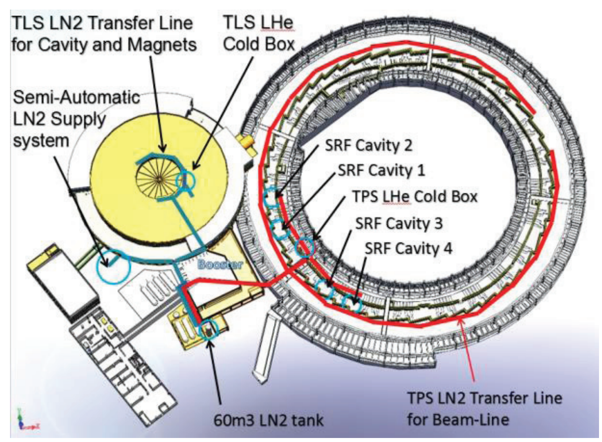

Figure 2: Configuration of LN_2 transfer line of NSRRC.

LN2 Consumption

Increasing numbers of users introduce a rapidly increasing consumption of LN2. Figure 3 shows the LN_2 consumption at NSRRC from 2005 to 2014. The average consumption is about 955 m^3 per year from 2005 to 2009, but the average consumption increased to 1777 m^3 per year from 2010 to 2014. The major increase was due to the TPS project. Many machines and systems were tested and commissioned during these five years. Figures 4 and 5 show the LN_2 ratio of users. It was easy to estimate the budget of TLS LN_2 consumption because of the stabilized operation in year 2009, but more than 51 % of the total amount LN_2 consumption was used to support the relevant testing of TPS in year 2013. It is difficult to estimate the LN_2 consumption under such conditions. To understand the LN_2 consumption of each user is an important issue for the stability of the LN_2 supply due to the budget control. A typical theory of valve sizing can help us to calculate the real-time consumption of LN_2

Content from this work may be used under the terms of the CC BY 3.0 licence (© 2015). Any distribution of this work must maintain attribution to the author(s), title of the work, publisher, and DOI.

ISBN: 978-3-95450-168-7 doi:10.18429/JACoW-IPAC2015-WEPHA033

ELECTRICAL POWER SCADA SYSTEM OF TAIWAN PHOTON SOURCE

Tzong-Shyan Ueng, Yung-Feng Chiu, Yu-Chih Lin, Kung-Cheng Kuo, Jui-Chi Chang, Wen Shuo Chan, NSRRC, Hsinchu, Taiwan

Abstract

The architecture of power SCADA system of TPS and its monitored real time data are described in this report. The on-line monitored and measured items include voltage/current, real power/reactive power, power factor, harmonic distortion, etc. These data are presented. The electric energy, the power quality and the harmonic distortion obtained with the SCADA system are used to study the status of the power system, and also provide information for the future improvement.

INTRODUCTION

The Taiwan Photon Source (TPS) is a newly constructed accelerator facility in National Synchrotron Radiation Research Center (NSRRC). It is adjacent to Taiwan Light Source (TLS). This new storage ring has 518 m in circumference and can deliver electron beam of 3.0 GeV and 500 mA, which is much more elaborate than the present TLS facility. During the last 20 years, the researchers have used TLS to produce many excellent scientific research results. Adding TPS to the present facility will provide the researchers with needed facility and resources to stay ahead in the scientific and technological competition. In order to keep this new synchrotron facility running smoothly for producing excellent experimental results, an electrical system with a good power quality is crucial.

ELECTRICAL POWER SYSTEM AND ITS LOADS

The electric power used in TPS is provided by Taiwan Power Company (Taipower) through two main distribution feeders, feeder A and B, to the main substations for TPS in NSRRC. These two feeders have rated voltage of 22.8 kV each. The power demand from Taipower is 12.5 kW. Two local generators can deliver 2000 kW for emergency need. There are 17 local substations for the power loads in TPS. All the loads are sorted and distributed evenly on the two feeders, Fig. 1. The loads of the accelerator facility are mostly for the subsystems of accelerator and the experimental stations, while the loads of the utility system are chillers, pumps, air handling units, smoke exhaust fans, hot water furnaces and those utilities for public use.

MONITORING AND DATA ACQUISITION SYSTEM

The real time monitoring and data acquisition system used for the TPS power system adopted the graphical programming approach but with one-line diagram in mind. This system has functions of I/O communication, storing trend data, real time alarm and remote GUI operation. In Fig. 2 the GUI of SCADA system shows the control panel of the main feeder A which displays the real time values of real power, maximum demand power and reactive power in main feeder A. It also displays voltage, current and power consumed at each substation. More information of the power system can be seen by further clicking the icon on the screen. The communication architecture adopts the Modbus RTU communication protocol, Fig. 3. The protection relays, digital multi-meters, thermal relays, automatic power factor regulators (APFR), DC chargers, generators and air circuit breakers (ACB) are connected to the I/O servers, then, the I/O servers convert the communication protocol to Modbus TCP protocol and communicate to the main server using optical fiber through Ethernet switch. The optical fiber is connected as a ring type which can transfer data in both directions to the two main servers. These two servers can access data from the I/O servers and monitor the status of devices simultaneously. Each server can also be used as backup of the other server in case one server is failed.

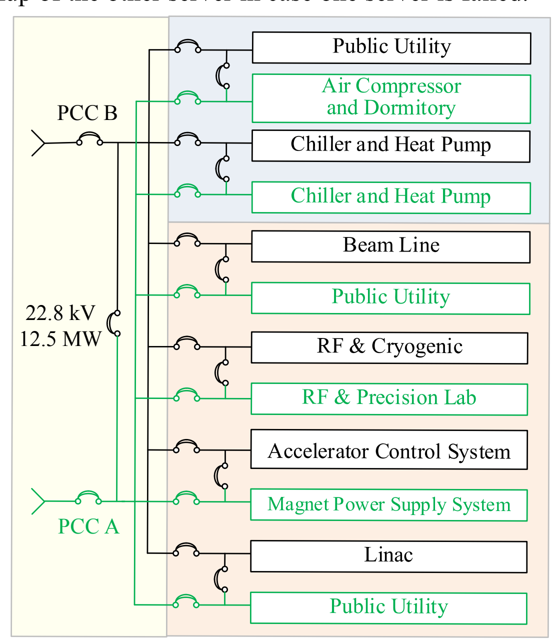

Figure 1: Block diagram shows the loads used at TPS.

MEASUREMENT AND ANALYSIS OF POWER QUALITY

The real time information of feeder B measured by the power SCADA system are shown in Fig. 4. The feeder B provides the power for most of the accelerator subsystems. It shows the voltage/current of each phase, real/reactive

Content from this work may be used under the terms of the CC BY 3.0 licence (© 2015). Any distribution of this work must maintain attribution to the author(s), title of the work, publisher, and DOI.

ISBN: 978-3-95450-168-7 doi:10.18429/JACoW-IPAC2015-WEPHA034

COMMISSIONING OF THE DE-IONIZED WATER SYSTEM FOR TAIWAN PHOTON SOURCE

W.S. Chan*, J.C. Chang, Y.C. Chang, C.S. Chen, Y.C. Chung, C.W. Hsu, C.Y. Liu, and Z.D. Tsai
National Synchrotron Radiation Research Center (NSRRC), Hsinchu 30076, Taiwan

Abstract

The de-ionized water (DIW) system plays a critical role in removing waste heat from an accelerator machine. Through years of design and constructs, the DIW system for Taiwan Photon Source (TPS) was complete at the end of 2013, but it is important to confirm that the quantity and quality of DIW comply with the requirements of the accelerator machine. Testing, adjustment and balancing methods have been applied to verify that the DIW system for TPS can provide flow rates greater than 1659, 380, 1284 and 1238 GPM in the individual Cu, Al, RF and booster subsystems. The proposed system can supply DIW of quality such that the resistivity is greater than 10 MΩ-cm at 25±0.1 °C; the concentration of dissolved oxygen (DO) is less than 10 ppb.

INTRODUCTION

The main utility equipment of TPS includes a deionized water (DIW) system installed in Utility Building III to avoid vibration and power noise induced by these cooling-water facilities, including cooling towers, chillers, heat pumps and water pumps [1]. A utility trench from Utility Building III connects to TPS for the piping system and electric power transmission [2]. Figure 1 has a schematic drawing of TPS and Utility Building III.

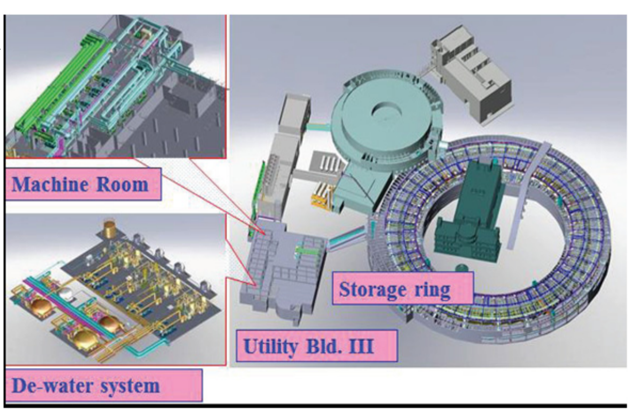

Figure 1: TPS storage ring and Utility Building III.

The DIW system for TPS has four subsystems -- Cu DIW for magnets and power devices, Al DIW for vacuum chambers, RF DIW for the RF facility, and booster DIW for booster devices and beamline optical instruments. The demanded flow rate that depends on the heat load for each portion of the TPS synchrotron accelerator is listed in Table 1.

Table 1: Flow Rate Requirements of DIW Subsystems

Point of use	flow rate /GPM			
	Cu	Al	RF	booster
magnet	594	-	-	136
power devices	501	-	-	-
vacuum	260	312	-	-
front end	296	68	-	-
RF facility	-	-	1284	-
cryogenics	-	-	-	17
Linac	-	-	-	435
mechanical	8	-	-	-
beamline	-	-	-	650
total	1659	380	1284	1238

All DIW flow circulates in a closed loop and removes heat within a stable range of temperature and pressure. Each return DIW flows through two plate heat exchangers for heating and cooling, then flows via a mixing buffer tank for highly precise temperature control. Respective DIW subsystems possess two pumps with variable-frequency drives (VFD) that achieve flow regulation, energy conservation and uninterrupted commission.

Water treatment is an important aspect of a DIW system. Impurities in DIW typically include particles, electrolytes, micro-organisms, organic substances and gases that must be removed with a physical or chemical mechanism. The activated carbon filter (ACF), reverse-osmosis equipment (RO), resin-mixed bed (MB), micro-filter (MF), ultraviolet sterilizer (UV) and dissolved oxygen membrane deaerator (MD) have been installed to sustain the water quality [3]. Of the primary loop flow, 5 % DIW flows through this recycle loop as shown in Fig. 2; the entire DIW system must meet specifications listed in Table 2.

In the TPS storage-ring building, an individual DIW subsystem has been divided into 48 manifolds for the 24 sections of the accelerator machine, as shown in Fig. 3. Every manifold has filters, flow-balance valves and sensors for temperature, pressure and flow, which provide an optimal flow balance and real-time DIW status. Every inlet and outlet piping connected with the accelerator machine has a flexible hose to prevent the propagation of vibration.

*Email: chan.ws@nsrrc.org.tw

Content from this work may be used under the terms of the CC BY 3.0 licence (© 2015). Any distribution of this work must maintain attribution to the author(s), title of the work, publisher, and DOI.

ISBN: 978-3-95450-168-7 doi:10.18429/JACoW-IPAC2015-WEPHA035

DEVELOPMENT OF AN IGBT PULSER FOR TPS LTB KICKER

C.L. Chen#, C.S. Fann, H.P. Chang, K.L. Tsai, Y.S. Cheng, S.Y. Hsu, K.T. Hsu, K.K. Lin
National Synchrotron Radiation Research Center, Hsinchu, Taiwan

Abstract

The Linac to Booster (LTB) injection kicker for Taiwan Photon Source (TPS) was first commissioned using Pulse Forming Network (PFN) pulser equipped with a thyratron switch. Although its bench-testing results fulfilled all specifications, the performance was degraded due to a couple of unavoidable integration difficulties. After evaluating several improving options in hand, an alternative pulser using IGBT switch is proposed for off-the-bench beneficial purpose. The results of the upgraded pulser satisfy the overall specifications with comfortable margins. Some major performance parameters, such as flattop and tail ringing, are emphasized concerning their influence on beam injection. This report describes the field-testing result of this new IGBT pulser.

INTRODUCTION

TPS LTB kicker pulser was installed for system test in 2014 using PFN- thyratron switch. This PFN pulser was designed and constructed in house, and it fulfils all the performance specifications, such as flattop width, pulse-to-pulse stability, and current pulse fall time with respect to the designed inductive load. The overall bench tested performance of the kicker pulser is listed in table 1. However, due to hardware design constrains, the load inductance (4.4 µH) exceeded the existing circuitry tuning limits of compromising margin, so the overall performance of PFN pulser was degraded, as illustrated in figure 1.

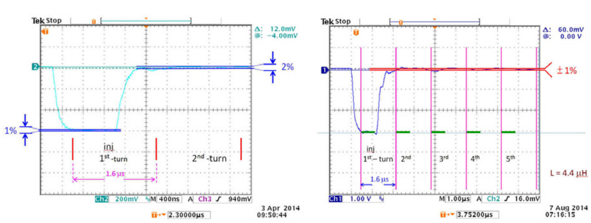

Figure 1: current pulse at (L) bench test; and (R) field test.

The contents in Table 1 indicate that the flattop, its ripple, and fall time, are consequently influenced. Several improving attempts have been studied in order to eliminate the postpulse oscillation, which has tail ripples and could induce extra kick, while the injected beam is circulating around in the booster ring. The urgent improvement attempt by modifying the electrical circuit and reducing the field inductance was made in time for booster injection system test in 2014 [1]. Yet, for the modified PFN circuitry, the available flattop region is reduced to 200 ns due to the unavoidable prolonged fall time. This reduction in the flattop duration does not only limits the bunch train tuning capability in the MB (multi-bunch) operation, but also restricts the bunch pattern manipulation flexibility in the MB+SB (single bunch) hybrid mode operation [2].

The initiation of this IGBT study is to improve TPS injection pulser by using an alternative approach. After evaluating several improvement options in hand, a pulser using IGBT switch is introduced. Comparing its performance with the modified PFN pulser [3] using same inductive load, the IGBT pulser provides a couple of advantages in this particular application, as follow:

1. Fall time can be reduced;
2. Flattop duration can be increased;
3. Small postpulse oscillation can be achieved;
4. Installation space is greatly reduced in the accelerator tunnel.

Some disadvantages are to be considered before implementing the IGBT pulser. There are: i) limitation of reducing fall time due to the existing inductive load; ii) noise interference with the low triggering threshold of IGBT switch. After examining the corresponding bench tested countermeasures, the results indicate that the performance of this IGBT pulser satisfies the specifications with comfortable margins. This report describes the field-testing result of this IGBT pulser in details.

Table 1: LTB Kicker Pulser Tested at Bench and Field

Booster Injection Kicker			
Parameter	**specifications**	**bench-test**	**field-test**
Pulse Shape	flat-top	flat-top	flat-top
Type	PFN	PFN	PFN
Pulse Length (µs)	1	1	0.7
Nominal Current (A)	280	280	280
Inductance (µH)	1.6	1.6	4.4
Fall Time (µs; 5-95%)	0.4	0.4	0.9
Pulse-to-pulse Stability (%)	0.1	0.1	0.1
Flatness (%)	± 1	± 1	± 2
Postpulse ripple (%)	± 1	± 1	± 1.5
Repetition Rate (Hz)	3	3	3

IGBT PULSER LAYOUT

The upgraded injection pulser consists of two parts: an IGBT switching unit and a DC charging power supply (DC-PS). Choosing the IGBT switch is primarily based on its capability of high delivery power and rapid switch-off ability [4]. A functional block diagram of using IGBT switch for the LTB kicker PS is shown in figure 2. A DC-PS charges the capacitor bank to a designated value. Then IGBT trigger is switched on by a control unit according to

#clchen@nsrrc.org.tw

Content from this work may be used under the terms of the CC BY 3.0 licence (© 2015). Any distribution of this work must maintain attribution to the author(s), title of the work, publisher, and DOI.

6th International Particle Accelerator Conference IPAC2015, Richmond, VA, USA JACoW Publishing
ISBN: 978-3-95450-168-7 doi:10.18429/JACoW-IPAC2015-WEPHA037

DESIGN STORAGE RING AND BOOSTER RING POWER SUPPLY CABLING IN TAIWAN PHOTON SOURCE

Yong-Seng Wong, Kuo-Bin Liu, Chen-Yao Liu, Yuan-Chen Chien, Bao-Sheng Wang
National Synchrotron Radiation Research Center
Hsinchu 30076, Taiwan

Abstract

For this paper is studies the storage ring and booster ring power supply cabling design, Papers can be divided into cabling design, control and instrument area construction (CIA), and testing; design including estimated cable length and arrangement, the CIA construction part site of the cable erection and overcome barriers of space; detection section is high resistance meter and insulation testing [1]. Circumference of booster ring is 496.8 meter and storage ring is 518.4 meter, TPS (Taiwan Photon Source) beam current is 500mA at 3GeV. Booster Ring dipole into BD and BH series 54 magnets, cable size is 250 mm^2 and total length of 5000m [2]. Booster Ring and storage ring quadrupole 150 magnets and cable size 250 mm^2, total length of 17000m. Storing Ring dipole 48 magnets cable size 325 mm^2, total length of 6000m. On the positive and negative voltage cables will produce magnetic interference effects generated through cabling overlapped technology eliminates magnetic interference [3]. Finally, using a high-impedance machine to detect cabling insulation effect. TPS power supply to the energy transfer is to ensure safe and correct magnet.

INTRODUCTION

"Taiwan Photon Source interdisciplinary laboratory facilities construction plan" to be executed in National Synchrotron Radiation Research Center. Subsystems must begin to build the system in the unfinished building structure; the degree of complexity is really unimaginable. Needed a software system can provide substantial help in a limited space, so that all of the equipment, planning to do effectively. National Synchrotron Radiation Research Center has embarked on a way to build 3D graphics module, virtual all parts through one to one 3D module, ensure that the planning can be more complete. Spatial planning magnet arrangement and cabling is a major work of this plan in the power supply group. The construction site using a 3D simulation module, early start magnet arrangement design and planning in civil engineering structures has not been completed, such as: cable length, procurement budget ..... Cabling works of various space-related configuration parameters refer to the values obtained in the 3D virtual environment module, essentially greatly enhance the efficiency of the design. 3D software will make the arrangement of the power supply to the magnet parts and models, including: Magnet coding, magnet placement, interference region. Model contains booster ring area, storage ring area, linac to Booster ring (LTB) and booster to storage ring (BTS) area; clearly show the main structure through 3D simulation software.

CONTROL AND INSTRUSMENT AREA

CIA is located in the inner circle adjacent to TPS tunnel. DC power supplies of magnets and ID controller are placed on the 1st floor. Figure 1 has shown cable tray design in CIA to tunnel magnets side. Colour tray is design by power supply group. It can separate to left and right hand side, power supply machine placed in CIA 1F and cable will through trench into the tunnel area of storing ring tray connect to magnets. Figure 2 has shown power rack and magnet placed on CIA cable tray, CIA place on 6 power rack that are 4 QF-SF rack and 2 corrector rack. Each side QF-SF rack will supplies energy to each 5 quadrupole magnets and 4 sextupole magnets.

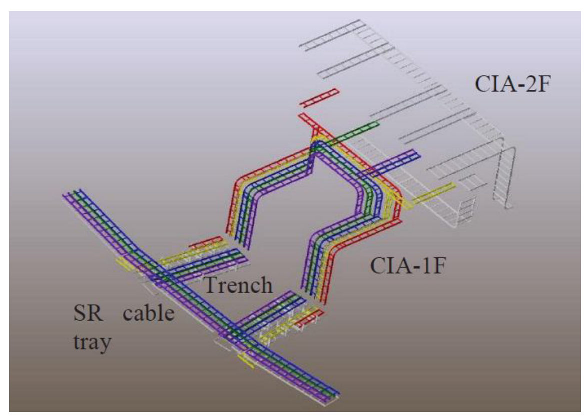

Figure 1: CIA power supply cable tray.

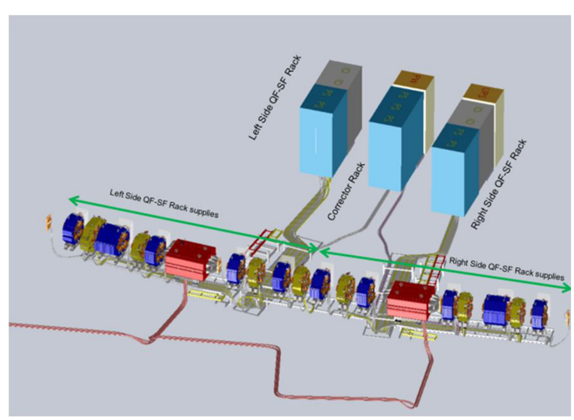

Figure 2: Power Rack and magnet simulation on CIA and Storing ring cable tray.

Content from this work may be used under the terms of the CC BY 3.0 licence (© 2015). Any distribution of this work must maintain attribution to the author(s), title of the work, publisher, and DOI.

ISBN: 978-3-95450-168-7 doi:10.18429/JACoW-IPAC2015-WEPHA038

UPGRADING THE PERFORMANCE OF THE POWER SUPPLY FOR THE TPS BOOSTER DIPOLE MAGNETS*

Chen-Yao Liu#, Yuan-Chen Chien, Bao-Sheng Wang, Yong-Seng Wong, Kuo-Bin Liu, NSRRC, Hisnchu 30076, Taiwan

Abstract

The performance of the power supply for the dipole magnet is important for the TPS booster ring. The output current of the power supply follows the beam current from 150 MeV ramping to 3 GeV. The frequency of the power supply is 3 Hz. The power supply must thus push enormous energy into the dipole magnets at $\pm$1000 V and $\pm$1200 A, and can handle this job. Because the TPS booster dipole supply is bipolar and the voltage is large, the lodged capacitors have large effects that produce common-mode high-frequency current noise, which drives the power supply beyond specification. The TPS booster ring hence fails to meet the dc and ramping specification.

We designed a common-mode filter to solve the high-frequency current noise by absorbing the current noise from the path of the lodged capacitors to the ground pad. The TPS booster dipole supply thus works within the specification when the power supply is in the dc or ramping mode. The beam current from the 150-MeV dc mode for the injection mode can ramp the beam current to 3 GeV. This paper reports the excellent results.

INTRODUCTION

The booster ring of Taiwan Photon Source (TPS) uses 48 dipole magnets in series connection to build the topology. A bipolar switching-mode power supply pushes the booster dipole magnets from 47 A to 980 A, which maps 150 MeV to 3 GeV.

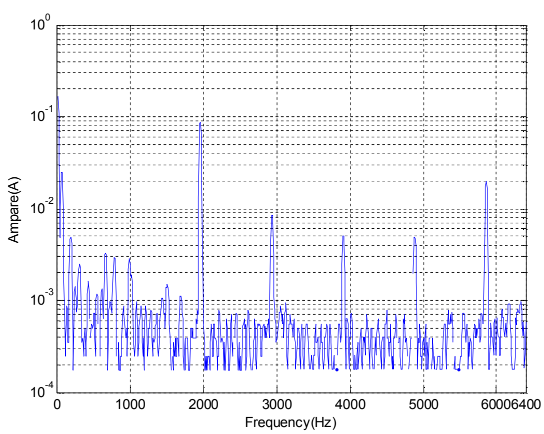

Figure 1: Current ripple in the dc mode (frequency from 0 to 6.4 kHz).

The current waveform follows the control system; the waveform is like a sine wave. Measured with instrument Agilent 35670A, the current ripple in the dc mode for the current set at 47 A for 150 MeV can be scanned from 0 to 51.2 kHz. When we read the current ripple in the frequency domain as shown in Fig. 1 and Fig. 2, we found that the current ripple is too large and beyond specification.

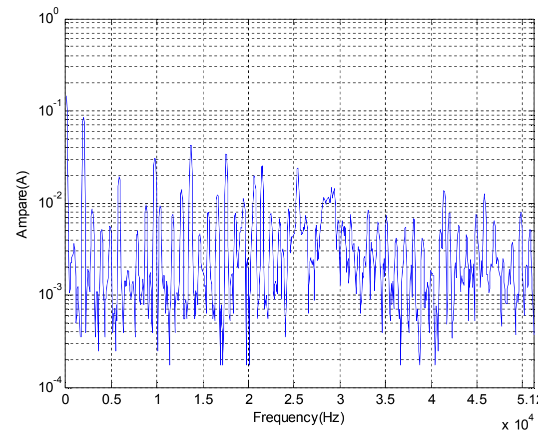

Figure 2: Current ripple in dc mode (frequency from 0 to 51.2 kHz).

As the dipole magnets act like a low-pass filter, the output current of the dipole power supply should possess a low-frequency current waveform, but the TPS booster ring has lodged capacitors that generate a high-frequency current ripple. The effect is especially large when the lodged capacitors for working voltage $\pm$1000 V are in the PWM mode. The ground current becomes large when the dipole power supply is in the ramping mode [1-2].

We added a common filter to the booster dipole power supply that can absorb the current noise in the path from the lodged capacitors to the ground pad. The filter is named a Y circuit. The TPS booster dipole supply can thus work within specification when the power supply is in both the dc and ramping modes. The beam current can proceed from the 150-MeV dc mode for the injection mode to ramp the beam current to 3 GeV, so the TPS booster ring can succeed in its task.

TOPOLOGY OF THE POWER SUPPLY

The topology of the booster dipole supply is an H bridge with a power bus at 1000 V. The power device is IGBT module. It can generate 1200 A to the dipole magnets. The power supply generates a unipolar current and a bipolar voltage to the magnets. The switching frequency is 2 kHz in the PWM mode. Figure 3 shows the topology of the H-Bridge.

*Work supported by Power Supply Group, NSRRC
#cyl@nsrrc.org.tw

Content from this work may be used under the terms of the CC BY 3.0 licence (© 2015). Any distribution of this work must maintain attribution to the author(s), title of the work, publisher, and DOI.

ISBN: 978-3-95450-168-7 doi:10.18429/JACoW-IPAC2015-WEPHA039

INRUSH CURRENT SUPPRESSION SCHEME OF HOT SWAP POWER MODULES

Yi-Ta Li, Kuo-Bin Liu, Chen-Yao Liu NSRRC, Hsinchu, Taiwan

Abstract

The corrected magnet power supplies apply modular designed for Taiwan Photon Source synchrotron project (TPS). If the module is damaged in the chassis, it must to be replaced without interrupting the power. However, the modular is a shared DC bus. If there is no good design and planning, it will cause the protection circuit into action.

In this article the theoretical derivation and implementation are used to prove the feasibility and necessity of the soft-start circuit. In the actual signal measurements it could be clearly seen the inrush currents is refrained and improved. Finally, the soft-start circuit is implemented applications in correction magnet power supply modular of Taiwan Photon Source synchrotron project (TPS).

INTRODUCTION

TPS corrected magnet power supplies apply modular designed, the architecture shown in Figure 1. A chassis can be installed eight corrected magnet power supplies module. These three busses in main power and operating voltage and control signals were shared by eight corrected magnet power supply modules. Shared these busses can effectively reduce the volume of the machine itself, and complexity of the hardware circuit, that also equivalent to achieved higher economic returns [1-2].

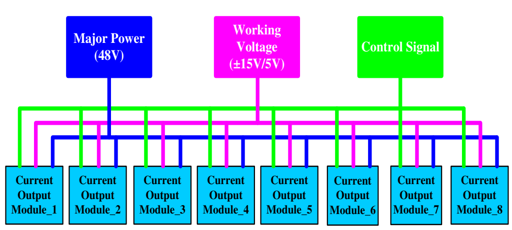

Figure 1: The architecture of TPS corrected magnet power supplies modular.

The modular power supply systems in practical applications, usually uninterrupted power supply of equipment systems. When the modules in the chassis were damaged, must replace the modules of the systems in uninterrupted power supplies.

The prototype of TPS corrected magnet power supply systems as an example. The waveform of the modules was plugged into the main systems, shown in Figure 2. The main power supply voltage 48V had plunged, which plunged about 9.2V (19%), the lowest voltage was 38.8V. When the main power supplies voltage was below 45V, corrected magnet power supply modules itself sent the mains input voltage failure signal and stopped working, it can be seen from the chart the voltage below the 45V duration approximately 2mS. The all of Corrected magnet power supply modules inside the chassis were stopped working, which was with the original modular designed concept different. It's worth noting that when the corrected magnet power supply modules plugged into main power bus, which main power supply output current swelled to 230A, shown in Figure 2. This current phenomenon was called Inrush current, Inrush current can cause to fuse was burned and damaged to other electronic components with the system can't operated normally.

In order to maintain the normal operation of the power supplies, so added the soft start design to the power supplies. The soft-start design can be ranged into active and passive two types, the active design must need a controller and a current sensor to control switches, so in this paper used passive design.

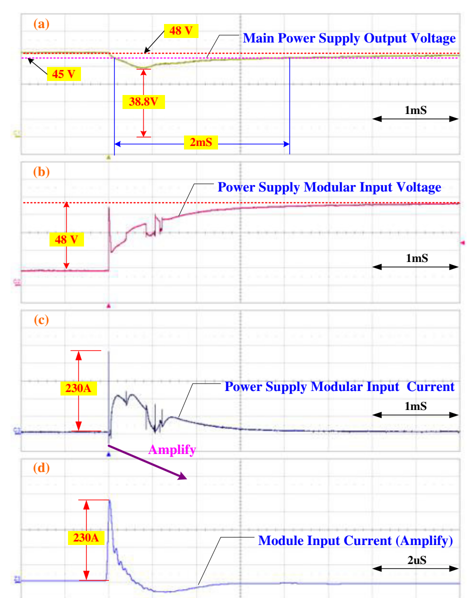

Figure 2: Corrected magnet power supplies modular plugged into the main system's waveform.

PRINCIPLE OF PASSIVE INRUSH CURRENT LIMTERING

Understand the impact caused by the inrush current, then in this section was proposed ways to improve the inrush current. Due to the charging of capacitors, so that were produced the inrush current when the corrected magnet power supply modules plugged into the chassis. Using the resister and capacitor (RC) charge circuit for the architecture is shown in Figure 3, the capacitor charging current formula such as the equation (1).

Content from this work may be used under the terms of the CC BY 3.0 licence (© 2015). Any distribution of this work must maintain attribution to the author(s), title of the work, publisher, and DOI.

ISBN: 978-3-95450-168-7 doi:10.18429/JACoW-IPAC2015-WEPHA040

STATUS OF AC POWER SUPPLIES FOR TPS BOOSTER RING

Yuan-Chen Chien, Bao-sheng Wang, Yong Seng Wong, Chen-Yao Liu, Kuo-Bin Liu, Chunyi Wu, Pei-Chen Chiu, Kuo-Tung Hsu, NSRRC, Hsinchu, Taiwan

Abstract

TPS is a third generation 3 GeV synchrotron light source under commission in Taiwan. The TPS Booster ring is concentric ring design sharing the same tunnel with storage ring. The booster ring power supplies are responsible of accelerating the 150 MeV Linac output energy to 3 GeV before the beam is preserved in the storage ring. The booster ring power supplies are required to operate at 3Hz sinusoidal waveform with 1000 A peak current for the dipole magnet. All power supplies' specifications and output performance are demonstrated here in this paper.

INTRODUCTION

Taiwan Photon Source (TPS) is a concentric ring with booster and storage ring allocated in the same tunnel. A combined function FODO lattice is chosen to be an optimal solution for the TPS booster ring lattice structure in terms of cost and performance. There are total six super-periods, in which each consists of 8 cells of combined–function FODO lattice. Figure 1 shows a portion of the super-period FODO lattice in the TPS ring [1].

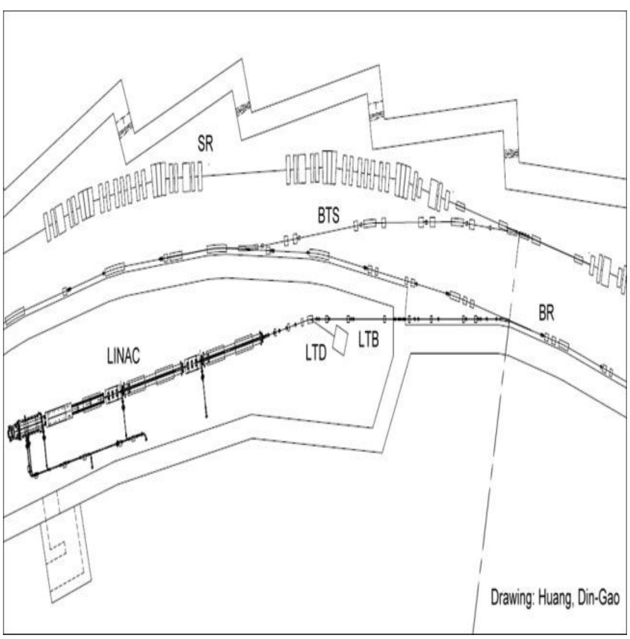

Figure 1: TPS concentric ring.

Based on this design, the TPS booster ring, with a circumference of 496.8m, includes 54 bending magnets, 72 quadruple magnets, 24 sextuple magnets and 96 corrector magnets. The detailed parameters of the booster magnets are listed in Table 1.

Table 1: Booster Magnet Specifications

Magnet	Qty	Load	Cable	Total
BD	48	1.973mH 9mΩ	29.18mΩ	94.854mH 467.2mΩ
BH	12	0.999mH 5mΩ		
Q1	12	4.683mH 49mΩ	67.86mΩ	56.196mH 655.8mΩ
Q2	12	2.298mH 33mΩ	67.86mΩ	27.567mH 463.8mΩ
QM	12	0.625mH 19mΩ	67.86mΩ	7.5mH 295.8mΩ
QF	48	4.683mH 49mΩ	67.86mΩ	224.78mH 2419.8mΩ

BOOSTER POWER SUPPLY

Dipole Power Supply

The two families of dipole bending magnets BD and BH are connected all together in series and driven by a single Dipole AC Power Supply (DPS). While, Q1, Q2, QM and QF of the quadruple magnets are powered independently by four quadruple power supplies (QPS1, QPS1, QPSM, QPSF). All magnets in the same family are also connected in series. The internal topology of the Dipole Power Supply is depicted in Figure 2.

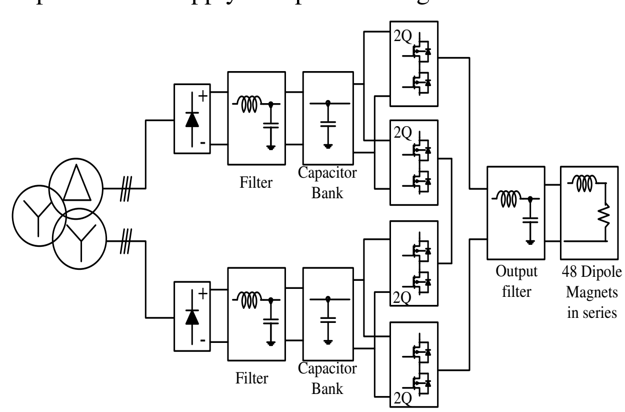

Figure 2: DPS functional diagram.

The DPS is composed of two identical DC voltage bank and 4-Quadrants IGBT switching module connected in series to boost up the output voltage as demanded. The 4-Quadrants IGBT switching module is made up of connecting two 2-Quadrants IGBT modules in parallel and the IGBT is switched with 4 kHz frequency.

The output filter is specially designed and fine-tuned to the magnet load with adequate cut-off frequency to minimize the output current ripple and earth leakage current due to the parasitic capacitance to earth ground from the magnet body.

Content from this work may be used under the terms of the CC BY 3.0 licence (© 2015). Any distribution of this work must maintain attribution to the author(s), title of the work, publisher, and DOI.

ISBN: 978-3-95450-168-7 doi:10.18429/JACoW-IPAC2015-WEPHA041

Content from this work may be used under the terms of the CC BY 3.0 licence (© 2015). Any distribution of this work must maintain attribution to the author(s), title of the work, publisher, and DOI.

ALGORITHM AND CIRCUIT TO IMPROVE ZERO-CROSSING STABILITY OF BIPOLAR TPS TRIM COIL POWER SUPPLY

Bao-Sheng Wang, Yuan-Chen Chien, Yong-Seng Wong, Chen-Yao Liu, Kuo-Bin Liu, Chun-Yi Wu, Pei-Chen Chiu, Kuo-Tung Hsu, NSRRC, Hsinchu, Taiwan

Abstract

In TPS (Taiwan Photon Source) project, 58 home-built small form factor bipolar power supplies are used to fine-tune the trim coil of booster ring bending dipole magnets. With the preliminary analog PI control loop design version, current output will tend to behave with poor linearity around zero current. By employing DSP chip, a full digital PI control loop design together with optimal MOSFT switching algorithm and 13bits PWM output capability is capable of improving the output current performance around zero current. Before the final realization, MATLAB SIMULINK is utilized to find out the optimal MOSFT switching algorithm, and then physical circuit is implemented and tested. The result and design will be demonstrated in this paper to show significant improvement around zero current.

INTRODUCTION

In TPS the sextuple and trim coil magnets converters of booster ring under operation are made by NSRRC and ITRI, the output current behaves nonlinearly at zero crossing with the analogy regulation control loop. In this paper, the original analog regulation loop is replaced by the fully digital regulation control one.

NI sb-RIO board is selected to implement digital PID controller and PWM command generation. NI sb-RIO board has FPGA built inside. All the digital control circuit are designed and written in VHDL code, thus design can be downloaded on the fly to the board for rapid verification.

The development of this NI sb-RIO board-based digital regulation control circuit of TPS's storage sextuple and corrector magnet power converters is based on the framework of NSRRC-ITRI CPS converter with a shunt as a current sensing component that could reduce the cost and less compromised performance to fulfill the fully digital regulation control implementation.

During the preliminary design phase, Matlab simulink is used to simulate the characteristic of the full bridge construction, the function of compensator and the PWM regulation algorism, and the accuracy of the control policy is confirmed.

With the NSRRC-ITRI CPS converter with the full bridge architecture as the test platform, the original analog regulation control loop circuit is replaced by the home-made digital regulation control circuit, including NI sb-RIO Board, Analog to Digital converter, Digital to Analog converter, gate drives of MOSFETs.

With digital regulation control is implemented, the long and short term output current stability and low current tracking error is largely improved.

THE STRUCTURE OF CORRECTOR MAGNET POWER CONVERTER

The full digital corrector magnet power converter could be roughly divided into six functional blocks: 1) Power regulation and L-C filter, 2) high resolution AD7767 24-bits analogy to digital converter, 3) four channel DA8734 16-bits digital to analogy converter, 4) high performance NI sb-RIO 9606 board controller, 5) DIO control trigger port and 6) USB, RS232, RS485, Ethernet and control page transmission interface. The functional blocks are shown in Fig. 1.

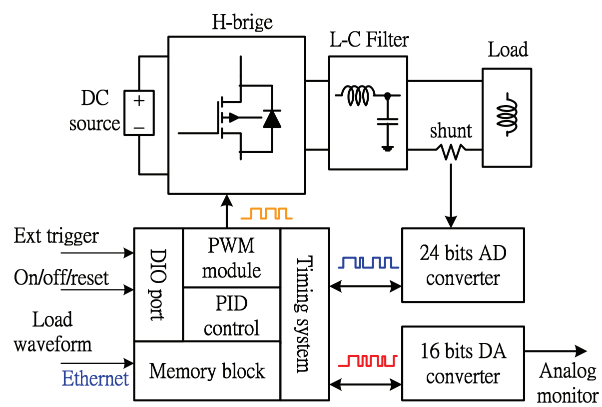

Figure 1: The structure of corrector magnet power converter.

PWM REGULATION METHOD

The PWM computation algorithm is done in the FPGA on the NI sb-RIO 9606 board. The compensated current command output from the PID block is exported to this PWM generation block, where the MOSFET switching signals S1, S2, S3 and S4 are generated by comparing the current command to two saw-tooth waveforms with 180 degree phase difference as illustrated in Fig. 2. It is shown in Fig. 2, the left waveforms are the MOSFET switching waveforms while the current setting is positive, while the waveforms when current is set to negative is depicted in the right [1].

The MOSFET Switch Modes with various load current flow are plotted in Fig. 3. There are 6 modes of load current flow. Mode Ⅰ～Ⅲ are positive current flows through the load, while in ModeⅣ~Ⅵ are modes when negative current occurs.

ISBN: 978-3-95450-168-7 doi:10.18429/JACoW-IPAC2015-WEPHA042

COMMISSIONING OF THE TPS COOLING SYSTEM: TESTING, ADJUSTING, BALANCING AND NUMERICAL SIMULATION

Z. D. Tsai,[#] W. S. Chan, C. S. Chen, C. Y. Liu, Y. C. Chung, C. W. Hsu, Y. C. Chang
National Synchrotron Radiation Research Center (NSRRC), Hsinchu 30076, Taiwan

Abstract

The civil construction and utility systems of the 3-GeV Taiwan Photon Source (TPS) at NSRRC are ready for machine commissioning in 2014. To achieve a highly precise control of temperature, the thermal load must be carefully controlled and balanced. On analysis of the characteristics between the water pipes and the balance valves, a specified control philosophy can effectively adjust the pressure load on the branch pipes to balance the water flow. With regard to the air flow, we use a damper, baffle plant or variable air-volume (VAV) box to balance the air flow of each diffuser. Here we discuss the mechanism through a numerical simulation of the hydrodynamics and verify the practical influences of the testing, adjusting and balancing (TAB) for de-ionized water and the heating, ventilation and air-conditioning (HVAC) system.

INTRODUCTION

The TPS infrastructure including civil and utility systems has been under construction since 2009 December and was completed in 2014 December [1]. The TPS facility is currently in the stage of commissioning. As the utility system is a most critical subsystem affecting the beam quality and reliability, much effort has been devoted to these designs [2]. Here we address mainly the testing, adjusting and balancing (TAB) design of the cooling system of the finalized utility system.

In the accelerator field in general, thermal waste can be treated through circulating deionized water (DIW) and air conditioning (AC). The main system for cooling water of TPS includes the cooling tower, chilled water, hot water, de-ionized water and HVAC system. Each manifold located near control-instrument areas (CIA) provides four loops for varied demand of facilities, including stable temperature, pressure and flow. The air-handling units (AHU) located at the inner and outer rings provide highly stable cooling air for the storage-ring tunnel, CIA, experimental hall and Linac area. Programmable automation controllers (PAC) and direct digital controllers (DDC) have been implemented in this hybrid utility system for highly precise control and status monitoring. To provide a stable cooling source, we must fine-tune the system to meet our requirements. The TAB process for de-ionized water and HVAC system is a critical procedure in the commissioning stage of the utility system. This paper reports that mechanism through numerical simulation of hydrodynamics and verifies the practical influences of the TAB process.

E-mail: zdtsai@nsrrc.org.tw

NUMERICAL SIMULATION OF HYDRODYNAMICS

We use a software package (fluent) to simulate the air flow in the air ducts with and without taper, as shown in Figures 1a and 1b. The boundary conditions are listed in Table 1. According to Bernoulli's principle, the system must maintain a constant total pressure. When the air flow encounters a divided flow, the dynamic pressure decreases and the static pressure increases, so that the end of the air duct has a larger static pressure, as shown in Figure 2. To overcome this problem with a consistent outlet airflow pressure, we must make tapers for the air duct or use a damper, baffle plant or VAV box to balance the air flow of each diffuser, as shown in Figure 1b. Figure 3 shows that each diffuser can downgrade the static pressure to match our requirement. If we use a damper or VAV box, we can efficiently control the air flow to balance the consistent outlet air pressure.

Aspects of the water system are shown in Figure 4; the water system flows through three loops for subsystem cooling and forms a closed-loop system. The pipe friction decreases the static pressure related to the distance; the divided flow can increase the static pressure as in the red line shown in Figure 5. In the return loop of the water, the pipe friction continually decreases the static pressure related to distance, and the merged flow also decreases the static pressure as in the white line shown in Figure 5. The pressure difference between the red and white lines is thus the actual pressure for each loop. The actual pressure is least in the latest part of the pipe loop, which even leads to no water flow at the end of the pipe. The TAB is so critical for a water system that we use a balance valve to fine-tune the water flow to meet each loop requirement.

Table 1: Boundary Conditions of Cases 1 and 2 of Air Duct

	case 1	case 2
length of air duct /m	20	20
diffuser area/m^2	0.14	0.14
cross-sectional area 1/m^2	1	1
cross-sectional area 2/m^2	1	0.757
cross-sectional area 3/m^2	1	0.49
cross-sectional area 4/m^2	1	0.303
inlet pressure of air duct /Pa	100	100

Content from this work may be used under the terms of the CC BY 3.0 licence (© 2015). Any distribution of this work must maintain attribution to the author(s), title of the work, publisher, and DOI.

6th International Particle Accelerator Conference IPAC2015, Richmond, VA, USA JACoW Publishing
ISBN: 978-3-95450-168-7 doi:10.18429/JACoW-IPAC2015-WEPHA044

Content from this work may be used under the terms of the CC BY 3.0 licence (© 2015). Any distribution of this work must maintain attribution to the author(s), title of the work, publisher, and DOI.

ALIGNMENT DESIGN AND STATUS OF TAIWAN PHOTON SOURCE

W.Y. Lai, C.J. Lin, P.S.D. Chuang, S.Y. Perng, M.L. Chen, H.S. Wang, C. W. Tsai, D. G. Huang, H.C. Ho, K.H. Hsu, C. K. Kuan, T.C. Tseng, J.R. Chen*
National Synchrotron Radiation Research Center, No 101, Hsin-Ann Road, Hsinchu 30076, Taiwan
*also at Department of Biomedical Engineering & Environmental Sciences,
National Tsing-Hua University, Taiwan

Abstract

After the construction of Taiwan Photon Source (TPS) was finished, the variation of the survey fiducials was stable. However, the following precise alignment work is concerned by the change of temperature critically. In this paper, the whole process of alignment work in the TPS storage ring with the relation of survey network and thermal issues of the environment will be described. We analysed these survey data so that the correction of survey network could be estimated by the change of temperature, thus all the elements for example, booster, pedestals, and girders could be positioned within the shortest time.

INTRODUCTION

Taiwan Photon Source is a new 3-GeV synchrotron ring under construction at the NSRRC in Taiwan. For stability reasons, the entire building has been constructed half underground. Since the construction is underground, it would take more time during the process of constructing the building's foundation and the transport of heavy machinery. In order to implement the operating test of the booster immediately after the building of TPS was constructed, we need to advance the schedule of the installation work. We carried out the installation work when the building was under construction. However, there are a lot of components (beam potion monitor in the vacuum system, pedestals of storage and booster ring, and the magnets) that needed to be installed, which could not be completed in a short time.

Since the work was carried out for a long time, the building was shape shifting due to the variation of thermal issues and the proceeding of the building's construction. To provide the precise fiducial points for positioning, those components will be critical. To achieve the purpose, the survey network of TPS was constructed since July 2012 until now. According to the historical survey data and the current temperature, we can conjecture the variable of shape shift of the building approximately during positioning.

Up to present, the major part of positioning work has been completed, and the booster system of TPS is under operating test. The fiducial points of TPS are still being surveyed periodically for constructing the coordinates of the survey network. In this paper, we also describe the process of survey and installation work and the results of the positioning work.

THE TPS NETWORK DESIGN

The network is the important foundation work to complete the alignment assignment of the TPS project. For stability reason, the TPS building is constructed half underground and has an outer wall blocking the measuring instrument from measuring one site to another directly. Thus, there are 8 fiducial points of global position system (GPS) set up around the building to confirm the location and the shape of TPS construction, as shown in Figure 1. By using these fiducial points of GPS, the primary fiducial points of survey network could be constructed.

Figure 1: The photo of TPS building.

Considering the variation of outdoor temperature, the GPS fiducial points are made by granite to reduce the effect of thermal variation. After the one year of construction, the GPS fiducial points seem to stabilize within time, as shown in Figure 2.

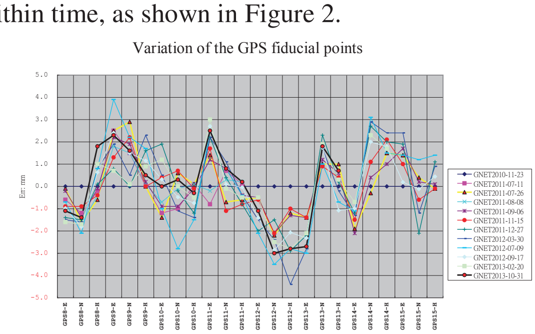

Figure 2: The variation of GPS fiducial points.

Since these fiducial points are stabilized, we can now then construct the primary survey network based on these fiducial points. The primary survey network is constructed by using theodolite and GPS due to environment issues during construction. By reasons of survey data of the altitude direction obtained from the GPS system is not sufficiently accurate. The 8 GPS

ISBN: 978-3-95450-168-7 doi:10.18429/JACoW-IPAC2015-WEPHA045

DESIGN AND CONSTRUCTION OF THE RF ELECTRONIC SYSTEM AT TAIWAN PHOTON SOURCE

F.-T. Chung#, M.-S. Yeh,T.-C. Yu ,Ch. Wang, L.-H. Chang, C.-H. Lo, M.-H. Tsai, M.-H. Chang, T.-C. Yu, L.-J. Chen, Z.-K. Liu, M.-C. Lin, P.-Y. Chen, C.-L. Tsai, National Synchrotron Radiation Research Center, Hsinchu 30076, Taiwan

Abstract

The RF electronic system at NSRRC was made fully in house by the RF group from design through construction to completion. The first RF electronic system includes an analogue LLRF system, a step motor, and an ARC module of a Petra cavity. It was successfully integrated with a 100-kW RF transmitter, high-power RF transfer system, and a cooling system and applied to the booster of TPS. Two duplicated RF electronic system were then applied to the storage ring but integrated with the 300-KW transmitters. With these RF systems, the TPS storage ring achieved beam current 100 mA on 2015 March 26.

INTRODUCTION

This article explains the architecture of the RF electronic system for Taiwan Photon Source (TPS). Modularization of the RF electronic subsystems can duplicate the subsequent second and third storage-ring RF electronic systems efficiently to operate individual RF plant in the first stage of TPS commissioning. The main objective of this article is the construction of the electronic system for booster RF plant, which has also a preliminary role for all RF plants.

The principle of this design is to realize both local and remote monitoring and control of the RF cavity. The booster RF system can provide maximum accelerating voltage 1200 kV to boost the electron beam with maximum RF power 100 kW for nominal operation of the TPS booster ring. The planning and allocation of electric power, cooling water, cooling air, cable tray and signal cabling would be shown as a preliminary preparation for construction of the booster RF plant. The complete construction of the booster and storage ring RF plants were designed to support the first-stage commissioning of the synchrotron accelerator with target beam current 100 mA; the parameters of TPS [1] are listed in Table I.

ELECTRIC UTILITY

To construct operating environment of the RF plants, firstly the AC power was allocated as follows:

(1) 3P4W (general AC power) 380V/220V 250/650A

(2) 3P4W (general AC power) 208V/120V 32/40A

(3) 3P4W (emergency AC power) 208V/120V 50/63A.

The components of the RF system are distributed around the building according to their function. To manage efficiently the electric power to each rack and module for all these components in a balanced and safe condition, the original power racks must their capacity with anti-EMI pipes to the load as shown in Figure 1.

Table 1: Parameters of the TPS Booster Ring

Parameter	Value
injection energy	150 Mev
extraction energy	3 GeV
circumference	496.8 m
harmonic number (h)	828
momentum compaction factor (alpha)	0.002474
repetition rate	3 Hz
RF frequency	499.65 MHz
energy spread (Linac to booster)	0.095 %

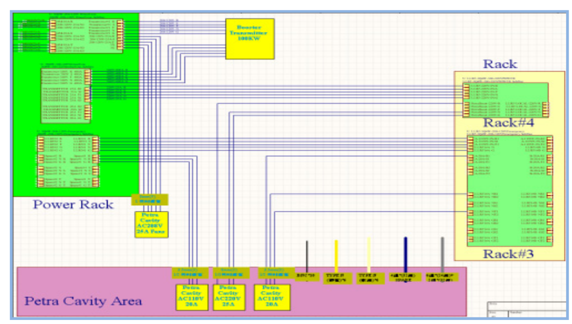

Figure 1: Allocation of AC power for the TPS booster RF system.

AC Power for Transmitter

The RF transmitter requires general AC power of capacity 380 V/400 A through a cable (200 mm^2, 400 A, Hypalon) and AC power (208 V/120 V) for the control panel through cable (22 mm^2, 50 A). As the transmitter rack has its own circuit breaker, the power line can be simply plugged in.

AC Power for Signal Controller

The controller rack area collects the entire control system; emergency power with an uninterruptible power supply is hence required. Racks 3 and 4 integrate a 3P4W AC power distributor to each rack. As the circulator part requires low AC power, this power is supplied by Rack 8.

AC Power for Cavity Control System

The cavity of the booster ring requires emergency electric power at 110 V/20 A for the controller rack, general electric power at 220 V/25 A for the controller rack and general electric power at 110 V/20 A for the main breaker. 220 VAC is supplied to ion pumps.

Content from this work may be used under the terms of the CC BY 3.0 licence (© 2015). Any distribution of this work must maintain attribution to the author(s), title of the work, publisher, and DOI.

ISBN: 978-3-95450-168-7 doi:10.18429/JACoW-IPAC2015-WEPHA046

OUTGASSING ANALYSIS DURING TRANSPORT FOR 14-m-LONG ARC-CELL VACUUM CHAMBERS OF THE TAIWAN PHOTON SOURCE

L. H. Wu#, T. Y. Lee, C. H. Chang, S. W. Chang, Y. C. Yang, Z. W. Chen, Y. P. Chang, C. S. Huang, Y. T. Huang, C. C. Chang, S. N. Hsu, C. K. Chan, C. M. Cheng, B. Y. Chen, H. P. Hsueh, G. Y. Hsiung, and J. R Chen, National Synchrotron Radiation Research Center, Hsinchu, Taiwan

Abstract

An outgassing analysis during transportation for the large, 14-m-long, ultra-high-vacuum aluminum arc-cell chambers of the Taiwan Photon Source (TPS) was performed using residual gas analysis (RGA). Each cell was baked to 150 °C in the laboratory to achieve ultra-high vacuum. Under pumping by primarily ion pumps (IP) and non-evaporable getter (NEG) pumps, the cells obtained pressures of 6.4×10^{-9} Pa on average, and the main residual gas was H_2. Here, vacuum pressure measurements and residual gas analyses were performed in situ while a cell chamber was being transported. It was found that the vibration of the arc-cell vacuum chamber caused the pressure to rise abruptly; in this case, the main outgassing gas was CH_4. Once the arc cell had been fully installed, the vacuum pressure gradually decreased to the original vacuum pressure because of the pumping effect of the ion gauges.

INTRODUCTION

Construction of the Taiwan Photon Source (TPS) began in 2010, and it is expected to begin operations in 2015. The TPS uses a medium-energy electron storage ring operating at 3 GeV. The vacuum chambers of the TPS storage ring are constructed of an aluminum (Al) alloy because of its high thermal conductivity, absence of magnetism, low residual radioactivity, and ease of machining [1]. The TPS contains 24 aluminum arc-cell vacuum chambers in the electron storage ring. Each arc-cell chamber is 14 m in length, including two straight chambers (S3 and S4) and two bending chambers (B1 and B2), as shown in Fig. 1. The straight chambers were constructed from extruded aluminum alloy and subjected to chemical cleaning in a sequential process [2]. The bending-chamber components were manufactured using computer numerical control (CNC) alcohol machining and cleaned with ozonated water [3-4]. Then, each chamber was assembled and jointed using tungsten inert gas (TIG) welding. A residual gas analyzer was installed in the arc-cell vacuum chamber to observe the outgassing of residual gases. According to previous research, [5] ozonated water effectively removes residual carbon from the surfaces of aluminum alloys, and the thermal outgassing rate of such alloys has been found to decrease to 6.7×10^{-12} Pa·m·s^{-1} after baking. Each cell was assembled in the laboratory to create the closed vacuum vessel with two sector gate valves and then pumped by turbo pumps and dry pumps, followed by a 24-hour bakeout. After bakeout and 24 hours of pumping, pressures of less than 1.0×10^{-8} Pa were achieved at room temperature for all cells. Once the vacuum pressure of the 14-m-long aluminum vacuum chamber had achieved UHV levels, the four ion pumps were turned off to investigate the outgassing and to analyze the residual gas using the pressure build-up method. The TPS cell vacuum system is described in detail below.

For one cell aluminum vacuum chamber, which is 14 m in length, the components of the vacuum assembly include two sector gate valves (SGVs) (comb-type RF shield; VAT), two pumping gate valves, bellows, beam position monitors (BPMs), extractor ionization gauges (IGs) (IE514, with an IM 540 gauge controller; Oerlikon), non-evaporable getters (NEGs) (MK5-type SAES getters), ion pumps (IPs) (Starcell 200 L·s^{-1} for nitrogen; Agilent), crotch absorbers, photon stoppers, front-end valves, angle valves, a residual gas analyzer (RGA) (Transpector 2, H100M, used with the control software Tware 32; Inficon), turbomolecular pumps (TMPs) (V81M; Agilent, STP 451; Edwards), and dry pumps (Drytel 1025; Adixen). The vacuum components were assembled in a clean room (class 10,000) under controlled dust-level and humidity conditions to minimize the outgassing rate from the chamber's inner surfaces.

The RGA spectrum was continuously recorded during pumping. In all experiments in this study, the following species were recorded: m/z = 2, 4, 12, 13, 14, 15, 16, 18, 28, 32, 40, and 44, associated with H_2^+, He^+, C^+, CH^+, CH_2^+, CH_3^+, CH_4^+/O^+, H_2O^+, N_2^+/CO^+, O_2^+, Ar^+, and $CO2^+$, respectively. The current I that is reported here represents a RGA spectrum rather than a partial pressure. Although the partial pressure could not be calculated exactly, the predominant component of the residual gas could be inferred by referring to the manufacturer's instructions for the RGA.

This paper focuses on the types of gases produced with increasing vacuum pressure during the cell transportation. While the cell was transported, the ion pumps were turned off and the ion gauges and RGA spectrums were both recorded. It is observed what kinds of gases were responsible for the variation of vacuum pressure. After the arc cell had been fully installed, the variation of the vacuum pressure was continuously observed and the pumping mechanism was discussed.

#wu.lh@nsrrc.org.tw

Content from this work may be used under the terms of the CC BY 3.0 licence (© 2015). Any distribution of this work must maintain attribution to the author(s), title of the work, publisher, and DOI.

ISBN: 978-3-95450-168-7 doi:10.18429/JACoW-IPAC2015-WEPHA048

Content from this work may be used under the terms of the CC BY 3.0 licence (© 2015). Any distribution of this work must maintain attribution to the author(s), title of the work, publisher, and DOI.

BEHAVIOR OF VACUUM PRESSURE IN TPS VACUUM SYSTEM

I-C Yang#, C-K Chan, B-Y Chen, C-K Kuan, I-C Sheng, G-Y Hsiung, L-H Wu, C-C Chang, C-M Cheng, J-Y Chuang, C-C Liang and J-R Chen
National Synchrotron Radiation Research Center (NSRRC), Hsinchu 30076, Taiwan

Abstract

Taiwan Photon source (TPS) is in its first stage commissioning in 2014-2015. The vacuum systems of TPS were installed for commissioning since August 2014. After four months performance testing and subsystem integration, the commissioning of booster ring began on 12 December and then the first 3 GeV beam was stored on 31 December. 100mA beam current, 35Ah accumulated beam dose was archived in March 2015 before machine shut down.

The average pressure in storage ring is 2.8×10^{-8} Pa before commissioning, rising to 1.33×10^{-7} Pa with 100mA beam current. In 35Ah accumulated beam dose, the target of beam cleaning effect has reached to 8.92×10^{-10} Pa/mA. The vacuum performance, experience and events during commissioning will be presented in this paper.

INTRODUCTION

TPS is a low-emittance 3-GeV synchrotron ring with the concentric storage and booster rings in the same tunnel. The storage ring, with 518.4m circumference, is divided into 48 sections by RF gate valves, including 24 arc cells and 24 straight sections [1]. The 14m arc cells, which were prebaked to ultra-high vacuum in NSRRC's facility during 2012 November to 2013 August, and installed into TPS tunnel under vacuum in 2013 October to 2014 March. The straight sections, six of length 12 m and 18 of length 7 m are assembled continually, including one injection section, one diagnostic section, two PETRA cavities and other dummy sections until 2014 August. During the installation of straight sections of storage ring, booster ring, the transfer line from the LINAC to the booster ring (LTB, LINAC to booster ring) and the transfer line from the booster ring to the storage ring (BTS, booster to storage ring) were also assembled at the same time.

Aluminium alloy was chosen as the material of vacuum chamber because of its lower thermal outgassing rate and good experience in Taiwan Light Source at NSRRC in the past 20 years. For the arc sections, the triangularly shaped vacuum chambers were designed and Cu crotch absorbers located downstream intercepts more than 70 % of the synchrotron radiation from the bending magnet. Pumping unit combined sputtering ion pump (SIP) with non-evaporable getter pump (NEG) was design and located at the antechamber so as to decrease the pumping ports and produce a smooth vacuum surface with small impedance. Besides, near the crotch absorbers and photon stoppers, NEG pumps were also installed to enhance pumping speed. In addition, exhaust pumping systems with turbo-molecular pumps were used to remove large amount of the photon stimulated desorption during machine commissioning. The geometric layout of bending chamber in arc section is shown in Figure1.

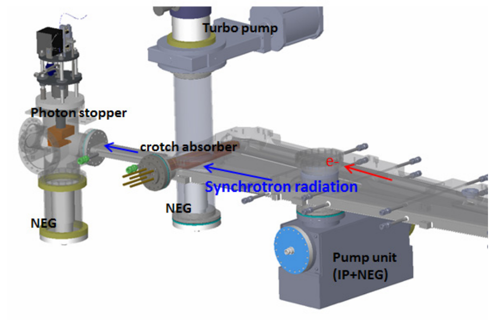

Figure 1: The geometric layout of bending chamber in arc section.

Extractor ion gauge (EIG) was used as pressure reading and safety interlock system in TPS storage ring while cold cathode gauges (CCG) were used in booster ring. Total 144 gauges installed averagely into 48 vacuum sections were planned; it means all 3 gauges were installed between two section gate valves (SGV). 1×10^{-4} Pa pressure trip was set as high limit for vacuum interlock. If any two gauges reach high limit or malfunction, the logic trigger signal would then be sent out to close the SGVs at this section. In order to extend the operation lifetime, self-protection mode of EIGs was set. In such mode, EIGs will be switched off automatically when the vacuum pressure raises higher than 1×10^{-3} Pa [2].

Due to impedance issue and reducing the interference from scatter electron, EIG was installed into pumping unit shown as EIG3 in Figure 2. In straight section, another one was installed near the orbit of electron beam, especially in out-of-vacuum insertion device which has no space to install. The reading of EIGs in different location was summarized in table1. In static pressure, the readings were similar; a 1.5x difference was found in dynamic condition with 100mA beam current.

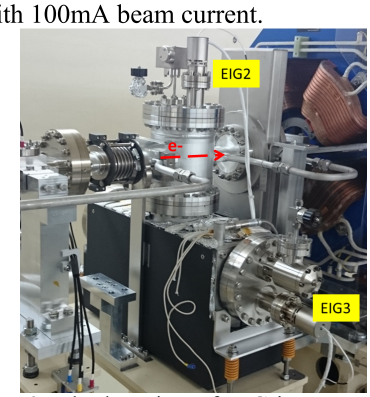

Figure 2: The location of EIG in storage ring.

#jolas@nsrrc.org.tw

ISBN: 978-3-95450-168-7 doi:10.18429/JACoW-IPAC2015-WEPHA049

DEMAGNETIZE BOOSTER CHAMBER IN TPS

I. C. Sheng#, C. K. Kuan, C.T.Chen, Y. C. Yang, National Synchrotron Radiation Research Center (NSRRC), HsinChu, Taiwan

Abstract

Taiwan Photon Source (TPS) project starts its booster commissioning starts from August 2014. Few issues have been discovered and fixed. Since the booster aperture is relatively small and number of magnets is barely sufficient. Therefore extreme precise control of booster chamber alignment and the corresponding chamber permeability is as well important.

In this paper, we present how the booster chamber is uninstalled, demagnetized and reinstalled within three weeks. This procedure is proven to result in the lowest booster chamber permeability in the world and a good high vacuum booster ring is built in 3 weeks.

INTRODUCTIONS

National Synchrotron Radiation Research Center (NSRRC) in Taiwan has just completed the construction of third generation synchrotron accelerator named Taiwan Photon Source (TPS) in second quarter of 2014, this 3GeV, 500mA designed energy machine will provide 48 beam lines in the future. The machine finished the Linac was commissioned in August 12, 2014 and the booster ring started its beam-based hardware testing right after that date.

However during the booster commissioning the operation group encountered several problems such as booster dipole magnet power overheated, even the power supply group quickly resolved the problem but the operation staff still had problem to store the beam in the 500m circumference concentric booster chamber. This 35mm x 20mm stainless steel 304 elliptical chamber was drawn from circular stainless steel tube and is 0.7mm thick, as shown in Figure 1.

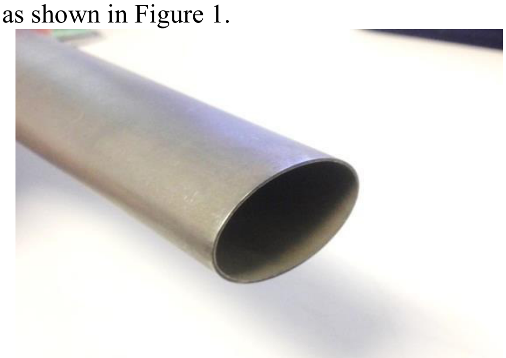

Figure 1: TPS booster chambers.

Beam dynamics staff had problem to fully control the electron beam even with correctors. Simulation shows that difference of closed orbit distortion (COD) can be up to $\pm 20\mathrm{mm}$ without corrections. While everyone was wondering what might be the causes. In November 12, 2014, one of engineering staff found that elliptical chambers attracted his small piece of NdFeB magnet. We further discovered that the chamber does meet our low permeability requirement (typically magnetic relative permeability for stainless steel $\mu_r = 1.01$ and some of them was found to be $\mu_r = 1.8$!). This explains why operation staff failed to store the electron beam in the booster no matter how hard they have tried to tweak the magnetic fields.

Since the target schedule is planning to have beam stored in the storage ring by the end of 2014, we have to demagnetize the booster chamber as soon as possible. As a matter of fact, vacuum group has to remove total 500m long booster chambers, demagnetize, reinstall and pumping down in three weeks.

Table 1: Heat Treatment Material Processing to Demagnetize Metals

Process	Pros	Cons
Continuous heat treat furnace	▪ Large size	▪Non-uniform heating, large deformation. ▪Not clean.
Demagnetizer	▪ Convenient to use. ▪ Cost effective	▪Temporarily demagnetize but not permanent.
Vacuum furnace	▪ Compliance with UHV	▪Limited heat treatment sizes.

The demagnetization process is to heat up stainless steel to Austenite (γ) phase at elevated temperature. This heat treatment process is to re-transform Martensitic structure back to Austenitic one. The carbon composition of SST304 we procured is 0.06, and the suggested demagnetized temperature is $1050\ ^{o}C$ [1], then cool down to room temperature. As shown in Table 1, there are several processes to demagnetize the stainless steel. It is clear that vacuum furnace is the only way to go, except we have many long tubes which are over 2-4meters long. And most of domestic heat treat companies have only less than 1.2m maximum size furnace.

Another challenging of this demagnetization task is how to efficiently sort out all the elliptical chambers, and restore them back within the time frame.

DEMAGNITIZATION

Table 2 indicates the original quantity of the booster chamber with their corresponding flange-to-flange length range.

#shengic@nsrrc.org.tw

Content from this work may be used under the terms of the CC BY 3.0 licence (© 2015). Any distribution of this work must maintain attribution to the author(s), title of the work, publisher, and DOI.

ISBN: 978-3-95450-168-7 doi:10.18429/JACoW-IPAC2015-WEPHA051

Content from this work may be used under the terms of the CC BY 3.0 licence (© 2015). Any distribution of this work must maintain attribution to the author(s), title of the work, publisher, and DOI.

DEVELOPMENT OF A HYBRID POWER SUPPLY AND RF TRANSMISSION LINE FOR SANAEM RFQ ACCELERATOR

S. Ogur *, Bogazici University, Istanbul, Turkey
G. Turemen, Ankara University, Ankara
F. Ahiska, EPROM Electronic Project & Microwave Ind. and Trade Ltd. Co., Ankara, Turkey
A. Alacakir, TAEK-SANAEM, Ankara, Turkey
G. Unel, UCI, Irvine, California, USA

Abstract

SANAEM Project Prometheus (SPP) has been building a proton beamline at MeV range. Its proton source, two solenoids, and a low energy diagnostic box have been already manufactured and installed. These are going to be followed by a 4-vane RFQ to be powered by two stage PSU. The first stage is a custom-built solid state amplifier providing 6 kW at 352.2 MHz operating frequency. The second stage, employing TH 595 tetrodes from Thales, will amplify this input to 160 kW in a short pulsed mode. The power transfer to the RFQ will be achieved by the means of a number of WR2300 full and half height waveguides, 3 1/8" rigid coaxial cables, joined by appropriate adapters and converters and by a custom design circulator. This paper summarizes the experience acquired during the design and the production of these components.

INTRODUCTION

SANAEM, Saraykoy Nuclear Research and Training Center of Turkish Atomic Energy Authority in Ankara, has begun to build a Proton Linac, under the name of SPP, with a modest target: aiming to get at least 1 mA of current at the energy of 1.3 MeV [1]. This low-energy proton linac is also going to serve as a domestic know-how build-up instrument by which young scientists and engineers, as well as the local industry, will get acquainted with accelerator technology. The RF power section of this linac consists of three main parts: the Power Supply Unit (PSU), a circulator, and the power transmission line including appropriate waveguide adapters and converters. The RF transmission system is to feed the 4-vane RFQ with the design parameters presented in elsewhere [1], [2]. The power requirement for the SPP RFQ is calculated by taking into account the ohmic losses on the RFQ walls (60 kW obtained after computer simulations) together with the transmission and coupling losses (30 kW a worst case scenario estimation). Folding in a safety factor of 1.3, one finds 120 kW as the required RF power under the assumption of continuous operation. SSP will initially operate with a duty factor less than 3% to reduce the requirements on the RF PSU. The entire RF power supply and transmission system is shown in Fig. 1.

* salim.ogur@boun.edu.tr

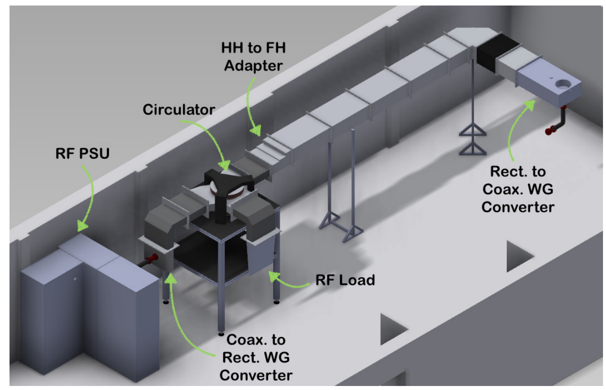

Figure 1: The overview of the SPP RF transmission line.

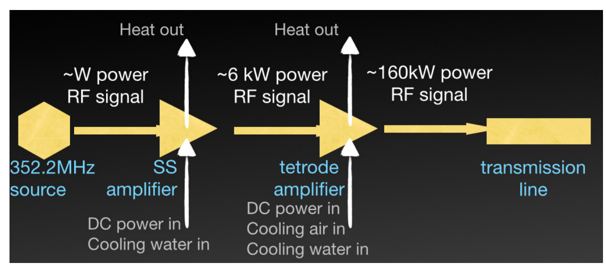

Figure 2: SPP PSU design.

POWER TRANSMISSION LINE

Power Supply Unit

The operating frequency of the SPP RFQ is 352.2 MHz. This operating frequency is chosen to be compatible with similar machines in Europe and to take advantage of already available RF amplifier market. The accelerator is intended to operate at a maximum duty factor of about 3%. To fulfill these requirements, two stage amplification has been selected, as summarized in Fig. 2. The power supply is designed by the SPP-team, and manufactured by a local company [3].

The construction of the first stage of the PSU started around the BLF-578XR high power transistor [4]. The water cooled solid state amplifier circuit designed around this transistor provides about 1.7 kW of RF power for a pulse length shorter than 500 milliseconds, with an amplification of about 18.3 dB. A photo of the SS amplifier unit test bench can be seen in Fig. 3. The combiner system, consisting of 8 such boards, achieves a total power of 6 kW in continuous mode and over 10 kW in pulsed mode. For this particular

ISBN: 978-3-95450-168-7 doi:10.18429/JACoW-IPAC2015-WEPHA052

TEST CAVITY AND CRYOSTAT FOR SRF THIN FILM EVALUATION

Philippe Goudket[1,3], Shrikant Pattalwar[1,3], Oleg B. Malyshev[1,3], Lewis Gurran[1,2], Graeme Burt[2], Edward S. Jordan[4], Thomas J. Jones[4], Dmitry O. Malyshev[1] and Reza Valizadeh[1,3]

[1] ASTeC, STFC Daresbury Laboratory, Daresbury, Warrington, Cheshire, UK
[2] Lancaster University, Cockcroft Institute, Lancaster, UK
[3] Cockcroft Institute, Warrington, Cheshire, UK
[4] TD, STFC Daresbury Laboratory, Daresbury, Warrington, Cheshire, UK

Abstract

In developing superconducting coatings for SRF cavities, the coated samples are tested using various techniques such as resistance measurements, AC, and DC magnetometry which provide information about the superconducting properties of the films such as RRR, H_{c1}, H_{c2} and vortex dynamics. However, these results do not allow the prediction of the superconducting properties at RF frequencies. A dedicated RF cavity was designed to evaluate surface resistive losses on a flat sample. The cavity contains two parts: a half-elliptical cell made of bulk niobium (Nb) and a flat Nb disc. The two parts can be thermally and electrically isolated via a vacuum gap, whereas the electromagnetic fields are constrained through the use of RF chokes. Both parts are conduction cooled hence the system is cryogen free. The flat disk can be replaced with a sample, such as a Cu disc coated with a Nb film. The RF test provides the cavity Q-factor and thermometric measurements of the losses on the sample. The design advantages are that the sample disc can be easily installed and replaced; installing a new sample requires no brazing/welding/vacuum or RF seal, so the sample preparation is simple and inexpensive.

INTRODUCTION

Superconducting coatings (SC) for radio-frequency (RF) cavities in particle accelerators have been used since the 1980s [1]. They provide many advantages such as combining the good thermal conductivity of copper and the superconducting properties provided by a thin niobium film. However, the RF performance of these SC cavities (such as Q_0 and E_{max}) has always been lower than those made of bulk niobium. Several research laboratories around the world have put in an effort to improve the quality of SC cavities [2-4]. This required understanding the correlation between (a) deposition parameters and conditions, (b) surface analysis, (c) superconducting properties and (d) performance in an RF field. To enable the UK capability in SC cavity production and to improve the quality of SC cavities the ASTeC team has employed a number of systems to evaluate the properties of the coated layer. Deposited samples are studied with surface analysis systems to study the film compositions and morphology, chemical bonding, grain size, crystal structure and phase. They then undergo the superconducting properties characterisation: measurements of quantities such as RRR, T_c, H_{c1} and H_{c2} (residual resistivity ratio, critical temperature, and critical H-fields 1 and 2) with DC and AC magnetic susceptibility methods [5–7]. However, these measurements do not allow the prediction of the behaviour of such a film in RF conditions. Depositing the coating on a different cavity for each type of film would be too expensive and time consuming; therefore a test cavity for quick evaluation of planar samples is required. This paper is devoted to the RF, cryogenic and mechanical design along with the implementation of such a cavity.

EXPERIMENT SETUP

As the cavity is not completely coated in the thin film, it is necessary to separate the losses on the bulk Nb walls from that on the sample. A convenient way of doing so is using a calorimetric method using a DC heater placed underneath the sample plate: the temperature of the sample is measured with no RF, then the RF is switched on while the DC heater is turned down to keep the sample at the same temperature, hence the losses on the sample are equal to the reduction in heater power. However for this measurement to be accurate it is necessary to thermally isolate the sample from the cavity.

Here we propose to have a vacuum gap between the two structures with RF chokes to prevent RF leakage. Both parts are conduction cooled to avoid having the cavity immersed in a LHe bath. The experiment is then placed in a large vacuum chamber, eliminating the need for any vacuum seals between the two parts. As such the cavity and the sample require no physical connection between them. The chokes increase the cavities transverse size hence a cavity frequency of 7.8 GHz is proposed in order to fit in the conduction cooling cryostat. The cavity will be used to measure BCS resistance as a function of cavity field. Due to the fact that R_{BCS} at 1.8 K will be 165 nΩ it will not be possible to measure the residual resistance.

RF CAVITY DESIGN

The project required the design of an RF structure capable of subjecting the sample surfaces to surface currents. In order to keep the sample as simple as possible, it was decided to design a cavity able to test a

Content from this work may be used under the terms of the CC BY 3.0 licence (© 2015). Any distribution of this work must maintain attribution to the author(s), title of the work, publisher, and DOI.

ISBN: 978-3-95450-168-7 doi:10.18429/JACoW-IPAC2015-WEPHA053

SURFACE RESISTANCE RF MEASUREMENTS OF MATERIALS USED FOR ACCELERATOR VACUUM CHAMBERS

Philippe Goudket[1,3], Lewis Gurran[1,2], Graeme Burt[2], Mark Roper[1,3], Stuart Wilde[1,4], Oleg B. Malyshev[1,3], Reza Valizadeh[1,3]
[1]ASTeC, STFC, Daresbury Laboratory, Daresbury, Warrington, Cheshire, UK
[2]Lancaster University, Cockcroft Institute, Lancaster, UK
[3]Cockcroft Institute, Warrington, Cheshire, UK
[4]Loughborough University, Loughborough, UK

Abstract

The RF surface resistance of accelerator vacuum chamber walls can have a significant impact on the beam quality. There is a need to know how the use of a new material, surface coating or surface treatment can affect the RF surface resistance. ASTeC and Lancaster University have designed and built two test cavities where one face can be replaced with a sample in the form of a flat plate. The measurements are performed with a network analyser at the resonant frequency of approximately 7.8 GHz.

INTRODUCTION

If one considers the formulation of the unloaded quality factor Q_0 of an RF cavity [1] one can write

$$Q_0 = \frac{2\pi f_0 \mu_0 \iiint_V |\boldsymbol{H}|^2.dV}{\iint_S R_S |\boldsymbol{H}|^2.dS} \quad (1)$$

where H is the magnetic field, R_S is the surface resistance of the cavity walls and f_0 is the resonant angular frequency of the cavity. To accommodate the possibility of a cavity being comprised of two parts (a cavity and a sample) which could be made of different metals or otherwise have different R_S values, one can most conveniently rewrite this as

$$Q_0 = \frac{G}{R_S^{sample} p_S + R_S^{cavity} p_C} \quad (2)$$

where G is the geometry constant of the cavity [1], defined as

$$G = \frac{2\pi f_0 \mu_0 \iiint_V |\boldsymbol{H}|^2.dV}{\iint_S |\boldsymbol{H}|^2.dS} \quad (3)$$

R_S^{sample} and R_S^{cavity} are the surface resistance of the sample and the cavity respectively, and p_S and p_c the sample and cavity ratios – the proportion of the total field dissipated over their respective surfaces, i.e.

$$p_S = \frac{\iint_{sample} |\boldsymbol{H}|^2.dS}{\iint_S |\boldsymbol{H}|^2.dS} \quad (4)$$

$$p_C = \frac{\iint_{cavity} |\boldsymbol{H}|^2.dS}{\iint_S |\boldsymbol{H}|^2.dS} = 1 - p_S \quad (5)$$

For any similarly-shaped cavity G and p_S are in principle constant, irrespective of the materials used.

This implies that, knowing R_S^{cavity}, G and p_S for a given cavity we can calculate R_S for any sample by placing it on top of the cavity and finding the unloaded Q-factor of the resulting RF resonance.

$$R_S^{sample} = \frac{G/Q_0 - R_S^{cavity}(1-p_S)}{p_S} \quad (6)$$

METHOD

Calculation of Q_0

Two double-choked pillbox-type cavities were used to take our measurements, one of which can be seen in Fig. 1. The choked cavity allows the testing of flat samples without the need for flanges and RF seals. Both cavities were manufactured to identical dimensions by Niowave Inc. [2], one being made from aluminium and one from niobium.

Figure 1: A two-choked 8 GHz Al test cavity.

In each case the samples, in the form of flat plates or discs of sufficient width to completely cover the outer choke, were placed on top of the cavity with spacers providing a gap of ~2 mm between the cavity and the sample. An axially-mounted coaxial antenna was attached to a calibrated network analyser to induce RF resonance, and the coefficient of signal reflection (S_{11}) measured against frequency. Initial setup required that the spacing between the sample and the cavity was adjusted to

Content from this work may be used under the terms of the CC BY 3.0 licence (© 2015). Any distribution of this work must maintain attribution to the author(s), title of the work, publisher, and DOI.

ISBN: 978-3-95450-168-7 doi:10.18429/JACoW-IPAC2015-WEPHA054

COMMISSIONING OF THE TRANSVERSE DEFLECTING CAVITY ON VELA AT DARESBURY LABORATORY

A.E. Wheelhouse#, R.K. Buckley, S.R. Buckley, L. Cowie[1], P. Goudket, L. Ma, J. McKenzie, A.J. Moss, STFC ASTeC, Daresbury, Warrington, Daresbury Laboratory, Sci-Tech Daresbury, Warrington, WA4 4AD, UK
G.C. Burt, M. Jenkins, Lancaster University, Cockcroft Institute, Lancaster, LA1 4YW, UK

Abstract

A 9-cell S-band transverse deflecting copper cavity (TDC) has been designed and built to provide a 5 MV transverse kick in order to perform longitudinal profile measurements of the electron bunch on the Versatile Electron Linear Accelerator (VELA) at Daresbury Laboratory. The cavity has been manufactured by industry and has been field flatness measured using a bead-pull system. The cavity has then been installed on to the VELA facility and commissioned for operation with the electron beam. This paper discusses the cold testing and the RF conditioning of the cavity.

INTRODUCTION

The Versatile Electron Linear Accelerator (VELA) [1] at Daresbury Laboratory is a facility which has been built for the investigation and development of novel and compact accelerator technology specifically aimed at medical, health, security, energy and industrial processing. For this purpose the facility consists of two separate user areas for scientific research.by industrial users. In addition VELA is to be used to study fundamental requirements for the next generation FEL as part of the development of the Compact Linear Accelerator for Research and Applications (CLARA) facility being built at Daresbury Laboratory [2].The VELA facility is designed to provide a 4 - 6 MeV electron beam with bunch charges between 10 - 250 pC, a short bunch length 0.1 – 3 ps) and low transverse emittance. The facility consists of an S-band photo-injector gun with a copper cathode which is driven by a Coherent Inc. UV laser providing a pseudo-Gaussian profile of 1 mm FWHM at the cathode. The beam is then transported to either of the user areas via a diagnostic line consisting of a transverse deflecting cavity (TDC), a wall current monitor, YAG screens, Faraday cup and slit/strip line beam position monitors (BPMs).

To accurately measure the longitudinal profile of the electron bunch an S-band 9-cell copper transverse deflecting cavity has been designed [3], built, characterised, installed (Fig.1) and commissioned. The cavity was manufactured by Research Instruments GmbH, Germany and was designed to provide a transverse kick of around 5 MV to the electron bunch which converts the longitudinal position into a transverse offset seen on a YAG screen enabling the bunch profile to be analysed [4]. The specifications of the TDC are shown in Table 1.

#Alan.Wheelhouse@stfc.ac.uk
[1] Lancaster University, Cockcroft Institute, Lancaster, LA1 4YW, UK

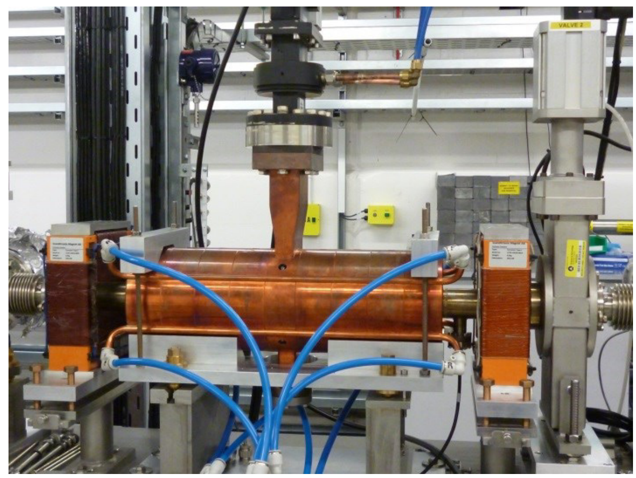

Figure 1: VELA Transverse Deflecting Cavity.

Table 1: VELA TDC Parameters

Parameter	Value	Units
Frequency	2998.5	MHz
Bunch energy	4-6	MeV
Time resolution	10	fs
Phase stability required	0.1	°
Operating mode	TM110-like	
Nearest mode separation	>5	MHz
Available RF power	5	MW
Pulse length	Up to 3	µs
Average RF power loss	<150	W
Input coupling	WR284	

CAVITY RF COLD TESTS

On delivery the frequency and field flatness of the cavity were measured. S-parameter measurements from the input coupler to the probe showed a room temperature operating mode frequency of 2999.1 MHz. This dictated an operating temperature of 55°C to achieve the required 2998.5 MHz. The water temperature will be reduced during RF operation to maintain the cavity frequency and to compensate for RF heating. An S21plot and the S11 Smith chart with the cavity at 55°C and under vacuum are shown in Figure 1. The bandwidth of the operating mode is 383 kHz and Q_0 is measured to be 13700.

The cavity has a vertical probe that couples to the operating mode, and a horizontal SOM coupler that couples to the orthogonal polarisation of the operating mode. The power in the cavity when in use is of the order

Content from this work may be used under the terms of the CC BY 3.0 licence (© 2015). Any distribution of this work must maintain attribution to the author(s), title of the work, publisher, and DOI.

ISBN: 978-3-95450-168-7 doi:10.18429/JACoW-IPAC2015-WEPHA057

HIGH GRADIENT TESTING OF AN X-BAND CRAB CAVITY AT XBOX2

B. Woolley, Cockcroft Institute, Lancaster, United Kingdom and CERN, Geneva Switzerland
P. Ambattu, R. Apsimon, G. Burt, A. C. Dexter, Cockcroft Institute, Lancaster, United Kingdom
A. Grudiev, I. Syratchev, R. Wegner, W. Wuensch, CERN, Geneva, Switzerland

Abstract

CERN's Compact linear collider (CLIC) will require crab cavities to align the bunches to provide effective head-on collisions. An X-band quasi-TM_{11} deflecting cavity has been designed and manufactured for testing at CERN's Xbox-2 high power standalone test stand.

The cavity is currently under test and has reached an input power level in excess of 40MW, with a measured breakdown rate of better than 10^{-5} breakdowns per pulse. This paper also describes surface field quantities which are important in assessing the expected BDR when designing high gradient structures.

INTRODUCTION

At the CLIC interaction region electron and positron bunches collide with a 20 mrad crossing angle and have an elongated shape (45 µm long and 45 nm wide). These two factors cause a 90% reduction in luminosity compared to a head on collision. Crab cavities on each linac are required to rotate each of the bunches before the interaction point. The luminosity can be restored to within 98% of which is attainable for a head on collision [1].

For cavities placed just before the final quadrupole doublets, the required voltage kick is 2.55MV per cavity. In order to reduce wakefields, a structure with a low cell count is preferred. Therefore, to obtain the required kick a high gradient design is needed. An 11.9942 GHz design was chosen in order to utilise the expertise and RF infrastructure already available within the CLIC project.

RF DESIGN

The cavity was designed at Lancaster University/Cockcroft Institute, UK. It is a travelling wave structure employing a quasi-TM11 dipole mode with $2\pi/3$ phase advance per cell. There are ten regular cells and two coupling cells. The cavity's specifications were finalised by considering the limits upon beam loading sensitivity, wakefields and peak power available from the high power RF network.

The iris radius is 5mm and was chosen to keep short range wakefields within acceptable limits. For long range wakefields, the same order mode (SOM) is actively damped by using a racetrack cell shape. The frequency of the SOM is shifted such that every other bunch damps the unwanted mode. The shifted frequency must be a factor of 3n/2 of the bunch reputation rate (2 GHz). A SOM frequency of 13GHz was chosen to this effect. In the final design, the lower order monopole mode and higher order modes also require damping. Studies have been conducted to design cavities with choke mode or waveguide damping. Waveguide damping was found to be superior [2] and two prototype cavities were commissioned to be built and tested at CERN; an un-damped prototype and a damped prototype (albeit without silicon carbide absorbers). The un-damped prototype has been built and is currently under high power test at CERN.

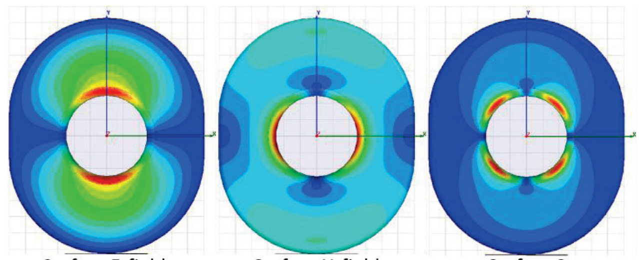

Figure 1 shows the cell geometry and the E-field, H-field and the modified pointing vector 'Sc' [3] of the un-damped crab cavity as simulated in HFSS.

As shown in Figure 1, the surface quantities affect breakdowns have peaks at different locations around the iris. For monopole mode structures all of the quantities shown in Figure 1 are distributed evenly around the iris. Therefore, this cavity provides an opportunity to test which surface quantities (electric field, magnetic field or power flow) contribute most strongly towards causing breakdowns. This can be achieved through a post-mortem inspection using optical and/or electron microscopy. A so called 'dark current spectrometer' can be used to look at the geometric source of emitted electrons during a BD in real-time. Both of these methods will be used with the latter being described in the following paper [4].

Table 1 shows the characteristics of the CLIC T24 un-damped accelerating structure, the LCLS deflector [5] and the CLIC crab cavity

Property	**CLIC T24 (unloaded)**	**LCLS deflector**	**CLIC Crab (un-damped)**
Input Power	37.2 MW	20 MW	13.35 MW
Transverse Kick	-	24 MV	2.55 MV
Peak surf. E-field	219 MV/m	115 MV/m	88.8 MV/m
Peak surf. H-field	410 kA/m	405 kA/m	292 kA/m
Peak Sc	3.4 MW/mm^2	-	1.83 MW/mm^2

Content from this work may be used under the terms of the CC BY 3.0 licence (© 2015). Any distribution of this work must maintain attribution to the author(s), title of the work, publisher, and DOI.

ISBN: 978-3-95450-168-7 doi:10.18429/JACoW-IPAC2015-WEPHA058

SUPERCONDUCTING COATINGS SYNTHETIZED BY CVD/PECVD FOR SRF CAVITIES

P. Pizzol[1,4], A. Hannah[1], O.B. Malyshev[1], S. Pattalwar[1], R. Valizadeh[1], G. B. G. Stenning[2], T. Heil[3], P. R. Chalker[4]
[1] ASTeC, STFC Daresbury Laboratory, Warrington, UK
[2] ISIS, STFC Rutherford Appleton Laboratory, Didcot, UK
[3] Nanoinvestigation Centre at Liverpool, University of Liverpool, Liverpool, UK
[4] Department of Material Science, University of Liverpool, Liverpool, UK

Abstract

Bulk niobium cavities are widely employed in particle accelerators to create high accelerating gradient despite their high material and operation cost.

In order to reduce this cost, thin layer of niobium are deposited on a copper cavity, which has lower material cost with higher availability and more importantly higher thermal conductivity.

The coating of superconducting cavities currently is synthesized by physical vapour deposition (PVD) method which suffers from lack of conformity. By using chemical vapour deposition (CVD) and plasma enhanced chemical vapour deposition (PECVD) it is possible to deposit thin Nb layers uniformly with density very close to bulk material. This project explores the use of PECVD / CVD techniques to deposit metallic niobium on copper using NbCl5 as precursor and hydrogen as a coreagent. The samples obtained were then characterized via SEM, TEM, SAD, XRD, XPS, and EDX as well as assessing their superconductivity characteristics (RRR and Tc) All the samples deposited are superconductive and polycrystalline; the sample obtained with CVD measured RRR=31 and Tc=7.9 K, while the sample obtained with PECVD exhibited RRR=9 and Tc= 9.4 K. In both cases the films grew in a (100) preferred orientation.

INTRODUCTION

Superconductive niobium cavities are widely used in particle accelerators to provide the gradient required to accelerate the desired particles via RF energy. Technology has caught up with the physical limits of bulk niobium, exploiting the material to its maximum potential [1]. Since the SRF requires less than 1 micron of material, it could be possible to obtain the same properties of niobium bulk with niobium thin films [2]. Thin films are a considerably cheaper option than bulk materials for the following reasons, firstly less material is being used and secondly, since SRF cavities operate at temperatures below 10K, the films can be deposited on high thermal conductivity materials such as copper making it easier to cool and maintain the low temperatures than with bulk superconductors [3]. Theoretical studies [4] have also suggested that the use of Superconductor / Insulator / Superconductor thin films (ISI) can lead to an increase in the accelerating gradient, surpassing the limits of bulk niobium. CVD [5] is a chemically driven technique that allows the coating of large areas with great control over the produced film. This technique is therefore being explored to verify the feasibility of depositing metallic superconductive niobium with a homogeneous and uniform structure.

The purpose of the present study is to deposit thin films of Nb using CVD and plasma enhanced CVD (PECVD) techniques. The use of plasma enables reduction of the deposition temperature and allows coating of shapes with a high degree of complexity, such as cavities [6].

After microstructural evaluation, the films have then been assessed for their superconducting properties showing their suitability for use in SRF cavities.

EXPERIMENTAL SETUP

A steel spherical chamber is kept at a base pressure of 10-6 mbar and constantly heated to 120 °C as shown in figure 1. The carrier gas (argon) and the reducing gas (hydrogen) are purified through a heated filters system to ensure that the presence of residual contaminants in the deposition chamber is kept as low as possible.

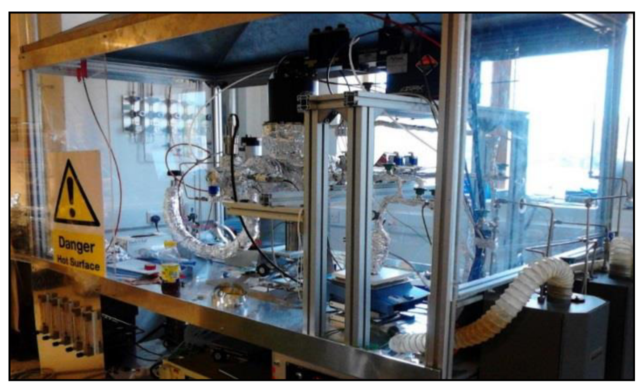

Figure 1: Deposition facility.

The chemical precursor ($NbCl_5$) is placed under controlled atmosphere in a two-legged steel bubbler. The bubbler is then connected to the deposition rig and maintained at the chamber base pressure. Oxygen free copper substrates are cleaned via in-house process (acetone – IPA- distilled water) to further reduce the quantity of contaminants. A substrate is introduced in the chamber and kept at the chamber base pressure for 24 hours prior deposition. The NbCl5 precursor is heated up until a vapor pressure suitable for the deposition is

Content from this work may be used under the terms of the CC BY 3.0 licence (© 2015). Any distribution of this work must maintain attribution to the author(s), title of the work, publisher, and DOI.

ISBN: 978-3-95450-168-7 doi:10.18429/JACoW-IPAC2015-WEPHA059

PHYSICAL VAPOUR DEPOSITION OF THIN FILMS FOR USE IN SUPERCONDUCTING RF CAVITIES

S. Wilde[1,3], R. Valizadeh[1], O.B. Malyshev[1], G. B. G. Stenning[2], A. Hannah[1], D.O. Malyshev[1], S. Pattalwar[1], B. Chesca[3]
[1]ASTeC, STFC Daresbury Laboratory, Warrington, UK
[2]ISIS, STFC Rutherford Appleton Laboratory, Didcot, UK
[3]Department of Physics, Loughborough University, Loughborough, UK

Abstract

The production of superconducting coatings for radio frequency cavities is a rapidly developing field that should ultimately lead to acceleration gradients greater than those obtained by bulk Nb RF cavities. Optimizing superconducting properties of Nb thin-films is therefore essential. Nb films were deposited by magnetron sputtering in pulsed DC mode onto Si (100) and MgO (100) substrates and also by high impulse magnetron sputtering (HiPIMS) onto Si (100), MgO (100) and polycrystalline Cu. The films were characterised using scanning electron microscopy, x-ray diffraction and DC SQUID magnetometry.

INTRODUCTION

Superconducting radio frequency (SRF) cavity technology in particle accelerators is now reaching the limit of performance achievable with bulk Nb cavities [1]. Since superconducting properties for SRF are confined to a penetration depth of less than one micron [2] then Nb thin-films offer an alternative to bulk Nb with the advantage of Cu substrates which have a factor of three higher thermal conductivity than Nb [3]. A Nb thin-film which is oriented parallel to a magnetic field can have a higher first critical magnetic field than bulk Nb if the film is thinner than the London penetration depth. There is also the possibility of multilayer films that provide greater magnetic shielding [4]. With better thermal stability and higher critical fields it is possible to have higher accelerating gradients within SRF cavities allowing for better performance, reduced cost and reduced volumes of Nb [5]. Physical vapour deposition by magnetron sputtering has been used as a preferred process due to its high deposition rate and ease of scalability in order to produce superconducting thin films within SRF cavities [6,7]. The purpose of the present study is to compare films deposited by both pulsed DC and HiPIMS and to compare films deposited onto Si (100), MgO (100) and polycrystalline Cu substrates. Nb thin films were deposited using the Advanced Energy Pinnacle + in pulsed DC mode. Films were then deposited by HiPIMS using an Ionautics HiPSTER 1000 power supply. HiPIMS has a characteristic peak current which is two orders of magnitude higher than pulsed DC at the expense of a reduction in deposition rate. The variable parameters are deposition current, voltage, pulsed duty cycle, pulsed frequency, substrate temperature, and substrate bias. After morphological evaluation the films have then been assessed for their superconducting properties showing their suitability for use in SRF cavities.

EXPERIMENTAL

Thin film samples were deposited simultaneously onto Si (100), MgO (100) and polycrystalline Cu substrates using Kr sputtering gas. Each substrate was prepared by cleaning in ultrasonic baths of acetone, methanol, IPA, then deionised water [8]. In the case of HiPIMS deposition, the substrate was then plasma cleaned using oxygen plasma, then ion bombarded for 30 minutes before deposition. The pulsed DC power was set to 400 W at 350 kHz with a 50% duty cycle. The HiPIMS power supply was varied between 100 and 400 W. Pulse lengths were operated between 100 and 300 µs at frequencies between 100 and 300 Hz. A typical current – voltage – time profile for the HiPIMS power supply is shown in Fig 1.

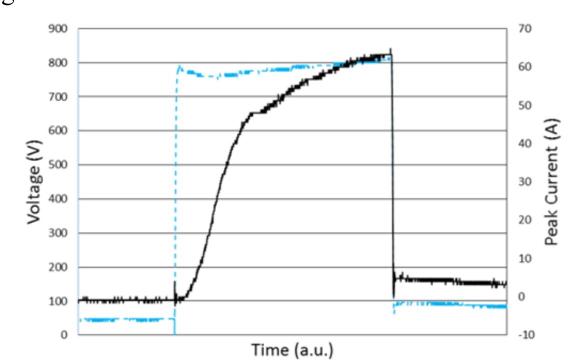

Figure 1: The current – voltage – time profile of a HiPIMS pulse. Peak current is shown in black and voltage in blue.

The current voltage characteristics of both power supplies are shown together in Fig 2. A DC bias voltage can be applied to the substrate and was varied between 0 and -100 V. RF biasing was used at 19 W. The base pressure of the unbaked UHV chamber reached ~10^{-8} mbar and the Kr pressure was set to 3 mbar.

Morphological analysis was performed by SEM and XRD. SEM analysis was used to determine the film structure and grain size at the surface. XRD analysis results show average grain size and lattice orientations within the film. RRR measurements have been performed using a purpose built cryostat housing a four point probe.

Content from this work may be used under the terms of the CC BY 3.0 licence (© 2015). Any distribution of this work must maintain attribution to the author(s), title of the work, publisher, and DOI.

ISBN: 978-3-95450-168-7 doi:10.18429/JACoW-IPAC2015-WEPHA060

5MW POWER UPGRADE STUDIES OF THE ISIS TS1 TARGET

Cristian Bungau, Adriana Bungau, Robert Cywinski, Thomas Robert Edgecock,
University of Huddersfield, Huddersfield, UK
Christopher Neal Booth, Lei Zang, Sheffield University, Sheffield, UK

Abstract

The increasing demand for neutron production at the ISIS neutron spallation source has motivated a study of an upgrade of the production target TS1. This study focuses on a 5 MW power upgrade and complete redesign of the ISIS TS1 spallation target, reflector and neutron moderators. The optimisation of the target-moderator arrangement was done in order to obtain the maximum neutron output per unit input power. In addition, at each step of this optimisation study, the heat load and thermal stresses were calculated to ensure the target can sustain the increase in the beam power.

INTRODUCTION

ISIS [1] is currently the world's most productive spallation neutron source hosting two target stations TS1 and TS2. The TS1 target station operates at proton beam powers of up to 200 kW. The goal of this study is to find the maximum beam power the TS1 target can sustain without changing the existing design concept of using fixed solid W plates. There are many factors that could limit the performance of a high power target therefore the design of such a target presents a major technical challenge in terms of the engineering constraints of heat removal and structural radiation damage while optimising the neutron yield. The ISIS accelerator has been upgraded to achieve the increased beam intensity necessary to provide a 10 pulses per second (pps) proton beam to TS2 at the same time as maintaining present intensity to TS1 where the repetition rate is reduced from 50 pps to 40 pps. The ISIS TS1 target is driven by an 800 MeV, 200 μA proton beam equivalent to almost 0.2 MW beam power.

THE TS1 TARGET

A schematic diagram of the ISIS target is shown in Fig. 1. It consists of a stack of 12 solid tungsten plates (105 $\times$ 80 mm) of different thicknesses (from 15 to 50 mm) enclosed in a stainless steel pressure vessel which contains heavy water for cooling the plates. Each tungsten plate is cladded in a 2 mm thick tantalum layer in order to avoid water corrosion of bare tungsten. The Ta/W interface must remain in close contact as developing gaps would restrict the coolant flow and create resistance to the heat evacuation generated by the target. The gaps between the plates is 2 mm and is used for cooling the plates with heavy water. The flow of heavy water is redistributed using stainless steel manifolds.

Four moderators are used to slow down fast neutrons escaping from the target to the lower speeds required for neutron scattering experiments. Two use water at room temperature, one uses liquid methane at 100 K and the fourth consists of liquid hydrogen at 20 K. The different temperatures result in different energy neutron beams. The moderators are small, about 0.5 l, and are surrounded by a water-cooled beryllium reflector which scatters neutrons back into the moderators and doubles the useful flux of neutrons. Surrounding radially the reflector are the neutron channels which conduct the neutrons to the instruments for neutron scattering applications.

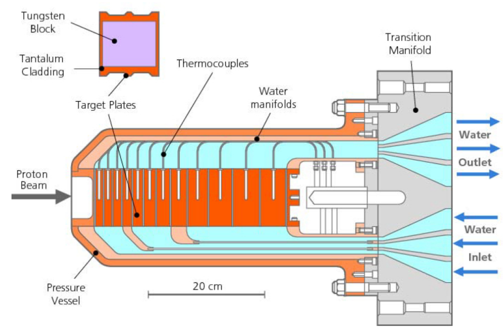

Figure 1: Layout of the ISIS-TS1 spallation target.

The ISIS TS1 target geometry was implemented into the Geant4 Monte Carlo code [2], and Fig. 2 shows the modelling of the target and the surrounding components. In this figure, the four neutron moderators that are used to thermalise the neutrons are shown in different colours: the two water moderators (blue), the liquid methane moderator (green) and the liquid hydrogen (yellow). The two water moderators are at ambient room temperature 300 K, the liquid methane moderator operates at 100 K and the liquid hydrogen moderator at 20 K. The liquid methane moderator has curved surfaces unlike the others. The target and the moderators are embedded in a beryllium reflector shown here in grey. Also the neutron beamlines are shown (lower right) which lead the neutrons to the experimental stations.

GEANT4 Versus MCNPX Simulations

The neutron yields energy spectra measured at various instruments pointing to the neutron moderators are shown in Fig. 3. Because the neutron moderators operate at different temperatures the neutron spectra show a strong dependence on the moderator temperature, resulting in an increase in the number of thermal neutrons for lower operating temperatures. This validation study shows an excellent agreement between the GEANT4 and MCNPX predictions for

Content from this work may be used under the terms of the CC BY 3.0 licence (© 2015). Any distribution of this work must maintain attribution to the author(s), title of the work, publisher, and DOI.

ISBN: 978-3-95450-168-7 doi:10.18429/JACoW-IPAC2015-WEPTY002

STUDIES INTO ELECTRON BEAM GENERATION, ACCELERATION AND DIAGNOSTICS WITHIN LA³NET*

C.P. Welsch#, Cockcroft Institute and the University of Liverpool, UK
on behalf of the LA³NET Consortium

Content from this work may be used under the terms of the CC BY 3.0 licence (© 2015). Any distribution of this work must maintain attribution to the author(s), title of the work, publisher, and DOI.

Abstract

The Laser Applications at Accelerators Network (LA³NET) is receiving funding of up to 4.6 M€ from the European Union within the 7th Framework Program to carry out R&D into laser-based particle sources, laser acceleration schemes and laser-based beam diagnostics. This international network joins universities, research centers and private companies and has been training 19 early stage researchers at network nodes across Europe since 2011. This contribution presents research outcomes from LA³NET's main work packages, covering electron beam generation, acceleration and diagnostics. Results from surface studies of photocathodes for photo injector applications in the framework of the CLIC project are presented along with information about expected accelerating gradients in dielectric laser-driven accelerators as identified for non-relativistic and relativistic electron beams using the CST and VSIM simulation codes. Initial results from energy measurements using Compton backscattering at the ANKA Synchrotron at KIT are also presented. In addition, a summary of recent and upcoming international events organized by the consortium is also given.

INTRODUCTION

The LA³NET Fellows are hosted by 11 partner institutions all over Europe and although their work focuses on research, they are provided not only with scientific supervision and opportunities of secondments to other institutions involved in the project, but also complementary training through network-wide events [1]. This includes international schools and topical workshops, as well as a final project conference and numerous outreach events. Through the involvement of almost 30 associated and adjunct partners the project gains an interdisciplinary dimension including strong links to industry. The network carries out many dissemination and outreach activities aimed at interesting a wide audience in science and to raise public awareness of the application of lasers and accelerators in many different fields that have influence on everyone's life, such as medicine, electronics, energy and the environment. LA³NET trains accelerator experts for academia and industry, joins the accelerator and laser communities and to raises public awareness of the importance of this research for society. In the following section examples of recent research results from across the consortium are given.

* This project has received funding from the European Union's Seventh Framework Programme for research, technological development and demonstration under grant agreement no 289191.
# carsten.welsch@cockcroft.ac.uk

RESEARCH

The Fellows carry ou research within one out of 5 thematic work packages within LA³NET. These are particle sources, acceleration, beam diagnostics, system integration and detector technology.

Surface Characterization of Photo Cathodes for Photoinjector Applications

Within the CLIC (Compact Linear Collider) project, feasibility studies of a photoinjector option for the drive beam are on-going, covering both, the laser and the photocathode side. The main challenge is to achieve high bunch charges, long trains and high bunch repetition rates together with sufficiently long cathode lifetimes. Cs_2Te cathodes, sensitive to ultra-violet (UV) laser beam that were produced at CERN showed good quantum efficiency and reasonable lifetime [2]. However, the available laser pulse energy in the UV for 140 µs long pulse trains is currently limited due to a degradation of the beam quality during the 4th harmonics conversion process. Using green laser beam in combination with Cs_3Sb cathodes would overcome this limitation. Cs_3Sb and Cs_2Te photocathodes were produced at CERN by co-deposition process and tested in the PHIN RF photoinjector, see [3]. LA³NET Fellow I. Martini who is based at CERN led a detailed analysis of cathode surface composition through X-ray Photoelectron Spectroscopy (XPS) and correlated the findings to the cathode performance [4]. The Quantum Efficiency (QE) map shows an overall efficiency reduction in used cathodes as compared to newly produced ones, see Fig. 1 as an example. This can be explained by changes in the composition of the photoemissive layer.

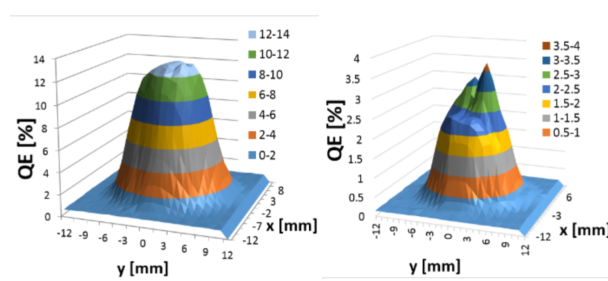

Figure 1: QE maps of Cathode #198 (Cs_2Te) as newly produced (left) and used in the RF photoinjector (right).

The XPS studies showed that both cathodes were oxidized during operation. Moreover, the detailed

ISBN: 978-3-95450-168-7 doi:10.18429/JACoW-IPAC2015-WEPTY003

MAGNET DESIGNS FOR THE MULTI-BEND ACHROMAT LATTICE AT THE ADVANCED PHOTON SOURCE*

M. Jaski, J. Liu, Argonne National Laboratory, Argonne, IL 60439, USA
A. Jain, C. Spataro, Brookhaven National Laboratory, Upton, NY 11973, USA
D. J. Harding, V. S. Kashikhin, M. L. Lopes, Fermi National Accelerator Laboratory, Batavia, IL 60510, USA

Abstract

The Advanced Photon Source (APS) is currently investigating replacing the existing two-bend 7 GeV lattice with a 6 GeV seven-bend achromat magnet lattice in order to achieve a low electron beam emittance [1]. This new lattice requires 1320 magnets, of which there are nine types. These include high strength quadrupoles (gradient up to ~97 T/m), sextupoles with second derivative of field up to ~7000 T/m^2, longitudinal gradient dipoles with field ratio of up to 5, and transverse gradient dipoles with gradients of ~50 T/m and central field of ~0.6 T. These field requirements and the limited space available pose several design challenges. This paper presents a summary of magnet designs for the various magnet types developed through a collaboration of APS with FNAL and BNL.

INTRODUCTION

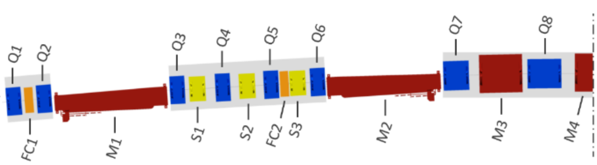

Figure 1: Half sector with magnet identifications.

The storage ring consists of forty sectors. There are 7 dipoles, 16 quadrupoles, 6 sextupoles, and 4 fast steering correctors, totalling 33 magnets in each sector. A representation of a half sector is shown in Fig. 1 along with magnet identifications. Table 1 lists the magnets and their respective lengths and maximum strengths. All magnets are solid core magnets with the exception of the corrector magnet, which requires a laminated core. The minimum pole tip radius for all magnets is 13 mm. For quadrupole, sextupole, and corrector magnets the minimum vertical gap between the poles is 10 mm and minimum vertical gap between the coils is 16 mm to allow for extraction of the photon beam. The fractional field deviation for each unwanted harmonic is limited to a maximum of 10^{-4} at a 10 mm reference radius. Any discrepancies in magnet harmonics are evaluated on a case-by-case basis.

VANADIUM PERMENDUR

Analysis shows that making quadrupole pole tips out of vanadium permendur (VP) can increase the field by 9% compared to steel core tips at the same magnetic efficiency. Figure 2 shows a plot of simulated integrated quadrupole field vs. insertion length for mushroom VP, mushroom steel, and straight steel tips. This plot was used in the lattice design to estimate obtainable quadrupole strengths for a given insertion length. Similar plots were developed for sextupole, Q7, and Q8 magnets. VP is expensive (~200x more than steel) so minimizing or eliminating the use of VP is desirable. During design, steel pole tips are the material of choice, unless the field could not be achieved for a given length.

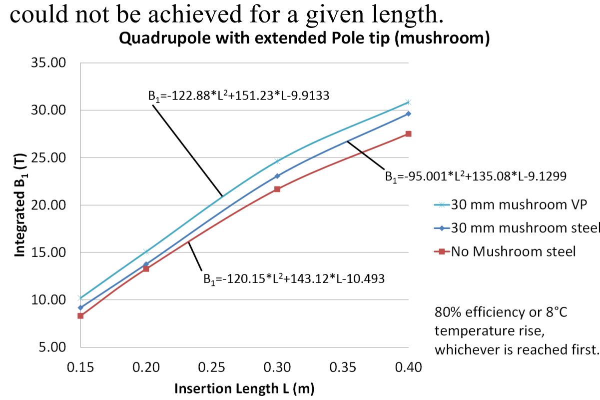

Figure 2: Quadrupole integrated field vs insertion length for VP and steel mushroom poles.

QUADRUPOLE MAGNETS

All quadrupole magnets are made of solid steel, two-piece (top and bottom) yokes with removable poles and pole tips. The Q1 through Q6 have long mushroom style pole tips. Figure 3a shows a magnet model of a Q1 magnet. The long mushroom style pole tips allow higher integrated field gradients at high saturation compared to straight pole tips at the same saturation. The Q1 quadrupole magnet operates at a high field gradient and requires VP pole tips. Prototypes of quadrupole magnets are under construction at APS and are expected to be ready for measurement in September 2015.

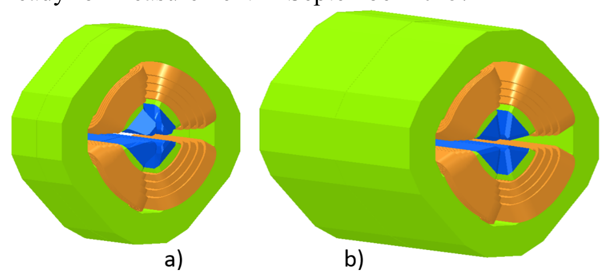

Figure 3: a) Q1 quadrupole magnet model. b) Q8 quadrupole magnet model.

* Work supported by the U.S. Department of Energy, Office of Science, under Contract No. DE-AC02-06CH11357.

Content from this work may be used under the terms of the CC BY 3.0 licence (© 2015). Any distribution of this work must maintain attribution to the author(s), title of the work, publisher, and DOI.

ISBN: 978-3-95450-168-7 doi:10.18429/JACoW-IPAC2015-WEPTY004

Content from this work may be used under the terms of the CC BY 3.0 licence (© 2015). Any distribution of this work must maintain attribution to the author(s), title of the work, publisher, and DOI.

MATHEMATICAL MODELING AND ANALYSIS OF A WIDE BANDWIDTH BIPOLAR POWER SUPPLY FOR THE FAST CORRECTORS IN THE APS UPGRADE CONTROLLER*

Byeong M. Song and Ju Wang
ANL, Argonne, IL 60439, USA

Abstract

This paper presents the mathematical modeling and analysis of a wide bandwidth bipolar power supply for the fast correctors in the APS Upgrade controller. A wide bandwidth current regulator with a combined PI and phase-lead compensator has been newly proposed, analyzed, and simulated through both a mathematical model and a physical electronic circuit model using MATLAB and PLECS. The proposed regulator achieves a bandwidth with a -1.23dB attenuation and a 32.40° phase-delay at 10 kHz for 0.3% AC component. The mathematical modeling and design, simulation results of a fast corrector power supply control system are presented in this paper.*

INTRODUCTION

Argonne National Laboratory's Advanced Photon Source (APS) Upgrade requires a bipolar power supply with a 10 kHz and -3dB small signal bandwidth for the fast correction magnets. In addition, low output current offset and DC drift to achieve a few hundred parts per million (ppm) output current stability are required. These requirements present a technical challenge to the design because the magnet load may have a significant inductance, making it difficult to achieve a high bandwidth for the current, and the input DC bus voltage may be limited. Until now, there have been no known commercial-off-the-shelf (COTS) power supplies that meet the 10kHz bandwidth requirement.

In order to meet the requirements, different circuit topologies and regulators are being investigated. One of the candidates is a standard full-bridge power circuit topology with a high switching frequency to provide a ±15A DC output current with an AC component less than 1% of the full DC scale with the required bandwidth.

In this paper, a 200kHz interleaved pulse-width-modulation (PWM) power supply circuit with a proportional-and-integral (PI) and phase-lead current regulator is proposed for the fast corrector power supply. The proposed current regulator is mathematically analyzed and optimized, so that it achieves the performance requirement of the power supply by minimizing the attenuation and phase-shift of the compensated closed-loop control system. The performance evaluation of the current regulator has been conducted through Matlab and PLECS simulations.

*This work is supported by the U.S. Department of Energy, Basic Energy Sciences, Office of Science, under contract # DE-AC02-06CH11357.

A WIDE BANDWIDTH BIPOLAR POWER SUPPLY

Main Circuit and Its PWM Operation

Figure 1(a) shows a bi-directional power circuit for fast corrector power supplies. The circuit consists of a 200kHz interleaved full-bridge MOSFET power circuit and a 50kHz low pass filter. The power circuit has four switches in two legs, S_1 and S_3, and S_2 and S_4.

Figure 1(b) shows the key PWM switching of the power circuit. Two references with the same amplitude but opposite sign, $+V_{ref}$ and $-V_{ref}$, are compared with a 100kHz triangular waveform, V_c, to generate two sets of PWM signals. The output voltage, V_o, is proportional to the duty cycle, $D*(1-D)$, and input voltage, V_{in}. With this switching pattern, the output current, i_o, has a ripple frequency that is twice the PWM frequency. Thus, this low current ripple can reduce the size of magnetic components and capacitors of the low pass filter in the power circuit.

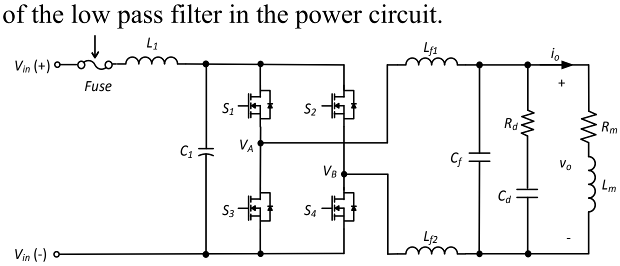

(a) Main circuit

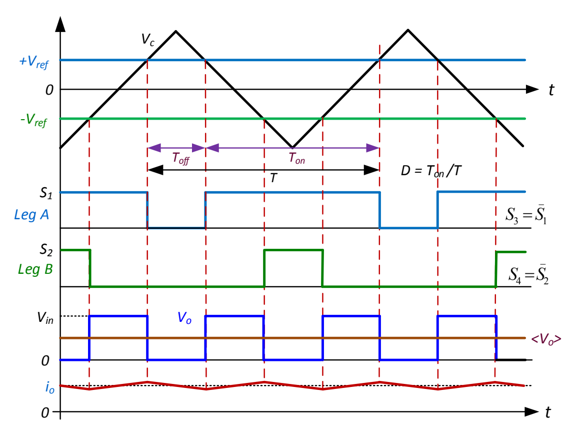

(b) PWM switching

Figure 1: Main circuit and its PWM switching for a fast corrector power supply.

ISBN: 978-3-95450-168-7 doi:10.18429/JACoW-IPAC2015-WEPTY008

SUPERCONDUCTING HARMONIC CAVITY FOR THE ADVANCED PHOTON SOURCE UPGRADE*

M.P. Kelly[1,#], A. Barcikowski[1], J. Carwardine[1], Z.A. Conway[1], D. Horan[1], M. Kedzie[1], S.H. Kim[1], P.N. Ostroumov[1], J.Rathke[2], T. Schultheiss[2], G. J. Waldschmidt[1]
[1)]Argonne National Laboratory, Argonne, IL 60439, U.S.A.
[2)]Advanced Energy Systems, Inc., Medford, NY 111763, U.S.A.

Abstract

A new bunch lengthening cryomodule using a single-cell 'higher-harmonic' superconducting cavity (HHC) based on the TESLA shape and operating at the 4th harmonic (1408 MHz) of the main RF is under development at Argonne. The system will be used to improve the Touschek lifetime and increase the single-bunch current limit in the upgraded multibend achromat lattice of the Advanced Photon Source electron storage ring. The 4 K cryomodule will fit within one half of a straight section, ~2.5 meters, of the ring. The system will use a pair of moveable 20 kW (each) CW RF power couplers to adjust the loaded Q and extract power from the beam. This will provide the flexibility to adjust the impedance presented to the beam and run at various beam currents. Higher-order modes (HOMs) induced by the circulating electron beam will be extracted along the beam axis and damped using a pair of room temperature beam line absorbers. Engineering designs and the prototyping status for the cavity, power couplers and HOM absorbers are discussed.

INTRODUCTION

The Advanced Photon Source Upgrade (APS-U) project [1] will have a relatively short Touschek lifetime [2] and a bunch lengthening cavity is required to mitigate the effect. Harmonic cavities provide lengthening by modifying the longitudinal potential to produce reduced slope near the bunch center [3] and are demonstrated and in use elsewhere [4,5].

Superconducting RF (SRF) cavities have major advantages over normal conducting cavities in many high-current, high-power CW applications, including for the 6 GeV, 200 mA electron storage ring in the APS-U:

- One beam-driven single-cell harmonic cavity easily provides all of the required voltage
- The large beam aperture and single-cell minimize the total beam-induced HOM power and the complexity of HOM power extraction
- The high quality factor, $Q_0>10^8$, combined with a variable coupler, permit adjustment of the loaded quality factor, Q_L, for near-optimal lengthening for various beam currents

* This work was supported by the U.S. Department of Energy, Office of Nuclear Physics, under Contract No. DE-AC02-06CH11357. This research used resources of ANL's ATLAS facility, which is a DOE Office of Science User Facility.
# mkelly@anl.gov

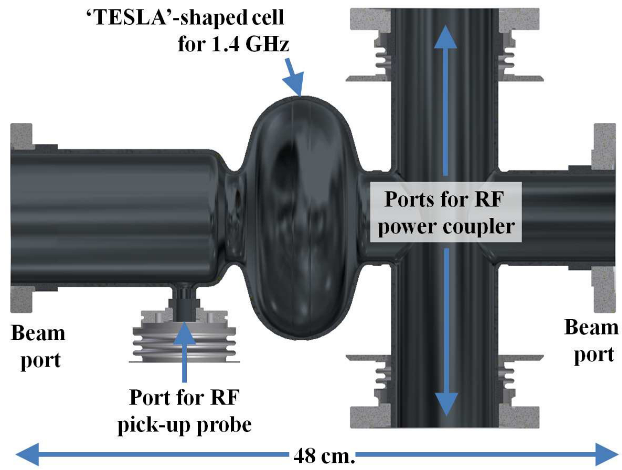

Figure 1: A higher-harmonic cavity for bunch lengthening in the Advanced Photon Source Upgrade.

A study of possible 3rd, 4th, and 5th harmonic SRF cavities has been performed based on analytical calculations. These assume 'optimal' bunch lengthening [6]. Differences are modest with the most lengthening, by ~20%, with the 3rd harmonic. However, the extracted power (through RF couplers) is double that for the 4th harmonic due to higher voltage and smaller detuning angle for the optimum condition. Multi-particle, collective effects and transients were not included. Tracking simulations [2] using ELEGANT, include these, and do not support a clear advantage with the 3rd harmonic. Finally, the 4th harmonic cavity choice (Figure 1) was influenced by practical considerations.

The 1.4 GHz frequency is sufficiently close to the 1.3 GHz linear collider frequency that existing infrastructure and techniques can be used to reduce development time. Performance needs are modest and are listed Table 1.

Table 1: Harmonic Cavity Main Parameters

Parameter	Value
Frequency, MHz	1408
Operating temperature, K	4.5
Beam induced voltage, MV	0.84
Cavity Q_0 at 4.5 K	2×10^8
R_{SH}/Q, Ω	109
G, Ω	270
E_{PEAK} at 0.9 MV, MV/m	16
B_{PEAK} at 0.9 MV, mT	33

Content from this work may be used under the terms of the CC BY 3.0 licence (© 2015). Any distribution of this work must maintain attribution to the author(s), title of the work, publisher, and DOI.

ISBN: 978-3-95450-168-7 doi:10.18429/JACoW-IPAC2015-WEPTY009

PRESERVATION OF QUALITY FACTOR OF HALF WAVE RESONATOR DURING QUENCHING IN THE PRESENCE OF SOLENOID FIELD*

S.H. Kim#, Z.A. Conway, M.P. Kelly, P.N. Ostroumov, S.M. Gerbick, T.C. Reid, M.J. Kedzie, S.W.T. MacDonald, D.M. Caldwell,
ANL, Argonne, IL 60439, USA

Abstract

The Proton Improvement Plan II at FNAL relies upon a 162.5 MHz superconducting half-wave resonator cryomodule to accelerate H- beams from 2.1 to 10 MeV. This cryomodule contains 8 resonators with 8 superconducting solenoid magnets interspersed between them. X-Y steering coils are integrated with a package of the superconducting solenoid magnets. The center of the solenoids is located within ~50 cm of the high surface magnetic field of the half-wave resonators and in this study we assess whether or not magnetic flux generated by this magnet is trapped into the half-wave resonators niobium surface and increases the RF losses to liquid helium. To test this we assembled a solenoid with a 162.5 MHz half-wave resonator spaced as they will be in the cryomodule. We measured the quality factor of the cavity before and after the cavity quenched as a function of field level in the coils. No measurable change in the quality factor was observed. In this paper, we will present details of the measurements and discuss the magnetic field map.

INTRODUCTION

Argonne has developed a 6 T superconducting solenoid (0.75 T·m field integral) with integral x-y dipole steering coils each producing a maximum 0.25 T steering field (30 T·mm field integral) [1,2]. This magnet will be used in the 162.5 MHz superconducting half-wave resonator (HWR) cryomodule which contains 8 resonators and 8 magnets and will be employed to accelerate H- beams from 2.1 to 10 MeV in the proposed Proton Improvement Plan II (PIP-II) at FNAL [3,4].

This solenoid integrates with bucking coils to minimize stray field such that the magnetic field on the cavity surface is much smaller than the (first) critical field for niobium. The intent is to avoid trapped magnetic flux and the associated increase of the surface resistance [1]. This minimization of the stray field reduces the possibility of flux trapped when cavity experiences thermal breakdown (quenching) [5,6]. Experimental studies show that magnetic flux can be trapped around the quench location where a normal region is present in the niobium for ~100 ms [6].

We assembled this solenoid with the 162.5 MHz HWR, which is the second cavity fabricated for PIP-II HWR cryomodule and the first one was reported on in ref. [7], and measured change of trapped magnetic flux after the cavity quenched in the presence of the solenoid/steering coil fields. We note that probability of cavity quenching during normal operation would be very low in the PIP-II HWR cryomodule because this cavity quenches at the accelerating gradient of E_{ACC}~18 MV/m while the operational accelerating field will be E_{ACC}=8 MV/m.

In the following sections, we will discuss the stray field generated by the solenoid and steering coils and then discuss measurement hardware and results.

STRAY FIELD

The stray field of the solenoid is minimized by integral bucking coils as shown in Fig. 1. These are wound in series with the main solenoid coil. Another pair of the dipole coils is located in the plane perpendicular to the cross-section shown in Fig. 1.

The simulated stray field generated by the solenoid, a combination of the main and bucking coil, is as shown in Fig. 2. We note that the unperturbed field is simply overlaid on the cavity and no Meissner effect is included. The stray field on the cavity surface is of the order 10 Gauss around the nosecone, placed in the high RF electric field region, and it is exponentially decayed along the surface toward the end torus of HWR so the stray field on a cavity surface in the high RF magnetic field region is much smaller than the lower critical field of the niobium [8]. The measured stray fields are in rough agreement with the design, differing by a factor of 3 [2].

The stray field generated by the steering coils at maximum deflection is estimated to be ~200 Gauss on the cavity niobium surface, relatively higher than for the main solenoid because these do not include bucking coils or shielding.

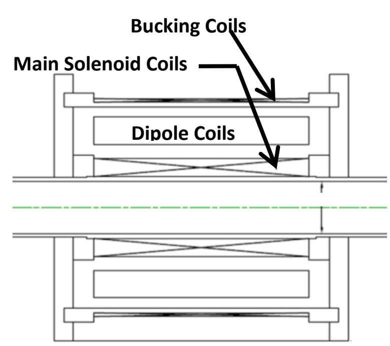

Figure 1: Structure of the coils in the superconducting solenoid magnet integrated with dipole steering coils. The bucking coil is wired in series with the main solenoid coils.

* This work was supported by the U.S. Department of energy, Offices of High-Energy Physics and Nuclear Physics, under Contract No. DE-AC02-76-CH03000 and DE-AC02-06CH11357.
#shkim121@anl.gov

Content from this work may be used under the terms of the CC BY 3.0 licence (© 2015). Any distribution of this work must maintain attribution to the author(s), title of the work, publisher, and DOI.

ISBN: 978-3-95450-168-7 doi:10.18429/JACoW-IPAC2015-WEPTY010

ELECTROPOLISHING FOR LOW-BETA AND QUASI-WAVEGUIDE SRF CAVITIES*

T. Reid[#], P.N. Ostroumov, M. P. Kelly, Z.A. Conway, S. M. Gerbick, M. Kedzie
Argonne National Laboratory, Argonne, IL 60439, U.S.A.

Abstract

Argonne National Laboratory (ANL) has extended high quality electropolishing techniques based on those developed for the International Linear Collider to several more complex superconducting RF cavities. These include the co-axial TEM-mode quarter-wave and half-wave cavities as well as a 2.815 GHz quasi-waveguide structure for beam bunch rotation. This system is an improved version of the one developed for 1.3 GHz 9-cell cavities and includes easy provision for direct water cooling using the helium jacket. The performance of these SRF cavities both in terms of RF fields and losses equals or exceeds that of most 9-cell elliptical cavities built and tested today.

INTRODUCTION

The Superconducting Surface Processing Facility (SCSPF) at ANL is a 200 m^2 laboratory which houses a pair of class 100 clean rooms for HPR and clean assembly, a class 1000 anteroom, and two separate chemistry rooms. The facility was originally designed to support processing of 1.3 GHz 9-cell cavities for the ILC, but has since expanded its capabilities to chemically process accelerating structures of various geometries.

In this paper we present the electropolishing and subsequent cold test results of three distinct cavity geometries. The first of which are β= 0.077, 72.75 MHz quarter-wave resonators (QWR) developed for the ANL ATLAS efficiency and intensity upgrade completed in 2014. The second are β= 0.11, 162.5 MHz half-wave resonators (HWR) currently being developed and fabricated for the PXIE injector experiment at Fermilab. Finally we will briefly review the tooling used to electropolish a 2.815 GHz deflecting cavity for novel beam manipulations.

LOW-BETA CAVITIES

Quarter-wave Cavities for ATLAS

A cryomodule containing seven 72 MHz quarter-wave resonators (QWRs) was recently installed into the ATLAS heavy-ion accelerator as part of the ATLAS Intensity Upgrade (AIU) project [1]. The prototype 72 MHz QWR was the cavity used to commission the newly built low-β EP tool at Argonne in 2011 [2], and developed the procedures generically employed for all of our cavities. The remaining six production cavities followed in 2012 [3]. The low-β EP tool was based on Argonne's experience with the horizontal electropolishing of 1.3 GHz 9-cell cavities for the global ILC effort [4]. One of the unique features of the ANL low-β tool is its versatility which enables the chemical polishing of many different cavity geometries. A QWR is shown in Figure 1. QWRs were the first cavities processed with this tool and the processing sequence used is described below.

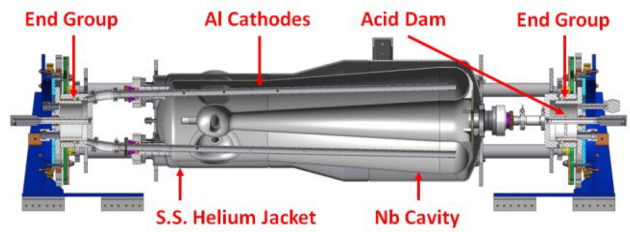

Figure 1: Section view of the low-β EP tool with 72 MHz quarter-wave cavities.

Prior to installation into the low-β EP tool, the finished cavities are ultrasonically cleaned for 60 minutes at 120°F in a 2% liquinox, 98% DI water solution. After the QWR is installed in the ANL low-β EP tool it receives a 20 µm buffered chemical polish (1:1:2; 48% HF: 70% HNO_3: 85% H_3PO_4) to remove the oxide layer formed during the final electrostatic discharge machining (EDM) of the cavity. This BCP step is necessary because the EDM oxide layer is not removed during EP. The BCP process has several similarities to the EP. The first is the helium jacket of the QWR is used for direct water cooling to keep the temperature of the niobium cavity below 17°C, minimizing the risk of contaminating the bulk niobium with hydrogen. Second, the BCP is done in the horizontal position and the cavity is rotated at 0.5 rpm. Since the cavity is not completely filled with the BCP electrolyte, the hydrogen gas which evolves during the procedure bubbles up through the bath and not along the cavity surface. This eliminates the surface pitting and groove formation inherent to the process when the hydrogen gas bubbles travel along the niobium surface.

After the BCP, a bulk 150 µm EP (1:9; 48% HF: 96% H_2SO_4) is performed using four 3003 series aluminium cathodes to achieve uniform polishing of the RF surface. With the low-β EP tool, cathodes are used to flow acid both into and out of the cavity, as well as flow N_2 gas into the cavity RF volume to purge the H_2 gas produced as part of the EP reaction. To accomplish this, a dam sets the acid level at ~60% of the cavity diameter, allowing there to be two cathodes submerged in the acid bath and two cathodes above the acid bath during the majority of the EP process. The two submerged cathodes are used to

* This work was supported by the U. S. Department of Energy, Office of Nuclear Physics, under contract number DE-AC02-06CH11357. This research used resources of ANL's ATLAS facility, which is a DOE Office of Science User Facility.
[#]treid@anl.gov

Content from this work may be used under the terms of the CC BY 3.0 licence (© 2015). Any distribution of this work must maintain attribution to the author(s), title of the work, publisher, and DOI.

ISBN: 978-3-95450-168-7 doi:10.18429/JACoW-IPAC2015-WEPTY011

POWER SUPPLY CONCEPTUAL DESIGN AND R&D FOR THE APS UPGRADE*

J. Wang, B. Deriy, T. Fors, R. Keane, B. Song
ANL, Argonne, IL 60439, USA

Content from this work may be used under the terms of the CC BY 3.0 licence (© 2015). Any distribution of this work must maintain attribution to the author(s), title of the work, publisher, and DOI.

Abstract

The multi-bend achromat (MBA) storage ring of the APS Upgrade (APS-U) requires more than 2200 power supplies with either unipolar or bipolar DC output currents. The power supply performance requirements are much more stringent than what can be achieved with commonly available and off-the-shelf commercial power supplies. The power supply output currents must be calibrated to the given specifications and confirmed with independent and accurate measurement. The bipolar power supplies for the fast correction magnets are required to have a wide bandwidth of 10 kHz. There are also new requirements for the power supply controls and communications that are much more demanding than those in the existing APS power supply systems. This paper reports on the conceptual designs of the power supply systems and the R&D programs that have been developed to find solutions to the technical challenges.

INTRODUCTION

The APS Upgrade with an MBA storage ring [1] requires power supplies with a stability better than 10 parts per million (ppm) of the full scale for the dipole, quadrupole, and sextupole magnets. This stability requirement is an order of magnitude more stringent than the original requirement of the existing power supplies, and a factor of two or more than what has been achieved today. The proposed real-time feedback (RTFB) beam orbit correction system has a designed bandwidth of 1 kHz, which requires the power supplies for the fast correctors to have a -3dB and small signal bandwidth at 10 kHz or higher in order to minimize the power supply's impact on the RTFB system. In addition to more demanding power supply performance requirements, there are other requirements to better facilitate the machine operations and the power supply fault identification. Those requirements include independent magnet current measurement, fast control and communication interfaces, and intensive data acquisition to monitor power supply operation status and conditions.

To meet these requirements, the conceptual designs and R&D programs are underway to investigate and evaluate commercial power supply options and to develop technical solutions.

UNIPOLAR DC POWER SUPPLY SYSTEM

The MBA storage ring needs 1000 unipolar power supplies with the output current up to 230 A, which is designated as DCU-230 in the conceptual design. The DCU-230 system is based on a 10 ppm stability-class commercial DC-to-DC power supply with modifications to satisfy the APS needs. The modifications are mostly in the input and output stages of the power supplies in order to utilize the existing APS DC distribution system.

Figure 1 shows a conceptual design of the unipolar power supply system. The system includes a commercial power supply, an external DCCT (DC current transducer) with a high precision measurement circuit for independent performance verification and calibration, and a power supply controller to provide the control and communication interfaces.

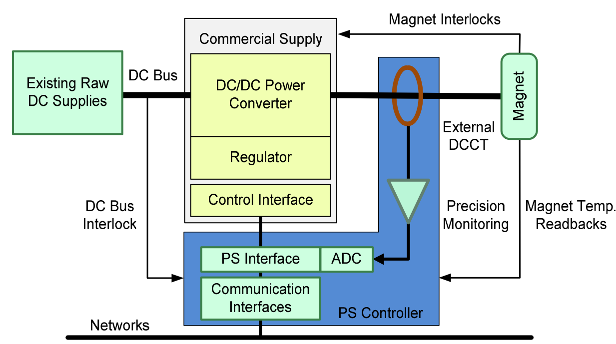

Figure 1: Unipolar power supply system.

Two different commercial power supply approaches have been evaluated through the R&D program. The first approach uses a 200A Danfysik 9100 power supply, which is a current-regulated power supply with a stability specification of 10 ppm. The second approach uses an external current regulator by BiRa Systems and SLAC to regulate a 250A TDK-Lambda Genesys power supply operating in the voltage mode. The evaluation results show that both approaches can meet the stability requirement. During a 7-day and 100A test, both approaches achieved a stability better than 0.5 ppm RMS and better than 5 ppm peak-to-peak. The two approaches were also tested for 24-hour runs with the output currents at 50 A, 100 A, and 200 A, respectively. The largest current deviation during the 24-hour runs is 0.7 ppm RMS and 4 ppm peak-to-peak.

In addition to DCU-230, there is also a requirement of two AC-to-DC power supplies for the L-bend, M1 and M2, dipole magnets. The maximum output currents are 880 A and 500 A, respectively, with the output voltage up to 450 volts. These sorts of power supplies – with a few ppm current stability – are available commercially.

*Work supported by the U.S. Department of Energy, Office of Science, Office of Basic Energy Sciences, under Contract No. DE-AC02-06CH11357.

ISBN: 978-3-95450-168-7 doi:10.18429/JACoW-IPAC2015-WEPTY012

MULTIPLE SCATTERING EFFECTS OF A THIN BERYLLIUM WINDOW ON A SHORT, 2 nC, 60 MeV BUNCHED ELECTRON BEAM

E.E. Wisniewski, M. Conde, W. Gai, J.G. Power, ANL/HEP, Argonne, IL USA
G. Ha, POSTECH, Pohang, Kyungbuk, S. Korea and ANL/HEP, Argonne, IL USA

Abstract

The Argonne Wakefield Accelerator (AWA) 75 MeV drive beamline at Argonne National Laboratory has as its electron source a Cesium telluride photocathode gun with a vacuum requirement on the order of 10^{-10} torr. In conflict with this, the experimental program at AWA sometimes requires beamline installation of experimental structures which due to materials and/or construction cannot meet the stringent vacuum requirement. One solution is to sequester these types of structures inside a separate vacuum chamber and inject the beam through a thin Beryllium window. The downside is that multiple scattering effects degrade the beam quality to some degree which is not well-known. This study was done in an effort to better understand and predict the multiple scattering effects of the Be thin window, particularly on the beam transverse size. The results of measurements are compared with GEANT4 simulations via G4beamline and analytical calculations via GPT.

MOTIVATION FOR USE OF BE WINDOWS AT AWA

The Argonne Wakefield Accelerator beamlines have a demanding vacuum environment, necessary to preserve the Cs_2Te photocathode in the drive gun. Cs_2Te photocathodes require vacuum pressures on the order of 10^{-10} torr, the upper range of Ultra-high vacuum (UHV). The strict vacuum requirements have a large impact on experimental design, severely limiting material choices to those that are UHV compatible. In addition, for all practical purposes, the UHV requirement completely prevents access to experimental structures after installation. Thus, the experiment must work "as installed". If it does not, at best, the consequences can include lengthy downtime while the device under test (DUT) area is vented and the experimental device is uninstalled, modified, cleaned, and re-installed. After this occurs, the experimental section of the beamline must then be pumped and baked to attain UHV vacuum pressure before the operations and the experiment may resume. This typically takes more than one week.

One way of easing the vacuum requirement and also allowing quick and easy access to make changes to the experimental setup is to place a vacuum chamber sequestered behind a Be window at the end of the beamline. The required vacuum pressure in this "dirty" vacuum chamber can be relaxed to 10^{-8} torr, which can be attained in a matter of hours with much fewer restrictions. The downside is the degradation of beam quality due to multiple scattering at the Be window. It is hoped to develop some guidance to be used in planning such installations in the future by trying to measure the effect on the beam and compare it to numerical and analytical predictions.

AWA has had some experience with this limiting effect of the increase in beam transverse size and emittance due to a Be window. Two recent experiments (RF choke cavity and a photonic-bandgap structure) come to mind. Both had an aperture I.D.=6 mm and required the beam to be moved within the aperture from an on-axis position to off-axis without significant beam loss inside the structure. In other words, a tightly focused beam was required with a fairly constant transverse size much less than the aperture I.D. Performing these experiments with a beam through a Be window was indeed a challenge.

SIMPLE FORMULA FOR MULTIPLE SCATTERING ANGLE

An electron beam traveling through matter primarily interacts with the nuclei via the Coulomb force. Electrons experience many mostly small deflections as they scatter multiple times within the media. The distribution of scattering events is described by Moliere's theory. The details of the theory are beyond the scope of this paper.

The Review of Particle Physics [1] presents a simplified equation based on a Gaussian approximation to Moliere's theory for the multiple scattering angle. For $\theta_0 = \theta_{rms\ plane} = \frac{1}{\sqrt{2}}\theta_{rms\ space}$. The width is:

$$\theta_0 = \frac{13.6\text{MeV}}{\beta pc} z \sqrt{\frac{x}{X_0}} \times (1 + 0.038) \ln\left(\frac{x}{X_0}\right)) \qquad (1)$$

for a relativistic electron beam of momentum p, velocity βc, charge number z, and scattering due to a foil of thickness x, made of material with radiation length X_0. Eq. 1 is accurate to 11% or better for the range $10^{-3} < x/X_0 < 100$ [1].

For the AWA drive beam during these tests, $p = 60$ MeV/c. And for the thin Be window: x = foil thickness (0.007" = 178 μm = 0.0178 cm) and X_0= 35.28 cm (beryllium) we finally have $\theta_0 = 0.0036 = 3.6$ mrad. This approximation was the basis of one of the simulations, the results of which are presented later in this paper. Note: This foil thickness results in a value of $x/X_0 = 0.0005$, just outside the quoted range of 11% accuracy, and that value will move further from that range as the foil is made thinner.

TESTING A Be WINDOW AT AWA

A vacuum chamber separate from the beamline vacuum was installed at the end of the drive beamline. The Be window (Materion) is circular with a 2" diameter aperture. The

Content from this work may be used under the terms of the CC BY 3.0 licence (© 2015). Any distribution of this work must maintain attribution to the author(s), title of the work, publisher, and DOI.

ISBN: 978-3-95450-168-7 doi:10.18429/JACoW-IPAC2015-WEPTY013

J/›“RPHOTOCATHODE PERFORMANCE IN THE AWA HIGH-CHARGE HIGH-GRADIENT DRIVE GUN

E.E. Wisniewski, M. Conde, D.S. Doran, W. Gai,
W. Liu, J.G. Power, and C. Whiteford, ANL/HEP, Argonne, IL USA
S.P. Antipov, C. Jing, ANL/HEP Argonne, IL, USA & Euclid TechLabs, LLC, Solon, OH, USA

Abstract

The unique high-charge L-band, 1.3 GHz, 1.5 cell gun for the new 75 MeV drive beam is in operation at the Argonne Wakefield Accelerator (AWA) facility (see M.E. Conde, this proceedings.) The high-field (> 80 MV/m) photoinjector has a large area, high QE Cesium telluride photocathode (diameter > 30 mm). The photocathode, a crucial component of the upgraded facility, is fabricated on-site. The photoinjector generates high-charge, short pulse, single bunches (Q > 100 nC) and long bunch-trains (Q > 600 nC) for wakefield experiments. The performance of the photocathode for the AWA drive gun is detailed. Quantum efficiency (QE) measurements indicate long, stable photocathode lifetime under demanding conditions.

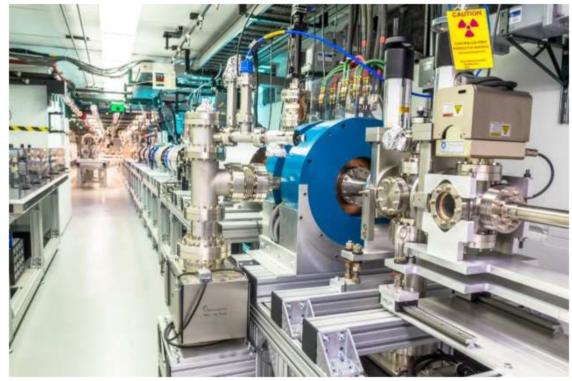

Figure 1: AWA upgrade: The new drive beam photocathode gun, looking in the direction of the beam. In the foreground is the cathode load-lock system.

THE ARGONNE WAKEFIELD ACCELERATOR (AWA) DRIVE PHOTOCATHODE GUN

The AWA L-band drive gun for the new 75 MeV drive linac has been commissioned and is operating. The 1.3 GHz photo-injector operates at high gradient (85 MV/m). The 31 mm dia. Cesium telluride photocathode, specifically designed for the production of high charge, is fabricated on-site. The photoinjector generates high-charge, short pulse, single bunches (Q > 100 nC) and long bunch-trains (Q > 600 nC) for wakefield experiments. A load-lock system was designed and built in-house for the required vacuum transport and installation of the cathode. The photocathode requirements at AWA were determined by the drive beam parameters. The AWA drive beam parameters are summarized in Table 1 [1].

Table 1: AWA Drive Beam Cathode Operating Parameters

Cathode peak RF field	>85 MV/m
RF pulse length	≈7.6 μs
Average dark current	<5 nC/RF pulse
QE%	>1%
QE lifetime	>1 month
Laser pulse width	1.5 – 8 ps FWHM
Single-bunch charge	100pC to >100nC
Multi-bunch mode:	• up to 50 nC/bunch • 2 to 32 bunches • bunch spacing = 770 ps • Max charge = 0.6 μC

PHOTOCATHODE FABRICATION

The method of fabrication used at AWA was based on and developed from methods published by researchers at LANL and INF and described in detail elsewhere [2, 3]. Using those sources for guidance, the AWA Cs_2Te photocathode is fabricated in a UHV chamber with a base pressure of 1.5×10^{-10} Torr.

The natural decline in QE of the photocathode while under UHV conditions can be reversed (up to a point) with a process referred to in the literature as rejuvenation. Previous studies on photocathode rejuvenation have shown a QE recovery up to about 60% of the original value [2, 4]. Two different rejuvenation methods have been reported. Reference [2] reported rejuvenation by heating the photocathode at 120-200°C for a period of several hours to a few days, while Ref. [4] reported that QE rejuvenation required simultaneous heating and illuminating with UV light.

Photocathodes have been rejuvenated at AWA many times, in most cases after the QE has dropped to about 5%. Rejuvenation was achieved by heating the photocathode in the deposition chamber at T=120°C for 1-3 days. The results have shown a minimum increase in QE of 60% above the QE measured just before heating. It was noted that the rejuvenated photocathodes also had a slower QE decay rate in the deposition chamber. This observation lead to applying the heating step immediately after fabrication in an attempt to retard QE decay. It was found that photocathodes formed with this post-deposition heating (annealing) step consistently showed improved QE lifetime. Figure 2 shows a comparison plot of QE lifetime for several photocathodes fabricated with and without the anneal. This plot indicates that QE decays

Content from this work may be used under the terms of the CC BY 3.0 licence (© 2015). Any distribution of this work must maintain attribution to the author(s), title of the work, publisher, and DOI.

ISBN: 978-3-95450-168-7 doi:10.18429/JACoW-IPAC2015-WEPTY014

DEVELOPMENT OF FAST KICKERS FOR THE APS MBA UPGRADE*

C. Yao#, L. Morrison, X. Sun, J. Wang, A. Cours, F. Westferro, R. Lindberg,
A. Xiao, F. Lenkszus, J. Carwardine, ANL, Argonne, IL 60439, USA

Abstract

The APS multi-bend achromat (MBA) upgrade storage ring will support two bunch fill patterns: 48 singlets and a 324 singlets. A “swap out” injection scheme is adopted. In order to minimize beam loss and residual oscillation of the injected beam and to minimize perturbation of the stored beam during a swap-on injection, the rise, fall, and flat-top parts of the kicker pulse must be held within a 22.8-ns interval. Traditional ferrite-core-type kickers can’t meet the timing requirements; therefore, we decided to use stripline-type kickers. We have completed a preliminary design of a prototype kicker geometry. Procurement of the pulser supply and other components of an evaluation system is under way. We report the specification and design of the fast kicker and current status.

2-D KICKER MODEL

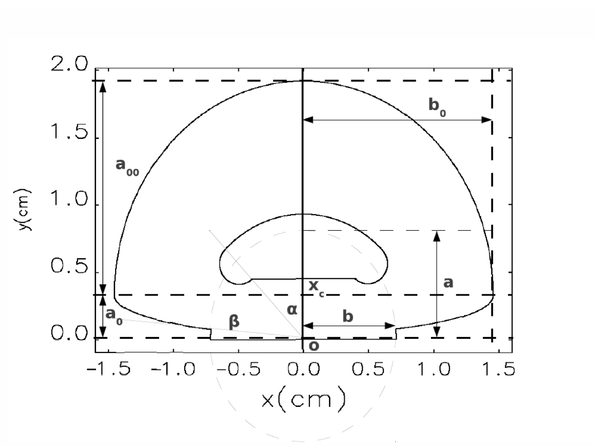

Figure 1: Geometry of the stripline kicker 2-D model.

The basic shape of the kicker stripline is shown in Figure 1. Specifications of the MBA injection/extraction kickers are listed in Table 1. Two-blade stripline type kickers with a line impedance of 50 Ω are selected, mainly due to fast rise and fall time, high voltage requirement and commercial availability of vacuum feedthroughs, connectors and cables. Similar devices have successfully been developed at KEK [1] and DAΦNE [2]. Impedance-matching plays an essential role in achieving maximum kicker strength, reducing local high-voltage concentration that can lead to breakdown, and minimizing beam impedances. Our optimization strategy is to match the differential impedance as close as possible to 50 Ω while allowing some mismatch in the common-mode impedance. A “vaned” outer body geometry is adopted to ease common-mode impedance-matching, while “D” shaped blades are used to improve field-uniformity in the good field region. The kicker has tapered end sections for matching impedance to the feedthroughs. Optimization is performed by running a multi-objective sddsoptimize [3] process with a 2-D simulation program [4]. Figure 1 shows the parametrization of geometry. The outer shell consists of two connected half-ellipses defined by the half axes (a0; b0) & (a00; b0), the center xc and the vanes on the horizontal axis. The inner blade is defined by an ellipse with axes (a, b), and by the thickness of the blade. Table 2 lists optimized parameters, and Figure 2 shows the 2-D E-field distribution. Results of the optimized parameters are shown in Table 2.

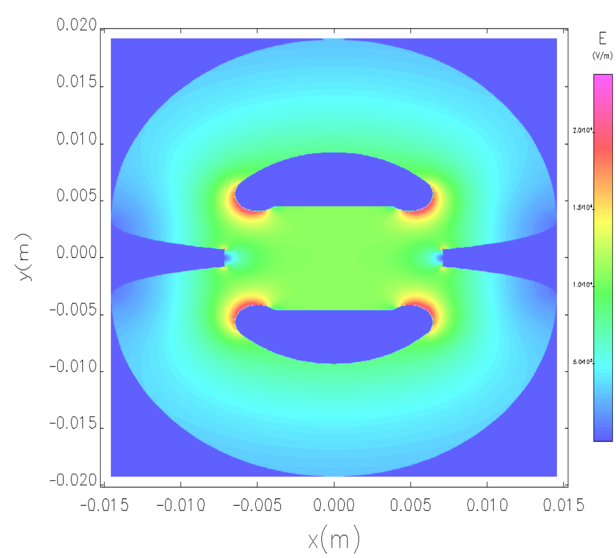

Figure 2: Field distribution of 2-D optimized model.

3-D MODELING

A 3-D simulation was performed with CST studio [5] in order to further verify 2-D result and to optimize the tapered part of the stripline kicker. The tapered parts are shown in Figure 3. Both the dimension of the body cavity and the width of the blades reduce gradually. The interface between the blade and the inner conductor of the feedthrough is under development. Optimization is performed on the blade width and the shape of the interface to minimize reflections. Figure 4 shows the TDR

*Work supported by the U.S. Department of Energy, Office of Science, under Contract No. DE-AC02-06CH11357.
#cyao@aps.anl.gov

Content from this work may be used under the terms of the CC BY 3.0 licence (© 2015). Any distribution of this work must maintain attribution to the author(s), title of the work, publisher, and DOI.

ISBN: 978-3-95450-168-7 doi:10.18429/JACoW-IPAC2015-WEPTY015

EXAMINATION OF BERYLLIUM UNDER INTENSE HIGH ENERGY PROTON BEAM AT CERN'S HIRADMAT FACILITY*

K. Ammigan†, B. Hartsell, P. Hurh, R. Zwaska, FNAL, Batavia, IL 60510, USA
A. Atherton, O. Caretta, T. Davenne, C. Densham, M. Fitton, P. Loveridge, J. O'Dell, RAL, Didcot, UK
S. Roberts, Oxford University, Oxford, and CCFE, Culham, UK
V. Kuksenko, Oxford University, Oxford, UK
M. Butcher, M. Calviani, M. Guinchard, R. Losito, CERN, Geneva, Switzerland

Abstract

Beryllium is extensively used in various accelerator beam lines and target facilities as material for beam windows, and to a lesser extent, as secondary particle production targets. With increasing beam intensities of future accelerator facilities, it is critical to understand the response of beryllium under extreme conditions to avoid compromising particle production efficiency by limiting beam parameters. As a result, the planned experiment at CERN's HiRadMat facility will take advantage of the test facility's tunable high intensity proton beam to probe and investigate the damage mechanisms of several grades of beryllium. The test matrix will consist of multiple arrays of thin discs of varying thicknesses as well as cylinders, each exposed to increasing beam intensities. Online instrumentations will acquire real time temperature, strain, and vibration data of the cylinders, while Post-Irradiation-Examination (PIE) of the discs will exploit advanced microstructural characterization and imaging techniques to analyze grain structures, crack morphology and surface evolution. Details on the experimental design, online measurements and planned PIE efforts are described in this paper.

INTRODUCTION

Beryllium is currently widely used as the material of choice for beam windows, as well as secondary particle production targets, in many accelerator beam lines and target facilities. With the increasing beam intensities of future accelerators [1,2], it is essential to evaluate the performance of beryllium under even more extreme conditions to successfully design and reliably operate windows and targets, without compromising particle production efficiency by limiting beam parameters.

An upcoming experiment at CERN's HiRadMat facility [3] will test beryllium specimens exposed to intense proton beams. The test facility is able to deliver high intensity proton beams, up to 4.9×10^{13} protons per 7.2 μs pulse (288 bunches), with a Gaussian beam sigma ranging from 0.1 mm to 2 mm [4]. The main objectives of the experiment are to explore the onset of failure modes of beryllium under controlled conditions at highly localized strain rates and temperatures, identify any thermal shock limits, and validate highly non-linear numerical models with experimental measurements.

EXPERIMENTAL SET-UP

The test rig is based on a double containment design to ensure containment of the beryllium specimens and any potential radioactive contamination created from beam interaction. The specimens will be arranged in four horizontal arrays aligned vertically in a single column. Figure 1 shows the test chamber positioned on the HiRadMat mobile table.

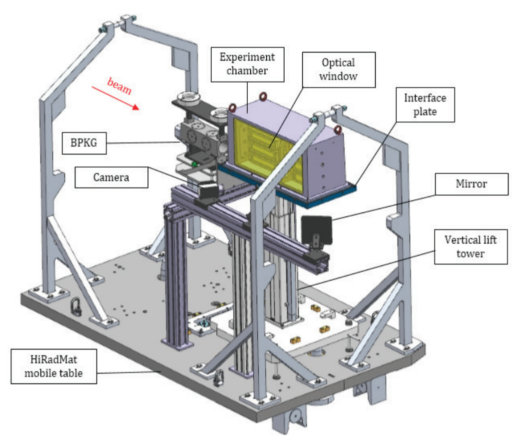

Figure 1: Test chamber positioned on mobile table.

The experiment chamber is an outer containment box, which encloses the specimen inner containment boxes. Small apertures on the outer box allow the beam to enter and exit, using a shutter system to provide post-experiment containment. Additionally, the internal volume of the outer chamber is continuously evacuated by a pump which draws the air out of the box via a HEPA filter (not shown in Figure 1). The continuous pumping and lower pressure within the outer chamber ensures no airborne particulate escapes the containment box. The HEPA filter will be analyzed upon completion of the experiment to check for any containment breach of the array boxes.

Specimen Housing

As shown in Figure 2, each specimen type within an array is enclosed in a separate containment box, sealed with glassy carbon beam windows [5]. Gafchromic foils are po-

* Work supported by Fermilab - Operated by Fermi Research Alliance, LLC, under Contract No. DE-AC02-07CH11359 with the U.S. Department of Energy
† ammikav@fnal.gov

Content from this work may be used under the terms of the CC BY 3.0 licence (© 2015). Any distribution of this work must maintain attribution to the author(s), title of the work, publisher, and DOI.

ISBN: 978-3-95450-168-7 doi:10.18429/JACoW-IPAC2015-WEPTY016

RF MODELLING OF A HELICAL KICKER FOR FAST CHOPPING*

M. Awida#, G. Sawert, A. Chen, T. Khabiboulline, and V. Yakovlev
Fermilab, Batavia, IL 60510, USA

Abstract

High intensity proton particle accelerators that support several simultaneous physics experiments require sharing the beam. A bunch by bunch beam chopper system located after the Radio Frequency Quadrupole (RFQ) is required in this case to structure the beam in the proper bunch format required by the several experiments. The unused beam will need to be kicked out of the beam path and is disposed in a beam dumb. In this paper, we report on the RF modelling results of a proposed helical kicker. Two beam kickers constitute the proposed chopper. The beam sequence is formed by kicking in or out the beam bunches from the streamline. The chopper was developed for Project X Injection Experiment (PXIE).

INTRODUCTION

PIP-II is a proposed high intensity superconducting accelerator to be built in Fermilab to replace the current 40 year old Linac injector of the accelerator complex. The new SRF Linac will secure the required Megawatt beam power required by the laboratory's future experiments, in particular by the Long Baseline Neutrino Experiment (LBNE) [1-2].

PXIE, Project-X injection experiment is planned to test the integrated systems of PIP-II (formerly called Project-X). Among those systems is the chopping mechanism in the Medium Energy Beam Transport (MEBT).

Having the beam shared between several experiments with different bunch sequences (as might happen in the future) puts a stringent specification on the overall bunch sequence supplied by the accelerator. In order to achieve the required bunch sequence, it is planned to have a bunch-by-bunch chopper located in the 2.1 MeV Medium Energy Beam Transport (MEBT) [3].

Figure 1 illustrates the function of the chopper in the MEBT section of PXIE. The beam originates from a 5 mA DC H- source and is then bunched and accelerated by a CW normal-conducting RFQ to energy of 2.1 MeV. A chopper system with a pre-programmed timeline is used then to format the bunch pattern and structure the beam.

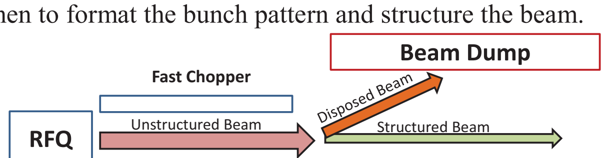

Figure 1: Simplified block-diagram of the Medium Energy Transport (MEBT) of PXIE indicating the function of the chopper.

*Operated by Fermi Research Alliance, LLC, under Contract DE-AC02-07CH11359 with the U.S. DOE
#mhassan@fnal.gov

Since the Linac pulsed beam current is limited to 2 mA and the beam current of the ion source can be as high as 5 mA, undesired beam bunches has to be removed by the chopper in normal operating conditions. The unused beam will get disposed in a beam dump.

GEOMETRY OF THE KICKER

The proposed kicker structure is a pair of traveling wave helices positioned on opposite sides of the beam [4]. The helices are wound with 13 gauge flat wire and are supported above a copper ground tube with four narrow ceramic spacer strips positioned every 90 degrees, as shown in in Fig. 2. Applied kicking voltages propagate along the helix at a speed matching the beam velocity having a beta = 0.0667. Flat, field-shaping electrodes are welded to every turn of wire on the side facing the beam. The resulting helix structure has a 200 Ω characteristic impedance.

Full 3D helical kicker models were built to carry out transient time electromagnetic simulation using CST microwave studio [5]. 200 Ohm excitation ports were used in the transient simulations.

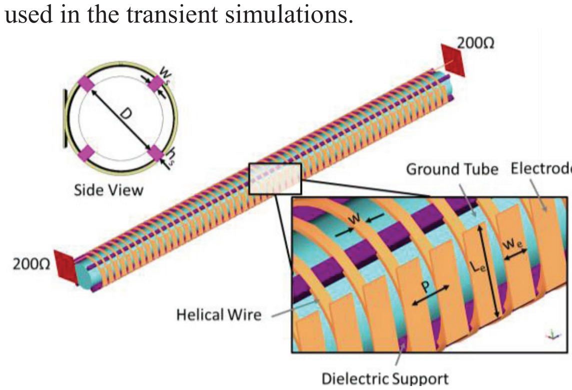

(a)

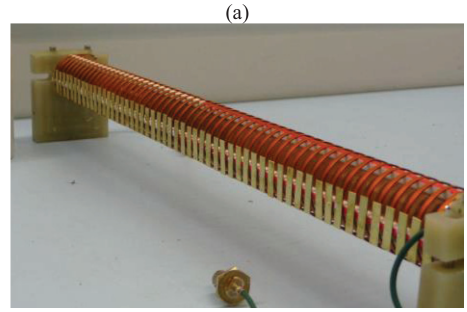

(b)

Figure 2: Geometry of the helical kicker. (a) CST microwave studio simulation model. (b) Picture of the fabricated prototype with N=55, p=0.333, D=0.563, w=0.105, w_s=0.135, h_s=0.189, w_e=0.220 and L_e=0.787 (all dimensions are in inches).

Content from this work may be used under the terms of the CC BY 3.0 licence (© 2015). Any distribution of this work must maintain attribution to the author(s), title of the work, publisher, and DOI.

ISBN: 978-3-95450-168-7 doi:10.18429/JACoW-IPAC2015-WEPTY017

DEVELOPMENT OF 650 MHz β=0.9 5-CELL ELLIPTICAL CAVITIES FOR PIP-II*

M. Awida#, M. Foley, C. Grimm, I. Gonin, T. Khabiboulline, A. Lunin, and V. Yakovlev
Fermilab, Batavia, IL 60510, USA

Abstract

5-cell 650 MHz elliptical cavities are being developed for the Proton Improvement Plan II (PIP-II) of Fermilab. The cavities are designed to accelerate protons of relative group velocity β=0.9 at the high energy part of the linear particle accelerator. In this paper, we report on the status of these cavities and summarize the results of the quality control measurements performed on four initial prototypes.

INTRODUCTION

Fermilab is proceeding with the Proton Improvement Plan PIP-II, which will revamp Fermilab's accelerator complex to meet future needs of Megawatt high intensity proton beam. PIP-II relies on replacing the current 40 years old 400 MeV normal conducting injector linear accelerator with an 800 MeV superconducting one with higher average beam current [1-2].

Two types of elliptical superconducting cavities are employed in the proposed superconductor Linac to accelerate the beam at relatively higher energies; specifically at a relative group velocity of 0.6 and 0.9 [2]. Both types of cavities consist of 5-cell and are operating at 650 MHz. Four prototypes of the 650 MHz β=0.9 5-cell cavity were fabricated by Advanced Energy Systems (AES) and were received at Fermilab. Prototype cavities passed the typical quality control process at Fermilab from visual inspection, and Coordinate Measurements (CMM). Meanwhile, RF measurements have been also performed on the prototype cavities.

In this paper, we report on the latest RF measurements results carried out to assess the spectrum, field flatness, and existence of trapped modes in the prototype cavities. In addition we present some of the latest simulations and analyses carried out to improve the performance of the 650 MHz β=0.9 5-cell cavity.

MICROPHONICS AND LFD DETUNING

We have studied both the frequency sensitivity to pressure fluctuation df/dP, and Lorentz Force Detuning LFD in the 650 MHz β=0.9 5-cell cavity dressed with helium vessel (HV) using Comsol Multipysics [3]. Upon coupling the electromagnetic problem to the solid mechanics one, we were able to calculate the frequency sensitivity coefficients. The resonance frequency of the π-mode is calculated before and after applying the pressure load. Deformation is calculated using the solid mechanics module then the mesh is deformed with the resultant displacement values to acquire the frequency change.

*Operated by Fermi Research Alliance, LLC, under Contract DE-AC02-07CH11359 with the U.S. DOE
#mhassan@fnal.gov

The mechanical design of the cavity's helium vessel underwent several iterations [4]-[6] in order to minimize the df/dP coefficient. The first generation of the HV design adopted a blade tuner with a 441 mm diameter bellows [4]. Later on a modified design was presented in [5]-[6] with an end tuner that can afford smaller diameter bellows.

Figure 1 depicts that cavity geometry with the blade and end tuner locations indicated. Also the stiffening ring size is an important factor that changes the stiffness of the cavity and thus affects the frequency sensitivity coefficients. Fig. 2(a) demonstrates how the df/dP coefficient and the stiffness changes versus the radius of the stiffening rings. It is clear that by increasing the stiffening ring radius, the cavities becomes stiffer reducing the frequency sensitivity coefficient df/dP.

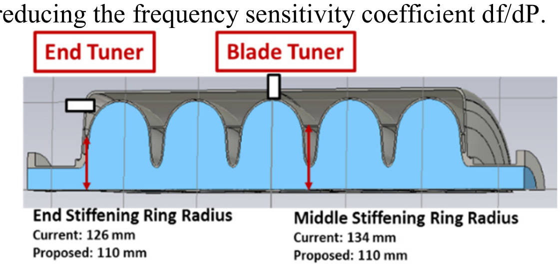

Figure 1: Geometry of the 650 MHz β=0.9 5-cell cavity.

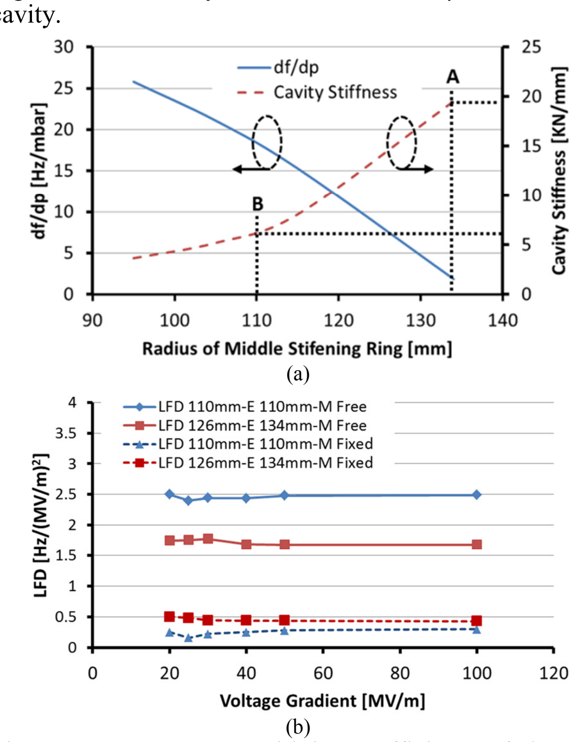

Figure 2: Frequency sensitivity coefficients of the 650 MHz β=0.9 5-cell cavity. (a) df/dP and cavity stiffness versus stiffening ring radius. (b) Lorentz Force Detuning (LFD).

Content from this work may be used under the terms of the CC BY 3.0 licence (© 2015). Any distribution of this work must maintain attribution to the author(s), title of the work, publisher, and DOI.

ISBN: 978-3-95450-168-7 doi:10.18429/JACoW-IPAC2015-WEPTY018

ANALYSIS OF A QUASI-WAVEGUIDE MULTICELL RESONATOR FOR SPX *

M. Awida#, I. Gonin, A. Lunin, T. Khabiboulline, and V. Yakovlev, Fermilab, Batavia, IL 60510
A. Zholents, ANL, Lemont, IL 60439, USA

Abstract

A compact deflecting cavity is needed for the Short Pulse X-rays (SPX) at the Advanced Photon Source (APS) of Argonne national laboratory. The deflecting cavity has to be quite efficient, providing a 2 MV kick voltage and satisfying stringent requirements on aperture size and total cavity length. Meanwhile, the cavity should allow operation up to 100 mT peak surface magnetic field before quenching. In this paper, we report on the latest analysis carried out on the cavity structure to investigate frequency sensitivity to pressure fluctuations, frequency sensitivity to tuning forces, mechanical resonances, and wakefield losses.

INTRODUCTION

A compact deflecting cavity was under development in a collaboration effort between Fermi and Argonne national laboratories to produce an efficient deflecting structure to be used in the Short Pulse X-rays (SPX) at the Advanced Proton Source (APS) of Argonne national laboratory. Using a deflecting cavity for SPX was initially suggested by Zholents, et al. in [1].

The cavity was designed to meet stringent requirements on both electromagnetic and mechanical performances. Table 1 lists the design parameters of the APS deflecting cavity, which operates at 2.815 GHz with an optimal group velocity of 1. The cavity should produce a nominal kick voltage of 2 MV, while keeping the peak surface electric field below 55 MV/m to avoid surface emission and the peak surface magnetic field below 80 mT to avoid thermal quench. Based on beam dynamics, the aperture of the cavity was required to be 12 mm x 30 mm.

Cavity design underwent several iterations to meet the specified design goals and in addition lower the higher order modes losses and simplify the fabrication process. Final electromagnetic design was reported in [2] with detailed higher order mode analysis. The cavity design named Quasi-waveguide Multicell Resonator (QMiR) is shown in Fig. 1. The proposed design meets the requirements and sustains a peak surface electric field of 54 MV/m and a peak surface magnetic field of 75 mT at the nominal operating kick of 2 MV. The designed cavity has a G-factor of 130 Ω.

Argonne successfully constructed a cavity prototype for the QMiR structure and initial testing results were reported in [3].

In this paper, we present the analysis carried out on the QMiR structure to examine the frequency sensitivity to pressure fluctuations and tuning forces. In addition modal and wakefield analyses are also reported.

QMIR DEFLECTING CAVITY

Figure 1 shows the geometry of the QMiR cavity. The cavity consist of 3-cells. Each cell shape was optimized to lower the surface fields as explained in [2]. The cavity operates at 2.815 GHz in the transverse electric TE dipole mode, which is needed to produce the required transverse kick. The power coupler is located on the side of the cavity and its position was optimized to lower the external quality factor of higher order modes (HOM).

The cavity prototype was machined from a solid brick of Niobium. Fig. 1(b) shows a section of the cavity with the Niobium walls highlighted. Series of blind holes is to be used for cooling the high magnetic field areas at the cell centers.

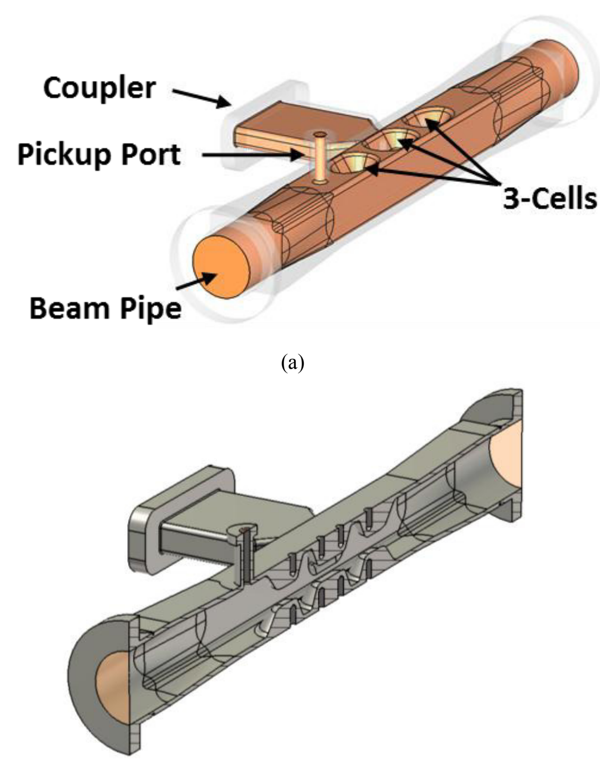

(a)

(b)

Figure 1: Geometry of the quasi multimode resonator. (a) RF domain is highlighted. (b) Section of the cavity with the Niobium walls highlighted.

* Operated by Fermi Research Alliance, LLC, under Contract DE-AC02-07CH11359 with the U.S. DOE
# mhassan@fnal.gov

Content from this work may be used under the terms of the CC BY 3.0 licence (© 2015). Any distribution of this work must maintain attribution to the author(s), title of the work, publisher, and DOI.

ISBN: 978-3-95450-168-7 doi:10.18429/JACoW-IPAC2015-WEPTY019

Content from this work may be used under the terms of the CC BY 3.0 licence (© 2015). Any distribution of this work must maintain attribution to the author(s), title of the work, publisher, and DOI.

TRANSVERSE FIELD PERTURBATION FOR PIP-II SRF CAVITIES*

P. Berrutti#, T. N. Khabiboulline, V. Lebedev, V. P. Yakovlev, Fermilab, Batavia, IL, 60510 USA

Abstract

Proton Improvement Plan II (PIP-II) consists in a plan for upgrading the Fermilab proton accelerator complex to a beam power capability of at least 1 MW delivered to the neutrino production target. A room temperature section accelerates H- ions to 2.1 MeV and creates the desired bunch structure for injection into the superconducting (SC) linac. Five cavity types, operating at three different frequencies 162.5, 325 and 650 MHz, provide acceleration to 800 MeV. This paper presents the studies on transverse field perturbation on particle dynamic for all the superconducting cavities in the linac. The effects studied include quadrupole defocusing for coaxial resonators, and dipole kick due to couplers for elliptical cavities. A multipole expansion has been performed for each of the cavity designs including effects up to octupole.

INTRODUCTION

PIP-II stands for Proton Improvement Plan-II [1] which is Fermilab plan for future improvements to the accelerator complex. The upgrade is aimed at providing LBNE (Long Base Neutrino Experiment) operations with a beam power of at least 1 MW on target. The central element of the PIP-II is a new 800 MeV superconducting linac, injecting into the existing Booster. The PIP-II 800 MeV linac is a derivative of the Project X Stage 1 design. The room temperature (RT) section includes a Low Energy Beam Transport (LEBT), RFQ and Medium Energy Beam Transport (MEBT), accelerating H- ions to 2.1 MeV and it creates the desired bunch structure for injection into the superconducting (SC) linac. This article focuses on the SC linac and its five cavity types, half wave resonator (HWR), single spoke resonator (SSR1 and SSR2), low beta (LB) and high beta (HB) elliptical cavities. The technology map of the PIP-II linac, Fig. 1, shows the transition energies between accelerating structures, and the transition in frequency, HWR operates at 162.5 MHz (same as RT section), SSR1 and SSR2 at 325 MHz, LB and HB elliptical cavities at 650 MHz.

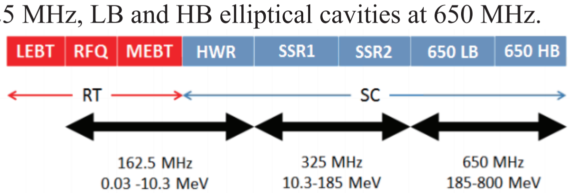

Figure 1: PIP-II linac technology map.

The three families of coaxial resonators show quadrupole perturbation to the transverse fields [2], this is due to the inner electrode which breaks the azimuthal symmetry of the cavity. Elliptical cavities do not have inner posts, but the transverse symmetry is broken by the coupler port on top of the beam tube, leading to a dipole perturbation to the transverse fields. All the results presented are based on EM fields simulated with Comsol multi-physics, the simulation technique requires local mesh refinement around the beam axis to improve transverse field quality. In this article transverse field perturbation is calculated and analyzed for all the cavities in the SC linac of PIP-II, multipole expansion has been performed to show if any higher order effect on the beam dynamic can be present, e.g. sextupole and octupole.

TRANSVERSE KICK

The transverse momentum gain is calculated by direct integration of the electric and magnetic fields transverse to the beam direction. Considering the z axis as the longitudinal (beam) direction, electric and magnetic fields will have x and y components. Assuming the particle velocity constant along z axis, β is constant, one can write:

$$\Delta p_x(r,\alpha)c = \int_{z_i}^{z_f}\left(\frac{E_{x(r,\alpha)}}{\beta} - \boldsymbol{Z}_0 iH_y(r,\alpha)\right)e^{i\frac{kz}{\beta}}dz \qquad (1)$$

$$\Delta p_y(r,\alpha)c = \int_{z_i}^{z_f}\left(\frac{E_y(r,\alpha)}{\beta} + \boldsymbol{Z}_0 iH_x(r,\alpha)\right)e^{i\frac{kz}{\beta}}dz \qquad (2)$$

$\Delta p_x(r,\alpha)c$ and $\Delta p_y(r,\alpha)c$ are functions of the radius and the angle α on the x-y plane, α is taken with respect to the x axis: α=0 corresponds to x axis and α=π/2 refers to y axis. For low-beta structures, the radial component variation will be maximum between the kick on x and on y axis; to have an estimation of the asymmetry one can define a parameter called Q:

$$Q = \frac{\Delta p_x(r,0)c - \Delta p_y(r,\pi/2)c}{(\Delta p_x(r,0)c + \Delta p_y(r,\pi/2)c)/2}. \qquad (3)$$

Asymmetry parameter Q gives partial information on the transverse kick, evaluating $\Delta p_R c$ on the whole x-y plane, it is possible to calculate the multipole expansion of the transverse momentum gain:

$$\Delta p_R c(r,\alpha) = A_0(r) + \sum_{n=1}^{\infty} A_n(r)\cos(n\alpha) + B_n(r)\sin(n\alpha) \qquad (4)$$

where $A_n(r) \propto nr^{n-1}$ and $B_n(r) \propto nr^{n-1}$ are the Fourier series coefficient of $\Delta p_R c$ while $A_0(r) \propto r$ and it is the mean value. One coefficient set out of two has non zero values and the other vanishes. Normal or skew components are due to the symmetry of the problem and to the choice frame of reference to define x-y plane. The transverse kick has been expanded up to octupole, corresponding to $n = 4$.

*Work supported by D.O.E. Contract No. DE-AC02-07CH11359
#berrutti@fnal.gov

ISBN: 978-3-95450-168-7 doi:10.18429/JACoW-IPAC2015-WEPTY020

Content from this work may be used under the terms of the CC BY 3.0 licence (© 2015). Any distribution of this work must maintain attribution to the author(s), title of the work, publisher, and DOI.

DESIGN OF A MARX-TOPOLOGY MODULATOR FOR FNAL LINAC*

T.A. Butler#, F.G. Garcia, M.R. Kufer, H. Pfeffer, D. Wolff, FNAL, Batavia, IL 60510, USA

Abstract

The Fermilab Proton Improvement Plan (PIP) was formed in late 2011 to address important and necessary upgrades to the Proton Source machines (Injector line, Linac and Booster). The goal is to increase the proton flux by doubling the Booster beam cycle rate while maintaining the same intensity per cycle, the same uptime, and the same residual activation in the enclosure. For the Linac, the main focus within PIP is to address reliability. One of the main tasks is to replace the present hard-tube modulator used on the 200 MHz RF system. Plans to replace this high power system with a Marx-topology modulator, capable of providing the required waveform shaping to stabilize the accelerating gradient and compensate for beam loading, will be presented, along with development data from the prototype unit.

INTRODUCTION

The Fermi National Accelerator Laboratory (FNAL) Linear accelerator accelerates H^- beam pulses from 750 keV up to 400 MeV. The lower energy Linac section, built in 1969, uses 201.25 MHz Alvarez style drift tube cavities powered by a 5 MW triode power tube (therein referred as 7835) accelerating beam up to 116 MeV, while the higher energy section uses 805 MHz side coupled cavities powered by a klystron to boost the beam energy to 400 MeV. The 7835 is plate modulated using a hard-tube topology modulator where a high voltage capacitor bank provides energy that is switched via three parallel grid-controlled electron tubes to regulate the anode on the triode. These series-pass tubes were discontinued in the early 2000s, so in order to sustain operations, these tubes required the development and management of a dedicated maintenance schedule in order to rebuild depleted tubes. This approach has been extending the life of the present modulator, but is not sustainable for long term operations.

Within the Proton Improvement Plan (PIP) [1], the chosen path to mitigate this reliability issue was to replace the hard-tube modulator with a modern solid state modulator which improves reliability, lowers operational costs while maintaining the same waveform accuracy required to accelerate the beam. The main challenge in designing a replacement for the present hard-tube modulator is achieving the waveform shaping that is required to regulate the accelerating cavity fields. Unlike other Linac RF systems, which typically use direct feedback (driving the RF input to the power amplifier to regulate gradient), the 7835 triode amplifier uses the plate voltage to regulate the cavity field, requiring a modulator capable of creating an adaptable waveform to compensate for beam loading and overshoot for filling the cavity.

*Operated by Fermi Research Alliance, LLC under Contract No. De-AC02-07CH11359 with the United States Department of Energy.
tbutler@fnal.gov

PRESENT MODULATOR TOPOLOGY AND SPECIFICATIONS

The present tube based modulator acts essentially as a large operational amplifier with finite gain. When operated in an analog feedback loop, it has the ability to regulate its output to any desired shape, which is presently chosen as a trapezoidal ramped waveform. Furthermore, this system compensates in real time for pulse-to-pulse gain changes, which are present in many amplifier stages. By choosing the feedback signal as the peak detected accelerating cavity gradient, the feedback system is able to regulate the cavity fields with ~0.2%. In Table 1, a subset of the most critical parameters for the modulator are listed.

Table 1: Linac Modulator Specifications

Parameter	Value	Units
Maximum Voltage	35	kV
Maximum Current	375	A
Voltage Regulation	±25	V
Minimum Slew Rate	15	kV/µs
Maximum Rise/Fall Step	1.5	kV
Maximum Beam Step	8	kV
Maximum Beam Tilt	±5	kV
Maximum Pulse Width	460	µs
Variable Rise/Fall Time	50-150	µs
Pulse Repetition Rate	15	Hz

NEW MODULATOR DESIGN

A careful study of the numerous alternative options were conducted and down-selected to the two best designs. Among the alternative options were 1) replace the modulator with another hard-tube modulator; 2) replace with industry developed solid state modulator and 3) adapt the Marx-topology modulator developed by SLAC for the International Linear Collider (ILC) project [2]. Despite having strong features most of the options would involve significant development costs in order to meet the desired operational requirements. In particular, the later was extensively studied, but it had slightly higher cost and more engineering time required to convert the design to operate in real time feedback, which is critical for meeting the desired operational requirements [3]. Therefore, the best option chosen for Linac was to design a new system, based on Marx-topology modulator which was designed to meet the critical specifications with the ability to run in real time feedback without compromising any other requirements.

ISBN: 978-3-95450-168-7 doi:10.18429/JACoW-IPAC2015-WEPTY021

ORIGIN OF TRAPPED FLUX CAUSED BY QUENCH IN SUPERCONDUCTING NIOBIUM CAVITIES*

M. Checchin†, M. Martinello
Fermilab, Batavia, IL 60510, USA / Illinois Institute of Technology, Chicago, IL 60616, USA
A. Grassellino, O. Melnychuk, A. Romanenko and D.A. Sergatskov
Fermilab, Batavia, IL 60510, USA

Abstract

In this study we prove that the mechanism at the basis of quality factor degradation due to quench involves the entrapment of ambient magnetic field. The cavity quench in the absence of magnetic field does not introduce any extra losses, and a clear trend between the external field and the extra losses introduced by the quench was observed.

It is demonstrated that the quality factor can be totally recovered by quenching in zero applied magnetic field. A dependence of the amount of quality factor degradation on the orientation of the magnetic field with respect to the cavity was also found.

INTRODUCTION

Superconducting accelerator cavities are devices used in accelerator physics to accelerate charged particles [1, 2]. Such accelerating structures are limited in field (E_{acc}) by the quench of the superconductive state, which leads to the break-down of the resonating electromagnetic field. During such phenomenon a normal conducting region is created on the cavity wall, whose dimension is related to the stored energy of the cavity at the moment of quench. When this normal conductive hole opens, some magnetic flux may be trapped [3], adding extra losses to the resonator and lowering its quality factor (Q_0).

Several different hypotheses where formulated in the past regarding the origin of trapped magnetic field during the quench, such as: thermocurrents driven by the local thermogradient in the quench zone [3], RF field trapped in the penetration depth, or ambient magnetic field. In this study the results obtained at Fermilab, indicate that trapping of ambient magnetic field is the principal cause of the quench-related Q_0 degradation, ruling out the other two proposed mechanisms.

EXPERIMENTAL SET-UP

In this study we used a bulk niobium 1.3 GHz TESLA type cavity nitrogen-doped with the recipe adopted for LCLS-II: 2 min at 800°C in 20 mTorr of N_2 plus a diffusion step of 6 min at 800°C followed by 5 μm EP removal. All the vertical tests were performed at the Fermilab vertical test facility.

The schematic of the setup is shown in Fig. 1. In order to resemble as much as possible the cryomodule situation, the cavity was hanged in the cryostat horizontally, so the cooling started at the very bottom equator point to the very top - also equator - point of the cavity. The cavity was equipped with two Helmholtz coils, capable of creating the magnetic field parallel and orthogonal with respect to the cavity axis, and the magnetic field was measured by means of four single-axis Bartington Mag-01H cryogenic flux-gates magnetometers. Two flux-gates were aligned axially to the cavity, one on top and the other at the middle position, while the other two were set vertically, one on top and one at the bottom.

The helium bath temperature was always maintained around 1.5 K, so the temperature dependent part of the surface resistance can be neglected. The quench study was performed by recording the degradation of Q_0 at the fixed accelerating field after RF quenching the cavity ($E_{quench} \simeq 29 MV/m$) in the presence of external magnetic field. After every quench we also tried to recover the Q_0 by quenching in zero magnetic field.

RESULTS AND DISCUSSION

We performed two series of quenching with either non-zero axial or non-zero orthogonal components of the ambient field H only. The change in the residual resistance

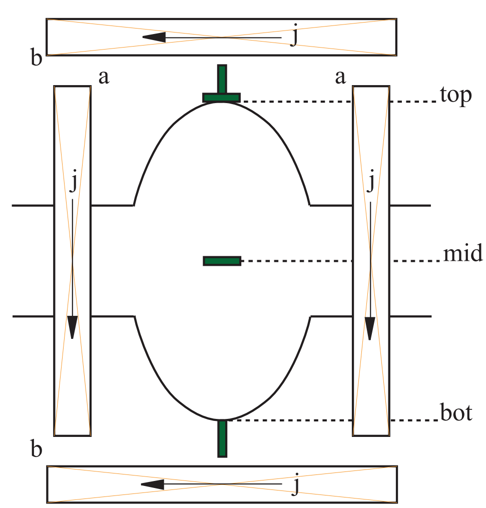

Figure 1: Experimental set-up. The flux-gates are represented by green rectangles, while the letters *a* and *b* indicate the two Helmholtz coils: axial and orthogonal respectively.

* Work supported by the US Department of Energy, Office of High Energy Physics.
† checchin@fnal.gov

Content from this work may be used under the terms of the CC BY 3.0 licence (© 2015). Any distribution of this work must maintain attribution to the author(s), title of the work, publisher, and DOI.

ISBN: 978-3-95450-168-7 doi:10.18429/JACoW-IPAC2015-WEPTY022

Content from this work may be used under the terms of the CC BY 3.0 licence (© 2015). Any distribution of this work must maintain attribution to the author(s), title of the work, publisher, and DOI.

MODIFICATIONS OF SUPERCONDUCTING PROPERTIES OF NIOBIUM CAUSED BY NITROGEN DOPING RECIPES FOR HIGH Q CAVITIES*

A. Vostrikov#, Y.-K. Kim, University of Chicago, Chicago, IL 60637, USA
A. Romanenko, A. Grassellino, FNAL, Batavia, IL 60510, USA

Abstract

A study is presented on the superconducting properties of niobium used for the fabrication of the SRF cavities after treating by recently discovered nitrogen doping methods. Cylindrical niobium samples have been subjected to the standard surface treatments applied to the cavities (electropolishing, 120C bake) and compared with samples treated by additional nitrogen doping recipes routinely used to reach ultra-high quality factor values ($>3\cdot10^{10}$ at 2K, 16MV/m). The DC magnetization curves and the complex magnetic AC susceptibility have been measured.

Evidence for the lowered field of first flux penetration after nitrogen doping is found suggesting a correlation with the lowered quench fields. Superconducting critical temperatures T_c = 9.25 K are found to be in agreement with previous measurements, and no strong effect on the critical surface field (B_{c3}) from nitrogen doping was found.

INTRODUCTION

Superconducting radio frequency (SRF) cavities are the key technology for future particle accelerators for high-energy physics, nuclear physics, light sources, and accelerator-driven subcritical reactors. Several decades of SRF research and development at laboratories and universities worldwide have led to the successful realization of niobium cavities that reliably achieve very high gradients and quality factors.

Recent breakthrough discovery at Fermilab demonstrated positive impact on cavity's quality factor from the doping of certain amount of nitrogen into niobium cavity walls. However, this treatment reduces somewhat the maximum gradient achievable in the cavity, i.e. reduction of quench field takes place. It was demonstrated that SRF cavities, which surfaces prepared with electrolytic polishing (EP) method and low temperature (120ºC) bake-out for 48 hours, can have quench fields over 40 MV/m, while cavities which undergone nitrogen doping are limited by a quench field of 25-30 MV/m. [1]

Magnetic measurements on niobium samples are a useful tool to investigate the effect of nitrogen doping on niobium critical fields. The experimental studies on the magnetization and susceptibility of niobium samples presented in the paper have been carried out with the aim to gain an understanding of superconducting properties change by nitrogen doping.

*Work supported by DOE HEP.
#vostrikov@uchicago.edu

EXPERIMENTAL PROCEDURE

The samples for the magnetization and susceptibility measurements are cylinders with diameter of 2.85 mm and a height of 7.0 mm, which are cut from RRR~300 fine grain niobium sheets used for SRF cavity production. Bulk EP of ~120 um removal was done on all samples. After that, one of the samples was baked for 48 hours at 120ºC in the vacuum. Such surface preparation in SRF cavities typically leads to maximum accelerating fields of 40 MV/m and above. Two other samples are prepared using different nitrogen doping recipes, which found to deliver SRF cavities with optimal quality factor ($>2.7\cdot10^{10}$ and above at 16 MV/m and 2 K). The procedure of surface treatment (after initial bulk EP) is the following:

- high temperature bake at 800ºC for 3 hours in vacuum;
- bake at 800ºC for time t_1 with nitrogen gas in the chamber (diffusion of nitrogen into niobium happens);
- after diffusion bake at 800ºC for time t_2 in vacuum (diffused nitrogen redistributes inside the niobium walls to produce desired nitrogen concentration profile);
- 5 µm surface layer removal by EP (nitrides formed at the surface removed, desired surface concentration of nitrogen is achieved).

Time parameters t_1 and t_2 are subject to optimization. Optimal in terms of quality factor recipes have the following parameters: t_1 = 2 min, t_2 = 6 min and t_1 = 20 min, t_2 = 30 min. Cavities prepared with the first recipe have quench fields of up to ~30 MV/m. Cavities prepared with the second recipe have quench fields of up to~25 MV/m. One more presented sample had no extra treatment after bulk EP.

Sample DC magnetization is measured with a commercial magnetometer (Quantum Design PPMS) at 2 K in external DC magnetic field between zero and 1 T. The same system is also used for AC susceptibility measurements. A frequency of 10 Hz and AC field amplitude of 0.2 mT allow good noise suppression and an acceptable measurement time. In all measurements external magnetic fields are aligned parallel to the symmetry axis of the cylindrical samples.

The demagnetization factor was calculated according to the theoretical expression [2]

$$N_Z = 1 - \frac{1}{1 + \frac{d}{h}\left(\frac{4}{3\pi} + \frac{2}{3\pi}\tanh\left(1.27\frac{h}{d}\ln\left(1 + \frac{d}{h}\right)\right)\right)},$$

ISBN: 978-3-95450-168-7 doi:10.18429/JACoW-IPAC2015-WEPTY023

LBNF 1.2 MW TARGET: CONCEPTUAL DESIGN & FABRICATION*

C. Crowley#, K. Ammigan, K. Anderson, B. Hartsell, P. Hurh, J. Hylen, R. Zwaska
FNAL, Batavia, IL 60510, USA

Abstract

Fermilab's Long-Baseline Neutrino Facility (LBNF) will utilize a modified design based on the NuMI low energy target that is reconfigured to accommodate beam operation at 1.2 MW. Achieving this power with a graphite target material and ancillary systems originally rated for 400 kW requires several design changes and R&D efforts related to material bonding and electrical isolation. Target cooling, structural design, and fabrication techniques must address higher stresses and heat loads that will be present during 1.2 MW operation, as the assembly will be subject to cyclic loads and thermal expansion. Mitigations must be balanced against compromises in neutrino yield. Beam monitoring and subsystem instrumentation will be updated and added to ensure confidence in target positioning and monitoring. Remote connection to the target hall support structure must provide for the eventual upgrade to a 2.4 MW target design, without producing excessive radioactive waste or unreasonable exposure to technicians during reconfiguration. Current designs and assembly layouts will be presented, in addition to current findings on processes and possibilities for prototype and final assembly fabrication.

CONCEPTUAL DESIGN

The 1.2 MW fin width has increased from 6.4 mm to 10 mm, with a roughly 5.5 mm expansion in height to accommodate accident conditions and prevent errant beam with a 1.7mm spot size from striking a cooling line. To mitigate the increased heat generation, cooling loop count was doubled. The outer containment tube also increased in size, gaining a 20% larger O.D., (see Fig. 1).

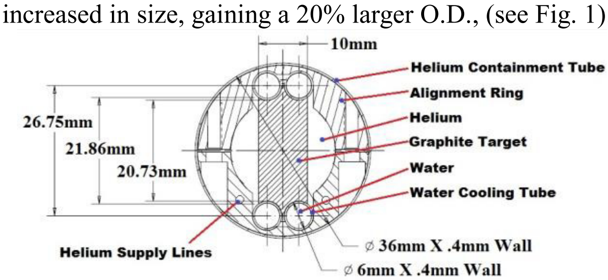

Figure 1: Target core cross section.

Since the design is rooted in a target used on a similar experiment, and with identical focusing horns, some design boundaries apply:

1. Target must be capable of being inserted into horn 1 inner conductor for a low-energy neutrino spectrum.
2. Mass should be kept to a minimum to reduce effects of beam energy deposition on horn conductors.

Target Braze Assembly

The braze assembly consists of twin continuous cooling loops, and forty-seven 20 mm long graphite fins, the first three of which are flared. TiCuNi braze foil at the interface, measuring .05 mm (.002") thick, bonds the assembly by use of specialized fixturing in a vacuum brazing furnace.

Containment Tube

Requirements of the containment tube are that it provide alignment stability, as well as enable the target to withstand a +/-1 atm pressure differential. The target must be pumped down to vacuum for initial installation, then backfilled with helium. This helium flow is piped to the D.S. window for cooling and back out from the target can.

Transition to Down Stream Window

The down stream (D.S.) window will be fabricated from .5 mm (.020") thick beryllium foil, then diffusion bonded to a 3000 series aluminum frame. Transitioning from 3000 series aluminium to grade 2 (CP) titanium requires the use of an explosion bonded or roll bonded Ti-Al bimetal ring. This ring can be fused to the mating halves by means of E-beam welding or micro-TIG welding to achieve a leak tight interface.

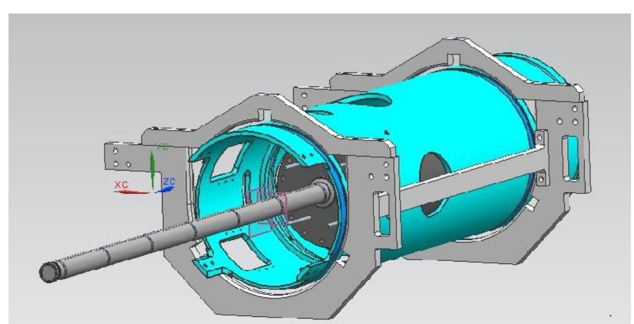

Figure 2: Target core assembly in alignment tube & support frame.

GENERAL LAYOUT & MATERIALS

A notable difference from the NuMI 400 kW design is the absence of a Budal monitor. It was made redundant by vertical & horizontal beam position thermometers located on the U.S. end of the target can. Also present in the 1.2 MW design are additional cooling passages: An outer can water jacket, and a U.S. window and beam position thermometer cooling loop, (see Figs. 2, 3 & Table 1).

* Work supported by Fermi Research Alliance, LLC under Contract No. DE-AC02-07CH11359 with the United States Department of Energy.
# crowley@fnal.gov

Content from this work may be used under the terms of the CC BY 3.0 licence (© 2015). Any distribution of this work must maintain attribution to the author(s), title of the work, publisher, and DOI.

ISBN: 978-3-95450-168-7 doi:10.18429/JACoW-IPAC2015-WEPTY025

Content from this work may be used under the terms of the CC BY 3.0 licence (© 2015). Any distribution of this work must maintain attribution to the author(s), title of the work, publisher, and DOI.

LBNF HADRON ABSORBER: MECHANICAL DESIGN AND ANALYSIS FOR 2.4 MW OPERATION*

B. Hartsell†, K. Anderson, J. Hylen, V. Sidorov, S. Tariq, FNAL, Batavia, IL 60510, USA

Abstract

Fermilab's Long-Baseline Neutrino Facility (LBNF) requires an absorber, essentially a large beam dump consisting of actively cooled aluminum and steel blocks, at the end of the decay pipe to stop leftover beam particles and provide radiation protection to people and groundwater. At LBNF's final beam power of 2.4 MW and assuming the worst case condition of a 204 m long helium filled decay pipe, the absorber is required to handle a heat load of about 750 kW. This results in significant thermal management challenges which have been mitigated by the addition of an aluminum 'spoiler' and 'sculpting' the central portion of the aluminum core blocks. These thermal effects induce structural stresses which can lead to fatigue and creep considerations. Various accident conditions are considered and safety systems are planned to monitor operation and any accident pulses. Results from these thermal and structural analyses will be presented as well as the mechanical design of the absorber. The design allows each of the core blocks to be remotely removed and replaced if necessary. A shielded remote handling structure is incorporated to hold the hadron monitor when it is removed from the beam.

DESIGN OVERVIEW

The absorber consists of two major sections, as shown in the left image of Figure 1. The core, a section consisting of replaceable water-cooled blocks, is shown inside the green box. It is enlarged in the right image of Figure 1. The core consists of an aluminum spoiler block to initiate the particle shower, five aluminum mask blocks with air space in the center to allow the shower to spread, nine sculpted aluminum blocks of reduced central density to further distribute the heat load, four solid aluminum blocks, and four solid A36 steel blocks. All aluminum in the core is 6061-T6. The beam power deposited into the core during 2.4 MW operation is approximately 520 kW, which is the majority of the incoming beam power into the absorber. Outside of the core is forced-air cooled steel and concrete shielding.

ANALYSIS

Using MARS15 [1] energy deposition results as a basis for heat load on the absorber and its core blocks, many iterative simulations between MARS and ANSYS have been carried out to determine the final configuration of the absorber. The main driver of this optimization is reduction of temperature and stress to acceptable levels for the materials during both normal operation and accident scenarios. Creep and fatigue effects have been considered when applicable.

Aluminum core blocks are all water cooled via four 1 inch diameter gun-drilled channels in the aluminum with 20 gallons per minute (gpm) volumetric flow rate through each channel. The water will be cooled to 10°C to help reduce steady state temperatures. Steel blocks are cooled via two 1 inch diameter stainless steel lines along the perimeter of the block with 20 gpm flow rate each.

Steady State Operation

Steady state temperatures and stresses were evaluated at the locations shown in Table 1 for both 120 GeV and 60 GeV operation. 120 GeV operation is by far the worst case due to the lower amount of beam scattering and higher overall beam power compared to 60 GeV operation. Further analysis shown will focus only on 120 GeV operation.

Table 1: Maximum Temperature and Von-Mises Stress for Steady State Operation

Location	Temperature (°C)	Von-Mises Stress (MPa)
Spoiler	60	34
Mask Block 1	25	-
Sculpt Al 3, Ctr	88	103
Sculpt Al 3, WL	25	74
Solid Al 2	84	48
Steel 1	225	199

Creep must be considered since the aluminum is being held at an elevated temperature under stress – 103 MPa at 88°C in the worst case. Creep data for 6061-T6 aluminum bus conductors [2] shows an average stress required to produce 1% creep at 100°C for 10 years to be 172 MPa. Other data [3] indicates the stress values are well below the 250 MPa needed to produce even 0.1% creep at 100°C, although this data only extends to 1000 hours.

A possible concern is losing the T6 temper of the aluminum due to elevated temperature for an extended period of time. After 100,000 hours (11.2 years) at 100°C, there is no change to tensile strength, yield strength, elastic modulus, or elongation [3].

Another consideration is the effect of a failed water line. In the case of the 3rd sculpted aluminum block, the downstream end of the block has a larger energy deposition than the upstream side. For this analysis, convection in the downstream inner water line is removed and the analysis is re-run. Maximum temperature and Von-Mises stress reach 109°C and 174 MPa respectively. At this temperature and stress level, the block would be at least temporarily operable while

* Work supported by Fermi Research Alliance, LLC under Contract No. DE-AC02-07CH11359 with the United States Department of Energy.
† hartsell@fnal.gov

ISBN: 978-3-95450-168-7 doi:10.18429/JACoW-IPAC2015-WEPTY026

DESIGN OF A COMPACT FATIGUE TESTER FOR TESTING IRRADIATED MATERIALS*

B. Hartsell†, M. Campbell, P. Hurh, FNAL, Batavia, IL 60510, USA
T. Ishida, T. Nakadaira, KEK, 1-1 Oho, Tsukuba 305-0801, Japan
M. Fitton, RAL, Didcot, UK

Abstract

A compact fatigue testing machine that can be easily inserted into a hot cell for characterization of irradiated materials is beneficial to help determine relative fatigue performance differences between new and irradiated material. Hot cell use has been carefully considered by limiting the size and weight of the machine, simplifying sample loading and test setup for operation via master-slave manipulator, and utilizing an efficient design to minimize maintenance. Funded from a US-Japan collaborative effort, the machine has been specifically designed to help characterize titanium material specimens. These specimens are flat cantilevered beams for initial studies, possibly utilizing samples irradiated at other sources of beam. The option to test spherically shaped samples cut from the T2K vacuum window is also available. The machine is able to test a sample to 10^7 cycles in under a week, with options to count cycles and sense material failure. The design of this machine will be presented along with current status.

JUSTIFICATION

Currently there is a lack of data concerning fatigue life for irradiated Titanium 6Al-4V, both standard (grade 5) and extra low interstitial (ELI, grade 23). This is of particular concern since a vacuum window with 6Al-4V titanium components directly interacting with the beam is currently installed in the T2K beam line, shown in Figure 1. When the current vacuum window is decommissioned and a new window is installed, it is possible that samples could be cut from the irradiated material. In addition, pre-machined flat samples are planned to be irradiated at other sources of particle beam. These samples can then be used in various tests to characterize irradiated 6Al-4V Ti. In order to estimate effects of irradiation on fatigue, a fatigue testing machine must be constructed that can fit within an existing hot cell design to provide radiation shielding. The results from these fatigue tests can then be compared to control samples run on the same machine prior to irradiation. Samples are expected to be run out to at least 10 million (10^7) cycles to approximate the number of beam pulses on a production window.

SYSTEM DESIGN

The fatigue testing machine used to test the samples must fit inside a hot cell due to sample radioactivity, with a maximum pass-through cross section of a square measuring 9 inches per side. The master-slave manipulators also impose restrictions on material handling, weight capacity, and machine operation. The machine must be able to withstand multiple fatigue runs of 10 million cycles or more with minimal maintenance.

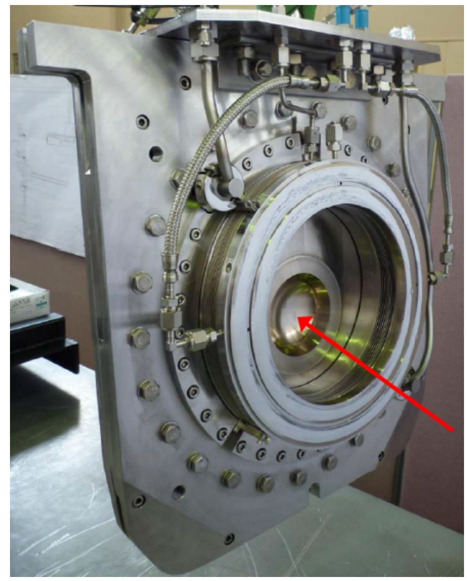

Figure 1: T2K vacuum window assembly, with a red arrow highlighting the approximately 15 cm diameter Ti window.

Sample Design

Two different fatigue samples were designed to accommodate two different test setups. First, a flat fatigue sample was designed in order to simplify the commissioning process of the fatigue testing machine as well as provide the ability to test samples irradiated at other particle beam facilities. Second, a sample with a spherical profile was designed to approximate samples cut from the T2K vacuum window.

Flat fatigue samples are designed as cantilever beams similar to the ASTM D671 standard. While the standard is meant for evaluating flexural fatigue of plastics, the geometry works well for all materials. Flat sample geometry can be seen in Figure 2. It features a wide area for clamping of the material, a transition to a narrower section through a curved profile, and a narrow gauge length. This geometry ensures that the maximum stress occurs away from the clamp and in the region transitioning to the thin gauge length. The effective testing length of the sample, which is the distance from the edge of the clamp to the point where the sample is

* Work supported by Fermi Research Alliance, LLC under Contract No. DE-AC02-07CH11359 with the United States Department of Energy.
† hartsell@fnal.gov

Content from this work may be used under the terms of the CC BY 3.0 licence (© 2015). Any distribution of this work must maintain attribution to the author(s), title of the work, publisher, and DOI.

ISBN: 978-3-95450-168-7 doi:10.18429/JACoW-IPAC2015-WEPTY027

KICKER PULSERS FOR RECYCLER NOVA UPGRADES

Chris C. Jensen, FNAL, Batavia IL, USA

Abstract

An upgrade of the Recycler injection kicker system required a faster rise time pulser. This system required a field rise and fall time of < 57 ns and a field flattop of 1.6 µs. This paper describes the variety of improvements made over the years that have resulted in this latest thyratron pulser. The effects of the trigger, the reservoir and the load impedance on delay and rise time will be discussed.

OVERVIEW

These pulsed power supplies have a fairly high peak power (25 kV, 1 kA), modest repetition rate (15 Hz), very fast rise times (15 ns), very flat pulse tops (+/- 1% for 1.6 us), operate around the clock for many years with limited downtime (1 extended maintenance per year), and the magnets are in a significant radiation field (100 kRad / year). The rise time and flattop requirements are driven by the need for more beam power and maintaining low losses in the accelerator [1].

The topology chosen to meet all of these requirements is a floating switch in a remote service building and a resistive termination mounted at the traveling wave magnet. The high radiation field and limited downtime require the pulser to be located outside the beam line enclosure. The tight flat top requirement requires a low loss pulse forming line. Additionally, the load must be located on the magnet to remove reflections between the load, cable and magnet that reduce flattop stability. To meet the high peak power and fast rise time requirements a thyratron switch was chosen. Low timing jitter and drift are required to maintain stable accelerator operation.

The magnet [2] and load [3] for this system have been previously described. The charging system for a different pulser was briefly described in [4] and [5] and further details are presented herein. The thyatron trigger system described previously [6] has been updated, but the filament and reservoir systems have never been described. Finally, measurements of current rise time for the complete system, without magnet, are presented.

CABLE AND CHARGING SYSTEM

A pulse forming line (PFL) is used instead of a lumped pulse forming network to generate a very square pulse. Low dispersion is required to maintain the fast rise time for the cable run from the pulser to the magnet, about 45 m in this case, and to preserve the prompt fall time at the end of the pulse. The cable used has the same dimensions as RG220/U but with two additional features. First, two foil layers are bonded to the polyethylene core under the bare copper braid to reduce dispersion at higher frequencies. Second, the center conductor has stricter tolerance on dimensional stability and surface roughness to maintain tighter impedance control and increase voltage rating. High voltage pulse testing (60 kV) and impedance testing (±0.4 Ohm) are done on all cables to verify performance.

A two-step command resonant charging system is used. A capacitor, which stores slightly more energy than the PFL, is connected through a thyristor switch to a step up transformer, then through a diode to the PFL. The leakage inductance of the transformer and the capacitance determine the charging time. The capacitor charging supply fully charges the capacitor once a kicker fire is requested, typically to ~ 4 kV in ~ 30 ms. This reduces voltage stress on the capacitor and improves lifetime. The PFL is then charged, typically to ~ 55 kV in ~ 250 µs. This decreases the time there is voltage on the thyratron so that the reservoir can be substantially increased while maintaining a low self triggering rate. That is a critical adjustment for achieving fast rise time as is shown later. The step up transformer is also used because of the limited voltage range of commercial charging supplies.

The resonant charging time is significantly shorter than other applications and there have been no issues. The reduced time was due to accelerator transfer timing requirements and the jitter between different clock systems. A side benefit is the reduced size of the transformer. Balancing resistors of 6 Meg Ohm are used to insure equal voltage division across the thyratron gap during the rapid charging. The negative bias on the G2 voltage trigger must be low impedance to prevent thyratron self triggering.

THYRATRON SUBSYSTEMS

Filament and Reservoir

Stray capacitance from cathode to ground is one fundamental limit to the rise time. One contribution to this capacitance is the transformers used to couple filament, reservoir and trigger power to the cathode. At Fermilab, we have used high frequency (20 kHz) AC to couple power to a floating cathode since the early 1990s.

This is done with two series transformers with a common, grounded intermediate winding. Power is applied to the primary of the first transformer with low isolation voltage. The intermediate winding is formed with a single turn of the improved RG220 cable going through the center of both transformers and the thyratron enclosure serving as the return. The ground conductors are removed from the cable and the center conductor is at ground potential. The second transformer provides the high isolation voltage with the cathode enclosure forming an electrostatic shield at high voltage. The capacitance of

Fermilab is operated by Fermi Research Alliance, LLC under Contract No. DE-AC02-07CH11359 with the United States Department of Energy

Content from this work may be used under the terms of the CC BY 3.0 licence (© 2015). Any distribution of this work must maintain attribution to the author(s), title of the work, publisher, and DOI.

ISBN: 978-3-95450-168-7 doi:10.18429/JACoW-IPAC2015-WEPTY028

Content from this work may be used under the terms of the CC BY 3.0 licence (© 2015). Any distribution of this work must maintain attribution to the author(s), title of the work, publisher, and DOI.

FERMILAB LINAC LASER NOTCHER*

D.E Johnson#, T.R. Johnson, K. Duel, M. Gardner, V. Scarpine, R.J. Tesarek,
Fermilab, Batavia, IL, USA

Abstract

Synchrotrons or storage rings require a small section of their circumference devoid of any beam (i.e. a "notch") to allow for the rise time of an extraction kicker device. In multi-turn injection schemes, this notch in the beam may be generated either in the linac pulse prior to injection or in the accelerator itself after injection. In the case of the Fermilab Booster, the notch is created in the ring near injection energy by the use of fast kickers which deposit the beam in a shielded collimation region within the accelerator tunnel. With increasing beam powers, it is desirable to create this notch at the lowest possible energy to minimize activation. Fermilab has undertaken an R&D project to build a laser system to create the notch within a linac beam pulse at 750 keV, where activation issues are negligible. We will describe the concept for the laser notcher and discuss our current status and future plans for installation of the device.

MOTIVATION

The current Fermilab Booster utilizes multi-turn injection and adiabatic capture to populate all RF buckets in the ring. To minimize losses from the rise time of the 8 GeV extraction kicker, a portion of the beam (about 60 ns. out of 2.2 μs.) in the ring is removed by fast kickers at low energy into an absorber. This empty section of the circumference is called a "Notch". On Booster cycles that are ultimately injected into the MI for the Neutrino program this process takes place at approx.700 MeV. At the completion of the Proton Improvement Plan (PIP) these losses are expected to contribute approximately 300 W of the total administrative limit of 525W. Moving this process out of the Booster tunnel to the 750 keV Medium Energy Beam Transport (MEBT) of the linac is expected to reduce the loss to 17 W, assuming a 90% efficiency in the Linac Notch creation and 10% clean-up in the Booster ring.

LINAC & BOOSTER BEAM

At the completion of PIP, the Fermilab Booster will be operating at 15 Hz. The length of the linac pulse injected into Booster is N*τ where N is the number of injected turns and τ is the Booster revolution period at injection. Creating a notch in the linac pulse requires removing a number sections of the linac beam at the Booster revolution period, where the number of sections to be removed is N-1. The spacing between these removed sections should guarantee that when the H- is injected into the Booster, the empty sections fall on top of one another in the ring producing a single notch in the Booster. This process is shown in Fig. 1. The top pane shows the 15Hz linac pulses to be injected into Booster. The bottom pane shows a single linac pulse with 60 ns notches created within the pulse separated by ~2.2 μs, the Booster revolution period. Not shown is the 200 MHz bunch structure in the linac pulse.

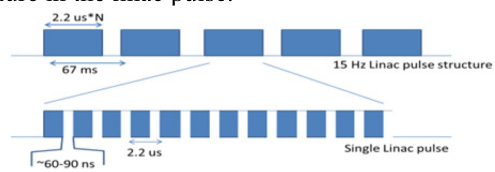

Figure 1: Linac pulse showing the notch structure for a single linac pulse.

LASER NOTCHER CONCEPT

The technique employed to produce the notch is to remove the outer electron of the H- ion using photoionization for the appropriate beam sections. There have been discussions on using lasers to create a notch in the linac beam for some time. [1-3] This technique was demonstrated in 2000. [1] The photoionization cross section has a broad peak centered at 1.51 eV (λ=821 nm) photon energy in the center-of-mass frame of the electron with a cross section of 4.2x10^{-17} cm^2. [4] The choice of the lab frame photon energy is dependent of the H- energy and the interaction angle through the standard Lorentz transformation. The laser technology for both solid state (Nd:YAG) and Yd doped fiber with a laser wavelength of 1064 nm has matured significantly over the last decade such that it is the natural choice for the laser system. The cross section for these photons with CM energy 1.165 eV is 3.66x10^{-17} cm^2, only 13% off the peak. When the probability of interaction between the photons and electrons is high and the mechanism does not depend on the electron intensity, the fraction of electrons that are detached from the moving H- ions is given by

$$F_{neut} = {}^{N}/_{N_0} = \left(1 - e^{-f_{CM}\sigma(E)\tau}\right),$$

where f_{CM} is the flux of photons at the interaction point in the rest frame of the H- [photons/cm^2/sec], σ(E) is the photoionization cross section for photon energy E, and τ is the interaction time of the photons and electrons. The center of mass flux can be expressed in lab frame parameters as

$$f_{CM} = \gamma\left(\frac{E_{laser}\lambda_{LAB}}{hc\tau_{laser}}\right)\left(\frac{1}{A_{laser}}\right)(1 - \beta\cos\theta),$$

where $\boldsymbol{E}_{\mathbf{laser}}$ is the laser pulse energy, $\boldsymbol{\lambda}_{\mathbf{LAB}}$ is the lab frame wavelength of the laser, τ_{laser} is the laser pulse length, $\boldsymbol{A}_{\mathbf{laser}}$ is the laser cross sectional area, γ and β are the usual relativistic parameters, and θ is the interaction angel between the photons and H-. Figure 2 shows the "single pass" neutralization fraction as a function of laser pulse energy to neutralize a single 60 ns section of the 750 keV H- linac pulse, assuming a 90° interaction angle.

*Operated by Fermi Research Alliance, LLC under contract No. DE-AC02-07CH11359 with the United States Department of Energy.
#DEJ@fnal.gov

ISBN: 978-3-95450-168-7 doi:10.18429/JACoW-IPAC2015-WEPTY029

MEASUREMENTS OF STRONTIUM FERRITE HYBRID PERMANENT MAGNET QUADRUPOLES AFTER REMOVAL FOR THE FERMILAB NOVA UPGRADE IN 2012

O. Kiemschies*, FNAL, Batavia, IL 60510 USA

Abstract

During the 2012 NOvA upgrade forty strontium ferrite hybrid permanent magnet quadrupoles from the injection, extraction and electron cooling regions of the Recycler accelerator, which had been measured in 2000 and subsequently installed in the tunnel, were replaced. The basic design of the quadrupoles [1] and expected decay rate [2] are described in design documents. Nine of these magnets, of varying strength were measured in 2014. Measurements were made with a rotating coil in a fashion similar to their initial pre-installation measurements in 2000. The 2014 measurements are compared to the 2000 measurements and the expected decay.

.

PERMANENT MAGNETS IN THE RECYCLER

The Fermilab Recycler contains approximately 500 permanent magnets [2] of several different types. These magnets use grade 8 Strontium Ferrite bricks to produce the magnetic field and machined steel poles to create the field shape [2]. Segments of a 4x6x1 bricks (cut to 2"x1" bricks of varying length) were used. To compensate for the change in magnetization as a function of temperature, 2"x1" thin pieces of 30% Ni 70% Fe alloy were interspersed among the ferrite segments [3].

During the initial years of the Recycler, measurements were made of several different magnets to understand the evolution of magnet strengths over time [2].

NOVA UPGRADE

For the 2012 NOvA upgrade, approximately forty 20" permanent quadrupole magnets (Figure 1) in the transfer lines and in the decommissioned electron cooling region of the Recycler needed to be modified or replaced because of new field strength requirements. The decision was made to replace them with new magnets [4]. This meant 40 magnets were uninstalled, allowing for the measurement of these magnets and the comparison of current measurement data with measurement data recorded prior to installation. Due to radiation these magnets remained an unused section of tunnel until 2014, at which time activation for nine magnets was low enough allowing for easier handling.

*ollie@fnal.gov
Work supported by the U.S. Department of Energy

ASSEMBLY AND INSTALLATION

Assembly

Assembly data was captured in "travelers" recorded during fabrication, and any modifications. Measurement data was captured in the Fermilab Magnet Test Facility system. The dates of measurements are correct, however dates of ferrite magnetization are approximate. The traveler records when the bricks were acquired from a pool of recently magnetized bricks. The time gap between magnetization and assembly is small (weeks to months range) compared to the time between these measurements. Initial strength specifications required the magnets to be within 5 units of grel [5].

Installation

Eight magnets listed were installed in the Recycler Ring and were in the proximity of Recycler Ring vacuum chamber "bake-outs". This typically involved baking sections of beam tubes in the range of 100^{o} C to 130^{o} C. Exact temperatures on the magnets were not measured. This is significant due to the potential effect of elevated temperature on the long-term decay of magnet strength [2]. RQMF009, however, was located in a transfer line so was not subjected to potential elevated temperatures.

ADDITIONAL STORED MAGNET MEASURED

PQP003

In addition to the removed quads, three additional magnets which had not been in the tunnel were measured. PQP003 was an early 20" permanent quadrupole prototype. Prior to 2009 there is uncertainty regarding modifications to this magnet. There are records of modifications as late as 1997. Because of the uncertainty, Measurements prior to 2009 were excluded. However, data from 1997 to 2009 would agree with the general trends in grel change since 2009. Since it is a form of 20" quad, PQP003 was included in Table 1.

RGF005

RGF005 is the first production gradient magnet which met Recycler specifications. It was kept as a standard magnet and was measured periodically since 1997 [2]. Continual measurements exist for this magnet. It was stored a temperature controlled building when not being measured.

Content from this work may be used under the terms of the CC BY 3.0 licence (© 2015). Any distribution of this work must maintain attribution to the author(s), title of the work, publisher, and DOI.

ISBN: 978-3-95450-168-7 doi:10.18429/JACoW-IPAC2015-WEPTY030

BREAKDOWN CHARACTERIZATION IN 805 MHz PILLBOX-LIKE CAVITY IN STRONG MAGNETIC FIELDS*

A. Kochemirovskiy, University of Chicago, IL, 60637, USA
D. Bowring, K. Yonehara, A. Moretti, D. Peterson, Fermilab, Batavia, IL, 60510, USA
G. Kazakevich, G. Flanagan, Muons, Inc. Batavia, IL, 60510, USA
M. Chung, UNIST, Ulsan 689-798, Korea
Y. Torun, B. Freemire, P. Hanlet, IIT, Chicago, IL, 60616, USA

Abstract

RF Breakdown in strong magnetic fields has a negative impact on a cavity performance. The MuCool Test Area at Fermilab has unique capabilities that that allow us to study the effects of static magnetic field on RF cavity operation. We have tested an 805 MHz pillbox-like cavity in external magnetic fields up to 5 T. Results confirm our basic model of breakdown in strong magnetic fields. We have measured maximum achievable surface gradient dependence on external static magnetic field. Damage inspection of cavity walls revealed a unique observed breakdown pattern. We present the analysis of breakdown damage distribution and propose the hypothesis to explain certain features of this distribution.

INTRODUCTION

Muon ionization cooling channel designs require RF cavities to be operated in strong magnetic fields up to several Tesla [1,2]. RF cavity performance is limited by breakdown: current discharge across a cavity accompanied by an abrupt drop in stored energy, light and x-ray emission, and a transient increase in vacuum pressure. It has been previously experimentally demonstrated that in strong magnetic fields the breakdown rate increases [3].

A model has been proposed which explains the effects of strong magnetic fields on breakdown-related cavity damage [4]. In the presence of a strong, solenoidal magnetic field, field-emitted electrons are focused into "beamlets" with current densities of 10^3 - 10^5A/m^2 at impact site. Space charge effects prevent further increase in beamlet current density above 0.5 T. These beamlets persist over multiple RF cycles and, through their impact on cavity surfaces, cause pulsed heating, cyclic material fatigue, and eventual breakdown. This type of damage may lead to increased breakdown probability. Materials with higher radiation length might be less prone to cyclic fatigue under such circumstances.

Cavity Design and Instrumentation

The cavity used in this study was designed to operate wither under vacuum or filled with high-pressure gas, in order to study the role of gas pressure in the suppression of breakdown [5]. Due to this flexibility, the cavity was described as "a cavity for all seasons". The walls of so-called All Seasons Cavity (ASC) are fastened with bolts and aluminum seals, allowing for relatively easy assembly and disassembly. The experimental goals of ASC program included determination of maximum achievable gradient for external magnetic fields between zero and five Tesla for cavity pressures between 10^{-8} Torr and 100 atmospheres, optimization conditioning scheme for stable cavity performance at high gradients, assessment of different cavity wall materials such as copper, aluminum, beryllium [6,7]. This paper presents results from vacuum operation of the ASC.

Figure 1 shows the cross section of the cavity with simulated electrical field distribution. The cavity was designed with two thick copper plated (25 μm) detachable end plates. Flat thin Al gaskets were used to make RF and vacuum seal. Coaxial capacitive coupling was used for power transmission into the cavity. The list of RF properties of ASC is presented in Table 1.

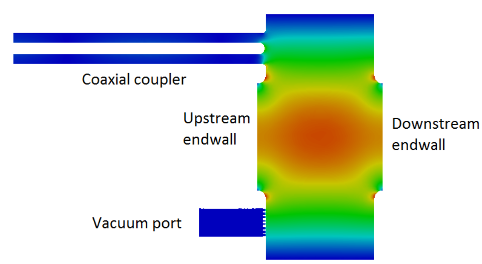

Figure 1: Cross section of ASC with electric fieldmap simulated in Omega3p.

Table 1: RF Properties of the Cavity

Parameter	Value
Frequency	810.4 MHz
Q_0, Q_L	28000, 15500
Coupling constant, β	0.8
Gap lenth	14.5 cm
Base vaccum pressure	3x10^{-8} Torr
Pulse length	30 μs
Stored energy at 20 MV/m	5 Joules
Rep rate	1Hz

Instrumentation and Data Acquisition

Fermilab's MuCool Test Area (MTA) is a unique facility, built specifically to test RF cavities' performance in strong magnetic fields [8]. ASC cavity instrumentation included

* Work supported in part by DOE STTR grant DE-FG02-08ER86352 and by Fermilab Research Alliance, LLC under Contract No. DE-AC02-07CH11359

Content from this work may be used under the terms of the CC BY 3.0 licence (© 2015). Any distribution of this work must maintain attribution to the author(s), title of the work, publisher, and DOI.

ISBN: 978-3-95450-168-7 doi:10.18429/JACoW-IPAC2015-WEPTY031

Content from this work may be used under the terms of the CC BY 3.0 licence (© 2015). Any distribution of this work must maintain attribution to the author(s), title of the work, publisher, and DOI.

ESTIMATION OF CRYOGENIC HEAT LOADS IN CRYOMODULE DUE TO THERMAL RADIATION *

A. Saini†, V. Lebedev, N.Solyak, V. Yakovlev, Fermilab, IL 60510, USA

Abstract

Cryogenic system is one of major cost drivers in high intensity superconducting (SC) continuous wave (CW) accelerators. Thermal radiations coming through the warm-ends of cryomodule and room temperature parts of the power coupler result in additional cryogenic heat loads. Excessive heat load in 2K environment may degrade overall performance of the cavity. In this paper we present studies performed to estimate additional heat load at 2K due to thermal radiation in 650 MHz cavity cryomodule in high energy section of PIP-II SC linac.

INTRODUCTION

The Proton Improvement Plan -II (PIP-II) is proposed to develop a high intensity proton beam facility at Fermilab. It is primarily based on construction of 800 MeV CW SC linac that would initially operate in the pulse mode. A schematic of linac baseline configuration is shown in Fig. 1. It consists of room temperature front-end and SC linac. Each superconducting section in Fig. 1 is represented by optimal beta of respective cavities except for LB and HB sections where geometrical beta of corresponding cavities are shown. A detail description of baseline configuration of PIP-II SC linac is presented elsewhere [1].

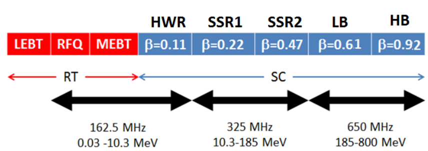

Figure 1: Technology map of PIP-II linac

All cryomodules in SC linac are connected by room temperature sections. This arrangement provides an option of possible beam collimation after each cryomodule which could help to minimize uncontrolled beam losses in cryogenic environment. Furthermore, it also provides space for additional beam diagnostics (transverse and longitudinal profile monitors, beam loss monitors, etc.).

GENERAL

The major infrastructure investment and the operational cost of a superconducting linear accelerator are outlined by its cryogenic requirements. As can be noticed from Table 1, the cryogenic efficiency is significantly lower at 2 K and it is required about 800 W of wall-plug power to remove every Watt of power dissipated in this environment. Consequently, cryogenic load at 2K derives size and therefore the cost of cryogenic-plant. While the dynamic cryogenic load at 2K

Table 1: Typical Cooling Efficiency at Different Cryogenic Temperatures

Temperature	2K	4K	70
Wall-plug power per Watt of power dissipation	800 W	250 W	25 W
Cryo- efficiency	0.125%	0.4%	4 %

is primarily determined by the RF power dissipation in an accelerating cavity, heat transfer due to conduction and radiation through various channels (Helium vessel supports, transfer lines, cables etc.) largely outlines the static heat load of cryomodule. Contribution of heat transfer through the convection is relatively negligible in cryomodule because of its vacuum vessel that maintain high vacuum for thermal insulation. A multilayer insulation using low emissivity material and intermediate temperature screenings (thermal shields) limit the radiation load in cryomodule. However, lateral radiation coming through the warm-ends of cryomodule and penetration of a room temperature surface into the cryogenic environment still result in an accountable radiation load. Heat transfer through the conduction can usually be estimated precisely, but estimation of the radiation heat load in a cryomodule is non-trivial and strongly affected by the geometry and the physical properties of a surface.

Insertions of warm section between cryomodules in PIP-II SC linac result in an increase of static cryogenic load due to lateral thermal radiation entering from both warm-ends of cryomodule. Room temperature parts of the power coupler also add radiation heat load. Radiation heat load in a cryomodule increases in proportion to cross-section area of beam pipe. Thus, radiation heat load for high beta (HB) 650 MHz cryomodules having beam pipe aperture of 118*mm* is higher than any other cryomodules in the SC linac. In this paper we present contribution of radiation to the cryogenic load at 2K in HB 650 MHz cryomodule and discuss its impact on overall performance of 5-cell elliptical shape HB 650 MHz cavity. This estimation allows us to take a decision on the requirement for 80 K thermal shield between HB cryomodules.

THERMAL RADIATION FROM CRYOMODULE WARM-ENDS

As shown in Fig. 2, niobium-beam pipe is not the part of helium jacket and it is cooled down by process of the conduction-cooling. Thus, heat removal in the niobium-beam pipe is not as efficient as in the cavity. Excessive heat deposition may rise temperature in the beam pipe that causes increase in the BCS surface resistance [2]. Consequently, RF

* Work supported by US DOE under contract DE- AC02-76CH03000.
† asaini@fnal.gov

ISBN: 978-3-95450-168-7 doi:10.18429/JACoW-IPAC2015-WEPTY032

MICE CAVITY INSTALLATION AND COMMISSIONING/OPERATION AT MTA*

M. Leonova, M. Backfish, D. Bowring, A. Kochemirovskiy, A. Moretti, D. Peterson, M. Popovic, Y. Torun, K. Yonehara, Fermilab, Batavia, IL, USA
B. Freemire, P. Lane, IIT, Chicago, IL, USA; T. Luo, LBNL, Berkley, CA, USA
C. Hunt, Imperial College, London, UK; T. Stanley, STFC/RAL, Didcot, UK
C. Speirs, C. Whyte, USTRAT/SUPA, Glasgow, UK

Abstract

A first electropolished 201-MHz RF cavity for the international Muon Ionization Cooling Experiment (MICE) has been assembled inside a special vacuum vessel and installed at the Fermilab's MuCool Test Area (MTA). The cavity and the MTA hall have been equipped with numerous instrumentation to characterize cavity operation. The cavity has been commissioned to run at 14 MV/m gradient with no external magnetic field; it is also being commissioned in presence of fringe field of a multi-Tesla superconducting solenoid magnet, the condition in which cavity modules will be operated in the MICE cooling channel. The assembly, installation and operation of the Single-Cavity Module gave valuable experience for operation of full-sized modules at MICE.

INTRODUCTION

The International Muon Ionization Cooling Experiment (MICE) is under construction at Rutherford Appleton Laboratory (RAL, UK). It is designed to demonstrate feasibility of an ionization cooling channel for use in such high-intensity muon sources like a Neutrino Factory or a Muon Collider [1].

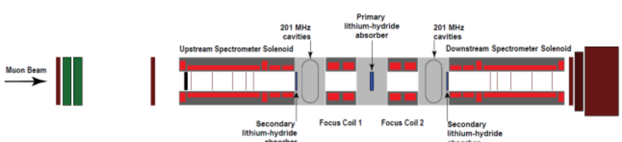

Figure 1: Final configuration of MICE cooling channel, showing two RF cavity modules.

Final MICE channel configuration [2] contains two RF Assembly (RFA) modules very similar to the module being tested at the MuCool Test Area (MTA). Each cavity will be driven by a 2-MW amplifier system to operate at a gradient of at 10.3 MV/m. The cavities also need to operate in fringe fields of multi-tesla solenoidal magnets.

MTA has a 5-T superconducting solenoid that provides operational conditions very similar to MICE channel. MTA Hall is also equipped with numerous detectors to monitor cavity environment and radiation levels, since radiation from RF cavities would affect various components of MICE channel [3] (e.g., radiation damage to detectors, thermal load on liquid hydrogen vessel, etc.). The cavity has also been equipped with instrumentation to characterize its behaviour during operation.

CAVITY INSTALLATION

RF Cavity body was manufactured in industry using techniques developed at LBNL, it was electropolished at LBNL and sent to Fermilab for installation and testing in a special vacuum vessel designed by LBNL, which is very similar to the final design to be used in MICE [4].

The cavity was initially installed and equipped with all the instrumentation in Lab 6 area, which has a class 100 (ISO 5) clean environment. All instrumentation, including the tuning system has been fully tested.

The tuner system consists of 6 stainless steel tuner forks driven by pneumatic actuators. Pneumatic system has a release valve at pressure of 120 PSI, and setup was tested up to 100 PSI at Lab 6, providing "pull" and "squeeze" with ~ 4 KHz/PSI tuning sensitivity [5].

The cavity was then moved to the MTA hall. It was removed from its vacuum vessel to reduce the dimensions during transport. The assembly installation in the vacuum vessel was finished in the MTA clean room [6].

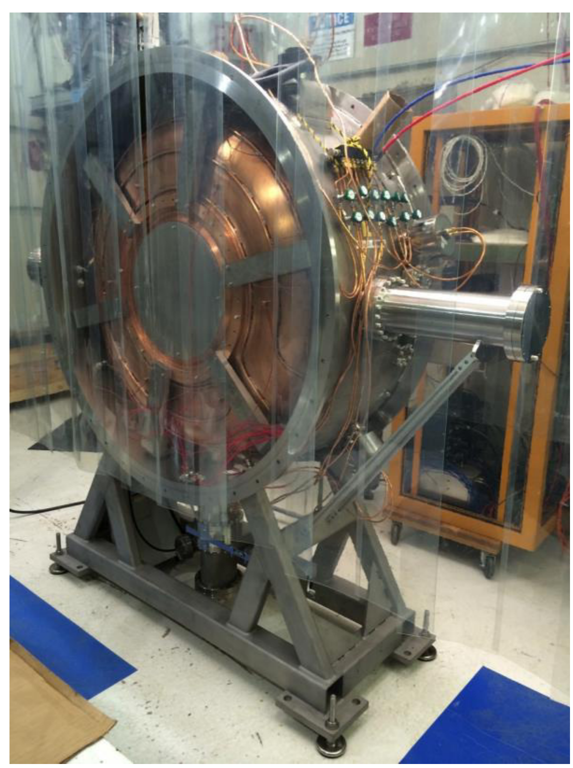

Figure 2: MICE Cavity in the MTA clean room, shortly after it was moved from Lab 6.

*Work supported by Fermilab Research Alliance, LLC under Contract No. DE-AC02-07CH11359.

Content from this work may be used under the terms of the CC BY 3.0 licence (© 2015). Any distribution of this work must maintain attribution to the author(s), title of the work, publisher, and DOI.

ISBN: 978-3-95450-168-7 doi:10.18429/JACoW-IPAC2015-WEPTY033

A CONCEPT FOR A HIGH-FIELD HELICAL SOLENOID

S. T. Krave#, N. Andreev, R. C. Bossert, M. L. Lopes, J. C. Tompkins, R. H. Wands, Fermi National Accelerator Laboratory, Batavia, IL 60510, USA
G. Flanagan, Muons Inc., Batavia, IL, 60510, USA
K. Melconian, Texas A&M University, College Station, TX 77845 USA

Abstract

Helical cooling channels have been proposed for highly efficient 6D muon cooling to produce the required helical solenoidal, dipole, and gradient field components. The channel is divided into sections, each subsequent section with higher field. Simulations have shown that for the high-field sections the use of Nb3Sn superconductor is needed. A continuous winding method and novel stainless steel collaring system has been developed for use in the high field section of a helical cooling channel. Each collar layer is identical, for ease of fabrication, and assembled by both flipping and rotating the subsequent layers. Mechanical and magnetic simulations were performed using a combination of ANSYS and OPERA. The winding and collaring method has been demonstrated on a three coil prototype using a Nb_3Sn Rutherford cable. Details of the mechanical design and winding method are presented.

INTRODUCTION

Helical cooling channels (HCC) based on a magnet system with a pressurized gas absorber in the aperture have been proposed as a highly efficient way to achieve 6D muon beam cooling [1-2]. The magnet system superimposes solenoid (*Bs*), helical dipole (*Bt*), and helical gradient (*G*) fields. The cooling channel was divided into several sections to provide the total phase space reduction of muon beams on the level of 10^5-10^6, and to reduce the equilibrium emittance each consequent section has a smaller aperture and stronger magnetic fields. The field components (*Bt* and *G*) are a function of many geometric parameters as it was presented in [3-6].

The Helical Solenoids (HS) are formed by transverse displacements of short solenoid rings following a helix. Due to this unusual geometry, large transverse forces are generated. In order to intercept the forces a support structure must be designed accordingly. HS prototypes based on NbTi super-conductor were developed and are presented in [7-8]. HS models based on YBCO tape are presented in [9]. These materials do not need a reaction cycle, therefore the winding and impregnation are straight forward.

Nb_3Sn is required for the medium field sections of the HCC. That material requires a reaction cycle to the temperature of 650°C, which restricts the material choices for the support dramatically. In particular the outer support should allow for expansion during the reaction at the same time it should pre-stress the coil during the cool-down. A collar approach allows different materials to be used in each stage of the coil manufacturing and coil operation.

*Work supported in part by Fermi Research Alliance under DOE Contract DE-AC02-07CH11359.
#skrave@fnal.gov

MECHANICAL DESIGN

Nb_3Sn presents a more difficult path to finished product than either NbTi or HTS Tapes as it requires a reaction cycle to ~650°C before use. This is typically implemented in a wind and react configuration in which magnet coils are wound onto a temporary fixture and undergo a reaction cycle in an inert atmosphere. After the reaction cycle, the superconductor becomes extremely brittle and strain intolerant. Coils are typically transferred into an impregnation fixture then impregnated with epoxy, setting the final size of the coil. After impregnation, it is traditionally possible to assemble coils into the final magnet configuration.

As the concept for the helical solenoid as presented is for a long array of multilayer coils, the magnet assembly would ideally be splice-less, leading to a stepped structure that becomes impractical to remove the winding mandrel after winding. For this reason, the inner mandrel of the coil is integrated into the structure and must be able to withstand the reaction cycle with no ill-effects. As the superconductor is not tolerant of strain, the differential thermal expansion of the superconductor during reaction should be well matched to the inner support. For this reason, 316L Stainless Steel has been chosen as the material of the winding mandrel which is also the reaction fixture.

The Collaring Concept

A similar difficulty appears during coil winding in that while hoops may be installed after each layer of coil winding, they must be sufficient to support the hoop and shear forces generated during operation. Using a series of bolt on half structures was rejected due to the complex nature of the helical shape of the coil and the level of forces involved.

A novel mechanical structure has been developed to provide coil alignment and support along both the base helix of the solenoid system and the center axis of the helix. A collared lamination system with locking load keys has been explored to enable the fabrication of a continuously wound helical magnet while maintaining the ability to expand the helical solenoid indefinitely. The collared structure also allows for a temporary support structure to be used during reaction. The basis of the

Content from this work may be used under the terms of the CC BY 3.0 licence (© 2015). Any distribution of this work must maintain attribution to the author(s), title of the work, publisher, and DOI.

ISBN: 978-3-95450-168-7 doi:10.18429/JACoW-IPAC2015-WEPTY034

T-MAP STUDIES ON GRADIENT-LIMITING MECHANISM IN NITROGEN DOPED CAVITIES*

M. Martinello†, M. Checchin, FNAL, Batavia, IL 60510, USA and IIT, Chicago, IL 60616, USA
A. Grassellino, A. Romanenko, FNAL, Batavia, IL 60510, USA

Content from this work may be used under the terms of the CC BY 3.0 licence (© 2015). Any distribution of this work must maintain attribution to the author(s), title of the work, publisher, and DOI.

Abstract

Nitrogen doping results in ultra-high quality factors in SRF niobium cavities but currently achievable gradients in doped cavities are, on average, somewhat lower than in EP/120 °C baked cavities. The origin of this difference is explored in the reported work by detailed temperature mapping studies on several single cell nitrogen doped cavities.

INTRODUCTION

Superconducting accelerating cavities have recently received a large improvement in terms of quality factor, thanks to the discovery of nitrogen doping treatment. Before this beneficial treatment was discovered, the performance of niobium cavities were limited, in terms of Q-factor, to $2 \cdot 10^{10}$ at 16 MV/m (at 2 K, for 1.3 GHz cavities). Nitrogen doped (N doped) cavities can instead reach quality factors of $4 \cdot 10^{10}$ at 16 MV/m [1]. On the other hand, the performance achieved in terms of accelerating field is nowadays lower for N doped cavities, that is in the range of $20 - 30$ MV/m, compared with EP/120 °C baked cavities which reach even 40 MV/m.

In this paper the quench mechanism is analyzed using temperature maps [2] captured before and during the quench of nitrogen doped cavities, allowing the localization of the quench spot. The study is done taking into account cavities with different doping treatment, in order to see if any differences appear between them, or if something systematically occurs before or during their quenches.

EXPERIMENTAL SET-UP

For the doping treatment, niobium cavities are typically treated with 800 °C degassing in HV for 2-3 hours, followed by injection of niotrogen (N_2) at high temperature. The N_2 flow is set to a specific partial pressure for a certain amount of time. During this step nitrogen reacts with the niobium at the surface and diffuses inside. After that, it is possible to perform a second, optional, step in which the cavity is maintained at high temperature, without nitrogen, in order to promote the diffusion of the nitrogen atoms inside the bulk, smoothing the concentration profile. Then, the heating is shut off and the cavity is let cooling till room temperature.

In Table 1 the nitrogen doping treatment of the analyzed cavities is listed. Only the cavity TE1AES011 is doped including the second step which promote the nitrogen diffusion. Depending on the doping treatment the cavity can be under-doped, for example increasing the time of the second step, or over-doped, for example increasing the time of the first step [3].

Table 1: Doping Treatment of the Analyzed Cavities

Cavity	Doping Treatment
TE1AES003	28 mTorr of N_2 for 10 min at 1000 °C
TE1NR005	25 mTorr of N_2 for 10 min at 800 °C
TE1AES011	25 mTorr of N_2 for 2 min at 800 °C plus 6 min without N_2 at 800 °C
TE1ACC002	25 mTorr of N_2 for 20 min at 800 °C

After the doping treatment the cavities are electropolished with a total removal of about $5\mu m$ for all the cavity analyzed except for TE1AES003 in which the removal is about $60\mu m$.

The temperature map system was used to capture the cavity temperature before and during the quench, in order to understand the mechanism responsible to the quench. The T-map system used in this experiment is shown in Fig. 1. It consists on 36 board placed around the cavity every 10°, and 16 thermometers are placed on each board, for a total of 576 thermal sensors all around the cavity.

RESULTS AND DISCUSSION

The Q-factor versus accelerating field of the nitrogen doped cavities for the T-map runs analyzed in this paper is shown in Fig. 2. The RF test of one EP and one EP/120 °C cavities are also shown as reference. It is important to notice that some of the N doped cavities do not show very high Q performance during these T-map runs because these tests were done with some imposed magnetic field and under not full flux expulsion cooling regimes. In particular the TE1ACC002 cavity had showed significant flux trapped under 10 mGauss field applied via Helmholtz coils.

Comparing TE1AES011 with the EP cavity, they reached almost the same accelerating field, but it is possible to notice that TE1AES011 is not affect by high-field Q-slope

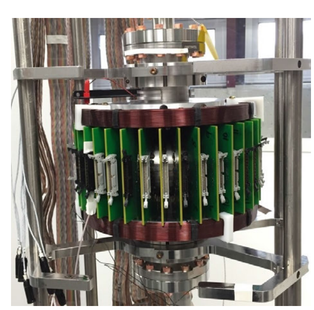

Figure 1: Picture of the T-map system.

* Work supported by the US Department of Energy, Office of High Energy Physics.
† mmartine@fnal.gov

ISBN: 978-3-95450-168-7 doi:10.18429/JACoW-IPAC2015-WEPTY035

DESIGN AND TEST OF COMPACT TUNER FOR NARROW BANDWIDTH SRF CAVITIES

Y. Pischalnikov, E. Borissov, I. Gonin, J. Holzbauer, T. Khabiboulline, W. Schappert, S.Smith, J.C. Yun.
FNAL, Batavia, IL 60510, USA

Abstract

The design of the compact tuner for 1.3 GHz 9-cell elliptical cavity will be presented. This compact tuner is designed for future accelerators that will operate in CW and pulsed RF-power modes. The major design features include highly reliable active components (electromechanical actuators and piezo-actuators) and the ability to replace tuner active components through designated ports in the cryomodule vacuum vessel. Results of tuner testing with cold cavity will also be presented.

TUNER DESIGN

Schematics of the tuner design are shown in Figure 1. The coarse tuner is a double lever tuner (with a 20:1 ratio) similar to the design of the SACLAY I tuner. The tuner works by compressing the cavity. The piezo-stack is installed close to the cavity end flange. This means that the piezo stroke is translated directly to the cavity, not through flex and/or bearing connections. This configuration will deliver better piezo-tuner resolution and decrease group delay of the fast tuner. Safety rods have been designed between the cavity end flange and main lever of the tuner. These safety rods protect the cavity from non-elastic deformation during cavity/helium vessel system leak check.

A split ring is attached to the conical flange welded to the cavity beam-pipe (Purple in Figures 2&3). All forces/stroke from the tuner to the cavity are translated through this split ring. The tuner is anchored to the helium vessel with two strong horizontal arms (Yellow in Figure 2). These arms have adjustment capabilities to accommodate differences (+3mm/-7mm) in the length of the 9-cell cavities after final tuning. The electromechanical actuator connects to the left arm and the lever system is attached through the bearings to the right arm. To decrease the cost of the tuner assembly, it was designed in several parts that are connected by welding or using screws. Set-screws and special washers were included to prevent loosening of the assembly screws during warmup and cool-down cycles.

A special adjustment screw (Figure 1) to hold the left side of the lever system to the left arm was introduced into the design. This addition allows the release of forces between the cavity and tuner system when either the electromechanical actuator or piezo-stack needs to be replaced through the designated port in the cryomodule.

Balls connections were chosen for the connections between the top & bottom encapsulated piezo-stack and the main lever. This prevents the build-up of shearing forces on the piezo-stack during tuner operation which are detrimental to piezo lifetime. Two adjustment screws (one in each main arm) help to uniformly preload piezo-stacks during assembly.

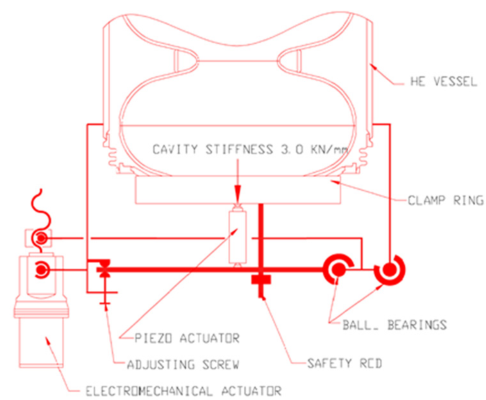

Figure 1: Schematic of the Tuner.

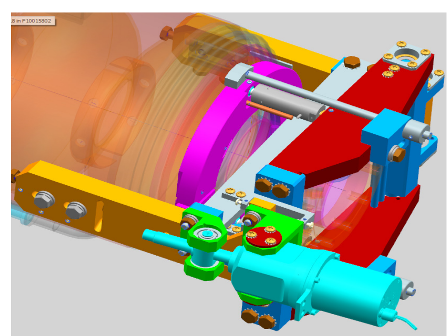

Figure 2: 3-D model of the Tuner, assembled on the cavity/helium vessel system.

ACTIVE COMPONENTS OF THE TUNER

The electromechanical actuator is the active element of the slow/coarse tuner. The electromechanical actuator translates rotation of the stepper motor to linear motion of the tuner arms. The tuner is equipped with a Phytron actuator (LVA 52-LCLS II-UHVC-X1) [1] designed for the FNAL linear SRF project. The Phytron actuator is built from:

- Stepper motor XXX
- Planetary gear (1:50 ratio)
- M12X1 spindle made from titanium
- Traveling nut made from stainless steel and radiation hard plastic material

*This manuscript has been authorized by Fermi Research Alliance, LLC under Contract N. DE-AC02-07CH11359 with U.S. Department of Energy.
#pischaln@fnal.gov

Content from this work may be used under the terms of the CC BY 3.0 licence (© 2015). Any distribution of this work must maintain attribution to the author(s), title of the work, publisher, and DOI.

ISBN: 978-3-95450-168-7 doi:10.18429/JACoW-IPAC2015-WEPTY036

PROGRESS AT FNAL IN THE FIELD OF THE ACTIVE RESONANCE CONTROL FOR NARROW BANDWIDTH SRF CAVITIES*

W. Schappert#, J. Holzbauer, Yu. Pischalnikov, FNAL, Batavia, IL 60510, USA

Abstract

Recent efforts at FNAL to actively compensate microphonics in narrow bandwidth cavities are discussed. Feed-forward compensation of Lorentz force detuning in combination with feedback of the forward/probe phase difference to a piezo actuator successfully stabilized the resonance of a 325 MHz spoke resonator to within 11 mHz of the frequency of the open-loop CW RF drive over a two hour interval.

INTRODUCTION

Many of the next generation of particle accelerators (ERLs, XFELs) are designed for relatively low beam loading. The cavities are designed to operate with narrow cavity bandwidths to minimize capital and operational costs of the RF plant. With such narrow bandwidths, cavity detuning from microphonics becomes a significant factor, and in some cases can drive the cost of the machine [1]. Piezo actuators have been successfully used to actively stabilize cavity resonant frequencies. This paper will present the results of ongoing detuning compensation efforts at FNAL using prototype 325 MHz SRF single spoke resonators designed for the PIP-II project at Fermilab [2].

PREVIOUS EFFORTS

Active compensation of both Lorentz force detuning and microphonics had been previously studied using an earlier SSR1 prototype with two different power couplers. An adaptive feedforward algorithm developed for pulsed 1.3 GHz 9-cell elliptical cavities [3] was able to reduce detuning in the spoke resonator from several kHz to 50 Hz or better during pulsed operation with a 150 Hz bandwidth power coupler (see Fig. 1). Feedback to the piezo actuator during CW operation at 4.3 K with a 0.5 Hz bandwidth coupler was able to limit detuning due to helium pressure variations to 0.4 Hz RMS. [4].

SECOND PROTOTYPE SSR1 SPOKE RESONATOR

A second SSR1 prototype was installed in the Spoke Test Cryostat (STC) in late 2014. The cavity was equipped with a matched coupler (0.6 Hz bandwidth) to allow quality factor measurements. The cavity was also equipped with two piezoelectric actuators that could provide dynamic tuning. The piezos were held in place by a dummy slow tuner that did not allow static tuning of the cavity. This cavity had been the focus on an active design effort to reduce and minimize pressure sensitivity [2]. During these tests the cavity was powered with CW at an operating temperature of 4.5 K. Despite the much lower measured value of df/dP (5 Hz/torr), the cavity would still not remain on resonance for any extended period without active stabilization.

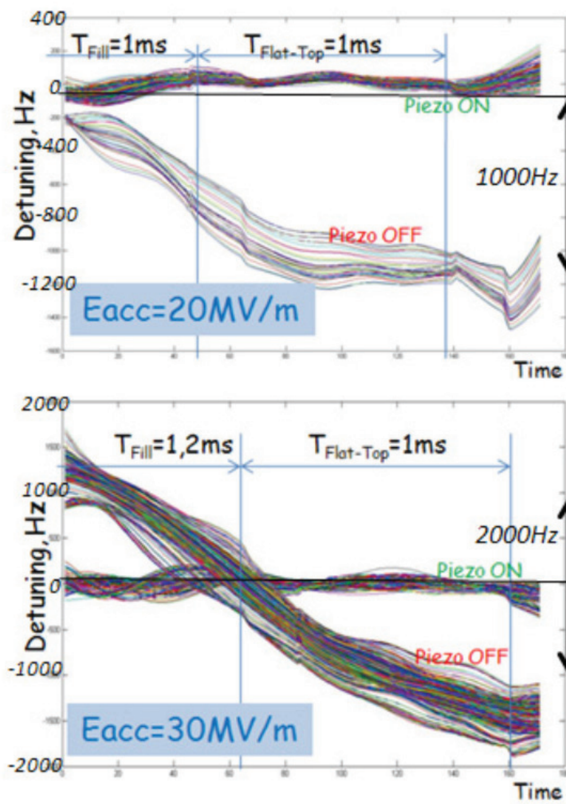

Figure 1: Pulsed compensation of Lorentz force detuning in an SSR1 cavity by adaptive algorithm.

FEED FORWARD COMPENSATION OF PONDEROMOTIVE EFFECTS

Radiation pressure from the EM fields in a powered resonator induces a mechanical deformation which in turn leads to shifts the cavity resonance frequency. The frequency shift is proportional to the square of the gradient as shown in Fig. 2.

*This manuscript has been authorized by Fermi Research Alliance, LLC under Contract N. DE-AC02-07CH11359 with U.S. Department of Energy.
warren@fnal.gov

Content from this work may be used under the terms of the CC BY 3.0 licence (© 2015). Any distribution of this work must maintain attribution to the author(s), title of the work, publisher, and DOI.

ISBN: 978-3-95450-168-7 doi:10.18429/JACoW-IPAC2015-WEPTY037

Content from this work may be used under the terms of the CC BY 3.0 licence (© 2015). Any distribution of this work must maintain attribution to the author(s), title of the work, publisher, and DOI.

A PERPENDICULAR BIASED 2ND HARMONIC CAVITY FOR THE FERMILAB BOOSTER*

C.Y. Tan†, J. Dey, R.L. Madrak, W. Pellico, G. Romanov, D. Sun, I. Terechkine,
Fermilab, Batavia, IL 60510, USA

Abstract

A perpendicular biased 2nd harmonic cavity is currently being designed for the Fermilab Booster. Its purpose cavity is to flatten the bucket at injection and thus change the longitudinal beam distribution so that space charge effects are decreased. It can also with transition crossing. The reason for the choice of perpendicular biasing over parallel biasing is that the Q of the cavity is much higher and thus allows the accelerating voltage to be a factor of two higher than a similar parallel biased cavity. This cavity will also provide a higher accelerating voltage per meter than the present folded transmission line cavity. However, this type of cavity presents technical challenges that need to be addressed. The two major issues are cooling of the garnet material from the effects of the RF and the cavity itself from eddy current heating because of the 15 Hz bias field ramp. This paper will address the technical challenge of preventing the garnet from overheating.

INTRODUCTION

It is well known that the addition of a 2nd harmonic cavity (in this paper, 2nd harmonic means the frequency is twice that of the fundamental) can be used to improve capture of the beam at injection. It is also possible to use this type of cavity at transition as well, to aid in crossing transition. For example, see ref. [1]. Simulations have shown that, in order, to increase capture, the voltage of the 2nd harmonic must be greater than 10% of the total accelerating voltage of the fundamental. This value sets the minimum voltage for the 2nd harmonic design, which for Booster means that it is about 100 kV.

In order to achieve this voltage in the limited space in the Fermilab Booster tunnel, it was decided to pursue a cavity design that is perpendicularly biased rather than parallel biased. [2] The reason is that the high Q of the garnet material used for a perpendicular biased cavity allows this voltage to be achieved with a single gap rather than with a double gap that is required for a parallel biased cavity. A double gap cavity essentially means a doubling of the length w.r.t. a perpendicular biased cavity (PPBC).

However, this choice is not without risk. PPBC's have been proposed and built before, for example, for the SSC low energy booster [3] and the kaon factory at TRIUMF [4]. Although the TRIUMF prototype did achieve its required specifications [5], it eventually developed a vacuum problem. And the SSC cavity never achieved its design power because localized heating in the garnet caused it to fail. [6] The repair and postmortems of these failures are also challenging because safety requirements have to be met. For example, the handling of beryllium oxide (BeO) cooling disks that are sandwiched between the garnet disks.

Besides localized heating of the garnet from the RF, there are other challenges, like the eddy current heating from the magnetic bias field ramp that will not be discussed here.

NEW DESIGN

The new design is shown in Fig. 1. The goal is to exploit the SSC and TRIUMF experiences to create a cavity that can work reliably without overheating. Although this new cavity looks similar to the SSC and TRIUMF designs, it is actually quite different: (a) Removal of BeO cooling disks — cooling is achieved by water paths that are outside the cavity. This design allows cooling of the inside circumference and outside circumference of the garnets. (b) The garnet is no longer symmetric about the RF neck region.

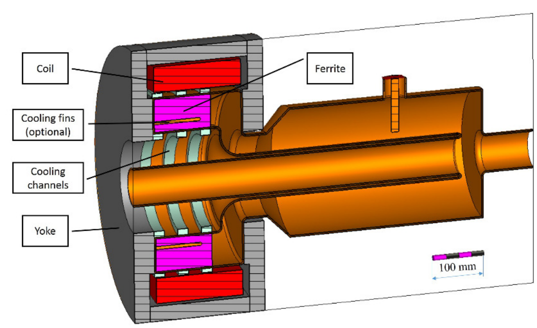

Figure 1: The cavity model.

Localized Heating

Localized hotspots are the major problem with all PPBC's designed and built so far. In order to mitigate this problem, it is essential that MWS be able to correctly calculate the heat density and the hot spots in the garnet material. Unfortunately, the magnetic and electric characteristics of the garnet material, AL800, that is used in the present design from published sources are insufficient for this application and thus, the AL800 properties have to be measured at Fermilab.

AL800 PROPERTIES

The biggest challenge in designing a workable cavity of this type is due to unavoidable nonuniformities in the garnet internal magnetic field. As the real and the imaginary parts of the biased garnet permeability are strong non-linear

---
* Operated by Fermi Research Alliance, LLC under Contract No. DE-AC02-07CH11359 with the United States Department of Energy.
† cytan@fnal.gov

ISBN: 978-3-95450-168-7 doi:10.18429/JACoW-IPAC2015-WEPTY040

QUENCH PERFORMANCE OF THE FIRST TWIN-APERTURE 11 T DIPOLE FOR LHC UPGRADES*

A.V. Zlobin#, N. Andreev, G. Apollinari, E. Barzi, G. Chlachidze, A. Nobrega, I. Novitski, S. Stoynev, D. Turrioni, FNAL, Batavia, IL 60510, USA
B. Auchmann, S. Izquierdo Bermudez, M. Karppinen, L. Rossi, F. Savary, D. Smekens, CERN, CH-1211 Geneva 23, Switzerland

Abstract

FNAL and CERN are developing a twin-aperture 11 T Nb_3Sn dipole suitable for installation in the LHC. A single-aperture 2-m long dipole demonstrator and two 1-m long dipole models have been fabricated and tested at FNAL in 2012-2014. The two 1 m long collared coils were then assembled into the first twin-aperture Nb_3Sn demonstrator dipole and tested. Test results of this twin-aperture Nb_3Sn dipole model are reported and discussed.

INTRODUCTION

The planned upgrades of the Large Hadron Collider (LHC) call for additional collimators in the dispersion suppressor (DS) areas around points 2, 3, 7, and CMS and ATLAS detectors [1]. The work on the development of the 11 T Nb_3Sn dipole for the LHC collimation system upgrade, started in 2011 [2], continues at FNAL [3] and at CERN [4]. Seven 1 m long coils were fabricated at FNAL since 2012. Four coils were assembled in two collared coil blocks and tested in a single-aperture configuration [5]-[7]. Both collared coils were trained above the LHC nominal operation current of 11.85 kA to a field in the magnet aperture of ~11.6 T at 1.9 K, or 97% of the dipole design field of 12 T. During the tests important information on the magnet quench performance and field quality, including geometrical harmonics, coil magnetization, iron saturation and dynamic effects in 11 T dipole models, was obtained [5]. These collared coils have been assembled in a first twin-aperture dipole model MBHDP01 and tested in February-March 2015. This paper summarizes the twin-aperture magnet design and construction, and reports test results of this Nb_3Sn dipole model focusing on magnet quench performance including training, ramp rate sensitivity and temperature dependence of the magnet quench current. The twin-aperture dipole quench performance is compared with the data for the single-aperture models MBHSP02 and MBHSP03.

MAGNET DESIGN AND CONSTRUCTION

The design concepts of the 11 T Nb_3Sn dipole in single-aperture and twin-aperture configurations, developed at FNAL and at CERN, are described in [2]-[8]. The calculated 2D design parameters for single- and twin-aperture dipoles (FNAL design) at I_{nom} of 11.85 kA, T_{op} of 1.9 K, nominal strand J_c(12T,4.2K) of 2750 A/mm^2 and cable I_c degradation of 10% are reported in Table 1.

Table 1: 11 T Dipole Design Parameters

Parameter	Single-aperture	Twin-aperture
Yoke outer diameter, mm	400	550
Nominal bore field at I_{nom}, T	10.88	11.23
Short sample field B_{SSL} at T_{op}, T	13.4	13.9
Margin B_{nom}/B_{SSL} at T_{op}, %	81	83
Stored energy at I_{nom}, kJ/m	424	969
F_x/quadrant at I_{nom}, MN/m	2.89	3.16
F_y/quadrant at I_{nom}, MN/m	-1.58	-1.59

In a twin-aperture configuration, two collared coils are placed inside a vertically split iron yoke with an iron spacer in between, and are surrounded by a thick welded stainless steel skin. Two thick stainless steel end plates, welded to the skin, restrict the axial motion of both collared coils.

MBHDP01 uses two collared coils: one, tested in MBHSP02, consists of coils 05 and 07 and the other one, tested in MBHSP03, consists of coils 09 and 10. Based on the test results in a single-aperture configuration, the collared coil with coils 09 and 10, was re-collared with a slightly larger radial shim of 0.075 mm installed in between coil and collar to increase the coil pre-stress. The midplane collar-yoke shims, the same for both collared coils, were reduced to the minimum size necessary to compensate for the difference in collar and yoke thermal contraction. These midplane shims, the same as in MBHSP03, provide some small collared coil bending at room temperature to keep contact between the collar and the yoke after cooling down. All the coils are electrically conneted in series as shown in Fig. 1 (left). The assembled twin-aperture dipole model MBHDP01 before end plate welding and coil splicing is shown in Fig.1 (right).

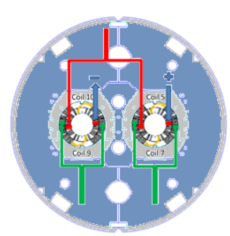

Figure 1: The coil electrical connection (left) and the assembled MBHDP01 cold mass before end plate welding and coil splicing (right).

* Work supported by Fermi Research Alliance, LLC, under contract No. DE-AC02-07CH11359 with the U.S. Department of Energy and European Commission under FP7 project HiLumi LHC, GA no.284404
# zlobin@fnal.gov

Content from this work may be used under the terms of the CC BY 3.0 licence (© 2015). Any distribution of this work must maintain attribution to the author(s), title of the work, publisher, and DOI.

ISBN: 978-3-95450-168-7 doi:10.18429/JACoW-IPAC2015-WEPTY041

DESIGN CONCEPT AND PARAMETERS OF A 15 T Nb_3Sn DIPOLE DEMONSTRATOR FOR A 100 TeV HADRON COLLIDER*

A.V. Zlobin#, N. Andreev, E. Barzi, V.V. Kashikhin, I. Novitski, FNAL, Batavia, IL 60510, USA

Abstract

FNAL has started the development of a 15 T Nb_3Sn dipole demonstrator for a 100 TeV scale hadron collider. This paper describes the design concept and parameters of the 15 T Nb_3Sn dipole demonstrator. The dipole magnetic, mechanical and quench protection concept and parameters are presented and discussed.

INTRODUCTION

Hadron Colliders (HC) are the most powerful discovery tools in modern high energy physics. Interest to a HC with energy above the LHC reach gained further momentum in the strategic plans recently developed in the U.S., Europe and China [1-3]. To build a ~100 TeV HC in a ~100 km tunnel, ~15 T dipoles operating at 1.9 or 4.5 K with 15-20% margin are needed. A nominal operation field up to 15-16 T can be provided by the Nb_3Sn technology. A practical demonstration of this field level in accelerator-quality magnets and a substantial reduction of magnet costs are key conditions for the realization of such a machine.

The main challenges for 15 T Nb_3Sn magnets include significantly stronger Lorentz forces and larger stored energy. The stronger forces generate higher stresses in the coil and mechanical structure and, thus, may need stress control to maintain them below 150 MPa, which is acceptable for brittle Nb_3Sn. The larger stored energy leads to further complications in the magnet quench protection.

FNAL has started the development of a 15 T Nb_3Sn dipole demonstrator for a 100 TeV scale HC based on the optimized "cos-theta" coil design. As a first step, the existing 11 T dipole, developed for LHC upgrades [4], will be modified by adding two layers to achieve the field of 15 T in a 60 mm aperture. Then, to increase the field margin the innermost 2-layer coil will be replaced with an optimized coil using the conductor grading approach. This paper describes the design concept and parameters of the 15 T Nb_3Sn dipole demonstrator.

MAGNET DESIGN STUDIES

The coil width w, needed to generate the bore field $B0_{max}$, could be estimated from the following equation for the cos-theta dipole coil with an azimuthal angle of 60 degrees

$$B0_{max} = \frac{\sqrt{3}\,\mu_0}{\pi} \cdot \lambda J_c(B_{max\_coil}) \cdot w$$

where λ is the fraction of superconductor in a coil (λ=0.25) and $J_c(B_{max\_coil})$ is the superconductor critical current density at B_{max_coil} in the coil (usually B_{max_coil} is ~ $1.05 \cdot B0_{max}$). Thus, to achieve $B0_{max}$=15 T using Nb_3Sn strands with a realistic $J_c(15\ T)$ of 1500 A/mm^2, the coil width w has to be ~60 mm. When using the same 15 mm wide cables as in the FNAL 11 T dipole [4], this requires a 4-layer coil design.

The chosen coil aperture of 60 mm, convenient for re-using the 11 T dipole coils, provides also enough room for a beam screen to intercept the large synchrotron radiation expected in a 100 TeV scale HC. To reduce the demonstrator cost, a collarless design with 2 mm thick spacer between the coil and the yoke was adopted. The standard thickness of the insulation between the coil layers as well as the coil ground insulation thickness are 0.5 mm. The mid-plane insulation is 0.2 mm.

Several four-layer coils were designed using two cables with a width of 15 mm and different thickness. The cable parameters are listed in Table 1. The cables use 1.0 and 0.7 mm Nb_3Sn strands with a critical current density $J_c(15T;4.2K)$ of 1500 A/mm^2 and a nominal Cu/SC ratio of 1.13. Nb_3Sn cables with these or similar parameters have already been developed at FNAL and used in HFDA and 11 T dipole models [5], [6].

Table 1: Reacted Cable Parameters

Parameter	Cable 1	Cable 2
Number of strands	28	40
Mid-thickness, mm	1.870	1.319
Width, mm	15.10	15.10
Keystone angle, degree	0.805	0.805

The coil cross-sections were optimized using the ROXIE code [7]. The goal was to achieve a maximum dipole field of 15 T or higher at 4.3 K and geometrical field harmonics below the 10^{-4} level at R_{ref}=17 mm, reduce the coil volume and inductance, and control the coil azimuthal stress. Five 4-layer coil designs with graded coils were analyzed. The main parameters of these coils are summarized in Table 2. The coil cross-sections with relative field errors in the aperture (dark blue area) and numbers of turns per coil layer N_L are shown in Fig. 1.

Table 2: Coil Parameters

Parameter	Coil design				
	4L-1	4L-2	4L-3	4L-4	4L-5
N_{L1}	15	17	18	18	18
N_{L2}	25	25	25	25	26
N_{L3}	47	40	39	36	33
N_{L4}	54	43	38	35	32
N_{tot} coil	141	125	120	114	109
S_{coil}, cm^2	31.4	28.4	27.5	26.3	25.4
$B0_{max}$(4.3K), T	16.3	16.1	16.0	15.8	15.7
I_{max}(4.3K), kA	9.89	10.34	10.52	10.84	11.10
L, mH/m	39.9	33.8	31.5	28.7	26.5
$W(B_{max})$, MJ/m	1.95	1.81	1.74	1.69	1.63

* Work supported by Fermi Research Alliance, LLC, under contract No. DE-AC02-07CH11359 with the U.S. Department of Energy
# zlobin@fnal.gov

Content from this work may be used under the terms of the CC BY 3.0 licence (© 2015). Any distribution of this work must maintain attribution to the author(s), title of the work, publisher, and DOI.

ISBN: 978-3-95450-168-7 doi:10.18429/JACoW-IPAC2015-WEPTY042

PULSED POWER SYSTEMS FOR ESS KLYSTRONS

I. Roth, M. P.J. Gaudreau, M. Kempkes, Diversified Technologies, Inc., Bedford, MA 01730 USA
J.L. Lancelot, P. Dupire, J.D. Holzmann, SigmaPhi Electronics, 67500 Haguenau, France

Abstract

Diversified Technologies, Inc. (DTI) is building three long pulse solid-state klystron transmitters to meet spallation source requirements. Two of the three will be installed at CEA Saclay and the National Institute of Nuclear and Particle Physics (IN2P3) in 2015, to be used as test stands for the European Spallation Source (ESS), The third system will be installed at Oak Ridge National Laboratory (ORNL) for the Spallation Neutron Source (SNS).

INTRODUCTION

Diversified Technologies, Inc. (DTI), in partnership with SigmaPhi Electronics, has designed an advanced, high voltage solid-state modulator for the European Spallation Source (ESS) klystron tubes (Figure 1). The ESS modulator uses a series-switch design driving a pulse transformer, with an advanced, patent pending regulator design to maintain a highly regulated cathode voltage as well as a constant load to the external power grid. The success of the design in meeting the ESS pulse requirements (Table 1) is shown in Figure 2.

The ESS modulator is a proven design, delivering significant advantages in klystron performance through:

- Highly reliable operation, demonstrated in hundreds of systems worldwide, and predicted to significantly exceed ESS requirements
- Flicker- and droop-free operation over a range of operating parameters
- All active electronics in air for easy maintenance

Table 1: ESS Modulator Requirements

Specification	
Voltage	-115 kV
Current	50 A
Pulse Width	3.5 ms
Frequency	14 Hz (max)
Average Power	290 kW
Droop	< 1%
Pulse Repeatability	< 0.1%

Figure 1: System designed for Oak Ridge National Laboratory Spallation Neutron Source. Design is optimized for long pulse operation with highest possible reliability and availabilityrequired for particle accelerator user facilities and test stands. High voltage cables connect to dummy load or klystrons not shown in figure.

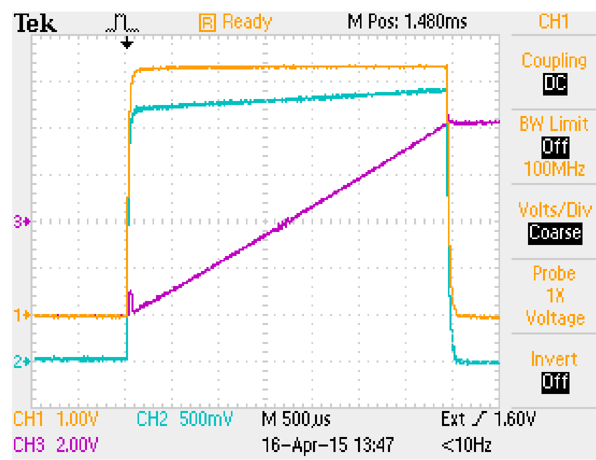

Figure 2: 106 kV, 58 A test pulse showing output voltage (yellow, 20 kV/div), current (blue, 10 A/div) and regulator voltage (purple, 200 V/div). Current increases slightly with time due to heating of the resistive load.

DESIGN

The heart of the ESS modulator is a high voltage solid-state switch. The switch is made of seven series-connected IGBT modules, and operates at 6.7 kV. The IGBTs in the switch give N+2 redundancy: two of the devices can fail without affecting the ability of the switch

Content from this work may be used under the terms of the CC BY 3.0 licence (© 2015). Any distribution of this work must maintain attribution to the author(s), title of the work, publisher, and DOI.

ISBN: 978-3-95450-168-7 doi:10.18429/JACoW-IPAC2015-WEPTY043

SHORT PULSE MARX MODULATOR*

R. Phillips, M. P.J. Gaudreau, M. Kempkes, R. Simpson,
Diversified Technologies, Inc., Bedford, MA 01730, USA
J. Casey, Rockfield Research, Inc., Las Vegas, NV, 89135, USA

Abstract

Under a U.S. Department of Energy grant, Diversified Technologies, Inc. (DTI) has developed a short pulse, solid-state Marx modulator. The modulator is designed for high efficiency in the 100 kV to 500 kV range, for currents up to 250 A, pulse lengths of 0.2 to 5.0 µs, and risetimes <300 ns. Key objectives of the development effort are modularity and scalability, combined with low cost and ease of manufacture. For short-pulse modulators, this Marx topology provides a means to achieve fast risetimes and flattop control that are not available with hard switch or transformer-coupled topologies.

INTRODUCTION

Under a DOE SBIR grant and based on research begun under the Next Generation Linear Collider (NLC) program, Diversified Technologies, Inc. (DTI) has developed a short pulse, solid-state Marx modulator relevant to the Compact Linear Collider (CLIC) and numerous X-Band accelerator designs (Fig. 1). The modulator is designed for high efficiency in the 100 kV to 500 kV range, for currents up to 250 A, pulse lengths of 0.2 to 5.0 µs, and risetimes <300 ns (Table 1). This fully optimized, transformer-less modulator design is capable of meeting the demanding requirements of very high voltage pulses at short pulsewidths.

Table 1: Yale Marx Design Parameters

Item	Specification
Pulse Voltage	500 kV
Pulse Current	250 A
Pulse Width	1.8 us
Repetition Rate	20 Hz
Module Voltage	12.5 kV
Module Capacitance	0.6 µF
# Modules for Base Pulse	40
Total # Modules in System	48 – 50
Expected Risetime	300 ns
Heater Voltage	24 VDC
Heater Current	21 A
Insulation	Oil

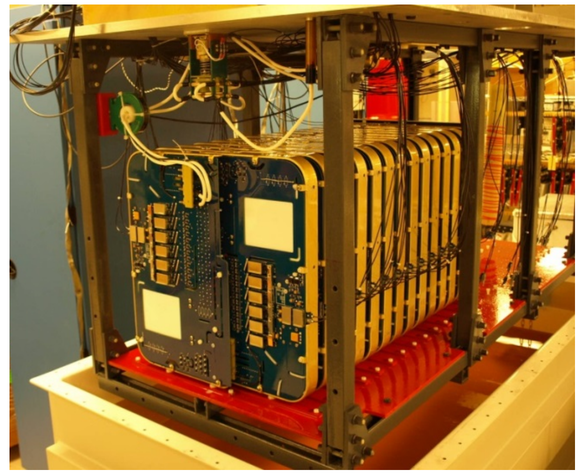

Figure 1: The Yale Marx 500 kV modulator charges many stages in parallel at low voltage, then discharges in series at high voltage. Each 12.5 kV, 250 A “flat pack” module is identical, providing for low fabrication and assembly cost.

A Marx generator is a system with energy storage capacitors which are charged in parallel at low voltage and discharged in series to provide high voltage output. This is a legacy idea, practiced for decades using resistor charging networks and spark-gaps for discharge. Constrained by the limits of closing switches, such systems required pulse forming networks and crowbars, with their attendant limitations.

The Marx topology allows a new degree of freedom unavailable to other architectures – DTI can intentionally underdamp the series snubbing within the pulse circuit. This cannot be done conventionally – the reactive overshoot endangers the load. In a Marx, we can compensate for the overshoot by initially firing only a subset of the switches – thus “sling-shotting” the leading edge faster than otherwise possible. We can tune the number and timing of subsequent module firings to counter the reactive ringing, and hold a flattop pulse to the desired voltage and accuracy.

Similarly, additional modules may be added to fire sequentially later in the pulse to compensate for capacitor droop. This is a critical enabling technology motivating Marx use for long-pulse accelerators (such as ILC), and yields valuable optimization even for very short-pulse systems. The reduction of capacitor size afforded by this flexibility further reduces parasitic capacitance, and thus reduces equipment size and cost while increasing power efficiency.

*Work supported by U.S. Department of Energy SBIR Award DESC0004251

Content from this work may be used under the terms of the CC BY 3.0 licence (© 2015). Any distribution of this work must maintain attribution to the author(s), title of the work, publisher, and DOI.

ISBN: 978-3-95450-168-7 doi:10.18429/JACoW-IPAC2015-WEPTY044

PHASE TRANSIENTS IN THE HIGHER HARMONIC RF SYSTEM FOR THE ALS-U PROPOSAL*

J. M. Byrd, S. De Santis, T. Luo, C. Steier, LBNL, Berkeley, CA, USA

Abstract

The proposed upgrade of the ALS to a diffraction limited light source (ALS-U) requires lengthening the bunch by a factor up to four in order to limit the emittance growth due to intra-beam scattering, increase the Touschek lifetime to a value consistent with a on-axis swap-out period of about 30 seconds, improve beam stability, and lower the peak current with consequent reduction of high-frequency wakefields and beampipe heating.

To obtain the necessary bunch lengthening factor, a higher harmonic RF system will be used to flatten the total accelerating voltage seen by the circulating bunches. A fourfold increase of the bunch length requires operating the harmonic RF system near the optimum flat condition, which corresponds to cancellation of first and second derivatives of the main RF voltage waveform at the time of the bunch passage (i.e. at the synchronous phase). Such a situation presents particular challenges since a significantly stretched bunch covers a large interval of RF phases and it deviates considerably from the usual gaussian longitudinal density distribution. Furthermore, in the case of a passive harmonic system, gaps in the fill pattern may cause part of the bunch train to miss the lengthening target. At this time, two options, 500 and 100 MHz, are being evaluated for the main RF frequency and we have calculated the main parameters for a harmonic system in each case. The 500 MHz option requires gaps at least 10 ns long in the fill pattern for the rise time of the on-axis injection kickers, while with a 100 MHz main RF frequency it is possible to use a perfectly uniform beam. Since the first one is the favoured option for several reasons, ensuring that gaps are not a limiting factor in lengthening the bunch is necessary before committing to this solution. In this paper we present our studies, using both computer simulations and experiments on the ALS, that show that a 500 MHz main RF system, together with a 1.5 GHz harmonic system is a viable solution for the ALS-U requirements.

INTRODUCTION

The ALS-U proposal envisions the upgrade of the present ALS synchrotron light source into a new ultra-low emittance machine for the production of diffraction-limited soft X-rays. The details of the proposal are reported in [1]. At our 2 GeV beam energy, intra-beam scattering becomes a serious limitation in achieving the desired ultra-low beam transverse emittance, of the order of 50 picometers, without decreasing the stored current. Therefore harmonic RF cavities are included in the machine design, to lengthen the bunch. In addition to reducing intra-beam scattering, longer bunches have a longer Touschek lifetime, which allows to increase the interval between bunch train swap-outs. The spread in synchrotron frequency caused by the flattened accelerating voltage waveform introduces Landau damping, thus improving beam stability. Finally, the lower peak current reduces beam heating of vacuum chamber elements and the high-frequency components of the beam power spectrum are also eliminated. At present, we are investigating two different options for the main RF frequency, as detailed in [2]. Depending on the frequency chosen the harmonic system would operate at 1.5 GHz (third harmonic of 500 MHz), or at 500 MHz (fifth harmonic of 100 MHz). Fill patterns are also different between the two options: in order to allow 10 ns long gaps for the operation of the injection/extraction kickers, the 500 MHz main RF machine would store 11 trains of 26 bunches each, while in the 100 MHz main RF case all the 66 RF buckets would be filled. The RF main parameters are summarized in Table 1.

Table 1: Main RF Parameters

Parameter	Value	
Beam Energy (E_b)		2 GeV
Circumference (L_R)		196.44 m
Beam Current (I_b)		500 mA
Main RF Frequency (f_{RF})	500 MHz	100 MHz
Number of Bunches (N_b)	275	66
Energy Loss/Turn (U_0)		165 keV (260 keV with ID's)
Energy Spread ($\Delta\varepsilon$)		$8{\cdot}10^{-4}$
Mom. Compaction (α)		$2.69{\cdot}10^{-4}$
Nat. Sync. Tune (Q_s)		0.002
Main RF Voltage (V_{RF})	760 kV	420 kV
Nat. Bunch Length (σ_b)	11 ps	35 ps
Higher Harm. Freq. (f_H)	1.5 GHz (3rd harm.)	500 MHz (5th harm.)
Req. Lengthening Factor		3-4

*Work supported by the Laboratory Directed Research and Development Program of Lawrence Berkeley National Laboratory under U.S. Department of Energy Contract No. DE-AC02-05CH11231

Content from this work may be used under the terms of the CC BY 3.0 licence (© 2015). Any distribution of this work must maintain attribution to the author(s), title of the work, publisher, and DOI.

ISBN: 978-3-95450-168-7 doi:10.18429/JACoW-IPAC2015-WEPTY045

HIGH-INTENSITY PROTON RFQ ACCELERATOR FABRICATION STATUS FOR PXIE*

A.R. Lambert#, A.J. DeMello, M.D. Hoff, D. Li, T. Luo, J.W. Staples, and S.P. Virostek
Lawrence Berkeley National Laboratory, Berkeley, CA 94720, USA
R. Andrews, C. Baffes, P. Berrutti, T. Khabiboulline, G. Romanov, D. Snee, and J. Steimel
Fermi National Accelerator Laboratory, Batavia, IL 60510, USA

ABSTRACT

PXIE is a prototype front end system [1] for the proposed PIP-II accelerator upgrade at Fermilab. An integral component of the front end is a 162.5 MHz, normal conducting, continuous wave (CW), radio-frequency quadrupole (RFQ) cavity that was designed and is being fabricated by LBNL. This RFQ will accelerate a continuous stream of up to 10mA of H- ions from 30 keV to 2.1 MeV. The four-vane, 4.45 meter long RFQ consists of four modules, each constructed from 2 pairs of identical modulated vanes. Vane modulations are machined using a custom carbide cutter designed at LBNL. Other machined features include ports for slug tuners, pi-mode rods, sensing loops, vacuum pumps and RF couplers. Vanes at the entrance and exit possess cutbacks for RF matching to the end plates. The vanes and pi-mode rods are bonded via hydrogen brazing with Cusil wire alloy. The brazing process mechanically bonds the RFQ vanes together and vacuum seals the module along its length. Vane fabrication is successfully completed, and the braze process has proved successful. Delivery of the full RFQ beam-line is expected in the middle of 2015.

VANE FABRICATION

For details on the PXIE RFQ design, please refer to [2]. Fabrication began with end machining of all vanes, followed by rough machining on all sides. Each vane was then sent out for gun-drilling ~ 1.0 meter long cooling channels. After gun drilling was complete, copper plugs were electron-beam welded to seal the cooling channels at the drilled end. The vanes then returned to LBNL where flow and leak tests were performed to verify the integrity of the e-beam weld, as well as check for any flow blockages in the cooling channels. After this, machining of tuner, pi-mode rod, sensing loop, and vacuum ports began. In addition to port features, several tapped hole patterns were machined in the backside for vane handling and mounting, which proved critical for handling and restraining the vanes later in the fabrication process. Once finished, each vane underwent CMM inspection of the backside to verify tolerances for flatness and port locations, as seen in Figure 1.

*Work supported by the Office of Science, U.S. Department of Energy under DOE contract number DE-AC02-05CH11231
#arlambert@lbl.gov

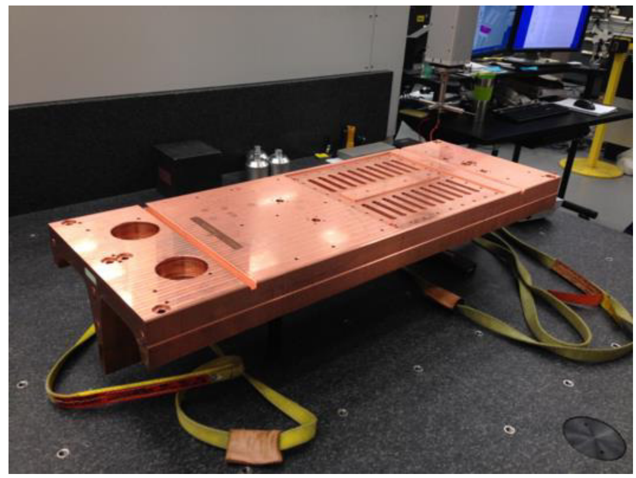

Figure 1: Backside port CMM check.

The vanes were then mounted to 3 in. thick stainless steel plates that restrained the copper during inner cavity rough machining, as well as subsequent final cavity machining. CMM inspection was then performed after rough machining of the cavity, followed by machining of the cavity walls to their final dimension. Vanes for modules 1 and 4 then had their cutbacks machined, as well the radial matcher for module 1 vanes. The cutback machining is initially checked with aluminum blanks to verify the machine program, as seen in Figure 2.

Figure 2: Aluminum test pieces to verify cutback machining program, if acceptable the program is saved on machine to be duplicated on the production part.

The vanes are again submitted to CMM inspection; after which the modulation machining begins. Each modulation program is initially verified using test pieces

Content from this work may be used under the terms of the CC BY 3.0 licence (© 2015). Any distribution of this work must maintain attribution to the author(s), title of the work, publisher, and DOI.

ISBN: 978-3-95450-168-7 doi:10.18429/JACoW-IPAC2015-WEPTY046

Content from this work may be used under the terms of the CC BY 3.0 licence (© 2015). Any distribution of this work must maintain attribution to the author(s), title of the work, publisher, and DOI.

PROGRESS ON THE MICE 201 MHz CAVITIES AT LBNL*

T. Luo†, A. DeMello, A. Lambert, D. Li, S. Prestemon, S. Virostek
LBNL, Berkeley, CA 94720, USA

Abstract

The international Muon Ionization Cooling Experiment aims to demonstrate the transverse cooling of a muon beam by ionization in energy absorbers. The final MICE cooling channel configuration has two RF modules, each housing a 201 MHz RF cavity used to compensate the longitudinal energy loss in the absorbers. The LBNL team has designed and fabricated all of the MICE RF cavities. The cavities will be post-processed and RF measured before being installed in the RF modules. We present the recent progress on this work, including the low level RF measurement on cavity body and Be windows, the electro-polishing (EP) on the cavity surface, the numerical simulation on cavity Be window detuning, and the ongoing mechanical designing work of cavity components.

INTRODUCTION

The international Muon Ionization Cooling Experiment (MICE) [1] aims to demonstrate the transverse cooling of a muon beam by ionization in energy absorbers. The final MICE cooling channel configuration has two RF modules, each housing a 201 MHz RF cavity to compensate the longitudinal energy loss in absorbers [2]. Recently a lot of work has been done at LBNL on the cavity production, including the characteristic frequencies measurement of cavity bodies and beryllium windows, electro-polishing of cavity inner surface, simulation of frequency detuning due to Be windows, modification of cavity coupler design, actuator design and prototype test, etc. In this paper, we will report these progresses.

CAVITY BODY AND BE WINDOW FREQUENCY MEASUREMENT

The MICE cavity is composed of a copper cavity body and two Be windows. Due to the production process, each cavity body and window has slightly different characteristic frequency. Under the first order approximation, the cavity frequency can be decomposed into the linear combination of cavity body frequency f_b and each window frequency f_{w1} and f_{w2}:

$$f_c = f_b \pm f_{w1} \pm f_{w2},$$

where the "+" corresponds to the curved-out window and "-" the curved-in. Once we know all the f_b and f_w, we can predict the cavity frequency with any combination of cavity body and Be windows without assembling one. The accuracy of this prediction is proved to be within 5kHz by Omega3P [3] simulation.

To measure the characteristic frequencies, we assemble a cavity, flip the direction of the Be windows one at a time and measure the cavity frequency for each assembly. With the linear approximation:

$$\begin{aligned} f_{c1} &= f_b - f_{w1} - f_{w2}, \\ f_{c2} &= f_b - f_{w1} + f_{w2}, \\ f_{c3} &= f_0 + f_{w1} - f_{w2} \end{aligned}$$

, and with the measured f_{c1}, f_{c2} and f_{c3}, we can calculate f_b, f_{w1} and f_{w2}. The measurement set up and the S11 measurement on a Network Analyzer are shown in Figure 1. The frequency results are shown in Table 1. After the electropolishing, we will select the two cavities bodies with the best surface condition, then pick up a pair of Be windows for each body to achieve the desired cavity frequency.

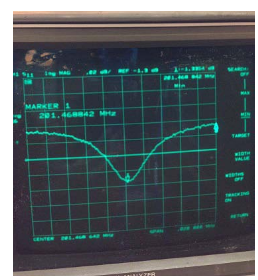

Figure 1: Cavity frequency measurement Left: Set up; Right: S11 measurement on Network Analyzer.

Table 1: Characteristic Frequency of Cavity Body and Be Window

Cavity #	Frequency (MHz)	Window #	Frequency (MHz)
5	201.510	1	0.674
6	200.976	2	0.581
7	200.675	3	0.640
8	200.874	4	0.537
9	200.970	5	0.517
10	200.999	6	0.557
		7	0.541
		8	0.623
		9	0.623
		10	0.663

* Work supported by the Office of Science, U.S. Department of Energy under DOE contract number DE-AC02-05CH11231
† tluo@lbl.gov

ISBN: 978-3-95450-168-7 doi:10.18429/JACoW-IPAC2015-WEPTY047

THERMAL AND LORENTZ FORCE ANALYSIS OF BERYLLIUM WINDOWS FOR A RECTILINEAR MUON COOLING CHANNEL*

T. Luo†, D. Li, S. Virostek, LBNL, Berkeley, CA 94720, USA
R. Palmer, D. Stratakis, BNL, Upton, NY 11973, USA
D. Bowring, FNAL, Batavia, IL 60510, USA

Abstract

Reduction of the 6-dimensional phase-space of a muon beam by several orders of magnitude is a key requirement for a Muon Collider. Recently, a 12-stage rectilinear ionization cooling channel has been proposed to achieve that goal. The channel consists of a series of low frequency (325 MHz-650 MHz) normal conducting pillbox cavities, which are enclosed with thin beryllium windows (foils) to increase shunt impedance and give a higher field on-axis for a given amount of power. These windows are subject to ohmic heating from RF currents and Lorentz force from the EM field in the cavity, both of which will produce out of the plane displacements that can detune the cavity frequency. In this study, using the TEM3P code, we report on a detailed thermal and mechanical analysis for the actual Be windows used on a 325 MHz cavity in a vacuum ionization cooling rectilinear channel for a Muon Collider.

INTRODUCTION

Recently, interest has increased in the possibility of using muon in high-energy physics as the colliding particles in μ^+-μ^- colliders [1]. The liability of muons is that they are created in a diffuse phase-space. As a result, the volume of the 6-Dimensional (6D) phase-space must be rapidly reduced via ionization cooling [2] by several orders of magnitude in order to be able to further accelerate it.

To reduce the transverse emittance, the beam is strongly focused with high magnetic fields and subsequently sent through an absorber material to reduce the overall momentum. The beam regains longitudinal momentum in RF cavities, resulting in an overall loss in transverse emittance. Longitudinal emittance reduction is achieved by shaping the absorbers into wedges and providing a bending magnetic field, generating a dispersion such that particles with higher energy are sent through more material. Recently, a 12-stage tapered rectilinear scheme for cooling a muon beam sufficiently for use in a Muon Collider has been designed and simulated [3].

Thin Be windows may be utilized in the cooling channel to increase shunt impedance of the closed-cell rf cavities. In this study, using the TEM3P code, we report on a detailed thermal and mechanical analysis for the actual Be windows used on the first stage (stage A1), which is the most challenging due to its large beam aperture (30 cm).

* Work supported by the Office of Science, U.S. Department of Energy under DOE contract number DE-AC02-05CH11231 and DE-AC02-98CH10886
† tluo@lbl.gov

RF CAVITY WITH BERYLLIUM WINDOW

The cavities in the rectilinear Muon Cooling channel are of pillbox type. The Be windows enclose the cavity on both sides to increase the cavity shunt impedance significantly.

The Be window needs to be thin enought to be almost transparent to the muon beam. However, the thinner the window, the poorer its thermal conduction. Besides, there is no extra cooling on the window with all the heat transfered out by thermal conduction. A "step" window design is proposed as a compromise between emittance dilution and the thermal heating. The window parameters of the first four stages are shown in Table 1.

Table 1: Window Parameters for the Frst 4 Stages of the Cooling Channel

Stg	f (MHz)	rWin (cm)	rStep (mm)	t0 (mm)	t1 (mm)
A1	325	30.0	16.0	0.300	1.40
A2	325	25.0	15.0	0.200	0.80
A3	650	19.0	10.0	0.200	0.60
A4	650	13.2	11.4	0.125	0.38

In this paper, we will focus on the cavity for A1 stage, which has the largest aperture, thus most challenging for the thermal heating. A schematic drawing of A1 stage lattice cell and its RF cavity model are shown in Figure 1.

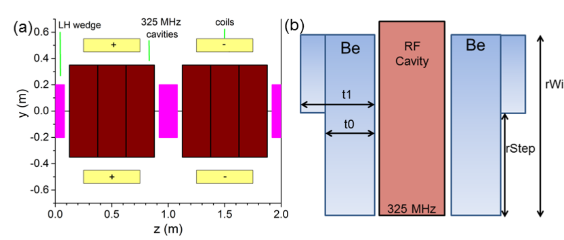

Figure 1: (a) Schematic drawing of Stage A1, and (b) RF cavity model.

Like MICE cavity, the Be windows are designed into a curved profile to control the direction of thermal expansion and reduce the thermal stress. Based on the parameters in Table 1 and the window curvature from MICE cavity, we build a 3D cavity model, as shown in Figure 2, for further study.

Content from this work may be used under the terms of the CC BY 3.0 licence (© 2015). Any distribution of this work must maintain attribution to the author(s), title of the work, publisher, and DOI.

ISBN: 978-3-95450-168-7 doi:10.18429/JACoW-IPAC2015-WEPTY048

Content from this work may be used under the terms of the CC BY 3.0 licence (© 2015). Any distribution of this work must maintain attribution to the author(s), title of the work, publisher, and DOI.

AN RFQ DIRECT INJECTION SCHEME FOR THE ISODAR HIGH INTENSITY H_2^+ CYCLOTRON*

D. Winklehner, MIT, Cambridge, MA, USA
R. Hamm, R&M Technical Enterprises, Pleasanton, CA, USA
J. Alonso, J. Conrad, MIT, Cambridge, MA, USA

Abstract

IsoDAR is a novel experiment designed to measure neutrino oscillations through $\bar{\nu}_e$ disappearance, thus providing a definitive search for sterile neutrinos. In order to generate the necessary anti-neutrino flux, a high intensity primary proton beam is needed. In IsoDAR, H_2^+ is accelerated and is stripped into protons just before the target, to overcome space charge issues at injection. As part of the design, we have refined an old proposal to use an RFQ to axially inject bunched H_2^+ ions into the driver cyclotron. This method has several advantages over a classical low energy beam transport (LEBT) design: (1) The bunching efficiency is higher than for the previously considered two-gap buncher and thus the overall injection efficiency is higher. This relaxes the constraints on the H_2^+ current required from the ion source. (2) The overall length of the LEBT can be reduced. (3) The RFQ can also accelerate the ions. This enables the ion source platform high voltage to be reduced from 70 kV to 30 kV, making underground installation easier. We are presenting the preliminary RFQ design parameters and first beam dynamics simulations from the ion source to the spiral inflector entrance.

INTRODUCTION

In the IsoDAR (Isotope Decay-At-Rest) experiment [1], H_2^+ ions will be delivered by a high performance ion source, accelerated to 60 MeV/amu in a compact cyclotron, and then stripped to protons and dumped on a beryllium target surrounded by a lithium sleeve. Neutrons generated by the protons hitting ^{9}Be will be captured on ^{7}Li, and the resulting ^{8}Li will then beta decay-at-rest, producing a very pure $\bar{\nu}_e$ beam. This accelerator and target system will be placed close (16 m from the center) to an existing neutrino detector (e.g. KamLAND) to measure $\bar{\nu}_e$ disappearance from neutrino oscillations via inverse beta decay. This process is depicted in Figure 1. The short baseline will allow tracing out more than a full period of the oscillation wave inside the detector, thus presenting a definitive search for proposed sterile neutrinos that may participate in the oscillation but not in the weak interaction. In order to get definitive results over the course of a few years, a high neutrino flux is necessary; hence a very high primary proton beam is desired.

In the summer months of 2013 and 2014, tests of high intensity H_2^+ production, transport, and injection into a cyclotron were conducted at Best Cyclotron Systems, Inc.

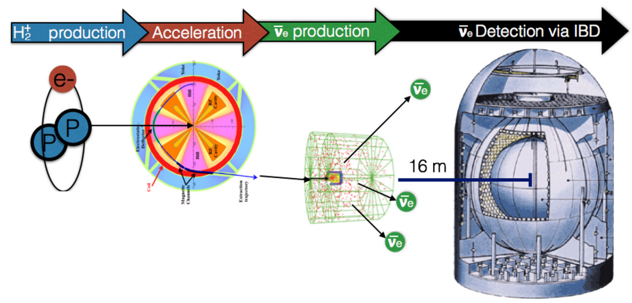

Figure 1: Cartoon of the IsoDAR experiment. Detector image courtesy of the KamLAND collaboration.

(BCS) in Vancouver, Canada. The ion source, borrowed from INFN Catania in Italy, was the "versatile ion source" (VIS), an off-resonance 2.45 GHz ECR ion source. From the VIS, it was possible to extract 12 mA of H_2^+. The main objective was to test the extent to which space charge will be a limiting factor in the low energy beam transport and the injection into the cyclotron through a spiral inflector. It was possible to show that the transmission through the spiral inflector at beam currents on the order of 10 mA was $\approx$ 95%. The typical acceptance of an unbunched beam into the cyclotron RF bucket is on the order of 5%, and with a 2-gap multiharmonic buncher, this acceptance can be increased to 10-20%. Considering the present performance of the VIS and suggested improvements to the source, the nominal 5 mA of H_2^+ extracted from the cyclotron is achievable, but pushing the limits. We are exploring two avenues to improve the situation: (1) We are constructing a new ion source (multicusp) dedicated to the production of H_2^+, and (2) we are investigating the use of an RFQ to replace the LEBT. The RFQ is a linear accelerator that can focus, bunch, and accelerate a continuous beam of charged particles at low energies with high bunching and transmission efficiencies. RFQs are very attractive for low energy ion accelerators, e.g. for applications with high current beams or in combination with sources such as an ECR, because the source can be close to ground potential and is easy to operate and to service. Because the basic RFQ concept can be implemented over a wide range of frequencies, voltages, and physical dimensions, it is an ideal structure to use for bunching an intense ion beam for injection into a cyclotron and has already been used in several cyclotron systems for radial injection of input beams [2]. It can also be used for axial injection at much lower energies as first proposed in 1981 [3]. However, to date, direct axial injection into a compact cyclotron using an RFQ has not yet been realized. For high acceptance into

* Work supported by grant NSF-PHY-1148134 and the Massachusetts Institute of Technology.

ISBN: 978-3-95450-168-7 doi:10.18429/JACoW-IPAC2015-WEPTY050

LOW POWERED RF MEASUREMENTS OF DIELECTRIC MATERIALS FOR USE IN HIGH PRESSURE GAS FILLED RF CAVITIES

B. Freemire*, Yagmur Torun, Illinois Institute of Technology, Chicago, IL 60563, USA
D. Bowring, A. Moretti, A.V. Tollestrup, K. Yonehara,
Fermi National Accelerator Laboratory, Batavia, IL 60510, USA
A. Kochemirovskiy, University of Chicago, Chicago, IL 60637, USA
H. Phan, McDaniel College, Westminster, MD 21157
G. Arriaga, Northern Illinois University, DeKalb, IL 60115, USA

Abstract

The Helical Cooling Channel scheme envisioned for a Muon Collider or Neutrino Factory requires high pressure gas filled radio frequency cavities to operate in superconducting magnets. One method to shrink the radii of the cavities is to load them with a dielectric material. The dielectric constant, loss tangent, and dielectric strength are important in determining the most suitable material. Low powered RF measurements of the dielectric constant and loss tangent were taken for multiple purities of alumina and magnesium calcium titanate, as well as cordierite, forsterite, and aluminum nitride. Measurements of alumina were consistent with previously reported results. The results were used to design an insert for a high powered RF test that will include sending beam through the cavity.

INTRODUCTION

One muon cooling channel scheme, the Helical Cooling Channel (HCC), utilizes high pressure gas filled radio frequency (HPRF) normal conducting cavities placed within superconducting solenoids [1]. Current magnet technology dictates the radial size of these cavities be smaller than that of a pillbox cavity filled with hydrogen gas in the TM_{010} mode at 325 or 650 MHz [2]. Loading the cavities with a dielectric material is one solution with which to shrink the radii of the cavities. An experiment to determine the dielectric strength of 99.8% pure alumina has already been performed [3]. This paper will present an expansion of those results, including the dielectric constant and loss tangent of different purites of alumina, as well as magnesium calcium titanate (MCT), cordierite, forsterite, and aluminum nitride (AlN).

MATERIAL SELECTION

For a simple pillbox filled with a dielectic, the resonant frequency is

$$f_{nml} = \frac{c}{2\pi\sqrt{\mu_r\,\epsilon_r}}\sqrt{\left(\frac{p_{nm}}{R}\right)^2 + \left(\frac{l\pi}{L}\right)^2} \qquad (1)$$

where c is the speed of light, μ_r and ϵ_r are the relative permeability and permittivity, respectively, and R and L are the radius and length of the cavity, respectively. Therefore in order to maintain a constant resonant frequency, one may add a dielectric in order to decrease the radius of the cavity. The loss tangent, $\tan\delta$, of a dielectric is related to the permittivity by

$$\epsilon = \epsilon_0\,\epsilon_r(1 - j\,\tan\delta) \qquad (2)$$

where ϵ_0 is the permittivity of free space.

The choice of material is important in designing a cooling channel in that an appropriate amount of material, based on its permittivity, must be inserted in order to bring the radius of the cavity down while minimizing the energy dissipation in the dielectric material.

Samples of alumina of various purities were obtained from Morgan Advanced Ceramics [4], CoorsTek [5], and Accuratus [6]. Samples of cordierite, forsterite, and magnesium calcium titanate were obtained from Euclid Techlabs [7]. A sample of aluminum nitride was obtained from Sienna Technologies, Inc. [8]. Table 1 lists the quoted properties of each sample by the manufacturer. The dielectric constant and loss tangent of each were measured in order to design a realistic cooling channel dielectric insert.

Table 1: Dielectric Constant and Loss Tangent Values (including the Frequencies) Reported by Each Manufacturer. 1 = Morgan, 2 = Accuratus, 3 = CoorsTek, 4 = Euclid, 5 = Sienna

Material	**Man.**	**Purity (%)**	ϵ_r	$\tan\delta$ **(10^{-4})**	**Freq. (MHz)**
Alumina	1	94	9.04	6.2	1000
Alumina	1	96	9.20	4.4	1000
Alumina	1	97.6	9.00	3.0	1000
Alumina	2	97.6	9.00	3.0	1000
Alumina	1	99.5	9.30	1.4	1000
Alumina	3	99.5	9.70	1.0	1
Cordierite	4	N/A	4.6	<10	1300
Forsterite	4	N/A	6.64	<10	1300
MCT	4	N/A	20	<10	1300
MCT	4	N/A	35	<10	1300
AlN	5	95	8.5	10	1

DIELECTRIC SAMPLE TEST

A modified pillbox cavity was designed such that small rods or tubes of each dielectric material could be placed on a

* freeben@hawk.iit.edu

Content from this work may be used under the terms of the CC BY 3.0 licence (© 2015). Any distribution of this work must maintain attribution to the author(s), title of the work, publisher, and DOI.

ISBN: 978-3-95450-168-7 doi:10.18429/JACoW-IPAC2015-WEPTY051

STRIPLINE KICKER FOR INTEGRABLE OPTICS TEST ACCELERATOR

Sergey A. Antipov, University of Chicago, Chicago, Illinois, USA
Alexander Didenko, Valeri Lebedev, Alexander Valishev, Fermilab, Batavia, Illinois, USA

Abstract

We present a design of a stripline kicker for Integrable Optics Test Accelerator (IOTA). For its experimental program IOTA needs two full-aperture kickers, capable to create an arbitrary controllable kick in 2D. For that reason their strengths are variable in a wide range of amplitudes up to 16 mrad, and the pulse length 100 ns is less than a revolution period for electrons. In addition, the kicker should have a physical aperture of 40 mm for a proposed operation with proton beam, and an outer size of 70 mm to fit inside existing quadrupole magnets to save space in the ring. Computer simulations using CST Microwave Studio® show high field uniformity and wave impedance close to 50 Ω.

KICKER DESCRIPTION

Integrable Optics Test Accelerator is a relatively small research storage ring with the circumference of 40 m. It will operate with short bunches of 150 MeV electrons injected from the ASTA linac [1], and later with 2.5 MeV protons from HINS RFQ [2]. The ring has a flexible linear optics to allow for a variety of physics experiments [3], including nonlinear integrable optics, the concept of which is described in [4]

The nonlinear dynamics research program at IOTA involves construction of Poincare maps of phase space, and that requires two kickers: a horizontal and a vertical to be able to place the beam at an arbitrary initial amplitudes in the transverse phase space. The kickers have to be tunable in a wide range from small to full-aperture, with the physical aperture of the machine being quite large: beam pipe inner radius is 24 mm or 40 sigma of horizontal size of electron beam at the place with maximum beta-function [3]. In addition, the vertical kicker will also serve as an injection kicker.

To support the required short length of kicker pulse a stripline kicker was preferred. It is also relatively simple in design and fabrication. The kickers are going to be fed by recommissioned power supplies from Fermilab's Tevatron injection kickers, which are capable of producing variable voltage pulses up to 25 kV. The power supplies have rise/fall time of about 20 ns, and are capable of producing a 100 ns-long pulse, which is slightly shorter than a revolution period of the ring – 130 ns. That allows us to make sure that the beam is affected on one turn only, and that is critical for the accuracy of experiments. The kickers are loaded with 50 Ω external resistive load.

Position of kickers in the ring is depicted in Fig. 1. Both kickers are located in the injection straight, downstream to injection Lambertson magnet. To minimize the required space one of the kickers is placed inside a quadrupole doublet. Their aperture of 72 mm determines a limit on the outer dimensions of the kicker's pipe. Table 1 lists basic parameters of the ring and its kickers.

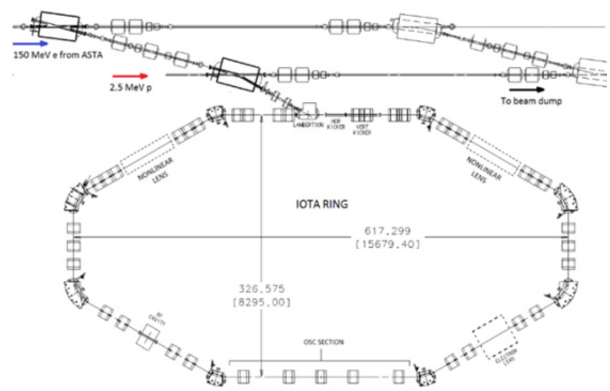

Figure 1: IOTA Ring, configuration for nonlinear optics.

Table 1: Parameters of IOTA Ring and its Kickers for Electron Operation. Proton Parameters are in Parentheses

Beam energy	150 MeV (2.5 MeV)
Revolution period	130 ns (1.8 μs)
RMS beam size at kicker	~ 0.2 mm (~ 3 mm)
Max plate voltage	±25 kV
Pulse duration, rep. rate	100 ns, < 1 Hz
Max. kick angle: hor., vert.	16, 8 mrad

DESIGN

The design of the kickers was inspired by a work carried out at the Budker Institute (BINP), Russia [5]. The geometry was adjusted to fit inside the existing quadrupole magnets. Since IOTA ring hosts several different experiments, requiring their own set of optics, it was crucial to minimize limitation of physical aperture, while meeting the requirements on the strength, field quality, wave impedance, and spatial constraints. The physical aperture was tentatively set to be at least 40 mm for future experiments with a proton beam. The kicker cross-section is depicted in Fig. 2.

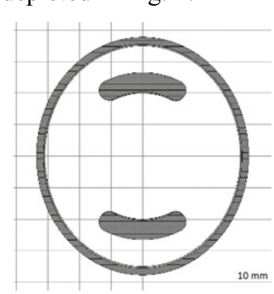

Figure 2: Kicker cross-section (vertical kicker).

Content from this work may be used under the terms of the CC BY 3.0 licence (© 2015). Any distribution of this work must maintain attribution to the author(s), title of the work, publisher, and DOI.

ISBN: 978-3-95450-168-7 doi:10.18429/JACoW-IPAC2015-WEPTY054

GRID WINDOW TESTS ON AN 805-MHz PILLBOX CAVITY*

Y. Torun†, Illinois Institute of Technology, Chicago, IL 60616, USA
A. Moretti, Fermilab, Batavia, IL 60510, USA

Abstract

Muon ionization cooling channel designs use pillbox shaped RF cavities for improved power efficiency and fine control over phasing of individual cavities. For minimum scattering of the muon beam, the ends should be made out of a small thickness of high radiation length material. Good electrical and thermal conductivity are required to reduce power dissipation and remove the heat efficiently. Thin curved beryllium windows with TiN coating have been used successfully in the past. We have built an alternative window set consisting of grids of tubes and tested these on a pillbox cavity previously used with both thin Be and thick Cu windows. The cavity was operated with a pair of grids as well as a single grid against a flat endplate.

CAVITY WINDOWS FOR MUON COOLING

Muon ionization cooling requires sections of RF acceleration at fairly low muon energy ($\beta \simeq 0.85$) interspersed with energy absorbers at low-$\beta_\perp$ locations in a strong focusing magnetic lattice. Since there is already material in the beam path and muons do not interact strongly, additional material at high-$\beta_\perp$ locations where the RF cavities are can be acceptable as long as the contribution to beam scattering is small compared to the absorbers. Thus, the pillbox cavity geometry can be used for muon beams if electrical termination of cavity irises is done with high radiation length material. This typically yields a factor of two or higher gain in the ratio of accelerating to peak surface field compared to the standard elliptical cavity geometry with open irises. The requirements for the windows are:

- thickness that is a small fraction of radiation length for minimal beam scattering
- high electrical conductivity for reduced RF power dissipation
- high thermal conductivity to carry away the heat
- mechanical strength to withstand pulsed heating from the RF field
- mechanical strength to limit Lorentz force detuning
- low secondary electron yield to avoid multipacting
- low dark current
- ultra high vacuum compatibility

Thin curved beryllium windows with TiN coating have been used in 805- and 201-MHz prototype cavities with excellent results [1]. However, beryllium is expensive and requires special precautions due to personnel safety issues. Thermal stress at the center of the window as well as Lorentz force detuning can force a gradient limit that is lower than that due to surface breakdown considerations alone [2]. Table 1 shows a summary of window configurations used in the past on cavities built for muon cooling R&D.

Table 1: Window Configurations Tested for Muon Cooling

Window type	Application: 805-MHz pillbox	Application: 201-MHz MICE prototype
Flat thick Cu endplates	OK	OK
Flat thin pre-stressed Be	Unstable at high power	–
Curved thin Be foils	OK	OK

GRID WINDOWS

A solid conductor is not needed to achieve a pillbox-like field pattern at RF frequencies. An alternative window layout has been studied [3] and consists of a grid of tubes. This configuration has the following useful features:

- Mechanical strength
  - less prone to electromagnetic impulse detuning for the same thickness
  - can be made thinner than solid windows for the same strength
- Cooling: hollow tubes can accommodate active cooling
- Holes: beam aperture can be left open in the middle
- Cost: cheaper than curved Be foils
- Safety: no Be

There are potential disadvantages as well:

- Electric field enhancement
  - smaller radius of curvature than solid curved window means higher surface field on the grids which may lead to higher field emission and breakdown probability
- Irregular material distribution in beam path
  - the effect on the beam needs to be evaluated for a cooling channel application

TEST SETUP

In order to carry out a first test of the concept on an actual pillbox type cavity, we have built a pair of 16-cm-diameter windows consisting of 1-cm-diameter solid tubes spaced 3.2-cm apart. These prototype windows were made out of aluminum, their surfaces were electropolished after fabrication and one of the windows was TiN coated on one side. They were designed to fit on an existing pillbox type cavity used in the past with Be windows.

* Work supported by the US Department of Energy Office of Science through the Muon Accelerator Program.
† torun@iit.edu

Content from this work may be used under the terms of the CC BY 3.0 licence (© 2015). Any distribution of this work must maintain attribution to the author(s), title of the work, publisher, and DOI.

ISBN: 978-3-95450-168-7 doi:10.18429/JACoW-IPAC2015-WEPTY055

INSTALLATION AND COMMISSIONING OF THE MICE RF MODULE PROTOTYPE*

Y. Torun†, P. Lane, Illinois Institute of Technology, Chicago, IL 60616, USA
T. Anderson, D. Bowring, M. Chung, J. H. Gaynier, M. Leonova, A. Moretti,
R. J. Pasquinelli, D. W. Peterson, R. Schultz, Fermilab, Batavia, IL 60510, USA
L. Somaschini, INFN-Pisa, Pisa, Italy
A. J. DeMello, D. Li, S. Virostek, LBNL, Berkeley, CA 94720, USA

Abstract

A special vacuum vessel prototype was built [1] to house the first electropolished 201-MHz RF cavity for the International Muon Ionization Cooling Experiment (MICE) [2]. The resulting prototype RF module has been assembled, instrumented, installed and commissioned at Fermilab's MuCool Test Area (MTA) [3] and the effort has provided valuable experience for design and assembly of modules that will be used in the cooling channel for the experiment.

MECHANICAL ASSEMBLY AND INSTALLATION

Cavity Insertion

There is little clearance between the dressed cavity assembly (with the tuner forks installed) and the vacuum vessel. The cavity was inserted into the vacuum vessel using a material lift with a custom fabricated attachment to match the stiffener ring. The setup is shown in Fig. 1. During adjustment of the suspension struts that form the six-axis platform to center the cavity in the vessel, several of the rod ends seized. This was most likely due to the lubricant film on the threaded rods being removed during cleaning or stripped during adjustment under load. The strut bodies and threaded rods were both made of stainless steel which increases the likelihood of galling. New strut bodies were machined out of aluminum bronze to avoid this problem. Magnetic permeability of the new parts were measured to confirm that they would be acceptable for use in a strong magnetic field. In addition, a test fixture was designed and built in order to gain some familiarity with the adjustment procedure without a heavy load. This fixture consisted of a hoop with identical attachment points as the cavity so it could be used with the same struts and fasteners. After successful testing of the system with the fixture, the cavity was reinstalled in the vessel using the new struts and adjustments could be made easily by turning the strut bodies by hand while the full weight of the cavity assembly was suspended.

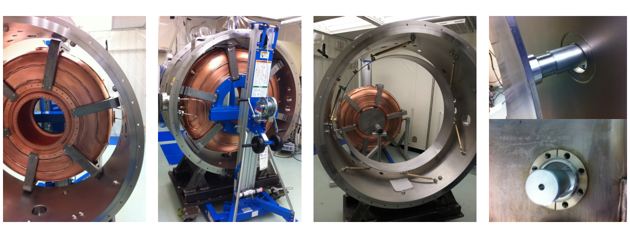

Figure 1: Left to right: cavity insertion, lift, test fixture with the new struts, and an alignment rod on the test fixture seen from inside (top) and outside (bottom) the vessel.

Tuner System

Initial tests of the pneumatic actuators were made on a separate fixture [4]. Alignment rods screwed into the tuner forks were used to center the tuner actuator shafts with respect to the corresponding vessel ports while adjusting the cavity position. Each actuator consists of a concentric inner and outer shaft pair with threaded sections at their tips. The shafts have identical thread spacing and are screwed into corresponding holes in the fork body. Initial installation of the actuators on the vessel revealed another issue; most actuator vacuum flanges would not mate up with the vessel port flanges before the inner actuator shafts bottomed out on the forks. This was resolved by removing a short section (about one thread) from the end of each inner shaft. After the cavity was aligned inside the vessel, detailed measurements of the mechanical (pressure to displacement) and RF control (pressure to frequency) transfer functions were carried out [5, 6] (Fig. 2). While the vessel was under vacuum in the MTA experimental hall, one of the actuators developed a vacuum leak during testing. No spare unit was available at the time, so the faulty actuator was removed and the corresponding port blocked off. This unit was repaired and reinstalled during reconfiguration of the module. Testing under vacuum revealed a vacuum leak in another unit which was replaced with a spare. The actuator design was modified to eliminate the weak joint responsible for the leak.

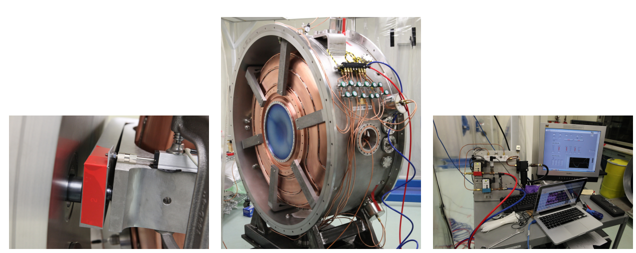

Figure 2: Tuner test setup: potentiometer on tuner fork (left) for displacement measurement, dressed cavity inside vessel (center), actuator pressure control (right).

* Work supported by the US Department of Energy Office of Science through the Muon Accelerator Program.
† torun@iit.edu

Content from this work may be used under the terms of the CC BY 3.0 licence (© 2015). Any distribution of this work must maintain attribution to the author(s), title of the work, publisher, and DOI.

ISBN: 978-3-95450-168-7 doi:10.18429/JACoW-IPAC2015-WEPTY056

NOVEL HIGH POWER SOURCES FOR THE PHYSICS OF IONOSPHERIC MODIFICATION*

B.L. Beaudoin, T.M. Antonsen Jr., I. Haber, T.W. Koeth, A.H. Narayan, G. Nusinovich, K. Ruisard,
Institute for Research in Electronics & Applied Physics,
University of Maryland, College Park, MD 20742-3511, USA
J.C. Rodgers, U.S. Naval Research Laboratory, SW Washington, DC 20375, USA

Abstract

The ionosphere plays a controlling role in the performance of critical civilian and DoD systems including the ELF-ULF communications, radars, navigation (including GPS) and geo-location systems. Ionospheric Modification (IM) is a complementary approach to passively studying the ionosphere that has intensified over the last 30 years with the construction of the High-Frequency Active Auroral Research Program (HAARP). The objective of IM is to control and exploit triggered ionospheric and magnetospheric processes to improve the performance of trans-ionospheric Command, Control, Communications and Intelligence (C3I) systems and to develop new applications that take advantage of the ionosphere as an active plasma medium. A key instrument in IM is the Ionospheric Heater (IH), a powerful High Frequency transmitter that modifies the properties of the ionospheric plasma by modulating the electron temperature at preselected altitudes.

A major reason for the development of a Mobile IH source (MIHs) is that it would allow investigators to conduct the needed research at different latitudes without building permanent installations. As part of a multi-university research initiative (MURI), UMD will develop a powerful RF source utilizing Inductive Output Tube (IOT) technology running in class-D amplifier mode. This technology was chosen because it has the potential to operate at high efficiencies. Some of the technical challenges presented in this paper will include: a gun design that minimizes intercepted current, a compact tunable hybrid cavity operating in the 1-10 MHz range, and an efficient modulator system capable of modulating a high power electron beam.

MAGNETRON INJECTION GUN (MIG) IOT DESIGN

A major concern with the gridded class-D operation of an IOT device is the heating of the grid due to intercepted electrons. A design using a MIG-type cathode that produces a hollow beam avoids this complication, as a small mod-anode local to the thin annular cathode can be used to bias the beam on and off without intercepting any electrons. We already possess a MIG-type cathode with a negative injection angle for this purpose. The proposed source with a Pierce-type geometry has been characterized with the Michelle code [1] with 2D axisymmetric geometry as shown in Fig. 1a. Steady state electrostatic PIC simulations show that for 60 kV on the anode and 200 V on the mod-anode, we can expect approximately 2 A of beam current from a 4.7 cm^2 emitter. The magnetic field design was identified by using Maxwell 2D (axisymmetric geometry) code to simulate solenoid coils/pole piece geometries. Iterations over several geometries maximized the dot product of the field lines with the unmagnetized beam trajectory (to minimize conversion of longitudinal to transverse momentum). The most recent iteration is shown below in Fig. 1b. The field lines follow the unmagnetized beam trajectory closely, except near the cathode surface. An additional set of coils or iron field shapers behind the cathode may be used to adjust the field lines in this region. As seen in simulation (Fig. 1b), with a 1.4 kGauss field (shown in Fig. 1c), the beam ripple due to transverse energy gain is minimal. This field simulation assumes ideal iron.

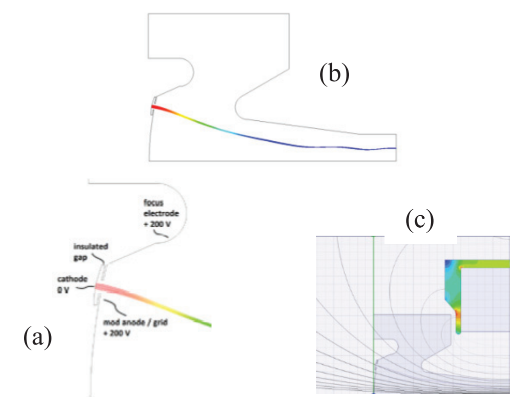

Figure 1: (a) Geometry of cathode, focusing electrode and mod-anode of a MIG-type gun and the particle trajectories. (b) Beam trajectory with field from a solenoid (c), with a peak on-axis field of 1.4 kGauss.

Steady state Michelle simulations were used to estimate the capacitance seen by the grid driver due to the focus electrode-mod anode spacing in the vicinity of the cathode. Calculations were done with and without beam in a 2D axisymmetric Michelle simulation, and the no-beam case was verified against a Maxwell 3D model of the gun assembly. Michelle and Maxwell measurements agreed to within 2 %, with the most likely discrepancy being a difference in mesh density. Additional comparisons of Michelle simulations with and without beam, predicts a 1 % increase in capacitance due to beam loading. We predict that the capacitance due to the inner surface of the mod-anode is 15.6 pF, requiring the grid driver to pull 2 A for a 5 ns rise time on a 600 V swing.

*Work supported by the Air Force Office of Scientific Research under grant FA95501410019.

Content from this work may be used under the terms of the CC BY 3.0 licence (© 2015). Any distribution of this work must maintain attribution to the author(s), title of the work, publisher, and DOI.

ISBN: 978-3-95450-168-7 doi:10.18429/JACoW-IPAC2015-WEPTY057

Content from this work may be used under the terms of the CC BY 3.0 licence (© 2015). Any distribution of this work must maintain attribution to the author(s), title of the work, publisher, and DOI.

ADAPTABLE MACHINE PROTECTION ARCHITECTURE FOR CW, HIGH INTENSITY ACCELERATORS

Saeed Assadi, Texas A&M University, College Station, TX 77843, USA

Abstract

An adaptable architecture of a machine protection system (MPS) suitable for continuous wave (CW), high intensity accelerators like those proposed for Accelerator Driven Systems (ADS) for subcritical reactor strategies and heavy ion accelerators for the production of rare isotopes is presented. A system of databases, networks and nodes that can systematically and flexibly be reconfigured to rebalance the required metadata is used. Additional features include reconfigurable machine setup templates that can rigorously be tested with mirror redundant online backups, the utilization of external reconfigurable geometric algorithms for the data channels and the network distribution, and the inclusion of initial system requirements as well as envisioned upgrades.

BACKGROUND

High power, high intensity proton drivers (Fig. 1) for nuclear fuel transmutation are required to have *High Availability* (Table 1) or better performance - otherwise the electric utilities do not consider these drivers as a viable solution. The implementation progress has been steady- however it has stalled at low 90%. The driving forces behind fourth generation superconducting accelerator machine protection system [MPS] is avoid incremental gain but structural.

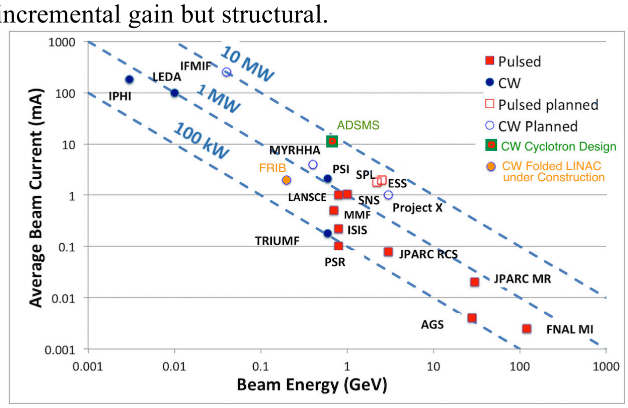

Figure 1: High Power Accelerator History

Table 1: Beam Availability Score

System Type	Availability	Unavailability
Fair	90%	37 days/year
Well-managed	99.9%	526 (min/year)
Fault-tolerant	99.99%	53 (min/year)
High-availability	99.999%	5 (min/year)

The generations are based on beam interaction with accelerator surrounding, beam power, technology and management mandate as systems have come to existence from the Tevatron and PSI to SNS and LHC. Although the MPS of each of these accelerators has significantly improved from its predecessor, the up time is in ~92% after four decades of operations, and cannot be sustained due to the complexity of tens of thousands of variables without a complete overhaul. Databases have become overwhelmed, and at times have become mere warehouses of information, that often provides valuable information, after accidents to discover a catastrophe in developing from days. In this paper I address one systematic approach that all MPS designers have considered but its implementation has fallen short due to cost, available technology and or integration framework factors. Data management is one aspect of high availability accelerator operation, automation, instrumentation and control, which are integral parts of forming the framework of MPS as machine performance manager.

METHODOLOGY

To achieve much better than 99% availability, one cannot simply attempt to squeeze efficiency without major architectural re-evaluation, and the bottom up systematics of running accelerators is even more model-driven with beam-hardware dynamic feedback. Moreover, the MPS has to provide reliable, redundant valid information from the start of the commissioning, rather than relying on limited physics studies to debug massive MPS on reliability, as it's failure will be the demise of an

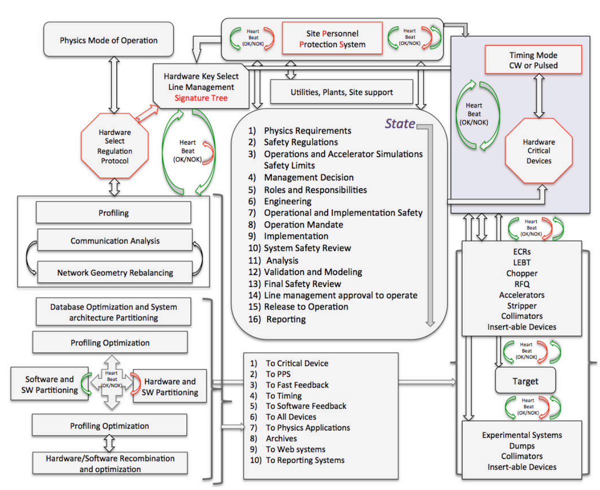

Figure 2: Database foundation setup for project dynamic integrated MPS in advance of hardware selection and parameterization.

Accelerator, such as the Texas A&M 800 MeV, Accelerator Driven Subcritical Molten Salt [ADSMS] or Facility for Rare Isotope Beam designed by Professor Richard York at FRIB. The first step is to integrate

ISBN: 978-3-95450-168-7 doi:10.18429/JACoW-IPAC2015-WEPTY058

DIAGNOSTICS FOR HIGH POWER CW ACCELERATORS*

Saeed Assadi#, Texas A&M University, College Station, TX, USA

Abstract

High power, continuous wave (CW) accelerators are proposed for applications such as Accelerator Driven Systems (ADS) for subcritical reactor strategies and heavy ion accelerators for the production of rare isotopes. Because of the high beam powers and high energy loss with beam interception of material, the beam diagnostic designs are necessarily shifting to non-intercepting, real-time feedback devices that can be fully integrated with the accelerator machine protection system (MPS) and operation control system including online models. Appropriate for these applications, three types of beam diagnostics (lanthanum bromide scintillation coincidence detectors, GaN neutron and gamma detectors, and beam position monitors) are presented.

BACKGOUND

Next generation of high power accelerators are more than ever in need of seamless integrated beam instrumentation, online models, controls system and agile beam characterization of particle losses and feedback systems. Role of beam diagnostics have shifted from a collection of exotic instruments with multiple platforms run individually by engineers and scientists adapted to an accelerator to base lattice from inception optimized specifically for operation. This methodology, not only requires inline beam instruments to be 3D multi-particle integrated modelled with lattice optimized as the accelerator being optimized in lattice but it has to foresee in advance the expected commissioning, operation and upgrade scenarios. To keep up with all expected modes of operations, we have limited choices to preserve design integrity, reliability, safety, and performance. (A) Design and test in collaboration of experts as soon as the project is formalized in an integrated form the fundamental beam instruments such as beam position electrodes and their expected signal delivery. (B) Tools for software development such as complete test stations. In this paper, I report on two such accelerator systems. (1) At Texas A&M University, a complete conceptual Accelerator Driven Subcritical Molten Reactor System is designed. The 100-800 MeV Cyclotron with strong focusing channels of twenty-three helical orbits (Figure 1) is embedded in more than 100 tons of iron preventing any externally accessible beam instrumentation such as loss monitors. It requires active beam orbit feedback system for 10 MW of CW proton beam with the possibility of aborting and landing segmentation loaded beam in numerous aborts located at the missing cavity extraction channel. There is about 0.75 Cm spacing at the inner radii for 100 MeV 400 W faraday cup abort dumps. This highly challenging cyclotron is compact, flexible and can be reconfigured to run if one of the ten superconducting cavities fails [1]. Second is the most versatile version of a CW Rare Isotope LINACs that have an added complexity of lattice change over to accelerate different radioactive species of same atomic mass to charge ratio as often as once every 4-6 weeks. These LINACS such as the one being considered by Jlab for MEIC or Facility for Rare Isotope Beam designed by R. York in 2009 [2] require full integration of beam diagnostics and operation changeover databases and online applications.

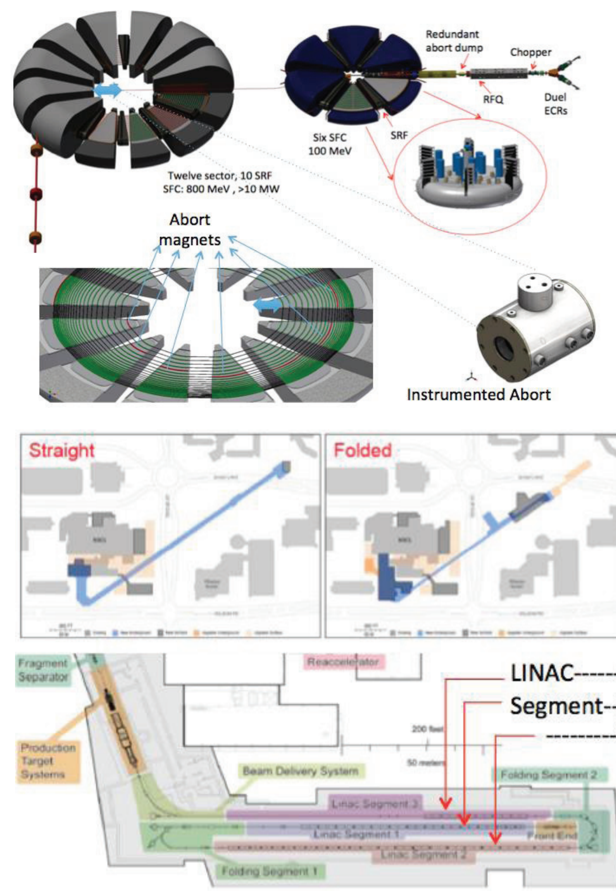

Figure 1: Top shows SFC at Texas, bottom is FRIB design status at MSU in 2010.

Both ADSMS and FRIB require specialized directional beam loss monitors such with energy discrimination, which will be discussed.

*Work supported by HiTek ESE LLC INC
#assadi@tamu.edu

Content from this work may be used under the terms of the CC BY 3.0 licence (© 2015). Any distribution of this work must maintain attribution to the author(s), title of the work, publisher, and DOI.

ISBN: 978-3-95450-168-7 doi:10.18429/JACoW-IPAC2015-WEPTY059

ALTERNATE METHODS FOR FIELD CORRECTIONS IN HELICAL SOLENOIDS*

M. L. Lopes#, S. T. Krave, J. C. Tompkins, K. Yonehara, Fermi National Accelerator Laboratory, Batavia, IL 60510, USA
G. Flanagan, S. A. Kahn, Muons Inc., Batavia, IL, 60510, USA
K. Melconian, Texas A&M University, College Station, TX 77845 USA

Abstract

Helical cooling channels have been proposed for highly efficient 6D muon cooling. Helical solenoids produce solenoidal, helical dipole, and helical gradient field components. Previous studies explored the geometric tunability limits on these main field components. In this paper we present two alternative correction schemes, tilting the solenoids and the addition of helical lines, to reduce the required strength of the anti-solenoid and add an additional tuning knob.

INTRODUCTION

Helical cooling channels (HCC) based on a magnet system with a pressurized gas absorber in the aperture have been proposed as a highly efficient way to achieve 6D muon beam cooling [1-2]. The cooling channel was divided into four sections to provide the total phase space reduction of muon beams on the level of 10^5-10^6, and to reduce the equilibrium emittance each consequent section has a smaller aperture and stronger magnetic fields.

The strength of the solenoid (*Bs*), helical dipole (*Bt*), and helical gradient (*G*) fields are strongly dependent on the coil and helix geometry [3-6]. The ratio *Bt*/*G* is fixed by the geometry but the absolute value can be adjusted independently from *Bs* by the means of an external anti-solenoid. However, this can be quite challenging due to the required magnetic field strength of this solenoid [4]. An additional knob capable of adjusting the ratio *Bt*/*G* independently of the coil geometry is highly desirable.

TILTED COILS

The coils for the helical cooling channel produce a dipole and gradient which rotates with the period of the helix. Two tilting schemes, shown in figure1, and their effect on the two transverse field components, were studied. In the "pitch" tilting arrangement, the coils were rotated about an axis at each coil which was tangent to the helix. The "yaw" tilting is about the axis of the angle to the rotated coil position, or an axis that is perpendicular to the pitch tilting.

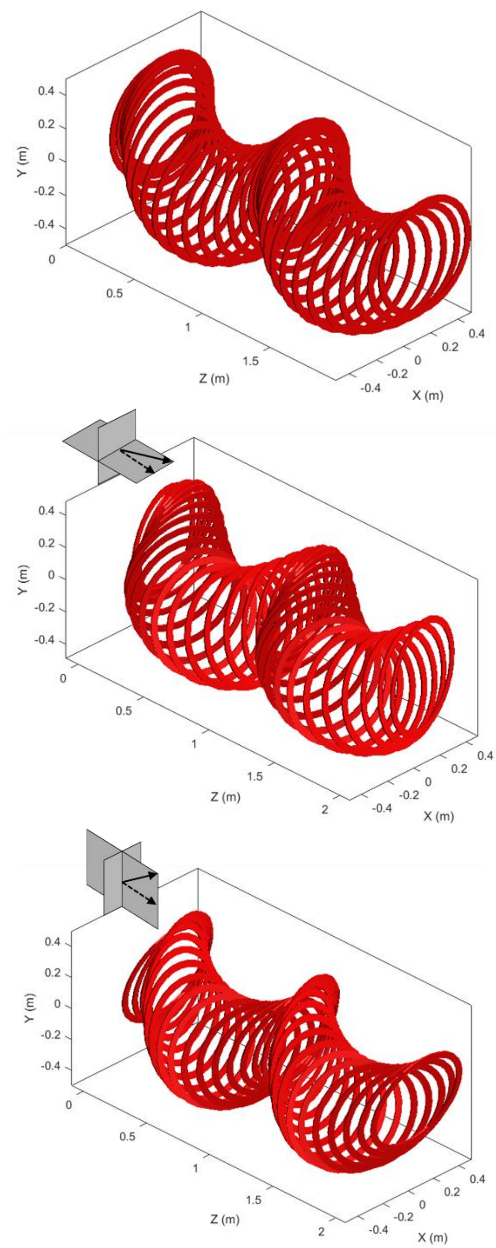

Figure 1: Helical coil arrangement of the non-tilted coil (top), Yaw tilt (middle), and Pitch tilt (bottom). The spacing between the coils and tilt were exaggerated for clarity.

*Work supported in part by Fermi Research Alliance under DOE Contract DE-AC02-07CH11359.
#mllopes@fnal.gov

Content from this work may be used under the terms of the CC BY 3.0 licence (© 2015). Any distribution of this work must maintain attribution to the author(s), title of the work, publisher, and DOI.

ISBN: 978-3-95450-168-7 doi:10.18429/JACoW-IPAC2015-WEPTY060

VIRTUAL WELDING AS A TOOL FOR SUPERCONDUCTING CAVITY COARSE TUNING *

A. Facco[1,2], C. Compton[1], J. Popielarski[1], G. J. Velianoff[1]
[1] Facility for Rare Isotope Beams, Michigan State University, East Lansing, MI 48824, USA
[2] Istituto Nazionale di Fisica Nucleare - Laboratori Nazionali di Legnaro, Padova, Italy

Abstract

Reaching the final frequency in the construction of Superconducting Half-Wave Resonators (HWR), either coaxial or spoke, is often a painful and time consuming process which requires several intermediate frequency tests and parts machining between subsequent welding steps. In spite of that, the final frequency error after final welding is often far from the target due to difficult to predict material contraction and cavity deformation induced by electron beam welding (EBW). Final coarse tuning is required by plastic deformation or differential etching. In coaxial HWR, both can decrease the cavity frequency but are not easily suitable to increase it. A novel method developed at MSU is "virtual" welding, i.e. deformation of the cavity shape by applying systematically EBW on the cavity outer surface to induce controlled Nb material contraction in strategic positions. This technique allows to increase the cavity frequency with excellent precision and predictability, thus simplifying and making less expensive and more reliable HWR coarse tuning. Method and experimental results will be described and discussed.

INTRODUCTION

Superconducting Half-Wave Resonators (HWR), in their coaxial and spoke versions, after being confined for decades in the R&D environment, have been recently used in a real accelerator [1] and are becoming fundamental components of large proton and ion linear accelerators under construction or planned [2]. These low- and medium-β resonators are closed cavities with relatively small apertures and their frequency is mostly determined by the length of their inner conductor. A common problem is the difficulty of building them with the right frequency, because it is not always easy to predict contraction of the Niobium material and thus the final cavity size after welding together its different parts. Coarse tuning of HWR cavities requires intermediate frequency measurements and length adjustments throughout the welding procedure. A large fine tuning range of the mechanical tuner is usually required to compensate for possible errors.

A typical problem is the difficulty of correcting the center frequency after the cavity is completely welded and closed. Two main methods are used, both well suitable for lowering the frequency:

1) Plastic deformation. It is often used in the beam port region for coarse tuning, but its application in HWRs is not always easy due to their structural stiffness and, for large frequency corrections, it can be dangerous for cavity mechanical integrity. Corrections are not very precise, nor smooth: initial elastic response is followed by a sudden adjustment to a new frequency, and the risk of going beyond the desired point is not negligible. Moreover, while it is easy to plastically push the beams ports in and lower the frequency, in HWRs it is rather difficult to pull them out safely to obtain the opposite effect.

2) Differential etching. Material from the rf surface inside the resonator is removed selectively by Chemical Polishing (CP). This is routinely applied since several years in QWRs [3][4], where it is possible to remove material either in the high B or in the high E region, causing frequency decrease or increase, respectively. It is easy to realize that in HWRs differential etching can be used without difficulty only to remove material from the end (shorting) plates, making the resonator longer and its frequency lower, while it seems almost impossible to increase the frequency by removing material only from the high E region near the beam port axis. So, at present, frequency corrections in closed HWRs are safely feasible only in the down direction, making final coarse tuning somehow difficult and time consuming.

TUNING BY VIRTUAL WELDING

In the original FRIB HWR construction plan, the beam ports were the last parts welded and their position was adjusted to reach the final goal frequency. We soon realized, however, that the mechanical contraction caused by such difficult full penetration weld from outside was moving the beam ports far from the initially planned position, and that a large and rather unpredictable frequency error was finally left. This method was then abandoned: the beam ports are now safely welded to the outer conductor from inside, at an early stage. Coarse tuning is made by adjusting the inner and outer conductor length before welding them to the shorting plates. Due to material contraction, however, this procedure is still leaving a large uncertainty on final frequency of several hundreds of kHz. It became clear that a good coarse tuning sequence required also a viable method to increase the final frequency.

* Work supported by the U.S. Department of Energy Office of Science under Cooperative Agreement DE-SC0000661

Content from this work may be used under the terms of the CC BY 3.0 licence (© 2015). Any distribution of this work must maintain attribution to the author(s), title of the work, publisher, and DOI.

ISBN: 978-3-95450-168-7 doi:10.18429/JACoW-IPAC2015-WEPTY061

PROGRESS ON THE CRYOGENIC AND CURRENT TESTS OF THE MSU CYCLOTRON GAS-STOPPER SUPERCONDUCTING MAGNET*

M. A. Green, S. S. Chouhan, G. Bollen, J. DeKamp, C. Magsig, and A. F. Zeller, FRIB, and D. Morrissey, J. Ottarson and S. Schwarz, NSCL, MSU, East Lansing, MI 48824, USA

Abstract

The Michigan State University (MSU) cyclotron gas stopper magnet is a warm iron superconducting cyclotron dipole. The desired field shape is obtained by the pole iron profile. Each coil of the two halves is in a separate cryostat and connected in series through a warm electrical connection. The entire system is mounted on a high voltage platform, and is cooled using six two-stage 4.2 K pulse tube coolers. This paper presents the progress on the magnet fabrication, cooling, and current testing.

INTRODUCTION

The fragmentation of fast heavy-ion particles enables fast chemistry-independent production, separation and delivery of exotic isotope beams. The resulting beams have high energies (<100 MeV/A) and large emittances. The range of experiments can be extended by slowing the fast ions, extracting them, and then re-accelerating them. The ReA3 [1] re-accelerator under construction at MSU will reaccelerate thermalized ions (~10 keV) to provide low emittance exotic ion beams over a range of energies.

A solution to thermalize and extract light to medium mass beams is to apply a strong gradient dipole magnetic field in a large magnetic gap that forces the ions into a spiral path while slowing them down in He gas at 80 K. Low energy ions near the extraction port are transported in a central extraction orifice by an RF carpet [2], [3]. The ions are transformed into low-energy beams using a differentially pumped ion guide. The low-energy low-emittance beams are transported directly to experiments or to other accelerators for reacceleration. The super-ferric cyclotron gas-stopper magnet at MSU will enable the capture of short-lived rare isotopes.

THE GAS-STOPPER MAGNET

The cyclotron gas-stopper magnet has evolved since it was first proposed in 2007 [4]. The gradient dipole field is produced in a gap of 180 mm between sector cyclotron poles. The peak field in the gap is ~2.6 T. A pair of superconducting solenoid coils produce the field. The warm iron poles and flux return can be separated so that the deceleration system can be maintained. Each pole has its own coil and liquid helium cryostat. The two 300 K magnet poles are connected through the iron return path. The coils are not connected at 4 K. Forces to the yoke are transmitted by the cold mass supports. The common axis of the magnet coils is horizontal.

The work reported in this paper was supported in part by an NSF grant PHY-09-58726 and PHY-11-02511.

The space between the poles is evacuated to provide an insulating vacuum for the 80 K magnet beam chamber. Figure 1 shows the assembled magnet with the iron poles closed. Figure 2 shows the magnet poles open. The magnet cryostat on the right has the cylindrical part of the beam chamber vacuum vessel attached. There is a double o-ring seal between the cylindrical portion of the vacuum vessel and the magnet cryostat installed in the left pole piece. One can see the shaped face of the shaped sector cyclotron pole on the pole to the right of Fig. 2.

Figure 1: The assembled magnet is shown fully closed.

Figure 2: The magnet is shown with poles separated. The beam chamber insulating vacuum chamber is visible along with one of the shaped cyclotron poles.

Content from this work may be used under the terms of the CC BY 3.0 licence (© 2015). Any distribution of this work must maintain attribution to the author(s), title of the work, publisher, and DOI.

ISBN: 978-3-95450-168-7 doi:10.18429/JACoW-IPAC2015-WEPTY062

MULTIPACTOR BREAKDOWN MODELLING USING AN AVERAGED VERSION OF FURMAN'S SEY MODEL*

S. Rice, J. Verboncoeur#, Michigan State University, East Lansing, MI USA

Abstract

Furman's seconday electron yield model is commonly used for the simulation of multipactor in accelerating cavities and other resonant structures. While accurate, the stochastic model requires many Monte Carlo simulations in order to characterize susceptibility to multipactor. This paper generalizes our previous research in characterizing a reduced-order Furman model, in which we replace the stochastic Furman model with a deterministic model based upon the Furman model's underlying statistics. Favorable comparisons between the full Furman model and the reduced-order Furman model are shown for multipactor simulations in a coaxial cavity, and the results are expected to generalize to other geometries.

INTRODUCTION

Multipactor [1, 2] is a resonant phenomenon in which an electromagnetic field causes free electrons to impact a surface, resulting in the surface emitting secondary electrons which can sustain the cyclic process. The formation of multipactor is strongly dependent upon the secondary electron yield (SEY) of a surface, and the emission velocities of the emitted electrons. A popular SEY model proposed by Furman and Pivi [3] is frequently used to simulate multipactor. This model is based around a stochastic scattering process, which necessitates computationally costly Monte-Carlo simulations in order to simulate the formation of multipactor in a given system.

In our previous work [4], we presented an approximation to Furman's model, in which for a given particle impact velocity, a single weighted particle is emitted deterministically, thus avoiding Monte Carlo simulations to model multipactor current; this particle was chosen to be simply the median of the underlying stochastic parameters in the SEY model. In this present work, we examine other cumulative probability statistics other than the 50th percentile (median) statistic. The results were obtained through simulations in a coaxial geometry, but are expected to be generalizable to other geometries.

SIMULATION DESCRIPTIONS

Consider a coaxial cavity shorted at both ends as shown in Fig. 1, which is excited by a TEM mode specified by $V_o \cdot \cos(\omega t+\theta) \cdot \sin(\pi z/L)$, where V_o is the peak instantaneous voltage, θ is the phase, ω is the cavity-dependent resonant angular frequency, z is the position along the axial direction as measured from the cavity end, L = 1.86 m is the cavity length, a = 1 cm is the cavity inner radius, b = 5.65 cm is the cavity outer radius. These dimensions were chosen to yield maximum multipactor response for $V_o \approx 1000$ V at the fundamental TEM mode resonant frequency of 80.5 MHz.

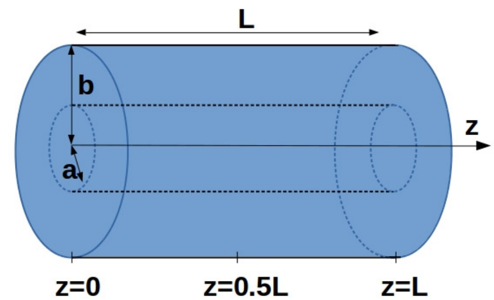

Figure 1: Coaxial Geometry

For each voltage V_o and phase θ to be simulated, particle-tracking (single particle) simulations were performed for 10 cycles, where a cycle is defined to end whenever either a boundary strike or a complete RF period elapses, whichever occurs first. For each simulation, an electron starts from rest from the outer wall at the z=0.5L position, and the following loop is carried out for each cycle:

(1) Electron is accelerated by the cavity fields until it strikes a boundary.
(2) Record SEY for the impact.
(3) Generate a secondary electron from emission energy and angle distributions.
(4) Repeat from step #2.

For Furman's full model, the number of secondary electrons can randomly range from 0 to a maximum integer value. If no electrons are emitted, then the SEY is set to 0, and the simulation terminates. If more than one electron is emitted, then one of these electrons are randomly chosen to continue propagating the multipactor simulation. For more sophisticated multipactor simulations, we would need to track each emitted electron, but by running a large number of Monte Carlo trials (1000 for this investigation), we are still able to sample the entire multipactor initiation space while tracking only one particle for each simulation.

The net SEY is defined to be the product of all the single-impact SEY values, with the adjustment that if less than two boundary impacts occurred over the 10 simulation cycles, then the net SEY is automatically set to 0. This net SEY gives a proxy measure of whether or not multipactor can initiate, since net SEY less than unity

*Work supported by a MSU Strategic Partnership Grant.
#iohnv@msu.edu

Content from this work may be used under the terms of the CC BY 3.0 licence (© 2015). Any distribution of this work must maintain attribution to the author(s), title of the work, publisher, and DOI.

ISBN: 978-3-95450-168-7 doi:10.18429/JACoW-IPAC2015-WEPTY063

CO-LINEAR X-BAND ENERGY BOOSTER (XCEB) CAVITY AND RF SYSTEM DETAILS

T. Sipahi, S. V. Milton, S. G. Biedron, Colorado State University (CSU), Electrical & Computer Engineering Dept., Fort Collins, CO, 80523, USA

Abstract

Due to their higher intrinsic shunt impedance X-band accelerating structures offer significant gradients with relatively modest input powers. At the Colorado State University Accelerator Laboratory (CSUAL) we would like to adapt this technology to our 1.3-GHz, L-band accelerator system in order to increase our overall beam energy in a manner that does not require investment in an expensive, custom, high-power X-band klystron system. Here we provide the design details of the X-band structures that will allow us to achieve our goal of reaching the maximum practical net potential across the X-band accelerating structure while driven solely by the beam from the L-band system.

GENERAL CONCEPT

The Colorado State University Accelerator and FEL Laboratory has an L-band system capable of generating 6 MeV electron bunches [1]. We would like to further increase the electron beam energy without additional significant investment. Our idea is to utilize the electron beam from our linac as a drive source for an otherwise unpowered (passive) X-band linac structure, thus allowing us to increase the beam energy by using the L-band power together with the inherent high shunt impedance of the X-band structure.

For our proposed Co-linear X-band Energy Booster system we start with the power extraction mechanism using the beam from the L-band linac passing through the power extraction cavity (PEC). This power is then delivered to the X-band main accelerating cavity (MAC) structures. One can then periodically pass a bunch through the whole system and achieve significantly higher beam energies. This is done by simple switching of the photocathode drive laser pulses and shifting the phase onto the cathode such that it puts the bunch into the accelerating phase of all accelerator structures. Finally, we describe a possible use of this high-energy electron beam using our existing undulator at CSU.

While we have presented this concept before in other conference papers [2,3,4], we would like to reiterate the idea as well as add some additional information that has been accomplished since our last publication on the topic.

X-BAND POWER EXTRACTION CAVITY DESIGN

Here we choose to use a $2\pi/3$ mode TW X-band structure with parameters given in Table 1 and as computed by the design code SUPERFISH [5] (Figure 1). As we found in our earlier paper even for moderate shunt impedance the structure is relatively short as we are limited by the maximum amount of energy we can remove from the drive beam [6]. Based on our previous study the length of this cavity should be 15.4 cm in order to decelerate the beam from 6 MeV down to 1 MeV. Under such conditions the net X-band rf power that can be generated is 1.42 MW.

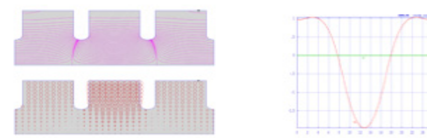

(a)

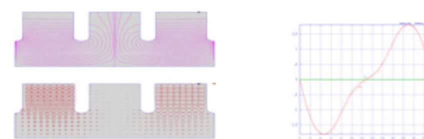

(b)

Figure 1: Electric and magnetic field patterns for $a/\lambda = 0.2$ in (a) Neumann boundary condition at end walls for $2\pi/3$mode (b) Dirichlet boundary condition at end walls for $2\pi/3$ mode

Table 1: Parameters for X-band PEC Structure

a/λ	0.2
Phase Advance per cell (ψ)	$2\pi/3$ Radian
Iris radius (a)	0.00512466 m
Cavity Radius (R)	0.0110955 m
Disk Thickness (h= $2r_1$)	0.002 m
Quality factor	6656 .15
Length	0.154 m
Frequency	11.7 GHz
Shunt impedance	57.15 MΩ

X-BAND MAIN ACCELERATING CAVITY DESIGN

The optimization for the X-band MAC design follows a different path. In this design we wish to maximize the energy gain in an optimum length and get the highest integrated potential through one or more cavities; therefore, we chose to design a new geometry, and change the phase advance from $2\pi/3$ to a higher mode, $5\pi/6$. This slows the group velocity and allows us to increase the length of the structure and provide more opportunity to increase the integrated potential [7,8,9].

Table 2 gives the resulting geometry parameters for a $5\pi/6$ phase advance MAC structure. This cavity will see a single, relatively low charge electron bunch, so the aperture requirements are not as severe as with the PEC. Further, we wish to maximize the overall integrated voltage seen by the beam during its passage. This clearly argues for high shunt impedance and as long a structure as reasonable.

Content from this work may be used under the terms of the CC BY 3.0 licence (© 2015). Any distribution of this work must maintain attribution to the author(s), title of the work, publisher, and DOI.

ISBN: 978-3-95450-168-7 doi:10.18429/JACoW-IPAC2015-WEPTY064

THERMAL-MECHANICAL ANALYSIS OF THE FRIB NUCLEAR FRAGMENT SEPARATOR DIPOLE MAGNET*

S.A. Kahn#, A. Dudas, G. Flanagan, Muons, Inc., Batavia, IL, 60510, USA
R.C. Gupta, BNL, Upton, NY 11973, USA

Abstract

Dipole magnets in the Facility for Rare Isotope Beams (FRIB) fragment separator are critical elements used to select the desired isotopes. These magnets are subjected to high radiation and heat loads. High temperature superconductors (HTS), which have been shown to be radiation resistant and can operate at 40 K where heat removal is substantially more efficient than at 4.5 K where conventional superconductors such as NbTi and Nb_3Sn operate, are proposed for the magnet coils. The magnet coils carry large currents and will be subject to large Lorentz forces that must be constrained to avoid deformations of the coils. It is desirable to minimize the use of organic materials in the fabrication of this magnet because of the radiation environment. This paper will describe an approach to support the coils to minimize coil deformation and cryogenic heat loss.

INTRODUCTION

The FRIB facility at MSU will provide intense isotope beams for physics research [1]. Large quantities of various isotopes are produced when a 400 kW linac beam hits the target. A variety of secondary nuclides with various ionic charge states is produced. Following the target are the fragmentation separator magnets which consists of three quadrupole magnets to provide focusing and two dipole magnets to select the desired nuclei. The beam enters the first dipole magnet with a spread of rigidities. The undesired nuclides are removed with a beam dump between the two dipole magnets.

To collect a sufficient sample of the rare isotopes the magnets in the fragment separator will have large apertures and strong. The radiation level in the fragment separator magnets is quite high and these magnets need to be radiation resistant. The radiation dose seen by the first quadrupole after the target is estimated to be 2.5×10^{15} neutrons/cm^2 per year [2] which corresponds to 10 kW/m of deposited power. The deposited power will drop by a factor of 10 when it reaches the bending dipole. The radiation environment influences the choice of materials used. Although NbTi and Nb_3Sn are robust conductors in radiation, they must operate at 4.5 K which is not practical, since the anticipated heat load would be difficult and costly to remove efficiently at that temperature. HTS conductors are reasonably resistant to radiation and can carry a significant current at 40 K where the heat capacity of the refrigerant is much larger and the Carnot efficiency is greater making heat removal and refrigeration easier. Also we would like to minimize the use of organic materials, both for conductor insulation and for coil support as these materials can degrade in the radiation environment.

Brookhaven National Laboratory has been involved in an R&D program to develop the quadrupole magnets for fragment separator at FRIB [3-6] using HTS conductor. The design of the fragment separator dipole magnets has relied on the technology learned from the quadrupole project. Previous articles [7-9] describing design aspects of this dipole magnet have been published.

MAGNET DESIGN

A superferric design has been chosen for this magnet where HTS coils are used to magnetize the iron which provides the desired field. The coils surround the iron poles and each coil is enclosed in its individual cryostat. Because of the large bend angle and the desire to avoid winding a coil with negative curvature the coil is wound with a "D" shape [10] with the inner section straight and the outer section curved. The coil and cryostat package is recessed behind the iron pole to protect them from direct exposure from the beam. Most of the radiation and the associated heat deposition will be deposited into the iron pole and flux return which are at room temperature and water cooled. The main source of radiation into the coils comes from neutrons that can penetrate deeply into material. It is estimated that ~700 W will be deposited into the coil cryostats [9]. The design parameters of the fragment separator magnet are shown in Table 1.

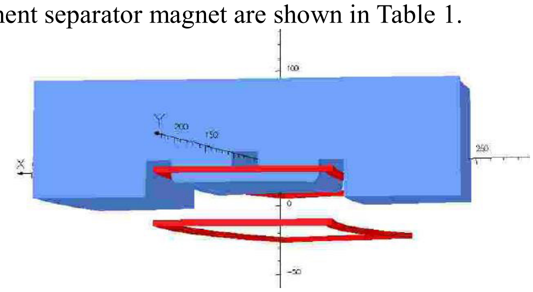

Figure 1: Model of the upper quarter of the magnet geometry.

*Work supported by US DOE grants DE-SC-0006273 and DE-AC02-98CH10886
#kahn@muonsinc.com

Content from this work may be used under the terms of the CC BY 3.0 licence (© 2015). Any distribution of this work must maintain attribution to the author(s), title of the work, publisher, and DOI.

ISBN: 978-3-95450-168-7 doi:10.18429/JACoW-IPAC2015-WEPTY065

Content from this work may be used under the terms of the CC BY 3.0 licence (© 2015). Any distribution of this work must maintain attribution to the author(s), title of the work, publisher, and DOI.

QUADRUPOLE MAGNET FOR A RAPID CYCLING SYNCHROTRON*

H. Witte†, J. S. Berg, Brookhaven National Laboratory, Upton, NY, USA

Abstract

Rapid Cycling Synchrotrons (RCS) feature interleaved warm and cold dipole magnets; the field of the warm magnets is used to modulate the average bending field depending on the particle energy. It has been shown that RCS can be an attractive option for fast acceleration of particles, for example muons which decay quickly.

In previous studies it was demonstrated that in principle warm dipole magnets can be designed which can provide the required ramp rates, which are equivalent to frequencies of about 1 kHz. To reduce the losses it is beneficial to employ two separate materials for the yoke; it was also shown that by employing an optimized excitation coil geometry the eddy current losses are acceptable.

In this paper we show that the same principles can be applied to quadrupole magnets targeting 30 T/m with a repetition rate of 1kHz and good field quality.

INTRODUCTION

A number of accelerators have been proposed recently to facilitate rapid acceleration. One application which requires extremely fast acceleration is a potential future Muon Collider; the rapid acceleration here is necessary due to the short lifetime of the particles.

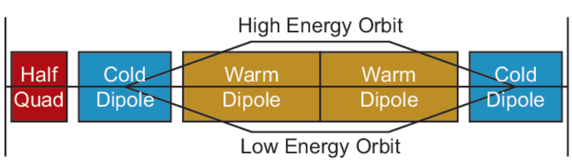

Figure 1: Rapid Cycling Synchrotron - Lattice.

Hybrid synchrotrons have been shown to be an attractive alternative to accelerate muons [1]. A hybrid synchrotron features interleaved warm and cold dipole magnets as shown in Fig. 1; the warm dipole magnets are expected to be ramped at rates equivalent to 400–1000 Hz with a repetition rate of 15 Hz in order to achieve the correct integrated bending strength for the particles.

In previous papers we have outlined solutions for those dipole magnets [2–4]; in this paper we show that the same design ideas are applicable to quadrupole magnets.

MAGNET REQUIREMENTS AND CONCEPT

The lattice requires 35 T/m quadrupole magnets, but 30 T/m are acceptable even though this increases the total installed length of the quads from 520 m to 606 m. The good field region is ±30 mm horizontally and ±12.5 mm vertically. The RCS for the muon collider requires a gradient quality of $1 \cdot 10^{-3}$ or better.

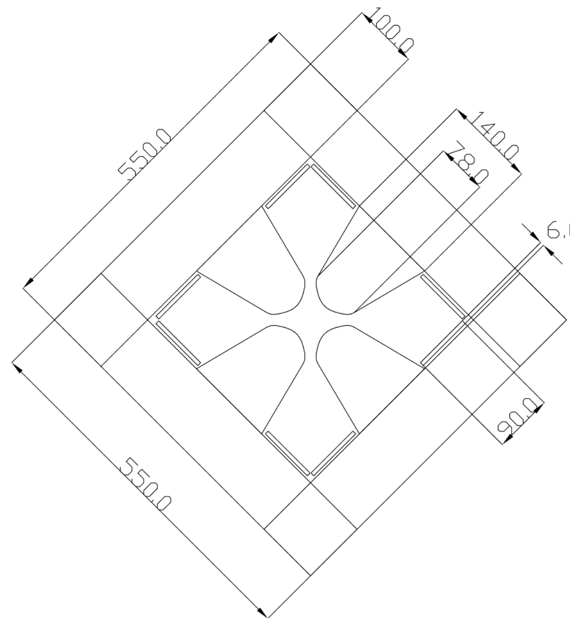

Figure 2: Magnet Geometry (all dimensions in mm).

Due to the high frequency it is of vital importance to minimize the losses in the quadrupole. In general there are two contributions:core losses in the yoke and eddy current losses in the excitation coil.

We employ two different materials for the yoke of the magnet in order to lower the overall losses. One material (3% SiFe) is used for the pole due to its higher saturation value [5]. The rest of yoke is made of 6.5% SiFe, which has very low losses at high frequencies [6]. The yoke of the magnet is assumed to be made of laminations with 100 μm (6.5% SiFe) and 127 μ (3% SiFe) thickness. In addition, the poles of the quadrupole are tapered to minimize the amount of iron at higher saturation.

To minimize the eddy current losses in the excitation coils thin current sheets are employed. Each sheet is 2 mm thick; three of these sheets (with Kapton insulation in between) are bundled together to form a bus-bar with total dimensions of 90×6 mm^2.

Figure 2 shows the geometry of the magnet; the pole shape is hyperbolic with an inscribed radius a of 30 mm ($y = a^2/2/x$).

SIMULATION RESULTS

For computer simulations we employ the commercial software package COMSOL Multiphysics[1]. 2D magnetostatic

* Work supported by Brookhaven Science Associates, LLC under Contract No. DE-AC02-98CH10886 with the U.S. Department of Energy.
† hwitte@bnl.gov

[1] COMSOL AB, Tegnergatan 23, SE-111 40 Stockholm, Sweden

ISBN: 978-3-95450-168-7 doi:10.18429/JACoW-IPAC2015-WEPTY066

T-MAPS TAKEN DURING COOL-DOWN OF AN SRF CAVITY: A TOOL TO UNDERSTAND FLUX TRAPPING

R. Eichhorn#, M. Ge, F. Furuta,
Cornell University, Ithaca, NY, 14853, USA

Abstract

During the past years a new effect has puzzled the community working in the field of superconducting RF cavities. I was found that the RF losses of the cavities are impacted by the cool-down procedures. On the flux trapping properties of superconducting cavities have been under investigation. We have measured temperature distributions of a multi-cell cavity using a T-map set-up to understand the transition to superconductivity in detail. We will report how the spatial disorder is affected by the cool-down speed and relate our findings to data on flux pinning.

INTRODUCTION

Continuous wave mode operation of future accelerators haven driven the research on achieving high quality factor SRF cavities to keep operation cost low. As the surface resistance of superconducting cavities approaches the theoretical limits parasitic effects limiting the performance came into focus of research. One interesting finding was that the quality factor of a cavity is impacted by the cool-down speed under which the cavity transits into the superconducting state.

This effect was first reported in 2011 by HZB [1]. With respect to magnetic flux pinning, they observed on samples that a slow cool-down can enable better external flux expulsion. Similar results were gained at Cornell, seeing that an initial cool-down to 4 K, followed by a thermo-cycle warming to 20 K and a slow re-cool through the critical temperature increased the quality factor significantly[2].

In contrast to this, FNAL [3] saw an increase of the quality factor of nitrogen doped cavities after a fast cool-down and claimed that – in contrast to [1]- flux expulsion is more efficient during a fast cool-down. In [4], it was proclaimed that the cool-down is more uniform during a fast cycle, which seems counter-intuitive.

As Cornell's multi-cell temperature-mapping system has unique capabilities [5], we started investigating cool-down dynamics of multi-cell cavities to get an understanding how the transition region between the normal and the superconducting state moves along the cavity.

THE EXPERIMENTAL SET-UP

The Cornell multi-cell Temperature-map system [6] has nearly two thousand thermometers, able to cover 7 cells with 11 sensors along the perimeter times 24 azimuthal angles. The temperature sensors are 100 Ω carbon Allen-Bradley resistor (5%, 1/8 W). To ensure good thermal contact, each sensor is pushed tightly against the cavity surface by a spring. APIEZON® type N grease, which has good thermal conductivity at low temperature, is applied to fill the gap between the sensors and the surface. Our data was taken on a TESLA-shape 9-cell cavity with the T-map place to cover the centre cells, shown in Figure 1.

In this paper, we only consider the T-map covered cells and define the cell numbers 1 to 7 from top to bottom. A read-out of all sensors takes about one minute when using 2^{14} samples per sensor which gives an accuracy in the temperature reading of 1.5 mK at 2 K. Usually, this system is operated at a constant bath temperature to identify heating spots and/ or quench locations of cavities. Under these conditions, calibration of the resistors is done against the Cernox sensors.

To take data during a cool-down, the system had to be modified: the sampling rate had to be reduced (to get shorter sampling times) and a careful recalibration had to be done.

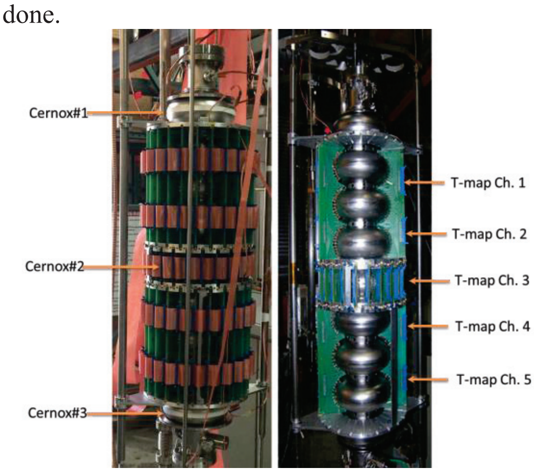

Figure 1: (Left):The multi-cell temperature-mapping system mounted on a TESLA-shape 9-cell SRF cavity. (Right): Several T-map boards have been removed to expose the cavity.

CALIBRATION

Cornell's T-map data acquisition system usually measures the resistance of each sensor which is converted into a temperature using calibration data. During calibration, the ambient temperature surrounding the T-map resistors, measured with calibrated cernox sensors mounted on the equator of top, middle, and bottom cell, is varied and the resistance curve of each T-map sensor is taken and calibrated against the nearest cernox sensor. For Our measurement, the calibration was performed during a slow warm-up, going from 4.2 K to 50 K in about 3 hours. The maximum temperature gradient along the cavity was 0.2 K.

---
r.eichhorn@cornell.edu

Content from this work may be used under the terms of the CC BY 3.0 licence (© 2015). Any distribution of this work must maintain attribution to the author(s), title of the work, publisher, and DOI.

ISBN: 978-3-95450-168-7 doi:10.18429/JACoW-IPAC2015-WEPTY067

Content from this work may be used under the terms of the CC BY 3.0 licence (© 2015). Any distribution of this work must maintain attribution to the author(s), title of the work, publisher, and DOI.

THERMAL AND MECHANICAL ANALYSIS OF A WAVEGUIDE TO COAX SYMMETRIC COUPLER FOR SUPERCONDUCTING CAVITIES

R. Eichhorn *, J. Robbins and V. Veshcherevich
CLASSE Cornell University, Ithaca, NY 14853, USA

Abstract

As kicks from fundamental power couplers become a concern for low emittance future accelerators, a design of a symmetric coupler for superconducting accelerating cavities has been started. In this coupler, a rectangular waveguide transforms into a coaxial line inside the beam pipe to feed the cavity. So far the RF design revealed an extremely low transversal kick but concerns about cooling and the thermal stability of the coaxial transition line remained. This contribution addresses this. We calculated the heat, heat transfer and thermal stability of this coupler and evaluated the risk of quenching due to particle losses on the coupler.

INTRODUCTION

The low energy section of a superconducting linac can significantly contribute to the emittance increase of the accelerated beam. One component of that can be asymmetric fields coming from the fundamental power coupler. Usually, power couplers are antenna type couplers attached to a side port of the beam pipe near the cavity, usually placed on one side, generating a strong dipole kick. With a symmetric arrangement like in the Cornell injector one can avoid emittance increase due to the dipole kicks. However, quadrupole kicks remain, which guided us in designing a waveguide-to-coaxial type coupler resulting in super-symmetric fields [1]. In this paper, we will complement our earlier findings with investigations on the thermal stability of the coupler under different conditions and report on mechanical properties.

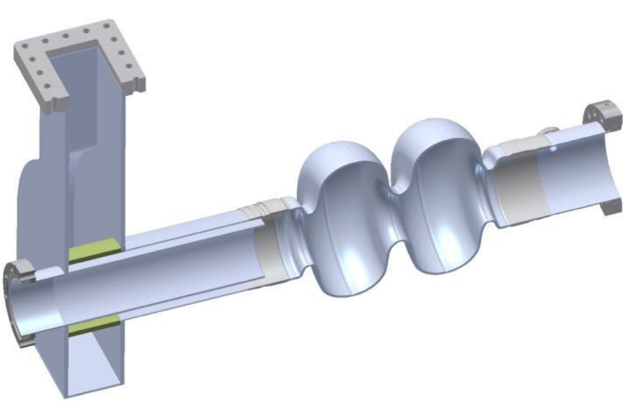

Figure 1: Cornell ERL injector cavity with symmetric coupler taken from [1]

* r.eichhorn@cornell.edu

Table 1: Parameters for Theoretical Thermal Conductivity Model Taken From [2]

param.	value	definition
RRR	400	resid. res. ratio
ρ_{295K}	$14.5 \times 10^{-8}\ \Omega m$	res. at $295K$
l	$50\ \mu m$	Nb. phonon mfp
T_c	9.2 K	Nb. crit. temp.
L	$2.45 \times 10^{-8}\ WK^{-2}$	param. of Eq. 1
a	$2.30 \times 10^{-5}\ mW^{-1}K^{-1}$	param. of Eq. 1
B	$7.0 \times 10^{3}\ Wm^{-2}K^{-4}$	param. of Eq. 1
$\frac{1}{D}$	$300\ mK^{-3}W^{-1}$	param. of Eq. 1
α	1.76	param. of Eq. 1

THERMAL ANALYSIS

Niobium Parameters

The thermal conductivity values that we used in our simulations were taken from a combination of theoretical models and experimental data. The theoretical model that we used was the thermal conductivity equation given by [2].

$$K_s(T) = \frac{K_{es}}{K_{en}}\left(\frac{\rho_{295K}}{L \cdot RRR \cdot T} + aT^2\right)^{-1} + \left(\frac{1}{D\, e^{\frac{\alpha T_c}{T}}\, T^2} + \frac{1}{B\, l T^3}\right)^{-1} \quad (1)$$

$K_{es}/K_{en}(T)$ is the ratio of superconducting to normal-conducting electron contributions to thermal conductivity. Constant parameters are given in Table 1. This model is valid for $T < 5.8$ K. For temperatures above 5.8 K, an experimental data set was used [3].

The specific heat of the niobium cylinder was assumed to follow the Debye model $C_v = \gamma T + AT^3$. Using experimental data from [4], values for the parameters were calculated as $\gamma = 0.0946 \frac{J}{kg\,K^2}$ and $A = 1.28 \times 10^{-3} \frac{J}{kg\,K^4}$ (for $T > T_c$) and $\gamma = 0$ and $A = 5.01 \times 10^{-3} \frac{J}{kg\,K^4}$ for $T < T_c$.

Analysis

Thermal calculations were performed using the transient thermal analysis system in ANSYS®. The front face of the cylinder was fixed at 2 K, assumed being perfectly cooled by the helium. To model the power deposition from the electron beam halo hitting the niobium surface, a heat flux of 0.5 W was applied to the rear face of the cylinder, which would be the worst case scenario.

Due to the RF field, there is additional heating along the cylinder surfaces which follows the equation

$$\frac{dP}{dA} = \frac{1}{2} R_s |\mathbf{H}|^2 \quad (2)$$

ISBN: 978-3-95450-168-7 doi:10.18429/JACoW-IPAC2015-WEPTY068

ASYMMETRIC THERMO-CURRENTS DIMINISHING SRF CAVITY PERFORMANCE

R. Eichhorn#, J, May-Mann
Cornell Laboratory for Accelerator-Based Sciences and Education, Ithaca, NY 14853-5001, USA

Abstract

Over the past years it became evident that the quality factor of a superconducting cavity is not only determined by its surface preparation procedure, but is also influenced by the way the cavity is cooled down. In this paper we will present results from numerical field calculations of magnetic fields produced by thermo-currents, driven by temperature gradients and material transitions. We will show how they can impact the quality factor of a cavity by producing a magnetic field at the RF surface of the cavity.

INTRODUCTION

The need to reduce the cost of the cryogenic infrastructure for future CW accelerators has driven the research on achieving high quality factor superconducting cavities. As a result, state of the art treated cavities display surface resistance approaches the theoretical limits. This allowed a deeper insight into the physics of parasitic effects, as they now become a prominent factor in limiting the performance of SRF cavities. One interesting finding, reproduced in different labs was that the quality factor of a cavity is impacted by the details of the cool-down procedure [1-3].

As of now, there seem to be two contributions resulting in the cool-down dependency of the cavity performance. One is flux pinning, the other is thermo-current.

Flux pinning describes the effect that a residual magnetic field is not fully expelled as the cavity becomes superconducting, resulting in an only partial Meissner effect. The trapped flux then concentrates in vortices which stay normal conducting and as a result, increases the losses of the cavity, denoted by a drop in the quality factor.

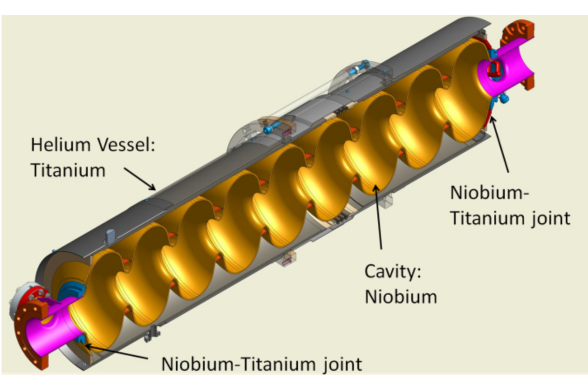

Figure 1: A superconducting cavity, welded into its helium vessel (dressed cavity).

#r.eichhorn@cornell.edu

Thermo-currents on the other hand have no direct effect. They are a result of the Seebeck effect that exist if material joints are held at different temperatures. As shown in fig.1, a superconducting cavity, welded into its helium vessel, is essentially a Seebeck current loop. As of their nature, thermo-currents generate a magnetic field-which then may be pinned during cool-down. In the past, an analytical analysis argued that the axial symmetry of SRF cavities leads to no (or when considering the potential asymmetry from vessel or cavity port: negligible small) thermo-electric induced magnetic fields in the relevant RF penetration layer at the inner cavity surface [4]. The author concluded that thermo-electric currents are not a concern for the performance of SRF cavities. However, our findings indicated early-on [5] that thermo-electric currents may have a more severe impact on the SRF performance as so far predicted [6].

SEEBECK EFFECT

Thermo-currents are the result of the Seebeck-effect, which is well known in physics for more than a century: Discovered in 1826, Seebeck found that a current will flow in a closed circuit made of two dissimilar metals when the two junctions are maintained at different temperatures. The voltage is dependent on the material, leading to the definition of the Seebeck coefficient *S*:

$$\Delta U = S \cdot \Delta T\,. \tag{1}$$

Seebeck coefficients of metals can have either sign as they are defined relative to platinum. In a single metal arrangement, this voltage exists across the metal but does not result in a current flowing other than simply building up the charges, initially. If there is a material transition, where two different metals are joined, not only does a potential difference exist, there might also be a persistent current, driven by the temperature difference, if the loop is closed. As superconducting cavities are made out of niobium while the helium vessel enclosing them is typically titanium this effect is relevant for accelerator physics: During the cool-down of a dressed cavity (a cavity welded into its helium vessel) it is easy to imagine that both ends of the cavity (where the Nb-Ti transition is located) have different temperatures. Seebeck coefficients are temperature dependent, as given in tab. 1 for niobium and titanium. With the more general definition of the Seebeck coefficient, the thermo-voltage becomes

$$U_{th} = \int_{T_1}^{T_2} \left(S_{Nb}(T) - S_{Ti}(T) \right) dT \tag{2}$$

Content from this work may be used under the terms of the CC BY 3.0 licence (© 2015). Any distribution of this work must maintain attribution to the author(s), title of the work, publisher, and DOI.

ISBN: 978-3-95450-168-7 doi:10.18429/JACoW-IPAC2015-WEPTY069

COMPLECTION OF THE CORNELL HIGH Q CW FULL LINAC CRYO-MODULE

R. Eichhorn#, F. Furuta, Y. He, G. Hoffstaetter, T. O'Connell, P. Quigley, D. Sabol, J. Sears, E. Smith, M. Liepe, B. Bullock, B. Elmore, J. Kaufman, J. Conway, V. Veshcherevich
Cornell Laboratory for Accelerator-Based Sciences and Education, Cornell University
Ithaca, NY 14853-5001, USA

Content from this work may be used under the terms of the CC BY 3.0 licence (© 2015). Any distribution of this work must maintain attribution to the author(s), title of the work, publisher, and DOI.

Abstract

Cornell University has finished building a 10 m long superconducting accelerator module as a prototype of the main linac of a proposed ERL facility. This module houses 6 superconducting cavities- operated at 1.8 K in continuous wave (CW) mode - with individual HOM absorbers and one magnet/ BPM section. In pushing the limits, a high quality factor of the cavities ($2 \bullet 10^{10}$) and high beam currents (100 mA accelerated plus 100 mA decelerated) were targeted. We will review the design shortly and present the results of the components tested before the assembly. This includes data of the quality-factors of all 6 cavities that we produced and treated in-house, the HOM absorber performance measured with beam on a test set-up lessons learned during assembly.

INTRODUCTION

Energy-Recovery Linacs (ERLs) can provide beams with high currents, small emittances, and low energy spread. The current can be as large as typically in rings, 100mA in the case of Cornell's x-ray ERL, while the emittances and the energy spread can stay as small as only possible in linacs. While the current limit for conventional linacs is determined by the available acceleration power, ERLs recapture the energy of the spent beam and the current then becomes limited by other effects like higher order mode (HOM) heating and beam-break up (BBU). Cornell University has started an extensive R&D program to address these questions and proposed an ERL as a driver for hard x-ray sources [1].

One part of that R&D program was building a linac cryo-module, based on 1.3 GHz cavities, optimized for a high BBU-limit and good HOM damping, with extraordinary high quality factors to reduce operating cost. This module, show in Fig.1, has been completed recently which allows us to highlight our findings within this paper.

CRYOMODULE CONCEPT

The Main Linac Cryomodule (MLC) prototype houses six superconducting 7-cell cavities and has an overall length of 10 m. The design has been guided by the ILC Cryomodule while necessary modifications have been made to allow CW operation. In addition, we decided to align all components inside the module by reference surfaces on the helium gas return pipe (HGRP). As a consequence, the cold-mass as a whole will shrink during cool-down, requiring the power couplers to flex.

#r.eichhorn@cornell.edu

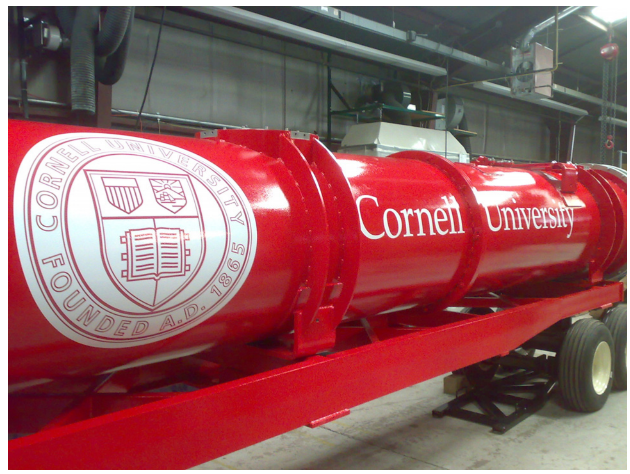

Figure 1: Cornell's Main linac cryo-module.

Due to the high beam current combined with the short bunch operation a careful control and efficient damping of the HOMs is essential, leading to the installation of dampers next to each cavity. There are more comprehensive details on the design in [2-5].

CAVITY PRODUCTION AND RESULTS

For the cavities, a 7-cells, 1.3 GHz design was made while an envisaged Q of $2x10^{10}$ was targeted at a gradient of 16 MV/m. All 6 cavities for the MLC module have been produced in-house starting from flat metal niobium sheets. To investigate microphonics, we decided to build 3 unstiffened cavities as well as 3 cavities with stiffening rings. All cavities were tested vertically, the summary of these test are given in Fig. 2. All six cavities exceeded the design quality factor, averaging to $2.9*10^{10}$ at 1.8K. At 2 K, the average Q was $1.8*10^{10}$, at 1.6 K we found $4.3*10^{10}$[6]. It should be noted that the Q we measured on the prototype cavity at 1.8 K was $2.5 *10^{10}$ in the vertical test, but $6*10^{10}$ in the horizontal test where magnetic shielding is more efficient [7].

The reproducibility of the Q versus E curves for all cavities is remarkable, also the fact that none of the cavities needed additional processing- giving a 100 % yield.

ISBN: 978-3-95450-168-7 doi:10.18429/JACoW-IPAC2015-WEPTY071

TIME RESOLVED CRYOGENIC COOLING ANALYSIS OF THE CORNELL INJECTOR CRYOMODULE

R. Eichhorn#, S. Markham, E. Smith, P. Quigley
Cornell Laboratory for Accelerator-Based Sciences and Education, Cornell University
Ithaca, NY 14853-5001, USA

Abstract

Managing parallel cryogenic flows has become a key challenge in designing efficient and smart cryo-modules for particle accelerators. In analyzing the heating dynamics of the Cornell high current injector module a power-full computational tool has been set-up allowing time resolved analysis and optimization. We will describe the computational methods and data sets we have used, report the results and compare them to measured data from the module being in good agreement. Mitigation strategies developed on basis of this model have helped pushing the operational limitations..

INTRODUCTION

In preparation for full ERL at Cornell [1], an injector cryomodule was designed and built to demonstrate high current generation and achieving low emittances. The construction of the Cornell injector was completed in the summer of 2007 when initial beam commissioning experiments revealed an issue with charging up of one set of ferrites in the higher-order mode (HOM) absorbers. After a rebuilt taking out the troublesome material, commissioning resumed leading to a world record performance in achieving 75 mA beam current [2]. However, the goal set for the ERL was 100 mA and in pushing for that we realized that heating of the 80 K thermal intercept of the power couplers is the limitation. As beam power ramps up, RF power transmitted by the coupler increases. Even though the couplers are designed for 60 kW we observe a significant heating which at the level of around 40-50 kW leads to temperatures around 140 K at an intercept which should be hold cold at 80 K.

Even though the heating itself is not an issue, the increase in vacuum pressure in the coupler leads to breakdowns- eventually limiting us in increasing the beam current. A careful analysis of the insufficient cooling of the 80 K intercept of the coupler revealed an adequate sizing of the heat exchanger but a deficient mass flow through the cooling channel, which happened to be a parallel flow to the cooling of the higher order mode absorbers. This cryogenic flow diagram is symbolized in fig.1.

Having parallel cooling flows is one of the key concepts to be used in designing highly cryogenically efficient accelerator modules, and we have investigated the stability of parallel flows under variations of operating parameters in the past [3]. In this paper, we describe the iterative numerical method we used to investigate and understand the transient heating issue and find a solutions which finally helped us to resolve the problem: We found that by adding a high impedance inlet pipe to each of the HOMs, we can reduce the flow rate of the whole system by 50%, while both improving the stability of the flow and reducing the operating equilibrium temperature of the couplers.

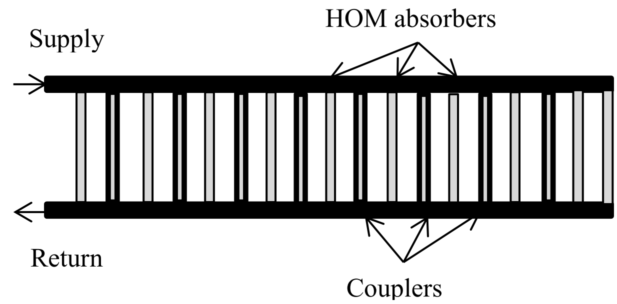

Figure 1: The 80 K cryogenic cooling piping: The thermal intercept of the ten coupler and the 12 channels to cool the higher order mode absorbers a fed in parallel.

METHOD

ICM Setup and Model Specifications

The focus of this paper is to outline the setup and results to a computational simulation intended to understand time dependent heating an their impact in diverting mas flows in parallel cooling channels. This paper focuses specifically on the HOM and coupler 80 K parallel flow channels of the injector cryo module (ICM) but our method is more general and can be applied to other scenarios, too.

In the ICM, the cooling helium is supplied at 80K. The fluid undergoes heat transfer as well as pressure drop as it flows across the couplers or the HOMs from the supply to the return pipe. Each of the HOM absorbers are represented in fig. 1 by thinly outlined channels, while the couplers are represented with thicker outlines. Because each coupler and HOM is geometrically identical, and as there is negligible head loss in the supply and return manifolds we can model this cryogenic system as a two pipe parallel system, shown in fig 2.

Accommodating this simplification, the total mass flow has to be calculated as $\dot{m_{tot}} = 10\, \dot{m_{coupler}} + 12\, \dot{m_{HOM}}$. To conduct the calculation, the following geometrical data describing the cooling piping was used: In the ICM,

#r.eichhorn@cornell.edu

Content from this work may be used under the terms of the CC BY 3.0 licence (© 2015). Any distribution of this work must maintain attribution to the author(s), title of the work, publisher, and DOI.

ISBN: 978-3-95450-168-7 doi:10.18429/JACoW-IPAC2015-WEPTY072
Content from this work may be used under the terms of the CC BY 3.0 licence (© 2015). Any distribution of this work must maintain attribution to the author(s), title of the work, publisher, and DOI.

UPDATE ON NITROGEN-DOPED 9-CELL CAVITY PERFORMANCE IN THE CORNELL HORIZONTAL TEST CRYOMODULE*

D. Gonnella†[1], R. Eichhorn[1], F. Furuta[1], M. Ge[1], A. Grassellino[2], C. Grimm[2], D. Hall[1], Y. He[1], V. Ho[1], G. Hoffstaetter[1], M. Liepe[1], J.T. Maniscalco[1], O. Melnychuk[2], T. O'Connell[1], S. Posen[2], P. Quigley[1], A. Romanenko[2], J. Sears[1], and V. Veshcherevich[1]

[1]CLASSE, Cornell University, Ithaca, NY 14853, USA
[2]FNAL, Batavia, IL 60510, USA

Abstract

The Linac Coherent Light Source-II (LCLS-II) is a new x-ray source that is planned to be constructed in the existing SLAC tunnel. To meet the quality factor specifications (2.7×10^{10} at 2.0 K and 16 MV/m), nitrogen-doping has been proposed as a preparation method for the SRF cavities. In order to demonstrate the feasibility of these goals, four 9-cell cavity tests have been completed in the Cornell Horizontal Test Cryomodule (HTC), which serves as a test bench for the full LCLS-II cryomodule. Here we report on the most recent two cavity tests in the HTC: one cavity nitrogen-doped at Cornell and tested with high Q input coupler and then again tested with high power LCLS-II input coupler. Transition to test in horizontal cryomodule resulted in no degradation in Q_0 from vertical test. Additionally, increased dissipated power due to the high power input coupler was small and in good agreement with simulations. These results represent a crucial step on the way to demonstrating technical readiness for LCLS-II.

INTRODUCTION

The Linac Coherent Light Source-II (LCLS-II) Project will construct a 4 GeV CW superconducting linac in the first kilometer of the existing SLAC tunnel [1]. In order to maximize cryogenic efficiency of the linac and ensure economic feasibility, the superconducting RF (SRF) cavities must reach an intrinsic quality factor (Q_0) of 2.7×10^{10} at 2.0 K and 16 MV/m. To meet this high Q_0, nitrogen-doping [2] of the SRF cavities has been proposed. Cornell has recently recommissioned the Horizontal Test Cryomodule (HTC) [3] to hold a 9-cell ILC shaped cavity. As part of the LCLS-II R& D program, four 9-cell tests have been completed so far in the HTC. The first two (using ILC helium tanks) were discussed thoroughly in [4]. This paper will focus on the most recent cavity and compare its performance vertically and un-dressed, vertically and dressed (in LCLS-II helium tank), horizontally with high Q input coupler, and horizontally with high power input coupler.

EXPERIMENTAL METHOD

The Cornell HTC is a full cryomodule that can hold one 9-cell ILC shaped cavity, see Fig. 1. It was designed as

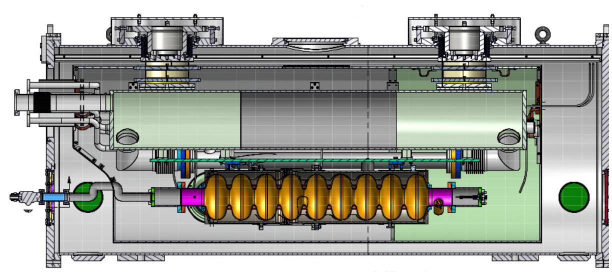

Figure 1: A schematic of a 9-cell cavity in the HTC.

a prototype to test SRF cavities under realistic cryomodule conditions. The cryomodule design is very similar to the LCLS-II cryomodule that will be used in the full machine. Ambient magnetic fields in the HTC are less than 5 mG. A 9-cell cavity (TB9AES018) was prepared with nitrogen-doping at Cornell. This consisted of a bulk vertical electropolish (VEP) of 120 μm, heat treatment in vacuum at 800°C for three hours, heat treatment in 60 mTorr of nitrogen gas for 20 minutes at 800°C, an annealing stage in vacuum at 800°C for 30 minutes, and finally an additional 24 μm VEP. It was then welded into a prototype LCLS-II helium tank at FNAL. The dressed cavity was assembled into the HTC with a high Q input coupler ($Q_{ext}\approx 3\times 10^{10}$). The cavity was also surrounded by a solenoid in order to induce a uniform external magnetic field parallel to the cavity axis for the purposes of studying cavity Q_0 sensitivity to ambient magnetic fields. A total of 13 cool downs were completed with various cool down rates, spatial temperature gradients, and applied external magnetic fields. After the first cool down, Q_0 vs E_{acc} was measured at different temperatures between 1.6 and 2.0 K in order to extract R_{BCS} vs. field (details of the method used to extract material properties are discussed in [5]). For each subsequent cool down, Q_0 vs E_{acc} was measured at 2.0 and 1.6 K. From this data, we were able to extract residual resistance and evaluate its dependence on cool down gradient and applied magnetic field. This test of TB9AES018 with high Q input coupler will be referred to as HTC9-3.

Following the HTC9-3 test, the cavity was removed from the HTC and an LCLS-II high power input coupler was installed [6] before re-assembly in the HTC. This test will be referred to as HTC9-4. This coupler has an adjustable

* Work supported by the US DOE and the LCLS-II High Q0 Program
† dg433@cornell.edu

ISBN: 978-3-95450-168-7 doi:10.18429/JACoW-IPAC2015-WEPTY073

Content from this work may be used under the terms of the CC BY 3.0 licence (© 2015). Any distribution of this work must maintain attribution to the author(s), title of the work, publisher, and DOI.

UPDATE ON NITROGEN-DOPING: QUENCH STUDIES AND SAMPLE ANALYSIS*

D. Gonnella†, F. Furata, M. Ge, J. Kaufman, M. Liepe, J. Maniscalco
CLASSE, Cornell University, Ithaca, NY 14853, USA

Abstract

Recently, nitrogen-doping of niobium has emerged as a promising preparation method for SRF cavities to reach higher intrinsic quality factors than can be reached with typical cavity preparation. Nitrogen-doped cavities prepared at Cornell have shown quality factors higher than 4×10^{10} at 2.0 K and 16 MV/m. While Q results have been very exciting, a reduced quench field currently limits nitrogen-doped cavities with quench typically occurring between 15 and 25 MV/m. Here we report on recent results from Cornell on single-cell and 9-cell cavities, focusing on new preparations and maximum and critical fields. First we discuss results from over-doping niobium with nitrgoen, baking nitrogen-doped cavities at 120°C, and doping with Argon. For a subset of these cavities we show results from quench studies that have been completed using temperature mapping. Finally, we present the first measurements of the higher critical field, H_{c2}, for nitrogen-doped niobium samples.

INTRODUCTION

Nitrogen-doping has been shown to increase the intrinsic quality factor, Q_0, of niobium SRF cavities to levels previously unreachable. Doping consists of giving cavities a heat treatment at high temperatures in a gaseous atmosphere [1]. An ongoing effort has been undertaken at Cornell, Jefferson Lab, and Fermilab to understand the benefits of nitrogen-doping and to create an optimal recipe for cavity preparation. Unfortunately, many cavities prepared with nitrogen-doping have shown a lower quench field than cavities prepared by other means. Cornell has recently been focusing on studying the cause of this lower quench field by systematically preparing cavities by different methods. Furthermore, we have employed the use of both single and 9-cell temperature mapping systems for quench detection along with OSTs. We have also measured the higher critical field, H_{c2} of nitrogen-doped niobium samples using Physical Property Measurement System (PPMS). Additionally, we have continued studying different preparation techniques such as doping with argon instead of nitrogen and subjecting a nitrogen-doped cavity to a 48 hours 120°C bake. These latest measurements push us closer to understanding the mechanisms behind higher Q_0's, lower quench fields, and other unique properties of nitrogen-doped cavities.

* Work supported by the US DOE and the LCLS-II High Q0 Program and NSF Grants NSF-PHY-1305500 and NSF-PHY-1416318. This work made use of the Cornell Center for Materials Research Shared Facilities which are supported through the NSF MRSEC program (DMR-1120296).
† dg433@cornell.edu

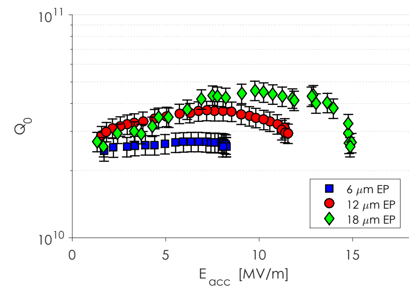

Figure 1: 2.0 K Q_0 vs E_{acc} performance for the over-doped cavity. Quench field increases with more material removal.

SINGLE-CELL STUDIES

Over-Doping

A single-cell 1.3 GHz ILC shaped cavity was given an "overdoping" of nitrogen. This consisted of a bulk electropolish (EP), followed by a heat treatment in vacuum at 900° for 3 hours, followed by 900°C heat treatment in 60 mTorr of nitrogen gas for 20 minutes, followed by an additional 900°C heat treatment in vacuum for 30 minutes. Finally, the cavity was given a series of 3 additional EPs in steps of 6 μm with tests in between. Typically, cavities have been treated at 800°C [1, 2]. By increasing the temperature by 100°C, we saw an increase in nitrogen uptake of ∼ 1.75× that for previous cavities. The 2.0 K Q_0 vs E_{acc} results are shown in Fig. 1. We can see that initially (after 6 μm EP), the cavity quenched at 8.3 MV/m with a maximum Q_0 of 2.7×10^{10}. After an additional 6 μm EP (total of 12 μm) the quench field increases to 11.5 MV/m with a maximum Q_0 of 3.7×10^{10}. Finally, after another additional 6 μm (total of 18 μm), the quench field increases to 15 MV/m with a maximum Q_0 of 4.6×10^{10}.

The increase in Q_0 with additional material removal is fairly well understood. Nitrogen-doping has been shown to optimize the BCS material properties and thus minimize the BCS resistance of SRF cavities [3]. By removing more material, we are reaching a more optimial place on the BCS curve. Nitrogen-doping has also been shown to form a lossy nitride layer on the surface. It is possible that this layer (which is now significantly thicker due to the higher temperature doping) causes the quench field to be even lower in this cavity than in previous cavities. This is consistent with the quench field increasing as more material is removed. A discussion of the quench location will be presented in a later section.

ISBN: 978-3-95450-168-7 doi:10.18429/JACoW-IPAC2015-WEPTY074

RECENT STUDIES ON THE CURRENT LIMITATIONS OF STATE-OF-THE-ART Nb_3Sn CAVITIES*

D.L. Hall†, M. Liepe, J.T. Maniscalco, S. Posen‡
Cornell Laboratory for Accelerator-Based Sciences and Education (CLASSE), Ithaca, NY 14853, USA
T. Proslier
Argonne National Laboratory, Argonne, Illinois 60439, USA

Abstract

Recent advances in the study of Nb_3Sn at Cornell University have yielded single-cell cavities that show excellent performance without the limiting Q-slope seen in previous work. This performance has been shown to be repeatable across multiple cavities. However, they are still limited by a quench field of approximately 16 MV/m, as well as residual resistance. In this work we present results quantifying the impact of ambient magnetic fields on Nb_3Sn cavities, as well as discuss the impact of cavity cooldown procedures on cavity performance. Finally, we will briefly discuss XRD results that shed light on the composition of the Nb_3Sn layer and how this relates to the current limits of these cavities.

INTRODUCTION

Studies on the fabrication and use of Nb_3Sn in superconducting radio-frequency (SRF) cavities at Cornell University have recently made considerable progress in developing Nb_3Sn as an alternative to niobium [1–4]. In this work we present results from the most recent work on Nb_3Sn at Cornell, with particular emphasis on measurements to determine the impact of ambient magnetic fields on the residual resistance of Nb_3Sn cavities. We also present data from two different cavity tests that demonstrate the impact that the procedure used to cool the cavity below its superconducting transition temperature has upon the cavity's performance. These measurements are critical in predicting how a Nb_3Sn cavity will behave when placed inside a cryomodule assembly, and what, if any, modifications will need to be made to accommodate it. Finally, we will briefly describe other recent measurements that have been made to determine both the fundamental properties and material parameters of Nb_3Sn fabricated at Cornell University using the vapour deposition method.

EXPERIMENTAL PROCEDURE

Cooldown Procedure

It is critical that niobium cavities coated with Nb_3Sn be cooled slowly through the transition temperature T_c of 18 K down to below 6 K to minimise the effects of magnetic fields generated by electric currents induced from thermal gradients. The method used to cool the cavities below their transition temperature is more completely described in Ref. [1], although a condensed version will be surmised here: the cavity is mounted upon an insert that is placed into a magnetically shielded cryostat, whereupon liquid helium is passed at a low flow rate through an injection port that is lined with heating elements, warming the incoming helium and thus allowing fine control of the temperature inside the cryostat. As the power of the heating elements is slowly reduced, the rate of the temperature decrease inside the cryostat is carefully controlled to ensure a minimal impact from thermal currents. This control system allows a rate control of between 2-30 min/K, with spatial gradients across the cavity of < 50-1000 mK (the latter being dependent upon the rate with time).

Flux Trapping Measurements

The method used to quantify the impact of external DC magnetic fields has been used in previous studies to investigate both standard niobium cavities as well as niobium cavities that have been doped with nitrogen [5]. Two solenoid coils are placed above and below the cavity in a Helmholtz configuration, to generate a magnetic field parallel to the cavity axis. Two flux gate magnetometers are placed on the cavity, one placed on the upper iris in parallel with the cavity z-axis (considering a cylindrical coordinate system in which the z-axis is placed along the path of the beam through the cavity), and one placed next to the previous pointing in the $\hat{\phi}$ direction. These are used to measure the field that is applied by use of the solenoids. As the cavity passes into the superconducting state and a fraction of the magnetic flux is expelled from the bulk of the cavity, these measurements are used to determine the amount of magnetic flux that has been trapped. A subsequent measurement of the cavity quality factor Q as a function of both temperature T and accelerating gradient E_{acc} is then used to quantify the impact of the externally applied magnetic field on residual surface resistance and its field dependence.

XRD and Phase Determination

XRD measurements were carried out at the APS at Argonne National Lab on Nb_3Sn samples fabricated at Cornell. The XRD provides a diffraction pattern from a region of spatial extent of approximately 1 mm wide and deep. The diffraction spectrum is used to determine the lattice parameter of the Nb_3Sn crystals, which is in turn used to infer

* This work is supported by NSF grants PHY-1305500 and PHY-14116318, and DOE grant ER41802
† dlh269@cornell.edu
‡ Now at Fermi National Laboratory

Content from this work may be used under the terms of the CC BY 3.0 licence (© 2015). Any distribution of this work must maintain attribution to the author(s), title of the work, publisher, and DOI.

ISBN: 978-3-95450-168-7 doi:10.18429/JACoW-IPAC2015-WEPTY075

H_{c2} MEASUREMENTS OF Nb_3Sn AND NITROGEN-DOPED NIOBIUM USING PHYSICAL PROPERTY MEASUREMENT SYSTEM*†

J. T. Maniscalco‡, D. Gonnella, D. L. Hall, M. Liepe, and S. Posen
CLASSE, Cornell University, Ithaca, NY, 14853, USA

Abstract

The measurement of the upper critical field of a type-II superconductor, H_{c2}, is an important step in determining its superconducting properties, and therefore its suitability as a material in SRF cavities. However, measuring H_{c2} directly can be challenging, as performing electrical measurements causes changes in the very properties one seeks to measure. We present a method for extracting H_{c2} from resistivity measurements made near the transition temperature for varied applied fields and excitation currents. We also present first results of these measurements made on Nb_3Sn and nitrogen-doped niobium.

INTRODUCTION

In the field of superconducting radio frequency (SRF) accelerators, niobium has had a long and successful career as the fabrication material of choice. However, as accelerator demands increase, the field is behooved to find new materials with improved qualities. One promising type of new material is surface-treated niobium, *i.e.* bulk niobium with a thin layer of a different material on the RF-active surface. In this paper we investigate the properties of two such materials, namely Nb_3Sn and nitrogen-doped niobium; we develop a method for finding the upper critical field of a material, from which one can calculate many other figures of merit, including the coherence length ξ and the mean free path ℓ.

The upper critical field H_{c2} of a type-II superconductor is the minimum magnetic field at which the material cannot superconduct, regardless of temperature. This field is very difficult to observe directly, as it requires holding the temperature of the sample at absolute zero while measurements are made. Instead, it must be extrapolated from measurements of the superconducting transition at higher temperatures.

The Physical Property Measurement System (PPMS, Quantum Design) and machines like it allow the researcher to perform low-temperature electrical and magnetic measurements with direct control over the temperature and applied magnetic field at the sample. Using such a machine, we can set a magnetic field and measure the resistivity of a sample of the material of interest, for a chosen magnetic field and temperature, with a lower bound of 1.9 K for the temperature and an upper bound of 9 T for the field.

* Funding provided by NSF grants PHY-1305500 and PHY-1416318.
† This work made use of the Cornell Center for Materials Research Shared Facilities which are supported through the NSF MRSEC program (DMR-1120296).
‡ jtm288@cornell.edu

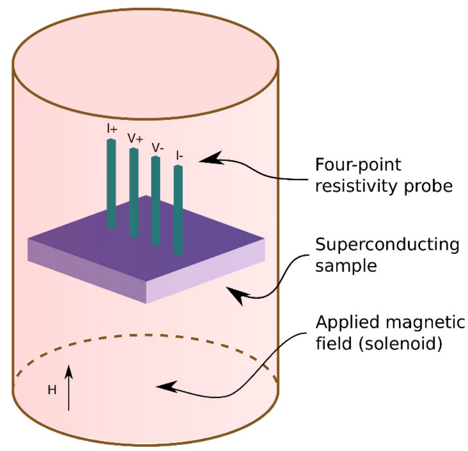

Figure 1: Schematic of testing environment inside PPMS. Spring-loaded press contacts act as a four-point resistivity probe on the surface of the superconducting material. The apparatus sits inside a solenoid, which applies an external magnetic field.

METHOD

At a given applied magnetic field strength, a superconductor will transition to its normal-conducting state at some temperature T. We can invert this function to get $H_{c2}(T)$, the magnetic field where, for a given temperature, the material makes its phase transition. Given a set of measurements of transitions with values of T and $H_{c2}(T)$, we can extrapolate the upper critical field $H_{c2} = H_{c2}(0)$ and the critical temperature T_c using Eq. 1 [1][1]:

$$H_{c2}(0) = H_{c2}(T)\left[1 - \left(\frac{T}{T_c(0)}\right)^2\right]^{-1} \tag{1}$$

In order to perform these measurements, we use the PPMS to perform four-point resistivity measurements on the sample at fixed magnetic fields and varying temperature. For these measurements, four needles are pressed against the surface of the sample and a 17 Hz AC signal is applied between the first and fourth pins for a short time. While the current is being applied, the voltage across the two center pins is measured, and the PPMS calculates and records the resistivity. Figure 1 shows the typical experimental setup. In the superconducting

[1] This dependence is approximate, see for example [2]

Content from this work may be used under the terms of the CC BY 3.0 licence (© 2015). Any distribution of this work must maintain attribution to the author(s), title of the work, publisher, and DOI.

ISBN: 978-3-95450-168-7 doi:10.18429/JACoW-IPAC2015-WEPTY076

RF PERFORMANCE STUDIES OF THIN-FILM SUPERCONDUCTORS USING A SAMPLE HOST CAVITY *

J. T. Maniscalco†, D. L. Hall, M. Liepe
CLASSE, Cornell University, Ithaca, NY, 14853, USA

Content from this work may be used under the terms of the CC BY 3.0 licence (© 2015). Any distribution of this work must maintain attribution to the author(s), title of the work, publisher, and DOI.

Abstract

Thin-film superconductors have the potential for reducing cost and for improved SRF performance over traditional bulk niobium superconducting cavities. Materials such as Nb3Sn, multilayer NbN/MgO, and thin-film Nb are currently under investigation for cost reduction or possible improvements in RF losses and accelerating gradients. Due to the complex geometries of traditional RF cavities, it is preferable to use a sample host cavity to study flat samples of the novel materials. The Cornell sample host cavity has been commissioned and has now reached peak magnetic surface fields of 100 mT. We present updates on the recent performance of the cavity.

INTRODUCTION

In the field of superconducting radio frequency (SRF) accelerators, many materials are currently being studied as alternatives to bulk niobium for RF operation. Particularly, thin film materials such as Nb_3Sn, nitrogen-doped niobium, and thin-film niobium show promise as future materials.

In order to study the material properties of candidate SRF materials, Cornell has developed a series of versatile sample host cavities [1–4]. The third and most recent of these cavities operates at a frequency of 4 GHz. Recent tests of the cavity have reached peak fields of 100 mT on the surface of the sample plate.

The sample host cavity operates in a TE mode, with a coupler extended upwards through the single beam tube. The clamp at the top of the cavity holds a removable sample plate in place. The plate, a flat five-inch disk, is mounted with an indium seal and can be manufactured, treated, and examined separately from the rest of the cavity. Figure 1 shows the assembled cavity.

RECENT RESULTS

The sample host cavity has now reached peak fields of over 100 mT on the sample plate. This is a significant step towards the empirically inferred limit of 120 mT, based on thermal runaway in previous TE cavities [4].

Recent tests of the sample host cavity have shown a Q-slope, as shown in Fig. 2. This is problematic, since the utility of the sample host cavity relies on achieving high Q at all fields: reaching high Q increases the sensitivity of the measurements of sample performance by reducing the background signal from the rest of the cavity.

* This work supported by NSF Career grant PHY-0841213 awarded to Matthias Liepe.
† jtm288@cornell.edu

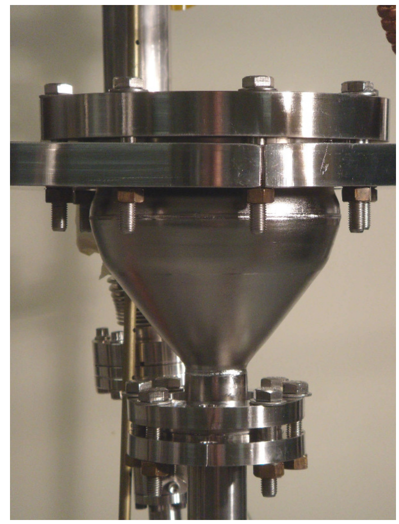

Figure 1: Third-generation Cornell TE sample host cavity.

It was speculated that the observed Q-slope effect was caused by indium losses, which can occur if the indium sealant approaches the RF surface at the cavity-sample plate interface. In order to investigate this possibility, we examined the relation between the quality factor Q and the temperature T for this high-field test, shown in Fig. 3. If the indium used as a sealant between the sample plate and cavity was interfering enough to bring rise to RF losses, we would expect that Q would decrease significantly above the superconducting critical temperature of indium, 3.4 K. However, the data do not suggest any such change in Q, implying that the observed Q-slope was not caused by indium losses. More work is needed to investigate this Q-slope.

A more recent test featuring a niobium-tipped coupler (discussed below), also seen in Fig. 2, aligns with the Q-slope of the high-field test, though the test did not reach fields high enough to make a direct comparison.

NIOBIUM COUPLER TIP

Previous tests of the sample host cavity suggested that the copper coupler assembly was introducing losses and affecting the intrinsic quality factor of the cavity [4,5]. In light of this, and in an effort to increase the Q of the system, the tip of the coupler for the sample host cavity was replaced with a duplicate made with niobium. In theory, a superconducting coupler tip would lower coupler losses significantly due to the strongly decreased resistance.

As Fig. 4 shows, to first order this coupler tip replacement does not appear to decrease the impact of the coupler on the

ISBN: 978-3-95450-168-7 doi:10.18429/JACoW-IPAC2015-WEPTY077

Content from this work may be used under the terms of the CC BY 3.0 licence (© 2015). Any distribution of this work must maintain attribution to the author(s), title of the work, publisher, and DOI.

ON QUENCH PROPAGATION, QUENCH DETECTION AND SECOND SOUND IN SRF CAVITIES

R. Eichhorn# and S. Markham
Cornell Laboratory for Accelerator-Based Sciences and Education, Cornell University
Ithaca, NY 14853-5001, USA

Abstract

The detection of a second sound wave, excited by a quench, has become a valuable tool in diagnosing hot spots and performance limitations of superconducting cavities. Several years ago, Cornell developed an oscillating super-leak transducer (OST) for these waves that nowadays are used world-wide. In a usual set-up, several OSTs surround the cavity, and the quench location is determined by triangulation of the different OST signals. Convenient as the method is there is a small remaining mystery: taking the well-known velocity of the second sound wave, the quench seems to come from a place slightly above the cavity's outer surface. We will present a model based on numerical quench propagation simulations and analytic geometrical calculations that help explain the discrepancy.

INTRODUCTION

Superconducting Radio Frequency (SRF) cavities are fabricated carefully to make a smooth, uniform surface. This ensures that electric current flows uniformly on the surface of the cavity, so that minimal heating of the cavity surface occurs. Despite precautions taken, it is still common for cavities to bear small (sub-millimeter) surface defects that impede cavity performance. These defects cause localized excess heating. If severe enough, this can heat the surrounding superconducting material (in most cases niobium) to above its critical temperature. When this happens, the niobium becomes normal conducting and begins to heat even more rapidly. This causes a runaway effect wherein all the cavity's stored energy is quickly converted into heat, called a quench. Because defects cause quenching, which severely detriments a cavity's performance, it is important to be able to locate the defect so that it can be removed.

One method of locating a defect involves using oscillating superleak transducers (OSTs,[1]) to detect second sound waves emitted from the cavity. Second sound is a phenomenon observed in superfluid helium[2] wherein heat propagates as a wave with properties comparable to that of a classical sonic wave. The speed of the second sound depends somewhat on the parameters of the fluid, but is almost a constant of 20 m/s, within the temperature range of 1.6 to 2 K.

Once the second sound wave has been produced, the signal propagates through the helium until it reaches an OST. A typical arrangement is given in Fig. 1. By calculating the difference in time between when the quench occurred, which one can measure as the time at which the cavity begins to lose its stored energy, one can use trilateration to deduce the location of the defect [1]. Problematically, when this procedure is performed, there is a discrepancy between the predicted location of the defect and the defect's actual location. In fact, the defect is often detected to be off the surface of the cavity entirely. Also, others [3] have noted that the quench expands faster enough that it may not behave as a point-like emitter of a second sound wave.

Previously, we investigated the possibility of a delay between the loss of stored energy in the cavity and the triggering of a second sound wave [4]. As we did so we could explain a discrepancy in the order of 2-3 mm.

In this paper we will investigate how heat propagation in the niobium can contribute to the quench signal propagation and its effect on quench location.

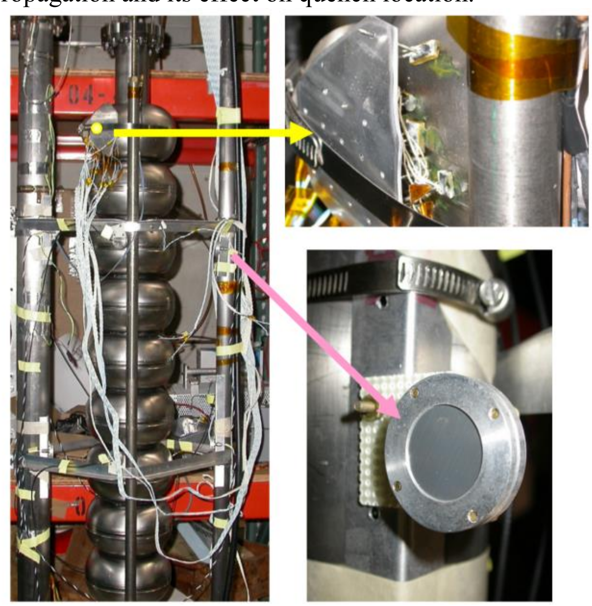

Figure 1: Basic layout of OST quench detection setup. OSTs are set up in an array around the exterior of the cavities, and submerged in He-II (Image from [1]).

GEOMETRICAL SETUP

Calculating Propagation Time

Figure 2 illustrates the basic geometry of the problem. For simplicity, the niobium is assumed to exist simply on a plane. The niobium is in thermal contact with a bath of helium-II. The OST is placed at a distance R from defect and an angle θ from the normal.

Naively, one would assume a signal propagates to the

#r.eichhorn@cornell.edu

ISBN: 978-3-95450-168-7 doi:10.18429/JACoW-IPAC2015-WEPTY078

HIGH Q_0 AT MEDIUM FIELDS IN Nb_3Sn SRF CAVITIES AT 4.2 K*

S. Posen†, Daniel Leslie Hall, and M. Liepe
Cornell Laboratory for Accelerator-Based Sciences and Education, Ithaca, NY, 14853, USA
T. Proslier
Argonne National Laboratory, Argonne, Illinois 60439, USA

Abstract

Nb_3Sn has proven itself to be a very promising alternative SRF material. With twice the critical temperature of niobium cavities, 1.3 GHz Nb_3Sn cavities can achieve quality factors on the order of 10^{10} even at 4.2 K, significantly reducing cryogenic infrastructure and operational costs. In addition, its large predicted superheating field may allow for maximum accelerating gradients up to twice that of niobium for high energy applications. In this work, we report on new cavity results from the Cornell Nb_3Sn SRF program demonstrating a significant improvement in the maximum field achieved with high Q_0 in a Nb_3Sn cavity. At 4.2 K, accelerating gradients above 16 MV/m were obtained with Q_0 of 8×10^9, showing the potential of this material for future applications. In addition to this result, current limitations are discussed.

INTRODUCTION

For decades, niobium has been the material of choice for superconducting RF cavities in particle accelerators. It has excellent superconducting properties and is relatively easy to work with to fabricate cavities. However, because it has a critical temperature T_c of ~9.2 K, it is usually necessary to cool niobium cavities with subatmospheric helium at ~2 K in order to achieve high quality factor Q_0. Furthermore, while accelerating gradients E_{acc} in niobium cavities have been steadily increasing over years of development, cavities are now regularly being produced with fields close to the ultimate limit set by the superheating field B_{sh} of niobium.

Nb_3Sn is an alternative SRF material currently under development that already is showing great promise. It has a T_c of 18 K, approximately twice that of niobium, allowing for high Q_0 operation even at 4.2 K, opening up the possibility of operation with atmospheric helium, reducing the infrastructure costs for cryogenic plants, and increasing their efficiency. Nb_3Sn is also is predicted [1] to have a B_{sh} of 400 mT, approximately twice that of niobium, which could halve the number of cavities required to reach a given energy.

Many laboratories contributed to pioneering research in the 1970s-1990s into Nb_3Sn SRF cavities [2–8]. Building on their work based on the vapor diffusion process [9], a Nb_3Sn SRF program was started at Cornell University in 2009. After a successful program to demonstrate high quality coatings on small samples [10], the cavity program began.

RF TESTING

A coating chamber built for an ulta-high vacuum furnace (see details in [11]) was used to coat two single cell 1.3 GHz niobium cavities with Nb_3Sn. Cavity 1 received BCP chemical removal before coating, and Cavity 2 received EP. The performance of the cavities was evaluated in vertical RF test. After evaluation, the coating layer of Cavity 1 was removed with BCP, then it was coated and tested again. This was repeated a total of four times. Details of the coating are presented elsewhere [12]. The performance curves of these coatings are presented in Fig. 1.

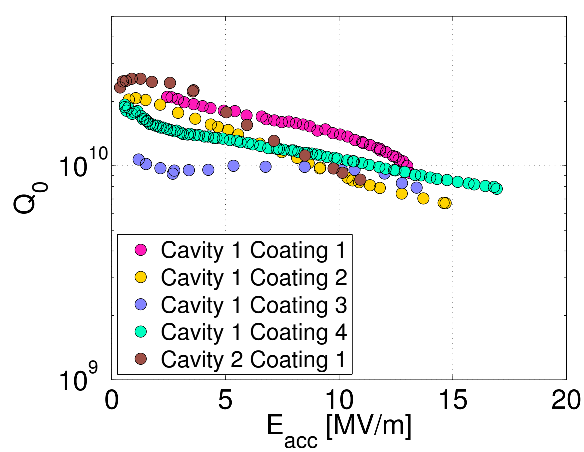

Figure 1: Q_0 vs E_{acc} at 4.2 K for single cell 1.3 GHz cavities over a series of five Nb_3Sn coatings.

In each test, Q_0 at 4.2 K on the order of 10^{10} is measured up to E_{acc} above 10 MV/m. Maximum fields are limited by quench without x-rays. An average quench field of 14 MV/m was measured, with an average Q_0 at quench of 8×10^9. The maximum field achieved was 17 MV/m. Moderate Q-slope was observed in each case, but it is far less strong than that observed by previous researchers studying Nb_3Sn accelerator cavities [13].

Material parameters were extracted during RF testing from fits to Q_0 versus temperature T data and resonant frequency f versus T data, as described in [14]. The results are shown in Table 1, along with the maximum fields in each test.

Q_0 on the order of 10^{10} at 4.2 K is a significant development in the effort to reduce power consumption in cryogenic

* Work supported by NSF Career award PHY-0841213 and DOE award ER41628.
† Now at Fermi National Accelerator Laboratory, Batavia, Illinois, 60510, USA. Email: sposen@fnal.gov

Content from this work may be used under the terms of the CC BY 3.0 licence (© 2015). Any distribution of this work must maintain attribution to the author(s), title of the work, publisher, and DOI.

ISBN: 978-3-95450-168-7 doi:10.18429/JACoW-IPAC2015-WEPTY082

HIGH GRADIENT TESTING OF THE FIVE-CELL SUPERCONDUCTING RF MODULE WITH A PBG COUPLER CELL*

S. Arsenyev†, Massachusetts Institute of Technology, Cambridge, MA 02139, USA
W.B. Haynes, D. Shchegolkov, E. Simakov, T. Tajima, Los Alamos National Laboratory, PO Box 1663, Los Alamos, NM 87545, USA
C.H. Boulware, T.L. Grimm, A.R. Rogacki, Niowave, Inc., 1012 North Walnut Street, Lansing, MI 48906, USA

Abstract

We report results of high-gradient testing of the first 5-cell superconducting radio frequency (SRF) module with a photonic band gap cell (PBG).

Higher order mode (HOM) damping is vital for preserving the quality of high-current electron beams in novel SRF accelerators. Because HOMs are not confined by the PBG array, they can be effectively damped in order to raise the current threshold for beam instabilities. The PBG design increases the real-estate gradient of the linac because both HOM damping and the fundamental power coupling can be done through the PBG cell instead of via the beam pipe at the ends of the cavity. A superconducting multi-cell cavity with a PBG damping cell is therefore an attractive option for high-current linacs.

The first-ever SRF multi-cell cavity incorporating a PBG cell was designed a LANL and built at Niowave Inc. The cavity was tuned to a desired gradient profile and underwent surface treatment at Niowave. A vertical test (VTS) was then performed at LANL, demonstrating an abnormally low cavity quality factor in the accelerating mode of 1.6×10^6. Future tests are proposed to determine the source of the losses and resolve the problem.

INTRODUCTION

Superconducting radio frequency (SRF) cavities are the natural choice for future generations of high energy linacs, especially for high-duty-factor machines where the heat produced in the accelerating structure cannot be effectively extracted [1]. Going to higher frequencies in SRF cavities is desirable in some applications for various reasons. First, it allows us to lower cost and increase achievable luminosity of an electron beam. Second, it is necessary for harmonic cavities operating at multiples of accelerator frequency. However, higher-order-mode (HOM) wakefields excited by a beam scale as the frequency cubed and can easily destroy the beam in a high-frequency machine. One high-current linac of relatively high frequency is the proposed SRF harmonic linac for eRHIC [2], which would be used to undo nonlinear distortion of the beam's longitudinal phase space induced by the main linac waveform.

Photonic band gap (PBG) cavities are of interest to the particle accelerator community because they have reduced

Figure 1: 2.1 GHz 5-cell module with a PBG center cell, made from bulk niobium.

higher-order modes that can degrade beam quality [3,4]. Unlike a room temperature PBG cell, the superconducting cell must be closed in the transverse plane and utilizes waveguide couplers to extract the HOMs (Fig. 1). Waveguide couplers are commonly used as an HOM suppression mechanism but are usually attached to the beam pipe (see, for example, [5]). In contrast, low field at the periphery of the PBG cell allows us to attach the waveguide couplers directly to the outside wall of the cell. This is beneficial to HOM damping and increases real estate gradient by saving space on the beampipes [6].

One of the three waveguides is also utilized as a fundamental power coupler (FPC). This particular 5-cell module was originally designed for the LANL Navy FEL beamline with high beam current (100 mA), and therefore requires a strongly coupled FPC, which is achieved by removing one of the PBG rods. Accelerating properties of the module are similar to that of a design with 5 elliptical "low loss" cells [7].

Previous superconducting tests of single PBG cells have achieved high gradients and high quality factors [8]. However, building a 5-cell module involved new challenges such

* Work supported by the U.S. Department of Energy (DOE) Office of Science Early Career Research Program
† arsenyev@mit.edu

Content from this work may be used under the terms of the CC BY 3.0 licence (© 2015). Any distribution of this work must maintain attribution to the author(s), title of the work, publisher, and DOI.

ISBN: 978-3-95450-168-7 doi:10.18429/JACoW-IPAC2015-WEPTY083

FIVE-CELL SUPERCONDUCTING RF MODULE WITH A PBG COUPLER CELL: DESIGN AND COLD TESTING OF THE COPPER PROTOTYPE*

S. Arsenyev†, Massachusetts Institute of Technology, Cambridge, MA 02139, USA
D. Shchegolkov, E. Simakov,
Los Alamos National Laboratory, PO Box 1663, Los Alamos, NM 87545, USA
C.H. Boulware, T.L. Grimm, A.R. Rogacki, Niowave, Inc.,
1012 North Walnut Street, Lansing, MI 48906, USA

Abstract

We report the design and experimental data for a copper prototype of a superconducting radio-frequency (SRF) accelerator module. The five-cell module has an incorporated photonic band gap (PBG) cell with couplers. The purpose of the PBG cell is to achieve better higher order mode (HOM) damping which is vital for preserving the quality of high-current electron beams. Better HOM damping raises the current threshold for beam instabilities in novel SRF accelerators. The PBG design also increases the real-estate gradient of the linac because both HOM damping and the fundamental power coupling can be done through the PBG cell instead of on the beam pipe via complicated end assemblies.

First, we will discuss the design and accelerating properties of the structure. The five-cell module was optimized to provide good HOM damping while maintaining the same accelerating properties as conventional elliptical-cell modules. We will then discuss the process of tuning the structure to obtain the desired accelerating gradient profile. Finally, we will list measured quality factors for the accelerating mode and the most dangerous HOMs.

INTRODUCTION

Superconducting radio frequency (SRF) cavities are the natural choice for future generations of high energy linacs, especially for high-duty-factor machines where the heat produced in the accelerating structure cannot be effectively extracted [1]. Going to higher frequencies in SRF cavities is desirable in some applications for various reasons. First, it allows us to lower cost and increase achievable luminosity of an electron beam. Second, it is necessary for harmonic cavities operating at multiples of accelerator frequency. However, higher-order-mode (HOM) wakefields excited by a beam scale as the frequency cubed and can easily destroy the beam in a high-frequency machine. One high-current linac of relatively high frequency is the proposed SRF harmonic linac for eRHIC [2], which would be used to undo nonlinear distortion of the beam's longitudinal phase space induced by the main linac waveform.

Photonic band-gap (PBG) cavities are of interest to the particle accelerator community because they have reduced higher-order modes that can degrade beam quality [3, 4]. Unlike a room temperature PBG cell, the superconducting cell is closed in the transverse plane and utilizes waveguide couplers to extract the HOMs. Waveguide couplers are commonly used as an HOM suppression mechanism but are usually attached to the beam pipe (see, for example, [5]). In contrast, low field at the periphery of the PBG cell lets the waveguide couplers be connected directly to the outside wall of the cell. This is beneficial to HOM damping and increases real estate gradient by saving space on the beampipes [6].

Figure 1: Copper prototype of the 5-cell accelerating module.

A niobium cavity was fabricated to test the maximum achievable accelerating gradient at superconducting temperature [7]. It was decided, however, that a much cheaper copper prototype (Fig. 1) would be fabricated prior to the niobium cavity for two reasons. This prototype serves to demonstrate the novel tuning required for the multi-cell structure with the PBG coupling cell, applied later to the niobium cavity. Also, HOM damping can be analyzed in the copper cavity by measuring external quality factors Q_e for the most dangerous HOMs. At room temperature, the Q_e can be calculated more accurately in the copper prototype because the conductivity of copper is about 10 times higher than that of niobium at room temperature. Mode overlapping, which is an issue for measurements in the niobium cavity at room temperature, is less of a problem. Unloaded Q factors for the copper prototype are in the order of 1.5×10^4 which is

* Work supported by the U.S. Department of Energy (DOE) Office of Science Early Career Research Program
† arsenyev@mit.edu

Content from this work may be used under the terms of the CC BY 3.0 licence (© 2015). Any distribution of this work must maintain attribution to the author(s), title of the work, publisher, and DOI.

ISBN: 978-3-95450-168-7 doi:10.18429/JACoW-IPAC2015-WEPTY084

COOLING SYSTEMS FOR THE NEW 201.25 MHz FINAL POWER AMPLIFIERS AT LOS ALAMOS NEUTRON SCIENCE CENTER (LANSCE)*

W.C. Barkley#, C.E. Buechler, J.T.M. Lyles, A.C. Naranjo, LANL, Los Alamos, NM 87544, USA
D. Baca, R.E. Bratton, Compa Industries, Los Alamos, NM 87544, USA

Abstract

Two new 201.25 MHz RF Final Power Amplifiers (FPAs) have been designed, assembled, installed and successfully tested at the Los Alamos Neutron Science Center (LANSCE), in Module 2 of the Drift Tube Linac (DTL). These production units were fabricated at Continental Electronics Corporation. In this paper, we summarize the FPA air and water cooling requirements and cooling systems [1].

Description of Systems

Figure 1 shows a CAD model of the FPA installation.

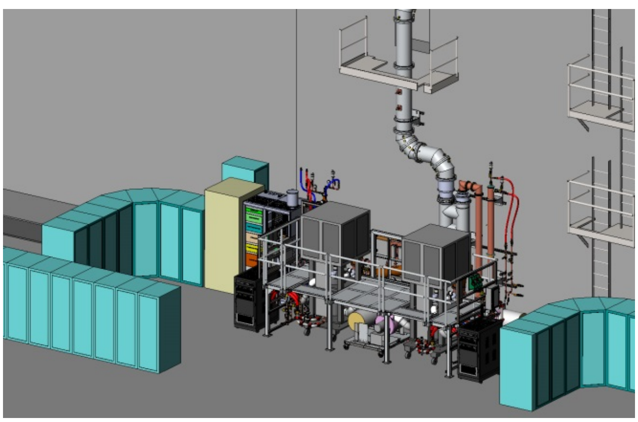

Figure 1: Model of FPA Installation.

Three separate water systems were required to fully cool each FPA and its auxiliary components. Two existing systems were modified and a new system was installed to meet the cooling requirements. A deionized water system (A01), cools the two power-combined FPAs and Intermediate Power Amplifier (IPA) directly. A chilled water system (A05), cools the RF reference source for the LANSCE accelerator and ignitrons in each of the four capacitor rooms. A treated water system (A06), cools the solid state driver amplifier (Rack 5), FPA and IPA water loads.

Flow requirements for the three water systems were developed for combined amplifier power, 3.4 MW at 13% duty factor or 442 kW each [2]. In addition, air cooling was implemented where water cooling was not practical.

The A01 System

The A01 system is an existing deionized water system that served the obsolete power amplifier that was previously located at Module 2 of the DTL. Centrifugal pumps, located in an adjacent mechanical room, deliver 88 psi, 1,250 gpm for the four DTL modules. One pump operates while the other serves as a backup. Adaptation of this water system consists of demolishing the existing plumbing at the module and installing the new plumbing as depicted in Fig. 2. Deionized water is required to eliminate the potential electrical path to ground in an ionized system. The A01 system is adapted to cool both FPAs and the IPA which is not shown in Fig. 2.

*Work supported by the United States Department of Energy, National Nuclear Security Agency, under contract DE-AC52-06NA25396
#barkley@lanl.gov

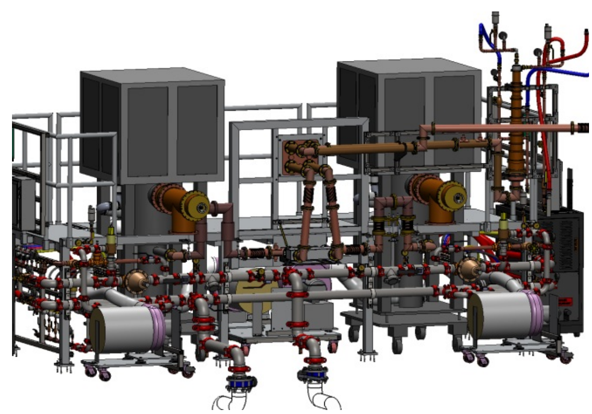

Figure 2: A01 Water System Adapted to the FPA Installation.

Note that the gray-colored piping and associated components in Fig. 2 are the distribution hardware for the A01 water system, and the brown colored piping is the 3 1/8 inch coax RF transmission lines. The A01 piping is mounted to the legs of the platform, and the legs of the platform are anchored to the concrete.

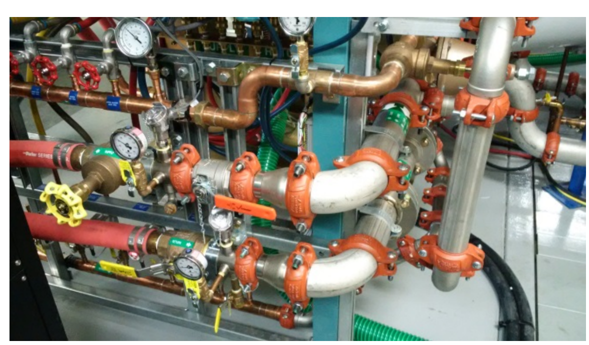

Figure 3: Side View of A01 Water System Mounted to Platform.

Content from this work may be used under the terms of the CC BY 3.0 licence (© 2015). Any distribution of this work must maintain attribution to the author(s), title of the work, publisher, and DOI.

ISBN: 978-3-95450-168-7 doi:10.18429/JACoW-IPAC2015-WEPWI001

Content from this work may be used under the terms of the CC BY 3.0 licence (© 2015). Any distribution of this work must maintain attribution to the author(s), title of the work, publisher, and DOI.

AN OVERVIEW OF THE MaRIE X-FEL AND ELECTRON RADIOGRAPHY LINAC RF SYSTEMS

J. Bradley III, D. Rees, A. Scheinker, R. Sheffield - Los Alamos National Laboratory, USA

Abstract

The purpose of the Matter-Radiation Interactions in Extremes (MaRIE) facility at Los Alamos National Laboratory is to investigate the performance limits of materials in extreme environments. The MaRIE facility will utilize a 12 GeV linac to drive an X-ray Free-Electron Laser (FEL). Most of the same linac will also be used to perform electron radiography. The main linac is driven by two shorter linacs; one short linac optimized for X-FEL pulses and one for electron radiography. The RF systems have historically been the one of the largest single component costs of a linac. We will describe the details of the different types of RF systems required by each part of the linacs. Starting with the High Power RF system, we will present our methodology for the choice of RF system peak power and pulselength with respect to klystrons parameters, modulator parameters, performance requirements and relative costs. We will also present an overview of the Low Level RF systems that are proposed for MaRIE and briefly describe their use with some proposed control schemes [1].

THE MaRIE FACILITY

The MaRIE facility will include a 12 GeV linac to provide a suite of measurement devices to investigate the performance limits of materials in extreme environments. One of MaRIE's most powerful tools will be the ability to multiplex an X-ray FEL, electron, and proton radiography onto a target material to study dynamic events as they develop.

The existing LANSCE proton linac will be used to provide proton radiography (pRad) [2]. The MaRIE electron linacs will be built in a new tunnel north of the existing LANSCE proton linac tunnel as shown in Figure 1.

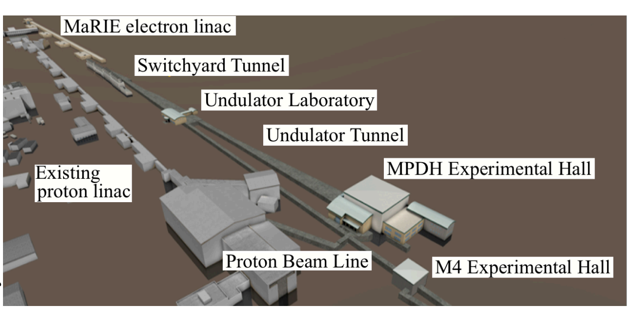

Figure 1: The MaRIE Facility layout.

MaRIE BEAM REQUIREMENTS

The MaRIE electron beams consist of micropulses for an X-ray FEL (XFEL) undulator and micropulses for electron radiography (eRad). A feature of the MaRIE facility is the ability to provide unevenly spaced XFEL and eRad micropulses distributed over a macropulse of up to 100 µs. The macropulse repetition rate is 60 Hz.

Each XFEL micropulse includes up to 0.2 nC of charge. Each 100µs long macropulse can include up to 30 XFEL micropulses. Each eRad micropulse includes up to 2 nC of charge. Each 100µs long macropulse can include up to 10 eRad micropulses.

The spacing between micropulses is determined by the experimental needs. The minimum separation between micropulses is determined by the time for cavity wakefields to decay. The minimum spacing after each eRad micropulse is 25 ns, while the minimum spacing after each XFEL micropulse is 2.5 ns.

COMBINATION LINAC DESIGN

Linac Layout

The XFEL and eRad micropulses are produced by and accelerated on separate injectors and initial linac sections. Both sections include an injector and L1 linac section, but the XFEL side also includes two bunch compressors and a short L2 linac section. The outputs of these parallel beamlines feed the L3 main linac as shown in Figure 2. A switchyard at the end of the L3 linac splits the XFEL and eRad beams off to go through undulators or directly to the target.

RF Cavity Details

The MaRIE linacs will use proven RF cavity designs. Four hundred sixty cavities will be of the 1.3 GHz TESLA type used in the FLASH [3], LCLS-II [4] and European XFEL [5] projects. The L3 linac includes 360 of these cavities. The L2 linac includes 78 of these cavities and the L1 linacs each include 11 of these cavities. Like the International Linear Collider (ILC), the 460 TESLA cavities are run at an average cavity field of 31.5MV/m [6].

The 22 third harmonic linearizer cavities will be of the 3.9 GHz type used in the FLASH linearizer [3]. Each L1 linac includes 7 of these cavities and the L2 linac includes 8 of these cavities. The average cavity gradient is 20 MV/m.

For beam diagnostics, the facility will use three transverse deflection cavities (TCAV) at 1.3 GHz and one normal conducting, traveling wave TCAV at 11.4 GHz.

ISBN: 978-3-95450-168-7 doi:10.18429/JACoW-IPAC2015-WEPWI002

INSTALLATION AND OPERATION OF REPLACEMENT 201 MHz HIGH POWER RF SYSTEM AT LANSCE

J. T. M. Lyles[#], W. Barkley, J. Davis, D. Rees, G. Sandoval,
AOT Division, Los Alamos National Laboratory, Los Alamos, NM
R. Bratton, R. Summers, Compa Industries, Los Alamos, NM

Abstract

The LANSCE RM project has restored the linac to high power capability after the power tube manufacturer could no longer provide triodes that consistently met our high average power requirement. Diacrodes® now supply RF power to two of the four DTL tanks. These tetrodes reuse the existing infrastructure including water-cooling systems, coaxial transmission lines, high voltage power supplies and capacitor banks. The power amplifier system uses a combined pair of LANL-designed cavity amplifiers using the TH628L Diacrode® to produce up to 3.5 MW peak and 420 kW of mean power. Design and prototype testing was completed in 2012, with commercialization following in 2013. The first installation was completed in 2014 and a second installed system is ready to test. The remaining replacement will follow in 2016. Meanwhile, there is a hybrid of old/new amplifiers until the changeover is complete. Operating results of the replacement system are summarized, along with observations from the rapid-paced installation project.

RF SYSTEM IMPROVEMENTS

The LANSCE drift tube linac (DTL) uses four Alvarez cavities powered at 201.25 MHz, to accelerate both protons (H^+) and negative hydrogen ions (H^-) from 0.75 to 100 MeV before injection into a coupled-cavity linac (CCL). Pulsed RF power must be capable of 12% duty factor (DF) and as high as 3.5 MW of peak RF power, with corresponding average power capability of 420 kW per cavity. This is in contrast to the high-peak/low-average power machines at 200 MHz proton injector linacs at Fermilab, CERN, RAL and BNL. Over the past 25 years, manufacture of reliable RF amplifier triodes operating at this high average power has been unpredictable. Both premature loss of cathode emission and ceramic cracking have occurred in some tubes when operated at LANL.

In 2006, the operating point of the power amplifiers (PA) had to be reduced in order to hold operating costs on budget (for all-too-frequent tube replacements) and prevent excess downtime. This led to the decision to operate LANSCE at half of its design original duty factor. A primary goal of the LANSCE Risk Mitigation project has been to double the linac duty factor by replacing the original 201.25 MHz amplifiers with modern power amplifier circuits with new generation tetrodes. Another goal has been to modernize the low level RF controls. Finally, end-of-life klystrons for the CCL are being replaced with forty-five new CPI VA862A1 1.3 MW klystrons [1].

Gridded Tube Cavity Amplifier

A previous report [2] explained the reasoning behind the choice of the TH628L Diacrode® from Thales Electron Tubes as the active device for this application. Combining the outputs of two PAs (Fig. 1) provides suitable headroom in peak and average power, allowing the tubes to operate well within their rating. Increased amplifier reliability and tube lifetime results from this pairing.

The caveat for gridded tubes is that a matching cavity amplifier circuit must be developed around a chosen device. The solution was to develop a commercially buildable PA design by our team, with technical assistance from the Thales tube product engineering team. The common-grid PA configuration uses a full wavelength double-ended coaxial line output circuit, in order to double the RF power available over a traditional single-ended tetrode. Progress on the mechanical and electrical design of the PA, supporting electronics and intermediate power amplifier (IPA) are discussed elsewhere [3][4][5]. Months of testing in 2012-13 ran up to 2.5 MW peak power at 12% duty factor and up to 3 MW into water loads to demonstrate design capability and to test the cathode emission capabilities of the tube. Each PA operates at < 1.85 MW at the DTL.

A tender for manufacturing the LANL-designed PA was issued in 2012 and the work was subsequently awarded to Continental Electronics Corporation [6]. Five PAs were delivered in 2013-2014 and tested at LANL. Two additional units are being manufactured for delivery in late 2015. Six TH628L Diacrodes® from Thales Electron Tubes have been received and tested. Two more are coming in late 2015. Three intermediate power amplifiers (IPA) have been produced by Betatron Electronics, Inc. with a fourth to be delivered in May. This amplifier assembly uses a Thales TH781 tetrode and matching TH18781 cavity amplifier. One IPA drives two final PAs (FPA) at each DTL RF station. All amplifiers conveniently reuse the same cooling water plant, the HV power supplies, capacitor banks and the 35.5 cm diameter coaxial transmission lines of the old RF powerplant.

Coaxial Transmission Lines

The 7.9 cm (3 1/8 inch) diameter coaxial transmission line from the 175 kW IPA is split by a λ/4 hybrid into two

* Work supported by the United States Department of Energy, National Nuclear Security Agency, under contract DE-AC52-06NA25396
# jtml@lanl.gov

Content from this work may be used under the terms of the CC BY 3.0 licence (© 2015). Any distribution of this work must maintain attribution to the author(s), title of the work, publisher, and DOI.

ISBN: 978-3-95450-168-7
doi:10.18429/JACoW-IPAC2015-WEPWI003

DESIGN OF A RADIAL KLYSTRON*

Massimo Dal Forno**, Sami G. Tantawi, Ronald D. Ruth, Aaron Jensen,
SLAC National Accelerator Laboratory, CA 94025, USA

Abstract

The radial klystron is a multidimensional rf source where the beam is generated by a cylindrical gun and it propagates in the radial dimension. The advantage of this design is that the space charge effects are balanced in the azimuthal dimension and a lower magnetic fields is required to focus the electron beam. The bunching is made with concentric coaxial resonators, connected by drift tube. The electron beam interaction with the cavity fields has been analyzed by means of particle tracking software in order to evaluate the beam bunching and the beam dynamics. This paper shows the klystron design, optimizing the shape and the position of each cavity, in order to maximize the efficiency of the device.

INTRODUCTION

The traditional klystron is a linear-beam rf source, where a focused electron beam interacts with resonant cavities. The beam must be focused by a solenoid, to compensate the space charge forces. Gain and efficiencies are limited by the space-charge. It is possible to reduce the space charge effects by allowing the electrons to propagate in the natural expansion according to the space charge forces. This can happen if the beam is generated from a central source (cathode) and it expands in the three-dimensional space (Fig. 1). In this ideal case, the transversal space-charge forces are

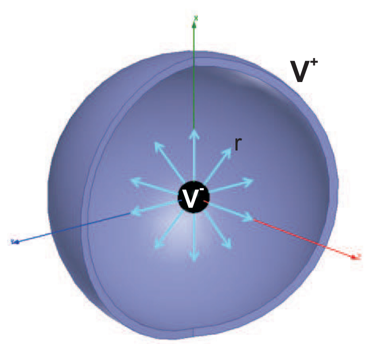

Figure 1: Three-dimensional natural expansion of electrons.

fully balanced (where the transverse dimension is the orthogonal to the propagation of each electron). No magnet is required to compensate space charge effects. This approach uses the multidimensional beam motion to avoid or reduce the space-charge effects.

This paper analyzes a radial klystron [1], which is a cylindrical device. It is the simplest case of multidimensional rf source. The electrons are generated by a cylindrical gun and propagate in the radial direction (Fig. 2(a)). The cavities are coaxial resonators endowed by drift tubes (Fig. 2(b)). The space charge effects are reduced since the

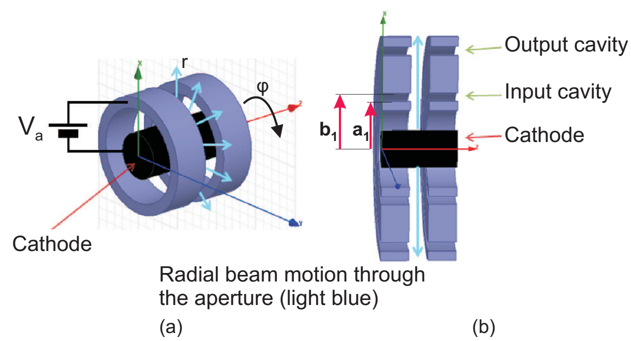

Figure 2: Cylindrical gun with expansion of electrons (a), Radial klystron with two coaxial resonators (b).

electron beam is balanced along the azimuthal direction (Indicated in Fig. 2(a)). Remnant space charge effects will decay when the beam is expanding. A lower magnetic field will be required to keep the beam focused.

This paper presents the ballistic design of a radial klystron. A coaxial mode stability test in presence of electrons have been analyzed. The electron beam interaction with the cavities has been analyzed with an in-house developed particle tracking software. The maximum efficiency of the output cavity has been evaluated with a Dirac delta beam test. Afterwards the whole klystron has been designed.

MODES STABILITY ANALYSIS

This section reports the single cavity stability results. A single cavity crossed by a DC beam can behave as an oscillator. This happens when the noise starts bunching the electron beam. The latter releases energy to the cavity, contributing to further bunching. If the feedback is positive, the released energy overcomes the losses and the cavity self-oscillates. To guarantee the stability a method has been proposed in [2, 3] to evaluate the stability function. When the cavity is stable, the stability function is negative.

A coaxial resonator has been considered. It approximates the input cavity of Fig. 2(b). The fundamental mode is the TEM_1 and its resonant frequency in vacuum is given by: $f_{TEM1} = c/(2L)$. High order resonant modes exist,

* Work supported by the US DOE under contract DE-AC03-76SF00515.
** dalforno@slac.stanford.edu

Content from this work may be used under the terms of the CC BY 3.0 licence (© 2015). Any distribution of this work must maintain attribution to the author(s), title of the work, publisher, and DOI.

ISBN: 978-3-95450-168-7 doi:10.18429/JACoW-IPAC2015-WEPWI004

Content from this work may be used under the terms of the CC BY 3.0 licence (© 2015). Any distribution of this work must maintain attribution to the author(s), title of the work, publisher, and DOI.

FPC AND HI-PASS FILTER HOM COUPLER DESIGN FOR THE RF DIPOLE CRAB CAVITY FOR THE LHC HILUMI UPGRADE*

Zenghai Li[1], SLAC, Menlo Park, CA 94025, USA
J. R. Delayen, S. U. De Silva, HyeKyoung Park, and R. G. Olave, ODU, Norfolk, VA 23529, USA

Abstract

A 400-MHz compact RF dipole (RFD) crab cavity design was jointly developed by Old Dominion University and SLAC under the support of US LARP program for the LHC HiLumi upgrade. The RFD cavity design is consisted of a rounded-square tank and two ridged deflecting poles, operating with a TE11-like dipole mode, which is the lowest mode of the cavity. A prototype RFD cavity is being manufactured and will be tested on the SPS beam line at CERN. The coaxial fundamental Power Coupler (FPC) of the prototype cavity was re-optimized to minimizing the power heating on the coupler internal antenna. A hi-pass filter HOM damping coupler was developed to achieve the required wakefield damping while maintaining a compact size to fit into the beam line space. In this paper, we will discuss the details of the RF optimization and tolerance analyses of the FPC and HOM couplers.

INTRODUCTION

A crabbing scheme [1] has been adopted as the baseline tool for the LHC HiLumi upgrade. The nominal scheme for the HL-LHC is the local crabbing with the 400 MHz superconducting deflecting cavities. Due to the small beam line separation close to the IP, the transverse size of the crab cavity is limited to 145-mm. To meet such a space constraint, an RF dipole (RFD) cavity [2-6] is being developed by a SLAC and ODU joint effort. The RFD design in concern is shown in Fig. 1. It consists of a rounded-square tank and two ridged deflecting poles. The operating mode is a TE11-like dipole mode, which is the fundamental mode. The frequency of the TE11-like mode is in principle not constrained by the cavity dimension in the deflecting plane, so the cavity dimension can be very compact. The rounded-square shape chosen for the present design is to accommodate for both the horizontal and vertical crabbing schemes. The present design also incorporates a curved pole profile as shown in Fig. 1 to improve the field uniformity within the beam aperture. Table 1 lists the major dimensions and RF parameters of the cavity. The lowest HOM frequency is more than 230 MHz above the operating mode. This large mode separation provides flexibilities of implementing different damping schemes for the HOMs using either waveguide [5] or high-pass filter HOM couplers. In this paper, we present a newly developed high-pass filter HOM coupler and the optimized FPC coupler design for the RFD cavity. This cavity design is being manufactured and will be tested on the SPS at CERN [7,8].

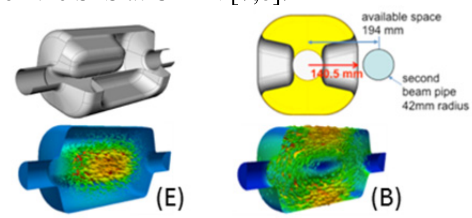

Figure 1: RFD crab cavity and the field patterns.

Table 1: RFD Crab Cavity RF Parameters

Frequency (MHz)	400
Operating Mode	TE11
Lowest dipole HOM (MHz)	634
Lowest acc HOM (MHz)	715
Iris aperture (diameter) (mm)	84
Transverse dimension (mm)	281x281
Longitudinal dimension (w/o couplers) (mm)	556
R_T (ohm/cavity)	433
V_T (MV/cavity)	3.34
Bs (mT)	55.6
Es (MV/m)	33.4

HOM COUPLERS

The HOM mode spectrum calculated using Omega3P [9,10] up to 2 GHz is shown in Fig. 2. The first HOM is a horizontal dipole mode at 634 MHz. The first important accelerating mode is at 761 MHz and the first vertical dipole mode is at 783 MHz.

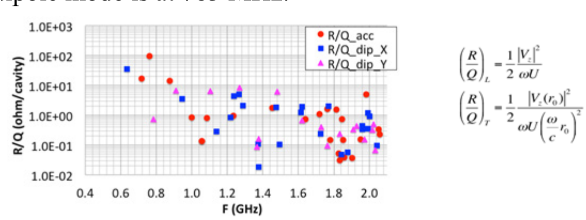

Figure 2: HOM mode spectrum.

The HOM and FPC coupler design were to meet the following design requirements: 1) be clear of the second beam line which is 194 mm away; 2) all coupler ports are oriented in the up-vertical direction to simplify the cryostat design; 3) the HOM couplers need be able to handle high HOM power that could potentially be generated by the beam. For example, the maximum beam (σ_z=76 mm) induced power by the first major accelerating mode at 761 MHz (R/Q~200) is $48I_b^2Q_{ext}$. A half-ampere beam would produce a power of 3.6 kW for a Q_{ext} of 300

* This work was supported by DOE Contract No. DE-AC02-76SF00515 and was partially supported by the DOE through the US LHC Accelerator Research Program (LARP). Computations used computer resources at NERSC, LBNL.
[1] lizh@slac.stanford.edu

ISBN: 978-3-95450-168-7 doi:10.18429/JACoW-IPAC2015-WEPWI005

NOVEL APPROACH TO VARIABLE VOLTAGE SUBSTATION PROTECTION

C. Jach, M. Mehtabuddin, S. Olek, SLAC, Menlo Park, CA 94025, USA

Abstract

Conventional electrical system protection of variable voltage substations (medium voltage rated) of using fuses and phase overcurrent and/or phase time overcurrent protection is not adequate. This was evident from the recent variable voltage substation (VVS) electrical fire at SLAC. Using information obtained from the fire investigation, ETAP simulations, and event reports of the faults which led to the fire, SLAC put into action a fast, feasible, and economical relay protection plan into adequately protecting VVS until long term plan of replacements is implemented. The plan utilizes the existing microprocessor protection relays on the upstream breakers and included the following adjustments: Adjusting the long-time overcurrent according to the de-rated cable ampacities, dual-fed arc flash fault protection, adding negative sequence settings and relay control logic to allow for two sets of settings for inrush mode and normal mode.

INTRODUCTION

The challenges we met were repetitive low fault currents in short durations not being protected by the fuses. At the same time, according to the protection coordination study results, the transformers' damage curves are positioned very close to the transformers' full load amps (FLA). It would not be possible to find a fuse fitting such configuration without creation of a significant risk of unintended tripping, as the transformers operated very close to the FLA. The ideal solution would be replacement of fuses by breakers controlled by protection relays equipped with differential protection elements and temperature monitoring. Use of the protection relays would also give us an opportunity to fine-tune the overcurrent time-current curve to fit it precisely between the full load amps point and the damage curve. This however would not be feasible in the short term due to restriction to capital resources and schedule impact to sciences.

An alternative solution presented in this document has been worked out and implemented instead. Thanks to the implemented protection system modification the transformers' protection at the low fault current range has been significantly improved in a very short period of time and at very low cost.

THE VARIABLE VOLTAGE SUBSTATIONS (VVS)

There are a total of 16 VVS in the SLAC linear accelerator. They are powered from breakers at the Master Substation with 3-500 MCM EPR insulated copper feeder cables. Each of the individual feeders can supply up to several (from 1 to 4) VVS substations, thus several 12.47/0.6 kV transformers may be powered by a single 12.47 kV breaker. The load break disconnect switches are deemed not operable due to their age and condition. The energizing of VVS is instead done at upstream breakers at Master Substation through the use of SEL 751A relays.

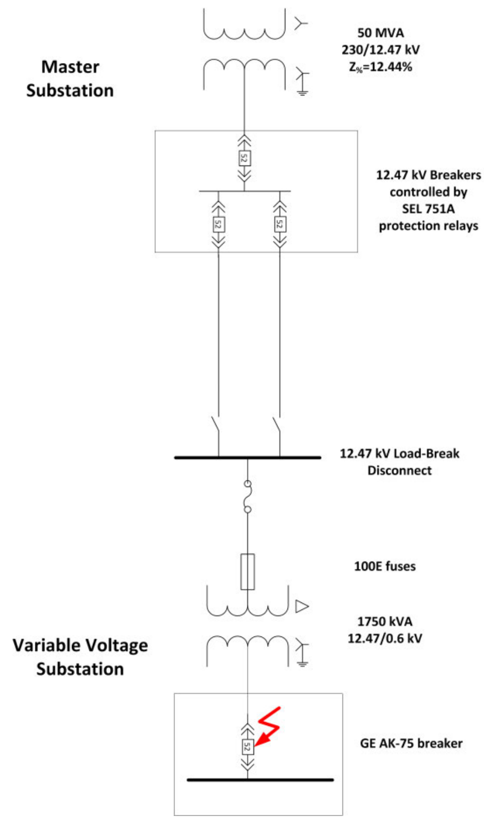

Figure 1: Simplified single line diagram of the VVS substation powering system.

VVS SUBSTATIONS PROTECTION SYSTEM AT THE TIME OF THE FIRE

The VVS substation protection system coordination plot is presented at Fig. 2. The 12.47/0.6 kV transformer damage curve has been shifted to reflect the overcurrent protection ability to see the fault current on the primary side of the transformer for secondary side faults. The plot shows that VVS 12.47 kV fuses do not ensure proper protection of the VVS 12.47/0.6 kV transformer for the range of currents below 220 A, which corresponds to time over 50 seconds on the 100E fuse time-current curve. The SEL 751A protection relay overcurrent settings were following.

- Function 50: I = 4.8 kA, time delay: 0.02 s.
- Function 51: extremely inverse U4 time-current curve, I = 451 A, time dial: 5.3 s

Content from this work may be used under the terms of the CC BY 3.0 licence (© 2015). Any distribution of this work must maintain attribution to the author(s), title of the work, publisher, and DOI.

ISBN: 978-3-95450-168-7 doi:10.18429/JACoW-IPAC2015-WEPWI006

Content from this work may be used under the terms of the CC BY 3.0 licence (© 2015). Any distribution of this work must maintain attribution to the author(s), title of the work, publisher, and DOI.

DITHER COILS FOR THE SUPERKEKB FAST COLLISION FEEDBACK SYSTEM*

U. Wienands†, S.D. Anderson, S. Gierman, M. Kosovsky, C.M. Spencer, M.K. Sullivan, SLAC, Menlo Park, CA 94025, USA
Y. Funakoshi, M. Masuzawa, T. Oki, KEK, Ibaraki, JP

Abstract

The collision feedback system for the SuperKEKB electron-positron collider at KEK will employ a dither feedback with a roughly 100 Hz excitation frequency to generate a signal proportional to the offset of the two beams. The excitation will be provided by a local bump across the interaction point (IP) that is generated by a set of eight air-core solid-wire magnet coil assemblies, each of which provides a horizontal and/or vertical deflection of the beam, to be installed around the vacuum system of the SuperKEKB Low Energy Ring. The design of the coils was challenging as large antechambers had to be accommodated and a 0.1% relative field uniformity across a good-field region of Âś1 cm was aimed for, while keeping reasonable dimensions of the coils. This led to non-symmetric, non-flat designs of the coils. The paper describes the magnetic design and the method used to calculate the magnetic field of the coils, the mechanical design and the field measurement results. Tracking in the lattice model has indicated acceptable performance.

INTRODUCTION

The SuperKEKB asymmetric e^+e^- collider [1] will employ a fast dither feedback scheme similar to the one developed for PEP-II [2, 3] to maintain collision between the two beams. [4] "Dither coils" are air-core magnet coils used to wiggle one of the two beams across the collision point by a small distance at a frequency near 100 Hz. Any offset between the two beams reveals itself in a modulation of the luminosity signal with the dither frequency. The coils are mounted around the vacuum chamber near the interaction point. Each coil assembly is to provide both horizontal and vertical deflection. In SuperKEKB, there are 8 coil assemblies to be able to independently vary the beam coordinates at the interaction point (IP) independently in position and angle in both directions while keeping the orbit change localized and correct for any coupling. The parameters of the coils are given in Table 1.

The coils will be mounted onto the vacuum chamber. The vertically deflecting coils have to go around the antechamber of the vacuum system. If flat rectangular coils were to be used, this would lead to very large coils with a large gap in between; inefficient magnetically and requiring a large support structure, and causing significant stray field. In order to keep the coils compact, a wrap-around design was adopted that brings the conductor relatively close to the vacuum chamber. Figure 1 shows the two different chamber cross sections that were accommodated and the schematic shape of the coils. Three different coil shapes had to be wound: a common shape for the horizontal deflectors and a narrow and a wide shape for the vertical deflectors depending on the chamber they are to be placed around.

Table 1: Design Parameters of the Coils

Parameter	Unit	Value
Overall Length	cm	25
Aperture radius	cm	5.24
Wire diameter	mm	1.291 (#16 AWG)
# of turns per coil		39
Coil cross section (h×v)	mm^2	19×3.8
Resistance/coil (vert. field, 20°C)	Ω	0.36
Resistance/coil* (horiz. field, small, 20°C)	Ω	0.40
Coil resistance* (horiz. field, large, 20°C)	Ω	0.53
Coil inductance (approx.)	mH	1…2
Field integral* (horizontal)	Tm	4.51×10^{-4}
Field integral* (vertical)	Tm	5.92×10^{-4}
Good-field region	cm	1
Field uniformity (rel.)	1	$\pm 1 \times 10^{-3}$

*: Measured parameter

COIL MODELLING AND DESIGN

The magnetic design of the coils was done in *Maple*®. [5] We use equations (4), (5) and (6) given by Misakian [6] for the field of a flat, rectangular coil with vanishing wire size. The complex shape of each coil is modeled as a sum of flat rectangular subcoils in the proper orientation with respect to each other. This required us to be able, programmatically, to rotate and translate the subcoils in space thus building a whole coil assembly from the individual pieces. Maple's "Record" data structure allows one to do this by defining a general prototype (which knows about its orientation in space) and creating and translating/rotating/reflecting each instance until the assembly model is complete. Each horizontal-field coil is modeled as three subcoils; the field at each point in space is then the sum of the contributions from each individual subcoil per coil and the two coils making

* This work performed under DOE Contract DE-AC02-76SF00515 and by the US/Japan Program for Cooperation in High Energy Physics.
† uli@slac.stanford.edu

ISBN: 978-3-95450-168-7 doi:10.18429/JACoW-IPAC2015-WEPWI007

TTF3 POWER COUPLER THERMAL ANALYSIS FOR LCLS-II CW OPERATION*

L. Xiao, C. Adolphsen, Z. Li, C. Nantista and T. Raubenheimer, SLAC, Menlo Park, CA, USA,
N. Solyak and I. Gonin, FNAL, Batavia, IL, USA

Abstract

The TESLA 9-cell SRF cavity design has been adopted for use in the LCLS-II SRF Linac. Its TTF3 coaxial fundamental power coupler (FPC), optimized for pulsed operation in European XFEL and ILC, requires modest changes to make it suitable for LCLS-II continuous-wave (CW) operation. For LCLS-II it must handle up to 7 kW of power, fully reflected, with the maximum temperature around 450 K, the coupler bake temperature. In order to improve TTF3 FPC cooling, an increased copper plating thickness will be used on the inner conductor of the 'warm' section of the coupler. Also the antenna will be shortened to achieve higher cavity Qext values. Fully 3D FPC thermal analysis has been performed using the SLAC-developed parallel finite element code suite ACE3P, which includes electromagnetic codes and an integrated electromagnetic, thermal and mechanical multi-physics code. In this paper, we present TTF3 FPC thermal analysis simulation results obtained using ACE3P as well as a comparison with measurement results.

INTRODUCTION

The TTF3 FPC, depicted in Fig. 1, brings 1.3 GHz RF power from an external waveguide feed to an SRF cavity inside a cryomodule via a coaxial structure incorporating two cylindrical vacuum windows and bellows for Qext tuning. The design was developed for pulsed operation, as in XFEL and ILC.

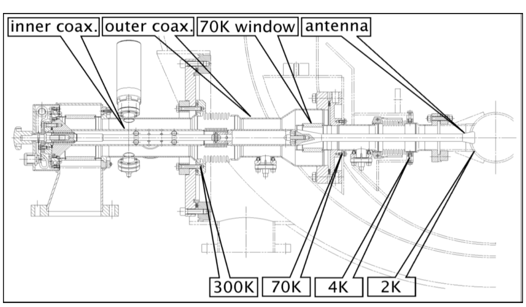

Figure 1: TTF3 FPC design. The FPC is made of copper plated stainless steel except for the cold-part center conductor antenna, which is made of solid copper (courtesy of DESY).

Past studies suggest its suitability up to at most 5 kW in standing-wave CW operation [1], less than the 7 kW required (worst case) for LCLS-II. The plating on the stainless steel inner conductor of the warm section will be increased from 30 μm to 150 μm to significantly lower its peak temperature to a level comparable to that during its bake-out (450 K). In addition, the antenna tip will be trimmed by 8.5 mm to increase the mid-range Qext value. For the low-current LCLS-II beams, Qext will be set to 4×10^7, about 10 times higher than for ILC.

Fully 3D LCLS-II FPC thermal analysis was performed using the SLAC developed ACE3P, a comprehensive set of conformal, higher-order, parallel finite-element electromagnetic codes with multi-physics capabilities in integrated electromagnetic, thermal and mechanical simulation [2]. TEM3P is ACE3P's multi-physics module. Its thermal capabilities include non-linear thermal conductivity in near superconducting condition, non-linear heat flux and convective boundary conditions for fluid-solid interface, shell elements for surface coating and volume RF heating for ceramic window loss.

2D SIMULATION BENCHMARKING

TTF3 FPC thermal simulations have been carried out using commercial software, such as ANSYS and COMSOL [3][4]. Because of single processor memory limitation, the FPC thermal simulations have been limited to its 2D model. In order to benchmark with COMSOL, a one-sixteenth slice of the FPC 2D structure, as shown in Fig. 2, was simulated using TEM3P. The second order tetrahedral meshes having 100k and 660k mesh elements for RF and thermal modelling, respectively are shown in Fig. 3.

Figure 2: A wedge model of the LCLS-II FPC.

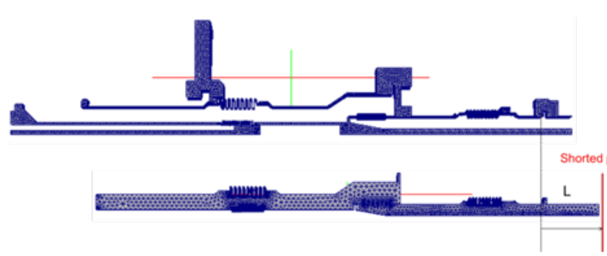

Figure 3: LCLS-II FPC meshes for thermal (upper) and RF (lower) simulations.

A shorting plane at varied locations was used to simulate cavity reflection for various frequency detunings. For this study, a 10 μm and 100 μm copper layer was assumed on the outer and inner stainless steel

* Work supported by the Department of Energy under Contract Number: DE-AC02-76SF00515.

Content from this work may be used under the terms of the CC BY 3.0 licence (© 2015). Any distribution of this work must maintain attribution to the author(s), title of the work, publisher, and DOI.

ISBN: 978-3-95450-168-7 doi:10.18429/JACoW-IPAC2015-WEPWI009

NITROGEN DOPING STUDY IN INGOT NIOBIUM CAVITIES*

Pashupati Dhakal#, Gianluigi Ciovati, Peter Kneisel, and Ganapati Rao Myneni
Jefferson Lab, Newport News, VA 23606, USA
Junki Makita, Old Dominion University, Norfolk, VA 23529, USA

Abstract

Thermal diffusion of nitrogen in niobium superconducting radio frequency cavities at temperature ~800 °C has resulted in the increase in quality factor with a low-field Q-rise extending to B_p > 90 mT. However, the maximum accelerating gradient of these doped cavities often deteriorates below the values achieved by standard treatments prior to doping. Here, we present the results of the measurements on ingot niobium cavities doped with nitrogen at 800 °C. The rf measurements were carried out after the successive electropolishing to remove small amount of material from the inner surface layer. The result showed higher breakdown field with lower quality factor as material removal increases.

INTRODUCTION

In the past few years much progress has been made in the development of the high quality factor superconducting radio frequency (SRF) cavities via the material diffusion in the thin layer of inner surface of the cavities. The motivation behind this process development is to reduce the cryogenic operating cost of current and future accelerators with reliable operation. The possibilities of higher quality factor in SRF cavities were first realized by the titanium doping [1, 2, 3] during annealing (~1400 °C) without any post-annealing chemistry and later by nitrogen doping at 800 °C [4], followed by electropolishing (EP). The diffusion process not only showed the increase in quality factor at low field levels, but also an increase in quality factor with increasing accelerating gradient, contrary to the previously observed Q-slope; except some anodized cavities showed the extended Q-rise in the past [5,6]. Possible explanation for the high quality factors are trapping of hydrogen due to the diffused materials [7,8] at interstitial sites, prohibiting the formation of lossy hydrides; the Q-rise phenomenon is a result of the broadening of the peaks at the gap edges in the electronic density of states by the rf current within the rf penetration depth [9,10].

A project-driven collaboration between Jefferson Lab, Fermi Lab and Cornell University began to investigate the robustness of the nitrogen doping process to meet the specifications for cavities for the LCLS-II, requiring a Q_0 value of at least 2.7×10^{10} at 2.0 K and a gradient of E_{acc}=16.0 MV/m in 9-cell, 1.3 GHz cavities [11]. The work of this collaboration was focused on developing the process on fine-grain (ASTM > 5), high purity (RRR>300) Nb cavities. In this contribution, we present the results of the rf measurements on high-purity single cell ingot niobium SRF cavities doped with nitrogen at 800 °C followed by the successive EP steps in small increments to understand the effects of nitrogen diffusion on ingot niobium and its correlation to the cavity performances.

CAVITY PREPERATION AND TEST RESULTS

Ingot Nb is an alternative material for the fabrication of SRF cavities having grain size of few cm^2. Cavities made from ingot have potential for material cost reduction and tend to have higher quality factor [12] even after the standard treatments [13]. Two single-cell 1.3 GHz cavities (labeled TD #3 and #4) with B_p/E_{acc} = 4.12 mT/(MV/m) made from ingot niobium with RRR~300 supplied by Tokyo-Denkai are used in this present study. The cavities have been processed thru several steps of typical cavity processing technique including the high temperature heat treatment (800-1250 °C) and buffer chemical processing. The baseline rf measurements were done after ~40 μm surface removal by buffer chemical polishing (BCP). The breakdown field at 2.0K was measured >150 mT during the baseline rf measurements. After the baseline rf measurements, cavities were heat treated at 800 °C for 3 hours followed by 20 minutes of exposure to nitrogen at pressure of ~25 mTorr at this temperature. The nitrogen is then evacuated and the cavities were further annealed at 800 °C for 30 min. The duration of the nitrogen exposure and subsequent annealing time were explored on several single and multi-cell fine grain cavities [14]. The cavities' inner surface was electropolished to remove the inner surface layer, followed by high pressure rinse with ultra-pure water. The rf test consisted of the measurements of $Q_0(T)$ at different constant B_p from 4.3−1.6 K and $Q_0(B_p)$ at different temperature between 2.1−1.6K. In some measurements the temperature maps of the outer cavity surface were also taken during the rf tests [15].

Cavity TD#3 was measured after the successive (10, 20, 30 and 35 μm) EP of the inner surface. In all cases the temperature dependence of surface resistance is measured at B_p~10 mT of peak rf field and material parameters such as the energy gap, electronic mean free path and residual resistance were extracted using the measured surface resistance to the calculation of surface resistance using the BCS theory [16] as shown in Table 1. No significant change in material parameters are observed regardless of

* This manuscript has been authored by Jefferson Science Associates, LLC under U.S. DOE Contract No. DE-AC05-06OR23177. The U.S. Government retains a non-exclusive, paid-up, irrevocable, world-wide license to publish or reproduce this manuscript for U.S. Government purposes.
#dhakal@jlab.org

Content from this work may be used under the terms of the CC BY 3.0 licence (© 2015). Any distribution of this work must maintain attribution to the author(s), title of the work, publisher, and DOI.

ISBN: 978-3-95450-168-7 doi:10.18429/JACoW-IPAC2015-WEPWI010

RESULTS FROM THE FIRST SINGLE-CELL Nb_3Sn CAVITY COATINGS AT JLAB*

G. Eremeev†
Thomas Jefferson National Accelerator Facility, Newport News, VA 23606, U.S.A.

Abstract

Nb_3Sn is a promising superconducting material for SRF applications and has the potential to exceed the limitations of niobium. We have used the recently commissioned Nb_3Sn coating system to investigate Nb_3Sn coatings on several single-cell cavities. We attempted to use the same coating procedure on several different single-cells with different 'genetics' and pre-coating surface preparation. We report on our findings with four 1.5 GHz CEBAF-shape single cell and one 1.3 GHz ILC single cavities that were coated, inspected, and tested.

CAVITY MATERIAL AND COATING PROCEDURE

Five cavities were used in these experiments. The cavity details are summarized in Table 1. Each cavity was measured at 2.0 K after the latest chemical treatment and the standard RF test preparation. After baseline tests, cavities were disassembled and prepared for Nb_3Sn coating. Following our experience with the first coated cavity C3C4, we adopted the following procedure:

- High pressure water rinsing, the cavity is left drying over the weekend
- Cleanroom assembly for Nb_3Sn coating
- Loading into the insert of Nb_3Sn coating system
- Nb_3Sn coating: 6 °C/min, 500 °C x 1 hr soak, 12 °C/min, 1200 °C x 3 hr soak. 3 gr of Sn and 3 gr of $SnCl_2$ used for each coating
- Visual inspection and KEK camera inspection
- Lapping of cavity flanges
- Low pressure water rinse
- Ultrasonic cleaning with 2% Liquinox detergent
- Assembly of the pick-up flange
- High pressure water rinsing
- Final assembly
- Slow pump down
- Leak check to $2{\cdot}10^{-10}$ ATM-CC/sec or better
- Cooldown to 4.3 K. ΔT across the cavity is maintained at less than 0.1K from 17.0 to 18.3 K.
- RF test at 4.3 K
- Warm up to above 18.3 K and cooldown to 2.0 K. ΔT across the cavity is maintained less than 0.1K from 17.0 to 18.3 K.
- RF test at 2.0 K

Because of the roughing pump failure, the coating of C1C2 had to be stopped, when the chamber was at about 1000 °C. The cavity then sat in the insert, until the heating profile was re-run a few days later.

OPTICAL INSPECTION

After the coating each cavity was moved to the optical inspection bench for optical inspection with KEK-style optical inspection bench [1, 2]. The focus of the inspection was largely the equatorial region, but pictures of beam tubes were also collected in several cases. The optical inspections of C3C4 and C1C2 revealed uniform complete coverage of the surface. In one place at the equator area of C3C4 we found several $\approx 100\ \mu$m-size features, Fig. 1. We did not find any outstanding features during the inspection of C1C2.

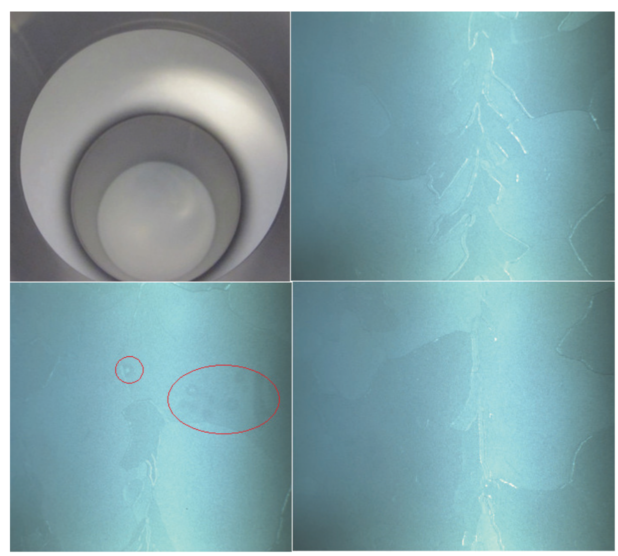

Figure 1: Optical inspection pictures of C3C4. Top left picture shows the coated surface of the cavity looking from one of the beam tubes. Top right and bottom right pictures show characteristic equatorial weld regions of the coated cavity. Bottom left picture shows the equatorial region with several observed features (marked with red circles).

* Authored by Jefferson Science Associates, LLC under U.S. DOE Contract No. DE-AC05-06OR23177. The U.S. Government retains a non-exclusive, paid-up, irrevocable, world-wide license to publish or reproduce this manuscript for U.S. Government purposes.
† grigory@jlab.org

Content from this work may be used under the terms of the CC BY 3.0 licence (© 2015). Any distribution of this work must maintain attribution to the author(s), title of the work, publisher, and DOI.

ISBN: 978-3-95450-168-7 doi:10.18429/JACoW-IPAC2015-WEPWI011

COMMISSIONING OF Nb_3Sn CAVITY VAPOR DIFFUSION DEPOSITION SYSTEM AT JLAB*

G. Eremeev†, W. Clemens, K. Macha, H. Park, R. Williams
Thomas Jefferson National Accelerator Facility, Newport News, VA 23606, U.S.A.

Abstract

Nb_3Sn as a BCS superconductor with a superconducting critical temperature higher than that of niobium offers potential benefit for SRF cavities via a lower-than-niobium surface resistance at the same temperature and frequency. A Nb_3Sn vapor diffusion deposition system designed for coating of 1.5 and 1.3 GHz single-cell cavities was built and commissioned at JLab. As the part of the commissioning, RF performance at 2.0 K of a single-cell 1.5 GHz CEBAF-shaped cavity was measured before and after coating in the system. Before Nb_3Sn coating the cavity had a Q_0 of about 10^{10} and was limited by the high field Q-slope at $E_{acc} \cong 27$ MV/m. Coated cavity exhibited the superconducting transition at about 17.9 K. The low-field quality factor was about $5{\cdot}10^9$ at 4.3 K and $7{\cdot}10^9$ at 2.0 K decreasing with field to about $1{\cdot}10^9$ at $E_{acc} \cong 8$ MV/m at both temperatures. The highest field was limited by the available RF power.

INTRODUCTION

Niobium is the the material of choice for the present SRF accelerators. Advances in the material fabrication and treatment has brought SRF niobium technology close to the superconducting limit of niobium material. Recent advances with mean free path variation has improved surface resistance by a factor 2-3[1, 2]. However, the present state-of-the-art for niobium is believed to be close to the fundamental limit of the material. Among other materials that have been considered for SRF applications, the most promising results in SRF cavities have been shown with Nb_3Sn[3, 4]. The Nb_3Sn transition temperature of about 18 K offers the opportunity of RF dissipation lower than that of niobium at the same temperature, while its superheating field expected at about 400 mT promises a higher breakdown field. In pursuit of Nb_3Sn coating on Nb cavities, we have built and commissioned a coating system that features a coating chamber of about 11" in diameter and 22" long.

* Authored by Jefferson Science Associates, LLC under U.S. DOE Contract No. DE-AC05-06OR23177. The U.S. Government retains a non-exclusive, paid-up, irrevocable, world-wide license to publish or reproduce this manuscript for U.S. Government purposes.
† grigory@jlab.org

CAVITY DEPOSITION SYSTEM

The deposition chamber comprises two main parts: the furnace that provides a clean heating environment to the coating chamber and the coating chamber that hosts the process vapors. The furnace was procured from T-M Vacuum Products Inc. The furnace was requested to be able to reach 1250 °C with the vacuum in 10^{-7} Torr range empty and the vacuum must be established by dry pumps. The furnace must be able to fit a 33" long by 11.5" diameter coating chamber with 24" long uniform (±5 °C) hot zone. A 14" mating conflat on the top must be provided for mating the insert to the furnace.

The coating chamber was built at JLab. The coating chamber was built as a cylinder 32" long x 11.5" diameter out of niobium, Fig. 1. Initially, the chamber was built to be inserted into JLab existing horizontal furnace 'Big Blue'. A

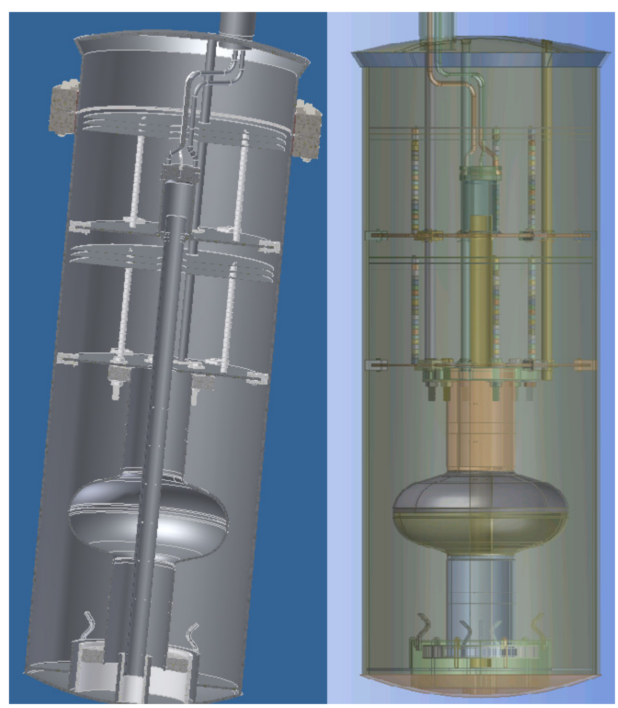

Figure 1: The Nb_3Sn insert drawing with a 1.3 GHz single cell cavity after(to the left) and before(to the right) conversion to vertical position. Note that Nb cylinder was split at the top with wire EDM to allow for 14" conflat stainless steel flange.

3" viewing port opening on the furnace door was adopted to allow niobium tube to extend from furnace space to the

Content from this work may be used under the terms of the CC BY 3.0 licence (© 2015). Any distribution of this work must maintain attribution to the author(s), title of the work, publisher, and DOI.

ISBN: 978-3-95450-168-7 doi:10.18429/JACoW-IPAC2015-WEPWI012

FIRST ATTEMPT OF AT-CAVITY CRYOGENIC X-RAY DETECTION IN A CEBAF CRYOMODULE FOR FIELD EMISSION MONITORING*

R.L. Geng#, E. Daly, M. Drury, A. Palczewski, JLAB, Newport News, VA 23606, USA

Abstract

We report on the first result of at-cavity X-ray detection in a CEBAF cryomodule for field emission monitoring. In the 8-cavity cryomodule F100, two silicon diodes were installed near the end flange of each cavity. Each cavity was individually tested during the cryomodule test in JLab's cryomodule test facility. The behaviors of these at-cavity cryogenic X-ray detectors were compared with those of the standard "in air" Geiger-Muller (G-M) tubes. Our initial experiments establish correlation between X-ray response of near diodes and the field emission source cavity in the 8-cavity string. For two out of these eight cavities, we also carried out at-cavity X-ray detection experiments during their vertical testing. The aim is to track field emission behavior uniquely from vertical cavity testing to horizontal cavity testing in the cryomodule. These preliminary results confirmed our expectation and warrant further effort toward the establishment of permanent at-cavity cryogenic X-ray detection for SRF development and operation.

INTRODUCTION

Field emission is a known mechanism in loading a superconducting radio frequency (SRF) cavity [1-3]. The consequence of field emission can vary, depending on the nature and location of field emitters. In the least harmful scenario, field emitted electrons form a small current and gain little energy from the stored energy in the cavity, therefore there is hardly detectable impact to the quality factor of the cavity, although there might be clearly detectable X-rays by high-sensitivity radiation detectors placed in the vicinity of the cavity. Most of the time however, field emitted electrons form a large enough current and/or gain a high enough energy, resulting in significant impact to the quality factor. Due to the exponential field dependence of the current density, raising the gradient further in this scenario becomes quickly prohibitive as the RF power dissipation is dominated by the process of "accelerating" the unwanted stray electrons. Energetic electrons striking the cavity wall also raise the local cavity wall temperature and eventually may trigger the cavity to quench, setting a hard limit to the attainable gradient. SRF cavities are oftentimes assembled into a long "string" which is in turn embedded in a cryomodule for installation in accelerators. In case of such a long string, electrons field emitted from one cavity can traverse the full length of the cavity and continue to travel into the next cavity, resulting in high energy stray electrons. When these electrons ultimately get lost from striking cavity walls or beam line components, energetic gamma rays are resulted, which in turn generate neutrons via photo-nuclear reactions [4].

While the body of knowledge about the field emitters inside SRF cavities is well established and avoidance of field emission has been quite successful for individual cavity qualification by applying the state-of-the-art cavity surface processing and handling techniques, there remain some open questions regarding field emission from a successfully qualified cavity to a performing cavity in a cryomodule installed in an accelerator. Notable ones are:

- Why do some cavities degrade in performance due to field emission from single-cavity vertical qualification test to integrated cavity string horizontal test in a cryomodule? Where are the active field emitters located? What is the origin of active field emitters?
- Is it possible to gauge the severity of field emission in a "common language" that is unique to the cavity and independent of the testing facilities?
- Why do new field emitters turn on during beam operation of cavities in CEBAF [5]?

In order to address these questions, a concept of permanent at-cavity cryogenic X-ray detection (ACCXD) is introduced. Following the successful validation of X-ray detectors attached to cavities immersed in liquid helium for vertical testing at JLab's VTA facility, we carried out initial experiments of at-cavity X-ray detection during single-cavity qualification tests. We tested the concept in a 8-cavity cryomodule for CEBAF. First results of these efforts are reported in this contribution.

DETECTOR VALIDATION FROM VERTICAL CAVITY TESTING

Silicon diodes have long been used in the field for cryogenic X-ray instrumentation for field emission studies [6,7]. The Hamamatsu S12230-1 PIN diode has been chosen based on evaluation among several candidates [8]. The same diode has been recently used at JLab for field emitter localization by combining the measured X-ray distribution with the computed electron trajectories [9].

The standard X-ray monitoring for cavity field emission in JLab's VTA facility is realized by placing an ion chamber (Canberra AM-IP 100) in the air at a location outside the cavity vertical testing dewar but within the dewar radiation shield. The distance between the ion chamber and the top flange of a 9-cell ILC cavity is approximately 3 meters. We carried out vertical tests of several different cavities with simultaneous X-ray monitoring by at-cavity cryogenic diodes and in-air ion

* Authored by Jefferson Science Associates, LLC under U.S. DOE Contract No. DE-AC05-06OR23177. The U.S. Government retains a non-exclusive, paid-up, irrevocable, world-wide license to publish or reproduce this manuscript for U.S. Government purposes.
Work partially supported by the US-Japan Collaboration Fund.
#geng@jlab.org

Content from this work may be used under the terms of the CC BY 3.0 licence (© 2015). Any distribution of this work must maintain attribution to the author(s), title of the work, publisher, and DOI.

ISBN: 978-3-95450-168-7 doi:10.18429/JACoW-IPAC2015-WEPWI013

Content from this work may be used under the terms of the CC BY 3.0 licence (© 2015). Any distribution of this work must maintain attribution to the author(s), title of the work, publisher, and DOI.

NEW RESULTS OF DEVELOPMENT ON HIGH EFFICIENCY HIGH GRADIENT SUPERCONDUCTING RF CAVITIES*

R.L. Geng[#], JLAB, Newport News, VA 23606, U.S.A.
J.K. Hao, K.X. Liu, Peking University, Beijing 100871, China
H.Y. Zhao, OTIC, Ningxia 753000, China
C. Adolphsen, Z. Li, SLAC, Menlo Park, CA 94025, USA

Abstract

We report on the latest results of development on high efficiency high gradient superconducting radio frequency (SRF) cavities. Several 1-cell cavities made of large-grain niobium (Nb) were built, processed and tested. Two of these cavities are of the Low Surface Field (LSF) shape. Series of tests were carried out following controlled thermal cycling. Experiments toward zero-field cooling were carried out. The best experimentally achieved results are E_{acc} = 41 MV/m at $Q_0 = 6.5\times10^{10}$ at 1.4 K by a 1-cell 1.3 GHz large-grain Nb TTF shape cavity and E_{acc} = 49 MV/m at $Q_0 = 1.5\times10^{10}$ at 1.8 K by a 1-cell 1.5 GHz large-grain Nb CEBAF upgrade low-loss shape cavity.

INTRODUCTION

Following the six-year (2006-2012) high-gradient SRF cavity R&D for ILC [1] and over a year of interruption due to SRF infrastructure upgrade at Jefferson Lab, we resumed the high gradient SRF R&D with an emphasis not only on gradient but also on efficiency. Initial results reported earlier in 2013 [2] were mixed due to the presence of strong field emission, consequential of irregularities in the SRF facilities before the full recovery in February 2014. After a 2-year hiatus, the high gradient SRF R&D at JLab was finally re-started for 1-cell testing. The new results since IPAC13 will be presented in this contribution.

Five L-band single-cell cavities, including two 1.3 GHz Low-Surface-Field (LSF) shape cavities, are fabricated using large-grain Nb. The choice of large-grain Nb is encouraged by the experimental demonstration of higher Q_0 at medium- and high- gradient regimes [3-5]. This gain in large-grain Nb cavity Q_0 is due to a lower residual surface resistance (roughly by a factor of 2) as compared to its fine-grain niobium counterpart [6]. The reason behind this difference may originate from different flux trapping behaviors [7]. Prior experimental results have established an average of residual resistance of 3-4 nΩ in 1.3-1.5 GHz large-grain Nb cavities.

Various surface processing and treatment techniques are adopted for comparison. The effect of cryogenic thermal cycling on the quality factor is studied. Higher values of Q_0 are realized at high as well as medium gradients. Several cavities achieved a $Q_0 \sim 3\times10^{10}$ at 15 MV/m, 2×10^{10} at 35 MV/m at 2K. A 1.5 GHz CEBAF upgrade low-loss shape cavity achieved a best result of E_{acc} = 49 MV/m at $Q_0 = 1.5\times10^{10}$ at 1.8 K. A 1-cell 1.3 GHz large-grain Nb TTF shape cavity achieved a best result of E_{acc} = 41 MV/m at $Q_0 = 6.5\times10^{10}$ at 1.4 K

* Authored by Jefferson Science Associates, LLC under U.S. DOE Contract No. DE-AC05-06OR23177. The U.S. Government retains a non-exclusive, paid-up, irrevocable, world-wide license to publish or reproduce this manuscript for U.S. Government purposes.
Work partially supported by the US-Japan Collaboration Fund.
[#]geng@jlab.org

CAVITY DESIGN, MATERIAL, FABRICATION AND PROCESSING

All cavities are built by using the standard forming and electron beam welding techniques. Table 1 gives a summary on the design, material and fabrication facilities.

Table 1: Niobium Cavity Design, Material and Fabrication

Cavity	Freq	Shape	Material*	EBW facility
G2	1.3 GHz	TTF EC[#]	TD**	JLAB
PJ1-1	1.3 GHz	TTF CC[##]	Ningxia	JLAB
PJ1-2	1.5 GHz	LL[###]	Ningxia	Ningxia
LSF1-2	1.3 GHz	LSF	Ningxia	JLAB
LSF1-3	1.3 GHz	LSF	Ningxia	JLAB

[#] EC: end cell; [##]CC: center cell; [###]LL: CEBAF upgrade low-loss shape. * All large-grain Nb disks are made from high RRR >300 ingot; ** TD: Tokyo Denkai.

Figure 1 shows the first completed LSF shape cavity (LSF1-2) along with cavity PJ1-1, parked in clean room, ready for final prepartion prior to vertical test.

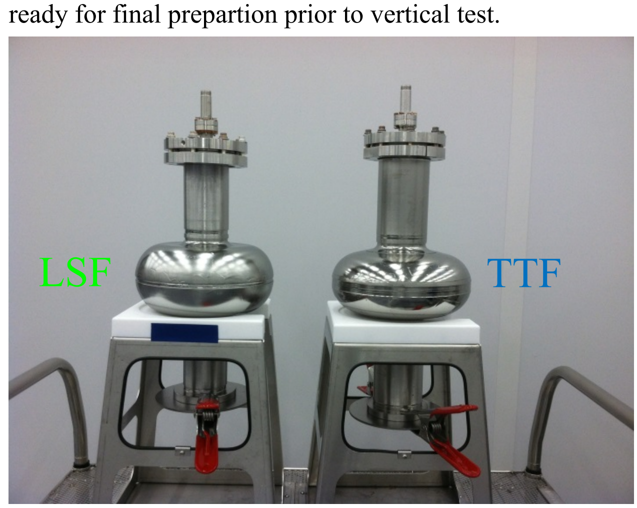

Figure 1: First 1-cell 1.3 GHz LSF shape cavity (L) made of large-grain Nb. A TTF shape 1-cell large-grain Nb cavity (R) is also shown for comparison.

ISBN: 978-3-95450-168-7 doi:10.18429/JACoW-IPAC2015-WEPWI015

BNL 56 MHz HOM DAMPER PROTOTYPE FABRICATION AT JLAB

N. Huque, E. F. Daly, W. Clemens, JLab, Newport News, VA 23606, USA
G. McIntyre, Q. Wu, S. Seberg, S. Bellavia, BNL, Upton, NY 11973, USA

Abstract

A prototype Higher-Order Mode (HOM) Damper was fabricated at JLab for the Relativistic Heavy-Ion Collider's (RHIC) 56 MHz cavity at Brookhaven National Laboratory (BNL). Primarily constructed from high RRR Niobium and Sapphire, the coaxial damper presented significant challenges in electron-beam welding (EBW), brazing and machining via acid etching. The results of the prototype operation brought about changes in the damper design, due to overheating braze alloys and possible multi-pacting. Five production HOM dampers are currently being fabricated at JLab. This paper outlines the challenges faced in the fabrication process, and the solutions put in place.

INTRODUCTION

Work on the prototype 56 MHz HOM Damper was started at JLab in July, 2013[1]. The agreement between BNL and JLab called for the following to be completed at JLab:

- Determine an assembly and fabrication sequence and plan
- Fabricate required components
- Conduct required welding, chemistry, brazing and inspection
- Tune fabricated damper
- Perform pressure and leak checks as required

The prototype was delivered to BNL in December, 2013.

DESIGN

A cut-away view of the prototype damper is shown in Fig. 1. The two main subsections of the damper are the Main Inductor and Filter Assembly.

Main Inductor

The Main Inductor connects to the Loop at the cavity end of the damper, and supports the Filter Assembly at the other end. The Inductor acts as the primary cooling mechanism for the damper. Essentially, it is a Niobium tube, through which a copper rod runs. The rod is connected via an interference fit at the Loop (the area of highest heat generation) and is immersed in flowing liquid helium at the Cooling Turret.

Filter Assembly

The Filter Assembly is a capacitor consisting of three Niobium and three Sapphire rings. The Niobium rings are connected to the outer shell of the damper via three inductor rods, and to the N-Type connected via another inductor rod. In the prototype, the rings were joined together by means of Stycast™. The final tuning of the damper was achieved by moving the entire Filter Assembly in an axial direction along the Main Inductor. The response frequency was measured by a network analyser coupling to the Loop. Figure 2 shows the tuning response. Once in the proper position, it was fixed in place using more Stycast™.

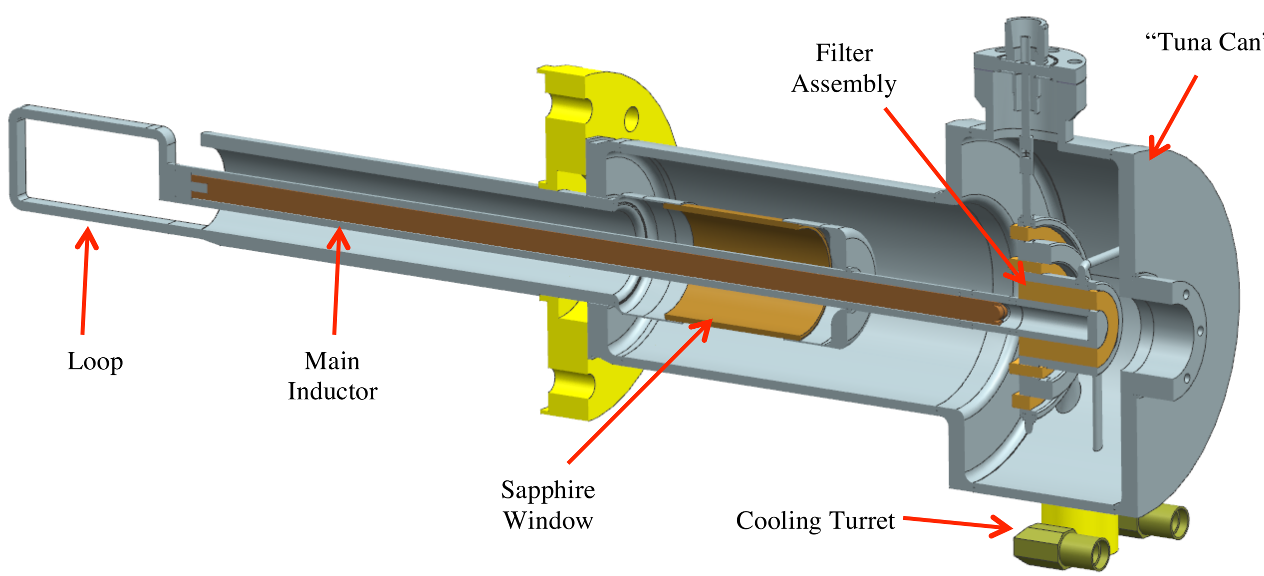

Figure 1. Cut-away view of the prototype damper, showing main components

Content from this work may be used under the terms of the CC BY 3.0 licence (© 2015). Any distribution of this work must maintain attribution to the author(s), title of the work, publisher, and DOI.

ISBN: 978-3-95450-168-7 doi:10.18429/JACoW-IPAC2015-WEPWI016

INVESTIGATION OF DIFFERENTIAL SURFACE REMOVAL DUE TO ELECTROPOLISHING AT JLAB*

F. Marhauser[#], J. Follkie, C.E. Reece, Jefferson Laboratory, Newport News, VA, USA

Abstract

The surface removal of JLab's present electropolishing process has been analyzed utilizing experimental data of six nine-cell 1.3 GHz superconducting radio frequency cavities that have been chemically post-processed in the frame of the LCLS-II high-Q development plan.

INRODUCTION

Surface chemistry carried out for superconducting radio frequency (SRF) cavities such as buffered chemical polishing (BCP) and electropolishing (EP) aims to uniformly remove the interior surface of a cavity along the entire structure and within each cell from equator to iris. A uniform removal is not readily achievable for either BCP or EP - though conceptually different - due to the complex chemical processes and varying process parameters (e.g. fluid flow, temperatures). The process-specific differential surface removal for instance impacts the cavity cell target frequency defined at the manufacturing stage. Quantifying the non-uniform removal helps to concurrently obtain the desired frequency and field flatness of an SRF cavity with minimum tuning effort and within tight tolerances [1]. An assessment of JLab's BCP system has been done in the past. The differential surface removal as experienced in the EP system has been quantified more recently as described in the following. It is based on experimental data in conjunction with numerical simulations. This includes the impact of EP on a cavity's fundamental mode field flatness.

MEASURMENTS

Removal from Integrated Current

Six LCLS-II (TESLA-type) R&D cavities (AES031-036) have been processed in the frame of the high-Q development plan [2]. The cavities have received a main (bulk) EP in preparation of the Nitrogen-doping, which is carried out as part of the 800°C vacuum furnace bake-out. A final (light) EP is applied after the doping process. The rather slow EP generally polishes the interior with a mixture of hydrofluoric acid and concentrated sulfuric acid. The EP at JLab is carried out horizontally (see Fig. 1). To stabilize process temperatures along the cavity, the external surface is constantly water-cooled via spray nozzles from below the cavity, while the cavity rotates (1 rpm). Cavity wall temperatures can typically be controlled within 20-25°C. To estimate the removal during the EP process, the accumulated charge is determined by recording the current over time flowing from the inserted cathode to the anode (cavity) taking into account the surface area of the cavity. With five electrons per niobium atom removed from anode and cathode reactions, the bulk removal rate is 2.247e-5 cm^3 Nb/Cb. The nominal voltage between cathode and anode is 13.5 ± 0.2 V. The EP process is stopped once the prospected removal is achieved. The assessed wall removal based on this method is summarized in Table 1. The main rather slow EP was carried out in two steps for operational convenience since the duration consumes more than a normal workday. The total removal by EP was around 140 µm at this point of time and well controlled among cavities.

Figure 1: Left: LCLS-II R&D cavity prepared for EP at JLab. Right: Arrangement of water-spray nozzles for external cooling of cavity walls.

Table 1: Wall Removal Evaluated from the Integrated Current for the Main (1st And 2nd Pass) and Final EP

Cavity ID	Main EP 1st pass (µm)	Main EP 2nd pass (µm)	Final EP (µm)	Total (µm)
AES-031	106.9	21.4	16.1	144.4
AES-032	96.2	26.7	16.1	139.0
AES-033	96.2	26.7	16.0	139.0
AES-034	96.2	26.7	16.1	139.0
AES-035	90.9	32.1	16.1	139.0
AES-036	96.2	26.7	16.1	139.0

Ultra-sonic Thickness Measurements

Though the assessment based on the integrated current is sufficiently accurate to control the EP process, it does not provide information with regard to the differential removal between irises and equators. Therefore, wall thickness measurements utilizing an ultra-sonic (US) gauge have been performed before and after the main EP. The measurements include one location close to the equator and one close the stiffening ring for each half cell. Locations below stiffening rings and close to irises are not accessible. Yet, measurements have been done directly on the beam tubes adjacent to end cells. Figure 2 plots the removal averaged for four repetitive measurements per location along each cavity to consider systematic errors. A quite uniform removal among equators has been

*Authored by Jefferson Science Associates, LLC under U.S. DOE Contract No. DE-AC05-06OR23177
marhause@jlab.org

Content from this work may be used under the terms of the CC BY 3.0 licence (© 2015). Any distribution of this work must maintain attribution to the author(s), title of the work, publisher, and DOI.

ISBN: 978-3-95450-168-7 doi:10.18429/JACoW-IPAC2015-WEPWI019

Content from this work may be used under the terms of the CC BY 3.0 licence (© 2015). Any distribution of this work must maintain attribution to the author(s), title of the work, publisher, and DOI.

QUENCH STUDIES OF SIX HIGH TEMPERATURE NITROGEN DOPED 9 CELL CAVITIES FOR USE IN THE LCLS-II BASELINE PROTOTYPE CRYO-MODULE AT JEFFERSON LABORATORY

A. D. Palczewski*, G. Eremeev, R.L. Geng, and C. E. Reece
Jefferson Lab (SRF R&D), Newport News, VA, USA

Abstract

Jefferson Lab (JLab) processed six nine-cell cavities as part of a small-scale production for LCLS-II cavity processing development utilizing the promising nitrogen-doping process. [1] Various nitrogen-doping recipes have been scrutinized to optimize process parameters with the aim to guarantee an unloaded quality factor (Q_0) of 2.7e10 at an accelerating field (Eacc) of 16 MV/m at 2.0 K in the cryomodule. During the R&D phase the characteristic Q0 vs. Eacc performance curve of the cavities has been measured in JLab's vertical test area at 2 K. The findings showed the characteristic rise of the Q0 with Eacc as expected from nitrogen-doping. Initially, five cavities achieved an average Q0 of 3.3e10 at the limiting Eacc averaging to 16.8 MV/m, while one cavity experienced an early quench accompanied by an unusual Q_0 vs. Eacc curve. The project accounts for a cavity performance loss from the vertical dewar test (with or without the helium vessel) to the horizontal performance in a cryomodule, such that these results leave no save margin to the cryomodule specification. Consequently, a refinement of the nitrogen-doping has been initiated to guarantee an average quench field above 20 MV/m without impeding the Q_0. This paper covers the refinement work performed for each cavity, which depends on the initial results, as well as a quench analysis carried out before and after the rework during the vertical RF tests as far as applicable.

INTRODUCTION

JLab is collaborating with FNAL and Cornell to expedite the development and exploitation of methods to produce dramatically lower-loss SRF cavities using the nitrogen-doping (N-doping) technique discovered by FNAL. [1] The LCLS-II project is eager to take advantage of these developments to minimize cryogenic capital and operating costs. JLab's contribution to this effort centered on systematic processing and tests of a set of single-cell 1.3 GHz cavities, followed by a "'production-style"' run treating six existing TESLA-style nine-cell cavities (AES031-036) to assess the performance in dependence on various nitrogen-doping recipes. Based on the single cell tests, a recipe for the nine-cell cavities has been determined which meets the desired project specifications. The initial nine-cell surface processing consisted of a UHV furnace heat treatment at 800 deg. C for 3 hours followed by controlled nitrogen injection for 20 minute at an average N2-pressure of 26 mTorr with an additional 30 minute annealing time under vacuum before letting the furnace cool down unconstrained with active pumping. After the N-doping each cavity received a 16 μm interior surface removal by Electropolishing (EP) to remove the topical highly nitrogen-enriched surface layer. [3] The nomenclature used in the following refers to the nitrogen injection time (N), annealing time (A) and EP surface removal, e.g. here **N20A30_EP16**. Three of the first nine-cell tests were published already. [4]

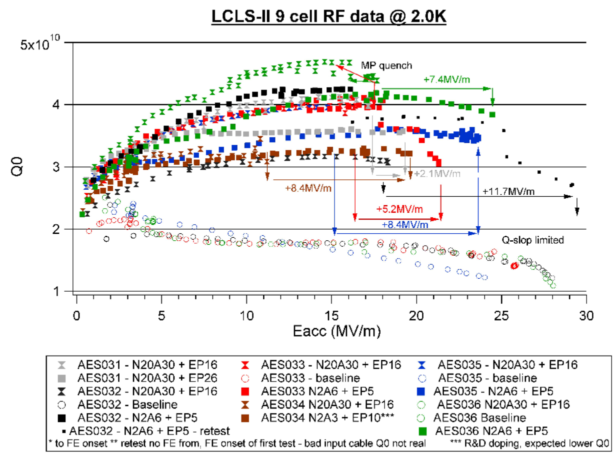

Figure 1: All RF test results for the 6 - 9 cell cavities.

At this time is became clear that although a sufficiently high Q_0 could be guaranteed at 16 MV/m, but the average quench field (Q_o >16=MV/m) was too close to the LCLS-II operating specification. In addition one has to consider that all N-doped cavities quenched at a much lower field than routinely achievable with conventional post-processing methods. [5] Consequently, an alternate recipe is scrutinized to obtain an average quench field beyond 20 MV/m without reducing the high Q0 already achieved. An N-doping refinement program resulted in a N2A6 EP5 recipe, which in fact resulted into quench fields 20 MV/m. [6] As a consequence, four of the six cavities at JLab were 'reset' by removing 50 μm from the

* ari@jlab.org, Authored by Jefferson Science Associates, LLC under U.S. DOE Contract No. DE-AC05-06OR23177, with support from the LCLS-II Project.
[1] Qo for cavities has an additional 1.4nohms residual removed for all data because of stainless steel flanged present on cavity. [2]

ISBN: 978-3-95450-168-7 doi:10.18429/JACoW-IPAC2015-WEPWI021

AN ANALYSIS OF THE TEMPERATURE AND FIELD DEPENDENCE OF THE RF SURFACE RESISTANCE OF NITROGEN-DOPED NIOBIUM SRF CAVITIES WITH RESPECT TO EXISTING THEORETICAL MODELS*

C. E. Reece#, A. D. Palczewski, JLab, Newport News, VA 23606, USA
B. P. Xiao, BNL, Upton, NY 11973, USA

Abstract

Recent progress with the reduction of rf surface resistance (R_s) of niobium SRF cavities via the use of high temperature surface doping by nitrogen has opened a new regime for energy efficient accelerator applications. For particular doping conditions one observes dramatic decreases in R_s with increasing surface magnetic fields. The observed variations as a function of temperature may be analyzed in the context of recent theoretical treatments in hopes of gaining insight into the underlying beneficial mechanism of the nitrogen treatment. Systematic data sets of Q_0 vs. E_{acc} vs. temperature acquired during the high Q_0 R&D work of the past year will be compared with theoretical model predictions.

INTRODUCTION

For many years the SRF community has informally assumed that the best performance to be obtained from SRF cavities was an rf surface with linear dissipation properties over the full dynamic range up until magnetic flux penetration phenomenon begins to create fundamental field limitations. The "best possible" performance was described by BCS losses produced by quasi-particle scattering according to the Mattis-Bardeen theory[1] for the surface resistance of a superconductor, and most conveniently calculated using the SRIMP code constructed by Halbritter[2] in the 1970's.

This changed in 2012-2014 when reports of experimental observation of unprecedentedly low $R_s(B)$ appeared with distinctly *decreasing* dependence on surface magnetic field appeared[3-5], as did first theoretical predictions of such a phenomenon[6, 7]. A fresh attempt at developing a theoretical expectation for $R_s(B,T)$ was a simplified theory that sought to extend Mattis-Bardeen theory to higher fields[6]. This analysis addressed rf current induced pair breaking, but principally noted the effects of anisotropies in the distribution function of quasiparticles due to significant current flow, in the limit of thermal equilibrium. This latter constraint implies that the quasiparticle inelastic scattering time is short compared with the rf cycle. The anisotropic Fermi surface effectively induces a broadening of the peaks in the quasiparticle density of states without significant modification of the gap. This simplified theory, while limited in scope, perhaps provides some conceptual guidance for understanding the rather surprising decrease in $R_s(B)$, which had previously been analyzed only for very thin superconducting films[8].

A more rigorous and general theoretical treatment has recently been proposed by Gurevich[9]. This treatment allows for non-equilibrium distribution functions and overheated quasiparticles.

It is interesting to examine the correspondence of these theoretical treatments with the field and temperature performance of some cavities that have received "nitrogen doping" to see if one may thereby gain insight into both mechanism and optimization strategies for best cavity performance.

DOPING NB

Evidence to date indicates that the beneficially "alloyed" N in Nb by thermal diffusion takes up residence interstitially with a concentration in the surface of ~0.1%[10, 11]. Analyses indicate that such N would first populate vacancies, then octahedral symmetry sites[12]. An expected effect of the interstitial nitrogen is lowering of the electron mean free path, l. It has been well recognized that a minimum in R_s with l ~ 35 nm is both experimentally observed and predicted by Mattis-Bardeen theory. Temperature dependent properties of the high-Q N-doped cavities have been consistent with l = 7–12 nm[13], significantly lower than would be the predicted optimum.

It has also been suggested that a beneficial role of the interstitial N is its ability to stabilize interstitial H, so that NbH nano-precipitates do not form. Previous work established that each N atom in an octahedral site will stabilized one H in a tetrahedral site[12, 14-16]. Creating conditions at elevated temperatures which give energetic preference to populating vacancies with N rather than O or multiple H, and adequate additional N distributed in octahedral sites to bind the available H during cavity cooldown (H diffusion length estimated at ~30 µm[17]) thus inhibiting the formation of Nb hydrides. Similar trapping of H by substitutional Ti diffused to fill vacancies is attributed to the comparable high-Q cavities realized by that technique[5, 18].

It is interesting to note that a very similar phenomenon was reported by Ballantini *et al.* in 1999[19], with dry oxidation of a niobium cavity after high temperature heat treatment. One may speculate that perhaps that also populated the near surface in a way which effectively inhibited the formation of particular hydride forms within the rf surface. The decrease of $R_s(B)$ to ~70 mT was

*Authored by Jefferson Science Associates, LLC under U.S. DOE Contract No. DE-AC05-06OR23177 .
#reece@jlab.org

Content from this work may be used under the terms of the CC BY 3.0 licence (© 2015). Any distribution of this work must maintain attribution to the author(s), title of the work, publisher, and DOI.

ISBN: 978-3-95450-168-7 doi:10.18429/JACoW-IPAC2015-WEPWI022

RF SYSTEM REQUIREMENTS FOR A MEDIUM-ENERGY ELECTRON-ION COLLIDER (MEIC) AT JLAB *

R. A. Rimmer#, J. Guo, J. Henry, Y. Huang, H. Wang, S. Wang, JLab, Newport News, VA 23606 USA

Abstract

JLab is studying options for a medium energy electron-ion collider that could fit on the JLab site and use CEBAF as a full-energy electron injector. A new ion source, linac and booster would be required, together with collider storage rings for the ions and electrons. In order to achieve the maximum luminosity these will be high current storage rings with many bunches. We present the high level RF system requirements for the storage rings, ion booster ring and high-energy ion beam cooling system, and describe the technology options under consideration to meet them. We also present options for staging that might reduce the initial capital cost while providing a smooth upgrade path to a higher final energy. The technologies under consideration may also be useful for other proposed storage ring colliders or ultimate light sources.

INTRODUCTION

The Medium-energy Electron Ion Collider (MEIC) proposed by JLab requires a very high luminosity to meet the physics goals [1,2]. The collider will be a "ring-ring" configuration [3,4], figure 1, with polarized electrons coming from CEBAF [5], and polarized ions from a new ion complex. The general design philosophy is closer to that used for the B-factories [6,7] than for traditional hadron colliders, namely employing a large number of bunches with short bunch length, reasonable charge per bunch, and acceptable beam-beam tune shift. Due to the large crossing angle envisaged in the detectors a crab crossing scheme is proposed. These parameter choices define the RF system requirements that, though demanding, can be fulfilled by existing state of the art systems or reasonable extrapolations thereof. Recent re-baselining of the project has resulted in the adoption of the former PEP-II high-energy ring (HER) as the basis for the MEIC electron collider storage ring. This necessitates a change in the baseline RF frequency so the other storage ring RF systems must now also be harmonics of the PEP-II frequency (476 ± 0.5 MHz). Tables 1 and 2 list the high-level parameters of the new RF systems for MEIC.

MAJOR SYSTEMS

Electron Ring

The electron ring will be based on the PEP-II HER, reusing major components such as the magnets, vacuum chambers and RF systems, and operate up to 10 GeV [8].

* Authored by Jefferson Science Associates, LLC under U.S. DOE Contract No. DE-AC05-06OR23177.
#rarimmer@jlab.org

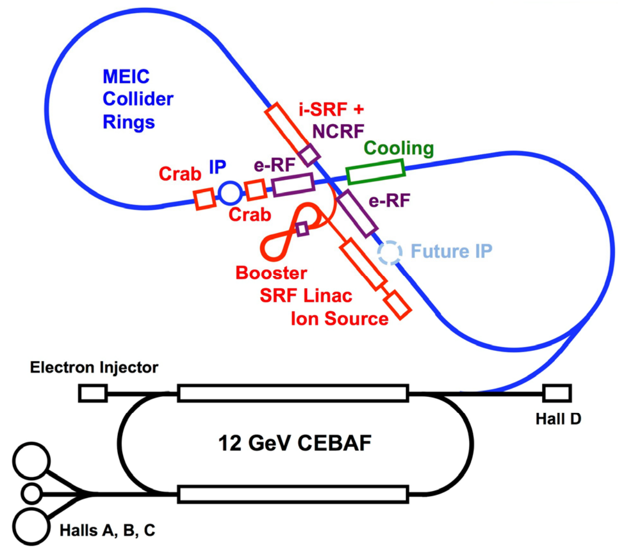

Figure 1: Schematic layout of figure-8 MEIC.

The circumference of the new baseline design figure-8 ring is similar to the PEP-II ring but since there is more total curvature the bending in each dipole is slightly higher than for PEP-II. At high energy the synchrotron radiation power density on the vacuum chamber wall in the arcs limits the current. The assumed vacuum chamber limit is 10 kW/m, and the maximum total synchrotron radiation power is chosen to not exceed 10 MW. 34 single-cell HOM-damped cavities and 13 1.2 MW klystrons are available from PEP-II, figure 2. At least 26 cavities and 10 klystrons will be needed for MEIC, though more may be installed to give operational margin.

Table 1: High Level MEIC RF Parameters

System	Frequency MHz	Total Voltage	Total Power
Booster	0.817-1.274	32 kV	98.5 kW
Ion capture	1.248-1.255	111 kV	357.4 kW
Ion-ring	952.6	18.94 MV	1.65 MW
e-ring	476.3	20.56 MV	12.8 MW
Crabbing	952.6	32.48 MV	~200 kW
Cooler ERL	952.6	56 MV	120 kW
Cooler inj.	952.6	10 MV	2.00 MW

Content from this work may be used under the terms of the CC BY 3.0 licence (© 2015). Any distribution of this work must maintain attribution to the author(s), title of the work, publisher, and DOI.

ISBN: 978-3-95450-168-7 doi:10.18429/JACoW-IPAC2015-WEPWI024

Content from this work may be used under the terms of the CC BY 3.0 licence (© 2015). Any distribution of this work must maintain attribution to the author(s), title of the work, publisher, and DOI.

VACUUM CHARACTERIZATION AND IMPROVEMENT FOR THE JEFFERSON LAB POLARIZED ELECTRON SOURCE*

M.L.Stutzman#, P.A.Adderley, M.Poelker, Jefferson Lab, Newport News, VA 23606, USA
Md.A.Mamun, Old Dominion University, Norfolk, VA 23529 USA

Abstract

Operating the JLab polarized electron source with high reliability and long lifetime requires vacuum near the XHV level, defined as pressure below 7.5×10^{-13} Torr. This paper describes ongoing vacuum research at Jefferson Lab including characterization of outgassing rates for surface coatings and heat treatments, ultimate pressure measurements, investigation of pumping including an XHV cryopump, and characterization of ionization gauges designed for this pressure regime.

MOTIVATION

The Jefferson Lab polarized electron source delivers an electron beam with polarization near 90% from a 130 kV DC high voltage electron gun. Lifetime is limited by the residual gasses in the system. These gasses are ionized by the electron beam and accelerated into the strained-superlattice photocathode, causing both ion implantation and affecting surface chemistry [1]. To enhance photocathode lifetime, and with the goal of developing higher current guns for future applications, a series of vacuum research measurements is underway. The pressure in a system is determined by the amount of gas entering the system and the effective removal of gas with pumps. As such, lower pressure can be obtained by reducing the gas load, which is dominated by hydrogen outgassing in UHV systems like photoguns, and/or increasing the pump speed. We describe our efforts to reduce outgassing and enhance pumping below. Furthermore, we discuss the challenges associated accurate pressure monitoring near the XHV regime.

OUTGASSING RATE STUDIES

Once a stainless steel vacuum chamber is baked to remove water vapor, the dominant gas in the chamber is hydrogen that originates from outgassing from the chamber walls. Measurements of the outgassing rate of small steel test chambers were made to determine the efficacy of reducing outgassing via medium temperature bakeouts, and by applying coatings to the chamber walls [2]. Two coatings were studied: titanium nitride (TiN) and amorphous silica (a-Si). Outgassing rates were measured for each system using a spinning rotor gauge and a gas accumulation method [3]. The lowest outgassing rates (at the room temperature of 25°C) are shown in Figure 1. Each value represents a significant outgassing rate reduction compared to the $1\text{x}10^{-12}$ $\text{TorrLs}^{-1}\text{cm}^{-2}$ outgassing rate typical of stainless steel that has undergone conventional 250°C bakeout.

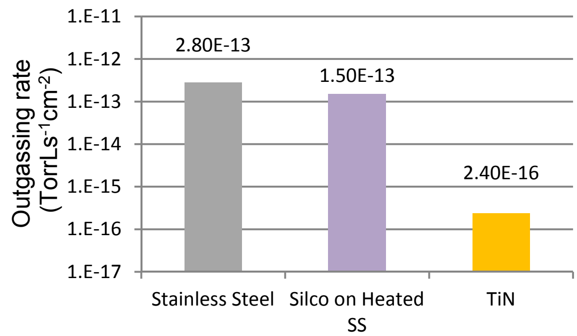

Figure 1: Best outgassing rate achieved for each chamber at room temperature of 25°C: the bare steel (304L stainless steel), the a-Si coating on 400°C heat treated steel, and the TiN coating.

BASE PRESSURE MEASUREMENTS

These outgassing rate values were inserted into the simple equation, $P = \frac{qA}{S}$, to predict the expected ultimate pressure P (Torr) that could be achieved for a given pump speed S (L/s), where q is the outgassing rate in $\text{TorrLs}^{-1}\text{cm}^{-2}$, and A is the internal area of the chamber in cm^2. Pumping for each chamber was provided by an ion pump [4] and non-evaporable getter modules [5], for a total pump speed of 1680 L/s. Following installation of pumps and bakeout, the pressure was measured using gauges with commercially rated for the XHV pressure range.

Table 1

Chamber	Expected Pressure (Torr)	Measured Pressure (Torr)
Stainless Steel	$8.6\times10^{-13} \pm 3\times10^{-13}$	$9.4\times10^{-13} \pm 4\times10^{-13}$
TiN Coating	$7.3\times10^{-16} \pm 3\times10^{-13}$	$1.0\times10^{-12} \pm 5\times10^{-13}$
a-Si coating	$4.6\times10^{-13} \pm 2\times10^{-13}$	$1.7\times10^{-12} \pm 8\times10^{-13}$

From Table 1, measured and predicted pressures are in reasonable agreement for the bare stainless steel and a-Si chambers. However, the measured pressure for the TiN system is greater than predicted pressure by three orders of magnitude. This can be understood by a careful examination of both the TiN coating chemical

*Work supported by U.S. DOE Contract No. DE-AC05-06OR23177 and with funding from the DOE R&D for Next Generation Nuclear Physics Accelerator Facilities Funding Opportunity Number: DE-FOA-0000339.
#marcy@jlab.org

ISBN: 978-3-95450-168-7 doi:10.18429/JACoW-IPAC2015-WEPWI028

Content from this work may be used under the terms of the CC BY 3.0 licence (© 2015). Any distribution of this work must maintain attribution to the author(s), title of the work, publisher, and DOI.

SIMULATION STUDY USING AN INJECTION PHASE-LOCKED MAGNETRON AS AN ALTERNATIVE SOURCE FOR SRF ACCELERATORS

H. Wang, T. Plawski, R.A. Rimmer
Thomas Jefferson Lab, Newport News, VA 23606, USA

Abstract

As a drop-in replacement for the CEBAF CW klystron system, a 1497 MHz, CW type high efficiency magnetron using injection phase lock and amplitude variation is attractive. Amplitude control using magnetic field trimming and anode voltage modulation has been studied using analytical models and MATLAB/Simulink simulations. Since the 1497 MHz magnetron has not been built yet, previously measured characteristics of a 2.45GHz cooker magnetron are used as reference. The results of linear responses to the amplitude and phase control of a superconducting RF (SRF) cavity, and the expected overall benefit for the current CEBAF and future MEIC RF systems are presented in this paper.

MAGNETRONS VERSUS KLYSTRONS

Magnetrons used in industrial and medical accelerators normally have 85-95% electronic efficiency, much higher than typical klystrons within the same perveances [1]. As a comparison shown in Fig. 1, this advantage is independent of the wavelengths (which are given in Fig. 1 in cm marked up next to their data points). The pictures show the two types of klystrons used at CEBAF, one 2.45GHz cooker magnetron (used in our experiment in ref. [2]) and one family of L3 magnetrons (potential candidate for MEIC SRF system) for the reference data points. The fundamental difference between the two types of devices is the electron bunch formation: linear motion in the klystron; circular motion in the magnetron. Space charge effects in the motion dominate the efficiency. The spoke-on-hub bunches in a magnetron interact with the anode RF cavity in multi-gaps over multiple-passes. Space charge de-bunching effect on the spokes is reduced. The beam bunching and power extraction in a klystron is a linear interaction with cavity gaps and only one pass. Also the spent energy from decelerated electrons in a magnetron is returned to the cathode which further helps the emission. But in a klystron, it is dumped into a collector which reduces efficiency further.

The traditional klystron works as a high gain linear amplifier driven by a low level signal. Its output phase and amplitude can be controlled at both low and high levels. It can be also operated in either CW or pulsed mode with a modulator. The capital cost is in the range $5-25/output Watt depending on the power and production quantity. The magnetron is a saturated oscillator which does not need a drive for oscillation at high power output, but can be seeded by a back injection signal through its output waveguide, in which case its output phase will follow the injection phase. It can be also both operated in CW or pulsed modes as long as the pulse width is longer than the magnetron starting time. If it is designed properly, it can be operated in both high gain and high efficiency as well as low production cost, e.g. less than $1/output Watt for a typical oven magnetron.

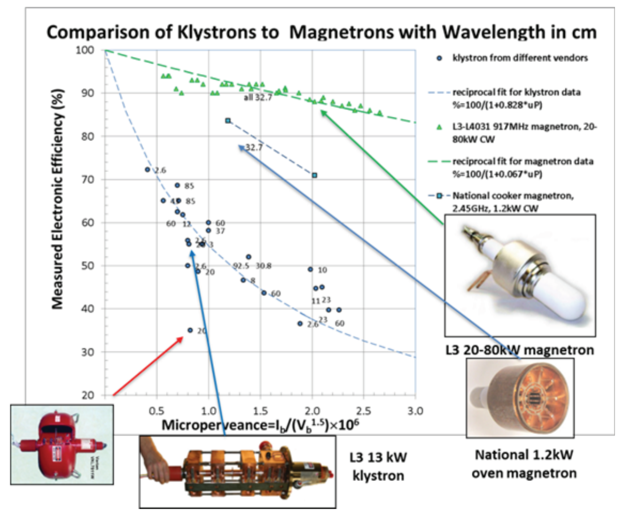

Figure 1: Comparison of electronic efficiencies between klystrons and magnetrons

BENEFITS TO CEBAF AND MEIC

The ultimate goal of using magnetrons instead of klystrons for the current CEBAF and future MEIC machines is the both capital and operation cost reduction in the electric power. Using the numbers from the RF power requirement for the current designed MEIC complex [3], a total DC power saving of 7.2-9.7MW has been estimated. This results $3.9-5.2M annual power cost saving if 41 weeks operation is assumed. Savings for CEBAF operation and other MEIC systems are shown in Table 1.

First demonstration and performance of an injection locked CW magnetron to phase control a SRF cavity was done at JLab in conjunction with Lancaster University, UK, in 2010 [1] with accuracy of 0.95° rms, -23.5dB injection input and 540W output.

However, using magnetrons to drive MEIC or other SRF accelerators like CEBAF still needs more R&D work particularly to demonstrate the amplitude control of a magnetron while preserving the high efficiency. If the magnetron can be operated as a voltage controlled oscillator while maintaining the injection phase lock, then this cost benefit will be significant to the accelerator community.

ISBN: 978-3-95450-168-7 doi:10.18429/JACoW-IPAC2015-WEPWI029

Content from this work may be used under the terms of the CC BY 3.0 licence (© 2015). Any distribution of this work must maintain attribution to the author(s), title of the work, publisher, and DOI.

CAVITY DESIGN, FABRICATION AND TEST PERFORMANCE OF 750MHz, 4-ROD SEPARATORS FOR CEBAF 4-HALL BEAM DELIVERY SYSTEM

H. Wang, G. Cheng, L. Turlington, M. Wissmann
Thomas Jefferson Lab, Newport News, VA 23606, USA

Abstract

A short version of the original CEBAF normal conducting 4-rod separator cavity has been developed into a 750 MHz one [1] since the concept of simultaneous 4-hall operation for CEBAF is introduced [2]. This work has been advanced further based on the EM design optimization, bench measurement and by conducting RF-thermal coupled simulation using CST and ANSYS to confirm the cavity tuning and thermal performance. The cavity fabrication used matured technology like copper plating and machining. The cavity flanges, couplers, tuners and cooling channels adopted consistent /compatible hardware with the existing 500 MHz cavities. The electromagnetic and thermal design simulations have greatly reduced the prototyping and bench tuning time of the first prototype. Four production cavities have reached a typical 1.94 MV kick voltage or 3.0 kW wall loss on each cavity after a minor multipactoring or no processing, 7.5 % overhead power than the design specification.

INTRODUCTION

Delivering CEBAF electron beam simultaneously to four experimental halls A-B-C-D scheme has been proposed by Kazimi in 2013 [2]. In this scheme, all halls have to run 250MHz repetition rate and one of A-B-C halls has to share the 5^{th} beam pass with Hall D as shown in Fig. 1. To achieve this goal and not dismount existing 500MHz beam separation systems for Halls A-B-C, a 750 MHz RF separator system to kick beam bunches horizontally as the way shown in Fig. 2 is needed. Other hardware development and initial 750 MHz 4-rod type separator cavity were recognized [2].

Primary electromagnetic design optimization was done immediately after this proposal based on the existing 500 MHz, 4-rod type, normal conducting, deflecting cavities used at the CEBAF for 3-hall beam delivery system [1].

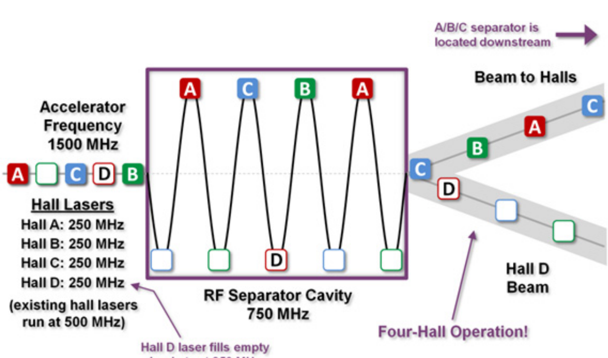

Figure 1: 4-hall beam operation with 750 MHz separator system proposed in ref. [2].

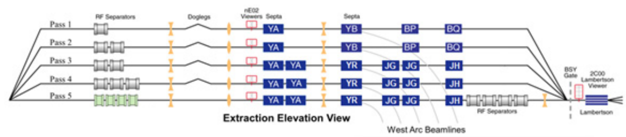

Figure 2: Four 750MHz separator cavities (in green colour) are installed on the 5^{th} pass of CEBAF beam extraction system for horizontal deflection.

CAVITY DESIGN AND SPECIFICATION

Primary design optimization shows that the TEM 4-rod type deflecting cavity has a relative high shunt impedance R_t compared to elliptical and TE type cavities as long as the beam aperture to wavelength ratio is small. So we used the same aperture diameter (15 mm) as the 500 MHz cavities for the new 750 MHz design. By varying the rod diameters from 2 cm, 2.5 cm, 3 cm to 4 cm, we found the 2 cm's design gives the highest R_t versus the thicker rod diameters. Using the same cavity structure, tuner, body, mid and end flanges hardware as the original 500 MHz's cavity, only shortening the rods and body lengths were needed for the new design. So we were able to quickly prototype and produce these new cavities.

The cavity design parameters and specification are listed in the Table 1. To get a 170μrad kick angle for the 11 GeV beam, the total peak transverse kick voltage is 1.87 MV. If 4 cavities are to be used, each cavity has to run at 2.79 kW in peak power.

Table 1: Cavity Design Parameters

Frequency (π mode, MHz)	748.5
0-mode frequency separation (MHz)	+5.944
Cell-to-cell coupling (%)	1.21
Beam aperture (mm)	15
R_t/Q including TTF ($=V_t^2/(\omega U)$, kΩ)	17.71
Q_0 (calculated, for room temp. copper)	4426
Q_{ext}	4426
Klystron Power/cavity (KW)	2.79
Peak power loss density (W/cm^2)	28.1
Total cavity number	4
Total deflecting angle (μrad)	±170
Deflecting beam energy (GeV)	11.0

Both the 500 MHz and 750 MHz cavities' CAD models were generated started from the early engineering drawings. The electromagnetic (EM) and thermal

ISBN: 978-3-95450-168-7 doi:10.18429/JACoW-IPAC2015-WEPWI030

INJECTOR CAVITIES FABRICATION, VERTICAL TEST PERFORMANCE AND PRIMARY CRYOMODULE DESIGN

H. Wang#, G. Cheng, B. Clemens, K. Davis, K. Macha, R. Overton, D. Spell
Thomas Jefferson Lab, Newport News, VA 23606, USA

Abstract

After the electromagnetic design [1] and the mechanical design [2] of a beta=0.6, 2-cell elliptical SRF cavity, the cavity has been fabricated. Then both 2-cell and 7-cell cavities have been bench tuned to the target values of frequency, coupling external Q and field flatness. After buffer chemistry polishing (BCP) and high pressure rinses (HPR), Vertical 2K cavity test results have been satisfied the specifications and ready for the string assembly. We will report the cavity performance including Lorentz Force Detuning (LFD) and Higher Order Modes (HOM) damping data. Its integration with cavity tuners to the cryomodule design will be reported.

SPECIFICATION AND STRING LAYOUT

The new SRF cryomodule construction for the CEBFA injector has been restarted and built until the string assembly. This cryomodule used to be two 5-cell cavities built within a quarter CEBAF cryomodule. Now it is going to be placed after the chopper, buncher and capture sections and before R100 (C100 prototype) cryomodule. In order to overcome the difficulties during the beam tuning up operation for the CEBAF injection particularly for the new 12 GeV machine, this new cryomodule contains a low beta cavity which can handle the low injection energy beam (~200 keV) well both in bunching and acceleration processes without blowing emittance up. After electrons reaching nearly relativistic ($\beta \approx 0.99$), acceleration can be taken by the R100, $\beta=1$ cryomodule up to 130MeV. Table 1 lists the cryomodule design specification derived from the beam dynamic analysis and beam user requirement. This derivation has been documented in a project note [3]. The minimization of transverse RF kick induced by the FPCs without a skew quadruple effect (x-y coupling) on the beam trajectory is critical for the cavity design. This achievement has been described in publication [1] and its references.

After the electromagnetic design [1] and the mechanical design [2] of the 2-cell cavity, the cavity has been fabricated in 2013. After delay holds due to funding, the project was restarted in April 2014. First step is to qualify both cavities in vertical tests. The second step is to advance the cryomodule design for primary components including cavity tuners, magnetic shields, and beam pipe components by taking the advantage of C100 type design for the 12GeV Upgrade. The third step will be hardware preparation for the clean room string assembly like the design layout in Figure 1.

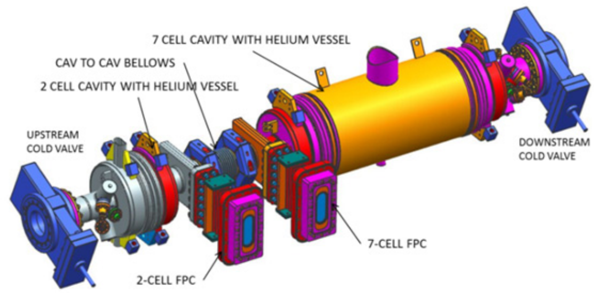

Figure 1: String assembly design of injector cryomodule electrons beam runs from 2-cell to 7cell cavity.

Table 1: Injector Cryomodule Design Specification

Cavity type	2-cell	7-cell
End beam energy (MeV)	0.533	5
Peak on axis E field (MV/m) nominal / (range)	4.6 (2-8)	13.2 (8-26)
E_{acc} including TTF (MV/m) nominal / (range)	2.6 (1.1-4.5)	7.1 (4.3-14.1)
Beam voltage V_a (MV) nominal / (range)	0.33 (0.13-0.54)	4.9 (3-10)
Beam current I (mA) nominal/max	0.38/1.0	
Geometry β_g	0.6	0.97
Q_0 at nominal gradient	>4E9	>8E9
Off-crest phase setup Φ_b (deg)	-17	-15
FPC Qext for max. beam current	6E6	9E6
FPC Qext for nominal beam current by using stub tuner	1.3E7	2.0E7
Klystron power for max E_{acc} 1mA beam current (kW)	0.547	14.6
HOMs dipole Imp.[1] $R_\perp$, Ω/m	<2.4E10	<2.4E10
FPC RF kick dP_y/P_z (mrad)	<1	<2
Tuning Sensitivity, (MHz/mm) ANSYS	2.63 cold	0.592 cold 0.431 warm m.
Helium Pressure Sensitivity (Ref. only, Hz/Torr)	382	320

CAVITIES' FABRICATION

The specification for two cavities for the vertical cold test acceptance criteria has been developed in Table 2.

* Authored by Jefferson Science Associates, LLC under U.S. DOE Contract No. DE-AC05-06OR23177. The U.S. Government retains a non-exclusive, paid-up, irrevocable, world-wide license to publish or reproduce this manuscript for U.S. Government purpose.
# haipeng@jlab.org

Content from this work may be used under the terms of the CC BY 3.0 licence (© 2015). Any distribution of this work must maintain attribution to the author(s), title of the work, publisher, and DOI.

ISBN: 978-3-95450-168-7 doi:10.18429/JACoW-IPAC2015-WEPWI032

Content from this work may be used under the terms of the CC BY 3.0 licence (© 2015). Any distribution of this work must maintain attribution to the author(s), title of the work, publisher, and DOI.

MECHANICAL PROPERTIES OF NIOBIUM CAVITIES*

G. Ciovati#, P. Dhakal, J. Matalevich, G. R. Myneni, JLab, Newport News, VA 23606, USA

Abstract

The mechanical stability of bulk Nb cavity is an important aspect to be considered in relation to cavity material, geometry and treatments. Mechanical properties of Nb are typically obtained from uniaxial tensile tests of small samples. In this contribution we report the results of measurements of the resonant frequency and local strain along the contour of single-cell cavities made of ingot and fine-grain Nb of different purity subjected to increasing uniform differential pressure, up to 6 atm. Measurements have been done on cavities subjected to different heat treatments. Good agreement between finite element analysis simulations and experimental data in the elastic regime was obtained with a single set of values of Young's modulus and Poisson's ratio. The experimental results indicate that the yield strength of medium-purity ingot Nb cavities is higher than that of fine-grain, high-purity Nb.

INTRODUCTION

An important aspect of cavity design is a structural analysis under different load conditions to verify that the maximum stress is well below the yield strength of the material. Typically, the highest load applied to the cavities occurs at the beginning of a cavity cool-down from 300 K to liquid He temperature inside a cryomodule, when loading due to a mechanical tuner attached to the cavity and pressurized helium gas flowing around the cavity occurs [1]. In recent years, it was also realized that cavities can be considered part of a "pressure vessel", as they are part of the boundary of a liquid helium reservoir, and therefore the structural and material analysis should comply with "pressure vessel code" specifications, which are different in different regions of the world [2-4].

The structural analysis of cavities is typically done using commercial finite-element analysis (FEA) computer software, with user-defined stress versus strain curves for the niobium material. Such stress versus strain curves are derived from "conservative" reviews of literature data from uniaxial tensile tests of flat samples which had been subjected to different treatments. The literature data show a progressive reduction of both yield and tensile strength of fine-grain (ASTM ≥ 5) Nb after heat-treatment at increasingly higher temperature, above ~600 °C [5-7]. Large variations in the values of yield and tensile strength have been reported even for samples subjected to the same treatment, depending on batches of material and/or material supplier [8-11]. The situation is even more complicated when considering ingot Nb material, for which tensile test samples only have a very small number of grains, if any, which results in a large variability in tensile test results, depending on the crystal orientation of the samples [7, 12-14]. Furthermore, the Nb material is subjected to a plastic deformation during the deep-drawing into half-cells and, as a result of the subsequent annealing of the entire Nb cavity, the behaviour of the material under mechanical loading can, in general, be different than for the case of flat tensile test samples which have no initial plastic deformation [15].

In the following section we present some results on the measurements of the local strain and resonant frequency of single-cell elliptical Nb cavities of the same shape subjected to an increasing uniform external pressure at room temperature. The experimental data have been used to guide the FEA of the cavity.

EXPERIMENTAL RESULTS

The single-cell cavities used for this study have the same shape as that of the original cavities for the CEBAF accelerator [16]. A schematic drawing of the cavity is shown in Fig. 1 along with a schematic of the location of the strain gages. The strain gages attached near the iris are "tee rosettes", allowing to measure strain in the longitudinal (gages No. 1 and 3) and azimuthal directions (gages No. 2 and 4). The strain gages attached on the side wall (gage No. 5) and close to the equator (gage No. 6) measured strain in the longitudinal direction. Further details about the strain gages and the experimental setup can be found in Ref. [17] and in a forthcoming publication.

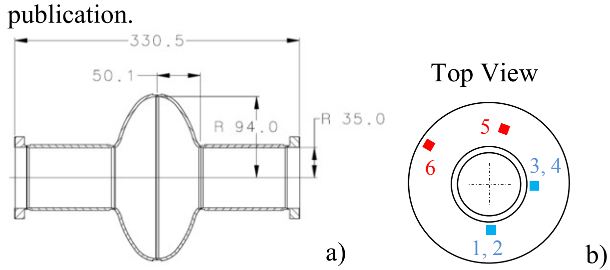

Figure 1: Schematic drawing of the single-cell cavity (a) and approximate location of the strain gages (b). Dimensions are in mm.

Cavities were placed inside a pressure tank. The inside volume of the cavity was filled with air at 1 atm. Uniform pressure is applied to the outside surface of the cavity by pumping DI water into the pressure tank. Strain, Δε, and frequency shift, Δf, as a function of applied pressure, P, were measured on four single-cell cavities made of Nb material with different properties, listed in Table 1. The fine-grain material was from ATI Wah Chang, the ingot

* This manuscript has been authored by Jefferson Science Associates, LLC under U.S. DOE Contract No. DE-AC05-06OR23177. The U.S. Government retains a non-exclusive, paid-up, irrevocable, world-wide license to publish or reproduce this manuscript for U.S. Government purposes.

#gciovati@jlab.org

ISBN: 978-3-95450-168-7 doi:10.18429/JACoW-IPAC2015-WEPWI033

EFFECTS OF PLASMA PROCESSING ON SECONDARY ELECTRON YIELD OF NIOBIUM SAMPLES

M. Basovic, S. Popovic, M. Tomovic, L. Vuskovic, Center for Accelerator Science, Old Dominion University, Norfolk, VA 23529, USA
A. Samolov, F. Cuckov, Department of Engineering, University of Massachusetts, Boston, MA 02125, USA

Abstract

Impurities deposited on the surface of niobium (Nb) during both the forming and welding of accelerator cavities add to the imperfections of the sheet metal, which then affects the overall performance of the cavities. This leads to a drop in the Q factor and limits the maximum acceleration gradient achievable per unit length of the cavities. The performance can be improved either by adjusting the fabrication and preparation parameters, or by mitigating the effects of fabrication and preparation techniques used. We have developed the experimental setup to determine the Secondary Electron Yield (SEY) from the surface of Nb samples. Our aim is to show the effect of plasma processing on the SEY of Nb. The setup measures the secondary electron energy distribution at various incident angles as measured between the electron beam and the surface of the sample. The goal is to determine SEY on non-treated and plasma treated surface of electron beam welded samples. Here we describe the experimental setup, plasma treatment device, and fabrication and processing of the Nb samples.

INTRODUCTION

Apart from the accelerated beam particles, cavities under operating conditions contain a small amount of free charged particles. The number of particles inside the cavity is increased due to the Secondary Electron Emission (SEE). Free particles are accelerated by receiving energy from the electromagnetic field confined inside the cavities. Under specific conditions those particles can impact the surface of cavities and create additional free electrons. An increase in the quantity of the free electrons in a confined space of a cavity can cause a detrimental effect on the accelerated particles and thus limit the effectiveness of cavities. Multiplication of electrons is called multipacting (MP) and leads to the high power losses and heating of the cavity walls [1]. Energy consumed by the increasing number of electrons prevents the increase of the accelerating field by increasing the power input.

Substantial research effort on the topic of SEE to date has determined that SEY is highly dependent on the surface treatment. It has been shown that exposure of the material surface to increased temperatures progressively reduces the SEY [2, 3]. Various surface coatings have also shown the ability to reduce the SEY on various substrate materials [4, 5, 6, 7]. The scrubbing effect of the continuous exposure of the surface to electron beam has been noticed on the copper samples [8]. The effect of air exposed metal surfaces on SEY is shown in [9]. Exposure of the Nb to glow discharges of various gasses changed the SEY curve compared to the untreated surface [2].

SEE depends on the energy dissipated by the primary electrons near the surface. Our analysis of energy spectra of secondary electrons indicates that the fraction of the dissipated energy of primary electrons reaches the maximum at the primary energies that produce the maximum yield. It can be illustrated by a case of typical SEE energy distribution and SEY from a clean Nb coupon.

Total energy returned to the field has been carried equally by true, back-diffused, and elastically reflected secondary electrons, although their number distribution is more shifted toward low energy. Overall relative energy feedback carried by the secondary electrons is

$$\Gamma = \frac{1}{E_p}\int_0^{E_p} f_P\left(E_p, E\right) dE \cong 0.3 \quad for \quad E_p = 200\,eV. \qquad (1)$$

That is, only 30% of the primary energy has been returned to the field and 70% is dissipated in the Nb coupon. We have analyzed this energy balance for a number of metal targets, whereby we have been restricted only to experimental data on the secondary electron energy distribution. For example, the available data for copper show that maximum dissipation into the target coincides with the maximum yield (see Fig. 1).

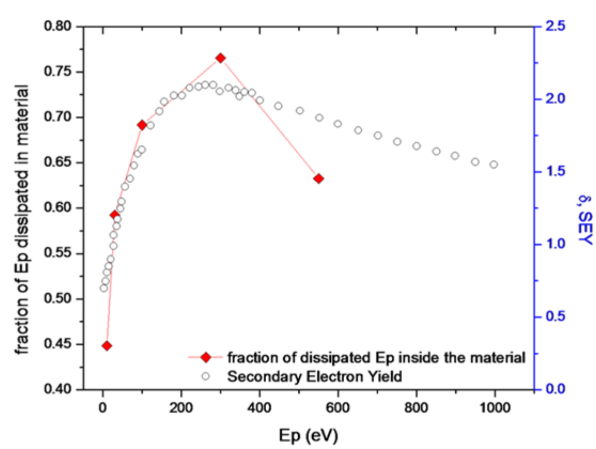

Figure 1: Energy dependence of the fraction of dissipated primary electron energy compared to the SEY curve for conditioned copper.

Content from this work may be used under the terms of the CC BY 3.0 licence (© 2015). Any distribution of this work must maintain attribution to the author(s), title of the work, publisher, and DOI.

ISBN: 978-3-95450-168-7 doi:10.18429/JACoW-IPAC2015-WEPWI034

EFFECTS OF CRAB CAVITIES' MULTIPOLE CONTENT IN AN ELECTRON-ION COLLIDER*

A. Castilla[1,2,3†], V. S. Morozov[2], T. Satogata[1,2], J. R. Delayen[1,2].
[1]Center for Accelerator Science, Old Dominion University, Norfolk, VA 23529, USA.
[2]Thomas Jefferson National Accelerator Facility, Newport News, VA 23606, USA.
[3]Universidad de Guanajuato (DCI-UG), Departamento de Fisica, Leon, Gto. 37150, Mex.

Abstract

The impact on the beam dynamics of the Medium Energy Electron-Ion Colider (MEIC) due to the multipole content of the 750 MHz crab cavity was studied using thin multipole elements for 6D phase space particle tracking in ELEGANT. Target values of the sextupole component for the cavity's field expansion were used to perform preliminary studies on the proton beam stability when compared to the case of pure dipole content of the rf kicks. Finally, important effects on the beam sizes due to non-linear components of the crab cavities' fields were identified and some criteria for their future study were proposed.

INTRODUCTION

Strong interest has been generated among the nuclear physics comunity for building an Electron-Ion Collider with a broad range of center of mass energy ($\sqrt{s} = 20 - 70$ GeV) and high luminosities ($\sim 10^{34}\mathrm{cm}^{-2}\mathrm{s}^{-1}$) per interaction point (IP) [1]. In order to have a full acceptance detector, a relatively large crossing angle (50 mrad) of the colliding beams has to be introduced. Then, the only way to reach the high luminosity required is to implement crab crossing correctors. A crab cavity suitable for this application is an rf deflector that operates at the transverse voltages needed to restore this angle for both protons up to 150 GeV and electrons up to 20 GeV. The design proposed as crab cavity candidate for the MEIC at Jefferson Lab is an rf dipole geometry that operates on a fundamental TE-like mode. The exercises performed in the present paper use the former MEIC baseline frequency of 750 MHz to analyze the effect of the sextupole component of the rf kick given by such a cavity on the proton bunches at 60 GeV as a case study, even when the baseline frequency of collision may be changed, the methods developed here can easily be implemented for different beam energies and frequencies without major difficulties.

ANALYTICAL CONSIDERATIONS

If we treat the horizontal crabbing of the bunch as a chirp in x, then we can express the change in emittance due to this chirp [2] as:

$$\frac{\Delta\epsilon_x}{\epsilon_x} = \frac{\sqrt{\sigma_{x'}^2 + \sigma_{\Delta x'}^2}}{\sigma_{x'}^2} - 1. \qquad (1)$$

Using a definition of the thin-lense rf multipole transverse kick, such as:

$$\begin{aligned} \Delta x' &= \frac{\Delta p_x}{p_z} \\ &\approx \mathcal{V}_0 \left(b_1 + b_3\left(x^2 - y^2\right) + ...\right)\cos(\phi). \qquad (2) \end{aligned}$$

Where $\mathcal{V}_0 \equiv \frac{eV_x}{p_z mc^2 k}$, with V_x as the total crabbing voltage, p_z the particle momentum, $k = \frac{\omega_{rf}}{\beta c}$, b_1 and b_3 are the dipole and sextupole coefficients respectively, and $\phi = 270^o$ as the rf phase with respect to the bunch centroid.

Then we can write:

$$\sigma_{\Delta x'} \approx \frac{\mathcal{V}_0 b_3}{2}\sqrt{\sigma_{x^2}^2 + \sigma_{y^2}^2}, \qquad (3)$$

thus, using Eqns. 1 and 3 we express in this notation the change on emittance per turn as:

$$\frac{\Delta\epsilon_x}{\epsilon_x} = \frac{\sqrt{\sigma_{x'}^2 + \frac{\mathcal{V}_0^2 b_3^2}{4}\left(\sigma_{x^2}^2 + \sigma_{y^2}^2\right)}}{\sigma_{x'}} - 1. \qquad (4)$$

Which shows that the change in the emittance will depend on the transverse second momenta of the bunches and the sextupole component. This shows how geometrically the sextupole content on the crabbing kicks may have repercussions on the beam luminosity or even the beam lifetime. For this reason we will compare the cases with a pure dipole kick to some cases where there is a sextupole component to the rf kick to look for possible resonances or relative stability conditions for the crab cavities' operation.

TRACKING METHODS

In this section we will first describe the simplifications made to the lattice to focus our numerical studies on the section of the interaction region (IR), proposing a linear map for the proton storage ring that properly accounts for the transverse and longitudinal dynamics of the machine, leaving the IR description as a separate block. Secondly, we will discuss the tracking elements and basic calculations performed in different sections of the IR.

Modeling the Lattice

As mentioned above, we used linear maps for the 6D dynamics of the entire proton storage ring, excluding the interaction region as seen in the schematic on Fig. 1, while the interaction region and its transverse Twiss functions are described in Fig. 2

* Authored by Jefferson Science Associates, LLC under U.S. DOE Contract No. DE-AC05-06OR23177.
† acastill@jlab.org

Content from this work may be used under the terms of the CC BY 3.0 licence (© 2015). Any distribution of this work must maintain attribution to the author(s), title of the work, publisher, and DOI.

ISBN: 978-3-95450-168-7 doi:10.18429/JACoW-IPAC2015-WEPWI035

Content from this work may be used under the terms of the CC BY 3.0 licence (© 2015). Any distribution of this work must maintain attribution to the author(s), title of the work, publisher, and DOI.

BEAM DYNAMICS STUDIES OF 499 MHz SUPERCONDUCTING RF-DIPOLE DEFLECTING CAVITY SYSTEM*

S. U. De Silva#, K. Deitrick, H. Park, J. R. Delayen
Old Dominion University, VA 23529, USA

Abstract

A 499 MHz deflecting cavity has been designed as a three-way beam spreader to separate an electron beam into 3 beams. The rf tests carried out on the superconducting rf-dipole cavity have demonstrated that a transverse voltage of 4.2 MV can be achieved with a single cavity. This paper discusses the beam dynamics on a deflecting structure operating in continuous-wave mode with a relativistic beam. The study includes the analysis on emittance growth, energy spread, and change in bunch size including effects due to field non-uniformities.

INTRODUCTION

A deflecting cavity system separates a single beam into multiple beams by applying a transverse momentum to the center of each bunch that displaces the bunch off axis at an angle. The Panofsky-Wenzel Theorem [1] describes the concept of producing a transverse momentum using the electromagnetic fields in an rf structure. A single beam can be separated into multiple beams depending on the rf phase at which the transverse kick is applied.

Jefferson Lab currently uses a three-way beam spreader system that separates the oncoming electron beam with a repetition rate of 1497 MHz in to 3 beams, that are delivered to the 3 experimental halls (Hall A, B and C) [2]. The rf separators system operating at 499 MHz will apply the transverse kick as shown in Fig. 1, that enables the delivery of the highest energy beam simultaneously to hall the 3 experimental halls.

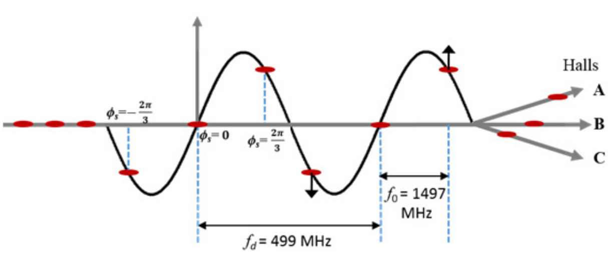

Figure 1: Bunch separation in the Jefferson Lab three-way beam spreader.

The rf separation for the 6 GeV CEBAF machined was achieved with the set of normal conducting cavities. The 4-rod cavity operating in TEM mode are also being used in the 12 GeV machine [2]. The optics in the beam switch yard region had been reworked that relaxed the transverse kick requirement for the 12 GeV upgrade [3]. The rf separators are required to deliver a transverse kick of 3.3 MV in order to deliver the required separation of 297 μrad in vertical direction. The required separation gives a ±17 mm separation at the extraction magnets [4].

RF-DIPOLE CAVITY

A superconducting rf deflecting cavity was initially proposed for the Jefferson Lab 12 GeV upgrade. The optimized 499 MHz rf-dipole cavity design shown in Fig. 2 was successfully fabricated and rf tested [5, 6, 7]. The rf properties of the cavity are listed in Table 1.

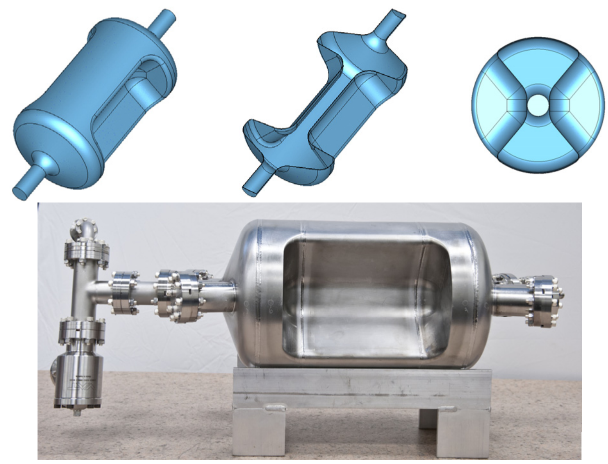

Figure 2: 499 MHz rf-dipole cavity design (top-left) with cross sections along z axis (top-center) and y axis (top-right), and the fabricated cavity (bottom).

Table 1: RF Properties of the 499 MHz rf-Dipole Cavity

Parameter	Value	Units
$\lambda/2$ of π mode	300.4	mm
Cavity length	440.0	mm
Cavity diameter	242.2	mm
Aperture diameter (d)	40.0	mm
Deflecting voltage (V_T*)	0.3	MV
Peak electric field (E_P*)	2.86	MV/m
Peak magnetic field (B_P*)	4.38	mT
B_P* / E_P*	1.53	mT/(MV/m)
Energy content (U*)	0.029	J
Geometrical factor	105.9	Ω
$[R/Q]_T$	982.5	Ω
$R_T R_S$	1.0×10^5	Ω^2
Operating Parameters		
Deflecting voltage (V_T)	3.3	MV
Peak electric field (E_P)	32	MV/m
Peak magnetic field (B_P)	49	mT
Power dissipation (P_{diss})	1.31	W

At E_T* = 1 MV/m

*Authored by Jefferson Science Associates, LLC under U.S. DOE Contract No. DE-AC05-06OR23177. The U.S. Government retains a non-exclusive, paid-up, irrevocable, world-wide license to publish or reproduce this manuscript for U.S. Government purposes.
#sdesilva@jlab.org

ISBN: 978-3-95450-168-7 doi:10.18429/JACoW-IPAC2015-WEPWI036

Content from this work may be used under the terms of the CC BY 3.0 licence (© 2015). Any distribution of this work must maintain attribution to the author(s), title of the work, publisher, and DOI.

DESIGN AND PROTOTYPING OF A 400 MHz RF-DIPOLE CRABBING CAVITY FOR THE LHC HIGH-LUMINOSITY UPGRADE*

S. U. De Silva#, H. Park, J. R. Delayen, Old Dominion University, Norfolk, VA, USA
Z. Li, SLAC National Accelerator Laboratory, Menlo Park, CA, USA
T. H. Nicol, Fermi National Accelerator Laboratory, Batavia, IL, USA

Abstract

LHC High Luminosity Upgrade is in need of two crabbing systems that deflects the beam in both horizontal and vertical planes. The 400 MHz rf-dipole crabbing cavity system is capable of crabbing the proton beam in both planes. At present we are focusing our efforts on a complete crabbing system in the horizontal plane. Prior to LHC installation the crabbing system will be installed for beam test at SPS. The crabbing system consists of two rf-dipole cavities in the cryomodule. This paper discusses the electromagnetic design and mechanical properties of the rf-dipole crabbing system for SPS beam test.

INTRODUCTION

The LHC High Luminosity Upgrade will be using crabbing cavities to increase the luminosity for the operation with 14 TeV proton beam collision. These crabbing systems will also reduce the pile up at the interaction point. Two crabbing systems will be installed at the ATLAS and CMS experiments where the former will be crabbing in vertical plane and the latter in the horizontal plane. The two parallel beam lines set a very tight dimensional constraint in designing a crabbing cavity operating at 400 MHz [1].

A compact 400 MHz crabbing cavity has been designed jointly by ODU and SLAC to meet the system requirements for LHC. A proof-of-principle cavity has been fabricated and tested [2, 3]. Currently the cavity design is being integrated into a cryomodule design intended for SPS test.

RF-DIPOLE CRABBING CAVITY

The 400 MHz proof-of-principle (P-o-P) rf-dipole cavity shown in Fig. 1-(left) is a cylindrical shaped cavity with trapezoidal shaped loading elements that operates in a TE-11 like mode. The prototype cavity sown in Fig. 1-(right) has a fundamental operating mode identical to the cylindrical shaped cavity. The cavity is designed with a square shaped outer body to reduce the transverse cavity size and have improved rf properties shown in Table 1.

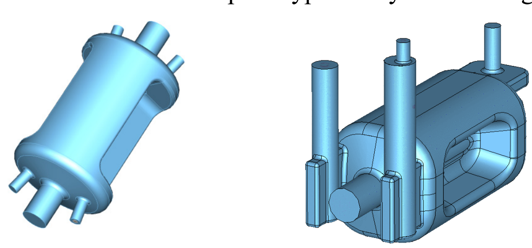

Figure 1: 400 MHz proof-of-principle (left) and prototype (right) rf-dipole cavities.

Table 1: RF Properties of Cylindrical Shaped P-o-P and Square Shaped Prototype rf-Dipole Cavities

Parameter	P-o-P Cavity	Prototype Cavity	Units
Cavity length	542	775	mm
Cavity diameter	340	281	mm
Aperture diameter	84	84	mm
Deflecting voltage (V_T*)	0.375	0.375	MV
Peak electric field (E_P*)	4.02	3.7	MV/m
Peak magnetic field (B_P*)	7.06	6.3	mT
B_P* / E_P*	1.76	1.71	mT/(MV/m)
Energy content (U*)	0.195	0.13	J
Geometrical factor	106	107	Ω
$[R/Q]_T$	287	430	Ω
$R_T R_S$	4.0×10^4	4.6×10^4	Ω^2

At E_T* = 1 MV/m

The P-o-P cavity was fabricated and rf tested at both 4.2 K and 2.0 K. The measured intrinsic quality factor (Q_0) as a function of V_T, E_T, E_P, B_P is shown in Fig. 2. The cavity achieved a V_T of 7 MV that exceeded the required V_T of 3.4 MV. The performance achieved by the P-o-P cavity shows that the rf-dipole cavity can be operated at 5.0 MV that would reduce the number of cavities required to achieve the total V_T of 13.4 MV. The Q_0 achieved during the first set of tests were low due to the surface losses at the SS blank flanges on the beam ports. The cavity was retested with Nb coated SS blank flanges and the cavity achieved a Q_0 of 1.25×10^{10} with reduced residual surface resistance (R_{res}) of 10 nΩ.

Table 2: Operating Parameters at 3.4 MV and 5.0 MV

Parameter	(A)	(B)	Units
Deflecting voltage (V_T)	3.4	5.0	MV
Peak electric field (E_P)	34	50	MV/m
Peak magnetic field (B_P)	57	84	mT
Power dissipation (P_{diss})	2.8	6.2	W

*Work supported by DOE via US LARP Program and by the High Luminosity LHC Project. Work was also supported by DOE Contract No. DE-AC02-76SF00515
#sdesilva@jlab.org

ISBN: 978-3-95450-168-7 doi:10.18429/JACoW-IPAC2015-WEPWI037

IMPERFECTION AND TOLERANCE ANALYSIS OF HOM COUPLERS FOR ODU/SLAC 400 MHz CRABBING CAVITY*

S. U. De Silva#, R. G. Olave, H. Park, J. R. Delayen, Old Dominion University, Norfolk, VA, USA
Z. Li, SLAC, Menlo Park, CA, USA

Abstract

In preparation for the LHC High Luminosity upgrade, a 400 MHz crab cavity has been developed jointly at ODU/SLAC, including two higher order mode couplers designed to damp the wakefields in order to comply with the impedance budget specified for the LHC system. During fabrication, assembly, and processing of the couplers, a number of imperfections may arise that could modify the higher order mode spectrum and the associated impedance for each mode. We present here a detailed study of the imperfections of the horizontal- and vertical- HOM couplers, and the associated allowed tolerances for manufacture, assembly and processing.

INTRODUCTION

A crabbing cavity system for the LHC High Luminosity Upgrade has been designed including the ancillary components such as the fundamental power coupler (FPC), higher order mode (HOM) couplers [1]. The corresponding high current operation demands extraction of 1 kW of HOM power and also impose a strict impedance budget. The full impedance study for the 7 TeV per beam LHC operation is ongoing.

The rf-dipole crabbing cavity is designed with a horizontal (H-HOM) and a vertical (V-HOM) HOM coupler set to meet the design specifications and dimensional requirements for LHC operation [2, 3]. The cavity design with the FPC and HOM couplers are shown in Fig. 1.

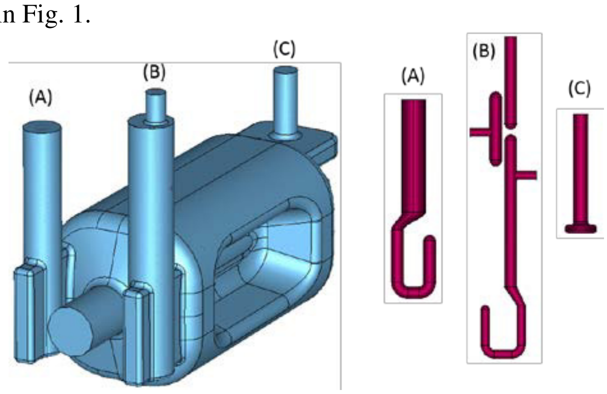

Figure 1: Complete rf-dipole cavity with (A) FPC, (B) HHOM filter, and (C) VHOM probe.

The rf-dipole geometry does not have any lower order modes or similar order modes. The H-HOM coupler is a high pass filter that cuts off the fundamental operating mode, and damps the horizontal dipole modes and accelerating modes. The high pass filter has excellent broad band transmission above 630 MHz up to 2 GHz [3]. The V-HOM coupler damps the vertical dipole modes and some of the accelerating modes. One attractive feature of the HOM couplers of the rf-dipole cavity is that all the couplers are at the end plates in the low field region. This reduces the rf heating at the HOM couplers.

HOM TOLERANCES

The fabrication procedure for the high pass filter is outlined in Ref. [4]. The H-HOM filter consists of three parts as shown in Fig. 1 with a hook, probe and T. The gap between T with the probe and hook is 2.8 mm, which needs to be controlled for precision during fabrication to minimize fundamental mode leakage through the filter.

The manufacturing, assembly, and processing may introduce deviations from the ideal filter shape. This may further have an impact to the effectiveness in HOM damping. Figure 2 shows the important tolerance parameters that have been investigated for the H-HOM high pass filter. HOM tolerances include translational in both vertical (gap probe, gap top, y tip) and transverse (gap bar P, gap bar H, gap T) directions and rotations around x and z axes.

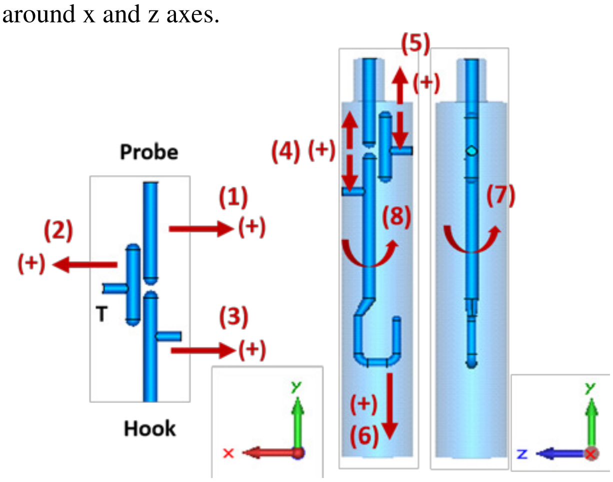

Figure 2: H-HOM tolerances: (1) gap bar P (2) gap bar T (3) gap bar H (4) gap probe (5) gap top (6) y tip (7) rotation about x axis (7) rotation about z axis.

Any variations on gap bar thickness in the T, probe and hook may be caused during fabrication of parts and chemical processing, which are the most crucial parameters for performance. The vertical and rotational deviations may be introduced during assembly of the components and electron beam welding (EBW) process. Extra measures are taken in using a collapsible fixture to hold parts during EBW. The welded parts will be measured to ensure the tolerances are met.

*Work supported by DOE via US LARP Program and by the High Luminosity LHC Project. Work was also supported by DOE Contract No. DE-AC02-76SF00515
#sdesilva@jlab.org

Content from this work may be used under the terms of the CC BY 3.0 licence (© 2015). Any distribution of this work must maintain attribution to the author(s), title of the work, publisher, and DOI.

ISBN: 978-3-95450-168-7 doi:10.18429/JACoW-IPAC2015-WEPWI038

TEMPERATURE MAPPING OF NITROGEN-DOPED NIOBIUM SUPERCONDUCTING RADIOFREQUENCY CAVITIES*

Junki Makita†, Old Dominion University, Norfolk, VA 23529, USA
Gianluigi Ciovati, Pashupati Dhakal, Jefferson Lab, Newport News, VA 23606, USA

Abstract

It was recently shown that diffusing nitrogen on the inner surface of superconducting radiofrequency (SRF) cavities at high temperature can improve the quality factor of the niobium cavity. However, a reduction of the quench field is also typically found. To better understand the location of rf losses and quench, we used a thermometry system to map the temperature of the outer surface of ingot Nb cavities after nitrogen doping and electropolishing. Surface temperature of the cavities was recorded while increasing the rf power and also during quenching. The results of the thermal mapping showed no precursor heating on the cavities and quenching to be ignited near the equator where the surface magnetic field is maximum. Hot-spots at the equator area during multipacting were also detected by thermal mapping.

INTRODUCTION

Over the last few years, much progress has been made on building superconducting rf resonator with high quality factor (Q_0). Achieving higher values of Q_0 could mean substantial reduction in the operational cost of an accelerator. Recent discovery to anneal Nb cavities in the presence of nitrogen or titanium have shown suppression of surface resistance up to ~ 50% − 70% with increase of the low rf field [1, 2]. Analysis of the experimental field and temperature dependence of the surface resistance and a theory explaining the unconventional reduction of surface resistance by the rf field have been recently published [3–5]. Although the cavities doped with nitrogen or titanium have been tested to reach higher Q_0, they are limited by the quench field almost 40% lower than that of conventional undoped cavities [2].

In an attempt to understand the quench mechanism of the doped cavities, we have used an array of thermometers to map the temperatures of the outer surface of the 1.3GHz nitrogen doped single cell cavities. The thermometers are carbon resistors, whose resistance increases nearly exponentially with decreasing temperature. Fast response of the resistors and use of large number of thermometers that span the entire cavity outer surface provide powerful tool for diagnosing the quench and hot spot locations while in its operation below 4.2K. We present here the result of the temperature mappings of the nitrogen doped cavities.

* Work supported by U.S. DOE Contract No. DE-SC0010081, and Jefferson Science Associates, LLC under U.S. DOE Contract No. DE-AC05-06OR23177

† jmaki002@odu.edu

EXPERIMENTAL METHOD

The thermometry system consists of 36 arrays of circuit boards each containing 16 thermometers fixed around the outer cavity surface and is based on the design developed at Cornell [6]. The boards run azimuthally around the cavity, with 10° separations, and each resistor on the board is labeled from 1 to 16, with the resistor 1 at the top iris of the cavity, 8 at the equator, and 16 at the beampipe. Temperature mapping was recorded on two single-cell ingot niobium cavities labeled TD#3 and TD#4 with resonant frequency of 1.3 GHz. After the cavities were heat treated at 800°C for 3 hours, nitrogen was injected at 25 mTorr partial pressure for 20 minutes and annealed for 30 minutes. The cavities then went through electropolishing and high-pressure rinse with ultra-pure water. On TD#3, a total of ~ 35 μm was removed from the inner surface by electropolishing, while on TD#4, only ~ 10 μm was removed. The first round of temperature mapping of the outer surface cavity was collected while ramping up the rf power up to a quench field in small increments at 2.0K and 1.6K. The temperature mapping was also recorded as rf power was ramped down from the break-down field. The cavity was then thermally cycled to above 100K, and tests were repeated.

EXPERIMENTAL RESULTS

Results of the Q_0 vs B_p measurements are summarized in Fig. 1. In both cavities, quality factors showed some improvements after the thermal cycle to above 100K. For TD#4, the cool down rate through T_c=9.25K of the cryogenic dewar was approximately 106mK/sec for the first test and 487mK/sec during the thermal cycle. For TD#3, the dewar measured the slow cooling rate of 11mK/sec for the first test and 119mK/sec during the second measurement. The vertical cryogenic dewar is cooled from the bottom, and at T_c, temperature gradients across the cavities were greater when the dewar was cooled at slower rate. During the slower cooldown, the temperature difference measured between the middle of the dewar and the bottom was ~ 180 K while the difference was ~ 60 K − 90 K during the faster cooldown when the bottom of the dewar reached T_c. Although this result seems to be consistent with the recent work published on dependence of the residual surface resistance on the cooling dynamics, further investigation is required to fully understand the mechanism of the effect [7].

TD#3 cavity which has gone through extra amount of electropolishing compared to TD#4 showed higher breakdown field, but lower quality factor. At 1.6K, TD#3 reached the breakdown field of ~ 130 ± 6 mT while TD#4 cavity quenched at ~ 88 ± 4 mT. On the other hand, the quality

Content from this work may be used under the terms of the CC BY 3.0 licence (© 2015). Any distribution of this work must maintain attribution to the author(s), title of the work, publisher, and DOI.

ISBN: 978-3-95450-168-7 doi:10.18429/JACoW-IPAC2015-WEPWI039

ENGINEERING STUDY OF CRAB CAVITY HOM COUPLERS FOR LHC HIGH LUMINOSITY UPGRADE*

HyeKyoung Park#, S.U. De Silva, R.G. Olave, J.R. Delayen
Center for Accelerator Science, ODU, Norfolk, VA 23529, USA
Z. Li, SLAC, Menlo Park, CA 94025, USA
T.H. Nicol, Fermilab, Batavia, IL 60510, USA
T. Capelli, CERN, Geneva, Switzerland
N.J. Templeton, STFC, Daresbury, UK

Abstract

The LHC is planning to employ crab cavities for the high luminosity upgrade. Old Dominion University and SLAC National Laboratory are developing a crab cavity completed with the HOM damping couplers [1]. The HOM couplers are coaxial type and perform over broadband up to 2 GHz. The amount of extracted power requires active cooling using liquid helium. The electromagnetic study has provided expected power dissipation on the coupler. Correlations between the fabrication tolerance and its damping performance have been studied and the results are providing guidelines on how to manufacture the HOM couplers. This paper summarizes the engineering studies; mechanical strength as a part of pressure system, thermal stability, and fabrication method to ensure the required tolerance.

HOM COUPLER DESIGN

The cavity is designed [2] to have the waveguide leading to the HOM coupler, of which cut off frequency is 945.8 MHz. Fig.1 is showing the overall cavity and the H-HOM coupler details inside.

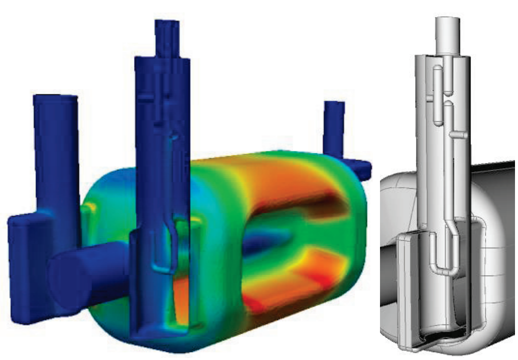

Figure 1: Cavity showing surface magnetic field distribution and H-HOM coupler internal structure.

There are two HOM couplers, one damping the horizontal HOM modes and the other damping the vertical HOM modes. The vertical HOM coupler is a simple coaxial probe type in the waveguide and the horizontal HOM (H-HOM) coupler is a high pass filter type comprised a hook and probes. This paper focuses on the horizontal HOM coupler.

THERMAL STUDY

The H-HOM coupler is designed with the niobium hook and probe. The dynamic and static heat loads must be dissipated by the liquid helium to ensure the niobium parts remain superconducting. To avoid a quench very conservative assumptions were used.

Thermal Properties of Material

The main property needed for the thermal study is the thermal conductivity of each material. Since the thermal conductivity is a temperature dependent property, a nonlinear thermal study was performed. The property curve of niobium is shown in Fig. 2 for example. Same type of nonlinear thermal conductivity was used for ceramic, stainless steel, and copper.

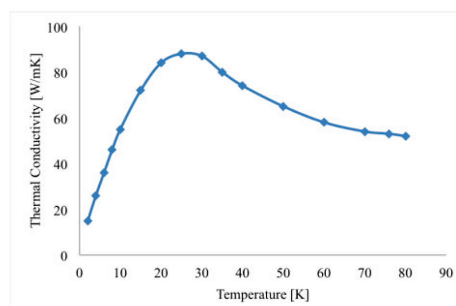

Figure 2: Temperature dependent thermal conductivity of niobium.

Dynamic Heat Load

The surface field is calculated from the finite element RF simulation, ACE3P developed at SLAC [2,3]. The heat load is Joule heating by this field and the surface resistance and it was numerically integrated as follows.

$$P = \frac{1}{2} R_s \int \left|\vec{H}\right|^2 da$$

where P is the power in Watt, Rs surface resistance in Ohm, H time averaged surface magnetic field in T. The power loss is scaled based on 1 kW of power extraction each mode. The surface resistance is assumed 10 nOhm, which is higher than typical niobium test results. For copper probe, the surface resistance was scaled to each frequency accounting for the anomalous limit of a normal conductor at the room temperature. Therefore, the

*Research supported by DOE via the US-LARP program and by the High Luminosity LHC project. Also supported by DOE Contract No. DE-AC02-76SF00515.
#hkpark@jlab.org

Content from this work may be used under the terms of the CC BY 3.0 licence (© 2015). Any distribution of this work must maintain attribution to the author(s), title of the work, publisher, and DOI.

ISBN: 978-3-95450-168-7 doi:10.18429/JACoW-IPAC2015-WEPWI040

EXPERIMENT AND RESULTS ON PLASMA ETCHING OF SRF CAVITIES

J. Upadhyay, Do Im, J. Peshl, S. Popović, and L. Vušković
Department of Physics, Center for Accelerator Science, Old Dominion University, Norfolk, VA 23529, USA
A.-M. Valente-Feliciano and L. Phillips
Thomas Jefferson National Accelerator Facility, Newport News, VA 23606, USA

Abstract

The inner surfaces of SRF cavities are currently chemically treated (etched or electro polished) to achieve the state of the art RF performance. We designed an apparatus and developed a method for plasma etching of the inner surface for SRF cavities. The process parameters (pressure, power, gas concentration, diameter and shape of the inner electrode, temperature and positive dc bias at inner electrode) are optimized for cylindrical geometry. To study the etching of the inner surface of the varied diameter cylindrical structure, a stainless steel pill box cavity has been made. The niobium samples placed inside this cavity has been studied for etch affects purposes. The inner electrode has been moved and plasma response to the movement of the powered electrode has been seen. Plasma characterization is done with the help of optical emission spectroscopy.

INTRODUCTION

Currently used technologies for superconductive radio-frequency (SRF) cavities processing are buffered chemical polishing or electro polishing. These technologies are based on the use of hydrogen fluoride (HF) in liquid acid baths [1], which poses major environmental and personal safety concern. Plasma etching would be a much more controllable, less expensive and more environment-friendly processing technology. It would also provide the unique opportunity to tailor the niobium surfaces for better superconducting rf properties.

We have been developing the plasma etching technology for SRF cavity in multiple stages. In the first stage, we demonstrated plasma etching of a flat coupon of niobium (Nb) in a microwave plasma of 2.45 GHz frequency inside a quartz tube with a gas mixture of 97% argon and 3% chlorine [2]. The effects of plasma etching on niobium surface on flat coupon samples were studied [3]. In the second stage, to demonstrate plasma etching on the inner surface of three dimensional structures, we designed a cylindrical cavity with diameter equal to the beam tube of single cell SRF cavity of 1497 MHz and length 15 cm. Ring shaped Nb samples were placed on the inner surface of this cylindrical cavity for etch rate measurements. Coaxial-type plasma was generated with the help of different diameter inner electrode and rf (13.56 MHz) power with a gas mixture of 85% argon and 15% chlorine. To overcome the asymmetry in ion energy bombarding the outer electrode wall and the inner electrode wall of this coaxial plasma, an external dc power supply is added. The etching of the samples placed on the outer wall was not possible without the help of the positive bias provided by an external dc power supply.

The dependence of the pressure, rf power, diameter of the inner electrode and chlorine concentration on the etch rate was measured [4]. The etch rate mechanism of Nb in the rf plasma of Ar/Cl_2 was determined by varying temperature, positive dc bias and gas conditions [5]. The variation of etch rate non-uniformity on two ring samples placed along gas flow direction on the process parameters were studied [5]. In this stage, the idea to change the inner electrode geometry for less asymmetric plasma production was implemented and a corrugated structured electrode was developed. The second stage addressed the problem of etching a cylindrical structure but an SRF cavity is a variable diameter cylindrical structure. In a third stage, we designed a steel pill box cavity with similar dimension as a single cell SRF cavity of 1497 MHz. The pill box cavity is filled with ring type and disk type Nb samples on the inner surface. The purpose of this stage is to study the etch rate behaviour of Nb on all the available surfaces of varied diameter cylindrical structure. In the fourth and final stage, single cell SRF cavities would be plasma etched and rf tested at cold temperatures.

MOVING INNER ELECTRODE IN CYLINDRICAL CAVITY EXPERIMENT

It was found that the ring sample placed further from the gas entry point has substantially lower etching than the sample placed closer to the gas entry point. The depletion of active radicals (positive ions, excited neutrals, negative ions) along the gas flow direction due to consumption by Nb during the etching process is a critical challenge to uniform etching of a long cylindrical tube. Segment-wise plasma production can be a viable alternative to overcome this problem. The movement of the inner electrode in a coaxial plasma, where the inner electrode is rf powered and positively dc biased is applied to produce the plasma in the segmented fashion. To achieve this, inner electrode is attached to thin flexible cylindrical bellows. The compression in the bellows allows the movement of the inner electrode in the vacuum while the plasma is on. The gas flow is in the opposite direction of the rf power flow direction.

Content from this work may be used under the terms of the CC BY 3.0 licence (© 2015). Any distribution of this work must maintain attribution to the author(s), title of the work, publisher, and DOI.

ISBN: 978-3-95450-168-7 doi:10.18429/JACoW-IPAC2015-WEPWI042

A TABLE-TOP ALPHA-MAGNET*

A. V. Smirnov#, R. Agustsson, T. Campese, Y. Chen, J. Hartzell, F. O'Shea, and E. Spranza,

RadiaBeam Technologies LLC, Santa Monica, CA 90404, USA

Abstract

A compact electromagnetic alpha-magnet design, engineering, and operation are presented. The magnet was designed and engineered at RadiaBeam for a low-energy, laser-free, coherent Cherenkov THz-sub-THz source developed in collaboration with Argonne National Laboratory and integrated into the Injector Test Stand (ITS) of the Advanced Photon Source (APS). The magnet having 15 cm depth, 14" height, and up to 4 T/m gradient features a rectangular yoke, two on-axis coils, and substantially truncated, substantially non-hyperbolic poles. The profiled vacuum chamber for the magnet includes a motorized scraper and means of optical control.

INTRODUCTION

A growing number of low-energy electron beam applications impose serious limitations on the sizes of the beamline components that may include alpha-magnets. Among these applications are, e.g., compact ultra-short pulse X-ray radiation sources. In particular, an alpha-magnet can perform phase space rotation to enable a sub-ps microbunching of a few MeV electron beam injected from an RF electron gun (or small electron linac, "microlinac") having "natural" energy chirp. In that case a sub-ps laser photoinjector can be avoided allowing orders of magnitude higher average beam current. A substantial portion of the long RF bunch from the injector cannot contribute effectively into the microbunching in that case. That portion is usually filtered out (typically at low momentums) with a beam scraper placed inside the alpha-magnet chamber. RadiaBeam Technologies has developed such a compact alpha-magnet for 0.5 THz radiation source recently commissioned [1]. The experiment was jointly developed by RadiaBeam Technologies, LLC, and Accelerator Systems Division of Advanced Photon Source (APS) at Argonne National Laboratory (ANL) and performed in the Injector Test Stand (ITS) of the APS.

MAGNETIC DESIGN

Since the magnet to be deployable on the optical table of the existing ITS beamline, the main specification requirements to the magnet design are rather stringent: 360 mm magnet height (determined by beamline height ~180 mm), 4 T/m maximum gradient, ~15 cm maximum trajectory depth, and ~1% field quality.

*Work supported by the U.S. Department of Energy (award No. DE-SC-FOA-0000760)
#asmirnov@radiabeam.com

A novel design was introduced to satisfy the challenging requirements. It features co-axis coils and a rectangular frame yoke. Such an approach implies a pole profile that essentially deviates from the conventional hyperbolic shape, because the magnetic flux distribution within the core of the pole in such a C-shaped, dipole-like configuration acquires naturally some intrinsic gradient and also higher order multipole components. Corresponding distortions must be compensated all the way along the trajectory depth with a non-canonical pole shape.

A special algorithm has been developed to provide the compensation. It is integrated with the model and makes correction of the pole shape on each iteration step. It uses prediction-correction technique to minimize field deviation from the linear curve of an ideal magnet. The correction function balanced with "weights" is based on a magnetic circuit approach in which the gap is considered as an array of magnetic resistors. As an initial example the approach was applied to design a larger magnet with 34 cm trajectory depth, and 1.25" minimum gap. The iterative optimization enabled ~0.3% field inaccuracy. The second model of the magnet was designed using this approach specifically for the RadiaBeam-APS experiment. The Radia [2] code used for the simulations demonstrated exceptional efficiency and required only several iterations to converge (or achieve satisfactory field quality). The model is shown in Fig. 1.

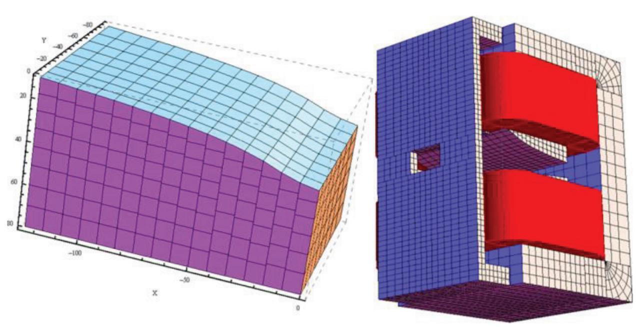

Figure 1: Radia model for the pole (left) and for the entire magnet (right).

The magnetization in the yoke is shown in Fig. 2. One can see that in spite of compactness the saturation effects in the yoke do not present the major limiting factor for the magnet performance. That enables gradients higher than 4 T/m for short periods of time.

In Fig. 3 and Fig. 4 the simulated magnetic field is plotted along the axis of symmetry and in the transverse direction respectively. The iterative simulation procedure

Content from this work may be used under the terms of the CC BY 3.0 licence (© 2015). Any distribution of this work must maintain attribution to the author(s), title of the work, publisher, and DOI.

ISBN: 978-3-95450-168-7 doi:10.18429/JACoW-IPAC2015-WEPWI044

HIGH-POWER MAGNETRON TRANSMITTER FOR THE ELECTRON COLLIDER RING OF THE MEIC FACILITY*

Grigory Kazakevich#, Euclid TechLabs LLC, Cleveland, OH, USA
Brian Chase, Vyacheslav Yakovlev, Fermilab, Batavia, IL, USA
Yaroslav Derbenev, JLab, Newport News, VA, USA

Abstract

Operation of the 3-12 GeV electron collider 8-shape ring of the MEIC facility causes a Synchrotron Radiation (SR) of electrons in arcs with energy loss of ~20 kW/m at beam current of ~3 A. The total SR loss up to 2 MW per a turn is presumed to compensate by Superconducting RF (SRF) accelerating cavities. To minimize the beam emittance, each individual SRF cavity is proposed to feed by an individual and independent CW RF source allowing a wide-band control in phase and power. Most efficient and less expensive in capital and maintenance costs the high-power transmitters based on magnetrons, injection-locked by phase-modulated signals, controlled in wide-band are proposed as the RF sources. The magnetron RF CW sources utilizing 2-cascade magnetrons allowing a wide-band phase and power control by the injection-locking phase-modulated signals were experimentally modelled by 2.45 GHz, CW, 1 kW magnetrons. Results of additional modelling and adequacy of the transmitters for the SRF cavities are discussed in the presented article.

INTRODUCTION

Compensation of the SR losses in arcs of the electron collider of the MEIC project requires high-power CW RF sources for acceleration of the electrons in SRF cavities keeping the accelerating voltage phase and amplitude deviations in each cavity significantly less than 1 degree and 1% of nominal, respectively. The strict requirements follow from necessity in a precise orientation and positioning of the highly compressed electron bunches relatively the proton/ion bunches. Therefore minimization of emittances of the electron bunches is one of general requirements at compencation of the SR losses. The low-noise RF sources with a precisely-stable carrier frequency allowing a wide-band dynamic phase and power control by a feedback within closed loops, eliminating the parasitic amplitude and phase modulation inherent in the SRF cavities, are necessary to compensate the SR losses.

The traditional CW RF amplifiers (klystrons, IOTs, solid-state amplifiers) are applicable for this task, but they associate with high capital and maintenance costs, [1, 2]. Utilization of high-power klystrons feeding groups of the SRF cavities decreases the costs in some degree, but does not allow minimizing the beam emittances because of non-optimized phase and amplitude of RF field in individual cavities. Capability of transmitters based on 2-cascade magnetrons, frequency-locked by phase-modulated signals for a dynamic phase and power control of RF field in SRF cavity was shown in [3]. A dynamic control of a CW magnetron, frequency-locked by wide-band phase-modulated signal, stabilizing RF field in the SRF cavity, in phase and power up to 0.26 deg. rms and 0.3% rms, respectively, was first demonstrated in [4].

The results reinforce our proposal on the use of the magnetron transmitters for feeding of the SRF cavities compensating SR losses in the electron ring of MEIC. The transmitter models capabilities and tests are considered in the presented work.

MAGNETRONS WITH A WIDE-BAND PHASE CONTROL

Operation of the phase-controlled frequency-locked magnetron one can represent considering the transient processes in the magnetron caused by frequency/phase pulling and pushing. Since the magnetron is assumed to be frequency-locked, the magnitude of the locking signal has to be significantly more than the signal reflected from the SRF cavity into magnetron. The standard ferrite circulators have inverse losses ≥20 dB, so the locking signal power of >-15 dB for the magnetron may be enough to obtain precisely-stable carrier frequency in the SRF cavity at variable beam loading.

As it is shown in [3], the equation, describing phase pulling/ pushing in the frequency-locked magnetron at a steady-state is transformed into the following expression:

$$\tilde{V}_M = \cos\psi \cdot \exp(i\psi)\cdot\left(\frac{2Q_{LM}}{Q_{EM}}\tilde{V}_{FM} - \frac{Q_{LM}\cdot R_{ShM}}{2\cdot Q_{0M}}\tilde{I}_M\right). \quad (1)$$

Here: Q_{0M}, Q_{LM} and Q_{EM} are unloaded, loaded and external Q-factors of the magnetron cavity, respectively, $\tilde{V}_M$, $\tilde{V}_{FM}$ and $\tilde{I}_M$ are phasors of the voltage in magnetron cavity, of the injection-locking signal, and of the magnetron current, respectively, β is the magnetron cavity coupling coefficient, R_{ShM} is the magnetron shunt impedance, and ψ is angle between sum of phasors $-(2Q_{LM}/Q_{EM})\cdot\tilde{V}_{FM}$, $(Q_{LM}\cdot R_{ShM}/2\cdot Q_{0M})\cdot\tilde{I}_M$ and $\tilde{V}_M$, Fig. 1, [5].

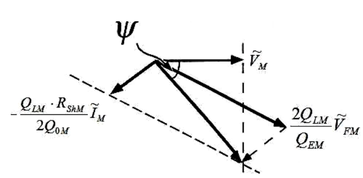

Figure 1: Phasor diagram of the injection-locked magnetron.

*Authored by Fermi Research Alliance, LLC under Contract No. De-AC02-07CH11359 with the United States Department of Energy.
gkazakevitch@yahoo.com

Content from this work may be used under the terms of the CC BY 3.0 licence (© 2015). Any distribution of this work must maintain attribution to the author(s), title of the work, publisher, and DOI.

ISBN: 978-3-95450-168-7 doi:10.18429/JACoW-IPAC2015-WEPWI045

STATUS OF SUPERCONDUCTING TRAVELLING WAVE CAVITY FOR HIGH GRADIENT LINAC*

Roman Kostin#, Pavel Avrakhov, Alexei Kanareykin, Euclid Techlabs, LLC, Solon, Ohio, USA
Nikolay Solyak, Vyacheslav Yakovlev, Timergali Khabiboulline, Yuriy Pischalnikov
Fermilab, Batavia, IL 60510, USA

Abstract

The use of a travelling wave (TW) accelerating structure with a small phase advance per cell instead of standing wave may provide a significant increase of accelerating gradient in a superconducting linear accelerator. The TW section achieves an accelerating gradient 1.2-1.4 times larger than TESLA-shaped standing wave cavities for the same surface electric and magnetic fields [1]. The final stage of a 3-cell superconducting travelling wave cavity development is presented. This cavity will be tested in travelling wave regime at cryogenic temperature.

INTRODUCTION

Accelerating gradient in RF cavities is one of the most important parameter of particle accelerator. It determines particle energy and accelerator length which is crucial for multi-kilometres accelerators such as International Linear Collider (ILC) [2]. The cost of this project highly depends on it. In order to reduce the cost with determined particle energy one should have a greater accelerating gradient. TESLA style superconducting standing wave (SW) cavity (180 degree phase advance per cell) is considered to be used as a current ILC design. Accelerating gradient shows the efficiency of acceleration and includes the multiplication of electric field gradient in a cavity and transit time factor which is around 0.7 for 180 degree phase advance. Standing wave cavities length is restricted to 1 meter in order have field flatness degradation less than 5% because of strong dependence on the cavity length. Thus, there is a gap between cavities (220 mm) which reduces accelerating rate by 22%. Superconducting traveling wave accelerating structure was proposed before in our previous publications [3, 4]. It requires feedback waveguide (WG) from one end of accelerating structure to another in order to make a closed loop for power distribution. Although, this cavity has more complicated design (additional waveguide) and tuning procedure (two tuners are required to tune operational frequency and compensate reflections along the loop) it has two urgent advantages. Firstly, field flatness has lower dependence on cavity length. If surface treatment and manufacturing process allow to build 10 meter long (cryomodule length) traveling wave cavity it will have better field flatness than 1 meter long standing wave cavity. This fact increases accelerating gradient by 22%. Secondly, traveling wave does not need to have 180 degree phase advance as it is required for standing waves cavities in order to have each cell filled with EM energy. Accelerating wave travels along the cavity together with accelerated particle. The geometry of TW cavity was optimized in order to obtain a higher accelerating gradient. 105 degree phase advance was found to have 24% higher accelerating gradient than in TESLA style SW cavity. The detailed information can be found in the following article [3, 4].

A 3-cell cavity was chosen to demonstrate traveling wave regime. It was optimized and is manufacturing in AES, Ink. This cavity will be processed and tested at Fermilab in the end of summer 2015. 3-cell tuning studies were presented in publications [5, 6]. They are the following for -30 dB reflections: WG deformation range is 90 um; WG deformation step is 20 nm; longitudinal position range ±4 mm, and longitudinal position step 0.5 um. WG deformation range was extended to 1 mm after some investigations with tuner design and tuning procedure. WG wall deformations were calculated by Ansys and 15 kN force was found to be required for 1 mm wall deformation at 2 K.

3-CELL TRAVELING WAVE CAVITY TUNER DESIGN

As was discussed in [6] 3-cell traveling wave cavity tuner must have the possibility to move the point of force application to the WG. This is the main feature which distinguishes it from conventional SW cavity tuners and the first attempt to make a design became SW tuners review. Cryogenic stepper motor actuator for vacuum application with a reinforced axial load was found in one of Fermilab tuner design. It consists of 200/1 stepper motor, 50/1 gearbox and a shaft with 1 mm thread. That means that 1 step of this actuator produce a 100 nm longitudinal displacement. This motor can withstand 1.3 kN of axial load (Fermilab experience shows 4 kN of axial force before nut failure), i.e. if 12/1 lever is involved 15 kN force and 8 nm step can be achieved by this motor. These numbers satisfy almost all of the requirements. The rest of them is the possibility of moving along the WG. That was solved by additional unit, called traverse, which is mounted to the active lever through linear guides and movable by the second actuator. The 3-cell tuner is depicted in Figure 1 with hidden front rib.

*Work supported by US Department of Energy # DE-SC0006300
r.kostin@euclidtechlabs.com

Content from this work may be used under the terms of the CC BY 3.0 licence (© 2015). Any distribution of this work must maintain attribution to the author(s), title of the work, publisher, and DOI.

ISBN: 978-3-95450-168-7 doi:10.18429/JACoW-IPAC2015-WEPWI046

Content from this work may be used under the terms of the CC BY 3.0 licence (© 2015). Any distribution of this work must maintain attribution to the author(s), title of the work, publisher, and DOI.

DEMONSTRATION OF COAXIAL COUPLING SCHEME AT 26 MV/m FOR 1.3 GHz TESLA-TYPE SRF CAVITIES*

Yi Xie†, A. Kanareykin, Euclid TechLabs, Solon, Ohio
T. Khabiboulline, A. Lunin, V. Poloubotko, A. Rowe,
N. Solyak, V. Yakovlev, Fermilab, Batavia, Illinois
J. Rathke, AES, Medford, New York

Abstract

Superconducting ILC-type cavities have an rf input coupler that is welded on. A detachable input coupler will reduce conditioning time (can be conditioned separately), reduce cost and improve reliability. The problem with placing an extra flange in the superconducting cavity is about creating a possible quench spot at the seal place. Euclid Techlabs LLC has developed a coaxial coupler which has an on the surface with zero magnetic field (hence zero surface current). By placing a flange in that area we are able to avoid disturbing surface currents that typically lead to a quench. The coupler is optimized to preserve the axial symmetry of the cavity and rf field. The surface treatments and rf test of the prototype coupler with a 1.3 GHz ILC-type single-cell cavity at Fermilab will be reported and discussed.

INTRODUCTION

The standard 1.3 GHz TESLA type SRF cavity has a fundamental power coupler and two asymmetric HOM couplers both upstream and downstream. The couplers break the cavity axial symmetry that in turn causes a rf field distortion and transverse wake field which may cause beam emittance dilution [1]. In order to preserve the axial symmetry of the acceleration channel, different schemes of coaxial coupler were proposed and developed [2], [3].

We suggested another design for the coupling unit, as shown in Figure 1. This coupler has the following features:

- The coupler unit preserves the axial symmetry of the acceleration channel. There are no RF kicks or wakes that lead to emittance dilution;
- It is a quarter-wave resonant coupler for the operating mode;
- The coupler is detachable, because in the operating mode the currents are small in the coupler corners, and non-welded superconducting joints may be used. Thus, the coupler unit can be a separate device that can be treated independently of the structure;
- It may be manufactured of low RRR niobium (reduced cost) compared with the main cavity;
- It is compact.

* This Work is supported by the US DOE SBIR Program DE-SC0002479.
† yixie@fnal.gov, now at Fermilab.

The magnetic field distribution for the operating mode is shown in Figure 2. One can see that the field in the corners is much smaller than in the main cavity. For the maximal acceleration gradient of 35 MeV/m the surface magnetic field is 147 mT. In this case in the corner it is about 0.15 mT, lower enough to definitely permit superconducting joints.

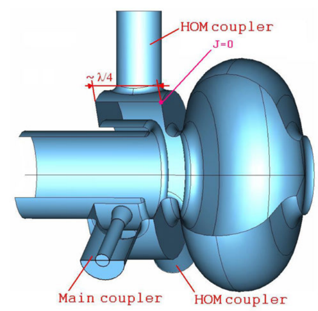

Figure 1: Schematic of Euclid proposed quarter-wave coaxial coupler.

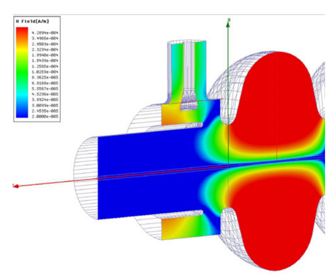

Figure 2: The magnetic field pattern in the coupler for the operating mode.

ELECTROMAGNETIC DESIGN

The first step in the coaxial coupler development was an adjustment of the shape to get the zero of the magnetic field at an accessible point for split flanges. The coaxial coupler which behaves like the coaxial resonator has an rf magnetic field and surface current minimum at the point $\lambda_{rf}/4$ from the corner (λ_{rf} is the wavelength in vacuum). This position can't be changed by appropriate choice of radii of the coaxial unit. Figure 3 shows the position of the magnetic field zero in the final design of the coaxial coupler. It satisfies the detachable design requirements.

The coupling to the fundamental mode has been modeled by the HFSS eigenmode solver for the shape depicted above.

ISBN: 978-3-95450-168-7 doi:10.18429/JACoW-IPAC2015-WEPWI049

COMMISSIONING OF THE 112 MHz SRF GUN AND 500 MHz BUNCHING CAVITIES FOR THE CeC PoP LINAC*

S. Belomestnykh[1,2,#], I. Ben-Zvi[1,2], J. C. Brutus[1], V. Litvinenko[1,2], P. McIntosh[3], A. Moss[3], G. Narayan[1], P. Orfin[1], I. Pinayev[1], T. Rao[1], J. Skaritka[1], K. Smith[1], R. Than[1], J. Tuozzolo[1], E. Wang[1], A. Wheelhouse[3], Q. Wu[1], B. Xiao[1], T. Xin[2], Wencan Xu[1], A. Zaltsman[1]

[1)] Brookhaven National Laboratory, Upton, NY 11973-5000, U.S.A.
[2)] Stony Brook University, Stony Brook, NY 11794, U.S.A.
[3)] STFC/DL/ASTeC, Daresbury, Warrington, Cheshire, UK

Abstract

The Coherent electron Cooling Proof-of-Principle (CeC PoP) experiment at BNL includes a short electron linac. During Phase I, a 112 MHz superconducting RF photo-emission gun and two 500 MHz normal conducting bunching cavities were installed and are under commissioning. The paper describes the Phase I linac layout and presents commissioning results for the cavities and associated RF, cryogenic and other sub-systems.

INTRODUCTION

The CeC PoP experiment is under construction at BNL to demonstrate feasibility of this cooling scheme for future colliders [1, 2]. The experiment is aimed to cool only one bunch in RHIC. A 22-MeV high-bunch-charge beam will be delivered by a short linac [3, 4]. Phase I of the project includes installation and commissioning of a 112 MHz Quarter Wave Resonator (QWR) photoemission electron gun and two normal conducting bunching cavities as well as generating first beam. The Phase I linac layout is shown in Figure 1. The SRF gun cryomodule and bunching cavities were installed in the Interaction Region 2 (IR2) of RHIC tunnel during summer shutdown of 2014. The installed hardware is illustrated in Figure 2. In this paper we describe the first commissioning results for the 112 MHz SRF gun and two bunching cavities.

INSTALLATION AND COMMISSIONING OF THE 112 MHz QWR SRF GUN

The 112 MHz SRF QWR quarter-wave resonator was developed by BNL in collaboration with Niowave, Inc. [5-7]. It is designed to generate electron bunches with a charge range from 1 to 5 nC and repetition rate of 78 kHz, matching the RHIC revolution frequency. Multi-alkali photocathodes will be illuminated with a green (532 nm) light from a laser. More details of the gun design can be found in the cited references.

The gun operates at 4.3 K with liquid helium supplied from a so-called quiet helium source [8], which isolates the 112 MHz cryomodule from noise coming from the RHIC magnet supply line and the local helium compressor that processes the boil-off. The gun cryomodule together with associated sub-systems (cryogenics, RF, cooling water, vacuum, fundamental power coupler/tuner motion, cathodes insertion) was installed in RHIC during summer of 2014. Its commissioning began in the fall.

We started conditioning without a photocathode puck. Initially, numerous multipacting zones were encountered at very low cavity voltages. They have been cleaned out after several days of conditioning and never presented a problem afterwards.

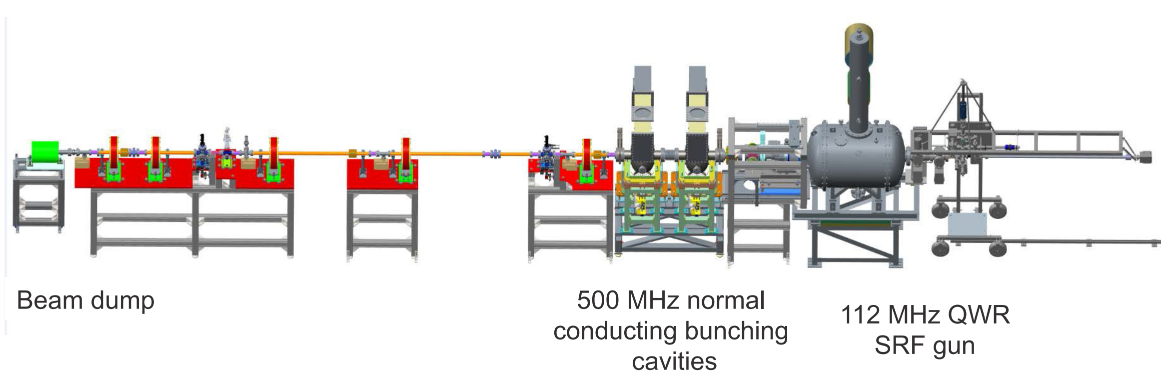

Figure 1: Layout of the Phase I of the CeC PoP linac installation.

* Work is supported by Brookhaven Science Associates, LLC under contract No. DE-AC02-98CH10886 with the US DOE.
#sbelomestnykh@bnl.gov

Content from this work may be used under the terms of the CC BY 3.0 licence (© 2015). Any distribution of this work must maintain attribution to the author(s), title of the work, publisher, and DOI.

ISBN: 978-3-95450-168-7 doi:10.18429/JACoW-IPAC2015-WEPWI050

SRF AND RF SYSTEMS FOR LEReC LINAC *

S. Belomestnykh[1,2,#], I. Ben-Zvi[1,2], J. C. Brutus[1], A. Fedotov[1], G. McIntyre[1], S. Polizzo[1], K. Smith[1], R. Than[1], J. Tuozzolo[1], V. Veshcherevich[3], Q. Wu[1], B. Xiao[1], Wencan Xu[1], A. Zaltsman[1]

[1)] Brookhaven National Laboratory, Upton, NY 11973-5000, U.S.A
[2)] Stony Brook University, Stony Brook, NY 11794, U.S.A
[3)] Cornell University, Ithaca, NY 14853, U.S.A

Abstract

The Low Energy RHIC electron Cooling (LEReC) is under development at BNL to improve RHIC luminosity at low energies. It will consist of a short electron linac and two cooling sections, one for blue and one for yellow rings. For the first stage of the project, LEReC-I, we will install a 704 MHz superconducting RF cavity and three normal conducting cavities operating at 9 MHz, 704 MHz and 2.1 GHz. The SRF cavity will boost the electron beam energy up to 2 MeV. The warm cavities will be used to correct the energy spread introduced in the SRF cavity. The paper describes layouts of the SRF and RF systems, their parameters and status.

INTRODUCTION

One of the highest priorities for the RHIC experimental program is to map the QCD phase diagram at center-of-mass collison energies below 20 GeV (γ = 10.7). However, at present the RHIC luminosity at these energies does not provide sufficient statistics. It was proposed to apply bunched beam electron cooling to significantly increase the luminosity. The Low Energy RHIC electron Cooling is under design at BNL [1].

There are two options under consideration for the LEReC electron linac: one based on a DC photoemission gun and another based on an SRF photoemission gun. During the first phase of the project, LEReC-I, electrons will be accelerated only to kinetic energies from 1.6 to 2 MeV. As the DC gun option was chosen as the baseline, in this paper we present only SRF and RF system parameters relevant to this option of LEReC-I.

The linac will be located in the RHIC tunnel near the Interaction Point 2 (IP2) where it will benefit from sharing cryogenic system and some RF infrastructure with the coherent electron cooling proof-of-principle experiment [2]. The linac will include a Cornell-type DC photoemission electron gun [3] operating at 400 kV. The gun will be followed by a 704-MHz SRF booster cavity, and three normal conducting cavities operating at frequencies 9 MHz, 704 MHz and 2.1 GHz. The latter two cavities will serve for beam energy spread correction. The Phase I linac layout is shown in Figure 1 and RF system parameters are listed in Table 1.

The 9-MHz cavity is an existing spare cavity available from RHIC together with an RF amplifier. This cavity will be used in LEReC to compensate bunch-to-bunch energy variation inside the 30-car long bunch trains. This variation is due to beam loading effect in other cavities. Other RF systems are described below.

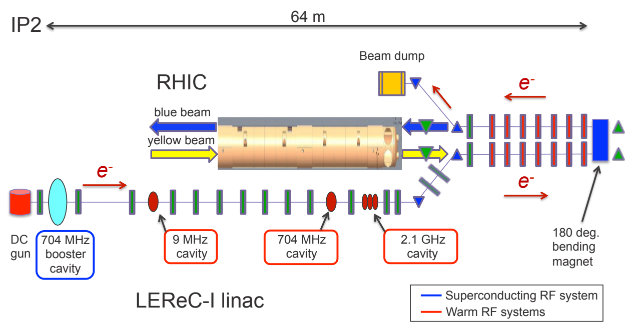

Figure 1: LEReC-I layout.

Table 1: Parameters of the LEReC-I RF Systems

Parameter	SRF booster	9 MHz	704 MHz	2.1 GHz
Cavity voltage	1.2 to 1.6 MV	3 kV	78 kV	7.5 kV
R/Q	96 Ω	190 Ω	247 Ω	487 Ω
Q_{ext}	5×10^5	35	2.6×10^4	1.09×10^4
Installed RF power	65 kW	1 kW	50 kW	10 kW

SRF BOOSTER

After generating a 400-keV beam in the DC gun, we need to boost its kinetic energy to 1.6 to 2 MeV. This will be achieved using a 704-MHz cryomodule converted from an SRF gun configuration to a booster cavity. At present, the cryomodule is installed in the R&D ERL at BNL and is under commissioning [4]. The SRF gun cavity has demonstrated very good performance, reaching its design voltage of 2 MV.

As soon as the R&D ERL beam experiments will be complete in 2016, the cryomodule will be removed and reconfigured to serve as a booster cavity for LEReC as illustrated in Figure 2. A photocathode stalk assembly will be removed and a specially designed beam pipe will be inserted in its place. In addition, the RF power coupling scheme will be modified to account much smaller beam loading in LEReC compared to R&D ERL. The booster will be powered from a 65-kW IOT-based high power RF amplifier.

* Work is supported by Brookhaven Science Associates, LLC under contract No. DE-AC02-98CH10886 with the US DOE.
#sbelomestnykh@bnl.gov

Content from this work may be used under the terms of the CC BY 3.0 licence (© 2015). Any distribution of this work must maintain attribution to the author(s), title of the work, publisher, and DOI.

ISBN: 978-3-95450-168-7 doi:10.18429/JACoW-IPAC2015-WEPWI051

UPDATE ON THE CeC PoP 704 MHz 5-CELL CAVITY CRYOMODULE DESIGN AND FABRICATION*

J. C. Brutus[#,1], S. Belomestnykh[1,2], I. Ben-Zvi[1,2], S. Gerbick[4], T. Grimm[3], Y. Huang[1,§], R. Jecks[3], M. Kelly[4], V. Litvinenko[1,2], I. Pinayev[1], T. Reid[4], J. Skaritka[1], L. Snydstrup[1], R. Than[1], J. Tuozzolo[1], Wencan Xu[1], J. Yancey[3]
[1)] Brookhaven National Laboratory, Upton, NY 11973-5000, U.S.A.
[2)] Stony Brook University, Stony Brook, NY 11794, U.S.A.
[3)] Niowave Inc., Lansing, MI 48906, U.S.A.
[4)] Argonne National Laboratory, Lemont, IL 60439, U.S.A.

Abstract

A 5-cell SRF cavity operating at 704 MHz will be used for the Coherent Electron Cooling Proof of Principle (CeC PoP) system under development for the Relativistic Heavy Ion Collider (RHIC) at Brookhaven National Laboratory. The CeC PoP experiment will demonstrate the new technique of cooling proton and ion beams that may increase the beam luminosity in certain cases, by as much as tenfold. The 704 MHz cavity will accelerate 2 MeV electrons from a 112 MHz SRF gun up to 22 MeV. This paper provides an overview of the design, the project status and schedule of the 704 MHz 5-cell SRF for CeC PoP experiment.

INTRODUCTION

The 5-cell 704 MHz SRF linac is being designed and fabricated in collaboration between BNL and Niowave. It will be the main 20 MeV electron accelerator for CeC PoP experiment under construction in RHIC at BNL [1]. The delivery of the 704 MHz SRF linac to BNL is scheduled for the end of June 2015. The 704 MHz SRF linac will be installed and ready for commissioning at the beginning of 2016 RHIC Run. An update on the layout of the fundamental power coupler , the tuner test results, the final buffer chemical polishing (BCP) and high pressure rinse (HPR) results, and the fabrication progress of several components including the completion of the helium vessel, magnetic shields, heat shield, cryogenic components and the ASME Code stamped cryostat are presented in this paper.

704 MHz COMPONENTS DESIGN

Fundamental Power Coupler

The 704 MHz SRF cryomodule [2] is powered by a coaxial coupler capable to deliver up to 20 kW CW RF power to the SRF cavity. The final model of the fundamental power coupler is shown in Fig. 1.

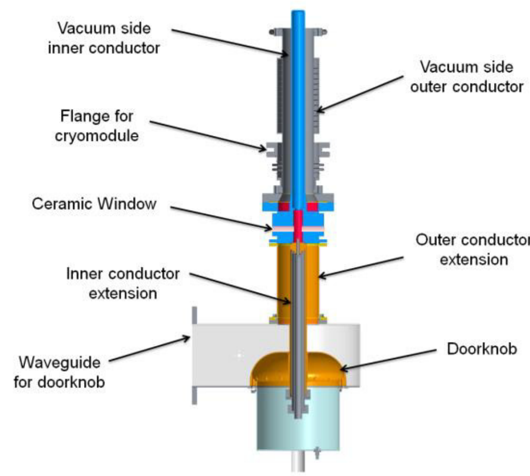

Figure 1: Fundamental power coupler design layout.

The FPC utilizes a coaxial RF window/antenna assembly from Toshiba Electron Tubes & Devices Co. [3], similar to the one currently in service on the 5-cell SRF cavity at the BNL's R&D ERL facility. On the vacuum side of the assembly, the outer conductor is a copper plated stainless steel tube with cooling channel used as a heat intercept and the inner conductor (antenna) is made of OFHC copper. The coaxial alumina window assembly has two instrumentation ports on the vacuum side: one for vacuum gauges the other one for an arc detector. The vacuum side outer conductor of the coaxial line will be cooled by 5 K helium gas, the vacuum side of the inner conductor will be cooled by air and the RF window will be cooled by water.

On the air side, the water–cooled inner extension is made of OFHC copper and the outer extension is made from copper-plated stainless steel. The FPC is coupled to a rectangular WR1150 waveguide via a waveguide doorknob transition supplied by Advanced Energy Systems, Inc. (AES) [4]. Custom conflat RF gaskets are used on all the outer conductor joints to provide good RF contact and at the same time a UHV joint.

TUNER MECHANISM

Mechanical Tuning System Design

The BNL3 cavity mechanical frequency tuning system was designed based on a tuner that has been successfully

* Work is supported by Brookhaven Science Associates, LLC under contract No. DE-AC02-98CH10886 with the US DOE.
# jcbrutus@bnl.gov
§ Present address: Fermi National Accelerator Laboratory, Batavia, IL 60510, U.S.A.

Content from this work may be used under the terms of the CC BY 3.0 licence (© 2015). Any distribution of this work must maintain attribution to the author(s), title of the work, publisher, and DOI.

ISBN: 978-3-95450-168-7 doi:10.18429/JACoW-IPAC2015-WEPWI052

Content from this work may be used under the terms of the CC BY 3.0 licence (© 2015). Any distribution of this work must maintain attribution to the author(s), title of the work, publisher, and DOI.

COMMISSIONING AND EARLY OPERATION EXPERIENCE OF THE NSLS-II STORAGE RING RF SYSTEM*

Feng Gao[#], James Rose, John Cupolo, Tom Dilgen, Ben Rose, Bill Gash, Vishy Ravindranath[§], Murali Yeddulla[¶], Joe Papu, Pete Davila, Brian Holub, Jueri Tagger, Bob Sikora, Gloria Ramirez and John Kulpin, Brookhaven National Laboratory, Upton, New York 11973, USA

Abstract

The National Synchrotron Light Source II (NSLS-II) is a 3 GeV electron X-ray user facility commissioned in 2014. The storage ring RF system, essential for replenishing energy loss per turn of the electrons, consists of digital low level RF controllers, 310 kW CW klystron transmitters, CESR-B type superconducting cavities, as well as a supporting cryogenic system. Here we will report on RF commissioning and early operation experience of the system for beam current up to 200mA.

INTRODUCTION

The NSLS-II storage ring was designed to maintain a 3GeV, 500mA circulating electron beam with very small horizontal (down to 0.5 nm-rad) and vertical (8 pm-rad) emittance [1]. There are fifteen 9.3 m straights and fifteen 6.6 m straight in the ring, where two of the 9.3 m straights were allocated for RF cavities. The fully built-out RF system is expected to have two CESR-B type 500 MHz superconducting cavities and one passive 1500 MHz superconducting Landau cavity on each RF straight.

To operate these superconducting cavities, an 840 watt liquid helium (LHe) refrigeration system has been commissioned [2]. Currently NSLS-II has two 500 MHz CESR-B type cavities on site, one of which is in the ring for daily operation, while the other is in the blockhouse (a test setup) for conditioning and studies. A prototype passive 1500 MHz Landau cavity is on site, whose construction is pending a cold test with LHe. Two 310 kW klystron transmitters, driven by FPGA based cavity field controllers (CFC) [3], have been commissioned to power the two 500MHz cavities. We will first briefly describe the status, then discuss a few interesting cases we have experienced, and finally the future plan and summary.

CURRENT STATUS

Figure 1 shows a simplified diagram of the storage ring RF system. The 500 MHz cavitiy design was optimized with flexibility for various scenarios with one to four operating cavities, and both first built cavities have measured Qext of 79,000. To reduce power reflection under operation with low beam current (< 200 mA), a 3-stub tuner has been added to raise the Qext of the cavity to 200,000. A cavity frequency tuner PLC was implemented to adjust tuner position based on the phase difference between the cavity field and the forward field.

*Work supported by DOE contract DE-SC0012704.
fgao@bnl.gov
§ Vishy is currently with SLAC.
¶ Murali is currently with Varian Medical Systems.

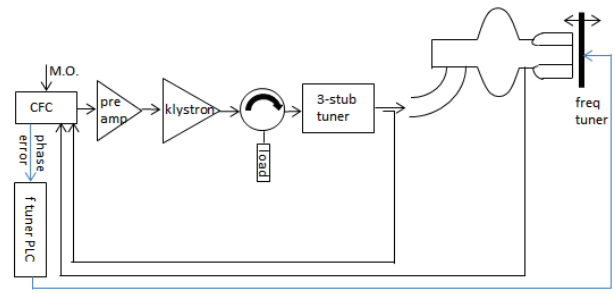

Figure 1: Simplified diagram of the NSLS-II storage ring RF system.

This PLC also monitors vacuum and water temperatures.

Table 1 shows typical operation parameters as of early April, 2015. The first cavity had been partially conditioned to 1.4 MV in the blockhouse before being moved to the ring. It then experienced frequent vacuum trips forcing the voltage to be lowered to 1.2 MV for reliability to accommodate optimization of other systems. In January 2015 the cavity was pulse conditioned to 1.87 MV with increasing duty cycles to CW, then the voltage was lowered to 1.778 MV for early operation.

Table 1: A Typical Set of Early Operation Parameters

M.O. frequency (MHz)	499.6815
r/Q (Ω)	89
Q0	2.7e+8
QL and Qext with 3-stub tuner	2.0e+5
Cavity voltage Vc (MV)	1.776
Cavity power (W)	131
Beam energy (GeV)	3.0
Beam energy loss per turn Va (kV)	288
Beam current (mA)	200
Revolution frequency (kHz)	378.55
Cavity detuning frequency (kHz)	-2.47
Momentum compaction	3.7e-4
Momentum acceptance	2.42e-2
Synchrotron frequency (Hz)	2550
Beam power (kW)	57.6
Forward power (kW)	77.8

ISBN: 978-3-95450-168-7 doi:10.18429/JACoW-IPAC2015-WEPWI053

HTS/LTS HYBRID HIGH FIELD SUPERCONDUCTING MAGNET DESIGNS FOR THE PROPOSED 100 TeV PROTON COLLIDERS*

R. Gupta#, M. Anerella, A. Ghosh, W. Sampson, J. Schmalzle,
Brookhaven National Laboratory, Upton, NY 11973, USA
J. Kolonko, D. Larson, R. Scanlan, R. Weggel, E. Willen,
Particle Beam Lasers, Inc., 18925 Dearborn Street, Northridge, CA 91324, USA
C. Rey, Energy to Power Solutions, 3958 W. Pensacola St., Tallahassee, FL 32304, USA

Abstract

Proposed proton-proton colliders with a center-of-mass energy up to 100 TeV in a tunnel of desired size require the dipole magnets to be of very high field—20 teslas in some proposals. This field is beyond the limit of present conventional Low Temperature Superconductors (LTS) and requires using High Temperature Superconductors (HTS). The preliminary magnetic design presented in this paper is an HTS/LTS hybrid design with high strength HTS tape used in higher field regions and less expensive LTS in lower field regions, with a goal of optimizing the performance while reducing the cost. A major concern in the magnets built with the HTS tape is the large field errors associated with the conductor magnetization. The strategy presented here aims to reduce those errors considerably. This paper also presents a proof-of-principle design and program to experimentally evaluate that concept.

INTRODUCTION

As a part of a recently funded Phase II Small Business Technology Transfer (STTR) award [1] by the U.S. Department of Energy (DOE), Particle Beam Lasers, Inc. (PBL), Brookhaven National Laboratory (BNL) and Energy to Power Solutions (E2P) are developing designs and technologies for accelerator magnets of very high field (20 T or more). Phase I of this STTR demonstrated this technology in a preliminary way [2]. To reduce cost, HTS/LTS hybrid designs are being examined. HTS is used in higher field regions, and conventional LTS in lower field regions. The designs are based on second generation (2G) ReBCO HTS tape with Hastelloy substrate, chosen primarily for its high strength and its ability to deal with large stresses. ReBCO is available in long lengths from several vendors around the world. The hybrid design presented here is based on a technique that is expected to keep the persistent current-induced harmonics to a manageable level despite the tape geometry of the conductor. These designs and technologies could be used in the proposed Future Circular Collider (FCC) at CERN [3] and/or the proposed Super proton-proton Collider (SppC) in China [4].

*Work supported by Brookhaven Science Associates, LLC under contract Number DE-SC0012704, with the U.S. Department of Energy and STTR contract DOE Grant Number DE-SC0011348.
#Corresponding author: Ramesh Gupta, gupta@bnl.gov.

MAGNETIC DESIGN

A preliminary magnetic design of a 21 T, 50 mm aperture HTS/LTS hybrid design is presented in Fig. 1, showing one quadrant of a magnet. The field contours and types of conductor used are shown in Fig. 2. Key design parameters are listed in Table 1. The block design allows easy conductor block segmentation and furthermore better magnetic and mechanical optimization. A segmented mechanical structure intercepts accumulated forces, similar to that used in an earlier design [5]. The space between the blocks will be adjusted to allow for an adequate space for structure. Ends will be lifted up to clear the bore or have an overpass/underpass configuration [6]. LTS coils will be simple and flat. Only the ends of a few HTS coils will need to be lifted to clear the bore in a common coil configuration [7].

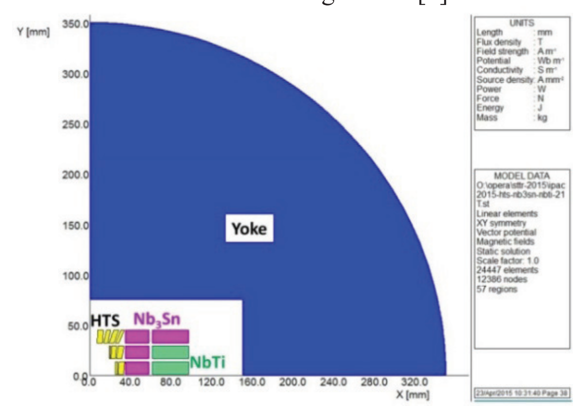

Figure 1: Quadrant of the magnetic model consisting of HTS, Nb_3Sn and NbTi (LTS) coil blocks and iron yoke.

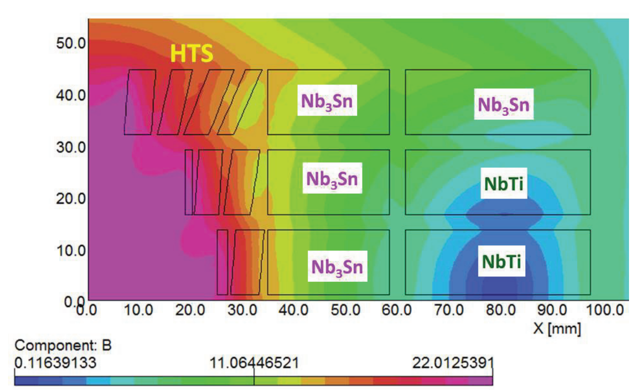

Figure 2: Field contours at central field of 21 T. Blocks with x<35mm use HTS (ReBCO tape); those with x>35mm use Nb3Sn or NbTi (LTS).

Content from this work may be used under the terms of the CC BY 3.0 licence (© 2015). Any distribution of this work must maintain attribution to the author(s), title of the work, publisher, and DOI.

ISBN: 978-3-95450-168-7 doi:10.18429/JACoW-IPAC2015-WEPWI054

DESIGN AND TEST OF THE RHIC CMD10 ABORT KICKER*

H. Hahn,# M. Blaskiewicz, A. Drees, W. Fischer, Jian-Lin Mi, Wuzheng Meng, Ch. Montag, Chien Pai, J. Sandberg, N. Tsoupas, J. E. Tuozzolo, Wu Zhang
BNL, Upton, NY 11973

Abstract

In recent RHIC operational runs, planned and unplanned pre-fire triggered beam aborts have been observed that resulted in quenches of SC main ring magnets, indicating a weakened magnet kick strength due to beam induced ferrite heating. An improvement program was initiated to reduce the longitudinal coupling impedance with changes to the ferrite material and the eddy-current strip geometry. Results of the impedance measurements and of magnet heating tests with CMD10 ferrite up to 190 °C are reported. All 10 abort kickers in the tunnel have been modified and were provided with a cooling system for the RUN 15.

INTRODUCTION

The original RHIC design provided a beam abort system for machine protection comprising five kicker magnets with the associated pulsers and pulse forming networks in each ring [1, 2]. The 5 kickers are serially located in the beam vacuum and must deflect the bunches by ≥ 3.55 cm to reach the dump absorber, corresponding to a beam kick of 1.5 mrad or 0.252 Tm/kicker [3]. The beam is deflected horizontally, and in essence the magnet defines a 7σ dynamic aperture. Each kicker is driven by a pulsed power supply during a 12 μs long pulse to eject 111 bunches. The kick starts with 1 μs rise time in the gap, formed by 9 missing bunches out of 120. The pulser is capable of 29 kV and at operation with 27 kV delivers 18 kA while modulating down to 11 kA. The required 1 μs rise time without thyratron pre-fire depends on the reservoir heater setting [4, 5].

The abort system performance as designed for the disposal of ~200 kJ was adequate until Run 13, when planned and thyratron pre-fired beam aborts resulted in quenching of SC main ring magnets [6, 7]. Retuning of the coiled-wire inductors in the pulse forming network provided temporary correction and allowed completion of the run. Various explanations were considered but the lowering of the pulser current bottom dip shown in Fig. 1 identified beam induced heating of the magnet inductance as the culprit. Planned p intensity increases in Run 15 from 1×10^{11} to beyond 2.5×10^{11} ppb [8] triggered the kicker redesign efforts.

*Work supported by Brookhaven Science Associates, LLC under contract no. DE-AC02-98CH10886 with the DOE.
hahnh@bnl.gov

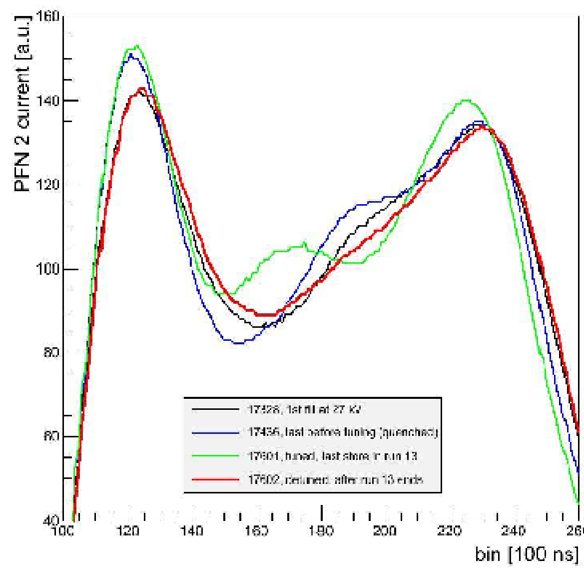

Figure 1: Pulser current at 27 kV in different operational stages: cold start, after quench, detuned in RUN13 and detuned cooled [6].

MAGNET INDUCTANCE

The magnet current sweep range results from an impedance mismatch between pulser and abort magnet impedance, ωL. The abort kicker inductance L has been largely determined by the dynamic beam aperture and by the power supply to be reasonably sized regarding voltage and peak current. The abort kickers are $\ell = 1.22$ m long and are constructed as window frame magnets with an aperture of $a = 5.08 \times b = 7.62$ cm in ferrite blocks, $w = 2.67$ cm wide. The inductance seen by the pulser can be estimated from $L \approx \mu_0 \frac{a\ell}{b} / \left(1 + a/\mu_F w\right)$ plus the feed-through inductance, that is the coaxial tube shown as Fig. 3 in Ref. [2]. The inductance is conveniently measured with a network analyzer via the bus bar input impedance as $L = Z_{BB}/\omega$ and is shown in Fig. 2 for the original magnet.

The kicker heating is dominated by the μ'' component of the ferrite and the search for better material beyond CMD5005 was done at many laboratories [9, 10], although limited here to the Ni-Zn ferrite CMD10 [11].

Content from this work may be used under the terms of the CC BY 3.0 licence (© 2015). Any distribution of this work must maintain attribution to the author(s), title of the work, publisher, and DOI.

ISBN: 978-3-95450-168-7 doi:10.18429/JACoW-IPAC2015-WEPWI055

COMMISSIONING AND EARLY OPERATION FOR THE NSLS-II BOOSTER RF SYSTEM*

C. Marques†, J. Cupolo, P. Davila, F. Gao, A.Goel‡, B. Holub, J. Kulpin, K. McDonald, J. Oliva, J. Papu, G. Ramirez, J. Rose, R. Sikora, C. Sorrentino, N. Towne, NSLS-II, BNL, Upton, NY 11973, USA

Abstract

The National Synchrotron Light Source II (NSLS-II) at Brookhaven National Laboratory (BNL) is a third generation 3GeV, 500mA synchrotron light source [1]. We discuss the booster synchrotron RF system responsible for providing power to accelerate an electron beam from 200MeV to 3GeV. The RF system design and construction are complete and is currently in the operational phase of the NSLS-II project. Preliminary operational data is also discussed.

INTRODUCTION

The booster synchrotron NSLS-II RF system is designed to efficiently accelerate a range of bunches from 0.5nC in single bunch mode up to 15nC in multi-bunch mode injected from the linac at 200MeV to the final acceptance energy of the storage ring of 3GeV once every second. The performance goals for the booster are derived from the beam acceptance requirements for the storage ring including an RF acceptance of 0.85% [1].

The booster RF system can be divided into five subsystems namely a 500MHz 7-Cell PETRA-like cavity, a 500MHz transmitter using a 90kW Inductive Output Tube (IOT), a 38kV/4A Pulse Step Modulated High Voltage Power Supply (HVPS), a Cavity Field Controller (CFC) and a high power circulator. Some relevant machine parameters are listed in Table 1 while the layout for the booster RF system is shown in Figure 1.

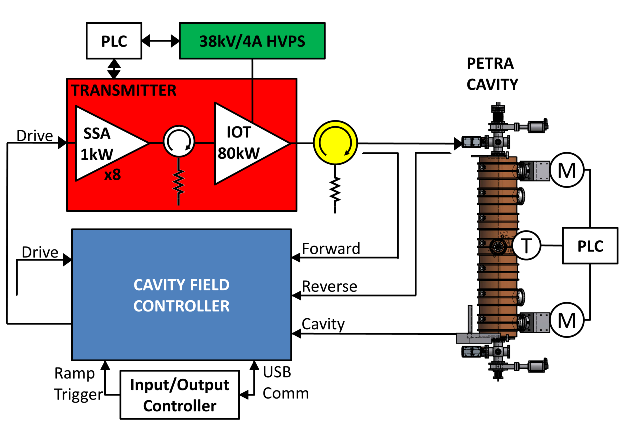

Figure 1: Simplified block diagram of the booster RF system.

* Work supported by the U.S. Department of Energy, Office of Science, Office of Basic Energy Sciences, under Contract No. DE-SC0012704.
† cmarques@bnl.gov ‡ Now at Argonne National Laboratory

Table 1: The NSLS-II Booster RF Parameters

Parameter	Value	Units
Frequency	499.68	MHz
Harmonic	264	
Bunch Train Charge	≤ 15	nC
Loss per turn @ 3GeV	625	keV
Gap Voltage @ Injection	200	kV
Gap Voltage @ Extraction	1200	kV
Injection Energy	200	MeV
Extraction Energy	3	GeV
RF Acceptance @ Extraction	0.85	%
Momentum Compaction	.0072	
Ramp Repetition Rate	1	Hz
Cavity Q_L	10^4	
Cavity Shunt Impedence	23	MΩ
HVPS Switching Frequency	93.75	kHz
HVPS Switching Modules	60	

SUB-SYSTEMS

Digital CFC

The Field Programmable Gate Array (FPGA) based CFC was developed as a common hardware platform for all NSLS-II RF systems and offers excellent versatility. A more detailed description of the CFC and the clock generating subsystem responsible for the FPGA clock, up/down conversions and timing can be found elsewhere [2, 3]. The booster CFC outputs a ramped RF waveform established by the host Input/Output Controller once a timing signal is initiated. The CFC uses a feedback control loop to stabilize the cavity field and phase throughout the ramp cycle.

Booster Transmitter

The 500MHz 90kW IOT is used to power the PETRA-like cavity. The cavity produces a ramped accelerating voltage from 200kV to 1200kV required for the acceleration from 200MeV to 3GeV. The measured output power of the IOT at extraction for a 3GeV acceleration was 47kW and is determined by the copper losses, beam loading and any external load. At peak operating levels the efficiency was measured to be 50%. The spectrum from the booster transmitter can be seen in Figure 2. The IOT is assembled on a cart which includes a focusing coil and input/output circuits. This modular approach allows switching out a tube assembly in about two hours. The transmitter is controlled via a Programmable Logic Controller (PLC) which communicates with the NSLS-II Experimental Physics and Industrial

Content from this work may be used under the terms of the CC BY 3.0 licence (© 2015). Any distribution of this work must maintain attribution to the author(s), title of the work, publisher, and DOI.

ISBN: 978-3-95450-168-7 doi:10.18429/JACoW-IPAC2015-WEPWI056

Content from this work may be used under the terms of the CC BY 3.0 licence (© 2015). Any distribution of this work must maintain attribution to the author(s), title of the work, publisher, and DOI.

A NUMBER OF UPGRADES ON RHIC POWER SUPPLY SYSTEM*

C. Mi#, D. Bruno, A. Di Lieto, J. Drozd, G. Heppner, T. Nolan, F. Orsatti, T. Samms, J. Sandberg, C. Schulthesis, R. Zapasek
Collider-Accelerator Dept., Brookhaven National Laboratory, Upton, NY 11973, USA

Abstract

This year marks the 15th run for the Relativistic Heavy Ion Collider (RHIC). Operation of a reliable superconducting magnet power supply system is a key factor of an accelerator's performance. Over the past 15 of years, the RHIC power supply group has made many improvements to increase the machine availability and reduce failures. During these past 15 years of operating RHIC a lot of problems have been solved or addressed. In this paper some of the essential upgrades/improvements are discussed.

INTRODUCTION

There are 6 above ground service buildings and 18 underground tunnel alcoves in the RHIC complex [1]. All power supplies and support instruments are in these locations around the RHIC ring. During the operations, the goal for all of the power supplies is to operate 24/7 without failure over the entire run. To achieve this high reliability a continuous improvement of the power supplies was required to reduce the failures over the years.

MACHINE PERFORMANCE OVER THE PAST SIX RUNS

Run 15 will be 22 weeks long. At the midway point of Run 15, the Mean-Time-Between-Failure (MTBF) rate is approximately 60 hours. This is the highest MTBF the power supply system has achieved. The MTBF has been improving steadily since Run 12. (See Table 1 for comparison)

Table 1: MTBF and Failures Over the Past Six Runs

Run	9	10	11	12	13	14
MTBF (hours)	15.1	35.4	17.7	39.0	40.4	41.1
# of Failures	215	117	205	89	61	82

UPGRADES AND IMPROVEMENTS

The upgrades and improvements were made in many different areas. They include adding new Print Circuit Boards (PCBs) into existing system, replacing power components, rework, adding redundant signal cables in the existing system, developing a drop in replacement power supply system for one type of power supply, swapping out old, obsolete PCBs and components to lengthen the power supply lifetime. All of the upgrades improved the power supplies reliability.

Replacement of Bipolar 300A and Bipolar 150A Power Supply

RHIC was commissioned in 1999. All of the original power supplies are still installed in the ring. Some of them are very reliable but some types have had more failures than other types. Some power supply types are easier to service than others due to the way they were packaged. Because of the serviceability issues, failures and aging a new replacement power supply is being installed.

Figure 1: 3 Kepco 10-100GL Units In Parallel.

There are a total 96 bipolar 150A model power supplies and 14 bipolar 300A model power supplies that are used in the RHIC superconducting power supply system. They are distributed in 6 service buildings. The topology of these power supplies is 3 phase AC input, full-bridge switch-mode pre-regulator with a linear output stage. The 150A model is the base unit and the 300A model is basically two 150A units paralleled to make a 300A unit. Due to the space constraints in the buildings, the packaging of these power supplies is extremely tight. The tight packaging of these power supplies means it is difficult to service them when a problem occurs.

*Work supported by Brookhaven Science Associates, LLC under Contract No. DE-AC02-98CH10886 with the U.S. Department of Energy.
#cmi@bnl.gov

ISBN: 978-3-95450-168-7 doi:10.18429/JACoW-IPAC2015-WEPWI057

A NEW BIPOLAR QTRIM POWER SUPPLY SYSTEM*

C. Mi#, D. Bruno, A. Di Lieto, J. Drozd, G. Heppner, T. Nolan, F. Orsatti, T. Samms, J. Sandberg, C. Schultheiss, R. Zapasek
Collider-Accelerator Dept., Brookhaven National Laboratory, Upton, NY 11973, USA

Abstract

This year marks the 15th run of RHIC (Relativistic Heavy Ion Collider) operations. The reliability of superconducting magnet power supplies is one of the essential factors in the entire accelerator complex. Besides maintaining existing power supplies and their associated equipment, newly designed systems are also required based on the physicist's latest requirements. [1] A bipolar power supply was required for this year's main quadrupole trim power supply. This paper will explain the design, prototype, testing, installation and operation of this recently installed power supply system.

INTRODUCTION

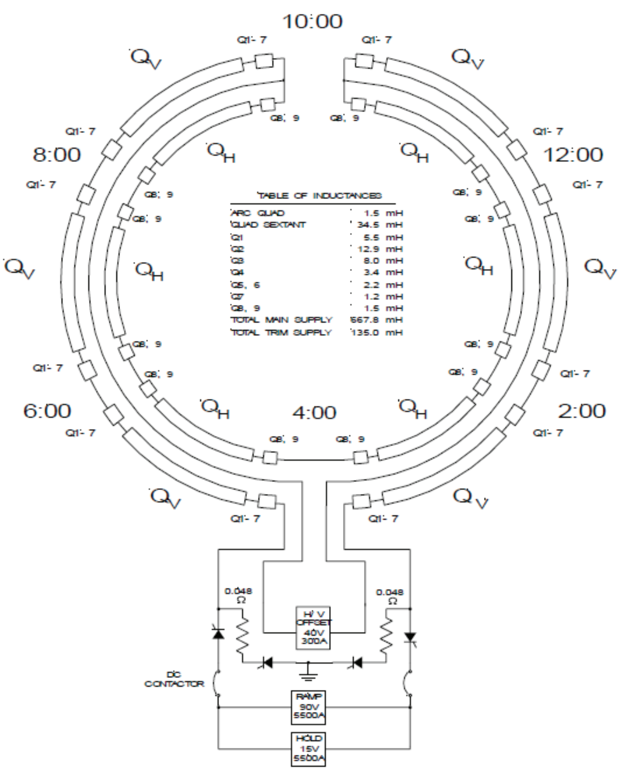

Figure 1: RHIC main quadrupole bus.

The existing quadrupole trim power supply (qtrim) was a unipolar power supply [2]. The power supply is connected in the middle of main quadruple magnet bus (Figure 1). The original qtrim power supply was a unipolar SCR type power supply. The accelerator physicist's required this new power supply to ramp up and down with bipolar capability. In order to keep the option of changing back to unipolar power supply setup in the future, it was decided to install a new power supply setup in an adjacent location.

*Work supported by Brookhaven Science Associates, LLC under Contract No. DE-AC02-98CH10886 with the U.S. Department of Energy.
#cmi@bnl.gov

DESIGN CONFIGURATION

System Consideration

We did not use the original AC power feed so we could easily revert back to the original unipolar power supply configuration if it was necessary. We have 2 qtrim power supplies installed and operating, one for blue ring and one for yellow ring. Both of them are 40V 300A unipolar SCR type power supplies. The new system is output +/-300A maximum current at 40V. However we don't need 40V based on our operational experience. A DC power supply that has 22V maximum output voltage was chosen. See maximum voltage required for ramp up in Table 1. As of the time of this writing the p.s. has been running at only a maximum of +10A during the second half of run 15 it will be operated at +130A. The voltage on the p.s. has been checked during a shutoff but this was only at 10A. [3]

Table 1: b-qtrim-ps Maximum Voltage Requirement During Ramp Up

Ramp Name	Operating Current (A)	V_{max} (V) @$I_{operating}$, calculated	V_{max} (V) @300A, calculated
Au14-v0	138.3	7.33	10.52
pp13-v2	183.6	8.56	10.86
pp13-v4	201	8.8	10.75
Au104	171	7.95	10.5

System Integration

The system is integrated in Figure 2 with all major components. Two DC power supplies [4] are connected in parallel for a maximum of +/-22V and +/-300A. Two h-bridge bipolar amplifiers are connected in parallel to make up the bipolar output stage, and each H-bridge amplifier is rated for +/-160A @ +/-25V [5].

AC Compartment

The main purpose of AC compartment is to pass the 3 phase 208V_{ac} into the rack and distribute the AC into 4 different AC outputs: 2 outputs for DC power supplies, 2 outputs for the H-bridge Amplifier and 1 output for the control chassis 110V_{ac} power. Also, the AC compartment interfaces with the control chassis to receive contactor ON command and it sends the contactor ON status back to control chassis. See figure 3 for rear panel view.

Content from this work may be used under the terms of the CC BY 3.0 licence (© 2015). Any distribution of this work must maintain attribution to the author(s), title of the work, publisher, and DOI.

ISBN: 978-3-95450-168-7 doi:10.18429/JACoW-IPAC2015-WEPWI058

NSLS-II RF CRYOGENIC SYSTEM*

J. Rose#, T. Dilgen, B. Gash, J. Gosman, J. Papu, V. Ravindranath, R. Sikora, A. Sitnikov,
BNL, Upton, NY 11786, USA
H. Wilhelm, Y. Jia LINDE, Pfungen, Switzerland
C. Monroe, Monroe Brothers, Moreton-in-Marsh, Gloucestershire GL56 9YX, UK

Content from this work may be used under the terms of the CC BY 3.0 licence (© 2015). Any distribution of this work must maintain attribution to the author(s), title of the work, publisher, and DOI.

Abstract

The National Synchrotron Light Source II is a 3 GeV X-ray user facility commissioned in 2014. A new helium refrigerator system has been installed and commissioned to support the superconducting RF cavities in the storage ring. Special care was taken to provide very stable helium and LN2 pressures and flow rates to minimize microphonics and thermal effects at the cavities. Details of the system design along with commissioning and early operations data will be presented.

INTRODUCTION

The NSLS-II RF cryogenic system, shown in Fig. 1, consists of a dedicated 4.5 K helium plant, LN2 system and RF system. The cryogenic system was designed for the complete build-out of the RF system, however only half of the RF is installed in the project scope. The cold box, compressors and dewar are all standard units, however boxes for helium and LN2 distribution are designed specifically with the application of superconducting RF in mind and have special features. Likewise the controls are split into two parts: one for the cryoplant operation, the second for the valve boxes that control the flow to and from the SRF cavities.

RF 4.5K COOLING REQUIREMENTS

The liquid helium cooling requirements for the NSLS-II RF cryogenic system was calculated for the full build out of two RF straights, each with two 500 MHz cavities and one 1500 MHz third harmonic cavity. The RF straights some 40 meters from the cold box and dewar, requiring some 45m each of vacuum jacketed transfer lines. In addition an RF test cave is located 20 m away. Each location requires valve boxes with 4 valves per cavity: LHe supply, cold GHe return, warm GHe return and LN2 supply. In addition the valve box for the RF test cave has valves for the transfer lines to the valve boxes (A and B) feeding the RF straights. Heat leaks were assigned to the rigid transfer lines (0.2 W/m), flexible VJ lines (1.6W/m), valve box and dewar losses. Dynamic heat loads from RF losses in the RF cavities were calculated as a function of cavity voltage. Since these losses are proportional to the square of the cavity voltage, and the required voltage of 3.3 MV per two cavities (1.5 MV each) and 4.8 MV per four cavities (1.2 MV each) the dynamic losses do not rise dramatically with the addition of the second RF straight. The 4.5K cooling requirements are summarized in Table 1.

Table 1: RF Cryogenic Requirements

Cryo=Plant Heat Load	Initial Project	Final Build
Total 500 MHz RF voltage (MV)	3.3	4.8
Number of 500-MHz cavities	2	4
R/Q (44.5 * # cavities)	89	178
Number of harmonic-cavities	1	2
R/Q (45 * # cavities)	90	180
Dynamic RF losses	(W)	(W)
500-MHz cavity Nb Q=7.5E8	69	71
500-MHz cavity Cu (W)	5	5
1500 MHz Nb (W) Q=3E8 (V= 1/3 V@500MHz)	20	31
1500 MHz Cu (W)	13	15
Dynamic Load Total	107	123
Static Heat Load	202	393
RF-ON, Total Load, W	309	516
150% Total Load	463	774

The total cryogenic load of 774 Watts is met by the largest of the Linde L280 series refrigerator/liquefier. Final specification was for a guaranteed 741 watts at 4.5 K as measured in the manifold box which is the central distribution point of the system.

CRYOGENIC PLANT

The cryogenic plant consists of the screw compressors, cold box with three (3) gas bearing turbo-expanders, 3500 L Dewar, gas management system, pure He gas storage tanks and helium purity analyser. The cold box includes integrated dual full flow 80 K adsorbers for manual regeneration, integrated single full flow 20 K adsorber for the removal of Neon and hydrogen, option of LN2 pre-cooling. The operation of the plant can be summarized as providing a full dewar of liquid Helium. The remainder of the cryogenic plant consists of the multichannel vacuum jacketed transfer lines, "manifold" valve box and two distribution valve boxes. The operation of the cavity side of the cryogenic system can be summarized as keeping the superconducting cavities helium vessel full of liquid with minimum of pressure and level variations which

* Work supported by DOE contract DE-SC0012704
#rose@bnl.gov

ISBN: 978-3-95450-168-7 doi:10.18429/JACoW-IPAC2015-WEPWI059

HIGHER ORDER MODE FILTER DESIGN FOR DOUBLE QUARTER WAVE CRAB CAVITY FOR THE LHC HIGH LUMINOSITY UPGRADE*

B. P. Xiao[1,†], S. Belomestnykh[1,2], I. Ben-Zvi[1,2], G. Burt[4], R. Calaga[3], O. Capatina[3], B. Hall[4], T. Jones[5,**], J. Skaritka[1], S. Verdú-Andrés[1], Q. Wu[1]
[1]Brookhaven National Laboratory, Upton, New York 11973-5000, USA
[2]Stony Brook University, Stony Brook, New York 11794, USA
[3]CERN, CH-1211 Geneva 23, Switzerland
[4]Lancaster University, Cockcroft Institute, Warrington, WA4 4AD, UK
[5]STFC, Daresbury Laboratory, Warrington WA4 4AD, UK

Abstract

A Double Quarter Wave Crab Cavity (DQWCC) was designed for the Large Hadron Collider (LHC) luminosity upgrade. A compact Higher Order Mode (HOM) filter with wide stop band at the deflecting mode is developed for this cavity. Multi-physics finite element simulation results are presented. The integration of this design to the cavity cryomodule is described.

INTRODUCTION

The LHC High Luminosity upgrade (HL-LHC) envisages the implementation of the crab-crossing technique [1-4] to correct the geometric effects of the wider crossing angles at which bunches collide, and hence maximize the LHC's luminosity. To fit the geometric limit of the LHC beam pipes, a compact HOM filter is designed for DQWCC to reflect the deflecting mode at 400 MHz back to the cavity, and to offer a pass band to the HOMs up to 2 GHz. Modes with frequencies above 2 GHz are expected to be Landau damped due to natural frequency spread, chromaticity, Landau octupoles and synchrotron oscillations [5].

CRAB CAVITY

The DQWCC, with its cross section shown in Fig. 1(a) [2, 6], can be considered as two quarter-wave resonators sharing a load capacitor, thus dubbed a double quarter wave cavity. For the 400 MHz fundamental mode, there is a transverse electric field between the two capacitive plates, offering the crabbing voltage when the beam passes at an appropriate phase. The frequency of the lowest HOM is 170 MHz higher than the fundamental mode frequency. Due to the installation of the thermal and magnetic shielding, shown in Fig. 1(c), the total height of the cavity plus HOM filter is confined within 350 mm from the beam axis.

* Work partly supported by US DOE through Brookhaven Science Associates LLC under contract No. DE-AC02-98CH10886 and by the US LHC Accelerator Research Program (LARP). This research used resources of the National Energy Research Scientific Computing Center, which is supported by US DOE under contract No. DE-AC02-05CH11231. Research supported by EU FP7 HiLumi LHC - Grant Agreement 284404.
†binping@bnl.gov
**Now at HZB Berlin, Germany

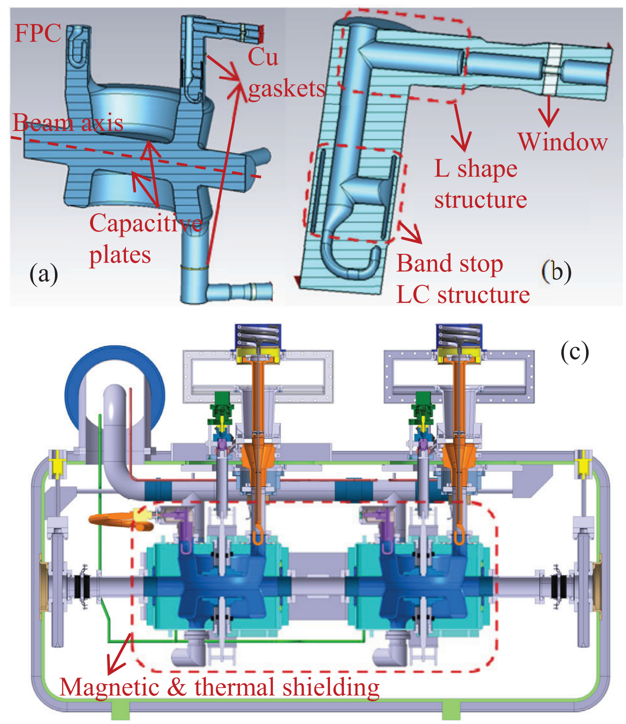

Figure 1: (a) DQWCC with 3 HOM filters, (b) HOM filter; (c) Cryomodule with two DQWCCs.

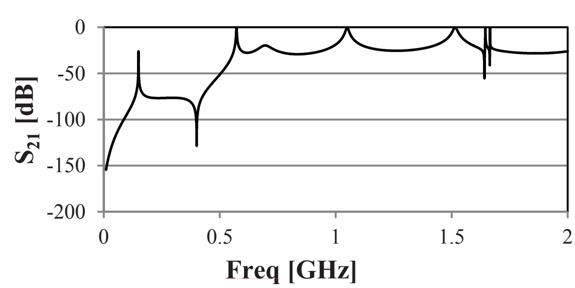

Figure 2: S_{21} of the HOM filter, with TE_{11} mode on the hook side and TEM mode on the port side.

RF DESIGN OF THE FILTER

The HOM filter, shown in Fig. 1(b), consists of a band stop LC structure right above the hook to minimize the RF loss on the Cu gasket that will be used to connect the cavity and the filter, shown in Fig. 1(a), and an L shape structure on the top to form a pass band starting from 570 MHz, the frequency of the first HOM. There are three

Content from this work may be used under the terms of the CC BY 3.0 licence (© 2015). Any distribution of this work must maintain attribution to the author(s), title of the work, publisher, and DOI.

ISBN: 978-3-95450-168-7 doi:10.18429/JACoW-IPAC2015-WEPWI060

Content from this work may be used under the terms of the CC BY 3.0 licence (© 2015). Any distribution of this work must maintain attribution to the author(s), title of the work, publisher, and DOI.

CYOGENIC TEST OF DOUBLE QUARTER WAVE CRAB CAVITY FOR THE LHC HIGH LUMINOSITY UPGRADE*

Binping Xiao[1,†], Luís Alberty[3], Sergey Belomestnykh[1,2], Ilan Ben-Zvi[1,2], Rama Calaga[3], Chris Cullen[1], Ofelia Capatina[3], Lee Hammons[1], Zenghai Li[4], Carlos Marques[1], John Skaritka[1], Silvia Verdú-Andres[1], Qiong Wu[1]
[1] Brookhaven National Laboratory, Upton, New York 11973-5000, USA
[2] Stony Brook University, Stony Brook, New York 11794, USA
[3] CERN, CH-1211 Geneva 23, Switzerland
[4] SLAC National Accelerator Laboratory, Menlo Park, CA 94025, USA

Abstract

A Proof-of-Principle (PoP) Double Quarter Wave Crab Cavity (DQWCC) was designed and fabricated for the Large Hadron Collider (LHC) luminosity upgrade. A vertical cryogenic test has been done at Brookhaven National Lab (BNL). The cavity achieved 4.5 MV deflecting voltage with a quality factor above 3×10^9. We report the test results of this design.

INTRODUCTION

The energy-frontier machine LHC at CERN is designed for high-energy particle physics, with energies up to 7 TeV per nucleon. Instead of upgrading the energies, the High Luminosity upgrade of the LHC (HL-LHC) will use the crab-crossing technique [1-4] to modify the angle at which bunches collide, and hence maximize the LHC's luminosity.

There are three phases for the LHC crab cavity project. The first one aims to validate the cryogenic performance of proof-of-principle (PoP) cavities. They must demonstrate a deflecting voltage of 3.34 MV per cavity. The second phase and the third phase will focus on fully dressed cavities in the Super Proton Synchrotron (SPS) and in the LHC. Eventually four cavities per beam will be needed at each side of the IP, i.e., 32 cavities in total plus spare ones.

The Quarter wave resonators (QWRs) first was proposed as a deflecting/crabbing cavity by Ben-Zvi [5, 6]. This design eventually evolved into a symmetric double quarter wave structure [1]. There is no lower order mode (LOM) or same order mode (SOM) exists in DQWCC, and its crabbing mode is the lowest resonant frequency, f_0. The first higher order mode (HOM) is well separated from the fundamental frequency f_0 by about $f_0/2$ due to the large capacitance. We describe the design, fabrication, and our results from testing the PoP DQWCC, built as part of the HL-LHC upgrade in this paper.

CAVITY DESIGN

The DQWCC shown in Fig. 1 can be considered as two quarter-wave resonators sharing a load capacitor. At the fundamental mode, there is a transverse electric field between capacitor's two plates, offering the crabbing voltage when the beam passes at an appropriate phase. Besides the two beam pipe ports, six extra ports are located on the top and bottom, with two on the top and four on the bottom, as shown in Fig. 1. These ports are designated for a fundamental power coupler (FPC), an RF pickup (PU) probe, and higher order mode couplers.

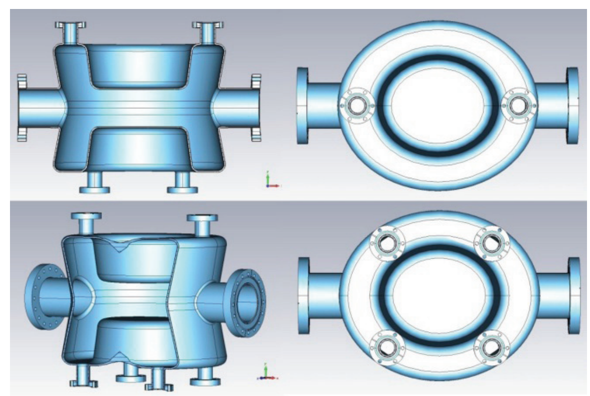

Figure 1: Geometry of the DQWCC. Top-left: Front sectional view; Top-right: Top view; Bottom-left: Front left sectional perspective view; Bottom-right: Bottom view.

Table 1 lists the key RF parameters of the DQWCC using CST Microwave Studio® with more than half a million tetrahedral meshes.

Table 1: Key RF Parameters of the Double Quarter Wave Crab Cavity

Fundamental mode frequency f_0 [MHz]	400
Nearest HOM frequency f_1 [MHz]	579
Deflection voltage V_t [MV]	3.34
R_t/Q (fundamental mode) [Ω]	406
Geometry factor [Ω]	85
Peak surface electric field E_{peak} [MV/m]	35.9
Peak surface magnetic field B_{peak} [mT]	83.9
Residual accelerating voltage V_{acc} [kV]	1.6
Stored energy [J]	10.9

* The work partly was supported by the US DOE through Brookhaven Science Associates, LLC under contract No. DE-AC02-98CH10886 with the US LHC Accelerator Research Porgram (LARP), and by the EU FP7 HiLumi LHC grant agreement No. 284404. This research used the resources of the National Energy Research Scientific Computing Center (NERSC), which is supported by the US DOE under contract No. DE-AC02-05CH11231
† binping@bnl.gov

ISBN: 978-3-95450-168-7 doi:10.18429/JACoW-IPAC2015-WEPWI061

Content from this work may be used under the terms of the CC BY 3.0 licence (© 2015). Any distribution of this work must maintain attribution to the author(s), title of the work, publisher, and DOI.

DESIGN OF NORMAL CONDUCTING 704 MHz AND 2.1 GHz CAVITIES FOR LEREC LINAC*

Binping Xiao[1,†], S. Belomestnykh[1,2], I. Ben-Zvi[1,2], J. C. Brutus[1], A. Fedotov[1], G. McIntyre[1]
K. Smith[1], J. Tuozzolo[1], V. Veshcherevich[3], Q. Wu[1], Wencan Xu[1], A. Zaltsman[1]
[1] Brookhaven National Laboratory, Upton, New York 11973-5000, USA
[2] Stony Brook University, Stony Brook, New York 11794, USA
[3] Cornell University, Ithaca, New York 14853, USA

Abstract

To improve RHIC luminosity for heavy ion beam energies below 10 GeV/nucleon, the Low Energy RHIC electron Cooler (LEReC) is currently under development at BNL. Two normal conducting cavities, a single cell 704 MHz cavity and a 3 cell 2.1 GHz third harmonic cavity, will be used in LEReC for energy spread correction. In this paper we report the design of these two cavities.

INTRODUCTION

To map the QCD phase diagram, especially to search the QCD critical point using the Relativistic Heavy Ion Collider (RHIC), significant luminosity improvement at energies below $\gamma = 10.7$ is required, which can be achieved with the help of an electron cooling upgrade called Low Energy RHIC electron Cooler (LEReC) [1].

An electron accelerator for LEReC (linac) consists of the photoemission gun (both the SRF and DC gun options are being developed) and the 5-cell 704 MHz SRF cavity. The SRF gun and 5-cell cavity are presently under commissioning in the R&D ERL [2]. In LEReC Phase I (electron kinetic energies up to 2 MeV) a one cell 704 MHz normal conducting cavity and a 3-cell third harmonic (2.1 GHz) normal conducting cavity will be added to de-chirp the energy spread and to compensate its non-linearity. An additional normal conducting cavity will be added in LEReC Phase II (energies up to 5 MeV with an accelerator working in the ERL mode), which is not covered in this paper.

CAVITY DESIGN

The optimization of the cavities is performed using CST Microwave Studio®, and the final designs are simulated using ACE3P package.

A. 2.1 GHz Cavity RF Design

The 2.1 GHz cavity will deliver 200 kV accelerating voltage. It will dissipate about 7.5 kW in its walls and will be fed from a 10 kW solid state RF amplifier. The design frequency is 2.1107 GHz, and the beam pipe diameter is 1.37 inches.

* Work is supported by Brookhaven Science Associates, LLC under contract No. DE-AC02-98CH10886 with the US DOE. This research used the resources of the National Energy Research Scientific Computing Center (NERSC), which is supported by the US DOE under contract No. DE-AC02-05CH11231.
† binping@bnl.gov

A pillbox shape cell is adopted as a baseline bare cell in this design. Nose cones with the height *h*, shown in Figure 1(c), are used to improve the cavity shunt impedance. Cell-to-cell coupling is determined by slots in the walls between adjacent cells, as shown in Figure 1(b). In this design four slots are added. Each slot has a width of 8 mm and an azimuthal length *phi*. 50 degrees is chosen for *phi* to get 1.2% cell-to-cell coupling for a 3-cell design. Cells with different height *h* were simulated, with *h* varied from 3 to 6 mm with a 0.5 mm step size. For each simulation the value of R_d is optimized so that resonance frequency can be set at 2.1107 GHz for π mode. The simulations showed a maximum shunt impedance at *h* = 4 mm.

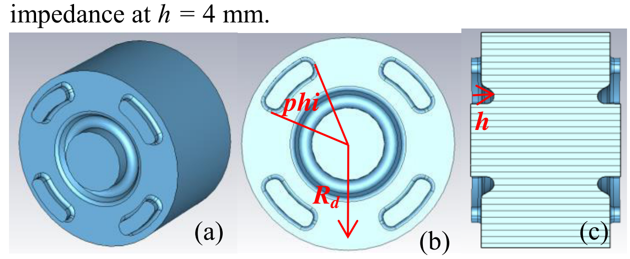

Figure 1: The 2.1 GHz bare cell: (a) perspective view; (b) front view; (c) side view.

This design provided a baseline for the 3-cell cavity. For the end cell with beam pipe, the *phi* value remains at 50 degree, the *h* value is re-optimized to maximize the shunt impedance, with a result of *h* = 4 mm.

For the center cell shown in Figure 2, a 30 mm diameter tuner is added at the bottom of the bare cell, with the tuner's penetration L_t to be negative while moving out of the cavity and to be positive while moving into the cavity. An FPC port is added opposite to the tuner. 134.42 mm × 25.04 mm JLab530 rectangular waveguide is used to deliver the RF power. This rectangular waveguide is connected to the cavity with a *WGHeight* + 5 mm long taper to a 25.04 mm × 25.04 mm coupling slot. 7.95 mm radius blending is applied to the transition edges. An RF window is not considered in this simulation and is added later to the 3-cell design. With *h* = 4 mm, *phi* = 50 degree, radius of the center cell R_d_c = 51.0 mm, the taper height *WGHeight* is chosen to be 92.0 mm to get the external quality factor Q_{ext}~3,300 from the FPC, so that the Q_{ext} for 3-cell cavity is about 10,000, with the assumption that the stored energy is evenly distributed between cells.

By assembling the two end cells (radius 52.5 mm and cone height 4 mm), and the center cell (radius 51.0 mm

ISBN: 978-3-95450-168-7 doi:10.18429/JACoW-IPAC2015-THXB1

Content from this work may be used under the terms of the CC BY 3.0 licence (© 2015). Any distribution of this work must maintain attribution to the author(s), title of the work, publisher, and DOI.

CEBAF SRF PERFORMANCE DURING INITIAL 12 GeV COMMISSIONING*

T. Allison, R. Bachimanchi#, E. Daly, M. Drury, C. Hovater, G. Lahti, C. Mounts, R. Nelson, and T. Plawski, Jefferson Lab, Newport News, Virginia 23606

Abstract

The Continuous Electron Beam Accelerator Facility (CEBAF) energy upgrade from 6 GeV to 12 GeV includes the installation of eleven new 100 MV cryomodules (88 cavities). The superconducting RF cavities are designed to operate CW at an accelerating gradient of 19.3 MV/m with a Q_L of 3×10^7. Not all the cavities were operated at the minimum gradient of 19.3 MV/m with the beam. Though the initial 12 GeV milestones were achieved during the initial commissioning of CEBAF, there are still some issues to be addressed for long term reliable operation of these modules. This paper reports the operational experiences during the initial commissioning and the path forward to improve the performance of C100 (100 MV) modules.

INTRODUCTION

In March of 2014 eleven new eight cavity high gradient cryomodules were operated for the first time in the CEBAF accelerator. The cryomodule design is a culmination of the lessons learned from three preproduction high gradient cryomodules and the original 42 CEBAF cryomodules [2]. To meet the 12 GeV energy goals the cryomodules must have an energy gain of 98 MeV. With that as a performance must, the cryomodule and cavities were designed to achieve 108 MV. Each cryomodule consists of eight 7-cell elliptical cavities. The cavities are tuned to 1.497 GHz, and individually controlled by both a mechanical stepper motor and a Piezo tuner (PZT).

Additionally the RF system is completely new for these cryomodules [3, 4]. Each cavity is powered and controlled by a single klystron and LLRF system. The klystrons produce 12 kW of linear power and up to 13 kW saturated. Four high voltage power supplies power two klystrons at a time. The eight klystrons are self-protected with their interlocks as part of the high power amplifier system. The RF controls use a traditional heterodyne scheme and digital down conversion at an intermediate frequency. Each cavity field and resonance control PI algorithm is contained in two FPGAs. One FPGA is in the field control chassis, controlling a single cavity. The resonance control chassis contains the other and controls up to eight cavities. The RF controls are unique incorporating a digital self excited loop (SEL) to quickly recover cavities. Controls and interfaces for both the HPA and the LLRF are provided through EPICS.

* Authored by JSA, LLC under U.S. DOE Contract DE-AC05-06OR23177. The U.S. Govt. retains a non-exclusive, paid-up, irrevocable, world-wide license to publish or reproduce this for U.S. Govt. purposes.
#bachiman@jlab.org

RF SYSTEM/CRYOMODULE COMMISSIONING

RF System Commissioning

The RF systems and cryomodules were installed and commissioned between 2011 and 2013, while the CEBAF accelerator was off for the energy upgrade. Typically they are commissioned in series, first with the RF systems and then followed by cryomodule commissioning.

The RF power systems (circulators and waveguide directional couplers) were commissioned by powering the klystrons up to their saturated power level of 13 kW. The LLRF system (field control chassis (FCC), stepper motor chassis, cavity interlocks, Piezo amplifier and heater controls) was simultaneously tested and calibrated [3]. The new digital RF control has made testing much simpler and easier since it replaces the RF sources and analog phase lock loops used in the past.

Table 1: C100 Cryomodule Energy Gain

Cryomodule	Beam Measurement	During CEBAF Commissioning
C100-1	104 MV	94.01 MV
C100-2	122	93.8
C100-3	108	76.58
C100-4	93	79.24
C100-5	121	100.31
C100-6	111	101.8
C100-7	104	103.81
C100-8	110	100.17
C100-9	105	101.15
C100-10	106	87.57
C100-0	104	89

Cryomodule Commissioning

All cavity/cryomodule performance aspects were tested in the CEBAF tunnel as part of commissioning [5]. Typical measured values include Qo, Qext and max

ISBN: 978-3-95450-168-7 doi:10.18429/JACoW-IPAC2015-THXB2

CRAB CAVITIES: PAST, PRESENT, AND FUTURE OF A CHALLENGING DEVICE*

Q. Wu#, BNL, Upton, NY 11973, USA

Abstract

In two-ring facilities operating with a crossing-angle collision scheme, luminosity can be limited due to an incomplete overlapping of the colliding bunches. Crab cavities then are introduced to restore head-on collisions by providing the destined opposite deflection to the head and tail of the bunch. An increase in luminosity was demonstrated at KEKB with global crab- crossing, while the Large Hadron Collider (LHC) at CERN currently is designing local crab crossing for the Hi-Lumi upgrade. Future colliders may investigate both approaches. In this paper, we review the challenges in the technology, and the implementation of crab cavities, while discussing experience in earlier colliders, ongoing R&D, and proposed implementations for future facilities, such as HiLumi-LHC, CERN's compact linear collider (CLIC), the international linear collider (ILC), and the electron-ion collider under design at BNL (eRHIC).

INTRODUCTION

Adopting head-on collision scheme is a straight-forward option for providing the highest possible luminosity at a given beam intensity. However, the particles and the debris from collisions travel towards the next bunch in the opposing beam after the interaction point (IP) [1]. To avoid long-range beam-beam collisions and possible damage to the instrumentation and detectors, it is necessary to separate bunches from their original travel orbit over a very short time. Depending on the bunch repetition rate, the substantial separation requirement could be within nano seconds, which is challenging for the designing the interaction region.

A crossing angle is introduced into colliders to avoid such drawbacks of the head-on collision; however, it also decreases luminosity due to reducing the geometric overlap of the colliding bunches. As shown in Figure 1, θ_c is defined as the full crossing angle.

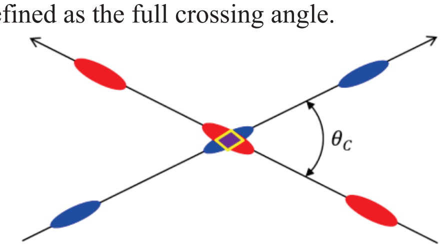

Figure 1: Beam collisions with crossing angle.

In 1988, Robert Palmer introduced the concept of crab cavity as a countermeasure to the geometric reduction in luminosity caused by the crossing angle in colliders [2]. The crab cavity imparts a transverse momentum kick, proportional to the longitudinal position of the particle. Transverse oscillation translates the longitudinally dependent kick to a transverse offset at IP. The offsets of the two beams cancel the reduction in luminosity caused by the crossing angle, and restore the head-on collision. Figure 2 illustrates the beam collision with the crab cavities [3]. The offset of the particles, x_{IP}, at the IP is a function of β_x at the crab cavity's location, $\beta_{x,cc}$, which is

$$x_{IP}=x'\sqrt{\beta_{x,cc}\beta_x^*}\sin\varphi$$

where φ is the phase advance from crab cavity to the IP.

The concept of the crab-crossing is appealing since it enables fast separation of the two colliding beam, has a compact interaction design, and small β^* at the interaction point (IP).

A few years after the concept was published, the first design of a superconducting RF (SRF) crab cavity started by KEK-Cornell University collaboration for CESR-B and later adopted at the High Energy Accelerator Research Organisation (KEK) in Japan for the electron-positron collider (KEKB). Since then, crab cavities have been added to many new collider designs as an essential element for pursuing higher luminosity.

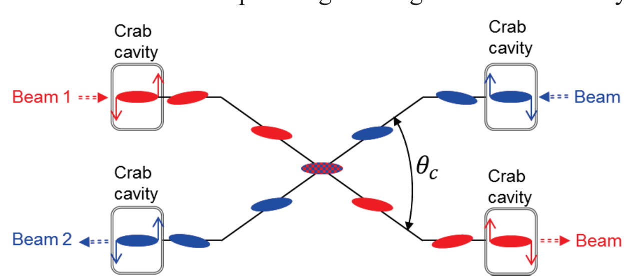

Figure 2: Beam collisions with crab cavity.

CRAB CAVITIES AT KEKB

In 2007, researchers at the KEKB demonstrated the first operational crab cavity, and observed a corresponding increase in luminosity [4][5].

The final configuration was a global crabbing scheme wherein a single cavity was used for each ring to compensate for a horizontal crossing angle of 22 mrad, Figure 3. In a global crabbing scheme, the crab cavity is installed at a particular location and generates transverse bunch oscillations around the ring. This scheme saved the cost by installing fewer cavities and utilization of the existing cryogenic system at Nikko.

*Work supported by Brookhaven Science Associates, LLC under Contract No. DE-AC02-98CH10886 with the U.S. Department of Energy and EU FP7 HiLumi LHC - Grant Agreement 284404
#qiowu@bnl.gov

Content from this work may be used under the terms of the CC BY 3.0 licence (© 2015). Any distribution of this work must maintain attribution to the author(s), title of the work, publisher, and DOI.

ISBN: 978-3-95450-168-7 doi:10.18429/JACoW-IPAC2015-THYB2

THE AUTO-ALIGNMENT GIRDER SYSTEM OF TPS STORAGE RING

T.C. Tseng, H.S. Wang, W.Y. Lai, S.Y. Perng, M.L. Chen, H.C. Ho, C.J. Lin, K.H. Hsu, D.G. Huang, C.S. Lin, P.S. Chuang, C.W. Tsai, C.K. Kuan and J.R. Chen
National Synchrotron Radiation Research Center, Hsinchu 30076, Taiwan

Abstract

To meet the stringent beam dynamic specs of TPS with high brilliance and low emittance characteristics, also to align the girders precisely and quickly with less manpower, the girder system for TPS (Taiwan Photon Source) storage ring is of an auto-tuning design. Each girder can be fine adjusted in 6 axes with 6 motorized cam movers of kinematic mounting design on 3 pedestals. With sensors between each girder, there are 72 girders to make up a whole ring auto-alignment girder system. All the sub-systems were carefully assembled and calibrated in a rented factory outside NSRRC during the civil construction period. Mock-up systems were set up and the auto–alignment processes were examined to modify interferences or mistakes between sub-systems. After the TPS building was nearly completed, the laser tracker alignment network was set up first and then the installation took place. When all the girders and sensors were installed into the tunnel, the auto-alignment procedures were carried out to fine tune all the girders. This paper describes the design, preparation, installation and implementation of this auto-alignment girder system for TPS storage ring.

INTRODUCTION

The TPS (Taiwan Photon Source) construction project started formally from 2006 while a feasibility study was initiated in 2004. It aimed to build a high brilliant and the very low emittance 3Gev ring with 518m circumference [1]. To meet the stringent beam dynamic specs, all the magnets should be located at precise positions and also firmly supported. However, considering the deformation of the floor and limited space in the tunnel also frequent earthquake in Taiwan, to align the girders precisely and quickly with less manpower is essential and an automatic-tuning girder system is thus proposed.

The design goal of the girders system for TPS is:

- To firm support and precise positioning of magnets
- Whole ring automatic alignment
- Precise resolution (μm)
- Beam based girder alignment (proposed)

In order to fulfill these challenging ambitions, a 6-axis motorized adjusting mechanism thus demanded. This girder system design is a modification from the girder system used in SLS (Swiss Light Source) by extending a 3 grooves type kinematic mounting from 3 balls to 6 balls and with a few major considerations:

- More contact points with locking system to raise natural frequency and reduce deflection.
- All contact points persist rolling contact when adjusting to reduce friction and remain high mobility.
- Contact stress is less than elastic limitation to reduce friction wear and keep high reliability.

In 2005, a preliminary study prototype bending section with 3 girders had been established for a test. This prototype proved the 6 axes adjustability with less than 1 μm resolution but the contact stress is exceed the elastic limitation due to point contact and wear occurred after a lifetime test [2-6].

In 2009, after the design stage of TPS is almost finished, a nearly real size testing mock-up system was set up in NSRRC fab for a system test and final examination [7-9]. After a few modifications, all hardware systems went into mass production processes.

From 2010, during the civil construction period, all the sub-systems were carefully assembled and calibrated in a rented factory outside NSRRC. A third mock-up system was set up again to modify interferences or mistakes [8-11].

After the tunnel completed, starting in January 2013, the pedestals were to be set out, anchor bolts drilling and installed with the accuracy around ±1mm. Upon completion of installation, the pedestals were grouted to the ground. There were 2 bending sections installed at July as an on-site mock-up testing system and the entire system installation began from October at a rate of 2 sections per week.

The whole storage ring girders were completed craned at March 2014 and finished control system installation test at May. In August, a whole ring girder automatic alignment was really performed the first time and it takes only 1900 seconds (32 minutes). In October, a second automatic alignment was performed to further minimize the deviations. Then, after the problem of high permeability booster vacuum chambers was discovered and solved, the commissioning of both rings were quick and accumulated beam took place at the end of 2014.

GIRDER SYSTEM DESIGN

According to the six-fold symmetric configuration DBA lattice design, 3 consecutive girders were used to accommodate one bending section magnets with the 2 dipole magnets assembled on side girders. With 4 bending sections to form a superperiod as in Fig. 1, there are 3 girder types and 72 girders total for the storage ring. With an electric levelling sensor (Leica Nevil 220) on each girder and touch sensors (Heidenhain Acanto AT1218 absolute length gauge) between consecutive girders in addition with a laser PSD (Position Sensitive Detector) system between straight section girders, a feedback controlled full ring automatic tuning girder system is established as in Fig. 2.

Content from this work may be used under the terms of the CC BY 3.0 licence (© 2015). Any distribution of this work must maintain attribution to the author(s), title of the work, publisher, and DOI.

ISBN: 978-3-95450-168-7 doi:10.18429/JACoW-IPAC2015-THXC2

ION BEAM THERAPY WITH IONS HEAVIER THAN PROTONS: PERFORMANCE AND PROSPECTS

U. Linz, Forschungszentrum Jülich, D-52425 Jülich, Germany

Content from this work may be used under the terms of the CC BY 3.0 licence (© 2015). Any distribution of this work must maintain attribution to the author(s), title of the work, publisher, and DOI.

Abstract

This presentation focuses on two aspects of the therapy with ions heavier than protons: technical equipment and rationale for the choice of ion. The part on equipment concentrates on accelerator and gantry. Biophysical, medical, and economical considerations will be discussed in the part featuring the choice of the proper ion.

INTRODUCTION

Whereas all ions have Bragg peak and magnetic deflectability in common, ions heavier than protons are characterized by a narrower dose peak, less lateral scattering, and an increased biological effectiveness. All of these properties render them interesting as ions for therapy. However, with increasing atomic mass ions tend to fragment after nuclear collision. The resulting lighter ions and neutrons cause tailing of the Bragg peak with a higher dose in the exit zone. The increasing number of neutrons per projectile are also a reason for increased cost due to shielding requirements. Another cost factor is the size of the accelerator and the gantry. Both are directly correlated with the choice of the ion. The question *which is the optimum ion* or *which ions do we need* is therefore one that influences future facility design.

ACCELERATORS FOR ION BEAM THERAPY

An accelerator system for ion beam therapy (IBT) has to be highly reliable, easy to operate and to maintain. In order to be competitive with other clinical treatment systems, the cost for operation, maintenance, and follow-up should be low.

All active IBT centers that utilize ions heavier than protons have opted for carbon ions and all these centers have a normal-conducting slow-cycling synchrotron (SCS) as accelerator. They value the established slow extraction method and the high beam stability of this accelerator type. A first design study of a compact (ø 6-10 m), superconducting SCS has been published by Noda et al. of NIRS [1]. A superconducting isochronous cyclotron is under development by IBA and intended for ARCHADE in France [2]. Plans for other accelerators such as the rapid-cycling synchrotron were presented in the past [3] but have not yet been put into action in any therapy center.

NECESSITY OF A GANTRY

State-of-the art for proton therapy, a gantry should also be conceived for an IBT center using ions heavier than protons, even though it is a significant cost factor. From a clinical point of view, external irradiation should be carried out from the optimum angle to reduce unnecessary radiation exposure, and the radiation beam should be directed to the target not the target to the beam.

The first IBT center with a rotating gantry for carbon ions has been HIT in Heidelberg, Germany. The gantry is 25 meters long, has a diameter of 13 meters, weighs 600 tons, moves with an accuracy of ±0.3°, and has a braking distance of only 1°. It is an engineering masterpiece but as a standard for IBT it is prohibitive.

A superconducting gantry is under development at NIRS which provides the same ion range but has only half the length and weight of the HIT gantry. The aperture size will be somewhat smaller than at HIT, but with 20x20 cm^2 it should be compatible with 3D scanning [4].

The non-scaling fixed-field alternating gradient gantry claims a reduction of the weight of the beam line by approx. 2 orders of magnitude (1.5 t vs. 135 t) [5]. Unfortunately, a working prototype of such a slimmed-down gantry has not yet been put into practice.

THE OPTIMUM ION

From a clinical point of view, a therapeutic ion beam should display as little as possible (low-LET) radiation in the entrance channel or plateau region to spare normal tissue. In the Bragg peak or target area the radiation quality should preferably be high-LET and of high relative biological effectiveness (RBE). Minimum fragmentation, a low neutron dose, and a high benefit-cost ratio are further requirements that the optimum therapeutic ion should meet. Despite decades of clinical experience with protons and carbon ions in particular, or helium and neon ions on a smaller scale, systematic experimental studies to find the optimum ion are lacking.

Simulation experiments illustrate that only ions up to boron (Z=5) stay significantly below an ionization density of 20 keV/µm in the entrance channel of a spread-out Bragg peak (SOBP) [6]. This is considered the lower limit of high-LET radiation. Carbon is borderline and oxygen and all heavier ions show definite unwanted high-LET behavior in this area with healthy tissue that should not be damaged.

Beyond the SOBP, ions up to boron show an insignificant dose tail of low-LET fragments. Carbon exhibits a short high-LET dose tail of 2-3 centimeters. For heavier ions, this unwanted fragmentation tail is further pronounced.

ISBN: 978-3-95450-168-7 doi:10.18429/JACoW-IPAC2015-THYC1

COMPARISON OF BEAM DIAGNOSTICS FOR 3RD AND 4TH GENERATION RING-BASED LIGHT SOURCES

H. Maesaka#, RIKEN SPring-8 Center, Kouto, Sayo, Hyogo, 679-5148, Japan

Abstract

Beam diagnostics for the fourth generation ring-based light sources (4GLSs) with a multi-bend achromat (MBA) lattice are discussed in comparison to the third generation light sources (3GLSs). While the MBA lattice enables small natural emittance of typically 100 pm rad, it has large non-linear effect that makes the machine operation difficult. In addition, stability requirements for the X-ray photon beam of the 4GLSs are stringent due to the small beam size and divergence. Therefore, novel diagnostic techniques are needed, such as highly accurate and stable beam position monitors, high resolution beam size monitors, and bunch-by-bunch feedback systems. We review beam diagnostic technologies implemented for 3GLSs and their application to the 4GLSs. To maximize the performance of the 4GLSs, R&D toward the photon-beam-oriented diagnostics is discussed.

INTRODUCTION

The third generation light sources (3GLSs) have been indispensable sources of brilliant X-rays for various science applications [1]. Several years ago, X-ray Free Electron Lasers (XFELs) became available [2,3], which was a significant breakthrough for photon science. The XFEL has excellent transverse coherence and extremely high peak brilliance. The success of the XFEL has stimulated 3GLSs to evolve the pursuit of higher brilliance and coherence.

The natural emittance of a 3GLS ranges from 1 to 10 nm rad and the average brilliance around 10^{20} photons/sec/mm^2/mrad^2/0.1%BW. Higher brilliance radiation can be obtained by reducing the natural emittance of the electron beam, if the emittance is larger than the diffraction limit [4]. Therefore, the goal of the emittance reduction for a ring-based light source is to achieve the diffraction limit. The diffraction limit for 10 keV X-rays, for example, is 10 pm rad, which is two orders of magnitude smaller than 3GLSs.

In order to approach the diffraction limit, a new type of lattice design, multi-bend achromat (MBA), has been established. The MBA is motivated by the emittance scaling formula [5]:

$$\epsilon_0 \propto \gamma^2 \theta^3,$$

where ϵ_0 is the natural emittance, γ is the Lorentz factor of the electron beam, and θ is the bending angle for each dipole magnet. In order to reduce θ, MBA uses more than 3 dipoles for each achromat cell. By using MBA, the natural emittance of around 100 pm rad can be achieved and the brilliance can be increased to around 10^{22} photons/sec/mm^2/mrad^2/0.1%BW. In this article, we call the light source using the MBA lattice as a fourth generation light source (4GLS).

At this moment, there are two 4GLS facilities, MAX IV [6] and Sirius [7], under construction. Many other projects, such as ESRF Upgrade [8], SPring-8-II [9], APS Upgrade [10], Diamond-II [11], ALS Upgrade [12], PEP-X [13], BAPS [14] and TauUSR [15], have been proposed so far. The main parameters of these facilities are tabulated in Table 1.

In this article, the characteristics of 4GLSs and 3GLSs are compared, and requirements for beam diagnostics for the 4GLSs are discussed. Novel beam instrumentations developed for 3GLSs are briefly reviewed with prospects of 4GLSs. Finally, diagnostic challenges for 4GLSs are discussed.

Table 1: 4GLS Facility Examples. E is the beam energy in GeV, ϵ_0 is the natural emittance in pm rad and C is the circumference in meter.

Facility	E	ϵ_0	C	Lattice
MAX IV	3.0	330	528	7BA
Sirius	3.0	280	518	5BA
ESRF-U	6.0	147	844	7BA
SPring-8-II	6.0	149	1435	5BA
APS-U	6.0	150	1104	7BA
Diamond-II	3.0	276	561	DDBA
ALS-U	1.9	50	196	9BA
PEP-X	4.5	50	2199	7BA
BAPS	5.0	75	1263	7BA
TauUSR	9.0	3	6210	7BA

COMPARISON OF 4GLS AND 3GLS

Accelerator Beam Parameters

The MBA lattice used in a 4GLS has many technological challenges compared with a 3GLS (DB lattice). Typical beam parameters of the 4GLS and the 3GLS are summarized in Table 2.

The beam size of a 4GLS is approximately 20 µm (H) x 5 µm (V), which is determined by the horizontal (vertical) emittance of 100 (10) pm rad and the beta function of several meters. The beam orbit should be stable within 1/10 of the beam size in order to maintain the stable optical axis of a photon beamline. Thus, stringent orbit stability is required for the 4GLS.

maesaka@spring8.or.jp

Content from this work may be used under the terms of the CC BY 3.0 licence (© 2015). Any distribution of this work must maintain attribution to the author(s), title of the work, publisher, and DOI.

ISBN: 978-3-95450-168-7 doi:10.18429/JACoW-IPAC2015-THYC2

Content from this work may be used under the terms of the CC BY 3.0 licence (© 2015). Any distribution of this work must maintain attribution to the author(s), title of the work, publisher, and DOI.

RECENT TRENDS IN BEAM SIZE MEASUREMENTS USING THE SPATIAL COHERENCE OF VISIBLE SYNCHROTRON RADIATION

T. Mitsuhashi, KEK, Tsukuba, Japan

Abstract

The optical method of measuring the transverse beam profile and size using visible synchrotron radiation (SR) began with simple imaging systems. The resolution was limited by both diffraction and wavefront errors making it difficult to resolve beam sizes less than 50 µm. Instead of imaging, an interferometric method for measuring the beam profile and size using spatial coherence was introduced. The method is based on Van Cittert-Zernike's theorem, and can resolve 4-5 µm beam sizes with an error of only 0.5 µm. In this presentation, the principle of the measurement, the SR interferometer design, and some resent measurement results are reviewed. The incoherent field depth effect for the horizontal beam size measurement is also described with some recent results. Design study calculations for the SR interferometer at the LHC will be presented.

INTRODUCTION

The synchrotron radiation (SR) monitor based on visible optics is one of the most fundamental diagnostic tools in high energy accelerators. The monitor gives a static and dynamic observation for the visible beam profile, beam size and with a streak camera, the longitudinal profile. These diagnostics greatly improve the efficiency of commissioning and operation of the accelerator. The discipline of monitoring began with simple imaging systems [1]. The resolution in the imaging systems was limited by both the diffraction and wavefront errors making it difficult to resolve beam sizes less than 50 µm. Instead of imaging, a method for measuring the beam profile taking advantage of inherent spatial coherence was introduced [2].

Nowadays, the SR interferometer is recognized as a powerful tool to easily measure small beam sizes [3]. Recent efforts to improve the measurable range down to 3-4µm have been reported [4]. In recent few years, an imbalance input technique was developed to introduce magnification into the interferometer [4][5][6]. The principal of the measurement, and some resent results are reviewed in this paper.

PRINCIPAL OF THE MEASUREMENT

In visible optics, interferometry is one of the standard methods to measure the profile or size of very small objects. The principle of measuring the profile of an object by means of spatial coherence was first proposed by H. Fizeau in 1898 [7], and is now known as the Van Cittert-Zernike theorem [8]. In other hand, it is well known that A. A. Michelson measured the angular dimension (extent) of a star with his stellar interferometer in 1920 [9]. With interferometry, all free parameters such as wavelength distance between object and interferometer and separation of double slit are measured by interferometry and a ruler. Due to this self-consistently, this method is classified as an *absolute* measurement.

Considering an incoherent light source as an ensemble of the single, independent modes of the emitted light, according to the van Cittert-Zernike theorem, the intensity distribution of the object is given by the Fourier transform of the complex degree of 1st order spatial coherence [8]. Mathematically, if we let f denotes the two dimensional transverse intensity distribution of beam profile as a function of coordinates x, y, the 1st order complex degree of spatial coherence γ as a function of spatial frequency υ_x and υ_y is given by ,

$$\gamma(\upsilon_x,\upsilon_y)=\int f(x,y)\exp\{-2\pi i(\upsilon_x x+\upsilon_y\cdot y)\}dxdy$$

$$\upsilon_x=\frac{2\pi D_x}{\lambda R},\ \upsilon_y=\frac{2\pi D_y}{\lambda R} \qquad (1)$$

where R denotes the distance between the source and the double slit. We can therefore obtain the beam profile and thus beam size via the inverse Fourier transform of complex degree of 1st order spatial coherence as measured with a 2-slit interferometer.

SR INTERFEROMETER

In order to measure the 1st order spatial coherence of a SR beam, a wavefront-division type interferometer using polarized, quasi-monochromatic rays is used. An outline of the interferometer is shown in Fig. 1 [2][3].

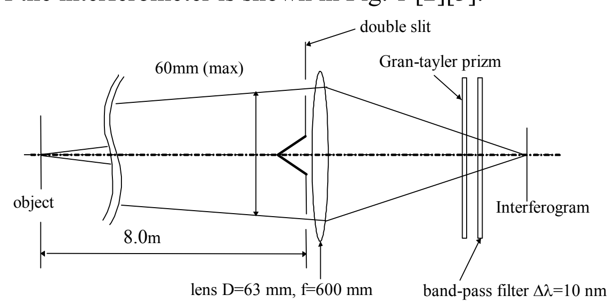

Figure 1: Outline of the 2 slit wavefront-division type of SR interferometer.

A diffraction-limited high quality lens (such as ED apochromat) is used to focus the beam onto the screen. In the vertical plane, there exists a π phase difference between the interference fringes relative to the σ-polarized fringes [2]. A Gran-Tayler prism is used to select the σ component of the SR. A band-pass filer is used for obtain quasi-monochromatic light. An eyepiece

toshiyuki.mitsuhashi@kek.jp

ISBN: 978-3-95450-168-7 doi:10.18429/JACoW-IPAC2015-THSMS2

THE CREATION OF THE PAC CONFERENCE SERIES*

Stan O. Schriber, Eagle, Idaho 83616, USA

Abstract

After much discussion in the early 1960s, the first Particle Accelerator Conference (PAC) was held in 1965 March at Washington, DC, using a particular format that the organizers determined should lead to a successful conference. In addition to focussing on all types of accelerators, the conference was organized to provide an environment for engineers, technologists, physicists and users/operators to interact and share information within an informal arrangement that promoted discussion and sharing information. The first conference was so successful that 50 years later we are using many of the concepts and procedures employed in the 1965 PAC, with improvements that have been added over the years. The initiation, development and operation/management of the successful PACs up to this 50th anniversary in 2015 are described in the following sections.

EARLY "TIMES"

With the advent of many accelerators being built and in operation in the USA, Europe and the Soviet Union, it was decided in the late 1950s to establish the International Conference on High Energy Accelerators – HEACC with sponsorship from the International Union of Pure and Applied Physics (IUPAP). Initially HEACCs were held every two years, but in 1971 this was changed to every three years. As an indication of the international nature of HEACCs, the 2nd was held at CERN in 1959, at BNL in 1961 and at Dubna in 1963. The author had the privilege of chairing the 16th HEACC in association with PAC'95 at Dallas, TX in March 1995. As chair, he worked with A.N. Skrinsky [1], Novosibirsk, Russian Federation for financial support from IUPAP to cover the costs for selected individuals to attend the conference from regions unable to provide funds for their attendance.

There are many excellent papers in the published records of this conference series, and several individuals in the accelerator community are investigating the possibility of having these conference records available through the popular Joint Accelerator Conferences Website (JACoW) [2].

Around 1960, the Institute of Electrical and Electronics Engineers (IEEE)[1] became more involved in various aspects of particle accelerators and their evolving technologies, especially for research and applications. For several years, the Technical Committee on Plasmas and the High Energy Physics sections of IEEE's Nuclear Science Group (precursor to the present IEEE-NPSS (Nuclear & Plasma Sciences Society)) was investigating ways to bring together individuals and teams interested in the technical and scientific aspects of particle accelerator design, engineering, construction, management and operations. At that time, there existed no opportunity for such accelerator specialists to forgather at one meeting covering all of these interrelated topics.

RATIONALE

Around 1963 a number of accelerator specialists felt that HEACC was becoming more of a dialogue between the high-energy facility designers and users. Because of this nature, they felt that an interdisciplinary conference (engineering/scientific) would complement the HEACC conference series, rather than create a conflict with it.

At the American Physical Society (APS)[2] meeting in Washington, DC in 1964, Louis Costrell [3,4], James E. Leiss [5,6] and H.W.(Bill) Koch [6,7] of NBS approached Robert S. Livingston [8] of ORNL regarding their desire to co-sponsor a particle accelerator meeting, using the decades old Scintillation Counter Symposium as a model for success. To achieve this interdisciplinary approach for the conference, with timely sharing of data/information, with ample time for discussion and with dissemination of important recent results, the program was organized to cover a large expanse of interests. In order to assist the broad accelerator community with the rapid development of scientific and technological advances, the following elements were considered important for success:

- To appeal to both scientists and engineers.
- To discuss the design of all sizes and types of accelerators, from the smallest to the largest.
- To include accelerators of both heavy and light particles.
- To review problems at both the input and output of the accelerator.
- To encourage participation of those who operate and build accelerators.

General Conference Layout

Many of the ideas and arrangements made for the first Particle Accelerator Conference (PAC) held in 1965 at the Shoreham Hotel in Washington DC have continued for the past 50 years, with some being modified to fit changes that have occurred within that timeframe, as described in later sections.

*Work supported by Schriber Consulting, Eagle, ID 83616, USA.

[1] IEEE is the world's largest professional association dedicated to advancing technological innovation and excellence for the benefit of humanity with >426,000 members in > 160 countries (~30% student members); >50% outside USA.

[2] APS is a non-profit membership organization working to advance and diffuse the knowledge of physics through its outstanding research journals, scientific meetings, and education, outreach, advocacy, and international activities with >51,000 members throughout the world.

Content from this work may be used under the terms of the CC BY 3.0 licence (© 2015). Any distribution of this work must maintain attribution to the author(s), title of the work, publisher, and DOI.

ISBN: 978-3-95450-168-7 doi:10.18429/JACoW-IPAC2015-THPF001

TOMOGRAPHY OF A HORIZONTAL PHASE SPACE DISTRIBUTION OF A SLOW EXTRACTED PROTON BEAM IN THE MedAustron HIGH ENERGY BEAM TRANSFER LINE

A. Wastl*, Atominstitut, Vienna, Austria
M. Benedikt, CERN, Geneva, Switzerland
A. Garonna, EBG MedAustron, Wiener Neustadt, Austria

Abstract

MedAustron is a synchrotron based hadron therapy and research center in Wiener Neustadt, Austria, which currently is under commissioning for the first patient treatment. The High Energy Beam Transfer Line (HEBT) consists of multiple functional modules amongst which the phase-shifter-stepper PSS is the most important module located where the dispersion from the synchrotron is zero and upstream of the switching magnet to the first irradiation room. The PSS is used to control the beam size for the downstream modules and for this scope rotates the beam in horizontal phase space by adjusting the phase advance. This functionality is used in this study to measure beam profiles for multiple phase space angles which act as input for a tomographic reconstruction. Simulation and measurement results are presented.

INTRODUCTION

The third order resonance slow extracted beam has a bar-like, non-gaussian phase space distribution in the plane of extraction (horizontal) called 'bar of charge' while in vertical phase space it has the usual distribution [1]. This particle distribution then propagates through the HEBT up to the PSS which is composed of six quadrupole magnets powered by independent power supplies. Its 'phase shifter' functionality adapts the horizontal phase advance μ_x keeping β_x at the end of the module (Fig. 1) constant while its 'shifter' function at the same time sets the needed variation of β_y.

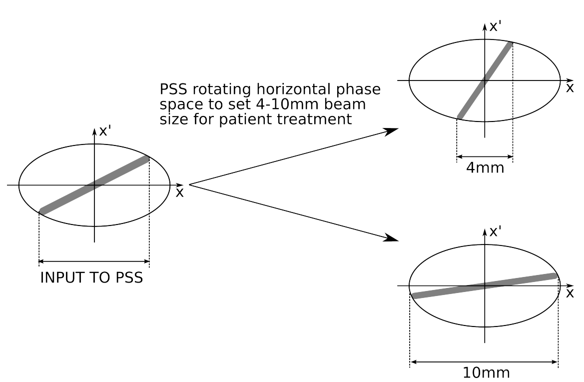

Figure 1: Adjusting the horizontal beam size [2].

Up to the entrance of the PSS the normalized strengths of optical components are independent of the required beam size at the beam line exit. Downstream the PSS 'telescope' modules project the adjusted beam size from the end of the PSS to the isocenter in the treatment room. This way the beam size is adapted to the required for patient treatment.

Using the PSS to rotate the bar in horizontal phase space and measuring the profiles downstream the module, the particle density distribution can be computed by a reconstruction techniques called tomography known from SPECT to compute the particle distribution at the monitor.

Figure 2 shows the horizontal and vertical β-functions for different horizontal phase advances and different β_y. In horizontal phase space the β-function at the PSS entrance and exit are identical. For medical purposes only four phase advance settings (representing 4mm, 6mm, 8mm and 10mm spot size at the isocenter in vacuum) are foreseen. For this study, MADX [3] was used to compute additional PSS magnet settings representing horizontal phase space rotation angles over a range of 180° (half a rotation) keeping β_y constant. Applying the different settings to the PSS, a scintillating fiber monitor SFX (64 fibers, 1mm resolution) downstream the PSS measured the different beam profiles.

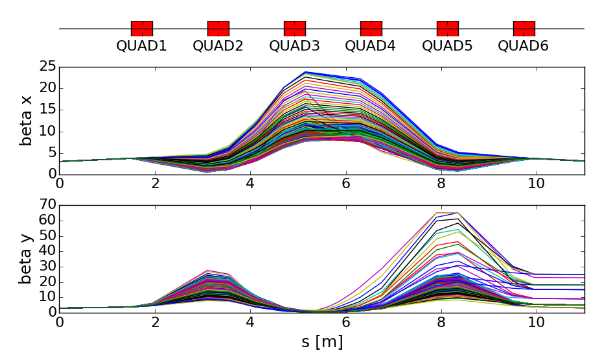

Figure 2: β_x and β_y for different beam sizes

RADON TRANSFORMATION

In modern medical diagnostics the computed tomography CT is a well-developed technique to recover information of the inner structure of the body. Density projections of a 2D 'slice' of the object of interest onto a 1D detector (the Radon transformation of the slice) performed from multiple angles around a perpendicular axis of rotation are taken as measurements and the inverse Radon transformation problem is solved to reconstruct an image of the inner structure. A medical CT performs the measurements by rotating an x-ray source and a detector around a patient who remains in place. In this study, this priciple is inverted using the PSS to rotate

* alexander.wastl@medaustron.at

Content from this work may be used under the terms of the CC BY 3.0 licence (© 2015). Any distribution of this work must maintain attribution to the author(s), title of the work, publisher, and DOI.

ISBN: 978-3-95450-168-7 doi:10.18429/JACoW-IPAC2015-THPF002

SPACE CHARGE EFFECT ESTIMATION FOR SYNCHROTRONS WITH THIRD-ORDER RESONANT EXTRACTION*

M. T. F. Pivi#, A. Garonna, EGB MedAustron, Wiener Neustadt, Austria

Abstract

In proton and ion storage rings using the third-order resonance extraction mechanism, beam particles are slowly extracted from the ring when reaching the resonance stop-band. Typically at beam injection, the horizontal tune is set to a value close to the resonance value. The tune is then moved towards the resonance value to trigger beam extraction in a controlled way. The tune shift generated by space charge forces needs to be taken into account. For this, the incoherent space-charge tune shift for protons of the MedAustron accelerator main ring has been evaluated. This has been performed by multi-particle tracking using an optics model based on MADX, considering a realistic Gaussian beam distribution and exact non-linear space charge electric field forces. The MedAustron accelerator is in the beam commissioning phase and is planned to start medical commissioning at the end of 2015.

INTRODUCTION

The recently constructed MedAustron synchrotron based accelerator in Austria is one of the novel therapy accelerators intended to use protons and light ions for clinical treatment, as already operating accelerators as e.g. CNAO in Italy and HIT in Germany. A collaboration was set up with CERN, TERA (CNAO), GSI in Germany and Onkologie Institute in Czech Republic. The design is based on the PIMMS study [1]. A report of the actual MedAustron beam commissioning can be found in [2].

For the clinical treatment a beam extracted in a slow controlled process over a couple of seconds is necessary to facilitate the measurement and control of the delivered radiation dose. The third-order resonance extraction method [1] can be used to extract particles from a synchrotron over a large number of turns and in a spill time period of 1-10 sec.

Third Order Resonance Extraction

In the slow extraction process, a sextupole field is turned on to excite the resonance. The extraction is activated by accelerating the beam into the resonance with a so called betatron core. By this mechanism, the horizontal tune is effectively moved towards the third order integer resonance tune Qx = 1.666. Thus, a precise control of the beam tune at extraction is necessary.

Space charge forces, in particular for protons, may induce an incoherent tune shift that may perturb the extraction process.

Furthermore, the space charge tune shift at beam injection into the ring, when the beam energy is low, may induce resonance crossing and beam losses.

#mauro.pivi@medaustron.at

Previous space charge estimations for the main ring have been performed as part of the design studies [1]. The estimation has been revisited with the assumption of a transverse Gaussian beam distribution, by modelling the space charge electric field and forces that are highly non-linear and to take into account recently updated machine design parameters, in particular an injected beam energy of 7 Mev [3, 4].

Possible space charge mitigations are vertical emittance dilution at injection and adjustment of the chromaticity to partially compensate for beam losses [1].

SPACE CHARGE EFFECT ESTIMATION

MedAustron Accelerator Parameters

During a cycle, the phases concerning the main ring are essentially four: injection, beam capture, acceleration using synchrotron radio frequency (RF) and slow beam extraction from the ring to the irradiation rooms. Main proton beam parameters assumed for the estimation of the effect in the MedAustron accelerator are listed in Table 1.

Table 1: MedAustron Ring Optics Parameters Assumed

Parameter	Value
Circumference (m)	77.65
Energy at injection/extraction (MeV)	7.0 / 250.3
Max. num. of particles per extracted spill	2×10^{10}
Normalized emittance ε_x, ε_y (π m rad)	0.519×10^{-6}
Q_x - Horizontal design tune inject./extract.	1.739→1.666
Q_y - Vertical design tune inject./extract.	1.79/1.79
Q_x' - Natural horizontal chromaticity at inj.	-0.6
Q_y' - Natural vertical chromaticity at inj.	-1.9
D_x -Horizontal dispersion maximum (m)	8.44

Analytic Estimation

The incoherent tune shift can be estimated analytically.

For this, one can use a linear approximation of the beam electric field, as given by

$$E_x = \frac{\lambda}{2\pi\varepsilon_0}\frac{x}{\sigma_x(\sigma_x+\sigma_y)} \quad E_y = \frac{\lambda}{2\pi\varepsilon_0}\frac{y}{\sigma_y(\sigma_x+\sigma_y)} \quad (1)$$

where λ is the linear charge distribution and using SI units. Using the linear electric field approximation and assuming a Gaussian charge distribution in the transverse plane, it is possible to derive the incoherent linear vertical

Content from this work may be used under the terms of the CC BY 3.0 licence (© 2015). Any distribution of this work must maintain attribution to the author(s), title of the work, publisher, and DOI.

ISBN: 978-3-95450-168-7 doi:10.18429/JACoW-IPAC2015-THPF003

BEST 70P CYCLOTRON FACTORY TEST

V. Sabaiduc, T. Boiesan, M. Carlson, D. Du, F. Grillet, F. Labrecque, B. Milton, L. AC Piazza
R. Ruegg, V. Ryjkov, M. Stazyk, S. Talmor, B. Versteeg, J. Zhu, R. Johnson, K. Suthanthiran
Best Cyclotron Systems Inc., Vancouver, BC, Canada
T. Evans, J. Harris, N. Matte, J. Panama, P. Zanetti, Best Theratronics Ltd., Ottawa, ON, Canada

Abstract

Best Cyclotron Systems Inc (BCSI) designed and manufactured a 70MeV compact cyclotron for radioisotope production and research applications. The cyclotron has been build at Best Theratronics facility in Ottawa, Canada for the INFN-LNL laboratory in Legnaro, Italy. The cyclotron has external negative hydrogen ion source, four radial sectors with two separated dees in opposite valleys, cryogenic vacuum system and simultaneous beam extraction on opposite lines. The beam intensity is 700μA with variable extraction energy between 35 and 70MeV. The beam acceleration to 1MeV results are reported as well as confirming the individual cyclotron systems performance.

ION SOURCE

The ion source for the BEST 70p cyclotron is a multi-cusp filament driven arc discharge ion source. The design parameters are chosen to closely follow, where possible, the published design parameters of the de facto reference design of this type of ion sources, the TRIUMF ion source [1]. Following the reference design, the walls of the plasma chamber contain 10-cusp magnetic structure confining the plasma to the centre portion of the chamber. The ion source emittance was found to be similar to that reported for the TRIUMF source as seen in Fig. 1. During the commissioning the ion source was operated at output currents greater than 8mA [3].

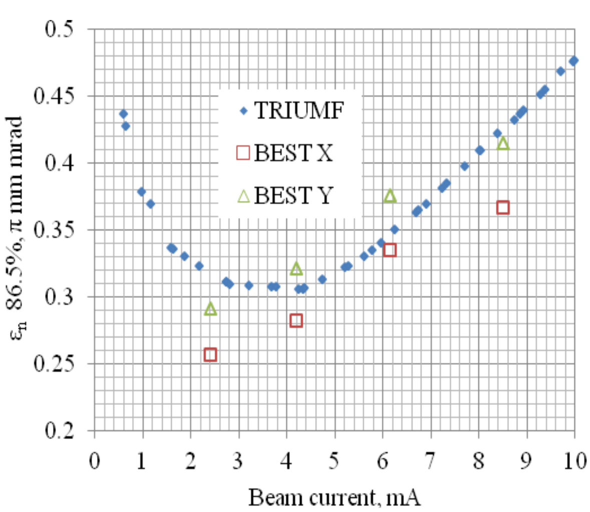

Figure 1: Emittance measurements (normalized emittance shown).

The ion source emittance was measured at the injection energy (40keV) in two perpendicular directions, one of them along the direction of the electron filter deflection. Sample emittance data is shown in Fig. 2, the "X" axis along the deflection direction. The dashed line boundaries outline emittance ellipses of 1σ, 4σ, and 9σ inclusion. While there are slight differences in the beam properties in x- and y- directions, they are not significant for transporting the beam through the injection line.

Further development of the ion source is continuing, a more detailed account of the ion source studies will be reported elsewhere.

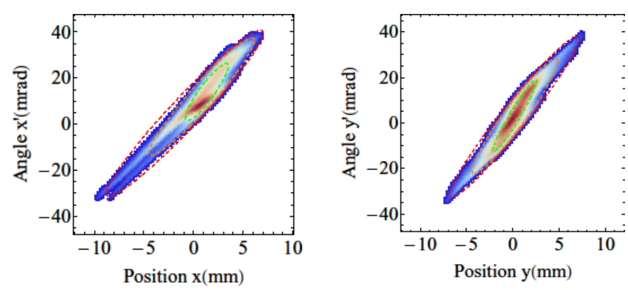

Figure 2: Ion source emittance at 6mA output (X and Y).

MAIN MAGNET

The magnet design has a good vertical focusing $\nu_z >$ 0.25 after the first few turns (0.4 at full extraction energy) and minimum magnet gap of 45mm to ensure low beam losses and high beam current acceleration. For a valley gap of 700mm the magnet operates with B Hill ≈1.6T and B Valley ≈0.12T.

The 70MeV magnet is shown in Fig. 3.

Figure 3: B70p Magnet.

Content from this work may be used under the terms of the CC BY 3.0 licence (© 2015). Any distribution of this work must maintain attribution to the author(s), title of the work, publisher, and DOI.

ISBN: 978-3-95450-168-7 doi:10.18429/JACoW-IPAC2015-THPF005

THE SARAF-LINAC PROJECT FOR SARAF-PHASE 2

N. Pichoff, P. Bredy, G. Ferrand, P. Girardot, F. Gougnaud, M. Jacquemet, A. Mosnier, CEA/IRFU, Gif-sur-Yvette, France
P. Bertrand, M. Di Giacomo, R. Ferdinand, CEA/GANIL, Caen, France
D. Berkovits, J. Luner, J. Rodnizki, Soreq NRC, Yavne, Israel

Abstract

SNRC and CEA collaborate to the upgrade of the SARAF accelerator to 5 mA CW 40 MeV deuteron and proton beams (Phase 2). This paper presents the reference design of the SARAF-LINAC Project including a four-vane 176 MHz RFQ, a MEBT and a superconducting linac made of four five-meter cryomodules housing 26 superconducting HWR cavities and 20 superconducting solenoids. The first two identical cryomodules house low-beta (β_{opt} = 0.091), 280 mm long (flange to flange), 176 MHz HWR cavities, the two identical last cryomodules house high-beta (β_{opt} = 0.181), 410 mm long, 176 MHz, HWR cavities. The beam is focused with superconducting solenoids located between cavities housing steering coils. A BPM is placed upstream each solenoid.

INTRODUCTION

SARAF [1] is an Israeli national project, announced in 2001, managed by SNRC and aiming to deliver 5 mA beams at 40 MeV (deuteron) or 35 MeV (proton). Its phase 1 consisted of an ECR source, a low energy beam transport (LEBT), a 176 MHz four-rod radiofrequency quadrupole (RFQ) and a prototype superconducting (SC) module (PSM) containing 3 SC solenoids and 6 SC HWR cavities. Its phase 2 consists in increasing the energy to final one. In this context, SNRC solicited CEA (France) to contribute to this phase.

The present CEA proposal at 176 MHz is based on its experiences on the 88 MHz SPIRAL2 [2], the 175 MHz IFMIF [3] the 352 MHz IPHI [4], ESS [5] and LINAC4 [6] projects. Beginning of 2014, CEA presented a cost-optimized design to the SARAF International Steering Committee which concluded that no major risk was foreseen, but suggested to make the design more robust in order to compensate possible loss of performances during the machine life-time.

During 2014, a new linac design has been studied, discussed between SNRC and CEA and finally accepted by both parts (Fig. 1). This paper summarises this last design: the SARAF-LINAC reference design.

SARAF PHASE 2 PROJECT

CEA is in charge of studying, delivering, and commissioning the SARAF-LINAC made of:

- an optional 4-vane RFQ bunching and accelerating 5 mA-cw beams from 20 keV/u to 1.3 MeV/u,
- a MEBT measuring, cleaning and matching the beams,
- a superconducting linac accelerating the beams to final energies within the limited bean loss criterion for Hands-On maintenance,
- and the associated local control systems.

SNRC is in charge of providing:

- the source and LEBT,
- the HEBT,
- the building,
- the main control systems,
- the auxiliaries for the linac (RF power, electricity, water, liquid helium, compressed air…).

The final commissioning is planned for mid-2022.

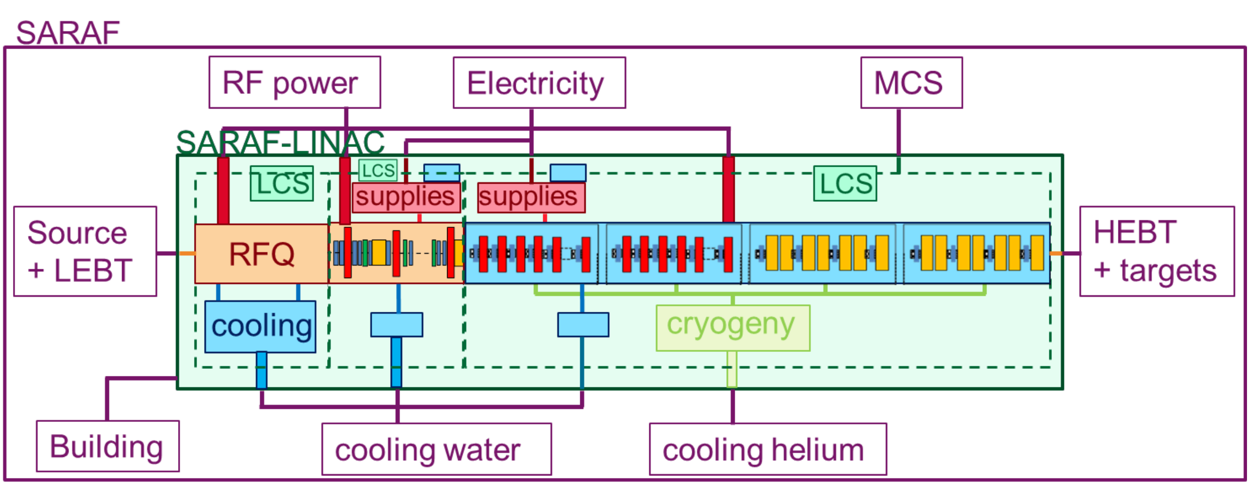

Figure 1: SARAF Phase 2 Project. In purples are SNRC deliverables, in other colours are the CEA deliverables.

Content from this work may be used under the terms of the CC BY 3.0 licence (© 2015). Any distribution of this work must maintain attribution to the author(s), title of the work, publisher, and DOI.

ISBN: 978-3-95450-168-7 doi:10.18429/JACoW-IPAC2015-THPF006

DESIGN AND MANUFACTURING STATUS OF THE IFMIF-LIPAC SRF LINAC

H. Dzitko, G. Devanz, N. Bazin, S. Chel, N. Berton, A. Bruniquel, P. Charon, G. Disset, P. Gastinel, P. Hardy, V. Hennion, H. Jenhani, J. Neyret, O. Piquet, J. Plouin, J. Relland, B. Renard, N. Sellami, IRFU CEA/Saclay, France
D. Regidor, F. Toral, CIEMAT, Madrid, Spain
D. Gex, G. Phillips, F4E, Garching, Germany

Content from this work may be used under the terms of the CC BY 3.0 licence (© 2015). Any distribution of this work must maintain attribution to the author(s), title of the work, publisher, and DOI.

Abstract

The IFMIF accelerator aims to provide an accelerator-based D-Li neutron source to produce high intensity high energy neutron flux for testing of candidate materials for use in fusion energy reactors. The first phase of the project, called EVEDA (Engineering Validation and Engineering Design Activities) aims at validating the technical options by constructing an accelerator prototype, called LIPAc (Linear IFMIF Prototype Accelerator) whose construction has begun [1], [2]. It is a full scale of one of the IFMIF accelerator from the injector to the first cryomodule. The cryomodule contains all the necessary equipment to transport and accelerate a 125 mA deuteron beam from an input energy of 5 MeV up to output energy of 9 MeV. It consists of a horizontal vacuum tank approximately 6 m long, 3 m high and 2.0 m wide, and includes 8 superconducting HWRs working at 175 MHz and at 4.45 K for beam acceleration. 8 Power Couplers provide RF power to the cavities up to 70 kW CW in the LIPAc case and 200 kW CW in the IFMIF case, with 8 Solenoid Packages acting as focusing elements. This paper gives an overview of the progress, achievements and status of the IFMIF SRF LINAC.

CRYOMODULE DESIGN

The SRF LINAC for the LIPAc phase mainly consists of a cryomodule designed to be as short as possible along the beam axis in order to meet the beam dynamics requirements [3]. Figure 1 shows the 12.5-ton cryomodule which consists of a rectangular section vacuum vessel, room temperature magnetic shield, MLI, thermal shield cooled down by GHe from the phase separator return line, and cold-mass wrapped in MLI.

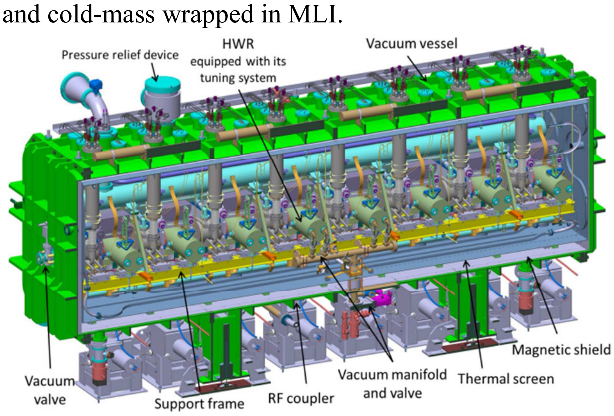

Figure 1: IFMIF LIPAc cryomodule cut view.

The cold mass is made up of the cylindrical phase separator; cryogenic circuit; titanium cavity support frame, attached to the vacuum vessel by TA6V rods ensuring lateral and horizontal positioning; 8 HWRs equipped with their frequency tuning system and power couplers; and 8 superconducting solenoids (see Figure 2). Due to their size and weight, the couplers are mounted vertically and connected to each HWR at their mid-plane.

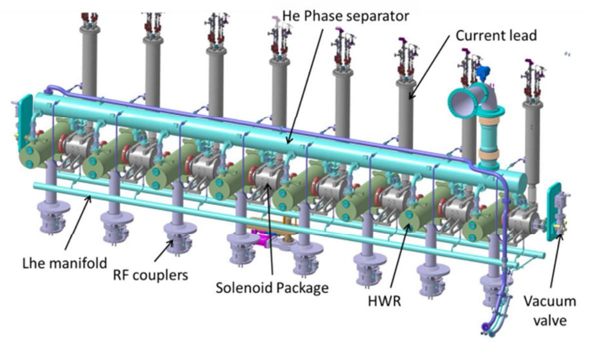

Figure 2: 3D view of the cold mass.

Several prototypes have been built during the design phase: One solenoid prototype was successfully tested [4]; the conditioning of the couplers was performed at room temperature by CIEMAT in April 2014, which qualified the design and fabrication respectively made by CEA and CPI for their use in CW mode up to 100 kW [5]; the superconducting HWR prototype, which was first equipped with a plunger for frequency tuning, was finally qualified in Dec. 2012 after removing the plunger and associated flanges [6], [7], [8], and replacing these with a more standard mechanical tuner including a disengagement system. Such a solution based on wall deformation of the half-wave resonator led to a lengthening of the cryomodule in order to accommodate it. The flange to flange length of the HWR was increased by 100 mm, and the total length of the cryomodule up to 5866 mm.

RISK MITIGATION STRATEGY

The new design of the cryomodule was submitted to a panel of international experts at a Detailed Design Review (DDR) held in June 2013 at Saclay. A detailed risk analysis taking into account the DDR remarks was also carried out. It highlighted the main risks which are related to safety, regulation, assembly, performance tests, connection, and transportation of the cryomodule. Mitigation measures to prevent the occurrence of the most

ISBN: 978-3-95450-168-7 doi:10.18429/JACoW-IPAC2015-THPF007

OPTIMIZATION OF MULTI-TURN INJECTION INTO A HEAVY-ION SYNCHROTRON USING GENETIC ALGORITHMS

S. Appel, O. Boine-Frankenheim, GSI, Darmstadt, Germany

Abstract

For heavy-ion synchrotrons an efficient multi-turn injection (MTI) from the injector linac is crucial in order to reach the specified currents using the available machine acceptance. The beam loss during the MTI must not exceed the limits determined by machine protection and vacuum requirements. Especially for low energy and intermediate charge state ions, the beam loss can cause a degradation of the vacuum and a corresponding reduction of the beam lifetime. In order to optimize the MTI a genetic algorithm based optimization is used to simultaneously minimize the loss and maximize the multiplication factor (e.g. stored currents in the synchrotron). The effect of transverse space charge force on the MTI has also been taken into account. The optimization resulted in injection parameters, which promise a significant improvement of the MTI performance for intense beams in the SIS18 synchrotron at GSI.

INTRODUCTION

The main goal during the design phase and later during operation of accelerators is to optimize and improve their performance. Unfortunately, accelerator problems are multi-dimensional, nonlinear, multi-objective and the quantities to be improved are often contradicting - improving one objective means worsening the others. A new approach to solve such difficult but realistic problems is the use of genetic algorithms (GA) [1,2]. The advantage of these optimization methods is that they allow finding globally optimal solutions with a large number of fit parameters, while showing the trade-offs in objective functions within a reasonable computing time. Over the years GA have been applied to optimize the performance of several accelerators.

In order to increase the space charge limit, heavy-ion synchrotrons are operated with intermediate charge state ions [3]. Therefore stripping injection is not an option and the MTI has to respect Liouville's theorem for the chosen charge state avoiding the already occupied phase space area. The MTI performance depends on various machine and beam parameters as well as on the contradicting quantities to be improved like multiplication of the injected current, the loss during injection and the required linac brilliance. Therefore, GA is well suited to optimize the injection.

GENETIC ALGORITHMS

Genetic algorithms are inspired by natural evolution. GA search for solutions using techniques such as *selection*, *mutation* and *crossover*. Due to the wide range of different algorithms GA are very flexible and can be adapted to a large range of different problems.

In GA terminology, a solution vector is called an *individual* and represents a set of variables; one variable is a *gene*. A group of individuals form a *population*, the following child populations are counted in *generations*. The first generation is created randomly. The crossover operator exchanges variables between two individuals - the parents - to discover with their offspring promising areas in the solution space. For the optimization within a promising area the mutation operator randomly changes the characteristics of individuals on the gene level. Reproduction of the individuals for the next generation involves selection. The *fitness* of an individual reflects how well an individual is adapted to the optimization problem and determines the probability of its survival for the next generation. The fitness is evaluated by the objective function, by a simulation code or by a real running system. During the single-objective optimization the most promising individuals are chosen to create the next generation. By allowing individuals with poor fitness to take part in the creation process the population is prevented to be dominated by a single individual. The most popular techniques are proportional selection, ranking and tournament selection [1,2].

In many real-life problems, multi-quantities have to be optimized. In addition, these quantities can be contradicting and there are more than one equally valid solutions. These solutions form a so-called *Pareto front* (PA front) in the solution space, see Figure 1. A solution is Pareto optimal if it is not dominated by any other solution. By using a non-dominated selection algorithm, one tries to find solutions near the optimal Pareto set. NSGA2 and SPEA2 are the most popular non-dominated selection algorithms.

As the SIS18 MTI model has been implemented in the particle tracking code pyORBIT - the python implementation of the ORBIT (Objective Ring Beam Injection and Tracking) code - and was carefully validated against experiments [4,5],

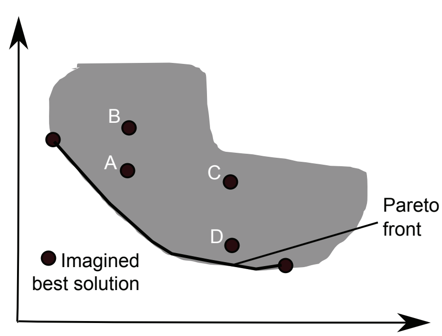

Figure 1: The Pareto front in the solution space. The solution A and D are be located near the Pareto front and non-dominated, while the solutions B and C are either dominates by the solution A or D. The solutions B and C do not dominate.

Content from this work may be used under the terms of the CC BY 3.0 licence (© 2015). Any distribution of this work must maintain attribution to the author(s), title of the work, publisher, and DOI.

ISBN: 978-3-95450-168-7 doi:10.18429/JACoW-IPAC2015-THPF008

U^{28+}-INTENSITY RECORD APPLYING A H_2-GAS STRIPPER CELL

W. Barth[1,2], A. Adonin[2], Ch. E. Düllmann[1,2,3], M. Heilmann[2], R. Hollinger[2], E. Jäger[2], J. Khuyagbaatar[1,2], J. Krier[2], P. Scharrer[1,2,3], H. Vormann[2], A. Yakushev[1,2]
[1] Helmholtz Institute Mainz, Germany
[2] GSI Helmholtzzentrum für Schwerionenforschung, Darmstadt, Germany
[3] Johannes Gutenberg-Universität Mainz, Germany

Abstract

To Meet the FAIR science requirements higher beam intensity has to be achieved in the present GSI-accelerator complex. An advanced upgrade program for the UNILAC aimed to meet the FAIR requirements is ongoing. Stripping is a key technology for all heavy ion accelerators. For this an extensive research and development program was carried out to optimize for high brilliance heavy ion operation. After upgrade of the supersonic N_2-gas jet (2007), implementation of high current foil stripping (2010 and 2011) and preliminary investigation of H_2-gas jet operation (2012), a new H_2-gas cell using a pulsed gas regime synchronized with arrival of the beam pulse was recently developed. An obviously enhanced stripper gas density at a simultaneously reduced gas load result in an increased stripping efficiency, while the beam emittance remains the same. A new record intensity (7.8 emA) for U^{28+} beams at 1.4 MeV/u has been achieved applying the pulsed high density H_2 stripper target, exploiting a high intensity U^{4+} beam from the VARIS ion source with a newly developed extraction system. The experimental results will be presented in detail.

STRIPPING OF HEAVY ION BEAMS

Suitable charge stripper technologies [1] are crucial to meet the challenging demands of state of the art heavy ion accelerator facilities. At FAIR - presently under construction at GSI - the existing linear accelerator UNILAC and the synchrotron SIS18 will serve as injector chain for the FAIR SIS100 synchrotron. Different approaches are investigated to increase the stripping efficiency of the heavy ion beam at 1.4 MeV/u and to generate higher charge states [2–5]. The stripper target at 1.4 MeV/u has to cope with a very high ion beam power of up to 1.5 MW for 18 emA U^{4+} beams during short beam pulses (100 µs) at low duty cycle (2.7 Hz rep. rate). Though for high beam powers gas or liquid strippers have clear advantages compared to foil strippers concerning durability and operational reliability, gas strippers lead to much lower equilibrium charge states due to the strongly reduced influence of the density effect [6–8] compared to solid strippers. Since electron capture cross sections of the heavy ions especially in the low-Z gases are considerably suppressed [8, 9], in particular hydrogen promises higher equilibrium charge states as compared to e.g. nitrogen, which is routinely used at the UNILAC gas stripper [10].

Thus a new setup, suitable for H_2 operation has been constructed. To enhance the gas density a pulsed gas injection [11] was implemented. This allows an increase of the maximum gas pressure and creates a high-pressure interaction zone for the stripping process. The time between two pulses is used to remove most of the gaseous particles from the system before injection of the next pulse.

UNILAC STRIPPER SECTION

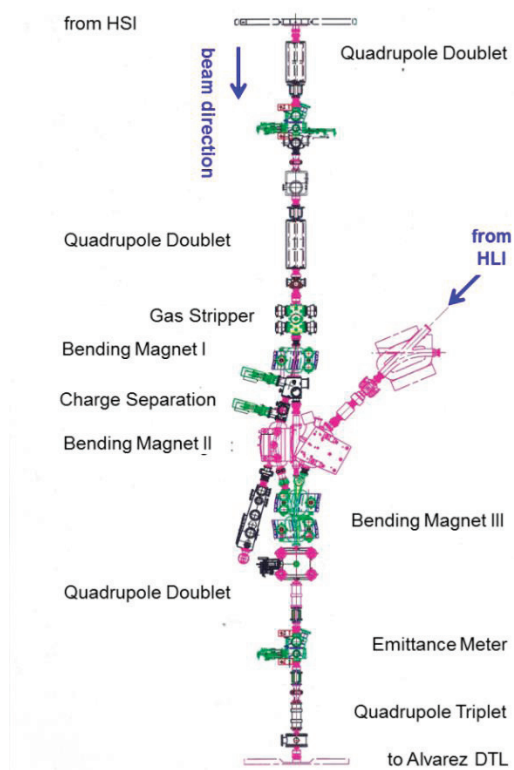

Figure 1: Layout of the 1.4 MeV/u stripper section; 14.0 m total length.

For the UNILAC a stripper section [12] was redesigned and installed in 1999 (Fig. 1). Charge separation and beam transport under highest space charge conditions and multi beam operation with pulsed magnets was established. A supersonic N_2-gas jet produced by a Laval nozzle crosses the ion beam in the central interaction region of the gas stripper chamber. Two sections of differential pumping upstream and downstream of the central region are pumped by four powerful turbo pumps (pumping speed 1200 l/s). The charge separator

Content from this work may be used under the terms of the CC BY 3.0 licence (© 2015). Any distribution of this work must maintain attribution to the author(s), title of the work, publisher, and DOI.

ISBN: 978-3-95450-168-7 doi:10.18429/JACoW-IPAC2015-THPF009

PUMPING PROPERTIES OF CRYOGENIC SURFACES IN SIS100*

L. Bozyk, GSI, Darmstadt, Germany†
F. Chill, IAP, Frankfurt am Main, Germany,
O. Kester, IAP, Frankfurt am Main, Germany, GSI, Darmstadt, Germany,
P. Spiller, GSI, Darmstadt, Germany

Abstract

The synchrotron SIS100 of the planned FAIR facility will provide heavy ion beams of highest intensities. The required low charge states are subject to enhanced charge exchange processes in collisions with residual gas molecules. Therefore, highest vacuum quality is crucial for a reliable operation and minimal beam loss. The generation of the required low gas densities relies on the pumping capabilities of the cryogenic beam pipe walls. Most typical gas components in ultra high vacuum are bound by cryocondensation at LHe temperatures, resulting in ultimate low pressures with almost infinite pumping capacity. Hydrogen can not be cryconden-sated to acceptable low pressures. But if the surface coverage is sufficiently low, it can get bound by cryoadsorption. The pumping capabilities of cryogenic walls for Hydrogen have been investigated for SIS100-like conditions. The measurement results have been used in dynamic vacuum simulations at heavy ion operation. The simulation results are presented.

EXPERIMENTAL SETUP

An experimental setup to measure the mean sojourn time and the sticking probability has been built at GSI. It consists of two parts: The warm part is made of an upper and a lower recipient, vacuum diagnostics, pumps, a defined vacuum conductance, a gate valve, and a gas inlet. The cold part consists of a cryogenic vacuum chamber inside a cryostat, which is cooled by a cryocooler, type RDK-408E2 by Sumitomo. This chamber is connected to the warm part via a cold-warm-transition (CWT), which minimizes the heat load onto the cryogenic system while providing a maximal vacuum conductance. The cold chamber is coated with copper on the outside, resulting in a homogeneous temperature distribution. The whole vacuum system can be baked at 150 °C to reduce the background by outgasing of the chamber walls.

Design considerations and concepts of the measurements, as well as measurements with the warm part have been described in [1]. Figure 1 shows a sectional view of the whole test setup.

A minimal temperature of 7.2 K was reached on the vacuum chamber. Two calibrated temperature sensors (Lakeshore silicon diodes, type DT-670, typical sensor accuracy: ±12 mK) are mounted on the chamber, one close to the cryocooler, the other close to the cold-warm-transition. A difference of 190 mK is measured, i.e. the temperature of the cryogenic chamber is homogeneous within 200 mK. The reason for not reaching the expected 4.2 K is still under inves-

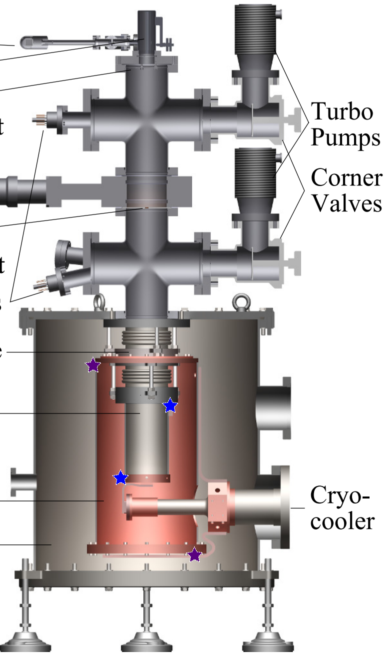

Figure 1: Sectional view of the experimental setup. Position of temperature sensors are marked with stars (blue: cryogenic vacuum chamber, purple: thermal shield).

tigation, a non-ideal connection to the cryocooler might be the reason. The thermal shield usually reaches a temperature of 36 K, measured with uncalibrated temperature sensors of the same type.

MEASUREMENTS OF CRYOGENIC PUMPING PROPERTIES

After evacuation of the UHV system, measurements are prepared by the following steps:

- Bakeout of the UHV system at 150 °C for about one week. Special care has to be taken to prevent damages by overheating of delicate components of the cold part. The cryocooler is removed during the bakeout. The cryostat is evacuated, the missing convection yields in a homogeneous temperature distribution.
- Cooldown to room temperature, meanwhile degassing of UHV diagnostics.
- Purging of the gas inlet system with hydrogen. Special care has to be taken to prevent the production of an explosive gas mixture in the exhaust system. The amount of gas in the gas pipes lasts for the whole measurements, the hydrogen bottle remains closed after purging.

* Work supported by Hic4Fair and BMBF (FKZ:05P12RDRBK).
† L.Bozyk@gsi.de

Content from this work may be used under the terms of the CC BY 3.0 licence (© 2015). Any distribution of this work must maintain attribution to the author(s), title of the work, publisher, and DOI.

ISBN: 978-3-95450-168-7 doi:10.18429/JACoW-IPAC2015-THPF010

SIMULATION AND EXPERIMENTAL INVESTIGATION OF HEAVY ION INDUCED DESORPTION FROM CRYOGENIC TARGETS*

Ch. Maurer†, D.H.H. Hoffmann, Institut für Kernphysik, TU Darmstadt, Germany
L.H.J. Bozyk, H. Kollmus, P.J. Spiller, GSI, Darmstadt, Germany

Abstract

Heavy-ion impact induced gas desorption is the key process that drives beam intensity limiting dynamic vacuum losses. Minimizing this effect, by providing low desorption yield surfaces, is an important issue for maintaining a stable ultra high vacuum during operation with medium charge state heavy ions. For room temperature targets, investigations show a scaling of the desorption yield with the beam's near-surface electronic energy loss, i.e. a decrease with increasing energy [1, 2]. An optimized material for a room temperature ion-catcher has been found. But for the planned superconducting heavy-ion synchrotron SIS100 at the FAIR accelerator complex, the ion catcher system has to work in a cryogenic environment. Desorption measurements with the prototype cryocatcher for SIS100 showed an unexpected energy scaling [3], which needs to be explained. Understanding this scaling might lead to a better suited choice of material, resulting in a lower desorption yield. Here, new experimental results will be presented along with insights gained from gas dynamics simulations.

MEASUREMENT OF CRYOGENIC DESORPTION

In this experiment, a cryogenic target is placed in a UHV environment and cooled by a coldhead. After the impact of a heavy ion beam, the resulting pressure evolution is measured. In combination with the beam intensity, a desorption yield η is calculated. It is defined as the number of desorbed gas particles divided by the number of impacting beam ions. A detailed description of the measurement setup can be found in [4].

While the beam's intensity can be measured with a beam current transformer, identifying the number of desorbed particles is more difficult. Up to now, the ideal gas law was employed to calculate this number by using the measured peak pressure after beam impact in a defined volume. A gas dynamics simulation can improve the analysis.

Another improvement compared to [4] is the extended range of experimental parameters, especially regarding the target. The target assembly is connected to a coldhead to facilitate a cryogenic environment and incorporates an optional thermal shield. Electrical insulation of the target is necessary to measure the ion current caused by the beam impact. It is achieved through a nonconducting tile, which unfortunately also limits the heat flow towards the coldhead. First results, obtained with a U^{73+} beam, an Al_2O_3-ceramic insulation plate, and a target made from gold coated copper have already been presented. Further experiments were conducted with a target made from uncoated stainless steel, but also without a thermal shield. In a later experiment, a Bi^{68+}-beam was used with the copper target and a thermal shield.

NEW EXPERIMENTAL RESULTS

Changing the target materials introduces several variations into the experiment. A modification in thermal conductivity leads to a shift of the thermal equilibrium between external heat load and heat transfer towards the coldhead. Thus, the lowest achievable temperature T_{min} rises when exchanging the copper target with a stainless steel target because copper has a higher thermal conductivity than steel.

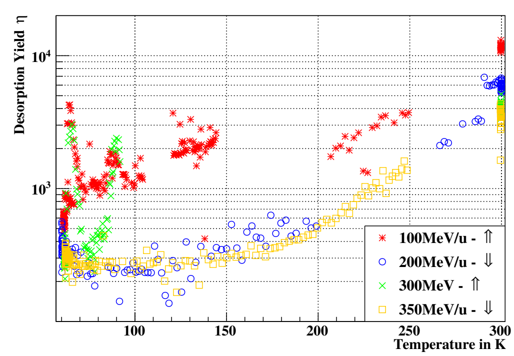

Figure 1: Temperature dependant desorption yield η for a U^{73+}-beam on a steel target.

The first modification was performed by exchanging the copper target with a stainless steel target. The results from this experiment are presented in Figs. 1 and 2.

The desorption yield decreases by an order of magnitude between room temperature and 100 K. The previously encountered desorption peak around 50 K can be found again when measuring with a deactivated coldhead on a rising temperature slope. After reaching room temperature, η again scales with $(\mathrm{d}E/\mathrm{d}x)^2$. Furthermore, a comparison of the absolute room temperature values with [1] and [3] shows a discrepancy by two orders of magnitude. The much higher η measured here might be a result of the milder bakeout process that had to be employed to protect the coldhead. Furthermore, the η measured with the copper target is twice as high as the η measured for the steel target at room temperature. This contradicts previous findings.

For cryogenic temperatures, the $(\mathrm{d}E/\mathrm{d}x)^2$ scaling can also be observed while the previously encountered, well

---

* This project is funded by the german ministry for education and research (FKZ 06DA7031)
† c.maurer@gsi.de

Content from this work may be used under the terms of the CC BY 3.0 licence (© 2015). Any distribution of this work must maintain attribution to the author(s), title of the work, publisher, and DOI.

ISBN: 978-3-95450-168-7 doi:10.18429/JACoW-IPAC2015-THPF011

STATUS OF THE FAIR PROTON LINAC

R. Brodhage, W. Vinzenz, M. Vossberg, M. Kaiser, GSI, Darmstadt, Germany
U. Ratzinger, IAP, Universität Frankfurt, Germany

Abstract

For the research program with cooled antiprotons at FAIR a dedicated 70 MeV, 70 mA proton injector is required. The main acceleration of this room temperature linac will be provided by six CH cavities operated at 325 MHz. Within the last years, the assembly and tuning of the first power prototype was finished. The cavity was tested with a preliminary aluminum drift tube structure, which was used for precise frequency and field tuning. Afterwards, the final drift tube structure has been welded inside the main tanks and the galvanic copper plating has taken place at GSI workshops. This paper will report on the recent advances with the prototype as well as on the current status of the overall p-Linac project.

INTRODUCTION

The proton linac for FAIR is mechanically grouped in two sections, each having a length of about 9 m. Based on the actual design the first section will consist of 3 coupled CH-cavities. Between both sections there will be a diagnostics area with a rebuncher for longitudinal beam matching. Investigations have shown that a simplified layout of the 2nd section of the proton linac will be an improvement. Therefore, three simple CH cavities without a coupling cell will be used, reducing the triplet lens number by three and simplifying the layout and tuning of the cavities a lot.

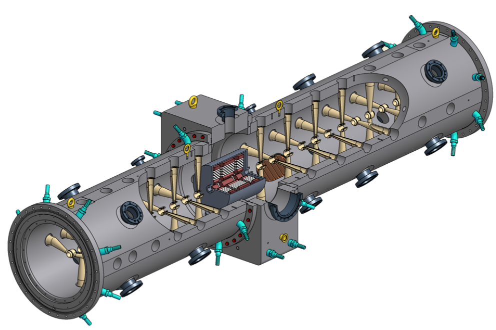

Figure 1: 3D-view of the coupled prototype cavity.

THE COUPLED PROTOTYPE CAVITY

Figure 1 shows the prototype cavity which corresponds to the second coupled cavity within the first section. The low energy part consists of 13 gaps, followed by the coupling cell and by the 14 gap high energy part. The whole cavity has an inner length of about 2.8 m and the cylindrical tanks have an inner diameter of about 360 mm. The coupling cell has a length of about $2\beta\lambda$ and hosts the focusing triplet lens within one large drift tube. The inter cavity tanks will also house triplet lenses and some beam diagnostics additionally (4 knob phase probes). They mechanically connect and support the neighbored cavities.

Table 1: Parameters of the Coupled CH Prototype Cavity

No. of gaps	13 + 14 = 27
Frequency [MHz]	325.2
Energy range [MeV]	11.7 - 24.3
Beam loading [kW]	882.6
Heat loss [MW]	1.35
Total power [MW]	2.2
Q_0-value	15300
Eff. shunt impedance [$M\Omega/m$]	60
Average $E_0T[MV/m]$	6.4 - 5.8
Kilpatrick factor	2.0
Coupling constant [%]	0.3
Aperture [mm]	20
Total inner length [mm]	2800
Inner diameter [mm]	360 / 434 / 364

Table 1 shows the main parameters of the prototype cavity. The prototype arrived at GSI in late 2013 and was prepared for galvanic copper plating. Unfortunately the plating process on long cavities with a complex inner structure is not trivial. Therefore lots of tests and investigations have been performed to realize a suitable copper layer. Figure 2 shows the final result after gavanic plating and polishing.

Figure 2: Picture of the copper plated inner surface of CH 3

This cavity is presently at the p-Linac RF test stand and is assembled with all tuners and the triplet lens. The first low level measurements were already performed and show a good accordance with theory and previous results. Copper plating and welding have not effected the performance and tolerances of the prototype. Further investigations and perturbation measurements of the field distribution will be performed within the next weeks.

Content from this work may be used under the terms of the CC BY 3.0 licence (© 2015). Any distribution of this work must maintain attribution to the author(s), title of the work, publisher, and DOI.

ISBN: 978-3-95450-168-7 doi:10.18429/JACoW-IPAC2015-THPF012

STATUS OF THE HIGH ENERGY BEAM TRANSPORT SYSTEM FOR FAIR

F. Hagenbuck*, L. Bozyk, S. Damjanovic, A. Krämer, B. Merk, C. Mühle, S. Ratschow,
B.R. Schlei, P.J. Spiller, B. Walasek-Höhne, H. Welker, C. Will
GSI, Helmholtzzentrum für Schwerionenforschung, Darmstadt, Germany

Abstract

The overall layout of the High Energy Beam Transport (HEBT) System of the Facility for Antiproton and Ion Research (FAIR) [1] did not change since its last presentation in 2008 [2]. All necessitated adaptions as for example due to the introduction of the Modularized Start Version (MSV, module 0-3) of FAIR [3] could be smoothly implemented. In the meanwhile the HEBT system is in its realisation phase with the procurement of its main components in progress.

In the following adaptions of the system layout not yet covered in [2] are summarized and an overview of the technical system design and procurement status are presented.

ADAPTIONS OF THE HEBT SYSTEM LAYOUT

Since its last presentation in 2008 [2] it has been confirmed several times that the HEBT system will be able to fulfill all requirements imposed on it. A new direct connection from SIS18 to the CR was included into the HEBT system without difficulties. For this the section TSN1 was modified in a way that the beam coming from SIS18 can be either injected straight via TSR1 into the end part of the Super-FRS ring branch (which is connected to the CR via the sections TFC1 and TCR1) or guided directly to the NESR as before via TSN2, see Fig. 1, 2. The new connection to the CR was included into the planning of the MSV, whereas the beam line to the NESR belongs to module 6. Modifications in the building planning were not required.

The RESR is not part of the MSV. As mitigating measure the transfer line to the HESR starts now at the CR (THS1) which could be implemented smoothly. After RESR is built in module 5, THS1 will be removed and replaced by a new transfer line from CR to RESR and a new beam line from RESR to HESR (TRH1). All components from the transfer line from CR to HESR can be reused for the connection from RESR to HESR. Dipole magnets will be operated with different bending angles by means of field adaption, merely their vacuum chambers have to be replaced.

Plasma physics (PP) and atomic physics (AP) experiments will share a common building (APPA building), which replaces the former PP and AP caves and will contain two beam lines. The eastern beam line, see Fig. 1, serves atomic physics, biophysics and material research experiments, the western beam line plasma physics experiments. As before the PP beam line provides the option for a perpendicular beam from SIS18 onto the same target.

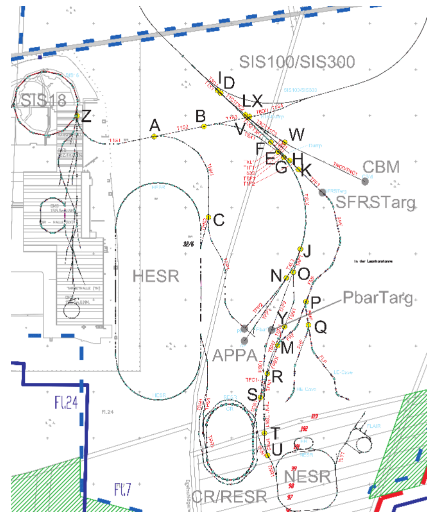

Figure 1: Top view of the beam line topology of FAIR (module 0-6).

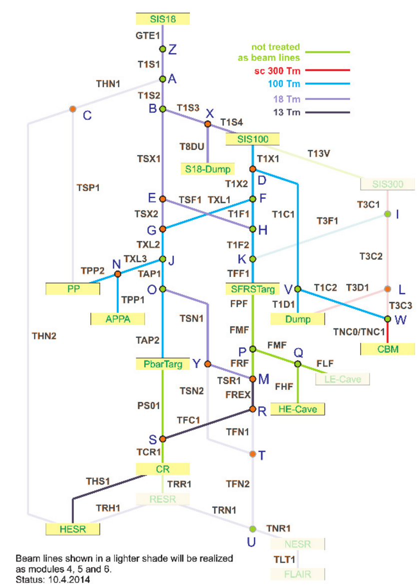

Figure 2: Beam line connection scheme.

The Super-FRS ring branch is not in line with the end of the Antiproton separator. The offset will be carried out now by use of in total four (module 0-6) dipole magnets similar to the ones used in the CR (different bending angle), which allows to use syneregies in magnet production, instead of two dipole magnets at two different bending angles, which turned out to be unpractical because their good field region

* f.hagenbuck@gsi.de

Content from this work may be used under the terms of the CC BY 3.0 licence (© 2015). Any distribution of this work must maintain attribution to the author(s), title of the work, publisher, and DOI.

ISBN: 978-3-95450-168-7 doi:10.18429/JACoW-IPAC2015-THPF013

UNILAC PROTON INJECTOR OPERATION FOR FAIR

M. Heilmann*[1], A. Adonin[1], S. Appel[1], W. Barth[1,2], P. Gerhard[1], F. Heymach[1], R. Hollinger[1], W. Vinzenz[1], H. Vormann[1], and S. Yaramyshev[1]

[1]GSI Helmholtzzentrum, 64291 Darmstadt, Germany
[2]HIM, Helmholtzinstitut, 55099 Mainz, Germany

Abstract

The pbar physics program at the Facility for Antiproton and Ion Research (FAIR) requires a high number of cooled pbars per hour [1]. The FAIR proton injector with coupled CH-cavities will provide for a high intensity (35 mA) pulsed 70 MeV proton beam at a repetition rate of 4 Hz [2, 3]. The recent heavy ion UNIversal Linear ACcelerator (UNILAC) at GSI is able to deliver proton as well as heavy ion beams for injection into the FAIR-synchrotrons. Recently GSI UNILAC could provide for a two orders of magnitude higher proton beam current in routine operation. A hydrocarbon beam (CH_3) from the MUCIS ion source [4] was accelerated inside the High Current Injector (HSI) and cracked in a supersonic nitrogen gas jet [5] into stripped protons and carbon ions. A new proton beam intensities record (3 mA) could be achieved during machine experiments in October 2014. Potentially up to 25% of the FAIR proton beam performance is achievable at a maximum UNILAC beam energy of 20 MeV and a maximum repetition rate of 2.7 Hz. The UNILAC can be used as a high performance proton injector for initial FAIR-commissioning and as a redundant option for the first FAIR-experiments [6].

INTRODUCTION

Two ion source terminals (PIG, MUCIS and MEVVA) deliver beam to a 36 MHz IH-RFQ and two IH-DTLs (up to 1.4 MeV/u). After acceleration the gas stripper and charge state separation four Alvarez DTL provide for end energies of 11.4 MeV/u; the eight installed Single Gap Resonators [7] could be used for energy fine adjustment. In the transfer line (TK) to the synchrotron SIS 18 [8, 9] a foil stripper and a second charge separator can be used.

The new FAIR proton linac delivers a high intensity proton beam with an energy of 70 MeV and a pulse current of up to 70 mA for injection into the SIS 18. The p-LINAC comprises of three new coupled CH-cavities with a compact and efficient design. The p-LINAC is connected to the TK (Fig. 1) by two 45 degree dipole magnets.

The first part of this machine experiment with the optimized mass spectrum (MUCIS), the gas stripper spectrum (HSI), emittance measurements and brillance for CH_3^+-operation are presented in [6].

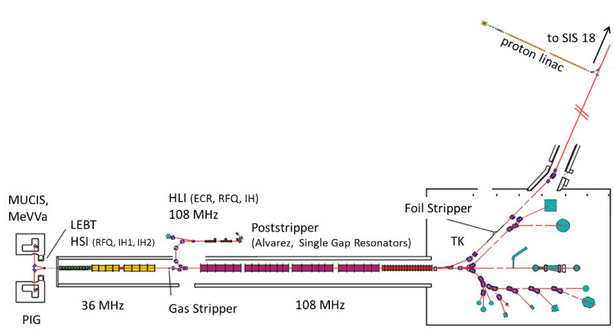

Figure 1: Schematic overview of the GSI UNILAC and FAIR proton linac.

RF CONTROL OPTIMIZATION

The proton acceleration with the current UNILAC implicates an optimization of the RF power control settings. The handling of low signal levels and in particular of the low level RF part (amplitude and phase control) is outside the predicable range of 100 kW up to 2 MW. The output power for the Alvarez tank (A3) is approximately 21 kW. The cavity voltage optimisation of a constant gap voltage (flat top) for the A3 (Fig. 2) was ensured with an adjustment of the rise time settings. While the beam pulse is passing the cavity, a flat top of the cavity voltage is required. The loop gain into to cavity has been optimized to increase up to a non-risky level.

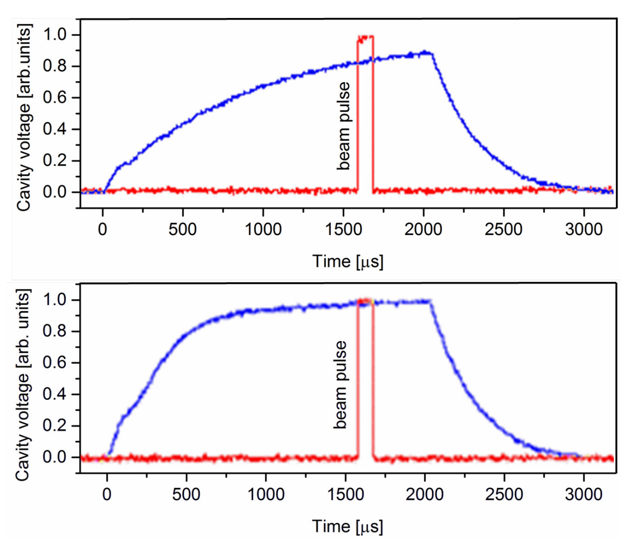

Figure 2: Shape of the cavity voltage before (top) and after (bottom) optimisation.

* manuel.heilmann@email.de

Content from this work may be used under the terms of the CC BY 3.0 licence (© 2015). Any distribution of this work must maintain attribution to the author(s), title of the work, publisher, and DOI.

ISBN: 978-3-95450-168-7 doi:10.18429/JACoW-IPAC2015-THPF014

Content from this work may be used under the terms of the CC BY 3.0 licence (© 2015). Any distribution of this work must maintain attribution to the author(s), title of the work, publisher, and DOI.

325 MHz HIGH POWER RF COUPLER FOR THE CH-CAVITIES OF THE FAIR p-LINAC

F. Maimone, R. Brodhage, M. Kaiser, W. Vinzenz, M. Vossberg
GSI, Planckstraße 1, 64291 Darmstadt, Germany

Abstract

In order to supply the input RF power to the Cross-bar H-mode (CH) cavities of the p-LINAC for FAIR an inductive RF coupler has been studied. The designed RF coupler, and its water cooled inductive loop, has to withstand up to a 3 MW pulsed power (at 325 MHz). At GSI a prototype has been manufactured and tests were performed. The prototype of the designed high power RF coupler is presented together with the results of the coupling measurements at the CH-prototype cavity.

INTRODUCTION

The Facility for Antiproton and Ion Research (FAIR) requires an intense proton beam at 70 MeV serving the SIS18. For this purpose a dedicated proton LINAC has been designed and will be produced by GSI. The room temperature DTL of the p-LINAC is composed by three coupled CH cavities, providing the acceleration up to 35 MeV, followed by three single CH cavities [1].

A prototype of the coupled CH cavity corresponding to the second accelerating unit, from 11.5 MeV to 24.2 MeV, has been manufactured, assembled and recently copper plated successfully at the GSI galvanic workshop [2-3]. The layout of the coupling cell for the coupled CH structures is designed to let it oscillate in an Alvarez E-mode at the same resonance frequency as the H-mode of the CH-cavities. In order to realize the coupling between the 6 1/8" coaxial line and the coupled CH-cavity, an inductive coupler has been studied. The advantage of an inductive coupler is the possibility to tune the coupling factor by rotating the loop inside the coupling cell. The design of the coupler inserted inside the coupling cell of the prototype of the CH cavity is shown in Figure 1. In the figure the coupler is oriented at 0° and the coupler area is perpendicular to the magnetic field lines.

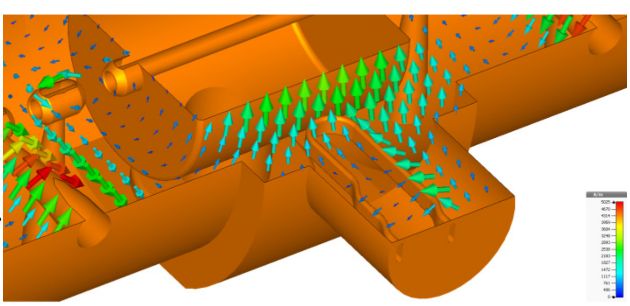

Figure 1: 3D-cut of the coupling cell of the second coupled CH cavity of the p-LINAC.

A prototype of the designed coupler has been assembled and tested. The mechanical construction steps of the prototype of the RF coupler are shown together with measurement results of the coupling to the coupled CH cavity.

INDUCTIVE COUPLER RF DESIGN

At GSI several inductive couplers are used for the UNILAC cavities at different frequencies (i.e. 36, 108 and 216 MHz) and also in other accelerator facilities (i.e. CERN Linac3, Heidelberg (HIT), Padova (CNAO) and at BNL). This design can be adapted to RFQs, IHs, Alvarez, Spirals and CH cavities covering a power range from some tens of kW up to 2 MW power (max 25% duty factor). Therefore a big number of flange-oriented types with respect to the dimensions of the used RF power lines can be realized [4]. The application of this type of coupler to the second coupled CH cavity of the p-LINAC has been studied with CST Microwave Studio. The coupling factor and the electromagnetic properties of the RF coupler insertion and rotation inside the coupling cell have been analysed for different effective loop areas [5]. However, the analysed solutions were not optimized to be used with a beam load. To take the cavity´s beam loading into account, the conventional parameter $\beta=Q_o/Q_{ext}$ has to be modified to include the contribution of the absorbed power by the beam:

$$\beta_{beam} = 1 + \frac{P_b}{P_{losses}} \tag{1}$$

Where P_{losses} is the average power dissipation at the cavity walls and P_b is the averagedelivered power to the beam as a function of the beam current [6]. For this reason the area of the loop was increased to enhance the coupling factor. Figure 2 shows the design of the inductive loop. The shape of the loop has been adopted in order to reduce the electric field between the coupler and the flange walls.

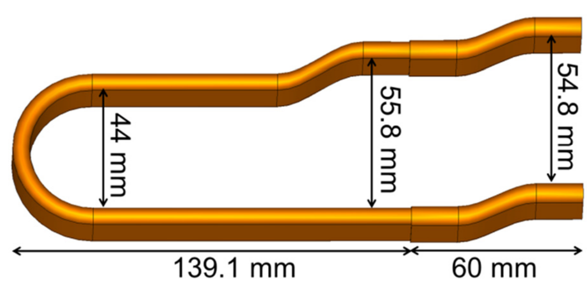

Figure 2: Inductive loop coupler.

ISBN: 978-3-95450-168-7 doi:10.18429/JACoW-IPAC2015-THPF015

STATUS OF THE FAIR HEAVY ION SYNCHROTRON PROJECT SIS100

P. Spiller, U. Blell, L. Bozyk, J. Ceballos Velasco, T. Eisel, E. Fischer, O. Kester, H.G. König, H. Kollmus, V. Kornilov, P. Kowina, J.P. Meier, A. Mierau, C. Mühle, C. Omet, D. Ondreka, N. Pyka, H. Ramakers, P. Rottländer, C. Roux, P. Schnizer, S. Wilfert
GSI, Darmstadt, Germany

Abstract

SIS100 is the main accelerator of the FAIR project. It is a worldwide unique heavy ion synchrotron dedicated to accelerate highest intensities of intermediate charge state heavy ion- and proton beams up to 100 Tm. From the technical point of view, most challenging issues are the fast ramped superconducting magnets and the acceleration of intense, intermediate charge state heavy ions beams. The latter required a unique lattice design (charge separator lattice) in combination with an ultra-high vacuum system based on distributed cryo-pumping with actively cooled magnet chambers, adsorption pumps and dedicated cryo-catchers for local suppression of gas desorption [1].

PROCUREMENT STATUS

The year 2014 was very much focused on completing, reviewing and finishing specifications and drawings for all kind of components. Finally, at the end of 2014, all contracts for the most demanding SIS100 components, the large series of superconducting magnets and RF systems, have been closed, which marks a major milestone in the project execution. This milestone corresponds to a bound value of about 50% of the SIS100 cost-book value. The last large in-kind contract regarding the quadrupole unit production has been successfully negotiated and closed with the Joint Institute for Nuclear Research (JINR, Dubna, Russia) and signed by the JINR, GSI and FAIR management at an official ceremony at JINR at 2015/02/20. This contract is accompanied by a number of contracts between GSI and JINR on quality assurance and magnet testing. Besides the major series with long production times, many other components have been tendered or contracted, e.g. the injection kicker system, the resonance sextupole magnets (awarded to DANFYSIK, Denmark) and the cryo-catcher system. The local cryogenics system will be delivered by the Wroclaw University of Technology (WrUT, Poland). The manufacturing design review for the first bypass line segment has been passed. The manufacturing design and preparation has been approved and the contract for the production of the bypass line has been awarded to the company KRIOSYSTEM, Poland.

BUILDING PLANNING

Detailed planning for the accelerator tunnel and the supply area (K0923A/T110) complex, including 3D DMU models of the accelerator and its technical infrastructure, has matured and is transitioning to execution planning, which will take place in 2015, see Figure 1. This will allow the finalization of the necessary building tendering documents and the start of the excavation in late 2015.

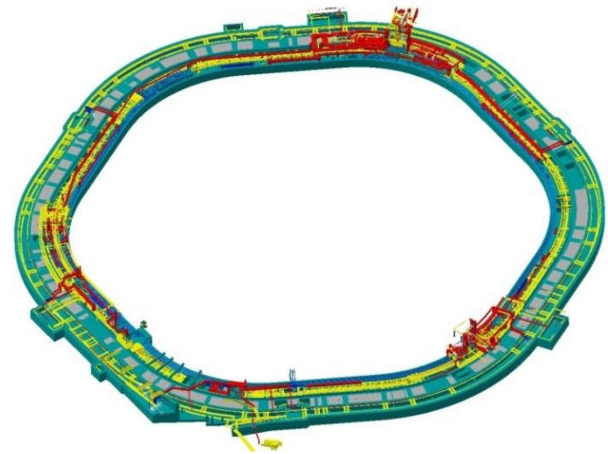

Figure 1: Design of T110, including the accelerator tunnel (outer tunnel) and the parallel supply tunnel (inner tunnel) with cable trays (yellow), cooling water supply lines (blue) and venting (red).

PROGRESS ON COMPONENT TENDERING AND DELIVERY

The first of the 109 superferric, 1.9 T dipole series magnets (FoS) [2] has already been delivered in June 2013 (Figure 2) and thoroughly tested under warm and cryogenic conditions. Although, the FoS dipole magnet has different to the previous prototype magnets, a completely new coil design and is operated at twice the electrical current, the quench training showed excellent behaviour. Nevertheless, the desired high beam currents allow only minimum mechanical errors in the series production of the yoke. Therefore, together with the manufacturer and the support by external experts, the production and welding process has been review and optimized. Meanwhile, significant progress in minimizing the deformation of the half yoke (before assembly) could be demonstrated by using a robot based laser welding. A new, mechanically further improved FoS yoke, providing the confidence in a high mechanical reproducibility of the series, will be produced and delivered until Q3/2015. In the frame of the side acceptance test of the FoS dipole, a number of precision measurement devices and technique could be developed, e.g. for high precision measurement of the inner magnet aperture (height, parallelism of pole surfaces, sag etc.), such that it will be able to release the

Content from this work may be used under the terms of the CC BY 3.0 licence (© 2015). Any distribution of this work must maintain attribution to the author(s), title of the work, publisher, and DOI.

ISBN: 978-3-95450-168-7 doi:10.18429/JACoW-IPAC2015-THPF017

DESIGN STUDIES FOR THE PROTON-LINAC RFQ FOR FAIR

M. Vossberg, R. Brodhage, M. Kaiser, F. Maimone, W. Vinzenz, S. Yaramyshev,
GSI, Darmstadt, Germany

Abstract

The planned 27 m long Proton-Linac (p-Linac) for FAIR (Facility for Antiproton and Ion Research) comprises a RFQ (Radio-Frequency Quadrupole) and six crossbar H-Mode cavities to accelerate a 70 mA proton beam up to 70 MeV. The FAIR Proton-Linac starts with a 325.2 MHz, from 95 keV to 3 MeV RFQ accelerator. The main RFQ for this Proton-Linac will be a 4-Vane type RFQ. RF analytics with varying and constant transverse focusing strength for the electrode parameters will be used. CST MWS (Microwave Studio) [1] simulations will help to find cavity parameters for the working frequency. This paper presents the main cavity design concepts and simulation results.

INTRODUCTION

A new international accelerator-based science center (FAIR) will be built in the near future at GSI, Germany [2, 3]. The FAIR facility is designed to provide antiproton and ion beams of worldwide unique intensity and quality for fundamental physics research.

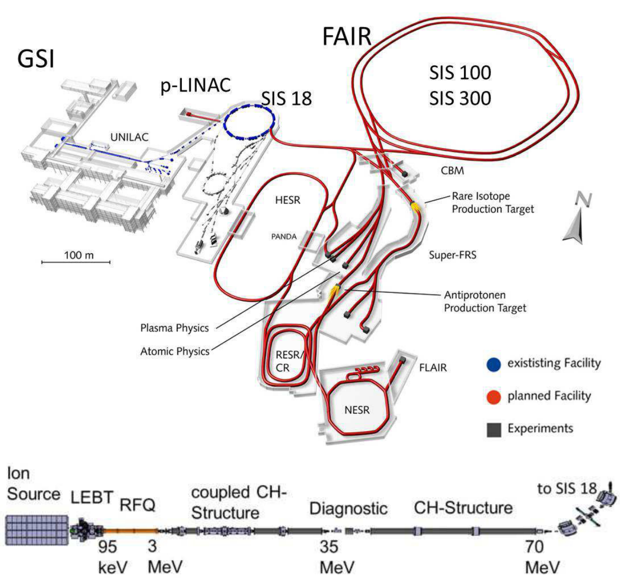

Figure 1: Layout of the FAIR facility and overview of the Proton-Linac.

Fig. 1 shows the planned Proton-Linac which is adjacent to the existing UNILAC. Both Linacs are injectors of the SIS 18 synchrotron, which delivers the SIS 100, the central accelerator component of FAIR. The Proton-Linac will mainly consist of an RFQ accelerator and two 9 m sections of Cross Bar H-Mode accelerators (CH structures) working at a frequency of 325.224 MHz. In the first section, there will be six CH cavities, which are pairwise RF-coupled. The second section consists of three separate long CH cavities. Each of those six cavities has its own klystron. It is required to provide a 70 MeV proton beam with a beam current up to 70 mA at a macro pulse length of 36 µs and a bunch length of 100 ps [4, 5]. The planned RFQ is between 3.2 m and 3.5 m long and will have an input energy W_{in} of 95 keV. After the acceleration in the RFQ the output energy W_{out} will be 3 MeV.

RFQ DESIGN STUDIES

One of the most important parameter for an RFQ design is the maximum electric field on the RFQ electrode surface. A high field is necessary for a reasonable and improved performance of the structure, but also a reliable and stable operation of the machine has a high priority [6]. The ongoing GSI Proton-Linac project requires such calculations for increased reliability.

Table 1: Design Requirements for the Proton-Linac RFQ for FAIR

Particle	proton (H^+)
Frequency	325.224 MHz
Input energy W_{in}	95 keV
Output energy W_{out}	3.0 MeV
Beam current (design)	70 mA
Length	> 3.2 m < 3.5 m
Kilpatrick factor	≤ 1.87
Rep. rate	≤ 4 Hz
Aperture (min)	≈ 2.2 mm
Modulation (max)	≈ 2
Average distance to beam	≈ 3.3 mm

The current design parameters for the Proton-Linac RFQ are listed in Table 1 [10]. These parameters are necessary for the beam dynamics design. For the RF-structure, a 4-Vane-RFQ is chosen [3]. The cavity geometry will be designed with the main parameters like aperture, modulation, frequency and the length of this cavity.

Content from this work may be used under the terms of the CC BY 3.0 licence (© 2015). Any distribution of this work must maintain attribution to the author(s), title of the work, publisher, and DOI.

ISBN: 978-3-95450-168-7 doi:10.18429/JACoW-IPAC2015-THPF018

SIMULATION STUDIES OF PLASMA-BASED CHARGE STRIPPERS

O. S. Haas*, TEMF TU-Darmstadt, Darmstadt, Germany
O. Boine-Frankenheim, TEMF TU-Darmstadt, Darmstadt, Germany, and GSI, Darmstadt, Germany

Abstract

Calculations on the charge state distributions in different charge stripping media are presented. The main focus of this work is the width and peak efficiency of the final charge state distribution. For equal number densities fully-stripped plasma stripping media achieve much higher charge states than gas stripping media of the same nuclear charge. This is due to the reduced electron capture rates of free target electrons compared to bound target electrons. Furthermore, targets with low nuclear charge like hydrogen achieve higher charge states than targets with high nuclear charge like nitrogen in the case of both a plasma and a gas target. Equal final mean charge states can thus be achieved with lower density for plasmas and targets with low nuclear charge. The widths of the charge state distributions are very similar, slightly smaller for plasmas due to the different scaling of the dielectronic recombination rate. In comparison with calculations and measurements published in literature this work underestimates the width of targets with higher nuclear charge like, e.g., nitrogen gas. This is mainly due to the omission of multiple loss processes in the presented calculations. In the future we intend to expand the methods and models used in this work to improve the agreement with different measurements on charge state distributions in plasmas and gases.

INTRODUCTION

Charge stripping of heavy ion beams at high intensities is a major challenge in current and future facilities with high intensity heavy ion beams. Conventional stripping techniques are often limited in their applicability, e.g. solid carbon foils suffer from short lifetimes at high intensities and common gas strippers usually achieve only low charge states. One possible alternative is the use of a plasma as a stripping medium. The presented work focuses on theoretical studies of the interaction of an heavy ion beam with a plasma and gases and accompanying effects in possible charge strippers. The main interest in the presented studies is the final charge state distribution of the ion beam, which determines the efficiency of the charge stripper as an accelerator component.

BASICS

The main focus of this work is on the charge state distribution or $F_q(t_{\text{eq}})$, where the latter is the relative fraction of the beam in charge state q at time t. The beam loses or captures electrons in several different processes with rates

$$\alpha_{q(q\pm n)}(q) = v_{\text{r}} n_{\text{t}} \sigma_{q(q\pm n)}(q) \,, \tag{1}$$

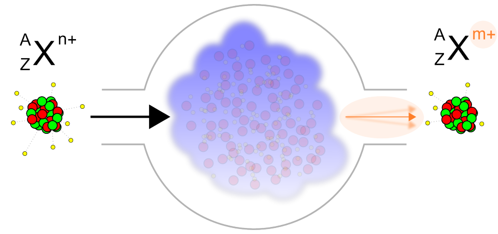

Figure 1: Sketch of a projectile getting stripped by a target.

where v_{r} is the relative velocity of projectile and target, n_{t} is the target density and $\sigma_{q(q\pm n)}(q)$ are the loss and capture cross sections. For every given beam energy the charge state distribution tends to an equilibrium. In the case of negligible multiple loss and capture rates the mean equilibrium charge q_{eq} is then given by

$$\alpha_{q(q+1)}(q_{\text{eq}}) = \alpha_{q(q-1)}(q_{\text{eq}}) \,. \tag{2}$$

Furthermore the rates can be approximated as $\alpha_{q(q\pm1)} \propto \exp(b_i(q - q_{\text{eq}}))$, leading to a Gaussian equilibrium charge state distribution with variance

$$\sigma^2_{q_{\text{eq}}} = \left(\left| \frac{\alpha'_{q(q+1)}(q_{\text{eq}})}{\alpha_{q(q+1)}(q_{\text{eq}})} \right| + \left| \frac{\alpha'_{q(q-1)}(q_{\text{eq}})}{\alpha_{q(q-1)}(q_{\text{eq}})} \right| \right)^{-1} \,, \tag{3}$$

where the prime denotes the derivative in respect to q. The peak efficiency is then given by $F_{q_{\text{eq}}}(t_{\text{eq}}) \approx 1/\left(\sigma_{q_{\text{eq}}}\sqrt{2\pi}\right)$. It should be noted that Eq. (3) implies that the width of the equilibrium charge state distribution does not depend on the absolute value of the rate, but on the scaling with the projectile charge q.

While the approximations above are useful for the discussions in this work, actual results in the presented work are calculated by solving the rate equations for the charge state evolution

$$\frac{\mathrm{d}F_q(t)}{\mathrm{d}t} = \sum_{q'} F_{q'}(t)\alpha_{q'q} - F_q(t) \sum_{q'} \alpha_{qq'} \,. \tag{4}$$

The system can be solved with a standard solver for differential equations, a Monte Carlo method or a matrix method (see Ref. [1]). The models used for the calculations of the rates are mostly summarized in Ref. [2] (which only includes single electron loss and capture) if not mentioned otherwise.

EQUAL DENSITY

As the basis of the theoretical discussion examples with parameters relevant for the GSI Unilac (see, e.g., Ref. [3]) are chosen. We assume an uranium projectile with energy $E = 1.4\,\text{MeV/u}$ in a fully-stripped hydrogen plasma and hydrogen, helium and nitrogen gas. For now the calculations

* haas@temf.tu-darmstadt.de

Content from this work may be used under the terms of the CC BY 3.0 licence (© 2015). Any distribution of this work must maintain attribution to the author(s), title of the work, publisher, and DOI.

ISBN: 978-3-95450-168-7 doi:10.18429/JACoW-IPAC2015-THPF019

Content from this work may be used under the terms of the CC BY 3.0 licence (© 2015). Any distribution of this work must maintain attribution to the author(s), title of the work, publisher, and DOI.

STATUS AND FIRST MEASUREMENT RESULTS FOR A HIGH GRADIENT CH-CAVITY *

Ali M. Almomani# and Ulrich Ratzinger, IAP, Frankfurt University, Germany

Abstract

The pulsed linac activity aims on compact designs and on a considerable increase of the voltage gain per meter. A high gradient CH – cavity operated at 325 MHz was developed and successfully built at IAP – Frankfurt. The mean effective accelerating field for this cavity is about 13.3 MV/m at β = 0.164. The results might influence the rebuilt and a later energy upgrade of the UNILAC – Alvarez section. Another motivation is the development of an efficient pulsed ion accelerator for significantly higher energies like 60 AMeV. The new GSI 3 MW Thales klystron test stand will be used for the cavity RF power tests. Detailed studies on two different types of copper plating can be performed on this cavity. The first measurement results of the frequency and the on axis electric field for this cavity will be presented.

INTRODUCTION

Conventional DTL's are limited in maximum field gain by thick walled drift tubes which are housing the focusing elements. Such geometries cause bigger parallel surfaces around the gaps which are loaded by high electric field levels. This leads to an increase of the stored field energies as well as the risk of spark damages on the cavity surfaces. Consequently, this results in reduced operable field levels.

Separated function DTL technology and strategies for a minimization of the consequences from transverse rf defocusing have been developed during the last decades of heavy ion linac development.

On the other hand, the combination between slim drift tubes and KONUS beam dynamics, in H – mode cavities allows to increase the effective field gain well above 10 MV/m. This has been tested successfully at CERN Linac 3, where the field gradient reached 10.7 MV/m at 1 ms pulse length and at low beam energy [1].

H – mode cavities profit very much from slim drift tubes (see Fig. 1), as they concentrate the electric field on the drift tube structure. Thus, the stored energy is reduced efficiently by a small outer drift tube diameter, reducing surface damages in case of sparking.

The development of CH – cavities towards a high field gradient [2-4] will be the main topic of this paper.

This aspect is important for cases, where a compact linac for low duty factor applications is needed. Also, for high current operation the high field acceleration provides the needed longitudinal focusing forces.

One main motivation of this work is to prepare the rebuilt and a later energy upgrade of the UNILAC – Alvarez section. Another motivation is the development of an efficient and compact ion accelerator for significantly higher energies for facilities like medical hospitals where available space is quite limited.

*This work supported by contract no. BMBF 05P12RFRB9
#a.almomani@iap.uni-frankfurt.de

CH – CAVITY FABRICATION

A high gradient, 7 gap CH – cavity has been developed and successfully built at IAP – Frankfurt and was fabricated at NTG, Gleisbau, Germany [2-5]. This cavity (Fig. 1) is expected to have a mean effective field gradient of about 13.3 MV/m at β = 0.164.

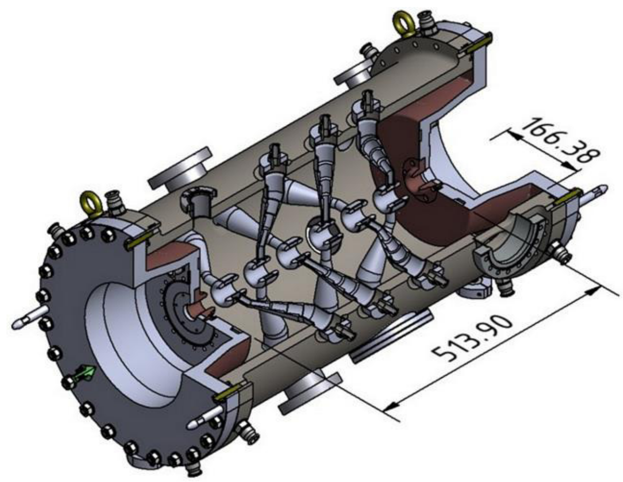

Figure 1: A 3D schematic view of the CH – cavity.

Table 1: Main Parameters of the High Field CH – cavity

Number of Gaps	7
Frequency (MHz)	325.2
Voltage Gain (MV)	6
Eff. Accel. Length (mm)	513.90
Mean eff. Accel. Field (MV/m)	13.3
Power Loss (MW)	1.76
Q_0 – value	12500
Effective Shunt impedance (MΩ/m)	52.15
Beam Aperture (mm)	27

The central part is a "monolithic" stainless steel element, where the drift tube structure was welded into a massive cylindrical tank. The drift tube stems with drift tubes are directly water cooled, the outer cylinder has eight cooling channels in longitudinal direction. The end plates have one cooling channel each, the quadrupole triplets will be positioned in the accessible outer volumes. Metal gaskets will be used at each bolted joint. Figure 2 shows the cavity tank, stems, end flanges and the massive drift tubes.

SURFACE ELECTRIC FIELD

The adaption of slim drift tubes for CH – cavity results in a very high sparking limit. The cavity geometry was

ISBN: 978-3-95450-168-7 doi:10.18429/JACoW-IPAC2015-THPF020

UPGRADE OF THE HSI-RFQ AT GSI TO FULFILL THE FAIR REQUIREMENTS

M. Baschke, H. Podlech
Institute for Applied Physics, Goethe University, Frankfurt am Main, Germany
Winfried Barth, GSI Helmholtzzentrum für Schwerionenforschung, Darmstadt, Germany

Abstract

In Darmstadt/Germany the existing accelerator facility GSI is expanding to one of the biggest joint research projects worldwide: FAIR, a new antiproton and ion research facility with so far unmatched intensities and quality. The existing accelerators will be used as pre-accelerator and therefor need to be upgraded. In a first step the 36 MHz-HSI-RFQ for high current beams will obtain new electrodes to fulfill the FAIR requirements. First simulation results for capacity and multipole components will be presented.

INTRODUCTION

The existing HSI-RFQ is part of the linear accelerator UNILAC at GSI which has a length of 120 m and consists of the RFQ (up to 120 keV/u), two IH-DTL (up to 1.395 MeV/u), four Alvarez cavities (up to 11.4 MeV/u) and 15 shiftable single gap resonators [1].

The facility is expanding with the FAIR project to one of the biggest joint research projects worldwide. With the physics at FAIR questions of the evolution of the universe, the structure of matter and its constituent parts will be approached [2]. Therefor the existing cite should be used as pre-injector. To fulfill the requirements (i.e. a huge range of beam intensities and energies, highest beam quality) a lot of modifications and updates are needed.

The RFQ was built in 1996 [3] and modified in the past years. With the actual structure the emittance is too high for the following IH-DTL which leads to unwanted beam losses and a low brilliance. The planned upgrade of the electrodes should result an increase of the brilliance.

THE RFQ STRUCTURE

The RFQ is designed as an IH-RFQ, it has a length of nearly 10 m and consists of 10 modules with 10 stems each (see Fig. 1). The electrodes are mounted on rings where only two of them are at the same ring on one stem (like in every RFQ). To tune the RFQ and to get a better voltage distribution it is possible to change every single ring to vary the capacity by adding correction rings (see Fig. 2). The parameters for the existing RFQ are listed in Table 1 (where $\bar{A}$ is the average aperture to the beam axis along the complete electrodes).

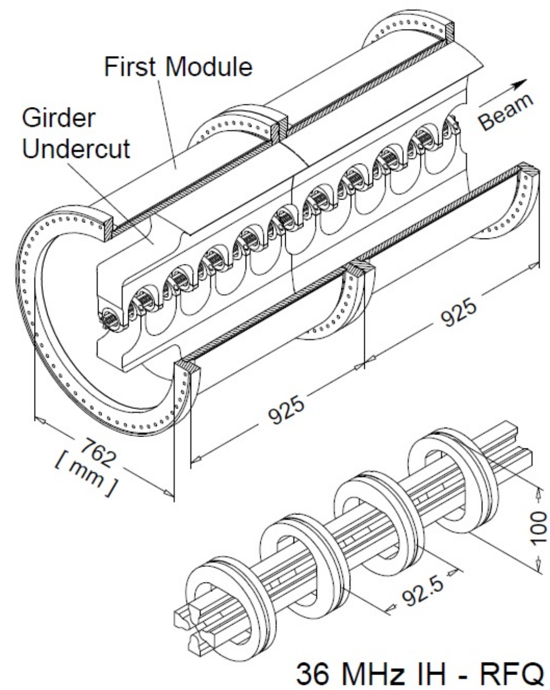

Figure 1: The IH-RFQ. [3]

Table 1: RFQ Parameters

parameter	value
$\bar{A}$	9.4 mm
R_0	4.2 mm
h	7 mm
L	14.8 mm

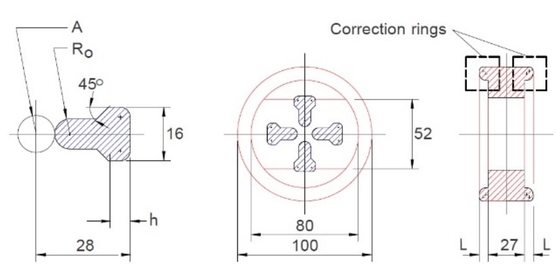

Figure 2: The electrodes with carrier and correction rings. [4]

Content from this work may be used under the terms of the CC BY 3.0 licence (© 2015). Any distribution of this work must maintain attribution to the author(s), title of the work, publisher, and DOI.

ISBN: 978-3-95450-168-7 doi:10.18429/JACoW-IPAC2015-THPF021

Content from this work may be used under the terms of the CC BY 3.0 licence (© 2015). Any distribution of this work must maintain attribution to the author(s), title of the work, publisher, and DOI.

STRUCTURAL MECHANICAL AND RF MEASUREMENTS ON THE SUPERCONDUCTING 217 MHz CH CAVITY FOR THE CW DEMONSTRATOR AT GSI*

F. Dziuba[†,1], M. Amberg[1,3], K. Aulenbacher[3,4], W. Barth[2,3], M. Basten[1], M. Busch[1], H. Podlech[1], S. Mickat[2,3]

[1]IAP University of Frankfurt, 60438 Frankfurt am Main, Germany
[2]GSI Helmholtzzentrum, 64291 Darmstadt, Germany
[3]Helmholtz Institute Mainz (HIM), 55099 Mainz, Germany
[4]KPH Mainz University, 55128 Mainz, Germany

Abstract

Together with the new horizontal cryomodule and two superconducting (sc) 9.5 T solenoids the sc 217 MHz Crossbar-H-mode (CH) cavity [1] represents the continuous wave (cw) demonstrator and brings sc rf technology to GSI. A reliable operability of the sc CH cavity is one major goal of the demonstrator project. Furthermore, the successful beam operation of the demonstrator will be a milestone on the way to a new sc cw linac at GSI for a competitive production of Super Heavy Elements (SHE) in the future. The production of the cryomodule and the solenoids is almost finished while the cavity has been completed except for the helium vessel. In this paper structural mechanical as well as related rf measurements on the sc 217 MHz CH cavity are presented.

INTRODUCTION

Currently, the production of the sc 217 MHz CH cavity [2] (see Fig. 1) for the cw demonstrator project is finished except for the titanium helium vessel. The cavity consists of 4 mm niobium sheets, has 15 equidistant arranged accelerating cells and a design gradient of 5.1 MV/m. It is equipped with nine static tuners, a 10 kW cw power coupler which is currently under development, several flanges for surface preparation and two fast frequency tuners. First performance tests of the cavity at 4 K with low rf power are expected in June 2015 at the Institute for Applied Physics (IAP), Frankfurt. As other sc cavities the 217 MHz CH structure is very susceptible to external influences like Lorentz-force detuning, microphonics or pressure variations as well. All caused mechanical deformations can change the resonance frequency of the cavity. Changes of the frequency due to evacuation and cooling down to 4 K have to be compensated by the static tuners during the respective production phase. Furthermore, the pressure sensitivity of the cavity is an important quantity regarding variations in the liquid helium bath as well as in the helium loop. These variations can be adjusted accordingly by the dynamic tuning system of the cavity [3]. Several rf measurements have been performed during each production step in order to adjust the cavity to its design frequency. Initially the frequency was designed higher than the operating frequency and lowered successively by reducing the end cap length and inserting static tuners. The following measurements have been performed before the last two remaining static tuners were welded into the cavity as the tuner ports were temporarily sealed with rings made from teflon.

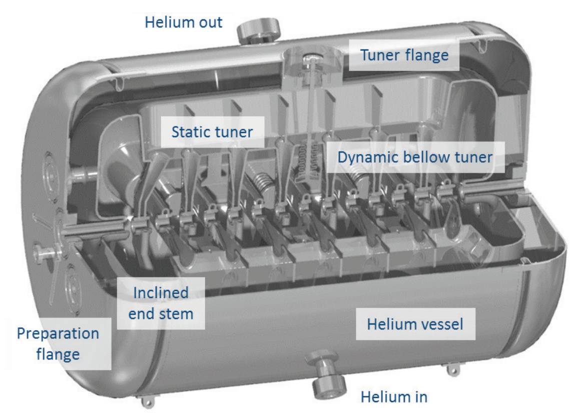

Figure 1: Layout of the sc 217 MHz CH cavity.

EVACUATION OF THE CAVITY

To study the cavity's resonance frequency change caused by evacuation and its pressure sensitivity, coupled structural - high frequency electromagnetic simulations [4] have been performed. For the analysis model the girders of the cavity were chosen as a fixed support while 1 bar pressure on the surface of the cavity walls was used as an applied load. These boundary conditions allow to simulate the mechanical behaviour of the self-supporting cavity during the evacuation process. The resulting deformations appear mainly at the central region of the cavity walls and at the end caps (see Fig. 2 top). As one can see, the results show that the maximum displacement at the end caps is around 0.23 mm while the deformation at the walls is about 0.17 mm. This leads to an increase of the resonance frequency and yields to a pressure sensitivity of 38 Hz/mbar. Additionally, the relative permittivity ϵ_r is decreasing during the evacuation pro-

* Work supported by GSI, HIM, BMBF Contr. No. 05P12RFRBL
† dziuba@iap.uni-frankfurt.de

ISBN: 978-3-95450-168-7 doi:10.18429/JACoW-IPAC2015-THPF022

DESIGN OF THE 325 MHz 4-ROD RFQ FOR THE FAIR PROTON LINAC*

B. Koubek†, H. Podlech, A. Schempp IAP,
Goethe University, Frankfurt, Germany

Abstract

Investigations on the 325 MHz 4-rod RFQ prototype for the FAIR proton linac have confirmed the feasibility of a 4-rod RFQ to work at frequencies above 300 MHz. This RFQ will accelerate protons from 95 keV to 3 MeV [1] within a length of 3.3 m and will be powered by a 2.5 MW klystron. The mechanical and rf design of this RFQ are presented in this paper.

325 MHz 4-ROD RFQ R & D

In simulations the dipole field, the fringe fields and higher order modes were investigated to find a solution for an rf design to fit a 4-rod RFQ to an operation frequency of 325 MHz. Based on this simulations a copper prototype was built and investigated as well. The results of the low level rf measurements confirmed the simulation work quite well and are presented in [2,3]. After the rf measurements the 6 stem prototype was power tested with 40 kW and a duty cycle of 0.3% that refers to a cw power of 400 W/m. At the FAIR project the 3.3 m RFQ will be powered at a duty cycle < 0.1% [4]. This tests have shown the feasability of the prototype to meet the FAIR requirements. Apart from this the input power was measured in comparison to the maximum electrodes voltage using gamma spectroscopy. From these measurements results the shunt impedance was determined and compared to other methods of determination of the shunt impedance to confirm their reliability. In summary these tests have demonstrated a working 325 MHz 4-rod RFQ without a dipole component that meets the FAIR requirements.

Challenges

Since higher frequencies refer to smaller dimensions of the resonant structure a 4-rod RFQ at 325 MHz becomes very small and sensitive with respect to parametric changes. This filigree and sensitive structure is very challenging for the engineering and requires very tight tolerances in manufacturing of every single part of the RFQ. In respect to rf this transversally small structure leads to a dipole component much stronger than at lower frequencies. In longitudinal direction the RFQ has a length above 3 m with approximately 60 rf cells. This leads to higher order modes in the region of the operation frequency that usually can be neglected at 4-rod RFQs. In addition this large number of rf cells makes the tuning procedure much more elaborate than usual.

ENGINEERING AND DESIGN

To reach a higher precision of the RFQ in the manufacturing process changes of the mechanical design, that worked very well over the last years on 4-rod RFQ at lower frequencies, were crucial. To reach a higher precision the idea was on the one hand to simplifiy all parts of the RFQ with respect to machining reasons and on the other hand to reduce the number of connected surfaces to increase the precision after assembly.

For example the stems and ground plate will be made of one piece of copper. This combination will be segmented in only few segments to form the support and resonant structure for the electrodes. To build this out of one or few pieces allow not only a higher precision in machining the surfaces that mount and connect the electrodes. In addition it provides also a better thermal and electrical connection of the single parts. Also the shape of the electrodes will be kept more simple to increase precision and stabillity of the filigree parts.

TUNING

General Tuning Process

In general the tuning of a 4-rod RFQ is an iterative process were a perturbance capacitor is placed on every single rf cell of the structure. From the frequency shift caused by this additive capacitance the longitudinal voltage distribution of the RFQ can be calculated. Then the tuning plates will be moved in such a way to minimize the longitudinal voltage deviation. This process has to be repeated several times to find a best match of the operating frequency and simultaneously a minimum longitudinal voltage deviation.

Additional to the large number of rf cells the frequency of 325 MHz causes a high sensitivity of the tuning plates that have to be placed very accurate (in sub millimeter range).

Simplification of the Tuning

In order to simplify and hence abbreviate the above mentioned process one can reduce the number of rf cells. This can be done by increasing the thickness of the stems but it only allows a limited reduction of the number of rf cells.

To reduce the sensitivity of the tuning plates the influence of plunger tuners instead has been investigated. While tuning plates change the inductivity of an rf cell by changing the length of the shortcut, plunger tuners are suppressing the field inside one rf cell. These kind of tuner have been used already as additional tuning possibilities at the FNAL RFQ [5]. Simulations of piston tuners have shown a strong reduction of the tuning range. The fact that the frequency is less sensitive on these plungers leads to a much higher precision of adjustment by keeping still enough frequency

* Work supported by BMBF & GSI
† koubek@physik.uni-frankfurt.de

Content from this work may be used under the terms of the CC BY 3.0 licence (© 2015). Any distribution of this work must maintain attribution to the author(s), title of the work, publisher, and DOI.

ISBN: 978-3-95450-168-7 doi:10.18429/JACoW-IPAC2015-THPF023

MASSLESS BEAM SEPARATION SYSTEM FOR INTENSE ION BEAMS

O. Payir*, M. Droba, O. Meusel, D. Noll, U. Ratzinger, P. P. Schneider, C. Wiesner,
IAP, Goethe University, Frankfurt am Main, Germany

Abstract

The ExB chopper [1] in the Low Energy Beam Transport (LEBT) section of the accelerator-driven neutron source FRANZ [2] will form the required pulses with a repetition rate of 257 kHz out of the primary 120 keV, 50 mA DC proton beam. A following beam separation system will extract the deflected beam out of the beamline and minimize the thermal load by beam losses in the vacuum chamber. To further avoid an uncontrolled production of secondary particles, a novel massless septum system is designed for the beam separation.

The septum system consists of a static C-magnet with optimized pole shapes, which will extract the beam with minimal losses, and a magnetic shielding tube, which will shield the transmitted pulsed beam from the fringing field of the dipole. The magnetic field and the beam transport properties of the system were numerically investigated. A main deflection field of about 250 mT was achieved, whereas the fringing field was reduced to below 0.3 mT on the beam axis at 60 mm distance from the dipole. With this settings, the beam was numerically transported through the system with minimal emittance growth. Manufacturing of the septum system has started.

INTRODUCTION

The ExB chopper system in the LEBT section of FRANZ consists of a dipole magnet and a pulsed electric deflector. The fields are oriented in a Wien filter configuration. During the flat top of the HV pulse of the electric deflector, the electric deflection of the beam compensates the magnetic deflection and the beam is transmitted in forward direction. Between two deflector pulses, i.e. when the deflector voltage is zero, the beam is deflected about 10 ° by the dipole magnet. To minimize the energy deposition of the beam on the vacuum chamber walls without increasing the magnetic field on the beam axis, a following septum magnet is under construction. During the rise and fall of the deflector voltage pulse the beam sweeps between the full field region and the zero field region of the septum magnet and forms the required pulsed beam. To minimize secondary particle emission during the deflector pulses, the possibility of using a massless septum system was investigated [3]. The most promising design regarding longitudinal and transversal magnetic field distributions on the transmitted beam axis is shown in Fig. 1. Table 1 shows the current specifications.

The C-magnet is tilted 12 ° to match the deflection angle of the deflected beam and to further reduce the magnetic field on the transmitted beam axis. To minimize beam losses, the pole shoes were modified with additional fittings, so that the deflected beam is exposed longer to the maximum magnetic field in the gap. With this fittings the C-magnet will deflect the beam into a beam dump, while the shielding tube made of high permeable material (VACUFLUX 50) will shield the 60 mm distant beamline of the transmitted pulsed beam from the fringing field of the C-Magnet (see Fig. 2). The varying proportions of the tube along the beam axis, particularly the widening at the ends, serve a more effective shielding of the magnetic field. A slit on the side assures a lossless beam sweep during the rise and fall of the deflector pulse.

* payir@iap.uni-frankfurt.de

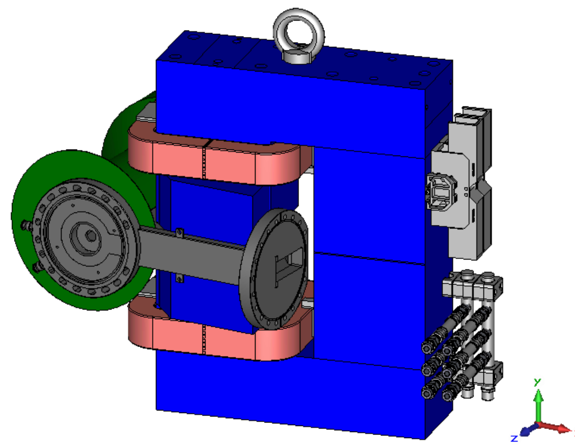

Figure 1: Model of the massless septum system for the FRANZ LEBT, consisting of a C-magnet and a shielding tube.

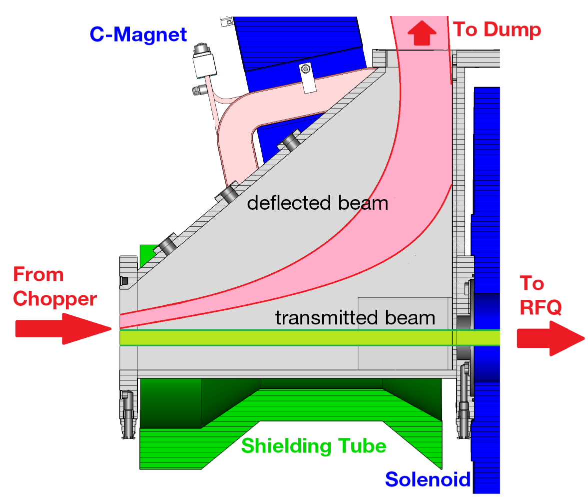

Figure 2: Horizontal cross section of the septum system including the vacuum chamber. The C-magnet will extract the deflected beam out of the beamline and guide it into a beam dump. The shielding tube will reduce the magnet's fringing field on the beam axis of the transmitted beam.

Content from this work may be used under the terms of the CC BY 3.0 licence (© 2015). Any distribution of this work must maintain attribution to the author(s), title of the work, publisher, and DOI.

ISBN: 978-3-95450-168-7 doi:10.18429/JACoW-IPAC2015-THPF024

LEBT DYNAMICS AND RFQ INJECTION

P. P. Schneider*, M. Droba, O. Meusel, H. Niebuhr, D. Noll, O. Payir,
H. Podlech, A. Schempp and C. Wiesner
IAP, Goethe-University, Frankfurt am Main, Germany

Abstract

The Low Energy Beam Transport (LEBT) section at the accelerator-driven neutron source FRANZ [1] consists of four solenoids, two of which match the primary proton beam into the chopper. The remaining two solenoids are intended to prepare the beam for injection into the RFQ. In the first commissioning phase, the LEBT successfully transported a 14 keV He^+ beam at low intensities [2]. In the current commissioning phase, the beam energy is increased to the RFQ injection energy of 120 keV. In the upcoming step, the intensity will be increased from 2 mA to 50 mA.

Beam dynamics calculations include effects of different source emittances, position and angle offsets and the effects of space charge compensation levels. In addition, the behavior of the undesired hydrogen fractions, H_2^+ and H_3^+, and their influence on the performance within the RFQ is simulated.

INTRODUCTION

A LEBT can satisfy several tasks within an accelerator. While the most important task is the transport of the beam at low energy from the ion source into the downstream RFQ, which expects well defined beam properties at the injection point, another important aspect is the matching of the beam properties, the “RFQ injection parameters”, which are usally given by the twiss parameters α_{Twiss}, β_{Twiss}, γ_{Twiss} and the emittance ε.

A possible additional task within a LEBT is to apply a time structure to the beam. A time structure is necessary to reduce the duty cycle of the RFQ or to provide the time structure required for the experimental needs.

Furthermore, beam diagnostics are an important task to ensure the required specifications and quality of the beam.

If the desired beam ion cannot be delivered in one fraction from the ion source, as, for example, for hydrogen beams, the LEBT should separate the unwanted fractions. Otherwise, these would be lost in an uncontrolled way within the RFQ or the later beamline, where high loss rates are intolerable.

This work will focus on the fraction separation within the FRANZ LEBT and gives an outlook on planned projects at the MYRRHA LEBT. Additionally the sucessful separation of an hydrogen beam at a solenoidal separation channel will be described.

FRACTION SEPARATION

Proton sources usually provide three fractions of charged hydrogen: H^+, H_2^+ and H_3^+. However, an RFQ is able to accelerate only one mass-to-charge ratio. Therefore, the two unwanted fractions have to be filtered by the LEBT in order to reduce their impact on the further accelerator. To perform this task, there are several possible solutions.

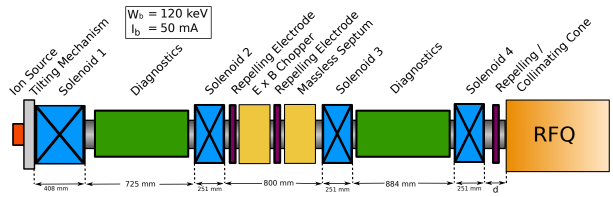

Figure 1: Schematic view of the FRANZ LEBT.

Dipole Separation

It is possible to separate the fractions with a dipole magnet, as is done for example at the SARAF LEBT [3].

⊕ separation efficiency up to 100 %
⊕ controlled dumping of separated beam possible

⊖ does not preserve beam symmetry
⊖ does not preserve space-charge compensation
⊖ small angle mismatches can lead to large offsets

Collimation System

Another possibility to separate the species is to exploit the momentum-dependent focusing of a solenoid in order to move every fraction to a different radius. A subsequent collimator system can scrape the fractions at high radii.

⊕ preserves beam symmetry
⊕ preserves space-charge compensation

⊖ separation efficiency always < 100 %
⊖ produces secondary particles
⊖ losses cause “hot spots”

Wien Filter

A third possibility is a Wien filter [4] composed of a magnetic dipole and an electric deflector. Particles that satisfy the Wien-ratio can pass, all others will be deflected.

⊕ preserves beam symmetry
⊕ controlled dumping of separated beam possible
⊕ separation efficiency up to 100 %

⊖ space-charge compensation is not preserved
⊖ complex to design and construct

FRANZ LEBT

The FRANZ LEBT (Fig. 1) consists of two sections. The first section ranges from the source to the chopper system, the second section from behind the chopper system to the entrance of the RFQ.

The first section has to transport the beam from the ion source into the chopper system. Between solenoid 1 and

* schneider@iap.uni-frankfurt.de

Content from this work may be used under the terms of the CC BY 3.0 licence (© 2015). Any distribution of this work must maintain attribution to the author(s), title of the work, publisher, and DOI.

ISBN: 978-3-95450-168-7 doi:10.18429/JACoW-IPAC2015-THPF025

Content from this work may be used under the terms of the CC BY 3.0 licence (© 2015). Any distribution of this work must maintain attribution to the author(s), title of the work, publisher, and DOI.

BEAM DYNAMICS FOR THE SC CW HEAVY ION LINAC AT GSI*

M. Schwarz[†,1], M. Amberg[1,3], K. Aulenbacher[3,4], W. Barth[2,3], M. Basten[1], F. Dziuba[1], V. Gettmann[2], M. Heilmann[2], S. Mickat[2,3], M. Miski-Oglu[3], A. Orzhekhovskaya[2], H. Podlech[1], U. Ratzinger[1], R. Tiede[1], S. Yaramyshev[2]
[1]IAP, Goethe University, Frankfurt am Main, Germany
[2]GSI Helmholtzzentrum, Darmstadt, Germany
[3]HIM, Helmholtzinstitut, Mainz, Germany
[4]KPH, Johannes Gutenberg University, Mainz, Germany

Abstract

For future experiments with heavy ions near the coulomb barrier within the SHE (super-heavy elements) research project a multi-stage R&D program of GSI, HIM and IAP is currently in progress [1]. It aims at developing a superconducting (sc) continuous wave (cw) LINAC with multiple CH cavities as key components downstream the High Charge Injector (HLI) at GSI (Fig. 1). The beam dynamics concept is based on EQUUS (equidistant multigap structure) constant-β cavities. Advantages of its periodicity are a high simulation accuracy, easy manufacturing and tuning with minimized costs as well as a straightforward energy variation. The next milestone will be a full performance beam test of the first LINAC section, comprising two solenoids and a 15-gap CH cavity inside a cryostat (Demonstrator).

INTRODUCTION

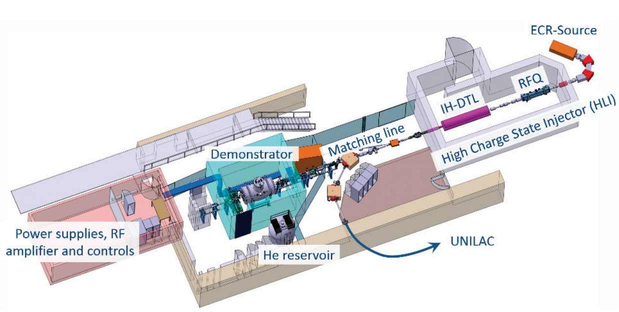

Figure 1: CH cavity test environment for a full performance test of the sc cw LINAC Demonstrator at GSI (first expansion stage with max. two cavities and one cryostat).

The beam dynamics concept for the sc cw LINAC is based on EQUUS, as proposed in [2]. It features high acceleration efficiency with longitudinal and transversal stability, as well as a straightforward energy variation. The latter can easily be achieved by varying the applied rf voltage (even down to "switched off" cavities) or the rf phase of the amplifier. Highly charged ions with a mass-to-charge ratio of up to 6 will be accelerated from 1.4 MeV/u up to 3.5 - 7.3 MeV/u. A typical ion species for acceleration is $^{48}Ca^{10+}$ (with an A/q of 4.8) as projectile for hot fusion reactions with actinide targets [3]. Energy variation whilst maintaining a high beam quality is the core issue with respect to beam dynamics. Therefore research has been started to optimize the present conceptual layout of a sc cw-LINAC by Minaev et al. [2].

BEAM DYNAMICS SIMULATIONS

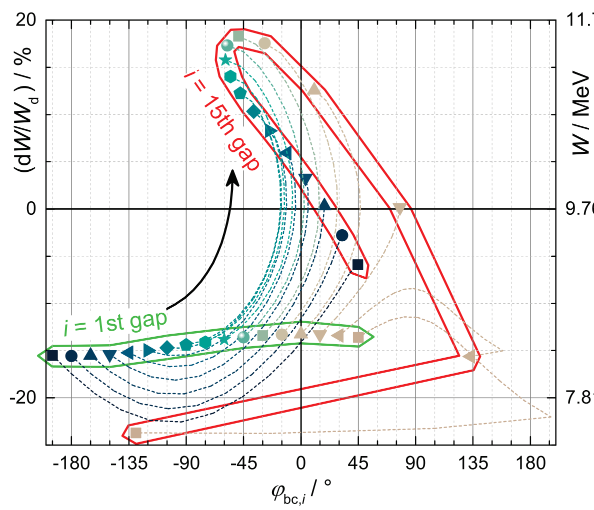

Figure 2: Movement of the bunch-center particle in longitudinal phase space in dependence of the initial phase $\varphi_{\mathrm{bc},1}$ while traversing the 15-gap CH cavity.

Inside an EQUUS cavity cell lengths are kept constant and are designed with a higher (geometrical) β than the one of the injected beam (also called "constant-β structure"). This leads to a sliding movement in longitudinal phase space. Trajectory and energy gain depend strongly on the initial phase at the first gap center $\varphi_{\mathrm{bc},1}$ and the difference between particle energy W and design energy W_{d}. Figure 2 shows this movement for the 15-gap CH cavity whose construction is nearly completed [4]. At $\varphi_{\mathrm{bc},1} = -30°$ the highest energy gain is achieved ($\Delta W = 3.1$ MeV), while at $-60°$ it has the highest symmetry. The corresponding emittance evolution is plotted in Fig. 3 showing a broad range of little growth. All simulations in this paper have been performed with LORASR [5] and will be prospectively benchmarked with TraceWin [6] and bender [7]. 10k particles with $q = 1$, $m = 6\,\mathrm{u}$ and $I = 0\,\mathrm{mA}$ were used as input distribution (Fig. 4), starting downstream the HLI IH-DTL (Fig. 5).

* Work supported by BMBF contr. No. 05P12RFRBL
† schwarz@iap.uni-frankfurt.de

ISBN: 978-3-95450-168-7 doi:10.18429/JACoW-IPAC2015-THPF026

DEVELOPMENT OF A 325 MHz LADDER-RFQ OF THE 4-ROD-TYPE*

M. Schütt, U. Ratzinger
Institut für Angewandte Physik, Johann Wolfgang Goethe Universität, Frankfurt, Germany
R. Brodhage, GSI, Darmstadt, Germany

Abstract

For the research program with cooled antiprotons at FAIR a dedicated 70 MeV, 70 mA proton injector is required. In the low energy section, between the Ion Source and the main linac an RFQ will be used. The 325 MHz RFQ will accelerate protons from 95 keV to 3 MeV. This particular high frequency for an 4-ROD type RFQ creates difficulties, which are challenging in developing this cavity. In order to define a satisfactory geometrical configuration for this resonator, both from the RF and the mechanical point of view, different designs have been examined and compared. Very promising results have been reached with a ladder type RFQ, which has been investigated since 2013 [1, 2]. We present recent 3D simulations of the general layout and of a complete cavity demonstrating the power of a ladder type RFQ as well as measurements of a 0.8 m prototype RFQ, which was manufactured in late 2014 and designed for RF power and vacuum tests. The prototype manufacturing was completed and first measurements are shown.

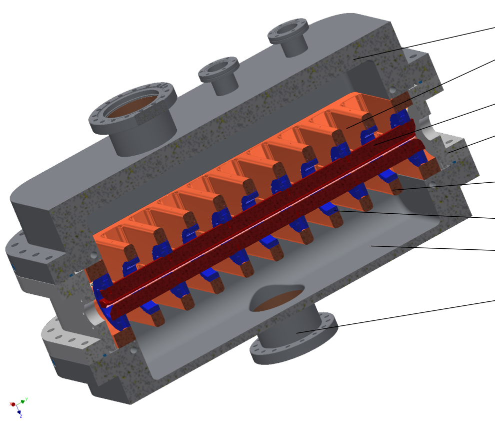

Figure 1: Isometric view of the Ladder-RFQ. The cooper carrier-rings (for a better view coloured in blue) guarantee the electrode positioning as well as the RF contact. The ladder structure consists of bulk copper components. Any brazing or welding processes are avoided.

INTRODUCTION

The idea of the Ladder-RFQ firstly came up in the late eighties [3, 4] and was realized successfully for the CERN Linac3 operating at 101 MHz [5] and for the CERN antiproton decelerator ASACUSA at 202 MHz [6]. Within the 4-ROD design the challange is to minimize dipole components and to have geometrical dimensions which are suitable for a mechanical manufacturing and assembling. At frequencies above 250 MHz the 4-Vane-type RFQ is used so far. Many versions for low and high duty factors have been realized successfully until now. Draw backs are the high costs per meter, the complexity as well as the challenging RF tuning procedure of that structure: The dipole modes tend to overlap with the quadrupole mode. Safe beam operation conditions result in ambitious mechanical vane tolerances. In the proposed ladder-RFQ version, the spokes show an extended width which increases the resonance frequency and which results in an homogeneous current flow towards the mini-vanes. The mini-vanes are embedded via precisely machined carrier rings into the copper shells (see Fig. 2). To proof the mentioned advantages and realizability of the Ladder RFQ a prototype was designed and built. The results of the simulation and comparision with the measurement are shown in this paper.

MECHANICAL LAYOUT

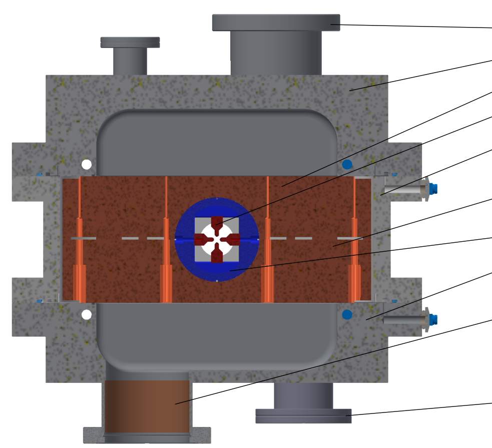

Figure 2: Sectional front view of the Ladder-RFQ.

The mechanical design consists of an inner copper ladder structure mounted into an outer stainless steel tank. The tank is divided into a base plate carrying the inner resonating structure, an intermediate part and the cover plate. The base will carry and adjust the position of the resonating structure. All parts are metal-sealed. Furthermore its task is to provide a vacuum at the level of 10^{-8} mbar. The rf is mainly determined by the resonating structure, while the dimensions of the tank have no significant influence to the frequency.

To lower the wall losses it is foreseen to copperplate the lower and upper half shells. The inner resonating structure consists of two symmetric half shells made of massive copper. They press and grout the carrier-rings in between. The

* Work funded by BMBF 05P12RFRB9

Content from this work may be used under the terms of the CC BY 3.0 licence (© 2015). Any distribution of this work must maintain attribution to the author(s), title of the work, publisher, and DOI.

ISBN: 978-3-95450-168-7 doi:10.18429/JACoW-IPAC2015-THPF027

TEN GAP MODEL OF A NEW ALVAREZ DTL CAVITY AT GSI

Anja Seibel, IAP University of Frankfurt, Germany
Xiaonan Du, Lars Groening, Oliver Kester, Sascha Mickat, GSI, Darmstadt, Germany

Abstract

In order to meet the challenges of the FAIR project at GSI requiring highest beam intensities an upgrade of the existing Universal Linear Accelerator (UNILAC) is planned. The 108 MHz cavities will be replaced by new rf-structures of the same frequency. Simulations are done to improve the rf-properties. The geometry of the drift tubes is to be changed to a smoother curvature to reach a homogeneous surface field distribution and higher shunt impedances. To check the necessity of cooling channels, simulations on the temperature distribution at the drift tubes and stems are conducted. A test bench for low power rf-measurements with a 10 gap aluminum model (scale 1:3) is under construction. The modular mechanical design of the model will allow probing experimentally a wide range of drift tube and stem geometries. With the bead pull method the electrical field distribution will be measured as well as the field stability with respect to parasitic modes. Additionally, appropriate locations along the cavity to place fixed and dynamic rf-frequency tuners will be determined.

THE FAIR PROJECT

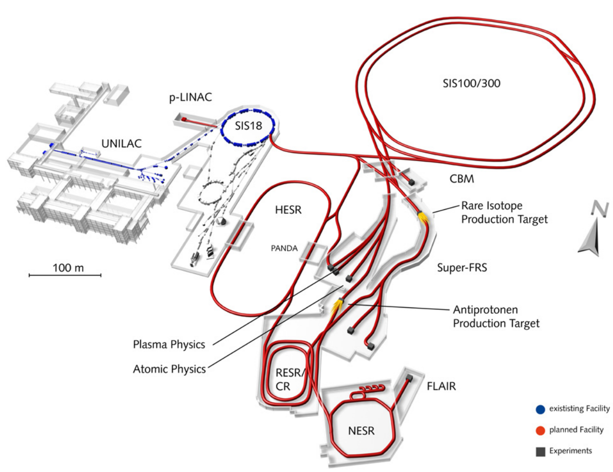

Figure 1: The FAIR facility in the full version [1].

The FAIR project (Fig. 1) will be a new international particle accelerator facility for antiprotons and heavy ions which is currently under construction [1]. This project will provide knowledge of still unknown subatomic components of matter in the Universe. In parallel the existing GSI facility is upgraded together with a new proton linear accelerator and will serve as pre-accelerator and injector for the new heavy ion synchrotron SIS100. The SIS100 beams are delivered to a complex of storage rings [2] and experimental stations reaching energies and intensities as required for FAIR [1].

As shown in Fig. 2, the existing HSI (high current injector) branch of the UNILAC consists of two ion source terminals, one RFQ, two IH cavities, a gas-stripper, and the poststripper with five Alvarez cavities and 10 single gap cavities. After the HSI the beam has an energy of 1.4 MeV/u. The operating frequency of the Alvarez DTL is 108.408 MHz accelerating the beam to the final energy of 11.4 MeV/u [3]. After almost 40 years in operation it is recommended to replace this section with an improved Alvarez DTL [4].

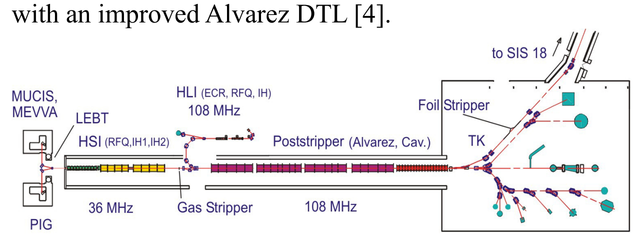

Figure 2: Existing UNILAC at GSI with the five Alvarez cavities working at 108.408 MHz [5].

DESIGN OF THE TEN GAP MODEL

A set of simulations has been performed using CST Microwave Studio [6] to improve the rf-properties of the existing Alvarez cavity [7]. Therefore a 1:3 scale ten gap model (Fig. 3) is simulated with a new design geometry inside. The frequency scales correspondingly to three times 108.408 MHz (= 325.224 MHz). To reach the exact frequency after fabrication, the tank is designed a bit larger in diameter, in accordance that the operating frequency is lower and can be shift up by tuners. The reasons for such procedure are small inaccuracies in fabrication which influence the frequency. The model design parameters are listed in Tab. 1.

The ten gap model with nine full and two half drift tubes at the end plate allows to vary the angle between the stems. With the rotating stem geometry the frequency of the TM011 mode (Fig. 4) can be pushed away in the simulations more than 5 MHz from the operating TM010 mode for the existing Alvarez 3 tank [7]. The stem configuration of each drift tube is used to damp parasitic modes and thus increase the field stability. In addition, the drift tube cabs are exchangeable to compare different drift tube geometries.

The goal is to optimize the rf-design geometry with respect to the field distribution stability. Therefore the above mentioned 10 gap aluminium model is under construction, to verify the simulated results using the bead pull method. The calculated electric field profile along the beam axis (Fig. 5) shows a flatness of better than 3 %.

Content from this work may be used under the terms of the CC BY 3.0 licence (© 2015). Any distribution of this work must maintain attribution to the author(s), title of the work, publisher, and DOI.

ISBN: 978-3-95450-168-7 doi:10.18429/JACoW-IPAC2015-THPF028

CONCEPTUAL DESIGN OF A NOVEL RFQ FOR MEDICAL ACCELERATORS

R. Cee*, E. Feldmeier, T. Haberer, A. Peters, T. Winkelmann

Abstract

At the Heidelberg Ion Beam Therapy Centre HIT we operate a 4-rod RFQ as first stage of a 7 MeV/u injector linac followed by an IH-DTL. During the first years of patient treatment the injector performance was perfectly adequate, even though the transmission of the linac remained below the theoretical expectations. New developments in dose delivery technology already realised or to come in the future increase the demand on higher beam intensities which will finally result in shorter irradiation times. As measurements performed at our test bench have confirmed that there is a margin for higher transmissions especially for the RFQ we are currently preparing for a new RFQ design. While keeping the original design parameters, the new RFQ should be optimised with respect to the transmission of beams from different ion sources such as electron cyclotron resonance or electron beam ion sources. All parts of the RFQ will be put up for discussion including electrodes, stems, tank and the integrated rebuncher. The design work will profit from new concepts that have evolved at our own and other medical heavy ion facilities in operation and from the progress modern simulation tools have run through.

MOTIVATION

As a new field of application radio-frequency-quadrupoles (RFQs) are nowadays used in medicine as part of injectors for subsequent circular accelerators (synchrotrons). One of the world's leading facilities for the treatment of cancer patients with ion beams is the Ion Beam Therapy Centre of the Heidelberg University Hospital (HIT) [1]. It comes along with an ion accelerator designed for carbon ions with a maximum energy of 430 MeV per nucleon. The range of available ion species is not limited to carbon ions. Both heavier elements, such as e.g. oxygen, as well as lighter ions, such as hydrogen or helium, are accelerated. Since patient treatment was established in 2009 the capacity of HIT could be continuously increased up to 750 carbon and proton patients per year. A further rise of the patient number will essentially depend on the achievable beam intensity.

One known source of particle losses is the HIT-RFQ. Its maximum achievable transmission ranges between 30 % and 40 % depending on the ion species and beam intensity. Measurements carried out at other therapy facilities such as the one in Marburg (now Marburg Ion Beam Therapy Centre [2]) obtain consistent results. Obviously it is not possible to achieve higher transmissions with the current RFQ design in combination with beams from the ion sources in operation, the electron cyclotron resonance ion sources (ECRIS). In order to further increase the efficiency of our ion beam therapy facility, it is necessary to increase the transmission of the RFQ accelerator by a factor of about 2.5. This can be achieved by optimising the RFQ in terms of design, fabrication and adjustment. The medium term objective of this work is therefore the design, construction and testing of a highly efficient RFQ structure with high transmission (desirably 90 %) maintaining the parameters of the original RFQ.

* rainer.cee@med.uni-heidelberg.de

RFQ IN OPERATION

The RFQ currently in operation is a 4-rod type RFQ developped at the IAP Frankfurt [3]. It accelerates ions from 8 keV/u to 400 keV/u. Further design parameters can be found in Table 1. The resonant structure, as shown in Fig. 1, consists of four electrodes held by 16 stems which are electrically connected via tuning plates with variable height. As a peculiarity the rebuncher for longitudinal beam focusing into the subsequent IH drift tube linac (IH-DTL) is placed within the RFQ tank and is coupled to the resonant structure. This unique design was chosen for the sake of compactness and cost efficiency but is attended by a loss of variability during operation.

Table 1: RFQ Design Parameters

Parameter	Value
input energy	8 keV/u
output energy	400 keV/u
operating frequency	216.816 MHz
max. power consumption (pulsed)	200 kW
max. mass-to-charge ratio	3

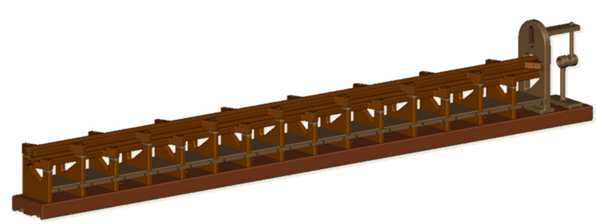

Figure 1: Resonant structure of the 4-rod RFQ with base plate, stems, tuning plates, electrodes and integrated rebuncher (beam direction from left to right).

CONCEPT FOR A NEW RFQ

Based on eight years of operational experience we see room for improvement for all major components of the RFQ.

Tank

The tank of the current RFQ essentially consists of a 250 mm diameter stainless steel tube equipped with sockets

Content from this work may be used under the terms of the CC BY 3.0 licence (© 2015). Any distribution of this work must maintain attribution to the author(s), title of the work, publisher, and DOI.

ISBN: 978-3-95450-168-7 doi:10.18429/JACoW-IPAC2015-THPF029

PREPARATION OF AN ION SOURCE FOR AN EXTRA LOW ENERGY SYNCHROTRON

Ralf Gebel, Olaf Felden, Rudolf Maier, Sebastian Mey, Dieter Prasuhn
Forschungszentrum Jülich GmbH, IKP-4, Jülich, Germany

Abstract

ELENA is a compact ring for cooling and further deceleration of 5.3 MeV antiprotons delivered by the CERN Antiproton Decelerator (AD) down to 100 keV. Because of the long AD cycle of 100 s, it is foreseen to use a source for protons and H^- with a kinetic energy of 100 keV for commissioning and start-ups. The source, designed to provide 0.2 to 2.0 μs pulses with 3×10^7 ions, is based on a proven multicusp volume source used at the COSY/Jülich injector cyclotron. The source and its auxiliaries were refurbished, upgraded to $+/-100$ keV operation at the Forschungszentrum Jülich and have been set in operation at CERN in April 2015 for first tests of new equipments.

INTRODUCTION

CERN has approved in 2011 the construction of the Extremely Low ENergy Antiproton ring ELENA [1] due to the growing scientific demand for low-energy antiprotons. ELENA is a small synchrotron with an electron cooler for further deceleration of 5.3 MeV antiprotons delivered by the antiproton decelerator AD [2]. Electron-cooling of antiprotons of about 100 keV energy will produce a beam quality that allows delivery of pulses in electrostatic beam lines to experiments in the AD hall. The ELENA Feasibility Study [1] constitutes the scientific and technical basis of the project. ELENA is also an accelerator test platform for developing new generation sources for antiprotons which may start with FLAIR [3], an addition to FAIR at the GSI in Darmstadt [4]. CERN's AD with ELENA is going to be the world's sole source for low-energy antiproton physics for the near future. The Institute for Nuclear Physics (IKP-4) of Forschungszentrum Jülich [5] has committed, like other parties, to contribute significantly to ELENA with manpower and equipment. Setting-up ELENA and experiments is foreseen with a dedicated H^- and proton source. This enables making part of the commissioning independent of the CERN schedule. A 100 keV source can be installed in a section of the transfer beam line between AD, experiments and ELENA. The ion source provides higher intensity and more frequent injections than possible with AD, about one bunch every 100 seconds, and improves efficiency.

SYSTEM LAYOUT AND STATUS

The 100 keV H^-/proton ion source with auxiliaries has been prepared in Jülich for delivery in an early stage of ELENA installation. The source is one of the first components installed in the AD hall at CERN in April 2015. All systems are operational and the source can be useful for validation of equipment prior and during their installation.

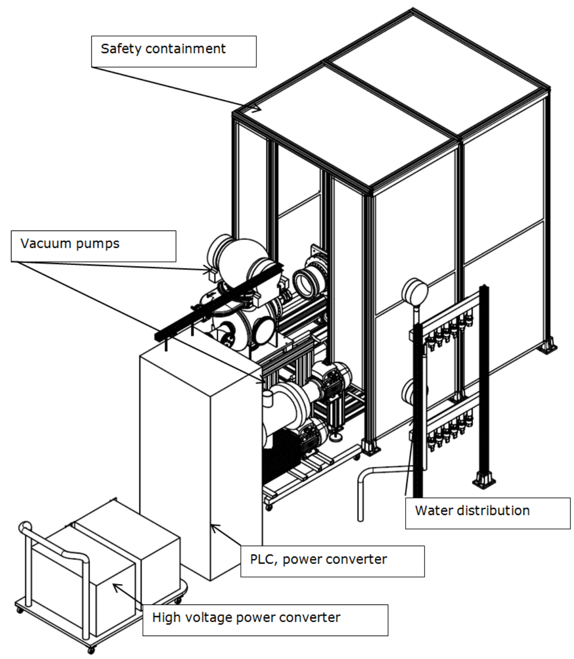

Figure 1: ELENA source set-up for commissioning, with its auxiliaries.

It is planned to test e.g. ion switch yard elements and diagnostic devices. In order to enable these activities the source has been delivered equipped with vacuum system, power converters, a local control computer and diagnostic tools. The ion source was successfully operated at 100 keV with both polarities in Jülich. Table 2 provides parameters first operation with 100 μA H^- and 150 μA proton ion beams. The first installation at CERN is very close to the opertional configuration used at Jülich. In a second step, after installation of the beam line elements between source to the ion switch after June 2015, the source is going to be installed at its final position. The faraday cage is already at its final position. The ion source system has been installed within the AD machine circumference and inside shielded areas. The position is fixed by the requirements of the switch yard for serving both ions and antiprotons to the ELENA ring and the experiments. The layout of the equipment integrates the HV cabinet which is enclosed inside a grounded safety cabinet of Faraday type and the ion source components. The ion source power supply is composed of four power supplies, filament driver to heat the filaments, arc power supply to create a discharge, two extraction power supplies for pulling out, or suppressing, ion beam and auxiliary power converters and high voltage solid state switches for pulsed operation.

Content from this work may be used under the terms of the CC BY 3.0 licence (© 2015). Any distribution of this work must maintain attribution to the author(s), title of the work, publisher, and DOI.

ISBN: 978-3-95450-168-7 doi:10.18429/JACoW-IPAC2015-THPF030

ANTIPROTON ACCELERATION AND DECELERATION IN THE HESR

B. Lorentz[#], T. Katayama, A.Lehrach, R. Maier, D. Prasuhn, R. Stassen, H. Stockhorst, and R. Tölle
Forschungszentrum Jülich GmbH, D 52425 Jülich, Germany.

Abstract

The High Energy Storage Ring (HESR) is a part of the future Facility for Antiproton and Ion Research (FAIR) in Darmstadt [1,2]. The ring is used for hadron physics experiments with a pellet target and the PANDA detector, and will supply antiprotons of momenta from 1.5 GeV/c to 15 GeV/c. To cover the whole energy range a flexible adjustment of transition energy and the corresponding γ_{tr} value is foreseen. For injection and accumulation of antiprotons delivered from the CR at a momentum of 3.8 GeV/c (γ=4.2), the HESR optics will be tuned to γ_{tr}=6.2. For deceleration down to a momentum of 1.5 GeV/c this optic is suitable as well. Stochastic cooling at an intermediate energy is required to avoid beam losses caused by adiabatic growth of the beam during deceleration. For acceleration to 8 GeV/c (γ=8.6) the optics will be changed after accumulation of the antiproton beam to γ_{tr}=14.6. For momenta higher than 8 GeV/c the beam will be debunched at 8 GeV/c, optics will be changed to γ_{tr}=6.2, and after adiabatic rebunching the beam will be accelerated to 15 GeV/c (γ=16). Simulations show the feasibility of the described procedures with practically no beam losses.

INTRODUCTION

The High Energy Storage Ring HESR is dedicated to the field of high energy antiproton physics with high quality beams over the broad momentum range from 1.5 to 15 GeV/c to explore the research areas of hadron structure and quark gluon dynamics, e.g. non perturbative QCD, confinement, and chiral symmetry. An important feature of the new facility is the combination of phase space cooled beams with internal targets which opens new capabilities for high precision experiments.

Wide international collaborations (e.g. PANDA [3]) with a rich scientific program are working on new experiments with antiprotons in the energy range between the CERN Antiproton Decelerator AD and the Tevatron energies.

Special equipment enables the high performance of this antiproton machine, which will make high precision experiments feasible that are not possible up to now. Key tasks for the design work to fulfil these requirements are:

- multi harmonic RF cavities [4],
- high sensitivity stochastic cooling pickups for the frequency range 2-4 and 4-6 GHz,
- powerful beam cooling systems to counteract beam heating (from beam target interaction and intra beam scattering) to achieve high luminosity and high beam quality.

[#] b.lorentz@fz-juelich.de

Stochastic cooling will be used for the injection and accumulation process and to counteract the beam heating caused by the target of the PANDA experiment.

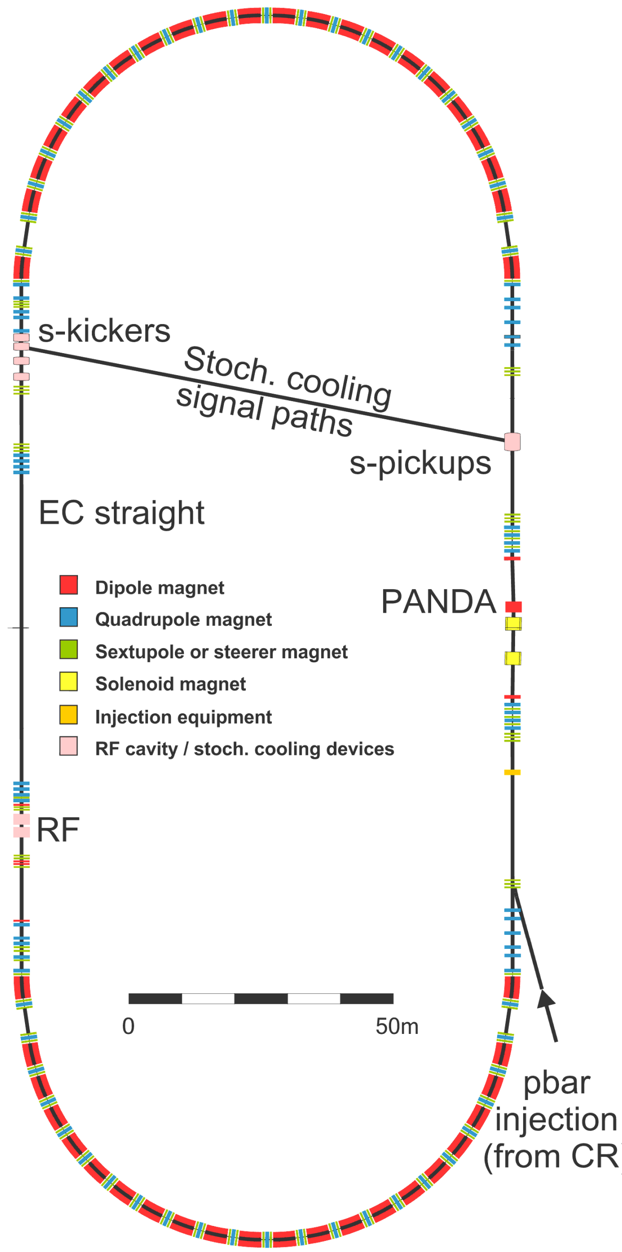

Figure 1: Schematic view of the HESR ring, the target position for PANDA is in the middle of the right straight section. Injection is placed on the bottom right, positions of stochastic cooling pickups and kickers are indicated.

Content from this work may be used under the terms of the CC BY 3.0 licence (© 2015). Any distribution of this work must maintain attribution to the author(s), title of the work, publisher, and DOI.

ISBN: 978-3-95450-168-7 doi:10.18429/JACoW-IPAC2015-THPF031

TOWARDS AN RF WIEN-FILTER FOR EDM EXPERIMENTS AT COSY

S. Mey[1,2] and R. Gebel[1] on behalf of the JEDI Collaboration

[1]Institut für Kernphysik, Forschungszentrum Jülich GmbH, 52425 Jülich, Germany
[2]III. Physikalisches Institut B, RWTH Aachen, Otto-Blumenthal-Str., Aachen, 52074, Germany

Abstract

The JEDI Collaboration (Jülich **E**lectric **D**ipole **M**oment (EDM) Investigations) is developing tools for the measurement of permanent EDMs of charged, light hadrons in storage rings. The Standard Model predicts unobservably small values for the EDM, but a non-vanishing EDM can be detected by measuring a tiny build-up of vertical polarization in a beforehand horizontally polarized beam. This technique requires a spin tune modulation by an RF Dipole without any excitation of beam oscillations.

In the course of 2014, a prototype RF ExB-Dipole has been successfully commissioned and tested. To determine the characteristics of the device, the force of a radial magnetic field is canceled out by a vertical electric one. In this configuration, the dipole fields form a *Wien*-Filter that directly rotates the particles' polarization vector. We verified that the device can be used to continuously flip the vertical polarization of a 970 MeV/c deuteron beam without exciting any coherent beam oscillations. For a first EDM Experiment, the RF ExB-Dipole in *Wien*-Filter Mode is going to be rotated by 90° around the beam axis and will be used for systematic investigations of sources for false EDM signals.

MOTIVATION

The motion of a relativistic particle's spin in an electromagnetic storage ring ($\vec{\beta}\cdot\vec{B} = \vec{\beta}\cdot\vec{E} = 0$) with non vanishing EDM contributions is given by the generalized *Thomas-BMT* Equation, $\mathrm{d}\vec{S}/\mathrm{d}t = \vec{S}\times(\vec{\Omega}_{\mathrm{MDM}} + \vec{\Omega}_{\mathrm{EDM}})$ [1,2], with

$$\begin{aligned}\vec{\Omega}_{\mathrm{MDM}} &= \frac{q}{m}\left((1+\gamma G)\vec{B} - \left(\gamma G + \frac{\gamma}{\gamma+1}\right)\vec{\beta}\times\frac{\vec{E}}{c}\right)\\ \vec{\Omega}_{\mathrm{EDM}} &= \frac{q}{m}\frac{\eta}{2}\left(\frac{\vec{E}}{c} + \vec{\beta}\times\vec{B}\right)\end{aligned} \quad (1)$$

Here, the anomalous magnetic moment G is given by the particle's **M**agnetic **D**ipole **M**oment (MDM), $\vec{\mu} = 2(G+1)\frac{q\hbar}{2m}\vec{S}$. This corresponds to $G = -0.142$ for deuterons. As an analogue, the dimensionless factor η describes the strength of the particle's permanent EDM relative to its MDM. For a Standard Model prediction of $d = \eta\frac{q\hbar}{2mc}\vec{S} \approx 10^{-32}$ ecm its value is $\eta \approx 10^{-16}$.

In a purely magnetic storage ring, all the terms containing electric fields in Eq. 1 vanish and the EDM contribution due to the interaction with the motional electric field ($\vec{\beta}\times\vec{B}$) will lead to a tiny tilt of the spin's precession axis. This leads to a very slow oscillation of the vertical polarization, but for $\eta \approx 10^{-16}$ its contribution is far below measurable. Adding an RF *Wien*-Filter with vertical magnetic field orientation to the ring's lattice yields a modulation of the horizontal spin precession by means of a phase kick without disturbing the beam dynamics. Together with the EDM's interaction with the motional electric field in the rest of the ring, the frequency modulation can lead to a continuous buildup of vertical polarization in a horizontally polarized beam [3].

SETUP OF THE PROTOTYPE

While the above described approach could provide a measurable EDM signal, it doesn't provide an observable to characterize the RF *Wien*-Filter itself. Therefore, a first prototype with a radial magnetic field ($\vec{B} = (B_x, 0, 0)^T$) compensated by a vertical electric field ($\vec{E} = (0, E_y, 0)^T$) has been commissioned. Here, the magnetic field directly manipulates the vertical beam polarization. Expressing the electric field in Eq. 1 in terms of the magnetic field leads to a simple formula for the spin precession in an ideal *Wien*-Filter [4]:

$$\vec{\Omega} = \frac{q}{m}\left((1+\gamma G)\vec{B} - \left(\gamma G + \frac{\gamma}{\gamma+1}\right)\beta^2\vec{B}\right) = \frac{1+G}{\gamma}\vec{B}. \quad (2)$$

The particles sample the localized RF fields once every turn. Their contribution may be approximated by the integrated field along the particles' path assigned to a point-like device at an orbital angle θ:

$$b(\theta) = \int \hat{B}_x\,\mathrm{d}l\,\cos(f_{\mathrm{RF}}/f_{\mathrm{rev}}\theta + \phi)\sum_{n=-\infty}^{\infty}\delta(\theta - 2\pi n). \quad (3)$$

The resonance strength $|\varepsilon_K|$ of such a device is given by the amount of spin rotation per turn and can be calculated by the *Fourier* integral over one turn in the accelerator [5,6]:

$$\begin{aligned}|\varepsilon_K| &= \frac{f_{\mathrm{spin}}}{f_{\mathrm{rev}}} = \frac{1+G}{2\pi\gamma}\oint\frac{b(\theta)}{B\rho}e^{iK\theta}\,\mathrm{d}\theta\\ &= \frac{1+G}{4\pi\gamma}\frac{\int\hat{B}_x\,\mathrm{d}l}{B\rho}\sum_n e^{\pm i\phi}\delta(n - K \mp f_{\mathrm{RF}}/f_{\mathrm{rev}}).\end{aligned} \quad (4)$$

An artificial spin resonance occurs at all side-bands with a frequency corresponding to the spin tune:

$$K \stackrel{!}{=} \gamma G = n \pm f_{\mathrm{RF}}/f_{\mathrm{rev}} \;\Leftrightarrow\; f_{\mathrm{RF}} = f_{\mathrm{rev}}|n - \gamma G|;\; n \in \mathbb{Z}. \quad (5)$$

In the scope of the current JEDI experiments, deuterons with a momentum of 970 MeV/c are stored at COSY [7]. In this case, $\gamma = 1.126$ and the resulting spin tune is $\gamma G = -0.1609$. The fundamental mode is located at $f_{\mathrm{RF}} = 121$ kHz with $n = \pm 1$ harmonics at 629 kHz and 871 kHz.

Content from this work may be used under the terms of the CC BY 3.0 licence (© 2015). Any distribution of this work must maintain attribution to the author(s), title of the work, publisher, and DOI.

ISBN: 978-3-95450-168-7 doi:10.18429/JACoW-IPAC2015-THPF032

SPIN TRACKING SIMULATIONS TOWARDS ELECTRIC DIPOLE MOMENT MEASUREMENTS AT COSY

M. Rosenthal*[1,2], A. Lehrach[1,2,3] for the JEDI collaboration
[1]Institut für Kernphysik, Forschungszentrum Jülich, 52425 Jülich, Germany
[2]III. Physikalisches Institut B, RWTH Aachen, 52056 Aachen, Germany
[3]JARA-FAME (Forces and Matter Experiments)

Abstract

A strong hint for physics beyond the Standard Model would be achieved by direct measurements of charged particles' Electric Dipole Moments (EDMs). Measurements in magnetic storage rings using a resonant spin interaction of a radiofrequency Wien filter are proposed and needs to be scrutinized. Therefore, the calculation of phase space transfer maps for time-varying fields has been implemented into an extensions for the software framework COSY INFINITY. Benchmarking with measured data and analytical estimates for rf solenoid induced spin resonances are in good agreement. The dependence of polarization oscillation damping on the solenoid frequency could be confirmed. First studies of the rf Wien filter method reveal systematic limitations: Uncorrected Gaussian distributed misalignments of the COSY lattice quadrupoles with a standard deviation of $\sigma = 0.1$ mm generate a similar buildup as an EDM $d \approx 5 \cdot 10^{-19}$ e $\cdot$ cm using this method.

INTRODUCTION

The JEDI collaboration investigates the feasibility of electric dipole moment (EDM) measurements of protons and deuterons in storage rings. Methods requiring radiofrequency fields to create an EDM related measurement signal in a magnetic storage ring like COSY [1] are proposed [2,3] . Systematic tracking studies needs to be performed to explore the limits of these methods. This requires the fast tracking of particles in radiofrequency fields in presence of an EDM. The software framework COSY INFINITY [4] is used to calculate transfer maps of the magnetic elements and perform tracking. Recent efforts extend the code by the EDM contribution and by calculation of maps for time-varying fields. Benchmarking of the new algorithms using measured data and analytical estimations is carried out. Based on the results systematic limitations of the measurement methods can be deduced.

BENCHMARKING USING AN RF SOLENOID INDUCED SPIN RESONANCE

First benchmarking is performed using calculations and measurements for an rf-B solenoid induced spin resonance at COSY. Preceding studies of this process can be found in [5]. For these studies a vector polarized deuteron beam was injected, electron cooled and accelerated up to $p = 970$ MeV/c.

* m.rosenthal@fz-juelich.de

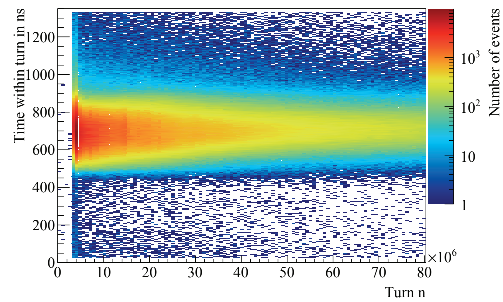

Figure 1: Event distribution within a turn vs. turn number for one measurement cycle.

The revolution time was roughly $T = 1332$ ns. After electron cooling had been turned off, a white noise electric signal was used to slowly extract the deuterons onto a carbon block target of the internal polarimeter. The scattering events were counted in four quadrants (up, down, left, right). The left-right-asymmetry is proportional to the vertical polarization. A more detailed description of the setup has been discussed in [6,7]. Figure 1 shows the event distribution during one measurement cycle. The timemarking system of the read-out electronics [6] allows to determine the event time with respect to the rf cavity period. The zero point is set to be shortly before the extraction starts. After about eleven million turns the rf-B solenoidal field was turned on:

$$B_{\text{sol}} = \hat{B}_{\text{sol}} \cos(2\pi\nu_{\text{sol}} + \phi_{\text{sol}}). \tag{1}$$

The spin tune for the particular setup is $\nu_s \approx G\gamma \approx -0.16$ [7], where G is the anomalous magnetic moment. The spin resonance condition for the solenoidal field is given by

$$\nu_{\text{sol}} = \nu_s + K, \quad K \in \mathbb{Z}. \tag{2}$$

Analytical estimations predict a vertical polarization $P_y(n)$ oscillation, which depends on the harmonic number K:

$$P_y(n) = \int_{-\infty}^{\infty} \rho(\hat{\tau}) S_y(n, \hat{\tau}) d\hat{\tau}, \tag{3}$$

$$S_y(n, \hat{\tau}) = \cos\left(\frac{\alpha_0}{2} \cdot J_0(C \cdot \hat{\tau}) \cdot n\right), \tag{4}$$

$$\alpha_0 = (1 + G)\frac{q}{p}\left(\hat{B} \cdot L\right)_{\text{sol}}, \tag{5}$$

$$C = \omega_{\text{rev}}\left(\nu_{\text{sol}} - \frac{G\gamma\beta^2}{\eta_{\text{ts}}}\right). \tag{6}$$

Here, S_y denotes the vertical spin component, $\left(\hat{B} \cdot L\right)_{\text{sol}}$ denotes the field amplitude times the length of the solenoid,

Content from this work may be used under the terms of the CC BY 3.0 licence (© 2015). Any distribution of this work must maintain attribution to the author(s), title of the work, publisher, and DOI.

ISBN: 978-3-95450-168-7 doi:10.18429/JACoW-IPAC2015-THPF033

THE FIRST OPERATION OF 56 MHz SRF CAVITY IN RHIC*

Q. Wu#, S. Belomestnykh, I. Ben-Zvi, M. Blaskiewicz, L. DeSanto, D. Goldberg, M. Harvey, T. Hayes, G. McIntyre, K. Mernick, P. Orfin, S. Seberg, F. Severino, K. Smith, R. Than, A. Zaltsman, BNL, Upton, NY 11973, USA

Abstract

A 56 MHz superconducting RF cavity has been designed, fabricated and installed in the Relativistic Heavy Ion Collider (RHIC). The cavity operates at 4.4 K with a "quiet helium source" to isolate the cavity from environmental acoustic noise. The cavity is a beam driven quarter wave resonator. It is detuned and damped during injection and acceleration cycles and is brought to operation only at store energy. For a first test operation, the cavity voltage was stabilized at 300 kV with full beam current. Within both Au + Au and asymmetrical Au + He3 collisions, luminosity improvement was detected from direct measurement, and the hourglass effect was reduced. One higher order mode (HOM) coupler was installed on the cavity. We report in this paper on our measurement of a broadband HOM spectrum excited by the Au beam.

INTRODUCTION

The RF system installed in RHIC includes two main accelerating cavities at 28.15 MHz and five storage cavities at 197.05 MHz for each ring, all operating at room temperature. The 197 MHz cavities are used to store bunches, after they have been accelerated to the top energy, for many hours. To accommodate the long ion bunches into the storage cavity bucket, which is ~50% shorter than the bunch length, rebucketing is adopted in the RHIC ramping procedure. However, longitudinal emittance increase due to nonlinearity and hardware complications during rebucketing will result in a 30% loss in the particles. A 56.3 MHz superconducting RF (SRF) cryomodule was installed near the interaction point (IP) 4 in RHIC, Figure 1, during the first quarter of 2014, to provide sufficient RF acceptance to long bunches [1].

To save cost on cryogenic system, the cavity location is in the common section of RHIC, and it is shared by ion bunches from both rings. The two colliding beams are synchronized at each IP. Therefore to achieve identical longitudinal beam dynamic effect, the cavity is installed at 1.25λ (6.66 m) away from IP 4.

CAVITY

The 56 MHz SRF cavity is a quarter-wave resonator with beam passing through its symmetrical axis, as shown in Figure 2. The cavity is designed to provide 2 MV at the 8.5 cm single gap, and the operation temperature is 4.4 K. Detailed cavity parameters can be found in Ref. [2].

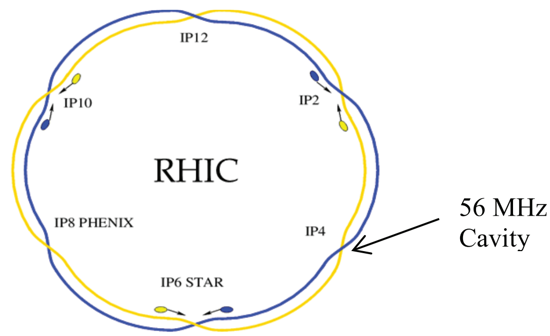

Figure 1: Location of the 56 MHz cavity in RHIC.

Mechanical tuning is achieved by pushing or pulling the end plate of the cavity that is close to the gap, as labeled in Figure 2 [3]. The tuning capability of this mechanism is 46.5 kHz, which is 60% of the revolution frequency of RHIC beam.

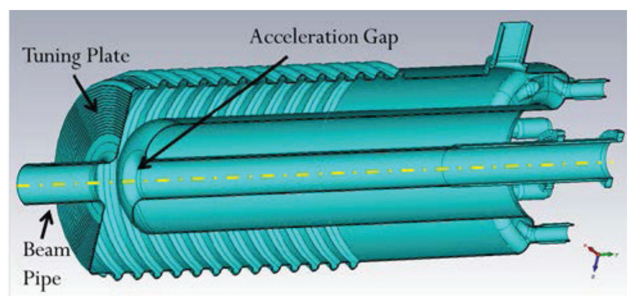

Figure 2: Crossection view of the 56 MHz SRF cavity.

Thirteen corrugations are added to the outer wall of the cavity to supress multipacting [4]. During the conditioning of the cavity, multipacting was encountered at 90 – 140 kV gap voltage, and was easily conditioned through after 30 minutes. During operation with beam, the cavity never encountered any multipacting issues.

Couplers

Since the cavity does not have sufficient tuning range to follow the large revolution frequency change during acceleration, it must be turned off during the energy ramp. In addition to full frequency detune from the tuning plate, a fundamental mode damper (FMD) is inserted into the cavity from a rectangular port. The port is opened perpendicular to the beam axis on the outer wall of the cavity, as shown in Figure 3. More information on the FMD can be found in Ref. [5].

*Work supported by by Brookhaven Science Associates, LLC under Contract No. DE-AC02-98CH10886 with the U.S. Department of Energy
#qiowu@bnl.gov

Content from this work may be used under the terms of the CC BY 3.0 licence (© 2015). Any distribution of this work must maintain attribution to the author(s), title of the work, publisher, and DOI.

ISBN: 978-3-95450-168-7 doi:10.18429/JACoW-IPAC2015-THPF034

INJECTION KICKER FOR HESR AT FAIR USING SEMI-CONDUCTOR SWITCHES*

R. Tölle†, N. Bongers, F. M. Esser, R. Gebel, S. Hamzic, H. Jagdfeld, F. Klehr, B. Laatsch, L. Reifferscheidt, M. Retzlaff, L. Semke, H. Soltner, H. Stockhorst, FZ Jülich, Jülich, Germany
S. Antoine, W. Beeckman, P. Bocher, O. Cosson, P. Jivkov, D. Ramauge, SigmaPhi, Vannes, France

Abstract

The High Energy Storage Ring for Antiprotons (HESR) is going to be built at FAIR in Darmstadt on the extended GSI campus. It will receive the antiprotons via the Collector Ring (CR). Using a barrier bucket, the circulating particles will be compressed into one half of the circumference. New particles have to be injected into the remaining half. Thus rise and fall time must not exceed 220 ns each with a flat top of 500 ns. A kick angle of 6.4 mrad is required at 13 Tm magnetic rigidity. The system must allow pole reversal for injection of positively charged particles. With a voltage lower than 40 kV a semi-conductor based pulser is going to be realized. Boundary conditions and the status of preparatory work are described. Simulation results and available measurements are presented.

INTRODUCTION

The HESR is a synchrotron and storage ring which is being built for FAIR on the GSI campus in Darmstadt in Germany. The Institute of Nuclear Physics 4 at Forschungszentrum Jülich (FZJ) has the overall responsibility for the complete HESR and will install it at the FAIR site when the buildings are ready. HESR will allow handling particles whose magnetic rigidity is in the range of 5 – 50 Tm. For protons or antiprotons this corresponds to momenta (energies) between 1.5 and 15 GeV/c (0.87 and 14.8 GeV), and for bare Uranium this corresponds to 579-5797 MeV/u/c. Injection is designed to operate at 3 GeV which is the production energy of antiprotons (12.76 Tm) to be injected via the collector ring CR which is needed for initial cooling. The injection equipment will be able to inject particles carrying positive or negative charge. For antiprotons each injected bunch might contain up to 10^8 particles, for heavy ions the intensity will be less.

INJECTION PROCESS

As the accumulator ring RESR will be postponed by several years, the proposed way of antiproton beam accumulation for the HESR is to use the already designed stochastic cooling system and the barrier bucket (BB) cavity of the HESR. The BB cavity of the HESR is used to separate the circumference of the HESR ring into two equal regions, one reserved for the injected beam and the other one for the accumulated beam. A beam bunch of 10^8 antiprotons delivered by the CR is kick-injected every 10 seconds into the central part of the two full wave barrier pulses (Fig. 1). The injection kicker rise time is 220 ns and the flat top time is 500 ns (Fig. 1). Just after beam injection the barrier voltages are switched off and the beam becomes coasting with a revolution period of 2 μs. Fast filter stochastic cooling is continuously applied during the whole accumulation process to avoid beam dilution due to Schottky noise diffusion. In the well cooled coasting beam again two full-wave barrier voltages are excited adiabatically and the right hand voltage moves to the injection position within the period of 0.5 sec. A new particle free gap with 1 μs duration for the injection of the next bunch is available. This procedure is repeated 100 times (1000 s) until 10^{10} antiprotons are accumulated. The beam accumulation and cooling processes have been studied in detail in [1, 2] and the corresponding proof of principle experiment has been successfully carried out at the GSI [3].

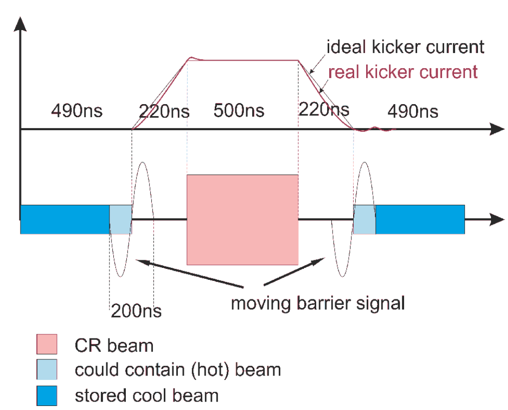

Figure 1: Injection timing of HESR.

SYSTEM DESIGN AND PARAMETERS

Preparatory studies at FZJ were carried out to specify mechanical properties, magnet properties and pulser properties. System design and the vacuum system are covered by FZJ, whereas the subsystems magnet and pulser are in the responsibility of the contractor. Requirements to build the coil (one single winding) with two horizontal slits on each side of the magnet and to make provisions to later install an eddy current strip (copper) into the slit in the bottom yoke have been accepted by the contractor (reduction of longitudinal impedance) [4]. The strip can be installed provided that in-vacuum dielectric tests are convincing.

The injection kicker system will have to deflect the incoming beam by 6.4 mrad using 4 individual 36 cm long

* Work supported by the Federal Government of Germany, Grant FAIR1118H
† r.toelle@fz-juelich.de

Content from this work may be used under the terms of the CC BY 3.0 licence (© 2015). Any distribution of this work must maintain attribution to the author(s), title of the work, publisher, and DOI.

ISBN: 978-3-95450-168-7 doi:10.18429/JACoW-IPAC2015-THPF035

STRIPPING OF HIGH INTENSITY HEAVY-ION BEAMS IN A PULSED GAS STRIPPER DEVICE AT 1.4 MeV/u

P. Scharrer[1,2,3], W. Barth[1,2], M. Bevcic[2], Ch. E. Düllmann[1,2,3], L. Groening[2], K. P. Horn[2], E. Jäger[2], J. Khuyagbaatar[1,2], J. Krier[2], A. Yakushev[2]
[1]Helmholtz Institute Mainz, Mainz, Germany
[2]GSI Helmholtzzentrum für Schwerionenforschung, Darmstadt, Germany
[3]Johannes Gutenberg-University, Mainz, Germany

Abstract

As part of an injector system for FAIR, the GSI UNILAC has to meet high demands in terms of beam brilliance at a low duty factor. To accomplish this goal an extensive upgrade program has started.

To increase the beam intensity behind the UNILAC, it is aimed to increase the efficiency of the 1.4 MeV/u gas stripper. A modification of the stripper setup was developed to replace the N_2-jet with a pulsed gas injection, synchronized with the transit of the beam pulse. The pulsed gas injection lowers the gas load for the differential pumping system, rendering possible the use of other promising gas targets.

In recent measurements the performance of the modified setup was tested using an ^{238}U-beam with various stripper media, including H_2, He, and N_2. The data provide a systematic basis for an improved understanding of slow heavy ions passing through gaseous media. The stripping performance of the current N_2-jet was excelled by using H_2 at increased gas densities, enabled by the new pulsed gas cell.

INTRODUCTION

The GSI UNIversal LInear ACcelerator (UNILAC) will serve as part of an injector system for the future Facility for Antiproton and Ion Research (FAIR), currently under construction at GSI in Darmstadt, Germany. Therefore it has to meet high demands in terms of beam brilliance at a very low duty cycle (100 µs beam pulse length, 2.7 Hz repetition rate) [1]. To achieve this goal, an extensive upgrade program of the UNILAC has been started [2].

After acceleration in the UNILAC High Current Injector the ion beams are passing a gas stripper section at 1.4 MeV/u. The ions are stripped of electrons and the charge state of the ion beam is increased. After stripping, a charge state distribution results, and charge separation is accomplished by a system of dipole magnets; thus, only ions with the desired charge state are selected for further acceleration. The current gas stripper uses a laval nozzle at a back-pressure of 0.4 MPa to apply a super-sonic N_2-jet [3].

A key projectile for FAIR is ^{238}U [1]. In the gas stripper, the charge state of the U-ions is increased from 4^+, with 28^+ being needed for further acceleration. Measurements with the N_2-jet show equilibrated charge state distributions for U on N_2 with an average charge state between 26^+ and 27^+ [4]. To increase the stripping efficiency into the desired charge state (28^+), the use of other stripper gases is explored. To use other promising stripper gases at sufficient gas density, the back-pressure on the gas inlet has to be increased. The limitations of the differential pumping system connecting the stripper to the accelerator hinder this approach using the laval nozzle [5].

For working with increased gas density with the current pumping setup, the laval nozzle was exchanged by a pulsed valve, which is the basis for a pulsed gas cell. The valve opens only when a beam pulse passes the gas stripper and closes immediately afterwards. Given the low beam duty cycle, this enables the use of much higher back-pressures on the gas inlet, which is assumed to lead to higher gas densities in the interaction zone. With this modified setup, the use of other stripper gases at sufficient gas densities appears possible.

The new modified setup was first tested early in 2014 with a Bi-beam using N_2 as a stripper gas [6]. Recently, another measurement series was conducted using an U-beam on H_2, He and N_2 and a yet improved setup.

EXPERIMENTAL SETUP

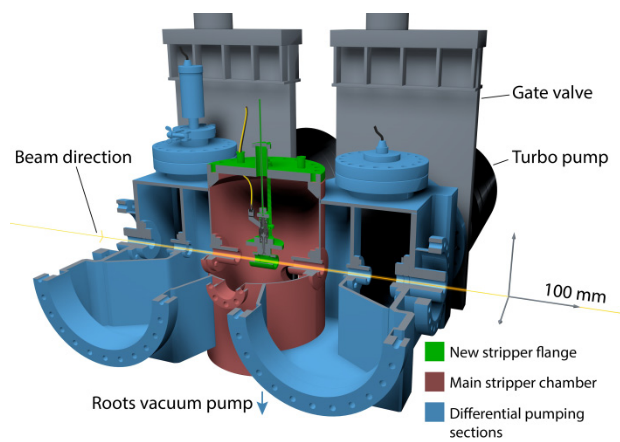

Figure 1: 3D model of the GSI UNILAC gas stripper.

The experimental setup that was used for these measurements is a modified version of the setup described in [6]. The basic parts of the GSI UNILAC gas stripper are depicted in Fig. 1. A four stage differential pumping system is used to achieve the required vacuum in the adjacent accelerator line. The major gas load is removed by a roots vacuum pump (2222 l/s) located directly below the main stripper chamber. The adjacent

Content from this work may be used under the terms of the CC BY 3.0 licence (© 2015). Any distribution of this work must maintain attribution to the author(s), title of the work, publisher, and DOI.

ISBN: 978-3-95450-168-7 doi:10.18429/JACoW-IPAC2015-THPF036

Content from this work may be used under the terms of the CC BY 3.0 licence (© 2015). Any distribution of this work must maintain attribution to the author(s), title of the work, publisher, and DOI.

A COMPACT CYCLOTRON FOR 35 MeV PROTONS AND 8 AMeV OF H_2^+

A. Calanna[1], T. Boiesan[2], L. Calabretta[1],
L. AC Piazza[2], R. Johnson[2], V. Sabaiduc[2]
[1] INFN-LNS, Catania, Italy
[2] BCSI, Vancouver, Canada

Abstract

The design characteristics and parameters of a compact cyclotron able to accelerate H^- ions up to an energy of 35 MeV and H_2^+ ions up to an energy of 8 AMeV are presented. This cyclotron is a 4-sector machine and its special feature is the possibility to modify the profiles of the sector hills to allow for the acceleration of the two different species. When equipped with two RF cavities and operated in harmonic mode 4, it accelerates the H- beam, which is extracted by stripping. The resulting proton beam is used for the commercial goal of radioisotope production. On the other hand, when equipped with four RF cavities, also operated in harmonic mode 4, it accelerates a high intensity H_2^+ beam that is of interest for the IsoDAR* experiment. Here, the presented cyclotron takes on the role of a prototype for the central region design of the final IsoDAR* cyclotron (60 A MeV H_2^+). By increasing the number of cavities, the energy gain per turn as well as the vertical focusing along the first orbit are increased, thereby optimizing the acceptance. Moreover, to minimize space-charge effects, the injection energy of H_2^+ is raised to 70 keV compared to the H- injection energy of 40 keV.

INTRODUCTION

A Memorandum of Understanding established a partnership between Best Theratronics Ltd. and LNS-INFN to develop a new high-power machine for proton and H_2^+. The study of this machine is based on the design of the central part of a bigger cyclotron studied for the DAEδALUS and IsoDAR experiments, respectively investigating the CP-violation and the existence of sterile neutrinos [1,2,3].

The primary goal of the project is the production of 1 mA proton beam at 35 MeV with cyclotron. The cyclotron here described and labelled B35P, accelerates H^- ions, which are extracted by stripping to deliver the proton beam. An additional feature of the cyclotron presented is the capability to accelerate ions with q/A=0.5 (H_2^+ hydrogen ionized molecule, deuteron and He^{++}) up to the maximum energy of 8 AMeV.

This feature is worth investigating, especially because one of the goals of the agreement is to check experimentally the acceleration of H_2^+ beams with currents up to 5mA. This feature is also of interest of Best Theratronics Ltd. because fine adjustments of the cyclotron central field and/or of the pole shims, allows the acceleration of He^{++} beams up to a maximum energy of 32 MeV (8 MeV/amu) and or deuteron beams up to 16 MeV.

The present magnetic circuit of the cyclotron is an evolution of the previous design presented at the Cyclotrons2014 [3]. The main differences are:

- the hill gap has been reduced to 5.4 cm from 6 cm;
- the maximum energy of H^- that has been increased from 28 MeV to 35 MeV;
- The iron size that was increased too;
- the coil sizes and the current to feed them have been optimized to reduce significantly the power consumption, which now is 7 kW;
- The stray field was significantly reduced to less than 20 Gauss on the cyclotron axis at a distance of 1.5 m from median plane, that is the position where the H^- source will be installed.

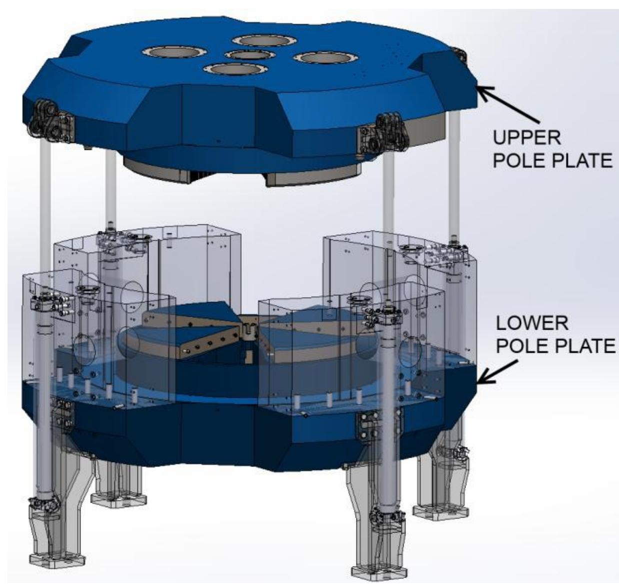

Figure 1: B35P layout.

These advantages have been achieved reducing the valley gap of the cyclotron from the previous value of 1400 mm to the present value of 1000 mm. The main change in respect to the September 2013 design is that the cyclotron here discussed is not a true dual machine for proton and H_2^+. That means, it is mandatory to open the cyclotron to switch from the proton operation mode to the H_2^+ mode.

[1] Present address: LNS-INFN, Catania, Italy

ISBN: 978-3-95450-168-7 doi:10.18429/JACoW-IPAC2015-THPF037

UPGRADE OF THE LNS SUPERCONDUCTING CYCLOTRON

A. Calanna, L. Calabretta, D. Rifuggiato, G. Cuttone, G. D'Agostino, INFN-LNS, Catania, Italy
M. Maggiore, INFN-LNL, Legnaro, Italy
A. Radovinsky, PSFC T&ED MIT, Cambridge, MA 02139, USA

Abstract

The INFN-LNS Superconducting Cyclotron (CS) has been working for about 20 years delivering ion beams from protons to gold in the wide energy range from 10 A MeV to 80 A MeV. The beam extraction is presently accomplished by means of two electrostatic deflectors and a set of magnetic channels. Recently, the experiment NUMEN [1, 2] has been highly recommended by the scientific community. The requirements on target are light ion beams (A<30 amu), within an energy range of 15-60 A MeV and a beam power of 5-10 kW, which means to increase the extracted power by a factor 10-100. To achieve this goal we have studied extraction by stripping using the existing extraction channel with an increased transversal section. In addition, a new extraction channel has been designed to broaden as much as possible the range of the extracted ions and energies. To allow the realization of these new channels, a new superconducting magnet is needed including a new cryostat. The major changes and the expected performances for the upgraded cyclotron, as well as the state-of-art of the design, are presented.

INTRODUCTION

The goal of this feasibility study is to investigate extraction by stripping in the Superconducting Cyclotron (CS) to achieve beam power intensity in the range 5-10 kW for light ions with A<30. Even if the NUMEN experiment, which proposes to measure the element of nuclear matrix using double charge exchange reactions [1, 2], is the main reason to increase the beam power, many other experiments currently accomplished at LNS will take advantage from this upgrade. These experiments make use of radioactive ions beam produced with in-flight technique at FRIBS@LNS [3]. Production of radioisotopes of medical interest can be considered too.

Presently, the vertical gap along the CS extraction channel is only +/- 12 mm, while the radial allowed beam dimension does not exceed +/- 5 mm. These mechanical constraints are not enough to plan an extraction of 5-10 kW of beam power. Moreover, a cold channel will be mandatory. For these reasons, we have to replace the whole cryostat. We have investigated the benefits of an increased cross-dimension of the existing channel as well as the feasibility of a complete new channel.

However, the CS peculiarity is its versatility, which has to be maintained since there is a consistent demand of beam types in a wide mass and energy range. For this reason, we plan to equip the CS with both extraction modes: extraction by stripping and extraction by electrostatic deflectors.

In this paper, we describe the approach and codes we used and we show few results that demonstrate we are ready to move towards the technical design. We have already committed to the Plasma Science and Fusion Centre of MIT a study on the feasibility of a new cryostat, which includes the new extraction channel. Some extract of the report they provided on the viability and costs have been reported too.

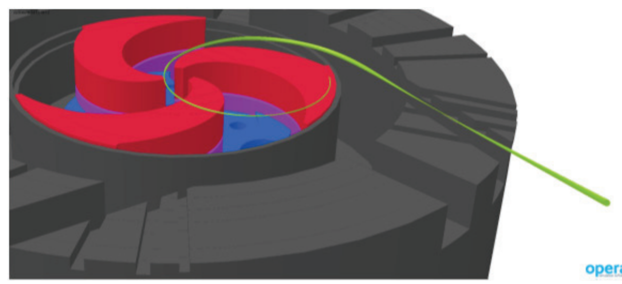

Figure 1: example of extraction trajectory of 12C at 45 AMeV achieved using the code OPERA.

TECHNICAL APPROCH

The main tools we used for this study of feasibility originate from two codes, GENSPE and ESTRAZ, developed at MSU by Gordon [4]. We updated them to suit and solve our needs. All the results have been validated and visualise through a FEM software, OPERA 3D.

Since this study is about an upgrade of an existing machine, measured magnetic maps are available. For this reason, we decided for an approach different from the usual. We created the magnetic model computing the components of the magnetic field outside the median plan solving the Maxwell equations. This 3D map can be visualised and analysed in the Post Processor module of OPERA 3D to track the particles both along the closed orbits and the extraction orbits.

Specifically, our procedure for each ion is now described.

At first, we identify the beam dynamics parameters along the closed orbits using GENSPE. Its input parameters are the magnetic map on the median plane, ion type, RF parameters, beam normalized emittance out of the inflector, which has been chosen to 1 π mm.mrad, about 2.5 larger than the value of the source emittance. The outputs of GENSPE give details on each closed orbit with a given step of energy. That means information on the radius, the radial component of the momentum, the isochronism, the phase slip and the axial and radial betatron oscillations.

Content from this work may be used under the terms of the CC BY 3.0 licence (© 2015). Any distribution of this work must maintain attribution to the author(s), title of the work, publisher, and DOI.

ISBN: 978-3-95450-168-7 doi:10.18429/JACoW-IPAC2015-THPF038

Content from this work may be used under the terms of the CC BY 3.0 licence (© 2015). Any distribution of this work must maintain attribution to the author(s), title of the work, publisher, and DOI.

RIB TRANSPORT AND SELECTION FOR THE SPES PROJECT

M. Comunian, A. Pisent, L. Bellan, INFN-LNL, Legnaro, Italy
A. D. Russo, INFN-LNS, Catania, Italy

Abstract

At LNL INFN is under construction a Rare Isotope Facility (SPES) based on a 35-70 MeV proton cyclotron, able to deliver two beams with a total current up to 0.5 mA, an ISOL fission target station and an existing ALPI superconducting accelerator as a post accelerator (up to 10 MeV/u for A/q=7). In this paper, some highlights are presented: the high resolution mass separator, the 5 MHz buncher performances and the voltage profile errors of the CW RFQ (80 MHz, 727 keV/u, internal bunching). The problems that have been solved during the design phase are partly common to all RIB facilities, like the necessity to have an high selectivity and high transmission for a beam of a very low intensity, plus the specific challenges related to the use of ALPI (with a reduced longitudinal acceptance) and related to the specific lay out. At present the design phase has been finalised, and the procurement procedure for the charge breeder, the transfer lines and the RFQ are in an advanced state.

INTRODUCTION

SPES, acronym of Selective Production of Exotic Species, is a CW radioactive ion beam facility under construction at LNL INFN in Italy. It will produce and accelerate neutron-rich radioactive ions, in order to perform nuclear physics experiments, which will require beams above Coulomb barrier.

The main functional steps of the facility are shown in Fig. 1: the primary beam delivered by the cyclotron, the beam from the fission target (as an example, up to 10^{10} particle/s of ^{132}Sn), the beam cooler, the separators, the charge breeder and the accelerator, the existing ALPI with a new RFQ injector. The use of the continuous beam from the +1 source, which can be of LIS, PIS, SIS type, maximizes the RNB efficiency but need a CW post accelerator (RFQ and ALPI); the charge breeder is chosen to be an ECR that woks in continuous. The energy on the transfer lines are determined by the chosen RFQ input energy (wRFQ=5.7 keV/u); for this reason, all the devices where the beam is approximately stopped (production target, charge breeder and RFQ cooler) lay at a voltage:

$$eV = (A/q)w_{rfq} \quad (1)$$

The charge state range (3.5<A/q<7) is bounded by the RFQ field level for the upper limit and by the minimum voltage on q=1 transport line. A full facility layout is shown on Fig. 2.

The beam preparation scheme satisfies various requirements:

- the zone with worst radiation protection issues is reduced by the first isobar selection (resolution R=1/200).
- after that an RFQ cooler reduces the beam energy spread and transverse emittance both for the isobar separation and to cope with the charge breeder acceptance (about 5 eV and 2 mm mrad rms normalized emittance).
- HRMS and MRMS (high and medium resolution mass separators, R=1/20000 and R=1/1000 respectively) are used to select the RNB (with good transmission) and to suppress the contaminants from the charge breeder source.
- both the HRMS and the MRMS are installed on a negative voltage platform, to decrease the beam geometrical emittance and the relative energy spread.
- the 7 m long RFQ is designed with an internal bunching and relatively high output energy; this easies the setting and allows 90% transmission into ALPI longitudinal acceptance.
- an external 5 MHz buncher placed 9 m before the RFQ will provide order of 100 ns beam length for specific experiments.
- the dispersion function is carefully managed in the various transport lines; where possible the transport is achromatic, otherwise the dispersion is kept low (in particular at RFQ input D=0).

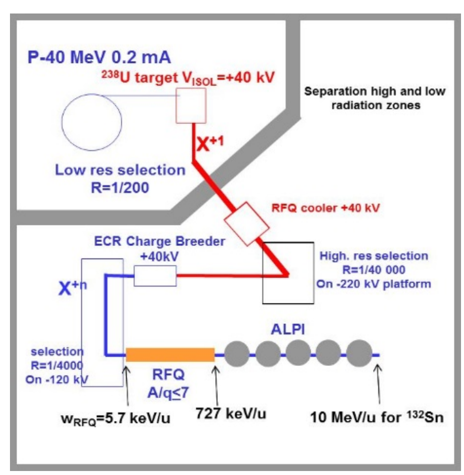

Figure 1: Functional scheme of the SPES facility. There are two main areas: the 1+ line and the n+ line, where 1+ and n+ indicates the beam charge state.

ISBN: 978-3-95450-168-7 doi:10.18429/JACoW-IPAC2015-THPF039

STABILITY STUDIES FOR J-PARC LINAC UPGRADE TO 50mA/400MeV

Y. Liu, T. Maruta, K. Futatsukawa, T. Miyao KEK/J-PARC, Ibaraki-ken, Japan
M. Ikegami, FRIB, East Lansing, USA
A. Miura, JAEA/J-PARC, Tokai-mura, Japan

Abstract

J-PARC linac applies the Equi-partitioning (EP) setting as the base-line design. And it is the first machine to adopt this approach at the design stage. EP condition is a natural solution for avoiding emittance exchange between transverse and longitudinal planes. At J-PARC linac it is also possible to explore off-EP settings. One of the motivations could be a lattice with relaxed envelope for mitigating the intra-beam stripping (IBSt) effects in high current H- beam. During and after the energy upgrade in Jan., 2014 and beam current upgrade in Oct., 2014, experiments were carried out to study the stability and emittance evolution for the EP and off-EP settings with high current H- beam at J-PARC linac for better choices of lattice and better understanding.

INTRODUCTION

The Japan Proton Accelerator Research Complex (J-PARC) is a high-intensity proton accelerator facility, which consists of a linac, a 3 GeV rapid cycling synchrotron (RCS), and a main ring synchrotron (MR).

The J-PARC linac consists of a 3 MeV RFQ, 50 MeV DTL (Drift Tube Linac), 181/190 MeV SDTL (Separate-type DTL) and 400 MeV ACS (Annular-ring Coupled Structure), as shown in Fig.1.

In Jan. 2014 the J-PARC linac energy was upgraded from 181 MeV to 400 MeV while the peak beam current was increased to 50 mA in Oct. 2014. These upgrades allowed the RCS to provide 1 MW equivalent beam powers, a major milestone in the development of J-PARC.

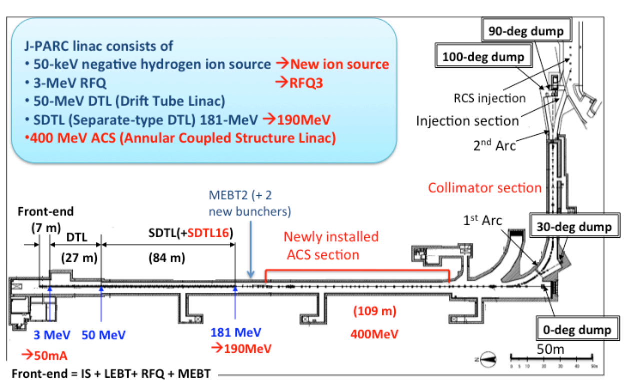

Figure 1: Layout of J-PARC linac.

During the design stage of J-PARC, there was sufficient evidence that an equi-partitioned (EP) lattice offers a natural solution for emittance conservation in high-intensity hadron accelerators, owing to pioneering work by R. A. Jameson, M. Reiser, I. Hofmann [1], and et al. J-PARC linac RF tank were arranged with consideration of a baseline design satisfying EP condition. It also has the flexibility for a wide range of off-EP operating points, offering the opportunities not only for investigating the basic physics principles but also for further optimizations of the machine operation.

As shown in Fig. 2, within the hardware capability, it is possible to set the DTL, the SDTL and the ACS in a wide range of Tx/Tz. Normally Tx=Ty is kept. Tx, Ty, Tz stand for the horizontal, vertical and longitudinal "temperature".

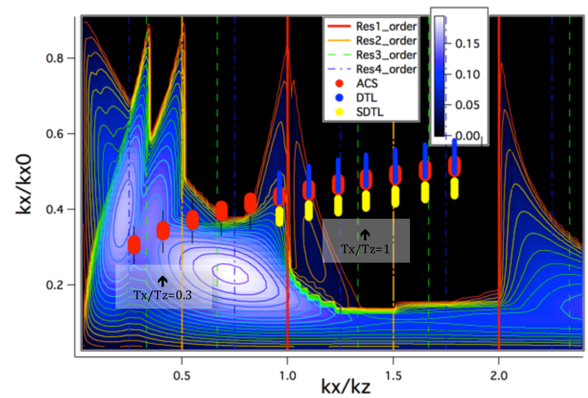

Figure 2: Tune-settings for J-PARC linac in Hofmann stability chart, at 50mA, with $\varepsilon_x / \varepsilon_z = 0.7$.

Tx/Tz is the ratio of oscillation energies in transverse and longitudinal plane, which is defined as,

$$\frac{T_x}{T_z} \equiv \frac{r_x^2 k_x^2}{r_z^2 k_z^2} = \frac{\epsilon_x k_x}{\epsilon_z k_z}. \qquad (1)$$

Here r stands for the beam rms envelop, ε the rms emittance, focusing is represented by the wave number k (with current) and k_0 (0-current). For instance settings to the left in Fig. 2 indicate less transverse focusing or more longitudinal focusing and vice versa. The EP condition generates largest stable area.

COMPLETION OF UPGRADES AND REMAINING QUESTIONS

Both energy [2] and beam current [3] upgrades were accomplished within the planned schedules with satisfying levels of beam loss and extinction rate. From 2015, J-PARC started ramping up of the RCS operation output power from 300 kW, in steps of 100 kW, towards the goal of 1MW in early 2016.

However, questions and difficulties remain. For example, the longitudinal measurement at MEBT2 was missing during the energy upgrade due to bunch shape monitor (BSM) vacuum problems. This measurement is

Content from this work may be used under the terms of the CC BY 3.0 licence (© 2015). Any distribution of this work must maintain attribution to the author(s), title of the work, publisher, and DOI.

6th International Particle Accelerator Conference IPAC2015, Richmond, VA, USA JACoW Publishing
ISBN: 978-3-95450-168-7 doi:10.18429/JACoW-IPAC2015-THPF040

RECENT PROGRESS OF THE BEAM COMMISSIONING IN J-PARC LINAC

T. Maruta*, Y. Liu, K. Futatsukawa, T. Miyao, KEK, Tsukuba, Japan
M. Ikegami, FRIB, East Lansing, MI, USA
A. Miura, JAEA, Tokai-mura, Japan

Abstract

The injector linac of Japan Proton Accelerator Research Complex (J-PARC) is recently conducted a front-end upgrade to increase the feasible peak current to 50 mA. Together with the beam energy upgrade in year 2013, we are ready for challenge into design beam power of 1 MW operation at the 3 GeV Rapid Cycling Synchrotron (RCS). The 1st commissioning after the upgrade began at September 29th, and then we successfully realized 50 mA beam acceleration on October 15th. In this paper, recent progress of linac beam commissioning, especially for after the front-end upgrade is described.

INTRODUCTION

J-PARC is a MW-class multi purpose proton accelerator facility in Japan. The accelerator is comprised from a 400 MeV linac, a 3 GeV RCS and a 50 GeV main ring (MR). The MR is currently operating at 30 GeV. The linac consists of 50 keV negative hydrogen (H^-) ion source (IS), a 3 MeV Radio Frequency Quadruple (RFQ), a 50 MeV Drift Tube Linac (DTL), an 191 MeV Separate-type DTL (SDTL) and a 400 MeV Annular-ring Coupled Structure (ACS) linac as shown in Fig.1 [1]. There are three beam transport sections; MEBT1 is between RFQ and DTL, MEBT2 is in SDTL and ACS and L3BT is from ACS to 3 GeV RCS, respectively. The RF frequency is 324 MHz in RFQ, DTL and SDTL, and ACS is threefold frequency of 972 MHz.

Outline of the Linac Upgrade

In the linac, a beam power upgrade project had been conducted in year 2013 - 2014 to achieve the design beam power of 1 MW at the RCS extraction. Before this upgrade, the beam energy and the peak current were 181 MeV and 30 mA, respectively. The upgrade is divided in two periods. The 1st period is a beam energy upgrade from 181 MeV to 400 MeV by introducing ACS after the existing linac. The aim of this upgrade is the alleviation of the Laslett incoherent tune shift at RCS. Since the shift amount is inversely proportional to $\beta^2\gamma^3$ (β, γ : Lorentz factor), This energy extension reduces the shift amount to be < 1/3, and it is settled in an acceptable range even in 50 mA.

In the 2nd period of the intensity upgrade, the IS is replaced to an RF-driven type and RFQ (RFQ III) is also replaced to new one which is designed for 50 mA. To handle the higher beam power from the RFQ III, we also upgraded the RF chopper system placed in MEBT1; introduction of a tandem scraper configuration and new chopper cavity.

* tmaruta@post.j-parc.jp

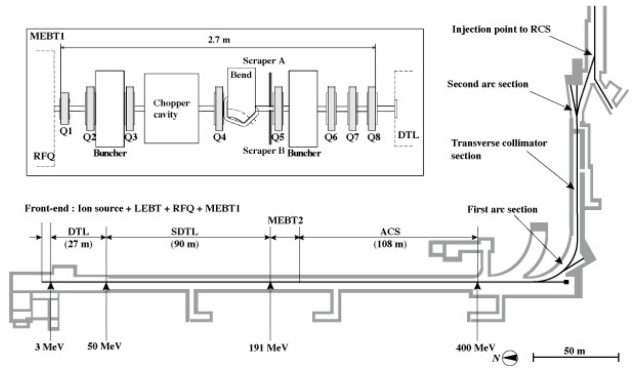

Figure 1: Outline of the J-PARC linac. The top-left Figure is the detail of MEBT1 between RFQ and DTL.

PROGRESS OF THE COMMISSIONING

The linac beam commissioning after the intensity upgrade began at September 29th, and continues till October 14th. There are main purposes; establishment of 400 MeV accelerator, a 50 mA tuning for a high power test and a 30 mA tuning for an user operation. We successfully accelerate a 50 mA beam at October 14th. In this section, the progress of the linac beam commissioning after the front-end upgrade is discussed.

MEBT1 Matching

It is needless to say that the replacement of the front-end results a variation of the beam distribution at RFQ exit, and this variation must be absorbed in MEBT1. Moreover, MEBT1 is the most severe matching section from the point of view of space-charge force due to its low energy. Therefore, an accurate matching is required for a beam halo mitigation. We firstly measured a transverse beam profile in MEBT1 by Q-scan. Then, the MEBT1 optics was determined from this measurement and simulated longitudinal profile at the RFQ III by PARMTEQM [2]. After setting a new lattice, we conducted a DTL acceptance scan [3] to check the consistency for longitudinal profile. We also measured a transverse beam profile at the SDTL entrance, because the beam profile at this region strongly depends on the accuracy of the MEBT1 matching.

The Q-scan is conducted by Q3 and the wire scanner monitor (WSM) between the RF chopper cavity and Q4 which is 0.62 m downstream from Q3. Since we turn off the chopper RF while a measurement, the lattice between them is quadrupole + drift. In the thin lens approximation, the square of beam size at the WSM (σ^2_{WSM}) is a 2nd order polynomial function described from the Twiss parameter at

Content from this work may be used under the terms of the CC BY 3.0 licence (© 2015). Any distribution of this work must maintain attribution to the author(s), title of the work, publisher, and DOI.

ISBN: 978-3-95450-168-7 doi:10.18429/JACoW-IPAC2015-THPF042

Content from this work may be used under the terms of the CC BY 3.0 licence (© 2015). Any distribution of this work must maintain attribution to the author(s), title of the work, publisher, and DOI.

RECTILINEAR COOLING SCHEME FOR BRIGHT MUON SOURCES*

Diktys Stratakis#, Brookhaven National Laboratory, Upton NY, USA

Abstract

A fast cooling technique is described that simultaneously reduces all six phase-space dimensions of a charged particle beam. In this process, cooling is accomplished by reducing the beam momentum through ionization energy loss in absorbers and replenishing the momentum loss only in the longitudinal direction rf cavities. In this work we review its main features and describe the main results.

INTRODUCTION

The initial muon beam occupies a relatively large phase-space volume which must be compressed by several orders of magnitude to obtain high-luminosity collisions. Furthermore, this phase-space reduction must be done within a time that is not long compared to the muon lifetime (2 μs in rest frame). Ionization cooling is currently the only feasible option for cooling a muon beam [1]. This technique is not very practical for protons, which would have frequent nuclear interactions, or electrons, which would have bremsstrahlung, but is practical for muons, and cooling rates compatible with muon lifetimes are possible. The main goal of this paper is to develop a potential baseline cooling lattice for a muon related applications and evaluate its performance. We also discuss a possible variant of this channel.

LATTICE DESIGN

Three different geometries for ionization cooling towards micron-scale emittances as required for a muon collider have been previously considered: (a) A ring, (b) a helix commonly known as a Guggenheim helix, and (c) a rectilinear channel. The common feature for all cases was that the solenoids were slightly tilted to generate upward dipole fields. In the third case, essentially the same cells from a ring or a Guggenheim, including their coil tilts and resulting upward dipole fields, are laid out in straight (rectilinear) geometry. The solenoid focusing is so strong, compared with the dipole deflections, that the closed orbits are merely displaced laterally, but continue down the now straight lattice. This rectilinear scheme was proposed for the first time by Balbekov [2] and is represented in Fig. 1. Despite its much simpler geometry, it was found [3] that its cooling performance was essentially the same as with rings or a helix. As a result, the rectilinear scheme will be considered our new baseline cooling lattice.

Figure 1(a) shows a cross section of a cell of the cooling rearly stage. The rf is at 325 MHz operating at 19 MV/m and a phase of approximately 41 degrees. The cell contains two coils of opposite polarity, yielding an approximate sinusoidal variation of the magnetic field in the channel with a peak on-axis value of 2.6 T. The coils are tilted in opposite directions by 0.9 degrees. Figure 1(b) shows a cell of a late cooling stage that is required to cool the beam transversely to ≤0.3 mm. The cell consists of six solenoids which surround four 650 MHz cavities in the cell center. As before, the geometry of the lattice is such that the absorber is located at beta minima (blue dashed curve).

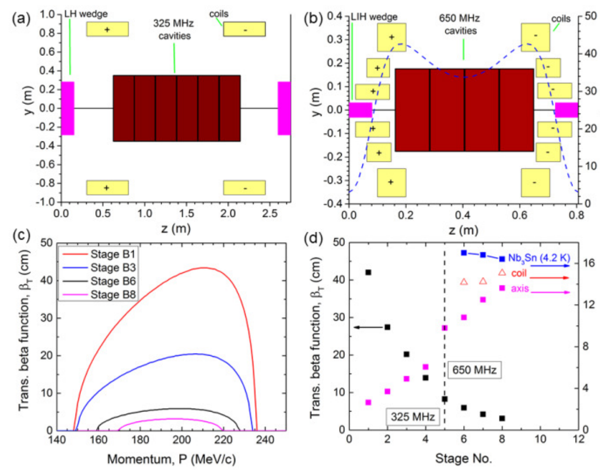

Figure 1: Lattice characteristics of the proposed rectilinear 6D cooling channel: (a) Early stage, (b) last cooling stage, (c) beta function for different stages, and (d) beta and maximum axial field per stage as well as allowable field limit for Nb_3Sn.

Figure 1(c) shows the transverse beta function at the absorber versus momentum for four stages out of the total 12 stages of the channel. Note that the transverse beta function becomes progressively smaller from stage to stage by scaling down the cell dimensions and raising the on-axis magnetic field [Fig. 1(d)]. As a result, the minimum beta function drops from 42.0 to 3.0 cm while the on-axis peak magnetic field increases from 2.6 to 13.6 T. This can become a challenge since the operating current in a superconducting magnet must be smaller than the critical current corresponding to the peak field in the coil. To highlight this last fact we also plot in Fig. 1(d) the maximum local fields in the coils for the last three stages (triangles) and compare them to the published maximum allowable field (squares) for the used coil current density, assuming a Nb3Sn conductor. Our findings indicate that the needed fields are consistent with the critical limits of existing conductor technology but the last stages are barely within the limits of Nb3Sn. A recent magnet feasibility study [4] revealed that for a more stable operation a 1.9 K operating magnet temperature is preferred for this stage. This would allow the Nb3Sn inner solenoids to operate at 85% of the load line at operational current.

*Work supported by Contract No, DE-AC02-07CH11359 with the US Department of Energy
#diktys@bnl.gov

ISBN: 978-3-95450-168-7 doi:10.18429/JACoW-IPAC2015-THPF043

PRELIMINARY STUDIES OF LASER-ASSISTED H⁻ STRIPPING AT 400 MeV

P.K. Saha*, H. Harada, M. Kinsho, T. Maruta, K. Okabe, M. Yoshimoto
J-PARC Center, KEK & JAEA, Tokai-mura, Naka-gun, Ibaraki-ken, Japan
Y. Irie, High Energy Accelerator Research Organization, Tsukuba, Ibaraki, Japan
T. Gorlov, Oak Ridge National Laboratory, Oak Ridge, TN, USA

Abstract

Laser-assisted H^- stripping is very essential to overcome real challenges of short lifetime and machine activation by using solid stripper foil for that purpose. Extensive studies on the laser stripping are in good progress at the Spallation Neutron Source (SNS) of Oak Ridge for an H^- energy of 1 GeV. It is therefore interesting to explore these studies for lower H^- energies. As an example, the 3-GeV Rapid Cycling Synchrotron (RCS) of Japan Proton Accelerator Research Complex (J-PARC) is considered, where H^- injection energy is 400 MeV. The present work is a preliminary study of the laser-assisted H^- stripping at this energy, where a set of optimized parameters are considered in order to realize a same level of stripping efficiency as in the SNS case. The feasibility and real challenges are discussed.

INTRODUCTION

Solid stripper foil is used for several hundred to thousand multi-turn H^- stripping injection in the proton accelerators in order to achieve MW-level beam power [1, 2]. However, lifetime and rapid foil failure due to overheating of the foil are serious concerns to maintain stable operation of the machine [3]. It is therefore a real challenge and may be the biggest limitation to realize a multi-MW user machine. Although continuous efforts on durable foil production made remarkable progress on the foil lifetime [4], it is still unclear how to deal with multi-MW beam. Other than foil lifetime, the residual activation near the stripper foil due to the foil scattering beam loss during multi-turn injection is also another uncontrollable factor and a serious issue for facility maintenance.

It is therefore essential that alternate technologies other than using solid foil for the charge-exchange injection have to be established in order to avoid these issues. The idea of laser-assisted H^- stripping, which is a three-step process of an H^- conversion to a proton (magnetic stripping + laser excitation + magnetic stripping) was originally proposed nearly two decades ago [5]. A schematic view of the concept is shown in Fig. 1. A little modified approach to reduce Doppler broadening in the second process of laser excitation was later proposed and also successfully demonstrated a proof-of-principle (POP) experiment at the Spallation Neutron Source (SNS) in Oak Ridge, achieving 90% stripping efficiency for a short pulse of 6 ns, 900 MeV H^- [6, 7]. Aiming for 3 orders of magnitude improvement by increasing

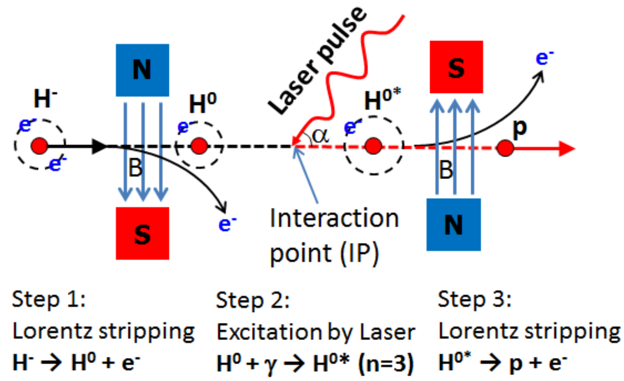

Figure 1: Schematic view of laser-assisted H^- stripping.

the H^- pulse length 5∼10 μs, preparations for the next experiment are in good stage and will be carried out in early 2016 [8, 9].

The present work is a preliminary study for laser-assisted H^- stripping at an energy quite lower that of SNS. For instance, the 3-GeV Rapid Cycling Synchrotron (RCS) of Japan Proton Accelerator Research Complex (J-PARC) is considered [1]. The injection energy is 400 MeV, while the extraction energy is 3 GeV. The designed beam power of the RCS is 1 MW at a repetition rate of 25 Hz. RCS beam power for the operation is 500 kW at present, while an equivalent beam power of 1 MW beam has already been demonstrated recently [10]. Although no foil failure occurred so far but based on measured foil degradation, it is worried that the real lifetime at 1 MW could be much shorter than expected. In order to realize further more than 1 MW beam power, it is therefor essential to study the possibility of laser-assisted H^- stripping at 400 MeV as foil may not survive beyond 1 MW. The present work has been done in the similar framework as in the SNS. The aim is to give an overview of the optimum parameters to realize laser-assisted H^- stripping at 400 MeV.

MAGNETIC FIELD STRIPPING

As shown in Fig. 1, the 1st and 3rd steps utilize Lorentz stripping by using high field magnets. In the former step, an H^- is stripped to an H^0, while H^0 excited by the laser is stripped to a proton by the 2nd magnet in the later step. The basic concept is similar to that already designed for 1 GeV H^- at SNS [11]. A detail is thus not discussed here. Figure 2 shows magnetic field configuration together with stripping functions. The magnetic field for each magnet is considered to be Gaussian shape with σ=0.03m for simplicity as shown

* E-mail address: saha.pranab@j-parc.jp

Content from this work may be used under the terms of the CC BY 3.0 licence (© 2015). Any distribution of this work must maintain attribution to the author(s), title of the work, publisher, and DOI.

ISBN: 978-3-95450-168-7 doi:10.18429/JACoW-IPAC2015-THPF044

STATUS OF THE J-PARC 3 GeV RCS

M. Kinsho#, J-PARC, KEK&JAEA, Tokai-mura, Naka-gun, Ibaraki-ken, 319-1195, Japan

Abstract

Beam power of routine operation of the J-PARC rapid cycling synchrotron (RCS) increased gradually for the MLF user operation, beam power of 400 kW was achieved on 10th March, and 500 kW user operation has been stably performed from 14th April this year. Beam studies were also performed to demonstrate the capability of the RCS to operate at powers in excess of 1 MW. The study produced a beam intensity of 8.41×10^{13} protons during short time, an intensity equivalent to 1.01 MW operation on 10th January 2015.

INTRODUCTION

The J-PARC rapid cycling synchrotron (RCS) has been operated for the neutron and MLF users program from December 23rd, 2008. The RCS operations not only in support of the MLF but also were providing beam for the MR user program (Hadron experiment and/or Neutrino experiment). The RCS has been deliver stable beam of beam power of 300 kW to the MLS and the MR until December 2013 with the linac energy of 181 MeV [1]. To achieve the nominal performance of 1 MW at the RCS and 0.75 MW at the MR, the full energy (400 MeV) and higher peak beam current of the linac is necessary for the J-PARC facility. J-PARC has been done upgrade their linac from 181 MeV to 400 MeV with new ACS (annular coupled structure) linca, and user operation started from February 2014[2].

Beam injection energy of the RCS in J-PARC was increased from 181 MeV to 400 MeV, and user operation with beam energy of 300 kW for both the MLF and the MR was performed with high availability from February to Jun in 2014. Beam losses during beam injection period was decreased by reduction of space charge effect due to increase of beam injection energy. Since an ion source and an RFQ of the LINAC are replaced to realize 1 MW beam power at the RCS in summer maintenance period, injection beam peak current was increased from 30 mA to 50 mA. User operation was restarted from November with beam power of 300 kW. The beam power for user operation will be gradually increased after getting radiation safety permission from government. High intensity beam study was also performed and it was successfully to accelerate beam of 1MW equivalent with small beam losses. In this beam study it was cleared issues to realize 1MW routine operation in the RCS. Status of user operation and issues to realize high power routine operation in the RCS are presented in this paper.

#kinsho.michikazu@jaea.go.jp

ROUTINE OPERATION FOR USERS

The RCS could be delivered beam whose power was 300 kW to both the MLF and the MR for their user operation with an average availability of more than 95 % before the linac energy upgrade. Figure 1 shows output beam power and availability of the RCS from February 2014 to January 2015. Summer maintenance period is usually three months (from July to September), but it was four months last summer for replacement of front-end (ion source and RFQ) of LINAC. Beam studies were performed in spare moments from routine operation in the end of June, and end of December and middle of January which are sighed (1) and (2), respectively in Fig. 1. User operation resumed from 17th February 2014 with 110 kW beam only for the MLF after the linac beam energy upgrade (400MeV injection). The beam power gradually increased, and then beam power achieved 300 kW for the MLF users in 27th February 2014. Since the MR started user operation for neutrino experiment from middle of May, the RCS also started to deliver beam to both the MLF and the MR with beam power of 300 kW.

Beam power was limited 300 kW for the MLF due to government permission of radiation safety, but it was possible to be 1 MW beam routine operation at the RCS from December 2014 because we could get the permission from government. Beam power increased gradually for the MLF user operation, beam power of 400 kW was achieved on 10th March, and 500 kW user operation has been stably performed from 14th April this year. The beam power will be increased to 600 kW in the middle of May.

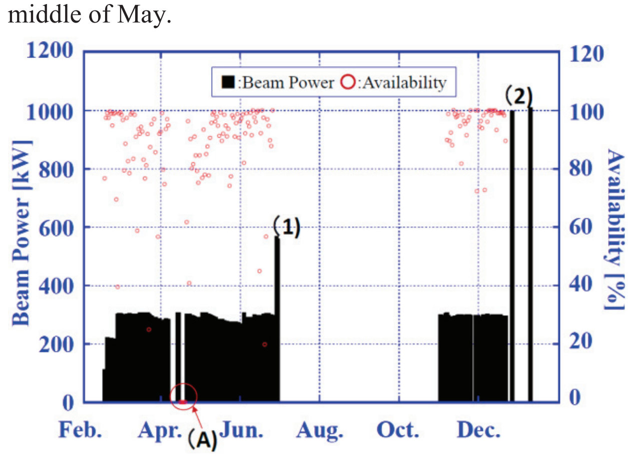

Figure 1: Output beam power and availability of the RCS from February 2014 to January 2015. Black line shows beam power and read circle shows availability. Beam studies were performed at the number (1) and (2) shown in this figure. Availability was zero at period of (A) shown in this figure due to failure of an oil cooling pump in the bending magnet choke transformer.

Content from this work may be used under the terms of the CC BY 3.0 licence (© 2015). Any distribution of this work must maintain attribution to the author(s), title of the work, publisher, and DOI.

ISBN: 978-3-95450-168-7 doi:10.18429/JACoW-IPAC2015-THPF045

SIMULATION STUDY OF MUON ACCELERATION USING RFQ FOR A NEW MUON G-2 EXPERIMENT AT J-PARC

Y. Kondo*, K. Hasegawa, JAEA, Tokai, Naka, Ibaraki, 319-1195, Japan
M. Otani, T. Mibe, N. Saito, KEK, Oho, Tsukuba, 305-0801, Japan
R. Kitamura, U. Tokyo, Tokyo, 113-0033, Japan

Abstract

A new muon g-2 experiment is planned at J-PARC. In this experiment, ultra cold muons will be generated and accelerated using a linear accelerator. As the first accelerating structure, an RFQ will be used. We are planning to use a spare RFQ of the J-PARC linac for the first acceleration test. In this paper, simulation studies of this muon acceleration test are presented. A design study of a muon dedicated RFQ is also shown.

INTRODUCTION

The J-PARC E34 experiment aims to investigate particle physics beyond the standard model by measuring the muon anomalous magnetic moment (g-2) and the electric dipole moment (EDM) with precision of 0.1 ppm and $1 \times 10^{-21} e\cdot$cm, respectively [1]. E34 will be conducted at the H-line [2] of J-PARC muon science facility. This experiment needs a low-emittance muon beam, and to this end, the idea of reacceleration of cooled muon is utilized. The reacceleration of cooled muon is already proposed in [3], in which a wedge-shaped energy absorber is used to cool the muons. On the contrary, we are planning to use ultra cold muons (UCMs) generated by laser-ionization of thermal muoniums (Mu: μ^+e^-) form an silica-aerogel target [4]. Generated UCMs are accelerated using a muon linac. As the first step, a spare RFQ of J-PARC linac (RFQ II [5]) will be used as a front-end accelerator. The resonant frequency of RFQ II is 324 MHz.

Prior to construct the muon linac, we are planning to conduct a muon acceleration experiment using RFQ II at the H-line. The accelerated particle for E34 experiment is μ^+, however, the ultra cold muon source will not be available when the initial stage acceleration experiment will be performed. Therefore, we are developing a negative muonium (Mu^-) source [6], with witch the Mu^-'s are generated by decelerating the muons from the H-line using an aluminum degrader.

RFQ II is originally designed to accelerate H^-'s, and the mass of the $H^-$is nine times larger than that of muon. To accelerate muons using RFQ II, the power should be reduced to 1/80 of the design power; this is very inefficient. Therefore, we are planning to develop a muon dedicated RFQ (muRFQ), and replace RFQ II when the following accelerators are ready.

In this paper, simulation studies of muon acceleration using RFQs are described.

UCM ACCELERATION USING J-PARC RFQ II

For the simulation of J-PARC RFQ II, PARMTEQM [7] is used because it was used for the optics design of RFQ II. To accelerate muons, the original input file should be modified as follows; 1) The particle mass is defined as muon. 2) Input and output energy are converted from the βs of the H^-. The muon mass and the input and output energy are summarized in Table 1 together with the original parameters for H^- acceleration.

Table 1: Parameter Conversion from H^- to μ

Beam species	H^-	μ
Mass (MeV/c^2)	939.302	105.658
Injection β	0.010318	
Injection energy (keV)	50.000	5.625
Extraction β	0.079732	
Extraction energy (MeV)	3.000	0.337
Inter vane voltage (V)	82.879	9.324
Nominal power (kW)	330	4.177

In this simulation, a particle distribution simulated using GEANT4 [6] is used, as shown in Fig. 1. The phase distribution is assumed to be uniform.

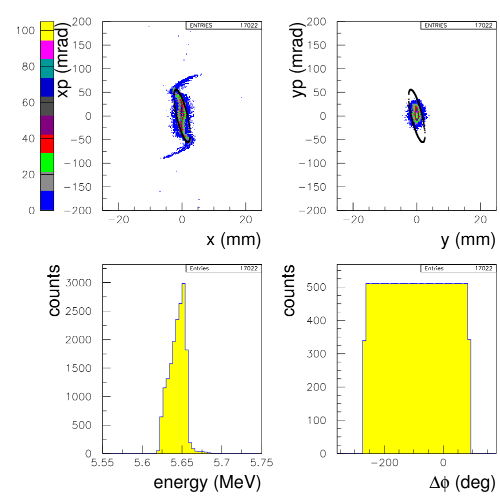

Figure 1: UCM distribution at the RFQ II entrance. The ellipses in upper figures represent the matched ellipses of $\varepsilon_{t,n,rms} = 0.167\pi$ mm mrad.

* yasuhiro.kondo@j-parc.jp

Content from this work may be used under the terms of the CC BY 3.0 licence (© 2015). Any distribution of this work must maintain attribution to the author(s), title of the work, publisher, and DOI.

ISBN: 978-3-95450-168-7 doi:10.18429/JACoW-IPAC2015-THPF046

Content from this work may be used under the terms of the CC BY 3.0 licence (© 2015). Any distribution of this work must maintain attribution to the author(s), title of the work, publisher, and DOI.

OPERATION OF THE RHIC INJECTOR CHAIN WITH IONS FROM EBIS*

C.J. Gardner†, K.L. Zeno, J. Alessi, E. Beebe, I. Blackler, M. Blaskiewicz, J.M. Brennan, K.A. Brown, J. Butler, C. Carlson, W. Fischer, D.M. Gassner, D. Goldberg, T. Hayes, H. Huang, P. Ingrassia, J.P. Jamilkowski, N. Kling, J.S. Laster, D. Maffei, M. Mapes, I. Marneris, G. Marr, A. Marusic, D. McCafferty, K. Mernick, M.G. Minty, J. Morris, C. Naylor, S. Nemesure, S. Perez, A. Pikin, D. Raparia, T. Roser, P. Sampson, J. Sandberg, V. Schoefer, F. Severino, T. Shrey, K. Smith, D. Steski, P. Thieberger, J. Tuozzolo, B. van Kuik, A. Zaltsman, W. Zhang,
BNL, Upton, NY 11973, USA

Abstract

Since 2012, gold and all other ions for the RHIC injector chain have been provided by an Electron-Beam Ion Source (EBIS). The source is followed by an RFQ, a short Linac, and a 30 m transport line. These components replace the Tandem van de Graaff and associated 840 m transport line. They provide ions at 2 MeV per nucleon (kinetic energy) for injection into the AGS Booster. The setup and performance of Booster and AGS with gold and other ions from the new source are reviewed.

INTRODUCTION

The RHIC injector chain, including both EBIS and Tandem, is shown in Figure 1 . Previous operation of the chain with ions from Tandem is documented in [1]. EBIS and associated components [2, 3] now provide essentially all ion species for both RHIC and the NASA Space Radiation Laboratory (NSRL), and allow both facilities to operate in parallel efficiently. Ions from EBIS are injected into Booster after acceleration by the RFQ and Linac. The EBIS, RFQ, and Linac output kinetic energies are 17 KeV, 300 KeV, and 2 MeV per nucleon, respectively. The nominal velocity of all ions at Booster injection is $c\beta$ where $\beta = 0.06505$. This gives a revolution period in Booster of 10.35 μs. EBIS delivers a short pulse of 10 to 40 μs, which amounts to 1-4 Booster turns.

The nominal un-normalized 95% transverse emittance of the beam at the end of the EBIS-to-Booster (ETB) transport line is 11π mm milliradians in both planes. This is an order of magnitude larger than the emittance of beams from Tandem, but with injection of EBIS beam occurring over just a few turns, the accumulated gross emittance after injection is somewhat less than that obtained with Tandem beam injected over some 60 turns. Injection proceeds by means of the same electrostatic inflector and four programmable dipoles that are used for Tandem beams. The dipoles move the closed orbit away from the inflector septum as beam is injected. In order to accommodate the larger emittance

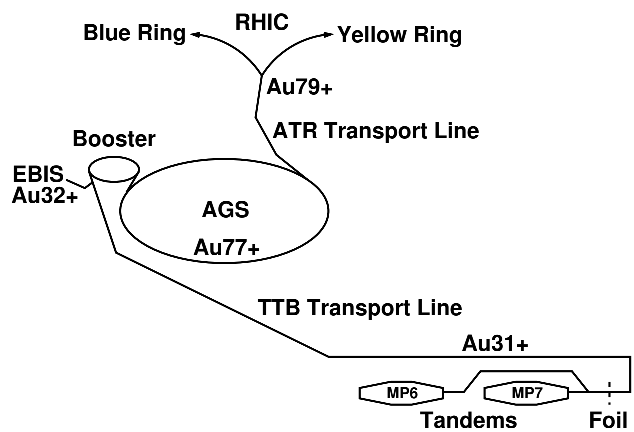

Figure 1: Acceleration of gold ions for RHIC.

of the incoming EBIS beam, the gap between the inflector cathode and septum was increased from 17 to 21 mm.

The number of gold ions delivered to Booster per EBIS pulse is roughly a factor of four less than that delivered per Tandem pulse. In order to make up for this shortfall, it is necessary to deliver 8 loads of Booster beam to AGS per AGS cycle instead of the usual 4 loads delivered for the setup with Tandem beams. Two bunch merges in Booster and two on the AGS injection porch are also required. One ends up with two bunches at AGS extraction, each of which contains 4 Booster loads. For the setup with Tandem one ends up with 4 bunches, each of which contains 1 Booster load. Thus, although there are half as many bunches at AGS extraction for the EBIS setup, each EBIS-setup bunch contains at least as many ions as each Tandem-setup bunch. The details of the setup with EBIS are given in the next section. Beam intensities and longitudinal emittances are discussed in the subsequent sections.

SETUP WITH IONS FROM EBIS

EBIS provided ions of Cu, Au, and U for Cu-Au and U-U collisions in RHIC during Run 12 [4], and for Au-Au collisions during Run 14 [5]. Helions (3He2+) were also provided for helion-Au collisions during Run 14. We focus here on the setup with gold ions. The setup is essentially

* Work performed under contract No. DE-SC0012704 with the auspices of the DoE of United States.
† cgardner@bnl.gov

ISBN: 978-3-95450-168-7 doi:10.18429/JACoW-IPAC2015-THPF047

NEW SERIES OF RFQ VANE SHAPES

Y. Iwashita, Y. Fuwa, ICR, Kyoto University, Uji, Kyoto, Japan

Abstract

New series of RFQ vane shapes are under investigation by introducing more terms in addition to the two term potential. Because they can incorporate with the feature of the trapezoidal shape modulation with less multipole components, higher acceleration efficiency is expected.

INTRODUCTION

RFQs have basically been designed with so-called two term potential [1]. The two term potential has the simplest form that has minimum terms of acceleration and focusing:

$$U_2(r,\psi,z) = \frac{V}{2}\{X\left(\frac{r}{a}\right)^2 \cos 2\psi + AI_0(kr)\cos(kz)\},$$

where $A = \dfrac{m^2-1}{m^2 I_0(ka)+I_0(mka)}, X = 1 - AI_0(ka), k = \pi / Lc$

and a is the minimum radius at z=0 (see Fig. 1). The vane surface profile can be defined by the equipotential surface of U_2. These parameters are defined at each cell, which may make discontinuities between cells.

The acceleration term A and the focusing term X are the functions of only m and Lc/a, whose contour plots are shown in Fig. 2. They are not monotonic with m in the short cell length region. This is the main reason why m is limited up to 2 or 3 for practical cases. The effective acceleration factor should include the transit time factor.

Typical vane profiles based on this expression are shown in Fig. 3. As can be seen, the vane shape becomes ugly when the modulation factor m becomes large since the large modulation at Lc/a is not realistic. Fringe areas have to be truncated for real vanes in any case. This will be discussed later in this paper.

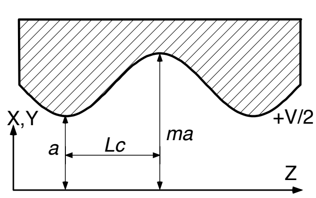

Figure 1: Definitions of vane parameter.

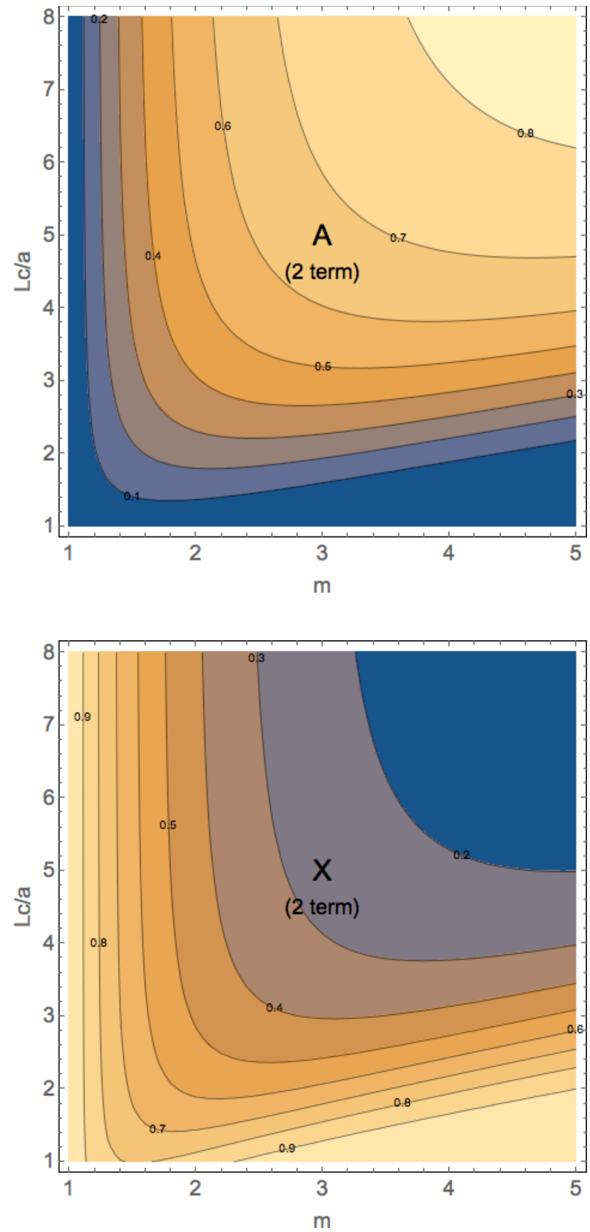

Figure 2: Acceleration term A and focusing term X.

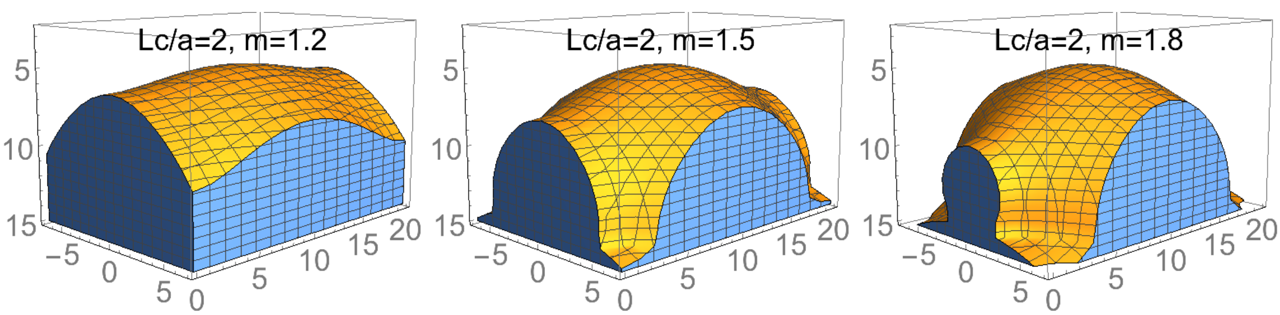

Figure 3: Typical vane profiles based on the two term potentials.

Content from this work may be used under the terms of the CC BY 3.0 licence (© 2015). Any distribution of this work must maintain attribution to the author(s), title of the work, publisher, and DOI.

ISBN: 978-3-95450-168-7 doi:10.18429/JACoW-IPAC2015-THPF049

THE SIMULATION AND MANUFACTURE OF THE ROOM TEMPERATURE CROSS-BAR H TYPE DRIFT TUBE LINAC*

Jinhai Li#, China Institute of Atomic Energy, Beijing, China
Zhihui Li, Institute of Nuclear Science and Technology, Sichuan University, Chengdu, China

Abstract

The room temperature Cross-bar H Type Drift Tube Linac (CH-DTL) is one of the candidate acceleration structures working in CW mode. In order to optimize the parameters, the 3 dimensional electromagnetic field of the CH-DTL cavity is simulated. The method of parameter sweeping with constraint variable is better than the method of parameter sweeping with only one variable during the optimization. In order to simplify the manufacture, the drift tube surface can be designed as spherical shape. The effective shunt impedance of the CH-DTL cavity with cylinder end cup is better than that with cone cup.

INTRODUCTON

An industrial scale ADS will require a 10 MW proton beam having an energy between 600 and 1500 MeV. To achieve the required power at this energy will require an average beam current of ≥10 mA. In 2010, a study program was initiated to develop the design a 10 mA, 1.5 GeV, CW superconducting proton linac for ADS. The Institute of High Energy Physics (IHEP) and the Institute of Modern Physics(IMP) are both developing superconducting accelerating structures which would follow an RFQ [1].

Although low AC power consumption and a large aperture favour superconducting structures following a 2–3.5MeV RFQ, normal-conducting accelerating structures have some advantages [2–5]. While the technology for normal-conducting structures in the energy range from 2 to a few tens of MeV is relatively mature, superconducting structures in this energy range are still under development. Normal-conducting structures in this energy range are more efficient than superconducting cavities and, when located downstream of the RFQ, can serve as a beam filter to reduce the potential for beam loss at higher energies.

Under the support of the National Nature Science Foundation of China, we have initiated the design of a 10 MeV CW proton injector, based on normal-conducting Cross-Bar H-type (CH) structure. The CH structure, initially proposed by IAP, Frankfurt University [6–9] belongs to the π-mode family of accelerating structures and is typically characterized by a high shunt impedance, low stored energy and a stable geometry that is relatively easy to cool. We are evaluating this structure as a potential candidate for CW operation. In this paper we present the results of geometry optimization of the CH structure using the method of parameter sweeping with constraint variable (PSCV).

*Work supported by NSFC (91126003)
#lijinhai@ciae.ac.cn

OPTIMIZATION PHILOSOPHY

The final energy of modern proton RFQs is typically 3 MeV, corresponding to a relativistic velocity β=0.08. The room-temperature CH-DTL can be used to accelerate the beam starting at this velocity. The CH structure belongs to the π-mode family of structures in which the cells are βλ/2 long, the cell length at β=0.08 being about 37mm. To save simulation time, the geometry of a single cell was first optimized followed by the optimization of the complete multi-cell cavity. The parameters of a single cell are shown in Fig.1. The outer drift tube radius (TR) and the radius of the drift tube aperture (HR) are fixed during the optimization.

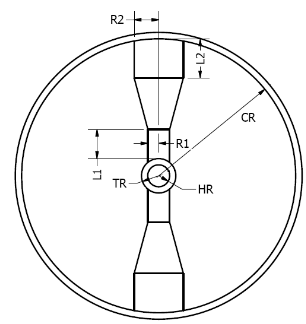

Figure 1: Geometry of a CH single cell.

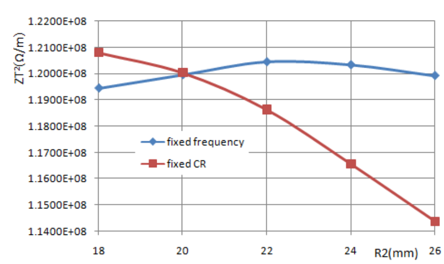

Figure 2: Shunt impedance as a function of outer stem radius using two methods of parameter sweeping

Typically we would sweep a single parameter while monitoring the cavity's RF properties. For example, we know that changing the length of a drift tube causes a corresponding change in the cavity's Q value [6]. However, by changing the length of a drift tube, the resonant frequency changes. Our objective is to optimize the cavity geometry at a fixed frequency (325 MHz). If the frequency changes during the optimization, the optimized value of the swept parameter will differ from the value corresponding to the correct frequency as shown in Fig. 2.

In Figure 2 we have swept the radius of the drift-tube stem base (R2) while fixing the cavity radius (CR). We see that the effective shunt impedance decreases with increasing R2 while the resonant frequency increases from 321.7 to 333.5 MHz. It is convenient to use the cavi-

Content from this work may be used under the terms of the CC BY 3.0 licence (© 2015). Any distribution of this work must maintain attribution to the author(s), title of the work, publisher, and DOI.

ISBN: 978-3-95450-168-7 doi:10.18429/JACoW-IPAC2015-THPF050

APPLICATIONS OF BEAM PARAMETER MEASUREMENTS IN TRANSPORT LINES AT CSNS

Z. Li, Y. Li, J. Peng, DINS/IHEP, Dongguan, 523803, China
L. S. Huang, S. Wang, IHEP, Beijing, 100049, China

Abstract

Several XAL-based applications for parameter measurements in Medium Energy Beam Transport line (MEBT) and Linac to Ring Beam Transport line (LRBT) at China Spallation Neutron Source (CSNS) have been developed. Algorithms and functions of these applications are introduced in this paper. Real Machine tests are carried out in the MEBT commissioning.

INTRODUCTION

China Spallation Neutron Source (CSNS) [1] has an H- linear accelerator as an injector and a rapid cycling synchrotron (RCS) of 1.6 GeV. The linac part consists of an H- ion source, a low energy beam transport line (LEBT), a four-vane RFQ linac of 3 MeV, a medium energy beam transport line (MEBT) and a four tank DTL linac working at RF frequency of 324MeV. The linac to ring beam transport line (LRBT) connects the DTL linac and the RCS and it reserves the space for linac upgrading in the further .

XAL[2] is a Java-based application framework which is developed at the Spallation Neutron Source (SNS) at first, then many other accelerator laboratories join the collaboration, including CSNS. XAL provides an accelerator physics programming interface to the accelerator, and it allows creation of general-purpose applications dedicated to various parts of the accelerator and various kinds of the accelerators. Although most tools in XAL application package can be transplanted directly for the use of CSNS, work of developing new essential tools to meets the distinct requirements of CSNS is still necessary.

XAL TOOLS FOR TRANSPORT LINE

Since the first accelerator device of CSNS was installed last October, the installations of ion source, LEBT, RFQ and MEBT have been finished. The commissioning of the front end is proceeding well and the MEBT transport line is going to start soon after. Applications for MEBT commissioning are based on XAL and some new tools have been developed for CSNS. In this paper some of the new developed tools for transport line parameter measurement are introduced, including tools for measuring twiss parameters at MEBT entrance, fudge factor measurement and dispersion function measurement. We are running tests of there tools on the real machine during the commissioning. Algorithms and functions of these applications are presented as follow.

Twiss Parameters Measurement Tool

MEBT of CSNS linac is located between RFQ and DTL, one of whose major functions is for beam matching both transversely and longitudinally. Figure 1 gives the schematic drawing of MEBT.

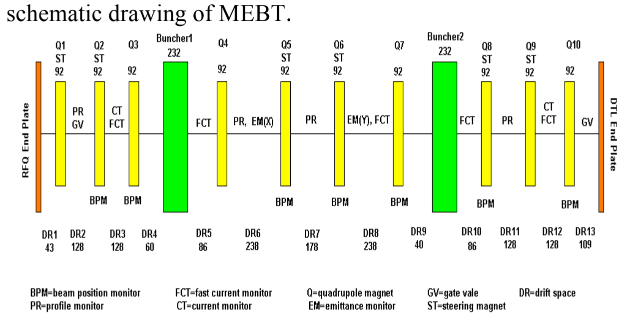

Figure 1: Schematic Drawing of CSNS MEBT.

The energy of MEBT is 3MeV and the peak current intensity is 15mA. Nonlinear space charge force must be considered seriously in the low-energy section of such a high intensity linac. Parmila[3] is an ion linac particle dynamics code. It is a versatile multi-particle code that generates the linac and transforms the beam, represented by a collection of particles, through a user-specified linac and/or transport system. It's widely used in linac designs and simulations, which have proved the accuracy in dealing with the low-energy optics calculation problems. To achieve good solution of MEBT optics matching, the twiss parameters at the MEBT entrance should be acquired first. By employing PARMILA code and 4 wire scanners devices installed in MEBT, a java-based tool was developed to fulfill this purpose. Figure 2 is the algorithm chart of the tool.

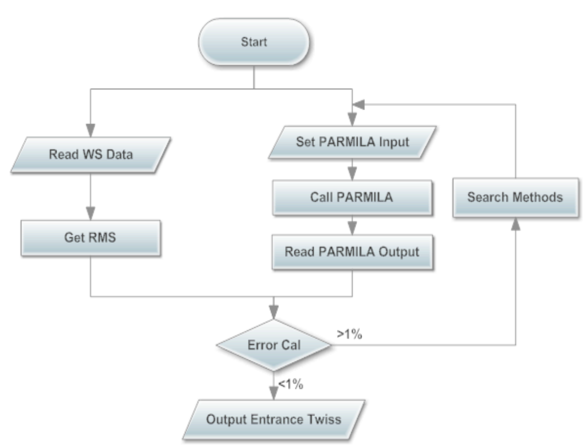

Figure 2: Algorithm Chart of Twiss Parameters Measurement Tool.

Content from this work may be used under the terms of the CC BY 3.0 licence (© 2015). Any distribution of this work must maintain attribution to the author(s), title of the work, publisher, and DOI.

ISBN: 978-3-95450-168-7 doi:10.18429/JACoW-IPAC2015-THPF051

BEAM-BASED ALIGNMENT SIMULATION ON TRANSPORT LINE OF CSNS

Yong Li, L.S.Huang, Z.P.Li, Y.W.An, X.H.Lu, W.B.Liu, S.Wang
Dongguan Campus, Institute of High Energy Physics，Dongguan 523803 China

Abstract

The China Spallation Neutron Source (CSNS) is a high beam power proton machine which needs high precise alignment. Compared to traditional optical alignment, the beam-based alignment (BBA) technique can implement higher precise alignment. This technique with two implementations is applied to the transport line of CSNS to get the transverse misalignments of beam position monitor (BPM) and quadrupole magnet by measuring BPM data under different conditions. The corresponding control system application programs were developed based on CSNS/XAL platform. The result shows the fitted result is consistent with the input result.

INTRODUCTION

CSNS is a high power proton machine which is composed of accelerator, target and spectrometer [1]. The accelerator mainly contained a linac with a modest but upgradable energy and a rapid cycling synchrotron (RCS) of the fixed energy at 1.6 GeV. The installation and beam commissioning of the front end of linac has been finished. The beam commissioning for MEBT is upcoming.

The control of beam loss is quite strict for the reason of high power proton. Orbit correction should be done to decreasing the beam loss. Besides, the orbit correction is normally the first and the most important work during beam commission. Other tasks can easily carry out with very small and smooth orbit. But unfortunately, the measured and the true orbit have difference for the error of alignment and resolution of the magnet and BPM. It can't reach the expected purpose with big errors. The calibration of BPM and quadrupole can be achieved through BBA method. In this paper, two kinds of methods and the detailed simulation based on XAL platform is presented.

REVIEW OF BEAM BASED ALIGNMENT METHOD

The study and application of BBA technique can be seen in many laboratories at home and abroad [2-4] and the way of implementation is diversity. Two kinds of implementations will be introduced in this section.

The principle of the first method is very easy. When the beam passes through the center of the magnet, the BPM data is the relative offset of BPM to the quadrupole. We can change the beam position at the entrance of the quadrupole and scan the gradient of the field in the quadrupole and measure the BPMs' responses on both transverse directions. In many situations, the error of alignment for quadrupole is very small; the measured offset can be approximately considered the offset of BPM. However, this method takes too much time.

The second approach looked more promising, which can get the quadrupole and BPM transverse misalignments simultaneously. This method also need to change orbit and scans the gradient of the field of quadrupole. Meanwhile, the liner optics between all beam line elements must be known.

Fig 1 is the beam orbit with misalignments. Based on the liner optics transmission theory, the beam position measurement (m_i) at BPM-i is assumed to be the sum of all upstream beam kicks from quadrupole offset, correctors, incoming launch conditions and BPM offset as in (1) and (2).

$$m_i = (\mathbf{x_i})_1 - \mathrm{b_i} \tag{1}$$

$$\boldsymbol{x_i} = \mathbf{R}^{(\mathrm{B_1}:\mathrm{i})}\boldsymbol{x_1} + \sum_{\mathrm{j}}^{\mathrm{N_{Ci}}} \mathbf{R}^{(\mathrm{C_j}:\mathrm{i})}\mathbf{c_j} + \sum_{\mathrm{j}}^{\mathrm{N_{Qi}}} \mathbf{R}^{(\mathrm{Q_j}:\mathrm{i})}\left(\mathbf{I} - \mathbf{R}^{(\mathrm{Q_j})}\right)\mathbf{q_j} \tag{2}$$

where x_1, $\mathrm{c_j}$ and $\mathrm{q_j}$ are, respectively, the incoming launch position/angle vector at the first BPM in the beam line, a corrector kick angle vector, and a quadrupole position offset vector defined as

$$\boldsymbol{x_1} = \begin{bmatrix} x_1 \\ x_1' \end{bmatrix}; \quad \boldsymbol{c_j} = \begin{bmatrix} 0 \\ \theta_\mathrm{j} \end{bmatrix}; \quad \boldsymbol{q_j} = \begin{bmatrix} \mathrm{q_j} \\ 0 \end{bmatrix}; \tag{3}$$

R is the 2x2 transfer matrix from the first BPM, or from corrector-j, or from quadrupole-j to the BPM-i, or simply the matrix across quadrupole-j.

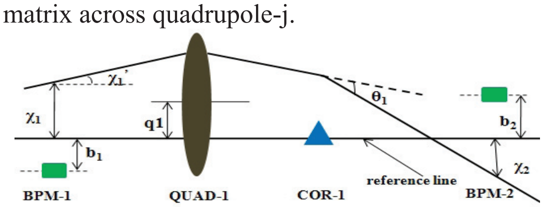

Figure 1: Beam based alignment scheme.

Based on Eq. 2, we can write a set of equations of each of BPM trajectory with different quadrupole strength settings and different incoming launch conditions. Quadrupole and BPM transverse misalignments can be calculated by the least square method.

SIMULATION RESULTS

This BBA application is developed based on the SNS/XAL [5], which is an open source development environment used for creating accelerator physics applications, scripts and services. There are many applications for beam commissioning like orbit correction, lattice calculation, lattice math and so on [6-7]. The result of XAL model for lattice calculation is consistent with the result used other accelerator code,

Content from this work may be used under the terms of the CC BY 3.0 licence (© 2015). Any distribution of this work must maintain attribution to the author(s), title of the work, publisher, and DOI.

ISBN: 978-3-95450-168-7 doi:10.18429/JACoW-IPAC2015-THPF054
Content from this work may be used under the terms of the CC BY 3.0 licence (© 2015). Any distribution of this work must maintain attribution to the author(s), title of the work, publisher, and DOI.

XAL DEVELOPMENT FOR CSNS/RCS COMMISSIONING

Y. An#, DINS/IHEP, Dongguan, 523803, P.R.C.
Y. Wei, S.Wang, Y. Liu, W. Liu, L. Huang, IHEP, Beijing, 100049, P.R.C.

Abstract

As a key component of the China Spallation Neutron Source (CSNS) Project, the Rapid Cycling Synchrotron (RCS) accumulates and accelerates the proton beam from 80MeV to 1.6GeV for extracting and striking the target with a repetition rate of 25Hz. A high level application programming framework code called XAL, based on Java Language with a well-performance online model, initially developed at the Spallation Neutron Source (SNS), has been installed as a part of control system via connection to EPICS for CSNS. Much of the applications have been initially established such as Tune Scan, Tune Monitor, Orbit Response Matrix Measurement, RCS Orbit Display, and Beta Function Measurement for preparing CSNS/RCS commissioning are showed in this paper.

INTRODUCTION

The CSNS accelerator consists of a low energy H^- Linac and high energy RCS. H^- beam with energy of 80MeV is scraped and transformed into proton beam by the carbon foil located in the injection region. After around four hundred turn accumulation, the proton beam is accelerated to 1.6GeV and then extracted to strike the target with the design power of 100kW. As a key component of CSNS, RCS consists of 4-fold symmetric structure, and each of which is constructed by a triplet cells. Table 1 shows the main parameters of RCS [1].

Table 1: Main Parameters of RCS

Parameters	Units	Values
Circumference	m	227.92
Repetition Rate	Hz	25
Average current	μA	62.5
Inj. Energy	MeV	80
Ext. Energy	GeV	1.6
Beam Power	kW	100
Quad		48
Dipole		24
Corrector		16/16
BPM		32/32
Nominal Tunes(H/V)	1	4.86/4.78

As a huge and complex accelerator, CSNS project needs a capable and well performance control system. As a high level application framework in control system, XAL is initially developed for SNS commissioning. After several years' development, and for better collaborating with other facilities and erasing the obsolete code, OPEN XAL formed out of XAL accelerator software about 5 years ago. Although XAL has capability, some modification or enhancement should be done to make the meets of the CSNS/RCS commissioning.

#anyw@ihep.ac.cn

XAL STRUCTURE AND FEATURES

As a device-oriented accelerator application based on java language, along with jython [2] and jruby [3] scripting languages, XAL provided numerous high level application frameworks with a common look and feel. However, the core of XAL is accelerator model. The hierarchy of accelerator model is initialized with a XML file, and that consists of a lot of accelerator sequences. The accelerator sequence is comprised of many ordered nodes which represent a kind of elements that affect the beam with different path, such as magnets, RF gap, and diagnosis elements and so on. The subclass of the nodes developed to distinguish the elements, like dipoles, quadrupoles, sextupoles, BPMs, CT and so on. XAL is also has capacity in doing real time physics simulation [4], and the online model is that application, and the accelerator parameters can be easily and quickly calculated from that.

XAL provides three principal java classes which are the application adaptor, document and document window [5], and all of which are extended from their corresponding abstract parent class. The application adaptor class is the main responsible for launching the main class and also receives the call back information. The document class is responsible for reading and writing the file as well as its associated main window. The document window class is responsible for creating and managing the views. However, in order to decouple the view and the controller as required by Model-View-Controller (MVC) compliance, the document window is now an optional for the developer after the bricks application frame [5] delivered, and that facilitates the application development.

APPLICATIONS

XAL tools have been used to create more than twenty applications in CSNS. And some of them, such that PV view, have been used to monitoring CT in LEBT (Low Energy Beam Transport Line) and MEBT (Medium Energy Beam Transport Line) to measure the beam current and beam energy for CSNS/RFQ tuning. However, we only discuss part of the applications framework for CSNS/RCS commissioning presented at next.

Tune Scan Application

As described in the previous paper, The Lattice of RCS is composed of 4 symmetric fold, and the nominal beta

ISBN: 978-3-95450-168-7 doi:10.18429/JACoW-IPAC2015-THPF055

STATUS OF THE SUPERCONDUCTING CAVITY DEVELOPMENT AT IHEP FOR THE CADS LINAC*

F.S. He#, J. Dai, J.P. Dai, H. Huang, X.F. Huang, L.H. Li, Z.Q. Li, H.Y. Lin, Q. Ma, Z.H. Mi, B.C. Ni, W.M. Pan, X.H. Peng, T.Z. Qi, P. Sha, G.W. Wang, Q.Y. Wang, Z. Xue, X.Y. Zhang, G.Y. Zhao, Key Laboratory of Particle Acceleration Physics and Technology, IHEP, CAS, Beijing, China

Abstract

IHEP (Institute of High Energy Physics) is developing a CW 10MeV proton injector and part of the 25MeV main linac for the CADS project. 14 SRF (superconducting radio frequency) spoke-012 cavities for the injector, as well as 6 SRF spoke-021 cavities for the main linac are to be beam commissioned before middle of 2016; meanwhile, VT (vertical test) of two more types of prototype cavities are to be finished with 2015, for the future phases of the project. In this paper, the VT statistics of 10 spoke012 cavities, 4 spoke021 cavities, and a 5-cell β0.82 elliptical cavity are reported; the cavity performance during beam commissioning of the TCM (test cryomodule) is reported as well.

INSTRUCTION

The C-ADS project is a strategic plan to help solve the nuclear waste problem and the resource problem for nuclear power plants in China [1]. For the first phase, the project goal is to build a CW proton linac of 25 MeV and 10 mA by about 2016. IHEP is developing one of the two 10-MeV injectors for the project, which is called Injector-I. The TCM, which contains two spoke-012 cavities, is under beam commissioning now. 8 more spoke0-12 cavities reached Ep of 60MV/m and Bp of 90 mT during VT, and 7 of them are being assembled to the CM1, which is the upstream cryomodule for the injector. 3 prototype spoke-021 cavities went through VT in 2014, and one more spoke-021 cavity for the cryomodule at the end of the 25MeV main linac reach specification during VT. Two spoke-040 cavities and two HMB cavities, which are 5cell β0.82 elliptical cavities, were fabricated, while one of the HMB cavities went through VT and reached specification. 8 more spoke-012 cavities and 7 more spoke-021 cavities are under fabrication now to catch up with the project schedule.

DESIGN AND FABRICATION OF THE CAVITIES

The Injector-I uses spoke012 cavities, which are 325MHz, β_0 of 0.14, single-spoke cavies. The main linac contains two types of 325MHz single-spoke cavities, i.e. spoke021 and spoke040, and two types of 650MHz multi-cell elliptical cavities, i.e. MB063 and HMB082. All types of cavities except for the MB063 have been designed and prototyped at IHEP, while three of them have reached the design specification during VT. The key parameters of these cavities are listed in Table 1.Note the effective length is defined as Leff = $\beta_0 \times \lambda$.for single-cell spoke cavities, while β_G is used for elliptical cavity instead of β_0.

Table 1: RF Parameters of the ADS SRF Cavities at IHEP

RF Parameters	Spoke -012	Spoke -021	Spoke -040	HMB 082
Frequency-MHz	325	325	325	650
β_0	0.14	0.24	0.46	0.82
Aperture-mm	35	40	50	100
Ep/Eacc	5.0	4.4	3.9	2.1
Bp/Eacc-mT/(MV/m)^2	6.9	9.4	9.2	4.1
G-Ω	60	71	104	236
R/Q-Ω	150	191	265	515
df/dp-Hz/mbar	+40	+0.6	+0.7	
df/dF-Hz/N	60	94	N/A	N/A
Leff -mm	129	221	424	945

The RF design of the spoke012 cavity was biased towards eliminating MP (multipacting); while stiffening rings and the helium vessel were designed to reduce pressure sensitivity. The spoke021 cavity was shaped to facilitate the fabrication, and the designed pressure sensitivity was significantly reduced by adopting a different helium vessel and tuner design. The spoke040 cavity is in the early phase of prototyping, and the RF properties are not fully optimized yet. The HMB082 cavity was designed to minimize surface field and to avoid MP. HOM (higher order modes) are not a concern for any type of these cavities.

The spoke012 cavities are in mass production phase now. The first two prototype spoke012 cavities were fabricated in 2012, and were VT in 2013. During the fabrication of the second batch of 4 cavities for TCM, the frequency errors of 2-4 MHz induced by inaccuracy in deep-drawing and machining were well understood and compensated by trimming the height of outer conductor. Though, a frequency scattering of 1.6 MHz induced by EBW were observed during the mass production of the third batch of 7 cavities for CM1 (see Fig. 1); since then the process flow of fabrication was adjusted to reduce the frequency error. The fourth batch of 8 cavities will be delivered from two vendors by September; they will be VT qualified after the He vessels are welded, and is

*Work supported by Chinese Academy of Science strategic Priority Research Program-Future Advanced Nuclear Fission Energy
#hefs@ihep.ac.cn

Content from this work may be used under the terms of the CC BY 3.0 licence (© 2015). Any distribution of this work must maintain attribution to the author(s), title of the work, publisher, and DOI.

ISBN: 978-3-95450-168-7 doi:10.18429/JACoW-IPAC2015-THPF057

BEAM COMMISSIONING OF C-ADS INJECTOR-I RFQ ACCELERATOR*

Cai Meng#, Shengchang Wang, Jianshe Cao, Yaoyao Du, Tongming Huang,
Huiping Geng, Rong Liu, Huafu Ouyang, Weimin Pan, Shilun Pei, Hua Shi,
Yanfeng Sui, Jianli Wang, Fang Yan, Qiang Ye, Lingda Yu, Ying Zhao
Key Laboratory of Particle Acceleration Physics & Technology,
Institute of High Energy Physics, Chinese Academy of Sciences, Beijing 100049, China

Abstract

The C-ADS accelerator is a CW (Continuous-Wave) proton linac with 1.5 GeV in beam energy, 10 mA in beam current, and 15 MW in beam power. C-ADS Injector-I accelerator is a 10-mA 10-MeV CW proton linac, which uses a 3.2-MeV normal conducting 4-Vane RFQ and superconducting single-spoke cavities for accelerating. The frequency of RFQ accelerator is 325 MHz. The test stand composed of an ECR ion source, LEBT, RFQ, MEBT and beam dump have been installed and the first stage of beam commissioning have been finished at IHEP in 2014 mid-year. At 90% duty factor, we got 11 mA proton beam at RFQ exit with 90% beam transmission efficiency, while 95% beam transmission efficiency at 70% duty factor. The energy after RFQ was measured by TOF method with FCTs. The transverse emittance measured by double-slits emittance meter was 0.135 π mm-mrad, which of detailed data analysis will be presented in this paper.

INTRODUCTION

The ADS project in China (C-ADS) is a strategic plan to solve the nuclear waste problem and the resource problem for nuclear power plants in China. For the C-ADS accelerator that is a CW proton linac with the proton beam of energy 1.5 GeV and current 10 mA [1]. The C-ADS accelerator uses superconducting acceleration structures, except for the RFQs and is composed of two major accelerating parts: the injector and the main linac. The rf frequencies for the main linac have been chosen as 325 MHz for the spoke cavity sections and 650 MHz for the elliptical cavity sections. However, two different designs employing different rf frequencies are pursued for the low-energy part of less than 10 MeV, namely, injectors in the technical developing phase, with 325 MHz for Injector Scheme-I [2] and 162.5 MHz for Injector Scheme-II.

For the first phase, the project goal is to build a CW proton linac of 25 MeV. The first phase itself will be executed progressively in several steps, with the first step to build two 5-MeV test stands of different front-end designs. Before the test stands of superconducting cavities, we have finished the first stage beam commissioning of the injector-I RFQ accelerator (Table 1), which composed of an ECR ion source, LEBT, RFQ, MEBT and beam dump line. There is an ACCT at the entrance of RFQ and a DCCT at the middle part of MEBT for transmission measurement, FCTs for energy measurement and double-slit for emittance measurement at the MEBT. Detailed analysis will be presented in this paper.

Table 1: Main RFQ design Parameters of Injector-I

Parameters	Value
RF Frequency (MHz)	325
Injection/Output energy (MeV)	0.035/3.2
Pulsed beam current (mA)	15
Beam duty factor	100%
Inter-vane voltage V (kV)	55
Average bore radius r0 (mm)	2.775
Maximum surface field (MV/m)	28.88 (1.62Kilp.)
Cavity power dissipation (kW)	272.94 (1.4*$P_{SUPERFISH}$)
Vane length (cm)	467.75

EXPERIMENTAL APPARATUS

The layout of the test stand is shown in Fig. 1. A 2.45 GHz electron cyclotron resonance (ECR) ion source was installed for the RFQ testing. The extraction energy is 35 keV and the typical pressure was 7.5×10^{-4} Pa. The low energy beam transport (LEBT) is equipped with two

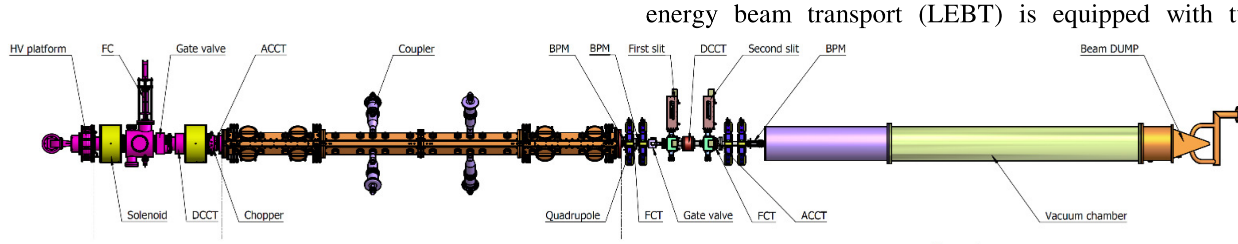

Figure 1: Layout of the test stand.

*Work supported by China ADS Project (XDA03020000)
#mengc@ihep.ac.cn

Content from this work may be used under the terms of the CC BY 3.0 licence (© 2015). Any distribution of this work must maintain attribution to the author(s), title of the work, publisher, and DOI.

6th International Particle Accelerator Conference IPAC2015, Richmond, VA, USA JACoW Publishing
ISBN: 978-3-95450-168-7 doi:10.18429/JACoW-IPAC2015-THPF059

Content from this work may be used under the terms of the CC BY 3.0 licence (© 2015). Any distribution of this work must maintain attribution to the author(s), title of the work, publisher, and DOI.

RHIC ELECTRON LENSES UPGRADES *

X. Gu#, Z. Altinbas, D. Bruno, S. Binello, M. Costanzo, A. Drees, W. Fischer, D.M. Gassner, J. Hock, K. Hock, M. Harvey, Y. Luo, A. Marusic, C. Mi, K. Mernick, M. Minty, R. Michnoff, T.A. Miller, A.I. Pikin, G. Robert-Demolaize, T. Samms, T. C. Shrey, V. Schoefer, Y. Tan, R. Than, P. Thieberger, and S.M. White
Brookhaven National Laboratory, Upton, NY 11973

Abstract

In the Relativistic Heavy Ion Collider (RHIC) 100 GeV polarized proton run in 2015[1], two electron lenses [2] were used to partially compensate for the head-on beam-beam effect for the first time. Here, we describe the design of the current electron lens, detailing the hardware modifications made after the 2014 commissioning run with heavy ions. A new electron gun with 15-mm diameter cathode is characterized. The electron beam transverse profile was measured using a YAG screen and fitted with a Gaussian distribution. During operation, the overlap of the electron and proton beams was achieved using the electron backscattering detector in conjunction with an automated orbit control program.

INTRODUCTION

Figure 1 schematically depicts the layout of the electron lens in the operational synoptic display and the parameters that we used during the 2015 run. At the top of the figure, we show the layout of magnets and their names, including their current controls. Vacuum values and proton-beam losses are also given. At the bottom of the figure, the parameters for the electron beam current, the energy and timing control, as well as the statuses of the e-lens system and the proton beam are displayed.

While in the commissioning run[3] , the electron beam was modulated at the 78 kHz revolution frequency to allow parasitic commissioning with the e-lens acting on only a few ion bunches, for the e-lens operation during the 2015 100 GeV polarized proton run, we used a DC electron beam for beam-beam compensation.

We developed a new lattice for the proton beam based on ATS optics [4], which assures the correct phase advance between the E-lenses and the PHENIX experiment and reduces the second order chromaticity so providing larger dynamic aperture. The lattice has $\beta_{x,y}$ = 15 m at the center of each lens where the electron beam and proton beam collide head-on. We designed a new cathode for the electron beam with a larger radius of 7. 5 mm (formerly, it was 4.1 mm) [5] and machined it to match the size of the proton beam.

After improving the blue superconducting magnet inner cooling system, both the blue and yellow solenoids can run at the design of 6 tesla magnetic field using the RHIC helium system.

NEW CATHODE

For the 2015 polarized proton run, the new cathode with 7.5 mm radius was installed. This cathode is a dispenser cathode [6], which consists of a porous tungsten matrix, impregnated with a barium-based emission-enhancing material.
To activate the cathode material, the pressure near the cathode should be kept below 5×10^{-6} Torr. However, the cathode should in principle be kept at a higher temperature than the rest of the structure during bake-out to avoid the deposition of poisons that may come from out-gassing. These two requirements compete against each other because during the e-lens bake-out, the

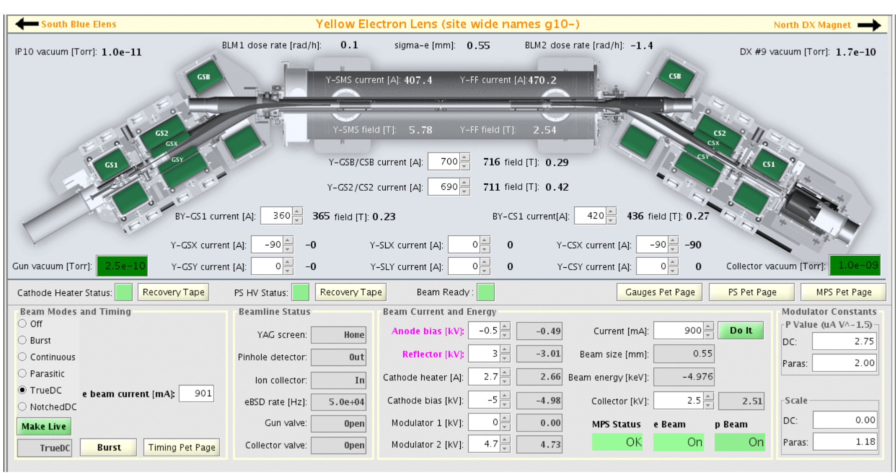

Figure 1: Schematic depiction of the layout and parameters of the electron lens during the 2015 run.

* Work supported by Brookhaven Science Associates, LLC under Contract No. DE-AC02-98CH10886 with the U.S. Department of Energy
#xgu@bnl.gov

ISBN: 978-3-95450-168-7 doi:10.18429/JACoW-IPAC2015-THPF060

THE SIMULATION STUDY OF SPACE CHARGE EFFECTS FOR CSNS LINAC

Y. Yuan[#,1,2], S. Wang[1,2], J. Peng[1,2], L. Huang[1,2]
[1]China Spallation Neutron Source, Institute of High Energy Physics, Chinese Academy of Sciences, Dongguan, China
[2]Dongguan Institute of Neutron Science, Dongguan, China

Abstract

China Spallation Neutron Source (CSNS) is a high intensity accelerator based facility. Its accelerator consists of an H- injector and a proton Rapid Cycling Synchrotron. The injector includes the front end and linac. The RFQ accelerates the beam to 3MeV, and then DTL accelerates it to 80MeV[1]. The space charge effect is the most important cause of emittance growth and beam loss due to the low beam energy and the high peak current. The paper performed simulation studies on the space charge effects at the LINAC by using three-dimensional code IMPACT-Z. The emittance evolution is studied in the point of view of the singe-particle dynamics and multi-particle dynamics with different peak beam current. The effect of mismatch is studied by simulation, and the emittance growth with different mismatch factor are given.

INTRODUCTION

The design beam power of the China Spallation Neutron Source (CSNS) is 100 kW at Phase Ⅰ, and it has upgrade potential of 500kW. Correspondingly, the design peak current of linac are 15mA and 30mA. In such a high intensity linear accelerator, the space chare effects is a very important research topic. The significance of the space-charge fields is not only that they reduce the effective focusing strength, but also the nonlinear terms, a consequence of the deviations from charge-density uniformity, cause growth of the rms emittance, which degrades the intrinsic beam quality. One consequence of space-charge-induced emittance growth is the formation of a low-density beam halo surrounding the core of the beam, which can be the cause of beam loss, resulting in radioactivation of the accelerating structure[2]. The interaction between a large number of charged particles is very complex, multi-particle tracking code provides a very effective means for the exploration of space charge effects. In this paper, three-dimensional code IMPACT-Z[3] is taken to study the space charge effects on MEBT and DTL, and this simulation also includes initial mismatch of beam.

SIMULATION STUDY OF SPACE-CHAREGE EFFECTS ON DTL

CSNS/DTL consists of four accelerating cavity with a total of 156 cell, the length among the cavities is designed to maintain longitudinal continuity. Transverse magnetic focusing lattice is FFDD, all quadrupole magnets arrangement can be approximated as periodic focusing structure. By tracking the position of the particle in phase space after each periodic structure, emittance growth can be analysed on microscopic view.

Beams that are in equilibrium in the focusing channel of a linac experience no emittance growth. Unfortunately, beams observed in linac numerical simulations are rarely in equilibrium. The space-chare force in high-current beams is typically the major cause of rms emittance growth. Four different space-charge mechanisms can be identified[4]: charge redistribution, the injected beam is not rms matched, space charge resonances that couple longitudinal and transverse oscillations, the periodic-focusing structure resonantly excite density oscillations in the beam.

Emittance Growth with Different Current

In the simulation, the initial distribution of particles is 6D water bag, the number of macro particles is 100,000, the currents of beams are respectively 0mA, 15mA and 30mA. Figure 1 is a comparison of the emittance evolution with different current of beam along linac.

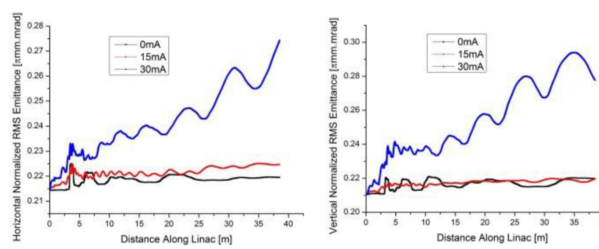

Figure 1: Left: beam horizontal RMS emittance growth along linac. Right: beam vertical RMS emittance growth along linac.

Figure 1 shows that beam's RMS emittance growth is very small with current of 15 mA , and oscillation of emittance is gradually levelling off. However, when the intensity reaches 30mA, emittance growth becomes apparent and increase the proportion of about 30%. In a strictly periodic focusing structure , without considering the impact of space charge effects, a single particle's trajectory after periodic cells is an ellipse in phase space. Because the particles are accelerated in DTL, the actual focusing structure is a quasi-periodic lattice. Therefore, without considering the space-charge effects, the trajectory of particles should be an approximation of an elliptical shape.

In the horizontal direction, for example, the position x and the spread angle x' of particles are normalized by

#yuanyue@ihep.ac.cn

Content from this work may be used under the terms of the CC BY 3.0 licence (© 2015). Any distribution of this work must maintain attribution to the author(s), title of the work, publisher, and DOI.

ISBN: 978-3-95450-168-7 doi:10.18429/JACoW-IPAC2015-THPF062

Content from this work may be used under the terms of the CC BY 3.0 licence (© 2015). Any distribution of this work must maintain attribution to the author(s), title of the work, publisher, and DOI.

CADS 650 MHz BETA=0.63 ELLIPTICAL CAVITY STUDY

Liangjian Wen, Shenghu Zhang, Yongming Li*, Yuan He, IMP, Lanzhou, China

Abstract

The China Accelerator Driven Sub-critical System (CADS) is a high intensity proton facility to dispose of nuclear waste and generate electric power. CADS is based on 1.5 GeV, 10mA CW superconducting (SC) linac as a driver. The high-energy section of the linac is composed of two families of SC elliptical cavities which are designed for the geometrical beta 0.63 and 0.82. In this paper, the 650 MHz β=0.63 SC elliptical cavity was studied, including cavity optimization, multipacting, high order modes (HOM) and generator RF power calculation.

INTRODUCTION

China strives to develop the nuclear energy and the nuclear power of China will reach to 58 million kilowatts in 2020. The nuclear waste will also accumulate to 10400 tons [1]. The demand of nuclear energy will grow further with economic development. The disposal of nuclear waste and nuclear fuel shortage are increasingly more serious in China. Accelerator Driven Sub-critical System (ADS) is the optimal way to dispose of nuclear waste and solves the problem of shortage of nuclear fuel. CADS is promoted and constructed by Chinese Academy of Sciences (CAS), as a long-term energy strategy for China.

CADS is composed of a SC linac, a spallation target and nuclear reactor operating in subcritical mod. The 650 MHz β=0.63 elliptical cavities accelerate proton beams from 180 MeV to 360 MeV. This paper is mainly concerned with the RF properties, multipacting, damping of the higher order modes and required generator power of the elliptical cavity

CAVITY RF DESIGN

The following consideration is needed for high-current SC elliptical cavity design:

1) HOM damping is primarily concerned in high-current SC elliptical cavity design. The larger cavity aperture reduces the interaction between the cavity and beam and improve the cell-to-cell coupling to reduce potential for the rapped HOM and beam instability.

2) The accelerating efficiency improves by increasing the numbers of cells per cavity, but also make it difficult to extract and damp the HOM. Five cells per cavity compromises among the accelerating efficiency, the particle acceptance of TTF, and damping the HOM.

A 650 MHzβ=0.63 superconducting cavity was designed by Superfish. The achieved cavity RF and geometry parameters are listed in Table 1. The final β=0.63 five-cell cavity design is depicted in Figure 1.

ymli@impcas.ac.cn

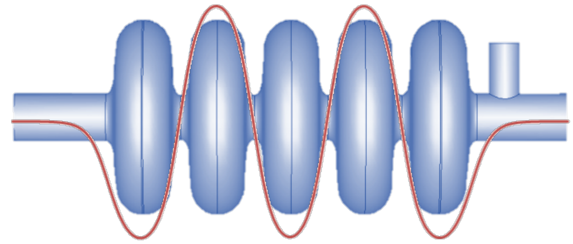

Figure 1: the final β=0.63 five-cell cavity design.

Table 1: The RF Parameters of the 650 MHz β=0.63 Elliptical Cavity

Parameter	unit	value
βg		0.63
frequency	MHz	650
equator diameter	mm	394.4
iris aperture	mm	90
beam pipe aperture	mm	96
cell-to-cell coupling	%	0.9
R/Q(βg)	Ω	333.5
G	Ω	192.7
Epeak/Eacc		2.34
Bpeak/Eacc	mT/(MV/m)	4.63

MULTIPACTING SIMULATION

Multipacting barriers restrict SC cavity performance and accelerating gradient enhanced since a great deal of electrons reach resonance and absorb RF power. Multipacting leads to temperature rise of SC cavity and eventually thermal breakdown. It is crucial to optimize the shape of cavity to eliminate the unexpected multipacting barriers. Multipac 2.1 code [2] was used to simulate the multipacting in the cavity. Fig. 2 shows the enhanced counter function. The result indicate that no hard multipacting was found and the cavity be processed by good cavity surface treatment.

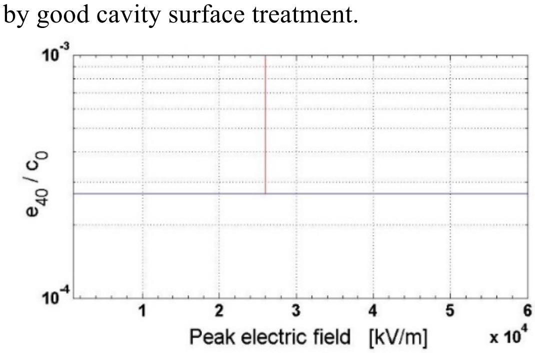

Figure 2: Enhanced counter function- ratio between the number of particles after the 40th impact and the initial number of particles.

ISBN: 978-3-95450-168-7 doi:10.18429/JACoW-IPAC2015-THPF069

THE EARLY RESULTS OF THE VERTICAL TEST FOR $\beta = 0.12$ HWR AT RISP

G.T. Park, H.C. Jung, Y.K. Kim, W.K. Kim, H.J. Cha, S. Choi, and H. Kim
Rare Isotope Science Project (RISP), Daejeon, Korea

Abstract

The facility for the vertical test at 2 K with the master frequency 81.25 MHz is being prepared at Rare Isotope Science Project (RISP) and the preliminary tests are being done as the preparation progresses. We briefly describe the vertical test system, the tests being done, and the future plan for the completion of the facility.

INTRODUCTION

At RISP [1], 4 different kinds of the superconducting cavities have been developed. Now the fabrication of the cavities is complete and their vertical test is being prepared. At the moment, as a beginning stage, the minimum facility is prepared with the prospect for further expansion and upgrade of the facility. For now, 4 K cryogenic system is prepared and no surface processing facility is available yet. The simple system check and the leak check at cryogenic temperature is examined and some RF measurement including critical coupling calibration and decay time measurement is made.

The future plan includes the construction for surface processing, the implementation of the magnetic shields, 2 K pumping station, LLRF system for the vertical test, adjustable coupler, radiation shields, and the interlock system.

SYSTEM PREPARATION

The vertical test stand consists of the cryostat, the pit, the test insert, the staging rack, and vacuum pump system.

The cryostat (See Fig. 1(a)) is made of the stainless steel STS304: The vacuum vessel is 3300 mm deep with 800 mm inner diameter. The helium vessel is 3000 mm deep 500 mm with inner diameter with about 250 L helium capacity. The helium vessel is surrounded by the thermal shield. The test insert was designed and fabricated. It consists of the top plate, the support cage, and the thermal baffle to reduce the static heat load through the conduction. The top plate is equipped with the pressure relief system, i.e., 8 cm diameter burst disk combined with a re-closable safety relief valve at a set pressure of 1 bar. The relief system is sized assuming complete helium vaporization due to a leak in insulating vacuum. It must also provide the various feedthroughs for the vacuum port (for the cavity), the temperature sensors, level sensors, N and SMA-type RF cables for the input and pick up couplers, LHe input port, and Gas output port. The vacuum pump system for the cavity evacuation was prepared. The system consists of the turbo molecular pump, the scroll pump, the controller, the compressor, the vacuum gauges (low range and the full range), and the residual gas analyzer (RGA) as shown in Fig. 1(c).

(a) Cryostat in the pit

(b) Test insert in the staging rack

(c) Vacuum pump system

Figure 1: Vertical test stand.

A simple cryogenic system to cool down the system to 77 K and 4 K using LN_2 and LHe, respectively, was prepared: The LHe dewar, GHe tank, LN_2 dewar, the thermometry sensors, the pressure transducer, and the level sensors. 2 K pump station will be added in near future.

The RF system is being installed to test the HWR with the resonant frequency of $f = 81.25$ MHz. The vertical test is generally done in critical coupling [2]. In the critical coupling, the bandwidths are very narrow and low power corresponding to the wall loss will be supplied.

The schematic of the RF system is given in Fig. 2. As shown in Fig. 2, the system consist of the signal generator, RF switch, the vertical test LLRF, the driving amplifier, the circulator, the directional coupler, the adjustable coupler, the power meters, and the oscilloscope with the diodes.

PRELIMINARY MEASUREMENTS

During the first cool down, the preliminary RF measurements were done using the vector network analyzer (VNA) only. Using the VNA, the frequency shift during the evacuation, the cool down (to 4 K), and the helium pressure pres-

Content from this work may be used under the terms of the CC BY 3.0 licence (© 2015). Any distribution of this work must maintain attribution to the author(s), title of the work, publisher, and DOI.

ISBN: 978-3-95450-168-7 doi:10.18429/JACoW-IPAC2015-THPF070

Content from this work may be used under the terms of the CC BY 3.0 licence (© 2015). Any distribution of this work must maintain attribution to the author(s), title of the work, publisher, and DOI.

PROTOTYPING PROGRESS OF SSR1 SINGLE SPOKE RESONATOR FOR RAON

H. J. Cha#, G. T. Park, H. Kim, W. Kim and H. J. Kim, IBS/RISP, Daejeon, South Korea

Abstract

We report the current status of prototyping of the SSR1 cavity (β = 0.3 and f = 325 MHz) for Korean heavy ion accelerator RAON. Simulation results on target frequency for vertical test of the cavity prototype are presented. Clamp-up tests for the cavity assembly are in progress.

INTRODUCTION

The RAON, an advanced heavy ion accelerator for basic sciences and multiple applications, is under construction in Daejeon, South Korea [1]. Based on the on-going technical designs, the prototyping for four different types of superconducting cavities (QWR [2], HWR [3], SSR1 [4], and SSR2) is in progress. In particular, the SSR1 cavities before the SSR2 section can reaccelerate the stable isotope heavy ion beams from the HWR cavities (β = 0.12) after the QWR section to higher energy (β = 0.3) with the resonant frequency of 325 MHz.

After completing the fabrication of the SSR1 cavity prototype, it will be qualified through vertical tests. Therefore, the target frequency considering the resonant frequency shifts by the followings: final electron beam welding (EBW) of an outer conductor with end walls, buffered chemical polishing (BCP), evacuation for ultra-high vacuum of the cavity, cooling to the temperature of 4 K and 2 K, and liquid helium (LHe) pressure acting on the cavity at the temperature should be determined before final trimming of the outer conductor and then EBW with end walls. The electromagnetic (EM) analyses with mechanical simulations will be given in the next section. In addition, the present status of clamp-up tests performing before final EBW is briefly introduced.

DETERMINATION OF TARGET FREQUENCY FOR VERTICAL TEST

The CST MWS and the CST MPhysics codes were utilized for predicting the target frequency of the SSR1 prototype. Figure 1 shows the variation of resonant frequency with respect to the width of the cylindrical outer conductor. Both sides of the outer conductor are simultaneously trimmed by the same length as shown in the inset. The positive sign at horizontal axis represents the decreasing width of the outer conductor and the negative one does the increasing that. Zero distance means the original design value of the outer conductor width. The slope was calculated to be -407.5 kHz/mm. It can be applied to the estimation of the resonant frequency shift by final EBW. Considering the shrinkage of 0.6 mm at each side in the case of niobium (Nb), the frequency shift by the EBW is -244.5 kHz.

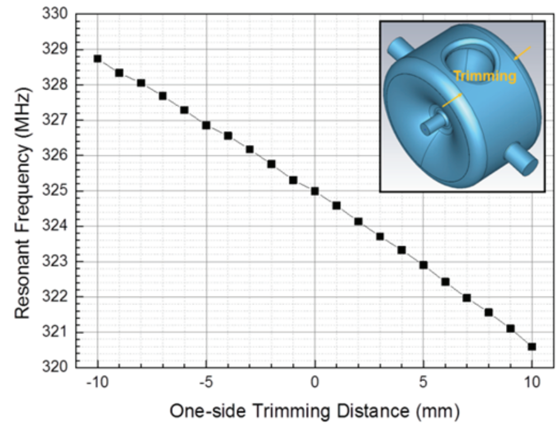

Figure 1: Variation of resonant frequency with changing the width of the outer conductor of the SSR1 cavity.

Figure 2 shows the variation of resonant frequency with respect to the BCP depth. Zero depth also means the original cavity design. The inset shows the simulation results in the narrower depth range. In both cases, it is expected that some fluctuations are caused by the limited mesh numbers. The frequency shift per unit depth calculated from linear fits of the data points is approximately -150 ~ -202 Hz/μm. For determining the target frequency, -150 Hz/μm was used.

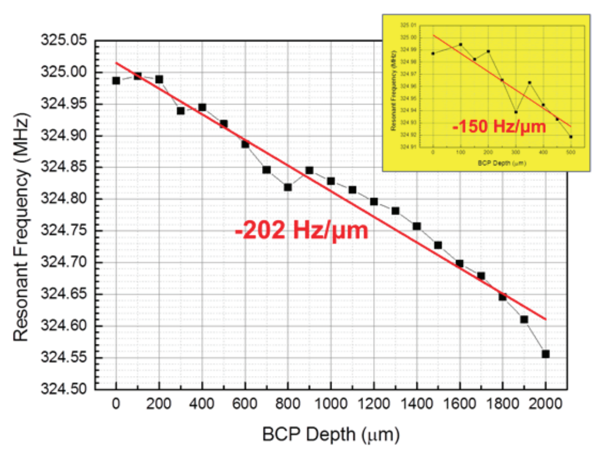

Figure 2: Variation of resonant frequency with changing the BCP depth of the SSR1 cavity.

The resonant frequency shift by vacuum in the cavity maintained during the vertical test should be considered. Figure 3(a) shows the deformation by pressure acting on the cavity due to the vacuum of the cavity inside. The pressure of 1 bar was assumed and the resultant maximum

#hjcha@ibs.re.kr

ISBN: 978-3-95450-168-7 doi:10.18429/JACoW-IPAC2015-THPF072

BEAM OPTICS OF RISP LINAC USING DYNAC CODE*

Ji-Ho Jang#, Hyo-Jae Jang, Hyun-Chang Jin, In-Seok Hong, Hyung-Jin Kim, Dong-O Jeon,
RISP/IBS, Daejeon, Korea

Abstract

The RISP (Rare Isotope Science Project) [1,2] is developing a superconducting linac which accelerates uranium beams up to 200MeV/u with the beam power of 400kW. The linac consists of an injector which includes an ECR ion source and an RFQ, and superconducting cavities which include SCL1 with QWR (Quarter Wave Resonator) and HWR (Half Wave Resonator), and SCL1 with two types of SSR (Single Spoke Resonator). Multiple charge state beams will be accelerated to achieve the required beam power and the charge stripper will be used to obtain the higher acceleration efficiency. This work focuses on the beam dynamics by using the DYNAC code[3] in order to study a possibility that the code can be used as an online model of RAON linac. We compared the results with the calculation by TRACK code [4].

INTRODUCTION

The DYNAC code is a good candidate for the online model of RAON Linac because it can simulates multiple charge states and fast enough. The beam specification of RAON diriver linac is summarized in Table 1. We focus on the uranium beam in this study.

Table 1: Beam Specification for the Driver Linac

Parameters	H^+	O^{8+}	Xe^{54+}	U^{79+}
Energy [MeV/u]	600	320	251	200
Current [pμA]	660	78	11	8.3
Power on target [kW]	>400	400	400	400

LEBT

The injection energy of RAON RFQ is 10 keV/u and we need to inject two charge states, 33+ and 34+ of uranium beams in order to achieve 400 kW of beam power on target. We will use a multi-harmonic buncher (MHB) and velocity equalizer in RAON LEBT to achieve it. The MHB uses three harmonics with 40.645 MHz and its two higher harmonic frequencies. The particle distributions in Δϕ-ΔW/W are given in Fig. 1 just after MHB. The rms beam envelope is given in Fig. 2. We found that the profile is consistent with TRACK simulation except bending magnet region.

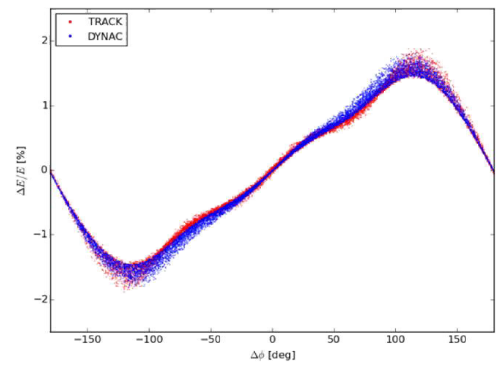

Figure 1: Particle distribution of DYNAC (blue) and TRACK (red) simulations in Δϕ-ΔW/W space.

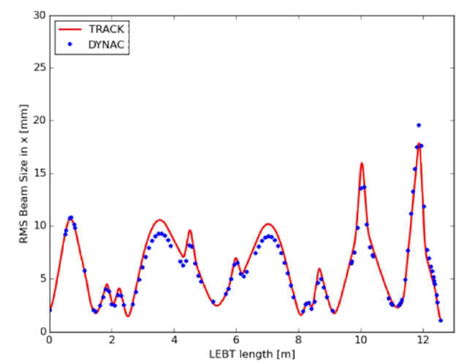

Figure 2: The rms beam envelope through RAON LEBT by DYNAC and TRACK codes.

The particle distribution at the entrance of the RFQ is given in Fig. 3 in the transverse phase space. The transverse beam parameters, twiss parameters and emittance, are summarized in Table 2.

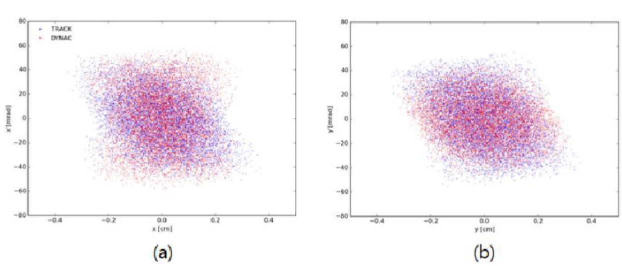

Figure 3: Particle distribution of DYNAC (blue) and TRACK (red) simulation results at the entrance of RFQ.

*Work supported by Ministry of Science, ICT and Future Planning.
#jhjang@ibs.re.kr

Content from this work may be used under the terms of the CC BY 3.0 licence (© 2015). Any distribution of this work must maintain attribution to the author(s), title of the work, publisher, and DOI.

ISBN: 978-3-95450-168-7 doi:10.18429/JACoW-IPAC2015-THPF073

Content from this work may be used under the terms of the CC BY 3.0 licence (© 2015). Any distribution of this work must maintain attribution to the author(s), title of the work, publisher, and DOI.

PROGRESS OF THE RAON HEAVY ION ACCELERATOR PROJECT*

Dong-O Jeon# representing the RAON
Institute for Basic Science, Daejeon, Republic of Korea

Abstract

Construction of the RAON heavy ion accelerator facility is progress in Korea with the In-flight Fragment (IF) and Isotope Separation On-Line (ISOL) facilities. Prototyping of major components and their tests are proceeding including the 28-GHz ECR ion source, RFQ, superconducting cavities, superconducting magnets and cryomodules. Superconducting magnets of the 28-GHz ECR ion source were fabricated and tested achieving 95% (80%) of design fields for the hexapole (solenoids) so far. Prototype superconducting cavities were fabricated through domestic vendors and delivered. Vertical tests showed good performance of the prototype cavities. Progress report of the RAON accelerator systems is presented.

INTRODUCTION

The RAON heavy ion accelerator facility is a unique facility that has the 400 kW In-flight Fragmentation (IF) facility and the 70 kW Isotope Separator On-Line (ISOL) facility providing wide range of rare isotope beams for users [1,2].

The driver accelerator for the IF facility is a superconducting linac (SCL) that can accelerate up to 200 MeV/u for the uranium beam delivering more than 400 kW of beam power to the IF target and various other targets. The driver for the ISOL facility is an H^- 70-MeV 1 mA cyclotron that delivers 70 kW beam power. The cyclotron has dual extraction ports with thin carbon foils for charge exchange extraction of H^- beam.

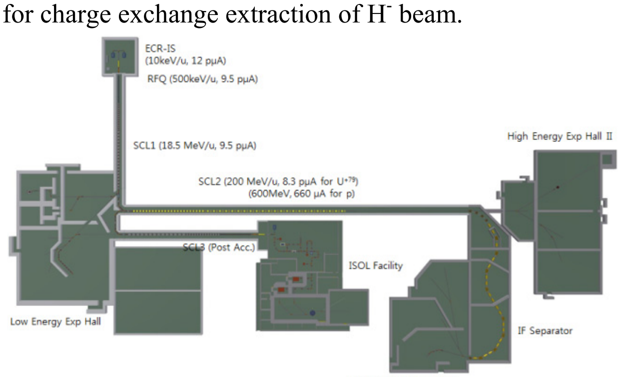

Figure 1: Plot of the RAON facility layout.

Rare isotope (RI) beams generated by the ISOL system is re-accelerated by a chain of post accelerators. The RI beams can be delivered to the low energy experimental hall or can be injected through P2DT to the SCL2 to accelerate to higher beam energy. The schematic layout of the facility is shown in Fig. 1.

The accelerator systems design is optimized to provide various high intensity stable ion beams and radioactive isotope (RI) beams from proton to uranium, while avoiding potential issues related with performance and operation.

Construction of the RAON heavy ion accelerator facility has begun December 2011 to be completed by December 2021. Detailed design of the accelerator systems has completed, and prototyping and testing of critical components and systems have been performed. In this paper, the status of the RAON accelerator systems is presented along with prototyping progress.

DRIVER LINAC

The driver linac consists of an injector (28-GHz ECR ion source, 500-keV/u RFQ) and SCL1 (QWR, HWR type), CSS (Charge Stripper Section) and SCL2 (SSR1, SSR2 type) that can accelerate a uranium beam to 200 MeV/u, delivering 400-kW beam power to the target. The driver linac can accelerate beams from proton to uranium.

Injector

28-GHz ECR ion source for the driver linac was designed [3] and its superconducting magnet assembly for the 28-GHz ECR ion source (ECRIS) was fabricated through domestic vendors. It consists of a saddle-type hexapole and four solenoids made of NbTi wires. Figure 2 shows the plot of the superconducting magnet assembly, the plot of ECRIS cryostat and actual ECRIS cryostat.

The cryostat for the 28-GHz ECRIS was put together and superconducting magnet tests have been carried out, achieving 95% (80%) of the design goal for the hexapole (solenoid) in a combined operation. Further magnet training is in progress. In parallel, beam extraction test is being prepared for of the 28-GHz ECRIS with a partial LEBT installed along with it.

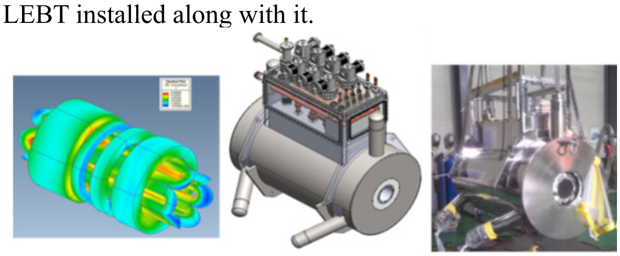

Figure 2: Plot of 28 GHz ECR ion source and its superconducting magnet assembly.

The 81.25-MHz RFQ is 5-meter long with a four-vane structure and its input and output beam energies are 10 keV/u and 500 keV/u respectively. RFQ prototype was successfully fabricated through a domestic vendor in September 2014, overcoming issues of the fabrication procedures and its photograph is shown in Fig. 3. The contract for the fabrication of the driver linac RFQ was

#jeond@ibs.re.kr

ISBN: 978-3-95450-168-7 doi:10.18429/JACoW-IPAC2015-THPF074

PROGRESS ON SUPERCONDUCTING LINAC FOR THE RAON HEAVY ION ACCELERATOR

H.J. Kim*, H.C. Jung, W.K. Kim, representing RAON, IBS, Daejeon, Korea

Abstract

The RISP (Rare Isotope Science Project) has been proposed as a multi-purpose accelerator facility for providing beams of exotic rare isotopes of various energies. It can deliver ions from proton to uranium. Proton and uranium ions are accelerated upto 600 MeV and 200 MeV/u respectively. The facility consists of three superconducting linacs of which superconducting cavities are independently phased. Requirement of the linac design is especially high for acceleration of multiple charge beams. In this paper, we present the RISP linac design, the prototyping of superconducting cavity and cryomodule.

INTRODUCTION

The RISP accelerator has been planned to study heavy ions in nuclear, material and medical science at the Institute for Basic Science (IBS). It can deliver ions from protons to uranium atoms with a final beam energy, for example, 200 MeV/u for uranium and 600 MeV for protons, and with a beam current range from 8.3 pμA (uranium) to 660 pμA (protons) [1, 2]. The facility consists of three superconducting linacs of which superconducting cavities are independently phased and operating at three different frequencies, namely, 81.25, 162.5 and 325 MHz.

SUPERCONDUCTING LINAC

Lattice Design

The configuration of the accelerator facility within the RISP is shown in Fig. 1. An injector system accelerates a heavy ion beam to 500 keV/u and creates the desired bunch structure for injection into the superconducting linac. The injector system comprises an electron cyclotron resonance ion source, a low-energy beam transport, a radio-frequency quadrupole, and a medium-energy beam transport. The superconducting driver linac accelerates the beam to 200 MeV/u. The driver linac is divided into three different sections, as shown in Fig. 2: a low-energy superconducting linac (SCL1), a charge stripper section (CSS) and a high-energy superconducting linac (SCL2). The SCL1 accelerates the beam to 18.5 MeV/u. The SCL1 uses two different families of superconducting resonators, i.e., a quarter wave resonator (QWR) and a half wave resonator (HWR). The SCL11 consists of 22 QWR's whose geometrical β is 0.047 and 22 quadrupole doublets. The resonance frequency of the QWR is 81.25 MHz. The cryomodule of the SCL11 hosts one superconducting cavity. The SCL12 consists of 102 HWR's whose geometrical β is 0.12 and 62 quadrupole doublets. The resonance frequency of the HWR is 162.5 MHz.

* hjkim@ibs.re.kr

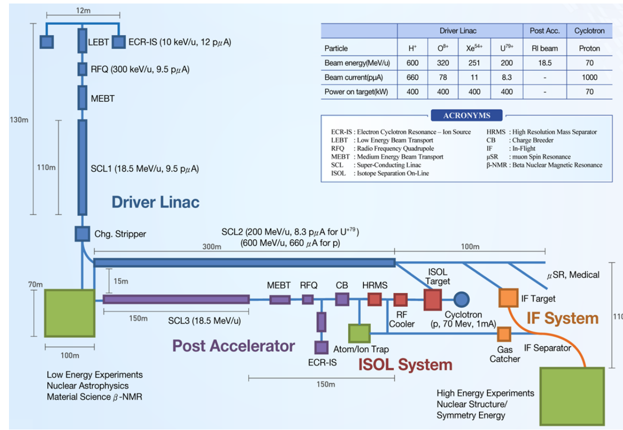

Figure 1: Layout of the RISP accelerator.

This segment has two families of cryomodules: one type of cryomodule hosts two superconducting cavities, and the other hosts four superconducting cavities. The CSS accepts beams at 18.5 MeV/u. The charge stripper strips electrons from the heavy-ion beams to enhance the acceleration efficiency in the high-energy linac section. The charge stripping section consists of normal conducting quadrupoles and room-temperature 45-degree bending magnets. The quadrupole magnets provide adequate transverse focusing and beam matching to the SCL2, and the bending magnet provides momentum dispersion for charge selection. The SCL2 accepts a beam at 18.5 MeV/u and accelerates it to 200 MeV/u. The SCL2 uses two types of single spoke resonators, i.e., SSR1 and SSR2. The SCL2 consists of the SCL21 and the SCL22, each with geometric β 0.30, resonance-frequency 325-MHz SSR and a geometric β 0.51, resonance-frequency 325-MHz SSR. The single-spoke-resonator type is chosen mainly because it can have a larger bore radius compared with the half-wave-resonator type, which is very important for reducing the uncontrolled beam loss in the high-energy linac section. The numbers of cavities in the SCL21 and the SCL22 is 69 and 138 respectively. The cryomodules of the SCL21 and SCL22 host 3 and 6 cavities, respectively. The SCL2 provides a beam into the in-flight fragmentation (IF) system via a high-energy beam transport (HEBT).

The post accelerator (SCL3) is designed to accelerate the rare isotopes produced in the ISOL (Isotope Separation On-Line) system. The SCL3 is, in principle, a duplicate of the driver linac up to low energy linear accelerator. The accelerated rare isotope beams are reaccelerated in the SCL2. Hence, the RISP accelerator provides a large number of rare isotopes with high intensity and with various beam energies.

Content from this work may be used under the terms of the CC BY 3.0 licence (© 2015). Any distribution of this work must maintain attribution to the author(s), title of the work, publisher, and DOI.

ISBN: 978-3-95450-168-7 doi:10.18429/JACoW-IPAC2015-THPF075

Content from this work may be used under the terms of the CC BY 3.0 licence (© 2015). Any distribution of this work must maintain attribution to the author(s), title of the work, publisher, and DOI.

PROTON BEAM OF 2 MeV 1.6 mA ON A TANDEM ACCELERATOR WITH VACUUM INSULATION*

S. Taskaev#, D. Kasatov, Novosibirsk State University, Russia
A. Kuznetsov, A. Makarov, I. Shudlo, I. Sorokin, BINP, Novosibirsk, Russia

Abstract

New type of charged particles accelerator, tandem accelerator with vacuum insulation, was proposed in BINP. The accelerator is characterized by fast acceleration of charged particles, long distance between ion beam and insulator (on which electrodes are mounted), big stored energy in the accelerating gaps and strong input electrostatic lens. High-voltage strength of vacuum gaps, dark currents, ion beam focusing, accelerating and stripping were investigated. Stationary proton beam with 2 MeV energy, 1.6 mA current has just been obtained. The beam is characterized by high-energy monochromaticity – 0.1%, and high current stability – 0.5%. Here we report the results of these investigations and discuss the proposal for obtaining 2.5 MeV 3 mA proton beam. The accelerator is considered to be a part of epithermal neutron source for boron neutron capture therapy and monoenergetic neutron source for calibration of dark matter detector.

INTRODUCTION

Currently, Boron Neutron Capture Therapy (BNCT) is considered as a promising technique for treatment of malignant tumours [1]. It provides selective destruction of tumour cells by prior accumulation inside them a stable boron-10 isotope and subsequent irradiation with epithermal neutrons. Because of the absorption of a neutron by boron, a nuclear reaction takes place with a large release of energy in the cell, leading to its death. Clinical trials on nuclear reactors showed that BNCT could treat glioblastoma, brain metastases of melanoma and several other tumours. For the widespread introduction of this technique in practice, compact sources of epithermal neutrons based on charged particle accelerators are required.

VACUUM-INSULATION TANDEM ACCELERATOR

The source of epithermal neutrons based on the original tandem accelerator with vacuum insulation and lithium neutron producing target was proposed and constructed in BINP [2]. Figure 1 shows the accelerator. Coming from the source *1* [3] negative hydrogen ion beam with 23 keV energy and 5 mA current is rotated in a magnetic field at an angle of 15 degrees, focused by a pair of magnetic lenses *2*, injected into the accelerator and accelerated up to 1 MeV. In the gas (argon) stripper *7*, which is installed inside the high-voltage electrode *5*, negative hydrogen ions are converted into protons. Then protons by the same 1 MV potential are accelerated to 2 MeV energy. The potential for the high-voltage *5* and five intermediate electrodes *6* of the accelerator is supplied by a high-voltage source *10* (most of the source is not shown) through the insulator *9*, wherein the resistive divider is set. Evacuation of gas is performed by turbomolecular pumps *8* mounted at the ion source and at the exit of the accelerator, and a cryogenic pump *4* via jalousies in the electrodes.

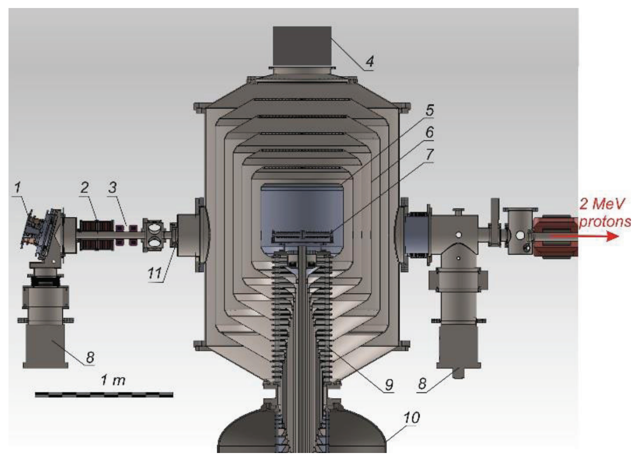

Figure 1: Tandem accelerator with vacuum insulation: *1* – source of negative hydrogen ions, *2* –magnetic lenses, *3* – correctors, *4* – cryogenic pump, *5* – high voltage electrode, *6* – intermediate electrodes, *7* – the gas stripper, *8* – turbomolecular pump, *9* – insulator, *10* – high-voltage power supply, *11* – inlet diaphragm.

A 50 kW sectitioned rectifier of industrial electron accelerator ELV is used as a high-voltage source providing voltage stability of 0.05% [4]. Vacuum part of the high-voltage feed-through insulator (Figure 2) is collected from 24 annular glass insulators with a diameter of 400 mm and a height of 35 mm, vacuum tightly strapped with intermediate electrodes through the rubber seals. The gas part of the insulator situated in a tank of a high voltage rectifier is composed of 14 ceramic rings with a diameter of 400 mm and a height of 60 mm, glued with their electrodes. The inner part of the feed-through insulator is filled with SF_6 gas at a pressure of 0.3 MPa, the high-voltage rectifier tank of 0.6 MPa. Maximum gradient along the surfaces of the insulators on the vacuum side is 12 kV/cm, on the sulfur hex side – 14 kV/cm, peak fields of the gaps in the gas region – 95 kV/cm.

* Work supported by Ministry of Education and Science of Russia (a unique identifier for applied scientific research – RFMEFI60414X0066)
# taskaev@inp.nsk.su

ISBN: 978-3-95450-168-7 doi:10.18429/JACoW-IPAC2015-THPF076

THERMAL AND STRUCTURAL ANALYSIS OF THE 72.75 MHz LINCE RFQ*

A.K. Orduz, C. Bontoiu, A. Berjillos, J.A. Dueñas, I. Martel, University of Huelva, Spain
A. Garbayo, AVS, Elgoibar, Gipuzkoa, Spain

Abstract

The 72.75 MHz LINCE RFQ [1] is designed to function at room temperature. Effective operation of the RFQ cavity requires efficient water cooling in order to dissipate significant resistive power non-uniformly distributed on the copper walls and vanes. This amounts to about 10 kW for one 0.5 m long RFQ section. Cylindrical cooling channels have been designed and optimized by varying their diameter and position in order to minimize the frequency shift generated by thermal displacements. The article reports results of power loss simulations coupled with electromagnetic modelling studies and their consequences on the RFQ performance in terms of resonant frequency and thermal deformations.

INTRODUCTION

The four-vanes RFQ is designed for LINCE high intensity accelerator complex [2]. The structure provides a 72.75 MHz resonating mode with a 1.3 MHz margin controlled by the tuners [1]. The initial beam is made of 2 ns long bunches of 40 keV/u and the aim of the design is to achieve 500 keV/u. The modulation was simulated using the DESRFQ code [3] with 82 kV inter-vane potential on a vane tip tested in ANL [4].

A complete loop of coupled numerical studies is achieved as shown in Fig. 1. The **RF Analysis** has been carried with COMSOL [5] resulting in an estimate for the resistive power losses. These are scaled and coupled with **Heat Transfer** model in order to obtain a temperature map at the vanes surface. The next step is the optimization of the cooling system according to the heat map. Two optimization for channel position, channel diameter, fluid and velocity temperature are carried out. The final heat flux is coupled to a **Solid Mechanics** study to estimates the stress and displacements due to thermal expansion. The frequency shift is obtained through a new RF study of the deformed structure.

RF ANALYSIS

The first study has been done with DESRFQ and Track [6] codes. Eigenfrequency studies have been done using COMSOL software, as shown before [1]. For the last version of the study the whole structure with modulated vanes was simulated and a 73.25 MHz for the quadrupole mode TE_{211} resonance is obtained.

Heat Map

Resistive power losses are calculated and that show the maximum loses are in the window corners as it is show in

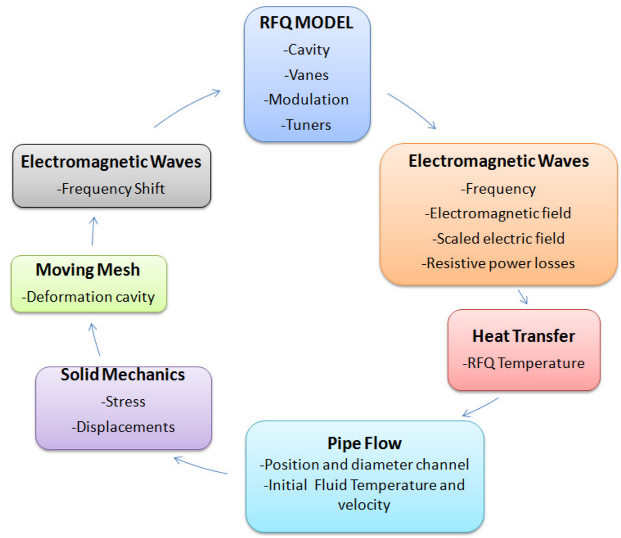

Figure 1: Study steps.

Fig. 2. This study is coupled with a non-isothermal pipe flow simulation in a quarter symmetry model (section) of the RFQ. The total resistive power dissipated by the RFQ working mode at 67.35 MHz is 10.67 kW. A cooling system must be design to control the heat dissipation in the RFQ.

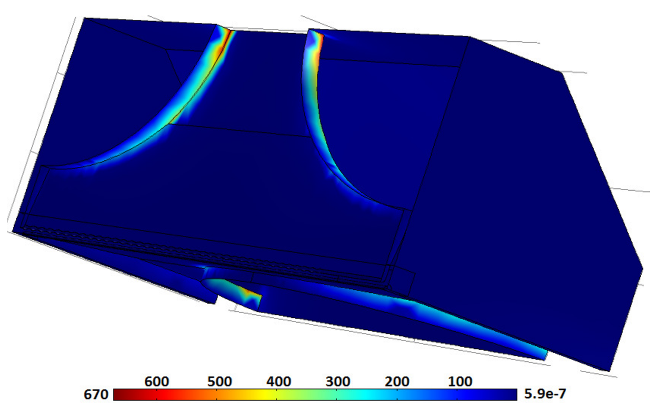

Figure 2: Resistive power losses [kW/m].

COOLING SYSTEM

According with the resistive power losses two models have been proposed as shown in Fig. 3. An initial cooling channel of rectangular profile has been considered due to its mechanical simplify as shown in Fig. 3(top) but proved unsatisfactory in the tip vanes. Therefore the second model Fig. 3(bottom) was studied whit better results.

* Work supported partially supported by the Spanish Government (MINECO-CDTI)under program FEDER INTERCONNECTA

Content from this work may be used under the terms of the CC BY 3.0 licence (© 2015). Any distribution of this work must maintain attribution to the author(s), title of the work, publisher, and DOI.

ISBN: 978-3-95450-168-7 doi:10.18429/JACoW-IPAC2015-THPF077

PROPOSAL FOR A 72.75 MH¿ RFQ FOR THE LINCE ACCELERATOR COMPLEX *

A.K. Orduz, C. Bontoiu, A. Berjillos, J.A. Dueñas, I. Martel, University of Huelva, Spain
A. Garbayo, AVS, Elgoibar, Gipuzkoa, Spain

Abstract

The low-energy part of the LINCE facility [1] can be based on a 72.75 MHz normal-conducting RFQ designed to give a 450 keV/u boost for A/Q=7 ions in about 5 m length. The vanes have been electromagnetically designed to accommodate dedicated RF windows producing effective separation of the RFQ modes in an octagonal-shaped resonance chamber [2]. This article outlines the optimization of the quality factor of the cavity by using numerical methods for electromagnetic calculations. Experimental results of RF test carried out on a prototype are also discussed.

INTRODUCTION

RFQ development, as a whole device is a very complex project which requires many iteration loops between physical concepts and engineering practices. Within the physical aspects, the development is carried out setting beam quality and specifications first. Considering a design mass-over-charge ratio A/Q=7 the RFQ must yield 460 keV/u energy gain working at a maximum inter-vane voltage of 82 kV. Results of the RF modelling process carried out in COMSOL [3], are outlined along the design stages from the shape of the resonator to the final modulated vanes including windows and tuners.

CAVITY OPTIMIZATION

Considering only two RFQ sections, the vanes and windows geometry can be optimized in order to produce the highest quality factor with a resonant frequency around 70 MHz such that adding modulation and tuners [2] would raise it in the 8 sections layout to about 72.75 MHz. This can be achieved in two stages:

- choice of the vane height and thickness in 2D with a predetermined cross-section in the beam region;
- optimization of the elliptical RF windows in 3D;

2D Optimization

The 2D optimization is achieved by doing a parametrization of the vane height which consists of several geometric pieces, namely a trapezoid, a rectangle, a stem and a half disk, all added on the top of the inter-vane radius R_0 = 6.16 mm. While the disk radius r_1 = 4.8 mm and stem height h_{stem} = 14 mm are kept constant, the rectangle and trapezoid height shown in Fig. 1 are taking values between 45 mm and 125 mm in steps of 2.5 mm.

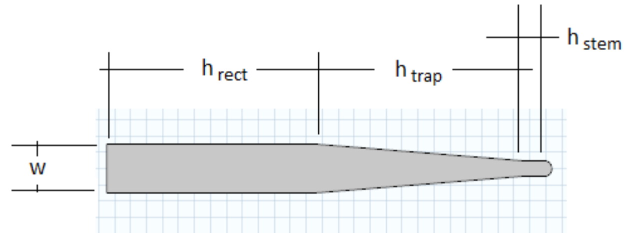

Figure 1: Transverse cross-section view of one vane.

Running the optimization process at three different values for the vane width w yields the quality factor and resonant frequency for the TM_{21} mode as shown in Fig. 2. For a given quality factor one must consider higher and thicker or shorter and thinner vanes. The trapezoid and rectangle heights are complementary in the sense that the same quality factor can be obtained decreasing any one of them and increasing the other one proportionally.

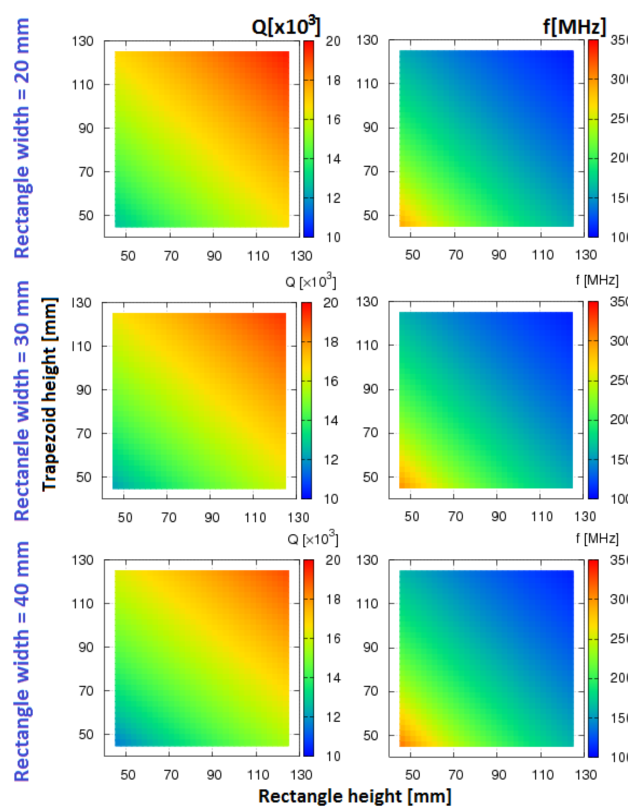

Figure 2: Evaluation of the quality factor and resonant frequency as function of rectangle and trapezoid height.

* Work partially supported by the Spanish Government (MINECO-CDTI) under program FEDER INTERCONNECTA

Content from this work may be used under the terms of the CC BY 3.0 licence (© 2015). Any distribution of this work must maintain attribution to the author(s), title of the work, publisher, and DOI.

ISBN: 978-3-95450-168-7 doi:10.18429/JACoW-IPAC2015-THPF078

Content from this work may be used under the terms of the CC BY 3.0 licence (© 2015). Any distribution of this work must maintain attribution to the author(s), title of the work, publisher, and DOI.

EFFECT OF THE FIELD MAPS ON THE BEAM DYNAMICS OF THE ESS DRIFT TUBE LINAC

R. De Prisco*, ESS, Lund, Sweden and Lund University, Lund, Sweden
M. Eshraqi, Y. I. Levinsen, R. Miyamoto, E. Sargsyan, ESS, Lund, Sweden
A. Karlsson, Lund University, Lund, Sweden

Abstract

In the beam dynamics design and modelling of the European Spallation Source (ESS) Drift Tube Linac (DTL) simplified models have been used for the focusing and accelerating elements. Since the high current requires precise control of the beam to analyze the losses it is useful to perform the beam dynamics simulations by using accurate field maps of the focusing and accelerating elements. In this paper the effects of the 3D-field maps on the beam dynamics of the ESS DTL are presented.

INTRODUCTION

The ESS DTL is an in-kind contribution from INFN/LNL [1]. Five Radio Frequency (RF) cavities (tanks) are used to accelerate a proton beam of 62.5 mA from 3.62 MeV to 89.68 MeV at 352.21 MHz; the transverse focusing system is composed by Permanent Magnet Quadrupoles (PMQs) arranged in a F0D0 lattice.

RF FIELD MAP OF THE ESS DTL

The design of the ESS DTL is defined in [2]. The cell numbers (and, consequently, the tank lengths) and the average electric accelerating field, E_0, are optimized simultaneously such that the sum of the power transferred to the beam, P_B, and the dissipated power on the internal tank surface, P_{Cu}, (including, on the last one, a factor 1.25 over the MDTfish computation) are slightly below 2.2 MW, that is the available RF power, P_{TOT}, per tank. The DTL parameters are summarized in Table 1 (E_{out} is the output energy of the beam at the end of each tank).

Table 1: DTL Parameters in Each Tank

Tank	1	2	3	4	5
E_0 [MV/m]	3.00	3.16	3.07	3.04	3.13
Cells	61	34	29	26	23
L_T [mm]	7618	7101	7583	7847	7687
P_B [kW]	1104	1114	1106	1064	1005
P_{Cu} [kW]	1088	1078	1090	1126	1190
P_{TOT} [kW]	2192	2191	2196	2189	2195
E_{out} [MeV]	21.29	39.11	56.81	73.83	89.68

Ideal and Nominal Accelerating Field

We define the average electric accelerating field, E_0, reported in the Table 1, as the *ideal* accelerating field, from now $E_{0,id}$. Even if all the cells, different in length, have the same frequency, *the accelerating field integral, cell by cell, is not constant* because of the imperfect mode matching between the adjacent cells. Thanks to algorithm presented in [3] it is possible to modify the geometry of the Drift Tubes (DTs) in order to calculate the electromagnetic field, solution of the Maxwell equations, inside each tank, such that the accelerating field is close to the ideal one. We call this field the *nominal* accelerating field, $E_{0,nom}$, shown in Fig. 1. From this moment all results are referred to the nominal accelerating field.

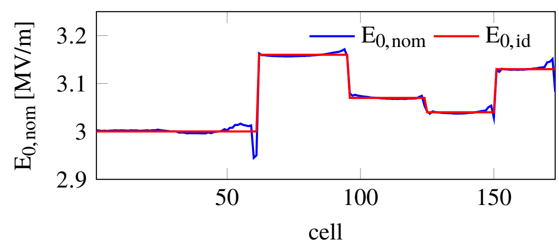

Figure 1: Nominal accelerating field in the DTL.

Self Perturbation Phenomena of the Post Couplers

The frequency perturbation due to the drift tube stems and the power couplers is compensated by tuning the cell face angles. Doing that the nominal accelerating field is achieved in the ESS DTL. Post Couplers (PCs) are used to stabilize the on axis accelerating electric field against tilts produced by mechanical errors (that, locally and randomly, change the resonant frequency of each cell). We define the *optimum lengths* of the PCs as the lengths for which there is the *confluence* [3]. The local frequency shift, due to the inserted PCs with their optimum lengths, must be compensated to avoid the *self perturbation* phenomena: uncompesated PCs produce, themselves, additional tilts of the accelerating electric field against which they are inserted.

FIELD MAP OF THE PMQs

The PMQ design is a modification of the segmented Halbach quadrupole.

The magnetic field into the beam pipe is given by the superposition of the magnetic fields of 16 parallelepiped permanent magnets of Sm_2Co_{17}. A transverse section of the PMQ is shown in Fig. 2. In each PMQ all the magnets (grey rectangles) have the same remanent magnetization along the appropriate direction.

The external radius of the PMQ housing is 30 mm. The transverse area of each of the 16 magnets is $w_m \times b_m$ =

* renato.deprisco@esss.se

ISBN: 978-3-95450-168-7 doi:10.18429/JACoW-IPAC2015-THPF079

A PLANNING AND SCHEDULING SYSTEM FOR THE ESS ACCELERATOR PROJECT

L. Lari, ESS, Lund, Sweden and CERN, Geneva, Switzerland
M. Conlon, H. Danared, L. Gunnarsson , G. Jacobsson, M. Jakobsson, M. Lindroos, E. Tanke
J.G. Weisend ESS, Lund, Sweden
P. Bonnal, CERN, Geneva, Switzerland

Abstract

Constructing a large, international research infrastructure is a complex task, especially when a large fraction of the equipment is delivered as in-kind contributions. A mature project management approach is essential to lead the planning and construction to deliver scientifically and technically.

The purpose of this paper is to present how the ESS accelerator project is managed in terms of planning and scheduling from the design phase until commissioning, keeping time, budgets and resources constraints, as well as creating and maintaining a strong and trust-based partnership with the external contributors.

INTRODUCTION

The European Spallation Source (ESS) is one of the largest science and technology infrastructure projects being built today. Bringing into successful operation this complex 1.8 billion-euro accelerator-based facility for neutron science implies collaborations among national institutions and nations. As a result, completing ESS, technically, financially and within schedule is strongly dependent from the capability of all the participants to meet delivery and performance specifications. In such a context of a complex project spanning over many years, a centralised project management team has been created in order to support the planning and scheduling activities of each macro project, such as the ESS Accelerator ones [1].

THE ESS CONSTRUCION PHASE

The ESS facility is currently under construction in Lund (Sweden). At present, the construction schedule is driven by the goals of producing neutrons by the end of 2019, completing the installation of the facility by the end of 2022 and installing/commissioning the neutron scattering instruments by the end of 2025.

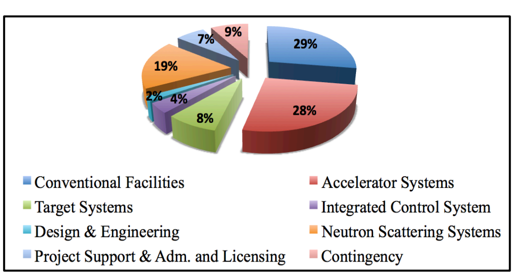

Figure 1: Distribution of the construction budget in % for the ESS macro-projects. The 510 million-euro accelerator project is shown in red.

The ESS construction phase is managed through seven macro project coordination schedules linked together. Five of the seven plans are machine and technically oriented, one is for tracking the civil engineering works, while two are used for administrative support (see Fig. 1). A centralized network-based is used for scheduling i.e. the Oracle's Primavera P6 software.

THE ESS ACCELERATOR PLAN

The ESS accelerator plan is a delivery oriented plan and an integrated cost-loaded multi-year and multi-level schedule. It covers from the start of the preliminary design of the accelerator components (2013) until the capability of delivering 2 GeV protons on Target (2022). It includes the design and industry preparation stages of the different accelerator systems, the development of the prototypes, the series production, the installation in gallery and tunnel buildings and the cold and beam commissioning of the ESS linac. The general services as well as the test stands for RF and cryomodules are also included in the accelerator budget and resource constraints of the schedule. The purpose of the plan is to give a complete and up-to-date picture of the whole Accelerator Project, including tracking the external partners contribution works.

The WBS of the ESS Accelerator Plan

A common Work Breakdown Structure (WBS) architecture is applied to all ESS projects during the construction phase. Work consists of activities and milestones, organized in a hierarchal structure (see Table 1). The WBS and levels do not necessary map in a one-to-one way the other breakdown structures, such as the ESS Product Breakdown Structure (PBS) of systems, sub-systems and components or the ESS Organizational Breakdown Structure (OBS).

Table 1: ESS Common WBS

WBS level	WBS element
1	ESS Programme
2	Projects
3	Work Packages (WP)
4	Work Unit (WU)
5	Activities/Milestones

Content from this work may be used under the terms of the CC BY 3.0 licence (© 2015). Any distribution of this work must maintain attribution to the author(s), title of the work, publisher, and DOI.

ISBN: 978-3-95450-168-7 doi:10.18429/JACoW-IPAC2015-THPF080

STATUS OF THE ESS ACCELERATOR CONSTRUCTION PROJECT

H. Danared, R. Garoby, D. McGinnis and E. Tanke, ESS AB, Lund, Sweden
M. Lindroos, ESS AB, Lund, Sweden and Lund University, Lund, Sweden

Content from this work may be used under the terms of the CC BY 3.0 licence (© 2015). Any distribution of this work must maintain attribution to the author(s), title of the work, publisher, and DOI.

Abstract

The European Spallation Source (ESS) is now under construction just outside in Lund in Sweden. The driver is a 5 MW linac operating at a duty factor of 4% and at 2 GeV. The detailed design of the buildings is just being completed, and the casting of the accelerator tunnel has started. The accelerator design is getting mature with the major parts under prototyping. A challenging aspect of the project is the large percentage of in-kind contributions. For the accelerator this is now reaching 50% in pre commitments by institutes and universities in the ESS member states. We will in this paper give an overview of the ESS accelerator design, the status of prototyping and the organization of the in-kind accelerator construction project.

THE ESS PROJECT

The ESS is a multi-disciplinary research centre based on the world's most powerful neutron source. This new facility will be 30–100 times brighter than today's leading facilities, enabling new opportunities for researchers in the fields of life sciences, energy, environmental technology, cultural heritage and fundamental physics. The facility is planned to have 570 MeV protons and first neutrons in 2019 and a user program starting in 2023.

ACCELERATOR BASELINE

The ESS accelerator high-level requirements are to provide a 2.86 ms long proton pulse at 2 GeV and a repetition rate of 14 Hz. This represents 5 MW of average beam power with a 4% duty cycle on target.

The ion source produces a proton beam that is transported through a Low Energy Beam Transport (LEBT) section to the Radio Frequency Quadrupole (RFQ) where it is bunched and accelerated up to 3.6 MeV. In the Medium Energy Beam Transport (MEBT) section the transverse and longitudinal beam characteristics are diagnosed and optimized for further acceleration in the Drift Tube Linac (DTL). The first superconducting section consists of 26 double-spoke cavities (SPK) with an optimum beta value of 0.50. The spoke cavities are followed by 36 Medium Beta Linac (MBL) elliptical cavities with β = 0.67 and 84 High Beta Linac (HBL) elliptical cavities, with β = 0.86. After acceleration the beam is transported to the target through the High Energy Beam Transport (HEBT) section and rastered on the target using an active fast magnet beam delivery system. A block diagram of the ESS accelerator design can be seen in Figure 1.

ACCELERATOR IN-KIND

Introduction

ESS is a new organization at a green field site set up in 2009. The design update of the ESS accelerator, undertaken from 2009 to 2013, was done in a collaboration including INFN in Italy, CEA and CNRS in France, ISA in Denmark, ESS-Bilbao in Spain, Uppsala University and Lund University in Sweden and the emerging ESS accelerator division. The design update resulted in a Technical Design Report [1] for the full facility, which has been the base of further negotiations for the funding of ESS. The funding for the construction is today secured but with a request from the member states for a very high proportion of in-kind financing. The target for the accelerator

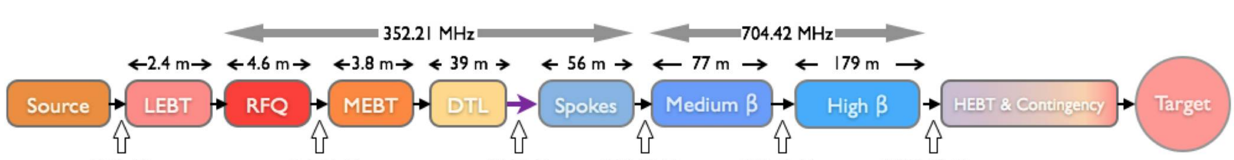

Figure 1: Schematic layout of the ESS linac [2]. Blue colour represents superconducting sections.

ISBN: 978-3-95450-168-7 doi:10.18429/JACoW-IPAC2015-THPF081

ON THE SUITABILITY OF A SOLENOID HORN FOR THE ESS NEUTRINO SUPERBEAM

M. Olvegård, T. Ekelöf, R. Ruber, V. Ziemann, Uppsala University, Sweden
J.-P. Koutchouk, Uppsala University, Sweden and CERN, Geneva, Switzerland

Abstract

The European Spallation Source (ESS), now under construction in Lund, Sweden, offers unique opportunities for experimental physics, not only in neutron science but potentially in particle physics. The ESS neutrino superbeam project plans to use a 5 MW proton beam from the ESS linac to generate a high intensity neutrino superbeam, with the final goal of detecting leptonic CP-violation in an underground megaton Cherenkov water detector. The neutrino production requires a second target station and a complex focusing system for the pions emerging from the target. The normal-conducting magnetic horns that are normally used for these applications cannot accept the 2.86 ms long proton pulses of the ESS linac, which means that pulse shortening in an accumulator ring would be required. That, in turn, requires H- operation in the linac to accommodate the high intensity. As an attractive alternative, we investigate the possibility of using superconducting solenoids for the pion focusing. This solenoid horn system needs to also separate positive and negative pion charge as completely as possible, in order to generate separately neutrino and anti-neutrino beams. We present here progress in the study of such a solenoid horn.

INTRODUCTION

The European Spallation Source (ESS) will provide neutrons to a variety of experiments in the applied sciences, starting 2019. The spallation neutrons are generated by a 5 MW proton beam impinging at 2 GeV on a rotating tungsten target. This world-unique intensity attracts projects beyond the neutron sciences, one of which is the ESS neutrino superbeam study, ESSnuSB [1]. The ESSnuSB plans to use a 5 MW beam from the ESS linac to produce an intense neutrino beam in a separate target station, as shown with the sketch in Fig. 1. These neutrinos will be directed towards an underground detector several hundreds of kilometers from the ESS site, where the number of electron and muon neutrinos will be counted. Placed at the second neutrino oscillation maximum, the megaton water Cherenkov detector is expected to help settle the existence of CP violation in the leptonic sector, by recording and comparing the amounts of neutrinos and anti-neutrinos.

The nuclear reactions that occur as the proton beam hits the target generate a shower of hadrons, mostly pions. These pions are to be collected and focused so that they travel in the direction of the far detector before they decay into muons and muon neutrinos. The established way of hadron collection is with a magnetic horn [2], which consists of a toroidal magnet structure where the pions need to traverse a thin metallic conductor layer in order to reach the magnetic field region. The structure is powered by 350 kA [3], which leads to heavy ohmic heat dissipation in the conductor layer. As a result, the horn cannot accept the 2.86 ms proton pulse directly from the ESS linac, but an accumulator ring for pulse compression down to a few microseconds, is required [4]. For efficient injection into the ring the linac must support acceleration of H^- as well as the protons for neutron production, which has additional implications for the linac optics, and for the minimum curvature of transfer lines, etc. In addition, it requires an H^- source. In total, the horn requirements lead to an increase of the project complexity and cost and there are strong motivations for an alternative hadron collection scheme using superconducting magnets.

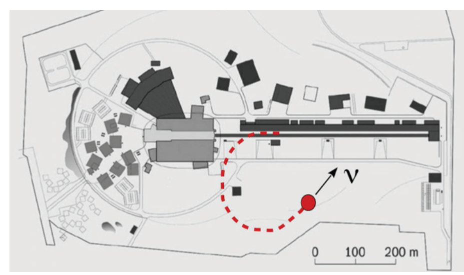

Figure 1: A sketch of the ESSnuSB layout at the ESS site.

BACKGROUND

An attractive alternative to the van der Meer horn is a superconducting solenoid. Earlier studies conducted for neutrino factories and muon colliders, as well as for neutrino superbeams, have shown that a solenoid horn could perform as well or better for certain neutrino energy ranges [5]. Here, we look specifically at the ESSnuSB case with a moderate proton beam energy of 2 GeV.

The pion distribution expected from the target was computed by N. Vassilopoulos for a van der Meer horn [3] and is shown in Fig. 2. We see a wide distribution both in total momentum and in emission angle θ with respect to the forward axis. The 2D distribution has its peak at around 500 MeV and 0.6 rad, which, with the strong tails, means that powerful collection directly at the target is necessary.

Figure 3 shows the decay scheme of the pions, whose life time in the rest frame is 26 ns. Since the detector cannot distinguish neutrinos from anti-neutrinos the pions of the wrong sign must be removed close to the source, before they have time to decay and contaminate the beam. Secondly, the length of the decay tunnel must be optimized so that the number of muons that have time to decay is mini-

Content from this work may be used under the terms of the CC BY 3.0 licence (© 2015). Any distribution of this work must maintain attribution to the author(s), title of the work, publisher, and DOI.

ISBN: 978-3-95450-168-7 doi:10.18429/JACoW-IPAC2015-THPF082

CONSIDERATIONS ON THE FAST PULSED MAGNET SYSTEMS FOR THE 2 GEV BEAM TRANSFER FROM THE CERN PSB TO PS

T. Kramer, J.L. Abelleira, W. Bartmann, J. Borburgh, L. Ducimetière, L.M. Feliciano, B. Goddard, L. Sermeus, CERN, Geneva, Switzerland

Abstract

Under the scope of the LIU project the CERN PS Booster to PS beam transfer will be modified to match the requirements for the future 2 GeV proton beam energy upgrade. This paper describes considerations on the PSB extraction and recombination kickers as well as on the injection kicker(s) into the PS. Different schemes of an injection into the PS have been outlined in the past and are reviewed under the aspect of individual transfer kicker rise and fall time performances. Recent measurements on the recombination kickers are presented and subsequently homogenous rise and fall time requirements in the whole PSB to PS transfer chain are discussed. New options for the PS injection kicker(s) are outlined and compared to the previously presented concepts.

INTRODUCTION

CERN's accelerator complex is undergoing a massive upgrade program in the framework of the LHC Injectors Upgrade (LIU) project [1]. In the CPS complex the Proton Synchrotron Booster (PSB) will see an energy upgrade to 2 GeV to enable the limitation in intensity due to the space-charge tune shift in the PS to be overcome [2]. The extraction systems of the PSB, the recombination beam lines and beam transfer elements, as well as the injection system of the PS will all need to function at the new higher beam energy. At the same time, the rise and fall times of the kickers must be compatible with the required bunch lengths and filling schemes for future HL-LHC beams, and with the specifications to reach the present performance for the existing 1.4 GeV beams for fixed-target users in the PS complex and the SPS. Table 1 gives an overview of the basic machine parameters.

Table 1: PSB and PS Main Beam Parameters

Parameter	Present	LIU upgrade
Beam energy [GeV]	1.4	2.0
Beam rigidity [T.m]	7.14	9.28
PSB t_{rev} [ns]	571	552
PS t_{rev} [ns]	2286	2210

Considerations on the Kicker Rise Times

The kicker rise/fall times (along with gap field) are key parameters, and affect strongly the technical choices, cost and performance of the planned upgrades, plus the overall feasibility and risk. The bunch lengths and gaps between bunches in the two machines are a function of the harmonic numbers, of the beam momentum and also of the beam type (intensity and longitudinal emittance/RF voltage). To alleviate the space charge limitations in the PS, the LHC type beams will be transferred at 2.0 GeV with the maximum possible bunch lengths and imposes together with the machine harmonic numbers the kicker rise and fall times. Table 2 shows an overview of the individual requirements for the involved kicker systems.

PSB EXTRACTION

The four BE.KFA14L1 kickers (one per ring) eject the beam from the PSB. The rise time must be short enough to fit into the shortest gap between the two longest bunches which is 105 ns for operation with PSB harmonic number 2 and PS harmonic numbers 7 or 8. Note that the PS harmonic number determines this shortest gap, and not the PSB one.

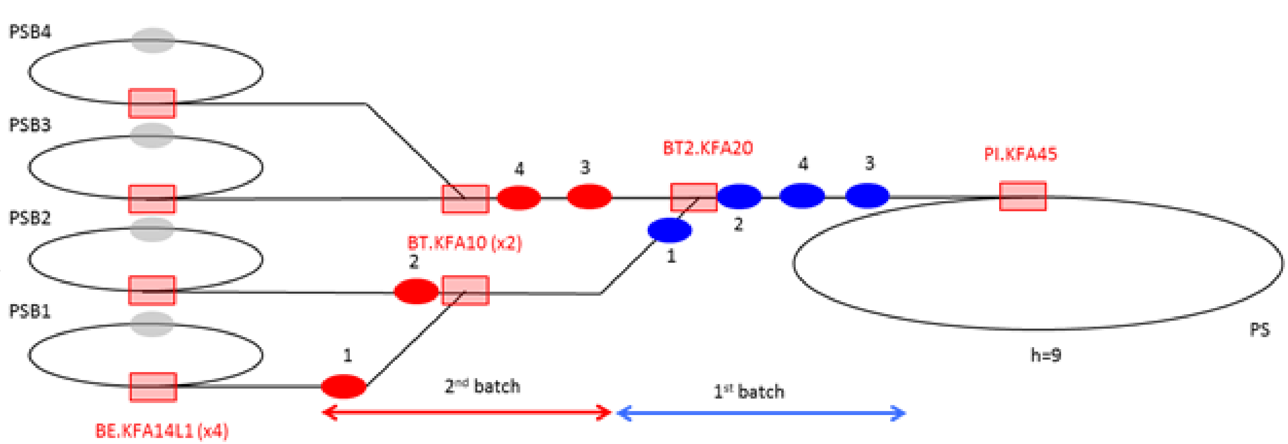

Figure 1: Schematic of beam transfer between PSB and PS, illustrated for the HL-LHC BCMS scheme [3].

Content from this work may be used under the terms of the CC BY 3.0 licence (© 2015). Any distribution of this work must maintain attribution to the author(s), title of the work, publisher, and DOI.

ISBN: 978-3-95450-168-7 doi:10.18429/JACoW-IPAC2015-THPF083

PAINTING SCHEMES FOR CERN PS BOOSTER H- INJECTION

J. L. Abelleira, W. Bartmann, E. Benedetto, C. Bracco, G.P. Di Giovanni, V. Forte, M. Meddahi, B. Mikulec, G. Rumolo, CERN, Geneva, Switzerland; M. Kowalska, EPFL, Lausanne, Switzerland.

Abstract

The present 50-MeV proton injection into the PS Booster will be replaced by a H$^-$ charge exchange injection at 160 MeV to be provided by Linac4. The higher energy will allow producing beams at higher brightness. A set of kicker magnets (KSW) will move the beam across the stripping foil to perform phase space painting in the horizontal plane to reduce space charge effects. The PSB must satisfy the different users with very different beams in terms of emittance and intensity. Therefore, the KSW waveforms must be adapted for each case to meet the beam characteristics while minimizing beam losses. Here we present the results of the simulations performed to optimise the injection system. A detailed analysis of the different painting schemes is discussed, including the effect of the working point on the painted beam, and variations in the offset of the injected beam.

INTRODUCTION

In this paper we present a description of the injection process and its influence on the profile for different beams. We assume that each pulse coming from the Linac4 and reaching the 4 rings of the PSB has 6.5x10^{13} protons over a length of 400 μs with an average current of 26 mA. The number of injection turns needed for each PSB user is adjusted according to the required intensity, taking into account that the revolution period of the PSB at injection is $\sim 1\mu s$. We will describe the injection for two particular cases: LHC beam and High Intensity beam (HI). In the latter case, an injection over 100 turns has been considered, in order to build up a final intensity of 1.6×10^{13} p^+. This means injecting in the PSB twice as much intensity as we do today for this kind of beam. with twice as much intensity. Also the beam brightness of the LHC beams would be doubled. Two scenarios have been analyzed for the simulations. We have called tune 1 the baseline working point, with tunes Q_x=4.28 and Q_y=4.55. The second scenario, called tune 2, is intended to reduce space-charge blow up during acceleration and corresponds to a working point of Q_x=4.43 and Q_y=4.60.

Table 1 summarizes the beam characteristics of the two different LIU [1] beams studied in this paper and compares it with the present values in operation.

SIMULATIONS

We simulated the H$^-$ charge exchange process with the ORBIT code [2]. The stripping foil is made of Carbon with a density of 200 $\mu g/cm^3$ and a dimension of 32 mm [H] and 58 mm [V]. The simulations include a complete aperture model that allows to analyze the particle losses around the PSB ring. We have assumed a matched (including dispersion) 0.4 μm normalized emittance beam and we have injected in each case a total of 5×10^5 macroparticles. The space-charge effects have been taken into account as well as the edge focusing of the chicane magnets. For the case of HI beams, we have simulated also a phase space painting in the longitudinal plane.

Table 1: Characteristics of LHC and HI Beams (Present and LIU). Injection Energy, Extraction Energy, Beam Intensity per Ring and Normalized Emittance (Horizontal and Vertical)

	Present		LIU	
Beam	LHC	HI	LHC	HI
E_{inj} [MeV]	50	50	160	160
E_{ext} [GeV]	1.4	1.4	2.0	1.4
N [$x10^{12}$]	1.8	8.0	3.4	16
$\epsilon_{N,x}[\mu m]$	2.1	15	1.7	13
$\epsilon_{N,y}[\mu m]$	2.1	8	1.7	6

LHC BEAMS

Other studies have been carried out to define the optimal brightness in the PSB, characterizing a relation (curve) between beam intensity and target emittance [3]. We have studied how the H$^-$ injection is able to reproduce each point of the so-mentioned curve. For this purpose we have assumed a maximum intensity of 3.4×10^{12} p^+. For this beam intensity we need to inject over 21 turns.

To enlarge the emittance of $\epsilon_N = 0.4\mu m$ provided by Linac4, the injected beam is off-centered with respect to the circulating one. For the vertical plane, the offset is applied using the steerers in the transfer line. For the horizontal one, we have varied instead the circulating orbit with respect to the injected beam (which is located at $x = -35$ mm) with the help of the KSW magnets. We have observed that for the same initial conditions, different tunes give different final emittances, as the particle distribution turns by a different angle in the respective phase space. For this reason the position of the circulating beam at the stripping foil must be adjusted for each tune. We have placed the KSW bump at $x = -31.5$ mm for tune 1 and $x = -33.5$ mm for tune 2. The vertical offset of 3 mm gives similar results as the tune difference in this case is very small (~ 0.05). Assuming an ideal machine, we have attained for both working points the target emittances at the end of injection of $\sim 1.2\mu m$; that would leave some margin ($\sim 0.5\mu m$) for other sources of emittance growth such as optics mismatch or blow up from space charge during acceleration [4].

Content from this work may be used under the terms of the CC BY 3.0 licence (© 2015). Any distribution of this work must maintain attribution to the author(s), title of the work, publisher, and DOI.

ISBN: 978-3-95450-168-7 doi:10.18429/JACoW-IPAC2015-THPF084

ProTec - A NORMAL-CONDUCTING CYCLINAC FOR PROTON THERAPY RESEARCH AND RADIOISOTOPE PRODUCTION

R. Apsimon*, G. Burt, J. Mitchell, S. Pitman, Lancaster University, Bailrigg, UK
H. Owen, University of Manchester, Manchester, UK
A. Degiovanni, CERN, Geneva, Switzerland

Abstract

The ProTec cyclinac proposes the use of a 24 MeV high-current cyclotron to inject protons into a normal-conducting linac pulsed at up to 1 kHz to give energies up to 150 MeV. As well as being able to produce radioisotopes such as ^{99m}Tc, the cyclinac can also provide protons at higher energy with beam properties relevant for proton therapy research. In this paper we present a comparison of linac designs in which S-band structures are used at lower energies, prior to injection into a high-gradient X-band structure; issues such as beam capture and transmission are evaluated.

INTRODUCTION

The ProTec cyclotron-linac, or cyclinac, is proposed as a multi-purpose facility which could simultaneously provide two proton beams [1]. Fed from a single high-current cyclotron that may generate extracted proton currents in excess of 500 μA to a single beamline, when that current is pulsed it may also feed a linac to obtain much higher energies albeit with lower currents. As such, such a facility could serve both as a regional site for production of medical radioisotopes whilst also being suitable for conducting research with higher-energy proton beams. In particular, we propose to utilise very high gradient X-band cavities to obtain 150 MeV protons suitable for testing methods and equipment to benefit particle radiotherapy. Whilst such research is possible at hospital proton therapy facilities, research time at such facilities is limited and this, a dedicated facility, provides much greater access.

We consider at present a cyclotron, such as the ACSI TR-24 [2], as a high-current cyclotron with multiple extraction ports which can obtain a suitably-high current for isotope production. One notable application is the volume production of ^{99m}Tc for nuclear medicine, in which a single c.1 mA cyclotron can, for example, provision sufficient numbers of technetium doses (around 250,000 per year per cyclotron) for about half of UK clinical demand [3, 4]. The TR-24 - similar to other multi-port cyclotrons - has two ports where we envisage providing up to four stations. Three of these are proposed to be at low energy to provide for radioisotope production; radiobiology research; irradiation experiments. The fourth station will feed the high-energy line that comprises both S- and X-band structures. S-band structures are proposed to accelerate the proton from 24 MeV up to ~100 MeV with an accelerating gradient of ~30 MV/m. High-gradient X-band structures will be used to further accelerate the beam to energies up to 150 MeV, with an accelerating gradient of at least ~50 MV/m.

We have chosen a cyclinac - that uses a cyclotron as its injector - for several reasons. Firstly, for protons energies up to 30 MeV and currents up to c.1 mA the cyclotron is a very mature technology that is compact, readily available commercially, and relatively inexpensive compared to alternative approaches such as linacs. Thus the low-energy stations can be obtained with minimal project risk. Although the extracted cyclotron beam is not naturally matched to the needs of a linac, the cyclinac concept has been explored at several institutions for a number of years and its technical issues have been well explored and addressed (see below). A summary of the extraction beam parameters of the TR-24 cyclotron are given in Table 1 [3, 5].

Table 1: TR-24 Extracted Beam Parameters

Parameter	Value
ε_x (90%, normalised)	10μm.rad
ε_y (90%, normalised)	17μm.rad
Beam energy	24 MeV
Energy spread (FWHM)	0.41 MeV
RF frequency	84.75 MHz
Bunch spacing	11.8 ns
Bunch length	2 ns

DESIGN CONSIDERATIONS

Transfer Line Optics

The 24 MeV protons extracted from the cyclotron must travel through a beam transfer system (BTS) some distance (~10 m) to the linac entrance. The protons have average relativistic parameters $\gamma_r = 1.026$ and $\beta_r = 0.222$; the velocity spread, σ_v, of the extracted bunches can be expressed in terms of energy spread, σ_E, as

$$\sigma_v = \frac{c\sigma_E}{\gamma_r^3 \beta_r mc^2}. \quad (1)$$

The velocity spread for low-energy bunches can therefore be quite large; which leads to ballistic (velocity) de-bunching that will lengthen the bunches from ~2 ns to ~3 ns. However, the bunches are then divided into sub-bunches in the higher frequency linac so this lengthening has no overall effect; the final pulse structure at the high-energy station will be insensitive to this.

* r.apsimon@lancaster.ac.uk

Content from this work may be used under the terms of the CC BY 3.0 licence (© 2015). Any distribution of this work must maintain attribution to the author(s), title of the work, publisher, and DOI.

ISBN: 978-3-95450-168-7 doi:10.18429/JACoW-IPAC2015-THPF085

Content from this work may be used under the terms of the CC BY 3.0 licence (© 2015). Any distribution of this work must maintain attribution to the author(s), title of the work, publisher, and DOI.

BEAM COMMISSIONING OF LINAC4 UP TO 12MeV

V. A. Dimov, E. Belli, G. Bellodi, J.B. Lallement, A. M. Lombardi, CERN, Geneva, Switzerland
M. Yarmohammadi Satri, IPM, Tehran, Iran

Abstract

CERN Linac4 is made of a 3 MeV front end including a 45 keV source , a 3 MeV Radio Frequency Quadrupole (RFQ) and a fast chopper, followed by a 50 MeV Drift Tube Linac (DTL), a 100 MeV Cell-Coupled Drift Tube Linac (CCDTL) and a 160 MeV Pi-Mode Structure (PIMS). The Linac4 beam commissioning is performed in 6 stages of increasing energy. Movable beam diagnostics benches, with various instruments, are used at each step to allow the detailed characterisation of operational parameters that will play a key role in the overall future performance. The first three stages of the commissioning, up to 12 MeV beam energy, have been completed at the end of 2014. The RFQ and the chopper line at 3 MeV, as well as the first tank of the DTL at 12 MeV were fully characterised, using permanent diagnostic instruments and a movable diagnostic bench equipped with a spectrometer, a slit-grid emittance meter, a Bunch Shape Monitor, Beam Position Monitors and a laser-emittance device. This paper reports on the strategy and the results of the commissioning up to 12 MeV. It also presents the validation of the set-up strategy, which is essential for the next stages of commissioning.

INTRODUCTION

Linac4 is a normal conducting, 160 MeV H- ions accelerator that is being constructed within the scope of the LHC Injectors Upgrade project. Linac4 will be connected to the Proton Synchrotron Booster during the next long LHC shutdown and it will replace the current 50 MeV proton linac, Linac2. Linac4 is being commissioned progressively with the installation of the accelerating structures into the Linac4 tunnel.

The first three stages of commissioning, which focused mainly on the characterisation of the RFQ (3MeV), the validation of the chopping system and the characterisation of the first DTL tank (12MeV), have been successfully performed by the end of 2014. A temporary version of the ion source, which gives about 20mA of beam current, was used during each stage.

Figure 1: The Linac4 basic architecture up to 12MeV.

Figure 1 shows the Linac4 basic architecture up to 12MeV and Fig. 2 shows the movable diagnostic bench, which was used for the beam commissioning at 3MeV and 12MeV. The bench was consecutively used for the beam measurements after the RFQ, the Medium Energy Beam Transport (MEBT) line and the DTL tank1. In addition to the temporary diagnostic instruments on the bench, the permanent diagnostic instruments of the MEBT line and between the DTL tank1 and tank2 were also used where necessary.

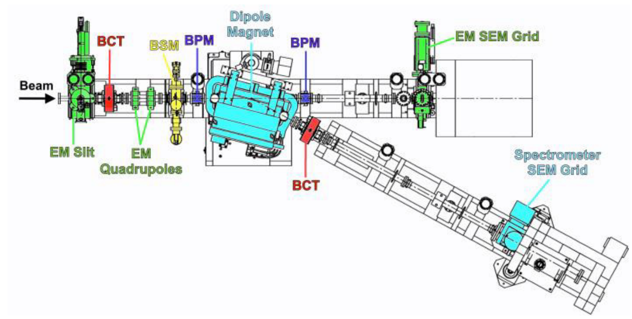

Figure 2: Movable diagnostic bench for 3MeV and 12MeV beam measurements.

During the 3MeV and 12MeV commissioning periods, the same beam properties were measured using different methods and instruments and then compared. In addition to the characterisation of the accelerating structures, these commissioning stages were particularly important for cross-calibration of the permanent diagnostic instruments with the temporary ones and validating the measurement methods, which are crucial for the high energy beam commissioning stages.

The following sections summarize the significant results of the 3MeV commissioning stage, with relevant references, and explain the measurement process and the results of the 12MeV commissioning in detail.

3MeV COMMISSIONING

During the 3MeV commissioning stage, many issues were addressed. The major ones were: confirming the RFQ performance, validating the chopping system operation and finding the RF phase and amplitude setting of the cavities on the MEBT line.

The performance of the RFQ and the calibration of the RF amplitude were confirmed by varying the power in the RFQ and measuring the transmission [1].

The chopping system is composed of four plates, followed by a cone shaped in-line dump. The correct operation of the chopping system was confirmed by measuring the transmission of the main and the chopped

ISBN: 978-3-95450-168-7 doi:10.18429/JACoW-IPAC2015-THPF086

A NEW HARDWARE DESIGN FOR PSB KICKER MAGNETS (KSW) FOR THE 35 mm TRANSVERSE PAINTING IN THE HORIZONTAL PLANE

L. Feliciano, C. Bracco, L. Ducimetière, A. Fowler,
G. Grawer, R. Noulibos, L. Sermeus,
W. Weterings, C. Zannini, CERN, Geneva, Switzerland

Abstract

The changeover from Linac2 to Linac4 in CERN's injector chain will allow increasing the injection energy into the PS Booster from 50 MeV to 160 MeV [1]. Transverse phase space painting will be performed in the horizontal plane, by means of four stacks of four KSW kicker magnets. The KSW magnets are located outside the injection region and will produce a 35 mm closed orbit bump, with falling amplitude during the injection to accomplish transverse phase space painting to the required emittance. New magnets with two different types of coils are being built using the existing design. The magnets are made of two halves, which are assembled together around a vacuum ceramic chamber. In order to reduce the beam impedance, the ceramic chamber is internally coated by a thin titanium layer. A new multiple-linear waveform generator has been developed to provide the high flexibility in the KSW kicker magnets current decay to fulfil the requirements of all the different users (LHC, nTOF, ISOLDE, CNGS, etc.).

INTRODUCTION

In the framework of the Linac4 – LIU (LHC Injectors Upgrade) project the European Organization for Nuclear Research (CERN) is designing a new layout for the transverse painting in the horizontal plane with kickers (KSW). The 160 MeV H^- ions beam from Linac4 will be distributed to four superposed rings of the PS Booster (PSB) and a new multi-turn H^- charge exchange injection system [2] will allow increasing the beam intensity in the PSB. A series of 4 horizontal kickers (KSW), outside the injection region, will produce a 35 mm closed orbit, with falling amplitude during injection, and uniformly fill the horizontal phase space (transverse painting) and move the circulating beam away from the stripping foil; this will allow the reduction of the emittance (ε_x) blow-up induced by space charge effects and scattering processes.

KICKER REQUIREMENTS

Two types of KSW magnets will be installed in the PSB layout to produce the transverse painting bump. Optics studies showed that, since the magnets are not symmetrically distributed around the stripping foil, each type of magnet has to give a slightly different kick to perfectly close the bump and prevent any orbit leakage around the ring. All the magnets will thus be individually powered.

A high flexibility in the KSW current decay waveform is needed to fulfil the requirements of all the different users. A multiple-linear waveform is chosen for the KSW generators as schematically shown in Fig 1.

For an "ideal painting" (red line in Fig 1), an initial fast decay over few turns (called in the following Slope 1) has to be followed by an almost constant slope (Slope 2) until the end of injection. This allows filling first the centre and then the outer area of the transverse phase space reducing the charge density in the core of the bunch and thus the space charge effects. Once injection is finished, the circulating beam is moved away from the foil (Slope 3), as fast as possible, until a negative bump of -9.2 mm (fixed for all the users) to avoid any further interaction with the foil. At this point also the chicane starts decaying and the KSW bump goes to zero in 1 ms.

For small emittance beams (i.e. LHC beams), no painting is applied during the full injection process, the bump stays constant at 35 mm (I_0 green line in Fig 1). This could vary between 10 μs and 20 μs, depending on the current delivered by Linac4. During injection, the deviation from the reference waveforms must be always kept smaller than 1%. After injection the beam has to be moved away from the foil as quickly as allowed by the HW. Studies with ORBIT [3] were performed assuming the fall of the injection bump from 35 mm to zero in 10 μs (cyan line in Figure 1; a 2 μs margin was considered to take into account possible delays induced by the eddy currents in the Titanium layer of the vacuum chambers as explained in above). Such decay speed allows keeping the number of foil crossings low enough to limit the emittance blow-up.

For the high intensity and large emittance beams (i.e. ISOLDE, nTOF, etc.) the "ideal painting" will be performed. In case of 40 mA average current delivered by Linac4 up to the PSB, the maximum target intensity (2.5×10^{13} protons per ring for ISOLDE) can be accumulated in 100 μs. The eventuality of a non-optimum performance of Linac4 (reduced current) and the consequent need to extend the injection process up to 150 μs to reach the target intensity is taken into account [4].

The envelope conditions for the KSW current decay (ΔI), depending on the user, are the following:

Content from this work may be used under the terms of the CC BY 3.0 licence (© 2015). Any distribution of this work must maintain attribution to the author(s), title of the work, publisher, and DOI.

ISBN: 978-3-95450-168-7 doi:10.18429/JACoW-IPAC2015-THPF087

NEW SHAVING SCHEME FOR LOW-INTENSITY BEAMS IN THE CERN PS BOOSTER AND FEASIBILITY AT 160 MeV

M. Kowalska, CERN, Geneva, Switzerland, EPFL, Lausanne, Switzerland
E. Benedetto, CERN, Geneva, Switzerland
V. Forte, CERN, Geneva, Switzerland, Université Blaise Pascal, Clermont-Ferrand, France
B. Mikulec, G. Rumolo, CERN, Geneva, Switzerland

Abstract

The PS Booster (PSB) is the first synchrotron in the CERN proton accelerator chain, serving all downstream machines. As part of the LHC Injector Upgrade (LIU) Project, the PSB injection energy will increase from 50 MeV to 160 MeV and a new H^- charge-exchange injection scheme will be implemented. Beam losses are a concern due to the increased injection energy, and mitigation scenarios are under investigation.

On the other hand it is desirable for low-intensity beams to have the possibility to precisely tailor sub-micron beam emittances through controlled scraping (transverse shaving process) towards a suitable aperture restriction. Challenges are the higher activation potential of the beam and the smaller transverse beam sizes around 160 MeV as compared to 63 MeV, at which the shaving is presently done.

This paper describes the proposal of a new shaving scheme, more robust with respect to the steering errors and the choice of the working point, which localizes the scraping losses on the main PS Booster aperture restriction. The robustness of the new method, together with the results of simulations and measurements are discussed for the current (50 MeV) and future (160 MeV) situation.

INTRODUCTION

Shaving is presently the main method to control the beam emittance and beam intensity in the PS Booster. The beam is supposed to be scraped on the aperture restriction of the machine, located in period 8 – called Window Beam Scope (WBS) [1]. It is a carbon, 40 mm thick absorber. Its physical dimensions are: 28.6 mm and 50 mm in the vertical and horizontal plane, respectively.

The global aperture limitations in the lattice are built by the quadrupoles in the horizontal plane (57 mm) and at the scrapers that protect the dipoles in the vertical plane (29.7 mm). A small difference between the dipoles aperture and the WBS aperture makes the vertical place fragile for any uncontrolled orbit perturbation or variation of working point with respect to the nominal one while shaving. Figure 1 is an example of an unsuccessful shaving due to the introduced closed orbit error.

The current shaving method, which consists in inducing closed orbit oscillations by a single kick (Figure 1), causes losses around the machine. In order to localize the losses at the PS Booster aperture restriction – Window Beam Scope (WBS), a new shaving scheme based on a closed bump was proposed and tested.

The closed bump scenario was first studied in simulations and then tested during the 2014 machine run. Dedicated measurements were performed in order to investigate the robustness of the method. Measurements of intensity, beam profiles and orbit excursion were made for both scenarios: at the future, foreseen upgraded injection energy - 160 MeV - and for the existing operational situation, at 63 MeV, when shaving occurs.

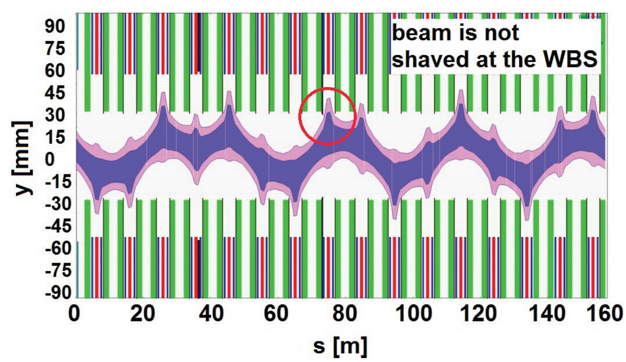

Figure 1: Lattice of the PSB and the illustration of the 3 sigma beam while conventional shaving. The 3-sigma beam is plotted in violet while 5 sigma is in magenta. The beam envelope is calculated for the vertical plane, with $Q_x = 4.37$ and $Q_y = 4.45$. Main lattice elements are shown in different colours: bending magnets in green, focusing quadrupoles in blue and defocusing quadrupoles in red. The scrapers are marked in maroon and WBS with the red circle.

EXISTING SITUATION IN OPERATION

Currently, operational shaving is performed by inducing a closed orbit global oscillation (Figure 1), using a single kick either in the horizontal or in the vertical plane. The vertical plane is preferred, mostly due to the absence of the dispersion and higher stability of the beam envelope in this plane. Closed orbit distortion (COD), induced during the shaving, depends strongly on the applied kick strength [2], which is adjusted independently for each type of the shaved beam. Moreover the shaving with the single kick is very sensitive to the working point and to steering errors.

Content from this work may be used under the terms of the CC BY 3.0 licence (© 2015). Any distribution of this work must maintain attribution to the author(s), title of the work, publisher, and DOI.

ISBN: 978-3-95450-168-7 doi:10.18429/JACoW-IPAC2015-THPF088

CERN PS BOOSTER UPGRADE AND LHC BEAMS EMITTANCE

E. Benedetto, J. L. Abelleira, C. Bracco, B. Mikulec, G. Rumolo, CERN, Geneva, Switzerland,
V. Forte, CERN, Geneva, Switzerland, and Université Blaise Pascal, Clermont-Ferrand, France

Abstract

By increasing the CERN PS Booster injection energy from 50 MeV to 160 MeV, the LHC Injector Upgrade Project aims at producing twice brighter beams for the LHC. Previous measurements showed a linear dependence of the transverse emittance with the beam intensity and space-charge simulations confirmed the linear scaling. This paper is discussing in detail the dependence on the longitudinal emittance and on the choice of the working point, with a special attention to the H^- injection process and to the beam dynamics in the first 5 ms, during the fall of the injection chicane bump.

INTRODUCTION

As part of the LHC Injectors Upgrade Project (LIU), the CERN PS Booster (PSB) will undergo an upgrade program [1], which includes the increase of injection energy from 50 MeV to 160 MeV and the implementation of an H^- charge-exchange injection from the new Linac4. Compared to the other rings with H^- injection and characterized by similar space-charge tune spreads at low energy ($\Delta Q \sim 0.5$ [2]), the peculiarity of the PSB is the required small transverse emittance. This needs to be produced and preserved in order to provide high brightness beams to the LHC. Being the first circular accelerator in the LHC proton injector chain, the PSB defines the minimum normalized transverse emittance.

The paper will review the measurements done in 2012 to characterize the operational LHC type beams in the PSB [3], which show a linear dependence of the transverse emittance with the beam intensity. The increase of injection energy with LIU should give about a factor $(\beta\gamma^2)^{160\mathrm{MeV}}/(\beta\gamma^2)^{50\mathrm{MeV}} = 2.04$ reduction of the space-charge tune spread for the present beams. Assuming the same tune spread as of today, which is in our baseline [4], with Linac4 it will be possible to inject twice the intensity in a given emittance (or to reduce the emittance by the same amount), i.e. the brightness curve should scale down by a factor 2. Simulation results will be presented to confirm these estimates and to discuss the dependence on the working point and on the longitudinal emittance of the minimum emittance achievable for a given intensity. Finally, the H^- injection scheme to produce in a controlled way 1-1.5 μm emittances will also be discussed.

MEASUREMENTS

Figure 1 shows the linear dependence of the transverse emittance on the beam intensity, found with the measurements done in 2012 for the LHC-type operational beams [3]. Two sets of points are plotted in the figure, for the standard LHC beam (LHC25ns) which has a required longitudinal emittance of 1.20 eVs (matched area at extraction), and for the so called BCMS LHC beam [5], which undergoes a special RF gymnastics in the downstream machine, the PS, and needs to be provided to the PS with a longitudinal emittance of maximum 0.9 eVs.

Different beam intensities have been produced by increasing the number of injected turns from 1 to 4 and by optimizing the injection parameters including the tune to minimize the transverse emittances. The horizontal and vertical profiles have been measured at extraction in Ring 3, which featured the best performances as the result of a careful optimization.

Additional measurements [3] showed that, provided that the working point is optimized all along the cycle, the transverse normalized emittance is constant during acceleration (however measurements at injection are difficult to read due to scattering at the wires, inducing 10% blow-up during the measurement itself). This indicates that the final values of the transverse emittance are dominated by space-charge effects at injection energy and by the multi-turn injection process itself.

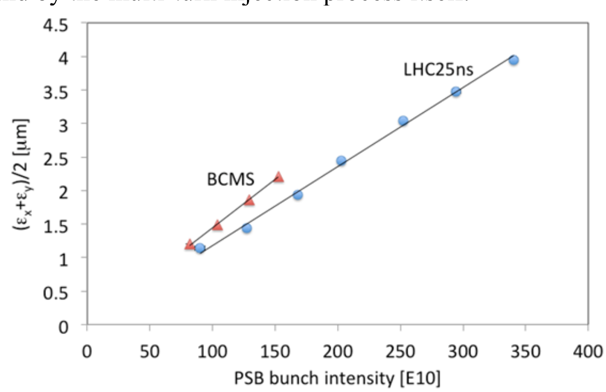

Figure 1: Emittance vs intensity curve for the LHC25ns beam (1.20 eVs) and the BCMS beam (0.86 eVs). Measurements of 2012 [3].

MINIMUM EMITTANCE SIMULATIONS

Simulations with PTC-Orbit [6] have been done to confirm the predictions of a factor 2 improvement in the brightness curve, assuming that the space-charge effects at injection energy in combination with machine errors are the cause of emittance blow-up.

The errors included in the model are the perturbations at the chicane magnets due to edge effect and Eddy currents [7]. Those provide the excitation of the half-integer and 20% vertical beta-beating, which is corrected down to a few % by special trims on two lattice quadrupoles. In addition to that, they induce the excitation

Content from this work may be used under the terms of the CC BY 3.0 licence (© 2015). Any distribution of this work must maintain attribution to the author(s), title of the work, publisher, and DOI.

ISBN: 978-3-95450-168-7 doi:10.18429/JACoW-IPAC2015-THPF089

BEAM TRANSFER TO THE FCC-hh COLLIDER FROM A 3.3 TeV BOOSTER IN THE LHC TUNNEL

W. Bartmann, M.J. Barnes, M. Fraser, B. Goddard, W. Herr, J. Holma, V. Kain, T. Kramer, M. Meddahi, A. Milanese, R. Ostojic, L.S. Stoel, J. Uythoven, F. Velotti, CERN, Geneva, Switzerland

Abstract

Transfer of the high brightness 3.3 TeV proton beams from the High Energy Booster (HEB) to the 100 TeV centre-of-mass proton collider in a new tunnel of 80–100 km circumference will be a major challenge. The extremely high stored beam energy means that machine protection considerations will constrain the functional design of the transfer, for instance in the amount of beam transferred, the kicker rise and fall times and hence the collider filling pattern. In addition the transfer lines may need dedicated insertions for passive protection devices. The requirements and constraints are described, and a first concept for the 3.3 TeV beam transfer between the machines is outlined. The resulting implications on the parameters and design of the various kicker systems are explored, in the context of the available technologies. The general features of the transfer lines between the machines are described, with the expected constraints on the collider layout and insertion lengths.

MACHINE PROTECTION LIMITS

Present investigations of the feasibility of absorber blocks for the LHC injection protection for High Luminosity-LHC (HL-LHC) beam parameters show two limitations. The foreseen high brigthness beams could cause mechanical stresses in the absorbers beyond their damage level. Also, attenuation of primary particles to provide protection of downstream elements would not be guaranteed with the present design [1–3]. The beam energy at the HEB to FCC transfer is a factor 130 higher than in case of the SPS to LHC transfer. Thus, a staggered transfer of batches with a reduced number of bunches is envisaged. The reachable bunch filling as a function of the injection kicker rise time for different transferred beam energies is shown in Fig. 1. In order to fill 80% of FCC and assuming 5 MJ as maximum energy per transfer leads to a required kicker rise time of less than 0.28 μs. A total of 120 batches with 90 bunches each need to be transferred. In case of LHC as HEB, there would be 4 times 30 batches of 90 bunches. The time between batch transfers is dominated by the synchronisation between the HEB and FCC and beam quality checks. Between each transferred batch both machines have to be synchronised on the common frequency:

$$f_c = \frac{f_{rev,HEB}}{C_{FCC}} = \frac{f_{rev,FCC}}{C_{HEB}} \tag{1}$$

In case of LHC as HEB the common frequency is about 111Hz which defines the required recharging frequency of HEB extraction and FCC injection kickers. With a total number of about 30 transferred batches from LHC the minimum injection time for one full LHC beam injected into FCC is 0.5 s.

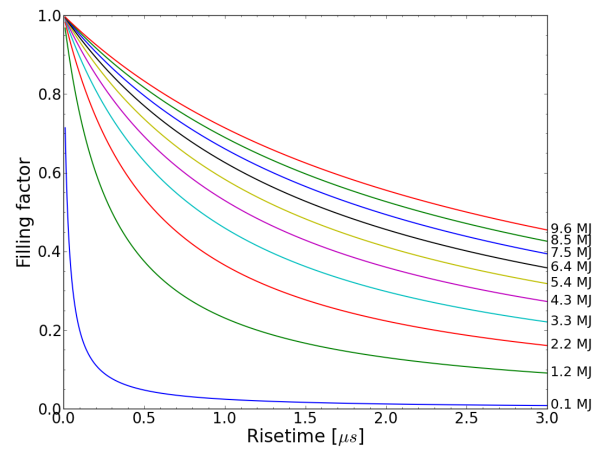

Figure 1: FCC bunch fill factor vs injection kickers rise time for different transferred beam energies. The foreseen filling of 80% is reached for HL-LHC energies (about 5 MJ) for a rise time of 0.28 μs.

INJECTION SYSTEM LAYOUT

The proposed injection system uses a Lambertson septum to deflect the beam horizontally onto the FCC orbit. The injected beam enters the septum with an offset in angle and position in both planes with respect to the ring orbit, Fig. 2. The vertical angle is reduced by off-centre passage through a quadrupole and finally compensated by a fast kicker system. In order to estimate the required kick angles we assume that the beam clearance at the level of the quadrupole is

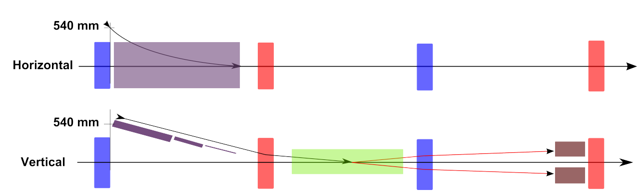

Figure 2: Layout of the injection system. Focussing (red) and defocussing (blue) quadrupoles build a FODO lattice. The Lambertson septum (violet), which is vertically aligned with the incoming trajectory angle, deflects the beam horizontally onto the orbit, and the kicker (green) compensates for the remaining angle in the vertical plane. The injection dump (brown) intercepts miskicked beam (red).

Content from this work may be used under the terms of the CC BY 3.0 licence (© 2015). Any distribution of this work must maintain attribution to the author(s), title of the work, publisher, and DOI.

ISBN: 978-3-95450-168-7 doi:10.18429/JACoW-IPAC2015-THPF090

STATUS AND PLANS FOR THE UPGRADE OF THE CERN PS BOOSTER

K. Hanke, D. Aguglia, M. E. Angoletta, W. Bartmann, C. Bedel, E. Benedetto, S. Bertolasi, C. Bertone, J. Betz, T. W. Birtwistle, A. Blas, J. Borburgh, C. Bracco, A. Butterworth, E. Carlier, S. Chemli, P. Dahlen, A. Dallocchio, G. P. Di Giovanni, T. Dobers, A. Findlay, R. Froeschl, A. Funken, S. Gabourin, J.-L. Grenard, D. Grenier, J. Hansen, D. Hay, J.-M. Lacroix, P. Le Roux, L. A. Lopez Hernandez, C. Martin, A. Masi, B. Mikulec, Y. Muttoni, A. Newborough, D. Nisbet, M. R. Obrecht, M. M. Paoluzzi, S. Pittet, B. Puccio, J. Tan, J. Vollaire, W. Weterings
CERN, Geneva, Switzerland

Abstract

CERN's Proton Synchrotron Booster (PSB) is undergoing a major upgrade program in the frame of the LHC Injectors Upgrade (LIU) project. During the first long LHC shutdown (LS1) some parts of the upgrade have already been implemented, and the machine has been successfully re-commissioned. More work is planned for the upcoming end-of-year technical stops, notably in 2016/17, while most of the upgrade is planned to take place during the second long LHC shutdown (LS2). We report on the upgrade items already completed and commissioned, the first Run 2 beam performance and give a status of the ongoing design and integration work.

INTRODUCTION

The upgrade of the PS Booster consists of two major parts. With the connection of Linac4, the injection scheme will be upgraded to charge exchange injection of H- ions. This change will significantly reduce beam loss in the injection area and allow for tailoring the transverse emittance by means of phase space painting. At the same time, the injection energy will be increased from 50 MeV to 160 MeV [1]. With this increase of beam energy the relativistic $\beta\gamma^2$ factor increases by a factor of 2. The incoherent space charge tune shift at Booster injection can be expressed as

$$\Delta Q_x = \frac{R_p N_b}{2\pi^{3/2}\gamma^3\beta^2\sigma_z}\oint\frac{\beta_x(s)ds}{\sigma_x(s)[\sigma_x(s)+\sigma_y(s)]}$$

$$\Delta Q_y = \frac{R_p N_b}{2\pi^{3/2}\gamma^3\beta^2\sigma_z\sqrt{\varepsilon_y}}\oint\frac{\sqrt{\beta_y(s)}ds}{\sigma_x(s)+\sigma_y(s)}$$

where R_p is the classical proton radius and N_b is the number of protons per bunch. With the increase of injection energy the space charge tune shift decreases by a factor 2, thus doubling the intensity that can be accumulated within a given emittance. The second component of the upgrade program is the increase of the extraction energy from presently 1.4 GeV to 2.0 GeV. The underlying idea is to reduce space charge effects at injection into the downstream Proton Synchrotron (PS), thus removing this bottleneck. The expected gain can again be deduced from the ratio of the $\beta\gamma^2$ factor at 1.4 GeV and 2.0 GeV, which is 1.63 and corresponds to an intensity increase of 60% within given emittance values.

LS1 WORK

While most of the upgrade activities are scheduled to be implemented during LS2, a number of LIU activities could be performed in the PSB during LS1 in 2013/14. Activities that could be completed comprise:

- implementation of the new digital RF controls
- installation of 5 additional prototype Finemet cavity cells (Fig. 1)
- upgrade of diagnostics (new beam loss monitors, new orbit measurement, new pick-ups and transformers in the transfer lines)
- renovation of the multipole power supplies
- installation of a new external dump
- limited cabling campaign and identification of obsolete cables
- controls upgrades (change of many front-end computers)
- consolidation of handling and lifting equipment
- new hardware interlock at extraction (Beam Interlock System - BIS)

Figure 1: Prototype Finemet cavity modules installed in Ring 4 of the PSB.

COMMISSIONING OF UPGRADE ITEMS

The PS Booster was re-started after LS1 in June 2014. Unlike in previous years, much more than standard

Content from this work may be used under the terms of the CC BY 3.0 licence (© 2015). Any distribution of this work must maintain attribution to the author(s), title of the work, publisher, and DOI.

ISBN: 978-3-95450-168-7 doi:10.18429/JACoW-IPAC2015-THPF091

Content from this work may be used under the terms of the CC BY 3.0 licence (© 2015). Any distribution of this work must maintain attribution to the author(s), title of the work, publisher, and DOI.

DETAILED STUDIES OF BEAM INDUCED SCRUBBING IN THE CERN-SPS

H. Bartosik, T. Bohl, B. Goddard, G. Iadarola*, G. Kotzian, K. Li, L. Mether,
G. Rumolo, E. Shaposhnikova, M. Schenk, M. Taborelli (CERN, Geneva)

Abstract

In the framework of the LHC Injectors Upgrade (LIU) project, it is foreseen to take all the necessary measures to avoid electron cloud effects in the CERN-SPS. This can be achieved by either relying on beam induced scrubbing or by coating the vacuum chambers with intrinsically low Secondary Electron Yield (SEY) material over a large fraction of the ring. To clearly establish the potential of beam induced scrubbing, and to eventually decide between the two above options, an extensive scrubbing campaign is taking place at the SPS. Ten days in 2014 and two full weeks in 2015 are devoted to machine scrubbing and scrubbing qualification studies. This paper summarizes the main findings in terms of scrubbing efficiency and reach so far, addressing also the option of using a special doublet beam and its implication for LHC.

INTRODUCTION

The electron cloud effect has been identified as a possible performance limitation for the SPS since LHC type beams with 25 ns spacing were injected into the machine for the first time in the early years of 2000. At that time a severe pressure rise was observed all around the machine together with transverse beam instabilities, significant losses and emittance blow-up on the trailing bunches of the train [1]. Since 2002, scrubbing runs with 25 ns beams were carried out almost every year of operation in order to condition the inner surfaces of the vacuum chambers and therefore mitigate the electron cloud. Extensive machine studies showed that by 2012 the conditioning state of the SPS was such to avoid any possible beam degradation due to electron cloud on the cycle timescale for 4 batches of 72 bunches with $N \approx 1.35{\times}10^{11}$ p/b and normalized transverse emittances of about 3 μm [2]. For higher intensities ($N \approx 1.45{\times}10^{11}$ p/b injected) a seemingly electron cloud driven transverse instability was observed after the injection of the third and the fourth batch, leading to emittance blow up and particle losses on the trailing bunches of the injected trains. Since the SPS was never scrubbed with such high beam intensities, an additional scrubbing step might be required for suppressing these effects. If scrubbing is not sufficient for suppressing the electron cloud effect with the high beam intensity and small transverse emittance produced with LIU, or in case the reconditioning process is very slow after large parts of the machine are vented (like during a long shutdown), the inner surface of the SPS vacuum chambers might have to be coated with a low Secondary Electron Yield (SEY) material. The solution developed at CERN is to produce a thin film of amorphous Carbon (a-C) using DC Hollow Cathode sputtering on the inner walls of the vacuum chamber [3]. The suppression of electron cloud in coated liners equipped with electron cloud strip monitors was already proved with beam in the SPS. An additional four SPS half cells (including quadrupoles) have been coated with a-C during Long Shutdown 1 (LS1), seeking for further experimental evidence of the coating efficiency with beam operation in Run 2.

The total or partial coating of the SPS machine with a-C is a major task, which requires careful preparation and planning of resources. The decision whether or how much of the SPS needs to be coated has therefore to be taken no later than mid 2015. After LS1, a first scrubbing run took place during the whole Week 45 in 2014 with the main goal of recovering the operational performance, as it was expected that the good conditioning state of the SPS will be degraded due to the long period without beam operation, partial venting, and the related interventions on the machine. Two and a half additional days of scrubbing in Week 50 were also used to start exploring the SPS behaviour with 25 ns beams with higher intensity as well as accelerated doublets and other LHC beam variants [4]. Two more weeks for scrubbing will be performed in the first half of 2015 in order to assess the potential to fully scrub the machine for high intensity 25 ns beams or the limitations of this approach. Only after collecting all the additional experience and the important information from the extensive experimental scrubbing from post-LS1 operation, the final choice between coating and scrubbing will be made in mid-2015.

WEEK 45: RECOVERY OF THE PRE-LS1 PERFORMANCE

The goals of the SPS scrubbing run in Week 45 were:

- Recover the 2012 performance with LHC 25 ns beams;
- Qualify the machine behaviour with LHC beams after long shutdown and extensive machine venting;
- Test doublet beams for SPS scrubbing and as preparation for LHC scrubbing in 2015.

In oder to make scrubbing efficient, the pressure interlocks on the injection kicker MKP-S and the beam dump (TIDVG), exchanged during LS1, had to be raised. The summary plot showing the maximum current per cycle (in

* Giovanni.Iadarola@cern.ch

ISBN: 978-3-95450-168-7 doi:10.18429/JACoW-IPAC2015-THPF092

EUROPEAN SPALLATION SOURCE LATTICE DESIGN STATUS

Y. Inntjore Levinsen*, H. Danared, M. Eshraqi,
R. Miyamoto, A. Ponton, R. de Prisco, E. Sargsyan, ESS, Lund, Sweden
H. Dølrath Thomsen, S. Pape-Møller, ISA, Aarhus Uni., Denmark

Abstract

The accelerator of the European Spallation Source (ESS) will deliver 62.5 mA proton beam of 2.0 GeV onto the target, offering an unprecedented beam power of 5 MW. Since the technical design report (TDR) was published in 2013, work has continued to further optimise the accelerator design. We report on the advancements in lattice design optimisations after the TDR to improve performance and flexibility, and reduce cost of the ESS accelerator.

INTRODUCTION

The ESS project is an ambitious project, which aims to provide a world leading 5 MW spallation neutron source, planned to be commissioned in 2019 [1]. The ESS is constructed in Lund, Sweden, in a collaboration between 17 partner countries. The neutrons are produced by shooting a high power proton beam onto a spallation target. The current accelerator design is assuming operation at 14 Hz, with 2.86 ms long pulses, corresponding to a duty cycle of 4 %. The accelerator can accelerate the beam up to 2 GeV, and a beam current of 62.5 mA is thus needed to reach the 5 MW requirement. The overall layout is shown in Fig. 1.

Since the TDR was published in 2013 [2], the beam energy has been reduced from 2.5 GeV to meet the budget requirements. Correspondingly the beam energy increased from 50 mA to 62.5 mA in order to keep the beam power constant. This was discussed last year in [3]. The high level parameters described within this reference remain unchanged this year.

The accelerator design is currently mainly limited by the amount of power that can be fed to the cavities (energy), beam loss limits (intensity), and space charge effects at low energy.

There has been ongoing work to further optimise and finalise the design of the lattice optics in the last year, and various error studies have been performed to better understand the limitations of the lattice and providing valuable input for the design constraints. The lattice and optics presented here will in the future be referenced to as the “2014 Baseline”.

FRONT END

The front end of the ESS linac will accelerate the high intensity beam from the 75 keV ion source and up to 90 MeV at the exit of the last DTL tank, before the beam is injected into the superconducting part of the linac. With a high power superconducting linac, it is important to provide a high quality beam to the superconducting section so as to minimise the losses (machine protection). In addition, it is important to generally keep the losses low, to reduce activation and keep a good machine reliability.

* yngve.levinsen@esss.se

Ion Source, LEBT, and RFQ

The proton beam is generated with a Microwave Discharge Ion Source (MDIS), delivering a 75 keV beam energy and more than 70 mA proton beam current to the low energy beam transport (LEBT) [4]. The LEBT is a 2.4 m long section matching the beam to the RFQ using two solenoids. In between the solenoids a chopper is installed to remove the transient of the beam pulse.

The four-vane RFQ acclerates and bunches the continuous pulse from the source into bunches at 352.21 MHz. The output beam energy of the RFQ is 3.62 MeV. The RFQ has a relatively long bunching section to allow for a higher transmission.

In Fig. 2, we show the transmission through the LEBT+RFQ for different strengths of the two solenoids in the LEBT lattice. The optimal setting found in this simulation is to have the two solenoids at 0.238 T and 0.244 T, providing a transmission of 97.8%. The working point is shown by the large dot in the figure.

MEBT and DTL

Between the RFQ and the start of the drift tubes, there is a section of 3.6 m called the Medium Energy Beam Transport (MEBT). Recent advancements in the MEBT layout was described in [5, 6]. The purpose of this section is to match the beam coming out of the RFQ to the drift tube linac, and to measure the beam properties with various beam diagnostics. The MEBT has 11 quadrupoles for the focusing of the beam, with one BPM per quadrupole. Three scrapers will be installed to clean the transverse halo, which will reduce the losses in the DTL and superconducting part of the linac [7].

A fast chopper is installed in the MEBT, which main purpose is to chop off the bad quality bunches at the beginning and end of the pulse which could not be removed by the LEBT chopper due to the space charge compensation recovery time. Both the LEBT and the MEBT choppers have a secondary purpose of providing an additional level of beam protection. The MEBT chopper is the last location where the beam can be dumped before the superconducting section.

The last accelerating section of the warm linac is the drift tube linac (DTL). The DTL consists of 5 tanks which brings the beam energy from 3.6 MeV to 90 MeV. The DTL has undergone a design optimisation since the TDR was published in 2013. One tank was added, and the output beam energy thus increased from the original 77.5 MeV to 90 MeV [8].

The FODO lattice is realised using permanent magnet quadrupoles (PMQ) in every second drift tube. There are also three horizontal, three vertical steerers, and three BPMs in each tank. The optimised locations of the steerers and BPMs are currently being studied [9].

Content from this work may be used under the terms of the CC BY 3.0 licence (© 2015). Any distribution of this work must maintain attribution to the author(s), title of the work, publisher, and DOI.

ISBN: 978-3-95450-168-7 doi:10.18429/JACoW-IPAC2015-THPF093

LHC INJECTORS UPGRADE (LIU) PROJECT AT CERN

M. Meddahi*, J. Coupard, H. Damerau, A. Funken, S. Gilardoni, B. Goddard, K. Hanke, I. Kobzeva, A. Lombardi, D. Manglunki, S. Mataguez, B. Mikulec, G. Rumolo, E. Shaposhnikova, M. Vretenar, CERN, Geneva, Switzerland

Abstract

CERN is currently carrying out an ambitious improvement programme of the full LHC Injectors chain in order to enable the delivery of beams with the challenging HL-LHC parameters. The LHC Injectors Upgrade project coordinates this massive upgrade program, and covers a new linac (Linac4 project) as well as upgrades to the Proton Synchrotron Booster, the Proton Synchrotron and Super Proton Synchrotron. The heavy ion injector chain is also included, adding the Linac3 and Low Energy Ion Ring to the list of accelerators concerned. The performance objectives and roadmap of the main upgrades will be presented, including the work status and outlook. The machine studies and milestones during LHC Run 2 will be discussed and a preliminary Long Shutdown 2 installation planning given. Finally, for the LHC Run 3, the beam performance across the full injector chain after all the upgrades will be estimated and the required commissioning stages outlined.

INTRODUCTION

The goal of the LHC Injectors Upgrade project (LIU) is to increase the intensity/brightness in the injectors in order to match the High Luminosity LHC (HL-LHC) requirements [1]. For protons, the Linac4/PSB/PS/SPS chain will be enabled to produce higher intensity beams (based on efficient production schemes, space charge and electron cloud mitigation, impedance reduction, feedback systems, hardware upgrade and improvement). For heavy ions, an important upgrade of the injector chain (Linac3, LEIR, PS, SPS) is planned to reach the beam parameters at the LHC injection that can meet the luminosity goal. In addition, the LIU project should ensure the increased injectors reliability and lifetime to cover the HL-LHC era (until 2035). This part, closely related to the CONSolidation, project [2], concerns the upgrade/replacement of ageing equipment (power supplies, magnets, RF) and the improvement of radioprotection measures (shielding, ventilation).

The timeline of the LIU project is sketched in Fig. 1. The simulation studies, beam measurements and equipment procurement will take place during Run 2 until the start of Long Shutdown 2 (LS2). During this time, key dates for pending decisions have been set in order to define the baseline program of all the interventions by end of 2016. All LIU installations and hardware works will then take place during LS2. For some of these installation activities, it is checked if they could be anticipated to Year-End-Technical-Stop (YETS) or Extended-Year-End-Technical-Stop (EYETS). Commissioning of LIU beams will take place in 2020 for the Pb ion beams, as the full beam performances are already needed for the 2020 ion run. The proton beam commissioning up to the LIU beam parameters will gradually be performed during Run 3 to be ready after LS3. This strategy would as well allow performing any further hardware corrective actions during the Run 3 technical stops or LS3, if needed.

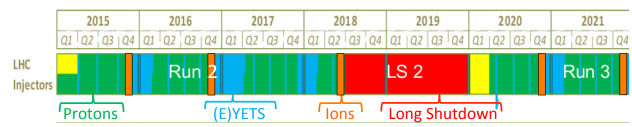

Figure 1: LHC (upper row) and Injectors (lower row) operation schedule (green: proton operation, blue: technical stops, orange: ion operation, red: long shutdown -LS).

LIU IONS

The main target of the LIU-IONS can be described in a simplified form as reaching 7 times the design peak luminosity [3]. This also translates into multiplying by about a factor 3 the peak luminosity extrapolated from beam parameters achieved during the 2013 p-Pb run. Table 1 summarises the desired versus achieved ion performance. The bunch intensity was already at the limit on the SPS flat bottom during the 2013 p-Pb run in terms of acceptable intra-beam scattering and space-charge effects. It is therefore needed to accumulate a larger number of bunches in LHC.

Table 1: Ion Beam Parameters at LHC Injection

	N (10^8 ions/b)	$\epsilon_{x,y}$ (μm)	Bunches
Achieved	1.4	1.2	358
HL-LHC (tbc)	1.4	1.2	960

The means to achieve the LIU-IONS target luminosity are the following:

- Increase the beam current from the source and Linac3 by improving both source and Low Energy Beam Transport (LEBT). This requires identifying and removing bottlenecks with the aid of beam dynamics simulations and beam measurements, and by installing new diagnostics. The increase of the injection rate from 5 to 10 Hz will allow injecting more intensity into LEIR, while keeping the same magnetic cycle duration;
- Increase the beam current out of LEIR by both increasing the amount of injected beam (compatibly with the electron cooling capabilities) and mitigating

* Malika.Meddahi@cern.ch

Content from this work may be used under the terms of the CC BY 3.0 licence (© 2015). Any distribution of this work must maintain attribution to the author(s), title of the work, publisher, and DOI.

ISBN: 978-3-95450-168-7 doi:10.18429/JACoW-IPAC2015-THPF094

POSSIBLE REUSE OF THE LHC AS A 3.3 TeV HIGH ENERGY BOOSTER FOR HADRON INJECTION INTO THE FCC-hh

B.Goddard, W. Bartmann, M. Benedikt, W. Herr, M. Lamont,
P. Lebrun, M. Meddahi, A. Milanese, M. Solfaroli Camillocci, L.S. Stoel
CERN, Geneva, Switzerland

Abstract

One option for the injector into a 100 TeV centre-of-mass energy frontier proton collider FCC-hh [1] in a new tunnel of 80–100 km circumference is to reuse a suitably modified LHC as 3.3 TeV High Energy Booster (HEB). The changes that would be required to the existing LHC insertions are described, including the types and numbers of new magnets and circuits. The limitations on the maximum LHC ramp rate and minimum cycle time discussed. The key question of the minimum FCC filling time achievable with technically possible upgrades is examined, together with the issues of decommissioning for the elements which would need to be removed from the machine. The potential performance reach of the modified LHC as 3.3 TeV HEB is quantified, and implications for FCC-hh discussed.

MAIN DESIGN CONSIDERATIONS

Initial studies have shown that beam transfer from both LHC P1 and P8 is preferable to optimise the orientation of the collider with respect to the local geology in the Geneva area and to minimise the length and overall bending angles of the new transfer lines. It is desirable to minimise changes to the LHC lattice and machine configuration, avoiding changes to highly activated zones. Beam parameters are summarised in Table 1. The low number of bunches per transfer is determined by the damage potential of the 3.3 TeV beam [2].

Table 1: Parameters of Beams to Inject into FCC-hh

Parameter	Unit	Value (option)
Beam energy	TeV	3.3
Bunch spacing	ns	25 (5)
Bunch population		1.0 (0.2)$\times 10^{11}$
H/V emittance (norm.)	mm.mrad	2.2 (0.44)
RMS bunch length	cm	8.0
Bunches per transfer		50-100
Turnaround time	h	5.0

Transfer Energy

The injection energy of the FCC-hh collider is assumed to be 3.3 TeV, based on the ratio of injection to collision dipole field. In view of possible changes to the baseline HEB energy e.g. as a result of the collider dipole magnet aperture optimisation, the LHC machine layout changes have been made to reach as high an energy as possible compatible with all other constraints.

Number and Length of Rings, and Crossing Points

The use of both LHC rings is assumed, both to decrease the filling time by a factor two and to minimise the length of transfer lines required (or avoid polarity reversal). The cost will be in the duplication of many circuits and instruments, higher complexity and lower availability. The lengths of the two rings should be identical to simplify the RF manipulations and re-phasing required for transfer to the collider, and from the SPS to the HEB. There thus need to be at least two crossings placed azimuthally opposite, which do not need to be at the centre of the respective LHC long straight sections. The lengths of both rings should be the same as the existing LHC 26.659 km, to maintain the present ratio of 27/7 with the 6.912 km circumference of SPS.

Machine System Locations

Injection should remain in P2 and P8, to avoid additional civil engineering for 450 GeV beamlines. With the layout proposed and only two crossings the injections would need to be into the inner rings, which is feasible but entails some reorganisation of the layouts in P2 and P8. The beam dump system should remain in P6, to avoid decommissioning of the highly active dump blocks, and to avoid additional civil engineering for the dump lines and dump caverns. The two collimation systems (betatron and momentum cleaning) are assumed to remain in their locations in P7 and P3 respectively. This avoids the issue of decommissioning or moving the highly activated systems, and having to modify the accelerator and its infrastructure in these activated areas. The 400 MHz RF accelerating system is assumed to remain in its present location in P4.

Extraction Towards FCC Collider

The two extraction systems for transfer of the beams to the FCC-hh collider are assumed to be located in P1 and P8. For an overall layout where the 100 km collider intersects the LHC machine, LHC Beam 1 would be extracted from P1 and Beam 2 from P8, Fig. 1 (top). For a layout where a 80 km collider does not intersect the LHC ring, the direction of extraction from these two points is inverted. Integration of the extraction system in P8 together with the existing injection is feasible for 3.3 TeV but is likely to rely on the HEB extraction energy being lower than 7 TeV. In P1 the accommodation of the extraction with crossing dipoles will also be likely to limit the transfer energy.

Content from this work may be used under the terms of the CC BY 3.0 licence (© 2015). Any distribution of this work must maintain attribution to the author(s), title of the work, publisher, and DOI.

ISBN: 978-3-95450-168-7 doi:10.18429/JACoW-IPAC2015-THPF095

LIMITS ON FAILURE SCENARIOS FOR CRAB CAVITIES IN THE HL-LHC *

A. Santamaría García, H. Burkhardt, K. Hernández Chahín, A. Macpherson, K. Sjobak, D. Wollmann, B. Yee-Rendón, CERN, Geneva, Switzerland

Abstract

The High Luminosity (HL) LHC upgrade aims for a tenfold increase in integrated luminosity compared to the nominal LHC, and for operation at a levelled luminosity of 5×10^{34} cm^{-2}s^{-1}, which is five times higher than the nominal LHC peak luminosity. Crab Cavities (CCs) are planned to compensate the geometric luminosity loss created by the increased crossing angle by rotating the bunch, allowing quasi head-on collisions at the Interaction Points (IP). The CCs work by creating transverse kicks, and their failure may have short time constants comparable to the reaction time of the Machine Protection System (MPS), producing significant coherent betatron oscillations and fast emittance growth. Simulations of CC failure modes have been carried out with the tracking code SIXTRACK [1], using the newly added functionality called DYNK [2], which allows to dynamically change the attributes of the CCs. We describe these simulations and discuss early, preliminary results.

INTRODUCTION

In order to produce ten times more collisions during the HL-LHC lifetime, the nominal levelled luminosity will be 5×10^{34}cm^{-2}s^{-1}. An increase in luminosity entails an increase in proton collisions per bunch crossing (pile-up) and a rapid decay of the beam current due to proton burning. In order to optimize the experimental detectors' efficiency, the pile-up has to be maintained at an acceptable level and the luminosity should remain constant over the length of the fill. It has been proposed to maintain the luminosity constant by reducing the transverse beam size by means of reducing β^*, called β^* levelling. A smaller beam size at the IP implies larger beam sizes in the triplet quadrupole magnets, which will need a larger aperture. The implementation of low β^* collision optics will be carried out with the Achromatic Telescopic Squeeze (ATS) scheme [3]. A smaller β^* requires a larger crossing angle θ, which in turn causes a reduction of the geometrical luminosity. The crossing angle will be increased by a factor of two for HL-LHC, causing a significant loss in luminosity and therefore delaying the integrated luminosity goal. CCs have been proposed to counteract this effect. They generate transverse electromagnetic fields, which rotate each bunch longitudinally by $\frac{\theta}{2}$ such that the bunches collide effectively head-on, compensating the geometric luminosity loss. CCs allow access to the full performance reach of the small β^* values offered by the ATS scheme and the larger triplet quadrupole magnets [4, Chapter 1].

* Research supported by the High Luminosity LHC project.

THE MPS AND CRAB CAVITY FAILURES

A variety of processes can cause unavoidable beam losses during normal and abnormal operation. Because of the high stored energy of the HL-LHC beams, above 700 MJ, the beams can be highly destructive. Even a local beam loss of a tiny fraction of the full beam into a superconducting magnet can cause a quench, and large beam losses can cause damage to accelerator components. Because of this, the MPS is designed with very high reliability to prevent an uncontrolled release of the energy and damage due to beam losses [4, Chapter 7].

With the installation of CCs, new failure scenarios that could cause beam losses have to be considered. Voltage or phase changes of the CCs will happen with a time constant τ, which is proportional to the time it takes to dissipate the energy stored in the cavity through the coupler when the RF sources are turned off (external Q factor):

$$\tau = \frac{2 \cdot Q_{\text{ext}}}{\omega},$$

where ω is the angular frequency of the CCs. For the HL-LHC parameters of $f_{\text{cc}} = 400.79$ MHz and $Q_{\text{ext}} = 3 \times 10^5 - 5 \times 10^5$, CC failures could happen with a time constant as fast as $\tau = 238 - 397$ μs $\approx 2 - 4$ LHC turns. These ultrafast failures are potentially dangerous, which motivates detailed studies as there may not be enough time to extract the beam in a controlled way [5].

SIMULATION SETTINGS

Tracking simulations have been carried out with the collimation version of SIXTRACK and the DYNK module, in order to estimate the beam loss distribution around the ring in case of CC failures. These simulations were carried out for Beam 1 and IP1, considering one bunch represented by 9.6×10^5 particles at collision energy. The relevant HL-LHC parameters considered are summarized in Table 1. Further studies including IP5 are foreseen.

Baseline Optics and Layout

The optics used for the whole machine is the HLLHCV1.0 collision optics, which includes the new Nb_3Sn triplet (140 T/m, 150 mm) with all the additional magnets needed to be compatible with $\beta^* = 0.15$ m and implementing the ATS scheme [6].

Crab Cavities

The HLLHCV1.0 optics include the installation of three CCs per IP, per side and per beam (n_{cc}). To simplify the opening and closing of the crab bump, the groups of $n_{\text{cc}} = 3$

Content from this work may be used under the terms of the CC BY 3.0 licence (© 2015). Any distribution of this work must maintain attribution to the author(s), title of the work, publisher, and DOI.

ISBN: 978-3-95450-168-7 doi:10.18429/JACoW-IPAC2015-THPF096

ORIGIN OF THE DAMAGE TO THE INTERNAL HIGH ENERGY BEAM DUMP IN THE CERN SPS

V. Kain, K. Cornelis, B. Goddard, M. Lamont, I. Leitao, R. Losito, C. Maglioni, M. Meddahi, F. Pasdeloup, G. Steele, F. Velotti, CERN, Geneva, Switzerland

Abstract

The high energy beam dump in the SPS has to deal with beams from 105 to 450 GeV/c and intensities of up to 4×10^{13} protons. An inspection during the last shutdown revealed significant damage to the Al section of the dump block. This paper summarizes the results of the analysis revealing the most likely cause of the damage to the beam dump. The implications for future SPS operation will also be briefly discussed, together with the short-term solution put in place.

INTRODUCTION

The SPS can provide a large variety of ion and proton beams in an energy range from 14 GeV to 450 GeV. The most demanding beams are the high intensity proton beams that are accelerated to 400 or 450 GeV with intensities of more than 4×10^{13} protons per shot. The characteristics of the high intensity proton beams relevant for the discussion in this paper are summarized in Table 1.

Table 1: Normalized emittance in horizontal and vertical plane, protons per bunch, number of bunches and cycle length of the achieved high intensity proton beams in the SPS: Fixed Target (FT) and CNGS beams are accelerated to 400 GeV and LHC beams to 450 GeV.

Beam	ε [μm]	ppb [10^{10}]	#bunches	T_{cycle} [s]
LHC 25 ns	2.6	12	288	21.6
LHC ultimate	3.5	17	288	21.6
FT	12/8	1.07	4200	14.4
CNGS	12/8	1.07	4200	6

The SPS Beam Dumping System

The beam dump system of the SPS is housed in the long straight section LSS1 along with the injection system. It is connected to the SPS interlocking system and has to be able to receive all types of SPS beam at all energies. The system consists of horizontal and vertical kicker magnets that are triggered together to move the beam down and then to sweep it across the beam dump block as indicated in Fig. 1. Due to limitations on the reachable minimum voltage for the kicker switches, two beam dump blocks are installed in long straight section LSS1. The low energy beam is dumped on the low energy beam dump TIDH. Beam above 102.2 GeV is dumped on the high energy beam dump, called TIDVG.

Whereas the concept of the SPS beam dump system is valid for all current and future beams in terms of aperture and

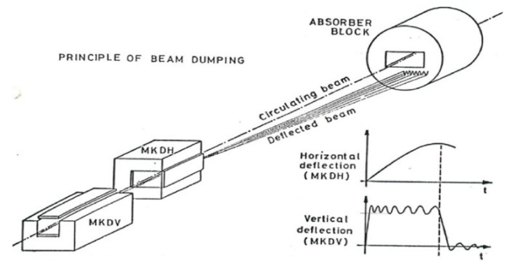

Figure 1: Principle of SPS beam dumping system.

technical feasibility for required kick strength, the radiation level in LSS1 due to the internal beam dump system and the robustness of the TIDVG dump block itself for high power loads have become a concern. In fact the TIDVG has suffered from beam induced damage during the years of the CNGS run.

TIDVG DAMAGE OBSERVATION

The absorber block of the high energy beam dump TIDVG is made of 2.5 m of Graphite, 1 m of Aluminum, 0.5 m of Copper and 0.3 m of Tungsten. The TIDVG Cu core is cooled with water and the absorber blocks are cooled through contact with the Cu core. Further information can be found in [1]. It was installed in 2006 before the CNGS run.

During the SPS shutdown from spring 2013 to September 2014 the equipment in LSS1 was dismantled and re-installed afterwards. When the TIDVG was ready to be re-connected, chunks of Aluminum close to its downstream end were detected. An endoscope inspection was carried out and the first Al block was found to have had melted and re-solidified, see Fig. 2. The damaged TIDVG was removed and the spare installed before the SPS start-up. The spare TIDVG absorber consists of the same materials as the original one, only that the graphite part is 2.7 m long and the Aluminum 0.8 m. As a consequence an analysis campaign was launched to understand the origin of the damage.

The TIDVG used between 1999 to 2005 was inspected as well. Also here the Al part of the absorber showed signs of damage.

SIMULATION RESULTS FOR ROBUSTNESS LIMITS

In 2009 possible power load limitations of the TIDVG absorber were investigated in simulation [2]. The weakest material in the sandwich absorber block is Aluminum with a melting point of only 660°C. With the assumptions used in the study for the thermal contact conductance of the Aluminum part, the maximum allowed temperature in

Content from this work may be used under the terms of the CC BY 3.0 licence (© 2015). Any distribution of this work must maintain attribution to the author(s), title of the work, publisher, and DOI.

ISBN: 978-3-95450-168-7 doi:10.18429/JACoW-IPAC2015-THPF097

FEASIBILITY STUDY OF A NEW SPS BEAM DUMP SYSTEM

F.M. Velotti, J.L. Abelleira, M.J. Barnes, C. Bracco, E. Carlier, F. Cerutti, K. Cornelis, R. Folch, B. Goddard, V. Kain, M. Meddahi, R.F. Morton, J. A. Osborne, F. Pasdeloup, V. Senaj, G.E. Steele, J. Uythoven, H. Vincke, CERN, Geneva, Switzerland

Abstract

The CERN Super Proton Synchrotron (SPS) presently uses an internal beam dump system with two separate blocks to cleanly dispose of low and high energy beams. In view of the increased beam power and brightness needed for the LHC Injector Upgrade project for High Luminosity LHC (HL-LHC), the performance of this internal beam dump system has been reviewed for future operation. Different possible upgrades of the beam dumping system have been investigated. The initially considered solution for the SPS Beam Dump System is to design a new, dedicated external system, with a dump block in a shielded cavern separated from the machine ring. Unfortunately this solution is not feasible with the present technology. In this paper, the design requirements and the possible solutions are investigated, including considering a new internal beam dump in the Long Straight Section 5 (LSS5).

INTRODUCTION

The internal SPS beam dump system (SBDS) is a concern for the upcoming HL-LHC upgrade and also, after the recent observed damage [1], during current operation. The system has been designed for very different beam parameters, compared to those that will be used after the Long Shut-down 2 (LS2). As shown in [2] the internal high-energy absorber block (TIDVG) will not survive the nominal HL-LHC beam, and hence an upgrade is necessary to fulfil the requirements.

The internal SBDS is installed in LSS1. It is composed of two kicker systems (MKDV to vertically deflect the beam onto the absorber blocks and MKDH to dilute it), two main absorber blocks (TIDVG and TIDH for high and low-energy beams respectively) and three displaced quadrupoles (dog-leg) [3]. The presence of the dump system in LSS1 makes this area the most activated in the SPS. The TIDVG receives the highest beam power (Fig. 1) of all the SPS absorbers, which causes severe material and air activation, as well as radiation triggered material damage (cables, beamlines equipment, etc.) in its surroundings. Therefore, the post-LS2 high-brightness beam requirements and the heavy radiation related problems caused by the dump system in LSS1, translate into investigating an external dedicated solution, or an upgraded internal one.

The design of a completely dedicated external beam dump could profit from the existing extraction channels in LSS4 and LSS6. In [4], these two possibilities have been documented and both considered unsuitable due to the operational and civil engineering complexity.

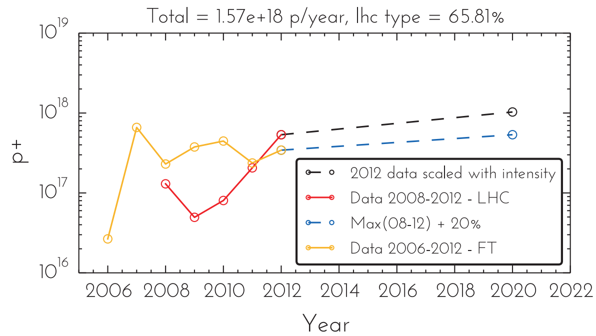

Figure 1: Extrapolation of the expected intensity to be dumped per year for post-LS2 era based on available data.

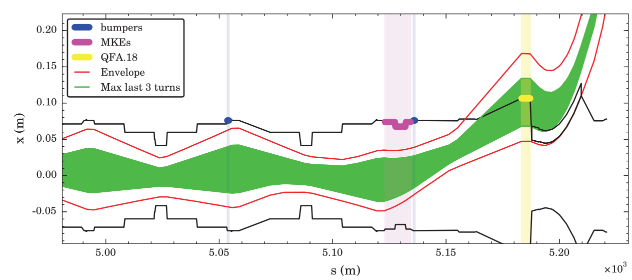

Figure 2: Proposed extraction channel in LSS5 using the same elements as in LSS4. In green the envelope of the last three turns trajectory of the particle with the maximum allowed amplitude at the extraction electrostatic septum ZS2 is shown. In red the beam envelope calculated as $A(s) = (D\delta_p + 1.2 \times \max\{6\sqrt{\epsilon\beta}, x_{3turns}\})1.1 + 6mm$.

It has also been studied to install a new external beam dump in LSS5 in order to fulfil all the requirements for a new beam dump. However this option suffers, as the other cited above, from the small extraction septum aperture and hence it will not be able to fulfil the design requirements within the time-line of the project.

In this paper the feasibility studies and main outcomes of an external dump using a new extraction system in LSS5 are presented. The design of a new internal system in LSS5 is also documented, covering most of the aspects that could undermine the feasibility of such a concept.

EXTERNAL SBDS IN LSS5

An extraction system for a beam dump exhibits several differences with respect to the classical fast extraction from the SPS, for example:

Content from this work may be used under the terms of the CC BY 3.0 licence (© 2015). Any distribution of this work must maintain attribution to the author(s), title of the work, publisher, and DOI.

ISBN: 978-3-95450-168-7 doi:10.18429/JACoW-IPAC2015-THPF098

SPS-TO-LHC TRANSFER LINES LOSS MAP GENERATION USING PYCOLLIMATE

F. M. Velotti[1,2], W. Bartmann[1], C. Bracco[1], M. A. Fraser[1], B. Goddard[1], V. Kain[1], M. Meddahi[1],
[1]CERN, Geneva, [2]EPFL, Lausanne, Switzerland

Abstract

The Transfer Lines (TL) linking the Super Proton Synchrotron (SPS) to the Large Hadron Collider (LHC) are both equipped with a complete collimation system to protect the LHC against mis-steered beams. During the setting up of these collimators, their gaps are positioned to nominal values and the phase-space coverage of the whole system is checked using a manual validation procedure. In order to perform this setting-up more efficiently and more reliably, the simulated loss maps of the TLs will be used to validate the collimator positions and settings. In this paper, the simulation procedure for the generation of TL loss maps is described, and a detailed overview of the new scattering routine (`pycollimate`) is given. Finally, the results of simulations benchmark with another scattering routine are presented.

INTRODUCTION

The SPS is the last accelerator of the LHC injector chain. The SPS and LHC are directly connected through two ≈3 km long TLs which allow the injection of the required 450 GeV beam.

Both transfer lines (TI2 and TI8) are equipped with a complete passive protection system; it is composed of three graphite (R4550 in 1.2 m of active length) collimators per transverse plane (TCDIs). TI2 differs from TI8 because it is also equipped with a momentum collimator installed at the beginning of the line.

Such collimation system is designed to protect the LHC aperture and the LHC injection septa, in case of any kind of failures of the TLs active elements, as well as the SPS extraction systems.

The complete phase-space coverage is ensured by placing the three collimators, on each plane, at about $\pi/3 + n\pi$ phase-advance from each other. They are located at the end of the TLs and are single-stage protection devices. In case of failure in the upstream part of the TL, only one TCDI will be completely hit by the beam; therefore, every collimator has to guarantee an attenuation of the beam intensity to a safe level for accelerator components, i.e. 2×10^{12} [1].

Phase-space Coverage

The main aim of the TL collimators is to ensure adequate protection of the LHC cold apertures. From the LHC Design Report [2], the minimum available aperture in the arc is $7\,\sigma$, hence this represents the target protection for the TL collimation system.

In order to define the collimator jaws aperture needed to guarantee the above cited protection, all possible sources of error have to be taken into account. All the considered errors are listed in Table 1; summing these contributions linearly, considering a typical beam size of 0.5 mm, the total error is $\approx 1.4\,\sigma$ [1]. The maximum escaping amplitude in a "three-phase" collimation system is given by pure geometrical considerations, i.e. $A_{max} = A_{jaw}/\cos(\pi/6)$; where A_{jaw} is the required jaw position, including errors. For the LHC $A_{max} = 7\,\sigma$, so the collimator half-gap has to be $A_{jaw} = 4.5\,\sigma$.

As an example, Fig. 1 shows the horizontal Poincaré portrait at the septum at the end of TI2 (MSI2). Here, all three collimators are sketched at their ideal position, i.e. $4.5\,\sigma$, together with the surviving particles at the MSI2 for two different amplitudes, 4.6/4.9 σ.

Table 1: Errors for the TL Collimator Jaws [1]

Error type	Unit	Value
Inter-jaw parallelism	μm	50
Jaw axis wrt tank	μm	100
Tank axis wrt beam size	μm	180
Surface flatness	μm	50
Knowledge of bema position	μm	44
Beam size errors	σ	0.5

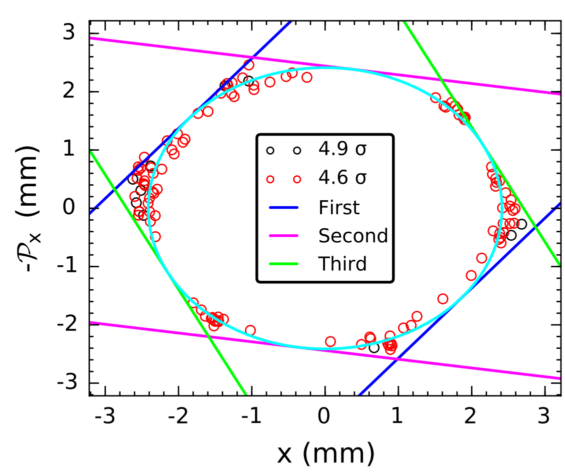

Figure 1: Horizontal phase-space at the LHC injection septum (MSI) downstream TI2.

Validation Methodology

In order to ensure the required protection, after setting up the TL collimators at their nominal apertures and centring them with respect to the measured beam trajectory,

Content from this work may be used under the terms of the CC BY 3.0 licence (© 2015). Any distribution of this work must maintain attribution to the author(s), title of the work, publisher, and DOI.

ISBN: 978-3-95450-168-7 doi:10.18429/JACoW-IPAC2015-THPF099

Content from this work may be used under the terms of the CC BY 3.0 licence (© 2015). Any distribution of this work must maintain attribution to the author(s), title of the work, publisher, and DOI.

UPGRADE OF THE SPS ION INJECTION SYSTEM

J. Uythoven, J. Borburgh, E. Bravin, S. Burger, E. Carlier, J.-M. Cravero, L. Ducimetière, S. Gilardoni, B. Goddard, J. Hansen, E.B. Holzer, M. Hourican, T. Kramer, F. Maciariello, D. Manglunki, F.-X. Nuiry, A. Perillo Marcone, G. Steele, F. Velotti, H. Vincke, CERN, Geneva, Switzerland

Abstract

As part of the LHC Injectors Upgrade Project (LIU) the injection system into the SPS will be upgraded for the use with ions. The changes will include the addition of a Pulse Forming Line parallel to the existing PFN to power the kicker magnets MKP-S. With the PFL a reduced magnetic field rise time of 100 ns should be reached. The missing deflection strength will be given by two new septum magnets MSI-V, to be installed between the existing septum MSI and the kickers MKP-S. A dedicated ion dump will be installed downstream of the injection elements. The parameter lists of the elements and studies concerning emittance blow-up coming from the injection system are presented. The feasibility of the 100 ns kicker rise time and the small ripple of the septum power converter are presented. Material studies of the ion dump are presented together with the radiation impact.

INTRODUCTION

The ALICE experiment in the LHC will be implementing a detector upgrade to reach higher luminosities with ion operation. The foreseen ALICE peak luminosity in Pb-Pb runs is 7×10^{27} Hz/cm^2. As part of the LHC Injector Upgrade Project (LIU), an upgrade of the LHC ion injection chain is ongoing to reach this ambitious goal [1]. The LIU ion project consists of upgrades throughout the ion injector complex and also of the injection system for the ions in the SPS, see Fig. 1.

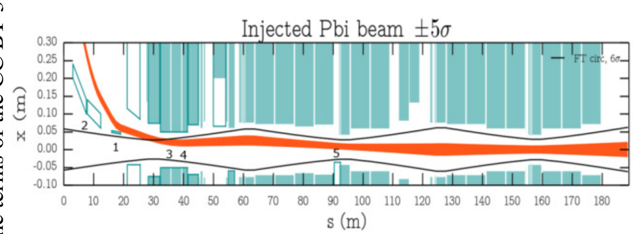

Figure 1: Trajectory and 5σ envelope of the injected ion beam together with the proposed layout: the new MSI-V septum (1), the existing septum MSI (2), the fast injection kickers MKP-S (3) and the slower injection kicker MKP-L (4) together with the new ion injection dump (5).

The new injection system for ions will allow a spacing of 100 ns between the ions batches in the SPS, due to an upgrade of the SPS injection kicker MKP, obtaining a faster pulse rise time. The resulting reduced kick strength will be compensated by the installation of an additional septum MSI-V. As the trajectory of the injected beam is different from the one of the protons, a new injection dump for ions will be installed. A new beam observation screen will be placed in front of the dump and additional beam loss monitors will be added. Details of some of the new or modified elements will be given below.

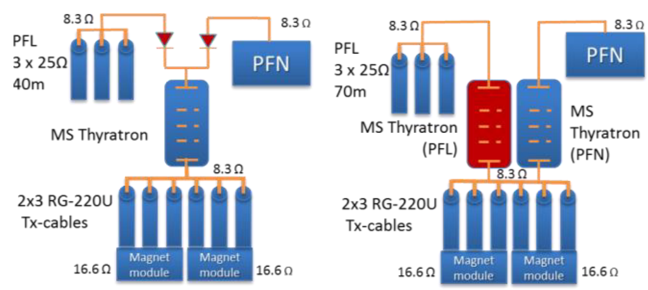

Figure 2: MKP 100 ns test set-up: Configuration 1with diode for separation between PFL and PFN (left) and configuration 2 with one thyratron per branch (right).

INJECTION KICKER UPGRADE

The upgrade of the existing SPS ion injection system by adding an additional PFL in parallel to the existing MKP-S PFN generators is outlined in [2]. In order to proof the feasibility of the 100 ns rise time (2-98%) and to validate the preliminary PSpice simulations a test stand for the 100 ns MKP-S upgrade was set up. Two basic options for a low impedance connection of the existing PFN to the PFL and the transmission cables, as shown in Fig. 2, were developed. Whilst configuration 1 considers only one main switch (MS) thyratron connected to the six parallel transmission cables (50 Ω RG-220U, 3 per magnet module) and separated for operation by two diode stacks, the same functionality is obtained in configuration 2 by using a 2nd thyratron for the PFL branch.

Measurements with the test system in configuration 1 have been performed and showed a significant increase of rise time due to the additional diode stack in the PFL branch. Rise times of around 350 ns were measured with a first test setup using switch tank connected to the spare MKP-S magnet via short transmission cables. Whilst optimization of the circuits (filters) would bring large improvements, it will not stay below the specified 100 ns rise time.

Activities will now focus on tests for configuration 2 which however requires mechanical modification on both switch tanks. Also more detailed PSpice simulations will be necessary to optimize the filter circuits mainly to

ISBN: 978-3-95450-168-7 doi:10.18429/JACoW-IPAC2015-THPF100

THE ACCUMULATOR OF THE ESSnuSB FOR NEUTRINO PRODUCTION

E. Wildner, B. Holzer, M. Martini, I. Papaphilippou, H. Schönauer, CERN, Geneva, Switzerland
M. Eshraqi, ESS, Lund, Sweden
T. Ekelöf, M. Olvegård, R. Ruber, Uppsala University, Uppsala, Sweden

Abstract

The European Spallation Source (ESS) is a research center based on the world's most powerful neutron source currently under construction in Lund, Sweden. 2.0 GeV, 2.86 ms long proton pulses at 14 Hz are produced for the spallation facility (5MW on target). The possibility to pulse the linac at higher frequency to deliver, in parallel with the spallation neutron production, a very intense, cost effective and high performance neutrino beam. Short pulses on the target require an accumulator ring. The optimization of the accumulator lattice to store these high intensity beams from the linac (1.1 10^{15} protons per pulse) has to take into account the space available on the ESS site, transport of H^- beams (charge exchange injection), radiation and shielding needs. Space must be available in the ring for collimation and an RF system for the extraction gap and loss control. We present the status of the accumulator for the ESS neutrino facility.

NEUTRINO PRODUCTION AT ESS

The European Spallation Source (ESS) [1] presently being built in Lund, Sweden, is a research centre that will have the world's most powerful neutron source. It is based on a 2.0 GeV superconducting linac, giving 2.86 ms long proton pulses at 14 Hz for the spallation facility (5MW on target). By pulsing the linac at 28 Hz, additional interleaved H^- pulses sent to a neutrino production target system, would give an opportunity to produce neutrino beams with unprecedented intensity [2]. The corresponding number of protons on target per year would be 12.7 10^{23}. However, the horn based hadron collector can not, for the time being, handle 2.86 ms long pulses due to ohmic heating of the magnet system current leads. Therefore the linac pulse has to be accumulated in a storage ring to produce pulses, a few μs long, on the neutrino production target.

THE ESS LINAC

The duty cycle of the ESS superconducting linac is relatively low (4%). This fact opens a possibility to add pulses in between those used for the spallation neutron production and use them to produce neutrinos. The linac would then be pulsed at 28 Hz, resulting in a total linac power of 10MW. The additional 5 MW that have to be provided for the neutrino production require an upgrade of the ESS linac, in particular of systems related to the acceleration of the H^-- beams needed for charge exchange injection into the accumulator. An additional H^--source would be added, probably including also additional LEBT, RFQ and MEBT sections for matching the H^--beam and the proton beams separately [1]. It is foreseen that focussing and steering elements necessary to tune the H^- beam may change setting between proton and H^- pulses. The ESS construction has started, therefore an urgent preliminary feasibility evaluation of the needed equipment and infrastructure upgrades has taken place, in particular concerning water, cryogenic distribution and capacity, radio frequency couplers, klystron modulators, and electric transformers and power capacity.

To fill the accumulator ring with 1.1 10^{15} protons is a challenging task and the possibility to split the 2.86 ms linac pulse in shorter linac pulses with the same current, still keeping the 5 MW total power for the neutrinos, would be a possibility to fill the accumulator with less number of particles but more often. The option of accelerating, for example, four shorter linac pulses for the neutrino production would make the Linac pulse at 70 Hz giving one 2.86 ms pulse for neutrons and four 0.72 ms pulses for neutrino production, see Fig. 1. 5MW beam power needs 13.3 MW wall plug power for one 2.86 ms long pulse. 4 pulses of 0.72 ms would need 17 MW power consequently there is an operational overhead for this option. To increase the duty cycle may lead to collective effects, which may limit the maximum usable duty cycle in the cavities. Extensive ongoing testing and future operational experience will show if higher duty cycles can be accepted. The aim is to operate the linac at the lowest possible frequency. The final design considerations and cost optimization of the accumulator will decide the optimal repetition rate.

The accumulator will be designed in order to profit from a possible linac upgrade to higher energy by designing the transfer line from the linac to the accumulator for 2.5 GeV and placing the extraction point in the contingency region of the linac, situated between the end f the linac and the spallation target region, where 2.5 GeV could be reached after adding more accelerating modules.

THE ACCUMULATOR

A preliminary lattice of 376 m circumference is described in [3] and summarized in Table 1. The accumulator has to be installed on the ESS site including the transfer lines and the target station. For the H^- beam transfer line the allowed minimum bending radius is limited by the Lorenz stripping of the H^--ions. The criterion we have used to design the transfer line is to have a beam loss corresponding to less than 0.1 W/m heat deposition. With a 66% dipole filling factor in the transfer line we would get, for 2.5 GeV, a radius of about 110 m (see [4]). The baseline layout for the accumulator, target, transfer lines, and the neutrino beam can be seen in

Content from this work may be used under the terms of the CC BY 3.0 licence (© 2015). Any distribution of this work must maintain attribution to the author(s), title of the work, publisher, and DOI.

ISBN: 978-3-95450-168-7 doi:10.18429/JACoW-IPAC2015-THPF101

DESIGN OF A PROTON TRAVELLING WAVE LINAC WITH A NOVEL TRACKING CODE

S. Benedetti[#], TERA, Novara, Italy and EPFL, Lausanne, Switzerland
A. Grudiev, A. Latina, CERN, Geneva, Switzerland
U. Amaldi, TERA, Novara, Italy

Abstract

A non-relativistic proton linac based on high gradient backward travelling wave accelerating structures was designed using a novel dedicated 3D particle tracking code. Together with the specific RF design approach adopted, the choice of a 2.9985 GHz backward travelling wave (BTW) structure with 150° RF phase advance per cell was driven by the goal of reaching an accelerating gradient of 50 MV/m, which is more than twice that achieved so far.

This choice dictated the need to develop a new code for tracking charged particles through travelling wave structures which were never used before in proton linacs. Nevertheless, the new code has the capability of tracking particles through any kind of accelerating structure, given its real and imaginary electromagnetic field map. This project opens a completely new field in the design of compact linacs for proton therapy, possibly leading to cost-effective and widespread single room facilities for cancer treatment.

INTRODUCTION

A collaboration between TERA Foundation and CLIC was established to study a novel linear accelerator for proton therapy. The main goal of the collaboration is to transfer the knowledge acquired by the CLIC group, mostly in terms of RF design, high-gradient limitations and linac optimization, to a medical linac.

Funds of the Knowledge Transfer group of CERN permitted the construction of a prototype based on the design discussed in [1]. High power RF test of this accelerating structure is under preparation at the present time, to validate its capability to reach the maximum accelerating gradient of 50 MV/m.

A backward travelling wave linac was never used for accelerating protons. Moreover, a medical linac has a certain number of peculiarities with respect to high energy physics linacs, as for instance the need to vary the kinetic energy of particles over a wide range to reach tumour tissues at different depth into the patient body. So it was decided to develop a completely new tracking code, called *RF-Track*. The main features of such code will be discussed in the present paper, together with the results of the benchmark study and a preliminary BTW linac design.

RF-TRACK

In order to evaluate and maximise the transmission through backward-travelling accelerating structures, a new *ad-hoc* tracking code was developed: *RF-Track*. The decision to develop a new code was motivated by the need to perform accurate tracking of continuous, unbunched, inherently relativistic beams of protons or ions (with beta = ~0.35 for the protons, even less for the ions), through 3D field maps of BTW structures. No code in our knowledge featured the required flexibility and had the capability to handle real and imaginary field maps of travelling-wave RF structures (forward or backward).

RF-Track can input and combine the 3D phasor maps of both electric and magnetic fields, in order to represent an RF field in all its complexity, as 3D solvers such as HFSS [2] generate. This possibility allows the accurate representation of (backward) travelling-wave structures, differently from most of the codes, which can only input static field maps or can only simulate standing wave structures (and require to overlap two standing waves to mimic a travelling wave).

RF-Track performs full 6D transport and maintains the proper time of each particle. This allows computing the correct timing of the RF fields felt by each particle. It must be noticed that, thanks to this strategic choice, the code is not bounded by the notion of "bunch" or "reference particle" and can track continuous beams consistently. It implements exact transfer maps for drifts, quadrupoles and sector bends in both the transverse plane and the longitudinal planes, with the exception of the quadrupole longitudinal map, which features a second-order expansion of the path length to take into account the particle's incoming position and angles. The approximated solution of the longitudinal quadrupole map (already better than the standard "drift-like" map adopted by many codes) doesn't undermine the tracking accuracy, because each element can be integrated in an arbitrary number of steps, recovering accuracy whenever a second-order tracking is not sufficient.

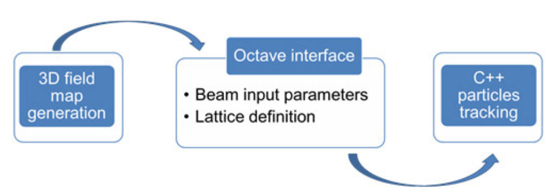

Figure 1: Simplified scheme of *RF-track* software architecture.

The code is written in modern, fast, parallel C++ that exploits multi-core CPUs. Its fast computational core is accessible by the user through a powerful SWIG Octave interface [3,4], which permits to write complex, yet readable and concise, simulation scripts that can directly benefit from a large number of optimization toolboxes

[#] stefano.benedetti@cern.ch

Content from this work may be used under the terms of the CC BY 3.0 licence (© 2015). Any distribution of this work must maintain attribution to the author(s), title of the work, publisher, and DOI.

ISBN: 978-3-95450-168-7 doi:10.18429/JACoW-IPAC2015-THPF102

VERIFICATION OF THE NEUTRON MIRROR CAPABILITIES IN MCNPX VIA GOLD FOIL MEASUREMENTS AT THE EIGER INSTRUMENT BEAMLINE AT THE SWISS SPALLATION NEUTRON SOURCE (SINQ) *

R.M. Bergmann†, U. Filges, S. Forss, E. Rantsiou, D. Reggiani, T. Reiss, U. Stuhr, V. Talanov, M. Wohlmuther
Paul Scherrer Institut, Villigen, Switzerland

Abstract

The EIGER triple-axis thermal neutron spectrometer beamline contains “supermirror” neutron guides, which preferentially reflect low-energy neutrons toward the EIGER spectrometer that come from the ambient temperature, light water neutron source in SINQ. Gold foil measurements have been performed at the EIGER beamline in 2013. This process can be modeled from incident proton to thermal neutron exiting the EIGER beamline by using the neutron mirror capabilities of MCNPX, which should be more accurate than simulations with simplified neutron source distributions and geometry representations. The supermirror reflectivity parameters have been measured previously and are used in MCNPX 2.7.0 to reproduce the activity measured from the gold foil irradiation, verifying the neutron mirror modeling capabilities in MCNPX 2.7.0.

INTRODUCTION

EIGER is a triple-axis thermal neutron spectrometer that looks at the light water scatterer inside SINQ, a spallation neutron source driven by a continuous 590 MeV proton beam at the Paul Scherrer Institut in Villigen, Switzerland. The incoming protons impinge on a lead target cooled with heavy water, producing high energy neutrons. These neutrons are moderated by the tank of D_2O surrounding the target. The “water scatterer” is a set of seven vertical aluminum tubes 25 cm away from the center of the target that contain ambient temperature light water. These tubes act as a scattering medium to send thermal neutrons streaming through low pressure nozzles towards neutron instruments.

The neutron guide that delivers thermal neutrons from the water scatterer towards the EIGER instrument is internally covered with neutron “supermirrors”. These mirrors are reflective to low-energy neutrons, and allow the guide to transport neutrons with small divergence instead of only neutrons with trajectories parallel to the guide axis, increasing neutron extraction efficiency. The reflectivity of the mirrors are described by Eq. 1 where R_0 is nominal reflectivity, Q_c is the critical momentum transfer, m is the angular extension parameter, α is reflectivity declination parameter, and W is the reflectivity edge width [1].

The reflectivity parameters of EIGER's supermirrors have been measured previously and determined to be $R_0 = 0.995$, $Q_c = 2.17 \times 10^{-2}$Å^{-1}, $m = 3.6$, $\alpha = 3.99$Å, and $W = 10^{-3}$Å^{-1} [2]. The guide is rectangular, tapers in the horizontal plane from 80 mm wide near the moderator tank to 30 mm wide at the guide exit, and is a constant 150 mm tall in the vertical plane. There is a 10 cm thick sapphire crystal near the moderator tank which acts as a neutron filter to preferentially scatter neutrons above 0.1 eV out of the beam [3].

$$R(Q) = \begin{cases} \text{if } Q > Q_c : \\ \frac{R_0}{2}\left\{1 - \tanh\left(\frac{Q-mQ_c}{W}\right)\right\}\{1-\alpha(Q-Q_c)\} \\ \\ \text{if } Q \le Q_c : \\ R_0 \end{cases} \tag{1}$$

This reflectivity model is used by McStas and has been previously implemented in patched version of MCNPX 2.5.0 [1]. The patch has recently been ported to MCNPX 2.7.0 [4] and debugged for MPI parallelism. The parallelized reflectivity capabilities now allow the neutron flux gains to be completely modeled in MCNPX 2.7.0. This capability is demonstrated by comparing the calculated activation of an array of gold foils exposed to the EIGER beam to experimental results.

GOLD FOIL MEASUREMENT

The vertical array of six gold foils shown in Figure 1 were exposed to the EIGER beam in December, 2013.

Figure 1: Gold foil array used in the measurements.

The foils were placed near the monochromator position at EIGER. The foils are 25 mm in diameter and 30 mm center-to-center. The blue marker lines in the figure show the approximate extent of the neutron guide. The average current on the SINQ target during the irradiation was 200μA, and the foils were exposed for 5 minutes. After irradiation, activation analysis was performed using a gamma spectrometer.

* Supported by Swiss National Science Foundation grant 200021_150048/1
† ryan.bergmann@psi.ch

Content from this work may be used under the terms of the CC BY 3.0 licence (© 2015). Any distribution of this work must maintain attribution to the author(s), title of the work, publisher, and DOI.

ISBN: 978-3-95450-168-7 doi:10.18429/JACoW-IPAC2015-THPF103

CURRENT STATUS OF THE SANAEM RFQ ACCELERATOR BEAMLINE

G. Turemen*, B. Yasatekin, Ankara University, Dept. of Physics, Ankara, Turkey
S. Ogur, V. Yildiz, Bogazici University, Dept. of Physics, Istanbul, Turkey
O. Mete, Cockcroft Institute and University of Manchester, School of Physics and Astronomy, UK
A. Ozbey, Istanbul University, Aircraft Technology Program, Istanbul, Turkey
H. Yildiz, Istanbul University, Machine Program, Istanbul, Turkey
S. Oz, Istanbul University, Dept. of Mechanical Engineering, Istanbul, Turkey
F. Yaman, IZTECH, Dept. of Electrical & Electronics Engineering, Izmir, Turkey
Y. Akgun, A. Alacakir, S. Bolukdemir, TAEK, SANAEM, Ankara, Turkey
A. Bozbey, A. Sahin, TOBB ETU, Dept. of Electrical and Electronics Engineering, Ankara, Turkey
G. Unel, University of California at Irvine, Physics Dept., CA, USA
S. Erhan, University of California at Los Angeles, Dept. of Physics and Astronomy, CA, USA

Abstract

The design and production studies of the proton beamline of SPP, which aims to acquire know-how on proton accelerator technology thru development of man power and serves as particle accelerator technologies test bench, continue at TAEK-SANAEM as a multi-phase project. For the first phase, 20 keV protons will be accelerated to 1.3 MeV by a single piece RFQ. Currently, the beam current and stability tests are ongoing for the Inductively Coupled Plasma ion source. The measured magnetic field maps of the Low Energy Beam Transport solenoids are being used for matching various beam configurations of the ion source to the RFQ by computer simulations. The installation of the low energy diagnostics box was completed in Q1 of 2015. The production of the RFQ cavity was started with aluminum 7075-T6 which will be subsequently coated by Copper to reduce the RF (Ohmic) losses. On the RF side, the development of the hybrid power supply based on solid state and tetrode amplifiers continues. All RF transmission components have already produced with the exception of the circulator and the power coupling antenna which are in the manufacturing and design phases, respectively. The acceptance tests of the produced RF components are ongoing. This work summarizes the design, production and test phases of the above-mentioned SPP proton beamline components.

INTRODUCTION

Turkish Atomic Energy Authority (TAEK) started the construction of a proton beamline at its Sarayköy Nuclear Research and Training Center, SANAEM. The SANAEM Prometheus Project (SPP) is designed and engineered with local resources enabling accelerator physicists to acquire know-how and it will serve as a particle accelerator technologies test bench. Currently some of the components are being manufactured (e.g. the single piece RFQ) or being assembled (e.g. the hybrid RF PSU). In the meantime, the stability tests and measurements continue with the already installed components such as the ion source, the LEBT line and the low energy diagnostics box (Fig. 1). The rest of this note details the ongoing work on the components of the SPP beamline.

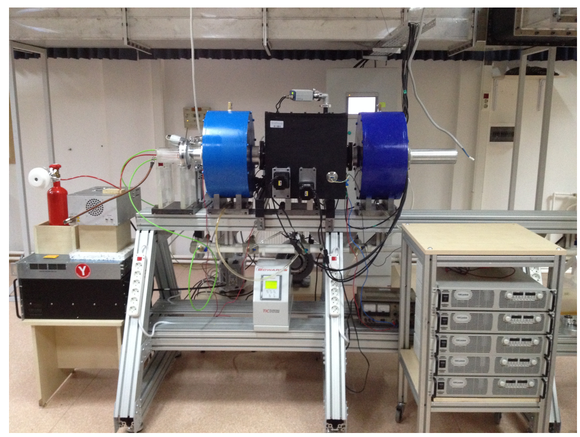

Figure 1: Currently installed parts of the SPP beamline.

ION SOURCE

An Inductively Coupled Plasma (ICP) type ion source was selected for its low production cost and its ability to match the relatively modest proton current requirements of the SPP project. Initially, a water cooled plasma chamber with 8 multicusp magnets was produced with an internal RF antenna [1]. Later, plasma generation method was changed because of the high voltage sparking between the alumina coated copper internal RF antenna and the high voltage plate. In the new design, a quartz tube with a gas injection nose is used as the plasma chamber. A 3.5 turn external RF antenna is used to produce hydrogen plasma and to prevent sparking. This RF antenna is sandwiched between the quartz plasma chamber and the plexi-glass water cooling chamber. With this setup, the ICP ion source is found to be suitable for longtime operation without overheating at an RF power below 500 W. The impedance matching between the RF antenna and the 13.56 MHz RF power supply was achieved using a matching network. The RF power coupling to the plasma was easily accomplished for a chamber diameter of 30 mm at 10^{-3} mBar.

* gorkem.turemen@ankara.edu.tr

Content from this work may be used under the terms of the CC BY 3.0 licence (© 2015). Any distribution of this work must maintain attribution to the author(s), title of the work, publisher, and DOI.

ISBN: 978-3-95450-168-7 doi:10.18429/JACoW-IPAC2015-THPF104

DESIGN OF A SCALED HIGH DUTY FACTOR HIGH CURRENT NEGATIVE PENNING SURFACE PLASMA SOURCE

D. Faircloth, S. Lawrie, T. Rutter, M. Whitehead, T. Wood
STFC/RAL/ISIS, Chilton, Oxfordshire, OX11 0QX, UK
V. Dudnikov
Muons Inc, Batavia, IL 60510, USA

Abstract

The Front End Test Stand (FETS) at the Rutherford Appleton Laboratory (RAL) requires a 60 mA, 2 ms, 50 Hz H^- beam. The present source can only deliver the current and pulse length requirements at 25 Hz. At 50 Hz there is too much droop in the beam current. To rectify this, a scaled source is being developed. This paper details the new source design and the experiments conducted that are guiding the design.

FETS

The FETS project aims to produce a very high quality, perfectly chopped H^- ion beam as required for high power proton drivers. The beam parameters are 3 MeV energy and 60 mA beam current at 50 Hz repetition rate and up to 2 ms pulse duration.

DUTY CYCLE LIMIT

FETS uses a Penning Surface Plasma Source (SPS) [1] (Fig. 1). The current FETS source uses the same plasma electrodes, and has the same plasma volume, as the ISIS operational source. The operational source has successfully delivered beam for ISIS operations for 30 years. It runs with a 760 µs discharge pulse length at a 50 Hz repetition rate.

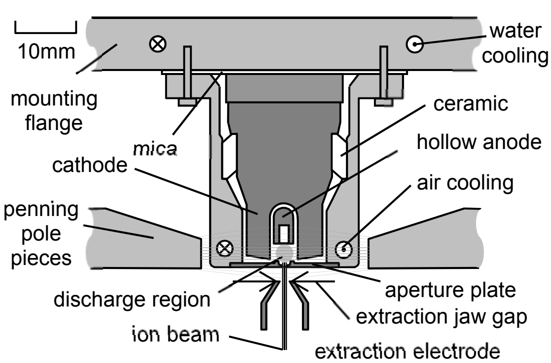

Figure 1: Existing FETS Penning SPS schematic.

FETS specifies a 2 ms 50 Hz 60 mA H^- beam. To cleanly extract a 2 ms beam it is necessary to produce a 2.2 ms long discharge pulse in the ion source. This gives the plasma 0.2 ms to stabilize before beam extraction begins. With increased cooling the maximum discharge pulse lengths achievable with the standard ISIS electrode geometry are 1.2 ms at 50 Hz or 2.2 ms at 25 Hz [1]. Beyond these duty cycles there is too much droop in the extracted beam current.

Although adequate for FETS commissioning, extra development work is required in order to meet the full FETS duty cycle requirements. ISIS is also interested in developing sources with longer lifetimes for ISIS operations.

NEW DESIGN

Scaled Source

Previous work [2,3] indicates that increasing the surface area of the electrodes presented to the plasma should solve the duty cycle limitations. Increasing the surface area will also reduce the sputtering rate and should yield longer source lifetimes. The proposed new design is shown in Fig. 2.

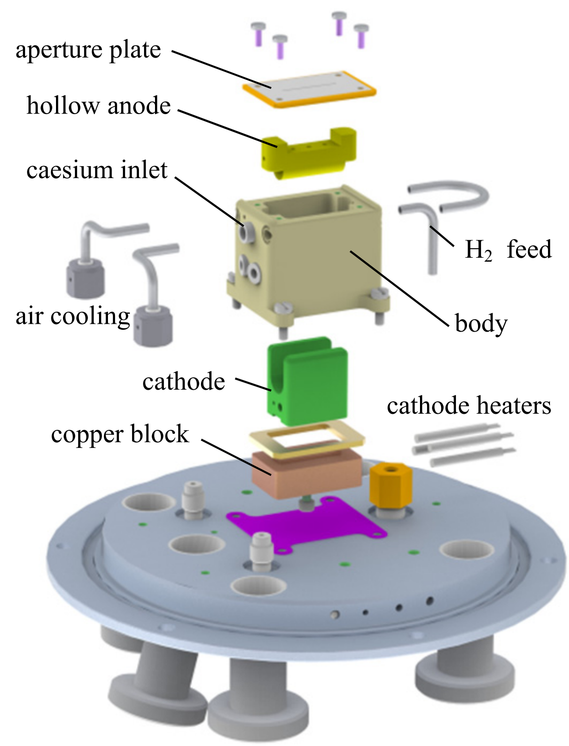

Figure 2: Scaled source exploded view.

The basis of the design is to double the plasma volume in each dimension, creating an 8 fold increase in plasma volume. Meanwhile, the external dimensions of the source are kept as compact as possible, limited by the

Content from this work may be used under the terms of the CC BY 3.0 licence (© 2015). Any distribution of this work must maintain attribution to the author(s), title of the work, publisher, and DOI.

ISBN: 978-3-95450-168-7 doi:10.18429/JACoW-IPAC2015-THPF105

STATUS OF THE RAL FRONT END TEST STAND

A. Letchford, M. Clarke-Gayther, M. Dudman, D. Faircloth, S. Lawrie, STFC RAL ISIS, UK
S.Alsari, M. Aslaninejad, P. Savage, Imperial College of Science and Technology, UK
J. Pozimski, STFC RAL, UK & Imperial College of Science and Technology, UK
G. Boorman, A. Bosco, S. Gibson, Royal Holloway University of London, UK
R. D'Arcy, S. Jolly, University College London, UK
J. Back, University of Warwick, UK

Abstract

The Front End Test Stand (FETS) under construction at RAL is a demonstrator of front end systems for future high power proton linacs. Possible applications include a linac upgrade for the ISIS spallation neutron source, new future neutron sources, accelerator driven sub-critical systems, high energy physics proton drivers etc. Designed to deliver a 60mA H-minus beam at 3MeV with a 10% duty factor, FETS consists of a high brightness surface plasma ion source, magnetic solenoid low energy beam transport (LEBT), 4-vane 324MHz radio frequency quadrupole and medium energy beam transport (MEBT) containing a high speed beam chopper and non-destructive laser diagnostics. This paper describes the current status of the project and future plans.

FRONT END TEST STAND

FETS was originally conceived as a chopper beam test facility but has since expanded its objectives to become a generic test stand for high power proton accelerator front end technologies. Applications include but are not limited to ISIS upgrades, future Spallation Neutron Sources, a Neutrino Factory, Muon Collider, Accelerator Driven Sub-critical Systems as well as exploitation of the low energy beam.

FETS has been extensively described elsewhere [1][2]. It consists of an H- ion source, magnetic low energy beam transport (LEBT), 324 MHz 4-vane Radio Frequency Quadrupole accelerator (RFQ), medium energy beam transport and chopper line (MEBT) and comprehensive diagnostics. The rest of this paper describes the status and future plans for each component of the test stand.

ION SOURCE

FETS uses a Penning Surface Plasma Source (SPS) [3]. A programme of continuous development over many years has resulted in source performance which is very close to the demanding FETS specification [4].

Having previously commissioned a new high voltage extraction power supply capable of 25 kV at the full 10% duty factor [5] and a redesigned downstream post-acceleration system which resulted in a considerably less divergent beam entering the LEBT, a beam emittance of 0.35 π mm mrad rms normalised was measured. The ion source systems have now been decommissioned to allow infrastructure installation and development has turned to the VESPA plasma test stand [6] where progress is being made towards a scaled version of the source capable of operating continuously at the full duty factor [7].

LEBT

The FETS LEBT consists of three identical magnetic solenoids with maximum on axis field of 0.4 T. Previous studies had shown high beam currents of up to 60 mA at the end of the LEBT with a reasonably small rms-emittance. However, large offsets of ~10mm in position and ~10 mrad in angle were observed in both transverse planes. These were traced to a lack of repeatability in mounting the ion source assembly following source changes or maintenance. An improved datum and alignment system has largely corrected this and although a perfect alignment cannot be achieved due to the length of ~2 m, minor offsets can be corrected with the dipole steerers integrated into the solenoids.

An extensive parametric evaluation of the LEBT has shown that a well aligned, well matched beam can be delivered to the RFQ injection point [8][9].

The LEBT is currently decommissioned to allow for infrastructure installations.

RFQ

The FETS RFQ is a 324 MHz, 4-vane type with a final energy of 3 MeV and a total length of ~4.0m. It employs a bolted, braze-free construction with a 3D O-ring for the vacuum seal and RF finger contacts [10]. The 4m long cavity consists of 4 sections each made up of 2 major and 2 minor vane segments.

Manufacturing of the RFQ is nearing completion. Inspection of the first section delivered to RAL showed a manufacturing error resulting in a transverse and longitudinal shift of the vane modulations. This error was traced to a changed datum setting in the 5-axis CNC machine. Simulations showed that the effect on the beam dynamics would have been acceptable however the resulting resonant frequency shift was beyond that which could be compensated for. Fortunately the internal surfaces have been re-machined and both major and minor vane segments recovered. Inspection of the second section showed a small (100 μm) curvature due to internals stresses introduced during rough machining. The outer datum surface was re-machined flat before finalising the internal surface. Similar corrective action will be performed on sections 3 and 4.

Resonant frequency measurements of section 1, including the error, showed good agreement with

Content from this work may be used under the terms of the CC BY 3.0 licence (© 2015). Any distribution of this work must maintain attribution to the author(s), title of the work, publisher, and DOI.

ISBN: 978-3-95450-168-7 doi:10.18429/JACoW-IPAC2015-THPF106

Content from this work may be used under the terms of the CC BY 3.0 licence (© 2015). Any distribution of this work must maintain attribution to the author(s), title of the work, publisher, and DOI.

REVIEW OF LINAC UPGRADE OPTIONS FOR THE ISIS SPALLATION NEUTRON SOURCE

C. Plostinar, C. Prior, G. Rees, STFC/ASTeC, Rutherford Appleton Laboratory, UK

Abstract

The ISIS Spallation Neutron Source at Rutherford Appleton Laboratory has recently celebrated 30 years of neutron production. However, with increasing demand for improved reliability and higher beam power it has become clear that a machine upgrade is necessary in the medium to long term. One of the upgrade options is to replace the existing 70 MeV H^- injector. In this paper we review the ongoing upgrade programme and highlight three linac upgrade scenarios now under study. The first option is to keep the existing infrastructure and replace the current linac with a higher frequency, more efficient machine. This would allow energies in excess of 100 MeV to be achieved in the same tunnel length. A second option is to replace the current linac with a new 180 MeV linac, requiring a new tunnel. A third option is part of a larger upgrade scenario and involves the construction of an 800 MeV superconducting linac.

ISIS UPGRADES

Over the last three decades, the ISIS spallation source has been delivering neutrons to generations of scientists from all over the world, creating a key centre for physical and life sciences research at Rutherford Appleton Laboratory in the UK. The accelerator consists of a 70 MeV H^- injector and an 800 MeV synchrotron delivering a total of ~200 kW beam power to two target stations. The injector starts with an H^- ion source, followed by a three solenoid low energy beam transport line (LEBT) and a 665 keV, four-rod RFQ operating at 202.5 MHz. A Drift Tube Linac (DTL) accelerates the beam to 70 MeV. The DTL consists of four tanks which have been recycled from previous high energy physics projects. Tanks 2 and 3 were commissioned in the 1950s for the RAL Proton Linear Accelerator, while tanks 1 and 4 were copies of the Fermilab DTL built in the 1970s, originally intended for the Nimrod accelerator, but first used in ISIS [1], [2].

While ISIS has been the most successful pulsed neutron spallation source in the world, it is also one of the oldest and the necessity for an upgrade has been made clear for some time. This involves not just maintaining or improving the current machine reliability, but also increasing its capabilities. With new facilities like the SNS in the USA and J-PARC in Japan now delivering MW class beams, a major power upgrade for ISIS has become a key strategic goal in the medium to long term.

Small upgrades are already taking place aimed mainly at improving the machine reliability and maintaining the current level of performance. A programme designed to improve the ion source lifetime, beam current, pulse length and reliability has been successfully taking place as part of the Front End Test Stand project [3]. The old Cockcroft-Walton linac injector was replaced a few years ago with a 665 keV, 202.5 MHz RFQ, the structure of choice for most modern proton injectors, while efforts are now underway to replace the fourth DTL tank, a structure soon to celebrate its 60th anniversary. In the ring, the installation of a dual harmonic system has taken place. By employing a combination of harmonic numbers two and four RF cavities, the stable area of longitudinal phase space can be lengthened, allowing more beam to be injected and accelerated, thus overcoming the old machine intensity space charge limit of $2.5\cdot10^{13}$ protons per pulse. Beam powers of ~240 kW have already been demonstrated [4].

In terms of major upgrades, the addition of a second target station at the end of 2008 saw the machine capabilities and user base greatly expanded. However, for power upgrades, the construction of new accelerators is necessary. There have been several proposals for a power increase ranging from injector to synchrotron upgrades, as well as for a multipurpose facility where a high power proton accelerator would be used both for a spallation source and as a driver for a neutrino factory [5].

Regarding linac developments, it has become clear that a major upgrade will be necessary. While plans for a new machine are welcomed, any proposal has to take into account several factors, of which two are essential. The first requirement is that any upgrade work should consider the high likelihood of a phased upgrade. This simply means that any design choice should be made as part of a broader, long term plan, such that later upgrade efforts are not hampered by early choices. The second requirement takes into account the wider context of neutron science in Europe. With several experimental reactors due to be retired and with ESS not being fully operational for another decade, ISIS remains the main source of neutrons. Indeed, demand for beam time is at an all time high. This makes machine availability the dominant user requirement and as a result, potential upgrades with minimum user disruption should be proposed. In this context, three linac upgrades routes will be further outlined.

100 MeV LINAC

A straightforward and by far the most economical upgrade is a new linac in the existing tunnel to replace the existing 70 MeV injector. By reusing the existing infrastructure, the civil engineering costs are dramatically reduced, the only constraint being the overall length restriction of ~50 m. By operating at a higher frequency, increased accelerating gradients and redesigning the RF structures for increased efficiency, energies in excess of 100 MeV can be achieved in the same length as the

ISBN: 978-3-95450-168-7 doi:10.18429/JACoW-IPAC2015-THPF107

Content from this work may be used under the terms of the CC BY 3.0 licence (© 2015). Any distribution of this work must maintain attribution to the author(s), title of the work, publisher, and DOI.

QUALITY AND STABILITY STUDIES OF THE BEAMS IN THE ELENA RING TRANSFER LINES

J. R. Hunt, O. Karamyshev, J. Resta-López, C. P. Welsch
Cockcroft Institute and The University of Liverpool, UK

Abstract

The Extra Low Energy Antiproton (ELENA) ring will initially provide eight different experiments at CERN with extra low energy (~100 keV) antiprotons by utilising electron cooling techniques. As a result, a system of transfer lines is being designed to ensure each experiment receives a beam consistent with specified properties. In this paper, particle tracking simulations are performed to explore the effects of different lattice imperfections, e.g. element misalignment, electric field errors and matching errors, on the beam quality and orbit stability. Specific values for the upper limits of inaccuracies are obtained as a guide for the construction of the transfer lines, and will enable further optimization.

INTRODUCTION

ELENA is a low energy storage ring designed to increase the efficiency of the antimatter experiments at CERN [1]. Currently under construction, ELENA will accept antiprotons from the Antiproton Decelerator (AD) [2] and employ the use of an electron cooler to further decelerate them from a kinetic energy of 5.3 MeV to 100 keV. At these lower energies, fewer antiprotons will be lost to degrader foils at the end of the deceleration process and as a result the anti-hydrogen experiments will receive higher intensity beams.

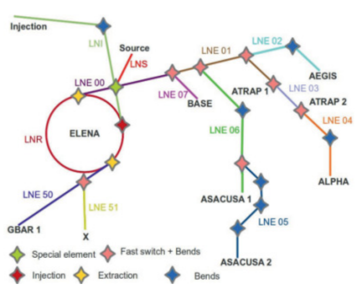

Figure 1: Schematic layout of transfer lines.

A system of transfer lines will carry these extra low energy beams to eight different locations within the AD hall. The low beam energy after ejection from ELENA allows the use of electrostatic elements. Reasons for this design choice include cost of construction, low power consumption, easy operation and good possibilities for shielding elements against stray magnetic fields. [1]

Nine separate lattices make up the transfer lines, two of which are directly connected to ELENA. The studies undertaken in this paper focus on the lattice 'LNE00' as it is connected directly to ELENA and the beams for all but one experiment will pass through this section,see Fig. 1. The only working optical elements present along LNE00 in these simulations are the quadrupoles in a configuration used to pass the beam through to LNE01.

TRACKING CODE

For this study Polymorphic Tracking Code (PTC) [3] was used to track a series of beams through a complete MAD-X [4] model of LNE00 obtained from [5]. For each simulation, a Gaussian beam of 10,000 particles with initial ε_x and ε_y = 1 mm·mrad, momentum spread = 5×10^{-4} and no x-y coupling, was generated using Monte-Carlo methods. After tracking, the beam data was passed to a custom Matlab code for analysis.

ELEMENT POSITION OFFSETS

The positions of the quadrupoles were offset in the x and y planes separately. Monte-Carlo methods were used to offset each element by a random amount corresponding to a Gaussian spread. The magnitude of the offsets was increased and the effect on the particle losses in the beam was observed (Fig. 2). For each point the result of 10 runs with varying random offsets were averaged to capture overall effect of the position errors.

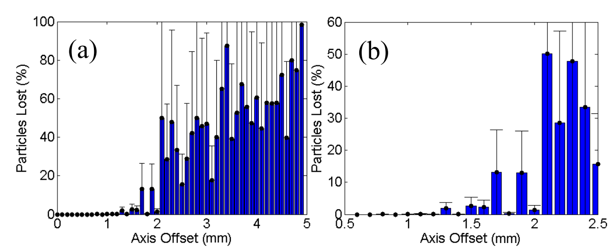

Figure 2: Horizontal losses at the end of LNE00 for increasing quadrupole offsets. The vertical losses results have similar features. (a) shows the full scan and (b) shows more detail around 1.5 mm.

The effects of the quadrupole offsets on the beam losses at the end of the transport line remain steady until they significantly increase around 1.8 mm, with the average reaching just below full beam loss by 5 mm. The first significant losses occur at 1.3 mm where for one particular run almost 18% of the beam was lost, however the other 9 runs lost only 0.56% in total, bringing the average down.

As this simulation only includes the physical aperture and we would expect a dynamic aperture at a smaller

Work supported by the EU under Grant Agreement 624854 and the STFC Cockcroft Institute core grant No. ST/G008248/1.
james.hunt@cockcroft.ac.uk

ISBN: 978-3-95450-168-7 doi:10.18429/JACoW-IPAC2015-THPF108

EBIS CHARGE BREEDER AT ANL AND ITS INTEGRATION INTO ATLAS

A. Perry#, A. Barcikowski, G. Cherry, C. Dickerson, B. Mustapha, P. N. Ostroumov,
Argonne National Laboratory, Argonne, IL 60439, USA

Abstract

An Electron Beam Ion source Charge Breeder (EBIS-CB) has been developed to charge breed CARIBU radioactive beams at ATLAS and it is now in the final stages of off-line commissioning. Within the next year, the EBIS-CB will replace the existing ECR charge breeder to increase the intensity and improve the purity of reaccelerated radioactive ion beams. The integration of the new EBIS-CB requires:

a. Building a new electrostatic low energy beam transport line (LEBT) from CARIBU to the EBIS-CB that will ensure successful seeding into the trap.
b. Modifications to the existing ATLAS LEBT to accommodate the injection of the charge bred ions into the post accelerator.

In this paper we will describe the beam line design and present beam dynamics simulation results.

INTRODUCTION

The CAlifornium Rare Isotope Breeder Upgrade (CARIBU) facility is capable of generating a wide variety of rare isotope beams (RIB) of heavy ions in the 80-160 mass range from the fission fragments of a ^{252}Cf source [1]. After thermalization in a helium gas catcher the ions are mass-separated using a magnetic spectrometer, charge bred in an electron-cyclotron resonance (ECR) ion source, and then injected into the Argonne Tandem Linear Accelerator System (ATLAS) for post acceleration. Plasma-surface interactions in the ECR chamber results in significant contamination of the extracted beams, which subsequently obscures the signature of low intensity RIBs. To address this, a charge breeder based on the electron beam ion source (EBIS) concept has been developed at ANL for the CARIBU system [2]. Higher breeding efficiency and most importantly, much better purity of radioactive ion beams are expected with the EBIS charge breeder. The CARIBU EBIS-CB utilizes technology recently developed at Brookhaven National Laboratory (BNL) [3].

The offline commissioning of the EBIS-CB is now approaching its final stages and 20% breeding efficiency into ^{133}Cs^{27} within 23 ms has already been demonstrated [4]. The integration into ATLAS is scheduled to commence later this year. This paper will focus on beam dynamics studies for the beam transport line from CARIBU to the EBIS-CB and from the EBIS-CB to ATLAS.

*This work was supported by the U.S. Department of Energy, Office of Nuclear Physics, under Contract DE-AC02-06CH11357. This Research used resources of ANL's ATLAS facility, which is a DOE Office of Science User Facility.
#aperry4@hawk.iit.edu

BEAM TRANSPORT FROM THE EBIS-CB TO ATLAS

The beam transport line from the EBIS-CB to the ATLAS RFQ is shown in Figure 2. In this section of the beam line it is necessary to separate the desired radioactive beams from the residual gas contaminants. The residual gas spectrum was measured during the EBIS offline commissioning and is depicted in Figure 1. Radioactive beams delivered from CARIBU will be charge-bred to a charge-to-mass ratio in the range $1/6 \leq Q/A \leq 1/4$ in every 10-30 ms breeding cycle. This corresponds to a dipole current between 36 A and 45 A in the figure. The intensity of the O^3 peak which lies in that range is estimated at $\sim 10^5$ ions per pulse. This should be compared to the intensity of radioactive beams delivered by CARIBU which will be in the order of 10^3-10^4 ions per pulse.

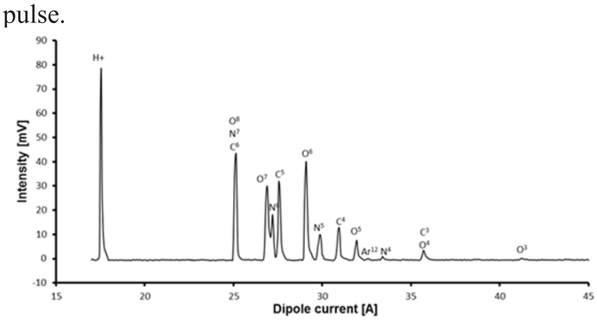

Figure 1: Residual gas spectrum after 30ms breeding.

It has already been noted by several authors that electron beam ion sources tend to generate beams with significant energy spreads [5]. This is due to heating of the ions in the trap by the electron beam [6], ionization heating [7], and heating by plasma instabilities [8] or as a result of the extraction process [9]. In order to handle the significant energy spread Nier-type spectrometers are usually employed, so the beam width at the mass selection slit does not depend on the energy spread at the first order [10]. However, in our case it was decided not to employ a Nier-type spectrometer due to the cost of replacing one of the existing dipole magnets with an electrostatic deflector capable of handling beams with relatively high electric rigidities (up to ~200 kV). Furthermore, the residual magnetic dispersion would prohibit the possible upgrade to a multi user facility, where beams with different magnetic rigidities will be transported simultaneously [11]. Instead, it was decided to use the existing dipoles and make the 180° bend doubly achromatic with the mass selection performed between the 90° dipoles. In addition, it was required that after the 180° bend the beam will be symmetric and focused into the small aperture of the Multi Harmonic Buncher (MHB)

Content from this work may be used under the terms of the CC BY 3.0 licence (© 2015). Any distribution of this work must maintain attribution to the author(s), title of the work, publisher, and DOI.

ISBN: 978-3-95450-168-7 doi:10.18429/JACoW-IPAC2015-THPF110

OFFLINE TESTING OF THE CARIBU EBIS CHARGE BREEDER*

C. Dickerson#, S. Kondrashev, P.N. Ostroumov, R. Vondrasek, ANL, Argonne, IL 60439, USA
A. Perry, IIT, Chicago, IL 60616, USA

Abstract

In 2015 an electron beam ion source (EBIS) will be installed at the ATLAS facility to charge breed radioactive beams from the Californium Rare Isotope Breeder Upgrade (CARIBU). Currently an ECR ion source is used to charge breed CARIBU beams. The EBIS will provide beams with much less contamination and higher breeding efficiencies. In preparation for its installation at ATLAS the EBIS has been successfully commissioned offline. The EBIS was configured in the offline facility to closely mimic the conditions expected in the ATLAS installation, so commissioning results should be representative of its performance with CARIBU. The EBIS breeding efficiency was tested with pulses of $^{133}Cs^{1+}$ from a surface ionization source, and for multiple operational modes relative breeding efficiencies greater than 25% could be achieved. After transmission losses the total efficiency of the system was 15-20%. The contaminants were expectedly very low for a UHV system with nominal pressures of ~1 – 3 x 10^{-10} Torr.

INTRODUCTION

Acceleration in the ATLAS facility requires an $A/q \leq 7$, so the ions produced by the CARIBU ^{252}Ca source in the mass range 80 – 160 amu with 1+ and 2+ charge states require charge breeding [1]. Presently an electron cyclotron resonance ion source (ECRIS) breeds the radioactive ion beams (RIB) from CARIBU. The combination of capture, breeding, and transport efficiencies of the ECR for CARIBU RIBs is typically 8-15%, but extracted beams can contain significant contamination which can be problematic for experiments with low intensity radioactive ions.

Later this year an electron beam ion source (EBIS) charge breeder will replace the ECRIS. Based on the performance achieved during offline testing and reported here, the EBIS will increase the intensity and reduce the contamination of RIBs accelerated in ATLAS.

OFFLINE CONFIGURATION AND OPERATING CONDITIONS

To take advantage of the higher breeding efficiencies an EBIS can reach when operated in a pulsed mode, ions from CARIBU will be cooled and bunched in a Radio Frequency Quadrupole (RFQ) prior to injection into the CARIBU EBIS. The offline configuration, shown in Figure 1, was designed to be able to closely match the injected ion beam expected in the final ATLAS installation. Instead of RIBs from CARIBU, pulses of stable $^{133}Cs^{1+}$ were created from a DC beam by pulsing the voltage of a deflector near the surface ionization source. Injected ion bunches were trapped, bred, extracted, and finally analysed with a 70° dipole magnet. Ion intensities were measured with standard Faraday cups and a Tektronix 3032B oscilloscope. Peak heights from the oscilloscope traces were recorded, and could be converted from voltage to charge with the measured capacitance of the cable and cup.

During commissioning two main operating modes were established. The EBIS was first operated in mode 1, for this was the initial commissioning configuration. Mode 1 was generally lower power; using a lower trap magnetic field, lower electron beam current, and lower trap current density. When it was clear better performance would be needed, the mode 2 configuration was established. The operating parameters for both modes are listed in Table 1.

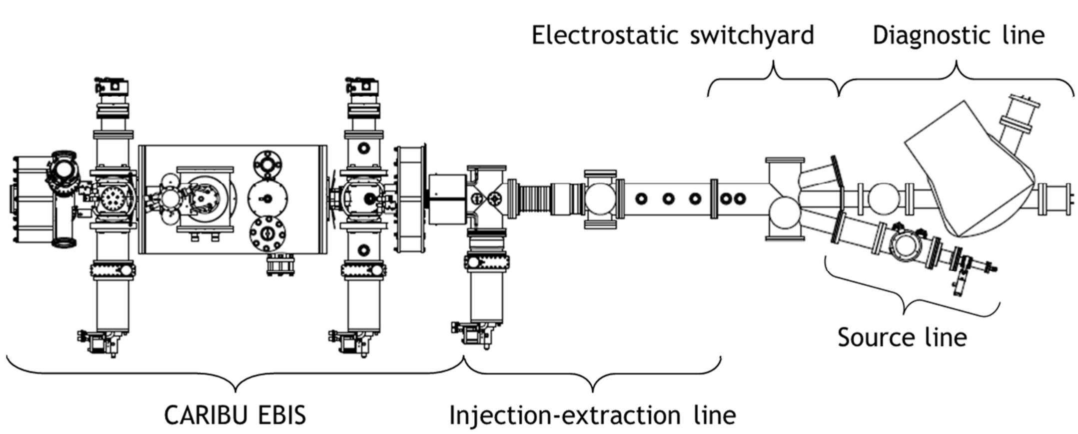

Figure 1: Offline EBIS configuration.

*Work supported by U.S. Department of Energy, Office of Nuclear Physics, under contract DE-AC02-06CH11357
#cdickerson@anl.gov

Content from this work may be used under the terms of the CC BY 3.0 licence (© 2015). Any distribution of this work must maintain attribution to the author(s), title of the work, publisher, and DOI.

ISBN: 978-3-95450-168-7 doi:10.18429/JACoW-IPAC2015-THPF112

Content from this work may be used under the terms of the CC BY 3.0 licence (© 2015). Any distribution of this work must maintain attribution to the author(s), title of the work, publisher, and DOI.

A NEW BEAM INJECTION SCHEME FOR THE FERMILAB BOOSTER *

C. M. Bhat#
Fermilab, Batavia, IL 60510, USA

Abstract

A new beam injection scheme is proposed for the Fermilab Booster to increase beam brightness. The beam is injected on the deceleration part of the sinusoidal magnetic ramp and capture is started immediately after the injection. During the entire capture process we impose $\dot{P} = 0$ in a changing B field. Beam dynamics simulations clearly show that this method is very efficient with no longitudinal beam emittance dilution and no beam loss. As a consequence of preserved emittance, the required RF power on a typical Booster cycle can be reduced by ~30% as compared with the scheme in current operation. Further, we also propose snap bunch rotation at extraction to reduce dP/P of the beam to improve the slip-stacking efficiency in MI/RR.

INTRODUCTION

The Fermilab Booster is one of the oldest rapid cycling proton synchrotron [1, 2] in the world. It uses a 15 Hz sinusoidal magnetic ramp for beam acceleration. The Booster receives H^- beam of 400 MeV kinetic energy from the LINAC while it is at B_{min} (minimum of the magnetic field ramp). H^- charge exchange injection scheme is adopted to accumulate multi-turn proton beam in the ring. Depending on the number of Booster Turns (BT), the duration of the beam injection varies in the range of 2-40 μsec. Ever since the Booster came into operation, the beam injection was carried out in the region of fairly constant magnetic field of the ramp i.e., close to B_{min}. The beam is allowed to debunch for a period of about 60-200 μsec and then captured with the help of a 37 MHz RF (para-phase) system. Since the magnetic field is continuously changing throughout this period, the beam is captured as quickly as possible with a considerably large RF bucket. This led to substantial beam filamentation in the RF bucket leading to longitudinal emittance dilution. Additional issue in the Booster is the observed jitter in B_{min} relative to the beam injection time which is of the order of 50 μsec. This jitter mainly arises from ComEd power-line frequency fluctuation. Further, the beam capture and acceleration found to partly overlap during this part of the cycle as shown in Fig. 1. A combination of all these effects led to undesirable decreased in beam capture efficiency. Over the years many improvements have been implemented to make the capture more efficient. Yet, the best capture efficiency observed so far is <95% with a longitudinal emittance dilution ≈50%.

Around 2000, the Fermilab long range accelerator program planning started focusing on increasing the beam power on targets for neutrino beams. A staged improvement approach is undertaken to inject beam on all of the Booster cycles and increase the BT per cycle [3, 4]. In this context, the Booster is found to play a significant role in the near future of Fermilab. In 2007, I started investigating possible advantages of beam injection on the deceleration part of the magnet ramp in the Booster and thereby, increase the beam brightness at extraction.

Tests of beam injection on the deceleration part of the magnet ramp in the Booster had been attempted in the past [5]. However, the beam transmission efficiencies turned out to be were very poor and the root causes of the problem were not understood at that time.

This paper proposes a fully developed *Early Beam Injection scheme* which has many advantages over the scheme in current operation. The general principle of the method, beam dynamics simulations and results of the proof of principle experiments are presented. Multi-particle beam dynamics simulations applied to the Booster injection convincingly validates the concepts and the proposed scheme's feasibility.

PRINCIPLE OF THE EARLY INJECTION SCHEME AND SIMULATIONS

Schematic views of the newly proposed early injection scheme (EIS) along with the currently used scheme (CIS) are shown in Fig. 1. In EIS, the beam is injected at about 150 μsec prior to $\dot{B} = 0$. Following the completion of the injection, the Booster RF system is turned on at a *matched* frequency. Debunching of the beam prior to the start of beam capture is eliminated. The RF capture voltage is increased by changing the para-phase angle from 180^0 to 0^0 in ≈ 260 μsec imposing $\dot{P} = 0$ to guarantee iso-adiabatic beam capture in stationary RF buckets with synchrotron oscillation period varying in the range of 125 μsec to 40 μsec. In an ideal case, one demands much longer capture time. Since, the magnetic field is continuously changing the capture time cannot be increased much further. Differential relationship between magnetic field B and the radius R of the orbit is given by, $\Delta R = (R/\gamma_T^2)(\Delta B/B)$ where, γ_T=5.47, $\Delta B/B = 3.74E-4$ and $R = 75.41$ m for the Booster. Then the radial displacement of the beam due to change in magnetic field is ≈0.9 mm, which is << the diameter of the RF cavity beam pipe (57.2 mm). However, the corresponding change in the RF frequency is ≈13.7 kHz. This RF frequency variation should be taken in to account during beam capture.

We have demonstrated the feasibility of the EIS in the Booster that includes i) beam capture with no emittance growths and no beam losses, ii) beam acceleration from injection energy to the extraction energy and iii) bunch rotation. The 2D- particle tracking simulation code ESME

* Work supported by Fermi Research Alliance, LLC under Contract No. De-AC02-07CH11359 with the United States Department of Energy
# cbhat@fnal.gov

ISBN: 978-3-95450-168-7 doi:10.18429/JACoW-IPAC2015-THPF113

ENERGY SPREAD OF THE PROTON BEAM IN THE FERMILAB BOOSTER AT ITS INJECTION ENERGY *

C. M. Bhat#, B. E. Chase, S. J. Chaurize, F. G. Garcia, K. Seiya,
W. A. Pellico, T. M. Sullivan, A. K. Triplett, Fermilab, Batavia, IL 60510, USA

Abstract

We have measured the total energy spread (≈ 99% energy spread) of the Booster beam at its injection energy of 400 MeV by three different methods - 1) creating a notch of about 40 nsec wide in the beam immediately after multiple turn injection and measuring the slippage time required for high and low momentum particles for a grazing touch in line-charge distribution, 2) injecting partial turn beam and letting it to debunch, and 3) comparing the beam profile monitor data with predictions from MAD simulations for the 400 MeV injection beam line. The measurements are repeated under varieties of conditions of RF systems in the ring and in the beam transfer line.

INTRODUCTION

The Booster is the oldest proton synchrotron in the Fermilab accelerator complex, operating at 8 GeV extraction energy since May 1971 [1, 2] (it was tested for 10 GeV extraction energy for a short time). Though it is a rapid cycling synchrotron (sinusoidal magnet ramp at 15 Hz with a frequency variation of ≈ 0.2% variation) the beam is not delivered on all of its cycles, all the time. Many improvements have been made over the past four decades to increase the beam intensity per Booster *batch* and to increase its average beam power to the down-stream accelerators and to the low energy neutrino program — full potential of the Booster is yet to be realized. One of the important goals of the "Proton Improvement Plan" at Fermilab [3] is to extract the beam at 15 Hz rate from the Booster all the time. Long range plan of Fermilab [4] is to increase the Booster beam delivery cycle rate from 15 Hz to 20 Hz. Hence, the current Booster plays a very significant role in the near future of the Fermilab.

In support of the proposed upgrades to the Fermilab facilities, a thorough investigation on the properties of the beam at the injection energy is extremely valuable. In the past, many attempts have been made in this regard (e.g., ref. [5]), in bits and pieces, often only soon after major upgrades in the upstream hardware. Nevertheless, we realized that a systematic and coherent set of measurements on beam properties at injection is highly needed to understand the beam dynamics.

The Booster receives 400 MeV (kinetic energy) proton beam from the LINAC with 200 MHz bunch structure, while it is at its minimum of sinusoidal ramp. The injection line is equipped with an 800 MHz debuncher cavity to reduce the energy spread of the injected beam. After the injection the beam is quickly captured with the help of a 37 MHz RF system. Typically the capture efficiency is < 97 %. Between the injection and RF capture the beam is debunched for ~100 µs. In this report, we primarily focus on the measurement of energy spread at this time of the beam cycle as a function of beam intensity which is measured in terms of Booster Turns (BT) (1BT ≈ 0.33× 10^{12} protons).

SIMULATIONS AND MEASUREMENTS

In the absence of any RF field, injected bunched beam into the synchrotron debunches (shears) forming a DC beam and maintains its initial energy spread. The energy spread of such a beam can be measured by producing a gap (notch) in the beam with the help of a fast kicker and measuring the time T_{Graz} required for a grazing touch of two sides of its line-charge distribution. Then the energy spread ΔE is given by,

$$\Delta E = \frac{\beta^2 E_s}{|\eta|} \frac{W_{notch}}{T_{Graz}} .$$

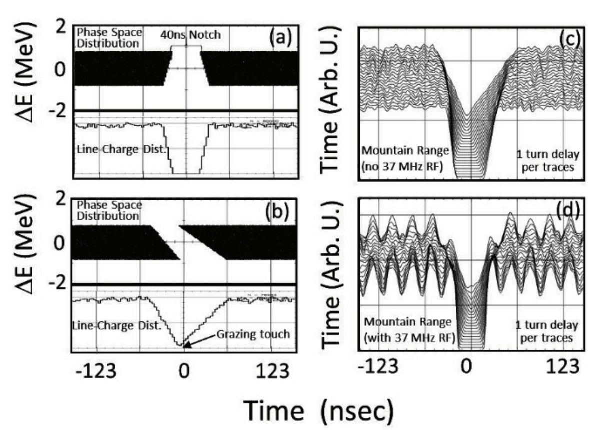

Figure 1: ESME[6] simulations for a) initial beam phase space distribution with a notch in the beam (top) and its line-charge distribution (bottom) b) same as "a" but at grazing touch, c) mountain range without 37 MHz RF and c) similar to "c" but with 37 MHz RF turned on at 25kV.

Where β, E_s, η and W_{notch} are relativistic velocity (0.713 for 400 MeV proton), synchronous energy of the beam (1338.3 MeV), slip factor (-0.4583) and the width of the notch in seconds (≈40 nsec), respectively. We have performed longitudinal beam dynamics simulations for the Booster injection scenario using the machine parameters [2] and for a notch of ≈40 ns width to understand the notch filling mechanism. Figure 1 depicts the predicted dynamics of the beam particle distribution

* Work supported by Fermi Research Alliance, LLC under Contract No. De-AC02-07CH11359 with the United States Department of Energy
# cbhat@fnal.gov

Content from this work may be used under the terms of the CC BY 3.0 licence (© 2015). Any distribution of this work must maintain attribution to the author(s), title of the work, publisher, and DOI.

ISBN: 978-3-95450-168-7 doi:10.18429/JACoW-IPAC2015-THPF116

Content from this work may be used under the terms of the CC BY 3.0 licence (© 2015). Any distribution of this work must maintain attribution to the author(s), title of the work, publisher, and DOI.

PIP-II STATUS AND STRATEGY

Stephen Holmes, Paul Derwent*, Valeri Lebedev, Shekhar Mishra, Donald Mitchell,
Vyacheslav P. Yakovlev, Fermi National Accelerator Laboratory, Batavia IL 60510, USA†

Abstract

Proton Improvement Plan-II (PIP-II) is the centerpiece of Fermilab's plan for upgrading the accelerator complex to establish the leading facility in the world for particle physics research based on intense proton beams. PIP-II has been developed to provide 1.2 MW of proton beam power at the start of operations of the Long Baseline Neutrino Facility (LBNF), while simultaneously providing a platform for eventual extension of LBNE beam power to >2 MW and enabling future initiatives in rare processes research based on high duty factor/higher beam power operations. PIP-II is based on the construction of a new 800 MeV superconducting linac, augmented by improvements to the existing Booster, Recycler, and Main Injector complex. PIP-II is currently in the development stage with an R&D program underway targeting the front end and superconducting RF acceleration technologies. This paper will describe the status of the PIP-II conceptual development, the associated technology R&D programs, and the strategy for project implementation.

OVERVIEW

The Proton Improvement Plan-II (PIP-II) is a high-intensity proton facility being developed to support a world-leading neutrino program over the next two decades at Fermilab. PIP-II is an integral part of the U.S. Intensity Frontier Roadmap as described in the Particle Physics Project Prioritization Panel (P5) report of May 2014 [1]. PIP-II is focused on upgrades to the Fermilab accelerator complex capable of providing a beam power in excess of 1 MW on target at the initiation of Long Baseline Neutrino Facility [1, 2] operations and is a part of a longer-term concept to achieve multi-MW capabilities at Fermilab. PIP-II is anticipated to be a Department of Energy project following the critical decision (CD) process and guidelines of DOE Order 413.3b [3]. At the present time, PIP-II is still in the development phase and is not a formal construction project.

Design Criteria and Considerations

The existing Fermilab accelerator complex could be upgraded using a number of different approaches in order to achieve beam power in excess of 1 MW on the LBNF target. The challenge is to identify solutions that provide an appropriate balance between minimizing near-term costs and maintaining the flexibility to support longer-term physics goals. In order to constrain consideration to a modest number of options the following criteria are applied to possible solutions:

- support the delivery of at least 1 MW of proton beam power from the Main Injector to the LBNF target at energies between 60-120 GeV.
- provide support to the currently envisioned 8 GeV program, including the Mu2e and g-2 experiments, as well as the suite of short-baseline experiments [4, 5].
- provide a platform for eventual extension of beam power to LBNF to more than 2 MW.
- include a future capability to support rare processes experiments with high duty factor and high beam power.

The ideal facility meeting the above criteria would be a modern 8 GeV superconducting linac for injection either into the Main Injector or Recycler as described in the Project X RDR [6], or the pairing of an ~2 GeV SRF linac with a modern Rapid Cycling Synchrotron. These options provide performance that would significantly exceed the first design criteria, and would meet all subsequent criteria, but also significantly exceed the likely available funding.

Design Approach

The goal of Proton Improvement Plan-II is to enhance the capabilities of the existing accelerator complex at Fermilab to support delivery of 1.2 MW beam power to the LBNF production target, while simultaneously providing a platform for subsequent upgrades of the accelerator complex to multi-MW capability. High-level goals, and supporting beam performance parameters, for PIP-II and their comparison to current Proton Improvement Plan (PIP) [7] parameters are given in Table 1. The central element of PIP-II is a new 800 MeV superconducting linac accelerating H- ions and located in close proximity to the existing Booster as shown in Figure 1. This siting offers several advantages in terms of minimizing cost while retaining options for future development; in particular, the site affords direct access to significant electrical, water, and cryogenic infrastructure.

The concept for PIP-II is described in a Reference Design Report [8] and includes the following scope:

- An 800 MeV superconducting linac (SC Linac), constructed of CW-capable accelerating structures and cryomodules, operating with a peak current of 2 mA and a beam duty factor of 1.1%.
- Beam transport from the end of the SC Linac to the new Booster injection point, and to a new 800 MeV beam dump.
- Upgrades to the Booster to accommodate 800 MeV injection, and acceleration of 6.5×10^{12} protons per pulse.

---
* derwent@fnal.gov
† Operated by Fermi Research Alliance, LLC under Contract No. DE-AC02-07CH11359 with the United States Department of Energy.

ISBN: 978-3-95450-168-7 doi:10.18429/JACoW-IPAC2015-THPF118

Content from this work may be used under the terms of the CC BY 3.0 licence (© 2015). Any distribution of this work must maintain attribution to the author(s), title of the work, publisher, and DOI.

FERMILAB BOOSTER INJECTION UPGRADE TO 800 MeV FOR PIP-II*

D.E. Johnson, V. Lebedev, I. Rakhno, Fermilab, Batavia, IL., USA.

Abstract

Fermilab is proposing to build an 800 MeV superconducting linac which will be used to inject H⁻ ions into the existing Booster synchrotron as part of the proposed PIP-II project. The injection energy of the Booster will be raised from the current 400 MeV to 800 MeV. Transverse phase space painting will be required due to the small linac transverse emittance ($\varepsilon_{ring}/\varepsilon_{linac}$ ~ 10) and low average linac current of 2 mA. The painting is also helpful with reduction of beam distribution resulting in a reduction of space charge effects. The injection will require approximately 300 turns corresponding to ~ 0.5 ms injection time. A factor of seven increase of the injected beam power (relative to present operation) requires an injection waste beam absorber. The paper describes the requirements for the injection insert, its design, and plans for transverse painting.

THE FNAL BOOSTER

The 40+ year old Booster contains 24 periods and can be described as a FoDooDoF lattice utilizing gradient magnet pairs (FD or DF) mounted on a girder with long straight sections (5.68 meters) between the defocusing gradient magnets and a short straight section (0.5 meters) between the F and D gradient magnets. Horizontal beta function varies from about 6 meters in the long straight to 33 m in the short straights while the vertical beta function varies from 20 m in the long straights to ~5.3 m in the short straights. The horizontal dispersion varies between approximately 1.8 (in the long straights) and 3.6 meters. The "nominal" ring optics is shown in Fig. 1.

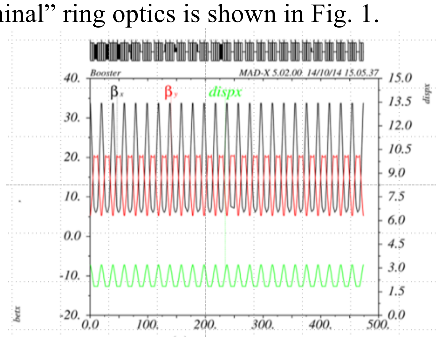

Figure 1: Booster lattice functions.

The current injection insert is located in one of the long straight sections (Long 1). The injection [1,2] is based on a three dipole (powered by a single supply) horizontal orbit bump moving the closed orbit by about 45mm onto a carbon stripping foil to match a trajectory of injected H⁻ beam for the duration of injection. The multi-turn injection time is $N_{turns}*\tau_{Booster}$ ~35μs for N_{turns}=16. Since the transverse emittance of the current 400 MeV linac is close to the Booster acceptance, no transverse phase space painting is used. Figure 2 shows the lattice functions for the injection straight with locations of the gradient and injection bump magnets shown at the top of the plot and the injection trajectories shown in the inset.

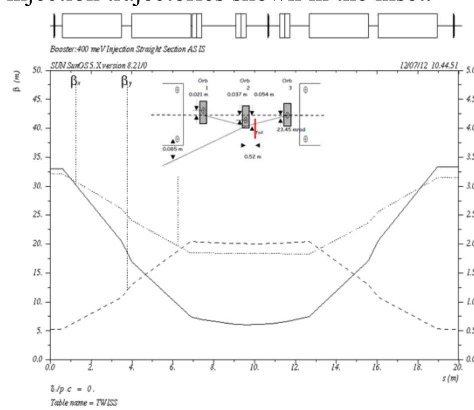

Figure 2: Current Booster injection straight section lattice.

800 MeV INJECTION

The goal of this effort is to verify that we can inject the PIP-II linac beam into the existing Booster at twice higher energy and to find the major issues to be addressed. The major challenges of the new injection system are related to (1) the ability to incorporate a well shielded injection absorber in the current straight section length to handle the factor of 7 increase in injection beam power (17 kW), (2) to introduce a dipole chicane capable to move the closed orbit onto the injection foil, and (3) to support both horizontal and vertical painting based on the control of closed orbit during injection. We also strive to limit the peak field in the single-turn ferrite loaded chicane dipoles to 3 kG due to ferrite saturation near the coils [3].

INITIAL CONCEPTUAL DESIGN

The initial conceptual design for the new injection insert, as described in the PIP-II RDR [4], utilizes an existing straight section (Long 11) with a flange-to-flange length of 5.68 m. The insert is located between gradient magnets and includes a vertical three bump chicane as shown in Fig. 3. The injection stripping foil is located after the two central chicane dipoles. Here, the vertical chicane dipoles not only move the closed orbit onto the foil, but serve as vertical painting magnets as well. The bending angle of each of the chicane dipoles is approximately 40 mrad. Horizontal painting magnets are located in the short straight sections on either side of the injection straight. The last injection line dipole located over the upstream gradient magnet directs the incoming H⁻ ions onto the foil. As the injected H⁻ beam passes

*Operated by Fermi Research Alliance, LLC under contract No. DE-AC02-07CH11359 with the United States Department of Energy.
#DEJ@fnal.gov

ISBN: 978-3-95450-168-7 doi:10.18429/JACoW-IPAC2015-THPF119

TRANSFER LINE DESIGN FOR PIP-II PROJECT*

A. Vivoli#, J. Hunt, D. E. Johnson, V. Lebedev, FNAL, Batavia, IL 60510, USA

Abstract

The recent U.S. Particle Physics Community P5 report encouraged the realization of the Proton Improvement Plan II (PIP-II) project to support future neutrino programs in the United States. PIP-II includes the construction of a new 800 MeV H$^-$ Superconducting (SC) Linac at Fermilab and an upgrade of its current accelerator complex mostly focused on upgrades of the Booster and Main Injector synchrotrons. The SC Linac will initially operate in pulsed mode at 20 Hz. The design should be compatible with upgrades to CW mode and higher energy. A new transport line will connect the Linac to the Booster. This line has to provide adequate collimation and be instrumented for beam parameter measurements. In addition, to support beam based Linac energy stabilization, the line should provide a mechanism to redirect the beam from the dump to the Booster within one pulse. In this paper we present the design of the transport line developed to meet the above requirements. Tracking simulations results are reported to confirm the validity of the design.

INTRODUCTION

PIP-II [1] immediate goal is to provide more than 1 MW of beam power on the target at the start of LBNF operations [2], maintaining the flexibility of the Fermilab accelerator complex necessary to support long-term neutrino physics and being cost-effective. The main limiting factor for an increase of beam power to LBNF is the current Linac/Booster system. Increasing the injection energy from the current 400 MeV to 800 MeV, together with some modifications in the existing Booster, Recycler and Main Injector, would allow higher beam intensity and power. To provide the 800 MeV proton beam, PIP-II assumes the construction of a new SC Linac operated in pulsed mode but built with CW-capable accelerating structures and cryomodules, minimizing the cost of a future upgrade to CW mode. The SC Linac will accelerate a 2 mA H$^-$ beam, requiring a multi-turn strip-injection in the Booster. The repetition frequency will be 20 Hz and the beam duty factor of 1.1%.

TRANSFER LINE DESIGN

The siting of the SC Linac has been selected because of its proximity to existing electrical, water and cryogenic infrastructure and the possibility it offers for future development. To connect the end of the Linac to the injection position in Booster a new beam line has been designed. Figure 1 shows a layout of the Fermilab site together with the existing beam lines. In green the footprint of the PIP-II SC Linac and Transfer Line are presented. In cyan the footprint of the alternate design is shown. The alternate design is around 24 m shorter than the baseline.

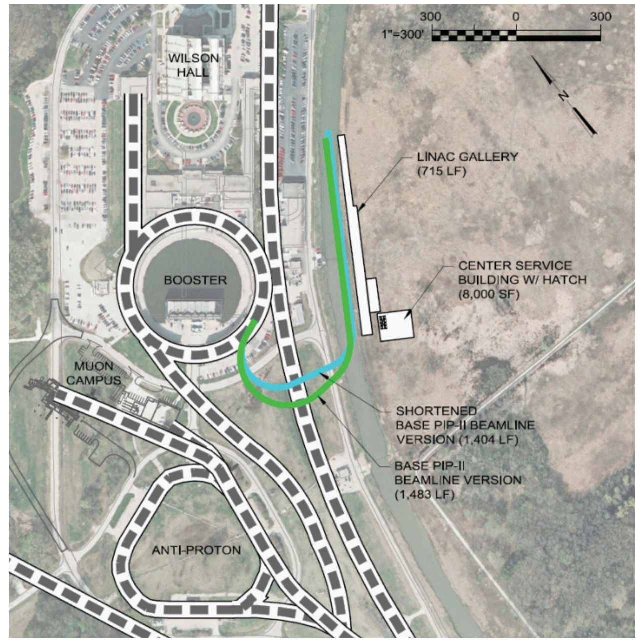

Figure 1: Layout of Fermilab site with PIP-II beam lines.

The direction of the Linac forms an angle of 217 deg. with the direction of injection in the Booster. In order to avoid Lorentz stripping, the magnetic field used to bend the beam has been chosen to be 2.36 kG, corresponding to a loss rate of $3{\cdot}10^{-13}$ m^{-1}. With these parameters the total bending angle can be completed with 32 bending dipole magnets of 2.45 m length (baseline) or with 24 dipoes 3.27 m long (alternate). To fit into the geometrical constraints of the site, the Transfer Line has been divided into a first matching straight section, a first arc, a second straight section, a second arc and an injection line to the Booster. The optics chosen for the transport is a FODO lattice for all the line but the first matching straight section, in which a doublet focusing system similar to the one in the Linac is used, and the injection line. The cell length has been determined by the geometrical constraints resulting in 12 m for both the options. The strength of the quadrupoles has been chosen to determine about 90 deg. phase advance per cell both horizontally and vertically. With this choice, the first arc is composed of 4 cells and the second arc of 12 or 8 cells for the baseline and alternate design respectively. Such choice assures achromaticity of the arcs. The vacuum chamber will be manufactured from 1.5” stainless steel pipe, leaving a transverse aperture of 17 mm for the beam. Figure 2 presents the optical functions of the Transfer Line (baseline) computed with the code OPTIM [3].

*Work supported by Fermi Research Alliance, LLC under Contract No. De-AC02-07CH11359 with the United States Department of Energy.
#vivoli@fnal.gov

Content from this work may be used under the terms of the CC BY 3.0 licence (© 2015). Any distribution of this work must maintain attribution to the author(s), title of the work, publisher, and DOI.

ISBN: 978-3-95450-168-7 doi:10.18429/JACoW-IPAC2015-THPF120

DESIGN OF THE LBNF BEAMLINE*

V. Papadimitriou#, R. Andrews, J. Hylen, T. Kobilarcik, G. Krafczyk, A. Marchionni, C. D. Moore, P. Schlabach, S. Tariq, Fermilab, Batavia, IL 60510, USA

Abstract

The Long Baseline Neutrino Facility (LBNF) will utilize a beamline located at Fermilab to carry out a compelling research program in neutrino physics. The facility will aim a wide band neutrino beam toward underground detectors placed at the SURF Facility in South Dakota, about 1,300 km away. The main elements of the facility are a primary proton beamline and a neutrino beamline. The primary proton beam (60-120 GeV) will be extracted from the MI-10 section of Fermilab's Main Injector. Neutrinos are produced after the protons hit a solid target and produce mesons which are subsequently focused by magnetic horns into a 204 m long decay pipe where they decay into muons and neutrinos. The parameters of the facility were determined taking into account the physics goals, spacial and radiological constraints and the experience gained by operating the NuMI facility at Fermilab. The initial proton beam power is expected to be 1.2 MW, however the facility is designed to be upgradeable to 2.4 MW. We discuss here the design status and the associated challenges as well as plans for improvements before baselining the facility.

INTRODUCTION

The Beamline is a central component of LBNF and its driving physics considerations are the long baseline neutrino oscillation analyses. On January 8, 2010 the Department of Energy approved the "Mission Need" (CD-0) for the Long Baseline Neutrino Experiment (LBNE) and on December 10, 2012 the conceptual design (CD-1). As of January 2015, the LBNE experiment had evolved to the Deep Underground Neutrino Experiment (DUNE) which uses the LBNF Facility at the Fermilab and Sanford Underground Research Facility (SURF) sites. Because of the increased scope for LBNF/DUNE we are preparing for a "CD-1 refresh" review in July 2015. For the Beamline, the change of scope consists of being ready to accept beam power of 1.2 MW (instead of 700 kW) at day one of operations.

The beamline facility is expected to be fully contained within Fermilab property. The primary proton beam, in the energy range of 60-120 GeV, will be extracted from the Main Injector's (MI) [1] MI-10 section using "single-turn" extraction. For 120 GeV operation and with the MI upgrades implemented for the NOvA experiment [2] as well as with the expected implementation of the accelerator Proton Improvement Plan, phase II (PIP-II) [3], the fast, single turn extraction will deliver all the protons (7.5 x 10^{13}) in one MI machine cycle (1.2 sec) to the LBNF target in 10 μs. The beam power is expected to be 1.03 to 1.20 MW in the energy range of 60 to 120 GeV [3]. The charged mesons produced by the interaction of the protons with the target are sign selected and focused by two magnetic horns into the decay pipe towards the far detector. These mesons are short-lived and decay into muons and neutrinos. At the end of the decay region, an absorber pile is needed to remove the residual hadrons remaining at the end of the decay pipe. The neutrino beam is aimed 4850 ft underground at SURF in South Dakota, about 1300 km away.

A wide band neutrino beam is needed to cover the first and second neutrino oscillation maxima, which for a 1300 km baseline are expected to be approximately at 2.4 and 0.8 GeV. The beam must provide a high neutrino flux at the energies bounded by the oscillation peaks and we are therefore optimizing the beamline design for neutrino energies between 0.5 and 5 GeV. The initial operation of the facility will be at a beam power incident on the production target of 1.2 MW, however some of the initial implementation will have to be done in such a manner that operation at 2.4 MW can be achieved without retrofitting. Such a higher beam power is expected to become available in the future with additional improvements in the Fermilab accelerator complex [4]. In general, components of the LBNF beamline system which cannot be replaced or easily modified after substantial irradiation at 1.2 MW operation are being designed for 2.4 MW. Examples of such components are the shielding of the target chase and the decay pipe, and the hadron absorber.

The LBNF Beamline design has to implement as well stringent limits on the radiological protection of the environment, workers and members of the public. The relevant radiological concerns, prompt dose, residual dose, air activation and water activation have been extensively modeled and the results are incorporated in the system design. A most important aspect of modeling at the present design stage is the determination of the necessary shielding thickness and composition in order to protect the ground water and the public and to control air emissions.

This paper is a snapshot of the present status of the design, detailed in the 2012 Conceptual Design Report [5] and the more recently published LBNE science document [6].

STATUS OF THE DESIGN

Figure 1 shows a longitudinal section of the LBNF beamline facility. At MI-10 there is no existing extraction enclosure and we are minimizing the impact on the MI by introducing a 15.6 m long beam carrier pipe to transport the beam through the MI tunnel wall into the new LBNF enclosure. The extraction and transport components send the proton beam through a man-made embankment/hill

*Work supported by DOE, contract No. DE-AC02-07CH11359
#vaia@fnal.gov

Content from this work may be used under the terms of the CC BY 3.0 licence (© 2015). Any distribution of this work must maintain attribution to the author(s), title of the work, publisher, and DOI.

ISBN: 978-3-95450-168-7 doi:10.18429/JACoW-IPAC2015-THPF121

OUT-OF-TIME BEAM EXTINCTION IN THE MU2E EXPERIMENT*

E.J. Prebys, S.Werkema, Fermilab, Batavia, IL 60510, USA

Abstract

The Mu2e Experiment at Fermilab will search for the conversion of a muon to an electron in the field of an atomic nucleus with unprecedented sensitivity. The experiment requires a beam consisting of proton bunches 250 ns FW long, separated by 1.7 μ sec, with no out-of-time protons at the 10^{-10} fractional level. Satisfying this "extinction" requirement is very challenging. The formation of the bunches is expected to result in an extinction on the order of 10^{-5}. The remaining extinction will be accomplished by a system of resonant magnets and collimators, configured such that only in-time beam is delivered to the experiment. Our simulations show that the total extinction achievable by the system is on the order of 10^{-12}, with an efficiency for transmitting in-time beam of 99.6%.

INTRODUCTION AND REQUIREMENTS

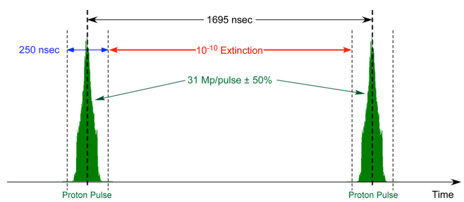

Figure 1: The proton bunch structure required by the Mu2e experiment.

The goal of the Mu2e experiment [1] is to search for the conversion into an electron of a muon which has been captured by a nucleus ($\mu N \rightarrow eN$). This manifestly violates the conservation of charged lepton flavor number, and therefore its observation would be an unambiguous indicator of physics beyond the Standard Model.

A key component of the experimental technique is the proton beam structure [2], which is illustrated in Figure 1. The primary beam consists of short (250 ns FW) proton bunches with 8 GeV kinetic energy, separated by approximately 1.7 μs, which are used to produce muons. To suppress backgrounds, it's vital that the interval between the bunches be free of protons at a level of at least 10^{-10}, relative to the beam in the bunches [3]. This will be achieved in two steps. The first step will be in the formation of the bunches, which - as we will show - we expect to achieve an extinction on the order of 10^{-5}. The remaining extinction will be provided by a system of resonant magnets and collimators in beam line, configured such that only the in-time beam is transmitted to the target. This system is designed to provide an additional extinction factor of below 10^{-7}. There is thus a safety margin of two orders of magnitude, which we feel is appropriately conservative, given the importance of the issue.

In the interest of minimizing radiation damage and secondary activation, we have also imposed the specification that less that 1% of the in-time beam be lost on the collimator.

* Work supported by the United States Department of Energy under Contract No. DE-AC02-07CH11359

BUNCH FORMATION

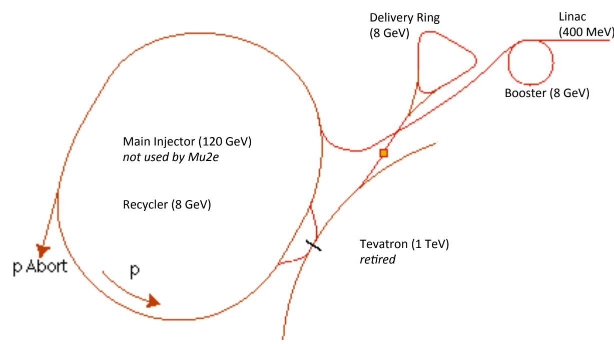

Figure 2: The parts of the Fermilab Accelerator Complex used for the Mu2e Experiment. The “Delivery Ring" was formerly the Antiproton Debuncher

The parts of the Fermilab accelerator complex which are required are shown in Figure 2.

Protons with 8 GeV of kinetic energy will be transferred from the Booster to the Recycler, an 8 GeV permanent magnet storage ring developed for the Tevatron program. In the Recycler, beam will be re-bunched into 2.5 MHz bunches. These will be transfered one at a time to the 8 GeV “Delivery Ring" (formerly the Antiproton Debucher"). Beam will then be resonantly extracted from this ring, which has a period of 1.7 μs, thus producing the bunch structure needed by the experiment.

BEAM LINE EXTINCTION

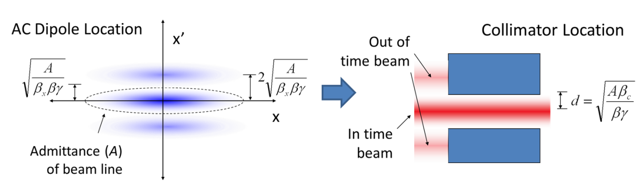

Figure 3: Effect of the AC dipole field in phase space. Beam line admittance A is indicated by the ellipse.

The AC dipole/collimator system and it's optimization has been described in detail elsewhere [4]. The principle is shown in Figure 3. A bending dipole deflects out-of-time beam, such that it will be absorbed by a collimator located 90° downstream in betatron phase advance. If the

Content from this work may be used under the terms of the CC BY 3.0 licence (© 2015). Any distribution of this work must maintain attribution to the author(s), title of the work, publisher, and DOI.

ISBN: 978-3-95450-168-7 doi:10.18429/JACoW-IPAC2015-THPF122

Content from this work may be used under the terms of the CC BY 3.0 licence (© 2015). Any distribution of this work must maintain attribution to the author(s), title of the work, publisher, and DOI.

THE STATUS OF MICE STEP IV

D. Rajaram*, Illinois Institute of Technology, Chicago, IL, USA
V. C. Palladino, INFN-Napoli, Napoli, Italy
on behalf of the MICE collaboration

Abstract

Muon (μ) beams of low emittance provide the basis for the intense, well-characterised neutrino beams of the Neutrino Factory and for lepton-antilepton collisions at energies of up to several TeV at the Muon Collider. The International Muon Ionization Cooling Experiment (MICE) will demonstrate ionization cooling – the technique by which it is proposed to reduce the μ phase-space volume. MICE is being constructed in a series of Steps. At Step IV, MICE will study the properties of liquid hydrogen and lithium hydride that affect cooling. A solenoidal spectrometer will measure emittance up and downstream of the absorber vessel into which a focusing coil will focus muons. The construction of Step IV at RAL is nearing completion. Its status will be described together with a summary of the performance of the principal components. Plans for the commissioning and operation and the Step IV measurement programme will be described.

INTRODUCTION

Stored muon beams for facilities such as a Neutrino Factory or a Muon Collider originate from decays of pions created in proton-target interactions. At production, occupy a large volume in phase space. For efficient acceleration the phase space volume (emittance) must be reduced (cooled) significantly. Due to the short lifetime of the muon, ionization cooling is the only practical technique by which to cool beams of muons.

In ionization cooling, a muon beam passes through an absorber material losing momentum in both transverse and longitudinal dimensions. Subsequently the muons are re-accelerated whereby only the longitudinal momentum is restored. This results in a net reduction of the transverse emittance. The dependence of the normalized 2D transverse emittance on path length in a medium is given by [1]:

$$\frac{d\varepsilon_N}{ds} \approx -\frac{1}{\beta^2}\frac{\varepsilon_N}{E_\mu}\left\langle\frac{dE}{ds}\right\rangle + \frac{1}{\beta^3}\frac{\beta_\perp(0.014\ \text{GeV})^2}{2E_\mu m_\mu X_0}, \qquad (1)$$

where ε_N is the normalized transverse emittance, β the velocity in units of c, E_μ the energy in GeV, $\beta_\perp$ the transverse betatron function, m_μ the muon mass in GeV/c^2, and X_0 the radiation length of the material. The first term on the right describes reduction of emittance per unit length ("cooling") while the second term describes the effect of multiple scattering ("heating"). Equilibrium emittance is reached when the terms are equal and an ideal cooling channel would provide the smallest equilibrium emittance.

* durga@fnal.gov

The Muon Ionization Cooling Experiment (MICE) [2] sited at the Rutherford Appleton Laboratory (RAL) will be the first demonstration of muon ionization cooling. A single cell of a realistic cooling channel will be built and its performance studied under a variety of conditions. The experiment was designed to be built and operated in a staged manner. In the first stage (Step I), which ended in 2013, the muon beamline was commissioned [3] and characterized [4]. The next stage – Step IV – will study the change in normalized transverse emittance using LH_2 and lithium hydride (LiH) absorbers under various optical configurations. Two 201 MHz rf cavities and a second focus-coil module will then be added to the Step IV configuration to allow the demonstration of ionization cooling.

STEP IV

A schematic layout of MICE Step IV is shown in Fig. 1. An absorber (LH_2 or LiH) is placed within a superconducting absorber/focus-coil (AFC) module.

The AFC module is sandwiched between two superconducting solenoids instrumented with scintillating-fiber trackers. The spectrometers measure the emittance of the beam upstream and downstream of the absorber precisely. Particle identification, to reject the small pion contamination in the MICE Muon Beam, upstream of the absorbers is performed using two time-of-flight hodoscope (TOF) stations, and two threshold Cherenkov (Ckov) counters. Downstream of the absorber, contamination from decay electrons is rejected using a TOF, a pre-shower calorimeter (KL) and a fully active scintillator calorimeter (EMR). More detailed descriptions and status of the components follow.

Diffuser

The diffuser is designed to allow varying the input emittance by inserting material into the beam. It sits just inside the upstream end of the first spectrometer solenoid and consists of four irises of different thicknesses, two made of brass and two of tungsten. The irises are pneumatically controlled from the MICE control room and provide 16 possible settings for the diffuser.

Spectrometer Modules

Two superconducting spectrometer solenoid magnets, one upstream and the other downstream of the absorber, house the scintillating fiber trackers. Each magnet consists of five coils wound on a common aluminum mandrel. A cross-sectional view of the magnet assembly is shown in Fig. 2. The center coil along with the end coils provide a uniform 4 T field over a 1 m long, 30 cm diameter volume. The two

ISBN: 978-3-95450-168-7 doi:10.18429/JACoW-IPAC2015-THPF123

MODELING PROTON- AND LIGHT ION-INDUCED REACTIONS AT LOW ENERGIES IN THE MARS15 CODE*

I.L. Rakhno#, N.V. Mokhov, Fermilab, Batavia, IL 60510, USA
K.K. Gudima, Institute of Applied Physics, National Academy of Sciences, Chisinau, Moldova

Abstract

An implementation of both ALICE code and TENDL evaluated nuclear data library in order to describe nuclear reactions induced by low-energy projectiles in the Monte Carlo code MARS15 is presented. Comparisons between results of modeling and experimental data on reaction cross sections and secondary particle distributions are shown.

INTRODUCTION

Correct prediction of secondary particles, both neutral and charged ones, generated in proton-nucleus interactions below a few tens of MeV is required for various applications. The latter include, e.g., radiation studies for front-end of many proton accelerators, energy deposition studies for detectors, residual activation and radiation damage calculations, etc. In medical accelerators, low energy primary proton or deuteron beams are used either directly or as a tool to generate secondary neutron beams. Cascade models of various flavours fail to properly describe this energy region (see Fig. 1). Therefore, we opted to use the TENDL library developed by the Nuclear Research and Consultancy Group [1]. The evaluated data is provided in the ENDF/B format in the projectile energy range from 1 to 200 MeV, and the library is annually updated since 2008. In addition, a much more time-consuming approach utilized in a modified code ALICE [2] was also looked at. For both the options, the energy and angle distributions of all secondary particles are described with the Kalbach-Mann systematics. The following secondaries are taken into account: gammas, neutrons, protons, deuterons, tritons, ^{3}He and ^{4}He. The energy and angular distributions of all generated residual nuclei—including unstable ones—are accounted for as well.

DETAILS OF THE IMPLEMENTATION AND FORMALISM

TENDL Library

The TALYS-based evaluated nuclear data library (TENDL) contains data for direct use in both basic physics and applications. The evaluations were performed for practically entire periodic table except for hydrogen and helium. The library contains data for both stable and unstable target nuclei—all isotopes which live longer than 1 second were taken into account. At present, the list includes about 2400 isotopes. In fact, the TENDL library contains data not only for protons as projectiles, but also for light ions (d, t, ^{3}He, ^{4}He), neutrons and gammas. In current implementation, the data for protons and light ions are used when modelling low-energy inelastic reactions in MARS15 code [4-5]. For every interaction the following information is extracted from the library: (i) total inelastic cross section; (ii) energy and angular distributions of all above mentioned secondary particles and residual nuclei; (iii) yields of all the secondaries.

The TENDL library is a collection of files in both ENDF/B and ACE format. We opted to use the source—ENDF/B format—because it is more easily readable which is a very important feature at the development and debugging stages. At the same time, there is little difference between the two formats with respect to computer memory requirements.

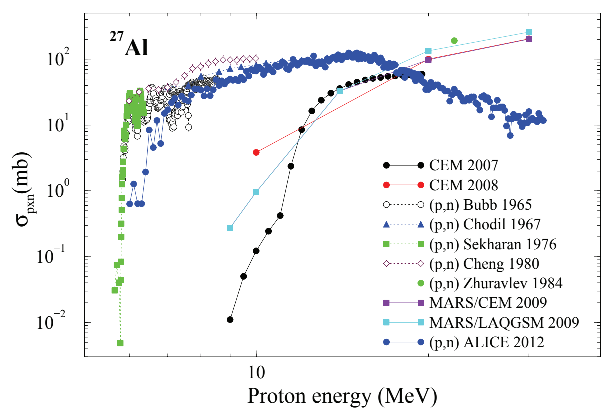

Figure 1: Calculated and measured [3] neutron production cross section on aluminum at low energies.

ALICE Code

An alternative approach—using an event generator—was explored as well. For this purpose, the nuclear model code ALICE [2] based on a hybrid model of pre-compound decay, Weisskopf-Ewing evaporation and Bohr-Wheeler fission models was employed. It was re-designed in order to be used as an event generator for nucleon, photon and heavy-ion nuclear reactions at incident energies from 1 to 20-30 MeV matching CEM and LAQGSM at energies above 20-30 MeV in MARS15. At present, this option looks much more time consuming, but potentially it can offer some advantages for applications where accuracy of the full exclusive modeling is of major importance, e.g. when modeling a detector performance.

Kalbach-Mann Systematics

Nowadays, continuum energy-angle distributions of secondary particles generated in low energy interactions

*Work supported by Fermi Research Alliance, LLC, under contract No. DE-AC02-07CH11359 with the U.S. Department of Energy
#rakhno@fnal.gov

Content from this work may be used under the terms of the CC BY 3.0 licence (© 2015). Any distribution of this work must maintain attribution to the author(s), title of the work, publisher, and DOI.

ISBN: 978-3-95450-168-7 doi:10.18429/JACoW-IPAC2015-THPF124

ENERGY DEPOSITION AND RADIOLOGICAL STUDIES FOR THE LBNF HADRON ABSORBER*

I.L. Rakhno#, N.V. Mokhov, I.S. Tropin, Fermilab, Batavia, IL 60510, USA
Y.I. Eidelman, Euclid TechLabs, LLC, Solon, OH 44139, USA

Abstract

Results of detailed Monte Carlo energy deposition and radiological studies performed for the LBNF hadron absorber [1] with the MARS15 code [2] are described. The model of the entire facility, that includes a pion-production target, focusing horns, target chase, decay channel, hadron absorber system – all with corresponding radiation shielding – was developed using the recently implemented ROOT-based geometry option in the MARS15 code. Both normal operation and accidental conditions were studied. Results of detailed thermal calculations with the ANSYS code helped to select the most viable design options.

INTRODUCTION

The Long-Baseline Neutrino Facility (LBNF) at Fermilab is supposed to provide the world's highest-intensity neutrino beam for the US and international programs in neutrino physics [1]. The corresponding incoming proton beam power can ultimately be as high as 2.4 MW, and the underground beam absorber at the end of the decay channel with related infrastructure is supposed to operate with little or no maintenance for about 20 years. Such a combination of long operation time and high deposited power imposes strict limitations on design.

UNIFIED COMPUTER MODEL

A very detailed model of the entire facility which includes a pion-production target, focusing horns, target chase, decay channel, and hadron absorber system was developed. A drawing that describes an elevation view of the entire facility and a fragment of the entire MARS model which shows the absorber hall are presented in Fig. 1. In the Figure, light blue and gray colors refer to air and concrete, respectively, and green color means soil. As a result of thorough optimization studies with MARS code, the system now consists of a spoiler aluminum block, five aluminum mask blocks, nine sculpted aluminum blocks, four solid aluminum blocks, and four central steel blocks, and all that is surrounded with sophisticated steel and concrete shielding. Total weight of the aluminum and steel is 39 and 2,500 ton, respectively. Volume of poured concrete is 24,000 ft^3.

BEAM PARAMETERS AND SCENARIOS

Table 1 summarizes the beam parameters used to study both the normal operation and two most severe credible accident scenarios. The beam starts at z=-7.3 m (this location is labelled as MC0 in Table 1) and emittance ε_{95} is 20π mm-mrad. The tilt downward is 0.101074 radian.

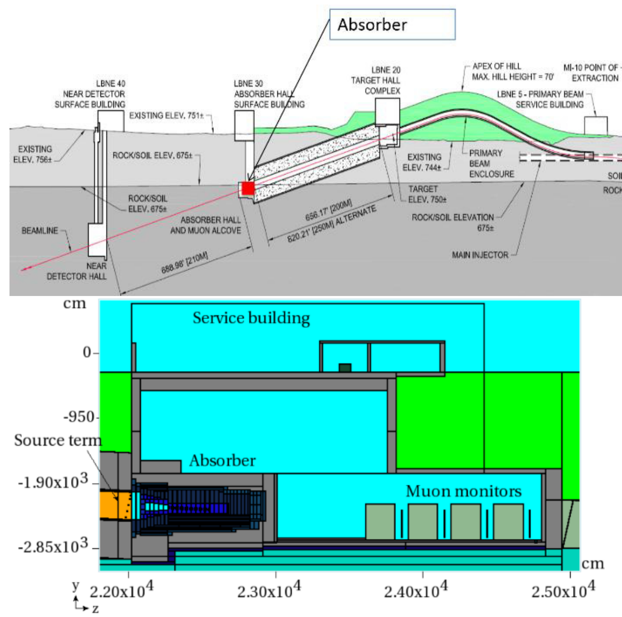

Figure 1: Elevation view of the entire facility (top) and a fragment of the MARS model that shows the hadron absorber and muon monitors in the hall with a service building above (bottom).

Table 1: Beam Parameters and Studied Scenarios

Parameter	Normal Operation	No-Target Accident On-Axis	Off-Axis Accident§
E_p(GeV)	120 60	120	120
P(MW) or Q(MJ)	2.40 MW 2.06 MW	2.88 MJ	2.88 MJ
σ_0 (mm) at MC0	1.7 1.7	2.4	2.4
β_0 (m) at MC0	110.8837 55.44	221.03	221.03
Cycle (s)	1.2 0.7	1.2	1.2
Intensity (10^{14})	1.25 p/s 2.14 p/s	1.5 p/pulse	1.5 p/pulse

§Beam points to absorber cooling water pipes.

*Work supported by Fermi Research Alliance, LLC, under contract No. DE-AC02-07CH11359 with the U.S. Department of Energy
#rakhno@fnal.gov

Content from this work may be used under the terms of the CC BY 3.0 licence (© 2015). Any distribution of this work must maintain attribution to the author(s), title of the work, publisher, and DOI.

ISBN: 978-3-95450-168-7 doi:10.18429/JACoW-IPAC2015-THPF125

Content from this work may be used under the terms of the CC BY 3.0 licence (© 2015). Any distribution of this work must maintain attribution to the author(s), title of the work, publisher, and DOI.

MARS TRACKING SIMULATIONS FOR THE MU2E SLOW EXTRACTED PROTON BEAM*

V. Nagaslaev#, I. Rakhno, Fermilab, USA

Abstract

Particle tracking taking into account interactions with fields and materials is necessary for proper evaluation of the resonant extraction losses and geometry optimization for the extraction beam line. This paper describes the tracking simulations for the Mu2e Resonant Extraction and discusses the geometry choices made based on these simulations.

INTRODUCTION

Mu2e experiment [1] uses the third integer resonant extraction from the Fermilab Delivery Ring to deliver the 8kW proton beam to the production target. Beam losses at the extraction location are a very serious concern of the design. Heavy in-tunnel shielding will be needed even for localized beam losses as low as 1% in order to keep prompt radiation dose levels on the surface within acceptable range and to reduce the residual doses in the tunnel to facilitate the machine maintenance. Another consequence of high beam losses is activation of hardware, which makes its servicing more difficult. Extraction channel geometry needs to be optimized for best extraction efficiency. We define the extraction channel here as the section of the beam line including two Electrostatic Septa (ESS) straddling a focusing quad Q203, defocusing quad Q204 and two magnetic septa straddling the large aperture quad Q205. The layout of this section is shown in Fig. 1. Extracted beam is separated from the circulating beam and deflected horizontally in the ESS and vertically in the Lambertson and the C-magnet. Quads Q204 and Q205 provide additional horizontal and vertical kicks outwards due to their defocusing and focusing functions correspondingly.

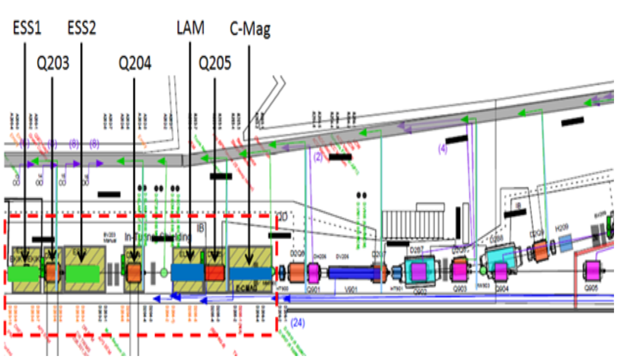

Figure 1: Extraction beam line, plan view. Extraction channel is marked by the red dashed line. Hatched yellow blocks are the in-tunnel shielding around the most activated elements.

* Work supported by Fermi Research Alliance, LLC, under contract No. DE-AC02-07CH11359 with the U.S. Department of Energy
#vnagasl@fnal.gov

The process of beam passage through the extraction channel and generation of losses in the ESS has been studied using tracking simulations with MARS program [2]. MARS provides a very detailed description of particle interaction with materials as well as tracking in the fields. Also MARS provides calculation of the prompt dose and residual activation maps, which are not discussed here.

MARS MODEL

Most of the beam line elements were described in the model using MARS "extended" and "nonstandard" types of geometry. Mixing these two types has to be done with care and should be avoided in volumes with thin objects. It is important that tracking in the ESS handles correctly transitions in and out the tiny foil strips, therefore only "extended" objects are used there. The volume recognition is verified in Fig. 2 that shows the proton beam crossing through the foil plane. Red dots on the plot indicate locations of the ends of steps along the particle path. The points are random outside the foil plane but in the plane they concentrate on the foil boundaries; this demonstrates that the volume transitions are properly recognized. The ESS planes are formed by the W/Re 50μ thick foils, of 1mm width, spaced at 2.6mm centre-centre. The foil shapes in Fig. 2 are exaggerated by the strong compression in z-direction along the beam path.

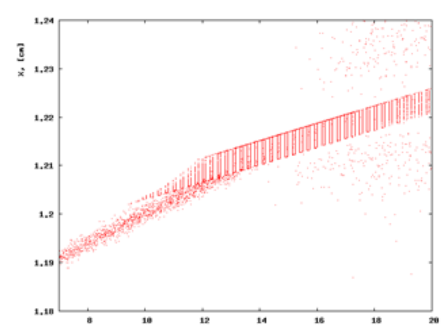

Figure 2: Beam tracking through the foil plane. Red dots show stopping points between two consecutive steps of a particle. They "light up" the foil strips boundaries.

Particle samples for the MARS tracking have been provided from the resonant extraction simulation in the Delivery Ring made with the Synergia program [3,4]. The phase space of two such samples is shown in Fig. 3. The green sample (Sample 1) represents particles at the entrance of the ESS1 that arrive beyond the nominal position of the septum foil plane in X - these are the extracted particles. The red sample (Sample 2) represents the outmost parts of the beam that still circulate in the ring but will be extracted after the next 1, 2 and 3 turns.

ISBN: 978-3-95450-168-7 doi:10.18429/JACoW-IPAC2015-THPF126

PXIE LOW ENERGY BEAM TRANSPORT COMMISSIONING*

L. Prost#, M. Alvarez, R. Andrews, J.-P. Carneiro, B. Hanna, V. Scarpine, A. Shemyakin, Fermilab, Batavia, IL 60510, USA
R. D'Arcy, University College London, London, WC1E 6BT, UK
C. Wiesner, IAP, Goethe University, Frankfurt am Main, Germany

Abstract

The Proton Improvement Plan II (PIP-II) at Fermilab is a program of upgrades to the injection complex [1]. At its core is the design and construction of a CW-compatible, pulsed H^- superconducting RF linac. To validate the concept of the front-end of such machine, a test accelerator (a.k.a. PXIE) is under construction [2]. It includes a 10 mA DC, 30 keV H^- ion source, a 2 m-long Low Energy Beam Transport (LEBT), a 2.1 MeV CW RFQ, followed by a Medium Energy Beam Transport (MEBT) that feeds the first of 2 cryomodules increasing the beam energy to ~ 25 MeV, and a High Energy Beam Transport section (HEBT) that takes the beam to a dump. The ion source and LEBT, which includes 3 solenoids, several clearing electrodes/collimators and a chopping system, have been built, installed, and commissioned to full specification parameters. This report presents the outcome of our commissioning activities, including phase-space measurements at the end of the beam line under various neutralization schemes obtained by changing the electrodes' biases and chopper parameters.

LEBT DESCRIPTION

The present layout of the PXIE beam line is shown on Fig. 1. It consists of an H^- Volume-Cusp Ion Source [3], capable of delivering up to 15 mA DC at 30 keV, 3 solenoids, a chopping system, Electrically Isolated Diaphragms (EID) (water-cooled, except for EID #4), an electrically isolated, water-cooled, vertical scraper assembly (a.k.a. "LEBT scraper"), and diagnostics [4]. Details about most of these components can be found in Ref. [5]. There is also a set of 4 electrically isolated scraper jaws (up, down, left and right) temporarily installed between the first two solenoids (not water-cooled). The LEBT only missing component is a switching dipole magnet which will eventually allow selecting between two ion sources (in PIP-II).

The EIDs can be biased to up to + 50V in order to prevent background ions from moving from one section of the LEBT to another. Depending on the relative potential of these electrodes, different neutralization patterns may be produced. The EIDs also act as scrapers to eliminate transverse tails particles and as a diagnostic tool for beam size and position measurements [4].

The chopper consists of two parallel plates. When the beam is interrupted, -6kV is applied to the bottom ('kicker') plate, and the beam is directed to the upper ('absorber') plate. In addition to the chopping system, a modulator was added to the ion source extraction electrode. Both can produce 1 μs-16.6 ms pulses at up to 60 Hz. Thus, for commissioning of the SRF modules, the initial nominal operation scenario will be to create 5-10 μs pulses with the LEBT chopper out of milliseconds-long ion source pulses. Then, the duty factor will be increased by extending the chopped pulse as the beam line is better understood.

One key aspect of the PXIE warm front-end is its vacuum management approach. For the RFQ, it was decided to keep the vacuum level in the 10^{-7}-10^{-6} Torr range, hence limiting the gas load allowed from the LEBT. The idea is that better vacuum will improve reliability and lifetime of the RFQ, which operates CW. Also, because of the relative proximity of the first superconducting structure, it is important to limit the number of fast neutrals that could potentially reach it.

A direct consequence from this choice is the design of a long (2.2 m) LEBT with extensive pumping to effectively isolate the inherently high pressure found near the ion source from the low pressure required in the RFQ. In measurements made with a configuration similar to the one shown on Fig. 1, the base pressure at the chopper assembly with the plasma on but without extracting beam is found to be < 10^{-7} Torr. With the entire beam being deflected onto the absorber, the vacuum remained < 2 × 10^{-7} Torr for beam currents of up to 6 mA DC.

Maintaining a low vacuum pressure also implies long neutralization times from the background ions; therefore the beam parameters may vary dramatically throughout the pulse, which in turn can cause large beam losses. In part to alleviate this issue, an atypical transport scheme has been proposed [6], where the major portion of the LEBT is kept neutralized while positive ions are cleared in the last ~1 m of the beam line before the RFQ by applying -300V DC voltage to the kicker plate.

A drawback foreseen with this scheme was the probable emittance growth that would result from the un-neutralized transport portion of the LEBT. However, simulations that used the ion source measured parameters indicated that the final emittance would remain within the RFQ specifications. In addition, the LEBT lattice is compatible with a fully neutralized transport solution, should the scheme with the un-neutralized section be found to be too detrimental to the beam quality.

COMMISSIONING MILESTONES

The LEBT was assembled and commissioned in phases, adding components as they were available [5].

* Operated by Fermi Research Alliance, LLC under Contract No. DEAC02-07CH11359 with the United States Department of Energy
#lprost@fnal.gov

Content from this work may be used under the terms of the CC BY 3.0 licence (© 2015). Any distribution of this work must maintain attribution to the author(s), title of the work, publisher, and DOI.

ISBN: 978-3-95450-168-7 doi:10.18429/JACoW-IPAC2015-THPF127

SCHEME FOR A LOW ENERGY BEAM TRANSPORT WITH A NON-NEUTRALIZED SECTION*

A. Shemyakin**, L. Prost, Fermilab, Batavia, IL 60510, USA

Abstract

A Low Energy Beam Transport (LEBT) line is the part of a modern ion accelerator between an ion source (IS) and a Radio-Frequency Quadrupole (RFQ). Its typical design includes 1-3 solenoidal lenses for focusing and relies on transport with nearly complete beam space charge neutralization over the entire length of the LEBT. In this paper, we discuss the possibility and rationality of imposing an un-neutralized transport in a portion of the LEBT adjacent to the RFQ. For estimations, we will use the parameters from PXIE [1], a test accelerator presently being constructed at Fermilab.

REASONING FOR A LEBT WITH AN UN-NEUTRALIZED SECTION

Often, a LEBT either operates with a pulsed ion source or is capable of creating pulses from an initially DC beam. Because the ionization process is not instantaneous, the front of the beam pulse is not neutralized as it propagates through the LEBT. Thus for long-pulse operation, when the accelerator optics is tuned for neutralized transport in the LEBT, the space charge at the beginning of the pulse may result in increased losses in the following beam line. In the case of PXIE, several microseconds pulses envisioned for tuning would not provide a representative envelope for CW operation.

Remedies include working at relatively high pressure to speed up the neutralization process, which, in turn shortens the time for the beam parameters to reach a steady state, and moving the chopping system as close as possible to the RFQ in order to decrease the distance that beam travels with full space charge and low energy. In both cases, reliability of the RFQ may suffer because of higher pressure and/or increased irradiation of the RFQ vanes during chopping.

Here we consider an alternative scheme, where the ion source works in the DC mode and the beam propagates through the first, 'high pressure' part of the LEBT being neutralized, but neutralization is stopped right upstream of an electrostatic chopper. Hence, in the ideal case with zero density for the neutralizing ions in the downstream part of the LEBT, the beam envelope is time-independent.

Applicability of such scheme depends on several factors, most importantly, the beam perveance $P_b = I_b / U_{IS}^{3/2}$, where I_b is the beam current and U_{IS} is the ion source bias voltage. If the perveance exceeds a certain limit, an un-neutralized beam simply cannot be transported in a LEBT with lumped focusing even in the linear approximation. In addition, even for a lower perveance, non-linear space charge effects can dramatically increase the beam emittance, making it not suitable for an accelerator.

LINEAR SPACE CHARGE EFFECT

To estimate the maximum perveance theoretically allowing lumped focusing, let's consider the space-charge dominated transport of a non-relativistic, round, completely un-neutralized H$^-$ beam with uniform transverse distribution of the charge density, i.e. neglecting the beam emittance and potential drop across the beam. The maximum length that the beam can propagate between two thin focusing elements while remaining within radius r_b can be expressed (using, for example, formulae from Ref. [2]) as

$$\frac{L_m}{r_b} = \sqrt{2.33\frac{\sqrt{2e/M_i}}{P_b}} = \sqrt{\frac{3.59\,\mu A/V^{3/2}}{P_b}}, \quad (1)$$

where e is the electrical charge and M_i the ion mass. In real-life, for a typical solenoid, the magnetic lens inner radius is at least twice the beam radius and its length is roughly equal to its inner diameter. One can argue that the maximum allowable perveance corresponds to the case when the minimum possible physical distance between lenses exceeds their length by only a factor of 2-3 (with a factor of '1' meaning that the lenses would be touching). Taking a factor of 3 for the lenses' distance-to-length ratio implies $L_{m\_sc}/r_b \approx 12$ and a value of the maximum allowable perveance of

$$P_{bm} \approx \left(\frac{L_{m\_sc}}{r_b}\right)^{-2} \cdot 3.59\,\mu A/V^{3/2} \approx 0.025\,\mu A/V^{3/2}. \quad (2)$$

In the case of PXIE's LEBT, the perveance of the 10mA, 30 kV H$^-$ beam is $1.9\cdot10^{-3}$ μA/V$^{3/2}$, significantly lower than the estimation from Eq. (2). Therefore, for these parameters, un-neutralized transport is not excluded in this simplest model.

NONLINEAR SPACE CHARGE EFFECT

A significantly more important limitation is an emittance growth due to space charge. For a beam with a Gaussian current density distribution, the space charge force is highly non-linear outside of the beam core. The tail particles experience a lower radial kick, which distorts the beam phase portrait and increases the beam emittance.

An obvious solution to avoid emittance dilution due to space charge is to create a beam with constant radial

* Operated by Fermi Research Alliance, LLC, under Contract DE-AC02-07CH11359 with the United States Department of Energy
** shemyakin@fnal.gov

Content from this work may be used under the terms of the CC BY 3.0 licence (© 2015). Any distribution of this work must maintain attribution to the author(s), title of the work, publisher, and DOI.

ISBN: 978-3-95450-168-7 doi:10.18429/JACoW-IPAC2015-THPF128

ACCELERATOR PHYSICS AND TECHNOLOGY RESEARCH TOWARD FUTURE MULTI-MW PROTON ACCELERATORS *

V. Shiltsev#, P. Hurh, A. Romanenko, A. Valishev, R. Zwaska, Fermilab, Batavia, IL 60510, USA

Abstract

Recent P5 report [1] indicated the accelerator-based neutrino and rare decay physics research as a centrepiece of the US domestic HEP program. Operation, upgrade and development of the accelerators for the near-term and longer-term particle physics program at the Intensity Frontier face formidable challenges. Here we discuss accelerator physics and technology research toward future multi-MW proton accelerators.

MULTI-MW ACCELERATORS: ISSUES

The 2014 Particle Physics Project and Prioritization Panel (P5) provided an updated strategic plan for the US HEP program necessary to realize a twenty-year global vision for the field. The near-term program of HEP research at the Intensity Frontier continuing throughout this decade includes the long-baseline neutrino experiments and a muon program focused on precision/rare processes. It requires: a) double the beam power capability of the Booster; b) double the beam power capability of the Main Injector; and c) build-out the muon campus infrastructure and capability based on the 8 GeV proton source. The long-term needs of the Intensity Frontier community are expected to be based on the following experiments: a) long-baseline neutrino experiments to unravel neutrino sector, CP-violation, etc.; and b) rare and precision measurements of muons, kaons, neutrons to probe mass-scales beyond LHC.

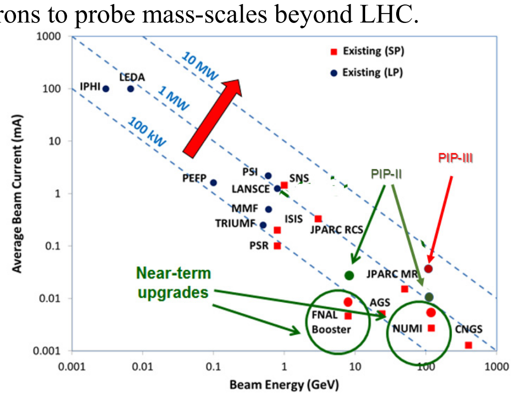

Figure 1: Accelerator beam power landscape.

Construction of the PIP-II SRF 800 MeV linac [2] is expected to address the near-term challenges. PIP-II will increase the Booster per pulse intensity by 50% and allow delivery 1.2 MW of the 120 GeV beam power from the Fermilab's Main Injector, with power approaching 1 MW at energies as low as 60 GeV, at the start of DUNE/LBNF operations ca 2023. It will also support the current 8 GeV program, including Mu2e, g-2, and the suite of short-baseline neutrino experiments; provide upgrade path for Mu2e and a platform for extension of beam power to DUNE/LBNF to multi-MW levels.

The P5 report sets longer-term sensitivity goals for the US long-baseline neutrino program. Those goals require an exposure of 600 kT*MW*yr (the product of the detector mass, beam power on target and exposure time). PIP-II offers a platform for the first 100 kt*MW*yr as in Table 1.

Table 1: Neutrino Physics Program Requirements

PIP-II Beyond PIP-II (mid-term)

	1st 10 years	2nd 10 years		
To Achieve :	100 kT-MW-year	500 kT-MW-year		
We combine :		Option 1	Option 2	Option 3
Mass	10 kT	50 kT	20 kT	10 kT
Power	1 MW	1 MW	2.5 MW	5 MW

The mid-term strategy towards an additional 500 kT*MW*yr after PIP-II depends on the technical feasibility of each option (see the Table) and the analysis of costs/kiloton of detector versus costs/MW of the beam power on target. To make an informed choice, extensive medium-term R&D on the effective control of beam losses in significantly higher current proton machines and on multi-MW targetry is needed [3].

There are two approaches for the multi-MW proton machine (currently tagged as PIP-III, see Fig. 1) – rapid cycling synchrotron and SRF linac. Attainment of the required beam intensities in synchrotrons is only possible with greatly reduced particle losses stemming from space-charge forces and coherent and incoherent beam instabilities. Modern SRF proton linacs can accelerate the needed currents but their cost/performance ratio needs to be significantly reduced compared to, e.g., the Project X facility [4] to be financially feasible. For both avenues, high-power targetry technology needs to be considerably enhanced to contribute to the cost and feasibility of any multi-MW superbeam facility.

In 2014-15, the HEPAP subpanel has developed *"A Strategic Plan for Accelerator R&D in the US"* [5] which recommends three R&D activities toward next step intensity frontier facility:

a) experimental studies of novel techniques to control beam instabilities and particle losses, such as integrable beam optics and space-charge compensation at IOTA ring at Fermilab;
b) exploration of the SRF capital and operating cost reductions through transformational R&D on high-Q cavities and innovative materials such as Nb-Cu composites, Nb films and Nb_3Sn; cavity performance upgrades through novel shapes and field emission elimination;

*Fermi Research Alliance, LLC operates Fermilab under contract No. DE-AC02-07CH11359 with the U.S. Department of Energy
#shiltsev@fnal.gov

Content from this work may be used under the terms of the CC BY 3.0 licence (© 2015). Any distribution of this work must maintain attribution to the author(s), title of the work, publisher, and DOI.

ISBN: 978-3-95450-168-7 doi:10.18429/JACoW-IPAC2015-THPF129

THE MICE DEMONSTRATION OF IONIZATION COOLING*

J. Pasternak#, V. Blackmore, C. Hunt, J-B. Lagrange, K. Long, Imperial College, London, UK
N. Collomb, DL-STFC,Warrington, UK
V. C. Palladino, INFN-Napoli, Napoli, Italy
R. Preece, C. Rogers, J. Tarrant, RAL-STFC, Harwell, UK
P. Snopok, FNAL, Batavia, IL, USA/IIT, Chicago, IL, USA
on behalf of the MICE Collaboration

Abstract

Muon beams of low emittance provide the basis for the intense, well-characterised neutrino beams necessary to elucidate the physics of flavour at the Neutrino Factory and to provide lepton-antilepton collisions at energies of up to several TeV at the Muon Collider. The International Muon Ionization Cooling Experiment (MICE) will demonstrate ionization cooling, the technique by which it is proposed to reduce the phase-space volume occupied by the muon beam at such facilities. In an ionization-cooling channel, the muon beam passes through a material (the absorber) in which it loses energy. The energy lost is then replaced using RF cavities. The combined effect of energy loss and re-acceleration is to reduce the transverse emittance of the beam (transverse cooling). A major revision of the scope of the project was carried out over the summer of 2014. The revised project plan, which has received the formal endorsement of the international MICE Project Board and the international MICE Funding Agency Committee, will deliver a demonstration of ionization cooling by September 2017. In the revised configuration a central lithium-hydride absorber provides the cooling effect. The magnetic lattice is provided by the two superconducting focus coils and acceleration is provided by two 201 MHz single-cavity modules. The phase space of the muons entering and leaving the cooling cell will be measured by two solenoidal spectrometers. All the superconducting magnets for the ionization cooling demonstration are available at the Rutherford Appleton Laboratory and the first single-cavity prototype is under test in the MuCool Test Area at Fermilab. The design of the cooling demonstration experiment will be described together with a summary of the performance of each of its components. The cooling performance of the revised configuration will also be presented.

INTRODUCTION

Stored muon beams have been proposed as the source of neutrinos at the Neutrino Factory and as the means to deliver multi-TeV lepton-antilepton collisions at the Muon Collider [1]. In such facilities the muon beam is produced from the decay of pions produced in the bombardment of a target by a high-power proton beam. The tertiary muon beam occupies a large volume in phase space. To optimise the muon yield while maintaining a suitably small aperture in the muon-acceleration systems requires that the muon-beam phase space be reduced (cooled) prior to acceleration. The short muon lifetime makes traditional cooling techniques unacceptably inefficient when applied to muon beams. Ionization cooling, in which the muon beam is passed through material (the absorber) and subsequently accelerated, is the technique by which it is proposed to cool the beam [2, 3].

The experimental configuration with which the MICE collaboration will study ionization cooling has been revised in the light of the recommendations of the US Particle Physics Projects Prioritization Panel [4] and subsequent national and international reviews of the project. This process culminated in November 2014 when the project was formally rebaselined to deliver the configuration presented in Fig 1. The cooling cell is formed of a central lithium-hydride (LiH) absorber sandwiched between two "focus-coil" (FC) modules. Acceleration is provided by two 201 MHz cavities. The emittance is measured upstream and downstream of the cooling channel by solenoidal spectrometers. Further instrumentation upstream and downstream of the magnetic channel serves to select a pure sample of muons passing through the channel and to measure the phase at which each muon passes through the RF cavities. The schedule for the rebaselined project shows that the initial demonstration of ionization cooling will be performed by the end of US fiscal year 2017, while preserving MICE measurements at Step IV [5] scheduled in 2015.

This paper describes the novel lattice configuration adopted for the MICE demonstration of ionization cooling and presents its performance.

LATTICE FOR COOLING DEMONSTRATION

The lattice that will be used for the demonstration of ionization cooling is shown in Fig. 1. The lattice has been optimised to maximise the reduction in transverse emittance using the primary (central) and secondary LiH absorbers. With this configuration, a small betatron function at the position of the primary absorber can be achieved together with an acceptable beam size at the position of the 201 MHz cavities. The spectrometer solenoids (SSs) house high-precision scintillating-fibre

*Work supported by the (UK) Science and Technology Facilities Council and the (US) Dept. of Energy and National Science Foundation
j.pasternak@imperial.ac.uk

Content from this work may be used under the terms of the CC BY 3.0 licence (© 2015). Any distribution of this work must maintain attribution to the author(s), title of the work, publisher, and DOI.

ISBN: 978-3-95450-168-7 doi:10.18429/JACoW-IPAC2015-THPF131

BEAM STUDIES FOR THE PROTON IMPROVEMENT PLAN (PIP) - REDUCING BEAM LOSS AT THE FERMILAB BOOSTER *

K. Seiya#, C. M. Bhat, D. E. Johnson, V. V. Kapin, W. A. Pellico, C. Y. Tan, R. J. Tesarek, FNAL, Batavia, IL 60510, USA

Abstract

The Fermilab Booster is being upgraded under the Proton Improvement Plan (PIP) to be capable of providing a proton flux of 2.25E17 protons per hour. [1] The intensity per cycle will remain at the present operational 4.3E12 protons per pulse, however the Booster beam cycle rate is going to be increased from 7.5 Hz to 15 Hz. One of the biggest challenges is to maintain the present beam loss power while the doubling the beam flux. Under PIP, there has been a large effort in beam studies and simulations to better understand the mechanisms of the beam loss. The goal is to reduce it by half by correcting and controlling the beam dynamics and by improving operational systems through hardware upgrades. This paper is going to present the recent beam study results and status of the Booster operations.

700 kW OPERATION

Fermilab is going to provide 700kW proton beam to the NOvA experiment. Booster is a 15 Hz resonant circuit synchrotron and accelerates proton beams from 400 MeV to 8 GeV. The required intensity in the Booster for NOvA is 4.3E12 ppp, the same as it was for 400 kW operation. [2] However, the cycle rate will be increased from ~7.5 Hz to 15 Hz to accommodate both NOvA and other users. The RF system and utilities are being upgraded to 15 Hz operations and are nearing completion. The plan is to start 15 Hz operations in FY15.

The beam loss limit has been set to 525W to allow workers to maintain all elements in the Booster tunnel without excessive radiation exposure. Figure 1 shows the historical beam loss in the Booster versus protons per hour. The total loss depends on the beam intensity.

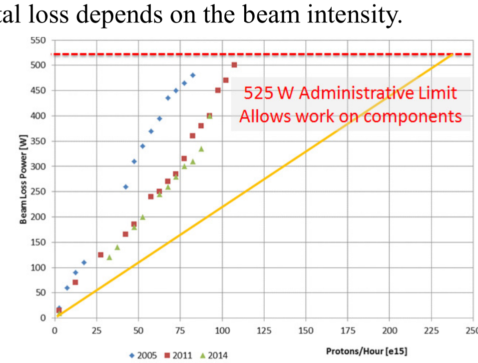

Figure 1: Beam power loss for 3 year operations (blue: 2005, red: 2011 and green: 2014).

*Work supported by Fermilab Research Alliance, LLC under Contract No. DE-AC02-07CH11359 with the United States Department of Energy.

#kiyomi@fnal.gov

The present operational beam intensity at injection is about 5E12 ppp and extraction is 4.5E12 ppp. The total energy loss is 0.075 kJ in one Booster cycle and hence 1150 W when the cycle rate is 15Hz. The loss has to be reduced to half by 2016. Figure 2 shows the intensity and loss during normal operations. Beam studies and upgrades that will be done to reduce the beam losses will be discussed in this paper.

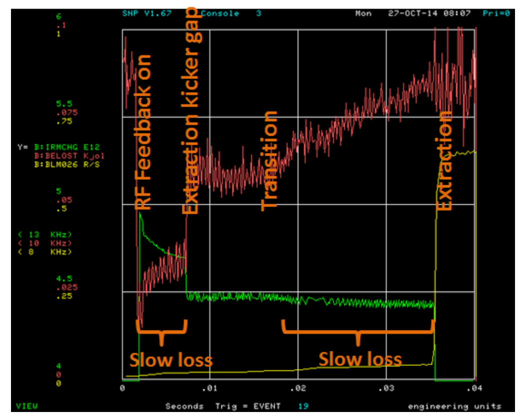

Figure 2: Beam intensity (green), energy loss (red) and extraction loss (yellow) signals.

COLLIMATORS

Two-stage collimator system which had horizontal and vertical primary collimators and three secondary collimators was installed in Booster in 2004. The primary collimators haven't been used and the secondary collimators have been used as single-stage collimators because the system never worked or implemented as designed which created much larger scatter than we expected from the simulation results.

Ramped corrector magnets, installed in the Booster during the 2007/2009 shutdowns, allowed us to control the beam orbit. In 2013, realignment of the main dipole magnets based on aperture scans and simulation increased aperture. RF Cogging changed the radial positon from cycle to cycle and it was replaced with Magnetic Cogging in 2015 which kept beam on central orbit. With the better understanding and control of the orbit, the operating parameters for the collimators will be optimized based on simulations and measurements.

A simulation was developed using MADX to replace an earlier STRUCT simulation and better optimize the material and thickness of the primary collimators. Assuming that 10^4 particles at the edge of horizontal

Content from this work may be used under the terms of the CC BY 3.0 licence (© 2015). Any distribution of this work must maintain attribution to the author(s), title of the work, publisher, and DOI.

ISBN: 978-3-95450-168-7 doi:10.18429/JACoW-IPAC2015-THPF133

TEXTURED-POWDER BI-2212/AG WIRE TECHNOLOGY DEVELOPMENT*

J.N. Kellams[#], K. Damborsky[1], P.M. McIntyre, J. Vandergrifft, Texas A&M University, College Station, TX 77840, USA
L. Motowidlo, Supramagnetics, Inc., Plantsville, CT 06479, USA
N. Pogue, Paul Scherrer Institute, Villigen, Switzerland

Abstract

Progress is reported in developing of textured-powder Bi-2212 cores as a new approach to Bi-2212/Ag wire technology. The process builds upon earlier work in which Bi-2212 fine powder can be highly textured in its a-b plane orientation and fabricated into square-cross-section bars. The current work concerns an Enhanced Textured Powder (ETP) process, in which silver nanopowder is homogeneously mixed with the Bi-2212 powder. We report studies of the effect of the addition on the phase dynamics near melt temperature. ETP cores are being prepared for compounding into a billet to fabricate multi-filament wire.

STATE-OF-ART: OPIT BI-2212 WIRE

Bi-2212 is the only one of the high-temperature superconductors that has been successfully fabricated into multi-filament round wire. The state-of-art fabrication route is oxide-powder-in-tube (OPIT), in which fine-powder ~phase-pure Bi-2212 is loaded into Ag or Ag alloy tubes, the tubes are drawn, stacked, and re-drawn to make multi-filament wire [1]. The wire is then cabled and wound into final-form windings, and the windings are subjected to a 'partial melt' (PM) heat treatment at ~887 C during which the Bi-2212 solid particles are fully melted and then gradually re-crystallized. Several properties of this PM heat treatment lead to difficulties and until recently limited engineering current density to je~200 A/mm^2:

- The void space among particles in the powder becomes bubbles in the liquid (porosity), and capillary forces coalesce the bubbles to form macro-voids that can block current transport.
- The liquid is chemically aggressive, and etches along grain boundaries in the silver matrix. This creates dendritic bridging among filaments (good and bad).
- Connectivity among grains remains a limit to performance.

A dramatic improvement in performance to je~800 A/mm^2 was obtained last year using overpressure processing at ~5-10 MPa during the formation heat treatment [2,3]. However, overpressure processing remains a challenging proposition for long dipoles of a future hadron collider.

TEXTURED POWDER BI-2212

We began several years ago to develop an alternative method for fabricating the Bi-2212 cores for wire, in which fine-powder Bi-2212 was uniaxially pressed to form square-cross-section rods [4]. The pressing aligns the orientation of the a-b planes in the micaceous powder to a remarkable degree. The motivation of the development is to achieve connectivity among textured grains of Bi-2212 within a core using solid-phase diffusion at a temperature slightly below melt. Conductivity is 100x greater in the a-b plane than in the c-axis, In a non-melt heat treatment the transition to liquid is never made and the favorable texture is preserved.

The procedure is summarized in the photos of Fig. 1: fine-powder Bi-2212 is loaded into the 4x150 mm^2 aperture of a female forming die. The male die is inserted into the aperture above the powder, the die assembly is loaded into a hydraulic press, and the powder is compressed by 200 MPa. Bi-2212 is micaceous, and therefore the powder particles are flat flakes, and they naturally align when compressed to yield ~80 % texture as measured using X-ray diffraction [4].

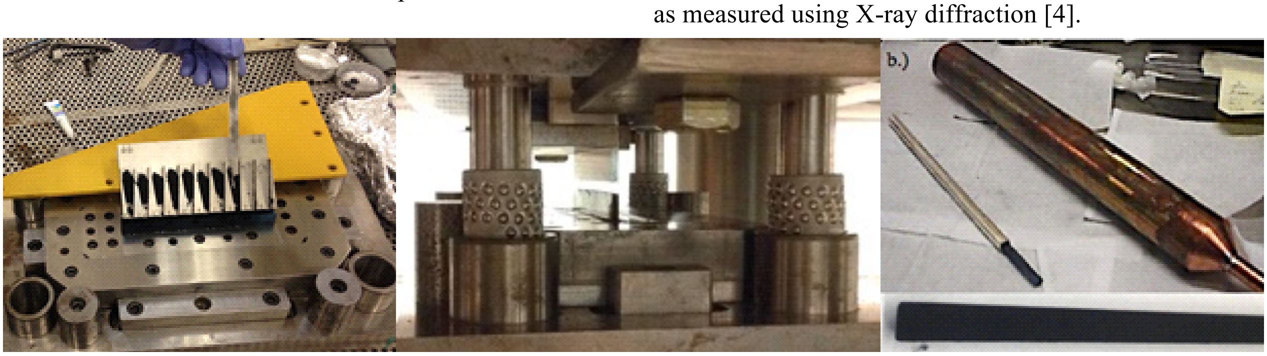

Figure 1: Fabrication of square-cross-section textured-powder Bi-2212 core a) load fine-powder Bi-2212 into rectangular die in oxygen atmosphere; b) compress to 200 MPa; insert bar into square hole in silver tube.

* This work supported by the George and Cynthia Mitchell Foundation.
# jnkellams@tamu.edu
1 Oxford Superconducting Technologies, Carteret, NJ 07008, USA

Content from this work may be used under the terms of the CC BY 3.0 licence (© 2015). Any distribution of this work must maintain attribution to the author(s), title of the work, publisher, and DOI.

ISBN: 978-3-95450-168-7 doi:10.18429/JACoW-IPAC2015-THPF134

MAGNET DESIGN AND SYNCHROTRON DAMPING CONSIDERATIONS FOR A 100 TeV HADRON COLLIDER*

S. Assadi, D. Chavez, J. Gerity, T. Mann, P. McIntyre#, N. Pogue[1], A. Sattarov,
Texas A&M University, College Station, TX 77845, USA
M. Tomsic, Hypertech, Columbus, OH 43228 USA

Abstract

A conceptual design is presented for a 100 TeV hadron collider based upon a 4.5 T NbTi cable-in-conduit dipole technology. It incorporates a side radiation channel to extract synchrotron radiation from the beam channel so that it does not produce limitations from heating on a beam liner or gas load limits on collider performance. Synchrotron damping can be used to support 'bottom-up' stacking to sustain maximum luminosity in the collisions.

INTRODUCTION

The importance of extending searches for new gauge fields by another order of magnitude has led to the suggestion by CERN to develop a Future Circular Collider (FCC) that could contain a 100 TeV hadron collider [1]. We report on development of a particular design for such a collider, motivated by a systematic optimization of its two major cost drivers – the dual ring of superconducting magnets and the tunnel. The two drivers optimize oppositely as a function of the choice of magnetic field.

The tunnel cost depends strongly upon the choice of site for the collider. An optimum case was the siting of the SSC near Dallas, for which the actual cost for the 39 km of completed 4 m diameter tunnels was \$3,300/m (1992). The advance rate for the tunnels averaged 40 m/day, the fastest rate of advance on any recorded large-bore tunnel project in history [2]. The favourable cost was the result of a favourable choice of rock: the Austin Chalk and Taylor Marl formations permit rapid excavation using tunnel boring machines and are self-supporting so that lining can be installed in coordination with excavation schedule [3].

The same site could accommodate a circular tunnel up to 270 km circumference and still remain entirely within those favourable rock strata. A 270 km circumference would require B_0 ~4.5 T to produce hadron collisions at 100 TeV. The tunnel cost today for a 100 TeV collider can be estimated from the SSC tunnel costs using the Construction Cost Index [4]: (270 km)(\$3,300/m)(2.04) = \$1.8 billion. Since this cost is almost certainly less than that of a superconducting magnet ring, it is reasonable to take 270 km as a working choice for collider design and to optimize the design of a superconducting dipole suitable for 4.5 T operating field.

*Work supported by the George and Cynthia Mitchell Foundation.
[1] current address PSI, Villigen, Switzerland.
#mcintyre@physics.tamu.edu

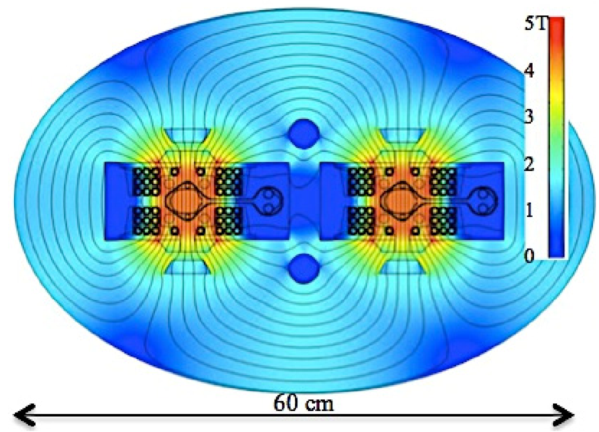

Figure 1: 4.5 T dipole for 100 TeV hadron collider.

4.5 T CABLE-IN-CONDUIT DIPOLE

Figure 1 shows the magnetic design of a 4.5 T dual dipole suitable for use in a 100 TeV hadron collider. The design uses a block winding of round NbTi cable-in-conduit (CIC). The design is inspired by the simplicity of the CIC dipoles that were developed at JINR for use in SIS-100 and FAIR [5]. Each dipole is configured in a C geometry so that the horizontal fan of synchrotron radiation exits the beam tube through a slot aperture and is absorbed in a separately cooled radiation channel as shown in Figure 2.

The main parameters of the dipole are summarized in Table 1. For a dipole field strength of 4.5 T, the C geometry shown requires no more superconductor than would a conventional dipole. A main benefit of the CIC conductor is that it simplifies the fabrication and support of end windings, as shown in Figure 2.

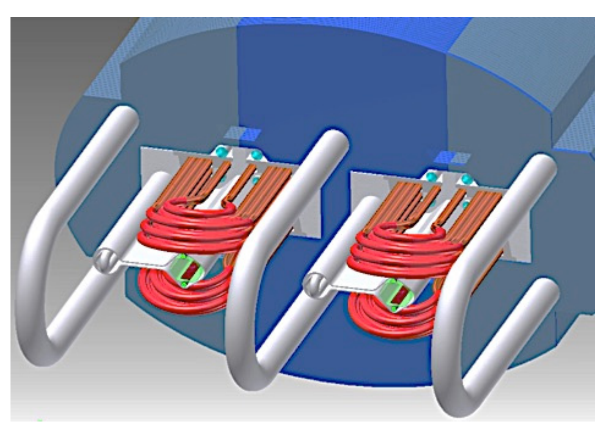

Figure 2: View of end windings in the CIC dipole.

Content from this work may be used under the terms of the CC BY 3.0 licence (© 2015). Any distribution of this work must maintain attribution to the author(s), title of the work, publisher, and DOI.

ISBN: 978-3-95450-168-7 doi:10.18429/JACoW-IPAC2015-THPF135

OPTIMIZATION OF ORBITS, SRF ACCELERATION, AND FOCUSING LATTICE FOR A STRONG-FOCUSING CYCLOTRON

K. Melconian#, J. Gerity, J. Kellams, P. M. McIntyre, A. Sattarov, S. Assadi, Texas A&M University, College Station, TX 77845 USA
N. Pogue, Paul Scherrer Institute, Villigen, Switzerland

Abstract

The strong-focusing cyclotron is an isochronous sector cyclotron designed to accelerate >10 mA CW beams of protons and ions up to >500 MeV/u with low loss and high efficiency. Superconducting RF cavities are used to provide enough energy gain per turn to fully separate orbits, and arc-shaped beam transport channels in the sector dipole apertures provide strong focusing of all orbits. A design methodology is being developed to optimize the sector dipoles, the focal lattice, and the SRF cavities so that betatron tunes can be locked to favorable operating point. Provision is made for correction of dispersion and chromaticity. The methodology will provide a framework on which we can then proceed to study and optimize the nonlinear beam dynamics for high-current transport.

INTRODUCTION

The Accelerator Research Laboratory at Texas A&M University is developing a strong-focusing cyclotron (SFC) for applications requiring high-current beams or micro-emittance beams [1]. Applications include an 800 MeV, >10 mA proton driver for accelerator-driven fission to destroy the transuranics and burn to completion the depleted uranium in spent nuclear fuel [2], a 100 MeV, >10 mA p/α driver for cost-effective production of medical isotopes [3], and a 100 MeV spallation driver for fast neutron damage studies [4].

A 100 MeV SFC is shown in cutaway in Figure 1. It contains 4 superconducting RF cavities [5] that provide enough energy gain to fully separate successive orbits (Δr>6 cm). Each sector dipole consists of a warm-iron flux return with a pair of cold-iron flux plates suspended in the mid-plane gap to define the magnetic field B(r) required for isochronicity [6]. An array of arc-shaped beam transport channels (BTCs, shown as blue in Figure 1) are located in the aperture between the flux plates, each aligned to define the equilibrium trajectory for one orbit in that sector [7]. Each BTC contains an F-D quadrupole doublet and a dipole correction winding, all fabricated as wire-wound superferric windings on a square beam channel. 80% of the 6 cm orbit spacing is available for particle trajectories.

In a previous study [8], we made a first design for a 100 MeV SFC and simulated several aspects of single-bunch dynamics of high-current proton bunches. That study validated that the SFC should be capable of accelerating >10 mA of CW beam without limitations from the effects that are known to limit beam current at PSI.

*This work supported by the George and Cynthia Mitchell Foundation.
#KarieMelconian@tamu.edu

The SFC design builds upon an earlier design for a separated-orbit cyclotron, TRITRON [9], which also used SRF cavities and quadrupole channels. Although TRITRON successfully demonstrated transport of beam through several orbits, the orbit separation was small (10 mm) and the fraction of aperture with usable field quality for orbits was ~40%. In order to avoid this limitation, the beam transport channels in the SFC have been designed with > 6 cm orbit separation and 4 cm good-field aperture in each BTC.

Table 1: Main Parameters of the SFC Design

Proton energy (inj/ext)	13/100	MeV
RF frequency	117	MHz
Orbit radius (inj/ext)		m
Dipole field (inj/ext)	0.60/0.45	T

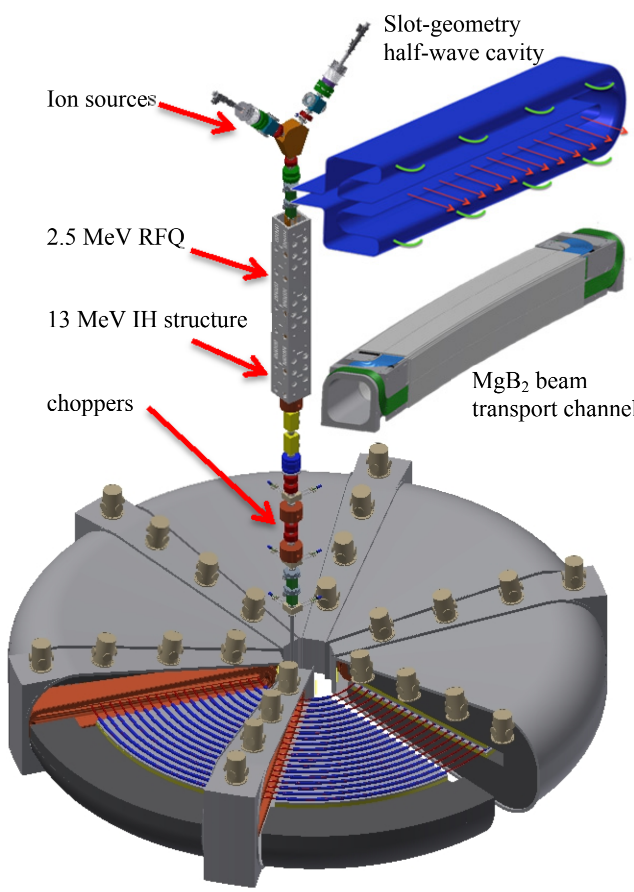

Figure 1: 100 MeV SFC, with cutaway to show SRF cavities and beam transport channels.

Content from this work may be used under the terms of the CC BY 3.0 licence (© 2015). Any distribution of this work must maintain attribution to the author(s), title of the work, publisher, and DOI.

6th International Particle Accelerator Conference IPAC2015, Richmond, VA, USA JACoW Publishing
ISBN: 978-3-95450-168-7 doi:10.18429/JACoW-IPAC2015-THPF136

Content from this work may be used under the terms of the CC BY 3.0 licence (© 2015). Any distribution of this work must maintain attribution to the author(s), title of the work, publisher, and DOI.

BEAM DYNAMICS OPTIMIZATION OF FRIB FOLDING SEGMENT 1 WITH A SINGLE TYPE OF REBUNCHER CRYOMODULE

Z. He*, Y. Zhang, T. Xu, Q. Zhao, M. Ikegami, F. Marti
FRIB, Michigan State University, USA

Abstract

The Facility for Rare Isotope Beams (FRIB) uses a charge stripper in folding segment 1 to increase the number of charge states of particles to enhance the acceleration efficiency. To control possible emittance growth after the charge stripper, the 3-dimensional on-stripper beam size should be as small as possible. The original 2-cavity-HWR (HWR stands for half wave resonator) rebuncher cryomodule is responsible for the longitudinal focusing before stripper. In order to accept and transport the beam downstream to linac segment 2, another kind of 3-cavity-QWR (QWR stands for quarter wave resonator) rebuncher cryomodule is baselined after the stripper. However, two kinds of cryomodules would increase the cost in design, therefore would be quite inefficient. In this paper, the FRIB lattice with only single-type 4-cavity-QWR rebuncher cryomodule in folding segment 1 is discussed. Positions of lattice elements are adjusted to accommodate the new type of cryomodule. Beam dynamics is optimized to meet the on-stripper beam requirement. The lattice is then adjusted and rematched.

INTRODUCTION

In the FRIB [1] baseline design of linac segment 1 (LS1) and folding segment 1 (FS1), there are two types of rebuncher cryomodules, one type is the 2-cavity-HWR rebuncher, and another is the 3-cavity-QWR rebuncher.And There are two rebuncher cryomodules for each type, two 2-cavity-HWR rebunchers and two 3-cavity-QWR rebunchers. The baseline design aims at decreasing the total number of RF cavities, however, further cost optimization favored the choice of decreasing the type of rebuncher cryomodules to a single type 4-cavity-QWR rebuncher, which can save design and manufacturing cost. A proposal was made to reduce the type of rebunchers from 2 to 1. And the feasibility of the new lattice with new type of rebuncher from beam dynamics point of view is studied and described in this paper.

NEW LATTICE DESIGN CONFIGURATION

This section mainly provides information on the new type of 4-cavity-QWR rebuncher and the two criteria of lattice design:

New Type of 4-cavity-QWR Rebuncher

Some pre-study shows that a single type of 4-cavity-QWR rebuncher is capable of replacing the two types of rebunchers. The drawing of the new 4-cavity-QWR rebuncher can

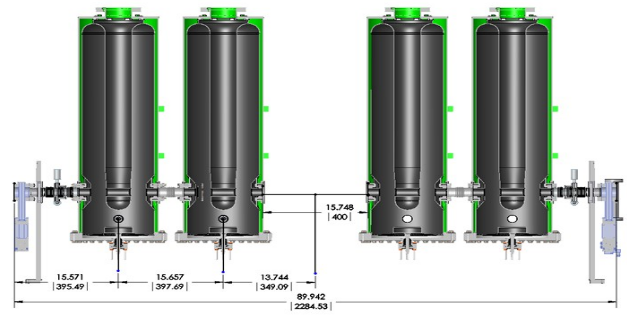

Figure 1: Mechanical drawing of the new 4-cavity-QWR rebuncher.

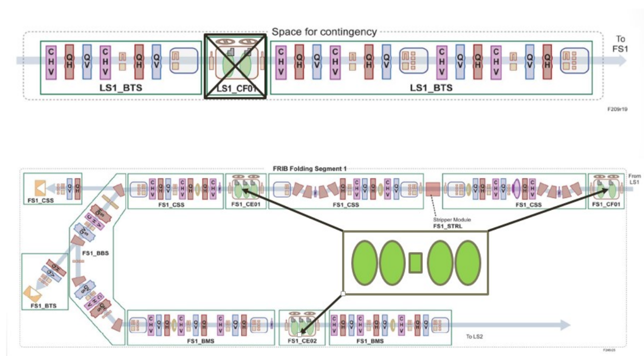

Figure 2: New lattice design with a single type of 4-cavity-QWR rebuncher (Criterion 1) [2].

be seen in Fig. 1. There are 4 $\beta = 0.085$ QWRs in one rebuncher cryomodule, and a 0.4 m reserved space at the center of the cryomodule for heat exchanger. The total length of the new rebuncher cryomodule is 2.285 m.

New Lattice Design Criterion 1

The first criterion of a new lattice design with a single type 4-cavity-QWR rebuncher can be seen in Fig. 2. The 2-cavity-HWR rebuncher LS1-CF01 is deleted, and the remaining rebunchers FS1-CF01, FS1-CE01, FS1-CE02 are changed into the 4-cavity-QWR rebuncher. In order to preserve cryogenic port position, center position of each rebuncher cryomodule is fixed.

The original 2-cavity-HWR rebuncher is 1.243 m long and the 3-cavity-QWR rebuncher is 1.589 m long, both kinds of old rebunchers are smaller in size. In order to accommodate the new rebuncher, lattice elements should be shifted around and drift spaces must be compressed to make room for the new rebuncher.

* hez@frib.msu.edu

ISBN: 978-3-95450-168-7 doi:10.18429/JACoW-IPAC2015-THPF137

BEAM DYNAMICS EFFECTS OF HIGH ORDER MULTIPOLES IN NON-AXISYMMETRIC SUPERCONDUCTING RF CAVITIES

Z. He*, Y. Zhang, J. Wei, FRIB, Michigan State University, USA

Abstract

Non-axisymmetric superconducting RF cavities have been widely used in accelerator facilities. Because of the geometry, electric and magnetic multipole components, including steering terms, quadrupole terms, and higher order terms, would arise and have potential effects on beam dynamics. In this paper, we start with a simple linac periodic structure to study the effects of higher order terms. The action is defined as a figure of merit to quantify the effects. After that, we move to a more realistic situation of FRIB linac segment 1 (LS1). Multipole terms of quarter wave resonators (QWRs) are firstly calculated using multipole expansion scheme. Then, the scheme is tested using the FRIB linac lattice with QWRs, and the effects of higher order terms on FRIB LS1 are estimated.

INTRODUCTION

The non-axisymmetric geometry of the superconducting RF cavities would produce all kinds of multipole components. In 1992, Marco Cavenago firstly described dipole and quadrupole terms in a non-axisymmetric QWR [1]. Then, Alberto Facco came up with an analytical approach to calculate steering terms in 2001 [2]. Later works [3–5], based on the idea of field multipole expansion, made several attempts to study the cavity multipole components under different scenarios. Even though efforts have been made to extract the higher order terms by multipole expansion, the beam dynamics effects coming from it have never received systematic study. In this paper, we are going to develop a systematic scheme to estimate beam dynamics effects coming from multipole components, and the scheme is then applied to FRIB LS1.

FIGURE OF MERIT

It is well known that the particle action, described in Eq.1, is a constant for a linear lattice with no error.

$$J = \frac{1}{2\beta}[y^2 + (\beta y' + \alpha y)^2]. \tag{1}$$

The transformation between action-angle coordinate system and x-x' phase space coordinate system is decribed in Eq.2. It can be easily found out that, the beam envelope of a beam bunch can be determined by the beta-function and the maximum particle action.

$$\begin{cases} y = \sqrt{2\beta J}\cos\psi \\ y' = -\sqrt{\frac{2J}{\beta}}[\sin\psi + \alpha\cos\psi] \end{cases} \tag{2}$$

Therefore, particle action can be chosen as the figure of merit [6–8].

ACTION KICK FOR SINGLE HIGH ORDER TERMS

Particle action is a constant for perfect linear lattice, however, when a non-linear high order kick occurs, particle action changes. The action kick coming from high order terms can be estimated by Eq.3 [7], where J represents particle action, $B_0\rho$ is the magnetic rigidity. B_{ref} and R_0 are reference magnetic field and radius. n is the multipole order. a_n is multipole coefficient, which can be both normal term or skewed term.

$$\frac{\Delta J_{x,y}}{J_{x,y}} \sim \frac{(2J)^{\frac{n-1}{2}}}{4\pi B_0\rho}\frac{B_{ref}}{R_0^n}\int a_n\beta_{x,y}^{\frac{n+1}{2}} \tag{3}$$

Subsequently, we take the specific example of sextupole to derivate the maximum action kick. Assume the sextupole kick is small, and take horizontal direction as an example, we can get Eq.4:

$$\begin{aligned}\Delta J_x &\sim \sqrt{2\beta_x J_x}\sin\psi_x\cdot g_2(2\beta_x\cos^2\psi_x - 2\beta_y J_y\cos^2\psi_y) \\ &\leq 2\sqrt{2}\beta_x^{\frac{3}{2}}J_x^{\frac{3}{2}}g_2\sin\psi_x\cos^2\psi_x\end{aligned} \tag{4}$$

Furthermore, we test Eq.4 using a simple lattice, which can be seen in Fig. 1(a). A sextupole kick is induced at 4.28 m with strength $g_2 = 0.05$. The red-plus line indicates the predicted maximum action after sextupole kick, which agrees pretty well with particle tracking result. Fig. 1(b) shows the predicted maximum action kick vs sextupole strength. Blue line is the result coming from 10000 particle tracking. The green star is the result coming from the model. We can see that, two results agree with each other pretty well.

ACTION KICK FOR MULTIPLE HIGH ORDER TERMS

Reference [7] has pointed out that, if phase advance can be neglected, multiple high order terms, after scaled by β-function, can be added up directly. However, in a superconducting linac, higher order multipoles caused by RF cavities would usually separate with each other by a certain phase advance. As a result, high order terms would not cancel out even with same absolute value and opposite sign.

We derive the formulism for multiple high order kicks separated by a non-negligible phase advance. We start with magnetic field and electric field can be treated similarly. We'll still based on the idea of small kick approximation and

* hez@frib.msu.edu

Content from this work may be used under the terms of the CC BY 3.0 licence (© 2015). Any distribution of this work must maintain attribution to the author(s), title of the work, publisher, and DOI.

ISBN: 978-3-95450-168-7 doi:10.18429/JACoW-IPAC2015-THPF139

Content from this work may be used under the terms of the CC BY 3.0 licence (© 2015). Any distribution of this work must maintain attribution to the author(s), title of the work, publisher, and DOI.

NONLINEAR OPTICS OF SOLENOID MAGNETS*

Steven M Lund†
Facility for Rare Isotope Beams, Michigan State University, East Lansing, MI , USA 48824

Abstract

Solenoid magnets are often employed for focusing in low energy beam transport lattices in the front-end of a machine. We derive a relatively simple analytic formula for the nonlinear angular focusing kick imparted to particles traversing the solenoid. Few approximations are made. The formula provides a clear expression of the well-known *Scherzer's Theorem* from electron optics that all nonlinear terms of an axisymmetric magnetic field provide more focusing and that nonlinear terms are non-removable. The formula suggests that for beam transport, little can be done to reduce nonlinearities in solenoid-type magnets other than take a simple design without abrupt changes as a function of axial coordinate and appropriately choose the aspect ratio (characteristic bore radius over axial length) of the magnet system and the beam filling factor within the aperture to limit nonlinear effects. Illustrative applications of the formula characterize nonlinear focusing effects in iron-free and iron type solenoid magnets.

INTRODUCTION

Solenoid magnets are appealing due to their simple field structure in idealized form. However, as the level of detail of the model description increases, the cross-coupled structure of the equations of motion describing particle focusing in a solenoid become increasingly complicated and difficult to analyze. In this study, we derive a closed analytic formula for the radial angular impulse imparted to a particle traversing an axisymmetric solenoid magnet including both linear and *all* nonlinear field components. The only approximation made is the paraxial approximation. The formula applies to particles with arbitrary (conserved) canonical angular momentum. This is important because in many cases particles are born from a source immersed in a magnetic field, and consequently, the particles can have finite canonical angular momentum. Near the source, particles are typically transported downstream using an axisymmetric solenoid focusing lattice where the particle canonical angular momentum is conserved. The surprisingly simple formula obtained for the focusing impulse provides insight on the nonlinear focusing properties of solenoid magnets. The formula is applied to better understand nonlinear focusing effects in solenoids, both as the radius of the particle within the magnet aperture increases and as the aspect ratio and structure of the solenoid is varied. The formula should be possible to exploit in future studies to estimate how statistical rms beam emittance (quality) evolves during transport in a nonlinear solenoid lattice.

* Work supported by the U.S. Department of Energy Office of Science under Cooperative Agreement DE-SC0000661 and the National Science Foundation under Grant No. PHY-1102511.
† lund@frib.msu.edu

DERIVATION

We consider the a single particle of charge q and mass m evolving in an axisymmetric ($\partial/\partial\theta = 0$) applied solenoid field $\mathbf{B}^a$ and employ r,θ,z cylindrical-polar coordinates. Because the magnetic field only bends particle trajectories, the kinetic energy of the particle is constant, or equivalently, the exact relativistic gamma factor ($\gamma = 1/\sqrt{1-\beta^2} = \text{const}$) and beta factors ($\beta = \text{const}$) are conserved. The applied magnetic field of the solenoid is assumed axisymmetric, so the particle evolves with a conserved angular momentum $P_\theta \equiv [\mathbf{x}\times(\mathbf{p}+q\mathbf{A})]\cdot\hat{\mathbf{z}} = r(p_\theta + qA_\theta) = \text{const}$. Here, $\mathbf{x}$ and $\mathbf{p} = m\gamma\dot{\mathbf{x}}$ are the coordinate and mechanical momentum of the particle, $\dot{} \equiv \frac{d}{dt}$ denotes a derivative with respect to the time t, and $\mathbf{A}$ is the vector potential that generates the applied field (i.e., $\mathbf{B}^a = \nabla\times\mathbf{A}$). Applying Stoke's theorem to the expression for P_θ obtains the so-called Bush's theorem expression [1, 2]

$$P_\theta = \gamma m r^2\dot{\theta} + \frac{q\psi}{2\pi} = \text{const.} \qquad (1)$$

Here, $\psi = \int_r d^2x\ B_z^a(r,\theta) = \oint_r \mathbf{A}\cdot d\ell = 2\pi r A_\theta$ is the magnetic flux bounded by a circle of radius r. In general, one cannot take $P_\theta = 0$ for orbits that do not go through the origin $r = 0$ (i.e., P_θ cannot in general be zeroed by coordinate choice for all particles) which corresponds to the axis of symmetry of the solenoid.

The static field Maxwell equations $\nabla\cdot\mathbf{B}^a = 0$ and $\nabla\times\mathbf{B}^a = 0$ allow $\mathbf{B}^a = \hat{\mathbf{r}}B_r(r,z) + \hat{\mathbf{z}}B_z(r,z)$ to be expanded as [1, 2]

$$\begin{aligned} B_r(r,z) &= \sum_{\nu=1}^{\infty} \frac{(-1)^\nu}{\nu!(\nu-1)!}\frac{\partial^{2\nu-1}B_{z0}(z)}{\partial z^{2\nu-1}}\left(\frac{r}{2}\right)^{2\nu-1}, \\ B_z(r,z) &= \sum_{\nu=0}^{\infty} \frac{(-1)^\nu}{(\nu!)^2}\frac{\partial^{2\nu}B_{z0}(z)}{\partial z^{2\nu}}\left(\frac{r}{2}\right)^{2\nu}, \end{aligned} \qquad (2)$$

where $B_{z0}(z) \equiv B_z(r=0,z)$ is the on-axis field. Thus, the 3D field of the axisymmetric magnet with all nonlinear terms can be regarded as specified by the on-axis ($z = 0$) field. The lowest-order terms in the sums in Eq. (2): $B_r \simeq -\frac{1}{2}\frac{\partial B_{z0}}{\partial z}r$ and $B_z \simeq B_{z0}$ provide linear focusing. All higher terms provide nonlinear focusing [1, 2].

The radial component of the Lorentz force equation for the particle evolving in the magnetic field $\ddot{\mathbf{x}} = [q/(\gamma m)]\mathbf{x}\times\mathbf{B}^a$ can be expressed as

$$\ddot{r} = r\dot{\theta}^2 - \frac{qr\dot{\theta}B_z^a}{\gamma m}. \qquad (3)$$

ISBN: 978-3-95450-168-7 doi:10.18429/JACoW-IPAC2015-THPF140

UNIQUE ACCELERATOR INTEGRATION FEATURES OF THE HEAVY ION CW DRIVER LINAC AT FRIB*

Y. Yamazaki#, N. Bultman, M. Ikegami, F. Marti, E. Pozdeyev, J. Wei, Y. Zhang, Q. Zhao, FRIB/MSU, East Lansing, MI 48824, USA
A. Facco, INFN-Laboratori Nazionali di Legnaro, Legnaro (Padova), Italy and FRIB/MSU, East Lansing, MI 48824, USA

Abstract

The FRIB driver linac is a front runner for the future high power hadron linacs, making full use of CW, superconducting acceleration from very low β. accelerator driven nuclear waste transmutation system (ADS), international fusion material irradiation facility (IFMIF), Project-X type proton accelerators for high energy physics and others may utilize the technologies developed for the design, construction, commissioning and power ramp up of the FRIB linac. Although each technology has been already well developed individually (except for charge stripper), their integration is another challenge. In addition, extremely high Bragg peak of uranium beams (several thousand times as high as that of proton beams) gives rise to one of the biggest challenges in many aspects. This report summarizes these challenges and mitigations, emphasizing the commonly overlooked features.

INTRODUCTION

The continuous wave (CW) heavy ion linac with a beam energy over 200 MeV/u and a beam power of 400 kW for Facility for Rare Isotope Beams (FRIB) [1] is a driver to produce various isotope species for nuclear physics study. The linac is to accelerate all the stable ions from proton to uranium by making full use of superconducting (SC) RF acceleration technology from a very low beam energy of 0.5 MeV/u. The linac is to use 330 SC cavities with four different types; β = 0.041 quarter wave resonator (QWR), β = 0.085 QWR, β = 0.29 half wave resonator (HWR) and β = 0.53. Most of the SC cavities are housed together with focusing SC solenoid magnets in 44 acceleration cryomodules (CMs), while the remaining 14 SC cavities in 5 rebuncher (matching) CMs (Recently, the rebuncher CMs and cavities therein were further optimized [2]). Needless to say, manufacturing of a great number of SC cavities and CMs of different kinds is one of the biggest challenges in this project. Also, it should be emphasized that the FRIB CMs equipped with the focusing SC solenoids and beam position monitors (BPMs) are much more complicated than those of SNS linacs and many electron SC linacs without the solenoids and BPMs inside. Furthermore, each of the FRIB CMs is equipped with many fundamental mode input couplers (FPCs) and each solenoid is with two SC corrector steering dipoles. The development of these FRIB SC technologies is detailed in Ref. [3, 4].

This driver is the first heavy ion linac to join the beam power front of an order of 1 MW as mentioned in Ref. [5], in which beam physics challenge in the FRIB driver linac is detailed. This article is a continuation of Ref. [5] in a sense that accelerator physics integration features of the FRIB driver linac is discussed.

MPS AND BEAM DUMPS

In order to contrast heavy ion beams against proton ones, take uranium beams as the most extreme example. One of the striking difference of the uranium beams from proton ones is their extremely high Bragg peak, that is, energy loss density dE/dx in materials. The uranium one is typically by several thousand times [5] as high as the proton one, depending upon their energy. The range is by several ten times smaller [5]. As a result heavy ion beam loss damage is significantly larger than proton one by this factor, while the radiation arising from the uranium beam loss is by several ten times lower than that of the proton one. The latter implies that the uranium beam loss is very hard to detect, in particular, at an energy below 100 MeV/u. It is one of the biggest challenges how to protect accelerator components from the beam impinge damage. For this reason, Machine Protection System (MPS) [6, 7] implements a redundant, multi-layer scheme, responding to fast events and slow losses.

The extremely high beam loss energy density gives rise to many technical challenges in the FRIB, like liquid lithium charge stripper [8], the target [9], the charge selector and others. In order to show the difficulty arising from high beam damage, take the beam dump design here as an example.

The linac beam dump is used for beam commissioning and beam tuning. For this purpose, we are going to use a beam pulse length of 50 μs and a repetition rate lower than 1 Hz in most cases in order to minimize the beam dump cost. However, after the commissioning and/or tuning, we have to increase the beam duty to CW. The difference between the 50 μs beam and the CW beam is the beam loading. Since the stored energy of SC cavities is very large, no beam loading can be observed with the 50 μs beam. In order to ramp up the beam to CW, we need to confirm the beam loading well compensated with low level RF control system. Since the filling time of the FRIB SC cavities is typically of 5 ms, we need the beam with a pulse length several times as long as this filling time, like 20 ms, in order to confirm the beam loading

*Work supported by the U.S. Department of Energy Office of Science under Cooperative Agreement DE-SC0000661.
#yamazaki@frib.msu.edu

Content from this work may be used under the terms of the CC BY 3.0 licence (© 2015). Any distribution of this work must maintain attribution to the author(s), title of the work, publisher, and DOI.

ISBN: 978-3-95450-168-7 doi:10.18429/JACoW-IPAC2015-THPF141

DESIGN OF A COMPACT ALL-PERMANENT MAGNET ECR ION SOURCE INJECTOR FOR REA AT THE MSU NSCL*

Alfonse N. Pham†, Daniela Leitner, Patrick Glennon, Jack Ottarson, Don Lawton, Mauricio Portillo, Guillaume Machicoane, John Wenstrom, Andrew Lajoie
Michigan State University National Superconducting Cyclotron Laboratory
East Lansing, MI 48824-1321, USA

Abstract

The design of a compact all-permanent magnet electron cyclotron resonance (ECR) ion source injector for the ReAccelerator Facility (ReA) at the Michigan State University (MSU) National Superconducting Cyclotron Laboratory (NSCL) is currently being carried out. The ECR ion source injector will augment the electron beam ion trap (EBIT) charge breeder as an off-line stable ion beam injector for the ReA linac. The objective of the ECR ion source injector will be to provide CW beams of heavy ions from hydrogen to masses up to ^{136}Xe within the ReA charge-to-mass ratio (Q/A) operational range from 0.2 to 0.5. The ECR ion source will be mounted on a high-voltage platform that can be adjusted to provide the required 12 keV/u injection energy into a room temperature radio-frequency quadrupole (RFQ) for further acceleration. The beam line consists of a 30 kV tetrode extraction system, mass analyzing section, and optical matching section for injection into the existing ReA Low Energy Beam Transport (LEBT) line. The design of the ECR ion source and the associated beam line are discussed.

INTRODUCTION

The Facility for Rare Isotope Beams (FRIB) is currently under construction at MSU [1]. FRIB consists of a heavy ion driver linac, target station to produce rare isotope, and fragment separator to purify the beam to be delivered to three large experimental areas for rare isotope nuclear physics research. The fast beam experimental area where the shortest-lived rare isotope beams (RIB) at energies >100 MeV/u are sent, and a stopped beam experimental area where RIBs are thermalized either in a gas cell or a cyclotron gas stopper before being transported to the trap and laser spectroscopy area or re-accelerated for low energy nuclear physics experiments with ReA [2]. Utilizing the modularity of the superconducting RF cyromodules, ReA currently re-accelerate thermal heavy ion beams from the gas stopper to 0.3–3 MeV/u for Q/A of 0.25 and up to 6 MeV/u for Q/A of 0.5. In its final configuration, ReA will reach kinetic energies of up to 12 MeV/u for the heaviest ions (e.g. ^{238}U) and 24 MeV/u for light ions (e.g. ^{4}He).

With the addition of an all-permanent magnet off-line ECR ion source, the existing beam delivery capabilities at ReA will be significantly expanded by providing a source of continuous-wave stable heavy ion beams for commissioning, beam preparation, detector testing, and stable beams experiments. The robust ECR ion source will be integrated with existing facility capabilities to allow for independent tuning of the linac with stable beams while optimizing the EBIT charge breeder during radioactive ion beam development for experiments.

* Work supported by MSU and NSF PHYS-1102511
† alfonse@nscl.msu.edu

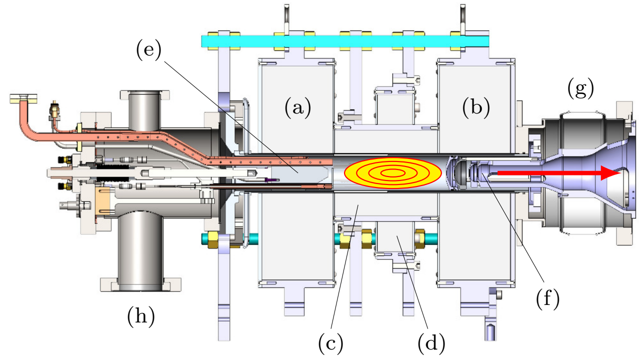

Figure 1: Cross-sectional diagram of the ECR ion source with (a) injection magnet, (b) extraction magnet, (c) hexapole magnet, (d) central magnet, (e) injection system, (f) extraction system, (g) high-voltage break, (h) injection vacuum port, ECR region, and direction of incident beam depicted.

Table 1: Requirements of the ECR Ion Source Injector

Parameter	Value
ReA Injection Energy	12 keV/u ± 5%
Q/A Range	0.2–0.5
Beam Current	~ 1–3 $e\mu$A
Optical Matching	$\alpha_x = 0.7$, $\beta_x = 8.4$ m/rad
Conditions	$\alpha_y = -1.1$, $\beta_y = 0.9$ m/rad

ECR ION SOURCE DESIGN

The design of the all-permanent magnet ECR ion source presented is based on a reference design developed at CEA-Grenoble, and later built for Oak Ridge National Laboratory and SOLAIRE [3]. The design allows for a compact, cost-effective ECR ion source with low power consumption that is optimized for the production of multiply charged heavy ions. A cross-sectional diagram of the ECR ion source is shown in Fig. 1 and Table 1 summarizes the injector requirements. The ECR ion source comprises of the injection, magnetic confinement, and extraction system to confine ions long

Content from this work may be used under the terms of the CC BY 3.0 licence (© 2015). Any distribution of this work must maintain attribution to the author(s), title of the work, publisher, and DOI.

ISBN: 978-3-95450-168-7 doi:10.18429/JACoW-IPAC2015-THPF142

HIGH INTENSITY SOURCE OF He NEGATIVE IONS

V. Dudnikov #, Muons, Inc., Batavia, IL 60510, USA, V. Morozov, Jefferson Laboratory, Newport News, VA 23606, USA and A. Dudnikov, BINP, Novosibirsk, Russia

Abstract

He- ion can be formed by an attachment of additional electron to the excited metastable 2^3S_1 He atom. Electron affinity in this metastable He^- ion is A=0.08 eV with excitation energy 19.8 eV. Production of He^- ions is difficult because the formation probability is very small but destruction probability is very high. Efficiency of He- ions generation was improved by using of an alkali vapor targets for charge exchange He^- sources. Low current He^- beams were used in tandem accelerators for research and technological diagnostics (Rutherford scattering). The development of high-intensity high-brightness arc-discharge ion sources at the Budker Institute of Nuclear Physics (BINP) has opened up an opportunity for efficient production of more intense and more brighter He- beam which can be used for alpha particles diagnostics in a fusion plasma and for realization of a new type of a polarized $^3He^−$ ion source. This report discusses the high intense He- beams production and a polarized $^3He^−$ ion source based on the large difference of extra-electron auto-detachment lifetimes of the different $^3He^−$ ion hyperfine states.

INTRODUCTION

The parameters of the Electron-Ion Collider projects that are being actively developed by BNL and JLab are discussed in Ref. [1]. Advanced spin control techniques used in these projects should provide very good polarization preservation including ^3He and D polarization. This means that the final beam polarization after acceleration will be determined by the beam polarization extracted from the ion source which must be made as high as possible. Polarized ^3He ions are particularly important for efficient electron-ion collider operation.

A review of the polarized ^3He ion beam production has been presented in Ref. [2]. Early ion sources have polarized ^3He ion beam intensities of nA scale. Since the efficiency of experiments is proportional to the square of the polarization, P^2, having the highest possible degree of polarization is very important. For polarized $^3He^{++}$ production, it was proposed to use ionization of nuclear-polarized $^3He^0$↑ by electrons in an electron beam ion source (EBIS) [2, 3]:

$$^3He^0\uparrow + e \rightarrow {}^3He^{++}\uparrow + 3e$$

The expected beam intensity is about $2.5\cdot10^{13}He^{++}$/pulse with nuclear polarization P >70 %.

For polarized $^3He^{++}$ production, one can also use the high-current arc-discharge source (developed at BINP [4] and used in the BNL OPPIS upgrade [5]) with pulsed injection of nuclear-polarized $^3He^0$↑ atoms (polarized by optical pumping) into an arc-discharge plasma source [6]. For protection of the nuclear polarization during the step-by-step ionization, a strong magnetic field can be used.

Another proposed technique [7] is to use resonant charge-exchange ionization of polarized $^3He^0$↑ in a storage tube by an incident $^4He^+$, $^4He^{++}$ plasma jet produced by an arc-discharge ion source [4]:

$$^3He^0\uparrow + {}^4He^{++} \Rightarrow {}^3He^{++}\uparrow + {}^4He^0$$

The proposed methods of polarized ^3He ion production were discussed but were never tested.

POTENTIAL OPTIONS FOR PRODUCTION OF POLARIZED $^3He^-$ IONS

An intense beam of polarized $^3He^−$ ions could be produced using the high-brightness arc-discharge ion source with geometrical focusing and low gas consumption developed at BINP and used in the BNL OPPIS upgrade [8]. Earlier this arc-discharge source was used for high-intensity (12 mA) $He^−$ beam production [9]. A schematic of this device is shown in Fig. 1. An intense high-brightness flow of He^+ ions is generated in the arc-discharge source (1) and formed into an ion beam by a multi-grid multi-slit flat extraction system of 4 cm in diameter. This intense space-charge-compensated beam is focused by a magnetic lens (2) into a sodium jet charge-exchange target (3). A part of He^+ ions captures two electrons from Na atoms and forms metastable $He^−$ ions. The beam of He^- ions is deflected from the more intense beams of He^+ and He^0 in an analyzing magnet (4) and detected by a FC (5). The secondary electron emission is suppressed by a suppression electrode. The beam profiles are controlled by profile monitors (6) and (7). Under the optimal conditions at the energy of 12 keV, up to 1.5% of He^+ ions were converted into He^- producing a 12 mA $He^−$ beam. The estimated He^+ beam intensity transferred to the FC is ~ 0.8 A. With a modern spherical multi-aperture extraction system, it is possible to have He^+ beam with an intensity of ~ 2 A.

With a 2 A $^3He^+$ beam current, up to 0.1 A of a $^3He^−$ beam can be produced by charge exchange in an alkali vapors target yielding up to 2 mA of highly polarized $^3He^−$ ions [4, 6].

A pulsed gas valve [10] can provide low gas consumption, which is important because ^3He gas is very expensive. The basic idea of this proposal can be traced back to the alpha particle diagnostics that is being developed for the ITER project in France.

#Vadim@muonsinc.com

Content from this work may be used under the terms of the CC BY 3.0 licence (© 2015). Any distribution of this work must maintain attribution to the author(s), title of the work, publisher, and DOI.

ISBN: 978-3-95450-168-7 doi:10.18429/JACoW-IPAC2015-THPF143

SADDLE ANTENNA RF ION SOURCES FOR EFFICIENT POSITIVE AND NEGATIVE IONS PRODUCTION*

V. Dudnikov#, R. Johnson, Muons, Inc., Batavia, IL 60510, USA
S. Murrey, B. Han, T. R. Pinnisi, C. Piller, M. Santana, M. Stockli, R. Welton, ORNL, Oak Ridge, TN 37831, USA
J. Breitschopf, Taxes Lutheran University, Seguin, TX 78155, USA
G. Dudnikova, UMD, College Park, MD 32611, USA

Abstract

Existing RF Ion Sources for accelerators have specific efficiencies for H^+ and H^- ion generation ~3- 5 mA/cm^2 kW, where about 50 kW of RF power is typically needed for 50 mA beam current production. The Saddle Antenna (SA) SPS described here was developed to improve H^- ion production efficiency, reliability and availability. In SA RF ion source the efficiency of positive ion generation in the plasma has been improved to 200 mA/cm^2 kW. After cesiation, the current of negative ions to the collector was increased from 1 mA to 10 mA with RF power ~1.5 kW in the plasma (6 mm diameter emission aperture) and up to 30 mA with ~4 kW RF. Continuous wave (CW) operation of the SA SPS has been tested on the test stand. The general design of the CW SA SPS is based on the pulsed version. Some modifications were made to improve the cooling and cesiation stability. CW operation with negative ion extraction was tested with RF power up to ~1.2 kW in the plasma with production up to Ic=7 mA. Long term operation was tested with ~0.8 kW in the plasma with production of I_c=5 mA, I_{ex} ~15 mA. A stable long time generation of H^- beam without degradation was demonstrated in RF discharge with AlN discharge chamber.

INTRODUCTION

Development of the saddle antenna RF surface plasma source (SA RF SPS) was proposed for improve efficiency of H- ion production and improve SPS reliability and availability [1-6]. RF SPS for accelerators have the efficiency of H- ion generation ~1 mA/kW and RF power ~ 50 kW is needed for 50 mA beam current production [7-8]. The high RF power required for the sources as well as triggering of the pulsed discharge can create problems for very long term operation. In tested version of SA RF SPS the specific efficiency of positive ion generation was increased to ~200 mA/ cm^2 kW and a specific efficiency of H- production was increased up to ~ 20 mA/cm^2 kW from previous ~2.5 mA/ cm^2 kW.

The total efficiency of the surface plasma produced fraction of the H^- beam is a product of the probability of secondary emission of H^- caused by plasma bombardment of the collar surface around the emission aperture, the probability of extraction of emitted H^-, and the rate of bombarding plasma flux [9-12].The coefficient of secondary emission of H^- is determined by surface properties (proper cesiation) and the spectrum of the plasma particles bombarding the collar surface around the emission aperture.

The cesiation was improved recently [7] and appears to be nearly optimal. The probability of extraction of H^- emitted from the collar surface is dependent on the surface collar shape [9-11], which was optimized recently to improve H^- emission [6]. The problem of efficient plasma generation is being addressed by the development of new RF plasma generators with higher plasma generation efficiency and better concentration of useful plasma flux onto the internal surfaces of the collar around the emission aperture for lower RF power [1-6]. In this project, we use the saddle antenna, which has its RF magnetic field transverse to the source axis, combined with an axial DC magnetic field, to concentrate the plasma on the collar where the negative ions are formed by secondary emission [1-6, 9-11].

SA SPS DESIGN

The schematic of a large RF SA SPS with the AlN ceramic discharge chamber, saddle antenna, and DC solenoid is shown in Fig. 1. The chamber has an ID=68 mm. The saddle antenna in this SPS with inductance L=3.5 µH is made from water cooled copper tube. RF assisted triggering plasma gun (TPG) is attached to discharge chamber from left. An extraction system is attached from right side.

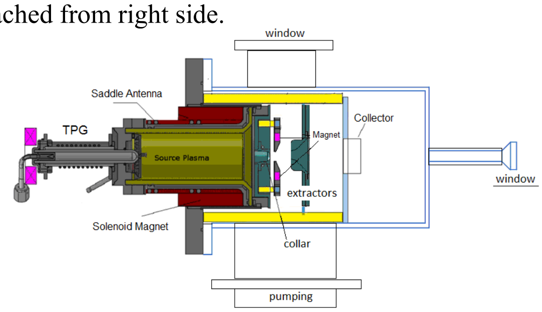

Figure 1: A schematic of the SA SPS with an extraction system and a collector.

A schematic of the extraction system is shown in Fig. 2. The strong transverse magnetic field (up to 1 kG) is created in the collar by permanent magnets (arrows) inserted into water cooled extractor attached to the plasma plate through ceramic insulators.

*Work supported in part by US DOE Contract DE-AC05-00OR22725 and by STTR grant DE-SC0011323
#Vadim@muonsinc.com

Content from this work may be used under the terms of the CC BY 3.0 licence (© 2015). Any distribution of this work must maintain attribution to the author(s), title of the work, publisher, and DOI.

ISBN: 978-3-95450-168-7 doi:10.18429/JACoW-IPAC2015-THPF144

ANALYSIS OF FEL-BASED CEC AMPLIFICATION AT HIGH GAIN LIMIT*

G. Wang#, V. N. Litvinenko and Y. Jing, BNL, Upton, NY 11973, U.S.A.

Abstract

An analysis of Coherent electron Cooling (CeC) amplifier based on 1D Free Electron Laser (FEL) theory was previously performed with exact solution of the dispersion relation, assuming electrons having Lorentzian energy distribution [1]. At high gain limit, the asymptotic behaviour of the FEL amplifier can be better understood by Taylor expanding the exact solution of the dispersion relation with respect to the detuning parameter [2, 3].

In this work, we make quadratic expansion of the dispersion relation for Lorentzian energy distribution [1, 4] and investigate how longitudinal space charge and electrons' energy spread affect the FEL amplification process.

INTRODUCTION

FEL instability plays a key role in a FEL-based CeC system: it determines the cooling force, the effective bandwidth, as well as the saturation level of the system[5]. An analytical analysis based on numerically solving the exact 1-D FEL dispersion relation had been previously performed for a warm electron beam with Lorentzian energy distribution [1]. Although the analysis in [1] is based on an exact solution of the FEL dispersion relation and takes into account both the warm beam and longitudinal space charge effects, the final solutions involve an inverse Fourier transformation that can only be evaluated numerically. During analysing and optimizing a CeC system, it is often beneficial to have analytical time-domain solutions, which provides scaling laws as well as more intuitive insights.

Recently, an analysis of CeC based on 1-D FEL at high gain limit has been performed [2] for cold electron beam. In the analysis, the solutions of 1-D FEL dispersion relation have been Taylor expanded up to the quadratic terms with respect to the detuning parameter. The approximation is valid if the FEL gain is large enough such that the beam spectrum is dominated by the components with small detuning parameter. The approximation significantly simplified the final results and allow for an analytical expression for the time-domain solution of the cooling force.

As an attempt to extend the analysis of [2], we start with the 1-D FEL dispersion relation of a warm electron beam as adopted in [1], and take the Taylor series of its solutions up to the quadratic terms in detuning as the approximate solutions. Similar to the results obtained in [2], the approximation leads to an electron density wave-packet with a Gaussian envelope in the time domain. Both the amplitude and the RMS width of the Gaussian envelope depend on the longitudinal space charge parameter and the energy spread parameter of the electron beam, which makes it possible to investigate how these beam parameters affect the cooling process.

The contents are organized as follows. In section II, we present the set of equations to be used to find the approximate solutions to the dispersion relation for arbitrary space charge and energy spread parameters. We then solve the equations for zero space charge parameter in section III, and investigate how energy spread parameter alone affects the gain and coherent length of the cooling force. For arbitrary space charge and energy-spread parameter, numerical method is required to solve the set of equations and we present our results in section IV. Section V consists our summary.

SOLUTION OF 1-D FEL DISPERSION RELATION AT HIGH GAIN LIMIT

Assuming the following energy distribution of the electron beam*: $\hat{F}\left(\hat{P}\right)=\hat{q}\Big/\left[\pi\left(\hat{P}^2+\hat{q}^2\right)\right]$, the 1-D FEL dispersion relation reads

$$s\left[\left(s+\hat{q}+i\hat{C}\right)^2+\hat{\Lambda}_p^2\right]=i \quad , \tag{1}$$

where s is the complex growth rate of 1-D FEL instability in unit of Γ, $\Gamma\equiv\left[\pi j_0\theta_s^2\omega\big/\left(c\gamma_z^2\gamma I_A\right)\right]^{\frac{1}{3}}$ is the 1-D gain parameter, $\hat{\Lambda}_p\equiv\sqrt{4\pi j_0\big/\left(\gamma_z^2\gamma I_A\right)}\Big/\Gamma$ is the normalized space charge parameter, $\hat{P}\equiv\left(E-E_0\right)/\left(\rho E_0\right)$ is the normalized energy deviation of an electron with energy E, ρ is the Pierce parameter, $\hat{q}$ is the normalized energy spread parameter, I_A is Alfven current, $\theta_s\equiv K/\gamma$ is the trajectory angle of electrons' motion, K is the undulator parameter, $\hat{C}\equiv\left[k_w-\omega\big/\left(2c\gamma_z^2\right)\right]\Big/\Gamma$ is the normalized detuning parameter and $\gamma_z=\gamma\Big/\sqrt{1+K^2}$.

Let the growing root of eq. (1) to be

$$s_1=\lambda_0+\lambda_1\Delta\hat{C}+\lambda_2\Delta\hat{C}^2+\ldots \tag{2}$$

where $\Delta\hat{C}\equiv\hat{C}-\hat{C}_0$ and $\hat{C}_0$ is the detuning corresponding to the maximal growth rate, i.e.

$$\left.\frac{d\,\mathrm{Re}\left(s\right)}{d\hat{C}}\right|_{\hat{C}_0}=0 \; . \tag{3}$$

Inserting eq. (2) into eq. (1) and using eq. (3) leads to

$$\lambda_0=\lambda_R+i\lambda_I \quad , \tag{4}$$

* Work supported by Brookhaven Science Associates, LLC under Contract No.DE-AC02-98CH10886 with the U.S. Department of Energy.
#gawang@bnl.gov

* We adopt the formalism and definition of variables of [4] .

Content from this work may be used under the terms of the CC BY 3.0 licence (© 2015). Any distribution of this work must maintain attribution to the author(s), title of the work, publisher, and DOI.

ISBN: 978-3-95450-168-7 doi:10.18429/JACoW-IPAC2015-THPF146

Content from this work may be used under the terms of the CC BY 3.0 licence (© 2015). Any distribution of this work must maintain attribution to the author(s), title of the work, publisher, and DOI.

SPIN COHERENCE TIME LENGTHENING FOR A POLARIZED DEUTERON BEAM USING SEXTUPOLE FIELDS

G. Guidoboni, University of Ferrara and INFN, Ferrara, Italy

Abstract

The possibility to use sextupole fields to increase the in-plane (ring plane) polarization lifetime of a deuteron beam is part of the feasiblity studies for a search for an electric dipole moment (EDM) of charged particles in storage rings. This experiment requires ring conditions that can ensure a lifetime of the in-plane polarization (spin coherence time, SCT) up to 1000 s. At the COoler SYnchrotron (COSY) located at the Forschungszentrum Jülich, the JEDI collaboration has begun to examine the effects of emittance and momentum spread on the SCT of a polarized deuteron beam at 0.97 GeV/c. The set of data presented here shows how second-order effects from emittance and momentum spread of the beam affect the lifetime of the horizontal polarization of a bunched beam. It has been observed that sextupole fields can correct for depolarizing sources and increase the spin coherence time up to hundreds of seconds while setting the chromaticities equal to zero.

INTRODUCTION

The spin coherence time (SCT) measurements presented here are part of feasibility studies [1, 2] for a new project searching for the electric dipole moment (EDM) of charged particles in storage rings. The EDM is a permanent charge separation within the particle volume, aligned along the spin axis. The EDM violates both parity conservation and time reversal invariance. Thus, assuming the validity of the CPT theorem, the EDM represents a source of CP violation that could explain why the universe evolved to a matter-dominated state. The Standard Model (SM) does not explain the observed baryon asymmetry and predicts unobservably small EDMs (*e.g.*, for the proton, $|d_p|_{\mathrm{SM}} < 10^{-32}\ e\cdot$cm). Models beyond the SM predict values within the sensitivity of current or planned experiments (for proton and deuteron $|d_{p,d}| \geq 10^{-29}$ e·cm), but no EDM has been observed yet. If an EDM is found within the present experimental limits it would be a clear and clean probe of new physics.

Since the EDM lies along the spin axis, the new detection method requires observing the polarization precession in an electric field while the charged particles are trapped in a storage ring. While keeping the horizontal component of the beam polarization along the velocity direction during the storage time, the EDM signal can be detected as a rotation of the polarization from the ring plane toward the vertical direction due to the interaction with the inward radial electric field that is always present in the particle frame. In a magnetic storage ring, the polarization will undergo a rotation relative to the velocity described by the Thomas-BMT equation [3]:

$$\vec{\omega}_a = \vec{\omega}_s - \vec{\omega}_c = -\frac{q}{m}\left\{G\vec{B} + \left[G - \left(\frac{m}{p}\right)^2\right]\frac{\vec{\beta}\times\vec{E}}{c}\right\} \quad (1)$$

where it is assumed that $\vec{\beta}\cdot\vec{B} = \vec{\beta}\cdot\vec{E} = 0$ and the EDM component has been omitted. $\vec{\omega}_s$ is the spin precession in the horizontal (ring) plane, $\vec{\omega}_c$ is the particle angular frequency and $G = \frac{g-2}{2}$ is the anomalous magnetic moment. In the deuteron case, where $G = -0.14$, the spin alignment along the velocity ($\vec{\omega}_a = 0$ in Eq. 1) is achieved with a combination of magnetic and outward electric fields. In order to reach a sensitivity of 10^{-29} e·cm, a good compromise for the experiment requires a polarimeter sensitivity of 10^{-6} rad and a horizontal polarization lifetime (SCT) of 1000 s. The SCT represents the time available to observe the EDM signal as a polarization precession toward the vertical direction. The aim of the feasibility studies made at COSY (COoler SYnchrotron at the Forschungszentrum Jülich, Germany) is to demonstrate the possibility to reach an SCT of 1000 s using sextupole field corrections and a dedicated beam preparation including beam bunching and electron cooling.

EXPERIMENTAL SETUP

The EDM feasibility studies started at COSY in 2012 using a polarized deuteron beam with a momentum of 0.97 GeV/c. The beam polarization was initially aligned along the vertical direction (orthogonal to the ring plane) and then rotated to the horizontal (ring) plane by exciting the $(1 - G\gamma)$ spin resonance with an RF-solenoid, where G is the anomalous magnetic moment and γ is the relativistic factor. With the development of a DAQ (Data AcQuisition system) capable of measuring the rapidly precessing polarization (≈ 120 kHz) in the ring plane [4], it was possible to continuosly measure the horizontal polarization as a function of time by slowly extracting the beam onto a thick carbon target and observing elastic scattering events at forward angles in the EDDA detector [5]. The beam was bunched at the first harmonic in order to remove the first order momentum spread ($\Delta p/p$) as a cause of the in-plane spin decoherence.

The SCT studies aimed to investigate the decoherence sources represented by the finite transverse beam size (emittance) and the second order momentum spread of the beam, ($(\Delta p/p)^2$), arising from synchrotron oscillations. With the combination of electron cooling, bunching and white noise applied to electric field plates, it was possibile to prepare different beam setups to separately study the single contributions. The sequence of doing electron cooling first, then bunching without cooling, was used to study the effect of $(\Delta p/p)^2$ alone. In another setup, electron cooling and

ISBN: 978-3-95450-168-7 doi:10.18429/JACoW-IPAC2015-THPF147

INCREASING THE BEAM BRIGHTNESS OF A DUOPLASMATRON PROTON ION SOURCE*

Y.K. Batygin#, I.N. Draganic, C.M. Fortgang, LANL, Los Alamos, NM 87545, USA

Abstract

The LANSCE accelerator facility operates with two independent ion injectors for H^+ and H^- particle beams. The H^+ ion beam is formed using a duoplasmatron source followed by a 750 keV Cockroft-Walton accelerating column. Formation of an optimal plasma meniscus is an important feature for minimizing beam emittance and maximizing beam brightness. An experimental study was performed to determine optimal conditions of extracted H^+ beam for maximizing beam brightness. Study was based on measurements of beam emittance versus variable beam current and extraction voltage. Measurements yielded 0.52 as the best ratio of beam perveance to Child - Langmuir perveance for maximizing beam brightness. As a result of optimization, beam brightness was increased by a factor of 2.

ION SOURCE AND BEAMLINE

The existing H^+ ion source is a duoplasmatron with a Pierce extraction geometry [1]. The source (see Fig. 1) has been operated successfully for many years at LANSCE [2]. Originally developed for production of 50 mA proton beam, the source was modified for production of a less intense, but brighter beam [3]. The Pierce anode was replaced with a modified electrode with an aperture radius of R = 2.5 mm. The extraction electrode was moved closer to the ion source. The extraction distance is now d =10.78 mm. Details of internal structure of LANSCE duoplasmatron are given in [2, page 28]. Presently the source delivers a proton beam current of I = 15 mA at 60 Hz x 625 μsec pulse length using 1.3 std cc/min gas flow. The source is mounted on a Cockroft-Walton accelerating column at 750 kV potential with respect to ground. The H^+ beamline (see Fig. 2) is equipped with two slit-collector emittance measurement stations. TAEM1 station is placed after the 750 keV Cockroft-Walton accelerating section, while TAEM2 is placed after the 81° bending magnet. An additional emittance measurement station, TDEM1, is common for both H^+ and H^- beams and is placed in front of Drift Tube Linear accelerator. Beam current is measured with 5 beam current monitors along the beamline. The beamline is operated at typical pressure of $9 \cdot 10^{-7}$ Torr.

CHARACTERISTICS OF EXTRACTED BEAM

Optimal operation of the accelerator facility critically depends on the emittance of the beam extracted

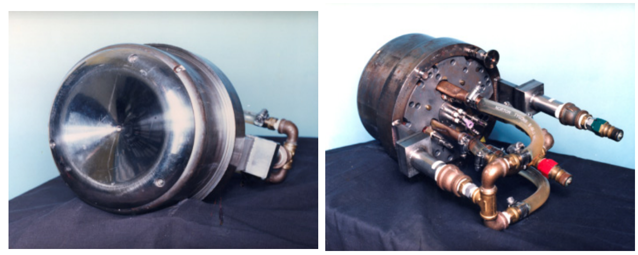

Figure 1: Side view of assembled LANSCE duoplasmatron ion source with Pierce electrode.

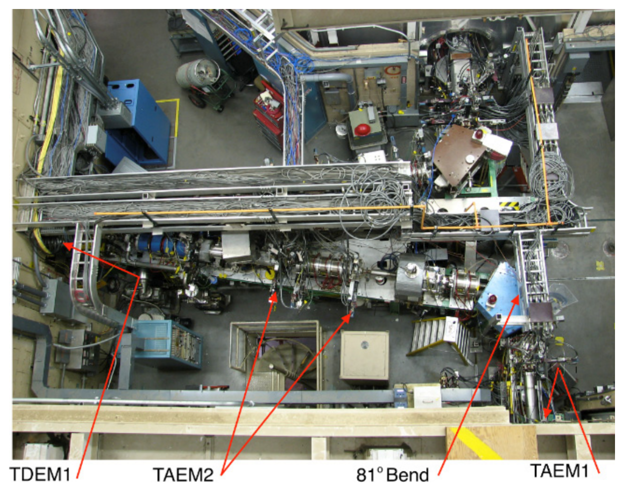

Figure 2: Layout of 750 keV H^+ Low Energy Beam Transport of LANSCE.

from the ion source. An intrinsic limitation in particle-source beam-emittance comes from the finite value of plasma temperature in the ion source and from the value of longitudinal magnetic field at extractor. Normalized emittance of the beam, extracted from a particle source with aperture radius R and plasma ion-temperature T with magnetic field B at extractor is estimated as [4]

$$4\varepsilon_{rms} = 2R\sqrt{\frac{kT}{mc^2} + \left(\frac{eBR}{4mc}\right)^2} \quad . \tag{1}$$

Besides emittance determined by Eq. (1), additional sources contributing to beam emittance are:

• irregularities in the plasma meniscus extraction surface
• aberrations due to ion-source extraction optics
• optical aberrations of the focusing elements of the Low Energy Beam Transport
• non-linearity of the electric field created by the beam space charge
• beam fluctuations due to ion-source instability or power regulation.

*Work supported by US DOE under contract DE-AC52-06NA25396
#batygin@lanl.gov

Content from this work may be used under the terms of the CC BY 3.0 licence (© 2015). Any distribution of this work must maintain attribution to the author(s), title of the work, publisher, and DOI.

ISBN: 978-3-95450-168-7 doi:10.18429/JACoW-IPAC2015-THPF148

LANSCE H$^+$ RFQ STATUS*

R. W. Garnett#, Y. K. Batygin, C. A. Chapman, I. N. Draganic, C. M. Fortgang, S. S. Kurennoy, R. C. McCrady, J. F. O'Hara, E. R. Olivas, L. J. Rybarcyk, and H. R. Salazar, LANL, Los Alamos, NM 87544, U.S.A., B. Koubek, A. Schempp, IAP, Goethe University, Frankfurt am Main, Germany, J. Haeuser, Kress GmbH, Biebergemuend, Germany

Abstract

The LANSCE linear accelerator at Los Alamos National Laboratory provides H$^-$ and H$^+$ beams to several user facilities that support Isotope Production, NNSA Stockpile Stewardship, and Basic Energy Science programs. These beams are initially accelerated to 750 keV using Cockcroft-Walton (CW) based injectors that have been in operation for over 37 years. To reduce long-term operational risks and to realize future beam performance goals for LANSCE we are completing fabrication of a 4-rod Radio-Frequency Quadrupole (RFQ) and design of an associated beam transport line that together will eventually become the modern injector replacement for the existing obsolete H$^+$ injector system. A similar H$^-$ system is also planned for future implementation. An update on the status and progress of the project will be presented.

INTRODUCTION

The present dual-beam CW-based injector scheme for the LANSCE linac is shown in Fig. 1. The two beam species are merged into a common beam transport line and bunched before injection into the drift-tube linac (DTL). The proton beam (H$^+$) is presently accelerated to 100 MeV for isotope production. The H$^-$-ion beam is accelerated to 800 MeV and used to produce neutrons for a wide variety of applications. Assessment of failure modes of our CW injectors revealed the potential for significant disruption of beam operations at LANSCE [1], primarily due to catastrophic failure of major components and unavailability of spare parts.

Our strategy to reduce operational risks associated with the current CW-based injector systems involves the eventual replacement of these systems with modern radio-frequency quadrupole (RFQ) based injectors. This approach is expected to improve reliability due to reduced overall complexity of the systems and by modernization. RFQ accelerators are employed worldwide and have demonstrated stable and reliable operation.

To meet both present and future, anticipated beam-delivery requirements, implementation of several RFQ-based injectors will be required at LANSCE [2]. Due to funding constraints and to minimize facility and operational impacts, this will be done in a phased manner with development of the H$^+$ RFQ having highest priority due to its impact on our near-term high-power performance goals [3, 4].

The RFQ is required to operate at a high duty factor of up to 15% and must meet strict beam performance requirements. Complementary simulations using the TRACE 2-D/3-D, PARMTEQM and PARMILA codes [5], Beampath [6], the CST Studio suite of codes [7] including Particle Studio, and the ANSYS [8] code were used to validate the design results prior to fabrication.

To ensure mechanical and operational robustness of the RFQ, several technical evaluations were completed prior to acceptance of the design [9]. These included: addressing potential structure cooling issues, evaluation of tuning range, impact of stem spacing on frequency and field flatness, impact of vane cross-section and stem geometry on dipole fields, and investigation of end-region field effects on emittance growth and final output energy.

The final physics design of the 4-rod RFQ was completed and verified through a joint effort between the Institute of Applied Physics (IAP) at Goethe University, Frankfurt, Germany, and Los Alamos in 2011[10]. A final mechanical design review was held in April 2013. Fabrication of the RFQ began in April 2014 in Germany by our project partner Kress, GmbH and was completed in December 2014.

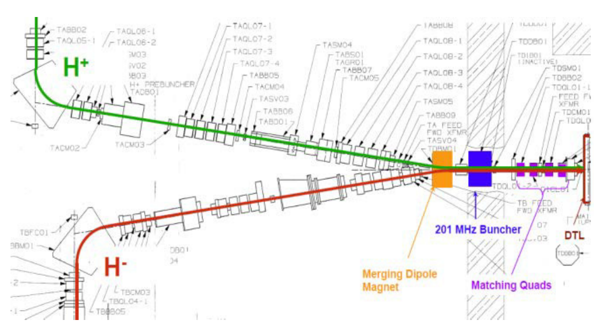

Figure 1: Present H$^+$/H$^-$ CW injector layout.

The H$^+$ RFQ and planned beam-transport layout will replace the existing H$^+$ CW injector and beam line, requiring no changes beyond the merging dipole upstream of the common H$^+$/H$^-$ beam transport section (See Fig.1). This enables early implementation of the new H$^+$ system, independent of the longer-term plans to implement multiple RFQ injectors. It is still our current plan to operate and commission the RFQ/beam transport system on a separate test stand prior to integration at the front end of the LANSCE linac. Figure 2 shows a preliminary layout of the new RFQ/ beam line configuration.

The RFQ has been delivered to Los Alamos. High-power RF testing is planned next. The ion source and high-voltage platform are being assembled in preparation for full assembly of an RFQ Test Stand that will include the ion source, low-energy beam transport (LEBT) to

* Work supported by the United States Department of Energy, National Nuclear Security Agency, under contract DE-AC52-06NA25396
# rgarnett@lanl.gov

Content from this work may be used under the terms of the CC BY 3.0 licence (© 2015). Any distribution of this work must maintain attribution to the author(s), title of the work, publisher, and DOI.

ISBN: 978-3-95450-168-7 doi:10.18429/JACoW-IPAC2015-THPF149

ELECTROMAGNETIC MODELING OF 4-ROD RFQ TUNING

S.S. Kurennoy, L.J. Rybarcyk, LANL, Los Alamos, NM 87545, USA

Abstract

Modern codes make possible detailed electromagnetic (EM) 3D modeling of RFQ accelerators. We have recently analyzed two 201.25-MHz 4-rod RFQs – one commissioned at FNAL [1] and a new design for LANL [2] – with CST Studio using imported manufacturer CAD files. The RFQ EM analysis with MicroWave Studio (MWS) was followed by beam dynamics modeling with Particle Studio as well as other multi-particle codes. Here we apply a similar approach to study the process of RFQ tuning in 3D CST models. In particular, the results will be used to better understand tuning the voltage flatness along the new LANL 4-rod RFQ.

INTRODUCTION

Radio-frequency quadrupole (RFQ) accelerators are now standard in front ends of modern ion linacs. They are usually designed with codes that rely on electrostatic field approximations, e.g., Parmteq [3]. While this is justified for classical 4-vane RFQs having perfect quadrupole symmetry, many modern RFQs contain elements that break such a symmetry. Additional RF field effects can be introduced by asymmetric elements like vane windows in split-coax designs or stem supports in 4-rod RFQs. Such effects are more complicated and can't be easily taken into account in electrostatic calculations, even in 3D, but can influence beam dynamics in some cases. We have discussed 3D RF effects in 4-rod RFQs in [4].

LANL is moving forward with replacing one of its aging Cockcroft-Walton injectors with an RFQ-based front end for the LANSCE proton linac [5]. The LANL H^+ RFQ, operating at 201.25 MHz at a duty factor up to 15%, with 35-keV injection and 750-keV final energy, should satisfy special requirements when incorporated into the existing medium-energy beam transfer that works with multiple beam species. The 4-rod type RFQ design was developed in collaboration between IAP (Frankfurt) and LANL. The RFQ was manufactured by Kress GmbH and recently delivered to LANL. The CAD files from Kress were imported into CST Studio [6] to create an RFQ model that was used to evaluate its performance [2].

4-ROD RFQ TUNING

RFQ CST Model

The imported CAD model was simplified by removing details nonessential for EM analysis such as external supports, etc. The RFQ cavity walls were also removed, leaving only the resonator vacuum volume in the CST model. The resulting model is shown in Fig. 1. Here the RFQ vacuum vessel, in gray-blue, is 175-cm long (wall-to-wall), 34-cm wide, and 30-cm high (along the stem direction, *z*). The model includes a frequency slug tuner (cyan cylinder) and two 5-cm-long beam pipes of radius 2 cm attached to the vacuum vessel, but other ports are ignored. The RFQ vanes are supported by 24 stems that are spaced longitudinally with variable period, 75 mm in the center and 69.5 mm for three periods near each end. There are 23 tuners that electrically short two adjacent stems and can be moved along them (in *z* direction) to adjust the mode frequency and voltage profile (flatness) along the structure length. The variable stem spacing simplifies tuning the voltage flatness along the structure. Our RFQ model uses the CAD model coordinates: *x* is along the RFQ axis, and the beam is moving in *-x* direction (right to left in Fig. 1).

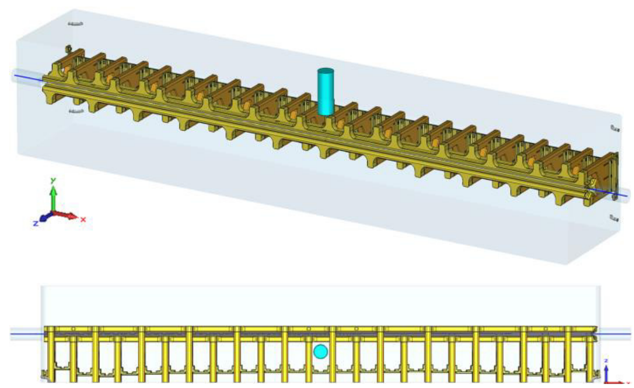

Figure 1: CST model of the LANSCE H^+ RFQ (top) and its side view (bottom).

One can see in Fig. 1 (bottom) that the tuners are at different heights: they are adjusted in the model to make the inter-vane voltage flat within ±1%. However, even with all tuners at the same height, the voltage is flat within ±5%, due to the variable stem spacing, see below.

RF Field Calculations with MWS

The fields in the RFQ model are calculated using the hexahedral AKS eigensolver; it approximates complicated surfaces well but is slow due to minimal parallelization. The efficient tetrahedral eigensolver fails to mesh the imported RFQ CAD model. The inter-vane voltages are obtained by integrating the electric field of the operating mode along short segments located in the middles of the RFQ stem periods between the vanes. The voltages calculated in different locations along one stem period show some variation (scalloping). The RFQ-model frequency is tuned to 201.226 MHz when all tuning plates are positioned at the same height, *h*=27.15 mm, from the ground plate. The voltage profiles calculated from the MWS eigenmode solution are plotted in Fig. 2 versus stem period number *n*; *n* = 0 is the middle of RFQ, negative *n* values correspond to the downstream end (left in Fig. 1). There are two profiles: V_y is calculated by integrating the field on both sides from the axis and averaging the two voltages to minimize errors – this is our usual procedure; for V_z the voltages are calculated

Content from this work may be used under the terms of the CC BY 3.0 licence (© 2015). Any distribution of this work must maintain attribution to the author(s), title of the work, publisher, and DOI.

ISBN: 978-3-95450-168-7 doi:10.18429/JACoW-IPAC2015-THPF150

3D ELECTROMAGNETIC AND BEAM DYNAMICS MODELING OF THE LANSCE DRIFT-TUBE LINAC

S.S. Kurennoy and Y.K. Batygin, LANL, Los Alamos, NM 87545, USA

Abstract

The LANSCE drift-tube linac (DTL) accelerates the proton or H- beam to 100 MeV. It consists of four tanks containing tens of drift tubes and post-couplers; for example, tank 2 is almost 20 m long and has 66 cells. We have developed 3D models of full tanks [1] in the DTL with CST Studio to accurately calculate the tank modes, their sensitivity to post-coupler positions and tilts, tuner effects, and RF-coupler influence. Electromagnetic analysis of the DTL tank models is performed using MicroWave Studio (MWS). The full-tank analysis allows tuning the field profile of the operating mode and adjusting the frequencies of the neighboring modes within a realistic CST model. Beam dynamics is modeled with Particle Studio for bunch trains with realistic initial beam distributions using the MWS-calculated and tuned RF fields and quadrupole magnetic fields to determine the output beam parameters and locations of particle losses.

INTRODUCTION

The drift-tube linac (DTL) structure, proposed by Alvarez in 1946, became the most popular type of low-energy proton linac for many decades. The DTL structure employs long cylindrical resonators (tanks) operating in the TM_{010} mode and containing a sequence of drift tubes (DTs) installed along the beam axis. DTL accelerators achieve their best efficiency for particle velocities from approximately 10% to 35% of the speed of light, i.e. $\beta = v/c = 0.1\text{-}0.35$. The Los Alamos Neutron Science Center (LANSCE) 201.25-MHz DTL covers a wide velocity range from $\beta = 0.04$ to 0.43, which corresponds to the proton energies from 750 keV to 100 MeV. The LANSCE DTL consists of four tanks. Some relevant parameters of the DTL tanks are listed in Table 1, where N_{DT} is the number of full DTs and N_{pc} is the number of post-couplers in the tank.

Table 1: LANSCE DTL Design Parameters [2]

Parameter	Tank 1	Tank 2	Tank 3	Tank 4
Energy in, MeV	0.75	5.39	41.33	72.72
β, in-out	0.04	0.107	0.287	.37-.43
Length L, m	3.26	19.688	18.75	17.92
N_{DT}	30	65	37	29
N_{pc}	0	65	37	29
Aperture r_b, cm	0.75	1-1.5	1.5	1.5
Grad. E_0, MV/m	1.6-2.3	2.4	2.4	2.5
Aver. ZT^2, MΩ/m	26.8	30.1	23.7	19.2

DTL TANK MODELS AND FIELDS

We have built 3D models of all four DTL tanks using CST Studio [3]. The EM fields in the tank models were calculated with CST MicroWave Studio (MWS), see [1, 4] for details. The CST model of tank 2 (T2) is shown in Fig. 1. This is the longest DTL tank (19.7 m) that contains 65 full DTs and two half-DTs on the end walls. The full DTs are supported by vertical stems. The tank cavity of radius 45 cm is shown in Fig. 1 as the blue-gray cylinder. Two upper insets in Fig. 1 show side views near the tank entrance (blue) and exit (green). The stabilizing post-couplers (gray) with rotating tabs can be seen in the end view of the tank in the right-bottom inset.

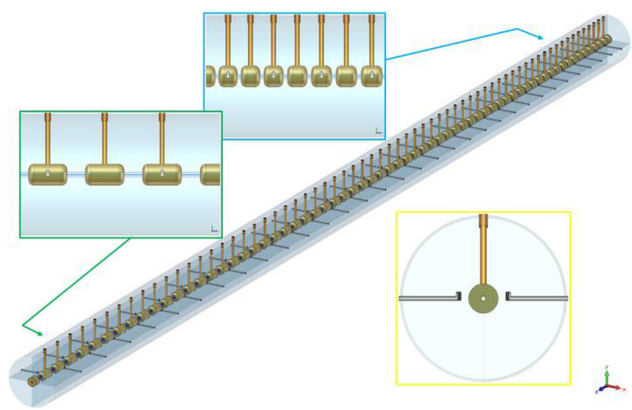

Figure 1: CST model of the LANSCE DTL tank 2. The cavity outer walls are removed for better view.

The shortest tank of the DTL, tank 1 (T1), does not have post-couplers, and its accelerating field is ramped: the average on-axis cell field E_0 increases along the tank from 1.6 to 2.3 MV/m. In T2-T4, the accelerating gradient E_0 is constant. Its flatness was tuned in the CST models by adjusting spacing between post-couplers and DTs, cf. [1, 4]. The RF fields in the tank models were calculated using primarily the MWS tetrahedral eigensolver. For accuracy, the meshes were refined locally, especially inside the DT apertures; details can be found in [4].

BEAM DYNAMICS

The MWS-calculated RF fields of the tuned operating mode in the tanks were used to study beam dynamics. The fields in the beam region were exported from MWS as text files in a format that can be imported into various multi-particle codes. We mainly use the CST Particle Studio (PS) particle-in-cell (PIC) solver. The static magnetic fields of the focusing quadrupoles, produced in Matlab as text files based on the hard-edge quad design values, were also imported into PS as external fields.

Content from this work may be used under the terms of the CC BY 3.0 licence (© 2015). Any distribution of this work must maintain attribution to the author(s), title of the work, publisher, and DOI.

ISBN: 978-3-95450-168-7 doi:10.18429/JACoW-IPAC2015-FRXB1

Content from this work may be used under the terms of the CC BY 3.0 licence (© 2015). Any distribution of this work must maintain attribution to the author(s), title of the work, publisher, and DOI.

THE DOE LONG-TERM ACCELERATOR R&D STEWARDSHIP PROGRAM*

E. Colby#, M. Zisman, DOE Office of High Energy Physics
E. Lessner, DOE Office of Basic Energy Sciences
M. Farkhondeh, DOE Office of Nuclear Physics

Abstract

Since the Accelerators for America's Future (AfAF) Symposium in 2009, the U. S. Dept. of Energy's Office of High Energy Physics (DOE-HEP) has worked to broaden its accelerator R&D activities beyond supporting only discovery science to include medicine, energy and environment, defense and security, and industry. Accelerators play a key role in many aspects of everyday life, and improving their capabilities will enhance U.S. economic competitiveness and the scientific research that drives it. Funded for the first time in 2014, the DOE Office of Science Accelerator Stewardship Program has launched initiatives to facilitate access to DOE accelerator infrastructure, develop innovative accelerator technologies that solve critical problems, and catalyze new partnerships across the accelerator user community. We will discuss the formulation and evolution of the Accelerator Stewardship program, the current status of initiatives, and plans for engagement with the accelerator and user communities for future stewardship activities.

INTRODUCTION

The mission of the DOE Long-Term Accelerator R&D Stewardship Program is to:

- Support fundamental accelerator science and technology R&D, and
- Disseminate accelerator knowledge and training.

This mission is implemented through:

- Facilitating access to national laboratory accelerator facilities and infrastructure† for industrial and U.S. government agency users and developers of accelerators and related technology,
- Developing innovative solutions to critical problems, to the benefit of both the broader user communities and the DOE discovery science community,
- Serving as a catalyst to broaden and strengthen the community that relies on accelerators and accelerator technology.

First funded in FY 2014 by redirection, the Stewardship program launched with two primary program elements: (1) a dedicated accelerator R&D user facility, and (2) a university-based R&D program. In response to (1), the Brookhaven Accelerator Test Facility ("ATF") was identified as a dedicated, central Accelerator Stewardship user facility. The initial university R&D program was created by redirecting ten university grants already awarded in the HEP General Accelerator R&D program.

The Brookhaven ATF [1] has for more than two decades supported experimental accelerator science that has led to world-first demonstrations of new high-gradient acceleration methods, SASE, HGHG, and Compton Scattering radiation generation, new beam diagnostic techniques, and more. The ATF supported 24 experiments in 2014, with a significant proportion of the experiments being funded by federal agencies other than High Energy Physics, and 25% led by industrial partners (primarily small businesses). In 2014, the Accelerator Stewardship program designated the Brookhaven ATF as a dedicated Stewardship accelerator R&D facility, broadening its mission to include accelerator technology development in addition to accelerator science. In 2015 the ATF's broad role has been recognized by the Office of Science by designating it as an Office of Science User Facility. This designation is a formalization of the merit-based approach to facility management that has been ATF's tradition, and raises the visibility of the facility to potential users.

This versatile facility provides medium energy electron beams (80 MeV) of very high quality, and high power CO_2 laser beams (up to 1 TW) together with an expert staff that supports the users. To accommodate the steadily growing demand for the ATF, an upgrade is also being funded through the Stewardship program which will result in a significantly expanded facility (~3x the space) with increased beam energy (~2x) and increased laser energy (~100x). The upgrade, dubbed "ATF-II", is planned to open for new users in 2018.

The ten redirected university grants for launching the Stewardship program were selected after discussions with the Offices of Basic Energy Sciences and Nuclear Physics to identify those with particular strategic long-term interest. The awards included fundamental R&D in beam physics, accelerator simulation codes, advanced superconductors, and cryogenics, with an emphasis on fundamental R&D that would have broad impact across multiple programs.

As a new program in the Office of Science, it is vital that the Accelerator Stewardship program demonstrate success in the near-term. As Accelerator Stewardship, by its definition, serves the needs of stakeholders other than High Energy Physics, it is essential that those stakeholders express an active interest in the R&D, and choose to make use of the results of the R&D when it is

*Work supported by U. S. Dept. of Energy
#Eric.Colby@science.doe.gov
†Limited to non-mission-critical accelerator R&D infrastructure

ISBN: 978-3-95450-168-7 doi:10.18429/JACoW-IPAC2015-FRXB3

ADVANCES IN CW ION LINACS*

P.N. Ostroumov#
ANL, Argonne, IL 60439, U.S.A.

Abstract

Substantial research and development related to continuous wave (CW) proton and ion accelerators is being performed at ANL. A 4-meter long 60.625-MHz normal conducting (NC) CW radio frequency quadrupole (RFQ) and a 4K cryomodule with seven 72.75-MHz quarter-wave resonators (QWR) and superconducting (SC) solenoids have been developed, built, commissioned and operated as an upgrade of the CW ion linac, ATLAS, to achieve higher efficiency and beam intensities [1]. Currently we are engaged in development of the first cryomodule for a CW H$^-$ linac being built at FNAL [2]. This work is well aligned with the development of a 1 GeV 25 MW linac as the driver of a sub-critical assembly for near-term spent nuclear fuel disposal.

The new CW RFQ and cryomodule were fully integrated into ATLAS and have been in routine operation for more than two years and one year, respectively. New design and fabrication techniques for QWRs resulted in the achievement of record accelerating voltages and low cryogenic losses. Since the very beginning the cryomodule provided 17.5 MV accelerating voltage or 2.5 MV per cavity. A 2K cryomodule with eight 162.5-MHz SC half wave resonators (HWR) and eight SC solenoids is being developed for FNAL and scheduled for commissioning in 2017. The testing of the first 2 HWRs demonstrated remarkable performance. Experience with the development and reliable operation of new NC and SC accelerating structures is an essential precursor for the future large scale high power CW accelerators.

INTRODUCTION

Technology required for both CW RFQ and SC RF accelerators was successfully developed for a recent ATLAS upgrade. This upgrade achieved greater efficiency and beam intensities than were previously obtained at ATLAS and in some cases a 10× improvement is observed [1]. Developments here can be applied to future high-power CW accelerators such as drivers for the production of rare isotope beams or for Accelerator Driven Systems (ADS). In this paper we present the description of major breakthroughs in technologies for CW linacs which have resulted in excellent performance in both normal conducting and SC accelerating structures. Details of our research and developments can be found in numerous conference publications and journal articles published by members of ANL's Physics Division. To save space only key publications will be referenced in this paper.

*This work was supported by the U.S. Department of Energy, Office of High Energy Physics and Nuclear Physics, under Contract DE-AC02-76CH03000, DE-AC02-06CH11357. This research used resources of ANL's ATLAS facility, which is a DOE Office of Science User Facility.
#ostroumov@anl.gov

CW ION LINACS

CW linear accelerators can be divided into two main categories: (1) low intensity ion linacs capable of accelerating the majority of ion species from hydrogen to uranium and (2) high intensity light ion linacs, primarily for acceleration of protons and/or deuterons. The linacs in the first category are not affected by the beam space charge and can deliver several hundred kilowatts of beam power; as is the case for FRIB or RAON [3,4]. There are many operational low energy (up to ~25 MeV/u) CW linacs worldwide which are being used for fundamental nuclear physics experiments. Currently, no high-power CW linac exists. Substantial research and development work has been performed in the past decade for several high-power CW linac projects worldwide [2,5-8] and the ability to accelerate several milliamp CW proton beams with SC cavities has been demonstrated in the prototype cryomodule at SARAF [9].

As we discussed in the recent review paper [10], independent of ion species, a CW hadron linac includes a room temperature RFQ accelerator. The transition energy from NC to SC structures depends upon the ion species and the beam intensity. A transition from NC to SC structures is accompanied with significant changes of two main accelerator lattice parameters: (1) the focusing period becomes longer and (2) higher accelerating gradients, E_{ACC}, are readily achievable when using SC cavities. These changes, if not mitigated, can easily lead to strong coupling of the transverse and longitudinal motions and may result in large emittance growth and beam halo formation. In heavy-ion linacs, the higher accelerating gradients available from SC cavities can be effectively used above ~300 keV/u. In high intensity proton linacs, the transition energy from normal conducting to SC structures must be pushed as high as possible not only to avoid transverse-longitudinal coupling but to supress space charge effects. Depending on the proton beam current, the transition energy can be in the range from 2 to 7 MeV/u and it is limited by the cost and complexity of CW RFQs.

CW RFQ

Starting in the 1990's, the ATLAS heavy ion linac included 48 MHz SC resonators capable of accelerating pre-bunched ions with an initial velocity of 0.008c. Due to the high velocity gain in the first 4 SC resonators, a significant distortion of both transverse and longitudinal emittance occurred and resulted in reduced beam transmission through the linac. To address this issue, we have developed and built a CW RFQ capable of accelerating any ion species from 30 keV/u to 295 keV/u. Several innovative ideas have been implemented in this CW RFQ. By selecting a multi-segment split-coaxial

Content from this work may be used under the terms of the CC BY 3.0 licence (© 2015). Any distribution of this work must maintain attribution to the author(s), title of the work, publisher, and DOI.

ISBN: 978-3-95450-168-7 doi:10.18429/JACoW-IPAC2015-FRXC1

THE LUMINOSITY UPGRADE AT RHIC*

G. Robert-Demolaize, Brookhaven National Laboratory, Upton, NY 11973, USA

Abstract

Starting with the high energy heavy ion run for Fiscal Year 07 (Run7), the Relativistic Heavy Ion Collider (RHIC) underwent a series of upgrades in all three tiers of its activities: machine hardware, lattice design and operational efficiency. The following presents a review of these upgrades and how their combined contributions to heavy ion operations lead to average store luminosities that exceed the initial RHIC design by a factor of 25.

INTRODUCTION

RHIC's main objective is to increase its ability to recreate quark-gluon plasma and study the rare processes associated with it. Run7 marked the first efforts towards the implementation of the components aimed at improving the design average store luminosity by a factor of 10. With Run14, all equipments designed for the heavy ion luminosity upgrade have been successfully commissioned with beam and used operationally. Table 1 presents an overview of the main performance parameters of all high energy heavy ion runs from Run7 to Run14, and includes the design, enhanced design and Run4 values as a reference point to the pre-upgrade machine conditions. When looking at the performances of the Au-Au runs alone, the average store luminosities have been improved by a factor of 25 from Run4, reaching a consistent $L_{avg.}$(Run14)=50.0x10^{26}cm^{-2}s^{-1} while keeping the beams for physics for twice as long. Figure 1 shows the evolution of the integrated luminosity of heavy ion runs at 100 GeV/u from Run1 to Run14 [1], where it can be seen that Run14 outperformed Run4 by over an order of magnitude.

Such a significant improvement can be attributed to the RHIC-II upgrade plans [2]. The next section will highlight the most signifcant changes and achievements in machine hardware and subsystems. New magnet settings for lattice design that allow for larger dynamic aperture and dynamic β^* squeeze for the STAR and PHENIX experiments are then presented. A review of the changes in machine operations and how the store-to-store turnaround time is pushed to maximize beam time in physics is also included.

HARDWARE AND SYSTEM UPGRADES

Injectors

The RHIC-II luminosity upgrade included plans to update the source where heavy ions are generated, from the Tandem Van de Graaf to a new Electron Beam Ion Source (EBIS) followed by an RFQ and a short linac [3]. This new, versatile source allows switching rapidly between various ion species while providing per-bunch intensities similar to the Au ion ones. EBIS was successfully commissioned in 2010 and has

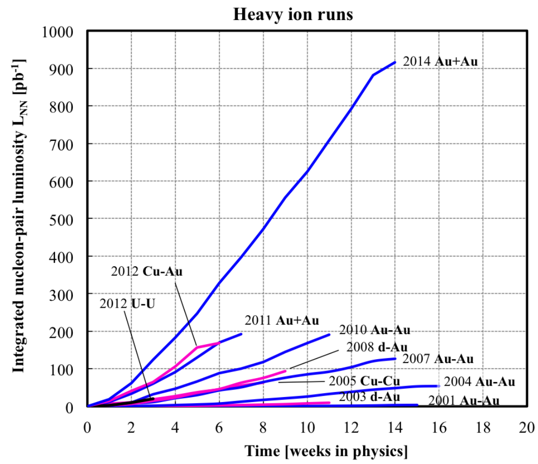

Figure 1: Integrated luminosity of the RHIC heavy ion runs at 100 GeV/nucleon as a function of the number of weeks in physics. The data is presented for the nucleon-pair luminosity $\mathcal{L}_{\text{N-N}}=N_1 N_2 \mathcal{L}$ from Run1 to Run14, where $\mathcal{L}$ is the luminosity and N_1,N_2 are the number of nucleons for the species in each beam. From [1].

since delivered beams to both RHIC and the NASA facility without slowing down operations for either programs. The ion species other than Au that have been used for RHIC physics are (to date) Cu, U and polarized ^{3}He.

Part of the limitations on the intensity of the heavy ion bunches injected into RHIC came from beam instabilities when crossing transition, due to impedance and electron clouds effects [4–6]. However starting with Run10 the intensity threshold was raised thanks to scrubbing runs with high intensity proton beams in 2009 and 2012, as evidenced by the new highs in bunch intensity reported in Table 1.

Stochastic Cooling

It is clear from the data shown in Table 1 that the main limitation to the luminosity lifetime comes from intrabeam scattering (IBS) which induces emittance blow-up during physics stores. The RHIC Stochastic Cooling (SC) system [7–9] was designed to counter this mechanism and reduce the beam emittance: for each of the three planes of motion, it uses a pickup and kicker magnet pair separated by a multiple of $\pi/2$ phase advance. The longitudinal SC system was installed for Run7, while the transverse one was implemented in stages: vertical plane only for Run10, both planes for Run11.

With a fully operational 3D SC system, the average store luminosity jumped by a factor 2.5 from Run7 to Run11 to 30.0x10^{26}cm^{-2}s^{-1} while reducing the transverse emittance in both planes by over 30%. Further upgrades were brought to all pickups and kickers prior to Run14, mainly for reliability purposes [10]. Figure 2 shows the improvement in transverse cooling efficiency from Run7 to Run14.

* Work supported by Brookhaven Science Associates, LLC under Contract No. DE-AC02-98CH10886 with the U.S. Department of Energy.

Content from this work may be used under the terms of the CC BY 3.0 licence (© 2015). Any distribution of this work must maintain attribution to the author(s), title of the work, publisher, and DOI.

ISBN: 978-3-95450-168-7 doi:10.18429/JACoW-IPAC2015-FRXC2

THE HIGH LUMINOSITY LHC PROJECT[1]

O. Brüning, CERN, Geneva, Switzerland

Abstract

This presentation reviews the status of the high luminosity LHC project, and highlights the main challenges from the technology and beam physics point of view. It will mention the outcome of the 2015 Cost and Schedule review for the HL-LHC project and summarizes the status of the high field quadrupole and crab cavity development.

HL-LHC PERFORMANCE GOALS AND SCHEDULE

The Large Hadron Collider (LHC) was successfully commissioned in 2010 for proton-proton collisions with a 7 TeV centre-of-mass energy and delivered 8 TeV centre-of-mass proton collisions from April 2012 to the end of 2012. The LHC underwent from 2013 to 2015 a general consolidation of the magnet bus bar interconnections and started the second operation phase, the LHC RunII, in 2015 with beam energies of 6.5 TeV (→ CM collision energy of 13 TeV).

The full exploitation of the LHC is the highest priority of the European Strategy for particle physics. This strategy has been adopted by the CERN Council, and is a reference point for the Particle Physics Strategy of the USA and, to a certain extent, Japan. To extend its discovery potential, the LHC will need a major upgrade in the 2020s to increase its luminosity (and thus event rate) by a factor of five beyond its design value. The integrated luminosity goal is a ten-fold increase of the nominal design value (300 fb^{-1} → 3000 fb^{-1}). The required machine modifications require new technologies and novel operation concepts. These include among others: cutting-edge 11-12 tesla superconducting magnets; very compact with ultra-precise phase control superconducting crab cavities for beam rotation; new technology for beam collimation; long high-power superconducting links with zero energy and the operation with novel optics schemes and leveled luminosity. The necessary developments require substantial prototyping and testing.

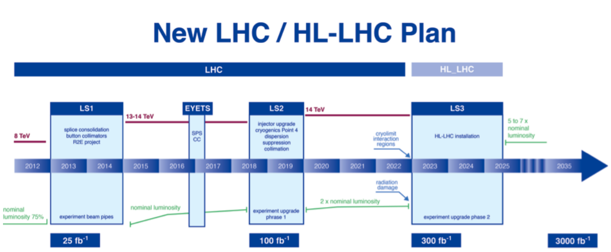

Figure 1: The LHC Baseline Program until 2025.

Figure 1 shows schematically the LHC baseline program until 2025 and Fig. 2 shows the potential evolution of the peak and integrated luminosities. After entering into the nominal energy regime of 13-14 TeV centre-of-mass energy in 2015, it is expected that the LHC will reach the design luminosity of $L = 10^{34}$ cm^{-2}s^{-1}. This peak value should give a total integrated luminosity of about 40 fb^{-1} per year. In the period from 2015 to 2022 the LHC will hopefully further increase the peak luminosity by exploiting upgrades implemented during the second long shutdown LS2. These upgrades include the Phase I upgrade of the LHC experiments and a full implementation of the LHC Injector complex Upgrade (LIU) project, opening the door to an operation beyond nominal bunch intensities and beam brightness. Margins in the design of the nominal LHC are expected to allow, in principle, about two times the nominal design performance.

After 2020 the statistical gain in running the accelerator without a significant luminosity increase beyond its design value will become marginal. The running time necessary to halve the statistical error in the measurements will be more than ten years after 2020. Therefore, to maintain scientific progress and to explore its full capability, the LHC will need to have a decisive increase of its luminosity.

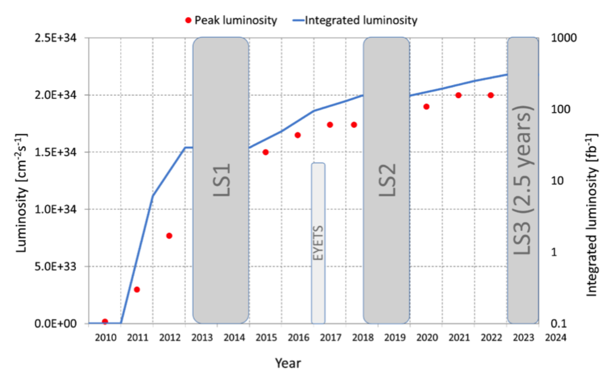

Figure 2: The projected evolution of peak and iterated luminosities over the LHC and HL-LHC project phases.

LHC LIMITATIONS AND HL-LHC CHALLENGES

The performance reach of the LHC beyond that of RunIII is limited by six fundamental limitations:

- Technical Bottle Necks
- Insertion Magnets: Lifetime and Aperture
- Crossing Angle and geometric reduction factor: Crab Cavities
- Performance optimization: Event rate and pileup density
- Beam power and particle losses
- Machine efficiency and availability

[1] Research supported by EU FP7 HiLumi LHC - Grant Agreement 284404

Content from this work may be used under the terms of the CC BY 3.0 licence (© 2015). Any distribution of this work must maintain attribution to the author(s), title of the work, publisher, and DOI.

ISBN: 978-3-95450-168-7 doi:10.18429/JACoW-IPAC2015-FRYGB1

HIGH POWER PROTON FACILITIES: OPERATIONAL EXPERIENCE, CHALLENGES, AND THE FUTURE*

S. Cousineau, ORNL, Oak Ridge, TN 37830, USA

Abstract

High power proton accelerators are increasingly popular as drivers for secondary beams with a large variety of applications, such as neutron sources for materials science and neutrino factories for high energy physics. In the last few decades, average beam powers have increased substantially, giving rise to an array of challenges centered on providing high beam power and availability while maintaining low activation levels. This talk summarizes the current status of high power proton accelerators. It discusses recent operational experiences and lessons learned, and identifies the primary hardware and beam dynamics limitations. A brief review of planned next generation facilities and driving technologies is also presented.

INTRODUCTION

Modern day high power proton facilities are employed primarily in the production of secondary and sometimes tertiary particle beams for various applications. In the past quarter of a century, the number of high power proton facilities and the range of applications have increased dramatically [1]. This has been driven in part by the desire for a new generation of high power neutron sources with various pulse structures for materials and life science applications, and in part the emerging focus in HEP on "intensity frontier" applications such as neutrino beam production.

The average beam power is a combination of both the energy and average beam current, and these parameters are optimized to suit the desired application. In general, HEP applications require higher energies in the 10^2 GeV range for production of particles such as neutrinos, while materials science applications require mid-range energies on the order of a few GeV for neutron production. In the last quarter century, beam powers for these types of facilities have increased approximately an order of magnitude, as demonstrated by Figure 1, which shows beam powers for several facilities in the era 1988-1993 compared with operational beam powers today. A number of advances in accelerator technology and accelerator physics have enabled this evolution, including H- charge exchange injection, phase space painting, superconducting linear accelerators, massively parallelized simulations, and liquid targets.

Regardless of the end application, all high power proton facilities are designed and operated with the goal of providing stable beams with minimal beam loss and activation that allow for hands-on maintenance. In addition, user facilities such as neutron sources place a high degree of emphasis on machine reliability. While reliability is most often tied to hardware performance, activation levels are tied to beam dynamics challenges. Increases in beam power have to respect the reliability and activation goals, and therefore require troubleshooting of present limitations rather than "turning the knob up" on either beam current or energy.

This paper discusses the operational experience of today's highest power proton accelerator facilities, and the challenges that limit increases in beam power. Finally, it summarizes the high power horizon with a preview of future facilities and their driving technologies.

OPERATIONAL EXPERIENCE

Operational Metrics

Table 1 shows the operational metrics for eight high power proton accelerator facilities. Sustained operation at high power relies on preventative hardware maintenance and tight control over beam losses. Most facilities shown in the table operate for 4000-4500 hours per year, which allows for one to two extended maintenance outages.

For user based facilities, reliability, as defined by the ratio of the number of hours operated divided by the number anticipated, is the highest figure of merit, trumping even the average beam power. The reliability metrics in Table 1 are averages over the last 2-3 years. As seen, the spread is small with all facilities operating between 80-92%. In practice, it is very difficult to break the 90-92% threshold, possibly because much of the accelerator hardware is R&D in nature, or operating near technological limits.

Perhaps the parameter of highest interest to accelerator physicists, because it is closely tied to beam control, is activation. The gold standard for beam loss in an accelerator is considered to be 1 Watt/meter, on average. In practical terms, activation levels should not exceed roughly 100 mrem/hr in order to allow for routine hands on maintenance of the accelerator. Table 1 shows the typical and peak activation levels for six high power machines. Note that the activation levels include facility-specific nuances in terms of measurement time and distance, and a direct comparison between values is not meaningful. However, one can draw a few general conclusions from the survey data. First, the activation in linacs is 30 to 60 times lower than in rings. Second, typical activation levels fall below the threshold for hands on maintenance. Third, peak activation levels are roughly an order of magnitude higher than typical levels. The peak activations levels occur in localized regions, usually injection or extraction, where measures can be taken to provide extra shielding and work-practice controls. Even so, peak activation levels can limit the beam power.

Content from this work may be used under the terms of the CC BY 3.0 licence (© 2015). Any distribution of this work must maintain attribution to the author(s), title of the work, publisher, and DOI.